

Konstantin K. Likharev

Essential Graduate Physics

Lecture Notes and Problems

Beta version



Essential Graduate Physics
Lecture Notes and Problems
Beta version, December 2013
with later problem additions and error corrections

© Copyright Konstantin K. Likharev

Open access to this material is provided online, at two mirror sites:

<http://commons.library.stonybrook.edu/egp/>

and

<https://sites.google.com/site/likharevegp/>

under the Creative Commons Attribution-NonCommercial-ShareAlike 4.0 International License



— see <http://creativecommons.org/licenses/by-nc-sa/4.0/>

The above copyright and license do not cover the figures adapted from published books and journal papers (with copyright holders listed in figure captions) and publicly-accessible Web sites (with URLs cited in figure captions). Using these materials beyond the “fair use”¹ boundaries requires obtaining permissions of the respective copyright holders.

¹ To the best of the author’s knowledge, the fair use clause of the U.S. copyright law (see, e.g., <http://www.copyright.gov/fls/fl102.html>) allows viewing, browsing, and/or downloading copyrighted materials for temporary, non-commercial, personal purposes, without requesting the copyright holder’s permission.

Preface

This is a series of lecture notes and problems on “Essential Graduate Physics”, consisting of the following four parts:

CM: Classical Mechanics (for a 1-semester course),

EM: Classical Electrodynamics (2 semesters),

QM: Quantum Mechanics (2 semesters), and

SM: Statistical Mechanics (1 semester).

The parts share a teaching style, structure, and (with a few exceptions) notation, and are interlinked by extensive cross-referencing. I believe that due to this unity, the notes may be used for teaching these courses not only in the (preferred) sequence shown above but in almost any order – or in parallel.

Each part is a two-component package consisting of:

- (i) *Lecture Notes* chapter texts,² with a list of exercise problems at the end of each chapter, and
- (ii) *Exercise and Test Problems with Model Solutions* files.

The series also includes this front matter, two brief reference appendices, *MA: Selected Mathematical Formulas* (16 pp.) and *CA: Selected Physics Constants* (2 pp.), and a list of references.

The series is a by-product of the so-called *core physics* courses I taught at Stony Brook University from 1991 to 2013. Reportedly, most physics departments require their graduate students to either take a set of similar courses or pass comprehensive exams based on an approximately similar body of knowledge. This is why I hope that my notes may be useful for both instructors and students of such courses, as well as for individual learners.

The motivation for composing the lecture notes (which had to be typeset because of my horrible handwriting) and their distribution to Stony Brook students was my desperation to find textbooks I could actually use for teaching. First of all, the textbooks I could find, including the most influential *Theoretical Physics* series by Landau and Lifshitz, did not match my class audiences, which included experiment-oriented students, some PhD candidates from other departments, some college graduates with substandard undergraduate background, and a few advanced undergraduates. Second, for the rigid time restrictions imposed on the core physics courses, most available textbooks are way too long, and using them would mean hopping from one topic to another, picking up a chapter here and a section there, at a high risk of losing the necessary background material and logical connections between course components – and students’ interest with them. On the other hand, many textbooks lack even brief discussions of several traditional and modern topics that I believe are necessary parts of *every* professional physicist’s education.^{3,4}

² The texts are saved as separate .pdf files of each chapter, optimized for two-page viewing and double-side printing; merged files for each part and the series as a whole, convenient for search purposes, are also provided.

³ To list just a few: statics and dynamics of elastic and fluid continua, basic notions of physical kinetics, turbulence and deterministic chaos, physics of reversible and quantum computation, energy relaxation and dephasing of open quantum systems, the van der Pol method (a.k.a. the Rotating-Wave Approximation, RWA) in classical and quantum mechanics, physics of electrons and holes in semiconductors, the weak-potential and tight-binding approximations in the energy band theory, optical fiber electrodynamics, macroscopic quantum effects in

The main goal of my courses was to make students familiar with the basic notions and ideas of physics (hence the series' title), and my main effort was to organize the material in a logical sequence the students could readily follow and enjoy, at each new step understanding why exactly they need to swallow the next knowledge pill. As a backside of such a minimalistic goal, I believe that my texts may be used by advanced undergraduate physics students as well. Moreover, I hope that selected parts of the series may be useful for graduate students of other disciplines, including astronomy, chemistry, mechanical engineering, electrical, computer and electronic engineering, and material science.

At least since Confucius and Sophocles, i.e. for the past 2,500 years, teachers have known that students can master a new concept or method only if they have seen its application to at least a few particular situations. This is why in my notes, the range of theoretical physics methods is limited to the approaches that are indeed necessary for the solution of the problems I had time to discuss, and the introduction of every new technique is always accompanied by an application example or two. Additional exercise problems are listed at the end of each chapter of the lecture notes; they may be used for homework assignments. Individual readers are strongly encouraged to solve as many of these problems as possible.⁵

Detailed model solutions of the exercise problems (some with additional expansion of the lecture material), and several shorter problems suitable for tests (also with model solutions), are gathered in six separate files – one per semester. These files are available for both university instructors and individual readers – free of charge, but in return for a signed commitment to avoid unlimited distribution of the solutions – see p. vii below. For instructors, these files are available not only in the Adobe Systems' Portable Document Format (*.pdf) but also in the Microsoft Office 1997-2003 format (*.doc) free of macros, so that the problem assignments and solutions may be readily grouped, edited, etc., before their distribution to students, using either virtually any version of Microsoft Word or independent software tools – e.g., the public-domain OpenOffice.org.

I know that my texts are far from perfection. In particular, some sacrifices made at the topic selection, always very subjective, were extremely painful. (Most regrettably, I could not find time for even a brief introduction to general relativity.⁶) Moreover, it is almost certain that despite all my effort and the great help from SBU students and teaching assistants, not all typos/errors have been weeded out. This is why all remarks (however candid) and suggestions by the readers would be highly appreciated; they may be sent to klikharev@gmail.com. All significant contributions will be gratefully acknowledged in future editions of the series.

Bose-Einstein condensates, Bloch oscillations and Landau-Zener tunneling, cavity QED, and the Density Functional Theory (DFT). All these topics are discussed, if only concisely, in these notes.

⁴ Recently, several high-quality graduate-level teaching materials became available online, including M. Fowler's *Graduate Quantum Mechanics Lectures* (<http://galileo.phys.virginia.edu/classes/751.mf1i.fall02/home.html>), R. Fitzpatrick's text on *Classical Electromagnetism* (farside.ph.utexas.edu/teaching/jk1/Electromagnetism.pdf), B. Simons' lecture notes on *Advanced Quantum Mechanics* (www.tcm.phy.cam.ac.uk/~bds10/aqp.html), and D. Tong's lecture notes on several topics (www.damtp.cam.ac.uk/user/tong/teaching.html).

⁵ The problems that require either longer calculations or more creative approaches (or both) are marked by asterisks.

⁶ For an introduction to that subject, I can recommend either its review by S. Carroll, *Spacetime and Geometry*, Addison-Wesley, 2003, or a longer text by A. Zee, *Einstein Gravity in a Nutshell*, Princeton U. Press, 2013.

Disclaimer

Since these materials are available free of charge, it is hard to imagine somebody blaming their author for deceiving “customers” for his commercial gain. Still, I would like to go a little bit beyond the usual litigation-avoiding claims,⁷ and offer a word of caution to potential readers, to preempt their possible later disappointment.

This is NOT a course of theoretical physics – at least in the contemporary sense of the term

Though much of the included material is similar to that in textbooks on “theoretical physics” (most notably in the famous series by L. Landau and E. Lifshitz), this lecture note series is different from them by its focus on the basic concepts and ideas of physics, their relation to experimental data, and most important applications – rather than on sophisticated theoretical techniques. Indeed, the set of theoretical methods discussed in the notes is limited to the minimum necessary for quantitative understanding of the key notions of physics and for solving a few (or rather about a thousand :-) core problems. Moreover, because of the notes’ shortness, I have not been able to cover some key fields of theoretical physics, most notably the general relativity and the quantum field theory – beyond some introductory elements of quantum electrodynamics in QM Chapter 9. If you want to work in modern theoretical physics, you need to know much more than what this series teaches!

Moreover, this is NOT a textbook – at least not the usual one

A usual textbook tries (though most commonly fails) to cover virtually all aspects of the addressed field. As a result, it is typically way too long for being fully read and understood by students during the time allocated for the corresponding course, so that the instructors are forced to pick up selected chapters and sections, frequently losing the narrative’s logic lines. In contrast, these notes are much shorter (about 200 pages per semester), enabling their thorough reading – perhaps with just a few later sections dropped, depending on the reader’s interests. I have tried to mitigate the losses due to this minimalistic approach by providing extensive further reading recommendations on the topics I had no time to cover. The reader is highly encouraged to use these sources (and/or the corresponding chapters of more detailed textbooks) on any topics of their special interest.

Then, what these notes ARE and why you may like to use them – I think

By tradition, graduate physics education consists of two main components: research experience and advanced physics courses. Unfortunately, the latter component is currently under pressure in many physics departments, apparently because of two reasons. On one hand, the average knowledge level of the students entering graduate school is not improving, so that bringing them up to the level of contemporary research becomes increasingly difficult. On the other hand, the research itself is becoming more fragmented, so that the students frequently do not feel an immediate need for a broad physics

⁷ Yes Virginia, these notes represent only my personal opinions, not necessarily those of the Department of Physics and Astronomy of Stony Brook University, the SBU at large, the SUNY system as a whole, the Empire State of New York, the federal agencies and private companies that funded my group’s research, etc. No dear, I cannot be held responsible for any harm, either bodily or mental, their reading may (?) cause.

knowledge base for their PhD project success. Some thesis advisors, trying to maximize the time they could use their students as a cheap laboratory workforce, do not help.

I believe that this trend toward the reduction of broad physics education in graduate school is irresponsible. Experience shows that during their future research career, a typical current student will change their research fields several times. Starting from scratch in a new field is hard – terribly hard in advanced age (believe me :-). However, physics is fortunate to have a stable *hard core* of knowledge, which many other sciences lack. With this knowledge, students will always feel in physics at home, while without it, they may not be able even to understand research literature in the new field, and would risk being reduced to auxiliary work roles – if any at all.

I have seen the main objective of my Stony Brook courses to give an introduction to this core of physics, at the same time trying to convey my own enchantment by the unparalleled beauty of the concepts and ideas of this science, and the remarkable logic of their fusion into a wonderful single construct. Let me hope that these notes relay not only the knowledge as such but also at least a part of this enchantment.

Acknowledgments

I am extremely grateful to my faculty colleagues and other readers who commented on certain sections of the notes; here is their list (in the alphabetic order):⁸

A. Abanov, P. Allen, D. Averin, S. Berkovich, P.-T. de Boer, M. Fernandez-Serra,
R. F. Hernandez, P. Johnson, T. Konstantinova, A. Korotkov, V. Semenov, F. Sheldon, E. Tikhonov,
O. Tikhonova, X. Wang.

(Evidently, these kind people are not responsible for the remaining deficiencies.)

The Department of Physics and Astronomy of Stony Brook University was very responsive to my kind requests of certain time ordering of my teaching assignments, that was beneficial for note writing and editing. The department, and the university as a whole, also provided a very friendly general environment for my work there for almost three decades.

A large part of my scientific background and experience, reflected in these materials, came from my education (and then research work) in the Department of Physics of Moscow State University.

And last but not least, I would like to thank my wife Lioudmila for several good bits of advice on aesthetic aspects of note typesetting, and more importantly for all her love, care, and patience – without them, this writing project would be impossible.

Konstantin K. Likharev
<https://you.stonybrook.edu/likharev/>

⁸ I am very much sorry that I have not kept proper records from the beginning of my lectures at Stony Brook, so I cannot list all the numerous students and TAs who had kindly attracted my attention to typos in earlier versions of these notes. Needless to say, I am very grateful to them all as well.

Problem Solution Request Templates

Requests should be sent to either klikharev@gmail.com or konstantin.likharev@stonybrook.edu in either of the following forms:

- an email from a valid university address,
- a scanned copy of a signed letter – as an email attachment.

Approximate contents:

A. Request from a Prospective Instructor

Dear Dr. Likharev,

I plan to use your lecture notes and problems of the *Essential Graduate Physics* series, part(s) <select: CM, EM, QM, SM>, in my course <title> during <semester, year> in the <department, university>. I would appreciate sending me the file(s) *Exercise and Test Problems with Model Solutions* of that part(s) of the series in the <select: .pdf, both .doc and .pdf> format(s).

I will avoid unlimited distribution of the solutions, in particular their posting on externally searchable websites. If I distribute the solutions among my students, I will ask them to adhere to the same restraint.

I will let you know of any significant typos/deficiencies I may find.

Sincerely, <signature, full name, university position, work phone number>

B. Request from an Individual Learner

Dear Dr. Likharev,

I plan to use your lecture notes and problems of the *Essential Graduate Physics* series, part(s) <select: CM, EM, QM, SM>, for my personal education. I would appreciate sending me the file(s) *Exercise and Test Problems with Model Solutions* of that part(s) of the series.

I will not share the material with anyone, and will not use it for passing courses that are officially based on your series.

I will let you know of any significant typos/deficiencies I may find.

Sincerely, <signature, full name, present home address (in English), acting phone number>

Notation

Abbreviations

Eq. any formula (e.g., equality)

Fig. figure

Sec. section

c.c. complex conjugate

h. c. Hermitian conjugate

Fonts

F, \mathcal{F} scalar variables⁹

\mathbf{F}, \mathcal{F} vector variables

$\hat{F}, \hat{\mathcal{F}}$ scalar operators

$\hat{\mathbf{F}}, \hat{\mathcal{F}}$ vector operators

\mathbf{F} matrix

$F_{jj'}$ matrix element

Symbols

\cdot time differentiation operator (d/dt)

∇ spatial differentiation vector (*del*)

\approx approximately equal to

\sim of the same order as

\propto proportional to

\equiv equal to by definition (or evidently)

\cdot scalar (“dot-”) product

\times vector (“cross-”) product¹⁰

$\bar{}$ time averaging

$\langle \rangle$ statistical averaging

$[,]$ commutator

$\{ , \}$ anticommutator

\mathbf{n} unit vector

Parts of the series

CM: Classical Mechanics

EM: Classical Electrodynamics

QM: Quantum Mechanics

SM: Statistical Mechanics

Appendices

MA: Selected Mathematical Formulas

CA: Selected Physical Constants

Prime signs

The prime signs ('', etc) are used to distinguish similar variables or indices (such as j and j' in the matrix element above), rather than to denote derivatives.

Formulas

The most general and/or important formulas are highlighted with blue frames and short titles on the margins.

Numbering

Chapter numbers are dropped in all references to formulas, figures, footnotes, and problems within the same chapter.

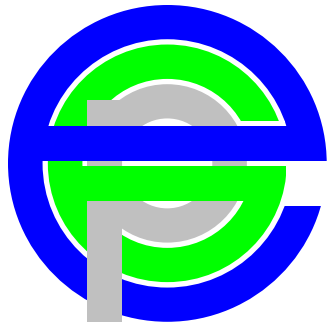
⁹ The same letter, typeset in different fonts, typically denotes different variables.

¹⁰ On a few occasions, the cross sign is used to emphasize the usual multiplication of scalars.

General Table of Contents

	<i>Pages</i>	<i>Exercise Problems</i>
CM: Classical Mechanics		
Table of Contents	4	—
Chapter 1. Review of Fundamentals	14	14
Chapter 2. Lagrangian Analytical Mechanics	14	11
Chapter 3. A Few Simple Problems	22	26
Chapter 4. Rigid Body Motion	32	36
Chapter 5. Oscillations	38	22
Chapter 6. From Oscillations to Waves	30	26
Chapter 7. Deformations and Elasticity	38	23
Chapter 8. Fluid Mechanics	30	25
Chapter 9. Deterministic Chaos	14	5
Chapter 10. A Bit More of Analytical Mechanics	16	10
CM TOTAL: 252		198
<i>Additional file</i> (available upon request):		
Exercise and Test Problems with Model Solutions	<i>Pages</i> 340	<i>Problems</i> $198 + 48 = 246$
EM: Classical Electrodynamics		
Table of Contents	4	—
Chapter 1. Electric Charge Interaction	20	19
Chapter 2. Charges and Conductors	68	47
Chapter 3. Dipoles and Dielectrics	28	30
Chapter 4. DC Currents	16	15
Chapter 5. Magnetism	42	29
Chapter 6. Electromagnetism	38	30
Chapter 7. Electromagnetic Wave Propagation	68	39
Chapter 8. Radiation, Scattering, Interference, and Diffraction	38	28
Chapter 9. Special Relativity	56	42
Chapter 10. Radiation by Relativistic Charges	40	15
EM TOTAL: 418		295
<i>Additional file</i> (available upon request):		
Exercise and Test Problems with Model Solutions	<i>Pages</i> 464	<i>Problems</i> $295 + 54 = 349$

	<i>Pages</i>	<i>Exercise Problems</i>
QM: Quantum Mechanics		
Table of Contents	4	—
Chapter 1. Introduction	28	15
Chapter 2. 1D Wave Mechanics	76	43
Chapter 3. Higher Dimensionality Effects	64	40
Chapter 4. Bra-ket Formalism	52	34
Chapter 5. Some Exactly Solvable Problems	48	48
Chapter 6. Perturbative Approaches	36	31
Chapter 7. Open Quantum Systems	50	14
Chapter 8. Multiparticle Systems	52	31
Chapter 9. Introduction to Relativistic Quantum Mechanics	36	21
Chapter 10. Making Sense of Quantum Mechanics	16	—
QM TOTAL:	462	277
<i>Additional file</i> (available upon request):		
Exercise and Test Problems with Model Solutions	<i>Pages</i> 518	<i>Problems</i> $277 + 70 = 347$
SM: Statistical Mechanics		
Table of Contents	4	—
Chapter 1. Review of Thermodynamics	24	16
Chapter 2. Principles of Physical Statistics	44	32
Chapter 3. Ideal and Not-So-Ideal Gases	34	29
Chapter 4. Phase Transitions	36	18
Chapter 5. Fluctuations	44	21
Chapter 6. Elements of Kinetics	38	15
SM TOTAL:	224	131
<i>Additional file</i> (available upon request):		
Exercise and Test Problems with Model Solutions	<i>Pages</i> 232	<i>Problems</i> $131 + 23 = 154$
Appendices		
MA: Selected Mathematical Formulas	16	
CA: Selected Physical Constants	2	
References		
A partial list of books used at work on the series	<i>Pages</i> 2	



Konstantin K. Likharev
Essential Graduate Physics
Lecture Notes and Problems

Beta version

Open online access at
<http://commons.library.stonybrook.edu/egp/>
and
<https://sites.google.com/site/likharevegp/>

Part CM: Classical Mechanics

Last corrections: August 22, 2022

A version of this material was published in 2017 under the title
Classical Mechanics: Lecture notes
IOPP, Essential Advanced Physics – Volume 1, ISBN 978-0-7503-1398-8,
with model solutions of the exercise problems published in 2018 under the title
Classical Mechanics: Problems with solutions
IOPP, Essential Advanced Physics – Volume 2, ISBN 978-0-7503-1401-5

However, by now this online version of the lecture notes, as well as the problem solutions available from the author by request, have been much better corrected

About the author:
<https://you.stonybrook.edu/likharev/>

Table of Contents

Chapter 1. Review of Fundamentals (14 pp.)

- 1.0. Terminology: Mechanics and dynamics
- 1.1. Kinematics: Basic notions
- 1.2. Dynamics: Newton laws
- 1.3. Conservation laws
- 1.4. Potential energy and equilibrium
- 1.5. OK, can we go home now?
- 1.6. Self-test problems (14)

Chapter 2. Lagrangian Analytical Mechanics (14 pp.)

- 2.1. Lagrange equation
- 2.2. Three simple examples
- 2.3. Hamiltonian function and energy
- 2.4. Other conservation laws
- 2.5. Exercise problems (11)

Chapter 3. A Few Simple Problems (22 pp.)

- 3.1. One-dimensional and 1D-reducible systems
- 3.2. Equilibrium and stability
- 3.3. Hamiltonian 1D systems
- 3.4. Planetary problems
- 3.5. Elastic scattering
- 3.6. Exercise problems (26)

Chapter 4. Rigid Body Motion (32 pp.)

- 4.1. Translation and rotation
- 4.2. Inertia tensor
- 4.3. Fixed-axis rotation
- 4.4. Free rotation
- 4.5. Torque-induced precession
- 4.6. Non-inertial reference frames
- 4.7. Exercise problems (36)

Chapter 5. Oscillations (38 pp.)

- 5.1. Free and forced oscillations
- 5.2. Weakly nonlinear oscillations
- 5.3. Reduced equations
- 5.4. Self-oscillations and phase locking
- 5.5. Parametric excitation
- 5.6. Fixed point classification
- 5.7. Numerical approaches
- 5.8. Higher-harmonic and subharmonic oscillations
- 5.9. Relaxation oscillations
- 5.10. Exercise problems (22)

Chapter 6. From Oscillations to Waves (30 pp.)

- 6.1. Two coupled oscillators
- 6.2. N coupled oscillators
- 6.3. 1D waves
- 6.4. Acoustic waves
- 6.5. Standing waves
- 6.6. Wave decay and attenuation
- 6.7. Nonlinear and parametric effects
- 6.8. Exercise problems (26)

Chapter 7. Deformations and Elasticity (38 pp.)

- 7.1. Strain
- 7.2. Stress
- 7.3. Hooke's law
- 7.4. Equilibrium
- 7.5. Rod bending
- 7.6. Rod torsion
- 7.7. 3D acoustic waves
- 7.8. Elastic waves in thin rods
- 7.9. Exercise problems (23)

Chapter 8. Fluid Mechanics (30 pp.)

- 8.1. Hydrostatics
- 8.2. Surface tension effects
- 8.3. Kinematics
- 8.4. Dynamics: Ideal fluids
- 8.5. Dynamics: Viscous fluids
- 8.6. Turbulence
- 8.7. Exercise problems (25)

Chapter 9. Deterministic Chaos (14 pp.)

- 9.1. Chaos in maps
- 9.2. Chaos in dynamic systems
- 9.3. Chaos in Hamiltonian systems
- 9.4. Chaos and turbulence
- 9.5. Exercise problems (5)

Chapter 10. A Bit More of Analytical Mechanics (16 pp.)

- 10.1. Hamilton equations
- 10.2. Adiabatic invariance
- 10.3. The Hamilton principle
- 10.4. The Hamilton-Jacobi equation
- 10.5. Exercise problems (10)

* * *

Additional file (available from the author upon request):

Exercise and Test Problems with Model Solutions (198 + 48 = 246 problems; 340 pp.)

This page is
intentionally left
blank

Chapter 1. Review of Fundamentals

After a brief discussion of the title and contents of the course, this introductory chapter reviews the basic notions and facts of the non-relativistic classical mechanics, that are supposed to be known to the reader from their undergraduate studies.¹ Due to this reason, the discussion is very short.

1.0. Terminology: Mechanics and dynamics

A more fair title for this course would be *Classical Mechanics and Dynamics*, because the notions of mechanics and dynamics, though much intertwined, are still somewhat different. The term *mechanics*, in its narrow sense, means the derivation of equations of motion of point-like particles and their systems (including solids and fluids), solution of these equations, and interpretation of the results. *Dynamics* is a more ambiguous term; it may mean, in particular:

- (i) the part of physics that deals with motion (in contrast to *statics*);
- (ii) the part of physics that deals with reasons for motion (in contrast to *kinematics*);
- (iii) the part of mechanics that focuses on its two last tasks, i.e. the solution of the equations of motion and discussion of the results.²

Because of this ambiguity, after some hesitation, I have opted to use the traditional name *Classical Mechanics*, with the word *Mechanics* in its broad sense that includes (similarly to *Quantum Mechanics* and *Statistical Mechanics*) studies of dynamics of some non-mechanical systems as well.

1.1. Kinematics: Basic notions

The basic notions of kinematics may be defined in various ways, and some mathematicians pay much attention to alternative systems of axioms and the relations between them. In physics, we typically stick to less rigorous ways (in order to proceed faster to solving particular problems) and end debating any definition as soon as “everybody in the room” agrees that we are all speaking about the same thing – at least in the context they are being discussed. Let me hope that the following notions used in classical mechanics do satisfy this criterion in our “room”:

¹ The reader is advised to perform (perhaps after reading this chapter as a reminder) a self-check by solving a few problems of those listed in Sec. 1.6. If the results are not satisfactory, it may make sense to start with some remedial reading. For that, I could recommend, e.g., J. Marion and S. Thornton, *Classical Dynamics of Particles and Systems*, 5th ed., Saunders, 2003; and D. Morin, *Introduction to Classical Mechanics*, Cambridge U., 2008.

² The reader may have noticed that the last definition of dynamics is suspiciously close to the part of mathematics devoted to differential equation analysis; what is the difference? An important bit of philosophy: physics may be defined as an art (and a bit of science :-) of describing Mother Nature by mathematical means; hence in many cases the approaches of a mathematician and a physicist to a problem are very similar. The main difference between them is that physicists try to express the results of their analyses in terms of the properties of the *systems* under study, rather than the *functions* describing them, and as a result develop a sort of intuition (“gut feeling”) about how other similar systems may behave, even if their exact equations of motion are somewhat different – or not known at all. The intuition so developed has an enormous heuristic power, and most discoveries in physics have been made through gut-feeling-based insights rather than by plugging one formula into another one.

(i) All the *Euclidean geometry* notions, including the *point*, the *straight line*, the *plane*, etc.³

(ii) *Reference frames*: platforms for observation and mathematical description of physical phenomena. A reference frame includes a *coordinate system* used for measuring the point's position (namely, its *radius vector* \mathbf{r} that connects the coordinate origin to the point – see Fig. 1) and a clock that measures *time* t . A coordinate system may be understood as a certain method of expressing the radius vector \mathbf{r} of a point as a set of its *scalar coordinates*. The most important of such systems (but by no means the only one) are the *Cartesian* (orthogonal, linear) *coordinates*⁴ r_j of a point, in which its radius vector may be represented as the following sum:

$$\mathbf{r} = \sum_{j=1}^3 \mathbf{n}_j r_j , \quad (1.1) \quad \text{Cartesian coordinates}$$

where \mathbf{n}_1 , \mathbf{n}_2 , and \mathbf{n}_3 are unit vectors directed along the coordinate axis – see Fig. 1.⁵

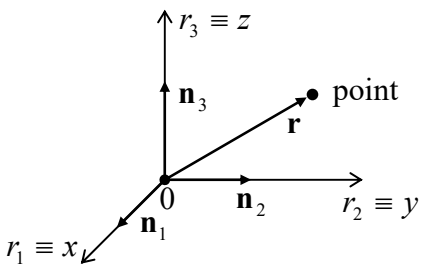


Fig. 1.1. Cartesian coordinates of a point.

(iii) The *absolute* (“Newtonian”) *space/time*,⁶ which does not depend on the matter distribution. The space is assumed to have the *Euclidean metric*, which may be expressed as the following relation between the length r of any radius vector \mathbf{r} and its Cartesian coordinates:

$$r^2 \equiv |\mathbf{r}|^2 = \sum_{j=1}^3 r_j^2 , \quad (1.2) \quad \text{Euclidean metric}$$

while time t is assumed to run similarly in all reference frames. These assumptions are critically revised in the relativity theory (which, in this series, is discussed only starting from EM Chapter 9.)

³ All these notions are of course abstractions: *simplified models* of the real objects existing in Nature. But please always remember that *any* quantitative statement made in physics (e.g., a formula) may be strictly valid only for an approximate model of a physical system. (The reader should not be disheartened too much by this fact: experiments show that many models make extremely precise predictions of the behavior of the real systems.)

⁴ In this series, the Cartesian coordinates (introduced in 1637 by René Descartes, a.k.a. Cartesius) are denoted either as either $\{r_1, r_2, r_3\}$ or $\{x, y, z\}$, depending on convenience in each particular case. Note that axis numbering is important for operations like the vector (“cross”) product; the “correct” (meaning generally accepted) numbering order is such that the rotation $\mathbf{n}_1 \rightarrow \mathbf{n}_2 \rightarrow \mathbf{n}_3 \rightarrow \mathbf{n}_1 \dots$ looks counterclockwise if watched from a point with all $r_j > 0$ – like the one shown in Fig. 1.

⁵ Note that the representation (1) is also possible for locally-orthogonal but *curvilinear* (for example, polar/cylindrical and spherical) coordinates, which will be extensively used in this series. However, such coordinates are not Cartesian, and for them some of the relations given below are invalid – see, e.g., MA Sec. 10.

⁶ These notions were formally introduced by Sir Isaac Newton in his main work, the three-volume *Philosophiae Naturalis Principia Mathematica* published in 1686-1687, but are rooted in earlier ideas by Galileo Galilei, published in 1632.

(iv) The (instant) *velocity* of the point,

Velocity

$$\mathbf{v}(t) \equiv \frac{d\mathbf{r}}{dt} \equiv \dot{\mathbf{r}}, \quad (1.3)$$

and its *acceleration*:

Acceleration

$$\mathbf{a}(t) \equiv \frac{d\mathbf{v}}{dt} \equiv \ddot{\mathbf{v}} = \ddot{\mathbf{r}}. \quad (1.4)$$

(v) *Transfer between reference frames.* The above definitions of vectors \mathbf{r} , \mathbf{v} , and \mathbf{a} depend on the chosen reference frame (are “reference-frame-specific”), and we frequently need to relate those vectors as observed in different frames. Within Euclidean geometry, the relation between the radius vectors in two frames with the corresponding axes parallel at the moment of interest (Fig. 2), is very simple:

Radius vector's transformation

$$\mathbf{r}|_{\text{in } 0'} = \mathbf{r}|_{\text{in } 0} + \mathbf{r}_0|_{\text{in } 0'}. \quad (1.5)$$

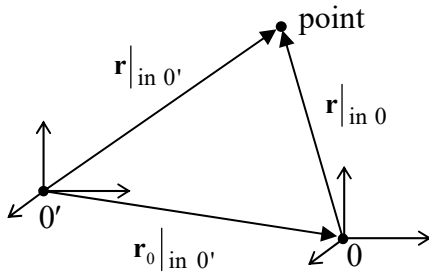


Fig. 1.2. Transfer between two reference frames.

If the frames move versus each other by *translation* only (no mutual rotation!), similar relations are valid for the velocities and accelerations as well:

$$\mathbf{v}|_{\text{in } 0'} = \mathbf{v}|_{\text{in } 0} + \mathbf{v}_0|_{\text{in } 0'}, \quad (1.6)$$

$$\mathbf{a}|_{\text{in } 0'} = \mathbf{a}|_{\text{in } 0} + \mathbf{a}_0|_{\text{in } 0'}. \quad (1.7)$$

Note that in the case of mutual rotation of the reference frames, the transfer laws for velocities and accelerations are more complex than those given by Eqs. (6) and (7). Indeed, in this case, the notions like $\mathbf{v}_0|_{\text{in } 0'}$ are not well defined: different points of an imaginary rigid body connected to frame 0 may have different velocities when observed in frame 0'. It will be more natural for me to discuss these more general relations at the end of Chapter 4 devoted to rigid body motion.

(vi) A *particle* (or “point particle”): a localized physical object whose size is negligible, and the shape is irrelevant *to the given problem*. Note that the last qualification is extremely important. For example, the size and shape of a spaceship are not too important for the discussion of its orbital motion but are paramount when its landing procedures are being developed. Since classical mechanics neglects the quantum mechanical uncertainties,⁷ in it, the position of a particle at any particular instant t , may be identified with a single geometrical point, i.e. with a single radius vector $\mathbf{r}(t)$. The formal final goal of classical mechanics is finding the *laws of motion* $\mathbf{r}(t)$ of all particles participating in the given problem.

⁷ This approximation is legitimate when the product of the coordinate and momentum scales of the particle motion is much larger than Planck’s constant $\hbar \sim 10^{-34}$ J·s. More detailed conditions of the classical mechanics’ applicability depend on a particular system – see, e.g., the QM part of this series.

1.2. Dynamics: Newton's laws

Generally, the classical dynamics is fully described (in addition to the kinematic relations discussed above) by three *Newton's laws*. In contrast to the impression some textbooks on theoretical physics try to create, these laws are experimental in nature, and cannot be derived from *purely* theoretical arguments.

I am confident that the reader of these notes is already familiar with Newton's laws,⁸ in one or another formulation. Let me note only that in some formulations, the *1st Newton's law* looks just a particular case of the *2nd law* – when the net force acting on a particle equals zero. To avoid this duplication, the *1st law* may be formulated as the following postulate:

There exists at least one reference frame, called *inertial*, in which any *free particle* (i.e. a particle fully isolated from the rest of the Universe) moves with $\mathbf{v} = \text{const}$, i.e. with $\mathbf{a} = 0$.

1st Newton law

Note that according to Eq. (7), this postulate immediately means that there is also an infinite number of inertial reference frames – because all frames $0'$ moving without rotation or acceleration relative to the postulated inertial frame 0 (i.e. having $\mathbf{a}_0|_{\text{in } 0'} = 0$) are also inertial.

On the other hand, the *2nd* and *3rd* Newton's laws may be postulated *together* in the following elegant way. Each particle, say number k , may be characterized by a scalar constant (called *mass* m_k), such that at any interaction of N particles (isolated from the rest of the Universe), in any inertial system,

$$\mathbf{P} \equiv \sum_{k=1}^N \mathbf{p}_k \equiv \sum_{k=1}^N m_k \mathbf{v}_k = \text{const.} \quad (1.8)$$

Total momentum and its conservation

(Each component of this sum,

$$\mathbf{p}_k \equiv m_k \mathbf{v}_k, \quad (1.9)$$

Particle's momentum

is called the *mechanical momentum*⁹ of the corresponding particle, while the sum \mathbf{P} , the *total momentum* of the system.)

Let us apply this postulate to just two interacting particles. Differentiating Eq. (8) written for this case, over time, we get

$$\dot{\mathbf{p}}_1 = -\dot{\mathbf{p}}_2. \quad (1.10)$$

Let us give the derivative $\dot{\mathbf{p}}_1$ (which is a vector) the name of the *force* \mathbf{F} exerted on particle 1. In our current case, when the only possible source of the force is particle 2, it may be denoted as \mathbf{F}_{12} : $\dot{\mathbf{p}}_1 \equiv \mathbf{F}_{12}$. Similarly, $\mathbf{F}_{21} \equiv \dot{\mathbf{p}}_2$, so that Eq. (10) becomes the *3rd Newton's law*

$$\mathbf{F}_{12} = -\mathbf{F}_{21}. \quad (1.11)$$

3rd Newton law

Plugging Eq. (1.9) into these force definitions, and differentiating the products $m_k \mathbf{v}_k$, taking into account that particle masses are constants,¹⁰ we get that for the k and k' taking any of values 1, 2,

⁸ Due to the genius of Sir Isaac, these laws were formulated in the same *Principia* (1687), well ahead of the physics of his time.

⁹ The more extended term *linear momentum* is typically used only in cases when there is a chance of confusion with the *angular momentum* of the same particle/system – see below. The present-day definition of the linear momentum and the term itself belong to John Wallis (1670), but the concept may be traced back to more vague notions of several previous scientists – all the way back to at least a 570 AD work by John Philoponus.

$$m_k \dot{\mathbf{v}}_k \equiv m_k \mathbf{a}_k = \mathbf{F}_{kk'}, \quad \text{where } k' \neq k.. \quad (1.12)$$

Now, returning to the general case of several interacting particles, and making an additional (but very natural) assumption that all partial forces $\mathbf{F}_{kk'}$ acting on particle k add up as vectors, we may generalize Eq. (12) into the *2nd Newton's law*

2nd Newton
law

$$m_k \mathbf{a}_k \equiv \dot{\mathbf{p}}_k = \sum_{k' \neq k} \mathbf{F}_{kk'} \equiv \mathbf{F}_k, \quad (1.13)$$

that allows a clear interpretation of the mass as a measure of a particle's *inertia*.

As a matter of principle, if the dependence of all pair forces $\mathbf{F}_{kk'}$ of particle positions (and generally of time as well) is known, Eq. (13) augmented with the kinematic relations (2) and (3) allows calculation of the laws of motion $\mathbf{r}_k(t)$ of all particles of the system. For example, for one particle the 2nd law (13) gives an ordinary differential equation of the second order:

$$m \ddot{\mathbf{r}} = \mathbf{F}(\mathbf{r}, t), \quad (1.14)$$

which may be integrated – either analytically or numerically.

In certain cases, this is very simple. As an elementary example, for local motions with $\Delta r \ll r$, Newton's gravity force¹¹

Newton's
gravity law

$$\mathbf{F} = -G \frac{mm'}{R^3} \mathbf{R} \quad (1.15)$$

(where $\mathbf{R} \equiv \mathbf{r} - \mathbf{r}'$ is the distance between particles of masses m and m')¹² may be approximated as

Uniform
gravity field

$$\mathbf{F} = m\mathbf{g}, \quad (1.16)$$

with the vector $\mathbf{g} \equiv -(Gm'/R^3)\mathbf{R}$ being constant.¹³ As a result, m in Eq. (13) cancels, it is reduced to just $\ddot{\mathbf{r}} = \mathbf{g} = \text{const}$, and may be easily integrated twice:

$$\dot{\mathbf{r}}(t) \equiv \mathbf{v}(t) = \int_0^t \mathbf{g} dt' + \mathbf{v}(0) = \mathbf{g}t + \mathbf{v}(0), \quad \mathbf{r}(t) = \int_0^t \mathbf{v}(t') dt' + \mathbf{r}(0) = \mathbf{g} \frac{t^2}{2} + \mathbf{v}(0)t + \mathbf{r}(0), \quad (1.17)$$

thus giving the generic solution to all those undergraduate problems on the projectile motion, which should be so familiar to the reader.

¹⁰ Note that this may not be true for composite bodies of varying total mass M (e.g., rockets emitting jets, see Problem 11), in these cases the momentum's derivative may differ from $M\mathbf{a}$.

¹¹ Introduced in the same famous *Principia*!

¹² The fact that the masses participating in Eqs. (14) and (16) are equal, the so-called *weak equivalence principle*, is actually highly nontrivial, but has been repeatedly verified experimentally with gradually improved relative accuracy, currently reaching $\sim 10^{-14}$ – see P. Touboul *et al.*, *Phys. Rev. Lett.* **119**, 231101 (2017).

¹³ Of course, the most important particular case of Eq. (16) is the gravity field near the Earth's surface. In this case, using the fact that Eq. (15) remains valid for the gravity field created by a spherically-uniform sphere, we get $\mathbf{g} = GM_E/R_E^2$, where M_E and R_E are the Earth's mass and radius. Plugging in their values, $M_E \approx 5.97 \times 10^{24}$ kg and $R_E \approx 6.37 \times 10^6$ m, we get $\mathbf{g} \approx 9.82$ m/s². The experimental value of \mathbf{g} varies from 9.78 to 9.83 m/s² at various locations on the surface (due to the deviations of Earth's shape from a sphere, and the location-dependent effect of the centrifugal "inertial force" – see Sec. 4.5 below), with an average value of approximately 9.807 m/s².

All this looks (and indeed is) very simple, but in most other cases, Eq. (13) leads to more complex calculations. As an example, let us think about how we would use it to solve another simple problem: a bead of mass m sliding, without friction, along a round ring of radius R in a gravity field obeying Eq. (16) – see Fig. 3. (This system is equivalent to the usual *point pendulum*, i.e. a point mass suspended from point 0 on a light rod or string, and constrained to move in one vertical plane.)

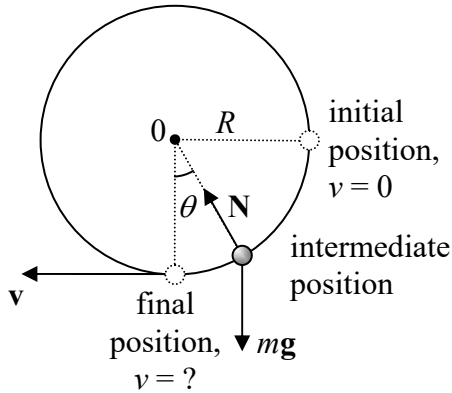


Fig. 1.3. A bead sliding along a vertical ring.

Suppose we are only interested in the bead's velocity v at the lowest point, after it has been dropped from the rest at the rightmost position. If we want to solve this problem using only the Newton laws, we have to make the following steps:

- (i) consider the bead in an arbitrary intermediate position on a ring, described, for example by the angle θ shown in Fig. 3;
- (ii) draw all the forces acting on the particle – in our current case, the gravity force mg and the reaction force N exerted by the ring – see Fig. 3 above
- (iii) write the Cartesian components of the 2nd Newton's law (14) for the bead acceleration: $ma_x = N_x$, $ma_y = N_y - mg$,
- (iv) recognize that in the absence of friction, the force N should be normal to the ring, so that we can use two additional equations, $N_x = -N \sin\theta$ and $N_y = N \cos\theta$;
- (v) eliminate unknown variables N , N_x , and N_y from the resulting system of four equations, thus getting a single second-order differential equation for one variable, for example, θ .

$$mR\ddot{\theta} = -mg \sin\theta; \quad (1.18)$$

- (vi) use the mathematical identity $\ddot{\theta} \equiv d(\dot{\theta}^2 / 2) / d\theta$ to integrate this equation over θ once to get an expression relating the velocity $\dot{\theta}$ and the angle θ ; and, finally,
- (vii) using our specific initial condition ($\dot{\theta} = 0$ at $\theta = \pi/2$), find the final velocity as $v = R\dot{\theta}$ at $\theta = 0$.

All this is very much doable, but please agree that the procedure is too cumbersome for such a simple problem. Moreover, in many other cases even writing equations of motion along relevant coordinates is very complex, and any help the general theory may provide is highly valuable. In many cases, such help is given by *conservation laws*; let us review the most general of them.

1.3. Conservation laws

(i) Energy conservation is arguably the most general law of physics, but in mechanics, it takes a more humble form of *mechanical energy conservation*, which has limited applicability. To derive it, we first have to define the *kinetic energy* of a particle as¹⁴

Kinetic energy

$$T \equiv \frac{m}{2} v^2, \quad (1.19)$$

and then recast its differential as¹⁵

$$dT \equiv d\left(\frac{m}{2} v^2\right) \equiv d\left(\frac{m}{2} \mathbf{v} \cdot \mathbf{v}\right) = m\mathbf{v} \cdot d\mathbf{v} = m \frac{d\mathbf{r} \cdot d\mathbf{v}}{dt} = d\mathbf{r} \cdot \frac{d\mathbf{p}}{dt}. \quad (1.20)$$

Now plugging in the momentum's derivative from the 2nd Newton's law, $d\mathbf{p}/dt = \mathbf{F}$, where \mathbf{F} is the full force acting on the particle, we get $dT = \mathbf{F} \cdot d\mathbf{r}$. The integration of this equality along the particle's trajectory connecting some points A and B gives the formula that is sometimes called the *work-energy principle*:

Work-energy principle

$$\Delta T \equiv T(\mathbf{r}_B) - T(\mathbf{r}_A) = \int_A^B \mathbf{F} \cdot d\mathbf{r}, \quad (1.21)$$

where the integral on the right-hand side is called the *work* of the force \mathbf{F} on the path from A to B.

The next step may be made only for a *potential* (also called “conservative”) force that may be represented as the (minus) gradient of some scalar function $U(\mathbf{r})$, called the *potential energy*.¹⁶ The vector operator ∇ (called either *del* or *nabla*) of spatial differentiation¹⁷ allows a very compact expression of this fact:

Force vs potential energy

$$\mathbf{F} = -\nabla U. \quad (1.22)$$

For example, for the uniform gravity field (16),

$$U = mgh + \text{const}, \quad (1.23)$$

where h is the vertical coordinate directed “up” – opposite to the direction of the vector \mathbf{g} .

Integrating the tangential component F_τ of the vector \mathbf{F} given by Eq. (22), along an arbitrary path connecting the points A and B, we get

$$\int_A^B F_\tau d\mathbf{r} \equiv \int_A^B \mathbf{F} \cdot d\mathbf{r} = U(\mathbf{r}_A) - U(\mathbf{r}_B), \quad (1.24)$$

¹⁴ In such quantitative form, the kinetic energy was introduced (under the name “living force”) by Gottfried Leibniz and Johann Bernoulli (circa 1700), though its main properties (21) and (27) had not been clearly revealed until an 1829 work by Gaspard-Gustave de Coriolis. The modern term “kinetic energy” was coined only in 1849–1851 by Lord Kelvin (born William Thomson).

¹⁵ In these notes, $\mathbf{a} \cdot \mathbf{b}$ denotes the scalar (or “dot–”) product of vectors \mathbf{a} and \mathbf{b} – see, e.g., MA Eq. (7.1).

¹⁶ Note that because of its definition via the gradient, the potential energy is only defined to an arbitrary additive constant. This notion had been used already by G. Leibniz, though the term we are using for it nowadays was introduced much later (in the mid-19th century) by William Rankine.

¹⁷ Its basic properties are listed in MA Sec. 8.

i.e. work of potential forces may be represented as the difference of values of the function $U(\mathbf{r})$ in the initial and final points of the path. (Note that according to Eq. (24), the work of a potential force on any closed path, with $\mathbf{r}_A = \mathbf{r}_B$, is zero.)

Now returning to Eq. (21) and comparing it with Eq. (24), we see that

$$T(\mathbf{r}_B) - T(\mathbf{r}_A) = U(\mathbf{r}_A) - U(\mathbf{r}_B), \quad \text{i.e. } T(\mathbf{r}_A) + U(\mathbf{r}_A) = T(\mathbf{r}_A) + U(\mathbf{r}_B), \quad (1.25)$$

so that the *total mechanical energy* E , defined as

$$E \equiv T + U, \quad (1.26)$$

is indeed conserved:

$$E(\mathbf{r}_A) \equiv E(\mathbf{r}_B), \quad (1.27)$$

Total
mechanical
energy

Mechanical
energy:
conservation

but for conservative forces only. (Non-conservative forces may change E by either transferring energy *from* its mechanical form to another form, e.g., to heat in the case of friction, or by pumping the energy *into* the system under consideration from another, “external” system.)

The mechanical energy conservation allows us to return for just a second to the problem shown in Fig. 3 and solve it in one shot by writing Eq. (27) for the initial and final points:¹⁸

$$0 + mgR = \frac{m}{2}v^2 + 0. \quad (1.28)$$

The (elementary) solution of Eq. (28) for v immediately gives us the desired answer. Let me hope that the reader agrees that this way of problem’s solution is much simpler, and I have earned their attention to discuss other conservation laws – which may be equally effective.

(ii) Linear momentum. The conservation of the full linear momentum of any system of particles isolated from the rest of the world was already discussed in the previous section, and may serve as the basic postulate of classical dynamics – see Eq. (8). In the case of one free particle, the law is reduced to the trivial result $\mathbf{p} = \text{const}$, i.e. $\mathbf{v} = \text{const}$. If a system of N particles is affected by external forces $\mathbf{F}^{(\text{ext})}$, we may write

$$\mathbf{F}_k = \mathbf{F}_k^{(\text{ext})} + \sum_{k=1}^N \mathbf{F}_{kk}. \quad (1.29)$$

If we sum up the resulting Eqs. (13) for all particles of the system then, due to the 3rd Newton’s law (11) valid for any indices $k \neq k'$, the contributions of all internal forces $\mathbf{F}_{kk'}$ to the resulting double sum on the right-hand side cancel, and we get the following equation:

$$\dot{\mathbf{P}} = \mathbf{F}^{(\text{ext})}, \quad \text{where } \mathbf{F}^{(\text{ext})} \equiv \sum_{k=1}^N \mathbf{F}_k^{(\text{ext})}. \quad (1.30)$$

System’s
momentum
evolution

It tells us that the translational motion of the system as the whole is similar to that of a single particle, under the effect of the *net external force* $\mathbf{F}^{(\text{ext})}$. As a simple sanity check, if the external forces have a zero sum, we return to the postulate (8). Just one reminder: Eq. (30), as its precursor Eq. (13), is only valid in an inertial reference frame.

¹⁸ Here the arbitrary constant in Eq. (23) is chosen so that the potential energy is zero at the final point.

I hope that the reader knows numerous examples of the application of the linear momentum's conservation law, including all these undergraduate problems on car collisions, where the large collision forces are typically not known so that the direct application of Eq. (13) to each car is impracticable.

(iii) The angular momentum of a particle¹⁹ is defined as the following vector:²⁰

$$\mathbf{L} \equiv \mathbf{r} \times \mathbf{p}, \quad (1.31)$$

where $\mathbf{a} \times \mathbf{b}$ means the vector (or “cross-“) product of the vector operands.²¹ Differentiating Eq. (31) over time, we get

$$\dot{\mathbf{L}} = \dot{\mathbf{r}} \times \mathbf{p} + \mathbf{r} \times \dot{\mathbf{p}}. \quad (1.32)$$

In the first product, $\dot{\mathbf{r}}$ is just the velocity vector \mathbf{v} , parallel to the particle momentum $\mathbf{p} = m\mathbf{v}$, so that this term vanishes since the vector product of any two parallel vectors equals zero. In the second product, $\dot{\mathbf{p}}$ is equal to the full force \mathbf{F} acting on the particle, so that Eq. (32) is reduced to

$$\dot{\mathbf{L}} = \boldsymbol{\tau}, \quad (1.33)$$

where the vector

$$\boldsymbol{\tau} \equiv \mathbf{r} \times \mathbf{F}, \quad (1.34)$$

is called the *torque* exerted by force \mathbf{F} .²² (Note that the torque is reference-frame specific – and again, the frame has to be inertial for Eq. (33) to be valid, because we have used Eq. (13) for its derivation.) For an important particular case of a *central* force \mathbf{F} that is directed along the radius vector \mathbf{r} of a particle, the torque vanishes, so that (in that particular reference frame only!) the angular momentum is conserved:

$$\mathbf{L} = \text{const.} \quad (1.35)$$

For a system of N particles, the total angular momentum is naturally defined as

$$\mathbf{L} \equiv \sum_{k=1}^N \mathbf{L}_k. \quad (1.36)$$

Differentiating this equation over time, using Eq. (33) for each $\dot{\mathbf{L}}_k$, and again partitioning each force per Eq. (29), we get

$$\dot{\mathbf{L}} = \sum_{\substack{k,k'=1 \\ k' \neq k}}^N \mathbf{r}_k \times \mathbf{F}_{kk'} + \boldsymbol{\tau}^{(\text{ext})}, \quad \text{where } \boldsymbol{\tau}^{(\text{ext})} \equiv \sum_{k=1}^N \mathbf{r}_k \times \mathbf{F}_k^{(\text{ext})}. \quad (1.37)$$

The first (double) sum may be always divided into pairs of the type $(\mathbf{r}_k \times \mathbf{F}_{kk'} + \mathbf{r}_{k'} \times \mathbf{F}_{k'k})$. With a natural assumption of the central forces, $\mathbf{F}_{kk'} \parallel (\mathbf{r}_k - \mathbf{r}_{k'})$, each of these pairs equals zero. Indeed, in this case,

¹⁹ Here we imply that the internal motions of the particle, including its rotation about its axis, are negligible. (Otherwise, it could not be represented by a point, as was postulated in Sec. 1.)

²⁰ This explicit definition of the angular momentum (in different mathematical forms, and under the name of “moment of rotational motion”) has appeared in scientific publications only in the 1740s, though the fact of its conservation (35) in the field of central forces, in the form of the 2nd Kepler law (see Fig. 3.4 below), had been proved already by I. Newton in his *Principia*.

²¹ See, e.g., MA Eq. (7.3).

²² Alternatively, especially in mechanical engineering, torque is called the *force moment*. This notion may be traced all the way back to Archimedes’ theory of levers developed in the 3rd century BC.

each component of the pair is a vector perpendicular to the plane containing the positions of both particles and the reference frame origin, i.e. to the plane of the drawing in Fig. 4.

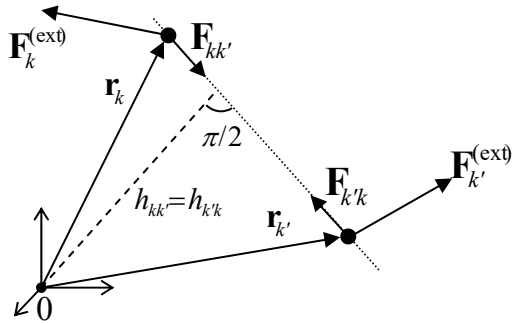


Fig. 1.4. Internal and external forces, and the internal torque cancellation in a system of two particles.

Also, due to the 3rd Newton's law (11), these two forces are equal and opposite, and the magnitude of each term in the sum may be represented as $|F_{kk}| h_{kk}$, with equal “lever arms” $h_{kk} = h_{k'k}$. As a result, each sum $(\mathbf{r}_k \times \mathbf{F}_{kk} + \mathbf{r}_{k'} \times \mathbf{F}_{k'k})$, and hence the whole double sum in Eq. (37) vanish, and it is reduced to a very simple result,

$$\dot{\mathbf{L}} = \boldsymbol{\tau}^{(\text{ext})}, \quad (1.38)$$

System's angular momentum: evolution

which is similar to Eq. (33) for a single particle, and is the angular analog of Eq. (30).

In particular, Eq. (38) shows that if the full external torque $\boldsymbol{\tau}^{(\text{ext})}$ vanishes for some reason (e.g., if the system of particles is isolated from the rest of the Universe), the conservation law (35) is valid for the full angular momentum \mathbf{L} even if its individual components \mathbf{L}_k are not conserved due to inter-particle interactions.

Please note again that since the conservation laws may be derived from Newton's laws (as was done above), they do not introduce anything new to the dynamics of any system. Indeed, from the mathematical point of view, the conservation laws discussed above are just the first integrals of the second-order differential equations of motion following from Newton's laws. However, for a physicist, thinking about particular systems in the terms of the conserved (or potentially conserved) quantities frequently provides decisive clues on their dynamics.

1.4. Potential energy and equilibrium

Another important role of the potential energy U , especially for dissipative systems whose total mechanical energy E is *not* conserved because it may be drained to the environment, is finding the positions of equilibrium (sometimes called the *fixed points*) of the system and analyzing their stability with respect to small perturbations. For a single particle, this is very simple: the force (22) vanishes at each extremum (either minimum or maximum) of the potential energy.²³ (Of those fixed points, only the minimums of $U(\mathbf{r})$ are stable – see Sec. 3.2 below for a discussion of this point.)

A slightly more subtle case is a particle with an internal potential energy $U(\mathbf{r})$, subjected to an *additional* external force $\mathbf{F}^{(\text{ext})}(\mathbf{r})$. In this case, the stable equilibrium is reached at the minimum of not the function $U(\mathbf{r})$, but of what is sometimes called the *Gibbs potential energy*

²³ Assuming that the additional, non-conservative forces (such as viscosity) responsible for the mechanical energy drain, vanish at equilibrium – as they typically do. (The static friction is one counter-example.)

Gibbs'
potential
energy

$$U_G(\mathbf{r}) \equiv U(\mathbf{r}) - \int^{\mathbf{r}} \mathbf{F}^{(ext)}(\mathbf{r}') \cdot d\mathbf{r}', \quad (1.39)$$

which is defined, just as $U(\mathbf{r})$ is, to an arbitrary additive constant.²⁴ The proof of Eq. (39) is very simple: in an extremum of this function, the total force acting on the particle,

$$\mathbf{F}^{(tot)} = \mathbf{F} + \mathbf{F}^{(ext)} \equiv -\nabla U + \nabla \int^{\mathbf{r}} \mathbf{F}^{(ext)}(\mathbf{r}') \cdot d\mathbf{r}' \equiv -\nabla U_G \quad (1.40)$$

vanishes, as it is necessary for equilibrium.

Physically, the difference $U_G - U$ specified by Eq. (39) is the \mathbf{r} -dependent part of the potential energy $U^{(ext)}$ of the external system responsible for the force $\mathbf{F}^{(ext)}$, so that U_G is just the total potential energy $U + U^{(ext)}$, excluding its part that does not depend on \mathbf{r} and hence is irrelevant for the analysis. According to the 3rd Newton's law, the force exerted by the particle on the external system equals $(-\mathbf{F}^{(ext)})$, so that its work (and hence the change of $U^{(ext)}$ due to the change of \mathbf{r}) is given by the second term on the right-hand side of Eq. (39). Thus the condition of equilibrium, $\nabla U_G = 0$, is just the condition of an extremum of the total potential energy, $U + U^{(ext)} + \text{const}$, of the two interacting systems.

For the simplest (and very frequent) case when the applied force is independent of the particle's position, the Gibbs potential energy (39) is just²⁵

$$U_G(\mathbf{r}) \equiv U(\mathbf{r}) - \mathbf{F}^{(ext)} \cdot \mathbf{r} + \text{const}. \quad (1.41)$$

As the simplest example, consider a 1D deformation of the usual elastic spring providing the returning force $(-\kappa x)$, where x is the deviation from its equilibrium. As follows from Eq. (22), its potential energy is $U = \kappa x^2/2 + \text{const}$, so that its minimum corresponds to $x = 0$. Now let us apply an additional external force F , say independent of x . Then the equilibrium deformation of the spring, $x_0 = F/\kappa$, corresponds to the minimum of not U , but rather of the Gibbs potential energy (41), in our particular case taking the form

$$U_G \equiv U - Fx = \frac{\kappa x^2}{2} - Fx. \quad (1.42)$$

1.5. OK, we've got it – can we go home now?

Sorry, not yet. In many cases, the conservation laws discussed above provide little help, even in systems without dissipation. As a simple example, consider a generalization of the bead-on-the-ring problem shown in Fig. 3, in which the ring is rotated by external forces, with a constant angular velocity ω , about its vertical diameter.²⁶ In this problem (to which I will repeatedly return below, using it as an

²⁴ Unfortunately, in most textbooks, the association of the (unavoidably used) notion of U_G with the glorious name of Josiah Willard Gibbs is postponed until a course of statistical mechanics and/or thermodynamics, where U_G is a part of the *Gibbs free energy*, in contrast to U , which is a part of the *Helmholtz free energy* – see, e.g., SM Sec. 1.4. I use this notion throughout my series, because the difference between U_G and U , and hence that between the Gibbs and Helmholtz free energies, has nothing to do with statistics or thermal motion, and belongs to the whole physics, including not only mechanics but also electrodynamics and quantum mechanics.

²⁵ Eq. (41) is a particular case of what mathematicians call the *Legendre transformations*.

²⁶ This is essentially a simplified model of the mechanical control device called the *centrifugal* (or “flyball”, or “centrifugal flyball”) *governor* – see, e.g., http://en.wikipedia.org/wiki/Centrifugal_governor. (Sometimes the

analytical mechanics “testbed”), none of the three conservation laws listed in the last section, holds. In particular, the bead’s energy,

$$E = \frac{m}{2}v^2 + mgh, \quad (1.43)$$

is *not* constant, because the external forces rotating the ring may change it. Of course, we still can solve the problem using Newton’s laws, but this is even more complex than for the above case of the ring at rest, in particular because the force \mathbf{N} exerted on the bead by the ring now may have three rather than two Cartesian components, which are not simply related. On the other hand, it is clear that the bead still has just one degree of freedom (say, the angle θ), so its dynamics should not be too complicated.

This case gives us a clue on how situations like this one can be simplified: if we only could exclude the so-called *reaction forces* such as \mathbf{N} , that take into account *external constraints* imposed on the particle motion, in advance, that should help a lot. Such a constraint exclusion may be provided by analytical mechanics, in particular its Lagrangian formulation, to which we will now proceed.

Of course, the value of the Lagrangian approach goes far beyond simple systems such as the bead on a rotating ring. Indeed, this system has just two externally imposed constraints: the fixed distance of the bead from the center of the ring, and the instant angle of rotation of the ring about its vertical diameter. Now let us consider the motion of a rigid body. It is essentially a system of a very large number, $N \gg 1$, of particles ($\sim 10^{23}$ of them if we think about atoms in a 1-cm-scale body). If the only way to analyze its motion would be to write Newton’s laws for each of the particles, the situation would be completely hopeless. Fortunately, the number of constraints imposed on its motion is almost similarly huge. (At negligible deformations of the body, the distances between each pair of its particles should be constant.) As a result, the number of actual degrees of freedom of such a body is small (at negligible deformations, just six – see Sec. 4.1), so that with the kind help from analytical mechanics, the motion of the body may be, in many important cases, analyzed even without numerical calculations.

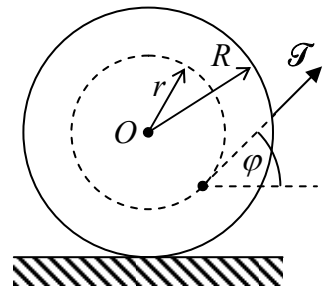
One more important motivation for analytical mechanics is given by the dynamics of “non-mechanical” systems, for example, of the electromagnetic field – possibly interacting with charged particles, conducting bodies, etc. In many such systems, the easiest (and sometimes the only practicable) way to find the equations of motion is to derive them from either the Lagrangian or Hamiltonian function of the system. Moreover, the Hamiltonian formulation of the analytical mechanics (to be reviewed in Chapter 10 below) offers a direct pathway to deriving quantum-mechanical Hamiltonian operators of various systems, which are necessary for the analysis of their quantum properties.

1.6. Self-test problems

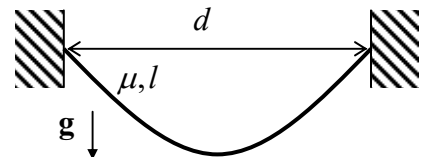
1.1. A bicycle, ridden with velocity v on wet pavement, has no mudguards on its wheels. How far behind should the following biker ride to avoid being splashed over? Neglect the air resistance effects.

device is called the “Watt’s governor”, after the famous James Watts who used it in 1788 in one of his first steam engines, though it had been used in European windmills at least since the early 1600s.) Just as a curiosity: the now-ubiquitous term *cybernetics* was coined by Norbert Wiener in 1948 from the word “governor” (or rather from its Ancient-Greek original κυβερνήτης) exactly in this meaning because the centrifugal governor had been the first well-studied control device.

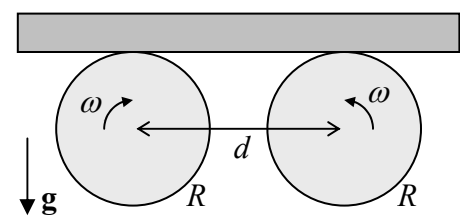
1.2. Two round disks of radius R are firmly connected with a coaxial cylinder of a smaller radius r , and a thread is wound on the resulting spool. The spool is placed on a horizontal surface, and the thread's end is being pooled out at angle φ – see the figure on the right. Assuming that the spool does not slip on the surface, what direction would it roll?



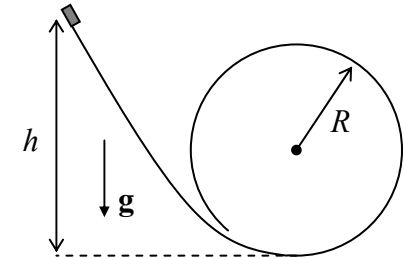
1.3.* Calculate the equilibrium shape of a flexible heavy rope of length l , with a constant mass μ per unit length, if it is hung in a uniform gravity field between two points separated by a horizontal distance d – see the figure on the right.



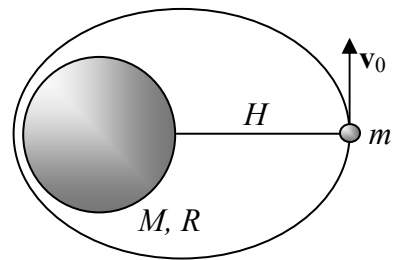
1.4. A uniform, long, thin bar is placed horizontally on two similar round cylinders rotating toward each other with the same angular velocity ω and displaced by distance d – see the figure on the right. Calculate the laws of relatively slow horizontal motion of the bar within the plane of the drawing, for both possible directions of cylinder rotation, assuming that the friction force between the slipping surfaces of the bar and each cylinder obeys the simple Coulomb approximation²⁷ $|F| = \mu N$, where N is the normal pressure force between them, and μ is a constant (velocity-independent) coefficient. Formulate the condition of validity of your result.



1.5. A small block slides, without friction, down a smooth slide that ends with a round loop of radius R – see the figure on the right. What smallest initial height h allows the block to make its way around the loop without dropping from the slide if it is launched with negligible initial velocity?



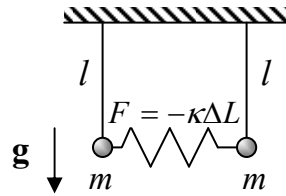
1.6. A satellite of mass m is being launched from height H over the surface of a spherical planet with radius R and mass $M \gg m$ – see the figure on the right. Find the range of initial velocities v_0 (normal to the radius) providing closed orbits above the planet's surface.



1.7. Prove that the thin-uniform-disk model of a galaxy describes small sinusoidal (“harmonic”) oscillations of stars inside it, along the direction normal to the disk, and calculate the frequency of these oscillations in terms of Newton’s gravitational constant G and density ρ of the disk’s matter.

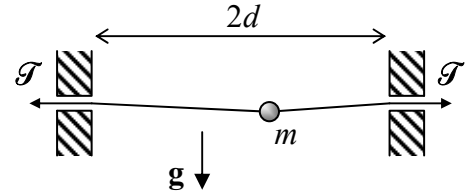
²⁷ It was suggested in 1785 by the same Charles-Augustin de Coulomb who has discovered the famous *Coulomb law* of electrostatics, and hence pioneered the whole quantitative science of electricity – see EM Ch. 1.

1.8. Derive differential equations of motion for small oscillations of two similar pendula coupled with a spring (see the figure on the right), within their common vertical plane. Assume that at the vertical position of both pendula, the spring is not stretched ($\Delta L = 0$).



1.9. One of the popular futuristic concepts of travel is digging a straight railway tunnel through the Earth and letting a train go through it, without initial velocity – driven only by gravity. Calculate the train's travel time through such a tunnel, assuming that the Earth's density ρ is constant, and neglecting the friction and planet-rotation effects.

1.10. A small bead of mass m may slide, without friction, along a light string stretched with force $\mathcal{T} \gg mg$, between two points separated by a horizontal distance $2d$ – see the figure on the right. Calculate the frequency of horizontal oscillations of the bead about its equilibrium position.



1.11. For a rocket accelerating due to its working jet motor (and hence spending the jet fuel), calculate the relation between its velocity and the remaining mass.

Hint: For the sake of simplicity, consider the 1D motion.

1.12. Prove the following *virial theorem*:²⁸ for a set of N particles performing a periodic motion,

$$\bar{T} = -\frac{1}{2} \sum_{k=1}^N \overline{\mathbf{F}_k \cdot \mathbf{r}_k},$$

where the top bar means averaging over time – in this case over the motion period. What does the virial theorem say about:

- (i) a 1D motion of a particle in the confining potential²⁹ $U(x) = ax^{2s}$, with $a > 0$ and $s > 0$, and
- (ii) an orbital motion of a particle in the central potential $U(r) = -C/r$?

Hint: Explore the time derivative of the following scalar function of time: $G(t) \equiv \sum_{k=1}^N \mathbf{p}_k \cdot \mathbf{r}_k$.

1.13. As will be discussed in Chapter 8, if a body moves through a fluid with a sufficiently high velocity v , the fluid's drag force is approximately proportional to v^2 . Use this approximation (introduced by Sir Isaac Newton himself) to find the velocity as a function of time during the body's vertical fall in the air near the Earth's surface.

1.14. A particle of mass m , moving with velocity u , collides head-on with a particle of mass M , initially at rest. Calculate the velocities of both particles after the collision, if the initial energy of the system is barely sufficient for an increase of its internal energy by ΔE .

²⁸ It was first stated by Rudolf Clausius in 1870.

²⁹ Here and below I am following the (regretful) custom of using the single word “potential” for the potential energy of the particle – just for brevity. This custom is also common in quantum mechanics, but in electrodynamics, these two notions should be clearly distinguished – as they are in the EM part of this series.

Chapter 2. Lagrangian Analytical Mechanics

The goal of this chapter is to describe the Lagrangian formalism of analytical mechanics, which is extremely useful for obtaining the differential equations of motion (and sometimes their first integrals) not only for mechanical systems with holonomic constraints but also for some other dynamic systems.

2.1. Lagrange equations

In many cases, the constraints imposed on the 3D motion of a system of N particles may be described by N vector (i.e. $3N$ scalar) algebraic equations

$$\mathbf{r}_k = \mathbf{r}_k(q_1, q_2, \dots, q_j, \dots, q_J, t), \quad \text{with } 1 \leq k \leq N, \quad (2.1)$$

where q_j are certain *generalized coordinates* that (together with constraints) completely define the system position. Their number $J \leq 3N$ is called the number of the actual *degrees of freedom* of the system. The constraints that allow such a description are called *holonomic*.¹

For example, for the problem already mentioned in Section 1.5, namely the bead sliding along a rotating ring (Fig. 1), $J = 1$, because with the constraints imposed by the ring, the bead's position is uniquely determined by just one generalized coordinate – for example, its polar angle θ .

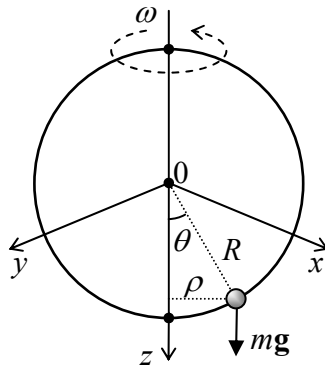


Fig. 2.1. A bead on a rotating ring as an example of a system with just one degree of freedom ($J=1$).

Indeed, selecting the reference frame as shown in Fig. 1 and using the well-known formulas for the spherical coordinates,² we see that in this case, Eq. (1) has the form

$$\mathbf{r} = \{x, y, z\} = \{R \sin \theta \cos \varphi, R \sin \theta \sin \varphi, R \cos \theta\}, \quad \text{where } \varphi = \omega t + \text{const}, \quad (2.2)$$

with the last constant depending on the exact selection of the axes x and y and the time origin. Since the angle φ , in this case, is a fixed function of time, and R is a fixed constant, the particle's position in space

¹ Possibly, the simplest counter-example of a *non-holonomic* constraint is a set of inequalities describing the hard walls confining the motion of particles in a closed volume. Non-holonomic constraints are better dealt by other methods, e.g., by imposing proper boundary conditions on the (otherwise unconstrained) motion.

² See, e.g., MA Eq. (10.7).

at any instant t is completely determined by the value of its only generalized coordinate θ . (Note that its dimensionality is different from that of Cartesian coordinates!)

Now returning to the general case of J degrees of freedom, let us consider a set of small *variations* (alternatively called “virtual displacements”) δq_j allowed by the constraints. Virtual displacements differ from the actual small displacements (described by *differentials* dq_j proportional to time variation dt) in that δq_j describes not the system’s motion as such, but rather its possible variation – see Fig. 1.

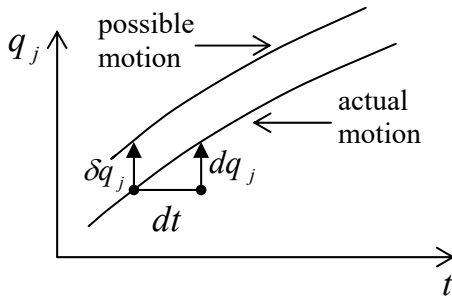


Fig. 2.2. Actual displacement dq_j vs. the virtual one (i.e. variation) δq_j .

Generally, operations with variations are the subject of a special field of mathematics, the calculus of variations.³ However, the only math background necessary for our current purposes is the understanding that operations with variations are similar to those with the usual differentials, though we need to watch carefully what each variable is a function of. For example, if we consider the variation of the radius vectors (1), at a fixed time t , as functions of independent variations δq_j , we may use the usual formula for the differentiation of a function of several arguments:⁴

$$\delta \mathbf{r}_k = \sum_j \frac{\partial \mathbf{r}_k}{\partial q_j} \delta q_j. \quad (2.3)$$

Now let us break the force acting upon the k^{th} particle into two parts: the frictionless, constraining part \mathbf{N}_k of the reaction force and the remaining part \mathbf{F}_k – including the forces from other sources and possibly the frictional part of the reaction force. Then the 2nd Newton’s law for the k^{th} particle of the system may be rewritten as

$$m_k \dot{\mathbf{v}}_k - \mathbf{F}_k = \mathbf{N}_k. \quad (2.4)$$

Since any variation of the motion has to be allowed by the constraints, its $3N$ -dimensional vector with N 3D-vector components $\delta \mathbf{r}_k$ has to be perpendicular to the $3N$ -dimensional vector of the constraining forces, also having N 3D-vector components \mathbf{N}_k . (For example, for the problem shown in Fig. 1, the virtual displacement vector $\delta \mathbf{r}_k$ may be directed only along the ring, while the constraining force \mathbf{N} exerted by the ring, has to be perpendicular to that direction.) This condition may be expressed as

³ For a concise introduction to the field see, e.g., either I. Gelfand and S. Fomin, *Calculus of Variations*, Dover, 2000, or L. Elsgolc, *Calculus of Variations*, Dover, 2007. An even shorter review may be found in Chapter 17 of Arfken and Weber – see MA Sec. 16. For a more detailed discussion, using many examples from physics, see R. Weinstock, *Calculus of Variations*, Dover, 2007.

⁴ See, e.g., MA Eq. (4.2). Also, in all formulas of this section, summations over j are from 1 to J , while those over the particle number k are from 1 to N , so that for the sake of brevity, these limits are not explicitly specified.

$$\sum_k \mathbf{N}_k \cdot \delta \mathbf{r}_k = 0, \quad (2.5)$$

where the scalar product of $3N$ -dimensional vectors is defined exactly like that of 3D vectors, i.e. as the sum of the products of the corresponding components of the operands. The substitution of Eq. (4) into Eq. (5) results in the so-called *D'Alembert principle*:⁵

D'Alembert principle

$$\sum_k (m_k \dot{\mathbf{v}}_k - \mathbf{F}_k) \cdot \delta \mathbf{r}_k = 0. \quad (2.6)$$

Plugging Eq. (3) into Eq. (6), we get

$$\sum_j \left\{ \sum_k m_k \dot{\mathbf{v}}_k \cdot \frac{\partial \mathbf{r}_k}{\partial q_j} - \mathcal{F}_j \right\} \delta q_j = 0, \quad (2.7)$$

where the scalars \mathcal{F}_j , called the *generalized forces*, are defined as follows:⁶

Generalized force

$$\mathcal{F}_j \equiv \sum_k \mathbf{F}_k \cdot \frac{\partial \mathbf{r}_k}{\partial q_j}. \quad (2.8)$$

Now we may use the standard argument of the calculus of variations: for the left-hand side of Eq. (7) to be zero for an arbitrary selection of independent variations δq_j , the expression in the curly brackets, for every j , should equal zero. This gives us the desired set of $J \leq 3N$ equations

$$\sum_k m_k \dot{\mathbf{v}}_k \cdot \frac{\partial \mathbf{r}_k}{\partial q_j} - \mathcal{F}_j = 0; \quad (2.9)$$

what remains is just to recast them in a more convenient form.

First, using the differentiation by parts to calculate the following time derivative:

$$\frac{d}{dt} \left(\mathbf{v}_k \cdot \frac{\partial \mathbf{r}_k}{\partial q_j} \right) = \dot{\mathbf{v}}_k \cdot \frac{\partial \mathbf{r}_k}{\partial q_j} + \mathbf{v}_k \cdot \frac{d}{dt} \left(\frac{\partial \mathbf{r}_k}{\partial q_j} \right), \quad (2.10)$$

we may notice that the first term on the right-hand side is exactly the scalar product in the first term of Eq. (9).

Second, let us use another key fact of the calculus of variations (which is, essentially, evident from Fig. 3): the differentiation of a variable over time and over the generalized coordinate variation (at a fixed time) are interchangeable operations. As a result, in the second term on the right-hand side of Eq. (10), we may write

$$\frac{d}{dt} \left(\frac{\partial \mathbf{r}_k}{\partial q_j} \right) = \frac{\partial}{\partial q_j} \left(\frac{d \mathbf{r}_k}{dt} \right) = \frac{\partial \mathbf{v}_k}{\partial q_j}. \quad (2.11)$$

⁵ It was spelled out in a 1743 work by Jean le Rond d'Alembert, though the core of this result has been traced to an earlier work by Jacob (Jean) Bernoulli (1667 – 1748) – not to be confused with his son Daniel Bernoulli (1700–1782) who is credited, in particular, for the *Bernoulli equation* for ideal fluids, to be discussed in Sec. 8.4 below.

⁶ Note that since the dimensionality of generalized coordinates may be arbitrary, that of generalized forces may also differ from the newton.

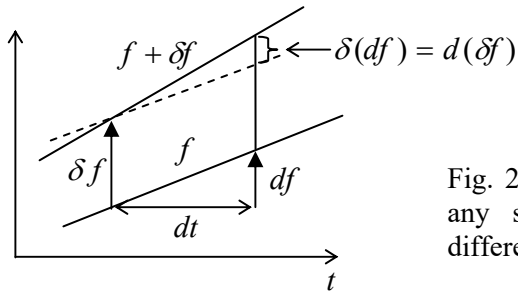


Fig. 2.3. The variation of the differential (of any smooth function f) is equal to the differential of its variation.

Finally, let us differentiate Eq. (1) over time:

$$\mathbf{v}_k \equiv \frac{d\mathbf{r}_k}{dt} = \sum_j \frac{\partial \mathbf{r}_k}{\partial q_j} \dot{q}_j + \frac{\partial \mathbf{r}_k}{\partial t}. \quad (2.12)$$

This equation shows that particle velocities \mathbf{v}_k may be considered to be linear functions of the generalized velocities \dot{q}_j *considered as independent variables*, with proportionality coefficients

$$\frac{\partial \mathbf{v}_k}{\partial \dot{q}_j} = \frac{\partial \mathbf{r}_k}{\partial q_j}. \quad (2.13)$$

With the account of Eqs. (10), (11), and (13), Eq. (9) turns into

$$\frac{d}{dt} \sum_k m_k \mathbf{v}_k \cdot \frac{\partial \mathbf{v}_k}{\partial \dot{q}_j} - \sum_k m_k \mathbf{v}_k \cdot \frac{\partial \mathbf{v}_k}{\partial q_j} - \mathcal{F}_j = 0. \quad (2.14)$$

This result may be further simplified by making, for the total kinetic energy of the system,

$$T \equiv \sum_k \frac{m_k}{2} \mathbf{v}_k^2 = \frac{1}{2} \sum_k m_k \mathbf{v}_k \cdot \mathbf{v}_k, \quad (2.15)$$

the same commitment as for \mathbf{v}_k , i.e. considering T a function of not only the generalized coordinates q_j and time t but also of the generalized velocities \dot{q}_i – as variables *independent* of q_j and t . Then we may calculate the partial derivatives of T as

$$\frac{\partial T}{\partial q_j} = \sum_k m_k \mathbf{v}_k \cdot \frac{\partial \mathbf{v}_k}{\partial q_j}, \quad \frac{\partial T}{\partial \dot{q}_j} = \sum_k m_k \mathbf{v}_k \cdot \frac{\partial \mathbf{v}_k}{\partial \dot{q}_j}, \quad (2.16)$$

and notice that they are exactly the two sums participating in Eq. (14). As a result, we get a system of J *Lagrange equations*,⁷

$$\frac{d}{dt} \frac{\partial T}{\partial \dot{q}_j} - \frac{\partial T}{\partial q_j} - \mathcal{F}_j = 0, \quad \text{for } j = 1, 2, \dots, J.$$

(2.17)

General
Lagrange
equations

Their big advantage over the initial Newton's-law equations (4) is that the Lagrange equations do not include the constraining forces \mathbf{N}_k , and thus there are only J of them – typically much fewer than $3N$.

⁷ They were derived in 1788 by Joseph-Louis Lagrange, who pioneered the whole field of analytical mechanics – not to mention his key contributions to the number theory and celestial mechanics.

This is as far as we can go for arbitrary forces. However, if all the forces may be expressed in the form similar to, but somewhat more general than Eq. (1.22), $\mathbf{F}_k = -\nabla_k U(\mathbf{r}_1, \mathbf{r}_2, \dots, \mathbf{r}_N, t)$, where U is the effective potential energy of the system,⁸ and ∇_k denotes the spatial differentiation over coordinates of the k^{th} particle, we may recast Eq. (8) into a simpler form:

$$\mathcal{F}_j \equiv \sum_k \mathbf{F}_k \cdot \frac{\partial \mathbf{r}_k}{\partial q_j} = - \sum_k \left(\frac{\partial U}{\partial x_k} \frac{\partial x_k}{\partial q_j} + \frac{\partial U}{\partial y_k} \frac{\partial y_k}{\partial q_j} + \frac{\partial U}{\partial z_k} \frac{\partial z_k}{\partial q_j} \right) \equiv - \frac{\partial U}{\partial q_j}. \quad (2.18)$$

Since we assume that U depends only on particle coordinates (and possibly time), but not velocities: $\partial U / \partial \dot{q}_j = 0$, with the substitution of Eq. (18), the Lagrange equation (17) may be represented in the so-called *canonical form*:

$$\frac{d}{dt} \frac{\partial L}{\partial \dot{q}_j} - \frac{\partial L}{\partial q_j} = 0, \quad (2.19a)$$

where L is the *Lagrangian function* (sometimes called just the “Lagrangian”), defined as

$$L \equiv T - U. \quad (2.19b)$$

(It is crucial to distinguish this function from the mechanical energy (1.26), $E = T + U$.)

Note also that according to Eq. (2.18), for a system under the effect of an additional generalized external force $\mathcal{F}(t)$ we have to use, in all these relations, not the internal potential energy $U^{(\text{int})}$ of the system, but its Gibbs potential energy $U \equiv U^{(\text{int})} - \mathcal{F}_j q_j$ – see the discussion in Sec. 1.4.

Using the Lagrangian approach in practice, the reader should always remember, first, that each system has only *one* Lagrange function (19b), but is described by $J \geq 1$ Lagrange equations (19a), with j taking values 1, 2, ..., J , and second, that differentiating the function L , we have to consider the generalized velocities as its independent arguments, ignoring the fact they are actually the time derivatives of the generalized coordinates.

2.2. Three simple examples

As the first, simplest example, consider a particle constrained to move along one axis (say, x):

$$T = \frac{m}{2} \dot{x}^2, \quad U = U(x, t). \quad (2.20)$$

In this case, it is natural to consider x as the (only) generalized coordinate, and \dot{x} as the generalized velocity, so that

$$L \equiv T - U = \frac{m}{2} \dot{x}^2 - U(x, t). \quad (2.21)$$

Considering \dot{x} and x as independent variables, we get $\partial L / \partial \dot{x} = m\dot{x}$, and $\partial L / \partial x = -\partial U / \partial x$, so that Eq. (19) (the only Lagrange equation in this case of the single degree of freedom!) yields

⁸ Note that due to the possible time dependence of U , Eq. (17) does not mean that the forces \mathbf{F}_k have to be conservative – see the next section for more discussion. With this understanding, I will still use for function U the convenient name of “potential energy”.

$$\frac{d}{dt}(m\dot{x}) - \left(-\frac{\partial U}{\partial x}\right) = 0, \quad (2.22)$$

evidently the same result as the x -component of the 2nd Newton's law with $F_x = -\partial U/\partial x$. This example is a good sanity check, but it also shows that the Lagrange formalism does not provide too much advantage in this particular case.

Such an advantage is, however, evident in our testbed problem – see Fig. 1. Indeed, taking the polar angle θ for the (only) generalized coordinate, we see that in this case, the kinetic energy depends not only on the generalized velocity but also on the generalized coordinate:⁹

$$\begin{aligned} T &= \frac{m}{2}R^2(\dot{\theta}^2 + \omega^2 \sin^2 \theta), & U &= -mgz + \text{const} \equiv -mgR \cos \theta + \text{const}, \\ L &\equiv T - U = \frac{m}{2}R^2(\dot{\theta}^2 + \omega^2 \sin^2 \theta) + mgR \cos \theta + \text{const}. \end{aligned} \quad (2.23)$$

Here it is especially important to remember that at substantiating the Lagrange equation, θ and $\dot{\theta}$ have to be treated as independent arguments of L , so that

$$\frac{\partial L}{\partial \dot{\theta}} = mR^2\dot{\theta}, \quad \frac{\partial L}{\partial \theta} = mR^2\omega^2 \sin \theta \cos \theta - mgR \sin \theta, \quad (2.24)$$

giving us the following equation of motion:

$$\frac{d}{dt}(mR^2\dot{\theta}) - (mR^2\omega^2 \sin \theta \cos \theta - mgR \sin \theta) = 0. \quad (2.25)$$

As a sanity check, at $\omega = 0$, Eq. (25) is reduced to the equation (1.18) of the usual pendulum:

$$\ddot{\theta} + \Omega^2 \sin \theta = 0, \quad \text{where } \Omega \equiv \left(\frac{g}{R}\right)^{1/2}. \quad (2.26)$$

We will explore Eq. (25) in more detail later, but please note how simple its derivation was – in comparison with writing the 3D Newton's law and then excluding the reaction force.

Next, though the Lagrangian formalism was derived from Newton's law for mechanical systems, the resulting equations (19) are applicable to other dynamic systems, especially those for which the kinetic and potential energies may be readily expressed via some generalized coordinates. As the simplest example, consider the well-known connection of a capacitor with capacitance C to an inductive coil with self-inductance \mathcal{L} ¹⁰ (Electrical engineers frequently call it the *LC tank circuit*.)

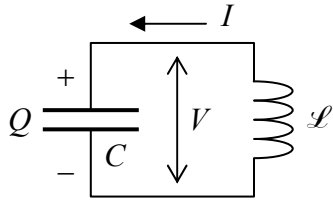


Fig. 2.4. *LC tank circuit*.

⁹ The above expression for $T \equiv (m/2)(\dot{x}^2 + \dot{y}^2 + \dot{z}^2)$ may be readily obtained either by the formal differentiation of Eq. (2) over time, or just by noticing that the velocity vector has two perpendicular components: one (of magnitude $R\dot{\theta}$) along the ring, and another one (of magnitude $\omega\rho = \omega R \sin \theta$) normal to the ring's plane.

¹⁰ A fancy font is used here to avoid any chance of confusion between the inductance and the Lagrange function.

As the reader (hopefully :-) knows from their undergraduate studies, at relatively low frequencies we may use the so-called lumped-circuit approximation, in which the total energy of this system is the sum of two components, the electric energy E_e localized inside the capacitor, and the magnetic energy E_m localized inside the inductance coil:

$$E_e = \frac{Q^2}{2C}, \quad E_m = \frac{\mathcal{L}I^2}{2}. \quad (2.27)$$

Since the electric current I through the coil and the electric charge Q on the capacitor are related by the charge continuity equation $dQ/dt = I$ (evident from Fig. 4), it is natural to declare Q the generalized coordinate of the system, and the current, its generalized velocity. With this choice, the electrostatic energy $E_e(Q)$ may be treated as the potential energy U of the system, and the magnetic energy $E_m(I)$, as its kinetic energy T . With this attribution, we get

$$\frac{\partial T}{\partial \dot{q}} \equiv \frac{\partial E_m}{\partial I} = \mathcal{L}I \equiv \mathcal{L}\dot{Q}, \quad \frac{\partial T}{\partial q} \equiv \frac{\partial E_m}{\partial Q} = 0, \quad \frac{\partial U}{\partial q} \equiv \frac{\partial E_e}{\partial Q} = \frac{Q}{C}, \quad (2.28)$$

so that the Lagrange equation (19) becomes

$$\frac{d}{dt}(\mathcal{L}\dot{Q}) - \left(-\frac{Q}{C}\right) = 0, \quad \text{i.e. } \ddot{Q} + \frac{1}{\mathcal{L}C}Q = 0. \quad (2.29)$$

Note, however, that the above choice of the generalized coordinate and velocity is not unique. Instead, one can use, as the generalized coordinate, the magnetic flux Φ through the inductive coil, related to the common voltage V across the circuit (Fig. 4) by Faraday's induction law $V = -d\Phi/dt$. With this choice, $(-V)$ becomes the generalized velocity, $E_m = \Phi^2/2\mathcal{L}$ should be understood as the *potential* energy, and $E_e = CV^2/2$ treated as the *kinetic* energy. For this choice, the resulting Lagrange equation of motion is equivalent to Eq. (29). If both parameters of the circuit, \mathcal{L} and C , are constant in time, Eq. (29) describes sinusoidal oscillations with the frequency

$$\omega_0 = \frac{1}{(\mathcal{L}C)^{1/2}}. \quad (2.30)$$

This is of course a well-known result, which may be derived in a more standard way – by equating the voltage drops across the capacitor ($V = Q/C$) and the inductor ($V = -\mathcal{L}dI/dt \equiv -\mathcal{L}d^2Q/dt^2$). However, the Lagrangian approach is much more convenient for more complex systems – for example, for the general description of the electromagnetic field and its interaction with charged particles.¹¹

2.3. Hamiltonian function and energy

The canonical form (19) of the Lagrange equation has been derived using Eq. (18), which is formally similar to Eq. (1.22) for a potential force. Does this mean that the system described by Eq. (19) always conserves energy? Not necessarily, because the “potential energy” U that participates in Eq. (18), may depend not only on the generalized coordinates but on time as well. Let us start the analysis of this issue with the introduction of two new (and very important!) notions: the *generalized momentum* corresponding to each generalized coordinate q_j ,

¹¹ See, e.g., EM Secs. 9.7 and 9.8.

$$p_j \equiv \frac{\partial L}{\partial \dot{q}_j}, \quad (2.31)$$

Generalized momentum

and the *Hamiltonian function*¹²

$$H \equiv \sum_j \frac{\partial L}{\partial \dot{q}_j} \dot{q}_j - L \equiv \sum_j p_j \dot{q}_j - L. \quad (2.32)$$

Hamiltonian function: definition

To see whether the Hamiltonian function is conserved during the motion, let us differentiate both sides of its definition (32) over time:

$$\frac{dH}{dt} = \sum_j \left[\frac{d}{dt} \left(\frac{\partial L}{\partial \dot{q}_j} \right) \dot{q}_j + \frac{\partial L}{\partial \dot{q}_j} \ddot{q}_j \right] - \frac{dL}{dt}. \quad (2.33)$$

If we want to make use of the Lagrange equation (19), the last derivative has to be calculated considering L as a function of independent arguments q_j , \dot{q}_j , and t , so that

$$\frac{dL}{dt} = \sum_j \left(\frac{\partial L}{\partial q_j} \dot{q}_j + \frac{\partial L}{\partial \dot{q}_j} \ddot{q}_j \right) + \frac{\partial L}{\partial t}, \quad (2.34)$$

where the last term is the derivative of L as an *explicit* function of time. We see that the last term in the square brackets of Eq. (33) immediately cancels with the last term in the parentheses of Eq. (34). Moreover, using the Lagrange equation (19a) for the first term in the square brackets of Eq. (33), we see that it cancels with the first term in the parentheses of Eq. (34). As a result, we arrive at a very simple and important result:

$$\frac{dH}{dt} = - \frac{\partial L}{\partial t}. \quad (2.35)$$

Hamiltonian function: time evolution

The most important corollary of this formula is that if the Lagrangian function does not depend on time *explicitly* ($\partial L / \partial t = 0$), the Hamiltonian function is an integral of motion:

$$H = \text{const.} \quad (2.36)$$

Let us see how this works, using the first two examples discussed in the previous section. For a 1D particle, the definition (31) of the generalized momentum yields

$$p_x \equiv \frac{\partial L}{\partial v} = mv, \quad (2.37)$$

so that it coincides with the usual linear momentum – or rather with its x -component. According to Eq. (32), the Hamiltonian function for this case (with just one degree of freedom) is

$$H \equiv p_x v - L = p_x \frac{p_x}{m} - \left(\frac{m}{2} \dot{x}^2 - U \right) = \frac{p_x^2}{2m} + U, \quad (2.38)$$

¹² It is named after Sir William Rowan Hamilton, who developed his approach to analytical mechanics in 1833, on the basis of the Lagrangian mechanics. This function is sometimes called just the “Hamiltonian”, but it is advisable to use the full term “Hamiltonian function” in classical mechanics, to distinguish it from the *Hamiltonian operator* used in quantum mechanics, whose abbreviation to *Hamiltonian* is extremely common. (The relation of these two notions will be discussed in Sec. 10.1 below.)

i.e. coincides with the particle's mechanical energy $E = T + U$. Since the Lagrangian does not depend on time explicitly, both H and E are conserved.

However, it is not always that simple! Indeed, let us return again to our testbed problem (Fig. 1). In this case, the generalized momentum corresponding to the generalized coordinate θ is

$$p_\theta \equiv \frac{\partial L}{\partial \dot{\theta}} = mR^2 \dot{\theta}, \quad (2.39)$$

and Eq. (32) yields:

$$\begin{aligned} H &\equiv p_\theta \dot{\theta} - L = mR^2 \dot{\theta}^2 - \left[\frac{m}{2} R^2 (\dot{\theta}^2 + \omega^2 \sin^2 \theta) + mgR \cos \theta \right] + \text{const} \\ &\equiv \frac{m}{2} R^2 (\dot{\theta}^2 - \omega^2 \sin^2 \theta) - mgR \cos \theta + \text{const}. \end{aligned} \quad (2.40)$$

This means that (as soon as $\omega \neq 0$), the Hamiltonian function *differs* from the mechanical energy

$$E \equiv T + U = \frac{m}{2} R^2 (\dot{\theta}^2 + \omega^2 \sin^2 \theta) - mgR \cos \theta + \text{const}. \quad (2.41)$$

The difference, $E - H = mR^2 \omega^2 \sin^2 \theta$ (besides an inconsequential constant), may change at bead's motion along the ring, so that although H is an integral of motion (since $\partial L/\partial t = 0$), the energy is generally *not* conserved.

In this context, let us find out when these two functions, E and H , do coincide. In mathematics, there is a notion of a *homogeneous function* $f(x_1, x_2, \dots)$ of degree λ , defined in the following way: for an arbitrary constant a ,

$$f(ax_1, ax_2, \dots) = a^\lambda f(x_1, x_2, \dots). \quad (2.42)$$

Such functions obey the following *Euler theorem*:¹³

$$\sum_j \frac{\partial f}{\partial x_j} x_j = \lambda f, \quad (2.43)$$

which may be simply proved by differentiating both parts of Eq. (42) over a and then setting this parameter to the particular value $a = 1$. Now, consider the case when the kinetic energy is a quadratic form of all generalized velocities \dot{q}_j :

$$T = \sum_{j,j'} t_{jj'}(q_1, q_2, \dots, t) \dot{q}_j \dot{q}_{j'}, \quad (2.44)$$

with no other terms. It is evident that such T satisfies the definition (42) of a homogeneous function of the velocities with $\lambda = 2$,¹⁴ so that the Euler theorem (43) gives

$$\sum_j \frac{\partial T}{\partial \dot{q}_j} \dot{q}_j = 2T. \quad (2.45)$$

¹³ This is just one of many theorems bearing the name of their author – the genius mathematician Leonhard Euler (1707–1783).

¹⁴ Such functions are called *quadratic-homogeneous*.

But since U is independent of the generalized velocities, $\partial L / \partial \dot{q}_j = \partial T / \partial \dot{q}_j$, and the left-hand side of Eq. (45) is exactly the first term in the definition (32) of the Hamiltonian function, so that in this case

$$H = 2T - L = 2T - (T - U) = T + U = E. \quad (2.46)$$

So, for a system with a kinetic energy of the type (44), for example, a free particle with T considered as a function of its Cartesian velocities,

$$T = \frac{m}{2} (v_x^2 + v_y^2 + v_z^2), \quad (2.47)$$

the notions of the Hamiltonian function and mechanical energy are identical. Indeed, some textbooks, very regrettably, do not distinguish these notions at all! However, as we have seen from our bead-on-the-rotating-ring example, these variables do not always coincide. For that problem, the kinetic energy, in addition to the term proportional to $\dot{\theta}^2$, has another, velocity-independent term – see the first of Eqs. (23) – and hence is *not* a quadratic-homogeneous function of the angular velocity, giving $E \neq H$.

Thus, Eq. (36) expresses a new conservation law, generally different from that of mechanical energy conservation.

2.4. Other conservation laws

Looking at the Lagrange equation (19), we immediately see that if $L \equiv T - U$ is independent of some generalized coordinate q_j , $\partial L / \partial q_j = 0$,¹⁵ then the corresponding generalized momentum is an integral of motion:¹⁶

$$p_j \equiv \frac{\partial L}{\partial \dot{q}_j} = \text{const.} \quad (2.48)$$

For example, for a 1D particle with the Lagrangian (21), the momentum p_x is conserved if the potential energy is constant (and hence the x -component of force is zero) – of course. As a less obvious example, let us consider a 2D motion of a particle in the field of central forces. If we use polar coordinates r and φ in the role of generalized coordinates, then the Lagrangian function¹⁷

$$L \equiv T - U = \frac{m}{2} (\dot{r}^2 + r^2 \dot{\varphi}^2) - U(r) \quad (2.49)$$

is independent of φ , and hence the corresponding generalized momentum,

$$p_\varphi \equiv \frac{\partial L}{\partial \dot{\varphi}} = mr^2 \dot{\varphi}, \quad (2.50)$$

¹⁵ Such coordinates are frequently called *cyclic*, because in some cases (like φ in Eq. (49) below) they represent periodic coordinates such as angles. However, this terminology is somewhat misleading, because some “cyclic” coordinates (e.g., x in our first example) have nothing to do with rotation.

¹⁶ This fact may be considered a particular case of a more general mathematical statement called the *Noether theorem* – named after its author, Emmy Nöther, sometimes called the “greatest woman mathematician ever lived”. Unfortunately, because of time/space restrictions, for its discussion I have to refer the interested reader elsewhere – for example to Sec. 13.7 in H. Goldstein *et al.*, *Classical Mechanics*, 3rd ed. Addison Wesley, 2002.

¹⁷ Note that here \dot{r}^2 is the square of the scalar derivative \dot{r} , rather than the square of the vector $\dot{\mathbf{r}} = \mathbf{v}$.

is conserved. This is just a particular (2D) case of the angular momentum conservation – see Eq. (1.24). Indeed, for the 2D motion within the $[x, y]$ plane, the angular momentum vector,

$$\mathbf{L} \equiv \mathbf{r} \times \mathbf{p} = \begin{vmatrix} \mathbf{n}_x & \mathbf{n}_y & \mathbf{n}_z \\ x & y & z \\ m\dot{x} & m\dot{y} & m\dot{z} \end{vmatrix}, \quad (2.51)$$

has only one component different from zero, namely the component normal to the motion plane:

$$L_z = x(m\dot{y}) - y(m\dot{x}). \quad (2.52)$$

Differentiating the well-known relations between the polar and Cartesian coordinates,

$$x = r \cos \varphi, \quad y = r \sin \varphi, \quad (2.53)$$

over time, and plugging the result into Eq. (52), we see that

$$L_z = mr^2\dot{\varphi} \equiv p_\varphi. \quad (2.54)$$

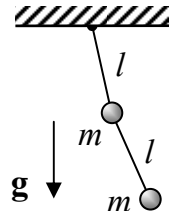
Thus the Lagrangian formalism provides a powerful way of searching for non-evident integrals of motion. On the other hand, if such a conserved quantity is obvious or known *a priori*, it is helpful for the selection of the most appropriate generalized coordinates, giving the simplest Lagrange equations. For example, in the last problem, if we knew in advance that p_φ had to be conserved, this could provide sufficient motivation for using the angle φ as one of the generalized coordinates.

2.5. Exercise problems

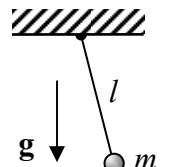
In each of Problems 2.1-2.11, for the given system:

- (i) introduce a convenient set of generalized coordinates q_j ,
- (ii) write down the Lagrangian L as a function of q_j, \dot{q}_j , and (if appropriate) time,
- (iii) write down the Lagrange equation(s) of motion,
- (iv) calculate the Hamiltonian function H ; find out whether it is conserved,
- (v) calculate the mechanical energy E ; is $E = H$?; is the energy conserved?
- (vi) any other evident integrals of motion?

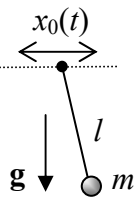
2.1. A double pendulum – see the figure on the right. Consider only the motion within the vertical plane containing the suspension point.



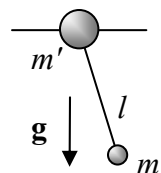
2.2. A stretchable pendulum (i.e. a massive particle hung on an elastic cord that exerts force $F = -\kappa(l - l_0)$, where κ and l_0 are positive constants), also confined to the vertical plane:



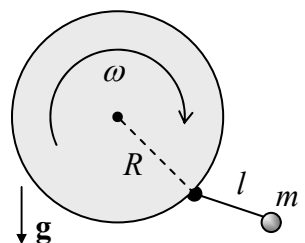
2.3. A fixed-length pendulum hanging from a horizontal support whose motion law $x_0(t)$ is fixed. (No vertical plane constraint here.)



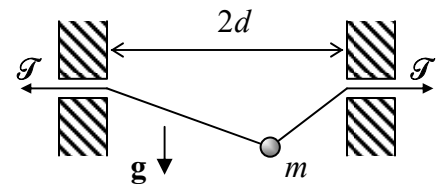
2.4. A pendulum of mass m , hung on another point mass m' that may slide, without friction, along a straight horizontal rail – see the figure on the right. The motion is confined to the vertical plane that contains the rail.



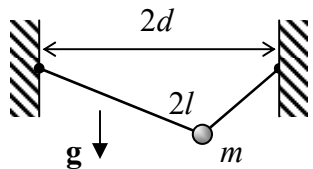
2.5. A point-mass pendulum of length l , attached to the rim of a disk of radius R , that is rotated in a vertical plane with a constant angular velocity ω – see the figure on the right. (Consider only the motion within the disk's plane.)



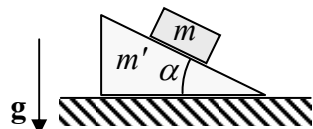
2.6. A bead of mass m , sliding without friction along a light string stretched by a fixed force \mathcal{T} between two horizontally displaced points – see the figure on the right. Here, in contrast to the similar Problem 1.10, the string's tension \mathcal{T} may be comparable with the bead's weight mg , and the motion is *not* restricted to the vertical plane.



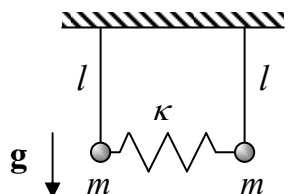
2.7. A bead of mass m , sliding without friction along a light string of a fixed length $2l$, that is hung between two points displaced horizontally by distance $2d < 2l$ – see the figure on the right. As in the previous problem, the motion is not restricted to the vertical plane.



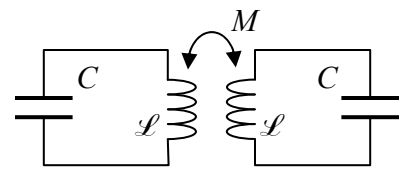
2.8. A block of mass m that can slide, without friction, along the inclined plane surface of a heavy wedge with mass m' . The wedge is free to move, also without friction, along a horizontal surface – see the figure on the right. (Both motions are within the vertical plane containing the steepest slope line.)



2.9. The two-pendula system that was the subject of Problem 1.8 – see the figure on the right.



2.10. A system of two similar, inductively-coupled LC circuits – see the figure on the right.



2.11.* A small *Josephson junction* – the system consisting of two superconductors (S) weakly coupled by Cooper-pair tunneling through a thin insulating layer (I) that separates them – see the figure on the right.



Hints:

- (i) At not very high frequencies (whose quantum $\hbar\omega$ is lower than the binding energy 2Δ of the Cooper pairs), the Josephson effect in a sufficiently small junction may be described by the following coupling energy:

$$U(\varphi) = -E_J \cos \varphi + \text{const},$$

where the constant E_J describes the coupling strength, while the variable φ (called the *Josephson phase difference*) is connected to the voltage V across the junction by the famous *frequency-to-voltage relation*

$$\frac{d\varphi}{dt} = \frac{2e}{\hbar} V,$$

where $e \approx 1.602 \times 10^{-19}$ C is the fundamental electric charge and $\hbar \approx 1.054 \times 10^{-34}$ J·s is the Planck constant.¹⁸

- (ii) The junction (as any system of two close conductors) has a substantial electric capacitance C .

¹⁸ More discussion of the Josephson effect and the physical sense of the variable φ may be found, for example, in EM Sec. 6.5 and QM Secs. 1.6 and 2.8 of this series, but the given problem may be solved without that additional information.

This page is
intentionally left
blank

Chapter 3. A Few Simple Problems

The objective of this chapter is to solve a few simple but very important particle dynamics problems that may be reduced to 1D motion. They notably include the famous “planetary” problem of two particles interacting via a spherically-symmetric potential, and the classical particle scattering problem. In the process of solution, several methods that will be very essential for the analysis of more complex systems are also discussed.

3.1. One-dimensional and 1D-reducible systems

If a particle is confined to motion along a straight line (say, axis x), its position is completely determined by this coordinate. In this case, as we already know, the particle’s Lagrangian function is given by Eq. (2.21):

$$L = T(\dot{x}) - U(x, t), \quad T(\dot{x}) = \frac{m}{2} \dot{x}^2, \quad (3.1)$$

so that the Lagrange equation of motion given by Eq. (2.22),

$$m\ddot{x} = -\frac{\partial U(x, t)}{\partial x} \quad (3.2)$$

is just the x -component of the 2nd Newton’s law.

It is convenient to discuss the dynamics of such *really-1D systems* as a part of a more general class of *effectively-1D systems*. This is a system whose position, due to either holonomic constraints and/or conservation laws, is also fully determined by one generalized coordinate q , and whose Lagrangian may be represented in a form similar to Eq. (1):

Effectively-
1D system

$$L = T_{\text{ef}}(\dot{q}) - U_{\text{ef}}(q, t), \quad T_{\text{ef}} = \frac{m_{\text{ef}}}{2} \dot{q}^2, \quad (3.3)$$

where m_{ef} is some constant which may be considered as the *effective mass* of the system, and the function U_{ef} , its *effective potential energy*. In this case, the Lagrange equation (2.19), describing the system’s dynamics, has a form similar to Eq. (2):

$$m_{\text{ef}} \ddot{q} = -\frac{\partial U_{\text{ef}}(q, t)}{\partial q}. \quad (3.4)$$

As an example, let us return to our testbed system shown in Fig. 2.1. We have already seen that for this system, having one degree of freedom, the genuine kinetic energy T , expressed by the first of Eqs. (2.23), is *not* a quadratically-homogeneous function of the generalized velocity. However, the system’s Lagrangian function (2.23) still may be represented in the form (3),

$$L = \frac{m}{2} R^2 \dot{\theta}^2 + \frac{m}{2} R^2 \omega^2 \sin^2 \theta + mgR \cos \theta + \text{const} \equiv T_{\text{ef}} - U_{\text{ef}}, \quad (3.5)$$

provided that we take

$$T_{\text{ef}} \equiv \frac{m}{2} R^2 \dot{\theta}^2, \quad U_{\text{ef}} \equiv -\frac{m}{2} R^2 \omega^2 \sin^2 \theta - mgR \cos \theta + \text{const.} \quad (3.6)$$

In this new partitioning of the function L , which is legitimate because U_{ef} depends only on the generalized coordinate θ , but not on the corresponding generalized velocity, T_{ef} includes only a part of the genuine kinetic energy T of the bead, while U_{ef} includes not only its real potential energy U in the gravity field but also an additional term related to ring rotation. (As we will see in Sec. 4.6, this term may be interpreted as the effective potential energy due to the inertial centrifugal “force” arising at the problem’s solution in the non-inertial reference frame rotating with the ring.)

Returning to the general case of effectively-1D systems with Lagrangians of the type (3), let us calculate their Hamiltonian function, using its definition (2.32):

$$H = \frac{\partial L}{\partial \dot{q}} \dot{q} - L = m_{\text{ef}} \dot{q}^2 - (T_{\text{ef}} - U_{\text{ef}}) = T_{\text{ef}} + U_{\text{ef}}. \quad (3.7)$$

So, H is expressed via T_{ef} and U_{ef} exactly as the energy E is expressed via genuine T and U .

3.2. Equilibrium and stability

Autonomous systems are defined as dynamic systems whose equations of motion do not depend on time explicitly. For the effectively-1D (and in particular the really-1D) systems obeying Eq. (4), this means that their function U_{ef} , and hence the Lagrangian function (3) should not depend on time explicitly. According to Eqs. (2.35), in such systems, the Hamiltonian function (7), i.e. the sum $T_{\text{ef}} + U_{\text{ef}}$, is an integral of motion. However, be careful! Generally, this conclusion is not valid for the genuine mechanical energy E of such a system; for example, as we already know from Sec. 2.2, for our testbed problem, with the generalized coordinate $q = \theta$ (Fig. 2.1), E is not conserved.

According to Eq. (4), an autonomous system, at appropriate initial conditions, may stay in equilibrium at one or several *stationary* (alternatively called *fixed*) points q_n , corresponding to either the minimum or a maximum of the effective potential energy (see Fig. 1):

$$\frac{dU_{\text{ef}}}{dq}(q_n) = 0. \quad (3.8)$$

Fixed-point condition

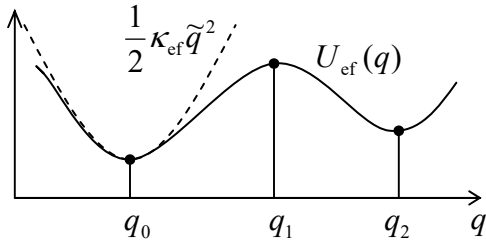


Fig. 3.1. An example of the effective potential energy profile near stable (q_0, q_2) and unstable (q_1) fixed points, and its quadratic approximation (10) near point q_0 .

In order to explore the *stability* of such fixed points, let us analyze the dynamics of small deviations

$$\tilde{q}(t) \equiv q(t) - q_n \quad (3.9)$$

from one of such points. For that, let us expand the function $U_{\text{ef}}(q)$ in the Taylor series at q_n :

$$U_{\text{ef}}(q) = U_{\text{ef}}(q_n) + \frac{dU_{\text{ef}}}{dq}(q_n)\tilde{q} + \frac{1}{2}\frac{d^2U_{\text{ef}}}{dq^2}(q_n)\tilde{q}^2 + \dots \quad (3.10)$$

The first term on the right-hand side, $U_{\text{ef}}(q_n)$, is an arbitrary constant and does not affect motion. The next term, linear in the deviation \tilde{q} , equals zero – see the fixed point’s definition (8). Hence the fixed point’s stability is determined by the next term, quadratic in \tilde{q} , more exactly by its coefficient,

$$\kappa_{\text{ef}} \equiv \frac{d^2U_{\text{ef}}}{dq^2}(q_n), \quad (3.11)$$

which is frequently called the *effective spring constant*. Indeed, neglecting the higher terms of the Taylor expansion (10),¹ we see that Eq. (4) takes the familiar form:

$$m_{\text{ef}}\ddot{\tilde{q}} + \kappa_{\text{ef}}\tilde{q} = 0. \quad (3.12)$$

I am confident that the reader of these notes knows everything about this equation, but since we will soon run into similar but more complex equations, let us review the formal procedure of its solution. From the mathematical standpoint, Eq. (12) is an ordinary linear differential equation of the second order, with constant coefficients. The general theory of such equations tells us that its general solution (for any initial conditions) may be represented as

$$\tilde{q}(t) = c_+ e^{\lambda_+ t} + c_- e^{\lambda_- t}, \quad (3.13)$$

where the constants c_{\pm} are determined by initial conditions, while the so-called *characteristic exponents* λ_{\pm} are completely defined by the equation itself. To calculate these exponents, it is sufficient to plug just one partial solution, $e^{\lambda t}$, into the equation. In our simple case (12), this yields the following *characteristic equation*:

$$m_{\text{ef}}\lambda^2 + \kappa_{\text{ef}} = 0. \quad (3.14)$$

If the ratio $k_{\text{ef}}/m_{\text{ef}}$ is positive, i.e. the fixed point corresponds to the minimum of potential energy (e.g., see points q_0 and q_2 in Fig. 1), the characteristic equation yields

$$\lambda_{\pm} = \pm i\omega_0, \quad \text{with } \omega_0 \equiv \left(\frac{\kappa_{\text{ef}}}{m_{\text{ef}}}\right)^{1/2}, \quad (3.15)$$

(where i is the imaginary unit, $i^2 = -1$), so that Eq. (13) describes *harmonic* (sinusoidal) oscillations of the system,²

$$\tilde{q}(t) = c_+ e^{+i\omega_0 t} + c_- e^{-i\omega_0 t} \equiv c_c \cos \omega_0 t + c_s \sin \omega_0 t, \quad (3.16)$$

¹ Those terms may be important only in very special cases then κ_{ef} is exactly zero, i.e. when a fixed point is also an *inflection point* of the function $U_{\text{ef}}(q)$.

² The reader should not be scared of the first form of (16), i.e. of the representation of a real variable (the deviation from equilibrium) via a sum of two complex functions. Indeed, any real initial conditions give $c_{-}^* = c_+$, so that the sum is real for any t . An even simpler way to deal with such complex representations of real functions will be discussed in the beginning of Chapter 5, and then used throughout this series.

with the frequency ω_0 , about the fixed point – which is thereby *stable*.³ On the other hand, at the potential energy maximum ($k_{\text{ef}} < 0$, e.g., at point q_1 in Fig. 1), we get

$$\lambda_{\pm} = \pm\lambda, \quad \text{where } \lambda \equiv \left(\frac{|k_{\text{ef}}|}{m_{\text{ef}}} \right)^{1/2}, \quad \text{so that } \tilde{q}(t) = c_+ e^{+\lambda t} + c_- e^{-\lambda t}. \quad (3.17)$$

Since the solution has an exponentially growing part,⁴ the fixed point is *unstable*.

Note that the *quadratic* expansion of function $U_{\text{ef}}(q)$, given by the truncation of Eq. (10) to the three displayed terms, is equivalent to a *linear* Taylor expansion of the effective force:

$$F_{\text{ef}} \equiv -\frac{dU_{\text{ef}}}{dq} \approx -\kappa_{\text{ef}} \tilde{q}, \quad (3.18)$$

immediately resulting in the linear equation (12). Hence, to analyze the stability of a fixed point q_n , it is sufficient to *linearize* the equation of motion with respect to small deviations from the point, and study possible solutions of the resulting linear equation. This linearization procedure is typically simpler to carry out than the quadratic expansion (10).

As an example, let us return to our testbed problem (Fig. 2.1) whose function U_{ef} we already know – see the second of Eqs. (6). With it, the equation of motion (4) becomes

$$mR^2 \ddot{\theta} = -\frac{dU_{\text{ef}}}{d\theta} = mR^2 (\omega^2 \cos \theta - \Omega^2) \sin \theta, \quad \text{i.e. } \ddot{\theta} = (\omega^2 \cos \theta - \Omega^2) \sin \theta, \quad (3.19)$$

where $\Omega \equiv (g/R)^{1/2}$ is the frequency of small oscillations of the system at $\omega = 0$ – see Eq. (2.26).⁵ From Eq. (8), we see that on any 2π -long segment of the angle θ ,⁶ the system may have four fixed points; for example, on the half-open segment $(-\pi, +\pi]$ these points are

$$\theta_0 = 0, \quad \theta_1 = \pi, \quad \theta_{2,3} = \pm \cos^{-1} \frac{\Omega^2}{\omega^2}. \quad (3.20)$$

The last two fixed points, corresponding to the bead shifted to either side of the rotating ring, exist only if the angular velocity ω of the rotation exceeds Ω . (In the limit of very fast rotation, $\omega \gg \Omega$, Eq. (20) yields $\theta_{2,3} \rightarrow \pm\pi/2$, i.e. the stationary positions approach the horizontal diameter of the ring – in accordance with our physical intuition.)

To analyze the fixed point stability, we may again use Eq. (9), in the form $\dot{\theta} = \theta_n + \tilde{\theta}$, plug it into Eq. (19), and Taylor-expand both trigonometric functions of θ up to the term linear in $\tilde{\theta}$:

$$\dot{\tilde{\theta}} = [\omega^2 (\cos \theta_n - \sin \theta_n \tilde{\theta}) - \Omega^2] (\sin \theta_n + \cos \theta_n \tilde{\theta}). \quad (3.21)$$

³ This particular type of stability, when the deviation from the equilibrium oscillates with a constant amplitude, neither growing nor decreasing in time, is called either the *orbital*, or “neutral”, or “indifferent” *stability*.

⁴ Mathematically, the growing part vanishes at some special (exact) initial conditions which give $c_+ = 0$. However, the futility of this argument for real physical systems should be obvious to anybody who has ever tried to balance a pencil on its sharp point.

⁵ Note that Eq. (19) coincides with Eq. (2.25). This is a good sanity check illustrating that the procedure (5)-(6) of moving a term from the potential to the kinetic energy within the Lagrangian function is indeed legitimate.

⁶ For this particular problem, the values of θ that differ by a multiple of 2π , are physically equivalent.

Generally, this equation may be linearized further by purging its right-hand side of the term proportional to $\tilde{\theta}^2$; however in this simple case, Eq. (21) is already convenient for analysis. In particular, for the fixed point $\theta_0 = 0$ (corresponding to the bead's position at the bottom of the ring), we have $\cos \theta_0 = 1$ and $\sin \theta_0 = 0$, so that Eq. (21) is reduced to a linear differential equation

$$\ddot{\tilde{\theta}} = (\omega^2 - \Omega^2) \tilde{\theta}, \quad (3.22)$$

whose characteristic equation is similar to Eq. (14) and yields

$$\lambda^2 = \omega^2 - \Omega^2, \quad \text{for } \theta \approx \theta_0. \quad (3.23a)$$

This result shows that if $\omega^2 < \Omega^2$, both roots λ are imaginary, so that this fixed point is orbitally stable. However, if the rotation speed is increased so that $\Omega^2 < \omega^2$, the roots become real: $\lambda_{\pm} = \pm(\omega^2 - \Omega^2)^{1/2}$, with one of them positive, so that the fixed point becomes unstable beyond this threshold, i.e. as soon as fixed points $\theta_{2,3}$ exist. Absolutely similar calculations for other fixed points yield

$$\lambda^2 = \begin{cases} \Omega^2 + \omega^2 > 0, & \text{for } \theta \approx \theta_1, \\ \Omega^2 - \omega^2, & \text{for } \theta \approx \theta_{2,3}. \end{cases} \quad (3.23b)$$

These results show that the fixed point θ_1 (the bead on the top of the ring) is always unstable – just as we could foresee, while the side fixed points $\theta_{2,3}$ are orbitally stable as soon as they exist – at $\Omega^2 < \omega^2$.

Thus, our fixed-point analysis may be summarized very simply: an increase of the ring rotation speed ω beyond a certain threshold value, equal to Ω given by Eq. (2.26), causes the bead to move to one of the ring sides, oscillating about one of the fixed points $\theta_{2,3}$. Together with the rotation about the vertical axis, this motion yields quite a complex (generally, open) spatial trajectory as observed from a lab frame, so it is fascinating that we could analyze it quantitatively in such a simple way.

Later in this course, we will repeatedly use the linearization of the equations of motion for the analysis of the stability of more complex dynamic systems, including those with energy dissipation.

3.3. Hamiltonian 1D systems

Autonomous systems that are described by time-independent Lagrangians are frequently called *Hamiltonian* ones because their Hamiltonian function H (again, not necessarily equal to the genuine mechanical energy E !) is conserved. In our current 1D case, described by Eq. (3),

$$H = \frac{m_{\text{ef}}}{2} \dot{q}^2 + U_{\text{ef}}(q) = \text{const.} \quad (3.24)$$

From the mathematical standpoint, this conservation law is just the first integral of motion. Solving Eq. (24) for \dot{q} , we get the first-order differential equation,

$$\frac{dq}{dt} = \pm \sqrt{\frac{2}{m_{\text{ef}}} [H - U_{\text{ef}}(q)]}, \quad \text{i.e. } \pm \left(\frac{m_{\text{ef}}}{2} \right)^{1/2} \frac{dq}{[H - U_{\text{ef}}(q)]^{1/2}} = dt, \quad (3.25)$$

which may be readily integrated:

$$\pm \left(\frac{m_{\text{ef}}}{2} \right)^{1/2} \int_{q(t_0)}^{q(t)} \frac{dq'}{H - U_{\text{ef}}(q')} = t - t_0. \quad (3.26)$$

Since the constant H (as well as the proper sign before the integral – see below) is fixed by initial conditions, Eq. (26) gives the reciprocal form, $t = t(q)$, of the desired law of system motion, $q(t)$. Of course, for any particular problem the integral in Eq. (26) still has to be worked out, either analytically or numerically, but even the latter procedure is typically much easier than the numerical integration of the initial, second-order differential equation of motion, because at the addition of many values (to which any numerical integration is reduced⁷) the rounding errors are effectively averaged out.

Moreover, Eq. (25) also allows a general classification of 1D system motion. Indeed:

(i) If $H > U_{\text{ef}}(q)$ in the whole range of our interest, the effective kinetic energy T_{ef} (3) is always positive. Hence the derivative dq/dt cannot change its sign, so that this effective velocity retains the sign it had initially. This is an unbound motion in one direction (Fig. 2a).

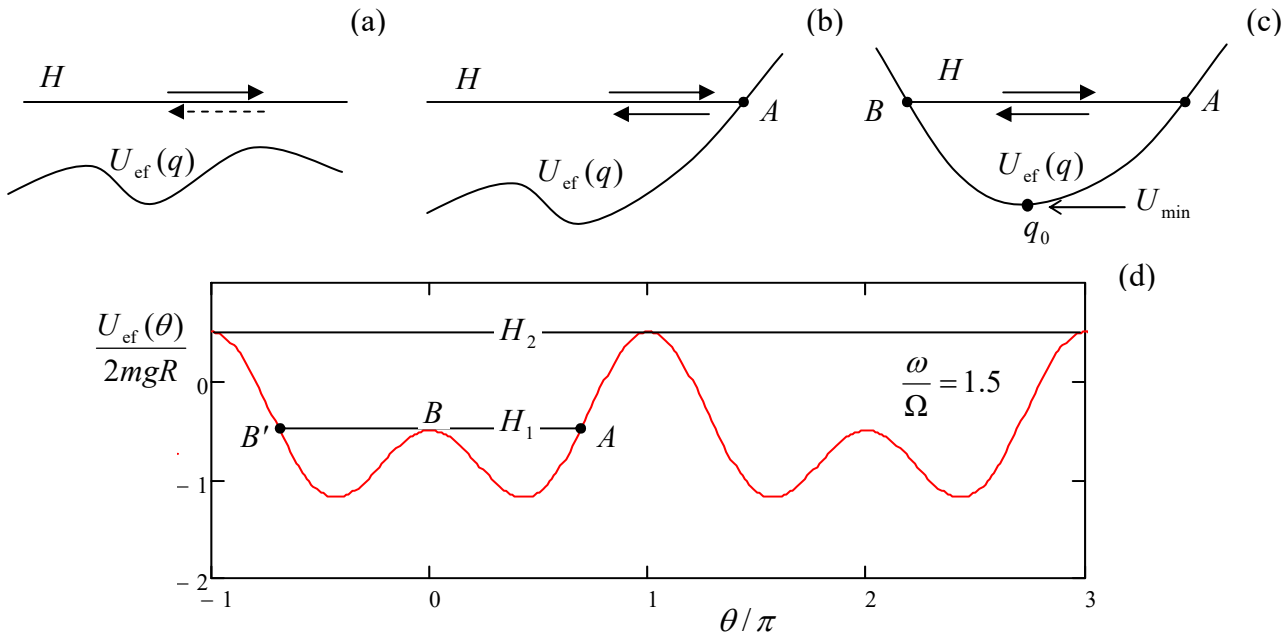


Fig. 3.2. Graphical representations of Eq. (25) for three different cases: (a) an unbound motion, with the velocity sign conserved, (b) a reflection from a “classical turning point”, accompanied by the velocity sign change, and (c) bound, periodic motion between two turning points – schematically. (d) The effective potential energy (6) of the bead on the rotating ring (Fig. 2.1) for a particular case with $\Omega^2 < \omega^2$.

(ii) Now let the particle approach a *classical turning point* A where $H = U_{\text{ef}}(q)$ – see Fig. 2b.⁸ According to Eq. (25), at that point the particle velocity vanishes, while its acceleration, according to Eq. (4), is still finite. This means that the particle’s velocity sign changes its sign at this point, i.e. it is *reflected* from it.

⁷ See, e.g., MA Eqs. (5.2) and (5.3).

⁸ This terminology comes from quantum mechanics, which shows that a particle (or rather its wavefunction) actually can, to a certain extent, penetrate “classically forbidden” regions where $H < U_{\text{ef}}(q)$.

(iii) If, after the reflection from some point A , the particle runs into another classical turning point B (Fig. 2c), the reflection process is repeated again and again, so that the particle is bound to a periodic motion between two turning points.

The last case of *periodic oscillations* presents a large conceptual and practical interest, and the whole Chapter 5 will be devoted to a detailed analysis of this phenomenon and numerous associated effects. Here I will only note that for an autonomous Hamiltonian system described by Eq. (4), Eq. (26) immediately enables the calculation of the oscillation period:

Oscillation period

$$\mathcal{T} = 2 \left(\frac{m_{\text{ef}}}{2} \right)^{1/2} \int_B^A \frac{dq}{[H - U_{\text{ef}}(q)]^{1/2}}, \quad (3.27)$$

where the additional front factor 2 accounts for two time intervals: of the motion from B to A and back – see Fig. 2c. Indeed, according to Eq. (25), at each classically allowed point q , the velocity's magnitude is the same, so these time intervals are equal to each other.

(Note that the dependence of points A and B on H is not necessarily continuous. For example, for our testbed problem, whose effective potential energy is plotted in Fig. 2d for a particular value of $\omega > \Omega$, a gradual increase of H leads to a sudden jump, at $H = H_1$, of the point B to a new position B' , corresponding to a sudden switch from oscillations about one fixed point $\theta_{2,3}$ to oscillations about two adjacent fixed points – before the beginning of a persistent rotation around the ring at $H > H_2$.)

Now let us consider a particular, but a very important limit of Eq. (27). As Fig. 2c shows, if H is reduced to approach U_{\min} , the periodic oscillations take place at the very bottom of this *potential well*, about a stable fixed point q_0 . Hence, if the potential energy profile is smooth enough, we may limit the Taylor expansion (10) to the displayed quadratic term. Plugging it into Eq. (27), and using the mirror symmetry of this particular problem about the fixed point q_0 , we get

$$\mathcal{T} = 4 \left(\frac{m_{\text{ef}}}{2} \right)^{1/2} \int_0^A \frac{d\tilde{q}}{[H - (U_{\min} + \kappa_{\text{ef}} \tilde{q}^2 / 2)]^{1/2}} = \frac{4}{\omega_0} I, \quad \text{with } I \equiv \int_0^1 \frac{d\xi}{(1 - \xi^2)^{1/2}}, \quad (3.28)$$

where $\xi \equiv \tilde{q} / A$, with $A \equiv (2/\kappa_{\text{ef}})^{1/2}(H - U_{\min})^{1/2}$ being the classical turning point, i.e. the oscillation amplitude, and ω_0 the frequency given by Eq. (15). Taking into account that the elementary integral I in that equation equals $\pi/2$,⁹ we finally get

$$\mathcal{T} = \frac{2\pi}{\omega_0}, \quad (3.29)$$

as it should be for the harmonic oscillations (16). Note that the oscillation period does not depend on the oscillation amplitude A , i.e. on the difference $(H - U_{\min})$ – while it is sufficiently small.

3.4. Planetary problems

Leaving a more detailed study of oscillations for Chapter 5, let us now discuss the so-called *planetary systems*¹⁰ whose description, somewhat surprisingly, may be also reduced to an effectively 1D

⁹Indeed, introducing a new variable ζ as $\xi \equiv \sin \zeta$, we get $d\xi = \cos \zeta d\zeta = (1 - \xi^2)^{1/2} d\zeta$, so that the function under the integral is just $d\zeta$, and its limits are $\zeta = 0$ and $\zeta = \pi/2$.

problem. Indeed, consider two particles that interact via a conservative central force $\mathbf{F}_{21} = -\mathbf{F}_{12} = \mathbf{n}_r F(r)$, where r and \mathbf{n}_r are, respectively, the magnitude and the direction of the *distance vector* $\mathbf{r} \equiv \mathbf{r}_1 - \mathbf{r}_2$ connecting the two particles (Fig. 3).

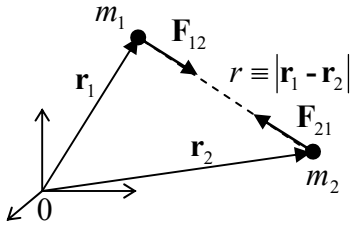


Fig. 3.3. Vectors in the planetary problem.

Generally, two particles moving without constraints in 3D space, have $3 + 3 = 6$ degrees of freedom, which may be described, e.g., by their Cartesian coordinates $\{x_1, y_1, z_1, x_2, y_2, z_2\}$. However, for this particular form of interaction, the following series of tricks allows the number of essential degrees of freedom to be reduced to just one.

First, the conservative force of particle interaction may be described by a time-independent potential energy $U(r)$, such that $F(r) = -\partial U(r)/\partial r$.¹¹ Hence the Lagrangian function of the system is

$$L \equiv T - U(r) = \frac{m_1}{2} \dot{\mathbf{r}}_1^2 + \frac{m_2}{2} \dot{\mathbf{r}}_2^2 - U(r). \quad (3.30)$$

Let us perform the transfer from the initial six scalar coordinates of the particles to the following six generalized coordinates: three Cartesian components of the distance vector

$$\mathbf{r} \equiv \mathbf{r}_1 - \mathbf{r}_2, \quad (3.31)$$

and three scalar components of the following vector:

$$\mathbf{R} \equiv \frac{m_1 \mathbf{r}_1 + m_2 \mathbf{r}_2}{M}, \quad \text{with } M \equiv m_1 + m_2,$$

(3.32)

Center of mass

which defines the position of the *center of mass* of the system, with the total mass M . Solving the system of two linear equations (31) and (32) for \mathbf{r}_1 and \mathbf{r}_2 , we get

$$\mathbf{r}_1 = \mathbf{R} + \frac{m_2}{M} \mathbf{r}, \quad \mathbf{r}_2 = \mathbf{R} - \frac{m_1}{M} \mathbf{r}. \quad (3.33)$$

Plugging these relations into Eq. (30), we see that it is reduced it to

$$L = \frac{M}{2} \dot{\mathbf{R}}^2 + \frac{m}{2} \dot{\mathbf{r}}^2 - U(r), \quad (3.34)$$

where m is the so-called *reduced mass*:

$$m \equiv \frac{m_1 m_2}{M}, \quad \text{so that } \frac{1}{m} \equiv \frac{1}{m_1} + \frac{1}{m_2}.$$

(3.35)

Reduced mass

¹⁰ This name is very conditional, because this group of problems includes, for example, charged particle scattering (see Sec. 3.7 below).

¹¹ See, e.g., MA Eq. (10.8) with $\partial/\partial\theta = \partial/\partial\varphi = 0$.

Note that according to Eq. (35), the reduced mass is lower than that of the lightest component of the two-body system. If one of $m_{1,2}$ is *much* less than its counterpart (like it is in most star-planet or planet-satellite systems), then with a good precision $m \approx \min [m_1, m_2]$.

Since the Lagrangian function (34) depends only on $\dot{\mathbf{R}}$ rather than \mathbf{R} itself, according to our discussion in Sec. 2.4, all Cartesian components of R are cyclic coordinates, and the corresponding generalized momenta are conserved:

$$P_j \equiv \frac{\partial L}{\partial \dot{R}_j} \equiv M \dot{R}_j = \text{const}, \quad j = 1, 2, 3. \quad (3.36)$$

Physically, this is just the conservation law for the full momentum $\mathbf{P} \equiv M\mathbf{R}$ of our system, due to the absence of external forces. Actually, in the axiomatics used in Sec. 1.3 this law is postulated – see Eq. (1.10) – but now we may attribute the momentum \mathbf{P} to a certain geometric point, with the center-of-mass radius vector \mathbf{R} . In particular, since according to Eq. (36) the center moves with a constant velocity in the inertial reference frame used to write Eq. (30), we may consider a new inertial frame with the origin at point \mathbf{R} . In this new frame, $\mathbf{R} \equiv 0$, so that the vector \mathbf{r} (and hence the scalar r) remain the same as in the old frame (because the frame transfer vector adds equally to \mathbf{r}_1 and \mathbf{r}_2 , and cancels in $\mathbf{r} = \mathbf{r}_1 - \mathbf{r}_2$), and the Lagrangian (34) is now reduced to

$$L = \frac{m}{2} \dot{\mathbf{r}}^2 - U(r). \quad (3.37)$$

Thus our initial problem has been reduced to just three degrees of freedom – three scalar components of the vector \mathbf{r} . In other words, Eq. (37) shows that the dynamics of the vector \mathbf{r} of our initial, two-particle system is identical to that of the radius vector of a *single particle* with the effective mass m , moving in the central potential field $U(r)$.

Two more degrees of freedom may be excluded from the planetary problem by noticing that according to Eq. (1.35), the angular momentum $\mathbf{L} = \mathbf{r} \times \mathbf{p}$ of our effective single particle of mass m is also conserved, both in magnitude and direction. Since the direction of \mathbf{L} is, by its definition, perpendicular to both \mathbf{r} and $\mathbf{v} = \mathbf{p}/m$, this means that the particle's motion is confined to the plane whose orientation is determined by the initial directions of the vectors \mathbf{r} and \mathbf{v} . Hence we can completely describe the particle's position by just two coordinates in that plane, for example by the distance r to the origin, and the polar angle φ . In these coordinates, Eq. (37) takes the form identical to Eq. (2.49):

$$L = \frac{m}{2} (\dot{r}^2 + r^2 \dot{\varphi}^2) - U(r). \quad (3.38)$$

Moreover, the latter coordinate, polar angle φ , may be also eliminated by using the conservation of angular momentum's magnitude, in the form of Eq. (2.50):¹²

$$L_z = mr^2 \dot{\varphi} = \text{const}. \quad (3.39)$$

A direct corollary of this conservation is the so-called *2^{nd Kepler's law}*:¹³ the radius vector \mathbf{r} sweeps equal areas A in equal time periods. Indeed, in the linear approximation in $dA \ll A$, the area

¹² Here index z stands for the coordinate perpendicular to the motion plane. Since other components of the angular momentum equal zero, this index is not really necessary, but I will still use it – just to make a clear distinction between the angular momentum L_z and the Lagrangian function L .

differential dA is equal to the area of a narrow right triangle with the base being the arc differential $rd\phi$, and the height equal to r – see Fig. 4. As a result, according to Eq. (39), the time derivative of the area,

$$\frac{dA}{dt} = \frac{r(rd\phi)/2}{dt} \equiv \frac{1}{2} r^2 \dot{\phi} = \frac{L_z}{2m}, \quad (3.40)$$

remains constant. Since the factor $L_z/2m$ is constant, integration of this equation over an arbitrary (not necessarily small!) time interval Δt proves the 2nd Kepler's law: $A \propto \Delta t$.

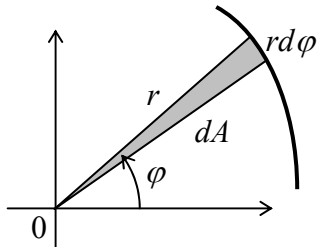


Fig. 3.4. The area differential dA in the polar coordinates.

Now note that since $\partial L/\partial t = 0$, the Hamiltonian function H is also conserved, and since, according to Eq. (38), the kinetic energy of the system is a quadratic-homogeneous function of the generalized velocities \dot{r} and $\dot{\phi}$, we have $H = E$, so that the system's energy E ,

$$E = \frac{m}{2} \dot{r}^2 + \frac{m}{2} r^2 \dot{\phi}^2 + U(r), \quad (3.41)$$

is also the first integral of motion.¹⁴ But according to Eq. (39), the second term on the right-hand side of Eq. (41) may be represented as

$$\frac{m}{2} r^2 \dot{\phi}^2 = \frac{L_z^2}{2mr^2}, \quad (3.42)$$

so that the energy (41) may be expressed as that of a 1D particle moving along axis r ,

$$E = \frac{m}{2} \dot{r}^2 + U_{\text{ef}}(r), \quad (3.43)$$

in the following effective potential:

$$U_{\text{ef}}(r) \equiv U(r) + \frac{L_z^2}{2mr^2}. \quad (3.44)$$

Effective potential energy

So the planetary motion problem has been reduced to the study of an effectively-1D system.¹⁵

¹³ This is one of the three laws deduced, from the extremely detailed astronomical data collected by Tycho Brahe (1546-1601), by Johannes Kepler in the early 17th century. In turn, the three Kepler's laws have become the main basis for Newton's discovery, a few decades later, of the gravity law (1.15). That relentless march of physics...

¹⁴ One may argue that this fact should have been evident earlier because the effective particle of mass m moves in a potential field $U(r)$, which conserves energy.

¹⁵ Note that this reduction has been done in a way different from that used for our testbed problem (Fig. 2.1) in Sec. 2 above. (The reader is encouraged to analyze this difference.) To emphasize this fact, I will keep writing E instead of H here, though for the planetary problem we are discussing now, these two notions coincide.

Now we may proceed just like we did in Sec. 3, with due respect to the very specific effective potential (44) which, in particular, diverges at $r \rightarrow 0$ – besides the very special case of an exactly radial motion, $L_z = 0$. In particular, we may solve Eq. (43) for dr/dt to get

$$dt = \left(\frac{m}{2} \right)^{1/2} \frac{dr}{[E - U_{\text{ef}}(r)]^{1/2}}. \quad (3.45)$$

This equation allows us not only to get a direct relation between time t and distance r , similarly to Eq. (26),

$$t = \pm \left(\frac{m}{2} \right)^{1/2} \int \frac{dr}{[E - U_{\text{ef}}(r)]^{1/2}} = \pm \left(\frac{m}{2} \right)^{1/2} \int \frac{dr}{[E - U(r) - L_z^2 / 2mr^2]^{1/2}}, \quad (3.46)$$

but also do a similar calculation of the angle φ of the effective particle. Indeed, integrating Eq. (39),

$$\varphi \equiv \int \dot{\varphi} dt = \frac{L_z}{m} \int \frac{dt}{r^2}, \quad (3.47)$$

and plugging dt from Eq. (45), we get an explicit expression for the particle's trajectory $\varphi(r)$:

$$\varphi = \pm \frac{L_z}{(2m)^{1/2}} \int \frac{dr}{r^2 [E - U_{\text{ef}}(r)]^{1/2}} = \pm \frac{L_z}{(2m)^{1/2}} \int \frac{dr}{r^2 [E - U(r) - L_z^2 / 2mr^2]^{1/2}}. \quad (3.48)$$

Note that according to Eq. (39), the derivative $d\varphi/dt$ does *not* change sign at the reflection from any classical turning point $r \neq 0$, so that, in contrast to Eq. (46), the sign on the right-hand side of Eq. (48) is uniquely determined by the initial conditions and cannot change during the motion.

Let us use these results, valid for any interaction law $U(r)$, for the planetary motion's classification. (Following a good tradition, in what follows I will select the arbitrary constant in the potential energy in the way to provide $U \rightarrow 0$ and hence $U_{\text{ef}} \rightarrow 0$, at $r \rightarrow \infty$.) The following cases should be distinguished.

If $U(r) < 0$, i.e. the particle interaction is *attractive* (as it always is in the case of gravity), and the divergence of the attractive potential at $r \rightarrow 0$ is faster than $1/r^2$, then $U_{\text{ef}}(r) \rightarrow -\infty$ at $r \rightarrow 0$, so that at appropriate initial conditions the particle may drop on the center even if $L_z \neq 0$ – the event called the *capture*.¹⁶ On the other hand, with $U(r)$ either converging or diverging slower than $1/r^2$, at $r \rightarrow 0$, the effective energy profile $U_{\text{ef}}(r)$ has the shape shown schematically in Fig. 5. This is true, in particular, for the very important case

$$U(r) = -\frac{\alpha}{r}, \quad \text{with } \alpha > 0, \quad (3.49)$$

which describes, in particular, the *Coulomb* (electrostatic) *interaction* of two particles with electric charges of opposite signs, and Newton's gravity law (1.15). This particular case will be analyzed in detail below, but for now let us return to the analysis of an arbitrary attractive potential $U(r) < 0$ leading to the effective potential shown in Fig. 5 when the angular-momentum term in Eq. (44) dominates at small distances r .

¹⁶ In order to analyze what exactly happens at the capture, i.e. at $r = 0$, we would need a model more specific than Eq. (30).

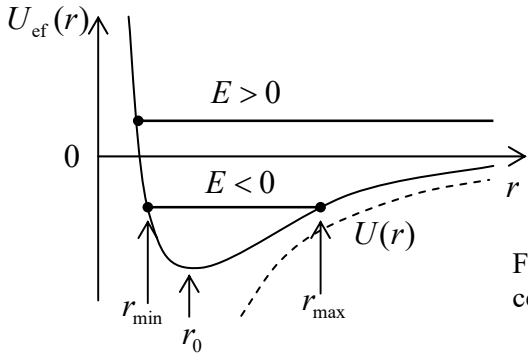


Fig. 3.5. Effective potential profile of an attractive central field, and two types of motion in it.

According to the analysis in Sec. 3, such potential profile, with a minimum at some distance r_0 , may sustain two types of motion, depending on the energy E (determined by initial conditions):

(i) If $E > 0$, there is only one classical turning point where $E = U_{\text{ef}}$, so that the distance r either grows with time from the very beginning or (if the initial value of \dot{r} was negative) first decreases and then, after the reflection from the increasing potential U_{ef} , starts to grow indefinitely. The latter case, of course, describes the *scattering* of the effective particle by the attractive center.¹⁷

(ii) On the opposite, if the energy is within the range

$$U_{\text{ef}}(r_0) \leq E < 0, \quad (3.50)$$

the system moves periodically between two classical turning points r_{\min} and r_{\max} – see Fig. 5. These oscillations of the distance r correspond to the bound orbital motion of our effective particle about the attracting center.

Let us start with the discussion of the bound motion, with the energy within the range (50). If the energy has its minimal possible value,

$$E = U_{\text{ef}}(r_0) \equiv \min[U_{\text{ef}}(r)], \quad (3.51)$$

the distance cannot change, $r = r_0 = \text{const}$, so that the particle's orbit is circular, with the radius r_0 satisfying the condition $dU_{\text{ef}}/dr = 0$. Using Eq. (44), we see that the condition for r_0 may be written as

$$\frac{L_z^2}{mr_0^3} = \frac{dU}{dr} \Big|_{r=r_0}. \quad (3.52)$$

Since at circular motion, the velocity \mathbf{v} is perpendicular to the radius vector \mathbf{r} , L_z is just mr_0v , the left-hand side of Eq. (52) equals mv^2/r_0 , while its right-hand side is just the magnitude of the attractive force, so that this equality expresses the well-known 2nd Newton's law for the circular motion. Plugging this result into Eq. (47), we get a linear law of angle change, $\varphi = \omega t + \text{const}$, with the angular velocity

$$\omega = \frac{L_z}{mr_0^2} = \frac{v}{r_0}, \quad (3.53)$$

and hence the rotation period $\mathcal{T}_\varphi \equiv 2\pi/\omega$ obeys the elementary relation

¹⁷ In the opposite case when the interaction is *repulsive*, $U(r) > 0$, the addition of the positive angular energy term only increases the trend, and the scattering scenario is the only one possible.

$$\mathcal{T}_\varphi = \frac{2\pi r_0}{v}. \quad (3.54)$$

Now let the energy be above its minimum value (but still negative). Using Eq. (46) just as in Sec. 3, we see that the distance r oscillates with the period

$$\mathcal{T}_r = 2 \left(\frac{m}{2} \right)^{1/2} \int_{r_{\min}}^{r_{\max}} \frac{dr}{[E - U(r) - L_z^2 / 2mr^2]^{1/2}}. \quad (3.55)$$

This period is not necessarily equal to another period, \mathcal{T}_φ , that corresponds to the 2π -change of the angle. Indeed, according to Eq. (48), the change of the angle φ between two sequential points of the nearest approach,

$$|\Delta\varphi| = 2 \frac{L_z}{(2m)^{1/2}} \int_{r_{\min}}^{r_{\max}} \frac{dr}{r^2 [E - U(r) - L_z^2 / 2mr^2]^{1/2}}, \quad (3.56)$$

is generally different from 2π . Hence, the general trajectory of the bound motion has a spiral shape – see, e.g., an illustration in Fig. 6.

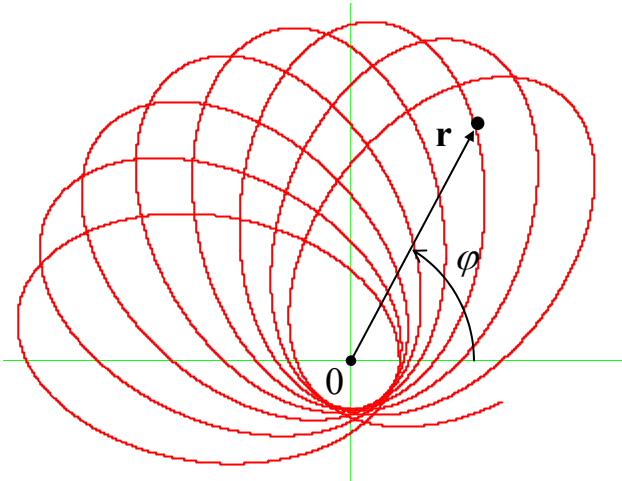


Fig. 3.6. A typical open orbit of a particle moving in a non-Coulomb central field.

The situation is special, however, for a very important particular case, namely that of the Coulomb potential described by Eq. (49).¹⁸ Indeed, plugging this potential into Eq. (48), we get

$$\varphi = \pm \frac{L_z}{(2m)^{1/2}} \int \frac{dr}{r^2 (E + \alpha/r - L_z^2 / 2mr^2)^{1/2}}. \quad (3.57)$$

This is a table integral,¹⁹ giving

$$\varphi = \pm \cos^{-1} \frac{L_z^2 / m\alpha r - 1}{(1 + 2EL_z^2 / m\alpha^2)^{1/2}} + \text{const.} \quad (3.58)$$

¹⁸ For the power-law interaction, $U \propto r^\nu$, the orbits are closed curves only if $\nu = -1$ (the Coulomb potential) or if $\nu = +2$ (the 3D harmonic oscillator) – the so-called *Bertrand theorem*, proved by J. Bertrand only in 1873.

¹⁹ See, e.g., MA Eq. (6.3a).

Hence the reciprocal function, $r(\varphi)$, is 2π -periodic:

$$r = \frac{p}{1 + e \cos(\varphi + \text{const})}, \quad (3.59)$$

so that at $E < 0$, the orbit is a closed line characterized by the following parameters:²⁰

$$p \equiv \frac{L_z^2}{m\alpha}, \quad e \equiv \left(1 + \frac{2EL_z^2}{m\alpha^2}\right)^{1/2}. \quad (3.60)$$

Elliptic orbit and its parameters

The physical meaning of these parameters is very simple. Indeed, the general Eq. (52), in the Coulomb potential for which $dU/dr = \alpha/r^2$, shows that p is just the circular orbit radius²¹ for the given L_z : $r_0 = L_z^2/m\alpha \equiv p$, so that

$$\min[U_{\text{ef}}(r)] \equiv U_{\text{ef}}(r_0) = -\frac{\alpha^2 m}{2L_z^2}. \quad (3.61)$$

Using this equality together with the second of Eqs. (60), we see that the parameter e (called the *eccentricity*) may be represented just as

$$e = \left\{1 - \frac{E}{\min[U_{\text{ef}}(r)]}\right\}^{1/2}. \quad (3.62)$$

Analytical geometry tells us that Eq. (59), with $e < 1$, is one of the canonical representations of an *ellipse*, with one of its two focuses located at the origin. The fact that planets have such trajectories is known as the *1st Kepler's law*. Figure 7 shows the relations between the dimensions of the ellipse and the parameters p and e .²²

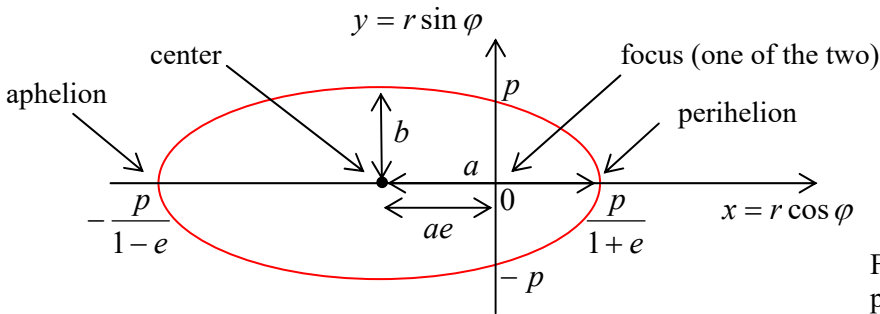


Fig. 3.7. Ellipse, and its special points and dimensions.

In particular, the *major semi-axis* a and the *minor semi-axis* b are simply related to p and e and hence, via Eqs. (60), to the motion integrals E and L_z :

$$a = \frac{p}{1 - e^2} = \frac{\alpha}{2|E|}, \quad b = \frac{p}{(1 - e^2)^{1/2}} = \frac{L_z}{(2m|E|)^{1/2}}. \quad (3.63)$$

²⁰ Let me hope that the difference between the parameter p and the particle momentum's magnitude is absolutely clear from the context, so that using the same (traditional) notation for both notions cannot lead to confusion.

²¹ Mathematicians prefer a more solemn terminology: the parameter $2p$ is called the *latus rectum* of the ellipse.

²² In this figure, the constant participating in Eqs. (58)-(59) is assumed to be zero. A different choice of the constant corresponds just to a different origin of φ , i.e. a constant turn of the ellipse about the origin.

As was mentioned above, at $E \rightarrow \min [U_{\text{ef}}(r)]$ the orbit is almost circular, with $r(\phi) \approx r_0 \approx p$. On the contrary, as E is increased to approach zero (its maximum value for the closed orbit), then $e \rightarrow 1$, so that the aphelion point $r_{\max} = p/(1 - e)$ tends to infinity, i.e. the orbit becomes extremely extended – see the magenta lines in Fig. 8.

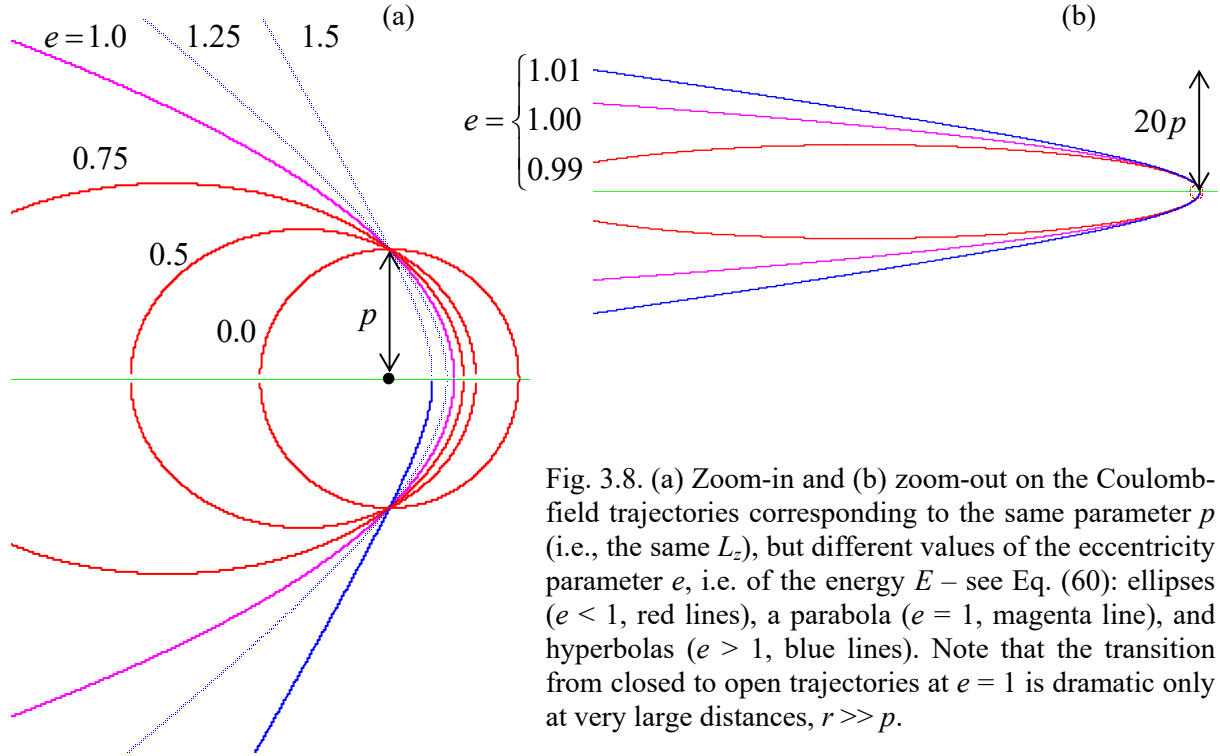


Fig. 3.8. (a) Zoom-in and (b) zoom-out on the Coulomb-field trajectories corresponding to the same parameter p (i.e., the same L_z), but different values of the eccentricity parameter e , i.e. of the energy E – see Eq. (60): ellipses ($e < 1$, red lines), a parabola ($e = 1$, magenta line), and hyperbolas ($e > 1$, blue lines). Note that the transition from closed to open trajectories at $e = 1$ is dramatic only at very large distances, $r \gg p$.

The above relations enable, in particular, a ready calculation of the rotation period $\mathcal{T} \equiv \mathcal{T}_r = \mathcal{T}_\phi$. (In the case of a closed trajectory, \mathcal{T}_r and \mathcal{T}_ϕ coincide.) Indeed, it is well known that the ellipse's area $A = \pi ab$. But according to the 2nd Kepler's law (40), $dA/dt = L_z/2m = \text{const}$. Hence

$$\mathcal{T} = \frac{A}{dA/dt} = \frac{\pi ab}{L_z/2m}. \quad (3.64a)$$

Using Eqs. (60) and (63), this important result may be represented in several other forms:

$$\mathcal{T} = \frac{\pi p^2}{(1-e^2)^{3/2}(L_z/2m)} = \pi \alpha \left(\frac{m}{2|E|^3} \right)^{1/2} = 2\pi a^{3/2} \left(\frac{m}{\alpha} \right)^{1/2}. \quad (3.64b)$$

Since for the Newtonian gravity (1.15), $\alpha = Gm_1m_2 = GmM$, at $m_1 \ll m_2$ (i.e. $m \ll M$) this constant is proportional to m , and the last form of Eq. (64b) yields the 3rd Kepler's law: periods of motion of different planets in the same central field, say that of our Sun, scale as $\mathcal{T} \propto a^{3/2}$. Note that in contrast to the 2nd Kepler's law (which is valid for any central field), the 1st and the 3rd Kepler's laws are potential-specific.

Now reviewing the above derivation of Eqs. (59)-(60), we see that they are also valid in the case of $E \geq 0$ – see the top horizontal line in Fig. 5 and its discussion above, if we limit the results to the

physically meaningful range $r \geq 0$. This means that if the energy is exactly zero, Eq. (59) (with $e = 1$) is still valid for all values of φ (except for one special point $\varphi = \pi$ where r becomes infinite) and describes a *parabolic* (i.e. open) trajectory – see the magenta lines in Fig. 8.

Moreover, if $E > 0$, Eq. (59) is still valid within a certain sector of angles φ ,

$$\Delta\varphi = 2\cos^{-1} \frac{1}{e} \equiv 2\cos^{-1} \left(1 + \frac{2EL_z^2}{m\alpha^2} \right)^{-1/2} < \pi, \quad \text{for } E > 0, \quad (3.65)$$

and describes an open, *hyperbolic* trajectory (see the blue lines in Fig. 8). As was mentioned earlier, such trajectories are typical, in particular, for particle scattering.

3.5. Elastic scattering

If $E > 0$, the motion is unbound for any realistic interaction potential. In this case, the two most important parameters of the particle trajectory are the *impact parameter* b and the *scattering angle* θ (Fig. 9), and the main task of the theory is to find the relation between them in the given potential $U(r)$.

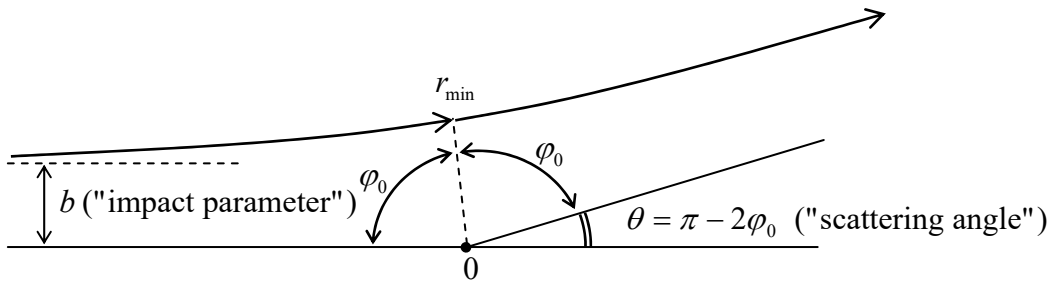


Fig. 3.9. Main geometric parameters of the scattering problem.

For that, it is convenient to note that b is related to the two conserved quantities, the particle's energy²³ E and its angular momentum L_z , in a simple way. Indeed, at $r \gg b$, the definition $\mathbf{L} = \mathbf{r} \times (\mathbf{v}m)$ yields $L_z = bm v_\infty$, where $v_\infty = (2E/m)^{1/2}$ is the initial (and hence the final) speed of the particle, so that

$$L_z = b(2mE)^{1/2}. \quad (3.66)$$

Hence the angular contribution to the effective potential (44) may be represented as

$$\frac{L_z^2}{2mr^2} = E \frac{b^2}{r^2}. \quad (3.67)$$

Next, according to Eq. (48), the trajectory sections going from infinity to the nearest approach point ($r = r_{\min}$) and from that point to infinity, have to be similar, and hence correspond to equal angle changes φ_0 – see Fig. 9. Hence we may apply the general Eq. (48) to just one of the sections, say $[r_{\min}, \infty]$, to find the scattering angle:

²³ The energy conservation law is frequently emphasized by calling such process *elastic scattering*.

$$\theta = \pi - 2\varphi_0 = \pi - 2 \frac{L_z}{(2m)^{1/2}} \int_{r_{\min}}^{\infty} \frac{dr}{r^2 [E - U(r) - L_z^2 / 2mr^2]^{1/2}} \equiv \pi - 2 \int_{r_{\min}}^{\infty} \frac{b dr}{r^2 [1 - U(r)/E - b^2/r^2]^{1/2}}. \quad (3.68)$$

In particular, for the Coulomb potential (49), now with an arbitrary sign of α , we can use the same table integral as in the previous section to get²⁴

$$|\theta| = \left| \pi - 2 \cos^{-1} \frac{\alpha/2Eb}{[1 + (\alpha/2Eb)^2]^{1/2}} \right|. \quad (3.69a)$$

This result may be more conveniently rewritten as

$$\tan \frac{|\theta|}{2} = \frac{|\alpha|}{2Eb}. \quad (3.69b)$$

Very clearly, the scattering angle's magnitude increases with the potential strength α , and decreases as either the particle energy or the impact parameter (or both) are increased.

The general result (68) and the Coulomb-specific relations (69) represent a formally complete solution of the scattering problem. However, in a typical experiment on elementary particle scattering, the impact parameter b of a single particle is unknown. In this case, our results may be used to obtain the statistics of the scattering angle θ , in particular, the so-called *differential cross-section*²⁵

Differential cross-section

$$\frac{d\sigma}{d\Omega} \equiv \frac{1}{n} \frac{dN}{d\Omega}, \quad (3.70)$$

where n is the average number of the *incident* particles per unit area, and dN is the average number of the particles *scattered* into a small solid angle interval $d\Omega$. For a uniform beam of initial particles, $d\sigma/d\Omega$ may be calculated by counting the average number of incident particles that have the impact parameters within a small range db :

$$dN = n 2\pi b db. \quad (3.71)$$

Scattered by a spherically-symmetric center, which provides an axially-symmetric scattering pattern, these particles are scattered into the corresponding small solid angle interval $d\Omega = 2\pi |\sin\theta d\theta|$. Plugging these two equalities into Eq. (70), we get the following general geometric relation:

$$\frac{d\sigma}{d\Omega} = b \left| \frac{db}{\sin\theta d\theta} \right|. \quad (3.72)$$

In particular, for the Coulomb potential (49), a straightforward differentiation of Eq. (69) yields the so-called *Rutherford scattering formula* (reportedly derived by R. H. Fowler):

Rutherford scattering formula

$$\frac{d\sigma}{d\Omega} = \left(\frac{\alpha}{4E} \right)^2 \frac{1}{\sin^4(\theta/2)}. \quad (3.73)$$

²⁴ Alternatively, this result may be recovered directly from the first form of Eq. (65), with the eccentricity e expressed via the same dimensionless parameter $(2Eb/\alpha)$: $e = [1 + (2Eb/\alpha)^2]^{1/2} > 1$.

²⁵ This terminology stems from the fact that an integral (74) of $d\sigma/d\Omega$ over the full solid angle, called the *total cross-section* σ , has the dimension of the area: $\sigma = N/n$, where N is the total number of scattered particles.

This result, which shows very strong scattering to small angles (so strong that the integral that expresses the total cross-section

$$\sigma \equiv \oint \frac{d\sigma}{d\Omega} d\Omega \quad (3.74)$$

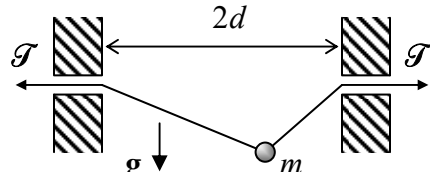
Total cross-section

is diverging at $\theta \rightarrow 0$),²⁶ and very weak *backscattering* (to angles $\theta \approx \pi$) was historically extremely significant: in the early 1910s, its good agreement with α -particle scattering experiments carried out by Ernest Rutherford's group gave a strong justification for his introduction of the *planetary model* of atoms, with electrons moving around very small nuclei – just as planets move around stars.

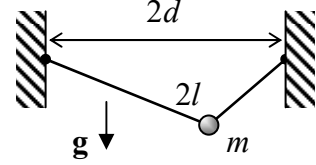
Note that elementary particle scattering is frequently accompanied by electromagnetic radiation and/or other processes leading to the loss of the initial mechanical energy of the system. Such *inelastic scattering* may give significantly different results. (In particular, the capture of an incoming particle becomes possible even for a Coulomb attracting center.) Also, quantum-mechanical effects may be important at the scattering of light particles with relatively low energies,²⁷ so that the above results should be used with caution.

3.6. Exercise problems

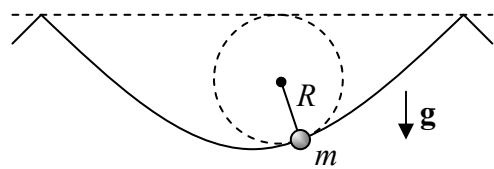
3.1. For the system considered in Problem 2.6 (a bead sliding along a string with fixed tension \mathcal{T} , see the figure on the right), analyze small oscillations of the bead near the equilibrium.



3.2. For the system considered in Problem 2.7 (a bead sliding along a string of a fixed length $2l$, see the figure on the right), analyze small oscillations near the equilibrium.



3.3. A bead is allowed to slide, without friction, along an inverted cycloid in a vertical plane – see the figure on the right. Calculate the frequency of its free oscillations as a function of their amplitude.



3.4. For a 1D particle of mass m , placed into potential $U(q) = \alpha q^{2n}$ (where $\alpha > 0$, and n is a positive integer), calculate the functional dependence of the particle oscillation period \mathcal{T} on its energy E . Explore the limit $n \rightarrow \infty$.

3.5. Two small masses m_1 and $m_2 \leq m_1$ may slide, without friction, over a horizontal surface. They are connected with a spring with equilibrium length l and elastic constant κ , and at $t < 0$ are at rest.

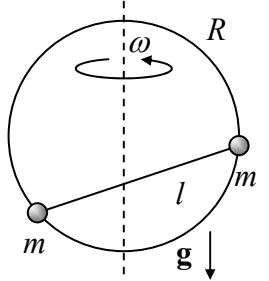
²⁶ This divergence, which persists at the quantum-mechanical treatment of the problem (see, e.g., QM Chapter 3), is due to particles with very large values of b , and disappears at an account, for example, of any non-zero concentration of the scattering centers.

²⁷ Their discussion may be found in QM Secs. 3.3 and 3.8.

At $t = 0$, the first of these masses receives a very short kick with impulse $\mathbf{P} \equiv \int \mathbf{F}(t)dt$ in the direction normal to the spring line. Calculate the largest and smallest magnitude of its velocity at $t > 0$.

3.6. Explain why the term $mr^2\dot{\phi}^2/2$, recast in accordance with Eq. (42), cannot be merged with $U(r)$ in Eq. (38), to form an effective 1D potential energy $U(r) - L_z^2/2mr^2$, with the second term's sign opposite to that given by Eq. (44). We have done an apparently similar thing for our testbed bead-on-rotating-ring problem at the very end of Sec. 1 – see Eq. (6); why cannot the same trick work for the planetary problem? Besides a formal explanation, discuss the physics behind this difference.

3.7. A system consisting of two equal masses m on a light rod of length l (frequently called a *dumbbell*) can slide without friction along a vertical ring of radius R , rotated about its vertical diameter with a constant angular velocity ω – see the figure on the right. Derive the condition of stability of the lower horizontal position of the dumbbell.



3.8. Analyze the dynamics of the so-called *spherical pendulum* – a point mass hung, in a uniform gravity field \mathbf{g} , on a light cord of length l , with no motion's confinement to a vertical plane. In particular:

- (i) find the integrals of motion and reduce the problem to a 1D one,
- (ii) calculate the time period of the possible circular motion around the vertical axis, and
- (iii) explore small deviations from the circular motion. (Are the pendulum orbits closed?)²⁸

3.9. If our planet Earth were suddenly stopped on its orbit around Sun, how long would it take it to fall on our star? Solve this problem using two different approaches, while neglecting the Earth's orbit eccentricity and the Sun's size.

3.10. The orbits of Mars and Earth around the Sun may be well approximated as circles,²⁹ with a radii ratio of 3/2. Use this fact, and the Earth's year duration (which you should know :-), to calculate the time of travel to Mars spending the least energy on the spacecraft's launch. Neglect the planets' size and the effects of their gravitational fields.

3.11. Derive first-order and second-order differential equations for the reciprocal distance $u \equiv 1/r$ as a function of φ , describing the trajectory of the particle's motion in a central potential $U(r)$. Spell out the latter equation for the particular case of the Coulomb potential (49) and discuss the result.

3.12. For the motion of a particle in the Coulomb attractive field ($U(r) = -\alpha/r$, with $\alpha > 0$), calculate and sketch the so-called *hodograph*³⁰ – the trajectory followed by the head of the velocity vector \mathbf{v} , provided that its tail is kept at the origin.

²⁸ Solving this problem is very good preparation for the analysis of the symmetric top's rotation in Sec. 4.5.

²⁹ Indeed, their eccentricities are close to, respectively, 0.093 and 0.0167.

³⁰ The use of this notion for the characterization of motion may be traced back at least to an 1846 treatise by W. Hamilton. Nowadays, it is most often used in applied fluid mechanics, in particular meteorology.

3.13. Prove that for arbitrary motion of a particle of mass m in the Coulomb field $U = -\alpha/r$, vector $\mathbf{A} \equiv \mathbf{p} \times \mathbf{L} - m\alpha \mathbf{n}_r$ is conserved.³¹ After that:

(i) spell out the scalar product $\mathbf{r} \cdot \mathbf{A}$ and use the result for an alternative derivation of Eq. (59), and for a geometric interpretation of the vector \mathbf{A} ;

(ii) spell out $(\mathbf{A} - \mathbf{p} \times \mathbf{L})^2$, and use the result for an alternative derivation of the hodograph diagram discussed in the previous problem.

3.14. For motion in the following central potential:

$$U(r) = -\frac{\alpha}{r} + \frac{\beta}{r^2},$$

(i) find the orbit $r(\phi)$, for positive α and β , and all possible ranges of energy E ;

(ii) prove that in the limit $\beta \rightarrow 0$, and for energy $E < 0$, the orbit may be represented as a slowly rotating ellipse;

(iii) express the angular velocity of this slow orbit rotation via the parameters α and β , the particle's mass m , its energy E , and the angular momentum L_z .

3.15. A star system contains a much smaller planet and an even much smaller amount of dust. Assuming that the attractive gravitational potential of the dust is spherically symmetric and proportional to the square of the distance from the star,³² calculate the slow precession it gives to a basically circular orbit of the planet.

3.16. A particle is moving in the field of an attractive central force, with potential

$$U(r) = -\frac{\alpha}{r^n}, \quad \text{where } \alpha n > 0.$$

For what values of n , the circular orbits are stable?

3.17. Determine the condition for a particle of mass m , moving under the effect of a central attractive force

$$\mathbf{F} = -\alpha \frac{\mathbf{r}}{r^3} \exp\left\{-\frac{r}{R}\right\},$$

where α and R are positive constants, to have a stable circular orbit.

3.18. A particle of mass m , with angular momentum L_z , moves in the field of an attractive central force with a distance-independent magnitude F . If the particle's energy E is slightly higher than the value E_{\min} corresponding to the circular orbit of the particle, what is the time period of its radial oscillations? Compare the period with that of the circular orbit at $E = E_{\min}$.

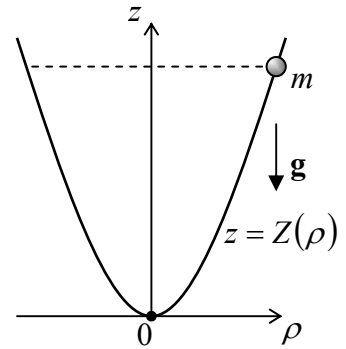
3.19. A particle may move without friction, in the uniform gravity field $\mathbf{g} = -g\mathbf{n}_z$, over an axially-symmetric surface that is described, in cylindrical coordinates $\{\rho, \varphi, z\}$, by a smooth function

³¹ This fact, first proved in 1710 by Jacob Hermann, was repeatedly rediscovered during the next two centuries. As a result, the most common name of \mathbf{A} is, rather unfairly, the *Runge-Lenz vector*.

³² As may be readily shown from the gravitation version of the Gauss law (see, e.g., the model solution of Problem 1.7), this approximation is exact if the dust density is constant between the star and the planet.

$Z(\rho)$ – see the figure on the right. Derive the condition of stability of circular orbits of the particle around the symmetry axis z with respect to small perturbations. For the cases when the condition is fulfilled, find out whether the weakly perturbed orbits are open or closed. Spell out your results for the following particular cases:

- (i) a conical surface with $Z = \alpha\rho$,
- (ii) a paraboloid with $Z = \kappa\rho^2/2$, and
- (iii) a spherical surface with $Z^2 + \rho^2 = R^2$, for $\rho < R$.



3.20. The gravitational potential (i.e. the gravitational energy of a unit probe mass) of our Milky Way galaxy, averaged over interstellar distances, is reasonably well approximated by the following axially-symmetric function:

$$\phi(r, z) = \frac{V^2}{2} \ln(r^2 + \alpha z^2),$$

where r is the distance from the galaxy's symmetry axis and z is the distance from its central plane, while V and $\alpha > 0$ are constants.³³ Prove that circular orbits of stars in this gravity field are stable, and calculate the frequencies of their small oscillations near such orbits, in the r - and z -directions.

3.21. For particle scattering by a repulsive Coulomb field, calculate the minimum approach distance r_{\min} and the velocity v_{\min} at that point, and analyze their dependence on the impact parameter b (see Fig. 9) and the initial velocity v_{∞} of the particle.

3.22. A particle is launched from afar, with impact parameter b , toward an attracting center with

$$U(r) = -\frac{\alpha}{r^n}, \quad \text{with } n > 2, \alpha > 0.$$

- (i) Express the minimum distance between the particle and the center via b , if the initial kinetic energy E of the particle is barely sufficient for escaping its capture by the attracting center.
- (ii) Calculate the capture's total cross-section; explore the limit $n \rightarrow 2$.

3.23. A meteorite with initial velocity v_{∞} approaches an atmosphere-free planet of mass M and radius R .

- (i) Find the condition on the impact parameter b for the meteorite to hit the planet's surface.
- (ii) If the meteorite barely avoids the collision, what is its scattering angle?

3.24. Calculate the differential and total cross-sections of the classical elastic scattering of small particles by a hard sphere of radius R .

3.25. The most famous³⁴ confirmation of Einstein's general relativity theory has come from the observation, by A. Eddington and his associates, of star light's deflection by the Sun, during the May

³³ Just for the reader's reference, these constants are close to, respectively, 2.2×10^5 m/s and 6.

1919 solar eclipse. Considering light photons as classical particles propagating with the speed of light, $v_0 \rightarrow c \approx 3.00 \times 10^8 \text{ m/s}$, and the astronomic data for the Sun's mass, $M_S \approx 1.99 \times 10^{30} \text{ kg}$, and radius, $R_S \approx 6.96 \times 10^8 \text{ m}$, calculate the non-relativistic mechanics' prediction for the angular deflection of the light rays grazing the Sun's surface.

3.26. Generalize the expression for the small angle of scattering, obtained in the solution of the previous problem, to a spherically-symmetric but otherwise arbitrary potential $U(r)$. Use the result to calculate the differential cross-section of small-angle scattering by potential $U = C/r^n$, with integer $n > 0$.

Hint: You may like to use the following table integral: $\int_1^\infty \frac{d\xi}{\xi^{n+1}(\xi^2 - 1)^{1/2}} = \pi^{1/2} \frac{\Gamma(n/2 + 1/2)}{n \Gamma(n/2)}$.

³⁴ It was not the first confirmation, though. The first one came four years earlier from Albert Einstein himself, who showed that his theory may qualitatively explain the difference between the rate of Mercury orbit's precession, known from earlier observations, and the non-relativistic theory of that effect.

Chapter 4. Rigid Body Motion

This chapter discusses the motion of rigid bodies, with a heavy focus on its most nontrivial part: rotation. Some byproducts of this analysis enable a discussion, at the end of the chapter, of the motion of point particles as observed from non-inertial reference frames.

4.1. Translation and rotation

It is natural to start a discussion of many-particle systems from a (relatively :-)) simple limit when the changes of distances $r_{kk'} \equiv |\mathbf{r}_k - \mathbf{r}_{k'}|$ between the particles are negligibly small. Such an abstraction is called the (*absolutely*) *rigid body*; it is a reasonable approximation in many practical problems, including the motion of solid samples. In other words, this model neglects *deformations* – which will be the subject of the next chapters. The rigid-body approximation reduces the number of degrees of freedom of the system of N particles from $3N$ to just six – for example, three Cartesian coordinates of one point (say, 0), and three angles of the system's rotation about three mutually perpendicular axes passing through this point – see Fig. 1.¹

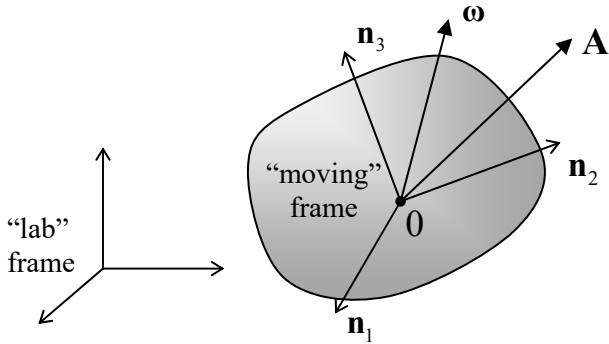


Fig. 4.1. Deriving Eq. (8).

As it follows from the discussion in Secs. 1.1-1.3, any purely *translational motion* of a rigid body, at which the velocity vectors \mathbf{v} of all points are equal, is not more complex than that of a point particle. Indeed, according to Eqs. (1.8) and (1.30), in an inertial reference frame, such a body moves exactly as a point particle upon the effect of the net external force $\mathbf{F}^{(\text{ext})}$. However, the rotation is a bit more tricky.

Let us start by showing that an arbitrary elementary displacement of a rigid body may be always considered as a sum of the translational motion and of what is called a *pure rotation*. For that, consider a “moving” reference frame $\{\mathbf{n}_1, \mathbf{n}_2, \mathbf{n}_3\}$, firmly bound to the body, and an arbitrary vector \mathbf{A} (Fig. 1). The vector may be represented by its Cartesian components A_j in that moving frame:

$$\mathbf{A} = \sum_{j=1}^3 A_j \mathbf{n}_j . \quad (4.1)$$

¹ An alternative way to arrive at the same number six is to consider three points of the body, which uniquely define its position. If movable independently, the points would have nine degrees of freedom, but since three distances $r_{kk'}$ between them are now fixed, the resulting three constraints reduce the number of degrees of freedom to six.

Let us calculate the time derivative of this vector as observed from a different (“lab”) frame, taking into account that if the body rotates relative to this frame, the directions of the unit vectors \mathbf{n}_j , as seen from the lab frame, change in time. Hence, in each product contributing to the sum (1), we have to differentiate both operands:

$$\frac{d\mathbf{A}}{dt} \Big|_{\text{in lab}} = \sum_{j=1}^3 \frac{dA_j}{dt} \mathbf{n}_j + \sum_{j=1}^3 A_j \frac{d\mathbf{n}_j}{dt}. \quad (4.2)$$

On the right-hand side of this equality, the first sum obviously describes the change of vector \mathbf{A} as observed from the moving frame. In the second sum, each of the infinitesimal vectors $d\mathbf{n}_j$ may be represented by its Cartesian components:

$$d\mathbf{n}_j = \sum_{j'=1}^3 d\varphi_{jj'} \mathbf{n}_{j'}, \quad (4.3)$$

where $d\varphi_{jj'}$ are some dimensionless scalar coefficients. To find out more about them, let us scalar-multiply each side of Eq. (3) by an arbitrary unit vector $\mathbf{n}_{j''}$, and take into account the obvious orthonormality condition:

$$\mathbf{n}_{j'} \cdot \mathbf{n}_{j''} = \delta_{j'j''}, \quad (4.4)$$

where $\delta_{j'j''}$ is the Kronecker delta symbol.² As a result, we get

$$d\mathbf{n}_j \cdot \mathbf{n}_{j''} = d\varphi_{jj''}. \quad (4.5)$$

Now let us use Eq. (5) to calculate the first differential of Eq. (4):

$$d\mathbf{n}_{j'} \cdot \mathbf{n}_{j''} + \mathbf{n}_{j'} \cdot d\mathbf{n}_{j''} \equiv d\varphi_{jj''} + d\varphi_{j''j'} = 0; \quad \text{in particular, } 2d\mathbf{n}_j \cdot \mathbf{n}_j = 2d\varphi_{jj} = 0. \quad (4.6)$$

These relations, valid for any choice of indices j, j' , and j'' of the set $\{1, 2, 3\}$, show that the matrix with elements $d\varphi_{jj'}$ is antisymmetric with respect to the swap of its indices; this means that there are not nine just three non-zero independent coefficients $d\varphi_{jj'}$, all with $j \neq j'$. Hence it is natural to renumber them in a simpler way: $d\varphi_{jj'} = -d\varphi_{j'j} \equiv d\varphi_{j''}$, where the indices j, j' , and j'' follow in the “correct” order – either $\{1,2,3\}$, or $\{2,3,1\}$, or $\{3,1,2\}$. It is straightforward to verify (either just by a component-by-component comparison or by using the Levi-Civita permutation symbol³) that in this new notation, Eq. (3) may be represented just as a vector product:

$$d\mathbf{n}_j = d\boldsymbol{\varphi} \times \mathbf{n}_j, \quad (4.7)$$

Elementary rotation

where $d\boldsymbol{\varphi}$ is the infinitesimal vector defined by its Cartesian components $d\varphi_j$ in the rotating reference frame $\{\mathbf{n}_1, \mathbf{n}_2, \mathbf{n}_3\}$.

This relation is the basis of all rotation kinematics. Using it, Eq. (2) may be rewritten as

$$\frac{d\mathbf{A}}{dt} \Big|_{\text{in lab}} = \frac{d\mathbf{A}}{dt} \Big|_{\text{in mov}} + \sum_{j=1}^3 A_j \frac{d\boldsymbol{\varphi}}{dt} \times \mathbf{n}_j \equiv \frac{d\mathbf{A}}{dt} \Big|_{\text{in mov}} + \boldsymbol{\omega} \times \mathbf{A}, \quad \text{where } \boldsymbol{\omega} \equiv \frac{d\boldsymbol{\varphi}}{dt}. \quad (4.8)$$

Vector's evolution in time

To reveal the physical sense of the vector $\boldsymbol{\omega}$, let us apply Eq. (8) to the particular case when \mathbf{A} is the radius vector \mathbf{r} of a point of the body, and the lab frame is selected in a special way: its origin has the

² See, e.g., MA Eq. (13.1).

³ See, e.g., MA Eq. (13.2). Using this symbol, we may write $d\varphi_{jj'} = -d\varphi_{j'j} \equiv \varepsilon_{jj'} d\varphi_{j''}$ for any choice of j, j' , and j'' .

same position and moves with the same velocity as that of the moving frame, in the particular instant under consideration. In this case, the first term on the right-hand side of Eq. (8) is zero, and we get

$$\frac{d\mathbf{r}}{dt} \Big|_{\text{in special lab frame}} = \boldsymbol{\omega} \times \mathbf{r}, \quad (4.9)$$

were vector \mathbf{r} itself is the same in both frames. According to the vector product definition, the particle velocity described by this formula has a direction perpendicular to the vectors $\boldsymbol{\omega}$ and \mathbf{r} (Fig. 2), and magnitude $\omega r \sin \theta$. As Fig. 2 shows, the last expression may be rewritten as $\omega \rho$, where $\rho = r \sin \theta$ is the distance from the line that is parallel to the vector $\boldsymbol{\omega}$ and passes through point 0. This is of course just the *pure rotation* about that line (called the *instantaneous axis of rotation*), with the angular velocity ω . According to Eqs. (3) and (8), the *angular velocity vector* $\boldsymbol{\omega}$ is defined by the time evolution of the moving frame alone, so it is the same for all points \mathbf{r} , i.e. for the rigid body as a whole. Note that nothing in our calculations forbids not only the magnitude but also the direction of the vector $\boldsymbol{\omega}$, and thus of the instantaneous axis of rotation, to change in time; hence the name.

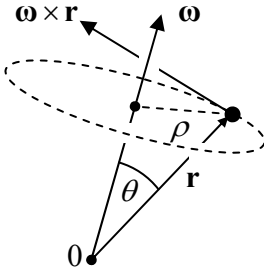


Fig. 4.2. The instantaneous axis and the angular velocity of rotation.

Now let us generalize our result a step further, considering two reference frames that do not rotate versus each other: one (“lab”) frame arbitrary, and another one selected in the special way described above, so that for it Eq. (9) is valid in it. Since their relative motion of these two reference frames is purely translational, we can use the simple velocity addition rule given by Eq. (1.6) to write

Body
point's
velocity

$$\mathbf{v}|_{\text{in lab}} = \mathbf{v}_0|_{\text{in lab}} + \mathbf{v}|_{\text{in special lab frame}} = \mathbf{v}_0|_{\text{in lab}} + \boldsymbol{\omega} \times \mathbf{r}, \quad (4.10)$$

where \mathbf{r} is the radius vector of a point is measured in the body-bound (“moving”) frame 0.

4.2. Inertia tensor

Since the dynamics of each point of a rigid body is strongly constrained by the conditions $r_{kk'} = \text{const}$, this is one of the most important fields of application of the Lagrangian formalism discussed in Chapter 2. For using this approach, the first thing we need to calculate is the kinetic energy of the body in an inertial reference frame. Since it is just the sum of the kinetic energies (1.19) of all its points, we can use Eq. (10) to write:⁴

$$T \equiv \sum \frac{m}{2} \mathbf{v}^2 = \sum \frac{m}{2} (\mathbf{v}_0 + \boldsymbol{\omega} \times \mathbf{r})^2 \equiv \sum \frac{m}{2} v_0^2 + \sum m \mathbf{v}_0 \cdot (\boldsymbol{\omega} \times \mathbf{r}) + \sum \frac{m}{2} (\boldsymbol{\omega} \times \mathbf{r})^2. \quad (4.11)$$

⁴ Actually, all symbols for particle masses, coordinates, and velocities should carry the particle’s index, over which the summation is carried out. However, in this section, for the notation simplicity, this index is just implied.

Let us apply to the right-hand side of Eq. (11) two general vector analysis formulas listed in the Math Appendix: the so-called *operad rotation rule* MA Eq. (7.6) to the second term, and MA Eq. (7.7b) to the third term. The result is

$$T = \sum \frac{m}{2} v_0^2 + \sum m \mathbf{r} \cdot (\mathbf{v}_0 \times \boldsymbol{\omega}) + \sum \frac{m}{2} [\omega^2 r^2 - (\boldsymbol{\omega} \cdot \mathbf{r})^2]. \quad (4.12)$$

This expression may be further simplified by making a specific choice of the point 0 (from which the radius vectors \mathbf{r} of all particles are measured), namely by using for this point the *center of mass* of the body. As was already mentioned in Sec. 3.4 for the two-point case, the radius vector \mathbf{R} of this point is defined as

$$M\mathbf{R} \equiv \sum m\mathbf{r}, \quad \text{with } M \equiv \sum m, \quad (4.13)$$

so that M is the total mass of the body. In the reference frame centered at this point, we have $\mathbf{R} = 0$, so that the second sum in Eq. (12) vanishes, and the kinetic energy is a sum of just two terms:

$$T = T_{\text{tran}} + T_{\text{rot}}, \quad T_{\text{tran}} \equiv \frac{M}{2} V^2, \quad T_{\text{rot}} \equiv \sum \frac{m}{2} [\omega^2 r^2 - (\boldsymbol{\omega} \cdot \mathbf{r})^2], \quad (4.14)$$

where $\mathbf{V} \equiv d\mathbf{R}/dt$ is the center-of-mass velocity in our inertial reference frame, and all particle positions \mathbf{r} are measured in the center-of-mass frame. Since the angular velocity vector $\boldsymbol{\omega}$ is common for all points of a rigid body, it is more convenient to rewrite the rotational part of the energy in a form in that the summation over the components of this vector is separated from the summation over the points of the body:

$$T_{\text{rot}} = \frac{1}{2} \sum_{j,j'=1}^3 I_{jj'} \omega_j \omega_{j'}, \quad (4.15)$$

Kinetic energy of rotation

where the 3×3 matrix with elements

$$I_{jj'} \equiv \sum m (r^2 \delta_{jj'} - r_j r_{j'}) \quad (4.16)$$

Inertia tensor

represents, in the selected reference frame, the *inertia tensor* of the body.⁵

Actually, the term “tensor” for the construct described by this matrix has to be justified, because in physics it implies a certain reference-frame-independent notion, whose matrix elements have to obey certain rules at the transfer between reference frames. To show that the matrix (16) indeed described such notion, let us calculate another key quantity, the total angular momentum \mathbf{L} of the same body.⁶ Summing up the angular momenta of each particle, defined by Eq. (1.31), and then using Eq. (10) again, in our inertial reference frame we get

$$\mathbf{L} \equiv \sum \mathbf{r} \times \mathbf{p} = \sum m \mathbf{r} \times \mathbf{v} = \sum m \mathbf{r} \times (\mathbf{v}_0 + \boldsymbol{\omega} \times \mathbf{r}) \equiv \sum m \mathbf{r} \times \mathbf{v}_0 + \sum m \mathbf{r} \times (\boldsymbol{\omega} \times \mathbf{r}). \quad (4.17)$$

We see that the momentum may be represented as a sum of two terms. The first one,

⁵ While the ABCs of the rotational dynamics were developed by Leonhard Euler in 1765, an introduction of the inertia tensor’s formalism had to wait very long – until the invention of the tensor analysis by Tullio Levi-Civita and Gregorio Ricci-Curbastro in 1900 – soon popularized by its use in Einstein’s general relativity.

⁶ Hopefully, there is very little chance of confusing the angular momentum \mathbf{L} (a vector) and its Cartesian components L_j (scalars with an index) on one hand, and the Lagrangian function L (a scalar without an index) on the other hand.

$$\mathbf{L}_0 \equiv \sum m\mathbf{r} \times \mathbf{v}_0 = M\mathbf{R} \times \mathbf{v}_0, \quad (4.18)$$

describes the possible rotation of the center of mass about the inertial frame's origin. This term vanishes if the moving reference frame's origin 0 is positioned at the center of mass (where $\mathbf{R} = 0$). In this case, we are left with only the second term, which describes a pure rotation of the body about its center of mass:

$$\mathbf{L} = \mathbf{L}_{\text{rot}} \equiv \sum m\mathbf{r} \times (\boldsymbol{\omega} \times \mathbf{r}). \quad (4.19)$$

Using one more vector algebra formula, the “bac minis cab” rule,⁷ we may rewrite this expression as

$$\mathbf{L} = \sum m[\boldsymbol{\omega} r^2 - \mathbf{r}(\mathbf{r} \cdot \boldsymbol{\omega})]. \quad (4.20)$$

Let us spell out an arbitrary Cartesian component of this vector:

$$L_j = \sum m \left[\omega_j r^2 - r_j \sum_{j'=1}^3 r_{j'} \omega_{j'} \right] \equiv \sum m \sum_{j'=1}^3 \omega_{j'} (r^2 \delta_{jj'} - r_j r_{j'}). \quad (4.21)$$

By changing the summation order and comparing the result with Eq. (16), the angular momentum may be conveniently expressed via the same matrix elements $I_{jj'}$ as the rotational kinetic energy:

$$L_j = \sum_{j'=1}^3 I_{jj'} \omega_{j'}. \quad (4.22)$$

Since \mathbf{L} and $\boldsymbol{\omega}$ are both legitimate vectors (meaning that they describe physical vectors independent of the reference frame choice), the matrix of elements $I_{jj'}$ that relates them is a legitimate tensor. This fact, and the symmetry of the tensor ($I_{jj'} = I_{j'j}$), evident from its definition (16), allow the tensor to be further simplified. In particular, mathematics tells us that by a certain choice of the coordinate axes' orientations, any symmetric tensor may be reduced to a diagonal form

$$I_{jj'} = I_j \delta_{jj'}, \quad (4.23)$$

where in our case

$$I_j = \sum m(r^2 - r_j^2) = \sum m(r_{j'}^2 + r_{j''}^2) \equiv \sum m\rho_j^2, \quad (4.24)$$

ρ_j being the distance of the particle from the j^{th} axis, i.e. the length of the perpendicular dropped from the point to that axis. The axes of such a special coordinate system are called the *principal axes*, while the diagonal elements I_j given by Eq. (24), the *principal moments of inertia* of the body. In such a special reference frame, Eqs. (15) and (22) are reduced to very simple forms:

$$T_{\text{rot}} = \sum_{j=1}^3 \frac{I_j}{2} \omega_j^2, \quad (4.25)$$

$$L_j = I_j \omega_j. \quad (4.26)$$

Both these results remind the corresponding relations for the translational motion, $T_{\text{tran}} = MV^2/2$ and $\mathbf{P} = M\mathbf{V}$, with the angular velocity $\boldsymbol{\omega}$ replacing the linear velocity \mathbf{V} , and the tensor of inertia playing the role of scalar mass M . However, let me emphasize that even in the specially selected reference frame, with

⁷ See, e.g., MA Eq. (7.5).

its axes pointing in principal directions, the analogy is incomplete, and rotation is generally more complex than translation, because the measures of inertia, I_j , are generally different for each principal axis.

Let me illustrate the last fact on a simple but instructive system of three similar massive particles fixed in the vertices of an equilateral triangle (Fig. 3).

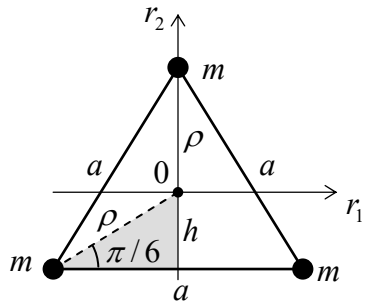


Fig. 4.3. Principal moments of inertia: a simple case study.

Due to the symmetry of the configuration, one of the principal axes has to pass through the center of mass O and be normal to the plane of the triangle. For the corresponding principal moment of inertia, Eq. (24) readily yields $I_3 = 3m\rho^2$. If we want to express this result in terms of the triangle's side a , we may notice that due to the system's symmetry, the angle marked in Fig. 3 equals $\pi/6$, and from the shaded right triangle, $a/2 = \rho\cos(\pi/6) \equiv \rho\sqrt{3}/2$, giving $\rho = a/\sqrt{3}$, so that, finally, $I_3 = ma^2$.

Let me use this simple case to illustrate the following general *axis shift theorem*, which may be rather useful – especially for more complex systems. For that, let us relate the inertia tensor elements $I_{jj'}$ and $I'_{jj'}$, calculated in two reference frames – one with its origin at the center of mass O , and another one (O') translated by a certain vector \mathbf{d} (Fig. 4a), so that for an arbitrary point, $\mathbf{r}' = \mathbf{r} + \mathbf{d}$. Plugging this relation into Eq. (16), we get

$$\begin{aligned} I'_{jj'} &= \sum m [(\mathbf{r} + \mathbf{d})^2 \delta_{jj'} - (r_j + d_j)(r_{j'} + d_{j'})] \\ &= \sum m [(r^2 + 2\mathbf{r} \cdot \mathbf{d} + d^2) \delta_{jj'} - (r_j r_{j'} + r_j d_{j'} + r_{j'} d_j + d_j d_{j'})]. \end{aligned} \quad (4.27)$$

Since in the center-of-mass frame, all sums $\sum mr_j$ equal zero, we may use Eq. (16) to finally obtain

$$I'_{jj'} = I_{jj'} + M(\delta_{jj'} d^2 - d_j d_{j'}). \quad (4.28)$$

In particular, this equation shows that if the shift vector \mathbf{d} is perpendicular to one (say, j^{th}) of the principal axes (Fig. 4b), i.e. $d_j = 0$, then Eq. (28) is reduced to a very simple formula:

$I'_{jj} = I_{jj} + M d^2.$

(4.29)

Principal
axis'
shift

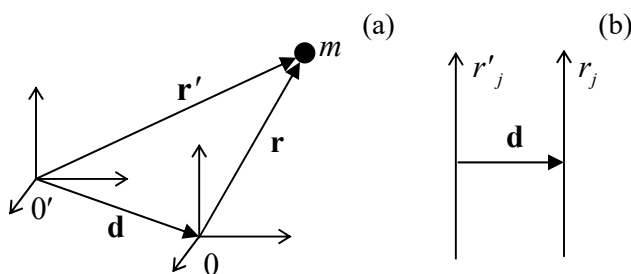


Fig. 4.4. (a) A general coordinate frame's shift from the center of mass, and (b) a shift perpendicular to one of the principal axes.

Now returning to the particular system shown in Fig. 3, let us perform such a shift to the new (“primed”) axis passing through the location of one of the particles, still perpendicular to their common plane. Then the contribution of that particular mass to the primed moment of inertia vanishes, and $I'_3 = 2ma^2$. Now, returning to the center of mass and applying Eq. (29), we get $I_3 = I'_3 - M\rho^2 = 2ma^2 - (3m)(a/\sqrt{3})^2 = ma^2$, i.e. the same result as above.

The symmetry situation inside the triangle’s plane is somewhat less obvious, so let us start by calculating the moments of inertia for the axes shown vertical and horizontal in Fig. 3. From Eq. (24), we readily get:

$$I_1 = 2mh^2 + m\rho^2 = m \left[2 \left(\frac{a}{2\sqrt{3}} \right)^2 + \left(\frac{a}{\sqrt{3}} \right)^2 \right] = \frac{ma^2}{2}, \quad I_2 = 2m \left(\frac{a}{2} \right)^2 = \frac{ma^2}{2}, \quad (4.30)$$

where h is the distance from the center of mass and any side of the triangle: $h = \rho \sin(\pi/6) = \rho/2 = a/2\sqrt{3}$. We see that $I_1 = I_2$, and mathematics tells us that in this case, *any* in-plane axis (passing through the center-of-mass 0) may be considered as principal, and has the same moment of inertia. A rigid body with this property, $I_1 = I_2 \neq I_3$, is called the *symmetric top*. (The last direction is called the *main principal axis* of the system.)

Despite the symmetric top’s name, the situation may be even more symmetric in the so-called *spherical tops*, i.e. highly symmetric systems whose principal moments of inertia are all equal,

$$I_1 = I_2 = I_3 \equiv I, \quad (4.31)$$

Mathematics says that in this case, the moment of inertia for rotation about *any* axis (but still passing through the center of mass) is equal to the same I . Hence Eqs. (25) and (26) are further simplified for any direction of the vector ω :

$$T_{\text{rot}} = \frac{I}{2}\omega^2, \quad \mathbf{L} = I\boldsymbol{\omega}, \quad (4.32)$$

thus making the analogy of rotation and translation complete. (As will be discussed in the next section, this analogy is also complete if the rotation axis is fixed by external constraints.)

Evident examples of a spherical top are a uniform sphere and a uniform spherical shell; its less obvious example is a uniform cube – with masses either concentrated in vertices, or uniformly spread over the faces, or uniformly distributed over the volume. Again, in this case *any* axis passing through the center of mass is a principal one and has the same principal moment of inertia. For a sphere, this is natural; for a cube, rather surprising – but may be confirmed by a direct calculation.

4.3. Fixed-axis rotation

Now we are well equipped for a discussion of the rigid body’s rotational dynamics. The general equation of this dynamics is given by Eq. (1.38), which is valid for dynamics of any system of particles – either rigidly connected or not:

$$\dot{\mathbf{L}} = \boldsymbol{\tau}, \quad (4.33)$$

where $\boldsymbol{\tau}$ is the net torque of external forces. Let us start exploring this equation from the simplest case when the axis of rotation, i.e. the direction of vector $\boldsymbol{\omega}$, is fixed by some external constraints. Directing

Symmetric top:
definition

Spherical top:
definition

Spherical top:
properties

the z -axis along this vector, we have $\omega_x = \omega_y = 0$. According to Eq. (22), in this case, the z -component of the angular momentum,

$$L_z = I_{zz} \omega_z, \quad (4.34)$$

where I_{zz} , though not necessarily one of the principal moments of inertia, still may be calculated using Eq. (24):

$$I_{zz} = \sum m \rho_z^2 = \sum m(x^2 + y^2), \quad (4.35)$$

with ρ_z being the distance of each particle from the rotation axis z . According to Eq. (15), in this case the rotational kinetic energy is just

$$T_{\text{rot}} = \frac{I_{zz}}{2} \omega_z^2. \quad (4.36)$$

Moreover, it is straightforward to show that if the rotation axis is fixed, Eqs. (34)-(36) are valid even if the axis does not pass through the center of mass – provided that the distances ρ_z are now measured from that axis. (The proof is left for the reader's exercise.)

As a result, we may not care about other components of the vector \mathbf{L} ,⁸ and use just one component of Eq. (33),

$$\dot{L}_z = \tau_z, \quad (4.37)$$

because it, when combined with Eq. (34), completely determines the dynamics of rotation:

$$I_{zz} \dot{\omega}_z = \tau_z, \quad \text{i.e. } I_{zz} \ddot{\theta}_z = \tau_z, \quad (4.38)$$

where θ_z is the angle of rotation about the axis, so that $\omega_z = \dot{\theta}_z$. The scalar relations (34), (36), and (38), describing rotation about a fixed axis, are completely similar to the corresponding formulas of 1D motion of a single particle, with ω_z corresponding to the usual (“linear”) velocity, the angular momentum component L_z – to the linear momentum, and I_z – to the particle’s mass.

The resulting motion about the axis is also frequently similar to that of a single particle. As a simple example, let us consider what is called the *physical* (or “compound”) *pendulum* (Fig. 5) – a rigid body free to rotate about a fixed horizontal axis that does not pass through the center of mass 0 , in a uniform gravity field \mathbf{g} .

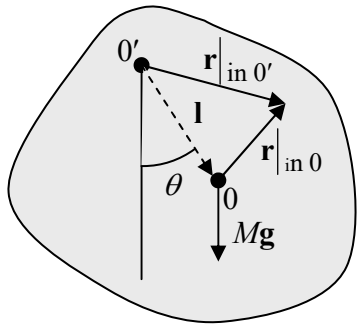


Fig. 4.5. Physical pendulum: a rigid body with a fixed (horizontal) rotation axis $0'$ that does not pass through the center of mass 0 . (The plane of drawing is normal to that axis.)

⁸ Note that according to Eq. (22), other Cartesian components of the angular momentum, L_x and L_y , may be different from zero, and even evolve in time. The corresponding torques τ_x and τ_y , which obey Eq. (33), are automatically provided by the external forces that keep the rotation axis fixed.

Let us drop the perpendicular from point 0 to the rotation axis, and call the oppositely directed vector \mathbf{l} – see the dashed arrow in Fig. 5. Then the torque (relative to the rotation axis 0') of the forces keeping the axis fixed is zero, and the only contribution to the net torque is due to gravity alone:

$$\tau|_{\text{in } 0'} \equiv \sum \mathbf{r}|_{\text{in } 0'} \times \mathbf{F} = \sum (\mathbf{l} + \mathbf{r}|_{\text{in } 0}) \times m\mathbf{g} = \sum m(\mathbf{l} \times \mathbf{g}) + \sum m\mathbf{r}|_{\text{in } 0} \times \mathbf{g} = M\mathbf{l} \times \mathbf{g}. \quad (4.39)$$

(The last step used the facts that point 0 is the center of mass, so that the second term on the right-hand side equals zero, and that the vectors \mathbf{l} and \mathbf{g} are the same for all particles of the body.)

This result shows that the torque is directed along the rotation axis, and its (only) component τ_z is equal to $-Mgl \sin \theta$, where θ is the angle between the vectors \mathbf{l} and \mathbf{g} , i.e. the angular deviation of the pendulum from the position of equilibrium – see Fig. 5 again. As a result, Eq. (38) takes the form,

$$I'\ddot{\theta} = -Mgl \sin \theta, \quad (4.40)$$

where I' is the moment of inertia for rotation about the axis 0' rather than about the center of mass. This equation is identical to Eq. (1.18) for the point-mass (sometimes called “mathematical”) pendulum, with small-oscillation frequency

$$\Omega = \left(\frac{Mgl}{I'} \right)^{1/2} \equiv \left(\frac{g}{l_{\text{ef}}} \right)^{1/2}, \quad \text{with } l_{\text{ef}} \equiv \frac{I'}{Ml}. \quad (4.41)$$

As a sanity check, in the simplest case when the linear size of the body is much smaller than the suspension length l , Eq. (35) yields $I' = Ml^2$, i.e. $l_{\text{ef}} = l$, and Eq. (41) reduces to the well-familiar formula $\Omega = (g/l)^{1/2}$ for the point-mass pendulum.

Now let us discuss the situations when a rigid body not only rotates but also moves as a whole. As was mentioned in the introductory chapter, the total linear momentum of the body,

$$\mathbf{P} \equiv \sum m\mathbf{v} = \sum m\dot{\mathbf{r}} = \frac{d}{dt} \sum m\mathbf{r}, \quad (4.42)$$

satisfies the 2nd Newton’s law in the form (1.30). Using the definition (13) of the center of mass, the momentum may be represented as

$$\mathbf{P} = M\dot{\mathbf{R}} = M\mathbf{V}, \quad (4.43)$$

so Eq. (1.30) may be rewritten as

$$M\dot{\mathbf{V}} = \mathbf{F}, \quad (4.44)$$

where \mathbf{F} is the vector sum of all external forces. This equation shows that the center of mass of the body moves exactly like a point particle of mass M , under the effect of the net force \mathbf{F} . In many cases, this fact makes the translational dynamics of a rigid body absolutely similar to that of a point particle.

The situation becomes more complex if some of the forces contributing to the vector sum \mathbf{F} depend on the rotation of the same body, i.e. if its rotational and translational motions are coupled. Analysis of such coupled motion is rather straightforward if the *direction* of the rotation axis does not change in time, and hence Eqs. (34)-(36) are still valid. Possibly the simplest example is a round cylinder (say, a wheel) rolling on a surface without slippage (Fig. 6). Here the no-slippage condition may be represented as the requirement to the net velocity of the particular wheel’s point A that touches the surface to equal zero – in the reference frame bound to the surface. For the simplest case of plane

surface (Fig. 6a), this condition may be spelled out using Eq. (10), giving the following relation between the angular velocity ω of the wheel and the linear velocity V of its center:

$$V + r\omega = 0. \quad (4.45)$$

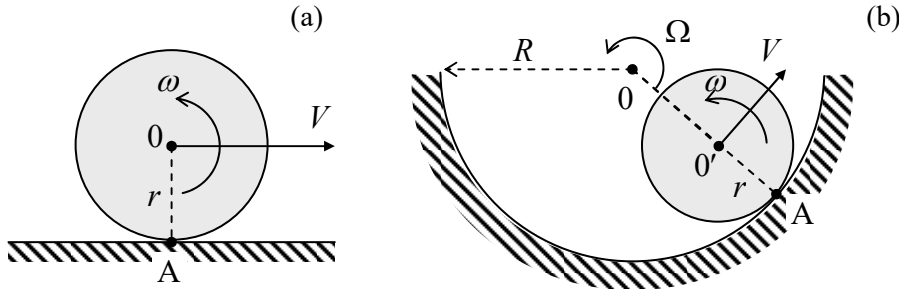


Fig. 4.6. Round cylinder rolling over (a) a plane surface and (b) a concave surface.

Such kinematic relations are essentially holonomic constraints, which reduce the number of degrees of freedom of the system. For example, without the no-slippage condition (45), the wheel on a plane surface has to be considered as a system with two degrees of freedom, making its total kinetic energy (14) a function of two independent generalized velocities, say V and ω :

$$T = T_{\text{tran}} + T_{\text{rot}} = \frac{M}{2}V^2 + \frac{I}{2}\omega^2. \quad (4.46)$$

Using Eq. (45) we may eliminate, for example, the linear velocity and reduce Eq. (46) to

$$T = \frac{M}{2}(\omega r)^2 + \frac{I}{2}\omega^2 \equiv \frac{I_{\text{ef}}}{2}\omega^2, \quad \text{where } I_{\text{ef}} \equiv I + Mr^2. \quad (4.47)$$

This result may be interpreted as the kinetic energy of pure rotation of the wheel about the instantaneous rotation axis A, with I_{ef} being the moment of inertia about that axis, satisfying Eq. (29).

Kinematic relations are not always as simple as Eq. (45). For example, if a wheel is rolling on a concave surface (Fig. 6b), we need to relate the angular velocities of the wheel's rotation about its axis $0'$ (say, ω) and that (say, Ω) of its axis' rotation about the center 0 of curvature of the surface. A popular error here is to write $\Omega = -(r/R)\omega$ [WRONG!]. A prudent way to derive the correct relation is to note that Eq. (45) holds for this situation as well, and on the other hand, the same linear velocity of the wheel's center may be expressed as $V = (R - r)\Omega$. Combining these formulas, we get the correct relation

$$\Omega = -\frac{r}{R - r}\omega. \quad (4.48)$$

Another famous example of the relation between translational and rotational motion is given by the “sliding-ladder” problem (Fig. 7). Let us analyze it for the simplest case of negligible friction, and the ladder’s thickness being small in comparison with its length l .

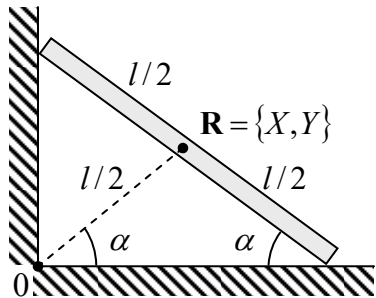


Fig. 4.7. The sliding-ladder problem.

To use the Lagrangian formalism, we may write the kinetic energy of the ladder as the sum (14) of its translational and rotational parts:

$$T = \frac{M}{2}(\dot{X}^2 + \dot{Y}^2) + \frac{I}{2}\dot{\alpha}^2, \quad (4.49)$$

where X and Y are the Cartesian coordinates of its center of mass in an inertial reference frame, and I is the moment of inertia for rotation about the z -axis passing through the center of mass. (For the uniformly distributed mass, an elementary integration of Eq. (35) yields $I = Ml^2/12$). In the reference frame with the center in the corner 0, both X and Y may be simply expressed via the angle α :

$$X = \frac{l}{2} \cos \alpha, \quad Y = \frac{l}{2} \sin \alpha. \quad (4.50)$$

(The easiest way to obtain these relations is to notice that the dashed line in Fig. 7 has length $l/2$, and the same slope α as the ladder.) Plugging these expressions into Eq. (49), we get

$$T = \frac{I_{\text{ef}}}{2}\dot{\alpha}^2, \quad I_{\text{ef}} \equiv I + M\left(\frac{l}{2}\right)^2 = \frac{1}{3}Ml^2. \quad (4.51)$$

Since the potential energy of the ladder in the gravity field may be also expressed via the same angle,

$$U = MgY = Mg\frac{l}{2} \sin \alpha, \quad (4.52)$$

α may be conveniently used as the (only) generalized coordinate of the system. Even without writing the Lagrange equation of motion for that coordinate, we may notice that since the Lagrangian function $L \equiv T - U$ does not depend on time explicitly, and the kinetic energy (51) is a quadratic-homogeneous function of the generalized velocity $\dot{\alpha}$, the full mechanical energy,

$$E \equiv T + U = \frac{I_{\text{ef}}}{2}\dot{\alpha}^2 + Mg\frac{l}{2} \sin \alpha = \frac{Mgl}{2}\left(\frac{l\dot{\alpha}^2}{3g} + \sin \alpha\right), \quad (4.53)$$

is conserved, giving us the first integral of motion. Moreover, Eq. (53) shows that the system's energy (and hence dynamics) is identical to that of a physical pendulum with an unstable fixed point $\alpha_1 = \pi/2$, a stable fixed point at $\alpha_2 = -\pi/2$, and frequency

$$\Omega = \left(\frac{3g}{2l}\right)^{1/2} \quad (4.54)$$

of small oscillations near the latter point. (Of course, this fixed point cannot be reached in the simple geometry shown in Fig. 7, where the ladder's fall on the floor would change its equations of motion. Moreover, even before that, the left end of the ladder may detach from the wall. The analysis of this issue is left for the reader's exercise.)

4.4. Free rotation

Now let us proceed to more complex situations when the rotation axis is *not* fixed. A good illustration of the complexity arising in this case comes from the case of a rigid body left alone, i.e. not subjected to external forces and hence with its potential energy U constant. Since in this case, according

to Eq. (44), the center of mass (as observed from any inertial reference frame) moves with a constant velocity, we can always use a convenient inertial reference frame with the origin at that point. From the point of view of such a frame, the body's motion is a pure rotation, and $T_{\text{tran}} = 0$. Hence, the system's Lagrangian function is just its rotational energy (15), which is, first, a quadratic-homogeneous function of the components ω_j (which may be taken for generalized velocities), and, second, does not depend on time explicitly. As we know from Chapter 2, in this case the mechanical energy, here equal to T_{rot} alone, is conserved. According to Eq. (15), for the principal-axes components of the vector $\boldsymbol{\omega}$, this means

$$T_{\text{rot}} = \sum_{j=1}^3 \frac{I_j}{2} \omega_j^2 = \text{const.} \quad (4.55)$$

Rotational energy's conservation

Next, as Eq. (33) shows, in the absence of external forces, the angular momentum \mathbf{L} of the body is conserved as well. However, though we can certainly use Eq. (26) to represent this fact as

$$\mathbf{L} = \sum_{j=1}^3 I_j \omega_j \mathbf{n}_j = \text{const}, \quad (4.56)$$

Angular momentum's conservation

where \mathbf{n}_j are the principal axes, this does not mean that all components ω_j are constant, because the principal axes are fixed relative to the rigid body, and hence may rotate with it.

Before exploring these complications, let us briefly mention two conceptually easy, but practically very important cases. The first is a spherical top ($I_1 = I_2 = I_3 = I$). In this case, Eqs. (55) and (56) imply that all components of the vector $\boldsymbol{\omega} = \mathbf{L}/I$, i.e. both the magnitude and the direction of the angular velocity are conserved, for any initial spin. In other words, the body conserves its rotation speed and axis direction, as measured in an inertial frame. The most obvious example is a spherical planet. For example, our Mother Earth, rotating about its axis with angular velocity $\omega = 2\pi/(1 \text{ day}) \approx 7.3 \times 10^{-5} \text{ s}^{-1}$, keeps its axis at a nearly constant angle of $23^\circ 27'$ to the *ecliptic pole*, i.e. to the axis normal to the plane of its motion around the Sun. (In Sec. 6 below, we will discuss some very slow motions of this axis, due to gravity effects.)

Spherical tops are also used in the most accurate gyroscopes, usually with gas-jet or magnetic suspension in vacuum. If done carefully, such systems may have spectacular stability. For example, the gyroscope system of the Gravity Probe B satellite experiment, flown in 2004-2005, was based on quartz spheres – round with a precision of about 10 nm and covered with superconducting thin films (which enabled their magnetic suspension and monitoring). The whole system was stable enough to measure the so-called *geodetic effect* in general relativity (essentially, the space curving by the Earth's mass), resulting in the axis' precession by only 6.6 arc seconds per year, i.e. with an angular velocity of just $\sim 10^{-11} \text{ s}^{-1}$, with experimental results agreeing with theory with a record $\sim 0.3\%$ accuracy.⁹

The second simple case is that of the symmetric top ($I_1 = I_2 \neq I_3$) with the initial vector \mathbf{L} aligned with the main principal axis. In this case, $\boldsymbol{\omega} = \mathbf{L}/I_3 = \text{const}$, so that the rotation axis is conserved.¹⁰ Such tops, typically in the shape of a *flywheel* (heavy, flat rotor), and supported by *gimbal systems* (also called the “Cardan suspensions”) that allow for virtually torque-free rotation about three mutually

⁹ Still, the main goal of this rather expensive ($\sim \$750M$) project, an accurate measurement of a more subtle relativistic effect, the so-called *frame-dragging drift* (also called “the Schiff precession”), predicted to be about 0.04 arc seconds per year, has not been achieved.

¹⁰ This is also true for an asymmetric top, i.e. an arbitrary body (with, say, $I_1 < I_2 < I_3$), but in this case the alignment of the vector \mathbf{L} with the axis \mathbf{n}_2 corresponding to the intermediate moment of inertia, is unstable.

perpendicular axes,¹¹ are broadly used in more common gyroscopes. Invented by Léon Foucault in the 1850s and made practical later by H. Anschütz-Kaempfe, such gyroscopes have become core parts of automatic guidance systems, for example, in ships, airplanes, missiles, etc. Even if its support wobbles and/or drifts, the suspended gyroscope sustains its direction relative to an inertial reference frame.¹²

However, in the general case with no such special initial alignment, the dynamics of symmetric tops is more complicated. In this case, the vector \mathbf{L} is still conserved, including its direction, but the vector $\boldsymbol{\omega}$ is not. Indeed, let us direct the \mathbf{n}_2 -axis normally to the common plane of the vector \mathbf{L} and the current instantaneous direction \mathbf{n}_3 of the main principal axis (in Fig. 8 below, the plane of the drawing); then, in that particular instant, $L_2 = 0$. Now let us recall that in a symmetric top, the axis \mathbf{n}_2 is a principal one. According to Eq. (26) with $j = 2$, the corresponding component ω_2 has to be equal to L_2/I_2 , so it is equal to zero. This means that in the particular instant we are considering, the vector $\boldsymbol{\omega}$ lies in this plane (the common plane of vectors \mathbf{L} and \mathbf{n}_3) as well – see Fig. 8a.

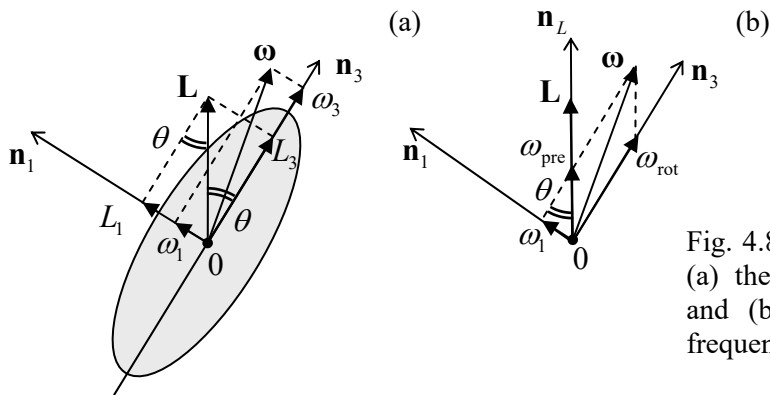


Fig. 4.8. Free rotation of a symmetric top:
(a) the general configuration of vectors,
and (b) calculating the free precession
frequency.

Now consider some point located on the main principal axis \mathbf{n}_3 , and hence on the plane $[\mathbf{n}_3, \mathbf{L}]$. Since $\boldsymbol{\omega}$ is the instantaneous axis of rotation, according to Eq. (9), the instantaneous velocity $\mathbf{v} = \boldsymbol{\omega} \times \mathbf{r}$ of the point is directed normally to that plane. This is true for each point of the main axis (besides only one, with $\mathbf{r} = 0$, i.e. the center of mass, which does not move), so the axis as a whole has to move normally to the common plane of the vectors \mathbf{L} , $\boldsymbol{\omega}$, and \mathbf{n}_3 , while still passing through point 0. Since this conclusion is valid for any moment of time, it means that the vectors $\boldsymbol{\omega}$ and \mathbf{n}_3 rotate about the space-fixed vector \mathbf{L} together, with some angular velocity ω_{pre} , at each moment staying within one plane. This effect is called the *free* (or “torque-free”, or “regular”) *precession*, and has to be clearly distinguished it from the completely different effect of the *torque-induced precession*, which will be discussed in the next section.

To calculate ω_{pre} , let us represent the instant vector $\boldsymbol{\omega}$ as a sum of not its Cartesian components (as in Fig. 8a), but rather of two non-orthogonal vectors directed along \mathbf{n}_3 and \mathbf{L} (Fig. 8b):

$$\boldsymbol{\omega} = \omega_{\text{rot}} \mathbf{n}_3 + \omega_{\text{pre}} \mathbf{n}_L, \quad \mathbf{n}_L \equiv \frac{\mathbf{L}}{L}. \quad (4.57)$$

¹¹ See, for example, a nice animation available online at <http://en.wikipedia.org/wiki/Gimbal>.

¹² Currently, optical gyroscopes are becoming more popular for all but the most precise applications. Much more compact but also much less accurate gyroscopes used, for example, in smartphones and tablet computers, are based on the effect of rotation on 2D mechanical oscillators (whose analysis is left for the reader’s exercise), and are implemented as micro-electro-mechanical systems (MEMS) – see, e.g., Chapter 22 in V. Kaajakari, *Practical MEMS*, Small Gear Publishing, 2009.

Fig. 8b shows that ω_{rot} has the meaning of the angular velocity of rotation of the body about its main principal axis, while ω_{pre} is the angular velocity of rotation of that axis about the constant direction of the vector \mathbf{L} , i.e. is exactly the frequency of precession that we are trying to find. Now ω_{pre} may be readily calculated from the comparison of two panels of Fig. 8, by noticing that the same angle θ between the vectors \mathbf{L} and \mathbf{n}_3 participates in two relations:

$$\sin \theta = \frac{L_1}{L} = \frac{\omega_1}{\omega_{\text{pre}}}. \quad (4.58)$$

Since the \mathbf{n}_1 -axis is a principal one, we may use Eq. (26) for $j = 1$, i.e. $L_1 = I_1 \omega_1$, to eliminate ω_1 from Eq. (58), and get a very simple formula

$$\omega_{\text{pre}} = \frac{L}{I_1}. \quad (4.59)$$

Free
precession:
lab frame

This result shows that the precession *frequency* is constant and independent of the alignment of the vector \mathbf{L} with the main principal axis \mathbf{n}_3 , while its *amplitude* (characterized by the angle θ) does depend on the initial alignment, and vanishes if \mathbf{L} is parallel to \mathbf{n}_3 .¹³ Note also that if all principal moments of inertia are of the same order, ω_{pre} is of the same order as the total angular speed $\boldsymbol{\omega} \equiv |\boldsymbol{\omega}|$ of the rotation.

Now let us briefly discuss the free precession in the general case of an “asymmetric top”, i.e. a body with arbitrary $I_1 \neq I_2 \neq I_3$. In this case, the effect is more complex because here not only the *direction* but also the *magnitude* of the instantaneous angular velocity $\boldsymbol{\omega}$ may evolve in time. If we are only interested in the relation between the instantaneous values of ω_j and L_j , i.e. the “trajectories” of the vectors $\boldsymbol{\omega}$ and \mathbf{L} as observed from the reference frame $\{\mathbf{n}_1, \mathbf{n}_2, \mathbf{n}_3\}$ of the principal axes of the body, rather than in the explicit law of their time evolution, they may be found directly from the conservation laws. (Let me emphasize again that the vector \mathbf{L} , being constant in an inertial reference frame, generally evolves in the frame rotating with the body.) Indeed, Eq. (55) may be understood as the equation of an ellipsoid in the Cartesian coordinates $\{\omega_1, \omega_2, \omega_3\}$, so that for a free body, the vector $\boldsymbol{\omega}$ has to stay on the surface of that ellipsoid.¹⁴ On the other hand, since the reference frame’s rotation preserves the *length* of any vector, the *magnitude* (but not the direction!) of the vector \mathbf{L} is also an integral of motion in the moving frame, and we can write

$$L^2 \equiv \sum_{j=1}^3 L_j^2 = \sum_{j=1}^3 I_j^2 \omega_j^2 = \text{const.} \quad (4.60)$$

Hence the trajectory of the vector $\boldsymbol{\omega}$ follows the closed curve formed by the intersection of two ellipsoids, (55) and (60) – the so-called *Poinsot construction*. It is evident that this trajectory is generally “taco-edge-shaped”, i.e. more complex than a planar circle, but never very complex either.¹⁵

The same argument may be repeated for the vector \mathbf{L} , for whom the first form of Eq. (60) describes a sphere, and Eq. (55), another ellipsoid:

¹³ For our Earth, free precession’s amplitude is so small (corresponding to sub-10-m linear deviations of the symmetry axis from the vector \mathbf{L} at the surface) that this effect is of the same order as other, more irregular motions of the axis, resulting from turbulent fluid flow effects in the planet’s interior and its atmosphere.

¹⁴ It is frequently called the *Poinsot’s ellipsoid*, named after Louis Poinsot (1777-1859) who has made several important contributions to rigid body mechanics.

¹⁵ Curiously, the “wobbling” motion along such trajectories was observed not only for macroscopic rigid bodies but also for heavy atomic nuclei – see, e.g., N. Sensharma *et al.*, *Phys. Rev. Lett.* **124**, 052501 (2020).

$$T_{\text{rot}} = \sum_{j=1}^3 \frac{1}{2I_j} L_j^2 = \text{const.} \quad (4.61)$$

On the other hand, if we are interested in the trajectory of the vector ω as observed from an *inertial* frame (in which the vector \mathbf{L} stays still), we may note that the general relation (15) for the same rotational energy T_{rot} may also be rewritten as

$$T_{\text{rot}} = \frac{1}{2} \sum_{j=1}^3 \omega_j \sum_{j'=1}^3 I_{jj'} \omega_{j'}. \quad (4.62)$$

But according to the Eq. (22), the second sum on the right-hand side is nothing more than L_j , so that

$$T_{\text{rot}} = \frac{1}{2} \sum_{j=1}^3 \omega_j L_j = \frac{1}{2} \boldsymbol{\omega} \cdot \mathbf{L}. \quad (4.63)$$

This equation shows that for a free body ($T_{\text{rot}} = \text{const}$, $\mathbf{L} = \text{const}$), even if the vector ω changes in time, its endpoint should stay on a plane normal to the angular momentum \mathbf{L} . Earlier, we have seen that for the particular case of the symmetric top – see Fig. 8b, but for an asymmetric top, the trajectory of the endpoint may not be circular.

If we are interested not only in the trajectory of the vector ω but also in the law of its evolution in time, it may be calculated using the general Eq. (33) expressed in the principal components ω_j . For that, we have to recall that Eq. (33) is only valid in an inertial reference frame, while the frame $\{\mathbf{n}_1, \mathbf{n}_2, \mathbf{n}_3\}$ may rotate with the body and hence is generally not inertial. We may handle this problem by applying, to the vector \mathbf{L} , the general kinematic relation (8):

$$\frac{d\mathbf{L}}{dt} \Big|_{\text{in lab}} = \frac{d\mathbf{L}}{dt} \Big|_{\text{in mov}} + \boldsymbol{\omega} \times \mathbf{L}. \quad (4.64)$$

Combining it with Eq. (33), in the moving frame we get

$$\frac{d\mathbf{L}}{dt} + \boldsymbol{\omega} \times \mathbf{L} = \boldsymbol{\tau}, \quad (4.65)$$

where $\boldsymbol{\tau}$ is the external torque. In particular, for the principal-axis components L_j , related to the components ω_j by Eq. (26), the vector equation (65) is reduced to a set of three scalar *Euler equations*

Euler equations (4.66)

$$I_j \dot{\omega}_j + (I_{j''} - I_{j'}) \omega_{j'} \omega_{j''} = \tau_j,$$

where the set of indices $\{j, j', j''\}$ has to follow the usual “right” order – e.g., $\{1, 2, 3\}$, etc.¹⁶

In order to get a feeling how do the Euler equations work, let us return to the particular case of a free symmetric top ($\tau_1 = \tau_2 = \tau_3 = 0$, $I_1 = I_2 \neq I_3$). In this case, $I_1 - I_2 = 0$, so that Eq. (66) with $j = 3$ yields $\omega_3 = \text{const}$, while the equations for $j = 1$ and $j = 2$ take the following simple form:

$$\dot{\omega}_1 = -\Omega_{\text{pre}} \omega_2, \quad \dot{\omega}_2 = \Omega_{\text{pre}} \omega_1, \quad (4.67)$$

where Ω_{pre} is a constant determined by both the system parameters and the initial conditions:

¹⁶ These equations are of course valid in the simplest case of the fixed rotation axis as well. For example, if $\omega = \mathbf{n}_z \omega$, i.e. $\omega_x = \omega_y = 0$, Eq. (66) is reduced to Eq. (38).

$$\Omega_{\text{pre}} \equiv \omega_3 \frac{I_3 - I_1}{I_1}. \quad (4.68)$$

Free precession:
body frame

The system of two equations (67) has a sinusoidal solution with frequency Ω_{pre} , and describes a uniform rotation of the vector $\boldsymbol{\omega}$, with that frequency, about the main axis \mathbf{n}_3 . This is just another representation of the free precession analyzed above, but this time as observed from the rotating body. Evidently, Ω_{pre} is substantially different from the frequency ω_{pre} (59) of the precession as observed from the lab frame; for example, Ω_{pre} vanishes for the spherical top (with $I_1 = I_2 = I_3$), while ω_{pre} , in this case, is equal to the rotation frequency.¹⁷

Unfortunately, for the rotation of an asymmetric top (i.e., an arbitrary rigid body) the Euler equations (66) are substantially nonlinear even in the absence of external torque, and may be solved analytically only in just a few cases. One of them is a proof of the already mentioned fact: the free top's rotation about one of its principal axes is stable if the corresponding principal moment of inertia is either the largest or the smallest one of the three. (This proof is easy, and is left for the reader's exercise.)

4.5. Torque-induced precession

The dynamics of rotation becomes even more complex in the presence of external forces. Let us consider the most counter-intuitive effect of *torque-induced precession*, for the simplest case of an axially-symmetric body (which is a particular case of the symmetric top, $I_1 = I_2 \neq I_3$), supported at some point A of its symmetry axis, that does not coincide with the center of mass 0 – see Fig. 9.

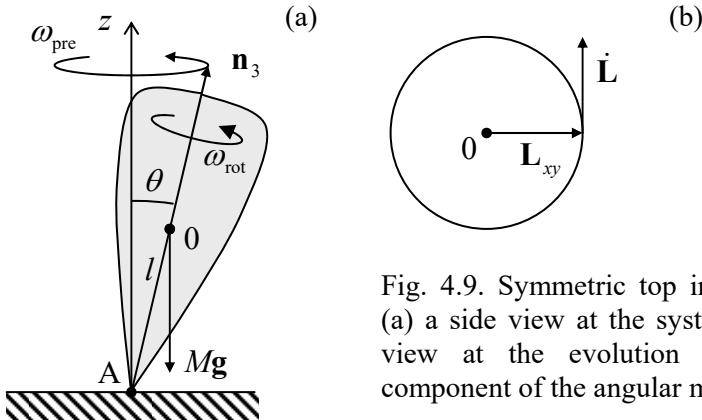


Fig. 4.9. Symmetric top in the gravity field:
(a) a side view at the system and (b) the top view at the evolution of the horizontal component of the angular momentum vector.

The uniform gravity field \mathbf{g} creates bulk-distributed forces that, as we know from the analysis of the physical pendulum in Sec. 3, are equivalent to a single force $M\mathbf{g}$ applied in the center of mass – in Fig. 9, point 0. The torque of this force relative to the support point A is

$$\tau = \mathbf{r}_0|_{\text{in } A} \times M\mathbf{g} = Ml\mathbf{n}_3 \times \mathbf{g}. \quad (4.69)$$

Hence the general equation (33) of the angular momentum evolution (valid in any inertial frame, for example the one with its origin at point A) becomes

¹⁷ For our Earth with its *equatorial bulge* (see Sec. 6 below), the ratio $(I_3 - I_1)/I_1$ is $\sim 1/300$, so that $2\pi/\Omega_{\text{pre}}$ is about 10 months. However, due to the fluid flow effects mentioned above, the observed precession is not very regular.

$$\dot{\mathbf{L}} = Ml\mathbf{n}_3 \times \mathbf{g}. \quad (4.70)$$

Despite the apparent simplicity of this (exact!) equation, its analysis is straightforward only in the limit when the top is spinning about its symmetry axis \mathbf{n}_3 with a very high angular velocity ω_{rot} . In this case, we may neglect the contribution to \mathbf{L} due to a relatively small precession velocity ω_{pre} (still to be calculated), and use Eq. (26) to write

$$\mathbf{L} = I_3\boldsymbol{\omega} = I_3\omega_{\text{rot}}\mathbf{n}_3. \quad (4.71)$$

Then Eq. (70) shows that the vector $\dot{\mathbf{L}}$ is perpendicular to both \mathbf{n}_3 (and hence \mathbf{L}) and \mathbf{g} , i.e. lies within a horizontal plane and is perpendicular to the horizontal component \mathbf{L}_{xy} of the vector \mathbf{L} – see Fig. 9b. Since, according to Eq. (70), the magnitude of this vector is constant, $|\dot{\mathbf{L}}| = Mgl \sin \theta$, the vector \mathbf{L} (and hence the body's main axis) rotates about the vertical axis with the following angular velocity:

$$\omega_{\text{pre}} = \frac{|\dot{\mathbf{L}}|}{L_{xy}} = \frac{Mgl \sin \theta}{L \sin \theta} \equiv \frac{Mgl}{L} = \frac{Mgl}{I_3 \omega_{\text{rot}}}. \quad (4.72)$$

Torque-induced precession: fast-rotation limit

Thus, rather counter-intuitively, the fast-rotating top does not follow the external, vertical force and, in addition to fast spinning about the symmetry axis \mathbf{n}_3 , performs a revolution, called the *torque-induced precession*, about the vertical axis.¹⁸ Note that, similarly to the free-precession frequency (59), the torque-induced precession frequency (72) does not depend on the initial (and sustained) angle θ . However, the torque-induced precession frequency is inversely (rather than directly) proportional to ω_{rot} . This fact makes the above simple theory valid in many practical cases. Indeed, Eq. (71) is quantitatively valid if the contribution of the precession into \mathbf{L} is relatively small: $I\omega_{\text{pre}} \ll I_3\omega_{\text{rot}}$, where I is a certain effective moment of inertia for the precession – to be calculated below. Using Eq. (72), this condition may be rewritten as

$$\omega_{\text{rot}} \gg \left(\frac{MglI}{I_3^2} \right)^{1/2}. \quad (4.73)$$

According to Eq. (16), for a body of not too extreme proportions, i.e. with all linear dimensions of the same length scale l , all inertia moments are of the order of Ml^2 , so that the right-hand side of Eq. (73) is of the order of $(g/l)^{1/2}$, i.e. comparable with the frequency of small oscillations of the same body as the physical pendulum at the absence of its fast rotation.

To develop a quantitative theory that would be valid beyond such approximate treatment, the Euler equations (66) may be used, but are not very convenient. A better approach, suggested by the same L. Euler, is to introduce a set of three independent angles between the principal axes $\{\mathbf{n}_1, \mathbf{n}_2, \mathbf{n}_3\}$ bound to the rigid body, and the axes $\{\mathbf{n}_x, \mathbf{n}_y, \mathbf{n}_z\}$ of an inertial reference frame (Fig. 10), and then express the basic equation (33) of rotation, via these angles. There are several possible options for the definition of such angles; Fig. 10 shows the set of *Euler angles*, most convenient for analyses of fast rotation.¹⁹ As one can see, the first Euler angle, θ , is the usual polar angle measured from the \mathbf{n}_z -axis to the \mathbf{n}_3 -axis. The second one is the azimuthal angle φ , measured from the \mathbf{n}_x -axis to the so-called *line of nodes* formed by the intersection of planes $[\mathbf{n}_x, \mathbf{n}_y]$ and $[\mathbf{n}_1, \mathbf{n}_2]$. The last Euler angle, ψ , is measured

¹⁸ A semi-quantitative interpretation of this effect is a very useful exercise, highly recommended to the reader.

¹⁹ Of the several choices more convenient in the absence of fast rotation, the most common is the set of so-called *Tait-Bryan angles* (called the *yaw*, *pitch*, and *roll*), which are broadly used for aircraft and maritime navigation.

within the plane $[\mathbf{n}_1, \mathbf{n}_2]$, from the line of nodes to the \mathbf{n}_1 -axis. For example, in the simple picture of slow force-induced precession of a symmetric top, that was discussed above, the angle θ is constant, the angle ψ changes rapidly, with the rotation velocity ω_{rot} , while the angle φ evolves with the precession frequency ω_{pre} (72).

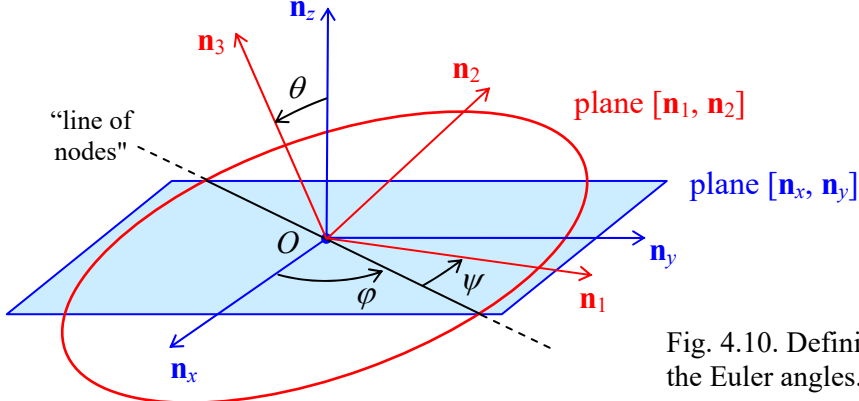


Fig. 4.10. Definition of the Euler angles.

Now we can express the principal-axes components of the instantaneous angular velocity vector, ω_1 , ω_2 , and ω_3 , as measured in the lab reference frame, in terms of the Euler angles. This may be readily done by calculating, from Fig. 10, the contributions of the Euler angles' evolution to the rotation about each principal axis, and then adding them up:

$$\begin{aligned}\omega_1 &= \dot{\varphi} \sin \theta \sin \psi + \dot{\theta} \cos \psi, \\ \omega_2 &= \dot{\varphi} \sin \theta \cos \psi - \dot{\theta} \sin \psi, \\ \omega_3 &= \dot{\varphi} \cos \theta + \dot{\psi}.\end{aligned}\tag{4.74}$$

ω via Euler angles

These relations enable the expression of the kinetic energy of rotation (25) and the angular momentum components (26) via the generalized coordinates θ , φ , and ψ and their time derivatives (i.e. the corresponding generalized velocities), and then using the powerful Lagrangian formalism to derive their equations of motion. This is especially simple to do in the case of symmetric tops (with $I_1 = I_2$), because plugging Eqs. (74) into Eq. (25) we get an expression,

$$T_{\text{rot}} = \frac{I_1}{2} (\dot{\theta}^2 + \dot{\varphi}^2 \sin^2 \theta) + \frac{I_3}{2} (\dot{\varphi} \cos \theta + \dot{\psi})^2,\tag{4.75}$$

which does not include explicitly either φ or ψ . (This reflects the fact that for a symmetric top we can always select the \mathbf{n}_1 -axis to coincide with the line of nodes, and hence take $\psi = 0$ at the considered moment of time. Note that this trick does *not* mean we can take $\dot{\psi} = 0$, because the \mathbf{n}_1 -axis, as observed from an inertial reference frame, moves!) Now we should not forget that at the torque-induced precession, the center of mass moves as well (see, e.g., Fig. 9), so that according to Eq. (14), the total kinetic energy of the body is the sum of two terms,

$$T = T_{\text{rot}} + T_{\text{tran}}, \quad T_{\text{tran}} = \frac{M}{2} V^2 = \frac{M}{2} l^2 (\dot{\theta}^2 + \dot{\varphi}^2 \sin^2 \theta),\tag{4.76}$$

while its potential energy is just

$$U = Mgl \cos \theta + \text{const}.\tag{4.77}$$

Now we could readily use Eqs. (2.19) to write the Lagrange equations of motion for the Euler angles, but it is simpler to immediately notice that according to Eqs. (75)-(77), the Lagrangian function, $T - U$, does not depend explicitly on the “cyclic” coordinates φ and ψ , so that the corresponding generalized momenta (2.31) are conserved:

$$p_\varphi \equiv \frac{\partial T}{\partial \dot{\varphi}} = I_A \dot{\varphi} \sin^2 \theta + I_3 (\dot{\varphi} \cos \theta + \dot{\psi}) \cos \theta = \text{const}, \quad (4.78)$$

$$p_\psi \equiv \frac{\partial T}{\partial \dot{\psi}} = I_3 (\dot{\varphi} \cos \theta + \dot{\psi}) = \text{const}, \quad (4.79)$$

where $I_A \equiv I_1 + Ml^2$. (According to Eq. (29), I_A is just the body’s moment of inertia for rotation about a horizontal axis passing through the support point A.) According to the last of Eqs. (74), p_ψ is just L_3 , i.e. the angular momentum’s component along the *precessing* axis \mathbf{n}_3 . On the other hand, by its very definition (78), p_φ is L_z , i.e. the same vector \mathbf{L} ’s component along the *stationary* axis z . (Actually, we could foresee in advance the conservation of both these components of \mathbf{L} for our system, because the vector (69) of the external torque is perpendicular to both \mathbf{n}_3 and \mathbf{n}_z .) Using this notation, and solving the simple system of two linear equations (78)-(79) for the angle derivatives, we get

$$\dot{\varphi} = \frac{L_z - L_3 \cos \theta}{I_A \sin^2 \theta}, \quad \dot{\psi} = \frac{L_3}{I_3} - \frac{L_z - L_3 \cos \theta}{I_A \sin^2 \theta} \cos \theta. \quad (4.80)$$

One more conserved quantity in this problem is the full mechanical energy²⁰

$$E \equiv T + U = \frac{I_A}{2} (\dot{\theta}^2 + \dot{\varphi}^2 \sin^2 \theta) + \frac{I_3}{2} (\dot{\varphi} \cos \theta + \dot{\psi})^2 + Mgl \cos \theta. \quad (4.81)$$

Plugging Eqs. (80) into Eq. (81), we get a first-order differential equation for the angle θ , which may be represented in the following physically transparent form:

$$\frac{I_A}{2} \dot{\theta}^2 + U_{\text{ef}}(\theta) = E, \quad U_{\text{ef}}(\theta) \equiv \frac{(L_z - L_3 \cos \theta)^2}{2I_A \sin^2 \theta} + \frac{L_3^2}{2I_3} + Mgl \cos \theta + \text{const}. \quad (4.82)$$

Thus, similarly to the planetary problems considered in Sec. 3.4, the torque-induced precession of a symmetric top has been reduced (without any approximations!) to a 1D problem of the motion of just one of its degrees of freedom, the polar angle θ , in the effective potential $U_{\text{ef}}(\theta)$. According to Eq. (82), very similar to Eq. (3.44) for the planetary problem, this potential is the sum of the actual potential energy U given by Eq. (77), and a contribution from the kinetic energy of motion along two other angles. In the absence of rotation about the axes \mathbf{n}_z and \mathbf{n}_3 (i.e., $L_z = L_3 = 0$), Eq. (82) is reduced to the first integral of the equation (40) of motion of a physical pendulum, with $I' = I_A$. If the rotation is present, then (besides the case of very special initial conditions when $\theta(0) = 0$ and $L_z = L_3$),²¹ the first contribution to $U_{\text{ef}}(\theta)$ diverges at $\theta \rightarrow 0$ and π , so that the effective potential energy has a minimum at some non-zero value θ_0 of the polar angle θ – see Fig. 11.

²⁰ Indeed, since the Lagrangian does not depend on time explicitly, $H = \text{const}$, and since the full kinetic energy T (75)-(76) is a quadratic-homogeneous function of the generalized velocities, we have $E = H$.

²¹ In that simple case, the body continues to rotate about the vertical symmetry axis: $\theta(t) = 0$. Note, however, that such motion is stable only if the spinning speed is sufficiently high – see Eq. (85) below.

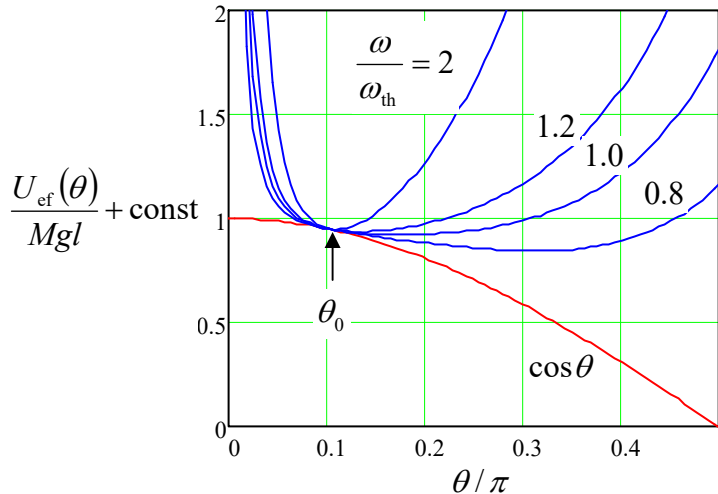


Fig. 4.11. The effective potential energy U_{ef} of the symmetric top, given by Eq. (82), as a function of the polar angle θ , for a particular value (0.95) of the ratio $r \equiv L_z/L_3$ (so that at $\omega_{\text{rot}} \gg \omega_{\text{th}}$, $\theta_0 = \cos^{-1} r \approx 0.1011 \pi$), and several values of the ratio $\omega_{\text{rot}}/\omega_{\text{th}}$ – see Eq. (85).

If the initial angle $\theta(0)$ is equal to this value θ_0 , i.e. if the initial effective energy is equal to its minimum value $U_{\text{ef}}(\theta_0)$, the polar angle remains constant through the motion: $\theta(t) = \theta_0$. This corresponds to the pure torque-induced precession whose angular velocity is given by the first of Eqs. (80):

$$\omega_{\text{pre}} \equiv \dot{\phi} = \frac{L_z - L_3 \cos \theta_0}{I_A \sin^2 \theta_0}. \quad (4.83)$$

The condition for finding θ_0 , $dU_{\text{ef}}/d\theta = 0$, is a transcendental algebraic equation that cannot be solved analytically for arbitrary parameters. However, in the high spinning speed limit (73), this is possible. Indeed, in this limit the Mgl -proportional contribution to U_{ef} is small, and we may analyze its effect by successive approximations. In the 0th approximation, i.e. at $Mgl = 0$, the minimum of U_{ef} is evidently achieved at $\cos \theta_0 = L_z/L_3$, turning the precession frequency (83) to zero. In the next, 1st approximation, we may require that at $\theta = \theta_0$, the derivative of the first term of Eq. (82) for U_{ef} over $\cos \theta$, equal to $-L_z(L_z - L_3 \cos \theta)/I_A \sin^2 \theta$ ²², is canceled with that of the gravity-induced term, equal to Mgl . This immediately yields $\omega_{\text{pre}} = (L_z - L_3 \cos \theta_0)/I_A \sin^2 \theta_0 = Mgl/L_3$, so that by identifying ω_{rot} with $\omega_3 \equiv L_3/I_3$ (see Fig. 8), we recover the simple expression (72).

The second important result that may be readily obtained from Eq. (82) is the exact expression for the threshold value of the spinning speed for a vertically rotating top ($\theta = 0$, $L_z = L_3$). Indeed, in the limit $\theta \rightarrow 0$ this expression may be readily simplified:

$$U_{\text{ef}}(\theta) \approx \text{const} + \left(\frac{L_3^2}{8I_A} - \frac{Mgl}{2} \right) \theta^2. \quad (4.84)$$

This formula shows that if $\omega_{\text{rot}} \equiv L_3/I_3$ is higher than the following threshold value,

$$\omega_{\text{th}} \equiv 2 \left(\frac{Mgl I_A}{I_3^2} \right)^{1/2},$$

(4.85)
Threshold rotation speed

²² Indeed, the derivative of the fraction $1/2I_A \sin^2 \theta$, taken at the point $\cos \theta = L_z/L_3$, is multiplied by the numerator, $(L_z - L_3 \cos \theta)^2$, which turns to zero at this point.

then the coefficient at θ^2 in Eq. (84) is positive, so that U_{ef} has a stable minimum at $\theta_0 = 0$. On the other hand, if ω_3 is decreased below ω_{th} , the fixed point becomes unstable, so that the top falls. As the plots in Fig. 11 show, Eq. (85) for the threshold frequency works very well even for non-zero but small values of the precession angle θ_0 . Note that if we take $I = I_A$ in the condition (73) of the approximate treatment, it acquires a very simple sense: $\omega_{\text{rot}} \gg \omega_{\text{th}}$.

Finally, Eqs. (82) give a natural description of one more phenomenon. If the initial energy is larger than $U_{\text{ef}}(\theta_0)$, the angle θ oscillates between two classical turning points on both sides of the fixed point θ_0 – see Fig. 11 again. The law and frequency of these oscillations may be found exactly as in Sec. 3.3 – see Eqs. (3.27) and (3.28). At $\omega_3 \gg \omega_{\text{th}}$, this motion is a fast rotation of the symmetry axis \mathbf{n}_3 of the body about its average position performing the slow torque-induced precession. Historically, these oscillations are called *nutations*, but their physics is similar to that of the free precession that was analyzed in the previous section, and the order of magnitude of their frequency is given by Eq. (59).

It may be proved that small friction (not taken into account in the above analysis) leads first to decay of these nutations, then to a slower drift of the precession angle θ_0 to zero, and finally, to a gradual decay of the spinning speed ω_{rot} until it reaches the threshold (85) and the top falls.

4.6. Non-inertial reference frames

Now let us use the results of our analysis of the rotation kinematics in Sec. 1 to complete the discussion of the transfer between two reference frames, which was started in the introductory Chapter 1. As Fig. 12 (which reproduces Fig. 1.2 in a more convenient notation) shows, even if the “moving” frame 0 rotates relative to the “lab” frame 0’, the radius vectors observed from these two frames are still related, at any moment of time, by the simple Eq. (1.5). In our new notation:

$$\mathbf{r}' = \mathbf{r}_0 + \mathbf{r}. \quad (4.86)$$

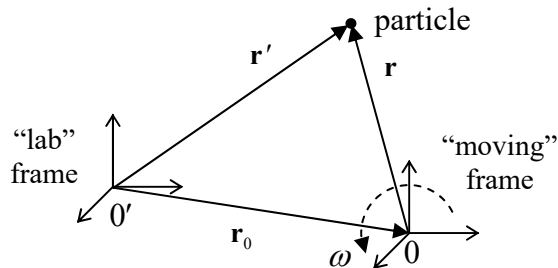


Fig. 4.12. The general case of transfer between two reference frames.

However, as was mentioned in Sec. 1, the general addition rule for velocities is already more complex. To find it, let us differentiate Eq. (86) over time:

$$\frac{d}{dt} \mathbf{r}' = \frac{d}{dt} \mathbf{r}_0 + \frac{d}{dt} \mathbf{r}. \quad (4.87)$$

The left-hand side of this relation is evidently the particle’s velocity as measured in the lab frame, and the first term on the right-hand side is the velocity \mathbf{v}_0 of point 0, as measured in the same lab frame. The last term is more complex: due to the possible mutual rotation of the frames 0 and 0’, that term may not vanish even if the particle does not move relative to the rotating frame 0 – see Fig. 12.

Fortunately, we have already derived the general Eq. (8) to analyze situations exactly like this one. Taking $\mathbf{A} = \mathbf{r}$ in it, we may apply the result to the last term of Eq. (87), to get

$$\mathbf{v}|_{\text{in lab}} = \mathbf{v}_0|_{\text{in lab}} + (\mathbf{v} + \boldsymbol{\omega} \times \mathbf{r}), \quad (4.88)$$

Transformation
of
velocity

where $\boldsymbol{\omega}$ is the instantaneous angular velocity of an imaginary rigid body connected to the moving reference frame (or we may say, of this frame as such), as measured in the *lab* frame 0', while \mathbf{v} is $d\mathbf{r}/dt$ as measured in the *moving* frame 0. The relation (88), on one hand, is a natural generalization of Eq. (10) for $\mathbf{v} \neq 0$; on the other hand, if $\boldsymbol{\omega} = 0$, it is reduced to simple Eq. (1.8) for the translational motion of the frame 0.

To calculate the particle's acceleration, we may just repeat the same trick: differentiate Eq. (88) over time, and then use Eq. (8) again, now for the vector $\mathbf{A} = \mathbf{v} + \boldsymbol{\omega} \times \mathbf{r}$. The result is

$$\mathbf{a}|_{\text{in lab}} \equiv \mathbf{a}_0|_{\text{in lab}} + \frac{d}{dt}(\mathbf{v} + \boldsymbol{\omega} \times \mathbf{r}) + \boldsymbol{\omega} \times (\mathbf{v} + \boldsymbol{\omega} \times \mathbf{r}). \quad (4.89)$$

Carrying out the differentiation in the second term, we finally get the goal relation,

$$\mathbf{a}|_{\text{in lab}} \equiv \mathbf{a}_0|_{\text{in lab}} + \mathbf{a} + \dot{\boldsymbol{\omega}} \times \mathbf{r} + 2\boldsymbol{\omega} \times \mathbf{v} + \boldsymbol{\omega} \times (\boldsymbol{\omega} \times \mathbf{r}), \quad (4.90)$$

Transformation
of
acceleration

where \mathbf{a} is particle's acceleration as measured in the moving frame. This result is a natural generalization of the simple Eq. (1.9) to the rotating frame case.

Now let the lab frame 0' be inertial; then the 2nd Newton's law for a particle of mass m is

$$m\mathbf{a}|_{\text{in lab}} = \mathbf{F}, \quad (4.91)$$

where \mathbf{F} is the vector sum of all forces exerted on the particle. This is simple and clear; however, in many cases it is much more convenient to work in a non-inertial reference frame. For example, when describing most phenomena on the Earth's surface, it is rather inconvenient to use a reference frame bound to the Sun (or to the galactic center, etc.). In order to understand what we should pay for the convenience of using a moving frame, we may combine Eqs. (90) and (91) to write

$$m\mathbf{a} = \mathbf{F} - m\mathbf{a}_0|_{\text{in lab}} - m\boldsymbol{\omega} \times (\boldsymbol{\omega} \times \mathbf{r}) - 2m\boldsymbol{\omega} \times \mathbf{v} - m\dot{\boldsymbol{\omega}} \times \mathbf{r}. \quad (4.92)$$

Inertial
"forces"

This result means that if we want to use an analog of the 2nd Newton's law in a non-inertial reference frame, we have to add, to the actual net force \mathbf{F} exerted on a particle, four pseudo-force terms, called *inertial forces*, all proportional to the particle's mass. Let us analyze them one by one, always remembering that these are just mathematical terms, not actual physical forces. (In particular, it would be futile to seek a 3rd-Newton's-law counterpart for any inertial force.)

The first term, $-m\mathbf{a}_0|_{\text{in lab}}$, is the only one not related to rotation and is well known from undergraduate mechanics. (Let me hope the reader remembers all these weight-in-the-accelerating-elevator problems.) However, despite its simplicity, this term has more subtle consequences. As an example, let us consider, semi-qualitatively, the motion of a planet, such as our Earth, orbiting a star and also rotating about its own axis – see Fig. 13. The bulk-distributed gravity forces, acting on a planet from its star, are not quite uniform, because they obey the $1/r^2$ gravity law (1.15), and hence are equivalent to a single force applied to a point A slightly offset from the planet's center of mass 0, toward

the star. For a spherically-symmetric planet, the direction from 0 to A would be exactly aligned with the direction toward the star. However, real planets are not absolutely rigid, so due to the centrifugal “force” (to be discussed momentarily), the rotation about their own axis makes them slightly ellipsoidal – see Fig. 13. (For our Earth, this equatorial bulge is about 10 km.) As a result, the net gravity force is slightly offset from the direction toward the center of mass 0. On the other hand, repeating all the arguments of this section for a body (rather than a point), we may see that, in the reference frame moving with the planet, the inertial force $-Ma_0$ (with the magnitude of the total gravity force, but directed *from* the star) is applied exactly to the center of mass. As a result, this pair of forces creates a torque τ perpendicular to both the direction toward the star and the vector 0A. (In Fig. 13, the torque vector is perpendicular to the plane of the drawing). If the angle δ between the planet’s “polar” axis of rotation and the direction towards the star was fixed, then, as we have seen in the previous section, this torque would induce a slow axis precession about that direction.

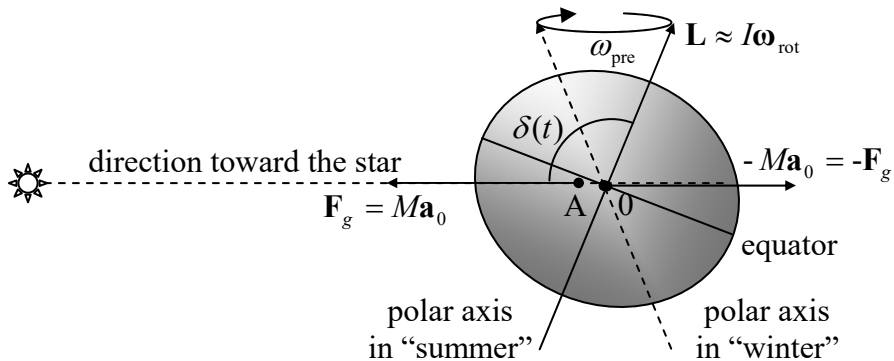


Fig. 4.13. The axial precession of a planet (with the equatorial bulge and the 0A-offset strongly exaggerated).

However, as a result of the orbital motion, the angle δ oscillates in time much faster (once a year) between values $(\pi/2 + \varepsilon)$ and $(\pi/2 - \varepsilon)$, where ε is the axis tilt, i.e. angle between the polar axis (the direction of vectors \mathbf{L} and $\boldsymbol{\omega}_{\text{rot}}$) and the normal to the *ecliptic plane* of the planet’s orbit. (For the Earth, $\varepsilon \approx 23.4^\circ$.) A straightforward averaging over these fast oscillations²³ shows that the torque leads to the polar axis’ precession about the axis *perpendicular* to the ecliptic plane, keeping the angle ε constant – see Fig. 13. For the Earth, the period $T_{\text{pre}} = 2\pi/\omega_{\text{pre}}$ of this *precession of the equinoxes*, corrected to a substantial effect of the Moon’s gravity, is close to 26,000 years.²⁴

Returning to Eq. (92), the direction of the second term of its right-hand side,

$$\mathbf{F}_{\text{cf}} \equiv -m\boldsymbol{\omega} \times (\boldsymbol{\omega} \times \mathbf{r}), \quad (4.93)$$

Centrifugal “force” called the *centrifugal force*, is always perpendicular to, and directed out of the instantaneous rotation axis – see Fig. 14. Indeed, the vector $\boldsymbol{\omega} \times \mathbf{r}$ is perpendicular to both $\boldsymbol{\omega}$ and \mathbf{r} (in Fig. 14, normal to the drawing plane and directed from the reader) and has the magnitude $\omega r \sin\theta = \omega\rho$, where ρ is the distance of the particle from the rotation axis. Hence the outer vector product, with the account of the minus sign, is normal to the rotation axis $\boldsymbol{\omega}$, directed from this axis, and is equal to $\omega^2 r \sin\theta = \omega^2 \rho$. The centrifugal “force” is of course just the result of the fact that the centripetal acceleration $\omega^2 \rho$, explicit in the inertial reference frame, disappears in the rotating frame. For a typical location of the Earth ($\rho \sim R_E \approx 6 \times 10^6$ m),

²³ Details of this calculation may be found, e.g., in Sec. 5.8 of the textbook by H. Goldstein *et al.*, *Classical Mechanics*, 3rd ed., Addison Wesley, 2002.

²⁴ This effect is known from antiquity, apparently discovered by Hipparchus of Rhodes (190-120 BC).

with its angular velocity $\omega_E \approx 10^{-4} \text{ s}^{-1}$, the acceleration is rather considerable, of the order of 3 cm/s^2 , i.e. $\sim 0.003 g$, and is responsible, in particular, for the largest part of the equatorial bulge mentioned above.

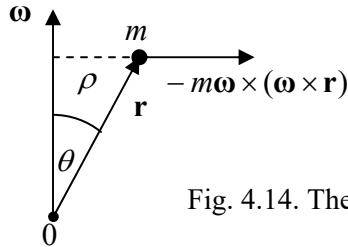


Fig. 4.14. The centrifugal force.

As an example of using the centrifugal force concept, let us return again to our “testbed” problem on the bead sliding along a rotating ring – see Fig. 2.1. In the non-inertial reference frame attached to the ring, we have to add, to the actual forces mg and \mathbf{N} exerted on the bead, the horizontal centrifugal force²⁵ directed from the rotation axis, with the magnitude $m\omega^2\rho$. Its component tangential to the ring equals $(m\omega^2\rho)\cos\theta = m\omega^2R\sin\theta\cos\theta$, and hence the component of Eq. (92) along this direction is $ma = -mgsin\theta + m\omega^2R\sin\theta\cos\theta$. With $a = R\ddot{\theta}$, this gives us an equation of motion equivalent to Eq. (2.25), which had been derived in Sec. 2.2 (in the inertial frame) using the Lagrangian formalism.

The third term on the right-hand side of Eq. (92),

$$\mathbf{F}_C \equiv -2m\omega \times \mathbf{v}, \quad (4.94)$$

Coriolis
“force”

is the so-called *Coriolis force*,²⁶ which is different from zero only if the particle moves in a rotating reference frame. Its physical sense may be understood by considering a projectile fired horizontally, say from the North Pole – see Fig. 15.

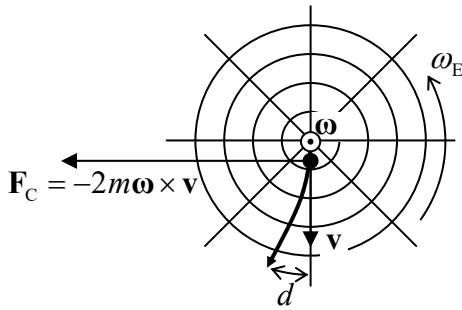


Fig. 4.15. The trajectory of a projectile fired horizontally from the North Pole, from the point of view of an Earth-bound observer looking down. The circles show parallels, while the straight lines mark meridians.

From the point of view of an Earth-based observer, the projectile will be affected by an additional Coriolis force (94), directed westward, with the magnitude $2m\omega_E v$, where \mathbf{v} is the main, southward component of the velocity. This force would cause the westward acceleration $a = 2\omega_E v$, and hence the westward deviation growing with time as $d = at^2/2 = \omega_E vt^2$. (This formula is exact only if d is much smaller than the distance $r = vt$ passed by the projectile.) On the other hand, from the point of

²⁵ For this problem, all other inertial “forces”, besides the Coriolis force (see below) vanish, while the latter force is directed normally to the ring and does not affect the bead’s motion along it.

²⁶ Named after G.-G. de Coriolis (already reverently mentioned in Chapter 1) who described its theory and applications in detail in 1835, though the first semi-quantitative analyses of this effect were given by Giovanni Battista Riccioli and Claude François Dechales already in the mid-1600s, and all basic components of the Coriolis theory may be traced to a 1749 work by Leonard Euler.

view of an inertial-frame observer, the projectile's trajectory in the horizontal plane is a straight line. However, during the flight time t , the Earth's surface slips eastward from under the trajectory by the distance $d = r\varphi = (vt)(\omega_E t) = \omega_E vt^2$, where $\varphi = \omega_E t$ is the azimuthal angle of the Earth's rotation during the flight). Thus, both approaches give the same result – as they should.

Hence, the Coriolis “force” is just a fancy (but frequently very convenient) way of description of a purely geometric effect pertinent to the rotation, from the point of view of the observer participating in it. This force is responsible, in particular, for the higher right banks of rivers in the Northern hemisphere, regardless of the direction of their flow – see Fig. 16. Despite the smallness of the Coriolis force (for a typical velocity of the water in a river, $v \sim 1$ m/s, it is equivalent to acceleration $a_C \sim 10^{-2}$ cm/s² $\sim 10^{-5}$ g), its multi-century effects may be rather prominent.²⁷

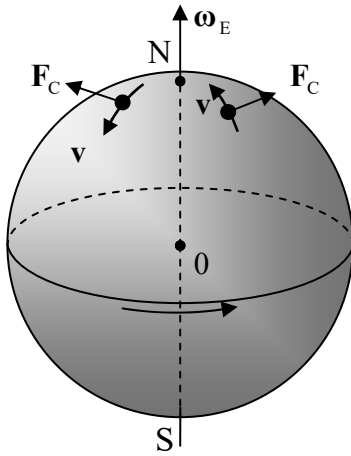


Fig. 4.16. Coriolis forces due to the Earth's rotation, in the Northern hemisphere.

Finally, the last, fourth term of Eq. (92), $-m\dot{\boldsymbol{\omega}} \times \mathbf{r}$, exists only when the rotation frequency changes in time, and may be interpreted as a local-position-specific addition to the first term.

The key relation (92), derived above from Newton's equation (91), may be alternatively obtained from the Lagrangian approach. Indeed, let us use Eq. (88) to represent the kinetic energy of the particle in an inertial “lab” frame in terms of \mathbf{v} and \mathbf{r} measured in a *rotating* frame:

$$T = \frac{m}{2} [\mathbf{v}_0|_{\text{in lab}} + (\mathbf{v} + \boldsymbol{\omega} \times \mathbf{r})]^2, \quad (4.95)$$

and use this expression to calculate the Lagrangian function. For the relatively simple case of a particle's motion in the field of potential forces, measured from a reference frame that performs a pure rotation (so that $\mathbf{v}_0|_{\text{in lab}} = 0$)²⁸ with a constant angular velocity $\boldsymbol{\omega}$, we get

$$L \equiv T - U = \frac{m}{2} \mathbf{v}^2 + \mathbf{m} \mathbf{v} \cdot (\boldsymbol{\omega} \times \mathbf{r}) + \frac{m}{2} (\boldsymbol{\omega} \times \mathbf{r})^2 - U \equiv \frac{m}{2} \mathbf{v}^2 + \mathbf{m} \mathbf{v} \cdot (\boldsymbol{\omega} \times \mathbf{r}) - U_{\text{ef}}, \quad (4.96a)$$

where the effective potential energy,²⁹

²⁷ The same force causes the counterclockwise circulation in the “Nor'easter” storms on the US East Coast, with the radial component of the air velocity directed toward the cyclone's center, due to lower pressure in its middle.

²⁸ A similar analysis of the cases with $\mathbf{v}_0|_{\text{in lab}} \neq 0$, for example, of a translational relative motion of the reference frames, is left for the reader's exercise.

$$U_{\text{ef}} \equiv U + U_{\text{cf}}, \quad \text{with } U_{\text{cf}} \equiv -\frac{m}{2}(\boldsymbol{\omega} \times \mathbf{r})^2, \quad (4.96\text{b})$$

is just the sum of the actual potential energy U of the particle and the so-called *centrifugal potential energy*, associated with the centrifugal “force” (93):

$$\mathbf{F}_{\text{cf}} = -\nabla U_{\text{cf}} = -\nabla \left[-\frac{m}{2}(\boldsymbol{\omega} \times \mathbf{r})^2 \right] = -m\boldsymbol{\omega} \times (\boldsymbol{\omega} \times \mathbf{r}). \quad (4.97)$$

It is straightforward to verify that the Lagrange equations (2.19), derived from Eqs. (96) considering the Cartesian components of \mathbf{r} and \mathbf{v} as generalized coordinates and velocities, coincide with Eq. (92) (with $\mathbf{a}_0|_{\text{in lab}} = 0$, $\dot{\boldsymbol{\omega}} = 0$, and $\mathbf{F} = -\nabla U$).

Now it is very informative to have a look at a by-product of this calculation, the generalized momentum (2.31) corresponding to the particle’s coordinate \mathbf{r} as measured in the rotating reference frame,³⁰

$$\boldsymbol{\mu} \equiv \frac{\partial L}{\partial \mathbf{v}} = m(\mathbf{v} + \boldsymbol{\omega} \times \mathbf{r}). \quad (4.98)$$

Canonical momentum at rotation

According to Eq. (88) with $\mathbf{v}_0|_{\text{in lab}} = 0$, the expression in the parentheses is just $\mathbf{v}|_{\text{in lab}}$. However, from the point of view of the moving frame, i.e. not knowing about the simple physical sense of the vector $\boldsymbol{\mu}$, we would have a reason to speak about two different linear momenta of the same particle, the so-called *kinetic momentum* $\mathbf{p} = m\mathbf{v}$ and the *canonical momentum* $\boldsymbol{\mu} = \mathbf{p} + m\boldsymbol{\omega} \times \mathbf{r}$.³¹ Let us calculate the Hamiltonian function H defined by Eq. (2.32), and the energy E as functions of the same moving-frame variables:

$$H \equiv \sum_{j=1}^3 \frac{\partial L}{\partial v_j} v_j - L = \boldsymbol{\mu} \cdot \mathbf{v} - L = m(\mathbf{v} + \boldsymbol{\omega} \times \mathbf{r}) \cdot \mathbf{v} - \left[\frac{m}{2}\mathbf{v}^2 + m\mathbf{v} \cdot (\boldsymbol{\omega} \times \mathbf{r}) - U_{\text{ef}} \right] = \frac{m\mathbf{v}^2}{2} + U_{\text{ef}}, \quad (4.99)$$

$$E \equiv T + U = \frac{m}{2}\mathbf{v}^2 + m\mathbf{v} \cdot (\boldsymbol{\omega} \times \mathbf{r}) + \frac{m}{2}(\boldsymbol{\omega} \times \mathbf{r})^2 + U = \frac{m}{2}\mathbf{v}^2 + U_{\text{ef}} + m\mathbf{v} \cdot (\boldsymbol{\omega} \times \mathbf{r}) + m(\boldsymbol{\omega} \times \mathbf{r})^2. \quad (4.100)$$

These expressions clearly show that E and H are *not* equal.³² In hindsight, this is not surprising, because the kinetic energy (95), expressed in the moving-frame variables, includes a term linear in \mathbf{v} , and hence

²⁹ For the attentive reader who has noticed the difference between the negative sign in the expression for U_{cf} , and the positive sign before the similar second term in Eq. (3.44): as was already discussed in Chapter 3, it is due to the difference of assumptions. In the planetary problem, even though the angular momentum \mathbf{L} and hence its component L_z are fixed, the corresponding angular velocity $\dot{\phi}$ is not. On the opposite, in our current discussion, the angular velocity $\boldsymbol{\omega}$ of the reference frame is assumed to be fixed, i.e. is independent of \mathbf{r} and \mathbf{v} .

³⁰ Here $\partial L / \partial \mathbf{v}$ is just a shorthand for a vector with Cartesian components $\partial L / \partial v_j$. In a more formal language, this is the gradient of the scalar function L in the velocity space.

³¹ A very similar situation arises at the motion of a particle with electric charge q in magnetic field \mathcal{B} . In that case, the role of the additional term $\boldsymbol{\mu} - \mathbf{p} = m\boldsymbol{\omega} \times \mathbf{r}$ is played by the product $q\mathcal{A}$, where \mathcal{A} is the vector potential of the field $\mathcal{B} = \nabla \times \mathcal{A}$ – see, e.g., EM Sec. 9.7, and in particular Eqs. (9.183) and (9.192).

³² Please note the last form of Eq. (99), which shows the physical sense of the Hamiltonian function of a particle in the rotating frame very clearly, as the sum of its kinetic energy (as measured in the moving frame), and the effective potential energy (96b), including that of the centrifugal “force”.

is not a quadratic-homogeneous function of this generalized velocity. The difference between these functions may be represented as

$$E - H = m\mathbf{v} \cdot (\boldsymbol{\omega} \times \mathbf{r}) + m(\boldsymbol{\omega} \times \mathbf{r})^2 \equiv m(\mathbf{v} + \boldsymbol{\omega} \times \mathbf{r}) \cdot (\boldsymbol{\omega} \times \mathbf{r}) = m\mathbf{v}|_{\text{in lab}} \cdot (\boldsymbol{\omega} \times \mathbf{r}). \quad (4.101)$$

Now using the operand rotation rule again, we may transform this expression into a simpler form:³³

$E - H$
at rotation

$$E - H = \boldsymbol{\omega} \cdot (\mathbf{r} \times m\mathbf{v}|_{\text{in lab}}) = \boldsymbol{\omega} \cdot (\mathbf{r} \times \boldsymbol{\mu}) = \boldsymbol{\omega} \cdot \mathbf{L}|_{\text{in lab}}. \quad (4.102)$$

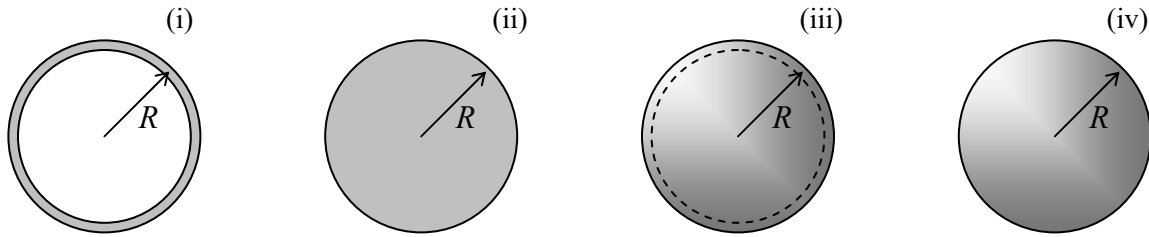
As a sanity check, let us apply this general expression to the particular case of our testbed problem – see Fig. 2.1. In this case, the vector $\boldsymbol{\omega}$ is aligned with the z -axis, so that of all Cartesian components of the vector \mathbf{L} , only the component L_z is important for the scalar product in Eq. (102). This component evidently equals $\omega L_z = \omega m\rho^2 = \omega m(R\sin\theta)^2$, so that

$$E - H = m\omega^2 R^2 \sin^2 \theta, \quad (4.103)$$

i.e. the same result that follows from the subtraction of Eqs. (2.40) and (2.41).

4.7. Exercise problems

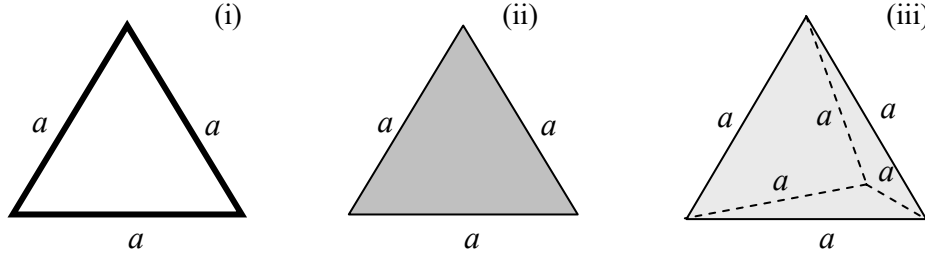
4.1. Calculate the principal moments of inertia for the following uniform rigid bodies:



(i) a thin, planar, round hoop, (ii) a flat round disk, (iii) a thin spherical shell, and (iv) a solid sphere.

Compare the results, assuming that all the bodies have the same radius R and mass M , and give an interpretation of their difference.

4.2. Calculate the principal moments of inertia for the rigid bodies shown in the figure below:



(i) an equilateral triangle made of thin rods with a uniform linear mass density μ ,

(ii) a thin plate in the shape of an equilateral triangle, with a uniform areal mass density σ , and

³³ Note that by the definition (1.36), the angular momenta \mathbf{L} of particles merely add up. As a result, the final form of Eq. (102) is valid for an arbitrary system of particles.

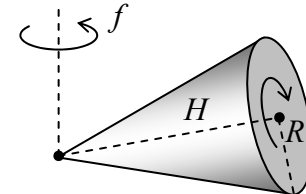
(iii) a tetrahedron with a uniform bulk mass density ρ .

Assuming that the total mass of the three bodies is the same, compare the results and give an interpretation of their difference.

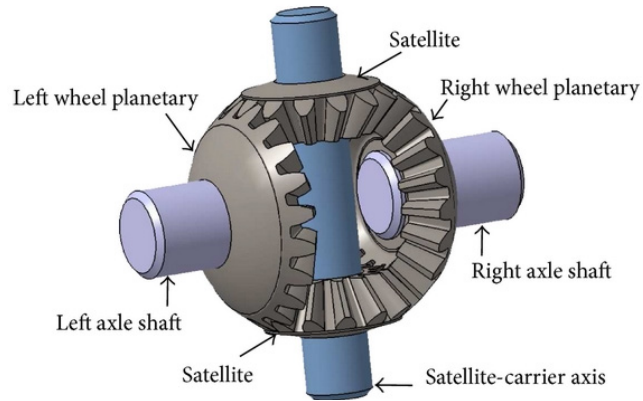
4.3. Calculate the principal moments of inertia of a thin uniform plate cut in the form of a right triangle with two $\pi/4$ angles.

4.4. Prove that Eqs. (34)-(36) are valid for rotation of a rigid body about a fixed axis z , even if it does not pass through its center of mass.

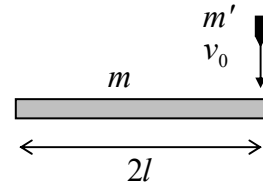
4.5. Calculate the kinetic energy of a right circular cone with height H , base radius R , and a constant mass density ρ , that rolls over a horizontal surface without slippage, making f turns per second about the vertical axis – see the figure on the right.



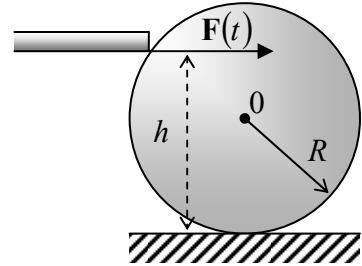
4.6. External forces exerted on a rigid body, rotating with an angular velocity ω , have zero vector sum but a non-vanishing net torque τ about its center of mass. Calculate the work of the forces on the body per unit time, i.e. their instantaneous power. Prove that the same result is valid for a body rotating about a fixed axis and the torque's component along this axis. Use the last result to prove that at negligible friction, the differential gear assembly (see the figure on the right)³⁴ distributes the external torque, applied to its satellite-carrier axis to rotate it about the common axis of two axle shafts, equally to both shafts, even if they rotate with different angular velocities.



4.7. The end of a uniform thin rod of length $2l$ and mass m , initially at rest, is hit by a bullet of mass m' , flying with velocity v_0 (see the figure on the right), which gets stuck in the rod. Use two different approaches to calculate the velocity of the opposite end of the rod right after the collision.



4.8. A ball of radius R , initially at rest on a horizontal table, is hit with a billiard cue in the horizontal direction, at height h above the table – see the figure on the right. Using the same Coulomb approximation for the friction force between the ball and the table as in Problem 1.4 ($|F|_{\max} = \mu N$), calculate the final linear velocity of the rolling ball as a function of h . Would it matter if the hit point is shifted horizontally (normally to the plane of the drawing)?



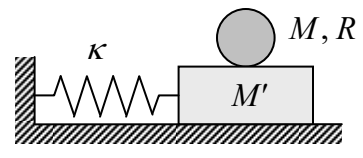
³⁴ Figure from G. Antoni, *Sci. World J.*, **2014**, 523281 (2014), adapted with permission. Both satellite gears may rotate freely about their carrier axis.

Hint: As in most solid body collision problems, during the short time of the cue hit, all other forces exerted on the ball may be considered negligibly small.

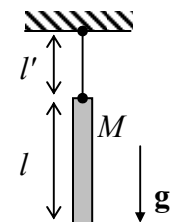
4.9. A round cylinder of radius R and mass M may roll, without slippage, over a horizontal surface. The mass density distribution inside the cylinder is not uniform, so that its center of mass is at some distance $l \neq 0$ from its geometrical axis, and the moment of inertia I (for rotation about the axis parallel to the symmetry axis but passing through the center of mass) is different from $MR^2/2$, where M is the cylinder's mass. Derive the equation of motion of the cylinder under the effect of the uniform vertical gravity field, and use it to calculate the frequency of its small oscillations of the cylinder near its stable equilibrium position.

4.10. A body may rotate about a fixed horizontal axis A – see Fig. 5. Find the frequency of its small oscillations, in a uniform gravity field, as a function of the distance l of the axis from the body's center of mass 0, and analyze the result.

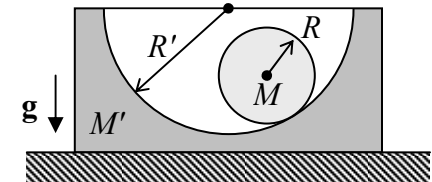
4.11. Calculate the frequency, and sketch the mode of oscillations of a round uniform cylinder of radius R and the mass M , that may roll, without slipping, on a horizontal surface of a block of mass M' . The block, in turn, may move in the same direction, without friction, on a horizontal surface, being connected to it with an elastic spring – see the figure on the right.



4.12. A thin uniform bar of mass M and length l is hung on a light thread of length l' (like a “chime” bell – see the figure on the right). Derive the equations of motion of the system within the plane of the drawing.

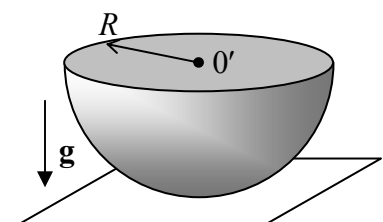


4.13. A solid, uniform, round cylinder of mass M can roll, without slipping, over a concave, round cylindrical surface of a block of mass M' , in a uniform gravity field – see the figure on the right. The block can slide without friction on a horizontal surface. Using the Lagrangian formalism,



- (i) find the frequency of small oscillations of the system near the equilibrium, and
- (ii) sketch the oscillation mode for the particular case $M' = M$, $R' = 2R$.

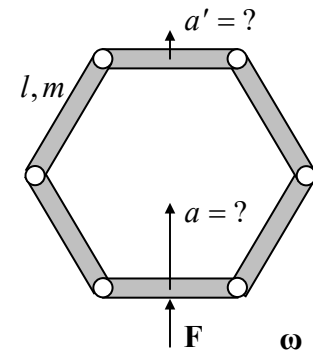
4.14. A uniform solid hemisphere of radius R is placed on a horizontal plane – see the figure on the right. Find the frequency of its small oscillations within a vertical plane, for two ultimate cases:



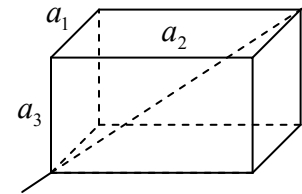
- (i) there is no *friction* between the hemisphere and plane surfaces;
- (ii) the static friction is so strong that there is no *slippage* between these surfaces.

4.15. For the “sliding ladder” problem started in Sec. 3 (see Fig. 7), find the critical value α_c of the angle α at that the ladder loses its contact with the vertical wall, assuming that it starts sliding from the vertical position, with a negligible initial velocity.

4.16. Six similar, uniform rods of length l and mass m are connected by light joints so that they may rotate, without friction, versus each other, forming a planar polygon. Initially, the polygon was at rest, and had the correct hexagon shape – see the figure on the right. Suddenly, an external force \mathbf{F} is applied to the middle of one rod, in the direction of the hexagon's symmetry center. Calculate the accelerations: of the rod to which the force is applied (a), and of the opposite rod (a'), immediately after the application of the force.



4.17. A rectangular cuboid (parallelepiped) with sides a_1 , a_2 , and a_3 , made of a material with a constant mass density ρ , is rotated, with a constant angular velocity ω , about one of its space diagonals – see the figure on the right. Calculate the torque τ necessary to sustain such rotation.



4.18. A uniform round ball moves, without slippage, over a “turntable”: a horizontal plane rotated about a vertical axis with a time-independent angular velocity Ω . Derive a self-consistent equation of motion of the ball’s center of mass, and discuss its solutions.

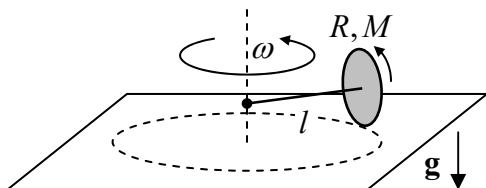
4.19. Calculate the free precession frequency of a flat round disk rotating with an angular velocity ω about a direction very close to its symmetry axis, from the point of view of:

- (i) an observer rotating with the disk, and
- (ii) a lab-based observer.

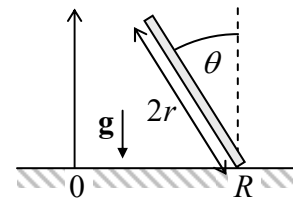
4.20. Use the Euler equations to prove the fact mentioned in Sec. 4: free rotation of an arbitrary body (“asymmetric top”) about its principal axes with the smallest and largest moments of inertia is stable with respect to small variations of initial conditions, while that about the intermediate- I_j axis is not. Illustrate the same fact using the Poinsot construction.

4.21. Give an interpretation of the torque-induced precession, explaining its direction, using any simple system exhibiting this effect, as a model.

4.22. One end of a light shaft of length l is firmly attached to the center of a thin uniform solid disk of radius $R \ll l$ and mass M , whose plane is perpendicular to the shaft. Another end of the shaft is attached to a vertical axis (see the figure on the right) so that the shaft may rotate about the axis without friction. The disk rolls, without slippage, over a horizontal surface, so that the whole system rotates about the vertical axis with a constant angular velocity ω . Calculate the (vertical) supporting force N exerted on the disk by the surface.



4.23. A coin of radius r is rolled over a horizontal surface, without slippage. Due to its tilt θ , it rolls around a circle of radius R – see the figure on the right. Modeling the coin as a very thin round disk, calculate the time period of its motion around the circle.



4.24. A symmetric top on point support (as shown see, e.g., Fig. 9), rotating around its symmetry axis with high angular velocity ω_{rot} , is subjected to not only its weight Mg , but also an additional force also applied to the top's center of mass, but directed normally to \mathbf{g} , with its vector rotating in the horizontal plane with a constant angular velocity $\omega \ll \omega_{\text{rot}}$. Derive the system of equations describing the top's motion. Analyze their solution for the simplest case when ω is exactly equal to the frequency (72) of the torque-induced precession in the gravity field alone.

4.25. Analyze the effect of small friction on the fast rotation of a symmetric top around its symmetry axis, using a simple model in that the lower end of the body is a right cylinder of radius R .

4.26. An air-filled balloon is placed inside a water-filled container, which moves by inertia in free space, at negligible gravity. Suddenly, force \mathbf{F} is applied to the container, pointing in a certain direction. What direction does the balloon move relative to the container?

4.27. Two planets are in a circular orbit around their common center of mass. Calculate the effective potential energy of a much lighter body (say, a spacecraft) rotating with the same angular velocity, on the line connecting the planets. Sketch the plot of the radial dependence of U_{ef} and find out the number of so-called *Lagrange points* in which the potential energy has local maxima. Calculate their position explicitly in the limit when one of the planets is much more massive than the other one.

4.28. Besides the three Lagrange points L_1 , L_2 , and L_3 discussed in the previous problem, which are located on the line connecting two planets on circular orbits about their mutual center of mass, there are two off-line points L_4 and L_5 – both within the pane of the planets' rotation. Calculate their positions.

4.29. The following simple problem may give additional clarity to the physics of the Coriolis “force”. Consider a bead of mass m , which may slide, without friction, along a straight rod that is rotated, within a horizontal plane with a constant angular velocity ω – see the figure on the right. Calculate the bead's linear acceleration and the force \mathbf{N} exerted on it by the rod, in:

- (i) an inertial (“lab”) reference frame, and
- (ii) the non-inertial reference frame rotating with the rod (but not moving with the bead), and compare the results.

4.30. Analyze the dynamics of the famous *Foucault pendulum*, used for spectacular demonstrations of the Earth's rotation. In particular, calculate the angular velocity of the rotation of its oscillation plane relative to the Earth's surface, at the location with the polar angle (“colatitude”) Θ . Assume that the pendulum oscillation amplitude is small enough to neglect nonlinear effects, and that its oscillation period is much shorter than 24 hours.

4.31. A small body is dropped down to the surface of Earth from height $h \ll R_E$, without initial velocity. Calculate the magnitude and direction of its deviation from the vertical, due to the Earth rotation. Estimate the effect's magnitude for a body dropped from the Empire State Building.

4.32. Calculate the height of solar tides on a large ocean, using the following simplifying assumptions: the tide period ($\frac{1}{2}$ of Earth's day) is much longer than the period of all ocean waves, the

Earth (of mass M_E) is a sphere of radius R_E , and its distance r_S from the Sun (of mass M_S) is constant and much larger than R_E .

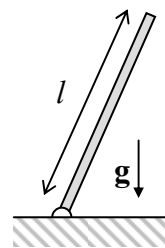
4.33. A satellite is on a circular orbit of radius R , around the Earth.

- (i) Write the equations of motion of a small body as observed from the satellite, and simplify them for the case when the motion is limited to the satellite's close vicinity.
- (ii) Use the equations to prove that the body may be placed on an elliptical trajectory around the satellite's center of mass, within its plane of rotation about Earth. Calculate the ellipse's orientation and eccentricity.

4.34. A non-spherical shape of an artificial satellite may ensure its stable angular orientation relative to Earth's surface, advantageous for many practical goals. Modeling the satellite as a strongly elongated, axially-symmetric body, moving around the Earth on a circular orbit of radius R , find its stable orientation.

4.35.^{*} A rigid, straight, uniform rod of length l , with the lower end on a pivot, falls in a uniform gravity field – see the figure on the right. Neglecting friction, calculate the distribution of the bending torque τ along its length, and analyze the result.

Hint: The bending torque is the net torque of the force \mathbf{F} acting between two parts of the rod, mentally separated by its cross-section, about a certain “neutral axis”.³⁵ As will be discussed in detail in Sec. 7.5, at the proper definition of this axis, the bending torque’s gradient along the rod’s length is equal to $(-F)$, where F is the rod-normal (“shear”) component of the force exerted by the top part of the rod on its lower part.



4.36. Let \mathbf{r} be the radius vector of a particle, as measured in a possibly non-inertial but certainly non-rotating reference frame. Taking its Cartesian components for the generalized coordinates, calculate the corresponding generalized momentum \mathbf{p} of the particle, and its Hamiltonian function H . Compare \mathbf{p} with $m\mathbf{v}$, and H with the particle’s energy E . Derive the Lagrangian equation of motion in this approach, and compare it with Eq. (92).

³⁵ Inadequate definitions of this torque are the main reason for numerous wrong solutions of this problem, posted online – readers beware!

Chapter 5. Oscillations

In this course, oscillations and waves are discussed in detail, because of their importance for fundamental and applied physics. This chapter starts with a discussion of the harmonic oscillator, whose differential equation of motion is linear and hence allows the full analytical solution, and then proceeds to so-called “nonlinear” and “parametric” systems whose dynamics may be only explored by either approximate analytical or numerical methods.

5.1. Free and forced oscillations

In Sec. 3.2 we briefly discussed oscillations in a keystone Hamiltonian system – a 1D *harmonic oscillator* described by a very simple Lagrangian¹

$$L \equiv T(\dot{q}) - U(q) = \frac{m}{2} \dot{q}^2 - \frac{\kappa}{2} q^2, \quad (5.1)$$

whose Lagrange equation of motion,²

Harmonic oscillator: motion

$$m\ddot{q} + \kappa q = 0, \quad \text{i.e. } \ddot{q} + \omega_0^2 q = 0, \quad \text{with } \omega_0^2 \equiv \frac{\kappa}{m} \geq 0, \quad (5.2)$$

is a *linear homogeneous* differential equation. Its general solution is given by Eq. (3.16), which is frequently recast into another, amplitude-phase form:

Harmonic oscillator: motion

$$q(t) = u \cos \omega_0 t + v \sin \omega_0 t \equiv A \cos(\omega_0 t - \varphi), \quad (5.3a)$$

where A is the *amplitude* and φ the *phase* of the oscillations, which are determined by the initial conditions. Mathematically, it is frequently easier to work with sinusoidal functions as complex exponents, by rewriting the last form of Eq. (3a) in one more form:³

$$q(t) = \operatorname{Re} \left[A e^{-i(\omega_0 t - \varphi)} \right] = \operatorname{Re} \left[a e^{-i\omega_0 t} \right], \quad (5.3b)$$

where a is the *complex amplitude* of the oscillations:

Real and complex amplitudes

$$a \equiv A e^{i\varphi}, \quad |a| = A, \quad \operatorname{Re} a = A \cos \varphi = u, \quad \operatorname{Im} a = A \sin \varphi = v. \quad (5.4)$$

For an autonomous, Hamiltonian oscillator, Eqs. (3) give the full classical description of its dynamics. However, it is important to understand that this *free-oscillation* solution, with a constant amplitude A ,

¹ For the notation brevity, in this chapter I will drop indices “ef” in the energy components T and U , and in parameters like m , κ , etc. However, the reader should still remember that T and U do not necessarily coincide with the actual kinetic and potential energies (even if those energies may be uniquely identified) – see Sec. 3.1.

² ω_0 is usually called the *own frequency* of the oscillator. In quantum mechanics, the Germanized version of the same term, *eigenfrequency*, is used more. In this series, I will use either of the terms, depending on the context.

³ Note that this is the so-called *physics convention*. Most engineering texts use the opposite sign in the imaginary exponent, $\exp\{-i\omega t\} \rightarrow \exp\{i\omega t\}$, with the corresponding sign implications for intermediate formulas, but (of course) similar final results for real variables.

means the conservation of the energy $E \equiv T + U = \kappa A^2/2$ of the oscillator. If its energy changes for any reason, the description needs to be generalized.

First of all, if the energy leaks out of the oscillator to its environment (the effect usually called the *energy dissipation*), the free oscillations decay with time. The simplest model of this effect is represented by an additional *linear drag* (or “kinematic friction”) *force*, proportional to the generalized velocity and directed opposite to it:

$$F_v = -\eta \dot{q}, \quad (5.5)$$

where constant η is called the *drag coefficient*.⁴ The inclusion of this force modifies the equation of motion (2) to become

$$m\ddot{q} + \eta \dot{q} + \kappa q = 0. \quad (5.6a)$$

This equation is frequently rewritten in the form

$$\ddot{q} + 2\delta \dot{q} + \omega_0^2 q = 0, \quad \text{with } \delta \equiv \frac{\eta}{2m},$$

(5.6b)

Free oscillator with damping

where the parameter δ is called the *damping coefficient* (or just “damping”). Note that Eq. (6) is still a linear homogeneous second-order differential equation, and its general solution still has the form of the sum (3.13) of two exponents of the type $\exp\{\lambda t\}$, with arbitrary pre-exponential coefficients. Plugging such an exponent into Eq. (6), we get the following algebraic characteristic equation for λ :

$$\lambda^2 + 2\delta\lambda + \omega_0^2 = 0. \quad (5.7)$$

Solving this quadratic equation, we get

$$\lambda_{\pm} = -\delta \pm i\omega'_0, \quad \text{where } \omega'_0 \equiv (\omega_0^2 - \delta^2)^{1/2}, \quad (5.8)$$

so that for not very high damping ($\delta < \omega_0$) we get the following generalization of Eq. (3):⁵

$$q_{\text{free}}(t) = c_+ e^{\lambda_+ t} + c_- e^{\lambda_- t} = (u_0 \cos \omega'_0 t + v_0 \sin \omega'_0 t) e^{-\delta t} = A_0 e^{-\delta t} \cos(\omega'_0 t - \varphi_0). \quad (5.9)$$

The result shows that, besides a certain correction to the free oscillation frequency (which is very small in the most interesting *low damping limit*, $\delta \ll \omega_0$), the energy dissipation leads to an exponential decay of oscillation amplitude with the time constant $\tau = 1/\delta$.

⁴ Here Eq. (5) is treated as a phenomenological model, but in statistical mechanics, such dissipative term may be *derived* as an average force exerted upon a system by its environment, at very general assumptions. As will be discussed in detail later in this series (QM Chapter 7 and SM Chapter 5), due to the numerous degrees of freedom of a typical environment (think about the molecules of air surrounding a macroscopic pendulum), its force also has a random component; as a result, the *dissipation* is fundamentally related to *fluctuations*. The latter effect may be neglected (as it is in this course) only if the oscillator’s energy E is much higher than the energy scale of its random fluctuations – in the thermal equilibrium at temperature T , the larger of $k_B T$ and $\hbar \omega_0 / 2$.

⁵ Systems with high damping ($\delta > \omega_0$) can hardly be called oscillators, and though they are used in engineering and physics experiment (e.g., for the shock and sound isolation), due to the lack of time/space, for their detailed discussion I have to refer the interested reader to special literature – see, e.g., C. Harris and A. Piersol, *Shock and Vibration Handbook*, 5th ed., McGraw Hill, 2002. Let me only note that according to Eq. (8), the dynamics of systems with very high damping ($\delta \gg \omega_0$) has two very different time scales: a relatively short “momentum relaxation time” $1/\lambda_- \approx 1/2\delta = m/\eta$, and a much longer “coordinate relaxation time” $1/\lambda_+ \approx 2\delta/\omega_0^2 = \eta/\kappa$.

$$A = A_0 e^{-t/\tau}, \quad \text{where } \tau \equiv \frac{1}{\delta} = \frac{2m}{\eta}. \quad (5.10)$$

A very popular dimensionless measure of damping is the so-called *quality factor* Q (or just the *Q-factor*) which is defined as $\omega_0/2\delta$, and may be rewritten in several other useful forms:

$$Q \equiv \frac{\omega_0}{2\delta} = \frac{m\omega_0}{\eta} = \frac{(m\kappa)^{1/2}}{\eta} = \pi \frac{\tau}{\mathcal{T}} = \frac{\omega_0 \tau}{2}, \quad (5.11)$$

where $\mathcal{T} \equiv 2\pi/\omega_0$ is the oscillation period in the absence of damping – see Eq. (3.29). Since the oscillation energy E is proportional to A^2 , i.e. decays as $\exp\{-2t/\tau\}$, i.e. with the time constant $\tau/2$, the last form of Eq. (11) may be used to rewrite the Q -factor in one more form:

$$Q = \omega_0 \frac{E}{(-\dot{E})} \equiv \omega_0 \frac{E}{\mathcal{P}}, \quad (5.12)$$

where \mathcal{P} is the energy dissipation rate. (Other practical ways to measure Q will be discussed below.) The range of Q -factors of important oscillators is very broad, all the way from $Q \sim 10$ for a human leg (with relaxed muscles), to $Q \sim 10^4$ of the quartz crystals used in electronic clocks and watches, all the way up to $Q \sim 10^{12}$ for carefully designed microwave cavities with superconducting walls.

In contrast to the decaying free oscillations, *forced oscillations* induced by an external force $F(t)$, may maintain their amplitude (and hence energy) infinitely, even at non-zero damping. This process may be described using a still linear but now *inhomogeneous* differential equation

$$m\ddot{q} + \eta\dot{q} + \kappa q = F(t), \quad (5.13a)$$

or, more usually, the following generalization of Eq. (6b):

$$\ddot{q} + 2\delta\dot{q} + \omega_0^2 q = f(t), \quad \text{where } f(t) \equiv F(t)/m. \quad (5.13b)$$

For a mechanical linear, dissipative 1D oscillator (6), under the effect of an additional external force $F(t)$, Eq. (13a) is just an expression of the 2nd Newton law. However, according to Eq. (1.41), Eq. (13) is valid for any dissipative, *linear*⁶ 1D system whose Gibbs potential energy (1.39) has the form $U_G(q, t) = \kappa q^2/2 - F(t)q$.

The forced-oscillation solutions to Eq. (13) may be analyzed by two mathematically equivalent methods whose relative convenience depends on the character of function $f(t)$.

(i) *Frequency domain*. Representing the function $f(t)$ as a Fourier sum of sinusoidal harmonics:⁷

$$f(t) = \sum_{\omega} f_{\omega} e^{-i\omega t}, \quad (5.14)$$

and using the linearity of Eq. (13), we may represent its general solution as a sum of the decaying free oscillations (9) with the frequency ω_0' , that are independent of the function $f(t)$, and forced oscillations due to each of the Fourier components of the force:⁸

⁶ This is a very unfortunate, but common jargon, meaning “the system described by linear equations of motion”.

⁷ Here, in contrast to Eq. (3b), we may drop the operator Re , assuming that $f_{-\omega} = f_{\omega}^*$, so that the imaginary components of the sum compensate for each other.

$$q(t) = q_{\text{free}}(t) + q_{\text{forced}}(t), \quad q_{\text{forced}}(t) = \sum_{\omega} a_{\omega} e^{-i\omega t}. \quad (5.15)$$

General solution of Eq. (13)

Plugging Eq. (15) into Eq. (13), and requiring the factors before each $e^{-i\omega t}$ on both sides to be equal, we get

$$a_{\omega} = f_{\omega} \chi(\omega), \quad (5.16)$$

where the complex function $\chi(\omega)$, in our particular case equal to

$$\chi(\omega) = \frac{1}{(\omega_0^2 - \omega^2) - 2i\omega\delta}, \quad (5.17)$$

is called either the *response function* or (especially for non-mechanical oscillators) the *generalized susceptibility*. From here, and Eq. (4), the amplitude of the oscillations under the effect of a sinusoidal force is

$$A_{\omega} \equiv |a_{\omega}| = |f_{\omega}| |\chi(\omega)|, \quad \text{with } |\chi(\omega)| = \frac{1}{[(\omega_0^2 - \omega^2)^2 + (2\omega\delta)^2]^{1/2}}. \quad (5.18)$$

Forced oscillations

This formula describes, in particular, an increase of the oscillation amplitude A_{ω} at $\omega \rightarrow \omega_0$ – see the left panel of Fig. 1. In particular, at the exact equality of these two frequencies,

$$|\chi(\omega)|_{\omega=\omega_0} = \frac{1}{2\omega_0\delta}, \quad (5.19)$$

so that, according to Eq. (11), the ratio of the response magnitudes at $\omega = \omega_0$ and $\omega = 0$ ($|\chi(\omega)|_{\omega=0} = 1/\omega_0^2$) is exactly equal to the Q -factor of the oscillator. Thus, the response increase is especially strong in the low-damping limit ($\delta \ll \omega_0$, i.e. $Q \gg 1$); moreover, at $Q \rightarrow \infty$ and $\omega \rightarrow \omega_0$, the response diverges. (This mathematical fact is very useful for the methods to be discussed later in this section.) This is the classical description of the famous phenomenon of *resonance*, so ubiquitous in physics.

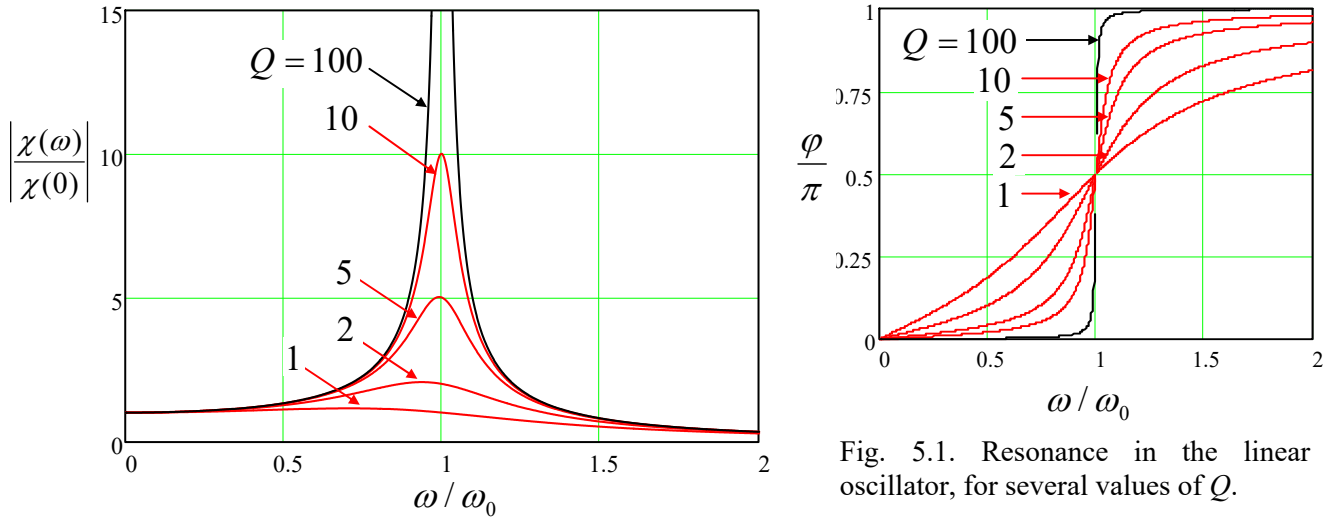


Fig. 5.1. Resonance in the linear oscillator, for several values of Q .

⁸ In physics, this mathematical property of linear equations is frequently called the *linear superposition principle*.

Due to the increase of the resonance peak height, its width is inversely proportional to Q . Quantitatively, in the most interesting low-damping limit, i.e. at $Q \gg 1$, the reciprocal Q -factor gives the normalized value of the so-called *full-width at half-maximum* (FWHM) of the resonance curve:⁹

$$\frac{\Delta\omega}{\omega_0} = \frac{1}{Q}. \quad (5.20)$$

Indeed, this $\Delta\omega$ is defined as the difference $(\omega_+ - \omega_-)$ between the two values of ω at that the square of the oscillator response function, $|\chi(\omega)|^2$ (which is proportional to the oscillation energy), equals a half of its resonance value (19). In the low damping limit, these points are very close to ω_0 , so that in the linear approximation in $|\omega - \omega_0| \ll \omega_0$, we may write $(\omega_0^2 - \omega^2) \equiv -(\omega + \omega_0)(\omega - \omega_0) \approx -2\omega\xi \approx -2\omega_0\xi$, where

$$\xi \equiv \omega - \omega_0 \quad (5.21)$$

is a very convenient parameter called *detuning*, which will be repeatedly used later in this chapter, and beyond it. In this approximation, the second of Eqs. (18) is reduced to¹⁰

$$|\chi(\omega)|^2 = \frac{1}{4\omega_0^2(\delta^2 + \xi^2)}. \quad (5.22)$$

As a result, the points ω_{\pm} correspond to $\xi^2 = \delta^2$, i.e. $\omega_{\pm} = \omega_0 \pm \delta = \omega_0(1 \pm 1/2Q)$, so that $\Delta\omega \equiv \omega_+ - \omega_- = \omega_0/Q$, thus proving Eq. (20).

(ii) *Time domain.* Returning to an arbitrary external force $f(t)$, one may argue that Eqs. (9), (15)-(17) provide a full solution of the forced oscillation problem even in this general case. This is formally correct, but this solution may be very inconvenient if the external force is far from a sinusoidal function of time, especially if it is not periodic at all. In this case, we should first calculate the complex amplitudes f_{ω} participating in the Fourier sum (14). In the general case of a non-periodic $f(t)$, this is actually the Fourier integral,¹¹

$$f(t) = \int_{-\infty}^{+\infty} f_{\omega} e^{-i\omega t} dt, \quad (5.23)$$

so that f_{ω} should be calculated using the reciprocal Fourier transform,

$$f_{\omega} = \frac{1}{2\pi} \int_{-\infty}^{+\infty} f(t') e^{i\omega t'} dt'. \quad (5.24)$$

Now we may use Eq. (16) for each Fourier component of the resulting forced oscillations, and rewrite the last of Eqs. (15) as

⁹ Note that the phase shift $\varphi \equiv \arg[\chi(\omega)]$ between the oscillations and the external force (see the right panel in Fig. 1) makes its steepest change, by $\pi/2$, within the same frequency interval $\Delta\omega$.

¹⁰ Such function of frequency may be met in many branches of science, frequently under special names, including the “Cauchy distribution”, “the Lorentz function” (or “Lorentzian line”, or “Lorentzian distribution”), “the Breit-Wigner function” (or “the Breit-Wigner distribution”), etc.

¹¹ Let me hope that the reader knows that Eq. (23) may be used for periodic functions as well; in such a case, f_{ω} is a set of equidistant delta functions. (A reminder of the basic properties of the Dirac δ -function may be found, for example, in MA Sec. 14.)

$$\begin{aligned}
q_{\text{forced}}(t) &= \int_{-\infty}^{+\infty} a_\omega e^{-i\omega t} d\omega = \int_{-\infty}^{+\infty} \chi(\omega) f_\omega e^{-i\omega t} d\omega = \int_{-\infty}^{+\infty} d\omega \chi(\omega) \frac{1}{2\pi} \int_{-\infty}^{+\infty} dt' f(t') e^{i\omega(t'-t)} \\
&\equiv \int_{-\infty}^{+\infty} dt' f(t') \left[\frac{1}{2\pi} \int_{-\infty}^{+\infty} d\omega \chi(\omega) e^{i\omega(t'-t)} \right],
\end{aligned} \tag{5.25}$$

with the response function $\chi(\omega)$ given, in our case, by Eq. (17). Besides requiring two integrations, Eq. (25) is conceptually uncomfortable: it seems to indicate that the oscillator's coordinate at time t depends not only on the external force exerted at earlier times $t' < t$, but also at future times. This would contradict one of the most fundamental principles of physics (and indeed, science as a whole), *causality*: no effect may precede its cause.

Fortunately, a straightforward calculation (left for the reader's exercise) shows that the response function (17) satisfies the following rule:¹²

$$\int_{-\infty}^{+\infty} \chi(\omega) e^{-i\omega\tau} d\omega = 0, \quad \text{for } \tau < 0. \tag{5.26}$$

This fact allows the last form of Eq. (25) to be rewritten in either of the following equivalent forms:

$$q_{\text{forced}}(t) = \int_{-\infty}^t f(t') G(t-t') dt' \equiv \int_0^\infty f(t-\tau) G(\tau) d\tau, \tag{5.27}$$

Linear system's response

where $G(\tau)$, defined as the Fourier transform of the response function,

$$G(\tau) \equiv \frac{1}{2\pi} \int_{-\infty}^{+\infty} \chi(\omega) e^{-i\omega\tau} d\omega, \tag{5.28}$$

Temporal Green's function

is called the (*temporal*) *Green's function* of the system. According to Eq. (26), $G(\tau) = 0$ for all $\tau < 0$.

While the second form of Eq. (27) is frequently more convenient for calculations, its first form is more suitable for physical interpretation of the Green's function. Indeed, let us consider the particular case when the force is a delta function

$$f(t) = \delta(t-t'), \quad \text{with } t' < t, \text{ i.e. } \tau \equiv t-t' > 0, \tag{5.29}$$

representing an ultimately short pulse at the moment t' , with unit "area" $\int f(t) dt$. Substituting Eq. (29a) into Eq. (27),¹³ we get

$$q(t) = G(t-t'). \tag{5.30}$$

Thus the Green's function $G(t-t')$ is just the oscillator's response, as measured at time t , to a short force pulse of unit "area", exerted at time t' . Hence Eq. (27) expresses the linear superposition principle in the time domain: the full effect of the force $f(t)$ on a linear system is a sum of the effects of short pulses of duration dt' and magnitude $f(t')$, each with its own "weight" $G(t-t')$ – see Fig. 2.

¹² Eq. (26) is true for any linear physical system in which $f(t)$ represents a cause, and $q(t)$ its effect. Following tradition, I discuss the frequency-domain expression of this causality relation (called the *Kramers-Kronig relations*) in the *Classical Electrodynamics* part of this lecture series – see EM Sec. 7.2.

¹³ Technically, for this integration, t' in Eq. (27) should be temporarily replaced with another letter, say t'' .

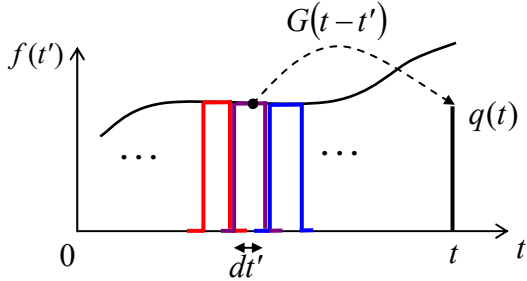


Fig. 5.2. A schematic, finite-interval representation of a force $f(t')$ as a sum of short pulses at all times $t' < t$, and their contributions to the linear system's response $q(t)$, as given by Eq. (27).

This picture may be used for the calculation of Green's function for our particular system. Indeed, Eqs. (29)-(30) mean that $G(\tau)$ is just the solution of the differential equation of motion of the system, in our case, Eq. (13), with the replacement $t \rightarrow \tau$, and a δ -functional right-hand side:

$$\frac{d^2 G(\tau)}{d\tau^2} + 2\delta \frac{dG(\tau)}{d\tau} + \omega_0^2 G(\tau) = \delta(\tau). \quad (5.31)$$

Since Eqs. (27) describes only the second term in Eq. (15), i.e. only the forced, rather than free oscillations, we have to exclude the latter by solving Eq. (31) with zero initial conditions:

$$G(-0) = \frac{dG}{d\tau}(-0) = 0, \quad (5.32)$$

where $\tau = -0$ means the instant immediately preceding $\tau = 0$.

This problem may be simplified even further. Let us integrate both sides of Eq. (31) over an infinitesimal interval including the origin, e.g. $[-d\tau/2, +d\tau/2]$, and then follow the limit $d\tau \rightarrow 0$. Since the Green's function has to be continuous because of its physical sense as the (generalized) coordinate, all terms on the left-hand side but the first one vanish, while the first term yields $dG/d\tau|_{+0} - dG/d\tau|_{-0}$. Due to the second of Eqs. (32), the last of these two derivatives has to equal zero, while the right-hand side of Eq. (31) yields 1 upon the integration. Thus, the function $G(\tau)$ may be calculated for $\tau > 0$ (i.e. for all times when it is different from zero) by solving the *homogeneous* version of the system's equation of motion for $\tau > 0$, with the following special initial conditions:

$$G(0) = 0, \quad \frac{dG}{d\tau}(0) = 1. \quad (5.33)$$

This approach gives us a convenient way for the calculation of Green's functions of linear systems. In particular for the oscillator with not very high damping ($\delta < \omega_0$, i.e. $Q > 1/2$), imposing the boundary conditions (33) on the homogeneous equation's solution (9), we immediately get

$$G(\tau) = \frac{1}{\omega_0'} e^{-\delta\tau} \sin \omega_0' \tau. \quad (5.34)$$

(The same result may be obtained directly from Eq. (28) with the response function $\chi(\omega)$ given by Eq. (19). This way is, however, a little bit more cumbersome, and is left for the reader's exercise.)

Relations (27) and (34) provide a very convenient recipe for solving many forced oscillations problems. As a very simple example, let us calculate the transient process in an oscillator under the effect of a constant force being turned on at $t = 0$, i.e. proportional to the theta-function of time:

$$f(t) = f_0 \theta(t) \equiv \begin{cases} 0, & \text{for } t < 0, \\ f_0, & \text{for } t > 0, \end{cases} \quad (5.35)$$

provided that at $t < 0$ the oscillator was at rest, so that in Eq. (15), $q_{\text{free}}(t) \equiv 0$. Then the second form of Eq. (27), together with Eq. (34), yield

$$q(t) = \int_0^\infty f(t-\tau) G(\tau) d\tau = f_0 \int_0^t \frac{1}{\omega_0'} e^{-\delta\tau} \sin \omega_0' \tau d\tau. \quad (5.36)$$

The simplest way to work out such integrals is to represent the sine function under it as the imaginary part of $\exp\{i\omega_0' t\}$, and merge the two exponents, getting

$$q(t) = f_0 \frac{1}{\omega_0'} \text{Im} \left[\frac{1}{-\delta + i\omega_0'} e^{-\delta\tau + i\omega_0' \tau} \right]_0^t = \frac{F_0}{k} \left[1 - e^{-\delta t} \left(\cos \omega_0' t + \frac{\delta}{\omega_0'} \sin \omega_0' t \right) \right]. \quad (5.37)$$

This result, plotted in Fig. 3, is rather natural: it describes nothing more than the transient from the initial position $q = 0$ to the new equilibrium position $q_0 = f_0/\omega_0^2 = F_0/\kappa$, accompanied by decaying oscillations. For this particular simple function $f(t)$, the same result might be also obtained by introducing a new variable $\tilde{q}(t) \equiv q(t) - q_0$ and solving the resulting *homogeneous* equation for \tilde{q} (with appropriate initial condition $\tilde{q}(0) = -q_0$). However, for more complicated functions $f(t)$, Green's function approach is irreplaceable.

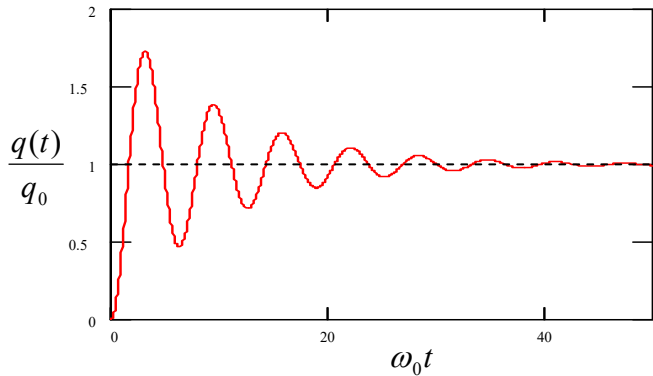


Fig. 5.3. The transient process in a linear oscillator, induced by a step-like force $f(t)$, for the particular case $\delta/\omega_0 = 0.1$ (i.e., $Q = 5$).

Note that for any particular linear system, its Green's function should be calculated only once, and then may be repeatedly used in Eq. (27) to calculate the system response to various external forces – either analytically or numerically. This property makes the Green's function approach very popular in many other fields of physics – with the corresponding generalization or re-definition of the function.¹⁴

5.2. Weakly nonlinear oscillations

In comparison with systems discussed in the last section, which are described by linear differential equations with constant coefficients and thus allow a complete and exact analytical solution, oscillations in nonlinear systems (very unfortunately but commonly called *nonlinear oscillations*) present a complex and, generally, analytically intractable problem. However, much insight on possible

¹⁴ See, e.g., Sec. 6.6, and also EM Sec. 2.7 and QM Sec. 2.2.

processes in such systems may be gained from a discussion of an important case of *weakly nonlinear* systems, which may be explored analytically. An important example of such systems is given by an *anharmonic oscillator* – a 1D system whose higher terms in the potential's expansion (3.10) cannot be neglected, but are small and may be accounted for approximately. If, in addition, damping is low (or negligible), and the external harmonic force exerted on the system is not too large, the equation of motion is a slightly modified version of Eq. (13):

Weakly
nonlinear
oscillator

$$\ddot{q} + \omega^2 q = f(t, q, \dot{q}, \dots), \quad (5.38)$$

where $\omega \approx \omega_0$ is the anticipated frequency of oscillations (whose choice may be to a certain extent arbitrary – see below), and the right-hand side f is small (say, scales as some small dimensionless parameter $\varepsilon \ll 1$), and may be considered as a small *perturbation*.

Since at $\varepsilon = 0$ this equation has the sinusoidal solution given by Eq. (3), one might naïvely think that at a nonzero but small ε , the approximate solution to Eq. (38) should be sought in the form

Perturbative
solution

$$q(t) = q^{(0)} + q^{(1)} + q^{(2)} + \dots, \quad \text{where } q^{(n)} \propto \varepsilon^n, \quad (5.39)$$

with $q^{(0)} = A \cos(\omega_0 t - \varphi) \propto \varepsilon^0$. This is a good example of an apparently impeccable mathematical reasoning that would lead to a very inefficient procedure. Indeed, let us apply it to the problem we already know the exact solution for, namely free oscillations in a linear but damped oscillator, for this occasion assuming the damping to be very low, $\delta/\omega_0 \sim \varepsilon \ll 1$. The corresponding equation of motion, Eq. (6), may be represented in form (38) if we take $\omega = \omega_0$ and

$$f = -2\delta\dot{q}, \quad \text{with } \delta \propto \varepsilon. \quad (5.40)$$

The naïve perturbation theory based on Eq. (39) would allow us to find *small* corrections, of the order of δ , to the free, non-decaying oscillations $A \cos(\omega_0 t - \varphi)$. However, we already know from Eq. (9) that the main effect of damping is a gradual decrease of the free oscillation amplitude to zero, i.e. a very *large* change of the amplitude, though at low damping, $\delta \ll \omega_0$, this decay takes large time $t \sim \tau \gg 1/\omega_0$. Hence, if we want our approximate method to be productive (i.e. to work at all time scales, in particular for forced oscillations with stationary amplitude and phase), we need to account for the fact that even a *small* right-hand side of Eq. (38) may eventually lead to *large* changes of oscillation's amplitude A (and sometimes, as we will see below, also of oscillation's phase φ) at large times, because of the *slowly accumulating* effects of the small perturbation.¹⁵

This goal may be achieved¹⁶ by the account of these slow changes already in the “0th approximation”, i.e. the basic part of the solution in the expansion (39):

¹⁵ The same flexible approach is necessary for approximations used in quantum mechanics. The method discussed here is closer in spirit (though not completely identical) to the *WKB approximation* (see, e.g., QM Sec. 2.4) rather than most perturbative approaches (QM Ch. 6).

¹⁶ This approach has a long history and, unfortunately, does not have a commonly accepted name. It had been gradually developed in celestial mechanics, but its application to 1D systems (on which I am focusing) was clearly spelled out only in 1926 by Balthasar van der Pol. So, I will follow several authors who call it the *van der Pol method*. Note, however, that in optics and quantum mechanics, this method is commonly called the *Rotating Wave Approximation* (RWA). In math-oriented texts, this approach, and especially its extensions to higher approximations, is usually called either the *small parameter method* or the *asymptotic method*. The list of other

$$q^{(0)} = A(t) \cos[\omega t - \varphi(t)], \quad \text{with } \dot{A}, \dot{\varphi} \rightarrow 0 \text{ at } \varepsilon \rightarrow 0. \quad (5.41)$$

0th
approximation

(It is evident that Eq. (9) is a particular case of this form.) Let me discuss this approach using a simple but representative example of a dissipative (but high- Q) pendulum driven by a weak sinusoidal external force with a nearly-resonant frequency:

$$\ddot{q} + 2\delta\dot{q} + \omega_0^2 \sin q = f_0 \cos \omega t, \quad (5.42)$$

with $|\omega - \omega_0|, \delta \ll \omega_0$, and the force amplitude f_0 so small that $|q| \ll 1$ at all times. From what we know about the forced oscillations from Sec. 1, in this case it is natural to identify ω on the left-hand side of Eq. (38) with the force's frequency. Expanding $\sin q$ into the Taylor series in small q , keeping only the first two terms of this expansion, and moving all small terms to the right-hand side, we can rewrite Eq. (42) in the following popular form (38):¹⁷

$$\ddot{q} + \omega^2 q = -2\delta\dot{q} + 2\xi\omega q + \alpha q^3 + f_0 \cos \omega t \equiv f(t, q, \dot{q}). \quad (5.43)$$

Duffing equation

Here $\alpha = \omega_0^2/6$ in the case of the pendulum (though the calculations below will be valid for any α), and the second term on the right-hand side was obtained using the approximation already employed in Sec. 1: $(\omega^2 - \omega_0^2)q \approx 2\omega(\omega - \omega_0)q = 2\omega\xi q$, where $\xi \equiv \omega - \omega_0$ is the detuning parameter that was already used earlier – see Eq. (21).

Now, following the general recipe expressed by Eqs. (39) and (41), in the 1st approximation in $f \propto \varepsilon$ we may look for the solution to Eq. (43) in the following form:

$$q(t) = A \cos \Psi + q^{(1)}(t), \quad \text{where } \Psi \equiv \omega t - \varphi, \quad q^{(1)} \sim \varepsilon. \quad (5.44)$$

Let us plug this solution into both parts of Eq. (43), keeping only the terms of the first order in ε . Thanks to our (smart :-) choice of ω on the left-hand side of that equation, the two zero-order terms in that part cancel each other. Moreover, since each term on the right-hand side of Eq. (43) is already of the order of ε , we may drop $q^{(1)} \propto \varepsilon$ from the substitution into that part at all, because this would give us only terms $O(\varepsilon^2)$ or higher. As a result, we get the following approximate equation:

$$\ddot{q}^{(1)} + \omega^2 q^{(1)} = f^{(0)}(t) \equiv -2\delta \frac{d}{dt}(A \cos \Psi) + 2\xi\omega(A \cos \Psi) + \alpha(A \cos \Psi)^3 + f_0 \cos \omega t. \quad (5.45)$$

According to Eq. (41), generally, A and φ should be considered (slow) functions of time. However, let us leave the analyses of the transient process and system's stability until the next section, and use Eq. (45) to find stationary oscillations in the system, that are established after an initial transient process. For that limited task, we may take $A = \text{const}$, $\varphi = \text{const}$, so that $q^{(0)}$ represents sinusoidal oscillations of frequency ω . Sorting the terms on the right-hand side according to their time dependence,¹⁸ we see that it has terms with frequencies ω and 3ω .

scientists credited for the development of this method, its variations, and extensions includes, most notably, N. Krylov, N. Bogolyubov, and Yu. Mitropolsky.

¹⁷ This equation is frequently called the *Duffing equation* (or the equation of the *Duffing oscillator*), after Georg Duffing who carried out its first (rather incomplete) analysis in 1918.

¹⁸ Using the second of Eqs. (44), $\cos \omega t$ may be rewritten as $\cos(\Psi + \varphi) \equiv \cos \Psi \cos \varphi - \sin \Psi \sin \varphi$. Then using the identity given, for example, by MA Eq. (3.4): $\cos^3 \Psi = (3/4)\cos \Psi + (1/4)\cos 3\Psi$, we get Eq. (46).

$$f^{(0)} = \left(2\xi\omega A + \frac{3}{4}\alpha A^3 + f_0 \cos \varphi \right) \cos \Psi + (2\delta\omega A - f_0 \sin \varphi) \sin \Psi + \frac{1}{4}\alpha A^3 \cos 3\Psi. \quad (5.46)$$

Now comes the main punch of the van der Pol approach: mathematically, Eq. (45) may be viewed as the equation of oscillations in a linear, *dissipation-free* harmonic oscillator of frequency ω (not ω_0 !) under the action of an external force $f^{(0)}(t)$. In our particular case, this force is given by Eq. (46) and has three terms: two “quadrature” components at that very frequency ω , and the third one of frequency 3ω . As we know from our analysis of this problem in Sec. 1, if any of the first two components is not equal to zero, $q^{(1)}$ grows to infinity – see Eq. (19) with $\delta=0$. At the same time, by the very structure of the van der Pol approximation, $q^{(1)}$ has to be finite – moreover, small! The only way to avoid these infinitely growing (so-called *secular*) terms is to require that the amplitudes of both quadrature components of $f^{(0)}$ with frequency ω are equal to zero:

$$2\xi\omega A + \frac{3}{4}\alpha A^3 + f_0 \cos \varphi = 0, \quad 2\delta\omega A - f_0 \sin \varphi = 0. \quad (5.47)$$

These two *harmonic balance equations* enable us to find both parameters of the forced oscillations: their amplitude A and phase φ . The phase may be readily eliminated from this system (most easily, by expressing $\sin \varphi$ and $\cos \varphi$ from Eqs. (47), and then requiring the sum $\sin^2 \varphi + \cos^2 \varphi$ to equal 1), and the solution for A recast in the following implicit but convenient form:

$$A^2 = \frac{f_0^2}{4\omega^2} \frac{1}{\xi^2(A) + \delta^2}, \quad \text{where } \xi(A) \equiv \xi + \frac{3}{8} \frac{\alpha A^2}{\omega} = \omega - \left(\omega_0 - \frac{3}{8} \frac{\alpha A^2}{\omega} \right). \quad (5.48)$$

This expression differs from Eq. (22) for the linear resonance in the low-damping limit only by the replacement of the detuning ξ with its effective amplitude-dependent value $\xi(A)$ – or, equivalently, the replacement of the frequency ω_0 of the oscillator with its effective, amplitude-dependent value

$$\omega_0(A) = \omega_0 - \frac{3}{8} \frac{\alpha A^2}{\omega}. \quad (5.49)$$

The physical meaning of $\omega_0(A)$ is simple: this is just the frequency of free oscillations of amplitude A in a similar nonlinear system, but with zero damping.¹⁹ Indeed, for $\delta=0$ and $f_0=0$ we could repeat our calculations, assuming that ω is an amplitude-dependent eigenfrequency $\omega_0(A)$. Then the second of Eqs. (47) is trivially satisfied, while the second of them gives Eq. (49). The implicit relation (48) enables us to draw the curves of this *nonlinear resonance* just by bending the linear resonance plots (Fig. 1) according to the so-called *skeleton curve* expressed by Eq. (49). Figure 4 shows the result of this procedure. Note that at small amplitude, $\omega_0(A) \rightarrow \omega_0$, i.e. we return to the usual, “linear” resonance (22).

To bring our solution to its logical completion, we should still find the first perturbation $q^{(1)}(t)$ from what is left of Eq. (45). Since the structure of this equation is similar to Eq. (13) with the force of frequency 3ω and zero damping, we may use Eqs. (16)-(17) to obtain

¹⁹ The effect of the pendulum’s frequency dependence on its oscillation amplitude was observed as early as 1673 by Christiaan Huygens – who by the way had invented the pendulum clock, increasing the timekeeping accuracy by about three orders of magnitude. (He also discovered the largest of Saturn’s moons, Titan).

$$q^{(1)}(t) = -\frac{1}{32\omega^2} \alpha A^3 \cos 3(\omega t - \varphi). \quad (5.50)$$

Adding this perturbation (note the negative sign!) to the sinusoidal oscillation (41), we see that as the amplitude A of oscillations in a system with $\alpha > 0$ (e.g., a pendulum) grows, their waveform becomes a bit more “blunt” near the largest deviations from the equilibrium.

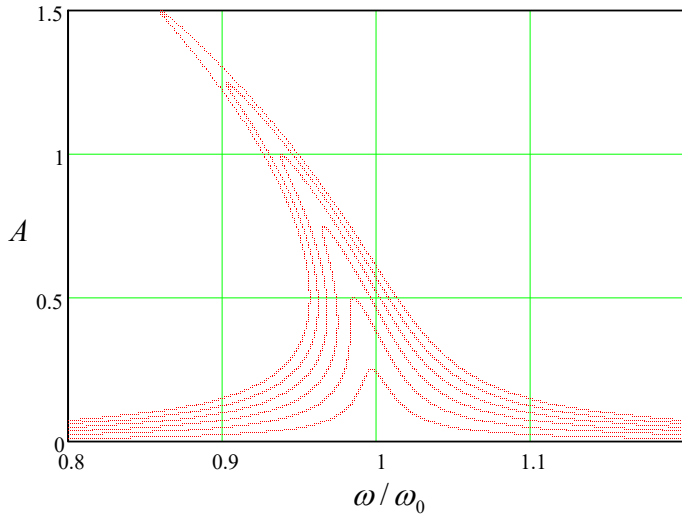


Fig. 5.4. The nonlinear resonance in the Duffing oscillator, as described by Eq. (48), for the particular case $\alpha = \omega_0^2/6$, $\delta/\omega = 0.01$ (i.e. $Q = 50$), and several values of the parameter f_0/ω_0^2 , increased by equal steps of 0.005 from 0 to 0.03.

The same Eq. (50) also enables an estimate of the range of validity of our first approximation: since it has been based on the assumption $|q^{(1)}| \ll |q^{(0)}| \leq A$, for this particular problem we have to require $\alpha A^2 / 32\omega^2 \ll 1$. For a pendulum (i.e. for $\alpha = \omega_0^2/6$), this condition becomes $A^2 \ll 192$. Though numerical coefficients in such strong inequalities should be taken with a grain of salt, the large magnitude of this particular coefficient gives a good hint that the method may give very accurate results even for relatively large oscillations with $A \sim 1$. In Sec. 7 below, we will see that this is indeed the case.

From the mathematical viewpoint, the next step would be to write the next approximation as

$$q(t) = A \cos \Psi + q^{(1)}(t) + q^{(2)}(t), \quad q^{(2)} \sim \varepsilon^2, \quad (5.51)$$

and plug it into the Duffing equation (43), which (thanks to our special choice of $q^{(0)}$ and $q^{(1)}$) would retain only the sum $\ddot{q}^{(2)} + \omega^2 q^{(2)}$ on its left-hand side. Again, requiring the amplitudes of two quadrature components of the frequency ω on the right-hand side to vanish, we may get second-order corrections to A and φ . Then we may use the remaining part of the equation to calculate $q^{(2)}$, and then go after the third-order terms, etc.²⁰ However, for most purposes, the sum $q^{(0)} + q^{(1)}$, and sometimes even just the crudest approximation $q^{(0)}$ alone, are completely sufficient. For example, according to Eq. (50), for a simple pendulum swinging as much as between the opposite horizontal positions ($A = \pi/2$), the 1st order correction $q^{(1)}$ is of the order of 0.5%. (Soon beyond this value, completely new dynamic phenomena

²⁰ For a mathematically rigorous treatment of higher approximations, see, e.g., Yu. Mitropolsky and N. Dao, *Applied Asymptotic Methods in Nonlinear Oscillations*, Springer, 2004. A more laymen (and, by today's standards, somewhat verbose) discussion of various oscillatory phenomena may be found in the classical text A. Andronov, A. Vitt, and S. Khaikin, *Theory of Oscillators*, first published in the 1960s and still available online as Dover's republication in 2011.

start – see Sec. 7 below – but they cannot be described by these successive approximations at all.) Due to such reasons, higher approximations are rarely pursued for particular systems.

5.3. Reduced equations

A much more important issue is the stability of the solutions described by Eq. (48). Indeed, Fig. 4 shows that within a certain range of parameters, these equations give three different values for the oscillation amplitude (and phase), and it is important to understand which of them are stable. Since these solutions are not the fixed points in the sense discussed in Sec. 3.2 (each point in Fig. 4 represents a nearly-sinusoidal oscillation), their stability analysis needs a more general approach that would be valid for oscillations with amplitude and phase slowly evolving in time. This approach will also enable the analysis of non-stationary (especially the initial transient) processes, which are of importance for some dynamic systems.

First of all, let us formalize the way the harmonic balance equations, such as Eqs. (47), should be obtained for the general case (38) – rather than for the particular Eq. (43) considered in the last section. After plugging in the 0th approximation (41) into the right-hand side of equation (38) we have to require the amplitudes of both quadrature components of frequency ω to vanish. From the standard Fourier analysis, we know that these requirements may be represented as

Harmonic
balance
equations

$$\overline{f^{(0)} \sin \Psi} = 0, \quad \overline{f^{(0)} \cos \Psi} = 0, \quad (5.52)$$

where the top bar means the time averaging – in our current case, over the period $2\pi/\omega$ of the right-hand side of Eq. (52), with the arguments calculated in the 0th approximation:

$$f^{(0)} \equiv f(t, q^{(0)}, \dot{q}^{(0)}, \dots) \equiv f(t, A \cos \Psi, -A \omega \sin \Psi, \dots), \quad \text{with } \Psi = \omega t - \varphi. \quad (5.53)$$

Now, for a transient process the contribution of $q^{(0)}$ to the left-hand side of Eq. (38) is not zero any longer, because its amplitude and phase may be both slow functions of time – see Eq. (41). Let us calculate this contribution. The exact result would be

$$\begin{aligned} \ddot{q}^{(0)} + \omega^2 q^{(0)} &\equiv \left(\frac{d^2}{dt^2} + \omega^2 \right) A \cos(\omega t - \varphi) \\ &= (\ddot{A} + 2\dot{\varphi}\omega A - \dot{\varphi}^2 A) \cos(\omega t - \varphi) - 2\dot{A}(\omega - \dot{\varphi}) \sin(\omega t - \varphi). \end{aligned} \quad (5.54)$$

However, in the first approximation in ε , we may neglect the second derivative of A , and also the squares and products of the first derivatives of A and φ (which are all of the second order in ε), so that Eq. (54) is reduced to

$$\ddot{q}^{(0)} + \omega^2 q^{(0)} \approx 2A\dot{\varphi}\omega \cos(\omega t - \varphi) - 2\dot{A}\omega \sin(\omega t - \varphi). \quad (5.55)$$

On the right-hand side of Eq. (53), we can neglect the time derivatives of the amplitude and phase at all, because this part is already proportional to the small parameter. Hence, in the first order in ε , Eq. (38) becomes

$$\ddot{q}^{(1)} + \omega^2 q^{(1)} = f_{\text{ef}}^{(0)} \equiv f^{(0)} - (2A\dot{\varphi}\omega \cos \Psi - 2\dot{A}\omega \sin \Psi). \quad (5.56)$$

Now, applying Eqs. (52) to the function $f_{\text{ef}}^{(0)}$, and taking into account that the time averages of $\sin^2\Psi$ and $\cos^2\Psi$ are both equal to $\frac{1}{2}$, while the time average of the product $\sin\Psi\cos\Psi$ vanishes, we get a pair of so-called *reduced equations* (alternatively called either “truncated”, or “RWA”, or “van der Pol” equations) for the time evolution of the amplitude and phase:

$$\dot{A} = -\frac{1}{\omega} \overline{f^{(0)} \sin \Psi}, \quad \dot{\varphi} = \frac{1}{\omega A} \overline{f^{(0)} \cos \Psi}. \quad (5.57a)$$

Reduced
(RWA)
equations

Extending the definition (4) of the complex amplitude of oscillations to their slow evolution in time, $a(t) \equiv A(t)\exp\{i\varphi(t)\}$, and differentiating this relation, the two equations (57a) may be also rewritten in the form of either one equation for a :

$$\dot{a} = \frac{i}{\omega} \overline{f^{(0)} e^{i(\Psi + \varphi)}} \equiv \frac{i}{\omega} \overline{f^{(0)} e^{i\omega t}}, \quad (5.57b)$$

Reduced
equations:
alternative
forms

or two equations for the real and imaginary parts of $a(t) = u(t) + iv(t)$:

$$\dot{u} = -\frac{1}{\omega} \overline{f^{(0)} \sin \omega t}, \quad \dot{v} = \frac{1}{\omega} \overline{f^{(0)} \cos \omega t}. \quad (5.57c)$$

The first-order harmonic balance equations (52) are evidently just the particular case of the reduced equations (57) for stationary oscillations ($\dot{A} = \dot{\varphi} = 0$).²¹

Superficially, the system (57a) of two coupled, first-order differential equations may look more complex than the initial, second-order differential equation (38), but actually, it is usually much simpler. For example, let us spell them out for the easy case of free oscillations a linear oscillator with damping. For that, we may reuse the ready Eq. (46) by taking $\alpha = f_0 = 0$, and thus turning Eqs. (57a) into

$$\dot{A} = -\frac{1}{\omega} \overline{f^{(0)} \sin \Psi} \equiv -\frac{1}{\omega} \overline{(2\xi\omega A \cos \Psi + 2\delta\omega A \sin \Psi) \sin \Psi} \equiv -\delta A, \quad (5.58a)$$

$$\dot{\varphi} = \frac{1}{\omega A} \overline{f^{(0)} \cos \Psi} \equiv \frac{1}{\omega A} \overline{(2\xi\omega A \cos \Psi + 2\delta\omega A \sin \Psi) \cos \Psi} \equiv \xi. \quad (5.58b)$$

The solution of Eq. (58a) gives us the same “envelope” law $A(t) = A(0)e^{-\delta t}$ as the exact solution (10) of the initial differential equation, while the elementary integration of Eq. (58b) yields $\varphi(t) = \xi t + \varphi(0) \equiv \omega t - \omega_0 t + \varphi(0)$. This means that our approximate solution,

$$q^{(0)}(t) = A(t) \cos[\omega t - \varphi(t)] = A(0) e^{-\delta t} \cos[\omega_0 t - \varphi(0)], \quad (5.59)$$

agrees with the exact Eq. (9), and misses only the correction (8) of the oscillation frequency. (This correction is of the second order in δ , i.e. of the order of ξ^2 , and hence is beyond the accuracy of our first approximation.) It is remarkable how nicely do the reduced equations recover the proper frequency of free oscillations in this autonomous system – in which the very notion of ω is ambiguous.

²¹ One may ask why we cannot stick to just one, most compact, complex-amplitude form (57b) of the reduced equations. The main reason is that when the function $f(q, \dot{q}, t)$ is nonlinear, we cannot replace its real arguments, such as $q = A \cos(\omega t - \varphi)$, with their complex-function representations like $a \exp\{-i\omega t\}$ (as could be done in the linear problems considered in Sec. 5.1), and need to use real variables, such as either $\{A, \varphi\}$ or $\{u, v\}$, anyway.

The result is different at forced oscillations. For example, for the (generally, nonlinear) Duffing oscillator described by Eq. (43) with $f_0 \neq 0$, Eqs. (57a) yield the reduced equations,

$$\dot{A} = -\delta A + \frac{f_0}{2\omega} \sin \varphi, \quad A\dot{\varphi} = \xi(A) A + \frac{f_0}{2\omega} \cos \varphi, \quad (5.60)$$

which are valid for an arbitrary function $\xi(A)$, provided that this nonlinear detuning remains much smaller than the oscillation frequency. Here (after a transient), the amplitude and phase tend to the stationary states described by Eqs. (47). This means that φ becomes a constant, so that $q^{(0)} \rightarrow A \cos(\omega t - \text{const})$, i.e. the reduced equations again automatically recover the correct frequency of the solution, in this case equal to the external force frequency.

Note that each stationary oscillation regime, with certain amplitude and phase, corresponds to a fixed point of the reduced equations, so that the stability of those fixed points determines that of the oscillations. In the next three sections, we will carry out such analyses for several simple systems of key importance for physics and engineering.

5.4. Self-oscillations and phase locking

B. van der Pol's motivation for developing his method was the analysis of one more type of oscillatory motion: *self-oscillations*. Several systems, e.g., electronic rf amplifiers with positive feedback and optical media with quantum level population inversion, provide convenient means for the compensation and even over-compensation of the intrinsic energy losses in oscillators. Phenomenologically, this effect may be described as the change of sign of the damping coefficient δ from positive to negative. Since for small oscillations the equation of motion is still linear, we may use Eq. (9) to describe its general solution. This equation shows that at $\delta < 0$, even infinitesimal deviations from equilibrium (say, due to unavoidable fluctuations) lead to oscillations with exponentially growing amplitude. Of course, in any real system such growth cannot persist infinitely, and shall be limited by this or that effect – e.g., in the above examples, respectively, by the amplifier's saturation and the quantum level population's exhaustion.

In many cases, the amplitude limitation may be described reasonably well by making the following replacement:

$$2\delta\ddot{q} \rightarrow 2\delta\ddot{q} + \beta\dot{q}^3, \quad (5.61)$$

with $\beta > 0$. Let us analyze the effects of such *nonlinear damping*, applying the van der Pol's approach²² to the corresponding differential equation:

$$\ddot{q} + 2\delta\ddot{q} + \beta\dot{q}^3 + \omega_0^2 q = 0. \quad (5.62)$$

Carrying out the dissipative and detuning terms to the right-hand side, and taking them for f in the canonical Eq. (38), we can easily calculate the right-hand sides of the reduced equations (57a), getting²³

$$\dot{A} = -\delta(A) A, \quad \text{where } \delta(A) \equiv \delta + \frac{3}{8}\beta\omega^2 A^2, \quad (5.63a)$$

²² In his original work, B. van der Pol considered a very similar equation (frequently called the *van der Pol oscillator*) that differs from Eq. (62) only by the nonlinear term: $\dot{q}^3 \rightarrow q^2 \dot{q}$, and has very similar properties.

²³ For that, one needs to use the trigonometric identity $\sin^3\Psi = (3/4)\sin\Psi - (1/4)\sin3\Psi$ – see, e.g., MA Eq. (3.4).

$$A\dot{\phi} = \xi A. \quad (5.63b)$$

The last of these equations has exactly the same form as Eq. (58b) for the case of decaying oscillations and hence shows that the self-oscillations (if they happen, i.e. if $A \neq 0$) have the own frequency ω_0 of the oscillator – cf. Eq. (59). However, Eq. (63a) is more substantive. If the initial damping δ is positive, it has only the trivial fixed point, $A_0 = 0$ (that describes the oscillator at rest), but if δ is negative, there is also another fixed point,

$$A_1 = \frac{2}{\sqrt{3}} q_0, \quad \text{where } q_0 \equiv \left(\frac{2|\delta|}{\beta\omega^2} \right)^{1/2}, \quad \text{for } \delta < 0, \quad (5.64)$$

which describes steady self-oscillations with a non-zero amplitude A_1 .

To understand which of these points is stable, let us apply the general approach discussed in Sec. 3.2, the linearization of equations of motion, to Eq. (63a). For the trivial fixed point $A_0 = 0$, its linearization is reduced to discarding the nonlinear term in the definition of the amplitude-dependent damping $\delta(A)$. The resulting linear equation evidently shows that the system's equilibrium point, $A = A_0 = 0$, is stable at $\delta > 0$ and unstable at $\delta < 0$. (This *self-excitation condition* was already discussed above.) On the other hand, the linearization of near the non-trivial fixed point A_1 requires a bit more math: in the first order in $\tilde{A} \equiv A - A_1 \rightarrow 0$, we get

$$\dot{\tilde{A}} \equiv \dot{A} = -\delta(A_1 + \tilde{A}) - \frac{3}{8}\beta\omega^2(A_1 + \tilde{A})^3 \approx -\delta\tilde{A} - \frac{3}{8}\beta\omega^2 3A_1^2\tilde{A} = (-\delta + 3\delta)\tilde{A} = 2\delta\tilde{A}, \quad (5.65)$$

where Eq. (64) has been used to eliminate A_1 . We see that the fixed point A_1 (and hence the self-oscillation process) is stable as soon as it exists ($\delta < 0$) – similarly to the situation in our “testbed problem” (Fig. 2.1), besides that in our current, dissipative system, the stability is “actual” rather than “orbital” – see Sec. 6 for more on this issue.

Now let us consider another important problem: the effect of an external oscillating force on a self-excited oscillator. If the force is sufficiently small, its effects on the self-excitation condition and the oscillation amplitude are negligible. However, if the frequency ω of such a weak force is close to the own frequency ω_0 of the oscillator, it may lead to *phase locking*²⁴ – also called “synchronization”, though the latter term also has a much broader meaning. At this effect, the oscillation frequency deviates from ω_0 , and becomes exactly equal to the external force’s frequency ω , within a certain range

$$-\Delta \leq \omega - \omega_0 < +\Delta. \quad (5.66)$$

To prove this fact, and also to calculate the phase-locking range width 2Δ , we may repeat the calculation of the right-hand sides of the reduced equations (57a), adding the term $f_0 \cos \omega t$ to the right-hand side of Eq. (62) – cf. Eqs. (42)-(43). This addition modifies Eqs. (63) as follows:²⁵

$$\dot{A} = -\delta(A)A + \frac{f_0}{2\omega} \sin \varphi, \quad (5.67a)$$

$$A\dot{\phi} = \xi A + \frac{f_0}{2\omega} \cos \varphi. \quad (5.67b)$$

²⁴ Apparently, the phase locking was first noticed by the same C. Huygens for pendulum clocks.

²⁵ Actually, this result should be evident, even without calculations, from the comparison of Eqs. (60) and (63).

If the system is self-excited, and the external force is weak, its effect on the oscillation amplitude is small, and in the first approximation in f_0 we can take A to be constant and equal to the value A_1 given by Eq. (64). Plugging this approximation into Eq. (67b), we get a very simple equation²⁶

Phase locking equation

where in our current case

$$\dot{\varphi} = \xi + \Delta \cos \varphi, \quad (5.68)$$

$$\Delta \equiv \frac{f_0}{2\omega A_1}. \quad (5.69)$$

Within the range $-|\Delta| < \xi < +|\Delta|$, Eq. (68) has two fixed points on each 2π -segment of the variable φ :

$$\varphi_{\pm} = \pm \cos^{-1} \left(-\frac{\xi}{\Delta} \right) + 2\pi n. \quad (5.70)$$

It is easy to linearize Eq. (68) near each point to analyze their stability in our usual way; however, let me use this case to demonstrate another convenient way to do this in 1D systems, using the so-called *phase plane* [$\varphi, \dot{\varphi}$] – see Fig. 5, where the red line shows the right-hand side of Eq. (68).

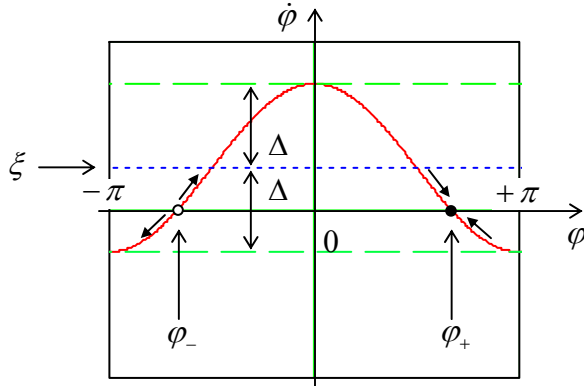


Fig. 5.5. The phase plane of a phase-locked oscillator, for the particular case $\xi = \Delta/2$, $f_0 > 0$.

Since according to Eq. (68), positive values of the plotted function correspond to the growth of φ in time and vice versa, we may draw the arrows showing the direction of phase evolution. From this graphics, it is clear that one of these fixed points (for $f_0 > 0$, φ_+) is stable, while its counterpart (in this case, φ_-) is unstable. Hence the magnitude of Δ given by Eq. (69) is indeed the phase-locking range (or rather its half) that we wanted to find. Note that the range is proportional to the amplitude of the phase-locking signal – perhaps the most important quantitative feature of this effect.

To complete our simple analysis, based on the assumption of fixed oscillation amplitude, we need to find the condition of its validity. For that, we may linearize Eq. (67a), for the stationary case, near the value A_1 , just as we have done in Eq. (65) for the transient process. The stationary result,

$$\tilde{A} \equiv A - A_1 = \frac{1}{2|\delta|} \frac{f_0}{2\omega} \sin \varphi_{\pm} \approx A_1 \left| \frac{\Delta}{2\delta} \right| \sin \varphi_{\pm}, \quad (5.71)$$

shows that our assumption, $|\tilde{A}| \ll A_1$, and hence the final result (69), are valid if the calculated phase-locking range 2Δ is much smaller than $4|\delta|$.

²⁶ This equation is ubiquitous in phase-locking system descriptions, including even some digital electronic circuits used for that purpose – at the proper re-definition of the phase difference φ .

5.5. Parametric excitation

In both problems solved in the last section, the stability analysis was easy because it could be carried out for just one slow variable, *either* amplitude *or* phase. More generally, such an analysis of the reduced equations involves both of these variables. A classical example of such a situation is provided by one important physical effect – the *parametric excitation* of oscillations. A simple example of such excitation is given by a pendulum with a variable parameter, for example, the suspension length $l(t)$ – see Fig. 6. Experiments²⁷ and numerical simulations show that if the length is changed periodically (*modulated*) with some frequency 2ω that is close to $2\omega_0$, and a sufficiently large depth Δl , the equilibrium position of the pendulum becomes unstable, and it starts oscillating with frequency ω equal *exactly* to the half of the modulation frequency – and hence only *approximately* equal to the average frequency ω_0 of the oscillator.

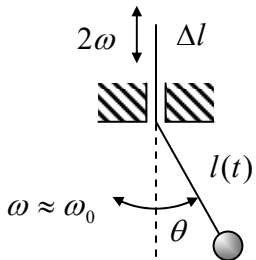


Fig. 5.6. Parametric excitation of a pendulum.

For an elementary analysis of this effect, we may consider the simplest case when the oscillations are small. At the lowest point ($\theta = 0$), where the pendulum moves with the highest velocity v_{\max} , the suspension string's tension \mathcal{T} is *higher* than mg by the centripetal force: $\mathcal{T}_{\max} = mg + mv_{\max}^2/l$. On the contrary, at the maximum deviation of the pendulum from the equilibrium, the force is *lower* than mg , because of the string's tilt: $\mathcal{T}_{\min} = mg\cos\theta_{\max}$. Using the energy conservation, $E = mv_{\max}^2/2 = mgl(1 - \cos\theta_{\max})$, we may express these values as $\mathcal{T}_{\max} = mg + 2E/l$ and $\mathcal{T}_{\min} = mg - E/l$. Now, if during each oscillation period the string is pulled up slightly by Δl (with $|\Delta l| \ll l$) at each of its two passages through the lowest point, and is let to go down by the same amount at each of two points of the maximum deviation, the net work of the external force per period is positive:

$$\mathcal{W} \approx 2(\mathcal{T}_{\max} - \mathcal{T}_{\min})\Delta l \approx 6\frac{\Delta l}{l}E, \quad (5.72)$$

and hence increases the oscillator's energy. If the parameter modulation depth Δl is sufficient, this increase may overcompensate the energy drained out by damping during the same period. Quantitatively, Eq. (10) shows that low damping ($\delta \ll \omega_0$) leads to the following energy decrease,

$$\Delta E \approx -4\pi\frac{\delta}{\omega_0}E, \quad (5.73)$$

per oscillation period. Comparing Eqs. (72) and (73), we see that the net energy flow into the oscillations is positive, $\mathcal{W} + \Delta E > 0$, i.e. oscillation amplitude has to grow if²⁸

²⁷ The simplest experiments of this kind may be done with the usual playground swings, where moving your body up and down moves the system's c.o.m. position, and hence the effective length l_{ef} of the support – see Eq. (4.41).

²⁸ Modulation of the pendulum's mass (say, by periodic pumping water in and out of a suspended bottle) gives a qualitatively similar result. Note, however, that parametric oscillations cannot be excited by modulating *every*

$$\frac{\Delta l}{l} > \frac{2\pi\delta}{3\omega_0} \equiv \frac{\pi}{3Q}. \quad (5.74)$$

Since this result is independent of the oscillation energy E , the growth of energy and amplitude is exponential (until E becomes so large that some of our assumptions fail), so that Eq. (74) is the condition of parametric excitation – in this simple model.

However, this result does not account for a possible difference between the oscillation frequency ω and the eigenfrequency ω_0 , and also does not clarify whether the best phase shift between the oscillations and parameter modulation, assumed in the above calculation, may be sustained automatically. To address these issues, we may apply the van der Pol approach to a simple but reasonable model:

$$\ddot{q} + 2\delta\dot{q} + \omega_0^2(1 + \mu \cos 2\omega t)q = 0, \quad (5.75)$$

describing the parametric excitation in a linear oscillator with a sinusoidal modulation of the parameter $\omega_0^2(t)$. Rewriting this equation in the canonical form (38),

$$\ddot{q} + \omega^2 q = f(t, q, \dot{q}) \equiv -2\delta\dot{q} + 2\xi\omega q - \mu\omega_0^2 q \cos 2\omega t, \quad (5.76)$$

and assuming that the dimensionless ratios δ/ω and $|\xi|/\omega$, and the modulation depth μ are all much less than 1, we may use general Eqs. (57a) to get the following reduced equations:

$$\begin{aligned} \dot{A} &= -\delta A - \frac{\mu\omega}{4} A \sin 2\varphi, \\ A\dot{\varphi} &= A\xi - \frac{\mu\omega}{4} A \cos 2\varphi. \end{aligned} \quad (5.77)$$

These equations evidently have a fixed point, with $A_0 = 0$, but its stability analysis (though possible) is not absolutely straightforward, because the phase φ of oscillations is undetermined at that point. In order to avoid this (technical rather than conceptual) difficulty, we may use, instead of the real amplitude and phase of oscillations, either their complex amplitude $a = A \exp\{i\varphi\}$, or its components u and v – see Eqs. (4). Indeed, for our function f , Eq. (57b) gives

$$\dot{a} = (-\delta + i\xi)a - i\frac{\mu\omega}{4}a^*, \quad (5.78)$$

while Eqs. (57c) yield

$$\begin{aligned} \dot{u} &= -\delta u - \xi v - \frac{\mu\omega}{4}v, \\ \dot{v} &= -\delta v + \xi u - \frac{\mu\omega}{4}u. \end{aligned} \quad (5.79)$$

We see that in contrast to Eqs. (77), in the “Cartesian coordinates” $\{u, v\}$ the trivial fixed point $A_0 = 0$ (i.e. $u_0 = v_0 = 0$) is absolutely regular. Moreover, equations (78)-(79) are already linear, so they do not require any additional linearization. Thus we may use the same approach as was already used in Secs. 3.2 and 5.1, i.e. look for the solution of Eqs. (79) in the exponential form $\exp\{\lambda t\}$. However, now

oscillator’s parameter – for example, the oscillator’s damping coefficient (at least if it stays positive at all times), because this does not change the system’s energy, just the energy drain rate.

we are dealing with two variables and should allow them to have, for each value of λ , a certain ratio u/v . For that, we may take the partial solution in the form

$$u = c_u e^{\lambda t}, \quad v = c_v e^{\lambda t}. \quad (5.80)$$

where the constants c_u and c_v are frequently called the *distribution coefficients*. Plugging this solution into Eqs. (79), we get from them the following system of two linear algebraic equations:

$$\begin{aligned} (-\delta - \lambda)c_u + \left(-\xi - \frac{\mu\omega}{4}\right)c_v &= 0, \\ \left(+\xi - \frac{\mu\omega}{4}\right)c_u + (-\delta - \lambda)c_v &= 0. \end{aligned} \quad (5.81)$$

The characteristic equation of this system, i.e. the condition of compatibility of Eqs. (81),

$$\begin{vmatrix} -\delta - \lambda & -\xi - \frac{\mu\omega}{4} \\ \xi - \frac{\mu\omega}{4} & -\delta - \lambda \end{vmatrix} \equiv \lambda^2 + 2\delta\lambda + \delta^2 + \xi^2 - \left(\frac{\mu\omega}{4}\right)^2 = 0, \quad (5.82)$$

has two roots:

$$\lambda_{\pm} = -\delta \pm \left[\left(\frac{\mu\omega}{4} \right)^2 - \xi^2 \right]^{1/2}. \quad (5.83)$$

Requiring the fixed point to be unstable, $\text{Re}\lambda_+ > 0$, we get the parametric excitation condition

$$\frac{\mu\omega}{4} > (\delta^2 + \xi^2)^{1/2}. \quad (5.84)$$

Thus the parametric excitation may indeed happen without any external phase control: the arising oscillations self-adjust their phase to pick up energy from the external source responsible for the periodic parameter variation.

Our key result (84) may be compared with two other calculations. First, in the case of negligible damping ($\delta = 0$), Eq. (84) turns into the condition $\mu\omega/4 > |\xi|$. This result may be compared with the well-developed theory of the so-called *Mathieu equation*, whose canonical form is

$$\frac{d^2y}{dv^2} + (a - 2b \cos 2v)y = 0. \quad (5.85)$$

With the substitutions $y \rightarrow q$, $v \rightarrow \omega t$, $a \rightarrow (\omega_0/\omega)^2$, and $b/a \rightarrow -\mu/2$, this equation is just a particular case of Eq. (75) for $\delta = 0$. In terms of Eq. (85), our result (84) may be re-written just as $b > |a - 1|$, and is supposed to be valid for $b \ll 1$. The boundaries given by this condition are shown with dashed lines in Fig. 7 together with the numerically calculated²⁹ stability boundaries for the Mathieu equation. One can see that the van der Pol approximation works just fine within its applicability limit (and a bit beyond :-), though it fails to predict some other important features of the Mathieu equation, such as the existence of higher, more narrow regions of parametric excitation (at $a \approx n^2$, i.e. $\omega_0 \approx \omega/n$, for all integer n), and some

²⁹ Such calculations are substantially simplified by the use of the so-called *Floquet theorem*, which is also the mathematical basis for the discussion of wave propagation in periodic media – see the next chapter.

spill-over of the stability region into the lower half-plane $a < 0$.³⁰ The reason for these failures is the fact that, as can be seen in Fig. 7, these phenomena do not appear in the first approximation in the parameter modulation amplitude $\mu \propto b$, which is the realm of the reduced equations (79).

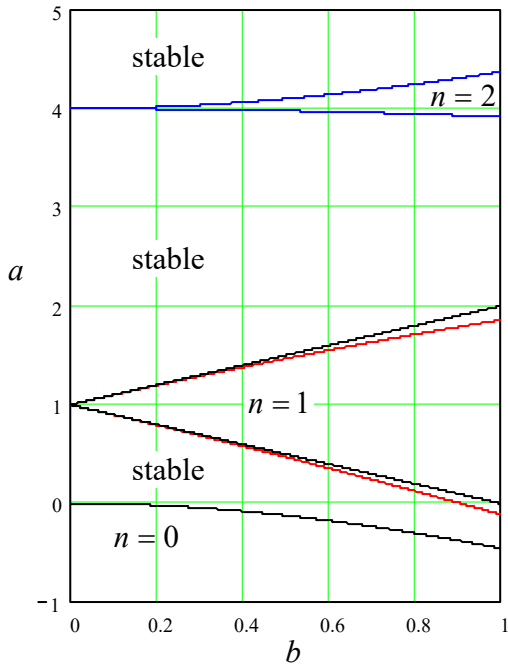


Fig. 5.7. Stability boundaries of the Mathieu equation (85), as calculated: numerically (solid curves) and using the reduced equations (79) (dashed straight lines). In the regions numbered by various n , the trivial solution $y = 0$ of the equation is unstable, i.e. its general solution $y(v)$ includes an exponentially growing term.

In the opposite case of non-zero damping but exact tuning ($\xi = 0, \omega \approx \omega_0$), Eq. (84) becomes

$$\mu > \frac{4\delta}{\omega_0} \equiv \frac{2}{Q}. \quad (5.86)$$

This condition may be compared with Eq. (74) by taking $\Delta l/l = 2\mu$. The comparison shows that while the structure of these conditions is similar, the numerical coefficients are different by a factor close to 2. The first reason for this difference is that the instant parameter change at optimal moments of time is more efficient than the smooth, sinusoidal variation described by (75). Even more significantly, the change of the pendulum's length modulates not only its frequency $\omega_0 \equiv (g/l)^{1/2}$ as Eq. (75) implies but also its *mechanical impedance* $Z \equiv (gl)^{1/2}$ – the notion to be discussed in detail in the next chapter. (The analysis of the general case of the simultaneous modulation of ω_0 and Z is left for the reader's exercise.)

To conclude this section, let me summarize the important differences between the excitation of the parametric and forced oscillations:

- (i) Parametric oscillations completely disappear outside of their excitation range, while the forced oscillations have a non-zero amplitude for any frequency and amplitude of the external force – see Eq. (18).
- (ii) While the parametric excitation may be described by linear equations such as Eq. (75), such equations cannot predict a finite oscillation amplitude within the excitation range, even at finite

³⁰ This region (for $b \ll 1, -b^2/2 < a < 0$) describes, in particular, the counter-intuitive stability of the so-called *Kapitza pendulum* – an inverted pendulum with the suspension point oscillated fast in the vertical direction – the effect first observed by Andrew Stephenson in 1908.

damping. In order to describe stationary parametric oscillations, some nonlinear effects have to be taken into account. (I am leaving analyses of such effects for the reader's exercise.)

One more important feature of parametric oscillations will be discussed in the next section.

5.6. Fixed point classification

The reduced equations (79) give us a good pretext for a brief discussion of an important general topic of dynamics: classification and stability of the fixed points of a system described by two time-independent, first-order differential equations with time-independent coefficients.³¹ After their linearization near a fixed point, the equations for deviations can always be expressed in the form similar to Eq. (79):

$$\begin{aligned}\dot{\tilde{q}}_1 &= M_{11}\tilde{q}_1 + M_{12}\tilde{q}_2, \\ \dot{\tilde{q}}_2 &= M_{21}\tilde{q}_1 + M_{22}\tilde{q}_2,\end{aligned}\quad (5.87)$$

where $M_{jj'}$ (with $j, j' = 1, 2$) are some real scalars, which may be viewed as the elements of a 2×2 matrix M . Looking for an exponential solution of the type (80),

$$\tilde{q}_1 = c_1 e^{\lambda t}, \quad \tilde{q}_2 = c_2 e^{\lambda t}, \quad (5.88)$$

we get a general system of two linear equations for the distribution coefficients $c_{1,2}$:

$$\begin{aligned}(M_{11} - \lambda)c_1 + M_{12}c_2 &= 0, \\ M_{21}c_1 + (M_{22} - \lambda)c_2 &= 0.\end{aligned}\quad (5.89)$$

These equations are consistent if

$$\begin{vmatrix} M_{11} - \lambda & M_{12} \\ M_{21} & M_{22} - \lambda \end{vmatrix} = 0, \quad (5.90)$$

giving us a quadratic characteristic equation:

$$\lambda^2 - \lambda(M_{11} + M_{22}) + (M_{11}M_{22} - M_{12}M_{21}) = 0. \quad (5.91)$$

Its solution,³²

$$\lambda_{\pm} = \frac{1}{2}(M_{11} + M_{22}) \pm \frac{1}{2}[(M_{11} - M_{22})^2 + 4M_{12}M_{21}]^{1/2}, \quad (5.92)$$

shows that the following situations are possible:

A. The expression under the square root, $(M_{11} - M_{22})^2 + 4M_{12}M_{21}$, is positive. In this case, both characteristic exponents λ_{\pm} are real, and we can distinguish three sub-cases:

³¹ Autonomous systems described by a single, second-order homogeneous differential equation, say $F(q, \dot{q}, \ddot{q}) = 0$, also belong to this class, because we may always treat the generalized velocity $\dot{q} \equiv v$ as a new variable, and use this definition as one first-order differential equation, while the initial equation, in the form $F(q, v, \dot{v}) = 0$, as the second first-order equation.

³² In the language of linear algebra, λ_{\pm} are the *eigenvalues*, and the corresponding sets of the distribution coefficients $[c_1, c_2]_{\pm}$ are the *eigenvectors* of the matrix M with elements $M_{jj'}$.

(i) Both λ_+ and λ_- are negative. As Eqs. (88) show, in this case the deviations \tilde{q} tend to zero at $t \rightarrow \infty$, i.e. the fixed point is stable. Because of generally different magnitudes of the exponents λ_{\pm} , the process represented on the phase plane $[\tilde{q}_1, \tilde{q}_2]$ (see Fig. 8a, with the solid arrows, for an example) may be seen as consisting of two stages: first, a faster (with the rate $|\lambda_-| > |\lambda_+|$) relaxation to a linear *asymptote*,³³ and then a slower decline, with the rate $|\lambda_+|$, along this line, i.e. at a virtually fixed ratio of the variables. Such a fixed point is called the *stable node*.

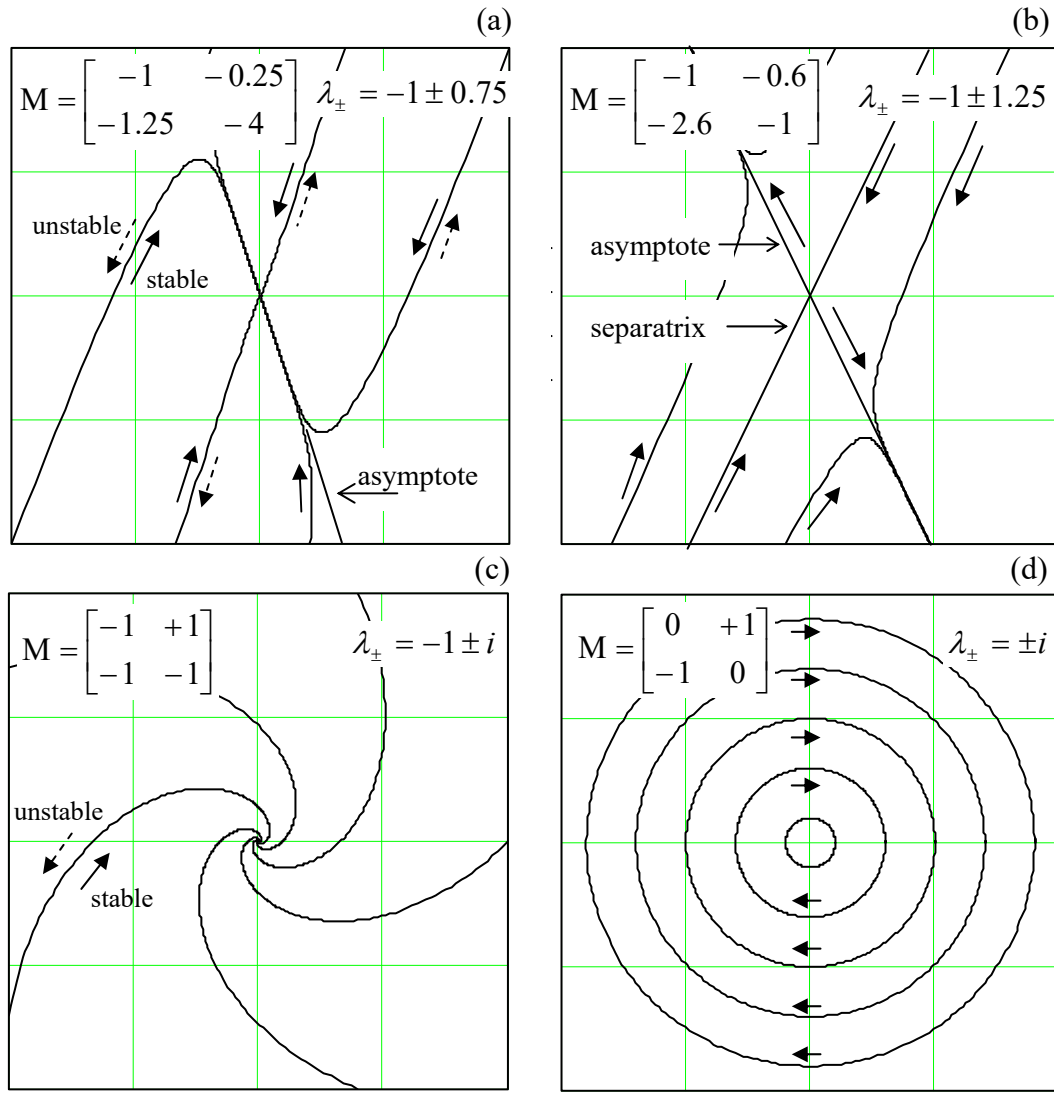


Fig. 5.8. Typical trajectories on the phase plane $[\tilde{q}_1, \tilde{q}_2]$ near fixed points of different types: (a) node, (b) saddle, (c) focus, and (d) center. The particular matrices M used for the first three panels correspond to Eqs. (81) for the parametric excitation, with $\xi = \delta$ and three different values of the ratio $\mu\omega/4\delta$: (a) 1.25, (b) 1.6, and (c) 0.

³³ The asymptote direction may be found by plugging the value λ_+ back into Eq. (89) and finding the corresponding ratio c_1/c_2 . Note that the separation of the system's evolution into the two stages is conditional, being most vivid in the case of a large difference between the exponents λ_+ and λ_- .

(ii) Both λ_+ and λ_- are positive. This case of an *unstable node* differs from the previous one only by the direction of motion along the phase plane trajectories – see the dashed arrows in Fig. 8a. Here the variable ratio is also approaching a constant soon, now the one corresponding to $\lambda_+ > \lambda_-$.

(iii) Finally, in the case of a *saddle* ($\lambda_+ > 0, \lambda_- < 0$), the system's dynamics is different (Fig. 8b): after the rate- $|\lambda_-|$ relaxation to an asymptote, the perturbation starts to grow, with the rate λ_+ , along one of two opposite directions. (The direction is determined on which side of another straight line, called the *separatrix*, the system has been initially.) So the saddle³⁴ is an unstable fixed point.

B. The expression under the square root in Eq. (92), $(M_{11} - M_{22})^2 + 4 M_{12}M_{21}$, is negative. In this case, the square root is imaginary, making the real parts of both roots equal, $\text{Re}\lambda_\pm = (M_{11} + M_{22})/2$, and their imaginary parts equal but opposite. As a result, here there can be just two types of fixed points:

(i) *Stable focus*, at $(M_{11} + M_{22}) < 0$. The phase plane trajectories are spirals going to the origin (i.e. toward the fixed point) – see Fig. 8c with the solid arrow.

(ii) *Unstable focus*, taking place at $(M_{11} + M_{22}) > 0$, differs from the stable one only by the direction of motion along the phase trajectories – see the dashed arrow in the same Fig. 8c.

C. Frequently, the border case, $M_{11} + M_{22} = 0$, corresponding to the orbital (“indifferent”) stability already discussed in Sec. 3.2, is also distinguished, and the corresponding fixed point is referred to as the *center* (Fig. 8d). Considering centers as a separate category makes sense because such fixed points are typical for Hamiltonian systems, whose first integral of motion may be frequently represented as the distance of the representing point from a certain center. For example, introducing new variables $\tilde{q}_1 \equiv \tilde{q}$ and $\tilde{q}_2 \equiv m\dot{\tilde{q}}_1$, we may rewrite Eq. (3.12) of a harmonic oscillator without dissipation (again, with indices “ef” dropped for brevity), as a system of two first-order differential equations:

$$\ddot{\tilde{q}}_1 = \frac{1}{m} \tilde{q}_2, \quad \ddot{\tilde{q}}_2 = -\kappa \tilde{q}_1, \quad (5.93)$$

i.e. as a particular case of Eq. (87), with $M_{11} = M_{22} = 0$, and $M_{12}M_{21} = -\kappa/m \equiv -\omega_0^2 < 0$, and hence $(M_{11} - M_{22})^2 + 4M_{12}M_{21} = -4\omega_0^2 < 0$, and $M_{11} + M_{22} = 0$. On the symmetrized phase plane $[\tilde{q}_1, \tilde{q}_2/Z]$, where the parameter $Z \equiv (\kappa m)^{1/2} \equiv m\omega_0$ is the oscillator's impedance, the sinusoidal oscillations of amplitude A are represented by a circle of radius A about the center-type fixed point $A = 0$. In the case when $\tilde{q}_1 \equiv \tilde{q}$ is the linear coordinate q of an actual mechanical oscillator, so that $\tilde{q}_2 \equiv m\dot{\tilde{q}}_1$ is its linear momentum $p = m\dot{q}$, such a circular trajectory corresponds to the conservation of the oscillator's energy

$$E \equiv T + U \equiv \frac{p^2}{2m} + \frac{\kappa q^2}{2} \equiv \frac{\kappa}{2} \left[\tilde{q}_1^2 + \left(\frac{\tilde{q}_2}{Z} \right)^2 \right] = \frac{\kappa A^2}{2} = \text{const.} \quad (5.94)$$

This is a convenient moment for a brief discussion of the so-called *Poincaré* (or “slow-variable”, or “stroboscopic”) *plane*.³⁵ From the point of view of the basic Eq. (41), the sinusoidal oscillations $q(t)$

³⁴ The term “saddle” is due to the fact that in this case, the system's dynamics is qualitatively similar to that of a heavily damped motion in a 2D potential $U(\tilde{q}_1, \tilde{q}_2)$ having the shape of a horse saddle (or a mountain pass).

³⁵ Named after Jules Henri Poincaré (1854–1912), who is credited, among many other achievements in physics and mathematics, for his contributions to special relativity (see, e.g., EM Chapter 9), and the basic idea of unstable trajectories responsible for the deterministic chaos – to be discussed in Chapter 9 of this course.

$= A \cos(\omega t - \varphi)$, described by a circular trajectory on the actual (symmetrized) phase plane, correspond to a fixed point $\{A, \varphi\}$, which may be conveniently represented by a stationary geometric point on the plane with these polar coordinates – see Fig. 9a. (As follows from Eq. (4), the Cartesian coordinates of the point on that plane are just the variables $u \equiv A \cos \varphi$ and $v \equiv A \sin \varphi$ that were used, in particular, in the last section.) The quasi-sinusoidal process (41), with slowly changing A and φ , may be represented by slow motion of that point on this Poincaré plane.

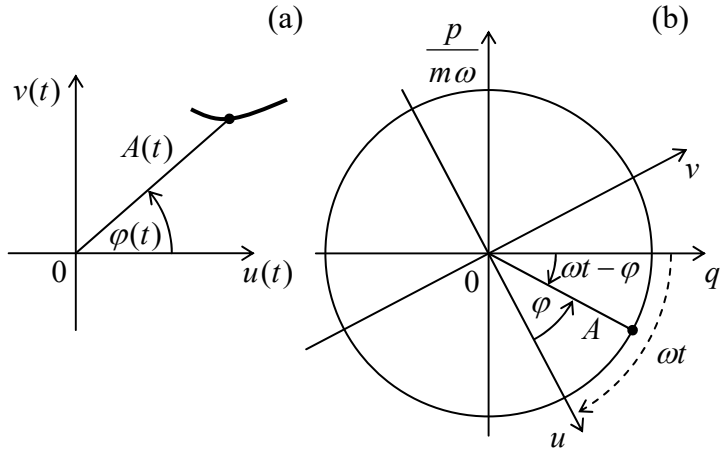


Fig. 5.9. (a) Representation of a sinusoidal oscillation (point) and a slow transient process (line) on the Poincaré plane, and (b) the relation between the “fast” phase plane and the “slow” (Poincaré) plane.

Figure 9b shows a convenient way to visualize the relation between the actual phase plane of an oscillator, with the “fast” symmetrized coordinates q and $p/m\omega$, and the Poincaré plane with the “slow” coordinates u and v : the latter plane rotates relative to the former one, about the origin, clockwise, with the angular velocity ω .³⁶ Another, “stroboscopic” way to generate the Poincaré plane pattern is to have a fast glance at the “real” phase plane just once during the oscillation period $\mathcal{T} = 2\pi/\omega$.

In many cases, the representation on the Poincaré plane is more convenient than that on the “real” phase plane. In particular, we have already seen that the reduced equations for such important phenomena as the phase locking and the parametric oscillations, whose original differential equations include time explicitly, are time-independent – cf., e.g., (75) and (79) describing the latter effect. This simplification brings the equations into the category considered earlier in this section, and enables an easy classification of their fixed points, which may shed additional light on their dynamic properties.

In particular, Fig. 10 shows the classification of the only (trivial) fixed point $A_1 = 0$ on the Poincaré plane of the parametric oscillator, which follows from Eq. (83). As the parameter modulation depth μ is increased, the type of this fixed point changes from a stable focus (pertinent to a simple oscillator with damping) to a stable node and then to a saddle describing the parametric excitation. In the last case, the two directions of the perturbation growth, so prominently featured in Fig. 8b, correspond to the two possible values of the oscillation phase φ , with the phase choice determined by initial conditions.

This double degeneracy of the parametric oscillation’s phase could already be noticed from Eqs. (77), because they are evidently invariant with respect to the replacement $\varphi \rightarrow \varphi + \pi$. Moreover, the degeneracy is not an artifact of the van der Pol approximation, because the initial equation (75) is already invariant with respect to the corresponding replacement $q(t) \rightarrow q(t - \pi/\omega)$. This invariance

³⁶ This notion of phase plane rotation is the origin of the term “Rotating Wave Approximation”, mentioned above. (The word “wave” is an artifact of this method’s wide application in classical and quantum optics.)

means that all other characteristics (including the amplitude) of the parametric oscillations excited with either of the two phases are *exactly* similar. At the dawn of the computer age (in the late 1950s and early 1960s), there were substantial attempts, especially in Japan, to use this property for storage and processing digital information coded in the binary-phase form. Though these attempts have not survived the competition with simpler approaches based on binary-voltage coding, some current trends in the development of prospective reversible and quantum computers may be traced back to that idea.

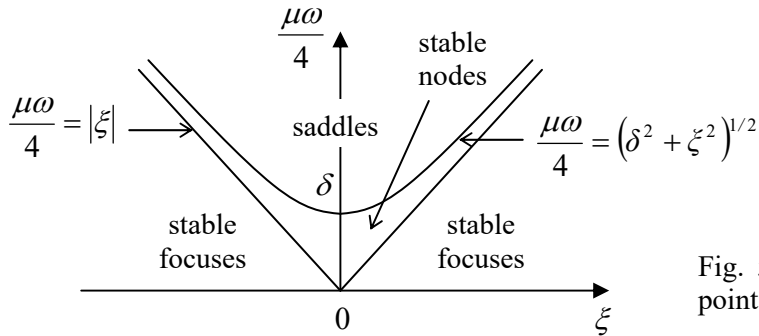


Fig. 5.10. Types of the trivial fixed point of a parametric oscillator.

5.7. Numerical approaches

If the amplitude of oscillations, for whatever reason, becomes so large that nonlinear terms in the equation describing an oscillator become comparable with its linear terms, numerical methods are virtually the only avenue available for their theoretical studies. In Hamiltonian 1D systems, such methods may be applied directly to Eq. (3.26), but dissipative and/or parametric systems typically lack such first integrals of motion, so that the initial differential equation has to be solved.

Let us discuss the general idea of such methods on the example of what mathematicians call the *Cauchy problem* (finding the solution for all moments of time, starting from the known initial conditions) for the first-order differential equation

$$\dot{q} = f(t, q). \quad (5.95)$$

(The generalization to a system of several such equations is straightforward.) Breaking the time axis into small equal steps h (Fig. 11) we can reduce the equation integration problem to finding the function's value at the next time point, $q_{n+1} \equiv q(t_{n+1}) \equiv q(t_n + h)$ from the previously found value $q_n = q(t_n)$ – and, if necessary, the values of q at other previous time steps.

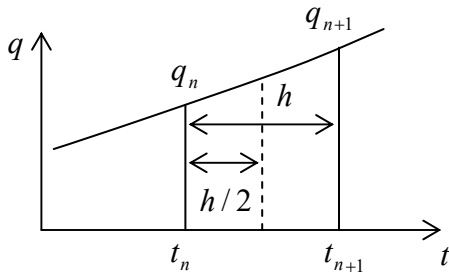


Fig. 5.11. The basic notions used at numerical integration of ordinary differential equations.

In the simplest approach (called the *Euler method*), q_{n+1} is found using the following formula:

$$q_{n+1} = q_n + k, \quad k \equiv h f(t_n, q_n). \quad (5.96)$$

This approximation is equivalent to the replacement of the genuine function $q(t)$, on the segment $[t_n, t_{n+1}]$, with the two first terms of its Taylor expansion in point t_n :

$$q(t_n + h) \approx q(t_n) + \dot{q}(t_n)h \equiv q(t_n) + hf(t_n, q_n). \quad (5.97)$$

This approximation has an error proportional to h^2 . One could argue that by making the step h sufficiently small, the Euler method's error might be made arbitrarily small, but even with all the number-crunching power of modern computer platforms, the CPU time necessary to reach sufficient accuracy may be too large for big problems.³⁷ Besides that, the increase of the number of time steps, which is necessary at $h \rightarrow 0$ at a fixed total time interval, increases the total rounding errors and eventually may cause an increase, rather than the reduction of the overall error of the computed result.

A more efficient way is to modify Eq. (96) to include the terms of the second order in h . There are several ways to do this, for example using the *2nd-order Runge-Kutta* method:

$$\begin{aligned} q_{n+1} &= q_n + k_2, \\ k_2 &\equiv h f\left(t_n + \frac{h}{2}, q_n + \frac{k_1}{2}\right), \quad k_1 \equiv h f(t_n, q_n). \end{aligned} \quad (5.98)$$

One can readily check that this method gives the exact result if the function $q(t)$ is a quadratic polynomial, and hence in the general case its errors are of the order of h^3 . We see that the main idea here is to first break the segment $[t_n, t_{n+1}]$ in half (see Fig. 11 again), evaluate the right-hand side of the differential equation (95) at the point intermediate (in both t and q) between the points number n and $(n+1)$, and then use this information to evaluate q_{n+1} .

The advantage of the Runge-Kutta approach over other second-order methods is that it may be readily extended to the 4th order, without an additional breakup of the interval $[t_n, t_{n+1}]$:

$$\begin{aligned} q_{n+1} &= q_n + \frac{1}{6}(k_1 + 2k_2 + 2k_3 + k_4), \\ k_4 &\equiv h f(t_n + h, q_n + k_3), \quad k_3 \equiv h f\left(t_n + \frac{h}{2}, q_n + \frac{k_2}{2}\right), \quad k_2 \equiv h f\left(t_n + \frac{h}{2}, q_n + \frac{k_1}{2}\right), \quad k_1 \equiv h f(t_n, q_n). \end{aligned} \quad (5.99)$$

This method has a much lower error, $O(h^5)$, without being not too cumbersome. These features have made the 4th-order Runge-Kutta the default method in most numerical libraries. Its extension to higher orders is possible, but requires more complex formulas, and is justified only for some special cases, e.g., very abrupt functions $q(t)$.³⁸ The most frequent enhancement of the method is an automatic adjustment of the step h to reach the pre-specified accuracy, but not make more calculations than necessary.

Figure 12 shows a typical example of an application of that method to the very simple problem of a damped linear oscillator, for two values of fixed time step h (expressed in terms of the number N of such steps per oscillation period). The black straight lines connect the adjacent points obtained by the

³⁷ In addition, the Euler method is not time-reversible – the handicap that may be essential for the integration of Hamiltonian systems described by systems of second-order differential equations. However, this drawback may be partly overcome by the so-called *leapfrogging* – the overlap of time steps h for a generalized coordinate and the corresponding generalized velocity.

³⁸ The most popular approaches in such cases are the *Richardson extrapolation*, the *Bulirsch-Stoer algorithm*, and a set of so-called *prediction-correction techniques*, e.g. the *Adams-Basforth-Moulton method* – see the literature recommended in MA Sec. 16(iii).

4^{th} -order Runge-Kutta method, while the points connected with the green straight lines represent the exact analytical solution (22). The plots show that a-few-percent errors start to appear only at as few as ~ 10 time steps per period, so that the method is indeed very efficient.

Let me hope that the discussion in the next section will make the conveniences and the handicaps of the numerical approach to problems of nonlinear dynamics very clear.

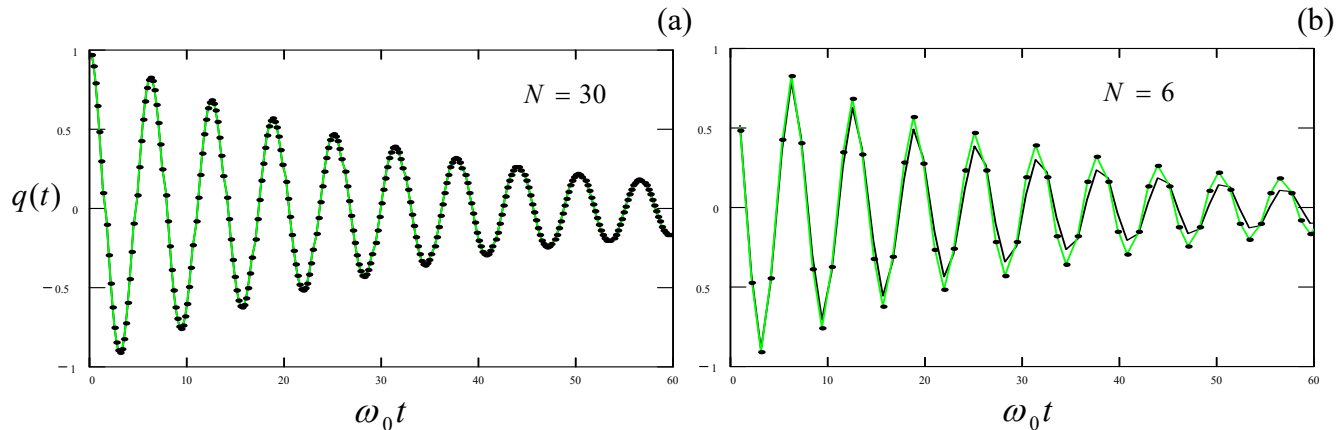


Fig. 5.12. Results of the Runge-Kutta solution of Eq. (6) (with $\delta/\omega_0 = 0.03$) for: (a) 30 and (b) 6 points per oscillation period. The results are shown by points; the black and green lines are only the guides for the eye.

5.8. Higher-harmonic and subharmonic oscillations

Figure 13 shows the numerically calculated³⁹ transient process and stationary oscillations in a linear oscillator and a very representative nonlinear system, the pendulum described by Eq. (42), both with the same ω_0 . Both systems are driven by a sinusoidal external force of the same amplitude and frequency – in this illustration, equal to the own small-oscillation frequency ω_0 of both systems. The plots show that despite a very substantial amplitude of the pendulum oscillations (the angle amplitude of about one radian), their waveform remains almost exactly sinusoidal.⁴⁰ On the other hand, the nonlinearity affects the oscillation amplitude very substantially. These results imply that the corresponding reduced equations (60), which are based on the assumption (41), may work very well far beyond its formal restriction $|q| \ll 1$.

Still, the waveform of oscillations in a nonlinear system always differs from that of the applied force – in our case, from the sine function of frequency ω . This fact is frequently formulated as the generation, by the system, of *higher harmonics*. Indeed, the Fourier theorem tells us that any non-sinusoidal periodic function of time may be represented as a sum of its basic harmonic of frequency ω , plus higher harmonics with frequencies $n\omega$, with integer $n > 1$.

Note that an effective generation of higher harmonics is only possible with adequate nonlinearity of the system. For example, consider the nonlinear term αq^3 used in the equations explored in Secs. 2

³⁹ All numerical results shown in this section have been obtained by the 4^{th} -order Runge-Kutta method with the automatic step adjustment that guarantees the relative error of the order of 10^{-4} – much smaller than the pixel size in the shown plots.

⁴⁰ In this particular case, the higher harmonic content is about 0.5%, dominated by the 3^{rd} harmonic, whose amplitude and phase are in a very good agreement with Eq. (50).

and 3. If the waveform $q(t)$ is sinusoidal, such term will have only the basic (1st) and the 3rd harmonics – see, e.g., Eq. (50). As another example, the “pendulum nonlinearity” $\sin q$ cannot produce, without a time-independent component (“bias”) in $q(t)$, any even harmonic, including the 2nd one. The most efficient generation of harmonics may be achieved using systems with the sharpest nonlinearities – e.g., semiconductor diodes whose current may follow an exponential dependence on the applied voltage through several orders of magnitude.⁴¹

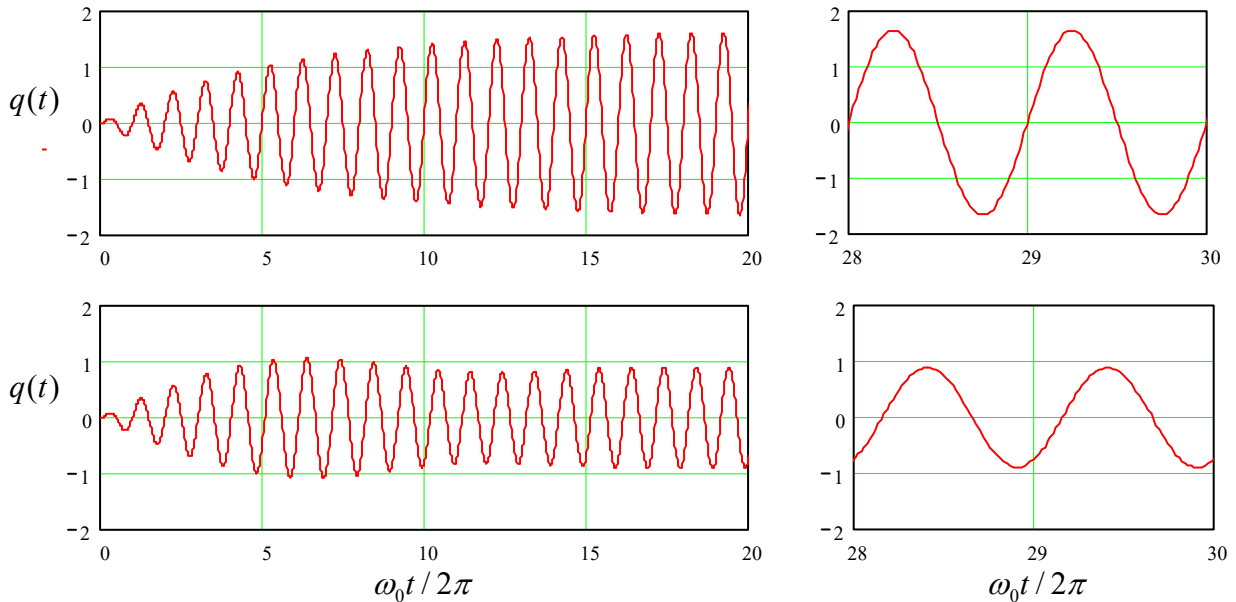


Fig. 5.13. The oscillations induced by a similar sinusoidal external force (turned on at $t = 0$) in two systems with the same small-oscillation frequency ω_0 and low damping: a linear oscillator (two top panels) and a pendulum (two bottom panels). In all cases, $\delta/\omega_0 = 0.03$, $f_0 = 0.1$, and $\omega = \omega_0$.

Another way to increase the contents of an n^{th} higher harmonic in a nonlinear oscillator is to reduce the excitation frequency ω to $\sim \omega_0/n$, so that the oscillator resonated at the frequency $n\omega \approx \omega_0$ of the desired harmonic. For example, Fig. 14a shows the oscillations in a pendulum described by the same Eq. (42), but driven at frequency $\omega = \omega_0/3$. One can see that the 3rd harmonic amplitude may be comparable with that of the basic harmonic, especially if the external frequency is additionally lowered (Fig. 14b) to accommodate for the deviation of the effective frequency $\omega_0(A)$ of own oscillations from its small-oscillation value ω_0 – see Eq. (49), Fig. 4, and their discussion in Sec. 2 above.

However, numerical modeling of nonlinear oscillators, as well as experiments with their physical implementations, bring more surprises. For example, the bottom panels of Fig. 15 show oscillations in a pendulum under the effect of a strong sinusoidal force with a frequency ω close to $3\omega_0$. One can see that at some parameter values and initial conditions, the system’s oscillation spectrum is heavily contributed (almost dominated) by the 3rd subharmonic, i.e. the Fourier component of frequency $\omega/3 \approx \omega_0$.

This counter-intuitive phenomenon of such *subharmonic generation* may be explained as follows. Let us assume that subharmonic oscillations of frequency $\omega/3 \approx \omega_0$ have somehow appeared, and coexist with the forced oscillations of frequency 3ω :

⁴¹ This method is used in practice, for example, for the generation of electromagnetic waves with frequencies in the terahertz range (10^{12} - 10^{13} Hz), which is still in wait for efficient electronic self-oscillators.

$$q(t) \approx A \cos \Psi + A_{\text{sub}} \cos \Psi_{\text{sub}}, \quad \text{where } \Psi \equiv \omega t - \varphi, \quad \Psi_{\text{sub}} \equiv \frac{\omega t}{3} - \varphi_{\text{sub}}. \quad (5.100)$$

Then the leading nonlinear term, αq^3 , of the Taylor expansion of the pendulum's nonlinearity $\sin q$, is proportional to

$$\begin{aligned} q^3 &= (A \cos \Psi + A_{\text{sub}} \cos \Psi_{\text{sub}})^3 \\ &\equiv A^3 \cos^3 \Psi + 3A^2 A_{\text{sub}} \cos^2 \Psi \cos \Psi_{\text{sub}} + 3AA_{\text{sub}}^2 \cos \Psi \cos^2 \Psi_{\text{sub}} + A_{\text{sub}}^3 \cos^3 \Psi_{\text{sub}}. \end{aligned} \quad (5.101)$$

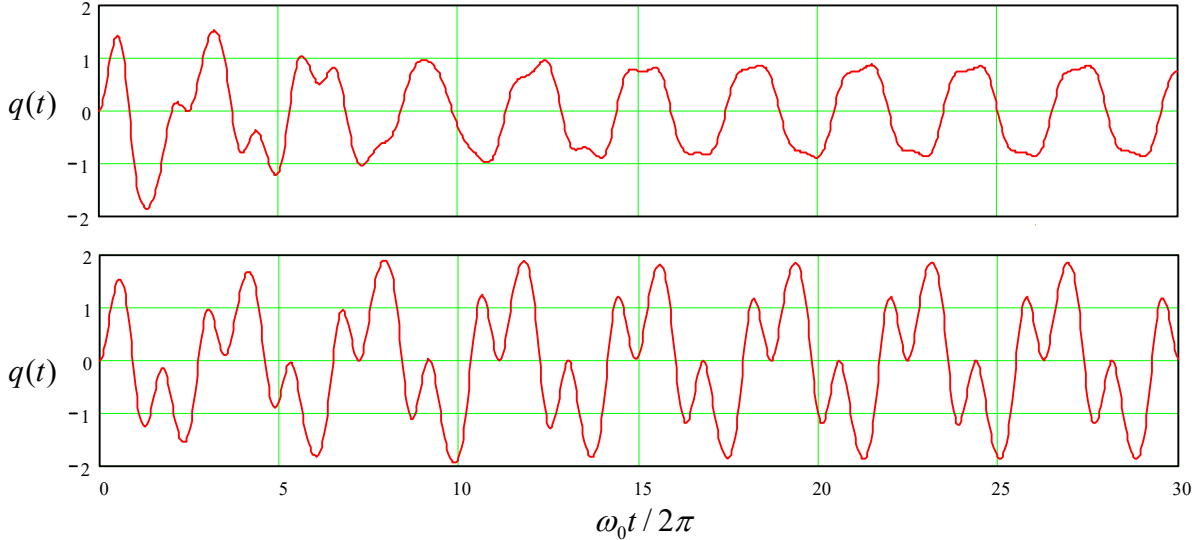


Fig. 5.14. The oscillations induced in a pendulum, with damping $\delta/\omega_0 = 0.03$, by a sinusoidal external force of amplitude $f_0 = 0.75$, and frequencies $\omega_0/3$ (top panel) and $0.8 \times \omega_0/3$ (bottom panel).

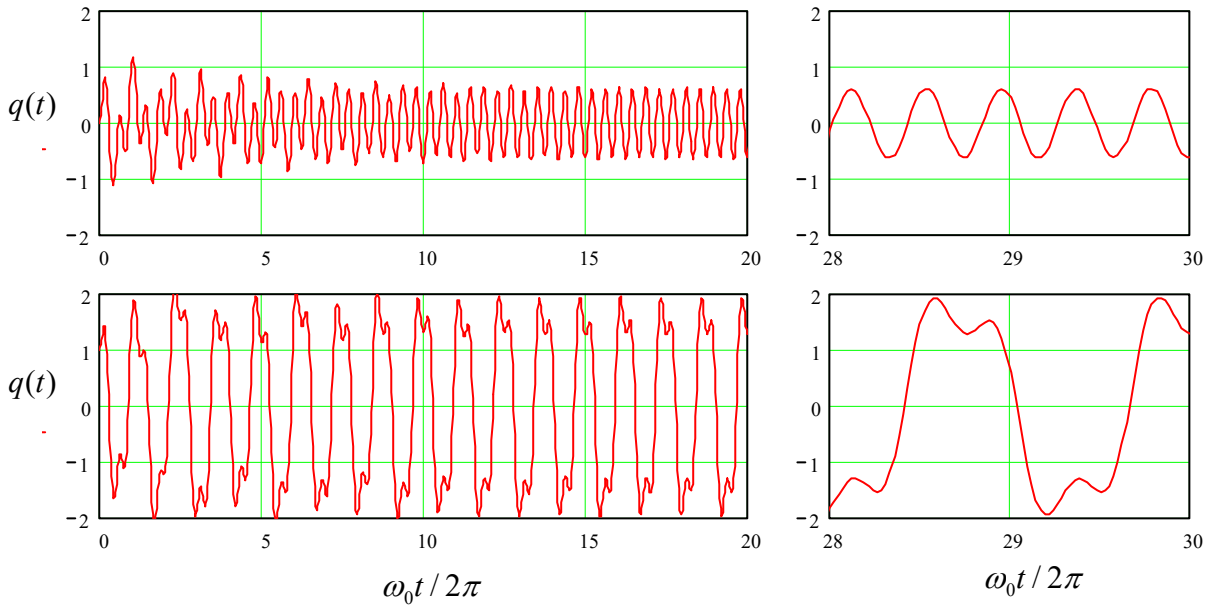


Fig. 5.15. The oscillations of a pendulum with $\delta/\omega_0 = 0.03$, driven by a sinusoidal external force of amplitude $f_0 = 3$ and frequency $0.8 \times 3\omega_0$, at initial conditions $q(0) = 0$ (the top panels) and $q(0) = 1$ (the bottom panels), with $dq/dt(0) = 0$ in both cases.

While the first and the last terms of the last expression depend only on the amplitudes of the individual components of oscillations, the two middle terms are more interesting, because they produce so-called *combinational frequencies* of the two components. For our case, the third term,

$$3A A_{\text{sub}}^2 \cos \Psi \cos^2 \Psi_{\text{sub}} = \frac{3}{4} A A_{\text{sub}}^2 \cos(\Psi - 2\Psi_{\text{sub}}) + \dots, \quad (5.102)$$

is of special importance, because it produces (besides other combinational frequencies) the subharmonic component with the total phase

$$\Psi - 2\Psi_{\text{sub}} = \frac{\omega t}{3} - \varphi + 2\varphi_{\text{sub}}. \quad (5.103)$$

Thus, this nonlinear contribution is synchronous with the subharmonic oscillations, and describes the interaction that can, within a certain range of the mutual phase shift between the Fourier components, deliver to them energy from the external force, so that the oscillations may be sustained. Note, however, that the amplitude of the term describing this energy exchange is proportional to the square of A_{sub} , and vanishes at the linearization of the equations of motion near the trivial fixed point. This means that the point is always stable, i.e., the 3rd subharmonic cannot be self-excited and always needs an initial ‘kick-off’ – compare the two panels of Fig. 15. The same is true for higher-order subharmonics.

Only the second subharmonic is a special case. Indeed, let us make a calculation similar to Eq. (102), by replacing Eq. (101) with

$$q(t) \approx A \cos \Psi + A_{\text{sub}} \cos \Psi_{\text{sub}}, \quad \text{where } \Psi \equiv \omega t - \varphi, \quad \Psi_{\text{sub}} \equiv \frac{\omega t}{2} - \varphi_{\text{sub}}, \quad (5.104)$$

for a nonlinear term proportional to q^2 :

$$q^2 = (A \cos \Psi + A_{\text{sub}} \cos \Psi_{\text{sub}})^2 = A^2 \cos^2 \Psi + 2AA_{\text{sub}} \cos \Psi \cos \Psi_{\text{sub}} + A_{\text{sub}}^2 \cos^2 \Psi_{\text{sub}}. \quad (5.105)$$

Here the combinational-frequency term capable of supporting the 2nd subharmonic,

$$2AA_{\text{sub}} \cos \Psi \cos \Psi_{\text{sub}} = AA_{\text{sub}} \cos(\Psi - \Psi_{\text{sub}}) = AA_{\text{sub}} \cos(\omega t - \varphi + \varphi_{\text{sub}}) + \dots, \quad (5.106)$$

is *linear* in the subharmonic’s amplitude, i.e. survives the linearization near the trivial fixed point. This means that the second subharmonic may arise spontaneously, from infinitesimal fluctuations.

Moreover, such excitation of the second subharmonic is very similar to the parametric excitation that was discussed in detail in Sec. 5, and this similarity is not coincidental. Indeed, let us redo the expansion (106) making a somewhat different assumption – that the oscillations are a sum of the forced oscillations at the external force’s frequency ω and an *arbitrary but weak* perturbation:

$$q(t) = A \cos(\omega t - \varphi) + \tilde{q}(t), \quad \text{with } |\tilde{q}| \ll A. \quad (5.107)$$

Then, neglecting the small term proportional to \tilde{q}^2 , we get

$$q^2 \approx A^2 \cos^2(\omega t - \varphi) + 2\tilde{q}(t)A \cos(\omega t - \varphi). \quad (5.108)$$

Besides the inconsequential phase shift φ , the second term in the last formula is *exactly* similar to the term describing the parametric effects in Eq. (75). This fact means that for a weak perturbation, a system with a quadratic nonlinearity in the presence of a strong ‘pumping’ signal of frequency ω is equivalent to a system with parameters changing in time with frequency ω . This fact is broadly used for the

parametric excitation at high (e.g., optical) frequencies, where the mechanical means of parameter modulation (see, e.g., Fig. 5) are not practicable. The necessary quadratic nonlinearity at optical frequencies may be provided by a *non-centrosymmetric nonlinear crystal*, e.g., the β -phase barium borate (BaB_2O_4).

Before finishing this section, let me elaborate a bit on a general topic: the relation between the numerical and analytical approaches to problems of dynamics – and to physics as a whole. We have just seen that sometimes numerical solutions, like those shown in Fig. 15b, may give vital clues for previously unanticipated phenomena such as the excitation of subharmonics. (The phenomenon of deterministic chaos, which will be discussed in Chapter 9 below, presents another example of such “numerical discoveries”.) One might also argue that for problems without exact analytical solutions, the numerical simulation may be an equally productive theoretical tool. These hopes are, however, muted by the general problem that is frequently called the *curse of dimensionality*,⁴² in which the last word refers to the number of parameters of the problem to be solved.⁴³

Indeed, let us have one more look at Fig. 15. OK, we have been lucky to find a new phenomenon, the 3rd subharmonic generation, for a particular set of parameters – in that case, five of them: $\delta/\omega_0 = 0.03$, $\omega/\omega_0 = 2.4$, $f_0 = 3$, $q(0) = 1$, and $dq/dt(0) = 0$. Could we tell anything about how common this effect is? Are subharmonics with different n possible in this system? The only way to address these questions computationally is to carry out similar numerical simulations at many points of the d -dimensional (in this case, $d = 5$) space of parameters. Say, we have decided that breaking the reasonable range of each parameter to $N = 100$ points is sufficient. (For many problems, even more points are necessary – see, e.g., Sec. 9.1.) Then the total number of numerical experiments to carry out is $N^d = (10^2)^5 = 10^{10}$ – not a simple task even for the powerful modern computing facilities. (Besides the pure number of required CPU cycles, consider the storage and analysis of the results.) For many important problems of nonlinear dynamics, e.g., turbulence, the parameter dimensionality d is substantially larger, and the computer resources necessary even for one numerical experiment, are much greater.

In view of the curse of dimensionality, approximate analytical considerations, like those outlined above for the subharmonic excitation, are invaluable. More generally, physics used to stand on two legs: experiment and analytical theory. The enormous progress of computer performance during the few last decades has provided it with one more support point (a tail? :-)) – numerical simulation. This does not mean we can afford to discard any of the legs we are standing on.

5.9. Relaxation oscillations

Such synthesis of the analytical and numerical approaches is also beneficial for the discussion of the last subject of this chapter: nonlinear oscillators with high damping. Perhaps the most interesting effect in such systems is the so-called *relaxation oscillations*, a type of self-oscillations with highly non-sinusoidal waveforms. Let me demonstrate them using our old friend, Eq. (62) with $\delta < 0$, whose

⁴² This term had been coined in 1957 by Richard Bellman in the context of the optimal control theory (where the dimensionality means the number of parameters affecting the system under control), but gradually has spread all over quantitative sciences using numerical methods.

⁴³ In EM Sec. 1.2, I discuss the implications of this “curse” for a different case, when both analytical and numerical solutions to the same problem are possible.

properties at $|\delta| \ll \omega_0$ were discussed in Sec. 4, because it will enable us to follow the crossover from the harmonic oscillations to the relaxation ones.

Figure 16 shows the results of the numerical solution of this equation for three characteristic values of its only substantial parameter⁴⁴

$$\mathcal{D} \equiv \frac{2|\delta|}{\omega_0} > 0. \quad (5.109)$$

(Indeed, if we introduce the natural dimensionless time $\tau \equiv \omega_0 t$, displacement $x \equiv q/q_0$, where q_0 is the scale defined in Eq. (64), and velocity $y \equiv dx/d\tau$, then the second-order differential equation (62) may be rewritten as the following system of two first-order equations:⁴⁵

$$\begin{aligned} \frac{dx}{d\tau} &= y, \\ \frac{dy}{d\tau} &= \mathcal{D}(1-y^2)y - x, \end{aligned} \quad (5.110)$$

with \mathcal{D} being its only parameter.) The left panels show phase planes $[x, dx/d\tau]$ of the oscillator, with their axes swapped⁴⁶ for the comparison with the right panels showing the displacement x as a function of time.

If the damping is low (top two panels), the system, launched from any initial state, gradually approaches the “limit cycle” of nearly-harmonic oscillations. Note that even for this, not extremely small value $\mathcal{D}=0.2$, deviations of the waveform $x(\tau)$ from a purely sinusoidal function of time are very small, its period (in the normalized time τ) is very close to the small-

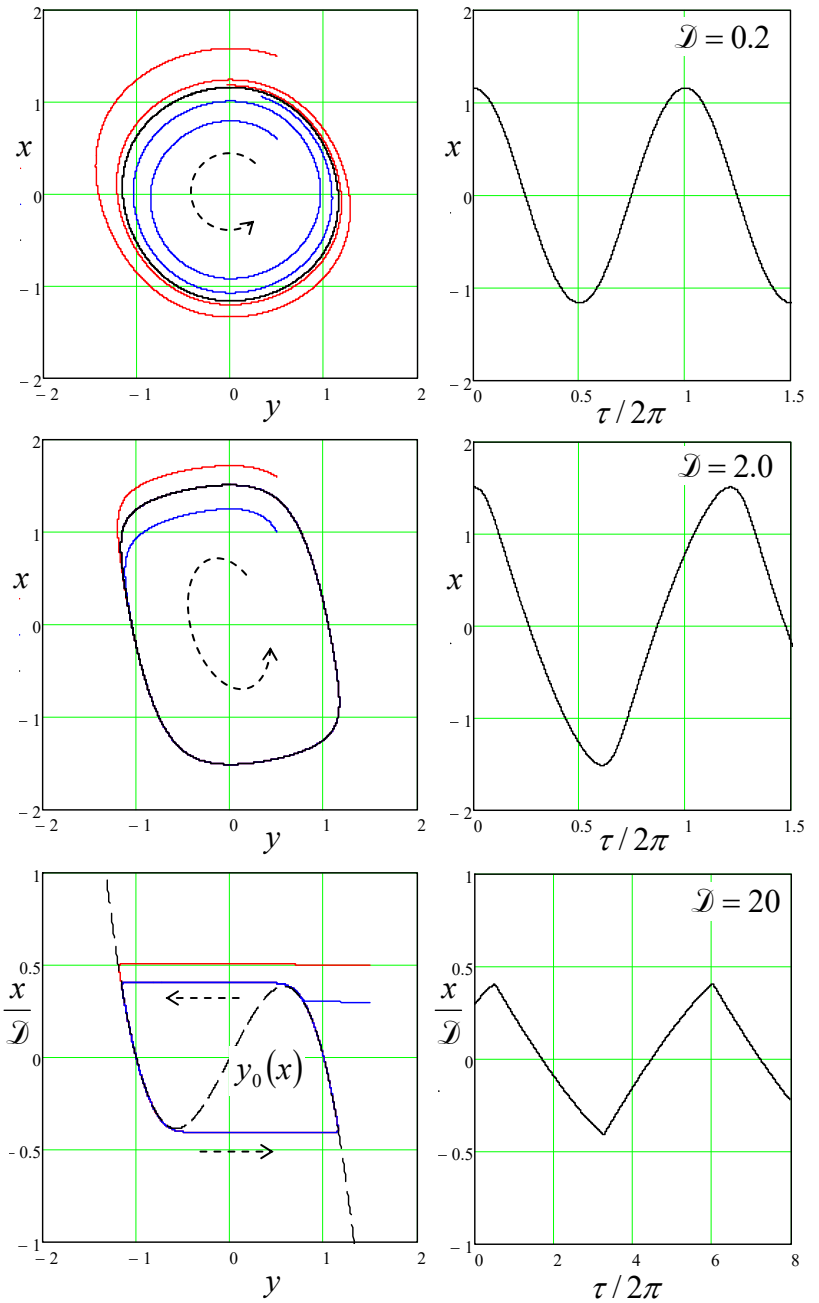


Fig. 5.16. The phase plane and time evolution of the self-oscillator described by Eqs. (62) and (110), for three values of the normalized damping (109). The red and blue lines show the system's dynamics for two representative initial conditions, while the black lines, its asymptotic behavior (the “limit cycles”).

⁴⁴ As Eq. (11) shows, for positive damping, this parameter is just the reciprocal Q -factor.

⁴⁵ A somewhat different equation used in 1926 by B. van der Pol to trace the harmonic-to-relaxation-oscillation crossover for the first time, may be also reduced to Eq. (110), using the so-called *Liénard's transformation*.

⁴⁶ Note that while on the usual phase plane, the free-oscillation process corresponds to a clockwise rotation of the representation point (see, e.g., Fig. 9), the axes' swap in Fig. 16 makes the rotation counterclockwise.

oscillation value 2π , and its amplitude is also very close to the value $2/\sqrt{3} \approx 1.15$ predicted by the van der Pol method – see Eq. (64).

As the damping is increased to $\mathcal{D} = 2$ (middle panels), the limit cycle's deviations from the circle, and hence the deviations of the waveform $x(\tau)$ from a sinusoidal function become obvious. Note also that while the oscillation period becomes somewhat *longer* than its small-oscillation value, the transient processes of approaching the limit cycle become *faster*.

The trend of these changes becomes evident on the bottom panels, showing case $\mathcal{D} = 20$. (The further increase of the damping does not change the results noticeably, only rescaling the displacements as $x \propto \mathcal{D}$ – note the vertical scale of the bottom panels of Fig. 16.) It shows that the oscillation period is dominated by two similar parts, of equal duration. During these two intervals of relatively slow evolution, the limit cycle closely follows the declining branches of the function

$$x = \mathcal{D}(1 - y_0^2)y_0, \quad (5.111)$$

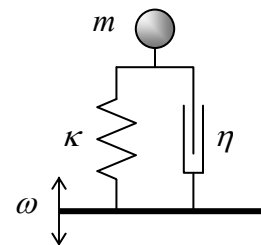
corresponding to the zero value of the first (and nominally, the largest) term in the second equation of the system (110) – see the dashed line on the left bottom panel. During these intervals, the displacement x grows in accordance with the first of these equations, with its right-hand part virtually equal to the y_0 corresponding to Eq. (111). Even without solving the resulting differential equation exactly,⁴⁷ we see that at these branches, with $y_0 \approx \pm 1$, $x(\tau)$ changes with a speed of the order of \mathcal{D} , and hence the path from the initial and final points of each branch, of a length $\Delta x \sim \mathcal{D}$, takes a time interval $\Delta\tau$ of the order of 1, just as the right panel shows.

As soon as the system reaches the branch's endpoint $x = \pm(2/3\sqrt{3})\mathcal{D} \approx \pm 0.385\mathcal{D}$, where the derivative dy_0/dx diverges, the balance of the terms on the right-hand part of the second Eq. (110) is not more possible, and its magnitude abruptly becomes of the order of $\mathcal{D} \gg 1$. As a result, the system jumps from this point to the opposite branch of the curve (111) very rapidly, during a time interval $\Delta\tau \sim \Delta y_0/\mathcal{D} \sim 1/\mathcal{D} \ll 1$, insufficient for x to change much. (The initial transient processes, i.e. the approaches to the limit cycle from almost arbitrary initial conditions, are equally fast, also with $x \approx \text{const.}$) Upon reaching the new branch, the system “relaxes” to a relatively slow evolution in the opposite direction (“relaxation oscillations”), and the process repeats again and again.

Such oscillations take place in a large number of practical mechanical systems and electronic devices, ranging from the bowed string musical instruments (including those of the violin family), to usual mechanical clocks, to car light blinkers. Many of them allow for simple analyses; to save time/space, let me leave a couple of problems of this type for the reader's exercise.

5.10. Exercise problems

5.1. A body of mass m is connected to its support not only with an elastic spring but also with a *damper* (say, an air brake) that provides a drag force obeying Eq. (5) – see the figure on the right.



⁴⁷ Its integration leads to an elementary function for $\tau(y)$, but transcendental equations for $y(\tau)$ and $x(\tau)$.

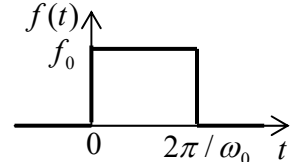
- (i) How to select the constants κ and η to minimize the body's vibrations caused by vertical oscillations of its support with frequency ω ?
(ii)^{*} What if the oscillations are random?

5.2. For a system with the response function given by Eq. (17):

- (i) prove Eq. (26), and
(ii) use an approach different from the one used in Sec. 1, to derive Eq. (34).

Hint: You may like to use the *Cauchy integral theorem* and the *Cauchy integral formula* for analytical functions of a complex variable.⁴⁸

- 5.3. A square-wave pulse of force (see the figure on the right) is exerted on a linear oscillator of frequency ω_0 (with no damping), initially at rest. Calculate the law of motion $q(t)$, sketch it, and interpret the result.



5.4. At $t = 0$, a sinusoidal external force $F(t) = F_0 \cos \omega t$, starts to be exerted on a linear oscillator with frequency ω_0 and damping δ , which was at rest at $t \leq 0$.

- (i) Derive the general expression for the time evolution of the oscillator's displacement, and interpret the result.
(ii) Spell out the result for the exact resonance ($\omega = \omega_0$) in a system with low damping ($\delta \ll \omega_0$), and, in particular, explore the limit $\delta \rightarrow 0$.

5.5. A pulse of external force $F(t)$, with a finite duration \mathcal{T} , is exerted on a linear oscillator, initially at rest in its equilibrium position. Neglecting dissipation, calculate the change of the oscillator's energy, using two different approaches, and compare the results.

5.6. A bead may slide, without friction, in a vertical plane along a parabolic curve $y = \alpha x^2/2$, in a uniform gravity field $\mathbf{g} = -g\mathbf{n}_y$. Calculate the frequency of its free oscillations as a function of their amplitude A , in the first nonvanishing approximation in $A \rightarrow 0$, using two different approaches.

5.7. For a system with the Lagrangian function

$$L = \frac{m}{2} \dot{q}^2 - \frac{\kappa}{2} q^2 + \varepsilon \dot{q}^4,$$

with small parameter ε , use the harmonic balance method to find the frequency of free oscillations as a function of their amplitude.

5.8. Use a different approach to derive Eq. (49) for the frequency of free oscillations of the system described by Eq. (43) with $\delta = 0$, in the first nonvanishing approximation in the small parameter $\alpha A^2/\omega_0^2 \ll 1$.

5.9. On the plane $[a_1, a_2]$ of two real, time-independent parameters a_1 and a_2 , find the regions in which the fixed point of the following system of equations,

⁴⁸ See, e.g., MA Eq. (15.1).

$$\begin{aligned}\dot{q}_1 &= a_1(q_2 - q_1), \\ \dot{q}_2 &= a_2 q_1 - q_2,\end{aligned}$$

is unstable, and sketch the regions of each fixed point type – stable and unstable nodes, focuses, etc.

5.10. Solve Problem 4(ii) using the reduced equations (57), and compare the result with the exact solution.

5.11. Use the reduced equations to analyze forced oscillations in an oscillator with weak nonlinear damping, described by the following equation:

$$\ddot{q} + 2\delta\dot{q} + \omega_0^2 q + \beta\dot{q}^3 = f_0 \cos \omega t,$$

with $\omega \approx \omega_0$; $\beta, \delta > 0$; and $\beta\omega A^2 \ll 1$. In particular, find the stationary amplitude of the forced oscillations and analyze their stability. Discuss the effect(s) of the nonlinear term on the resonance.

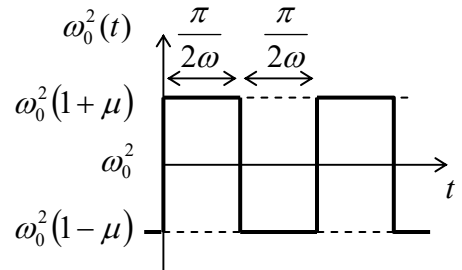
5.12. Within the approach discussed in Sec. 4, calculate the average frequency of a self-oscillator outside of the range of its phase-locking by a small external sinusoidal force.

5.13.* Use the reduced equations to analyze the stability of the forced nonlinear oscillations described by the Duffing equation (43). Relate the result to the slope of resonance curves (Fig. 4).

5.14. Use the van der Pol method to find the condition of parametric excitation of the oscillator described by the following equation:

$$\ddot{q} + 2\delta\dot{q} + \omega_0^2(t)q = 0,$$

where $\omega_0^2(t)$ is the square-wave function shown in the figure on the right, with $\omega \approx \omega_0$.



5.15. Use the van der Pol method to analyze parametric excitation of an oscillator with weak nonlinear damping, described by the following equation:

$$\ddot{q} + 2\delta\dot{q} + \beta\dot{q}^3 + \omega_0^2(1 + \mu \cos 2\omega t)q = 0,$$

with $\omega \approx \omega_0$; $\beta, \delta > 0$; and $\mu, \beta\omega A^2 \ll 1$. In particular, find the amplitude of stationary oscillations and analyze their stability.

5.16.* Adding nonlinear term αq^3 to the left-hand side of Eq. (75),

- (i) find the corresponding addition to the reduced equations,
- (ii) calculate the stationary amplitude A of the parametric oscillations,
- (iii) find the type and stability of each fixed point of the reduced equations,
- (iv) sketch the Poincaré phase planes of the system in major parameter regions.

5.17. Use the van der Pol method to find the condition of parametric excitation of an oscillator with weak modulation of both the effective mass $m(t) = m_0(1 + \mu_m \cos 2\omega t)$ and the effective spring constant $\kappa(t) = \kappa_0[1 + \mu_\kappa \cos(2\omega t - \psi)]$, with the same frequency $2\omega \approx 2\omega_0$, at arbitrary modulation depths

ratio μ_m/μ_k and phase shift ψ . Interpret the result in terms of modulation of the instantaneous frequency $\omega(t) \equiv [\kappa(t)/m(t)]^{1/2}$ and the mechanical impedance $Z(t) \equiv [\kappa(t)m(t)]^{1/2}$ of the oscillator.

5.18.* Find the condition of parametric excitation of a nonlinear oscillator described by the following equation:

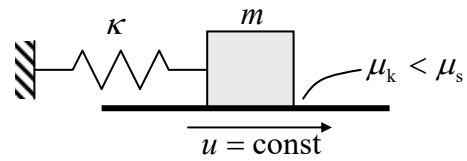
$$\ddot{q} + 2\delta\dot{q} + \omega_0^2 q + \gamma q^2 = f_0 \cos 2\omega t,$$

with sufficiently small δ , γ , f_0 , and $\xi \equiv \omega - \omega_0$.

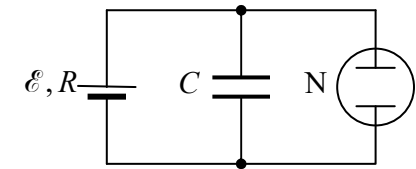
5.19. Find the condition of stability of the equilibrium point $q = 0$ of a parametric oscillator described by Eq. (75), in the limit when $\delta \ll |\omega_0| \ll \omega$ and $\mu \ll 1$. Use the result to analyze the stability of the Kapitza pendulum mentioned in Sec. 5.

5.20.* Use numerical simulation to explore phase-plane trajectories $[q, \dot{q}]$ of an autonomous pendulum described by Eq. (42) with $f_0 = 0$, for both low and high damping, and discuss their most significant features.

5.21. Analyze relaxation oscillations of the system shown in the figure on the right: an elastic spring prevents a block of mass m from being carried away by a horizontal conveyer belt moving with a constant velocity u . Assume that the coefficient μ_k of the kinematic friction between the block and the belt is lower than the static friction coefficient μ_s .



5.22. The figure on the right shows the electric circuit of the simplest relaxation oscillator. In it, N is a bistable circuit element that switches very rapidly from its very-high-resistance state to a very-low-resistance state as the voltage across it is increased beyond some value V_t , and switches back as the voltage is decreased below another value $V_t' < V_t$.⁴⁹ Calculate the waveform and the time period of voltage oscillations in the circuit.



Hint: The solution of this problem requires a very basic understanding of electric circuits, including the e.m.f. ϵ and internal resistance R of a dc current source such as an electric battery.

⁴⁹ This is a good model for many two-terminal gas-discharge devices (such as *glow lamps*), whose effective resistance may drop by up to 5 orders of magnitude when the discharge has been activated by voltage $V > V_t$. In usual neon glow lamps, V_t' is about 30% lower than V_t .

This page is
intentionally left
blank

Chapter 6. From Oscillations to Waves

In this chapter, the discussion of oscillations is extended to systems with two and more degrees of freedom. This extension naturally leads to another key notion of physics – waves, so far in simple, mostly 1D systems. (In the next chapter, this discussion will be extended to more complex elastic continua.) However, even the limited scope of the models analyzed in this chapter will still enable us to discuss such important general aspects of waves as their dispersion, phase and group velocities, impedance, reflection, and attenuation.

6.1. Two coupled oscillators

Let us discuss oscillations in systems with several degrees of freedom, starting from the simplest case of two linear (harmonic), dissipation-free, 1D oscillators. If the oscillators are independent of each other, the Lagrangian function of their system may be represented as a sum of two independent terms of the type (5.1):

$$L = L_1 + L_2, \quad L_{1,2} = T_{1,2} - U_{1,2} = \frac{m_{1,2}}{2} \dot{q}_{1,2}^2 - \frac{\kappa_{1,2}}{2} q_{1,2}^2. \quad (6.1)$$

Correspondingly, Eqs. (2.19) for $q_j = q_{1,2}$ yields two independent equations of motion of the oscillators, each one being similar to Eq. (5.2):

$$m_{1,2} \ddot{q}_{1,2} + m_{1,2} \Omega_{1,2}^2 q_{1,2} = 0, \quad \text{where } \Omega_{1,2}^2 = \frac{\kappa_{1,2}}{m_{1,2}}. \quad (6.2)$$

(In the context of what follows, $\Omega_{1,2}$ are sometimes called the *partial frequencies*.) This means that in this simplest case, an arbitrary motion of the system is just a sum of independent sinusoidal oscillations at two frequencies equal to the partial frequencies (2).

However, as soon as the oscillators are *coupled* (i.e. interact), the full Lagrangian L contains an additional *mixed* term L_{int} depending on both generalized coordinates q_1 and q_2 and/or generalized velocities. As a simple example, consider the system shown in Fig. 1, where two small masses $m_{1,2}$ are constrained to move in only one direction (shown horizontal), and are kept between two stiff walls with three springs.

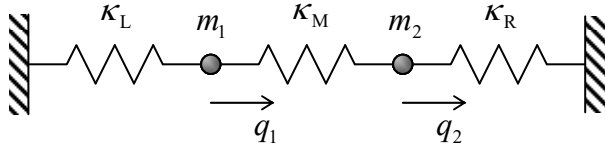


Fig. 6.1. A simple system of two coupled linear oscillators.

In this case, the kinetic energy is still separable, $T = T_1 + T_2$, but the total potential energy, consisting of the elastic energies of three springs, is not:

$$U = \frac{\kappa_L}{2} q_1^2 + \frac{\kappa_M}{2} (q_1 - q_2)^2 + \frac{\kappa_R}{2} q_2^2, \quad (6.3a)$$

where $q_{1,2}$ are the horizontal displacements of the particles from their equilibrium positions. It is convenient to rewrite this expression as

$$U = \frac{\kappa_1}{2}q_1^2 + \frac{\kappa_2}{2}q_2^2 - \kappa q_1 q_2, \quad \text{where } \kappa_1 \equiv \kappa_L + \kappa_M, \quad \kappa_2 \equiv \kappa_R + \kappa_M, \quad \kappa \equiv \kappa_M. \quad (6.3b)$$

This formula shows that the Lagrangian function $L = T - U$ of this system contains, besides the partial terms (1), a *bilinear* interaction term:

$$L = L_1 + L_2 + L_{\text{int}}, \quad L_{\text{int}} = \kappa q_1 q_2. \quad (6.4)$$

The resulting Lagrange equations of motion are as follows:

$$\begin{aligned} m_1 \ddot{q}_1 + m_1 \Omega_1^2 q_1 &= \kappa q_2, \\ m_2 \ddot{q}_2 + m_2 \Omega_2^2 q_2 &= \kappa q_1. \end{aligned} \quad (6.5)$$

Linearly
coupled
oscillators

Thus the interaction leads to an effective generalized force κq_2 exerted on subsystem 1 by subsystem 2, and the reciprocal effective force κq_1 .

Please note two important aspects of this (otherwise rather simple) system of equations. First, in contrast to the *actual* physical interaction forces (such as $F_{12} = -F_{21} = \kappa_M(q_2 - q_1)$ for our system¹) the *effective* forces on the right-hand sides of Eqs. (5) do not obey the 3rd Newton law. Second, the forces are proportional to the same coefficient κ ; this feature is a result of the general bilinear structure (4) of the interaction energy, rather than of any special symmetry.

From our prior discussions, we already know how to solve Eqs. (5), because it is still a system of linear and homogeneous differential equations, so that its general solution is a sum of particular solutions of the form similar to Eqs. (5.88),

$$q_1 = c_1 e^{\lambda t}, \quad q_2 = c_2 e^{\lambda t}, \quad (6.6)$$

with all possible values of λ . These values may be found by plugging Eq. (6) into Eqs. (5), and requiring the resulting system of two linear, homogeneous algebraic equations for the distribution coefficients $c_{1,2}$,

$$\begin{aligned} m_1 \lambda^2 c_1 + m_1 \Omega_1^2 c_1 &= \kappa c_2, \\ m_2 \lambda^2 c_2 + m_2 \Omega_2^2 c_2 &= \kappa c_1, \end{aligned} \quad (6.7)$$

to be self-consistent. In our particular case, we get a characteristic equation,

$$\begin{vmatrix} m_1(\lambda^2 + \Omega_1^2) & -\kappa \\ -\kappa & m_2(\lambda^2 + \Omega_2^2) \end{vmatrix} = 0, \quad (6.8)$$

that is quadratic in λ^2 , and thus has a simple analytical solution:

$$\begin{aligned} (\lambda^2)_{\pm} &= -\frac{1}{2}(\Omega_1^2 + \Omega_2^2) \mp \left[\frac{1}{4}(\Omega_1^2 + \Omega_2^2)^2 - \Omega_1^2 \Omega_2^2 + \frac{\kappa^2}{m_1 m_2} \right]^{1/2} \\ &\equiv -\frac{1}{2}(\Omega_1^2 + \Omega_2^2) \mp \left[\frac{1}{4}(\Omega_1^2 - \Omega_2^2)^2 + \frac{\kappa^2}{m_1 m_2} \right]^{1/2}. \end{aligned} \quad (6.9)$$

¹ Using these expressions, Eqs. (5) may be readily obtained from the Newton laws, but the Lagrangian approach used above will make their generalization, in the next section, more straightforward.

According to Eqs. (2) and (3b), for any positive spring constants, the product $\Omega_1\Omega_2 = (\kappa_L + \kappa_M)(\kappa_R + \kappa_M)/(m_1m_2)^{1/2}$ is always larger than $\kappa/(m_1m_2)^{1/2} = \kappa_M/(m_1m_2)^{1/2}$, so that the square root in Eq. (9) is always smaller than $(\Omega_1^2 + \Omega_2^2)/2$. As a result, both values of λ^2 are negative, i.e. the general solution to Eq. (5) is a sum of four terms, each proportional to $\exp\{\pm i\omega_{\pm}t\}$, where both *normal frequencies* (or “natural frequencies”, or “eigenfrequencies”) $\omega_{\pm} \equiv i\lambda_{\pm}$ are real:

Anticrossing:
example

$$\omega_{\pm}^2 \equiv -\lambda_{\pm}^2 = \frac{1}{2}(\Omega_1^2 + \Omega_2^2) \pm \left[\frac{1}{4}(\Omega_1^2 - \Omega_2^2)^2 + \frac{\kappa^2}{m_1m_2} \right]^{1/2}. \quad (6.10)$$

A plot of these eigenfrequencies as a function of one of the partial frequencies (say, Ω_1), with the other partial frequency fixed, gives us the famous *anticrossing* (also called the “avoided crossing” or “non-crossing”) *diagram* – see Fig. 2. One can see that at weak coupling, the normal frequencies ω_{\pm} are close to the partial frequencies $\Omega_{1,2}$ everywhere besides a narrow range near the anticrossing point $\Omega_1 = \Omega_2$. Most remarkably, at passing through this region, ω_{\pm} smoothly “switches” from following Ω_2 to following Ω_1 and vice versa.

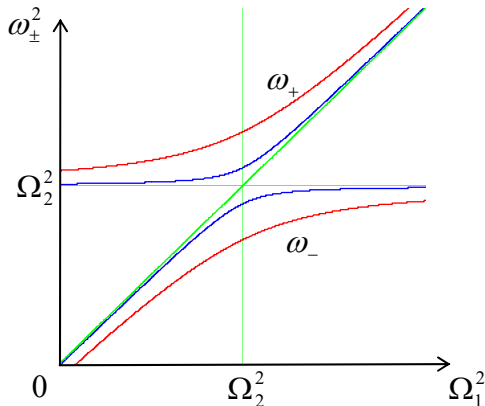


Fig. 6.2. The anticrossing diagram for two values of the normalized coupling strength $\kappa/(m_1m_2)^{1/2}\Omega_2^2$: 0.3 (red lines) and 0.1 (blue lines). In this plot, Ω_1 is assumed to be changed by varying κ_1 rather than m_1 , but in the opposite case, the diagram is qualitatively similar.

The reason for this counterintuitive behavior may be found by examining the distribution coefficients $c_{1,2}$ corresponding to each branch of the diagram, which may be obtained by plugging the corresponding value of $\lambda_{\pm} = -i\omega_{\pm}$ back into Eqs. (7). For example, at the anticrossing point $\Omega_1 = \Omega_2 \equiv \Omega$, Eq. (10) is reduced to

$$\omega_{\pm}^2 = \Omega^2 \pm \frac{\kappa}{(m_1m_2)^{1/2}} = \Omega^2 \left(1 \pm \frac{\kappa}{(\kappa_1\kappa_2)^{1/2}} \right). \quad (6.11)$$

Plugging this expression back into any of Eqs. (7), we see that for the two branches of the anticrossing diagram, the distribution coefficient ratio is the same by magnitude but opposite by sign:

$$\left(\frac{c_1}{c_2} \right)_{\pm} = \mp \left(\frac{m_2}{m_1} \right)^{1/2}, \quad \text{at } \Omega_1 = \Omega_2. \quad (6.12)$$

In particular, if the system is symmetric ($m_1 = m_2$, $\kappa_L = \kappa_R$), then at the upper branch, corresponding to $\omega_+ > \omega_-$, we get $c_1 = -c_2$. This means that in this so-called *hard mode*,² masses oscillate

² In physics, the term “mode” (or “normal mode”) is typically used to describe the distribution of a variable in space, at its oscillations with a single frequency. In our current case, when the notion of space is reduced to two oscillator numbers, each mode is fully specified by the corresponding ratio of two distribution coefficients $c_{1,2}$.

in anti-phase: $q_1(t) \equiv -q_2(t)$. The resulting substantial extension/compression of the middle spring (see Fig. 1 again) yields additional returning force which increases the oscillation frequency. On the contrary, at the lower branch, corresponding to ω_- , the particle oscillations are in phase: $c_1 = c_2$, i.e. $q_1(t) \equiv q_2(t)$, so that the middle spring is neither stretched nor compressed at all. As a result, in this *soft mode*, the oscillation frequency ω is lower than ω_+ , and does not depend on κ_M :

$$\omega_-^2 = \Omega^2 - \frac{\kappa}{m} = \frac{\kappa_L}{m} = \frac{\kappa_R}{m}. \quad (6.13)$$

Note that for both modes, the oscillations equally engage both particles.

Far from the anticrossing point, the situation is completely different. Indeed, a similar calculation of $c_{1,2}$ shows that on each branch of the diagram, the magnitude of one of the distribution coefficients is much larger than that of its counterpart. Hence, in this limit, any particular mode of oscillations involves virtually only one particle. A slow change of system parameters, bringing it through the anticrossing, leads, first, to a maximal delocalization of each mode at $\Omega_1 = \Omega_2$, and then to a restoration of the localization, but in a different partial degree of freedom.

We could readily carry out similar calculations for the case when the systems are coupled via their velocities, $L_{\text{int}} = m\dot{q}_1\dot{q}_2$, where m is a coupling coefficient – not necessarily a certain physical mass.³ The results are generally similar to those discussed above, again with the maximum level splitting at $\Omega_1 = \Omega_2 \equiv \Omega$:

$$\omega_\pm^2 = \frac{\Omega^2}{1 \mp |m|/(m_1 m_2)^{1/2}} \approx \Omega^2 \left[1 \pm \frac{|m|}{(m_1 m_2)^{1/2}} \right], \quad (6.14)$$

the last relation being valid for weak coupling. The generalization to the case of simultaneous coordinate and velocity coupling is also straightforward – see the next section.⁴

One more property of weakly coupled oscillators is a periodic slow transfer of energy between them, especially strong at or near the anticrossing point $\Omega_1 = \Omega_2$. Let me leave an analysis of such transfer for the reader's exercise. (Due to the importance of this effect for quantum mechanics, it will be discussed in detail in the QM part of this series.)

6.2. N coupled oscillators

The calculations of the previous section may be readily generalized to the case of an arbitrary number (say, N) of coupled harmonic oscillators, with an arbitrary type of coupling. It is obvious that in this case Eq. (4) should be replaced with

³ In mechanics, with $q_{1,2}$ standing for the actual displacements of particles, such coupling is not very natural, but there are many dynamic systems of non-mechanical nature in which such coupling is the most natural one. The simplest example is the system of two *LC* ("tank") circuits, with either capacitive or inductive coupling. Indeed, as was discussed in Sec. 2.2, for such a system, the very notions of the potential and kinetic energies are conditional and interchangeable.

⁴ Note that the anticrossing diagram shown in Fig. 2, is even more ubiquitous in quantum mechanics, because, due to the time-oscillatory character of the Schrödinger equation solutions, a weak coupling of any two quantum states leads to qualitatively similar behavior of the eigenfrequencies ω_\pm of the system, and hence of its *eigenenergies* ("energy levels") $E_\pm = \hbar\omega_\pm$ of the system.

$$L = \sum_{j=1}^N L_j + \sum_{j,j'=1}^N L_{jj'}. \quad (6.15)$$

Moreover, we can generalize the above expression for the mixed terms $L_{jj'}$, taking into account their possible dependence not only on the generalized coordinates but also on the generalized velocities, in a bilinear form similar to Eq. (4). The resulting Lagrangian may be represented in a compact form,

$$L = \sum_{j,j'=1}^N \left(\frac{m_{jj'}}{2} \dot{q}_j \dot{q}_{j'} - \frac{\kappa_{jj'}}{2} q_j q_{j'} \right), \quad (6.16)$$

where the off-diagonal terms are index-symmetric: $m_{jj'} = m_{j'j}$, $\kappa_{jj'} = \kappa_{j'j}$, and the factors $1/2$ compensate for the double-counting of each term with $j \neq j'$, at the summation over two independently running indices. One may argue that Eq. (16) is quite general if we still want to keep the equations of motion linear – as they always are if the oscillations are small enough.

Plugging Eq. (16) into the general form (2.19) of the Lagrange equation, we get N equations of motion of the system, one for each value of the index $j' = 1, 2, \dots, N$:

$$\sum_{j=1}^N (m_{jj'} \ddot{q}_j + \kappa_{jj'} q_j) = 0. \quad (6.17)$$

Just as in the previous section, let us look for a particular solution to this system in the form

$$q_j = c_j e^{\lambda t}. \quad (6.18)$$

As a result, we are getting a system of N linear, homogeneous algebraic equations,

$$\sum_{j=1}^N (m_{jj'} \lambda^2 + \kappa_{jj'}) c_j = 0, \quad (6.19)$$

for the set of N distribution coefficients c_j . The condition that this system is self-consistent is that the determinant of its matrix equals zero:

$$\text{Det}(m_{jj'} \lambda^2 + \kappa_{jj'}) = 0. \quad (6.20)$$

This characteristic equation is an algebraic equation of degree N for λ^2 , and so has N roots $(\lambda^2)_n$. For any Hamiltonian system with stable equilibrium, the matrices $m_{jj'}$ and $\kappa_{jj'}$ ensure that all these roots are real and negative. As a result, the general solution to Eq. (17) is the sum of $2N$ terms proportional to $\exp\{\pm i\omega_n t\}$, $n = 1, 2, \dots, N$, where all N normal frequencies ω_n are real.

Plugging each of these $2N$ values of $\lambda = \pm i\omega_n$ back into a particular set of linear equations (17), one can find the corresponding sets of distribution coefficients $c_{j\pm}$. Generally, the coefficients are complex, but to keep $q_j(t)$ real, the coefficients c_{j+} corresponding to $\lambda = +i\omega_n$, and c_{j-} corresponding to $\lambda = -i\omega_n$ have to be complex-conjugate of each other. Since the sets of the distribution coefficients may be different for each λ_n , they should be marked with two indices, j and n . Thus, at general initial conditions, the time evolution of the j^{th} generalized coordinate may be represented as

$$q_j = \frac{1}{2} \sum_{n=1}^N \left(c_{jn} \exp\{+i\omega_n t\} + c_{jn}^* \exp\{-i\omega_n t\} \right) \equiv \text{Re} \sum_{n=1}^N c_{jn} \exp\{i\omega_n t\}. \quad (6.21)$$

This formula shows very clearly again the physical sense of the distribution coefficients c_{jn} : a set of these coefficients, with different values of index j but the same mode number n , gives the complex amplitudes of oscillations of the coordinates in this mode, i.e. for the special initial conditions that ensure purely sinusoidal motion of all the system, with frequency ω_n .

The calculation of the normal frequencies and the corresponding modes (distribution coefficient sets) of a particular coupled system with many degrees of freedom from Eqs. (19)–(20) is a task that frequently may be only done numerically.⁵ Let us discuss just two particular but very important cases. First, let all the coupling coefficients be small in the following sense: $|m_{jj'}| \ll m_j \equiv m_{jj}$ and $|\kappa_{jj'}| \ll \kappa_j \equiv \kappa_{jj}$, for all $j \neq j'$, and all partial frequencies $\Omega_j \equiv (\kappa_j/m_j)^{1/2}$ be not too close to each other:

$$\frac{|\Omega_j^2 - \Omega_{j'}^2|}{\Omega_j^2} \gg \frac{|\kappa_{jj'}|}{\kappa_j}, \frac{|m_{jj'}|}{m_j}, \quad \text{for all } j \neq j'. \quad (6.22)$$

(Such situation frequently happens if parameters of the system are “random” in the sense that they do not follow any special, simple rule – for example, the one resulting from some simple symmetry of the system.) Results of the previous section imply that in this case, the coupling does not produce a noticeable change in the oscillation frequencies: $\{\omega_n\} \approx \{\Omega_j\}$. In this situation, oscillations at each eigenfrequency are heavily concentrated in one degree of freedom, i.e. in each set of the distribution coefficients c_{jn} (for a given n), one coefficient’s magnitude is much larger than all others.

Now let the conditions (22) be valid for all but one pair of partial frequencies, say Ω_1 and Ω_2 , while these two frequencies are so close that the coupling of the corresponding partial oscillators becomes essential. In this case, the approximation $\{\omega_n\} \approx \{\Omega_j\}$ is still valid for all other degrees of freedom, and the corresponding terms may be neglected in Eqs. (19) for $j = 1$ and 2. As a result, we return to Eqs. (7) (perhaps generalized for velocity coupling) and hence to the anticrossing diagram (Fig. 2) discussed in the previous section. As a result, an extended change of only one partial frequency (say, Ω_1) of a weakly coupled system produces a sequence of eigenfrequency anticrossings – see Fig. 3.

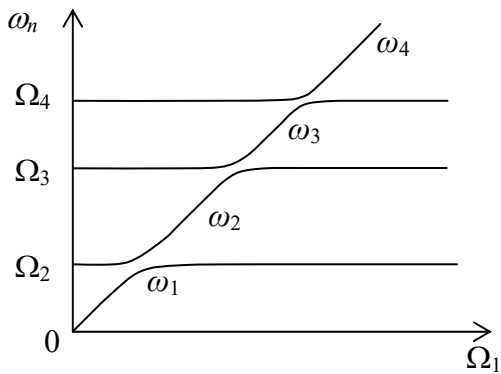


Fig. 6.3. The level anticrossing in a system of N weakly coupled oscillators – schematically.

6.3. 1D waves

The second case when the general results of the last section may be simplified are coupled systems with a considerable degree of symmetry. Perhaps the most important of them are uniform

⁵ Fortunately, very effective algorithms have been developed for this *matrix diagonalization* task – see, e.g., references in MA Sec. 16(iii)-(iv). For example, the popular MATLAB software package was initially created exactly for this purpose. (“MAT” in its name stood for “matrix” rather than “mathematics”).

systems that may sustain traveling and standing *waves*. Figure 4a shows a simple example of such a system – a long uniform chain of particles, of mass m , connected with light, elastic springs, pre-stretched with the tension force \mathcal{T} to have equal lengths d . (This system may be understood as a natural generalization of the two-particle system considered in Sec. 1 – cf. Fig. 1.)

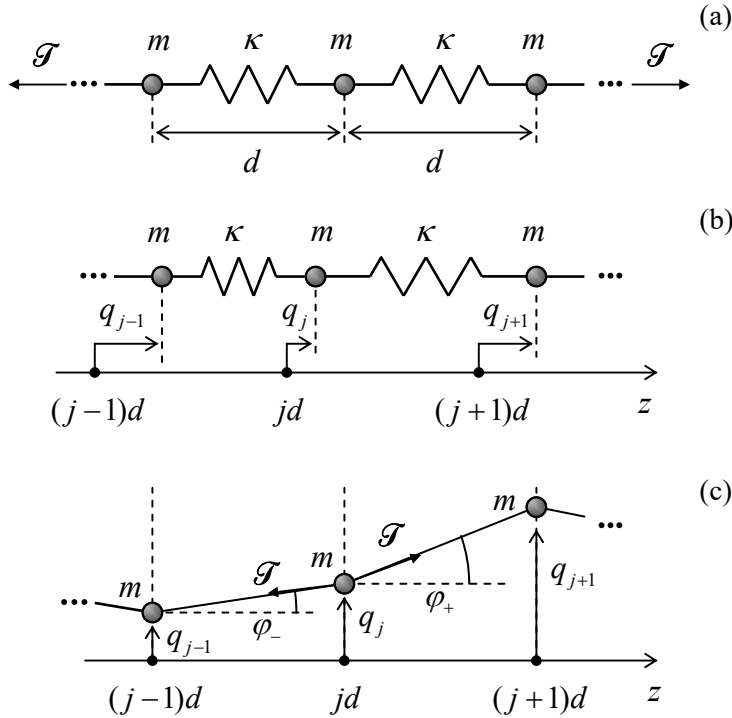


Fig. 6.4. (a) A uniform 1D chain of elastically coupled particles, and their small (b) longitudinal and (c) transverse displacements (much exaggerated for clarity).

The spring's pre-stretch does not affect small *longitudinal* oscillations q_j of the particles about their equilibrium positions $z_j = jd$ (where the integer j numbers the particles sequentially) – see Fig. 4b.⁶ Indeed, in the 2nd Newton law for such a longitudinal motion of the j^{th} particle, the forces \mathcal{T} and $-\mathcal{T}$ exerted by the springs on the right and the left of it, cancel. However, the elastic additions, $\kappa\Delta q$, to these forces are generally different:

$$m\ddot{q}_j = \kappa(q_{j+1} - q_j) - \kappa(q_j - q_{j-1}). \quad (6.23)$$

On the contrary, for *transverse* oscillations within one plane (Fig. 4c), the net transverse component of the pre-stretch force exerted on the j^{th} particle, $\mathcal{T}_t = \mathcal{T}(\sin\varphi_+ - \sin\varphi_-)$, where φ_\pm are the force direction angles, does not vanish. As a result, direct contributions to this force from small longitudinal oscillations, with $|q_j| \ll d$, \mathcal{T}/κ , are negligible. Also, due to the first of these strong conditions, the angles φ_\pm are small, and hence may be approximated, respectively, as $\varphi_+ \approx (q_{j+1} - q_j)/d$ and $\varphi_- \approx (q_j - q_{j-1})/d$. Plugging these expressions into a similar approximation, $\mathcal{T}_t \approx \mathcal{T}(\varphi_+ - \varphi_-)$ for the transverse force, we see that it may be expressed as $\mathcal{T}(q_{j+1} - q_j)/d - \mathcal{T}(q_j - q_{j-1})/d$, i.e. is absolutely similar

⁶ Note the need for a clear distinction between *the equilibrium position* z_j of the j^{th} point and its *deviation* q_j from it. Such distinction has to be sustained in the continuous limit (see below), where it is frequently called the *Eulerian description* – named after L. Euler, even though it was introduced to mechanics by J. d'Alembert. In this course, the distinction is emphasized by using different letters – respectively, z and q (in the 3D case, \mathbf{r} and \mathbf{q}).

to that in the longitudinal case, just with the replacement $\kappa \rightarrow \mathcal{T}/d$. As a result, we may write the equation of motion of the j^{th} particle for these two cases in the same form:

$$m\ddot{q}_j = \kappa_{\text{ef}}(q_{j+1} - q_j) - \kappa_{\text{ef}}(q_j - q_{j-1}), \quad (6.24)$$

where κ_{ef} is the “effective spring constant”, equal to κ for the longitudinal oscillations, and to \mathcal{T}/d for the transverse oscillations.⁷

Apart from the (formally) infinite size of the system, Eq. (24) is just a particular case of Eq. (17), and thus its particular solution may be looked for in the form (18), where, in light of our previous experience, we may immediately take $\lambda^2 \equiv -\omega^2$. With this substitution, Eq. (24) gives the following simple form of the general system of equations (19) for the distribution coefficients c_j :

$$(-m\omega^2 + 2\kappa_{\text{ef}})c_j - \kappa_{\text{ef}}c_{j+1} - \kappa_{\text{ef}}c_{j-1} = 0. \quad (6.25)$$

Now comes the most important conceptual step toward the wave theory. The *translational symmetry* of Eq. (25), i.e. its invariance with respect to the replacement $j \rightarrow j + 1$, allows it to have particular solutions of the following form:

$$c_j = ae^{i\alpha j}, \quad (6.26)$$

where the coefficient α may depend on ω (and system’s parameters), but not on the particle number j . Indeed, plugging Eq. (26) into Eq. (25) and canceling the common factor $e^{i\alpha j}$, we see that this *differential* equation is indeed identically satisfied, provided that α obeys the following *algebraic* characteristic equation:

$$(-m\omega^2 + 2\kappa_{\text{ef}}) - \kappa_{\text{ef}}e^{+i\alpha} - \kappa_{\text{ef}}e^{-i\alpha} = 0. \quad (6.27)$$

The physical sense of the solution (26) becomes clear if we use it and Eq. (18) with $\lambda = \mp i\omega$, to write

$$q_j(t) = \text{Re}[a \exp\{i(kz_j \mp \omega t)\}] = \text{Re}[a \exp\{ik(z_j \mp v_{\text{ph}}t)\}], \quad (6.28)$$

1D
traveling
wave

where the *wave number* k is defined as $k \equiv \alpha/d$. Eq. (28) describes a *sinusoidal*⁸ *traveling wave* of particle displacements, which propagates, depending on the sign before v_{ph} , to the right or the left along the particle chain, with the so-called *phase velocity*

$$v_{\text{ph}} \equiv \frac{\omega}{k}. \quad (6.29)$$

Phase
velocity

Perhaps the most important characteristic of a wave system is the so-called *dispersion relation*, i.e. the relation between the wave’s frequency ω and its wave number k – one may say, between the temporal and spatial frequencies of the wave. For our current system, this relation is given by Eq. (27) with $\alpha \equiv kd$. Taking into account that $(2 - e^{+i\alpha} - e^{-i\alpha}) \equiv 2(1 - \cos\alpha) \equiv 4\sin^2(\alpha/2)$, the dispersion relation may be rewritten in a simpler form:

⁷ The re-derivation of Eq. (24) from the Lagrangian formalism, with the simultaneous strict proof that the small oscillations in the longitudinal direction and the two mutually perpendicular transverse directions are all independent of each other, is a very good exercise, left for the reader.

⁸ In optics and quantum mechanics, such waves are usually called *monochromatic*; I will try to avoid this term until the corresponding parts (EM and QM) of my series.

$$\omega = \pm \omega_{\max} \sin \frac{\alpha}{2} \equiv \pm \omega_{\max} \sin \frac{kd}{2}, \quad \text{where } \omega_{\max} \equiv 2 \left(\frac{\kappa_{\text{ef}}}{m} \right)^{1/2}. \quad (6.30)$$

This result, sketched in Fig. 5, is rather remarkable in several aspects. I will discuss them in some detail, because most of these features are typical for waves of any type (including even the “de Broglie waves”, i.e. wavefunctions, in quantum mechanics), propagating in periodic structures.

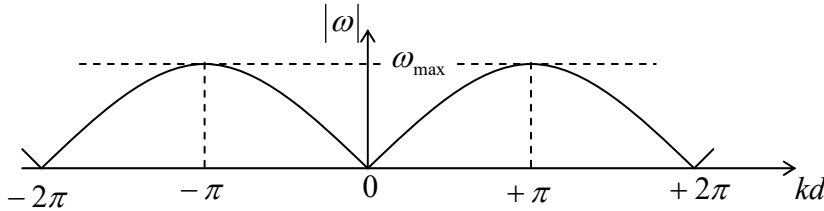


Fig. 6.5. The dispersion relation (30).

First, at low frequencies, $\omega \ll \omega_{\max}$, the dispersion relation (31) is linear:

$$\omega = \pm v k, \quad \text{where } v \equiv \left| \frac{d\omega}{dk} \right|_{k=0} = \frac{\omega_{\max} d}{2} = \left(\frac{\kappa_{\text{ef}}}{m} \right)^{1/2} d. \quad (6.31)$$

Plugging Eq. (31) into Eq. (29), we see that the constant v plays, in the low-frequency limit, the role of the same phase velocity for waves of any frequency. Due to its importance, this *acoustic-wave*⁹ limit will be the subject of the special next section.

Second, when the wave frequency *is* comparable with ω_{\max} , the dispersion relation is *not* linear, and the system is *dispersive*. This means that as a wave, whose Fourier spectrum has several essential components with frequencies of the order of ω_{\max} , travels along the structure, its *waveform* (which may be defined as the shape of the line connecting all points $q_j(z)$, at the same time) changes.¹⁰ This effect may be analyzed by representing the general solution of Eq. (24) as the sum (more generally, an integral) of the components (28) with different complex amplitudes a :

1D wave packet

$$q_j(t) = \operatorname{Re} \int_{-\infty}^{+\infty} a_k \exp\{i[kz_j - \omega(k)t]\} dk. \quad (6.32)$$

This notation emphasizes the possible dependence of the component wave amplitudes a_k and frequencies ω on the wave number k . While the latter dependence is given by the dispersion relation, in our current case by Eq. (30), the function a_k is determined by the initial conditions. For applications, the case when a_k is substantially different from zero only in a narrow interval, of a width $\Delta k \ll k_0$ around some central value k_0 , is of special importance. The Fourier transform reciprocal to Eq. (32) shows that this is true, in particular, for the so-called *wave packet* – a sinusoidal (“carrier”) wave modulated by a spatial *envelope* function of a large width $\Delta z \sim 1/\Delta k \gg 1/k_0$ – see, e.g., Fig. 6.

⁹ This term is purely historical. Though the usual sound waves in air, which are the subject of acoustics, belong to this class, the waves we are discussing may have frequencies both well below and well above the human ear’s sensitivity range.

¹⁰ The waveform’s deformation due to *dispersion* (which we are considering now) should be clearly distinguished from its possible change due to *attenuation* due to energy dissipation – which is *not* taken into account in our current energy-conserving model – cf. Sec. 6 below.

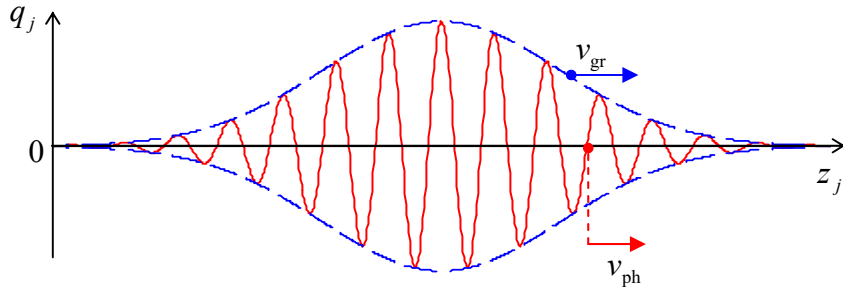


Fig. 6.6. The phase and group velocities of a wave packet.

Using the strong inequality $\Delta k \ll k_0$, the wave packet's propagation may be analyzed by expanding the dispersion relation $\omega(k)$ into the Taylor series at point k_0 , and, in the first approximation in $\Delta k/k_0$, restricting the expansion to its first two terms:

$$\omega(k) \approx \omega_0 + \frac{d\omega}{dk} \Big|_{k=k_0} \tilde{k}, \quad \text{where } \omega_0 = \omega(k_0), \text{ and } \tilde{k} = k - k_0. \quad (6.33)$$

In this approximation, Eq. (32) yields

$$\begin{aligned} q_j(t) &\approx \operatorname{Re} \int_{-\infty}^{+\infty} a_k \exp \left\{ i \left[(k_0 + \tilde{k}) z_j - \left(\omega_0 + \frac{d\omega}{dk} \Big|_{k=k_0} \tilde{k} \right) t \right] \right\} dk \\ &\equiv \operatorname{Re} \left[\exp \{i(k_0 z_j - \omega_0 t)\} \int_{-\infty}^{+\infty} a_k \exp \left\{ i \tilde{k} \left(z_j - \frac{d\omega}{dk} \Big|_{k=k_0} t \right) \right\} dk \right]. \end{aligned} \quad (6.34)$$

Comparing the last expression with the initial form of the wave packet,

$$q_j(0) = \operatorname{Re} \int_{-\infty}^{+\infty} a_k e^{ikz_j} dk \equiv \operatorname{Re} \left[\exp \{ik_0 z_j\} \int_{-\infty}^{+\infty} a_k \exp \{i\tilde{k}z_j\} dk \right], \quad (6.35)$$

and taking into account that the phase factors before the integrals in the last forms of Eqs. (34) and (35) do not affect its envelope, we see that in this approximation, the envelope sustains its initial form and propagates along the system with the so-called *group velocity*

$$v_{\text{gr}} \equiv \frac{d\omega}{dk} \Big|_{k=k_0}.$$

(6.36) Group velocity

Except for the acoustic wave limit (31), this velocity, which characterizes the propagation of the waveform's envelope, is different from the phase velocity (29), which describes the propagation of the carrier wave, e.g., the spatial position of one of its zeros – see the red and blue arrows in Fig. 6.¹¹

Next, for our particular dispersion relation (30), the difference between v_{ph} and v_{gr} increases as ω approaches ω_{\max} , with the group velocity (36) tending to zero, while the phase velocity stays almost constant. The physics of such a maximum frequency available for the wave propagation may be readily understood by noticing that according to Eq. (30), at $\omega = \omega_{\max}$, the wave number k equals $n\pi/d$, where n

¹¹ Taking into account the next term in the Taylor expansion of the function $\omega(q)$, proportional to $d^2\omega/dq^2$, we would find that the dispersion leads to a gradual change of the envelope's form. Such changes play an important role in quantum mechanics, so that they are discussed in detail in the QM part of these lecture notes.

is an odd integer, and hence the phase shift $\alpha \equiv kd$ is an odd multiple of π . Plugging this value into Eq. (28), we see that at $\omega = \omega_{\max}$, the oscillations of two adjacent particles are in anti-phase, for example:

$$q_0(t) = \operatorname{Re}[a \exp\{-i\omega t\}], \quad q_1(t) = \operatorname{Re}[a \exp\{i\pi - i\omega t\}] = -q_0(t). \quad (6.37)$$

It is clear, especially from Fig. 4b for longitudinal oscillations, that at such a phase shift, all the springs are maximally stretched/compressed (just as in the hard mode of the two coupled oscillators analyzed in Sec. 1), so that it is natural that this mode has the highest possible frequency.

This fact invites a natural question: what happens with the system if it is agitated at a frequency $\omega > \omega_{\max}$, say by an external force exerted on its boundary? Reviewing the calculations that have led to the dispersion relation (30), we see that they are all valid not only for real but also for any complex values of k . In particular, at $\omega > \omega_{\max}$ it gives

$$k = \frac{(2n-1)\pi}{d} \pm \frac{i}{\Lambda}, \quad \text{where } n = 1, 2, 3, \dots, \quad \Lambda \equiv \frac{d}{2\cosh^{-1}(\omega/\omega_{\max})}. \quad (6.38)$$

Plugging this relation into Eq. (28), we see that the wave's amplitude becomes an exponential function of the particle's position:

$$|q_j| = |a| e^{\pm j \operatorname{Im} k d} \propto \exp\{\pm z_j / \Lambda\}. \quad (6.39)$$

Physically this means that penetrating into the structure, the wave decays exponentially (from the excitation point), dropping by a factor of $e \approx 3$ at the so-called *penetration depth* Λ . (According to Eq. (38), at $\omega \sim \omega_{\max}$ this depth is of the order of the distance d between the adjacent particles, and decreases but rather slowly as the frequency is increased beyond ω_{\max} .) Such a limited penetration is a very common property of waves, including the electromagnetic waves penetrating into various plasmas and superconductors, and the quantum-mechanical de Broglie waves penetrating into classically-forbidden regions of space. Note that this effect of “wave expulsion” from the medium’s bulk does not require any energy dissipation.

Finally, one more fascinating feature of the dispersion relation (30) is its periodicity: if the relation is satisfied with some wave number $k_0(\omega)$, it is also satisfied with any $k_n(\omega) = k_0(\omega) + 2\pi n/d$, where n is an integer. This property is independent of the particular dynamics of the system and is a common property of all systems that are d -periodic in the usual (“direct”) space. It has especially important implications for the quantum de Broglie waves in periodic systems – for example, crystals – leading, in particular, to the famous band/gap structure of their energy spectrum.¹²

6.4. Acoustic waves

Now let us return to the limit of low-frequency, dispersion-free *acoustic waves*, with $|\omega| \ll \omega_0$, propagating with the frequency-independent velocity (31). Such waves are the general property of *any* elastic continuous medium and obey a simple (and very important) partial differential equation. To derive it, let us note that in the acoustic wave limit, $|kd| \ll 1$,¹³ the phase shift $\alpha \equiv kd$ is very close to

¹² For more detail see, e.g., QM Sec. 2.5.

¹³ Strictly speaking, per the discussion at the end of the previous section, in this reasoning k means the distance of the wave number from the closest point $2\pi n/d$ – see Fig. 5 again.

$2\pi n$. This means that the differences $q_{j+1}(t) - q_j(t)$ and $q_j(t) - q_{j-1}(t)$, participating in Eq. (24), are relatively small and may be approximated with $\partial q/\partial j \equiv \partial q/\partial(z/d) \equiv d(\partial q/\partial z)$, with the derivatives taken at middle points between the particles: respectively, $z_+ \equiv (z_{j+1} - z_j)/2$ and $z_- \equiv (z_j - z_{j-1})/2$. Let us now consider z as a continuous argument, and introduce the particle displacement $q(z, t)$ – a continuous function of space and time, satisfying the requirement $q(z_j, t) = q_j(t)$. In this notation, in the limit $kd \rightarrow 0$, the sum of the last two terms of Eq. (24) becomes $-\kappa d [\partial q/\partial z(z_+) - \partial q/\partial z(z_-)]$, and hence may be approximated as $-\kappa d^2 (\partial^2 q/\partial z^2)$, with the second derivative taken at point $(z_+ - z_-)/2 \equiv z_j$, i.e. exactly at the same point as the time derivative. As the result, the whole set of *ordinary* differential equations (24), for different j , is reduced to just *one partial* differential equation

$$m \frac{\partial^2 q}{\partial t^2} - \kappa_{\text{ef}} d^2 \frac{\partial^2 q}{\partial z^2} = 0. \quad (6.40a)$$

Using Eq. (31), we may rewrite this *1D wave equation* in a more general form

$$\left(\frac{1}{v^2} \frac{\partial^2}{\partial t^2} - \frac{\partial^2}{\partial z^2} \right) q(z, t) = 0.$$

(6.40b) 1D wave equation

The most important property of the wave equation (40), which may be verified by an elementary substitution, is that it is satisfied by either of two *traveling wave* solutions (or their linear superposition):

$$q_+(z, t) = f_+(t - z/v), \quad q_-(z, t) = f_-(t + z/v), \quad (6.41)$$

where f_\pm are *any* smooth functions of one argument. The physical sense of these solutions may be revealed by noticing that the displacements q_\pm do not change at the addition of an arbitrary change Δt to their time argument, provided that it is accompanied by an addition of the proportional addition of $\mp v\Delta t$ to their space argument. This means that with time, the waveforms just move (respectively, to the left or the right), with the constant speed v , retaining their form – see Fig. 7.¹⁴

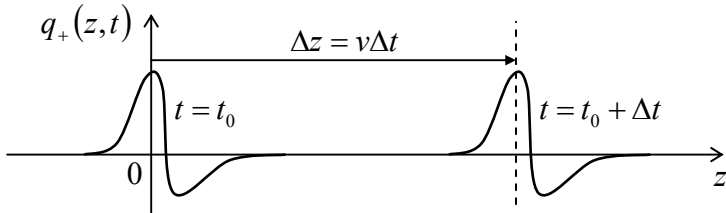


Fig. 6.7. Propagation of a traveling wave in a dispersion-free 1D system.

Returning to the simple model shown in Fig. 4, let me emphasize that the acoustic-wave velocity v is different for the waves of two types: for the longitudinal waves (with $\kappa_{\text{ef}} = \kappa$, see Fig. 4b),

$$v = v_l \equiv \left(\frac{\kappa}{m} \right)^{1/2} d, \quad (6.42)$$

while for the transverse waves (with $\kappa_{\text{ef}} = \mathcal{T}/d$, see Fig. 4c):

¹⁴ From the point of view of Eq. (40), the only requirement to the “smoothness” of the functions f_\pm is to be doubly differentiable. However, we should not forget that in our case the wave equation is only an approximation of the discrete Eq. (24), so that according to Eq. (30), the traveling waveform conservation is limited by the acoustic wave limit condition $\omega \ll \omega_{\text{max}}$, which should be fulfilled for all Fourier components of these functions.

$$v = v_t = \left(\frac{\mathcal{T}}{md} \right)^{1/2} d \equiv \left(\frac{\mathcal{T}d}{m} \right)^{1/2} \equiv \left(\frac{\mathcal{T}}{\mu} \right)^{1/2}, \quad (6.43)$$

where the constant $\mu \equiv m/d$ has a simple physical sense of the particle chain's mass per unit length. Evidently, these velocities, in the same system, may be rather different.

The wave equation (40), with its only parameter v , may conceal the fact that any wave-supporting system is characterized by one more key parameter. In our current model (Fig. 4), this parameter may be revealed by calculating the forces $F_{\pm}(z, t)$ accompanying any of the traveling waves (41) of particle displacements. For example, in the acoustic wave limit $kd \rightarrow 0$ we are considering now, the force exerted by the j^{th} particle on its right neighbor may be approximated as

$$F(z_j, t) \equiv \kappa_{\text{ef}} [q_j(t) - q_{j+1}(t)] \approx -\kappa_{\text{ef}} \frac{\partial q}{\partial z} \Big|_{z=z_j} d, \quad (6.44)$$

where, as was discussed above, κ_{ef} is equal to κ for the longitudinal waves, and to \mathcal{T}/d for the transverse waves. But for the traveling waves (41), the partial derivatives $\partial q_{\pm}/\partial z$ are equal to $\mp \dot{f}_{\pm}/v$ (where the dot means the differentiation over the full arguments of the functions f_{\pm}), so that the corresponding forces are equal to

$$F_{\pm} = \mp \frac{\kappa_{\text{ef}} d}{v} \dot{f}_{\pm}, \quad (6.45)$$

i.e. are proportional to the particle's velocities $u = \partial q/\partial t$ in these waves,¹⁵ $u_{\pm} = \dot{f}_{\pm}/v$, for the same z and t . This means that the ratio

$$\frac{F_{\pm}(z, t)}{u_{\pm}(z, t)} = -\kappa_{\text{ef}} d \frac{\partial q_{\pm}/\partial z}{\partial q_{\pm}/\partial t} = -\kappa_{\text{ef}} d \frac{(\mp \dot{f}_{\pm})/v}{\dot{f}_{\pm}} \equiv \pm \frac{\kappa_{\text{ef}} d}{v}, \quad (6.46)$$

depends only on the wave propagation direction, but is independent of z and t , and also of the propagating waveform. Its magnitude,

Wave impedance

$$Z \equiv \left| \frac{F_{\pm}(z, t)}{u_{\pm}(z, t)} \right| = \frac{\kappa_{\text{ef}} d}{v} = (\kappa_{\text{ef}} m)^{1/2}, \quad (6.47)$$

characterizing the dynamic "stiffness" of the system for the propagating waves, is called the *wave impedance*.¹⁶ Note that the impedance is determined by the *product* of the system's generic parameters κ_{ef} and m , while the wave velocity (31) is proportional to their *ratio*, so that these two parameters are completely independent, and both are important. According to Eq. (47), the wave impedance, just as the wave velocity, is also different for the longitudinal and transverse waves:

$$Z_l = \frac{\kappa d}{v_l} \equiv (\kappa m)^{1/2}, \quad Z_t = \frac{\mathcal{T}}{v_t} \equiv (\mathcal{T}\mu)^{1/2}. \quad (6.48)$$

¹⁵ Of course, the *particle's* velocity u (which is proportional to the wave amplitude) should not be confused with the *wave's* velocity v (which is independent of this amplitude).

¹⁶ This notion is regrettably missing from many physics (but not engineering!) textbooks.

(Note that the first of these expressions for Z coincides with the one used for a single oscillator in Sec. 5.6. In that case, Z may be also recast in a form similar to Eq. (46), namely, as the ratio of the force and velocity amplitudes at free oscillations.)

One of the wave impedance's key functions is to scale the power carried by a traveling wave:

$$\mathcal{P}_\pm \equiv F_\pm(z, t)u_\pm(z, t) = -\kappa_{\text{ef}}d \frac{\partial q_\pm}{\partial z} \frac{\partial q_\pm}{\partial t} = \pm \frac{\kappa_{\text{ef}}d}{v} \dot{f}_\pm^2 \equiv \pm Z\dot{f}_\pm^2. \quad (6.49)$$

Traveling wave's power

Two remarks about this important result. First, the sign of \mathcal{P} depends only on the direction of the wave propagation, but not on the waveform. Second, the instant value of the power does not change if we move with the wave in question, i.e. measure \mathcal{P} at points with $z \pm vt = \text{const}$. This is natural because in the Hamiltonian system we are considering, the wave energy is conserved. Hence, the wave impedance Z characterizes the energy *transfer* along the system rather than its *dissipation*.

Another important function of the wave impedance notion becomes clear when we consider waves in nonuniform systems. Indeed, our previous analysis assumed that the 1D system supporting the waves (Fig. 4) is exactly periodic, i.e. macroscopically uniform, and extends all the way from $-\infty$ to $+\infty$. Now let us examine what happens when this is not true. The simplest, and very important example of such nonuniform systems is a *sharp interface*, i.e. a point (say, $z = 0$) at which system parameters experience a jump while remaining constant on each side of the interface – see Fig. 8.

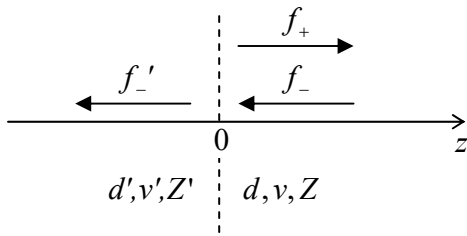


Fig. 6.8. Partial reflection of a wave from a sharp interface.

In this case, the wave equation (40) and its partial solutions (41) are still valid for $z < 0$ and $z > 0$ – in the former case, with primed parameters. However, the jump of parameters at the interface leads to a partial *reflection* of the incident wave from the interface, so that at least on the side of the incidence (in the case shown in Fig. 8, for $z \geq 0$), we need to use two such terms, one describing the incident wave and another one, the reflected wave:

$$q(z, t) = \begin{cases} f'_-(t + z/v'), & \text{for } z \leq 0, \\ f_-(t + z/v) + f_+(t - z/v), & \text{for } z \geq 0. \end{cases} \quad (6.50)$$

To find the relations between the functions f_- , f_+ , and f'_- (of which the first one, describing the incident wave, may be considered known), we may use two boundary conditions at $z = 0$. First, the displacement $q_0(t)$ of the particle at the interface has to be the same whether it is considered a part of the left or right sub-system, and it participates in Eqs. (50) for both $z \leq 0$ and $z \geq 0$. This gives us the first boundary condition:

$$f'_-(t) = f_-(t) + f_+(t). \quad (6.51)$$

On the other hand, the forces exerted on the interface from the left and the right should also have equal magnitude, because the interface may be considered as an object with a vanishing mass, and any

nonzero net force would give it an infinite (and hence unphysical) acceleration. Together with Eqs. (45) and (47), this gives us the second boundary condition:

$$Z' \dot{f}'_-(t) = Z [\dot{f}_-(t) - \dot{f}_+(t)]. \quad (6.52)$$

Integrating both parts of this equation over time, and neglecting the integration constant (which describes a common displacement of all particles rather than their oscillations), we get

$$Z f'_-(t) = Z [f_-(t) - f_+(t)]. \quad (6.53)$$

Now solving the system of two linear equations (51) and (53) for $f_+(t)$ and $f'_+(t)$, we see that both these functions are proportional to the incident waveform:

$$f_+(t) = \mathcal{R} f_-(t), \quad f'_+(t) = \mathcal{T} f_-(t), \quad (6.54)$$

with the following *reflection* (\mathcal{R}) and *transmission* (\mathcal{T}) coefficients:

Reflection
and
transmission
coefficients

$$\mathcal{R} = \frac{Z - Z'}{Z + Z'}, \quad \mathcal{T} = \frac{2Z}{Z + Z'}. \quad (6.55)$$

Later in this series, we will see that with the appropriate re-definition of the impedance, these relations are also valid for waves of other physical nature (including the de Broglie waves in quantum mechanics) propagating in 1D continuous structures, and also in continua of higher dimensions, at the normal wave incidence upon the interface.¹⁷ Note that the coefficients \mathcal{R} and \mathcal{T} give the ratios of wave *amplitudes*, rather than their *powers*. Combining Eqs. (49) and (55), we get the following relations for the powers – either at the interface or at the corresponding points of the reflected and transmitted waves:

$$\mathcal{P}_+ = \left(\frac{Z - Z'}{Z + Z'} \right)^2 \mathcal{P}_-, \quad \mathcal{P}'_- = \frac{4ZZ'}{(Z + Z')^2} \mathcal{P}_-. \quad (6.56)$$

Note that $\mathcal{P}_- + \mathcal{P}_+ = \mathcal{P}'_-$, again reflecting the wave energy conservation.

Perhaps the most important corollary of Eqs. (55)–(56) is that the reflected wave completely vanishes, i.e. the incident wave is completely transmitted through the interface ($\mathcal{P}'_- = \mathcal{P}_+$), if the so-called *impedance matching condition* $Z' = Z$ is satisfied, even if the wave velocities v (32) are different on the left and the right sides of it. On the contrary, the equality of the acoustic velocities in the two continua does *not* guarantee the full transmission of their interface. Again, this is a very general result.

Finally, let us note that for the important particular case of a sinusoidal incident wave:¹⁸

$$f_-(t) = \operatorname{Re}[a e^{-i\omega t}], \quad \text{so that } f_+(t) = \operatorname{Re}[\mathcal{R} a e^{-i\omega t}], \quad (6.57)$$

where a is its complex amplitude, the total wave (50) on the right of the interface is

$$q(z, t) = \operatorname{Re} \left[a e^{-i\omega(t+z/v)} + \mathcal{R} a e^{-i\omega(t-z/v)} \right] \equiv \operatorname{Re} \left[a (e^{-ikz} + \mathcal{R} e^{+ikz}) e^{-i\omega t} \right], \quad \text{for } z \geq 0, \quad (6.58)$$

¹⁷ See, e.g. the corresponding parts of this series: QM Sec. 2.3 and EM Sec. 7.3.

¹⁸ In the acoustic wave limit, when the impedances Z and Z' , and hence the reflection coefficient \mathcal{R} , are real, \mathcal{R} and Z may be taken from under the Re operators in Eqs. (57)–(59). However, in the current, more general form of these relations they are also valid for the case of arbitrary frequencies, $\omega \sim \omega_{\max}$, when \mathcal{R} and Z may be complex.

while according to Eq. (45), the corresponding force distribution is

$$F(z,t) = F_-(z,t) + F_+(z,t) = -Z\dot{f}_-(t - z/v) + Z\dot{f}_+(t - z/v) = \operatorname{Re} [i\omega Za(e^{-ikz} - \mathcal{R}e^{+ikz})e^{-i\omega t}]. \quad (6.59)$$

These expressions will be used in the next section.

6.5. Standing waves

Now let us consider the two limits in which Eqs. (55) predicts a *total wave reflection* ($\mathcal{T} = 0$): $Z'/Z \rightarrow \infty$ (when $\mathcal{R} = -1$) and $Z'/Z \rightarrow 0$ (when $\mathcal{R} = +1$). According to Eq. (53), the former limit corresponds to $f_-(t) + f_+(t) \equiv q(0, t) = 0$, i.e. to vanishing oscillations at the interface. This means that this particular limit describes a perfectly *rigid boundary*, not allowing the system's end to oscillate at all. In this case, Eqs. (58)-(59) yield

$$q(z,t) = \operatorname{Re} [a(e^{-ikz} - e^{+ikz})e^{-i\omega t}] \equiv -2\operatorname{Re} [a e^{-i\omega t}] \sin kz, \quad (6.60)$$

$$F(z,t) = \operatorname{Re} [i\omega Za(e^{-ikz} + e^{+ikz})e^{-i\omega t}] \equiv 2\omega Z \operatorname{Re} [a e^{-i(\omega t - \pi/2)}] \cos kz. \quad (6.61)$$

These equalities mean that we may interpret the process on the right of the interface using two mathematically equivalent, but physically different languages: either as the sum of two *traveling waves* (the incident one and the reflected one, propagating in opposite directions), or as a single *standing wave*. Note that in contrast with the traveling wave (Fig. 9a, cf. Fig. 7), in the standing sinusoidal wave (Fig. 9b) all particles oscillate in time with the same phase.

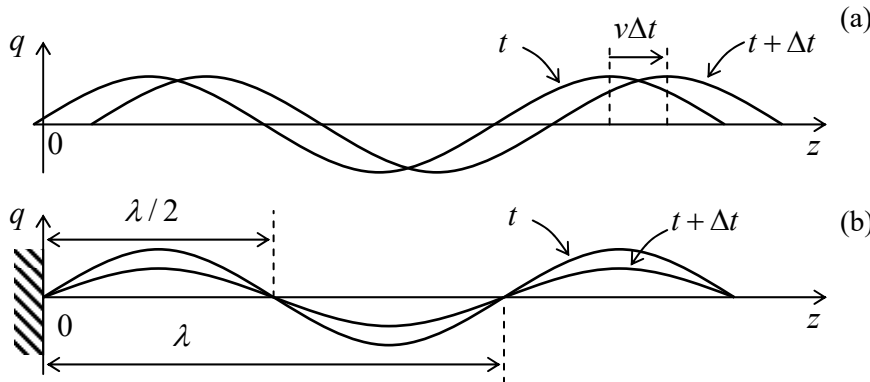


Fig. 6.9. The time evolution of (a) a traveling sinusoidal wave, and (b) a standing sinusoidal wave at a rigid boundary.

Note also that the phase of the force oscillations (61) is shifted, both in space and in time, by $\pi/2$ relatively to the particle displacement oscillations. (In particular, at the rigid boundary the force amplitude reaches its maximum.) As a result, the average power flow vanishes, so that the *average* energy of the standing wave does not change, though its *instant* energy still oscillates, at each spatial point, between its kinetic and potential components – just as at the usual harmonic oscillations of one particle. A similar standing wave, but with a maximum of the displacement q , and with a zero (“node”) of the force F , is formed at the open boundary, with $Z'/Z \rightarrow 0$, and hence $\mathcal{R} = +1$.

Now I have to explain why I have used the sinusoidal waveform for the wave reflection analysis. Let us consider a 1D wave system, which obeys Eq. (40), of a finite length l , limited by two rigid walls (located, say, at $z = 0$ and $z = l$), which impose the corresponding boundary conditions,

$$q(0,t) = q(l,t) = 0, \quad (6.62)$$

on its motion. Naturally, a sinusoidal traveling wave, induced in the system, will be reflected from both ends, forming the standing wave patterns of the type (60) near each of them. These two patterns are compatible if l is exactly equal to an integer number (say, n) of $\lambda/2$, where $\lambda \equiv 2\pi/k$ is the wavelength:

$$l = n \frac{\lambda}{2} \equiv n \frac{\pi}{k}. \quad (6.63)$$

This requirement yields the following spectrum of possible wave numbers:

$$k_n = n \frac{\pi}{l}, \quad (6.64)$$

where the list of possible integers n may be limited to non-negative values: $n = 1, 2, 3, \dots$ (Indeed, negative values give absolutely similar waves (60), while $n = 0$ yields $k_n = 0$, and the corresponding wave vanishes at all points: $\sin(0 \cdot z) \equiv 0$.) In the acoustic wave limit we are discussing, Eq. (31), $\omega = \pm v k$, may be used to translate this wave-number spectrum into an equally simple spectrum of possible standing-wave frequencies:¹⁹

$$\omega_n = v k_n = n \frac{\pi v}{l}, \quad \text{with } n = 1, 2, 3, \dots \quad (6.65)$$

Now let us notice that this spectrum, and the corresponding standing-wave patterns,²⁰

$$q^{(n)}(z,t) = 2 \operatorname{Re}[a_n \exp\{-i\omega_n t\}] \sin k_n z, \quad \text{for } 0 \leq z \leq l, \quad (6.66)$$

may be calculated in a different way, by a direct solution of the wave equation (41) with the boundary conditions (62). Indeed, let us look for the general solution of this partial differential equation in the so-called *variable-separated* form²¹

$$q(z,t) = \sum_n Z_n(z) T_n(t), \quad (6.67)$$

where each partial product $Z_n(z)T_n(t)$ is supposed to satisfy the equation on its own. Plugging such partial solution into Eq. (40), and then dividing all its terms by the same product, $Z_n T_n$, we may rewrite the result as

$$\frac{1}{v^2} \frac{1}{T_n} \frac{d^2 T_n}{dt^2} = \frac{1}{Z_n} \frac{d^2 Z_n}{dz^2}. \quad (6.68)$$

Here comes the punch line of the variable separation method: since the left-hand side of the equation may depend only on t , while its right-hand side, only on z , Eq. (68) may be valid only if both its sides are constant. Denoting this constant as $-k_n^2$, we get two similar ordinary differential equations,²²

$$\frac{d^2 Z_n}{dz^2} + k_n^2 Z_n = 0, \quad \frac{d^2 T_n}{dt^2} + \omega_n^2 T_n = 0, \quad \text{where } \omega_n^2 \equiv v^2 k_n^2, \quad (6.69)$$

¹⁹ Again, negative values of ω may be dropped, because they give similar real functions $q(z, t)$.

²⁰ They describe, in particular, the well-known transverse standing waves on a guitar string.

²¹ This *variable separation method* is very general and is discussed in all parts of this series, especially in EM Chapter 2.

²² The first of them is the 1D form of what is frequently called the *Helmholtz equation*.

with well-known (and similar) sinusoidal solutions

$$Z_n = c_n \cos k_n z + s_n \sin k_n z, \quad T_n = u_n \cos \omega_n t + v_n \sin \omega_n z \equiv \text{Re}[a_n \exp\{-i\omega_n t\}], \quad (6.70)$$

where c_n , v_n , u_n , and ω_n (or, alternatively, $a_n \equiv u_n + iv_n$) are constants. The first of these relations, with all k_n different, may satisfy the boundary conditions only if for all n , $c_n = 0$, and $\sin k_n l = 0$, giving the same wave number spectrum (64) and hence the own frequency spectrum (65), so that the general solution (67) of the so-called *boundary problem*, given by Eqs. (40) and (62), takes the form

$$q(z, t) = \text{Re} \sum_n a_n \exp\{-i\omega_n t\} \sin k_n z, \quad (6.71)$$

where the complex amplitudes a_n are determined by the initial conditions.

Hence such sinusoidal standing waves (Fig. 10a) are not just an assumption, but a natural property of the 1D wave equation. It is also easy to verify that the result (71) is valid for the same system with different boundary conditions, though with a modified wave number spectrum. For example, if the rigid boundary condition ($q = 0$) is implemented at $z = 0$, and the so-called *open* boundary condition ($F = 0$, i.e. $\partial q / \partial z = 0$) is imposed at $z = l$, the spectrum becomes

$$k_n = \left(n - \frac{1}{2} \right) \frac{\pi}{l}, \quad \text{with } n = 1, 2, 3, \dots, \quad (6.72)$$

so that the lowest standing waves look like Fig. 10b shows.²³

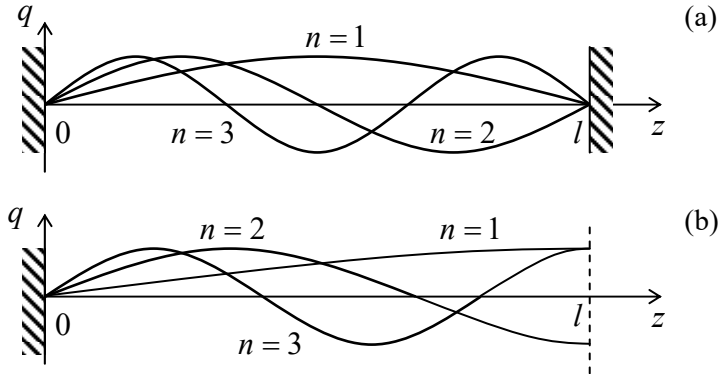


Fig. 6.10. The lowest standing wave modes for the 1D systems with (a) two rigid boundaries, and (b) one rigid and one open boundary.

Note that the difference between the sequential values of k_n is still a constant:

$$k_{n+1} - k_n = \frac{\pi}{l}, \quad (6.73)$$

the same one as for the spectrum (64). This is natural because in both cases the transfer from the n^{th} mode to the $(n + 1)^{\text{th}}$ mode corresponds just to an addition of one more half-wave – see Fig. 10. (This conclusion is valid for any combination of rigid and free boundary conditions.) As was discussed above, for the discrete-particle chain we have started with (Fig. 4), the wave equation (40), and hence the above derivation of Eq. (71), are only valid in the acoustic wave limit, i.e. when the distance d between the particles is much less than the wavelengths $\lambda_n \equiv 2\pi/k_n$ of the mode under analysis. For a chain of length l , this means that the number of particles, $N \sim l/d$, has to be much larger than 1. However, a remarkable

²³ The lowest standing wave of the system, with the smallest k_n and ω_n , is usually called its *fundamental mode*.

property of Eq. (71) is that it remains valid, with the same wave number spectrum (64), not only in the acoustic limit but also for arbitrary $N > 0$. Indeed, since $\sin k_n z \equiv (\exp\{+ik_n z\} - \exp\{-ik_n z\})/2$, each n^{th} term of Eq. (71) may be represented as a sum of two traveling waves with equal but opposite wave vectors. As was discussed in Sec. 3, such a wave is a solution of equation (24) describing the discrete-particle system for *any* k_n , with the only condition that its frequency obeys the general dispersion relation (30), rather than its acoustic limit (65).

Moreover, the expressions for k_n (with appropriate boundary conditions), such as Eq. (64) or Eq. (72), also survive the transition to arbitrary N , because their derivation above was based only on the sinusoidal form of the standing wave. The only new factor arising in the case of arbitrary N is that due to the equidistant property (73) of the wave number spectrum, as soon as n exceeds N , the waveforms (71), at particle locations $z_j = jd$, start to repeat. For example,

$$\sin k_{n+N} z_j = \sin(k_n + N\Delta k)jd = \sin\left(k_n + N\frac{\pi}{d}\right)jd = \sin(k_n z_j + \pi jN) \equiv \pm \sin k_n z_j. \quad (6.74)$$

Hence the system has only N different (linearly-independent) modes. But this result is in full compliance with the general conclusion made in Sec. 2, that *any* system of N coupled oscillators has exactly N own frequencies and corresponding oscillation modes. So, our analysis of a particular system shown in Fig. 4, just exemplifies this general conclusion. Fig. 11 below illustrates this result for a particular finite value of N ; the curve connecting the points shows exactly the same dispersion relation as was shown in Fig. 5, but now it is just a guide for the eye, because for a system with a finite length l , the wave number spectrum is discrete, and the intermediate values of k and ω do not have an immediate physical sense.²⁴ Note that the own frequencies of the system are generally not equidistant, while the wave numbers are.

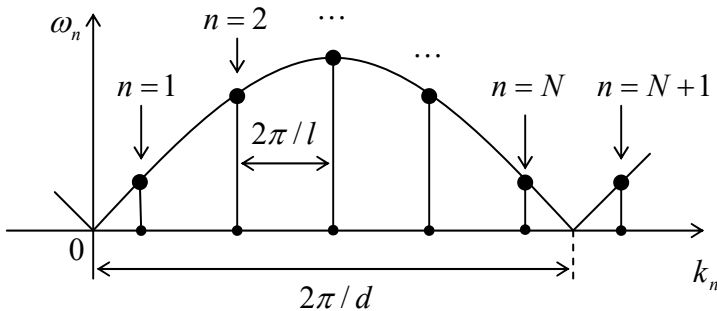


Fig. 6.11. The wave numbers and own frequencies of a chain of a finite number N of particles in a chain with one rigid and one open boundary – schematically.

This insensitivity of the spacing (73) between the adjacent wave numbers to the particular physics of a macroscopically uniform system is a very general fact, common for waves of any nature, and is broadly used for analyses of systems with a very large number of particles (such as human-size crystals, with $N \sim 10^{23}$). For N so large, the effect of the boundary conditions, e.g., the difference between the spectra (64) and (72) is negligible, and they may be summarized as the following rule for the number of different standing waves within some interval $\Delta k \gg \pi/l$:

²⁴ Note that Fig. 11 shows the case of one rigid and one open boundary (see Fig. 10b), where $l = Nd$; for a conceptually simpler system with two rigid boundaries (Fig. 10a) we would need to take $l = (N + 1)d$, because neither of the end points can oscillate.

$$\Delta N \equiv \frac{\Delta k|_{\text{standing}}}{k_{n+1} - k_n} = \frac{l}{\pi} \Delta k|_{\text{standing}} . \quad (6.75a)$$

For such analyses, it is frequently more convenient to work with traveling waves rather than the standing ones. In this case, we have to take into account that (as was just discussed above) each standing wave (66) may be decomposed into two traveling waves with wave numbers $\pm k_n$, so that the interval Δk doubles, and Eq. (75a) becomes²⁵

$$\boxed{\Delta N = \frac{l}{2\pi} \Delta k|_{\text{traveling}}} . \quad (6.75b)$$

Traveling
wave
number

Note that this counting rule is valid for waves of just one type. As was discussed above, for the model system we have studied (Fig. 4), there are 3 types of such waves – one longitudinal and two transverse, so that if we need to count them all, ΔN should be multiplied by 3.

6.6 Wave decay and attenuation

Now let us discuss the effects of energy dissipation on the 1D waves, on the example of the same uniform system shown in Fig. 4. The simplest description of this effect is the linear drag that may be described, as it was done for a single oscillator in Sec. 5.1, by adding the term $\eta dq_j/dt$, to Eq. (24) for each particle:

$$m\ddot{q}_j + \eta\dot{q}_j - \kappa_{\text{ef}}(q_{j+1} - q_j) + \kappa_{\text{ef}}(q_j - q_{j-1}) = 0 . \quad (6.76)$$

(In a uniform system, the drag coefficient η should be similar for all particles, though it may be different for the longitudinal and transverse oscillations.)

To analyze the dissipation effect on the *standing* waves, we may again use the variable separation method, i.e. look for the solution of Eq. (76) in the form similar to Eq. (67), naturally re-adjusting it for our current discrete case:

$$q(z_j, t) = \sum_n Z_n(z_j) T_n(t) . \quad (6.77)$$

After dividing all terms by $mZ_n(z_j)T_n(t)$ and separating the time-dependent and space-dependent terms, we get

$$\frac{\ddot{T}_n}{T_n} + \frac{\eta}{m} \frac{\dot{T}_n}{T_n} = \frac{\kappa_{\text{ef}}}{m} \left[\frac{Z_n(z_{j+1})}{Z_n(z_j)} + \frac{Z_n(z_{j+1})}{Z_n(z_j)} - 2 \right] = \text{const.} \quad (6.78)$$

As we know from the previous section, the resulting equation for the function $Z_n(z_j)$ is satisfied if the variable separation constant is equal to $-\omega_n^2$, where ω_n obeys the dispersion relation (30) for the wave number k_n , properly calculated for the *dissipation-free* system, with the account of the given boundary conditions – see, e.g. Eqs. (62) and (72). Hence for the function $T_n(t)$ we are getting the following ordinary differential equation:

²⁵ Note that this simple, but very important relation is frequently derived using the so-called *Born-Carman boundary condition* $q_0(t) \equiv q_N(t)$, which implies bending the system of interest into a closed loop. For a 1D system with $N \gg 1$, such mental exercise may be somehow justified, but for systems of higher dimension, it is hardly physically plausible – and is unnecessary.

$$\ddot{T}_n + 2\delta\dot{T}_n + \omega_n^2 T_n = 0, \quad \text{with } \delta \equiv \frac{\eta}{2m}, \quad (6.79)$$

which is absolutely similar to Eq. (5.6b) for a single linear oscillator, which was studied in Sec. 5.1. As we already know, it has the solution (5.9) describing the free oscillation decay with the relaxation time given by (5.10), $\tau = 1/\delta$, and hence similar for all modes.²⁶

Hence, the above analysis of the dissipation effect on *free* standing waves has not brought any surprises, but it gives us a hint of how their *forced* oscillations, induced by some external forces $F_j(t)$ exerted on the particles, may be analyzed. Indeed, representing each of the forces as a sum over the system's modes (spatial harmonics),

$$f(z_j, t) \equiv \frac{F_j(t)}{m} = \sum_n f_n(t) Z_n(z_j), \quad (6.80)$$

and using the variable separation (77), we arrive at the natural generalization of Eq. (79):

$$\ddot{T}_n + 2\delta\dot{T}_n + \omega_n^2 T_n = f_n(t), \quad (6.81)$$

which is identical to Eq. (5.13b) for a single oscillator. This fact enables us to use Eq. (5.27), with $G(\tau) \rightarrow G_n(\tau)$, for the calculation of each $T_n(t)$. Now finding the functions $f_n(t)$ from Eq. (80) by the usual reciprocal Fourier transform, and plugging these results into Eq. (77), we get the following generalization of Eq. (5.27):

$$q(z_j, t) = \sum_{j'=1}^N \int_0^\infty f(z_{j'}, t - \tau) \mathcal{G}(z_j, z_{j'}, \tau) d\tau, \quad \text{where } \mathcal{G}(z_j, z_{j'}, \tau) \equiv \sum_n G_n(\tau) Z_n(z_j) Z_n(z_{j'}). \quad (6.82)$$

(Here the mutually orthogonal functions $Z_n(z_j)$ are assumed to be normalized, i.e. the sums of their squares over $j = 1, 2, \dots, N$ to equal 1.) Such $\mathcal{G}(z_j, z_{j'}, \tau)$ is called the *spatial-temporal Green's function* of the system – in our current case, of a discrete, 1D set of N particles located at points $z_j = jd$. The reader is challenged to spell out this function for at least one of the particular cases discussed above and use it to solve at least one forced-oscillation problem.

Now let us discuss the dissipation effects on the *traveling* waves, where they may take a completely different form of *attenuation*. Let us discuss it on a simple example when one end (located at $z = 0$) of a very long chain ($l \rightarrow \infty$) is externally forced to perform sinusoidal oscillations of a certain frequency ω and a fixed amplitude A_0 . In this case, it is natural to look for a particular solution to Eq. (76) in a form very different from Eq. (77):

$$q(z_j, t) = \operatorname{Re} \left[c_j e^{-i\omega t} \right], \quad (6.83)$$

with time-independent but generally complex amplitudes c_j . As our discussion of a single oscillator in Sec. 5.1 implies, this is not the general, but rather a partial solution, which describes the forced

²⁶ Even an elementary experience with acoustic guitars shows that for their strings this particular conclusion of our theory is not valid: higher modes (“overtones”) decay substantially faster, leaving the fundamental mode oscillations for a slower decay. This is a result of another important energy dissipation (i.e. the wave decay) mechanism, not taken into account in Eq. (76) – the radiation of the sound into the guitar’s body through the string supports, mostly through the bridge. Such radiation may be described by a proper modification of the boundary conditions (62), in terms of the ratio of the wave impedance (47) of the string and those of the supports.

oscillations in the system, to that it settles after some initial transient process. (At non-zero damping, we may be sure that free oscillations fade after a finite time, and thus may be ignored for most purposes.)

Plugging Eq. (83) into Eq. (76), we reduce it to an equation for the amplitudes c_j ,

$$(-m\omega^2 - i\omega\eta + 2\kappa_{\text{ef}})c_j - \kappa_{\text{ef}}c_{j+1} - \kappa_{\text{ef}}c_{j-1} = 0, \quad (6.84)$$

which is a natural generalization of Eq. (25). As a result, partial solutions of the set of these equations (for $j = 0, 1, 2, \dots$) may be looked for in the form (26) again, but now, because of the new, imaginary term in Eq. (84), we should be ready to get a complex phase shift α , and hence a complex wave number $k \equiv \alpha/d$.²⁷ Indeed, the resulting characteristic equation for k ,

$$\sin^2 \frac{kd}{2} = \frac{\omega^2}{\omega_{\max}^2} + i \frac{2\omega\delta}{\omega_{\max}^2} \quad (6.85)$$

(where ω_{\max} is defined by Eq. (30), and the damping coefficient is defined just as in a single oscillator, $\delta \equiv \eta/2m$), does not have a real solution even at $\omega < \omega_{\max}$. Using the well-known expressions for the sine function of a complex argument,²⁸ Eq. (85) may be readily solved in the most important low-damping limit $\delta \ll \omega$. In the linear approximation in δ , it does not affect the real part of k , but makes its imaginary part different from zero:

$$k = \pm \frac{2}{d} \left(\sin^{-1} \frac{\omega}{\omega_{\max}} + i \frac{\delta}{\omega_{\max}} \right) \equiv \pm \left(\frac{2}{d} \sin^{-1} \frac{\omega}{\omega_{\max}} + i \frac{\delta}{v} \right), \quad \text{for } -\pi \leq \operatorname{Re} k \leq \pi, \quad (6.86)$$

with a periodic extension to other periods – see Fig. 5. Just as was done in Eq. (28), due to two values of the wave number, generally we have to take c_j in the form of not a single wave (26), but of a linear superposition of two partial solutions:

$$c_j = \sum_{\pm} c_{\pm} \exp \left\{ \pm i \operatorname{Re} kz_j \mp \frac{\delta}{v} z_j \right\}, \quad (6.87)$$

where the constants c_{\pm} should be found from the boundary conditions. In our particular case, when $|c_0| = A_0$ and $c_{\infty} = 0$, only one of these two waves, namely the wave exponentially decaying at its penetration into the system, is different from zero: $|c_+| = A_0$, $c_- = 0$. Hence our solution describes a single wave, with the real amplitude and the oscillation energy decreasing as

$$A_j \equiv |c_j| = A_0 \exp \left\{ -\frac{\delta}{v} z_j \right\}, \quad E_j \propto A_j^2 \propto \exp \left\{ -\alpha z_j \right\}, \quad \text{with } \alpha = \frac{2\delta}{v}, \quad (6.88)$$

Wave attenuation

i.e. with a frequency-independent *attenuation constant* $\alpha = 2\delta/v$,²⁹ so that the spatial scale of wave penetration into a dissipative system is given by $l_d \equiv 1/\alpha$. Certainly, our simple solution (88) is only valid for a system of length $l \gg l_d$; otherwise, we would need the second term in the sum (87) to describe the wave reflected from its opposite end.

²⁷ As a reminder, we have already met such a situation in the absence of damping, but at $\omega > \omega_{\max}$ – see Eq. (38).

²⁸ See, e.g., MA Eq. (3.5).

²⁹ I am sorry to use for the attenuation the same letter α as for the phase shift in Eq. (26) and a few of its corollaries, but both notations are traditional.

6.7 Nonlinear and parametric effects

Now let me discuss (because of the lack of time, very briefly, and on a semi-quantitative level), the new nonlinear and parametric phenomena that appear in oscillatory systems with more than one degree of freedom – cf. Secs. 5.4–5.8. One important new effect here is the *mutual phase locking* of (two or more) weakly coupled self-excited oscillators with close frequencies: if the own frequencies of the oscillators are sufficiently close, their oscillation frequencies “stick together” to become exactly equal. Though its dynamics of this process is very close to that of the phase locking of a single oscillator by an external signal, which was discussed in Sec. 5.4, it is rather counter-intuitive in view of the results of Sec. 1, and in particular, the anticrossing diagram shown in Fig. 2. The analysis of the effect using the van der Pol method (which is left for the reader’s exercise) shows that the origin of the difference is the oscillators’ nonlinearity, which makes oscillation amplitudes virtually independent of the phase evolution – see Eq. (5.68) and its discussion.

One more new effect is the so-called *non-degenerate parametric excitation*. It may be illustrated on the example of just two coupled oscillators – see Sec. 1 above. Let us assume that the coupling constant κ participating in Eqs. (5) is not constant, but oscillates in time – say with some frequency ω_p . In this case, the forces acting on each oscillator from its counterpart, described by the right-hand side of Eqs. (5), will be proportional to $\kappa q_{2,i}(1 + \mu \cos \omega_p t)$. Assuming that the oscillations of q_1 and q_2 are close to sinusoidal ones, with certain frequencies $\omega_{1,2}$, we see that the force exerted on each oscillator contains the so-called *combinational frequencies*

$$\omega_p \pm \omega_{2,1}. \quad (6.89)$$

If one of these frequencies is close to the own oscillation frequency of the oscillator, we can expect a substantial parametric interaction between the oscillators (on top of the constant coupling effects discussed in Sec. 1). According to Eq. (89), this may happen in two cases:

Parametric
interaction
conditions

$$\omega_p = \omega_1 + \omega_2, \quad (6.90a)$$

$$\omega_p = \omega_1 - \omega_2. \quad (6.90b)$$

The quantitative analysis (also highly recommended to the reader) shows that in the case (90a), the parameter modulation indeed leads to energy “pumping” into the oscillations.³⁰ As a result, a sufficiently large μ , at sufficiently small damping coefficients $\delta_{1,2}$ and the effective detuning

$$\xi \equiv \omega_p - (\Omega_1 + \Omega_2), \quad (6.91)$$

may lead to a simultaneous self-excitation of two frequency components $\omega_{1,2}$. These frequencies, while being approximately equal to the corresponding own frequencies $\Omega_{1,2}$ of the system, are related to the *pumping frequency* ω_p by the exact relation (90a), but otherwise are arbitrary, e.g., may be incommensurate (Fig. 12a), thus justifying the term *non-degenerate* parametric excitation.³¹ (The parametric excitation of a single oscillator, which was analyzed in Sec. 5.5, is a particular, *degenerate* case of such excitation, with $\omega_1 = \omega_2 = \omega_p/2$.) On the other hand, for the case described by Eq. (90b), the parameter modulation always extracts energy *from* the oscillations, effectively increasing the system’s damping.

³⁰ Hence the common name of ω_p – the pumping frequency.

³¹ Note that in some publications, the term *parametric down-conversion* (PDC) is used instead.

Somewhat counter-intuitively, this difference between the two cases (90) may be simpler interpreted using the basic notions of quantum mechanics. Namely, the equality $\omega_p = \omega_1 + \omega_2$ enables a decay of an external photon of energy $\hbar\omega_p$ into two photons of energies $\hbar\omega_1$ and $\hbar\omega_2$ of the oscillators. On the contrary, the complementary relation (90b), meaning that $\omega_1 = \omega_p + \omega_2$, results in a pumping-induced decay of photons of frequency ω_1 .

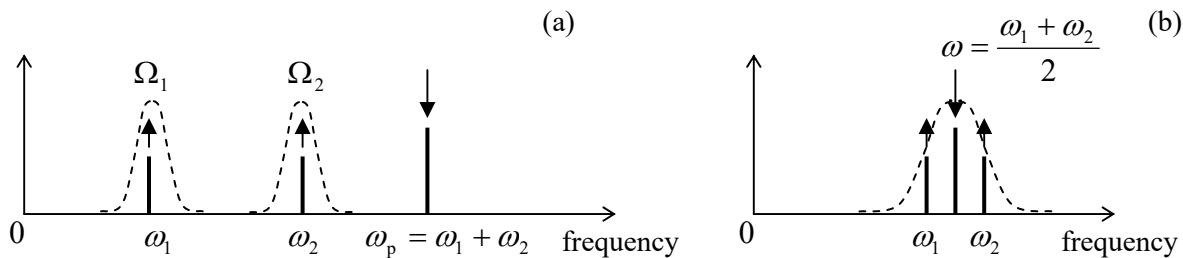


Fig. 6.12. Spectra of oscillations at (a) the non-degenerate parametric excitation, and (b) the four-wave mixing. The arrow directions symbolize the energy flows into and out of the system.

Note that even if the frequencies ω_1 and ω_2 of the parametrically excited oscillations are incommensurate, the oscillations are highly correlated. Indeed, the quantum-mechanical theory of this effect³² shows that the generated photons are *entangled*. This fact makes the parametric excitation very popular for a broad class of experiments in several currently active fields including quantum computation and encryption, and the Bell inequality/local reality studies.³³

Proceeding to nonlinear phenomena, let us note, first of all, that the simple reasoning that accompanied Eq. (5.108) in Sec. 5.8, is also valid in the case when oscillations consist of two (or more) sinusoidal components with incommensurate frequencies. Replacing the notation 2ω with ω_p , we see that the non-degenerate parametric excitation of the type (90a) is possible in a system of two coupled oscillators with a quadratic nonlinearity (of the type γq^2), “pumped” by an intensive external signal at frequency $\omega_p \approx \Omega_1 + \Omega_2$. In optics, it is often more convenient to have all three of these frequencies within the same, relatively narrow range. A simple calculation, similar to the one made in Eqs. (5.107)-(5.108), shows that this may be done using the cubic nonlinearity³⁴ of the type αq^3 , which allows a similar parametric energy exchange at the frequency relation shown in Fig. 12b:

$$2\omega = \omega_1 + \omega_2, \quad \text{with } \omega \approx \omega_1 \approx \omega_2. \quad (6.92a)$$

Four-wave mixing

This process is often called the *four-wave mixing*, because it may be interpreted quantum-mechanically as the transformation of *two* externally-delivered photons, each with energy $\hbar\omega$, into two other photons of energies $\hbar\omega_1$ and $\hbar\omega_2$. The word “wave” in this term stems from the fact that at optical frequencies, it is hard to couple a sufficient volume of a nonlinear medium with lumped-type resonators. It is much easier to implement the parametric excitation (as well as other nonlinear phenomena such as the higher harmonic generation) of light in *distributed systems* of a linear size much larger than the involved wavelengths. In such systems, the energy transfer from the incoming wave of frequency ω to

³² Which is, surprisingly, not much more complex than the classical theory – see, e.g., QM Sec.5.5.

³³ See, e.g., QM Secs. 8.5 and 10.3, respectively.

³⁴ In optics, such nonlinearity is implemented using transparent crystals such as lithium niobate (LiNbO_3), with the cubic-nonlinear dependence of the electric polarization on the applied electric field: $\mathcal{P} \propto \mathcal{E} + \alpha \mathcal{E}^3$.

generated waves of frequencies ω_1 and ω_2 is gradually accumulated at their joint propagation along the system. From the analogy between Eq. (85) (describing the evolution of the wave's amplitude *in space*), and the usual equation of the linear oscillator (describing its evolution *in time*), it is clear that this energy transfer accumulation requires not only the frequencies ω but also the wave numbers k be in similar relations. For example, the four-wave mixing requires that not only the frequency balance (92a) but also a similar relation

$$2k = k_1 + k_2, \quad (6.92b)$$

to be fulfilled. Since all three frequencies are close, this relation is easy to arrange. Unfortunately, due to the lack of time/space, for more discussion of this very interesting subject, called *nonlinear optics*, I have to refer the reader to special literature.³⁵

It may look like a dispersion-free media, with $\omega/k = v = \text{const}$, is the perfect solution for arranging the nonlinear/parametric interaction of waves, because in such media, for example, Eq. (92b) automatically follows from Eq. (92a). However, in such a medium, not only the desirable three parametrically interacting waves but also all their harmonics, have the same velocity. At these conditions, the energy transfer rates between all harmonics are of the same order. Perhaps the most important result of such a multi-harmonic interaction is that intensive incident traveling waves, interacting with a nonlinear medium, may develop sharply non-sinusoidal waveforms, in particular those with an almost instant change of the field at a certain moment. Such *shock waves*, especially those of mechanical nature, are of large interest for certain applications – some of them not quite innocent, e.g., the dynamics of explosion in the usual (chemical) and nuclear bombs.³⁶

To conclude this chapter, let me note that the above discussion of 1D acoustic waves will be extended, in Sec. 7.7, to elastic 3D media. There we will see that generally, the waves obey a more complex equation than the apparently natural generalization of Eq. (40):

$$\left(\frac{1}{v^2} \frac{\partial^2}{\partial t^2} - \nabla^2 \right) q(\mathbf{r}, t) = 0, \quad (6.93)$$

where ∇^2 is the 3D Laplace operator. This fact adds to the complexity of traveling-wave and standing-wave phenomena in higher dimensions. Moreover, in multi-dimensional systems, including such pseudo-1D systems as thin rods and pseudo-2D systems such as thin membranes, even static elastic deformations may be very nontrivial. An introduction to the general theory of small deformations, with a focus on elastic continua, will be the subject of the next chapter.

6.8 Exercise problems

For each of the systems specified in Problems 6.1-6.6:

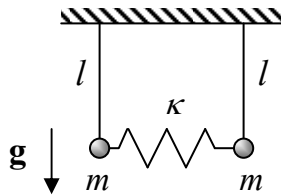
- (i) introduce convenient generalized coordinates q_j of the system,

³⁵ See, e.g., N. Bloembergen, *Nonlinear Optics*, 4th ed., World Scientific, 1996, or a more modern treatment by R. Boyd, *Nonlinear Optics*, 3rd ed., Academic Press, 2008. This field is currently very active. As just a single example, let me mention the recent experiments with parametric amplification of ultrashort ($\sim 20\text{-fs}$) optical pulses to peak power as high as $\sim 5 \times 10^{12} \text{ W}$ – see X. Zeng *et al.*, *Optics Lett.* **42**, 2014 (2017).

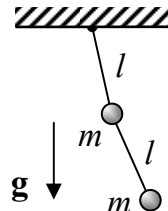
³⁶ The classical (and perhaps still the best) monograph on the subject is Ya. Zeldovich, *Physics of Shock Waves and High-Temperature Phenomena*, Dover, 2002.

- (ii) calculate the frequencies of its small harmonic oscillations near the equilibrium,
- (iii) calculate the corresponding distribution coefficients, and
- (iv) sketch the oscillation modes.

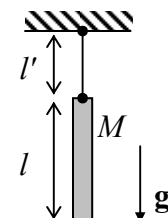
6.1. Two elastically coupled pendula, confined to a vertical plane, with the parameters shown in the figure on the right (see also Problems 1.8 and 2.9).



6.2. The double pendulum, confined to a vertical plane containing the support point (considered in Problem 2.1), with $m' = m$ and $l = l'$ – see the figure on the right.

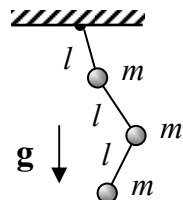


6.3 The chime bell considered in Problem 4.12 (see the figure on the right), for the particular case $l = l'$.

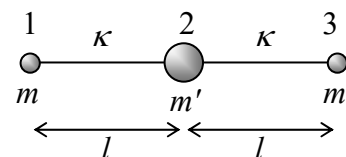


6.4. The triple pendulum shown in the figure on the right, with the motion confined to a vertical plane containing the support point.

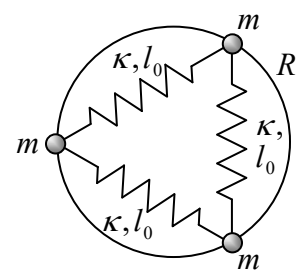
Hint: You may use any (e.g., numerical) method to calculate the characteristic equation's roots.



6.5. A symmetric system of three particles, shown in the figure on the right, where the connections between the particles not only act as usual elastic springs (giving potential energies $U = \kappa(\Delta l)^2/2$) but also resist bending, giving additional potential energy $U' = \kappa'(l\theta)^2/2$, where θ is the (small) bending angle.³⁷



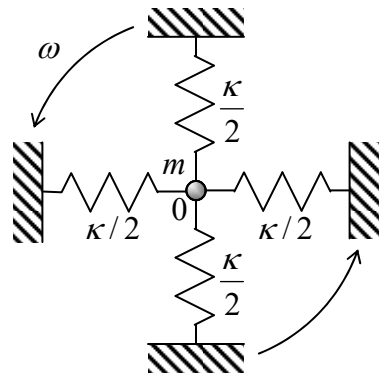
6.6. Three similar beads of mass m , which may slide along a circle of radius R without friction, connected with similar springs with elastic constants κ and equilibrium lengths l_0 (generally not equal to $\sqrt{3}R$) – see the figure on the right.



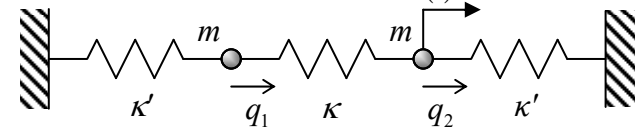
³⁷ This is a good model for small oscillations of linear molecules such as the now-infamous CO₂.

6.7. On the example of the model considered in Problem 1, explore free oscillations in a system of two similar and weakly coupled linear oscillators.

6.8. A small body is held by four similar elastic springs as shown in the figure on the right. Analyze the effect of rotation of the system as a whole about the axis normal to its plane, on the body's small oscillations within this plane. Assume that the oscillation frequency is much higher than the angular velocity ω of the rotation. Discuss the physical sense of your results, and possible ways of using such systems for measurement of the rotation.



6.9. An external longitudinal force $F(t)$ is applied to the right particle of the system shown in Fig. 1, with $\kappa_L = \kappa_R = \kappa'$ and $m_1 = m_2 \equiv m$ (see the figure on the right), and the response $q_1(t)$ of the left particle to this force is being measured.



(i) Calculate the temporal Green's function for this response.

(ii) Use this function to calculate the response to the following force:

$$F(t) = \begin{cases} 0, & \text{for } t < 0, \\ F_0 \sin \omega t, & \text{for } 0 \leq t, \end{cases}$$

with constant amplitude F_0 and frequency ω .

6.10. Use the Lagrangian formalism to re-derive Eqs. (24) for both the longitudinal and the transverse oscillations in the system shown in Fig. 4a.

6.11. Calculate the energy (per unit length) of a sinusoidal traveling wave propagating in the 1D system shown in Fig. 4a. Use your result to calculate the average power flow created by the wave, and compare it with Eq. (49) in the acoustic wave limit.

6.12. Calculate spatial distributions of the kinetic and potential energies in a standing, sinusoidal, 1D acoustic wave, and analyze their evolution in time.

6.13. The midpoint of a guitar string of length l has been slowly pulled off by distance $h \ll l$ from its equilibrium position, and then let go. Neglecting dissipation, use two different approaches to calculate the midpoint's displacement as a function of time.

Hint: You may like to use the following series: $\sum_{m=1}^{\infty} \frac{\cos(2m-1)\xi}{(2m-1)^2} = \frac{\pi^2}{8} \left(1 - \frac{\xi}{\pi/2}\right)$, for $0 \leq \xi \leq \pi$.

6.14. Spell out the spatial-temporal Green's function (82) for waves in a 1D uniform system of N points, with the rigid boundary conditions (62). Explore the acoustic limit of your result.

6.15. Calculate the dispersion law $\omega(k)$ and the maximum and minimum frequencies of small longitudinal waves in a long chain of similar, spring-coupled pendula – see the figure on the right.

6.16. Calculate and analyze the dispersion relation $\omega(k)$ for small waves in a long chain of elastically coupled particles with alternating masses – see the figure on the right. In particular, discuss the dispersion relation's period Δk , and its evolution at $m' \rightarrow m$.

6.17. Analyze the traveling wave's reflection from a “point inhomogeneity”: a single particle with a different mass $m_0 \neq m$, within an otherwise uniform 1D chain – see the figure on the right.

6.18.*

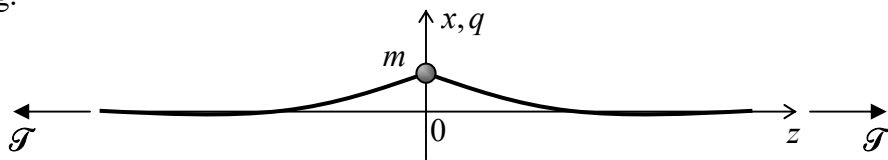
(i) Explore an approximate way to analyze waves in a continuous 1D system with parameters slowly varying along its length.

(ii) Apply this method to calculate the frequencies of transverse standing waves on a freely hanging heavy rope of length l , with a constant mass μ per unit length – see the figure on the right.

(iii) For the three lowest standing wave modes, compare the results with those obtained in the solution of Problem 4 for the triple pendulum.

Hint: The reader familiar with the WKB approximation in quantum mechanics (see, e.g., QM Sec. 2.4) is welcome to adapt it for this classical application. Another possible starting point is the van der Pol approximation discussed in Sec. 5.3, which should be translated from the time domain to the space domain.

6.19. A particle of mass m is attached to an infinite string, of mass μ per unit length, stretched with tension \mathcal{T} . The particle is confined to move along the x -axis normal to the string (see the figure below), in an additional potential $U(x)$ with a minimum at $x = 0$. Assuming that the waves on the string are excited only by the motion of the particle (rather than any external source), reduce the system of equations describing the system to an ordinary differential equation for the small displacements $x(t)$. For the case of a linear oscillator, when $U(x) = m\omega^2 x^2/2$, calculate its Q -factor due to the effective drag caused by the string.



6.20.* Use the van der Pol method to analyze the mutual phase locking of two weakly coupled self-oscillators with the dissipative nonlinearity, for the cases of:

- (i) the direct coordinate coupling described by Eq. (5), and
- (ii) a bilinear but otherwise arbitrary coupling of two similar oscillators.

Hint: In Task (ii), describe the coupling by a linear operator, and express the result via its Fourier image.

6.21.* Extend Task (ii) of the previous problem to the mutual phase locking of N similar self-oscillators. In particular, explore the in-phase mode's stability for the case of the so-called *global coupling* via a single force F contributed equally by all oscillators.

6.22.* Find the condition of non-degenerate parametric excitation in a system of two coupled oscillators described by Eqs. (5), but with a time-dependent coupling: $\kappa \rightarrow \kappa(1 + \mu \cos \omega_p t)$, with $\omega_p \approx \Omega_1 + \Omega_2$, and $\kappa/m \ll |\Omega_2 - \Omega_1|$.

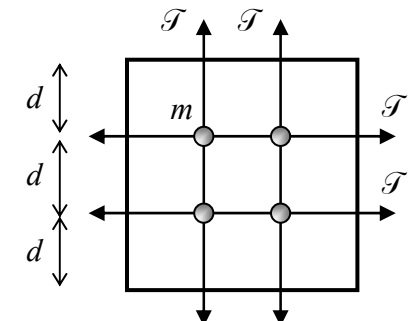
Hint: Assuming the modulation depth μ , the static coupling coefficient κ , and the detuning $\xi \equiv \omega_p - (\Omega_1 + \Omega_2)$ sufficiently small, use the van der Pol method for each of the coupled oscillators.

6.23. Show that the cubic nonlinearity of the type αq^3 indeed enables the parametric interaction (“four-wave mixing”) of oscillations with incommensurate frequencies related by Eqs. (92a).

6.24. In the first nonvanishing approximation in small oscillation amplitudes, calculate their effect on the own frequencies of the same double-pendulum system that was the subject of Problem 1.

6.25. Calculate the velocity of small transverse waves propagating on a thin, planar, elastic membrane, with mass m per unit area, pre-stretched with force τ per unit width.

6.26. A membrane discussed in the previous problem is stretched on a thin but firm plane frame of area $a \times a$. Calculate the frequency spectrum of small transverse standing waves in the system; sketch a few lowest wave modes. Compare the results with those for a discrete-point analog of this system, with four particles of equal masses m , connected with light flexible strings that are stretched, with equal tensions \mathcal{T} , on a similar frame – see the figure on the right. (The frames do not allow the membrane edges/string ends to deviate from their planes.)



This page is
intentionally left
blank

Chapter 7. Deformations and Elasticity

The objective of this chapter is a discussion of small deformations of 3D continua, with a focus on the elastic properties of solids. The reader will see that such deformations are nontrivial even in the absence of their evolution in time, so that several key problems of statics will need to be discussed before proceeding to such dynamic phenomena as elastic waves in infinite media and thin rods.

7.1. Strain

As was already discussed in Chapters 4-6, in a *continuum*, i.e. a system of particles so close to each other that the system discreteness may be neglected, particle displacements \mathbf{q} may be considered as a continuous function of not only time but also space. In this chapter, we will consider only *small* deviations from the rigid-body approximation discussed in Chapter 4, i.e. small *deformations*. The deformation smallness allows us to consider the displacement vector \mathbf{q} as a function of the *initial* (pre-deformation) position of the particle, \mathbf{r} , and time t – just as was done in Chapter 6 for 1D waves.

The first task of the deformation theory is to exclude from consideration the types of motion considered in Chapter 4, namely the body's translation and rotation, unrelated to deformations. This means, first of all, that the variables describing deformations should not depend on the displacement's part that is independent of the position \mathbf{r} (i.e. is common for the whole media), because that part corresponds to a translational shift rather than to a deformation (Fig. 1a). Moreover, even certain non-uniform displacements do not contribute to deformation. For example, Eq. (4.9) (with $d\mathbf{r}$ replaced with $d\mathbf{q}$ to comply with our current notation) shows that a small displacement of the type

$$d\mathbf{q}|_{\text{rotation}} = d\phi \times \mathbf{r}, \quad (7.1)$$

where $d\phi = \omega dt$ is an infinitesimal vector common for the whole continuum, corresponds to its elementary rotation of the body about the direction of that vector, and has nothing to do with its deformation (Fig. 1b).

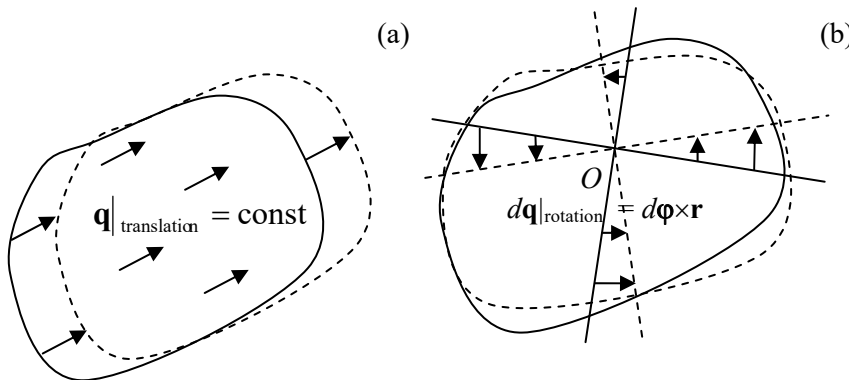


Fig. 7.1. Two types of displacement vector distributions that are unrelated to deformation: (a) translation and (b) rotation.

This is why to develop an adequate quantitative characterization of deformation, so far for fixed t , we should start with finding suitable functions of the spatial distribution of displacements, $\mathbf{q}(\mathbf{r})$, that exist only due to deformations. One of such measures is the change of the distance $dl \equiv |d\mathbf{r}|$ between two close points:

$$(dl)^2 \Big|_{\text{after deformation}} - (dl)^2 \Big|_{\text{before deformation}} = \sum_{j=1}^3 (dr_j + dq_j)^2 - \sum_{j=1}^3 (dr_j)^2 , \quad (7.2)$$

where dq_j is the j^{th} Cartesian component of the difference $d\mathbf{q}$ between the displacements \mathbf{q} of these close points. If the deformation is small in the sense $|d\mathbf{q}| \ll dl$, we may keep, in this expression, only the terms proportional to the first power of the infinitesimal vector $d\mathbf{q}$:

$$(dl)^2 \Big|_{\text{after deformation}} - (dl)^2 \Big|_{\text{before deformation}} = \sum_{j=1}^3 [2dr_j dq_j + (dq_j)^2] \approx 2 \sum_{j=1}^3 dr_j dq_j . \quad (7.3)$$

Since q_j is a function of three independent scalar arguments r_j , its full differential (at fixed time) may be represented as

$$dq_j = \sum_{j'=1}^3 \frac{\partial q_j}{\partial r_{j'}} dr_{j'} . \quad (7.4)$$

The coefficients $\partial q_j / \partial r_{j'}$ may be considered as elements of a tensor providing a linear relation between the vectors $d\mathbf{r}$ and $d\mathbf{q}$.¹ Plugging Eq. (4) into Eq. (2), we get

$$(dl)^2 \Big|_{\text{after deformation}} - (dl)^2 \Big|_{\text{before deformation}} = 2 \sum_{j,j'=1}^3 \frac{\partial q_j}{\partial r_{j'}} dr_j dr_{j'} . \quad (7.5)$$

The convenience of the tensor $\partial q_j / \partial r_{j'}$ for characterizing deformations is that it automatically excludes the translation displacement (Fig. 1a), which is independent of r_j . Its drawback is that its particular elements are still affected by the rotation of the body – even though the sum (5) is not. Indeed, according to the vector product's definition, Eq. (1) may be represented in Cartesian coordinates as

$$dq_j \Big|_{\text{rotation}} = (d\varphi_{j'} r_{j''} - d\varphi_{j''} r_{j'}) \varepsilon_{jj'j''} , \quad (7.6)$$

where $\varepsilon_{jj'j''}$ is the Levi-Civita symbol. Differentiating Eq. (6) over a particular Cartesian coordinate of vector \mathbf{r} , and taking into account that this partial differentiation (∂) is independent of (and hence may be swapped with) the differentiation (d) over the common rotation angle φ , we get the amounts

$$d \left(\frac{\partial q_j}{\partial r_{j'}} \right)_{\text{rotation}} = -\varepsilon_{jj'j''} d\varphi_{j''} \quad \text{and} \quad d \left(\frac{\partial q_{j'}}{\partial r_j} \right)_{\text{rotation}} = -\varepsilon_{j'jj''} d\varphi_{j''} = \varepsilon_{jj'j''} d\varphi_{j''} , \quad (7.7)$$

which may differ from 0. However, notice that the *sum* of these two differentials equals zero for any $d\varphi$, which is possible only if²

$$\left(\frac{\partial q_{j'}}{\partial r_j} + \frac{\partial q_j}{\partial r_{j'}} \right)_{\text{rotation}} = 0 , \quad \text{for } j \neq j' . \quad (7.8)$$

This is why it is convenient to rewrite Eq. (5) in a mathematically equivalent form,

¹ Since both $d\mathbf{q}$ and $d\mathbf{r}$ are legitimate physical vectors (whose Cartesian components are properly transformed as the transfer between reference frames), the 3×3 matrix with elements $\partial q_j / \partial r_{j'}$ is indeed a legitimate physical tensor – see the discussion in Sec. 4.2.

² As a result, the full sum (5), which includes three partial sums (8), is not affected by rotation – as we already know.

$$(dl)^2 \Big|_{\text{after deformation}} - (dl)^2 \Big|_{\text{before deformation}} = 2 \sum_{j,j'=1}^3 s_{jj'} dr_j dr_{j'}, \quad (7.9a)$$

where $s_{jj'}$ are the elements of the so-called *symmetrized strain tensor*, defined as

Strain tensor

$$s_{jj'} \equiv \frac{1}{2} \left(\frac{\partial q_j}{\partial r_{j'}} + \frac{\partial q_{j'}}{\partial r_j} \right). \quad (7.9b)$$

(Note that this modification does not affect the diagonal elements $s_{jj} = \partial q_j / \partial r_j$.) So, the advantage of the symmetrized tensor (9b) over the initial tensor with elements $\partial q_j / \partial r_j$ is that according to Eq. (8), at pure rotation, all elements of the symmetrized strain tensor vanish.

Now let us discuss the physical meaning of this tensor. As was already mentioned in Sec. 4.2, any symmetric tensor may be diagonalized by an appropriate selection of the reference frame axes. In such principal axes, $s_{jj'} = s_{jj} \delta_{jj'}$, so that Eq. (4) takes a simple form:

$$dq_j = \frac{\partial q_j}{\partial r_j} dr_j = s_{jj} dr_j. \quad (7.10)$$

We may use this expression to calculate the change of each side of an elementary cuboid (parallelepiped) with its sides dq_j parallel to the principal axes:

$$dr_j \Big|_{\text{after deformation}} - dr_j \Big|_{\text{before deformation}} \equiv dq_j = s_{jj} dr_j, \quad (7.11)$$

and of the cuboid's volume $dV = dr_1 dr_2 dr_3$:

$$dV \Big|_{\text{after deformation}} - dV \Big|_{\text{before deformation}} = \prod_{j=1}^3 (dr_j + s_{jj} dr_j) - \prod_{j=1}^3 dr_j = dV \left[\prod_{j=1}^3 (1 + s_{jj}) - 1 \right], \quad (7.12)$$

Since all our analysis is only valid in the linear approximation in small s_{jj} , Eq. (12) is reduced to

$$dV \Big|_{\text{after deformation}} - dV \Big|_{\text{before deformation}} \approx dV \sum_{j=1}^3 s_{jj} \equiv dV \text{Tr}(s), \quad (7.13)$$

where Tr (*trace*)³ of any matrix (in particular, any tensor) is the sum of its diagonal elements; in our current case

$$\text{Tr}(s) \equiv \sum_{j=1}^3 s_{jj}. \quad (7.14)$$

The tensor theory shows that the trace does not depend on the particular choice of the coordinate axes; so, the diagonal elements of the strain tensor characterize the medium's compression/extension.

Next, what is the meaning of its off-diagonal elements? It may be illustrated by the simplest example of a purely *shear deformation* shown in Fig. 2. (The geometry means to be uniform along the z -axis normal to the plane of the drawing.) In this case, all displacements (assumed small) have just one Cartesian component, in Fig. 2 along the x -axis: $\mathbf{q} = \mathbf{n}_x \alpha \mathbf{y}$ (with $\alpha \ll 1$), so that the only nonzero element of the initial strain tensor $\partial q_j / \partial r_j$ is $\partial q_x / \partial y = \alpha$, and the symmetrized tensor (9b) is

³ The traditional European notation for Tr is Sp (from the German *Spur* meaning “trace” or “track”).

$$\mathbf{s} = \begin{pmatrix} 0 & \alpha/2 & 0 \\ \alpha/2 & 0 & 0 \\ 0 & 0 & 0 \end{pmatrix}. \quad (7.15)$$

Evidently, the change of volume, given by Eq. (13), vanishes in this case. Thus, off-diagonal elements of the tensor \mathbf{s} characterize shear deformations.

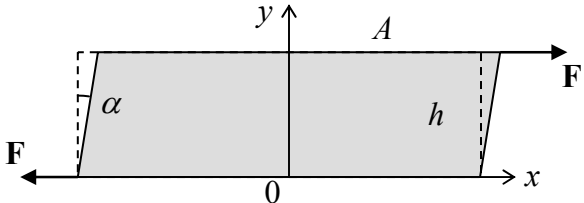


Fig. 7.2. An example of pure shear.

To conclude this section, let me note that Eq. (9) is only valid in Cartesian coordinates. For the solution of some important problems with the axial or spherical symmetry, it is frequently convenient to express six different elements of the symmetric strain tensor in either cylindrical or spherical coordinates via three components of the displacement vector \mathbf{q} in the same coordinates. A straightforward differentiation of the definitions of these curvilinear coordinates, similar to that used to derive the well-known expressions for spatial derivatives of arbitrary functions,⁴ yields, in particular, the following formulas for the diagonal elements of the tensor:

(i) in the cylindrical coordinates:

$$s_{\rho\rho} = \frac{\partial q_\rho}{\partial \rho}, \quad s_{\varphi\varphi} = \frac{1}{\rho} \left(q_\rho + \frac{\partial q_\varphi}{\partial \varphi} \right), \quad s_{zz} = \frac{\partial q_z}{\partial z}. \quad (7.16)$$

(ii) in the spherical coordinates:

$$s_{rr} = \frac{\partial q_r}{\partial r}, \quad s_{\theta\theta} = \frac{1}{r} \left(q_r + \frac{\partial q_\theta}{\partial \theta} \right), \quad s_{\varphi\varphi} = \frac{1}{r} \left(q_r + q_\theta \frac{\cos \theta}{\sin \theta} + \frac{1}{\sin \theta} \frac{\partial q_\varphi}{\partial \varphi} \right). \quad (7.17)$$

These expressions, which will be used below for the solution of some problems for symmetrical geometries, may be a bit counter-intuitive. Indeed, Eq. (16) shows that even for a purely radial, axially-symmetric deformation, $\mathbf{q} = q(\rho)\mathbf{n}_\rho$, the angular element of the strain tensor does not vanish: $s_{\varphi\varphi} = q/\rho$. (According to Eq. (17), in the spherical coordinates, both angular elements of the tensor exhibit the same property.) Note, however, that this relation describes a simple geometric fact: the change of the lateral distance $\rho d\varphi \ll \rho$ between two close points at the same distance from the symmetry axis, at a small change of ρ that keeps the angle $d\varphi$ between the directions towards these two points intact.

7.2. Stress

Now let us discuss the forces that cause the strain – or, from a legitimate alternative point of view, are caused by the strain. Internal forces acting inside (i.e. between arbitrarily defined parts of) a

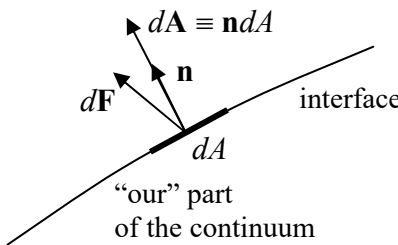
⁴ See, e.g., MA Eqs. (10.1)-(10.12).

continuum may be also characterized by a tensor. This *stress tensor*,⁵ with elements $\sigma_{jj'}$, relates the Cartesian components of the vector $d\mathbf{F}$ of the force acting on an elementary area dA of an (in most cases, just imagined) interface between two parts of a continuum, to the components of the elementary vector $d\mathbf{A} = \mathbf{n}dA$ normal to the area – see Fig. 3:

Stress tensor

$$dF_j = \sum_{j'=1}^3 \sigma_{jj'} dA_{j'} . \quad (7.18)$$

The usual sign convention here is to take the *outer* normal $d\mathbf{n}$, i.e. to direct $d\mathbf{A}$ out of “our” part of the continuum, i.e. the part on which the calculated force $d\mathbf{F}$ is exerted – by the complementary part.

Fig. 7.3. The definition of vectors $d\mathbf{A}$ and $d\mathbf{F}$.

In some cases, the stress tensor’s structure is very simple. For example, as will be discussed in detail in the next chapter, static and ideal *fluids* (i.e. liquids and gases) may only provide forces normal to any interface, and usually directed toward “our” part of the body, so that

Pressure

$$d\mathbf{F} = -P d\mathbf{A}, \quad \text{i.e. } \sigma_{jj'} = -P \delta_{jj'}, \quad (7.19)$$

where the scalar P (in most cases positive) is called *pressure*, and generally may depend on both the spatial position and time. This type of stress, with $P > 0$, is frequently called *hydrostatic compression* – even if it takes place in solids, as it may.

However, in the general case, the stress tensor also has off-diagonal terms, which characterize the shear stress. For example, if the shear strain in Fig. 2 is caused by the shown pair of forces $\pm F$, they create internal forces $F_x \mathbf{n}_x$, with $F_x > 0$ if we speak about the force acting upon a part of the sample below the imaginary horizontal interface we are discussing. To avoid a horizontal acceleration of each horizontal slice of the sample, the forces should not depend on y , i.e. $F_x = \text{const} = F$. Superficially, it may look that in this case, the only nonzero element of the stress tensor is $dF_x/dA_y = F/A = \text{const}$, so that tensor is asymmetric, in contrast to the strain tensor (15) of the same system. Note, however, that the displayed pair of forces $\pm F$ creates not only the shear stress but also a nonzero rotating torque $\tau = -Fh\mathbf{n}_z = -(dF_x/dA_y)Ah\mathbf{n}_z = -(dF_x/dA_y)V\mathbf{n}_z$, where $V = Ah$ is the sample’s volume. So, if we want to perform a static stress experiment, i.e. avoid the sample’s rotation, we need to apply some other forces, e.g., a pair of vertical forces creating an equal and opposite torque $\tau' = (dF_y/dA_x)V\mathbf{n}_z$, implying that $dF_y/dA_x = dF_x/dA_y = F/A$. As a result, the stress tensor becomes symmetric, and similar in structure to the symmetrized strain tensor (15):

⁵ It is frequently called the *Cauchy stress tensor*, partly to honor Augustin-Louis Cauchy who introduced this notion (and is responsible for the development, mostly in the 1820s, much of the theory described in this chapter), and partly to distinguish it from other possible definitions of the stress tensor, including the *1st* and *2nd* *Piola-Kirchhoff tensors*. For the small deformations discussed in this course, all these notions coincide.

$$\sigma = \begin{pmatrix} 0 & F/A & 0 \\ F/A & 0 & 0 \\ 0 & 0 & 0 \end{pmatrix}. \quad (7.20)$$

In many situations, the body may be stressed not only by forces applied to their surfaces but also by some volume-distributed (*bulk*) forces $d\mathbf{F} = \mathbf{f}dV$, whose certain effective *bulk density* \mathbf{f} . (The most evident example of such forces is gravity. If its field is uniform as described by Eq. (1.16), then $\mathbf{f} = \rho\mathbf{g}$, where ρ is the mass density.) Let us derive the key formula describing the summation of the interface and bulk forces. For that, consider again an elementary cuboid with sides dr_j parallel to the corresponding coordinate axes \mathbf{n}_j (Fig. 4) – now not necessarily the principal axes of the stress tensor.

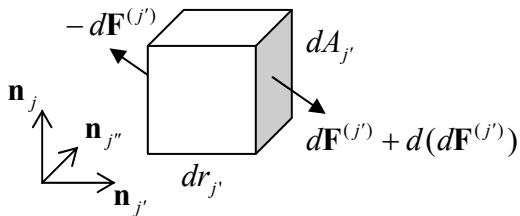


Fig. 7.4. Deriving Eq. (23).

If elements $\sigma_{jj'}$ of the tensor do not depend on position, the force $d\mathbf{F}^{(j')}$ acting on the j' -th face of the cuboid is exactly balanced by the equal and opposite force acting on its opposite face, because the vectors $d\mathbf{A}^{(j')}$ at these faces are equal and opposite. However, if $\sigma_{jj'}$ is a function of \mathbf{r} , then the net force $d(d\mathbf{F}^{(j)})$ does not vanish. (In this expression, the first differential sign refers to the elementary shift dr_j , while the second one, to the elementary area $dA_{j'}$.) Using the expression $\sigma_{jj'}dA_{j'}$ for the j' th contribution to the sum (18), in the first order in $d\mathbf{r}$ the j th components of the vector $d(d\mathbf{F}^{(j)})$ is

$$d(dF_j^{(j')}) = d(\sigma_{jj'}dA_{j'}) = \frac{\partial\sigma_{jj'}}{\partial r_{j'}} dr_{j'} dA_{j'} \equiv \frac{\partial\sigma_{jj'}}{\partial r_{j'}} dV, \quad (7.21)$$

where the cuboid's volume $dV = dr_j dA_{j'}$ evidently does not depend on the index j' . The addition of these force components for all three pairs of cuboid faces, i.e. the summation of Eqs. (21) over all three values of the upper index j' , yields the following relation for the j th Cartesian component of the net force exerted on the cuboid:

$$d(dF_j) = \sum_{j'=1}^3 d(dF_j^{(j')}) = \sum_{j'=1}^3 \frac{\partial\sigma_{jj'}}{\partial r_{j'}} dV. \quad (7.22)$$

Since any volume may be broken into such infinitesimal cuboids, Eq. (22) shows that the space-varying stress is equivalent to a volume-distributed force $d\mathbf{F}_{\text{ef}} = \mathbf{f}_{\text{ef}}dV$, whose *effective* (not real!) bulk density \mathbf{f}_{ef} has the following Cartesian components

$$(f_{\text{ef}})_j = \sum_{j'=1}^3 \frac{\partial\sigma_{jj'}}{\partial r_{j'}}, \quad (7.23)$$

Euler-Cauchy principle

so that in the presence of genuinely bulk forces $d\mathbf{F} = \mathbf{f}dV$, the densities \mathbf{f}_{ef} and \mathbf{f} just add up. This is the so-called *Euler-Cauchy stress principle*.

Let us use this addition rule to spell out the 2nd Newton law for a unit volume of a continuum:

$$\rho \frac{\partial^2 \mathbf{q}}{\partial t^2} = \mathbf{f}_{\text{ef}} + \mathbf{f}. \quad (7.24)$$

Using Eq. (23), the j^{th} Cartesian component of Eq. (24) may be represented as

$$\rho \frac{\partial^2 q_j}{\partial t^2} = \sum_{j'=1}^3 \frac{\partial \sigma_{jj'}}{\partial r_{j'}} + f_j. \quad (7.25)$$

This is the key equation of the continuum's dynamics (and statics), which will be repeatedly used below.

For the solution of some problems, it is also convenient to have a general expression for the work $\delta\mathcal{W}$ of the stress forces at a virtual deformation $\delta\mathbf{q}$ – understood in the same variational sense as the virtual displacements $\delta\mathbf{r}$ in Sec. 2.1. Using the Euler-Cauchy principle (23), for any volume V of a medium not affected by volume-distributed forces, we may write⁶

$$\delta\mathcal{W} = - \int_V \mathbf{f}_{\text{ef}} \cdot \delta\mathbf{q} d^3 r = - \sum_{j=1}^3 \int_V (f_{\text{ef}})_j \delta q_j d^3 r = - \sum_{j,j'=1}^3 \int_V \frac{\partial \sigma_{jj'}}{\partial r_{j'}} \delta q_j d^3 r. \quad (7.26)$$

Let us work out this integral by parts for a volume so large that the deformations δq_j on its surface are negligible. Then, swapping the operations of the variation and the spatial differentiation (just like it was done with the time differentiation in Sec. 2.1), we get

$$\delta\mathcal{W} = \sum_{j,j'=1}^3 \int_V \sigma_{jj'} \delta \frac{\partial q_j}{\partial r_{j'}} d^3 r. \quad (7.27)$$

Assuming that the tensor $\sigma_{jj'}$ is symmetric, we may rewrite this expression as

$$\delta\mathcal{W} = \frac{1}{2} \sum_{j,j'=1}^3 \int_V \left(\sigma_{jj'} \delta \frac{\partial q_j}{\partial r_{j'}} + \sigma_{j'j} \delta \frac{\partial q_j}{\partial r_{j'}} \right) d^3 r. \quad (7.28)$$

Now, swapping indices j and j' in the second expression, we finally get

$$\delta\mathcal{W} = \frac{1}{2} \sum_{j,j'=1}^3 \int_V \delta \left(\frac{\partial q_j}{\partial r_{j'}} \sigma_{jj'} + \frac{\partial q_{j'}}{\partial r_j} \sigma_{j'j} \right) d^3 r = - \sum_{j,j'=1}^3 \int_V \sigma_{jj'} \delta s_{jj'} d^3 r, \quad (7.29)$$

where $s_{jj'}$ are the elements of the strain tensor (9b). It is natural to rewrite this important formula as

$$\delta\mathcal{W} = \int_V \delta \mathbf{w}(\mathbf{r}) d^3 r, \quad \text{where } \delta \mathbf{w}(\mathbf{r}) \equiv \sum_{j,j'=1}^3 \sigma_{jj'} \delta s_{jj'}, \quad (7.30)$$

and interpret the locally-defined scalar function $\delta\mathbf{w}(\mathbf{r})$ as the work of the stress forces per unit volume, at a small variation of the deformation.

As a sanity check, for the pure pressure (19), Eq. (30) is reduced to the obviously correct result $\delta\mathcal{W} = -P\delta V$, where V is the volume of “our” part of the continuum.

⁶ Here the sign corresponds to the work of the “external” stress force $d\mathbf{F}$ exerted on “our” part of the continuum by its counterpart – see Fig. 3. Note that some texts make the opposite definition of $\delta\mathcal{W}$, leading to its opposite sign.

7.3. Hooke's law

In order to form a complete system of equations describing the continuum's dynamics, one needs to complement Eq. (25) with an appropriate *constitutive equation* describing the relation between the forces described by the stress tensor $\sigma_{jj'}$, and the deformations \mathbf{q} described (in the small deformation limit) by the strain tensor $s_{jj'}$. This relation depends on the medium, and generally may be rather complicated. Even leaving alone various anisotropic solids (e.g., crystals) and macroscopically-inhomogeneous materials (like ceramics or sand), strain typically depends not only on the current value of stress (possibly in a nonlinear way) but also on the previous history of stress application. Indeed, if strain exceeds a certain *plasticity threshold*, atoms (or nanocrystals) may slip to their new positions and never come back even if the strain is reduced. As a result, deformations become irreversible – see Fig. 5.

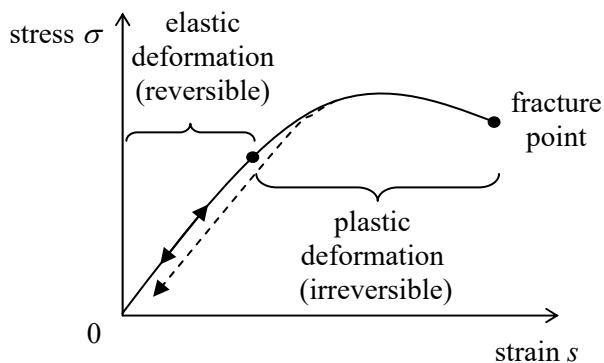


Fig. 7.5. A typical relation between the stress and strain in solids (schematically).

Only below the thresholds of nonlinearity and plasticity (which are typically close to each other), the strain is nearly proportional to stress, i.e. obeys the famous *Hooke's law*.⁷ However, even in this *elastic range*, the law is not quite simple, and even for an isotropic medium is described not by one but by two constants, called the *elastic moduli*. The reason for that is that most elastic materials resist the strain accompanied by a volume change (say, the hydrostatic compression) differently from how they resist a shear deformation.

To describe this difference, let us first represent the symmetrized strain tensor (9b) in the following mathematically equivalent form:

$$s_{jj'} = \left(s_{jj'} - \frac{1}{3} \delta_{jj'} \text{Tr}(s) \right) + \left(\frac{1}{3} \delta_{jj'} \text{Tr}(s) \right). \quad (7.31)$$

According to Eq. (13), the *traceless tensor* in the first parentheses does not give any contribution to the volume change, e.g., may be used to characterize a purely shear deformation, while the second term describes the hydrostatic compression alone. Hence we may expect that the stress tensor may be represented (again, within the elastic deformation range only!) as

$$\sigma_{jj'} = 2\mu \left(s_{jj'} - \frac{1}{3} \text{Tr}(s) \delta_{jj'} \right) + 3K \left(\frac{1}{3} \text{Tr}(s) \delta_{jj'} \right), \quad (7.32)$$

Hooke's law via μ and K

where K and μ are constants. (The inclusion of coefficients 2 and 3 into Eq. (32) is justified by the simplicity of some of its corollaries – see, e.g., Eqs. (36) and (41) below.) Indeed, experiments show that

⁷ Named after Robert Hooke (1635-1703), the polymath who was the first to describe the law in its simplest, 1D version.

Hooke's law in this form is followed, at small strain, by all isotropic materials. In accordance with the above discussion, the constant μ (in some texts, denoted as G) is called the *shear modulus*, while the constant K (sometimes denoted B), the *bulk modulus*. The two left columns of Table 1 show the approximate values of these moduli for typical representatives of several major classes of materials.⁸

Table 7.1. Elastic moduli, density, and sound velocities of a few representative materials (approximate values)

Material	K (GPa)	μ (GPa)	E (GPa)	ν	ρ (kg/m ³)	v_l (m/s)	v_t (m/s)
Diamond ^(a)	600	450	1,100	0.20	3,500	1,830	1,200
Hardened steel	170	75	200	0.30	7,800	5,870	3,180
Water ^(b)	2.1	0	0	0.5	1,000	1,480	0
Air ^(b)	0.00010	0	0	0.5	1.2	332	0

^(a) Averages over crystallographic directions (~10% anisotropy).

^(b) At the so-called *ambient conditions* ($T = 20^\circ\text{C}$, $\mathcal{P} = 1 \text{ bar} \equiv 10^5 \text{ Pa}$).

To better appreciate these values, let us first discuss the quantitative meaning of K and μ , using two simple examples of elastic deformation. However, in preparation for that, let us first solve the set of nine (or rather six different) linear equations (32) for $s_{jj'}$. This is easy to do, due to the simple structure of these equations: they relate the elements $\sigma_{jj'}$ and $s_{jj'}$ with the same indices, but the tensor's trace effect. This slight complication may be readily overcome by noticing that according to Eq. (32),

$$\text{Tr}(\sigma) \equiv \sum_{j=1}^3 \sigma_{jj} = 3K \text{Tr}(s), \quad \text{so that } \text{Tr}(s) = \frac{1}{3K} \text{Tr}(\sigma). \quad (7.33)$$

Plugging this result into Eq. (32) and solving it for $s_{jj'}$, we readily get the reciprocal relation, which may be represented in a similar form:

$$s_{jj'} = \frac{1}{2\mu} \left(\sigma_{jj'} - \frac{1}{3} \text{Tr}(\sigma) \delta_{jj'} \right) + \frac{1}{3K} \left(\frac{1}{3} \text{Tr}(\sigma) \delta_{jj'} \right). \quad (7.34)$$

Now let us apply Hooke's law, in the form of Eqs. (32) or (34), to two simple situations in which the strain and stress tensors may be found without using the full differential equation of the elasticity theory and boundary conditions for them. (That will be the subject of the next section.) The first situation is the hydrostatic compression when the stress tensor is diagonal, and all its diagonal elements are equal – see Eq. (19).⁹ For this case, Eq. (34) yields

$$s_{jj'} = -\frac{\mathcal{P}}{3K} \delta_{jj'}, \quad (7.35)$$

⁸ Since the strain tensor elements, defined by Eq. (9), are dimensionless, while the strain, defined by Eq. (18), has the dimensionality similar to pressure (of force per unit area), so do the elastic moduli K and μ .

⁹ It may be proved that such a situation may be implemented not only in a fluid with pressure \mathcal{P} but also in a solid sample of an *arbitrary* shape, for example by placing it into a compressed fluid.

i.e. regardless of the shear modulus, the strain tensor is also diagonal, with all diagonal elements equal. According to Eqs. (11) and (13), this means that all linear dimensions of the body are reduced by a similar factor, so that its shape is preserved, while the volume is reduced by

$$\frac{\Delta V}{V} = \sum_{j=1}^3 S_{jj} = -\frac{\mathcal{P}}{K}. \quad (7.36)$$

This formula clearly shows the physical sense of the bulk modulus K as the *reciprocal compressibility*. As Table 1 shows, the values of K may be dramatically different for various materials, and even for such “soft stuff” as water, this modulus is actually rather high. For example, even at the bottom of the deepest, 10-km ocean well ($\mathcal{P} \approx 10^3$ bar ≈ 0.1 GPa), the water’s density increases by just about 5%. As a result, in most human-scale experiments, water may be treated as an *incompressible fluid* – the approximation that will be widely used in the next chapter. Many solids are even much less compressible – see, for example, the first two rows of Table 1.

Quite naturally, the most compressible media are gases. For a portion of gas, a certain background pressure \mathcal{P} is necessary just for containing it within its volume V , so that Eq. (36) is only valid for small increments of pressure, $\Delta\mathcal{P}$:

$$\frac{\Delta V}{V} = -\frac{\Delta\mathcal{P}}{K}. \quad (7.37)$$

Moreover, the compression of gases also depends on thermodynamic conditions. (In contrast, for most condensed media, the temperature effects are very small.) For example, at ambient conditions, most gases are reasonably well described by the equation of state called the *ideal classical gas*:

$$\mathcal{P}V = Nk_B T, \quad \text{i.e. } \mathcal{P} = \frac{Nk_B T}{V}. \quad (7.38)$$

where N is the number of molecules in volume V , and $k_B \approx 1.38 \times 10^{-23}$ J/K is the Boltzmann constant.¹⁰ For a small volume change ΔV at a constant temperature T , this equation gives

$$\Delta\mathcal{P}|_{T=\text{const}} = -\frac{Nk_B T}{V^2} \Delta V = -\frac{\mathcal{P}}{V} \Delta V, \quad \text{i.e. } \frac{\Delta V}{V}|_{T=\text{const}} = -\frac{\Delta\mathcal{P}}{P}. \quad (7.39)$$

Comparing this expression with Eq. (36), we get a remarkably simple result for the isothermal compression of gases,

$$K|_{T=\text{const}} = \mathcal{P}, \quad (7.40)$$

which means in particular that the bulk modulus listed in Table 1 is actually valid, at the ambient conditions, for almost any gas. Note, however, that the change of thermodynamic conditions (say, from isothermal to adiabatic¹¹) may affect the compressibility of the gas..

Now let us consider the second, rather different, fundamental experiment: a purely shear deformation shown in Fig. 2. Since the traces of the matrices (15) and (20), which describe this situation, are equal to 0, for their off-diagonal elements, Eq. (32) gives merely $\sigma_{jj'} = 2\mu s_{jj'}$, so that the deformation angle α (see Fig. 2) is just

¹⁰ For the derivation and a detailed discussion of Eq. (37), see, e.g., SM Sec. 3.1.

¹¹ See, e.g., SM Sec. 1.3.

$$\alpha = \frac{1}{\mu} \frac{F}{A}. \quad (7.41)$$

Note that the angle does not depend on the thickness h of the sample, though of course the maximal linear deformation $q_x = \alpha h$ is proportional to the thickness. Naturally, as Table 1 shows, $\mu = 0$ for all fluids because they do not resist static shear stress.

However, not all situations, even apparently simple ones, involve just either K or μ . Let us consider stretching a long and thin elastic rod of a uniform cross-section of area A – the so-called *tensile stress experiment* shown in Fig. 6.¹²

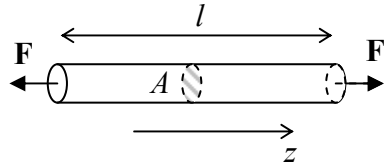


Fig. 7.6. The tensile stress experiment.

Though the deformation of the rod near its clamped ends depends on the exact way forces \mathbf{F} are applied (we will discuss this issue later on), we may expect that over most of its length the tension forces are directed virtually along the rod, $d\mathbf{F} = F_z \mathbf{n}_z$, and hence, with the coordinate choice shown in Fig. 6, $\sigma_{xj} = \sigma_{yj} = 0$ for all j , including the diagonal elements σ_{xx} and σ_{yy} . Moreover, due to the open lateral surfaces, on which, evidently, $dF_x = dF_y = 0$, there cannot be an internal stress force of *any* direction, acting on any elementary internal boundary parallel to these surfaces. This means that $\sigma_{zx} = \sigma_{zy} = 0$. So, of all elements of the stress tensor only one, σ_{zz} , is not equal to zero, and for a uniform sample, $\sigma_{zz} = \text{const} = F/A$. For this case, Eq. (34) shows that the strain tensor is also diagonal, but with different diagonal elements:

$$s_{zz} = \left(\frac{1}{9K} + \frac{1}{3\mu} \right) \sigma_{zz}, \quad (7.42)$$

$$s_{xx} = s_{yy} = \left(\frac{1}{9K} - \frac{1}{6\mu} \right) \sigma_{zz}. \quad (7.43)$$

Since the tensile stress is most common in engineering practice (including physical experiment design), both combinations of the elastic moduli participating in these two relations have earned their own names. In particular, the constant in Eq. (42) is usually denoted as $1/E$ (but in many texts, as $1/Y$), where E is called *Young's modulus*:¹³

$$\frac{1}{E} \equiv \frac{1}{9K} + \frac{1}{3\mu}, \quad \text{i.e. } E \equiv \frac{9K\mu}{3K + \mu}. \quad (7.44)$$

¹² Though the analysis of compression in this situation gives similar results, in practical experiments a strong compression of a long sample may lead to the loss of the horizontal stability – the so-called *buckling* – of the rod.

¹³ Named after another polymath, Thomas Young (1773–1829) – somewhat unfairly, because his work on elasticity was predicated by a theoretical analysis by L. Euler in 1727 and detailed experiments by Giordano Riccati in 1782.

As Fig. 6 shows, in the tensile stress geometry $s_{zz} \equiv \partial q_z / \partial z = \Delta l / l$, so that Young's modulus scales the linear relation between the relative extension of the rod and the force applied per unit area:¹⁴

$$\frac{\Delta l}{l} = \frac{1}{E} \frac{F}{A}. \quad (7.45)$$

The third column of Table 1 above shows the values of this modulus for two well-known solids: diamond (with the highest known value of E of all bulk materials¹⁵) and the steels (solid solutions of ~10% of carbon in iron) used in construction. Again, for all fluids, Young's modulus equals zero – as it follows from Eq. (44) for $\mu = 0$.

I am confident that most readers of these notes have been familiar with Eq. (42), in the form of Eq. (45), from their undergraduate studies. However, this can hardly be said about its counterpart, Eq. (43), which shows that at the tensile stress, the rod's cross-section dimensions also change. This effect is usually characterized by the following dimensionless *Poisson's ratio*:¹⁶

$$\nu \equiv -\frac{s_{xx}}{s_{zz}} = -\frac{s_{yy}}{s_{zz}} = -\left(\frac{1}{9K} - \frac{1}{6\mu}\right) \Bigg/ \left(\frac{1}{9K} + \frac{1}{3\mu}\right) \equiv \frac{1}{2} \frac{3K - 2\mu}{3K + \mu}. \quad (7.46)$$

Poisson ratio

According to this formula, for realistic materials with $K > 0$, $\mu \geq 0$, ν may vary from (-1) to (+1/2), but for the vast majority of materials,¹⁷ its values are between 0 and 1/2 – see the corresponding column of Table 1. The lower limit of this range is reached in porous materials like cork, whose *lateral dimensions* almost do not change at the tensile stress. Some soft materials such as natural and synthetic rubbers present the opposite case: $\nu \approx 1/2$.¹⁸ Since according to Eqs. (13) and (42), the volume change is

$$\frac{\Delta V}{V} = s_{xx} + s_{yy} + s_{zz} = \frac{1}{E} \frac{F}{A} (1 - 2\nu) \equiv (1 - 2\nu) \frac{\Delta l}{l}, \quad (7.47)$$

such materials virtually do not change their *volume* at the tensile stress. The ultimate limit of this trend, $\Delta V/V = 0$, is provided by fluids and gases, because, as it follows from Eq. (46) with $\mu = 0$, their Poisson's ratio ν is exactly 1/2. However, for most practicable construction materials such as various steels (see Table 1) the relative volume change (47) is as high as ~40% of that of the length.

Due to the tensile stress dominance in practice, the coefficients E and ν are frequently used as a pair of independent elastic moduli, instead of K and μ . Solving Eqs. (44) and (46) for them, we get

$$K = \frac{E}{3(1 - 2\nu)}, \quad \mu = \frac{E}{2(1 + \nu)}. \quad (7.48)$$

¹⁴ According to Eq. (47), E may be thought of as the force (per unit area) that would double the initial sample's length, if only Hooke's law was valid for deformations that large – as it typically isn't.

¹⁵ E is probably somewhat higher (up to 2,000 GPa) in such nanostructures as carbon nanotubes and monatomic sheets (*graphene*), though there is still substantial uncertainty in experimentally measured elastic moduli of these structures – for a review see, e.g., G. Dimitrios *et al.*, *Prog. Mater. Sci.* **90**, 75 (2017).

¹⁶ In some older texts, the Poisson's ratio is denoted σ , but its notation as ν dominates modern literature.

¹⁷ The only known exceptions are certain exotic solids with very specific internal microstructure – see, e.g., R. Lakes, *Science* **235**, 1038 (1987) and references therein.

¹⁸ For example, *silicone rubbers* (synthetic polymers broadly used in engineering and physics experiment design) have, depending on their particular composition, synthesis, and thermal curing, $\nu = 0.47 \div 0.49$, and as a result combine respectable bulk moduli $K = (1.5 \div 2)$ GPa with very low Young's moduli: $E = (0.0001 \div 0.05)$ GPa.

Using these formulas, the two (equivalent) formulations of Hooke's law, expressed by Eqs. (32) and (34), may be rewritten as

Hooke's
law via
 E and ν

$$\sigma_{jj'} = \frac{E}{1+\nu} \left(s_{jj'} + \frac{\nu}{1-2\nu} \text{Tr}(s)\delta_{jj'} \right), \quad (7.49a)$$

$$s_{jj'} = \frac{1+\nu}{E} \left(\sigma_{jj'} - \frac{\nu}{1+\nu} \text{Tr}(\sigma)\delta_{jj'} \right). \quad (7.49b)$$

The linear relation between the strain and stress tensor in elastic continua enables one more step in our calculation of the potential energy U due to deformation, which was started at the end of Sec. 2. Indeed, to each infinitesimal part of this strain increase, we may apply Eq. (30), with the elementary work $\delta\mathcal{W}$ of the surface forces increasing the potential energy of "our" part of the body by the equal amount δU . Let us slowly increase the deformation from a completely unstrained state (in which we may take $U = 0$) to a certain strained state, in the absence of bulk forces \mathbf{f} , keeping the deformation type, i.e. the relation between the elements of the stress tensor, intact. In this case, all elements of the tensor $\sigma_{jj'}$ are proportional to the same single parameter characterizing the stress (say, the total applied force), and according to Hooke's law, all elements of the tensor $s_{jj'}$ are proportional to that parameter as well. In this case, integration of Eq. (30) through the variation yields the following final value:¹⁹

Elastic
deformation
energy

$$U = \int_V u(\mathbf{r}) d^3 r, \quad u(\mathbf{r}) = \frac{1}{2} \sum_{j,j'=1}^3 \sigma_{jj'} s_{jj'}. \quad (7.50)$$

Evidently, this $u(\mathbf{r})$ may be interpreted as the volumic density of the potential energy of the elastic deformation.

7.4. Equilibrium

Now we are fully equipped to discuss the elastic deformation dynamics, but let us start with statics. The static (equilibrium) state may be described by requiring the right-hand side of Eq. (25) to vanish. To find the elastic deformation, we need to plug $\sigma_{jj'}$ from Hooke's law (49a), and then express the elements $s_{jj'}$ via the displacement distribution – see Eq. (9). For a uniform material, the result is²⁰

$$\frac{E}{2(1+\nu)} \sum_{j'=1}^3 \frac{\partial^2 q_j}{\partial r_{j'}^2} + \frac{E}{2(1+\nu)(1-2\nu)} \sum_{j'=1}^3 \frac{\partial^2 q_{j'}}{\partial r_j \partial r_{j'}} + f_j = 0. \quad (7.51)$$

Taking into account that the first sum is just the j^{th} component of $\nabla^2 \mathbf{q}$, while the second sum is the j^{th} component of $\nabla(\nabla \cdot \mathbf{q})$, we see that all three equations (51) for three Cartesian components ($j = 1, 2$, and 3) of the deformation vector \mathbf{q} , may be conveniently merged into one vector equation

$$\frac{E}{2(1+\nu)} \nabla^2 \mathbf{q} + \frac{E}{2(1+\nu)(1-2\nu)} \nabla(\nabla \cdot \mathbf{q}) + \mathbf{f} = 0. \quad (7.52)$$

Elastic
continuum:
equilibrium

¹⁹ To give additional clarity to the arising factor $\frac{1}{2}$, let me spell out this integration for the simple case of a 1D spring. In this case, Eq. (30) is reduced to $\delta U = \delta\mathcal{W} = F\delta x$, and if the spring's force is elastic, $F = \kappa x$, the integration over x from 0 to its final value yields $U = \kappa x^2/2 \equiv Fx/2$.

²⁰ As it follows from Eqs. (48), the coefficient before the first sum in Eq. (51) is just the shear modulus μ , while that before the second sum is equal to $(K + \mu/3)$.

For some applications, it is more convenient to recast this equation into a different form, using the well-known vector identity²¹ $\nabla^2 \mathbf{q} = \nabla(\nabla \cdot \mathbf{q}) - \nabla \times (\nabla \times \mathbf{q})$. The result is

$$\frac{E(1-\nu)}{(1+\nu)(1-2\nu)} \nabla(\nabla \cdot \mathbf{q}) - \frac{E}{2(1+\nu)} \nabla \times (\nabla \times \mathbf{q}) + \mathbf{f} = 0. \quad (7.53)$$

It is interesting that in problems without volume-distributed forces ($\mathbf{f} = 0$), Young's modulus E cancels out. Even more fascinating, in this case, the equation may be re-written in a form not involving the Poisson's ratio ν either. Indeed, calculating the divergence of the remaining terms of Eq. (53), taking into account MA Eqs. (9.2) and (11.2), we get a surprisingly simple equation

$$\nabla^2(\nabla \cdot \mathbf{q}) = 0. \quad (7.54)$$

A natural question here is how the elastic moduli affect the deformation distribution if they do not participate in the differential equation describing it. The answer is different in the following two cases. If what is fixed at the body's boundary are deformations, then the moduli are irrelevant, because the deformation distribution through the body does not depend on them. On the other hand, if the boundary conditions describe fixed stress (or a combination of stress and strain), then the elastic constants creep into the solution via the recalculation of these conditions into the strain. As a simple but representative example, let us calculate the deformation distribution in a (generally, thick) spherical shell under the effect of pressures inside and outside it – see Fig. 7a.

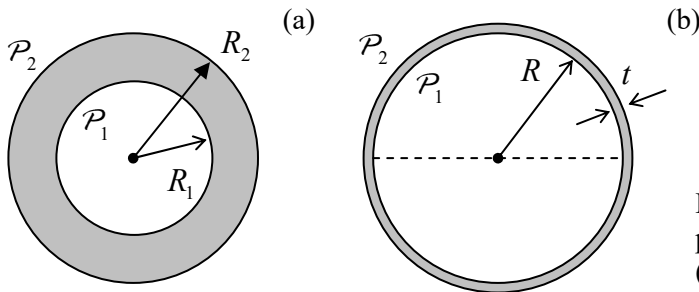


Fig. 7.7. The spherical shell problem: (a) the general case, and (b) the thin shell limit.

Due to the spherical symmetry of the problem, the deformation is obviously spherically-symmetric and radial, $\mathbf{q}(\mathbf{r}) = q(r)\mathbf{n}_r$, i.e. is completely described by one scalar function $q(r)$. Since the curl of such a radial vector field is zero,²² Eq. (53) is reduced to

$$\nabla(\nabla \cdot \mathbf{q}) = 0, \quad (7.55)$$

This means that the divergence of the function $q(r)$ is constant within the shell. In the spherical coordinates:²³

$$\frac{1}{r^2} \frac{d}{dr} (r^2 q) = \text{const.} \quad (7.56)$$

Naming this constant $3a$ (with the numerical factor chosen just for the later notation's convenience), and integrating Eq. (56) over r , we get its solution,

²¹ See, e.g., MA Eq. (11.3).

²² If this is not immediately evident, please have a look at MA Eq. (10.11) with $\mathbf{f} = f_r(r)\mathbf{n}_r$.

²³ See, e.g., MA Eq. (10.10) with $\mathbf{f} = q(r)\mathbf{n}_r$.

$$q(r) = ar + \frac{b}{r^2}, \quad (7.57)$$

which also includes another integration constant, b . The constants a and b may be determined from the boundary conditions. Indeed, according to Eq. (19),

$$\sigma_{rr} = \begin{cases} -\mathcal{P}_1, & \text{at } r = R_1, \\ -\mathcal{P}_2, & \text{at } r = R_2. \end{cases} \quad (7.58)$$

In order to relate this stress to strain, let us use Hooke's law, but for that, we first need to calculate the strain tensor components for the deformation distribution (57). Using Eqs. (17), we get

$$s_{rr} = \frac{\partial q}{\partial r} = a - 2\frac{b}{r^3}, \quad s_{\theta\theta} = s_{\varphi\varphi} = \frac{q}{r} = a + \frac{b}{r^3}, \quad (7.59)$$

so that $\text{Tr}(s) = 3a$. Plugging these relations into Eq. (49a) for σ_{rr} , we obtain

$$\sigma_{rr} = \frac{E}{1+\nu} \left[\left(a - 2\frac{b}{r^3} \right) + \frac{\nu}{1-2\nu} 3a \right]. \quad (7.60)$$

Now plugging this relation into Eqs. (58), we get a system of two linear equations for the coefficients a and b . An easy solution to this system yields

$$a = \frac{1-2\nu}{E} \frac{\mathcal{P}_1 R_1^3 - \mathcal{P}_2 R_2^3}{R_2^3 - R_1^3}, \quad b = \frac{1+\nu}{2E} \frac{(\mathcal{P}_1 - \mathcal{P}_2) R_1^3 R_2^3}{R_2^3 - R_1^3}. \quad (7.61)$$

Formulas (57) and (61) give a complete solution to our problem. (Note that the elastic moduli are back, as was promised.) This solution is rich in physical content and deserves at least some analysis. First of all, note that according to Eq. (48), the coefficient $(1-2\nu)/E$ in the expression for a is just $1/3K$, so that the first term in Eq. (57) for the net deformation describes the hydrostatic compression. Now note that the second of Eqs. (61) yields $b = 0$ if $R_1 = 0$. Thus for a solid sphere, we have only the hydrostatic compression that was discussed in the previous section. Perhaps less intuitively, making two pressures equal also gives $b = 0$, i.e. the purely hydrostatic compression, for arbitrary $R_2 > R_1$.

However, in the general case, $b \neq 0$, so that the second term in the deformation distribution (57), which describes the shear deformation,²⁴ is also substantial. In particular, let us consider the important thin-shell limit, when $R_2 - R_1 \equiv t \ll R_{1,2} \equiv R$ – see Fig. 7b. In this case, $q(R_1) \approx q(R_2)$ is just the change of the shell radius R , for which Eqs. (57) and (61) (with $R_2^3 - R_1^3 \approx 3R^2t$) give

$$\Delta R \equiv q(R) \approx aR + \frac{b}{R^2} \approx \frac{(\mathcal{P}_1 - \mathcal{P}_2)R^2}{3t} \left(\frac{1-2\nu}{E} + \frac{1+\nu}{2E} \right) = (\mathcal{P}_1 - \mathcal{P}_2) \frac{R^2}{t} \frac{1-\nu}{2E}. \quad (7.62)$$

Naively, one could think that at least in this limit the problem could be analyzed by elementary means. For example, the total force exerted by the pressure difference $(\mathcal{P}_1 - \mathcal{P}_2)$ on the diametrical cross-section of the shell (see, e.g., the dashed line in Fig. 7b) is $F = \pi R^2 (\mathcal{P}_1 - \mathcal{P}_2)$, giving the stress,

²⁴Indeed, according to Eq. (48), the material-dependent factor in the second of Eqs. (61) is just $1/4\mu$.

$$\sigma = \frac{F}{A} = \frac{\pi R^2 (\mathcal{P}_1 - \mathcal{P}_2)}{2\pi R t} = (\mathcal{P}_1 - \mathcal{P}_2) \frac{R}{2t}, \quad (7.63)$$

directed along the shell's walls. One can check that this simple formula may be indeed obtained, in this limit, from the strict expressions for $\sigma_{\theta\theta}$ and $\sigma_{\varphi\varphi}$, following from the general treatment carried out above. However, if we now tried to continue this approach by using the simple relation (45) to find the small change R_{sr} of the sphere's radius, we would arrive at a result with the general structure of Eq. (62), but without the factor $(1 - \nu) < 1$ in the numerator. The reason for this error (which may be as significant as $\sim 30\%$ for typical construction materials – see Table 1) is that Eq. (45), while being valid for *thin rods* of arbitrary cross-section, is invalid for *thin but broad sheets*, and in particular the thin shell in our problem. Indeed, while at the tensile stress both lateral dimensions of a thin rod may contract freely, in our last problem all dimensions of the shell are under stress – actually, under much more tangential stress than the radial one.²⁵

7.5. Rod bending

The general approach to the static deformation analysis, outlined at the beginning of the previous section, may be simplified not only for symmetric geometries but also for the uniform thin structures such as *thin plates* (also called “membranes” or “thin sheets”) and *thin rods*. Due to the shortage of time, in this course, I will demonstrate typical approaches to such systems only on the example of thin rods. (The theory of thin plates and shells is conceptually similar but mathematically more involved.²⁶)

Besides the tensile stress analyzed in Sec. 3, the two other major types of rod deformation are *bending* and *torsion*. Let us start from a “local” analysis of bending caused by a pair of equal and opposite external torques $\tau = \pm \mathbf{n}_y \tau_y$ perpendicular to the rod axis z (Fig. 8), assuming that the rod is “quasi-uniform”, i.e. that on the scale of this analysis (comparable with the linear scale a of the cross-section) its material parameters and the cross-section A do not change substantially.

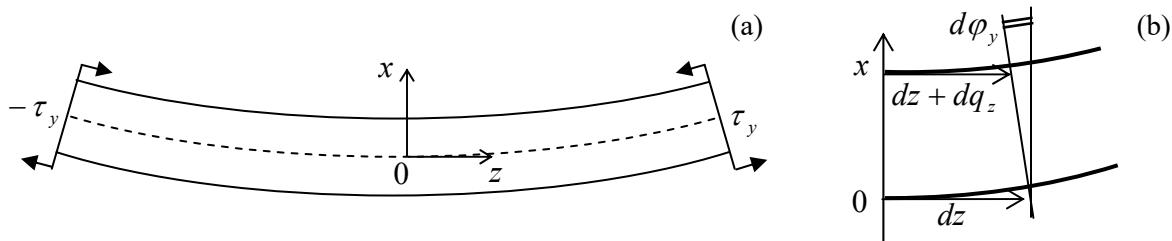


Fig. 7.8. Rod bending, in a local reference frame (specific for each cross-section). The bold arrows show the simplest way to create the two opposite torques τ_y : a couple of opposite forces for each torque.

Just as in the tensile stress experiment (Fig. 6), the components of the stress forces $d\mathbf{F}$, normal to the rod's length, have to equal zero on the surface of the rod. Repeating the arguments made for the tensile stress discussion, we have to conclude that only one diagonal element of the tensor (in Fig. 8, σ_{zz}) may differ from zero:

²⁵ Strictly speaking, this is only true if the pressure difference is not too small, namely, if $|\mathcal{P}_1 - \mathcal{P}_2| \gg \mathcal{P}_{1,2}t/R$.

²⁶ For its review see, e.g., Secs. 11-15 in L. Landau and E. Lifshitz, *Theory of Elasticity*, 3rd ed., Butterworth-Heinemann, 1986.

$$\sigma_{jj'} = \delta_{jz} \sigma_{zz}. \quad (7.64)$$

However, in contrast to the tensile stress, at pure static bending, the net force directed along the rod has to vanish:

$$F_z = \int_S \sigma_{zz} d^2 r = 0, \quad (7.65)$$

where S is the rod's cross-section, so that σ_{zz} has to change its sign at some point of the x -axis, selected to lie in the plane of the bent rod. Thus, the bending deformation may be viewed as a combination of a stretch of some layers of the rod (bottom layers in Fig. 8) with compression of other (top) layers.

Since it is hard to make more conclusions about the stress distribution immediately, let us turn over to strain, assuming that the rod's cross-section is virtually constant over the length of our local analysis. From the above representation of bending as a combination of stretching and compression, it is evident that the longitudinal deformation q_z has to vanish along some *neutral line* on the rod's cross-section – in Fig. 8, represented by the dashed line.²⁷ Selecting the origin of the x -coordinate on this line, and expanding the relative deformation in the Taylor series in x , due to the cross-section smallness we may keep just the first, linear term of the expansion:

$$s_{zz} \equiv \frac{dq_z}{dz} = -\frac{x}{R}. \quad (7.66)$$

The constant R has the sense of the *curvature radius* of the bent rod. Indeed, on a small segment dz , the cross-section turns by a small angle $d\varphi_y = -dq_z/x$ (Fig. 8b). Using Eq. (66), we get $d\varphi_y = dz/R$, which is the usual definition of the curvature radius R in the differential geometry, for our special choice of the coordinate axes.²⁸

Expressions for other elements of the strain tensor are harder to guess (like at the tensile stress, not all of them are equal to zero!), but what we already know about σ_{zz} and s_{zz} is already sufficient to start formal calculations. Indeed, plugging Eq. (64) into Hooke's law in the form (49b), and comparing the result for s_{zz} with Eq. (66), we find

$$\sigma_{zz} = -E \frac{x}{R}. \quad (7.67)$$

From the same Eq. (49b), we could also find the transverse elements of the strain tensor, and conclude that they are related to s_{zz} exactly as at the tensile stress:

$$s_{xx} = s_{yy} = -\nu s_{zz}, \quad (7.68)$$

and then, integrating these relations along the cross-section of the rod, find the deformation of the cross-section's shape. More important for us, however, is to calculate the relation between the rod's curvature and the net torque acting on a given cross-section S (taking $dA_z > 0$):

$$\tau_y \equiv \int_S (\mathbf{r} \times d\mathbf{F})_y = - \int_S x \sigma_{zz} d^2 r = \frac{E}{R} \int_S x^2 d^2 r \equiv \frac{EI_y}{R}, \quad (7.69)$$

²⁷ Strictly speaking, that dashed line is the intersection of the *neutral surface* (the continuous set of such neutral lines for all cross-sections of the rod) with the plane of the drawing.

²⁸ Indeed, for $(dx/dz)^2 \ll 1$, the general formula MA Eq. (4.3) for the curvature (with the appropriate replacements $f \rightarrow x$ and $x \rightarrow z$) is reduced to $1/R = d^2x/dz^2 = d(dx/dz)/dz = d(\tan\varphi_y)/dz \approx d\varphi_y/dz$.

where I_y is a geometric constant defined as

$$I_y \equiv \int_S x^2 dxdy. \quad (7.70)$$

Note that this factor, defining the bending rigidity of the rod, grows as fast as a^4 with the linear scale a of the cross-section.²⁹

In these expressions, x has to be referred to the neutral line. Let us see where exactly this line passes through the rod's cross-section. Plugging the result (67) into Eq. (65), we get the condition defining the neutral line:

$$\int_S x dxdy = 0. \quad (7.71)$$

This condition allows for a simple interpretation. Imagine a thin sheet of some material, with a constant mass density σ per unit area, cut in the form of the rod's cross-section. If we place a reference frame into its center of mass, then, by its definition,

$$\sigma \int_S \mathbf{r} dxdy = 0. \quad (7.72)$$

Comparing this condition with Eq. (71), we see that one of the neutral lines has to pass through the center of mass of the sheet, which may be called the “center of mass of the cross-section”. Using the same analogy, we see that the integral I_y given by Eq. (72) may be interpreted as the moment of inertia of the same imaginary sheet of material, with σ formally equal to 1, for its rotation about the neutral line – cf. Eq. (4.24). This analogy is so convenient that the integral is usually called the *moment of inertia of the cross-section* and denoted similarly – just as has been done above. So, our basic result (69) may be rewritten as

$$\frac{1}{R} = \frac{\tau_y}{EI_y}.$$

(7.73)

Rod
bending:
curvature
vs. torque

This relation is only valid if the deformation is small in the sense $R \gg a$. Still, since the deviations of the rod from its unstrained shape may accumulate along its length, Eq. (73) may be used for calculations of large “global” deviations of the rod from equilibrium, on a length scale much larger than a . To describe such deformations, Eq. (73) has to be complemented by conditions of the balance of the bending forces and torques. Unfortunately, a general analysis of such deformations requires a bit more differential geometry than I have time for, so I will only discuss this procedure for the simplest case of relatively small transverse deviations $q \equiv q_x$ of an initially horizontal rod from its straight shape that will be used for the z -axis (Fig. 9a), by some forces, possibly including bulk-distributed forces $\mathbf{f} = \mathbf{n}_x f_x(z)$. (Again, the simplest example is a uniform gravity field, for which $f_x = -\rho g = \text{const.}$) Note that in the forthcoming discussion the reference frame will be global, i.e. common for the whole rod, rather than local (pertaining to each cross-section) as it was in the previous analysis – cf. Fig. 8.

First of all, we may write a static relation for the total vertical force $\mathbf{F} = \mathbf{n}_x F_x(z)$ exerted on the part of the rod to the left of the considered cross-section – located at point z . The differential form of this relation expresses the balance of vertical forces exerted on a small fragment dz of the rod (Fig. 9a), necessary for the absence of its *linear* acceleration: $F_x(z + dz) - F_x(z) + f_x(z)Adz = 0$, giving

²⁹ In particular, this is the reason why the usual electric wires are made not of a solid copper core, but rather a twisted set of thinner sub-wires, which may slip relative to each other, increasing the wire flexibility.

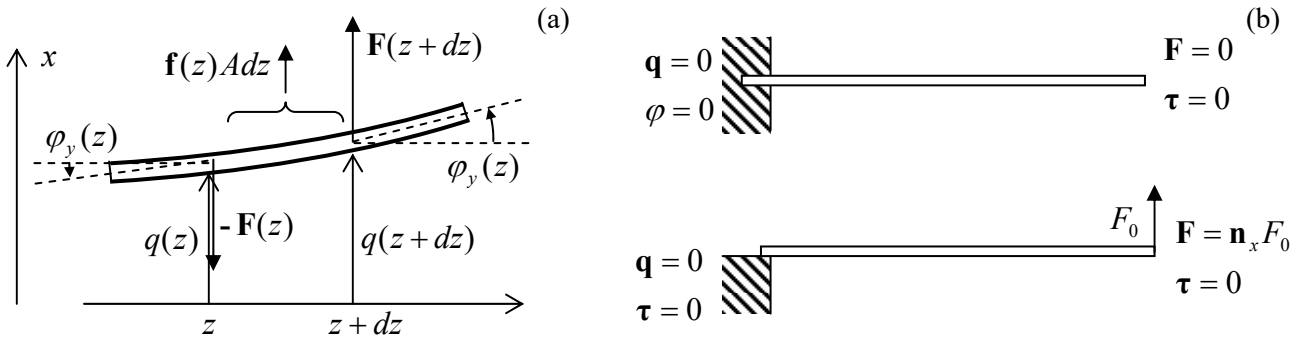


Fig. 7.9. A global picture of rod bending: (a) the forces acting on a small fragment of a rod, and (b) two bending problem examples, each with two typical but different boundary conditions.

$$\frac{dF_x}{dz} = -f_x A, \quad (7.74)$$

where A is the cross-section's area. Note that this vertical component of the internal forces has been neglected in our derivation of Eq. (73), and hence our final results will be valid only if the ratio F_x/A is much smaller than the magnitude of σ_{zz} described by Eq. (67). However, in reality, these are exactly the forces that create the very torque $\tau = \mathbf{n}_y \tau_y$ that in turn causes the bending, and thus have to be taken into account in the analysis of the global picture.

Such an account may be made by writing the balance of the components of the elementary torque exerted on the same rod fragment of length dz , necessary for the absence of its *angular* acceleration: $d\tau_y + F_x dz = 0$, so that

$$\frac{d\tau_y}{dz} = -F_x. \quad (7.75)$$

These two equations should be complemented by two geometric relations. The first of them is $d\varphi_y/dz = 1/R$, which has already been discussed above. We may immediately combine it with the basic result (73) of our local analysis, getting:

$$\frac{d\varphi_y}{dz} = \frac{\tau_y}{EI_y}. \quad (7.76)$$

The final equation is the geometric relation evident from Fig. 9a:

$$\frac{dq_x}{dz} = \varphi_y, \quad (7.77)$$

which is (as all expressions of our simple analysis) only valid for small bending angles, $|\varphi_y| \ll 1$.

The four differential equations (74)-(77) are sufficient for the full solution of the weak-bending problem, if complemented by appropriate boundary conditions. Figure 9b shows the conditions most frequently met in practice. Let us solve, for example, the problem shown on the top panel of Fig. 9b: bending of a rod, “clamped” at one end (say, immersed into a rigid wall), under its own weight. As should be clear from their derivation, Eqs. (74)-(77) are valid for any distribution of parameters A , E , I_y , and ρ over the rod's length, provided that the rod is *quasi-uniform*, i.e. its parameters' changes are so slow that the local relation (76) is still valid at any point. However, just for simplicity, let us consider a

uniform rod. The simple structure of Eqs. (74)-(77) allows for their integration one by one, each time using the appropriate boundary conditions. To start, Eq. (74) with $f_x = -\rho g = \text{const}$ yields

$$F_x = \rho g A z + \text{const} = \rho g A (z - l), \quad (7.78)$$

where the integration constant has been selected to satisfy the right-end boundary condition: $F_x = 0$ at $z = l$. As a sanity check, at the left wall ($z = 0$), $F_x = -\rho g A l = -mg$, meaning that the whole weight of the rod is exerted on the supporting wall – fine.

Next, by plugging Eq. (78) into Eq. (75) and integrating, we get

$$\tau_y = -\frac{\rho g A}{2} (z^2 - 2lz) + \text{const} = -\frac{\rho g A}{2} (z^2 - 2lz + l^2) \equiv -\frac{\rho g A}{2} (z - l)^2, \quad (7.79)$$

where the integration constant's choice ensures the second right-boundary condition: $\tau_y = 0$ at $z = l$ – see Fig. 9b again. Now proceeding in the same fashion to Eq. (76), we get

$$\varphi_y = -\frac{\rho g A}{2EI_y} \frac{(z - l)^3}{3} + \text{const} = -\frac{\rho g A}{6EI_y} [(z - l)^3 + l^3], \quad (7.80)$$

where the integration constant is selected to satisfy the *clamping condition* at the left end of the rod: $\varphi_y = 0$ at $z = 0$. (Note that this is different from the *support condition* illustrated on the lower panel of Fig. 9b, which allows the *angle* φ_y to be different from zero at $z = 0$, but requires the *torque* to vanish at that point.) Finally, integrating Eq. (77) with φ_y given by Eq. (80), we get the rod's global deformation law,

$$q_x(z) = -\frac{\rho g A}{6EI_y} \left[\frac{(z - l)^4}{4} + l^3 z + \text{const} \right] = -\frac{\rho g A}{6EI_y} \left[\frac{(z - l)^4}{4} + l^3 z - \frac{l^4}{4} \right], \quad (7.81)$$

where the integration constant is selected to satisfy the second left-boundary condition: $q = 0$ at $z = 0$. So, the bending law is sort of complicated even in this very simple problem. It is also remarkable how fast does the end's displacement grow with the increase of the rod's length:

$$q_x(l) = -\frac{\rho g A l^4}{8EI_y}. \quad (7.82)$$

To conclude this solution, let us discuss the validity of this result. First, the geometric relation (77) is only valid if $|\varphi_y(l)| \ll 1$, and hence if $|q_x(l)| \ll l$. Next, the local formula Eq. (76) is valid if $1/R = \tau(l)/EI_y \ll 1/a \sim A^{-1/2}$. Using the results (79) and (82), we see that the latter condition is equivalent to $|q_x(l)| \ll l^2/a$, i.e. is weaker than the former one, because all our analysis has been based on the assumption $l \gg a$. Another point of concern may be that the off-diagonal stress element $\sigma_{xz} \sim F_x/A$, which is created by the vertical gravity forces, has been ignored in our local analysis. For that approximation to be valid, this element must be much smaller than the diagonal element $\sigma_{zz} \sim aE/R = a\tau/I_y$ taken into account in that analysis. Using Eqs. (78) and (80), we are getting the following estimates: $\sigma_{xz} \sim \rho gl$, $\sigma_{zz} \sim a\rho g Al^2/I_y \sim a^3 \rho gl^2/I_y$. According to its definition (70), I_y may be crudely estimated as a^4 , so that we finally get the simple condition $a \ll l$, which has been assumed from the very beginning of our solution.

7.6. Rod torsion

One more class of analytically solvable elasticity problems is the torsion of quasi-uniform, straight rods by a couple of axially-oriented torques $\tau = \pm \mathbf{n}_z \tau_z$ – see Fig. 10.

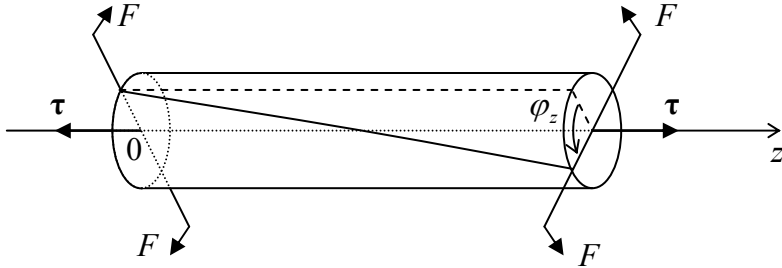


Fig. 7.10. Rod torsion. Just as in Fig. 8, the couples of forces \mathbf{F} are just vivid representations of the opposite torques $\pm\tau$.

This problem is simpler than the bending in the sense that due to its longitudinal uniformity, $d\varphi_z/dz = \text{const}$, it is sufficient to relate the torque τ_z to the so-called *torsion parameter*

$$\kappa \equiv \frac{d\varphi_z}{dz}. \quad (7.83)$$

If the deformation is elastic and small (in the sense $\kappa a \ll 1$, where a is again the characteristic size of the rod's cross-section), κ is proportional to τ_z . Hence our task is to calculate their ratio,

Torsional rigidity:
definition

$$C \equiv \frac{\tau_z}{\kappa} \equiv \frac{\tau_z}{d\varphi_z / dz}, \quad (7.84)$$

called the *torsional rigidity* of the rod.

As the first guess (as we will see below, of a limited validity), one may assume that the torsion does not change either the shape or size of the rod's cross-sections, but leads just to their mutual rotation about a certain central line. Using a reference frame with the origin on that line, this assumption immediately enables the calculation of Cartesian components of the displacement vector $d\mathbf{q}$, by using Eq. (6) with $d\varphi = \mathbf{n}_z d\varphi_z$:

$$dq_x = -y d\varphi_z = -\kappa y dz, \quad dq_y = x d\varphi_z = \kappa x dz, \quad dq_z = 0. \quad (7.85)$$

From here, we can calculate all Cartesian elements (9) of the symmetrized strain tensor:

$$s_{xx} = s_{yy} = s_{zz} = 0, \quad s_{xy} = s_{yx} = 0, \quad s_{xz} = s_{zx} = -\frac{\kappa}{2} y, \quad s_{yz} = s_{zy} = \frac{\kappa}{2} x. \quad (7.86)$$

The first of these equalities means that the elementary volume does not change, i.e. we are dealing with purely shear deformation. As a result, all nonzero elements of the stress tensor, calculated from Eqs. (32), are proportional to the shear modulus alone:³⁰

$$\sigma_{xx} = \sigma_{yy} = \sigma_{zz} = 0, \quad \sigma_{xy} = \sigma_{yx} = 0, \quad \sigma_{xz} = \sigma_{zx} = -\mu \kappa y, \quad \sigma_{yz} = \sigma_{zy} = \mu \kappa x. \quad (7.87)$$

³⁰ Note that for this problem, with a purely shear deformation, using the alternative elastic moduli E and ν would be rather unnatural. If needed, we may always use the second of Eqs. (48): $\mu = E/2(1 + \nu)$.

Now it is straightforward to use this result to calculate the full torque as an integral over the cross-section's area A :

$$\tau_z \equiv \int_A (\mathbf{r} \times d\mathbf{F})_z = \int_A (xdF_y - ydF_x) = \int_A (x\sigma_{yz} - y\sigma_{xz}) dx dy. \quad (7.88)$$

Using Eq. (87), we get $\tau_z = \mu\kappa I_z$, i.e.

$C = \mu I_z, \quad \text{where } I_z \equiv \int_A (x^2 + y^2) dx dy.$

(7.89) C at axial symmetry

Again, just as in the case of thin rod bending, we have got an integral, in this case I_z , similar to a moment of inertia, this time for the rotation about the z -axis passing through a certain point of the cross-section. For any axially-symmetric cross-section, this has to be its central point. Then, for example, for the practically important case of a uniform round pipe with internal radius R_1 and external radius R_2 , Eq. (89) yields

$$C = \mu 2\pi \int_{R_1}^{R_2} \rho^3 d\rho = \frac{\pi}{2} \mu (R_2^4 - R_1^4). \quad (7.90)$$

In particular, for the solid rod of radius R (which may be treated as a pipe with $R_1 = 0$ and $R_2 = R$), this result gives the following torsional rigidity

$$C = \frac{\pi}{2} \mu R^4, \quad (7.91a)$$

while for a hollow pipe of small thickness $t \ll R$, Eq. (90) is reduced to

$$C = 2\pi\mu R^3 t. \quad (7.91b)$$

Note that per unit cross-section area A (and hence per unit mass of the rod) the thin pipe's rigidity is twice higher than that of a solid rod:

$$\frac{C}{A} \Big|_{\text{thin round pipe}} = \mu R^2 > \frac{C}{A} \Big|_{\text{solid round rod}} = \frac{1}{2} \mu R^2. \quad (7.92)$$

This fact is one reason for the broad use of thin pipes in engineering and physical experiment design.

However, for rods with axially-asymmetric cross-sections, Eq. (89) gives *wrong* results. For example, for a narrow rectangle of area $A = w \times t$ with $t \ll w$, it yields the expression $C = \mu t w^3 / 12$ [WRONG!], which is even functionally different from the correct result – cf. Eq. (104) below. The reason for this error is that the above analysis does not describe possible bending $q_z(x, y)$ of the rod's cross-section in the direction *along* the rod. (For axially-symmetric rods, such bending is evidently forbidden by the symmetry, so that Eq. (89) is valid, and the results (90)-(92) are absolutely correct.)

Let us describe³¹ this counter-intuitive effect by taking

$$q_z = \kappa \psi(x, y), \quad (7.93)$$

³¹ I would not be terribly shocked if the reader skipped the balance of this section at the first reading. Though the calculation described in it is very elegant, instructive, and typical for the theory of elasticity (and for good physics as a whole!), its results will not be used in other chapters of this course or other parts of this series.

(where ψ is some function to be determined), but still keeping Eq. (87) for two other components of the displacement vector. The addition of ψ does not perturb the equality to zero of the diagonal elements of the strain tensor, as well as of s_{xy} and s_{yx} , but contributes to other off-diagonal elements:

$$s_{xz} = s_{zx} = \frac{\kappa}{2} \left(-y + \frac{\partial \psi}{\partial x} \right), \quad s_{yz} = s_{zy} = \frac{\kappa}{2} \left(x + \frac{\partial \psi}{\partial y} \right), \quad (7.94)$$

and hence to the corresponding elements of the stress tensor:

$$\sigma_{xz} = \sigma_{zx} = \mu \kappa \left(-y + \frac{\partial \psi}{\partial x} \right), \quad \sigma_{yz} = \sigma_{zy} = \mu \kappa \left(x + \frac{\partial \psi}{\partial y} \right). \quad (7.95)$$

Now let us find the requirement imposed on the function $\psi(x,y)$ by the fact that the stress force component parallel to the rod's axis,

$$dF_z = \sigma_{zx} dA_x + \sigma_{zy} dA_y = \mu \kappa dA \left[\left(-y + \frac{\partial \psi}{\partial x} \right) \frac{dA_x}{dA} + \left(x + \frac{\partial \psi}{\partial y} \right) \frac{dA_y}{dA} \right], \quad (7.96)$$

has to vanish at the rod's surface(s), i.e. at a cross-section's border. The coordinates $\{x, y\}$ of any point at the border may be considered as unique functions, $x(l)$ and $y(l)$, of the arc l of that line – see Fig. 11.

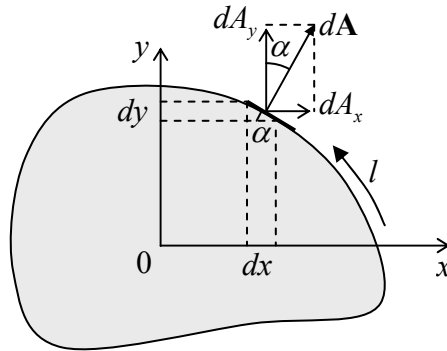


Fig. 7.11. Deriving Eq. (99).

As this sketch shows, the elementary area ratios participating in Eq. (96) may be readily expressed via the derivatives of these functions: $dA_x/dA = \sin \alpha = dy/dl$, $dA_y/dA = \cos \alpha = -dx/dl$, so that we may write

$$\left[\left(-y + \frac{\partial \psi}{\partial x} \right) \left(\frac{dy}{dl} \right) + \left(x + \frac{\partial \psi}{\partial y} \right) \left(-\frac{dx}{dl} \right) \right]_{\text{border}} = 0. \quad (7.97)$$

Introducing, instead of ψ , a new function $\chi(x,y)$, defined by its derivatives as

$$\frac{\partial \chi}{\partial x} \equiv \frac{1}{2} \left(-x - \frac{\partial \psi}{\partial y} \right), \quad \frac{\partial \chi}{\partial y} \equiv \frac{1}{2} \left(-y + \frac{\partial \psi}{\partial x} \right), \quad (7.98)$$

we may rewrite Eq. (97) as

$$2 \left(\frac{\partial \chi}{\partial y} \frac{dy}{dl} + \frac{\partial \chi}{\partial x} \frac{dx}{dl} \right)_{\text{border}} = 2 \frac{d\chi}{dl} \Big|_{\text{border}} = 0, \quad (7.99)$$

so that the function χ has to be constant at each border of the cross-section.

In particular, for a singly-connected cross-section, limited to just one continuous border line (as in Fig. 11), this constant is arbitrary, because according to Eqs. (98), its choice does not affect the longitudinal deformation function $\psi(x,y)$ and hence the deformation as a whole. Now let us use the definition (98) of $\chi(x,y)$ to calculate the 2D Laplace operator of this function:

$$\nabla_{x,y}^2 \chi \equiv \frac{\partial^2 \chi}{\partial x^2} + \frac{\partial^2 \chi}{\partial y^2} = \frac{1}{2} \frac{\partial}{\partial x} \left(-x - \frac{\partial \psi}{\partial y} \right) + \frac{1}{2} \frac{\partial}{\partial y} \left(-y + \frac{\partial \psi}{\partial y} \right) \equiv -1. \quad (7.100)$$

This is a 2D *Poisson equation* (frequently met, for example, in electrostatics), but with a very simple, constant right-hand side. Plugging Eqs. (98) into Eqs. (95), and those into Eq. (88), we may express the torque τ_z , and hence the torsional rigidity C , via the same function:

$$C \equiv \frac{\tau_z}{\kappa} = -2\mu \int_A \left(x \frac{\partial \chi}{\partial x} + y \frac{\partial \chi}{\partial y} \right) dx dy. \quad (7.101a)$$

C for
arbitrary
cross-
section

Sometimes, it is easier to use this result in either of its two different forms. The first of them may be readily obtained from Eq. (101a) using the integration by parts:

$$\begin{aligned} C &= -2\mu \left(\int dy \int x d\chi + \int dx \int y d\chi \right) = -2\mu \left[\int dy \left(x \chi_{\text{border}} - \int \chi dx \right) + \int dx \left(y \chi_{\text{border}} - \int \chi dy \right) \right] \\ &= 4\mu \left[\int_A \chi dx dy - \chi_{\text{border}} \int_A dx dy \right], \end{aligned} \quad (7.101b)$$

while the proof of one more form,

$$C = 4\mu \int_A (\nabla_{x,y} \chi)^2 dx dy, \quad (7.101c)$$

is left for the reader's exercise. Thus, if we need to know the rod's rigidity alone, it is sufficient to calculate the function $\chi(x,y)$ from Eq. (100) with the boundary condition $\chi|_{\text{border}} = \text{const}$, and then plug it into any of Eqs. (101). Only if we are also curious about the longitudinal deformation (93) of the cross-section, we may continue by using Eq. (98) to find the function $\psi(x,y)$ describing this deformation.

Let us see how does this recipe work for the two examples discussed above. For the round cross-section of radius R , both the Poisson equation (100) and the boundary condition, $\chi = \text{const}$ at $x^2 + y^2 = R^2$, are evidently satisfied by the following axially-symmetric function:

$$\chi = -\frac{1}{4}(x^2 + y^2) + \text{const}. \quad (7.102)$$

For this case, Eq. (101a) yields

$$C = 4\mu \int_A \left[\left(-\frac{1}{2}x \right)^2 + \left(-\frac{1}{2}y \right)^2 \right] dx dy = \mu \int_A (x^2 + y^2) d^2 r, \quad (7.103)$$

i.e. the same result (89) that we had for $\psi = 0$. Indeed, plugging Eq. (102) into Eqs. (98), we see that in this case $\partial\psi/\partial x = \partial\psi/\partial y = 0$, so that $\psi(x,y) = \text{const}$, i.e. the cross-section is not bent. (As was discussed in Sec. 1, a uniform translation $dq_z = \kappa\psi = \text{const}$ does not constitute a deformation.)

Now, turning to a rod with a narrow rectangular cross-section $A = w \times t$ with $t \ll w$, we may use this strong inequality to solve the Poisson equation (100) approximately, neglecting the second

derivative of χ along the wider dimension (say, y). The remaining 1D differential equation $d^2\chi/d^2x = -1$, with boundary conditions $\chi|_{x=+t/2} = \chi|_{x=-t/2}$, has an obvious solution: $\chi = -x^2/2 + \text{const.}$ Plugging this expression into any form of Eq. (101), we get the following (correct!) result for the torsional rigidity:

$$C = \frac{1}{3} \mu w t^3. \quad (7.104)$$

Now let us have a look at the cross-section bending law (93) for this particular case. Using Eqs. (98), we get

$$\frac{\partial \psi}{\partial y} = -x - 2 \frac{\partial \chi}{\partial x} = x, \quad \frac{\partial \psi}{\partial x} = y + 2 \frac{\partial \chi}{\partial y} = y. \quad (7.105)$$

Integrating these differential equations over the cross-section, and taking the integration constant (again, not contributing to the deformation) for zero, we get a beautifully simple result:

$$\psi = xy, \quad \text{i.e. } q_z = \kappa xy. \quad (7.106)$$

It means that the longitudinal deformation of the rod has a “propeller bending” form: while the regions near the opposite corners (on the same diagonal) of the cross-section bend toward one direction of the z -axis, the corners on the other diagonal bend in the opposite direction. (This qualitative conclusion remains valid for rectangular cross-sections with any “aspect ratio” t/w .)

For rods with several surfaces, i.e. with cross-sections limited by several boundaries (say, hollow pipes), finding the function $\chi(x, y)$ requires a bit more care, and Eq. (103b) has to be modified, because the function may be equal to a different constant at each boundary. Let me leave the calculation of the torsional rigidity for this case for the reader’s exercise.

7.7. 3D acoustic waves

Now moving from the statics to dynamics, we may start with Eq. (24), which may be transformed into the vector form exactly as this was done for the static case at the beginning of Sec. 4. Comparing Eqs. (24) and (52), we immediately see that the result may be represented as

$$\rho \frac{\partial^2 \mathbf{q}}{\partial t^2} = \frac{E}{2(1+\nu)} \nabla^2 \mathbf{q} + \frac{E}{2(1+\nu)(1-2\nu)} \nabla(\nabla \cdot \mathbf{q}) + \mathbf{f}(\mathbf{r}, t). \quad (7.107)$$

Let us use this general equation for the analysis of the perhaps most important type of time-dependent deformations: *acoustic waves*. First, let us consider the simplest case of a virtually infinite, uniform elastic medium, with no external forces: $\mathbf{f} = 0$. In this case, due to the linearity and homogeneity of the equation of motion, and taking clues from the analysis of the simple 1D model (see Fig. 6.4a) in Secs. 6.3-6.5,³² we may look for a particular time-dependent solution in the form of a sinusoidal, *linearly-polarized, plane traveling wave*

$$\mathbf{q}(\mathbf{r}, t) = \text{Re} \left[\mathbf{a} e^{i(\mathbf{k} \cdot \mathbf{r} - \omega t)} \right], \quad (7.108)$$

Elastic continuum:
dynamics

Plane,
sinusoidal
wave

³² Note though that Eq. (107) is more complex than the simple wave equation (6.40).

where \mathbf{a} is the constant complex amplitude of a wave (now a vector!), and \mathbf{k} is the *wave vector*, whose magnitude is equal to the wave number k . The direction of these two vectors should be clearly distinguished: while \mathbf{a} determines the wave's *polarization*, i.e. the direction of particle displacements, the vector \mathbf{k} is directed along the spatial gradient of the full phase of the wave

$$\Psi \equiv \mathbf{k} \cdot \mathbf{r} - \omega t + \arg a, \quad (7.109)$$

i.e. along the direction of the wave front propagation.

The importance of the angle between these two vectors may be readily seen from the following simple calculation. Let us point the z -axis of an (inertial) reference frame along the direction of vector \mathbf{k} , and the x -axis in such direction that the vector \mathbf{q} , and hence \mathbf{a} , lie within the $\{x, z\}$ plane. In this case, all variables may change only along the z -axis, i.e. $\nabla = \mathbf{n}_z(\partial/\partial z)$, and the amplitude vector may be represented as the sum of just two Cartesian components:

$$\mathbf{a} = a_x \mathbf{n}_x + a_z \mathbf{n}_z. \quad (7.110)$$

Let us first consider a *longitudinal* wave, with the particle motion along the wave direction: $a_x = 0$, $a_z = a$. Then the vector \mathbf{q} in Eq. (107) describing this wave, has only one (z -) component, so that $\nabla \cdot \mathbf{q} = \partial q_z / \partial z$ and $\nabla(\nabla \cdot \mathbf{q}) = \mathbf{n}_z(\partial^2 \mathbf{q} / \partial z^2)$, and the Laplace operator gives the same expression: $\nabla^2 \mathbf{q} = \mathbf{n}_z(\partial^2 \mathbf{q} / \partial z^2)$. As a result, Eq. (107), with $\mathbf{f} = 0$, is reduced to a 1D wave equation

$$\rho \frac{\partial^2 q_z}{\partial t^2} = \left[\frac{E}{2(1+\nu)} + \frac{E}{2(1+\nu)(1-2\nu)} \right] \frac{\partial^2 q_z}{\partial z^2} \equiv \frac{E(1-\nu)}{(1+\nu)(1-2\nu)} \frac{\partial^2 q_z}{\partial z^2}, \quad (7.111)$$

similar to Eq. (6.40). As we already know from Sec. 6.4, this equation is indeed satisfied with the solution (108), provided that ω and k obey a linear dispersion relation, $\omega = v_l k$, with the following longitudinal wave velocity:

$$v_l^2 = \frac{E(1-\nu)}{(1+\nu)(1-2\nu)\rho} \equiv \frac{K + (4/3)\mu}{\rho}. \quad (7.112)$$

Longitudinal waves:
velocity

The last expression allows for a simple interpretation. Let us consider a static experiment, similar to the tensile test experiment shown in Fig. 6, but with a sample much wider than l in both directions perpendicular to the force. Then the lateral contraction is impossible ($s_{xx} = s_{yy} = 0$), and we can calculate the only finite stress element, σ_{zz} , directly from Eq. (34) with $\text{Tr}(\mathbf{s}) = s_{zz}$:

$$\sigma_{zz} = 2\mu \left(s_{zz} - \frac{1}{3}s_{zz} \right) + 3K \left(\frac{1}{3}s_{zz} \right) \equiv \left(K + \frac{4}{3}\mu \right) s_{zz}. \quad (7.113)$$

We see that the numerator in Eq. (112) is nothing more than the static elastic modulus for such a uniaxial deformation, and it is recalculated into the velocity exactly as the spring constant in the 1D waves considered in Secs. 6.3-6.4 – cf. Eq. (6.42).

Formula (114) becomes especially simple in fluids, where $\mu = 0$, and the wave velocity is described by the well-known expression

$$v_l = \left(\frac{K}{\rho} \right)^{1/2}. \quad (7.114)$$

Longitudinal waves:
velocity
in fluids

Note, however, that for gases, with their high compressibility and temperature sensitivity, the value of K participating in this formula may differ, at high frequencies, from that given by Eq. (40), because fast compressions/extensions of gas are usually adiabatic rather than isothermal. This difference is noticeable in Table 1, one of whose columns lists the values of v_l for representative materials.

Now let us consider an opposite case of *transverse* waves with $a_x = a$, $a_z = 0$. In such a wave, the displacement vector is perpendicular to \mathbf{n}_z , so that $\nabla \cdot \mathbf{q} = 0$, and the second term on the right-hand side of Eq. (107) vanishes. On the contrary, the Laplace operator acting on such vector still gives the same non-zero contribution, $\nabla^2 \mathbf{q} = n_z (\partial^2 \mathbf{q} / \partial z^2)$, to Eq. (107) so that the equation yields

$$\rho \frac{\partial^2 q_x}{\partial t^2} = \frac{E}{2(1+\nu)} \frac{\partial^2 q_x}{\partial z^2}, \quad (7.115)$$

and we again get the linear dispersion relation, $\omega = v_t k$, but with a different velocity:³³

Transverse
waves:
velocity

$$v_t^2 = \frac{E}{2(1+\nu)\rho} = \frac{\mu}{\rho}. \quad (7.116)$$

We see that the speed of the transverse waves depends exclusively on the shear modulus μ of the medium.³⁴ This is also very natural: in such waves, the particle displacements $\mathbf{q} = \mathbf{n}_x q$ are perpendicular to the elastic forces $d\mathbf{F} = \mathbf{n}_z dF$, so that the only one element σ_{xz} of the stress tensor is involved. Also, the strain tensor $s_{jj'}$ has no diagonal elements, $\text{Tr } s = 0$, so that μ is the only elastic modulus actively participating in Hooke's law (32). In particular, fluids cannot carry transverse waves at all (formally, their velocity (116) vanishes), because they do not resist shear deformations. For all other materials, the longitudinal waves are faster than the transverse ones.³⁵ Indeed, for all known natural materials' Poisson's ratio is positive so that the velocity ratio that follows from Eqs. (112) and (116),

$$\frac{v_l}{v_t} = \left(\frac{2 - 2\nu}{1 - 2\nu} \right)^{1/2}, \quad (7.117)$$

is above $\sqrt{2} \approx 1.4$. For the most popular construction materials, with $\nu \approx 0.3$, Poisson's ratio is about 2 – see Table 1.

Let me emphasize again that for both the longitudinal and the transverse waves, the dispersion relation between the wave number and frequency is linear: $\omega = vk$. As was already discussed in Chapter 6, in this case of *acoustic waves* (or just “sound”), the phase and group velocities are equal, and waves of more complex form, consisting of several (or many) Fourier components of the type (108), preserve

³³ Just as in Chapter 6, let me emphasize that the *wave* velocities we are discussing in this section and Sec. 8 below have nothing to do with *particle* velocities $\partial \mathbf{q} / \partial t$. For example, in the transverse wave we are discussing now, v_t is the velocity in the z -direction, while the particles of the medium move across it, in the x -direction. Also, v_l and v_t do not depend on the wave amplitudes, while the particle velocities are proportional to them.

³⁴ Because of that, one can frequently meet the term *shear waves*. Note also that in contrast to the transverse waves in the simple 1D model analyzed in Chapter 6 (see Fig. 6.4a), those in a 3D continuum do not need a pre-stretch tension \mathcal{T} . We will return to the effect of tension in the next section.

³⁵ Because of this difference between v_l and v_t , in geophysics, the longitudinal waves are known as *P-waves* (with the letter P standing for “primary”) because they arrive at the detection site, say from an earthquake, first – before the transverse waves, called the *S-waves*, with S standing for “secondary”.

their form during propagation. This means that both Eqs. (111) and (115) are satisfied by solutions of the type (6.41):

$$q_{\pm}(z, t) = f_{\pm}\left(t \mp \frac{z}{v}\right), \quad (7.118)$$

where the functions f_{\pm} describe the propagating waveforms. (However, if the initial wave is a mixture, of the type (110), of the longitudinal and transverse components, then these components, propagating with different velocities, will “run from each other”.) As one may infer from the analysis of a periodic system model in Chapter 6, the wave dispersion becomes essential at very high (*hypersound*) frequencies where the wave number k becomes close to the reciprocal distance d between the particles of the medium (e.g., atoms or molecules), and hence the approximation of the medium as a continuum, used through this chapter, becomes invalid.

As we already know from Chapter 6, besides the velocity, the waves of each type are characterized by one more important parameter, the wave impedance Z – for acoustic waves frequently called the *acoustic impedance* of the medium. Generalizing Eq. (6.46) to the 3D case, we may define the impedance as the ratio of the force *per unit area* (i.e. the corresponding element of the stress tensor) exerted by the wave, and the particles’ velocity. For the longitudinal waves,

$$Z_l \equiv \left| \frac{\sigma_{zz}}{\partial q_z / \partial t} \right| = \left| \frac{\sigma_{zz}}{s_{zz}} \frac{s_{zz}}{\partial q_z / \partial t} \right| = \left| \frac{\sigma_{zz}}{s_{zz}} \frac{\partial q_z / \partial z}{\partial q_z / \partial t} \right|. \quad (7.119)$$

Plugging in Eqs. (108), (112), and (113), we get

$$Z_l = [(K + 4\mu/3)\rho]^{1/2}, \quad (7.120)$$

Longitudinal waves:
impedance

in a clear analogy with the first of Eqs. (6.48). Similarly, for the transverse waves, the appropriately modified definition, $Z_t \equiv |\sigma_{xz}/(\partial q_x/\partial z)|$, yields

$$Z_t = (\mu\rho)^{1/2}. \quad (7.121)$$

Transverse waves:
impedance

Just like in the 1D models studied in Chapter 6, one role of the wave impedance is to scale the power \mathcal{P} carried by the wave. For plane 3D waves in infinite media, with their infinite wave front area, it is more appropriate to speak about the *power density*, i.e. power $\mu = d\mathcal{P}/dA$ per unit area of the front, and characterize it by not only its magnitude,

$$\mu = \frac{d\mathbf{F}}{dA} \cdot \frac{\partial \mathbf{q}}{\partial t}, \quad (7.122)$$

but also the direction of the energy propagation, that (for a plane acoustic wave in an isotropic medium) coincides with the direction of the wave vector: $\boldsymbol{\mu} \equiv \mu \mathbf{n}_k$. Using the definition (18) of the stress tensor, the Cartesian components of this *Umov vector*³⁶ may be expressed as

³⁶ Named after N. A. Umov, who introduced this concept in 1874 – ten years before a similar notion for electromagnetic waves (see, e.g., EM Sec. 6.4) was suggested by J. Poynting. In a dissipation-free elastic medium, the Umov vector obeys the continuity equation $\partial(\rho v^2/2 + u)/\partial t + \nabla \cdot \boldsymbol{\mu} = 0$, with u given by Eq. (52), which expresses the conservation of the total (kinetic plus potential) energy of the elastic deformation.

$$\mu_j = \sum_{j'} \sigma_{jj'} \frac{\partial q_{j'}}{\partial t}. \quad (7.123)$$

Returning to plane waves propagating along axis z , and acting exactly like in Sec. 6., for both the longitudinal and transverse waves we again arrive at Eq. (6.49), but for μ rather than \mathcal{P} (due to a different definition of the wave impedance – per unit area rather than per particle chain). For the sinusoidal waves of the type (108), it yields

$$\mu_z = \frac{\omega^2 Z}{2} aa^*, \quad (7.124)$$

with Z being the corresponding impedance – either Z_l or Z_t .

Just as in the 1D case, one more important effect, in which the notion of impedance is crucial, is the partial *wave reflection* from at an interface between two media. The two boundary conditions, necessary for the analysis of the reflection, may be obtained from the continuity of the vectors \mathbf{q} and $d\mathbf{F}$. (The former condition is evident, while the latter one may be obtained by applying the 2nd Newton law to any infinitesimal volume $dV = dA dz$, where the segment dz straddles the interface.) Let us start from the simplest case of the *normal incidence* on a plane interface between two uniform media, each with its own elastic moduli and mass density. Due to the symmetry of the system, it is obvious that the longitudinal/transverse incident wave may only excite similarly polarized reflected and transferred waves. As a result, we may literally repeat the calculations of Sec. 6.4, again arriving at the fundamental relations (6.55) and (6.56), with the replacement of Z and Z' with the corresponding values of either Z_l (120) or Z_t (121). Thus, at the normal incidence, the wave reflection is determined solely by the acoustic *impedances* of the media, while the sound *velocities* are not involved.

The situation, however, becomes more complicated at a nonzero incidence angle $\theta_t^{(i)}$ (Fig. 12), where the transmitted wave is generally also *refracted*, i.e. propagates under a different angle, $\theta' \neq \theta_t^{(i)}$, beyond the interface. Moreover, at $\theta_t^{(i)} \neq 0$ the directions of particle motion (vector \mathbf{q}) and of the stress forces (vector $d\mathbf{F}$) in the incident wave are neither exactly parallel nor exactly perpendicular to the interface, and thus this wave may serve as an actuator for the reflected and refracted waves of both polarizations – see Fig. 12, drawn for the particular case when the incident wave is transverse. The corresponding four angles, $\theta_t^{(r)}, \theta_l^{(r)}, \theta'_l, \theta'_t$, may be readily related to $\theta_t^{(i)}$ by the “kinematic” condition that the incident wave, as well as the reflected and refracted waves of both types, must have the same spatial distribution along the interface plane, i.e. for the interface particles participating in all five waves. According to Eq. (108), the necessary boundary condition is the equality of the tangential components (in Fig. 12, k_x), of all five wave vectors:

$$k_t \sin \theta_t^{(r)} = k_l \sin \theta_l^{(r)} = k'_l \sin \theta'_l = k'_t \sin \theta'_t = k_x \equiv k_t \sin \theta_t^{(i)}. \quad (7.125)$$

Since the acoustic wave vector magnitudes k , at fixed frequency ω , are inversely proportional to the corresponding wave velocities, we immediately get the following relations:

$$\theta_t^{(r)} = \theta_t^{(i)}, \quad \frac{\sin \theta_l^{(r)}}{v_l} = \frac{\sin \theta'_l}{v'_l} = \frac{\sin \theta'_t}{v'_t} = \frac{\sin \theta_t^{(i)}}{v_t}, \quad (7.126)$$

so that generally all four angles are different. (This is of course an analog of the well-known *Snell law* in optics – where, however, only transverse waves are possible.) These relations show that, just like in optics, the direction of a wave propagating into a medium with lower velocity is closer to the normal (in

Fig. 12, to the z -axis). In particular, this means that if $v' > v$, the acoustic waves, at larger angles of incidence, may exhibit the effect of total internal reflection, so well known from optics³⁷, when the *refracted* wave vanishes. In addition, Eqs. (126) show that in acoustics, the *reflected* longitudinal wave, with velocity $v_l > v_t$, may vanish at sufficiently large angles of the transverse wave incidence.

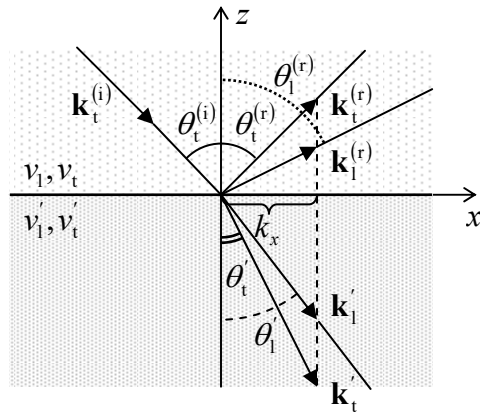


Fig. 7.12. Deriving the “kinematic” conditions (126) of the acoustic wave reflection and refraction (for the case of a transverse incident wave).

All these facts automatically follow from general expressions for amplitudes of the reflected and refracted waves via the amplitude of the incident wave. These relations are straightforward to derive (again, from the continuity of the vectors \mathbf{q} and $d\mathbf{F}$), but since they are much bulkier than those in the electromagnetic wave theory (where they are called the *Fresnel formulas*³⁸), I would not have time/space to spell out and discuss them. Let me only note that, in contrast to the case of normal incidence, these relations involve eight media parameters: the impedances Z, Z' , and the velocities v, v' on both sides of the interface, and for both the longitudinal and transverse waves.

There are other interface effects as well. Within certain frequency ranges, interfaces and surfaces of elastic solids may sustain so-called *surface acoustic waves* (SAW), in particular, the *Rayleigh waves* and the *Love waves*.³⁹ The main feature that distinguishes such waves from their *bulk* (longitudinal and transverse) counterparts discussed above, is that the displacement amplitudes are largest at the interface and decay exponentially into the bulk of both adjacent media, so that the waves cannot be plane in the usual sense of being independent of two Cartesian coordinates.

For an analysis of such waves, it is important that in a uniform medium, even non-plane elastic waves may be always separated into independent longitudinal and transverse components. Indeed, it is straightforward (and hence left for the reader) to prove that Eq. (107) may be satisfied by a vector sum $\mathbf{q}(\mathbf{r}, t) = \mathbf{q}_l(\mathbf{r}, t) + \mathbf{q}_t(\mathbf{r}, t)$, with the former component having zero curl ($\nabla \times \mathbf{q}_l = 0$) and propagating with the velocity (112), and the latter component having zero divergence ($\nabla \cdot \mathbf{q}_t = 0$) and propagating with the velocity (116). The plane waves $q_l \mathbf{n}_z$ and $q_t \mathbf{n}_x$ analyzed above certainly fall into these two categories, but in more general waves, there may be no clear association between the longitudinal and transverse components and their polarization.

This is true, in particular, in the Rayleigh waves, where the particle displacement vector \mathbf{q} may be represented as the sum $\mathbf{q}_l + \mathbf{q}_t$, each of the vectors having more than one Cartesian component. In

³⁷ See, e.g., EM Sec. 7.5.

³⁸ Their discussion may be also found in EM Sec. 7.5.

³⁹ Named, respectively, after Lord Rayleigh (born J. Strutt, 1842-1919) who has theoretically predicted the very existence of surface acoustic waves, and A. Love (1863-1940).

contrast to the bulk waves, the longitudinal and transverse components are coupled via their interaction with the interface, and as a result, propagate with a single velocity v_R . A straightforward analysis of the Rayleigh waves on the *surface* of an elastic solid (i.e. its interface with free space) yields the following equation for v_R :

$$\left(1 - \frac{v_R^2}{2v_t^2}\right)^4 = \left(1 - \frac{v_R^2}{v_t^2}\right) \left(1 - \frac{v_R^2}{v_l^2}\right). \quad (7.127)$$

According to this formula, and Eqs. (112) and (116), for realistic materials with the Poisson index between 0 and $\frac{1}{2}$, the Rayleigh waves are slightly (by 4 to 13%) slower than the bulk transverse waves – and hence substantially slower than the bulk longitudinal waves.

In the simplest case a “1D-plane” Rayleigh wave, independent of one Cartesian coordinate, the net vector \mathbf{q} has just two Cartesian components (each contributed by \mathbf{q}_l and \mathbf{q}_t): one parallel to the propagation direction and hence to the interface, and another one normal to it. As a result, the trajectory of each particle in the wave is an ellipse in the plane normal to the interface. In contrast, the Love waves are purely transverse, with \mathbf{q} oriented parallel to the interface. However, the interaction of these waves with the interface reduces their velocity v_L in comparison with that (v_t) of the bulk transverse waves, keeping it within the narrow interval between v_t and v_R :

$$v_R < v_L < v_t < v_l. \quad (7.128)$$

The practical importance of surface acoustic waves is that their amplitude decays very slowly with distance r from their point-like source: $a \propto 1/r^{1/2}$, while any bulk waves decay much faster, as $a \propto 1/r$. (Indeed, in the latter case the power $\mathcal{P} \propto a^2$, emitted by such source, is distributed over a spherical surface area proportional to r^2 , while in the former case all the power goes into a thin surface circle whose length scales as r .) At least two areas of applications of the surface acoustic waves have to be mentioned: geophysics (for the earthquake detection and the Earth crust seismology), and electronics (for signal processing, with a focus on frequency filtering). Unfortunately, I cannot dwell on these interesting topics and I have to refer the reader to special literature.⁴⁰

7.8. Elastic waves in restricted geometries

From what was discussed at the end of the last section, it should be pretty clear that generally, the propagation of acoustic waves in elastic bodies of finite size is rather complicated. There is, however, one important limit in which several important simple results may be readily obtained. This is the limit of (relatively) low frequencies, where the corresponding wavelength is much larger than at least one dimension of the system.

Let us consider, for example, various waves that may propagate along thin rods, in this case “thin” meaning that the characteristic size a of the rod’s cross-section is much smaller than not only the length of the rod but also the wavelength $\lambda = 2\pi/k$. In this case, there is a considerable range Δz of distances along the rod,

$$a \ll \Delta z \ll \lambda, \quad (7.129)$$

⁴⁰ See, for example, K. Aki and P. Richards, *Quantitative Seismology*, 2nd ed., University Science Books, 2002 and D. Morgan, *Surface Acoustic Waves*, 2nd ed., Academic Press, 2007.

in that we can neglect the material's inertia, and apply the results of our earlier static analyses. For example, for a *longitudinal* wave of stress, which is essentially a wave of periodic tensile extensions and compressions of the rod, within the range (129) we may use the static relation (42):

$$\sigma_{zz} = Es_{zz}. \quad (7.130)$$

In this simple case, it is easier to use the general equation of elastic dynamics not in its vector form (107), but rather in the precursor, Cartesian-component form (25), with $f_j = 0$. For the plane waves of stress, propagating along the z -axis, only one component (with $j' \rightarrow z$) of the sum on the right-hand side of that equation is not equal to zero, and it is reduced to

$$\rho \frac{\partial^2 q_j}{\partial^2 t^2} = \frac{\partial \sigma_{jz}}{\partial z}. \quad (7.131)$$

In our current case of longitudinal waves, all components of the stress tensor but σ_{zz} are equal to zero. With σ_{zz} from Eq. (130), and using the definition $s_{zz} = \partial q_z / \partial z$, Eq. (131) is reduced to a simple 1D wave equation,

$$\rho \frac{\partial^2 q_z}{\partial^2 t^2} = E \frac{\partial^2 q_z}{\partial z^2}, \quad (7.132)$$

which shows that the velocity of such *tensile waves* is

$$v = \left(\frac{E}{\rho} \right)^{1/2}. \quad (7.133)$$

Tensile waves: velocity

Comparing this result with Eq. (112), we see that the tensile wave velocity, for any realistic material with a positive Poisson's ratio, is lower than the velocity v_l of longitudinal waves in the bulk of the same material. The reason for this difference is simple: in thin rods, the cross-section is free to oscillate (e.g., shrink in the longitudinal extension phase of the passing wave),⁴¹ so that the effective force resisting the longitudinal deformation is smaller than in a border-free space. Since (as it is clearly visible from the wave equation), the scale of the force determines that of v^2 , this difference translates into slower waves in rods. Of course, as the wave frequency is increased to $ka \sim 1$, there is a (rather complicated and cross-section-depending) crossover from Eq. (133) to Eq. (112).

Proceeding to *transverse* waves on rods, let us first have a look at long *bending waves* for which the condition (129) is satisfied, so that the vector $\mathbf{q} = \mathbf{n}_x q_x$ (with the x -axis being the bending direction – see Fig. 8) is virtually constant in the whole cross-section. In this case, the only element of the stress tensor contributing to the net transverse force F_x is σ_{xz} , so that the integral of Eq. (131) over the cross-section is

$$\rho A \frac{\partial^2 q_x}{\partial t^2} = \frac{\partial F_x}{\partial z}, \quad \text{with } F_x = \int_A \sigma_{xz} d^2 r. \quad (7.134)$$

Now, if Eq. (129) is satisfied, we again may use the static local relations (75)-(77), with all derivatives d/dz duly replaced with their partial form $\partial/\partial z$, to express the force F_x via the bending deformation q_x . Plugging these relations into each other one by one, we arrive at a rather unusual differential equation

⁴¹ For this reason, the tensile waves can be called longitudinal only in a limited sense: while the stress wave is purely longitudinal: $\sigma_{xx} = \sigma_{yy} = 0$, the strain wave is not: $s_{xx} = s_{yy} = -\sigma_{zz} \neq 0$, i.e. $\mathbf{q}(\mathbf{r}, t) \neq \mathbf{n}_z q_z$.

$$\rho A \frac{\partial^2 q_x}{\partial t^2} = -EI_y \frac{\partial^4 q_x}{\partial z^4}. \quad (7.135)$$

Looking for its solution in the form of a sinusoidal wave (108), we get the following dispersion relation:⁴²

Bending waves:
dispersion relation

$$\omega^2 = \frac{EI_y}{\rho A} k^4. \quad (7.136)$$

Such relation means that the bending waves are not acoustic at *any* frequency, and cannot be characterized by a single velocity that would be valid for all wave numbers k , i.e. for all spatial Fourier components of a waveform. According to our discussion in Sec. 6.3, such *strongly dispersive* systems cannot pass non-sinusoidal waveforms too far without changing their waveform rather considerably.

This situation changes, however, if the rod is pre-stretched with a tension force \mathcal{T} – just as in the discrete 1D model that was analyzed in Sec. 6.3. The calculation of the effect of this force is essentially similar; let us repeat it for the continuous case, for a minute neglecting the bending stress – see Fig. 13.

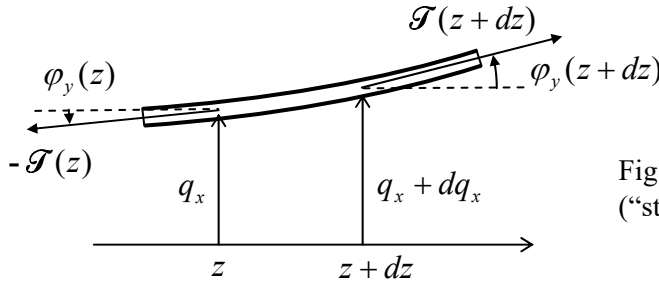


Fig. 7.13. Additional forces in a thin rod (“string”), due to the background tension \mathcal{T} .

Still sticking to the limit of small angles φ , the additional vertical component $d\mathcal{T}_x$ of the net force acting on a small rod fragment of length dz is $\mathcal{T}_x(z - dz) - \mathcal{T}_x(z) = \mathcal{T}\varphi_y(z + dz) - \mathcal{T}\varphi_y(z) \approx \mathcal{T}(\partial\varphi_y/\partial z)dz$, so that $\partial F_x/\partial z = \mathcal{T}(\partial\varphi_y/\partial z)$. With the geometric relation (77) in its partial-derivative form $\partial q_x/\partial z = \varphi_y$, this additional term becomes $\mathcal{T}(\partial^2 q_x/\partial z^2)$. Now adding it to the right-hand side of Eq. (135), we get the following dispersion relation

$$\omega^2 = \frac{1}{\rho A} (EI_y k^4 + \mathcal{T}k^2). \quad (7.137)$$

Since the product ρA in the denominator of this expression is just the rod’s mass per unit length (which was denoted μ in Chapter 6), at low k (and hence low frequencies), this expression is reduced to the linear dispersion law, with the velocity given by Eq. (6.43):

$$v = \left(\frac{\mathcal{T}}{\rho A} \right)^{1/2}. \quad (7.138)$$

So Eq. (137) describes a smooth crossover from the “guitar-string” acoustic waves to the highly dispersive bending waves (136).

⁴² Note that since the “moment of inertia” I_y , defined by Eq. (70), may depend on the bending direction (unless the cross-section is sufficiently symmetric), the dispersion relation (136) may give different results for different directions of the bending wave polarization.

Now let us consider another type of transverse waves in thin rods – the so-called *torsional waves*, which are essentially the dynamic propagation of the torsional deformation discussed in Sec. 6. The easiest way to describe these waves, again within the limits (129), is to write the equation of rotation of a small segment dz of the rod about the z -axis, passing through the “center of mass” of its cross-section, under the difference of torques $\tau = \mathbf{n}_z \tau_z$ applied on its ends – see Fig. 10:

$$\rho I_z dz \frac{\partial^2 \varphi_z}{\partial t^2} = d\tau_z, \quad (7.139)$$

where I_z is the “moment of inertia” defined by Eq. (91), which now, after its multiplication by ρdz , i.e. by the mass per unit area, has turned into the genuine moment of inertia of a dz -thick slice of the rod. Dividing both sides of Eq. (139) by dz , and using the static local relation (84), $\tau_z = C\kappa = C(\partial\varphi_z/\partial z)$, we get the following differential equation

$$\rho I_z \frac{\partial^2 \varphi_z}{\partial t^2} = C \frac{\partial^2 \varphi_z}{\partial z^2}. \quad (7.140)$$

Just as Eqs. (111), (115), and (132), this equation describes an acoustic (dispersion-free) wave, which propagates with the following frequency-independent velocity

$$v = \left(\frac{C}{\rho I_z} \right)^{1/2}. \quad (7.141)$$

Torsional waves:
velocity

As we have seen in Sec. 6, for rods with axially-symmetric cross-sections, the torsional rigidity C is described by the simple relation (89), $C = \mu I_z$, so that Eq. (141) is reduced to Eq. (116) for the transverse waves in infinite media. The reason for this similarity is straightforward: in a torsional wave, particles oscillate along small arcs (Fig. 14a), so that if the rod’s cross-section is round, its surface is stress-free, and does not perturb or modify the motion in any way, and hence does not affect the transverse velocity.

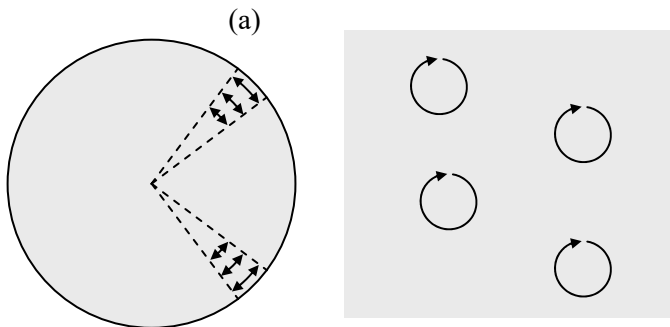


Fig. 7.14. Particle trajectories in two different transverse waves with the same velocity: (a) torsional waves in a thin round rod and (b) circularly-polarized waves in an infinite (or very broad) sample.

This fact raises an interesting issue of the relation between the torsional and *circularly-polarized* waves. Indeed, in Sec. 7, I have not emphasized enough that Eq. (116) is valid for a transverse wave polarized in any direction perpendicular to the wave vector \mathbf{k} (in our notation, directed along the z -axis). In particular, this means that such waves are doubly-degenerate: any isotropic elastic continuum can carry simultaneously two non-interacting transverse waves propagating in the same direction with the same velocity (116), with two mutually perpendicular linear polarizations (directions of the vector \mathbf{a}),

for example, directed along the x - and y -axes.⁴³ If both waves are sinusoidal (108), with the same frequency, each point of the medium participates in two simultaneous sinusoidal motions within the $[x, y]$ plane:

$$q_x = \operatorname{Re} \left[a_x e^{i(kz - \omega t)} \right] = A_x \cos \Psi, \quad q_y = \operatorname{Re} \left[a_y e^{i(kz - \omega t)} \right] = A_y \cos(\Psi + \varphi), \quad (7.142)$$

where $\Psi \equiv kz - \omega t + \varphi_x$, and $\varphi \equiv \varphi_y - \varphi_x$. Basic geometry tells us that the trajectory of such a motion on the $[x, y]$ plane is an ellipse (Fig. 15), so that such waves are called *elliptically polarized*. The most important particular cases of such polarization are:

- (i) $\varphi = 0$ or π : a *linearly-polarized* wave, with the displacement vector \mathbf{a} is directed at angle $\theta = \tan^{-1}(A_y/A_x)$ to the x -axis; and
- (ii) $\varphi = \pm \pi/2$ and $A_x = A_y$: two possible *circularly-polarized* waves, with the *right* or *left* polarization, respectively.⁴⁴

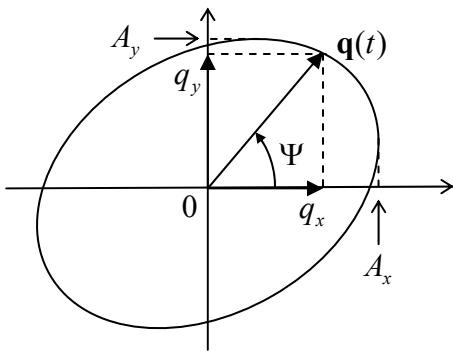


Fig. 7.15. The trajectory of a particle in an elliptically polarized transverse wave, within the plane perpendicular to the direction of wave propagation.

Now comparing the trajectories of particles in the torsional wave in a thin round rod (or pipe) and the circularly-polarized wave in a broad sample (Fig. 14), we see that, despite the same wave propagation velocity, these transverse waves are rather different. In the former case (Fig. 14a) each particle moves back and forth along an arc, with the arc's length different for different particles (and vanishing at the rod's center), so that the waves are *not* plane. On the other hand, in a circularly polarized wave, all particles move along similar, circular trajectories, so that such a wave *is* plane.

To conclude this chapter, let me briefly mention the opposite limit when the size of the body, from whose boundary the waves are completely reflected,⁴⁵ is much larger than the wavelength. In this case, the waves propagate almost as in an infinite 3D continuum (which was analyzed in Sec. 7), and the most important new effect is the finite number of wave modes in the body. Repeating the 1D analysis at the end of Sec. 6.5, for each dimension of a 3D cuboid of volume $V = l_1 l_2 l_3$, and taking into account that the numbers k_n in each of the three dimensions are independent, we get the following generalization of

⁴³ As was discussed in Sec. 6.3, this is also true in the simple 1D model shown in Fig. 6.4a.

⁴⁴ The circularly polarized waves play an important role in quantum mechanics, where they may be most naturally quantized, with their elementary excitations (in the case of mechanical waves we are discussing, called *phonons*) having either positive or negative angular momentum $L_z = \pm \hbar$.

⁴⁵ For acoustic waves, such a condition is easy to implement. Indeed, from Sec. 7 we already know that the strong inequality of the wave impedances Z is sufficient for such reflection. The numbers in Table 1 show that, for example, the impedance of a longitudinal wave in a typical metal (say, steel) is almost two orders of magnitude higher than that in air, ensuring their virtually full reflection from the surface.

Eq. (6.75) for the number ΔN of different traveling waves with wave vectors within a relatively small volume $d^3 k$ of the wave vector space:

$$dN = g \frac{V}{(2\pi)^3} d^3 k \gg 1, \quad \text{for } \frac{1}{V} \ll d^3 k \ll k^3, \quad (7.143)$$

3D
density
of modes

where $k \ggg 1/l_{1,2,3}$ is the center of this volume, and g is the number of different possible wave modes with the same wave vector \mathbf{k} . For the mechanical waves analyzed above, with one longitudinal mode, and two transverse modes with different polarizations, $g = 3$.

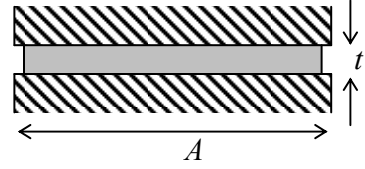
Note that since the derivation of Eqs. (6.75) and (143) does not use other properties of the waves (in particular, their dispersion relations), this mode counting rule is ubiquitous in physics, being valid, in particular, for electromagnetic waves (where $g = 2$) and quantum “de Broglie waves” (i.e. wavefunctions), whose degeneracy factor g is usually determined by the particle’s spin.⁴⁶

7.9. Exercise problems

7.1. Derive Eqs. (16).

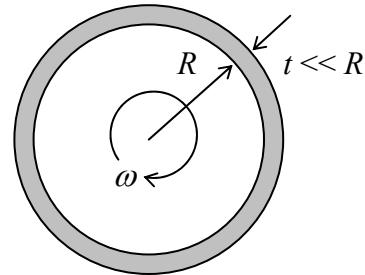
Hint: Besides the definition of the cylindrical coordinates and basic calculus, you may like to use Eq. (4.7) with $d\phi = (d\varphi)\mathbf{n}_z$.

7.2. A uniform thin sheet of an isotropic, elastic material, of thickness t and area $A \gg t^2$, is compressed by two plane, parallel, broad, rigid surfaces – see the figure on the right. Assuming that there is no slippage between the sheet and the surfaces, calculate the relative compression ($-\Delta t/t$) as a function of the compressing force. Compare the result with that for the tensile stress calculated in Sec. 3.



7.3. Two opposite edges of a thin, very wide sheet of an isotropic, elastic material have been clamped in two rigid, plane, parallel walls that are pulled apart with force F , along the sheet’s length l . Find the relative extension $\Delta l/l$ of the sheet in the direction of the force and its relative compression $\Delta t/t$ in the perpendicular direction, and compare the results with Eqs. (45)-(46) for the tensile stress and the solution of the previous problem.

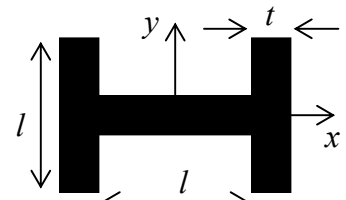
7.4. Calculate radial extension ΔR of a thin, long, round cylindrical pipe, due to its rotation with a constant angular velocity ω about its symmetry axis (see the figure on the right), in terms of the elastic moduli E and v . The external pressure both inside and outside the pipe is negligible.



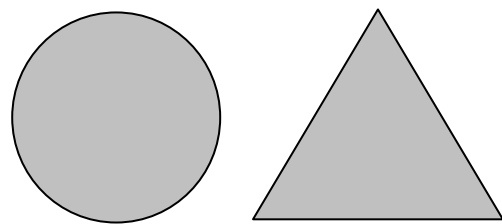
7.5.* A static force \mathbf{F} is exerted on an inner point of a uniform, isotropic elastic body. Calculate the spatial distribution of the deformation created by the force, assuming that far from the point of its application and the points we are interested in, the body’s position is kept fixed.

⁴⁶ See, e.g., EM Secs. 7.8 and QM Sec. 1.7.

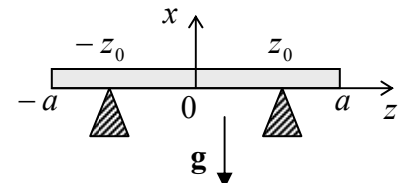
7.6. A long, uniform rail with the cross-section shown in the figure on the right, is being bent with the same (small) torque twice: first within the xz -plane and then within the yz -plane. Assuming that $t \ll l$, find the ratio of the rail bending deformations in these two cases.



7.7. Two thin rods of the same length and mass are made of the same elastic, isotropic material. The cross-section of one of them is a circle, while the other one is an equilateral triangle – see the figure on the right. Which of the rods is stiffer for bending along its length? Quantify the relation. Does the result depend on the bending plane orientation?



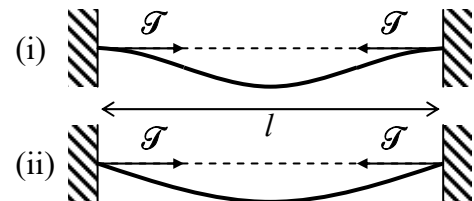
7.8. A thin, elastic, uniform, initially straight beam is placed on two point supports at the same height – see the figure on the right. Calculate the support placements that:



- (i) ensure that the beam ends are horizontal, and
- (ii) minimize the largest deviation of the beam from the horizontal baseline.

Hint: For Task (ii), an approximate answer (with an accuracy better than 1%) is acceptable.

7.9. Calculate the largest longitudinal compression force \mathcal{T} that may be withstood by a thin, straight, elastic rod without buckling (see the figure on the right) for two shown cases:



- (i) the rod's ends are clamped, and
- (ii) the rod is free to turn about the support points.

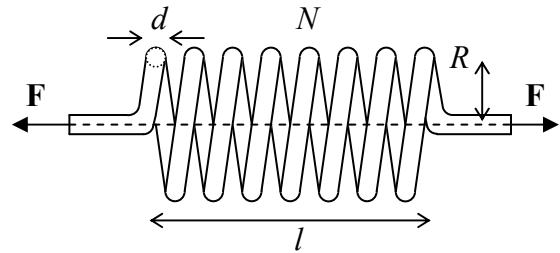
7.10. An elastic, light, thin poll with a square cross-section of area $A = a \times a$, had been firmly dug into the ground in the vertical position, sticking out by height $h \gg a$. What largest compact mass M may be placed straight on the top of the poll without the stability loss?

7.11. Calculate the potential energy of a small and slowly changing, but otherwise arbitrary bending deformation of a uniform, elastic, initially straight rod. Can the result be used to derive the dispersion relation (136)?

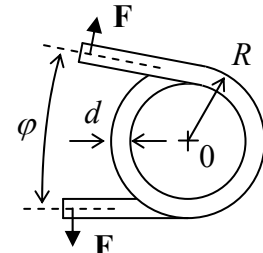
7.12. Calculate the torsional rigidity of a thin, uniform rod whose cross-section is an ellipse with semi-axes a and b .

7.13. Calculate the potential energy of a small but otherwise arbitrary torsional deformation $\varphi_z(z)$ of a uniform, straight, elastic rod.

7.14. Calculate the spring constant $\kappa \equiv dF/dl$ of a coil made of a uniform, elastic wire with a circular cross-section of diameter d , wound as a dense round spiral of $N \gg 1$ turns of radius $R \gg d$ – see the figure on the right.



7.15. The coil described in the previous problem is now used as what is sometimes called the *torsion spring* – see the figure on the right. Find the corresponding spring constant $d\tau/d\varphi$, where τ is the torque of the external forces \mathbf{F} relative to the center of the coil (point 0).



7.16. Use Eqs. (99) and (100) to recast Eq. (101b) for the torsional rigidity C of a thin rod into the form given by Eq. (101c).

7.17.* Generalize Eq. (101b) to the case of rods with more than one cross-section's boundary. Use the result to calculate the torsional rigidity of a thin round pipe, and compare it with Eq. (91).

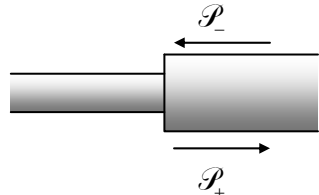
7.18. Prove that in a uniform medium, any (not necessarily plane) elastic wave may be decomposed into a longitudinal wave with $\nabla \times \mathbf{q}_l = 0$ and a transverse wave with $\nabla \cdot \mathbf{q}_t = 0$, and find the equations satisfied by these functions.

7.19.* Use the wave equations derived in the solution of the previous problem and the semi-quantitative description of the Rayleigh surface waves given in Sec. 7 of the lecture notes, to calculate the structure of the waves and derive Eq. (127).

7.20.* Calculate the modes and frequencies of free radial oscillations of a sphere with radius R , made of a uniform elastic material.

7.21. A long steel wire has a circular cross-section with a 3-mm diameter, and is pre-stretched with a constant force of 10 N. Which of the longitudinal and transverse waves with frequency 1 kHz has the largest group velocity in the wire? Accept the following parameters for the steel (see Table 1): $E = 170$ GPa, $\nu = 0.30$, $\rho = 7.8$ g/cm³.

7.22. Define and calculate the wave impedances for (i) tensile and (ii) torsional waves in a thin rod, appropriate in the long-wave limit. Use the results to calculate the fraction of each wave's power \mathcal{P} reflected from a firm connection of a long rod with a round cross-section to a similar rod, but with a twice smaller diameter – see the figure on the right.



7.23. Calculate the fundamental frequency of small transverse standing waves on a free and uniform thin rod, and the position of displacement nodes in this mode.

Hint: Numerical solution of the final transcendent equations is acceptable.

Chapter 8. Fluid Mechanics

This chapter describes the basic notions of fluid mechanics, discusses a few core problems of statics and dynamics of ideal and viscous fluids, and gives a very brief review of such a complicated phenomenon as turbulence. In addition, the viscous fluid flow discussion is used as a platform for an elementary introduction to numerical methods of the partial differential equation solution – whose importance extends well beyond this particular field.

8.1. Hydrostatics

The mechanics of *fluids* (defined as the materials that cannot keep their geometric form on their own, and include both liquids and gases) is both more simple and more complex than that of the elastic solids, with the simplifications mostly in *statics*.¹ Indeed, fluids, by definition, cannot resist static shear deformations. There are two ways to express this fact. First, we can formally take the shear modulus μ , describing this resistance, to equal zero. Then the Hooke's law (7.32) shows that the stress tensor is diagonal:

$$\sigma_{jj'} = \sigma_{jj} \delta_{jj'}. \quad (8.1)$$

Alternatively, the same conclusion may be reached just by looking at the stress tensor definition (7.19) and/or Fig. 7.3, and saying that in the absence of shear stress, the elementary interface $d\mathbf{F}$ has to be normal to the area element dA , i.e. parallel to the vector $d\mathbf{A}$.

Moreover, in fluids at equilibrium, all three diagonal elements σ_{jj} of the stress tensor have to be equal at each point. To prove that, it is sufficient to single out (mentally rather than physically), from a static fluid, a small volume in the shape of a right prism, with mutually perpendicular faces normal to the two directions we are interested in – in Fig. 1, along the x - and y -axes.

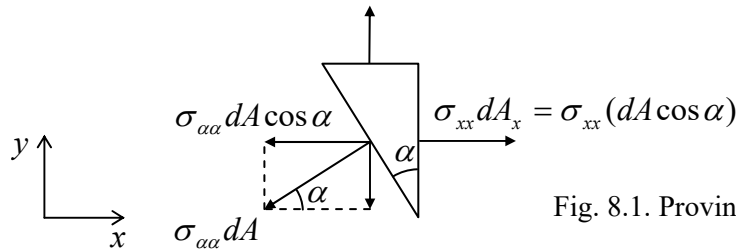


Fig. 8.1. Proving the pressure isotropy.

The prism is in equilibrium if each Cartesian component of the vector of the total force exerted on all its faces equals zero. For the x -component this balance may be expressed as $\sigma_{xx}dA_x - (\sigma_{\alpha\alpha}dA)\cos\alpha = 0$. However, from the geometry (Fig. 1), $dA_x = dA\cos\alpha$, so that the above expression yields $\sigma_{\alpha\alpha} = \sigma_{xx}$. A similar argument for the y -component gives $\sigma_{\alpha\alpha} = \sigma_{yy}$ so that $\sigma_{xx} = \sigma_{yy}$. Changing the orientation of the prism, we can get such equalities for any pair of diagonal elements of the stress tensor, σ_{jj} , so that all three of them have to be equal.

¹ It is often called *hydrostatics* because water has always been the most important liquid for the human race and hence for science and engineering.

This common diagonal element of the stress matrix is usually denoted as $(-\mathcal{P})$, because in the vast majority of cases, the parameter \mathcal{P} , called *pressure*, is positive. Thus we arrive at the key relation (which was already mentioned in Sec. 7.2):

$$\sigma_{jj'} = -\mathcal{P}\delta_{jj'}. \quad (8.2) \quad \text{Pressure}$$

In the absence of bulk forces, pressure should be constant through the volume of fluid, due to the translational symmetry. Let us see how this result is affected by bulk forces. With the simple stress tensor (2), the general condition of equilibrium of a continuous medium, expressed by Eq. (7.25) with the left-hand side equal to zero, becomes

$$-\frac{\partial \mathcal{P}}{\partial r_j} + f_j = 0, \quad (8.3)$$

and may be re-written in the following convenient vector form:

$$-\nabla \mathcal{P} + \mathbf{f} = 0. \quad (8.4)$$

In the simplest case of a heavy fluid with mass density ρ , in a uniform gravity field $\mathbf{f} = \rho \mathbf{g}$, the equation of equilibrium becomes,

$$-\nabla \mathcal{P} + \rho \mathbf{g} = 0, \quad (8.5)$$

with only one nonzero component – near the Earth's surface, the vertical one. If, in addition, the fluid may be considered *incompressible*, with its density ρ constant,² this equation may be readily integrated over the vertical coordinate (say, y) to give the so-called *Pascal equation*:³

$$\mathcal{P} + \rho g y = \text{const}, \quad (8.6) \quad \text{Pascal equation}$$

where the direction of the y -axis is taken opposite to that of vector \mathbf{g} .

Two manifestations of this key equation are well known. The first one is the fact that in interconnected vessels filled with a fluid, its pressure is equal at all points at the same height (y), regardless of the vessel shape, provided that the fluid is in equilibrium.⁴ In particular, if a heavy liquid has an open surface, then in equilibrium, it has to be horizontal – at least, not too close to the retaining walls (see Sec. 2).

The second manifestation of Eq. (6) is the *buoyant force* \mathbf{F}_b exerted by a liquid on a (possibly, partly) submerged body, i.e. the vector sum of the elementary pressure forces $d\mathbf{F} = \mathcal{P}d\mathbf{A}$ exerted on all elementary areas dA of the submerged part of the body's surface – see Fig. 2. According to Eq. (6), with the constant equal to zero (corresponding to zero pressure at the liquid's surface taken for $y = 0$, see Fig. 2a), the vertical component of this elementary force is

² As was discussed in Sec. 7.3 in the context of Table 7.1, this is an excellent approximation, for example, for human-scale experiments with water.

³ The equation, and the SI unit of pressure 1 Pa $\equiv 1\text{N/m}^2$, are named after Blaise Pascal (1623–1662) who has not only pioneered hydrostatics, but also invented the first mechanical calculator, and made several other important contributions to mathematics – and to Christian philosophy!

⁴ This simple fact opens wide opportunities for the engineering field of *hydraulics*, in particular enabling a very simple and efficient way to magnify forces, using interconnected *hydraulic cylinders* of different diameters.

$$dF_y = dF \cos \varphi = \mathcal{P}dA \cos \varphi = -\rho gy \cos \varphi dA = -\rho gy dA_h. \quad (8.7)$$

where $dA_h = \cos \varphi dA$ is the horizontal footprint (say, $dx dz$) of the elementary area dA . Now integrating this relation over all the surface, we get the total vertical buoyant force:⁵

Archimedes principle

$$F_b = \rho g \int_S (-y) dA_h \equiv \rho g V, \quad (8.8)$$

where V is the volume of the *submerged* part of the body's volume, while ρ is the liquid's density, so that by magnitude, F_b equals the weight of the liquid which *would* fill the submerged volume.

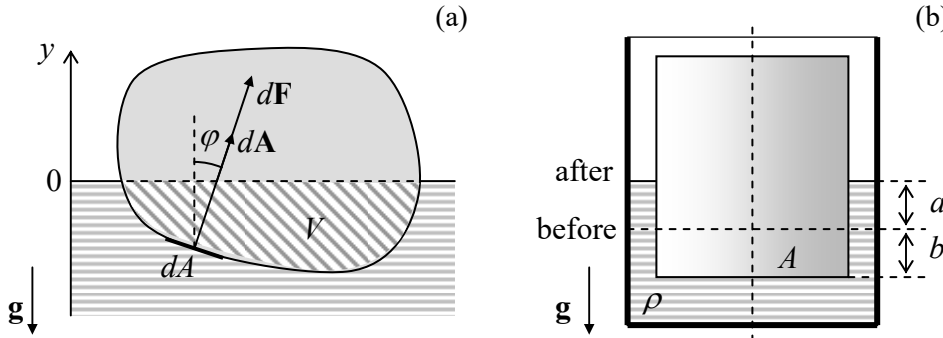


Fig. 8.2. Calculating the buoyant force.

This well-known *Archimedes principle* may be proved even more simply using the following argument: the liquid's pressure forces, and hence the resulting buoyant force, cannot depend on what is inside the body's volume. Hence F_b would be the same if we filled the volume V in question with a liquid similar to the surrounding one. But in this case, the liquid should be still in equilibrium even if the surface is completely flexible, so that both forces acting on its inner part, the buoyant force \mathbf{F}_b and the inner liquid's weight $m\mathbf{g} = \rho V \mathbf{g}$, have to be equal and opposite, thus proving Eq. (8) again.

Despite the simplicity of the Archimedes principle, its erroneous formulations, such as “*The buoyant force's magnitude is equal to the weight of the displaced liquid*” [WRONG!] creep from one undergraduate textbook to another, leading to application errors. A typical example is shown in Fig. 2b, where a solid vertical cylinder with the base area A is pressed into a liquid inside a container of comparable size, pushing the liquid's level up by distance a . The correct answer for the buoyant force, following from Eq. (8), is

$$F_b = \rho g V = \rho g A(a + b), \quad (8.9a)$$

because the volume V of the *submerged* part of the cylinder is evidently $A(a + b)$. But the wrong formulation cited above, using the term *displaced liquid*, would give a different answer:

$$F_b = \rho g V_{\text{displaced}} = \rho g A b. \quad [\text{WRONG!}] \quad (8.9b)$$

(The latter result is correct only asymptotically, in the limit $b/a \rightarrow \infty$.)

Another frequent error in hydrostatics concerns the angular stability of a freely floating body – the problem of vital importance for the boat/ship design. It is sometimes claimed that the body is stable

⁵ The force is vertical, because the horizontal components of the elementary forces $d\mathbf{F}$ exerted on opposite elementary areas dA , at the same height y , cancel.

only if the so-called *buoyancy center*, the effective point of buoyant force application (in Fig. 3, point B),⁶ is *above* the center of mass (C) of the floating body. However, as Fig. 3 shows, this is unnecessary; indeed in the shown case, point B remains *below* point C, even at a small tilt. Still, in this case, the torque created by the pair of forces F_b and mg tries to return the body to the equilibrium position, which is therefore stable. As Fig. 3 shows, the actual condition of the angular stability may be expressed as the requirement for point M (in shipbuilding, called the *metacenter* of the ship's hull) to be above the ship's center of mass C.⁷

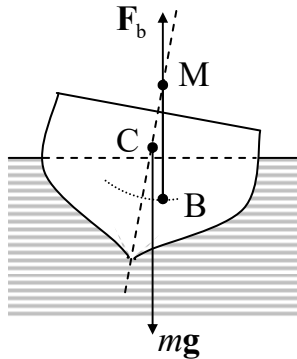


Fig. 8.3. Angular stability of a floating body.

To conclude this section, let me note that the integration of Eq. (4) may be more complex in the case if the bulk forces \mathbf{f} depend on position,⁸ and/or if the fluid is substantially compressible. In the latter case, Eq. (4) has to be solved together with the medium-specific *equation of state* $\rho = \rho(\mathcal{P})$ describing its compressibility law – whose example is given by Eq. (7.38) for ideal gases: $\rho \equiv mN/V = m\mathcal{P}/k_B T$, where m is the mass of one gas molecule.

8.2. Surface tension effects

Besides the bulk (volume-distributed) forces, one more possible source of pressure is *surface tension*. This effect results from the difference between the potential energy of atomic interactions on the interface between two different fluids and that in their bulks, and thus may be described by an additional potential energy

$$U_i = \gamma A, \quad (8.10)$$

Surface tension

where A is the interface area, and γ is called the *surface tension constant* – or just the “surface tension”. For a stable interface of any two fluids, γ is always positive.⁹ For surfaces of typical liquids (or their interfaces with air), at room temperature, the surface tension equals a few 10^{-2} J/m^2 ,¹⁰ corresponding to

⁶ A simple calculation, similar to the one resulting in Eq. (8), but for the total torque rather than the total force, shows that B is just the center of mass of the submerged volume V filled with any uniform material.

⁷ It is easy (and hence is left for the reader) to prove that a small tilt of the body leads to a small lateral displacement of point B, but does not affect the position of the metacenter M.

⁸ A simple example of such a problem is given by the fluid equilibrium in a container rotating with a constant angular velocity ω . If we solve such a problem in a reference frame rotating together with the container, the real bulk forces should be complemented by the centrifugal “force” (4.93), depending on \mathbf{r} .

⁹ Indeed, if the γ of the interface of certain two fluids is negative, it self-reconfigures to decrease U_i , i.e. to increase $|U_i|$, by increasing the interface area, i.e. fragments the system into a macroscopically-uniform solution.

¹⁰ For a better feeling of this number, one should remember that $1 \text{ J/m}^2 \equiv 1 \text{ N/m}$.

the potential energy U_i of a few 10^{-2} eV per surface molecule – i.e. just a fraction of the full *binding* (or “cohesive”) *energy* of the same liquid, which is typically of the order of 10^{-1} eV per molecule.

In the absence of other forces, the surface tension makes a liquid drop spherical to minimize its surface area A at a fixed volume. For the analysis of the surface tension effects for more complex geometries, and in the presence of other forces, it is convenient to reduce them to a certain additional effective pressure drop ΔP_{ef} at the interface. To calculate ΔP_{ef} , let us consider the condition of equilibrium of a small part dA of a smooth interface between two fluids (Fig. 2), in the absence of bulk forces.

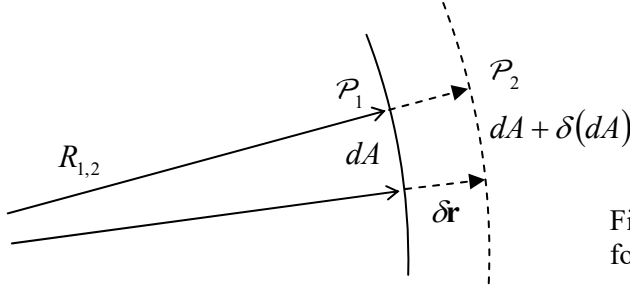


Fig. 8.4. Deriving the Young-Laplace formula (13).

If the pressures $P_{1,2}$ on the two sides of the interface are different, the work of stress forces on fluid 1 at a small virtual displacement $\delta r = \mathbf{n} \delta \mathbf{r}$ of the interface (where $\mathbf{n} = d\mathbf{A}/dA$ is the unit vector normal to the interface) equals¹¹

$$\delta \mathcal{W} = dA \delta r (\mathcal{P}_1 - \mathcal{P}_2). \quad (8.11)$$

For equilibrium, this work has to be compensated by an equal change of the interface energy, $\delta U_i = \gamma \delta(dA)$. Differential geometry tells us that in the linear approximation in δr , the relative change of the elementary surface area, corresponding to a fixed solid angle $d\Omega$, may be expressed as

$$\frac{\delta(dA)}{dA} = \frac{\delta r}{R_1} + \frac{\delta r}{R_2}, \quad (8.12)$$

where $R_{1,2}$ are the so-called *principal radii* of the interface curvature.¹² Combining Eqs. (10)-(12), we get the following *Young-Laplace formula*:¹³

$$\mathcal{P}_1 - \mathcal{P}_2 = \Delta P_{\text{ef}} \equiv \gamma \left(\frac{1}{R_1} + \frac{1}{R_2} \right).$$

(8.13)

Young-
Laplace
formula

¹¹ This equality follows from the general relation (7.30), with the stress tensor elements expressed by Eq. (2), but in this simple case of the net stress force $d\mathbf{F} = (\mathcal{P}_1 - \mathcal{P}_2)d\mathbf{A}$ parallel to the interface element vector $d\mathbf{A}$, it may be even more simply obtained just from the definition of work: $\delta \mathcal{W} = d\mathbf{F} \cdot \delta \mathbf{r}$ at the virtual displacement $\delta \mathbf{r} = \mathbf{n} \delta r$.

¹² This general formula may be readily verified for a sphere of radius r (for which $R_1 = R_2 = r$ and $dA = r^2 d\Omega$, so that $\delta(dA)/dA = \delta(r^2)/r^2 = 2\delta r/r$), and for a round cylindrical interface of radius R (for which $R_1 = r$, $R_2 = \infty$, and $dA = rd\varphi dz$, so that $\delta(dA)/dA = \delta r/r$). For more on curvature, see, for example, M. do Camo, *Differential Geometry of Curves and Surfaces*, 2nd ed., Dover, 2016.

¹³ This result (not to be confused with Eq. (15), called *Young's equation*) was derived in 1806 by Pierre-Simon Laplace (of the Laplace operator/equation fame) on the basis of the first analysis of the surface tension effects by Thomas Young (yes, the same Young who performed the famous two-slit experiment with light!) a year earlier.

In particular, this formula shows that the additional pressure created by surface tension inside a spherical drop of a liquid, of radius R , equals $2\gamma/R$, i.e. decreases with R . In contrast, according to Eqs. (5)-(6), the pressure effects of bulk forces, for example gravity, grow as $\rho g R$. The comparison of these two pressure components shows that if the drop radius (or more generally, the characteristic linear size of a liquid's sample) is much larger than the so-called *capillary length*

$$a_c \equiv \left(\frac{2\gamma}{\rho g} \right)^{1/2}, \quad (8.14)$$

Capillary length

the surface tension may be safely ignored – as will be done in all following sections of this chapter, besides a brief discussion at the end of Sec. 4. For the water surface, or more exactly its interface with air at ambient conditions, $\gamma \approx 0.073 \text{ J/m}^2$, while $\rho \approx 1,000 \text{ kg/m}^3$, so that $a_c \approx 4 \text{ mm}$.

On the other hand, in very narrow tubes, such as blood capillary vessels with radius $a \sim 1 \mu\text{m}$, i.e. $a \ll a_c$, the surface tension effects are very important. The key notion for the analysis of these effects is the *contact angle* θ_c (also called the “wetting angle”) at an equilibrium edge of a liquid wetting a solid – see Fig. 5.

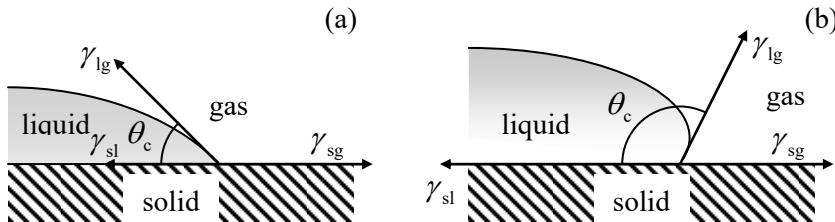


Fig. 8.5. Contact angles for (a) hydrophilic and (b) hydrophobic surfaces.

According to its definition (10), the constant γ may be interpreted as a force (per unit length of the interface boundary) directed normally to the boundary, and “trying” to reduce the interface area. As a result, the balance of horizontal components of the three such forces, shown in Fig. 5a, immediately yields the *Young's equation*

$$\gamma_{sl} + \gamma_{lg} \cos \theta_c = \gamma_{sg}, \quad (8.15)$$

Young's equation

where the indices of the three constants γ correspond to three possible interfaces between the liquid, solid, and gas. For the so-called *hydrophilic* surfaces that “like to be wet” by a particular liquid (not necessarily water), meaning that $\gamma_{sl} < \gamma_{sg}$, this relation yields $\cos \theta_c > 0$, i.e. $\theta_c < \pi/2$ – the situation shown in Fig. 5a. On the other hand, for *hydrophobic* surfaces with $\gamma_{sl} > \gamma_{sg}$, Eq. (15) yields larger contact angles, $\theta_c > \pi/2$ – see Fig. 5b.

Let us use this notion to solve the simplest and perhaps the most practically important problem of this field – find the height h of the fluid column lifted by the surface tension forces in a narrow vertical tube made of a hydrophilic material, assuming its internal surface to be a round cylinder of radius a – see Fig. 6. Inside an incompressible fluid, pressure drops with height according to the Pascal equation (6), so that just below the surface, $P \approx P_0 - \rho gh$, where P_0 is the background (e.g., atmospheric) pressure. This means that at $a \ll h$, the pressure variation along the concave surface (called the *meniscus*) of the liquid is negligible, so that according to the Young-Poisson equation (13), the sum $(1/R_1 + 1/R_2)$ has to be virtually constant along the surface. Due to the axial symmetry of the problem, this means that the surface has to be a part of a sphere. From the contact angle definition, the radius R of

the sphere is equal to $a/\cos\theta_c$ – see Fig. 6. Plugging this relation into Eq. (3) with $\mathcal{P}_1 - \mathcal{P}_2 = \rho gh$, we get the following result for h :

$$\rho gh = \frac{2\gamma \cos\theta_c}{a}. \quad (8.16a)$$

In hindsight, this result might be obtained more directly – by requiring the total weight $\rho gV = \rho g(\pi a^2 h)$ of the lifted liquid's column to be equal to the vertical component $F \cos\theta_c$ of the full surface tension force $F = \gamma p$, acting on the perimeter $p = 2\pi a$ of the meniscus. Using the definition (11) of the capillary length a_c , Eq. (16a) may be represented as the so-called *Jurin rule*:

$$h = \frac{a_c^2}{a} \cos\theta_c \leq \frac{a_c^2}{a};$$

(8.16b)

according to our initial assumption $h \gg a$, Eq. (16) is only valid for narrow tubes, with radius $a \ll a_c$.

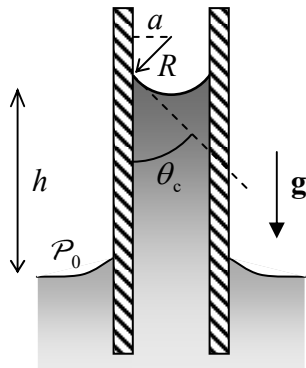


Fig. 8.6. Liquid's rise in a vertical capillary tube.

This capillary rise is the basic mechanism of lifting water with nutrients from roots to the branches and leaves of plants, so that the tallest tree heights correspond to the Jurin rule (16), with $\cos\theta_c \approx 1$, and the pore radius a limited from below by a few microns, because of the viscosity effects restricting the fluid discharge – see Sec. 5 below.

8.3. Kinematics

In contrast to the stress tensor, which is frequently very simple – see Eq. (2), the strain tensor is *not* a very useful notion in fluid mechanics. Indeed, besides a very few situations,¹⁴ typical problems of this field involve fluid *flow*, i.e. a state when the velocity of fluid particles has some nonzero time average. This means that the trajectory of each particle is a long line, and the very notion of its displacement \mathbf{q} from the initial position becomes impracticable. However, the particle's velocity $\mathbf{v} \equiv d\mathbf{q}/dt$ remains a very useful notion, especially if it is considered as a function of the *observation point* \mathbf{r} and (generally) time t . In an important class of fluid dynamics problems, the so-called *stationary* (or “steady”, or “static”) *flow*, the velocity defined in this way does not depend on time, $\mathbf{v} = \mathbf{v}(\mathbf{r})$.

¹⁴ One of them is sound propagation, where the particle displacements \mathbf{q} are typically small, so that the results of Sec. 7.7 are applicable. As a reminder, they show that in fluids, with $\mu = 0$, the transverse sound cannot propagate, while the longitudinal sound can – see Eq. (7.114).

There is, however, a price to pay for the convenience of this notion: namely, due to the difference between the vectors \mathbf{q} and \mathbf{r} , the particle's acceleration $\mathbf{a} = d^2\mathbf{q}/dt^2$ (that participates, in particular, in the 2nd Newton law) cannot be calculated just as the time derivative of the velocity $\mathbf{v}(\mathbf{r}, t)$. This fact is evident, for example, for the static flow case, in which the acceleration of individual fluid particles may be very significant even if $\mathbf{v}(\mathbf{r})$ does not depend on time – just think about the acceleration of a drop of water flowing over the Niagara Falls' rim, first accelerating fast and then virtually stopping below, while the water velocity \mathbf{v} at every particular point, as measured from a bank-based reference frame, is nearly constant. Thus the primary task of fluid kinematics is to express \mathbf{a} via \mathbf{v} ; let us do this.

Since each Cartesian component v_j of the velocity \mathbf{v} has to be considered as a function of four *independent* scalar variables: three Cartesian components r_j of the vector \mathbf{r} and time t , its full time derivative may be represented as

$$\frac{dv_j}{dt} = \frac{\partial v_j}{\partial t} + \sum_{j'=1}^3 \frac{\partial v_j}{\partial r_{j'}} \frac{dr_{j'}}{dt}. \quad (8.17)$$

Let us apply this *general* relation to a *specific* set of infinitesimal changes $\{dr_1, dr_2, dr_3\}$ that follows a small displacement $d\mathbf{q}$ of a certain particle of the fluid: $d\mathbf{r} = d\mathbf{q} = \mathbf{v}dt$, i.e.

$$dr_j = v_j dt. \quad (8.18)$$

In this case, dv_j/dt is the j^{th} component a_j of the particle's acceleration \mathbf{a} , so that Eq. (17) yields the following key relation of fluid kinematics:

$$a_j = \frac{\partial v_j}{\partial t} + \sum_{j'=1}^3 v_{j'} \frac{\partial v_j}{\partial r_{j'}}. \quad (8.19a)$$

Using the del operator ∇ , this result may be rewritten in the following compact vector form:¹⁵

$$\mathbf{a} = \frac{\partial \mathbf{v}}{\partial t} + (\mathbf{v} \cdot \nabla) \mathbf{v}. \quad (8.19b)$$

Fluid
particle's
acceleration

This relation already signals the main technical problem of the fluid dynamics: many equations involving particle's acceleration are nonlinear in velocity, excluding such a powerful tool as the linear superposition principle (which was used so frequently in the previous chapters of this course) from the applicable mathematical arsenal.

One more basic relation of fluid kinematics is the so-called *continuity equation*, which is essentially just the differential version of the mass conservation law. Let us mark, inside a fluid flow, an arbitrary volume V limited by a stationary (time-independent) surface S . The total mass of the fluid inside the volume may change only due to its flow through the boundary:

$$\frac{dM}{dt} \equiv \frac{d}{dt} \int_V \rho d^3r = - \int_S \rho v_n d^2r \equiv - \int_S \rho \mathbf{v} \cdot d\mathbf{A}, \quad (8.20a)$$

¹⁵ Note that the operator relation $d/dt = \partial/\partial t + (\mathbf{v} \cdot \nabla)$ is applicable to an arbitrary (scalar or vector) function; it is frequently called the *convective derivative*. (Alternative adjectives, such as “Lagrangian”, “substantial”, or “Stokes”, are sometimes used for this derivative as well.) The relation has numerous applications well beyond the fluid dynamics – see, e.g., EM Chapter 9 and QM Chapter 1.

where the elementary area vector $d\mathbf{A}$ is defined just as in Sec. 7.2 – see Fig. 7.

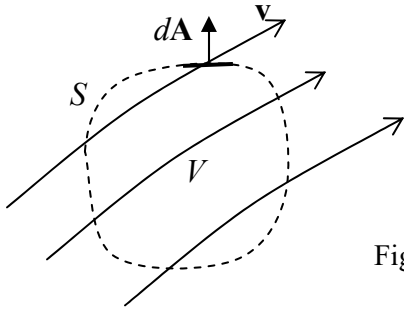


Fig. 8.7. Deriving the continuity equation.

Now using the same divergence theorem that has been used several times in this course,¹⁶ the surface integral in Eq. (20a) may be transformed into the integral of $\nabla(\rho\mathbf{v})$ over the volume V , so that relation may be rewritten as

$$\int_V \left(\frac{\partial \rho}{\partial t} + \nabla \cdot \mathbf{j} \right) d^3r = 0, \quad (8.20b)$$

where the vector $\mathbf{j} \equiv \rho\mathbf{v}$ is called either the *mass flux density* (or the “mass current”). Since Eq. (20b) is valid for an arbitrary stationary volume V , the function under the integral has to vanish at any point:

$\frac{\partial \rho}{\partial t} + \nabla \cdot \mathbf{j} = 0.$ (8.21)

Note that similar continuity equations are valid not only for mass but also for other conserved physics quantities (e.g., the electric charge, probability, etc.), with the proper re-definitions of ρ and \mathbf{j} .¹⁷

8.4. Dynamics: Ideal fluids

Let us start our discussion of fluid dynamics from the simplest case when the stress tensor obeys Eq. (2) even in motion. Physically, this means that the fluid viscosity effects, leading to mechanical energy loss, are negligible. (The conditions of this assumption will be discussed in the next section.) Then the equation of motion of such an *ideal fluid* (essentially the 2nd Newton law for its unit volume) may be obtained from Eq. (7.25) using the simplifications of its right-hand side, discussed in Sec. 1:

$$\rho\mathbf{a} = -\nabla\mathcal{P} + \mathbf{f}. \quad (8.22)$$

Now using the basic kinematic relation (19), we arrive at the following *Euler equation*:¹⁸

$\rho \frac{\partial \mathbf{v}}{\partial t} + \rho(\mathbf{v} \cdot \nabla)\mathbf{v} = -\nabla\mathcal{P} + \mathbf{f}.$ (8.23)

Generally, this equation has to be solved together with the continuity equation (21) and the equation of state of the particular fluid, $\rho = \rho(\mathcal{P})$. However, as we have already discussed, in many

¹⁶ If the reader still needs a reminder, see MA Eq. (12.1).

¹⁷ See, e.g., EM Sec. 4.1, QM Sec. 1.4, and SM Sec. 5.6.

¹⁸ It was derived in 1755 by the same Leonhard Euler whose name has already been (reverently) mentioned several times in this course.

situations the compressibility of water and other important liquids is very low and may be ignored, so that ρ may be treated as a given constant. Moreover, in many cases the bulk forces \mathbf{f} are conservative and may be represented as a gradient of a certain potential function $u(\mathbf{r})$ – the potential energy per unit volume:

$$\mathbf{f} = -\nabla u ; \quad (8.24)$$

for example, for a uniform, vertical gravity field, $u(\mathbf{r}) = \rho gy$, where y is referred to some (arbitrary) horizontal level. In this case, the right-hand side of Eq. (23) becomes $-\nabla(\mathcal{P} + u)$. For these cases, it is beneficial to recast the left-hand of that equation as well, using the following well-known identity of vector algebra¹⁹

$$(\mathbf{v} \cdot \nabla) \mathbf{v} = \nabla \left(\frac{v^2}{2} \right) - \mathbf{v} \times (\nabla \times \mathbf{v}). \quad (8.25)$$

As a result, the Euler equation takes the following form:

$$\rho \frac{\partial \mathbf{v}}{\partial t} - \rho \mathbf{v} \times (\nabla \times \mathbf{v}) + \nabla \left(\mathcal{P} + u + \rho \frac{v^2}{2} \right) = 0. \quad (8.26)$$

In a stationary flow, the first term of this equation vanishes. If the second term, describing fluid's vorticity, is zero as well, then Eq. (26) has the first integral of motion,

$$\mathcal{P} + u + \frac{\rho}{2} v^2 = \text{const},$$

(8.27)

Bernoulli
equation

called the *Bernoulli equation*.²⁰ Numerous examples of the application of Eq. (27) to simple problems of stationary flow in pipes, both with and without the Earth gravity field, should be well known to the readers from their undergraduate courses, so I hope I can skip their discussion without much harm.

In the general case, an ideal fluid may have vorticity, so that Eq. (27) is not always valid. Moreover, due to the absence of viscosity in an ideal fluid, the vorticity, once created, does not decrease along the so-called *streamline* – the fluid particle's trajectory, to which the velocity is tangential at every point.²¹ Mathematically, this fact²² is expressed by the following *Kelvin theorem*: $(\nabla \times \mathbf{v}) \cdot d\mathbf{A} = \text{const}$ along any small contiguous group of streamlines crossing an elementary area dA .²³

However, in many important cases, the vorticity is negligible. For example, even if the vorticity exists in some part of the fluid volume (say, induced by local turbulence, see Sec. 6 below), it may decay due to the fluid's viscosity, to be discussed in Sec. 5, well before it reaches the region of our interest. (If this viscosity is sufficiently small, its effects on the fluid's flow in the region of interest are

¹⁹ It readily follows, for example, from MA Eq. (11.6) with $\mathbf{g} = \mathbf{f} = \mathbf{v}$.

²⁰ Named after Daniel Bernoulli (1700-1782), not to be confused with Jacob Bernoulli or one of several Johanns of the same famous Bernoulli family, which gave the world so many famous mathematicians and scientists.

²¹ Perhaps the most spectacular manifestation of the vorticity conservation is the famous *toroidal vortex rings* (see, e.g., a nice photo and a movie at https://en.wikipedia.org/wiki/Vortex_ring), predicted in 1858 by H. von Helmholtz, and then demonstrated by P. Tait in a series of spectacular experiments with smoke in the air. The persistence of such a ring, once created, is only limited by the fluid's viscosity – see the next section.

²² This theorem was first formulated (verbally) by Hermann von Helmholtz.

²³ Its proof may be found, e.g., in Sec. 8 of L. Landau and E. Lifshitz, *Fluid Mechanics*, 2nd ed., Butterworth-Heinemann, 1987.

negligible, i.e. the ideal-fluid approximation is still acceptable.) Another important case is when a solid body of an arbitrary shape is embedded into an ideal fluid whose flow is uniform (meaning, by definition, that $\mathbf{v}(\mathbf{r}, t) = \mathbf{v}_0 = \text{const}$) at large distances,²⁴ its vorticity is zero everywhere. Indeed, since $\nabla \times \mathbf{v} = 0$ at the uniform flow, the vorticity is zero at distant points of any streamline, and according to the Kelvin theorem, should equal zero everywhere.

In such cases, the velocity distribution, as any curl-free vector field, may be represented as a gradient of some effective potential function,

$$\mathbf{v} = -\nabla\phi. \quad (8.28)$$

Such *potential flow* may be described by a simple differential equation. Indeed, the continuity equation (21) for a steady flow of an incompressible fluid is reduced to $\nabla \cdot \mathbf{v} = 0$. Plugging Eq. (28) into this relation, we get the scalar Laplace equation,

$$\nabla^2\phi = 0, \quad (8.29)$$

which should be solved with appropriate boundary conditions. For example, the fluid flow may be limited by solid bodies, inside which the fluid cannot penetrate. Then the fluid velocity \mathbf{v} at the solid body boundaries should not have a normal component; according to Eq. (28), this means

$$\frac{\partial\phi}{\partial n}\Big|_{\text{surfaces}} = 0. \quad (8.30)$$

On the other hand, if at large distances the fluid flow is known, e.g., uniform, then:

$$\nabla\phi = -\mathbf{v}_0 = \text{const}, \quad \text{at } r \rightarrow \infty. \quad (8.31)$$

As the reader may already know (for example, from a course on electrodynamics²⁵), the Laplace equation (29) is analytically solvable in several simple (symmetric) but important situations. Let us consider, for example, the case of a round cylinder, with radius R , immersed into a flow with the initial velocity \mathbf{v}_0 perpendicular to the cylinder's axis (Fig. 8). For this problem, it is natural to use the cylindrical coordinates, with the z -axis coinciding with the cylinder's axis. In this case, the velocity distribution is obviously independent of z , so that we may simplify the general expression of the Laplace operator in cylindrical coordinates²⁶ by taking $\partial/\partial z = 0$. As a result, Eq. (29) is reduced to²⁷

$$\frac{1}{\rho}\frac{\partial}{\partial\rho}\left(\rho\frac{\partial\phi}{\partial\rho}\right) + \frac{1}{\rho^2}\frac{\partial^2\phi}{\partial\theta^2} = 0, \quad \text{at } \rho \geq R. \quad (8.32)$$

The general solution of this equation may be obtained using the variable separation method, similar to that used in Sec. 6.5 – see Eq. (6.67). The result is²⁸

²⁴ This case is very important, because the motion of a solid body, with a constant velocity \mathbf{u} , in the otherwise stationary fluid, gives exactly the same problem (with $\mathbf{v}_0 = -\mathbf{u}$), in a reference frame bound to the body.

²⁵ See, e.g., EM Secs. 2.3-2.8.

²⁶ See, e.g., MA Eq. (10.3).

²⁷ Let me hope that the letter ρ , used here to denote the magnitude of the 2D radius vector $\mathbf{p} = \{x, y\}$, will not be confused with the fluid's density ρ – which does not participate in this boundary problem.

²⁸ See, e.g., EM Eq. (2.112). Note that the most general solution of Eq. (32) also includes a term proportional to φ , but in our geometry, this term should be zero for such a single-valued function as the velocity potential.

$$\phi = a_0 + b_0 \ln \rho + \sum_{n=1}^{\infty} (c_n \cos n\varphi + s_n \sin n\varphi) (a_n \rho^n + b_n \rho^{-n}), \quad (8.33)$$

where the coefficients a_n and b_n have to be found from the boundary conditions (30) and (31). Choosing the x -axis to be parallel to the vector \mathbf{v}_0 (Fig. 8a), so that $x = \rho \cos \varphi$, we may spell out these conditions in the following form:

$$\frac{\partial \phi}{\partial \rho} = 0, \quad \text{at } \rho = R, \quad (8.34)$$

$$\phi \rightarrow -v_0 \rho \cos \varphi + \phi_0, \quad \text{at } \rho \gg R, \quad (8.35)$$

where ϕ_0 is an arbitrary constant, which does not affect the velocity distribution and may be taken for zero. The condition (35) is incompatible with any term of the sum (33) except the term with $n = 1$ (with $s_1 = 0$ and $c_1 a_1 = -v_0$), so that Eq. (33) is reduced to

$$\phi = \left(-v_0 \rho + \frac{c_1 b_1}{\rho} \right) \cos \varphi. \quad (8.36)$$

Now, plugging this solution into Eq. (34), we get $c_1 b_1 = -v_0 R^2$, so that, finally,

$$\phi = -v_0 \left(\rho + \frac{R^2}{\rho} \right) \cos \varphi. \quad (8.37a)$$

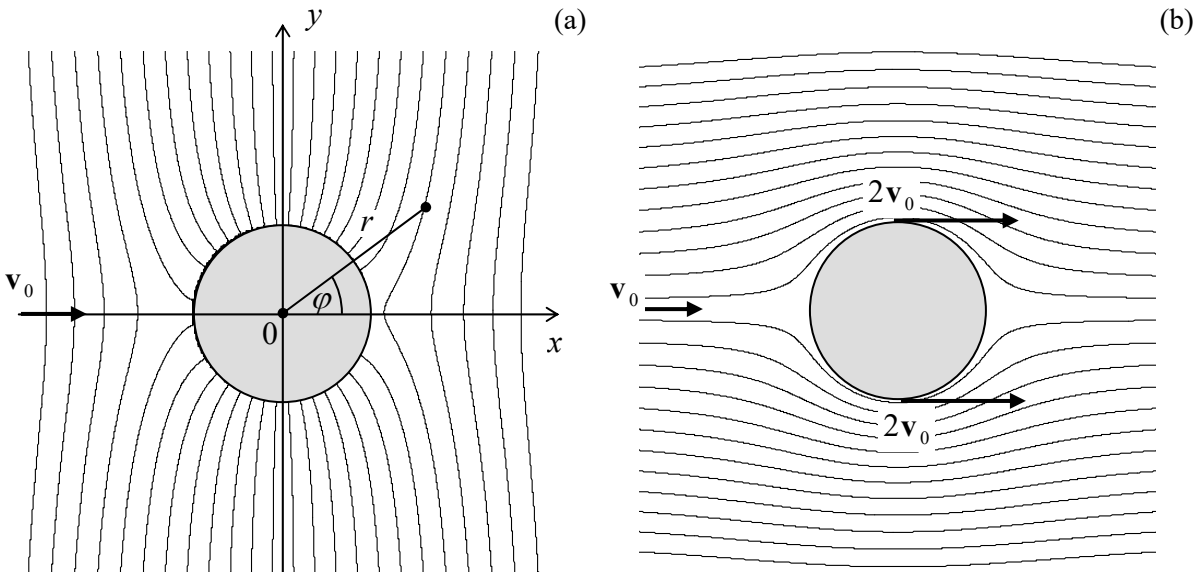


Fig. 8.8. The flow of an ideal, incompressible fluid around a cylinder: (a) equipotential surfaces and (b) streamlines.

Figure 8a shows the surfaces of constant velocity potential ϕ given by Eq. (37a). To find the fluid velocity, it is easier to rewrite that result in the Cartesian coordinates $x = \rho \cos \varphi$, $y = \rho \sin \varphi$:

$$\phi = -v_0 x \left(1 + \frac{R^2}{\rho^2} \right) = -v_0 x \left(1 + \frac{R^2}{x^2 + y^2} \right). \quad (8.37b)$$

From here, we may readily calculate the Cartesian components of the fluid's velocity:²⁹

$$\begin{aligned} v_x &= -\frac{\partial \phi}{\partial x} = v_0 \left[1 + R^2 \frac{y^2 - x^2}{(x^2 + y^2)^2} \right] \equiv v_0 \left(1 + \frac{R^2}{\rho^2} \cos 2\varphi \right), \\ v_y &= -\frac{\partial \phi}{\partial y} = -v_0 R^2 \frac{2xy}{(x^2 + y^2)^2} \equiv -v_0 \frac{R^2}{\rho^2} \sin 2\varphi. \end{aligned} \quad (8.38)$$

These expressions show that the maximum fluid's speed is achieved at the transverse diameter's ends ($\rho = R$, $\varphi = \pm \pi/2$), where $v = 2v_0$, while at the longitudinal diameter's ends ($\rho = R$, $\varphi = 0, \pm\pi$), the velocity vanishes – the so-called *stagnation points*.

Now the pressure distribution may be calculated by plugging Eqs. (38) into the Bernoulli equation (27) with $u(\mathbf{r}) = 0$. The result shows that the pressure reaches its maximum at the stagnation points, while at the ends of the transverse diameter $x = 0$, where the velocity is largest, it is lower by $2\rho v_0^2$. Note that the distributions of both the velocity and the pressure are symmetric with respect to the transverse axis $x = 0$, so that the fluid flow does not create any net drag force in its direction. It may be shown that this result, which stems from the conservation of the mechanical energy of an ideal fluid, remains valid for a solid body of arbitrary shape moving inside an infinite volume of an ideal fluid – the so-called *D'Alembert paradox*. However, if a body moves near an ideal fluid's surface, its energy may be transformed into that of the surface waves, and the drag becomes possible.

Speaking about the *surface waves*: the description of such waves in a gravity field³⁰ is one more classical problem of the ideal fluid dynamics.³¹ Let us consider an open surface of an ideal liquid of density ρ in a uniform gravity field $\mathbf{f} = \rho \mathbf{g} = -\rho g \mathbf{n}_y$ – see Fig. 9.

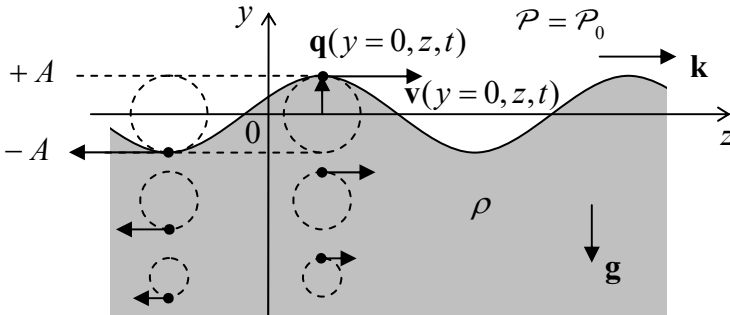


Fig. 8.9. Small surface wave on a deep heavy liquid. Dashed lines show particle trajectories. (For clarity, the displacement amplitude A is strongly exaggerated.)

If the wave amplitude A is sufficiently small, we may neglect the nonlinear term $(\mathbf{v} \cdot \nabla) \mathbf{v} \propto A^2$ in the Euler equation (23) in comparison with the first term, $\partial \mathbf{v} / \partial t$, which is linear in A . For a wave with

²⁹ Figure 8b shows the flow streamlines. They may be found by the integration of the obvious equation $dy/dx = v_y(x, y)/v_x(x, y)$. For our simple problem, this may be done analytically, giving $y(1 - R^2/\rho^2) = \text{const}$, where the constant is specific for each streamline.

³⁰ The alternative, historic term “gravity waves” for this phenomenon may nowadays lead to confusion with the relativistic effect of gravity waves – which may propagate in free space.

³¹ It was solved by Sir George Biddell Airy (1801–1892), of the Airy functions' fame. (He was also a prominent astronomer and, in particular, established Greenwich as the prime meridian.)

frequency ω and wave number k , the particle's velocity $\mathbf{v} = d\mathbf{q}/dt$ is of the order of ωA , so that this approximation is legitimate if $\omega^2 A \gg k(\omega A)^2$, i.e. when

$$kA \ll 1, \quad (8.39)$$

i.e. when the wave's amplitude A is much smaller than its wavelength $\lambda = 2\pi/k$. Due to this assumption, we may neglect the liquid vorticity effects, and (for an incompressible fluid) again use the Laplace equation (29) for the wave's analysis. Looking for its solution in the natural form of a sinusoidal wave, uniform in one of the horizontal directions (x),

$$\phi = \text{Re} \left[\Phi(y) e^{i(kz - \omega t)} \right], \quad (8.40)$$

we get a very simple equation

$$\frac{d^2\Phi}{dy^2} - k^2\Phi = 0, \quad (8.41)$$

with an exponential solution (properly decaying at $y \rightarrow -\infty$), $\Phi = \Phi_A \exp\{ky\}$, so that Eq. (40) becomes

$$\phi = \text{Re} \left[\Phi_A e^{ky} e^{i(kz - \omega t)} \right] = \Phi_A e^{ky} \cos(kz - \omega t), \quad (8.42)$$

where the last form is valid if Φ_A is real – which may be always arranged by a proper selection of the origins of z and/or t . Note that the rate k of the wave's decay in the vertical direction is exactly equal to the wave number of its propagation in the horizontal direction – along the fluid's surface. Because of that, the trajectories of fluid particles are exactly circular – see Fig. 9. Indeed, using Eqs. (28) and (42) to calculate velocity components,

$$v_x = 0, \quad v_y = -\frac{\partial \phi}{\partial y} = -k\Phi_A e^{ky} \cos(kz - \omega t), \quad v_z = -\frac{\partial \phi}{\partial z} = k\Phi_A e^{ky} \sin(kz - \omega t), \quad (8.43)$$

we see that v_y and v_z , at the same height y , have equal real amplitudes, and are phase-shifted by $\pi/2$. This result becomes even more clear if we use the velocity definition $\mathbf{v} = d\mathbf{q}/dt$ to integrate Eqs. (43) over time to recover the particle displacement law $\mathbf{q}(t)$. Due to the strong inequality (39), the integration may be done at fixed y and z :

$$q_y = q_A e^{ky} \sin(kz - \omega t), \quad q_z = q_A e^{ky} \cos(kz - \omega t), \quad \text{with } q_A \equiv \frac{k}{\omega} \Phi_A. \quad (8.44)$$

Note that the phase of oscillations of v_z coincides with that of q_y . This means, in particular, that at the wave's “crest”, particles are moving in the direction of the wave's propagation – see arrows in Fig. 9.

It is remarkable that all this picture follows from the Laplace equation alone! The “only” remaining feature to calculate is the dispersion law $\omega(k)$, and for that, we need to combine Eq. (42) with what remains, in our linear approximation, of the Euler equation (23). In this approximation, and with the bulk force potential $u = \rho gy$, the equation is reduced to

$$\nabla \left(-\rho \frac{\partial \phi}{\partial t} + \mathcal{P} + \rho gy \right) = 0. \quad (8.45)$$

This equality means that the function in the parentheses is constant in space; at the surface, and at negligible surface tension, it should be equal to the pressure P_0 above the surface (say, the atmospheric pressure), which we assume to be constant. This means that on the surface, the contributions to \mathcal{P} that come from the first and the third term in Eq. (45) have to compensate for each other. Let us take the average surface position for $y = 0$; then the surface with waves is described by the relation $y(z, t) = q_y(y, z, t)$ – see Fig. 9. Due to the strong relation (39), we can use Eqs. (42) and (44) with $y = 0$, so that the above compensation condition yields

$$-\rho\omega\Phi_A \sin(kz - \omega t) + \rho g \frac{k}{\omega} \Phi_A \sin(kz - \omega t) = 0. \quad (8.46)$$

This condition is identically satisfied on the whole surface (and for any Φ_A) as soon as

Surface
waves'
dispersion

$$\boxed{\omega^2 = gk}, \quad (8.47)$$

This equality is the dispersion relation we were looking for. Looking at this very simple result (which includes just one constant, g), note, first of all, that it does not involve the fluid's density. This is not too surprising, because due to the weak equivalence principle, particle masses always drop out from the solutions of problems involving gravitational forces alone. Second, the dispersion law (47) is strongly nonlinear, and in particular, does not have an acoustic wave limit at all. This means that the surface wave propagation is strongly dispersive, with both the phase velocity $u_{\text{ph}} \equiv \omega/k = g/\omega$ and the group velocity $u_{\text{gr}} \equiv d\omega/dk = g/2\omega \equiv u_{\text{ph}}/2$ diverging at $\omega \rightarrow 0$.³²

This divergence is an artifact of our assumption of the infinitely deep liquid. A rather straightforward generalization of the above calculations to a layer of a finite thickness h , using the additional boundary condition $v_y|_{y=-h} = 0$, yields a more general dispersion relation:³³

$$\omega^2 = gk \tanh kh. \quad (8.48)$$

It shows that relatively long waves, with $\lambda \gg h$, i.e. with $kh \ll 1$, propagate without dispersion (i.e. have $\omega/k = \text{const} \equiv u$), with the following velocity:

$$u = (gh)^{1/2}. \quad (8.49)$$

For the Earth's oceans, this velocity is rather high, close to 250 m/s (!) for the average ocean depth $h \approx 5$ km. This result explains, in particular, the very fast propagation of tsunami waves.

In the opposite limit of very short waves (large k), Eq. (47) also does not give a good description of typical experimental data, due to surface tension effects – see Sec. 2 above. Using Eq. (13), it is easy (and hence also left for the reader's exercise) to show that their account leads (at $kh \gg 1$) to the following modification of Eq. (47):

$$\omega^2 = gk + \frac{\gamma k^3}{\rho}. \quad (8.50)$$

³² Here, unlike in Chapters 6 and 7, the wave velocity is denoted by the letter u to avoid any chance of its confusion with the velocity \mathbf{v} (43) of the liquid's particles.

³³ This calculation (left for the reader's exercise), shows also that at finite h , the particle trajectories are elliptical rather than circular, becoming more and more stretched in the wave propagation direction near the bottom of the layer.

According to this formula, the surface tension is important at wavelengths smaller than the capillary constant a_c given by Eq. (14). Much shorter waves, for that Eq. (50) yields $\omega \propto k^{3/2}$, are called the *capillary waves* – or just “ripples”.

8.5. Dynamics: Viscous fluids

The viscosity of many fluids, at not overly high velocities, may be described surprisingly well by adding, to the static stress tensor (2), additional elements proportional to the velocity $\mathbf{v} \equiv d\mathbf{q}/dt$:

$$\sigma_{jj'} = -P\delta_{jj'} + \tilde{\sigma}_{jj'}(\mathbf{v}). \quad (8.51)$$

In view of our experience with the Hooke’s law (7.32) expressing a stress tensor proportional to particle displacements \mathbf{q} , we may expect a similar expression with the replacement $\mathbf{q} \rightarrow \mathbf{v} = d\mathbf{q}/dt$:

$$\tilde{\sigma}_{jj'} = 2\eta \left(e_{jj'} - \frac{1}{3} \delta_{jj'} \text{Tr}(\mathbf{e}) \right) + 3\zeta \left(\frac{1}{3} \delta_{jj'} \text{Tr}(\mathbf{e}) \right), \quad (8.52a)$$

where $e_{jj'}$ are the elements of the symmetrized strain derivative tensor:

$$e_{jj'} \equiv \frac{ds_{jj'}}{dt} = \frac{1}{2} \left(\frac{\partial v_j}{\partial r_{j'}} + \frac{\partial v_{j'}}{\partial r_j} \right). \quad (8.52b)$$

Experiment confirms that Eq. (52) gives a good description of the viscosity effects in a broad range of isotropic fluids. The coefficient η is called either the *shear viscosity*, or the *dynamic viscosity*, or just *viscosity*, while ζ is called the *second* (or *bulk*) viscosity.

In the most frequent case of virtually incompressible fluids, $\text{Tr}(\mathbf{e}) = d[\text{Tr}(\mathbf{s})]/dt = (dV/dt)/V = 0$, so that the term proportional to ζ vanishes, and η is the only important viscosity parameter.³⁴ Table 1 shows the approximate values of the viscosity, together with the mass density ρ , for several representative fluids.

Table 8.1. Important parameters of several representative fluids (approximate values)

Fluid (all at 300 K, until indicated otherwise)	η (mPa·s)	ρ (kg/m ³)
Glasses	$10^{21}\text{--}10^{24}$	2,200–2,500
Earth magmas (at 800 to 1,400 K)	$10^4\text{--}10^{14}$	2,200–2,800
Machine oils (SAE 10W – 40 W)	65–320	900
Water	0.89	1,000
Mercury	1.53	13,530
Liquid helium 4 (at 4.2K, 10 ⁵ Pa)	0.019	130
Air (at 10 ⁵ Pa)	0.018	1.3

³⁴ Probably the most important effect we miss by neglecting ζ is the attenuation of the (longitudinal) acoustic waves, into which the second viscosity makes a major contribution – whose (rather straightforward) analysis is left for the reader’s exercise.

One can see that η may vary in very broad limits; the extreme cases of fluids are glasses (which, somewhat counter-intuitively, are not stable solids even at room temperature, but rather may “flow”, though extremely slowly, until they eventually crystallize) and liquid helium (whose viscosity is of the order of that of gases,³⁵ despite its much higher density).

Incorporating the additional elements of σ_{ij} to the equation (23) of fluid motion, absolutely similarly to how it was done at the derivation of Eq. (7.107) of the elasticity theory, and with the account of Eq. (19), we arrive at the famous *Navier-Stokes equation*:³⁶

Navier-Stokes
equation

$$\rho \frac{\partial \mathbf{v}}{\partial t} + \rho(\mathbf{v} \cdot \nabla) \mathbf{v} = -\nabla P + \mathbf{f} + \eta \nabla^2 \mathbf{v} + \left(\zeta + \frac{\eta}{3} \right) \nabla (\nabla \cdot \mathbf{v}). \quad (8.53)$$

The apparent simplicity of this equation should not mask an enormous range of phenomena, notably including turbulence (see the next section) that are described by it, and the complexity of its solutions even for some simple geometries. In most problems interesting for practice, the only option is to use numerical methods, but due to a large number of parameters (ρ , η , ζ , plus geometrical parameters of the involved bodies, plus the distribution of bulk forces \mathbf{f} , plus boundary conditions), this way is strongly plagued by the *curse of dimensionality* that was discussed in the end of Sec. 5.8.

Let us see how the Navier-Stokes equation works, on several simple examples. As the simplest case, let us consider the so-called *Couette flow* of an incompressible fluid layer between two wide, horizontal plates (Fig. 10), caused by their mutual sliding with a constant relative velocity \mathbf{v}_0 .

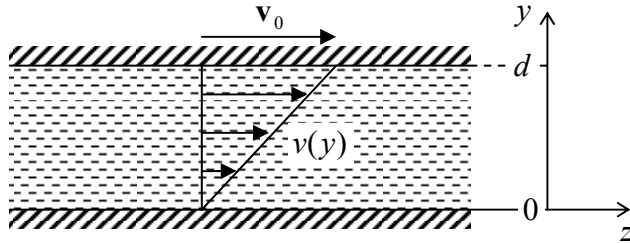


Fig. 8.10. The simplest problem of the viscous fluid flow.

Let us assume a *laminar* (vorticity-free) fluid flow. (As will be discussed in the next section, this assumption is only valid within certain limits.) Then we may use the evident symmetry of the problem, to take, in the coordinate frame shown in Fig. 10, $\mathbf{v} = \mathbf{n}_z v(y)$. Let the bulk forces be vertical, $\mathbf{f} = \mathbf{n}_y f$, so they do not give an additional drive to the fluid flow. Then for the stationary flow ($\partial \mathbf{v} / \partial t = 0$), the vertical, y -component of the Navier-Stokes equation is reduced to the static Pascal equation (6), showing that the pressure distribution is not affected by the plate (and fluid) motion. In the horizontal, z -component of the equation, only one term, $\nabla^2 v$, survives, so that for the only Cartesian component of the fluid's velocity we get the 1D Laplace equation

$$\frac{d^2 v}{dy^2} = 0. \quad (8.54)$$

³⁵ Actually, at even lower temperatures (for He 4, at $T < T_\lambda \approx 2.17$ K), helium becomes a *superfluid*, i.e. loses its viscosity completely, as a result of the Bose-Einstein condensation – see, e.g., SM Sec. 3.4.

³⁶ Named after Claude-Louis Navier (1785-1836) who had suggested the equation, and Sir George Gabriel Stokes (1819-1903) who has demonstrated its relevance by solving the equation for several key situations.

In contrast to the ideal fluid (see, e.g., Fig. 8b), the relative velocity of a viscous fluid and a solid wall it flows by should approach zero at the wall,³⁷ so that Eq. (54) should be solved with boundary conditions

$$v = \begin{cases} 0, & \text{at } y = 0, \\ v_0, & \text{at } y = d. \end{cases} \quad (8.55)$$

Using the evident solution to this boundary problem, $v(y) = (y/d)v_0$, illustrated by the arrows in Fig. 10, we can now calculate the horizontal *drag force* acting on a unit area of each plate. For the bottom plate,

$$\frac{F_z}{A_y} = \sigma_{zy} \Big|_{y=0} = \eta \frac{\partial v}{\partial y} \Big|_{y=0} = \eta \frac{v_0}{d}. \quad (8.56)$$

(For the top plate, the derivative $\partial v / \partial y$ has the same value, but the sign of dA_y has to be changed to reflect the direction of the outer normal to the solid surface so that we get a similar force but with the negative sign.) The well-known result (56) is often used, in undergraduate physics courses, for a definition of the dynamic viscosity η , and indeed shows its meaning very well.³⁸

As the next, slightly less trivial example let us consider the so-called *Poiseuille problem*:³⁹ finding the relation between the constant external pressure gradient $\chi \equiv -\partial P / \partial z$ applied along a round pipe with internal radius R (Fig. 11) and the so-called *discharge Q* – defined as the mass of fluid flowing through the pipe’s cross-section in unit time.

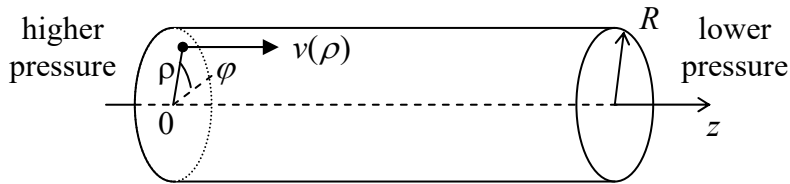


Fig. 8.11. The Poiseuille problem.

Again assuming a laminar flow, we can involve the problem’s uniformity along the z -axis and its axial symmetry to infer that $\mathbf{v} = \mathbf{n}_z v(\rho)$, and $P = -\chi z + f(\rho, \varphi) + \text{const}$ (where $\rho = \{\rho, \varphi\}$ is again the 2D radius vector rather than the fluid density) so that the Navier-Stokes equation (53) for an incompressible fluid (with $\nabla \cdot \mathbf{v} = 0$) is reduced to the following 2D Poisson equation:

$$\eta \nabla^2 v = -\chi. \quad (8.57)$$

After spelling out the 2D Laplace operator in polar coordinates for our axially-symmetric case $\partial/\partial\varphi = 0$, Eq. (57) becomes a simple ordinary differential equation,

³⁷ This is essentially an additional experimental fact, but may be understood as follows. The tangential component of the velocity should be continuous at the interface between two viscous fluids, in order to avoid infinite stress – see Eq. (52), and solid may be considered as an ultimate case of fluid, with infinite viscosity.

³⁸ The very notion of viscosity η was introduced (by nobody other than the same Sir Isaac Newton) via a formula similar to Eq. (56), so that any effect resulting in a drag force proportional to velocity is frequently called the *Newtonian viscosity*.

³⁹ It was solved by G. Stokes in 1845 to explain the experimental results obtained by Gotthilf Hagen in 1839 and (independently) by Jean Poiseuille in 1840-41.

$$\eta \frac{1}{\rho} \frac{d}{d\rho} (\rho \frac{dv}{d\rho}) = -\chi, \quad (8.58)$$

which has to be solved on the segment $0 \leq \rho \leq R$, with the following boundary conditions:

$$\begin{aligned} v &= 0, & \text{at } \rho = R, \\ \frac{dv}{d\rho} &= 0, & \text{at } \rho = 0. \end{aligned} \quad (8.59)$$

(The latter condition is required by the axial symmetry.) A straightforward double integration yields:

$$v = \frac{\chi}{4\eta} (R^2 - \rho^2), \quad (8.60)$$

so that the (easy) integration of the mass flow density over the cross-section of the pipe,

$$Q \equiv \int_A \rho v d^2 r = 2\pi \rho \frac{\chi}{4\eta} \int_0^R (R^2 - \rho^2) \rho d\rho, \quad (8.61)$$

immediately gives us the so-called *Poiseuille* (or “Hagen-Poiseuille”) law for the fluid discharge:

$$Q = \frac{\pi}{8} \rho \frac{\chi}{\eta} R^4. \quad (8.62)$$

Poiseuille
law

The most prominent (and practically important) feature of this result is the very strong dependence of the discharge on the pipe’s radius.

Of course, the 2D Poisson equation (57) is so readily solvable not for each cross-section shape. For example, consider a very simple, square-shaped cross-section with side a (Fig. 12).

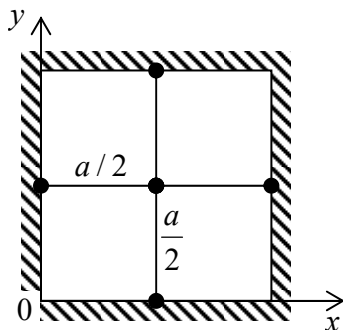


Fig. 8.12. Application of the finite-difference method with a very coarse mesh (with step $h = a/2$) to the problem of viscous fluid flow in a pipe with a square cross-section.

In this case, it is natural to use the Cartesian coordinates aligned with the cross-section’s sides, so that Eq. (57) becomes

$$\frac{\partial^2 v}{\partial x^2} + \frac{\partial^2 v}{\partial y^2} = -\frac{\chi}{\eta} = \text{const}, \quad \text{for } 0 \leq x, y \leq a, \quad (8.63)$$

and has to be solved with boundary conditions

$$v = 0, \quad \text{at } x, y = 0, a. \quad (8.64)$$

For this boundary problem, analytical methods such as the variable separation lead to answers in the form of infinite sums (series), which ultimately require computers anyway – at least for their plotting and comprehension. Let me use this pretext to discuss how explicitly numerical methods may be used for such problems – or for any partial differential equations involving the Laplace operator. The simplest of them is the *finite-difference* method⁴⁰ in which the function to be calculated, $f(\mathbf{r})$, is represented by its values $f(\mathbf{r}_1)$, $f(\mathbf{r}_2)$, ... in discrete points of a rectangular grid (frequently called *mesh*) of the corresponding dimensionality – Fig. 13.

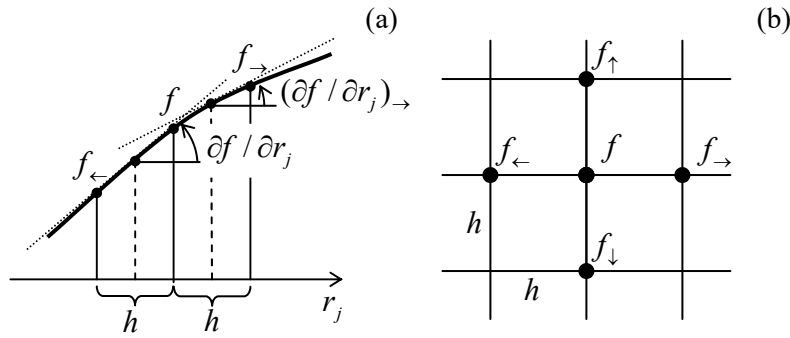


Fig. 8.13. The idea of the finite-difference method in (a) one and (b) two dimensions.

In Sec. 5.7, we have already discussed how to use such a grid to approximate the first derivative of the function – see Eq. (5.97). Its extension to the second derivative is straightforward – see Fig. 13a:⁴¹

$$\frac{\partial^2 f}{\partial r_j^2} \equiv \frac{\partial}{\partial r_j} \left(\frac{\partial f}{\partial r_j} \right) \approx \frac{1}{h} \left(\frac{\partial f}{\partial r_j} \Big|_{\rightarrow} - \frac{\partial f}{\partial r_j} \Big|_{\leftarrow} \right) \approx \frac{1}{h} \left[\frac{f_{\rightarrow} - f}{h} - \frac{f - f_{\leftarrow}}{h} \right] \equiv \frac{f_{\rightarrow} + f_{\leftarrow} - 2f}{h^2}. \quad (8.65)$$

The relative error of this approximation is of the order of $h^2 \partial^4 f / \partial r_j^4$, quite acceptable in many cases. As a result, the left-hand side of Eq. (63), treated on a square mesh with step h (Fig. 13b), may be approximated with the so-called *five-point scheme*:

$$\frac{\partial^2 v}{\partial x^2} + \frac{\partial^2 v}{\partial y^2} \approx \frac{v_{\rightarrow} + v_{\leftarrow} - 2v}{h^2} + \frac{v_{\uparrow} + v_{\downarrow} - 2v}{h^2} = \frac{v_{\rightarrow} + v_{\leftarrow} + v_{\uparrow} + v_{\downarrow} - 4v}{h^2}. \quad (8.66)$$

(The generalization to the *seven-point scheme*, appropriate for 3D problems, is straightforward.) Let us apply this scheme to the pipe with the square cross-section, using an extremely coarse mesh with step $h = a/2$, shown in Fig. 12. In this case, the fluid velocity v should equal zero at the walls, i.e. at all points of the five-point scheme except for the central point (in which the velocity obviously reaches its maximum), so that Eqs. (63) and (66) yield⁴²

⁴⁰ For more details see, e.g., R. Leveque, *Finite Difference Methods for Ordinary and Partial Differential Equations*, SIAM, 2007.

⁴¹ As a reminder, at the beginning of Sec. 6.4 we have already discussed the reciprocal transition – from a similar sum to the second derivative in the continuous limit ($h \rightarrow 0$).

⁴² Note that value (67) of v_{\max} is exactly the same as given by the analytical formula (60) for the round cross-section with the radius $R = a/2$. This is not an occasional coincidence. The velocity distribution given by (60) is a quadratic function of both x and y . For such functions, with all derivatives higher than $\partial^2 f / \partial r_j^2$ equal to zero, equation (66) is exact rather than approximate.

$$\frac{0+0+0+0-4v_{\max}}{(a/2)^2} \approx -\frac{\chi}{\eta}, \quad \text{i.e. } v_{\max} \approx \frac{1}{16} \frac{\chi a^2}{\eta} \quad (8.67)$$

This result for the maximal velocity is only $\sim 20\%$ different from the exact value. Using a slightly finer mesh with $h = a/4$, which gives a readily solvable system of three linear equations for three different velocity values (the exercise left for the reader), brings us within just a couple of percent from the exact result. So numerical methods may be practically more efficient than the “analytical” ones, even if the only available tool is a calculator app on your smartphone rather than an advanced computer.

Of course, many practical problems of fluid dynamics do require high-performance computing, especially in conditions of turbulence with its complex, irregular spatial-temporal structure – see the next section). In such cases, the finite-difference approach discussed above may become unsatisfactory, because it implies the same accuracy of the derivative approximation through the whole area of interest. A more powerful (but also much more complex for implementation) approach is the *finite-element method* in which the discrete-point mesh is based on triangles with unequal sides, and is (in most cases, automatically) generated from the system geometry, giving many more mesh points at the location(s) of the highest gradients of the calculated function (Fig. 14), and hence a better calculation accuracy for the same total number of points. Unfortunately, I do not have time for going into the details of that method, so the interested reader is referred to the special literature on this subject.⁴³

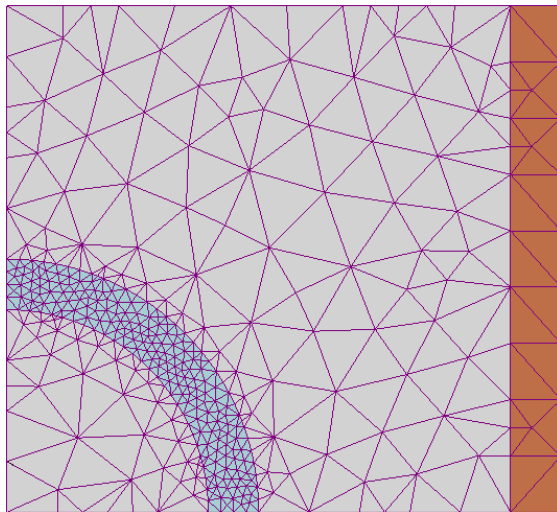


Fig. 8.14. A typical finite-element mesh generated automatically for a system with relatively complex geometry – a round cylindrical shell inside another one, with mutually perpendicular axes. (Adapted from the original by I. Zureks, <https://commons.wikimedia.org/w/index.php?curid=2358783>, under the CC license BY-SA 3.0.)

Before proceeding to our next topic, let me mention one more important problem that is analytically solvable using the Navier-Stokes equation: a slow motion of a solid sphere of radius R , with a constant velocity v_0 , through an incompressible viscous fluid – or equivalently, a slow flow of the fluid (uniform at large distances) around an immobile sphere. In the limit $v \rightarrow 0$, the second term on the left-hand side of Eq. (53) is negligible (just as at the surface wave analysis in Sec. 3), the equation takes the form

$$-\nabla P + \eta \nabla^2 \mathbf{v} = 0, \quad \text{for } R \leq r < \infty, \quad (8.68)$$

⁴³ I can recommend, e.g., C. Johnson, *Numerical Solution of Partial Differential Equations by the Finite Element Method*, Dover, 2009, or T. Hughes, *The Finite Element Method*, Dover, 2000.

and should be complemented with the incompressibility condition $\nabla \cdot \mathbf{v} = 0$ and the boundary conditions

$$\begin{aligned}\mathbf{v} &= 0, \quad \text{at } r = R, \\ \mathbf{v} &\rightarrow \mathbf{v}_0, \quad \text{at } r \rightarrow \infty.\end{aligned}\tag{8.69}$$

In spherical coordinates, with the polar axis directed along the vector \mathbf{v}_0 , this boundary problem has the axial symmetry (so that $\partial \mathbf{v}/\partial \varphi = 0$ and $v_\varphi = 0$), and allows the following analytical solution:

$$v_r = v_0 \cos \theta \left(1 - \frac{3R}{2r} + \frac{R^3}{2r^2} \right), \quad v_\theta = -v_0 \sin \theta \left(1 - \frac{3R}{4r} - \frac{R^3}{4r^2} \right), \quad \mathcal{P} = -\frac{3\eta v_0 R}{2r^2} \cos \theta. \tag{8.70}$$

Now calculating the tensor elements (52b) at $r = R$, using them to find the stress tensor elements from Eq. (52a), and integrating the elementary forces (7.18) over the surface of the sphere, it is straightforward to obtain the famous *Stokes formula* for the drag force acting on the sphere:⁴⁴

$$F = 6\pi\eta R v_0. \tag{8.71}$$

Stokes formula

For water drops with a 1-micron diameter, usually taken for the border between *aerosols* and *droplets*, descending in the ambient-condition air under their own weight, it predicts an equilibrium velocity v of close to 0.1 meter per hour, with the further scaling $v \propto R^2$.⁴⁵ (Note, however, that at R below $\sim 10 \mu\text{m}$, corrections due to air molecule discreteness become noticeable.)

For what follows in the next section, it is convenient to recast this result into the following form:

$$C_d = \frac{24}{Re}, \tag{8.72}$$

where C_d is the *drag coefficient* defined as

$$C_d \equiv \frac{F}{\rho v_0^2 A / 2}, \tag{8.73}$$

with $A \equiv \pi R^2$ being the sphere's cross-section "as seen by the incident fluid flow", and Re is the so-called *Reynolds number*.⁴⁶ In the general case, the number is defined as

$$Re \equiv \frac{\rho v l}{\eta}, \tag{8.74}$$

Reynolds number

where l is the linear-size scale of the problem, and v is its velocity scale. (In the particular case of Eq. (72) for the sphere, l is identified with the sphere's diameter $D = 2R$, and v with v_0). The physical sense of these two definitions will be discussed in the next section.

⁴⁴ This formula has played an important role in the first precise (better than 1%) calculation of the fundamental electric charge e by R. Millikan and H. Fletcher from their famous oil drop experiments in 1909-1913.

⁴⁵ These numbers are of key importance not only for the contagious disease transmission analysis, but also for many other fields including atmospheric physics. For example, for an average water droplet in clouds, with $R \sim 10 \mu\text{m}$, Eq. (71) (even with a due account of the slightly lower air viscosity at typical cloud heights) yields the equilibrium descent velocity of the order of 10 m/hr, substantiating the correct answer to the popular high-school question, "Why clouds do not fall?" (The answer is: each water droplet does descend, but so slowly that it has ample time to evaporate at the lower surface of the cloud, so that the cloud as a whole may maintain its height.)

⁴⁶ This notion was introduced in 1851 by the same G. Stokes but eventually named after O. Reynolds who popularized it three decades later.

8.6. Turbulence

As Fig. 15 shows, the Stokes result (71)-(72) is only valid at $Re \ll 1$, while for larger values of the Reynolds number, i.e. at higher velocities v_0 , the drag force is larger. This very fact is not quite surprising, because at the derivation of the Stokes' result, the nonlinear term $(\mathbf{v} \cdot \nabla) \mathbf{v}$ in the Navier-Stokes equation (53), which scales as v^2 , was neglected in comparison with the linear terms, scaling as v . What is more surprising is that the function $C_d(Re)$ exhibits such a complicated behavior over many orders of the velocity's magnitude, giving a hint that the fluid flow at large Reynolds numbers should be also very complicated. Indeed, the reason for this complexity is a gradual development of very intricate, time-dependent fluid patterns, called *turbulence*, rich with vortices – for example, see Fig. 16. These vortices are especially pronounced in the region behind the moving body (the so-called *wake*), while the region before the body remains almost unperturbed. As Fig. 15 indicates, the turbulence exhibits rather different behaviors at various velocities (i.e. values of Re), and sometimes changes rather abruptly – see, for example, the significant drag's drop at $Re \approx 5 \times 10^5$.

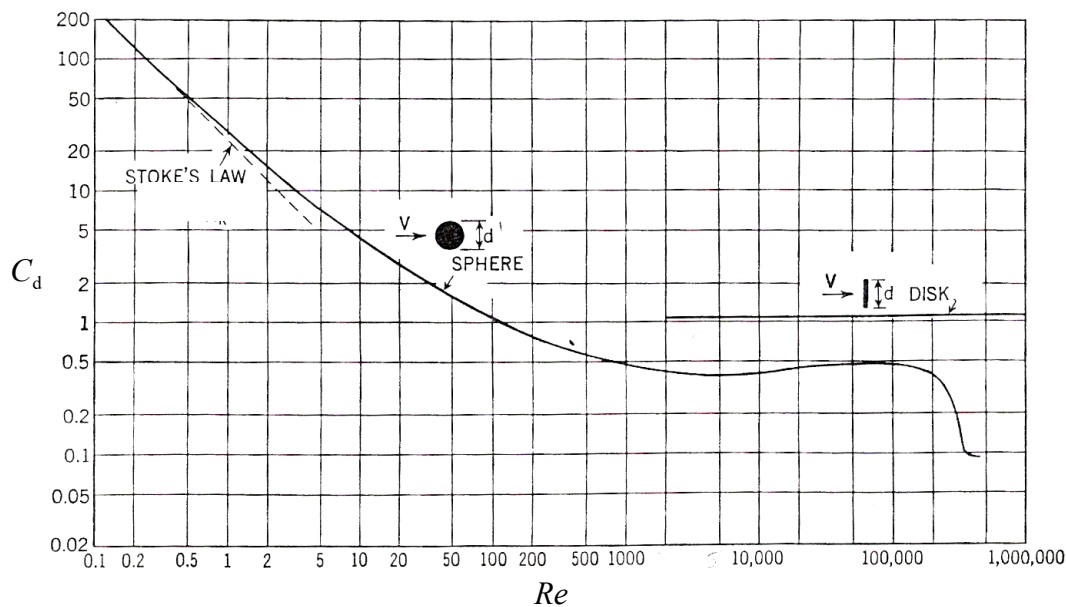


Fig. 8.15. The drag coefficient for a sphere and a thin round disk as functions of the Reynolds number.
Adapted from F. Eisner, *Das Widerstandsproblem*, Proc. 3rd Int. Cong. on Appl. Mech., Stockholm, 1931.

In order to understand the conditions of this phenomenon, let us estimate the scale of various terms of the Navier-Stokes equation (53) for a generic body with characteristic size l , moving in an otherwise static incompressible fluid, with velocity v . In this case, the time scale of possible non-stationary phenomena is given by the ratio l/v ,⁴⁷ so that we arrive at the following estimates:

⁴⁷ The time scale of phenomena in externally-driven systems may be different; for example, for forced oscillations with frequency ω , it may be the oscillation period $\mathcal{T} \equiv 2\pi/\omega$. For such problems, the ratio $S \equiv (l/v)/\mathcal{T}$, commonly called either the *Strouhal number* or the *reduced frequency*, serves as another dimensionless constant.

Equation term:	$\rho \frac{\partial \mathbf{v}}{\partial t}$	$\rho(\mathbf{v} \cdot \nabla)\mathbf{v}$	\mathbf{f}	$\eta \nabla^2 \mathbf{v}$	(8.75)
Order of magnitude:	$\rho \frac{v^2}{l}$	$\rho \frac{v^2}{l}$	ρg	$\eta \frac{v}{l^2}$	

(I have skipped the term ∇P because as we have seen in the previous section, in typical fluid flow problems, it balances the viscosity term, and hence is of the same order of magnitude.)

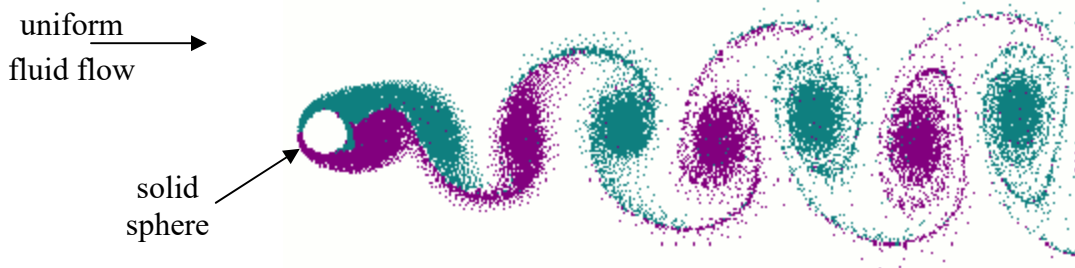


Fig. 8.16. A snapshot of the turbulent tail (wake) behind a sphere moving in a fluid with a high Reynolds number, showing the so-called von Kármán vortex street. Adapted from the original (actually, a very nice animation, <http://www.mcef.ep.usp.br/staff/jmeneg/cesareo/vort2.gif>) by Cesareo de La Rosa Siqueira, as a copyright-free material, available at <https://commons.wikimedia.org/w/index.php?curid=87351>.

Estimates (75) show that the relative importance of the terms may be characterized by two dimensionless ratios.⁴⁸ The first of them is the so-called *Froude number*⁴⁹

$$F \equiv \frac{\rho v^2 / l}{\rho g} \equiv \frac{v^2}{lg}, \quad (8.76)$$

which characterizes the relative importance of the gravity – or, upon appropriate modification, of other bulk forces. In most practical problems (with the important exception of surface waves, see Sec. 4 above), $F \gg 1$ so that the gravity effects may be neglected.

Much more important is another ratio, the Reynolds number (74), which may be rewritten as

$$Re \equiv \frac{\rho v l}{\eta} \equiv \frac{\rho v^2 / l}{\eta v / l^2}, \quad (8.77)$$

and hence is a measure of the relative importance of the fluid particle's inertia in comparison with the viscosity effects.⁵⁰ So again, it is natural that for a sphere, the role of the vorticity-creating term $(\mathbf{v} \cdot \nabla)\mathbf{v}$

⁴⁸ For substantially compressible fluids (e.g., gases), the most important additional dimensionless parameter is the *Mach number* $M \equiv v/v_l$, where $v_l = (K/\rho)^{1/2}$ is the velocity of the longitudinal sound – which is, as we already know from Chapter 7, the only wave mode possible in an infinite fluid. Especially significant for practice are *supersonic effects* (including the shock wave in the form of the famous *Mach cone* with half-angle $\theta_M = \sin^{-1} M^{1/2}$) that arise at $M > 1$. For a more thorough discussion of these issues, I have to refer the reader to more specialized texts – either Chapter IX of the Landau-Lifshitz volume cited above or Chapter 15 in I. Cohen and P. Kundu, *Fluid Mechanics*, 4th ed., Academic Press, 2007 – which is generally a good book on the subject.

⁴⁹ Named after William Froude (1810-1879), one of the applied hydrodynamics pioneers.

⁵⁰ Note that the “dynamic” viscosity η participates in this number (and many other problems of fluid dynamics) only in the combination η/ρ , which thereby has deserved a special name of *kinematic viscosity*.

becomes noticeable already at $Re \sim 1$ – see Fig. 15. What is very counter-intuitive is the onset of turbulence in systems where the laminar (turbulence-free) flow is formally an exact solution to the Navier-Stokes equation for any Re . For example, at $Re > Re_t \approx 2,100$ (with $l \equiv 2R$ and $v \equiv v_{\max}$) the laminar flow in a round pipe, described by Eq. (60), becomes unstable, and the resulting turbulence decreases the fluid discharge Q in comparison with the Poiseuille law (62). Even more strikingly, the critical value of Re is rather insensitive to the pipe wall roughness and does not diverge even in the limit of perfectly smooth walls.

Since $Re \gg 1$ in many real-life situations, turbulence is very important for practice. (Indeed, the values of η and ρ for water listed in Table 1 imply that even for a few-meter-sized object, such as a human body or a small boat, $Re > 1,000$ at any speed above just ~ 1 mm/s.) However, despite nearly a century of intensive research, there is no general, quantitative analytical theory of this phenomenon, and most results are still obtained either by rather approximate analytical treatments, or by the numerical solution of the Navier-Stokes equations using the approaches discussed in the previous section, or in experiments (e.g., on scaled models⁵¹ in *wind tunnels*). A rare exception is the relatively recent theoretical result by S. Orszag (1971) for the turbulence threshold in a flow of an incompressible fluid through a gap of thickness t between two parallel plane walls (see Fig. 10): $Re_t \approx 5,772$ (for $l \equiv t/2$ and $v \equiv v_{\max}$). However, even for this simplest geometry, the analytical theory still cannot predict the turbulence patterns at $Re > Re_t$. Only certain general, semi-quantitative features of turbulence may be understood from simple arguments.

For example, Fig. 15 shows that within a very broad range of Reynolds numbers, from $\sim 10^2$ to $\sim 3 \times 10^5$, C_d of a thin round disk perpendicular to the incident flow, C_d is very close to 1.1 for any $Re > 10^3$, and that of a sphere is not too far away. The approximate equality $C_d \approx 1$, meaning that the drag force F is close to $\rho v_0^2 A/2$, may be understood (in the picture where the object is moved by an external force F with the velocity v_0 through a fluid that was initially at rest) as the equality of the force-delivered power Fv_0 and the fluid's kinetic energy $(\rho v_0^2/2)V$ created in volume $V = v_0 A$ in unit time. This relation would be exact if the object gave its velocity v_0 to each and every fluid particle its cross-section runs into, for example by dragging all such particles behind itself. In reality, much of this kinetic energy goes into vortices, where the particle velocity may differ from v_0 , so that the equality $C_d \approx 1$ is only approximate.

Another important general effect is that at very high values of Re , fluid flow at the leading surface of solid objects forms a thin, highly turbulent *boundary layer* that matches the zero relative velocity of the fluid at the surface with its substantial velocity in the outer region, which is almost free of turbulence and many cases, of other viscosity effects. This fact, clearly visible in Fig. 16, enables semi-quantitative analyses of several effects, for example, the so-called *Magnus lift force*⁵² \mathbf{F}_l exerted (on top of the usual drag force \mathbf{F}_d) on rotating objects, and directed across the fluid flow – see Fig. 17.

An even more important application of this concept is an approximate analysis of the forces exerted on non-rotating *airfoils* (such as aircraft wings) with special cross-sections forming sharp angles at their back ends. Such a shape minimizes the airfoil's contacts with the vortex street it creates in its

⁵¹ The crucial condition of correct modeling is the equality of the Reynolds numbers (74) (and if relevant, also of the Froude numbers and/or the Mach numbers) of the object of interest and its model.

⁵² Named after G. Magnus, who studied this effect in detail in 1852, though it had been described much earlier (in 1672) by I. Newton, and by B. Robins after him (in 1742).

wake, and allows the thin boundary layer to extend over virtually all of its surface, enhancing the lift force.

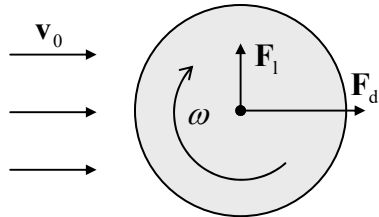


Fig. 8.17. The Magnus effect.

Unfortunately, due to the time/space restrictions, for a more detailed discussion of these results I have to refer the reader to more specialized literature,⁵³ and will conclude this chapter with a brief discussion of just one issue: can turbulence be explained by a single mechanism? (In other words, can it be reduced, at least on a semi-quantitative level, to a set of simpler phenomena that are commonly considered “well understood”?) Apparently the answer is *no*,⁵⁴ though nonlinear dynamics of simpler systems may provide some useful insights.

In the middle of the last century, the most popular qualitative explanation of turbulence had been the formation of an “energy cascade” that would transfer the energy from the regular fluid flow to a hierarchy of vortices of various sizes.⁵⁵ With our background, it is easier to retell that story in the time-domain language (with the velocity v serving as the conversion factor), using the fact that in a rotating vortex, each Cartesian component of a particle’s radius vector oscillates in time, so that to some extent the vortex plays the role of an oscillatory motion mode.

Let us consider the passage of a solid body between two, initially close, small parts of the fluid. The body pushes them apart, but after its passage, these partial volumes are free to return to their initial positions. However, the dominance of inertia effects at motion with $Re \gg 1$ means that the volumes continue to oscillate for a while about those equilibrium positions. (Since elementary volumes of an incompressible fluid cannot merge, these oscillations take the form of rotating vortices – see Fig. 16 again.)

Now, from Sec. 5.8 we know that intensive oscillations in a system with the quadratic nonlinearity, in this case, provided by the convective term $(\mathbf{v} \cdot \nabla) \mathbf{v}$, are equivalent, for small perturbations, to the oscillation of the system’s parameters at the corresponding frequency. On the other hand, as was briefly discussed in Sec. 6.7, in a system with two oscillatory degrees of freedom, a periodic parameter change with frequency ω_p may lead to the non-degenerate parametric excitation (“down-conversion”) of oscillations with frequencies $\omega_{1,2}$ satisfying the relation $\omega_1 + \omega_2 = \omega_p$. Moreover, the spectrum of oscillations in such a system also has higher combinational frequencies such as $(\omega_p + \omega_1)$, thus pushing the oscillation energy up the frequency scale (“up-conversion”). In the presence of other oscillatory modes, these oscillations may in turn produce, via the same nonlinearity, even higher frequencies, etc. In a fluid, the spectrum of these “oscillatory modes” (actually, vortex

⁵³ See, e.g., P. Davidson, *Turbulence*, Oxford U. Press, 2004.

⁵⁴ The following famous quote is attributed to Werner Heisenberg on his deathbed: “When I meet God, I will ask him two questions: Why relativity? And why turbulence? I think he will have an answer for the first question.” Though probably inaccurate, this story reflects rather well the frustration of the fundamental physics community, renown for their reductionist mentality, with the enormous complexity of phenomena that obey simple (e.g., the Navier-Stokes) equations, i.e. from their point of view, do not describe any new physics.

⁵⁵ This picture was suggested in 1922 by Lewis F. Richardson.

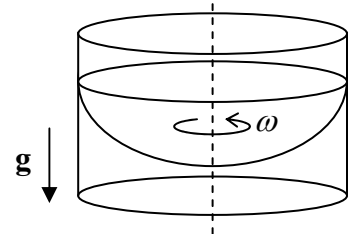
structures) is essentially continuous, so that the above arguments make very plausible a sequential transfer of the energy from the moving body to a broad range of oscillatory modes – whose frequency spectrum is limited from above by the energy dissipation due to the fluid's viscosity. When excited, these modes interact (in particular, mutually phase-lock) via the system's nonlinearity, creating the complex motion we call turbulence.

Though not having much quantitative predictive power, such handwaving explanations, which are essentially based on the excitation of a *large* number of effective degrees of freedom, had been dominating the turbulence reviews until the mid-1960s. At that point, the discovery (or rather re-discovery) of quasi-random motions in classical dynamic systems with just *a few* degrees of freedom altered the discussion substantially. Since this phenomenon, called the *deterministic chaos*, extends well beyond the fluid dynamics, I will devote to it a separate (albeit short) next chapter, and in its end will briefly return to the discussion of turbulence.

8.7. Exercise problems

8.1. For a mirror-symmetric but otherwise arbitrary shape of a ship's hull, derive an explicit expression for the height of metacenter M – see Fig. 3. Spell out this expression for a rectangular hull.

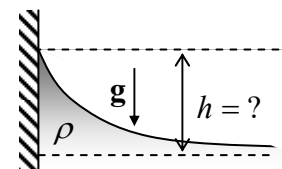
8.2. Find the stationary shape of the open surface of an incompressible, heavy fluid in a container rotated about its vertical axis with a constant angular velocity ω – see the figure on the right.



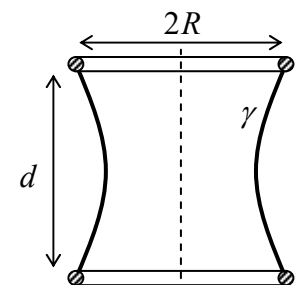
8.3. In the first order in the so-called *flattening* $f \equiv (R_e - R_p)/R_p \ll 1$ of the Earth (where R_e and R_p are, respectively, its equatorial and polar radii), calculate it within a simple model in that our planet is a uniformly-rotating nearly-spherical fluid ball, whose gravity field is dominated by a relatively small spherical core. Compare your result with the experimental value of f , and interpret the difference.

Hint: You may use experimental values $R_e \approx 6,378$ km, $R_p \approx 6,357$ km, and $g \approx 9.807$ m/s².

8.4.* Use two different approaches to calculate the stationary shape of the surface of an incompressible fluid of density ρ near a vertical plane wall, in a uniform gravity field – see the figure on the right. In particular, find the height h of liquid's rise at the wall surface as a function of the contact angle θ_c .



8.5.* A soap film with surface tension γ is stretched between two similar, coaxial, thin, round rings of radius R , separated by distance d – see the figure on the right. Neglecting gravity, calculate the equilibrium shape of the film, and the external force needed for keeping the rings at this distance.



8.6. A solid sphere of radius R is kept in a steady, vorticity-free flow of an ideal incompressible fluid, with velocity v_0 . Find the spatial distribution of velocity and pressure, and in particular their extreme values. Compare the results with those obtained in Sec. 4 for a round cylinder.

8.7.* Solve the same problem for a long and thin solid strip of width $2w$, with its plane normal to the unperturbed fluid flow.

Hint: You may like to use the so-called *elliptic coordinates* $\{\mu, \eta\}$ defined by their relations with the Cartesian coordinates $\{x, y\}$:

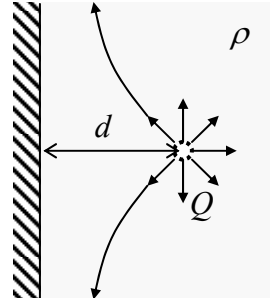
$$x = C \cosh \mu \cos \nu, \quad y = C \sinh \mu \sin \nu, \quad \text{with } 0 \leq \mu < \infty, \quad -\pi \leq \nu < +\pi,$$

where C is a constant; in these coordinates,

$$\nabla^2 = \frac{1}{C^2(\cosh^2 \mu - \cos^2 \nu)} \left(\frac{\partial^2}{\partial \mu^2} + \frac{\partial^2}{\partial \nu^2} \right).$$

8.8. A small source, located at distance d from a plain wall of a container filled with an ideal, incompressible fluid of density ρ , injects additional fluid isotropically, at a constant mass current (“discharge”) $Q \equiv dM/dt$ – see the figure on the right. Calculate the fluid’s velocity distribution, and its pressure on the wall, created by the flow.

Hint: Recall the charge image method in electrostatics,⁵⁶ and contemplate its possible analog.



8.9. Calculate the average kinetic, potential, and full energies (per unit area) of a traveling sinusoidal wave, of a small amplitude q_A , on the horizontal surface of an ideal, incompressible, deep fluid of density ρ , in a uniform gravity field \mathbf{g} .

8.10. Calculate the average power (per unit width of the wave’s front) carried by the surface wave discussed in the previous problem, and relate the result to the wave’s energy.

8.11. Derive Eq. (48) for the surface waves on a finite-thickness layer of a heavy liquid.

8.12. The utmost simplicity of Eq. (49) for the velocity of waves on a relatively shallow ($h \ll \lambda$) layer of an ideal incompressible liquid implies that they may be described using a very simple physical picture. Develop such a picture, and verify that it yields the same expression for the velocity.

8.13. Use the solution of the previous problem to calculate the energy and power of the shallow-layer waves, and use the result to explain the high tides on some ocean shores, using two models:

- (i) the water depth h decreases gradually toward the shore, and
- (ii) h decreases sharply, at some distance l from the shore – as it does on the ocean shelf border.

8.14.* Derive a 2D differential equation describing the propagation of relatively long ($\lambda \gg h$) waves on the surface of a broad, plane layer of thickness h , of an ideal, incompressible fluid, and use it

⁵⁶ See, e.g., EM Secs. 2.9, 3.3, and 4.3.

to calculate the longest standing wave modes and frequencies in a layer covering a spherical planet of radius $R \gg h$.

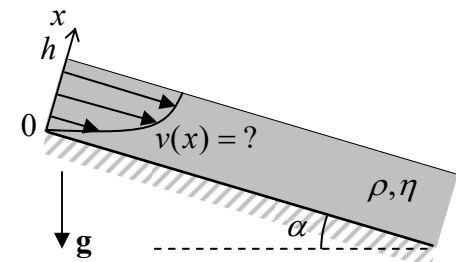
Hint: The second task requires some familiarity with the basic properties of spherical harmonics.⁵⁷

8.15. Calculate the velocity distribution and the dispersion relation of the waves propagating along the horizontal interface of two ideal, incompressible fluids of different densities.

8.16. Derive Eq. (50) for the capillary waves (“ripples”).

8.17. Use the finite-difference approximation for the Laplace operator, with the mesh step $h = a/4$, to find the maximum velocity and total mass flow Q of a viscous, incompressible fluid through a long pipe with a square-shaped cross-section of side a . Compare the results with those described in Sec. 5 for the same problem with the mesh step $h = a/2$, and for a pipe with the circular cross-section of the same area.

8.18. A layer, of thickness h , of a heavy, viscous, incompressible fluid flows down a long and wide inclined plane, under its own weight – see the figure on the right. Find the stationary velocity distribution profile, and the total fluid discharge (per unit width.)



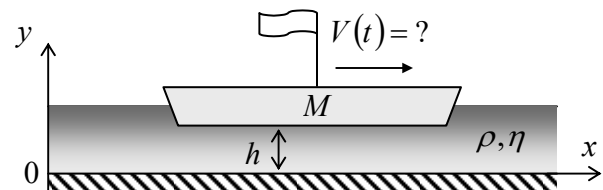
8.19. An external force moves two coaxial round disks of radius R , with an incompressible viscous fluid in the gap between them, toward each other with a constant velocity u . Calculate the applied force in the limit when the gap's thickness t is already much smaller than R .

8.20. Calculate the drag torque exerted on a unit length of a solid round cylinder of radius R that rotates about its axis, with angular velocity ω , inside an incompressible fluid with viscosity η , kept static far from the cylinder.

8.21. Solve a similar problem for a sphere of radius R , rotating about one of its principal axes.

8.22. Calculate the tangential force (per unit area) exerted by an incompressible fluid, with density ρ and viscosity η , on a broad solid plane placed over its surface and forced to oscillate, along the surface, with amplitude a and frequency ω .

8.23. A massive barge, with a flat bottom of area A , floats in shallow water, with clearance $h \ll A^{1/2}$ – see the figure on the right. Analyze the time dependence of the barge's velocity $V(t)$, and the water velocity profile, after the barge's engine has been turned off. Discuss the limits of large and small values of the dimensionless parameter $M/\rho Ah$.



⁵⁷ See, e.g., EM Sec. 2.8 and/or QM Sec. 3.6.

8.24.* Derive a general expression for mechanical energy loss rate in a viscous incompressible fluid that obeys the Navier-Stokes equation, and use this expression to calculate the attenuation coefficient of the surface waves, assuming that the viscosity is small. (Quantify this condition).

8.25. Use the Navier-Stokes equation to calculate the coefficient of attenuation of a plane, sinusoidal acoustic wave.

8.26.* Use two different approaches for a semi-quantitative calculation of the Magnus lift force \mathbf{F}_l exerted by an incompressible fluid of density ρ on a round cylinder of radius R , with its axis normal to the fluid's velocity \mathbf{v}_0 , and rotating about the axis with an angular velocity ω – see Fig. 17. Discuss the relation of the results.

Chapter 9. Deterministic Chaos

This chapter gives a very brief review of chaotic phenomena in deterministic maps and dynamic systems with and without dissipation, and an even shorter discussion of the possible role of chaos in fluid turbulence.

9.1. Chaos in maps

The possibility of quasi-random dynamics of deterministic systems with a few degrees of freedom (nowadays called the *deterministic chaos* – or just “chaos”) had been noticed before the 20th century,¹ but became broadly recognized only after the publication of a 1963 paper by theoretical meteorologist Edward Lorenz. In that work, he examined numerical solutions of the following system of three nonlinear, ordinary differential equations,

Lorenz system

$$\begin{aligned}\dot{q}_1 &= a_1(q_2 - q_1), \\ \dot{q}_2 &= a_2 q_1 - q_2 - q_1 q_3, \\ \dot{q}_3 &= q_1 q_2 - a_3 q_3,\end{aligned}\tag{9.1}$$

as a rudimentary model of heat transfer through a horizontal layer of fluid separating two solid plates. (Experiment shows that if the bottom plate is kept hotter than the top one, the fluid may exhibit turbulent convection.) He has found that within a certain range of the constants $a_{1,2,3}$, the solution to Eq. (1) follows complex, unpredictable, non-repeating trajectories in the 3D q -space. Moreover, the functions $q_j(t)$ (where $j = 1, 2, 3$) are so sensitive to initial conditions $q_j(0)$ that at sufficiently large times t , solutions corresponding to slightly different initial conditions become completely different.

Very soon it was realized that such behavior is typical for even simpler mathematical objects called *maps*, so that I will start my discussion of chaos from these objects. A 1D map is essentially a rule for finding the next number q_{n+1} of a discrete sequence numbered by the integer index n , in the simplest cases using only its last known value q_n . The most famous example is the so-called *logistic map*:²

Logistic map

$$q_{n+1} = f(q_n) \equiv r q_n (1 - q_n).\tag{9.2}$$

The basic properties of this map may be understood using its (hopefully, self-explanatory) graphical representation shown in Fig. 1.³ One can readily see that at $r < 1$ (Fig. 1a) the logistic map sequence rapidly converges to the trivial fixed point $q^{(0)} = 0$ because each next value of q is less than the previous one. However, if r is increased above 1 (as in the example shown in Fig. 1b), the fixed point

¹ It may be traced back at least to an 1892 paper by the same Jules Henri Poincaré who was already reverently mentioned in Chapter 5. Citing it: “...it may happen that small differences in the initial conditions produce very great ones in the final phenomena. [...] Prediction becomes impossible.”

² Its chaotic properties were first discussed in 1976 by Robert May, though the map itself is one of the simple ecological models repeatedly discussed much earlier, and may be traced back at least to the 1838 work by Pierre François Verhulst.

³ Since the maximum value of the function $f(q)$, achieved at $q = 1/2$, equals $r/4$, the mapping may be limited to segment $x = [0, 1]$, if the parameter r is between 0 and 4. Since all interesting properties of the map, including chaos, may be found within these limits, I will discuss only this range of r .

$q^{(0)}$ becomes unstable. Indeed, at $q_n \ll 1$, the map yields $q_{n+1} \approx rq_n$, so that at $r > 1$, the values q_n grow with each iteration. Instead of the unstable point $q^{(0)} = 0$, in the range $1 < r < r_1$, where $r_1 \equiv 3$, the map has a stable fixed point $q^{(1)}$ that may be found by plugging this value into both parts of Eq. (2):

$$q^{(1)} = f(q^{(1)}) \equiv rq^{(1)}(1 - q^{(1)}), \quad (9.3)$$

giving $q^{(1)} = 1 - 1/r$ – see the leftmost branch of the plot shown in Fig. 2.

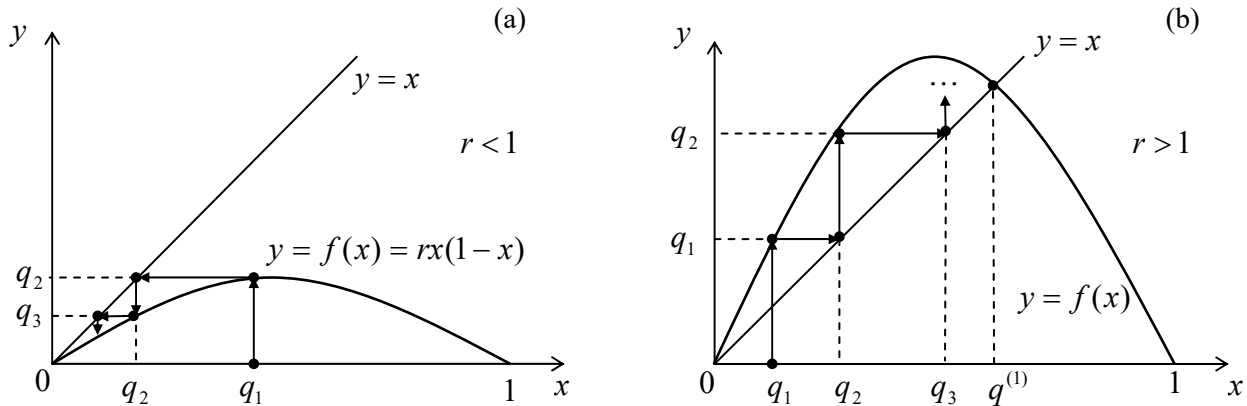


Fig. 9.1. Graphical analysis of the logistic map for: (a) $r < 1$ and (b) $r > 1$.

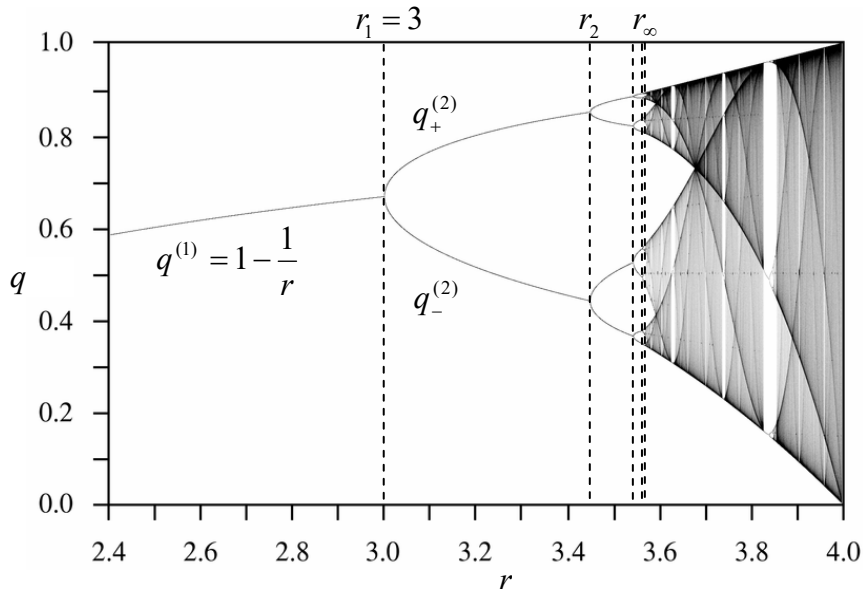


Fig. 9.2. The fixed points and chaotic regions of the logistic map. Adapted, under the CCO 1.0 Universal Public Domain Dedication, from the original by Jordan Pierce, available at http://en.wikipedia.org/wiki/Logistic_map. (A very nice live simulation of the map is also available on this website.)

However, at $r > r_1 = 3$, the fixed point $q^{(1)}$ also becomes unstable. To prove that, let us take $q_n \equiv q^{(1)} + \tilde{q}_n$, assume that the deviation \tilde{q}_n from the fixed point $q^{(1)}$ is small, and linearize the map (2) in \tilde{q}_n – just as we repeatedly did for differential equations earlier in this course. The result is

$$\tilde{q}_{n+1} = \frac{df}{dq} \Big|_{q=q^{(1)}} \tilde{q}_n = r(1 - 2q^{(1)})\tilde{q}_n \equiv (2 - r)\tilde{q}_n. \quad (9.4)$$

It shows that at $0 < 2 - r < 1$, i.e. at $1 < r < 2$, the deviations \tilde{q}_n decrease monotonically. At $-1 < 2 - r < 0$, i.e. in the range $2 < r < 3$, the deviations' sign alternates, but their magnitude still decreases – as in a stable focus, see Sec. 5.6. However, at $-1 < 2 - r$, i.e. $r > r_1 \equiv 3$, the deviations grow by magnitude, while still changing their sign, at each step. Since Eq. (2) has no other fixed points, this means that at $n \rightarrow \infty$, the values q_n do not converge to one point; rather, within the range $r_1 < r < r_2$, they approach a *limit cycle* of alternation of two points, $q_+^{(2)}$ and $q_-^{(2)}$, which satisfy the following system of algebraic equations:

$$q_+^{(2)} = f(q_-^{(2)}), \quad q_-^{(2)} = f(q_+^{(2)}). \quad (9.5)$$

These points are also plotted in Fig. 2, as functions of the parameter r . What has happened at the point $r_1 = 3$ is called the *period-doubling bifurcation*.

The story repeats at $r = r_2 \equiv 1 + \sqrt{6} \approx 3.45$, where the system goes from the 2-point limit cycle to a 4-point cycle, then at $r = r_3 \approx 3.54$, where the limit cycle begins to consist of 8 alternating points, etc. Most remarkably, the period-doubling bifurcation points r_n , at that the number of points in the limit cycle doubles from 2^{n-1} points to 2^n points, become closer and closer to each other. Numerical simulations show that at $n \rightarrow \infty$, these points obey the following asymptotic behavior:

$$r_n \rightarrow r_\infty - \frac{C}{\delta^n}, \quad \text{where } r_\infty = 3.5699..., \quad \delta = 4.6692... \quad (9.6)$$

Feigenbaum
bifurcation
sequence

The parameter δ is called the *Feigenbaum constant*; for other maps, and some dynamic systems (see the next section), period-doubling sequences follow a similar law, but with different values of δ .

More important for us, however, is what happens at $r > r_\infty$. Numerous numerical experiments, repeated with increasing precision,⁴ have confirmed that here the system is disordered, with no reproducible limit cycle, though (as Fig. 2 shows) at $r \approx r_\infty$, all sequential values q_n are still confined to a few narrow regions.⁵ However, as parameter r is increased well beyond r_∞ , these regions broaden and merge. This is the so-called *deep chaos*, with no apparent order at all.⁶

The most important feature of the chaos (in this and any other system) is the *exponential divergence of trajectories*. For a 1D map, this means that even if the initial conditions q_1 in two map implementations differ by a very small amount Δq_1 , the difference Δq_n between the corresponding sequences q_n is growing, on average, exponentially with n . Such exponents may be used to characterize chaos. Indeed, an evident generalization of the linearized Eq. (4) to an arbitrary point q_n is

$$\Delta q_{n+1} = e_n \Delta q_n, \quad e_n \equiv \left. \frac{df}{dq} \right|_{q=q_n}. \quad (9.7)$$

⁴ The reader should remember that just like the usual (“nature”) experiments, numerical experiments also have limited accuracy, due to unavoidable rounding errors.

⁵ The geometry of these regions is essentially *fractal*, i.e. has a dimensionality intermediate between 0 (which any final set of geometric points would have) and 1 (pertinent to a 1D continuum). An extensive discussion of fractal geometries and their relation to the deterministic chaos may be found, e.g., in the book by B. Mandelbrot, *The Fractal Geometry of Nature*, W. H. Freeman, 1983.

⁶ This does not mean that chaos’ depth is always a monotonic function of r . As Fig. 2 shows, within certain intervals of this parameter, the chaotic behavior suddenly disappears, being replaced, typically, with a few-point limit cycle, just to resume on the other side of the interval. Sometimes (but not always!) the “route to chaos” on the borders of these intervals follows the same Feigenbaum sequence of period-doubling bifurcations.

Let us assume that Δq_1 is so small that N first values q_n are relatively close to each other. Then using Eq. (7) iteratively for these steps, we get

$$\Delta q_N = \Delta q_1 \prod_{n=1}^N e_n, \quad \text{so that } \ln \left| \frac{\Delta q_N}{\Delta q_1} \right| = \sum_{n=1}^N \ln |e_n|. \quad (9.8)$$

Numerical experiments show that in most chaotic regimes, at $N \rightarrow \infty$ such a sum fluctuates about an average, which grows as λN , with the parameter

$$\lambda \equiv \lim_{\Delta q_1 \rightarrow 0} \lim_{N \rightarrow \infty} \frac{1}{N} \sum_{n=1}^N \ln |e_n|, \quad (9.9)$$

Lyapunov exponent

called the *Lyapunov exponent*,⁷ being independent of the initial conditions. The bottom panel in Fig. 3 shows λ as a function of the parameter r for the logistic map (2). (Its top panel shows the same pattern as Fig. 2, which is reproduced here just for the sake of comparison.)

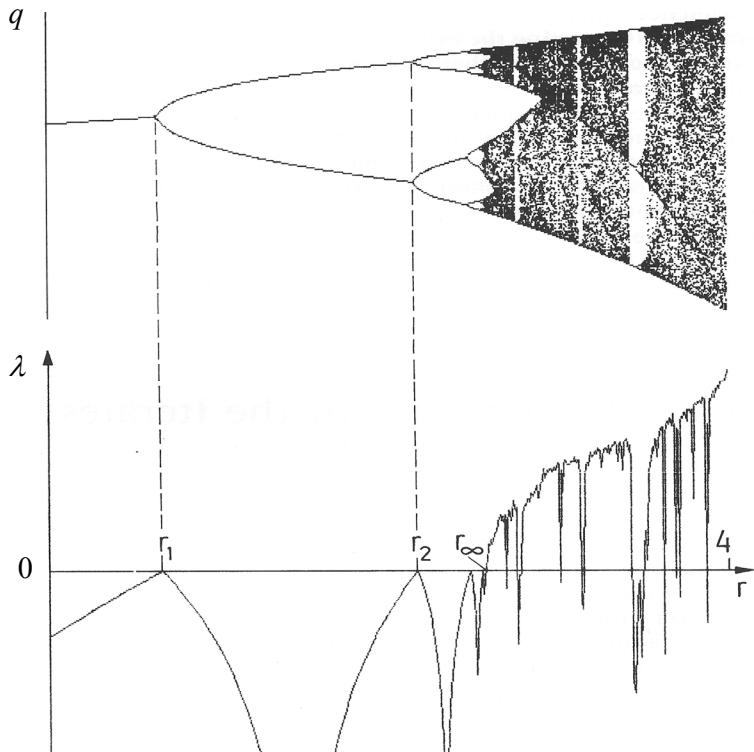


Fig. 9.3. The Lyapunov exponent for the logistic map. Adapted, with permission, from the monograph by Schuster and Just (cited below). © Wiley-VCH Verlag GmbH & Co. KGaA.

Note that at $r < r_\infty$, λ is negative, indicating the sequence's stability, besides the points r_1, r_2, \dots where λ would become positive if the limit cycle changes (bifurcations) had not brought it back into the negative territory. However, at $r > r_\infty$, λ becomes positive, returning to negative values only in limited intervals of stable limit cycles. It is evident that in numerical experiments (which dominate the studies of deterministic chaos) the Lyapunov exponent may be used as a good measure of the chaos' depth.⁸

⁷ After Alexandre Mikhailovich Lyapunov (1857-1918), famous for his studies of the stability of dynamic systems.

⁸ N -dimensional maps that relate N -dimensional vectors rather than scalars, may be characterized by N Lyapunov exponents rather than one. For chaotic behavior, it is sufficient for just one of them to become positive. For such systems, another measure of chaos, the *Kolmogorov entropy*, may be more relevant. This measure and its relation with the Lyapunov exponents are discussed, for example, in SM Sec. 2.2.

Despite the abundance of results published for particular maps,⁹ and several interesting observations (like the already discussed existence of the Feigenbaum bifurcation sequences), to the best of my knowledge, nobody can yet predict the patterns like those shown in Fig. 2 and 3 from just studying the mapping rule itself, i.e. without carrying out actual numerical experiments. Unfortunately, the understanding of deterministic chaos in other systems is not much better.

9.2. Chaos in dynamic systems

Proceeding to the discussion of chaos in dynamic systems, it is more natural, with our background, to illustrate this discussion not with the Lorenz equations, but with the system of equations describing a dissipative pendulum driven by a sinusoidal external force, which was repeatedly discussed in Chapter 5. Introducing two new variables, the normalized momentum $p \equiv (dq/dt)/\omega_0$, and the external force's full phase $\psi \equiv \omega t$, we may rewrite Eq. (5.42), describing the pendulum, in a form similar to Eq. (1), i.e. as a system of three first-order ordinary differential equations:

$$\begin{aligned}\dot{q} &= \omega_0 p, \\ \dot{p} &= -\omega_0 \sin q - 2\delta p + (f_0 / \omega_0) \cos \psi, \\ \dot{\psi} &= \omega.\end{aligned}\tag{9.10}$$

Figure 4 shows several results of a numerical solution of Eq. (10).¹⁰ In all cases, parameters δ , ω_0 , and f_0 are fixed, while the external frequency ω is gradually changed. For the case shown on the top two panels, the system still tends to a stable periodic solution, with very low contents of higher harmonics. If the external force frequency is reduced by a just few percent, the 3rd subharmonic may be excited. (This effect has already been discussed in Sec. 5.8 – see, e.g., Fig. 5.15.) The next row shows that just a small further reduction of the frequency ω leads to a new tripling of the period, i.e. the generation of a complex waveform with the 9th subharmonic. Finally (see the bottom panels of Fig. 4), even a minor further change of ω leads to oscillations without any visible period, e.g., to the chaos.

In order to trace this transition, a direct inspection of the oscillation waveforms $q(t)$ is not very convenient, and trajectories on the phase plane $[q, p]$ also become messy if plotted for many periods of the external frequency. In situations like this, the Poincaré (or “stroboscopic”) plane, already discussed in Sec. 5.6, is much more useful. As a reminder, this is essentially just the phase plane $[q, p]$, but with the points highlighted only once a period, e.g., at $\psi = 2\pi n$, with $n = 1, 2, \dots$. On this plane, periodic oscillations of frequency ω are represented just as one fixed point – see, e.g. the top panel in the right column of Fig. 4. The 3rd subharmonic generation, shown on the next panel, means the oscillation period's tripling and is represented as the splitting of the fixed point into three. It is evident that this transition is similar to the period-doubling bifurcation in the logistic map, besides the fact (already discussed in Sec. 5.8) that in systems with an antisymmetric nonlinearity, such as the pendulum (10), the 3rd subharmonic is easier to excite. From this point, the 9th harmonic generation (shown on the 3rd panel of Fig. 4), i.e. one more splitting of the points on the Poincaré plane, may be understood as one more step on the Feigenbaum-like route to chaos – see the bottom panel of that figure.

⁹ See, e.g., Chapters 2-4 in H. Schuster and W. Just, *Deterministic Chaos*, 4th ed., Wiley-VCH, 2005, or Chapters 8-9 in J. Thompson and H. Stewart, *Nonlinear Dynamics and Chaos*, 2nd ed., Wiley, 2002.

¹⁰ In the actual simulation, a small term εq , with $\varepsilon \ll 1$, has been added to the left-hand side of this equation. This term slightly tames the trend of the solution to spread along the q -axis, and makes the presentation of results easier, without affecting the system's dynamics too much.

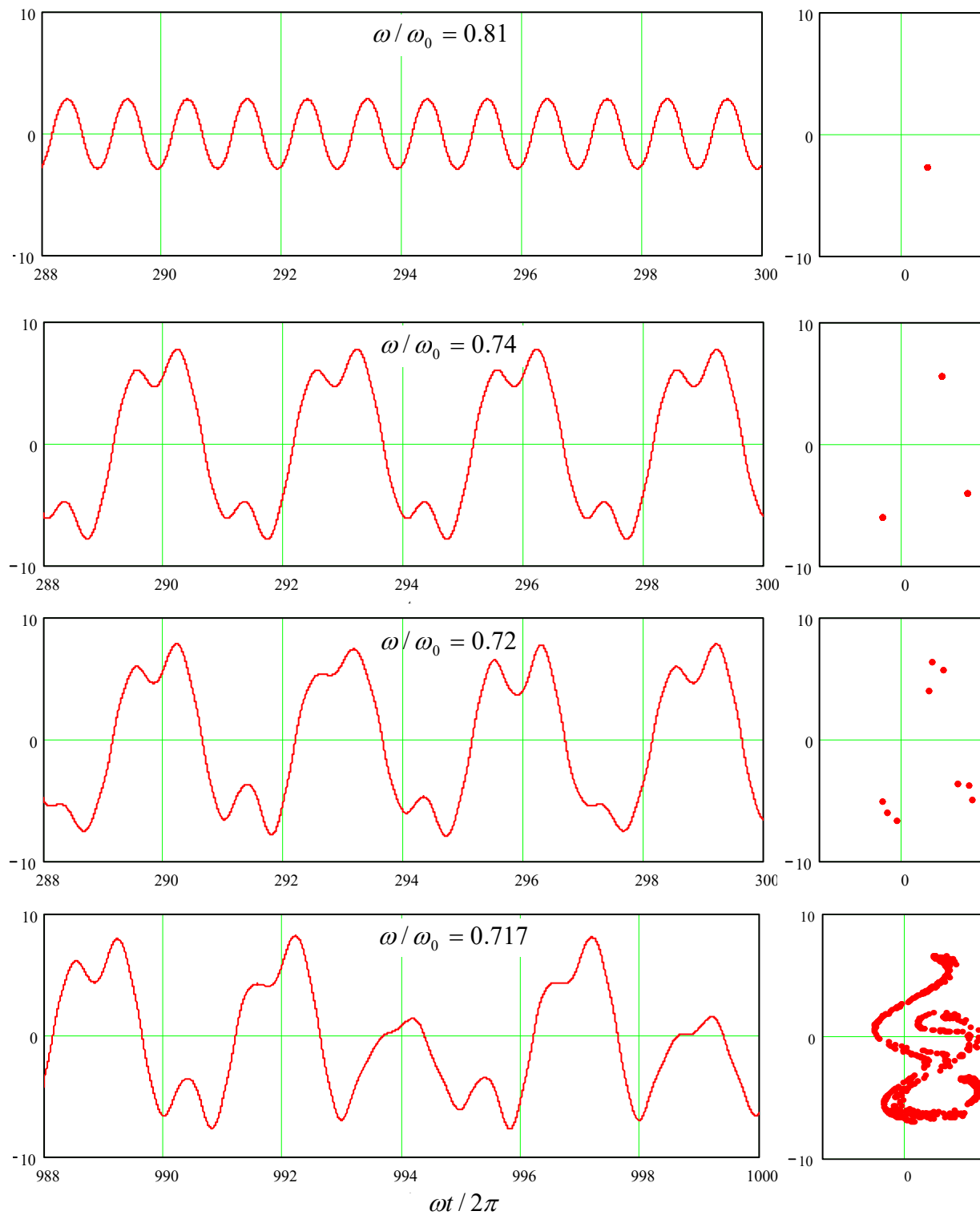


Fig. 9.4. Oscillations in a pendulum with weak damping, $\delta/\omega_0 = 0.1$, driven by a sinusoidal external force with a fixed effective amplitude $f_0/\omega_0^2 = 1$, and several close values of the frequency ω (listed on the panels). Left panel column: the oscillation waveforms $q(t)$ recorded after certain initial transient intervals. Right column: representations of the same processes on the Poincaré plane of the variables $[q, p]$, with the q -axis turned vertically, for the convenience of comparison with the left panels.

So, the transition to chaos in dynamic systems may be at least qualitatively similar to that in 1D maps, with a law similar to Eq. (6) for the critical values of some parameter of the system (in Fig. 4, frequency ω), though with a system-specific value of the coefficient δ . Moreover, we may consider the first two differential equations of the system (10) as a 2D map that relates the vector $\{q_{n+1}, p_{n+1}\}$ of the coordinate and momentum, measured at $\psi = 2\pi(n + 1)$, with the previous value $\{q_n, p_n\}$ of that vector, reached at $\psi = 2\pi n$.

Unfortunately, this similarity also implies that the deterministic chaos in dynamic systems is at least as complex, and is as little understood, as in maps. For example, Fig. 5 shows (a part of) the phase diagram of the externally-driven pendulum, with the red bar marking the route to chaos traced in Fig. 4, and shading/hatching styles marking different oscillation regimes. One can see that the pattern is at least as complex as that shown in Figs. 2 and 3, and, besides a few features,¹¹ is equally unpredictable from the form of the equation.

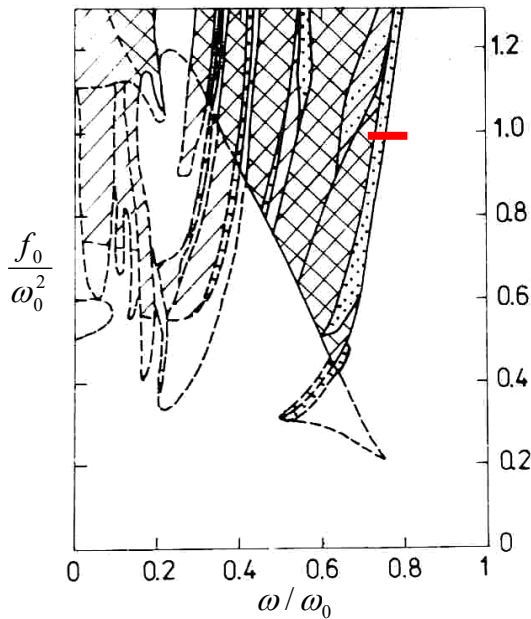


Fig. 9.5. The phase diagram of an externally-driven pendulum with weak damping ($\delta/\omega_0 = 0.1$). The regions of oscillations with the basic period are not shaded; the notation for other regions is as follows. Doted: subharmonic generation; cross-hatched: chaos; hatched: either chaos or the basic period (depending on the initial conditions); hatch-dotted: either the basic period or subharmonics. Solid lines show the boundaries of single-regime regions, while dashed lines are the boundaries of the regions where several types of motion are possible. (Figure courtesy by V. Kornev.)

Are there any valuable general results concerning the deterministic chaos in dynamic systems? The most important (though an almost evident) result is that this phenomenon is impossible in any system described by one or two first-order differential equations with time-independent right-hand sides. Indeed, let us start with a single equation

$$\dot{q} = f(q), \quad (9.11)$$

where $f(q)$ is any single-valued function. This equation may be directly integrated to give

$$t = \int \frac{dq'}{f(q')} + \text{const}, \quad (9.12)$$

showing that the relation between q and t is unique and hence does not leave any place for chaos.

¹¹ In some cases, it is possible to predict a parameter region where chaos *cannot* happen, due to the lack of any instability-amplification mechanism. Unfortunately, typically the analytically predicted boundaries of such a region form a rather loose envelope of the actual (numerically simulated) chaotic regions.

Next, let us explore a system of two such equations:

$$\begin{aligned}\dot{q}_1 &= f_1(q_1, q_2), \\ \dot{q}_2 &= f_2(q_1, q_2).\end{aligned}\tag{9.13}$$

Consider its phase plane shown schematically in Fig. 6. In a “usual” system, the trajectories approach either some fixed point (Fig. 6a) describing static equilibrium, or a limit cycle (Fig. 6b) describing periodic oscillations. (Both notions are united by the term *attractor* because they “attract” trajectories launched from various initial conditions.) On the other hand, phase plane trajectories of a chaotic system of equations that describe physical variables (which cannot be infinite), should be confined to a limited phase plane area, and simultaneously cannot start repeating each other. (This topology is frequently called the *strange attractor*.) For that, the 2D trajectories need to cross – see, e.g., point A in Fig. 6c.

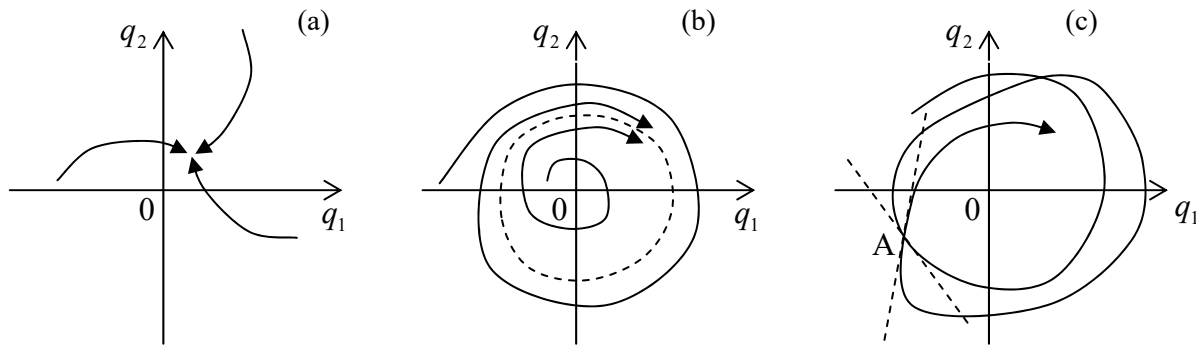


Fig. 9.6. Attractors in dynamical systems: (a) a fixed point, (b) a limit cycle, and (c) a strange attractor.

However, in the case described by Eqs. (13), such a crossing is clearly impossible, because according to these equations, the tangent of a phase plane trajectory is a unique function of the coordinates $\{q_1, q_2\}$:

$$\frac{dq_1}{dq_2} = \frac{f_1(q_1, q_2)}{f_2(q_1, q_2)}.\tag{9.14}$$

Thus, in this case, the deterministic chaos is impossible.¹² It becomes, however, readily possible if the right-hand sides of a system similar to Eq. (13) depend either on other variables of the system or time. For example, if we consider the first two differential equations of the system (10), in the case $f_0 = 0$ they have the structure of the system (13), and hence the chaos is impossible – even at $\delta < 0$ when (as we know from Sec. 5.4) the system allows self-excitation of oscillations, leading to a limit-cycle attractor. However, if $f_0 \neq 0$, this argument does not work any longer, and (as we have already seen) the system may have a strange attractor – which is, for dynamic systems, a synonym for the deterministic chaos.

Thus, chaos is only possible in autonomous dynamic systems described by three or more differential equations of the first order.¹³

¹² A mathematically strict formulation of this statement is called the *Poincaré-Bendixon theorem*, which was proved by Ivar Bendixon in 1901.

¹³ Since a typical dynamic system with one degree of freedom is described by two such equations, the number of first-order equations describing a dynamic system is sometimes called the number of its *half-degrees of freedom*. This notion is very useful and popular in statistical mechanics – see, e.g., SM Sec. 2.2 and on.

9.3. Chaos in Hamiltonian systems

The last conclusion is of course valid for Hamiltonian systems, which are just a particular type of dynamic systems. However, one may wonder whether these systems, that feature at least one first integral of motion, $H = \text{const}$, and hence are more “ordered” than the systems discussed above, can exhibit chaos at all. The answer is *yes* because such systems still can have mechanisms for the exponential growth of a small initial perturbation.

As the simplest way to show it, let us consider the so-called *mathematical billiard*, i.e. system with a ballistic particle (a “ball”) moving freely by inertia on a horizontal plane surface (“table”) limited by rigid walls. In this idealized model of the usual game of billiards, the ball’s velocity \mathbf{v} is conserved when it moves on the table, and when it runs into a wall, the ball is elastically reflected from it as from a mirror,¹⁴ with the reversal of the sign of the normal velocity v_n , and the conservation of the tangential velocity v_τ , and hence without any loss of its kinetic (and hence the full) energy

$$E = H = T = \frac{m}{2} v^2 = \frac{m}{2} (v_n^2 + v_\tau^2). \quad (9.15)$$

This model, while being a legitimate 2D dynamic system,¹⁵ allows geometric analyses for several simple table shapes. The simplest of them is a rectangular billiard of area $a \times b$ (Fig. 7), whose analysis may be readily carried out just by the replacement of each *ball* reflection event with the mirror reflection of the *table* in that wall – see the dashed lines on panel (a).

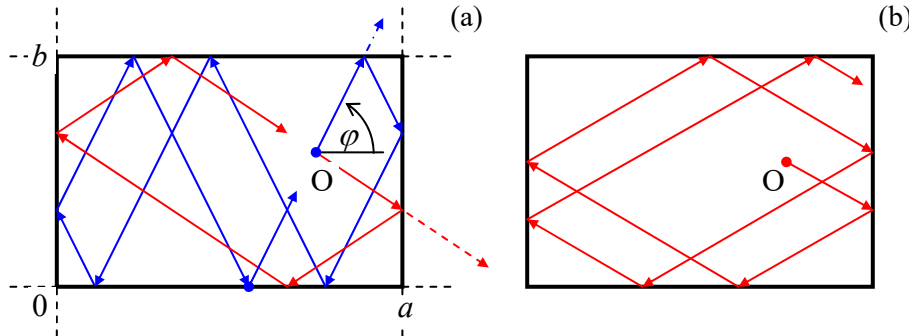


Fig. 9.7. Ball motion on a rectangular billiard at (a) a commensurate, and (b) an incommensurate launch angle.

Such analysis (left for the reader’s pleasure :-) shows that if the tangent of the ball launching angle φ is commensurate with the side length ratio:

$$\tan \varphi = \pm \frac{m}{n} \frac{b}{a}, \quad (9.16)$$

where n and m are non-negative integers without common integer multipliers, the ball returns exactly to the launch point O, after bouncing m times from each wall of length a , and n times from each wall of length b . (Red lines in Fig. 7a show an example of such a trajectory for $n = m = 1$, while blue lines, for $m = 3, n = 1$.) The larger is the sum $(m + n)$, the more complex is such a closed “orbit”.

¹⁴ A more scientific-sounding name for such a reflection is *specular* – from the Latin word “speculum” meaning a metallic mirror.

¹⁵ Indeed, it is fully described by the following Lagrangian function: $L = mv^2/2 - U(\mathbf{p})$, with $U(\mathbf{p}) = 0$ for the 2D radius vectors \mathbf{p} belonging to the table area, and $U(\mathbf{p}) = +\infty$ outside the area.

Finally, if $(n + m) \rightarrow \infty$, i.e. $\tan\varphi$ and b/a are incommensurate (meaning that their ratio is an irrational number), the trajectory covers all of the table area, and the ball never returns exactly to the launch point. Still, this is not genuine chaos. Indeed, a small shift of the launch point O shifts all the trajectory fragments by the same displacement. Moreover, at any time t , each of Cartesian components $v_j(t)$ of the ball's velocity (with coordinate axes parallel to the table sides) may take only two values, $\pm v_j(0)$, and hence may vary only as much as the initial velocity is being changed.

In 1963, i.e. well before E. Lorenz's work, Yakov Sinai showed that the situation changes completely if an additional wall, in the shape of a circle, is inserted into the rectangular billiard (Fig. 8). For most initial conditions, the ball's trajectory eventually runs into the circle (see the red line on panel (a) as an example), and the further trajectory becomes essentially chaotic. Indeed, let us consider the ball's reflection from a circle-shaped wall – Fig. 8b. Due to the conservation of the tangential velocity, and the sign change of the normal velocity component, the reflection obeys a simple law: $\theta_r = \theta_i$. Figure 8b shows that as the result, the magnitude of a small difference $\delta\varphi$ between the angles of two close trajectories (as measured in the lab system), doubles at each reflection from the curved wall. This means that the small deviation grows along the ball trajectory as

$$|\delta\varphi(N)| \sim |\delta\varphi(0)| \times 2^N \equiv |\delta\varphi(0)| e^{N \ln 2}, \quad (9.17)$$

where N is the number of reflections from the convex wall.¹⁶ As we already know, such exponential divergence of trajectories, with a positive Lyapunov exponent, is the main feature of deterministic chaos.¹⁷

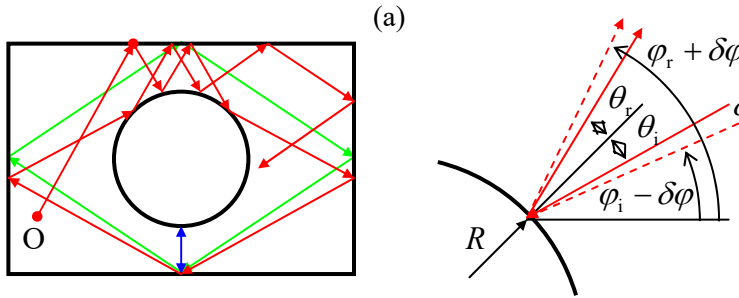


Fig. 9.8. (a) Motion on a Sinai billiard table, and (b) the mechanism of the exponential divergence of close trajectories.

The most important new feature of the dynamic chaos in Hamiltonian systems is its dependence on initial conditions. (In the systems discussed in the previous two sections, that lack the integrals of motion, the initial conditions are rapidly “forgotten”, and the chaos is usually characterized after an initial transient period – see, e.g., Fig. 4.) Indeed, even a Sinai billiard allows periodic motion, along closed orbits, under certain initial conditions – see the blue and green lines in Fig. 8a as examples. Thus

¹⁶ Superficially, Eq. (17) is also valid for a plane wall, but as was discussed above, a billiard with such walls features a full correlation between sequential reflections, so that angle φ always returns to its initial value. In a Sinai billiard, such correlation disappears. Concave walls may also make a billiard chaotic; a famous example is the *stadium billiard*, suggested by Leonid Bunimovich in 1974, with two straight, parallel walls connecting two semi-circular, concave walls. Another example, which allows a straightforward analysis (first carried out by Martin Gutzwiller in the 1980s), is the so-called *Hadamard billiard*: an infinite (or rectangular) table with a non-horizontal surface of negative curvature.

¹⁷ Curved-wall billiards are also a convenient platform for studies of quantum properties of classically chaotic systems (for their conceptual discussion, see QM Sec. 3.5), in particular, the features called “quantum scars” – see, e.g., the spectacular numerical simulation results by E. Heller, *Phys. Rev. Lett.* **53**, 1515 (1984).

the chaos “depth” in such systems may be characterized by the “fraction”¹⁸ of the phase space of initial parameters (for a 2D billiard, of the 3D space of the initial values of x , y , and ϕ) resulting in chaotic trajectories.

This conclusion is also valid for Hamiltonian systems that are met in physics much more frequently than exotic billiards, for example, coupled nonlinear oscillators without damping. Perhaps the earliest and the most popular example is the so-called *Hénon-Heiles* system,¹⁹ which may be described by the following Lagrangian function:

$$L = \frac{m_1}{2}(\dot{q}_1^2 - \omega_1^2 q_1^2) + \frac{m_2}{2}(\dot{q}_2^2 - \omega_2^2 q_2^2) - \varepsilon \left(q_1^2 - \frac{1}{3}q_2^2 \right) q_2. \quad (9.18)$$

Hénon-
Heiles
system

It is straightforward to use this function to derive the corresponding Lagrange equations of motion,

$$\begin{aligned} m_1(\ddot{q}_1 + \omega_1^2 q_1) &= -2\varepsilon q_1 q_2, \\ m_2(\ddot{q}_2 + \omega_2^2 q_2) &= -\varepsilon(q_1^2 - q_2^2), \end{aligned} \quad (9.19)$$

and find their first integral of motion (physically, the energy conservation law):

$$H = E = \frac{m_1}{2}(\dot{q}_1^2 + \omega_1^2 q_1^2) + \frac{m_2}{2}(\dot{q}_2^2 + \omega_2^2 q_2^2) + \varepsilon \left(q_1^2 - \frac{1}{3}q_2^2 \right) q_2 = \text{const}. \quad (9.20)$$

In the context of our discussions in Chapters 5 and 6, Eqs. (19) may be readily interpreted as those describing two oscillators, with small-oscillation frequencies ω_1 and ω_2 , coupled only by the quadratic terms on the right-hand sides of the equations. This means that as the oscillation amplitudes $A_{1,2}$, and hence the total energy E of the system, are close to zero, the oscillator subsystems are virtually independent, each performing sinusoidal oscillations at its own frequency. This observation suggests a convenient way to depict the system’s motion.²⁰ Let us consider a Poincaré plane for one of the oscillators (say, with coordinate q_2), similar to that discussed in Sec. 2 above, with the only difference is that (because of the absence of an explicit function of time in the system’s equations), the trajectory on the phase plane [q_2, \dot{q}_2] is highlighted at the moments when $q_1 = 0$.

Let us start from the limit $A_{1,2} \rightarrow 0$ when the oscillations of q_2 are virtually sinusoidal. As we already know (see Fig. 5.9 and its discussion), if the representation point highlighting was perfectly synchronous with frequency ω_2 of the oscillations, there would be only one point on the Poincaré plane – see, e.g. the right top panel of Fig. 4. However, at the q_1 – initiated highlighting, there is no such synchronism, so that each period, a different point of the elliptical (at the proper scaling of the velocity,

¹⁸ Actually, quantitative characterization of the fraction is not trivial, because it may have *fractal dimensionality*. Unfortunately, due to lack of time I have to refer the reader interested in this issue to special literature, e.g., the monograph by B. Mandelbrot (cited above) and references therein.

¹⁹ It was first studied in 1964 by M. Hénon and C. Heiles as a simple model of star rotation about a galactic center. Most studies of this equation have been carried out for the following particular case: $m_2 = 2m_1$, $m_1\omega_1^2 = m_2\omega_2^2$. In this case, by introducing new variables $x \equiv \varepsilon q_1$, $y \equiv \varepsilon q_2$, and $\tau \equiv \omega_1 t$, it is possible to rewrite Eqs. (19) in a parameter-free form. All the results shown in Fig. 9 below are for this case.

²⁰ Generally, the system has a trajectory in 4D space, e.g., that of coordinates $q_{1,2}$ and their time derivatives, although the first integral of motion (20) means that for each fixed energy E , the motion is limited to a 3D subspace. Still, this is one dimension too many for a convenient representation of the motion.

circular) trajectory is highlighted, so that the resulting points, for certain initial conditions, reside on a circle of radius A_2 . If we now vary the initial conditions, i.e. redistribute the initial energy between the oscillators, but keep the total energy E constant, on the Poincaré plane we get a set of ellipses.

Now, if the initial energy is increased, the nonlinear interaction of the oscillations starts to deform these ellipses, causing also their crossings – see, e.g., the top left panel of Fig. 9. Still, below a certain threshold value of E , all Poincaré points belonging to a certain initial condition sit on a single closed contour. Moreover, these contours may be calculated approximately, but with pretty good accuracy, using straightforward generalization of the method discussed in Sec. 5.2.²¹

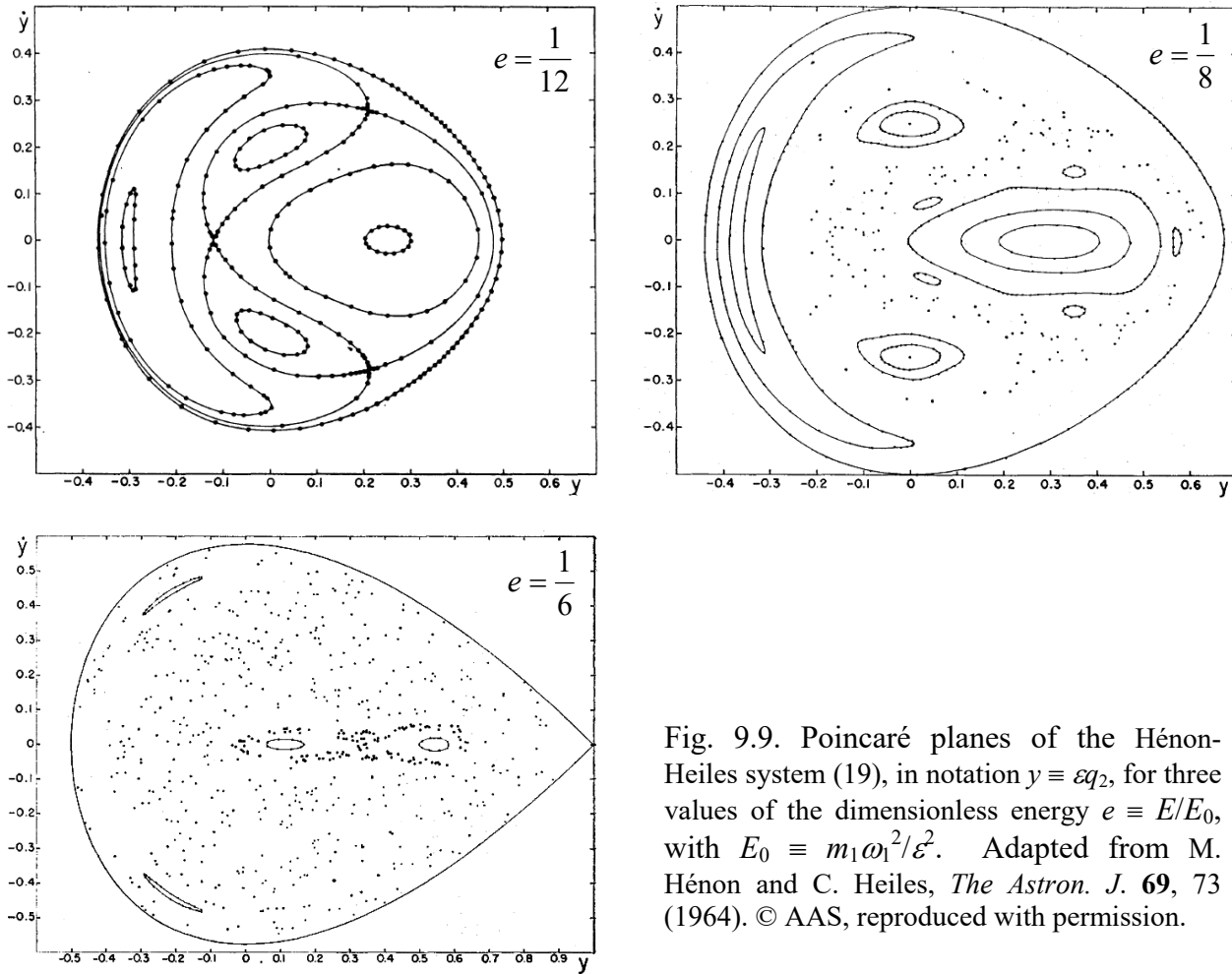


Fig. 9.9. Poincaré planes of the Hénon-Heiles system (19), in notation $y \equiv \varepsilon q_2$, for three values of the dimensionless energy $e \equiv E/E_0$, with $E_0 \equiv m_1 \omega_1^2 / \varepsilon^2$. Adapted from M. Hénon and C. Heiles, *The Astron. J.* **69**, 73 (1964). © AAS, reproduced with permission.

However, starting from some value of energy, certain initial conditions lead to sequences of points scattered over parts of the Poincaré plane, with a nonzero area – see the top right panel of Fig. 9. This means that the corresponding oscillations $q_2(t)$ do not repeat from one (quasi-) period to the next one – cf. Fig. 4 for the dissipative, forced pendulum. This is chaos.²² However, some other initial

²¹ See, e.g., M. Berry, in: S. Jorna (ed.), *Topics in Nonlinear Dynamics*, AIP Conf. Proc. No. 46, AIP, 1978, pp. 16-120.

²² This fact complies with the necessary condition of chaos, discussed at the end of Sec. 2, because Eqs. (19) may be rewritten as a system of four differential equations of the first order.

conditions still lead to closed contours. This feature is similar to that in Sinai billiards, and is typical for Hamiltonian systems. As the energy is increased, larger and larger parts of the Poincaré plane correspond to the chaotic motion, signifying deeper and deeper chaos – see the bottom panel of Fig. 9.

9.4. Chaos and turbulence

This extremely short section consists of essentially just one statement, extending the discussion in Sec. 8.5. The (re-) discovery of the deterministic chaos in systems with just a few degrees of freedom in the 1960s has changed the tone of the debates concerning turbulence origins, very considerably. At first, an extreme point of view that equated the notions of chaos and turbulence, became the debate's favorite.²³ However, after the initial excitement, a significant role of the Richardson-style energy-cascade mechanisms, involving many degrees of freedom, has been rediscovered and could not be ignored any longer. To the best knowledge of this author, who is a very distant albeit interested observer of that field, most experimental and numerical-simulation data carry features of both mechanisms, so that the debate continues.²⁴ Due to the age difference, most readers of these notes have much better chances than the author to see where would this discussion eventually lead.²⁵

9.5. Exercise problems

9.1. Generalize the reasoning of Sec. 1 to an arbitrary 1D map $q_{n+1} = f(q_n)$, with a function $f(q)$ differentiable at all points of interest. In particular, derive the condition of stability of an N -point limit cycle $q^{(1)} \rightarrow q^{(2)} \rightarrow \dots \rightarrow q^{(N)} \rightarrow q^{(1)} \dots$

9.2. Use the stability condition derived in the previous problem, to analyze the possibility of the deterministic chaos in the so-called *tent map*, with

$$f(q) = \begin{cases} rq, & \text{for } 0 \leq q \leq 1/2, \\ r(1-q), & \text{for } 1/2 \leq q \leq 1, \end{cases} \quad \text{with } 0 \leq r \leq 2.$$

9.3. Find the conditions of existence and stability of fixed points of the so-called *standard circle map*:

$$q_{n+1} = q_n + \Omega - \frac{K}{2\pi} \sin 2\pi q_n,$$

where q_n are real numbers defined modulo 1 (i.e. with $q_n + 1$ identified with q_n), while Ω and K are constant parameters. Discuss the relevance of the result for phase locking of self-oscillators – see, e.g., Sec. 5.4.

²³ An important milestone in that way was the work by S. Newhouse *et al.*, *Comm. Math. Phys.* **64**, 35 (1978), who proved the existence of a strange attractor in a rather abstract model of fluid flow.

²⁴ See, e.g., U. Frisch, *Turbulence: The Legacy of A. N. Kolmogorov*, Cambridge U. Press, 1996.

²⁵ The reader interested in the deterministic chaos as such may like to have a look at a very popular book by S. Strogatz, *Nonlinear Dynamics and Chaos*, Westview, 2001.

9.4. Find the conditions of existence and stability of fixed points of the so-called *Hénon map*:²⁶

$$\begin{aligned}q_{n+1} &= 1 - aq_n^2 + p_n, \\p_{n+1} &= bq_n, \quad \text{with } a, b > 0.\end{aligned}$$

9.5. Is the deterministic chaos possible in our “testbed” problem shown in Fig. 2.1? What if an additional periodic external force is applied to the bead? Explain your answers.

²⁶ This map, first explored by M. Hénon in 1976 (for a particular set of constants a and b), has played an important historic role in the study of strange attractors.

Chapter 10. A Bit More of Analytical Mechanics

This concluding chapter reviews two alternative approaches to analytical mechanics, whose major value is a closer parallel to quantum mechanics in general and its quasiclassical (WKB) approximation in particular. One of them, the Hamiltonian formalism, is also convenient for the derivation of an important asymptotic result, the adiabatic invariance, for classical systems with slowly changing parameters.

10.1. Hamilton equations

Throughout this course, we have seen how analytical mechanics, in its Lagrangian form, is invaluable for solving various particular problems of classical mechanics. Now let us discuss several alternative formulations¹ that may not be much more useful for this purpose, but shed additional light on possible extensions of classical mechanics, most importantly to quantum mechanics.

As was already discussed in Sec. 2.3, the partial derivative $p_j \equiv \partial L / \partial \dot{q}_j$ participating in the Lagrange equation (2.19),

$$\frac{d}{dt} \frac{\partial L}{\partial \dot{q}_j} - \frac{\partial L}{\partial q_j} = 0, \quad (10.1)$$

may be considered as the generalized momentum corresponding to the generalized coordinate q_j , and the full set of these momenta may be used to define the Hamiltonian function (2.32):

$$H \equiv \sum_j p_j \dot{q}_j - L. \quad (10.2)$$

Now let us rewrite the full differential of this function² in the following form:

$$\begin{aligned} dH &= d\left(\sum_j p_j \dot{q}_j - L\right) = \sum_j [d(p_j) \dot{q}_j + p_j d(\dot{q}_j)] - dL \\ &= \sum_j [d(p_j) \dot{q}_j + p_j d(\dot{q}_j)] - \left[\frac{\partial L}{\partial t} dt + \sum_j \left(\frac{\partial L}{\partial q_j} d(q_j) + \frac{\partial L}{\partial \dot{q}_j} d(\dot{q}_j) \right) \right]. \end{aligned} \quad (10.3)$$

According to the definition of the generalized momentum, the second terms of each sum over j in the last expression cancel each other, while according to the Lagrange equation (1), the derivative $\partial L / \partial \dot{q}_j$ is equal to \dot{p}_j , so that

$$dH = -\frac{\partial L}{\partial t} dt + \sum_j (\dot{q}_j dp_j - \dot{p}_j dq_j). \quad (10.4)$$

So far, this is just a universal identity. Now comes the main trick of Hamilton's approach: let us consider H as a function of the following independent arguments: time t , the generalized coordinates q_j ,

¹ Due to not only William Rowan Hamilton (1805-1865), but also Carl Gustav Jacob Jacobi (1804-1851).

² Actually, this differential was already spelled out (but partly and implicitly) in Sec. 2.3 – see Eqs. (2.33)-(2.35).

and the generalized *momenta* p_j – rather than generalized *velocities* \dot{q}_j as in the Lagrangian formalism. With this new commitment, the general “chain rule” of differentiation of a function of several arguments gives

$$dH = \frac{\partial H}{\partial t} dt + \sum_j \left(\frac{\partial H}{\partial q_j} dq_j + \frac{\partial H}{\partial p_j} dp_j \right), \quad (10.5)$$

where dt , dq_j , and dp_j are independent differentials. Since Eq. (5) should be valid for any choice of these argument differentials, it should hold in particular if they correspond to the real law of motion, for which Eq. (4) is valid as well. The comparison of Eqs. (4) and (5) gives us three relations:

$$\frac{\partial H}{\partial t} = -\frac{\partial L}{\partial t}. \quad (10.6)$$

$$\dot{q}_j = \frac{\partial H}{\partial p_j}, \quad p_j = -\frac{\partial H}{\partial q_j}. \quad (10.7)$$

Hamilton equations

Comparing the first of them with Eq. (2.35), we see that

$$\frac{dH}{dt} = \frac{\partial H}{\partial t}, \quad (10.8)$$

meaning that the function $H(t, q_j, p_j)$ can change in time only via its explicit dependence on t . Two Eqs. (7) are even more substantial: provided that such function $H(t, q_j, p_j)$ has been calculated, they give us two first-order differential equations (called the *Hamilton equations*) for the time evolution of the generalized coordinate and generalized momentum of each degree of freedom of the system.³

Let us have a look at these equations for the simplest case of a system with one degree of freedom, with the Lagrangian function (3.3):

$$L = \frac{m_{\text{ef}}}{2} \dot{q}^2 - U_{\text{ef}}(q, t). \quad (10.9)$$

In this case, $p \equiv \partial L / \partial \dot{q} = m_{\text{ef}} \dot{q}$, and $H \equiv p \dot{q} - L = m_{\text{ef}} \dot{q}^2 / 2 + U_{\text{ef}}(q, t)$. To honor our new commitment, we need to express the Hamiltonian function explicitly via t , q , and p (rather than \dot{q}). From the above expression for p , we immediately have $\dot{q} = p / m_{\text{ef}}$; plugging this expression back to Eq. (9), we get

$$H = \frac{p^2}{2m_{\text{ef}}} + U_{\text{ef}}(q, t). \quad (10.10)$$

Now we can spell out Eqs. (7) for this particular case:

$$\dot{q} \equiv \frac{\partial H}{\partial p} = \frac{p}{m_{\text{ef}}}, \quad (10.11)$$

$$\dot{p} \equiv -\frac{\partial H}{\partial q} = -\frac{\partial U_{\text{ef}}}{\partial q}. \quad (10.12)$$

³ Of course, the right-hand side of each equation (7) may include coordinates and momenta of other degrees of freedom as well, so that the equations of motion for different j are generally coupled.

While the first of these equations just repeats the definition of the generalized momentum corresponding to the coordinate q , the second one gives the equation of momentum's change. Differentiating Eq. (11) over time, and plugging Eq. (12) into the result, we get:

$$\ddot{q} = \frac{\dot{p}}{m_{\text{ef}}} = -\frac{1}{m_{\text{ef}}} \frac{\partial U_{\text{ef}}}{\partial q}. \quad (10.13)$$

So, we have returned to the same equation (3.4) that had been derived from the Lagrangian approach.⁴

Thus, the Hamiltonian formalism does not give much help for the solution of this problem – and indeed most problems of classical mechanics. (This is why its discussion had been postponed until the very end of this course.) Moreover, since the Hamiltonian function $H(t, q_j, p_j)$ does not include generalized velocities explicitly, the phenomenological introduction of dissipation in this approach is less straightforward than that in the Lagrangian equations, whose precursor form (2.17) is valid for dissipative forces as well. However, the Hamilton equations (7), which treat the generalized coordinates and momenta in a manifestly symmetric way, are heuristically fruitful – besides being very appealing aesthetically. This is especially true in the cases where these arguments participate in H in a similar way. For example, in the very important case of a dissipation-free linear (“harmonic”) oscillator, for which $U_{\text{ef}} = \kappa_{\text{ef}} q^2/2$, Eq. (10) gives the symmetric form

$$H = \frac{p^2}{2m_{\text{ef}}} + \frac{\kappa_{\text{ef}} x^2}{2} \equiv \frac{p^2}{2m_{\text{ef}}} + \frac{m_{\text{ef}} \omega_0^2 x^2}{2}, \quad \text{where } \omega_0^2 \equiv \frac{\kappa_{\text{ef}}}{m_{\text{ef}}}. \quad (10.14)$$

The Hamilton equations (7) for this system preserve that symmetry, especially evident if we introduce the normalized momentum $\rho \equiv p/m_{\text{ef}}\omega_0$ (already used in Secs. 5.6 and 9.2):

$$\frac{dq}{dt} = \omega_0 \rho, \quad \frac{d\rho}{dt} = -\omega_0 q. \quad (10.15)$$

More practically, the Hamilton approach gives additional tools for the search for the integrals of motion. To see that, let us consider the full time derivative of an arbitrary function $f(t, q_j, p_j)$:

$$\frac{df}{dt} = \frac{\partial f}{\partial t} + \sum_j \left(\frac{\partial f}{\partial q_j} \dot{q}_j + \frac{\partial f}{\partial p_j} \dot{p}_j \right). \quad (10.16)$$

Plugging in \dot{q}_j and \dot{p}_j from the Hamilton equations (7), we get

$$\frac{df}{dt} = \frac{\partial f}{\partial t} + \sum_j \left(\frac{\partial H}{\partial p_j} \frac{\partial f}{\partial q_j} - \frac{\partial H}{\partial q_j} \frac{\partial f}{\partial p_j} \right) \equiv \frac{\partial f}{\partial t} + \{H, f\}. \quad (10.17)$$

The last term on the right-hand side of this expression is the so-called *Poisson bracket*,⁵ and is defined, for two arbitrary functions $f(t, q_j, p_j)$ and $g(t, q_j, p_j)$, as

⁴ The reader is strongly encouraged to perform a similar check for a few more problems, for example those listed at the end of the chapter, to get a better feeling of how the Hamiltonian formalism works.

⁵ Named after Siméon Denis Poisson (1781–1840), of the Poisson equation and the Poisson statistical distribution fame.

$$\{g, f\} \equiv \sum_j \left(\frac{\partial g}{\partial p_j} \frac{\partial f}{\partial q_j} - \frac{\partial f}{\partial p_j} \frac{\partial g}{\partial q_j} \right). \quad (10.18)$$

Poisson bracket

From this definition, one can readily verify that besides evident relations $\{f, f\} = 0$ and $\{f, g\} = -\{g, f\}$, the Poisson brackets obey the following important *Jacobi identity*:

$$\{f, \{g, h\}\} + \{g, \{h, f\}\} + \{h, \{f, g\}\} = 0. \quad (10.19)$$

Now let us use these relations for a search for integrals of motion. First, Eq. (17) shows that if a function f does not depend on time explicitly, and

$$\{H, f\} = 0, \quad (10.20)$$

then $df/dt = 0$, i.e. that function is an integral of motion. Moreover, it turns out that if we already know two integrals of motion, say f and g , then the following function,

$$F \equiv \{f, g\}, \quad (10.21)$$

is also an integral of motion – the so-called *Poisson theorem*. In order to prove it, we may use the Jacobi identity (19) with $h = H$. Next, using Eq. (17) to express the Poisson brackets $\{g, H\}$, $\{H, g\}$, and $\{H, \{f, g\}\} = \{H, F\}$ via the full and partial time derivatives of the functions f , g , and F , we get

$$\left\{ f, \frac{\partial g}{\partial t} - \frac{dg}{dt} \right\} + \left\{ g, \frac{df}{dt} - \frac{\partial f}{\partial t} \right\} + \frac{dF}{dt} - \frac{\partial F}{\partial t} = 0, \quad (10.22)$$

so that if f and g are indeed integrals of motion, i.e., $df/dt = dg/dt = 0$, then

$$\frac{dF}{dt} = \frac{\partial F}{\partial t} + \left\{ g, \frac{\partial f}{\partial t} \right\} - \left\{ f, \frac{\partial g}{\partial t} \right\} = \frac{\partial F}{\partial t} - \left[\left\{ \frac{\partial f}{\partial t}, g \right\} + \left\{ f, \frac{\partial g}{\partial t} \right\} \right]. \quad (10.23)$$

Plugging Eq. (21) into the first term of the right-hand side of this equation, and differentiating it by parts, we get $dF/dt = 0$, i.e. F is indeed an integral of motion as well.

Finally, one more important role of the Hamilton formalism is that it allows one to trace the close formal connection between classical and quantum mechanics. Indeed, using Eq. (18) to calculate the Poisson brackets of the generalized coordinates and momenta, we readily get

$$\{q_j, q_{j'}\} = 0, \quad \{p_j, p_{j'}\} = 0, \quad \{q_j, p_{j'}\} = -\delta_{jj'}. \quad (10.24)$$

In quantum mechanics, the operators of these variables (“observables”) obey commutation relations⁶

$$[\hat{q}_j, \hat{q}_{j'}] = 0, \quad [\hat{p}_j, \hat{p}_{j'}] = 0, \quad [\hat{q}_j, \hat{p}_{j'}] = i\hbar\delta_{jj'}, \quad (10.25)$$

where the definition of the commutator, $[\hat{g}, \hat{f}] \equiv \hat{g}\hat{f} - \hat{f}\hat{g}$, is to a certain extent⁷ similar to that (18) of the Poisson bracket. We see that the classical relations (24) are similar to the quantum-mechanical relations (25) if the following parallel has been made:

⁶ See, e.g., QM Sec. 2.1.

$$\{g, f\} \leftrightarrow \frac{i}{\hbar} [\hat{g}, \hat{f}]. \quad (10.26)$$

This analogy extends well beyond Eqs. (24)-(25). For example, making the replacement (26) in Eq. (17), we get

$$\frac{d\hat{f}}{dt} = \frac{\partial \hat{f}}{\partial t} + \frac{i}{\hbar} [\hat{H}, \hat{f}], \quad \text{i.e. } i\hbar \frac{d\hat{f}}{dt} = i\hbar \frac{\partial \hat{f}}{\partial t} + [\hat{f}, \hat{H}], \quad (10.27)$$

which is the correct equation of operator evolution in the Heisenberg picture of quantum mechanics.⁸ The parallel (26) may give important clues in the search for the proper quantum-mechanical operator of a given observable – which is not always elementary.

10.2. Adiabatic invariance

One more application of the Hamiltonian formalism in classical mechanics is the solution of the following problem.⁹ Earlier in the course, we already studied some effects of time variation of parameters of a single oscillator (Sec. 5.5) and coupled oscillators (Sec. 6.5). However, those discussions were focused on the case when the parameter variation speed is comparable with the own oscillation frequency (or frequencies) of the system. Another practically important case is when some system's parameter (let us call it λ) is changed much more slowly (*adiabatically*¹⁰),

$$\left| \frac{\dot{\lambda}}{\lambda} \right| \ll \frac{1}{\tau}, \quad (10.28)$$

where τ is a typical period of oscillations in the system. Let us consider a 1D system whose Hamiltonian $H(q, p, \lambda)$ depends on time only via such a slow evolution of such parameter $\lambda = \lambda(t)$, and whose initial energy restricts the system's motion to a finite coordinate interval – see, e.g., Fig. 3.2c.

Then, as we know from Sec. 3.3, if the parameter λ is constant, the system performs a periodic (though not necessarily sinusoidal) motion back and forth the q -axis, or, in a different language, along a closed trajectory on the phase plane $[q, p]$ – see Fig. 1.¹¹ According to Eq. (8), in this case, H is constant along the trajectory. (To distinguish this particular *value* of H from the Hamiltonian *function* as such, I will call it E , implying that this constant coincides with the full mechanical energy E – as does for the Hamiltonian (10), though this assumption is not necessary for the calculation made below.)

The oscillation period τ may be calculated as a contour integral along this closed trajectory:

⁷ There is, of course, a conceptual difference between the “usual” products of the function derivatives participating in the Poisson brackets, and the operator “products” (meaning their sequential action on a state vector) forming the commutator.

⁸ See, e.g., QM Sec. 4.6.

⁹ Various aspects of this problem and its quantum-mechanical extensions were first discussed by L. Le Cornu (1895), Lord Rayleigh (1902), H. Lorentz (1911), P. Ehrenfest (1916), and M. Born and V. Fock (1928).

¹⁰ This term is also used in thermodynamics and statistical mechanics, where it implies not only a slow parameter variation (if any) but also thermal insulation of the system – see, e.g., SM Sec. 1.3. Evidently, the latter condition is irrelevant in our current context.

¹¹ As a reminder, we discussed such phase-plane representations in Chapter 5 – see, e.g., Figs. 5.5, 5.9, and 5.16.

$$\tau \equiv \int_0^\tau dt = \oint \frac{dt}{dq} dq \equiv \oint \frac{1}{\dot{q}} dq . \quad (10.29)$$

Using the first of the Hamilton equations (7), we may represent this integral as

$$\tau = \oint \frac{1}{\partial H / \partial p} dq . \quad (10.30)$$

At each given point q , $H = E$ is a function of p alone, so that we may flip the partial derivative in the denominator just as the full derivative, and rewrite Eq. (30) as

$$\tau = \oint \frac{\partial p}{\partial E} dq . \quad (10.31)$$

For the particular Hamiltonian (10), this relation is immediately reduced to Eq. (3.27), now in the form of a contour integral:

$$\tau = \left(\frac{m_{\text{ef}}}{2} \right)^{1/2} \oint \frac{1}{[E - U_{\text{ef}}(q)]^{1/2}} dq . \quad (10.32)$$

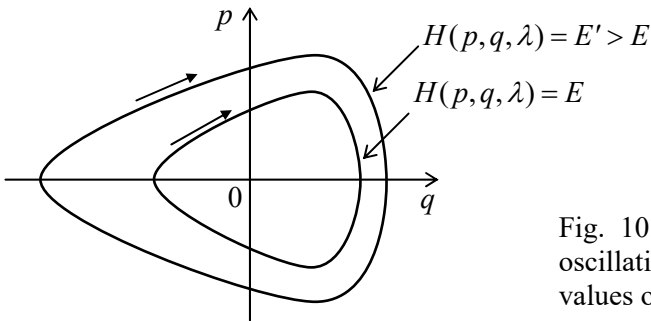


Fig. 10.1. Phase-plane representation of periodic oscillations of a 1D Hamiltonian system, for two values of energy (schematically).

Naively, it may look that these formulas may be also used to find the motion period's change when the parameter λ is being changed adiabatically, for example, by plugging the given functions $m_{\text{ef}}(\lambda)$ and $U_{\text{ef}}(q, \lambda)$ into Eq. (32). However, there is no guarantee that the energy E in that integral would stay constant as the parameter changes, and indeed we will see below that this is not necessarily the case. Even more interestingly, in the most important case of the harmonic oscillator ($U_{\text{ef}} = \kappa_{\text{ef}} q^2/2$), whose oscillation period τ does not depend on E (see Eq. (3.29) and its discussion), its variation in the adiabatic limit (28) may be readily predicted: $\tau(\lambda) = 2\pi/\omega_0(\lambda) = 2\pi[m_{\text{ef}}(\lambda)/\kappa_{\text{ef}}(\lambda)]^{1/2}$, but the dependence of the oscillation energy E (and hence of the oscillation amplitude) on λ is not immediately obvious.

In order to address this issue, let us use Eq. (8) (with $E = H$) to represent the rate of the energy change with $\lambda(t)$, i.e. in time, as

$$\frac{dE}{dt} = \frac{\partial H}{\partial t} = \frac{\partial H}{\partial \lambda} \frac{d\lambda}{dt} . \quad (10.33)$$

Since we are interested in a very slow (adiabatic) time evolution of energy, we can average Eq. (33) over fast oscillations in the system, for example over one oscillation period τ , treating $d\lambda/dt$ as a constant during this averaging. (This is the most critical point of this argumentation, because at any non-

vanishing rate of parameter change the oscillations are, strictly speaking, non-periodic.¹²⁾ The averaging yields

$$\overline{\frac{dE}{dt}} = \frac{d\lambda}{dt} \overline{\frac{\partial H}{\partial \lambda}} \equiv \frac{d\lambda}{dt} \frac{1}{\mathcal{T}} \int_0^{\mathcal{T}} \frac{\partial H}{\partial \lambda} dt. \quad (10.34)$$

Transforming this time integral to the contour one, just as we did at the transition from Eq. (29) to Eq. (30), and then using Eq. (31) for \mathcal{T} , we get

$$\overline{\frac{dE}{dt}} = \frac{d\lambda}{dt} \frac{\oint \frac{\partial H / \partial \lambda}{\partial H / \partial p} dq}{\oint \frac{\partial p}{\partial E} dq}. \quad (10.35)$$

At each point q of the contour, H is a function of not only λ , but also of p , which may be also λ -dependent, so that if E is fixed, the partial differentiation of the relation $E = H$ over λ yields

$$\frac{\partial H}{\partial \lambda} + \frac{\partial H}{\partial p} \frac{\partial p}{\partial \lambda} = 0, \quad \text{i.e. } \frac{\partial H / \partial \lambda}{\partial H / \partial p} = -\frac{\partial p}{\partial \lambda}. \quad (10.36)$$

Plugging the last relation to Eq.(35), we get

$$\overline{\frac{dE}{dt}} = -\frac{d\lambda}{dt} \frac{\oint \frac{\partial p}{\partial \lambda} dq}{\oint \frac{\partial p}{\partial E} dq}. \quad (10.37)$$

Since the left-hand side of Eq. (37) and the derivative $d\lambda/dt$ do not depend on q , we may move them into the integrals over q as constants, and rewrite Eq. (37) as

$$\oint \left(\frac{\partial p}{\partial E} \frac{\overline{dE}}{dt} + \frac{\partial p}{\partial \lambda} \frac{d\lambda}{dt} \right) dq = 0. \quad (10.38)$$

Now let us consider the following integral over the same phase-plane contour,

$$J \equiv \frac{1}{2\pi} \oint pdq, \quad (10.39)$$

Action variable called the *action variable*. Just to understand its physical sense, let us calculate J for a harmonic oscillator (14). As we know very well from Chapter 5, for such an oscillator, $q = A\cos\Psi$, $p = -m_{\text{ef}}\omega_0 A\sin\Psi$ (with $\Psi = \omega_0 t + \text{const}$), so that J may be easily expressed either via the oscillations' amplitude A , or via their energy $E = H = m_{\text{ef}}\omega_0^2 A^2/2$:

$$J = \frac{1}{2\pi} \oint pdq = \frac{1}{2\pi} \int_{\Psi=0}^{\Psi=2\pi} (-m_{\text{ef}}\omega_0 A\sin\Psi) d(A\cos\Psi) = \frac{m_{\text{ef}}\omega_0}{2} A^2 = \frac{E}{\omega_0}. \quad (10.40)$$

¹² Because of the implied nature of this conjecture (which is very close to the assumptions made at the derivation of the reduced equations in Sec. 5.3), new, more strict (but also much more cumbersome) proofs of the final Eq. (42) are still being offered in literature – see, e.g., C. Wells and S. Siklos, *Eur. J. Phys.* **28**, 105 (2007) and/or A. Lobo *et al.*, *Eur. J. Phys.* **33**, 1063 (2012).

Returning to a general system with adiabatically changed parameter λ , let us use the definition of J , Eq. (39), to calculate its time derivative, again taking into account that at each point q of the trajectory, p is a function of E and λ :

$$\frac{dJ}{dt} = \frac{1}{2\pi} \oint \frac{dp}{dt} dq = \frac{1}{2\pi} \oint \left(\frac{\partial p}{\partial E} \frac{dE}{dt} + \frac{\partial p}{\partial \lambda} \frac{d\lambda}{dt} \right) dq . \quad (10.41)$$

Within the accuracy of our approximation, in which the contour integrals (38) and (41) are calculated along a closed trajectory, the factor dE/dt is indistinguishable from its time average, and these integrals coincide so that the result (38) is applicable to Eq. (41) as well. Hence, we have finally arrived at a very important result: at a slow parameter variation, $dJ/dt = 0$, i.e. the action variable remains constant:

$$J = \text{const} . \quad (10.42)$$

Adiabatic invariance

This is the famous *adiabatic invariance*.¹³ In particular, according to Eq. (40), in a harmonic oscillator, the energy of oscillations changes proportionately to its own (slowly changed) frequency.

Before moving on, let me briefly note that the adiabatic invariance is not the only application of the action variable J . Since the initial choice of generalized coordinates and velocities (and hence the generalized momenta) in analytical mechanics is arbitrary (see Sec. 2.1), it is almost evident that J may be taken for a new generalized momentum corresponding to a certain new generalized coordinate Θ ,¹⁴ and that the pair $\{J, \Theta\}$ should satisfy the Hamilton equations (7), in particular,

$$\frac{d\Theta}{dt} = \frac{\partial H}{\partial J} . \quad (10.43)$$

Following the commitment of Sec. 1 (made there for the “old” arguments q_j, p_j), before the differentiation on the right-hand side of Eq. (43), H should be expressed as a function (besides t) of the “new” arguments J and Θ . For time-independent Hamiltonian systems, H is uniquely defined by J – see, e.g., Eq. (40). Hence in this case the right-hand side of Eq. (43) does not depend on either t or Θ , so according to that equation, Θ (called the *angle variable*) is a linear function of time:

$$\Theta = \frac{\partial H}{\partial J} t + \text{const} . \quad (10.44)$$

For a harmonic oscillator, according to Eq. (40), the derivative $\partial H / \partial J = \partial E / \partial J$ is just $\omega_0 \equiv 2\pi/\mathcal{T}$, so that $\Theta = \omega_0 t + \text{const}$, i.e. it is just the full phase Ψ that was repeatedly used in this course – especially in Chapter 5. It may be shown that a more general form of this relation,

$$\frac{\partial H}{\partial J} = \frac{2\pi}{\mathcal{T}} , \quad (10.45)$$

¹³ For certain particular oscillators, e.g., a point pendulum, Eq. (42) may be also proved directly – an exercise highly recommended to the reader.

¹⁴ This, again, is a plausible argument but not a strict proof. Indeed: though, according to its definition (39), J is nothing more than a sum of several (formally, the infinite number of) values of the momentum p , they are not independent, but have to be selected on the same closed trajectory on the phase plane. For more mathematical vigor, the reader is referred to Sec. 45 of *Mechanics* by Landau and Lifshitz (which was repeatedly cited above), which discusses the general rules of the so-called *canonical transformations* from one set of Hamiltonian arguments to another one – say from $\{p, q\}$ to $\{J, \Theta\}$.

is valid for an arbitrary system described by Eq. (10). Thus, Eq. (44) becomes

$$\Theta = 2\pi \frac{t}{T} + \text{const.} \quad (10.46)$$

This means that for an arbitrary (nonlinear) 1D oscillator, the angle variable Θ is a convenient generalization of the full phase Ψ . Due to this reason, the variables J and Θ present a convenient tool for discussion of certain fine points of the dynamics of strongly nonlinear oscillators – for whose discussion I, unfortunately, do not have time/space.¹⁵

10.3. The Hamilton principle

Now let me show that the Lagrange equations of motion, that were derived in Sec. 2.1 from the Newton laws, may be also obtained from the so-called *Hamilton principle*,¹⁶ namely the condition of a minimum (or rather an extremum) of the following integral called *action*:

Action

$$S \equiv \int_{t_{\text{ini}}}^{t_{\text{fin}}} L dt, \quad (10.47)$$

where t_{ini} and t_{fin} are, respectively, the initial and final moments of time, at which all generalized coordinates and velocities are considered fixed (not varied) – see Fig. 2.

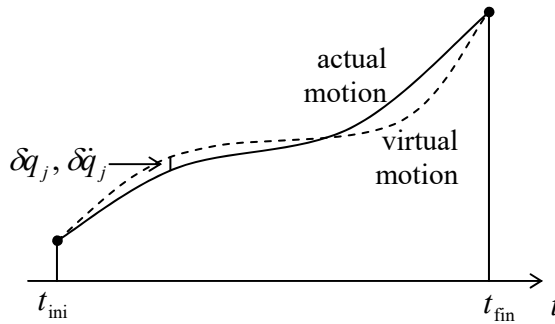


Fig. 10.2. Deriving the Hamilton principle.

The proof of that statement is rather simple. Considering, similarly to Sec. 2.1, a possible virtual variation of the motion, described by infinitesimal deviations $\{\delta q_j(t), \delta \dot{q}_j(t)\}$ from the real motion, the necessary condition for S to be minimal is

Hamilton principle

$$\delta S \equiv \int_{t_{\text{ini}}}^{t_{\text{fin}}} \delta L dt = 0, \quad (10.48)$$

where δS and δL are the variations of the action and the Lagrange function, corresponding to the set $\{\delta q_j(t), \delta \dot{q}_j(t)\}$. As has been already discussed in Sec. 2.1, we can use the operation of variation just

¹⁵ An interested reader may be referred, for example, to Chapter 6 in J. Jose and E. Saletan, *Classical Dynamics*, Cambridge U. Press, 1998.

¹⁶ It is also called the “principle of least action”. (This name may be fairer in the context of a long history of the development of the principle, starting from its simpler particular forms, which includes the names of P. de Fermat, P. Maupertuis, L. Euler, and J.-L. Lagrange.)

as the usual differentiation (but at a fixed time, see Fig. 2), swapping these two operations if needed – see Fig. 2.3 and its discussion. Thus, we may write

$$\delta L = \sum_j \left(\frac{\partial L}{\partial q_j} \delta q_j + \frac{\partial L}{\partial \dot{q}_j} \delta \dot{q}_j \right) = \sum_j \frac{\partial L}{\partial q_j} \delta q_j + \sum_j \frac{\partial L}{\partial \dot{q}_j} \frac{d}{dt} \delta q_j. \quad (10.49)$$

After plugging the last expression into Eq. (48), we can integrate the second term by parts:

$$\begin{aligned} \delta S &= \int_{t_{\text{ini}}}^{t_{\text{fin}}} \sum_j \frac{\partial L}{\partial q_j} \delta q_j dt + \sum_j \int_{t_{\text{ini}}}^{t_{\text{fin}}} \frac{\partial L}{\partial \dot{q}_j} \frac{d}{dt} \delta q_j dt \\ &= \int_{t_{\text{ini}}}^{t_{\text{fin}}} \sum_j \frac{\partial L}{\partial q_j} \delta q_j dt + \sum_j \left[\frac{\partial L}{\partial \dot{q}_j} \delta q_j \right]_{t_{\text{ini}}}^{t_{\text{fin}}} - \sum_j \int_{t_{\text{ini}}}^{t_{\text{fin}}} \delta q_j d \left(\frac{\partial L}{\partial \dot{q}_j} \right) = 0. \end{aligned} \quad (10.50)$$

Since the generalized coordinates in the initial and final points are considered fixed (not affected by the variation), all $\delta q_j(t_{\text{ini}})$ and $\delta q_j(t_{\text{fin}})$ vanish, so that the second term in the last form of Eq. (50) vanishes as well. Now multiplying and dividing the last term of that expression by dt , we finally get

$$\delta S = \int_{t_{\text{ini}}}^{t_{\text{fin}}} \sum_j \frac{\partial L}{\partial q_j} \delta q_j dt - \sum_j \int_{t_{\text{ini}}}^{t_{\text{fin}}} \delta q_j \frac{d}{dt} \left(\frac{\partial L}{\partial \dot{q}_j} \right) dt = - \int_{t_{\text{ini}}}^{t_{\text{fin}}} \sum_j \left[\frac{d}{dt} \left(\frac{\partial L}{\partial \dot{q}_j} \right) - \frac{\partial L}{\partial q_j} \right] \delta q_j dt = 0. \quad (10.51)$$

This relation should hold for an arbitrary set of functions $\delta q_j(t)$, and for any time interval, and this is only possible if the expressions in the square brackets equal zero for all j , giving us the set of the Lagrange equations (2.19). So, the Hamilton principle indeed gives the Lagrange equations of motion.

It is fascinating to see how the Hamilton principle works for particular cases. As a very simple example, let us consider the usual 1D linear oscillator, with the Lagrangian function used so many times before in this course:

$$L = \frac{m}{2} \dot{q}^2 - \frac{m\omega_0^2}{2} q^2. \quad (10.52)$$

As we know very well, the Lagrange equations of motion for this L are exactly satisfied by any sinusoidal function with the frequency ω_0 , in particular by a symmetric function of time

$$q_e(t) = A \cos \omega_0 t, \quad \text{so that } \dot{q}_e(t) = -A \omega_0 \sin \omega_0 t. \quad (10.53)$$

On a limited time interval, say $0 \leq \omega_0 t \leq +\pi/2$, this function is rather smooth and may be well approximated by another simple, reasonably selected functions of time, for example

$$q_a(t) = A(1 - \lambda t^2), \quad \text{so that } \dot{q}_a(t) = -2A\lambda t, \quad (10.54)$$

provided that the parameter λ is also selected reasonably. Let us take $\lambda = (\pi/2\omega_0)^2$, so that the approximate function $q_a(t)$ coincides with the exact function $q_e(t)$ at both ends of our time interval (Fig.3):

$$q_a(t_{\text{ini}}) = q_e(t_{\text{ini}}) = A, \quad q_a(t_{\text{fin}}) = q_e(t_{\text{fin}}) = 0, \quad \text{where } t_{\text{ini}} \equiv 0, \quad t_{\text{fin}} \equiv \frac{\pi}{2\omega_0}, \quad (10.55)$$

and check which of them the Hamilton principle “prefers”, i.e. which function gives the least action.

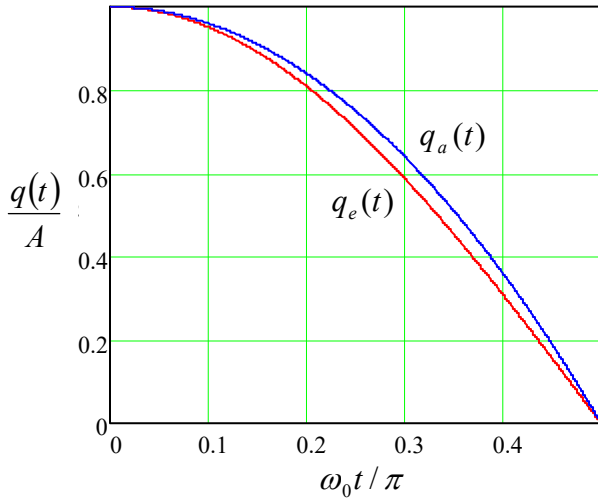


Fig. 10.3. Plots of the functions $q(t)$ given by Eqs. (53) and (54).

An elementary calculation of the action (47) corresponding to these two functions, yields

$$S_e = \left(\frac{\pi}{8} - \frac{\pi}{8} \right) m\omega_0 A^2 = 0, \quad S_a = \left(\frac{4}{3\pi} - \frac{2\pi}{15} \right) m\omega_0 A^2 \approx (0.4244 - 0.4189)m\omega_0 A^2 > 0, \quad (10.56)$$

with the first terms in all the parentheses coming from the time integrals of the kinetic energy, and the second terms, from those of the potential energy.

This result shows, first, that the exact function of time, for which these two contributions *exactly* cancel,¹⁷ is indeed “preferable” for minimizing the action. Second, for the approximate function, the two contributions to the action are rather close to the exact ones, and hence *almost* cancel each other, signaling that this approximation is very reasonable. It is evident that in some cases when the exact analytical solution of the equations of motion cannot be found, the minimization of S by adjusting one or more free parameters, incorporated into a guessed “trial” function, may be used to find a reasonable approximation for the actual law of motion.¹⁸

It is also very useful to make the notion of action S , defined by Eq. (47), more transparent by calculating it for the simple case of a single particle moving in a potential field that conserves its energy $E = T + U$. In this case, the Lagrangian function $L = T - U$ may be represented as

$$L = T - U = 2T - (T + U) = 2T - E = mv^2 - E, \quad (10.57)$$

with a time-independent E , so that

$$S = \int L dt = \int mv^2 dt - Et + \text{const.} \quad (10.58)$$

Recasting the expression under the remaining integral as $mv \cdot \mathbf{v} dt = \mathbf{p} \cdot (d\mathbf{r}/dt) dt = \mathbf{p} \cdot d\mathbf{r}$, we finally get

$$S = \int \mathbf{p} \cdot d\mathbf{r} - Et + \text{const} = S_0 - Et + \text{const}, \quad (10.59)$$

¹⁷ Such cancellation, i.e. the equality $S = 0$, is of course not the general requirement; it is specific only for this particular example, with a specific choice of the arbitrary constant in the potential energy of the system.

¹⁸ This is essentially a classical analog of the variational method of quantum mechanics – see, e.g., QM Sec. 2.9.

where the time-independent integral

$$S_0 \equiv \int \mathbf{p} \cdot d\mathbf{r} \quad (10.60)$$

is frequently called the *abbreviated action*.¹⁹

This expression may be used to establish one more important connection between the classical and quantum mechanics – now in its Schrödinger picture. Indeed, in the quasiclassical (WKB) approximation of that picture²⁰ a particle of fixed energy E is described by a de Broglie wave

$$\Psi(\mathbf{r}, t) \propto \exp\left\{i\left(\int \mathbf{k} \cdot d\mathbf{r} - \omega t + \text{const}\right)\right\}, \quad (10.61)$$

where the wave vector \mathbf{k} is proportional to the particle's momentum (which is possibly a slow function of \mathbf{r}) and the frequency ω , to its energy:

$$\mathbf{k} = \frac{\mathbf{p}}{\hbar}, \quad \omega = \frac{E}{\hbar}. \quad (10.62)$$

Plugging these expressions into Eq. (61) and comparing the result with Eq. (59), we see that the WKB wavefunction may be represented as

$$\Psi \propto \exp\{iS/\hbar\}. \quad (10.63)$$

Hence the Hamilton principle (48) means that the total phase of the quasiclassical wavefunction should be minimal along the particle's real trajectory. But this is exactly the so-called *eikonal minimum principle* well known from the optics (though it is valid for any other waves as well), where it serves to define the ray paths in the geometric optics limit – similar to the WKB approximation. Thus, the ratio S/\hbar may be considered just as the eikonal, i.e. the total phase accumulation, of the de Broglie waves.²¹

Now, comparing Eq. (60) with Eq. (39), we see that the action variable J is just the change of the abbreviated action S_0 along a single phase-plane contour, divided by 2π . This means, in particular, that in the WKB approximation, J is the number of de Broglie waves along the classical trajectory of a particle, i.e. an integer value of the corresponding quantum number. If the system's parameters are changed slowly, the quantum number has to stay integer, and hence J cannot change, giving a quantum-mechanical interpretation of the adiabatic invariance. The reader should agree that this is really fascinating: a fact of classical mechanics may be “derived” (or at least understood) more easily from the quantum mechanics' standpoint. (As a reminder, we have run into a similarly pleasant surprise at our discussion of the non-degenerate parametric excitation in Sec. 6.7.)

¹⁹ Comparing Eq. (59) with the Hamilton principle (48), we see that if the variational trajectories are limited to those of only one (actual) energy E , the real motion corresponds to the minimum of not only S but S_0 as well. This fact is called the *Maupertuis principle*. (Historically, this result rather than Eq. (48), was called the “principle of least action”, and some authors still use this terminology, so the reader's caution is advised.)

²⁰ See, e.g., QM Sec. 3.1.

²¹ Indeed, Eq. (63) was the starting point for R. Feynman's development of his path-integral formulation of quantum mechanics – see, e.g., QM Sec. 5.3.

10.4. The Hamilton-Jacobi equation

The action S , defined by Eq. (47), may be used for one more analytical formulation of classical mechanics. For that, we need to make one more, different commitment: S has to be considered as a function of the following independent arguments: the final time point t_{fin} (which I will, for brevity, denote as t in this section), and the set of generalized coordinates (but not of the generalized velocities!) at that point:

Hamilton-Jacobi action

$$S \equiv \int_{t_{\text{ini}}}^t L dt = S[t, q_j(t)]. \quad (10.64)$$

Let us calculate the variation of this (from the variational point of view, new!) function, resulting from an arbitrary combination of variations of the final values $q_j(t)$ of the coordinates while keeping t fixed. Formally this may be done by repeating the variational calculations described by Eqs. (49)-(51), besides that now the variations δq_j at the finite point (t) do not necessarily equal zero. As a result, we get

$$\delta S = \sum_j \frac{\partial L}{\partial \dot{q}_j} \delta q_j \Big|_t - \int_{t_{\text{ini}}}^t dt \sum_j \left[\frac{d}{dt} \left(\frac{\partial L}{\partial \dot{q}_j} \right) - \frac{\partial L}{\partial q_j} \right] \delta q_j. \quad (10.65)$$

For the motion along the real trajectory, i.e. satisfying the Lagrange equations (2.19), the second term of this expression equals zero. Hence Eq. (65) shows that, for (any) fixed time t ,

$$\frac{\partial S}{\partial q_j} = \frac{\partial L}{\partial \dot{q}_j}. \quad (10.66)$$

But the last derivative is nothing else than the generalized momentum p_j , so that

$$\frac{\partial S}{\partial q_j} = p_j. \quad (10.67)$$

(As a reminder, both parts of this relation refer to the final moment t of the trajectory.) As a result, the full derivative of the action $S[t, q_j(t)]$ over time takes the form

$$\frac{dS}{dt} = \frac{\partial S}{\partial t} + \sum_j \frac{\partial S}{\partial q_j} \dot{q}_j = \frac{\partial S}{\partial t} + \sum_j p_j \dot{q}_j. \quad (10.68)$$

Now, by the definition of S , the full derivative dS/dt is nothing more than the Lagrangian function L , so that Eq. (67) yields

$$\frac{\partial S}{\partial t} = L - \sum_j p_j \dot{q}_j. \quad (10.69)$$

However, according to the definition (2) of the Hamiltonian function H , the right-hand side of Eq. (69) is just $(-H)$, and we get an extremely simply-looking *Hamilton-Jacobi equation*

$$\frac{\partial S}{\partial t} = -H. \quad (10.70)$$

This simplicity is, however, rather deceiving, because to use this equation for the calculation of the function $S(t, q_j)$ for any particular problem, the Hamiltonian function has to be first expressed as a function of time t , generalized coordinates q_j , and the generalized momenta p_j (which may be, according

Hamilton-Jacobi equation

to Eq. (67), represented just as the derivatives $\partial S/\partial q_j$). Let us see how this procedure works for the simplest case of a 1D system with the Hamiltonian function given by Eq. (10). In this case, the only generalized momentum is $p = \partial S/\partial q$, so that

$$H = \frac{p^2}{2m_{\text{ef}}} + U_{\text{ef}}(q, t) = \frac{1}{2m_{\text{ef}}} \left(\frac{\partial S}{\partial q} \right)^2 + U_{\text{ef}}(q, t), \quad (10.71)$$

and Eq. (70) is reduced to the following partial differential equation,

$$\frac{\partial S}{\partial t} + \frac{1}{2m_{\text{ef}}} \left(\frac{\partial S}{\partial q} \right)^2 + U_{\text{ef}}(q, t) = 0. \quad (10.72)$$

Its solution may be readily found in the easiest case of time-independent potential energy $U_{\text{ef}} = U_{\text{ef}}(q)$. In this case, Eq. (72) is evidently satisfied by the following variable-separated solution:

$$S(t, q) = S_0(q) + \text{const} \times t. \quad (10.73)$$

Plugging this solution into Eq. (72), we see that since the sum of the two last terms on the left-hand side of that equation represents the full mechanical energy E , the constant in Eq. (73) is nothing but $(-E)$. Thus for the function $S_0(q)$ we get an ordinary differential equation

$$-E + \frac{1}{2m_{\text{ef}}} \left(\frac{dS_0}{dq} \right)^2 + U_{\text{ef}}(q) = 0. \quad (10.74)$$

Integrating it, we get

$$S_0 = \int \{2m_{\text{ef}}[E - U_{\text{ef}}(q)]\}^{1/2} dq + \text{const}, \quad (10.75)$$

so that, finally, the action is equal to

$$S = \int \{2m_{\text{ef}}[E - U_{\text{ef}}(q)]\}^{1/2} dq - Et + \text{const}. \quad (10.76)$$

For the case of 1D motion of a single 1D particle, i.e. for $q = x$, $m_{\text{ef}} = m$, $U_{\text{ef}}(q) = U(x)$, this solution is just the 1D case of the more general Eqs. (59)-(60), which were obtained above in a much more simple way. (In particular, S_0 is just the abbreviated action.)

This particular example illustrates that the Hamilton-Jacobi equation is not the most efficient way for the solution of most practical problems of classical mechanics. However, it may be rather useful for studies of certain mathematical aspects of dynamics.²² Moreover, in the early 1950s this approach was extended to a completely different field – the optimal control theory, in which the role of the action S is played by the so-called *cost function* – a certain functional of a system (understood in a very general sense of this term), that should be minimized by an optimal choice of a *control signal* – a function of time that affects the system’s evolution in time. From the point of view of this theory, Eq. (70) is a particular case of a more general *Hamilton-Jacobi-Bellman* equation.²³

²² See, e.g., Chapters 6-9 in I. C. Percival and D. Richards, *Introduction to Dynamics*, Cambridge U. Press, 1983.

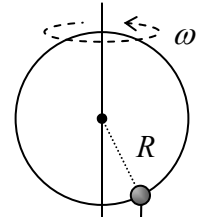
²³ See, e.g., T. Bertsekas, *Dynamic Programming and Optimal Control*, vols. 1 and 2, Aetna Scientific, 2005 and 2007. The reader should not be intimidated by the very unnatural term “dynamic programming”, which was invented by the founding father of this field, Richard Bellman, to lure government bureaucrats into funding his research, deemed too theoretical at that time. (Presently, it has a broad range of important applications.)

10.5. Exercise problems

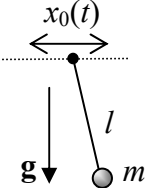
In each of Problems 10.1-10.3, for the given system:

- (i) derive the Hamilton equations of motion, and
- (ii) check whether these equations are equivalent to those derived from the Lagrangian formalism.

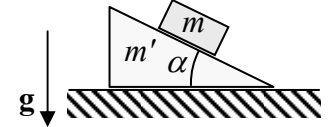
10.1. Our “testbed” system: a bead on a ring, being rotated with a fixed angular velocity ω about its vertical diameter – see Fig. 2.1, reproduced on the right.



10.2. The system considered in Problem 2.3: a pendulum hanging from a horizontal support whose motion law $x_0(t)$ is fixed – see the figure on the right. (No vertical-plane constraint.)



10.3. The system considered in Problem 2.8: a block of mass m that can slide, without friction, along the inclined surface of a heavy wedge of mass m' . The wedge is free to move, also without friction, along a horizontal surface – see the figure on the right. (Both motions are within the vertical plane containing the steepest slope line.)



10.4. Derive and solve the equations of motion of a particle with the following Hamiltonian function:

$$H = \frac{1}{2m}(\mathbf{p} + a\mathbf{r})^2,$$

where a is a constant scalar.

10.5. Let L be the Lagrangian function, and H the Hamiltonian function, of the same system. What three of the following four statements,

$$(i) \frac{dL}{dt} = 0, \quad (ii) \frac{\partial L}{\partial t} = 0, \quad (iii) \frac{dH}{dt} = 0, \quad (iv) \frac{\partial H}{\partial t} = 0,$$

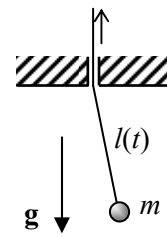
are equivalent? Give an example when those three equalities hold, but the fourth one does not.

10.6. Calculate the Poisson brackets of a Cartesian component of the angular momentum \mathbf{L} of a particle moving in a central force field and its Hamiltonian function H , and discuss the most evident implication of the result.

10.7. After small oscillations had been initiated in the point pendulum shown in Fig. on the right, the supporting string is being pulled up slowly, so that the pendulum's length l is being reduced. Neglecting dissipation,

(i) prove by a direct calculation that the oscillation energy is indeed changing proportionately to the oscillation frequency, as it follows from the constancy of the corresponding adiabatic invariant (40); and

(ii) find the l -dependence of the amplitudes of the angular and linear deviations from the equilibrium.



10.8. The mass m of a small body that performs 1D oscillations in the potential well $U(x) = ax^{2n}$, with $n > 0$, is being changed slowly. Calculate the oscillation energy E as a function of m .

10.9. A stiff ball is bouncing vertically from the floor of an elevator whose upward acceleration changes very slowly. Neglecting the energy dissipation, calculate how much the bounce height h changes during the acceleration's increase from 0 to g . Is your result valid for an equal but abrupt increase of the elevator's acceleration?

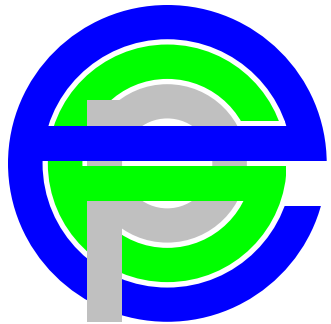
10.10.* A 1D particle of a constant mass m moves in a time-dependent potential $U(q, t) = m\omega^2(t)q^2/2$, where $\omega(t)$ is a slow function of time, with $|\dot{\omega}| \ll \omega^2$. Develop the approximate method for the solution of the corresponding equation of motion, similar to the WKB approximation used in quantum mechanics.²⁴ Use the approximation to confirm the conservation of the action variable (40) for this system.

Hint: You may like to look for the solution to the equation of motion in the form

$$q(t) = \exp\{\Lambda(t) + i\Psi(t)\},$$

where Λ and Ψ are some real functions of time, and then make proper approximations in the resulting equations for these functions.

²⁴ See, e.g., QM Sec. 2.4.



Konstantin K. Likharev
Essential Graduate Physics
Lecture Notes and Problems

Beta version

Open online access at
<http://commons.library.stonybrook.edu/egp/>
and
<https://sites.google.com/site/likharevegp/>

Part EM:

Classical Electrodynamics

Last corrections: September 30, 2022

A version of this material was published in 2018 under the title

Classical Electrodynamics: Lecture notes
IOPP, Essential Advanced Physics – Volume 3, ISBN 978-0-7503-1405-3,
with the model solutions of the exercise problems published under the title
Classical Electrodynamics: Problems with solutions
IOPP, Essential Advanced Physics – Volume 4, ISBN 978-0-7503-1408-4

However, by now this online version of the lecture notes
and the problem solutions available from the author, have been better corrected

About the author:

<https://you.stonybrook.edu/likharev/>

Table of Contents

Chapter 1. Electric Charge Interaction (20 pp.)

- 1.1. The Coulomb law
- 1.2. The Gauss law
- 1.3. Scalar potential and electric field energy
- 1.4. Exercise problems (20)

Chapter 2. Charges and Conductors (68 pp.)

- 2.1. Polarization and screening
- 2.2. Capacitance
- 2.3. The simplest boundary problems
- 2.4. Using other orthogonal coordinates
- 2.5. Variable separation – Cartesian coordinates
- 2.6. Variable separation – polar coordinates
- 2.7. Variable separation – cylindrical coordinates
- 2.8. Variable separation – spherical coordinates
- 2.9. Charge images
- 2.10. Green's functions
- 2.11. Numerical approach
- 2.12. Exercise problems (47)

Chapter 3. Dipoles and Dielectrics (28 pp.)

- 3.1. Electric dipole
- 3.2. Dipole media
- 3.3. Polarization of dielectrics
- 3.4. Electrostatics of linear dielectrics
- 3.5. Electric field energy in a dielectric
- 3.6. Exercise problems (30)

Chapter 4. DC Currents (16 pp.)

- 4.1. Continuity equation and the Kirchhoff laws
- 4.2. The Ohm law
- 4.3. Boundary problems
- 4.4. Energy dissipation
- 4.5. Exercise problems (15)

Chapter 5. Magnetism (42 pp.)

- 5.1. Magnetic interaction of currents
- 5.2. Vector potential and the Ampère law
- 5.3. Magnetic flux, energy, and inductance
- 5.4. Magnetic dipole moment, and magnetic dipole media
- 5.5. Magnetic materials
- 5.6. Systems with magnetic materials
- 5.7. Exercise problems (29)

Chapter 6. Electromagnetism (38 pp.)

- 6.1. Electromagnetic induction
- 6.2. Magnetic energy revisited
- 6.3. Quasistatic approximation, and the skin effect
- 6.4. Electrodynamics of superconductivity, and the gauge invariance
- 6.5. Electrodynamics of macroscopic quantum phenomena
- 6.6. Inductors, transformers, and ac Kirchhoff laws
- 6.7. Displacement currents
- 6.8. Finally, the full Maxwell equation system
- 6.9. Exercise problems (30)

Chapter 7. Electromagnetic Wave Propagation (68 pp.)

- 7.1. Plane waves
- 7.2. Attenuation and dispersion
- 7.3. Reflection
- 7.4. Refraction
- 7.5. Transmission lines: TEM waves
- 7.6. Waveguides: H and E waves
- 7.7. Dielectric waveguides, optical fibers, and paraxial beams
- 7.8. Resonance cavities
- 7.9. Energy loss effects
- 7.10. Exercise problems (39)

Chapter 8. Radiation, Scattering, Interference, and Diffraction (38 pp.)

- 8.1. Retarded potentials
- 8.2. Electric dipole radiation
- 8.3. Wave scattering
- 8.4. Interference and diffraction
- 8.5. The Huygens principle
- 8.6. Fresnel and Fraunhofer diffraction patterns
- 8.7. Geometrical optics placeholder
- 8.8. Fraunhofer diffraction from more complex scatterers
- 8.9. Magnetic dipole and electric quadrupole radiation
- 8.10. Exercise problems (28)

Chapter 9. Special Relativity (56 pp.)

- 9.1. Einstein postulates and the Lorentz transform
- 9.2. Relativistic kinematic effects
- 9.3. 4-vectors, momentum, mass, and energy
- 9.4. More on 4-vectors and 4-tensors
- 9.5. The Maxwell equations in the 4-form
- 9.6. Relativistic particles in electric and magnetic fields
- 9.7. Analytical mechanics of charged particles
- 9.8. Analytical mechanics of electromagnetic field
- 9.9. Exercise problems (42)

Chapter 10. Radiation by Relativistic Charges (40 pp.)

- 10.1. Liénard-Wiechert potentials
- 10.2. Radiation power
- 10.3. Synchrotron radiation
- 10.4. Bremsstrahlung
- 10.5. Coulomb losses
- 10.6. Density effects and the Cherenkov radiation
- 10.7. Radiation's back-action
- 10.8. Exercise problems (15)

* * *

Additional file (available from the author upon request):

Exercise and Test Problems with Model Solutions (295 + 54 = 349 problems; 464 pp.)

Chapter 1. Electric Charge Interaction

This chapter reviews the basics of electrostatics – the description of interactions between stationary (or relatively slowly moving) electric charges. Much of this material should be known to the reader from their undergraduate studies;¹ because of that, the explanations are very brief.

1.1. The Coulomb law

A quantitative discussion of classical electrodynamics, starting from the electrostatics, requires common agreement on the meaning of the following notions:²

- *electric charges* q_k , as revealed, most explicitly, by observation of *electrostatic interaction* between the charged particles;
- *point charges* – the charged particles so small that their position in space, for the given problem, may be completely described (in the given reference frame) by their radius-vectors \mathbf{r}_k ; and
- *electric charge conservation* – the fact that the algebraic sum of all charges q_k inside any closed volume is conserved unless the charged particles cross the volume's border.

I will assume that these notions are well known to the reader. Using them, the *Coulomb law*³ for the interaction of two stationary point charges may be formulated as follows:

$$\mathbf{F}_{kk'} = \kappa q_k q_{k'} \frac{\mathbf{r}_k - \mathbf{r}_{k'}}{|\mathbf{r}_k - \mathbf{r}_{k'}|^3} \equiv \kappa \frac{q_k q_{k'}}{R_{kk'}^2} \mathbf{n}_{kk'},$$

with $\mathbf{R}_{kk'} \equiv \mathbf{r}_k - \mathbf{r}_{k'}$, $\mathbf{n}_{kk'} \equiv \frac{\mathbf{R}_{kk'}}{R_{kk'}}$, $R_{kk'} \equiv |\mathbf{R}_{kk'}|$,

Coulomb
law
(1.1)

where $\mathbf{F}_{kk'}$ denotes the electrostatic (*Coulomb*) force exerted on the charge number k by the charge number k' , separated from it by distance $R_{kk'}$ – see Fig. 1.

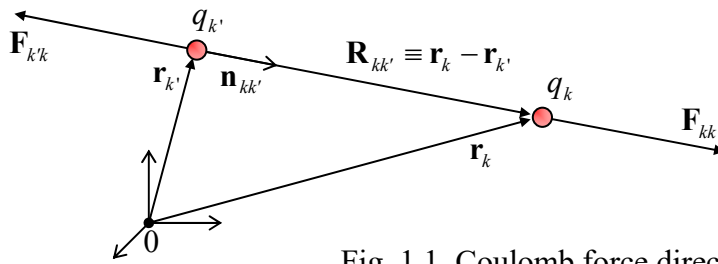


Fig. 1.1. Coulomb force directions (for the case $q_k q_{k'} > 0$).

¹ For remedial reading, I can recommend, for example, D. Griffiths, *Introduction to Electrodynamics*, 4th ed., Pearson, 2015.

² On top of the more general notions of the *classical Newtonian space*, *point particles* and *forces*, as used in classical mechanics – see, e.g., CM Sec. 1.1.

³ Formulated in 1785 by Charles-Augustin de Coulomb, on basis of his earlier experiments, in turn rooting in prior studies of electrostatic phenomena, with notable contributions by William Gilbert, Otto von Guericke, Charles François de Cisternay Du Fay, Benjamin Franklin, and Henry Cavendish.

I am confident that this law is very familiar to the reader, but a few comments may still be due:

(i) Flipping the indices k and k' , we see that Eq. (1) complies with the 3rd Newton law: the reciprocal force is equal in magnitude but opposite in direction: $\mathbf{F}_{k'k} = -\mathbf{F}_{kk'}$.

(ii) Since the vector $\mathbf{R}_{kk'} \equiv \mathbf{r}_k - \mathbf{r}_{k'}$, by its definition, is directed from point $\mathbf{r}_{k'}$ toward point \mathbf{r}_k (Fig. 1), Eq. (1) correctly describes the experimental fact that charges of the same sign (i.e. with $q_k q_{k'} > 0$) repulse, while those with opposite signs ($q_k q_{k'} < 0$) attract each other.

(iii) In some textbooks, the Coulomb law (1) is given with the qualifier “in free space” or “in vacuum”. However, actually, Eq. (1) remains valid even in the presence of any other charges – for example, of internal charges in a quasi-continuous medium that may surround the two charges (number k and k') under consideration. The confusion stems from the fact, to be discussed in detail in Chapter 3 below, that in some cases it is convenient to *formally* represent the effect of the other charges as an *effective* (rather than actual!) modification of the Coulomb law.

(iv) The constant κ in Eq. (1) depends on the system of units we use. In the *Gaussian* units, κ is set to 1, for the price of introducing a special unit of charge (the *statcoulomb*) that would make experimental data compatible with Eq. (1) if the force $\mathbf{F}_{kk'}$ is measured in the Gaussian units (*dynes*). On the other hand, in the *International System* (“SI”) of units, the charge’s unit is one *coulomb* (abbreviated C), and κ is different from 1:

$$\kappa|_{\text{SI}} = \frac{1}{4\pi\epsilon_0}, \quad (1.2) \quad \begin{matrix} \kappa \text{ in} \\ \text{SI units} \end{matrix}$$

where $\epsilon_0 \approx 8.854 \times 10^{-12}$ is called the *electric constant*.⁴

Unfortunately, the continuing struggle between zealous proponents of these two systems of units bears all not-so-nice features of a religious war, with a similarly slim chance for any side to win it in any foreseeable future. In my humble view, each of these systems has its advantages and handicaps (to be noted on several occasions below), and every educated physicist should have no problem with using any of them. Following insisting recommendations of international scientific unions, I am using the SI units throughout my series. However, for the readers’ convenience, in this course (where the difference between the Gaussian and SI systems is especially significant) I will write the most important formulas with the constant (2) clearly displayed – for example, Eq. (1) as

$$\mathbf{F}_{kk'} = \frac{1}{4\pi\epsilon_0} q_k q_{k'} \frac{\mathbf{r}_k - \mathbf{r}_{k'}}{|\mathbf{r}_k - \mathbf{r}_{k'}|^3}, \quad (1.3)$$

so that the transfer to the Gaussian units may be performed just by the formal replacement $4\pi\epsilon_0 \rightarrow 1$. (In the rare cases when the transfer is not obvious, I will duplicate formulas in the Gaussian units.)

Besides Eq. (3), another key experimental law of electrostatics is the *linear superposition principle*: the electrostatic forces exerted on some point charge (say, q_k) by other charges add up as vectors, forming the net force

⁴ Since 2018, one coulomb is defined, in the “legal” metrology, as a certain, exactly fixed number of the fundamental electric charges e , and the “legal” SI value of ϵ_0 is not more exactly equal to $10^7/4\pi c^2$ (where c is the speed of light) as it was before that, but remains extremely close to that fraction, with the relative difference of the order of 10^{-10} – see appendix *CA: Selected Physical Constants*. In this series, this minute difference is ignored.

$$\mathbf{F}_k = \sum_{k' \neq k} \mathbf{F}_{kk'}, \quad (1.4)$$

where the summation is extended over all charges but q_k , and the partial force $\mathbf{F}_{kk'}$ is described by Eq. (3). The fact that the sum is restricted to $k' \neq k$ means that a *point charge, in statics, does not interact with itself*. This fact may look obvious from Eq. (3), whose right-hand side diverges at $\mathbf{r}_k \rightarrow \mathbf{r}_{k'}$, but becomes less evident (though still true) in quantum mechanics – where the charge of even an elementary particle is effectively spread around some volume, together with the particle’s wavefunction.⁵

Now we may combine Eqs. (3) and (4) to get the following expression for the net force \mathbf{F} acting on a *probe charge* q located at point \mathbf{r} :

$$\mathbf{F}(\mathbf{r}) = q \frac{1}{4\pi\epsilon_0} \sum_{\mathbf{r}_k \neq \mathbf{r}} q_{k'} \frac{\mathbf{r} - \mathbf{r}_{k'}}{|\mathbf{r} - \mathbf{r}_{k'}|^3}. \quad (1.5)$$

This equality implies that it makes sense to introduce the notion of the *electric field* (as an entity independent of q), whose distribution in space is characterized by the following vector:

Electric field:
definition

$$\mathbf{E}(\mathbf{r}) \equiv \frac{\mathbf{F}(\mathbf{r})}{q}, \quad (1.6)$$

formally called the *electric field strength* – but much more frequently, just the “electric field”. In these terms, Eq. (5) becomes

Electric field of
point charges

$$\mathbf{E}(\mathbf{r}) = \frac{1}{4\pi\epsilon_0} \sum_{\mathbf{r}_k \neq \mathbf{r}} q_{k'} \frac{\mathbf{r} - \mathbf{r}_{k'}}{|\mathbf{r} - \mathbf{r}_{k'}|^3}. \quad (1.7)$$

Just convenient is electrostatics, the notion of the field becomes virtually unavoidable for the description of time-dependent phenomena (such as electromagnetic waves, see Chapter 7 and on), where the electromagnetic field shows up as a specific form of matter, different from the usual “material” particles – even though quantum electrodynamics (to be reviewed in QM Chapter 9) offers their joint description.

Many real-world problems involve multiple point charges located so closely that it is possible to approximate them with a continuous charge distribution. Indeed, let us consider a group of many ($dN \gg 1$) close charges, located at points $\mathbf{r}_{k'}$, all within an elementary volume $d^3 r'$. For relatively distant field observation points, with $|\mathbf{r} - \mathbf{r}_{k'}| \gg dr'$, the geometrical factor in the corresponding terms of Eq. (7) is essentially the same. As a result, these charges may be treated as a single elementary charge $dQ(\mathbf{r}')$. Since at $dN \gg 1$, this elementary charge is proportional to the elementary volume $d^3 r'$, we can define the local 3D *charge density* $\rho(\mathbf{r}')$ by the following relation:

$$\rho(\mathbf{r}') d^3 r' \equiv dQ(\mathbf{r}') \equiv \sum_{\mathbf{r}_{k'} \in d^3 r'} q_{k'}, \quad (1.8)$$

and rewrite Eq. (7) as an integral (over the volume containing all essential charges):

Electric field of
continuous
charge

$$\mathbf{E}(\mathbf{r}) = \frac{1}{4\pi\epsilon_0} \int \rho(\mathbf{r}') \frac{\mathbf{r} - \mathbf{r}'}{|\mathbf{r} - \mathbf{r}'|^3} d^3 r'. \quad (1.9)$$

⁵ Note that some widely used approximations, e.g., the density functional theory (DFT) of multiparticle systems, essentially violate this law, thus limiting their accuracy and applicability – see, e.g., QM Sec. 8.4.

Note that for a continuous, smooth charge density $\rho(\mathbf{r}')$, the integral in Eq. (9) does not diverge at $\mathbf{R} \equiv \mathbf{r} - \mathbf{r}' \rightarrow 0$, because in this limit, the fraction under the integral increases as R^{-2} , i.e. slower than the decrease of the elementary volume d^3r' , proportional to R^3 .

Let me emphasize the dual use of Eq. (9). In the case when $\rho(\mathbf{r})$ is a continuous function representing the average charge defined by Eq. (8), Eq. (9) is not valid at distances $|\mathbf{r} - \mathbf{r}_k'|$ of the order of the distance between the adjacent point charges, i.e. does not describe rapid variations of the electric field at these distances. Such *approximate*, smoothly changing field $\mathbf{E}(\mathbf{r})$, is called *macroscopic*; we will repeatedly return to this notion in the following chapters. On the other hand, Eq. (9) may be also used for the description of the *exact* (frequently called *microscopic*) field of discrete point charges, by employing the notion of Dirac's delta function, which is the mathematical description of a very sharp function equal to zero everywhere but one point, and still having a finite integral (equal to 1).⁶ Indeed, in this formalism, a set of point charges q_k located in points \mathbf{r}_k may be represented by the pseudo-continuous density

$$\rho(\mathbf{r}') = \sum_{k'} q_{k'} \delta(\mathbf{r}' - \mathbf{r}_{k'}). \quad (1.10)$$

Plugging this expression into Eq. (9), we return to its exact, discrete version (7). In this sense, Eq. (9) is exact, and we may use it as the general expression for the electric field.

1.2. The Gauss law

Due to the extension of Eq. (9) to point ("discrete") charges, it may seem that we do not need anything besides it for solving any problem of electrostatics. In practice, however, this is not quite true – first of all, because the direct use of Eq. (9) frequently leads to complex calculations. Indeed, let us try to solve a problem that is conceptually very simple: find the electric field induced by a spherically-symmetric charge distribution with density $\rho(r')$ – see Fig. 2.

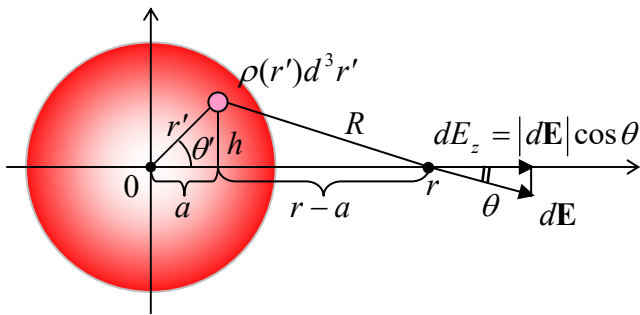


Fig. 1.2. One of the simplest problems of electrostatics: the electric field produced by a spherically-symmetric charge distribution.

We may immediately use the problem's symmetry to argue that the electric field should be also spherically-symmetric, with only one component in the spherical coordinates: $\mathbf{E}(\mathbf{r}) = E(r)\mathbf{n}_r$, where $\mathbf{n}_r \equiv \mathbf{r}/r$ is the unit vector in the direction of the field observation point \mathbf{r} . Taking this direction for the polar

⁶ See, e.g., MA Sec. 14. The 2D (*areal*) charge density σ and the 1D (*linear*) density λ may be defined absolutely similarly to the 3D (*volumic*) density ρ : $dQ = \sigma d^2r$, $dQ = \lambda dr$. Note that the approximations in that either $\sigma \neq 0$ or $\lambda \neq 0$ imply that ρ is formally infinite at the charge location; for example, the model in that a plane $z = 0$ is charged with areal density $\sigma \neq 0$, means that $\rho = \sigma \delta(z)$, where $\delta(z)$ is Dirac's delta function.

axis of a spherical coordinate system, we can use the evident axial symmetry of the system to reduce Eq. (9) to

$$E = \frac{1}{4\pi\epsilon_0} 2\pi \int_0^\pi \sin\theta' d\theta' \int_0^\infty r'^2 dr' \frac{\rho(r')}{R^2} \cos\theta, \quad (1.11)$$

where θ , θ' , and R are the geometrical parameters marked in Fig. 2. Since θ and R may be readily expressed via r' and θ' , using the auxiliary parameters a and h ,

$$\cos\theta = \frac{r-a}{R}, \quad R^2 = h^2 + (r - r'\cos\theta)^2, \quad \text{where } a \equiv r'\cos\theta', \quad h \equiv r'\sin\theta', \quad (1.12)$$

Eq. (11) may be eventually reduced to an explicit integral over r' and θ' , and worked out analytically, but that would require some effort.

For other problems, the integral (9) may be much more complicated, defying an analytical solution. One could argue that with the present-day abundance of computers and numerical algorithm libraries, one can always resort to numerical integration. This argument may be enhanced by the fact that numerical *integration* is based on the replacement of the required integral by a discrete sum, and the summation is much more robust to the (unavoidable) rounding errors than the finite-difference schemes typical for the numerical solution of *differential* equations. These arguments, however, are only partly justified, since in many cases the numerical approach runs into a problem sometimes called the *curse of dimensionality* – the exponential dependence of the number of needed calculations on the number of independent parameters of the problem.⁷ Thus, despite the proliferation of numerical methods in physics, analytical results have an everlasting value, and we should try to get them whenever we can. For our current problem of finding the electric field generated by a fixed set of electric charges, large help may come from the so-called *Gauss law*.

To derive it, let us consider a single point charge q inside a smooth closed surface S (Fig. 3), and calculate the product $E_n d^2r$, where d^2r is an elementary area of the surface (which may be well approximated with a plane fragment of that area), and $E_n \equiv \mathbf{E} \cdot \mathbf{n}$ is the component of the electric field at that point, normal to the plane.

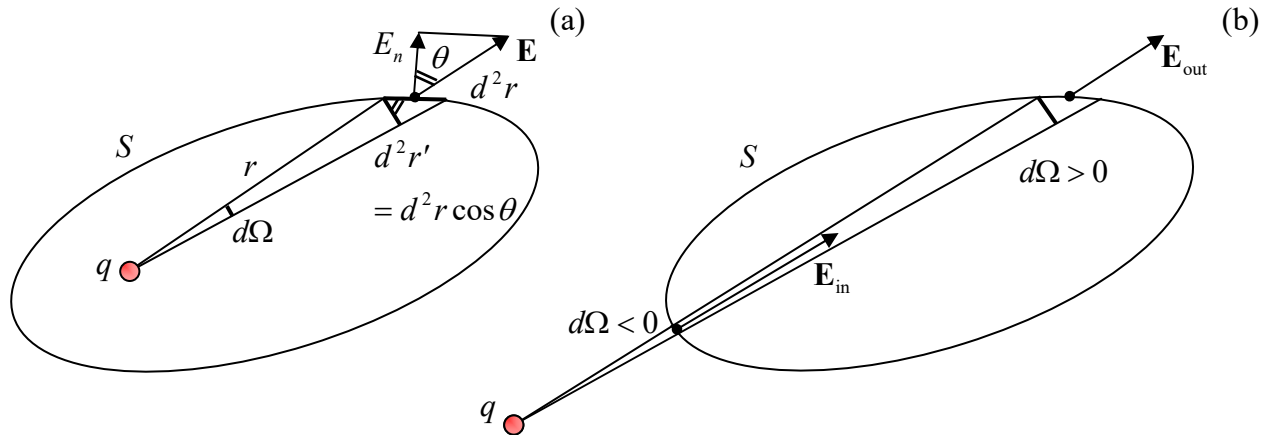


Fig. 1.3. Deriving the Gauss law: a point charge q (a) inside the volume V , and (b) outside of that volume.

⁷ For a more detailed discussion of this problem, see, e.g., CM Sec. 5.8.

This component may be calculated as $E \cos \theta$, where θ is the angle between the vector \mathbf{E} and the unit vector \mathbf{n} normal to the surface. Now let us notice that the product $\cos \theta d^2r$ is nothing more than the area d^2r' of the projection of d^2r onto the plane normal to the vector \mathbf{r} connecting the charge q with the considered point of the surface (Fig. 3), because the angle between the elementary areas d^2r' and d^2r is also equal to θ . Using the Coulomb law for \mathbf{E} , we get

$$E_n d^2r = E \cos \theta d^2r = \frac{1}{4\pi\epsilon_0} \frac{q}{r^2} d^2r'. \quad (1.13)$$

But the ratio d^2r'/r^2 is nothing more than the elementary solid angle $d\Omega$ under which the areas d^2r' and d^2r are seen from the charge point, so that $E_n d^2r$ may be represented just as a product of $d\Omega$ by a constant ($q/4\pi\epsilon_0$). Summing these products over the whole surface, we get

$$\oint_S E_n d^2r = \frac{q}{4\pi\epsilon_0} \oint_S d\Omega \equiv \frac{q}{\epsilon_0}, \quad (1.14)$$

since the full solid angle equals 4π . (The integral on the left-hand side of this relation is called the *flux of electric field through the surface S*.)

Relation (14) expresses the Gauss law for one point charge. However, it is only valid if the charge is located *inside* the volume V limited by the surface S . To find the flux created by a charge located *outside* of this volume, we still can use Eq. (13), but have to be careful with the signs of the elementary contributions $E_n dA$. Let us use the common convention to direct the unit vector \mathbf{n} out of the closed volume we are considering (the so-called *outer normal*), so that the elementary product $E_n d^2r = (\mathbf{E} \cdot \mathbf{n}) d^2r$ and hence $d\Omega = E_n d^2r'/r^2$ is positive if the vector \mathbf{E} is pointing out of the volume (like in the example shown in Fig. 3a and at the upper-right area in Fig. 3b), and negative in the opposite case (for example, at the lower-left area in Fig. 3b). As the latter panel shows, if the charge is located outside of the volume, for each positive contribution $d\Omega$ there is always an equal and opposite contribution to the integral. As a result, at the integration over the solid angle, the positive and negative contributions cancel exactly, so that

$$\oint_S E_n d^2r = 0. \quad (1.15)$$

The real power of the Gauss law is revealed by its generalization to the case of several, especially many charges. Since the calculation of flux is a linear operation, the linear superposition principle (4) means that the flux created by several charges is equal to the (algebraic) sum of individual fluxes from each charge, for which either Eq. (14) or Eq. (15) are valid, depending on whether the charge is in or out of the volume. As the result, for the total flux we get:

$$\oint_S E_n d^2r = \frac{Q_V}{\epsilon_0} \equiv \frac{1}{\epsilon_0} \sum_{\mathbf{r}_j \in V} q_j \equiv \frac{1}{\epsilon_0} \int_V \rho(\mathbf{r}') d^3r', \quad (1.16)$$

Gauss law

where Q_V is the net charge inside volume V . This is the full version of the Gauss law.⁸

In order to appreciate the problem-solving power of the law, let us revisit the problem shown in Fig. 2, i.e. the field of a spherical charge distribution. Due to its symmetry, which had already been

⁸ The law is named after the famed Carl Gauss (1777-1855), even though it was first formulated earlier (in 1773) by Joseph-Louis Lagrange who was also the father-founder of analytical mechanics – see, e.g., CM Chapter 2.

discussed above, if we apply Eq. (16) to a sphere of a certain radius r , the electric field has to be normal to the sphere at each its point (i.e., $E_n = E$), and its magnitude has to be the same at all points: $E_n = E(r)$. As a result, the flux calculation is elementary:

$$\oint E_n d^2r = 4\pi r^2 E(r). \quad (1.17)$$

Now applying the Gauss law (16), we get:

$$4\pi r^2 E(r) = \frac{1}{\epsilon_0} \int_{r'<r} \rho(r') d^3r' = \frac{4\pi}{\epsilon_0} \int_0^r r'^2 \rho(r') dr', \quad (1.18)$$

so that, finally,

$$E(r) = \frac{1}{r^2 \epsilon_0} \int_0^r r'^2 \rho(r') dr' \equiv \frac{1}{4\pi \epsilon_0} \frac{Q_r}{r^2}, \quad (1.19)$$

where Q_r is the full charge inside the sphere of radius r :

$$Q_r \equiv \int_{r'<r} \rho(r') d^3r' = 4\pi \int_0^r \rho(r') r'^2 dr'. \quad (1.20)$$

In particular, this formula shows that the field *outside* of a sphere of a finite radius R is exactly the same as if all its charge $Q = Q(R)$ is concentrated in the sphere's center. (Note that this important result is only valid for a spherically-symmetric charge distribution.) For the field *inside* the sphere, finding the electric field still requires the explicit integration (20), but this 1D integral is much simpler than the 2D integral (11), and in some important cases may be readily worked out analytically. For example, if the charge Q is uniformly distributed inside a sphere of radius R ,

$$\rho(r') = \rho = \frac{Q}{V} = \frac{Q}{(4\pi/3)R^3}, \quad (1.21)$$

then the integration is elementary:

$$E(r) = \frac{\rho}{r^2 \epsilon_0} \int_0^r r'^2 dr' = \frac{\rho r}{3\epsilon_0} = \frac{1}{4\pi \epsilon_0} \frac{Qr}{R^3}. \quad (1.22)$$

We see that in this case, the field is growing linearly from the center to the sphere's surface, and only at $r > R$ starts to decrease in agreement with Eq. (19) with constant $Q(r) = Q$. Note also that the electric field is continuous for all r (including $r = R$) – as for all systems with finite volumic density,

In order to underline the importance of the last condition, let us consider one more elementary but very important example of Gauss law's application. Let a thin plane sheet (Fig. 4) be charged uniformly, with a finite *areal* density $\sigma = \text{const}$. In this case, it is fruitful to use the Gauss volume in the form of a planar “pillbox” of thickness $2z$ (where z is the Cartesian coordinate perpendicular to the plane) and certain area A – see the dashed lines in Fig. 4. Due to the symmetry of the problem, it is evident that the electric field should be: (i) directed along the z -axis, (ii) constant on each of the upper and bottom sides of the pillbox, (iii) equal and opposite on these sides, and (iv) parallel to the side surfaces of the box. As a result, the full electric field flux through the pillbox's surface is just $2AE(z)$, so the Gauss law (16) yields $2AE(z) = Q_A/\epsilon_0 \equiv \sigma A/\epsilon_0$, and we get a very simple but important formula

$$E(z) = \frac{\sigma}{2\epsilon_0} = \text{const.} \quad (1.23)$$

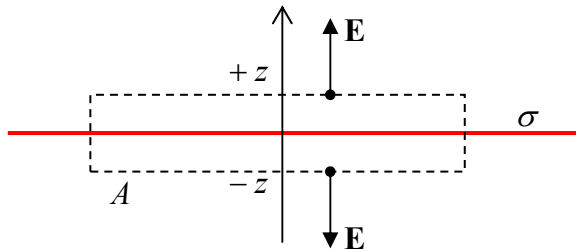


Fig. 1.4. The electric field of a charged plane.

Notice that, somewhat counter-intuitively, the field magnitude does not depend on the distance from the charged plane. From the point of view of the Coulomb law (5), this result may be explained as follows: the farther the observation point from the plane, the weaker the effect of each elementary charge, $dQ = \sigma d^2 r$, but the more such elementary charges give contributions to the z -component of vector \mathbf{E} , because they are “seen” from the observation point at relatively small angles to the z -axis.

Note also that though the magnitude $E \equiv |\mathbf{E}|$ of this electric field is constant, its component E_n normal to the plane (for our coordinate choice, E_z) changes its sign at the plane, experiencing a *discontinuity* (jump) equal to

$$\Delta E_z \equiv E_z(z=+0) - E_z(z=-0) = \frac{\sigma}{\epsilon_0}. \quad (1.24)$$

This jump disappears if the surface is not charged. Returning for a split second to our charged sphere problem (Fig. 2), solving it we have considered the volumic charge density ρ to be finite everywhere, including the sphere’s surface, so that on it $\sigma = 0$, and the electric field should be continuous – as it is.

Admittedly, the *integral form* (16) of the Gauss law is immediately useful only for highly symmetrical geometries, such as in the two problems discussed above. However, it may be recast into an alternative, *differential form* whose field of useful applications is much wider. This form may be obtained from Eq. (16) using the *divergence theorem* of the vector algebra, which is valid for any space-differentiable vector, in particular \mathbf{E} , and for the volume V limited by any closed surface S :⁹

$$\oint_S E_n d^2 r = \int_V (\nabla \cdot \mathbf{E}) d^3 r, \quad (1.25)$$

where ∇ is the *del* (or “nabla”) operator of spatial differentiation.¹⁰ Combining Eq. (25) with the Gauss law (16), we get

$$\int_V \left(\nabla \cdot \mathbf{E} - \frac{\rho}{\epsilon_0} \right) d^3 r = 0. \quad (1.26)$$

For a given spatial distribution of electric charge (and hence of its electric field), this equation should be valid for any choice of the volume V . This can hold only if the function under the integral vanishes at each point, i.e. if¹¹

⁹ See, e.g., MA Eq. (12.2). Note also that the scalar product under the volumic integral in Eq. (25) is nothing else than the divergence of the vector \mathbf{E} – see, e.g., MA Eq. (8.4), hence the theorem’s name.

¹⁰ See, e.g., MA Secs. 8-10.

¹¹ In the Gaussian units, just as in the initial Eq. (6), ϵ_0 has to be replaced with $1/4\pi$, so that the Maxwell equation (27) looks like $\nabla \cdot \mathbf{E} = 4\pi\rho$, while Eq. (28) stays the same.

Inhomogeneous Maxwell equation for \mathbf{E}

$$\nabla \cdot \mathbf{E} = \frac{\rho}{\epsilon_0}. \quad (1.27)$$

Note that in sharp contrast with the integral form (16), Eq. (27) is *local*: it relates the electric field's divergence to the charge density *at the same point*. This equation, being the differential form of the Gauss law, is frequently called one of the famed *Maxwell equations*¹² – to be discussed again and again later in this course.

In the mathematical terminology, Eq. (27) is *inhomogeneous*, because it has a right-hand side independent (at least explicitly) of the field \mathbf{E} that it describes. Another, *homogeneous* Maxwell equation's “embryo” (this one valid for the stationary case only!) may be obtained by noticing that the curl of the point charge's field, and hence that of *any* system of charges, equals zero:¹³

$$\nabla \times \mathbf{E} = 0. \quad (1.28)$$

Homo-geneous Maxwell equation for \mathbf{E}

(We will arrive at two other Maxwell equations, for the magnetic field, in Chapter 5, and then generalize all the equations to their full, time-dependent form at the end of Chapter 6. However, Eq. (27) will stay the same.)

Just to get a better gut feeling of Eq. (27), let us apply it to the same example of a uniformly charged sphere (Fig. 2). Vector algebra tells us that the divergence of a spherically symmetric vector function $\mathbf{E}(\mathbf{r}) = E(r)\mathbf{n}_r$ may be simply expressed in spherical coordinates:¹⁴ $\nabla \cdot \mathbf{E} = [d(r^2 E)/dr]/r^2$. As a result, Eq. (27) yields a linear ordinary differential equation for the scalar function $E(r)$:

$$\frac{1}{r^2} \frac{d}{dr} (r^2 E) = \begin{cases} \rho/\epsilon_0, & \text{for } r \leq R, \\ 0, & \text{for } r \geq R, \end{cases} \quad (1.29)$$

which may be readily integrated on each of these segments:

$$E(r) = \frac{1}{\epsilon_0} \frac{1}{r^2} \times \begin{cases} \rho \int r^2 dr = \rho r^3 / 3 + c_1, & \text{for } r \leq R, \\ c_2, & \text{for } r \geq R. \end{cases} \quad (1.30)$$

To determine the integration constant c_1 , we can use the following boundary condition: $E(0) = 0$. (It follows from the problem's spherical symmetry: in the center of the sphere, the electric field has to vanish, because otherwise, where would it be directed?) This requirement gives $c_1 = 0$. The second constant, c_2 , may be found from the continuity condition $E(R - 0) = E(R + 0)$, which has already been discussed above, giving $c_2 = \rho R^3 / 3 \equiv Q/4\pi$. As a result, we arrive at our previous results (19) and (22).

We can see that in this particular, highly symmetric case, using the differential form of the Gauss law is a bit more complex than its integral form. (For our second example, shown in Fig. 4, it would be even less natural.) However, Eq. (27) and its generalizations are more convenient for asymmetric charge

¹² Named after the genius of classical electrodynamics and statistical physics, James Clerk Maxwell (1831-1879).

¹³ This follows, for example, from the direct application of MA Eq. (10.11) to any spherically-symmetric vector function of type $\mathbf{f}(\mathbf{r}) = f(r)\mathbf{n}_r$ (in particular, to the electric field of a point charge placed at the origin), giving $f_\theta = f_\phi = 0$ and $\partial f_r / \partial \theta = \partial f_r / \partial \phi = 0$ so that all components of the vector $\nabla \times \mathbf{f}$ vanish. Since nothing prevents us from placing the reference frame's origin at the point charge's location, this result remains valid for any position of the charge.

¹⁴ See, e.g., MA Eq. (10.10) for the particular case $\partial/\partial\theta = \partial/\partial\phi = 0$.

distributions, and are invaluable in the cases where the distribution $\rho(\mathbf{r})$ is not known *a priori* and has to be found in a self-consistent way. (We will start discussing such cases in the next chapter.)

1.3. Scalar potential and electric field energy

One more help for solving problems of electrostatics (and electrodynamics as a whole) may be obtained from the notion of the *electrostatic potential*, which is just the electrostatic potential energy U of a probe point charge q placed into the field in question, normalized by its charge:

$$\phi \equiv \frac{U}{q}. \quad (1.31)$$

Electro-static potential

As we know from classical mechanics,¹⁵ the notion of U (and hence ϕ) makes the most sense for the case of *potential forces* – for example, those depending just on the particle's position. Eqs. (6) and (9) show that stationary electric fields fall into this category. For such a field, the potential energy may be defined as a scalar function $U(\mathbf{r})$ that allows the force to be calculated as its gradient (with the opposite sign):

$$\mathbf{F} = -\nabla U. \quad (1.32)$$

Dividing both sides of this equation by the probe charge, and using Eqs. (6) and (31), we get¹⁶

$$\mathbf{E} = -\nabla \phi. \quad (1.33)$$

Electrostatic field as a gradient

To calculate the scalar potential, let us start from the simplest case of a single point charge q placed at the origin. For it, Eq. (7) takes the simple form

$$\mathbf{E} = \frac{1}{4\pi\epsilon_0} q \frac{\mathbf{r}}{r^3} \equiv \frac{1}{4\pi\epsilon_0} q \frac{\mathbf{n}_r}{r^2}. \quad (1.34)$$

It is straightforward to verify that the last fraction in the last form of Eq. (34) is equal to $-\nabla(1/r)$.¹⁷ Hence, according to the definition (33), for this particular case

$$\phi = \frac{1}{4\pi\epsilon_0} \frac{q}{r}. \quad (1.35)$$

Potential of a point charge

(In the Gaussian units, this result is spectacularly simple: $\phi = q/r$.) Note that we could add an arbitrary constant to this potential (and indeed to *any* other distribution of ϕ discussed below) without changing the field, but it is convenient to define the potential energy so it would approach zero at infinity.

In order to justify the introduction and the forthcoming exploration of U and ϕ , let me demonstrate (I hope, unnecessarily :-) how useful the notions are, on a very simple example. Let two similar charges q be launched from afar, with the same initial speed $v_0 \ll c$ each, straight toward each other (i.e. with the zero impact parameter) – see Fig. 5. Since, according to the Coulomb law, the

¹⁵ See, e.g., CM Sec. 1.4.

¹⁶ Eq. (28) could be also derived from this relation because according to vector algebra, any gradient field has no curl – see, e.g., MA Eq. (11.1).

¹⁷ This may be done either by Cartesian components or using the well-known expression $\nabla f = (df/dr)\mathbf{n}_r$, valid for any spherically-symmetric scalar function $f(r)$ – see, e.g., MA Eq. (10.8) for the particular case $\partial/\partial\theta = \partial/\partial\phi = 0$.

charges repel each other with increasing force, they will stop at some minimum distance r_{\min} from each other, and then fly back. We could of course find r_{\min} directly from the Coulomb law. However, for that, we would need to write the 2nd Newton law for each particle (actually, due to the problem symmetry, they would be similar), then integrate them over time to find the particle velocity v as a function of distance, and only then recover r_{\min} from the requirement $v = 0$.

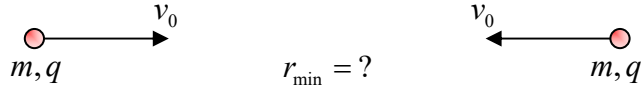


Fig. 1.5. A simple problem of charged particle motion.

The notion of potential allows this problem to be solved in one line. Indeed, in the field of potential forces, the system's total energy $\mathcal{E} = T + U \equiv T + q\phi$ is conserved. In our non-relativistic case $v \ll c$, the kinetic energy T is just $mv^2/2$. Hence, equating the total energy of two particles at the points $r = \infty$ and $r = r_{\min}$, and using Eq. (35) for ϕ , we get

$$2 \frac{mv_0^2}{2} + 0 = 0 + \frac{1}{4\pi\epsilon_0} \frac{q^2}{r_{\min}}, \quad (1.36)$$

immediately giving us the final answer: $r_{\min} = q^2/4\pi\epsilon_0 mv_0^2$. So, the notion of scalar potential is indeed very useful.

With this motivation, let us calculate ϕ for an arbitrary configuration of charges. For a single charge in an arbitrary position (say, at point \mathbf{r}_k), $r \equiv |\mathbf{r}|$ in Eq. (35) should be evidently replaced with $|\mathbf{r} - \mathbf{r}_k|$. Now, the linear superposition principle (3) allows for an easy generalization of this formula to the case of an arbitrary set of discrete charges,

$$\phi(\mathbf{r}) = \frac{1}{4\pi\epsilon_0} \sum_{\mathbf{r}_k \neq \mathbf{r}} \frac{q_k}{|\mathbf{r} - \mathbf{r}_k|}. \quad (1.37)$$

Finally, using the same arguments as in Sec. 1, we can use this result to argue that in the case of an arbitrary continuous charge distribution

$$\phi(\mathbf{r}) = \frac{1}{4\pi\epsilon_0} \int \frac{\rho(\mathbf{r}')}{|\mathbf{r} - \mathbf{r}'|} d^3r'. \quad (1.38)$$

Again, Dirac's delta function allows using the last equation to recover Eq. (37) for discrete charges as well, so that Eq. (38) may be considered as the general expression for the electrostatic potential.

For most practical calculations, using this expression and then applying Eq. (33) to the result, is preferable to using Eq. (9), because ϕ is a scalar, while \mathbf{E} is a 3D vector, mathematically equivalent to three scalars. Still, this approach may lead to technical problems similar to those discussed in Sec. 2. For example, applying it to the spherically-symmetric distribution of charge (Fig. 2), we get the integral

$$\phi = \frac{1}{4\pi\epsilon_0} 2\pi \int_0^\pi \sin\theta' d\theta' \int_0^\infty r'^2 dr' \frac{\rho(r')}{R} \cos\theta', \quad (1.39)$$

which is not much simpler than Eq. (11).

The situation may be much improved by recasting Eq. (38) into a differential form. For that, it is sufficient to plug the definition of ϕ , Eq. (33), into Eq. (27):

$$\nabla \cdot (-\nabla \phi) = \frac{\rho}{\epsilon_0}. \quad (1.40)$$

The left-hand side of this equation is nothing else than the Laplace operator of ϕ (with the minus sign), so that we get the famous *Poisson equation*¹⁸ for the electrostatic potential:

$$\boxed{\nabla^2 \phi = -\frac{\rho}{\epsilon_0}}. \quad (1.41)$$
Poisson
equation
for ϕ

(In the Gaussian units, the Poisson equation is $\nabla^2 \phi = -4\pi\rho$.) This differential equation is so convenient for applications that even its particular case for $\rho = 0$,

$$\boxed{\nabla^2 \phi = 0}, \quad (1.42)$$
Laplace
equation
for ϕ

has earned a special name – the *Laplace equation*.¹⁹

In order to get a gut feeling of the Poisson equation's value as a problem-solving tool, let us return to the spherically-symmetric charge distribution (Fig. 2) with a constant charge density ρ . Exploiting this symmetry, we can represent the potential as $\phi(r)$, and hence use the following simple expression for its Laplace operator:²⁰

$$\nabla^2 \phi = \frac{1}{r^2} \frac{d}{dr} \left(r^2 \frac{d\phi}{dr} \right), \quad (1.43)$$

so that for the points inside the charged sphere ($r \leq R$) the Poisson equation yields

$$\frac{1}{r^2} \frac{d}{dr} \left(r^2 \frac{d\phi}{dr} \right) = -\frac{\rho}{\epsilon_0}, \quad \text{i.e. } \frac{d}{dr} \left(r^2 \frac{d\phi}{dr} \right) = -\frac{\rho}{\epsilon_0} r^2. \quad (1.44)$$

Integrating the last form of the equation over r once, with the natural boundary condition $d\phi/dr|_{r=0} = 0$ (because of the condition $E(0) = 0$, which has been discussed above), we get

$$\frac{d\phi}{dr}(r) = -\frac{\rho}{r^2 \epsilon_0} \int_0^r r'^2 dr' = -\frac{\rho r}{3\epsilon_0} \equiv -\frac{1}{4\pi\epsilon_0} \frac{Qr}{R^3}. \quad (1.45)$$

Since this derivative is nothing more than $-E(r)$, in this formula we can readily recognize our previous result (22). Now we may like to carry out the second integration to calculate the potential itself:

$$\phi(r) = -\frac{Q}{4\pi\epsilon_0 R^3} \int_0^r r' dr' + c_1 = -\frac{Qr^2}{8\pi\epsilon_0 R^3} + c_1. \quad (1.46)$$

¹⁸ Named after Siméon Denis Poisson (1781-1840), also famous for the *Poisson distribution* – one of the central results of the probability theory – see, e.g., SM Sec. 5.2.

¹⁹ Named after the famous mathematician (and astronomer) Pierre-Simon Laplace (1749-1827) who, together with Alexis Clairault, is credited for the development of the very concept of potential.

²⁰ See, e.g., MA Eq. (10.8) for $\partial/\partial\theta = \partial/\partial\varphi = 0$.

Before making any judgment on the integration constant c_1 , let us solve the Poisson equation (in this case, just the Laplace equation) for the range outside the sphere ($r > R$):

$$\frac{1}{r^2} \frac{d}{dr} \left(r^2 \frac{d\phi}{dr} \right) = 0. \quad (1.47)$$

Its first integral,

$$\frac{d\phi}{dr}(r) = \frac{c_2}{r^2}, \quad (1.48)$$

also gives the electric field (with the minus sign). Now using Eq. (45) and requiring the field to be continuous at $r = R$, we get

$$\frac{c_2}{R^2} = -\frac{Q}{4\pi\epsilon_0 R^2}, \quad \text{i.e. } \frac{d\phi}{dr}(r) = -\frac{Q}{4\pi\epsilon_0 r^2}, \quad (1.49)$$

in an evident agreement with Eq. (19). Integrating this result again,

$$\phi(r) = -\frac{Q}{4\pi\epsilon_0} \int \frac{dr}{r^2} = \frac{Q}{4\pi\epsilon_0 r} + c_3, \quad \text{for } r > R, \quad (1.50)$$

we can select $c_3 = 0$, so that $\phi(\infty) = 0$, in accordance with the usual (though not compulsory) convention. Now we can finally determine the constant c_1 in Eq. (46) by requiring that this equation and Eq. (50) give the same value of ϕ at the boundary $r = R$. (According to Eq. (33), if the potential had a jump, the electric field at that point would be infinite.) The final answer may be represented as

$$\phi(r) = \frac{Q}{4\pi\epsilon_0 R} \left(\frac{R^2 - r^2}{2R^2} + 1 \right), \quad \text{for } r \leq R. \quad (1.51)$$

This calculation shows that using the Poisson equation to find the electrostatic potential distribution for highly symmetric problems may be a bit more cumbersome than directly finding the electric field – say, from the Gauss law. However, we will repeatedly see below that if the electric charge distribution is not fixed in advance, using Eq. (41) may be the only practicable way to proceed.

Returning now to the general theory of electrostatic phenomena, let us calculate the potential energy U of an arbitrary system of point electric charges q_k . Despite the apparently simple relation (31) between U and ϕ , the result is not that straightforward. Indeed, let us assume that the charge distribution has a finite spatial extent, so that at large distances from it (formally, at $\mathbf{r} = \infty$) the electric field tends to zero, so that the electrostatic potential tends to a constant. Selecting this constant, for convenience, to equal zero, we may calculate U as a sum of the energy increments ΔU_k created by bringing the charges, one by one, from infinity to their final positions \mathbf{r}_k – see Fig. 6.²¹ According to the integral form of Eq. (32), such a contribution is

$$\Delta U_k = - \int_{\infty}^{\mathbf{r}_k} \mathbf{F}(\mathbf{r}) \cdot d\mathbf{r} = -q_k \int_{\infty}^{\mathbf{r}_k} \mathbf{E}(\mathbf{r}) \cdot d\mathbf{r} \equiv q_k \phi(\mathbf{r}_k), \quad (1.52)$$

²¹ Indeed, by the very definition of the potential energy of a system, it should not depend on the way we are arriving at its final configuration.

where $\mathbf{E}(\mathbf{r})$ is the total electric field, and $\phi(\mathbf{r})$ is the total electrostatic potential during this process, besides the field created by the very charge q_k that is being moved.

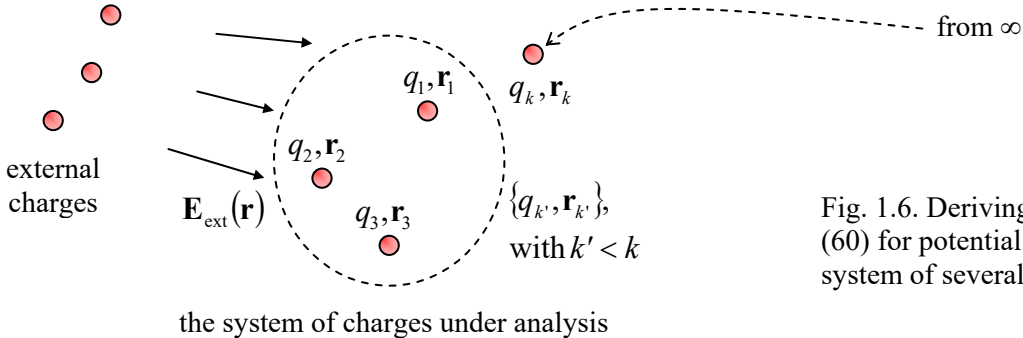


Fig. 1.6. Deriving Eqs. (55) and (60) for potential energies of a system of several point charges.

This expression shows that the increment ΔU_k , and hence the total potential energy U , depend on the source of the electric field \mathbf{E} . If the field is dominated by an *external field* \mathbf{E}_{ext} , induced by some *external charges*, not being a part of the charge configuration under our analysis (whose energy we are calculating, see Fig. 6), then the spatial distribution $\phi(\mathbf{r})$ is determined by this field, i.e. does not depend on how many charges we have already brought in, so that Eq. (52) is reduced to

$$\Delta U_k = q_k \phi_{\text{ext}}(\mathbf{r}_k), \quad \text{where } \phi_{\text{ext}}(\mathbf{r}) \equiv - \int_{\infty}^{\mathbf{r}} \mathbf{E}_{\text{ext}}(\mathbf{r}') \cdot d\mathbf{r}'. \quad (1.53)$$

Summing up these contributions, we get what is called the charge system's energy *in the external field*:²²

$$U_{\text{ext}} \equiv \sum_k \Delta U_k = \sum_k q_k \phi_{\text{ext}}(\mathbf{r}_k). \quad (1.54)$$

Now repeating the argumentation that has led us to Eq. (9), we see that for a continuously distributed charge, this sum turns into an integral:

$$U_{\text{ext}} = \int \rho(\mathbf{r}) \phi_{\text{ext}}(\mathbf{r}) d^3 r. \quad (1.55)$$

Energy:
external
field

(As was discussed above, using the delta-functional representation of point charges, we may always return from here to Eq. (54), so that Eq. (55) may be considered as a final, universal result.)

The result is different in the opposite limit when the electric field $\mathbf{E}(\mathbf{r})$ is created only by the very charges whose energy we are calculating. In this case, $\phi(\mathbf{r}_k)$ in Eq. (52) is the potential created only by the charges with numbers $k' = 1, 2, \dots, (k-1)$ that are already in place when the k^{th} charge is moved in (in Fig. 6, the charges inside the dashed boundary), and we may use the linear superposition principle to write

$$\Delta U_k = q_k \sum_{k' < k} \phi_{k'}(\mathbf{r}_k), \quad \text{so that } U = \sum_k U_k = \sum_{k, k' \atop (k' < k)} q_k \phi_{k'}(\mathbf{r}_k). \quad (1.56)$$

This result is so important that it is worthy of rewriting in several other forms. First, we may use Eq. (35) to represent Eq. (56) in a more symmetric form:

²² An alternative, perhaps more accurate term for U_{ext} is the energy of the system's *interaction with the external field*.

$$U = \frac{1}{4\pi\epsilon_0} \sum_{\substack{k,k' \\ (k' \neq k)}} \frac{q_k q_{k'}}{|\mathbf{r}_k - \mathbf{r}_{k'}|}. \quad (1.57)$$

The expression under this sum is evidently symmetric with respect to the index swap, so that it may be extended into a different form,

$$U = \frac{1}{4\pi\epsilon_0} \frac{1}{2} \sum_{\substack{k',k \\ (k' \neq k)}} \frac{q_k q_{k'}}{|\mathbf{r}_k - \mathbf{r}_{k'}|}, \quad (1.58)$$

where the interaction between each couple of charges is described by two equal terms under the sum, and the front coefficient $\frac{1}{2}$ is used to compensate for this *double-counting*. The convenience of the last form is that it may be readily generalized to the continuous case:

$$U = \frac{1}{4\pi\epsilon_0} \frac{1}{2} \int d^3 r \int d^3 r' \frac{\rho(\mathbf{r})\rho(\mathbf{r}')}{|\mathbf{r} - \mathbf{r}'|}. \quad (1.59)$$

(As before, in this case the restriction expressed in the discrete charge case as $k \neq k'$ is not important, because if the charge density is a continuous function, the integral (59) does not diverge at point $\mathbf{r} = \mathbf{r}'$.)

To represent this result in one more form, let us notice that according to Eq. (38), the inner integral over r' in Eq. (59), divided by $4\pi\epsilon_0$, is just the full electrostatic potential at point \mathbf{r} , and hence

$$U = \frac{1}{2} \int \rho(\mathbf{r})\phi(\mathbf{r})d^3 r. \quad (1.60)$$

Energy:
charge
interaction

For the discrete charge case, this result is

$$U = \frac{1}{2} \sum_k q_k \phi(\mathbf{r}_k), \quad (1.61)$$

but here it is important to remember that here the “full” potential’s value $\phi(\mathbf{r}_k)$ should exclude the (infinite) contribution from the point charge k itself. Comparing the last two formulas with Eqs. (54) and (55), we see that the electrostatic energy of charge interaction within the system, as expressed via the charge-by-potential product, is twice less than that of the energy of charge interaction with a fixed (“external”) field. This is the result of the fact that in the case of mutual interaction of the charges, the electric field \mathbf{E} in the basic Eq. (52) is proportional to the charge’s magnitude, rather than constant.²³

Now we are ready to address an important conceptual question: can we locate this interaction energy in space? This task may seem trivial: Eqs. (58)-(61) seem to imply that non-zero contributions to U come only from the regions where the electric charges are located. However, one of the most beautiful features of physics is that sometimes completely different interpretations of the same mathematical result are possible. To get an alternative view of our current result, let us write Eq. (60) for a volume V so large that the electric field on the limiting surface S is negligible, and plug into it the charge density expressed from the Poisson equation (41):

²³ The nature of this additional factor $\frac{1}{2}$ is absolutely the same as in the well-known formula $U = (\frac{1}{2})\kappa x^2$ for the potential energy of an elastic spring providing the returning force $F = -\kappa x$, proportional to its displacement x from the equilibrium position.

$$U = -\frac{\epsilon_0}{2} \int_V \phi \nabla^2 \phi d^3 r. \quad (1.62)$$

This expression may be integrated by parts as²⁴

$$U = -\frac{\epsilon_0}{2} \left[\oint_S \phi (\nabla \phi)_n d^2 r - \int_V (\nabla \phi)^2 d^3 r \right]. \quad (1.63)$$

According to our condition of negligible field $\mathbf{E} = -\nabla \phi$ at the surface, the first integral vanishes, and we get a very important formula

$$U = \frac{\epsilon_0}{2} \int (\nabla \phi)^2 d^3 r = \frac{\epsilon_0}{2} \int E^2 d^3 r. \quad (1.64)$$

This result, represented in the following equivalent form:²⁵

$$U = \int u(\mathbf{r}) d^3 r, \quad \text{with } u(\mathbf{r}) \equiv \frac{\epsilon_0}{2} E^2(\mathbf{r}),$$

(1.65)

Energy:
electric
field

certainly invites an interpretation very much different than Eq. (60): it is natural to consider $u(\mathbf{r})$ as the *spatial density of the electric field energy*, which is continuously distributed over all the space where the field exists – rather than just its part where the charges are located.

Let us have a look at how these two alternative pictures work for our testbed problem, a uniformly charged sphere. If we start with Eq. (60), we may limit the integration by the sphere volume ($0 \leq r \leq R$) where $\rho \neq 0$. Using Eq. (51), and the spherical symmetry of the problem (giving $d^3 r = 4\pi r^2 dr$), we get

$$U = \frac{1}{2} 4\pi \int_0^R \rho \phi r^2 dr = \frac{1}{2} 4\pi \rho \frac{Q}{4\pi\epsilon_0 R} \int_0^R \left(\frac{R^2 - r^2}{2R^2} + 1 \right) r^2 dr = \frac{6}{5} \frac{1}{4\pi\epsilon_0} \frac{Q^2}{2R}. \quad (1.66)$$

On the other hand, if we use Eq. (65), we need to integrate the energy density everywhere, i.e. both inside and outside of the sphere:

$$U = \frac{\epsilon_0}{2} 4\pi \left(\int_0^R E^2 r^2 dr + \int_R^\infty E^2 r^2 dr \right). \quad (1.67)$$

Using Eqs. (19) and (22) for, respectively, the external and internal regions, we get

$$U = \frac{\epsilon_0}{2} 4\pi \left[\int_0^R \left(\frac{Qr}{4\pi\epsilon_0} \right)^2 r^2 dr + \int_R^\infty \left(\frac{Q}{4\pi\epsilon_0 r^2} \right)^2 r^2 dr \right] = \left(\frac{1}{5} + 1 \right) \frac{1}{4\pi\epsilon_0} \frac{Q^2}{2R}. \quad (1.68)$$

This is (fortunately :-) the same answer as given by Eq. (66), but to some extent, Eq. (68) is more informative because it shows how exactly the electric field's energy is distributed between the interior and exterior of the charged sphere.²⁶

²⁴ This transformation follows from the divergence theorem MA (12.2) applied to the vector function $\mathbf{f} = \phi \nabla \phi$, taking into account the differentiation rule MA Eq. (11.4a): $\nabla \cdot (\phi \nabla \phi) = (\nabla \phi) \cdot (\nabla \phi) + \phi \nabla \cdot (\nabla \phi) = (\nabla \phi)^2 + \phi \nabla^2 \phi$.

²⁵ In the Gaussian units, the standard replacement $\epsilon_0 \rightarrow 1/4\pi$ turns the last of Eqs. (65) into $u(\mathbf{r}) = E^2/8\pi$.

²⁶ Note that $U \rightarrow \infty$ at $R \rightarrow 0$. Such divergence appears at the application of Eq. (65) to any point charge. Since it does not affect the force acting on the charge, the divergence does not create any technical difficulty for analysis

We see that, as we could expect, within the realm of *electrostatics*, Eqs. (60) and (65) are equivalent. However, when we examine *electrodynamics* (in Chapter 6 and beyond), we will see that the latter equation is more general and that it is more adequate to associate the electric energy with the field itself rather than its sources – in our current case, the electric charges.

Finally, let us calculate the potential energy of a system of charges in the general case when both the internal interaction of the charges and their interaction with an external field are important. One might fancy that such a calculation should be very hard since, in both ultimate limits, when one of these interactions dominates, we have got different results. However, once again we get help from the almighty linear superposition principle: in the general case, for the total electric field we may write

$$\mathbf{E}(\mathbf{r}) = \mathbf{E}_{\text{int}}(\mathbf{r}) + \mathbf{E}_{\text{ext}}(\mathbf{r}), \quad \phi(\mathbf{r}) = \phi_{\text{int}}(\mathbf{r}) + \phi_{\text{ext}}(\mathbf{r}), \quad (1.69)$$

where the index “int” now marks the field induced by the charge system under analysis, i.e. the variables participating (without indices) in Eqs. (56)-(65). Now let us imagine that our system is being built up in the following way: first, the charges are brought together at $\mathbf{E}_{\text{ext}} = 0$, giving the potential energy U_{int} expressed by Eq. (60), and then \mathbf{E}_{ext} is slowly increased. Evidently, the energy contribution from the latter process cannot depend on the internal interaction of the charges, and hence may be expressed in the form (55). As the result, the total potential energy²⁷ is the sum of these two components:

$$U = U_{\text{int}} + U_{\text{ext}} = \frac{1}{2} \int \rho(\mathbf{r}) \phi_{\text{int}}(\mathbf{r}) d^3 r + \int \rho(\mathbf{r}) \phi_{\text{ext}}(\mathbf{r}) d^3 r. \quad (1.70)$$

Now making the transition from the potentials to the fields, absolutely similar to that performed in Eqs. (62)-(65), we may rewrite this expression as

$$U = \int u(\mathbf{r}) d^3 r, \quad \text{with } u(\mathbf{r}) \equiv \frac{\epsilon_0}{2} [E_{\text{int}}^2(\mathbf{r}) + 2\mathbf{E}_{\text{int}}(\mathbf{r}) \cdot \mathbf{E}_{\text{ext}}(\mathbf{r})]. \quad (1.71)$$

One might think that this result, more general than Eq. (65) and perhaps less familiar to the reader, is something entirely new; however, it is not. Indeed, let us add to, and subtract $E_{\text{ext}}^2(\mathbf{r})$ from the sum in the brackets, and use Eq. (69) for the total electric field $\mathbf{E}(\mathbf{r})$; then Eq. (71) takes the form

$$U = \frac{\epsilon_0}{2} \int E^2(\mathbf{r}) d^3 r - \frac{\epsilon_0}{2} \int E_{\text{ext}}^2(\mathbf{r}) d^3 r. \quad (1.72)$$

Hence, in the most important case when we are using the potential energy to analyze the statics and dynamics of a system of charges in a fixed external field, i.e. when the second term on the right-hand side of Eq. (72) may be considered as a constant, we may still use for U an expression similar to the familiar Eq. (65), but with the field $\mathbf{E}(\mathbf{r})$ being the sum (69) of the internal and external fields.

Let us see how this works in a very simple situation. A uniform external electric field \mathbf{E}_{ext} is applied normally to a very broad, plane layer that contains a very large and equal number of free electric charges of both signs – see Fig. 7. What is the equilibrium distribution of the charges over the layer?

of charge statics or non-relativistic dynamics, but it points to a possible conceptual problem of classical electrodynamics as the whole at describing point charges. This issue will be discussed at the very end of the course (Sec. 10.6).

²⁷ This total U (or rather its part dependent on our system of charges) is sometimes called the *Gibbs potential energy* of the system. (I will discuss this notion in detail in Sec. 3.5.)

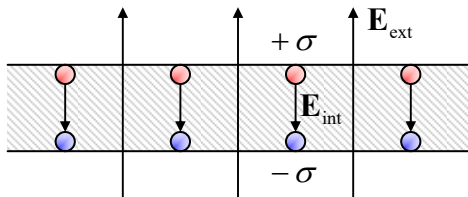


Fig. 1.7. A simple model of the electric field screening in a conductor. Here (and in all figures below) the red and blue colors are used to denote the opposite charge signs.

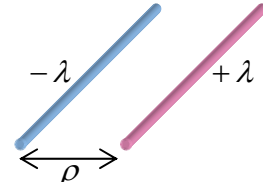
Since any area-uniform distribution of the charge inside the layer does not affect the field (and hence its energy) outside it, and the equilibrium distribution has to minimize the total potential energy of the system, Eq. (72) immediately gives the answer: the distribution should provide $\mathbf{E} \equiv \mathbf{E}_{\text{int}} + \mathbf{E}_{\text{ext}} = 0$ inside the whole layer – the effect called the electric field *screening*. The only way to ensure this equality is to have enough free charges of opposite signs residing on the layer's surfaces to induce a uniform field $\mathbf{E}_{\text{int}} = -\mathbf{E}_{\text{ext}}$, exactly compensating the external field at each point inside the layer – see Fig. 7. According to Eq. (24), the areal density of these surface charges should equal $\pm\sigma$, with $\sigma = E_{\text{ext}}/\epsilon_0$. This is a rudimentary but reasonable model of conductors' *polarization* – to be discussed in detail in the next chapter.

1.4. Exercise problems

1.1. Calculate the electric field of a thin, long, straight filament, electrically charged with a constant linear density λ , using two approaches:

- (i) directly from the Coulomb law, and
- (ii) using the Gauss law.

1.2. Two thin, straight parallel filaments, separated by distance ρ , carry equal and opposite uniformly distributed charges with linear density λ – see the figure on the right. Calculate the force (per unit length) of the Coulomb interaction of the wires. Compare its dependence on ρ with the Coulomb law for the force between two point charges, and interpret their difference.



1.3. Calculate the electric field of the following spherically-symmetric charge distribution: $\rho(r) = \rho_0 \exp\{-\lambda r\}$.

1.4. A sphere of radius R , whose volume had been charged with a constant density ρ , is split with a very narrow planar gap passing through its center. Calculate the force of the mutual electrostatic repulsion of the resulting two hemispheres.

1.5. A thin spherical shell of radius R , which had been charged with a constant areal density σ , is split into two equal halves with a very narrow, planar cut passing through the sphere's center. Calculate the force of electrostatic repulsion between the resulting hemispheric shells, and compare the result with that of the previous problem.

1.6. Calculate the distribution of the electrostatic potential created by a straight, thin filament of a finite length $2l$, charged with a constant linear density λ , and explore the result in the limits of very small and very large distances from the filament.

1.7. A thin plane sheet, perhaps of an irregular shape, carries an electric charge with a constant areal density σ .

(i) Express the electric field's component normal to the plane, at a certain distance from it, via the solid angle Ω at which the sheet is visible from the observation point.

(ii) Use the result to calculate the field in the center of a cube, with one face charged with a constant density σ .

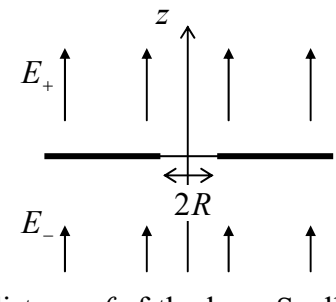
1.8. Can one create, in an extended region of space, electrostatic fields with the Cartesian components proportional to the following products of Cartesian coordinates $\{x, y, z\}$:

- (i) $\{yz, xz, xy\}$,
- (ii) $\{xy, xy, yz\}$?

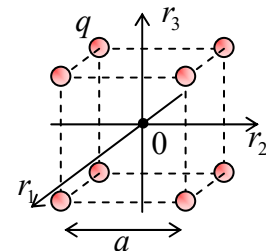
1.9. Distant sources have been used to create different uniform electric fields in two semi-spaces:

$$\mathbf{E}(\mathbf{r}) \Big|_{r \gg R} = \mathbf{n}_z \times \begin{cases} E_+, & \text{at } z < 0, \\ E_-, & \text{at } z > 0, \end{cases}$$

everywhere except for a transitional region of scale R near the origin, where the field is perturbed but still axially-symmetric. (As will be discussed in the next chapter, this may be done, for example, using a thin conducting membrane with a round hole of radius R in it – see the figure on the right.) Prove that such field may serve as an electrostatic lens for charged particles flying along the z -axis, at distances $\rho \ll R$ from it, and calculate the focal distance f of the lens. Spell out the conditions of validity of your result.

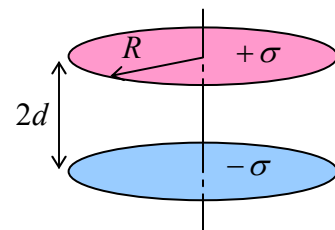


1.10. Eight equal point charges q are located at the corners of a cube of side a . Calculate all Cartesian components E_j of the electric field, and their spatial derivatives $\partial E_j / \partial r_j$, at the cube's center, where r_j are the Cartesian coordinates oriented along the cube's sides – see the figure on the right. Are all your results valid for the center of a plane square, with four equal charges at its corners?



1.11. By a direct calculation, find the average electric potential of a spherical surface of radius R , created by a point charge q located at a distance $r > R$ from the sphere's center. Use the result to prove the following general *mean value theorem*: the electric potential at any point is always equal to its average value on any spherical surface with the center at that point, and containing no electric charges inside it.

1.12. Two similar thin, circular, coaxial disks of radius R , separated by distance $2d$, are uniformly charged with equal and opposite areal densities $\pm\sigma$ – see the figure on the right. Calculate and sketch the distribution of the electrostatic potential and the electric field of the disks along their common axis.



1.13. The electrostatic potential created by some electric charge distribution, is

$$\phi(\mathbf{r}) = C \left(\frac{1}{r} + \frac{1}{2r_0} \right) \exp \left\{ -\frac{r}{r_0} \right\},$$

where C and r_0 are constants, and $r \equiv |\mathbf{r}|$ is the distance from the origin. Calculate the charge distribution in space.

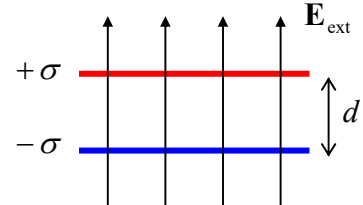
1.14. A thin flat sheet cut in the form of a rectangle of size $a \times b$, is electrically charged with a constant areal density σ . Without an explicit calculation of the spatial distribution $\phi(\mathbf{r})$ of the electrostatic potential induced by this charge, find the ratio of its values at the center and at the corners of the rectangle.

Hint: Consider partitioning the rectangle into several similar parts and using the linear superposition principle.

1.15. Calculate the electrostatic energy per unit area of the system of two thin, parallel planes with equal and opposite charges of a constant areal density σ , separated by distance d .

1.16. The system analyzed in the previous problem (two thin, parallel, oppositely charged planes) is now placed into an external, uniform, normal electric field $E_{\text{ext}} = \sigma/\epsilon_0$ – see the figure on the right. Find the force (per unit area) acting on each plane, by two methods:

- (i) directly from the electric field distribution, and
- (ii) from the potential energy of the system.



1.17. Explore the relationship between the Laplace equation (42) and the condition of the minimum of the electrostatic field energy (65).

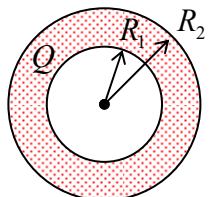
1.18. Prove the following *reciprocity theorem of electrostatics*:²⁸ if two spatially-confined charge distributions $\rho_1(\mathbf{r})$ and $\rho_2(\mathbf{r})$ create respective distributions $\phi_1(\mathbf{r})$ and $\phi_2(\mathbf{r})$ of the electrostatic potential, then

$$\int \rho_1(\mathbf{r}) \phi_2(\mathbf{r}) d^3 r = \int \rho_2(\mathbf{r}) \phi_1(\mathbf{r}) d^3 r.$$

Hint: Consider the integral $\int \mathbf{E}_1 \cdot \mathbf{E}_2 d^3 r$.

1.19. Calculate the energy of electrostatic interaction of two spheres, of radii R_1 and R_2 , each with a spherically-symmetric charge distribution, separated by distance $d > R_1 + R_2$.

1.20. Calculate the electrostatic energy U of a (generally, thick) spherical shell, with charge Q uniformly distributed through its volume – see the figure on the right. Analyze and interpret the dependence of U on the inner cavity's radius R_1 , at fixed Q and R_2 .



²⁸ This is only the simplest one of several reciprocity theorems in electromagnetism – see, e.g., Sec. 6.8 below.

Chapter 2. Charges and Conductors

This chapter starts our discussion of the very common situations when the electric charge distribution in space is not known *a priori*, but rather should be calculated in a self-consistent way together with the electric field it creates. The simplest situations of this kind involve conductors and lead to the so-called boundary problems in that the partial differential equations describing the field distribution have to be solved with appropriate boundary conditions. Such problems are also typical for other parts of electrodynamics (and indeed for other fields of physics as well), so that following tradition, I will use this chapter's material as a playground for a discussion of various methods of boundary problem solution, and the special functions most frequently encountered on that way.

2.1. Polarization and screening

The basic principles of electrostatics outlined in Chapter 1 present the conceptually full solution of the problem of finding the electrostatic field (and hence Coulomb forces) induced by electric charges distributed over space with some density $\rho(\mathbf{r})$. However, in most practical situations, this function is not known but should be found self-consistently with the field. For example, if a sample of relatively dense material is placed into an external electric field, it is typically *polarized*, i.e. acquires some local charges of its own, which contribute to the total electric field $\mathbf{E}(\mathbf{r})$ inside, and even outside it – see Fig. 1a.

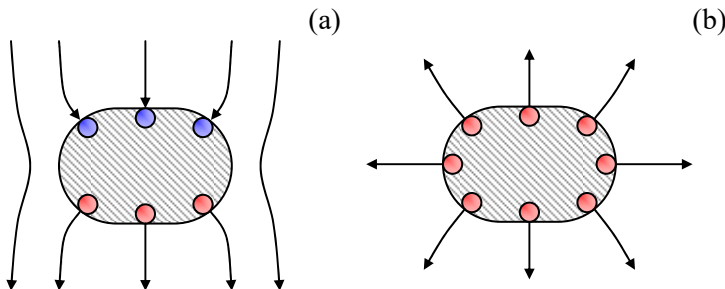


Fig. 2.1. Two typical electrostatic situations involving conductors: (a) polarization by an external field, and (b) re-distribution of conductor's own charge over its surface – schematically. Here and below, the red and blue points denote charges of opposite signs.

The full solution of such problems should satisfy not only the fundamental Eq. (1.7) but also the so-called *constitutive relations* between the macroscopic variables describing the sample's material. Due to the atomic character of real materials, such relations may be very involved. In this part of my series, I will have time to address these relations, for various materials, only rather superficially,¹ focusing on their simple approximations. Fortunately, in most practical cases such approximations work very well.

In particular, for the polarization of good conductors, a very reasonable approximation is given by the so-called *macroscopic model*, in which the free charges in the conductor are treated as a charged continuum that is free to move under the effect of the force $\mathbf{F} = q\mathbf{E}$ exerted by the *macroscopic* electric field \mathbf{E} , i.e. the field averaged over space on the atomic scale – see also the discussion at the end

¹ A more detailed discussion of the electrostatic field screening may be found, e.g., in SM Sec. 6.4. (Alternatively, see either Sec. 13.5 of J. Hook and H. Hall, *Solid State Physics*, 2nd ed., Wiley, 1991; or Chapter 17 of N. Ashcroft and N. Mermin, *Solid State Physics*, Brooks Cole, 1976.)

of Sec. 1.1. In electrostatics (which excludes the case dc currents, to be discussed in Chapter 4 below), there should be no such motion, so that everywhere inside the conductor the macroscopic electric field should vanish:

$$\mathbf{E} = 0. \quad (2.1a)$$

Conductor:
macroscopic
model

This is the *electric field screening*² effect, meaning, in particular, that conductors' polarization in an external electric field has the extreme form shown (rather schematically) in Fig. 1a, with the field of the induced surface charges completely compensating the external field in the conductor's bulk. Note that Eq. (1a) may be rewritten in another, frequently more convenient form:

$$\phi = \text{const}, \quad (2.1b)$$

where ϕ is the *macroscopic* electrostatic potential related to the macroscopic field by Eq. (1.33).³ (If a problem includes several unconnected conductors, the constant in Eq. (1b) may be specific for each of them.)

Now let us examine what we can say about the electric field in free space just *outside* a conductor, within the same macroscopic model. At close proximity, any smooth surface (in our current case, that of a conductor) looks planar. Let us integrate Eq. (1.28) over a narrow ($d \ll l$) rectangular loop C encircling a part of such plane conductor's surface (see the dashed line in Fig. 2a), and apply it to the electric field vector \mathbf{E} the well-known vector algebra equality – the *Stokes theorem*⁴

$$\oint_S (\nabla \times \mathbf{E})_n d^2 r = \oint_C \mathbf{E} \cdot d\mathbf{r}, \quad (2.2)$$

where S is any surface limited by the contour C .

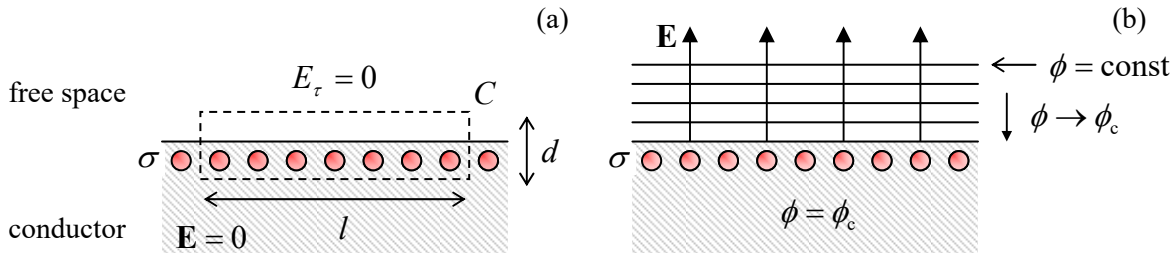


Fig. 2.2. (a) The surface charge layer at a conductor's surface, and
(b) the electric field lines and equipotential surfaces near it.

In our current case, the contour is dominated by two straight lines of length l , so that if l is much smaller than the characteristic spatial scale of field's changes but much larger than the interatomic distances, the right-hand side of Eq. (2) may be well approximated as $[(E_\tau)_{\text{in}} - (E_\tau)_{\text{out}}] l$, where E_τ is the tangential component of the corresponding macroscopic field, parallel to the surface. On the other hand, according to Eq. (1.28), the left-hand side of Eq. (2) equals zero. Hence, the macroscopic field's

² This term, used for the *electric* field, should not be confused with *shielding* – the term used for the description of *magnetic* field's reduction by magnetic materials – see Chapter 5 below.

³ Since averaging of a function over space is a linear operation, any linear relation between genuine (microscopic) variables, including Eq. (1.33), is also valid for the corresponding macroscopic variables.

⁴ See, e.g., MA Eq. (12.1).

component E_τ should be continuous at the surface, and to satisfy Eq. (1a) inside the conductor, the component has to vanish immediately outside it: $(E_\tau)_{\text{out}} = 0$. This means that the electrostatic potential immediately outside of a conducting surface cannot change along it. In other words, the equipotential surfaces outside a conductor should “lean” to the conductor’s surface, with their potential values approaching the constant potential of the conductor – see Fig. 2b.

So, the electrostatic field just outside any conductor has to be normal to its surface. To find this normal field, we may apply the universal relation (1.24) to our macroscopic field \mathbf{E} . Since in our current case $E_n = 0$ inside the conductor, we get

Surface
charge
density

$$\sigma = \epsilon_0 (E_n)_{\text{out}} \equiv -\epsilon_0 (\nabla \phi)_n \equiv -\epsilon_0 \frac{\partial \phi}{\partial n}, \quad (2.3)$$

where σ is the macroscopic areal density of the conductor’s surface charge. Note that deriving this universal relation between the normal component of the field and the surface charge density, we have not used any cause-vs-effect arguments, so that Eq. (3) is valid regardless of whether the surface charge is induced by an externally applied field (as in the case of conductor’s polarization, shown in Fig. 1a), or the electric field is induced by the electric charge placed on the conductor and then self-redistributed over its surface (Fig. 1b), or it is some combination of both effects.

Before starting to use the macroscopic model for the solution of particular problems of electrostatics, let me use the balance of this section to briefly discuss its limitations. (The reader in a rush may skip this discussion and proceed to Sec. 2; however, I believe that every educated physicist has to understand when this model works, and when it does not.)

Since the argumentation which has led us to Eq. (1.24) and hence to Eq. (3) is valid for any thickness d of the Gauss pillbox, within the macroscopic model, the whole surface charge is located within an infinitely thin surface layer. This is of course impossible physically: for one, this would require an infinite volumic density ρ of the charge. In reality, the charged layer (and hence the region of the electric field’s crossover from the finite value (3) to zero) has a nonzero thickness λ . At least three effects contribute to λ .

(i) *Atomic structure of matter.* Within each atom, and frequently between the adjacent atoms as well, the genuine (“microscopic”) electric field is highly nonuniform. Thus, as was already stated above, Eq. (1) is valid only for the *macroscopic field*, i.e. the field averaged over distances of the order of the atomic size scale $a_0 \sim 10^{-10}$ m,⁵ and cannot be applied to the field changes on that scale. As a result, the surface layer of charges cannot be much thinner than a_0 .

(ii) *Thermal excitation.* According to Eq. (1.9), in the whole field-free bulk of a conductor, the net charge density, $\rho = e(n - n_e)$,⁶ has to vanish, so that the numbers of protons in atomic nuclei (n) and electrons (n_e) per unit volume have to be balanced. However, if an external electric field penetrates a conductor, free electrons can shift in or out of its affected part, depending on the field’s contribution to their potential energy, $\Delta U = q_e \phi = -e \phi$. (Here the arbitrary constant in ϕ is chosen to give $\phi = 0$ well inside the conductor.) In classical statistics, this change is described by the Boltzmann distribution:⁷

⁵ This scale originates from the quantum-mechanical effects of electron motion, characterized by the *Bohr radius* $r_B \equiv \hbar^2/m_e(e^2/4\pi\epsilon_0) \approx 0.53 \times 10^{-10}$ m – see, e.g., QM Eq. (1.10). It also defines the scale $E_B = e/4\pi\epsilon_0 r_B^2 \sim 10^{12}$ SI units (V/m) of the microscopic electric fields inside atoms. (Please note how large these fields are.)

⁶ In this series, e denotes the fundamental charge, $e \approx 1.6 \times 10^{-19}$ C > 0, so that the electron’s charge equals $(-e)$.

⁷ See, e.g., SM Sec. 3.1.

$$n_e(\mathbf{r}) = n \exp\left\{-\frac{U(\mathbf{r})}{k_B T}\right\}, \quad (2.4)$$

where T is the absolute temperature in kelvins (K), and $k_B \approx 1.38 \times 10^{-23}$ J/K is the Boltzmann constant. As a result, the net charge density is

$$\rho(\mathbf{r}) = en \left(1 - \exp\left\{\frac{e\phi(\mathbf{r})}{k_B T}\right\} \right). \quad (2.5)$$

The penetrating electric field polarizes the atoms as well. As will be discussed in the next chapter, such polarization results in the reduction of the electric field by a material-specific dimensionless factor κ (larger, but typically not too much larger than 1), called the *dielectric constant*. As a result, the Poisson equation (1.41) takes the so-called *Poisson-Boltzmann* form,⁸

$$\frac{d^2\phi}{dz^2} = -\frac{\rho}{\kappa\epsilon_0} = \frac{en}{\kappa\epsilon_0} \left(\exp\left\{\frac{e\phi}{k_B T}\right\} - 1 \right), \quad (2.6)$$

where we have taken advantage of the 1D geometry of the system to simplify the Laplace operator, with the z -axis normal to the surface.

Even with this simplification, Eq. (6) is a nonlinear differential equation allowing an analytical but rather bulky solution. Since our current goal is just to estimate the field penetration depth λ , let us simplify the equation further by considering the low-field limit: $e|\phi| \sim e|E|\lambda \ll k_B T$. In this limit, we may extend the exponent into the Taylor series, and keep only two leading terms (of which the first one cancels with the following unity). As a result, Eq. (6) becomes linear,

$$\frac{d^2\phi}{dz^2} = \frac{en}{\kappa\epsilon_0} \frac{e\phi}{k_B T}, \quad \text{i.e. } \frac{d^2\phi}{dz^2} = \frac{1}{\lambda^2} \phi, \quad (2.7)$$

where the constant λ , in this case, is called the *Debye* (or “*Debye-Hückel*”) *screening length* λ_D :

$$\lambda_D^2 \equiv \frac{\kappa\epsilon_0 k_B T}{e^2 n}. \quad (2.8)$$

Debye
screening
length

As the reader certainly knows, Eq. (7) describes an exponential decrease of the electric potential, with the characteristic length λ_D : $\phi \propto \exp\{-z/\lambda_D\}$, where the z -axis is directed into the conductor. Plugging in the involved fundamental constants into Eq. (8), we get the following estimate: $\lambda_D[\text{m}] \approx 70 \times (\kappa \times T[\text{K}] / n[\text{m}^{-3}])^{1/2}$. According to this formula, in semiconductors at room temperature, the Debye length may be rather substantial. For example, in silicon ($\kappa \approx 12$) doped to the free charge carrier concentration $n = 3 \times 10^{18} \text{ cm}^{-3}$ (the value typical for modern integrated circuits),⁹ $\lambda_D \approx 2 \text{ nm}$, still well

⁸ This equation and/or its straightforward generalization to the case of charged particles (ions) of several kinds is also (especially in the theories of electrolytes and plasmas) called the *Debye-Hückel equation*.

⁹ There is a good reason for making an estimate of λ_D for this case: the electric field created by the gate electrode of a field-effect transistor, penetrating into doped silicon by a depth $\sim \lambda_D$, controls the electric current in this most important electronic device – on whose back all our information technology rides. Because of that, λ_D establishes the possible scale of semiconductor circuit shrinking, which is the basis of the well-known Moore’s law. (Practically, the scale is determined by integrated circuit patterning techniques, and Eq. (8) may be used to find the proper charge carrier density n and hence the necessary level of silicon doping – see, e.g., SM Sec. 6.4.)

above the atomic size scale a_0 , thus justifying the estimate. However, for typical good metals ($n \sim 10^{29} \text{ m}^{-3}$, $\kappa \sim 10$) the same formula gives $\lambda_D \sim 10^{-11} \text{ m}$, less than a_0 . In this case, Eq. (8) should not be taken literally, because it is based on the assumption of a continuous charge distribution.

(iii) *Quantum statistics.* Actually, the last estimate is not valid for good metals (and highly doped semiconductors) for one more reason: their free electrons obey the quantum (*Fermi-Dirac*) statistics rather than the Boltzmann distribution (4).¹⁰ As a result, at all realistic temperatures the electrons form a degenerate quantum gas, occupying all available energy states below some energy level $\mathcal{E}_F \gg k_B T$, called the *Fermi energy*. In these conditions, the screening of relatively low electric field may be described by replacing Eq. (5) with

$$\rho \equiv e(n - n_e) = eg(\mathcal{E}_F)(-U) = -e^2 g(\mathcal{E}_F)\phi, \quad (2.9)$$

where $g(\mathcal{E})$ is the density of quantum states (per unit volume per unit energy) at the electron's energy \mathcal{E} . At the Fermi surface, the density is of the order of n/\mathcal{E}_F .¹¹ As a result, we again get the second of Eqs. (7), but with a different characteristic scale λ , defined by the following relation:

Thomas-Fermi screening length

$$\lambda_{TF}^2 \equiv \frac{\kappa \mathcal{E}_0}{e^2 g(\mathcal{E}_F)} \sim \frac{\kappa \mathcal{E}_0 \mathcal{E}_F}{e^2 n}, \quad (2.10)$$

and called the *Thomas-Fermi screening length*. Since for most good metals, n is of the order of 10^{29} m^{-3} , and \mathcal{E}_F is of the order of 10 eV, Eq. (10) typically gives λ_{TF} close to a few a_0 , and makes the Thomas-Fermi screening theory valid at least semi-quantitatively.

To summarize, the electric field penetration into good conductors is limited to a depth λ ranging from a fraction of a nanometer to a few nanometers, so that for problems with a characteristic linear size much larger than that scale, the macroscopic model (1) gives a very good accuracy, and we will use them in the rest of this chapter. However, the reader should remember that in many situations involving semiconductors, as well as at some nanoscale experiments with metals, the electric field penetration should be taken into account.

Another important condition of the macroscopic model's validity is imposed on the electric field's magnitude, which is especially significant for semiconductors. Indeed, as Eq. (6) shows, Eq. (7) is only valid if $e|\phi| \ll k_B T$, so that $|E| \sim |\phi|/\lambda_D$ should be much lower than $k_B T/e\lambda_D$. In the example given above ($\lambda_D \approx 2 \text{ nm}$, $T = 300 \text{ K}$), this means $|E| \ll E_t \sim 10^7 \text{ V/m} \equiv 10^5 \text{ V/cm}$ – the value readily reachable in the lab. In larger fields, the field penetration becomes nonlinear, leading in particular to the very important effect of *carrier depletion*; it will be discussed in SM Sec. 6.4. For typical metals, such linearity limit, $E_t \sim \mathcal{E}_F/e\lambda_{TF}$ is much higher, $\sim 10^{11} \text{ V/m}$, but the model may be violated at lower fields by other effects, such as the impact-ionization leading to *electric breakdown*, which may start at $\sim 10^6 \text{ V/m}$.

2.2. Capacitance

Let us start using the macroscopic model from systems consisting of charged conductors only, with no so-called *stand-alone* charges in the free space outside them.¹² Our goal here is to calculate the

¹⁰ See, e.g., SM Sec. 2.8. For a more detailed derivation of Eq. (10), see SM Chapter 3.

¹¹ See, e.g., SM Sec. 3.3.

distributions of the electric field \mathbf{E} and potential ϕ in space, and the distribution of the surface charge density σ over the conductor surfaces. However, before doing that for particular situations, let us see if there are any integral measures of these distributions, which should be our primary focus.

The simplest case is of course a single conductor in the otherwise free space. According to Eq. (1b), all its volume should have the same electrostatic potential ϕ , evidently providing one convenient global measure of the situation. Another integral measure is provided by the total charge

$$Q \equiv \int_V \rho d^3r \equiv \oint_S \sigma d^2r, \quad (2.11)$$

where the last integral is extended over the whole surface S of the conductor. In the general case, what can we tell about the relation between Q and ϕ ? At $Q = 0$, there is no electric field in the system, and it is natural (though not absolutely necessary) to select the arbitrary constant in the electrostatic potential to have $\phi = 0$ everywhere. Then, if the conductor is charged with a non-zero Q , according to the linear Eq. (1.7), the electric field at any point of space has to be proportional to that charge. Hence the electrostatic potential at all points, including its value ϕ inside the conductor, is also proportional to Q :

$$\phi = pQ. \quad (2.12)$$

The proportionality coefficient p , which depends on the conductor's size and shape, but on neither ϕ nor Q , is called its *reciprocal capacitance* (or, not too often, "electric elastance"). Usually, Eq. (12) is rewritten in a different form,

$$Q = C\phi, \quad \text{with } C \equiv \frac{1}{p} \quad (2.13)$$

Self-capacitance

where C is called *self-capacitance*. (Frequently, C is called just *capacitance*, but as we will see very soon, for more complex situations the latter term may be ambiguous.)

Before calculating C for particular geometries, let us have a look at the electrostatic energy U of a single conductor. To calculate it, of the several relations discussed in Chapter 1, Eq. (1.61) is most convenient, because all elementary charges q_k are now parts of the conductor charge, and hence reside at the same potential ϕ – see Eq. (1b) again. As a result, the equality becomes very simple:

$$U = \frac{1}{2} \phi \sum_k q_k = \frac{1}{2} \phi Q. \quad (2.14)$$

Moreover, using the linear relation (13), the same result may be re-written in two more forms:

$$U = \frac{Q^2}{2C} = \frac{C}{2} \phi^2. \quad (2.15)$$

Electrostatic energy

We will discuss several ways to calculate C in the next sections, and right now will have a quick look at just the simplest example for that we have calculated everything necessary in the previous chapter: a conducting sphere of radius R . Indeed, we already know the electric field distribution: according to Eq. (1), $E = 0$ inside the sphere, while Eq. (1.19), with $Q(r) = Q$, describes the field distribution outside it, because of the evident spherical symmetry of the surface charge distribution.

¹² In some texts, these charges are called "free". This term is somewhat misleading, because they may well be bound, i.e. unable to move freely.

Moreover, since the latter formula is exactly the same as for the point charge placed in the sphere's center, the potential's distribution in space may be obtained from Eq. (1.35) by replacing q with the sphere's full charge Q . Hence, on the surface of the sphere (and, according to Eq. (1b), through its interior),

$$\phi = \frac{1}{4\pi\epsilon_0} \frac{Q}{R}. \quad (2.16)$$

Comparing this result with the definition (13), for the sphere's self-capacitance we obtain a very simple formula¹³

C: sphere

$$C = 4\pi\epsilon_0 R. \quad (2.17)$$

This formula, which should be well familiar to the reader, is convenient to get some feeling of how large the SI unit of capacitance (1 *farad*, abbreviated as F) is: the self-capacitance of Earth ($R_E \approx 6.34 \times 10^6$ m) is below 1 mF! Another important note is that while Eq. (17) is not exactly valid for a conductor of arbitrary shape, it implies an important general estimate

$$C \sim 2\pi\epsilon_0 a \quad (2.18)$$

where a is the scale of the linear size of any conductor.¹⁴

Now proceeding to a system of *two* arbitrary conductors, we immediately see why we should be careful with the capacitance definition: one constant C is insufficient to describe all electrostatic properties of such a system. Indeed, here we have two, generally different conductor potentials, ϕ_1 and ϕ_2 , that may depend on both conductor charges, Q_1 and Q_2 . Using the same arguments as for the single-conductor case, we may conclude that the dependence is always linear:

$$\begin{aligned} \phi_1 &= \rho_{11}Q_1 + \rho_{12}Q_2, \\ \phi_2 &= \rho_{21}Q_1 + \rho_{22}Q_2, \end{aligned} \quad (2.19)$$

but now has to be described by more than one coefficient. Actually, it turns out that there are three rather than four different coefficients in these relations, because

$$\rho_{12} = \rho_{21}. \quad (2.20)$$

This equality may be proved in several ways, for example, using the general *reciprocity theorem of electrostatics* (whose proof was the subject of Problem 1.17):

$$\int \rho_1(\mathbf{r})\phi^{(2)}(\mathbf{r})d^3r = \int \rho_2(\mathbf{r})\phi^{(1)}(\mathbf{r})d^3r, \quad (2.21)$$

¹³ In the Gaussian units, using the standard replacement $4\pi\epsilon_0 \rightarrow 1$, this relation takes an even simpler form: $C = R$, very easy to remember. Generally, in the Gaussian units (but not in the SI system!) the capacitance has the dimensionality of length, i.e. is measured in centimeters. Note also that a fractional SI unit, 1 picofarad (10^{-12} F), is very close to the Gaussian unit: $1 \text{ pF} = [(1 \times 10^{-12}) / (4\pi\epsilon_0 \times 10^{-2})] \text{ cm} \approx 0.8998 \text{ cm}$. So, 1 pF is close to the capacitance of a metallic ball with a 1-cm radius, making this unit very convenient for human-scale systems.

¹⁴ These arguments are somewhat insufficient to say which size should be used for a in the case of narrow, extended conductors, e.g., a thin, long wire. Very soon we will see that in such cases the electrostatic energy, and hence C , depends mostly on the *larger* size of the conductor.

where $\phi^{(1)}(\mathbf{r})$ and $\phi^{(2)}(\mathbf{r})$ are the potential distributions induced, respectively, by two electric charge distributions, $\rho_1(\mathbf{r})$ and $\rho_2(\mathbf{r})$. In our current case, each of these integrals is limited to the volume (or, more exactly, the surface) of the corresponding conductor, where each potential is constant and may be taken out of the integral. As a result, Eq. (21) is reduced to

$$Q_1\phi^{(2)}(\mathbf{r}_1) = Q_2\phi^{(1)}(\mathbf{r}_2). \quad (2.22)$$

In terms of Eq. (19), $\phi^{(2)}(\mathbf{r}_1)$ is just $p_{12}Q_2$, while $\phi^{(1)}(\mathbf{r}_2)$ equals $p_{21}Q_1$. Plugging these expressions into Eq. (22), and canceling the product Q_1Q_2 , we arrive at Eq. (20).

Hence the 2×2 matrix of coefficients p_{jj} (called the *reciprocal capacitance matrix*) is always symmetric, and using the natural notation $p_{11} \equiv p_1$, $p_{22} \equiv p_2$, $p_{12} = p_{21} \equiv p$, we may rewrite it in a simpler form:

$$\begin{pmatrix} p_1 & p \\ p & p_2 \end{pmatrix}. \quad (2.23)$$

Plugging the relation (19), in this new notation, into Eq. (1.61), we see that the full electrostatic energy of the system may be expressed as a quadratic form of its charges:

$$U = \frac{p_1}{2}Q_1^2 + pQ_1Q_2 + \frac{p_2}{2}Q_2^2. \quad (2.24)$$

It is evident that the middle term on the right-hand side of this equality describes the electrostatic coupling of the conductors. (Without it, the energy would be just a sum of two independent electrostatic energies of conductors 1 and 2.)¹⁵ Still, even with this simplification, Eqs. (19) and (20) show that in the general case of arbitrary charges Q_1 and Q_2 , the system of two conductors should be characterized by three, rather than just one coefficient (“the capacitance”). This is why we may attribute a single capacitance to the system only in some particular cases.

For practice, the most important of them is when the system as the whole is electrically neutral: $Q_1 = -Q_2 \equiv Q$. In this case, the most important function of Q is the difference between the conductors’ potentials, called the *voltage*:¹⁶

$$V \equiv \phi_1 - \phi_2, \quad (2.25)$$

Voltage:
definition

For that function, the subtraction of two Eqs. (19) gives

$$V = \frac{Q}{C}, \quad \text{with } C \equiv \frac{1}{p_1 + p_2 - 2p}, \quad (2.26)$$

Mutual
capacitance

where the coefficient C is called the *mutual capacitance* between the conductors – or, again, just “capacitance” if the term’s meaning is absolutely clear from the context. The same coefficient describes

¹⁵ This is why systems with $p \ll p_1, p_2$ are called *weakly coupled*, and may be analyzed using approximate methods – see, e.g., Fig. 4 and its discussion below.

¹⁶ A word of caution: in condensed matter physics and electrical engineering, voltage is most commonly defined as the difference between *electrochemical* rather than *electrostatic* potentials. These two notions coincide if the conductors have equal *workfunctions* – for example if they are made of the same material. In this course, this condition will be implied, and the difference between the two voltages ignored – to be discussed in detail in SM Sec. 6.3.

the electrostatic energy of the system. Indeed, plugging Eqs. (19) and (20) into Eq. (24), we see that both forms of Eq. (15) are reproduced if ϕ is replaced with V , Q_1 with Q , and with C meaning the mutual capacitance:

Capacitor's energy

$$U = \frac{Q^2}{2C} = \frac{C}{2}V^2. \quad (2.27)$$

The best-known system for that the mutual capacitance C may be readily calculated is the *plane* (or “parallel-plate”) *capacitor*: a system of two conductors separated with a narrow plane gap of a constant thickness d and an area $A \sim a^2 \gg d^2$ – see Fig. 3.

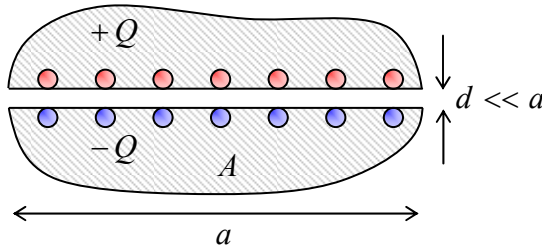


Fig. 2.3. Plane capacitor – schematically.

Since the surface charges that contribute to the opposite charges $\pm Q$ of the conductors of this system, attract each other, in the limit $d \ll a$ they sit entirely on the opposite surfaces limiting the gap, so there is virtually no electric field outside of the gap, while (according to the discussion in Sec. 1) inside the gap it is normal to the surfaces. According to Eq. (3), the magnitude of this field is $E = \sigma/\epsilon_0$. Integrating this field across thickness d of the narrow gap, we get $V \equiv \phi_1 - \phi_2 = Ed = \sigma d/\epsilon_0$, so that $\sigma = \epsilon_0 V/d$. But due to the constancy of the potential of each electrode, V should not depend on the position in the gap area. As a result, σ should be also constant over all the gap area A , regardless of the external geometry of the conductors (see Fig. 3 again), and hence $Q = \sigma A = \epsilon_0 V/d$. Thus we may write $V = Q/C$, with

$$C = \frac{\epsilon_0 A}{d}. \quad (2.28)$$

C: Plane capacitor

Let me offer a few comments on this well-known formula. First, it is valid even if the gap is not quite planar – for example, if it gently curves on a scale much larger than d , but retains its thickness. Second, Eq. (28), which is valid only if $A \sim a^2$ is much larger than d^2 , ignores the nonuniform electric fields spreading to distances $\sim d$ beyond the gap edges. Such *fringe fields* result in an additional *stray capacitance* $C' \sim \epsilon_0 a \ll C \sim \epsilon_0 a \times (a/d)$.¹⁷ Finally, the same condition ($A \gg d^2$) assures that C is much larger than the self-capacitance C_j of each conductor – see Eq. (18).

The opportunities opened by the last fact for electronic engineering and experimental physics practice are rather astonishing. For example, a very realistic 3-nm layer of high-quality aluminum oxide, which may provide a nearly perfect electric insulation between two thin conducting films, with an area of 0.1 m^2 (a typical area of silicon wafers used in the semiconductor industry) provides $C \sim 1 \text{ mF}$,¹⁸ larger than the self-capacitance of the whole planet Earth!

¹⁷ The exact value of C' depends on the shape of the conductors. In a rare case when it has been calculated analytically, two thin round concentric disks of radius R , $C' = \epsilon_0 R [\ln(16\pi R/d) - 1]$.

¹⁸ Just as in Sec. 1, for the estimate to be realistic, I took into account the additional factor κ (for aluminum oxide, close to 10) which should be included in the numerator of Eq. (28) to make it applicable to dielectrics – see Chapter 3 below.

In a plane capacitor with $d \ll a$, the electrostatic coupling of the two conductors is evidently very *strong*. As an opposite example of a *weakly* coupled system, let us consider two conducting spheres of the same radius R , separated by a much larger distance d (Fig. 4).

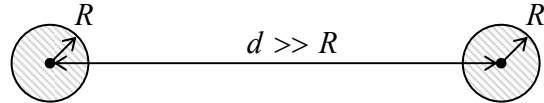


Fig. 2.4. A system of two far-separated, similar conducting spheres.

In this case, the diagonal components of the matrix (23) may be approximately found from Eq. (16), i.e. by neglecting the coupling altogether:

$$\rho_1 = \rho_2 \approx \frac{1}{4\pi\epsilon_0 R}. \quad (2.29)$$

Now, if we had just one sphere (say, number 1), the electric potential at distance d from its center would be given by Eq. (16): $\phi = Q_1/4\pi\epsilon_0 d$. If we move to this point a small ($R \ll d$) sphere without its own charge, we may expect that its potential should not be too far from this result, so that $\phi_2 \approx Q_1/4\pi\epsilon_0 d$. Comparing this expression with the second of Eqs. (19) (taken for $Q_2 = 0$), we get

$$\rho \approx \frac{1}{4\pi\epsilon_0 d} \ll \rho_{1,2}. \quad (2.30)$$

From here and Eq. (26), the mutual capacitance

$$C \approx \frac{1}{\rho_1 + \rho_2} \approx 2\pi\epsilon_0 R. \quad (2.31)$$

We see that (somewhat counter-intuitively), in this limit C does not depend substantially on the distance between the spheres, i.e. does *not* describe their electrostatic coupling. The off-diagonal coefficients of the *reciprocal* capacitance matrix (20) play this role much better – see Eq. (30).

Now let us consider the case when only one conductor of the two is charged, for example $Q_1 \equiv Q$, while $Q_2 = 0$. Then Eqs. (19)-(20) yield

$$\phi_1 = \rho_1 Q_1. \quad (2.32)$$

Now, we may follow Eq. (13) and define $C_1 \equiv 1/\rho_1$ (and $C_2 \equiv 1/\rho_2$), just to see that such *partial capacitances* of the conductors of the system differ from its mutual capacitance C – cf. Eq. (26). For example, in the case shown in Fig. 4, $C_1 = C_2 \approx 4\pi\epsilon_0 R \approx 2C$.

Finally, let us consider one more frequent case when one of the conductors carries a certain charge (say, $Q_1 = Q$), but the potential of its counterpart is sustained constant, say $\phi_2 = 0$.¹⁹ (This condition is especially easy to implement if the second conductor is much larger than the first one. Indeed, as the estimate (18) shows, in this case it would take a much larger charge Q_2 to make the potential ϕ_2 comparable with ϕ_1 .) In this case the second of Eqs. (19), with the account of Eq. (20), yields $Q_2 = -(\rho/\rho_2)Q_1$. Plugging this relation into the first of those equations, we get

¹⁹ In electrical engineering, such a constant-potential conductor is called the *ground*. This term stems from the fact that in many cases the electrostatic potential of the (weakly) conducting ground at the Earth's surface is virtually unaffected by laboratory-scale electric charges.

$$Q_1 = C_1^{\text{ef}} \phi_1, \quad \text{with } C_1^{\text{ef}} \equiv \left(p_1 - \frac{p^2}{p_2} \right)^{-1} \equiv \frac{p_2}{p_1 p_2 - p^2}. \quad (2.33)$$

Thus, this *effective capacitance* of the first conductor is generally different both from both its partial capacitance C_1 and the mutual capacitance C of the system, emphasizing again how accurate one should be using the term “capacitance” without a qualifier.

Note also that none of these capacitances is equal to any element of the matrix reciprocal to the matrix (23):

$$\begin{pmatrix} p_1 & p \\ p & p_2 \end{pmatrix}^{-1} = \frac{1}{p^2 - p_1 p_2} \begin{pmatrix} -p_2 & p \\ p & -p_1 \end{pmatrix}. \quad (2.34)$$

Because of this reason, this *physical capacitance matrix*, which expresses the vector of conductor charges via the vector of their potentials, is less convenient for most applications than the reciprocal capacitance matrix (23). The same conclusion is valid for multi-conductor systems, which are most conveniently characterized by an evident generalization of Eq. (19). Indeed, in this case, even the mutual capacitance between two selected conductors may depend on the electrostatic conditions of other components of the system.

Logically, at this point I would need to discuss the particular, but practically very important case when the regions where the electric field between each pair of conductors is most significant do not overlap – such as in the example shown in Fig. 5a. In this case, the system’s properties may be discussed using the *equivalent-circuit* language, representing each such region as a *lumped* (localized) *capacitor*, with a certain mutual capacitance C , and the whole system as some connection of these capacitors by conducting “wires”, whose length and geometry are not important – see Fig. 5b.

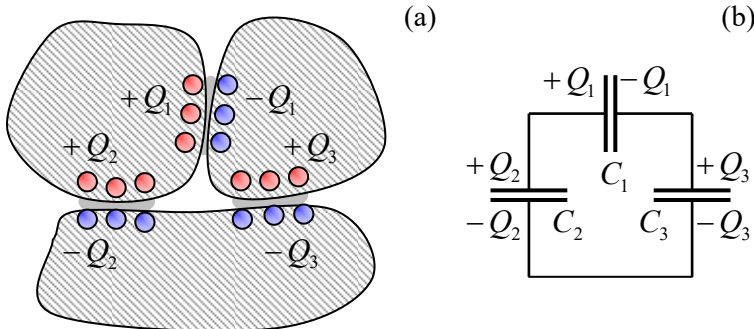


Fig. 2.5. (a) A simple system of conductors, with three well-localized regions of high electric field (and hence surface charge) concentration, and (b) its representation with an equivalent circuit of three lumped capacitors.

Since the analysis of such equivalent circuits is covered in typical introductory physics courses, I will save time by skipping their discussion. However, since such circuits are very frequently met in the physical experiment and electrical engineering practice, I would urge the reader to self-test their understanding of this topic by solving a couple of problems offered at the end of this chapter,²⁰ and if their solution presents any difficulty, review the corresponding section in an undergraduate textbook.

²⁰ These problems have been selected to emphasize the fact that not every circuit may be reduced to the simplest connections of the capacitors in parallel and/or in series.

2.3. The simplest boundary problems

In the general case when the electric field distribution in the free space between the conductors cannot be easily found from the Gauss law or a particular symmetry, the best approach is to try to solve the differential Laplace equation (1.42), with the boundary conditions (1b):

$$\nabla^2 \phi = 0, \quad \phi|_{S_k} = \phi_k, \quad (2.35)$$

Typical
boundary
problem

where S_k is the surface of the k^{th} conductor of the system. After this *boundary problem* has been solved, i.e. the spatial distribution $\phi(\mathbf{r})$ has been found at all points outside the conductors, it is straightforward to use Eq. (3) to find the surface charge density, and finally the total charge

$$Q_k = \oint_{S_k} \sigma d^2 r \quad (2.36)$$

of each conductor, and hence any component of the reciprocal capacitance matrix. As an illustration, let us implement this program for three very simple problems.

(i) Plane capacitor (Fig. 3). In this case, the easiest way to solve the Laplace equation is to use the linear (Cartesian) coordinates with one axis (say, z) normal to the conductor surfaces – see Fig. 6.

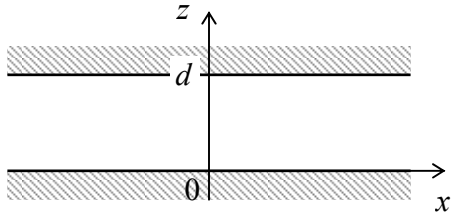


Fig. 2.6. The plane capacitor as the system for the simplest illustration of the boundary problem (35) and its solution.

In these coordinates, the Laplace operator is just the sum of three second derivatives.²¹ It is evident that due to the problem's translational symmetry within the $[x, y]$ plane, deep inside the gap (i.e. at any lateral distance from the edges much larger than d) the electrostatic potential may only depend on the coordinate normal to the gap surfaces: $\phi(\mathbf{r}) = \phi(z)$. For such a function, the derivatives over x and y vanish, and the boundary problem (35) is reduced to a very simple ordinary differential equation

$$\frac{d^2 \phi}{dz^2}(z) = 0, \quad (2.37)$$

with boundary conditions

$$\phi(0) = 0, \quad \phi(d) = V. \quad (2.38)$$

(For the sake of notation simplicity, I have used the discretion of adding a constant to the potential, to make one of the potentials vanish, and also the definition (25) of the voltage V .) The general solution of Eq. (37) is a linear function: $\phi(z) = c_1 z + c_2$, whose constant coefficients $c_{1,2}$ may be readily found from the boundary conditions (38). The final solution is

$$\phi = V \frac{z}{d}. \quad (2.39)$$

²¹ See, e.g. MA Eq. (9.1).

From here the only nonzero component of the electric field is

$$E_z = -\frac{d\phi}{dz} = -\frac{V}{d}, \quad (2.40)$$

and the surface charge of the capacitor plates is

$$\sigma = \epsilon_0 E_n = \mp \epsilon_0 E_z = \pm \epsilon_0 \frac{V}{d}, \quad (2.41)$$

where the upper and lower signs correspond to the upper and lower plate, respectively. Since σ does not depend on x and y , we can get the full charges $Q_1 = -Q_2 \equiv Q$ of the surfaces by its multiplication by the gap area A , giving us again the already obtained result (28) for the mutual capacitance $C \equiv Q/V$. I believe that this calculation, though very easy, may serve as a good illustration of the boundary problem solution approach, which will be used below for more complex cases.

(ii) Coaxial-cable capacitor. *Coaxial cable* is a system of two round cylindrical, coaxial conductors, with the cross-section shown in Fig. 7.

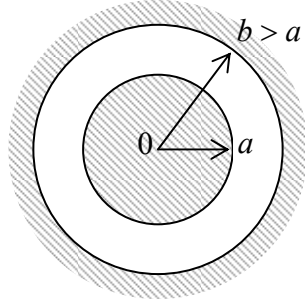


Fig. 2.7. The cross-section of a coaxial cable.

Evidently, in this case the cylindrical coordinates $\{\rho, \varphi, z\}$, with the z -axis coinciding with the common axis of the cylinders, are most convenient.²² Due to the axial symmetry of the problem, in these coordinates $\mathbf{E(r)} = \mathbf{n}_\rho E(\rho)$, $\phi(\mathbf{r}) = \phi(\rho)$, so that in the general expression for the Laplace operator²³ we may take $\partial/\partial\varphi = \partial/\partial z = 0$. As a result, only the radial term of the operator survives, and the boundary problem (35) takes the form

$$\frac{1}{\rho} \frac{d}{d\rho} \left(\rho \frac{d\phi}{d\rho} \right) = 0, \quad \phi(a) = V, \quad \phi(b) = 0. \quad (2.42)$$

The sequential double integration of this ordinary linear differential equation is elementary (and similar to that of the Poisson equation in spherical coordinates, carried out in Sec. 1.3), giving

$$\rho \frac{d\phi}{d\rho} = c_1, \quad \phi(\rho) = c_1 \int_a^\rho \frac{d\rho''}{\rho''} + c_2 = c_1 \ln \frac{\rho}{a} + c_2. \quad (2.43)$$

The constants $c_{1,2}$ may be found using boundary conditions (42):

²² I am sorry for using for the 2D radius the same letter ρ as for the volumic density of charge. (Both notations are too common to refuse.) I do not believe this may lead to confusion, because the letter will not be used in two different meanings during any particular discussion.

²³ See, e.g., MA Eq. (10.3).

$$c_2 = V, \quad c_1 \ln \frac{b}{a} + c_2 = 0, \quad (2.44)$$

giving $c_1 = -V/\ln(b/a)$, so that Eq. (43) takes the following form:

$$\phi(\rho) = V \left[1 - \frac{\ln(\rho/a)}{\ln(b/a)} \right]. \quad (2.45)$$

Next, for our axial symmetry, the general expression for the gradient of a scalar function is reduced to its radial derivative, so that

$$E(\rho) \equiv -\frac{d\phi(\rho)}{d\rho} = \frac{V}{\rho \ln(b/a)}. \quad (2.46)$$

This expression, plugged into Eq. (2), allows us to find the density of conductors' surface charge. For example, for the inner electrode

$$\sigma_a = \epsilon_0 E(a) = \frac{\epsilon_0 V}{a \ln(b/a)}, \quad (2.47)$$

so that its full charge (per unit length of the system) is

$$\frac{Q}{l} = 2\pi a \sigma_a = \frac{2\pi \epsilon_0 V}{\ln(b/a)}. \quad (2.48)$$

(It is straightforward to check that the charge of the outer electrode is equal and opposite.) Hence, by the definition of the mutual capacitance, its value per unit length is

$$\boxed{\frac{C}{l} \equiv \frac{Q}{lV} = \frac{2\pi \epsilon_0}{\ln(b/a)}}. \quad (2.49)$$

C: Coaxial cable

This expression shows that the total capacitance C is proportional to the systems length l (if $l \gg a, b$), while being only logarithmically dependent on the dimensions of its cross-section. Since the logarithm of a large argument is an extremely slow function (sometimes called a *quasi-constant*), if the external conductor is made very large ($b \gg a$), the capacitance diverges, but very weakly. Such *logarithmic divergence* may be cut by any minuscule additional effect, for example by the finite length l of the system. This fact yields the following very useful estimate of the self-capacitance of a *single* round wire of radius a :

$$C \approx \frac{2\pi \epsilon_0 l}{\ln(l/a)}, \quad \text{for } l \gg a. \quad (2.50)$$

On the other hand, if the gap d between the conductors is very narrow: $d \equiv b - a \ll a$, then $\ln(b/a) \equiv \ln(1 + d/a)$ may be approximated as d/a , and Eq. (49) is reduced to $C \approx 2\pi \epsilon_0 a l / d$, i.e. to Eq. (28) for the plane capacitor, of the appropriate area $A = 2\pi a l$.

(iii) Spherical capacitor. This is a system of two conductors, with the *central* cross-section similar to that of the coaxial cable (Fig. 7), but now with the spherical rather than axial symmetry. This symmetry implies that we may be better off using spherical coordinates, so that the potential ϕ depends only on one of them: the distance r from the common center of the conductors: $\phi(\mathbf{r}) = \phi(r)$. As we already know from Sec. 1.3, in this case the general expression for the Laplace operator is reduced to its

first (radial) term, so that the Laplace equation takes the simple form (1.47). Moreover, we have already found the general solution of this equation – see Eq. (1.50):

$$\phi(r) = \frac{c_1}{r} + c_2, \quad (2.51)$$

Now acting exactly as above, i.e. determining the (only essential) constant c_1 from the boundary condition $\phi(a) - \phi(b) = V$, we get

$$c_1 = V \left(\frac{1}{a} - \frac{1}{b} \right)^{-1}, \quad \text{so that } \phi(r) = \frac{V}{r} \left(\frac{1}{a} - \frac{1}{b} \right)^{-1} + c_2. \quad (2.52)$$

Next, we can use the spherical symmetry to find the electric field, $\mathbf{E}(\mathbf{r}) = \mathbf{n}_r E(r)$, with

$$E(r) = -\frac{d\phi}{dr} = \frac{V}{r^2} \left(\frac{1}{a} - \frac{1}{b} \right)^{-1}, \quad (2.53)$$

and hence its values on conductors' surfaces, and then the surface charge density σ from Eq. (3). For example, for the inner conductor's surface,

$$\sigma_a = \epsilon_0 E(a) = \epsilon_0 \frac{V}{a^2} \left(\frac{1}{a} - \frac{1}{b} \right)^{-1}, \quad (2.54)$$

so that, finally, for the full charge of that conductor we get the following result:

$$Q = 4\pi a^2 \sigma = 4\pi \epsilon_0 \left(\frac{1}{a} - \frac{1}{b} \right)^{-1} V. \quad (2.55)$$

(Again, the charge of the outer conductor is equal and opposite.) Now we can use the definition (26) of the mutual capacitance to get the final result:

$$C \equiv \frac{Q}{V} = 4\pi \epsilon_0 \left(\frac{1}{a} - \frac{1}{b} \right)^{-1} \equiv 4\pi \epsilon_0 \frac{ab}{b-a}. \quad (2.56)$$

For $b \gg a$, it coincides with Eq. (17) for the self-capacitance of the inner conductor. On the other hand, if the gap d between two conductors is narrow, $d \equiv b - a \ll a$, then

$$C = 4\pi \epsilon_0 \frac{a(a+d)}{d} \approx 4\pi \epsilon_0 \frac{a^2}{d}, \quad (2.57)$$

i.e. the capacitance approaches that of the planar capacitor of the area $A = 4\pi a^2$ – as it should.

All this seems (and indeed is) very straightforward, but let us contemplate what was the reason for such easy successes. In each of the cases (i)-(iii) we have managed to find such coordinates that both the Laplace equation and the boundary conditions involved only one of them. The necessary condition for the former fact is for the coordinates to be *orthogonal*. This means that the three vector components of the local differential $d\mathbf{r}$, due to small variations of the new coordinates (say, dr , $d\theta$, and $d\varphi$ for the spherical coordinates), are mutually perpendicular.

2.4. Using other orthogonal coordinates

The cylindrical and spherical coordinates used above are only the simplest examples of the *curvilinear orthogonal* (or just “orthogonal”) coordinates, and that approach may be extended to other

coordinate systems of this type. As an example, let us calculate the self-capacitance of a thin, round conducting disk. The cylindrical or spherical coordinates would not give much help here, because while they have the appropriate axial symmetry, they would make the boundary condition on the disk too complicated: involving two coordinates, either ρ and z , or r and θ . Help comes from noting that the flat disk, i.e. the area with $z = 0, r < R$, may be viewed as the limiting case of an *axially-symmetric ellipsoid* (or “degenerate ellipsoid”, or “ellipsoid of rotation”, or “spheroid”) – the surface formed by rotation of the usual ellipse about one of its major axes – which would be also the symmetry axis of the disk – in Fig. 8, the z -axis.

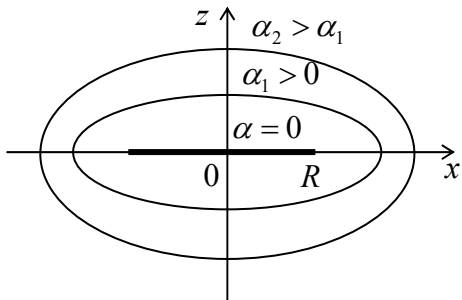


Fig. 2.8. Solving the disk’s capacitance problem. (The cross-section of the system by the vertical plane $y = 0$.)

Analytically, this ellipsoid may be described by the following equation:

$$\frac{x^2 + y^2}{a^2} + \frac{z^2}{b^2} = 1, \quad (2.58)$$

where a and b are the so-called *major semi-axes*, whose ratio determines the ellipse’s *eccentricity* – the degree of its “squeezing”. For our problem, we will only need *oblate* ellipsoids with $a \geq b$; according to Eq. (58), they may be represented as surfaces of constant α in the *oblate spheroidal* (also called “degenerate ellipsoidal”) *coordinates* $\{\alpha, \beta, \varphi\}$ that are related to the Cartesian coordinates as follows:²⁴

$$\begin{aligned} x &= R \cosh \alpha \sin \beta \cos \varphi, & 0 \leq \alpha < \infty, \\ y &= R \cosh \alpha \sin \beta \sin \varphi, & \text{with } 0 \leq \beta \leq \pi, \\ z &= R \sinh \alpha \cos \beta, & 0 \leq \varphi \leq 2\pi. \end{aligned} \quad (2.59)$$

Such spheroidal coordinates are an evident generalization of the spherical coordinates, which correspond to the limit $\alpha \gg 1$ (i.e. $r \gg R$). In the opposite limit, the surface of constant $\alpha = 0$ describes our thin disk of radius R , with the coordinate β describing the distance $\rho \equiv (x^2 + y^2)^{1/2} = R \sin \beta$ of its point from the z -axis. It is almost evident (and easy to prove) that the curvilinear coordinates (59) are also orthogonal; the Laplace operator in them is:

$$\nabla^2 = \frac{1}{R^2(\cosh^2 \alpha - \sin^2 \beta)} \times \left[\begin{array}{l} \frac{1}{\cosh \alpha} \frac{\partial}{\partial \alpha} \left(\cosh \alpha \frac{\partial}{\partial \alpha} \right) \\ + \frac{1}{\sin \beta} \frac{\partial}{\partial \beta} \left(\sin \beta \frac{\partial}{\partial \beta} \right) + \left(\frac{1}{\sin^2 \beta} - \frac{1}{\cosh^2 \alpha} \right) \frac{\partial^2}{\partial \varphi^2} \end{array} \right]. \quad (2.60)$$

Though this expression may look a bit intimidating, let us notice that since in our current problem, the boundary conditions depend only on α :²⁵

²⁴ For solution of some problems, it is convenient to use Eqs. (59) with $-\infty < \alpha < +\infty$ and $0 \leq \beta \leq \pi/2$.

²⁵ I have called the disk’s potential V , to distinguish it from the potential ϕ at an arbitrary point of space.

$$\phi|_{\alpha=0} = V, \quad \phi|_{\alpha=\infty} = 0, \quad (2.61)$$

there is every reason to assume that the electrostatic potential in all space is a function of α alone; in other words, that all ellipsoids $\alpha = \text{const}$ are the equipotential surfaces. Indeed, acting on such a function $\phi(\alpha)$ by the Laplace operator (60), we see that the two last terms in the square brackets vanish, and the Laplace equation (35) is reduced to a simple ordinary differential equation

$$\frac{d}{d\alpha} \left[\cosh \alpha \frac{d\phi}{d\alpha} \right] = 0. \quad (2.62)$$

Integrating it twice, just as we did in the three previous problems, we get

$$\phi(\alpha) = c_1 \int \frac{d\alpha}{\cosh \alpha}. \quad (2.63)$$

This integral may be readily worked out using the substitution $\xi \equiv \sinh \alpha$ (which gives $d\xi \equiv \cosh \alpha d\alpha$, i.e. $d\alpha = d\xi / \cosh \alpha$, and $\cosh^2 \alpha = 1 + \sinh^2 \alpha \equiv 1 + \xi^2$):

$$\phi(\alpha) = c_1 \int_0^{\sinh \alpha} \frac{d\xi}{1 + \xi^2} + c_2 = c_1 \tan^{-1}(\sinh \alpha) + c_2. \quad (2.64)$$

The integration constants $c_{1,2}$ may be simply found from the boundary conditions (61), and we arrive at the following final expression for the electrostatic potential:

$$\phi(\alpha) = V \left[1 - \frac{2}{\pi} \tan^{-1}(\sinh \alpha) \right] \equiv \frac{2V}{\pi} \tan^{-1}\left(\frac{1}{\sinh \alpha}\right). \quad (2.65)$$

This solution satisfies both the Laplace equation and the boundary conditions. Mathematicians tell us that the solution of any boundary problem of the type (35) is *unique*, so we do not need to look any further.

Now we may use Eq. (3) to find the surface density of electric charge, but in the case of a thin disk, it is more natural to add up such densities on its top and bottom surfaces at the same distance $\rho = (x^2 + y^2)^{1/2}$ from the disk's center. The densities are evidently equal, due to the problem symmetry about the plane $z = 0$, so that the total density is $\sigma = 2\epsilon_0 E_n|_{z=+0}$. According to Eq. (65), and the last of Eqs. (59), the electric field on the upper surface is

$$E_n|_{z=+0} = -\frac{\partial \phi}{\partial z}|_{z=+0} = -\frac{\partial \phi(\alpha)}{\partial(R \sinh \alpha \cos \beta)}|_{\alpha=0} = \frac{2}{\pi} V \frac{1}{R \cos \beta} = \frac{2}{\pi} V \frac{1}{(R^2 - \rho^2)^{1/2}}, \quad (2.66)$$

and we see that the charge is distributed over the disk very nonuniformly:

$$\sigma = \frac{4}{\pi} \epsilon_0 V \frac{1}{(R^2 - \rho^2)^{1/2}}, \quad (2.67)$$

with a singularity at the disk edge. Below we will see that such singularities are very typical for sharp edges of conductors. Fortunately, in our current case the divergence is integrable, giving a finite disk charge:

$$Q = \int_{\text{disk surface}} \sigma d^2 \rho = \int_0^R \sigma(\rho) 2\pi \rho d\rho = \frac{4}{\pi} \epsilon_0 V \int_0^R \frac{2\pi \rho d\rho}{(R^2 - \rho^2)^{1/2}} = 4\epsilon_0 V R \int_0^1 \frac{d\xi}{(1 - \xi)^{1/2}} = 8\epsilon_0 RV. \quad (2.68)$$

Thus, for the disk's self-capacitance we get a very simple result,

$$C = 8\epsilon_0 R \equiv \frac{2}{\pi} 4\pi\epsilon_0 R, \quad (2.69)$$

a factor of $\pi/2 \approx 1.57$ lower than that for the conducting sphere of the same radius, but still complying with the general estimate (18).

Can we always find such a “good” system of orthogonal coordinates? Unfortunately, the answer is *no*, even for highly symmetric geometries. This is why the practical value of this approach is limited, and other, more general methods of boundary problem solution are clearly needed. Before proceeding to their discussion, however, let me note that in the case of 2D problems (i.e. cylindrical geometries²⁶), the orthogonal coordinate method gets much help from the following *conformal mapping* approach.

Let us consider a pair of Cartesian coordinates $\{x, y\}$ of the cylinder's cross-section plane as a complex variable $z \equiv x + iy$,²⁷ where i is the imaginary unit ($i^2 = -1$), and let $\mathbf{w}(z) = u + iv$ be an *analytic complex function* of z .²⁸ For our current purposes, the most important property of an analytic function is that its real and imaginary parts obey the following *Cauchy-Riemann relations*:²⁹

$$\frac{\partial u}{\partial x} = \frac{\partial v}{\partial y}, \quad \frac{\partial v}{\partial x} = -\frac{\partial u}{\partial y}. \quad (2.70)$$

For example, for the function

$$\mathbf{w} = z^2 \equiv (x + iy)^2 \equiv (x^2 - y^2) + 2ixy, \quad (2.71)$$

whose real and imaginary parts are

$$u \equiv \operatorname{Re} \mathbf{w} = x^2 - y^2, \quad v \equiv \operatorname{Im} \mathbf{w} = 2xy, \quad (2.72)$$

we immediately see that $\partial u / \partial x = 2x = \partial v / \partial y$, and $\partial v / \partial x = 2y = -\partial u / \partial y$, in accordance with Eq. (70).

Let us differentiate the first of Eqs. (70) over x again, then change the order of differentiation, and after that use the latter of those equations:

$$\frac{\partial^2 u}{\partial x^2} = \frac{\partial}{\partial x} \frac{\partial u}{\partial x} = \frac{\partial}{\partial x} \frac{\partial v}{\partial y} = \frac{\partial}{\partial y} \frac{\partial v}{\partial x} = -\frac{\partial}{\partial y} \frac{\partial u}{\partial y} = -\frac{\partial^2 u}{\partial y^2}, \quad (2.73)$$

²⁶ Let me remind the reader that the term *cylindrical* describes any surface formed by a translation, along a straight line, of an *arbitrary* curve, and hence more general than the usual circular cylinder. (In this terminology, for example, a prism is also a cylinder of a particular type, formed by a translation of a polygon.)

²⁷ The complex variable z should not be confused with the (real) 3rd spatial coordinate z ! We are considering 2D problems now, with the potential independent of z .

²⁸ An analytic (or “holomorphic”) function may be defined as the one that may be expanded into the Taylor series in its complex argument, i.e. is infinitely differentiable in the given point. (Almost all “regular” functions, such as z^n , $z^{1/n}$, $\exp z$, $\ln z$, etc., and their linear combinations are analytic at all z , maybe besides certain special points.) If the reader needs to brush up on their background on this subject, I can recommend a popular textbook by M. Spiegel *et al.*, *Complex Variables*, 2nd ed., McGraw-Hill, 2009.

²⁹ These relations may be used, in particular, to prove the Cauchy integral formula – see, e.g., MA Eq. (15.1).

and similarly for v . This means that the sum of second-order partial derivatives of each of the real functions $u(x, y)$ and $v(x, y)$ is zero, i.e. that both functions obey the 2D Laplace equation. This mathematical fact opens a nice way of solving problems of electrostatics for (relatively simple) 2D geometries. Imagine that for a particular boundary problem we have found a function $w(z)$ for that either $u(x, y)$ or $v(x, y)$ is constant on all electrode surfaces. Then all lines of constant u (or v) represent equipotential surfaces, i.e. the problem of the potential distribution has been essentially solved.

As a simple example, let us consider a problem important for practice: the *quadrupole electrostatic lens* – a system of four cylindrical electrodes with hyperbolic cross-sections, whose boundaries are described by the following relations:

$$x^2 - y^2 = \begin{cases} +a^2, & \text{for the left and right electrodes,} \\ -a^2, & \text{for the top and bottom electrodes,} \end{cases} \quad (2.74)$$

voltage-biased as shown in Fig. 9a.

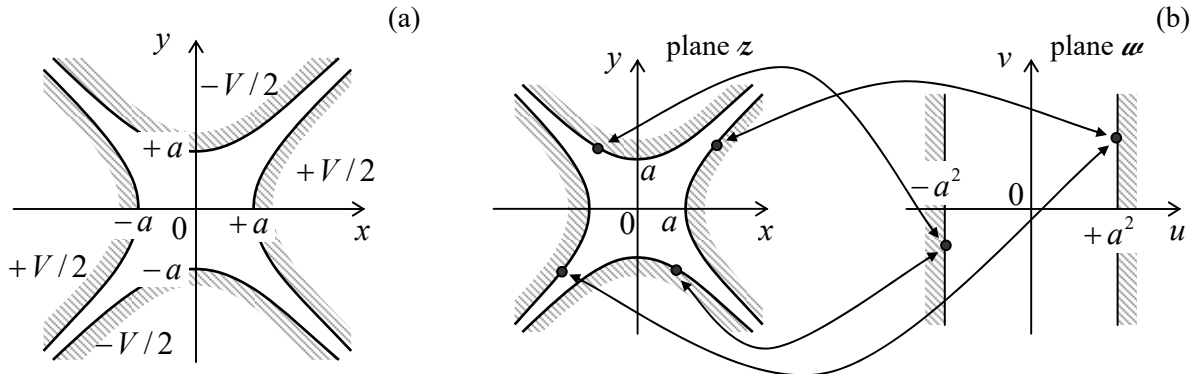


Fig. 2.9. (a) The quadrupole electrostatic lens' cross-section and (b) its conformal mapping.

Comparing these relations with Eqs. (72), we see that each electrode surface corresponds to a constant value of the real part $u(x, y)$ of the function given by Eq. (71): $u = \pm a^2$. Moreover, the potentials of both surfaces with $u = +a^2$ are equal to $+V/2$, while those with $u = -a^2$ are equal to $-V/2$. Hence we may conjecture that the electrostatic potential at each point is a function of u alone; moreover, a simple linear function,

$$\phi = c_1 u + c_2 \equiv c_1 (x^2 - y^2) + c_2, \quad (2.75)$$

is a valid (and hence the unique) solution of our boundary problem. Indeed, it does satisfy the Laplace equation, while the constants $c_{1,2}$ may be readily selected in a way to satisfy all the boundary conditions shown in Fig. 9a:

$$\phi = \frac{V}{2} \frac{x^2 - y^2}{a^2}. \quad (2.76)$$

so that the boundary problem has been solved.

According to Eq. (76), all equipotential surfaces are hyperbolic cylinders, similar to those of the electrode surfaces. What remains is to find the electric field at an arbitrary point inside the system:

$$E_x = -\frac{\partial \phi}{\partial x} = -V \frac{x}{a^2}, \quad E_y = -\frac{\partial \phi}{\partial y} = V \frac{y}{a^2}. \quad (2.77)$$

These formulas show, in particular, that if charged particles (e.g., electrons in an electron-optics system) are launched to fly ballistically through such a lens, along the z -axis, they experience a force pushing them toward the symmetry axis and proportional to the particle's deviation from the axis (and thus equivalent in action to an optical lens with a positive refraction power) in one direction, and a force pushing them out (negative refractive power) in the perpendicular direction. One can show that letting the particles fly through several such lenses, with alternating voltage polarities, in series, enables beam focusing.³⁰

Hence, we have reduced the 2D Laplace boundary problem to that of finding the proper analytic function $\mathbf{w}(z)$. This task may be also understood as that of finding a *conformal map*, i.e. a correspondence between components of any point pair, $\{x, y\}$ and $\{u, v\}$, residing, respectively, on the initial Cartesian plane z and the plane \mathbf{w} of the new variables. For example, Eq. (71) maps the real electrode configuration onto a plane capacitor of an infinite area (Fig. 9b), and the simplicity of Eq. (75) is due to the fact that for the latter system the equipotential surfaces are just parallel planes $u = \text{const}$.

For more complex geometries, the suitable analytic function $\mathbf{w}(z)$ may be hard to find. However, for conductors with piece-linear cross-section boundaries, substantial help may be obtained from the following *Schwarz-Christoffel integral*

$$\mathbf{w}(z) = \text{const} \times \int \frac{dz}{(z - x_1)^{k_1} (z - x_2)^{k_2} \dots (z - x_{N-1})^{k_{N-1}}}. \quad (2.78)$$

that provides a conformal mapping of the interior of an *arbitrary* N -sided polygon on the plane $\mathbf{w} = u + iv$, onto the upper-half ($y > 0$) of the plane $z = x + iy$. In Eq. (78), x_j ($j = 1, 2, N-1$) are the points of the $y = 0$ axis (i.e., of the boundary of the mapped region on plane z) to which the corresponding polygon vertices are mapped, while k_j are the exterior angles at the polygon vertices, measured in the units of π , with $-1 \leq k_j \leq +1$ – see Fig. 10.³¹ Of the points x_j , two may be selected arbitrarily (because their effects may be compensated by the multiplicative constant in Eq. (78), and the additive constant of integration), while all the others have to be adjusted to provide the correct mapping.

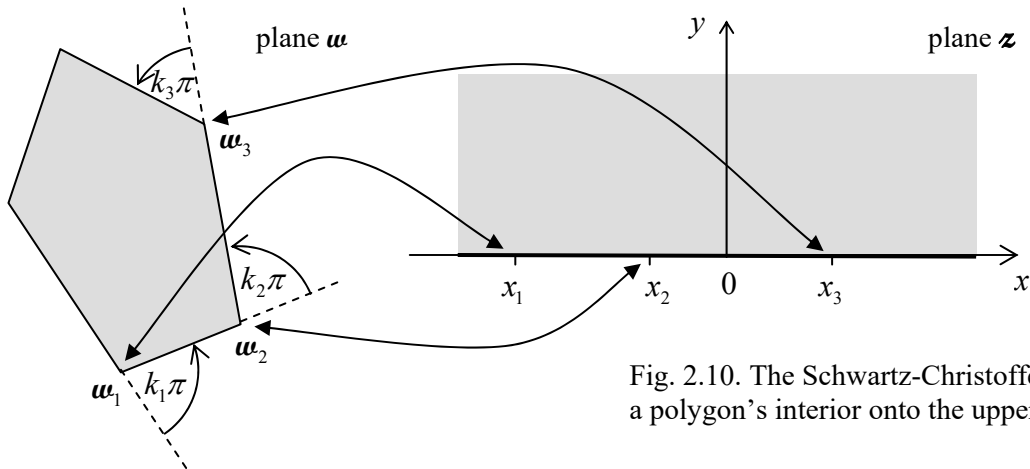


Fig. 2.10. The Schwartz-Christoffel mapping of a polygon's interior onto the upper half-plane.

³⁰ See, e.g., textbook by P. Grivet, *Electron Optics*, 2nd ed., Pergamon, 1972.

³¹ The integral (78) includes only $(N-1)$ rather than N poles because a polygon's shape is fully determined by $(N-1)$ positions \mathbf{w}_j of its vertices and $(N-1)$ angles πk_j . In particular, since the algebraic sum of all external angles of a polygon equals 2π , the last angle parameter $k_j = k_N$ is uniquely determined by the set of the previous ones.

In the general case, the complex integral (78) may be hard to tackle. However, in some important cases, in particular those with right angles ($k_j = \pm\frac{1}{2}$) and/or with some points \mathbf{w}_j at infinity, the integrals may be readily worked out, giving explicit analytical expressions for the mapping functions $\mathbf{w}(z)$. For example, let us consider a semi-infinite strip defined by restrictions $-1 \leq u \leq +1$ and $0 \leq v$, on the \mathbf{w} -plane – see the left panel of Fig. 11.

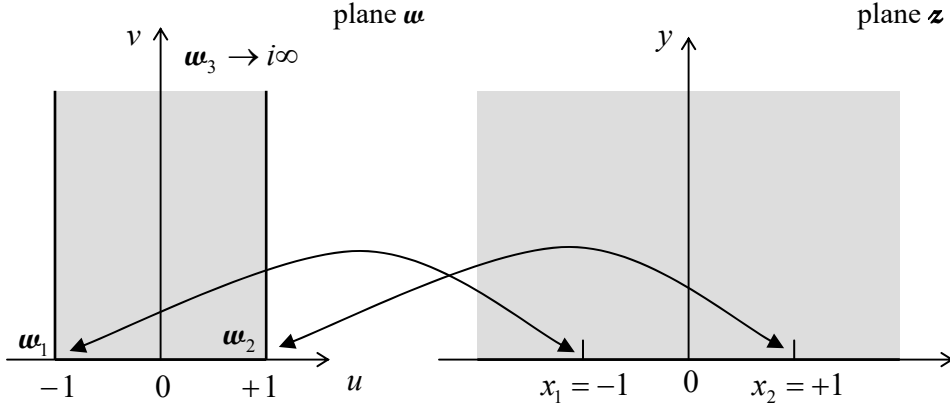


Fig. 2.11. A semi-infinite strip mapped onto the upper half-plane.

The strip may be considered as a triangle, with one vertex at the infinitely distant vertical point $\mathbf{w}_3 = 0 + i\infty$. Let us map the polygon on the upper half of plane z , shown on the right panel of Fig. 11, with the vertex $\mathbf{w}_1 = -1 + i0$ mapped onto the point $z_1 = -1 + i0$, and the vertex $\mathbf{w}_2 = +1 + i0$ mapped onto the point $z_2 = +1 + i0$. Since the external angles at both these vertices are equal to $+\pi/2$, and hence $k_1 = k_2 = +\frac{1}{2}$, Eq. (78) is reduced to

$$\mathbf{w}(z) = \text{const} \times \int \frac{dz}{(z+1)^{1/2}(z-1)^{1/2}} \equiv \text{const} \times \int \frac{dz}{(z^2-1)^{1/2}} \equiv \text{const} \times i \int \frac{dz}{(1-z^2)^{1/2}}. \quad (2.79)$$

This complex integral may be worked out, just as for real z , with the substitution $z = \sin \xi$, giving

$$w(z) = \text{const}' \times \int d\xi \stackrel{\sin^{-1} z}{=} c_1 \sin^{-1} z + c_2. \quad (2.80)$$

Determining the constants $c_{1,2}$ from the required mapping, i.e. from the conditions $\mathbf{w}(-1 + i0) = -1 + i0$ and $\mathbf{w}(+1 + i0) = +1 + i0$ (see the arrows in Fig. 11), we finally get³²

$$\mathbf{w}(z) = \frac{2}{\pi} \sin^{-1} z, \quad \text{i.e. } z = \sin \frac{\pi \mathbf{w}}{2}. \quad (2.81a)$$

Using the well-known expression for the sine of a complex argument,³³ we may rewrite this elegant result in either of the following two forms for the real and imaginary components of z and \mathbf{w} :

$$u = \frac{2}{\pi} \sin^{-1} \frac{2x}{[(x+1)^2 + y^2]^{1/2} + [(x-1)^2 + y^2]^{1/2}}, \quad v = \frac{2}{\pi} \cosh^{-1} \frac{[(x+1)^2 + y^2]^{1/2} + [(x-1)^2 + y^2]^{1/2}}{2},$$

³² Note that this function differs only by a linear transformation of variables from the function $\mathbf{z} = c \cosh \mathbf{w}$, which is the canonical form of the definition of the so-called *elliptic* (not ellipsoidal!) orthogonal coordinates.

³³ See, e.g., MA Eq. (3.5).

$$x = \sin \frac{\pi u}{2} \cosh \frac{\pi v}{2}, \quad y = \cos \frac{\pi u}{2} \sinh \frac{\pi v}{2}. \quad (2.81b)$$

It is amazing how perfectly does the last formula manage to keep $y \equiv 0$ at the different borders of our ω -region (Fig. 11): at its side borders ($u = \pm 1, 0 \leq v < \infty$), this is performed by the first multiplier, while at the bottom border ($-1 \leq u \leq +1, v = 0$), the equality is enforced by the second multiplier.

This mapping may be used to solve several electrostatics problems with the geometry shown in Fig. 11a; probably the most surprising of them is the following one. A straight gap of width $2t$ is cut in a very thin conducting plane, and voltage V is applied between the resulting half-planes – see the bold straight lines in Fig. 12.

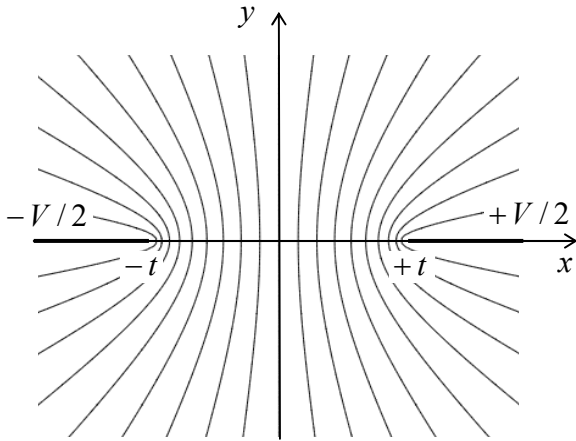


Fig. 2.12. The equipotential surfaces of the electric field between two thin conducting semi-planes (or rather their cross-sections by the plane $z = \text{const}$).

Selecting a Cartesian coordinate system with the z -axis directed along the cut, the y -axis normal to the plane, and the origin in the middle of the cut (Fig. 12), we can write the boundary conditions of this Laplace problem as

$$\phi = \begin{cases} +V/2, & \text{for } x > +t, y = 0, \\ -V/2, & \text{for } x < -t, y = 0. \end{cases} \quad (2.82)$$

(Due to the problem's symmetry, we may expect that in the middle of the gap, i.e. at $-t < x < +t$ and $y = 0$, the electric field is parallel to the plane and hence $\partial\phi/\partial y = 0$.) The comparison of Figs. 11 and 12 shows that if we normalize our coordinates $\{x, y\}$ to t , Eqs. (81) provide the conformal mapping of our system on the plane z to a plane capacitor on the plane ω , with the voltage V between two conducting planes located at $u = \pm 1$. Since we already know that in that case $\phi = (V/2)u$, we may immediately use the first of Eqs. (81b) to write the final solution of the problem:³⁴

$$\phi = \frac{V}{2}u = \frac{V}{\pi} \sin^{-1} \frac{2x}{[(x+t)^2 + y^2]^{1/2} + [(x-t)^2 + y^2]^{1/2}}. \quad (2.83)$$

The thin lines in Fig. 12 show the corresponding equipotential surfaces;³⁵ it is evident that the electric field concentrates at the gap edges, just as it did at the edge of the thin disk (Fig. 8). Let me

³⁴ This result may be also obtained by the Green's function method, to be discussed in Sec. 10 below.

³⁵ Another graphical representation of the electric field distribution, by *field lines*, is less convenient. (It is more useful for the magnetic field, which may be represented by a scalar potential only in particular cases, so there is no surprise that the field lines were introduced only by Michael Faraday in the 1830s.) As a reminder, the field

leave the remaining calculation of the surface charge distribution and the mutual capacitance between the half-planes (per unit length of the system in the z -direction) for the reader's exercise.

2.5. Variable separation – Cartesian coordinates

The general approach of the methods discussed in the last two sections was to satisfy the Laplace equation by a function of a single variable that also satisfies the boundary conditions. Unfortunately, in many cases this cannot be done – at least, using reasonably simple functions. In this case, a very powerful method called the *variable separation*,³⁶ may work, typically producing “semi-analytical” results in the form of series (infinite sums) of either elementary or well-studied special functions. Its main idea is to look for the solution of the boundary problem (35) as the sum of partial solutions,

$$\phi = \sum_k c_k \phi_k , \quad (2.84)$$

where each function ϕ_k satisfies the Laplace equation, and then select the set of coefficients c_k to satisfy the boundary conditions. More specifically, in the variable separation method, the partial solutions ϕ_k are looked for in the form of a product of functions, each depending on just one spatial coordinate.

Let us discuss this approach on the classical example of a rectangular box with conducting walls (Fig. 13), with the same potential (that I will take for zero) at all its sidewalls and the lower lid, but a different potential V at the top lid ($z = c$). Moreover, to demonstrate the power of the variable separation method, let us carry out all the calculations for a more general case when the top lid's potential is an arbitrary 2D function $V(x, y)$.³⁷

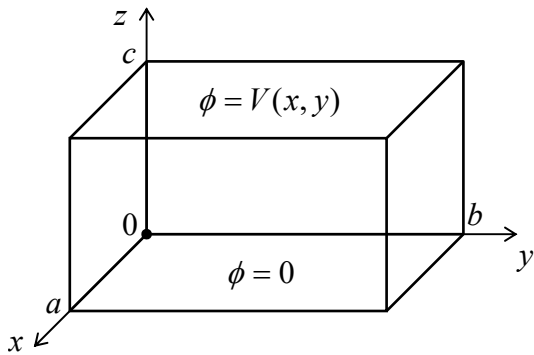


Fig. 2.13. The standard playground for the variable separation discussion: a rectangular box with five conducting, grounded walls and a fixed potential distribution $V(x, y)$ on the top lid.

For this geometry, it is natural to use the Cartesian coordinates $\{x, y, z\}$, representing each of the partial solutions in Eq. (84) as the following product

line is the curve to which the field vectors are tangential at each point. Hence the electric field lines are always normal to the equipotential surfaces, so that it is always straightforward to sketch them, if desirable, from the equipotential surface pattern – like the one shown in Fig. 12.

³⁶ This method was already discussed in CM Sec. 6.5 and then used also in Secs. 6.6 and 8.4 of that course. However, it is so important that I need to repeat its discussion in this part of my series, for the benefit of the readers who have skipped the Classical Mechanics course for whatever reason.

³⁷ Such voltage distributions may be implemented in practice, for example, using the so-called *mosaic electrodes* consisting of many electrically-insulated and individually-biased panels.

$$\phi_k = X(x)Y(y)Z(z). \quad (2.85)$$

Plugging it into the Laplace equation expressed in the Cartesian coordinates,

$$\frac{\partial^2 \phi_k}{\partial x^2} + \frac{\partial^2 \phi_k}{\partial y^2} + \frac{\partial^2 \phi_k}{\partial z^2} = 0, \quad (2.86)$$

and dividing the result by XYZ , we get

$$\frac{1}{X} \frac{d^2 X}{dx^2} + \frac{1}{Y} \frac{d^2 Y}{dy^2} + \frac{1}{Z} \frac{d^2 Z}{dz^2} = 0. \quad (2.87)$$

Here comes the punch line of the variable separation method: since the first term of this sum may depend only on x , the second one only of y , etc., Eq. (87) may be satisfied everywhere in the volume only if each of these terms equals a constant. In a minute we will see that for our current problem (Fig. 13), these constant x - and y -terms have to be negative; hence let us denote these *variable separation constants* as $(-\alpha^2)$ and $(-\beta^2)$, respectively. Now Eq. (87) shows that the constant z -term has to be positive; denoting it as γ^2 we get the following relation:

$$\alpha^2 + \beta^2 = \gamma^2. \quad (2.88)$$

Now the variables are separated in the sense that for the functions $X(x)$, $Y(y)$, and $Z(z)$ we have got separate ordinary differential equations,

$$\frac{d^2 X}{dx^2} + \alpha^2 X = 0, \quad \frac{d^2 Y}{dy^2} + \beta^2 Y = 0, \quad \frac{d^2 Z}{dz^2} - \gamma^2 Z = 0, \quad (2.89)$$

which are related only by Eq. (88) for their constant parameters.

Let us start from the equation for $X(x)$. Its general solution is the sum of functions $\sin \alpha x$ and $\cos \alpha x$, multiplied by arbitrary coefficients. Let us select these coefficients to satisfy our boundary conditions. First, since $\phi \propto X$ should vanish at the back vertical wall of the box (i.e., with the coordinate origin choice shown in Fig. 13, at $x = 0$ for any y and z), the coefficient at $\cos \alpha x$ should be zero. The remaining coefficient (at $\sin \alpha x$) may be included in the general factor c_k in Eq. (84), so that we may take X in the form

$$X = \sin \alpha x. \quad (2.90)$$

This solution satisfies the boundary condition at the opposite wall ($x = a$) only if the product αa is a multiple of π , i.e. if α is equal to any of the following numbers (commonly called *eigenvalues*):³⁸

$$\alpha_n = \frac{\pi}{a} n, \quad \text{with } n = 1, 2, \dots \quad (2.91)$$

(Terms with negative values of n would not be linearly-independent from those with positive n , and may be dropped from the sum (84). The value $n = 0$ is formally possible, but would give $X = 0$, i.e. $\phi_k = 0$, at

³⁸ Note that according to Eqs. (91)-(92), as the spatial dimensions a and b of the system are increased, the distances between the adjacent eigenvalues tend to zero. This fact implies that for spatially-infinite systems, the eigenvalue spectra are continuous, so that the sums of the type (84) become integrals; however, the general approach remains the same. A few problems of this type are provided in Sec. 9 for the reader's exercise.

any x , i.e. no contribution to sum (84), so it may be dropped as well.) Now we see that we indeed had to take α real, i.e. α^2 positive – otherwise, instead of the oscillating function (90) we would have a sum of two exponential functions, which cannot equal zero at two independent points of the x -axis.

Since the equation (89) for function $Y(y)$ is similar to that for $X(x)$, and the boundary conditions on the walls perpendicular to axis y ($y = 0$ and $y = b$) are similar to those for x -walls, the absolutely similar reasoning gives

$$Y = \sin \beta y, \quad \beta_m = \frac{\pi}{b} m, \quad \text{with } m = 1, 2, \dots, \quad (2.92)$$

where the integer m may be selected independently of n . Now we see that according to Eq. (88), the separation constant γ depends on two integers n and m , so that the relationship may be rewritten as

$$\gamma_{nm} = [\alpha_n^2 + \beta_m^2]^{1/2} = \pi \left[\left(\frac{n}{a} \right)^2 + \left(\frac{m}{b} \right)^2 \right]^{1/2}. \quad (2.93)$$

The corresponding solution of the differential equation for Z may be represented as a linear combination of two exponents $\exp\{\pm \gamma_{nm} z\}$, or alternatively of two hyperbolic functions, $\sinh \gamma_{nm} z$ and $\cosh \gamma_{nm} z$, with arbitrary coefficients. At our choice of coordinate origin, the latter option is preferable because $\cosh \gamma_{nm} z$ cannot satisfy the zero boundary condition at the bottom lid of the box ($z = 0$). Hence we may take Z in the form

$$Z = \sinh \gamma_{nm} z, \quad (2.94)$$

which automatically satisfies that condition.

Now it is the right time to merge Eqs. (84)-(85) and (90)-(94), replacing the temporary index k with the full set of possible eigenvalues, in our current case of two integer indices n and m :

Variable
separation
in Cartesian
coordinates
(example)

$$\phi(x, y, z) = \sum_{n,m=1}^{\infty} c_{nm} \sin \frac{\pi n x}{a} \sin \frac{\pi m y}{b} \sinh \gamma_{nm} z, \quad (2.95)$$

where γ_{nm} is given by Eq. (93). This solution satisfies not only the Laplace equation but also the boundary conditions on all walls of the box, besides the top lid, for arbitrary coefficients c_{nm} . The only job left is to choose these coefficients from the top-lid requirement:

$$\phi(x, y, c) \equiv \sum_{n,m=1}^{\infty} c_{nm} \sin \frac{\pi n x}{a} \sin \frac{\pi m y}{b} \sinh \gamma_{nm} c = V(x, y). \quad (2.96)$$

It may look bad to have just one equation for the infinite set of coefficients c_{nm} . However, the decisive help comes from the fact that the functions of x and y that participate in Eq. (96), form *full, orthogonal* sets of 1D functions. The last term means that the integrals of the products of the functions with different integer indices over the region of interest equal zero. Indeed, a direct integration gives

$$\int_0^a \sin \frac{\pi n x}{a} \sin \frac{\pi n' x}{a} dx = \frac{a}{2} \delta_{nn'}, \quad (2.97)$$

where $\delta_{nn'}$ is the Kronecker symbol, and similarly for y (with the evident replacements $a \rightarrow b$, and $n \rightarrow m$). Hence, a fruitful way to proceed is to multiply both sides of Eq. (96) by the product of the basis functions, with arbitrary indices n' and m' , and integrate the result over x and y :

$$\sum_{n,m=1}^{\infty} c_{nm} \sinh \gamma_{nm} c \int_0^a \sin \frac{\pi n x}{a} \sin \frac{\pi n' x}{a} dx \int_0^b \sin \frac{\pi m y}{b} \sin \frac{\pi m' y}{b} dy = \int_0^a dx \int_0^b dy V(x,y) \sin \frac{\pi n x}{a} \sin \frac{\pi m y}{b}. \quad (2.98)$$

Due to Eq. (97), all terms on the left-hand side of the last equation, besides those with $n = n'$ and $m = m'$, vanish, and (replacing n' with n , and m' with m , for notation brevity) we finally get

$$c_{nm} = \frac{4}{ab \sinh \gamma_{nm} c} \int_0^a dx \int_0^b dy V(x,y) \sin \frac{\pi n x}{a} \sin \frac{\pi m y}{b}. \quad (2.99)$$

The relations (93), (95), and (99) give the complete solution of the posed boundary problem; we can see both good and bad news here. The first bit of bad news is that in the general case we still need to work out the integrals (99) – formally, the infinite number of them. In some cases, it is possible to do this analytically, in one shot. For example, if the top lid in our problem is a single conductor, i.e. has a constant potential V_0 , we may take $V(x,y) = V_0 = \text{const}$, and both 1D integrations are elementary; for example

$$\int_0^a \sin \frac{\pi n x}{a} dx = \frac{a}{\pi n} \int_0^{\pi n} \sin \xi d\xi = \frac{a}{\pi n} \times \begin{cases} 2, & \text{for } n \text{ odd,} \\ 0, & \text{for } n \text{ even,} \end{cases} \quad (2.100)$$

and similarly for the integral over y , so that

$$c_{nm} = \frac{16V_0}{\pi^2 nm \sinh \gamma_{nm} c} \times \begin{cases} 1, & \text{if both } n \text{ and } m \text{ are odd,} \\ 0, & \text{otherwise.} \end{cases} \quad (2.101)$$

The second bad news is that even on such a happy occasion, we still have to sum up the series (95), so that our result may only be called analytical with some reservations because in most cases we need to perform numerical summation to get the final numbers or plots.

Now the first *good* news. Computers are very efficient for both operations (95) and (99), i.e. for the summation and integration. (As was discussed in Sec. 1.2, random errors are averaged out at these operations.) As an example, Fig. 14 shows the plots of the electrostatic potential in a cubic box ($a = b = c$), with an equipotential top lid ($V = V_0 = \text{const}$), obtained by a numerical summation of the series (95), using the analytical expression (101). The remarkable feature of this calculation is a very fast convergence of the series; for the middle cross-section of the cubic box ($z/c = 0.5$), already the first term (with $n = m = 1$) gives an accuracy of about 6%, while the sum of four leading terms (with $n, m = 1, 3$) reduces the error to just 0.2%. (For a longer box, $c > a, b$, the convergence is even faster – see the discussion below.) Only very close to the corners between the top lid and the sidewalls, where the potential changes rapidly, several more terms are necessary to get a reasonable accuracy.

The related piece of good news is that our “semi-analytical” result allows its ultimate limits to be explored analytically. For example, Eq. (93) shows that for a very flat box (with $c \ll a, b$), $\gamma_{n,m} z \leq \gamma_{n,m} c \ll 1$ at least for the lowest terms of series (95), with $n, m \ll c/a, c/b$. In this case, the sinh functions in Eqs. (96) and (99) may be well approximated with their arguments, and their ratio by z/c . So if we limit the summation to these terms, Eq. (95) gives a very simple result

$$\phi(x,y) \approx \frac{z}{c} V(x,y), \quad (2.102)$$

which means that each elementary segment of the flat box behaves just as a plane capacitor. Only near the sidewalls, the higher terms in the series (95) are important, producing some deviations from Eq.

(102). (For the general problem with an arbitrary function $V(x,y)$, this is also true in all regions where this function changes sharply.)

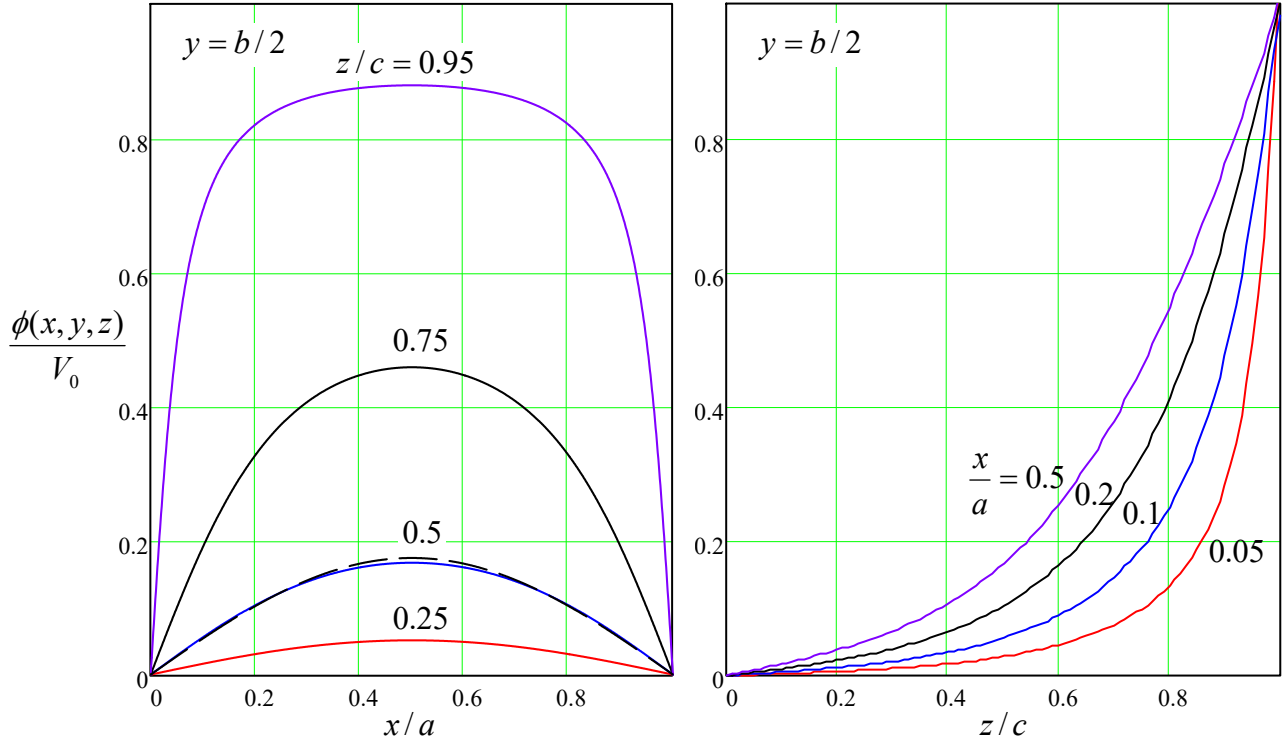


Fig. 2.14. The electrostatic potential's distribution inside a cubic box ($a = b = c$) with a constant voltage V_0 on the top lid (Fig. 13), calculated numerically from Eqs. (93), (95), and (101). The dashed line on the left panel shows the contribution of the main term of the series (with $n = m = 1$) to the full result, for $z/c = 0.5$.

In the opposite limit ($a, b \ll c$), Eq. (93) shows that on the contrary, $\gamma_{n,m}c \gg 1$ for all n and m . Moreover, the ratio $\sinh\gamma_{n,m}z/\sinh\gamma_{n,m}c$ drops sharply if either n or m is increased, provided that z is not too close to c . Hence in this case a very good approximation may be obtained by keeping just the leading term, with $n = m = 1$, in Eq. (95), so that the challenge of summation disappears. (As was discussed above, this approximation works reasonably well even for a cubic box.) In particular, for the constant potential of the upper lid, we can use Eq. (101) and the exponential asymptotic for both sinh functions, to get a very simple formula:

$$\phi = \frac{16}{\pi^2} \sin \frac{\pi x}{a} \sin \frac{\pi y}{b} \exp \left\{ -\pi \frac{(a^2 + b^2)^{1/2}}{ab} (c - z) \right\}. \quad (2.103)$$

These results may be readily generalized to some other problems. For example, if all walls of the box shown in Fig. 13 have an arbitrary potential distribution, we may use the linear superposition principle to represent the electrostatic potential distribution as the sum of six partial solutions of the type of Eq. (95), each with one wall biased by the corresponding voltage, and all other grounded ($\phi = 0$).

To summarize, the results given by the variable separation method in the Cartesian coordinates are closer to what we could call a genuinely analytical solution than to a purely numerical solution.

Now, let us explore the issues that arise when this method is applied in other orthogonal coordinate systems.

2.6. Variable separation – polar coordinates

If a system of conductors is cylindrical, the potential distribution is independent of the z -coordinate along the cylinder axis: $\partial\phi/\partial z = 0$, and the Laplace equation becomes two-dimensional. If the conductor's cross-section is rectangular, the variable separation method works best in Cartesian coordinates $\{x, y\}$, and is just a particular case of the 3D solution discussed above. However, if the cross-section is circular, much more compact results may be obtained by using the polar coordinates $\{\rho, \varphi\}$. As we already know from Sec. 3(ii), these 2D coordinates are orthogonal, so that the two-dimensional Laplace operator is a sum of two separable terms.³⁹ Requiring, just as we have done above, each component of the sum (84) to satisfy the Laplace equation, we get

$$\frac{1}{\rho} \frac{\partial}{\partial \rho} \left(\rho \frac{\partial \phi_k}{\partial \rho} \right) + \frac{1}{\rho^2} \frac{\partial^2 \phi_k}{\partial \varphi^2} = 0. \quad (2.104)$$

In a full analogy with Eq. (85), let us represent each particular solution ϕ_k as a product $\mathcal{R}(\rho)\mathcal{A}(\varphi)$. Plugging this expression into Eq. (104) and then dividing all its parts by $\mathcal{R}\mathcal{A}/\rho^2$, we get

$$\frac{\rho}{\mathcal{R}} \frac{d}{d\rho} \left(\rho \frac{d\mathcal{R}}{d\rho} \right) + \frac{1}{\mathcal{A}} \frac{d^2\mathcal{A}}{d\varphi^2} = 0. \quad (2.105)$$

Following the same reasoning as for the Cartesian coordinates, we get two separated ordinary differential equations

$$\rho \frac{d}{d\rho} \left(\rho \frac{d\mathcal{R}}{d\rho} \right) = \nu^2 \mathcal{R}, \quad (2.106)$$

$$\frac{d^2\mathcal{A}}{d\varphi^2} + \nu^2 \mathcal{A} = 0, \quad (2.107)$$

where ν^2 is the variable separation constant.

Let us start their analysis from Eq. (106), plugging into it a probe solution $\mathcal{R} = c\rho^\alpha$ where c and α are some constants. The elementary differentiation shows that if $\alpha \neq 0$, the equation is indeed satisfied for any c , with just one requirement imposed on the constant α , namely $\alpha^2 = \nu^2$. This means that the following linear superposition

$$\mathcal{R} = a_\nu \rho^{+\nu} + b_\nu \rho^{-\nu}, \quad \text{for } \nu \neq 0, \quad (2.108)$$

with any constant coefficients a_ν and b_ν , is also a solution of Eq. (106). Moreover, the general theory of linear ordinary differential equations tells us that the solution of a second-order equation like Eq. (106) may only depend on just two constant factors that scale two linearly-independent functions. Hence, for all values $\nu^2 \neq 0$, Eq. (108) presents the *general* solution of that equation. The case when $\nu = 0$, in which the functions $\rho^{+\nu}$ and $\rho^{-\nu}$ are just constants and hence are *not* linearly independent, is special, but in this case, the integration of Eq. (106) is straightforward,⁴⁰ giving

³⁹ See, e.g., MA Eq. (10.3) with $\partial/\partial z = 0$.

⁴⁰ Actually, we have already performed it in Sec. 3 – see Eq. (43).

$$\mathcal{R} = a_0 + b_0 \ln \rho, \quad \text{for } \nu = 0. \quad (2.109)$$

In order to specify the separation constant, let us explore Eq. (107), whose general solution is

$$\mathcal{F} = \begin{cases} c_\nu \cos \nu \varphi + s_\nu \sin \nu \varphi, & \text{for } \nu \neq 0, \\ c_0 + s_0 \varphi, & \text{for } \nu = 0. \end{cases} \quad (2.110)$$

There are two possible cases here. In many boundary problems solvable in cylindrical coordinates, the free-space region, in which the Laplace equation is valid, extends continuously around the origin point $\rho = 0$. In this region, the potential has to be continuous and uniquely defined, so that \mathcal{F} has to be a 2π -periodic function of φ . For that, one needs the product $\nu(\varphi + 2\pi)$ to equal $\nu\varphi + 2\pi n$, with n being an integer, immediately giving us a discrete spectrum of possible values of the variable separation constant:

$$\nu = n = 0, \pm 1, \pm 2, \dots \quad (2.111)$$

In this case, both functions \mathcal{R} and \mathcal{F} may be labeled with the integer index n . Taking into account that the terms with negative values of n may be summed up with those with positive n , and that s_0 has to equal zero (otherwise the 2π -periodicity of function \mathcal{F} would be violated), we see that the general solution of the 2D Laplace equation for such geometries may be represented as

Variable separation in polar coordinates

$$\phi(\rho, \varphi) = a_0 + b_0 \ln \rho + \sum_{n=1}^{\infty} \left(a_n \rho^n + \frac{b_n}{\rho^n} \right) (c_n \cos n\varphi + s_n \sin n\varphi). \quad (2.112)$$

Let us see how all this machinery works on the famous problem of a round cylindrical conductor placed into an electric field that is uniform and perpendicular to the cylinder's axis at large distances (see Fig. 15a), as if it is created by a large plane capacitor. First of all, let us explore the effect of the system's symmetries on the coefficients in Eq. (112). Selecting the coordinate system as shown in Fig. 15a, and taking the cylinder's potential for zero, we immediately get $a_0 = 0$.

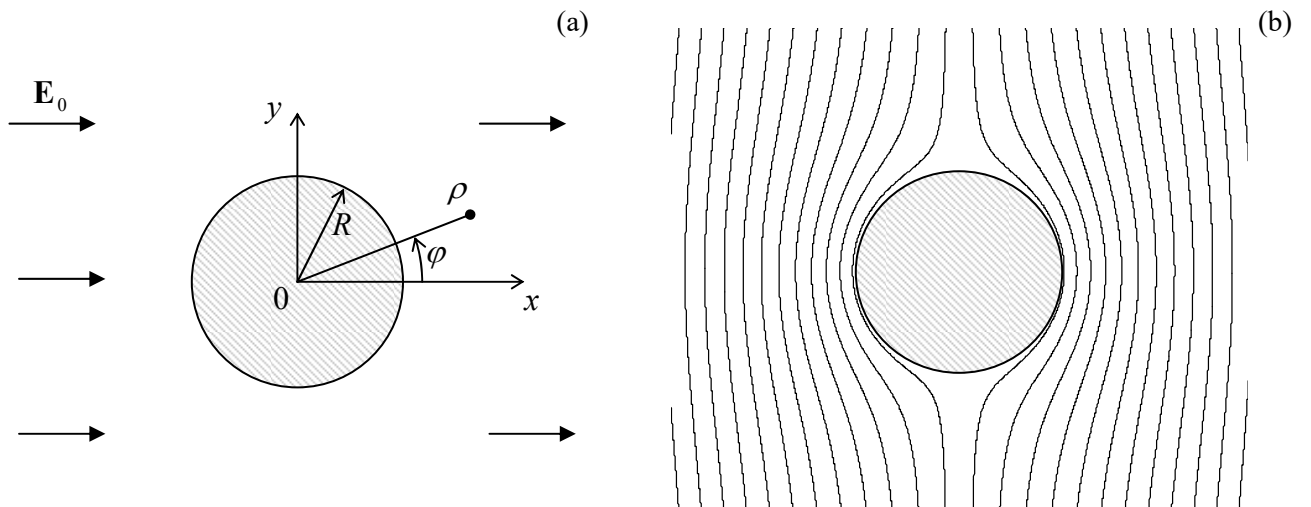


Fig. 2.15. A conducting cylinder inserted into an initially uniform electric field perpendicular to its axis: (a) the problem's geometry, and (b) the equipotential surfaces given by Eq. (117).

Moreover, due to the mirror symmetry about the plane $[x, z]$, the solution has to be an even function of the angle φ , and hence all coefficients s_n should also equal zero. Also, at large distances ($\rho \gg R$) from the cylinder, its effect on the electric field should vanish, and the potential should approach that of the uniform external field $\mathbf{E} = E_0 \mathbf{n}_x$:

$$\phi \rightarrow -E_0 x \equiv -E_0 \rho \cos \varphi, \quad \text{for } \rho \rightarrow \infty. \quad (2.113)$$

This is only possible if in Eq. (112), $b_0 = 0$, and also all coefficients a_n with $n \neq 1$ vanish, while the product $a_1 c_1$ should be equal to $(-E_0)$. Thus the solution is reduced to the following form

$$\phi(\rho, \varphi) = -E_0 \rho \cos \varphi + \sum_{n=1}^{\infty} \frac{B_n}{\rho^n} \cos n\varphi, \quad (2.114)$$

in which the coefficients $B_n \equiv b_n c_n$ should be found from the boundary condition at $\rho = R$:

$$\phi(R, \varphi) = 0. \quad (2.115)$$

This requirement yields the following equation,

$$\left(-E_0 R + \frac{B_1}{R} \right) \cos \varphi + \sum_{n=2}^{\infty} \frac{B_n}{R^n} \cos n\varphi = 0, \quad (2.116)$$

which should be satisfied for all φ . This equality, read backward, may be considered as an expansion of a function identically equal to zero into a series over mutually orthogonal functions $\cos n\varphi$. It is evidently valid if all coefficients of the expansion, including $(-E_0 R + B_1/R)$, and all B_n for $n \geq 2$ are equal to zero. Moreover, mathematics tells us that such expansions are unique, so this is the only possible solution of Eq. (116). So, $B_1 = E_0 R^2$, and our final answer (valid only outside of the cylinder, i.e. for $\rho \geq R$), is

$$\phi(\rho, \varphi) = -E_0 \left(\rho - \frac{R^2}{\rho} \right) \cos \varphi \equiv -E_0 \left(1 - \frac{R^2}{x^2 + y^2} \right) x. \quad (2.117)$$

This result, which may be graphically represented with the equipotential surfaces shown in Fig. 15b, shows a smooth transition between the uniform field (113) far from the cylinder, to the equipotential surface of the cylinder (with $\phi = 0$). Such smoothening is very typical for Laplace equation solutions. Indeed, as we know from Chapter 1, these solutions correspond to the lowest integral of the potential gradient's square, i.e. to the lowest potential energy (1.65) possible at the given boundary conditions.

To complete the problem, let us use Eq. (3) to calculate the distribution of the surface charge density over the cylinder's cross-section:

$$\sigma = \epsilon_0 E_n \Big|_{\text{surface}} \equiv -\epsilon_0 \frac{\partial \phi}{\partial \rho} \Big|_{\rho=R} = \epsilon_0 E_0 \cos \varphi \frac{\partial}{\partial \rho} \left(\rho - \frac{R^2}{\rho} \right) \Big|_{\rho=R} = 2\epsilon_0 E_0 \cos \varphi. \quad (2.118)$$

This very simple formula shows that with the field direction shown in Fig. 15a ($E_0 > 0$), the surface charge is positive on the right-hand side of the cylinder and negative on its left-hand side, thus creating a field directed from the right to the left, which exactly compensates the external field inside the conductor, where the net field is zero. (Please take one more look at the schematic Fig. 1a.) Note also that the net electric charge of the cylinder is zero, in correspondence with the problem symmetry.

Another useful by-product of the calculation (118) is that the surface electric field equals $2E_0\cos\varphi$, and hence its largest magnitude is twice the field far from the cylinder. Such electric field concentration is very typical for all convex conducting surfaces.

The last observation gets additional confirmation from the second possible topology, when Eq. (110) is used to describe problems with no angular periodicity. A typical example of this situation is a cylindrical conductor with a cross-section that features a corner limited by two straight-lines segments (Fig. 16). Indeed, we may argue that at $\rho < R$ (where R is the radial extension of the planar sides of the corner, see Fig. 16), the Laplace equation may be satisfied by a sum of partial solutions $\mathcal{R}(\rho)\mathcal{A}(\varphi)$, if the angular components of the products satisfy the boundary conditions on the corner sides. Taking (just for the simplicity of notation) the conductor's potential to be zero, and one of the corner's sides as the x -axis ($\varphi = 0$), these boundary conditions are

$$\mathcal{A}(0) = \mathcal{A}(\beta) = 0, \quad (2.119)$$

where the angle β may be anywhere between 0 and 2π – see Fig. 16.

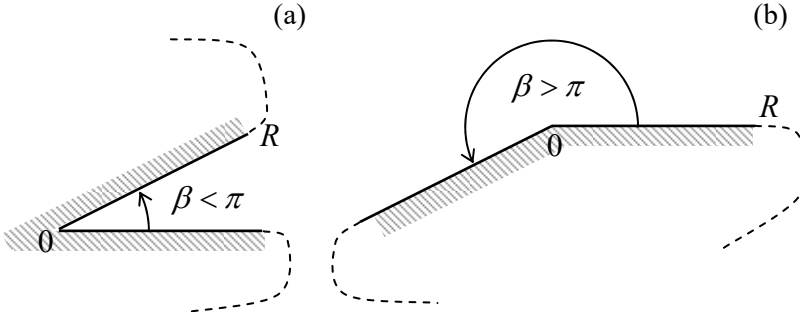


Fig. 2.16. The cross-sections of cylindrical conductors with (a) a corner and (b) a wedge.

Comparing this condition with Eq. (110), we see that it requires s_0 and all c_v to vanish, and v to take one of the values of the following discrete spectrum:

$$v_m \beta = \pi m, \quad \text{with } m = 1, 2, \dots \quad (2.120)$$

Hence the full solution of the Laplace equation for this geometry takes the form

$$\phi = \sum_{m=1}^{\infty} a_m \rho^{\pi m / \beta} \sin \frac{\pi m \varphi}{\beta}, \quad \text{for } \rho < R, \quad 0 \leq \varphi \leq \beta, \quad (2.121)$$

where the constants s_v have been incorporated into a_m . The set of coefficients a_m cannot be universally determined, because it depends on the exact shape of the conductor outside the corner, and the externally applied electric field. However, whatever the set is, in the limit $\rho \rightarrow 0$, the solution (121) is almost⁴¹ always dominated by the term with the lowest $m = 1$:

$$\phi \rightarrow a_1 \rho^{\pi / \beta} \sin \frac{\pi}{\beta} \varphi, \quad (2.122)$$

because the higher terms go to zero faster. This potential distribution corresponds to the surface charge density

⁴¹ Exceptions are possible only for highly symmetric configurations when the external field is specially crafted to make $a_1 = 0$. In this case, the solution at $\rho \rightarrow 0$ is dominated by the first nonzero term of the series (121).

$$\sigma = \epsilon_0 E_n \Big|_{\text{surface}} = -\epsilon_0 \frac{\partial \phi}{\partial (\rho \varphi)} \Big|_{\rho=\text{const}, \varphi \rightarrow +0} = -\epsilon_0 \frac{\pi a_1}{\beta} \rho^{(\pi/\beta - 1)}. \quad (2.123)$$

(It is similar, with the opposite sign, on the opposite face of the angle.)

The result (123) shows that if we are dealing with a concave corner ($\beta < \pi$, see Fig. 16a), the charge density (and the surface electric field) tends to zero. On the other case, at a “convex corner” with $\beta > \pi$ (actually, a wedge – see Fig. 16b), both the charge and the field’s strength concentrate, formally diverging at $\rho \rightarrow 0$. (So, do not sit on a roof’s ridge during a thunderstorm; rather hide in a ditch!) We have already seen qualitatively similar effects for the thin round disk and the split plane.

2. 7. Variable separation – cylindrical coordinates

Now, let us discuss how to generalize the approach discussed in the previous section to problems whose geometry is still axially-symmetric, but where the electrostatic potential depends not only on the radial and angular coordinates but also on the axial coordinate: $\partial \phi / \partial z \neq 0$. The classical example of such a problem is shown in Fig. 17. Here the sidewall and the bottom lid of a hollow round cylinder are kept at a fixed potential (say, $\phi = 0$), but the potential V fixed at the top lid is different. Evidently, this problem is qualitatively similar to the rectangular box problem solved above (Fig. 13), and we will also try to solve it first for the case of arbitrary voltage distribution over the top lid: $V = V(\rho, \varphi)$.

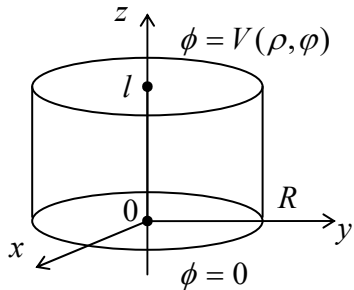


Fig. 2.17. A cylindrical volume with conducting walls.

Following the main idea of the variable separation method, let us require that each partial function ϕ_k in Eq. (84) satisfies the Laplace equation, now in the full cylindrical coordinates $\{\rho, \varphi, z\}$:⁴²

$$\frac{1}{\rho} \frac{\partial}{\partial \rho} \left(\rho \frac{\partial \phi_k}{\partial \rho} \right) + \frac{1}{\rho^2} \frac{\partial^2 \phi_k}{\partial \varphi^2} + \frac{\partial^2 \phi_k}{\partial z^2} = 0. \quad (2.124)$$

Plugging ϕ_k in the form of the product $\mathcal{R}(\rho)\mathcal{A}(\varphi)\mathcal{Z}(z)$ into Eq. (124) and then dividing all resulting terms by this product, we get

$$\frac{1}{\rho \mathcal{R}} \frac{d}{d\rho} \left(\rho \frac{d\mathcal{R}}{d\rho} \right) + \frac{1}{\rho^2 \mathcal{A}} \frac{d^2 \mathcal{A}}{d\varphi^2} + \frac{1}{\mathcal{Z}} \frac{d^2 \mathcal{Z}}{dz^2} = 0. \quad (2.125)$$

Since the first two terms of Eq. (125) can only depend on the polar variables ρ and φ , while the third term, only on z , at least that term should equal a constant. Denoting it (just like we did in the rectangular box problem) by γ^2 , we get the following set of two equations:

⁴² See, e.g., MA Eq. (10.3).

$$\frac{d^2\mathcal{Z}}{dz^2} = \gamma^2 \mathcal{Z}, \quad (2.126)$$

$$\frac{1}{\rho\mathcal{R}} \frac{d}{d\rho} \left(\rho \frac{d\mathcal{R}}{d\rho} \right) + \gamma^2 + \frac{1}{\rho^2 \mathcal{R}} \frac{d^2\mathcal{R}}{d\varphi^2} = 0. \quad (2.127)$$

Now, multiplying all the terms of Eq. (127) by ρ^2 , we see that the last term of the result, $(d^2\mathcal{R}/d\varphi^2)/\mathcal{R}$, may depend only on φ , and thus should equal a constant. Calling that constant ν^2 (just as in Sec. 6 above), we separate Eq. (127) into an angular equation,

$$\frac{d^2\mathcal{R}}{d\varphi^2} + \nu^2 \mathcal{R} = 0, \quad (2.128)$$

and a radial equation:

$$\frac{d^2\mathcal{R}}{d\rho^2} + \frac{1}{\rho} \frac{d\mathcal{R}}{d\rho} + (\gamma^2 - \frac{\nu^2}{\rho^2}) \mathcal{R} = 0. \quad (2.129)$$

We see that the ordinary differential equations for the functions $\mathcal{Z}(z)$ and $\mathcal{R}(\rho)$ (and hence their solutions) are identical to those discussed earlier in this chapter. However, Eq. (129) for the radial function $\mathcal{R}(\rho)$ (called the *Bessel equation*) is more complex than in the 2D case and depends on two independent constant parameters, γ and ν . The latter challenge may be readily overcome if we notice that any change of γ may be reduced to the corresponding re-scaling of the radial coordinate ρ . Indeed, introducing a dimensionless variable $\xi \equiv \gamma\rho$,⁴³ Eq. (129) may be reduced to an equation with just one parameter, ν :

$$\frac{d^2\mathcal{R}}{d\xi^2} + \frac{1}{\xi} \frac{d\mathcal{R}}{d\xi} + \left(1 - \frac{\nu^2}{\xi^2}\right) \mathcal{R} = 0. \quad (2.130)$$

Bessel
equation

Moreover, we already know that for angle-periodic problems, the spectrum of eigenvalues of Eq. (128) is discrete: $\nu = n$, with integer n .

Unfortunately, even in this case, Eq. (130), which is the canonical form of the Bessel equation, cannot be satisfied by a single “elementary” function. Its solutions that we need for our current problem are called the *Bessel function of the first kind of order ν* , commonly denoted as $J_\nu(\xi)$. Let me review in brief those properties of these functions that are most relevant for our problem – and many other problems discussed in this series.⁴⁴

First of all, the Bessel function of a negative integer order is very simply related to that with the positive order:

$$J_{-n}(\xi) = (-1)^n J_n(\xi), \quad (2.131)$$

enabling us to limit our discussion to the functions with $n \geq 0$. Figure 18 shows four of these functions with the lowest positive n .

⁴³ Note that this normalization is specific for each value of the variable separation parameter γ . Also, please notice that the normalization is meaningless for $\gamma = 0$, i.e. for the case $Z(z) = \text{const}$. However, if we need the partial solutions for this particular value of γ , we can always use Eqs. (108)-(109).

⁴⁴ For a more complete discussion of these functions, see the literature listed in MA Sec. 16, for example, Chapter 6 (written by F. Olver) in the famous collection compiled and edited by Abramowitz and Stegun, available online.

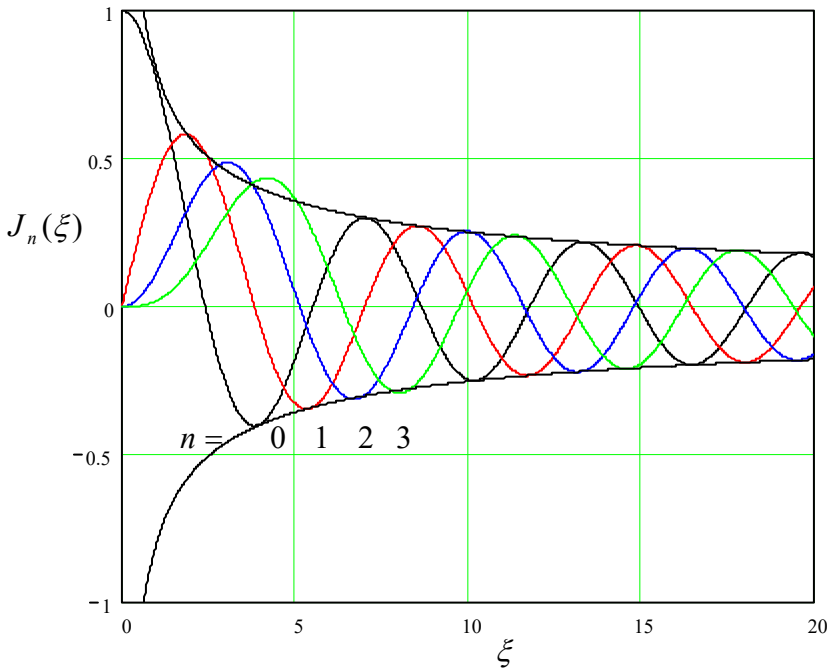


Fig. 2.18. Several Bessel functions $J_n(\xi)$ of integer order. The dashed lines show the envelope of the asymptotes (135).

As its argument is increased, each function is initially close to a power law: $J_0(\xi) \approx 1$, $J_1(\xi) \approx \xi/2$, $J_2(\xi) \approx \xi^2/8$, etc. This behavior follows from the Taylor series

$$J_n(\xi) = \left(\frac{\xi}{2}\right)^n \sum_{k=0}^{\infty} \frac{(-1)^k}{k!(n+k)!} \left(\frac{\xi}{2}\right)^{2k}, \quad (2.132)$$

which is formally valid for any ξ , and may even serve as an alternative definition of the functions $J_n(\xi)$. However, the series is converging fast only at small arguments, $\xi \ll n$, where its leading term is

$$J_n(\xi) \Big|_{\xi \rightarrow 0} \rightarrow \frac{1}{n!} \left(\frac{\xi}{2}\right)^n. \quad (2.133)$$

At $\xi \approx n + 1.86n^{1/3}$, the Bessel function reaches its maximum⁴⁵

$$\max_{\xi} [J_n(\xi)] \approx \frac{0.675}{n^{1/3}}, \quad (2.134)$$

and then starts to oscillate with a period gradually approaching 2π , a phase shift that increases by $\pi/2$ with each unit increment of n , and an amplitude that decreases as $\xi^{-1/2}$. All these features are described by the following asymptotic formula:

$$J_n(\xi) \Big|_{\xi \rightarrow \infty} \rightarrow \left(\frac{2}{\pi\xi}\right)^{1/2} \cos\left(\xi - \frac{\pi}{4} - \frac{n\pi}{2}\right), \quad (2.135)$$

which starts to give a reasonable approximation soon after the function peaks – see Fig. 18.⁴⁶

⁴⁵ These two approximations for the Bessel function peak are strictly valid for $n \gg 1$, but may be used for reasonable estimates starting already from $n = 1$. For example, $\max_{\xi} [J_1(\xi)]$ is close to 0.58 and is reached at $\xi \approx 2.4$, just about 30% away from the values given by the asymptotic formulas.

Now we are ready for our case study (Fig. 17). Since the functions the $Z(z)$ have to satisfy not only Eq. (126) but also the bottom-lid boundary condition $Z(0) = 0$, they are proportional to $\sinh \gamma z$ – cf. Eq. (94). Then Eq. (84) becomes

$$\phi = \sum_{n=0}^{\infty} \sum_{\gamma} J_n(\gamma\rho) (c_{n\gamma} \cos n\varphi + s_{n\gamma} \sin n\varphi) \sinh \gamma z. \quad (2.136)$$

Next, we need to satisfy the zero boundary condition at the cylinder's side wall ($\rho = R$). This may be ensured by taking

$$J_n(\gamma R) = 0. \quad (2.137)$$

Since each function $J_n(x)$ has an infinite number of positive zeros (see Fig. 18 again), which may be numbered by an integer index $m = 1, 2, \dots$, Eq. (137) may be satisfied with an infinite number of discrete values of the parameter γ :

$$\gamma_{nm} = \frac{\xi_{nm}}{R}, \quad (2.138)$$

where ξ_{nm} is the m -th zero of the function $J_n(x)$ – see the top numbers in the cells of Table 1. (Very soon we will see what we need the bottom numbers for.)

Table 2.1. Approximate values of a few first zeros, ξ_{nm} , of a few lowest-order Bessel functions $J_n(\xi)$ (the top number in each cell), and the values of $dJ_n(\xi)/d\xi$ at these points (the bottom number).

	$m = 1$	2	3	4	5	6
$n = 0$	2.40482 -0.51914	5.52008 +0.34026	8.65372 -0.27145	11.79215 +0.23245	14.93091 -0.20654	18.07106 +0.18773
	1	3.83171 -0.40276	7.01559 +0.30012	10.17347 -0.24970	13.32369 +0.21836	16.47063 -0.19647
1	5.13562 -0.33967	8.41724 +0.27138	11.61984 -0.23244	14.79595 +0.20654	17.95982 -0.18773	21.11700 +0.17326
	2	6.38016 -0.29827	9.76102 +0.24942	13.01520 -0.21828	16.22347 +0.19644	19.40942 -0.18005
2	7.58834 -0.26836	11.06471 +0.23188	14.37254 -0.20636	17.61597 +0.18766	20.82693 -0.17323	24.01902 +0.16168
	3	8.77148 -0.24543	12.33860 +0.21743	15.70017 -0.19615	18.98013 +0.17993	22.21780 -0.16712
3	10.98631 -0.21526	14.62656 +0.19188	18.87295 -0.16915	22.17800 +0.15669	26.43034 -0.14543	30.63333 +0.13426
	4	13.19911 -0.18504	18.07571 +0.16823	22.33210 -0.14543	26.58471 +0.13426	30.83730 -0.12304
4	15.41189 -0.15482	21.42496 +0.15143	25.68155 -0.13063	29.93426 +0.12082	34.18685 -0.11063	38.43944 +0.10143
	5	17.62467 -0.12460	24.77421 +0.14123	29.03980 -0.11980	33.29251 +0.11123	37.54510 -0.10123
5	19.83745 -0.09438	28.12346 +0.12183	32.30545 -0.09700	36.55816 +0.08800	40.81075 -0.07800	45.06334 +0.06800
	6	22.05023 -0.06416	31.47271 +0.10243	35.77000 -0.08220	39.92271 +0.07320	44.17530 -0.06320

Hence, Eq. (136) may be represented in a more explicit form:

$$\phi(\rho, \varphi, z) = \sum_{n=0}^{\infty} \sum_{m=1}^{\infty} J_n\left(\xi_{nm} \frac{\rho}{R}\right) (c_{nm} \cos n\varphi + s_{nm} \sin n\varphi) \sinh\left(\xi_{nm} \frac{z}{R}\right). \quad (2.139)$$

Variable separation in cylindrical coordinates (example)

⁴⁶ Eq. (135) and Fig. 18 clearly show the close analogy between the Bessel functions and the usual trigonometric functions, sine and cosine. To emphasize this similarity, and help the reader to develop more gut feeling of the Bessel functions, let me mention one result of the elasticity theory: while the sinusoidal functions describe, in particular, transverse standing waves on a guitar string, the functions $J_n(\xi)$ describe, in particular, transverse standing waves on an elastic round membrane (say, a round drum), with $J_0(\xi)$ describing their lowest (fundamental) mode – the only mode with a nonzero amplitude of the membrane center's oscillations.

Here the coefficients c_{nm} and s_{nm} have to be selected to satisfy the only remaining boundary condition – that on the top lid:

$$\phi(\rho, \varphi, l) \equiv \sum_{n=0}^{\infty} \sum_{m=1}^{\infty} J_n\left(\xi_{nm} \frac{\rho}{R}\right) (c_{nm} \cos n\varphi + s_{nm} \sin n\varphi) \sinh\left(\xi_{nm} \frac{l}{R}\right) = V(\rho, \varphi). \quad (2.140)$$

To use it, let us multiply both sides of Eq. (140) by the product $J_n(\xi_{nm} \cdot \rho/R) \cos n'\varphi$, integrate the result over the lid area, and use the following property of the Bessel functions:

$$\int_0^1 J_n(\xi_{nm} s) J_n(\xi_{nm} s) s ds = \frac{1}{2} [J_{n+1}(\xi_{nm})]^2 \delta_{mm}. \quad (2.141)$$

As a small but important detour, the last relation expresses a very specific (“2D”) orthogonality of the Bessel functions with different indices m – do not confuse them with the function orders n , please!⁴⁷ Since it relates two Bessel functions of the same order n , it is natural to ask why its right-hand side contains the function with a different order ($n + 1$). Some gut feeling of that may come from one more very important property of the Bessel functions, the so-called *recurrence relations*:⁴⁸

$$J_{n-1}(\xi) + J_{n+1}(\xi) = \frac{2n J_n(\xi)}{\xi}, \quad (2.142a)$$

$$J_{n-1}(\xi) - J_{n+1}(\xi) = 2 \frac{d J_n(\xi)}{d\xi}, \quad (2.142b)$$

which in particular yield the following formula (convenient for working out some Bessel function integrals):

$$\frac{d}{d\xi} [\xi^n J_n(\xi)] = \xi^n J_{n-1}(\xi). \quad (2.143)$$

Let us apply the recurrence relations at the special points ξ_{nm} . At these points, J_n vanishes, and the system of two equations (142) may be readily solved to get, in particular,

$$J_{n+1}(\xi_{nm}) = -\frac{d J_n}{d\xi}(\xi_{nm}), \quad (2.144)$$

so that the square bracket on the right-hand side of Eq. (141) is just $(d J_n / d\xi)^2$ at $\xi = \xi_{nm}$. Thus the values of the Bessel function derivatives at the zero points of the function, given by the lower numbers in the cells of Table 1, are as important for boundary problem solutions as the zeros themselves.

Now returning to our problem: since the angular functions $\cos n\varphi$ are also orthogonal – both to each other,

⁴⁷ The Bessel functions of the *same argument* but *different orders* are also orthogonal, but differently:

$$\int_0^{\infty} J_n(\xi) J_{n'}(\xi) \frac{d\xi}{\xi} = \frac{1}{n+n'} \delta_{nn'}.$$

⁴⁸ These relations provide, in particular, a convenient way for numerical computation of all $J_n(\xi)$ – after $J_0(\xi)$ has been computed. (The latter task is usually performed using Eq. (132) for smaller ξ and an extension of Eq. (135) for larger ξ .) Note that most mathematical software packages, including all those listed in MA Sec. 16(iv), include ready subroutines for calculation of the functions $J_n(\xi)$ and other special functions used in this lecture series. In this sense, the conditional line separating these “special functions” from “elementary functions” is rather fine.

$$\int_0^{2\pi} \cos(n\varphi) \cos(n'\varphi) d\varphi = \pi \delta_{nn'}, \quad (2.145)$$

and to all functions $\sin n\varphi$, the integration over the lid area kills all terms of both series in Eq. (140), besides just one term proportional to $c_{n'm'}$, and hence gives an explicit expression for that coefficient. The counterpart coefficients $s_{n'm'}$ may be found by repeating the same procedure with the replacement of $\cos n'\varphi$ by $\sin n'\varphi$. This evaluation (left for the reader's exercise) completes the solution of our problem for an arbitrary lid potential $V(\rho, \varphi)$.

Still, before leaving the Bessel functions behind (for a while only :-), let me address two important issues. First, we have seen that in our cylinder problem (Fig. 17), the set of functions $J_n(\xi_{nm}\rho/R)$ with different indices m (which characterize the degree of Bessel function's stretch along axis ρ) play a role similar to that of functions $\sin(\pi nx/a)$ in the rectangular box problem shown in Fig. 13. In this context, what is the analog of functions $\cos(\pi nx/a)$ – which may be important for some boundary problems? In a more formal language, are there any functions of the same argument $\xi \equiv \xi_{nm}\rho/R$, that would be linearly independent of the Bessel functions of the first kind, while satisfying the same Bessel equation (130)?

The answer is yes. For the definition of such functions, we first need to generalize our prior formulas for $J_n(\xi)$, and in particular Eq. (132), to the case of arbitrary, not necessarily real order ν . Mathematics says that the generalization may be performed in the following way:

$$J_\nu(\xi) = \left(\frac{\xi}{2}\right)^\nu \sum_{k=0}^{\infty} \frac{(-1)^k}{k! \Gamma(\nu + k + 1)} \left(\frac{\xi}{2}\right)^{2k}, \quad (2.146)$$

where $\Gamma(s)$ is the so-called *gamma function* that may be defined as⁴⁹

$$\Gamma(s) \equiv \int_0^{\infty} \xi^{s-1} e^{-\xi} d\xi. \quad (2.147)$$

The simplest, and the most important property of the gamma function is that for integer values of its argument, it gives the factorial of the number smaller by one:

$$\Gamma(n+1) = n! \equiv 1 \cdot 2 \cdot \dots \cdot n, \quad (2.148)$$

so it is essentially a generalization of the notion of the factorial to all real numbers.

The Bessel functions defined by Eq. (146) satisfy, after the replacements $n \rightarrow \nu$ and $n! \rightarrow \Gamma(n+1)$, virtually all the relations discussed above, including the Bessel equation (130), the asymptotic formula (135), the orthogonality condition (141), and the recurrence relations (142). Moreover, it may be shown that $\nu \neq n$, functions $J_\nu(\xi)$ and $J_{-\nu}(\xi)$ are linearly independent of each other, and hence their linear combination may be used to represent the general solution of the Bessel equation. Unfortunately, as Eq. (131) shows, for $\nu = n$ this is not true, and a solution linearly independent of $J_n(\xi)$ has to be formed differently. The most common way to do that is first to define, for all $\nu \neq n$, the following functions:

$$Y_\nu(\xi) \equiv \frac{J_\nu(\xi) \cos \nu \pi - J_{-\nu}(\xi)}{\sin \nu \pi}, \quad (2.149)$$

⁴⁹ See, e.g., MA Eq. (6.7a). Note that $\Gamma(s) \rightarrow \infty$ at $s \rightarrow 0, -1, -2, \dots$

called the *Bessel functions of the second kind*, or more often the *Weber functions*,⁵⁰ and then to follow the limit $\nu \rightarrow n$. At this, both the numerator and denominator of the right-hand side of Eq. (149) tend to zero, but their ratio tends to a finite value called $Y_n(x)$. It may be shown that the resulting functions are still the solutions of the Bessel equation and are linearly independent of $J_n(x)$, though are related just as those functions if the sign of n changes:

$$Y_{-n}(\xi) = (-1)^n Y_n(\xi). \quad (2.150)$$

Figure 19 shows a few Weber functions of the lowest integer orders.

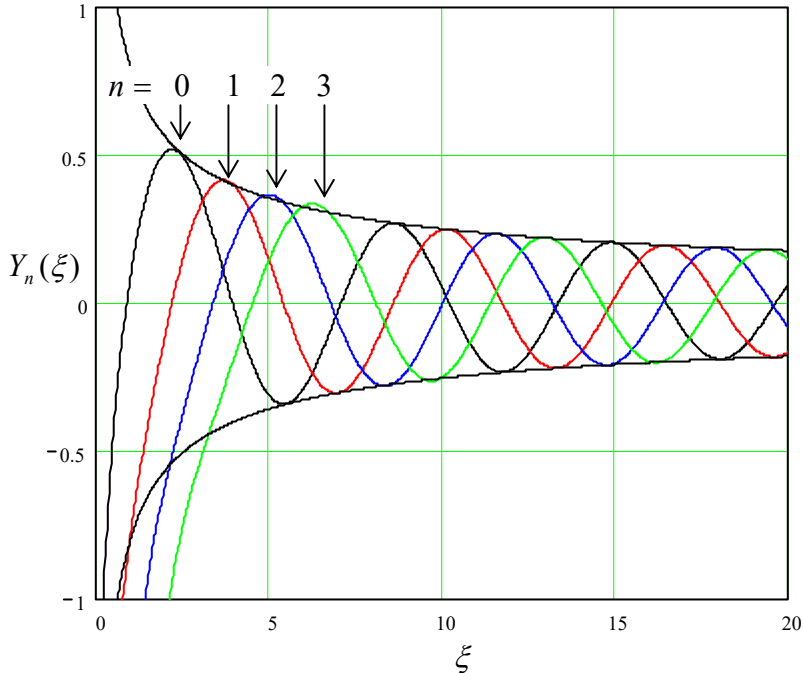


Fig. 2.19. A few Bessel functions of the second kind (a.k.a. the Weber functions, a.k.a. the Neumann functions).

The plots show that their asymptotic behavior is very much similar to that of the functions $J_n(\xi)$:

$$Y_n(\xi) \rightarrow \left(\frac{2}{\pi \xi} \right)^{1/2} \sin \left(\xi - \frac{\pi}{4} - \frac{n\pi}{2} \right), \quad \text{for } \xi \rightarrow \infty, \quad (2.151)$$

but with the phase shift necessary to make these Bessel functions orthogonal to those of the first order – cf. Eq. (135). However, for small values of argument ξ , the Bessel functions of the second kind behave completely differently from those of the first kind:

$$Y_n(\xi) \rightarrow \begin{cases} \frac{2}{\pi} \left(\ln \frac{\xi}{2} + \gamma \right), & \text{for } n = 0, \\ -\frac{(n-1)!}{\pi} \left(\frac{\xi}{2} \right)^{-n}, & \text{for } n \neq 0, \end{cases} \quad (2.152)$$

where γ is the so-called *Euler constant*, defined as follows:

⁵⁰ Sometimes, they are called the *Neumann* functions and denoted as $N_n(\xi)$.

$$\gamma \equiv \lim_{n \rightarrow \infty} \left(1 + \frac{1}{2} + \frac{1}{3} + \dots + \frac{1}{n} - \ln n \right) \approx 0.577157\dots \quad (2.153)$$

As Eqs. (152) and Fig. 19 show, the functions $Y_n(\xi)$ diverge at $\xi \rightarrow 0$ and hence cannot describe the behavior of any physical variable, in particular the electrostatic potential.

One may wonder: if this is true, when do we need these functions in physics? Figure 20 shows an example of a simple boundary problem of electrostatics, whose solution by the variable separation method involves both functions $J_n(\xi)$ and $Y_n(\xi)$.

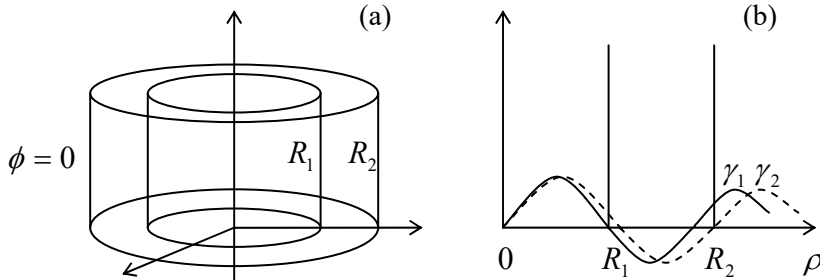


Fig. 2.20. A simple boundary problem that cannot be solved using just one kind of Bessel functions.

Here two round, conducting coaxial cylindrical tubes are kept at the same (say, zero) potential, but at least one of two lids has a different potential. The problem is almost completely similar to that discussed above (Fig. 17), but now we need to find the potential distribution in the free space between the tubes, i.e. for $R_1 < \rho < R_2$. If we use the same variable separation as in the simpler counterpart problem, we need the radial functions $\mathcal{R}(\rho)$ to satisfy two zero boundary conditions: at $\rho = R_1$ and $\rho = R_2$. With the Bessel functions of just the first kind, $J_n(\gamma\rho)$, it is impossible to do, because the two boundaries would impose two independent (and generally incompatible) conditions, $J_n(\gamma R_1) = 0$, and $J_n(\gamma R_2) = 0$, on one “stretching parameter” γ . The existence of the Bessel functions of the second kind immediately saves the day, because if the radial function solution is represented as a linear combination,

$$\mathcal{R} = c_J J_n(\gamma\rho) + c_Y Y_n(\gamma\rho), \quad (2.154)$$

two zero boundary conditions give two equations for γ and the ratio $c \equiv c_Y/c_J$.⁵¹ (Due to the oscillating character of both Bessel functions, these conditions would be typically satisfied by an infinite set of discrete pairs $\{\gamma, c\}$.) Note, however, that generally none of these pairs would correspond to zeros of either J_n or Y_n , so that having an analog of Table 1 for the latter function would not help much. Hence, even the simplest problems of this kind (like the one shown in Fig. 20) typically require the numerical solution of transcendental algebraic equations.

⁵¹ A pair of independent linear functions, used for the representation of the general solution of the Bessel equation, may be also chosen differently, using the so-called *Hankel functions*

$$H_n^{(1,2)}(\xi) \equiv J_n(\xi) \pm iY_n(\xi).$$

For representing the general solution of Eq. (130), this alternative is completely similar, for example, to using the pair of complex functions $\exp\{\pm i\alpha x\} \equiv \cos \alpha x \pm i \sin \alpha x$ instead of the pair of real functions $\{\cos \alpha x, \sin \alpha x\}$ for the representation of the general solution of Eq. (89) for $X(x)$.

In order to complete the discussion of variable separation in the cylindrical coordinates, one more issue to address is the so-called *modified Bessel functions*: of the *first kind*, $I_\nu(\xi)$, and of the *second kind*, $K_\nu(\xi)$. They are two linearly-independent solutions of the *modified Bessel equation*,

$$\frac{d^2\mathcal{R}}{d\xi^2} + \frac{1}{\xi} \frac{d\mathcal{R}}{d\xi} - \left(1 + \frac{\nu^2}{\xi^2}\right) \mathcal{R} = 0, \quad (2.155)$$

Modified
Bessel
equation

which differs from Eq. (130) “only” by the sign of one of its terms. Figure 21 shows a simple problem that leads (among many others) to this equation: a round thin conducting cylindrical pipe is sliced, perpendicular to its axis, to rings of equal height h , which are kept at equal but sign-alternating potentials.

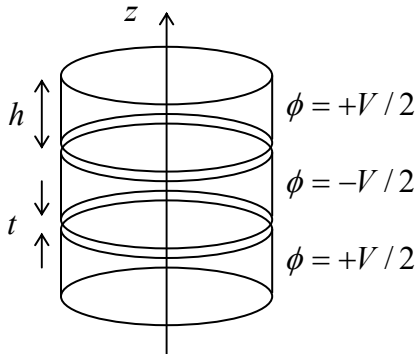


Fig. 2.21. A typical boundary problem whose solution may be conveniently described in terms of the modified Bessel functions.

If the system is very long (formally, infinite) in the z -direction, we may use the variable separation method for the solution of this problem, but now evidently need periodic (rather than exponential) solutions along the z -axis, i.e. linear combinations of $\sin kz$ and $\cos kz$ with various real values of the constant k . Separating the variables, we arrive at a differential equation similar to Eq. (129), but with the negative sign before the separation constant:

$$\frac{d^2\mathcal{R}}{d\rho^2} + \frac{1}{\rho} \frac{d\mathcal{R}}{d\rho} - (k^2 + \frac{\nu^2}{\rho^2}) \mathcal{R} = 0. \quad (2.156)$$

The same radial coordinate’s normalization, $\xi \equiv k\rho$, immediately leads us to Eq. (155), and hence (for $\nu = n$) to the modified Bessel functions $I_n(\xi)$ and $K_n(\xi)$.

Figure 22 shows the behavior of such functions, of a few lowest orders. One can see that at $\xi \rightarrow 0$ the behavior is virtually similar to that of the “usual” Bessel functions – cf. Eqs. (132) and (152), with $K_n(\xi)$ multiplied (by purely historical reasons) by an additional coefficient, $\pi/2$:

$$I_n(\xi) \rightarrow \frac{1}{n!} \left(\frac{\xi}{2}\right)^n, \quad K_n(\xi) \rightarrow \begin{cases} -\left[\ln\left(\frac{\xi}{2}\right) + \gamma\right], & \text{for } n = 0, \\ \frac{(n-1)!}{2} \left(\frac{\xi}{2}\right)^{-n}, & \text{for } n \neq 0, \end{cases} \quad (2.157)$$

However, the asymptotic behavior of the modified functions is very much different, with $I_n(x)$ exponentially growing, and $K_n(\xi)$ exponentially dropping at $\xi \rightarrow \infty$:

$$I_n(\xi) \rightarrow \left(\frac{1}{2\pi\xi} \right)^{1/2} e^{\xi}, \quad K_n(\xi) \rightarrow \left(\frac{\pi}{2\xi} \right)^{1/2} e^{-\xi}. \quad (2.158)$$

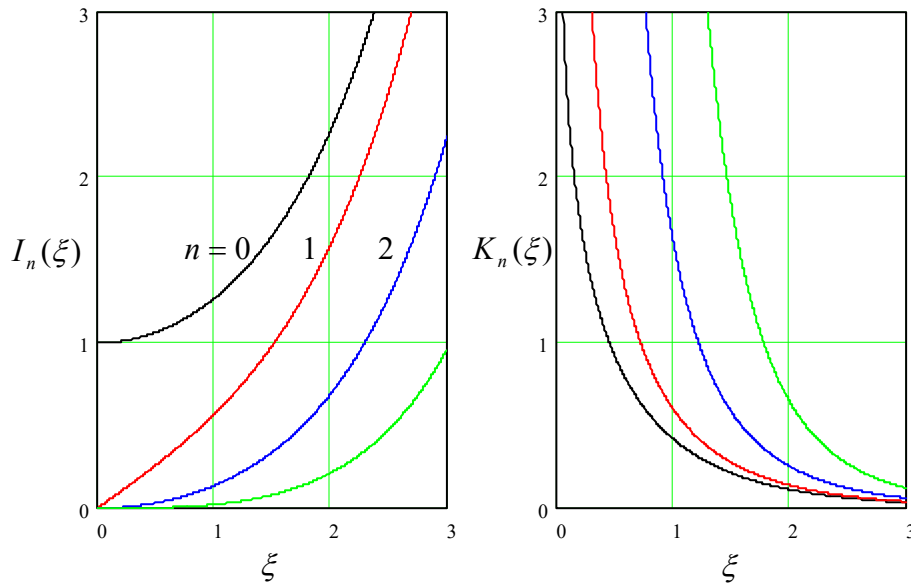


Fig. 2.22. The modified Bessel functions of the first kind (left panel) and the second kind (right panel).

This behavior is completely natural in the context of the problem shown in Fig. 21, in which the electrostatic potential may be represented as a sum of terms proportional to $I_n(\gamma\rho)$ inside the thin pipe, and of terms proportional to $K_n(\gamma\rho)$ outside it.

To complete our brief survey of the Bessel functions, let me note that all of them discussed so far may be considered as particular cases of *Bessel functions of the complex argument*, say $J_n(z)$ and $Y_n(z)$, or, alternatively, $H_n^{(1,2)}(z) \equiv J_n(z) \pm iY_n(z)$.⁵² At that, the “usual” Bessel functions $J_n(\xi)$ and $Y_n(\xi)$ may be considered as the sets of values of these generalized functions on the real axis ($z = \xi$), while the modified functions as their particular case on the imaginary axis, i.e. at $z = i\xi$, also with real ξ :

$$I_\nu(\xi) = i^{-\nu} J_\nu(i\xi), \quad K_\nu(\xi) = \frac{\pi}{2} i^{\nu+1} H_\nu^{(1)}(i\xi). \quad (2.159)$$

Moreover, this generalization of the Bessel functions to the whole complex plane z enables the use of their values along other directions on that plane, for example under angles $\pi/4 \pm \pi/2$. As a result, one arrives at the so-called *Kelvin functions*:

$$\begin{aligned} \text{ber}_\nu \xi + i \text{bei}_\nu \xi &\equiv J_\nu(\xi e^{-i\pi/4}), \\ \text{ker}_\nu \xi + i \text{kei}_\nu \xi &\equiv i \frac{\pi}{2} H_\nu^{(1)}(\xi e^{-i3\pi/4}), \end{aligned} \quad (2.160)$$

which are also useful for some important problems in physics and engineering. Unfortunately, I do not have time/space to discuss these problems in this course.⁵³

⁵² These complex functions still obey the general relations (143) and (146), with ξ replaced with z .

⁵³ In the QM part of this series we will run into the so-called *spherical Bessel functions* $j_n(\xi)$ and $y_n(\xi)$, which may be expressed via the Bessel functions of semi-integer orders. Surprisingly enough, these functions turn out to be simpler than $J_n(\xi)$ and $Y_n(\xi)$.

2. 8. Variable separation – spherical coordinates

The spherical coordinates are very important in physics, because of the (at least approximate) spherical symmetry of many physical objects – from nuclei and atoms, to water drops in clouds, to planets and stars. Let us again require each component ϕ_k of Eq. (84) to satisfy the Laplace equation. Using the full expression for the Laplace operator in spherical coordinates,⁵⁴ we get

$$\frac{1}{r^2} \frac{\partial}{\partial r} \left(r^2 \frac{\partial \phi_k}{\partial r} \right) + \frac{1}{r^2 \sin \theta} \frac{\partial}{\partial \theta} \left(\sin \theta \frac{\partial \phi_k}{\partial \theta} \right) + \frac{1}{r^2 \sin^2 \theta} \frac{\partial^2 \phi_k}{\partial \varphi^2} = 0. \quad (2.161)$$

Let us look for a solution of this equation in the following variable-separated form:

$$\phi_k = \frac{\mathcal{R}(r)}{r} \mathcal{P}(\cos \theta) \mathcal{A}(\varphi), \quad (2.162)$$

Separating the variables one by one, starting from φ , just like this has been done in cylindrical coordinates, we get the following equations for the partial functions participating in this solution:

$$\frac{d^2 \mathcal{R}}{dr^2} - \frac{l(l+1)}{r^2} \mathcal{R} = 0, \quad (2.163)$$

$$\frac{d}{d\xi} \left[(1-\xi^2) \frac{d\mathcal{P}}{d\xi} \right] + \left[l(l+1) - \frac{\nu^2}{1-\xi^2} \right] \mathcal{P} = 0, \quad (2.164)$$

$$\frac{d^2 \mathcal{A}}{d\varphi^2} + \nu^2 \mathcal{A} = 0, \quad (2.165)$$

where $\xi \equiv \cos \theta$ is a new variable used in lieu of θ (so that $-1 \leq \xi \leq +1$), while ν^2 and $l(l+1)$ are the separation constants. (The reason for selection of the latter one in this form will be clear in a minute.)

One can see that Eq. (165) is very simple, and is absolutely similar to the Eq. (107) we have got for the polar and cylindrical coordinates. Moreover, the equation for the radial functions is *simpler* than in the cylindrical coordinates. Indeed, let us look for its partial solution in the form cr^α – just as we have done with Eq. (106). Plugging this solution into Eq. (163), we immediately get the following condition on the parameter α :

$$\alpha(\alpha-1) = l(l+1). \quad (2.166)$$

This quadratic equation has two roots, $\alpha = l+1$ and $\alpha = -l$, so that the general solution of Eq. (163) is

$$\mathcal{R} = a_l r^{l+1} + \frac{b_l}{r^l}. \quad (2.167)$$

However, the general solution of Eq. (164) (called either the *general* or *associated Legendre equation*) cannot be expressed via what is usually called elementary functions.⁵⁵ Let us start its discussion from the axially-symmetric case when $\partial\phi/\partial\varphi=0$. This means $\mathcal{A}(\varphi) = \text{const}$, and thus $\nu = 0$, so that Eq. (164) is reduced to the so-called *Legendre differential equation*:

⁵⁴ See, e.g., MA Eq. (10.9).

⁵⁵ Again, there is no generally accepted line between the “elementary” and “special” functions.

Legendre
equation

$$\frac{d}{d\xi} \left[(1 - \xi^2) \frac{d\mathcal{P}}{d\xi} \right] + l(l+1)\mathcal{P} = 0. \quad (2.168)$$

One can readily verify that the solutions of this equation for integer values of l are specific (*Legendre*) polynomials⁵⁶ that may be described by the following *Rodrigues' formula*:

Legendre
polynomials

$$\mathcal{P}_l(\xi) = \frac{1}{2^l l!} \frac{d^l}{d\xi^l} (\xi^2 - 1)^l, \quad \text{with } l = 0, 1, 2, \dots \quad (2.169)$$

According to this formula, the first few Legendre polynomials are pretty simple:

$$\begin{aligned} \mathcal{P}_0(\xi) &= 1, \\ \mathcal{P}_1(\xi) &= \xi, \\ \mathcal{P}_2(\xi) &= \frac{1}{2}(3\xi^2 - 1), \\ \mathcal{P}_3(\xi) &= \frac{1}{2}(5\xi^3 - 3\xi), \\ \mathcal{P}_4(\xi) &= \frac{1}{8}(35\xi^4 - 30\xi^2 + 3), \end{aligned} \quad (2.170)$$

though such explicit expressions become more and more bulky as l is increased. As Fig. 23 shows, all these polynomials, which are defined on the $[-1, +1]$ segment, end at the same point: $\mathcal{P}_l(+1) = +1$, while starting either at the same point or at the opposite point: $\mathcal{P}_l(-1) = (-1)^l$. Between these two endpoints, the l^{th} Legendre polynomial has l zeros. It is straightforward to use Eq. (169) for proving that these polynomials form a full, orthogonal set of functions, with the following normalization rule:

$$\int_{-1}^{+1} \mathcal{P}_l(\xi) \mathcal{P}_{l'}(\xi) d\xi = \frac{2}{2l+1} \delta_{ll'}, \quad (2.171)$$

so that any function $f(\xi)$ defined on the segment $[-1, +1]$ may be represented as a unique series over the polynomials.⁵⁷

Thus, taking into account the additional division by r in Eq. (162), the general solution of any axially-symmetric Laplace problem may be represented as

$$\phi(r, \theta) = \sum_{l=0}^{\infty} \left(a_l r^l + \frac{b_l}{r^{l+1}} \right) \mathcal{P}_l(\cos \theta). \quad (2.172)$$

Variable
separation
in spherical
coordinates
(for axial
symmetry)

Note a strong similarity between this solution and Eq. (112) for the 2D Laplace problem in the polar coordinates. However, besides the difference in the angular functions, there is also a difference (by one) in the power of the second radial function, and this difference immediately shows up in problem solutions.

⁵⁶ Just for the reference: if l is not an integer, the general solution of Eq. (2.168) may be represented as a linear combination of the so-called *Legendre functions* (not polynomials!) of the first and second kind, $\mathcal{P}_l(\xi)$ and $\mathcal{Q}_l(\xi)$.

⁵⁷ This is why, at least for the purposes of this course, there is no good reason for pursuing (more complicated) solutions to Eq. (168) for non-integer values of l , mentioned in the previous footnote.

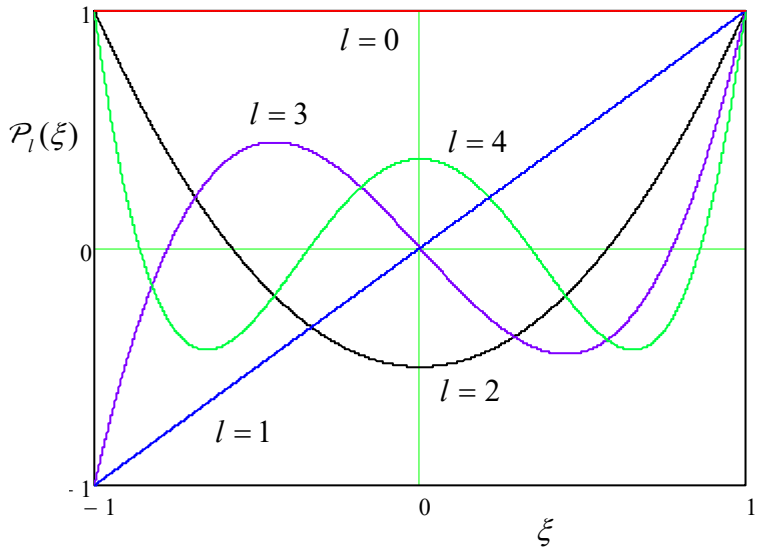


Fig. 2.23. A few lowest Legendre polynomials $\mathcal{P}_l(\xi)$.

Indeed, let us solve a problem similar to that shown in Fig. 15: find the electric field around a conducting sphere of radius R , placed into an initially uniform external field \mathbf{E}_0 (whose direction I will now take for the z -axis) – see Fig. 24a.

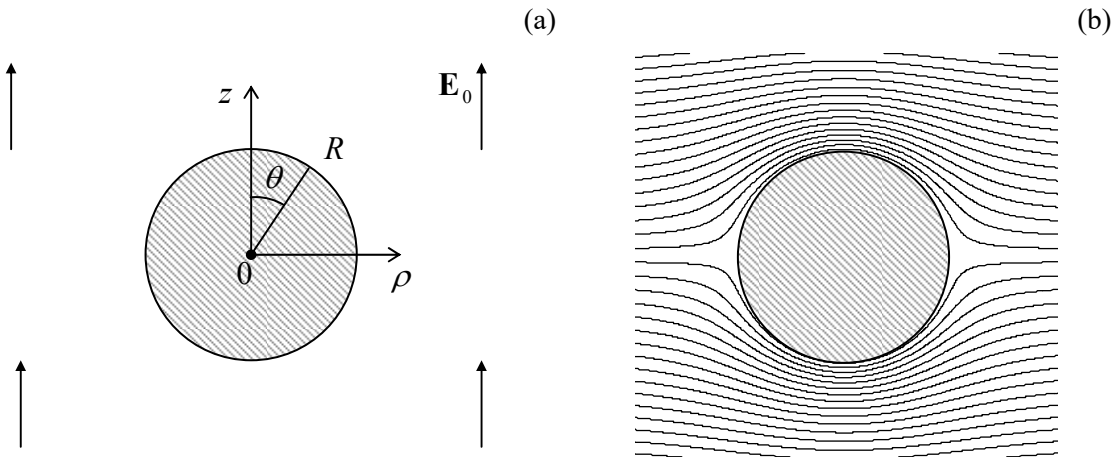


Fig. 2.24. Conducting sphere in a uniform electric field: (a) the problem's geometry, and (b) the equipotential surface pattern given by Eq. (176). The pattern is qualitatively similar but quantitatively different from that for the conducting cylinder in a perpendicular field – cf. Fig. 15.

If we select the arbitrary constant in the electrostatic potential so that $\phi|_{z=0} = 0$, then in Eq. (172) we should take $a_0 = b_0 = 0$. Now, just as has been argued for the cylindrical case, at $r \gg R$ the potential should approach that of the uniform field:

$$\phi \rightarrow -E_0 z = -E_0 r \cos \theta, \quad (2.173)$$

so that in Eq. (172), only one of the coefficients a_l survives: $a_l = -E_0 \delta_{l,1}$. As a result, from the boundary condition on the surface, $\phi(R, \theta) = 0$, we get the following equation for the coefficients b_l :

$$\left(-E_0 R + \frac{b_1}{R^2} \right) \cos \theta + \sum_{l \geq 2} \frac{b_l}{R^{l+1}} \mathcal{P}_l(\cos \theta) = 0. \quad (2.174)$$

Now repeating the argumentation that led to Eq. (117), we may conclude that Eq. (174) is satisfied if

$$b_l = E_0 R^3 \delta_{l,1}, \quad (2.175)$$

so that, finally, Eq. (172) is reduced to

$$\phi = -E_0 \left(r - \frac{R^3}{r^2} \right) \cos \theta. \quad (2.176)$$

This distribution, shown in Fig. 24b, is very much similar to Eq. (117) for the cylindrical case (cf. Fig. 15b, with the account for a different plot orientation), but with a different power of the radius in the second term. This difference leads to a quantitatively different distribution of the surface electric field:

$$E_n = -\frac{\partial \phi}{\partial r} \Big|_{r=R} = 3E_0 \cos \theta, \quad (2.177)$$

so that its maximal value is a factor of 3 (rather than 2) larger than the external field.

Now let me briefly (mostly just for the reader's reference) mention the Laplace equation solutions in the general case – with no axial symmetry. If the conductor-free space surrounds the origin from all sides, the solutions to Eq. (165) have to be 2π -periodic, and hence $\nu = n = 0, \pm 1, \pm 2, \dots$. Mathematics says that Eq. (164) with integer $\nu = n$ and a fixed integer l has a solution only for a limited range of n :⁵⁸

$$-l \leq n \leq +l. \quad (2.178)$$

These solutions are called *associated Legendre functions* (generally, they are *not* polynomials). For $n \geq 0$, these functions may be defined via the Legendre polynomials, using the following formula:⁵⁹

$$\mathcal{P}_l^n(\xi) = (-1)^n (1 - \xi^2)^{n/2} \frac{d^n}{d\xi^n} \mathcal{P}_l(\xi). \quad (2.179)$$

On the segment $\xi \in [-1, +1]$, each set of the associated Legendre functions with a fixed index n and non-negative values of l form a full, orthogonal set, with the normalization relation,

$$\int_{-1}^{+1} \mathcal{P}_l^n(\xi) \mathcal{P}_{l'}^n(\xi) d\xi = \frac{2}{2l+1} \frac{(l+n)!}{(l-n)!} \delta_{ll'}, \quad (2.180)$$

that is evidently a generalization of Eq. (171).

Since these relations may seem a bit intimidating, let me write down explicit expressions for a few $\mathcal{P}_l^n(\cos \theta)$ with the three lowest values of l and $n \geq 0$, which are most important for applications.

$$l=0: \quad \mathcal{P}_0^0(\cos \theta) = 1; \quad (2.181)$$

⁵⁸ In quantum mechanics, the letter n is typically reserved for the “principal quantum number”, while the azimuthal functions are numbered by index m . However, here I will keep using n as their index because for this course’s purposes, this seems more logical, in view of the similarity of the spherical and cylindrical functions.

⁵⁹ Note that some texts use different choices for the front factor (called the *Condon-Shortley phase*) in the functions \mathcal{P}_l^m , which do not affect the final results for the spherical harmonics Y_l^m .

$$l=1: \begin{cases} \mathcal{P}_1^0(\cos\theta) = \cos\theta, \\ \mathcal{P}_1^1(\cos\theta) = -\sin\theta; \end{cases} \quad (2.182)$$

$$l=2: \begin{cases} \mathcal{P}_2^0(\cos\theta) = (3\cos^2\theta - 1)/2, \\ \mathcal{P}_2^1(\cos\theta) = -2\sin\theta\cos\theta, \\ \mathcal{P}_2^2(\cos\theta) = -3\cos^2\theta. \end{cases} \quad (2.183)$$

The reader should agree there is not much to fear in these functions – they are just certain sums of products of $\cos\theta \equiv \xi$ and $\sin\theta \equiv (1 - \xi^2)^{1/2}$. Fig. 25 shows the plots of a few lowest functions $\mathcal{P}_l^n(\xi)$.

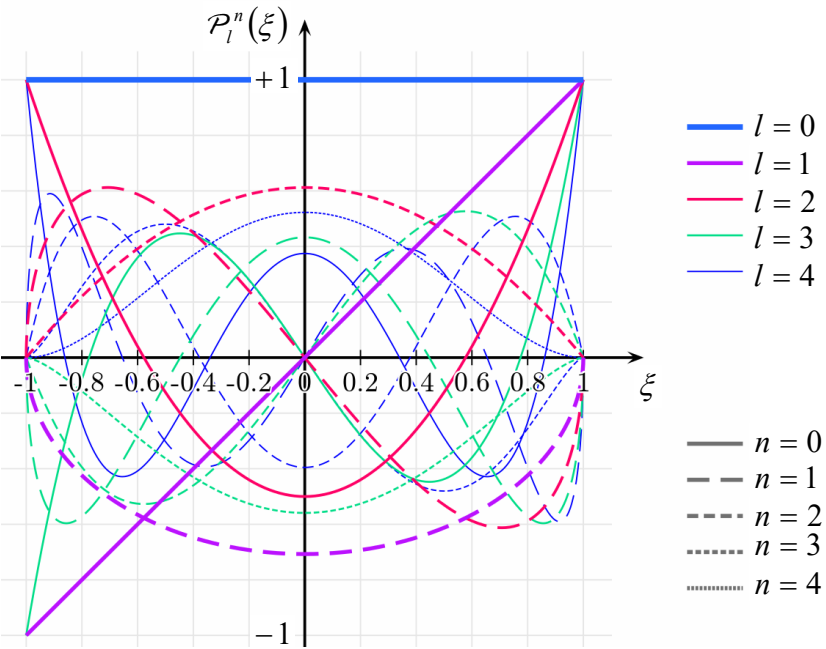


Fig. 2.25. A few lowest associated Legendre functions. (Adapted from an original by Geek3, available at https://en.wikipedia.org/wiki/Associated_Legendre_polynomials, under the GNU Free Documentation License.)

Using the associated Legendre functions, the general solution (162) to the Laplace equation in the spherical coordinates may be expressed as

$$\phi(r, \theta, \varphi) = \sum_{l=0}^{\infty} \left(a_l r^l + \frac{b_l}{r^{l+1}} \right) \sum_{n=0}^l \mathcal{P}_l^n(\cos\theta) \mathcal{J}_n(\varphi), \quad \mathcal{J}_n(\varphi) = c_n \cos n\varphi + s_n \sin n\varphi. \quad (2.184)$$

Variable separation in spherical coordinates (general case)

Since the difference between the angles θ and φ is somewhat artificial, physicists prefer to think not in terms of the functions \mathcal{P} and \mathcal{J} in separation, but directly about their products that participate in this solution.⁶⁰

⁶⁰ In quantum mechanics, it is more convenient to use a slightly different alternative set of basic functions of the same problem, namely the following complex functions called the *spherical harmonics*:

$$Y_l^n(\theta, \varphi) \equiv \left[\frac{2l+1}{4\pi} \frac{(l-n)!}{(l+n)!} \right]^{1/2} \mathcal{P}_l^n(\cos\theta) e^{in\varphi},$$

which are defined for both positive and negative n (within the limits $-l \leq n \leq +l$) – see, e.g., QM Secs. 3.6 and 5.6. (Note again that in that field, our index n is traditionally denoted as m , and called the *magnetic quantum number*.)

As a rare exception for my courses, to save time I will skip giving an example of using the associated Legendre functions in electrostatics, because quite a few examples of these functions' applications will be given in the quantum mechanics part of this series.

2.9. Charge images

So far, we have discussed various methods of solution of the *Laplace* boundary problem (35). Let us now move on to the discussion of its generalization, the *Poisson* equation (1.41). We need it when besides conductors, we also have stand-alone charges with a known spatial distribution $\rho(\mathbf{r})$. (Its discussion will also allow us, better equipped, to revisit the Laplace problem in the next section.)

Let us start from a somewhat limited, but very useful *charge image* (or “image charge”) method. Consider a very simple problem: a single point charge near a conducting half-space – see Fig. 26.

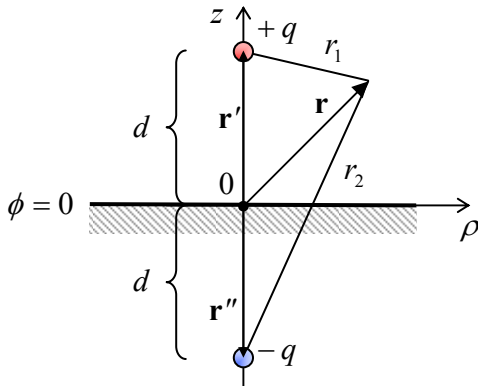


Fig. 2.26. The simplest problem readily solvable by the charge image method. The points' colors are used, as before, to denote the charges of the original (red) and opposite (blue) sign.

Let us prove that its solution, above the conductor's surface ($z \geq 0$), may be represented as:

$$\phi(\mathbf{r}) = \frac{1}{4\pi\epsilon_0} \left(\frac{q}{r_1} - \frac{q}{r_2} \right) \equiv \frac{q}{4\pi\epsilon_0} \left(\frac{1}{|\mathbf{r} - \mathbf{r}'|} - \frac{1}{|\mathbf{r} - \mathbf{r}''|} \right), \quad (2.185)$$

or in a more explicit form, using the cylindrical coordinates shown in Fig. 26:

$$\phi(\mathbf{r}) = \frac{q}{4\pi\epsilon_0} \left\{ \frac{1}{[\rho^2 + (z-d)^2]^{1/2}} - \frac{1}{[\rho^2 + (z+d)^2]^{1/2}} \right\}, \quad (2.186)$$

where ρ is the distance of the field observation point \mathbf{r} from the “vertical” line on which the charge is located. Indeed, this solution satisfies both the boundary condition $\phi = 0$ at the surface of the conductor ($z = 0$), and the Poisson equation (1.41), with the single δ -functional source at point $\mathbf{r}' = \{0, 0, +d\}$ on its right-hand side, because the second singularity of the solution, at point $\mathbf{r}'' = \{0, 0, -d\}$, is outside the region of the solution's validity ($z \geq 0$). Physically, this solution may be interpreted as the sum of the fields of the actual charge ($+q$) at point \mathbf{r}' , and an equal but opposite charge ($-q$) at the “mirror image” point \mathbf{r}'' (Fig. 26). This is the basic idea of the charge image method.

Before moving on to more complex problems, let us discuss the situation shown in Fig. 26 in a little bit more detail, due to its fundamental importance. First, we can use Eqs. (3) and (186) to calculate the surface charge density:

$$\sigma = -\epsilon_0 \frac{\partial \phi}{\partial z} \Big|_{z=0} = -\frac{q}{4\pi} \frac{\partial}{\partial z} \left(\frac{1}{[\rho^2 + (z-d)^2]^{1/2}} - \frac{1}{[\rho^2 + (z+d)^2]^{1/2}} \right)_{z=0} = -\frac{q}{4\pi} \frac{2d}{(\rho^2 + d^2)^{3/2}}. \quad (2.187)$$

From this, the total surface charge is

$$Q = \int_S \sigma d^2 r = 2\pi \int_0^\infty \sigma(\rho) \rho d\rho = -\frac{q}{2} \int_0^\infty \frac{2d}{(\rho^2 + d^2)^{3/2}} \rho d\rho. \quad (2.188)$$

This integral may be easily worked out using the substitution $\xi \equiv \rho^2/d^2$ (giving $d\xi = 2\rho d\rho/d^2$):

$$Q = -\frac{q}{2} \int_0^\infty \frac{d\xi}{(\xi + 1)^{3/2}} = -q. \quad (2.189)$$

This result is very natural: the conductor brings as much surface charge from its interior to the surface as necessary to fully compensate for the initial charge ($+q$) and hence kill the electric field at large distances as efficiently as possible, hence reducing the total electrostatic energy (1.65) to the lowest possible value.

For a better feeling of this *polarization charge* of the surface, let us take our calculations to the extreme – to the q equal to one elementary charge e , and place a particle with this charge (for example, a proton) at a macroscopic distance – say 1 m – from the conductor’s surface. Then, according to Eq. (189), the total polarization charge of the surface equals that of an electron, and according to Eq. (187), its spatial extent is of the order of $d^2 = 1 \text{ m}^2$. This means that if we consider a much smaller part of the surface, $\Delta A \ll d^2$, its polarization charge magnitude $\Delta Q = \sigma \Delta A$ is much *less than one electron!* For example, Eq. (187) shows that the polarization charge of quite a macroscopic area $\Delta A = 1 \text{ cm}^2$ right under the initial charge ($\rho = 0$) is $e \Delta A / 2\pi d^2 \approx 1.6 \times 10^{-5} e$. Can this be true, or our theory is somehow limited to the charges q much larger than e ? (After all, the theory is substantially based on the approximate macroscopic model (1); maybe it is the culprit?)

Surprisingly enough, the answer to this question has become clear (at least to some physicists :-) only as late as in the mid-1980s when several experiments demonstrated, and theorists accepted (some of them rather grudgingly) that the usual polarization charge formulas are valid for elementary charges as well, i.e., such the polarization charge ΔQ of a macroscopic surface area may differ from a multiple of e . The underlying reason for this paradox is the physical nature of the polarization charge of a conductor’s surface: as was discussed in Sec. 1, it is due not to new charged particles brought into the conductor (such charge would be in fact a multiple of e), but to a small *shift* of the free charges of a conductor by a very small distance from their equilibrium positions that they had in the absence of the external field induced by charge q . This shift is not quantized, at least on the scale relevant to our problem, and hence neither is ΔQ .

This understanding has paved the way toward the invention and experimental demonstration of several new devices including so-called *single-electron transistors*,⁶¹ which may be used, in particular, for ultrasensitive measurement of polarization charges as small as $\sim 10^{-6} e$. Another important class of single-electron devices is the dc and ac current standards based on the fundamental relation $I = -ef$,

⁶¹ Actually, this term (for which the author of these notes may be blamed :-) is misleading: the operation of the “single-electron transistor” is based on the interplay of discrete charges (multiples of e) transferred between conductors, and *sub-single-electron* polarization charges – see, e.g., K. Likharev, *Proc. IEEE* **87**, 606 (1999).

where I is the dc current carried by electrons transferred with the frequency f . The experimentally achieved⁶² relative accuracy of such standards is of the order of 10^{-7} , and is not too far from that provided by the competing approach based on a combination of the Josephson effect and the quantum Hall effect.⁶³

Second, let us find the potential energy U of the charge-to-surface interaction. For that, we may use the value of the electrostatic potential (185) at the point of the charge itself ($\mathbf{r} = \mathbf{r}'$), of course ignoring the infinite potential created by the real charge, so that the remaining potential is that of the image charge

$$\phi_{\text{image}}(\mathbf{r}') = -\frac{1}{4\pi\epsilon_0} \frac{q}{2d}. \quad (2.190)$$

Looking at the electrostatic potential's definition given by Eq. (1.31), it may be tempting to immediately write $U = q\phi_{\text{image}} = -(1/4\pi\epsilon_0)(q^2/2d)$ [WRONG!], but this would be incorrect. The reason is that the potential ϕ_{image} is not independent of q , but is actually induced by this charge. This is why the correct approach is to calculate U from Eq. (1.61), with just one term:

$$U = \frac{1}{2}q\phi_{\text{image}} = -\frac{1}{4\pi\epsilon_0} \frac{q^2}{4d}, \quad (2.191)$$

giving twice lower energy than the wrong result cited above. To double-check Eq. (191), and also get a better feeling of the factor $\frac{1}{2}$ that distinguishes it from the wrong guess, we can calculate U as the integral of the force exerted on the charge by the conductor's surface charge (i.e., in our formalism, by the image charge):

$$U = -\int_{-\infty}^d F(z)dz = \frac{1}{4\pi\epsilon_0} \int_{-\infty}^d \frac{q^2}{(2z)^2} dz = -\frac{1}{4\pi\epsilon_0} \frac{q^2}{4d}. \quad (2.192)$$

This calculation clearly accounts for the gradual build-up of the force F , as the real charge is being brought from afar (where we have opted for $U=0$) toward the surface.

This result has several important applications. For example, let us plot the electrostatic energy U of an electron, i.e. a particle with charge $q = -e$, near a metallic surface, as a function of d . For that, we may use Eq. (191) until our macroscopic model (1) becomes invalid, and U transitions to some negative constant value ($-\psi$) inside the conductor – see Fig. 27a. Since our calculation was for an electron with zero potential energy at infinity, at relatively low temperatures, $k_B T \ll \psi$, electrons in metals may occupy only the states with energies below $-\psi$ (the so-called *Fermi level*⁶⁴). The positive constant ψ is called the *workfunction* because it describes the smallest work needed to remove the electron from a metal. As was discussed in Sec. 1, in good metals the electric field screening takes place at interatomic distances $a_0 \sim 10^{-10}$ m. Plugging $d = 1 \times 10^{-10}$ m and $q = -e \approx -1.6 \times 10^{-19}$ C into Eq. (191), we get $\psi \approx 6 \times 10^{-19}$ J ≈ 3.5 eV. This crude estimate is in surprisingly good agreement with the experimental values of the workfunction, ranging between 4 and 5 eV for most metals.⁶⁵

⁶² See, e.g., M. Keller *et al.*, *Appl. Phys. Lett.* **69**, 1804 (1996); F. Stein *et al.*, *Metrologia* **54**, 1 (2017).

⁶³ J. Brun-Pickard *et al.*, *Phys. Rev. X* **6**, 041051 (2016).

⁶⁴ More discussion of these states may be found in SM Secs. 3.3 and 6.3.

⁶⁵ More discussion of the workfunction, and its effect on the electrons' kinetics, is given in SM Sec. 6.3.

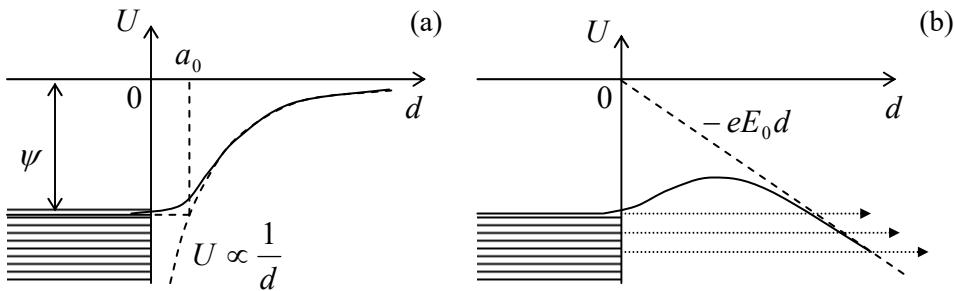


Fig. 2.27. (a) The origin of the workfunction, and (b) the field emission of electrons (schematically).

Next, let us consider the effect of an additional uniform external electric field E_0 applied normally to a metallic surface, on this potential profile. For that, we may add the potential energy that the field gives to the electron at distance d from the surface, $U_{\text{ext}} = -eE_0 d$, to that created by the image charge. (As we know from Eq. (1.53), since the field E_0 is independent of the electron's position, its recalculation into the potential energy does not require the coefficient $\frac{1}{2}$.) As the result, the potential energy of an electron near the surface becomes

$$U(d) = -eE_0 d - \frac{1}{4\pi\epsilon_0} \frac{e^2}{4d}, \quad \text{for } d \gg a_0, \quad (2.193)$$

with a similar crossover to $U = -\psi$ inside the conductor – see Fig. 27b. One can see that at the appropriate sign, and a sufficient magnitude of the applied field, it lowers the potential barrier that prevents electrons from leaving the conductor. At $E_0 \sim \psi/a_0$ (for metals, $\sim 10^{10}$ V/m), this suppression becomes so strong that electrons with energies at, and just below the Fermi level start quantum-mechanical tunneling through the remaining thin barrier. This is the *field electron emission* (or just “field emission”) effect, which is used in vacuum electronics to provide efficient cathodes that do not require heating to high temperatures.⁶⁶

Returning to the basic electrostatics, let us find some other conductor geometries where the method of charge images may be effectively applied. First, let us consider a right-angle corner (Fig. 28a). Reflecting the initial charge in the vertical plane, we get the image shown in the top left corner of that panel. This image makes the boundary condition $\phi = \text{const}$ satisfied on the vertical surface of the corner. However, for the same to be true on the horizontal surface, we have to reflect *both* the initial charge *and* the image charge in the horizontal plane, flipping their signs. The final configuration of four charges, shown in Fig. 28a, satisfies all boundary conditions. The resulting potential distribution may be readily written as an evident generalization of Eq. (185). From it, the electric field and electric charge distributions, and the potential energy and forces acting on the charge may be calculated exactly as above – an easy exercise left for the reader.

Next, consider a corner with the angle $\pi/4$ (Fig. 28b). Here we need to repeat the reflection operation not two but four times before we arrive at the final pattern of eight positive and negative charges. (Any attempt to continue this process would lead to overlap with the already existing charges.)

⁶⁶ The practical use of such “cold” cathodes is affected by the fact that, as it follows from our discussion in Sec. 4, any nanoscale irregularity of a conducting surface (a protrusion, an atomic cluster, or even a single “adatom” stuck to it) may cause a strong increase of the local field well above the applied uniform field E_0 , making the electron emission reproducibility and stability in time significant challenges. In addition, the impact-ionization effects may lead to avalanche-type electric breakdown at dc fields as low as $\sim 3 \times 10^6$ V/m.

This reasoning may be readily extended to corners of angles $\beta = \pi/n$, with any integer n , which require $2n$ charges (including the initial one) to satisfy all the boundary conditions.

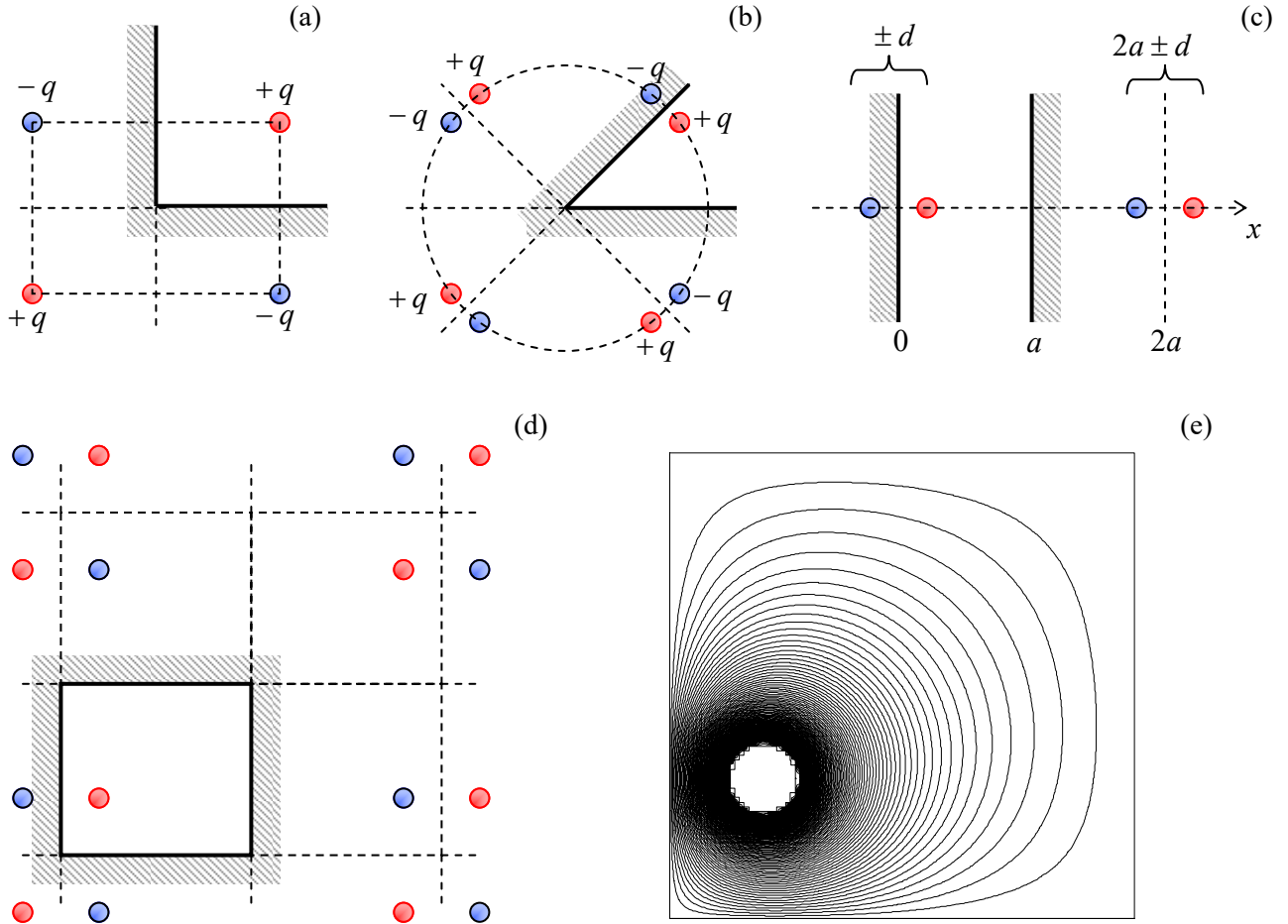


Fig. 2.28. The charge images for (a, b) the corners with angles $\pi/2$ and $\pi/4$, (c) a plane capacitor, and (d) a rectangular box; (e) typical equipotential surfaces for the last system.

Some configurations require an infinite number of images but are still tractable. The most important of them is a system of two parallel conducting surfaces, i.e. an unbiased plane capacitor of infinite area (Fig. 28c). Here the repeated reflection leads to an infinite system of charges $\pm q$ at points

$$x_j^\pm = 2aj \pm d, \quad (2.194)$$

where d (with $0 < d < a$) is the position of the initial charge, and j is an arbitrary integer. The resulting infinite sum for the potential of the real charge q , created by the field of its images,

$$\phi(d) = \frac{1}{4\pi\epsilon_0} \left[-\frac{q}{2d} + \sum_{j \neq 0} \sum_{\pm} \frac{\pm q}{|d - x_j^\pm|} \right] \equiv -\frac{q}{4\pi\epsilon_0} \left\{ \frac{1}{2d} + \frac{d^2}{a^3} \sum_{j=1}^{\infty} \frac{1}{j[j^2 - (d/a)^2]} \right\}, \quad (2.195)$$

is converging (in its last form) very fast. For example, the exact value, $\phi(a/2) = -2\ln 2 (q/4\pi\epsilon_0 a)$, differs by less than 5% from the approximation using just the first term of the sum.

The same method may be applied to 2D (cylindrical) and 3D rectangular conducting boxes that require, respectively, 2D or 3D infinite rectangular lattices of images; for example in a 3D box with sides a , b , and c , charges $\pm q$ are located at points (Fig. 28d)

$$\mathbf{r}_{jkl}^{\pm} = 2ja + 2kb + 2lc \pm \mathbf{r}', \quad (2.196)$$

where \mathbf{r}' is the location of the initial (real) charge, and j , k , and l are arbitrary integers. Figure 28e shows a typical result of the summation of the potentials of such charge set, including the real one, in a 2D box (within the plane of the real charge). One can see that the equipotential surfaces, concentric near the charge, are naturally leaning along the conducting walls of the box, which have to be equipotential.

Even more surprisingly, the image charge method works very efficiently not only for rectilinear geometries but also for spherical ones. Indeed, let us consider a point charge q at distance d from the center of a conducting, grounded sphere of radius R (Fig. 29a), and try to satisfy the boundary condition $\phi = 0$ for the electrostatic potential on the sphere's surface using an imaginary charge q' located at some point beyond the surface, i.e. inside the sphere.

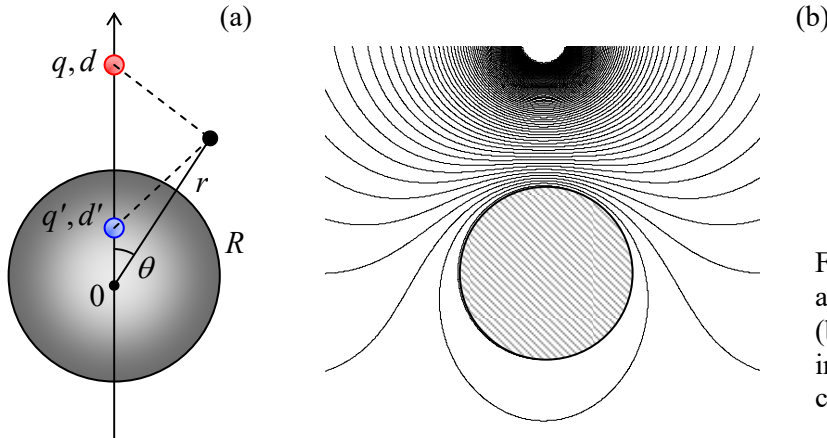


Fig. 2.29. Method of charge images for a conducting sphere: (a) the idea, and (b) the resulting potential distribution in the central plane containing the charge, for the particular case $d = 2R$.

From the problem's symmetry, it is clear that the point should be at the line passing through the real charge and the sphere's center, at some distance d' from the center. Then the total potential created by the two charges at an arbitrary point of free space, i.e. at $r \geq R$ (Fig. 29a) is

$$\phi(r, \theta) = \frac{1}{4\pi\epsilon_0} \left[\frac{q}{(r^2 + d^2 - 2rd \cos \theta)^{1/2}} + \frac{q'}{(r^2 + d'^2 - 2rd' \cos \theta)^{1/2}} \right]. \quad (2.197)$$

This expression shows that we can make the two involved fractions equal and opposite at all points on the sphere's surface (i.e. for any θ at $r = R$) if we take⁶⁷

$$d' = \frac{R^2}{d}, \quad q' = -\frac{R}{d}q. \quad (2.198)$$

Since the solution of any Poisson boundary problem is unique, Eqs. (197) and (198) give us the final solution for this problem. Fig. 29b shows a typical equipotential pattern following from this solution. It may be surprising how formulas that simple may describe such an elaborate field distribution.

⁶⁷ In geometry, such points with $dd' = R^2$, are referred to as the result of mutual *inversion* in a sphere of radius R .

Now we can calculate the total charge Q on the grounded sphere's surface, induced by the external charge q . We could do this, as we have done for the conducting plane, by the brute-force integration of the surface charge density $\sigma = -\epsilon_0 \partial \phi / \partial r|_{r=R}$. It is more elegant, however, to use the following Gauss law argument. Equality (197) is valid (at $r \geq R$) regardless of whether we are dealing with our real problem (charge q and the conducting sphere) or with the equivalent charge configuration – with the point charges q and q' , but no sphere at all. Hence, according to Eq. (1.16), the Gaussian integral over a surface with radius $r = R + 0$, and the total charge inside the sphere should be also the same. Hence we immediately get

$$Q = q' = -\frac{R}{d} q. \quad (2.199)$$

A similar argumentation may be used to calculate the charge-to-sphere interaction force:

$$F = q E_{\text{image}}(d) = q \frac{q'}{4\pi\epsilon_0(d-d')^2} = -\frac{q^2}{4\pi\epsilon_0} \frac{R}{d} \frac{1}{(d-R^2/d)^2} = -\frac{q^2}{4\pi\epsilon_0} \frac{Rd}{(d^2-R^2)^2}. \quad (2.200)$$

(Note that this expression is legitimate only at $d > R$.) At large distances, $d \gg R$, this attractive force decreases as $1/d^3$. This unusual dependence arises because, as Eq. (199) specifies, the induced charge of the sphere, responsible for the force, is not constant but decreases as $1/d$. In the next chapter, we will see that such force is also typical for the interaction between a point charge and a *dipole*.

All previous formulas were for a sphere that is grounded to keep its potential equal to zero. But what if we keep the sphere galvanically insulated, so that its *net charge* is fixed, for example, equals zero? Instead of solving this problem from scratch, let us use (again!) the almighty linear superposition principle. For that, we may add to the previous problem an additional charge, equal to $-Q = -q'$, to the sphere, and argue that this addition gives, at all points, an additional, spherically-symmetric potential that does not depend on the potential induced by the external charge q , and was calculated in Sec. 1.2 – see Eq. (1.19). For the interaction force, such addition yields

$$F = \frac{qq'}{4\pi\epsilon_0(d-d')^2} + \frac{qq'}{4\pi\epsilon_0 d^2} = -\frac{q^2}{4\pi\epsilon_0} \left[\frac{Rd}{(d^2-R^2)^2} - \frac{R}{d^3} \right]. \quad (2.201)$$

At large distances, the two terms proportional to $1/d^3$ cancel each other, giving $F \propto 1/d^5$, so that the potential energy of such interaction behaves as $U \propto 1/d^4$. Such a rapid force decay is due to the fact that the field of the uncharged sphere is equivalent to that of two (equal and opposite) induced charges $+q'$ and $-q'$, and the distance between them ($d - d' = d - R^2/d$) tends to zero at $d \rightarrow \infty$.

2.10. Green's functions

I have spent so much time/space discussing potential distributions created by a single point charge in various conductor geometries because for any of the geometries, the generalization of these results to the arbitrary distribution $\rho(\mathbf{r})$ of free charges is straightforward. Namely, if a single charge q , located at some point \mathbf{r}' , creates at point \mathbf{r} the electrostatic potential

$$\phi(\mathbf{r}) = \frac{1}{4\pi\epsilon_0} q G(\mathbf{r}, \mathbf{r}'), \quad (2.202)$$

then, due to the linear superposition principle, an arbitrary charge distribution creates the potential

$$\phi(\mathbf{r}) = \frac{1}{4\pi\epsilon_0} \sum_j q_j G(\mathbf{r}, \mathbf{r}_j) = \frac{1}{4\pi\epsilon_0} \int \rho(\mathbf{r}') G(\mathbf{r}, \mathbf{r}') d^3 r'. \quad (2.203)$$

Spatial
Green's
function

The function $G(\mathbf{r}, \mathbf{r}')$ is called the (spatial) *Green's function* – the notion very fruitful and hence popular in all fields of physics.⁶⁸ Evidently, as Eq. (1.35) shows, in the unlimited free space

$$G(\mathbf{r}, \mathbf{r}') = \frac{1}{|\mathbf{r} - \mathbf{r}'|}, \quad (2.204)$$

i.e. the Green's function depends only on one scalar argument – the distance between the field-observation point \mathbf{r} and the field-source (charge) point \mathbf{r}' . However, as soon as there are conductors around, the situation changes. In this course, I will only discuss the Green's functions defined to vanish as soon as the radius-vector \mathbf{r} points to the surface (S) of any conductor:⁶⁹

$$G(\mathbf{r}, \mathbf{r}') \Big|_{\mathbf{r} \in S} = 0. \quad (2.205)$$

With this definition, it is straightforward to deduce the Green's functions for the solutions of the last section's problems in which conductors were grounded, i.e. had potential $\phi = 0$. For example, for a semi-space $z \geq 0$ limited by a grounded conducting plane $z = 0$ (Fig. 26), Eq. (185) yields

$$G = \frac{1}{|\mathbf{r} - \mathbf{r}'|} - \frac{1}{|\mathbf{r} - \mathbf{r}''|}, \quad \text{with } \mathbf{r}'' = \mathbf{r}' \text{ and } z'' = -z', \quad (2.206)$$

where \mathbf{r} is the 2D radius vector. We see that in the presence of conductors (and, as we will see later, any other polarizable media), the Green's function may depend not only on the difference $\mathbf{r} - \mathbf{r}'$, but on each of these two arguments in a specific way.

So far, this is just re-naming our old results. The really non-trivial result of the Green's function formalism in electrostatics is that, somewhat counter-intuitively, the knowledge of this function for a system with *grounded* conductors (Fig. 30a) enables the calculation of the field created by *voltage-biased* conductors (Fig. 30b), with the same geometry. To show this, let us use the so-called *Green's theorem* of the vector calculus.⁷⁰ The theorem states that for any two scalar, differentiable functions $f(\mathbf{r})$ and $g(\mathbf{r})$, and any volume V ,

$$\int_V (f \nabla^2 g - g \nabla^2 f) d^3 r = \oint_S (f \nabla g - g \nabla f)_n d^2 r, \quad (2.207)$$

where S is the surface limiting the volume. Applying the theorem to the electrostatic potential $\phi(\mathbf{r})$ and the Green's function G (also considered as a function of \mathbf{r}), let us use the Poisson equation (1.41) to replace $\nabla^2 \phi$ with $(-\rho/\epsilon_0)$, and notice that G , considered as a function of \mathbf{r} , obeys the Poisson equation with the δ -functional source:

$$\nabla^2 G(\mathbf{r}, \mathbf{r}') = -4\pi\delta(\mathbf{r} - \mathbf{r}'). \quad (2.208)$$

⁶⁸ See, e.g., CM Sec. 5.1, QM Secs. 2.2 and 7.4, and SM Sec. 5.5.

⁶⁹ G so defined is sometimes called the *Dirichlet function*.

⁷⁰ See, e.g., MA Eq. (12.3). Actually, this theorem is a ready corollary of the better-known divergence ("Gauss") theorem, MA Eq. (12.2).

(Indeed, according to its definition (202), this function may be formally considered as the field of a point charge $q = 4\pi\epsilon_0$.) Now swapping the notation of the radius-vectors, $\mathbf{r} \leftrightarrow \mathbf{r}'$, and using the Green's function symmetry, $G(\mathbf{r}, \mathbf{r}') = G(\mathbf{r}', \mathbf{r})$,⁷¹ we get

$$-4\pi\phi(\mathbf{r}) - \int_V \left(-\frac{\rho(\mathbf{r}')}{\epsilon_0} \right) G(\mathbf{r}, \mathbf{r}') d^3 r' = \oint_S \left[\phi(\mathbf{r}') \frac{\partial G(\mathbf{r}, \mathbf{r}')}{\partial n'} - G(\mathbf{r}, \mathbf{r}') \frac{\partial \phi(\mathbf{r}')}{\partial n'} \right] d^2 r'. \quad (2.209)$$

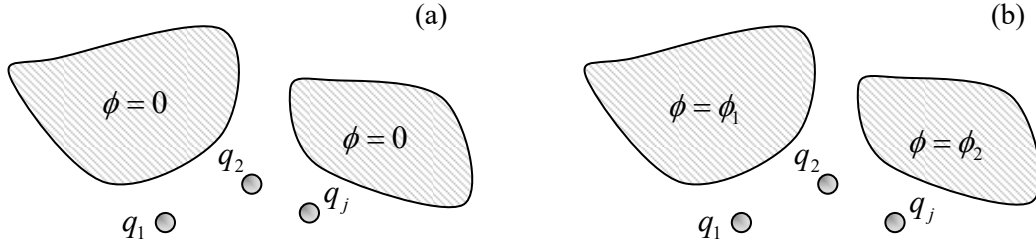


Fig. 2.30. Green's function method allows the solution of a simpler boundary problem (a) to be used for the solution of a more complex problem (b), for the same conductor geometry.

Let us apply this relation to the volume V of *free space* between the conductors, and the boundary S drawn immediately outside of their surfaces. In this case, by its definition, Green's function $G(\mathbf{r}, \mathbf{r}')$ vanishes at the conductor surface, i.e. at $\mathbf{r} \in S$ – see Eq. (205). Now changing the sign of $\partial n'$ (so that it would be the outer normal for *conductors*, rather than free space volume V), dividing all terms by 4π , and partitioning the total surface S into the parts (numbered by index j) corresponding to different conductors (possibly, kept at different potentials ϕ_k), we finally arrive at the famous result:⁷²

Potential via Green's function

$$\phi(\mathbf{r}) = \frac{1}{4\pi\epsilon_0} \int_V \rho(\mathbf{r}') G(\mathbf{r}, \mathbf{r}') d^3 r' + \frac{1}{4\pi} \sum_k \phi_k \oint_{S_k} \frac{\partial G(\mathbf{r}, \mathbf{r}')}{\partial n'} d^2 r'. \quad (2.210)$$

While the first term on the right-hand side of this relation is a direct and evident expression of the superposition principle, given by Eq. (203), the second term is highly non-trivial: it describes the effect of conductors with *arbitrary* potentials ϕ_k (Fig. 30b), using the Green's function calculated for the similar system with *grounded* conductors, i.e. with all $\phi_k = 0$ (Fig. 30a). Let me emphasize that since our volume V excludes conductors, the first term on the right-hand side of Eq. (210) includes only the stand-alone charges in the system (in Fig. 30, marked q_1, q_2 , etc.), but not the surface charges of the conductors – which are taken into account, indirectly, by the second term.

In order to illustrate what a powerful tool Eq. (210) is, let us use to calculate the electrostatic field in two systems. In the first of them, a plane, circular, conducting disk of radius R , separated with a very thin cut from the remaining conducting plane, is biased with potential $\phi = V$, while the rest of the plane is grounded – see Fig. 31.

⁷¹ This symmetry, evident for the particular cases (204) and (206), may be readily proved for the general case by applying Eq. (207) to the functions $f(\mathbf{r}) \equiv G(\mathbf{r}, \mathbf{r}')$ and $g(\mathbf{r}) \equiv G(\mathbf{r}, \mathbf{r}'')$. With this substitution, the left-hand side of that equality becomes equal to $-4\pi [G(\mathbf{r}'', \mathbf{r}') - G(\mathbf{r}', \mathbf{r}'')]$, while the right-hand side is zero, due to Eq. (205).

⁷² In some textbooks, the sign before the surface integral is negative, because their authors use the outer normal to the *free-space* region V rather than those *occupied by conductors* – as I do.

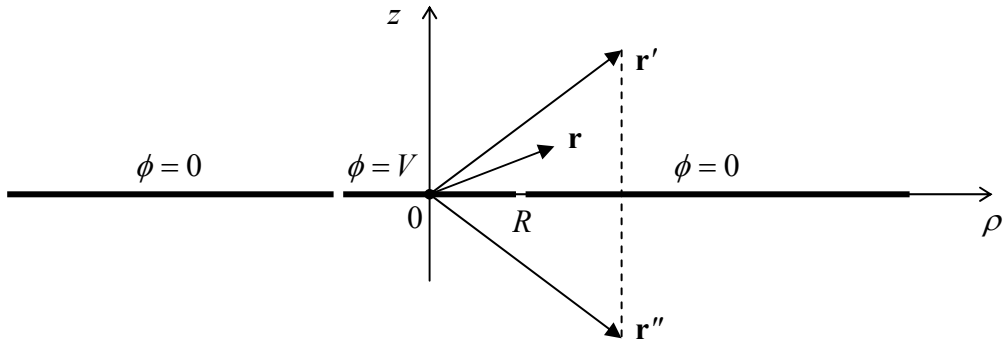


Fig. 2.31. A voltage-biased conducting disk separated from the rest of a conducting plane.

If the width of the gap between the disk and the rest of the plane is negligible, we may apply Eq. (210) without stand-alone charges, $\rho(\mathbf{r}') = 0$, and the Green's function for the uncut plane – see Eq. (206).⁷³ In the cylindrical coordinates, with the origin at the disk's center (Fig. 31), the function is

$$G(\mathbf{r}, \mathbf{r}') = \frac{1}{[\rho^2 + \rho'^2 - 2\rho\rho' \cos(\phi - \phi') + (z - z')^2]^{1/2}} - \frac{1}{[\rho^2 + \rho'^2 - 2\rho\rho' \cos(\phi - \phi') + (z + z')^2]^{1/2}}. \quad (2.211)$$

(The sum of the first three terms under each square root in Eq. (211) is just the squared distance between the horizontal projections ρ and ρ' of the vectors \mathbf{r} and \mathbf{r}' (or \mathbf{r}'') correspondingly, while the last terms are the squares of their vertical displacements.)

Now we can readily calculate the derivative participating in Eq. (210), for $z \geq 0$:

$$\frac{\partial G}{\partial n'}|_S = \frac{\partial G}{\partial z'}|_{z'=+0} = \frac{2z}{(\rho^2 + \rho'^2 - 2\rho\rho' \cos(\phi - \phi') + z^2)^{3/2}}. \quad (2.212)$$

Due to the axial symmetry of the system, we may take ϕ for zero. With this, Eqs. (210) and (212) yield

$$\phi = \frac{V}{4\pi} \oint_S \frac{\partial G(\mathbf{r}, \mathbf{r}')}{\partial n'} d^2 r' = \frac{Vz}{2\pi} \int_0^{2\pi} d\phi' \int_0^R \frac{\rho' d\rho'}{(\rho^2 + \rho'^2 - 2\rho\rho' \cos\phi' + z^2)^{3/2}}. \quad (2.213)$$

This integral is not overly pleasing, but may be readily worked out at least for points on the symmetry axis ($\rho = 0, z \geq 0$):⁷⁴

$$\phi = Vz \int_0^R \frac{\rho' d\rho'}{(\rho'^2 + z^2)^{3/2}} = \frac{V}{2} \int_0^{R^2/z^2} \frac{d\xi}{(\xi + 1)^{3/2}} = V \left[1 - \frac{z}{(R^2 + z^2)^{1/2}} \right], \quad (2.214)$$

This result shows that if $z \rightarrow 0$, the potential tends to V (as it should), while at $z \gg R$,

$$\phi \rightarrow V \frac{R^2}{2z^2}. \quad (2.215)$$

⁷³ Indeed, if all parts of the cut plane are grounded, a narrow cut does not change the field distribution, and hence the Green's function, significantly.

⁷⁴ There is no need to repeat the calculation for $z \leq 0$: from the symmetry of the problem, $\phi(-z) = \phi(z)$.

Now let us use the same Eq. (210) to solve the (in :-)-famous problem of the cut sphere (Fig. 32). Again, if the gap between the two conducting semi-spheres is very thin ($t \ll R$), we may use Green's function for the grounded (and uncut) sphere. For a particular case $\mathbf{r}' = d\mathbf{n}_z$, this function follows from Eqs. (197)-(198); generalizing the former relation for an arbitrary direction of vector \mathbf{r}' , we get

$$G = \frac{1}{[r^2 + r'^2 - 2rr' \cos \gamma]^{1/2}} - \frac{R/r'}{[r^2 + (R^2/r')^2 - 2r(R^2/r') \cos \gamma]^{1/2}}, \quad \text{for } r, r' \geq R, \quad (2.216)$$

where γ is the angle between the vectors \mathbf{r} and \mathbf{r}' , and hence \mathbf{r}'' – see Fig. 32.

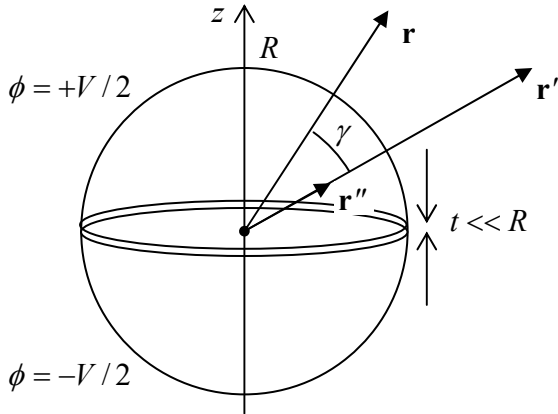


Fig. 2.32. A system of two separated, oppositely biased semi-spheres.

Now, calculating the Green's function's derivative,

$$\frac{\partial G}{\partial r'}|_{r'=R+0} = -\frac{(r^2 - R^2)}{R[r^2 + R^2 - 2Rr \cos \gamma]^{3/2}}, \quad (2.217)$$

and plugging it into Eq. (210), we see that the integration is again easy only for the field on the symmetry axis (where $\mathbf{r} = z\mathbf{n}_z$, and $\gamma = \theta'$), giving:

$$\phi = \frac{V}{2} \left[1 - \frac{z^2 - R^2}{z(z^2 + R^2)^{1/2}} \right], \quad \text{for } \theta = 0. \quad (2.218)$$

For $z \rightarrow R$, this relation yields $\phi \rightarrow V/2$ (as it should), while for $z/R \rightarrow \infty$,

$$\phi \rightarrow \frac{3R^2}{4z^2}V. \quad (2.219)$$

As will be discussed in the next chapter, such a field is typical for an electric dipole.

2.11. Numerical methods

Despite the richness of analytical methods, for many boundary problems (especially in geometries without a high degree of symmetry), the numerical approach is the only way to the solution.

Though software packages offering their automatic numerical solution are abundant nowadays,⁷⁵ it is important for every educated physicist to understand “what is under the hood”, at least because most universal programs exhibit mediocre performance in comparison with custom codes written for particular problems, and sometimes do not converge at all, especially for fast-changing (say, exponential) functions. The very brief discussion presented here⁷⁶ is a (hopefully, useful) fast glance under the hood, though it is certainly insufficient for professional numerical research work.

The simplest of the numerical approaches to the solution of partial differential equations, such as the Poisson or the Laplace equations (1.41)-(1.42), is the *finite-difference* method,⁷⁷ in which the sought continuous scalar function $f(\mathbf{r})$, such as the potential $\phi(\mathbf{r})$, is represented by its values in discrete points of a rectangular grid (frequently called *mesh*) of the corresponding dimensionality – see Fig. 33.

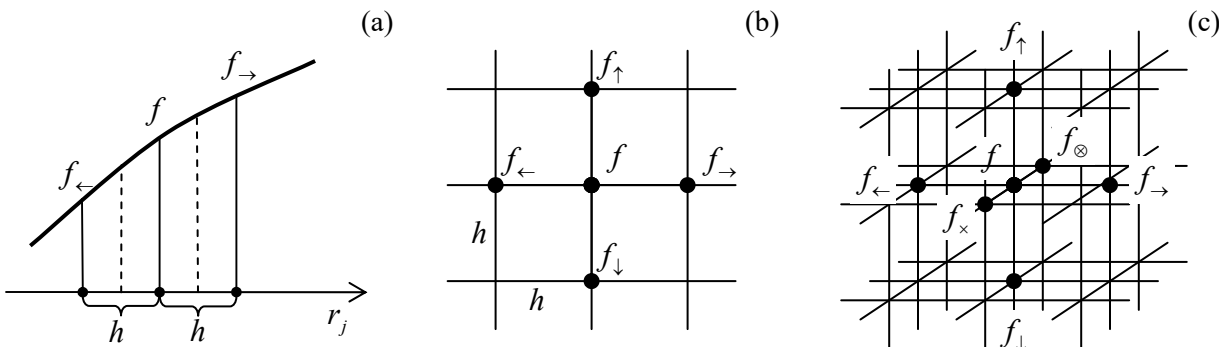


Fig. 2.33. The general idea of the finite-difference method in (a) one, (b) two, and (c) three dimensions.

Each partial second derivative of the function is approximated by the formula that readily follows from linear approximations of the function f and then its partial derivatives – see Fig. 33a:

$$\frac{\partial^2 f}{\partial r_j^2} \equiv \frac{\partial}{\partial r_j} \left(\frac{\partial f}{\partial r_j} \right) \approx \frac{1}{h} \left(\frac{\partial f}{\partial r_j} \Big|_{r_j+h/2} - \frac{\partial f}{\partial r_j} \Big|_{r_j-h/2} \right) \approx \frac{1}{h} \left[\frac{f_{\rightarrow} - f}{h} - \frac{f - f_{\leftarrow}}{h} \right] = \frac{f_{\rightarrow} + f_{\leftarrow} - 2f}{h^2}, \quad (2.220)$$

where $f_{\rightarrow} \equiv f(r_j + h)$ and $f_{\leftarrow} \equiv f(r_j - h)$. (The relative error of this approximation is of the order of $h^4 \partial^4 f / \partial r_j^4$.) As a result, the action of a 2D Laplace operator on the function f may be approximated as

$$\frac{\partial^2 f}{\partial x^2} + \frac{\partial^2 f}{\partial y^2} \approx \frac{f_{\rightarrow} + f_{\leftarrow} - 2f}{h^2} + \frac{f_{\uparrow} + f_{\downarrow} - 2f}{h^2} = \frac{f_{\rightarrow} + f_{\leftarrow} + f_{\uparrow} + f_{\downarrow} - 4f}{h^2}, \quad (2.221)$$

and of the 3D operator, as

$$\frac{\partial^2 f}{\partial x^2} + \frac{\partial^2 f}{\partial y^2} + \frac{\partial^2 f}{\partial z^2} \approx \frac{f_{\rightarrow} + f_{\leftarrow} + f_{\uparrow} + f_{\downarrow} + f_{\otimes} + f_x - 6f}{h^2}. \quad (2.222)$$

(The notation used in Eqs. (221)-(222) should be clear from Figs. 33b and 33c, respectively.)

⁷⁵ See, for example, MA Secs. 16 (iii) and (iv).

⁷⁶ It is almost similar to that given in CM Sec. 8.5 and is reproduced here for the reader's convenience, illustrated with examples from this (EM) course.

⁷⁷ For more details see, e.g., R. Leveque, *Finite Difference Methods for Ordinary and Partial Differential Equations*, SIAM, 2007.

As a simple example, let us use this scheme to find the electrostatic potential distribution inside a cylindrical box with conducting walls and square cross-section $a \times a$, using an extremely coarse mesh with step $h = a/2$ (Fig. 34). In this case, our function, the electrostatic potential $\phi(x, y)$, equals zero at the side and bottom walls, and V_0 at the top lid, so that, according to Eq. (221), the 2D Laplace equation may be approximated as

$$\frac{0 + 0 + V_0 + 0 - 4\phi}{(a/2)^2} = 0. \quad (2.223)$$

The resulting value for the potential in the center of the box is $\phi = V_0/4$.

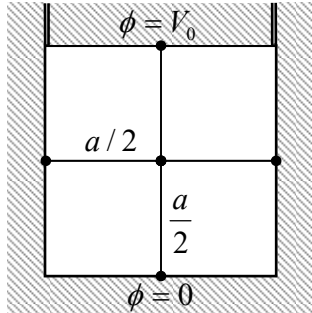


Fig. 2.34. Numerically solving an internal 2D boundary problem for a conducting, cylindrical box with a square cross-section, using a very coarse mesh (with $h = a/2$).

Surprisingly, this is the *exact* value! This may be proved either by solving this problem by the variable separation method, just as this has been done for a similar 3D problem in Sec. 5, or just from the following Green's-function argument. If all four walls of our 2D volume were biased to the voltage V_0 , there would be no electric field in it at all, so that the middle-point potential would be equal V_0 as well. However, from the point of view of Eq. (210) with no bulk charge, $\rho(\mathbf{r}) = 0$, this result may be legitimately viewed as the linear superposition of the four contributions of the potentials $\phi_k = V_0$ of each wall. Since for this symmetric geometry, the corresponding geometrical factors are equal, the contribution of one wall, with $\phi_k = 0$ on all other walls (as in our current problem), has to equal $V_0/4$.

For a similar 3D problem (a cubic box), with a similar 3D mesh, Eq. (222) yields

$$\frac{0 + 0 + V_0 + 0 + 0 + 0 - 6\phi}{(a/2)^2} = 0, \quad (2.226)$$

so that $\phi = V_0/6$. Using the same Green's-function argument, now for six wall of the cube, we see that this result is also exact! (This fact also follows from our variable-separation result expressed by Eqs. (95) and (99) with $a = b = c$.)

Though such exact results should be considered as a happy coincidence rather than the general law, they still show that numerical methods, even with relatively crude meshes, may be more computationally efficient than some “analytical” approaches, like the variable separation method with its infinite-sum results that, in most cases, require computers anyway – at least for the result’s comprehension and analysis.

A more powerful (but also much more complex) approach is the *finite-element* method in which the discrete point mesh, typically with triangular cells, is (automatically) generated in accordance with the system geometry.⁷⁸ Such mesh generators provide higher point concentration near sharp convex

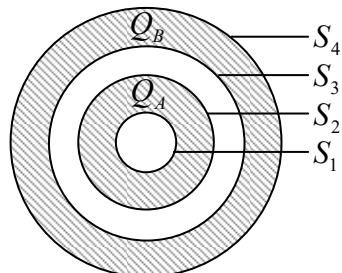
⁷⁸ See, e.g., CM Fig. 8.14.

parts of conductor surfaces, where the field concentrates and hence the potential changes faster, thus ensuring a better accuracy-to-speed tradeoff than the finite-difference methods on a uniform grid. The price to pay for this improvement is the algorithm's complexity which makes its adjustments much harder. Unfortunately, in this series, I do not have time for going into the details of that method and have to refer the reader to the special literature on this subject.⁷⁹

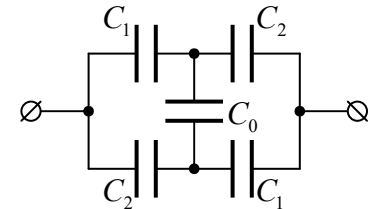
2.12. Exercise problems

2.1. Calculate the force (per unit area) exerted on a conducting surface by an external electric field normal to it. Compare the result with the electric field's definition given by Eq. (1.6), and comment.

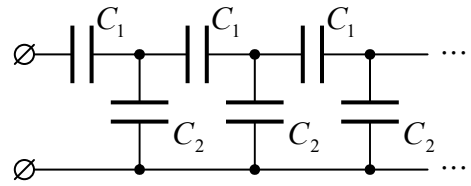
2.2. Electric charges Q_A and Q_B have been placed on two conducting concentric spherical shells – see the figure on the right. What is the full charge of each of the surfaces S_1-S_4 ?



2.3. Calculate the mutual capacitance between the terminals of the lumped-capacitor circuit shown in the figure on the right. Analyze and interpret the result for major particular cases.

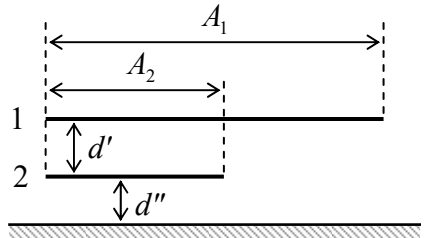


2.4. Calculate the mutual capacitance between the terminals of the semi-infinite lumped-capacitor circuit shown in the figure on the right, and the law of the applied voltage's decay along the system. Analyze and interpret the result.



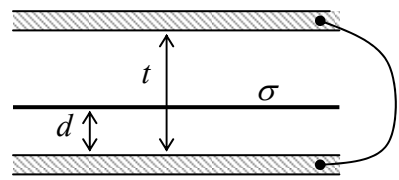
2.5. A system of two thin conducting plates is located over a ground plane as shown in the figure on the right, where A_1 and A_2 are the areas of the indicated plate parts, while d' and d'' are the distances between them. Neglecting the fringe effects, calculate:

- (i) the effective capacitance of each plate, and
- (ii) their mutual capacitance.

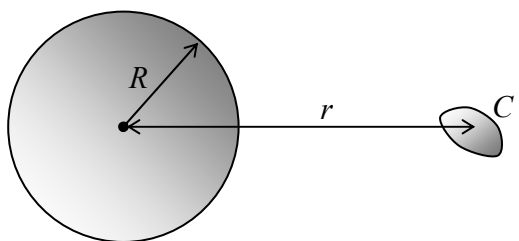


⁷⁹ See, e.g., either C. Johnson, *Numerical Solution of Partial Differential Equations by the Finite Element Method*, Dover, 2009, or T. Hughes, *The Finite Element Method*, Dover, 2000.

2.6. A wide and thin film, carrying a uniform electric charge density σ , is placed inside a plane capacitor whose plates are connected with a wire (see the figure on the right), and were initially electroneutral. Neglecting the fringe effects, calculate the surface charges of the plates, and the net force exerted on the film (per unit area).

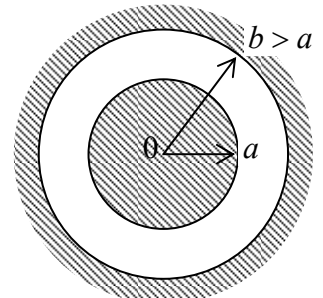


2.7. A relatively small conductor (possibly, of an irregular shape) with self-capacitance C is located at distance r from the center of a conducting sphere of radius R – see the figure on the right. In the first approximation in C , find the reciprocal capacitance matrix of the system. Use the matrix to calculate its potential energy and the force of the conductor interaction for two cases:



- (i) the conductor *charges* Q are equal, and
- (ii) the conductors are connected with a thin wire, so that their *potentials* ϕ are equal.

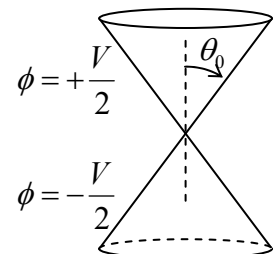
2.8. Use the Gauss law to calculate the mutual capacitance of the following two-electrode systems, with the cross-section shown in Fig. 7 (reproduced on the right):



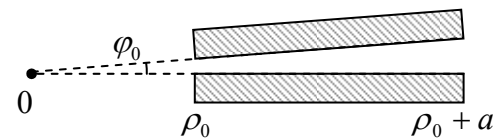
- (i) a conducting sphere inside a concentric spherical cavity inside another conductor, and
- (ii) a long conducting cylinder inside a coaxial cavity inside another conductor, i.e. a coaxial cable. (In this case, we speak about the capacitance per unit length).

Compare the results with those obtained in Sec. 2.2 using the Laplace equation.

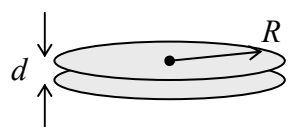
2.9. Calculate the electrostatic potential distribution around two barely separated conductors in the form of coaxial, round cones (see the figure on the right), with voltage V between them. Compare the result with that of a similar 2D problem, with the cones replaced by plane-face wedges. Can you calculate the mutual capacitances between the conductors in these systems? If not, can you estimate them?



2.10. Calculate the mutual capacitance between two rectangular, plane electrodes of area $A = a \times l$, with a small angle $\varphi_0 \ll a/\rho_0$ between them – see the figure on the right.



2.11. Using the results for a single thin round disk, obtained in Sec. 4, consider a system of two such disks at a small distance $d \ll R$ from each other – see the figure on the right. In particular, calculate:



- (i) the reciprocal capacitance matrix of the system,

- (ii) the mutual capacitance between the disks,
- (iii) the partial capacitance of one disk, and
- (iv) the effective capacitance of one disk,

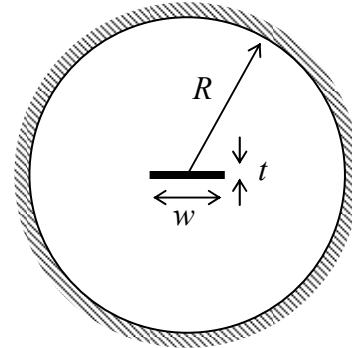
(all in the first nonvanishing approximation in $d/R \ll 1$). Compare the results (ii)-(iv) and interpret their similarities and differences.

2.12.* Calculate the mutual capacitance (per unit length) between two cylindrical conductors forming a system with the cross-section shown in the figure on the right, in the limit $t \ll w \ll R$.

Hint: You may like to use the elliptic coordinates mentioned in Sec. 4. They are defined by the following equality:

$$x + iy = c \cosh(\mu + i\nu), \quad (*)$$

where c is a constant.



2.13. Calculate the mutual capacitance (per unit length) between two similar, long, parallel wires, each with a round cross-section of radius R , whose axes are separated by distance $d > 2R$. Explore and interpret the result in the limits $R \rightarrow 0$ and $R \rightarrow 2d$.

Hint: You may like to use the 2D orthogonal *bipolar coordinates* $\{\tau, \sigma\}$ defined by the following relations with the Cartesian coordinates $\{x, y\}$:

$$x = a \frac{\sinh \tau}{\cosh \tau - \cos \sigma}, \quad y = a \frac{\sin \sigma}{\cosh \tau - \cos \sigma}, \quad \text{with } -\infty < \tau < +\infty, \quad -\pi \leq \sigma \leq +\pi.$$

In these coordinates, the Laplace operator is

$$\nabla^2 = \frac{1}{a^2} (\cosh \tau - \cos \sigma) \left(\frac{\partial^2}{\partial \tau^2} + \frac{\partial^2}{\partial \sigma^2} \right).$$

2.14. Formulate 2D electrostatic problems that can be solved using each of the following analytic functions of the complex variable $z \equiv x + iy$:

- (i) $u = \ln z$,
- (ii) $u = z^{1/2}$,
- (iii) $u = z + 1/z$,

and solve these problems.

2.15. On each side of a cylindrical volume with a rectangular cross-section $a \times b$, with no electric charges inside it, the electric field's component normal to the side's plane is constant, and opposite to that on the opposite side. Calculate the distribution of the electric potential inside the volume, provided that the magnitude of the normal components on the sides of length b equals E . Suggest a practicable method to implement such potential distribution.

2.16. Complete the solution of the problem shown in Fig. 12, by calculating the distribution of the surface charge of the semi-planes. Can you calculate the mutual capacitance between the semi-planes (per unit length of the system)? If not, can you estimate it?

2.17. A straight, long, thin, round-cylindrical metallic pipe has been cut, along its axis, into two equal parts – see the figure on the right.

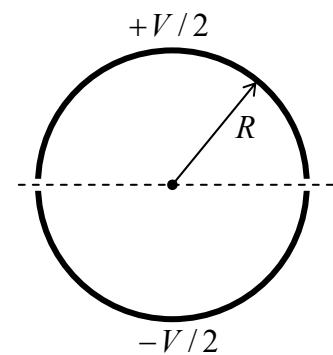
(i) Use the conformal mapping method to calculate the distributions of the electrostatic potential created by voltage V applied between the two parts, both outside and inside the pipe, and of the surface charge.

(ii)* Calculate the mutual capacitance between pipe's halves (per unit length), taking into account a small width $2t \ll R$ of the cut.

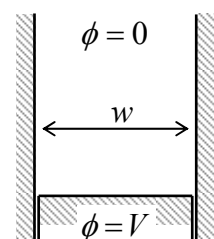
Hints: In Task (i), you may like to use the complex function

$$w = \ln \frac{R+z}{R-z},$$

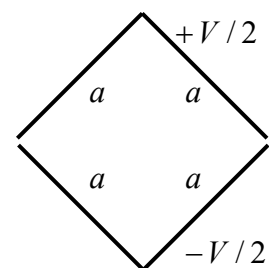
while in Task (ii), you may use the solution of the previous problem.



2.18. A gap of constant width w between two grounded conducting semi-spaces is closed, from one side, with a conducting plunger biased with voltage V , so that the cross-section of the system looks like the figure on the right shows. Use the variable separation method to calculate the distribution of the electrostatic potential within the gap.

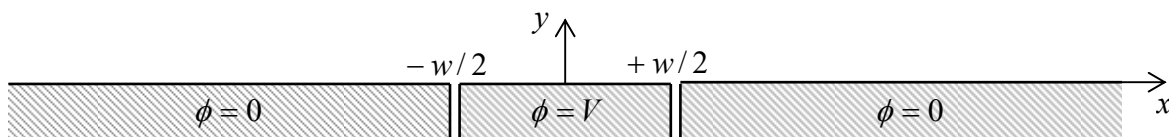


2.19. Use the variable separation method to calculate the electrostatic potential's distribution inside a very long thin-wall metallic box with a quadratic cross-section, cut and voltage-biased as shown in the figure on the right. (The cut's width is negligibly small.)



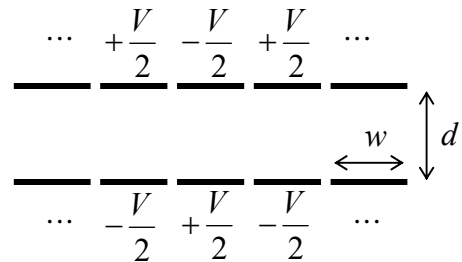
2.20. Solve Problem 17(i) using the variable separation method, and compare the results.

2.21. Use the variable separation method to calculate the potential distribution above the plane surface of a conductor, with a strip of width w separated by very thin cuts, and biased with voltage V – see the figure below.



2.22. The previous problem is now modified: the cut-out and voltage-biased part of the conducting plane is now not a strip, but a square with side w . Calculate the potential distribution above the conductor's surface.

2.23. Each electrode of a large plane capacitor is cut into long strips of equal width w , with very narrow gaps between them. These strips are kept at alternating potentials, as shown in the figure on the right. Use the variable separation method to calculate the electrostatic potential distribution in space, and explore the limit $w \ll d$.



2.24. Complete the cylinder problem started in Sec. 7 (see Fig. 17), for the cases when the top lid's voltage is fixed as follows:

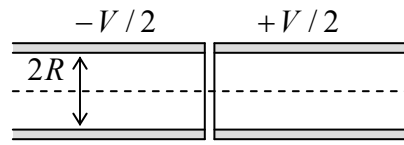
- (i) $V = V_0 J_1(\xi_{11}\rho/R) \sin\varphi$, where $\xi_{11} \approx 3.832$ is the first root of the Bessel function $J_1(\xi)$;
- (ii) $V = V_0 = \text{const}$.

For both cases, calculate the electric field at the centers of the lower and upper lids. (For Task (ii), an answer including series and/or integrals is acceptable.)

2.25. For an infinitely long system sketched in Fig. 21:

- (i) calculate and sketch the distribution of the electrostatic potential inside the system for various values of the ratio R/h , and
- (ii) simplify the results for the limit $R/h \rightarrow 0$.

2.26. A long round cylindrical conducting pipe is split, with a very narrow cut normal to its axis, into two parts that are voltage-biased as the figure on the right shows. Use two different approaches to calculate the force exerted by the resulting field upon a charged particle flying along the pipe close to its axis. Can the system work as an electrostatic lens?



2.27. Use the variable separation method to find the potential distribution inside and outside of a thin spherical shell of radius R , with a fixed potential distribution: $\phi(R, \theta, \varphi) = V_0 \sin\theta \cos\varphi$.

2.28. A thin spherical shell carries an electric charge with areal density $\sigma = \sigma_0 \cos\theta$. Calculate the spatial distribution of the electrostatic potential and the electric field, both inside and outside the shell.

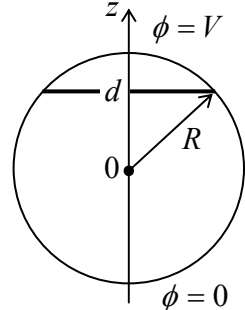
2.29. Use the variable separation method to solve the problem already addressed in Sec. 10: calculate the potential distribution both inside and outside of a thin spherical shell of radius R , separated with a very thin cut, along the central plane $z = 0$, into two halves, with voltage V applied between them – see Fig. 32. Analyze the solution; compare the field at the axis z , for $z > R$, with Eq. (218).

Hint: You may like to use the following integral of a Legendre polynomial with odd index $l = 1, 3, 5, \dots = 2n - 1$:⁸⁰

⁸⁰ As a reminder, the *double factorial* (also called “semifactorial”) operator (!!) is similar to the usual factorial operator (!), but with the product limited to numbers of the same parity as its argument – in our particular case, of the odd numbers in the numerator, and even numbers in the denominator.

$$I_n \equiv \int_0^1 P_{2n-1}(\xi) d\xi = \frac{1}{n!} \cdot \left(\frac{1}{2}\right) \cdot \left(-\frac{3}{2}\right) \cdot \left(-\frac{5}{2}\right) \cdots \left(\frac{3}{2} - n\right) \equiv (-1)^{n-1} \frac{(2n-3)!!}{2n(2n-2)!!}.$$

2.30. Calculate, up to the terms $O(1/r^2)$, the long-range electric field induced by a split and voltage-biased conducting sphere – similar to that discussed in Sec. 10 (see Fig. 32) and in the previous problem, but with the cut's plane at an arbitrary distance $d < R$ from the center – see the figure on the right.



2.31. Calculate the field distribution in the simple electrostatic lens that was the subject of Problem 1.9.

Hint: You may like to use the fact that a general axially-symmetric solution of the Laplace equation in the oblate ellipsoidal coordinates (see Eqs. (2.59)-(2.60) of the lecture notes) may be represented in the following variable-separation form:

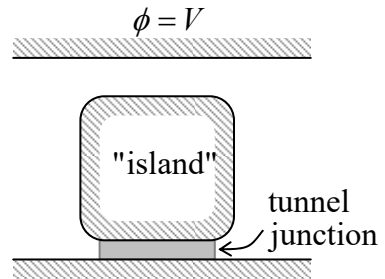
$$\phi = \sum_{n=0}^{\infty} [P_n \mathcal{P}_n(i \sinh \alpha) + Q_n \mathcal{Q}_n(i \sinh \alpha)] \mathcal{P}_n(\cos \beta),$$

where \mathcal{P}_n are the Legendre polynomials (2.169) that are sometimes called the *Legendre functions of the first kind*, while \mathcal{Q}_n are the *Legendre functions of the second kind* (briefly mentioned in Sec. 2.8) that may be defined by the following recurrence relations:

$$\mathcal{Q}_0(\xi) = \frac{1}{2} \ln \frac{1+\xi}{1-\xi}, \quad \mathcal{Q}_1(\xi) = \mathcal{P}_1(\xi) \mathcal{Q}_0(\xi) - 1, \quad \mathcal{Q}_{n>2}(\xi) = \frac{2n-1}{n} \xi \mathcal{Q}_{n-1}(\xi) - \frac{n-1}{n} \mathcal{Q}_{n-2}(\xi).$$

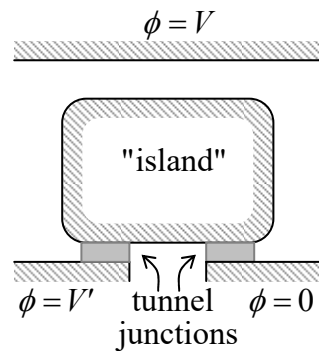
2.32. A small conductor (in this context, usually called *single-electron island*) is placed between two conducting electrodes, with voltage V applied between them. The gap between the island and one of the electrodes is so narrow that electrons may tunnel quantum-mechanically through this “junction” – see the figure on the right. Neglecting thermal excitations, calculate the equilibrium charge of the island as a function of V .

Hint: To solve this problem, you do not need to know much about the quantum-mechanical tunneling between conductors, besides that such tunneling of an electron, followed by energy relaxation of the resulting excitations, may be considered as a single inelastic (energy-dissipating) event.⁸¹ At negligible thermal excitations, such an event takes place only if it decreases the total potential energy of the system.



⁸¹ Strictly speaking, this statement, implying negligible quantum-mechanical coherence of the tunneling events, is correct only if the junction transparency is sufficiently low, so that its effective electric resistance is much higher than the fundamental quantum unit of resistance, $R_Q \equiv \pi \hbar / 2e^2 \approx 6.5 \text{ k}\Omega$ (see, e.g., QM Sec. 3.2). However, this condition is satisfied in most experimental tunnel junctions.

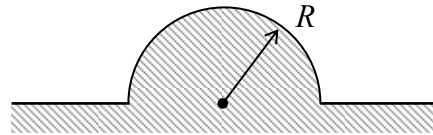
2.33. The system discussed in the previous problem is now generalized as the figure on the right shows. If the voltage V' applied between the two bottom electrodes is sufficiently large, electrons can successively tunnel through two junctions of this system (called the *single-electron transistor*), carrying dc current between these electrodes. Neglecting thermal excitations, calculate the region of voltages V and V' where such a current is fully suppressed (*Coulomb-blocked*).



2.34. Use the charge image method to calculate the full surface charges induced in the plates of a very broad, voltage-unbiased plane capacitor of thickness D by a point charge q separated from one of the electrodes by distance d . Suggest at least one alternative method to obtain the same result.

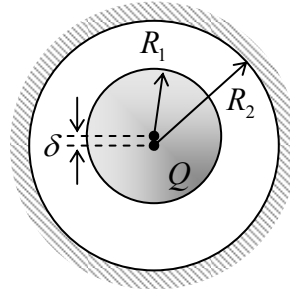
2.35. Use the charge image method to calculate the potential energy of the electrostatic interaction between a point charge placed in the center of a spherical cavity that had been carved inside a grounded conductor, and the cavity's walls. Looking at the result, could it be obtained in a simpler way (or ways)?

2.36. Use the method of charge images to find the Green's function of the system shown in the figure on the right, where the bulge on the conducting plane has the shape of a semi-sphere of radius R .



2.37.* Use the spherical inversion expressed by Eq. (198), to develop an iterative method for a more and more precise calculation of the mutual capacitance between two similar metallic spheres of radius R , with their centers separated by distance $d > 2R$.

2.38.* A conducting sphere of radius R_1 , carrying electric charge Q , is placed inside a spherical cavity of radius $R_2 > R_1$, carved inside another metal. Calculate the electric force exerted on the sphere if its center is displaced by a small distance $\delta \ll R_1, R_2 - R_1$ from that of the cavity – see the figure on the right.



2.39. Within the simple models of the electric field screening in conductors, discussed in Sec. 2.1, analyze the partial screening of the electric field of a point charge q by a plane conducting film of constant thickness $t \ll \lambda$, where λ is (depending on charge carrier statistics) either the Debye or the Thomas-Fermi screening length – see, respectively, Eqs. (8) or (10). Assume that the distance d between the charge and the film is much larger than t .

2.40. It is sometimes convenient to use representations of the Green's functions as series of the Legendre polynomials. Derive such representation for the function expressed by Eq. (204).

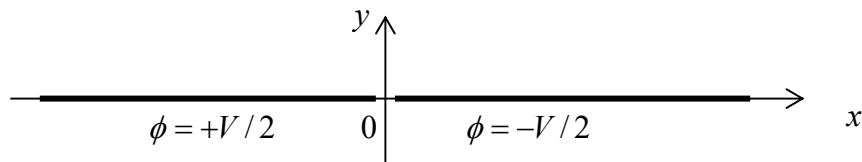
2.41. Use the result of the previous problem to confirm the solution (197)-(198) of the problem illustrated in Fig. 29: a grounded conducting sphere of radius R , and a point charge q located at distance $d > R$ from its center.

2.42. Suggest a convenient definition of the Green's function for 2D electrostatic problems, and calculate it for:

- (i) the unlimited free space, and
- (ii) the free space above a conducting plane.

Use the latter result to re-solve Problem 21.

2.43. A conducting plane located at $y = 0$ is separated into two parts with a very narrow, straight cut along the z -axis, and voltage V is applied between the resulting half-planes, as shown in the figure below. Use the Green's function method to find the distribution of the electrostatic potential and the electric field everywhere in the space. Compare the result with Eq. (83). In hindsight, could the problem be solved in an even simpler way?



2.44. Use the last result of Problem 42 and one of the conformal mappings discussed in Sec. 4 to find one more solution of Problem 18.

2.45. Calculate the 2D Green's functions for the free spaces:

- (i) outside a round conducting cylinder, and
- (ii) inside a round cylindrical hole in a conductor.

2.46. Solve Problem 17(i) using the Green's function method.

2.47. Solve the 2D boundary problem that was discussed in Sec. 11 (Fig. 34), using:

- (i) the finite difference method with a finer square mesh: $h = a/3$, and
- (ii) the variable separation method.

Compare the results at the mesh points, and comment.

This page is
intentionally left
blank

Chapter 3. Dipoles and Dielectrics

In contrast to conductors, the motion of charges in dielectrics is restricted to the atom/molecule interiors, so that the electric polarization of these materials by an external field takes a different form. This issue is the main subject of this chapter, but in preparation for its analysis, we have to start with a general discussion of the electric field induced by spatially-restricted systems of charges.

3.1. Electric dipole

Let us consider a localized system of charges, of a linear scale a , and derive a simple approximate expression for the electrostatic field induced by the system at a distant point \mathbf{r} . For that, let us select a reference frame with the origin either somewhere inside the system, or at a distance of the order of a from it (Fig. 1).

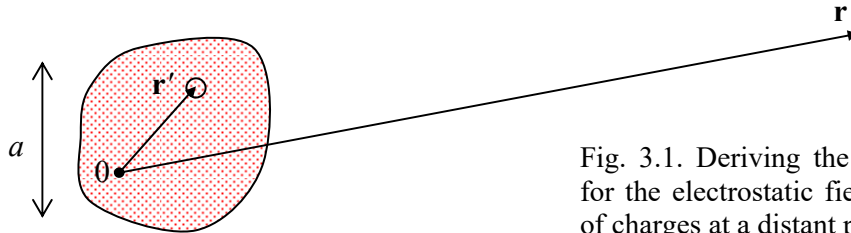


Fig. 3.1. Deriving the approximate expression for the electrostatic field of a localized system of charges at a distant point ($r \gg r' \sim a$).

Then positions of all charges of the system satisfy the following condition:

$$r' \ll r. \quad (3.1)$$

Using this condition, we can expand the general expression (1.38) for the electrostatic potential $\phi(\mathbf{r})$ of the system into the Taylor series in small parameter r' . For any function of type $f(\mathbf{r} - \mathbf{r}')$, the expansion may be represented as¹

$$f(\mathbf{r} - \mathbf{r}') = f(\mathbf{r}) - \sum_{j=1}^3 r_j' \frac{\partial f}{\partial r_j}(\mathbf{r}) + \frac{1}{2!} \sum_{j,j'=1}^3 r_j' r_{j'}' \frac{\partial^2 f}{\partial r_j \partial r_{j'}}(\mathbf{r}) - \dots \quad (3.2)$$

Applying this formula to the fraction $1/|\mathbf{r} - \mathbf{r}'|$ in Eq. (1.38) (i.e. essentially to the free-space Green's function), we get the so-called *multipole expansion* of the electrostatic potential:

$$\phi(\mathbf{r}) = \frac{1}{4\pi\epsilon_0} \left(\frac{1}{r} Q + \frac{1}{r^3} \sum_{j=1}^3 r_j p_j + \frac{1}{2r^5} \sum_{j,j'=1}^3 r_j r_{j'} \mathcal{Q}_{jj'} + \dots \right), \quad (3.3)$$

whose \mathbf{r} -independent parameters are defined as follows:

$$Q \equiv \int \rho(\mathbf{r}') d^3 r', \quad p_j \equiv \int \rho(\mathbf{r}') r_j' d^3 r', \quad \mathcal{Q}_{jj'} \equiv \int \rho(\mathbf{r}') (3r_j' r_{j'}' - r'^2 \delta_{jj'}) d^3 r'. \quad (3.4)$$

¹ See, e.g., MA Eq. (2.11b).

(Indeed, the two leading terms of the expansion (2) may be rewritten in the vector form $f(\mathbf{r}) - \mathbf{r}' \cdot \nabla f(\mathbf{r})$, and the gradient of such a spherically-symmetric function $f(r) = 1/r$ is just $\mathbf{n}_r d\mathbf{f}/dr$, so that

$$\frac{1}{|\mathbf{r} - \mathbf{r}'|} \approx \frac{1}{r} - \mathbf{r}' \cdot \mathbf{n}_r \frac{d}{dr} \left(\frac{1}{r} \right) = \frac{1}{r} + \mathbf{r}' \cdot \frac{\mathbf{r}}{r^3}, \quad (3.5)$$

immediately giving the two first terms of Eq. (3). The proof of the third, *quadrupole* term in Eq. (3) is similar but a bit longer, and is left for the reader's exercise.)

Evidently, the scalar parameter Q in Eqs. (3)-(4) is just the total charge of the system. The constants p_j may be considered as Cartesian components of the following vector:

$$\mathbf{p} \equiv \int \rho(\mathbf{r}') \mathbf{r}' d^3 r', \quad (3.6)$$

Electric dipole moment

called the system's *electric dipole moment*, and $Q_{jj'}$ are Cartesian elements of a tensor – system's *electric quadrupole moment*. If $Q \neq 0$, all higher terms on the right-hand side of Eq. (3), at large distances (1), are just small corrections to the first one, and in many cases may be ignored. However, the net charge of many systems is exactly zero, the most important examples being neutral atoms and molecules. For such neutral systems, the second (*dipole*) term in Eq. (3) is, most frequently, the leading one. Such systems are called *electric dipoles*. Due to their importance, let us rewrite the expression for the dipole term in three other, mathematically equivalent forms:

$$\phi_d \equiv \frac{1}{4\pi\epsilon_0} \frac{\mathbf{r} \cdot \mathbf{p}}{r^3} \equiv \frac{1}{4\pi\epsilon_0} \frac{p \cos \theta}{r^2} \equiv \frac{1}{4\pi\epsilon_0} \frac{pz}{(x^2 + y^2 + z^2)^{3/2}}, \quad (3.7)$$

Electric dipole's potential

that are more convenient for some applications. Here θ is the angle between the vectors \mathbf{p} and \mathbf{r} , and in the last (Cartesian) representation, the z -axis is directed along the vector \mathbf{p} . Fig. 2a shows equipotential surfaces of the dipole field – or rather their cross-sections by any plane in which the vector \mathbf{p} resides.

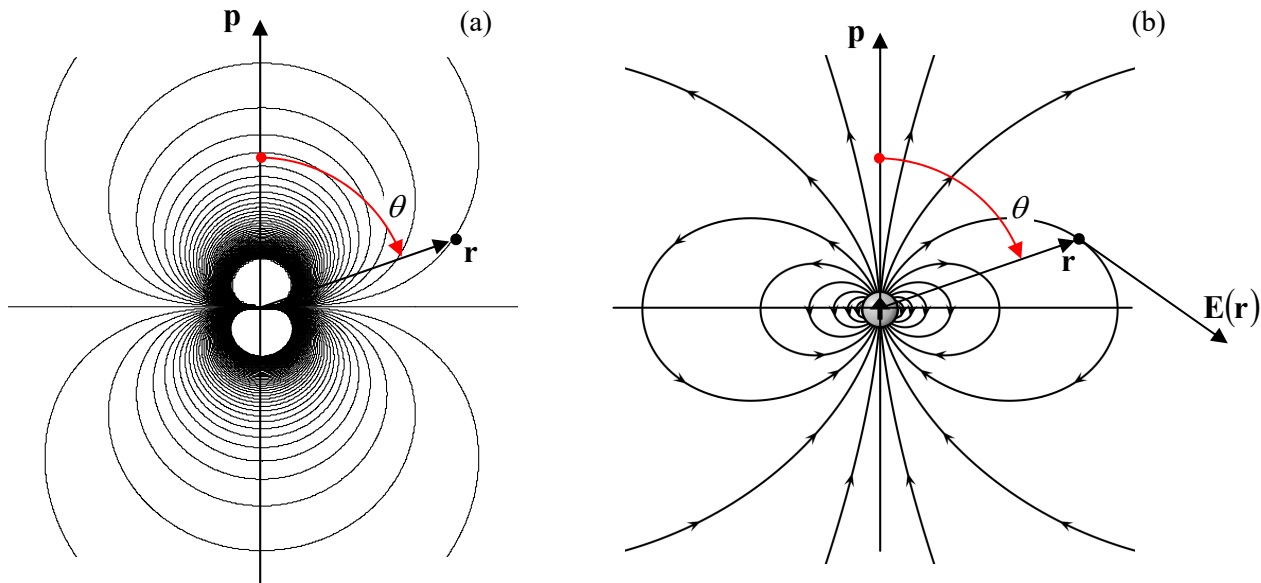


Fig. 3.2. (a) The equipotential surfaces and (b) the electric field lines of a dipole. (Panel (b) adapted from <http://en.wikipedia.org/wiki/Dipole> under the GNU Free Documentation License.)

The simplest example of a system whose field, at large distances, approaches the dipole field (7), is two equal but opposite point charges (“poles”), $+q$ and $-q$, with the radius-vectors, respectively, \mathbf{r}_+ and \mathbf{r}_- :

$$\rho(\mathbf{r}) = (+q)\delta(\mathbf{r} - \mathbf{r}_+) + (-q)\delta(\mathbf{r} - \mathbf{r}_-). \quad (3.8)$$

For this system (sometimes called the *physical dipole*), Eq. (4) yields

$$\mathbf{p} = (+q)\mathbf{r}_+ + (-q)\mathbf{r}_- = q(\mathbf{r}_+ - \mathbf{r}_-) = q\mathbf{a}, \quad (3.9)$$

where \mathbf{a} is the vector connecting the points \mathbf{r}_- and \mathbf{r}_+ . Note that in this case (and indeed for all systems with $Q = 0$), the dipole moment does not depend on the choice of the reference frame’s origin.

A less trivial example of a dipole is a conducting sphere of radius R in a uniform external electric field \mathbf{E}_0 . As a reminder, its field was calculated in Sec. 2.8, and its result is expressed by Eq. (2.176). The first term in the parentheses of that relation describes just the external field (2.173), so that the field of the sphere itself (i.e. that of the surface charge induced by \mathbf{E}_0) is given by the second term:

$$\phi_s = \frac{E_0 R^3}{r^2} \cos \theta. \quad (3.10)$$

Comparing this expression with the second form of Eq. (7), we see that the sphere has an *induced* dipole moment

$$\mathbf{p} = 4\pi\epsilon_0 \mathbf{E}_0 R^3. \quad (3.11)$$

This is an interesting example of a *virtually* pure dipole field: at all points outside the sphere ($r > R$), the field has neither a quadrupole moment nor any higher moments.

Other examples of dipole fields are given by two more systems discussed in Chapter 2 – see Eqs. (2.215) and (2.219). Those systems, however, do have higher-order multipole moments, so for them, Eq. (7) gives only the long-distance approximation.

Now returning to the general properties of the dipole field (7), let us calculate its major characteristics. First of all, we may use Eq. (7) to calculate the electric field of a dipole:

$$\mathbf{E}_d = -\nabla\phi_d = -\frac{1}{4\pi\epsilon_0} \nabla \left(\frac{\mathbf{r} \cdot \mathbf{p}}{r^3} \right) = -\frac{1}{4\pi\epsilon_0} \nabla \left(\frac{p \cos \theta}{r^2} \right). \quad (3.12)$$

This differentiation is easiest in the spherical coordinates, using the well-known expression for the gradient of a scalar function in these coordinates² and taking the z -axis parallel to the dipole moment \mathbf{p} . From the last form of Eq. (12), we immediately get

$$\mathbf{E}_d = \frac{p}{4\pi\epsilon_0 r^3} (2\mathbf{n}_r \cos \theta + \mathbf{n}_\theta \sin \theta) \equiv \frac{1}{4\pi\epsilon_0} \frac{3\mathbf{r}(\mathbf{r} \cdot \mathbf{p}) - \mathbf{p}r^2}{r^5}. \quad (3.13)$$

Fig. 2b above shows the electric field lines given by Eqs. (13). The most important features of this result are a faster drop of the field’s magnitude ($E_d \propto 1/r^3$, rather than $E \propto 1/r^2$ for a point charge), and the change of the signs of its radial component as a function of the polar angle $\theta \in [0, \pi]$.

² See, e.g., MA Eq. (10.8) with $\partial/\partial\varphi = 0$.

Next, let us use Eq. (1.55) to calculate the potential energy of interaction between a dipole and an external electric field. Assuming that this field does not change much at distances of the order of a (Fig. 1), we may expand its potential $\phi_{\text{ext}}(\mathbf{r})$ into the Taylor series, and keep only two leading terms:

$$U = \int \rho(\mathbf{r}) \phi_{\text{ext}}(\mathbf{r}) d^3 r \approx \int \rho(\mathbf{r}) [\phi_{\text{ext}}(0) + \mathbf{r} \cdot \nabla \phi_{\text{ext}}(0)] d^3 r \equiv Q \phi_{\text{ext}}(0) - \mathbf{p} \cdot \mathbf{E}_{\text{ext}}. \quad (3.14)$$

The first term is the potential energy the system would have if it were just a point charge. If the net charge Q is zero, that term disappears, and the leading contribution is due to the dipole moment:

$$U = -\mathbf{p} \cdot \mathbf{E}_{\text{ext}}, \quad \text{for } \mathbf{p} = \text{const.} \quad (3.15a)$$

Dipole's
energy in
external
field

Note that this result is only valid for a *fixed* dipole, with \mathbf{p} independent of \mathbf{E}_{ext} . In the opposite limit, when the dipole is *induced* by the field, i.e. $\mathbf{p} \propto \mathbf{E}_{\text{ext}}$ (you may have one more look at Eq. (11) to see an example of such a proportionality), we need to start with Eq. (1.60) rather than Eq. (1.55), getting

$$U = -\frac{1}{2} \mathbf{p} \cdot \mathbf{E}_{\text{ext}}, \quad \text{for } \mathbf{p} \propto \mathbf{E}_{\text{ext}}. \quad (3.15b)$$

In particular, combining Eqs. (13) and Eq. (15a), we may get the following important formula for the interaction of two independent dipoles:

$$U_{\text{int}} = \frac{1}{4\pi\epsilon_0} \frac{\mathbf{p}_1 \cdot \mathbf{p}_2 r^2 - 3(\mathbf{r} \cdot \mathbf{p}_1)(\mathbf{r} \cdot \mathbf{p}_2)}{r^5} = \frac{1}{4\pi\epsilon_0} \frac{p_{1x}p_{2x} + p_{1y}p_{2y} - 2p_{1z}p_{2z}}{r^3}, \quad (3.16)$$

where \mathbf{r} is the vector connecting the dipoles, and the z -axis is directed along this vector. It is easy to prove (this exercise is left for the reader) that if the magnitude p of each dipole moment is fixed (the approximation valid, in particular, for weak interaction of so-called *polar molecules*), this potential energy reaches its minimum at the parallel orientation of the dipoles along the line connecting them. Note also that in this case, U_{int} is proportional to $1/r^3$. On the other hand, if each moment \mathbf{p} has a random value plus a component due to its polarization by the electric field of its counterpart: $\Delta\mathbf{p}_{1,2} \propto \mathbf{E}_{2,1} \propto 1/r^3$, their average interaction energy (which may be calculated from Eq. (16) with the additional factor $1/2$) is always negative and is proportional to $1/r^6$. Such negative potential describes, in particular, the long-range, attractive part (the so-called *London dispersion force*) of the interaction between electrically neutral atoms and molecules.³

According to Eqs. (15), the electric field should “try” to reach the minimum of U by aligning the dipole vector’s direction with its own. The direct quantitative description of this effect is the torque $\boldsymbol{\tau}$ exerted by the field. The simplest way to calculate it is to sum up all the elementary torques $d\boldsymbol{\tau} = \mathbf{r} \times d\mathbf{F}_{\text{ext}} = \mathbf{r} \times \mathbf{E}_{\text{ext}}(\mathbf{r}) \rho(\mathbf{r}) d^3 r$ exerted on all elementary charges of the system:

$$\boldsymbol{\tau} = \int \mathbf{r} \times \mathbf{E}_{\text{ext}}(\mathbf{r}) \rho(\mathbf{r}) d^3 r \approx \mathbf{p} \times \mathbf{E}_{\text{ext}}(0), \quad (3.17)$$

where at the last step, the spatial dependence of the external field $\mathbf{E}_{\text{ext}}(\mathbf{r})$ was again neglected. This dependence cannot, however, be ignored at the calculation of the *total force* exerted by the field on the dipole (with $Q = 0$). Indeed, Eqs. (15) shows that if the field is constant, the dipole’s energy is

³ Several calculations of this force, using various models, are described in the QM and SM parts of this series.

independent of its spatial location and hence the net force is zero. However, if the field has a non-zero gradient, a total force does appear; for a field-independent dipole,

$$\mathbf{F} = -\nabla U = \nabla(\mathbf{p} \cdot \mathbf{E}_{\text{ext}}), \quad (3.18)$$

where the derivative has to be taken at the dipole's position (in our notation, at $\mathbf{r} = 0$). If the dipole that is being moved in a field retains its magnitude and orientation, then the last formula is equivalent to⁴

$$\mathbf{F} = (\mathbf{p} \cdot \nabla) \mathbf{E}_{\text{ext}}. \quad (3.19)$$

Alternatively, the last expression may be obtained similarly to Eq. (14):

$$\mathbf{F} = \int \rho(\mathbf{r}) \mathbf{E}_{\text{ext}}(\mathbf{r}) d^3 r \approx \int \rho(\mathbf{r}) [\mathbf{E}_{\text{ext}}(0) + (\mathbf{r} \cdot \nabla) \mathbf{E}_{\text{ext}}] d^3 r = Q \mathbf{E}_{\text{ext}}(0) + (\mathbf{p} \cdot \nabla) \mathbf{E}_{\text{ext}}. \quad (3.20)$$

Finally, let me add a note on the so-called *coarse-grain model* of the dipole. The dipole approximation explored above is asymptotically correct only at large distances, $r \gg a$. However, for some applications (including the forthcoming discussion of the molecular field effects in Sec. 3) it is beneficial to have an expression that might be formally used *everywhere* in space, though maybe without exact details at $r \sim a$, giving the correct result for the space average of the electric field,

$$\bar{\mathbf{E}} \equiv \frac{1}{V} \int_V \mathbf{E} d^3 r, \quad (3.21)$$

where V is a regularly-shaped volume much larger than a^3 , for example, a sphere of a radius $R \gg a$, with the dipole at its center. For the field \mathbf{E}_d given by Eq. (13), such an average is zero. Indeed, let us consider the Cartesian components of that vector in a reference frame with the z -axis directed along the vector \mathbf{p} . Due to the axial symmetry of the field, the averages of the components E_x and E_y vanish. Let us use Eq. (13) to spell out the “vertical” component of the field (parallel to the dipole moment vector):

$$E_z \equiv \mathbf{E}_d \cdot \frac{\mathbf{p}}{p} = \frac{1}{4\pi\epsilon_0 r^3} (2\mathbf{n}_r \cdot \mathbf{p} \cos\theta - \mathbf{n}_\theta \cdot \mathbf{p} \sin\theta) = \frac{p}{4\pi\epsilon_0 r^3} (2\cos^2\theta - \sin^2\theta). \quad (3.22)$$

Integrating this expression over the whole solid angle $\Omega = 4\pi$, at fixed r , using a convenient variable substitution $\cos\theta \equiv \xi$, we get

$$\oint_{4\pi} E_z d\Omega = 2\pi \int_0^\pi E_z \sin\theta d\theta = \frac{p}{2\epsilon_0 r^3} \int_0^\pi (2\cos^2\theta - \sin^2\theta) \sin\theta d\theta = \frac{p}{2\epsilon_0 r^3} \int_{-1}^{+1} (3\xi^2 - 1) d\xi = 0. \quad (3.23)$$

On the other hand, the *exact* electric field of an *arbitrary* charge distribution, with the total dipole moment \mathbf{p} , obeys the following equality:

$$\int_V \mathbf{E}(\mathbf{r}) d^3 r = -\frac{\mathbf{p}}{3\epsilon_0} \equiv -\frac{1}{4\pi\epsilon_0} \frac{4\pi}{3} \mathbf{p}, \quad (3.24)$$

where the integration is over *any* sphere containing all the charges. A proof of this formula for the general case requires a straightforward, but somewhat tedious integration (which is, therefore, left for the reader's exercise). The origin of Eq. (24) is illustrated in Fig. 3 on the example of the physical

⁴ The equivalence may be proved, for example, by using MA Eq. (11.6) with $\mathbf{f} = \mathbf{p} = \text{const}$ and $\mathbf{g} = \mathbf{E}_{\text{ext}}$, taking into account that according to the general Eq. (1.28), $\nabla \times \mathbf{E}_{\text{ext}} = 0$.

dipole, i.e. the system of two equal but opposite charges – see Eqs. (8)-(9). The zero average (23) of the dipole field (13) does not take into account the contribution from the region between the charges (where Eq. (13) is not valid), where the field is directed mostly against the dipole vector (9).

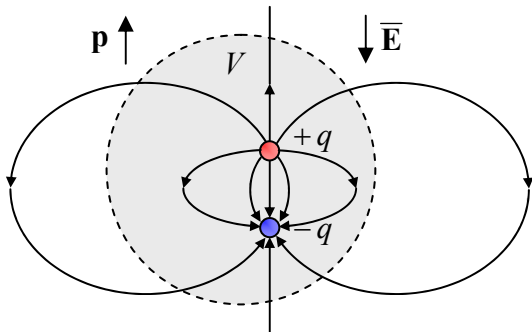


Fig. 3.3. A sketch illustrating the origin of Eq. (24) for a physical dipole.

So, in order to be used as a reasonable coarse-grain model, Eq. (13) may be modified as follows:

$$\mathbf{E}_{\text{cg}} = \frac{1}{4\pi\epsilon_0} \left[\frac{3(\mathbf{r} \cdot \mathbf{p}) - \mathbf{p}r^2}{r^5} - \frac{4\pi}{3} \mathbf{p} \delta(\mathbf{r}) \right], \quad (3.25)$$

with the average (21) satisfying Eq. (24). Evidently, such a modification does not change the field at large distances $r \gg a$, i.e. in the region where the expansion (3), and hence Eq. (13), are valid.

3.2. Dipole media

Now let us generalize Eq. (7) to the case of several (possibly, many) dipoles \mathbf{p}_j located at arbitrary points \mathbf{r}_j . Using the linear superposition principle, we get

$$\phi_d(\mathbf{r}) = \frac{1}{4\pi\epsilon_0} \sum_j \mathbf{p}_j \cdot \frac{\mathbf{r} - \mathbf{r}_j}{|\mathbf{r} - \mathbf{r}_j|^3}. \quad (3.26)$$

If our system (medium) contains many similar dipoles, distributed in space with density $n(\mathbf{r})$, we may approximate the last sum with a *macroscopic potential*, which is the average of the genuine (“microscopic”) potential (26) over a local volume much larger than the distance between the dipoles, and as a result, is given by the integral

$$\phi_d(\mathbf{r}) = \frac{1}{4\pi\epsilon_0} \int \mathbf{P}(\mathbf{r}') \cdot \frac{\mathbf{r} - \mathbf{r}'}{|\mathbf{r} - \mathbf{r}'|^3} d^3 r', \quad \text{with } \mathbf{P}(\mathbf{r}) \equiv n(\mathbf{r}) \mathbf{p}, \quad (3.27)$$

where the vector $\mathbf{P}(\mathbf{r})$, called the *electric polarization*, has the physical meaning of the net dipole moment per unit volume. (Note that by its definition, $\mathbf{P}(\mathbf{r})$ is also a “macroscopic” field.)

Now comes a very impressive trick, which is the basis of all the theory of “macroscopic” electrostatics (and eventually, “macroscopic” electrodynamics). Just as was done at the derivation of Eq. (5), Eq. (27) may be rewritten in the equivalent form

$$\phi_d(\mathbf{r}) = \frac{1}{4\pi\epsilon_0} \int \mathbf{P}(\mathbf{r}') \cdot \nabla' \frac{1}{|\mathbf{r} - \mathbf{r}'|} d^3 r', \quad (3.28)$$

where ∇' means the del operator (in this particular case, the gradient) acting in the “source space” of vectors \mathbf{r}' . The right-hand side of Eq. (28), applied to any volume V limited by a closed surface S , may be integrated by parts to give⁵

$$\phi_d(\mathbf{r}) = \frac{1}{4\pi\epsilon_0} \oint_S \frac{P_n(\mathbf{r}')}{|\mathbf{r} - \mathbf{r}'|} d^2 r' - \frac{1}{4\pi\epsilon_0} \int_V \frac{\nabla' \cdot \mathbf{P}(\mathbf{r}')}{|\mathbf{r} - \mathbf{r}'|} d^3 r'. \quad (3.29)$$

If the surface does not carry an infinitely dense (δ -functional) sheet of additional dipoles,⁶ or it is just very distant, the first term on the right-hand side is negligible. Now comparing the second term with the basic equation (1.38) for the electric potential, we see that this term may be interpreted as the field of certain *effective* electric charges with density

$$\rho_{ef} = -\nabla \cdot \mathbf{P}. \quad (3.30)$$

Effective
charge
density

Figure 4 illustrates the physics of this key relation for a cartoon model of a simple multi-dipole system: a layer of uniformly-distributed two-point-charge units oriented perpendicular to the layer surface. (In this case $\nabla \cdot \mathbf{P} = dP/dx$.) One can see that the ρ_{ef} defined by Eq. (30) may be interpreted as the density of the uncompensated surface charges of polarized elementary dipoles.

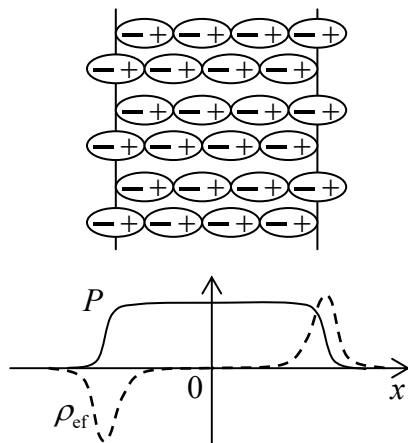


Fig. 3.4. The spatial distributions of the polarization and effective charges in a layer of similar elementary dipoles (schematically).

Next, from Sec. 1.2, we already know that Eq. (1.38) is equivalent to the inhomogeneous Maxwell equation (1.27) for the electric field, so that the *macroscopic* electric field of the dipoles (defined as $\mathbf{E}_d = -\nabla\phi_d$, where ϕ_d is given by Eq. (27)) obeys a similar equation, with the effective charge density (30).

Now let us consider a more general case when a system, besides the compensated charges of the dipoles, also has certain stand-alone charges – not parts of the dipoles already taken into account in the polarization \mathbf{P} . As was discussed in Sec. 1.1, if we average this charge over the inter-point-charge distances, i.e. approximate it with a continuous “macroscopic” density $\rho(\mathbf{r})$, then its macroscopic

⁵ To prove this (almost evident) formula strictly, it is sufficient to apply the divergence theorem given by MA Eq. (12.2), to the vector function $\mathbf{f} = \mathbf{P}(\mathbf{r}')/|\mathbf{r} - \mathbf{r}'|$, in the “source space” of radius-vectors \mathbf{r}' .

⁶ Just like in the case of Eq. (1.9), we may always describe such a dipole sheet using the second term in Eq. (29), by including a delta-functional part into the polarization distribution $\mathbf{P}(\mathbf{r}')$.

electric field also obeys Eq. (1.27), but with the stand-alone charge density. Due to the linear superposition principle, for the *total macroscopic field* \mathbf{E} of these charges and dipoles, we may write

$$\nabla \cdot \mathbf{E} = \frac{1}{\epsilon_0} (\rho + \rho_{\text{ef}}) = \frac{1}{\epsilon_0} (\rho - \nabla \cdot \mathbf{P}). \quad (3.31)$$

This is already the main result of the “macroscopic” electrostatics. However, it is evidently tempting (and very convenient for applications) to rewrite Eq. (31) in a different form by carrying the dipole-related term of this equality over to its left-hand side. The resulting formula is called the *macroscopic Maxwell equation for \mathbf{D}* :

$$\nabla \cdot \mathbf{D} = \rho, \quad (3.32)$$

Maxwell equation for \mathbf{D}

where $\mathbf{D}(\mathbf{r})$ is a new “macroscopic” field, called the *electric displacement* (in some older texts, “electric induction”), defined as⁷

$$\mathbf{D} \equiv \epsilon_0 \mathbf{E} + \mathbf{P}. \quad (3.33)$$

Electric displacement

The comparison of Eqs. (32) and (1.27) shows that \mathbf{D} (or more strictly, the fraction \mathbf{D}/ϵ_0) may be interpreted as the “would-be electric field” that *would be* created by stand-alone charges in the absence of the dipole medium polarization. It should be distinguished from the \mathbf{E} participating in Eqs. (31) and (33), i.e. from the genuine electric field, if averaged over a spatial scale of the order of the distance between elementary charges and dipoles.

In order to get an even better gut feeling of the fields \mathbf{E} and \mathbf{D} , let us first rewrite the macroscopic Maxwell equation (32) in the integral form. Applying the divergence theorem to an arbitrary volume V limited by surface S , we get the following *macroscopic Gauss law*:

$$\oint_S D_n d^2 r = \int_V \rho d^3 r \equiv Q, \quad (3.34)$$

Macroscopic Gauss law

where Q is the *stand-alone* charge inside volume V .

This general result may be used to find the boundary conditions for \mathbf{D} at a sharp interface between two different dielectrics. (The analysis is applicable to a dielectric/free-space boundary as well.) For that, let us apply Eq. (34) to a flat pillbox formed at the interface (see the solid rectangle in Fig. 5), which is sufficiently small on the spatial scales of the dielectric’s nonuniformity and the interface’s curvature, but still containing many elementary dipoles. Assuming that the interface does not have stand-alone surface charges, we immediately get

$$(D_n)_1 = (D_n)_2, \quad (3.35)$$

Boundary condition for \mathbf{D}

i.e. the normal component of the electric displacement has to be continuous. Note that a similar statement for the macroscopic electric field \mathbf{E} is generally not valid, because the polarization vector \mathbf{P} may have, and typically does have a leap at a sharp interface (say, due to the different polarizability of

⁷ Note that according to its definition (33), the dimensionality of \mathbf{D} in the SI units is different from that of \mathbf{E} . In contrast, in the Gaussian units, the electric displacement is defined as $\mathbf{D} = \mathbf{E} + 4\pi\mathbf{P}$, so that $\nabla \cdot \mathbf{D} = 4\pi\rho$ (the relation $\rho_{\text{ef}} = -\nabla \cdot \mathbf{P}$ remains the same as in SI units), and the dimensionalities of \mathbf{D} and \mathbf{E} coincide. This coincidence is a certain perceptual handicap because it is frequently convenient to consider the scalar components of \mathbf{E} as generalized forces, and those of \mathbf{D} as generalized coordinates (see Sec. 5 below), and it is somewhat comforting to have their dimensionalities different, as they are in the SI units.

the two different dielectrics), providing a surface layer of the effective charges (30) – see again the example shown in Fig. 4.

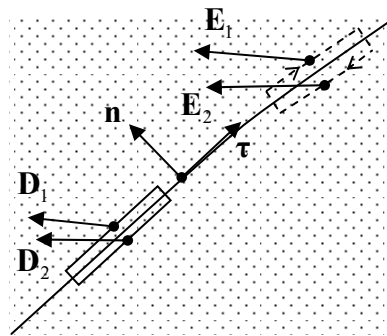


Fig. 3.5. Deriving the boundary conditions at an interface between two dielectrics, using a Gauss pillbox (shown as a solid-line rectangle) and a circulation contour (dashed-line rectangle). Here \mathbf{n} and τ are the unit vectors that are, respectively, normal and tangential to the interface. Note that due to the leap of polarization, the field lines are generally “refracted” at the interface – see Fig. 11b for an example.

However, we still can make an important statement about the behavior of \mathbf{E} at the interface. Indeed, the macroscopic electric fields defined by Eqs. (29) and (31), are evidently still potential ones, and hence obey the macroscopic Maxwell equation similar to Eq. (1.28):

$$\nabla \times \mathbf{E} = 0. \quad (3.36)$$

Integrating this equality along a narrow contour stretched along the interface (see the dashed rectangle in Fig. 5), we get

$$(E_\tau)_1 = (E_\tau)_2. \quad (3.37)$$

Note that this condition is compatible with (and may be derived from) the continuity of the macroscopic electrostatic potential ϕ related to the macroscopic field \mathbf{E} by the relation similar to Eq. (1.33), $\mathbf{E} = -\nabla\phi$, at each point of the interface: $\phi_1 = \phi_2$.

In order to see how these boundary conditions work, let us consider the simple problem shown in Fig. 6. A very broad plane capacitor, with zero voltage between its conducting plates (as may be enforced, for example, by their connection with an external wire), is partly filled with a material with a uniform polarization \mathbf{P}_0 ,⁸ oriented normal to the plates. Let us calculate the spatial distribution of the fields \mathbf{E} and \mathbf{D} , and also the surface charge density of each conducting plate.

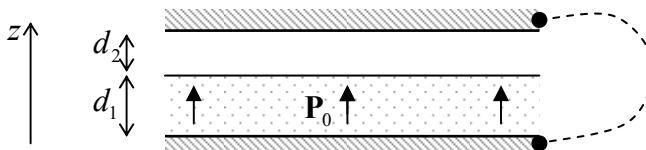


Fig. 3.6. A simple system whose analysis requires Eq. (35).

Due to the symmetry of the system, the vectors \mathbf{E} and \mathbf{D} are both normal to the plates and do not depend on the position in the capacitor’s plane, so we can limit the fields’ analysis to the calculation of their z -components $E(z)$ and $D(z)$. In this case, the Maxwell equation (32) is reduced to $dD/dz = 0$ inside each layer (but not at their border!), so that within each of them, D is constant – say, some D_1 in the layer with $\mathbf{P} = \mathbf{P}_0$, and certain D_2 in the free-space layer, where $\mathbf{P} = 0$. As a result, according to Eq. (33), the (macroscopic) electric field inside each layer is also constant:

⁸ As will be discussed in the next section, this is a good approximation for the so-called *electrets*, and also for *hard ferroelectrics* in not very high electric fields.

$$D_1 = \epsilon_0 E_1 + P_0, \quad D_2 = \epsilon_0 E_2. \quad (3.38)$$

Since the voltage between the plates is zero, we may also require the integral of E , taken along a path connecting the plates, to vanish. This gives us one more relation:

$$E_1 d_1 + E_2 d_2 = 0. \quad (3.39)$$

Still, the three equations (38)-(39) are insufficient to calculate the four fields in the system ($E_{1,2}$ and $D_{1,2}$). The decisive help comes from the boundary condition (35):

$$D_1 = D_2. \quad (3.40)$$

(Note that it is valid because the layer interface does not carry *stand-alone* electric charges, even though it has a *polarization surface charge*, whose areal density may be calculated by integrating Eq. (30) across the interface: $\sigma_{\text{ef}} = P_0$. Note also that in our simple system, Eq. (37) is identically satisfied due to the system's symmetry, and hence does not give any additional information.)

Now solving the resulting system of four equations (38)-(40), we readily get

$$E_1 = -\frac{P_0}{\epsilon_0} \frac{d_2}{d_1 + d_2}, \quad E_2 = \frac{P_0}{\epsilon_0} \frac{d_1}{d_1 + d_2}, \quad D_1 = D_2 = D = P_0 \frac{d_1}{d_1 + d_2}. \quad (3.41)$$

The areal densities of the electrode surface charges may now be readily calculated by the integration of Eq. (32) across each surface:

$$\sigma_1 = -\sigma_2 = D = P_0 \frac{d_1}{d_1 + d_2}. \quad (3.42)$$

Note that due to the spontaneous polarization of the lower layer's material, the capacitor plates are charged even in the absence of voltage between them, and that this charge is a function of the second electrode's position (d_2).⁹ Also notice a substantial similarity between this system (Fig. 6), and the one whose analysis was the subject of Problem 2.6.

3.3. Polarization of dielectrics

The general relations derived in the previous section may be used to describe the electrostatics of any dielectrics – materials with bound electric charges (and hence with negligible dc electric conduction). However, to form a full system of equations necessary to solve electrostatics problems, they have to be complemented by certain constitutive relations between the vectors \mathbf{P} and \mathbf{E} .¹⁰

In most materials, in the absence of an external electric field, the elementary dipoles \mathbf{p} either equal zero or have a random orientation in space, so that the net dipole moment of each macroscopic volume (still containing many such dipoles) equals zero: $\mathbf{P} = 0$ at $\mathbf{E} = 0$. Moreover, if the field changes

⁹ This effect is used in most modern microphones. In such a device, the sensed sound wave's pressure bends a thin conducting membrane playing the role of one of the capacitor's plates, and thus modulates the thickness (in Fig. 6, d_2) of the air gap adjacent to the electret layer. This modulation produces proportional variations of the charges (42), and hence some electric current in the wire connecting the plates, which is picked up by readout electronics.

¹⁰ In the problem solved at the end of the previous section, the role of such relation was played by the equality $\mathbf{P}_0 = \text{const.}$

are sufficiently slow, most materials may be characterized by a unique dependence of \mathbf{P} on \mathbf{E} . Then using the Taylor expansion of function $\mathbf{P}(\mathbf{E})$, we may argue that in relatively low electric fields the function should be well approximated by a linear dependence between these two vectors. Such dielectrics are called *linear* (or “simple”). In an isotropic media, the coefficient of proportionality should be just a scalar. In the SI units, this scalar is defined by the following relation:

Electric susceptibility

$$\mathbf{P} = \chi_e \epsilon_0 \mathbf{E}, \quad (3.43)$$

with the dimensionless constant χ_e called the *electric susceptibility*. However, it is much more common to use, instead of χ_e , another dimensionless parameter,¹¹

Dielectric constant

$$\kappa \equiv 1 + \chi_e, \quad (3.44)$$

which is sometimes called the “relative electric permittivity”, but much more often, the *dielectric constant*. This parameter is very convenient, because combining Eqs. (43) and (44),

$$\mathbf{P} = (\kappa - 1) \epsilon_0 \mathbf{E}. \quad (3.45)$$

and then plugging the resulting relation into the general Eq. (33), we get simply

$$\mathbf{D} = \kappa \epsilon_0 \mathbf{E}, \quad \text{or} \quad \mathbf{D} = \epsilon \mathbf{E}, \quad (3.46)$$

where another popular parameter,¹²

$$\epsilon \equiv \kappa \epsilon_0 \equiv (1 + \chi_e) \epsilon_0. \quad (3.47)$$

ϵ is called the *electric permittivity* of the material.¹³ Table 1 gives the approximate values of the dielectric constant for several representative materials.

In order to understand the range of these values, let me discuss (briefly and rather superficially¹⁴) the two simplest mechanisms of electric polarization. The first of them is typical for liquids and gases of *polar* atoms/molecules, which have their own, spontaneous dipole moments \mathbf{p} . (A typical example is the water molecule H_2O , with the negative oxygen ion offset from the line connecting two positive hydrogen ions, thus producing a spontaneous dipole moment $p = ea$, with $a \approx 0.38 \times 10^{-10} \text{ m} \sim r_{\text{B}}$.) In the absence of an external electric field, the orientation of such dipoles may be random, with the average polarization $\mathbf{P} = n\langle \mathbf{p} \rangle$ equal to zero – see the top panel of Fig. 7a.

¹¹ In older physics literature, the dielectric constant is often denoted by the letter ϵ_r (with the index “r” meaning “relative”), while in electrical engineering publications, its notation is frequently K .

¹² The reader may be perplexed by the use of three different but uniquely related parameters (χ_e , $\kappa \equiv 1 + \chi_e$, and $\epsilon \equiv \kappa \epsilon_0$) for the description of just one scalar property. Unfortunately, such redundancy is typical for physics, whose different sub-field communities have different, well-entrenched traditions.

¹³ In the Gaussian units, χ_e is defined by the following relation: $\mathbf{P} = \chi_e \mathbf{E}$, while ϵ is defined just as in the SI units, $\mathbf{D} = \epsilon \mathbf{E}$. Because of that, in the Gaussian units, the constant ϵ is dimensionless and equals $(1 + 4\pi\chi_e)$. As a result, $\epsilon_{\text{Gaussian}} = (\epsilon/\epsilon_0)_{\text{SI}} \equiv \kappa$, so that $(\chi_e)_{\text{Gaussian}} = (\chi_e)_{\text{SI}}/4\pi$, sometimes creating confusion between the numerical values of the latter parameter – dimensionless in both systems.

¹⁴ While I believe this discussion is very useful, it is quantitatively valid only for relatively sparse media, with low concentration ($n \ll 1/a^3$) of elementary atomic/molecular dipoles of size scale a . Indeed, in some condensed materials, with $na^3 \sim 1$, even the notion of the dipole moment \mathbf{p} with a single atomic cell is ambiguous.

Table 3.1. Dielectric constants of a few representative (and/or practically important) dielectrics

Material	κ
Air (at ambient conditions)	1.00054
Teflon (polytetrafluoroethylene, $[C_2F_4]_n$)	2.1
Silicon dioxide (amorphous)	3.9
Glasses (of various compositions)	3.7–10
Castor oil	4.5
Silicon ^(a)	11.7
Water (at 100°C)	55.3
Water (at 20°C)	80.1
Barium titanate ($BaTiO_3$, at 20°C)	~1,600

^(a) Anisotropic materials, such as silicon crystals, require a *susceptibility tensor* to give an exact description of the linear relation of the vectors \mathbf{P} and \mathbf{E} . However, most important crystals (including Si) are only weakly anisotropic, so they may be reasonably well characterized with a scalar (angle-average) susceptibility.

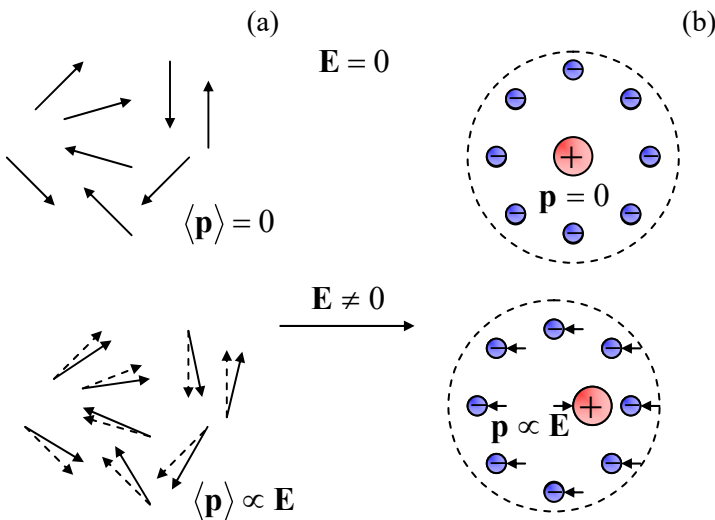


Fig. 3.7. Crude cartoons of two mechanisms of the induced electrical polarization: (a) a partial ordering of spontaneous elementary dipoles, and (b) an elementary dipole induction. The upper two panels correspond to $E = 0$, and the lower two panels, to $E \neq 0$.

A relatively weak external field does not change the magnitude of the dipole moments significantly, but according to Eqs. (15a) and (17), tries to orient them along the field, creating a non-zero vector average $\langle \mathbf{p} \rangle$ directed along the vector \mathbf{E}_m , where \mathbf{E}_m is the microscopic field at the point of the dipole's location – cf. two panels of Fig. 7a. If the field is not too high ($p\langle E_m \rangle \ll k_B T$), the induced average polarization $\langle \mathbf{p} \rangle$ is proportional to \mathbf{E}_m . If we write this proportionality relation in the following traditional form,

$$\langle \mathbf{p} \rangle = \alpha \mathbf{E}_m, \quad (3.48)$$

Atomic polarizability

where α is called the *atomic* (or, sometimes, “*molecular*”) *polarizability*, this means that α is positive. If the concentration n of such elementary dipoles is low, the contribution of their own fields into the

microscopic field acting on each dipole is negligible, and we may identify \mathbf{E}_m with the macroscopic field \mathbf{E} . As a result, the second of Eqs. (27) yields

$$\mathbf{P} \equiv n \langle \mathbf{p} \rangle = \alpha n \mathbf{E}. \quad (3.49)$$

Comparing this relation with Eq. (45), we get

$$\kappa = 1 + \frac{\alpha n}{\epsilon_0}, \quad (3.50)$$

so that $\kappa > 1$ (i.e. $\chi_e = \alpha n / \epsilon_0 > 0$). Note that at this particular polarization mechanism (illustrated on the lower panel of Fig. 7a), the thermal motion “tries” to randomize the dipole orientation, i.e. reduce its ordering by the field, so that we may expect α , and hence $\chi_e \equiv \kappa - 1$ to increase as temperature T is decreased – the so-called *paraelectricity*. Indeed, the basic statistical mechanics¹⁵ shows that in this case, the electric susceptibility follows the so-called *Curie law* $\chi_e \propto 1/T$.

The materials of the second, much more common class consist of *non-polar* atoms without intrinsic spontaneous polarization. A crude classical image of such an atom is an isotropic cloud of negatively charged electrons surrounding a positively charged nucleus – see the top panel of Fig. 7b. The external electric field shifts the positive charge in the direction of the vector \mathbf{E} , and the negative charges in the opposite direction, thus creating a similarly directed average dipole moment $\langle \mathbf{p} \rangle$.¹⁶ At relatively low fields, this average moment is proportional to \mathbf{E} , so that we again arrive at Eq. (48), with $\alpha > 0$, and if the dipole concentration n is sufficiently low, also at Eq. (50), with $\kappa - 1 > 0$. So, the dielectric constant is larger than 1 for both polarization mechanisms – please have one more look at Table 1.

In order to make a crude but physically transparent estimate of the difference $\kappa - 1$, let us consider the following toy model of a non-polar dielectric: a set of similar conducting spheres of radius R , distributed in space with a low density $n \ll 1/R^3$. At such density, the electrostatic interaction of the spheres is negligible, and we can use Eq. (11) for the induced dipole moment of a single sphere. Then the polarizability definition (48) yields $\alpha = 4\pi\epsilon_0 R^3$, so that Eq. (50) gives

$$\kappa = 1 + 4\pi R^3 n. \quad (3.51)$$

Let us use this result for a crude estimate of the dielectric constant of air at the so-called *ambient conditions*, meaning the normal atmospheric pressure $P = 1.013 \times 10^5$ Pa and temperature $T = 300$ K. At these conditions the molecular density n may be, with a few-percent accuracy, found from the well-known equation of state of an ideal gas:¹⁷ $n \approx P/k_B T \approx (1.013 \times 10^5)/(1.38 \times 10^{-23} \times 300) \approx 2.45 \times 10^{25} \text{ m}^{-3}$. The molecule of the air’s main component, N₂, has a van-der-Waals radius¹⁸ of 1.55×10^{-10} m. Taking this radius for the R of our crude model, we get $\chi_e \equiv \kappa - 1 \approx 1.15 \times 10^{-3}$. Comparing this number with the

¹⁵ See, e.g., SM Chapter 2.

¹⁶ Realistically, these effects are governed by quantum mechanics, so the average here should be understood not only in the statistical-mechanical but also (and mostly) in the quantum-mechanical sense. Because of that, for non-polar atoms, α is typically a very weak function of temperature, at least on the usual scale $T \sim 300$ K.

¹⁷ If needed, see, e.g., SM Secs. 1.4 and 3.1.

¹⁸ Such radius is defined by the requirement that the volume of the corresponding sphere, if used in the van-der-Waals equation (see, e. g., SM Sec. 4.1), gives the best fit to the experimental equation of state $n = n(P, T)$.

first line of Table 1, we see that the model gives a surprisingly reasonable result: to get the experimental value, it is sufficient to decrease the effective R of the sphere by just $\sim 30\%$, to $\sim 1.2 \times 10^{-10}$ m.¹⁹

This result may encourage us to try using Eq. (51) for a larger density n . For example, as a crude model for a non-polar crystal, let us assume that the conducting spheres form a simple cubic lattice with the period $a = 2R$ (i.e., the neighboring spheres virtually touch). With this, $n = 1/a^3 = 1/8R^3$ and Eq. (44) yields $\kappa = 1 + 4\pi/8 \approx 2.5$. This estimate provides a reasonable semi-qualitative explanation for the values of κ listed in a few middle rows of Table 1. However, at such small distances, the electrostatic dipole-dipole interaction should be already essential, so that this simple model cannot even approximately describe the values of κ much larger than 1, listed in the last rows of the table.

Such high values may be explained by the so-called *molecular field effect*: each elementary dipole is polarized not only by the external field, as Eq. (49) assumes, but by the field of neighboring dipoles as well. Ottavino-Fabrizio Mossotti in 1850 and (but almost 30 years later) Rudolf Clausius suggested what is now known, rather unfairly, as the *Clausius-Mossotti formula*, which describes this effect reasonably well in many non-polar materials.²⁰ In our notation, it reads²¹

$$\frac{\kappa - 1}{\kappa + 2} = \frac{\alpha n}{3\epsilon_0}, \quad \text{so that } \kappa = 1 + \frac{\alpha n / \epsilon_0}{1 - \alpha n / 3\epsilon_0}. \quad (3.52)$$

Clausius-Mossotti formula

If the dipole density is low in the sense $n \ll \epsilon_0/\alpha$, this relation is reduced to Eq. (50) corresponding to independent dipoles. However, at higher dipole density, both κ and χ_e increase faster and tend to infinity as the density-polarizability product approaches some critical value n_c , in the simple Clausius-Mossotti model equal to $3\epsilon_0/\alpha$.²² This means that the zero-polarization state becomes unstable even in the absence of an external electric field.

This instability is a linear-theory (i.e. low-field) manifestation of a substantially nonlinear effect – the formation, in some materials, of spontaneous polarization even in the absence of an external electric field. Such materials are called *ferroelectrics*, and may be experimentally recognized by the hysteretic behavior of their polarization as a function of the applied (external) electric field – see Fig. 8. As the plots show, the polarization of a ferroelectric depends on the applied field's history. For example, the direction of its spontaneous *remnant polarization* P_R may be switched by first applying, and then removing a sufficiently high field (larger than the so-called *coercive field* E_C – see Fig. 8) of the opposite orientation. The physics of this switching is rather involved; the polarization vector \mathbf{P} of a ferroelectric material is typically constant only within each of spontaneously formed spatial regions (called *domains*), with a typical size of a few tenths of a micron, and different (frequently, opposite) directions of the vector \mathbf{P} in adjacent domains. The change of the applied electric field results not in the

¹⁹ As will be discussed in QM Chapter 6, for a hydrogen atom in its ground state, the low-field polarizability may be calculated analytically: $\alpha = (9/2) \times 4\pi\epsilon_0 r_B^3$, corresponding to our metallic-ball model with a close value of the effective radius: $R = (9/2)^{1/3} r_B \approx 1.65 r_B \approx 0.87 \times 10^{-10}$ m.

²⁰ Applied to the high-frequency electric field, with κ replaced by the square of the refraction coefficient n at the field's frequency (see Chapter 7), this formula is known as the *Lorenz-Lorentz relation*.

²¹ I am leaving the approximate proof of Eq. (52), using Eq. (3.24), for the reader's exercise.

²² The Clausius-Mossotti formula does not give quantitatively correct results for most ferroelectric materials. For a review of modern approaches to the theory of their polarization, see, e.g., the paper by R. Resta and D. Vanderbilt in the review collection by K. Rabe, C. Ahn, and J.-M. Triscone (eds.), *Physics of Ferroelectrics: A Modern Perspective*, Springer, 2010.

switching of the direction of \mathbf{P} inside each domain, but rather in a shift of the domain walls, resulting in the change of the average polarization of the sample.

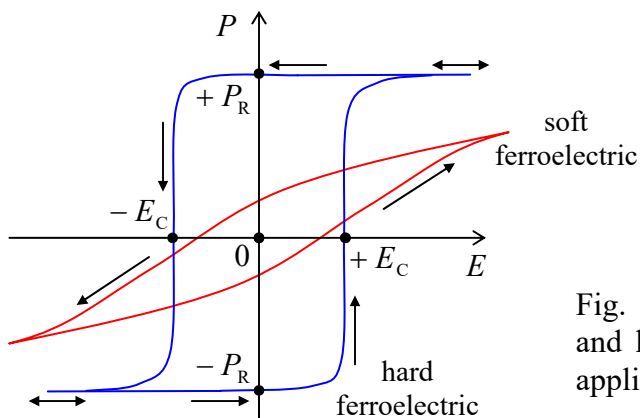


Fig. 3.8. The average polarization of soft and hard ferroelectrics as functions of the applied electric field (schematically).

Depending on the ferroelectric's material, temperature, and the sample's geometry (a solid crystal, a ceramic material, or a thin film), the hysteretic loops may be rather different, ranging from a rather smooth form in the so-called *soft ferroelectrics* (which include most ferroelectric thin films) to an almost rectangular form in *hard ferroelectrics* – see Fig. 8. In low fields, soft ferroelectrics behave essentially as linear paraelectrics, but with a very high average dielectric constant – see the bottom line of Table 1 for such a classical material as BaTiO₃ (which is a soft ferroelectric at temperatures below $T_c \approx 120^\circ\text{C}$, and a paraelectric above this critical temperature). On the other hand, the polarization of a hard ferroelectric in the fields below its coercive field remains virtually constant, and the analysis of their electrostatics may be based on the condition $\mathbf{P} = \mathbf{P}_R = \text{const}$ – already used in the problem discussed in the end of the previous section.²³ This condition is even more applicable to the so-called *electrets* – synthetic polymers with a spontaneous polarization that remains constant even in very high electric fields.

Some materials exhibit even more complex polarization effects, for example, *antiferroelectricity*, *helielectricity*, and (practically very valuable) *piezoelectricity*. Unfortunately, I do not have time for a discussion of these exotic phenomena in this course;²⁴ the main reason I am mentioning them is to emphasize again that the constitutive relation $\mathbf{P} = \mathbf{P}(\mathbf{E})$ is material-specific rather than fundamental. However, most insulators, in practicable fields, behave as linear dielectrics, so the next section will be committed to the discussion of their electrostatics.

²³ Due to this property, hard ferroelectrics, such as the lead zirconate titanate (PZT) and strontium bismuth tantalite (SBT), with high remnant polarization P_R (up to $\sim 1 \text{ C/m}^2$), may be used in nonvolatile random-access memories (dubbed either FRAM or FeRAM) – see, e.g., J. Scott, *Ferroelectric Memories*, Springer, 2000. In a cell of such a memory, binary information is stored in the form of one of two possible directions of spontaneous polarization at $\mathbf{E} = 0$ (see Fig. 8). Unfortunately, the time of spontaneous depolarization of ferroelectric thin films is typically well below 10 years – the industrial standard for data retention in nonvolatile memories, and this time may be decreased even more by “fatigue” from the repeated polarization recycling at information recording. Due to these reasons, the industrial production of FRAM is currently just a tiny fraction of the nonvolatile memory market, which is dominated by floating-gate memories – see, e.g., Sec. 4.2 below.

²⁴ For detailed coverage of ferroelectrics, I can recommend the encyclopedic monograph by M. Lines and A. Glass, *Principles and Applications of Ferroelectrics and Related Materials*, Oxford U. Press, 2001, and the recent review collection edited by K. Rabe *et al.*, that was cited above.

3.4. Electrostatics of linear dielectrics

First, let us consider the simplest but very important problem: how is the electrostatic field of a set of stand-alone charges of density $\rho(\mathbf{r})$ modified if it is placed into a uniform linear dielectric medium that obeys Eq. (46) with a dielectric constant κ constant in the whole region we are interested in. In this case, we may combine Eqs. (32) and (46) to write

$$\nabla \cdot \mathbf{E} = \frac{\rho}{\epsilon}. \quad (3.53)$$

As a reminder, in the free space we had a similar equation (1.27), but with a different constant, $\epsilon_0 = \epsilon/\kappa$. Hence all the results discussed in Chapter 1 are valid inside a uniform linear dielectric, for the macroscopic field the \mathbf{E} (and the corresponding macroscopic electrostatic potential ϕ), if they are reduced by the factor of $\kappa > 1$. Thus, the most straightforward result of the induced polarization of a dielectric medium is the *electric field reduction*. This is a very important effect, especially taking into account the very high values of κ in such common dielectrics as water – see Table 1. Indeed, it is the reduction of the attraction between positive and negative ions (called, respectively, *cations* and *anions*) in water that enables their substantial dissociation and hence almost all biochemical reactions, which are the basis of the biological cell functions – and hence of the life itself.

Let us apply this general result to the important particular case of the plane capacitor (Fig. 2.3) filled with a linear, uniform dielectric. Applying the macroscopic Gauss law (34) to a pillbox-shaped volume on the conductor surface, we get the following relation,

$$\sigma = D_n = \epsilon E_n = -\epsilon \frac{\partial \phi}{\partial n}, \quad (3.54)$$

which differs from Eq. (2.3) only by the replacement $\epsilon_0 \rightarrow \epsilon \equiv \kappa \epsilon_0$. Hence, for a fixed field E_n , the charge density calculated for the free-space case should be increased by the factor of κ – that's it. In particular, this means that the capacitance (2.28) has to be increased by this factor:

$$C = \frac{\kappa \epsilon_0 A}{d} \equiv \frac{\epsilon A}{d}. \quad (3.55)$$

C of a
planar
capacitor

(As a reminder, this increase of C by κ has been already incorporated, without proof, into some estimates made in Secs. 2.1 and 2.2, to make them realistic.)

If a linear dielectric is nonuniform, the situation is more complex. For example, let us consider the case of a sharp interface between two otherwise uniform dielectrics, free of stand-alone charges. In this case, we still may use Eq. (37) for the tangential component of the macroscopic electric field, and also Eq. (36), with $D_n = \epsilon E_n$, for its normal component, getting

$$(\epsilon E_n)_1 = (\epsilon E_n)_2, \quad \text{i.e. } \epsilon_1 \frac{\partial \phi_1}{\partial n} = \epsilon_2 \frac{\partial \phi_2}{\partial n}. \quad (3.56)$$

Boundary
condition
for E_n

Let us apply these boundary conditions, first of all, to consider how carving a slit of some width d and a much smaller thickness $t \ll d$ from inside a dielectric, changes an initially uniform electric field \mathbf{E}_0 , depending on its orientation – see Fig. 9.

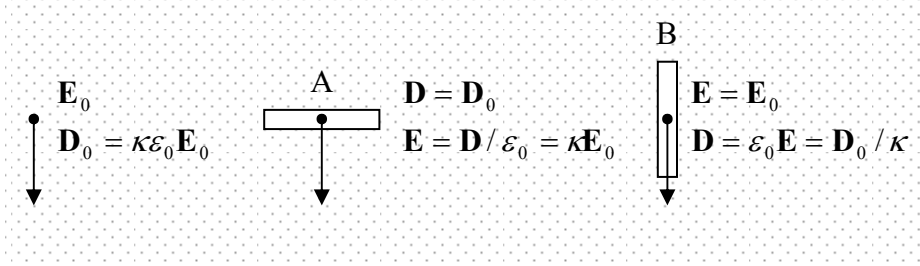


Fig. 3.9. Fields inside two narrow slits cut in a linear dielectric.

First of all, intuition tells us that regardless of its orientation, a slit cannot change the field far from it; moreover, at $t \rightarrow 0$, it cannot modify substantially even the field right outside its “major” (broader) surfaces. This conclusion may be supported either by direct calculations (see, e.g., the problem illustrated by Fig. 11 below), or by energy arguments: at $t \ll d$, any potential energy decrease due to the field change inside the slit’s volume (proportional to td) cannot compensate its increase in the outer volume proportional to d^2 . However, it may induce some local field changes – inside the slit, and even outside it, close to its “minor” surfaces.

To calculate the inner field for case A, with the slit’s plane normal to the applied field, we may apply Eq. (56) to its major surfaces (shown horizontal), to prove that the vector \mathbf{D} should be continuous. But according to Eq. (46), this means that in the free space inside the slit, the electric field should equal \mathbf{D}/ϵ_0 , and hence be κ times higher than the field $\mathbf{E}_0 = \mathbf{D}/\kappa\epsilon_0$ far from the slit. This field, and hence \mathbf{D} , may be measured by a sensor placed inside the gap, so that the electric displacement is not an entirely mathematical construct.²⁵ On the contrary, for case B, with the slit’s plane parallel to the initial field, we may apply Eq. (37) to the major (now, vertical) interfaces of the slit, to see that now the electric field \mathbf{E} is continuous, while the electric displacement $\mathbf{D} = \epsilon_0\mathbf{E}$ inside the gap is a factor of κ lower than its value in the dielectric. (Similarly to case A, any perturbations of the field uniformity, caused by the compliance with Eq. (56) at the minor surfaces, settle down at distances $\sim t$ from them.)

For other problems with piecewise-constant ϵ , with more complex geometries, we may need to apply the methods studied in Chapter 2. In particular, in the simplest cases we can select such a set of orthogonal coordinates that the electrostatic potential depends on just one of them. Consider, for example, two types of filling a plane capacitor with two different dielectrics – see Fig. 10.

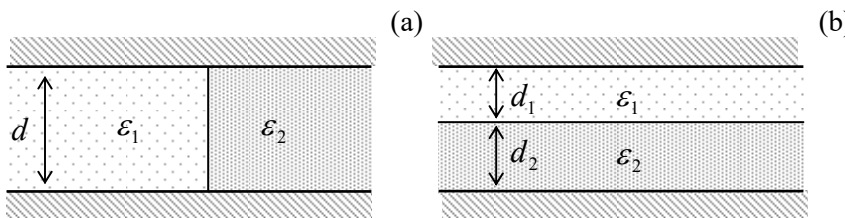


Fig. 3.10. Plane capacitors filled with two different dielectrics.

In case (a), the voltage V between the electrodes is the same for each part of the capacitor, telling us that at least far from the dielectric interface, the electric field is vertical, uniform, and constant ($E = V/d$). Hence the boundary condition (37) is satisfied even if such a distribution is valid near the surface

²⁵ Superficially, this result violates the boundary condition (37) at the vertical (“minor”) surfaces of the gap. This apparent contradiction is resolved by the fact the thin slit can deform the field both inside and outside it, at distances of the order of t around these interfaces, but not far beyond them, so that the above relations for \mathbf{E} and \mathbf{D} are valid at most of the slit area.

as well, i.e. at any point of the system. The only effect of different values of ϵ in the two parts is that the electric displacement $D = \epsilon E$ and hence electrodes' surface charge density $\sigma = D$ are different in them. Thus we can calculate the electrode charges $Q_{1,2}$ of the two parts independently, and then add up the results to get the total mutual capacitance

$$C = \frac{Q_1 + Q_2}{V} = \frac{1}{d} (\epsilon_1 A_1 + \epsilon_2 A_2). \quad (3.57)$$

Note that this formula may be interpreted as the total capacitance of two separate lumped capacitors connected (by wires) *in parallel*. This is natural, because we may cut the system along the dielectric interface, without any effect on the fields in either part, and then connect the corresponding electrodes by external wires, again without any effect on the system – besides very close vicinities of the capacitor's edges, where the fringe

Case (b) may be analyzed just as in the problem illustrated by Fig. 6, by applying Eq. (34) to a Gaussian pillbox with one lid inside the (for example) bottom electrode, and the other lid inside any of the layers. As a result, we see that D anywhere inside the system should be equal to the surface charge density σ of the electrode, i.e. constant. Hence, according to Eq. (46), the electric field E inside each dielectric layer is also constant: in the top layer, it is $E_1 = D_1/\epsilon_1 = \sigma/\epsilon_1$, while in bottom layer, $E_2 = D_2/\epsilon_2 = \sigma/\epsilon_2$. Integrating the field E across the whole capacitor, we get

$$V = \int_0^{d_1+d_2} E(z) dz = E_1 d_1 + E_2 d_2 = \left(\frac{d_1}{\epsilon_1} + \frac{d_2}{\epsilon_2} \right) \sigma, \quad (3.58)$$

so that the mutual capacitance per unit area

$$\frac{C}{A} \equiv \frac{\sigma}{V} = \left[\frac{d_1}{\epsilon_1} + \frac{d_2}{\epsilon_2} \right]^{-1}. \quad (3.59)$$

Note that this result is similar to the total capacitance of an *in-series* connection of two plane capacitors based on each of the layers. This is also natural because we could insert an uncharged, thin conducting sheet (rather than a cut as in the previous case) at the layer interface, which is an equipotential surface, without changing the field distribution in any part of the system. Then we could thicken the conducting sheet as much as we liked (and possibly shape its internal part into a thin wire), also without changing the fields in the dielectric parts of the system, and hence the capacitance.

Proceeding to problems with more complex geometry, let us consider the system shown in Fig. 11a: a dielectric sphere placed into an initially uniform external electric field \mathbf{E}_0 . According to Eq. (53) for the macroscopic electric field, and the definition of the macroscopic electrostatic potential, $\mathbf{E} = -\nabla\phi$, the potential satisfies the Laplace equation both inside and outside the sphere, though not at its border. Due to the spherical symmetry of the dielectric sample, this problem invites the variable separation method in spherical coordinates, which was discussed in Sec. 2.8. From that discussion, we already know, in particular, the general solution (2.172) of the Laplace equation outside of the sphere. To satisfy the uniform-field condition at $r \rightarrow \infty$, we have to reduce this solution to

$$\phi_{r \geq R} = -E_0 r \cos \theta + \sum_{l=1}^{\infty} \frac{b_l}{r^{l+1}} P_l(\cos \theta). \quad (3.60)$$

Inside the sphere, we can also use Eq. (2.172), but keeping only the radial functions finite at $r \rightarrow 0$:

$$\phi_{r \leq R} = \sum_{l=1}^{\infty} a_l r^l \mathcal{P}_l(\cos \theta). \quad (3.61)$$

Now, spelling out the boundary conditions (37) and (56) at $r = R$, we see that for all coefficients a_l and b_l with $l \geq 2$, we get homogeneous linear equations (just like for the conducting sphere discussed in Sec. 2.8) that have only trivial solutions. Hence, all these terms may be dropped, while for the only surviving terms with $l = 1$, proportional to the Legendre polynomial $\mathcal{P}_1(\cos \theta) \equiv \cos \theta$, we get two equations:

$$-E_0 - \frac{2b_1}{R^3} = \kappa a_1, \quad -E_0 R + \frac{b_1}{R^2} = a_1 R. \quad (3.62)$$

Solving this simple system of linear equations for a_1 and b_1 , and plugging the result into Eqs. (60) and (61), we get the final solution of the problem:

$$\phi_{r \geq R} = E_0 \left(-r + \frac{\kappa-1}{\kappa+2} \frac{R^3}{r^2} \right) \cos \theta, \quad \phi_{r \leq R} = -E_0 \frac{3}{\kappa+2} r \cos \theta. \quad (3.63)$$

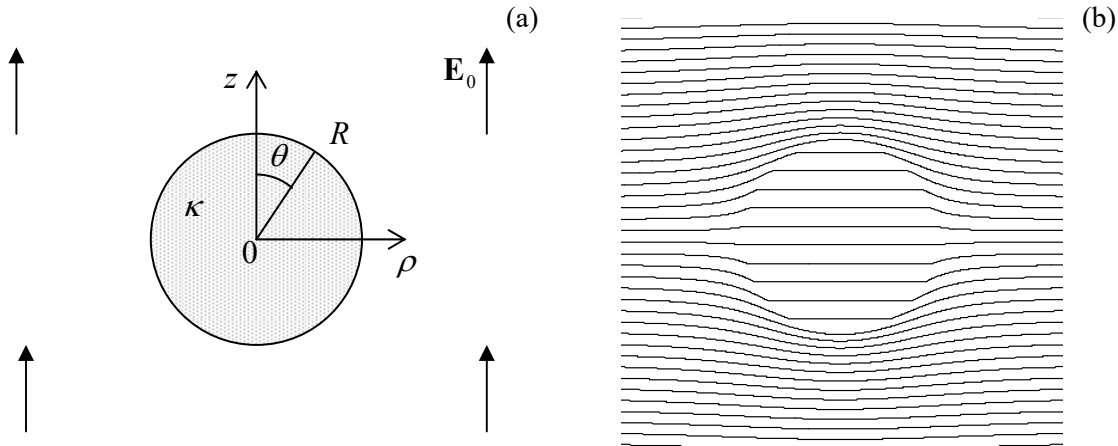


Fig. 3.11. A dielectric sphere in an initially uniform electric field: (a) the problem, and (b) the equipotential surfaces, as given by Eq. (63), for $\kappa = 3$.

Figure 11b shows the equipotential surfaces given by this solution, for a particular value of the dielectric constant κ . Note that according to Eq. (62), at $r \geq R$ the dielectric sphere, just as the conducting sphere in a similar problem, produces (on top of the uniform external field) a pure dipole field, with the dipole moment

$$\mathbf{p} = 4\pi R^3 \frac{\kappa-1}{\kappa+2} \epsilon_0 \mathbf{E}_0 \equiv 3V \frac{\kappa-1}{\kappa+2} \epsilon_0 \mathbf{E}_0, \quad \text{where } V = \frac{4\pi}{3} R^3. \quad (3.64)$$

This is an evident generalization of Eq. (11), to which Eq. (64) tends at $\kappa \rightarrow \infty$. By the way, this property is common: for their electrostatic properties, conductors may be adequately described as dielectrics with $\kappa \rightarrow \infty$.

Another remarkable feature of Eqs. (63) is that the electric field and polarization inside the sphere are uniform, with R -independent values

$$\mathbf{E} = \frac{3}{\kappa+2} \mathbf{E}_0, \quad \mathbf{D} \equiv \kappa \epsilon_0 \mathbf{E} = \epsilon_0 \frac{3\kappa}{\kappa+2} \mathbf{E}_0, \quad \mathbf{P} \equiv \mathbf{D} - \epsilon_0 \mathbf{E} = 3\epsilon_0 \frac{\kappa-1}{\kappa+2} \mathbf{E}_0. \quad (3.65)$$

In the limit $\kappa \rightarrow 1$ (for example, the “sphere made of free space”, i.e. no sphere at all), the electric field inside it naturally tends to the external one, and its polarization vanishes. In the opposite limit $\kappa \rightarrow \infty$, the electric field inside the sphere vanishes. Curiously enough, in this limit the electric displacement inside the sphere remains finite: $\mathbf{D} \rightarrow 3\epsilon_0 \mathbf{E}_0$.

More complex problems with piecewise-uniform dielectrics also may be addressed by the methods discussed in Chapter 2, and hopefully, the reader will be able to use them to solve a few such problems offered in Sec. 6, on their own. Let me discuss just one of such problems because it exhibits a new feature of the charge image method that was discussed in Secs 2.9 (and is the basis of Green’s function approach – see Sec. 2.10). Consider the system shown in Fig. 12: a point charge near a dielectric half-space; it obviously parallels the system discussed in Sec. 2.9 – see Fig. 2.26.

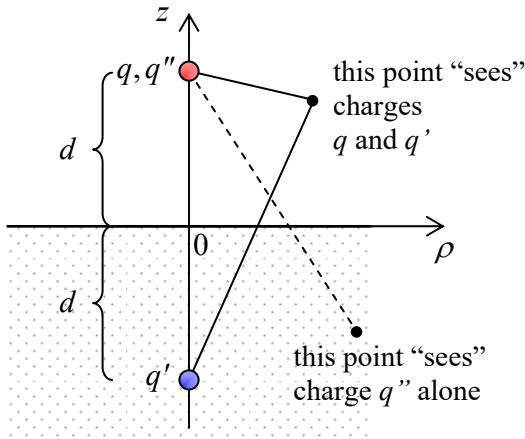


Fig. 3.12. Charge images for a dielectric half-space.

As for the case of a conducting half-space, the Laplace equation for the electrostatic potential in the upper half-space $z > 0$ (besides the charge point $\rho = 0, z = d$) may be satisfied using a single image charge q' at the point with $\rho = 0$ and $z = -d$, but now q' may differ from $(-q)$. In addition, in contrast to the case analyzed in Sec. 2.9, we should also calculate the field inside the dielectric ($z \leq 0$). This field cannot be contributed by the image charge q' , because that would give a potential divergence at its location. Thus, in the dielectric-filled half-space we should try to use the real point source only, but with a re-normalized charge q'' rather than the genuine charge q – see Fig. 12. As a result, we may look for the potential distribution in the form

$$\phi(\rho, z) = \frac{1}{4\pi\epsilon_0} \times \begin{cases} \left[\frac{q}{(\rho^2 + (z-d)^2)^{1/2}} + \frac{q'}{(\rho^2 + (z+d)^2)^{1/2}} \right], & \text{for } z \geq 0, \\ \frac{q''}{(\rho^2 + (z-d)^2)^{1/2}}, & \text{for } z \leq 0, \end{cases} \quad (3.66)$$

at this stage of solution, with unknown q' and q'' . Plugging this equality into the boundary conditions (37) and (56) at $z = 0$ (with $\partial/\partial n = \partial/\partial z$), we see that they are indeed satisfied (so that Eq. (66) does express the solution of the boundary problem), provided that the effective charges q' and q'' obey the following relations:

$$q - q' = \kappa q'', \quad q + q' = q''. \quad (3.67)$$

Solving this simple system of linear equations, we get

$$q' = -\frac{\kappa-1}{\kappa+1}q, \quad q'' = \frac{2}{\kappa+1}q. \quad (3.68)$$

If $\kappa \rightarrow 1$, then $q' \rightarrow 0$, and $q'' \rightarrow q$ – both facts very natural because in this limit (no polarization at all) we have to recover the unperturbed field of the initial point charge in both semi-spaces. In the opposite limit $\kappa \rightarrow \infty$ (which, as was discussed above, may describe a conducting half-space), $q' \rightarrow -q$ (repeating the result we have discussed in detail in Sec. 2.9), and $q'' \rightarrow 0$. The last result means that in this limit, the electric field \mathbf{E} in the dielectric tends to zero – as it should.

In conclusion of this section, please note that if the permittivity ε of a linear dielectric is a continuous rather than piecewise function of coordinates, the distribution of the electrostatic potential ϕ may be found from Eq. (32) with the electric displacement given by Eq. (46): $\mathbf{D} = \varepsilon(\mathbf{r})\mathbf{E} = -\varepsilon(\mathbf{r})\nabla\phi$. However, analytical solutions of the resulting partial differential equation of the second order may be found only for rare particular cases; one of them is offered in Sec. 6 for the reader's exercise.

3.5. Electric field energy in a dielectric

In Chapter 1, we have obtained two key results for the electrostatic energy: Eq. (1.55) for a charge interaction with an independent (“external”) field, and a similarly structured formula (1.60), but with an additional factor $1/2$, for the field induced by the charges under consideration. These relations are universal, i.e. valid for dielectrics as well, provided that the charge density includes *all* charges – including those bound into the elementary dipoles. However, for most applications, it is convenient to recast them into a form where these bound charges participate not explicitly, but only via the macroscopic polarization effects they create.

If a field is created only by the stand-alone charges under consideration and is proportional to $\rho(\mathbf{r})$ (requiring that we deal with linear dielectrics), we can repeat all the argumentation of the beginning of Sec. 1.3, and again arrive at Eq. (1.60), provided that ϕ is now the macroscopic field’s potential. Now we can recast this result in the terms of fields – essentially as this was done in Eqs. (1.62)-(1.64), but now making a clear difference between the macroscopic electric field $\mathbf{E} = -\nabla\phi$ and the electric displacement field \mathbf{D} , which obeys the macroscopic Maxwell equation (32). Plugging $\rho(\mathbf{r})$ expressed from that equation, into Eq. (1.60), we get

$$U = \frac{1}{2} \int (\nabla \cdot \mathbf{D}) \phi \, d^3 r. \quad (3.69)$$

Using the fact²⁶ that for differentiable functions ϕ and \mathbf{D} ,

$$(\nabla \cdot \mathbf{D})\phi = \nabla \cdot (\phi \mathbf{D}) - (\nabla\phi) \cdot \mathbf{D}, \quad (3.70)$$

we may rewrite Eq. (69) as

$$U = \frac{1}{2} \int \nabla \cdot (\phi \mathbf{D}) d^3 r - \frac{1}{2} \int (\nabla\phi) \cdot \mathbf{D} d^3 r. \quad (3.71)$$

²⁶ See, e.g., MA Eq. (11.4a).

The divergence theorem, applied to the first term on the right-hand side, reduces it to a surface integral of ϕD_n . (As a reminder, in Eq. (1.63) the integral was of $\phi(\nabla\phi)_n \propto \phi E_n$.) If the surface of the volume we are considering is sufficiently far, this surface integral vanishes. On the other hand, the gradient in the second term of Eq. (71) is just (minus) field **E**, so it gives

$$U = \frac{1}{2} \int \mathbf{E} \cdot \mathbf{D} d^3r = \frac{1}{2} \int E(\mathbf{r}) \epsilon(\mathbf{r}) E(\mathbf{r}) d^3r \equiv \frac{\epsilon_0}{2} \int \kappa(\mathbf{r}) E^2(\mathbf{r}) d^3r. \quad (3.72)$$

This expression is a natural generalization of Eq. (1.65), and shows that we can, as we did in free space, represent the electrostatic energy in a local form:²⁷

$$U = \int u(\mathbf{r}) d^3r, \quad \text{with } u = \frac{1}{2} \mathbf{E} \cdot \mathbf{D} = \frac{\epsilon}{2} E^2 = \frac{D^2}{2\epsilon}. \quad (3.73)$$

Field
energy in
a linear
dielectric

As a sanity check, in the trivial case $\epsilon = \epsilon_0$ (i.e. $\kappa = 1$), this result is reduced to Eq. (1.65).

Of course, Eq. (73) is valid only for linear dielectrics, because our starting point, Eq. (1.60), is only valid if ϕ is proportional to ρ . To make our calculation more general, we should intercept the calculations of Sec. 1.3 at an earlier stage, at which this proportionality had not yet been used. For example, the first of Eqs. (1.56) may be rewritten, in the continuous form, as

$$\delta U = \int \phi(\mathbf{r}) \delta \rho(\mathbf{r}) d^3r, \quad (3.74)$$

where the symbol δ means a small variation of the function – e.g., its change in time, sufficiently slow to ignore the relativistic and magnetic-field effects. Applying such variation to Eq. (32), and plugging the resulting relation $\delta \rho = \nabla \cdot \delta \mathbf{D}$ into Eq. (74), we get

$$\delta U = \int (\nabla \cdot \delta \mathbf{D}) \phi d^3r. \quad (3.75)$$

(Note that in contrast to Eq. (69), this expression does not have the front factor $1/2$.) Now repeating the same calculations as in the linear case, for the energy density's *variation* we get a remarkably simple (and general!) expression,

$$\delta u = \mathbf{E} \cdot \delta \mathbf{D} \equiv \sum_{j=1}^3 E_j \delta D_j, \quad (3.76)$$

Energy
density's
variation

where the last expression uses the Cartesian components of the vectors **E** and **D**. This is as far as we can go for the general dependence **D(E)**. If the dependence is linear and isotropic, as in Eq. (46), then $\delta \mathbf{D} = \epsilon \delta \mathbf{E}$ and

$$\delta u = \epsilon \mathbf{E} \cdot \delta \mathbf{E} = \epsilon \delta \left(\frac{E^2}{2} \right). \quad (3.77)$$

The integration of this expression over the whole variation, from the field equal to zero to a certain final distribution **E(r)**, brings us back to Eq. (73).

An important role of Eq. (76), in its last form, is to indicate that from the point of view of analytical mechanics, the Cartesian coordinates of **E** may be interpreted as generalized forces, and those

²⁷ In the Gaussian units, each of the last three expressions should be divided by 4π .

of \mathbf{D} as generalized coordinates of the field's effect on a unit volume of the dielectric. This allows one, in particular, to form the proper *Gibbs potential energy*²⁸ of a system with an electric field $\mathbf{E}(\mathbf{r})$ fixed, at every point, by some external source:

Gibbs potential energy

$$U_G = \int_V u_G(\mathbf{r}) d^3r, \quad u_G(\mathbf{r}) = u(\mathbf{r}) - \mathbf{E}(\mathbf{r}) \cdot \mathbf{D}(\mathbf{r}). \quad (3.78)$$

The essence of this notion is that if the generalized external force (in our case, \mathbf{E}) is fixed, the stable equilibrium of the system corresponds to the minimum of U_G , rather than of the potential energy U as such – in our case, that of the field in our system.

As the simplest illustration of this important concept, let us consider a very long cylinder (with an arbitrary cross-section's shape), made of a uniform linear dielectric, placed into a uniform external electric field parallel to the cylinder's axis – see Fig. 13.

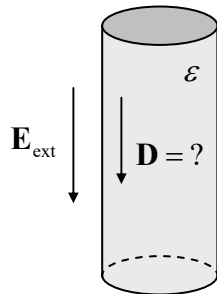


Fig. 3.13. A cylindrical dielectric sample in a longitudinal external electric field.

For this simple problem, the equilibrium value of \mathbf{D} inside the cylinder may be, of course, readily found without any appeal to energies. Indeed, the solution of the Laplace equation inside the cylinder, with the boundary condition (37) is evident: $\mathbf{E}(\mathbf{r}) = \mathbf{E}_{\text{ext}}$, and so that Eq. (46) immediately yields $\mathbf{D}(\mathbf{r}) = \epsilon \mathbf{E}_{\text{ext}}$. One may wonder why does the minimum of the potential energy U , given by Eq. (73) in its last form,

$$\frac{U}{V} = \frac{D^2}{2\epsilon}, \quad (3.79)$$

correspond to a different (zero) value of \mathbf{D} , but let us recall that Eq. (73) was derived for the case when the electric field is created by the stand-alone charges in the system under consideration. If it is created by external sources, we have to use the Gibbs potential energy (78) instead. For our current uniform case, this energy per unit volume of the cylinder is

$$\frac{U_G}{V} = \frac{U}{V} - \mathbf{E} \cdot \mathbf{D} = \frac{D^2}{2\epsilon} - \mathbf{E} \cdot \mathbf{D} \equiv \sum_{j=1}^3 \left(\frac{D_j^2}{2\epsilon} - E_j D_j \right), \quad (3.80)$$

and its minimum as a function of every Cartesian component of \mathbf{D} corresponds to the correct value of the displacement: $D_j = \epsilon E_j$, i.e. to $\mathbf{D} = \epsilon \mathbf{E} = \epsilon \mathbf{E}_{\text{ext}}$. So, the systems' equilibrium indeed corresponds to the minimum of the Gibbs potential energy (78) rather than of the energy (73).

²⁸ See, e.g., CM Sec. 1.4, in particular Eq. (1.41). Note that as Eq. (78) clearly illustrates, once again, that the difference between the potential energies U_G and U , usually discussed in courses of thermodynamics and statistical physics as the difference between the Gibbs and Helmholtz free energies (see, e.g., SM 1.4), is more general than the effects of random thermal motion addressed by these disciplines.

Now note that Eq. (80), at this equilibrium point (only!), may be rewritten as

$$\frac{U_G}{V} = \frac{U}{V} - \mathbf{E} \cdot \mathbf{D} = \frac{D^2}{2\epsilon} - \frac{\mathbf{D} \cdot \mathbf{D}}{\epsilon} \equiv -\frac{D^2}{2\epsilon}, \quad (3.81)$$

i.e. formally coincides with Eq. (79), besides the (perhaps, somewhat counter-intuitive) *opposite sign*. A similar but more general relation (not limited to linear dielectrics and uniform fields) may be obtained by taking the variation of the u_G expressed by Eq. (78), and then using Eq. (76):

$$\delta u_G = \delta u - \delta(\mathbf{E} \cdot \mathbf{D}) = \mathbf{E} \cdot \delta \mathbf{D} - (\delta \mathbf{E} \cdot \mathbf{D} + \mathbf{E} \cdot \delta \mathbf{D}) \equiv -\mathbf{D} \cdot \delta \mathbf{E}. \quad (3.82)$$

In order to see how this expression works, let us plug \mathbf{D} from Eq. (33):

$$\delta u_G = -(\epsilon_0 \mathbf{E} + \mathbf{P}) \cdot \delta \mathbf{E} \equiv -\delta \left(\frac{\epsilon_0 E^2}{2} \right) - \mathbf{P} \cdot \delta \mathbf{E}. \quad (3.83)$$

So far, this relation is general. In the particular case when the polarization \mathbf{P} is field-independent, we may integrate Eq. (83) over the full electric field's variation, say from 0 to some finite value \mathbf{E} , getting

$$u_G = -\frac{\epsilon_0 E^2}{2} - \mathbf{P} \cdot \mathbf{E}. \quad (3.84)$$

Again, the Gibbs energy is relevant only if \mathbf{E} is dominated by an external field \mathbf{E}_{ext} independent of the orientation of \mathbf{P} . If, in addition, $\mathbf{P}(\mathbf{r}) \neq 0$ only in some finite volume V , we may integrate Eq. (84) over that volume, getting

$$U_G = -\mathbf{p} \cdot \mathbf{E}_{\text{ext}} + \text{const}, \quad \text{with } \mathbf{p} \equiv \int_V \mathbf{P}(\mathbf{r}) d^3 r, \quad (3.85)$$

where the “const” means the terms independent of \mathbf{p} . In this expression, we may readily recognize Eq. (15a) for an electric dipole \mathbf{p} of a fixed magnitude, which was obtained in Sec. 1 in a different way. This comparison illustrates again that U_G is nothing mysterious; it is just the relevant part of the potential energy of the system in a fixed external field, including the energy of its interaction with the field.

Finally, in the other important case of a linear dielectric, when according to Eqs. (45) and (47), $\mathbf{P} = (\epsilon - \epsilon_0)\mathbf{E}$, the similar integration of the general Eq. (83) over the field yields the additional factor $\frac{1}{2}$:

$$U_G = -\frac{1}{2} \int_V \mathbf{P} \cdot \mathbf{E}_{\text{ext}} d^3 r + \text{const}. \quad (3.86)$$

This expression may be very convenient for analyses of the forces exerted by electric fields on linear dielectric media – see, for example, a few exercises on this topic, offered at the end of this chapter.

3.6. Exercise problems

3.1. Prove Eqs. (3)-(4), starting from Eqs. (1.38) and (3.2).

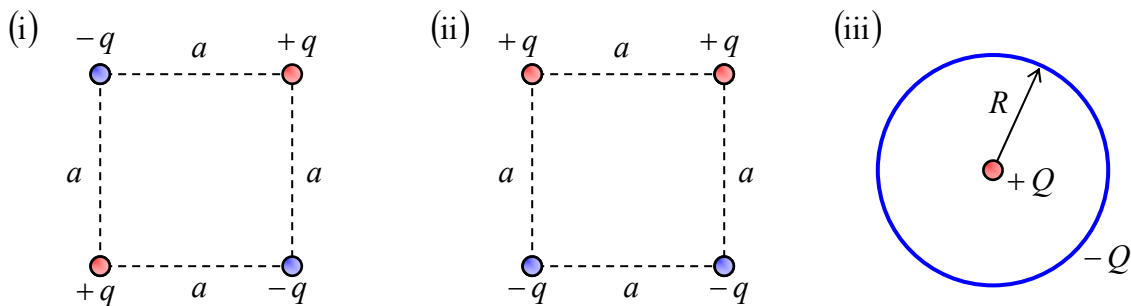
3.2. A plane thin ring of radius R is charged with a constant linear density λ . Calculate the exact electrostatic potential distribution along the symmetry axis of the ring, and prove that at large distances, $r \gg R$, the three leading terms of its multipole expansion are indeed correctly described by Eqs. (3)-(4).

3.3. In suitable reference frames, calculate the dipole and quadrupole moments of the following systems (see the figures below):

(i) four point charges of the same magnitude, but alternating signs, placed in the corners of a square;

(ii) a similar system, but with a pair charge sign alternation; and

(iii) a point charge in the center of a thin ring carrying a similar but opposite charge, uniformly distributed along its circumference.



3.4. Calculate the dipole and quadrupole moments of a thin spherical shell of radius R , carrying an electric charge with areal density $\sigma = \sigma_0 \cos\theta$. Discuss the relation between the results and the solution of Problem 2.28.

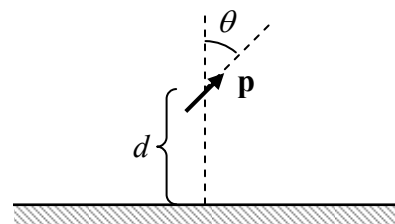
3.5. For a regular cubic lattice of similarly oriented identical dipoles, calculate the electric field it creates at the location of each dipole.

3.6. Without carrying out an exact calculation, can you predict the spatial dependence of the interaction between various electric multipoles, including point charges (in this context, frequently called electric *monopoles*), dipoles, and quadrupoles? Based on these predictions, what is the functional dependence of the interaction between diatomic molecules such as H_2 , N_2 , O_2 , etc., on the distance between them, if the distance is much larger than the molecular size?

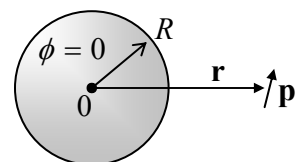
3.7. Two similar electric dipoles, of fixed magnitude p , located at a fixed distance r from each other, are free to change their directions. What stable equilibrium position(s) they may take as a result of their electrostatic interaction?

3.8. An electric dipole is located above an infinite, grounded conducting plane (see the figure on the right). Calculate:

- (i) the distribution of the induced charge in the conductor,
- (ii) the dipole-to-plane interaction energy, and
- (iii) the force and the torque exerted on the dipole.



3.9. Calculate the net charge Q induced in a grounded conducting sphere of radius R by a dipole \mathbf{p} located at point \mathbf{r} outside the sphere – see the figure on the right.



3.10. Use two different approaches to calculate the energy of interaction between a grounded conductor and an electric dipole \mathbf{p} placed in the center of a spherical cavity of radius R , carved in the conductor.

3.11. A plane separating two parts of otherwise free space is densely and uniformly (with a constant areal density n) covered with electric dipoles, with similar moments \mathbf{p} oriented normally to the plane.

(i) Use two different approaches to calculate the electrostatic potential at distances $d \gg 1/n^{1/2}$ on both sides of the plane.

(ii) Give a physical interpretation of your result.

(iii) Use the result to calculate the potential distribution created in space by a spherical surface of radius R , densely and uniformly covered with radially-oriented dipoles.

3.12. Prove Eq. (24).

Hint: You may like to use the basic Eq. (1.9) to spell out the left-hand side of Eq. (1.24), change the order of integration over \mathbf{r} and \mathbf{r}' , and then contemplate the physical sense of the inner integral.

3.13. A sphere of radius R is made of a material with a uniform spontaneous polarization \mathbf{P}_0 . Calculate the electric field everywhere in space – both inside and outside the sphere, and compare the result for the internal field with Eq. (24).

3.14. Calculate the electric field at the center of a cube made of a material with the uniform spontaneous polarization \mathbf{P}_0 of arbitrary orientation.

3.15. Derive the Clausius-Mossotti formula (52), using Eq. (24) for an approximate evaluation of the field created by an elementary atomic/molecular dipole.

3.16. Stand-alone charge Q is distributed, in some way, in the volume of a body made of a uniform linear dielectric with a dielectric constant κ . Calculate the total polarization charge Q_{ef} residing on the surface of the body, provided that it is surrounded by free space.

3.17. In two separate experiments, a thin plane sheet of a linear dielectric with $\kappa = \text{const}$ is placed into a uniform external electric field \mathbf{E}_0 :

(i) with the sheet's surfaces parallel to the electric field, and

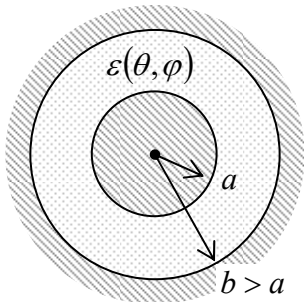
(ii) with the surfaces normal to the field.

For each case, find the electric field \mathbf{E} , the electric displacement \mathbf{D} , and the polarization \mathbf{P} inside the dielectric (sufficiently far from the sheet's edges).

3.18. A fixed dipole \mathbf{p} is placed in the center of a spherical cavity of radius R , carved inside a uniform, linear dielectric. Calculate the electric field distribution everywhere in the system (both at $r < R$ and at $r > R$).

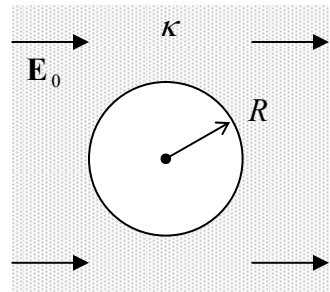
Hint: You may start with the assumption that the field at $r > R$ has a distribution typical for a dipole (but be ready for surprises :-).

3.19. A spherical capacitor (see the figure on the right) is filled with a linear dielectric whose permittivity ϵ depends on the spherical angles θ and φ , but not on the distance r from the system's center. Derive an explicit expression for its capacitance C .



3.20. A spherical capacitor similar to that considered in the previous problem is now filled with a linear dielectric whose permittivity depends only on the distance from the center. Obtain a closed expression for its capacitance, and spell it out for the particular case $\epsilon(r) = \epsilon(a)(r/a)^n$.

3.21. A uniform electric field \mathbf{E}_0 has been created (by distant external sources) inside a uniform linear dielectric. Find the change of the electric field, created by carving out a cavity in the shape of a round cylinder of radius R , with its axis normal to the external field – see the figure on the right.



3.22. Similar small spherical particles, made of a linear dielectric, are dispersed in free space with a low concentration $n \ll 1/R^3$, where R is the particle's radius. Calculate the average dielectric constant of such a medium. Compare the result with the apparent but wrong answer

$$\bar{\kappa} - 1 = (\kappa - 1)nV, \quad (\text{WRONG!})$$

(where κ is the dielectric constant of the particle's material and $V = (4\pi/3)R^3$ is its volume), and explain the origin of the difference.

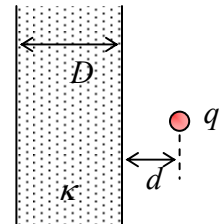
3.23. A straight thin filament, uniformly charged with linear density λ , is stretched parallel to the plane separating two uniform linear dielectrics, at a distance d from it. Calculate the electric potential's distribution everywhere in the system.

3.24. A point charge q is located at a distance $d > R$ from the center of a sphere of radius R , made of a uniform linear dielectric with permittivity ϵ .

(i) Calculate the electrostatic potential's distribution in all space for arbitrary ratio d/R .

(ii) For large d/R , use two different approaches to calculate the interaction force and the energy of interaction between the sphere and the charge, in the first nonzero approximation in $R/d \ll 1$.

3.25. Calculate the spatial distribution of the electrostatic potential induced by a point charge q placed at distance d from a very wide parallel plate, of thickness D , made of a uniform linear dielectric – see the figure on the right.

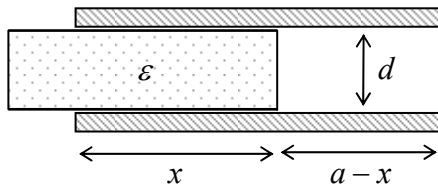


3.26. Discuss the physical nature of Eq. (76). Apply your conclusions to a material with a fixed (field-independent) polarization \mathbf{P}_0 , and calculate the electric field's energy of a uniformly polarized sphere (see Problem 13).

3.27. Use Eqs. (73) and (82) to calculate the force of attraction of plane capacitor's plates (per unit area), for two cases:

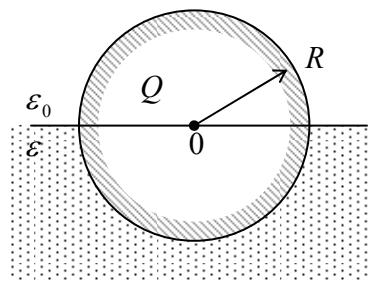
- (i) the capacitor is charged to voltage V , and then disconnected from the battery,²⁹ and
- (ii) the capacitor remains connected to the battery.

3.28. A slab made of a linear dielectric is partly inserted into a plane capacitor – see the figure on the right. Assuming the simplest (cylindrical) geometry of the system, calculate the force exerted by the field on the slab, for the same two cases as in the previous problem



3.29. For each of the two capacitors shown in Fig. 10, calculate the electric force exerted on the interface between two different dielectrics, in terms of the fields in the system.

3.30. One half of a conducting sphere of radius R , carrying electric charge Q , is submerged into a half-space filled with a linear dielectric with permittivity ϵ – see the figure on the right. Calculate the electric force exerted on the sphere.



²⁹ “Battery” is a common if misleading term for what is usually a single *galvanic element*. (The last term stems from the name of Luigi Galvani, a pioneer of electric current studies. Another term derived from his name is the *galvanic connection*, meaning a direct connection of two conductors, enabling a dc current flow – see the next chapter.) The term “battery” had to be, in all fairness, reserved for the connection of several galvanic elements in series – as was pioneered in 1800 by L. Galvani’s friend Alexander Volta.

Chapter 4. DC Currents

The goal of this chapter is to discuss the distribution of stationary (“dc”) currents in conducting samples and their “global” characteristics such as resistance. In the most important case of linear (“Ohmic”) conductivity, the current distribution is governed by the same Laplace and Poisson equations whose solution methods were discussed in detail in the previous chapters. Because of that, we can piggyback on most approaches discussed earlier, enabling me to keep this chapter rather brief.

4.1. Continuity equation and the Kirchhoff laws

Until this point, our discussion of conductors has been limited to the cases when they are separated with *insulators* (meaning either the free space or some dielectric media), preventing any continuous motion of charges from one conductor to another, even if there is a non-zero voltage (and hence electric field) between them – see Fig. 1a.

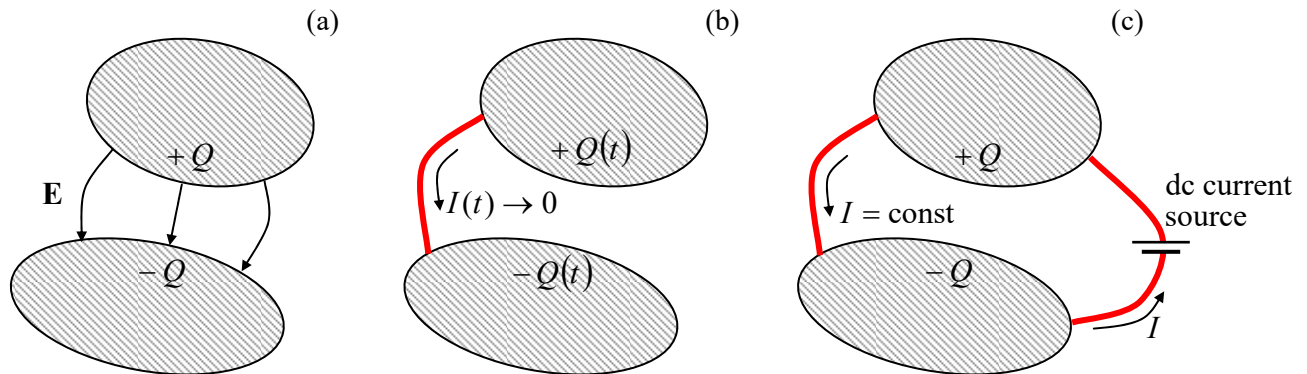


Fig. 4.1. Two oppositely charged conductors: (a) in the electrostatic situation, (b) at the charge relaxation through an additional narrow conductor (“wire”), and (c) in a system sustaining a dc current I .

Now let us connect the two conductors with a *wire* – a thin, elongated conductor (Fig. 1b). Then the electric field causes the motion of charge carriers in the wire, from the conductor with a higher electrostatic potential toward that with lower potential, until the potentials equilibrate. Such a process is called *charge relaxation*. The main equation governing this process may be obtained from the fundamental experimental fact (already mentioned in Sec. 1.1) that electric charges cannot appear or disappear – though opposite charges may recombine with the conservation of the net charge. As a result, the charge Q in a conductor may change only due to the *electric current* I through the wire:

$$\frac{dQ}{dt} = -I(t); \quad (4.1)$$

this relation may be understood as the definition of the current.¹

¹ Just as a (hopefully, unnecessary :-) reminder, in the SI units the current is measured in amperes (A). In legal metrology, the ampere (rather than the coulomb, which is defined as $1C = 1A \times 1s$) is a primary unit. (Its formal definition will be discussed in the next chapter.) In the Gaussian units, Eq. (1) remains the same, so that the current’s unit is the statcoulomb per second – the so-called *statampere*.

Let us express Eq. (1) in a differential form, introducing the notion of the *current density* $\mathbf{j}(\mathbf{r})$. This vector may be defined via the following relation for the elementary current dI crossing an elementary area dA (Fig. 2):

$$dI = j dA \cos \theta \equiv (j \cos \theta) dA \equiv j_n dA, \quad (4.2)$$

where θ is the angle between the direction normal to the surface and the charge carrier motion direction, which is taken for the direction of the vector \mathbf{j} .

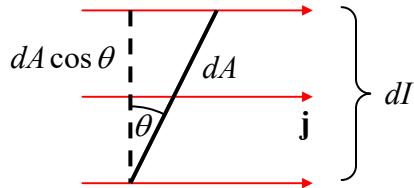


Fig. 4.2. The current density vector \mathbf{j} .

With that definition, Eq. (1) may be rewritten as

$$\frac{d}{dt} \int_V \rho d^3 r = - \oint_S j_n d^2 r, \quad (4.3)$$

where V is an arbitrary but stationary volume limited by the closed surface S . Applying to this volume the same divergence theorem as was repeatedly used in previous chapters, we get

$$\int_V \left[\frac{\partial \rho}{\partial t} + \nabla \cdot \mathbf{j} \right] d^3 r = 0. \quad (4.4)$$

Since the volume V is arbitrary, this equation may be true only if

$$\boxed{\frac{\partial \rho}{\partial t} + \nabla \cdot \mathbf{j} = 0.} \quad (4.5)$$

Continuity
equation

This is the fundamental *continuity equation* – which is true even for time-dependent phenomena.²

The charge relaxation, illustrated by Fig. 1b, is of course a dynamic, time-dependent process. However, electric currents may also exist in stationary situations, when a certain *current source*, for example a battery, drives the current against the electric field, and thus replenishes the conductor charges and sustains currents at a certain time-independent level – see Fig. 1c. (This process requires a persistent replenishment of the electrostatic energy of the system from either a source or a large storage of energy of a different kind – say, the chemical energy of the battery.) Let us discuss the laws governing the distribution of such *dc currents*. In this case ($\partial/\partial t = 0$), Eq. (5) reduces to a very simple equation

$$\nabla \cdot \mathbf{j} = 0. \quad (4.6)$$

This relation acquires an even simpler form in the particular but important case of *dc electric circuits* (Fig. 3) – the systems that may be fairly represented as direct (“galvanic”) connections of components of two types:

² Similar differential relations are valid for the density of any conserved quantity, for example for mass in classical dynamics (see, e.g., CM Sec. 8.3), and for the probability, as it is defined in statistical physics (SM Sec. 5.6) and in quantum mechanics (QM Sec. 1.4).

(i) relatively-small-size (*lumped*) *circuit elements*, meaning either a passive resistor, or a current source, etc. – generally, any “black box” with two or more *terminals*, and

(ii) *perfectly conducting wires*, with a negligible drop of the electrostatic potential along them, that are galvanically connected at certain points called *nodes* (or “junctions”).

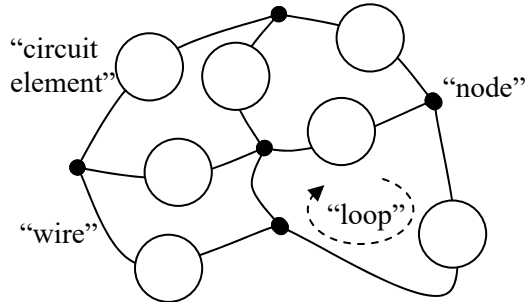


Fig. 4.3. A typical system obeying Kirchhoff laws.

In the standard circuit theory, the electric charges of the nodes are considered negligible,³ and we may integrate Eq. (6) over the closed surface drawn around any node to get a simple equality

$$\sum_j I_j = 0, \quad (4.7a)$$

where the summation is over all the wires (numbered with index j) connected in the node. On the other hand, according to its definition (2.25), the voltage V_k across each circuit element may be represented as the difference of the electrostatic potentials of the adjacent nodes, $V_k = \phi_k - \phi_{k-1}$. Summing such differences around any closed loop of the circuit (Fig. 3), we get all terms canceled, so that

$$\sum_k V_k = 0. \quad (4.7b)$$

These relations are called, respectively, the *1st* and *2nd* *Kirchhoff laws*⁴ – or sometimes the *node rule* (7a) and the *loop rule* (7b). They may seem elementary, and their genuine power is in the mathematical fact that any set of Eqs. (7) covering every node and every circuit element of the system at least once, gives a system of equations sufficient for the calculation of all currents and voltages in it – provided that the relation between the current and voltage is known for each circuit element.

It is almost evident that in the absence of current sources, the system of equations (7) has only the trivial solution: $I_j = 0$, $V_k = 0$ – with the exotic exception of superconductivity, to be discussed in Sec. 6.3. The current sources that allow non-zero current flows may be described by their *electromotive forces* (*e.m.f.*) \mathcal{V}_k , having the dimensionality of voltage, which have to be taken into account in the corresponding terms V_k of the sum (7b). Let me hope that the reader has some experience of using Eqs. (7) for analyses of simple circuits – say, consisting of several resistors and batteries, so that I can save our time by skipping their discussion. Still, due to their practical importance, I would recommend the reader to carry out a self-test by solving a couple of problems offered at the beginning of Sec. 6.

³ In many cases, the charge accumulation/relaxation may be described without an explicit violation of Eq. (7a), just by adding other circuit elements, *lumped capacitors* (see Fig. 2.5 and its discussion), to the circuit under analysis. The resulting circuit may be used to describe not only the transient processes but also periodic ac currents. However, it is convenient for me to postpone the discussion of such *ac circuits* until Chapter 6, where one more circuit element type, *lumped inductances*, will be introduced.

⁴ Named after Gustav Kirchhoff (1824-1887) – who also suggested the differential form (8) of the Ohm law.

4.2. The Ohm law

As was mentioned above, the relations spelled out in Sec. 1 are sufficient for forming a closed system of equations for finding electric current and field in a system only if they are complemented with some constitutive relations between the scalars I and V in each lumped circuit element, or alternatively between the macroscopic (atomic-scale-averaged) vectors \mathbf{j} and \mathbf{E} at each point of the material of such an element. The simplest of such relations is the famous *Ohm law* whose differential (or “local”) form is

$$\mathbf{j} = \sigma \mathbf{E}, \quad (4.8)$$

Ohm
law

where σ is a constant called the *Ohmic conductivity* (or just the “conductivity” for short).⁵ Though the Ohm law (discovered, in its simpler form, by Georg Simon Ohm in 1827) is one of constitutive rather than fundamental relations, and is approximate for *any* conducting medium, we can argue that if:

- (i) the medium carries no current at $\mathbf{E} = 0$ (mind superconductors!),
 - (ii) the medium is isotropic or virtually isotropic (a notable exception: some organic conductors),
 - (iii) the *mean free path* l of the current carriers (the notion to be discussed in detail in SM Ch. 6) in this medium is much smaller than the characteristic scale a of the spatial variations of \mathbf{j} and \mathbf{E} ,
- then the law may be viewed as the leading, linear term of the Taylor expansion of the local relation $\mathbf{j}(\mathbf{E})$, and thus is general for relatively low fields.

Table 1 gives approximate experimental values of σ for some representative (and/or practically important) materials. Note that the range of these values is very broad, even without going to such extremes as very pure metallic crystals at very low temperatures, where σ may reach $\sim 10^{12}$ S/m.

Table 4.1. Ohmic dc conductivities for some materials at 20°C.

Material	σ (S/m)
Teflon (PTFE, $[C_2F_4]_n$)	10^{-22} - 10^{-24}
Silicon dioxide	10^{-16} - 10^{-19}
Various glasses	10^{-10} - 10^{-14}
Deionized water	$\sim 10^{-6}$
Seawater	5
Silicon n -doped to 10^{16}cm^{-3}	2.5×10^2
Silicon n -doped to 10^{19}cm^{-3}	1.6×10^4
Silicon p -doped to 10^{19}cm^{-3}	1.1×10^4
Nichrome (alloy 80% Ni + 20% Cr)	0.9×10^6
Aluminum	3.8×10^7
Copper	6.0×10^7
Zinc crystal along a -axis	1.65×10^7
Zinc crystal along c -axis	1.72×10^7

⁵ In SI units, the conductivity is measured in S/m, where one siemens (S) is the reciprocal of the ohm: $1\text{S} \equiv (1\Omega)^{-1} \equiv 1\text{A}/1\text{V}$. The constant reciprocal to conductivity, $1/\sigma$, is called *resistivity* and is commonly denoted by the letter ρ . I will, however, try to avoid using this notion, because in these notes this letter is already overused.

In order to get a better feeling of what do these values mean, let us consider a very simple system (Fig. 4): a plane capacitor of area $A \gg d^2$, filled with a material that has not only a dielectric constant κ , but also some Ohmic conductivity σ , with much more conductive electrodes.

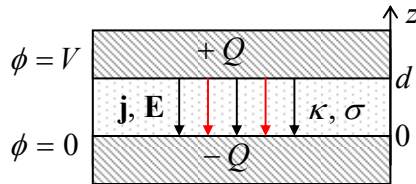


Fig. 4.4. A “leaky” plane capacitor.

Assuming that these properties are compatible with each other,⁶ we may assume that the distribution of the electric potential (not too close to the capacitor’s edges) still obeys Eq. (2.39), so that the electric field is normal to the electrode surfaces and uniform, with $E = V/d$. Then, according to Eq. (6), the current density is also uniform, $j = \sigma E = \sigma V/d$. From here, the total current between the plates is

$$I = jA = \sigma EA = \sigma \frac{V}{d} A. \quad (4.9)$$

On the other hand, from Eqs. (2.26) and (3.45), the instantaneous value of the total charge of the top electrode is $Q = CV = (\kappa\epsilon_0 A/d)V$. Plugging these relations into Eq. (1), we see that the speed of charge (and voltage) relaxation is independent of the geometric parameters A and d of the capacitor:

$$\frac{dV}{dt} = -\frac{V}{\tau_r}, \quad \text{with } \tau_r \equiv \frac{\epsilon_0 \kappa}{\sigma} \equiv \frac{\epsilon}{\sigma}, \quad (4.10)$$

so that the *relaxation time constant* τ_r may be used to characterize the gap-filling material as such.

As we already know (see Table 3.1), for most practical materials the dielectric constant κ is within one order of magnitude from 10, so that the numerator in the second of Eqs. (10) is of the order of 10^{-10} (SI units). As a result, according to Table 1, the charge relaxation time ranges from $\sim 10^{14}$ s (more than a million years!) for the best insulators like Teflon (polytetrafluoroethylene, PTFE),⁷ to $\sim 10^{-18}$ s for the least resistive metals. What is the physics behind such a huge range of σ , and why, for some materials, Table 1 gives them with such a large uncertainty? As in Chapters 2 and 3, in this course I have time only for a brief, admittedly superficial discussion of these issues.⁸

If the charge carriers move almost as classical particles (e.g., in plasmas or non-degenerate semiconductors), a very reasonable description of the conductivity is given by the famous *Drude formula*.⁹ In his picture, due to a weak electric field, the charge carriers are accelerated in its direction (on top of their random motion in all directions, with the average velocity vector equal zero):

$$\frac{d\mathbf{v}}{dt} = \frac{q}{m} \mathbf{E}, \quad (4.11)$$

and as a result, their velocity acquires the average value

⁶ As will be discussed in Chapter 6, this is true only if σ is not too high.

⁷ This polymer is broadly used in engineering and physical experiment, due to its many remarkable properties.

⁸ A more detailed discussion of this issue may be found in SM Chapter 6.

⁹ It was suggested by Paul Drude in 1900.

$$\mathbf{v} = \frac{d\mathbf{v}}{dt} \tau = \frac{q}{m} \mathbf{E} \tau, \quad (4.12)$$

where the phenomenological parameter $\tau = l/2v$ (not to be confused with τ_r !) may be understood as half the average time between carrier scattering events. From here, the current density:¹⁰

$$\mathbf{j} = qn\mathbf{v} = \frac{q^2 n \tau}{m} \mathbf{E}, \quad \text{i.e. } \sigma = \frac{q^2 n \tau}{m}. \quad (4.13a)$$

(Notice the independence of σ of the charge sign.) Another form of the same result, more popular in the physics of semiconductors, is

$$\sigma = q^2 n \mu, \quad \text{with } \mu = \frac{\tau}{m}, \quad (4.13b)$$

where the parameter μ , defined by the relation $\mathbf{v} \equiv \mu \mathbf{E}$, is called the *charge carrier mobility*.

Most good conductors (e.g., metals) are essentially degenerate Fermi gases (or liquids), in which the average thermal energy of a particle, $k_B T$ is much lower than the Fermi energy ϵ_F . In this case, a quantum theory is needed for the calculation of σ . Such theory was developed by the quantum physics' godfather A. Sommerfeld in 1927 (and is sometimes called the *Drude-Sommerfeld model*). I have no time to discuss it in this course,¹¹ and here will only notice that for a nearly-ideal, isotropic Fermi gas the result is reduced to Eq. (13), with a certain effective value of τ , so it may be used for estimates of σ , with due respect to the quantum theory of scattering. In a typical metal, n is very high ($\sim 10^{23} \text{ cm}^{-3}$) and is fixed by the atomic structure, so the sample quality may only affect σ via the scattering time τ .

At room temperature, the scattering of electrons by thermally-excited lattice vibrations (*phonons*) dominates, so that τ and σ are high but finite, and do not change much from one sample to another. (Hence the relatively accurate values given for metals in Table 1.) On the other hand, at $T \rightarrow 0$, quantum mechanics says a perfect crystal should not exhibit scattering at all, and its conductivity should be infinite. In practice, this is never true (for one, due to electron scattering from imperfect boundaries of finite-size samples), and the effective conductivity σ is infinite (or practically infinite, at least above the largest measurable values $\sim 10^{20} \text{ S/m}$) only in superconductors.¹²

On the other hand, the conductivity of quasi-insulators (including deionized water) and semiconductors depends mostly on the carrier density n , which is much lower than in metals. From the point of view of quantum mechanics, this happens because the ground-state wavefunctions of charge carriers are localized within an atom (or molecule), and their energies are separated from those of excited states, with space-extended wavefunctions, by a large energy gap – often called the *bandgap*. For example, in SiO₂ the bandgap approaches 9 eV, equivalent to $\sim 4,000$ K. This is why even at room temperatures the density of thermally-excited free charge carriers in good insulators is negligible. In these materials, n is determined by impurities and vacancies, and may depend on a particular chemical synthesis or other fabrication technology, rather than on the fundamental properties of the material. (On the contrary, the carrier mobility μ in these materials is almost technology-independent.)

¹⁰ Note that \mathbf{j} in Eq. (8) is defined as an already macroscopic variable, averaged over inter-particle distances, so that no additional average sign is necessary in the first of Eqs. (13a).

¹¹ For such a discussion see, e.g., SM Sec. 6.3.

¹² The electrodynamic properties of superconductors are so interesting (and fundamentally important) that I will discuss them in more detail in Chapter 6.

Drude formula:
two versions

The practical importance of the fabrication technology may be illustrated by the following example. In the cells of the so-called *floating-gate memories*, in particular the *flash memories*, which currently dominate the nonvolatile digital memory technology, data bits are stored as small electric charges ($Q \sim 10^{-16}$ C $\sim 10^3$ e) of highly doped silicon islands (so-called *floating gates*) separated from the rest of the integrated circuit with ~ 10 -nm-thick layers of silicon dioxide, SiO₂. Such layers are fabricated by high-temperature oxidation of virtually perfect silicon crystals. The conductivity of the resulting high-quality (though amorphous) material is so low, $\sigma \sim 10^{-19}$ S/m, that the relaxation time τ_r , defined by Eq. (10), is well above 10 years – the industrial standard for data retention in nonvolatile memories. To appreciate how good this technology is, the cited value should be compared with the typical conductivity $\sigma \sim 10^{-16}$ S/m of the usual, bulk SiO₂ ceramics.¹³

To conclude this chapter, let me note that the Ohm law, for all its importance, is not a universal law of nature. As a reminder of this fact, in Sec. 5 below I describe two very simple systems (leaving their analysis for the reader's exercise) whose *I-V* relation is nonlinear even for very small currents.

4.3. Boundary problems

For an Ohmic conducting medium, we may combine Eqs. (6) and (8) to get the following differential equation

$$\nabla \cdot (\sigma \nabla \phi) = 0. \quad (4.14)$$

For a uniform conductor ($\sigma = \text{const}$), Eq. (14) is reduced to the Laplace equation for the (macroscopic) electrostatic potential ϕ . As we already know from Chapters 2 and 3, its solution depends on the boundary conditions. These conditions, in turn, depend on the interface type.

(i) Conductor-conductor interface. Applying the continuity equation (6) to a Gauss-type pillbox at the interface of two different conductors (Fig. 5), we get

$$(j_n)_1 = (j_n)_2, \quad (4.15)$$

so that if the Ohm law (8) is valid inside each medium, then

$$\sigma_1 \frac{\partial \phi_1}{\partial n} = \sigma_2 \frac{\partial \phi_2}{\partial n}. \quad (4.16)$$

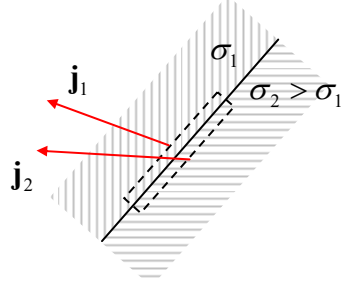


Fig. 4.5. DC current's “refraction” at the interface between two different conductors.

¹³ This course is not an appropriate platform to discuss details of the floating-gate memory technology. However, I think that every educated physicist should know its basics, because such memories are presently the driver of all semiconductor integrated circuit technology development, and hence of the whole information technology progress. Perhaps the best available general book on this topic is still the relatively old review collection by J. Brewer and M. Gill (eds.), *Nonvolatile Memory Technologies with Emphasis on Flash*, IEEE Press, 2008.

Also, since the electric field should be finite, its potential ϕ has to be continuous across the interface – the condition that may also be written as

$$\frac{\partial\phi_1}{\partial\tau} = \frac{\partial\phi_2}{\partial\tau}. \quad (4.17)$$

Both these conditions (and hence the solutions of the boundary problems using them) are similar to those for the interface between two dielectrics – cf. Eqs. (3.46)-(3.47). Note that using the Ohm law, Eq. (17) may be rewritten as

$$\frac{1}{\sigma_1}(j_\tau)_1 = \frac{1}{\sigma_2}(j_\tau)_2. \quad (4.18)$$

Comparing it with Eq. (15) we see that, generally, the current density's magnitude changes at the interface: $j_1 \neq j_2$. It is also curious that if $\sigma_1 \neq \sigma_2$, the current line slope changes at the interface (Fig. 5), qualitatively similar to the refraction of light rays in optics – see Chapter 7.

(ii) Conductor-electrode interface. An *electrode* is defined as a body made of a “perfect conductor”, i.e. of a medium with $\sigma \rightarrow \infty$. Then, at a fixed current density at the interface, the electric field in the electrode tends to zero, and hence it may be described by the equality

$$\phi = \phi_j = \text{const}, \quad (4.19)$$

where constants ϕ_j may be different for different electrodes (numbered with index j). Note that with such boundary conditions, the Laplace boundary problem becomes exactly the same as in electrostatics – see Eq. (2.35) – and hence we can use the methods (and some solutions :-) discussed in Chapter 2 for finding the dc current distribution.

(iii) Conductor-insulator interface. For the description of a good insulator, we can use the equality $\sigma = 0$, so that Eq. (16) yields the following boundary condition,

$$\frac{\partial\phi}{\partial n} = 0, \quad (4.20)$$

for the potential derivative *inside the conductor*. From the Ohm law (8) in the form $\mathbf{j} = -\sigma\nabla\phi$, we see that this is just the very natural requirement for the dc current not to flow into an insulator. Now note that this condition makes the Laplace problem inside the conductor completely well-defined, and independent of the potential distribution in the adjacent insulator. On the contrary, due to the continuity of the electrostatic potential at the border, its distribution inside the surrounding insulator has to follow that inside the conductor.

Let us discuss this conceptual issue on the following (apparently, trivial) example: dc current in a uniform wire of length l and a cross-section of area A . The reader certainly knows the answer:

$I = \frac{V}{R}, \quad \text{where } R \equiv \frac{V}{I} = \frac{l}{\sigma A},$

(4.21)

Uniform
wire's
resistance

where the constant R is called the wire's *resistance*.¹⁴

¹⁴ The first of Eqs. (21) is essentially the (historically, initial) integral form of the Ohm law, and is valid not only for a uniform wire but also for Ohmic conductors of any geometry in that I and V may be clearly defined.

However, let us derive this result formally from our theoretical framework. For the simple geometry shown in Fig. 6a, this is easy to do. Here the potential evidently has a linear 1D distribution

$$\phi = \text{const} - \frac{x}{l} V, \quad (4.22)$$

both in the conductor and the surrounding free space, with both boundary conditions (16) and (17) satisfied at the conductor-insulator interfaces, and the condition (20) satisfied at the conductor-electrode interfaces. As a result, the electric field is constant and has only one Cartesian component: $E_x = V/l$, so that inside the conductor

$$j_x = \sigma E_x, \quad I = j_x A, \quad (4.23)$$

giving us the well-known Eq. (21).

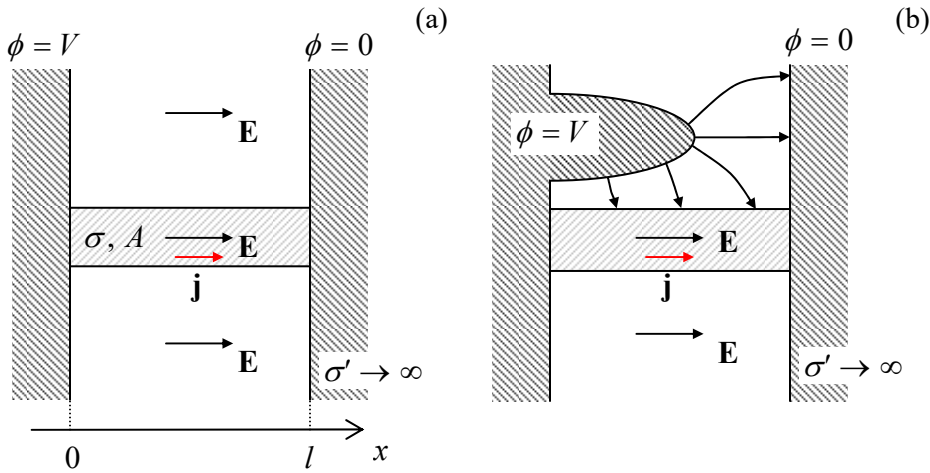


Fig. 4.6. (a) An elementary problem and (b) a (slightly) less obvious problem of the field distribution at dc current flow (schematically).

However, what about the geometry shown in Fig. 6b? In this case, the field distribution in the free space around the conductor is dramatically different, but according to the boundary problem defined by Eqs. (14) and (20), inside the conductor, the solution is exactly the same as it was in the former case. Now, the Laplace equation in the surrounding insulator has to be solved with the boundary values of the electrostatic potential, “dictated” by the distribution of the current (and hence potential) in the conductor. Note that as the result, the electric field lines are generally *not* normal to the conductor’s surface, because the surface is not equipotential – see Eq. (22) again.

Let us solve a problem in that this *conduction hierarchy* may be followed analytically to the very end. Consider an empty spherical cavity carved in a conductor with an initially uniform current flow with a constant density $\mathbf{j}_0 = \mathbf{n}_0 j_0$ (Fig. 7a). Following the hierarchy, we have to solve the boundary problem in the conducting part of the system, i.e. outside the sphere (at $r \geq R$), first. Since the problem is evidently axially symmetric, we already know the general solution of the Laplace equation – see Eq. (2.172). Moreover, we know that in order to match the uniform field distribution at $r \rightarrow \infty$, all coefficients a_l but one ($a_1 = -E_0 = -j_0/\sigma$) have to be zero, and that the boundary conditions at $r = R$ will give zero solutions for all coefficients b_l but one (b_1), so that

$$\phi = -\frac{j_0}{\sigma} r \cos \theta + \frac{b_1}{r^2} \cos \theta, \quad \text{for } r \geq R. \quad (4.24)$$

In order to find the remaining coefficient b_1 , we have to use the boundary condition (20) at $r = R$:

$$\frac{\partial \phi}{\partial r} \Big|_{r=R} = \left(-\frac{j_0}{\sigma} - \frac{2b_1}{R^3} \right) \cos \theta = 0. \quad (4.25)$$

This gives $b_1 = -j_0 R^3 / 2\sigma$, so that, finally,

$$\phi(r, \theta) = -\frac{j_0}{\sigma} \left(r + \frac{R^3}{2r^2} \right) \cos \theta, \quad \text{for } r \geq R. \quad (4.26)$$

(Note that this potential distribution corresponds to the dipole moment $\mathbf{p} = -\mathbf{E}_0 R^3 / 2$. It is straightforward to check that if the spherical cavity was cut in a dielectric, the potential distribution outside it would be similar, with $\mathbf{p} = -\mathbf{E}_0 R^3 (\kappa - 1) / (\kappa + 2)$. In the limit $\kappa \rightarrow \infty$, these two results coincide, despite the rather different type of the problem: in the dielectric case, there is no current at all.)

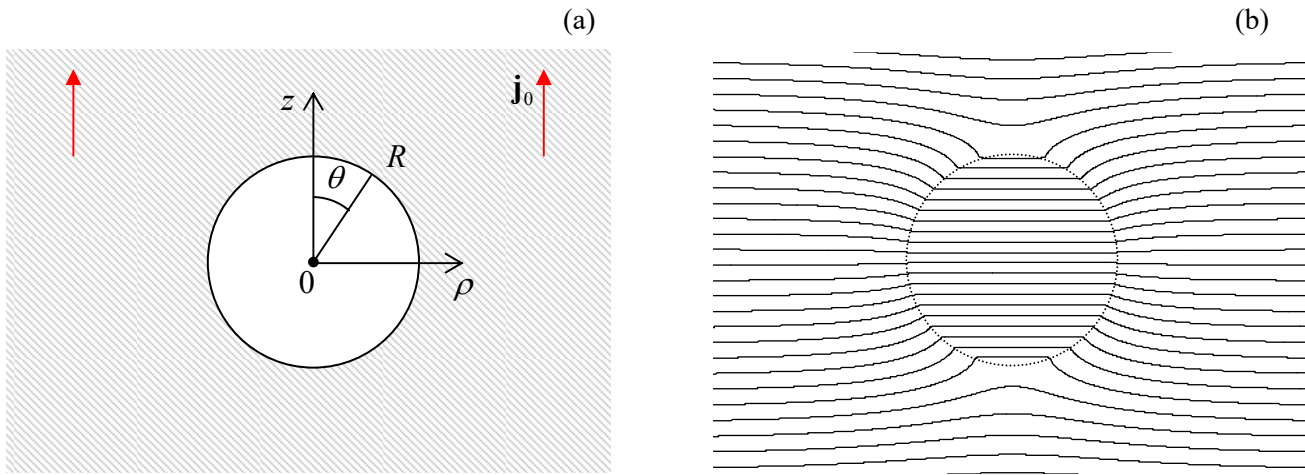


Fig. 4.7. A spherical cavity carved in a uniform conductor: (a) the problem's geometry, and (b) the equipotential surfaces as given by Eqs. (26) and (28).

Now, as the second step in the conductivity hierarchy, we may find the electrostatic potential distribution $\phi(r, \theta)$ in the insulator, in this particular case inside the empty cavity (at $r \leq R$). It should also satisfy the Laplace equation with the boundary values at $r = R$, “dictated” by the distribution (26):

$$\phi(R, \theta) = -\frac{3}{2} \frac{j_0}{\sigma} R \cos \theta. \quad (4.27)$$

We could again solve this problem by the formal variable separation (keeping in the general solution (2.172) only the term proportional to a_l , which does not diverge at $r \rightarrow 0$), but if we notice that the boundary condition (27) depends on just one Cartesian coordinate, $z = R \cos \theta$, the solution may be just guessed:

$$\phi(r, \theta) = -\frac{3}{2} \frac{j_0}{\sigma} z = -\frac{3}{2} \frac{j_0}{\sigma} r \cos \theta, \quad \text{at } r \leq R. \quad (4.28)$$

Indeed, it evidently satisfies the Laplace equation and the boundary condition (27), and corresponds to a constant electric field parallel to the vector \mathbf{j}_0 , and equal to $3j_0/2\sigma$ – see Fig. 7b. Again, the cavity surface is *not* equipotential, and the electric field lines at $r \leq R$ are *not* normal to it at almost all points.

More generally, the conductivity hierarchy says that static electrical fields and charges outside conductors (e.g., electric wires) do not affect currents flowing in the wires, and it is physically very clear

why. For example, if a charge in the free space is slowly moved close to a wire, it (in accordance with the linear superposition principle) only induces an additional surface charge (see Sec. 2.1) that screens the external charge's field, without participating in the current flow inside the conductor.

Besides this conceptual issue, the two examples given above may be considered as applications of the first two methods discussed in Chapter 2 – the orthogonal coordinates (Fig. 6) and the variable separation (Fig. 7) – to dc current distribution problems. As the reader may recall, in that chapter we also discussed the method of charge images. It turns out that its analog may be also used for the solution of some dc conductivity problems. Indeed, let us consider a spherically-symmetric potential distribution of the electrostatic potential, similar to that given by the basic Eq. (1.35):

$$\phi = \frac{c}{r}. \quad (4.29)$$

As we know from Chapter 1, this is a particular solution of the 3D Laplace equation at all points but $r = 0$. In free space, this distribution would correspond to a point charge $q = 4\pi\epsilon_0 c$; but what about a uniform Ohmic conductor? Calculating the corresponding electric field and current density,

$$\mathbf{E} = -\nabla\phi = \frac{c}{r^3}\mathbf{r}, \quad \mathbf{j} = \sigma\mathbf{E} = \sigma\frac{c}{r^3}\mathbf{r}, \quad (4.30)$$

we see that the total current flowing from the origin through a sphere of an arbitrary radius r does not depend on the radius:

$$I = Aj = 4\pi r^2 j = 4\pi\sigma c. \quad (4.31)$$

Plugging the resulting coefficient c into Eq. (29), we get

$$\phi = \frac{I}{4\pi\sigma r}. \quad (4.32)$$

Hence the Coulomb-type distribution of the electric potential in a conductor is possible (at least at some distance from the singular point $r = 0$), and describes the dc current I flowing out of a small-size electrode – or *into* such an electrode if the coefficient c is negative. Such *current injection* may be readily implemented experimentally; think for example about an insulated wire with a small bare end, inserted into a poorly conducting soil – an important method in geophysical research. Such point injection is even simpler in 2D situations – think about a wire attached, within a small spot, to a thin resistive layer, such as the thin films used for wiring in microelectronics.¹⁵

Now let the current injection point \mathbf{r}' be close to a plane interface between the conductor and an insulator (Fig. 8). In this case, besides the Laplace equation, we should satisfy the boundary condition,

$$j_n = \sigma E_n = -\sigma \frac{\partial \phi}{\partial n} = 0, \quad (4.33)$$

at the interface. It is clear that this can be done by replacing the insulator with an imaginary similar conductor with an additional current injection point, at the mirror image point \mathbf{r}'' . Note, however, that in contrast to charge images, the sign of the imaginary current has to be *similar*, not opposite, to the initial one, so that the total electrostatic potential inside the conducting semi-space is

¹⁵ Note that in such layers, the current distribution near the injection point is different, $j \propto 1/r$ rather than $1/r^2$.

$$\phi(\mathbf{r}) = \frac{I}{4\pi\sigma} \left(\frac{1}{|\mathbf{r} - \mathbf{r}'|} + \frac{1}{|\mathbf{r} - \mathbf{r}''|} \right). \quad (4.34)$$

(The image current's sign would be opposite at the interface between a conductor with a moderate conductivity and a perfect conductor ("electrode"), whose potential should be virtually constant.)

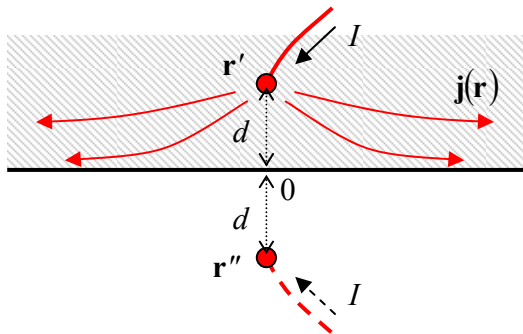


Fig. 4.8. Applying the method of images for the current injection analysis.

This result may be readily used, for example, to calculate the current density at a plane surface of a uniform conductor, as a function of distance ρ from point 0 – the surface's point closest to the current injection site – see Fig. 8. At such surface, Eq. (34) yields

$$\phi = \frac{I}{2\pi\sigma} \frac{1}{(\rho^2 + d^2)^{1/2}}, \quad (4.35)$$

so that the current density is:

$$j_\rho = \sigma E_\rho = -\sigma \frac{\partial \phi}{\partial \rho} = \frac{I}{2\pi} \frac{\rho}{(\rho^2 + d^2)^{3/2}}. \quad (4.36)$$

Deviations from Eqs. (35) and (36) may be used to find and characterize conductance inhomogeneities, say, those due to mineral deposits in the Earth's crust.¹⁶

So, the methods used in electrostatics to calculate the potential distribution in linear dielectrics may be also used to find such distributions in Ohmic conductors. Moreover, some of these methods are more valuable in this field. For example, in electrostatics the effective methods of solution of the 2D Laplace equation, discussed in Secs. 2.3-2.6, could be only applied to cylindrical geometries. At Ohmic conduction, this equation is also valid in some 3D cases. A practically important example is the current flow in thin resistive layers where, due to the conductivity hierarchy principle, the 3D-distributed field outside a layer, induced by the 2D-distributed current in it, does not affect the flow and in many cases is not important. A few problems of this kind, formulated in Sec. 5, are left for the reader's exercise.

4.4. Energy dissipation

Let me conclude this brief chapter with an ultra-short discussion of energy dissipation in conductors. In contrast to the electrostatic situations in insulators (vacuum or dielectrics), at dc

¹⁶ The current injection may be also produced, due to electrochemical reactions, by an ore mass itself, so that one need only measure (and correctly interpret :-) the resulting potential distribution – the so-called *self-potential method* – see, e.g., Sec. 6.1 in W. Telford *et al.*, *Applied Geophysics*, 2nd ed., Cambridge U. Press, 1990.

conduction, the electrostatic energy U is “dissipated” (i.e. transferred to heat) at a certain rate $\mathcal{P} \equiv -dU/dt$, with the dimensionality of power.¹⁷ This so-called *energy dissipation* may be evaluated by calculating the power of the electric field’s work on a single moving charge:

$$\mathcal{P}_i = \mathbf{F} \cdot \mathbf{v} = q\mathbf{E} \cdot \mathbf{v}. \quad (4.37)$$

After the summation over all charges, Eq. (37) gives us the average dissipation power. If the charge density n is uniform, multiplying by it both parts of this relation, and taking into account that $q\mathbf{v} = \mathbf{j}$, for the energy dissipation in a unit volume we get the differential form of the *Joule law*¹⁸

General Joule law

$$\mu \equiv \frac{\mathcal{P}}{V} = \frac{\mathcal{P}_i N}{V} = \mathcal{P}_i n = q\mathbf{E} \cdot \mathbf{v}n = \mathbf{E} \cdot \mathbf{j}. \quad (4.38)$$

In the case of the Ohmic conductivity (8), this expression may be also rewritten in two other forms:

Joule law for Ohmic conductivity

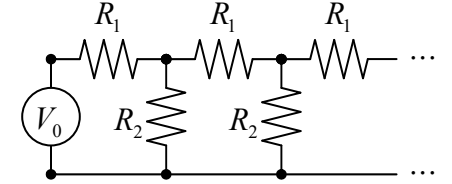
$$\mu = \sigma E^2 = \frac{j^2}{\sigma}. \quad (4.39)$$

With our electrostatics background, it is also straightforward (and hence left for the reader’s exercise) to prove that the dc current distribution in a uniform Ohmic conductor, at a fixed voltage distribution along its borders, corresponds to the minimum of the total dissipation in the sample,

$$\mathcal{P} \equiv \int_V \mu d^3r = \sigma \int_V E^2 d^3r. \quad (4.40)$$

4.5. Exercise problems

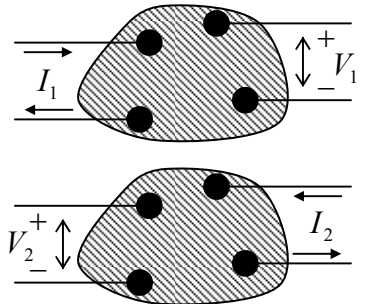
4.1. DC voltage V_0 is applied to the end of a semi-infinite chain of lumped Ohmic resistors, shown in the figure on the right. Calculate the voltage across the j^{th} link of the chain.



4.2. It is well known that properties of many dc current sources (e.g., batteries) may be reasonably well represented as a connection in series of a *perfect voltage source* and an Ohmic *internal resistance*. Discuss the option, and possible advantages, of using a different equivalent circuit that would include a *perfect current source*.

4.3. Prove the following *Rayleigh-Lorentz-Carson reciprocity relation*: Results of two reciprocal experiments shown schematically in the figure on the right, with an arbitrary Ohmic conductor with four electrodes/terminals, are related as $I_1 V_2 = I_2 V_1$.

Hint: Try to apply the same approach as was used to prove Green’s reciprocity relation in electrostatics in Problem 1.18, but with proper modifications.

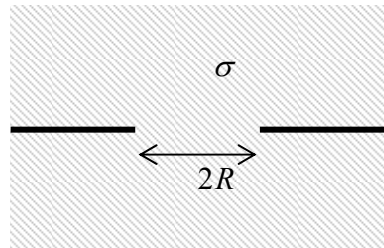


¹⁷ If this electric field and hence the electrostatic energy are time-independent, the energy is replenished at the same rate from the current source(s).

¹⁸ Named after James Prescott Joule, who quantified this effect in 1841.

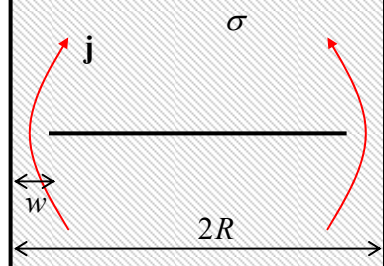
4.4. Calculate the resistance between two large, uniform Ohmic conductors separated by a very thin, plane, insulating partition, with a circular hole of radius R in it – see the figure on the right.

Hint: You may like to use the oblate spheroidal coordinates which were discussed in Sec. 2.4.



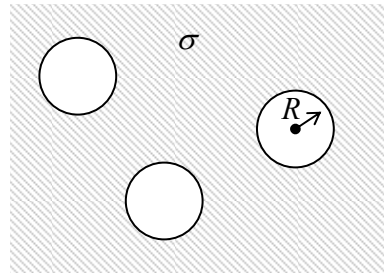
4.5. A very narrow plane crack inside a round conducting wire of radius R does not reach its surface by a small distance w – see the figure on the right. Assuming that the Ohmic conductivity σ of the wire's material is otherwise constant, calculate the electric resistance of the obstacle in the first approximation in small $w/R \ll 1$.

Hint: You may like to use the same elliptic coordinates as were employed at the solution of Problem 2.12.



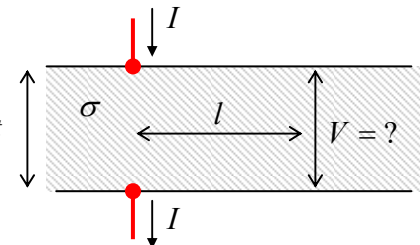
4.6. Calculate the effective (average) conductivity σ_{ef} of a medium with many empty spherical cavities of radius R , carved at random positions in a uniform Ohmic conductor (see the figure on the right), in the limit of a low density $n \ll R^{-3}$ of the spheres.

Hint: You may like to use the analogy with a dipole medium – see, e.g., Sec. 3.2.



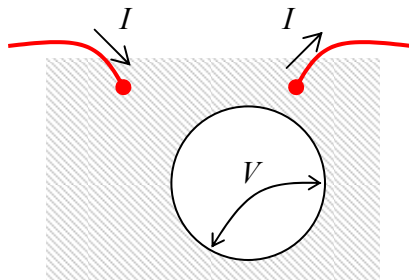
4.7. In two separate experiments, a narrow gap, possibly of irregular width, between two close, perfectly conducting electrodes is filled with some material: in the first case, with a uniform linear dielectric with an electric permittivity ϵ , and in the second case, with a uniform conducting material with an Ohmic conductivity σ . Neglecting the fringe effects, calculate the relation between the mutual capacitance C between the electrodes (in the first case) and the dc resistance R between them (in the second case).

4.8. Calculate the voltage V across a uniform, wide resistive slab of thickness t , at distance l from the points of injection/pickup of the dc current I passed across the slab – see the figure on the right.

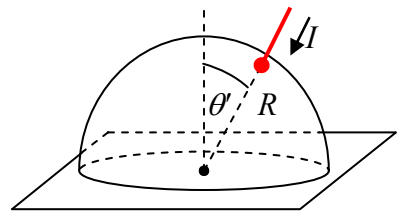


4.9. Calculate the distribution of the dc current's density in a thin, round, uniform resistive disk, if the current is inserted into some point at its rim, and picked up at the center.

4.10. DC current is passed between two point electrodes connected to a wide, thin, uniform resistive sheet – see the figure on the right. Use the model solution of the previous problem to prove, without much new calculation, that cutting a round hole in the sheet (outside of the current injection/extraction points) doubles the voltage between any two points on its border.

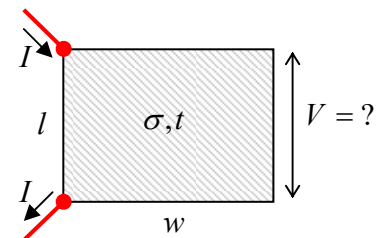


4.11. The rim of a hemispherical thin shell, of radius R and thickness $t \ll R$, made of a uniform Ohmic conductor, is connected to a plane grounded electrode. Calculate the distribution of the electrostatic potential created in the shell by a dc current I injected into it through a small-size electrode located at a polar angle $\theta' < \pi/2$ from the symmetry axis – see the figure on the right.



Hint: You may like to use the variable substitution $\rho \equiv \tan(\theta/2)$ to map the hemisphere onto a unit circle.

4.12. A rectangle of area $l \times w$ is cut from a resistive sheet of thickness $t \ll l, w$. Use two different approaches to calculate the voltage V between its two adjacent corners, induced by the dc current I passed between the two other corners – see the figure on the right.



Hint: Besides the charge/current image method, you may like to consider using the variable separation method, with due respect to the current injection/extraction points.

4.13.* The simplest reasonable model of a vacuum diode consists of two plane, parallel metallic electrodes of area A , separated by a gap of thickness $d \ll A^{1/2}$: a “cathode” that emits electrons into the gap, and an “anode” that absorbs the electrons arriving from the gap at its surface. Calculate the dc $I-V$ curve of the diode, i.e. the stationary relation between the current I flowing between the electrodes and the voltage V applied between them, using the following simplifying assumptions:

- (i) due to the effect of the negative space charge of the emitted electrons, the current I is much lower than the emission ability of the cathode,
- (ii) the initial velocity of the emitted electrons is negligible, and
- (iii) the direct Coulomb interaction of electrons (besides the space charge effect) is negligible.

4.14.* Calculate the space-charge-limited current in a system with the same geometry as in the previous problem, and using the same assumptions besides that now the emitted charge carriers move not ballistically, but drift in accordance with the Ohm law, with the conductivity given by Eq. (13): $\sigma = q^2 \mu n$, with a constant mobility μ .¹⁹

Hint: In order to get a realistic result, assume that the medium in that the charge carriers move has a certain dielectric constant κ unrelated to the carriers.

4.15. Prove that the distribution of dc currents in a uniform Ohmic conductor with a given voltage distribution along its boundaries, corresponds to the minimum of the total energy dissipation rate (“Joule heat”).

¹⁹ As was mentioned in Sec. 2, the approximation of a constant (in particular, field- and charge-density-independent) mobility is most suitable for semiconductors.

This page is
intentionally left
blank

Chapter 5. Magnetism

Even though this chapter addresses a completely new type of electric charge interaction, its discussion (for the stationary case) will take not too much time/space, because it recycles many ideas and methods of electrostatics, though with a twist or two.

5.1. Magnetic interaction of currents

DC currents in conductors usually leave them *electroneutral*, $\rho(\mathbf{r}) = 0$, with very good precision, because even a minute imbalance of positive and negative charge density results in extremely strong Coulomb forces that restore the electroneutrality by a very fast additional shift of free charge carriers. This is why let us start the discussion of magnetism from the simplest case of two spatially-separated, dc-current-carrying, electroneutral conductors (Fig. 1).

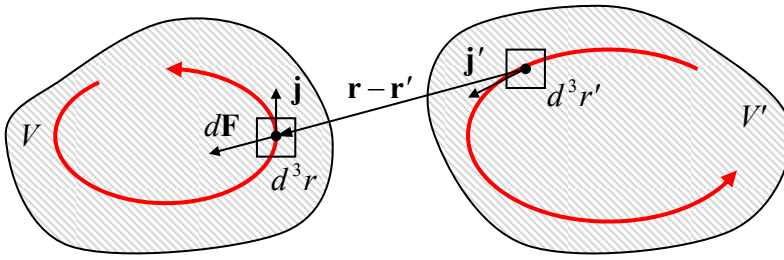


Fig. 5.1. Magnetic interaction of two currents.

According to the Coulomb law, there is no electrostatic force between them. However, several experiments carried out in 1820¹ proved that there is a different, *magnetic* interaction between the currents. In the present-day notation, the results of all such experiments may be summarized with just one formula, in SI units expressed as

Magnetic force

$$\mathbf{F} = -\frac{\mu_0}{4\pi} \int_V d^3 r \int_{V'} d^3 r' [\mathbf{j}(\mathbf{r}) \cdot \mathbf{j}'(\mathbf{r}')] \frac{\mathbf{r} - \mathbf{r}'}{|\mathbf{r} - \mathbf{r}'|^3}. \quad (5.1)$$

Here the coefficient $\mu_0/4\pi$ (where μ_0 is called either the *magnetic constant* or the *free space permeability*) equals to almost exactly 10^{-7} SI units, with the product $\epsilon_0 \mu_0$ equal to exactly $1/c^2$.²

Note a close similarity of this expression to the Coulomb law (1.1) rewritten for the interaction of two continuously distributed charges, with the account of the linear superposition principle (1.4):

Electric force

$$\mathbf{F} = \frac{1}{4\pi\epsilon_0} \int_V d^3 r \int_{V'} d^3 r' \rho(\mathbf{r}) \rho'(\mathbf{r}') \frac{\mathbf{r} - \mathbf{r}'}{|\mathbf{r} - \mathbf{r}'|^3}. \quad (5.2)$$

¹ Most notably, by Hans Christian Ørsted who discovered the effect of electric currents on magnetic needles, and André-Marie Ampère who extended this work by finding the magnetic interaction between two currents.

² For details, see Appendix CA: Selected Physical Constants. In the Gaussian units, the coefficient $\mu_0/4\pi$ in Eq. (1) and beyond is replaced with $1/c^2$.

Besides the different coefficient and a different sign, the “only” difference of Eq. (1) from Eq. (2) is the scalar product of the current densities, evidently necessary because of their vector character. We will see soon that this difference brings certain complications in applying the approaches discussed in the previous chapters, to magnetostatics.

Before going to their discussion, let us have one more glance at the coefficients in Eqs. (1) and (2). To compare them, let us consider two objects with *uncompensated* charge distributions $\rho(\mathbf{r})$ and $\rho'(\mathbf{r})$, each moving parallel to each other as a whole, with certain velocities \mathbf{v} and \mathbf{v}' , as measured in the same inertial (“laboratory”) reference frame. In this case, $\mathbf{j}(\mathbf{r}) = \rho(\mathbf{r})\mathbf{v}$, so that $\mathbf{j}(\mathbf{r}) \cdot \mathbf{j}'(\mathbf{r}) = \rho(\mathbf{r})\rho'(\mathbf{r})vv'$, and the integrals in Eqs. (1) and (2) become functionally similar, differing only by the factor

$$\frac{F_{\text{magnetic}}}{F_{\text{electric}}} = -\frac{\mu_0 vv'}{4\pi} \left/ \frac{1}{4\pi\epsilon_0} \right. \equiv -\frac{vv'}{c^2}. \quad (5.3)$$

(The last expression is valid in any consistent system of units.) We immediately see that the magnetism is an essentially relativistic phenomenon, very weak in comparison with the electrostatic interaction at the human scale velocities, $v \ll c$, and may dominate only if the latter interaction vanishes – as it does in electroneutral systems.³ The discovery and initial studies⁴ of such a subtle, relativistic phenomenon as magnetism were much facilitated by the relative abundance of natural *ferromagnets*: materials with a spontaneous magnetic polarization, whose strong magnetic field is due to relativistic effects (such as spin) inside the constituent atoms – see Sec. 5 below.

Also, Eq. (3) points to an interesting paradox. Consider two electron beams moving parallel to each other, with the same velocity v with respect to a lab reference frame. Then, according to Eq. (3), the net force of their total (electric plus magnetic) interaction is proportional to $(1 - v^2/c^2)$, tending to zero in the limit $v \rightarrow c$. However, in the reference frame moving together with the electrons, they are not moving at all, i.e. $v = 0$. Hence, from the point of view of such a moving observer, the electron beams should interact only electrostatically, with a repulsive force independent of the velocity v . Historically, this had been one of several paradoxes that led to the development of special relativity; its resolution will be discussed in Chapter 9 devoted to this theory.

Returning to Eq. (1), in some simple cases the double integration in it may be carried out analytically. First of all, let us simplify this expression for the case of two thin, long conductors (“wires”) separated by a distance much larger than their thickness. In this case, we may integrate the products $\mathbf{j}d^3r$ and $\mathbf{j}'d^3r'$ over the wires’ cross-sections first, neglecting the corresponding change of the factor $(\mathbf{r} - \mathbf{r}')$. Since the integrals of the current density over the cross-sections of the wires are just the currents I and I' flowing in the wires, and cannot change along their lengths (say, l and l' , respectively), they may be taken out of the remaining integrals, reducing Eq. (1) to

$$\mathbf{F} = -\frac{\mu_0 II'}{4\pi} \oint_l \oint_{l'} (\mathbf{dr} \cdot \mathbf{dr}') \frac{\mathbf{r} - \mathbf{r}'}{|\mathbf{r} - \mathbf{r}'|^3}. \quad (5.4)$$

³ An important case when the electroneutrality may not hold is the motion of electrons in vacuum. (However, in this case, the electron speed is often comparable with the speed of light, so that the magnetic forces may be comparable in strength with electrostatic forces, and hence important.) Local violations of electroneutrality also play an important role in some semiconductor devices – see, e.g., SM Chapter 6.

⁴ The first detailed book on this subject, *De Magnete* by William Gilbert (a.k.a. Gilberd), was published as early as 1600.

As the simplest example, consider two straight, parallel wires (Fig. 2) separated by distance d , both with length $l \gg d$.

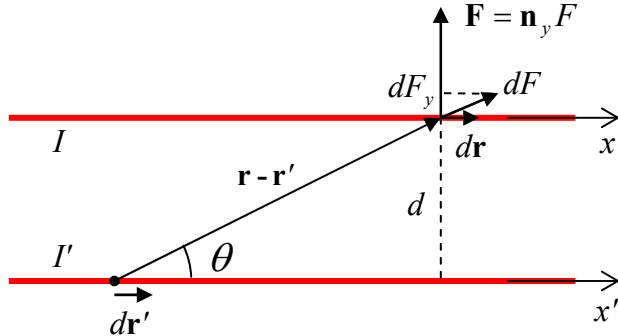


Fig. 5.2. The magnetic force between two straight parallel currents.

Due to the symmetry of this system, the vector of the magnetic interaction force has to:

- (i) lie in the same plane as the currents, and
- (ii) be normal to the wires – see Fig. 2.

Hence we may limit our calculations to just one component of the force – normal to the wires. Using the fact that with the coordinate choice shown in Fig. 2, the scalar product $d\mathbf{r} \cdot d\mathbf{r}'$ is just $dx dx'$, we get

$$F = -\frac{\mu_0 II'}{4\pi} \int_{-\infty}^{+\infty} dx \int_{-\infty}^{+\infty} dx' \frac{\sin \theta}{d^2 + (x - x')^2} = -\frac{\mu_0 II'}{4\pi} \int_{-\infty}^{+\infty} dx \int_{-\infty}^{+\infty} dx' \frac{d}{[d^2 + (x - x')^2]^{3/2}}. \quad (5.5)$$

Now introducing, instead of x' , a new, dimensionless variable $\xi \equiv (x - x')/d$, we may reduce the internal integral to a table one, which we have already encountered in this course:

$$F = -\frac{\mu_0 II'}{4\pi d} \int_{-\infty}^{+\infty} dx \int_{-\infty}^{+\infty} \frac{d\xi}{(1 + \xi^2)^{3/2}} = -\frac{\mu_0 II'}{2\pi d} \int_{-\infty}^{+\infty} dx. \quad (5.6)$$

The integral over x formally diverges, but it gives a finite interaction force *per unit length* of the wires:

$$\frac{F}{l} = -\frac{\mu_0 II'}{2\pi d}. \quad (5.7)$$

Note that the force drops rather slowly (only as $1/d$) as the distance d between the wires is increased, and is attractive (rather than repulsive as in the Coulomb law) if the currents are of the same sign.

This is an important result,⁵ but again, the problems so simply solvable are few and far between, and it is intuitively clear that we would strongly benefit from the same approach as in electrostatics, i.e., from decomposing Eq. (1) into a product of two factors via the introduction of a suitable field. Such decomposition may be done as follows:

$$\mathbf{F} = \int_V \mathbf{j}(\mathbf{r}) \times \mathbf{B}(\mathbf{r}) d^3 r, \quad (5.8)$$

⁵ In particular, until very recently (2018), Eq. (7) was used for the legal definition of the SI unit of current, the ampere (A), via the SI unit of force (the newton, N), with the coefficient μ_0 considered exactly fixed. (A brief description of the recent changes in legal metrology is given in Appendix CA.)

where the vector \mathbf{B} is called the *magnetic field*.⁶ In the case when it is induced by the current \mathbf{j}' :

$$\mathbf{B}(\mathbf{r}) \equiv \frac{\mu_0}{4\pi} \int_V \mathbf{j}'(\mathbf{r}') \times \frac{\mathbf{r} - \mathbf{r}'}{|\mathbf{r} - \mathbf{r}'|^3} d^3 r'. \quad (5.9)$$

Biot-Savart law

The last relation is called the *Biot-Savart law*,⁷ while the force \mathbf{F} expressed by Eq. (8) is sometimes called the *Lorentz force*.⁸ However, more frequently the latter term is reserved for the full force,

$$\mathbf{F} = q(\mathbf{E} + \mathbf{v} \times \mathbf{B}), \quad (5.10)$$

Lorentz force: particle

exerted by electric and magnetic fields field on a point charge q , moving with velocity \mathbf{v} .⁹

Now we have to prove that the new formulation, given by Eqs. (8)-(9), is equivalent to Eq. (1). At the first glance, this seems unlikely. Indeed, first of all, Eqs. (8) and (9) involve vector products, while Eq. (1) is based on a scalar product. More profoundly, in contrast to Eq. (1), Eqs. (8) and (9) do *not* satisfy the 3rd Newton's law applied to elementary current components $\mathbf{j}d^3r$ and $\mathbf{j}'d^3r'$, if these vectors are not parallel to each other. Indeed, consider the situation shown in Fig. 3.

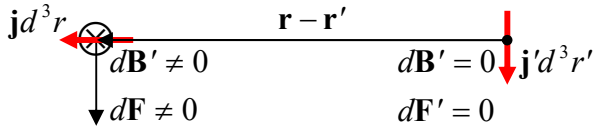


Fig. 5.3. The apparent violation of the 3rd Newton law in magnetism.

Here the vector \mathbf{j}' is perpendicular to the vector $(\mathbf{r} - \mathbf{r}')$, and hence, according to Eq. (9), produces a non-zero contribution $d\mathbf{B}'$ to the magnetic field directed (in Fig. 3) normally to the plane of the drawing, i.e. perpendicular to the vector \mathbf{j} . Hence, according to Eq. (8), this field provides a non-zero contribution to \mathbf{F} . On the other hand, if we calculate the reciprocal force \mathbf{F}' by swapping the prime indices in Eqs. (8) and (9), the latter equation immediately shows that $d\mathbf{B}(\mathbf{r}') \propto \mathbf{j} \times (\mathbf{r}' - \mathbf{r}) = 0$, because the two operand vectors are parallel – see Fig. 3 again. Hence, the current component $\mathbf{j}'d^3r'$ does exert a force on its counterpart, while $\mathbf{j}d^3r$ does not.

⁶ The SI unit of the magnetic field is called *tesla* (T) – after Nikola Tesla, a pioneer of electrical engineering. In the Gaussian units, the already discussed constant $1/c^2$ in Eq. (1) is equally divided between Eqs. (8) and (9), so that in them both, the constant before the integral is $1/c$. The resulting Gaussian unit of the field \mathbf{B} is called *gauss* (G); taking into account the difference of units of electric charge and length, and hence of the current density, 1 G equals exactly 10^{-4} T. Note also that in some textbooks, especially old ones, \mathbf{B} is called either the *magnetic induction* or the *magnetic flux density*, while the term “magnetic field” is reserved for the field \mathbf{H} that will be introduced in Sec. 5 below.

⁷ Named after Jean-Baptiste Biot and Félix Savart who made several key contributions to the theory of magnetic interactions – in the same notorious 1820.

⁸ Named after Hendrik Antoon Lorentz, famous mostly for his numerous contributions to the development of special relativity – see Chapter 9 below. To be fair, the magnetic part of the Lorentz force was implicitly described in a much earlier (1865) paper by J. C. Maxwell, and then spelled out by Oliver Heaviside (another genius of electrical engineering – and mathematics!) in 1889, i.e. also before the 1895 work by H. Lorentz.

⁹ From the magnetic part of Eq. (10), Eq. (8) may be derived by the elementary summation of all forces acting on $n \gg 1$ particles in a unit volume, with $\mathbf{j} = qn\mathbf{v}$ – see the footnote on Eq. (4.13a). On the other hand, the reciprocal derivation of Eq. (10) from Eq. (8) with $\mathbf{j} = q\mathbf{v}\delta(\mathbf{r} - \mathbf{r}_0)$, where \mathbf{r}_0 is the current particle's position (so that $d\mathbf{r}_0/dt = \mathbf{v}$), requires certain mathematical care and will be performed in Chapter 9.

Despite this apparent problem, let us still go ahead and plug Eq. (9) into Eq. (8):

$$\mathbf{F} = \frac{\mu_0}{4\pi} \int_V d^3r \int_{V'} d^3r' \mathbf{j}(\mathbf{r}) \times \left(\mathbf{j}'(\mathbf{r}') \times \frac{\mathbf{r} - \mathbf{r}'}{|\mathbf{r} - \mathbf{r}'|^3} \right). \quad (5.11)$$

This double vector product may be transformed into two scalar products, using the vector algebraic identity called the *bac minus cab rule*, $\mathbf{a} \times (\mathbf{b} \times \mathbf{c}) = \mathbf{b}(\mathbf{a} \cdot \mathbf{c}) - \mathbf{c}(\mathbf{a} \cdot \mathbf{b})$.¹⁰ Applying this relation, with $\mathbf{a} = \mathbf{j}$, $\mathbf{b} = \mathbf{j}'$, and $\mathbf{c} = \mathbf{R} \equiv \mathbf{r} - \mathbf{r}'$, to Eq. (11), we get

$$\mathbf{F} = \frac{\mu_0}{4\pi} \int_{V'} d^3r' \mathbf{j}'(\mathbf{r}') \left(\int_V d^3r \frac{\mathbf{j}(\mathbf{r}) \cdot \mathbf{R}}{R^3} \right) - \frac{\mu_0}{4\pi} \int_V d^3r \int_{V'} d^3r' \mathbf{j}(\mathbf{r}) \cdot \mathbf{j}'(\mathbf{r}') \frac{\mathbf{R}}{R^3}. \quad (5.12)$$

The second term on the right-hand side of this equality coincides with the right-hand side of Eq. (1), while the first term equals zero because its internal integral vanishes. Indeed, we may break the volumes V and V' into narrow *current tubes* – the stretched elementary volumes whose walls are not crossed by current lines (so that on their walls, $j_n = 0$). As a result, the elementary current in each tube, $dI = jdA = jd^2r$, is the same along its length, and, just as in a thin wire, jd^2r may be replaced with $dId\mathbf{r}$, with the vector $d\mathbf{r}$ directed along \mathbf{j} . Because of this, each tube's contribution to the internal integral in the first term of Eq. (12) may be represented as

$$dI \oint_l d\mathbf{r} \cdot \frac{\mathbf{R}}{R^3} = -dI \oint_l d\mathbf{r} \cdot \nabla \frac{1}{R} = -dI \oint_l dr \frac{\partial}{\partial r} \frac{1}{R}, \quad (5.13)$$

where the operator ∇ acts in the \mathbf{r} -space, and the integral is taken along the tube's length l . Due to the current continuity expressed by Eq. (4.6), each loop should follow a closed contour, and an integral of a full differential of some scalar function (in our case, of $1/R$) along such contour equals zero.

So we have recovered Eq. (1). Returning for a minute to the paradox illustrated in Fig. 3, we may conclude that the apparent violation of the 3rd Newton law was the artifact of our interpretation of Eqs. (8) and (9) as the sums of independent elementary components. In reality, due to the dc current continuity, these components are *not* independent. For the whole currents, Eqs. (8)-(9) do obey the 3rd law – as follows from their already proved equivalence to Eq. (1).

Thus it is possible to break the magnetic interaction into two effects: the induction of the magnetic field \mathbf{B} by one current (in our notation, \mathbf{j}'), and the effect of this field on the other current (\mathbf{j}). Now comes an additional experimental fact: other elementary components $\mathbf{j}d^3r'$ of the current $\mathbf{j}(\mathbf{r})$ also contribute to the magnetic field (9) acting on the component $\mathbf{j}d^3r$.¹¹ This fact allows us to drop the prime sign after \mathbf{j} in Eq. (9), and rewrite Eqs. (8) and (9) as

$$\mathbf{B}(\mathbf{r}) = \frac{\mu_0}{4\pi} \int_{V'} \mathbf{j}(\mathbf{r}') \times \frac{\mathbf{r} - \mathbf{r}'}{|\mathbf{r} - \mathbf{r}'|^3} d^3r', \quad (5.14)$$

$$\mathbf{F} = \int_V \mathbf{j}(\mathbf{r}) \times \mathbf{B}(\mathbf{r}) d^3r. \quad (5.15)$$

¹⁰ See, e.g., MA Eq. (7.5).

¹¹ Just as in electrostatics, one needs to exercise due caution in transforming these expressions for the limit of discrete classical particles, and extended wavefunctions in quantum mechanics, to avoid the (non-existing) magnetic interaction of a charged particle with itself.

Again, the field *observation* point \mathbf{r} and the field *source* point \mathbf{r}' have to be clearly distinguished. We immediately see that these expressions are close to, but still different from the corresponding relations of the electrostatics, namely Eq. (1.9) and the distributed-charge version of Eq. (1.6):

$$\mathbf{E}(\mathbf{r}) = \frac{1}{4\pi\epsilon_0} \oint_V \rho(\mathbf{r}') \frac{\mathbf{r} - \mathbf{r}'}{|\mathbf{r} - \mathbf{r}'|^3} d^3 r', \quad (5.16)$$

$$\mathbf{F} = \oint_V \rho(\mathbf{r}) \mathbf{E}(\mathbf{r}) d^3 r. \quad (5.17)$$

(Note that the sign difference has disappeared, at the cost of the replacement of scalar-by-vector multiplications in electrostatics with cross-products of vectors in magnetostatics.)

For the frequent particular case of a thin wire of length l' , Eq. (14) may be re-written as

$$\mathbf{B}(\mathbf{r}) = \frac{\mu_0 I}{4\pi} \oint_{l'} d\mathbf{r}' \times \frac{\mathbf{r} - \mathbf{r}'}{|\mathbf{r} - \mathbf{r}'|^3}. \quad (5.18)$$

Let us see how this formula works for the simplest case of a straight wire (Fig. 4a). The magnetic field contributions $d\mathbf{B}$ due to all small fragments $d\mathbf{r}'$ of the wire's length are directed along the same line (perpendicular to both the wire and the shortest distance d from the observation point to the wire's line), and its magnitude is

$$dB = \frac{\mu_0 I}{4\pi} \frac{dx'}{|\mathbf{r} - \mathbf{r}'|^2} \sin \theta = \frac{\mu_0 I}{4\pi} \frac{dx'}{(d^2 + x^2)} \frac{d}{(d^2 + x^2)^{1/2}}. \quad (5.19)$$

Summing up all such elementary contributions, we get

$$B = \frac{\mu_0 I \rho}{4\pi} \int_{-\infty}^{\infty} \frac{dx}{(x^2 + d^2)^{3/2}} = \frac{\mu_0 I}{2\pi d}. \quad (5.20)$$

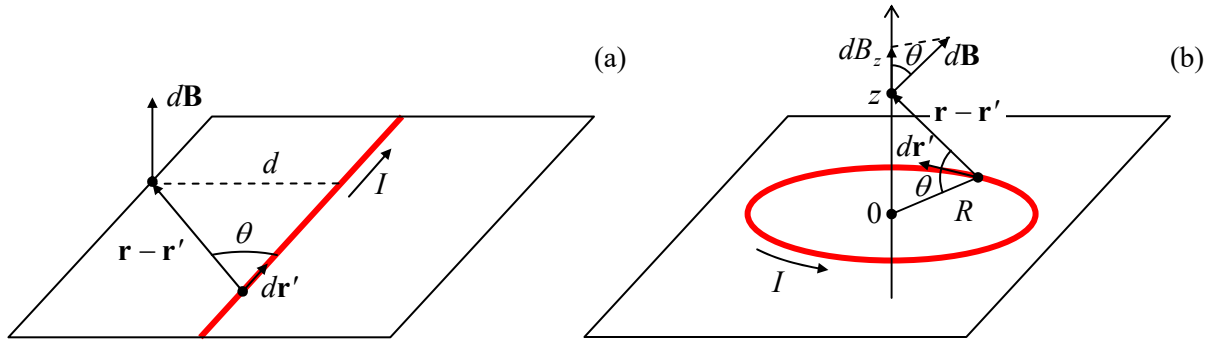


Fig. 5.4. Calculating magnetic fields: (a) of a straight current, and (b) of a current loop.

This is a simple but important result. (Note that it is only valid for very long ($l \gg d$), straight wires.) It is especially crucial to note the “vortex” character of the field: its lines go around the wire, forming rings with the centers on the current line. This is in sharp contrast to the electrostatic field lines, which can only begin and end on electric charges and never form closed loops (otherwise the Coulomb force $q\mathbf{E}$ would not be conservative). In the magnetic case, the vortex structure of the *field* may be reconciled with the potential character of the magnetic *forces*, which is evident from Eq. (1), due to the vector products in Eqs. (14)-(15).

Now we may readily use Eq. (15), or rather its thin-wire version

$$\mathbf{F} = I \oint_l d\mathbf{r} \times \mathbf{B}(\mathbf{r}), \quad (5.21)$$

to apply Eq. (20) to the two-wire problem (Fig. 2). Since for the second wire, the vectors $d\mathbf{r}$ and \mathbf{B} are perpendicular to each other, we immediately arrive at our previous result (7), which was obtained directly from Eq. (1).

The next important example of the application of the Biot-Savart law (14) is the magnetic field at the axis of a circular current loop (Fig. 4b). Due to the problem's symmetry, the net field \mathbf{B} has to be directed along the axis, but each of its elementary components $d\mathbf{B}$ is tilted by the angle $\theta = \tan^{-1}(z/R)$ to this axis, so that its axial component is

$$dB_z = dB \cos \theta = \frac{\mu_0 I}{4\pi} \frac{dr'}{R^2 + z^2} \frac{R}{(R^2 + z^2)^{1/2}}. \quad (5.22)$$

Since the denominator of this expression remains the same for all wire components dr' , the integration over \mathbf{r}' is easy ($\int dr' = 2\pi R$), giving finally

$$B = \frac{\mu_0 I}{2} \frac{R^2}{(R^2 + z^2)^{3/2}}. \quad (5.23)$$

Note that the magnetic field in the loop's center (i.e., for $z = 0$),

$$B = \frac{\mu_0 I}{2R}, \quad (5.24)$$

is π times higher than that due to a similar current in a straight wire, at distance $d = R$ from it. This difference is readily understandable, since all elementary components of the loop are at the same distance R from the observation point, while in the case of a straight wire, all its points but one are separated from the observation point by distances larger than d .

Another notable fact is that at large distances ($z^2 \gg R^2$), the field (23) is proportional to z^{-3} :

$$B \approx \frac{\mu_0 I}{2} \frac{R^2}{|z|^3} \equiv \frac{\mu_0}{4\pi} \frac{2m}{|z|^3}, \quad \text{with } m \equiv IA, \quad (5.25)$$

where $A = \pi R^2$ is the loop area. Comparing this expression with Eq. (3.13), for the particular case $\theta = 0$, we see that such field is similar to that of an electric dipole (at least along its direction), with the replacement of the electric dipole moment magnitude p with the m so defined – besides the front factor. Indeed, such a plane current loop is the simplest example of a system whose field, at distances much larger than R , is that of a *magnetic dipole*, with a *dipole moment* \mathbf{m} – the notions to be discussed in much more detail in Sec. 4 below.

5.2. Vector potential and the Ampère law

The reader could see that the calculations of the magnetic field using Eq. (14) or (18) are still somewhat cumbersome even for the very simple systems we have examined. As we saw in Chapter 1, similar calculations in electrostatics, at least for several important highly symmetric systems, could be

substantially simplified using the Gauss law (1.16). A similar relation exists in magnetostatics as well, but has a different form, due to the vortex character of the magnetic field.

To derive it, let us notice that in an analogy with the scalar case, the vector product under the integral (14) may be transformed as

$$\frac{\mathbf{j}(\mathbf{r}') \times (\mathbf{r} - \mathbf{r}')}{|\mathbf{r} - \mathbf{r}'|^3} = \nabla \times \frac{\mathbf{j}(\mathbf{r}')}{|\mathbf{r} - \mathbf{r}'|}, \quad (5.26)$$

where the operator ∇ acts in the \mathbf{r} -space. (This equality may be readily verified by Cartesian components, noticing that the current density is a function of \mathbf{r}' and hence its components are independent of \mathbf{r} .) Plugging Eq. (26) into Eq. (14), and moving the operator ∇ out of the integral over \mathbf{r}' , we see that the magnetic field may be represented as the curl of another vector field – the so-called *vector potential*, defined as:¹²

$$\mathbf{B}(\mathbf{r}) \equiv \nabla \times \mathbf{A}(\mathbf{r}), \quad (5.27)$$

and in our current case equal to

$$\mathbf{A}(\mathbf{r}) = \frac{\mu_0}{4\pi} \int_V \frac{\mathbf{j}(\mathbf{r}')}{|\mathbf{r} - \mathbf{r}'|} d^3 r'. \quad (5.28)$$

Vector potential

Please note a beautiful analogy between Eqs. (27)-(28) and, respectively, Eqs. (1.33) and (1.38).¹³ This analogy implies that the vector potential \mathbf{A} plays, for the magnetic field, essentially the same role as the scalar potential ϕ plays for the electric field (hence the name “potential”), with due respect to the vortex character of \mathbf{B} . This notion will be discussed in more detail below.

Now let us see what equations we may get for the spatial derivatives of the magnetic field. First, vector algebra says that the divergence of any curl is zero.¹⁴ In application to Eq. (27), this means that

$$\nabla \cdot \mathbf{B} = 0. \quad (5.29)$$

No magnetic monopoles

Comparing this equation with Eq. (1.27), we see that Eq. (29) may be interpreted as the absence of a magnetic analog of an electric charge, on which magnetic field lines could originate or end. Numerous searches for such hypothetical magnetic charges, called *magnetic monopoles*, using very sensitive and sophisticated experimental setups, have not given any reliable evidence of their existence in Nature.

Proceeding to the alternative, vector derivative of the magnetic field, i.e. to its curl, and using Eq. (28), we obtain

$$\nabla \times \mathbf{B}(\mathbf{r}) = \frac{\mu_0}{4\pi} \nabla \times \left(\nabla \times \int_V \frac{\mathbf{j}(\mathbf{r}')}{|\mathbf{r} - \mathbf{r}'|} d^3 r' \right). \quad (5.30)$$

This expression may be simplified by using the following general vector identity:¹⁵

$$\nabla \times (\nabla \times \mathbf{c}) = \nabla(\nabla \cdot \mathbf{c}) - \nabla^2 \mathbf{c}, \quad (5.31)$$

applied to vector $\mathbf{c}(\mathbf{r}) \equiv \mathbf{j}(\mathbf{r}')/|\mathbf{r} - \mathbf{r}'|$:

¹² In the Gaussian units, Eq. (27) remains the same, and hence in Eq. (28), $\mu_0/4\pi$ is replaced with $1/c$.

¹³ In Eq. (1.38), there was no real need for the additional clarification provided by the integration volume label V' .

¹⁴ See, e.g., MA Eq. (11.2).

¹⁵ See, e.g., MA Eq. (11.3).

$$\nabla \times \mathbf{B} = \frac{\mu_0}{4\pi} \nabla \int_{V'} \mathbf{j}(\mathbf{r}') \cdot \nabla \frac{1}{|\mathbf{r} - \mathbf{r}'|} d^3 r' - \frac{\mu_0}{4\pi} \int_{V'} \mathbf{j}(\mathbf{r}') \nabla^2 \frac{1}{|\mathbf{r} - \mathbf{r}'|} d^3 r'. \quad (5.32)$$

As was already discussed during our study of electrostatics in Sec. 3.1,

$$\nabla^2 \frac{1}{|\mathbf{r} - \mathbf{r}'|} = -4\pi\delta(\mathbf{r} - \mathbf{r}'), \quad (5.33)$$

so that the last term of Eq. (32) is just $\mu_0 \mathbf{j}(\mathbf{r})$. On the other hand, inside the first integral we can replace ∇ with $(-\nabla')$, where prime means differentiation in the space of the radius vectors \mathbf{r}' . Integrating that term by parts, we get

$$\nabla \times \mathbf{B} = -\frac{\mu_0}{4\pi} \nabla \oint_{S'} j_n(\mathbf{r}') \frac{1}{|\mathbf{r} - \mathbf{r}'|} d^2 r' + \nabla \int_{V'} \frac{\nabla' \cdot \mathbf{j}(\mathbf{r}')}{|\mathbf{r} - \mathbf{r}'|} d^3 r' + \mu_0 \mathbf{j}(\mathbf{r}). \quad (5.34)$$

Applying this equality to the volume V' limited by a surface S' either sufficiently distant from the field concentration, or with no current crossing it, we may neglect the first term on the right-hand side of Eq. (34), while the second term always equals zero in statics, due to the dc charge continuity – see Eq. (4.6). As a result, we arrive at a very simple differential equation¹⁶

$$\nabla \times \mathbf{B} = \mu_0 \mathbf{j}. \quad (5.35)$$

This is (the dc form of) the inhomogeneous Maxwell equation – which in magnetostatics plays a role similar to Eq. (1.27) in electrostatics. Let me display, for the first time in this course, this fundamental system of equations (at this stage, for statics only), and give the reader a minute to stare, in silence, at their beautiful symmetry – which has inspired so much of the later development of physics:

$$\begin{aligned} \nabla \times \mathbf{E} &= 0, & \nabla \times \mathbf{B} &= \mu_0 \mathbf{j}, \\ \nabla \cdot \mathbf{E} &= \frac{\rho}{\epsilon_0}, & \nabla \cdot \mathbf{B} &= 0. \end{aligned} \quad (5.36)$$

Maxwell
equations:
statics

Their only asymmetry, two zeros on the right-hand sides (for the magnetic field's divergence and electric field's curl), is due to the absence in the Nature of magnetic monopoles and their currents. I will discuss these equations in more detail in Sec. 6.7, after the first two equations (for the fields' curls) have been generalized to their full, time-dependent versions.

Returning now to our current, more mundane but important task of calculating the magnetic field induced by simple current configurations, we can benefit from an integral form of Eq. (35). For that, let us integrate this equation over an arbitrary surface S limited by a closed contour C , and apply to the result the Stokes theorem.¹⁷ The resulting expression,

$$\oint_C \mathbf{B} \cdot d\mathbf{r} = \mu_0 \oint_S j_n d^2 r \equiv \mu_0 I, \quad (5.37)$$

Ampère
law

where I is the net electric current crossing surface S , is called the *Ampère law*.

¹⁶ As in all earlier formulas for the magnetic field, in the Gaussian units, the coefficient μ_0 in this relation is replaced with $4\pi/c$.

¹⁷ See, e.g., MA Eq. (12.1) with $\mathbf{f} = \mathbf{B}$.

As the first example of its application, let us return to the current in a straight wire (Fig. 4a). With the Ampère law in our arsenal, we can readily pursue an even more ambitious goal than that achieved in the previous section, namely to calculate the magnetic field both outside and inside of a wire of an arbitrary radius R , with an arbitrary (albeit axially-symmetric) current distribution $j(\rho)$ – see Fig. 5.

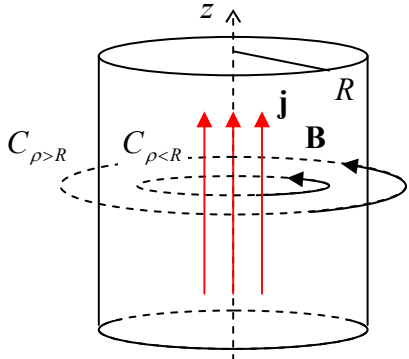


Fig. 5.5. The simplest application of the Ampère law: the magnetic field of a straight current.

Selecting the Ampère-law contour C in the form of a ring of some radius ρ in the plane normal to the wire's axis z , we have $\mathbf{B} \cdot d\mathbf{r} = B\rho d\varphi$, where φ is the azimuthal angle, so that Eq. (37) yields:

$$2\pi\rho B(\rho) = \mu_0 \times \begin{cases} 2\pi \int_0^\rho j(\rho')\rho' d\rho', & \text{for } \rho \leq R, \\ 2\pi \int_0^R j(\rho')\rho' d\rho' \equiv I, & \text{for } \rho \geq R. \end{cases} \quad (5.38)$$

Thus we have not only recovered our previous result (20), with the notation replacement $d \rightarrow \rho$, in a much simpler way but also have been able to calculate the magnetic field's distribution inside the wire. In the most common particular case when the current is uniformly distributed along its cross-section, $j(\rho) = \text{const}$, the first of Eqs. (38) immediately yields $B \propto \rho$ for $\rho \leq R$.

Another important system is a straight, long *solenoid* (Fig. 6a), with dense winding: $n^2A \gg 1$, where n is the number of wire turns per unit length, and A is the area of the solenoid's cross-section.

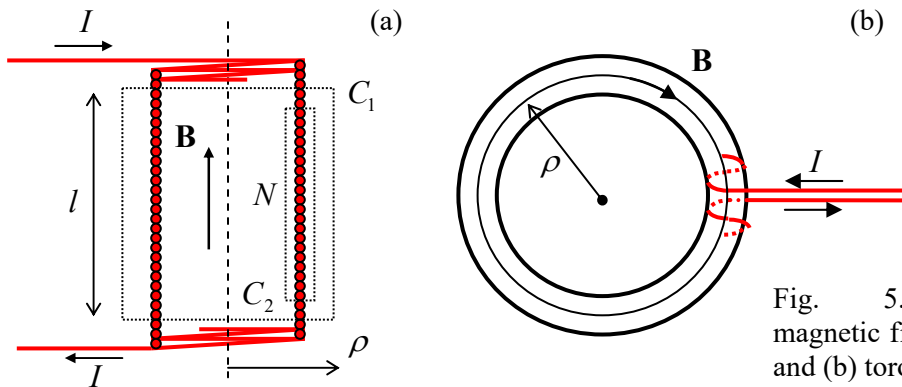


Fig. 5.6. Calculating magnetic fields of (a) straight and (b) toroidal solenoids.

From the symmetry of this problem, the longitudinal (in Fig. 6a, vertical) component B_z of the magnetic field may only depend on the distance ρ of the observation point from the solenoid's axis. First taking a plane Ampère contour C_1 , with both long sides outside the solenoid, we get $B_z(\rho_2) - B_z(\rho_1) = 0$,

because the total current piercing the contour equals zero. This is only possible if $B_z = 0$ at any ρ outside of the solenoid, provided that it is infinitely long.¹⁸ With this result on hand, from the Ampère law applied to the contour C_2 , we get the following relation for the only (z -) component of the internal field:

$$Bl = \mu_0 NI, \quad (5.39)$$

where N is the number of wire turns passing through the contour of length l . This means that regardless of the exact position of the internal side of the contour, the result is the same:

$$B = \mu_0 \frac{N}{l} I \equiv \mu_0 nI. \quad (5.40)$$

Thus, the field inside an infinitely long solenoid (with an arbitrary shape of its cross-section) is uniform; in this sense, a long solenoid is a magnetic analog of a wide plane capacitor, explaining why this system is so widely used in physical experiment.

As should be clear from its derivation, the obtained results, especially that the field outside of the solenoid equals zero, are conditional on the solenoid length being very large in comparison with its lateral size. (From Eq. (25), we may predict that for a solenoid of a finite length l , the close-range external field is a factor of $\sim A/l^2$ lower than the internal one.) A much better suppression of such “fringe” fields may be obtained using *toroidal solenoids* (Fig. 6b). The application of the Ampère law to this geometry shows that in the limit of dense winding ($N \gg 1$), there is no fringe field at all (for any relation between the two radii of the torus), while inside the solenoid, at distance ρ from the system’s axis,

$$B = \frac{\mu_0 NI}{2\pi\rho}. \quad (5.41)$$

We see that a possible drawback of this system for practical applications is that the internal field does depend on ρ , i.e. is not quite uniform; however, if the torus is relatively thin, this deficiency is minor.

Next let us discuss a very important question: how can we solve the problems of magnetostatics for systems whose low symmetry does not allow getting easy results from the Ampère law? (The examples are of course too numerous to list; for example, we cannot use this approach even to reproduce Eq. (23) for a round current loop.) From the deep analogy with electrostatics, we may expect that in this case, we could calculate the magnetic field by solving a certain boundary problem for the field’s potential – in our current case, the vector potential \mathbf{A} defined by Eq. (28). However, despite the similarity of this formula and Eq. (1.38) for ϕ , which was noticed above, there is an additional issue we should tackle in the magnetic case – besides the obvious fact that calculating the vector potential distribution means determining three scalar functions (say, A_x , A_y , and A_z), rather than just one (ϕ).

To reveal the issue, let us plug Eq. (27) into Eq. (35):

$$\nabla \times (\nabla \times \mathbf{A}) = \mu_0 \mathbf{j}, \quad (5.42)$$

and then apply to the left-hand side of this equation the same identity (31). The result is

¹⁸ Applying the Ampère law to a circular contour of radius ρ , coaxial with the solenoid, we see that the field outside (but not inside!) it has an azimuthal component B_ϕ , similar to that of the straight wire (see Eq. (38) above) and hence (at $N \gg 1$) much weaker than the longitudinal field inside the solenoid – see Eq. (40).

$$\nabla(\nabla \cdot \mathbf{A}) - \nabla^2 \mathbf{A} = \mu_0 \mathbf{j}. \quad (5.43)$$

On the other hand, as we know from electrostatics (please compare Eqs. (1.38) and (1.41)), the vector potential $\mathbf{A}(\mathbf{r})$ given by Eq. (28) has to satisfy a simpler (“vector-Poisson”) equation

$$\boxed{\nabla^2 \mathbf{A} = -\mu_0 \mathbf{j}}, \quad (5.44)$$

Poisson
equation
for \mathbf{A}

which is just a set of three usual Poisson equations for each Cartesian component of \mathbf{A} .

To resolve the difference between these results, let us note that Eq. (43) is reduced to Eq. (44) if $\nabla \cdot \mathbf{A} = 0$. In this context, let us discuss what discretion we have in the choice of the potential. In electrostatics, we may add, to the scalar function ϕ' that satisfies Eq. (1.33) for the given field \mathbf{E} , not only an arbitrary constant but even an arbitrary function of time:

$$-\nabla[\phi' + f(t)] = -\nabla\phi' = \mathbf{E}. \quad (5.45)$$

Similarly, using the fact that the curl of the gradient of any scalar function equals zero,¹⁹ we may add to any vector function \mathbf{A}' that satisfies Eq. (27) for the given field \mathbf{B} , not only any constant but even a gradient of an arbitrary scalar function $\chi(\mathbf{r}, t)$, because

$$\nabla \times (\mathbf{A}' + \nabla\chi) = \nabla \times \mathbf{A}' + \nabla \times (\nabla\chi) = \nabla \times \mathbf{A}' = \mathbf{B}. \quad (5.46)$$

Such additions, which keep the fields intact, are called *gauge transformations*.²⁰ Let us see what such a transformation does to $\nabla \cdot \mathbf{A}'$:

$$\nabla \cdot (\mathbf{A}' + \nabla\chi) = \nabla \cdot \mathbf{A}' + \nabla^2 \chi. \quad (5.47)$$

For any choice of such a function \mathbf{A}' , we can always choose the function χ in such a way that it satisfies the Poisson equation $\nabla^2 \chi = -\nabla \cdot \mathbf{A}'$, and hence makes the divergence of the transformed vector potential, $\mathbf{A} \equiv \mathbf{A}' + \nabla\chi$, equal to zero everywhere,

$$\boxed{\nabla \cdot \mathbf{A} = 0}, \quad (5.48)$$

Coulomb
gauge

thus reducing Eq. (43) to Eq. (44).

To summarize, the set of distributions $\mathbf{A}'(\mathbf{r})$ that satisfy Eq. (27) for a given field $\mathbf{B}(\mathbf{r})$, is not limited to the vector potential $\mathbf{A}(\mathbf{r})$ given by Eq. (44), but is reduced to it upon the additional *Coulomb gauge condition* (48). However, as we will see in a minute, even this condition still leaves some degrees of freedom in the choice of the vector potential. To illustrate this fact, and also to get a better gut feeling of the vector potential’s distribution in space, let us calculate $\mathbf{A}(\mathbf{r})$ for two very basic cases.

First, let us revisit the straight wire problem shown in Fig. 5. As Eq. (28) shows, in this case the vector potential \mathbf{A} has just one component (along the axis z). Moreover, due to the problem’s axial symmetry, its magnitude may only depend on the distance from the axis: $\mathbf{A} = \mathbf{n}_z A(\rho)$. Hence, the gradient of \mathbf{A} is directed across the z -axis, so that Eq. (48) is satisfied at all points. For our symmetry ($\partial/\partial\varphi = \partial/\partial z = 0$), the Laplace operator, written in cylindrical coordinates, has just one term,²¹ reducing Eq. (44) to

¹⁹ See, e.g., MA Eq. (11.1).

²⁰ The use of the term “gauge” (originally meaning “a measure” or “a scale”) in this context is purely historic, so the reader should not try to find too much hidden sense in it.

²¹ See, e.g., MA Eq. (10.3).

$$\frac{1}{\rho} \frac{d}{d\rho} \left(\rho \frac{dA}{d\rho} \right) = -\mu_0 j(\rho). \quad (5.49)$$

Multiplying both sides of this equation by ρ and integrating them over the coordinate once, we get

$$\rho \frac{dA}{d\rho} = -\mu_0 \int_0^\rho j(\rho') \rho' d\rho' + \text{const.} \quad (5.50)$$

Since in the cylindrical coordinates, for our symmetry, $B = -dA/d\rho$,²² Eq. (50) is nothing else than our old result (38) for the magnetic field.²³ However, let us continue the integration, at least for the region outside the wire, where the function $A(\rho)$ depends only on the full current I rather than on the current distribution. Dividing both parts of Eq. (50) by ρ , and integrating them over this argument again, we get

$$A(\rho) = -\frac{\mu_0 I}{2\pi} \ln \rho + \text{const}, \quad \text{where } I = 2\pi \int_0^R j(\rho) \rho d\rho, \quad \text{for } \rho \geq R. \quad (5.51)$$

As a reminder, we had similar logarithmic behavior for the electrostatic potential outside a uniformly charged straight line. This is natural because the Poisson equations for both cases are similar.

Now let us find the vector potential for the long solenoid (Fig. 6a), with its uniform magnetic field. Since Eq. (28) tells us that the vector \mathbf{A} should follow the direction of the inducing current, we may start with looking for it in the form $\mathbf{A} = \mathbf{n}_\varphi A(\rho)$. (This is especially natural if the solenoid's cross-section is circular.) With this orientation of \mathbf{A} , the same general expression for the curl operator in cylindrical coordinates yields $\nabla \times \mathbf{A} = \mathbf{n}_z (1/\rho) d(\rho A)/d\rho$. According to Eq. (27), this expression should be equal to \mathbf{B} – in our current case to $\mathbf{n}_z B$, with a constant B – see Eq. (40). Integrating this equality, and selecting such integration constant that $A(0)$ is finite, we get

$$A(\rho) = \frac{B\rho}{2}, \quad \text{i.e. } \mathbf{A} = \frac{B\rho}{2} \mathbf{n}_\varphi. \quad (5.52)$$

Plugging this result into the general expression for the Laplace operator in the cylindrical coordinates,²⁴ we see that the Poisson equation (44) with $\mathbf{j} = 0$ (i.e. the Laplace equation) is satisfied again – which is natural since, for this distribution, the Coulomb gauge condition (48) is satisfied: $\nabla \cdot \mathbf{A} = 0$.

However, Eq. (52) is not the unique (or even the simplest) vector potential that gives the same uniform field $\mathbf{B} = \mathbf{n}_z B$. Indeed, using the well-known expression for the curl operator in Cartesian coordinates,²⁵ it is straightforward to check that each of the vector functions $\mathbf{A}' = \mathbf{n}_y Bx$ and $\mathbf{A}'' = -\mathbf{n}_x By$ also has the same curl, and also satisfies the Coulomb gauge condition (48).²⁶ If such solutions do not look very natural because of their anisotropy in the $[x, y]$ plane, please consider the fact that they represent the uniform magnetic field regardless of its source – for example, regardless of the shape of the long solenoid's cross-section. Such choices of the vector potential may be very convenient for some

²² See, e.g., MA Eq. (10.5) with $\partial/\partial\varphi = \partial/\partial z = 0$.

²³ Since the magnetic field at the wire's axis has to be zero (otherwise, being normal to the axis, where would it be directed?), the integration constant in Eq. (50) has to equal zero.

²⁴ See, e.g., MA Eq. (10.6).

²⁵ See, e.g., MA Eq. (8.5).

²⁶ The axially-symmetric vector potential (52) is just a weighted sum of these two functions: $\mathbf{A} = (\mathbf{A}' + \mathbf{A}'')/2$.

problems, for example for the quantum-mechanical analysis of the 2D motion of a charged particle in the perpendicular magnetic field, giving the famous Landau energy levels.²⁷

5.3. Magnetic energy, flux, and inductance

Considering the currents flowing in a system as generalized coordinates, the magnetic forces (1) between them are their unique functions, and in this sense, the energy U of their magnetic interaction may be considered the potential energy of the system. The apparent (but somewhat deceptive) way to derive an expression for this energy is to use the analogy between Eq. (1) and its electrostatic analog, Eq. (2). Indeed, Eq. (2) may be transformed into Eq. (1) with just three replacements:

- (i) $\rho(\mathbf{r})\rho'(\mathbf{r}')$ should be replaced with $[\mathbf{j}(\mathbf{r}) \cdot \mathbf{j}'(\mathbf{r}')]$,
- (ii) ϵ_0 should be replaced with $1/\mu_0$, and
- (iii) the sign before the double integral has to be replaced with the opposite one.

Hence we may avoid repeating the calculation made in Chapter 1, by making these replacements in Eq. (1.59), which gives the electrostatic potential energy of the system with $\rho(\mathbf{r})$ and $\rho'(\mathbf{r}')$ describing the same charge distribution, i.e. with $\rho'(\mathbf{r}) = \rho(\mathbf{r})$, to get the following expression for the magnetic potential energy in the system with, similarly, $\mathbf{j}'(\mathbf{r}) = \mathbf{j}(\mathbf{r})$:²⁸

$$U_j = -\frac{\mu_0}{4\pi} \frac{1}{2} \int d^3r \int d^3r' \frac{\mathbf{j}(\mathbf{r}) \cdot \mathbf{j}(\mathbf{r}')}{|\mathbf{r} - \mathbf{r}'|}. \quad (5.53)$$

But this is *not* the unique answer! Indeed, Eq. (53) describes the proper potential energy of the system (in particular, giving the correct result for the current interaction forces) only in the case when the interacting currents are fixed – just as Eq. (1.59) is adequate when the interacting charges are fixed. Here comes a substantial difference between electrostatics and magnetostatics: due to the fundamental fact of electric charge conservation (already discussed in Secs. 1.1 and 4.1), keeping electric charges fixed does not require external work, while the maintenance of currents generally does. As a result, Eq. (53) describes the energy of the magnetic interaction *plus* of the system keeping the currents constant – or rather of its part depending on the system under our consideration. In this situation, using the terminology already used in Sec. 3.5 (see also a general discussion in CM Sec. 1.4.), U_j may be called the Gibbs potential energy of our magnetic system.

Now to exclude from U_j the contribution due to the interaction with the current-supporting system(s), i.e. calculate the potential energy U of our system as such, we need to know this contribution. The simplest way to do this is to use the *Faraday induction law* that describes this interaction and will be discussed at the beginning of the next chapter. This is why let me postpone the derivation until that point, and for now ask the reader to believe me that the removal of the interaction leads to an expression similar to Eq. (53), but with the opposite sign:

$$U = \frac{\mu_0}{4\pi} \frac{1}{2} \int d^3r \int d^3r' \frac{\mathbf{j}(\mathbf{r}) \cdot \mathbf{j}(\mathbf{r}')}{|\mathbf{r} - \mathbf{r}'|}, \quad (5.54)$$

Magnetic
interaction
energy

²⁷ See, e.g., QM Sec. 3.2.

²⁸ Just as in electrostatics, for the interaction of two *independent* current distributions $\mathbf{j}(\mathbf{r})$ and $\mathbf{j}'(\mathbf{r}')$, the factor $1/2$ should be dropped.

I will prove this result in Sec. 6.2, but actually, this sign dichotomy should not be quite surprising to the attentive reader, in the context of a similar duality of Eqs. (3.73) and (3.81) for the electrostatic energies including and excluding the interaction with the field source.

Due to the importance of Eq. (54), let us rewrite it in several other forms, convenient for various applications. First of all, just as in electrostatics, it may be recast into a potential-based form. Indeed, with the definition (28) of the vector potential $\mathbf{A}(\mathbf{r})$, Eq. (54) becomes

$$U = \frac{1}{2} \int \mathbf{j}(\mathbf{r}) \cdot \mathbf{A}(\mathbf{r}) d^3 r . \quad (5.55)$$

This formula, which is a clear magnetic analog of Eq. (1.60) of electrostatics, is very popular among field theorists, because it is very handy for their manipulations; it is also useful for some practical applications. However, for many calculations, it is more convenient to have a direct expression of the energy via the magnetic field. Again, this may be done very similarly to what had been done for electrostatics in Sec. 1.3, i.e. by plugging into Eq. (55) the current density expressed from Eq. (35) and then transforming it as²⁹

$$U = \frac{1}{2} \int \mathbf{j} \cdot \mathbf{A} d^3 r = \frac{1}{2\mu_0} \int \mathbf{A} \cdot (\nabla \times \mathbf{B}) d^3 r = \frac{1}{2\mu_0} \int \mathbf{B} \cdot (\nabla \times \mathbf{A}) d^3 r - \frac{1}{2\mu_0} \int \nabla \cdot (\mathbf{A} \times \mathbf{B}) d^3 r . \quad (5.56)$$

Now using the divergence theorem, the second integral may be transformed into a surface integral of $(\mathbf{A} \times \mathbf{B})_n$. According to Eqs. (27)-(28) if the current distribution $\mathbf{j}(\mathbf{r})$ is localized, this vector product drops, at large distances, faster than $1/r^2$, so that if the integration volume is large enough, the surface integral is negligible. In the remaining first integral in Eq. (56), we may use Eq. (27) to rewrite $\nabla \times \mathbf{A}$ as \mathbf{B} . As a result, we get a very simple and fundamental formula.

$$U = \frac{1}{2\mu_0} \int B^2 d^3 r . \quad (5.57a)$$

Just as with the electric field, this expression may be interpreted as a volume integral of the *magnetic energy density* u :

$$U = \int u(\mathbf{r}) d^3 r, \quad \text{with } u(\mathbf{r}) \equiv \frac{1}{2\mu_0} \mathbf{B}^2(\mathbf{r}), \quad (5.57b)$$

clearly similar to Eq. (1.65).³⁰ Again, the conceptual choice between the spatial localization of magnetic energy – either at the location of electric currents only, as implied by Eqs. (54) and (55), or in all regions where the magnetic field exists, as apparent from Eq. (57b), cannot be done within the framework of magnetostatics, and only the electrodynamics gives a decisive preference for the latter choice.

For the practically important case of currents flowing in several thin wires, Eq. (54) may be first integrated over the cross-section of each wire, just as was done at the derivation of Eq. (4). As before, since the integral of the current density over the k^{th} wire's cross-section is just the current I_k in the wire, and cannot change along its length, it may be taken from the remaining integrals, giving

²⁹ For that, we may use MA Eq. (11.7) with $\mathbf{f} = \mathbf{A}$ and $\mathbf{g} = \mathbf{B}$, giving $\mathbf{A} \cdot (\nabla \times \mathbf{B}) = \mathbf{B} \cdot (\nabla \times \mathbf{A}) - \nabla \cdot (\mathbf{A} \times \mathbf{B})$.

³⁰ The transfer to the Gaussian units in Eqs. (57) may be accomplished by the usual replacement $\mu_0 \rightarrow 4\pi$, thus giving, in particular, $u = B^2/8\pi$.

$$U = \frac{\mu_0}{4\pi} \frac{1}{2} \sum_{k,k'} I_k I_{k'} \oint \oint \frac{d\mathbf{r}_k \cdot d\mathbf{r}_{k'}}{l_k l_{k'}} , \quad (5.58)$$

where l_k is the full length of the k^{th} wire loop. Note that Eq. (58) is valid if all currents I_k are independent of each other, because the double sum counts each current pair twice, compensating the coefficient $\frac{1}{2}$ in front of the sum. It is useful to decompose this relation as

$$U = \frac{1}{2} \sum_{k,k'} I_k I_{k'} L_{kk'} , \quad (5.59)$$

where the coefficients $L_{kk'}$ are independent of the currents:

$$L_{kk'} \equiv \frac{\mu_0}{4\pi} \oint \oint \frac{d\mathbf{r}_k \cdot d\mathbf{r}_{k'}}{l_k l_{k'}} , \quad (5.60)$$

Mutual
inductance
coefficients

The coefficient $L_{kk'}$ with $k \neq k'$, is called the *mutual inductance* between current the k^{th} and k'^{th} loops, while the diagonal coefficient $L_k \equiv L_{kk}$ is called the *self-inductance* (or just *inductance*) of the k^{th} loop.³¹ From the symmetry of Eq. (60) with respect to the index swap, $k \leftrightarrow k'$, it is evident that the matrix of coefficients $L_{kk'}$ is symmetric:³²

$$L_{kk'} = L_{k'k} , \quad (5.61)$$

so that for the practically most important case of two interacting currents I_1 and I_2 , Eq. (59) reads

$$U = \frac{1}{2} L_1 I_1^2 + M I_1 I_2 + \frac{1}{2} L_2 I_2^2 , \quad (5.62)$$

where $M \equiv L_{12} = L_{21}$ is the *mutual inductance coefficient*.

These formulas clearly show the importance of the self- and mutual inductances, so I will demonstrate their calculation for at least a few basic geometries. Before doing that, however, let me recast Eq. (58) into one more form that may facilitate such calculations. Namely, let us notice that for the magnetic field induced by current I_k in a thin wire, Eq. (28) is reduced to

$$\mathbf{A}_k(\mathbf{r}) = \frac{\mu_0}{4\pi} I_k \int_{l'} \frac{d\mathbf{r}_k}{|\mathbf{r} - \mathbf{r}_k|} , \quad (5.63)$$

so that Eq. (58) may be rewritten as

$$U = \frac{1}{2} \sum_{k,k'} I_k \oint_{l_k} \mathbf{A}_{k'}(\mathbf{r}_k) \cdot d\mathbf{r}_{k'} . \quad (5.64)$$

But according to the same Stokes theorem that was used earlier in this chapter to derive the Ampère law, and Eq. (27), the integral in Eq. (64) is nothing else than the *magnetic field's flux* Φ (more frequently called just the *magnetic flux*) through a surface S limited by the contour l :

³¹ As evident from Eq. (60), these coefficients depend only on the geometry of the system. Moreover, in the Gaussian units, in which Eq. (60) is valid without the factor $\mu_0/4\pi$, the inductance coefficients have the dimension of length (centimeters). The SI unit of inductance is called the *henry*, abbreviated H – after Joseph Henry, who in particular discovered the effect of electromagnetic induction (see Sec. 6.1) independently of Michael Faraday.

³² Note that the matrix of the mutual inductances $L_{jj'}$ is very much similar to the matrix of *reciprocal capacitance* coefficients $p_{kk'}$ – for example, compare Eq. (62) with Eq. (2.21).

Magnetic flux

$$\oint_l \mathbf{A}(\mathbf{r}) \cdot d\mathbf{r} = \int_S (\nabla \times \mathbf{A})_n d^2 r = \int_S B_n d^2 r \equiv \Phi \quad (5.65)$$

– in the particular case of Eq. (64), the flux $\Phi_{kk'}$ of the field induced by the k' th current through the loop of the k th current.³³ As a result, Eq. (64) may be rewritten as

$$U = \frac{1}{2} \sum_{k,k'} I_k \Phi_{kk'}. \quad (5.66)$$

Comparing this expression with Eq. (59), we see that

$$\Phi_{kk'} \equiv \int_{S_k} (\mathbf{B}_{k'})_n d^2 r = L_{kk'} I_{k'}, \quad (5.67)$$

This expression not only gives us one more means for calculating the coefficients $L_{kk'}$, but also shows their physical sense: the mutual inductance characterizes what part of the magnetic flux (colloquially, “what fraction of field lines”) induced by the current $I_{k'}$ pierces the k th loop’s area S_k – see Fig. 7.

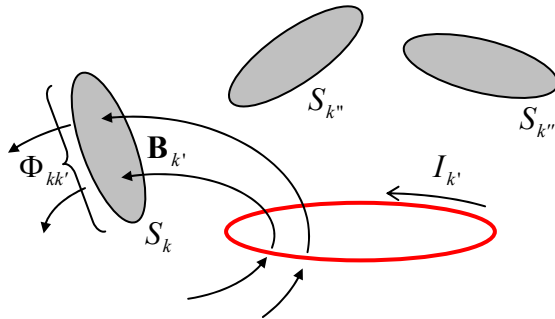


Fig. 5.7. The physical sense of the mutual inductance coefficient $L_{kk'} \equiv \Phi_{kk'}/I_{k'}$ – schematically.

Due to the linear superposition principle, the total flux piercing the k th loop may be represented as

$$\Phi_k \equiv \sum_{k'} \Phi_{kk'} = \sum_{k'} L_{kk'} I_{k'} \quad (5.68)$$

Magnetic flux from currents

For example, for the system of two currents, this expression is reduced to a clear analog of Eqs. (2.19):

$$\begin{aligned} \Phi_1 &= L_1 I_1 + M I_2, \\ \Phi_2 &= M I_1 + L_2 I_2. \end{aligned} \quad (5.69)$$

For the even simpler case of a single current,

Φ of a single current

$$\Phi = LI, \quad (5.70)$$

so that the magnetic energy of the current may be represented in several equivalent forms:

³³ The SI unit of magnetic flux is called *weber*, abbreviated Wb – after Wilhelm Edward Weber (1804-1891), who in particular co-invented (with Carl Gauss) the electromagnetic telegraph. More importantly for this course, in 1856 he was the first (together with Rudolf Kohlrausch) to notice that the value of (in modern terms) $1/(\epsilon_0 \mu_0)^{1/2}$, derived from electrostatic and magnetostatic measurements, coincides with the independently measured speed of light c . This observation gave an important motivation for Maxwell’s theory.

$$U = \frac{L}{2} I^2 = \frac{1}{2} I\Phi = \frac{1}{2L} \Phi^2. \quad (5.71)$$

U of a single current

These relations, similar to Eqs. (2.14)-(2.15) of electrostatics, show that the self-inductance L of a current loop may be considered a measure of the system's magnetic energy. However, as we will see in Sec. 6.1, this measure is adequate only if the flux Φ , rather than the current I , is fixed.

Now we are well equipped for the calculation of inductance coefficients for particular systems, having three options. The first one is to use Eq. (60) directly.³⁴ The second one is to calculate the magnetic field energy from Eq. (57) as the function of all currents I_k in the system, and then use Eq. (59) to find all coefficients $L_{kk'}$. For example, for a system with just one current, Eq. (71) yields

$$L = \frac{U}{I^2 / 2}. \quad (5.72)$$

Finally, if the system consists of thin wires, so that the loop areas S_k and hence the fluxes $\Phi_{kk'}$ are well defined, we may calculate them from Eq. (65), and then use Eq. (67) to find the inductances.

Usually, the third option is simpler, but the first two one may be very useful even for thin-wire systems, if the notion of magnetic flux in them is not quite apparent. As an important example, let us find the self-inductance of a long solenoid – see Fig. 6a again. We have already calculated the magnetic field inside it – see Eq. (40) – so that, due to the field uniformity, the magnetic flux piercing each turn of the wire is just

$$\Phi_1 = BA = \mu_0 nIA, \quad (5.73)$$

where A is the area of the solenoid's cross-section – for example πR^2 for a round solenoid, though Eq. (40), and hence Eq. (73) are valid for cross-sections of any shape. Comparing Eqs. (73) with Eq. (70), one might wrongly conclude that $L = \Phi_1/I = \mu_0 nA$ (**WRONG!**), i.e. that the solenoid's inductance is independent of its length. Actually, the magnetic flux Φ_1 pierces *each* wire turn, so that the total flux through the *whole* current loop, consisting of N turns, is

$$\Phi = N\Phi_1 = \mu_0 n^2 lAI, \quad (5.74)$$

and the correct expression for the long solenoid's self-inductance is

$$L = \frac{\Phi}{I} = \mu_0 n^2 lA \equiv \frac{\mu_0 N^2 A}{l}, \quad (5.75)$$

L of a solenoid

i.e. at fixed A and l , the inductance scales as N^2 , not as N . Since this reasoning may seem not quite evident, it is prudent to verify this result by using Eq. (72), with the full magnetic energy inside the solenoid (neglecting minor fringe field contributions), given by Eq. (57) with $\mathbf{B} = \text{const}$ within the internal volume $V = lA$, and zero outside of it:

$$U = \frac{1}{2\mu_0} B^2 Al = \frac{1}{2\mu_0} (\mu_0 nI)^2 Al \equiv \mu_0 n^2 lA \frac{I^2}{2}. \quad (5.76)$$

Plugging this relation into Eq. (72) immediately confirms the result (75).

³⁴ Numerous applications of that *Neumann formula* (derived in 1845 by F. Neumann) to electrical engineering problems may be found, for example, in the classical text by F. Grover, *Inductance Calculations*, Dover, 1946.

This energy-based approach becomes virtually inevitable for continuously distributed currents. As an example, let us calculate the self-inductance L of a long coaxial cable with the cross-section shown in Fig. 8,³⁵ and the full current in the outer conductor equal and opposite to that (I) in the inner conductor.

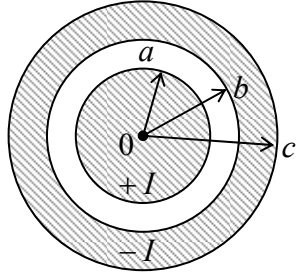


Fig. 5.8. The cross-section of a coaxial cable.

Let us assume that the current is uniformly distributed over the cross-sections of both conductors. (As we know from the previous chapter, this is indeed the case if both the internal and external conductors are made of a uniform resistive material.) First, we should calculate the radial distribution of the magnetic field – which has only one, azimuthal component because of the axial symmetry of the problem. This distribution may be immediately found applying the Ampère law (37) to circular contours of radii ρ within four different ranges:

$$2\pi\rho B = \mu_0 I \Big|_{\text{piercing the contour}} = \mu_0 I \times \begin{cases} \rho^2/a^2, & \text{for } \rho < a, \\ 1, & \text{for } a < \rho < b, \\ (c^2 - \rho^2)/(c^2 - b^2), & \text{for } b < \rho < c, \\ 0, & \text{for } c < \rho. \end{cases} \quad (5.77)$$

Now, an easy integration yields the magnetic energy per unit length of the cable:

$$\begin{aligned} \frac{U}{l} &= \frac{1}{2\mu_0} \int B^2 d^2r = \frac{\pi}{\mu_0} \int_0^\infty B^2 \rho d\rho = \frac{\mu_0 I^2}{4\pi} \left[\int_0^a \left(\frac{\rho}{a^2} \right)^2 \rho d\rho + \int_a^b \left(\frac{1}{\rho} \right)^2 \rho d\rho + \int_b^c \left(\frac{c^2 - \rho^2}{\rho(c^2 - b^2)} \right)^2 \rho d\rho \right] \\ &= \frac{\mu_0}{2\pi} \left[\ln \frac{b}{a} + \frac{c^2}{c^2 - b^2} \left(\frac{c^2}{c^2 - b^2} \ln \frac{c}{b} - \frac{1}{2} \right) \right] \frac{I^2}{2}. \end{aligned} \quad (5.78)$$

From here, and Eq. (72), we get the final answer:

$$\frac{L}{l} = \frac{\mu_0}{2\pi} \left[\ln \frac{b}{a} + \frac{c^2}{c^2 - b^2} \left(\frac{c^2}{c^2 - b^2} \ln \frac{c}{b} - \frac{1}{2} \right) \right]. \quad (5.79)$$

Note that for the particular case of a thin outer conductor, $c - b \ll b$, this expression reduces to

$$\frac{L}{l} \approx \frac{\mu_0}{2\pi} \left(\ln \frac{b}{a} + \frac{1}{4} \right), \quad (5.80)$$

where the first term in the parentheses is due to the contribution of the magnetic field energy in the free space between the conductors. This distinction is important for some applications because in

³⁵ As a reminder, the mutual capacitance C between the conductors of such a system was calculated in Sec. 2.3.

superconductor cables, as well as the normal-metal cables at high frequencies (to be discussed in the next chapter), the field does not penetrate the conductor's bulk, so that Eq. (80) is valid without the last term $\frac{1}{4}$ in the parentheses – for any $b < c$.

As the last example, let us calculate the *mutual* inductance between a long straight wire and a round wire loop adjacent to it (Fig. 9), neglecting the thickness of both wires.

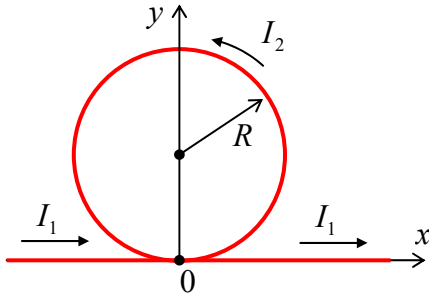


Fig. 5.9. An example of the mutual inductance calculation.

Here there is no problem with using the last approach discussed above, based on the direct calculation of the magnetic flux. Indeed, as was discussed in Sec. 1, the field \mathbf{B}_1 induced by the current I_1 at any point of the round loop is normal to its plane – e.g., to the plane of drawing of Fig. 9. In the Cartesian coordinates shown in that figure, Eq. (20) reads $B_1 = \mu_0 I_1 / 2\pi y$, giving the following magnetic flux through the loop:

$$\Phi_{21} = \frac{\mu_0 I_1}{2\pi} \int_{-R}^{+R} dx \int_{R - (R^2 - x^2)^{1/2}}^{R + (R^2 - x^2)^{1/2}} \frac{dy}{y} = \frac{\mu_0 I_1}{\pi} \int_0^R \ln \frac{R + (R^2 - x^2)^{1/2}}{R - (R^2 - x^2)^{1/2}} dx \equiv \frac{\mu_0 I_1 R}{\pi} \int_0^1 \ln \frac{1 + (1 - \xi^2)^{1/2}}{1 - (1 - \xi^2)^{1/2}} d\xi. \quad (5.81)$$

This is a table integral equal to π ,³⁶ so that $\Phi_{21} = \mu_0 I_1 R$, and the final answer for the mutual inductance $M \equiv L_{12} = L_{21} = \Phi_{21}/I_1$ is finite (and very simple):

$$M = \mu_0 R, \quad (5.82)$$

despite the magnetic field's divergence at the lowest point of the loop ($y = 0$).

Note that in contrast with the finite *mutual* inductance of this system, the *self*-inductances of both its wires are formally infinite in the thin-wire limit – see, e.g., Eq. (80), which in the limit $b/a \gg 1$ describes a thin straight wire. However, since this divergence is very weak (logarithmic), it is quenched by any deviation from this perfectly axial geometry. For example, a fair estimate of the inductance of a wire of a large but finite length $l \gg a$ may be obtained from Eq. (80) by the replacement of b with l :

$$L \approx \frac{\mu_0 l}{2\pi} \ln \frac{l}{a}. \quad (5.83)$$

(Note, however, that the exact result depends on where from/to the current flows beyond that segment.) It turns out that a similar approximate result, with l replaced with $2\pi R$ in the front factor, and with R under the logarithm, is valid for the self-inductance of a round loop with $a \ll R$. (A proof of this fact is a very useful exercise, highly recommended to the reader.)

³⁶ See, e.g., MA Eq. (6.13), with $a = 1$.

5.4. Magnetic dipole moment, and magnetic dipole media

The most natural way of the magnetic media description parallels that for dielectrics in Chapter 3, and is based on the properties of *magnetic dipoles* – the notion close (but not identical!) to that of the electric dipoles discussed in Sec. 3.1. To introduce this notion quantitatively, let us consider, just as in Sec. 3.1, a spatially-localized system with a current distribution $\mathbf{j}(\mathbf{r}')$, whose magnetic field is measured at relatively large distances $r \gg r'$ (Fig. 10).

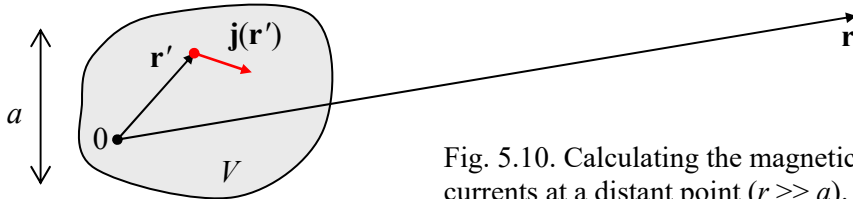


Fig. 5.10. Calculating the magnetic field of localized currents at a distant point ($r \gg a$).

Applying the truncated Taylor expansion (3.5) of the fraction $1/|\mathbf{r} - \mathbf{r}'|$ to the vector potential given by Eq. (28), we get

$$\mathbf{A}(\mathbf{r}) \approx \frac{\mu_0}{4\pi} \left[\frac{1}{r} \int_V \mathbf{j}(\mathbf{r}') d^3 r' + \frac{1}{r^3} \int_V (\mathbf{r} \cdot \mathbf{r}') \mathbf{j}(\mathbf{r}') d^3 r' \right]. \quad (5.84)$$

Now, due to the vector character of this potential, we have to depart somewhat from the approach of Sec. 3.1 and use the following vector algebra identity:³⁷

$$\int_V [f(\mathbf{j} \cdot \nabla g) + g(\mathbf{j} \cdot \nabla f)] d^3 r = 0, \quad (5.85)$$

that is valid for any pair of smooth (differentiable) scalar functions $f(\mathbf{r})$ and $g(\mathbf{r})$, and any vector function $\mathbf{j}(\mathbf{r})$ that, as the dc current density, satisfies the continuity condition $\nabla \cdot \mathbf{j} = 0$ and whose normal component vanishes on the surface of the volume V . First, let us use Eq. (85) with f equal to 1, and g equal to any Cartesian component of the radius-vector \mathbf{r} : $g = r_l$ ($l = 1, 2, 3$). Then it yields

$$\int_V (\mathbf{j} \cdot \mathbf{n}_l) d^3 r = \int_V j_l d^3 r = 0, \quad (5.86)$$

so that for the vector as the whole

$$\int_V \mathbf{j}(\mathbf{r}) d^3 r = 0, \quad (5.87)$$

showing that the first term on the right-hand side of Eq. (84) equals zero. Next, let us use Eq. (85) again, but now with $f = r_l$, $g = r_{l'}$ (where $l, l' = 1, 2, 3$); then it yields

$$\int_V (r_l j_{l'} + r_{l'} j_l) d^3 r = 0, \quad (5.88)$$

so that the l^{th} Cartesian component of the second integral in Eq. (84) may be transformed as

³⁷ See, e.g., MA Eq. (12.3) with the additional condition $j_n|_S = 0$, pertinent to space-restricted currents.

$$\begin{aligned} \int_V (\mathbf{r} \cdot \mathbf{r}') j_l d^3 r' &= \int_V \sum_{l'=1}^3 r_{l'} r'_{l'} j_l d^3 r' = \frac{1}{2} \sum_{l'=1}^3 r_{l'} \int_V (r'_{l'} j_l + r'_{l'} j_{l'}) d^3 r' \\ &= \frac{1}{2} \sum_{l'=1}^3 r_{l'} \int_V (r'_{l'} j_l - r'_{l'} j_{l'}) d^3 r' = -\frac{1}{2} \left[\mathbf{r} \times \int_V (\mathbf{r}' \times \mathbf{j}) d^3 r' \right]_l. \end{aligned} \quad (5.89)$$

As a result, Eq. (84) may be rewritten as

$$\boxed{\mathbf{A}(\mathbf{r}) = \frac{\mu_0}{4\pi} \frac{\mathbf{m} \times \mathbf{r}}{r^3}}, \quad (5.90)$$

where the vector \mathbf{m} , defined as³⁸

$$\boxed{\mathbf{m} \equiv \frac{1}{2} \int_V \mathbf{r} \times \mathbf{j}(\mathbf{r}) d^3 r}, \quad (5.91)$$

Magnetic dipole and its potential

is called the *magnetic dipole moment* of a field source – that itself, within the long-rang approximation (90), is called the *magnetic dipole*.

Note a close analogy between the \mathbf{m} defined by Eq. (91), and the orbital³⁹ angular momentum of a non-relativistic particle with mass m_k :

$$\mathbf{L}_k \equiv \mathbf{r}_k \times \mathbf{p}_k = \mathbf{r}_k \times m_k \mathbf{v}_k, \quad (5.92)$$

where $\mathbf{p}_k = m_k \mathbf{v}_k$ is its linear momentum. Indeed, for a continuum of such particles with equal electric charges q , distributed with spatial density n , we have $\mathbf{j} = qn\mathbf{v}$, and Eq. (91) yields

$$\mathbf{m} = \int_V \frac{1}{2} \mathbf{r} \times \mathbf{j} d^3 r = \int_V \frac{nq}{2} \mathbf{r} \times \mathbf{v} d^3 r, \quad (5.93)$$

while the total angular momentum of such a system of particles of equal masses m_0 , is

$$\mathbf{L} = \int_V n m_0 \mathbf{r} \times \mathbf{v} d^3 r,$$

so that we get a very straightforward relation

$$\boxed{\mathbf{m} = \frac{q}{2m_0} \mathbf{L}.} \quad (5.95) \quad \text{m vs. L}$$

For the orbital motion, this classical relation survives in quantum mechanics for linear operators, and hence for eigenvalues of the observables. Since the orbital angular momentum is quantized in the units of the Planck constant \hbar , the orbital magnetic moment of an electron is always a multiple of the so-called *Bohr magneton*

$$\boxed{\mu_B \equiv \frac{e\hbar}{2m_e},} \quad (5.96)$$

Bohr magneton

where m_e is the free electron mass.⁴⁰ However, for particles with spin, such a universal relation between the vectors \mathbf{m} and \mathbf{L} is no longer valid. For example, the electron's spin $s = \frac{1}{2}$ gives a contribution of $\hbar/2$ to its mechanical angular momentum, but a contribution very close to μ_B to its magnetic moment.

³⁸ In the Gaussian units, the definition (91) is kept valid “as is”, so that Eq. (90) is stripped of the factor $\mu_0/4\pi$.

³⁹ This adjective is used, especially in quantum mechanics, to distinguish the motion of a particle as a whole (not necessarily along a closed orbit!) from its intrinsic angular momentum, the spin – see, e.g., QM Chapters 3-6.

⁴⁰ In the SI units, $m_e \approx 0.91 \times 10^{-30}$ kg, so that $\mu_B \approx 0.93 \times 10^{-23}$ J/T.

The next important example of a magnetic dipole is a *planar* thin-wire loop, limiting area A (of arbitrary shape), and carrying current I , for which \mathbf{m} has a surprisingly simple form,

$$\mathbf{m} = IA, \quad (5.97)$$

where the modulus of the vector \mathbf{A} equals the loop's area A , and its direction is normal to the loop's plane. This formula may be readily proved by noticing that if we select the coordinate frame origin on the plane of the loop (Fig. 11), then the elementary component of the magnitude of the integral (91),

$$dm = \frac{1}{2} \left| \oint_C \mathbf{r} \times I d\mathbf{r} \right| \equiv I \oint_C \left| \frac{1}{2} \mathbf{r} \times d\mathbf{r} \right| = I \oint_C \frac{1}{2} r^2 d\varphi, \quad (5.98)$$

is just the elementary area $dA = (1/2)rd(r\varphi) = r^2d\varphi/2$ – the equality already used in CM Eq. (3.40).

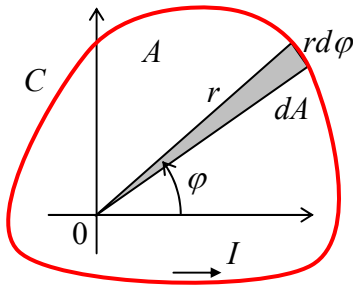


Fig. 5.11. Calculating the magnetic dipole moment of a planar current loop.

The comparison of Eqs. (96) and (97) allows a useful estimate of the scale of atomic currents, by finding what current I should flow in a circular loop of the atomic size scale (the Bohr radius) $r_B \sim 0.5 \times 10^{-10}$ m, i.e. of an area $A \sim 10^{-20}$ m², to produce a magnetic moment of the order of μ_B .⁴¹ The result is surprisingly macroscopic: $I \sim 1$ mA – quite comparable to the currents driving the sound in your phone's earbuds. Though due to the quantum-mechanical spread of electron's wavefunctions, this estimate should not be taken too literally, it is very useful for getting a gut feeling of how significant the atomic magnetism is, and hence why ferromagnets may provide such strong magnetic fields.

After these illustrations, let us return to the discussion of the general Eq. (90). Plugging it into (also general) Eq. (27), we may calculate the magnetic field of a magnetic dipole:⁴²

⁴¹ Another way to arrive at the same estimate is to take $I \sim ef = e\omega/2\pi$ with $\omega \sim 10^{16}$ s⁻¹ being the typical frequency of radiation due to atomic interlevel quantum transitions.

⁴² Similarly to the situation with the electric dipoles (see Eq. (3.24) and its discussion), it may be shown that the magnetic field of any closed current loop (or any system of such loops) satisfies the following equality:

$$\int_V \mathbf{B}(\mathbf{r}) d^3r = (2/3)\mu_0 \mathbf{m},$$

where the integral is over any sphere confining all the currents. On the other hand, as we know from Sec. 3.1, for a field with the structure (99), derived from the long-range approximation (90), such an integral vanishes. As a result, to get a coarse-grain description of the magnetic field of a small system located at $r = 0$, that would give the correct average value of the magnetic field, Eq. (99) should be modified as follows:

$$\mathbf{B}_{cg}(\mathbf{r}) = \frac{\mu_0}{4\pi} \left(\frac{3\mathbf{r}(\mathbf{r} \cdot \mathbf{m}) - \mathbf{m}r^2}{r^5} + \frac{8\pi}{3} \mathbf{m}\delta(\mathbf{r}) \right),$$

in a conceptual (though not quantitative) similarity to Eq. (3.25).

$$\boxed{\mathbf{B}(\mathbf{r}) = \frac{\mu_0}{4\pi} \frac{3\mathbf{r}(\mathbf{r} \cdot \mathbf{m}) - \mathbf{m}r^2}{r^5}.} \quad (5.99)$$

Magnetic dipole's field

The structure of this formula *exactly* replicates that of Eq. (3.13) for the electric dipole field – including the sign). Because of this similarity, the energy of a dipole of a fixed magnitude m in an external field, and hence the torque and the force exerted on it by a fixed external field, are given by expressions fully similar to those for an electric dipole – see Eqs. (3.15)-(3.19):⁴³

$$\boxed{U = -\mathbf{m} \cdot \mathbf{B}_{\text{ext}},} \quad (5.100)$$

Magnetic dipole in external field

and as a result,

$$\boldsymbol{\tau} = \mathbf{m} \times \mathbf{B}_{\text{ext}}, \quad (5.101)$$

$$\mathbf{F} = \nabla(\mathbf{m} \cdot \mathbf{B}_{\text{ext}}). \quad (5.102)$$

Now let us consider a system of many magnetic dipoles (e.g., atoms or molecules), distributed in space with an atomic-scale-averaged density n . Then we can use Eq. (90) generalized in an evident way for an arbitrary position \mathbf{r}' of the dipole, and the linear superposition principle, to calculate the macroscopic vector potential \mathbf{A} :

$$\mathbf{A}(\mathbf{r}) = \frac{\mu_0}{4\pi} \int \frac{\mathbf{M}(\mathbf{r}') \times (\mathbf{r} - \mathbf{r}')}{|\mathbf{r} - \mathbf{r}'|^3} d^3 r', \quad (5.103)$$

where $\mathbf{M} \equiv n\mathbf{m}$ is the *magnetization*: the average magnetic moment per unit volume. Transforming this integral absolutely similarly to how Eq. (3.27) had been transformed into Eq. (3.29), we get:

$$\mathbf{A}(\mathbf{r}) = \frac{\mu_0}{4\pi} \int \frac{\nabla' \times \mathbf{M}(\mathbf{r}')}{|\mathbf{r} - \mathbf{r}'|} d^3 r'. \quad (5.104)$$

Comparing this result with Eq. (28), we see that $\nabla \times \mathbf{M}$ is equivalent, in its magnetic effect, to the density \mathbf{j}_{ef} of a certain effective “magnetization current”. Just as the electric-polarization charge ρ_{ef} discussed in Sec. 3.2 (see Fig. 3.4), the vector $\mathbf{j}_{\text{ef}} = \nabla \times \mathbf{M}$ may be interpreted as the uncompensated part of the loop currents representing single magnetic dipoles \mathbf{m} – see Fig. 12. Note, however, that since the atomic magnetic dipoles may be due to particles’ spins, rather than the actual electric currents due to the orbital motion, the magnetization current’s nature is not as direct as that of the polarization charge.

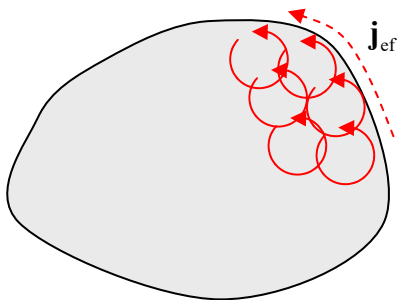


Fig. 5.12. A cartoon illustrating the physical nature of the effective magnetization current $\mathbf{j}_{\text{ef}} = \nabla \times \mathbf{M}$.

⁴³ Note that the fixation of m and \mathbf{B}_{ext} effectively means that the currents producing them are fixed – please have one more look at Eqs. (35) and (97). As a result, Eq. (100) is a particular case of Eq. (53) rather than (54) – hence the minus sign.

Now, using Eq. (28) to add the possible contribution from the *stand-alone currents* \mathbf{j} not included in the currents of microscopic magnetic dipoles, we get the general expression for the vector potential of the macroscopic field:

$$\mathbf{A}(\mathbf{r}) = \frac{\mu_0}{4\pi} \int \frac{[\mathbf{j}(\mathbf{r}') + \nabla' \times \mathbf{M}(\mathbf{r}')] d^3 r'}{|\mathbf{r} - \mathbf{r}'|}. \quad (5.105)$$

Repeating the calculations that have led us from Eq. (28) to the Maxwell equation (35), with the account of the magnetization current term, for the macroscopic magnetic field \mathbf{B} we get

$$\nabla \times \mathbf{B} = \mu_0 (\mathbf{j} + \nabla \times \mathbf{M}). \quad (5.106)$$

Following the same reasoning as in Sec. 3.2, we may recast this equation as

$$\nabla \times \mathbf{H} = \mathbf{j}, \quad (5.107)$$

where the field defined as

$$\mathbf{H} \equiv \frac{\mathbf{B}}{\mu_0} - \mathbf{M}, \quad (5.108)$$

for historic reasons (and very unfortunately) is also called the *magnetic field*.⁴⁴ This is why it is crucial to remember that the physical sense of field \mathbf{H} is very much different from field \mathbf{B} . To understand this difference better, let us use Eq. (107) to bring Eqs. (3.32), (3.36), (29), and (107) together, writing them as the following system of *macroscopic Maxwell equations* (again, so far for the stationary case $\partial/\partial t = 0$):⁴⁵

$$\boxed{\begin{aligned} \nabla \times \mathbf{E} &= 0, & \nabla \times \mathbf{H} &= \mathbf{j}, \\ \nabla \cdot \mathbf{D} &= \rho, & \nabla \cdot \mathbf{B} &= 0. \end{aligned}} \quad (5.109)$$

These equations clearly show that the roles of the vector fields \mathbf{D} and \mathbf{H} are very similar: they both may be called “would-be fields” – meaning the fields that *would be* induced by the stand-alone charges ρ and currents \mathbf{j} , if the medium had not modified them by its dielectric and magnetic polarization.

Despite this similarity, let me note an important difference of signs in the relation (3.33) between \mathbf{E} , \mathbf{D} , and \mathbf{P} , on one hand, and the relation (108) between \mathbf{B} , \mathbf{H} , and \mathbf{M} , on the other hand. This is *not* just a matter of definition. Indeed, due to the similarity of Eqs. (3.15) and (100), including similar signs, the electric and magnetic fields both try to orient the corresponding dipole moments along the field. Hence, in the media that allow such an orientation (and as we will see momentarily, for magnetic media it is not always the case), the induced polarizations \mathbf{P} and \mathbf{M} are directed along, respectively, the vectors \mathbf{E} and \mathbf{B} of the genuine (though macroscopic, i.e. atomic-scale-averaged) fields. According to Eq. (3.33), if the would-be field \mathbf{D} is fixed – say, by a fixed stand-alone charge distribution $\rho(\mathbf{r})$ – such a polarization *reduces* the electric field $\mathbf{E} = (\mathbf{D} - \mathbf{P})/\epsilon_0$. On the other hand, Eq. (108) shows that in a magnetic media with a fixed would-be field \mathbf{H} , the magnetic polarization making \mathbf{M} parallel to \mathbf{B} ,

⁴⁴ This confusion is exacerbated by the fact that in Gaussian units, Eq. (108) has the form $\mathbf{H} = \mathbf{B} - 4\pi\mathbf{M}$, and hence the fields \mathbf{B} and \mathbf{H} have the same dimensionality (and are formally equal in free space!) – though the unit of \mathbf{H} has a different name (*oersted*, abbreviated as Oe). Mercifully, in the SI units, the dimensionality of \mathbf{B} and \mathbf{H} is different, with the unit of \mathbf{H} called the *ampere per meter*.

⁴⁵ Let me remind the reader once again that in contrast with the system (36) of the Maxwell equations for the genuine (microscopic) fields, the right-hand sides of Eqs. (109) represent only the stand-alone charges and currents, not included in the microscopic electric and magnetic dipoles.

enhances the magnetic field $\mathbf{B} = \mu_0(\mathbf{H} + \mathbf{M})$. This difference may be traced back to the sign difference in the basic relations (1) and (2), i.e. to the fundamental fact that the electric charges of the same sign repulse, while the currents of the same direction attract each other.

5.5. Magnetic materials

In order to form a complete system, sufficient for the calculation of all fields from given $\rho(\mathbf{r})$ and $\mathbf{j}(\mathbf{r})$, the macroscopic Maxwell equations (109) have to be complemented with the constitutive relations describing the medium: $\mathbf{D} \leftrightarrow \mathbf{E}$, $\mathbf{j} \leftrightarrow \mathbf{E}$, and $\mathbf{B} \leftrightarrow \mathbf{H}$. The first two of them were discussed, in brief, in the last two chapters; let us proceed to the last one.

A major difference between the dielectric and magnetic constitutive relations $\mathbf{D}(\mathbf{E})$ and $\mathbf{B}(\mathbf{H})$ is that while a dielectric medium always *reduces* the external field, magnetic media may *either reduce or enhance* it. To quantify this fact, let us consider the most common case – *linear magnetic materials* in that \mathbf{M} (and hence \mathbf{H}) is proportional to \mathbf{B} . For isotropic materials, this proportionality is characterized by a scalar – either the *magnetic permeability* μ defined by the following relation:

$$\mathbf{B} \equiv \mu \mathbf{H}, \quad (5.110) \quad \text{Magnetic permeability}$$

or the *magnetic susceptibility*⁴⁶ defined as

$$\mathbf{M} = \chi_m \mathbf{H}. \quad (5.111) \quad \text{Magnetic susceptibility}$$

Plugging these relations into Eq. (108), we see that these two parameters are not independent, but are related as

$$\mu = (1 + \chi_m) \mu_0. \quad (5.112) \quad \chi_m \text{ vs. } \mu$$

Note that despite the superficial similarity between Eqs. (110)-(112) and the corresponding relations (3.43)-(3.47) for linear dielectrics:

$$\mathbf{D} = \epsilon \mathbf{E}, \quad \mathbf{P} = \chi_e \epsilon_0 \mathbf{E}, \quad \epsilon = (1 + \chi_e) \epsilon_0, \quad (5.113)$$

there is an important conceptual difference between them. Namely, while the vector \mathbf{E} on the right-hand sides of Eqs. (113) is the actual (though macroscopic) electric field, the vector \mathbf{H} on the right-hand side of Eqs. (110)-(111) represents a “would-be” magnetic field, in most aspects similar to \mathbf{D} rather than \mathbf{E} – see, for example, Eqs. (109). This historic difference in the traditional form of the constitutive relations for the electric and magnetic fields is not without its physical reasons. Most experiments with electric and magnetic materials are performed by placing their samples into nearly-uniform electric and magnetic fields, and the simplest systems for their implementation are, respectively, plane capacitors (Fig. 2.3) and long solenoids (Fig. 6). The field in the former system may be most conveniently

⁴⁶ According to Eqs. (110) and (112), i.e. in the SI units, χ_m is dimensionless, while μ has the same dimensionality as μ_0 . In the Gaussian units, μ is dimensionless: $(\mu)_{\text{Gaussian}} = (\mu)_{\text{SI}}/\mu_0$, and χ_m is also introduced differently, as $\mu = 1 + 4\pi\chi_m$. Hence, just as for the electric susceptibilities, these dimensionless coefficients are different in the two systems: $(\chi_m)_{\text{SI}} = 4\pi(\chi_m)_{\text{Gaussian}}$. Note also that χ_m is formally called the *volumic* magnetic susceptibility, to distinguish it from the *atomic* (or “molecular”) susceptibility χ defined by a similar relation, $\langle \mathbf{m} \rangle \equiv \chi \mathbf{H}$, where \mathbf{m} is the induced magnetic moment of a single dipole – e.g., an atom. (χ is an analog of the electric atomic polarizability α – see Eq. (3.48) and its discussion.) In a dilute medium, i.e. in the absence of substantial dipole-dipole interactions, $\chi_m = n\chi$, where n is the dipole density.

controlled by fixing the voltage V between its plates, which is proportional to the electric field \mathbf{E} . On the other hand, the field provided by the solenoid may be fixed by the current I in it, and according to Eq. (107), the field proportional to this stand-alone current is \mathbf{H} , rather than \mathbf{B} .⁴⁷

Table 1 lists the approximate magnetic susceptibility values for several materials. It shows that in contrast to linear dielectrics whose susceptibility χ_e is always positive, i.e. the dielectric constant $\kappa = \chi_e + 1$ is always larger than 1 (see Table 3.1), linear magnetic materials may be either *paramagnets* (with $\chi_m > 0$, i.e. $\mu > \mu_0$) or *diamagnets* (with $\chi_m < 0$, i.e. $\mu < \mu_0$).

Table 5.1. Susceptibility (χ_m)_{SI} of a few representative and/or important magnetic materials^(a)

“Mu-metal” (75% Ni + 15% Fe + a few %% of Cu and Mo)	$\sim 20,000^{(b)}$
Permalloy (80% Ni + 20% Fe)	$\sim 8,000^{(b)}$
“Electrical” (or “transformer”) steel (Fe + a few %% of Si)	$\sim 4,000^{(b)}$
Nickel	~ 100
Aluminum	$+2 \times 10^{-5}$
Oxygen (at ambient conditions)	$+0.2 \times 10^{-5}$
Water	-0.9×10^{-5}
Diamond	-2×10^{-5}
Copper	-7×10^{-5}
Bismuth (the strongest non-superconducting diamagnet)	-17×10^{-5}

^(a)The table does not include bulk superconductors, which may be described, in a so-called *coarse-scale approximation*, as perfect diamagnets (with $\mathbf{B} = 0$, i.e. formally with $\chi_m = -1$ and $\mu = 0$), though the actual physics of this phenomenon is different – see Sec. 6.3 below.

^(b)The exact values of $\chi_m \gg 1$ for soft ferromagnetic materials (see, e.g., the upper three rows of the table) depend not only on their composition but also on their thermal processing (“annealing”). Moreover, due to unintentional vibrations, the extremely high values of χ_m of such materials may decay with time, though they may be restored to the original values by new annealing. The reason for such behavior is discussed in the text below.

The reason for this difference is that in dielectrics, two different polarization mechanisms (schematically illustrated by Fig. 3.7) lead to the same sign of the average polarization – see the discussion in Sec. 3.3. One of these mechanisms, illustrated by Fig. 3.7b, i.e. the ordering of spontaneous dipoles by the applied field, is also possible for magnetization – for the atoms and molecules with spontaneous internal magnetic dipoles of magnitude $m_0 \sim \mu_B$, due to their net spins. Again, in the absence of an external magnetic field the spins, and hence the dipole moments \mathbf{m}_0 may be disordered, but according to Eq. (100), the external magnetic field tends to align the dipoles along its direction. As a result, the average direction of the spontaneous elementary moments \mathbf{m}_0 , and hence the direction of the arising magnetization \mathbf{M} , is the same as that of the microscopic field \mathbf{B} at the points of the dipole location (i.e., for a diluted media, of $\mathbf{H} \approx \mathbf{B}/\mu_0$), resulting in a positive susceptibility χ_m , i.e. in the paramagnetism, such as that of oxygen and aluminum – see Table 1.

⁴⁷ This fact also explains the misleading term “magnetic field” for \mathbf{H} .

However, in contrast to the electric polarization of atoms/molecules with no spontaneous electric dipoles, which gives the same sign of $\chi_e \equiv \kappa - 1$ (see Fig. 3.7a and its discussion), the magnetic materials with no spontaneous atomic magnetic dipole moments have $\chi_m < 0$ – the effect called the *orbital* (or “Larmor”⁴⁸) *diamagnetism*. As the simplest model of this effect, let us consider the orbital motion of an atomic electron about an atomic nucleus as that of a classical particle of mass m_0 , with an electric charge q , about an immobile attracting center. As classical mechanics tells us, the central attractive force does not change the particle’s angular momentum $\mathbf{L} \equiv m_0 \mathbf{r} \times \mathbf{v}$, but the applied magnetic field \mathbf{B} (that may be taken uniform on the atomic scale) does, due to the torque (101) it exerts on the magnetic moment (95):

$$\frac{d\mathbf{L}}{dt} = \boldsymbol{\tau} = \mathbf{m} \times \mathbf{B} = \frac{q}{2m_0} \mathbf{L} \times \mathbf{B}. \quad (5.114)$$

The diagram in Fig. 13 shows that in the limit of a relatively weak field, when the magnitude of the angular momentum \mathbf{L} may be considered constant, this equation describes the rotation (called the *torque-induced precession*⁴⁹) of the vector \mathbf{L} about the direction of the vector \mathbf{B} , with the angular frequency $\Omega = -q\mathbf{B}/2m_0$, independent of the angle θ . According to Eqs. (91) and (114), the resulting additional (field-induced) magnetic moment $\Delta\mathbf{m} \propto q\Omega \propto -q^2\mathbf{B}/m_0$ has, irrespectively of the sign of q , a direction *opposite* to the field. Hence, according to Eq. (111) with $\mathbf{H} \approx \mathbf{B}/\mu_0$, the susceptibility $\chi_m \propto \chi \equiv \Delta\mathbf{m}/\mathbf{H}$ is indeed negative. (Let me leave its quantitative estimate within this classical model for the reader’s exercise.) The quantum-mechanical treatment confirms this qualitative picture of the Larmor diamagnetism, giving only quantitative corrections to the classical result for χ_m .⁵⁰

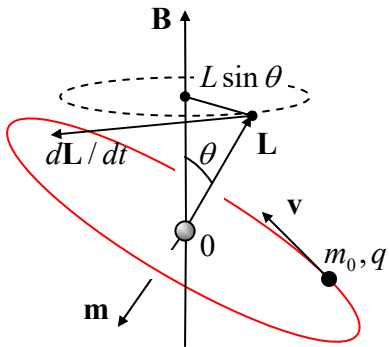


Fig. 5.13. The torque-induced precession of a classical charged particle in a magnetic field.

A simple estimate (also left for the reader’s exercise) shows that in atoms with spontaneous non-zero net spins, the magnetic dipole orientation mechanism prevails over the orbital diamagnetism, so that the materials incorporating such atoms usually exhibit net paramagnetism – see Table 1. Due to possible strong quantum interaction between the spin dipole moments, the magnetism of such materials is rather complex, with numerous interesting phenomena and elaborate theories. Unfortunately, all this physics is well outside the framework of this course, and I have to refer the interested reader to special literature,⁵¹ but still will mention some key facts.

⁴⁸ Named after Sir Joseph Larmor who was the first (in 1897) to describe this effect mathematically.

⁴⁹ For a detailed discussion of this effect see, e.g., CM Sec. 4.5.

⁵⁰ See, e.g., QM Sec. 6.4. Quantum mechanics also explains why in most common (*s*-) ground states, the average contribution (95) of the orbital angular momentum \mathbf{L} to the net vector \mathbf{m} vanishes.

⁵¹ See, e.g., D. J. Jiles, *Introduction to Magnetism and Magnetic Materials*, 2nd ed., CRC Press, 1998, or R. C. O’Handley, *Modern Magnetic Materials*, Wiley, 1999.

Most importantly, a sufficiently strong magnetic dipole-dipole interaction may lead to their spontaneous ordering, even in the absence of the applied field. This ordering may correspond to either parallel alignment of the dipoles (*ferromagnetism*) or anti-parallel alignment of the adjacent dipoles (*antiferromagnetism*). Evidently, the external effects of ferromagnetism are stronger, because this phase corresponds to a substantial spontaneous magnetization \mathbf{M} even in the absence of an external magnetic field. (The corresponding magnitude of $\mathbf{B} = \mu_0\mathbf{M}$ is called the *remanence field*, B_R .) The direction of the vector \mathbf{B}_R may be switched by the application of an external magnetic field, with a magnitude above a certain value H_C called *coercivity*, leading to the well-known hysteretic loops on the $[H, B]$ plane (see Fig. 14 for a typical example) – similar to those in ferroelectrics, already discussed in Sec. 3.3.

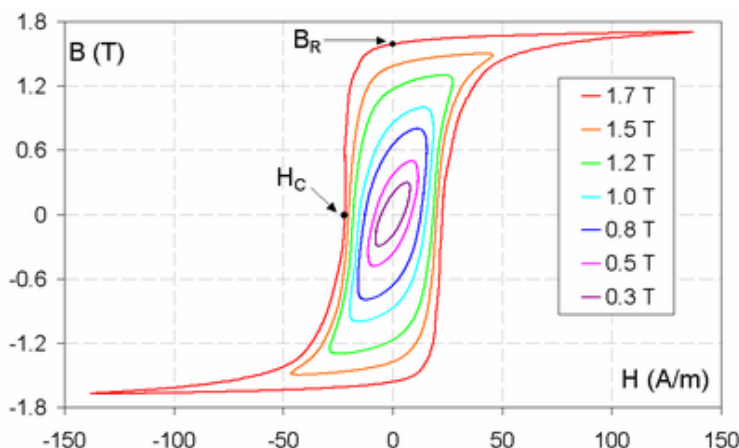


Fig. 5.14. Experimental magnetization curves of specially processed (cold-rolled) electrical steel – a solid solution of $\sim 10\%$ C and $\sim 6\%$ Si in Fe. (Reproduced from www.thefullwiki.org/Hysteresis under the Creative Commons BY-SA 3.0 license.)

Just as the ferroelectrics, the ferromagnets may also be *hard* or *soft* – in the magnetic rather than mechanical sense. In hard ferromagnets (also called *permanent magnets*), the dipole interaction is so strong that B stays close to B_R in all applied fields below H_C , so that the hysteretic loops are virtually rectangular. Hence, in lower fields, the magnetization \mathbf{M} of a permanent magnet may be considered constant, with the magnitude B_R/μ_0 . Such hard ferromagnetic materials (notably, rare-earth compounds such as SmCo_5 , $\text{Sm}_2\text{Co}_{17}$, and especially $\text{Nd}_2\text{Fe}_{14}\text{B}$), with high remanence fields (~ 1 T) and high coercivity ($\sim 10^6$ A/m), have numerous practical applications.⁵² Let me give just two, most important examples.

First, permanent magnets are the core components of most *electric motors*. By the way, this venerable (~ 150 -years-old) technology is currently experiencing a quiet revolution, driven mostly by the electric car development. In the most advanced type of motors, called *permanent-magnet synchronous machines* (PMSM), the remanence magnetic field B_R of a permanent-magnet rotating part of the machine (called the *rotor*) interacts with the magnetic field of ac currents passed through wire windings in the external, static part of the motor (called the *stator*). The resulting torque may drive the rotor to extremely high speeds, exceeding 10,000 rotations per minute, enabling the motor to deliver several kilowatts of mechanical power from each kilogram of its mass.

As the second important example, despite the decades of the exponential (*Moore's-law*) progress of semiconductor electronics, most computer data storage systems (e.g., in data centers) are still based

⁵² Currently, the neodymium-iron-boron compound holds nearly 95% percent of the world permanent-magnet application market, due to its combination of high B_R and H_C with lower fabrication costs.

on *hard disk drives* whose active media are submicron-thin layers of hard ferromagnets, with the data bits stored in the form of the direction of the remanent magnetization of small film spots. This technology has reached fantastic sophistication, with the recorded data density of the order of 10^{12} bits per square inch.⁵³ (Only recently it started to be seriously challenged by *solid-state drives* based on the floating-gate semiconductor memories already mentioned in Chapter 3.)⁵⁴

In contrast, in soft ferromagnets, with their lower magnetic dipole interactions, the magnetization is constant only inside each of the spontaneously formed magnetic domains, while the volume and shape of the domains are affected by the applied magnetic field. As a result, the hysteresis loop's shape of soft ferromagnets is dependent on the cycled field's amplitude and cycling history – see Fig. 14. At high fields, their \mathbf{B} (and hence \mathbf{M}) is driven into saturation, with $B \approx B_R$, but at low fields, they behave essentially as linear magnetics with very high values of χ_m and hence μ – see the top rows of Table 1. (The magnetic domain interaction, and hence the low-field susceptibility of such soft ferromagnets are highly dependent on the material's fabrication technology and its post-fabrication thermal and mechanical treatments.) Due to these high values of μ , soft ferromagnets, especially iron and its alloys (e.g., various special steels), are extensively used in electrical engineering – for example in the cores of transformers – see the next section.

Due to the relative weakness of the magnetic dipole interaction in some materials, their ferromagnetic ordering may be destroyed by thermal fluctuations, if the temperature is increased above some value called the *Curie temperature* T_C , specific for each material. The transition between the ferromagnetic and paramagnetic phases at $T = T_C$ is a classical example of a *continuous phase transition*, with the average polarization \mathbf{M} playing the role of the so-called *order parameter* that (in the absence of external fields) becomes different from zero only at $T < T_C$, increasing gradually at the further temperature reduction.⁵⁵

5.6. Systems with magnetic materials

Just as the electrostatics of linear dielectrics, the magnetostatics is very simple in the particular case when all essential stand-alone currents are embedded into a linear magnetic medium with a constant permeability μ . Indeed, let us assume that we know the solution $\mathbf{B}_0(\mathbf{r})$ of the magnetic pair of

⁵³ “A magnetic head slider [the read/write head – KKL] flying over a disk surface with a flying height of 25 nm with a relative speed of 20 meters/second [all realistic parameters – KKL] is equivalent to an aircraft flying at a physical spacing of 0.2 μm at 900 kilometers/hour.” B. Bhushan, as quoted in the (generally good) book by G. Hadjipanayis, *Magnetic Storage Systems Beyond 2000*, Springer, 2001.

⁵⁴ The high-frequency properties of hard ferromagnets are also very non-trivial. For example, according to Eq. (101), an external magnetic field \mathbf{B}_{ext} exerts torque $\boldsymbol{\tau} = \mathbf{M} \times \mathbf{B}_{\text{ext}}$ on the spontaneous magnetic moment \mathbf{M} of a unit volume of a ferromagnet. In some nearly-isotropic, mechanically fixed ferromagnetic samples, this torque causes the precession, around the direction of \mathbf{B}_{ext} (very similar to that illustrated in Fig. 13), of not the sample as such, but of the magnetization \mathbf{M} inside it, with a certain frequency ω_r . If the frequency ω of an additional ac field becomes very close to ω_r , its absorption sharply increases – the so-called *ferromagnetic resonance*. Moreover, if ω is somewhat higher than ω_r , the effective magnetic permeability $\mu(\omega)$ of the material for the ac field may become *negative*, enabling a series of interesting effects and practical applications. Very unfortunately, I could not find time for their discussion in this series and have to refer the interested reader to literature, for example the monograph by A. Gurevich and G. Melkov, *Magnetization Oscillations and Waves*, CRC Press, 1996.

⁵⁵ In this series, a quantitative discussion of such transitions is given in SM Chapter 4.

the genuine (“microscopic”) Maxwell equations (36) in free space, i.e. when the genuine current density \mathbf{j} coincides with that of stand-alone currents. Then the macroscopic Maxwell equations (109) and the linear constitutive equation (110) are satisfied with the pair of functions

$$\mathbf{H}(\mathbf{r}) = \frac{\mathbf{B}_0(\mathbf{r})}{\mu_0}, \quad \mathbf{B}(\mathbf{r}) = \mu \mathbf{H}(\mathbf{r}) = \frac{\mu}{\mu_0} \mathbf{B}_0(\mathbf{r}). \quad (5.115)$$

Hence the only effect of the complete filling of a fixed-current system with a uniform, linear magnetic medium is the change of the magnetic field \mathbf{B} at all points by the same constant factor $\mu/\mu_0 \equiv 1 + \chi_m$, which may be either larger or smaller than 1. (As a reminder, a similar filling of a system of fixed stand-alone charges with a uniform, linear dielectric always leads to a reduction of the electric field \mathbf{E} by a factor of $\epsilon/\epsilon_0 \equiv 1 + \chi_e$ – the difference whose physics was already discussed at the end of Sec. 4.)

However, this simple result is generally invalid in the case of nonuniform (or piecewise-uniform) magnetic samples. To analyze this case, let us first integrate the macroscopic Maxwell equation (107) along a closed contour C limiting a smooth surface S . Now using the Stokes theorem just as at the derivation of Eq. (37), we get the macroscopic version of the Ampère law (37):

Macroscopic
Ampère
law

$$\oint_C \mathbf{H} \cdot d\mathbf{r} = I. \quad (5.116)$$

Let us apply this relation to a sharp boundary between two regions with different magnetic materials, with no stand-alone currents on the interface, similarly to how this was done for the field \mathbf{E} in Sec. 3.4 – see Fig. 3.5. The result is similar as well:

$$H_\tau = \text{const}. \quad (5.117)$$

On the other hand, the integration of the Maxwell equation (29) over a Gaussian pillbox enclosing a border fragment (again just as shown in Fig. 3.5 for the field \mathbf{D}) yields a result similar to Eq. (3.35):

$$B_n = \text{const}. \quad (5.118)$$

For linear magnetic media, with $\mathbf{B} = \mu \mathbf{H}$, the latter boundary condition is reduced to

$$\mu H_n = \text{const}. \quad (5.119)$$

Let us use these boundary conditions, first of all, to see what happens with a long cylindrical sample of a uniform magnetic material, placed parallel to a uniform external magnetic field \mathbf{B}_0 – see Fig. 15. Such a sample cannot noticeably disturb the field in the free space outside it, at most of its length: $\mathbf{B}_{\text{ext}} = \mathbf{B}_0$, $\mathbf{H}_{\text{ext}} = \mu_0 \mathbf{B}_{\text{ext}} = \mu_0 \mathbf{B}_0$. Now applying Eq. (117) to the dominating surfaces of the sample, we get $\mathbf{H}_{\text{int}} = \mathbf{H}_0$.⁵⁶ For a linear magnetic material, these relations yield $\mathbf{B}_{\text{int}} = \mu \mathbf{H}_{\text{int}} = (\mu/\mu_0) \mathbf{B}_0$.⁵⁷ For the high- μ media, this means that $B_{\text{int}} \gg B_0$. This effect may be vividly represented as the concentration of the magnetic field lines in high- μ samples – see Fig. 15 again. (The concentration affects the external field

⁵⁶ The independence of \mathbf{H} on magnetic properties of the sample in this geometry explains why this field’s magnitude is commonly used as the argument in the plots like Fig. 14: such measurements are typically carried out by placing an elongated sample of the material under study into a long solenoid with a controllable current I , so that according to Eq. (116), $H_0 = nI$, regardless of the sample.

⁵⁷ The reader is highly encouraged to carry out a similar analysis of the fields inside narrow gaps cut in a linear magnetic material, similar to that carried in Sec. 3.3 out for linear dielectrics – see Fig. 3.6 and its discussion.

distribution only at distances of the order of $(\mu/\mu_0) t \ll l$ near the sample's ends.) Such concentration is widely used in such practically important devices as transformers, in which two multi-turn coils are wound on a ring-shaped (e.g., toroidal, see Fig. 6b) core made of a soft ferromagnetic material (such as the *transformer steel*, see Table 1) with $\mu \gg \mu_0$. This minimizes the number of "stray" field lines, and makes the magnetic flux Φ piercing each wire turn of either coil virtually the same – the equality important for the secondary voltage induction – see the next chapter.

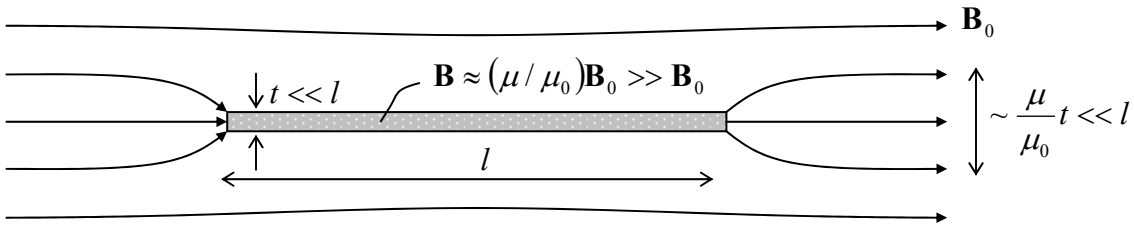


Fig. 5. 15. Magnetic field concentration in long, high- μ magnetic samples (schematically).

Samples of other geometries may create strong perturbations of the external field, extended to distances of the order of the sample's dimensions. To analyze such problems, we may benefit from a simple, partial differential equation for a scalar function, e.g., the Laplace equation, because in Chapter 2 we have learned how to solve it for many simple geometries. In magnetostatics, the introduction of a scalar potential is generally impossible due to the vortex-like magnetic field lines. However, if there are no stand-alone currents within the region we are interested in, then the macroscopic Maxwell equation (107) for the field \mathbf{H} is reduced to $\nabla \times \mathbf{H} = 0$, similar to Eq. (1.28) for the electric field, showing that we may introduce the scalar potential of the magnetic field, ϕ_m , using a relation similar to Eq. (1.33):

$$\mathbf{H} = -\nabla \phi_m. \quad (5.120)$$

Combining it with the homogenous Maxwell equation (29) for the magnetic field, $\nabla \cdot \mathbf{B} = 0$, and Eq. (110) for a linear magnetic material, we arrive at a single differential equation, $\nabla \cdot (\mu \nabla \phi_m) = 0$. For a uniform medium ($\mu(\mathbf{r}) = \text{const}$), it is reduced to our beloved Laplace equation:

$$\nabla^2 \phi_m = 0. \quad (5.121)$$

Moreover, Eqs. (117) and (119) give us very familiar boundary conditions: the first of them

$$\frac{\partial \phi_m}{\partial \tau} = \text{const}, \quad (5.122a)$$

being equivalent to

$$\phi_m = \text{const}, \quad (5.122b)$$

while the second one giving

$$\mu \frac{\partial \phi_m}{\partial n} = \text{const}. \quad (5.123)$$

Indeed, these boundary conditions are absolutely similar for (3.37) and (3.56) of electrostatics, with the replacement $\epsilon \rightarrow \mu$.⁵⁸

⁵⁸ This similarity may seem strange because earlier we have seen that the parameter μ is physically more similar to $1/\epsilon$. The reason for this paradox is that in magnetostatics, the magnetic potential ϕ_m is traditionally used to

Let us analyze the geometric effects on magnetization, first using the (too?) familiar structure: a sphere, made of a linear magnetic material, placed into a uniform external field $\mathbf{H}_0 \equiv \mathbf{B}_0/\mu_0$. Since the differential equation and the boundary conditions are similar to those of the corresponding electrostatics problem (see Fig. 3.11 and its discussion), we can use the above analogy to reuse the solution we already have – see Eqs. (3.63). Just as in the electric case, the field outside the sphere, with

$$(\phi_m)_{r>R} = H_0 \left(-r + \frac{\mu - \mu_0}{\mu + 2\mu_0} \frac{R^3}{r^2} \right) \cos \theta, \quad (5.124)$$

is a sum of the uniform external field \mathbf{H}_0 , with the potential $-H_0 r \cos \theta \equiv -H_0 z$, and the dipole field (99) with the following induced magnetic dipole moment of the sphere:⁵⁹

$$\mathbf{m} = 4\pi \frac{\mu - \mu_0}{\mu + 2\mu_0} R^3 \mathbf{H}_0. \quad (5.125)$$

On the contrary, the internal field is perfectly uniform, and directed along the external one:

$$(\phi_m)_{r < R} = -H_0 \frac{3\mu_0}{\mu + 2\mu_0} r \cos \theta, \quad \text{so that} \quad \frac{H_{\text{int}}}{H_0} = \frac{3\mu_0}{\mu + 2\mu_0}, \quad \frac{B_{\text{int}}}{B_0} = \frac{\mu H_{\text{int}}}{\mu_0 H_0} = \frac{3\mu}{\mu + 2\mu_0}. \quad (5.126)$$

Note that the field \mathbf{H}_{int} inside the sphere is *not* equal to the applied external field \mathbf{H}_0 . This example shows that the interpretation of \mathbf{H} as the “would-be” magnetic field generated by external stand-alone currents \mathbf{j} should not be exaggerated by saying that its distribution is independent of the magnetic bodies in the system. In the limit $\mu \gg \mu_0$, Eqs. (126) yield $H_{\text{int}}/H_0 \ll 1$, $B_{\text{int}}/H_0 = 3\mu_0$, the factor 3 being specific for the particular geometry of the sphere. If a sample is strongly stretched along the applied field, with its length l much larger than the scale t of its cross-section, this geometric effect is gradually decreased, and B_{int} tends to its value $\mu H_0 \gg B_0$, as was discussed above – see Fig. 15.

Now let us calculate the field distribution in a similar, but slightly more complex (and practically important) system: a round cylindrical shell, made of a linear magnetic material, placed into a uniform external field \mathbf{H}_0 normal to its axis – see Fig. 16.

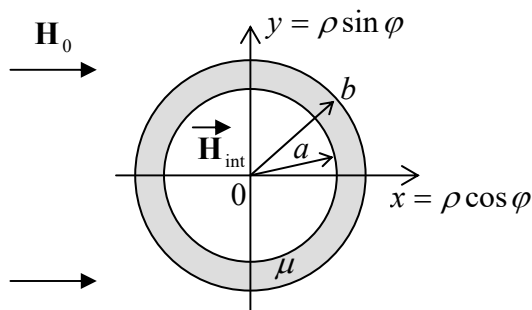


Fig. 5.16. Cylindrical magnetic shield.

describe the “would-be field” \mathbf{H} , while in electrostatics, the potential ϕ describes the actual electric field \mathbf{E} . (This tradition persists from the days when \mathbf{H} was perceived as a genuine magnetic field.)

⁵⁹ To derive Eq. (125), we may either calculate the gradient of the ϕ_m given by Eq. (124), or use the similarity of Eqs. (3.13) and (99), to derive from Eq. (3.17) a similar expression for the magnetic dipole’s potential:

$$\phi_m = \frac{1}{4\pi} \frac{m \cos \theta}{r^2}.$$

Now comparing this formula with the second term of Eq. (124), we immediately get Eq. (125).

Since there are no stand-alone currents in the region of our interest, we can again represent the field $\mathbf{H}(\mathbf{r})$ by the gradient of the magnetic potential ϕ_m – see Eq. (120). Inside each of three constant- μ regions, i.e. at $\rho < b$, $a < \rho < b$, and $b < \rho$ (where ρ is the 2D distance from the cylinder's axis), the potential obeys the Laplace equation (121). In the convenient, polar coordinates (see Fig. 16), we may, guided by the general solution (2.112) of the Laplace equation and our experience in its application to axially-symmetric geometries, look for ϕ_m in the following form:

$$\phi_m = \begin{cases} (-H_0\rho + b_1'/\rho)\cos\varphi, & \text{for } b \leq \rho, \\ (a_1\rho + b_1/\rho)\cos\varphi, & \text{for } a \leq \rho \leq b, \\ -H_{\text{int}}\rho\cos\varphi, & \text{for } \rho \leq a. \end{cases} \quad (5.127)$$

Plugging this solution into the boundary conditions (122)-(123) at both interfaces ($\rho = b$ and $\rho = a$), we get the following system of four equations:

$$\begin{aligned} -H_0b + b_1'/b &= a_1b + b_1/b, & (a_1a + b_1/a) &= -H_{\text{int}}a, \\ \mu_0(-H_0 - b_1'/b^2)H_0 &= \mu(a_1 - b_1/b^2), & \mu(a_1 - b_1/a^2) &= -\mu_0H_{\text{int}}, \end{aligned} \quad (5.128)$$

for four unknown coefficients a_1 , b_1 , b_1' , and H_{int} . Solving the system, we get, in particular:

$$\frac{H_{\text{int}}}{H_0} = \frac{\alpha_c - 1}{\alpha_c - (a/b)^2}, \quad \text{with } \alpha_c \equiv \left(\frac{\mu + \mu_0}{\mu - \mu_0} \right)^2. \quad (5.129)$$

According to these formulas, at $\mu > \mu_0$, the field in the free space inside the cylinder is lower than the external field. This fact allows using such structures, made of high- μ materials such as permalloy (see Table 1), for passive shielding⁶⁰ from unintentional magnetic fields (e.g., the Earth's field) – the task very important for the design of many physical experiments. As Eq. (129) shows, the larger is μ , the closer is α_c to 1, and the smaller is the ratio H_{int}/H_0 , i.e. the better is the shielding, for the same a/b ratio. On the other hand, for a given magnetic material, i.e. for a fixed parameter α_c , the shielding is improved by making the ratio $a/b < 1$ smaller, i.e. the shield thicker. On the other hand, as Fig. 16 shows, smaller a leaves less space for the shielded samples, calling for a compromise.

Note that in the limit $\mu/\mu_0 \rightarrow \infty$, both Eq. (126) and Eq. (129), describing different geometries yield $H_{\text{int}}/H_0 \rightarrow 0$. Indeed, as it follows from Eq. (119), in this limit the field \mathbf{H} tends to zero inside magnetic samples of virtually geometry. (The formal exception is the longitudinal cylindrical geometry shown in Fig. 15, with $t/l \rightarrow 0$, where $\mathbf{H}_{\text{int}} = \mathbf{H}_0$ for any finite μ , but even in it, the last equality holds only if $t/l \ll \mu_0/\mu$.)

Now let us discuss a curious (and practically important) approach to systems with relatively thin, closed magnetic cores made of several sections of high- μ magnetic materials, with the cross-section areas A_k much smaller than the squared lengths l_k of the sections – see Fig. 17. If all $\mu_k \gg \mu_0$, virtually all field lines are confined to the interior of the core. Then, applying the macroscopic Ampère law (116) to a contour C that follows a magnetic field line inside the core (see, for example, the dashed line in Fig. 17), we get the following approximate expression (exactly valid only in the limit $\mu_k/\mu_0, l_k^2/A_k \rightarrow \infty$):

⁶⁰ Another approach to the undesirable magnetic fields' reduction is the "active shielding" – the external field's compensation with the counter-field induced by controlled currents in specially designed wire coils.

$$\oint_C H_l dl \approx \sum_k l_k H_k \equiv \sum_k l_k \frac{B_k}{\mu_k} = NI . \quad (5.130)$$

However, since the magnetic field lines stay in the core, the magnetic flux $\Phi_k \approx B_k A_k$ should be the same ($\equiv \Phi$) for each section, so that $B_k = \Phi/A_k$. Plugging this condition into Eq. (130), we get

Magnetic Ohm law and reluctance

$$\Phi = \frac{NI}{\sum_k \mathcal{R}_k}, \quad \text{where } \mathcal{R}_k \equiv \frac{l_k}{\mu_k A_k} . \quad (5.131)$$

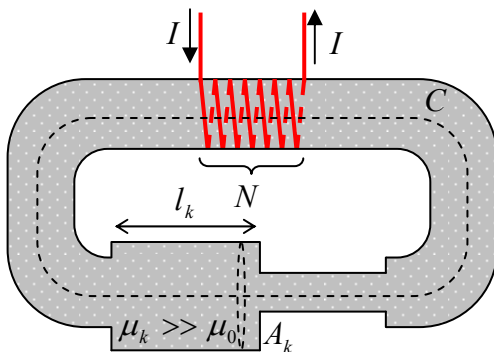


Fig. 5.17. Deriving the “magnetic Ohm law” (131).

Note a close analogy of the first of these equations with the usual Ohm law for several resistors connected in series, with the magnetic flux playing the role of electric current, while the product NI , the role of the voltage applied to the chain of resistors. This analogy is fortified by the fact that the second of Eqs. (131) is similar to the expression for the resistance $R = l/\sigma A$ of a long, uniform conductor, with the magnetic permeability μ playing the role of the electric conductivity σ . (To sound similar, but still different from the resistance R , the parameter \mathcal{R} is called *reluctance*.) This is why Eq. (131) is called the *magnetic Ohm law*; it is very useful for approximate analyses of systems like ac transformers, magnetic energy storage systems, etc.

Now let me proceed to a brief discussion of systems with permanent magnets. First of all, using the definition (108) of the field \mathbf{H} , we may rewrite the Maxwell equation (29) for the field \mathbf{B} as

$$\nabla \cdot \mathbf{B} \equiv \mu_0 \nabla \cdot (\mathbf{H} + \mathbf{M}) = 0, \quad \text{i.e. as } \nabla \cdot \mathbf{H} = -\nabla \cdot \mathbf{M} , \quad (5.132)$$

While this relation is general, it is especially convenient in permanent magnets, where the magnetization vector \mathbf{M} may be approximately considered field-independent.⁶¹ In this case, Eq. (132) for \mathbf{H} is an exact analog of Eq. (1.27) for \mathbf{E} , with the fixed term $-\nabla \cdot \mathbf{M}$ playing the role of the fixed charge density (more exactly, of ρ/ϵ_0). For the scalar potential ϕ_m , defined by Eq. (120), this gives the Poisson equation

$$\nabla^2 \phi_m = \nabla \cdot \mathbf{M} , \quad (5.133)$$

similar to those solved, for quite a few geometries, in the previous chapters.

⁶¹ Note that in this approximation, there is no difference between the *remanence magnetization* $M_R \equiv B_R/\mu_0$, of the magnet and its *saturation magnetization* $M_S \equiv \lim_{H \rightarrow \infty} [B(H)/\mu_0 - H]$.

In the case when \mathbf{M} is not only field-independent but also uniform inside a permanent magnet's volume, then the right-hand sides of Eqs. (132) and (133) vanish both inside the volume and in the surrounding free space, and give a non-zero effective charge only on the magnet's surface. Integrating Eq. (132) along a short path normal to the surface and crossing it, we get the following boundary conditions:

$$\Delta H_n \equiv (H_n)_{\text{in free space}} - (H_n)_{\text{in magnet}} = M_n \equiv M \cos \theta, \quad (5.134)$$

where θ is the angle between the magnetization vector and the outer normal to the magnet's surface. This relation is an exact analog of Eq. (1.24) for the normal component of the field \mathbf{E} , with the effective surface charge density (or rather σ/ϵ_0) equal to $M \cos \theta$.

This analogy between the magnetic field induced by a fixed, constant magnetization and the electric field induced by surface electric charges enables one to reuse the solutions of quite a few problems considered in Chapters 1-3. Leaving a few such problems for the reader's exercise (see Sec. 7), let me demonstrate the power of this analogy on just two examples specific to magnetic systems. First, let us calculate the force necessary to detach the flat ends of two long, uniform rod magnets, of length l and cross-section area $A \ll l^2$, with the saturated remanent magnetization \mathbf{M}_0 directed along their length – see Fig. 18.

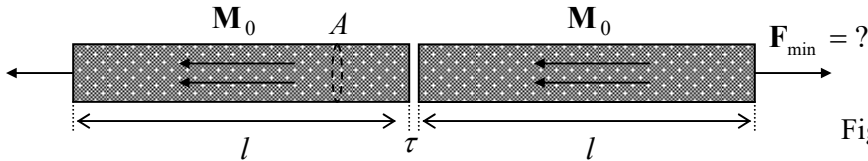


Fig. 5.18. Detaching two magnets.

Let us assume we have succeeded to detach the magnets by an infinitesimal distance $\tau \ll A^{1/2}, l$. Then, according to Eqs. (133)-(134), the distribution of the magnetic field near this small gap should be similar to that of the electric field in a system of two equal by opposite surface charges with the surface density σ proportional to M_0 . From Chapters 1-3, we know the properties of such a system very well: within the gap, the field is virtually constant, uniform, proportional to σ , and independent of τ . For its magnitude in the magnetic case, Eq. (134) gives simply $H = M_0$, and hence $B = \mu_0 M_0$. (Just outside of the gap, the field is very low, because due to the condition $A \ll l^2$, the effect of the similar effective charges at the "outer" ends of the rods on the field near the gap τ is negligible.)

From here, we can readily calculate F_{\min} as the force exerted by this field on the effective surface "charges". However, it is even easier to find it from the following energy argument. Since the magnetic field energy localized inside the magnets and near their outer ends cannot depend on τ , this small detachment may only alter the energy inside the gap. For this part of the energy, Eq. (57) yields:

$$\Delta U = \frac{B^2}{2\mu_0} V = \frac{(\mu_0 M_0)^2}{2\mu_0} A \tau. \quad (5.135)$$

The gradient of this potential energy is equal to the attraction force $\mathbf{F} = -\nabla(\Delta U)$, trying to reduce ΔU by decreasing the gap, with the following magnitude:

$$|F| = \frac{\partial(\Delta U)}{\partial \tau} = \frac{\mu_0 M_0^2 A}{2}. \quad (5.136)$$

The magnet detachment requires an equal and opposite external force. For a typical permanent magnet, with $\mu_0 M_0 \approx B_R \sim 1\text{T}$, the force corresponds to a ratio $|F|/A$ close to $4 \times 10^5 \text{ Pa}$, a few times the normal atmospheric pressure.

Now let us consider the situation when similar long permanent magnets (such as the *magnetic needles* used in magnetic compasses) are separated, in otherwise free space, by a larger distance $d \gg A^{1/2}$ – see Fig. 19. For each needle (Fig. 19a), of a length $l \gg A^{1/2}$, the right-hand side of Eq. (133) is substantially different from zero only in two relatively small areas at the needle's ends. Integrating the equation over each area, we see that at distances $r \gg A^{1/2}$ from each end, we may reduce Eq. (132) to

$$\nabla \cdot \mathbf{H} = q_m \delta(\mathbf{r} - \mathbf{r}_+) - q_m \delta(\mathbf{r} - \mathbf{r}_-), \quad (5.137)$$

where \mathbf{r}_{\pm} are ends' positions, and $q_m \equiv M_0 A$, with A being the needle's cross-section area. This equation is completely similar to Eq. (3.32) for the electric displacement \mathbf{D} , for the particular case of two equal and opposite point charges, i.e. with $\rho = q \delta(\mathbf{r} - \mathbf{r}_+) - q \delta(\mathbf{r} - \mathbf{r}_-)$, with the only replacement $q \rightarrow q_m$. Since we know the resulting electric field all too well (see, e.g., Eq. (1.7) for $\mathbf{E} \equiv \mathbf{D}/\epsilon_0$), we may immediately write a similar expression for the field \mathbf{H} :

$$\mathbf{H}(\mathbf{r}) = \frac{1}{4\pi} q_m \left(\frac{\mathbf{r} - \mathbf{r}_+}{|\mathbf{r} - \mathbf{r}_+|^3} - \frac{\mathbf{r} - \mathbf{r}_-}{|\mathbf{r} - \mathbf{r}_-|^3} \right). \quad (5.138)$$

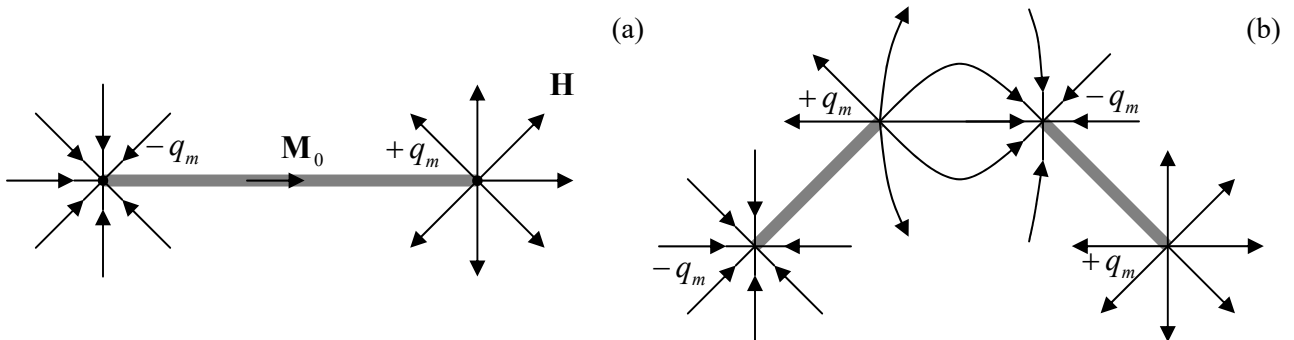


Fig. 5.19. (a) “Magnetic charges” at the ends of a thin permanent-magnet needle and (b) the result of its breaking into two parts (schematically).

The resulting magnetic field $\mathbf{B}(\mathbf{r}) = \mu_0 \mathbf{H}(\mathbf{r})$ exerts on another “magnetic charge” q'_m , located at some point \mathbf{r}' , the force $\mathbf{F} = q'_m \mathbf{B}(\mathbf{r}')$.⁶² Hence if two ends of different needles are separated by an intermediate distance R ($A^{1/2} \ll R \ll l$, see Fig. 19b), we may neglect one term in Eq. (138), and get the following “magnetic Coulomb law” for the interaction of the nearest ends:

$$\mathbf{F} = \pm \frac{\mu_0}{4\pi} q_m q'_m \frac{\mathbf{R}}{R^3}. \quad (5.139)$$

The “only” (but conceptually, crucial!) difference between this interaction and that of the electric point charges is that the two “magnetic charges” (quasi-monopoles) of a magnetic needle cannot be fully

⁶² The simplest way to verify this (perhaps, obvious) expression is to check that for a system of two “charges” $\pm q'_m$, separated by vector \mathbf{a} , placed into a uniform external magnetic field \mathbf{B}_{ext} , it yields the potential energy (100) with the correct magnetic dipole moment $\mathbf{m} = q_m \mathbf{a}$ – cf. Eq. (3.9) for an electric dipole.

separated. For example, if we break a needle in the middle in an attempt to bring its two ends further apart, two new “point charges” appear – see Fig. 19b.

There are several solid-state systems where more flexible structures, similar in their magnetostatics to the needles, may be implemented. First of all, certain (“type-II”) superconductors may carry so-called *Abrikosov vortices* – flexible tubes with field-suppressed superconductivity inside, each carrying one quantum $\Phi_0 = \pi\hbar/e \approx 2 \times 10^{-15}$ Wb of the magnetic flux. Ending on superconductor’s surfaces, these tubes let their magnetic field lines spread into the surrounding free space, essentially forming magnetic monopole analogs – of course, with equal and opposite “magnetic charges” q_m on each end of the tube – just as Fig. 19a shows. Such flux tubes are not only flexible but also stretchable, resulting in several peculiar effects – see Sec. 6.4 for more detail. Another recently found example of such paired quasi-monopoles is *spin chains* in the so-called *spin ices* – crystals with paramagnetic ions arranged into a specific (pyrochlore) lattice – such as dysprosium titanate $Dy_2Ti_2O_7$.⁶³ Let me emphasize again that any reference to magnetic monopoles in such systems should not be taken literally.

In order to complete this section (and this chapter), let me briefly discuss the magnetic field energy U , for the simplest case of systems with linear magnetic materials. In this case, we still may use Eq. (55), but if we want to operate only with macroscopic fields, and hence only stand-alone currents, we should repeat the manipulations that have led us to Eq. (57), using \mathbf{j} not from Eq. (35), but from Eq. (107). As a result, instead of Eq. (57) we get

$$U = \int_V u(\mathbf{r}) d^3r, \quad \text{with } u = \frac{\mathbf{B} \cdot \mathbf{H}}{2} = \frac{B^2}{2\mu} = \frac{\mu H^2}{2}, \quad (5.140)$$

Magnetic field
energy:
linear medium

This result is evidently similar to Eq. (3.73) of electrostatics.

As a simple but important example of its application, let us again consider a long solenoid (Fig. 6a), but now filled with a linear magnetic material with permeability μ . Using the macroscopic Ampère law (116), just as we used Eq. (37) for the derivation of Eq. (40), we get

$$H = In, \quad \text{and hence } B = \mu In, \quad (5.141)$$

where $n \equiv N/l$, just as in Eq. (40), is the winding density, i.e. the number of wire turns per unit length. (At $\mu = \mu_0$, we immediately return to that old result.) Now we may plug Eq. (141) into Eq. (140) to calculate the magnetic energy stored in the solenoid:

$$U = uV = \frac{\mu H^2}{2} lA = \frac{\mu(nI)^2 lA}{2}, \quad (5.142)$$

and then use Eq. (72) to calculate its self-inductance:⁶⁴

$$L = \frac{U}{I^2/2} = \mu n^2 lA \quad (5.143)$$

We see that $L \propto \mu V$, so filling a solenoid with a high- μ material may allow making it more compact while preserving the same value of inductance. In addition, as the discussion of Fig. 15 has

⁶³ See, e.g., L. Jaubert and P. Holdsworth, *J. Phys. – Cond. Matt.* **23**, 164222 (2011), and references therein.

⁶⁴ Admittedly, we could get the same result simpler, just by arguing that since the magnetic material fills the whole volume of a substantial magnetic field in this system, the filling simply increases the vector \mathbf{B} at all points, and hence its flux Φ , and hence $L \equiv \Phi/I$ by the factor μ/μ_0 in comparison with the free-space value (75).

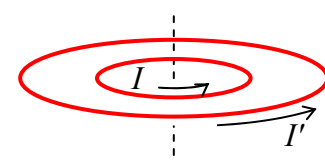
shown, such filling reduces the fringe fields near the solenoid's ends, which may be detrimental for some applications, especially in physical experiments striving for high measurement precision.

However, we still need to explore the issue of magnetic energy beyond Eq. (140), not only to get a general expression for it in materials with an arbitrary dependence $\mathbf{B}(\mathbf{H})$, but also to finally prove Eq. (54) and explore its relation with Eq. (53). I will do this at the beginning of the next chapter.

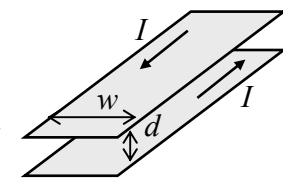
5.7. Exercise problems

5.1. DC current I flows around a thin wire loop bent into the form of a plane equilateral triangle with side a . Calculate the magnetic field in the center of the loop.

5.2. A circular wire loop, carrying a fixed dc current, has been placed inside a similar but larger loop, carrying a fixed current in the same direction – see the figure on the right. Use semi-quantitative arguments to analyze the mechanical stability of the coaxial and coplanar position of the inner loop with respect to its possible angular, axial, and lateral displacements relative to the outer loop.



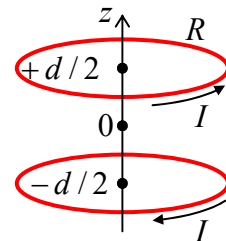
5.3. Two straight, plane, parallel, long, thin conducting strips of width w , separated by distance d , carry equal but oppositely directed currents I – see the figure on the right. Calculate the magnetic field in the plane located in the middle between the strips, assuming that the flowing currents are uniformly distributed across the strip widths.



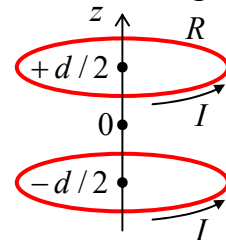
5.4. For the system studied in the previous problem, but now only in the limit $d \ll w$, calculate:

- the distribution of the magnetic field in space,
- the vector potential of the field,
- the magnetic force (per unit length) exerted on each strip, and
- the magnetic energy and self-inductance of the loop formed by the strips (per unit length).

5.5. Calculate the magnetic field distribution near the center of the system of two similar, plane, round, coaxial wire coils, carrying equal but oppositely directed currents – see the figure on the right.

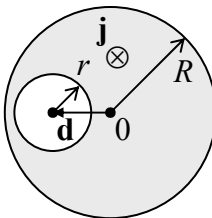


5.6. The two-coil-system considered in the previous problem, now carries equal and similarly directed currents – see the figure on the right.⁶⁵ Calculate what should be the ratio d/R for the second derivative $\partial^2 B_z / \partial z^2$ to equal zero at $z = 0$.

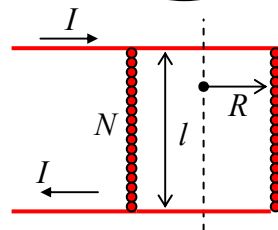


⁶⁵ This system (called the *Helmholtz coils*), producing a highly uniform field near its center, is broadly used in physical experiment.

5.7. DC current of a constant density j flows along a round cylindrical wire of radius R , with a round cylindrical cavity of radius r cut in it. The cavity's axis is parallel to that of the wire but offset from it by a distance $d < R - r$ (see the figure on the right). Calculate the magnetic field inside the cavity.



5.8. Calculate the magnetic field's distribution along the axis of a straight solenoid (see Fig. 6a, partly reproduced on the right) with a finite length l , and round cross-section of radius R . Assume that the solenoid has many ($N \gg 1$, l/R) wire turns, uniformly distributed along its length.



5.9. A thin round disk of radius R , carrying an electric charge of a constant areal density σ , rotates around its axis with a constant angular velocity ω . Calculate:

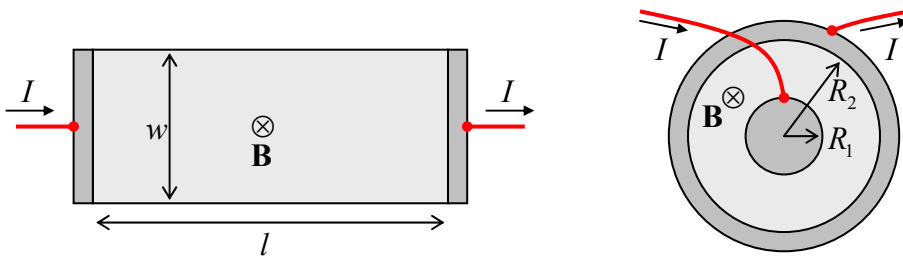
- (i) the induced magnetic field on the disk's axis,
- (ii) the magnetic moment of the disk,

and relate these results.

5.10. A thin spherical shell of radius R , with charge Q uniformly distributed over its surface, rotates about its diameter with a constant angular velocity ω . Calculate the distribution of the magnetic field everywhere in space.

5.11. A sphere of radius R , made of an insulating material with a uniform electric charge density ρ , rotates about its diameter with a constant angular velocity ω . Calculate the magnetic field distribution inside the sphere and outside it.

5.12. The reader is hopefully familiar with the classical Hall effect in the usual rectangular *Hall bar* geometry – see the left panel of the figure below. However, the effect takes a different form in the so-called *Corbino disk* – see the right panel of the figure below. (Dark shading shows electrodes, with no appreciable resistance.) Analyze the effect in both geometries, assuming that in both cases, the conductors are thin and planar, have a constant Ohmic conductivity σ and charge carrier density n , and that the applied magnetic field \mathbf{B} is uniform and normal to conductors' planes.

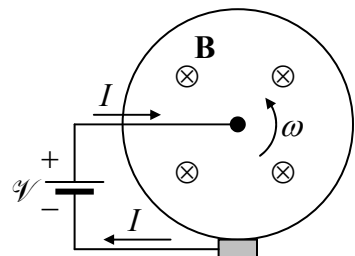


5.13.* The simplest version of the famous *homopolar* (or “unipolar”) *motor* is a thin, round conducting disk, placed into a uniform magnetic field normal to its plane, with dc current passed between the disk's center and a sliding electrode (“brush”) on its rim – see the figure below.

(i) Express the torque rotating the disk via its radius R , the magnetic field \mathbf{B} , and the current I .

(ii) If the disk is allowed to rotate about its axis, and the motor is driven by a battery with e.m.f. \mathcal{V} , calculate its stationary angular velocity ω , neglecting friction and the electric circuit's resistance.

(iii) Now assuming that the current circuit (battery + wires + contacts + disk itself) has a non-zero resistance \mathcal{R} , derive and solve the equation for the time evolution of ω , and analyze the solution.



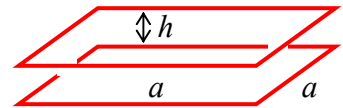
5.14. Current I flows in a thin wire bent into a plane round loop of radius R . Calculate the net magnetic flux through the plane in which the loop is located.

5.15. A wire with a round cross-section of radius a has been bent into a round loop of radius $R \gg r$. Prove the formula for its self-inductance, mentioned at the end of Sec. 5.3 of the lecture notes: $L = \mu_0 R \ln(cR/a)$, with $c \sim 1$.

5.16. Prove that:

- (i) the self-inductance L of a current loop cannot be negative, and
- (ii) any inductance coefficient $L_{kk'}$, defined by Eq. (60), cannot be larger than $(L_{kk} L_{k'k'})^{1/2}$.

5.17. Calculate the mutual inductance of two similar thin-wire square-shaped loops, offset by distance h in the direction normal to their planes – see the figure on the right.



5.18.* Estimate the values of magnetic susceptibility due to

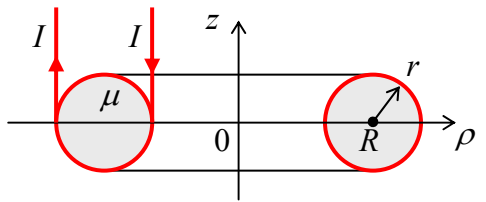
- (i) orbital diamagnetism, and
- (ii) spin paramagnetism,

for a medium with negligible interaction between the induced molecular dipoles. Compare the results.

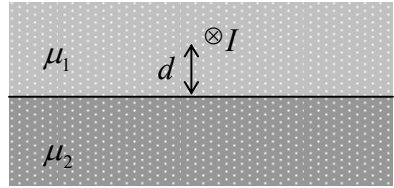
Hints: For Task (i), you may use the classical model described by Eq. (114) – see Fig. 13. For Task (ii), assume the mechanism of ordering of spontaneous magnetic dipoles \mathbf{m}_0 , with a magnitude m_0 of the order of the Bohr magneton μ_B , similar to the one sketched for electric dipoles in Fig. 3.7a.

5.19.* Use the classical picture of the orbital (“Larmor”) diamagnetism, discussed in Sec. 5, to calculate its (small) contribution $\Delta\mathbf{B}(0)$ to the magnetic field \mathbf{B} felt by an atomic nucleus, treating the electrons of the atom as a spherically-symmetric cloud with an electric charge density $\rho(r)$. Express the result via the value $\phi(0)$ of the electrostatic potential of the electron cloud, and use this expression for a crude numerical estimate of the ratio $\Delta B(0)/B$ for the hydrogen atom.

5.20. Calculate the self-inductance of a toroidal solenoid (see Fig. 6b) with the round cross-section of radius $r \sim R$ (see the figure on the right), with many ($N \gg 1, R/r$) wire turns uniformly distributed along the perimeter, and filled with a linear magnetic material of permeability μ . Check your results by analyzing the limit $r \ll R$.



5.21. A long straight, thin wire carrying current I , passes parallel to the plane boundary between two uniform, linear magnetic media – see the figure on the right. Calculate the magnetic field everywhere in the system, and the force (per unit length) exerted on the wire.

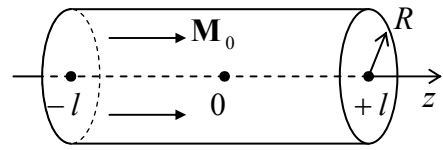


5.22. Solve the magnetic shielding problem similar to that discussed in Sec. 5.6 of the lecture notes, but for a *spherical* rather than cylindrical shell, with the same central cross-section as shown in Fig. 16. Compare the efficiency of those two shields, for the same shell's permeability μ , and the same b/a ratio.

5.23. Calculate the magnetic field distribution around a spherical permanent magnet with a uniform magnetization $\mathbf{M}_0 = \text{const}$.

5.24. A limited volume V is filled with a magnetic material with a fixed (field-independent) magnetization $\mathbf{M}(\mathbf{r})$. Write explicit expressions for the magnetic field induced by the magnetization, and its potential, and recast these expressions into the forms more convenient when $\mathbf{M}(\mathbf{r}) = \mathbf{M}_0 = \text{const}$ inside the volume V .

5.25. Use the results of the previous problem to calculate the distribution of the magnetic field \mathbf{H} along the axis of a straight permanent magnet of length $2l$, with a round cross-section of radius R , and a uniform magnetization \mathbf{M}_0 parallel to the axis – see the figure on the right.



5.26. A flat end of a long straight permanent magnet, similar to that considered in the previous problem but of an arbitrary cross-section of area A , is stuck to a flat surface of a large sample of a linear magnetic material with a very high permeability $\mu \gg \mu_0$. Calculate the normally-directed force needed to detach them.

5.27. A permanent magnet with a uniform magnetization \mathbf{M}_0 has the form of a spherical shell with an internal radius R_1 and an external radius $R_2 > R_1$. Calculate the magnetic field inside the shell.

5.28. A very broad film of thickness $2t$ is permanently magnetized normally to its plane, with a periodic checkerboard pattern, with the square of area $a \times a$:

$$\mathbf{M} \Big|_{|z| < t} = \mathbf{n}_z M(x, y), \quad \text{with } M(x, y) = M_0 \times \text{sgn} \left(\cos \frac{\pi x}{a} \cos \frac{\pi y}{a} \right).$$

Calculate the magnetic field's distribution in space.

5.29.* Based on the discussion of the quadrupole electrostatic lens in Sec. 2.4, suggest the permanent-magnet systems that may similarly focus particles moving close to the system's axis, for the cases when each particle carries:

- (i) an electric charge,
- (ii) no net electric charge, but a spontaneous magnetic dipole moment \mathbf{m} of a certain orientation.

Chapter 6. Electromagnetism

This chapter discusses two major effects that arise when electric and magnetic fields change over time: the “electromagnetic induction” of an additional electric field by changing magnetic field, and the reciprocal effect of the “displacement currents”—actually, the induction of an additional magnetic field by changing electric field. These two phenomena, which make time-dependent electric and magnetic fields inseparable (hence the term “electromagnetism”¹), are reflected in the full system of Maxwell equations, valid for an arbitrary electromagnetic process. On the way toward this system, I will make a brief detour to review the electrodynamics of superconductivity, which (besides its own significance), provides a perfect platform for discussion of the important general issue of gauge invariance.

6.1. Electromagnetic induction

As Eqs. (5.36) show, in static situations ($\partial/\partial t = 0$) the Maxwell equations describing the electric and magnetic fields are independent – more exactly, coupled only implicitly, via the continuity equation (4.5) relating their right-hand sides ρ and \mathbf{j} . In dynamics, when the fields change in time, the situation is different.

Historically, the first discovered explicit coupling between the electric and magnetic fields was the effect of electromagnetic induction. Although this effect was discovered independently by Joseph Henry, it was a brilliant series of experiments by Michael Faraday, carried out mostly in 1831, that resulted in the first general formulation of the induction law. The summary of Faraday’s numerous experiments has turned out to be very simple: if the magnetic flux defined by Eq. (5.65),

$$\Phi \equiv \int_S B_n d^2 r, \quad (6.1)$$

through a surface S limited by a closed contour C , changes in time by whatever reason (e.g., either due to a change of the magnetic field \mathbf{B} (as in Fig. 1), or the contour’s motion, or its deformation, or any combination of the above), it induces an additional, vortex-like electric field \mathbf{E}_{ind} directed along the contour – see Fig. 1.

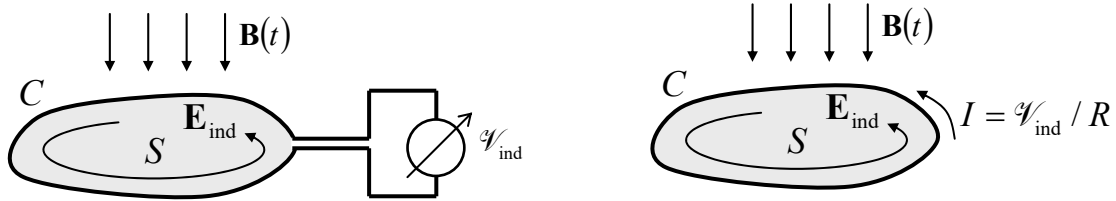


Fig. 6.1. Two simplest ways to observe the Faraday electromagnetic induction.

The exact distribution of \mathbf{E}_{ind} in space depends on the system’s details, but its integral along the contour C , called the *inductive electromotive force* (e.m.f.), obeys a very simple *Faraday induction law*:

¹ It was coined by H. Ørsted in 1820 in the context of his experiments – see the previous chapter.

$$\mathcal{V}_{\text{ind}} \equiv \oint_C \mathbf{E}_{\text{ind}} \cdot d\mathbf{r} = -\frac{d\Phi}{dt}. \quad (6.2)$$

Faraday
induction
law

(In the Gaussian units, the right-hand side of this formula has an additional coefficient of $1/c$.)

It is straightforward (and hence left for the reader's exercise) to show that this e.m.f. may be measured, for example, either by inserting a voltmeter into a conducting loop following the contour C or by measuring the small current $I = \mathcal{V}_{\text{ind}}/R$ it induces in a thin wire with a sufficiently large Ohmic resistance R ,² whose shape follows that contour – see Fig. 1. (Actually, these methods are not entirely different, because a typical voltmeter measures voltage by the small Ohmic current it drives through the pre-calibrated high internal resistance of the device.) In the context of the latter approach, the minus sign in Eq. (2) may be described by the following *Lenz rule*: the magnetic field of the induced current I provides a partial compensation of the *change* of the original flux $\Phi(t)$ with time.³

In order to recast Eq. (2) in a differential form, more convenient in many cases, let us apply to the contour integral in it the Stokes theorem, which was repeatedly used in Chapter 5. The result is

$$\mathcal{V}_{\text{ind}} = \int_S (\nabla \times \mathbf{E}_{\text{ind}})_n d^2 r. \quad (6.3)$$

Now combining Eqs. (1)-(3), for a contour C whose shape does not change in time (so that the integration along it is interchangeable with the time derivative), we get

$$\int_S \left(\nabla \times \mathbf{E}_{\text{ind}} + \frac{\partial \mathbf{B}}{\partial t} \right)_n d^2 r = 0. \quad (6.4)$$

Since the induced electric field is an addition to the gradient field (1.33) created by electric charges, for the net field we may write $\mathbf{E} = \mathbf{E}_{\text{ind}} - \nabla\phi$. However, since the curl of any gradient field is zero,⁴ $\nabla \times (\nabla\phi) = 0$, Eq. (4) remains valid even for the net field \mathbf{E} . Since this equation should be correct for *any* closed area S , we may conclude that

$$\nabla \times \mathbf{E} + \frac{\partial \mathbf{B}}{\partial t} = 0 \quad (6.5)$$

Faraday law:
differential
form

at any point. This is the final (time-dependent) form of this Maxwell equation. Superficially, it may look that Eq. (5) is less general than Eq. (2); for example, it does not describe any electric field, and hence any e.m.f. in a moving loop, if the field \mathbf{B} is constant in time, even if the magnetic flux (1) through the loop does change in time. However, this is not true; in Chapter 9 we will see that in the reference frame moving with the loop such e.m.f. does appear.⁵

² Such induced current is sometimes called the *eddy current*, though most often this term is reserved for the distributed currents induced by changing magnetic fields in bulk conductors – see Sec. 3 below.

³ Let me also hope that the reader is familiar with the paradox arising at attempts to measure \mathcal{V}_{ind} with a voltmeter without its insertion into the wire loop; if not, I would highly recommend them to solve the offered Problem 2.

⁴ See, e.g., MA Eq. (11.1).

⁵ I have to admit that from the beginning of the course, I was carefully sweeping under the rug a very important question: in what exactly reference frame(s) all the equations of electrodynamics are valid? I promise to discuss this issue in detail later in the course (in Chapter 9), and for now would like to get away with a very short answer: all the formulas discussed so far are valid in *any inertial* reference frame, as defined in classical mechanics – see, e.g., CM Sec. 1.3; however, the fields \mathbf{E} and \mathbf{B} have to be measured *in the same* reference frame.

Now let us reformulate Eq. (5) in terms of the vector potential \mathbf{A} . Since the induction effect does not alter the fundamental relation $\nabla \cdot \mathbf{B} = 0$, we still may represent the magnetic field as prescribed by Eq. (5.27), i.e. as $\mathbf{B} = \nabla \times \mathbf{A}$. Plugging this expression into Eq. (5), and changing the order of the temporal and spatial differentiation, we get

$$\nabla \times \left(\mathbf{E} + \frac{\partial \mathbf{A}}{\partial t} \right) = 0. \quad (6.6)$$

Hence we can use the same argumentation as in Sec. 1.3 (there applied to the vector \mathbf{E} alone) to represent the expression in the parentheses as $-\nabla\phi$, so that we get

Fields via potentials

$$\boxed{\mathbf{E} = -\frac{\partial \mathbf{A}}{\partial t} - \nabla\phi, \quad \mathbf{B} = \nabla \times \mathbf{A}.} \quad (6.7)$$

It is very tempting to interpret the first term of the right-hand side of the expression for \mathbf{E} as the one describing the electromagnetic induction alone, and the second term as representing a purely electrostatic field induced by electric charges. However, the separation of these two terms is, to a certain extent, conditional. Indeed, let us consider the gauge transformation already mentioned in Sec. 5.2,

$$\mathbf{A} \rightarrow \mathbf{A} + \nabla\chi, \quad (6.8)$$

that, as we already know, does not change the magnetic field. According to Eq. (7), to keep the full electric field intact (*gauge-invariant*) as well, the scalar electric potential has to be transformed simultaneously, as

$$\phi \rightarrow \phi - \frac{\partial\chi}{\partial t}, \quad (6.9)$$

leaving the choice of an addition to ϕ restricted only by the Laplace equation – since the full ϕ should satisfy the Poisson equation (1.41) with a gauge-invariant right-hand side. We will return to the discussion of the gauge invariance in Sec. 4.

6.2. Magnetic energy revisited

Now we are sufficiently equipped to revisit the issue of magnetic energy, in particular, to finally prove Eqs. (5.57) and (5.140), and discuss the dichotomy of the signs in Eqs. (5.53) and (5.54). For that, let us consider a sufficiently slow and small magnetic field variation $\delta\mathbf{B}$. If we want to neglect the kinetic energy of the system of electric currents under consideration, as well as the wave radiation effects, we need to prevent its significant acceleration by the arising induction field \mathbf{E}_{ind} . Let us suppose that we do this by virtual balancing of this field by an external electric field $\mathbf{E}_{\text{ext}} = -\mathbf{E}_{\text{ind}}$. According to Eq. (4.38), the work of that field⁶ on the stand-alone currents of the system during a small time interval δt , and hence the change of the potential energy of the system, is

$$\delta U = \delta t \int_V \mathbf{j} \cdot \mathbf{E}_{\text{ext}} d^3r, \quad \text{so that } \delta U = -\delta t \int_V \mathbf{j} \cdot \mathbf{E}_{\text{ind}} d^3r, \quad (6.10)$$

⁶ As a reminder, the magnetic component of the Lorentz force (5.10), $\mathbf{v} \times \mathbf{B}$, is always perpendicular to the particle velocity \mathbf{v} , so the magnetic field \mathbf{B} itself cannot perform any work on moving charges, i.e. on currents.

where the integral is over the volume of the system. Now expressing the current density \mathbf{j} from the macroscopic Maxwell equation (5.107), $\mathbf{j} = \nabla \times \mathbf{H}$, and then applying the vector algebra identity⁷

$$(\nabla \times \mathbf{H}) \cdot \mathbf{E}_{\text{ind}} \equiv \mathbf{H} \cdot (\nabla \times \mathbf{E}_{\text{ind}}) - \nabla \cdot (\mathbf{E}_{\text{ind}} \times \mathbf{H}), \quad (6.11)$$

we get

$$\delta U = -\delta t \int_V \mathbf{H} \cdot (\nabla \times \mathbf{E}) d^3 r + \delta t \int_V \nabla \cdot (\mathbf{E} \times \mathbf{H}) d^3 r. \quad (6.12)$$

According to the divergence theorem, the second integral in the right-hand of this equality is equal to the flux of the so-called *Poynting vector* $\mathbf{S} \equiv \mathbf{E} \times \mathbf{H}$ through the surface limiting the considered volume V . Later in the course we will see that this flux represents, in particular, the power of electromagnetic radiation through the surface. If such radiation is negligible (as it always is if the field variation is sufficiently slow), the surface may be selected sufficiently far, so that the flux of \mathbf{S} vanishes. In this case, we may express $\nabla \times \mathbf{E}$ from the Faraday induction law (5) to get

$$\delta U = -\delta t \int_V \left(-\frac{\partial \mathbf{B}}{\partial t} \right) \cdot \mathbf{H} d^3 r = \int_V \mathbf{H} \cdot \delta \mathbf{B} d^3 r. \quad (6.13)$$

Just as in the electrostatics (see Eqs. (1.65) and (3.73), and their discussion), this relation may be interpreted as the variation of the magnetic field energy U of the system, and represented in the form

$$\delta U = \int_V \delta u(\mathbf{r}) d^3 r, \quad \text{with } \delta u \equiv \mathbf{H} \cdot \delta \mathbf{B}. \quad (6.14)$$

Magnetic
energy's
variation

This is a keystone result; let us discuss it in some detail.

First of all, for a system filled with a linear and isotropic magnetic material, we may use Eq. (14) together with Eq. (5.110): $\mathbf{B} = \mu \mathbf{H}$. Integrating the result over the variation of the field from 0 to a certain final value \mathbf{B} , we get Eq. (5.140) – so important one that it deserves rewriting it again:

$$U = \int_V u(\mathbf{r}) d^3 r, \quad \text{with } u = \frac{B^2}{2\mu}. \quad (6.15)$$

In the simplest case of free space (no magnetics at all, so that \mathbf{j} above is the complete current density), we may take $\mu = \mu_0$, and reduce Eq. (15) to Eq. (5.57). Now performing backward the transformations that took us, in Sec. 5.3, to derive that relation from Eq. (5.54), we finally have the latter formula proved – as was promised in the last chapter.

It is very important, however, to understand the limitations of Eq. (15). For example, let us try to apply it to a very simple problem, which was already analyzed in Sec. 5.6 (see Fig. 5.15): a very long cylindrical sample of a linear magnetic material placed into a fixed external field \mathbf{H}_{ext} parallel to the sample's length. It is evident that in this simple geometry, the field \mathbf{H} and hence the field $\mathbf{B} = \mu \mathbf{H}$ have to be uniform inside the sample, besides negligible regions near its ends, so that Eq. (15) is reduced to

$$U = \frac{B^2}{2\mu} V, \quad (6.16)$$

⁷ See, e.g., MA Eq. (11.7) with $\mathbf{f} = \mathbf{E}_{\text{ind}}$ and $\mathbf{g} = \mathbf{H}$.

where $V = Al$ is the cylinder's volume. Now if we try to calculate the static (equilibrium) value of the field from the minimum of this potential energy, we get evident nonsense: $\mathbf{B} = 0$ (**WRONG!**).⁸

The situation may be readily rectified by using the notion of the Gibbs potential energy, just as it was done for the electric field in Sec. 3.5 (and implicitly in the end of Sec. 1.3). According to Eq. (14), in magnetostatics, the Cartesian components of the field $\mathbf{H}(\mathbf{r})$ play the role of the generalized forces, while those of the field $\mathbf{B}(\mathbf{r})$, of the generalized coordinates (per unit volume).⁹ As the result, the Gibbs potential energy, whose minimum corresponds to the stable equilibrium of the system under the effect of a fixed generalized force (in our current case, of the fixed external field \mathbf{H}_{ext}), is

Gibbs
potential
energy

$$U_G = \int_V u_G(\mathbf{r}) d^3r, \quad \text{with } u_G(\mathbf{r}) \equiv u(\mathbf{r}) - \mathbf{H}_{\text{ext}}(\mathbf{r}) \cdot \mathbf{B}(\mathbf{r}), \quad (6.17)$$

– the expression parallel to Eq. (3.78). For a system with linear magnetics, we may use for u our result (15), getting the following Gibbs energy's density:

$$u_G(\mathbf{r}) = \frac{1}{2\mu} \mathbf{B} \cdot \mathbf{B} - \mathbf{H}_{\text{ext}} \cdot \mathbf{B} \equiv \frac{1}{2\mu} (\mathbf{B} - \mu \mathbf{H}_{\text{ext}})^2 + \text{const}, \quad (6.18)$$

where “const” means a term independent of the field \mathbf{B} inside the sample. For our simple cylindrical system, with its uniform fields, Eqs. (17)-(18) gives the following full Gibbs energy of the sample:

$$U_G = \frac{(\mathbf{B}_{\text{int}} - \mu \mathbf{H}_{\text{ext}})^2}{2\mu} V + \text{const}, \quad (6.19)$$

whose minimum immediately gives the correct stationary value $\mathbf{B}_{\text{int}} = \mu \mathbf{H}_{\text{ext}}$, i.e. $\mathbf{H}_{\text{int}} \equiv \mathbf{B}_{\text{int}}/\mu = \mathbf{H}_{\text{ext}}$, which was already obtained in Sec. 5.6 in a different way, from the boundary condition (5.117).

Now notice that with this result on hand, Eq. (18) may be rewritten in a different form:

$$u_G(\mathbf{r}) = \frac{1}{2\mu} \mathbf{B} \cdot \mathbf{B} - \frac{\mathbf{B}}{\mu} \cdot \mathbf{B} \equiv -\frac{B^2}{2\mu}, \quad (6.20)$$

similar to Eq. (15) for $u(\mathbf{r})$, but with an opposite sign. This sign dichotomy explains that of Eqs. (5.53) and Eq. (5.54); indeed, as was already noted in Sec. 5.3, the former of these expressions gives the potential energy whose minimum corresponds to the equilibrium of a system with fixed currents. (In our current example, these are the external stand-alone currents inducing the field \mathbf{H}_{ext} .) So, the energy U_j given by Eq. (5.53) is essentially the Gibbs energy U_G defined by Eqs. (17) and (for the equilibrium state of linear magnetic media) by Eq. (20), while Eq. (5.54) is just another form of Eq. (15) – as was explicitly shown in Sec. 5.3.¹⁰

⁸ This erroneous result cannot be corrected by just adding the energy of the field outside the cylinder because in the limit $A \rightarrow 0$, this field is not affected by the internal field \mathbf{B} .

⁹ Note an aspect in that the analogy with electrostatics is not quite complete. Indeed, according to Eq. (3.76), in electrostatics, the role of a generalized coordinate is played by the “would-be” field \mathbf{D} , and that of the generalized force, by the actual (if macroscopic) electric field \mathbf{E} . This difference may be traced back to the fact that the electric field \mathbf{E} may perform work on a moving charged particle, while the magnetic field cannot. However, this difference does not affect the full analogy of the expressions (3.73) and (15) for the field energy density in *linear* media.

¹⁰ As was already noted in Sec. 5.4, one more example of the energy U_j (i.e. U_G) is given by Eq. (5.100).

Let me complete this section by stating that the difference between the energies U and U_G is not properly emphasized (or even left obscure) in some textbooks, so that the reader is advised to get additional clarity by solving a few additional simple problems – for example, by spelling out these energies for a long straight solenoid (Fig. 5.6a), and then using the results to calculate the pressure exerted by the magnetic field on the solenoid's walls (windings) and the longitudinal forces exerted on its ends.

6.3. Quasistatic approximation and skin effect

Perhaps the most surprising experimental fact concerning the time-dependent electromagnetic phenomena is that unless they are so fast that one more new effect of the *displacement currents* (to be discussed in Sec. 7 below) becomes noticeable, all formulas of electrostatics and magnetostatics remain valid, with the only exception: the generalization of Eq. (3.36) to Eq. (5), describing the Faraday induction. As a result, the system of macroscopic Maxwell equations (5.109) is generalized to

$$\boxed{\begin{aligned}\nabla \times \mathbf{E} + \frac{\partial \mathbf{B}}{\partial t} &= 0, & \nabla \times \mathbf{H} &= \mathbf{j}, \\ \nabla \cdot \mathbf{D} &= \rho, & \nabla \cdot \mathbf{B} &= 0.\end{aligned}} \quad (6.21)$$

Quasistatic approximation

(As it follows from the discussions in chapters 3 and 5, the corresponding system of microscopic Maxwell equations for the genuine, “microscopic” fields \mathbf{E} and \mathbf{B} may be obtained from Eq. (21) by the formal substitutions $\mathbf{D} = \epsilon_0 \mathbf{E}$ and $\mathbf{H} = \mathbf{B}/\mu_0$, and the replacement of the stand-alone charge and current densities ρ and \mathbf{j} with their full densities.¹¹⁾ These equations, whose range of validity will be quantified in Sec. 7, define the so-called *quasistatic approximation* of electromagnetism and are sufficient for an adequate description of a broad range of physical effects.

In order to form a complete system of equations, Eqs. (21) should be augmented by constituent equations describing the medium under consideration. For a linear isotropic material, they may be taken in the simplest (and simultaneously, most common) linear and isotropic forms already discussed in Chapters 4 and 5:

$$\mathbf{j} = \sigma \mathbf{E}, \quad \mathbf{B} = \mu \mathbf{H}. \quad (6.22)$$

If the conductor is uniform, i.e. the coefficients σ and μ are constant inside it, the whole system of Eqs. (21)-(22) may be reduced to just one simple equation. Indeed, a sequential substitution of these equations into each other, using a well-known vector-algebra identity¹² in the middle, yields:

$$\begin{aligned}\frac{\partial \mathbf{B}}{\partial t} &= -\nabla \times \mathbf{E} = -\frac{1}{\sigma} \nabla \times \mathbf{j} = -\frac{1}{\sigma} \nabla \times (\nabla \times \mathbf{H}) = -\frac{1}{\sigma \mu} \nabla \times (\nabla \times \mathbf{B}) \equiv -\frac{1}{\sigma \mu} [\nabla(\nabla \cdot \mathbf{B}) - \nabla^2 \mathbf{B}] \\ &= \frac{1}{\sigma \mu} \nabla^2 \mathbf{B}.\end{aligned} \quad (6.23)$$

Thus we have arrived, without any further assumptions, at a rather simple partial differential equation. Let us use it for an analysis of the so-called *skin effect*, the phenomenon of an Ohmic

¹¹ Obviously, in free space, the last replacement is unnecessary, because all charges and currents may be treated as “stand-alone” ones.

¹² See, e.g., MA Eq. (11.3).

conductor's self-shielding from the alternating (*ac*) magnetic field. In its simplest geometry (Fig. 2a), an external source (which, at this point, does not need to be specified) produces, near a plane surface of a bulk conductor, a spatially-uniform ac magnetic field $\mathbf{H}^{(0)}(t)$ parallel to the surface.¹³

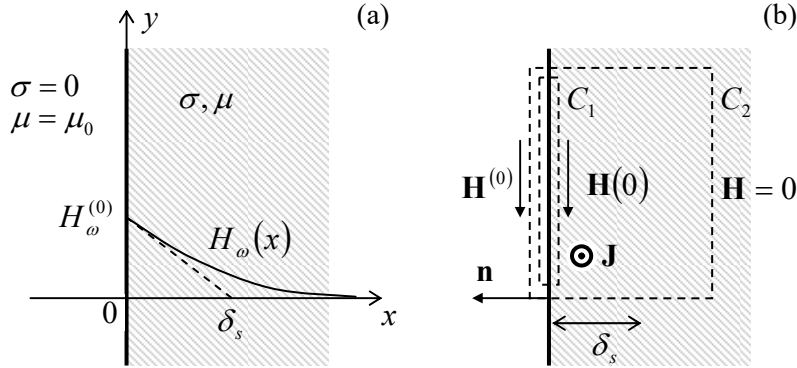


Fig. 6.2. (a) The skin effect in the simplest, planar geometry, and (b) two Ampère contours, C_1 and C_2 , for deriving the “macroscopic” (C_1) and the “coarse-grain” (C_2) boundary conditions for \mathbf{H} .

Selecting the coordinate system as shown in Fig. 2a, we may express this condition as

$$\mathbf{H}|_{x=-0} = H^{(0)}(t)\mathbf{n}_y . \quad (6.24)$$

The translational symmetry of our simple problem within the surface plane [y, z] implies that inside the conductor, $\partial/\partial y = \partial/\partial z = 0$ as well, and $\mathbf{H} = H(x, t)\mathbf{n}_y$ even at $x \geq 0$, so that Eq. (23) for the conductor's interior is reduced to a differential equation for just one scalar function $H(x, t) = B(x, t)/\mu$:

$$\frac{\partial H}{\partial t} = \frac{1}{\sigma\mu} \frac{\partial^2 H}{\partial x^2}, \quad \text{for } x \geq 0 . \quad (6.25)$$

This equation may be further simplified by noticing that due to its linearity, we may use the linear superposition principle for the time dependence of the field,¹⁴ via expanding it, as well as the external field (24), into the Fourier series:

$$\begin{aligned} H(x, t) &= \sum_{\omega} H_{\omega}(x) e^{-i\omega t}, \quad \text{for } x \geq 0, \\ H^{(0)}(t) &= \sum_{\omega} H_{\omega}^{(0)} e^{-i\omega t}, \quad \text{for } x = -0, \end{aligned} \quad (6.26)$$

and arguing that if we know the solution for each frequency component of the series, the whole field may be found through the straightforward summation (26) of these solutions.

For each single-frequency component, Eq. (25) is immediately reduced to an ordinary differential equation for the complex amplitude $H_{\omega}(x)$:¹⁵

¹³ Due to the simple linear relation $\mathbf{B} = \mu\mathbf{H}$ between the fields \mathbf{B} and \mathbf{H} , it does not matter too much which of them is used for the solution of this problem, with a slight preference for \mathbf{H} , due to the simplicity of Eq. (5.117) – the only boundary condition relevant for this simple geometry.

¹⁴ Another way to exploit the linearity of Eq. (6.25) is to use the *spatial-temporal Green's function* approach to explore the dependence of its solutions on various initial conditions. Unfortunately, because of a lack of time, I have to leave an analysis of this opportunity for the reader's exercise.

$$-i\omega H_\omega = \frac{1}{\sigma\mu} \frac{d^2}{dx^2} H_\omega. \quad (6.27)$$

From the theory of linear ordinary differential equations, we know that Eq. (27) has the following general solution:

$$H_\omega(x) = H_+ e^{\kappa_+ x} + H_- e^{\kappa_- x}, \quad (6.28)$$

where the constants κ_\pm are the roots of the characteristic equation that may be obtained by the substitution of any of these two exponents into the initial differential equation. For our particular case, the characteristic equation following from Eq. (27) is

$$-i\omega = \frac{\kappa^2}{\sigma\mu} \quad (6.29)$$

and its roots are

$$\kappa_\pm = (-i\mu\omega\sigma)^{1/2} \equiv \pm \frac{1-i}{\sqrt{2}} (\mu\omega\sigma)^{1/2}. \quad (6.30)$$

For our problem, the field cannot grow exponentially at $x \rightarrow +\infty$, so only one of the coefficients, namely the H_- corresponding to the decaying exponent, with $\text{Re } \kappa_- < 0$, may be different from zero, i.e. $H_\omega(x) = H_\omega(0)\exp\{\kappa_- x\}$. To find the constant factor $H_\omega(0)$, we can integrate the macroscopic Maxwell equation $\nabla \times \mathbf{H} = \mathbf{j}$ along a pre-surface contour – say, the contour C_1 shown in Fig. 2b. The right-hand side's integral is negligible because the stand-alone current density \mathbf{j} does not include the “genuinely-surface” currents responsible for the magnetic permeability μ – see Fig. 5.12. As a result, we get the boundary condition similar to Eq. (5.117) for the stationary magnetic field: $H_\tau = \text{const}$ at $x = 0$, giving us

$$H(0, t) = H^{(0)}(t), \quad \text{i.e. } H_\omega(0) = H_\omega^{(0)}, \quad (6.31)$$

so that the final solution of our boundary problem may be represented as

$$H_\omega(x) = H_\omega^{(0)} \exp\{\kappa_- x\} = H_\omega^{(0)} \exp\left\{-\frac{x}{\delta_s}\right\} \exp\left\{-i\left(\omega t - \frac{x}{\delta_s}\right)\right\}, \quad (6.32)$$

where the constant δ_s , with the dimension of length, is called the *skin depth*:

$$\delta_s \equiv -\frac{1}{\text{Re } \kappa_-} = \left(\frac{2}{\mu\sigma\omega}\right)^{1/2}. \quad (6.33)$$

Skin depth

This solution describes the *skin effect*: the penetration of the ac magnetic field, and the eddy currents \mathbf{j} , into a conductor only to a finite depth of the order of δ_s . Let me give a few numerical examples of this depth: for copper at room temperature, $\delta_s \approx 1$ cm at the usual ac power distribution frequency of 60 Hz, and is of the order of just 1 μm at a few GHz, i.e. at typical frequencies of cell

¹⁵ Let me hope that the reader is not intimidated by the (very convenient) use of such complex variables for describing real fields; their imaginary parts always disappear at the final summation (26). For example, if the external field is purely sinusoidal, with the actual (positive) frequency ω , each sum in Eq. (26) has just two terms, with complex amplitudes H_ω and $H_{-\omega} = H_\omega^*$, so that their sum is always real. (For a more detailed discussion of this issue, see, e.g., CM Sec. 5.1.)

phone signals and kitchen microwave magnetrons. On the other hand, for lightly salted water, δ_s is close to 250 m at just 1 Hz (with significant implications for radio communications with submarines), and of the order of 1 cm at a few GHz (explaining, in particular, the nonuniform heating of a soup bowl in a microwave oven).¹⁶

Let me hope that the equality chain (23) makes the physics of this effect very clear: the external electric field \mathbf{E} , which is Faraday-induced by an external ac magnetic field, drives the eddy currents \mathbf{j} , which in turn induce their own magnetic field that eventually (at $x \sim \delta_s$) compensates the external one. Let us quantify these \mathbf{E} and \mathbf{j} . Since we have used, in particular, relations $\mathbf{j} = \nabla \times \mathbf{H} = \nabla \times \mathbf{B}/\mu$, and $\mathbf{E} = \mathbf{j}/\sigma$, and spatial differentiation of an exponent yields a similar exponent, the electric field and current density have the same spatial dependence as the magnetic field, i.e. penetrate the conductor only by distances of the order of $\delta_s(\omega)$. Their vectors are directed normally to \mathbf{B} , while still being parallel to the conductor's surface:¹⁷

$$\mathbf{j}_\omega(x) = \kappa_- H_\omega(x) \mathbf{n}_z, \quad \mathbf{E}_\omega(x) = \frac{\kappa_-}{\sigma} H_\omega(x) \mathbf{n}_z. \quad (6.34)$$

We may use these expressions, in particular, to calculate the time-averaged power density (4.39) of the energy dissipation, for the important case of a sinusoidal ("monochromatic") field $H(x, t) = |H_\omega(x)| \cos(\omega t + \varphi)$, and hence sinusoidal eddy currents: $j(x, t) = |j_\omega(x)| \cos(\omega t + \varphi')$:

$$\bar{\mu}(x) = \frac{\overline{j^2(x, t)}}{\sigma} = \frac{|j_\omega(x)|^2 \overline{\cos^2(\omega t + \varphi')}}{\sigma} = \frac{|j_\omega(x)|^2}{2\sigma} = \frac{|\kappa_-|^2 |H_\omega(x)|^2}{2\sigma} = \frac{|H_\omega(x)|^2}{\delta_s^2 \sigma}. \quad (6.35)$$

Now the (elementary) integration of this expression along the x -axis (through all the skin depth), using the exponential law (6.32), gives us the following average power of the energy loss per unit area:

Energy loss
at skin effect

$$\frac{d\bar{\mathcal{P}}}{dA} \equiv \int_0^\infty \bar{\mu}(x) dx = \frac{1}{2\delta_s \sigma} |H_\omega^{(0)}|^2 \equiv \frac{\mu \omega \delta_s}{4} |H_\omega^{(0)}|^2. \quad (6.36)$$

We will extensively use this expression in the next chapter to calculate the energy losses in microwave waveguides and resonators with conducting (practically, metallic) walls, and for now let me note only that according to Eqs. (33) and (36), for a fixed magnetic field amplitude, the losses grow with frequency as $\omega^{1/2}$.

One more important remark concerning Eqs. (34): integrating the first of them over x , with the help of Eq. (32), we may see that the *linear density* \mathbf{J} of the surface currents (measured in A/m), is simply and fundamentally related to the applied magnetic field:

$$\mathbf{J}_\omega \equiv \int_0^\infty \mathbf{j}_\omega(x) dx = H_\omega^{(0)} \mathbf{n}_z. \quad (6.37)$$

Since this relation does not have any frequency-dependent factors, we may sum it up for all frequency components, and get a universal relation

¹⁶ Let me hope that the reader's physical intuition makes it evident that the skin effect remains conceptually the same for samples of any *shape*, besides possibly some quantitative details of the field distribution.

¹⁷ The loop (vortex) character of the induced current lines, responsible for the term "eddy", is not very apparent in the 1D geometry explored above, with the near-surface currents (Fig. 2b) looping only implicitly, at $z \rightarrow \pm\infty$.

$$\mathbf{J}(t) = H^{(0)}(t)\mathbf{n}_z \equiv H^{(0)}(t)(-\mathbf{n}_y \times \mathbf{n}_x) = \mathbf{H}^{(0)}(t) \times (-\mathbf{n}_x) = \mathbf{H}^{(0)}(t) \times \mathbf{n}, \quad (6.38a)$$

(where $\mathbf{n} = -\mathbf{n}_x$ is the outer normal to the surface – see Fig. 2b) or, in a different form,

$$\Delta\mathbf{H}(t) = \mathbf{n} \times \mathbf{J}(t), \quad (6.38b)$$

where $\Delta\mathbf{H}$ is the full change of the field through the skin layer. This simple *coarse-grain relation* (independent of the choice of coordinate axes), is also independent of the used constituent relations (22), and is by no means occasional. Indeed, it may be readily obtained from the macroscopic Ampère law (5.116), by applying it to a contour drawn around a fragment of the surface, extending under it substantially deeper than the skin depth – see the contour C_2 in Fig. 2b. Hence, Eq. (38) is valid regardless of the exact law of the field penetration.

Coarse-grain
boundary
relation

For the skin effect, this fundamental relationship between the linear current density and the external magnetic field implies that the skin effect's implementation does not necessarily require a dedicated ac magnetic field source. For example, the effect takes place in any wire that carries an ac current, leading to a current's concentration in a surface sheet of thickness $\sim\delta_s$. (Of course, the quantitative analysis of this problem in a wire with an arbitrary cross-section may be technically complicated, because it requires solving Eq. (23) for the corresponding 2D geometry; even for the round cross-section, the solution involves the Bessel functions.) In this case, the ac magnetic field outside the conductor, which still obeys Eq. (38), may be better interpreted as the effect, rather than the cause, of the ac current flow.

Finally, please mind the limited validity of all the above results. First, for the quasistatic approximation to be valid, the field frequency ω should not be too high, so that the displacement current effects are negligible. (Again, this condition will be quantified in Sec. 7 below; it will show that for metals, the condition is violated only at extremely high frequencies above $\sim 10^{18} \text{ s}^{-1}$.) A more practical upper limit on ω is that the skin depth δ_s should stay much larger than the mean free path l of charge carriers,¹⁸ because beyond this point, the constituent relation between the vectors $\mathbf{j}(\mathbf{r})$ and $\mathbf{E}(\mathbf{r})$ becomes essentially *non-local*. Both theory and experiment show that at δ_s below l , the skin effect persists, but acquires a frequency dependence slightly different from Eq. (33): $\delta_s \propto \omega^{-1/3}$ rather than $\omega^{-1/2}$. Historically, this *anomalous skin effect* has been very useful for the measurements of the Fermi surfaces of metals.¹⁹

6.4. Electrodynamics of superconductivity, and the gauge invariance

The effect of superconductivity²⁰ takes place (in certain materials only, mostly metals) when temperature T is reduced below a certain *critical temperature* T_c specific for each material. For most metallic superconductors, T_c is of the order of typically a few kelvins, though several compounds (the so-called *high-temperature superconductors*) with T_c above 100 K have been found since 1987. The most notable property of superconductors is the absence, at $T < T_c$, of measurable resistance to (not very high) dc currents. However, the electromagnetic properties of superconductors cannot be described by

¹⁸ A discussion of the mean free path may be found, for example, in SM Chapter 6. In very clean metals at very low temperatures, δ_s may approach l at frequencies as low as $\sim 1 \text{ GHz}$, but at room temperature, the crossover between the normal to the anomalous skin effect takes place only at $\sim 100 \text{ GHz}$.

¹⁹ See, e.g., A. Abrikosov, *Introduction to the Theory of Normal Metals*, Academic Press, 1972.

²⁰ Discovered experimentally in 1911 by Heike Kamerlingh Onnes.

just taking $\sigma = \infty$ in our previous results. Indeed, for this case, Eq. (33) would give $\delta_s = 0$, i.e., no ac magnetic field penetration at all. Experiment shows something substantially different: weak magnetic fields do penetrate into superconductors by a material-specific distance $\delta_L \sim 10^{-7}\text{-}10^{-6}$ m, the so-called *London's penetration depth*,²¹ which is virtually frequency-independent until the skin depth δ_s , of the same material in its “normal” state, i.e. the absence of superconductivity, becomes less than δ_L . (This crossover happens typically at frequencies $\omega \sim 10^{13}\text{-}10^{14}$ s⁻¹.) The smallness of δ_L on the human scale means that the magnetic field is pushed out from macroscopic samples at their transition into the superconducting state.

This *Meissner-Ochsenfeld effect*, discovered experimentally in 1933,²² may be partly understood using the following classical reasoning. Our discussion of the Ohm law in Sec. 4.2 implied that the current’s (and hence the electric field’s) frequency ω is either zero or sufficiently low. In the classical Drude reasoning, this is acceptable while $\omega\tau \ll 1$, where τ is the effective carrier scattering time participating in Eqs. (4.12)-(4.13). If this condition is not satisfied, we should take into account the charge carrier inertia; moreover, in the opposite limit $\omega\tau \gg 1$, we may neglect the scattering at all. Classically, we can describe the charge carriers in such a “perfect conductor” as particles with a non-zero mass m , which are accelerated by the electric field following the 2nd Newton law (4.11),

$$m\dot{\mathbf{v}} = \mathbf{F} = q\mathbf{E}, \quad (6.39)$$

so that the current density $\mathbf{j} = qn\mathbf{v}$ that they create, changes in time as

$$\dot{\mathbf{j}} = qn\dot{\mathbf{v}} = \frac{q^2 n}{m} \mathbf{E}. \quad (6.40)$$

In terms of the Fourier amplitudes of the functions $\mathbf{j}(t)$ and $\mathbf{E}(t)$, this means

$$-i\omega \mathbf{j}_\omega = \frac{q^2 n}{m} \mathbf{E}_\omega. \quad (6.41)$$

Comparing this formula with the relation $\mathbf{j}_\omega = \sigma \mathbf{E}_\omega$ implied in the last section, we see that we can use all its results with the following replacement:

$$\sigma \rightarrow i \frac{q^2 n}{m\omega}. \quad (6.42)$$

This change replaces the characteristic equation (29) with

$$-i\omega = \frac{\kappa^2 m\omega}{iq^2 n\mu}, \quad \text{i.e. } \kappa^2 = \frac{\mu q^2 n}{m}, \quad (6.43)$$

i.e. replaces the skin effect with the field penetration by the following frequency-independent depth:

$$\delta \equiv \frac{1}{\kappa} = \left(\frac{m}{\mu q^2 n} \right)^{1/2}. \quad (6.44)$$

Superficially, this means that the field decay into the superconductor does not depend on frequency:

²¹ Named so to acknowledge the pioneering theoretical work of brothers Fritz and Heinz London – see below.

²² It is hardly fair to shorten this name to just the “Meissner effect” as it is frequently done, because of the reportedly crucial contribution by Robert Ochsenfeld, then a Walther Meissner’s student, to the discovery.

$$H(x,t) = H(0,t)e^{-x/\delta}, \quad (6.45)$$

thus explaining the Meissner-Ochsenfeld effect.

However, there are two problems with this result. First, for the parameters typical for good metals ($q = -e$, $n \sim 10^{29} \text{ m}^{-3}$, $m \sim m_e$, $\mu \approx \mu_0$), Eq. (44) gives $\delta \sim 10^{-8} \text{ m}$, one or two orders of magnitude lower than the experimental values of δ_L . Experiment also shows that the penetration depth diverges at $T \rightarrow T_c$, which is not predicted by Eq. (44).

The second, much more fundamental problem with Eq. (44) is that it has been derived for $\omega\tau \gg 1$. Even if we assume that somehow there is no scattering at all, i.e. $\tau = \infty$, at $\omega \rightarrow 0$ both parts of the characteristic equation (43) vanish, and we cannot make any conclusion about κ . This is not just a mathematical artifact we could ignore. For example, let us place a non-magnetic metal into a static external magnetic field at $T > T_c$. The field would completely penetrate the sample. Now let us cool it. As soon as temperature is decreased below T_c , the above calculations would become valid, forbidding the penetration into the superconductor of any *change* of the field, so that the initial field would be “frozen” inside the sample. The Meissner-Ochsenfeld experiments have shown something completely different: as T is lowered below T_c , the initial field is being expelled out of the sample.

The resolution of these contradictions is provided by quantum mechanics. As was explained in 1957 in a seminal work by J. Bardeen, L. Cooper, and J. Schrieffer (commonly referred to as the *BCS theory*), superconductivity is due to the correlated motion of electron pairs, with opposite spins and nearly opposite momenta. Such *Cooper pairs*, each with the electric charge $q = -2e$ and zero spin, may form only in a narrow energy layer near the Fermi surface, of a certain thickness $\Delta(T)$. This parameter $\Delta(T)$, which may be also interpreted as the binding energy of the pair, tends to zero at $T \rightarrow T_c$, while at $T \ll T_c$ it has a virtually constant value $\Delta(0) \approx 3.5 k_B T_c$, of the order of a few meV for most superconductors. This fact readily explains the relatively low spatial density of the Cooper pairs: $n_p \sim n\Delta(T)/\epsilon_F \sim 10^{26} \text{ m}^{-3}$. With the correction $n \rightarrow n_p$, Eq. (44) for the penetration depth becomes

$$\delta \rightarrow \delta_L = \left(\frac{m}{\mu q^2 n_p} \right)^{1/2}. \quad (6.46)$$

London's penetration depth

This result diverges at $T \rightarrow T_c$, and generally fits the experimental data reasonably well, at least for the so-called “clean” superconductors with the mean free path $l = v_F \tau$ (where $v_F \sim (2m\epsilon_F)^{1/2}$ is the r.m.s. velocity of electrons on the Fermi surface) much longer than the Cooper pair size ξ —see below.

The smallness of the coupling energy $\Delta(T)$ is also a key factor in the explanation of the Meissner-Ochsenfeld effect. Because of Heisenberg’s quantum uncertainty relation $\delta r \delta p \sim \hbar$, the spatial extension of the Cooper-pair’s wavefunction (the so-called *coherence length* of the superconductor) is relatively large: $\xi \sim \delta r \sim \hbar/\delta p \sim \hbar v_F/\Delta(T) \sim 10^{-6} \text{ m}$. As a result, $n_p \xi^3 \gg 1$, meaning that the wavefunctions of the pairs are strongly overlapped in space. Due to their integer spin, Cooper pairs behave like bosons, which means in particular that at low temperatures they exhibit the so-called *Bose-Einstein condensation* onto the same ground energy level ϵ_g .²³ This means that the quantum frequency ω

²³ A quantitative discussion of the Bose-Einstein condensation of bosons may be found in SM Sec. 3.4, though the full theory of superconductivity is more complicated because it has to describe the condensation taking place simultaneously with the formation of effective bosons (Cooper pairs) from fermions (single electrons). For a

$= \epsilon_g/\hbar$ of the time evolution of each pair's wavefunction $\Psi = \psi \exp\{-i\omega t\}$ is exactly the same, and that the phases φ of the wavefunctions, defined by the relation

$$\psi = |\psi| e^{i\varphi}, \quad (6.47)$$

coincide, so that the electric current is carried not by individual Cooper pairs but rather their *Bose-Einstein condensate* described by a single wavefunction (47). Due to this coherence, the quantum effects (which are, in the usual Fermi-gases of single electrons, masked by the statistical spread of their energies, and hence of their phases), become very explicit – “macroscopic”.

To illustrate this, let us write the well-known quantum-mechanical formula for the probability current density of a free, non-relativistic particle,²⁴

$$\mathbf{j}_w = \frac{i\hbar}{2m} (\psi \nabla \psi^* - \text{c.c.}) \equiv \frac{1}{2m} [\psi^* (-i\hbar \nabla) \psi - \text{c.c.}], \quad (6.48)$$

where c.c. means the complex conjugate of the previous expression. Now let me borrow one result that will be proved later in this course (in Sec. 9.7) when we discuss the analytical mechanics of a charged particle moving in an electromagnetic field. Namely, to account for the magnetic field effects, the particle's *kinetic momentum* $\mathbf{p} \equiv m\mathbf{v}$ (where $\mathbf{v} \equiv d\mathbf{r}/dt$ is the particle's velocity) has to be distinguished from its *canonical momentum*,²⁵

$$\mathbf{P} \equiv \mathbf{p} + q\mathbf{A}. \quad (6.49)$$

where \mathbf{A} is the field's vector potential defined by Eq. (5.27). In contrast with the Cartesian components $p_j = mv_j$ of the kinetic momentum \mathbf{p} , the canonical momentum's components are the generalized momenta corresponding to the Cartesian components r_j of the radius-vector \mathbf{r} , considered as generalized coordinates of the particle: $P_j = \partial \mathcal{L} / \partial v_j$, where \mathcal{L} is the particle's Lagrangian function. According to the general rules of transfer from classical to quantum mechanics,²⁶ it is the vector \mathbf{P} whose operator (in the coordinate representation) equals $-i\hbar \nabla$, so that the operator of the kinetic momentum $\mathbf{p} = \mathbf{P} - q\mathbf{A}$ is $-i\hbar \nabla + q\mathbf{A}$. Hence, to account for the magnetic field²⁷ effects, we should make the following replacement,

$$-i\hbar \nabla \rightarrow -i\hbar \nabla - q\mathbf{A}, \quad (6.50)$$

in all quantum-mechanical relations. In particular, Eq. (48) has to be generalized as

$$\mathbf{j}_w = \frac{1}{2m} [\psi^* (-i\hbar \nabla - q\mathbf{A}) \psi - \text{c.c.}] \quad (6.51)$$

This expression becomes more transparent if we take the wavefunction in form (47); then

detailed, but still very readable coverage of the physics of superconductors, I can recommend the reader the monograph by M. Tinkham, *Introduction to Superconductivity*, 2nd ed., McGraw-Hill, 1996.

²⁴ See, e.g., QM Sec. 1.4, in particular Eq. (1.47).

²⁵ I am sorry to use traditional notations \mathbf{p} and \mathbf{P} for the momenta – the same symbols which were used for the electric dipole moment and polarization in Chapter 3. I hope there will be no confusion because the latter notions are not used in this section.

²⁶ See, e.g., CM Sec. 10.1, in particular Eq. (10.26).

²⁷ The account of the electric field is easier, because the related energy $q\phi$ of the particle may be directly included in the potential energy operator.

$$\mathbf{j}_w = \frac{\hbar}{m} |\psi|^2 \left(\nabla \varphi - \frac{q}{\hbar} \mathbf{A} \right). \quad (6.52)$$

This relation means, in particular, that in order to keep \mathbf{j}_w gauge-invariant, the transformation (8)-(9) has to be accompanied by a simultaneous transformation of the wavefunction's phase:

$$\varphi \rightarrow \varphi + \frac{q}{\hbar} \chi. \quad (6.53)$$

It is fascinating that the quantum-mechanical wavefunction (or more exactly, its phase) is *not* gauge-invariant, meaning that you may change it in your mind – at your free will! Again, this does not change any observable (such as \mathbf{j}_w or the probability density $|\psi|^2$), i.e. any experimental results.

Now for the *electric* current density of the whole superconducting condensate, Eq. (52) yields the following constitutive relation:

$$\mathbf{j} \equiv \mathbf{j}_w q n_p = \frac{\hbar q n_p}{m} |\psi|^2 \left(\nabla \varphi - \frac{q}{\hbar} \mathbf{A} \right), \quad (6.54)$$

Supercurrent density

The formula shows that this *supercurrent* may be induced by the dc magnetic field alone and does not require any electric field. Indeed, for the simple 1D geometry shown in Fig. 2a, $\mathbf{j}(\mathbf{r}) = j(x) \mathbf{n}_z$, $\mathbf{A}(\mathbf{r}) = A(x) \mathbf{n}_z$, and $\partial/\partial z = 0$, so that the Coulomb gauge condition (5.48) is satisfied for any choice of the gauge function $\chi(x)$. For the sake of simplicity we can choose this function to provide $\varphi(\mathbf{r}) \equiv \text{const}$,²⁸ so that

$$\mathbf{j} = -\frac{q^2 n_p}{m} \mathbf{A} \equiv -\frac{1}{\mu \delta_L^2} \mathbf{A}. \quad (6.55)$$

where δ_L is given by Eq. (46), and the field is assumed to be small and hence not affecting the probability $|\psi|^2$ (here normalized to 1 in the absence of the field). This is the so-called *London equation*, proposed (in a different form) by F. and H. London in 1935 for the Meissner-Ochsenfeld effect's explanation. Combining it with Eq. (5.44), generalized for a linear magnetic medium by the replacement $\mu_0 \rightarrow \mu$, we get

$$\nabla^2 \mathbf{A} = \frac{1}{\delta_L^2} \mathbf{A}, \quad (6.56)$$

This simple differential equation, similar to Eq. (23), for our 1D geometry has an exponential solution similar to Eq. (32):

$$A(x) = A(0) \exp \left\{ -\frac{x}{\delta_L} \right\}, \quad B(x) = B(0) \exp \left\{ -\frac{x}{\delta_L} \right\}, \quad j(x) = j(0) \exp \left\{ -\frac{x}{\delta_L} \right\}, \quad (6.57)$$

which shows that the magnetic field and the supercurrent penetrate into a superconductor only by London's penetration depth δ_L , regardless of frequency.²⁹ By the way, integrating the last result through the penetration layer, and using the vector potential's definition, $\mathbf{B} = \nabla \times \mathbf{A}$ (for our geometry, giving

²⁸ This is the so-called *London gauge*; for our simple geometry, it is also the Coulomb gauge (5.48).

²⁹ Since at $T > 0$, not all electrons in a superconductor form Cooper pairs, at any frequency $\omega \neq 0$ the unpaired electrons provide energy-dissipating Ohmic currents, which are not described by Eq. (54). These losses become very substantial when the frequency ω becomes so high that the skin-effect length δ_s of the material becomes less than δ_L . For typical metallic superconductors, this crossover takes place at frequencies of a few hundred GHz, so that even for microwaves, Eq. (57) still gives a fairly accurate description of the field penetration.

$B(x) = dA(x)/dx = -\delta A(x)$) we may readily verify that the linear density \mathbf{J} of the surface supercurrent still satisfies the universal coarse-grain relation (38).

This universality should bring to our attention the following common feature of the skin effect (in “normal” conductors) and the Meissner-Ochsenfeld effect (in superconductors): if the linear size of a bulk sample is much larger than, respectively, δ_s or δ_L , than $\mathbf{B} = 0$ in the dominating part of its interior. According to Eq. (5.110), a formal description of such conductors (valid only on a coarse-grain scale much larger than either δ_s or δ_L), may be achieved by formally treating the sample as an *ideal diamagnet*, with $\mu = 0$. In particular, we can use this description and Eq. (5.124) to immediately obtain the magnetic field’s distribution outside of a bulk sphere:

$$\mathbf{B} = \mu_0 \mathbf{H} = -\mu_0 \nabla \phi_m, \quad \text{with } \phi_m = H_0 \left(-r - \frac{R^3}{2r^2} \right) \cos \theta, \quad \text{for } r \geq R. \quad (6.58)$$

Figure 3 shows the corresponding surfaces of equal potential ϕ_m . It is evident that the magnetic field lines (which are normal to the equipotential surfaces) bend to become parallel to the surface near it.

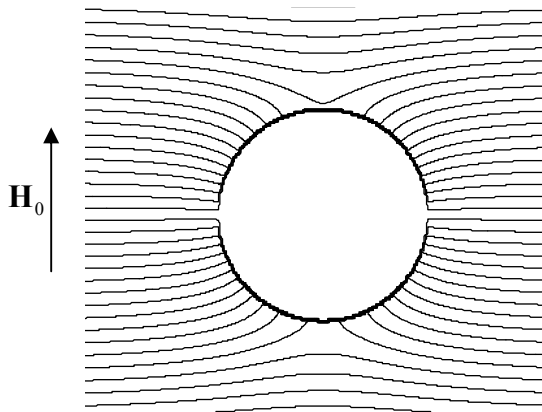


Fig. 6.3. Equipotential surfaces $\phi_m = \text{const}$ around a conducting sphere of radius $R \gg \delta_s$ (or δ_L), placed into a uniform magnetic field, calculated within the coarse-grain (ideal-diamagnet) approximation $\mu = 0$.

This pattern also helps to answer the question that might arise at making the assumption (24): what happens to bulk conductors placed into a *normal* ac magnetic field – and to superconductors in a normal dc magnetic field as well? The answer is: the field is deformed outside of the conductor to sustain the following *coarse-grain boundary condition*:³⁰

$$B_n|_{\text{surface}} = 0, \quad (6.59)$$

which follows from Eq. (5.118) and the coarse-grain requirement $\mathbf{B}|_{\text{inside}} = 0$.

This answer should be taken with reservations. For normal conductors it is only valid at sufficiently high frequencies where the skin depth (33) is sufficiently small: $\delta_s \ll a$, where a is the scale of the conductor’s linear size – for a sphere, $a \sim R$. In superconductors, this simple picture requires not only that $\delta_s \ll a$, but also that magnetic field is relatively low because strong fields *do* penetrate

³⁰ Sometimes this boundary condition, as well as the (compatible) Eq. (38), are called “macroscopic”. However, this term may lead to confusion with the genuine macroscopic boundary conditions (5.117)-(5.118), which also ignore the atomic-scale microstructure of the “effective currents” $\mathbf{j}_{\text{ef}} = \nabla \times \mathbf{M}$, but (as was shown earlier in this section) still allow explicit, detailed accounts of the skin-current (34) and supercurrent (55) distributions.

superconductors, destroying superconductivity (either completely or partly), and as a result violating the Meissner-Ochsenfeld effect – see the next section.

6.5. Electrodynamics of macroscopic quantum phenomena³¹

Despite the superficial similarity of the skin effect and the Meissner-Ochsenfeld effect, the electrodynamics of superconductors is much richer. For example, let us use Eq. (54) to describe the fascinating effect of *magnetic flux quantization*. Consider a closed ring/loop (not necessarily a round one) made of a superconducting “wire” with a cross-section much larger than δ_L^2 (Fig. 4a).

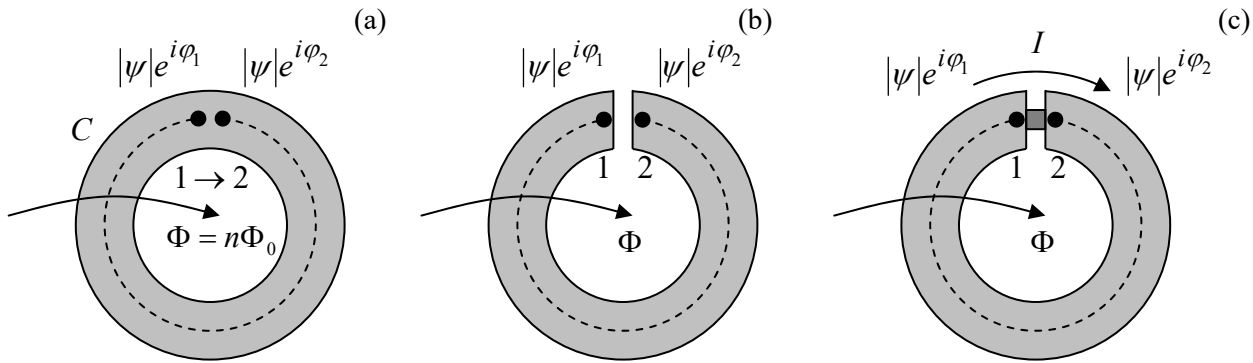


Fig. 6.4. (a) A closed, flux-quantizing superconducting ring, (b) a ring with a narrow slit, and (c) a Superconducting QUantum Interference Device (SQUID).

From the last section’s discussion, we know that deep inside the wire the supercurrent is exponentially small. Integrating Eq. (54) along any closed contour C that does not approach the surface closer than a few δ_L at any point (see the dashed line in Fig. 4), so that with $\mathbf{j} = 0$ at all its points, we get

$$\oint_C \nabla \varphi \cdot d\mathbf{r} - \frac{q}{\hbar} \oint_C \mathbf{A} \cdot d\mathbf{r} = 0. \quad (6.60)$$

The first integral, i.e. the difference of φ in the initial and final points, has to be equal to either zero or an integer number of 2π because the change $\varphi \rightarrow \varphi + 2\pi n$ does not change the Cooper pair’s condensate’s wavefunction:

$$\psi' \equiv |\psi|e^{i(\varphi+2\pi n)} = |\psi|e^{i\varphi} \equiv \psi. \quad (6.61)$$

On the other hand, according to Eq. (5.65), the second integral in Eq. (60) is just the magnetic flux Φ through the contour.³² As a result, we get a wonderful result:

³¹ The material of this section is not covered in most E&M textbooks, and will not be used in later sections of this course. Thus the “only” loss due to the reader’s skipping this section would be the lack of familiarity with one of the most fascinating fields of physics. Note also that we already have virtually all formal tools necessary for its discussion, so reading this section should not require much effort.

³² Due to the Meissner-Ochsenfeld effect, the exact path of the contour is not important, and we may discuss Φ just as the magnetic flux through the ring.

Magnetic flux quantization

$$\Phi = n\Phi_0, \quad \text{where } \Phi_0 \equiv \frac{2\pi\hbar}{|q|}, \quad \text{with } n = 0, \pm 1, \pm 2, \dots, \quad (6.62)$$

saying that the magnetic flux inside any superconducting loop can only take values multiple of the *flux quantum* Φ_0 . This effect, predicted in 1950 by the same Fritz London (who expected q to be equal to the electron charge $-e$), was observed experimentally in 1961,³³ but with $|q| = 2e$ – so that $\Phi_0 \approx 2.07 \times 10^{-15}$ Wb. Historically, this observation gave decisive support to the BCS theory of superconductivity (implying Cooper pairs with charge $q = -2e$) that had been put forward just four years earlier.

Note the truly macroscopic character of this quantum effect: it has been repeatedly observed in human-scale superconducting loops, and from what is known about superconductors, there is no doubt that if we had made a giant superconducting wire loop extending, say, over the Earth's equator, the magnetic flux through it would still be quantized – though with a very large flux quanta number n . This means that the quantum coherence of Bose-Einstein condensates may extend over, using H. Casimir's famous expression, “miles of dirty lead wire”. (Lead is a typical superconductor, with $T_c \approx 7.2$ K, and indeed retains its superconductivity even being highly contaminated by impurities.)

Moreover, hollow rings are not entirely necessary for flux quantization. In 1957, A. Abrikosov explained the counter-intuitive high-field behavior of superconductors with $\delta_L > \xi\sqrt{2}$, known experimentally as their *mixed* (or “Shubnikov”) *phase* since the 1930s. He showed that a sufficiently high magnetic field may penetrate such superconductors in the form of self-formed magnetic field “threads” (or “tubes”) surrounded by vortex-shaped supercurrents – the so-called *Abrikosov vortices*. In the simplest case, the core of such a vortex is a straight line, on which the superconductivity is completely suppressed ($|\psi| = 0$), surrounded by circular, axially-symmetric, persistent supercurrents $j(\rho)$, where ρ is the distance from the vortex axis – see Fig. 5a. At the axis, the current vanishes, and with the growth of ρ , it first rises and then falls (with $j(\infty) = 0$), reaching its maximum at $\rho \sim \xi$, while the magnetic field $B(\rho)$, directed along the vortex axis, is largest at $\rho = 0$, and drops monotonically at distances of the order of δ_L (Fig. 5b).

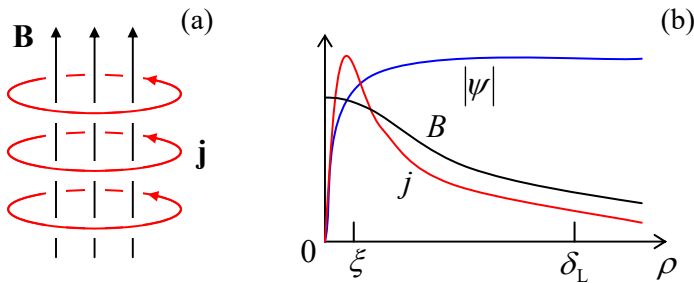


Fig. 6.5. The Abrikosov vortex:
(a) a 3D structure's sketch, and
(b) the main variables as functions of the distance ρ from the axis (schematically).

The total flux of the field equals exactly one flux quantum Φ_0 , given by Eq. (62). Correspondingly, the wavefunction's phase φ performs just one $\pm 2\pi$ revolution along *any* contour drawn around the vortex's axis, so that $\nabla\varphi = \pm \mathbf{n}_\varphi / \rho$, where \mathbf{n}_φ is the azimuthal unit vector.³⁴ This topological feature of the wavefunction's phase is sometimes called the *fluxoid quantization* – to

³³ Independently and virtually simultaneously by two groups: B. Deaver and W. Fairbank, and R. Doll and M. N  bauer; their reports were published back-to-back in the same issue of the *Physical Review Letters*.

³⁴ The last (perhaps, evident) expression for $\nabla\varphi$ follows from MA Eq. (10.2) with $f = \pm\varphi + \text{const.}$

distinguish it from the magnetic *flux* quantization, which is valid only for relatively large contours, not approaching the axis by distances $\sim \delta_L$.

A quantitative analysis of Abrikosov vortices requires, besides the equations we have discussed, one more constituent relation that would describe the suppression of the number of Cooper pairs (quantified by $|\psi|^2$) by the magnetic field – or rather by the field-induced supercurrent. In his original work, Abrikosov used for this purpose the famous *Ginzburg-Landau* equation,³⁵ which is quantitatively valid only at $T \approx T_c$. The equation may be conveniently represented in either of the following two forms:

$$\frac{1}{2m}(-i\hbar\nabla - q\mathbf{A})^2\psi = a\psi - b\psi|\psi|^2, \quad \xi^2\psi * \left(\nabla - i\frac{q}{\hbar}\mathbf{A}\right)^2\psi = (1 - |\psi|^2)|\psi|^2, \quad (6.63)$$

where a and b are certain temperature-dependent coefficients, with $a \rightarrow 0$ at $T \rightarrow T_c$. The first of these forms clearly shows that the Ginzburg-Landau equation (as well as the similar *Gross-Pitaevskii* equation describing electrically-neutral Bose-Einstein condensates) belongs to a broader class of *nonlinear Schrödinger equations*, differing only by the additional nonlinear term from the usual Schrödinger equation, which is linear in ψ . The equivalent, second form of Eq. (63) is more convenient for applications and shows more clearly that if the superconductor's condensate density, proportional to $|\psi|^2$, is suppressed only locally, it self-restores to its unperturbed value (with $|\psi|^2 = 1$) at the distances of the order of the coherence length $\xi \equiv \hbar/(2ma)^{1/2}$.

This fact enables a simple quantitative analysis of the Abrikosov vortex in the most important limit $\xi \ll \delta_L$. Indeed, as Fig. 5 shows, in this case, $|\psi|^2 = 1$ at most distances ($\rho \sim \delta_L$) where the field and current are distributed, so that these distributions may be readily calculated without any further involvement of Eq. (63), just from Eq. (54) with $\nabla\varphi = \pm\mathbf{n}_\varphi/\rho$, and the Maxwell equations (21) for the magnetic field, giving $\nabla \times \mathbf{B} = \mu\mathbf{j}$, and $\nabla \cdot \mathbf{B} = 0$. Indeed, combining these equations just as this was done at the derivation of Eq. (23), for the only Cartesian component of the vector $\mathbf{B}(\mathbf{r}) = B(\rho)\mathbf{n}_z$ (where the z -axis is directed along the vortex' symmetry axis), we get a simple equation

$$\delta_L^2 \nabla^2 B - B = -\frac{\hbar}{q} \nabla \times (\nabla \times \varphi) \equiv \mp \Phi_0 \delta_2(\rho), \quad \text{at } \rho \gg \xi, \quad (6.64)$$

which coincides with Eq. (56) at all regular points $\rho \neq 0$. Spelling out the Laplace operator for our current case of axial symmetry,³⁶ we get an ordinary differential equation,

$$\delta_L^2 \frac{1}{\rho} \frac{d}{d\rho} \left(\rho \frac{dB}{d\rho} \right) - B = 0, \quad \text{for } \rho \neq 0. \quad (6.65)$$

Comparing this equation with Eq. (2.155) with $v = 0$, and taking into account that we need the solution decreasing at $\rho \rightarrow \infty$, making any contribution proportional to the function I_0 unacceptable, we get

³⁵ This equation was derived by Vitaly Lazarevich Ginzburg and Lev Davidovich Landau from phenomenological arguments in 1950, i.e. before the advent of the “microscopic” BSC theory, and may be used for simple analyses of a broad range of nonlinear effects in superconductors. The Ginzburg-Landau and Gross-Pitaevskii equations will be further discussed in SM Sec. 4.3.

³⁶ See, e.g., MA Eq. (10.3) with $\partial/\partial\varphi = \partial/\partial z = 0$.

$$B = CK_0\left(\frac{\rho}{\delta_L}\right) \quad (6.66)$$

– see the plot of this Bessel function on the right panel of Fig. 2.22 (black line). The constant C should be calculated from fitting the 2D delta function on the right-hand side of Eq. (64), i.e. by requiring

$$\int_{\text{vortex}} B(\rho) d^2\rho \equiv 2\pi \int_0^\infty B(\rho) \rho d\rho \equiv 2\pi \delta_L^2 C \int_0^\infty K_0(\zeta) \zeta d\zeta = \mp \Phi_0. \quad (6.67)$$

The last, dimensionless integral equals 1,³⁷ so that finally

$$B(\rho) = \frac{\Phi_0}{2\pi\delta_L^2} K_0\left(\frac{\rho}{\delta_L}\right), \quad \text{at } \rho \gg \xi. \quad (6.68)$$

So the magnetic field of the vortex drops exponentially at distances ρ much larger than δ_L , and diverges at $\rho \rightarrow 0$ – see, e.g., the second of Eqs. (2.157). However, this divergence is very slow (logarithmic), and, as was repeatedly discussed in this series, is avoided by the account of virtually any other factor. In our current case, this factor is the decrease of $|\psi|^2$ to zero at $\rho \sim \xi$ (see Fig. 5), not taken into account in Eq. (68). As a result, we may estimate the field on the axis of the vortex as

$$B(0) \approx \frac{\Phi_0}{2\pi\delta_L^2} \ln \frac{\delta_L}{\xi}; \quad (6.69)$$

the exact (and much more involved) solution of the problem confirms this estimate with a minor correction: $\ln(\delta_L/\xi) \rightarrow \ln(\delta_L/\xi) - 0.28$, i.e. $\xi \rightarrow 1.3\xi$.

The current density distribution may be now calculated from the Maxwell equation $\nabla \times \mathbf{B} = \mu \mathbf{j}$, giving $\mathbf{j} = j(\rho) \mathbf{n}_\phi$, with³⁸

$$j(\rho) = -\frac{1}{\mu} \frac{\partial B}{\partial \rho} = -\frac{\Phi_0}{2\pi\mu\delta_L^2} \frac{\partial}{\partial \rho} K_0\left(\frac{\rho}{\delta_L}\right) \equiv \frac{\Phi_0}{2\pi\mu\delta_L^3} K_1\left(\frac{\rho}{\delta_L}\right), \quad \text{at } \rho \gg \xi, \quad (6.70)$$

where the same identity (2.158), with $J_n \rightarrow K_n$ and $n = 1$, was used. Now looking at Eqs. (2.157) and (2.158), with $n = 1$, we see that the supercurrent's density is exponentially low at $\rho \gg \delta_L$ (thus outlining the vortex' periphery), and is proportional to $1/\rho$ within the broad range $\xi \ll \rho \ll \delta_L$. This rise of the current at $\rho \rightarrow 0$ (which could be readily predicted directly from Eq. (54) with $\nabla\varphi = \pm \mathbf{n}_\phi/\rho$, and the \mathbf{A} -term negligible at $\rho \ll \delta_L$) is quenched at $\rho \sim \xi$ by a rapid drop of the factor $|\psi|^2$ in the same Eq. (54), i.e. by the suppression of the superconductivity near the axis (by the same supercurrent!) – see Fig. 5 again.

This structure of the Abrikosov vortex may be used to calculate, in a straightforward way, its energy per unit length (i.e. its linear tension)

³⁷ This fact follows, for example, from the integration of both sides of Eq. (2.143) (which is valid for any Bessel functions, including K_n) with $n = 1$, from 0 to ∞ , and then using the asymptotic values given by Eqs. (2.157)-(2.158): $K_1(\infty) = 0$, and $K_1(\zeta) \rightarrow 1/\zeta$ at $\zeta \rightarrow 0$.

³⁸ See, e.g., MA Eq. (10.5), with $f_\rho = f_\phi = 0$, and $f_z = B(\rho)$.

$$\mathcal{T} \equiv \frac{U}{l} \approx \frac{\Phi_0^2}{4\pi\mu\delta_L^2} \ln \frac{\delta_L}{\xi}, \quad (6.71)$$

and hence the so-called “first critical” value H_{c1} of the external magnetic field,³⁹ at that the vortex formation becomes possible (in a long cylindrical sample parallel to the field):

$$H_{c1} = \frac{\mathcal{T}}{\Phi_0} \approx \frac{\Phi_0}{4\pi\mu\delta_L^2} \ln \frac{\delta_L}{\xi}. \quad (6.72)$$

Let me leave the proof of these two formulas for the reader’s exercise.

The flux quantization and the Abrikosov vortices discussed above are just two of several *macroscopic quantum effects* in superconductivity. Let me discuss just one more, but perhaps the most interesting of such effects. Let us consider a superconducting ring/loop interrupted with a very narrow slit (Fig. 4b). Integrating Eq. (54) along any current-free path from point 1 to point 2 (see, e.g., dashed line in Fig. 4b), we get

$$0 = \int_1^2 \left(\nabla \varphi - \frac{q}{\hbar} \mathbf{A} \right) \cdot d\mathbf{r} = \varphi_2 - \varphi_1 - \frac{q}{\hbar} \Phi. \quad (6.73)$$

Using the flux quantum definition (62), this result may be rewritten as

$$\varphi \equiv \varphi_1 - \varphi_2 = \frac{2\pi}{\Phi_0} \Phi, \quad (6.74)$$

Josephson
phase
difference

where φ is called the *Josephson phase difference*. Note that in contrast to each of the phases $\varphi_{1,2}$, their difference φ is gauge-invariant: Eq. (74) directly relates it to the gauge-invariant magnetic flux Φ .

Can this φ be measured? Yes, for example, using the *Josephson effect*.⁴⁰ Let us consider two (for the argument simplicity, similar) superconductors, connected with some sort of *weak link*, for example, a small tunnel junction, or a point contact, or a narrow thin-film bridge, through that a weak Cooper-pair supercurrent can flow. (Such a system of two weakly coupled superconductors is called a *Josephson junction*.) Let us think about what this supercurrent I may be a function of. For that, reverse thinking is helpful: let us imagine that we change the current; what parameter of the superconducting condensate can it affect? If the current is very weak, it cannot perturb the superconducting condensate’s density, proportional to $|\psi|^2$; hence it may only change the Cooper condensate phases $\varphi_{1,2}$. However, according to Eq. (53), the phases are not gauge-invariant, while the current should be. Hence the current may affect (or, if you like, may be affected by) only the phase difference φ defined by Eq. (74). Moreover, just has already been argued during the flux quantization discussion, a change of any of $\varphi_{1,2}$ (and hence of φ) by 2π or any of its multiples should not change the current. Also, if the wavefunction is the same in both superconductors ($\varphi = 0$), the supercurrent should vanish due to the system’s symmetry. Hence the function $I(\varphi)$ should satisfy the following conditions:

³⁹ This term is used to distinguish H_{c1} from the higher “second critical field” H_{c2} , at which the Abrikosov vortices are pressed to each other so tightly (to distances $d \sim \xi$) that they merge, and the remains of superconductivity vanish: $\psi \rightarrow 0$. Unfortunately, I do not have time/space to discuss these effects; the interested reader may be referred, for example, to Chapter 5 of M. Tinkham’s monograph cited above.

⁴⁰ It was predicted in 1961 by Brian David Josephson (then a PhD student!) and observed experimentally by several groups soon after that.

$$I(0) = 0, \quad I(\varphi + 2\pi) = I(\varphi). \quad (6.75)$$

With these conditions on hand, we should not be terribly surprised by the following Josephson's result that for the weak link provided by tunneling,⁴¹

Josephson
(super)current

$$I(\varphi) = I_c \sin \varphi, \quad (6.76)$$

where constant I_c , which depends on the weak link's strength and temperature, is called the *critical current*. Actually, Eqs. (54) and (63) enable not only a straightforward calculation of this relation but even obtaining a simple expression of the critical current I_c via the link's normal-state resistance – the task left for the (creative :-) reader's exercise.

Now let us see what happens if a Josephson junction is placed into the gap in a superconductor loop – see Fig. 4c. In this case, we may combine Eqs. (74) and (76), getting

Macroscopic
quantum
interference

$$I = I_c \sin\left(2\pi \frac{\Phi}{\Phi_0}\right). \quad (6.77)$$

This effect of a periodic dependence of the current on the magnetic flux is called *macroscopic quantum interference*,⁴² while the system shown in Fig. 4c, the *superconducting quantum interference device – SQUID* (with all letters capital, please :-). The low value of the magnetic flux quantum Φ_0 , and hence the high sensitivity of φ to external magnetic fields, allows using such SQUIDs as ultrasensitive magnetometers. Indeed, for a superconducting ring of area $\sim 1 \text{ cm}^2$, one period of the change of the supercurrent (77) is produced by a magnetic field change of the order of 10^{-11} T (10^{-7} Gs), while sensitive electronics allows measuring a tiny fraction of this period – limited by thermal noise at a level of the order of a few fT. Such sensitivity allows measurements, for example, of the minuscule magnetic fields induced outside of the body by the beating human heart, and even by brain activity.⁴³

An important aspect of quantum interference is the so-called *Aharonov-Bohm (AB) effect* – which actually takes place for single quantum particles as well.⁴⁴ Let the magnetic field lines be limited to the central, hollow part of the SQUID loop so that no appreciable magnetic field ever touches the ring itself. (This may be done experimentally with very good accuracy, for example using high- μ magnetic cores – see their discussion in Sec. 5.6.) As predicted by Eq. (77), and confirmed by several careful experiments carried out in the mid-1960s,⁴⁵ this restriction does not matter – the interference is observed

⁴¹ For some other types of weak links, the function $I(\varphi)$ may deviate from the sinusoidal form Eq. (76) rather considerably, while still satisfying the general conditions (75).

⁴² The name is due to a deep analogy between this phenomenon and the interference between two coherent waves, to be discussed in detail in Sec. 8.4.

⁴³ Other practical uses of SQUIDs include MRI signal detectors, high-sensitive measurements of magnetic properties of materials, and weak field detection in a broad variety of physical experiments – see, e.g., J. Clarke and A. Braginski (eds.), *The SQUID Handbook*, vol. II, Wiley, 2006. For a comparison of these devices with other sensitive magnetometers see, e.g., the review collection by A. Grosz *et al.* (eds.), *High Sensitivity Magnetometers*, Springer, 2017.

⁴⁴ For a more detailed discussion of the AB effect see, e.g., QM Sec. 3.2.

⁴⁵ Similar experiments have been carried out with single (unpaired) electrons – moving either ballistically, in vacuum, or in “normal” (non-superconducting) conducting rings. In the last case, the effect is much harder to observe than in SQUIDs: the ring size has to be very small, and temperature very low, to avoid the so-called

anyway. This means that not only the magnetic field \mathbf{B} but also the vector potential \mathbf{A} represents physical reality, albeit in a quite peculiar way – remember the gauge transformation (5.46), which you may carry out in your head, without changing any physical reality? (Fortunately, this transformation does not change the contour integral participating in Eq. (5.65), and hence the magnetic flux Φ , and hence the interference pattern.)

Actually, the magnetic flux quantization (62) and the macroscopic quantum interference (77) are not completely different effects, but just two manifestations of the interrelated macroscopic quantum phenomena. To show that, one should note that if the critical current I_c (or rather its product by the loop's self-inductance L) is high enough, the flux Φ in the SQUID loop is due not only to the external magnetic field flux Φ_{ext} but also has a self-field component – cf. Eq. (5.68):⁴⁶

$$\Phi = \Phi_{\text{ext}} - LI, \quad \text{where } \Phi_{\text{ext}} \equiv \int_S (B_{\text{ext}})_n d^2r. \quad (6.78)$$

Now the relation between Φ and Φ_{ext} may be readily found by solving this equation together with Eq. (77). Figure 6 shows this relation for several values of the dimensionless parameter $\lambda \equiv 2\pi LI_c/\Phi_0$.

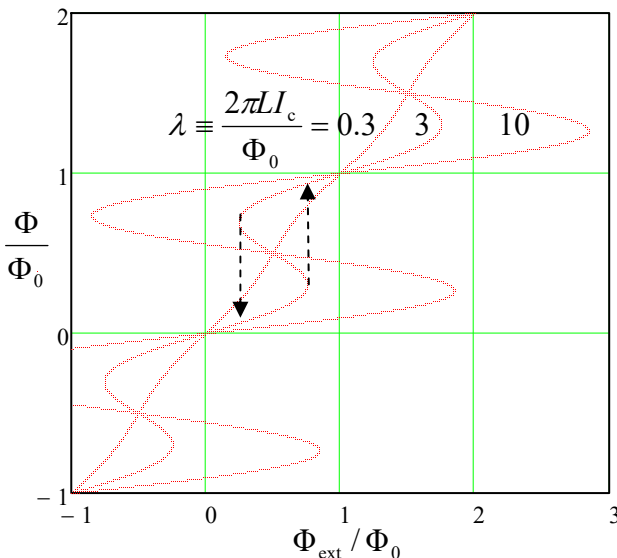


Fig. 6.6. The function $\Phi(\Phi_{\text{ext}})$ for SQUIDS with various values of the normalized LI_c product. Dashed arrows show the flux leaps as the external field is changed. (The branches with $d\Phi/d\Phi_{\text{ext}} < 0$ are unstable.)

These plots show that if the critical current (and/or the inductance) is low, $\lambda \ll 1$, the self-field effects are negligible, and the total flux follows the external field (i.e., Φ_{ext}) faithfully. However, at $\lambda > 1$, the function $\Phi(\Phi_{\text{ext}})$ becomes hysteretic, and at $\lambda \gg 1$, its stable (positive-slope) branches are nearly flat, with the total flux values corresponding to Eq. (62). Thus, a superconducting ring closed with a high- I_c Josephson junction exhibits a nearly-perfect flux quantization.

The self-field effects described by Eq. (78) create certain technical problems for SQUID magnetometry, but they are the basis for one more useful application of these devices: ultrafast

dephasing effects due to unavoidable interactions of the electrons with their environment – see, e.g., QM Chapter 7.

⁴⁶ The sign before LI would be positive, as in Eq. (5.70), if I was the current flowing *into* the inductance. However, in order to keep the sign in Eq. (76) intact, I should mean the current flowing into the Josephson junction, i.e. *from* the inductance, thus changing the sign of the LI term in Eq. (78).

computing. Indeed, Fig. 6 shows that at the values of λ modestly above 1 (e.g., $\lambda \approx 3$), and within a certain range of applied field, the SQUID has two stable flux states, which differ by $\Delta\Phi \approx \Phi_0$ and may be used for coding binary 0 and 1. For practical superconductors (like Nb), the time of switching between these states (see dashed arrows in Fig. 4) is of the order of a picosecond, while the energy dissipated at such event may be as low as $\sim 10^{-19}$ J. (This bound is determined not by device's physics, by the fundamental requirement for the energy barrier between the two states to be much higher than the thermal fluctuation energy scale $k_B T$, ensuring a sufficiently long information retention time.) While the picosecond switching speed may be also achieved with some semiconductor devices, the power consumption of the SQUID-based digital devices may be 5 to 6 orders of magnitude lower, enabling large-scale digital integrated circuits with 100-GHz-scale clock frequencies. Unfortunately, the range of practical applications of these *Rapid Single-Flux-Quantum* (RSFQ) digital circuits is still very narrow, due to the inconvenience of their deep refrigeration to temperatures below T_c .⁴⁷

Since we have already got the basic relations (74) and (76) describing the macroscopic quantum phenomena in superconductivity, let me mention in brief two other prominent members of this group, called the *dc* and *ac Josephson effects*. Differentiating Eq. (74) over time, and using the Faraday induction law (2), we get⁴⁸

$$\frac{d\varphi}{dt} = \frac{2e}{\hbar} V. \quad (6.79)$$

Josephson
phase-to-
voltage
relation

This famous *Josephson phase-to-voltage relation* should be valid regardless of the way how the voltage V has been created,⁴⁹ so let us apply Eqs. (76) and (79) to the simplest circuit with a non-superconducting source of dc voltage – see Fig. 7.

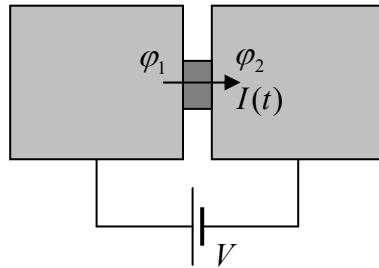


Fig. 6.7. DC-voltage-biased Josephson junction.

If the current's magnitude is below the critical value, Eq. (76) allows phase φ to have the time-independent value

$$\varphi = \sin^{-1} \frac{I}{I_c}, \quad \text{if } -I_c < I < +I_c, \quad (6.80)$$

and hence, according to Eq. (79), a vanishing voltage drop across the junction: $V = 0$. This *dc Josephson effect* is not quite surprising – indeed, we have postulated from the very beginning that the Josephson junction may pass a certain supercurrent. Much more fascinating is the so-called *ac Josephson effect* that occurs if the voltage across the junction has a non-zero average (dc) component V_0 . For simplicity, let us

⁴⁷ For more on that technology, see, e.g., the review paper by P. Bunyk *et al.*, *Int. J. High Speed Electron. Syst.* **11**, 257 (2001), and references therein.

⁴⁸ Since the induced e.m.f. \mathcal{E}_{ind} cannot drop on the superconducting path between the Josephson junction electrodes 1 and 2 (see Fig. 4c), it should be equal to $(-V)$, where V is the voltage across the junction.

⁴⁹ Indeed, it may be also obtained from simple Schrödinger-equation-based arguments – see, e.g., QM Sec. 1.6.

assume that this is the *only* voltage component: $V(t) = V_0 = \text{const}$ ⁵⁰ then Eq. (79) may be easily integrated to give $\varphi = \omega_J t + \varphi_0$, where

$$\omega_J \equiv \frac{2e}{\hbar} V_0. \quad (6.81)$$

Josephson
oscillation
frequency

This result, plugged into Eq. (76), shows that the supercurrent oscillates,

$$I = I_c \sin(\omega_J t + \varphi_0), \quad (6.82)$$

with the so-called *Josephson frequency* ω_J (81) proportional to the applied dc voltage. For practicable voltages (above the typical noise level), the frequency $f_J = \omega_J/2\pi$ corresponds to the GHz or even THz ranges, because the proportionality coefficient in Eq. (81) is very high: $f_J/V_0 = e/\pi\hbar \approx 483 \text{ MHz}/\mu\text{V}$.⁵¹

An important experimental fact is the universality of this coefficient. For example, in the mid-1980s, a Stony Brook group led by J. Lukens proved that this factor is material-independent with a relative accuracy of at least 10^{-15} . Very few experiments, especially in solid-state physics, have ever reached such precision. This fundamental nature of the Josephson voltage-to-frequency relation (81) allows an important application of the ac Josephson effect in metrology. Namely, phase-locking⁵² the Josephson oscillations with an external microwave signal from an atomic frequency standard, one can get a more precise dc voltage than from any other source. In NIST and other metrological institutions around the globe, this effect is used for the calibration of simpler “secondary” voltage standards that can operate at room temperature.

6.6. Inductors, transformers, and ac Kirchhoff laws

Let a *wire coil* (meaning either a single loop illustrated in Fig. 5.4b or a series of such loops, such as one of the solenoids shown in Fig. 5.6) have a self-inductance L much larger than that of the wires connecting it to other components of our system: ac voltage sources, voltmeters, etc. (Since, according to Eq. (5.75), L scales as the square of the number N of wire turns, this condition is easier to satisfy at $N \gg 1$.) Then in a quasistatic system consisting of such *lumped induction coils*, external wires, and other lumped circuit elements such as resistors, capacitances, etc., we may neglect the electromagnetic induction effects everywhere outside the coil, so that the electric field in those external regions is potential. Then the voltage V between the coil’s terminals may be defined, just as in electrostatics, as the difference of values of ϕ between the terminals, i.e. as the integral

$$V = \int \mathbf{E} \cdot d\mathbf{r} \quad (6.83)$$

between the coil terminals along any path outside the coil. This voltage has to be balanced by the induction e.m.f. (2) in the coil, so that if the Ohmic resistance of the coil is negligible, we may write

⁵⁰ In experiment, this condition is hard to implement, due to relatively high inductances of the current leads providing the dc voltage supply. However, this technical complication does not affect the main conclusion of the simple analysis described here.

⁵¹ This 1962 prediction (by the same B. Josephson) was confirmed experimentally – in 1963 indirectly, by phase-locking of the oscillations (82) with an external microwave signal, and in 1967 explicitly, by the direct detection of the emitted microwave radiation.

⁵² For a discussion of this very important (and general) effect, see, e.g., CM Sec. 5.4.

$$V = \frac{d\Phi}{dt}, \quad (6.84)$$

where Φ is the magnetic flux in the coil.⁵³ If the flux is due to the current I in the same coil only (i.e. if it is magnetically uncoupled from other coils), we may use Eq. (5.70) to get the well-known relation

Voltage drop on
inductance
coil

$$V = L \frac{dI}{dt}, \quad (6.85)$$

where compliance with the Lenz sign rule is achieved by selecting the relations between the assumed voltage polarity and the current direction as shown in Fig. 8a.

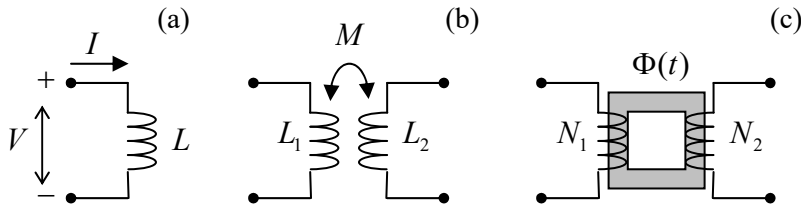


Fig. 6.8. Some lumped ac circuit elements: (a) an induction coil, (b) two inductively coupled coils, and (c) an ac transformer.

If similar conditions are satisfied for two magnetically coupled coils (Fig. 8b), then, in Eq. (84), we need to use Eqs. (5.69) instead, getting

$$V_1 = L_1 \frac{dI_1}{dt} + M \frac{dI_2}{dt}, \quad V_2 = L_2 \frac{dI_2}{dt} + M \frac{dI_1}{dt}. \quad (6.86)$$

Such systems of inductively coupled coils have numerous applications in electrical engineering and physical experiment. Perhaps the most important of them is the *ac transformer*, in which the coils share a common soft-ferromagnetic core of the toroidal (“doughnut”) topology – see Fig. 8c.⁵⁴ As we already know from the discussion in Sec. 5.6, such cores, with $\mu \gg \mu_0$, “try” to absorb all magnetic field lines, so that the magnetic flux $\Phi(t)$ in the core is nearly the same in each of its cross-sections. With this, Eq. (84) yields

$$V_1 \approx N_1 \frac{d\Phi}{dt}, \quad V_2 \approx N_2 \frac{d\Phi}{dt}, \quad (6.87)$$

so that the voltage ratio is completely determined by the ratio N_1/N_2 of the number of wire turns.

Now we may generalize, to the ac current case, the Kirchhoff laws already discussed in Sec. 4.1 – see Fig. 4.3 reproduced in Fig. 9a below. Let not only inductances but also capacitances and resistances of the wires be negligible in comparison with those of the lumped (compact) circuit elements, whose list now would include not only resistors and current sources (as in the dc case), but also the induction coils (including magnetically coupled ones) and capacitors – see Fig. 9b. In the quasistatic approximation, the current flowing in each wire is conserved, so that the “node rule”, i.e. the 1st Kirchhoff law (4.7a),

⁵³ If the resistance is substantial, it may be represented by a separate lumped circuit element (resistor) connected in series with the coil.

⁵⁴ The first practically acceptable form of this device, called the *Stanley transformer*, was invented in 1886. In it, multi-turn windings could be easily mounted onto a toroidal ferromagnetic (at that time, silicon-steel-plate) core.

$$\sum_j I_j = 0. \quad (6.88a)$$

remains valid. Also, if the electromagnetic induction effect is restricted to the interior of lumped induction coils as discussed above, the voltage drops V_k across each circuit element may be still represented, just as in dc circuits, with differences between the adjacent node potentials. As a result, the “loop rule”, i.e. 2nd Kirchhoff law (4.7b),

$$\sum_k V_k = 0, \quad (6.88b)$$

is also valid. Now, in contrast to the dc case, Eqs. (88) may be the (ordinary) differential equations. However, if all circuit elements are linear (as in the examples presented in Fig. 9b), these equations may be readily reduced to linear algebraic equations, using the Fourier expansion. (In the common case of sinusoidal ac sources, the final stage of the Fourier series summation is unnecessary.)

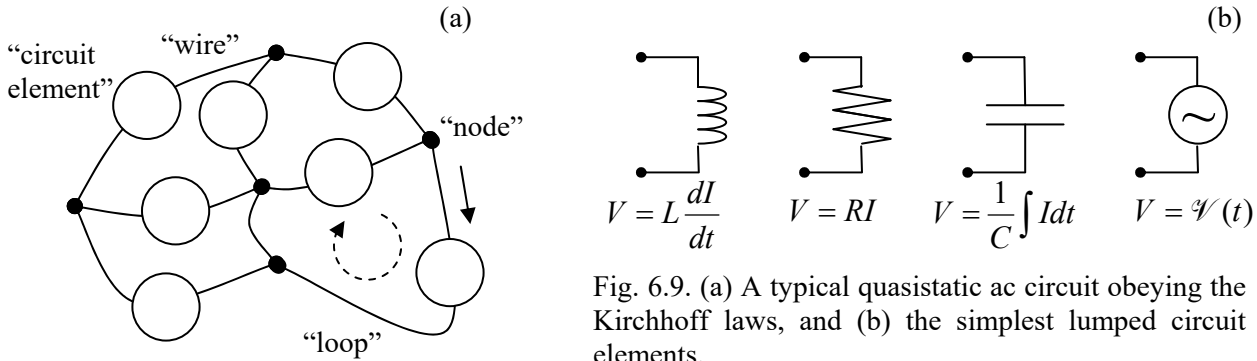


Fig. 6.9. (a) A typical quasistatic ac circuit obeying the Kirchhoff laws, and (b) the simplest lumped circuit elements.

My teaching experience shows that the potential readers of these notes are well familiar with the application of Eqs. (88) to such problems from their undergraduate studies, so I will save time/space by skipping discussions of even the simplest examples of such circuits, such as LC , LR , RC , and LRC loops and periodic structures.⁵⁵ However, since such problems are very important for practice, my sincere advice to the reader is to carry out a self-test by solving a few problems of this type, provided in Sec. 9 below, and if they cause any difficulty, pursue some remedial reading.

6.7. Displacement currents

Electromagnetic induction is not the only new effect arising in non-stationary electrodynamics. Indeed, though Eqs. (21) are adequate for the description of quasistatic phenomena, a deeper analysis shows that one of these equations, namely $\nabla \times \mathbf{H} = \mathbf{j}$, cannot be exact. To see that, let us take the divergence of its both sides:

$$\nabla \cdot (\nabla \times \mathbf{H}) = \nabla \cdot \mathbf{j}. \quad (6.89)$$

But, as the divergence of any curl,⁵⁶ the left-hand side should equal zero. Hence we get

⁵⁵ Curiously enough, these effects include wave propagation in periodic LC circuits, even within the quasistatic approximation! However, the speed $1/(LC)^{1/2}$ of these waves in lumped circuits is much lower than the speed $1/(\epsilon\mu)^{1/2}$ of electromagnetic waves in the surrounding medium – see Sec. 8 below.

⁵⁶ Again, see MA Eq. (11.2) – if you need it.

$$\nabla \cdot \mathbf{j} = 0. \quad (6.90)$$

This is fine in statics, but in dynamics, this equation forbids any charge accumulation, because according to the continuity relation (4.5),

$$\nabla \cdot \mathbf{j} = -\frac{\partial \rho}{\partial t}. \quad (6.91)$$

This discrepancy had been recognized by James Clerk Maxwell who suggested, in the 1860s, a way out of this contradiction. If we generalize the equation for $\nabla \times \mathbf{H}$ by adding to the term \mathbf{j} (that describes the density of real electric currents) the so-called *displacement current density* term,

Displacement
current
density

$$\mathbf{j}_d \equiv \frac{\partial \mathbf{D}}{\partial t}, \quad (6.92)$$

(which of course vanishes in statics), then the equation takes the form

$$\nabla \times \mathbf{H} = \mathbf{j} + \mathbf{j}_d \equiv \mathbf{j} + \frac{\partial \mathbf{D}}{\partial t}. \quad (6.93)$$

In this case, due to the equation (3.22), $\nabla \cdot \mathbf{D} = \rho$, the divergence of the right-hand side equals zero due to the continuity equation (92), and the discrepancy is removed. This incredible theoretical feat,⁵⁷ confirmed by the 1886 experiments carried out by Heinrich Hertz (see below) was perhaps the main triumph of theoretical physics of the 19th century.

Maxwell's displacement current concept, expressed by Eq. (93), is so important that it is worthwhile to have one more look at its derivation using a particular model shown in Fig. 10.⁵⁸

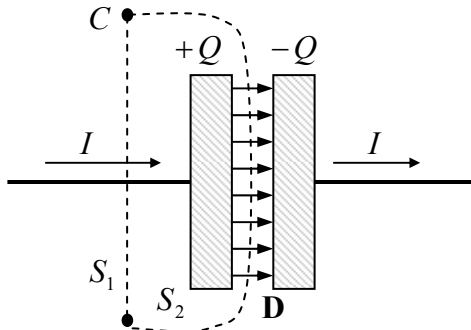


Fig. 6.10. The Ampère law applied to capacitor recharging.

Neglecting the fringe field effects, we may use Eq. (4.1) to describe the relationship between the current I flowing through the wires and the electric charge Q of the capacitor:⁵⁹

$$\frac{dQ}{dt} = I. \quad (6.94)$$

⁵⁷ It looks deceptively simple now – after the fact, and with the current mathematical tools (especially the del operator), which are much superior to those that were available to J. Maxwell.

⁵⁸ No physicist should be ashamed of doing this. For example, J. Maxwell's main book, *A Treatise of Electricity and Magnetism*, is full of drawings of plane capacitors, inductance coils, and voltmeters. More generally, the whole history of science teaches us that snobbery regarding particular examples and practical systems is a virtually certain path toward producing nothing of either practical value or fundamental importance.

⁵⁹ This is of course just the integral form of the continuity equation (91).

Now let us consider a closed contour C drawn around the wire. (Solid points in Fig. 10 show the places where the contour intercepts the plane of the drawing.) This contour may be seen as the line limiting either surface S_1 (crossed by the wire) or surface S_2 (avoiding such crossing by passing through the capacitor's gap). Applying the macroscopic Ampère law (5.116) to the former surface, we get

$$\oint_C \mathbf{H} \cdot d\mathbf{r} = \int_{S_1} j_n d^2 r = I, \quad (6.95)$$

while for the latter surface the same law gives a different result,

$$\oint_C \mathbf{H} \cdot d\mathbf{r} = \int_{S_2} j_n d^2 r = 0, \quad [\text{WRONG!}] \quad (6.96)$$

for the same integral. This is just an integral-form manifestation of the discrepancy outlined above, but it shows clearly how serious the problem is (or rather it was – before Maxwell).

Now let us see how the introduction of the displacement currents saves the day, considering for the sake of simplicity a plane capacitor of area A , with a small and constant electrode spacing. In this case, as we already know, the field inside it is uniform, with $D = \sigma$, so that the total capacitor's charge $Q = A\sigma = AD$, and the current (94) may be represented as

$$I = \frac{dQ}{dt} = A \frac{dD}{dt}. \quad (6.97)$$

So, instead of the wrong Eq. (96), the Ampère law modified following Eq. (93), gives

$$\oint_C \mathbf{H} \cdot d\mathbf{r} = \int_{S_2} (j_d)_n d^2 r = \int_{S_2} \frac{\partial D_n}{\partial t} d^2 r = \frac{dD}{dt} A = I, \quad (6.98)$$

i.e. the Ampère integral becomes independent of the choice of the surface limited by the contour C – as it has to be.

6.8. Finally, the full Maxwell equation system

. This is a very special moment in this course: with the displacement currents in, i.e. with the replacement of Eq. (5.107) with Eq. (93), we have finally arrived at the full set of macroscopic Maxwell equations for time-dependent fields,⁶⁰

$$\nabla \times \mathbf{E} + \frac{\partial \mathbf{B}}{\partial t} = 0, \quad \nabla \times \mathbf{H} - \frac{\partial \mathbf{D}}{\partial t} = \mathbf{j}, \quad (6.99a)$$

$$\nabla \cdot \mathbf{D} = \rho, \quad \nabla \cdot \mathbf{B} = 0, \quad (6.99b)$$

Macroscopic
Maxwell
equations

whose validity has been confirmed by an enormous body of experimental data. Indeed, despite numerous efforts, no other corrections (e.g., additional terms) to the Maxwell equations have been ever found, and these equations are still considered exact within the range of their validity, i.e. while the electric and magnetic fields may be considered classically. Moreover, even in quantum theory, these

⁶⁰ This vector form of the Maxwell equations, magnificent in its symmetry and simplicity, was developed in 1884-85 by Oliver Heaviside, with substantial contributions by H. Lorentz. (The original Maxwell's result circa 1864 looked like a system of 20 equations for Cartesian components of the vector and scalar potentials.)

equations are believed to be *strictly* valid as relations between the Heisenberg operators of the electric and magnetic fields.⁶¹ (Note that the *microscopic* Maxwell equations for the genuine fields \mathbf{E} and \mathbf{B} may be formally obtained from Eqs. (99) by the substitutions $\mathbf{D} = \epsilon_0 \mathbf{E}$ and $\mathbf{H} = \mathbf{B}/\mu_0$, and the simultaneous replacement of the stand-alone charge and current densities on their right-hand sides with the full ones.)

Perhaps the most striking feature of these equations is that, even in the absence of stand-alone charges and currents inside the region of our interest, when the equations become fully homogeneous,

$$\nabla \times \mathbf{E} = -\frac{\partial \mathbf{B}}{\partial t}, \quad \nabla \times \mathbf{H} = \frac{\partial \mathbf{D}}{\partial t}, \quad (6.100a)$$

$$\nabla \cdot \mathbf{D} = 0, \quad \nabla \cdot \mathbf{B} = 0, \quad (6.100b)$$

they still describe something very non-trivial: *electromagnetic waves*, including light. The physics of the waves may be clearly seen from Eqs. (100a): according to the first of them, the change of the magnetic field in time creates a vortex-like (divergence-free) electric field. On the other hand, the second of Eqs. (100a) describes how the changing electric field, in turn, creates a vortex-like magnetic field. So-coupled electric and magnetic fields may propagate as waves – even very far from their sources.

We will carry out a detailed quantitative analysis of the waves in the next chapter, and here I will only use this notion to make good on the promise given in Sec. 3, namely to establish the condition of validity of the quasistatic approximation (21). For simplicity, let us consider an electromagnetic wave with a time period \mathcal{T} , velocity v , and hence the wavelength⁶² $\lambda = v\mathcal{T}$ in a linear medium with $\mathbf{D} = \epsilon \mathbf{E}$, $\mathbf{B} = \mu \mathbf{H}$. Then the magnitude of the left-hand side of the first of Eqs. (100a) is of the order of $E/\lambda = E/v\mathcal{T}$, while that of its right-hand side may be estimated as $B/\mathcal{T} \sim \mu H/\mathcal{T}$. Using similar estimates for the second of Eqs. (100a), we arrive at the following two requirements:⁶³

$$\frac{E}{H} \sim \mu v \sim \frac{1}{\epsilon v}. \quad (6.101)$$

To insure the compatibility of these two relations, the wave's speed should satisfy the estimate

$$v \sim \frac{1}{(\epsilon \mu)^{1/2}}, \quad (6.102)$$

reduced to $v \sim 1/(\epsilon_0 \mu_0)^{1/2} \equiv c$ in free space, while the ratio of the electric and magnetic field amplitudes should be of the following order:

$$\frac{E}{H} \sim \mu v \sim \mu \frac{1}{(\epsilon \mu)^{1/2}} \equiv \left(\frac{\mu}{\epsilon} \right)^{1/2}. \quad (6.103)$$

(In the next chapter we will see that for plane electromagnetic waves, these results are exact.)

Now, let a system of a linear size $\sim a$ carry currents producing a certain magnetic field H . Then, according to Eqs. (100a), their magnetic field Faraday-induces the electric field of magnitude $E \sim \mu Ha/\mathcal{T}$, whose displacement currents, in turn, produce an additional magnetic field with magnitude

⁶¹ See, e.g., QM Chapter 9.

⁶² Let me hope the reader knows that the relation $\lambda = v\mathcal{T}$ is universal, valid for waves of any nature – see, e.g., CM Chapter 6. (In the case of substantial dispersion, v means the phase velocity.)

⁶³ The fact that \mathcal{T} has canceled, shows that these estimates are valid for waves of any frequency.

$$H' \sim \frac{a\epsilon}{\tau} E \sim \frac{a\epsilon}{\tau} \frac{\mu a}{\tau} H \equiv \left(\frac{a\lambda}{v\tau\lambda} \right)^2 H \equiv \left(\frac{a}{\lambda} \right)^2 H. \quad (6.104)$$

Hence, the displacement current effects are negligible for a system of size $a \ll \lambda$.⁶⁴

In particular, the quasistatic picture of the skin effect, discussed in Sec. 3, is valid while the skin depth (33) remains much *smaller* than the corresponding wavelength,

$$\lambda = v\tau = \frac{2\pi\nu}{\omega} = \left(\frac{4\pi^2}{\epsilon\mu\omega^2} \right)^{1/2}. \quad (6.105)$$

The wavelength decreases with the frequency as $1/\omega$, i.e. faster than $\delta_s \propto 1/\omega^{1/2}$, so that they become comparable at the crossover frequency

$$\omega_r = \frac{\sigma}{\epsilon} \equiv \frac{\sigma}{\kappa\epsilon_0}, \quad (6.106)$$

which is nothing else than the reciprocal charge relaxation time (4.10). As was discussed in Sec. 4.2, for good metals this frequency is extremely high (about 10^{18} s^{-1}), so the validity of Eq. (33) is typically limited by the anomalous skin effect (which was briefly discussed in Sec. 3), rather than the wave effects.

Before going after the analysis of the full Maxwell equations for particular situations (that will be the main goal of the next chapters of this course), let us have a look at the energy balance they yield for a certain volume V , which may include both some charged particles and the electromagnetic field. Since, according to Eq. (5.10), the magnetic field performs no work on charged particles even if they move, the total power \mathcal{P} being transferred from the field to the particles inside the volume is due to the electric field alone – see Eq. (4.38):

$$\mathcal{P} = \int_V \mu d^3r, \quad \text{with } \mu = \mathbf{j} \cdot \mathbf{E}, \quad (6.107)$$

Expressing \mathbf{j} from the corresponding Maxwell equation of the system (99), we get

$$\mathcal{P} = \int_V \left[\mathbf{E} \cdot (\nabla \times \mathbf{H}) - \mathbf{E} \cdot \frac{\partial \mathbf{D}}{\partial t} \right] d^3r. \quad (6.108)$$

Let us pause here for a second, and transform the divergence of $\mathbf{E} \times \mathbf{H}$, using the well-known vector algebra identity:⁶⁵

$$\nabla \cdot (\mathbf{E} \times \mathbf{H}) = \mathbf{H} \cdot (\nabla \times \mathbf{E}) - \mathbf{E} \cdot (\nabla \times \mathbf{H}). \quad (6.109)$$

The last term on the right-hand side of this equality is exactly the first term in the square brackets of Eq. (108), so we may rewrite that formula as

$$\mathcal{P} = \int_V \left[-\nabla \cdot (\mathbf{E} \times \mathbf{H}) + \mathbf{H} \cdot (\nabla \times \mathbf{E}) - \mathbf{E} \cdot \frac{\partial \mathbf{D}}{\partial t} \right] d^3r. \quad (6.110)$$

⁶⁴ Let me emphasize that if this condition is *not* fulfilled, the lumped-circuit representation of the system (see Fig. 9 and its discussion) is typically inadequate – besides some special cases, to be discussed in the next chapter.

⁶⁵ See, e.g., MA Eq. (11.7) with $\mathbf{f} = \mathbf{E}$ and $\mathbf{g} = \mathbf{H}$.

However, according to the Maxwell equation for $\nabla \times \mathbf{E}$, this curl is equal to $-\partial \mathbf{B} / \partial t$, so that the second term in the square brackets of Eq. (110) equals $-\mathbf{H} \cdot \partial \mathbf{B} / \partial t$ and, according to Eq. (14), is just the (minus) time derivative of the magnetic energy per unit volume. Similarly, according to Eq. (3.76), the third term under the integral is the (minus) time derivative of the electric energy per unit volume. Finally, we can use the divergence theorem to transform the integral of the first term in the square brackets to a 2D integral over the surface S limiting the volume V . As a result, we get the so-called *Poynting theorem*⁶⁶ for the power balance in the system:

Poynting theorem

$$\int_V \left(\mu + \frac{\partial u}{\partial t} \right) d^3 r + \oint_S S_n d^2 r = 0. \quad (6.111)$$

Here u is the density of the total (electric plus magnetic) energy of the electromagnetic field, with

Field's energy variation

$$\delta u \equiv \mathbf{E} \cdot \delta \mathbf{D} + \mathbf{H} \cdot \delta \mathbf{B} \quad (6.112)$$

– just the sum of the expressions given by Eqs. (3.76) and (14). For the particular case of an isotropic, linear, and dispersion-free medium, with $\mathbf{D}(t) = \epsilon \mathbf{E}(t)$, $\mathbf{B}(t) = \mu \mathbf{H}(t)$, Eq. (112) yields

Field's energy

$$u = \frac{\mathbf{E} \cdot \mathbf{D}}{2} + \frac{\mathbf{H} \cdot \mathbf{B}}{2} \equiv \frac{\epsilon E^2}{2} + \frac{B^2}{2\mu}. \quad (6.113)$$

Another key notion participating in Eq. (111) is the *Poynting vector*, defined as⁶⁷

Poynting vector

$$\mathbf{S} \equiv \mathbf{E} \times \mathbf{H}. \quad (6.114)$$

The first integral in Eq. (111) is evidently the net change of the energy of the system (particles + field) per unit time, so that the second (surface) integral has to be the power flowing out from the system through the surface. As a result, it is tempting to interpret the Poynting vector \mathbf{S} locally, as the power flow density at the given point. In many cases, such a local interpretation of vector \mathbf{S} is legitimate; however, in other cases, it may lead to wrong conclusions. Indeed, let us consider the simple system shown in Fig. 11: a charged plane capacitor placed into a static and uniform external magnetic field, so that the electric and magnetic fields are mutually perpendicular.

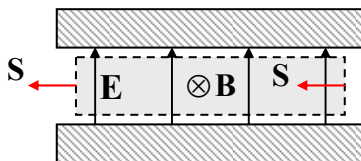


Fig. 6.11. The Poynting vector paradox.

In this static situation, with no charges moving, both μ and $\partial/\partial t$ are equal to zero, and there should be no power flow in the system. However, Eq. (114) shows that the Poynting vector is not equal

⁶⁶ It is named after John Henry Poynting for his work published in 1884, though this fact was independently discovered by O. Heaviside in 1885 in a simpler form, while a similar result for the intensity of mechanical elastic waves had been obtained earlier (in 1874) by Nikolay Alekseevich Umov – see, e.g., CM Sec. 7.7.

⁶⁷ Actually, an addition to \mathbf{S} of the curl of an arbitrary vector function $\mathbf{f}(\mathbf{r}, t)$ does not change Eq. (111). Indeed, we may use the divergence theorem to transform the corresponding change of the surface integral in Eq. (111) to a volume integral of scalar function $\nabla \cdot (\nabla \times \mathbf{f})$ that equals zero at any point – see, e.g., MA Eq. (11.2).

to zero inside the capacitor, being directed as the red arrows in Fig. 11 show. From the point of view of the only unambiguous corollary of the Maxwell equations, Eq. (111), there is no contradiction here, because the fluxes of the vector \mathbf{S} through the side boundaries of the volume shaded in Fig. 11 are equal and opposite (and they are zero for other faces of this rectilinear volume), so that the total flux of the Poynting vector through the volume boundary equals zero, as it should. It is, however, useful to recall this example each time before giving a local interpretation of the vector \mathbf{S} .

The paradox illustrated in Fig. 11 is closely related to the *radiation recoil effects*, due to the electromagnetic field's momentum – more exactly, its *linear momentum*. Indeed, acting as at the Poynting theorem derivation, it is straightforward to use the *microscopic* Maxwell equations⁶⁸ to prove that, neglecting the boundary effects, the vector sum of the mechanical linear momentum of the particles in an arbitrary volume, and the integral of the following vector,

$$\mathbf{g} \equiv \frac{\mathbf{S}}{c^2}, \quad (6.115)$$

Electro-magnetic field's momentum

over the same volume, is conserved, enabling an interpretation of \mathbf{g} as the density of the linear momentum of the electromagnetic field. (It will be more convenient for me to prove this relation, and discuss the related issues, in Sec. 9.8, using the 4-vector formalism of the special relativity.) Due to this conservation, if some static fields coupled to mechanical bodies are suddenly decoupled from them and are allowed to propagate in space, i.e. to change their local integral of \mathbf{g} , they give the bodies an equal and opposite impulse of force.

Finally, to complete our initial discussion of the Maxwell equations,⁶⁹ let us rewrite them in terms of potentials \mathbf{A} and ϕ , because this is more convenient for the solution of some (though not all!) problems. Even when dealing with the system (99) of the more general Maxwell equations than discussed before, Eqs. (7) are still used for the definition of the potentials. It is straightforward to verify that with these definitions, the two homogeneous Maxwell equations (99b) are satisfied automatically. Plugging Eqs. (7) into the inhomogeneous equations (99a), and considering, for simplicity, a linear, uniform medium with frequency-independent ϵ and μ , we get

$$\nabla^2\phi + \frac{\partial}{\partial t}(\nabla \cdot \mathbf{A}) = -\frac{\rho}{\epsilon}, \quad \nabla^2\mathbf{A} - \epsilon\mu\frac{\partial^2\mathbf{A}}{\partial t^2} - \nabla\left(\nabla \cdot \mathbf{A} + \epsilon\mu\frac{\partial\phi}{\partial t}\right) = -\mu\mathbf{j}. \quad (6.116)$$

This is a more complex result than what we would like to get. However, let us select a special gauge, which is frequently called (especially for the free space case, when $v = c$) the *Lorenz gauge condition*⁷⁰

$$\nabla \cdot \mathbf{A} + \epsilon\mu\frac{\partial\phi}{\partial t} = 0, \quad (6.117)$$

Lorenz gauge condition

⁶⁸ The situation with the *macroscopic* Maxwell equations is more complex, and is still a subject of some lingering discussions (usually called the *Abraham-Minkowski controversy*, despite contributions by many other scientists including A. Einstein), because of the ambiguity of the momentum's division between its field and particle components – see, e.g., the review paper by R. Pfeiffer *et al.*, *Rev. Mod. Phys.* **79**, 1197 (2007).

⁶⁹ We will return to their general discussion (in particular, to the analytical mechanics of the electromagnetic field, and its stress tensor) in Sec. 9.8, after we have got equipped with the special relativity theory.

⁷⁰ This condition, named after *Ludwig Lorenz*, should not be confused with the so-called *Lorentz invariance condition* of relativity, due to *Hendrik Lorentz*, to be discussed in Sec. 9.4. (Note the last names' spelling.)

which is a natural generalization of the Coulomb gauge (5.48) to time-dependent phenomena. With this condition, Eqs. (107) are reduced to a simpler, beautifully symmetric form:

Potentials'
dynamics

$$\nabla^2 \phi - \frac{1}{v^2} \frac{\partial^2 \phi}{\partial t^2} = -\frac{\rho}{\epsilon}, \quad \nabla^2 \mathbf{A} - \frac{1}{v^2} \frac{\partial^2 \mathbf{A}}{\partial t^2} = -\mu \mathbf{j}, \quad (6.118)$$

where $v^2 \equiv 1/\epsilon\mu$. Note that these equations are essentially a set of 4 similar equations for 4 scalar functions (namely, ϕ and three Cartesian components of \mathbf{A}) and thus clearly invite the 4-component vector formalism of the relativity theory; it will be discussed in Chapter 9.⁷¹

If ϕ and \mathbf{A} depend on just one spatial coordinate, say z , then in a region without field sources: $\rho = 0$, $\mathbf{j} = 0$, Eqs. (118) are reduced to the following 1D wave equations

$$\frac{\partial^2 \phi}{\partial z^2} - \frac{1}{v^2} \frac{\partial^2 \phi}{\partial t^2} = 0, \quad \frac{\partial^2 \mathbf{A}}{\partial z^2} - \frac{1}{v^2} \frac{\partial^2 \mathbf{A}}{\partial t^2} = 0. \quad (6.119)$$

It is well known⁷² that these equations describe waves, with arbitrary waveforms (including sinusoidal waves of any frequency), propagating with the same speed v in either of the z -axis directions. According to the definitions of the constants ϵ_0 and μ_0 , in free space, v is just the speed of light:

$$v = \frac{1}{(\epsilon_0 \mu_0)^{1/2}} \equiv c. \quad (6.120)$$

Historically, the experimental observation of relatively low-frequency (GHz-scale) electromagnetic waves, with their speed equal to that of light, was the decisive proof (actually, a real triumph!) of the Maxwell theory and his prediction of such waves.⁷³ This was first accomplished in 1886 by Heinrich Rudolf Hertz, using the electronic circuits and antennas he had invented for this purpose.

Before proceeding to the detailed analysis of these waves in the following chapters, let me mention that the invariance of Eqs. (119) with respect to the wave propagation direction is not occasional; it is just a manifestation of one more general property of the Maxwell equations (99), called the *Lorentz reciprocity*. We have already met its simplest example, for time-independent electrostatic fields, in one of the problems of Chapter 1. In a much more general case when two monochromatic electromagnetic fields of the same frequency, with complex amplitudes, say, $\{\mathbf{E}_1(\mathbf{r}), \mathbf{H}_1(\mathbf{r})\}$ and $\{\mathbf{E}_2(\mathbf{r}),$

⁷¹ Here I have to mention in passing the so-called *Hertz vector potentials* Π_e and Π_m (whose introduction may be traced back at least to the 1904 work by E. Whittaker). They may be defined by the following relations:

$$\mathbf{A} = \mu \frac{\partial \Pi_e}{\partial t} + \mu \nabla \times \Pi_m, \quad \phi = -\frac{1}{\epsilon} \nabla \cdot \Pi_e,$$

which make the Lorentz gauge condition (117) automatically satisfied. These potentials are especially convenient for the solution of problems in which the electromagnetic field is induced by sources characterized by field-independent electric and magnetic polarizations \mathbf{P} and \mathbf{M} – rather than by field-independent charge and current densities ρ and \mathbf{j} . Indeed, it is straightforward to check that both Π_e and Π_m satisfy the equations similar to Eqs. (118), but with their right-hand sides equal to, respectively, $-\mathbf{P}$ and $-\mathbf{M}$. Unfortunately, I would not have time/space to discuss such problems and have to refer interested readers elsewhere – for example, to a classical text by J. Stratton, *Electromagnetic Theory*, Adams Press, 2008.

⁷² See, e.g., CM Secs. 6.3-6.4 and 7.7-7.8.

⁷³ By that time, the speed of light (estimated very reasonably by Ole Rømer as early as 1676) has been experimentally measured, by Hippolyte Fizeau and then Léon Foucault, with an accuracy better than 1%.

$\mathbf{H}_2(\mathbf{r})\}$ are induced, separately, by stand-alone currents with complex amplitudes $\mathbf{j}_1(\mathbf{r})$ and $\mathbf{j}_2(\mathbf{r})$ of their densities. Then it may be proved⁷⁴ that if the medium is linear and either isotropic or even anisotropic but with symmetric tensors $\varepsilon_{jj'}$ and $\mu_{jj'}$, then for any volume V limited by a closed surface S ,

$$\int_V (\mathbf{j}_1 \cdot \mathbf{E}_2 - \mathbf{j}_2 \cdot \mathbf{E}_1) d^3 r = \oint_S (\mathbf{E}_1 \times \mathbf{H}_2 - \mathbf{E}_2 \times \mathbf{H}_1)_n d^2 r. \quad (6.121)$$

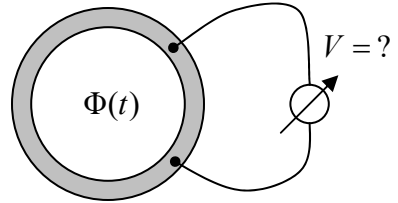
This property implies, in particular, that the waves propagate similarly in two reciprocal directions even in situations much more general than the 1D case described by Eqs. (119). For some important practical applications (e.g., for low-noise amplifiers and detectors) such reciprocity is rather inconvenient. Fortunately, Eq. (121) may be violated in anisotropic media with asymmetric tensors $\varepsilon_{jj'}$ and/or $\mu_{jj'}$. The simplest case of such an anisotropy, the *Faraday rotation* of the wave polarization in plasma, will be discussed in the next chapter.

6.9. Exercise problems

6.1. Prove that the electromagnetic induction e.m.f. \mathcal{V}_{ind} in a conducting loop may be measured as shown on two panels of Fig. 1:

- (i) by measuring the current $I = \mathcal{V}_{\text{ind}}/R$ induced in the loop closed with an Ohmic resistor R , or
- (ii) using a voltmeter inserted into the loop.

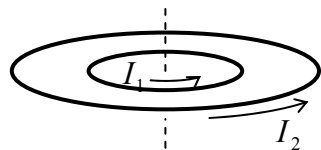
6.2. The flux Φ of the magnetic field that pierces a resistive ring is being changed in time, while the field outside of the ring is negligibly low. A voltmeter is connected to a part of the ring, as shown in the figure on the right. What would the voltmeter show?



6.3. A weak, uniform, time-independent magnetic field \mathbf{B} is applied to an axially-symmetric permanent magnet with the dipole magnetic moment \mathbf{m} directed along its axis, rapidly rotating about the same axis, with an angular momentum \mathbf{L} . Calculate the electric field resulting from the magnetic field's application, and formulate the conditions of your result's validity.

6.4. The similarity of Eq. (5.53) obtained in Sec. 5.3 without any use of the Faraday induction law, and Eq. (5.54) proved in Sec. 2 of this chapter using the law, implies that the law may be derived from magnetostatics. Prove that this is indeed true for a particular case of a current loop, being slowly deformed in a fixed magnetic field \mathbf{B} .

6.5. Could Problem 5.2 (i.e. the analysis of the mechanical stability of the system shown in the figure on the right) be solved using potential energy arguments?



⁷⁴ It will be more convenient for me to give this proof (or rather offer it for the reader's exercise :-) in the next chapter, after we have discussed the Fourier expansion of the fields in linear media.

6.6. Use energy arguments to calculate the pressure exerted by the magnetic field \mathbf{B} inside a long uniform solenoid of length l , and a cross-section of area $A \ll l^2$, with $N \gg l/A^{1/2} \gg 1$ turns, on its “walls” (windings), and the forces exerted by the field on the solenoid’s ends, for two cases:

(i) the current through the solenoid is fixed by an external source, and

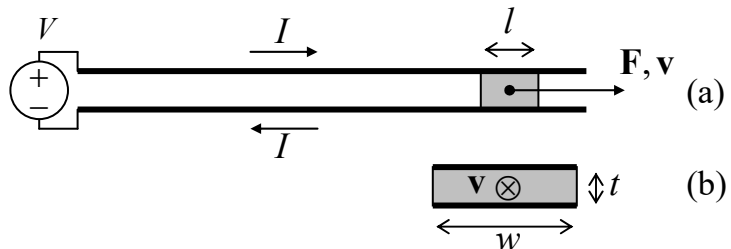
(ii) after the initial current setting, the ends of the solenoid’s wire, with negligible resistance, are connected, so that it continues to carry a non-zero current.

Compare the results, and give a physical interpretation of the direction of these forces.

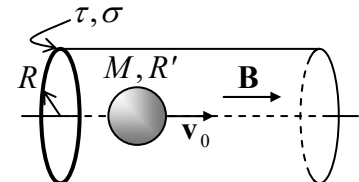
6.7. The *electromagnetic railgun* is a projectile launch system consisting of two long, parallel conducting rails and a sliding conducting projectile, shorting the current I fed into the system by a powerful source – see panel (a) in the figure on the right. Calculate the force exerted on the projectile, using two approaches:

(i) by a direct calculation, assuming that the cross-section of the system has the simple shape shown on panel (b) of the figure above, with $t \ll w, l$, and

(ii) using the energy balance (for simplicity, neglecting the Ohmic resistances in the system), and compare the results.



6.8. A uniform, static magnetic field \mathbf{B} is applied along the axis of a long round pipe of a radius R and a very small thickness τ , made of a material with Ohmic conductivity σ . A sphere of mass M and radius $R' \ll R$, made of a linear magnetic material with permeability $\mu \gg \mu_0$, is launched, with an initial velocity v_0 , to fly ballistically along the pipe’s axis – see the figure on the right. Use the quasistatic approximation to calculate the distance the sphere would pass before it stops. Formulate the conditions of validity of your result.



6.9. A plane thin-wire loop with inductance L , resistance R , and area A is launched to fly ballistically into a region where the magnetic field \mathbf{B} is constant. Calculate the final change of the kinetic energy of the loop, assuming that the time of its entry into the field region is much shorter than the relaxation time constant L/R , and that the loop cannot rotate.

6.10. AC current of frequency ω is being passed through a long uniform wire with a round cross-section of radius R comparable with the skin depth δ_s . In the quasistatic approximation, find the current’s distribution across the cross-section, and analyze it in the limits $R \ll \delta_s$ and $\delta_s \ll R$. Calculate the effective ac resistance of the wire (per unit length) in these two limits.

6.11. A very long, round cylinder of radius R , made of a uniform conductor with an Ohmic conductivity σ and magnetic permeability μ , has been placed into a uniform ac magnetic field $\mathbf{H}_{\text{ext}}(t) = \mathbf{H}_0 \cos \omega t$, directed along its symmetry axis. Calculate the spatial distribution of the magnetic field’s amplitude, and in particular its value on the cylinder’s axis. Spell out the last result in the limits of relatively small and large R .

6.12.* Define and calculate an appropriate spatial-temporal Green's function for Eq. (25), and then use this function to analyze the dynamics of propagation of the external magnetic field that is suddenly turned on at $t = 0$ and then kept constant:

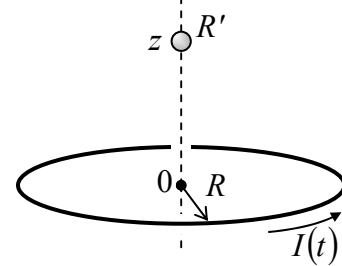
$$H(x < 0, t) = \begin{cases} 0, & \text{at } t < 0, \\ H_0, & \text{at } t > 0, \end{cases}$$

into an Ohmic conductor occupying the semi-space $x > 0$ – see Fig. 2.

Hint: Try to use a function proportional to $\exp\{-(x-x')^2/(2(\delta x)^2)\}$, with a suitable time dependence of the parameter δx , and a properly selected pre-exponential factor.

6.13. Solve the previous problem using the variable separation method, and compare the results.

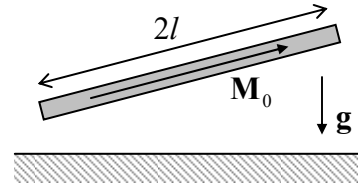
6.14. Calculate the average force exerted by ac current $I(t)$ of amplitude I_0 , flowing in a planar round coil of radius R , on a conducting sphere with a much smaller radius R' (which is still much larger than the skin depth δ_s at the ac current's frequency), located on the loop's axis, at distance z from its center – see the figure on the right.



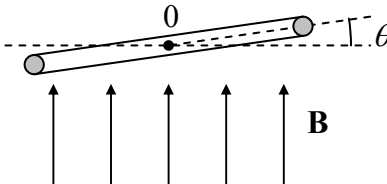
6.15. A small, planar wire loop carrying current I , is located far from a plane surface of a superconductor. Within the coarse-grain (ideal-diamagnetic) description of the Meissner-Ochsenfeld effect, calculate:

- (i) the energy of the loop-superconductor interaction,
- (ii) the force and torque acting on the loop, and
- (iii) the distribution of supercurrents on the superconductor surface.

6.16. A straight, uniform magnet of length $2l$, cross-section area $A \ll l^2$, and mass m , with a permanent longitudinal magnetization M_0 , is placed over a horizontal surface of a superconductor – see the figure on the right. Within the ideal-diamagnet description of the Meissner-Ochsenfeld effect, find the stable equilibrium position of the magnet.



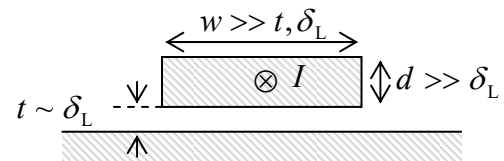
6.17. A plane superconducting wire loop of area A and inductance L may rotate, without friction, about a horizontal axis 0 (in the figure on the right, normal to the plane of the drawing) passing through its center of mass. Initially, the loop had been horizontal (with $\theta = 0$), and carried supercurrent I_0 in such a direction that its magnetic dipole vector had been directed down. Then a uniform magnetic field \mathbf{B} , directed vertically up, was applied. Using the ideal-diamagnet description of the Meissner-Ochsenfeld effect, find all possible equilibrium positions of the loop, analyze their stability, and give a physical interpretation of the results.



6.18. Use the London equation to analyze the penetration of a uniform external magnetic field into a thin ($t \sim \delta_L$) planar superconducting film, whose plane is parallel to the field.

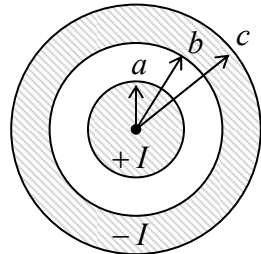
6.19. Use the London equation to calculate the distribution of supercurrent density \mathbf{j} inside a long, straight superconducting wire, with a circular cross-section of radius $R \sim \delta_L$, carrying dc current I .

6.20. Use the London equation to calculate the inductance (per unit length) of a long, uniform superconducting strip placed close to the surface of a similar superconductor – see the figure on the right, which shows the structure's cross-section.



6.21. Calculate the inductance (per unit length) of a superconducting cable with the round cross-section shown in the figure on the right, in the following limits:

- (i) $\delta_L \ll a, b, c - b$, and
- (ii) $a \ll \delta_L \ll b, c - b$.



6.22. Use the London equation to analyze the magnetic field shielding by a superconducting thin film of thickness $t \ll \delta_L$, by calculating the penetration of the field induced by current I in a thin wire that runs parallel to a wide planar thin film, at a distance $d \gg t$ from it, into the space behind the film.

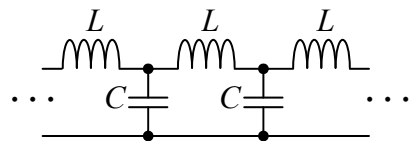
6.23. Use the Ginzburg-Landau equations (54) and (63) to calculate the largest (“critical”) value of supercurrent in a uniform, long superconducting wire of a small cross-section $A_w \ll \delta_L^2$.

6.24. Use the discussion of a long, straight Abrikosov vortex, in the limit $\xi \ll \delta_L$, in Sec. 5 to prove Eqs. (71)-(72) for its energy per unit length, and the first critical field.

6.25.* Use the Ginzburg-Landau equations (54) and (63) to prove the Josephson relation (76) for a small superconducting weak link, and express its critical current I_c via the Ohmic resistance R_n of the same weak link in its normal state.

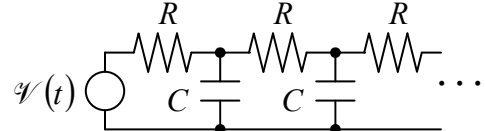
6.26. Use Eqs. (76) and (79) to calculate the coupling energy of a Josephson junction and the full potential energy of the SQUID shown in Fig. 4c.

6.27. Analyze the possibility of wave propagation in a long, uniform chain of lumped inductances and capacitances – see the figure on the right.



Hint: Readers without prior experience with electromagnetic wave analysis may like to use a substantial analogy between this effect and mechanical waves in a 1D chain of elastically coupled particles.⁷⁵

6.28. A sinusoidal e.m.f. of amplitude V_0 and frequency ω is applied to an end of a long chain of similar lumped resistors and capacitors, shown in the figure on the right. Calculate the law of decay of the ac voltage amplitude along the chain.

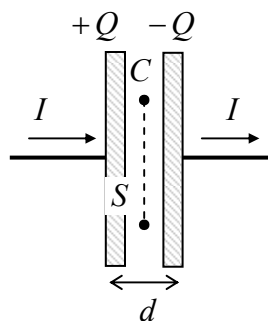


⁷⁵ See, e.g., CM Sec. 6.3.

6.29. As was discussed in Sec. 7, the displacement current concept allows one to generalize the Ampère law to time-dependent processes as

$$\oint_C \mathbf{H} \cdot d\mathbf{r} = I_S + \frac{\partial}{\partial t} \int_S D_n d^2 r .$$

We also have seen that such generalization makes the integral $\oint \mathbf{H} \cdot d\mathbf{r}$ over an external contour, such as the one shown in Fig. 10, independent of the choice of the surface S limited by the contour. However, it may look like the situation is different for a contour drawn inside the capacitor – see the figure on the right. Indeed, if the contour's size is much larger than the capacitor's thickness, the magnetic field \mathbf{H} created by the linear current I on the contour's line is virtually the same as that of a continuous wire, and hence the integral $\oint \mathbf{H} \cdot d\mathbf{r}$ along the contour apparently does not depend on its area, while the magnetic flux $\int D_n d^2 r$ does, so that the equation displayed above seems invalid. (The current I_S piercing this contour evidently equals zero.) Resolve the paradox, for simplicity considering an axially-symmetric system.



6.30. A straight, uniform, long wire with a circular cross-section of radius R is made of an Ohmic conductor with conductivity σ , and carries dc current I . Calculate the flux of the Poynting vector through its surface, and compare it with the Joule rate of energy dissipation.

Chapter 7. Electromagnetic Wave Propagation

This (rather extensive) chapter focuses on the most important effect that follows from the time-dependent Maxwell equations, namely the electromagnetic waves, at this stage avoiding the issue of their origin, i.e. of the wave radiation process – which will be the subject of Chapters 8 and 10. We will start from the simplest, plane waves in uniform and isotropic media, and then proceed to a discussion of nonuniform systems, bringing up such effects as reflection and refraction. Then we will discuss the so-called guided waves, propagating along various transmission lines – such as cables, waveguides, and optical fibers. Finally, the end of the chapter is devoted to final-length fragments of such lines, serving as resonant cavities, and to the effects of energy dissipation in transmission lines and cavities..

7.1. Plane waves

Let us start by considering a spatial region that does not contain field sources ($\rho = 0, \mathbf{j} = 0$), and is filled with a linear, uniform, isotropic medium, which obeys Eqs. (3.46) and (5.110):

$$\mathbf{D} = \epsilon \mathbf{E}, \quad \mathbf{B} = \mu \mathbf{H}. \quad (7.1)$$

Moreover, let us assume for a while that these constitutive equations hold for all frequencies of interest. (Of course, these relations are *exactly* valid for the very important particular case of free space, where we may formally use the macroscopic Maxwell equations (6.100), but with $\epsilon = \epsilon_0$ and $\mu = \mu_0$.) As was already shown in Sec. 6.8, in this case, the Lorenz gauge condition (6.117) allows the Maxwell equations to be recast into the wave equations (6.118) for the scalar and vector potentials. However, for most purposes, it is more convenient to use the homogeneous Maxwell equations (6.100) for the electric and magnetic fields – which are independent of the gauge choice. After an elementary elimination of \mathbf{D} and \mathbf{B} using Eqs. (1),¹ these equations take a simple, very symmetric form:

Maxwell
equations
for uniform
linear
media

$$\nabla \times \mathbf{E} + \mu \frac{\partial \mathbf{H}}{\partial t} = 0, \quad \nabla \times \mathbf{H} - \epsilon \frac{\partial \mathbf{E}}{\partial t} = 0, \quad (7.2a)$$

$$\nabla \cdot \mathbf{E} = 0, \quad \nabla \cdot \mathbf{H} = 0. \quad (7.2b)$$

Now, acting by operator $\nabla \times$ on each of Eqs. (2a), i.e. taking their curl, and then using the vector algebra identity (5.31), whose first term, for both \mathbf{E} and \mathbf{H} , vanishes due to Eqs. (2b), we get fully similar wave equations for the electric and magnetic fields:²

EM wave
equations

$$\left(\nabla^2 - \frac{1}{v^2} \frac{\partial^2}{\partial t^2} \right) \mathbf{E} = 0, \quad \left(\nabla^2 - \frac{1}{v^2} \frac{\partial^2}{\partial t^2} \right) \mathbf{H} = 0, \quad (7.3)$$

where the parameter v is defined as

¹ Though \mathbf{B} rather than \mathbf{H} is the actual magnetic field, mathematically it is a bit more convenient (just as it was in Sec. 6.2) to use the vector pair $\{\mathbf{E}, \mathbf{H}\}$ in the following discussion, because at sharp media boundaries, it is \mathbf{H} that obeys the boundary condition (5.117) similar to that for \mathbf{E} – cf. Eq. (3.37).

² The two vector equations (3) are of course just a shorthand for six similar equations for three Cartesian components of \mathbf{E} and \mathbf{H} , and hence for their magnitudes E and H .

$$v^2 \equiv \frac{1}{\epsilon\mu}.$$

(7.4) Wave velocity

with $v^2 = 1/\epsilon_0\mu_0 \equiv c^2$ in free space – see Eq. (6.120) again.

These equations allow, in particular, solutions of the following type;

$$E \propto H \propto f(z - vt),$$

(7.5) Plane wave

where z is the Cartesian coordinate along a certain (*arbitrary*) direction \mathbf{n} , and f is an *arbitrary* function of one argument. Note that this solution, first of all, describes a *traveling wave* – meaning a certain field pattern moving, without deformation, along the z -axis, with the constant velocity v . Second, according to Eq. (5), both \mathbf{E} and \mathbf{H} have the same values at all points of each plane perpendicular to the direction $\mathbf{n} \equiv \mathbf{n}_z$ of the wave propagation; hence the second name – *plane wave*.

According to Eqs. (2), the independence of the wave *equations* (3) for vectors \mathbf{E} and \mathbf{H} does not mean that their plane-wave *solutions* are independent. Indeed, plugging any solution of the type (5) into Eqs. (2a), we get

$$\mathbf{H} = \frac{\mathbf{n} \times \mathbf{E}}{Z}, \quad \text{i.e. } \mathbf{E} = Z \mathbf{H} \times \mathbf{n},$$

Field vector relationship

where

$$Z \equiv \frac{E}{H} = \left(\frac{\mu}{\epsilon} \right)^{1/2}.$$

Wave impedance

The vector relationship (6) means, first of all, that at any point of space and at any time instant, the vectors \mathbf{E} and \mathbf{H} are perpendicular not only to the propagation vector \mathbf{n} (such waves are called *transverse*) but also to each other — see Fig. 1.

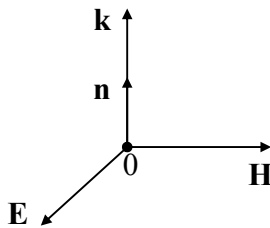


Fig. 7.1. Field vectors in a plane electromagnetic wave propagating along direction \mathbf{n} .

Second, this equality does not depend on the function f , meaning that the electric and magnetic fields increase and decrease *simultaneously*. Finally, the field magnitudes are related by the constant Z called the *wave impedance* of the medium. Very soon we will see that this impedance plays a pivotal role in many problems, in particular at the wave reflection from the interface between two media. Since the dimensionality of E , in SI units, is V/m, and that of H is A/m, Eq. (7) shows that Z has the dimensionality of V/A, i.e. ohms (Ω).³ In particular, in free space,

³ In the Gaussian units, E and H have a similar dimensionality (in particular, in a free-space wave, $E = H$), making the (very useful) notion of the wave impedance less manifestly exposed – so that in some older physics textbooks it is not mentioned at all!

Wave
impedance
of free
space

$$Z = Z_0 \equiv \left(\frac{\mu_0}{\epsilon_0} \right)^{1/2} = 4\pi \times 10^{-7} c \approx 377 \Omega. \quad (7.8)$$

Next, plugging Eq. (6) into Eqs. (6.113) and (6.114), we get:

$$u = \epsilon E^2 = \mu H^2, \quad (7.9a)$$

Wave's
energy

Wave's
power

$$\mathbf{S} \equiv \mathbf{E} \times \mathbf{H} = \mathbf{n} \frac{E^2}{Z} = \mathbf{n} Z H^2, \quad (7.9b)$$

so that, according to Eqs. (4) and (7), the wave's energy and power densities are universally related as

$$\mathbf{S} = \mathbf{n} u v. \quad (7.9c)$$

In view of the Poynting vector paradox discussed in Sec. 6.8 (see Fig. 6.11), one may wonder whether the last equality may be interpreted as the actual density of power flow. In contrast to the static situation shown in Fig. 6.11, which limits the electric and magnetic fields to the vicinity of their sources, waves may travel far from them. As a result, they can form *wave packets* of a finite length in free space – see Fig. 2.

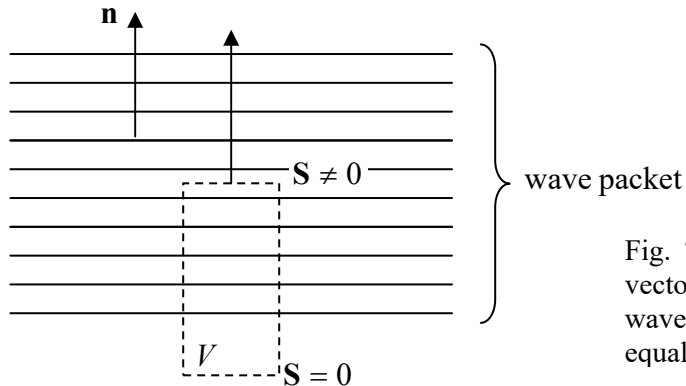


Fig. 7.2. Interpreting the Poynting vector in a plane electromagnetic wave. (Horizontal lines show equal-field planes.)

Let us apply the Poynting theorem (6.111) to the cylinder shown with dashed lines in Fig. 2, with one lid inside the wave packet, and another lid in the region already passed by the wave. Then, according to Eq. (6.111), the rate of change of the full field energy ϵ inside the volume is $d\epsilon/dt = -SA$ (where A is the lid area), so that S may be indeed interpreted as the power flow (per unit area) from the volume. Making a reasonable assumption that the finite length of a sufficiently long wave packet does not affect the physics inside it, we may indeed interpret the \mathbf{S} given by Eqs. (9b-c) as the power flow density inside a plane electromagnetic wave.

As we will see later in this chapter, the free-space value Z_0 of the wave impedance, given by Eq. (8), establishes the scale of Z of virtually all wave transmission lines, so we may use it, together with Eq. (9), to get a better feeling of how much different are the electric and magnetic field amplitudes in the waves – on the scale of typical electrostatics and magnetostatics experiments. For example, according to Eqs. (9), a wave of a modest intensity $S = 1 \text{ W/m}^2$ (this is what we get from a usual electric bulb a few meters away from it) has $E \sim (SZ_0)^{1/2} \sim 20 \text{ V/m}$, quite comparable with the dc field created by a standard AA battery right outside it. On the other hand, the wave's magnetic field $H = (S/Z_0)^{1/2} \approx 0.05 \text{ A/m}$. For this particular case, the relation following from Eqs. (1), (4), and (7),

$$B = \mu H = \mu \frac{E}{Z} = \mu \frac{E}{(\mu/\epsilon)^{1/2}} \equiv (\epsilon\mu)^{1/2} E = \frac{E}{v}, \quad (7.10)$$

gives $B = \mu_0 H = E/c \sim 7 \times 10^{-8}$ T, i.e. a magnetic field a thousand times lower than the Earth's field, and about 7 orders of magnitude lower than the field of a typical permanent magnet. This huge difference may be interpreted as follows: the scale $B \sim E/c$ of magnetic fields in the waves is "normal" for electromagnetism, while the permanent magnet fields are abnormally high because they are due to the ferromagnetic alignment of electron spins, essentially relativistic objects – see the discussion in Sec. 5.5.

The fact that Eq. (5) is valid for an arbitrary function f means, in the standard terminology, that a medium with frequency-independent ϵ and μ supports the propagation of plane waves without either decay (*attenuation*) or waveform deformation (*dispersion*). However, for any real medium but pure vacuum, this approximation is valid only within limited frequency intervals. We will discuss the effects of attenuation and dispersion in the next section and will see that all our prior formulas remain valid even for an arbitrary linear media, provided that we limit them to single-frequency (i.e. sinusoidal, frequently called *monochromatic*) waves. Such waves may be most conveniently represented as⁴

$$f = \text{Re} \left[f_\omega e^{i(kz - \omega t)} \right], \quad (7.11)$$

Mono-chromatic wave

where f_ω is the *complex amplitude* of the wave, and k is its *wave number* (the magnitude of the *wave vector* $\mathbf{k} \equiv \mathbf{n}k$), sometimes called the *spatial frequency*. The last term is justified by the fact, evident from Eq. (11), that k is related to the wavelength λ exactly as the usual ("temporal") frequency ω is related to the time period T :

$$k = \frac{2\pi}{\lambda}, \quad \omega = \frac{2\pi}{T}. \quad (7.12)$$

Spatial and temporal frequencies

In the dispersion-free case (5), the compatibility of that relation with Eq. (11) requires the argument $(kz - \omega t) \equiv k[z - (\omega/k)t]$ to be proportional to $(z - vt)$, so that $\omega/k = v$, i.e.

$$k = \frac{\omega}{v} \equiv (\epsilon\mu)^{1/2} \omega, \quad (7.13)$$

Dispersion relation

so that in that particular case, the *dispersion relation* $\omega(k)$ is linear.

Now note that Eq. (6) does not mean that the vectors \mathbf{E} and \mathbf{H} retain their direction in space. (The wave in that they do is called *linearly polarized*.⁵) Indeed, nothing in the Maxwell equations prevents, for example, a joint rotation of this vector pair around the fixed vector \mathbf{n} , while still keeping all these three vectors perpendicular to each other at any instant – see Fig. 1. However, an arbitrary rotation law or even an arbitrary constant frequency of such rotation would violate the single-frequency (monochromatic) character of the elementary sinusoidal wave (11). To understand what is the most general type of polarization the wave may have without violating that condition, let us represent two

⁴ As we have already seen in the previous chapter (see also CM Sec. 1), such complex-exponential representation of sinusoidally-changing variables is more convenient for mathematical manipulation with than using sine and cosine functions, especially because in all linear relations, the operator Re may be omitted (implied) until the very end of the calculation. Note, however, that this is *not* valid for the quadratic forms such as Eqs. (9).

⁵ The possibility of different polarizations of electromagnetic waves was discovered (for light) in 1699 by Rasmus Bartholin, a.k.a. Erasmus Bartholinus.

Cartesian components of one of these vectors (say, \mathbf{E}) along any two fixed axes x and y , perpendicular to each other and the z -axis (i.e. to the vector \mathbf{n}), in the same form as used in Eq. (11):

$$E_x = \operatorname{Re} [E_{\omega x} e^{i(kz - \omega t)}], \quad E_y = \operatorname{Re} [E_{\omega y} e^{i(kz - \omega t)}]. \quad (7.14)$$

To keep the wave monochromatic, the complex amplitudes $E_{\omega x}$ and $E_{\omega y}$ have to be constant in time; however, they may have different magnitudes and an arbitrary phase shift between them.

In the simplest case when the arguments of these complex amplitudes are equal,

$$E_{\omega x,y} = |E_{\omega x,y}| e^{i\varphi}. \quad (7.15)$$

the real field components have the same phase:

$$E_x = |E_{\omega x}| \cos(kz - \omega t + \varphi), \quad E_y = |E_{\omega y}| \cos(kz - \omega t + \varphi), \quad (7.16)$$

so that their ratio is constant in time – see Fig. 3a. This means that the wave is linearly polarized, with the polarization plane defined by the relation

$$\tan \theta = |E_{\omega y}| / |E_{\omega x}|. \quad (7.17)$$

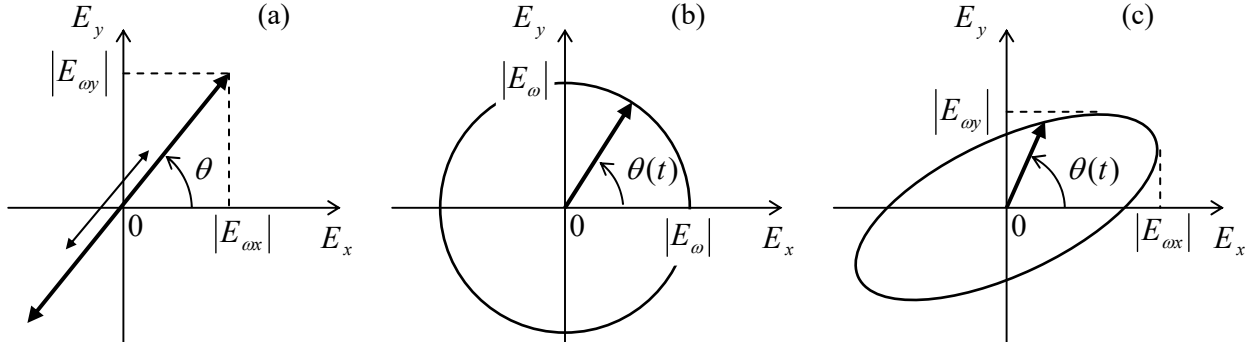


Fig. 7.3. Time evolution of the instantaneous electric field vector in monochromatic waves with:
(a) a linear polarization, (b) a circular polarization, and (c) an elliptical polarization.

Another simple case is when the moduli of the complex amplitudes $E_{\omega x}$ and $E_{\omega y}$ are equal, but their phases are shifted by $+\pi/2$ or $-\pi/2$:

$$E_{\omega x} = |E_\omega| e^{i\varphi}, \quad E_{\omega y} = |E_\omega| e^{i(\varphi \pm \pi/2)}. \quad (7.18)$$

In this case

$$E_x = |E_\omega| \cos(kz - \omega t + \varphi), \quad E_y = |E_\omega| \cos\left(kz - \omega t + \varphi \pm \frac{\pi}{2}\right) \equiv \mp |E_\omega| \sin(kz - \omega t + \varphi). \quad (7.19)$$

This means that on the wave's plane (normal to \mathbf{n}), the end of the vector \mathbf{E} moves, with the wave's frequency ω , either clockwise or counterclockwise around a circle – see Fig. 3b:

$$\theta(t) = \mp(\omega t - \varphi). \quad (7.20)$$

Such waves are called *circularly polarized*. In the dominant convention, the wave is called *right-polarized* (RP) if it is described by the lower sign in Eqs. (18)-(20), i.e. if the vector ω of the angular frequency of the field vector's rotation coincides with the wave propagation's direction \mathbf{n} , and *left-polarized* (LP) in the opposite case. These particular solutions of the Maxwell equations are very convenient for quantum electrodynamics, because single electromagnetic field quanta with a certain (positive or negative) spin direction may be considered as elementary excitations of the corresponding circularly-polarized wave.⁶ (This fact does not exclude, from the quantization scheme, waves of other polarizations, because any monochromatic wave may be presented as a linear combination of two opposite circularly-polarized waves – just as Eqs. (14) represent it as a linear combination of two linearly-polarized waves.)

Finally, in the general case of arbitrary complex amplitudes $E_{\omega x}$ and $E_{\omega y}$, the field vector's end moves along an ellipse (Fig. 3c); such wave is called *elliptically polarized*. The elongation (“eccentricity”) and orientation of the ellipse are completely described by one complex number, the ratio $E_{\omega x}/E_{\omega y}$, i.e. by two real numbers, for example, $|E_{\omega x}/E_{\omega y}|$ and $\varphi = \arg(E_{\omega x}/E_{\omega y})$.⁷

7.2. Attenuation and dispersion

Let me start the discussion of the dispersion and attenuation effects by considering a particular case of the time evolution of the electric polarization $\mathbf{P}(t)$ of a dilute, non-polar medium, with negligible interaction between its elementary dipoles $\mathbf{p}(t)$. As was discussed in Sec. 3.3, in this case, the local electric field acting on each elementary dipole, may be taken equal to the macroscopic field $\mathbf{E}(t)$. Then, the dipole moment $\mathbf{p}(t)$ may be caused not only by the values of the field \mathbf{E} at the same moment of time (t), but also by those at the earlier moments $t' < t$. Due to the linear superposition principle, the macroscopic polarization $\mathbf{P}(t) = n\mathbf{p}(t)$ should be a sum (practically, an integral) of the values of $\mathbf{E}(t')$ at all moments $t' \leq t$, weighed by some function of t and t' :⁸

$$P(t) = \int_{-\infty}^t E(t')G(t,t')dt'. \quad (7.21)$$

Temporal
Green's
function

⁶ This issue is closely related to that of the wave's angular momentum; it will be more convenient for me to discuss it later in this chapter (in Sec. 7).

⁷ Note that the same information may be expressed via four so-called *Stokes parameters* s_0 , s_1 , s_2 , and s_3 , which are popular in practical optics, because they may be used for the description of not only completely coherent waves that are discussed here, but also of partly coherent or even fully incoherent waves – including the *natural light* emitted by thermal sources such as our Sun. (In contrast to the coherent waves (14), whose complex amplitudes are deterministic numbers, the amplitudes of incoherent waves should be treated as random variables.) For more on the Stokes parameters, as well as many other optics topics I will not have time to cover, I can recommend the classical text by M. Born *et al.*, *Principles of Optics*, 7th ed., Cambridge U. Press, 1999.

⁸ In an isotropic media, the vectors \mathbf{E} , \mathbf{P} , and hence $\mathbf{D} = \epsilon_0\mathbf{E} + \mathbf{P}$, are all parallel, and for notation simplicity, I will drop the vector sign in the following formulas of this section. I am also assuming that \mathbf{P} at any point \mathbf{r} is only dependent on the electric field at the same point, and hence drop the factor $\exp\{ikz\}$, the same for all variables. This last assumption is valid if the wavelength λ is much larger than the elementary dipole's size a . In most systems of interest, the scale of a is atomic ($\sim 10^{-10}\text{m}$), so that this approximation is valid up to extremely high frequencies, $\omega \sim c/a \sim 10^{18}\text{ s}^{-1}$, corresponding to hard X-rays.

The condition $t' \leq t$, which is implied by this relation, expresses a keystone principle of all science, the *causal relation* between a cause (in our case, the electric field $E(t')$ applied to each dipole) and its effect (the polarization $P(t)$ it creates). The function $G(t, t')$ is called the *temporal Green's function* for the electric polarization.⁹ To reveal its physical sense, let us consider the case when the applied field $E(t)$ is a very short pulse at the moment $t_0 < t$, which may be well approximated with Dirac's delta function:

$$E(t) = \delta(t - t''). \quad (7.22)$$

Then Eq. (21) yields just $P(t) = G(t, t'')$, so that the Green's function $G(t, t')$ is just the polarization at moment t , created by a unit δ -functional pulse of the applied field at moment t' (Fig. 4).

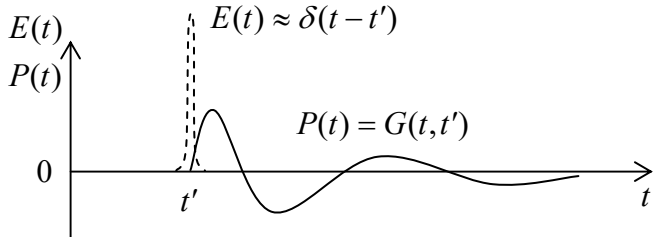


Fig. 7.4. An example of the temporal Green's function for the electric polarization (schematically).

What are the general properties of the temporal Green's function? First, for systems without infinite internal “memory”, G should tend to zero at $t - t' \rightarrow \infty$, although the type of this approach (e.g., whether the function G oscillates approaching zero, as in Fig. 4, or not) depends on the medium's properties. Second, if parameters of the medium do not change in time, the polarization response to an electric field pulse should be dependent not on its absolute timing, but only on the time difference $\theta \equiv t - t'$ between the pulse and observation instants, when Eq. (21) is reduced to

$$P(t) = \int_{-\infty}^t E(t') G(t - t') dt' \equiv \int_0^\infty E(t - \theta) G(\theta) d\theta. \quad (7.23)$$

For a sinusoidal waveform, $E(t) = \text{Re}[E_\omega e^{-i\omega t}]$, this equation yields

$$P(t) = \text{Re} \int_0^\infty E_\omega e^{-i\omega(t-\theta)} G(\theta) d\theta \equiv \text{Re} \left[\left(E_\omega \int_0^\infty G(\theta) e^{i\omega\theta} d\theta \right) e^{-i\omega t} \right]. \quad (7.24)$$

The expression in the last parentheses is of course nothing else than the complex amplitude P_ω of the polarization. This means that though even if the static linear relation (3.43), $P = \chi_e \epsilon_0 E$, is invalid for an arbitrary time-dependent process, we may still keep its Fourier analog,

$$P_\omega = \chi_e(\omega) \epsilon_0 E_\omega, \quad \text{with } \chi_e(\omega) \equiv \frac{1}{\epsilon_0} \int_0^\infty G(\theta) e^{i\omega\theta} d\theta, \quad (7.25)$$

for each sinusoidal component of the process, using it as the definition of the frequency-dependent electric susceptibility $\chi_e(\omega)$. Similarly, the frequency-dependent electric permittivity may be defined using the Fourier analog of Eq. (3.46):

⁹ The idea of these functions is very similar to that of the spatial Green's functions (see Sec. 2.10), but with a new twist, due to the causality principle. A discussion of the temporal Green's functions in application to classical mechanics (which to some extent overlaps with our current discussion) may be found in CM Sec. 5.1.

$$D_\omega \equiv \epsilon(\omega)E_\omega. \quad (7.26a)$$

Then, according to Eq. (3.47), the complex permittivity is related to the temporal Green's function by the usual Fourier transform:

$$\epsilon(\omega) \equiv \epsilon_0 + \frac{P_\omega}{E_\omega} = \epsilon_0 + \int_0^\infty G(\theta)e^{i\omega\theta}d\theta. \quad (7.26b)$$

This relation shows that the function $\epsilon(\omega)$ may be complex,

$$\epsilon(\omega) = \epsilon'(\omega) + i\epsilon''(\omega), \quad \text{with } \epsilon'(\omega) = \epsilon_0 + \int_0^\infty G(\theta)\cos\omega\theta d\theta, \quad \epsilon''(\omega) = \int_0^\infty G(\theta)\sin\omega\theta d\theta, \quad (7.27)$$

and that its real part $\epsilon'(\omega)$ is always an even function of frequency, while the imaginary part $\epsilon''(\omega)$ is an odd function of ω . Note that though the particular causal relationship (21) between $P(t)$ and $E(t)$ is conditioned by the elementary dipole independence, the frequency-dependent complex electric permittivity $\epsilon(\omega)$ may be introduced, in a similar way, if *any* two linear combinations of these variables are related by a similar formula.

Absolutely similar arguments show that magnetic properties of a linear, isotropic medium may be characterized by a frequency-dependent, complex permeability $\mu(\omega)$. Now rewriting Eqs. (1) for the complex amplitudes of the fields at a particular frequency, we may readily repeat all calculations of Sec. 1, and verify that all its results are valid for monochromatic waves even for a dispersive (but necessarily linear!) medium. In particular, Eqs. (7) and (13) now become

$$Z(\omega) = \left(\frac{\mu(\omega)}{\epsilon(\omega)} \right)^{1/2}, \quad k(\omega) = \omega[\epsilon(\omega)\mu(\omega)]^{1/2}, \quad (7.28)$$

so that the wave impedance and the wave number may be both complex functions of frequency.¹⁰

This fact has important consequences for electromagnetic wave propagation. First, plugging the representation of the complex wave number as the sum of its real and imaginary parts, $k(\omega) \equiv k'(\omega) + ik''(\omega)$, into Eq. (11):

$$f = \operatorname{Re} \left\{ f_\omega e^{i[k(\omega)z - \omega t]} \right\} = e^{-k''(\omega)z} \operatorname{Re} \left\{ f_\omega e^{i[k'(\omega)z - \omega t]} \right\}, \quad (7.29)$$

we see that $k''(\omega)$ describes the rate of wave *attenuation* in the medium at frequency ω .¹¹ Second, if the waveform is not sinusoidal (and hence should be represented as a sum of several/many sinusoidal components), the frequency dependence of $k'(\omega)$ provides for wave *dispersion*, i.e. the waveform deformation at the propagation, because the propagation velocity (4) of component waves is now different.¹²

¹⁰ The first unambiguous observations of dispersion (for the case of light refraction) were described by Sir Isaac Newton in his *Optics* (1704) – even though this genius has never recognized the wave nature of light!

¹¹ It may be tempting to attribute this effect to wave *absorption*, i.e. the dissipation of the wave's energy, but we will see very soon that wave attenuation may be due to different effects as well.

¹² The reader is probably familiar with the most noticeable effect of the dispersion: the difference between the *group velocity* $v_{\text{gr}} \equiv d\omega/dk'$ giving the speed of the envelope of a wave packet with a narrow frequency spectrum, and the *phase velocity* $v_{\text{ph}} \equiv \omega/k'$ of the component waves. The second-order dispersion effect, proportional to $d^2\omega/dk'^2$, leads to the deformation (gradual broadening) of the envelope itself. Following tradition, these effects

As an example of such a dispersive medium, let us consider a simple but very representative *Lorentz oscillator model*.¹³ In dilute atomic or molecular systems (e.g., gases), electrons respond to the external electric field especially strongly when its frequency ω is close to certain frequencies ω_j corresponding to the spectrum of quantum interstate transitions of a single atom/molecule. A phenomenological description of this behavior may be obtained from a classical model of several externally-driven harmonic oscillators, generally with non-zero damping. For a single oscillator, driven by the electric field's force $F(t) = qE(t)$, we can write the 2nd Newton law as

$$m(\ddot{x} + 2\delta_0 \dot{x} + \omega_0^2 x) = qE(t), \quad (7.30)$$

where ω_0 is the own frequency of the oscillator, and δ_0 is its damping coefficient. For the electric field of a monochromatic wave, $E(t) = \text{Re}[E_\omega \exp\{-i\omega t\}]$, we may look for a particular, *forced-oscillation* solution of this equation in a similar form $x(t) = \text{Re}[x_\omega \exp\{-i\omega t\}]$.¹⁴ Plugging this solution into Eq. (30), we readily find the complex amplitude of these oscillations:

$$x_\omega = \frac{q}{m} \frac{E_\omega}{(\omega_0^2 - \omega^2) - 2i\omega\delta_0}. \quad (7.31)$$

Using this result to calculate the complex amplitude of the dipole moment as $p_\omega = qx_\omega$, and then the electric polarization $P_\omega = np_\omega$ of a dilute medium with n independent oscillators for unit volume, for its frequency-dependent permittivity (26) we get

$$\epsilon(\omega) = \epsilon_0 + n \frac{q^2}{m} \frac{1}{(\omega_0^2 - \omega^2) - 2i\omega\delta_0}. \quad (7.32)$$

Lorentz oscillator model

This result may be readily generalized to the case when the system has several types of oscillators with different masses and frequencies:

$$\epsilon(\omega) = \epsilon_0 + nq^2 \sum_j \frac{f_j}{m_j[(\omega_j^2 - \omega^2) - 2i\omega\delta_j]}, \quad (7.33)$$

where $f_j \equiv n_j/n$ is the fraction of oscillators with frequency ω_j , so that the sum of all f_j equals 1. Figure 5 shows a typical behavior of the real and imaginary parts of the complex dielectric constant, described by Eq. (33), as functions of frequency. The oscillator resonances' effect is clearly visible, and dominates the media response at $\omega \approx \omega_j$, especially in the case of low damping, $\delta_j \ll \omega_j$. Note that in the low-damping limit, the imaginary part of the dielectric constant ϵ'' , and hence the wave attenuation k'' , are negligibly small at all frequencies besides small vicinities of ω_j , where the derivative $d\epsilon'(\omega)/d\omega$ is

are discussed in more detail in the quantum-mechanics part of this series (QM Sec. 2.2), because they are a crucial factor of Schrödinger's wave mechanics. (See also a brief discussion in CM Sec. 6.3.)

¹³ This example is focused on the frequency dependence of ϵ rather than μ , because electromagnetic waves interact with “usual” media via their electric field much more than via the magnetic field. Indeed, according to Eq. (7), the magnetic field of the wave is of the order of E/c , so that the magnetic component of the Lorentz force (5.10), acting on a non-relativistic particle, $F_m \sim quB \sim (u/c)qE$, is much smaller than that of its electric component, $F_e = qE$, and may be neglected. However, as will be discussed in Sec. 6, forgetting about the possible dispersion of $\mu(\omega)$ may result in missing some remarkable opportunities for manipulating the waves.

¹⁴ If this point and Eq. (30) are not absolutely clear, please see CM Sec. 5.1 for a more detailed discussion.

negative.¹⁵ Thus, for a system of weakly-damped oscillators, Eq. (33) may be well approximated by a sum of singularities (“poles”):

$$\varepsilon(\omega) \approx \varepsilon_0 + n \frac{q^2}{2} \sum_j \frac{f_j}{m_j \omega_j (\omega_j - \omega)}, \quad \text{for } \delta_j \ll |\omega - \omega_j| \ll |\omega_j - \omega_{j'}|. \quad (7.34)$$

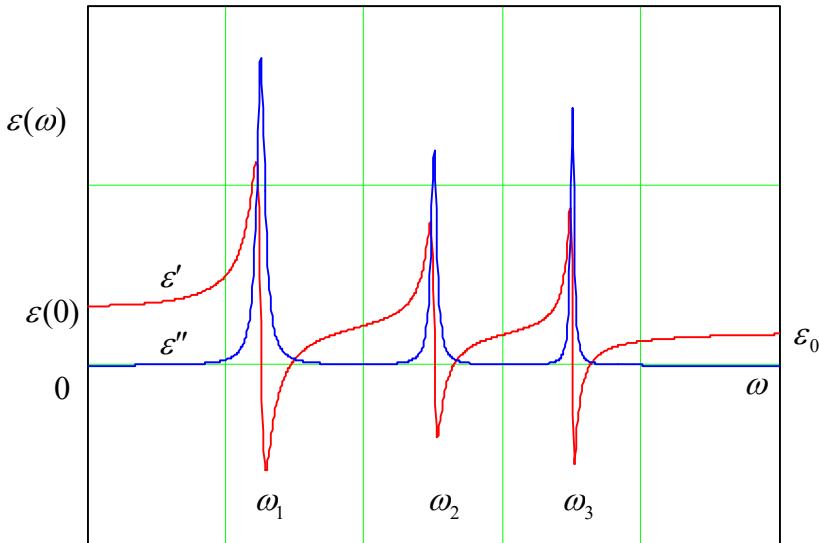


Fig. 7.5. Typical frequency dependence of the real and imaginary parts of the complex electric permittivity, according to the generalized Lorentz oscillator model.

This result is especially important because according to quantum mechanics,¹⁶ Eq. (34) (with all m_j equal) is also valid for a set of non-interacting, similar quantum systems (whose dynamics may be completely different from that of a harmonic oscillator!), provided that ω_j are replaced with frequencies of possible quantum interstate transitions, and coefficients f_j are replaced with the so-called *oscillator strengths* of the transitions – which obey the same *sum rule*, $\sum_j f_j = 1$.

At $\omega \rightarrow 0$, the imaginary part of the complex permittivity (33) also vanishes (for any δ_j), while its real part approaches its electrostatic (“dc”) value

$$\varepsilon(0) = \varepsilon_0 + q^2 \sum_j \frac{n_j}{m_j \omega_j^2}. \quad (7.35)$$

Note that according to Eq. (30), the denominator of the fraction in Eq. (35) is just the effective spring constant $\kappa_j = m_j \omega_j^2$ of the j^{th} oscillator, so that the oscillator masses m_j as such are actually (and quite naturally) not involved in the static dielectric response.

In the opposite limit of very high frequencies, $\omega \gg \omega_j, \delta_j$, the permittivity also becomes real and may be represented as

$$\varepsilon(\omega) = \varepsilon_0 \left(1 - \frac{\omega_p^2}{\omega^2} \right), \quad \text{where } \omega_p^2 \equiv \frac{q^2}{\varepsilon_0} \sum_j \frac{n_j}{m_j}. \quad (7.36)$$

ε(ω) in plasma

¹⁵ In optics, such behavior is called *anomalous dispersion*.

¹⁶ See, e.g., QM Chapters 5-6.

This result is very important because it is also valid at *all* frequencies if all ω_j and δ_j vanish, for example for gases of free charged particles, in particular for *plasmas* – ionized atomic gases, provided that the ion collision effects are negligible. (This is why the parameter ω_p defined by Eq. (36) is called the *plasma frequency*.) Typically, the plasma as a whole is neutral, i.e. the density n of positive atomic ions is equal to that of the free electrons. Since the ratio n_j/m_j for electrons is much higher than that for ions, the general formula (36) for the plasma frequency is usually well approximated by the following simple expression:

$$\omega_p^2 = \frac{ne^2}{\epsilon_0 m_e}. \quad (7.37)$$

This expression has a simple physical sense: the effective spring constant $\kappa_{\text{ef}} \equiv m_e \omega_p^2 = ne^2/\epsilon_0$ describes the Coulomb force that appears when the electron subsystem of the plasma is shifted, as a whole, from its positive-ion subsystem, thus violating the electroneutrality.¹⁷ Hence, there is no surprise that the function $\epsilon(\omega)$ given by Eq. (36) vanishes at $\omega = \omega_p$: at this resonance frequency, the polarization electric field \mathbf{E} may oscillate, i.e. have a non-zero amplitude $E_\omega = D_\omega/\epsilon(\omega)$, even in the absence of external forces induced by external (stand-alone) charges, i.e. in the absence of the field \mathbf{D} these charges induce – see Eq. (3.32).

The behavior of electromagnetic waves in a medium that obeys Eq. (36), is very remarkable. If the wave frequency ω is above ω_p , the dielectric constant $\epsilon(\omega)$ and hence the wave number (28) are positive and real, and waves propagate without attenuation, following the dispersion relation,

Plasma
dispersion
relation

$$k(\omega) = \omega [\epsilon(\omega) \mu_0]^{1/2} = \frac{1}{c} (\omega^2 - \omega_p^2)^{1/2}, \quad (7.38)$$

whose plot is shown in Fig. 6.

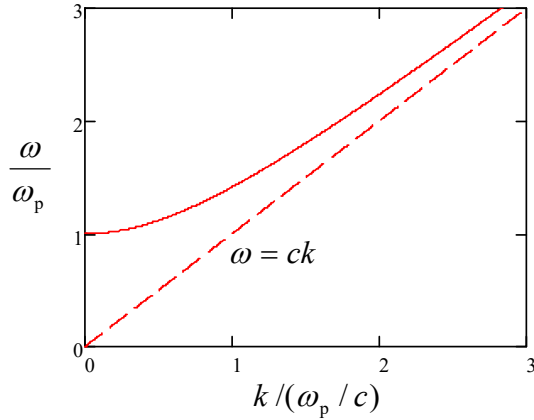


Fig. 7.6. The plasma dispersion law (solid line) in comparison with the linear dispersion in the free space (dashed line).

At $\omega \rightarrow \omega_p$ the wave number k tends to zero. Beyond that point (i.e. at $\omega < \omega_p$), we still can use Eq. (38), but it is instrumental to rewrite it in the mathematically equivalent form

¹⁷ Indeed, let us consider such a small shift Δx , perpendicular to the plane surface of a broad, plane slab filled with plasma. The uncompensated ion charges, with equal and opposite surface densities $\sigma = \pm en\Delta x$, that appear at the slab surfaces, create inside it, according to Eq. (2.3), a uniform electric field with $E_x = en\Delta x/\epsilon_0$. This field exerts the force $-eE_x = -(ne^2/\epsilon_0)\Delta x \equiv -\kappa_{\text{ef}}\Delta x$ on each electron, pulling it back to its equilibrium position.

$$k(\omega) = \frac{i}{c} \left(\omega_p^2 - \omega^2 \right)^{1/2} = \frac{i}{\delta}, \quad \text{where } \delta \equiv \frac{c}{\left(\omega_p^2 - \omega^2 \right)^{1/2}}. \quad (7.39)$$

At $\omega < \omega_p$, the so-defined parameter δ is real, and Eq. (29) shows that the electromagnetic field exponentially decreases with distance:

$$f = \operatorname{Re} f_\omega e^{i(kz - \omega t)} \equiv \exp \left\{ -\frac{z}{\delta} \right\} \operatorname{Re} f_\omega e^{-i\omega t}. \quad (7.40)$$

Does this mean that the wave is being absorbed in the plasma? Answering this question is a good pretext to calculate the time average of the Poynting vector $\mathbf{S} = \mathbf{E} \times \mathbf{H}$ of a monochromatic electromagnetic wave in an *arbitrary* dispersive (but still linear and isotropic) medium. First, let us spell out the real fields' time dependences:

$$E(t) = \operatorname{Re}[E_\omega e^{-i\omega t}] \equiv \frac{1}{2} [E_\omega e^{-i\omega t} + \text{c.c.}], \quad H(t) = \operatorname{Re}[H_\omega e^{-i\omega t}] \equiv \frac{1}{2} \left[\frac{E_\omega}{Z(\omega)} e^{-i\omega t} + \text{c.c.} \right]. \quad (7.41)$$

Now, a straightforward calculation yields¹⁸

$$\bar{S} = \overline{E(t)H(t)} = \frac{E_\omega E_\omega^*}{4} \left[\frac{1}{Z(\omega)} + \frac{1}{Z^*(\omega)} \right] \equiv \frac{E_\omega E_\omega^*}{2} \operatorname{Re} \frac{1}{Z(\omega)} \equiv \frac{|E_\omega|^2}{2} \operatorname{Re} \left[\frac{\epsilon(\omega)}{\mu(\omega)} \right]^{1/2}. \quad (7.42)$$

Let us apply this important general formula to our simple model of plasma at $\omega < \omega_p$. In this case, the magnetic permeability equals μ_0 , i.e. $\mu(\omega) = \mu_0$ is positive and real, while $\epsilon(\omega)$ is real and negative, so that $1/Z(\omega) = [\epsilon(\omega)/\mu(\omega)]^{1/2}$ is purely imaginary, and the average Poynting vector (42) vanishes. This means that the energy, on average, does not flow along the z -axis. So, the waves with $\omega < \omega_p$ are not absorbed in plasma. (Indeed, the Lorentz model with $\delta_l = 0$ does not describe any energy dissipation mechanism.) Instead, as we will see in the next section, the waves are rather *reflected* from the plasma's boundary, more exactly from its surface layer of a thickness $\sim \delta$.

Note also that in the limit $\omega \ll \omega_p$, Eq. (39) yields

$$\delta \rightarrow \frac{c}{\omega_p} = \left(\frac{c^2 \epsilon_0 m_e}{ne^2} \right)^{1/2} = \left(\frac{m_e}{\mu_0 ne^2} \right)^{1/2}. \quad (7.43)$$

But this is just a particular case (for $q = e$, $m = m_e$, and $\mu = \mu_0$) of Eq. (6.44) that was derived in Sec. 6.4 for the depth of the magnetic field's penetration into a lossless (collision-free) conductor in the quasistatic approximation. This fact shows again that, as was already discussed in Sec. 6.7, this

¹⁸ For an arbitrary plane wave, the total average power flow may be calculated as an integral of Eq. (42) over all frequencies. By the way, combining this integral and the Poynting theorem (6.111), is it straightforward to prove the following interesting expression for the average electromagnetic energy density of a narrow ($\Delta\omega \ll \omega$) wave packet propagating in an arbitrary dispersive (but linear and isotropic) medium:

$$\bar{u} = \frac{1}{2} \int_{\text{packet}} \left\{ \frac{d[\omega\epsilon'(\omega)]}{d\omega} E_\omega E_\omega^* + \frac{d[\omega\mu'(\omega)]}{d\omega} H_\omega H_\omega^* \right\} d\omega.$$

approximation (in which the displacement currents are neglected) gives an adequate description of the time-dependent phenomena at $\omega \ll \omega_p$, i.e. at $\delta \ll c/\omega = 1/k = \lambda/2\pi$.¹⁹

There are two most important examples of natural plasmas. For the Earth's ionosphere, i.e. the upper part of its atmosphere, which is almost completely ionized by the ultra-violet and X-ray components of the Sun's radiation, the maximum value of n , reached about 300 km over the Earth's surface, is between 10^{10} and 10^{12} m^{-3} (depending on the time of the day and the Sun's activity phase), so that the maximum plasma frequency (37) is between 1 and 10 MHz. This is much higher than the particles' typical reciprocal collision time τ^{-1} , so that Eq. (38) gives a good description of wave dispersion in this plasma. The effect of reflection of electromagnetic waves with $\omega < \omega_p$ from the ionosphere enables the long-range (over-the-globe) radio communications and broadcasting at the so-called *short waves*, with cyclic frequencies of the order of 10 MHz:²⁰ they may propagate in the flat channel formed by the Earth's surface and the ionosphere, being reflected repeatedly by these parallel "walls". Unfortunately, due to the random variations of the Sun's activity, and hence of ω_p , this natural radio communication channel is not too reliable, and in our age of transworld optical-fiber cables (see Sec. 7 below), its practical importance has diminished.

Another important example of plasmas is free electrons in metals and other conductors. For a typical metal, n is of the order of $10^{23} \text{ cm}^{-3} \equiv 10^{29} \text{ m}^{-3}$, so that Eq. (37) yields $\omega_p \sim 10^{16} \text{ s}^{-1}$. This value of ω_p is somewhat higher than the mid-optical frequencies ($\omega \sim 3 \times 10^{15} \text{ s}^{-1}$), explaining why planar, clean metallic surfaces, such as the aluminum and silver films used in mirrors, are so shiny: at these frequencies, their complex permittivity $\epsilon(\omega)$ is almost exactly real and negative, leading to light reflection, with very little absorption.

The simple model (36), which neglects electron scattering, becomes inadequate at lower frequencies, $\omega\tau \sim 1$. A good phenomenological way of extending the model to the account of scattering is to take, in Eq. (33), the lowest frequency ω_j equal zero (to describe the free electrons), while keeping the damping coefficient δ_0 of this mode larger than zero, to account for the energy dissipation due to their scattering. Then Eq. (33) is reduced to

$$\epsilon_{\text{ef}}(\omega) = \epsilon_{\text{opt}}(\omega) + \frac{n_0 q^2}{m} \frac{1}{-\omega^2 - 2i\omega\delta_0} \equiv \epsilon_{\text{opt}}(\omega) + i \frac{n_0 q^2}{2\delta_0 m \omega} \frac{1}{1 - i\omega/2\delta_0}, \quad (7.44)$$

where the response $\epsilon_{\text{opt}}(\omega)$ at high (in practice, optical) frequencies is still given by Eq. (33), but now with $j > 0$. The result (44) allows for a simple interpretation. To show that, let us incorporate into our calculations the Ohmic conduction of the medium, generalizing Eq. (4.7) as $\mathbf{j}_\omega = \sigma(\omega)\mathbf{E}_\omega$ to account for the possible frequency dependence of the Ohmic conductivity. Plugging this relation into the Fourier image of the relevant macroscopic Maxwell equation, $\nabla \times \mathbf{H}_\omega = \mathbf{j}_\omega - i\omega\mathbf{D}_\omega \equiv \mathbf{j}_\omega - i\omega\epsilon(\omega)\mathbf{E}_\omega$, we get

$$\nabla \times \mathbf{H}_\omega = [\sigma(\omega) - i\omega\epsilon(\omega)]\mathbf{E}_\omega. \quad (7.45)$$

¹⁹ One more convenience of the simple model of a collision-free plasma, which has led us to Eq. (36), is that it may be readily generalized to the case of an additional strong dc magnetic field \mathbf{B}_0 (much higher than that of the wave) applied in the direction \mathbf{n} of wave propagation. It is straightforward (and hence left for the reader) to show that such plasma exhibits the *Faraday effect* of the polarization plane's rotation, and hence gives an example of an anisotropic media that violates the Lorentz reciprocity relation (6.121).

²⁰ These frequencies are an order of magnitude lower than those used for TV and FM-radio broadcasting.

This relation shows that for a monochromatic wave, the addition of the Ohmic current density \mathbf{j}_ω to the displacement current density is equivalent to the addition of $\sigma(\omega)$ to $-i\omega\epsilon(\omega)$, i.e. to the following change of the ac electric permittivity:²¹

$$\epsilon(\omega) \rightarrow \epsilon_{\text{ef}}(\omega) \equiv \epsilon_{\text{opt}}(\omega) + i \frac{\sigma(\omega)}{\omega}. \quad (7.46)$$

Now the comparison of Eqs. (44) and (46) shows that they coincide if we take

$$\sigma(\omega) = \frac{n_0 q^2 \tau}{m_0} \frac{1}{1 - i\omega\tau} \equiv \sigma(0) \frac{1}{1 - i\omega\tau}, \quad (7.47)$$

Generalized Drude formula

where the dc conductivity $\sigma(0)$ is described by the Drude formula (4.13), and the phenomenologically introduced coefficient δ_0 is associated with $1/2\tau$. Eq. (47), which is frequently called the *generalized* (or “ac”, or “rf”) *Drude formula*,²² gives a very reasonable (semi-quantitative) description of the ac conductivity of many metals almost up to optical frequencies.

Now returning to our discussion of the generalized Lorentz model (33), we see that the frequency dependences of the real (ϵ') and imaginary (ϵ'') parts of the complex permittivity it yields are not quite independent. For example, let us have one more look at the resonance peaks in Fig. 5. Each time the real part drops with frequency, $d\epsilon'/d\omega < 0$, its imaginary part ϵ'' has a positive peak. Ralph Kronig (in 1926) and Hendrik (“Hans”) Kramers (in 1927) independently showed that this is not an occasional coincidence pertinent only to this particular model. Moreover, the full knowledge of the function $\epsilon'(\omega)$ enables the *calculation* of the function $\epsilon''(\omega)$, and vice versa. The mathematical reason for this fact is that both these functions are always related to a single real function $G(\theta)$ – see Eqs. (27).

To derive these relations, let us consider Eq. (26b) on the complex frequency plane, $\omega \rightarrow \mathbf{\Omega} \equiv \omega' + i\omega''$:

$$f(\mathbf{\Omega}) \equiv \epsilon(\mathbf{\Omega}) - \epsilon_0 = \int_0^\infty G(\theta) e^{i\mathbf{\Omega}\theta} d\theta \equiv \int_0^\infty G(\theta) e^{i\omega'\theta} e^{-\omega''\theta} d\theta. \quad (7.48)$$

For all stable physical systems, $G(\theta)$ has to be finite for all important values of the real integration variable ($\theta > 0$), and tend to zero at $\theta \rightarrow 0$ and $\theta \rightarrow \infty$. (Indeed, according to Eq. (23), a non-zero $G(0)$ would mean an instantaneous response of the medium to the external force, while $G(\infty) \neq 0$ would mean that it has an infinitely long memory.) Because of that, and thanks to the factor $e^{-\omega''\theta}$, the expression under the integral in Eq. (48) tends to zero at $|\mathbf{\Omega}| \rightarrow \infty$ in all upper half-plane ($\omega'' \geq 0$). As a result, we may claim that the complex function $f(\mathbf{\Omega})$ given by this relation, is analytical in that half-plane. This fact allows us to apply to it the general *Cauchy integral* formula²³

$$f(\mathbf{\Omega}) = \frac{1}{2\pi i} \oint_C f(\mathbf{\Omega}) \frac{d\mathbf{\Omega}}{\mathbf{\Omega} - \mathbf{\Omega}}, \quad (7.49)$$

²¹ Alternatively, according to Eq. (45), it is possible (and in the field of infrared spectroscopy, conventional) to attribute the ac response of a medium at *all* frequencies to its effective complex conductivity: $\sigma_{\text{ef}}(\omega) \equiv \sigma(\omega) - i\omega\epsilon(\omega) \equiv -i\omega\epsilon_{\text{ef}}(\omega)$.

²² It may be also derived from the Boltzmann kinetic equation in the so-called relaxation-time approximation (RTA) – see, e.g., SM Sec. 6.2.

²³ See, e.g., MA Eq. (15.2).

where $\Omega \equiv \Omega' + i\Omega''$ is also a complex variable. Let us take the integration contour C of the form shown in Fig. 7, with the radius R of the larger semicircle tending to infinity, and the radius r of the smaller semicircle (around the singular point $\Omega = \omega$) tending to zero. Due to the exponential decay of $|f(\Omega)|$ at $|\Omega| \rightarrow \infty$, the contribution to the right-hand side of Eq. (49) from the larger semicircle vanishes,²⁴ while the contribution from the small semicircle, where $\Omega = \omega + r \exp\{i\varphi\}$, with $-\pi \leq \varphi \leq 0$, is

$$\lim_{r \rightarrow 0} \frac{1}{2\pi i} \int_{\Omega=\omega+r \exp\{i\varphi\}} f(\Omega) \frac{d\Omega}{\Omega - \omega} = \frac{f(\omega)}{2\pi i} \int_{-\pi}^0 \frac{ir \exp\{i\varphi\} d\varphi}{r \exp\{i\varphi\}} \equiv \frac{f(\omega)}{2\pi} \int_{-\pi}^0 d\varphi = \frac{1}{2} f(\omega). \quad (7.50)$$

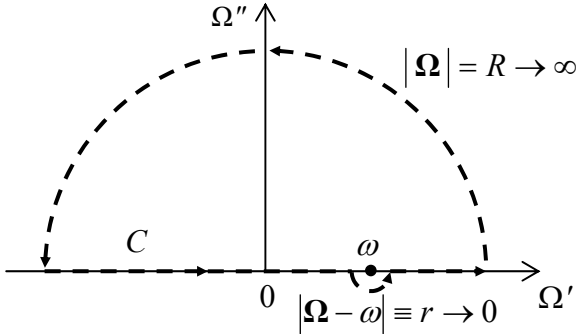


Fig. 7.7. Deriving the Kramers-Kronig dispersion relations.

As a result, for our contour C , Eq. (49) yields

$$f(\omega) = \lim_{r \rightarrow 0} \frac{1}{2\pi i} \left(\int_{-\infty}^{\omega-r} + \int_{\omega+r}^{+\infty} \right) f(\Omega) \frac{d\Omega}{\Omega - \omega} + \frac{1}{2} f(\omega), \quad (7.51)$$

where $\Omega \equiv \Omega'$ on the real axis (where $\Omega'' = 0$). Such an integral, excluding a symmetric infinitesimal vicinity of a pole singularity, is called the *principal value* of the (formally, diverging) integral from $-\infty$ to $+\infty$, and is denoted by the letter P before it.²⁵ Using this notation, subtracting $f(\omega)/2$ from both parts of Eq. (51), and multiplying them by 2, we get

$$f(\omega) = \frac{1}{\pi i} P \int_{-\infty}^{+\infty} f(\Omega) \frac{d\Omega}{\Omega - \omega}. \quad (7.52)$$

Now plugging into this complex equality the polarization-related difference $f(\omega) \equiv \varepsilon(\omega) - \varepsilon_0$ in the form $[\varepsilon'(\omega) - \varepsilon_0] + i[\varepsilon''(\omega)]$, and requiring both real and imaginary components of the two sides of Eq. (52) to be equal separately, we get the famous *Kramers-Kronig dispersion relations*

$$\varepsilon'(\omega) = \varepsilon_0 + \frac{1}{\pi} P \int_{-\infty}^{+\infty} \varepsilon''(\Omega) \frac{d\Omega}{\Omega - \omega}, \quad \varepsilon''(\omega) = -\frac{1}{\pi} P \int_{-\infty}^{+\infty} [\varepsilon'(\Omega) - \varepsilon_0] \frac{d\Omega}{\Omega - \omega}. \quad (7.53)$$

Kramers-Kronig dispersion relations

We may use the already mentioned fact that $\varepsilon'(\omega)$ is always an even function, while $\varepsilon''(\omega)$ an odd function of frequency, to rewrite these relations in the following equivalent form,

²⁴Strictly speaking, this also requires $|f(\Omega)|$ to decrease faster than Ω^{-1} at the real axis (at $\Omega'' = 0$), but due to the inertia of charged particles, this requirement is fulfilled for all realistic models of dispersion – see, e.g., Eq. (36).

²⁵I am typesetting this symbol in a Roman (upright) font, to avoid any possibility of confusion with the medium's polarization.

$$\varepsilon'(\omega) = \varepsilon_0 + \frac{2}{\pi} P \int_0^{+\infty} \varepsilon''(\Omega) \frac{\Omega d\Omega}{\Omega^2 - \omega^2}, \quad \varepsilon''(\omega) = -\frac{2\omega}{\pi} P \int_0^{+\infty} [\varepsilon'(\Omega) - \varepsilon_0] \frac{d\Omega}{\Omega^2 - \omega^2}, \quad (7.54)$$

which is more convenient for most applications, because it involves only physical (positive) frequencies.

Though the Kramers-Kronig relations are “global” in frequency, in certain cases they allow an approximate calculation of dispersion from experimental data for absorption, collected even within a limited (“local”) frequency range. Most importantly, if a medium has a sharp absorption peak at some frequency ω_j , we may describe it as

$$\varepsilon''(\omega) \approx c\delta(\omega - \omega_j) + \text{a more smooth function of } \omega, \quad (7.55)$$

and the first of Eqs. (54) immediately gives

$$\varepsilon'(\omega) \approx \varepsilon_0 + \frac{2c}{\pi} \frac{\omega_j}{\omega_j^2 - \omega^2} + \text{another smooth function of } \omega, \quad (7.56)$$

Dispersion
near an
absorption
line

thus predicting the anomalous dispersion near such a point. This calculation shows that such behavior observed in the Lorentz oscillator model (see Fig. 5) is by no means occasional or model-specific.

Let me emphasize again that the Kramers-Kronig relations (53)-(54) are much more general than the Lorentz model (33), and require only a causal linear relation (21) between the polarization $P(t)$ with the electric field $E(t)$.²⁶ Hence, these relations are also valid for the complex functions relating Fourier images of any cause/effect-related pair of variables. In particular, at a measurement of *any* linear response $r(t)$ of *any* experimental sample to *any* external field $f(t')$, whatever the nature of this response and physics behind it, we may be confident that there is a causal relationship between the variables r and f , so that the corresponding complex function $\chi(\omega) \equiv r_\omega/f_\omega$ does obey the Kramers-Kronig relations. However, it is still important to remember that a linear relationship between the Fourier amplitudes of two variables does *not* necessarily imply a causal relationship between them.²⁷

7.3. Reflection

The most important new effect arising in nonuniform media is wave *reflection*. Let us start its discussion from the simplest case of a plane electromagnetic wave that is normally incident on a sharp interface between two uniform, linear, isotropic media.

Moreover, let us first consider an even simpler sub-case when one of the two media (say, that located at $z > 0$, see Fig. 8) cannot sustain any electric field at all – as implied, in particular, by the macroscopic model of a perfect conductor – see Eq. (2.1):

²⁶ Actually, in mathematics, the relations even somewhat more general than Eqs. (53), valid for an arbitrary analytic function of complex argument, are known at least from 1868 – the *Sokhotski-Plemelj theorem*.

²⁷ For example, the function $\varphi(\omega) \equiv E_\omega/P_\omega$ in the Lorentz oscillator model, does not obey the Kramers-Kronig relations. This is evident not only physically, from the fact that $E(t)$ is *not* a causal function of $P(t)$, but even mathematically. Indeed, Green’s function describing a causal relationship has to tend to zero at small time delays $\theta \equiv t - t'$, so that its Fourier image has to tend to zero at $\omega \rightarrow \pm\infty$. This is certainly true for the function $f(\omega)$ given by Eq. (32), but not for the reciprocal function $\varphi(\omega) \equiv 1/f(\omega) \propto (\omega^2 - \omega_0^2) - 2i\delta\omega$, which diverges at large frequencies.

$$E|_{z \geq 0} = 0. \quad (7.57)$$

This condition is evidently incompatible with the single traveling wave (5). However, this solution may be readily generalized using the fact that the dispersion-free 1D wave equation,

$$\left(\frac{\partial^2}{\partial z^2} - \frac{1}{v^2} \frac{\partial^2}{\partial t^2} \right) E = 0, \quad (7.58)$$

supports waves propagating, with the same speed, in any of two opposite directions. As a result, the following linear superposition of two such waves,

$$E|_{z \leq 0} = f(z - vt) - f(-z - vt), \quad (7.59)$$

satisfies both the equation and the boundary condition (57), for an arbitrary function f . The second term on the right-hand side of Eq. (59) may be interpreted as a result of *total reflection* of the incident wave (described by its first term) – in this particular case, with the change of the electric field's sign. This means, in particular, that within the macroscopic model, a conductor acts as a perfect mirror. By the way, since the vector \mathbf{n} of the reflected wave is opposite to that of the incident one (see the arrows in Fig. 8), Eq. (6) shows that the magnetic field of the wave does *not* change its sign at the reflection:

$$H|_{z \leq 0} = \frac{1}{Z} [f(z - vt) + f(-z - vt)]. \quad (7.60)$$

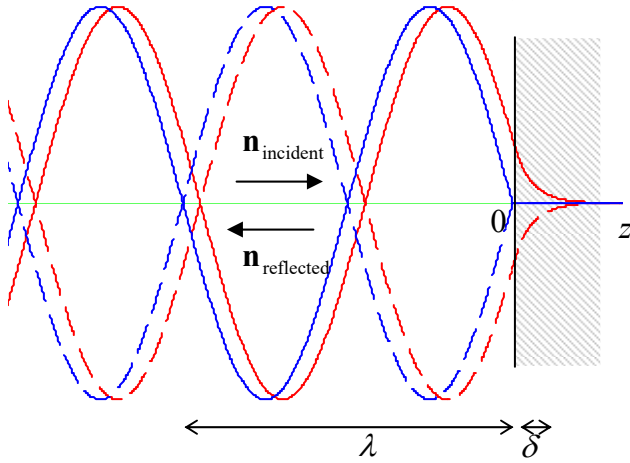


Fig. 7.8. A snapshot of the electric field at the reflection of a sinusoidal wave from a perfect conductor: a realistic pattern (red lines) and its macroscopic, ideal-mirror approximation (blue lines). Dashed lines show the snapshots after a half-period time delay ($\omega\Delta t = \pi$).

The blue lines in Fig. 8 show the resulting pattern (59) for the simplest, monochromatic wave:

$$E|_{z \leq 0} = \operatorname{Re} [E_\omega e^{i(kz - \omega t)} - E_\omega e^{i(-kz - \omega t)}]. \quad (7.61a)$$

Depending on convenience in a particular context, this pattern may be legitimately represented and interpreted either as the linear superposition (61a) of two *traveling* waves or as a single *standing* wave:

$$E|_{z \leq 0} = -2 \operatorname{Im}(E_\omega e^{-i\omega t}) \sin kz \equiv 2 \operatorname{Re}(iE_\omega e^{-i\omega t}) \sin kz \equiv 2 \operatorname{Re}[E_\omega e^{-i(\omega t - \pi/2)}] \sin kz, \quad (7.61b)$$

in which the electric and magnetic field oscillate with phase shifts by $\pi/2$ both in time and space:

$$H|_{z \leq 0} = \operatorname{Re} \left[\frac{E_\omega}{Z} e^{i(kz - \omega t)} + \frac{E_\omega}{Z} e^{i(-kz - \omega t)} \right] = 2 \operatorname{Re} \left(\frac{E_\omega}{Z} e^{-i\omega t} \right) \cos kz. \quad (7.62)$$

As a result of this shift, the time average of the Poynting vector's magnitude,

$$S(z, t) = EH = \frac{1}{Z} \operatorname{Re} [E_\omega^2 e^{-2i\omega t}] \sin 2kz, \quad (7.63)$$

equals zero, showing that at the total reflection there is no *average* power flow. (This is natural because the perfect mirror can neither transmit the wave nor absorb it.) However, Eq. (63) shows that the standing wave features local oscillations of energy, transferring it periodically between the concentrations of the electric and magnetic fields, separated by the distance $\Delta z = \pi/2k = \lambda/4$.

In the case of the sinusoidal waves, the reflection effects may be readily explored even for the more general case of dispersive and/or lossy (but still linear) media in which $\alpha(\omega)$ and $\mu(\omega)$, and hence the wave vector $k(\omega)$ and the wave impedance $Z(\omega)$, defined by Eqs. (28), are certain complex functions of frequency. The “only” new factor we have to account for is that in this case, the reflection may not be total, so that inside the second medium we have to use the traveling-wave solution as well. This factor may be taken care of by looking for the solution to our boundary problem in the form

$$E|_{z \leq 0} = \operatorname{Re} [E_\omega (e^{ik_- z} + R e^{-ik_- z}) e^{-i\omega t}], \quad E|_{z \geq 0} = \operatorname{Re} [E_\omega T e^{ik_+ z} e^{-i\omega t}], \quad (7.64)$$

Wave's
partial
reflection

and hence, according to Eq. (6),

$$H|_{z \leq 0} = \operatorname{Re} \left[\frac{E_\omega}{Z_-(\omega)} (e^{ik_- z} - R e^{-ik_- z}) e^{-i\omega t} \right], \quad H|_{z \geq 0} = \operatorname{Re} \left[\frac{E_\omega}{Z_+(\omega)} T e^{ik_+ z} e^{-i\omega t} \right]. \quad (7.65)$$

(The indices + and – correspond to the media located at $z > 0$ and $z < 0$, respectively.) Please note the following important features of Eqs. (64)-(65):

(i) They satisfy the Maxwell equations in both media. (Historically, the fact that at $z > 0$, these solutions do not include any components proportional to $\exp\{ik_- z\}$, looked surprising and was called the *wave extinction paradox*.)

(ii) Due to the problem's linearity, we could (and did :-)) take the complex amplitudes of the reflected and transmitted wave proportional to that (E_ω) of the incident wave, while scaling them with dimensionless, generally complex coefficients R and T . As a comparison of Eqs. (64)-(65) with Eqs. (61)-(62) shows, the total reflection from an ideal mirror corresponds to $R = -1$ and $T = 0$.

(iii) Since in our current problem, the incident wave arrives from one side only (from $z = -\infty$), there is no need to include a term proportional to $\exp\{-ik_+ z\}$ into Eqs. (64)-(65) – even though this term is also a legitimate solution of our wave equation. However, we would need to add such a term if the medium at $z > 0$ had been nonuniform (e.g., had at least one more interface or any other inhomogeneity), because the wave reflected from that additional inhomogeneity would be incident on our interface (located at $z = 0$) from the right.

(iv) Eqs. (64)-(65) may be used even for the description of the cases when waves cannot propagate to $z \geq 0$, for example, a conductor or a plasma with $\omega_p > \omega$. Indeed, the exponential drop of the field amplitude at $z > 0$ in such cases is automatically described by the imaginary part of the wave number k_+ – see Eq. (29).

In order to calculate the coefficients R and T , we need to use boundary conditions at $z = 0$. Since in our current case of the normal incidence, the reflection does not change the transverse character of the partial waves, both vectors \mathbf{E} and \mathbf{H} remain tangential to the interface plane (in our notation, $z = 0$). Reviewing the arguments that have led us, in statics, to the boundary conditions (3.37) and (5.117) for these components, we see that they remain valid for the time-dependent situation as well,²⁸ so that for our current case of normal incidence we may write:

$$E|_{z=-0} = E|_{z=+0}, \quad H|_{z=-0} = H|_{z=+0}. \quad (7.66)$$

Plugging Eqs. (64)-(65) into these conditions, we readily get two equations for the coefficients R and T :

$$1 + R = T, \quad \frac{1}{Z_-}(1 - R) = \frac{1}{Z_+}T. \quad (7.67)$$

Solving this simple system of linear equations, we get²⁹

Reflection
and
transmission:
sharp interface

$$R = \frac{Z_+ - Z_-}{Z_+ + Z_-}, \quad T = \frac{2Z_+}{Z_+ + Z_-}. \quad (7.68)$$

These formulas are very important, and much more general than one might think because they are applicable for virtually any 1D waves – electromagnetic or not, provided that the impedance Z is defined properly.³⁰ Since in the general case the wave impedances Z_{\pm} defined by Eq. (28) with the corresponding indices, are complex functions of frequency, Eqs. (68) show that R and T may have imaginary parts as well. This fact has important consequences at $z < 0$, where the reflected wave, proportional to R , combines (“interferes”) with the incident wave. Indeed, with $R = |R| e^{i\varphi}$ (where $\varphi \equiv \arg R$ is a real phase shift), the expression in the parentheses in the first of Eqs. (64) becomes

$$\begin{aligned} e^{ik_- z} + R e^{-ik_- z} &= (1 - |R| + |R|) e^{ik_- z} + |R| e^{i\varphi} e^{-ik_- z} \\ &\equiv (1 - |R|) e^{ik_- z} + 2|R| e^{i\varphi/2} \sin[k_-(z - \delta_-)], \quad \text{where } \delta_- \equiv \frac{\varphi - \pi}{2k_-}. \end{aligned} \quad (7.69)$$

This means that the field may be represented as a sum of a traveling wave and a standing wave, with an amplitude proportional to $|R|$, shifted by the distance δ_- toward the interface, relatively to the ideal-mirror pattern (61b) – see Fig. 8. This effect is frequently used for the experimental measurements of an unknown impedance Z_+ of some medium, provided than Z_- is known – most often, it is the free space, where $Z_- = Z_0$. For that, a small antenna (the *probe*), not disturbing the fields’ distribution too much, is placed into the wave field, and the amplitude of the ac voltage induced in it by the wave is measured with a detector (e.g., a semiconductor diode with a nearly-quadratic I - V curve), as a function of z (Fig.

²⁸ For example, the first of Eqs. (66) may be obtained by integrating the full (time-dependent) Maxwell equation $\nabla \times \mathbf{E} + \partial \mathbf{B} / \partial t = 0$ over a narrow and long rectangular contour with dimensions l and d ($d \ll l$) stretched along the interface. At the application of the Stokes theorem to this integral, the first term gives $\Delta E l$, while the contribution of the second term is proportional to the product ld , so that its contribution at $d/l \rightarrow 0$ is negligible. The proof of the second boundary condition is similar – as was already discussed in Sec. 6.2.

²⁹ Please note that only the media impedances (rather than their wave velocities) are important for reflection in this case! Unfortunately, this fact is not clearly emphasized in some textbooks that discuss only the case $\mu_{\pm} = \mu_0$, when $Z = (\mu_0/\epsilon)^{1/2}$ and $v = 1/(\mu_0\epsilon)^{1/2}$ are proportional to each other.

³⁰ See, e.g., the discussion of elastic waves of mechanical deformations in CM Secs. 6.3, 6.4, 7.7, and 7.8.

9). From the results of such a measurement, it is straightforward to find both $|R|$ and δ , and hence restore the complex R , and then use Eq. (68) to calculate both the modulus and the argument of Z_+ . (Before computers became ubiquitous, a specially lined paper called the *Smith chart*, had been frequently used for performing this recalculation graphically; even nowadays, it is still used for result presentation.)

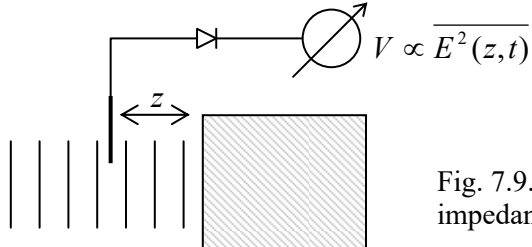


Fig. 7.9. Measurement of the complex impedance of a medium (schematically).

Now let us discuss what these results give for waves incident from the free space ($Z_-(\omega) = Z_0 = \text{const}$, $k_- = k_0 = \omega/c$) onto the surfaces of two particular important media.

(i) For a collision-free plasma (with negligible magnetization) we may use Eq. (36) with $\mu(\omega) = \mu_0$, to represent the impedance (28) in either of two equivalent forms:

$$Z_+ = Z_0 \frac{\omega}{(\omega^2 - \omega_p^2)^{1/2}} \equiv -iZ_0 \frac{\omega}{(\omega_p^2 - \omega^2)^{1/2}}. \quad (7.70)$$

The first of these forms is more convenient in the case $\omega > \omega_p$, when the wave vector k_+ and the wave impedance Z_+ of the plasma are real, so that a part of the incident wave does propagate into it. Plugging this expression into the latter of Eqs. (68), we see that T is real as well:

$$T = \frac{2\omega}{\omega + (\omega^2 - \omega_p^2)^{1/2}}. \quad (7.71)$$

Note that according to this formula, and somewhat counter-intuitively, $T > 1$ for any frequency (above ω_p), inviting the question: how can the transmitted wave be more intensive than the incident one that has induced it? For answering this question, we need to compare the powers (rather than the electric field amplitudes) of these two waves, i.e. their average Poynting vectors (42):

$$\overline{S_{\text{incident}}} = \frac{|E_\omega|^2}{2Z_0}, \quad \overline{S}_+ = \frac{|TE_\omega|^2}{2Z_+} = \frac{|E_\omega|^2}{2Z_0} \frac{4\omega(\omega^2 - \omega_p^2)^{1/2}}{\left[\omega + (\omega^2 - \omega_p^2)^{1/2}\right]^2}. \quad (7.72)$$

The ratio of these two values³¹ is always below 1 (and tends to zero at $\omega \rightarrow \omega_p$), so that only a fraction of the incident wave power may be transmitted. Hence the result $T > 1$ may be interpreted as follows: an interface between two media may be an *impedance transformer*: it can never transmit more *power* than the incident wave provides, i.e. can only decrease the product $S = EH$, but since the ratio $Z = E/H$ changes at the interface, the amplitude of *one of the fields* may increase at the transmission.

Now let us proceed to case $\omega < \omega_p$ when the waves cannot propagate in the plasma. In this case, the second of the expressions (70) is more convenient, because it immediately shows that Z_+ is purely

³¹ This ratio is sometimes also called the “wave transmission coefficient”, but to avoid its confusion with the T defined by Eq. (64), it is better to call it the *power transmission coefficient*.

imaginary, while $Z_- = Z_0$ is purely real. This means that $(Z_{+-} Z_-) = (Z_+ + Z_-)^*$, i.e. according to the first of Eqs. (68), $|R| = 1$, so that the reflection is total, i.e. no incident power (on average) is transferred into the plasma – as was already discussed in Sec. 2. However, the complex R has a finite argument,

$$\varphi \equiv \arg R = 2 \arg(Z_+ - Z_0) = -2 \tan^{-1} \frac{\omega}{(\omega_p^2 - \omega^2)^{1/2}}, \quad (7.73)$$

and hence provides a finite spatial shift (69) of the standing wave toward the plasma surface:

$$\delta_- = \frac{\varphi - \pi}{2k_0} = \frac{c}{\omega} \tan^{-1} \frac{\omega}{(\omega_p^2 - \omega^2)^{1/2}}. \quad (7.74)$$

On the other hand, we already know from Eq. (40) that the solution at $z > 0$ is exponential, with the decay length δ described by Eq. (39). Calculating, from the coefficient T , the exact coefficient before this exponent, it is straightforward to verify that the electric and magnetic fields are indeed continuous at the interface, completing the pattern shown with red lines in Fig. 8. This wave penetration into a fully reflecting material may be experimentally observed, for example, by thinning its sample. Even without solving this problem exactly, it is evident that if the sample's thickness d becomes comparable to δ , a part of the exponential “tail” of the field reaches its second interface, and induces a propagating wave. This is a classical-electromagnetic analog of the quantum-mechanical tunneling through a potential barrier.³²

Note that at low frequencies, both δ_- and δ tend to the same frequency-independent value,

$$\delta, \delta_- \rightarrow \frac{c}{\omega_p} = \left(\frac{c^2 \epsilon_0 m_e}{ne^2} \right)^{1/2} = \left(\frac{m_e}{\mu_0 ne^2} \right)^{1/2}, \quad \text{at } \frac{\omega}{\omega_p} \rightarrow 0, \quad (7.75)$$

which is just the field penetration depth (6.44) calculated for a perfect conductor model (assuming $m = m_e$ and $\mu = \mu_0$) in the quasistatic limit. This is natural, because the condition $\omega \ll \omega_p$ may be recast as $\lambda_0 \equiv 2\pi c/\omega \gg 2\pi c/\omega_p \equiv 2\pi\delta$, i.e. as the quasistatic approximation's validity condition.

(ii) Now let us consider electromagnetic wave's reflection from an Ohmic, non-magnetic conductor. In the simplest low-frequency limit, when $\omega\tau$ is much less than 1, the conductor may be described by a frequency-independent conductivity σ .³³ According to Eq. (46), in this case we can take

$$Z_+ = \left(\frac{\mu_0}{\epsilon_{\text{opt}}(\omega) + i\sigma/\omega} \right)^{1/2}. \quad (7.76)$$

With this substitution, Eqs. (68) immediately give us all the results of interest. In particular, in the most important quasistatic limit when $\delta_s \equiv (2/\mu_0\sigma\omega)^{1/2} \ll \lambda_0 \equiv 2\pi c/\omega$, i.e. $\sigma/\omega \gg \epsilon_0 \sim \epsilon_{\text{opt}}$, the conductor's impedance is low:

$$Z_+ \approx \left(\frac{\mu_0 \omega}{i\sigma} \right)^{1/2} \equiv \pi \left(\frac{2}{i} \right)^{1/2} \frac{\delta_s}{\lambda_0} Z_0, \quad \text{i.e. } \left| \frac{Z_+}{Z_0} \right| \ll 1. \quad (7.77)$$

³² See, e.g., QM Sec. 2.3.

³³ In a typical metal, $\tau \sim 10^{-13}$ s, so that this approximation works well up to $\omega \sim 10^{13}$ s⁻¹, i.e. up to the far-infrared frequencies.

This impedance is complex, and hence some fraction ℓ of the incident wave is absorbed by the conductor. The fraction may be found as the ratio of the dissipated power (either calculated, as was done above, from Eqs. (68), or just taken from Eq. (6.36), with the magnetic field amplitude $|H_\omega| = 2|E_\omega|/Z_0$ – see Eq. (62)) to the incident wave's power given by the first of Eqs. (72). The result,

$$\ell = \frac{2\omega\delta_s}{c} \equiv 4\pi \frac{\delta_s}{\lambda_0} \ll 1. \quad (7.78)$$

is used for crude estimates of the energy dissipation in metallic-wall waveguides and resonators. It shows that to keep the energy losses low, the characteristic size of such systems (which gives a scale of the free-space wavelengths λ_0 at which they are used) should be much larger than δ_s . A more detailed theory of these structures, and of the energy loss in them, will be discussed later in this chapter.

7.4. Refraction

Now let us consider the effects arising at a plane interface between two uniform media when the wave's incidence angle θ (Fig. 10) is arbitrary rather than equal to zero as in our previous analysis, for the simplest case of fully transparent media, with real $\varepsilon_\pm(\omega)$ and $\mu_\pm(\omega)$. (For the sake of notation simplicity, in most formulas below, the argument of these functions will be dropped, i.e. just implied.)

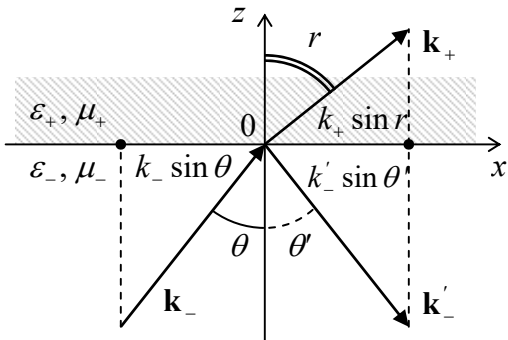


Fig. 7.10. Plane wave's reflection, transmission, and refraction at a plane interface. The plane of the drawing is selected to contain all three wave vectors: \mathbf{k}_+ , \mathbf{k}_- , and \mathbf{k}'_- .

In contrast with the case of normal incidence, here the wave vectors \mathbf{k}_- , \mathbf{k}'_- , and \mathbf{k}_+ of the three components (incident, reflected, and transmitted) waves may have different directions. (Such change of the transmitted wave's direction is called *refraction*.) Hence let us start our analysis by writing a general expression for a single plane, monochromatic wave for the case when its wave vector \mathbf{k} has all three Cartesian components, rather than one. An evident generalization of Eq. (11) for this case is

$$f(\mathbf{r}, t) = \text{Re} \left[f_\omega e^{i(k_x x + k_y y + k_z z) - \omega t} \right] \equiv \text{Re} \left[f_\omega e^{i(\mathbf{k} \cdot \mathbf{r} - \omega t)} \right]. \quad (7.79)$$

This expression enables a ready analysis of “kinematic” relations, which are independent of the media impedances. Indeed, it is sufficient to notice that to satisfy *any* linear, homogeneous boundary conditions at the interface ($z = 0$), all partial plane waves must have the same temporal and spatial dependence on this plane. Hence if we select the x - z plane so that the vector \mathbf{k}_- lies in it, then $(k_-)_y = 0$, and \mathbf{k}_+ and \mathbf{k}'_- cannot have any y -component either, i.e. all three wave vectors lie in the same plane –

that is selected as the plane of the drawing in Fig. 10. Moreover, because of the same reason, their x -components should be equal:

$$k_- \sin \theta = k'_- \sin \theta' = k_+ \sin r. \quad (7.80)$$

From here we immediately get two well-known laws: of reflection

Reflection angle

$$\theta' = \theta, \quad (7.81)$$

and of refraction:³⁴

Snell law

$$\frac{\sin r}{\sin \theta} = \frac{k_-}{k_+}. \quad (7.82)$$

In this form, the laws are valid for plane waves of any nature. In optics, the Snell law (82) is frequently represented in the form

$$\frac{\sin r}{\sin \theta} = \frac{n_-}{n_+}, \quad (7.83)$$

where n_{\pm} is the *index of refraction* (also called the “refractive index”) of the corresponding medium, defined as its wave number normalized to that of the free space (at the particular wave’s frequency):

Index of refraction

$$n_{\pm} \equiv \frac{k_{\pm}}{k_0} \equiv \left(\frac{\epsilon_{\pm} \mu_{\pm}}{\epsilon_0 \mu_0} \right)^{1/2}. \quad (7.84)$$

Perhaps the most famous corollary of the Snell law is that if a wave propagates from a medium with a higher index of refraction to that with a lower one (i.e. if $n_- > n_+$ in Fig. 10), for example from water to air, there is always a certain *critical* value θ_c of the incidence angle,

Critical angle

$$\theta_c = \sin^{-1} \frac{n_+}{n_-} \equiv \sin^{-1} \left(\frac{\epsilon_+ \mu_+}{\epsilon_- \mu_-} \right)^{1/2}, \quad (7.85)$$

at which the refraction angle r (see Fig. 10 again) reaches $\pi/2$. At a larger θ , i.e. within the range $\theta_c < \theta < \pi/2$, the boundary conditions (80) cannot be satisfied by a refracted wave with a real wave vector, so that the wave experiences the so-called *total internal reflection*. This effect is very important for practice because it means that dielectric surfaces may be used as optical mirrors, in particular in optical fibers – to be discussed in more detail in Sec. 7 below. This is very fortunate for telecommunication technology because light’s reflection from metals is rather imperfect. Indeed, according to Eq. (78), in the optical range ($\lambda_0 \sim 0.5 \text{ } \mu\text{m}$, i.e. $\omega \sim 10^{15} \text{ s}^{-1}$), even the best conductors (with $\sigma \sim 6 \times 10^8 \text{ S/m}$ and hence the normal skin depth $\delta_s \sim 1.5 \text{ nm}$) provide power loss of at least a few percent at each reflection.

Note, however, that even within the range $\theta_c < \theta < \pi/2$, the field at $z > 0$ is not identically equal to zero: it penetrates into the lower- n media by a distance of the order of λ_0 , exponentially decaying inside it, just as it does at the normal incidence – see Fig. 8. However, at $\theta \neq 0$ the penetrating field still propagates, with the wave number (80), along the interface. Such a field, exponentially dropping in one direction but still propagating as a wave in another direction, is commonly called the *evanescent wave*.

³⁴ The latter relation is traditionally called the *Snell law*, after a 17th-century astronomer Willebrord Snellius, but it has been traced all the way back to a circa 984 work by Abu Saad al-Ala ibn Sahl. (Claudius Ptolemy who performed pioneering experiments on light refraction in the 2nd century AD, was just one step from this result.)

One more remark: just as at the normal incidence, the field's penetration into another medium causes a phase shift of the reflected wave – see, e.g., Eq. (69) and its discussion. A new feature of this phase shift, arising at $\theta \neq 0$, is that it also has a component parallel to the interface – the so-called *Goos-Hänchen effect*. In geometric optics, this effect leads to an image shift (relative to that its position in a perfect mirror) with components both normal and parallel to the interface.

Now let us carry out an analysis of “dynamic” relations that determine amplitudes of the refracted and reflected waves. For this, we need to write explicitly the boundary conditions at the interface (i.e. the plane $z = 0$). Since now the electric and/or magnetic fields may have components normal to the plane, in addition to the continuity of their tangential components, which were repeatedly discussed above,

$$E_{x,y}|_{z=-0} = E_{x,y}|_{z=+0}, \quad H_{x,y}|_{z=-0} = H_{x,y}|_{z=+0}, \quad (7.86)$$

we also need relations for the normal components. As it follows from the homogeneous macroscopic Maxwell equations (6.99b), they are also the same as in statics, i.e. $D_n = \text{const}$, and $B_n = \text{const}$, for our coordinate choice (Fig. 10) giving

$$\varepsilon_- E_z|_{z=-0} = \varepsilon_+ E_z|_{z=+0}, \quad \mu_- H_z|_{z=-0} = \mu_+ H_z|_{z=+0}. \quad (7.87)$$

The expressions of these components via the amplitudes E_ω , RE_ω , and TE_ω of the incident, reflected, and transmitted waves depend on the incident wave's polarization. For example, for a linearly-polarized wave with the electric field vector *normal* to the plane of incidence, i.e. *parallel* to the interface plane, the reflected and refracted waves are similarly polarized – see Fig. 11a.

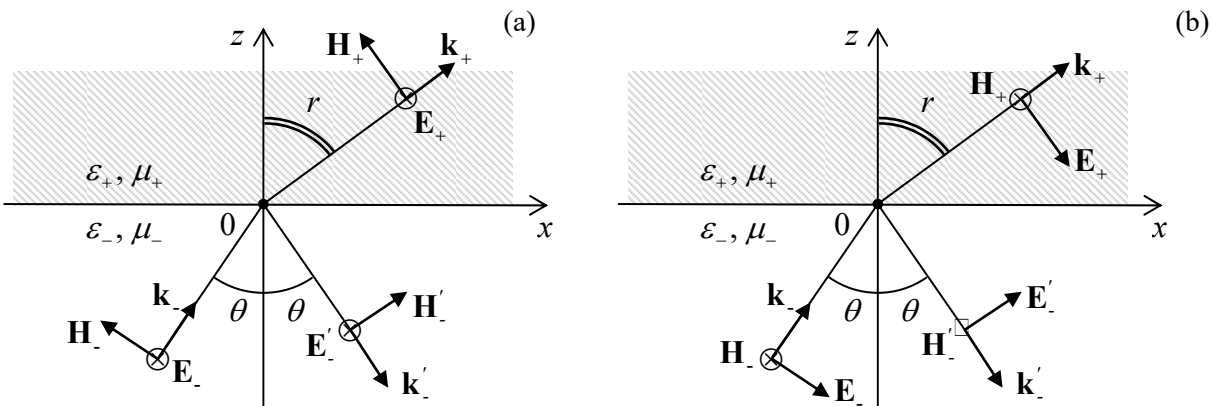


Fig. 7.11. Reflection and refraction at two different linear polarizations of the incident wave.

As a result, all E_z are equal to zero (so that the first of Eqs. (87) is inconsequential), while the tangential components of the electric field are equal to their full amplitudes, just as at the normal incidence, so we still can use Eqs. (64) expressing these components via the coefficients R and T . However, at $\theta \neq 0$ the magnetic fields have not only tangential components

$$H_x|_{z=-0} = \text{Re} \left[\frac{E_\omega}{Z_-} (1-R) \cos \theta e^{-i\omega t} \right], \quad H_x|_{z=+0} = \text{Re} \left[\frac{E_\omega}{Z_+} T \cos r e^{-i\omega t} \right], \quad (7.88)$$

but also normal components (see Fig. 11a):

$$H_z|_{z=-0} = \operatorname{Re} \left[\frac{E_\omega}{Z_-} (1+R) \sin \theta e^{-i\omega t} \right], \quad H_z|_{z=+0} = \operatorname{Re} \left[\frac{E_\omega}{Z_+} T \sin r e^{-i\omega t} \right]. \quad (7.89)$$

Plugging these expressions into the boundary conditions expressed by Eqs. (86) (in this case, for the y -components only) and the second of Eqs. (87), we get *three* equations for *two* unknown coefficients R and T . However, two of these equations duplicate each other because of the Snell law, and we get just two independent equations,

$$1+R=T, \quad \frac{1}{Z_-}(1-R)\cos\theta=\frac{1}{Z_+}T\cos r, \quad (7.90)$$

which are a very natural generalization of Eqs. (67), with the replacements $Z_- \rightarrow Z_- \cos r$, $Z_+ \rightarrow Z_+ \cos \theta$. As a result, we can immediately use Eq. (68) to write the solution of the system (90):³⁵

$$R = \frac{Z_+ \cos \theta - Z_- \cos r}{Z_+ \cos \theta + Z_- \cos r}, \quad T = \frac{2Z_+ \cos \theta}{Z_+ \cos \theta + Z_- \cos r}. \quad (7.91a)$$

If we want to express these coefficients via the angle of incidence alone, we should use the Snell law (82) to eliminate the angle r , getting frequently quoted bulkier expressions:

$$R = \frac{Z_+ \cos \theta - Z_- [1 - (k_-/k_+)^2 \sin^2 \theta]^{1/2}}{Z_+ \cos \theta + Z_- [1 - (k_-/k_+)^2 \sin^2 \theta]^{1/2}}, \quad T = \frac{2Z_+ \cos \theta}{Z_+ \cos \theta + Z_- [1 - (k_-/k_+)^2 \sin^2 \theta]^{1/2}}. \quad (7.91b)$$

However, conceptually it is preferable to use the kinematic relation (82) and the dynamic relations (91a) separately, because Eq. (91b) obscures the very important physical fact that the ratio of k_\pm , i.e. of the wave velocities of the two media, is only involved in the Snell law, while Eqs. (91b) explicitly include only the wave impedances – just as in the case of normal incidence.

In the opposite case of the linear polarization of the electric field within the plane of incidence (Fig. 11b), it is the magnetic field that does not have a normal component, so it is now the second of Eqs. (87) that does not participate in the solution. However, now the electric fields in the two media have not only tangential components,

$$E_x|_{z=-0} = \operatorname{Re} [E_\omega (1+R) \cos \theta e^{-i\omega t}], \quad E_x|_{z=+0} = \operatorname{Re} [E_\omega T \cos r e^{-i\omega t}], \quad (7.92)$$

but also normal components (Fig. 11b):

$$E_z|_{z=-0} = E_\omega (-1+R) \sin \theta, \quad E_z|_{z=+0} = -E_\omega T \sin r. \quad (7.93)$$

As a result, instead of Eqs. (90), the reflection and transmission coefficients are related as

$$(1+R)\cos\theta = T\cos r, \quad \frac{1}{Z_-}(1-R) = \frac{1}{Z_+}T. \quad (7.94)$$

Again, the solution of this system may be immediately written using the analogy with Eq. (67):

³⁵ Note that we may calculate the reflection and transmission coefficients R' and T' for the wave traveling in the opposite direction just by making the following parameter swaps: $Z_+ \leftrightarrow Z_-$ and $\theta \leftrightarrow r$, and that the resulting coefficients satisfy the following *Stokes relations*: $R' = -R$, and $R'^2 + TT' = 1$, for any Z_\pm .

$$R = \frac{Z_+ \cos r - Z_- \cos \theta}{Z_+ \cos r + Z_- \cos \theta}, \quad T = \frac{2Z_+ \cos \theta}{Z_+ \cos r + Z_- \cos \theta}, \quad (7.95a)$$

or, alternatively, using the Snell law, in a more bulky form:

$$R = \frac{Z_+ [1 - (k_- / k_+)^2 \sin^2 \theta]^{1/2} - Z_- \cos \theta}{Z_+ [1 - (k_- / k_+)^2 \sin^2 \theta]^{1/2} + Z_- \cos \theta}, \quad T = \frac{2Z_+ \cos \theta}{Z_+ [1 - (k_- / k_+)^2 \sin^2 \theta]^{1/2} + Z_- \cos \theta}. \quad (7.95b)$$

For the particular case $\mu_+ = \mu_- = \mu_0$, when $Z_+/Z_- = (\varepsilon_+/\varepsilon_-)^{1/2} = k_-/k_+ = n_-/n_+$ (which is approximately correct for traditional optical media), Eqs. (91b) and (95b) are called the *Fresnel formulas*.³⁶ Most textbooks are quick to point out that there is a major difference between them: while for the electric field polarization within the plane of incidence (Fig. 11b), the reflected wave's amplitude (proportional to the coefficient R) turns to zero³⁷ at a special value of θ (called the *Brewster angle*):³⁸

$$\theta_B = \tan^{-1} \frac{n_+}{n_-}, \quad (7.96)$$

while there is no such angle in the opposite case (shown in Fig. 11a). However, note that this statement, as well as Eq. (96), is true only for the case $\mu_+ = \mu_-$. In the general case of different ε and μ , Eqs. (91) and (95) show that the reflected wave vanishes at $\theta = \theta_B$ with

$$\tan^2 \theta_B = \frac{\varepsilon_- \mu_+ - \varepsilon_+ \mu_-}{\varepsilon_+ \mu_+ - \varepsilon_- \mu_-} \times \begin{cases} (\mu_+ / \mu_-), & \text{for } \mathbf{E} \perp \mathbf{n}_z \text{ (Fig. 11a),} \\ (-\varepsilon_+ / \varepsilon_-), & \text{for } \mathbf{H} \perp \mathbf{n}_z \text{ (Fig. 11b).} \end{cases} \quad (7.97)$$

Brewster angle

Note the natural $\varepsilon \leftrightarrow \mu$ symmetry of these relations, resulting from the $\mathbf{E} \leftrightarrow \mathbf{H}$ symmetry for these two polarization cases (Fig. 11). These formulas also show that for any set of parameters of the two media (with $\varepsilon_{\pm}, \mu_{\pm} > 0$), $\tan^2 \theta_B$ is positive (and hence a real Brewster angle θ_B exists) only for one of these two polarizations. In particular, if the interface is due to the change of μ alone (i.e. if $\varepsilon_+ = \varepsilon_-$), the first of Eqs. (97) is reduced to the simple form (96) again, while for the polarization shown in Fig. 11b, there is no Brewster angle, i.e. the reflected wave has a non-zero amplitude for any θ .

Such an account of both media parameters, ε and μ , on an equal footing is necessary to describe several interesting effects. The first of them is the so-called *negative refraction*.³⁹ As was shown in Sec.

³⁶ Named after Augustin-Jean Fresnel (1788-1827), one of the wave optics pioneers, who is credited, among many other contributions (see, in particular, discussions in Ch. 8), for the concept of light as a purely transverse wave.

³⁷ This effect is used in practice to obtain linearly polarized light, with the electric field vector perpendicular to the plane of incidence, from the natural light with its random polarization. An even more widespread application of the effect is a partial reduction of undesirable glare from wet pavement (for the water/air interface, $n_+/n_- \approx 1.33$, giving $\theta_B \approx 50^\circ$) by covering glasses and car headlights with thin vertically-polarizing layers.

³⁸ A very simple interpretation of Eq. (96) is based on the fact that, together with the Snell law (82), it gives $r + \theta = \pi/2$. As a result, the vector \mathbf{E}_+ is parallel to the vector \mathbf{k}'_- , and hence the oscillating electric dipoles of the medium do not have the Cartesian component that could induce the transverse electric field \mathbf{E}'_- of the potential reflected wave.

³⁹ Despite some important background theoretical work by A. Schuster (1904), L. Mandelstam (1945), D. Sivikhin (1957), and especially V. Veselago (1966-67), the negative refractivity effects became a subject of intensive scientific research and engineering development only in the 2000s.

2, in a medium with electric-field-driven resonances, the function $\epsilon(\omega)$ may be almost real and negative, at least within limited frequency intervals – see, in particular, Eq. (34) and Fig. 5. As has already been discussed, if, at these frequencies, the function $\mu(\omega)$ is real and positive, then $k^2(\omega) = \omega^2 \epsilon(\omega) \mu(\omega) < 0$, and k may be represented as i/δ with a real δ , meaning the exponential field decay into the medium. However, let us consider the case when both $\epsilon(\omega) < 0$ and $\mu(\omega) < 0$ at a certain frequency. (This is possible in a medium with both **E**-driven and **H**-driven resonances, at a proper choice of their resonance frequencies.) Since in this case $k^2(\omega) = \omega^2 \epsilon(\omega) \mu(\omega) > 0$, the wave vector is real, so that Eq. (79) describes a traveling wave, and one could think that there is nothing new in this case. Not so!

First of all, for a sinusoidal plane wave (79), the operator ∇ is equivalent to the multiplication by $i\mathbf{k}$. As the Maxwell equations (2a) show, this means that at a fixed direction of vectors **E** and **k**, the simultaneous reversal of signs of ϵ and μ means the reversal of the direction of the vector **H**. Namely, if both ϵ and μ are positive, these equations are satisfied with mutually orthogonal vectors $\{\mathbf{E}, \mathbf{H}, \mathbf{k}\}$ forming the usual, *right-hand* system (see Fig. 1 and Fig. 12a), the name stemming from the popular “right-hand rule” used to determine the vector product’s direction. However, if both ϵ and μ are negative, the vectors form a *left-hand* system – see Fig. 12b. (Due to this fact, the media with $\epsilon < 0$ and $\mu < 0$ are frequently called the *left-handed materials*, LHM for short.) According to the basic relation (6.114), which does not involve media parameters, this means that for a plane wave in a left-hand material, the Poynting vector **S** = $\mathbf{E} \times \mathbf{H}$, i.e. the energy flow, is directed *opposite* to the wave vector **k**.

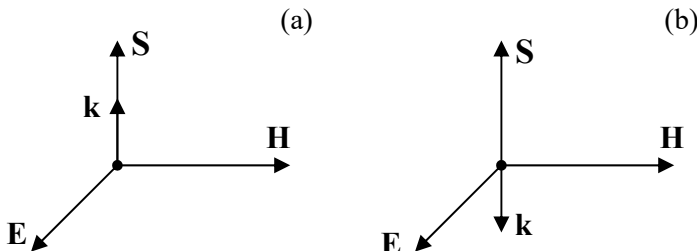


Fig. 7.12. Directions of the main vectors of a plane wave inside a medium with (a) positive and (b) negative values of ϵ and μ .

This fact may look strange but is in no contradiction with any fundamental principle. Let me remind you that, according to the definition of the vector **k**, its direction shows the direction of the *phase* velocity $v_{ph} = \omega/k$ of a sinusoidal (and hence infinitely long) wave, which cannot be used, for example, for signaling. Such signaling (by sending wave packets – see Fig. 13) is possible only with the *group* velocity $v_{gr} = d\omega/dk$. This velocity in left-hand materials is always directed (as in the right-hand materials) along the vector **S**, i.e. along the wave’s energy flow.

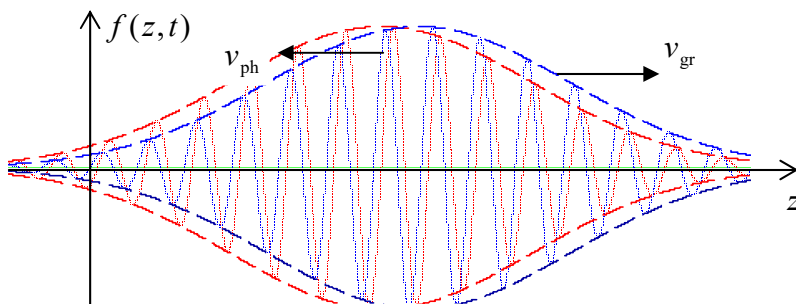


Fig. 7.13. An example of a wave packet moving along axis z with a negative phase velocity, but positive group velocity. Blue lines show a packet’s snapshot a short time interval after the first snapshot (red lines).

Perhaps the most fascinating effect possible with left-hand materials is the wave refraction at their interfaces with the usual, right-handed materials – first predicted by V. Veselago in 1960. Consider the example shown in Fig. 14a. In the incident wave, arriving from a usual material, the directions of the vectors \mathbf{k}_- and \mathbf{S}_- coincide, and so they are in the reflected wave with vectors \mathbf{k}'_- and \mathbf{S}'_- . This means that the electric and magnetic fields in the interface plane ($z = 0$) are, at our choice of the coordinate axes, proportional to $\exp\{ik_x x\}$, with a positive component $k_x = k_- \cos \theta$. To satisfy any linear boundary conditions, the refracted wave, propagating into the left-handed material, has to match that dependence, i.e. have a positive x -component of its wave vector \mathbf{k}_+ . But in this medium, this vector has to be antiparallel to the vector \mathbf{S}_+ , which in turn should be directed out of the interface, because it represents the power flow from the interface into the material's bulk. These conditions cannot be reconciled by the refracted wave propagating along the usual Snell-law direction (shown with the dashed line in Fig. 13a), but are all satisfied at refraction in the direction given by Snell's angle with the opposite sign. (Hence the term “negative refraction”).⁴⁰

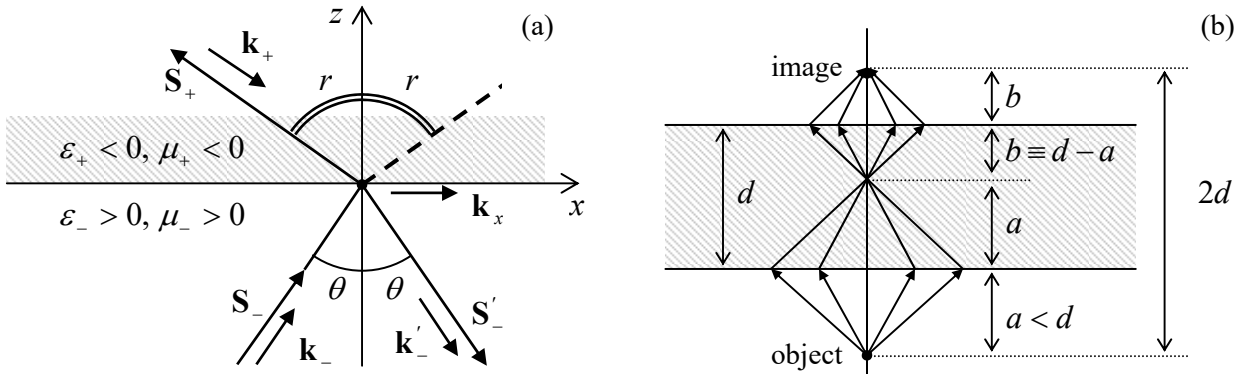


Fig. 7.14. Negative refraction: (a) waves at the interface between media with positive and negative values of $\epsilon\mu$, and (b) the hypothetical *perfect lens*: a parallel plate made of a material with $\epsilon = -\epsilon_0$ and $\mu = -\mu_0$.

In order to understand how unusual the results of the negative refraction may be, let us consider a parallel slab of thickness d , made of a hypothetical left-handed material with exactly selected values $\epsilon = -\epsilon_0$, and $\mu = -\mu_0$ (see Fig. 14b). For such a material, placed in free space, the refraction angle $r = -\theta$, so that the rays from a point source, located in free space at a distance $a < d$ from the slab's surface, propagate as shown on that panel, i.e. all meet again at the distance a beyond the surface, and then continue to propagate to the second surface of the slab. Repeating our discussion for this surface, we see that a point's image is also formed beyond the slab, at distance $2a + 2b = 2a + 2(d - a) = 2d$ from the object.

Superficially, this system looks like a usual lens, but the well-known lens formula, which relates a and b with the focal length f , is *not* satisfied. (In particular, a parallel beam is *not* focused into a point at any finite distance.) As an additional difference from the usual lens, the system shown in Fig. 14b *does not reflect* any part of the incident light. Indeed, it is straightforward to check that for all the above formulas for R and T to be valid, the sign of the wave impedance Z in left-handed materials has to be kept positive. Thus, for our particular choice of parameters ($\epsilon = -\epsilon_0$, $\mu = -\mu_0$), Eqs. (91a) and (95a) are

⁴⁰ In some publications inspired by this fact, the left-hand materials are prescribed a negative index of refraction n . However, this prescription should be treated with care. For example, it complies with the first form of Eq. (84), but not its second form, and the sign of n , in contrast to that of the wave vector \mathbf{k} , is a matter of convention.

valid with $Z_+ = Z_- = Z_0$ and $\cos r = \cos \theta = 1$, giving $R = 0$ for any linear polarization, and hence for any other wave polarization – circular, elliptic, natural, etc.

The perfect lens suggestion has triggered a wave of efforts to implement left-hand materials experimentally. (Attempts to find such materials in nature have failed so far.) Most progress in this direction has been achieved using the so-called *metamaterials*, which are essentially quasi-periodic arrays of specially designed electromagnetic resonators, ideally with high density $n \gg \lambda^3$. For example, Fig. 15 shows the metamaterial that was used for the first demonstration of negative refractivity in the microwave region – for ~ 10 -GHz waves.⁴¹ It combines straight strips of a metallic film, working as lumped resonators with a large electric dipole moment (and hence strongly coupled to the wave's electric field \mathbf{E}), and several almost-closed film loops (so-called *split rings*), working as lumped resonators with large magnetic dipole moments, strongly coupled to the field \mathbf{H} . The negative refractivity is achieved by designing the resonance frequencies close to each other. More recently, metamaterials with negative refractivity were demonstrated in the optical range as well,⁴² although to the best of my knowledge, their relatively large absorption still prevents practical applications.

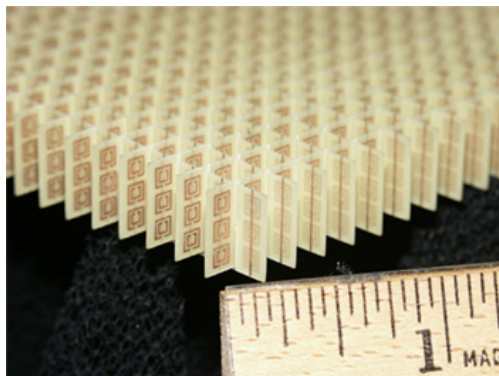


Fig. 7.15. An artificial left-hand material providing negative refraction at microwave frequencies ~ 10 GHz. The original by Jeffrey D. Wilson (in the public domain) is available at <https://en.wikipedia.org/wiki/Metamaterial>.

This progress has stimulated the development of other potential uses of metamaterials (not necessarily the left-handed ones), in particular, designs of nonuniform systems with handcrafted distributions $\epsilon(\mathbf{r}, \omega)$ and $\mu(\mathbf{r}, \omega)$ that may provide electromagnetic wave propagation along the desired paths, e.g., around a certain region of space, making it virtually invisible for an external observer – so far, within very limited frequency ranges.⁴³

As was mentioned in Sec. 5.5, another way to reach negative values of $\mu(\omega)$ is to place a ferromagnetic material into such an external dc magnetic field that the frequency ω_r of the ferromagnetic resonance is somewhat lower than ω . If thin layers of such a material (e.g., nickel) are interleaved with layers of a non-magnetic good conductor (such as copper), the average value of $\mu(\omega)$ of the resulting metamaterial may be positive but substantially below μ_0 . According to Eq. (6.33), the skin-depth δ_s of such a material may be larger than that of the good conductor alone, enforcing a more uniform distribution of the ac current flowing along the layers, and hence making the energy losses lower than in the good conductor alone. This effect may be useful, in particular, for electronic circuit interconnects.⁴⁴

⁴¹ R. Shelby *et al.*, *Science* **292**, 77 (2001); J. Wilson and Z. Schwartz, *Appl. Phys. Lett.* **86**, 021113 (2005).

⁴² See, e.g., J. Valentine *et al.*, *Nature* **455**, 376 (2008).

⁴³ For a review of such “invisibility cloaks”, see, e.g., B. Wood, *Comptes Rendus Physique* **10**, 379 (2009).

⁴⁴ See, for example, N. Sato *et al.*, *J. Appl. Phys.* **111**, 07A501 (2012), and references therein.

7.5. Transmission lines: TEM waves

So far, we have analyzed plane electromagnetic waves, implying that their cross-section is infinite – evidently, an unrealistic assumption. The cross-section may be limited, still sustaining wave propagation, using *wave transmission lines*:⁴⁵ long, uniform structures made of either good conductors or dielectrics. Let us first discuss the first option, using the following simplifying assumptions:

(i) the structure is a cylinder (not necessarily with a round cross-section, see Fig. 16) filled with a usual (right-handed), uniform dielectric material with negligible energy losses ($\epsilon'' = \mu'' = 0$), and

(ii) the wave attenuation due to the skin effect is also negligibly low. (As Eq. (78) indicates, for that the characteristic size a of the line's cross-section has to be much larger than the skin-depth δ_s of its wall material. The energy dissipation effects will be analyzed in Sec. 9 below.)

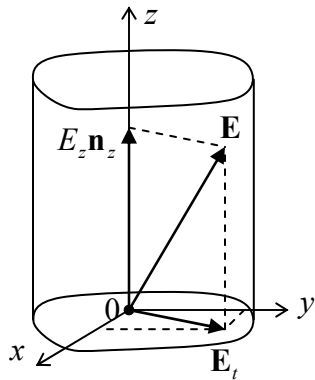


Fig. 7.16. Electric field's decomposition in a transmission line (in particular, a waveguide).

With such exclusion of energy losses, we may look for a particular solution of the macroscopic Maxwell equations in the form of a monochromatic wave traveling along the line:

$$\mathbf{E}(\mathbf{r}, t) = \text{Re}[\mathbf{E}_\omega(x, y) e^{i(k_z z - \omega t)}], \quad \mathbf{H}(\mathbf{r}, t) = \text{Re}[\mathbf{H}_\omega(x, y) e^{i(k_z z - \omega t)}], \quad (7.98)$$

with real k_z , where the z -axis is directed along the transmission line – see Fig. 16. Note that this form allows a substantial coordinate dependence of the electric and magnetic field within the plane $[x, y]$ of the transmission line's cross-section, as well as nonvanishing longitudinal components E_z and/or H_z of the fields, so that the solution (98) is substantially more general than the plane waves discussed above. We will see in a minute that as a result, the parameter k_z may be very much different from its plane-wave value (13), $k \equiv \omega(\epsilon\mu)^{1/2}$, in the same material, at the same frequency.

In order to describe these effects quantitatively, let us decompose the complex amplitudes of the wave's fields into their longitudinal and transverse components (Fig. 16):⁴⁶

$$\mathbf{E}_\omega = E_z \mathbf{n}_z + \mathbf{E}_t, \quad \mathbf{H}_\omega = H_z \mathbf{n}_z + \mathbf{H}_t. \quad (7.99)$$

⁴⁵ Another popular term is the *waveguide*, but it is typically reserved for the transmission lines with singly-connected cross-sections, to be analyzed in the next section. The first structure for guiding waves was proposed by J. J. Thomson in 1893, and experimentally tested by O. Lodge in 1894.

⁴⁶ For the notation simplicity, I am dropping index ω in the complex amplitudes of the field components, and also have dropped the argument ω in k_z and Z , even though these parameters may depend on the wave's frequency rather substantially – see below.

Plugging Eqs. (98)-(99) into the source-free Maxwell equations (2), and requiring the longitudinal and transverse components to be balanced separately, we get

$$\begin{aligned} ik_z \mathbf{n}_z \times \mathbf{E}_t - i\omega\mu \mathbf{H}_t &= -\nabla_t \times (E_z \mathbf{n}_z), & ik_z \mathbf{n}_z \times \mathbf{H}_t + i\omega\epsilon \mathbf{E}_t &= -\nabla_t \times (H_z \mathbf{n}_z), \\ \nabla_t \times \mathbf{E}_t &= i\omega\mu H_z \mathbf{n}_z, & \nabla_t \times \mathbf{H}_t &= -i\epsilon\omega E_z \mathbf{n}_z, \\ \nabla_t \cdot \mathbf{E}_t &= -ik_z E_z, & \nabla_t \cdot \mathbf{H}_t &= -ik_z H_z. \end{aligned} \quad (7.100)$$

where ∇_t is the 2D del operator acting in the transverse plane $[x, y]$ only, i.e. the usual ∇ , but with $\partial/\partial z = 0$. The system (100) looks even bulkier than the original equations (2), but it is much simpler for analysis. Indeed, by eliminating the transverse components from these equations (or, even simpler, just by plugging Eq. (99) into Eqs. (3) and keeping only their z -components), we get a pair of self-consistent equations for the longitudinal components of the fields,⁴⁷

$$\boxed{(\nabla_t^2 + k_t^2) E_z = 0, \quad (\nabla_t^2 + k_t^2) H_z = 0}, \quad (7.101)$$

where k is still defined by Eq. (13), $k \equiv (\epsilon\mu)^{1/2}\omega$, while

$$\boxed{k_t^2 \equiv k^2 - k_z^2 = \omega^2 \epsilon\mu - k_z^2}. \quad (7.102)$$

After the distributions $E_z(x, y)$ and $H_z(x, y)$ have been found from these equations, they provide right-hand sides for the rather simple, closed system of equations (100) for the transverse components of field vectors. Moreover, as we will see below, each of the following three types of solutions:

- (i) with $E_z = 0$ and $H_z = 0$ (called the *transverse electromagnetic*, or *TEM waves*),
- (ii) with $E_z = 0$, but $H_z \neq 0$ (called either the *TE waves* or, more frequently, *H-modes*), and
- (iii) with $E_z \neq 0$, but $H_z = 0$ (the so-called *TM waves* or *E-modes*),

has its own dispersion law and hence its own wave propagation velocity; as a result, these *modes* (i.e. the field distribution patterns) may be considered separately.

In the balance of this section, we will focus on the simplest, TEM waves (i), with *no longitudinal components* of either field. For them, the top two equations of the system (100) immediately give Eqs. (6) and (13), and $k_z = k$. In plain English, this means that $\mathbf{E} = \mathbf{E}_t$ and $\mathbf{H} = \mathbf{H}_t$ are proportional to each other and are mutually perpendicular (just as in the plane wave) at each point of the cross-section, and that the TEM wave's impedance $Z \equiv E/H$ and dispersion law $\omega(k)$, and hence the propagation speed, are the same as in a plane wave in the same material. In particular, if ϵ and μ are frequency-independent within a certain frequency range, the dispersion law within this range is linear, $\omega = k/(\epsilon\mu)^{1/2}$, and the wave's speed does not depend on its frequency. For practical applications to telecommunications, this is a very important advantage of the TEM waves over their TM and TE counterparts – to be discussed in the next sections.

Unfortunately for practice, such waves cannot propagate in every transmission line. To show this, let us have a look at the two last lines of Eqs. (100). For the TEM waves ($E_z = 0, H_z = 0, k_z = k$), they are reduced to merely

⁴⁷ The wave equation represented in the form (101), even with the 3D Laplace operator, is called the *Helmholtz equation*, named after Hermann von Helmholtz (1821-1894) – the mentor of H. Hertz and M. Planck, among many others.

$$\begin{aligned}\nabla_t \times \mathbf{E}_t &= 0, & \nabla_t \times \mathbf{H}_t &= 0, \\ \nabla_t \cdot \mathbf{E}_t &= 0, & \nabla_t \cdot \mathbf{H}_t &= 0.\end{aligned}\tag{7.103}$$

Within the coarse-grain description of the conducting walls of the line (i. e., neglecting not only the screening depth but also the skin depth in comparison with the cross-section dimensions), we have to require that inside them, $\mathbf{E} = \mathbf{H} = 0$. Close to a wall but outside it, the normal component E_n of the electric field may be different from zero, because surface charges may sustain its jump – see Sec. 2.1, in particular Eq. (2.3). Similarly, the tangential component H_t of the magnetic field may have a finite jump at the surface due to skin currents – see Sec. 6.3, in particular Eq. (6.38). However, the tangential component of the electric field and the normal component of the magnetic field cannot experience such jumps, and to have them equal to zero inside the walls they have to equal zero just outside the walls as well:

$$\mathbf{E}_t = 0, \quad H_n = 0. \tag{7.104}$$

But the left columns of Eqs. (103)-(104) coincide with the formulation of the 2D boundary problem of electrostatics for the electric field induced by electric charges of the conducting walls, with the only difference that in our current case the value of ϵ actually means $\epsilon(\omega)$. Similarly, the right columns of those relations coincide with the formulation of the 2D boundary problem of magnetostatics for the magnetic field induced by currents in the walls, with $\mu \rightarrow \mu(\omega)$, with the only difference is that in our current coarse-grain approximation, the magnetic fields cannot penetrate into the conductors.

Now we immediately see that in waveguides with a singly-connected wall, for example, a hollow conducting tube (see, e.g., Fig. 16), the TEM waves are impossible, because there is no way to create a non-zero electrostatic field inside a conductor with such cross-section. However, such fields (and hence the TEM waves) are possible in structures with cross-sections consisting of two or more disconnected (galvanically-insulated) parts – see, e.g., Fig. 17.

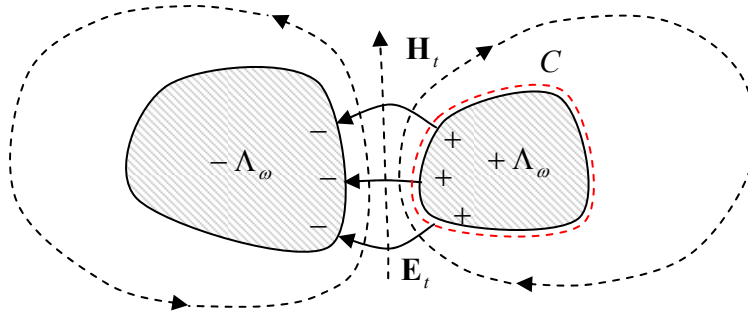


Fig. 7.17. An example of the cross-section of a transmission line that may support the TEM wave propagation.

In order to derive “global” relations for such a transmission line, let us consider the contour C drawn very close to the surface of one of its conductors – see, e.g., the red dashed line in Fig. 17. We can consider it, on one hand, as the cross-section of a cylindrically-shaped Gaussian volume of a certain elementary length $dz \ll \lambda \equiv 2\pi/k$. Using the generalized Gauss law (3.34), we get

$$\oint_C (\mathbf{E}_t)_n dr = \frac{\Lambda_\omega}{\epsilon}, \tag{7.105}$$

where Λ_ω (not to be confused with the wavelength λ !) is the complex amplitude of the linear density of the electric charge of the conductor. On the other hand, the same contour C may be used in the generalized Ampère law (5.116) to write

$$\oint_C (\mathbf{H}_t)_\tau dr = I_\omega, \quad (7.106)$$

where I_ω is the total current flowing along the conductor (or rather its complex amplitude). But, as was mentioned above, in the TEM wave the ratio E_t/H_t of the field components participating in these two integrals is constant and equal to $Z = (\mu/\epsilon)^{1/2}$, so that Eqs. (105)-(106) give the following simple relation between the “global” variables of the conductor:

$$I_\omega = \frac{\Lambda_\omega / \epsilon}{Z} \equiv \frac{\Lambda_\omega}{(\epsilon\mu)^{1/2}} \equiv \frac{\omega}{k} \Lambda_\omega. \quad (7.107)$$

This important relation may be also obtained in a different way; let me describe it as well, because (as we will see below) it has an independent heuristic value. Let us consider a small segment $dz \ll \lambda = 2\pi/k$ of the line’s conductor, and apply the electric charge conservation law (4.1) to the *instant* values of the linear charge density and current. The cancellation of dz in both parts yields

$$\frac{\partial \Lambda(z, t)}{\partial t} = -\frac{\partial I(z, t)}{\partial z}. \quad (7.108)$$

If we accept the sinusoidal waveform, $\exp\{i(kz - \omega t)\}$, for both these variables, we immediately recover Eq. (107) for their complex amplitudes, showing that this relation expresses just the charge continuity law.

The global equation (108) may be made more specific in the case when the frequency dependence of ϵ and μ is negligible, and the transmission line consists of just two isolated conductors – see, e.g., Fig. 17. In this case, to have the wave localized in the space near the two conductors, we need a sufficiently fast decrease of its electric field at large distances. For that, their linear charge densities for each value of z should be equal and opposite, and we can simply relate them to the potential difference V between the conductors:

$$\frac{\Lambda(z, t)}{V(z, t)} = C_0, \quad (7.109)$$

where C_0 is the mutual capacitance of the conductors (per unit length) – which was repeatedly discussed in Chapter 2. Then Eq. (108) takes the following form:

$$C_0 \frac{\partial V(z, t)}{\partial t} = -\frac{\partial I(z, t)}{\partial z}. \quad (7.110)$$

Next, let us consider the contour shown with the red dashed line in Fig. 18 (which shows a different cross-section of the transmission line – by a plane containing the wave propagation axis z), and apply to it the Faraday induction law (6.3).

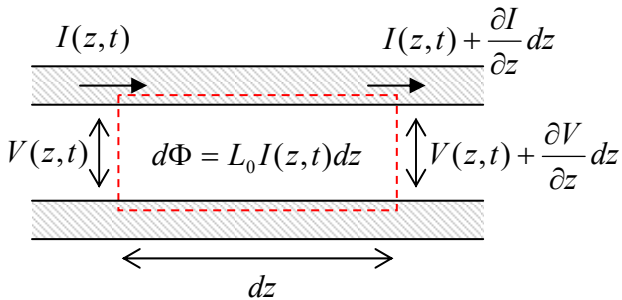


Fig. 7.18. Electric current, magnetic flux, and voltage in a two-conductor transmission line.

Since, in the coarse-grain approximation, the electric field inside the conductors (in Fig. 18, on the horizontal segments of the contour) vanishes, the total e.m.f. equals the difference of the voltages V at the ends of the segment dz , while the only sources of the magnetic flux through the area limited by the contour are the (equal and opposite) currents $\pm I$ in the conductors, we can use Eq. (5.70) to express the flux. As a result, canceling dz in both parts of the equation, we get

$$L_0 \frac{\partial I(z,t)}{\partial t} = -\frac{\partial V(z,t)}{\partial z}, \quad (7.111)$$

where L_0 is the mutual inductance of the conductors per unit length. The only difference between this L_0 and the dc mutual inductances discussed in Chapter 5 is that at the high frequencies we are analyzing now, L_0 should be calculated neglecting the magnetic field penetration into the conductors. (In the dc case, we had the same situation for superconductor electrodes within their coarse-grain, ideal-diamagnet description.)

The system of Eqs. (110) and (111) is frequently called the *telegrapher's equations*. Combined, they give for any “global” variable f (either V , or I , or Λ) the usual 1D wave equation,

$$\frac{\partial^2 f}{\partial z^2} - L_0 C_0 \frac{\partial^2 f}{\partial t^2} = 0, \quad (7.112)$$

which describes dispersion-free TEM wave’s propagation. Again, this equation is only valid within the frequency range where the frequency dependence of both ϵ and μ is negligible. If this is not so, the global approach may still be used for sinusoidal waves $f = \text{Re}[f_\omega \exp\{i(kz - \omega t)\}]$. Repeating the above arguments, instead of Eqs. (110)-(111) we get a more general system of two algebraic equations

$$\omega C_0 V_\omega = k I_\omega, \quad \omega L_0 I_\omega = k V_\omega, \quad (7.113)$$

in which $L_0 \propto \mu$ and $C_0 \propto \epsilon$ may now depend on frequency. These equations are consistent only if

$$L_0 C_0 = \frac{k^2}{\omega^2} \equiv \frac{1}{v^2} \equiv \epsilon \mu. \quad (7.114)$$

$L_0 C_0$
product
invariance

Besides the fact we have already known (that the TEM wave’s speed is the same as that of the plane wave), Eq. (114) gives us the result that I confess was not emphasized enough in Chapter 5: the product $L_0 C_0$ does not depend on the shape or size of line’s cross-section, provided that the magnetic field’s penetration into the conductors is negligible). Hence, if we have calculated the mutual capacitance C_0 of a system of two cylindrical conductors, the result immediately gives us their mutual inductance: $L_0 = \epsilon \mu / C_0$. This relationship stems from the fact that both the electric and magnetic fields may be expressed via the solution of the same 2D Laplace equation for the system’s cross-section.

With Eq. (114) satisfied, any of Eqs. (113) gives the same result for the following ratio:

$$Z_W \equiv \frac{V_\omega}{I_\omega} = \left(\frac{L_0}{C_0} \right)^{1/2}, \quad (7.115)$$

Transmission
line’s TEM
Impedance

which is called the *transmission line’s impedance*. This parameter has the same dimensionality (in SI units – ohms, denoted Ω) as the wave impedance (7),

$$Z \equiv \frac{E_\omega}{H_\omega} = \left(\frac{\mu}{\epsilon} \right)^{1/2}, \quad (7.116)$$

but these parameters should not be confused, because Z_W depends on the cross-section's geometry, while Z does not. In particular, Z_W is the only important parameter of a transmission line for its matching with a lumped load circuit (Fig. 19) in the important case when both the cable cross-section's size and the load's linear dimensions are much smaller than the wavelength.⁴⁸

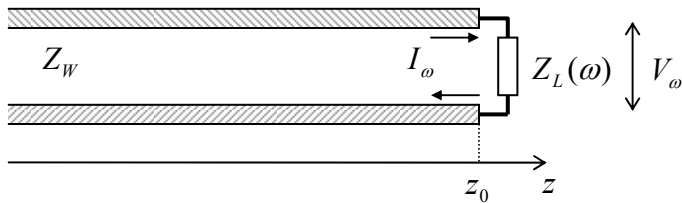


Fig. 7.19. Passive, lumped termination of a TEM transmission line.

Indeed, in this case, we may consider the load in the quasistatic limit and write

$$V_\omega(z_0) = Z_L(\omega)I_\omega(z_0), \quad (7.117)$$

where $Z_L(\omega)$ is the (generally complex) impedance of the load. Taking $V(z,t)$ and $I(z,t)$ in the form similar to Eqs. (61) and (62), and writing the two Kirchhoff's circuit laws for the point $z = z_0$, we get for the reflection coefficient a result similar to Eq. (68):

$$R = \frac{Z_L(\omega) - Z_W}{Z_L(\omega) + Z_W}. \quad (7.118)$$

This formula shows that for the perfect matching (i.e. the total wave absorption in the load), the load's impedance $Z_L(\omega)$ should be real and equal to Z_W – but not necessarily to Z .

As an example, let us consider one of the simplest (and most practically important) transmission lines: the coaxial cable (Fig. 20).⁴⁹

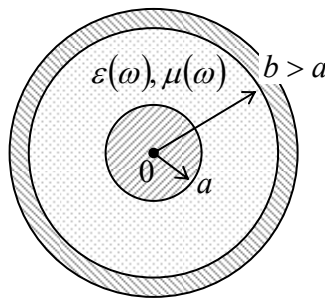


Fig. 7.20. The cross-section of a coaxial cable with (possibly, dispersive) dielectric filling.

For this geometry, we already know the expressions for both C_0 and L_0 ,⁵⁰ though they have to be modified for the account of arbitrary dielectric and magnetic constants, and the magnetic field's non-penetration into the conductors. As a result of this (elementary) modification, we get the formulas,

⁴⁸ The ability of TEM lines to have such a small cross-section is another important practical advantage.

⁴⁹ It was invented by the same O. Heaviside in 1880.

⁵⁰ See, respectively, Eqs. (2.49) and (5.79).

$$C_0 = \frac{2\pi\epsilon}{\ln(b/a)}, \quad L_0 = \frac{\mu}{2\pi} \ln(b/a), \quad (7.119)$$
Coaxial cable's C_0 and L_0

illustrating that the universal relationship (114) is indeed valid. For the cable's impedance (115), Eqs. (119) yield a geometry-dependent value

$$Z_w = \left(\frac{\mu}{\epsilon} \right)^{1/2} \frac{\ln(b/a)}{2\pi} \equiv Z \frac{\ln(b/a)}{2\pi} \neq Z. \quad (7.120)$$

For the standard TV antenna cables (such as RG-6/U, with $b/a \sim 3$, $\epsilon/\epsilon_0 \approx 2.2$), $Z_w = 75 \Omega$, while for most computer component connections, coaxial cables with $Z_w = 50 \Omega$ (such as RG-58/U) are prescribed by electronic engineering standards. Such cables are broadly used for the transmission of electromagnetic waves with frequencies up to 1 GHz over distances of a few km, and up to ~ 20 GHz on the tabletop scale (a few meters), limited by wave attenuation – see Sec. 9 below.

Moreover, the following two facts enable a wide application, in electrical engineering and physical experiment, of coaxial-cable-*like* systems. First, as Eq. (5.78) shows, in a cable with $a \ll b$, most energy of the wave is localized near the internal conductor. Second, the theory to be discussed in the next section shows that excitation of other (H - and E -) waves in the cable is impossible until the wavelength λ becomes smaller than $\sim \pi(a + b)$. As a result, the TEM mode propagation in a cable with $a \ll b < \lambda/\pi$ is not much affected even if the internal conductor is not straight, but bent – for example, into a helix – see, e.g., Fig. 21.

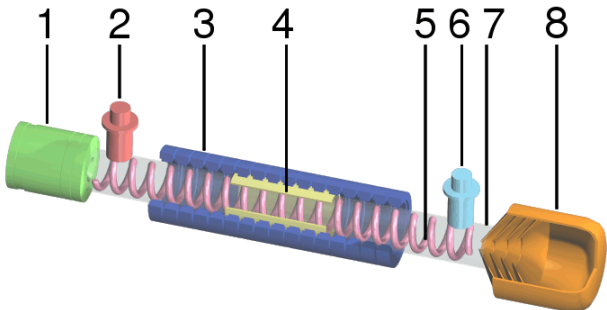


Fig. 7.21. A typical traveling-wave tube: (1) electron gun, (2) ac input, (3) beam-focusing magnets, (4) wave attenuator, (5) helix coil, (6) ac output, (7) vacuum tube, (8) electron collector. Adapted from https://en.wikipedia.org/wiki/Traveling-wave_tube under the Creative Commons BY-SA 3.0 license.

In such a system, called the *traveling-wave tube* (TWT), a quasi-TEM wave propagates with velocity $v \approx c$ along the helix's length, so that the velocity's component along the cable's axis may be made close to the velocity $u \ll c$ of the electron beam moving ballistically along the tube's axis, enabling their effective interaction, and as a result, a length-accumulating amplification of the wave.⁵¹

Another important example of a TEM transmission line is a set of two parallel wires. In the form of *twisted pairs*,⁵² they allow communications, in particular long-range telephone and DSL Internet

⁵¹ Despite the current prevalence of semiconductor devices in electronics, TWTs are still used in satellite TV and radio systems, because they may work at very high microwave power – e.g., up to 200W at 20 GHz and pulsed 50W at 200 GHz. Very unfortunately, in this course, I will not have time/space to discuss even the (rather elegant) basic theory of such devices. The reader interested in this field may be referred, for example, to the detailed monograph by J. Whitaker, *Power Vacuum Tubes Handbook*, 3rd ed., CRC Press, 2017.

⁵² Such twisting, around the line's direction axis, reduces the crosstalk between adjacent lines, and the parasitic radiation at their bends.

connections, at frequencies up to a few hundred kHz, as well as relatively short, multi-line Ethernet and TV cables at frequencies up to ~ 1 GHz, limited mostly by the mutual interference (“crosstalk”) between the individual lines of the same cable, and the unintentional radiation of the wave into the environment.

7.6. Waveguides: H and E waves

Let us now return to Eqs. (100) and explore the H - and E -waves – with, respectively, either H_z or E_z different from zero. At the first sight, they may seem more complex. However, Eqs. (101), which determine the distribution of these longitudinal components over the cross-section, are just the 2D Helmholtz equations for scalar functions. For simple cross-section geometries, they may be readily solved using the methods discussed for the Laplace equation in Chapter 2, in particular the variable separation. After the solution of such an equation has been found, the transverse components of the fields may be calculated by differentiation, using the simple formulas,

$$\mathbf{E}_t = \frac{i}{k_t^2} [k_z \nabla_t E_z - kZ(\mathbf{n}_z \times \nabla_t H_z)], \quad \mathbf{H}_t = \frac{i}{k_t^2} \left[k_z \nabla_t H_z + \frac{k}{Z} (\mathbf{n}_z \times \nabla_t E_z) \right], \quad (7.121)$$

which follow from the first line of Eqs. (100).⁵³

In comparison with the boundary problems of electro- and magnetostatics, the only conceptually new feature of Eqs. (101) is that they form the so-called *eigenproblems*, with typically many solutions (*eigenfunctions*), each describing a specific wave mode, and corresponding to a specific *eigenvalue* of the parameter k_t . The good news here is that these values of k_t are determined by this 2D boundary problem and hence do not depend on k_z . As a result, the dispersion law $\omega(k_z)$ of any mode, which follows from the last form of Eq. (102),

$$\omega = \left(\frac{k_z^2 + k_t^2}{\epsilon\mu} \right)^{1/2} \equiv (v^2 k_z^2 + \omega_c^2)^{1/2}, \quad (7.122)$$

Universal dispersion relation

is functionally similar for all modes. It is also similar to that of plane waves in plasma (see Eq. (38), Fig. 6, and their discussion in Sec. 2), with the only differences that the speed in light c is generally replaced with $v = 1/(\epsilon\mu)^{1/2}$ – the speed of the plane or TEM waves in the medium filling the waveguide, and that ω_p is replaced with the so-called *cutoff frequency*

$$\omega_c \equiv v k_t, \quad (7.123)$$

specific for each mode. (As Eq. (101) implies, and as we will see from several examples below, k_t has the order of $1/a$, where a is the characteristic dimension of the waveguide’s cross-section, so that the critical value of the free-space wavelength $\lambda \equiv 2\pi c/\omega$ is of the order of a .) Below the cutoff frequency of each particular mode, such wave cannot propagate in the waveguide.⁵⁴ As a result, the modes with the

⁵³ For the derivation of Eqs. (121), one of these two linear equations should be first vector-multiplied by \mathbf{n}_z . Note also that this approach could not be used to analyze the TEM waves, because for them $k_t = 0$, $E_z = 0$, $H_z = 0$, and Eqs. (121) yield uncertainty.

⁵⁴ An interesting twist in the ideas of electromagnetic metamaterials (mentioned in Sec. 5 above) is the so-called ϵ -near-zero materials, designed to have the effective product $\epsilon\mu$ much lower than $\epsilon_0\mu_0$ within certain frequency ranges. Since at these frequencies the speed v (4) becomes much lower than c , the cutoff frequency (123) virtually

lowest values of ω_c present special practical interest, because the choice of the signal frequency ω between the two lowest values of the cutoff frequency (123) guarantees that the waves propagate in the form of only one mode, with the lowest k_t . Such a choice enables engineers to simplify the excitation of the desired mode by wave generators and to avoid the unintentional transfer of electromagnetic wave energy to undesirable modes by (virtually unavoidable) small inhomogeneities of the system.

The boundary conditions for the Helmholtz equations (101) depend on the propagating wave type. For the E -modes, with $H_z = 0$ but $E_z \neq 0$, the condition $E_\tau = 0$ immediately gives

$$E_z|_C = 0, \quad (7.124)$$

where C is the inner contour limiting the conducting wall's cross-section. For the H -modes, with $E_z = 0$ but $H_z \neq 0$, the boundary condition is slightly less obvious and may be obtained using, for example, the second equation of the system (100), vector-multiplied by \mathbf{n}_z . Indeed, for the component normal to the conductor surface, the result of such multiplication is

$$ik_z(\mathbf{H}_t)_n - i\frac{k}{Z}(\mathbf{n}_z \times \mathbf{E}_t)_n = \frac{\partial H_z}{\partial n}. \quad (7.125)$$

But the first term on the left-hand side of this relation must be zero on the wall surface, because of the second of Eqs. (104), while according to the first of Eqs. (104), the vector \mathbf{E}_t in the second term cannot have a component tangential to the wall. As a result, the vector product in that term cannot have a normal component, so that the term should equal zero as well, and Eq. (125) is reduced to

$$\frac{\partial H_z}{\partial n}|_C = 0. \quad (7.126)$$

Let us see how all this machinery works for a simple but practically important case of a metallic-wall waveguide with a rectangular cross-section – see Fig. 22

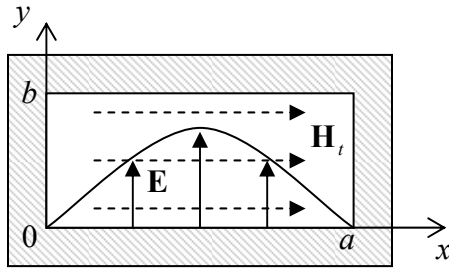


Fig. 7.22. A rectangular waveguide, and the transverse field distribution in its fundamental mode H_{10} (schematically).

In the natural Cartesian coordinates shown in this figure, both Eqs. (101) take the simple form

$$\left(\frac{\partial^2}{\partial x^2} + \frac{\partial^2}{\partial y^2} + k_t^2 \right) f = 0, \quad \text{where } f = \begin{cases} E_z, & \text{for } E\text{-modes,} \\ H_z, & \text{for } H\text{-modes.} \end{cases} \quad (7.127)$$

From Chapter 2, we know that the most effective way of solution of such equations in a rectangular region is the variable separation, in which the general solution is represented as a sum of partial solutions of the type

vanishes. As a result, the waves may “tunnel” through very narrow sections of metallic waveguides filled with such materials – see, e.g., M. Silveirinha and N. Engheta, *Phys. Rev. Lett.* **97**, 157403 (2006).

$$f = X(x)Y(y). \quad (7.128)$$

Plugging this expression into Eq. (127), and dividing each term by XY , we get the equation,

$$\frac{1}{X} \frac{d^2 X}{dx^2} + \frac{1}{Y} \frac{d^2 Y}{dy^2} + k_t^2 = 0, \quad (7.129)$$

which should be satisfied for all values of x and y within the waveguide's interior. This is only possible if each term of the sum equals a constant. Taking the X -term and Y -term constants in the form $(-k_x^2)$ and $(-k_y^2)$, respectively, and solving the corresponding ordinary differential equations,⁵⁵ for the eigenfunction (128) we get

$$f = (c_x \cos k_x x + s_x \sin k_x x)(c_y \cos k_y y + s_y \sin k_y y), \quad \text{with } k_x^2 + k_y^2 = k_t^2, \quad (7.130)$$

where the constants c and s should be found from the boundary conditions. Here the difference between the H -modes and E -modes kicks in.

For the H -modes, Eq. (130) is valid for H_z , and we should use the boundary condition (126) on all metallic walls of the waveguide, i.e. at $x = 0$ and a ; and $y = 0$ and b – see Fig. 22. As a result, we get very simple expressions for eigenfunctions and eigenvalues:

$$(H_z)_{nm} = H_l \cos \frac{\pi n x}{a} \cos \frac{\pi m y}{b}, \quad (7.131)$$

$$k_x = \frac{\pi n}{a}, \quad k_y = \frac{\pi m}{b}, \quad \text{so that } (k_t)_{nm} = (k_x^2 + k_y^2)^{1/2} = \pi \left[\left(\frac{n}{a} \right)^2 + \left(\frac{m}{b} \right)^2 \right]^{1/2}, \quad (7.132)$$

where H_l is the longitudinal field's amplitude, and n and m are two integer numbers – each of them arbitrary besides that they cannot be equal to zero simultaneously.⁵⁶ Assuming, just for certainty, that $a \geq b$ (as shown in Fig. 22), we see that the lowest eigenvalue of k_t and hence the lowest cutoff frequency (123) are achieved for the so-called H_{10} mode with $n = 1$ and $m = 0$, and hence with

$$(k_t)_{10} = \frac{\pi}{a}, \quad (7.133)$$

thus confirming our prior estimate of k_t .

Depending on the a/b ratio, the second-lowest k_t (and hence ω_c) belongs to either the H_{11} mode with $n = 1$ and $m = 1$:

$$(k_t)_{11} = \pi \left(\frac{1}{a^2} + \frac{1}{b^2} \right)^{1/2} \equiv \left[1 + \left(\frac{a}{b} \right)^2 \right]^{1/2} (k_t)_{10}, \quad (7.134)$$

or to the H_{20} mode with $n = 2$ and $m = 0$:

⁵⁵ Let me hope that the solution of equations of the type $d^2 X/dx^2 + k_x^2 X = 0$ does not present any problem for the reader, at least due to their prior experience with problems such as standing waves on a guitar string, wavefunctions in a flat 1D quantum well, or (with the replacement $x \rightarrow t$) a classical harmonic oscillator.

⁵⁶ Otherwise, the function $H_z(x,y)$ would be constant, so that, according to Eq. (121), the transverse components of the electric and magnetic field would equal zero. As a result, as the last two lines of Eqs. (100) show, the whole field would be zero for any $k_z \neq 0$.

$$(k_t)_{20} = \frac{2\pi}{a} \equiv 2(k_t)_{10}. \quad (7.135)$$

These values become equal at $a/b = \sqrt{3} \approx 1.7$; in practical waveguides, the a/b ratio is not too far from this value. For example, in the standard X-band (~ 10 -GHz) waveguide WR90, $a \approx 2.3$ cm ($f_c \equiv \omega_c/2\pi \approx 6.5$ GHz), and $b \approx 1.0$ cm.

Now let us have a look at the alternative E -modes. For them, we still should use the general solution (130) with $f = E_z$, but now with the boundary condition (124). This gives us the eigenfunctions

$$(E_z)_{nm} = E_l \sin \frac{\pi nx}{a} \sin \frac{\pi my}{b}, \quad (7.136)$$

and the same eigenvalue spectrum (132) as for the H modes. However, now neither n nor m can be equal to zero; otherwise, Eq. (136) would give the trivial solution $E_z(x,y) = 0$. Hence the lowest cutoff frequency of TM waves is achieved at the so-called E_{11} mode with $n=1$, $m=1$, and with the eigenvalue given by Eq. (134), always higher than $(k_t)_{10}$.

Thus the fundamental H_{10} mode is certainly the most important wave in rectangular waveguides; let us have a better look at this field distribution. Plugging the corresponding solution (131) with $n=1$ and $m=0$ into the general relation (121), we easily get

$$(H_x)_{10} = -i \frac{k_z a}{\pi} H_l \sin \frac{\pi x}{a}, \quad (H_y)_{10} = 0, \quad (7.137)$$

$$(E_x)_{10} = 0, \quad (E_y)_{10} = i \frac{ka}{\pi} Z H_l \sin \frac{\pi x}{a}. \quad (7.138)$$

This field distribution is (schematically) shown in Fig. 22. Neither of the fields depends on the coordinate y – the feature very convenient, in particular, for microwave experiments with small samples. The electric field has only one (in Fig. 22, vertical) component that vanishes at the side walls and reaches its maximum at the waveguide's center; its field lines are straight, starting and ending on wall surface charges (whose distribution propagates along the waveguide together with the wave). In contrast, the magnetic field has two non-zero components (H_x and H_z), and its field lines are shaped as horizontal loops wrapped around the electric field maxima.

An important question is whether the H_{10} wave may be usefully characterized by a unique impedance introduced similarly to Z_W of the TEM modes – see Eq. (115). The answer is *not*, because the main value of Z_W is a convenient description of the impedance matching of a transmission line with a lumped load – see Fig. 19 and Eq. (118). As was discussed above, such a simple description is possible (i.e., does not depend on the exact geometry of the connection) only if both dimensions of the line's cross-section are much less than λ . But for the H_{10} wave (and more generally, any non-TEM mode) this is impossible – see, e.g., Eq. (129): its lowest frequency corresponds to the TEM wavelength $\lambda_{\max} = 2\pi/(k_t)_{\min} = 2\pi/(k_t)_{10} = 2a$. (The reader is challenged to find a simple interpretation of this equality.)

Now let us consider metallic-wall waveguides with a round cross-section (Fig. 23a). In this single-connected geometry, the TEM waves are impossible again, while for the analysis of H -modes and E -modes, the polar coordinates $\{\rho, \varphi\}$ are most natural. In these coordinates, the 2D Helmholtz equation (101) takes the following form:

$$\left[\frac{1}{\rho} \frac{\partial}{\partial \rho} \left(\rho \frac{\partial}{\partial \rho} \right) + \frac{1}{\rho^2} \frac{\partial^2}{\partial \varphi^2} + k_t^2 \right] f = 0, \quad \text{where } f = \begin{cases} E_z, & \text{for } E\text{-modes,} \\ H_z, & \text{for } H\text{-modes.} \end{cases} \quad (7.139)$$

Separating the variables as $f = \mathcal{R}(\rho)\mathcal{H}(\varphi)$, we get

$$\frac{1}{\rho \mathcal{R}} \frac{d}{d\rho} \left(\rho \frac{d\mathcal{R}}{d\rho} \right) + \frac{1}{\rho^2 \mathcal{H}} \frac{d^2 \mathcal{H}}{d\varphi^2} + k_t^2 = 0. \quad (7.140)$$

But this is exactly the Eq. (2.127) that was studied in Sec. 2.7 in the context of electrostatics, just with a replacement of notation: $\gamma \rightarrow k_t$. So we already know that to have 2π -periodic functions $\mathcal{H}(\varphi)$ and finite values $\mathcal{R}(0)$ (which are evidently necessary for our current case – see Fig. 23a), the general solution must have the form given by Eq. (2.136), i.e. the eigenfunctions are expressed via integer-order Bessel functions of the first kind:

$$f_{nm} = J_n(k_{nm}\rho)(c_n \cos n\varphi + s_n \sin n\varphi) \equiv \text{const} \times J_n(k_{nm}\rho) \cos n(\varphi - \varphi_0), \quad (7.141)$$

with the eigenvalues k_{nm} of the transverse wave number k_t to be determined from appropriate boundary conditions, and an arbitrary constant φ_0 .

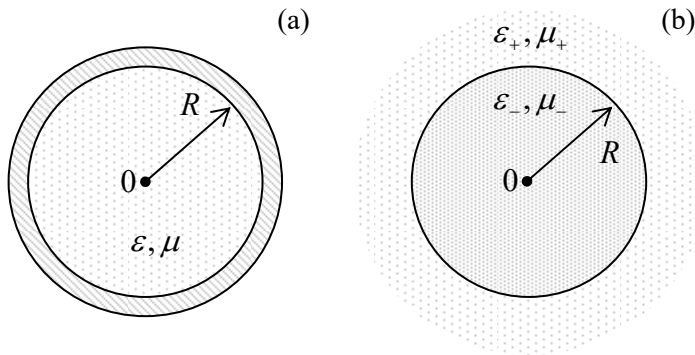


Fig. 7.23. (a) Metallic and (b) dielectric waveguides with circular cross-sections.

As for the rectangular waveguide, let us start from the H -modes ($f = H_z$). Then the boundary condition on the wall surface ($\rho = R$) is given by Eq. (126), which, for the solution (141), takes the form

$$\frac{d}{d\xi} J_n(\xi) = 0, \quad \text{where } \xi \equiv kR. \quad (7.142)$$

This means that the eigenvalues of Eq. (139) are

$$k_t = k_{nm} = \frac{\xi'_{nm}}{R}, \quad (7.143)$$

where ξ'_{nm} is the m^{th} zero of the function $dJ_n(\xi)/d\xi$. Approximate values of these zeros for several lowest n and m may be read out from Fig. 2.18; their more accurate values are given in Table 1 below.

Table 7.1. Zeros ξ'_{nm} of the function $dJ_n(\xi)/d\xi$ for a few lowest values of the Bessel function's index n and the root's number m .

	$m = 1$	2	3
$n = 0$	3.83171	7.015587	10.1735
1	1.84118	5.33144	8.53632
2	3.05424	6.70613	9.96947
3	4.20119	8.01524	11.34592

The table shows, in particular, that the lowest of the zeros is $\xi'_{11} \approx 1.84$.⁵⁷ Thus, perhaps a bit counter-intuitively, the fundamental mode, providing the lowest cutoff frequency $\omega_c = v k_{nm}$, is H_{11} , corresponding to $n = 1$ rather than $n = 0$:

$$H_z = H_1 J_1 \left(\xi'_{11} \frac{\rho}{R} \right) \cos(\varphi - \varphi_0). \quad (7.144)$$

It has the transverse wave number is $k_t = k_{11} = \xi'_{11}/R \approx 1.84/R$, and hence the cutoff frequency corresponding to the TEM wavelength $\lambda_{\max} = 2\pi/k_{11} \approx 3.41 R$. Thus the ratio of λ_{\max} to the waveguide's diameter $2R$ is about 1.7, i.e. is close to the ratio $\lambda_{\max}/a = 2$ for the rectangular waveguide. The origin of this proximity is clear from Fig. 24, which shows the transverse field distribution in the H_{11} mode. (It may be readily calculated from Eqs. (121) with $E_z = 0$, and H_z given by Eq. (144).)

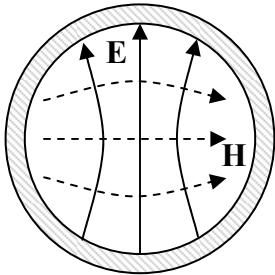


Fig. 7.24. Transverse field components in the fundamental H_{11} mode of a metallic, circular waveguide (schematically).

One can see that the field structure is actually very similar to that of the fundamental mode in the rectangular waveguide, shown in Fig. 22, despite the different nomenclature (which is due to the different coordinate system used for the solution). However, note the arbitrary constant angle φ_0 , indicating that in circular waveguides, the transverse field's polarization is arbitrary. For some practical applications, such degeneracy of these “quasi-linearly-polarized” waves creates problems; some of them may be avoided by using waves with circular polarization.

As Table 1 shows, the next lowest H -mode is H_{21} , for which $k_t = k_{21} = \xi'_{21}/R \approx 3.05/R$, almost twice larger than that of the fundamental mode, and only then comes the first mode with no angular dependence of any field, H_{01} , with $k_t = k_{01} = \xi'_{01}/R \approx 3.83/R$,⁵⁸ followed by several angle-dependent modes: H_{31}, H_{12} , etc.

For the E modes, we may still use Eq. (141) (with $f = E_z$), but with the boundary condition (124) at $\rho = R$. This gives the following equation for the problem eigenvalues:

$$J_n(k_{nm}R) = 0, \text{ i.e. } k_{nm} = \frac{\xi_{nm}}{R}, \quad (7.145)$$

where ξ_{nm} is the m^{th} zero of function $J_n(\xi)$ – see Table 2.1. That table shows that the lowest k_t is equal to $\xi_{01}/R \approx 2.405/R$. Hence the corresponding mode (E_{01}), with no angular dependence of its fields, e.g.

⁵⁷ Mathematically, the lowest root of Eq. (142) with $n = 0$ equals 0. However, it would yield $k = 0$ and hence a constant field H_z , which, according to the first of Eqs. (121), would give a vanishing electric field.

⁵⁸ The electric field lines in the H_{01} mode (as well as all higher H_{0m} modes) are directed straight from the symmetry axis to the walls, reminding those of the TEM waves in the coaxial cable. Due to this property, these modes provide, at $\omega \gg \omega_c$, much lower energy losses (see Sec. 9 below) than the fundamental H_{11} mode, and are sometimes used in practice, despite the inconvenience of working in the multimode frequency range.

$$E_z = E_i J_0 \left(\xi_{01} \frac{\rho}{R} \right), \quad (7.146)$$

has the second-lowest cutoff frequency, $\sim 30\%$ higher than that of the fundamental mode H_{11} .

Finally, let us discuss one more topic of general importance – the number N of electromagnetic modes that may propagate in a waveguide within a certain range of relatively large frequencies $\omega \gg \omega_c$. It is easy to calculate for a rectangular waveguide, with its simple expressions (132) for the eigenvalues of $\{k_x, k_y\}$. Indeed, these expressions describe a rectangular mesh on the $[k_x, k_y]$ plane, so that each point corresponds to the plane area $\Delta A_k = (\pi/a)(\pi/b)$, and the number of modes in a large k -plane area $A_k \gg \Delta A_k$ is $N = A_k / \Delta A_k = ab A_k / \pi^2 = AA_k / \pi^2$, where A is the waveguide's cross-section area.⁵⁹ However, it is frequently more convenient to discuss transverse wave vectors \mathbf{k}_t of arbitrary direction, i.e. with an arbitrary sign of their components k_x and k_y . Taking into account that the opposite values of each component actually give the same wave, the actual number of different modes of each type (E - or H -) is a factor of $2^2 \equiv 4$ lower than was calculated above. This means that the number of modes of *both* types is

$$N = 2 \frac{A_k A}{(2\pi)^2}. \quad (7.147)$$

Let me leave it for the reader to find hand-waving (but convincing :-) arguments that this *mode counting rule* is valid for waveguides with cross-sections of any shape, and any boundary conditions on the walls, provided that $N \gg 1$.

7.7. Dielectric waveguides, optical fibers, and paraxial beams

Now let us discuss electromagnetic wave propagation in *dielectric waveguides*. The simplest, *step-index* waveguide (see Figs. 23b and 25) consists of an inner *core* and an outer shell (in the optical fiber technology lingo, called *cladding*) with a higher wave propagation speed, i.e. a lower index of refraction:

$$v_+ > v_-, \quad \text{i.e. } n_+ < n_-, \quad k_+ < k_-, \quad \epsilon_+ \mu_+ < \epsilon_- \mu_-. \quad (7.148)$$

at the same frequency. (In most cases the difference is achieved due to that in the electric permittivity, $\epsilon_+ < \epsilon_-$, while magnetically both materials are virtually passive: $\mu \approx \mu_+ \approx \mu_0$, so that their refraction indices n_\pm , defined by Eq. (84), are very close to $(\epsilon_\pm/\epsilon_0)^{1/2}$; I will limit my discussion to this approximation.)

The basic idea of the waveguide's operation may be readily understood in the limit when the wavelength λ is much smaller than the characteristic size R of the core's cross-section. In this “geometric-optics” limit, at distances of the order of λ from the core-cladding interface, which provides the wave reflection, we can neglect the interface's curvature and approximate its geometry with a plane. As we know from Sec. 4, if the angle θ of the wave's incidence on such a plane interface is larger than the critical value θ_c specified by Eq. (85), the wave is totally reflected. As a result, the waves launched into the fiber core at such “grazing” angles, propagate inside the core, being repeatedly reflected from the cladding – see Fig. 25.

⁵⁹ This formula ignores the fact that, according to the above analysis, some modes (with $n = 0$ and $m = 0$ for the H modes, and $n = 0$ or $m = 0$ for the E modes) are forbidden. However, for $N \gg 1$, the associated corrections of Eq. (147) are negligible.

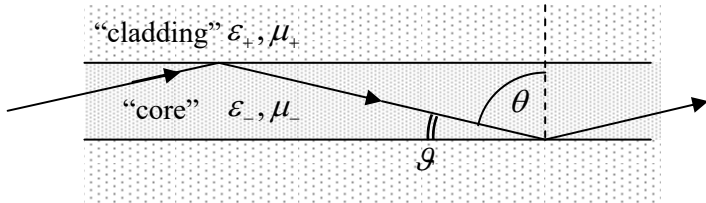


Fig. 7.25. Wave propagation in a thick optical fiber at $\theta > \theta_c$.

The most important type of dielectric waveguides is *optical fibers*.⁶⁰ Due to a heroic technological effort over three decades starting from the mid-1960s, the attenuation of such fibers has been decreased from values of the order of 20 db/km (typical for a window glass) to the fantastically low values of ~ 0.2 db/km (meaning virtually perfect transparency of 10-km-long fiber segments!), combined with the extremely low plane-wave (“chromatic”) dispersion below 10 ps/km·nm.⁶¹ In conjunction with the development of inexpensive erbium-based quantum amplifiers, this breakthrough has enabled inter-city and inter-continental (undersea), broadband⁶² optical cables, which are the backbone of all modern telecommunication infrastructure.

The only bad news is that these breakthroughs were achieved for just one kind of materials (silica-based glasses)⁶³ within a very narrow range of their chemical composition. As a result, the dielectric constants $\kappa_{\pm} \equiv \epsilon_{\pm}/\epsilon_0$ of the cladding and core of practical optical fibers are both close to 2.2 ($n_{\pm} \approx 1.5$) and hence very close to each other, so that the relative difference of the refraction indices,

$$\Delta \equiv \frac{n_- - n_+}{n_-} = \frac{\epsilon_-^{1/2} - \epsilon_+^{1/2}}{\epsilon_-^{1/2}} \approx \frac{\epsilon_- - \epsilon_+}{2\epsilon_{\pm}}, \quad (7.149)$$

is typically below 0.5%. This factor limits the fiber bandwidth. Indeed, let us use the geometric-optics picture to calculate the number of quasi-plane-wave modes that may propagate in the fiber. For the complementary angle (Fig. 25)

$$\vartheta \equiv \frac{\pi}{2} - \theta, \quad \text{so that } \sin \theta = \cos \vartheta, \quad (7.150)$$

Eq. (85) gives the following propagation condition:

$$\cos \vartheta > \frac{n_+}{n_-} = 1 - \Delta. \quad (7.151)$$

⁶⁰ For a comprehensive discussion of this vital technology see, e.g., A. Yariv and P. Yeh, *Photonics*, 6th ed., Oxford U. Press, 2007.

⁶¹ Both these parameters have their best values not in the visible light range (with wavelengths from 380 to 740 nm), but in the near-infrared, with the attenuation lowest between approximately 1,500 and 1,630 nm. As a result, most modern communication systems use two spectral windows – the so-called C-band (1,530-1,565 nm) and L-band (1,570-1,610 nm) within that range.

⁶² Each of the spectral bands mentioned above, at a typical signal-to-noise ratio $S/N > 10^5$, corresponds to the Shannon bandwidth $\Delta f \log_2(S/N)$ exceeding 10^{14} bits per second, some five orders of magnitude (!) higher than that of a modern Ethernet cable. The practically usable bandwidth of each fiber is somewhat lower, but a typical optical cable, with many fibers in parallel, has a proportionately higher aggregate bandwidth. A relatively recent (circa 2017) example is the C-band transatlantic (6,600-km-long) cable *Marea*, with eight fiber pairs and an aggregate useable bandwidth of 160 terabits per second.

⁶³ The silica-based fibers were developed in 1966 by an industrial research group led by Charles Kao (who shared the 2009 Nobel Prize in physics), but the very idea of using optical fibers for long-range communications may be traced back at least to the 1963 work by Jun-ichi Nishizawa – who also invented semiconductor lasers.

In the limit $\Delta \ll 1$, when the incidence angles $\theta > \theta_c$ of all propagating waves are very close to $\pi/2$, and hence the complementary angles are ϑ small, we may keep only two first terms in the Taylor expansion of the left-hand side of Eq. (151) and get

$$\vartheta_{\max}^2 \approx 2\Delta. \quad (7.152)$$

(Even for the higher-end value $\Delta = 0.005$, this critical angle is only ~ 0.1 radian, i.e. is close to 5° .) Due to this smallness, we may approximate the maximum transverse component of the wave vector as

$$(k_t)_{\max} = k(\sin \vartheta)_{\max} \approx k\vartheta_{\max} \approx \sqrt{2}\Delta, \quad (7.153)$$

and use Eq. (147) to calculate the number N of propagating modes:

$$N \approx 2 \frac{(\pi R^2)(\pi k^2 \vartheta_{\max}^2)}{(2\pi)^2} = (kR)^2 \Delta. \quad (7.154)$$

For typical values $k = 0.73 \times 10^7 \text{ m}^{-1}$ (corresponding to the free-space wavelength $\lambda_0 = n\lambda = 2\pi n/k \approx 1.3 \mu\text{m}$), $R = 25 \mu\text{m}$, and $\Delta = 0.005$, this formula gives $N \approx 150$.

Now we can calculate the *geometric dispersion* of such a fiber, i.e. the difference in the mode propagation speed, which is commonly characterized in terms of the difference between the wave delay times (traditionally measured in picoseconds per kilometer) of the fastest and slowest modes. Within the geometric optics approximation, the difference in time delays of the fastest mode (with $k_z = k$) and the slowest mode (with $k_z = k \sin \theta_c$) at distance l is

$$\Delta t = \Delta \left(\frac{l}{v_z} \right) = \Delta \left(\frac{k_z l}{\omega} \right) = \frac{l}{\omega} \Delta k_z = \frac{l}{v} (1 - \sin \theta_c) = \frac{l}{v} \left(1 - \frac{n_+}{n_-} \right) \equiv \frac{l}{v} \Delta. \quad (7.155)$$

For the example considered above, the TEM wave's speed in the glass, $v = c/n \approx 2 \times 10^8 \text{ m/s}$, and the geometric dispersion $\Delta t/l$ is close to 25 ps/m, i.e. 25,000 ps/km. (This means, for example, that a 1-ns pulse, being distributed between the modes, would spread to a ~ 25 -ns pulse after passing a just 1-km fiber segment.) This result should be compared with the chromatic dispersion mentioned above, below 10 ps/km·nm, which gives dt/l is of the order of only 1,000 ps/km in the whole communication band $d\lambda \sim 100 \text{ nm}$. Due to this high geometric dispersion, such relatively thick ($2R \sim 50 \text{ nm}$) *multi-mode fibers* are used for the transfer of signals over only short distances below $\sim 100 \text{ m}$. (As compensation, they may carry relatively large power, beyond 10 mW, without being damaged by the field.)

Long-range telecommunications are based on *single-mode fibers*, with thin cores (typically with diameters $2R \sim 5 \mu\text{m}$, i.e. of the order of $\lambda/\Delta^{1/2}$). For such structures, Eq. (154) yields $N \sim 1$, but in this case, the geometric optics approximation is not quantitatively valid, and for the fiber analysis, we should get back to the Maxwell equations. In particular, this analysis should take into explicit account the evanescent wave in the cladding, because its penetration depth may be comparable with R .⁶⁴

⁶⁴ The following quantitative analysis of the single-mode fibers is very valuable – both for practice and as a very good example of Maxwell equations' solution. However, I have to confess that its results will not be used in the following parts of the course. So, if the reader is not interested in this topic, they may safely jump to the text following Eq. (181). (I believe that the discussion of the angular momentum of electromagnetic radiation, starting at that point, is compulsory for every professional physicist.)

Since the cross-section of an optical fiber lacks metallic walls, the Maxwell equations describing them cannot be exactly satisfied with either TEM-wave, or H -mode, or E -mode solutions. Instead, the fibers can carry the so-called HE and EH modes, with both vectors \mathbf{H} and \mathbf{E} having longitudinal components simultaneously. In such modes, both E_z and H_z inside the core ($\rho \leq R$) have a form similar to Eq. (141):

$$f_- = f_l J_n(k_t \rho) \cos n(\varphi - \varphi_0), \quad \text{where } k_t^2 = k_-^2 - k_z^2 > 0, \text{ and } k_-^2 \equiv \omega^2 \epsilon_- \mu_-, \quad (7.156)$$

where the constant angles φ_0 may be different for each field. On the other hand, for the evanescent wave in the cladding, we may rewrite Eqs. (101) as

$$(\nabla^2 - \kappa_t^2) f_+ = 0, \quad \text{where } \kappa_t^2 \equiv k_z^2 - k_+^2 > 0, \text{ and } k_+^2 \equiv \omega^2 \epsilon_+ \mu_+. \quad (7.157)$$

Figure 26 illustrates these relations between k_t , κ_t , k_z , and k_\pm ; note that the following sum,

$$k_t^2 + \kappa_t^2 = \omega^2 (\epsilon_- - \epsilon_+) \mu_0 = 2k^2 \Delta, \quad (7.158)$$

Universal relation between k_t and κ_t

is fixed (at a given frequency) and, for typical fibers, is very small ($\ll k^2$). In particular, Fig. 26 shows that neither k_t nor κ_t can be larger than $\omega[(\epsilon_- - \epsilon_+) \mu_0]^{1/2} = (2\Delta)^{1/2} k$. This means that the depth $\delta = 1/\kappa_t$ of the wave penetration into the cladding is at least $1/k(2\Delta)^{1/2} = \lambda/2\pi(2\Delta)^{1/2} \gg \lambda/2\pi$. This is why the cladding layers in practical optical fibers are made as thick as $\sim 50 \mu\text{m}$, so that only a negligibly small tail of this evanescent wave field reaches their outer surfaces.

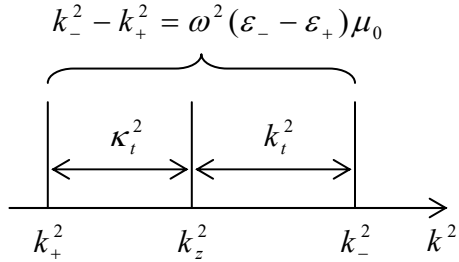


Fig. 7.26. The relation between the transverse exponents k_t and κ_t for waves in optical fibers.

In the polar coordinates, Eq. (157) becomes

$$\left[\frac{1}{\rho} \frac{\partial}{\partial \rho} \left(\rho \frac{\partial}{\partial \rho} \right) + \frac{1}{\rho^2} \frac{\partial^2}{\partial \varphi^2} - \kappa_t^2 \right] f_+ = 0, \quad (7.159)$$

- the equation to be compared with Eq. (139) for the circular metallic-wall waveguide. From Sec. 2.7, we know that the eigenfunctions of Eq. (159) are the products of the sine and cosine functions of $n\varphi$ by a linear combination of the modified Bessel functions I_n and K_n , shown in Fig. 2.22, now of the argument $\kappa_t \rho$. The fields have to vanish at $\rho \rightarrow \infty$, so that only the latter functions (of the second kind) can participate in the solution:

$$f_+ \propto K_n(\kappa_t \rho) \cos n(\varphi - \varphi_0). \quad (7.160)$$

Now we have to reconcile Eqs. (156) and (160), using the boundary conditions at $\rho = R$ for both longitudinal and transverse components of both fields, with the latter components first calculated using Eqs. (121). Such a conceptually simple, but a bit bulky calculation (which I am leaving for the reader's exercise), yields a system of two linear, homogeneous equations for the complex amplitudes E_l and H_l , which are compatible if

$$\left(\frac{k_-^2 J_n'}{k_t J_n} + \frac{k_+^2 K_n'}{\kappa_t K_n} \right) \left(\frac{1}{k_t} \frac{J_n'}{J_n} + \frac{1}{\kappa_t} \frac{K_n'}{K_n} \right) = \frac{n^2}{R^2} \left(\frac{k_-^2}{k_t^2} + \frac{k_+^2}{\kappa_t^2} \right) \left(\frac{1}{k_t^2} + \frac{1}{\kappa_t^2} \right), \quad (7.161)$$

where the prime signs denote (as a rare exception in this series) the derivatives of each function over its full argument: $k_t \rho$ for J_n , and $\kappa_t \rho$ for K_n .

For any given frequency ω , the system of equations (158) and (161) determines the values of k_t and κ_t , and hence k_z . Actually, for any $n > 0$, this system provides two different solutions: one corresponding to the so-called *HE* wave, with a larger ratio E_z/H_z , and the *EH* wave, with a smaller value of that ratio. For angular-symmetric modes with $n = 0$ (for whom we might naively expect the lowest cutoff frequency), the equations may be satisfied by the fields having just one non-zero longitudinal component (either E_z or H_z), so that the *HE* wave are the usual *E*-modes, while the *EH* modes are the *H*-waves. For the *H*-modes, the characteristic equation is reduced to the requirement that the expression in the second parentheses on the left-hand side of Eq. (161) is equal to zero. Using the Bessel function identities $J_0' = -J_1$ and $K_0' = -K_1$, this equation may be rewritten in a simpler form:

$$\frac{1}{k_t} \frac{J_1(k_t R)}{J_0(k_t R)} = -\frac{1}{\kappa_t} \frac{K_1(\kappa_t R)}{K_0(\kappa_t R)}. \quad (7.162)$$

Using the universal relation between k_t and κ_t given by Eq. (158), we may plot both sides of Eq. (162) as functions of the same argument, say, $\xi \equiv k_t R$ – see Fig. 27.

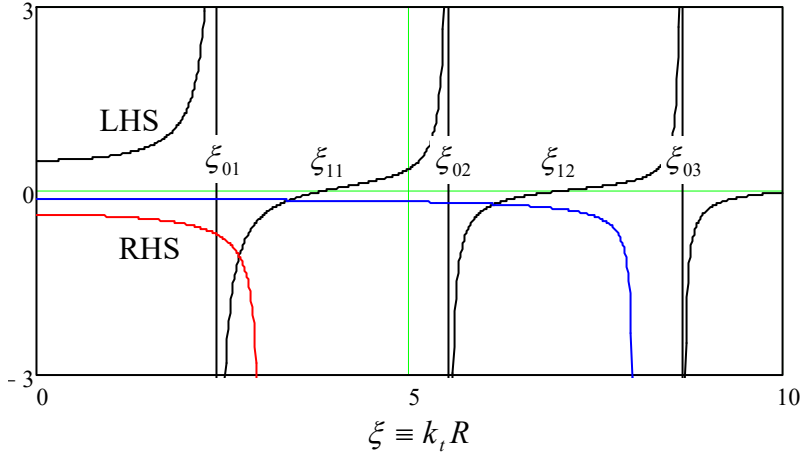


Fig. 7.27. Two sides of the characteristic equation (162), plotted as functions of $k_t R$, for two values of its dimensionless parameter: $V = 8$ (blue line) and $V = 3$ (red line). Note that according to Eq. (158), the argument of the functions K_0 and K_1 is $\kappa_t R = [V^2 - (k_t R)^2]^{1/2} \equiv (V^2 - \xi^2)^{1/2}$.

The right-hand side of Eq. (162) depends not only on ξ , but also on the dimensionless parameter V defined as the normalized right-hand side of Eq. (158):

$$V^2 \equiv \omega^2 (\epsilon_- - \epsilon_+) \mu_0 R^2 \approx 2 \Delta k_\pm^2 R^2. \quad (7.163)$$

(According to Eq. (154), if $V \gg 1$, it gives twice the number N of the fiber modes – the conclusion confirmed by Fig. 27, taking into account that it describes only the *H*-modes.) Since the ratio K_1/K_0 is positive for all values of the functions' argument (see, e.g., the right panel of Fig. 2.22), the right-hand side of Eq. (162) is always negative, so that the equation may have solutions only in the intervals where the ratio J_1/J_0 is negative, i.e. at

$$\xi_{01} < k_t R < \xi_{11}, \quad \xi_{02} < k_t R < \xi_{12}, \dots, \quad (7.164)$$

where ξ_{nm} is the m -th zero of the function $J_n(\xi)$ – see Table 2.1. The right-hand side of the characteristic equation (162) diverges at $k_t R \rightarrow 0$, i.e. at $k_t R \rightarrow \mathcal{V}$, so that no solutions are possible if \mathcal{V} is below the critical value $\mathcal{V}_c = \xi_{01} \approx 2.405$. At this cutoff point, Eq. (163) yields $k_{\pm} \approx \xi_{01}/R(2\Delta)^{1/2}$. Hence, the cutoff frequency of the lowest H mode corresponds to the TEM wavelength

$$\lambda_{\max} = \frac{2\pi R}{\xi_{01}} (2\Delta)^{1/2} \approx 3.7 R \Delta^{1/2}. \quad (7.165)$$

For typical parameters $\Delta = 0.005$ and $R = 2.5 \mu\text{m}$, this result yields $\lambda_{\max} \sim 0.65 \mu\text{m}$, corresponding to the free-space wavelength $\lambda_0 \sim 1 \mu\text{m}$. A similar analysis of the first parentheses on the left-hand side of Eq. (161) shows that at $\Delta \rightarrow 0$, the cutoff frequency for the E modes is similar.

This situation may look exactly like that in metallic-wall waveguides, with no waves possible at frequencies below ω_c , but this is not so. The basic reason for the difference is that in the metallic waveguides, the approach to ω_c results in the divergence of the longitudinal wavelength $\lambda_z \equiv 2\pi/k_z$. On the other hand, in dielectric waveguides, the approach leaves λ_z finite ($k_z \rightarrow k_+$). Due to this difference, a certain linear superposition of HE and EH waves with $n = 1$ can propagate at frequencies well below the cutoff frequency for $n = 0$, which we have just calculated.⁶⁵ This mode, in the limit $\varepsilon_+ \approx \varepsilon_-$ (i.e. $\Delta \ll 1$) allows a very interesting and simple description using the *Cartesian* (rather than polar) components of the fields, but still expressed as functions of the *polar* coordinates ρ and φ . The reason is that this mode is very close to a linearly polarized TEM wave. (Due to this reason, this mode is referred to as LP_{01} .)

Let us select the x -axis parallel to the transverse component of the magnetic field vector at $\rho = 0$, so that $E_x|_{\rho=0} = 0$, but $E_y|_{\rho=0} \neq 0$, and $H_x|_{\rho=0} \neq 0$, but $H_y|_{\rho=0} = 0$. The only suitable solutions of the 2D Helmholtz equation (that should be obeyed not only by the z -components of the fields but also their x - and y -components) are proportional to $J_0(k_t \rho)$, with zero coefficients for E_x and H_y :

$$E_x = 0, \quad E_y = E_0 J_0(k_t \rho), \quad H_x = H_0 J_0(k_t \rho), \quad H_y = 0, \quad \text{for } \rho \leq R. \quad (7.166) \quad LP_{01} \text{ mode}$$

Now we can use the last two equations of Eqs. (100) to calculate the longitudinal components of the fields:

$$E_z = -\frac{1}{ik_z} \frac{\partial E_y}{\partial y} = -i \frac{k_t}{k_z} E_0 J_1(k_t \rho) \sin \varphi, \quad H_z = -\frac{1}{ik_z} \frac{\partial H_x}{\partial x} = -i \frac{k_t}{k_z} H_0 J_1(k_t \rho) \cos \varphi, \quad (7.167)$$

where I have used the following mathematical identities: $J_0 = -J_1'$, $\partial \rho / \partial x = x/\rho = \cos \varphi$, and $\partial \rho / \partial y = y/\rho = \sin \varphi$. As a sanity check, we see that the longitudinal component of each field is a (legitimate!) eigenfunction of the type (141), with $n = 1$. Note also that if $k_t \ll k_z$ (this relation is always true if $\Delta \ll 1$ – see either Eq. (158) or Fig. 26), the longitudinal components of the fields are much smaller than their transverse counterparts, so that the wave is indeed very close to the TEM one. Because of that, the ratio of the electric and magnetic field amplitudes is also close to that in the TEM wave: $E_0/H_0 \approx Z_- \approx Z_+$.

Now to satisfy the boundary conditions at the core-to-cladding interface ($\rho = R$), we need to have a similar angular dependence of these components at $\rho \geq R$. The longitudinal components of the fields

⁶⁵ This fact becomes less surprising if we recall that in the circular metallic waveguide, discussed in Sec. 6, the fundamental mode (H_{11} , see Fig. 23) also corresponded to $n = 1$ rather than $n = 0$.

are tangential to the interface and thus should be continuous. Using the solutions similar to Eq. (160) with $n = 1$, we get

$$E_z = -i \frac{k_t}{k_z} \frac{J_1(k_t R)}{K_1(\kappa_t R)} E_0 K_1(\kappa_t \rho) \sin \varphi, \quad H_z = -i \frac{k_t}{k_z} \frac{J_1(k_t R)}{K_1(\kappa_t R)} H_0 K_1(\kappa_t \rho) \cos \varphi, \quad \text{for } \rho \geq R. \quad (7.168)$$

For the transverse components, we should require the continuity of the normal magnetic field μH_n , for our simple field structure equal to just $\mu H_x \cos \varphi$, of the tangential electric field $E_\tau = E_y \sin \varphi$, and of the normal component of $D_n = \epsilon E_n = \epsilon E_y \cos \varphi$. Assuming that $\mu = \mu_+ = \mu_0$, and $\epsilon_+ \approx \epsilon_-$ ⁶⁶ we can satisfy these conditions with the following solutions:

$$E_x = 0, \quad E_y = \frac{J_0(k_t R)}{K_0(\kappa_t R)} E_0 K_0(\kappa_t \rho), \quad H_x = \frac{J_0(k_t R)}{K_0(k_t R)} H_0 K_0(\kappa_t \rho), \quad H_y = 0, \quad \text{for } \rho \geq R. \quad (7.169)$$

From here, we can calculate components from E_z and H_z , using the same approach as for $\rho \leq R$:

$$\begin{aligned} E_z &= \frac{1}{-ik_z} \frac{\partial E_y}{\partial y} = -i \frac{\kappa_t}{k_z} \frac{J_0(k_t R)}{K_0(\kappa_t R)} E_0 K_1(\kappa_t \rho) \sin \varphi, \\ H_z &= \frac{1}{-ik_z} \frac{\partial H_x}{\partial x} = -i \frac{\kappa_t}{k_z} \frac{J_0(k_t R)}{K_0(\kappa_t R)} H_0 K_1(\kappa_t \rho) \cos \varphi, \quad \text{for } \rho \geq R. \end{aligned} \quad (7.170)$$

These relations provide the same functional dependence of the fields as Eqs. (167), i.e. the internal and external fields are compatible, but their amplitudes at the interface coincide only if

$$\boxed{k_t \frac{J_1(k_t R)}{J_0(k_t R)} = \kappa_t \frac{K_1(\kappa_t R)}{K_0(\kappa_t R)}}. \quad (7.171)$$

LP₀₁ mode:
characteristic
equation

This characteristic equation (which may be also derived from Eq. (161) with $n = 1$ in the limit $\Delta \rightarrow 0$) looks close to Eq. (162), but functionally is much different from it – see Fig. 28. Indeed, its right-hand side is always positive, and the left-hand side tends to zero at $k_t R \rightarrow 0$. As a result, Eq. (171) may have a solution for arbitrary small values of the parameter \mathcal{V} defined by Eq. (163), i.e. for *arbitrary low frequencies* (large wavelengths). This is why this mode is used in practical single-mode fibers: there are no other modes with wavelengths larger than the λ_{\max} given by Eq. (165), so that they cannot be unintentionally excited on small inhomogeneities of the fiber.

It is easy to use the Bessel function approximations by the first terms of the Taylor expansions (2.132) and (2.157) to show that in the limit $\mathcal{V} \rightarrow 0$, $\kappa_t R$ tends to zero much faster than $k_t R \approx \mathcal{V}$: $\kappa_t R \rightarrow 2\exp\{-1/\mathcal{V}\} \ll \mathcal{V}$. This means that the scale $\rho_c \equiv 1/\kappa_t$ of the radial distribution of the *LP₀₁* wave's fields in the cladding becomes very large. In this limit, this mode may be interpreted as a virtually TEM wave propagating in the cladding, just slightly deformed (and guided) by the fiber's core. The drawback of this feature is that it requires very thick cladding, to avoid energy losses in its outer (“buffer” and “jacket”) layers that defend the silica layers from the elements and mechanical damages, but lack their

⁶⁶ This is the core assumption of this approximate theory, which accounts only for the most important effect of the small difference of the dielectric constants ϵ_+ and ϵ_- : the difference between $(k_+^2 - k_z^2) = k_t^2 > 0$ and $(k_-^2 - k_z^2) = -\kappa_t^2 < 0$. For more discussion of the accuracy of this approximation and some exact results, the interested reader may be referred either to the monograph by A. Snyder and D. Love, *Optical Waveguide Theory*, Chapman and Hill, 1983, or to Chapter 3 and Appendix B in the monograph by Yariv and Yeh, that was cited above.

low optical absorption. Due to this reason, the core radius is usually selected so that the parameter \mathcal{V} is just slightly less than the critical value $\mathcal{V}_c = \xi_{01} \approx 2.4$ for higher modes, thus ensuring the single-mode operation.

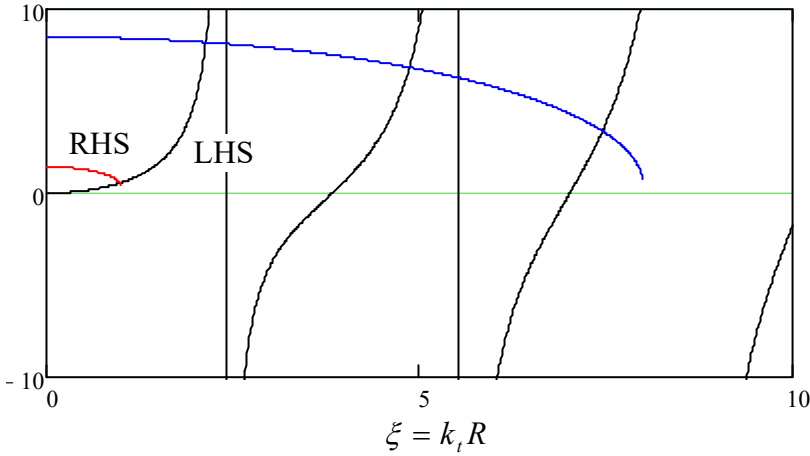


Fig. 7.28. Two sides of the characteristic equation (171) for the LP_{01} mode, plotted as a function of $k_t R$, for two values of the dimensionless parameter: $\mathcal{V} = 8$ (blue line) and $\mathcal{V} = 1$ (red line).

In order to reduce the field spread into the cladding, the step-index fibers discussed above may be replaced with *graded-index* fibers whose dielectric constant ε is gradually and slowly decreased from the center to the periphery.⁶⁷ Keeping only the main two terms in the Taylor expansion of the function $\varepsilon(\rho)$ at $\rho = 0$, we may approximate such reduction as⁶⁸

$$\varepsilon(\rho) \approx \varepsilon(0)(1 - \zeta\rho^2), \quad (7.172)$$

where $\zeta \equiv -[(d^2\varepsilon/d\rho^2)/2\varepsilon]_{\rho=0}$ is a positive constant characterizing the fiber composition gradient. Moreover, if this constant is sufficiently small ($\zeta \ll k^2$), the field distribution across the fiber's cross-section may be described by the same 2D Helmholtz equation (101), but with a space-dependent transverse wave vector:⁶⁹

$$[\nabla_t^2 + k_t^2(\rho)]f = 0, \quad (7.173)$$

where

$$k_t^2(\rho) = k^2(\rho) - k_z^2 \equiv k_t^2(0) - k^2(0)\zeta\rho^2, \quad \text{and } k^2(0) \equiv \omega^2\varepsilon(0)\mu_0.$$

Surprisingly for such an axially-symmetric problem, because of its special dependence on the radius, this equation may be most readily solved in the Cartesian coordinates. Indeed, rewriting it as

$$\left[\frac{\partial^2}{\partial x^2} + \frac{\partial^2}{\partial y^2} + k_t^2(0) - k^2(0)\zeta(x^2 + y^2) \right] f = 0, \quad (7.174)$$

and separating the variables as $f = X(x)Y(y)$, we get

⁶⁷ Due to the difficulty of fabrication of graded-index fibers with wave attenuation below a few dm/km, they are not used as broadly as the step-index ones.

⁶⁸ For an axially-symmetric smooth function $\varepsilon(\rho)$, the first derivative $d\varepsilon/d\rho$ always vanishes at $\rho = 0$, so that Eq. (172) does not have a term linear in ρ .

⁶⁹ This approach is invalid at arbitrary (large) ζ because in the macroscopic Maxwell equations, $\varepsilon(\mathbf{r})$ is under the differentiation sign, and the exact Helmholtz-type equations for fields have additional terms containing $\nabla\varepsilon$.

$$\frac{1}{X} \frac{d^2 X}{dx^2} + \frac{1}{Y} \frac{d^2 Y}{dy^2} + k_t^2(0) - k^2(0)\zeta(x^2 + y^2) = 0, \quad (7.175)$$

so that the functions X and Y obey similar differential equations, for example

$$\frac{d^2 X}{dx^2} + [k_x^2 - k^2(0)\zeta x^2]X = 0, \quad (7.176)$$

with the separation constants satisfying the following condition:

$$k_x^2 + k_y^2 = k_t^2(0) \equiv k^2(0) - k_z^2. \quad (7.177)$$

The ordinary differential equation (176) is well known from quantum mechanics, because the stationary Schrödinger equation for one of the most important basic quantum systems, a 1D harmonic oscillator, may be rewritten in this form. Its eigenvalues are very simple:

$$(k_x^2)_n = k(0)\zeta^{1/2}(2n+1), \quad (k_y^2)_m = k(0)\zeta^{1/2}(2m+1), \quad \text{with } n, m = 0, 1, 2, \dots, \quad (7.178)$$

but the corresponding eigenfunctions $X_n(x)$ and $Y_m(y)$ are expressed via not quite elementary functions – the Hermite polynomials.⁷⁰ For most practical purposes, however, the lowest eigenfunctions $X_0(x)$ and $Y_0(y)$ are sufficient, because they correspond to the lowest $k_{x,y}$, and hence the lowest

$$[k_t^2(0)]_{\min} = (k_x^2)_0 + (k_y^2)_0 = 2k(0)\zeta^{1/2}, \quad (7.179)$$

and the lowest cutoff frequency. As may be readily verified by the substitution to Eq. (176), the eigenfunctions corresponding to this fundamental mode are also simple:

$$X_0(x) = \text{const} \times \exp\left\{-\frac{k(0)\zeta^{1/2}x^2}{2}\right\}, \quad (7.180)$$

and similarly for $Y_0(y)$, so that the field distribution follows the Gaussian function

$$f_0(\rho) = f_0(0) \exp\left\{-\frac{k(0)\zeta^{1/2}\rho^2}{2}\right\} \equiv f_0(0) \exp\left\{-\frac{\rho^2}{2a^2}\right\}, \quad \text{with } a \equiv 1/k^{1/2}(0)\zeta^{1/4}, \quad (7.181)$$

where $a \gg 1/k(0)$ has the sense of the effective width of the field's extension in the radial direction, normal to the wave's propagation axis z . This is the so-called *Gaussian beam*, very convenient for some applications.

The Gaussian beam (181) is just one example of the so-called *paraxial beams*, which may be represented as a result of modulation of a plane wave with a wave number k , by an axially-symmetric *envelope function* $f(\rho)$, where $\rho \equiv \{x, y\}$, with a relatively large effective radius $a \gg 1/k$.⁷¹ Such beams give me a convenient opportunity to deliver on the promise made in Sec. 1: calculate the angular momentum \mathbf{L} of a circularly polarized wave propagating in free space, and prove its fundamental relation to the wave's energy U . Let us start from the calculation of U for a paraxial beam (with an

⁷⁰ See, e.g., QM Sec. 2.9.

⁷¹ Note that propagating in a uniform medium, i.e. outside of grade-index fibers or other focusing systems, such beams gradually increase their width a due to diffraction – the effect to be analyzed in the next chapter.

arbitrary, but spatially-localized envelope f) of a circularly polarized wave, with the transverse electric field components given by Eq. (19):

$$E_x = E_0 f(\rho) \cos \psi, \quad E_y = \mp E_0 f(\rho) \sin \psi, \quad (7.182a)$$

where E_0 is the real amplitude of the wave's electric field at the propagation axis, $\psi \equiv kz - \omega t + \varphi$ is its total phase, and the two signs correspond to two possible directions of the circular polarization.⁷² According to Eq. (6), the corresponding transverse components of the magnetic field are

$$H_x = \pm \frac{E_0}{Z_0} f(\rho) \sin \psi, \quad H_y = \frac{E_0}{Z_0} f(\rho) \cos \psi. \quad (7.182b)$$

These expressions are sufficient to calculate the energy density (6.113) of the wave,⁷³

$$u = \frac{\epsilon_0 (E_x^2 + E_y^2)}{2} + \frac{\mu_0 (H_x^2 + H_y^2)}{2} = \frac{\epsilon_0 E_0^2 f^2}{2} + \frac{\mu_0 E_0^2 f^2}{2 Z_0^2} \equiv \epsilon_0 E_0^2 f^2, \quad (7.183)$$

and hence the full energy (per unit length in the direction z of the wave's propagation) of the beam:

$$U = \int u d^2r \equiv 2\pi \int_0^\infty u \rho d\rho = 2\pi \epsilon_0 E_0^2 \int_0^\infty f^2 \rho d\rho. \quad (7.184)$$

However, the transverse fields (182) are insufficient to calculate a non-zero average of \mathbf{L} . Indeed, following the angular momentum's definition in mechanics,⁷⁴ $\mathbf{L} \equiv \mathbf{r} \times \mathbf{p}$, where \mathbf{p} is the particle's (linear) momentum, we may use Eq. (6.115) for the electromagnetic field momentum's density \mathbf{g} in free space, to define the field's angular momentum's density as

$$\mathbf{l} \equiv \mathbf{r} \times \mathbf{g} \equiv \frac{1}{c^2} \mathbf{r} \times \mathbf{S} \equiv \frac{1}{c^2} \mathbf{r} \times (\mathbf{E} \times \mathbf{H}). \quad (7.185)$$

EM field's
angular
momentum

Let us use the familiar *bac minus cab* rule of the vector algebra⁷⁵ to transform this expression to

$$\mathbf{l} = \frac{1}{c^2} [\mathbf{E}(\mathbf{r} \cdot \mathbf{H}) - \mathbf{H}(\mathbf{r} \cdot \mathbf{E})] \equiv \frac{1}{c^2} \{ \mathbf{n}_z [E_z(\mathbf{r} \cdot \mathbf{H}) - H_z(\mathbf{r} \cdot \mathbf{E})] + [\mathbf{E}_t(\mathbf{r} \cdot \mathbf{H}) - \mathbf{H}_t(\mathbf{r} \cdot \mathbf{E})] \}. \quad (7.186)$$

If the field is purely transverse ($E_z = H_z = 0$), as it is in a strictly plane wave, the first square brackets in the last expression vanish, while the second bracket gives an azimuthal component of \mathbf{l} , which oscillates in time and vanishes at its time averaging. (This is exactly the reason why I have not tried to calculate \mathbf{L} during our first discussion of the circularly polarized waves in Sec. 1.)

⁷² For our task of calculating two *quadratic* forms of the fields (\mathbf{L} and U), their real representation (182) is more convenient than the complex-exponent one. However, for *linear* manipulations, the latter representation of the circularly-polarized waves, $\mathbf{E}_t = E_0 f(\rho) \text{Re}[(\mathbf{n}_x \pm i\mathbf{n}_y) \exp\{i\psi\}]$, $\mathbf{H}_t = (E_0/Z_0) f(\rho) \text{Re}[(\mp i\mathbf{n}_x + \mathbf{n}_y) \exp\{i\psi\}]$, is usually more convenient, and is broadly used.

⁷³ Note that, in contrast to a linearly-polarized wave (16), the energy density of a circularly-polarized wave does not depend on the full phase ψ – in particular, on t at fixed z , or vice versa. This is natural because its field vectors rotate (keeping their magnitude) rather than oscillate – see Fig. 3b.

⁷⁴ See, e.g., CM Eq. (1.31).

⁷⁵ See, e.g., MA Eq. (7.5).

Fortunately, our discussion of optical fibers, in particular, the derivation of Eqs. (167), (168), and (170), gives us a clear clue on how to resolve this paradox. If the envelope function $f(\rho)$ differs from a constant, the transverse wave components (182) alone do *not* satisfy the Maxwell equations (2b), which necessitates longitudinal components E_z and H_z of the fields, with⁷⁶

$$\frac{\partial E_z}{\partial z} = -\frac{\partial E_x}{\partial x} - \frac{\partial E_y}{\partial y}, \quad \frac{\partial H_z}{\partial z} = -\frac{\partial H_x}{\partial x} - \frac{\partial H_y}{\partial y}. \quad (7.187)$$

However, as these expressions show, if the envelope function f changes very slowly in the sense $df/d\rho \sim f/a \ll kf$, the longitudinal components are very small and do not have a back effect on the transverse components. Hence, the above calculation of U is still valid (asymptotically, at $ka \rightarrow 0$), and we may still use Eqs. (182) on the right-hand side of Eqs. (187),

$$\frac{\partial E_z}{\partial z} = E_0 \left(-\frac{\partial f}{\partial x} \cos \psi \pm \frac{\partial f}{\partial x} \sin \psi \right), \quad \frac{\partial H_z}{\partial z} = \frac{E_0}{Z_0} \left(\mp \frac{\partial f}{\partial x} \sin \psi - \frac{\partial f}{\partial x} \cos \psi \right), \quad (7.188)$$

and integrate them over z as

$$\begin{aligned} E_z &= E_0 \int \left(-\frac{\partial f}{\partial x} \cos \psi \pm \frac{\partial f}{\partial x} \sin \psi \right) dz = \frac{E_0}{k} \left(-\frac{\partial f}{\partial x} \int \cos \psi d\psi \pm \frac{\partial f}{\partial x} \int \sin \psi d\psi \right) \\ &\equiv \frac{E_0}{k} \left(-\frac{\partial f}{\partial x} \sin \psi \mp \frac{\partial f}{\partial x} \cos \psi \right). \end{aligned} \quad (7.189a)$$

Here the integration constant is taken for zero because no wave field component may have a time-independent part. Integrating, absolutely similarly, the second of Eqs. (188), we get

$$H_z = \frac{E_0}{kZ_0} \left(\pm \frac{\partial f}{\partial x} \cos \psi - \frac{\partial f}{\partial y} \sin \psi \right). \quad (7.189b)$$

With the same approximation, we may calculate the longitudinal (z -) component of \mathbf{I} , given by the first term of Eq. (186), keeping only the dominating, transverse fields (182) in the scalar products:

$$l_z = E_z (\mathbf{r} \cdot \mathbf{H}_t) - H_z (\mathbf{r} \cdot \mathbf{E}_t) \equiv E_z (xH_x + yH_y) - H_z (xE_x + yE_y). \quad (7.190)$$

Plugging in Eqs. (182) and (189), and taking into account that in free space, $k = \omega/c$, and hence $1/Z_0 c^2 k = \epsilon_0/\omega$, we get:

$$l_z = \mp \frac{\epsilon_0 E_0^2}{\omega} \left(xf \frac{\partial f}{\partial x} + y \frac{\partial f}{\partial y} \right) \equiv \mp \frac{\epsilon_0 E_0^2}{2\omega} \left[x \frac{\partial(f^2)}{\partial x} + y \frac{\partial(f^2)}{\partial y} \right] \equiv \mp \frac{\epsilon_0 E_0^2}{2\omega} \mathbf{p} \cdot \nabla(f^2) \equiv \mp \frac{\epsilon_0 E_0^2}{2\omega} \rho \frac{d(f^2)}{d\rho}. \quad (7.191)$$

Hence the total angular momentum of the beam (per unit length), is

$$L_z = \int l_z d^2 r \equiv 2\pi \int_0^\infty l_z \rho d\rho = \mp \pi \frac{\epsilon_0 E_0^2}{\omega} \int_0^\infty \rho^2 \frac{d(f^2)}{d\rho} d\rho \equiv \mp \pi \frac{\epsilon_0 E_0^2}{\omega} \int_{\rho=0}^{\rho=\infty} \rho^2 d(f^2). \quad (7.192)$$

Taking this integral by parts, with the assumption that $\rho f \rightarrow 0$ at $\rho \rightarrow 0$ and $\rho \rightarrow \infty$ (at it is true for the Gaussian beam (181) and all realistic paraxial beams), we finally get

⁷⁶ The complex-exponential versions of these equalities are given by the bottom line of Eq. (100).

$$L_z = \pm \pi \frac{\epsilon_0 E_0^2}{\omega} \int_0^\infty f^2 d(\rho^2) \equiv \pm 2\pi \frac{\epsilon_0 E_0^2}{\omega} \int_0^\infty f^2 \rho d\rho. \quad (7.193)$$

Now comparing this expression with Eq. (184), we see that remarkably, the ratio L_z/U does not depend on the shape and the width of the beam (and of course on the wave's amplitude E_0), so these parameters are very simply and universally related:

$$L_z = \pm \frac{U}{\omega}. \quad (7.194)$$

Angular momentum at circular polarization

Since this relation is valid in the plane-wave limit $a \rightarrow \infty$, it may be attributed to plane waves as well, with the understanding that in real life they always have some width (“aperture”) restriction.

As the reader certainly knows, in quantum mechanics the energy excitations of any harmonic oscillator of frequency ω are quantized in the units of $\hbar\omega$, while the internal angular momentum of a particle is quantized in the units of $s\hbar$, where s is its spin. In this context, the classical relation (194) is used in quantum electrodynamics as the basis for treating the electromagnetic field excitation quanta (*photons*) as some sort of quantum particles with spin $s = 1$. (Such integer spin also fits the Bose-Einstein statistics of the electromagnetic radiation.)

Unfortunately, I do not have time/space for a further discussion of the (very interesting) physics of paraxial beams but cannot help noticing, at least in passing, the very curious effect of *helical waves* – the beams carrying not only the “spin” momentum (194), but also an additional “orbital” angular momentum. The distribution of their energy in space is not monotonic, as it is in the Gaussian beam (181), but reminds several threads twisted around the propagation axis – hence the term “helical”.⁷⁷ Mathematically, their field structure is described by the *associate Laguerre polynomials* – the same special functions that are used for the quantum-mechanical description of hydrogen-like atoms.⁷⁸ Presently, there are efforts to use such beams for the so-called *orbital angular momentum* (OAM) multiplexing for high-rate information transmission.⁷⁹

7.8. Resonant cavities

Generally, *resonators* are structures that may sustain oscillations (in electrodynamics, of the electromagnetic field) even without an external source, until the oscillation amplitude slowly decreases in time due to unavoidable energy losses. If the resonator quality (described by the so-called *Q-factor*, which will be defined and discussed in the next section) is high, $Q \gg 1$, this decay takes many oscillation periods. Alternatively, high- Q resonators may sustain high oscillating fields permanently, if driven by relatively weak incident waves. In contrast to lumped-element resonators, say, the well-known *LC tank circuit*, the subject of this section is *resonant cavities* (or “distributed resonators”) limited by either conducting or dielectric walls that contain distributed standing waves inside them.

⁷⁷ Noticing such solutions of the Maxwell equations may be traced back to at least a 1943 theoretical work by J. Humbert; however, this issue had not been discussed in literature too much until experiments carried out in 1992 – see, e.g. L. Allen *et al.*, *Optical Angular Momentum*; IOP, 2003.

⁷⁸ See, e.g., QM Sec. 3.7.

⁷⁹ See, e.g., J. Wang *et al.*, *Nature Photonics* **6**, 488 (2012).

Conceptually the simplest resonant cavity is the *Fabry-Pérot interferometer*⁸⁰ that may be obtained by placing two well-conducting planes parallel to each other.⁸¹ Indeed, in Sec. 3 we have seen that if a plane wave is normally incident on such a “perfect mirror”, located at $z = 0$, its reflection, at negligible skin depth, results in a standing wave described by Eq. (61b):

$$E(z, t) = \operatorname{Re} \left(2E_\omega e^{-i\omega t + i\pi/2} \right) \sin kz. \quad (7.195)$$

This wave would not change if we place the second mirror (isolating the segment of length l from the external wave source) at any position $z = l$ with $\sin kl = 0$, i.e. with

$$kl = p\pi, \quad \text{where } p = 1, 2, \dots \quad (7.196)$$

This condition, which determines the spectrum of *own* (or *resonance*, or *eigen-*) *frequencies* of the resonator of fixed length l ,

$$\omega_p = \nu k_p = \frac{\pi\nu}{a} p, \quad \text{with } \nu = \frac{1}{(\epsilon\mu)^{1/2}}, \quad (7.197)$$

has a simple physical sense: the resonator’s length l equals exactly p half-waves of the frequency ω_p . Though this is all very simple, please note a considerable change of philosophy from what we have been doing in the previous sections: the main task of the resonator’s analysis is finding its own frequencies ω_p , which are now determined by the system’s geometry rather than by an external wave source.

Before we move to cavities of more complex shapes, let us use Eq. (62) to represent the magnetic field in the Fabry-Pérot interferometer:

$$H(z, t) = \operatorname{Re} \left(2 \frac{E_\omega}{Z} e^{-i\omega t} \right) \cos kz. \quad (7.198)$$

Expressions (195) and (198) show that in contrast to traveling waves, each field of the standing wave changes simultaneously (proportionately) at all points of the Fabry-Pérot resonator, turning to zero everywhere twice a period. At these instants, the energy of the corresponding field vanishes, but the total energy of the two fields stays constant because the counterpart field oscillates with the phase shift $\pi/2$. Such behavior is typical for all electromagnetic resonators.

A more technical remark is that we can readily get the same results (195)-(198) by solving the Maxwell equations from scratch. For example, we already know that in the absence of dispersion, losses, and sources, they are reduced to wave equations (3) for any field components. For the Fabry-Pérot resonator’s analysis, we can use the 1D form of these equations, say, for the transverse component of the electric field:

$$\left(\frac{\partial^2}{\partial z^2} - \frac{1}{\nu^2} \frac{\partial^2}{\partial t^2} \right) E = 0, \quad (7.199)$$

and solve it as a part of an eigenvalue problem with the corresponding boundary conditions. Indeed, by separating time and space variables as $E(z, t) = Z(z)\mathcal{T}(t)$, we obtain

⁸⁰ This device, named after its inventors, Charles Fabry and Alfred Pérot; is also called the *Fabry-Pérot étalon* (meaning “gauge”), because of its initial usage for light wavelength measurements.

⁸¹ The resonators formed by well conducting (usually, metallic) walls are frequently called *resonant cavities*.

$$\frac{1}{Z} \frac{d^2 Z}{dz^2} - \frac{1}{v^2} \frac{1}{\mathcal{T}} \frac{d^2 \mathcal{T}}{dt^2} = 0. \quad (7.200)$$

Calling the separation constant k^2 , we get two similar ordinary differential equations,

$$\frac{d^2 Z}{dz^2} + k^2 Z = 0, \quad \frac{d^2 \mathcal{T}}{dt^2} + k^2 v^2 \mathcal{T} = 0, \quad (7.201)$$

both with sinusoidal solutions, so that the product $Z(z)\mathcal{T}(t)$ is a standing wave with the wave vector k and frequency $\omega = kv$. (In this form, the equations are valid even in the presence of dispersion, but with a frequency-dependent wave speed: $v^2 = 1/\epsilon(\omega)\mu(\omega)$.) Now using the boundary conditions $E(0, t) = E(l, t) = 0$,⁸² we get the eigenvalue spectrum for k_p and hence for $\omega_p = vk_p$, given by Eqs. (196) and (197).

Lessons from this simple case study may be readily generalized to any cavity formed as a transmission line's section:⁸³ there are two approaches to finding the resonant frequency spectrum:

(i) We may look at a traveling wave solution and find where reflecting mirrors may be inserted without affecting the wave's structure.

(ii) We may solve the general 3D wave equations,

$$\left(\nabla^2 - \frac{1}{v^2} \frac{\partial^2}{\partial t^2} \right) f(\mathbf{r}, t) = 0, \quad (7.202)$$

for field components, as an eigenvalue problem with appropriate boundary conditions. If the system's parameters (and hence the coefficient v) do not change in time, the spatial and temporal variables of Eq. (202) may be *always* separated by taking

$$f(\mathbf{r}, t) = \sum_k f_k(\mathbf{r}) \mathcal{T}_k(t), \quad (7.203)$$

where each function $\mathcal{T}_k(t)$ *always* obeys the same equation as in Eq. (201), having the sinusoidal solution of frequency $\omega_k = vk$. Plugging this solution back into Eqs. (202), for the spatial distribution of the field, we get the *3D Helmholtz equation*,

$$\boxed{\left(\nabla^2 + k^2 \right) f_k(\mathbf{r}) = 0,} \quad (7.204)$$

3D
Helmholtz
equation

whose eigenfunctions $f_k(\mathbf{r})$ may be much more involved, especially for non-symmetric geometries.

Let us use these approaches to find the resonant frequency spectrum of a few simple, but practically important cavities. First of all, the first method is completely sufficient for the analysis of any resonator formed as a fragment of a uniform TEM transmission line (e.g., a coaxial cable), confined with two conducting lids normal to the line's direction. Indeed, since in such lines $k_z = k = \omega/v$, and the electric field is perpendicular to the propagation axis, e.g., parallel to the lid surface, the boundary conditions are exactly the same as in the Fabry-Pérot resonator, and we again arrive at the eigenfrequency spectrum (197).

⁸² This is of course the expression of the first of the general boundary conditions (104). The second of these conditions (for the magnetic field) is satisfied automatically for the transverse waves we are considering.

⁸³ The resonators may have different geometries as well, and in many cases, only the second approach may be used.

Now let us analyze a slightly more complex system: a rectangular metallic-wall cavity of volume $a \times b \times l$ – see Fig. 29. To use the first approach outlined above, let us consider the resonator as a finite-length ($\Delta z = l$) section of the rectangular waveguide extended along the z -axis, which was analyzed in detail in Sec. 6. As a reminder, at $a < b$, in the fundamental H_{10} traveling wave mode, both vectors \mathbf{E} and \mathbf{H} do not depend on y , with \mathbf{E} having only a y -component. In contrast, \mathbf{H} has two components, H_x and H_z , with the phase shift $\pi/2$ between them, and with H_x having the same phase as E_y – see Eqs. (131), (137), and (138). Hence, if a plane perpendicular to the z -axis, is placed so that the electric field vanishes on it, H_x also vanishes, so that both boundary conditions (104), pertinent to a perfect metallic wall, are fulfilled simultaneously.

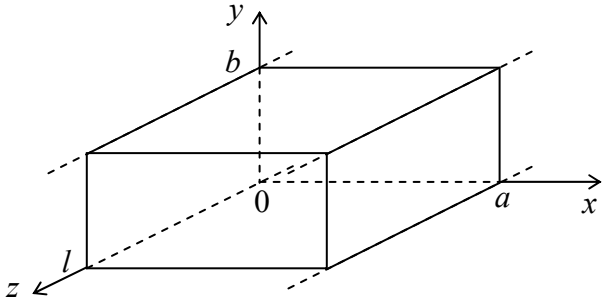


Fig. 7.29. Rectangular metallic-wall resonator as a finite section of a waveguide with the cross-section shown in Fig. 22.

As a result, the H_{10} wave would not be perturbed by two metallic walls separated by an integer number of half-wavelengths $\lambda_z/2$ corresponding to the wave number given by the combination of Eqs. (102) and (133):

$$k_z = (k^2 - k_t^2)^{1/2} = \left(\frac{\omega^2}{v^2} - \frac{\pi^2}{a^2} \right)^{1/2}. \quad (7.205)$$

Using this expression, we see that the smallest of these distances, $l = \lambda_z/2 = \pi/k_z$, gives the resonance frequency⁸⁴

$$\omega_{101} = v \left[\left(\frac{\pi}{a} \right)^2 + \left(\frac{\pi}{l} \right)^2 \right]^{1/2}, \quad (7.206)$$

where the indices of ω show the numbers of half-waves along each dimension of the system, in the order $[a, b, l]$. This is the lowest (“fundamental”) frequency of the resonator (if $b < a, l$).

The field distribution in this mode is close to that in the corresponding waveguide mode H_{10} (Fig. 22), with the important difference that the magnetic and electric fields are now shifted by phase $\pi/2$ both in space and time, just as in the Fabry-Pérot resonator – see Eqs. (195) and (198). Such a time shift allows for a very simple interpretation of the H_{101} mode, which is especially adequate for very flat resonators, with $b \ll a, l$. At the instant when the electric field reaches its maximum (Fig. 30a), i.e. when the magnetic field vanishes in the whole volume, the surface electric charge of the broadest (in Fig. 30, horizontal) walls of the resonator is largest, being localized mostly near the centers of the walls. At the immediate later times, the walls start to recharge via surface currents, whose density J is largest in the side walls, and reaches its maximal value in a quarter of the oscillation period $\tau = 2\pi/\omega_{101}$ – see Fig. 30b. The currents generate the vortex magnetic field, with looped field lines in the plane of the

⁸⁴ In most electrical engineering handbooks, the index corresponding to the shortest side of the resonator is listed last, so that the fundamental mode is nominated as H_{110} and its eigenfrequency as ω_{110} .

broadest face of the resonator. The surface currents continue to flow in this direction until (in one more quarter period) the broader walls of the resonator are fully recharged in the polarity opposite to that shown in Fig. 30a. After that, the surface currents start to flow in the direction opposite to that shown in Fig. 30b. This process, which repeats again and again, is conceptually similar to the well-known oscillations in a lumped *LC* circuit, with the role of (now, distributed) capacitance played mostly by the broadest walls of the resonator, and that of (now, distributed) inductance, by its narrower walls.

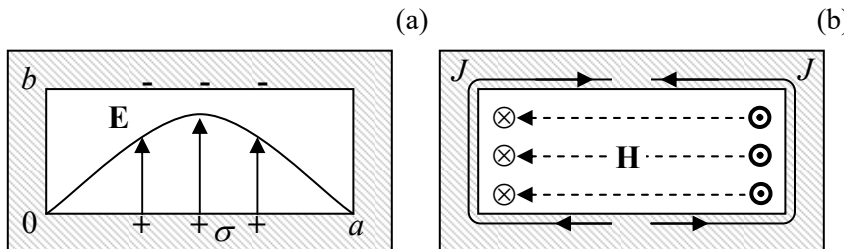


Fig. 7.30. Fields, charges, and currents in the fundamental (H_{101}) mode of a rectangular metallic resonator, at two instants separated by $\Delta t = \pi/2\omega_{101}$ – schematically.

In order to generalize Eq. (206) to higher oscillation modes, the second of the approaches discussed above is more prudent. Separating the variables in the Helmholtz equation (204) as $\mathcal{R}(\mathbf{r}) = X(x)Y(y)Z(z)$, we see that X , Y , and Z have to be either sinusoidal or cosinusoidal functions of their arguments, with the wave vector components satisfying the characteristic equation

$$k_x^2 + k_y^2 + k_z^2 = k^2 \equiv \frac{\omega^2}{v^2}. \quad (7.207)$$

In contrast to the wave propagation problem, now we are dealing with standing waves along all three dimensions, and have to satisfy the macroscopic boundary conditions (104) on all sets of parallel walls. It is straightforward to check that these conditions ($E_\tau = 0$, $H_n = 0$) are fulfilled at the following field component distribution:

$$\begin{aligned} E_x &= E_1 \cos k_x x \sin k_y y \sin k_z z, & H_x &= H_1 \sin k_x x \cos k_y y \cos k_z z, \\ E_y &= E_2 \sin k_x x \cos k_y y \sin k_z z, & H_y &= H_2 \cos k_x x \sin k_y y \cos k_z z, \\ E_z &= E_3 \sin k_x x \sin k_y y \cos k_z z, & H_z &= H_3 \cos k_x x \cos k_y y \sin k_z z, \end{aligned} \quad (7.208)$$

with each of the wave vector components having an equidistant spectrum similar to Eq. (196):

$$k_x = \frac{\pi n}{a}, \quad k_y = \frac{\pi m}{b}, \quad k_z = \frac{\pi p}{l}, \quad (7.209)$$

so that the full spectrum of resonance frequencies is given by the following formula:

$$\omega_{nmp} = \nu k = \nu \left[\left(\frac{\pi n}{a} \right)^2 + \left(\frac{\pi m}{b} \right)^2 + \left(\frac{\pi p}{l} \right)^2 \right]^{1/2}, \quad (7.210)$$

which is a natural generalization of Eq. (206). Note, however, that of the three integers m , n , and p , at least two have to be different from zero to keep the fields (208) from vanishing at all points.

We may use Eq. (210), in particular, to evaluate the number of different modes in a relatively small range $d^3 k \ll k^3$ of the wave vector space volume that is, on the other hand, much larger than the reciprocal volume, $1/V = 1/abl$, of the cavity. Taking into account that each eigenfrequency (210), with

$nml \neq 0$, corresponds to two field modes with different polarizations,⁸⁵ the argumentation absolutely similar to the one used for the 2D case at the end of Sec. 7, yields

Oscillation mode density

$$dN = 2V \frac{d^3 k}{(2\pi)^3}. \quad (7.211)$$

This property, valid for resonators of arbitrary shape, is broadly used in classical and quantum statistical physics,⁸⁶ in the following form. If some electromagnetic mode functional $f(\mathbf{k})$ is a smooth function of the wave vector \mathbf{k} , and the volume V is large enough, then Eq. (211) may be used to approximate the sum of the functional's values over the modes by an integral:

$$\sum_{\mathbf{k}} f(\mathbf{k}) \approx \int_N f(\mathbf{k}) dN \equiv \int_{\mathbf{k}} f(\mathbf{k}) \frac{dN}{d^3 k} d^3 k = 2 \frac{V}{(2\pi)^3} \int_{\mathbf{k}} f(\mathbf{k}) d^3 k. \quad (7.212)$$

Leaving similar analyses of resonant cavities of some other simple shapes for the reader's exercises, let me finish this section by noting that low-loss resonators may be also formed by finite-length sections of not only metallic-wall waveguides of various cross-sections but also of dielectric waveguides. Moreover, even a simple slab of a dielectric material with a μ/ϵ ratio substantially different from that of its environment (say, of the free space) may be used as a high- Q Fabry-Pérot interferometer (Fig. 31), due to an effective wave reflection from its surfaces at the normal and especially an inclined incidence – see, respectively, Eqs. (68), and Eqs. (91) and (95).

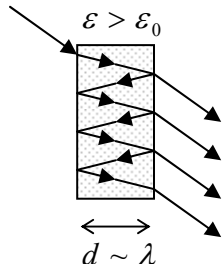


Fig. 7.31. A dielectric Fabry-Pérot interferometer.

Actually, such dielectric Fabry-Pérot interferometers are frequently more convenient for practical purposes than metallic-wall resonators, not only due to possibly lower losses (especially in the optical range), but also due to a natural coupling to the environment, which offers a ready way of wave insertion and extraction – see Fig. 31 again. The backside of the same medal is that this coupling to the environment provides an additional mechanism of power losses, limiting the resonance's quality factor – see the next section.

7.9. Energy loss effects

The inevitable energy losses (“dissipation”) in passive media lead, in two basic situations, to two different effects. In a long transmission line fed by a constant wave source, the losses lead to a gradual

⁸⁵ This fact becomes evident from plugging Eqs. (208) into the Maxwell equation $\nabla \cdot \mathbf{E} = 0$. The resulting equation, $k_x E_1 + k_y E_2 + k_z E_3 = 0$, with the discrete, equidistant spectrum (209) for each wave vector component, may be always satisfied by two linearly-independent sets of the constants $E_{1,2,3}$.

⁸⁶ See, e.g., QM Sec. 1.1 and SM Sec. 2.6.

attenuation of the wave, i.e. to a decrease of its amplitude, and hence its power \mathcal{P} , with the growing distance z from the source. In linear materials, the power losses are proportional to the power \mathcal{P} carried by the wave, so that the energy balance on a small segment dz takes the form

$$d\mathcal{P}_{\text{loss}} \equiv -d\mathcal{P} \equiv -\frac{d\mathcal{P}}{dz} dz = \alpha \mathcal{P} dz. \quad (7.213)$$

The coefficient α participating in the last form of Eq. (213), and hence defined as

$$\alpha \equiv -\frac{d\mathcal{P}/dz}{\mathcal{P}}, \quad (7.214)$$

is called the *attenuation constant*.⁸⁷ Comparing the solution of Eq. (213),

$\mathcal{P}(z) = \mathcal{P}(0)e^{-\alpha z},$

(7.215) Wave's attenuation

with Eq. (29), where k is replaced with k_z , we see that α may be expressed as

$$\alpha = 2 \operatorname{Im} k_z, \quad (7.216)$$

where k_z is the component of the wave vector along the transmission line. In the most important limit when the losses are low in the sense $\alpha \ll |k_z| \approx \operatorname{Re} k_z$, its effects on the field distribution along the line's cross-section are negligible, making the calculation of α rather straightforward. In particular, in this limit, the contributions to attenuation from two major sources, the energy losses in the filling dielectric and the skin-effect losses in conducting walls, are independent and additive.

The dielectric losses are especially simple to describe. Indeed, a review of our calculations in Secs. 5-7 shows that all of them remain valid if either $\epsilon(\omega)$, or $\mu(\omega)$, or both, and hence $k(\omega)$, have small imaginary parts:

$$k'' = \omega \operatorname{Im} [\epsilon^{1/2}(\omega) \mu^{1/2}(\omega)] \ll k'. \quad (7.217)$$

In TEM transmission lines, $k_z = k$, and hence Eq. (216) yields

$\alpha_{\text{filling}} = 2k'' = 2\omega \operatorname{Im} [\epsilon^{1/2}(\omega) \mu^{1/2}(\omega)].$

(7.218) Attenuation due to filling

For dielectric waveguides, in particular optical fibers, these losses are the main attenuation mechanism. As was discussed in Sec. 7, in practical optical fibers $\kappa_i R \gg 1$, i.e. most of the field propagates (as an evanescent wave) in the cladding, with a field distribution very close to the TEM wave. This is why Eq. (218) is approximately valid if it is applied to the cladding material alone. In waveguides with non-TEM waves, we can use the relations between k_z and k , derived in the previous sections, to re-calculate k'' into $\operatorname{Im} k_z$. (Note that at this recalculation, the values of k , have to be kept real, because they are just the eigenvalues of the Helmholtz equation (101), which does not include the filling media parameters.).

⁸⁷ In engineering, attenuation is frequently measured in *decibels per meter*, abbreviated as db/m (the term not to be confused with dBm standing for decibel-milliwatt):

$$\alpha|_{\text{db/m}} \equiv 10 \log_{10} \frac{\mathcal{P}(z)}{\mathcal{P}(z+1 \text{ m})} = 10 \log_{10} e^{\alpha[1/\text{m}]} \equiv \frac{10}{\ln 10} \alpha [\text{m}^{-1}] \approx 4.34 \alpha [\text{m}^{-1}].$$

In transmission lines and waveguides and with metallic walls, higher energy losses may come from the skin effect. If the wavelength λ is much larger than δ_s , as it usually is,⁸⁸ the losses may be readily evaluated using Eq. (6.36):

$$\frac{d\mathcal{P}_{\text{loss}}}{dA} \equiv -\frac{d\mathcal{P}}{dA} = H_{\text{wall}}^2 \frac{\mu\omega\delta_s}{4}, \quad (7.219)$$

where H_{wall} is the real amplitude of the tangential component of the magnetic field at the wall's surface. The total power loss $\mathcal{P}_{\text{loss}}/dz$ per unit length of a waveguide, i.e. the right-hand side of Eq. (213), now may be calculated by the integration of this expression along the contour(s) limiting the cross-section of all conducting walls. Since our calculation is only valid for low losses, we may ignore their effect on the field distribution, so that the unperturbed distributions may be used both in Eq. (219), i.e. in the numerator of Eq. (214), and also for the calculation of the average propagating power, i.e. the denominator of Eq. (214) – as the integral of the Poynting vector over the cross-section of the waveguide.

Let us see how this approach works for the TEM mode in one of the simplest transmission lines, the coaxial cable (Fig. 20). As we already know from Sec. 5, in the coarse-grain approximation, implying negligible power loss, the TEM mode field distributions between the two conductors are the same as in statics, namely:

$$H_z = 0, \quad H_\rho = 0, \quad H_\varphi(\rho) = H_0 \frac{a}{\rho}, \quad (7.220)$$

where H_0 is the field's amplitude on the surface of the inner conductor, and

$$E_z = 0, \quad E_\rho(\rho) = ZH_\varphi(\rho) = ZH_0 \frac{a}{\rho}, \quad E_\varphi = 0, \quad \text{where } Z \equiv \left(\frac{\mu}{\epsilon} \right)^{1/2}. \quad (7.221)$$

Neglecting the power losses for a minute, we may plug these expressions into Eq. (42) to calculate the time-averaged Poynting vector:

$$\bar{S} = \frac{Z|H_\varphi(\rho)|^2}{2} = \frac{Z|H_0|^2}{2} \left(\frac{a}{\rho} \right)^2, \quad (7.222)$$

and from it, the total wave power flow through the cross-section:

$$\mathcal{P} = \int_A \bar{S} d^2r = \frac{Z|H_0|^2 a^2}{2} 2\pi \int_a^b \frac{\rho d\rho}{\rho^2} = \pi Z|H_0|^2 a^2 \ln \frac{b}{a}. \quad (7.223)$$

Next, for this particular system (Fig. 20), the contours limiting the wall cross-section are circles of radii $\rho = a$ (where the surface field amplitude H_{walls} equals, in our notation, H_0), and $\rho = b$ (where, according to Eq. (214), the field is a factor of b/a lower). As a result, for the power loss per unit length, Eq. (219) yields

$$\frac{d\mathcal{P}_{\text{loss}}}{dz} = \oint_{C_a + C_b} \frac{d\mathcal{P}_{\text{loss}}}{dA} dl = \left(2\pi a |H_0|^2 + 2\pi b \left| H_0 \frac{a}{b} \right|^2 \right) \frac{\mu_0 \omega \delta_s}{4} = \frac{\pi}{2} a \left(1 + \frac{a}{b} \right) \mu \omega \delta_s |H_0|^2. \quad (7.224)$$

⁸⁸ As follows from Eq. (78), which may be used for crude estimates even in cases of arbitrary wave incidence, this condition is necessary for low attenuation: $\alpha \ll k$ only if $\beta \ll 1$.

Note that at $a \ll b$, the losses in the inner conductor dominate, despite its smaller surface, because of the higher surface field.

Now we may plug Eqs. (223) and (224) into the definition (214) of α , to calculate the skin-effect contribution to the attenuation constant:

$$\alpha_{\text{skin}} \equiv \frac{d\mathcal{P}_{\text{loss}} / dz}{\mathcal{P}} = \frac{1}{2 \ln(b/a)} \left(\frac{1}{a} + \frac{1}{b} \right) \frac{\mu \omega \delta_s}{Z} \equiv \frac{k \delta_s}{2 \ln(b/a)} \left(\frac{1}{a} + \frac{1}{b} \right). \quad (7.225)$$

This result shows that the relative (dimensionless) attenuation, α/k , scales approximately as the ratio $\delta_s/\min[a, b]$, in a semi-quantitative agreement with the plane-wave result (78).

Let us use this result to evaluate α for the standard TV cable RG-6/U, with copper conductors of diameters $2a = 1$ mm, $2b = 4.7$ mm, and $\epsilon \approx 2.2\epsilon_0$ and $\mu \approx \mu_0$. According to Eq. (6.33), for $f = 100$ MHz (i.e. $\omega \approx 6.3 \times 10^8$ s $^{-1}$) the skin depth of pure copper at room temperature (with $\sigma \approx 6.0 \times 10^7$ S/m) is close to 6.5×10^{-6} m, while $k = \omega(\epsilon\mu)^{1/2} = (\epsilon/\epsilon_0)^{1/2}(\omega/c) \approx 3.1$ m $^{-1}$. As a result, the attenuation is rather low: $\alpha_{\text{skin}} \approx 0.016$ m $^{-1}$, so that the attenuation length scale $l_d \equiv 1/\alpha$ is about 60 m. Hence the attenuation in a cable connecting a roof TV antenna or a cable distribution box to a TV set is not a big problem, though using a worse conductor, e.g., steel, would make the losses rather noticeable. (Hence the current worldwide shortage of copper.) However, the use of such cable in the X-band ($f \sim 10$ GHz) is more problematic. Indeed, though the skin depth $\delta_s \propto \omega^{-1/2}$ decreases with frequency, the wavelength drops, i.e. k increases, even faster ($k \propto \omega$), so that the attenuation $\alpha_{\text{skin}} \propto \omega^{1/2}$ becomes close to 0.16 m $^{-1}$, i.e. l_d to ~ 6 m. This is why at such frequencies, it may be necessary to use rectangular waveguides, with their larger internal dimensions $a, b \sim 1/k$, and hence lower attenuation. Let me leave the calculation of this attenuation, using Eq. (219) and the results derived in Sec. 7, for the reader's exercise.

The main effect of dissipation on free oscillations in *resonators* is different: here it leads to a gradual decay of the oscillating fields' energy U in time. A useful dimensionless measure of this decay, called the *Q-factor*, is commonly defined by writing the following temporal analog of Eq. (213):⁸⁹

$$-dU \equiv \mathcal{P}_{\text{loss}} dt = \frac{\omega}{Q} U dt, \quad (7.226)$$

where ω is the resonance frequency in the loss-free limit, and

$$\frac{\omega}{Q} \equiv \frac{\mathcal{P}_{\text{loss}}}{U}. \quad (7.227)$$

Q-factor

The solution of Eq. (226),

$$U(t) = U(0) e^{-t/\tau}, \quad \text{with } \tau \equiv \frac{Q}{\omega} \equiv \frac{Q/2\pi}{\omega/2\pi} = \frac{Q\tau}{2\pi}, \quad (7.228)$$

which is the temporal analog of Eq. (215), shows the physical meaning of the *Q*-factor: the characteristic time τ of the oscillation energy's decay is $(Q/2\pi)$ times longer than the oscillation period $\tau = 2\pi/\omega$. (Another useful interpretation of *Q* comes from the universal relation⁹⁰

⁸⁹ As losses grow, the oscillation waveform deviates from the sinusoidal one, and the very notion of "oscillation frequency" becomes vague. As a result, the parameter *Q* is well-defined only if it is much higher than 1.

⁹⁰ See, e.g., CM Sec. 5.1.

$$Q = \frac{\omega}{\Delta\omega}, \quad (7.229)$$

where $\Delta\omega$ is the so-called *FWHM*⁹¹ *bandwidth* of the resonance, namely the difference between the two values of the external signal frequency, one above and one below ω , at which the energy of the oscillations induced in the resonator by an input signal is twice lower than its resonance value.)

In the important particular case of a resonant cavity formed by the insertion of metallic walls into a TEM transmission line of a small cross-section (with the linear size scale a much less than the wavelength λ), there is no need to calculate the Q -factor directly, provided that the line attenuation coefficient α is already known. In fact, as was discussed in Sec. 8 above, the standing waves in such a resonator, of the length given by Eq. (196): $l = p(\lambda/2)$ with $p = 1, 2, \dots$, may be understood as an overlap of two TEM waves propagating in opposite directions, or in other words, a traveling wave plus its reflection from one of the ends, the whole roundtrip taking time $\Delta t = 2l/v = p\lambda/v = 2\pi p/\omega = p\tau$. According to Eq. (215), at this distance, the wave's power drops by a factor of $\exp\{-2\alpha l\} = \exp\{-p\alpha\lambda\}$. On the other hand, the same decay may be viewed as taking place in time, and according to Eq. (228), results in the drop by a factor of $\exp\{-\Delta t/\tau\} = \exp\{-(p\tau)/(Q/\omega)\} = \exp\{-2\pi p/Q\}$. Comparing these two exponents, we get

Q vs. α

$$Q = \frac{2\pi}{\alpha\lambda} = \frac{k}{\alpha}. \quad (7.230)$$

This simple relation neglects the losses at the wave reflection from the walls limiting the resonator length. This approximation is indeed legitimate at $a \ll \lambda$; if this relation is violated, or if we are dealing with more complex resonator modes (such as those based on the reflection of E or H waves), the Q -factor may be different from that given by Eq. (230), and needs to be calculated directly from Eq. (227). A substantial relief for such a direct calculation is that, just at the calculation of small attenuation in waveguides, in the low-loss limit ($Q \gg 1$), both the numerator and denominator of the right-hand side of that formula may be calculated neglecting the effects of the power loss on the field distribution in the resonator. I am leaving such a calculation, for the simplest (rectangular and circular) resonant cavities, for the reader's exercise.

To conclude this chapter, the last remark: in some distributed resonators (including certain dielectric resonators and metallic cavities with holes in their walls), additional losses due to the wave radiation into the environment are also possible. In some simple cases (say, the Fabry-Pérot interferometer shown in Fig. 31) the calculation of these *radiative losses* is straightforward, but sometimes it requires more elaborated approaches that will be discussed in the next chapter.

7.10. Exercise problems

7.1.* Find the temporal Green's function of a medium whose complex dielectric constant obeys the Lorentz oscillator model given by Eq. (32), using:

- (i) the Fourier transform, and
- (ii) the direct solution of Eq. (30).

Hint: For the Fourier-transform approach, you may like to use the Cauchy integral.⁹²

⁹¹ FWHM is the acronym for *Full Width at Half-Maximum*.

7.2. The electric polarization of some material responds in the following way to an electric field step:⁹³

$$P(t) = \epsilon_1 E_0 (1 - e^{-t/\tau}), \quad \text{if } E(t) = E_0 \times \begin{cases} 0, & \text{for } t < 0, \\ 1, & \text{for } 0 < t, \end{cases}$$

where $\tau > 0$ and ϵ_1 are some constants. Calculate the complex permittivity $\epsilon(\omega)$ of this material, and discuss a possible simple physical model giving such dielectric response.

7.3. Calculate the complex permittivity $\epsilon(\omega)$ of a material whose dielectric-response Green's function defined by Eq. (23), is

$$G(\theta) = G_0 (1 - e^{-\theta/\tau}),$$

with some positive constants G_0 and τ . What is the difference between this dielectric response and the apparently similar one considered in the previous problem?

7.4. Use the Lorentz oscillator model of an atom, given by Eq. (30), to calculate the average potential energy of the atom in a uniform, sinusoidal ac electric field, and use the result to calculate the potential profile created for the atom by a standing electromagnetic wave with the electric field amplitude $E_\omega(\mathbf{r})$.

7.5. The solution of the previous problem shows that a standing, plane electromagnetic wave exerts a time-averaged force on an otherwise free non-relativistic charged particle. Reveal the physics of this force by writing and solving the equations of motion of the particle in:

- (i) a linearly-polarized, monochromatic, plane traveling wave, and
- (ii) a similar but standing wave.

7.6. Use the first of Eqs. (54) to relate the integral

$$\int_0^\infty \epsilon''(\Omega) \Omega d\Omega$$

to the plasma frequency for the Lorentz oscillator model of a system of non-interacting atoms.

7.7. Calculate, sketch, and discuss the dispersion relation for electromagnetic waves propagating in a medium described by Eq. (32), for the case of negligible damping.

7.8. As was briefly discussed in Sec. 2,⁹⁴ a wave pulse of a finite but relatively large spatial extension $\Delta z \gg \lambda \equiv 2\pi/k$ may be formed as a *wave packet* – a sum of sinusoidal waves with wave vectors \mathbf{k} within a relatively narrow interval. Consider an electromagnetic plane wave packet of this type, with the electric field distribution

$$\mathbf{E}(\mathbf{r}, t) = \operatorname{Re} \int_{-\infty}^{+\infty} \mathbf{E}_k e^{i(kz - \omega_k t)} dk, \quad \text{with } \omega_k [\epsilon(\omega_k) \mu(\omega_k)]^{1/2} \equiv |k|,$$

⁹² See, e.g., MA Eq. (15.2).

⁹³ This function $E(t)$ is of course proportional to the well-known step function $\theta(t)$ – see, e.g., MA Eq. (14.3). I am not using this notion just to avoid possible confusion between two different uses of the Greek letter θ .

⁹⁴ For even more detail, see CM Sec. 5.3 and especially QM Sec. 2.2.

propagating along the z -axis in an isotropic, linear, and loss-free (but not necessarily dispersion-free) medium. Express the full energy of the packet (per unit area of the wave's front) via the complex amplitudes \mathbf{E}_k , and discuss its dependence on time.

7.9. Prove the Lorentz reciprocity relation expressed by Eq. (6.121), for a linear isotropic medium.

7.10. A plane wave of frequency ω is normally incident, from free space, on the surface of a collision-free plasma with the electron density growing linearly with the distance from the surface: $n = \gamma z$ for $z \geq 0$, where $\gamma > 0$ is a constant. Calculate the functional form of the resulting standing wave's "tail" deep inside the plasma, i.e. at $z \rightarrow \infty$.

7.11.* Analyze the effect of a time-independent uniform magnetic field \mathbf{B}_0 , parallel to the direction \mathbf{n} of electromagnetic wave propagation, on the wave's dispersion in plasma, within the same simple model that was used in Sec. 2 for the derivation of Eq. (38). (Limit your analysis to relatively weak waves, whose magnetic field is negligible in comparison with \mathbf{B}_0 .)

Hint: You may like to represent the incident wave as a linear superposition of two circularly polarized waves, with opposite polarization directions.

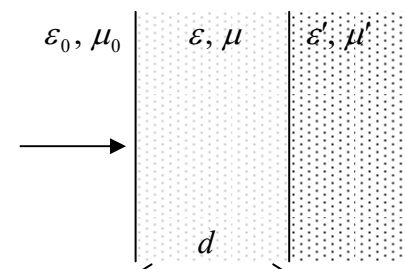
7.12. A monochromatic plane electromagnetic wave is normally incident, from free space, on a uniform slab with electric permittivity ϵ and magnetic permeability μ , with the slab's thickness d comparable with the wavelength.

(i) Calculate the power transmission coefficient \mathcal{T} , i.e. the fraction of the incident wave's power, that is transmitted through the slab.

(ii) Assuming that ϵ and μ are frequency-independent and positive, analyze in detail the frequency dependence of \mathcal{T} . In particular, how does the function $\mathcal{T}(\omega)$ depend on the slab's thickness d and the wave impedance $Z \equiv (\mu/\epsilon)^{1/2}$ of its material?

7.13. A plane electromagnetic wave, with free-space wave number k_0 , is normally incident on a plane, conducting film of thickness $d \sim \delta_s \ll 1/k_0$. Calculate the power transmission coefficient of the system, i.e. the fraction of the incident wave's power propagating beyond the film. Analyze the result in the limits of small and large ratio d/δ_s .

7.14. A plane wave of frequency ω is normally incident, from free space, on a plane surface of a material with real electric permittivity ϵ' and magnetic permeability μ' . To minimize the wave's reflection from the surface, it may be covered with a layer, of thickness d , of another transparent material – see the figure on the right. Calculate the optimal values of ϵ , μ , and d .

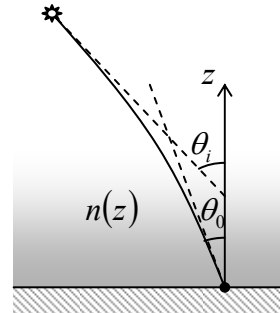


7.15. A monochromatic plane wave is incident from inside a medium with $\epsilon\mu > \epsilon_0\mu_0$ onto its plane surface, at an angle of incidence θ larger than the critical angle $\theta_c = \sin^{-1}(\epsilon_0\mu_0/\epsilon\mu)^{1/2}$. Calculate

the depth δ of the evanescent wave penetration into the free space, and analyze its dependence on θ . Does the result depend on the wave's polarization?

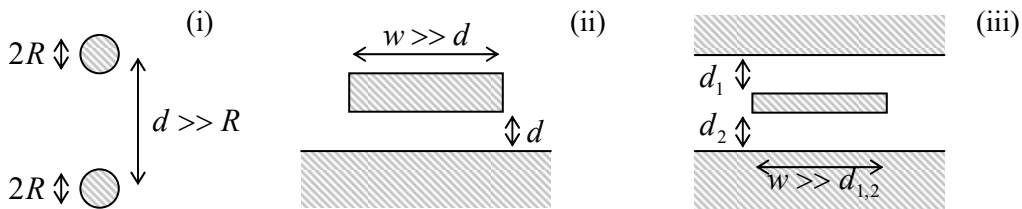
7.16. Analyze the possibility of propagation of surface electromagnetic waves along a plane boundary between plasma and free space. In particular, calculate and analyze the dispersion relation of the waves.

Hint: Assume that the magnetic field of the wave is parallel to the boundary and perpendicular to the wave's propagation direction. (After solving the problem, justify this mode choice.)



7.17. Light from a very distant source arrives to an observer through a plane layer of nonuniform medium with a certain 1D gradient of its refraction index $n(z)$, at angle θ_0 – see the figure on the right. What is the genuine direction θ_i to the source, if $n(z) \rightarrow 1$ at $z \rightarrow \infty$? (This problem is evidently important for high-precision astronomical measurements from the Earth's surface.)

7.18. Calculate the impedance Z_W of the long, straight TEM transmission lines formed by metallic electrodes with the cross-sections shown in the figure below:



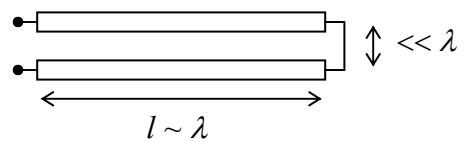
- (i) two round, parallel wires separated by distance $d \gg R$,
- (ii) a *microstrip line* of width $w \gg d$,
- (iii) a *stripline* with $w \gg d_1 \sim d_2$,

in all cases using the coarse-grain boundary conditions on the metallic surfaces. Assume that the conductors are embedded into a linear dielectric with constant ϵ and μ .

7.19. Modify the solution of Task (ii) of the previous problem for a superconductor microstrip line, taking into account the magnetic field's penetration into both the strip and the ground plane.

7.20.* What lumped ac circuit would be equivalent to the TEM-line system shown in Fig. 19, with an incident wave's power \mathcal{P}_i ? Assume that the wave reflected from the lumped load circuit does not return to it.

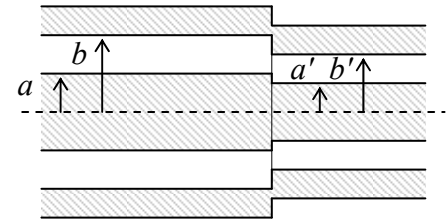
7.21. Find the lumped ac circuit equivalent to a loss-free TEM transmission line of length $l \sim \lambda$, with a small cross-section area $A \ll \lambda^2$, as “seen” (measured) from one end, if the line's conductors are galvanically connected (“shortened”) at the other end – see the figure on the right. Discuss the result's dependence on the signal frequency.



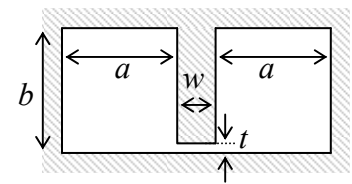
7.22. Represent the fundamental H_{10} wave in a rectangular waveguide (Fig. 22) with a sum of two plane waves, and discuss the physics behind such a representation.

7.23.* For the metallic coaxial cable (Fig. 20), find the lowest non-TEM mode and calculate its cutoff frequency.

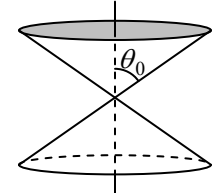
7.24. Two coaxial cable sections are connected coaxially – see the figure on the right, which shows the system's cut along its symmetry axis. Relations (118) and (120) seem to imply that if the ratios b/a of these sections are equal, their impedance matching is perfect, i.e. a TEM wave incident from one side on the connection would pass it without any reflection at all: $R = 0$. Is this statement correct?



7.25. Calculate the cutoff frequencies ω_c of the fundamental mode and the next lowest mode in the so-called *ridge waveguide* with the cross-section shown in the figure on the right, in the limit $t \ll a, b, w$. Briefly discuss possible advantages and drawbacks of such waveguides for signal transfer and physical experiment.



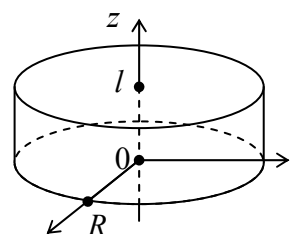
7.26. Prove that TEM-like waves may propagate, in the radial direction, in the free space between two coaxial, round, metallic cones – see the figure on the right. Can this system be characterized by a certain transmission line impedance Z_W , as defined by Eq. (115)?



7.27. Use the recipe outlined in Sec. 7 to prove the characteristic equation (161) for the *HE* and *EH* waves in step-index optical fiber with a round cross-section.

7.28. Derive an approximate equation describing spatial variations of the complex amplitude of a general monochromatic paraxial beam propagating in a uniform medium, for the case when these variations are sufficiently slow. Is the Gaussian beam described by Eq. (181) one of possible solutions of this equation? Give your interpretation of the last result.

7.29. Neglecting the skin-effect depth δ_s in comparison with l and R , find the lowest resonance frequencies, and the corresponding field distributions, of standing electromagnetic waves inside a round cylindrical cavity with metallic walls – see the figure on the right.



7.30. Analyze long-wave electromagnetic waves that may propagate inside a relatively narrow gap between two well-conducting concentric shells of radii R and $R + d$, in the limit $d \ll R$.

(i) Within the coarse-grain approximation, derive the 2D equation describing such waves with relatively large wavelengths $\lambda \sim R \gg d$.

(ii)* Calculate the lowest resonance frequencies of the system.

Hint: The last task requires some familiarity with the basic properties of spherical harmonics.

7.31. A plane monochromatic wave propagates through a medium with an Ohmic conductivity σ , and negligible electric and magnetic polarization effects. Calculate the wave's attenuation, and relate the result with a certain calculation carried out in Chapter 6.

7.32. Generalize the telegrapher's equations (110)-(111) by accounting for small energy losses:

- (i) in the transmission line's conductors, and
- (ii) in the medium separating the conductors,

using their simplest (Ohmic) models. Formulate the conditions of validity of the resulting equations.

7.33. Calculate the skin-effect contribution to the attenuation constant α of a TEM wave in the microstrip line discussed in Problem 18 (ii).

7.34. Calculate the skin-effect contribution to the attenuation coefficient α defined by Eq. (214), for the fundamental (H_{10}) mode propagating in a metallic-wall waveguide with a rectangular cross-section – see Fig. 22. Use the results to evaluate the wave decay length $l_d \equiv 1/\alpha$ of a 10 GHz wave in the standard X-band waveguide WR-90 (with copper walls, $a = 23$ mm, $b = 10$ mm, and no dielectric filling), at room temperature. Compare the result with that (obtained in Sec. 9) for the standard TV coaxial cable, at the same frequency.

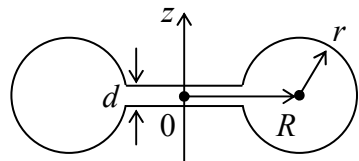
7.35. Calculate the skin-effect contribution to the attenuation coefficient α of

- (i) the fundamental (H_{11}) wave, and
- (ii) the H_{01} wave,

in a metallic-wall waveguide with the circular cross-section (see Fig. 23a), and analyze the low-frequency ($\omega \rightarrow \omega_c$) and high-frequency ($\omega \gg \omega_c$) behaviors of α for each of these modes.

7.36. For a rectangular metallic-wall resonant cavity with dimensions $a \times b \times l$ ($b \leq a$, l), calculate the Q -factor of the fundamental oscillation mode, due to the skin-effect losses in the walls. Evaluate the factor for a $23 \times 23 \times 10$ mm³ cavity with copper walls, at room temperature.

7.37.* Calculate the lowest eigenfrequency and the Q -factor (due to the skin-effect losses) of the toroidal (axially-symmetric) resonant cavity with metallic walls, and the interior's cross-section shown in the figure on the right, in the case when $d \ll r, R$.



7.38. Express the contribution to the damping coefficient (the reciprocal Q -factor) of a resonant cavity, by small energy losses in the dielectric that fills it, via the complex functions $\epsilon(\omega)$ and $\mu(\omega)$ of the material.

7.39. For the dielectric Fabry-Pérot resonator (Fig. 31) with the normal wave incidence, calculate the Q -factor due to radiation losses, in the limit of a strong impedance mismatch ($Z \gg Z_0$), using two approaches:

- (i) from the energy balance, using Eq. (227), and
- (ii) from the frequency dependence of the power transmission coefficient, using Eq. (229).

Compare the results.

Chapter 8. Radiation, Scattering, Interference, and Diffraction

This chapter continues the discussion of electromagnetic wave propagation, now focusing on the results of wave incidence on various objects of more complex shapes. Depending on the shape, the resulting wave pattern is called either “scattering”, or “diffraction”, or “interference”. However, as the reader will see, the boundaries between these effects may be blurry, and their basic mathematical description may be conveniently based on the same key calculation – the electric-dipole radiation of a spherical wave by a localized source. Naturally, I will start the chapter from this calculation, deriving it from an even more general result – the “retarded-potential” solution of the Maxwell equations.

8.1. Retarded potentials

Let us start by finding the general solution of the macroscopic Maxwell equations (6.99) in a dispersion-free, linear, uniform, isotropic medium characterized by frequency-independent real ϵ and μ .¹ The easiest way to perform this calculation is to use the scalar (ϕ) and vector (\mathbf{A}) potentials defined by Eqs. (6.7):

$$\mathbf{E} = -\nabla\phi - \frac{\partial\mathbf{A}}{\partial t}, \quad \mathbf{B} = \nabla \times \mathbf{A}. \quad (8.1)$$

As was discussed in Sec. 6.8, by imposing upon the potentials the Lorenz gauge condition (6.117),

$$\nabla \cdot \mathbf{A} + \frac{1}{v^2} \frac{\partial\phi}{\partial t} = 0, \quad \text{with } v^2 \equiv \frac{1}{\epsilon\mu}, \quad (8.2)$$

which does not affect the fields \mathbf{E} and \mathbf{B} , the Maxwell equations are reduced to a pair of very similar, simple equations (6.118) for the potentials:

$$\nabla^2\phi - \frac{1}{v^2} \frac{\partial^2\phi}{\partial t^2} = -\frac{\rho}{\epsilon}, \quad (8.3a)$$

$$\nabla^2\mathbf{A} - \frac{1}{v^2} \frac{\partial^2\mathbf{A}}{\partial t^2} = -\mu\mathbf{j}. \quad (8.3b)$$

Let us find the general solution of these equations, for now thinking of the densities $\rho(\mathbf{r}, t)$ and $\mathbf{j}(\mathbf{r}, t)$ of the stand-alone charges and currents as known functions. (This will not prevent the results from being valid for the cases when $\rho(\mathbf{r}, t)$ and $\mathbf{j}(\mathbf{r}, t)$ should be calculated self-consistently.) The idea of such a solution may be borrowed from electro- and magnetostatics. Indeed, for the stationary case ($\partial/\partial t = 0$), the solutions of Eqs. (8.3) are given by a ready generalization of, respectively, Eqs. (1.38) and (5.28) to a uniform, linear medium:

$$\phi(\mathbf{r}) = \frac{1}{4\pi\epsilon} \int \rho(\mathbf{r}') \frac{d^3r'}{|\mathbf{r} - \mathbf{r}'|}, \quad (8.4a)$$

$$\mathbf{A}(\mathbf{r}) \equiv \frac{\mu}{4\pi} \int \mathbf{j}(\mathbf{r}') \frac{d^3r'}{|\mathbf{r} - \mathbf{r}'|}. \quad (8.4b)$$

¹ When necessary (e.g., at the discussion of the Cherenkov radiation in Sec. 10.5), it will be not too hard to generalize these results to a dispersive medium.

As we know, these expressions may be derived by, first, calculating the potential of a point source, and then using the linear superposition principle for a system of such sources.

Let us do the same for the time-dependent case, starting from the field induced by a time-dependent point charge at the origin:²

$$\rho(\mathbf{r}, t) = q(t)\delta(\mathbf{r}), \quad (8.5)$$

In this case, Eq. (3a) is homogeneous everywhere but the origin:

$$\nabla^2\phi - \frac{1}{v^2}\frac{\partial^2\phi}{\partial t^2} = 0, \quad \text{for } r \neq 0. \quad (8.6)$$

Due to the spherical symmetry of the problem, it is natural to look for a spherically-symmetric solution to this equation.³ Thus, we may simplify the Laplace operator correspondingly (as was repeatedly done earlier in this course), so that Eq. (6) becomes

$$\left[\frac{1}{r^2}\frac{\partial}{\partial r}\left(r^2\frac{\partial}{\partial r}\right) - \frac{1}{v^2}\frac{\partial^2}{\partial t^2} \right]\phi = 0, \quad \text{for } r \neq 0. \quad (8.7)$$

By introducing a new variable $\chi(r, t) \equiv r\phi(r, t)$, Eq. (7) is reduced to the 1D wave equation

$$\left(\frac{\partial^2}{\partial r^2} - \frac{1}{v^2}\frac{\partial^2}{\partial t^2} \right)\chi = 0, \quad \text{for } r \neq 0. \quad (8.8)$$

From discussions in Chapter 7,⁴ we know that its general solution may be represented as

$$\chi(r, t) = \chi_{\text{out}}\left(t - \frac{r}{v}\right) + \chi_{\text{in}}\left(t + \frac{r}{v}\right), \quad (8.9)$$

where χ_{in} and χ_{out} are (so far) arbitrary functions of one variable. The physical sense of $\phi_{\text{out}} = \chi_{\text{out}}/r$ is a spherical wave propagating from our source (located at $r = 0$) to outer space, i.e. exactly the solution we are looking for. On the other hand, $\phi_{\text{in}} = \chi_{\text{in}}/r$ describes a spherical wave that could be created by some distant spherically-symmetric source, that converged exactly on our charge located at the origin – evidently not the effect we want to consider here. Discarding this term, and returning to $\phi = \chi/r$, we get

$$\phi(r, t) = \frac{1}{r}\chi_{\text{out}}\left(t - \frac{r}{v}\right), \quad \text{for } r \neq 0. \quad (8.10)$$

In order to calculate the function χ_{out} , let us consider the solution (10) at distances r so small ($r \ll vt$) that the time-derivative term in Eq. (3a), with the right-hand side (5),

$$\nabla^2\phi - \frac{1}{v^2}\frac{\partial^2\phi}{\partial t^2} = -\frac{q(t)}{\epsilon}\delta(\mathbf{r}), \quad (8.11)$$

² Admittedly, this expression does *not* satisfy the continuity equation (4.5), but this deficiency will be corrected imminently, at the linear superposition stage – see Eq. (17) below.

³ Let me emphasize that this is *not* the general solution to Eq. (6). For example, it does not describe the possible waves created by other sources, that pass by the considered charge $q(t)$. However, such fields are irrelevant for our current task: to calculate the field *induced* by the charge $q(t)$. The solution becomes general when it is integrated (as it will be) over all relevant charges.

⁴ See also CM Sec. 6.3.

is much smaller than the spatial derivative term (which diverges at $r \rightarrow 0$) . Then Eq. (11) is reduced to the Poisson equation, whose solution (4a), for the source (5), is

$$\phi(r \rightarrow 0, t) = \frac{q(t)}{4\pi\epsilon r}. \quad (8.12)$$

Now requiring the two solutions, Eqs. (10) and (12), to coincide at $r \ll vt$, we get $\chi_{\text{out}}(t) = q(t)/4\pi\epsilon r$, so that Eq. (10) becomes

$$\phi(r, t) = \frac{1}{4\pi\epsilon r} q \left(t - \frac{r}{v} \right). \quad (8.13)$$

Just as was repeatedly done in statics, this result may be readily generalized for the arbitrary position \mathbf{r}' of the point charge:

$$\rho(\mathbf{r}, t) = q(t)\delta(\mathbf{r} - \mathbf{r}') \equiv q(t)\delta(\mathbf{R}), \quad (8.14)$$

where R is the distance between the field observation point \mathbf{r} and the source position point \mathbf{r}' , i.e. the length of the vector,

$$\mathbf{R} \equiv \mathbf{r} - \mathbf{r}', \quad (8.15)$$

connecting these points – see Fig. 1.

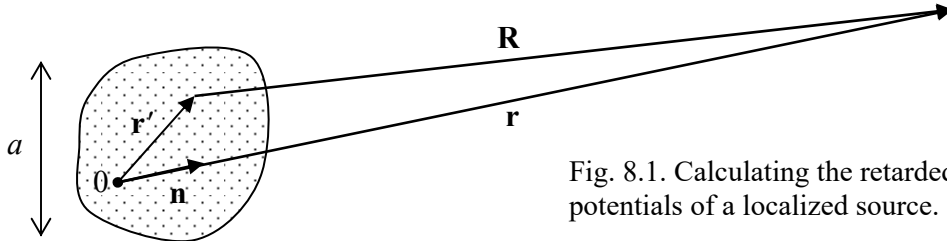


Fig. 8.1. Calculating the retarded potentials of a localized source.

Obviously, now Eq. (13) becomes

$$\phi(\mathbf{r}, t) = \frac{1}{4\pi\epsilon R} q \left(t - \frac{R}{v} \right). \quad (8.16)$$

Finally, we may use the linear superposition principle to write, for the arbitrary charge distribution,

Retarded scalar potential

$$\boxed{\phi(\mathbf{r}, t) = \frac{1}{4\pi\epsilon} \int \rho \left(\mathbf{r}', t - \frac{R}{v} \right) \frac{d^3 r'}{R}}, \quad (8.17a)$$

where the integration is extended over all charges of the system under analysis. Solving Eq. (4b) absolutely similarly, for the vector potential we get⁵

Retarded vector potential

$$\boxed{\mathbf{A}(\mathbf{r}, t) = \frac{\mu}{4\pi} \int \mathbf{j} \left(\mathbf{r}', t - \frac{R}{v} \right) \frac{d^3 r'}{R}}. \quad (8.17b)$$

⁵ As should be clear from the analogy of Eqs. (17) with their stationary forms (4), which were discussed, respectively, in Chapters 1 and 5, in the Gaussian units the retarded potential formulas are valid with the coefficient $1/4\pi$ dropped in Eq. (17a), and replaced with $1/c$ in Eq. (17b).

(Now nothing prevents the functions $\rho(\mathbf{r}, t)$ and $\mathbf{j}(\mathbf{r}, t)$ from satisfying the continuity equation.)

The solutions expressed by Eqs. (17) are traditionally called the *retarded potentials*, the name signifying the fact that the observed fields are “retarded” (in the meaning “delayed”) in time by $\Delta t = R/v$ relative to the source variations – physically, because of the finite speed v of the electromagnetic wave propagation. Note that, very remarkably, these simple expressions are *exact* solutions of the macroscopic Maxwell equations (again, in a uniform, linear, dispersion-free medium) for an *arbitrary* distribution of stand-alone charges and currents. They also may be considered as the *general* solutions of these equations, provided that the integration has been extended over all field sources in the Universe – or at least over those ones that affect our observations.

Note also that due to the mathematical similarity of the microscopic and macroscopic Maxwell equations, Eqs. (17) are valid, with the coefficient replacement $\epsilon \rightarrow \epsilon_0$ and $\mu \rightarrow \mu_0$, for the exact, rather than the macroscopic fields, provided that the functions $\rho(\mathbf{r}, t)$ and $\mathbf{j}(\mathbf{r}, t)$ describe not only stand-alone but all charges and currents in the system. (Alternatively, this statement may be formulated as the validity of Eqs. (17), with the same coefficient replacement, in free space.)

Finally, note that Eqs. (17) may be plugged into Eqs. (1), giving (after an explicit differentiation) the so-called *Jefimenko equations*⁶ for fields \mathbf{E} and \mathbf{B} – similar in structure to Eqs. (17), but more cumbersome. Conceptually, the existence of such equations is good news, because they are free from the gauge ambiguity pertinent to the potentials ϕ and \mathbf{A} . However, the practical value of these explicit expressions for the fields is not overly high: for all applications I am aware of, it is easier to use Eqs. (17) to calculate the particular expressions for the potentials first, and only then calculate the fields from Eqs. (1). Let me now present an (arguably, the most important) example of this approach.

8.2. Electric dipole radiation

Consider again the problem that was discussed in electrostatics (Sec. 3.1), namely the field of a localized source with linear dimensions $a \ll r$ (see Fig. 1 again), but now with time-dependent charge and/or current distributions. Using all the arguments of that discussion, in particular the condition expressed by Eq. (3.1), $r' \ll r$, we may apply the Taylor expansion (3.3), truncated to two leading terms,

$$f(\mathbf{R}) = f(\mathbf{r}) - \mathbf{r}' \cdot \nabla f(\mathbf{r}) + \dots, \quad (8.18)$$

to the scalar function $f(\mathbf{R}) \equiv R$ (for which $\nabla f(\mathbf{r}) = \nabla R = \mathbf{n}$, where $\mathbf{n} \equiv \mathbf{r}/r$ is the unit vector directed toward the observation point – see Fig. 1) to approximate the distance R as

$$R \approx r - \mathbf{r}' \cdot \mathbf{n}. \quad (8.19)$$

In each of the retarded potential formulas (17), R participates in two places: in the denominator and in the source’s time argument. If ρ and \mathbf{j} change in time on the scale $\sim 1/\omega$, where ω is some characteristic frequency, then any change of the argument $(t - R/v)$ on that time scale, for example due to a change of R on the spatial scale $\sim v/\omega = 1/k$, may substantially change these functions. Thus, the expansion (19) may be applied to R in the argument $(t - R/v)$ only if $ka \ll 1$, i.e. if the system’s size a

⁶ They were published by O. D. Jefimenko only in 1966, but the Fourier representation of the same result was obtained much earlier (in 1912) by G. A. Scott.

is much smaller than the radiation wavelength $\lambda = 2\pi/k$. On the other hand, the function $1/R$ changes relatively slowly, and for it even the first term of the expansion (19) gives a good approximation as soon as $a \ll r, R$. In the latter approximation alone, Eq. (17a) yields

$$\phi(\mathbf{r}, t) \approx \frac{1}{4\pi\epsilon_0 r} \int \rho \left(\mathbf{r}', t - \frac{R}{v} \right) d^3 r' \equiv \frac{1}{4\pi\epsilon_0 r} Q \left(t - \frac{R}{v} \right), \quad (8.20)$$

where $Q(t)$ is the net electric charge of the localized system. Due to the charge conservation, this charge cannot change with time, so that the approximation (20) describes just a static Coulomb field of our localized source, rather than a radiated wave.

Let us, however, apply a similar approximation to the vector potential (17b):

$$\mathbf{A}(\mathbf{r}, t) \approx \frac{\mu}{4\pi r} \int \mathbf{j} \left(\mathbf{r}', t - \frac{R}{v} \right) d^3 r'. \quad (8.21)$$

According to Eq. (5.87), the right-hand side of this expression vanishes in statics, but in dynamics, this is no longer true. For example, if the current is due to some non-relativistic motion⁷ of a system of point charges q_k , we can write

$$\int \mathbf{j}(\mathbf{r}', t) d^3 r' = \sum_k q_k \dot{\mathbf{r}}_k(t) = \frac{d}{dt} \sum_k q_k \mathbf{r}_k(t) \equiv \dot{\mathbf{p}}(t), \quad (8.22)$$

where $\mathbf{p}(t)$ is the dipole moment of the localized system, defined by Eq. (3.6). Now, after the integration, we may keep only the first term of the approximation (19) in the argument $(t - R/v)$ as well, getting

$$\mathbf{A}(\mathbf{r}, t) \approx \frac{\mu}{4\pi r} \dot{\mathbf{p}} \left(t - \frac{r}{v} \right), \quad \text{for } a \ll R, \frac{1}{k}. \quad (8.23)$$

Let us analyze what exactly this result describes. The second of Eqs. (1) allows us to calculate the magnetic field by the spatial differentiation of \mathbf{A} . At large distances $r \gg \lambda$ (i.e. in the so-called *far-field zone*), where Eq. (23) describes a locally-plane wave, the dominating contribution to this derivative is given by the dipole moment factor:

Far-field
wave

$$\boxed{\mathbf{B}(\mathbf{r}, t) = \frac{\mu}{4\pi r} \nabla \times \dot{\mathbf{p}} \left(t - \frac{r}{v} \right) = -\frac{\mu}{4\pi r v} \mathbf{n} \times \ddot{\mathbf{p}} \left(t - \frac{r}{v} \right)}. \quad (8.24)$$

This expression means that the magnetic field, at the observation point, is perpendicular to the vectors \mathbf{n} and (the retarded value of) $\ddot{\mathbf{p}}$, and its magnitude is

$$B = \frac{\mu}{4\pi r v} \ddot{p} \left(t - \frac{r}{v} \right) \sin \Theta, \quad \text{i.e. } H = \frac{1}{4\pi r v} \ddot{p} \left(t - \frac{r}{v} \right) \sin \Theta, \quad (8.25)$$

where Θ is the angle between those two vectors – see Fig. 2.⁸

⁷ For relativistic particles, moving with velocities of the order of speed of light, one has to be more careful. As the result, I will postpone the discussion of their radiation until Chapter 10, i.e. until after the detailed discussion of special relativity in Chapter 9.

⁸ From the first of Eqs. (1) for the electric field, in the first approximation (23), we would get $-\partial \mathbf{A} / \partial t = -(1/4\pi\epsilon_0 r v) \ddot{\mathbf{p}}(t - r/v) = -(Z/4\pi r) \ddot{\mathbf{p}}(t - r/v)$. The transverse component of this vector (see Fig. 2) is the proper electric field \mathbf{E}

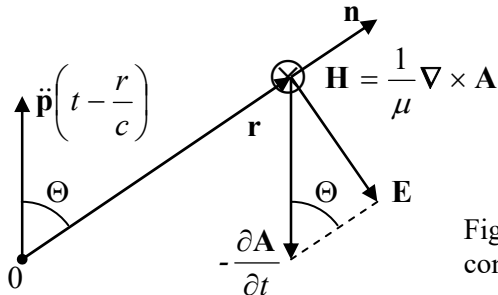


Fig. 8.2. Far-fields of a localized source, contributing to its electric dipole radiation.

The most important feature of this result is that the time-dependent field decreases very slowly (only as $1/r$) with the distance from the source, so that the radial component of the corresponding Poynting vector (7.9b),⁹

$$S_r = ZH^2 = \frac{Z}{(4\pi v)^2} \left[\ddot{p} \left(t - \frac{r}{v} \right) \right]^2 \sin^2 \Theta, \quad (8.26)$$

Instant power density

drops only as $1/r^2$, i.e. the full instant power \mathcal{P} of the emitted wave,

$$\mathcal{P} \equiv \oint S_r r^2 d\Omega = \frac{Z}{(4\pi v)^2} \ddot{p}^2 2\pi \int_0^\pi \sin^3 \Theta d\Theta = \frac{Z}{6\pi v^2} \ddot{p}^2. \quad (8.27)$$

Larmor formula

does not depend on the distance from the source – as it should for radiation.¹⁰

This is the famous *Larmor formula*¹¹ for the *electric dipole radiation*; it is the dominating component of radiation by a localized system of charges – unless $\ddot{p} = 0$. Please notice its angular dependence: the radiation vanishes at the axis of the retarded vector \ddot{p} (where $\Theta = 0$), and reaches its maximum in the plane normal to that axis.

In order to find the average power, Eq. (27) has to be averaged over a sufficiently long time. In particular, if the source is monochromatic, $\mathbf{p}(t) = \text{Re}[\mathbf{p}_\omega \exp\{-i\omega t\}]$, with a time-independent vector amplitude \mathbf{p}_ω , such averaging may be carried out just over one period, giving an extra factor 2 in the denominator:

$$\overline{\mathcal{P}} = \frac{Z\omega^4}{12\pi v^2} |\mathbf{p}_\omega|^2. \quad (8.28)$$

Average radiation power

The easiest application of this formula is to a point charge oscillating, with frequency ω , along a straight line (which we may take for the z -axis), with amplitude a . In this case, $\mathbf{p} = qz(t)\mathbf{n}_z = qa \text{Re}[\exp\{-i\omega t\}]\mathbf{n}_z$, and if the charge velocity amplitude, $a\omega$, is much less than the electromagnetic wave's speed v , we may use Eq. (28) with $p_\omega = qa$, giving

= $Z\mathbf{H} \times \mathbf{n}$ of the radiated wave, while its longitudinal component is exactly compensated by $(-\nabla\phi)$ in the next term of the Taylor expansion of Eq. (17a) in small parameter $ka \sim a/\lambda \ll 1$.

⁹ Note the “doughnut” dependence of S_r on the direction \mathbf{n} , frequently used to visualize the dipole radiation.

¹⁰ In the Gaussian units, for free space ($v = c$), Eq. (27) reads $\mathcal{P} = (2/3c^3)\ddot{p}^2$.

¹¹ Named after Joseph Larmor, who was the first to derive this formula (in 1897) for the particular case of a single point charge q moving with acceleration $\ddot{\mathbf{r}}$, when $\ddot{\mathbf{p}} = q\ddot{\mathbf{r}}$.

$$\overline{\mathcal{P}} = \frac{Zq^2 a^2 \omega^4}{12\pi v^2}. \quad (8.29)$$

Applied to a classical picture of an electron (with $q = -e \approx 1.6 \times 10^{-19} \text{ C}$), initially rotating about an atom's nucleus at an atomic distance $a \sim 10^{-10} \text{ m}$, Eq. (29) shows¹² that the energy loss due to the dipole radiation is so large that it would cause the electron to collapse on the nucleus in just $\sim 10^{-11} \text{ s}$. In the beginning of the 1900s, this result was one of the main arguments for the development of quantum mechanics, which prevents such a collapse of electrons for their lowest-energy (ground) quantum state.

Another useful application of Eq. (28) is the radio wave radiation by a short, straight, symmetric antenna which is fed, for example, by a TEM transmission line such as a coaxial cable – see Fig. 3.

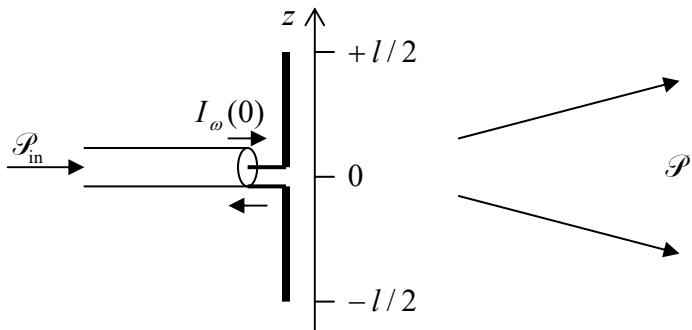


Fig. 8.3. The dipole antenna.

The exact solution of this problem is rather complicated because the law $I_\omega(z)$ of the current variation along the antenna's length should be calculated self-consistently with the distribution of the electromagnetic field induced by the current in the surrounding space. (Unfortunately, this fact is not mentioned in some textbooks.) However, the current should be largest in the feeding point (in Fig. 3, taken for $z = 0$) and vanish at antenna's ends ($z = \pm l/2$), and hence we may guess that at $l \ll \lambda$, the linear function

$$I_\omega(z) = I_\omega(0) \left(1 - \frac{2}{l}|z|\right), \quad (8.30)$$

should be a good approximation of the actual distribution – as it indeed is. Now we can use the continuity equation $\partial Q/\partial t = I$, i.e. $-i\omega Q_\omega = I_\omega$, to calculate the complex amplitude $Q_\omega(z) = iI_\omega(z)\operatorname{sgn}(z)/\omega$ of the electric charge $Q(z, t) = \operatorname{Re}[Q_\omega \exp\{-i\omega t\}]$ of the wire's segment $[0, z]$, and from it, the amplitude of the charge's linear density:

$$\lambda_\omega(z) \equiv \frac{dQ_\omega(z)}{dz} = -i \frac{2I_\omega(0)}{\omega l} \operatorname{sgn} z. \quad (8.31)$$

From here, the dipole moment's amplitude is

$$p_\omega = 2 \int_0^{l/2} \lambda_\omega(z) z dz = -i \frac{I_\omega(0)}{2\omega} l, \quad (8.32)$$

so that Eq. (28) yields

¹² Actually, the formula needs a numerical coefficient adjustment to account for the electron's orbital (rather than linear) motion – the task left for the reader's exercise. However, this adjustment does not affect the order-of-magnitude estimate given above.

$$\overline{\mathcal{P}} = Z \frac{\omega^4}{12\pi v^2} \frac{|I_\omega(0)|^2}{4\omega^2} l^2 = \frac{Z(kl)^2}{24\pi} \frac{|I_\omega(0)|^2}{2}, \quad (8.33)$$

where $k = \omega/v$. The analogy between this result and the dissipation power $\mathcal{P} = \text{Re}Z |I_\omega|^2/2$ in a lumped linear circuit element, enables the interpretation of the first fraction in the last form of Eq. (33) as the real part of the antenna's impedance:

$$\text{Re}Z_A = Z \frac{(kl)^2}{24\pi}, \quad (8.34)$$

as felt by the transmission line.

According to Eq. (7.118), the wave traveling along the line toward the antenna is fully radiated, i.e. not reflected back, only if Z_A equals to Z_W of the line. As we know from Sec. 7.5 (and the solution of the related problems), for typical TEM lines, $Z_W \sim Z_0$, while Eq. (34), which is only valid in the limit $kl \ll 1$, shows that for the radiation into free space ($Z = Z_0$), $\text{Re}Z_A$ is much less than Z_0 . Hence to reach the impedance matching condition $Z_W = Z_A$, the antenna's length should be increased – as a more involved theory shows, to $l \approx \lambda/2$. However, in many cases, practical considerations make short antennas necessary. The example most often met nowadays is the cell phone antennas, which use frequencies close to 1 or 2 GHz, with free-space wavelengths λ between 15 and 30 cm, i.e. much larger than the phone size.¹³ The quadratic dependence of the antenna's efficiency on l , following from Eq. (34), explains why every millimeter counts in the design of such antennas, and why the designs are carefully optimized using software packages for the (virtually exact) numerical solution of the Maxwell equations for the specific shape of the antenna and other phone parts.¹⁴

To conclude this section, let me note that if the wave source is not monochromatic, so that $\mathbf{p}(t)$ should be represented as a Fourier series,

$$\mathbf{p}(t) = \text{Re} \sum_{\omega} \mathbf{p}_{\omega} e^{-i\omega t}, \quad (8.35)$$

the terms corresponding to the interference of spectral components with different frequencies ω are averaged out at the time averaging of the Poynting vector, and the *average* radiated power is just a sum of contributions (28) from all substantial frequency components.

8.3. Wave scattering

The Larmor formula may be used as the basis of the theory of *scattering* – the phenomenon illustrated by Fig. 4. Generally, scattering is a complex problem. However, in many cases it allows the so-called *Born approximation*,¹⁵ in which the scattered wave field's effect on the scattering object is assumed to be much weaker than that of the incident wave, and is neglected.

¹³ The situation will be partly remedied by the transfer of the wireless mobile technology to its next generations, with the frequencies moved up to the 28 GHz, 37-39 GHz, and possibly even the 64-71 GHz bands.

¹⁴ A partial list of popular software packages of this kind includes both publicly available codes such as Nec2 (whose various versions are available online, e.g., at <http://www.qsl.net/4nec2/>), and proprietary packages – such as *Momentum* from Agilent Technologies (now owned by Hewlett-Packard), *FEKO* from EM Software & Systems, and *XFdtd* from Remcom.

¹⁵ Named after Max Born, one of the founding fathers of quantum mechanics. However, the basic idea of this approach to EM waves was developed much earlier (in 1881) by Lord Rayleigh – born John William Strutt.

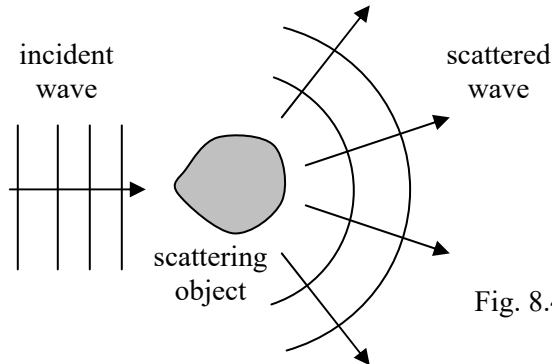


Fig. 8.4. Wave scattering (schematically).

As the first example of this approach, let us consider the scattering of a plane wave, propagating in free space ($Z = Z_0$, $\nu = c$), by an otherwise free¹⁶ charged particle whose motion may be described by non-relativistic classical mechanics. (This requires, in particular, the incident wave to be not too powerful, so that the speed of the charge's motion induced by the wave remains much lower than c .) As was already discussed at the derivation of Eq. (7.32), in this case, the magnetic component of the Lorentz force (5.10) is negligible in comparison with the force $\mathbf{F}_e = q\mathbf{E}$ exerted by the wave's electric field. Thus, assuming that the incident wave is linearly polarized along some axis x , the equation of particle's motion in the Born approximation is just $m\ddot{x} = qE(t)$, so that for the x -component $p_x = qx$ of its dipole moment we can write

$$\ddot{p} = q\ddot{x} = \frac{q^2}{m} E(t). \quad (8.36)$$

As we already know from Sec. 2, oscillations of the dipole moment lead to radiation of a wave with a wide angular distribution of intensity; in our case, this is the scattered wave – see Fig. 4. Its full power may be found by plugging Eq. (36) into Eq. (27):

$$\mathcal{P} = \frac{Z_0}{6\pi c^2} \dot{p}^2 = \frac{Z_0 q^4}{6\pi c^2 m^2} E^2(t), \quad (8.37)$$

so that for the average power we get

$$\overline{\mathcal{P}} = \frac{Z_0 q^4}{12\pi c^2 m^2} |E_\omega|^2. \quad (8.38)$$

Since this power is proportional to the incident wave's intensity S , it is customary to characterize the scattering ability of an object by the ratio,

$$\sigma \equiv \frac{\overline{\mathcal{P}}}{S_{\text{incident}}} \equiv \frac{\overline{\mathcal{P}}}{|E_\omega|^2 / 2Z_0},$$

(8.39)

which has the dimensionality of area, and is called the *total cross-section* of scattering.¹⁷ For this measure, Eq. (38) yields the famous result

¹⁶ As Eq. (7.30) shows, this calculation is also valid for an oscillator with a low own frequency, $\omega_0 \ll \omega$.

¹⁷ This definition parallels those accepted in the classical and quantum theories of *particle* scattering – see, e.g., respectively, CM Sec. 3.5 and QM Sec. 3.3.

$$\sigma = \frac{Z_0^2 q^4}{6\pi c^2 m^2} = \frac{\mu_0^2 q^4}{6\pi m^2}, \quad (8.40)$$

which is called the *Thomson scattering formula*,¹⁸ especially when applied to an electron. This relation is most frequently represented in the form¹⁹

$$\sigma = \frac{8\pi}{3} r_c^2, \quad \text{with } r_c \equiv \frac{q^2}{4\pi\epsilon_0} \cdot \frac{1}{mc^2}. \quad (8.41)$$

Thomson scattering

This constant r_c is called the *classical radius of the particle* (or sometimes the “Thomson scattering length”); for the electron ($q = -e$, $m = m_e$) it is close to 2.82×10^{-15} m. Its possible interpretation is evident from Eq. (41) for r_c : at that distance between two similar particles, the potential energy $q^2/4\pi\epsilon_0 r$ of their electrostatic interaction is equal to the particle’s rest-mass energy mc^2 .²⁰

Now we have to go back and establish the conditions at which the Born approximation, when the field of the scattered wave is negligible, is indeed valid for a point-object scattering. Since the scattered wave’s intensity described by Eq. (26) diverges at $r \rightarrow 0$ as $1/r^2$, according to the definition (39) of the cross-section, it may become comparable to S_{incident} at $r^2 \sim \sigma$. However, Eq. (38) itself is only valid if $r \gg \lambda$, so that the Born approximation does not lead to a contradiction only if

$$\sigma \ll \lambda^2. \quad (8.42)$$

For the Thompson scattering by an electron, this condition means $\lambda \gg r_c \sim 3 \times 10^{-15}$ m and is fulfilled for all frequencies up to very hard γ -rays with photon energies ~ 100 MeV.

Possibly the most notable feature of the result (40) is its independence of the wave frequency. As it follows from its derivation, particularly from Eq. (37), this independence is intimately related to the unbound character of charge motion. For bound charges, say for electrons in gas molecules, this result is only valid if the wave frequency ω is much higher than the frequencies ω_j of most important quantum transitions. In the opposite limit, $\omega \ll \omega_j$, the result is dramatically different. Indeed, in this limit we may approximate the molecule’s dipole moment by its static value (3.48):

$$\mathbf{p} = \alpha \mathbf{E}. \quad (8.43)$$

In the Born approximation, and in the absence of the molecular field effects mentioned in Sec. 3.3, \mathbf{E} in this expression is just the incident wave’s field, and we can use Eq. (28) to calculate the power of the wave scattered by a single molecule:

¹⁸ Named after Sir Joseph John (“JJ”) Thomson, the discoverer of the electron – and isotopes as well! He should not be confused with his son, G. P. Thomson, who discovered (simultaneously with C. Davisson and L. Germer) quantum-mechanical wave properties of the same electron.

¹⁹ In the Gaussian units, this formula looks like $r_c = q^2/mc^2$ (giving, of course, the same numerical values: for the electron, $r_c \approx 2.82 \times 10^{-13}$ cm). This *classical* quantity should not be confused with the particle’s *Compton wavelength* $\lambda_C \equiv 2\pi\hbar/mc$ (for the electron, close to 2.24×10^{-12} m), which naturally arises in *quantum* electrodynamics – see a brief discussion in the next chapter, and also QM Sec. 1.1.

²⁰ It is fascinating how smartly the *relativistic* expression mc^2 sneaked into the result (40)-(41), which was obtained using the *non-relativistic* equation (36) of the particle motion. This was possible because the calculation engaged electromagnetic waves, which propagate with the speed of light, and whose quanta (*photons*), as a result, may be frequently treated as relativistic (moreover, ultra-relativistic) particles – see the next chapter.

$$\bar{\mathcal{P}} = \frac{Z_0 \omega^4}{4\pi c^2} \alpha^2 |E_\omega|^2. \quad (8.44)$$

Now, using the last form of the definition (39) of the cross-section, we get a very simple result,

$$\sigma = \frac{Z_0^2 \omega^4}{6\pi c^2} \alpha^2, \quad (8.45)$$

showing that in contrast to Eq. (40), at low frequencies σ changes as fast as ω^4 .

Now let us explore the effect of such *Rayleigh scattering* on wave propagation in a gas, with a relatively low volumic density n . We may expect (and will prove in the next section) that due to the randomness of molecule positions, the waves scattered by individual molecules may be treated as *incoherent* ones, so that the total scattering power may be calculated just as the sum of those scattered by each molecule. We can use this fact to write the balance of the incident's wave intensity in a small volume dV of length (along the incident wave direction) dz , and area A across it. Since such a segment includes $ndV = nAdz$ molecules, and according to Eq. (39), each of them scatters power $S\sigma = \mathcal{P}\sigma/A$, the total scattered power is $n\mathcal{P}\sigma dz$; hence the incident power's change is

$$d\mathcal{P} \equiv -n\sigma\mathcal{P} dz. \quad (8.46)$$

Comparing this equation with the definition (7.213) of the wave attenuation constant, applied to the scattering,²¹

$$d\mathcal{P} \equiv -\alpha_{\text{scat}}\mathcal{P} dz. \quad (8.47)$$

we see that this effect gives the following contribution to attenuation: $\alpha_{\text{scat}} = n\sigma$. From here, using Eq. (3.50) to write $\alpha = \epsilon_0(\kappa - 1)/n$, where κ is the dielectric constant, and Eq. (45) for σ , we get

$$\alpha_{\text{scat}} = \frac{k^4}{6\pi n} (\kappa - 1)^2, \quad \text{where } k \equiv \frac{2\pi}{\lambda_0} = \frac{\omega}{c}. \quad (8.48)$$

Rayleigh scattering This is the famous *Rayleigh scattering formula*, which in particular explains the colors of blue sky and red sunsets. Indeed, through the visible light spectrum, ω changes almost two-fold; as a result, the scattering of blue components of sunlight is an order of magnitude higher than that of its red components. For the air near the Earth's surface, $\kappa - 1 \approx 6 \times 10^{-4}$, and $n \sim 2.5 \times 10^{25} \text{ m}^{-3}$ – see Sec. 3.3. Plugging these numbers into Eq. (48), we see that the effective length $l_{\text{scat}} \equiv 1/\alpha_{\text{scat}}$ of scattering is ~ 30 km for the blue light and ~ 200 km for the red light.²² The effective thickness h of the Earth's atmosphere is ~ 10 km, so that the Sun looks just a bit yellowish during most of the day. However, an elementary geometry shows that on sunset, the light has to pass the length $l \sim (R_E h)^{1/2} \approx 300$ km to reach an Earth-surface observer; as a result, the blue components of the Sun's light spectrum are almost completely scattered out, and even the red components are weakened very substantially.

²¹ I am sorry for using the same letter (α) for both the molecular polarizability and the wave attenuation, but both notations are traditional. Hopefully, the subscript “scat”, marking α in the latter meaning, minimizes the possibility of confusion.

²² These values are approximate because both n and $(\kappa - 1)$ vary through the atmosphere's thickness.

8.4. Interference and diffraction

Now let us discuss scattering by objects with a size of the order of, or even larger than λ . For such extended objects, the phase difference factors (neglected above) step in, leading in particular to the important effects of *interference* and *diffraction*. These effects show up not as much in the total power of the scattered radiation, as in its angular distribution. It is common to characterize this distribution by the *differential cross-section* defined as

$$\frac{d\sigma}{d\Omega} \equiv \frac{\bar{S}_r r^2}{S_{\text{incident}}}, \quad (8.49)$$

Differential cross-section

where r is the distance from the scatterer, at which the scattered wave is observed.²³ Both the definition and the notation may become more clear if we notice that according to Eq. (26), at large distances ($r \gg a$), the numerator of the right-hand side of Eq. (49), and hence the differential cross-section as a whole, do not depend on r , and that its integral over the total solid angle $\Omega = 4\pi$ coincides with the total cross-section defined by Eq. (39):

$$\oint \frac{d\sigma}{d\Omega} d\Omega = \frac{1}{S_{\text{incident}}} r^2 \oint \bar{S}_r d\Omega = \frac{1}{S_{\text{incident}}} \int_{r=\text{const}} \bar{S}_r d^2 r = \frac{\bar{\mathcal{P}}}{S_{\text{incident}}} = \sigma. \quad (8.50)$$

For example, according to Eq. (26), the angular distribution of the radiation scattered by a single dipole is rather broad; in particular, in the quasistatic case (43), within the Born approximation,

$$\frac{d\sigma}{d\Omega} = \left(\frac{\alpha k^2}{4\pi\epsilon_0} \right)^2 \sin^2 \Theta. \quad (8.51)$$

If the wave is scattered by a small dielectric body, with a characteristic size $a \ll \lambda$ (i.e., $ka \ll 1$), then all its parts re-radiate the incident wave coherently. Hence, we can calculate it similarly, just replacing the molecular dipole moment (43) with the total dipole moment of the object – see Eq. (3.45):

$$\mathbf{p} = \mathbf{P}V = (\kappa - 1)\epsilon_0 \mathbf{E}V, \quad (8.52)$$

where $V \sim a^3$ is the body's volume. As a result, the differential cross-section may be obtained from Eq. (51) with the replacement $\alpha_{\text{mol}} \rightarrow (\kappa - 1)\epsilon_0 V$:

$$\frac{d\sigma}{d\Omega} = \left(\frac{k^2 V}{4\pi} \right)^2 (\kappa - 1)^2 \sin^2 \Theta, \quad (8.53)$$

i.e. follows the same $\sin^2 \Theta$ law.

The situation for extended objects, with at least one dimension of the order of (or larger than) the wavelength, is different: here we have to take into account the phase shifts between the wave's re-radiation by various parts of the body. Let us analyze this issue first for an arbitrary collection of similar point scatterers located at points \mathbf{r}_j . If the wave vector of the incident plane wave is \mathbf{k}_0 , the wave's field has the phase factor $\exp\{i\mathbf{k}_0 \cdot \mathbf{r}\}$ – see Eq. (7.79). At the location \mathbf{r}_j of the j^{th} scattering center, this factor equals $\exp\{i\mathbf{k}_0 \cdot \mathbf{r}_j\}$, defining the time dependence of the dipole vector \mathbf{p} , and hence of the scattered wave.

²³ Just as in the case of the total cross-section, this definition is also similar to that accepted at the *particle* scattering – see, e.g., CM Sec. 3.5 and QM Sec. 3.3.

According to Eq. (17), the scattered wave with a wave vector \mathbf{k} (with $k = k_0$) acquires, on its way from the source point \mathbf{r}_j to the observation point \mathbf{r} , an additional phase factor $\exp\{i\mathbf{k}\cdot(\mathbf{r} - \mathbf{r}_j)\}$, so that the scattered wave field is proportional to

$$\exp\{i\mathbf{k}_0 \cdot \mathbf{r}_j + i\mathbf{k}(\mathbf{r} - \mathbf{r}_j)\} \equiv e^{i\mathbf{k}\cdot\mathbf{r}} \exp\{-i(\mathbf{k} - \mathbf{k}_0) \cdot \mathbf{r}_j\}. \quad (8.54)$$

Since the first factor in the last expression does not depend on \mathbf{r}_j , to calculate the total scattering wave, it is sufficient to sum up the last phase factors, $\exp\{-i\mathbf{q}\cdot\mathbf{r}_j\}$, where the vector

$$\mathbf{q} \equiv \mathbf{k} - \mathbf{k}_0 \quad (8.55)$$

has the physical sense of the wave vector change at scattering.²⁴ It may look like the phase factor depends on our choice of the reference frame. However, according to Eq. (7.42), the average *intensity* of the scattered wave is proportional to $E_\omega E_\omega^*$, i.e. to the following real scalar function of the vector \mathbf{q} :

Scattering function

$$F(\mathbf{q}) = \left(\sum_j \exp\{-i\mathbf{q}\cdot\mathbf{r}_j\} \right) \left(\sum_{j'} \exp\{-i\mathbf{q}\cdot\mathbf{r}_{j'}\} \right)^* \equiv \sum_{j,j'} \exp\{i\mathbf{q}\cdot(\mathbf{r}_j - \mathbf{r}_{j'})\} = |I(\mathbf{q})|^2, \quad (8.56)$$

where the complex function

Phase sum

$$I(\mathbf{q}) \equiv \sum_j \exp\{-i\mathbf{q}\cdot\mathbf{r}_j\} \quad (8.57)$$

is called the *phase sum*, and may be calculated in any reference frame without affecting the final result given by Eq. (56).

So, besides the $\sin^2\Theta$ factor, the differential cross-section (49) of scattering by an extended object is also proportional to the scattering function (56). Its double-sum form is convenient to notice that for a system of *many* ($N \gg 1$) similar but randomly located scatterers, only the terms with $j = j'$ accumulate at summation, so that $F(\mathbf{q})$, and hence $d\sigma/d\Omega$, scale as N , rather than N^2 – thus justifying again our treatment of the Rayleigh scattering problem in the previous section.

Now let us apply Eq. (56) to a simple problem of just *two* similar small scatterers, separated by a fixed distance a :

$$F(\mathbf{q}) = \sum_{j,j'=1}^2 \exp\{i\mathbf{q}\cdot(\mathbf{r}_j - \mathbf{r}_{j'})\} = 2 + \exp\{-iq_a a\} + \exp\{iq_a a\} = 2(1 + \cos q_a a) = 4 \cos^2 \frac{q_a a}{2}, \quad (8.58)$$

where $q_a \equiv \mathbf{q}\cdot\mathbf{a}/a$ is the component of the vector \mathbf{q} along the vector \mathbf{a} connecting the scatterers. The apparent simplicity of this result may be a bit misleading because the mutual plane of the vectors \mathbf{k} and \mathbf{k}_0 (and hence of the vector \mathbf{q}) does not necessarily coincide with the mutual plane of the vectors \mathbf{k}_0 and \mathbf{E}_ω , so that the *scattering angle* θ between \mathbf{k} and \mathbf{k}_0 is generally different from $(\pi/2 - \Theta)$ – see Fig. 5. Moreover, the angle between the vectors \mathbf{q} and \mathbf{a} (within their common plane) is one more parameter independent of both θ and Θ . As a result, the angular dependence of the scattered wave's intensity (and hence $d\sigma/d\Omega$), which depends on all three angles, may be rather involved, but some of its details are irrelevant for the basic physics of interference/diffraction.

²⁴ In quantum mechanics, $\hbar\mathbf{q}$ has a very clear sense of the momentum transferred from the scattering object to the scattered particle (for example, a photon), and this terminology is sometimes smuggled even into classical electrodynamics texts.

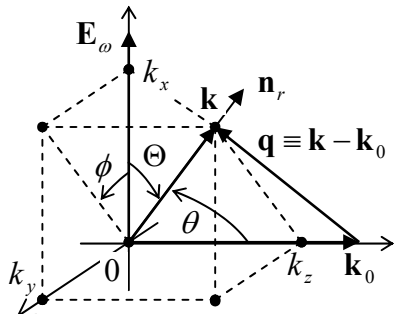


Fig. 8.5. The angles important for the general scattering problem.

This is why let me consider in detail only the simple cases when the vectors \mathbf{k} , \mathbf{k}_0 , and \mathbf{a} all reside in the same plane, with \mathbf{k}_0 normal to \mathbf{a} – see Fig. 6a.

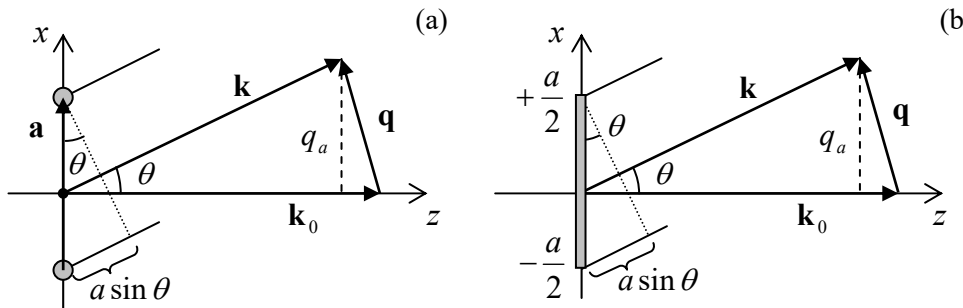


Fig. 8.6. The simplest cases of (a) interference and (b) diffraction.

In this case, $q_a = k \sin \theta$, and Eq. (58) is reduced to

$$F(\mathbf{q}) = 4 \cos^2 \frac{ka \sin \theta}{2}. \quad (8.59)$$

This function always has two maxima, at $\theta = 0$ and $\theta = \pi$, and, if the product ka is large enough, other maxima²⁵ at the special angles θ_n that satisfy the simple *Bragg condition*

$$ka \sin \theta_n = 2\pi n, \quad \text{i.e. } a \sin \theta_n = n\lambda. \quad (8.60)$$

Bragg condition

As Fig. 6a shows, this condition may be readily understood as that of the in-phase addition (the *constructive interference*) of two coherent waves scattered from the two points, when the difference between their paths toward the observer, $a \sin \theta$, is equal to an integer number of wavelengths. At each such maximum, $F = 4$, due to the doubling of the wave amplitude and hence quadrupling its power.

If the distance between the point scatterers is large ($ka \gg 1$), the first maxima (60) correspond to small scattering angles, $\theta \ll 1$. For this region, Eq. (59) is reduced to a simple periodic dependence of function F on the angle θ . Moreover, within the range of small θ , the wave polarization factor $\sin^2 \Theta$ is virtually constant, so that the angular dependence of the scattered wave's intensity, and hence of the differential cross-section are also very simple:

$$\frac{d\sigma}{d\Omega} \propto F(\mathbf{q}) = 4 \cos^2 \frac{ka\theta}{2}. \quad (8.61)$$

Young's interference pattern

²⁵ In optics especially, such intensity maxima/minima patterns are called *interference fringes*.

This simple *interference pattern* is well known from Young's two-slit experiment.²⁶ (As will be discussed in the next section, the theoretical description of the two-slit experiment is more complex than that of the Born scattering, but is preferable experimentally because, at such scattering, the wave of intensity (61) has to be observed on the backdrop of a much stronger incident wave that propagates in almost the same direction, $\theta = 0$.)

A very similar analysis of scattering from $N > 2$ similar, equidistant scatterers, located along the same straight line shows that the positions (60) of the constructive interference maxima do not change (because the derivation of this condition is still applicable to each pair of adjacent scatterers), but the increase of N makes these peaks sharper and sharper. Leaving the quantitative analysis of this system for the reader's exercise, let me jump immediately to the limit $N \rightarrow 0$, in which we may ignore the scatterers' discreteness. The resulting pattern is similar to that at scattering by a continuous thin rod (see Fig. 6b), so let us first spell out the Born scattering formula for an arbitrary extended, continuous, uniform dielectric body. Transferring Eq. (56) from the sum to an integral, for the differential cross-section we get

$$\frac{d\sigma}{d\Omega} = \left(\frac{k^2}{4\pi} \right)^2 (\kappa - 1)^2 F(\mathbf{q}) \sin^2 \Theta = \left(\frac{k^2}{4\pi} \right)^2 (\kappa - 1)^2 |I(\mathbf{q})|^2 \sin^2 \Theta, \quad (8.62)$$

where $I(\mathbf{q})$ now becomes the *phase integral*,²⁷

Phase integral

$$I(\mathbf{q}) = \int_V \exp\{-i\mathbf{q} \cdot \mathbf{r}'\} d^3 r', \quad (8.63)$$

with the dimensionality of volume.

Now we may return to the particular case of a thin rod (with both dimensions of the cross-section's area A much smaller than λ , but an arbitrary length a), otherwise keeping the same simple geometry as for two point scatterers – see Fig. 6b. In this case, the phase integral is just

Fraunhofer diffraction integral

$$I(\mathbf{q}) = A \int_{-a/2}^{+a/2} \exp\{-iq_a x'\} dx' = A \frac{\exp\{-iq_a a/2\} - \exp\{iq_a a/2\}}{-iq} \equiv V \frac{\sin \xi}{\xi}, \quad (8.64)$$

where $V = Aa$ is the volume of the rod, and ξ is the dimensionless argument defined as

$$\xi \equiv \frac{q_a a}{2} \equiv \frac{ka \sin \theta}{2}. \quad (8.65)$$

The fraction participating in the last form of Eq. (64) is met in physics so frequently that it has deserved the special name of the *sinc* (not “sync”, please!) *function* (see Fig. 7):

²⁶ This experiment was described in 1803 by Thomas Young – one more universal genius of science, who also introduced the Young modulus in the elasticity theory (see, e.g., CM Chapter 7), besides numerous other achievements – including deciphering Egyptian hieroglyphs! It is fascinating that the first clear observation of wave interference was made as early as 1666 by another genius, Sir Isaac Newton, in the form of so-called *Newton's rings*. Unbelievably, Newton failed to give the most natural explanation of his observations – perhaps because he was vehemently opposed to the very idea of light as a wave, which was promoted in his times by others, notably by Christian Huygens. Due to Newton's enormous authority, only Young's two-slit experiments more than a century later have firmly established the wave picture of light – to be replaced by the dualistic wave/photon picture formalized by quantum electrodynamics (see, e.g., QM Ch. 9), in one more century.

²⁷ Since the observation point's position \mathbf{r} does not participate in this formula explicitly, the prime sign in \mathbf{r}' could be dropped, but I keep it as a reminder that the integral is taken over points \mathbf{r}' of the *scattering object*.

$$\text{sinc}\xi \equiv \frac{\sin \xi}{\xi}.$$

(8.66)

Sinc
function

It vanishes at all points $\xi_n = \pi n$ with integer n , besides such point with $n = 0$: $\text{sinc}\xi_0 \equiv \text{sinc } 0 = 1$.

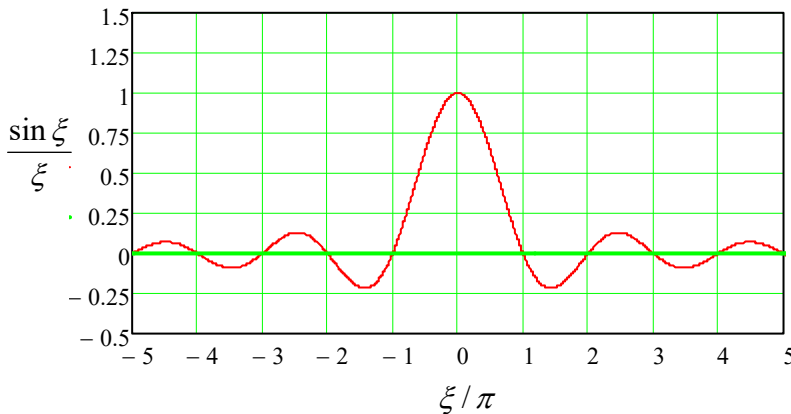


Fig. 8.7. The sinc function.

The function $F(\mathbf{q}) = V^2 \text{sinc}^2 \xi$, given by Eq. (64) and plotted with the red line in Fig. 8, is called the *Fraunhofer diffraction pattern*.²⁸

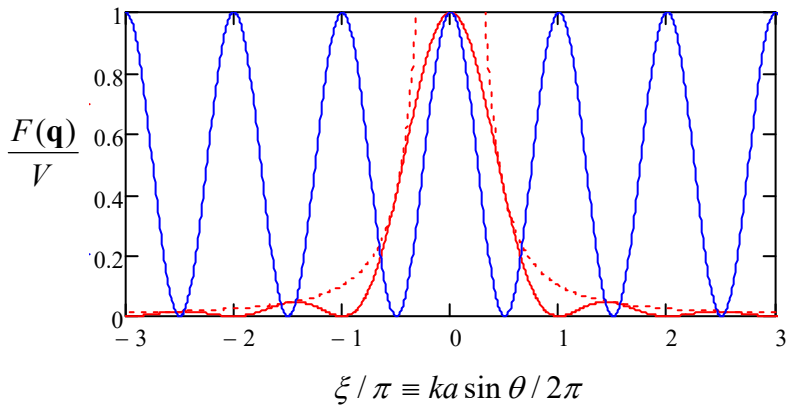


Fig. 8.8. The Fraunhofer diffraction pattern (solid red line) and its envelope $1/\xi^2$ (dashed red line). For comparison, the blue line shows the basic interference pattern $\cos^2 \xi$ – cf. Eq. (61).

Note that it oscillates with the same argument's period $\Delta(k \sin \theta) = 2\pi/ka$ as the interference pattern (61) from two-point scatterers (shown with the blue line in Fig. 8). However, at the interference, the scattered wave intensity vanishes at angles θ_n' that satisfy the condition

$$\frac{k \sin \theta_n'}{2\pi} = n + \frac{1}{2}, \quad (8.67)$$

i.e. when the optical paths difference $a \sin \alpha$ is equal to a semi-integer number of wavelengths $\lambda/2 = \pi/k$, and hence the two waves from the scatterers reach the observer in anti-phase – the so-called *destructive interference*. On the other hand, for the diffraction on a continuous rod the minima occur at a different set of scattering angles:

$$\frac{k \sin \theta_n}{2\pi} = n, \quad (8.68)$$

²⁸ It is named after Joseph von Fraunhofer (1787-1826) – who has invented the spectroscope, developed the diffraction grating (see below), and also discovered the dark *Fraunhofer lines* in Sun's spectrum.

i.e. exactly where the two-point interference pattern has its maxima – please have a look at Fig. 8 again. The reason for this relation is that the wave diffraction on the rod may be considered as a simultaneous interference of waves from all its elementary fragments, and exactly at the observation angles when the rod edges give waves with phases shifted by $2\pi n$, the interior points of the rod give waves with all phases within this difference, with their algebraic sum equal to zero. As even more visible in Fig. 8, at the diffraction, the intensity oscillations are limited by a rapidly decreasing envelope function $1/\xi^2$ – while at the two-point interference, the oscillations retain the same amplitude. The reason for this fast decrease is that with each Fraunhofer diffraction period, a smaller and smaller fraction of the road gives an unbalanced contribution to the scattered wave.

If the rod's length is small ($ka \ll 1$, i.e. $a \ll \lambda$), then the sinc function's argument ξ is small at all scattering angles θ , so $I(\mathbf{q}) \approx V$, and Eq. (62) is reduced to Eq. (53). In the opposite limit, $a \gg \lambda$, the first zeros of the function $I(\mathbf{q})$ correspond to very small angles θ , for which $\sin\Theta \approx 1$, so that the differential cross-section is just

$$\frac{d\sigma}{d\Omega} = \left(\frac{k^2}{4\pi} \right)^2 (\kappa - 1)^2 \text{sinc}^2 \frac{ka\theta}{2}, \quad (8.69)$$

i.e. Fig. 8 shows the scattering intensity as a function of the direction toward the observation point – if this point is within the plane containing the rod.

Finally, let us discuss a problem of large importance for applications: calculate the positions of the maxima of the interference pattern arising at the incidence of a plane wave on a very large 3D periodic system of point scatterers. For that, first of all, let us quantify the notion of 3D periodicity. The periodicity in one dimension is simple: the system we are considering (say, the positions of point scatterers) should be invariant with respect to the linear translation by some period a , and hence by any multiple sa of this period, where s is any integer. Anticipating the 3D generalization, we may require any of the possible *translation vectors* \mathbf{R} to that the system is invariant, to be equal $s\mathbf{a}$, where the *primitive vector* \mathbf{a} is directed along the (so far, the only) axis of the 1D system.

Now we are ready for the common definition of the 3D periodicity – as the invariance of the system with respect to the translation by any vector of the following set:

$$\boxed{\mathbf{R} = \sum_{l=1}^3 s_l \mathbf{a}_l,} \quad (8.70)$$

Bravais
lattice

where s_l are three independent integers, and $\{\mathbf{a}_l\}$ is a set of three linearly-independent *primitive vectors*. The set of geometric points described by Eq. (70) is called the *Bravais lattice* (first analyzed in detail, circa 1850, by Auguste Bravais). Perhaps the most nontrivial feature of this relation is that the vectors \mathbf{a}_l should not necessarily be orthogonal to each other. (That requirement would severely restrict the set of possible lattices and make it unsuitable for the description, for example, of many solid-state crystals.) For the scattering problem we are considering, we will assume that the position \mathbf{r}_j of each point scatterer coincides with one of the points \mathbf{R} of some Bravais lattice, with a given set of primitive vectors \mathbf{a}_l , so that in the basic Eq. (57), the index j is coding the set of three integers $\{s_1, s_2, s_3\}$.

Now let us consider a similarly defined Bravais lattice, but in the reciprocal (wave-number) space, numbered by three independent integers $\{t_1, t_2, t_3\}$:

$$\boxed{\mathbf{Q} = \sum_{m=1}^3 t_m \mathbf{b}_m, \quad \text{with } \mathbf{b}_m = 2\pi \frac{\mathbf{a}_{m''} \times \mathbf{a}_{m'}}{\mathbf{a}_m \cdot (\mathbf{a}_{m''} \times \mathbf{a}_{m'})},} \quad (8.71)$$

Reciprocal
lattice

where in the last expression, the indices m , m' , and m'' are all different. This is the so-called *reciprocal lattice*, which plays an important role in all physics of periodic structures, in particular in the quantum energy-band theory.²⁹ To reveal its most important property, and thus justify the above introduction of the primitive vectors \mathbf{b}_m , let us calculate the following scalar product:

$$\mathbf{R} \cdot \mathbf{Q} \equiv \sum_{l,m=1}^3 s_l t_m \mathbf{a}_l \cdot \mathbf{b}_m \equiv 2\pi \sum_{l,m=1}^3 s_l t_m \mathbf{a}_l \cdot \frac{\mathbf{a}_{m''} \times \mathbf{a}_{m'}}{\mathbf{a}_m \cdot (\mathbf{a}_{m''} \times \mathbf{a}_{m'})} \equiv 2\pi \sum_{l,m=1}^3 s_l t_k \frac{\mathbf{a}_l \cdot (\mathbf{a}_{m''} \times \mathbf{a}_{m'})}{\mathbf{a}_m \cdot (\mathbf{a}_{m''} \times \mathbf{a}_{m'})}. \quad (8.72)$$

Applying to the numerator of the last fraction the *operand rotation rule* of vector algebra,³⁰ we see that it is equal to zero if $l \neq m$, while for $l = m$ the whole fraction is evidently equal to 1. Thus the double sum (72) is reduced to a single sum:

$$\mathbf{R} \cdot \mathbf{Q} = 2\pi \sum_{l=1}^3 s_l t_l = 2\pi \sum_{l=1}^3 n_l, \quad (8.73)$$

where each of the products $n_l \equiv s_l t_l$ is an integer, and hence their sum,

$$n \equiv \sum_{l=1}^3 n_l \equiv s_1 t_1 + s_2 t_2 + s_3 t_3, \quad (8.74)$$

is an integer as well, so that the main property of the direct/reciprocal lattice couple is very simple:

$$\mathbf{R} \cdot \mathbf{Q} = 2\pi n, \quad \text{and hence } \exp\{-i\mathbf{R} \cdot \mathbf{Q}\} = 1. \quad (8.75)$$

Now returning to the scattering function (56) for a Bravais lattice of point scatters, we see that if the vector $\mathbf{q} \equiv \mathbf{k} - \mathbf{k}_0$ coincides with *any* vector \mathbf{Q} of the reciprocal lattice, then all terms of the phase sum (57) take their largest possible values (equal to 1), and hence the sum as the whole is largest as well, giving a constructive interference maximum. This equality, $\mathbf{q} = \mathbf{Q}$, where \mathbf{Q} is given by Eq. (71), is called the *von Laue condition* (named after Max von Laue) of the constructive interference; it is, in particular, the basis of the whole field of the X-ray crystallography of solids and polymers – the main tool for revealing their atomic/molecular structure.³¹

In order to recast the von Laue condition in a more vivid geometric form, let us consider one of the vectors \mathbf{Q} of the reciprocal lattice, corresponding to a certain integer n in Eq. (75), and notice that if that relation is satisfied for one point \mathbf{R} of the direct Bravais lattice (70), i.e. for one set of the integers $\{s_1, s_2, s_3\}$, it is also satisfied for a 2D system of other integer sets, which may be parameterized, for example, by two integers S_1 and S_2 :

$$s'_1 = s_1 + S_1 t_3, \quad s'_2 = s_2 + S_2 t_3, \quad s'_3 = s_3 - S_1 t_1 - S_2 t_2. \quad (8.76)$$

Indeed, each of these sets has the same value of the integer n , defined by Eq. (74), as the original one:

$$n' \equiv s'_1 t_1 + s'_2 t_2 + s'_3 t_3 \equiv (s_1 + S_1 t_3) t_1 + (s_2 + S_2 t_3) t_2 + (s_3 - S_1 t_1 - S_2 t_2) t_3 = n. \quad (8.77)$$

Since according to Eq. (75), the vector of the distance between any pair of the corresponding points of the direct Bravais lattice (70),

²⁹ See, e.g., QM Sec. 3.4, where several particular Bravais lattices \mathbf{R} , and their reciprocals \mathbf{Q} , are considered.

³⁰ See, e.g., MA Eq. (7.6).

³¹ For more reading on this important topic, I can recommend, for example, the classical monograph by B. Cullity, *Elements of X-Ray Diffraction*, 2nd ed., Addison-Wesley, 1978. (Note that its title uses the alternative name of the field, once again illustrating how blurry the boundary between the interference and diffraction is.)

$$\Delta \mathbf{R} = \Delta S_1 t_3 \mathbf{a}_1 + \Delta S_2 t_3 \mathbf{a}_2 - (\Delta S_1 t_1 + \Delta S_2 t_2) \mathbf{a}_3, \quad (8.78)$$

satisfies the condition $\Delta \mathbf{R} \cdot \mathbf{Q} = 2\pi \Delta n = 0$, this vector is normal to the (fixed) vector \mathbf{Q} . Hence, all the points corresponding to the 2D set (76) with arbitrary integers S_1 and S_2 , are located on one geometric plane, called the *crystal* (or “lattice”) *plane*. In a 3D system of $N \gg 1$ scatterers (such as $N \sim 10^{20}$ atoms in a $\sim 1\text{-mm}^3$ solid crystal), with all linear dimensions comparable, such a plane contains $\sim N^{2/3} \gg 1$ points. As a result, the constructive interference peaks are very sharp.

Now rewriting Eq. (75) as a relation for the vector \mathbf{R} ’s component along the vector \mathbf{Q} ,

$$R_Q = \frac{2\pi}{Q} n, \quad \text{where } R_Q \equiv \mathbf{R} \cdot \mathbf{n}_Q \equiv \mathbf{R} \cdot \frac{\mathbf{Q}}{|Q|}, \quad \text{and } Q \equiv |\mathbf{Q}|, \quad (8.79)$$

we see that the parallel crystal planes corresponding to different numbers n (but the same \mathbf{Q}) are located in space periodically, with the smallest distance

$$d = \frac{2\pi}{Q}, \quad (8.80)$$

so that the von Laue condition $\mathbf{q} = \mathbf{Q}$ may be rewritten as the following rule for the possible magnitudes of the scattering vector $\mathbf{q} \equiv \mathbf{k} - \mathbf{k}_0$:

$$q = \frac{2\pi n}{d}. \quad (8.81)$$

Figure 9a shows the diagram of the three wave vectors \mathbf{k} , \mathbf{k}_0 , and \mathbf{q} , taking into account the elastic scattering condition $|\mathbf{k}| = |\mathbf{k}_0| = k \equiv 2\pi/\lambda$. From the diagram, we immediately get the famous *Bragg rule*³² for the (equal) angles $\alpha \equiv \theta/2$ between the crystal plane and each of the vectors \mathbf{k} and \mathbf{k}_0 :

$k \sin \alpha = \frac{q}{2} = \frac{\pi n}{d}, \quad \text{i.e. } 2d \sin \alpha = n\lambda. \quad (8.82)$

Bragg
rule

The physical sense of this relation is very simple – see Fig. 9b drawn in the “direct” space of the radius-vectors \mathbf{r} , rather than in the reciprocal space of the wave vectors, as Fig. 9a. It shows that if the Bragg condition (82) is satisfied, the total difference $2d \sin \alpha$ of the optical paths of two waves, partly reflected from the adjacent crystal planes, is equal to an integer number of wavelengths, so these waves interfere constructively.

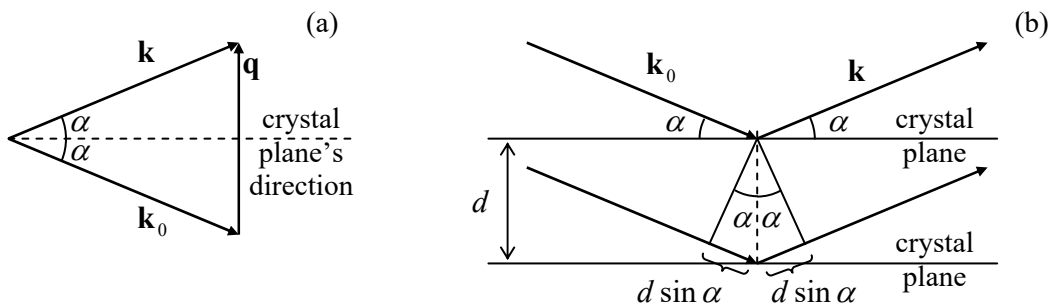


Fig. 9.9. Deriving the Bragg rule: (a) from the von Laue condition (in the reciprocal space), and (b) from a direct-space diagram. Note that the scattering angle θ equals 2α .

³² Named after Sir William Bragg and his son, Sir William Lawrence Bragg, who were the first to demonstrate (in 1912) the X-ray diffraction by atoms in crystals. The Braggs’ experiments have made the existence of atoms (before that, a somewhat hypothetical notion ignored by many physicists) indisputable.

Finally, note that the von Laue and Bragg rules, as well as the similar condition (60) for the 1D system of scatterers, are valid not only in the Born approximation but also follow from any adequate theory of scattering, because the phase sum (57) does not depend on the magnitude of the wave propagating from each elementary scatterer, provided that they are all equal.

8.5. The Huygens principle

As the reader could see, the Born approximation is very convenient for tracing the basic features of (and the difference between) the phenomena of interference and diffraction. Unfortunately, this approximation, based on the relative weakness of the scattered wave, cannot be used to describe more typical experimental implementations of these phenomena, for example, Young's two-slit experiment, or diffraction on a single slit or orifice – see, e.g. Fig. 10. Indeed, at such experiments, the orifice size a is typically much larger than the light's wavelength λ , and as a result, no clear decomposition of the fields to the “incident” and “scattered” waves is possible inside it.³³

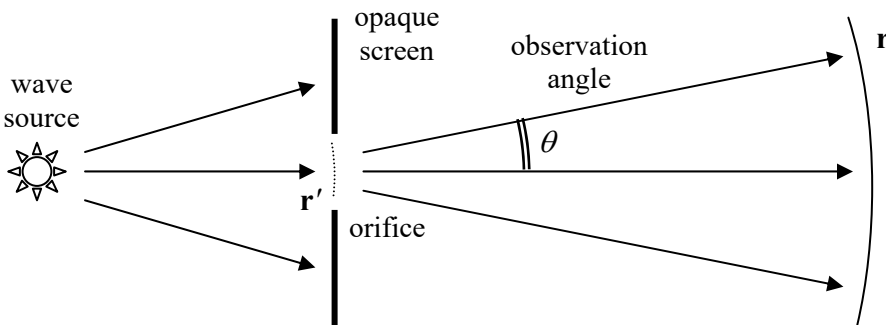


Fig. 8.10. Deriving the Huygens principle.

However, another approximation called the *Huygens* (or “Huygens-Fresnel”) *principle*,³⁴ is very instrumental for the description of such situations. In this approach, the wave beyond the screen is represented as a linear superposition of spherical waves of the type (17), as if they were emitted by every point of the incident wave’s front that has arrived at the orifice. This approximation is valid if the following strong conditions are satisfied:

$$\lambda \ll a \ll r, \quad (8.83)$$

where r is the distance of the observation point from the orifice. In addition, as we have seen in the last section, at small λ/a the diffraction phenomena are confined to angles $\theta \sim 1/ka \sim \lambda/a \ll 1$. For observation at such small angles, the mathematical expression of the Huygens principle, for the complex amplitude $f_\omega(\mathbf{r})$ of a monochromatic wave $f(\mathbf{r}, t) = \text{Re}[f_\omega e^{-i\omega t}]$, is given by the following simple formula

$$f_\omega(\mathbf{r}) = C \int_{\text{orifice}} f_\omega(\mathbf{r}') \frac{e^{ikR}}{R} d^2 r'. \quad (8.84)$$

³³ Another complaint against the Born approximation is that it does not satisfy the so-called *optical* (or “forward scattering”) *theorem* relating σ to scattering with $\mathbf{k} = \mathbf{k}_0$. This relation is especially important for quantum-mechanical description of particle scattering, and in this series, will be discussed in its QM part (Sec. 3.3).

³⁴ Named after Christian Huygens (1629-1695) who had conjectured the wave nature of light (which remained controversial for more than a century, until T. Young’s experiments), and Augustin-Jean Fresnel (1788-1827) who developed a quantitative theory of diffraction, and in particular gave a mathematical formulation of the Huygens principle. (Note that Eq. (91), sufficient for the purposes of this course, is not its most general form.)

Here f is any transverse component of any of the wave's fields (either \mathbf{E} or \mathbf{H}),³⁵ R is the distance between point \mathbf{r}' at the orifice and the observation point \mathbf{r} (i.e. the magnitude of vector $\mathbf{R} \equiv \mathbf{r} - \mathbf{r}'$), and C is a complex constant.

Before describing the proof of Eq. (84), let me carry out its sanity check – which also will give us the constant C . Let us see what the Huygens principle gives for the case when the field under the integral is a plane wave with the complex amplitude $f_\omega(z)$, propagating along axis z , with an unlimited x - y front, (i.e. when there is no opaque screen at all), so that in Eq. (84) we should take the whole $[x, y]$ plane, say with $z' = 0$, as the integration area—see Fig. 11.

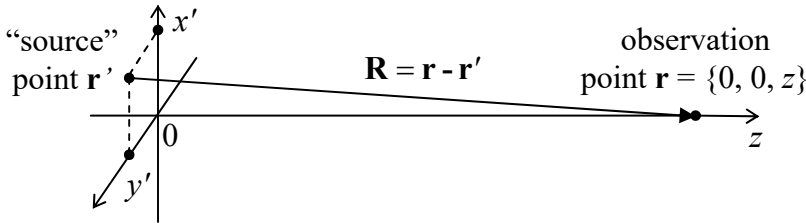


Fig. 8.11. Applying the Huygens principle to a plane incident wave.

Then, for the observation point with coordinates $x = 0, y = 0$, and $z > 0$, Eq. (84) yields

$$f_\omega(z) = Cf_\omega(0) \int dx' \int dy' \frac{\exp\left\{ik(x'^2 + y'^2 + z^2)^{1/2}\right\}}{(x'^2 + y'^2 + z^2)^{1/2}}. \quad (8.85)$$

Before specifying the integration limits, let us consider the range $|x'|, |y'| \ll z$. In this range, the square root participating in Eq. (85) twice, may be approximated as

$$(x'^2 + y'^2 + z^2)^{1/2} \equiv z \left(1 + \frac{x'^2 + y'^2}{z^2}\right)^{1/2} \approx z \left(1 + \frac{x'^2 + y'^2}{2z^2}\right) \equiv z + \frac{x'^2 + y'^2}{2z}. \quad (8.86)$$

At $z \gg \lambda$, the denominator of Eq. (85) is a much slower function of x' and y' than the exponent in the nominator, and in the former case, it is sufficient (as we will check *a posteriori*) to keep just the main, first term of expansion (86). With that, Eq. (85) becomes

$$f_\omega(z) = Cf_\omega(0) \frac{e^{ikz}}{z} \int dx' \int dy' \exp\frac{ik(x'^2 + y'^2)}{2z} = Cf_\omega(0) \frac{e^{ikz}}{z} I_x I_y, \quad (8.87)$$

where I_x and I_y are two similar integrals; for example,

$$I_x = \int \exp\frac{ikx'^2}{2z} dx' = \left(\frac{2z}{k}\right)^{1/2} \int \exp\{i\xi^2\} d\xi \equiv \left(\frac{2z}{k}\right)^{1/2} \left[\int \cos(\xi^2) d\xi + i \int \sin(\xi^2) d\xi \right], \quad (8.88)$$

where $\xi \equiv (k/2z)^{1/2} x'$. These are the so-called *Fresnel integrals*. I will discuss them in more detail in the next section (see, in particular, Fig. 13), and for now, only one property³⁶ of these integrals is important

³⁵ The fact that the Huygens principle is valid for any field component should not too surprising. In the limit $a \gg \lambda$, the real boundary conditions at the orifice edges are not important; it is only important for the screen that limits the orifice, to be opaque. Because of this, the Huygens principle (84) is a part of the so-called *scalar theory of diffraction*. (I will not have time to discuss the *vector theory* of these effects, which is more accurate at smaller a – see, e.g., Chapter 11 of the monograph by M. Born and E. Wolf, cited at the end of Sec. 7.1.)

for us: if taken in symmetric limits $[-\xi_0, +\xi_0]$, both of them rapidly converge to the same value, $(\pi/2)^{1/2}$, as soon as ξ_0 becomes much larger than 1. This means that even if we do not impose any exact limits on the integration area in Eq. (85), this integral converges to the value

$$f_\omega(z) = Cf_\omega(0) \frac{e^{ikz}}{z} \left\{ \left(\frac{2z}{k} \right)^{1/2} \left[\left(\frac{\pi}{2} \right)^{1/2} + i \left(\frac{\pi}{2} \right)^{1/2} \right] \right\}^2 \equiv \left(C \frac{2\pi i}{k} \right) f_\omega(0) e^{ikz}, \quad (8.89)$$

due to contributions from the central area with a linear size corresponding to $\Delta\xi \sim 1$, i.e. to

$$\Delta x \sim \Delta y \sim \left(\frac{z}{k} \right)^{1/2} \sim (\lambda z)^{1/2}, \quad . \quad (8.90)$$

so that the net contribution from the front points \mathbf{r}' well beyond the range (90) is negligible.³⁷ (Within our assumptions (83), which in particular require λ to be much less than z , the *diffraction angle* $\Delta x/z \sim \Delta y/z \sim (\lambda/z)^{1/2}$, corresponding to the important area of the front, is small.) According to Eq. (89), to sustain the unperturbed plane wave propagation, $f_\omega(z) = f_\omega(0)e^{ikz}$, the constant C has to be taken equal to $k/2\pi i$. Thus, the Huygens principle's prediction (84), in its final form, reads

$$f_\omega(\mathbf{r}) = \frac{k}{2\pi i} \int_{\text{orifice}} f_\omega(\mathbf{r}') \frac{e^{ikR}}{R} d^2 r', \quad (8.91)$$

Huygens principle

and describes, in particular, the straight propagation of the plane wave (in a uniform medium).

Let me pause to emphasize how nontrivial this result is. It would be a natural corollary of Eqs. (25) (and the linear superposition principle) if all points of the orifice were filled with point scatterers that re-emit all the incident waves as spherical waves. However, as it follows from the above example, the Huygens principle also works if there is nothing in the orifice but the free space!

This is why let us discuss a proof of this principle,³⁸ based on Green's theorem (2.207). Let us apply it to the function $f = f_\omega$ where f_ω is the complex amplitude of a scalar component of one of the wave's fields, which satisfies the Helmholtz equation (7.204),

$$(\nabla^2 + k^2) f_\omega(\mathbf{r}) = 0, \quad (8.92)$$

and the function $g = G_\omega$ is the temporal Fourier image of the corresponding Green's function. The latter function may be defined, as usual, as the solution of the same equation with the added delta-functional right-hand side with an arbitrary coefficient, for example,

$$(\nabla^2 + k^2) G_\omega(\mathbf{r}, \mathbf{r}') = -4\pi\delta(\mathbf{r} - \mathbf{r}'). \quad (8.93)$$

Using Eqs. (92) and (93) to express the Laplace operators of the functions f_ω and G_ω , we may rewrite Eq. (2.207) as

³⁶ See, e.g., MA Eq. (6.10).

³⁷ This result very is natural, because the function $\exp\{ikR\}$ oscillates fast with the change of \mathbf{r}' , so that the contributions from various front points are averaged out. Indeed, the only reason why the central part of the plane $[x', y']$ gives a non-zero contribution (89) to $f_\omega(z)$ is that the phase exponents stop oscillating as $(x'^2 + y'^2)$ is reduced below $\sim z/k$ – see Eq. (86).

³⁸ This proof was given in 1882 by the same G. Kirchhoff whose circuit rules were discussed in Sec. 4.1 and 6.6.

$$\int_V \left\{ f_\omega \left[-k^2 G_\omega(\mathbf{r}, \mathbf{r}') - 4\pi \delta(\mathbf{r} - \mathbf{r}') \right] - G_\omega(\mathbf{r}, \mathbf{r}') \left[-k^2 f_\omega \right] \right\} d^3 r = \oint_S \left[f_\omega \frac{\partial G_\omega(\mathbf{r}, \mathbf{r}')}{\partial n} - G_\omega(\mathbf{r}, \mathbf{r}') \frac{\partial f_\omega}{\partial n} \right] d^2 r, \quad (8.94)$$

where \mathbf{n} is the outward normal to the surface S limiting the integration volume V . Two terms on the left-hand side of this relation cancel, so that after swapping the arguments \mathbf{r} and \mathbf{r}' , we get

$$-4\pi f_\omega(\mathbf{r}) = \oint_S \left[f_\omega(\mathbf{r}') \frac{\partial G_\omega(\mathbf{r}', \mathbf{r})}{\partial n'} - g_\omega(\mathbf{r}', \mathbf{r}) \frac{\partial G_\omega(\mathbf{r}')}{\partial n'} \right] d^2 r'. \quad (8.95)$$

This relation is only correct if the selected volume V includes the point \mathbf{r} (otherwise we would not get its left-hand side from the integration of the delta function), but does not include the genuine source of the wave – otherwise, Eq. (92) would have a non-zero right-hand side. Now let \mathbf{r} be the field observation point, V be all the source-free half-space (for example, the space right of the screen in Fig. 10), so that S is the surface of the screen, including the orifice. Then the right-hand side of Eq. (95) describes the field (at the observation point \mathbf{r}) induced by the wave passing through the orifice points \mathbf{r}' . Since no waves are emitted by the opaque parts of the screen, we can limit the integration by the orifice area.³⁹ Assuming also that the opaque parts of the screen do not re-emit the waves “radiated” by the orifice, we can take the solution of Eq. (93) to be the retarded potential for the free space:⁴⁰

$$G_\omega(\mathbf{r}, \mathbf{r}') = \frac{e^{ikR}}{R}. \quad (8.96)$$

Plugging this expression into Eq. (82), we get

$$-4\pi f_\omega(\mathbf{r}) = \oint_{\text{orifice}} \left[f_\omega(\mathbf{r}') \frac{\partial}{\partial n'} \left(\frac{e^{ikR}}{R} \right) - \left(\frac{e^{ikR}}{R} \right) \frac{\partial f_\omega(\mathbf{r}')}{\partial n'} \right] d^2 r'. \quad (8.97)$$

This is the so-called *Kirchhoff* (or “Fresnel-Kirchhoff”) *integral*. (Again, with the integration extended over *all* boundaries of the volume V , this would be an exact mathematical result.) Now, let us make two additional approximations. The first of them stems from Eq. (83): at $ka \gg 1$, the wave’s spatial dependence in the orifice area may be represented as

$$f_\omega(\mathbf{r}') = (\text{a slow function of } \mathbf{r}') \times \exp\{i\mathbf{k}_0 \cdot \mathbf{r}'\}, \quad (8.98)$$

where “slow” means a function that changes on the scale of a rather than λ . If, also, $kR \gg 1$, then the differentiation in Eq. (97) may be, in both instances, limited to the rapidly changing exponents, giving

$$-4\pi f_\omega(\mathbf{r}) = \oint_{\text{orifice}} i(\mathbf{k} + \mathbf{k}_0) \cdot \mathbf{n}' \frac{e^{ikR}}{R} f(\mathbf{r}') d^2 r'. \quad (8.99)$$

Second, if all observation angles are small, we may take $\mathbf{k} \cdot \mathbf{n}' \approx \mathbf{k}_0 \cdot \mathbf{n}' \approx -k$. With that, Eq. (99) is reduced to the Huygens principle in its form (91).

³⁹ Actually, this is a nontrivial point of the proof. Indeed, it may be shown that the exact solution of Eq. (94) identically is equal to zero if $f(\mathbf{r}')$ and $\partial f(\mathbf{r}')/\partial n'$ vanish together at any *part* of the boundary, of a non-zero area. A more careful analysis of this issue (it is the task of the formal vector theory of diffraction, which I will not have time to pursue) confirms the validity of the described intuition-based approach at $a \gg \lambda$.

⁴⁰ It follows, e.g., from Eq. (16) with a monochromatic source $q(t) = q_\omega \exp\{-i\omega t\}$, with the amplitude $q_\omega = 4\pi\varepsilon$ that fits the right-hand side of Eq. (93).

It is clear that the principle immediately gives a very simple description of the interference of waves passing through two small holes in the screen. Indeed, if the holes' sizes are negligible in comparison with the distance a between them (though still are much larger than the wavelength!), Eq. (91) yield

$$f_\omega(\mathbf{r}) = c_1 e^{ikR_1} + c_2 e^{ikR_2}, \quad \text{with } c_{1,2} \equiv kf_{1,2} A_{1,2} / 2\pi i R_{1,2}, \quad (8.100)$$

where $R_{1,2}$ are the distances between the holes and the observation point, and $A_{1,2}$ are the hole areas. For the wave intensity, Eq. (100) gives

$$\bar{S} \propto f_\omega f_\omega^* = |c_1|^2 + |c_2|^2 + 2|c_1||c_2|\cos[k(R_1 - R_2) + \varphi], \quad \text{where } \varphi \equiv \arg c_1 - \arg c_2. \quad (8.101)$$

The first two terms in the last expression clearly represent the intensities of the partial waves passed through each hole, while the last one is the result of their interference. The interference pattern's *contrast ratio*

$$\frac{\bar{S}_{\max}}{\bar{S}_{\min}} = \left(\frac{|c_1| + |c_2|}{|c_1| - |c_2|} \right)^2, \quad (8.102)$$

is the largest (infinite) when both waves have equal amplitudes.

The analysis of the interference pattern is simple if the line connecting the holes is perpendicular to wave vector $\mathbf{k} \approx \mathbf{k}_0$ – see Fig. 6a. Selecting the coordinate axes as shown in that figure, and using for the distances $R_{1,2}$ the same expansion as in Eq. (86), for the interference term in Eq. (101) we get

$$\cos[k(R_1 - R_2) + \varphi] \approx \cos\left(\frac{kxa}{z} + \varphi\right). \quad (8.103)$$

This means that the term does not depend on y , i.e. the interference pattern in the plane of constant z is a set of straight, parallel strips, perpendicular to the vector \mathbf{a} , with the period given by Eq. (60), i.e. by the Bragg law.⁴¹ This result is strictly valid only at $y^2 \ll z^2$; it is straightforward to use the next term in the Taylor expansion (73) to show that farther on from the interference plane $y = 0$, the strips start to diverge.

8.6. Fresnel and Fraunhofer diffraction patterns

Now let us use the Huygens principle to analyze a slightly more complex problem: plane wave's diffraction on a long, straight slit of a constant width a (Fig. 12). According to Eq. (83), to use the Huygens principle for the problem's analysis we need to have $\lambda \ll a \ll z$. Moreover, the simple version (91) of the principle is only valid for small observation angles, $|x| \ll z$. Note, however, that the relation between two dimensionless parameters of the problem, z/a and a/λ , which are both much less than 1, is so far arbitrary; as we will see in a minute, this relation determines the type of the observed diffraction pattern.

⁴¹ The phase shift φ vanishes at the normal incidence of a plane wave on the holes. Note, however, that the spatial shift of the interference pattern following from Eq. (103), $\Delta x = -(z/ka)\varphi$, is extremely convenient for the experimental measurement of the phase shift between two waves, especially if it is induced by some factor (such as insertion of a transparent object into one of the interferometer's arms) that may be turned on/off at will.

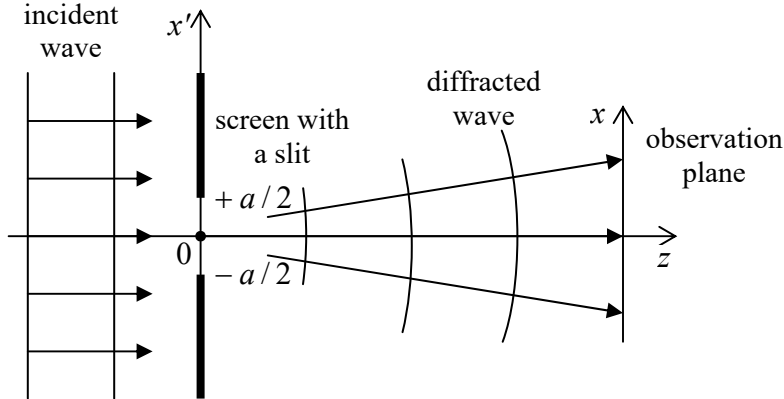


Fig. 8.12. Diffraction on a slit.

Let us apply Eq. (91) to our current problem (Fig. 12), for the sake of simplicity assuming the normal wave incidence, and taking $z' = 0$ at the screen plane:

$$f_\omega(x, z) = f_0 \frac{k}{2\pi i} \int_{-a}^{+a} dx' \int_{-\infty}^{+\infty} dy' \frac{\exp\left\{ik[(x-x')^2 + y'^2 + z^2]^{1/2}\right\}}{[(x-x')^2 + y'^2 + z^2]^{1/2}}, \quad (8.104)$$

where $f_0 \equiv f_\omega(x', 0) = \text{const}$ is the incident wave's amplitude. This is the same integral as in Eq. (85), except for the finite limits for the integration variable x' , and may be simplified similarly, using the small-angle condition $(x-x')^2 + y'^2 \ll z^2$:

$$f_\omega(x, z) \approx f_0 \frac{k}{2\pi i} \frac{e^{ikz}}{z} \int_{-a/2}^{+a/2} dx' \int_{-\infty}^{+\infty} dy' \exp\frac{ik[(x-x')^2 + y'^2]}{2z} \equiv f_0 \frac{k}{2\pi i} \frac{e^{ikz}}{z} I_x I_y. \quad (8.105)$$

The integral over y' is the same as in the last section:

$$I_y \equiv \int_{-\infty}^{+\infty} \exp\frac{iky'^2}{2z} dy' = \left(\frac{2\pi iz}{k}\right)^{1/2}, \quad (8.106)$$

but the integral over x' is more general, because of its finite limits:

$$I_x \equiv \int_{-a/2}^{+a/2} \exp\frac{ik(x-x')^2}{2z} dx'. \quad (8.107)$$

It may be simplified in the following two (opposite) limits.

(i) *Fraunhofer diffraction* takes place when $z/a \gg a/\lambda$ – the relation which may be rewritten either as $a \ll (z\lambda)^{1/2}$, or as $ka^2 \ll z$. In this limit, the ratio kx^2/z is negligibly small for all values of x' under the integral, and we can approximate it as

$$\begin{aligned} I_x &= \int_{-a/2}^{+a/2} \exp\frac{ik(x^2 - 2xx' + x'^2)}{2z} dx' \approx \int_{-a/2}^{+a/2} \exp\frac{ik(x^2 - 2xx')}{2z} dx' \\ &\equiv \exp\frac{ikx^2}{2z} \int_{-a/2}^{+a/2} \exp\left\{-\frac{ikxx'}{z}\right\} dx' = \frac{2z}{kx} \exp\left\{\frac{ikx^2}{2z}\right\} \sin\frac{kxa}{2z}, \end{aligned} \quad (8.108)$$

so that Eq. (105) yields

$$f_\omega(x, z) \approx f_0 \frac{k}{2\pi i} \frac{e^{ikz}}{z} \frac{2z}{kx} \left(\frac{2\pi iz}{k} \right)^{1/2} \exp \left\{ \frac{ikx^2}{2z} \right\} \sin \frac{kxa}{2z}, \quad (8.109)$$

and hence the relative wave intensity is

$$\frac{\bar{S}(x, z)}{S_0} = \left| \frac{f_\omega(x, z)}{f_0} \right|^2 = \frac{8z}{\pi kx^2} \sin^2 \frac{kxa}{2z} \equiv \frac{2}{\pi} \frac{ka^2}{z} \text{sinc}^2 \left(\frac{ka\theta}{2} \right), \quad (8.110)$$

Fraunhofer diffraction pattern

where S_0 is the intensity of the incident wave, and $\theta \equiv x/z \ll 1$ is the observation angle. Comparing this expression with Eq. (69), we see that this diffraction pattern is exactly the same as that for a similar (uniform, 1D) object in the Born approximation – see the red line in Fig. 8. Note again that the angular width $\delta\theta$ of the Fraunhofer pattern is of the order of $1/ka$, so that its linear width $\delta x = z\delta\theta$ is of the order of $z/ka \sim z\lambda/a$.⁴² Hence the condition of the Fraunhofer approximation's validity may be also represented as $a \ll \delta x$.

(ii) *Fresnel diffraction.* In the opposite limit of a relatively wide slit, with $a \gg \delta x = z\delta\theta \sim z/ka \sim z\lambda/a$, i.e. $ka^2 \gg z$, the diffraction patterns at two edges of the slit are well separated. Hence, near each edge (for example, near $x' = -a/2$) we may simplify Eq. (107) as

$$I_x(x) \approx \int_{-a/2}^{+\infty} \exp \frac{ik(x-x')^2}{2z} dx' \equiv \left(\frac{2z}{k} \right)^{1/2} \frac{\int_{(k/2z)^{1/2}(x+a/2)}^{+\infty} \exp(i\xi^2) d\xi}{(k/2z)^{1/2}}, \quad (8.111)$$

and express it via the special functions called the Fresnel integrals:⁴³

$$\mathcal{C}(\xi) \equiv \left(\frac{2}{\pi} \right)^{1/2} \int_0^\xi \cos(\zeta^2) d\zeta, \quad \mathcal{S}(\xi) \equiv \left(\frac{2}{\pi} \right)^{1/2} \int_0^\xi \sin(\zeta^2) d\zeta, \quad (8.112)$$

Fresnel integrals

whose plots are shown in Fig. 13a. As was mentioned above, at large values of their argument (ξ), both functions tend to $1/2$.

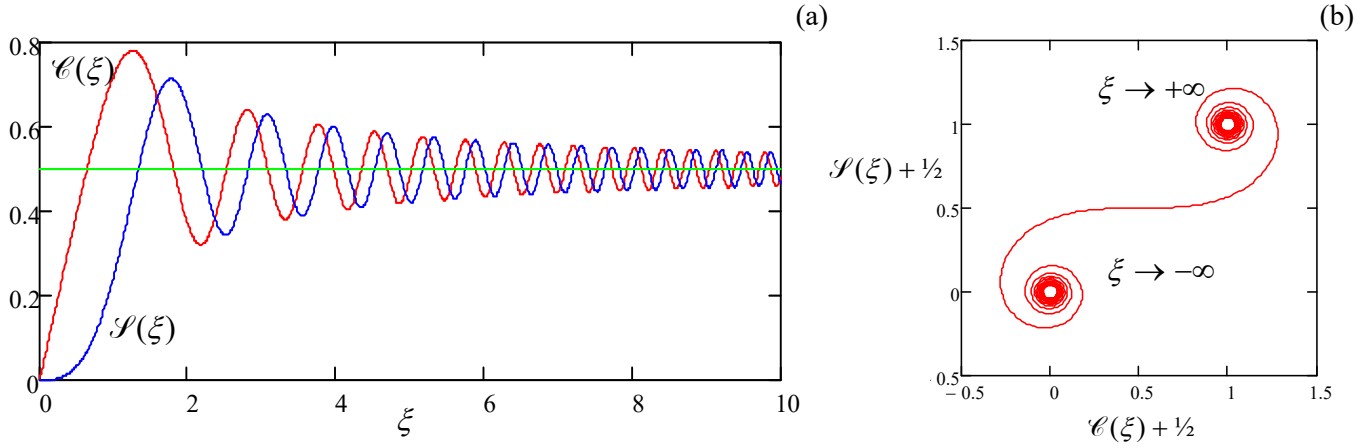


Fig. 8.13. (a) The Fresnel integrals and (b) their parametric representation.

⁴² Note also that since in this limit $ka^2 \ll z$, Eq. (97) shows that even the maximum value $S(0, z)$ of the diffracted wave's intensity is much lower than that (S_0) of the incident wave. This is natural because the incident power $S_0 a$ per unit length of the slit is now distributed over a much larger width $\delta x \gg a$, so that $S(0, z) \sim S_0 (a/\delta x) \ll S_0$.

⁴³ Slightly different definitions of these functions, affecting the constant factors, may also be met in literature.

Plugging this expression into Eqs. (105) and (111), for the diffracted wave intensity, in the Fresnel limit (i.e. at $|x + a/2| \ll a$), we get

Fresnel
diffraction
pattern

$$\frac{\bar{S}(x, z)}{S_0} = \frac{1}{2} \left\{ \left[\mathcal{C}\left(\left(\frac{k}{2z}\right)^{1/2}\left(x + \frac{a}{2}\right)\right) + \frac{1}{2} \right]^2 + \left[\mathcal{S}\left(\left(\frac{k}{2z}\right)^{1/2}\left(x + \frac{a}{2}\right)\right) + \frac{1}{2} \right]^2 \right\}. \quad (8.113)$$

A plot of this function (Fig. 14) shows that the diffraction pattern is very peculiar: while in the “dark” region $x < -a/2$ the wave intensity fades monotonically, the transition to the “bright” region within the gap ($x > -a/2$) is accompanied by intensity oscillations, just as at the Fraunhofer diffraction – cf. Fig. 8.

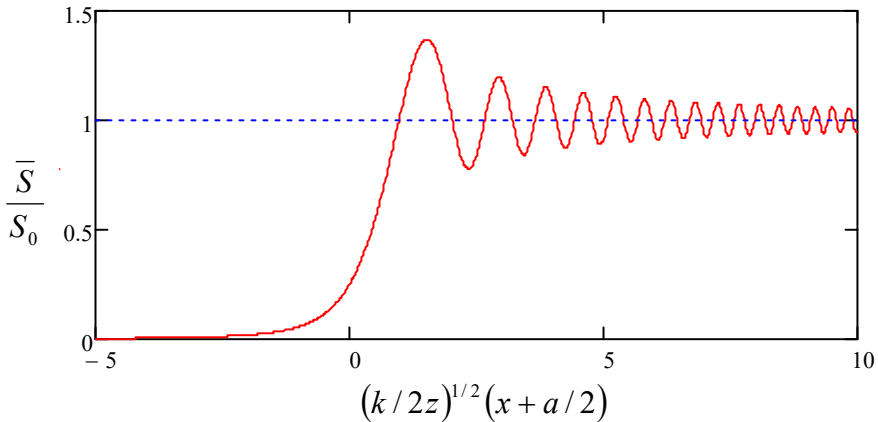


Fig. 8.14. The Fresnel diffraction pattern.

This behavior, which is described by the following asymptotes,

$$\frac{\bar{S}}{S_0} \rightarrow \begin{cases} 1 + \frac{1}{\sqrt{\pi}} \frac{\sin(\xi^2 - \pi/4)}{\xi}, & \text{for } \xi \equiv \left(\frac{k}{2z}\right)^{1/2}\left(x + \frac{a}{2}\right) \rightarrow +\infty, \\ \frac{1}{4\pi\xi^2}, & \text{for } \xi \rightarrow -\infty, \end{cases} \quad (8.114)$$

is essentially an artifact of “observing” just the wave intensity (i.e. its real amplitude) rather than its phase as well. Indeed, as may be seen even more clearly from the parametric representation of the Fresnel integrals, shown in Fig. 13b, these functions oscillate similarly at large positive and negative values of their argument. (This famous pattern is called either the *Euler spiral* or the *Cornu spiral*.) Physically, this means that the wave diffraction at the slit edge leads to similar oscillations of its phase at $x < -a/2$ and $x > -a/2$; however, in the latter region (i.e. inside the slit) the diffracted wave overlaps the incident wave passing through the slit directly, and their interference reveals the phase oscillations, making them visible in the observed intensity as well.

Note that according to Eq. (113), the linear scale δx of the Fresnel diffraction pattern is of the order of $(2z/k)^{1/2}$, i.e. it complies with the estimate given by Eq. (90). If the slit is gradually narrowed so that its width a becomes comparable to δx ,⁴⁴ the Fresnel diffraction patterns from both edges start to “collide” (interfere). The resulting wave, fully described by Eq. (107), is just a sum of two contributions of the type (111) from both edges of the slit. The resulting interference pattern is somewhat complicated, and only when a becomes substantially less than δx , it is reduced to the simple Fraunhofer pattern (110).

⁴⁴ Note that this condition may be also rewritten as $a \sim \delta x$, i.e. $z/a \sim a/\lambda$.

Of course, this crossover from the Fresnel to Fraunhofer diffraction may be also observed, at fixed wavelength λ and slit width a , by increasing z , i.e. by measuring the diffraction pattern farther and farther away from the slit.

Note also that the Fraunhofer limit is always valid if the diffraction is measured as a function of the diffraction angle θ alone. This may be done, for example, by collecting the diffracted wave with a “positive” (converging) lens and observing the diffraction pattern in its focal plane.

8.7. Geometrical optics placeholder

I would not like the reader to miss, behind all these details, the main feature of the Fresnel diffraction, which has an overwhelming practical significance. Namely, besides narrow diffraction “cones” (actually, parabolic-shaped regions) with the lateral scale $\delta x \sim (\lambda z)^{1/2}$, the wave far behind a slit of width $a \gg \lambda$, δx , reproduces the field just behind the slit, i.e. reproduces the unperturbed incident wave inside it, and has a negligible intensity in the shade regions outside it. An evident generalization of this fact is that when a plane wave (in particular an electromagnetic wave) passes any opaque object of a large size $a \gg \lambda$, it propagates around it, by distances z up to $\sim a^2/\lambda$, along straight lines, with virtually negligible diffraction effects. This fact gives the strict foundation for the notion of the wave *ray* (or *beam*), as the line perpendicular to the local front of a quasi-plane wave. In a uniform media such a ray follows a straight line,⁴⁵ but it refracts in accordance with the Snell law at the interface of two media with different values of the wave speed v , i.e. different values of the refraction index. The concept of rays enables the whole field of *geometric optics*, devoted mostly to ray tracing in various (sometimes very sophisticated) optical systems.

This is why, at this point, an E&M course that followed the scientific logic more faithfully than this one, would give an extended discussion of the geometric and quasi-geometric optics, including (as a minimum⁴⁶) such vital topics as

- the so-called *lensmaker's equation* expressing the focus length f of a lens via the curvature radii of its spherical surfaces and the refraction index of the lens material,
- the *thin lens formula* relating the image distance from the lens via f and the source distance,
- the concepts of basic optical instruments such as *glasses*, *telescopes*, and *microscopes*,
- the concepts of the spherical, angular, and chromatic *aberrations* (image distortions).

However, since I have made a (possibly, wrong) decision to follow the common tradition in selecting the main topics for this course, I do not have time/space left for such discussion. Still, I am using this “placeholder” pseudo-section to relay my deep conviction that any educated physicist has to know the geometric optics basics. If the reader has not been exposed to this subject during their undergraduate studies, I highly recommend at least browsing one of the available textbooks.⁴⁷

⁴⁵ In application to optical waves, this notion may be traced back to at least the work by Hero (a.k.a. Heron) of Alexandria (circa 170 AD). Curiously, he correctly described light reflection from one or several plane mirrors, starting from the completely wrong idea of light propagation *from* the eye of the observer *to* the observed object.

⁴⁶ Admittedly, even this list leaves aside several spectacular effects, including such a beauty as *conical refraction* in biaxial crystals – see, e.g., Chapter 15 of the textbook by M. Born and E. Wolf, cited in the end of Sec. 7.1.

⁴⁷ My top recommendation for that purpose would be Chapters 3-6 and Sec. 8.6 in Born and Wolf. A simpler alternative is Chapter 10 in G. Fowles, *Introduction to Modern Optics*, 2nd ed., Dover, 1989. Note also that the venerable field of optical microscopy is currently revitalized by holographic/tomographic methods, using the

8.8. Fraunhofer diffraction from more complex scatterers

So far, our quantitative analysis of diffraction has been limited to a very simple geometry – a single slit in an otherwise opaque screen (Fig. 12). However, in the most important Fraunhofer limit, $z \gg ka^2$, it is easy to get a very simple expression for the plane wave diffraction/interference by a plane orifice (with a linear size scale a) of arbitrary shape. Indeed, the evident 2D generalization of the approximation (106)-(107) is

$$\begin{aligned} I_x I_y &= \int_{\text{orifice}} \exp \frac{ik[(x-x')^2 + (y-y')^2]}{2z} dx' dy' \\ &\approx \exp \left\{ \frac{ik(x^2 + y^2)}{2z} \right\} \int_{\text{orifice}} \exp \left\{ -i \frac{kxx'}{z} - i \frac{kyy'}{z} \right\} dx' dy', \end{aligned} \quad (8.115)$$

so that besides the inconsequential total phase factor, Eq. (105) is reduced to

$$f(\rho) \propto f_0 \int_{\text{orifice}} \exp \{-i\kappa \cdot \rho'\} d^2 \rho' \equiv f_0 \int_{\text{all screen}} T(\rho') \exp \{-i\kappa \cdot \rho'\} d^2 \rho'. \quad (8.116)$$

General
Fraunhofer
diffraction
pattern

Here the 2D vector κ (not to be confused with wave vector \mathbf{k} , which is virtually perpendicular to κ !) is defined as

$$\kappa \equiv k \frac{\rho}{z} \approx \mathbf{q} \equiv \mathbf{k} - \mathbf{k}_0, \quad (8.117)$$

and $\rho = \{x, y\}$ and $\rho' = \{x', y'\}$ are 2D radius-vectors in the, respectively, observation and orifice planes – both nearly normal to the vectors \mathbf{k} and \mathbf{k}_0 .⁴⁸ In the last form of Eq. (116), the function $T(\rho')$ describes the screen's transparency at point ρ' , and the integral is over the whole screen plane $z' = 0$. (Though the two forms of Eq. (116) are strictly equivalent only if $T(\rho')$ is equal to either 1 or 0, its last form may be readily obtained from Eq. (91) with $f(\mathbf{r}') = T(\rho')/f_0$ for any transparency profile, provided that $T(\rho')$ is any function that changes substantially only at distances much larger than $\lambda \equiv 2\pi/k$.)

From the mathematical point of view, the last form of Eq. (116) is just the 2D spatial Fourier transform of the function $T(\rho')$, with the variable κ defined by the observation point's position: $\rho \equiv (z/k) \kappa \equiv (z\lambda/2\pi) \kappa$. This interpretation is useful because of the experience we all have with the Fourier transform, if only in the context of its time/frequency applications. For example, if the orifice is a single small hole, $T(\rho')$ may be approximated by a delta function, so that Eq. (116) yields $|f(\rho)| \approx \text{const}$. This result corresponds (at least for the small diffraction angles $\theta \equiv \rho/z$, for which the Huygens approximation is valid) to a spherical wave spreading from the point-like orifice. Next, for two small holes, Eq. (116) immediately gives the interference pattern (103). Let me now use Eq. (116) to analyze other simplest (and most important) 1D transparency profiles, leaving a few 2D cases for the reader's exercise.

(i) A single slit of width a (Fig. 12) may be described by transparency

scattered wave's phase information. These methods are especially productive in biology and medicine – see, e.g., M. Brezinski, *Optical Coherence Tomography*, Academic Press, 2006, and G. Popescu, *Quantitative Phase Imaging of Cells and Tissues*, McGraw-Hill (2011).

⁴⁸ Note that for a thin uniform plate of the same shape as the orifice we are discussing now, the Born phase integral (63) with $q \ll k$ gives a result functionally similar to Eq. (116).

$$T(\mathbf{p}') = \begin{cases} 1, & \text{for } |x'| < a/2, \\ 0, & \text{otherwise.} \end{cases} \quad (8.118)$$

Its substitution into Eq. (116) yields

$$f(\mathbf{p}) \propto f_0 \int_{-a/2}^{+a/2} \exp\{-i\kappa_x x'\} dx' = f_0 \frac{\exp\{-i\kappa_x a/2\} - \exp\{i\kappa_x a/2\}}{-i\kappa_x} \propto \text{sinc}\left(\frac{\kappa_x a}{2}\right) = \text{sinc}\left(\frac{kxa}{2z}\right), \quad (8.119)$$

naturally returning us to Eqs. (64) and (110), and hence to the red lines in Fig. 8 for the wave intensity. (Please note again that Eq. (116) describes only the Fraunhofer, but not the Fresnel diffraction!)

(ii) Two infinitely narrow, similar, parallel slits with a larger distance a between them (i.e. the simplest model of Young's two-slit experiment) may be described by taking

$$T(\mathbf{p}') \propto \delta\left(x' - \frac{a}{2}\right) + \delta\left(x' + \frac{a}{2}\right), \quad (8.120)$$

so that Eq. (116) yields the generic 1D interference pattern,

$$f(\mathbf{p}) \propto f_0 \left[\exp\left\{-\frac{i\kappa_x a}{2}\right\} + \exp\left\{\frac{i\kappa_x a}{2}\right\} \right] \propto \cos \frac{\kappa_x a}{2} = \cos \frac{kxa}{2z}, \quad (8.121)$$

whose intensity is shown with the blue line in Fig. 8.

(iii) In a more realistic model of Young's experiment, each slit has a width (say, w) that is much larger than the light wavelength λ , but still much smaller than the slit spacing a . This situation may be described by the following transparency function

$$T(\mathbf{p}') = \sum_{\pm} \begin{cases} 1, & \text{for } |x' \pm a/2| < w/2, \\ 0, & \text{otherwise,} \end{cases} \quad (8.122)$$

for which Eq. (116) yields a natural combination of the results (119) (with a replaced with w) and (121):

$$f(\mathbf{r}) \propto \text{sinc}\left(\frac{kxw}{2z}\right) \cos\left(\frac{kxa}{2z}\right). \quad (8.123)$$

This is the usual interference pattern, but modulated with a Fraunhofer-diffraction envelope – shown in Fig. 15 with the dashed blue line. Since the function $\text{sinc}^2 \xi$ decreases very fast beyond its first zeros at $\xi = \pm\pi$, the practical number of observable interference fringes is close to $2a/w$.

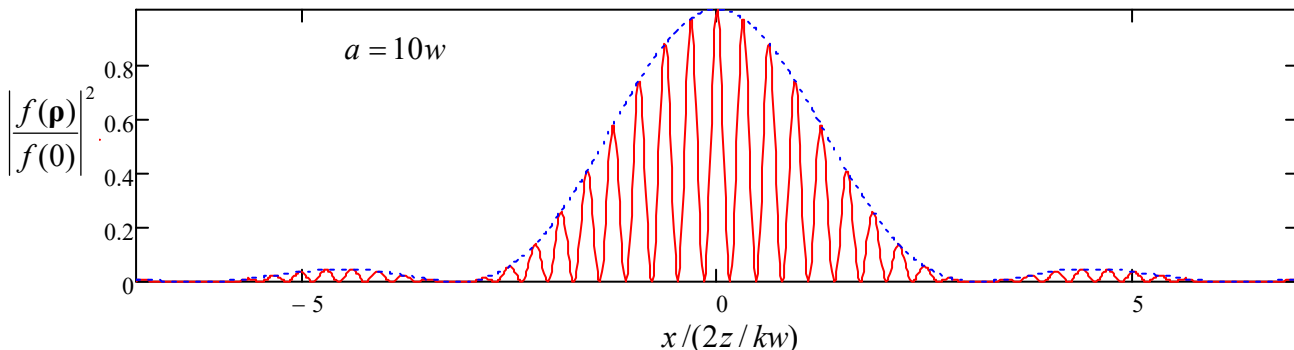


Fig. 8.15. Young's double-slit interference pattern for a finite-width slit.

(iv) A structure very useful for experimental and engineering practice is a set of many parallel, similar slits, called the *diffraction grating*.⁴⁹ If the slit's width is much smaller than period d of the grating, its transparency function may be approximated as

$$T(\mathbf{p}') \propto \sum_{n=-\infty}^{+\infty} \delta(x' - nd), \quad (8.124)$$

and Eq. (116) yields

$$f(\mathbf{p}) \propto \sum_{n=-\infty}^{+\infty} \exp\{-in\kappa_x d\} = \sum_{n=-\infty}^{+\infty} \exp\left\{-i \frac{n k x d}{z}\right\}. \quad (8.125)$$

This sum vanishes for all values of $\kappa_x d$ that are not multiples of 2π , so that the result describes sharp intensity peaks at the following diffraction angles:

$$\theta_m \equiv \left(\frac{x}{z} \right)_m = \left(\frac{\kappa_x}{k} \right)_m = \frac{2\pi}{kd} m = \frac{\lambda}{d} m. \quad (8.126)$$

Taking into account that this result is only valid for small angles $|\theta_m| \ll 1$, it may be interpreted exactly as Eq. (59) – see Fig. 6a. However, in contrast with the interference (121) from two slits, the destructive interference from many slits kills the net wave as soon as the angle is even slightly different from each value (60). This is very convenient for spectroscopic purposes because the diffraction lines produced by multi-frequency waves do not overlap even if the frequencies of their adjacent components are very close.

Two unavoidable features of practical diffraction gratings make their properties different from this simple, ideal picture. First, the finite number N of slits, which may be described by limiting the sum (125) to the interval $n = [-N/2, +N/2]$, results in a non-zero spread, $\delta\theta/\theta \sim 1/N$, of each diffraction peak, and hence in the reduction of the grating's spectral resolution. (Unintentional variations of the inter-slit distance d have a similar effect, so that before the advent of high-resolution photolithography, special high-precision mechanical tools had been used for grating fabrication.)

Second, a finite slit width w leads to the diffraction peak pattern modulation by the $\text{sinc}^2(kw\theta/2)$ envelope, similar to the pattern shown in Fig. 15. Actually, for spectroscopic purposes, such modulation is sometimes a plus, because only one diffraction peak (say, with $m = \pm 1$) is practically used, and if the frequency spectrum of the analyzed wave is very broad (covers more than one octave), the higher peaks produce undesirable hindrance. Because of this reason, w is frequently selected to be equal exactly to $d/2$, thus suppressing each other diffraction maximum. Moreover, sometimes semi-transparent films are used to make the transparency function $T(\mathbf{r}')$ continuous and close to a sinusoidal one:

$$T(\mathbf{p}') \approx T_0 + T_1 \cos \frac{2\pi x'}{d} \equiv T_0 + \frac{T_1}{2} \left(\exp\left\{i \frac{2\pi x'}{d}\right\} + \exp\left\{-i \frac{2\pi x'}{d}\right\} \right). \quad (8.127)$$

Plugging the last expression into Eq. (116) and integrating, we see that the output wave consists of just 3 components: the direct-passing wave (proportional to T_0) and two diffracted waves (proportional to T_1) propagating in the directions of the two lowest Bragg angles, $\theta_{\pm 1} = \pm \lambda/d$.⁵⁰

⁴⁹ The rudimentary diffraction grating effect, produced by the parallel fibers of a bird's feather, was discovered as early as 1673 by James Gregory (who also invented the “Gregorian” telescope – one of the basic designs for reflecting telescopes).

The same Eq. (116) may be also used to obtain one more general (and rather curious) result, called the *Babinet principle*.⁵¹ Consider two experiments with the diffraction of similar plane waves on two “complementary” screens – such that together they would cover the whole plane, without a hole or an overlap. (Think, for example, about an opaque disk of radius R and a large opaque screen with a round orifice of the same radius.) Then, according to the Babinet principle, the diffracted wave patterns produced by these two screens in all directions with $\theta \neq 0$ are *identical*.

The proof of this principle is straightforward: since the transparency functions produced by the screens are complementary:

$$T(\mathbf{p}') \equiv T_1(\mathbf{p}') + T_2(\mathbf{p}') = 1, \quad (8.128)$$

and the diffracted wave is (in the Fraunhofer approximation only!) a Fourier transform of $T(\mathbf{p}')$, which is a linear operation, we get

$$f_1(\mathbf{p}) + f_2(\mathbf{p}) = f_0(\mathbf{p}), \quad (8.129)$$

where f_0 is the wave “scattered” by the composite screen with $T_0(\mathbf{p}') \equiv 1$, i.e. the unperturbed initial wave propagating in the initial direction ($\theta = 0$). In all other directions, $f_1 = -f_2$, i.e. the diffracted waves are indeed similar besides the difference in sign – which is equivalent to a phase shift by $\pm\pi$. However, it is important to remember that the Babinet principle notwithstanding, in real experiments, with screens at finite distances, the diffracted waves may interfere with the unperturbed plane wave $f_0(\mathbf{p})$, leading to different diffraction patterns in cases 1 and 2 – see, e.g., Fig. 14 and its discussion.

8.9. Magnetic dipole and electric quadrupole radiation

Throughout this chapter, we have seen how many important results may be obtained from Eq. (26) for the electric dipole radiation by a small-size source (Fig. 1). Only in rare cases when this radiation is absent, for example, if the dipole moment \mathbf{p} of the source equals zero (or does not change in time – either at all or at the frequency of our interest), higher-order effects may be important. I will now discuss the main two of them, *quadrupole electric radiation* and *dipole magnetic radiation*.

In Sec. 2 above, the electric dipole radiation was calculated by plugging the expansion (19) into the exact formula (17b) for the retarded vector potential $\mathbf{A}(\mathbf{r}, t)$. Let us make a more exact calculation, by keeping the second term of that expansion as well:

$$\mathbf{j}\left(\mathbf{r}', t - \frac{R}{v}\right) \approx \mathbf{j}\left(\mathbf{r}', t - \frac{r}{v} + \frac{\mathbf{r}' \cdot \mathbf{n}}{v}\right) \equiv \mathbf{j}\left(\mathbf{r}', t' + \frac{\mathbf{r}' \cdot \mathbf{n}}{v}\right), \quad \text{where } t' \equiv t - \frac{r}{v}. \quad (8.130)$$

Since the expansion is only valid if the last term in the time argument of \mathbf{j} is relatively small, in the Taylor expansion of \mathbf{j} with respect to that argument we may keep just two leading terms:

$$\mathbf{j}\left(\mathbf{r}', t' + \frac{\mathbf{r}' \cdot \mathbf{n}}{v}\right) \approx \mathbf{j}(\mathbf{r}', t') + \frac{\partial \mathbf{j}(\mathbf{r}', t')}{\partial t'} \frac{(\mathbf{r}' \cdot \mathbf{n})}{v}, \quad (8.131)$$

⁵⁰ Similar tricks are used in the so-called *phased-array antennas*, broadly used in radar systems and radioastronomy, in which electronically controlled mutual phase shifts of microwave signals feeding many similar component antennas are used to steer the direction of the resulting narrow beam. For more on this important technology, see, e.g. T. Milligan, *Modern Antenna Design*, 2nd ed., Wiley (2005).

⁵¹ Named after Jacques Babinet (1784-1874) who made several important contributions to optics.

so that Eq. (17b) yields $\mathbf{A} = \mathbf{A}_d + \mathbf{A}'$, where \mathbf{A}_d is the electric dipole contribution as given by Eq. (23), and \mathbf{A}' is the new term of the next order in the small parameter $r' \ll r$:

$$\mathbf{A}'(\mathbf{r}, t) = \frac{\mu}{4\pi r v} \frac{\partial}{\partial t'} \int \mathbf{j}(\mathbf{r}', t') (\mathbf{r}' \cdot \mathbf{n}) d^3 r'. \quad (8.132)$$

Just as it was done in Sec. 2, let us evaluate this term for a system of non-relativistic particles with electric charges q_k and radius vectors $\mathbf{r}_k(t)$:

$$\mathbf{A}'(\mathbf{r}, t) = \frac{\mu}{4\pi r v} \left[\frac{d}{dt} \sum_k q_k \dot{\mathbf{r}}_k (\mathbf{r}_k \cdot \mathbf{n}) \right]_{t=t'}. \quad (8.133)$$

Using the “bac minus cab” identity of the vector algebra again,⁵² the vector operand of Eq. (133) may be rewritten as

$$\begin{aligned} \dot{\mathbf{r}}_k (\mathbf{r}_k \cdot \mathbf{n}) &\equiv \frac{1}{2} \dot{\mathbf{r}}_k (\mathbf{r}_k \cdot \mathbf{n}) + \frac{1}{2} \dot{\mathbf{r}}_k (\mathbf{n} \cdot \mathbf{r}_k) = \frac{1}{2} (\mathbf{r}_k \times \dot{\mathbf{r}}_k) \times \mathbf{n} + \frac{1}{2} \mathbf{r}_k (\mathbf{n} \cdot \dot{\mathbf{r}}_k) + \frac{1}{2} \dot{\mathbf{r}}_k (\mathbf{n} \cdot \mathbf{r}_k) \\ &\equiv \frac{1}{2} (\mathbf{r}_k \times \dot{\mathbf{r}}_k) \times \mathbf{n} + \frac{1}{2} \frac{d}{dt} [\mathbf{r}_k (\mathbf{n} \cdot \mathbf{r}_k)], \end{aligned} \quad (8.134)$$

so that the right-hand side of Eq. (133) may be represented as a sum of two terms, $\mathbf{A}' = \mathbf{A}_m + \mathbf{A}_q$, where

$$\mathbf{A}_m(\mathbf{r}, t) = \frac{\mu}{4\pi r v} \dot{\mathbf{m}}(t') \times \mathbf{n} \equiv \frac{\mu}{4\pi r v} \dot{\mathbf{m}} \left(t - \frac{r}{v} \right) \times \mathbf{n}, \quad \text{with } \mathbf{m}(t) \equiv \frac{1}{2} \sum_k \mathbf{r}_k(t) \times q_k \dot{\mathbf{r}}_k(t); \quad (8.135)$$

$$\mathbf{A}_q(\mathbf{r}, t) = \frac{\mu}{8\pi r v} \left[\frac{d^2}{dt^2} \sum_k q_k \mathbf{r}_k (\mathbf{n} \cdot \mathbf{r}_k) \right]_{t=t'}. \quad (8.136)$$

Comparing the second of Eqs. (135) with Eq. (5.91), we see that \mathbf{m} is just the total magnetic moment of the source. On the other hand, the first of Eqs. (135) is absolutely similar in structure to Eq. (23), with \mathbf{p} replaced with $(\mathbf{m} \times \mathbf{n})/v$, so that for the corresponding component of the magnetic field it gives (in the same approximation $r \gg \lambda$) a result similar to Eq. (24):

$$\mathbf{B}_m(\mathbf{r}, t) = \frac{\mu}{4\pi r v} \nabla \times \left[\dot{\mathbf{m}} \left(t - \frac{r}{v} \right) \times \mathbf{n} \right] = -\frac{\mu}{4\pi r v^2} \mathbf{n} \times \left[\ddot{\mathbf{m}} \left(t - \frac{r}{v} \right) \times \mathbf{n} \right]. \quad (8.137)$$

According to this expression, just as at the electric dipole radiation, the vector \mathbf{B} is perpendicular to the vector \mathbf{n} , and its magnitude is also proportional to $\sin \Theta$, where Θ is now the angle between the direction toward the observation point and the second time derivative of the vector \mathbf{m} – rather than \mathbf{p} :

$$B_m = \frac{\mu}{4\pi r v^2} \ddot{m} \left(t - \frac{r}{v} \right) \sin \Theta. \quad (8.138)$$

As the result, the intensity of this *magnetic dipole radiation* has a similar angular distribution:

$$S_r = ZH^2 = \frac{Z}{(4\pi v^2 r)^2} \left[\ddot{m} \left(t - \frac{r}{v} \right) \right]^2 \sin^2 \Theta \quad (8.139)$$

⁵² If you still need it, see MA Eq. (7.5).

- cf. Eq. (26), besides the (generally) different meaning of the angle Θ .

Note, however, that this radiation is usually much weaker than its electric-dipole counterpart. For example, for a non-relativistic particle with electric charge q , moving on a trajectory of linear size $\sim a$, the electric dipole moment is of the order of qa , while its magnetic moment scales as $qa^2\omega$, where ω is the motion frequency. As a result, the ratio of the magnetic and electric dipole radiation intensities is of the order of $(a\omega/v)^2$, i.e. the squared ratio of the particle's speed to the speed of the emitted waves – that has to be much smaller than 1 for our non-relativistic calculation to be valid.

The angular distribution of the *electric quadrupole radiation*, described by Eq. (136), is more complicated. To show this, we may add to \mathbf{A}_q a vector parallel to \mathbf{n} (i.e. along the wave's propagation), getting

$$\mathbf{A}_q(\mathbf{r}, t) \rightarrow \frac{\mu}{24\pi rv} \ddot{\mathcal{Q}} \left(t - \frac{r}{v} \right), \quad \text{where } \mathcal{Q} \equiv \sum_k q_k \{ 3\mathbf{r}_k (\mathbf{n} \cdot \mathbf{r}_k) - \mathbf{n} r_k^2 \}, \quad (8.140)$$

because this addition does not give any contribution to the transverse component of the electric and magnetic fields, i.e. to the radiated wave. According to the above definition of the vector \mathcal{Q} , its Cartesian components may be represented as

$$\mathcal{Q}_j = \sum_{j'=1}^3 \mathcal{Q}_{jj'} n_{j'}, \quad (8.141)$$

where $\mathcal{Q}_{jj'}$ are the elements of the electric quadrupole tensor of the system – see the last of Eqs. (3.4):⁵³

$$\mathcal{Q}_{jj'} = \sum_k q_k (3r_j r_{j'} - r^2 \delta_{jj'})_k. \quad (8.142)$$

Now taking the curl of the first of Eqs. (140) at $r \gg \lambda$, we get

$$\boxed{\mathbf{B}_q(\mathbf{r}, t) = -\frac{\mu}{24\pi rv^2} \mathbf{n} \times \ddot{\mathcal{Q}} \left(t - \frac{r}{v} \right)}. \quad (8.143)$$

Electric
quadrupole
radiation:
field

This expression is similar to Eqs. (24) and (137), but according to Eqs. (140) and (142), components of the vector \mathcal{Q} do depend on the direction of the vector \mathbf{n} , leading to a different angular dependence of S_r .

As the simplest example, let us consider the system of two equal point electric charges moving symmetrically, at equal distances $d(t) \ll \lambda$ from a stationary center – see Fig. 16.

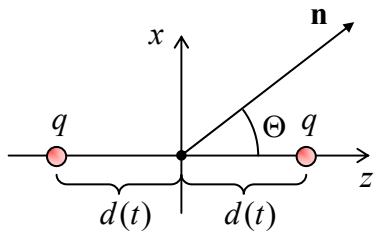


Fig. 8.16. The simplest system emitting electric quadrupole radiation.

Due to the symmetry of the system, its dipole moments \mathbf{p} and \mathbf{m} (and hence its electric and magnetic dipole radiation) vanish, but the quadrupole tensor (142) still has non-zero elements. With the coordinate choice shown in Fig. 16, these elements are diagonal:

⁵³ Let me hope that the reader has already acquired some experience in the calculation of this tensor's elements – e.g., for the simple systems specified in Problems 3.2-3.4.

$$\mathcal{Q}_{xx} = \mathcal{Q}_{yy} = -2qd^2, \quad \mathcal{Q}_{zz} = 4qd^2. \quad (8.144)$$

With the x -axis selected within the common plane of the z -axis and the direction \mathbf{n} toward the observation point (Fig. 16), so that $n_x = \sin\Theta$, $n_y = 0$, and $n_z = \cos\Theta$, Eq. (141) yields

$$\mathcal{Q}_x = -2qd^2 \sin\Theta, \quad \mathcal{Q}_y = 0, \quad \mathcal{Q}_z = 4qd^2 \cos\Theta, \quad (8.145)$$

and the vector product in Eq. (143) has only one non-vanishing Cartesian component:

$$(\mathbf{n} \times \ddot{\mathcal{Q}})_y = n_z \ddot{\mathcal{Q}}_x - n_x \ddot{\mathcal{Q}}_z = -6q \sin\Theta \cos\Theta \frac{d^3}{dt^3} [d^2(t)]. \quad (8.146)$$

As a result, the quadrupole radiation intensity, $S \propto B_q^2$, is proportional to $\sin^2\Theta \cos^2\Theta$, i.e. vanishes not only along the symmetry axis of the system (as the electric-dipole and the magnetic-dipole radiations would), but also in all directions perpendicular to this axis, reaching its maxima at $\Theta = \pm\pi/4$.

For more complex systems, the angular distribution of the electric quadrupole radiation may be different, but it may be proved that its total (instant) power always obeys the following simple formula:

$$\mathcal{P}_q = \frac{Z}{720\pi\nu^4} \sum_{j,j'=1}^3 (\ddot{\mathcal{Q}}_{jj'})^2. \quad (8.147)$$

Electric
quadrupole
radiation:
power

Let me finish this section by giving, also without proof, one more fact important for some applications: due to their different spatial structure, the magnetic-dipole and electric-quadrupole radiation fields do not interfere, i.e. the total power of radiation (neglecting the electric-dipole and higher multipole terms) may be found as the sum of these components, calculated independently. On the contrary, the electric-dipole and magnetic-dipole radiations of the same system they typically interfere coherently, so that their radiation fields (rather than powers) should be summed up.

8.10. Exercise problems

8.1. Equation (8.8) of the lecture notes obviously has standing-wave solutions $\chi(r, t) = \text{Re}[Csinkr \exp\{-i\omega t\}]$, turning the scalar potential $\phi = \chi/r$ into a finite constant at $r = 0$ and into zero at $kr = \pi n$, with $n = 0, 1, 2, \dots$. This fact seems to imply that a metallic cavity of radius R has resonant modes with a purely radial electric field $\mathbf{E}(\mathbf{r}) = \mathbf{n}_r E(r)$, and the lowest nonvanishing of them, with $k = \pi/R$, gives the lowest (fundamental) frequency $\omega \equiv \nu k = \pi(\nu/R)$ of the cavity. Is this conclusion correct?

8.2. Simplify the Lorentz reciprocity theorem (6.121) for space-localized field sources. Then find out what it says about the fields of two compact, well-separated sources of the electric-dipole radiation.

8.3. In the electric-dipole approximation, calculate the angular distribution and the total power of electromagnetic radiation by the hydrogen atom within the following classical model: an electron rotates, at a constant distance R , about a much heavier proton. Use this result to calculate the law of a gradual reduction of R in time. Finally, evaluate the classical lifetime of the atom, borrowing the initial value of R from quantum mechanics: $R(0) = r_B \approx 0.53 \times 10^{-10} \text{ m}$.

8.4. A non-relativistic particle of mass m , with electric charge q , is placed into a uniform, time-independent magnetic field \mathbf{B} . Derive the law of decrease of the particle's kinetic energy due to its

electromagnetic radiation at the *cyclotron frequency* $\omega_c = qB/m$. Evaluate the rate of such *radiation cooling* of electrons in a magnetic field of 1 T, and estimate the energy interval in which this result is quantitatively correct.

Hint: The cyclotron motion will be discussed in detail (for arbitrary particle velocities $v \sim c$) in Sec. 9.6 below, but I hope that the reader knows that in the non-relativistic case ($v \ll c$) the above formula for ω_c may be readily obtained by combining the 2nd Newton law $mv_{\perp}^2/R = qv_{\perp}B$ for the circular motion of the particle under the effect of the magnetic component of the Lorentz force (5.10), and the geometric relation $v_{\perp} = R\omega_c$. (Here v_{\perp} is the particle's velocity in the plane normal to the vector \mathbf{B} .)

8.5. A particle with mass m and electric charge q and kinetic energy T collides head-on with a much more massive particle of charge $\mathcal{T}q$, in free space. Calculate the total energy of electromagnetic radiation during this collision, assuming it to much lower than T .

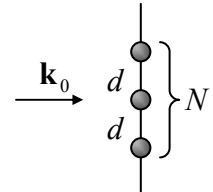
8.6. Solve the dipole antenna radiation problem discussed in Sec. 2 (see Fig. 3) for the optimal length $l = \lambda/2$, assuming that the current distribution in each of its arms is sinusoidal: $I(z, t) = I_0 \cos(\pi z/l) \cos\omega t$.⁵⁴

8.7. A plane wave is scattered by a localized object in free space. Relate the differential cross-section of the wave's scattering to the average force it exerts on the object. Use this general relation to calculate the force exerted by a plane monochromatic wave on a free non-relativistic particle, compare the result with those obtained in Problems 7.4 and 7.5, and discuss the comparison.

8.8. Use the Lorentz oscillator model of a bound charge, given by Eq. (7.30), to explore the transition between the two scattering limits discussed in Sec. 3, and in particular, the *resonant scattering* taking place at $\omega \approx \omega_0$. In this context, discuss the contribution of scattering to the oscillator's damping.

8.9.* A sphere of radius R , made of a material with a uniform permanent electric polarization \mathbf{P}_0 and a constant mass density ρ , is free to rotate about its center. Calculate the average total cross-section of scattering, by the sphere, of a linearly polarized electromagnetic wave of frequency $\omega \ll R/c$, propagating in free space, in the limit of small wave amplitude, assuming that the initial orientation of the polarization vector \mathbf{P}_0 is random.

8.10. Use Eq. (56) to analyze the interference/diffraction pattern produced by a plane wave's scattering on a set of N similar, equidistant points on a straight line normal to the direction of the incident wave's propagation – see the figure on the right. Discuss the trend(s) of the pattern in the limit $N \rightarrow \infty$.



8.11. Use the Born approximation to calculate the differential cross-section of the plane wave scattering by a uniform dielectric sphere of an arbitrary radius R . In the limits $kR \ll 1$ and $1 \ll kR$ (where k is the wave number), analyze the angular dependence of the differential cross-section and calculate the total cross-section of scattering.

⁵⁴ As was emphasized in Sec. 2, this is a reasonable guess rather than a controllable approximation. The exact (rather involved!) theory shows that this assumption gives errors ~5%, depending on the wire's diameter.

8.12. A sphere of radius R is made of a uniform dielectric material, with an arbitrary dielectric constant. Derive an exact expression for its total cross-section of scattering of a linearly-polarized low-frequency ($k \ll 1/R$) wave and compare the result with the solution of the previous problem.

8.13. Use the Born approximation to calculate the differential cross-section of the plane wave scattering on a right, circular cylinder of length l and radius R , for an arbitrary angle of incidence.

8.14. Formulate the quantitative condition of the Born approximation's validity for a uniform dielectric scatterer, with all linear dimensions of the order of the same scale a .

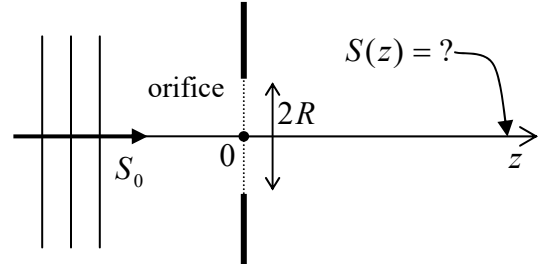
8.15. If a scatterer absorbs some part of the incident wave's power, it may be characterized by an *absorption cross-section* σ_a defined similarly to Eq. (39) for the scattering cross-section:

$$\sigma_a \equiv \frac{\bar{\mathcal{P}}_a}{|E_\omega|^2 / 2Z_0},$$

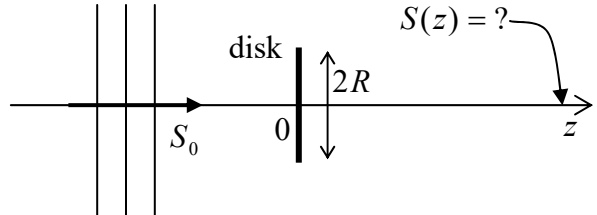
where the numerator is the time-averaged power absorbed in the scatterer. Use two different approaches to calculate σ_a of a very small sphere of radius $R \ll k^{-1}$, δ_s , made of a nonmagnetic material with an Ohmic conductivity σ and the high-frequency permittivity $\epsilon_{\text{opt}} = \epsilon_0$. Can σ_a of such a sphere be larger than its geometric cross-section πR^2 ?

8.16. Use the Huygens principle to calculate the wave's intensity on the symmetry plane of the slit diffraction experiment (i.e. at $x = 0$ in Fig. 12), for arbitrary ratio z/ka^2 .

8.17. A plane wave with wavelength λ is normally incident on an opaque, plane screen, with a round orifice of radius $R \gg \lambda$. Use the Huygens principle to calculate the passing wave's intensity distribution along the system's symmetry axis, at distances $z \gg R$ from the screen (see the figure on the right), and analyze the result.



8.18. A plane monochromatic wave is now normally incident on an opaque circular disk of radius $R \gg \lambda$. Use the Huygens principle to calculate the wave's intensity at a distance $z \gg R$ behind the disk's center (see the figure on the right). Discuss the result.

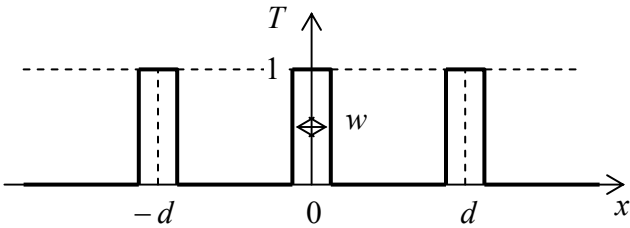


8.19. Use the Huygens principle to analyze the Fraunhofer diffraction of a plane wave normally incident on a square-shaped hole, of size $a \times a$, in an opaque screen. Sketch the diffraction pattern you would observe at a sufficiently large distance, and quantify the expression "sufficiently large" for this case.

8.20. Use the Huygens principle to analyze the propagation of a monochromatic Gaussian beam described by Eq. (7.181), with the initial characteristic width $a_0 \gg \lambda$, in a uniform, isotropic medium. Use the result for a semi-quantitative derivation of the so-called *Abbe limit* for the spatial resolution of

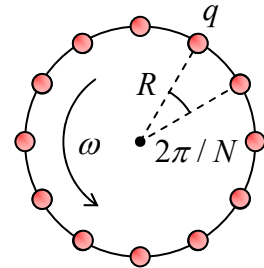
an optical system: $w_{\min} = \lambda/2\sin\theta$, where θ is the half-angle of the wave cone propagating from the object, and captured by the system.

8.21. Within the Fraunhofer approximation, analyze the pattern produced by a 1D diffraction grating with the periodic transparency profile shown in the figure on the right, for the normal incidence of a plane, monochromatic wave.



8.22. N equal point charges are attached, at equal intervals, to a circle rotating with a constant angular velocity about its center – see the figure on the right. For what values of N does the system emit:

- (i) the electric dipole radiation?
- (ii) the magnetic dipole radiation?
- (iii) the electric quadrupole radiation?



8.23. What general statements can you make about:

- (i) the electric dipole radiation, and
- (ii) the magnetic dipole radiation,

due to a collision of an arbitrary number of similar classical, non-relativistic particles?

8.24. Calculate the angular distribution and the total power radiated by a small round loop antenna with radius R , fed with ac current $I(t)$ with frequency ω and amplitude I_0 , into the free space.

8.25. The orientation of a magnetic dipole \mathbf{m} , of a fixed magnitude, is rotating about a certain axis with angular velocity ω , with the angle α between them staying constant. Calculate the angular distribution and the average power of its radiation (into the free space).

8.26. Solve Problem 12 (also in the low-frequency limit $kR \ll 1$), for the case when the sphere's material has a frequency-independent Ohmic conductivity σ , and $\epsilon_{\text{opt}} = \epsilon_0$, in two limits:

- (i) of a very large skin depth ($\delta_s \gg R$), and
- (ii) of a very small skin depth ($\delta_s \ll R$).

8.27. Complete the solution of the problem started in Sec. 9, by calculating the full power of radiation of the system of two charges oscillating in antiphase along the same straight line – see Fig. 16. Also, calculate the average radiation power for the case of harmonic oscillations, $d(t) = a \cos\omega t$, compare it with the case of a single charge performing similar oscillations, and interpret the difference.

8.28. The system of four alternating charges located at the angles of a square, considered in Problem 3.3(i), is now being rotated around the axis normal to their plane and passing through the square's center, with a constant angular frequency $\omega \ll a/v$. Calculate the time-averaged angular distribution and the total power of the resulting radiation.

Chapter 9. Special Relativity

This chapter starts with a review of special relativity's basics, including its very convenient 4-vector formalism. This background is then used for the analysis of the relation between the electromagnetic field's values measured in different inertial reference frames moving relative to each other. The results enable us to discuss relativistic particle dynamics in the electric and magnetic fields, and the analytical mechanics of the particles – and of the electromagnetic field as such.

9.1. Einstein postulates and the Lorentz transform

As was emphasized at the derivation of expressions for the dipole and quadrupole radiation in the last chapter, they are only valid for systems of non-relativistic particles moving with velocities \mathbf{u} much lower than c . In order to generalize these results to particles moving with arbitrary \mathbf{u} , we need help from the relativity theory. Moreover, an analysis of the motion of charged relativistic particles in electric and magnetic fields is also a natural part of electrodynamics. This is why I will follow the tradition of using this course for a (by necessity, brief) introduction to the special relativity theory. This theory is based on the fundamental idea that measurements of physical variables (including the spatial and even temporal intervals between two events) may give different results in different reference frames, in particular in two inertial frames moving relative to each other translationally (i.e. without rotation), with a certain constant velocity \mathbf{v} (Fig. 1).

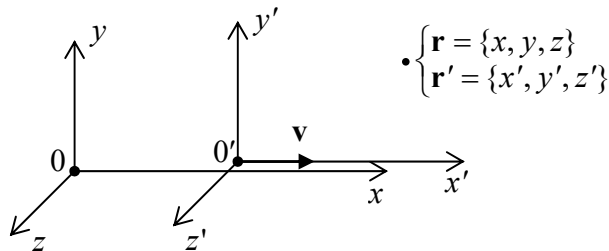


Fig. 9.1. The translational, uniform mutual motion of two reference frames.

In the non-relativistic (Newtonian) mechanics the problem of transfer between such reference frames has a simple solution at least in the limit $v \ll c$, because the basic equation of particle dynamics (the 2nd Newton law)¹

$$m_k \ddot{\mathbf{r}}_k = -\nabla_k \sum_{k'} U(\mathbf{r}_k - \mathbf{r}_{k'}) , \quad (9.1)$$

where U is the potential energy of inter-particle interactions, is invariant with respect to the so-called *Galilean transformation* (or just “transform” for short).² Choosing the coordinates in both frames so that their axes x and x' are parallel to the vector \mathbf{v} (as in Fig. 1), the transform may be represented as

¹ Let me hope that the reader does not need a reminder that for Eq. (1) to be valid, the reference frames 0 and 0' have to be inertial – see, e.g., CM Sec. 1.2.

² It had been first formulated by Galileo Galilei, if only rather informally, as early as in 1638 – four years before Isaac Newton was born! Note also the very unfortunate term “boost”, used sometimes to describe such translational transformations. (It is especially unnatural in the special relativity, not describing accelerations.) In my course, this term is avoided, with the equivalent “transform” used instead.

$$x = x' + vt', \quad y = y', \quad z = z', \quad t = t', \quad (9.2a)$$

Galilean transform

and plugging Eq. (2a) into Eq. (1), we get an absolutely similarly looking equation of motion in the “moving” reference frame $0'$. Since the reciprocal transform,

$$x' = x - vt, \quad y = y', \quad z' = z, \quad t' = t, \quad (9.2b)$$

is similar to the direct one, with the replacement of $(+v)$ with $(-v)$, we may say that the Galilean invariance means that there is no “master” (*absolute*) spatial reference frame in classical mechanics, although the spatial and temporal intervals between different instant events are absolute, i.e. reference-frame invariant: $\Delta x = \Delta x', \dots, \Delta t = \Delta t'$.

However, it is straightforward to use Eq. (2) to check that the form of the wave equation

$$\left(\frac{\partial^2}{\partial x^2} + \frac{\partial^2}{\partial y^2} + \frac{\partial^2}{\partial z^2} - \frac{1}{c^2} \frac{\partial^2}{\partial t^2} \right) f = 0, \quad (9.3)$$

describing, in particular, the electromagnetic wave propagation in free space,³ is *not* Galilean-invariant.⁴ For the “usual” (say, elastic) waves, which obey a similar equation albeit with a different speed,⁵ this lack of Galilean invariance is natural and is compatible with the invariance of Eq. (1), from which the wave equation originates. This is because the elastic waves are essentially the oscillations of interacting particles of a certain medium (e.g., an elastic solid), making the reference frame connected to this medium, special. So, if the electromagnetic waves were oscillations of a certain special medium (which was first called the “luminiferous aether”⁶ and later *aether* – or just “ether”), similar arguments might be applicable to reconcile Eqs. (2) and (3).

The detection of such a medium was the goal of the measurements carried out between 1881 and 1887 (with better and better precision) by Albert Abraham Michelson and Edward Williams Morley, which are sometimes called “the most famous failed experiments in physics”. Figure 2 shows a crude scheme of these experiments.

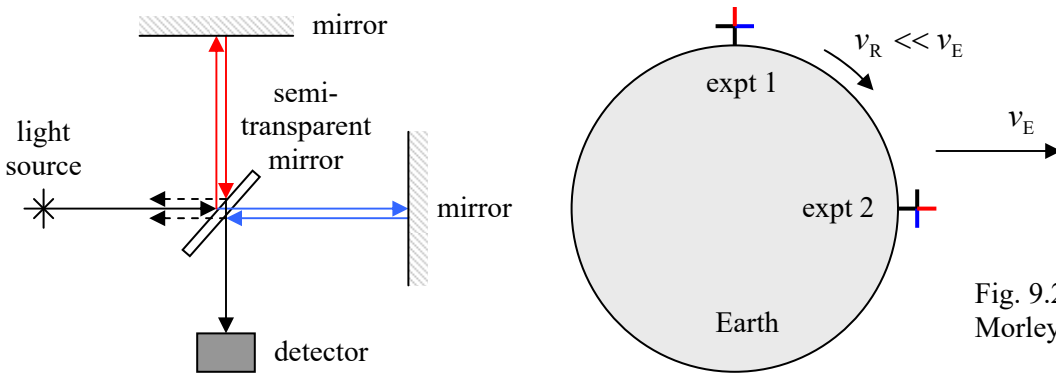


Fig. 9.2. The Michelson-Morley experiment.

³ The discussions in this chapter and most of the next chapter will be restricted to the free-space (and hence dispersion-free) case; some media effects on the radiation by relativistic particles will be discussed in Sec. 10.4.

⁴ It is interesting that the usual (non-relativistic) Schrödinger equation, whose fundamental solution for a free particle is a similar monochromatic wave (albeit with a different dispersion law), *is* Galilean-invariant, with a certain change of the wavefunction’s phase – see, e.g., QM Chapter 1.

⁵ See, e.g., CM Secs. 6.5 and 7.7.

⁶ In ancient Greek mythology, aether is the clean air breathed by the gods residing on Mount Olympus.

A nearly-monochromatic wave from a light source is split into two parts (optimally, of equal intensity), using a semi-transparent mirror tilted by angle $\pi/4$ to the incident wave direction. These two partial waves are reflected back by two fully-reflecting mirrors and arrive at the same semi-transparent mirror again. Here a half of each wave is directed toward the light source (they vanish there without affecting the source), but another half is passed toward an intensity detector, forming, with its counterpart, an interference pattern similar to that in the Young experiment. Thus each of the interfering waves has traveled twice (back and forth) each of two mutually perpendicular “arms” of the interferometer. Assuming that the aether, in which light propagates with speed c , moves with speed $v < c$ along one of the arms, of length l_l , it is straightforward (and hence left for the reader’s exercise :-)) to get the following expression for the difference between the light roundtrip times:

$$\Delta t = \frac{2}{c} \left[\frac{l_t}{\left(1 - v^2/c^2\right)^{1/2}} - \frac{l_l}{1 - v^2/c^2} \right] \approx \frac{l}{c} \left(\frac{v}{c} \right)^2, \quad (9.4)$$

where l_t is the length of the second, “transverse” arm of the interferometer (perpendicular to \mathbf{v}), and the last, approximate expression is valid at $l_t \approx l_l \equiv l$ and $v \ll c$.

Since the Earth moves around the Sun with a speed $v_E \approx 30 \text{ km/s} \approx 10^{-4} c$, the arm positions relative to this motion alternate, due to the Earth’s rotation about its axis, every 6 hours – see the right panel of Fig. 2. Hence if we assume that the aether rests in the Sun’s reference frame, then Δt (and the corresponding shift of the interference fringes), has to change its sign with this half-period as well. The same alternation may be achieved, at a smaller time scale, by a deliberate rotation of the instrument by $\pi/2$. In the most precise version of the Michelson-Morley experiment (circa 1887), this shift was expected to be close to 0.4 of the interference pattern period. The results of the search for such a shift were negative, with the error bar about 0.01 of the period.⁷

The most prominent immediate explanation of this zero result⁸ was suggested in 1889 by George Francis Fitzgerald and (independently and more qualitatively) by H. Lorentz in 1892: as evident from Eq. (4), if the longitudinal arm of the interferometer itself experiences the so-called *length contraction*,

$$l_l(v) = l_l(0) \left(1 - \frac{v^2}{c^2} \right)^{1/2}, \quad (9.5)$$

while the transverse arm’s length is not affected by its motion through the aether, this effect kills the shift Δt . This radical idea received strong support from the proof, in 1887-1905, that the Maxwell equations, and hence the wave equation (3), are form-invariant under the so-called *Lorentz transform*,⁹ which in particular describes Eq. (5). For the choice of coordinates shown in Fig. 1, the transform reads

⁷ Through the 20th century, the Michelson-Morley-type experiments were repeated using more and more refined experimental techniques, always with zero results for the apparent aether motion speed. For example, recent experiments using cryogenically cooled optical resonators have reduced the upper limit for such speed to just $3 \times 10^{-15} c$ – see H. Müller *et al.*, *Phys. Rev. Lett.* **91**, 020401 (2003).

⁸ The zero result of a slightly later experiment, namely a precise measurement of the torque which should be exerted by the moving aether on a charged capacitor, carried out in 1903 by F. Trouton and H. Noble (following G. Fitzgerald’s suggestion), seconded the Michelson and Morley’s conclusions.

⁹ The theoretical work toward this result included important contributions by Woldemart Voigt (in 1887), Hendrik Lorentz (in 1892-1904), Joseph Larmor (in 1897 and 1900), and Henri Poincaré (in 1900 and 1905).

$$x = \frac{x' + vt'}{\left(1 - v^2/c^2\right)^{1/2}}, \quad y = y', \quad z = z', \quad t = \frac{t' + (v/c^2)x'}{\left(1 - v^2/c^2\right)^{1/2}}. \quad (9.6a)$$

Lorentz transform

It is elementary to solve these equations for the primed coordinates to get the reciprocal transform

$$x' = \frac{x - vt}{\left(1 - v^2/c^2\right)^{1/2}}, \quad y' = y, \quad z' = z, \quad t' = \frac{t - (v/c^2)x}{\left(1 - v^2/c^2\right)^{1/2}}. \quad (9.6b)$$

(I will soon represent Eqs. (6) in a more elegant form – see Eqs. (19) below.)

The Lorentz transform relations (6) are evidently reduced to the Galilean transform formulas (2) at $v^2 \ll c^2$. However, all attempts to give a reasonable interpretation of these equalities while keeping the notion of the aether have failed, in particular because of the restrictions imposed by results of earlier experiments carried out in 1851 and 1853 by Hippolyte Fizeau – which were repeated with higher accuracy by the same Michelson and Morley in 1886. These experiments have shown that if one sticks to the aether concept, this hypothetical medium has to be partially “dragged” by any moving dielectric material with a speed proportional to $(\kappa - 1)$. Such local drag would be irreconcilable with the assumed continuity of the aether.

In his famous 1905 paper, Albert Einstein suggested a bold resolution of this contradiction, essentially removing the concept of the aether altogether.¹⁰ Moreover, he argued that the Lorentz transform is the general property of time and space, rather than of the electromagnetic field alone. He started with two postulates, the first one essentially repeating the relativity principle formulated a bit earlier (in 1904) by H. Poincaré in the following form:

*“...the laws of physical phenomena should be the same, whether for an observer fixed or for an observer carried along in a uniform movement of translation; so that we have not and could not have any means of discerning whether or not we are carried along in such a motion.”*¹¹

The second Einstein postulate was that the speed of light c , in free space, should be constant in all reference frames. (This is essentially a denial of the aether’s existence.)

Then, Einstein showed that the Lorenz transform relations (6) naturally follow from his postulates, with a few (very natural) additional assumptions. Let a point source emit a short flash of light, at the moment $t = t' = 0$ when the origins of the reference frames shown in Fig. 1 coincide. Then, according to the second of Einstein’s postulates, in each of the frames, the spherical wave propagates with the same speed c , i.e. the coordinates of points of its front, measured in the two frames, have to obey the following equalities:

$$(ct)^2 - (x^2 + y^2 + z^2) = 0, \\ (ct')^2 - (x'^2 + y'^2 + z'^2) = 0. \quad (9.7)$$

¹⁰ In hindsight, this was much relief, because the aether had been a very awkward construct to start with. In particular, according to the basic theory of elasticity (see, e.g., CM Ch. 7), in order to carry such transverse waves as the electromagnetic ones, this medium would need to have a non-zero shear modulus, i.e. behave as an elastic solid – rather than as a rarified gas hypothesized initially by C. Huygens.

¹¹ Note that though the relativity principle excludes the notion of the special (“absolute”) spatial reference frame, its quoted verbal formulation still leaves the possibility of the Galilean “absolute time” $t = t'$ open. The quantitative relativity theory kills this option – see Eqs. (6) and their discussion below.

What may be the general relation between the combinations in the left-hand side of these equations – not for this particular wave's front, but in general? A very natural (essentially, the only justifiable) choice is

$$[(ct)^2 - (x^2 + y^2 + z^2)] = f(v^2)[(ct')^2 - (x'^2 + y'^2 + z'^2)]. \quad (9.8)$$

Now, according to the first postulate, the same relation should be valid if we swap the reference frames ($x \leftrightarrow x'$, etc.) and replace v with $(-v)$. This is only possible if $f^2 = 1$, so that excluding the option $f = -1$ (which is incompatible with the Galilean transform in the limit $v/c \rightarrow 0$), we are left with $f = +1$, i.e.

$$(ct)^2 - (x^2 + y^2 + z^2) = (ct')^2 - (x'^2 + y'^2 + z'^2). \quad (9.9)$$

For the line with $y = y' = 0$ and $z = z' = 0$, Eq. (9) is reduced to

$$(ct)^2 - x^2 = (ct')^2 - x'^2. \quad (9.10)$$

It is very illuminating to interpret this relation as the one resulting from a mutual rotation of the reference frames (that now have to include clocks to measure time) on the plane of the coordinate x and the so-called *imaginary time* $\tau \equiv ict$ – see Fig. 3.

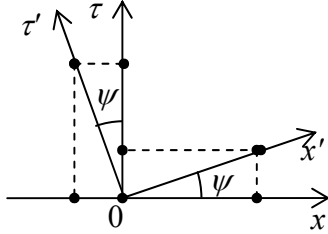


Fig. 9.3. The Lorentz transform as a mutual rotation of two reference frames on the $[x, \tau]$ plane.

Indeed, rewriting Eq. (10) as

$$\tau^2 + x^2 = \tau'^2 + x'^2, \quad (9.11)$$

we may consider it as the invariance of the squared radius at the rotation shown in Fig. 3 and described by the following geometric relations:

$$\begin{aligned} x &= x' \cos \psi - \tau' \sin \psi, \\ \tau &= x' \sin \psi + \tau' \cos \psi, \end{aligned} \quad (9.12a)$$

with the reciprocal relations

$$\begin{aligned} x' &= x \cos \psi + \tau \sin \psi, \\ \tau' &= -x \sin \psi + \tau \cos \psi. \end{aligned} \quad (9.12b)$$

So far, the angle ψ has been arbitrary. In the spirit of Eq. (8), a natural choice is $\psi = \psi(v)$, with the requirement $\psi(0) = 0$. To find this function, let us write the definition of the velocity v of frame $0'$, as measured in frame 0 (which was implied above): for $x' = 0$, $x = vt$. In the variables x and τ , this means

$$\frac{x}{\tau} \Big|_{x'=0} \equiv \frac{x}{ict} \Big|_{x'=0} = \frac{v}{ic}. \quad (9.13)$$

On the other hand, for the same point $x' = 0$, Eqs. (12a) yield

$$\frac{x}{\tau} \Big|_{x'=0} = -\tan \psi . \quad (9.14)$$

These two expressions are compatible only if

$$\tan \psi = \frac{iv}{c}, \quad (9.15)$$

so that

$$\sin \psi \equiv \frac{\tan \psi}{(1 + \tan^2 \psi)^{1/2}} = \frac{iv/c}{(1 - v^2/c^2)^{1/2}} \equiv i\beta\gamma, \quad \cos \psi \equiv \frac{1}{(1 + \tan^2 \psi)^{1/2}} = \frac{1}{(1 - v^2/c^2)^{1/2}} \equiv \gamma, \quad (9.16)$$

where β and γ are two very convenient and commonly used dimensionless parameters defined as

$$\beta \equiv \frac{v}{c}, \quad \gamma \equiv \frac{1}{(1 - v^2/c^2)^{1/2}} \equiv \frac{1}{(1 - \beta^2)^{1/2}} . \quad (9.17)$$

Relativistic parameters
 β and γ

(The vector β is called the *normalized velocity*, while the scalar γ , the *Lorentz factor*).¹²

Using the above relations for ψ , Eqs. (12) become

$$x = \gamma(x' - i\beta\tau'), \quad \tau = \gamma(i\beta x' + \tau'), \quad (9.18a)$$

$$x' = \gamma(x + i\beta\tau), \quad \tau' = \gamma(-i\beta x + \tau). \quad (9.18b)$$

Now returning to the real variables $[x, ct]$, we get the Lorentz transform relations (6), in a more compact form:

$$x = \gamma(x' + \beta ct'), \quad y = y', \quad z = z', \quad ct = \gamma(ct' + \beta x'), \quad (9.19a)$$

$$x' = \gamma(x - \beta ct), \quad y' = y, \quad z' = z, \quad ct' = \gamma(ct - \beta x). \quad (9.19b)$$

Lorentz transform - again

An immediate corollary of Eqs. (19) is that for γ to stay real, we need $v^2 \leq c^2$, i.e. that the speed of any physical body (to which we could connect a meaningful reference frame) cannot exceed the speed of light, as measured in *any* other meaningful reference frame.¹³

9.2. Relativistic kinematic effects

Before proceeding to other corollaries of Eqs. (19), let us spend a few minutes discussing what these relations actually mean. Evidently, they are trying to tell us that the spatial and temporal intervals are not absolute (as they are in the Newtonian space), but do depend on the reference frame they are measured in. So, we have to understand very clearly what exactly may be measured – and thus may be discussed in a meaningful physics theory. Recognizing this necessity, A. Einstein introduced the notion of numerous imaginary *observers* that may be distributed all over each reference frame. Each observer

¹² Note the following identities: $\gamma^2 \equiv 1/(1 - \beta^2)$ and $(\gamma^2 - 1) \equiv \beta^2/(1 - \beta^2) \equiv \gamma^2\beta^2$, which are frequently handy in relativity-related algebra. One more function of β , the *rapidity* $\varphi \equiv \tanh^{-1}\beta$ (so that $\psi = i\varphi$), is also useful for some calculations.

¹³ All attempts to rationally conjecture particles moving with $v > c$ (called *tachyons*) have failed – so far, at least. Possibly the strongest objection against their existence is the fact that the tachyons could be used to communicate back in time, thus violating the causality principle – see, e.g., G. Benford *et al.*, *Phys. Rev. D* **2**, 263 (1970).

has a clock and may use it to measure the instants of *local* events, taking place at the observer's location. He also conjectured, very reasonably, that:

- (i) all observers within the same reference frame may agree on a common length measure ("a scale"), i.e. on their relative positions in that frame, and synchronize their clocks,¹⁴ and
- (ii) the observers belonging to different reference frames may agree on the nomenclature of *world events* (e.g., short flashes of light) to which their respective measurements refer.

Actually, these additional postulates have been already implied in our "derivation" of the Lorentz transform in Sec. 1. For example, by the set $\{x, y, z, t\}$ we mean the results of space and time measurements of a certain world event, about that all observers belonging to frame 0 agree. Similarly, all observers of frame 0' have to agree about the results $\{x', y', z', t'\}$. Finally, when the origin of frame 0' passes by some sequential points x_k of frame 0, the observers in the latter frame may measure its passage times t_k without a fundamental error, and know that all these times belong to $x' = 0$.

Now we can analyze the major corollaries of the Lorentz transform, which are rather striking from the point of view of our everyday (rather non-relativistic) experience.

- (i) Length contraction. Let us consider a thin rigid rod oriented along the x -axis, with its length $l \equiv x_2 - x_1$, where $x_{1,2}$ are the coordinates of the rod's ends, as measured in its rest frame 0, at any instant t (Fig. 4). What would be the rod's length l' measured by the Einstein observers in the moving frame 0'?

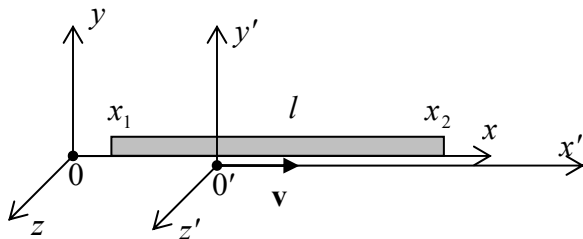


Fig. 9.4. The relativistic length contraction.

At a time instant t' agreed upon in advance, the observers who find themselves exactly at the rod's ends, may register that fact, and then subtract their coordinates $x'_{1,2}$ to calculate the apparent rod length $l' \equiv x'_2 - x'_1$ in the moving frame. According to Eq. (19a), l may be expressed via this l' as

$$l \equiv x_2 - x_1 = \gamma(x'_2 + \beta c t') - \gamma(x'_1 + \beta c t') = \gamma(x'_2 - x'_1) \equiv \gamma l'. \quad (9.20a)$$

Hence, the rod's length, as measured in the *moving* reference frame is

$$l' = \frac{l}{\gamma} = l \left(1 - \frac{v^2}{c^2}\right)^{1/2} \leq l,$$

(9.20b)

in accordance with the FitzGerald-Lorentz hypothesis (5). This is the *relativistic length contraction* effect: an object is always the longest (has the so-called *proper length* l) if measured in its *rest frame*.

¹⁴ A posteriori, the Lorenz transform may be used to show that consensus-creating procedures (such as clock synchronization) are indeed possible. The basic idea of the proof is that since at $v \ll c$, the relativistic corrections to space and time intervals are of the order of $(v/c)^2$, they have negligible effects on clocks being brought together into the same point for synchronization slowly, with a speed $u \ll c$. The reader interested in a detailed discussion of this and other fine points of special relativity may be referred to, e.g., either H. Arzeliès, *Relativistic Kinematics*, Pergamon, 1966, or W. Rindler, *Introduction to Special Relativity*, 2nd ed., Oxford U. Press, 1991.

Note that according to Eqs. (19), the length contraction takes place only in the direction of the relative motion of two reference frames. As was noted in Sec. 1, this result immediately explains the zero result of the Michelson-Morley-type experiments, so that they give very convincing evidence (if not irrefutable proof) of Eqs. (18)-(19).

(ii) Time dilation. Now let us use Eqs. (19a) to find the time interval Δt , as measured in some reference frame 0, between two world events – say, two ticks of a clock moving with another frame 0' (Fig. 5), i.e. having fixed values of x' , y' , and z' .

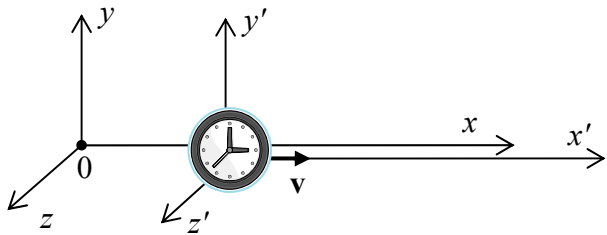


Fig. 9.5. The relativistic time dilation.

Let the time interval between these two events, measured in the clock's rest frame 0', be $\Delta t' \equiv t_2' - t_1'$. At these two moments, the clock would fly by certain two Einstein's observers at rest in frame 0, so that they can record the corresponding moments $t_{1,2}$ shown by their clocks, and then calculate Δt as their difference. According to the last of Eqs. (19a),

$$c\Delta t \equiv ct_2 - ct_1 = \gamma[(ct_2' + \beta x') - (ct_1' + \beta x')] \equiv \gamma c\Delta t', \quad (9.21a)$$

so that, finally,

$$\boxed{\Delta t = \gamma \Delta t' \equiv \frac{\Delta t'}{(1 - v^2/c^2)^{1/2}} \geq \Delta t'}. \quad (9.21b)$$
Time dilation

This is the famous *relativistic time dilation* (or “dilatation”) effect: a time interval is *longer* if measured in a frame (in our case, frame 0) *moving relative to the clock*, while that in the clock's rest frame is the shortest possible – the so-called *proper time interval*.

This rather counter-intuitive effect is the everyday reality in experiments with high-energy elementary particles. For example, in a typical (and by no means record-breaking) experiment carried out in Fermilab, a beam of charged 200 GeV pions with $\gamma \approx 1,400$ traveled a distance of $l = 300$ m with the measured loss of only 3% of the initial beam intensity due to the pion decay (mostly, into muon-neutrino pairs) with the proper lifetime $t_0 \approx 2.56 \times 10^{-8}$ s. Without the time dilation, only an $\exp\{-l/ct_0\} \sim 10^{-17}$ fraction of the initial pions would survive, while the relativity-corrected number, $\exp\{-l/c\gamma t_0\} = \exp\{-l/c\gamma t_0\} \approx 0.97$, was in full accordance with experimental measurements.

As another example, the global positioning systems (say, the GPS) are designed with the account of the time dilation due to the velocity of their satellites (and also some gravity-induced, i.e. general-relativity corrections, which I would not have time to discuss) and would give large errors without such corrections. So, there is no doubt that time dilation (21) is a reality, though the precision of its experimental tests I am aware of¹⁵ has been limited to a few percent, because of the almost unavoidable involvement of less controllable gravity effects – which provide a time interval change of the opposite sign in most experiments near the Earth's surface.

¹⁵ See, e.g., J. Hafele and R. Keating, *Science* **177**, 166 (1972).

Before the first reliable observation of time dilation (by B. Rossi and D. Hall in 1940), there had been serious doubts about the reality of this effect, the most famous being the *twin paradox* first posed (together with an immediate suggestion of its resolution) by P. Langevin in 1911. Let us send one of two twins on a long space roundtrip with the maximum speed approaching c . Upon his return to Earth, who of the twins would be older? The naïve approach is to say that due to the relativity principle, not one can be (and hence there is no time dilation) because each twin could claim that their counterpart rather than them, was moving, with the same speed but in the opposite direction. The resolution of the paradox is that one of the twins had to be accelerated to be brought back, and hence the reference frames have to be dissimilar: only one of them may stay inertial all the time. As a result, the twin who had been accelerated (“actually traveling”) would be younger than their sibling when they finally come together. Constructive proof of this conclusion for the particular case of straight-line travel with a piecewise-constant acceleration, is simple and hence left for the reader’s exercise.

(iii) Velocity transformation. Now let us calculate the velocity \mathbf{u} of a moving point, as observed in reference frame 0, provided that its velocity, as measured in frame 0', is \mathbf{u}' (Fig. 6).

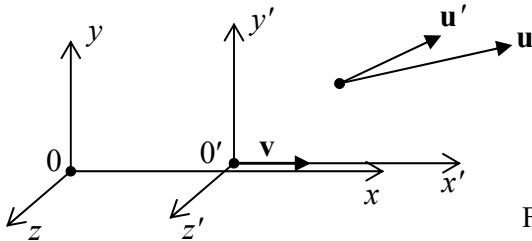


Fig. 9.6. The relativistic velocity addition.

Keeping the usual definition of velocity, but with due attention to the relativity of not only spatial but also temporal intervals, we may write

$$\mathbf{u} \equiv \frac{d\mathbf{r}}{dt}, \quad \mathbf{u}' \equiv \frac{d\mathbf{r}'}{dt'}. \quad (9.22)$$

Plugging in the differentials of the Lorentz transform relations (6a) into these definitions, we get

$$u_x \equiv \frac{dx}{dt} = \frac{dx' + vdt'}{dt' + vdx'/c^2} \equiv \frac{u'_x + v}{1 + u'_x v/c^2}, \quad u_y \equiv \frac{dy}{dt} = \frac{1}{\gamma} \frac{dy'}{dt' + vdx'/c^2} \equiv \frac{1}{\gamma} \frac{u'_y}{1 + u'_x v/c^2}, \quad (9.23)$$

with a similar formula for u_z . In the classical limit $v/c \rightarrow 0$, these relations are reduced to

$$u_x = u'_x + v, \quad u_y = u'_y, \quad u_z = u'_z, \quad (9.24a)$$

and may be merged into the familiar Galilean form

$$\mathbf{u} = \mathbf{u}' + \mathbf{v}, \quad \text{for } v \ll c. \quad (9.24b)$$

In order to see how unusual the full relativistic rules (23) are at $u \sim c$, let us first consider a purely longitudinal motion, $u_y = u_z = 0$; then¹⁶

¹⁶ With an account of the identity $\tanh(a + b) = (\tanh a + \tanh b)/(1 + \tanh a \tanh b)$, which readily follows from MA Eq. (3.5), Eq. (25) shows that rapidities $\varphi \equiv \tanh^{-1}\beta$ add up exactly as longitudinal velocities at non-relativistic motion, making that notion very convenient for the analysis of transfer between several frames.

$$u = \frac{u' + v}{1 + u'v/c^2}, \quad (9.25)$$

Longitudinal
velocity
addition

where $u \equiv u_x$ and $u' \equiv u'_x$. Figure 7 shows this u as the function of u' , for several values of the reference frames' relative velocity v .

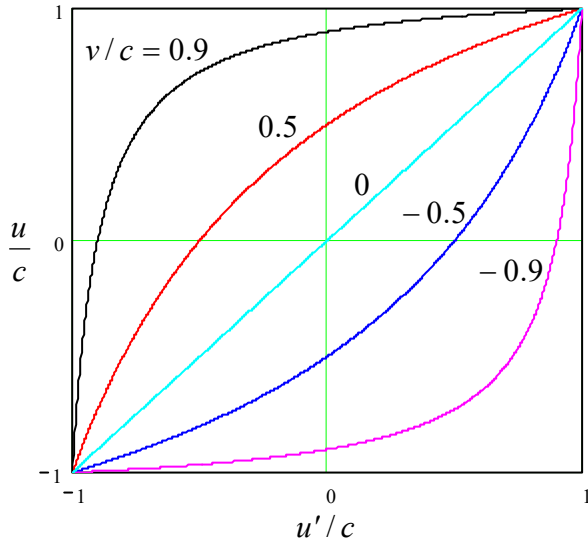


Fig. 9.7. The addition of longitudinal velocities.

The first sanity check is that if $v = 0$, i.e. if the reference frames are at rest relative to each other, then $u = u'$, as it should be – see the diagonal straight line in Fig. 7. Next, if magnitudes of u' and v are both below c , so is the magnitude of u . (Also good, because otherwise ordinary particles in one frame would be tachyons in the other one, and the theory would be in big trouble.) Now strange things begin: even as u' and v are both approaching c , then u is also close to c , but does not exceed it. As an example, if we fired forward a bullet with the relative speed of $0.9c$, from a spaceship moving from the Earth also at $0.9c$, Eq. (25) predicts the speed of the bullet relative to the Earth to be just $[(0.9 + 0.9)/(1 + 0.9 \times 0.9)]c \approx 0.994c < c$, rather than $(0.9 + 0.9)c = 1.8c > c$ as in the Galilean kinematics. Actually, we could expect this strangeness, because it is necessary to fulfill the 2nd Einstein's postulate: the independence of the speed of light in any reference frame. Indeed, for $u' = \pm c$, Eq. (25) yields $u = \pm c$, regardless of v .

In the opposite case of a purely transverse motion, when a point moves across the relative motion of the frames (for example, at our choice of coordinates, $u'_{\text{x}} = u'_{\text{z}} = 0$), Eqs. (23) yield a much less spectacular result

$$u_y = \frac{1}{\gamma} u'_{\text{y}} \leq u'_{\text{y}}. \quad (9.26)$$

This effect comes purely from the time dilation because the transverse spatial intervals are Lorentz-invariant.

In the case when both u_x' and u_y' are substantial (but u_z' is still zero), we may divide Eqs. (23) by each other to relate the angles θ of the point's propagation, as observed in the two reference frames:

$$\tan \theta \equiv \frac{u_y}{u_x} = \frac{u'_{\text{y}}}{\gamma(u'_{\text{x}} + v)} = \frac{\sin \theta'}{\gamma(\cos \theta' + v/u')}. \quad (9.27)$$

Stellar
aberration
effect

This expression describes, in particular, the so-called *stellar aberration* effect: the dependence of the observed direction θ toward a star on the speed v of the telescope's motion relative to the star – see Fig. 8. (The effect is readily observable experimentally as the *annual aberration* due to the periodic change of speed v by $2v_E \approx 60$ km/s because of the Earth's rotation about the Sun. Since the aberration's main part is of the first order in $v_E/c \sim 10^{-4}$, this effect is very significant and has been known since the early 1700s.)

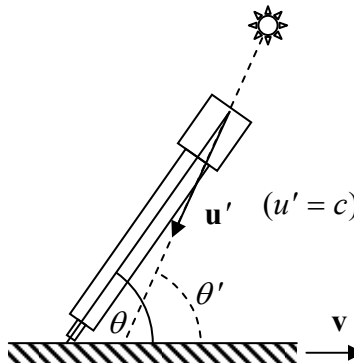


Fig. 9.8. The stellar aberration.

For the analysis of this effect, it is sufficient to take, in Eq. (27), $u' = c$, i.e. $v/u' = \beta$, and interpret θ' as the “proper” direction to the star, that would be measured at $v = 0$.¹⁷ At $\beta \ll 1$, both Eq. (27) and the Galilean result (which the reader is invited to derive directly from Fig. 8),

$$\tan \theta = \frac{\sin \theta'}{\cos \theta' + \beta}, \quad (9.28)$$

may be well approximated by the first-order term

$$\Delta\theta \equiv \theta - \theta' \approx -\beta \sin \theta'. \quad (9.29)$$

Unfortunately, it is not easy to use the difference between Eqs. (27) and (28), of the second order in β , for special relativity's confirmation, because other components of the Earth's motion, such as its rotation, nutation, and torque-induced precession,¹⁸ give masking first-order contributions to the aberration.

Finally, for a completely arbitrary direction of the vector \mathbf{u}' , Eqs. (22) may be readily used to calculate the velocity's magnitude. The most popular form of the resulting expression is the following expression for the square of the relative velocity (or rather the reduced relative velocity β) of two points,

$$\beta^2 = \frac{(\beta_1 - \beta_2)^2 - |\beta_1 \cdot \beta_2|}{(1 - \beta_1 \cdot \beta_2)^2} \leq 1. \quad (9.30)$$

where $\beta_{1,2} \equiv \mathbf{v}_{1,2}/c$ are their normalized velocities as measured in the same reference frame.

¹⁷ Strictly speaking, to reconcile the geometries shown in Fig. 1 (for which all our formulas, including Eq. (27), are valid) and Fig. 8 (giving the traditional scheme of the stellar aberration), it is necessary to invert the signs of \mathbf{u} (and hence of $\sin \theta'$ and $\cos \theta'$) and \mathbf{v} , but as it is evident from Eq. (27), all the minus signs cancel, and the formula is valid “as is”.

¹⁸ See, e.g., CM Secs. 4.4-4.5.

(iv) The Doppler effect. Let us consider a monochromatic plane wave of some physical nature, traveling along the x -axis:

$$f = \operatorname{Re}[f_\omega \exp\{i(kx - \omega t)\}] \equiv |f_\omega| \cos(kx - \omega t + \arg f_\omega) \equiv |f_\omega| \cos \Psi. \quad (9.31)$$

Its total phase, $\Psi \equiv kx - \omega t + \arg f_\omega$ (in contrast to its amplitude $|f_\omega|$ – see Sec. 5 below) cannot depend on the observer's reference frame, because the variable f vanishes completely at $\Psi = \pi(n + \frac{1}{2})$ (for all integer n), and such “world events” should be observable in all reference frames. The only way to keep $\Psi = \Psi'$ at all times is to have¹⁹

$$kx - \omega t = k'x' - \omega't'. \quad (9.32)$$

First, let us use this general relation to consider the Doppler effect in the usual non-relativistic mechanical waves, e.g., oscillations of particles of a certain medium. Using the Galilean transform (2), we may rewrite Eq. (32) as

$$k(x' + vt) - \omega t = k'x' - \omega't'. \quad (9.33)$$

Since this transform leaves all space intervals (including the wavelength $\lambda = 2\pi/k$) intact, we can take $k = k'$, so that Eq. (33) yields

$$\omega' = \omega - kv. \quad (9.34)$$

For a dispersion-free medium, the wave number k is the ratio of its frequency ω , as measured in the reference frame bound to the medium, and the wave velocity v_w . In particular, if the wave source rests in the medium, we may bind the reference frame 0 to the medium as well, and frame 0' to the wave's receiver (i.e. $v = v_r$), so that

$$k = \frac{\omega}{v_w}, \quad (9.35)$$

and for the frequency perceived by the receiver, Eq. (34) yields

$$\omega' = \omega \frac{v_w - v_r}{v_w}. \quad (9.36)$$

On the other hand, if the receiver and the medium are at rest in the reference frame 0', while the wave source is bound to the frame 0 (so that $v = -v_s$), Eq. (35) should be replaced with

$$k = k' = \frac{\omega'}{v_w}, \quad (9.37)$$

and Eq. (34) yields a different result:

$$\omega' = \omega \frac{v_w}{v_w - v_s}, \quad (9.38)$$

Finally, if both the source and detector are moving, it is straightforward to combine these two results to get the general relation

$$\omega' = \omega \frac{v_w - v_r}{v_w - v_s}. \quad (9.39)$$

¹⁹ Strictly speaking, Eq. (32) is valid to an additive constant, but for notation simplicity, it may be always made equal to zero by selecting (as has already been done in all relations of Sec. 1) the reference frame origins and/or clock turn-on times so that at $t = 0$ and $x = 0$, $t' = 0$ and $x' = 0$ as well.

At low speeds of both the source and the receiver, this result simplifies,

$$\omega' \approx \omega(1 - \beta), \quad \text{with } \beta \equiv \frac{v_r - v_s}{v_w}, \quad (9.40)$$

but at speeds comparable to v_w we have to use the more general Eq. (39). Thus, the usual Doppler effect is generally affected not only by the relative speed ($v_r - v_s$) of the wave's source and detector but also by their speeds relative to the medium in which the waves propagate.

Somewhat counter-intuitively, for the electromagnetic waves the calculations are *simpler* because for them the propagation medium (aether) does not exist, the wave velocity equals $\pm c$ in any reference frame, and there are no two separate cases: we can always take $k = \pm \omega/c$ and $k' = \pm \omega'/c$. Plugging these relations, together with the Lorentz transform (19a), into the phase-invariance condition (32), we get

$$\pm \frac{\omega}{c} \gamma(x' + \beta ct') - \omega \gamma \frac{ct' + \beta x'}{c} = \pm \frac{\omega'}{c} x' - \omega' t'. \quad (9.41)$$

This relation has to hold for any x' and t' , so we may require that the net coefficients before these variables vanish. These two requirements yield the same equality:

$$\omega' = \omega \gamma(1 \mp \beta). \quad (9.42)$$

This result is already quite simple, but may be transformed further to be even more illuminating:

$$\omega' = \omega \frac{1 \mp \beta}{(1 - \beta^2)^{1/2}} \equiv \omega \left[\frac{(1 \mp \beta)(1 \mp \beta)}{(1 + \beta)(1 - \beta)} \right]^{1/2}. \quad (9.43)$$

At any sign before β , one pair of parentheses cancel, so that²⁰

$$\omega' = \omega \left(\frac{1 \mp \beta}{1 \pm \beta} \right)^{1/2}. \quad (9.44)$$

Thus the Doppler effect for electromagnetic waves depends only on the relative velocity $v = \beta c$ between the wave source and detector – as it should be, given the aether's absence. At velocities much lower than c , Eq. (44) may be approximated as

$$\omega' \approx \omega \frac{1 \mp \beta/2}{1 \pm \beta/2} \approx \omega(1 \mp \beta), \quad (9.45)$$

i.e. in the first approximation in $\beta \equiv v/c$ it tends to the corresponding limit (40) of the usual Doppler effect.

If the wave vector \mathbf{k} is tilted by angle θ to the vector \mathbf{v} (as measured in frame 0), then we have to repeat the calculations, with k replaced by k_x , and components k_y and k_z left intact at the Lorentz transform. As a result, Eq. (42) is generalized as

²⁰ It may look like the reciprocal expression of ω via ω' is different, violating the relativity principle. However, in this case, we have to change the sign of β , because the relative velocity of the system is opposite, so that we return to Eq. (44) again.

$$\omega' = \omega\gamma(1 - \beta \cos \theta). \quad (9.46)$$

For the case $\cos\theta = \pm 1$, Eq. (46) reduces to our previous result (42). However, at $\theta = \pi/2$ (i.e. $\cos\theta = 0$), the relation is rather different:

$$\boxed{\omega' = \gamma\omega \equiv \frac{\omega}{(1 - \beta^2)^{1/2}}.} \quad (9.47)$$

Transverse
Doppler
effect

This is the *transverse Doppler effect* – which is absent in non-relativistic physics. Its first experimental evidence was obtained using electron beams (as had been suggested in 1906 by J. Stark), by H. Ives and G. Stilwell in 1938 and 1941. Later, similar experiments were repeated several times, but the first unambiguous measurements were performed only in 1979 by D. Hasselkamp *et al.* who confirmed Eq. (47) with a relative accuracy of about 10%. This precision may not look too spectacular, but besides the special tests discussed above, the Lorentz transform formulas have been also confirmed, less directly, by a huge body of other experimental data, especially in high energy physics, agreeing with calculations incorporating this transform as their part. This is why, with due respect to the spirit of challenging authority, I should warn the reader: if you decide to challenge the relativity theory (called “theory” by tradition only), you would also need to explain all these data. Best luck with that!²¹

9.3. 4-vectors, momentum, mass, and energy

Before proceeding to the relativistic dynamics, let us discuss the mathematical formalism that makes all calculations more compact – and more beautiful. We have already seen that the three spatial coordinates $\{x, y, z\}$ and the product ct are Lorentz-transformed similarly – see Eqs. (18)-(19) again. So it is natural to consider them as components of a single four-component vector (or, for short, *4-vector*),

$$\{x_0, x_1, x_2, x_3\} \equiv \{ct, \mathbf{r}\}, \quad (9.48)$$

with components

$$\boxed{x_0 \equiv ct, \quad x_1 \equiv x, \quad x_2 \equiv y, \quad x_3 \equiv z.} \quad (9.49)$$

Space
-time
4-vector

According to Eqs. (19), its components are Lorentz-transformed as

$$\boxed{x_j = \sum_{j'=0}^3 L_{jj'} x'_{j'},} \quad (9.50)$$

Lorentz
transform:
4-form

where $L_{jj'}$ are the elements of the following *4×4 Lorentz transform matrix*

$$\boxed{\begin{pmatrix} \gamma & \beta\gamma & 0 & 0 \\ \beta\gamma & \gamma & 0 & 0 \\ 0 & 0 & 1 & 0 \\ 0 & 0 & 0 & 1 \end{pmatrix}.} \quad (9.51)$$

Lorentz
transform
matrix

Since such 4-vectors are a new notion for this course and will be used for many more purposes than just the space-time transform, we need to discuss the general mathematical rules they obey. Indeed,

²¹ The same fact, ignored by crackpots, is also valid for other favorite directions of their attacks, including the Universe expansion, quantum measurement uncertainty, and entropy growth in physics, and the evolution theory in biology.

as was already mentioned in Sec. 8.9, the usual (three-component) vector is not just any ordered set (*string*) of three scalars $\{A_x, A_y, A_z\}$; if we want it to represent a reference-frame-independent physical reality, the vector's components have to obey certain rules at the transfer from one reference frame to another. In particular, in the non-relativistic limit the vector's *norm* (its magnitude squared),

$$A^2 = A_x^2 + A_y^2 + A_z^2, \quad (9.52)$$

should be invariant with respect to the transfer between different reference frames. However, a naïve extension of this approach to 4-vectors would not work, because, according to the calculations of Sec. 1, the Lorentz transform keeps intact the combinations of the type (7), with one sign negative, rather than the sum of all components squared. Hence for the 4-vectors, all the rules of the game have to be reviewed and adjusted – or rather redefined from the very beginning, for example as follows.²²

An arbitrary 4-vector is a string of 4 scalars,²³

$$\boxed{\{A_0, A_1, A_2, A_3\}}, \quad (9.53)$$

whose components A_j , as measured in the reference frames 0 and 0' shown in Fig. 1, obey the Lorentz transform relations similar to Eq. (50):

$$\boxed{A_j = \sum_{j'=0}^3 L_{jj'} A'_{j'}}. \quad (9.54)$$

As we have already seen in the example of the space-time 4-vector (48), this means in particular that

$$\boxed{A_0^2 - \sum_{j=1}^3 A_j^2 = (A'_0)^2 - \sum_{j=1}^3 (A'_{j'})^2}. \quad (9.55)$$

This is the so-called *Lorentz invariance* condition for the 4-vector's *norm*. (The difference between this relation and Eq. (52), pertaining to the Euclidian geometry, is the reason why the Minkowski space is called *pseudo-Euclidian*.) It is also straightforward to use Eqs. (51) and (54) to check that the evident generalization of the norm, the *scalar product* of two arbitrary 4-vectors,

$$\boxed{A_0 B_0 - \sum_{j=1}^3 A_j B_j}, \quad (9.56)$$

is also Lorentz-invariant.

Now consider the 4-vector corresponding to a small *interval* between two close world events:

$$\{dx_0, dx_1, dx_2, dx_3\} = \{cdt, d\mathbf{r}\}; \quad (9.57)$$

its norm,

$$\boxed{(ds)^2 \equiv dx_0^2 - \sum_{j=1}^3 dx_j^2 = c^2(dt)^2 - (dr)^2}, \quad (9.58)$$

²² The most prominent alternative, which has both advantages and drawbacks, is to use 4-vectors with one imaginary component – for example, the imaginary time ict instead of the real product ct in Eq. (48).

²³ Such vectors are said to reside in so-called 4D *Minkowski spaces* – called after Hermann Minkowski who was the first one to recast (in 1907) the special relativity relations in a form in which the spatial coordinates and time (or rather ct) are treated on an equal footing.

is of course also Lorentz-invariant. Since the speed of any particle (or signal) cannot be larger than c , for any pair of world events that are in a causal relation with each other, $(dr)^2$ cannot be larger than $(cdt)^2$, i.e. such *time-like* interval $(ds)^2$ cannot be negative. The 4D surface separating such intervals from *space-like* intervals $(ds)^2 < 0$ is called the light cone (Fig. 9).

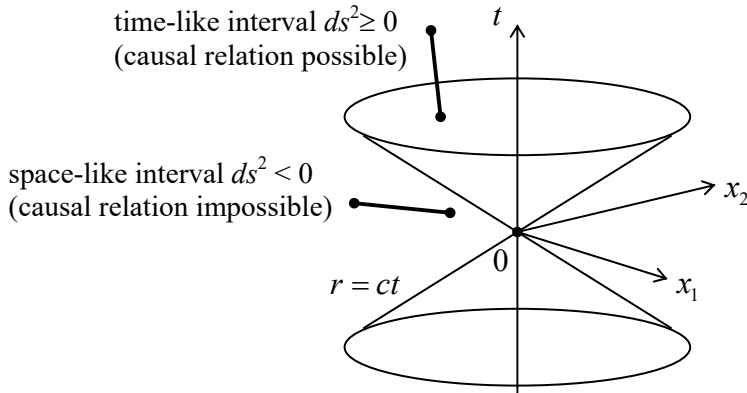


Fig. 9.9. A 2+1 dimensional image of the light cone – which is actually 3+1 dimensional.

Now let us consider two close world events that happen with the same point moving with velocity \mathbf{u} . Then in the frame moving with the point ($\mathbf{v} = \mathbf{u}$), the last term on the right-hand side of Eq. (58) equals zero, while the involved time is the proper one, so that

$$ds = cdt, \quad (9.59)$$

where dt is the proper time interval. But according to Eq. (21), this means that we can write

$$d\tau = \frac{dt}{\gamma}, \quad (9.60)$$

where $d\tau$ is the time interval in an *arbitrary* (besides being inertial) reference frame, while

$$\beta \equiv \frac{\mathbf{u}}{c} \quad \text{and} \quad \gamma \equiv \frac{1}{(1 - \beta^2)^{1/2}} = \frac{1}{(1 - u^2/c^2)^{1/2}} \quad (9.61)$$

are the parameters (17) corresponding to the *point's* velocity (\mathbf{u}) in that frame, so that $ds = cdt/\gamma$.²⁴

Let us use Eq. (60) to explore whether a 4-vector may be formed using the spatial Cartesian components of the point's velocity

$$\mathbf{u} = \left\{ \frac{dx}{d\tau}, \frac{dy}{d\tau}, \frac{dz}{d\tau} \right\}. \quad (9.62)$$

Here we have some problem: as Eqs. (22) show, these components do not obey the Lorentz transform. However, let us use $d\tau \equiv dt/\gamma$, the proper time interval of the point, to form the following string:

$$\left\{ \frac{dx_0}{d\tau}, \frac{dx_1}{d\tau}, \frac{dx_2}{d\tau}, \frac{dx_3}{d\tau} \right\} \equiv \gamma \left\{ c, \frac{dx}{dt}, \frac{dy}{dt}, \frac{dz}{dt} \right\} \equiv \gamma \{c, \mathbf{u}\}.$$

(9.63)

4-velocity

²⁴ I have opted against using special indices (e.g., β_u and γ_u) to distinguish Eqs. (17) and (61) here and below, in a hope that the suitable velocity (of either a reference frame or a particle) will be always clear from the context.

As it follows from the comparison of the middle form of this expression with Eq. (48), since the time-space vector obeys the Lorentz transform, and τ is Lorentz-invariant, the string (63) is a legitimate 4-vector; it is called the *4-velocity* of a point – or of a point particle.

Now we are well equipped to proceed to relativistic dynamics. Let us start with such basic notions as the momentum \mathbf{p} and the energy \mathcal{E} – so far, for a free particle.²⁵ Perhaps the most elegant way to “derive” (or rather guess²⁶) the expressions for \mathbf{p} and \mathcal{E} as functions of the particle’s velocity \mathbf{u} , is based on analytical mechanics. Due to the conservation of \mathbf{v} , the trajectory of a free particle in the 4D Minkowski space $\{ct, \mathbf{r}\}$ is always a straight line. Hence, from the Hamilton principle,²⁷ we may expect its action \mathcal{S} , between points 1 and 2, to be a linear function of the space-time interval (59):

Free
particle:
action

$$\mathcal{S} = \alpha \int_1^2 ds \equiv \alpha c \int_1^2 d\tau \equiv \alpha c \int_{t_1}^{t_2} \frac{dt}{\gamma}, \quad (9.64)$$

where α is some constant. On the other hand, in analytical mechanics, the action is defined as

$$\mathcal{S} \equiv \int_{t_1}^{t_2} \mathcal{L} dt, \quad (9.65)$$

where \mathcal{L} is the particle’s Lagrangian function.²⁸ Comparing these two expressions, we get

$$\mathcal{L} = \frac{\alpha c}{\gamma} \equiv \alpha c \left(1 - \frac{u^2}{c^2}\right)^{1/2}. \quad (9.66)$$

In the non-relativistic limit ($u \ll c$), this function tends to

$$\mathcal{L} \approx \alpha c \left(1 - \frac{u^2}{2c^2}\right) \equiv \alpha c - \frac{\alpha u^2}{2c}. \quad (9.67)$$

In order to correspond to the Newtonian mechanics,²⁹ the last (velocity-dependent) term should equal $mu^2/2$. From here we find $\alpha = -mc$, so that, finally,

Free
particle:
Lagrangian
function

$$\mathcal{L} = -mc^2 \left(1 - \frac{u^2}{c^2}\right)^{1/2} \equiv -\frac{mc^2}{\gamma}. \quad (9.68)$$

Now we can find the Cartesian components p_j of the particle’s momentum as the generalized momenta corresponding to the corresponding components r_j ($j = 1, 2, 3$) of the 3D radius-vector \mathbf{r} :³⁰

²⁵ I am sorry for using, just as in Sec. 6.3, the same traditional notation (\mathbf{p}) for the particle’s momentum as had been used earlier for the electric dipole moment. However, since the latter notion will be virtually unused in the balance of this course, this may hardly lead to confusion.

²⁶ Indeed, such a derivation uses additional assumptions, however natural (such as the Lorentz-invariance of \mathcal{S}), i.e. it can hardly be considered as a real proof of the final results, so that they require experimental confirmation. Fortunately, such confirmations have been numerous – see below.

²⁷ See, e.g., CM Sec. 10.3.

²⁸ See, e.g., CM Sec. 2.1.

²⁹ See, e.g., CM Eq. (2.19b).

³⁰ See, e.g., CM Sec. 2.3, in particular Eq. (2.31).

$$p_j = \frac{\partial \mathcal{L}}{\partial \dot{r}_j} \equiv \frac{\partial \mathcal{L}}{\partial u_j} = -mc^2 \frac{\partial}{\partial u_j} \left(1 - \frac{u_1^2 + u_2^2 + u_3^2}{c^2} \right)^{1/2} = \frac{mu_j}{\left(1 - u^2/c^2 \right)^{1/2}} \equiv m\gamma u_j. \quad (9.69)$$

Thus for the 3D vector of momentum, we can write the result in the same form as in non-relativistic mechanics,

$$\mathbf{p} = m\gamma \mathbf{u} \equiv M\mathbf{u}, \quad (9.70)$$

Relativistic momentum

using the reference-frame-dependent scalar M (called the *relativistic mass*) defined as

$$M \equiv m\gamma = \frac{m}{\left(1 - u^2/c^2 \right)^{1/2}} \geq m, \quad (9.71)$$

Relativistic mass

m being the non-relativistic mass of the particle. (More often, m is called the *rest mass*, because in the reference frame in which the particle rests, Eq. (71) yields $M = m$.)

Next, let us return to analytical mechanics to calculate the particle's energy \mathcal{E} (which for a free particle coincides with its Hamiltonian function \mathcal{H}):³¹

$$\mathcal{E} = \mathcal{H} \equiv \sum_{j=1}^3 p_j u_j - \mathcal{L} = \mathbf{p} \cdot \mathbf{u} - \mathcal{L} = \frac{mu^2}{\left(1 - u^2/c^2 \right)^{1/2}} + mc^2 \left(1 - \frac{u^2}{c^2} \right)^{1/2} \equiv \frac{mc^2}{\left(1 - u^2/c^2 \right)^{1/2}}. \quad (9.72)$$

Thus, we have arrived at the most famous of Einstein's formulas – and probably of physics as a whole:

$$\mathcal{E} = m\gamma c^2 \equiv Mc^2, \quad (9.73)$$

$\mathcal{E} = Mc^2$

which expresses the relation between the free particle's mass and its energy.³² In the non-relativistic limit, it reduces to

$$\mathcal{E} = \frac{mc^2}{\left(1 - u^2/c^2 \right)^{1/2}} \approx mc^2 \left(1 + \frac{u^2}{2c^2} \right) = mc^2 + \frac{mu^2}{2}, \quad (9.74)$$

the first term mc^2 being called the *rest energy* of a particle.

Now let us consider the following string of 4 scalars:

$$\left\{ \frac{\mathcal{E}}{c}, p_1, p_2, p_3 \right\} \equiv \left\{ \frac{\mathcal{E}}{c}, \mathbf{p} \right\}. \quad (9.75)$$

4-vector of energy-momentum

Using Eqs. (70) and (73) to represent this expression as

$$\left\{ \frac{\mathcal{E}}{c}, \mathbf{p} \right\} = m\gamma \{c, \mathbf{u}\}, \quad (9.76)$$

³¹ See, e.g., CM Eq. (2.32).

³² Let me hope that the reader understands that all the layman talk about the “mass to energy conversion” is only valid in a very limited sense of the word. While the Einstein relation (73) does allow the conversion of “massive” particles (with $m \neq 0$) into particles with $m = 0$, such as photons, each of the latter particles also has a non-zero relativistic mass M , and simultaneously the energy \mathcal{E} related to this M by Eq. (73).

and comparing the result with Eq. (63), we immediately see that, since m is a Lorentz-invariant constant, this string is a legitimate 4-vector of *energy-momentum*. As a result, its norm,

$$\left(\frac{\mathcal{E}}{c}\right)^2 - p^2, \quad (9.77a)$$

is Lorentz-invariant, and in particular, has to be equal to the norm in the particle-bound frame. But in that frame, $p = 0$, and according to Eq. (73), $\mathcal{E} = mc^2$, and the norm is just

$$\left(\frac{\mathcal{E}}{c}\right)^2 = \left(\frac{mc^2}{c}\right)^2 \equiv (mc)^2, \quad (9.77b)$$

so that in an arbitrary frame

$$\left(\frac{\mathcal{E}}{c}\right)^2 - p^2 = (mc)^2. \quad (9.78a)$$

This very important relation³³ between the relativistic energy and momentum (valid for free particles only!) is usually represented in the form³⁴

$$\mathcal{E}^2 = (mc^2)^2 + (pc)^2.$$

(9.78b)

According to Eq. (70), in the so-called *ultra-relativistic limit* $u \rightarrow c$, p tends to infinity, while mc^2 stays constant so that $pc/mc^2 \rightarrow \infty$. As follows from Eq. (78), in this limit $\mathcal{E} \approx pc$. Though the above discussion was for particles with finite m , the 4-vector formalism allows us to consider compact objects with zero rest mass as ultra-relativistic particles for which the above energy-to-moment relation,

$$\mathcal{E} = pc, \quad \text{for } m = 0, \quad (9.79)$$

is exact. Quantum electrodynamics³⁵ tells us that under certain conditions, the electromagnetic field quanta (photons) may be also considered as such *massless particles* with momentum $\mathbf{p} = \hbar\mathbf{k}$. Plugging (the modulus of) the last relation into Eq. (78), for the photon's energy we get $\mathcal{E} = pc = \hbar kc = \hbar\omega$. Please note again that according to Eq. (73), the relativistic mass of a photon is not equal to zero: $M = \mathcal{E}/c^2 = \hbar\omega/c^2$, so that the term “massless particle” has a limited meaning: $m = 0$. For example, the relativistic mass of an optical phonon is of the order of 10^{-36} kg. On the human scale, this is not too much, but still a noticeable (approximately one-millionth) part of the rest mass m_e of an electron.

The fundamental relations (70) and (73) have been repeatedly verified in numerous particle collision experiments, in which the total energy and momentum of a system of particles are conserved – at the same conditions as in non-relativistic dynamics. (For the momentum, this is the absence of external forces, and for the energy, the elasticity of particle interactions – in other words, the absence of alternative channels of energy escape.) Of course, generally only the total energy of the system is conserved, including the potential energy of particle interactions. However, at typical high-energy

³³ Please note one more simple and useful relation following from Eqs. (70) and (73): $\mathbf{p} = (\mathcal{E}/c^2)\mathbf{u}$.

³⁴ It may be tempting to interpret this relation as the perpendicular-vector-like addition of the rest energy mc^2 and the “kinetic energy” pc , but from the point of view of the total energy conservation (see below), a better definition of the kinetic energy is $T(u) \equiv \mathcal{E}(u) - \mathcal{E}(0)$.

³⁵ It is briefly reviewed in QM Chapter 9.

particle collisions, the potential energy vanishes so rapidly with the distance between them that we can use the momentum and energy conservation laws using Eq. (73).

As an example, let us calculate the minimum energy \mathcal{E}_{\min} of a proton (p_a), necessary for the well-known high-energy reaction that generates a new proton-antiproton pair, $p_a + p_b \rightarrow p + p + p + \bar{p}$, provided that before the collision, proton p_b had been at rest in the lab frame. This minimum corresponds to the vanishing relative velocity of the reaction products, i.e. their motion with virtually the same velocity (\mathbf{u}_{fin}), as seen from the lab frame – see Fig. 10.

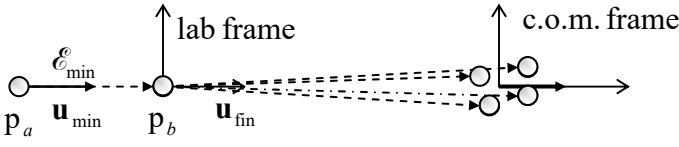


Fig. 9.10. A high-energy proton reaction at $\mathcal{E} \approx \mathcal{E}_{\min}$ – schematically.

Due to the momentum conservation, this velocity should have the same direction as the initial velocity (\mathbf{u}_{\min}) of proton p_a . This is why two scalar equations: for energy conservation,

$$\frac{mc^2}{(1-u_{\min}^2/c^2)^{1/2}} + mc^2 = \frac{4mc^2}{(1-u_{\text{fin}}^2/c^2)^{1/2}}, \quad (9.80a)$$

and for momentum conservation,

$$\frac{mu}{(1-u_{\min}^2/c^2)^{1/2}} + 0 = \frac{4mu_{\text{fin}}}{(1-u_{\text{fin}}^2/c^2)^{1/2}}, \quad (9.80b)$$

are sufficient to find both u_{\min} and u_{fin} . After a rather tedious solution of this system of two nonlinear equations, we get

$$u_{\min} = \frac{4\sqrt{3}}{7}c \approx 0.990c, \quad u_{\text{fin}} = \frac{\sqrt{3}}{2}c \approx 0.866c. \quad (9.81)$$

Finally, we can use Eq. (72) to calculate the required energy; the result is $\mathcal{E}_{\min} = 7mc^2$. (Note that at this threshold, only a minor $2mc^2$ part of the kinetic energy $T_{\min} = \mathcal{E}_{\min} - mc^2 = 6mc^2$ of the initially moving particle, goes into the “useful” proton-antiproton pair production.) The proton’s rest mass, $m_p \approx 1.67 \times 10^{-27}$ kg, corresponds to $m_p c^2 \approx 1.502 \times 10^{-10}$ J ≈ 0.938 GeV, so that $\mathcal{E}_{\min} \approx 6.57$ GeV.

The second, more intelligent way to solve the same problem is to use the center-of-mass (c.o.m.) reference frame that, in relativity, is defined as the frame in which the total momentum of the system vanishes.³⁶ In this frame, at $\mathcal{E} = \mathcal{E}_{\min}$, the velocity and momenta of all reaction products are vanishing, while the velocities of the protons p_a and p_b before the collision are equal and opposite, with an initially unknown magnitude u' . Hence the energy conservation law becomes

$$\frac{2mc^2}{(1-u'^2/c^2)^{1/2}} = 4mc^2, \quad (9.82)$$

³⁶ Note that according to this definition, the c.o.m.’s radius-vector is $\mathbf{R} = \sum_k M_k \mathbf{r}_k / \sum_k M_k \equiv \sum_k \gamma_k m_k \mathbf{r}_k / \sum_k \gamma_k m_k$, i.e. is generally different from the well-known non-relativistic expression $\mathbf{R} = \sum_k m_k \mathbf{r}_k / \sum_k m_k$.

readily giving $u'/c = \sqrt{3}/2$. (This is of course the same result as Eq. (81) gives for $u_{\text{fin.}}$.) Now we can use the fact that the velocity of the proton p_a in the c.o.m. frame is $(-u')$, to find its lab-frame speed, using the velocity transform (25):

$$u_{\min} = \frac{2u'}{1 + u'^2/c^2}. \quad (9.83)$$

With the above result for u' , this relation gives the same result as the first method, $u_{\min}/c = 4\sqrt{3}/7$, but in a simpler way.

9.4. More on 4-vectors and 4-tensors

This is a good moment to introduce a formalism that will allow us, in particular, to solve the same proton collision problem in one more (and arguably, the most elegant) way. Much more importantly, this formalism will be virtually necessary for the description of the Lorentz transform of the electromagnetic field, and its interaction with relativistic particles – otherwise the formulas would be too cumbersome.

Let us call the 4-vectors we have used before,

Contravariant
4-vectors

$$A^\alpha \equiv \{A_0, \mathbf{A}\}, \quad (9.84)$$

contravariant, and denote them with top indices, and introduce also *covariant* vectors,

Covariant
4-vectors

$$A_\alpha \equiv \{A_0, -\mathbf{A}\}, \quad (9.85)$$

marked by bottom indices. Now if we form a scalar product of these two vectors using the *standard* (3D-like) rule, just as a sum of the products of the corresponding components, we immediately get

$$A_\alpha A^\alpha \equiv A^\alpha A_\alpha \equiv A_0^2 - \mathbf{A}^2. \quad (9.86)$$

Here and below the sign of the sum of four components of the product has been dropped.³⁷ The scalar product (86) is just the norm of the 4-vector in our former definition, and as we already know, is Lorentz-invariant. Moreover, the scalar product of two different vectors (also a Lorentz invariant), may be rewritten in any of two similar forms:³⁸

Scalar
product's
forms

$$A_0 B_0 - \mathbf{A} \cdot \mathbf{B} \equiv A_\alpha B^\alpha = A^\alpha B_\alpha; \quad (9.87)$$

again, the only caveat is to take one vector in the covariant, and the other one in the contravariant form.

Now let us return to our sample problem (Fig. 10). Since all components (\mathcal{E}/c and \mathbf{p}) of the total 4-momentum of our system are conserved at the collision, its norm is conserved as well:

$$(p_a + p_b)_\alpha (p_a + p_b)^\alpha = (4p)_\alpha (4p)^\alpha. \quad (9.88)$$

³⁷ This compact notation may take some time to be accustomed to, but is very convenient (compact) and can hardly lead to any confusion, due to the following rule: the summation is implied when (and only when) the same index is repeated twice, once on the top and another at the bottom. In this course, this shorthand notation will be used only for 4-vectors, but not for the usual (3D spatial) vectors.

³⁸ Note also that, by definition, for any two 4-vectors, $A_\alpha B^\alpha = B^\alpha A_\alpha$.

Since now the vector product is the usual math construct, we know that the parentheses on the left-hand side of this equation may be multiplied as usual. We may also swap the operands and move constant factors through products as convenient. As a result, we get

$$(p_a)_\alpha (p_a)^\alpha + (p_b)_\alpha (p_b)^\alpha + 2(p_a)_\alpha (p_b)^\alpha = 16 p_\alpha p^\alpha. \quad (9.89)$$

Thanks to the Lorentz invariance of each of the terms, we may calculate it in the reference frame we like. For the first two terms on the left-hand side, as well as for the right-hand side term, it is beneficial to use the frames in which that particular proton is at rest; as a result, according to Eq. (77b), each of the two left-hand-side terms equals $(mc)^2$, while the right-hand side equals $16(mc)^2$. On the contrary, the last term on the left-hand side is more easily evaluated in the lab frame, because in it, the three spatial components of the 4-momentum p_b vanish, and the scalar product is just the product of the scalars \mathcal{E}/c for protons a and b . For the latter proton, being at rest, this ratio is just mc so that we get a simple equation,

$$(mc)^2 + (mc)^2 + 2 \frac{\mathcal{E}_{\min}}{c} mc = 16(mc)^2, \quad (9.90)$$

immediately giving the final result $\mathcal{E}_{\min} = 7 mc^2$, already obtained earlier in two more complex ways.

Let me hope that this example was a convincing demonstration of the convenience of representing 4-vectors in the contravariant (84) and covariant (85) forms,³⁹ with Lorentz-invariant norms (86). To be useful for more complex tasks, this formalism should be developed a little bit further. In particular, it is crucial to know how the 4-vectors change under the Lorentz transform. For contravariant vectors, we already know the answer (54); let us rewrite it in our new notation:

$$A^\alpha = L_\beta^\alpha A'^\beta. \quad (9.91)$$

where L_β^α is the matrix (51), generally called the *mixed Lorentz tensor*:⁴⁰

$$L_\beta^\alpha = \begin{pmatrix} \gamma & \beta\gamma & 0 & 0 \\ \beta\gamma & \gamma & 0 & 0 \\ 0 & 0 & 1 & 0 \\ 0 & 0 & 0 & 1 \end{pmatrix}, \quad (9.92)$$

Lorentz transform:
contravariant vectors

Mixed Lorentz tensor

Note that though the position of the indices α and β in the Lorentz tensor notation is not crucial, because this tensor is symmetric, it is convenient to place them using the general *index balance rule*: the difference of the numbers of the upper and lower indices should be the same in both parts of any 4-vector/tensor equality. (You may check that all the formulas above do satisfy this rule.)

³⁹ These forms are 4-vector extensions of the notions of contravariance and covariance, introduced in the 1850s by J. Sylvester (who also introduced the term “matrix” in its mathematical sense) for the description of the change of the usual 3-component spatial vectors at the transfer between different reference frames – e.g., resulting from the frame rotation. In this case, the contravariance or covariance of a vector is uniquely determined by its nature: if the Cartesian coordinates of a vector (such as the non-relativistic velocity $\mathbf{v} = d\mathbf{r}/dt$) are transformed similarly to the radius-vector \mathbf{r} , it is called contravariant, while the vectors (such as ∇f) that require the reciprocal transform, are called covariant. In the 4D Minkowski space, both forms may be used for any 4-vector.

⁴⁰ Just as the 4-vectors, 4-tensors with two top indices are called contravariant, and those with two bottom indices, covariant. The tensors with one top and one bottom index are called *mixed*.

In order to rewrite Eq. (91) in a more general form that would not depend on the particular orientation of the coordinate axes (Fig. 1), let us use the contravariant and covariant forms of the 4-vector of the time-space interval (57),

$$dx^\alpha = \{cdt, d\mathbf{r}\}, \quad dx_\alpha = \{cdt, -d\mathbf{r}\}; \quad (9.93)$$

then its norm (58) may be represented as⁴¹

$$(ds)^2 \equiv (cdt)^2 - (dr)^2 = dx^\alpha dx_\alpha = dx_\alpha dx^\alpha. \quad (9.94)$$

Applying Eq. (91) to the first, contravariant form of the 4-vector (93), we get

$$dx^\alpha = L_\beta^\alpha dx'^\beta. \quad (9.95)$$

But with our new shorthand notation, we can also write the usual rule of differentiation of each component x^α , considering it a function (in our case, linear) of four arguments x'^β , as follows:⁴²

$$dx^\alpha = \frac{\partial x^\alpha}{\partial x'^\beta} dx'^\beta. \quad (9.96)$$

Comparing Eqs. (95) and (96), we can rewrite the general Lorentz transform rule (92) in a new form,

Lorentz
transform:
general form

$$A^\alpha = \frac{\partial x^\alpha}{\partial x'^\beta} A'^\beta. \quad (9.97a)$$

which does not depend on the coordinate axes' orientation.

It is straightforward to verify that the reciprocal transform may be represented as

Reciprocal
Lorentz
transform

$$A'^\alpha = \frac{\partial x'^\alpha}{\partial x^\beta} A^\beta. \quad (9.97b)$$

However, the reciprocal transform has to differ from the direct one only by the sign of the relative velocity of the frames, so that for the coordinate choice shown in Fig. 1, its matrix is

⁴¹ Another way to write this relation is $(ds)^2 = g_{\alpha\beta} dx^\alpha dx^\beta = g^{\alpha\beta} dx_\alpha dx_\beta$, where double summation over indices α and β is implied, and g is the so-called *metric tensor*,

$$g^{\alpha\beta} \equiv g_{\alpha\beta} \equiv \begin{pmatrix} 1 & 0 & 0 & 0 \\ 0 & -1 & 0 & 0 \\ 0 & 0 & -1 & 0 \\ 0 & 0 & 0 & -1 \end{pmatrix},$$

which may be used, in particular, to transfer a covariant vector into the corresponding contravariant one and back: $A^\alpha = g^{\alpha\beta} A_\beta$, $A_\alpha = g_{\alpha\beta} A^\beta$. The metric tensor plays a key role in general relativity, in which it is affected by gravity – “curved” by particles’ masses.

⁴² Note that in the index balance rule, the top index in the denominator of a fraction is counted as a bottom index in the numerator, and vice versa.

$$\frac{\partial x'^\alpha}{\partial x^\beta} = \begin{pmatrix} \gamma & -\beta\gamma & 0 & 0 \\ -\beta\gamma & \gamma & 0 & 0 \\ 0 & 0 & 1 & 0 \\ 0 & 0 & 0 & 1 \end{pmatrix}, \quad (9.98)$$

Since according to Eqs. (84)-(85), covariant 4-vectors differ from the contravariant ones by the sign of their spatial components, their direct transform is given by matrix (98). Hence their direct and reciprocal transforms may be represented, respectively, as

$$A_\alpha = \frac{\partial x'^\beta}{\partial x^\alpha} A'_\beta, \quad A'_\alpha = \frac{\partial x^\beta}{\partial x'^\alpha} A_\beta, \quad (9.99)$$

Lorentz
transform:
covariant
vectors

evidently satisfying the index balance rule. (Note that primed quantities are now multiplied, rather than divided as in the contravariant case.) As a sanity check, let us apply this formalism to the scalar product $A_\alpha A^\alpha$. As Eq. (96) shows, the implicit-sum notation allows us to multiply and divide any equality by the same partial differential of a coordinate, so that we can write:

$$A_\alpha A^\alpha = \frac{\partial x'^\beta}{\partial x^\alpha} \frac{\partial x^\alpha}{\partial x'^\gamma} A'_\beta A'^\gamma = \frac{\partial x'^\beta}{\partial x'^\gamma} A'_\beta A'^\gamma = \delta_{\beta\gamma} A'_\beta A'^\gamma = A'_\gamma A'^\gamma, \quad (9.100)$$

i.e. the scalar product $A_\alpha A^\alpha$ (as well as $A^\alpha A_\alpha$) is Lorentz-invariant, as it should be.

Now, let us consider the 4-vectors of derivatives. Here we should be very careful. Consider, for example, the following 4-vector operator

$$\frac{\partial}{\partial x^\alpha} \equiv \left\{ \frac{\partial}{\partial(ct)}, \nabla \right\}, \quad (9.101)$$

As was discussed above, the operator is not changed by its multiplication and division by another differential, e.g., $\partial x'^\beta$ (with the corresponding implied summation over all four values of β), so that

$$\frac{\partial}{\partial x^\alpha} = \frac{\partial x'^\beta}{\partial x^\alpha} \frac{\partial}{\partial x'^\beta}. \quad (9.102)$$

But, according to the first of Eqs. (99), this is exactly how the covariant vectors are Lorentz-transformed! Hence, we have to consider the derivative over a *contravariant* space-time interval as a *covariant* 4-vector, and vice versa.⁴³ (This result might be also expected from the index balance rule.) In particular, this means that the scalar product

$$\frac{\partial}{\partial x^\alpha} A^\alpha \equiv \frac{\partial A_0}{\partial(ct)} + \nabla \cdot \mathbf{A} \quad (9.103)$$

should be Lorentz-invariant for any legitimate 4-vector. A convenient shorthand for the covariant derivative, which complies with the index balance rule, is

$$\frac{\partial}{\partial x^\alpha} \equiv \partial_\alpha, \quad (9.104)$$

⁴³ As was mentioned above, this is also a property of the reference-frame transform of the “usual” 3D vectors.

so that the invariant scalar product may be written just as $\partial_\alpha A^\alpha$. A similar definition of the contravariant derivative,

$$\partial^\alpha \equiv \frac{\partial}{\partial x_\alpha} = \left\{ \frac{\partial}{\partial(ct)}, -\nabla \right\}, \quad (9.105)$$

allows us to write the Lorentz-invariant scalar product (103) in any of the following two forms:

$$\frac{\partial A_0}{\partial(ct)} + \nabla \cdot \mathbf{A} = \partial^\alpha A_\alpha = \partial_\alpha A^\alpha. \quad (9.106)$$

Finally, let us see how the general Lorentz transform changes 4-tensors. A second-rank 4×4 matrix is a legitimate 4-tensor if the 4-vectors it relates obey the Lorentz transform. For example, if two legitimate 4-vectors are related as

$$A^\alpha = T^{\alpha\beta} B_\beta, \quad (9.107)$$

we should require that

$$A'^\alpha = T'^{\alpha\beta} B'_\beta, \quad (9.108)$$

where A^α and A'^α are related by Eqs. (97), while B_β and B'_β , by Eqs. (99). This requirement immediately yields

$$T^{\alpha\beta} = \frac{\partial x^\alpha}{\partial x'^\gamma} \frac{\partial x'^\beta}{\partial x^\delta} T'^{\gamma\delta}, \quad T'^{\alpha\beta} = \frac{\partial x'^\alpha}{\partial x^\gamma} \frac{\partial x^\beta}{\partial x'^\delta} T^{\gamma\delta}, \quad (9.109)$$

Lorentz
transform
of 4-tensors

with the implied summation over two indices, γ and δ . The rules for the covariant and mixed tensors are similar.⁴⁴

9.5. Maxwell equations in the 4-form

This 4-vector formalism background is sufficient to analyze the Lorentz transform of the electromagnetic field. Just to warm up, let us consider the continuity equation (4.5),

$$\frac{\partial \rho}{\partial t} + \nabla \cdot \mathbf{j} = 0, \quad (9.110)$$

which expresses the electric charge conservation, and as we already know, is compatible with the Maxwell equations. If we now define the contravariant and covariant 4-vectors of electric current as

$$j^\alpha \equiv \{\rho c, \mathbf{j}\}, \quad j_\alpha \equiv \{\rho c, -\mathbf{j}\}, \quad (9.111)$$

then Eq. (110) may be represented in the form

$$\partial^\alpha j_\alpha = \partial_\alpha j^\alpha = 0, \quad (9.112)$$

showing that the continuity equation is *form-invariant*⁴⁵ with respect to the Lorentz transform.

4-vector
of electric
current

Continuity
equation:
4-form

⁴⁴ It is straightforward to check that transfer between the contravariant and covariant forms of the same tensor may be readily achieved using the metric tensor g : $T_{\alpha\beta} = g_{\alpha\gamma} T^{\gamma\delta} g_{\delta\beta}$, $T^{\alpha\beta} = g^{\alpha\gamma} T_{\gamma\delta} g^{\delta\beta}$.

⁴⁵ In some texts, the formulas preserving their form at a transform are called “covariant”, creating a possibility for confusion with the covariant vectors and tensors. On the other hand, calling such formulas “invariant” would not distinguish them properly from invariant *quantities*, such as the scalar products of 4-vectors.

Of course, such a form-invariance of a relation does not mean that all component *values* of the 4-vectors participating in it are the same in both frames. For example, let us have some static charge density ρ in frame 0; then Eq. (97b), applied to the contravariant form of the 4-vector (111), reads

$$j'^\alpha = \frac{\partial x'^\alpha}{\partial x^\beta} j^\beta, \quad \text{with } j^\beta = \{\rho c, 0, 0, 0\}. \quad (9.113)$$

Using the particular form (98) of the reciprocal Lorentz matrix for the coordinate choice shown in Fig. 1, we see that this relation yields

$$\rho' = \gamma\rho, \quad j'_x = -\gamma\beta\rho c = -\gamma\rho, \quad j'_y = j'_z = 0. \quad (9.114)$$

Lorentz transforms of ρ and \mathbf{j}

Since the charge velocity, as observed from frame 0', is $(-\mathbf{v})$, the non-relativistic results would be $\rho' = \rho$, $\mathbf{j}' = -\mathbf{v}\rho$. The additional γ factor in the relativistic results is caused by the length contraction: $dx' = dx/\gamma$, so that to keep the total charge $dQ = \rho d^3r = \rho dx dy dz$ inside the elementary volume $d^3r = dx dy dz$ intact, ρ (and hence j_x) should increase proportionally.

Next, at the end of Chapter 6 we have seen that Maxwell equations for the electromagnetic potentials ϕ and \mathbf{A} may be represented in similar forms (6.118), under the Lorenz (again, not “Lorentz”, please!) gauge condition (6.117). For free space, this condition takes the form

$$\nabla \cdot \mathbf{A} + \frac{1}{c^2} \frac{\partial \phi}{\partial t} = 0. \quad (9.115)$$

This expression gives us a hint of how to form the 4-vector of electromagnetic potentials:⁴⁶

$$A^\alpha \equiv \left\{ \frac{\phi}{c}, \mathbf{A} \right\}, \quad A_\alpha \equiv \left\{ \frac{\phi}{c}, -\mathbf{A} \right\}; \quad (9.116)$$

4-vector of potentials

indeed, this vector satisfies Eq. (115) in its 4-form:

$$\partial^\alpha A_\alpha = \partial_\alpha A^\alpha = 0. \quad (9.117)$$

Lorenz gauge: 4-form

Since this scalar product is Lorentz-invariant, and the derivatives (104)-(105) are legitimate 4-vectors, this implies that the 4-vector (116) is also legitimate, i.e. obeys the Lorentz transform formulas (97), (99). Even more convincing evidence of this fact may be obtained from the Maxwell equations (6.118) for the potentials. In free space, they may be rewritten as

$$\left[\frac{\partial^2}{\partial(ct)^2} - \nabla^2 \right] \frac{\phi}{c} = \frac{\rho c}{\epsilon_0 c^2} \equiv \mu_0 (\rho c), \quad \left[\frac{\partial^2}{\partial(ct)^2} - \nabla^2 \right] \mathbf{A} = \mu_0 \mathbf{j}. \quad (9.118)$$

Using the definition (116), these equations may be merged to one:⁴⁷

$$\square A^\alpha = \mu_0 j^\alpha, \quad (9.119)$$

Maxwell equation for 4-potential

where \square is the *d'Alembert operator*,⁴⁸ which may be represented as either of two scalar products,

⁴⁶ In the Gaussian units, the scalar potential should not be divided by c in this relation.

⁴⁷ In the Gaussian units, the coefficient μ_0 in Eq. (119) should be replaced, as usual, with $4\pi/c$.

D'Alembert operator

$$\square \equiv \frac{\partial^2}{\partial(ct)^2} - \nabla^2 = \partial^\beta \partial_\beta = \partial_\beta \partial^\beta. \quad (9.120)$$

and hence is Lorentz-invariant. Because of that, and the fact that the Lorentz transform changes both 4-vectors A^α and j^α in a similar way, Eq. (119) does not depend on the reference frame choice. Thus we have arrived at a key point of this chapter: we see that the Maxwell equations are indeed form-invariant with respect to the Lorentz transform. As a by-product, the 4-vector form (119) of these equations (for potentials) is extremely simple – and beautiful!

However, as we have seen in Chapter 7, for many applications the Maxwell equations for the field vectors are more convenient; so let us represent them in the 4-form as well. For that, we may express all Cartesian components of the usual (3D) field vector vectors (6.7),

$$\mathbf{E} = -\nabla\phi - \frac{\partial\mathbf{A}}{\partial t}, \quad \mathbf{B} = \nabla \times \mathbf{A}, \quad (9.121)$$

via those of the potential 4-vector A^α . For example,

$$E_x = -\frac{\partial\phi}{\partial x} - \frac{\partial A_x}{\partial t} \equiv -c\left(\frac{\partial\phi}{\partial x} + \frac{\partial A_x}{\partial(ct)}\right) \equiv -c(\partial^0 A^1 - \partial^1 A^0), \quad (9.122)$$

$$B_x = \frac{\partial A_z}{\partial y} - \frac{\partial A_y}{\partial z} \equiv -(\partial^2 A^3 - \partial^3 A^2). \quad (9.123)$$

Completing similar calculations for other field components (or just generating them by appropriate index shifts), we find that the following antisymmetric, contravariant *field-strength tensor*,

$$F^{\alpha\beta} \equiv \partial^\alpha A^\beta - \partial^\beta A^\alpha, \quad (9.124)$$

may be expressed via the field components as follows:⁴⁹

Field-strength tensors

$$F^{\alpha\beta} = \begin{pmatrix} 0 & -E_x/c & -E_y/c & -E_z/c \\ E_x/c & 0 & -B_z & B_y \\ E_y/c & B_z & 0 & -B_x \\ E_z/c & -B_y & B_x & 0 \end{pmatrix}, \quad (9.125a)$$

so that the covariant form of the tensor is

$$F_{\alpha\beta} \equiv g_{\alpha\gamma} F^{\gamma\delta} g_{\delta\beta} = \begin{pmatrix} 0 & E_x/c & E_y/c & E_z/c \\ -E_x/c & 0 & -B_z & B_y \\ -E_y/c & B_z & 0 & -B_x \\ -E_z/c & -B_y & B_x & 0 \end{pmatrix}. \quad (9.125b)$$

⁴⁸ Named after Jean-Baptiste le Rond d'Alembert (1717-1783), who has made several pioneering contributions to the general theory of waves – see, e.g., CM Chapter 6. (Some older textbooks use notation \square^2 for this operator.)

⁴⁹ In Gaussian units, this formula, as well as Eq. (131) for $G^{\alpha\beta}$, do not have the factor c in all the denominators.

If Eq. (124) looks a bit too bulky, please note that as a reward, the pair of *inhomogeneous* Maxwell equations, i.e. two equations of the system (6.99), which in free space ($\mathbf{D} = \epsilon_0 \mathbf{E}$, $\mathbf{B} = \mu_0 \mathbf{H}$) may be rewritten as

$$\nabla \cdot \frac{\mathbf{E}}{c} = \mu_0 c \rho, \quad \nabla \times \mathbf{B} - \frac{\partial}{\partial(ct)} \frac{\mathbf{E}}{c} = \mu_0 \mathbf{j}, \quad (9.126)$$

may now be expressed in a very simple (and manifestly form-invariant) way,

$$\boxed{\partial_\alpha F^{\alpha\beta} = \mu_0 j^\beta}, \quad (9.127)$$

Maxwell equation for tensor F

which is comparable with Eq. (119) in its simplicity – and beauty. Somewhat counter-intuitively, the pair of *homogeneous* Maxwell equations of the system (6.99),

$$\nabla \times \mathbf{E} + \frac{\partial \mathbf{B}}{\partial t} = 0, \quad \nabla \cdot \mathbf{B} = 0, \quad (9.128)$$

look, in the 4-vector notation, a bit more complicated:⁵⁰

$$\boxed{\partial_\alpha F_{\beta\gamma} + \partial_\beta F_{\gamma\alpha} + \partial_\gamma F_{\alpha\beta} = 0}. \quad (9.129)$$

Note, however, that Eqs. (128) may be also represented in a much simpler 4-form,

$$\partial_\alpha G^{\alpha\beta} = 0, \quad (9.130)$$

using the so-called *dual tensor*

$$G^{\alpha\beta} = \begin{pmatrix} 0 & B_x & B_y & B_z \\ -B_x & 0 & -E_z/c & E_y/c \\ -B_y & E_z/c & 0 & -E_x/c \\ -B_z & -E_y/c & E_x/c & 0 \end{pmatrix}, \quad (9.131)$$

which may be obtained from $F^{\alpha\beta}$, given by Eq. (125a), by the following replacements:

$$\frac{\mathbf{E}}{c} \rightarrow -\mathbf{B}, \quad \mathbf{B} \rightarrow \frac{\mathbf{E}}{c}. \quad (9.132)$$

Besides the proof of the form-invariance of the Maxwell equations with respect to the Lorentz transform, the 4-vector formalism allows us to achieve our initial goal: to find out how the electric and magnetic field components change at the transfer between two (inertial!) reference frames. For that, let us apply to the tensor $F^{\alpha\beta}$ the reciprocal Lorentz transform described by the second of Eqs. (109). Generally, it gives, for each field component, a sum of 16 terms, but since (for our choice of coordinates, shown in Fig. 1) there are many zeros in the Lorentz transform matrix, and the diagonal components of $F^{\gamma\delta}$ equal zero as well, the calculations are rather doable. Let us calculate, for example, $E'_x \equiv -cF^{01}$. The only non-zero terms on the right-hand side are

$$E'_x = -cF^{01} = -c \left(\frac{\partial x'^0}{\partial x^1} \frac{\partial x'^1}{\partial x^0} F^{10} + \frac{\partial x'^0}{\partial x^0} \frac{\partial x'^1}{\partial x^1} F^{01} \right) \equiv -c\gamma^2 (\beta^2 - 1) \frac{E_x}{c} \equiv E_x. \quad (9.133)$$

⁵⁰ To be fair, note that just as Eq. (127), Eq. (129) this is also a set of four scalar equations – in the latter case with the indices α , β , and γ taking any three *different* values of the set {0, 1, 2, 3}.

Repeating the calculation for the other five components of the fields, we get very important relations

$$\begin{aligned} E'_x &= E_x, & B'_x &= B_x, \\ E'_y &= \gamma(E_y - vB_z), & B'_y &= \gamma(B_y + vE_z / c^2), \\ E'_z &= \gamma(E_z + vB_y), & B'_z &= \gamma(B_z - vE_y / c^2), \end{aligned} \quad (9.134)$$

whose more compact “semi-vector” form is

$$\boxed{\begin{aligned} E'_{||} &= E_{||}, & B'_{||} &= B_{||}, \\ \mathbf{E}'_{\perp} &= \gamma(\mathbf{E} + \mathbf{v} \times \mathbf{B})_{\perp}, & \mathbf{B}'_{\perp} &= \gamma(\mathbf{B} - \mathbf{v} \times \mathbf{E} / c^2)_{\perp}, \end{aligned}} \quad (9.135)$$

Lorentz
transform
of field
components

where the indices $||$ and \perp stand, respectively, for the field components parallel and normal to the relative velocity \mathbf{v} of the two reference frames. In the non-relativistic limit, the Lorentz factor γ tends to 1, and Eqs. (135) acquire an even simpler form

$$\mathbf{E}' \rightarrow \mathbf{E} + \mathbf{v} \times \mathbf{B}, \quad \mathbf{B}' \rightarrow \mathbf{B} - \frac{1}{c^2} \mathbf{v} \times \mathbf{E}. \quad (9.136)$$

Thus we see that the electric and magnetic fields are transformed to each other even in the first order of the v/c ratio. For example, if we fly across the field lines of a uniform, static, purely electric field \mathbf{E} (e.g., the one in a plane capacitor) we will see not only the electric field’s renormalization (in the second order of the v/c ratio), but also a non-zero dc magnetic field \mathbf{B}' perpendicular to both the vector \mathbf{E} and the vector \mathbf{v} , i.e. to the direction of our motion. This is of course what might be expected from the relativity principle: from the point of view of the moving observer (which is as legitimate as that of a stationary observer), the surface charges of the capacitor’s plates, that create the field \mathbf{E} , move back creating the dc currents (114), which induce the magnetic field \mathbf{B}' . Similarly, motion across a magnetic field creates, from the point of view of the moving observer, an electric field.

This fact is very important conceptually. One may say there is no such thing in Mother Nature as an electric field (or a magnetic field) all by itself. Not only can the electric field induce the magnetic field (and vice versa) in dynamics, but even in an apparently static configuration, what exactly we measure depends on our speed relative to the field sources – justifying once again the term *electromagnetism* for the field of physics we are studying in this course.

Another simple but very important application of Eqs. (134)-(135) is the calculation of the fields created by a charged particle moving in free space by inertia, i.e. along a straight line with constant velocity \mathbf{u} , at the *impact parameter*⁵¹ (the closest distance) b from the observer. Selecting the reference frame $0'$ to move with the particle in its origin, and the reference frame 0 to reside in the “lab” in which the fields \mathbf{E} and \mathbf{B} are measured, we can use the above formulas with $\mathbf{v} = \mathbf{u}$. In this case, the fields \mathbf{E}' and \mathbf{B}' may be calculated from, respectively, electro- and magnetostatics:

$$\mathbf{E}' = \frac{q}{4\pi\epsilon_0 r'^3} \frac{\mathbf{r}'}{r'^3}, \quad \mathbf{B}' = 0, \quad (9.137)$$

because in frame $0'$, the particle does not move. Selecting the coordinate axes so that at the measurement point, $x = 0$, $y = b$, $z = 0$ (Fig. 11a), for this point we may write $x' = -ut'$, $y' = b$, $z' = 0$, so that $r' = (u^2 t'^2 + b^2)^{1/2}$, and the Cartesian components of the fields (137) are:

⁵¹ This term is very popular in the theory of particle scattering – see, e.g., CM Sec. 3.7.

$$E'_x = -\frac{q}{4\pi\epsilon_0} \frac{ut'}{(u^2 t'^2 + b^2)^{3/2}}, \quad E'_y = \frac{q}{4\pi\epsilon_0} \frac{b}{(u^2 t'^2 + b^2)^{3/2}}, \quad E'_z = 0, \quad (9.138)$$

$$B'_x = B'_y = B'_z = 0.$$

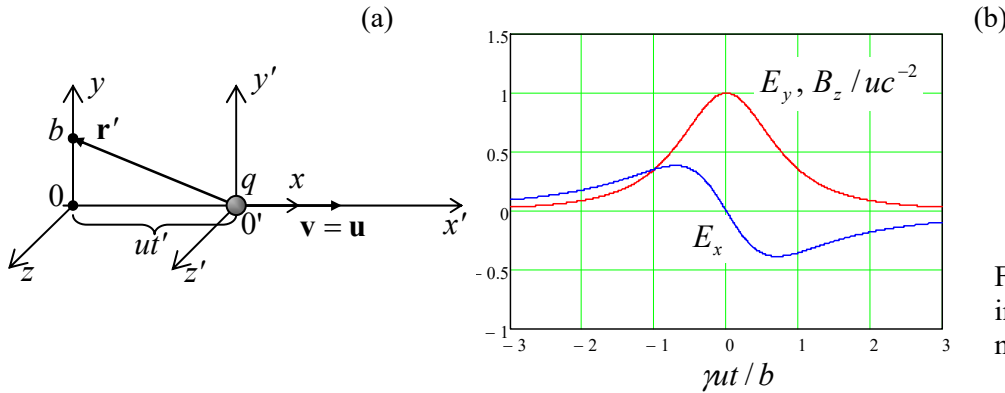


Fig. 9.11. The field pulses induced by a uniformly moving charge.

Now using the last of Eqs. (19b) with $x = 0$, giving $t' = \gamma t$, and the relations reciprocal to Eqs. (134) for the field transform (they are similar to the direct transform but with v replaced with $-v = -u$), in the lab frame we get

$$E_x = E'_x = -\frac{q}{4\pi\epsilon_0} \frac{u\gamma t}{(u^2 \gamma^2 t^2 + b^2)^{3/2}}, \quad E_y = \gamma E'_y = \frac{q}{4\pi\epsilon_0} \frac{\gamma b}{(u^2 \gamma^2 t^2 + b^2)^{3/2}}, \quad E_z = 0, \quad (9.139)$$

$$B_x = 0, \quad B_y = 0, \quad B_z = \frac{\mu}{c^2} E'_y = \frac{u}{c^2} \frac{q}{4\pi\epsilon_0} \frac{\gamma b}{(u^2 \gamma^2 t^2 + b^2)^{3/2}} \equiv \frac{u}{c^2} E_y. \quad (9.140)$$

These results,⁵² plotted in Fig. 11b in the units of $\gamma q^2 / 4\pi\epsilon_0 b^2$, reveal two major effects. First, the charge passage by the observer generates not only an electric field pulse but also a magnetic field pulse. This is natural, because, as was repeatedly discussed in Chapter 5, any charge motion is essentially an electric current.⁵³ Second, Eqs. (139)-(140) show that the pulse duration scale is

$$\Delta t = \frac{b}{\gamma u} \equiv \frac{b}{u} \left(1 - \frac{u^2}{c^2}\right)^{1/2}, \quad (9.141)$$

i.e. shrinks to virtually zero as the charge's velocity u approaches the speed of light. This is of course a direct corollary of the relativistic length contraction. Indeed, in the frame $0'$ moving with the charge, the longitudinal spread of its electric field at distance b from the motion line is of the order of $\Delta x' = b$. When observed from the lab frame 0 , this interval, in accordance with Eq. (20), shrinks to $\Delta x = \Delta x' / \gamma = b/\gamma$, and hence so does the pulse duration scale $\Delta t = \Delta x/u = b/\gamma u$.

⁵² In the next chapter, we will re-derive them in a different way.

⁵³ It is straightforward to use Eqs. (140) and the linear superposition principle to calculate, for example, the magnetic field of a string of charges moving along the same line and separated by equal distances $\Delta x = a$ (so that the average current, as measured in frame 0 , is qu/a), and to show that the time-average of the magnetic field is given by the familiar Eq. (5.20) of magnetostatics, with b instead of ρ .

9.6. Relativistic particles in electric and magnetic fields

Now let us analyze the dynamics of charged particles in electric and magnetic fields. Inspired by “our” success in forming the 4-vector (75) of energy-momentum, with the contravariant form

$$p^\alpha = \left\{ \frac{\mathcal{E}}{c}, \mathbf{p} \right\} = \gamma \{mc, \mathbf{p}\} = m \frac{dx^\alpha}{d\tau} \equiv mu^\alpha, \quad (9.142)$$

where u^α is the contravariant form of the 4-velocity (63) of the particle,

$$u^\alpha \equiv \frac{dx^\alpha}{d\tau}, \quad u_\alpha \equiv \frac{dx_\alpha}{d\tau}, \quad (9.143)$$

we may notice that the non-relativistic equation of motion, resulting from the Lorentz-force formula (5.10) for the three spatial components of p^α , for a charged particle’s motion in an electromagnetic field,

$$\boxed{\frac{d\mathbf{p}}{dt} = q(\mathbf{E} + \mathbf{u} \times \mathbf{B})}, \quad (9.144)$$

is fully consistent with the following 4-vector equality (which is evidently form-invariant with respect to the Lorentz transform):

$$\boxed{\frac{dp^\alpha}{d\tau} = qF^{\alpha\beta}u_\beta}. \quad (9.145)$$

For example, according to Eq. (125), the $\alpha = 1$ component of this equation reads

$$\frac{dp^1}{d\tau} = qF^{1\beta}u_\beta = q \left[\frac{E_x}{c} \gamma c + 0 \cdot (-\gamma u_x) + (-B_z)(-\gamma u_y) + B_y(-\gamma u_z) \right] = q\gamma [\mathbf{E} + \mathbf{u} \times \mathbf{B}]_x, \quad (9.146)$$

and similarly for two other spatial components ($\alpha = 2$ and $\alpha = 3$). It may look that these expressions differ from the 2nd Newton law (144) by an extra factor of γ . However, plugging into Eq. (146) the definition of the proper time interval, $d\tau = dt/\gamma$, and canceling γ in both parts, we recover Eq. (144) exactly – for *any* velocity of the particle! The only caveat is that if u is comparable with c , the vector \mathbf{p} in Eq. (144) has to be understood as the relativistic momentum (70), proportional to the velocity-dependent mass $M = \gamma m \geq m$ rather than to the rest mass m .

The only remaining general task is to examine the meaning of the 0th component of Eq. (145). Let us spell it out:

$$\frac{dp^0}{d\tau} = qF^{0\beta}u_\beta = q \left[0 \cdot \gamma c + \left(-\frac{E_x}{c} \right) (-\gamma u_x) + \left(-\frac{E_y}{c} \right) (-\gamma u_y) + \left(-\frac{E_z}{c} \right) (-\gamma u_z) \right] = q\gamma \frac{\mathbf{E}}{c} \cdot \mathbf{u}. \quad (9.147)$$

Recalling that $p^0 = \mathcal{E}/c$, and using the basic relation $d\tau = dt/\gamma$ again, we see that Eq. (147) looks exactly like the non-relativistic relation for the kinetic energy change (what is sometimes called the *work-energy principle*, in our case for the Lorentz force only⁵⁴):

⁵⁴ See, e.g., CM Eq. (1.20) divided by dt , and with $d\mathbf{p}/dt = \mathbf{F} = q\mathbf{E}$. (As a reminder, the magnetic field cannot affect the particle’s energy, because the magnetic component of the Lorentz force is perpendicular to its velocity.)

$$\boxed{\frac{d\mathcal{E}}{dt} = q\mathbf{E} \cdot \mathbf{u},} \quad (9.148)$$
Particle's
energy:
evolution

besides that in the relativistic case, the energy has to be taken in the general form (73).

Without question, the 4-component equation (145) of the relativistic dynamics is absolutely beautiful in its simplicity. However, for the solution of particular problems, Eqs. (144) and (148) are frequently more convenient. As an illustration of this point, let us now use these equations to explore relativistic effects at charged particle motion in uniform, time-independent electric and magnetic fields. In doing that, we will, for the time being, neglect the contributions into the field by the particle itself.⁵⁵

(i) Uniform magnetic field. Let the magnetic field be constant and uniform in the “lab” reference frame 0 that is used for measurements. Then in this frame, Eqs. (144) and (148) yield

$$\frac{d\mathbf{p}}{dt} = q\mathbf{u} \times \mathbf{B}, \quad \frac{d\mathcal{E}}{dt} = 0. \quad (9.149)$$

From the second equation, $\mathcal{E} = \text{const}$, we get $u = \text{const}$, $\beta \equiv u/c = \text{const}$, $\gamma \equiv (1 - \beta^2)^{-1/2} = \text{const}$, and $M \equiv \gamma m = \text{const}$, so that the first of Eqs. (149) may be rewritten as

$$\frac{d\mathbf{u}}{dt} = \mathbf{u} \times \boldsymbol{\omega}_c, \quad (9.150)$$

where $\boldsymbol{\omega}_c$ is the vector directed along the magnetic field \mathbf{B} , with the magnitude equal to the following *cyclotron frequency* (sometimes called “gyrofrequency”):

$$\boxed{\boldsymbol{\omega}_c \equiv \frac{qB}{M} = \frac{qB}{\gamma m} = \frac{qc^2 B}{\mathcal{E}}.} \quad (9.151)$$
Cyclotron
frequency

If the particle’s initial velocity \mathbf{u}_0 is perpendicular to the magnetic field, Eq. (150) describes its circular motion, with a constant speed $u = u_0$, in a plane normal to \mathbf{B} , with the angular velocity (151). In the non-relativistic limit $u \ll c$, when $\gamma \rightarrow 1$, i.e. $M \rightarrow m$, the cyclotron frequency $\boldsymbol{\omega}_c$ equals qB/m , i.e. is independent of the speed. However, as the kinetic energy of the particle is increased to become comparable with its rest energy mc^2 , the frequency decreases, and in the ultra-relativistic limit,

$$\boldsymbol{\omega}_c \approx qc \frac{B}{p} \ll \frac{qB}{m}, \quad \text{for } u \approx c. \quad (9.152)$$

The cyclotron motion’s radius may be calculated as $R = u/\boldsymbol{\omega}_c$; in the non-relativistic limit, it is proportional to the particle’s speed, i.e. to the square root of its kinetic energy. However, as Eq. (151) shows, in the general case the radius is proportional to the particle’s relativistic momentum rather than its speed:

$$\boxed{R = \frac{u}{\boldsymbol{\omega}_c} = \frac{Mu}{qB} = \frac{m\gamma u}{qB} = \frac{1}{q} \frac{p}{B},} \quad (9.153)$$
Cyclotron
radius

so that in the ultra-relativistic limit, when $p \approx \mathcal{E}/c$, R is proportional to the kinetic energy.

⁵⁵ As was emphasized earlier in this course, in statics this contribution is formally infinite and has to be ignored. In dynamics, this is generally not true; these *self-action effects* (which are, in most cases, negligible) will be discussed in the next chapter.

These dependencies of ω_c and R on energy are the major factors in the design of circular accelerators of charged particles. In the simplest of these machines (the *cyclotron*, invented in 1929 by Ernest Orlando Lawrence), the frequency ω of the accelerating ac electric field is constant, so that even if it is tuned to the ω_c of the initially injected particles, the drop of the cyclotron frequency with energy eventually violates this tuning. Due to this reason, the largest achievable particle's speed is limited to just $\sim 0.1 c$ (for protons, corresponding to the kinetic energy of just ~ 15 MeV). This problem may be addressed in several ways. In particular, in *synchrotrons* (such as Fermilab's Tevatron and the CERN's Large Hadron Collider, LHC⁵⁶) the magnetic field is gradually increased in time to compensate for the momentum increase ($B \propto p$), so that both R (148) and ω_c (147) stay constant, enabling proton acceleration to energies as high as ~ 7 TeV, i.e. $\sim 2,000 mc^2$ ⁵⁷.

Returning to our initial problem, if the particle's initial velocity has a component u_{\parallel} along the magnetic field, then it is conserved in time, so that the trajectory is a spiral around the magnetic field lines. As Eqs. (149) show, in this case, Eq. (150) remains valid but in Eqs. (151) and (153) the full speed and momentum have to be replaced with magnitudes of their (also time-conserved) components, u_{\perp} and p_{\perp} , normal to \mathbf{B} , while the Lorentz factor γ in those formulas still includes the full speed of the particle.

Finally, in the special case when the particle's initial velocity is directed *exactly* along the magnetic field's direction, it continues to move straight along the vector \mathbf{B} . In this case, the cyclotron frequency still has the non-zero value (151) but does not correspond to any real motion, because $R = 0$.

(ii) Uniform electric field. This problem is (technically) more complex than the previous one because in the electric field, the particle's energy changes. Directing the z -axis along the field \mathbf{E} , from Eq. (144) we get

$$\frac{dp_z}{dt} = qE, \quad \frac{d\mathbf{p}_{\perp}}{dt} = 0. \quad (9.154)$$

If E does not change in time, the first integration of these equations is elementary,

$$p_z(t) = p_z(0) + qEt, \quad \mathbf{p}_{\perp}(t) = \text{const} = \mathbf{p}_{\perp}(0), \quad (9.155)$$

but the further integration requires care because the effective mass $M = \gamma m$ of the particle depends on its full speed u , with

$$u^2 = u_z^2 + u_{\perp}^2, \quad (9.156)$$

making the two motions, along and across the field, mutually dependent.

If the initial velocity is perpendicular to the field \mathbf{E} , i.e. if $p_z(0) = 0$, $p_{\perp}(0) = p(0) \equiv p_0$, the easiest way to proceed is to calculate the kinetic energy first:

$$\mathcal{E}^2 = (mc^2)^2 + c^2 p^2(t) \equiv \mathcal{E}_0^2 + c^2 (qEt)^2, \quad \text{where } \mathcal{E}_0 \equiv [(mc^2)^2 + c^2 p_0^2]^{1/2}. \quad (9.157)$$

On the other hand, we can calculate the same energy by integrating Eq. (148),

⁵⁶ See <https://home.cern/topics/large-hadron-collider>.

⁵⁷ I am sorry I have no more time/space to discuss particle accelerator physics, and have to refer the interested reader to special literature, for example, either S. Lee, *Accelerator Physics*, 2nd ed., World Scientific, 2004, or E. Wilson, *An Introduction to Particle Accelerators*, Oxford U. Press, 2001.

$$\frac{d\mathcal{E}}{dt} = q\mathbf{E} \cdot \mathbf{u} \equiv qE \frac{dz}{dt}, \quad (9.158)$$

over time, with a simple result:

$$\mathcal{E} = \mathcal{E}_0 + qEz(t), \quad (9.159)$$

where (just for the notation simplicity) I took $z(0) = 0$. Requiring Eq. (159) to give the same \mathcal{E}^2 as Eq. (157), we get a quadratic equation for the function $z(t)$,

$$\mathcal{E}_0^2 + c^2(qEt)^2 = [\mathcal{E}_0 + qEz(t)]^2, \quad (9.160)$$

whose solution (with the sign before the square root corresponding to $E > 0$, i.e. to $z \geq 0$) is

$$z(t) = \frac{\mathcal{E}_0}{qE} \left\{ \left[1 + \left(\frac{cqEt}{\mathcal{E}_0} \right)^2 \right]^{1/2} - 1 \right\}. \quad (9.161)$$

Now let us find the particle's trajectory. Directing the x -axis so that the initial velocity vector (and hence the velocity vector at any further instant) is within the $[x, z]$ plane, i.e. that $y(t) = 0$ identically, we may use Eqs. (155) to calculate the trajectory's slope, at its arbitrary point, as

$$\frac{dz}{dx} \equiv \frac{dz/dt}{dx/dt} \equiv \frac{Mu_z}{Mu_x} \equiv \frac{p_z}{p_x} = \frac{qEt}{p_0}. \quad (9.162)$$

Now let us use Eq. (160) to express the numerator of this fraction, qEt , as a function of z :

$$qEt = \frac{1}{c} [(\mathcal{E}_0 + qEz)^2 - \mathcal{E}_0^2]^{1/2}. \quad (9.163)$$

Plugging this expression into Eq. (161), we get

$$\frac{dz}{dx} = \frac{1}{cp_0} [(\mathcal{E}_0 + qEz)^2 - \mathcal{E}_0^2]^{1/2}. \quad (9.164)$$

This differential equation may be readily integrated separating the variables z and x , and using the following substitution: $\xi \equiv \cosh^{-1}(qEz/\mathcal{E}_0 + 1)$. Selecting the origin of axis x at the initial point, so that $x(0) = 0$, we finally get the trajectory:

$$z = \frac{\mathcal{E}_0}{qE} \left(\cosh \frac{qEx}{cp_0} - 1 \right). \quad (9.165)$$

This curve is usually called the *catenary*, but sometimes the “chainette”, because it (with the proper constant replacement) describes, in particular, the stationary shape of a heavy, uniform chain in a uniform gravity field directed along the z -axis. At the initial part of the trajectory, where $qEx \ll cp_0(0)$, this expression may be approximated with the first non-zero term of its Taylor expansion in small x , giving the following parabola:

$$z = \frac{\mathcal{E}_0 q E}{2} \left(\frac{x}{cp_0} \right)^2, \quad (9.166)$$

so that if the initial velocity of the particle is much lower than c (i.e. $p_0 \approx mu_0$, $\mathcal{E}_0 \approx mc^2$), we get the very familiar non-relativistic formula:

$$z = \frac{qE}{2mu_0^2} x^2 \equiv \frac{a}{2} t^2, \quad \text{with } a = \frac{F}{m} = \frac{qE}{m}. \quad (9.167)$$

The generalization of this solution to the case of an arbitrary direction of the particle's initial velocity is left for the reader's exercise.

(iii) Crossed uniform magnetic and electric fields ($\mathbf{E} \perp \mathbf{B}$). In view of the somewhat bulky solution of the previous problem (i.e. the particular case of the current problem for $\mathbf{B} = 0$), one might think that this problem, with $\mathbf{B} \neq 0$, should be forbiddingly complex for an analytical solution. Counter-intuitively, this is not the case, due to the help from the field transform relations (135). Let us consider two possible cases.

Case 1: $E/c < B$. Let us consider an inertial reference frame $0'$ moving (relatively the "lab" reference frame 0 in that the fields \mathbf{E} and \mathbf{B} are measured) with the following velocity:

$$\mathbf{v} = \frac{\mathbf{E} \times \mathbf{B}}{B^2}, \quad (9.168)$$

and hence the speed $v = c(E/c)/B < c$. Selecting the coordinate axes as shown in Fig. 12, so that

$$E_x = 0, \quad E_y = E, \quad E_z = 0; \quad B_x = 0, \quad B_y = 0, \quad B_z = B, \quad (9.169)$$

we see that the Cartesian components of this velocity are $v_x = v, v_y = v_z = 0$.

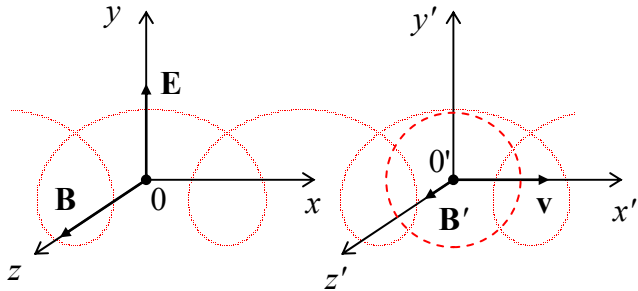


Fig. 9.12. Particle's trajectory in crossed electric and magnetic fields (at $E/c < B$).

Since this choice of the coordinates complies with the one used to derive Eqs. (134), we can readily use that simple form of the Lorentz transform to calculate the field components in the moving reference frame:

$$E'_x = 0, \quad E'_y = \gamma(E - vB) \equiv \gamma\left(E - \frac{E}{B}B\right) \equiv 0, \quad E'_z = 0, \quad (9.170)$$

$$B'_x = 0, \quad B'_y = 0, \quad B'_z = \gamma\left(B - \frac{vE}{c^2}\right) = \gamma B\left(1 - \frac{vE}{Bc^2}\right) = \gamma B\left(1 - \frac{v^2}{c^2}\right) = \frac{B}{\gamma} \leq B, \quad (9.171)$$

where the Lorentz parameter $\gamma \equiv (1 - v^2/c^2)^{-1/2}$ corresponds to the velocity (168) rather than that of the particle. These relations show that in this special reference frame, the particle only "sees" the renormalized uniform magnetic field $B' \leq B$, parallel to the initial field, i.e. normal to the velocity (168). Using the result of the above case (i), we see that in this frame the particle moves along either a circle or a spiral winding about the direction of the magnetic field, with the angular velocity (151):

$$\omega'_c = \frac{qB'}{\epsilon'/c^2}, \quad (9.172)$$

and the radius (153):

$$R' = \frac{p'_\perp}{qB'}. \quad (9.173)$$

Hence in the lab frame, the particle performs this orbital/spiral motion plus a “drift” with the constant velocity v (Fig. 12). As a result, the lab-frame trajectory of the particle (or rather its projection onto the plane normal to the magnetic field) is a *trochoid*-like curve⁵⁸ that, depending on the initial velocity, may be either *prolate* (self-crossing), as in Fig. 12, or *curtate* (drift-stretched so much that it is not self-crossing).

Such looped motion of electrons is used, in particular, in *magnetrons* – very popular generators of microwave radiation. In such a device (Fig. 13), the magnetic field, usually created by specially-shaped permanent magnets, is nearly uniform (in the region of electron motion) and directed along the magnetron’s axis (in Fig. 13, normal to the plane of the drawing), while the electric field of magnitude $E \ll cB$, created by the dc voltage applied between the anode and the cathode, is virtually radial.

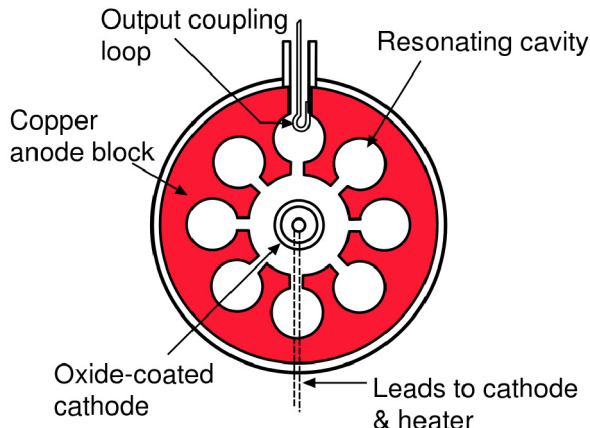


Fig. 9.13. Schematic cross-section of a typical magnetron. (Figure adapted from https://en.wikipedia.org/wiki/Cavity_magnetron under the Free GNU Documentation License.)

As a result, the above simple theory is only approximately valid, and the electron trajectories are close to *epicycloids* rather than trochoids. The applied electric field is adjusted so that these looped trajectories pass close to the anode’s surface, and hence to the gap openings of the cylindrical microwave cavities drilled in the anode’s bulk. The fundamental mode of such a cavity is quasi-lumped, with the cylindrical walls working mostly as inductances, and the gap openings as capacitances, with the microwave electric field concentrated in these openings. This is why the mode is strongly coupled to the electrons “licking” the anode’s surface, and their interaction creates large positive feedback (equivalent to negative damping), which results in intensive microwave self-oscillations at the cavities’ own frequency.⁵⁹ The oscillation energy, of course, is taken from the dc-field-accelerated electrons; due to this energy loss, the looped trajectory of each electron gradually moves closer to the anode and finally

⁵⁸ As a reminder, a trochoid may be described as the trajectory of a point on a rigid disk rolled along a straight line. Its canonical parametric representation is $x = \Theta + a \cos \Theta$, $y = a \sin \Theta$. (For $a > 1$, the trochoid is *prolate*, if $a < 1$, it is *curtate*, and if $a = 1$, it is called the *cyclid*.) Note, however, that for our problem, the trajectory in the lab frame is exactly trochoidal only in the non-relativistic limit $v \ll c$ (i.e. $E/c \ll B$).

⁵⁹ See, e.g., CM Sec. 5.4.

lands on its surface. The wide use of such generators (in particular, in microwave ovens, which operate in a narrow frequency band around 2.45 GHz, allocated for these devices to avoid their interference with wireless communication systems) is due to their simplicity and high (up to 65%) efficiency of the dc-to-rf energy transfer.

Case 2: $E/c > B$. In this case, the speed given by Eq. (168) would be above the speed of light, so let us introduce a reference frame moving with a different velocity,

$$\mathbf{v} = \frac{\mathbf{E} \times \mathbf{B}}{(E/c)^2}, \quad (9.174)$$

whose direction is the same as before (Fig. 12), and magnitude $v = c \times B / (E/c)$ is again below c . A calculation absolutely similar to the one performed above for Case 1, yields

$$E'_x = 0, \quad E'_y = \gamma(E - vB) = \gamma E \left(1 - \frac{vB}{E}\right) = \gamma E \left(1 - \frac{v^2}{c^2}\right) = \frac{E}{\gamma} \leq E, \quad E'_z = 0, \quad (9.175)$$

$$B'_x = 0, \quad B'_y = 0, \quad B'_z = \gamma \left(B - \frac{vE}{c^2}\right) = \gamma \left(B - \frac{EB}{E}\right) = 0. \quad (9.176)$$

so that in the moving frame the particle “sees” only the electric field $E' \leq E$. According to the solution of our previous problem (ii), the trajectory of the particle in the moving frame is the catenary (165), so that in the lab frame it has an “open”, hyperbolic character as well.

To conclude this section, let me note that if the electric and magnetic fields are nonuniform, the particle motion may be much more complex, and in most cases, the integration of the system of equations (144) and (148) may be carried out only numerically. However, if the field’s nonuniformity is small, approximate analytical methods may be very effective. For example, if $\mathbf{E} = 0$, and the magnetic field has a small *transverse* gradient ∇B in a direction normal to the vector \mathbf{B} itself, such that

$$\eta \equiv \frac{|\nabla B|}{B} \ll \frac{1}{R}, \quad (9.177)$$

where R is the cyclotron radius (153), then it is straightforward to use Eq. (150) to show⁶⁰ that the cyclotron orbit drifts perpendicular to both \mathbf{B} and ∇B , with the drift speed

$$v_d \approx \frac{\eta}{\omega_c} \left(\frac{1}{2} u_{\perp}^2 + u_{||}^2 \right) \ll u. \quad (9.178)$$

The physics of this drift is rather simple: according to Eq. (153), the instant curvature of the cyclotron orbit is proportional to the local value of the field. Hence if the field is nonuniform, the trajectory bends slightly more on its parts passing through a stronger field, thus acquiring a shape close to a curate trochoid.

For experimental physics and engineering practice, the effects of *longitudinal* gradients of magnetic field on the charged particle motion are much more important, but it is more convenient for me to postpone their discussion until we have developed a little bit more analytical tools in the next section.

⁶⁰ See, e.g., Sec. 12.4 in J. Jackson, *Classical Electrodynamics*, 3rd ed., Wiley, 1999.

9.7. Analytical mechanics of charged particles

The general Eq. (145) gives a full description of relativistic particle dynamics in electric and magnetic fields, just as the 2nd Newton law (1) does it in the non-relativistic limit. However, we know that in the latter case, the Lagrange formalism of analytical mechanics allows an easier solution of many problems.⁶¹ We can expect that to be true in relativistic mechanics as well, so let us expand the analysis of Sec. 3 (which was valid only for free particles) to particles in the field.

For a free particle, our main result was Eq. (68), which may be rewritten as

$$\gamma \mathcal{L} = -mc^2, \quad (9.179)$$

with $\gamma \equiv (1 - u^2/c^2)^{-1/2}$, showing that the product on the left-hand side is Lorentz-invariant. How can the electromagnetic field affect this relation? In non-relativistic electrostatics, we could write

$$\mathcal{L} = T - U = T - q\phi. \quad (9.180)$$

However, in relativity, the scalar potential ϕ is just one component of the potential 4-vector (116). The only way to get from this full 4-vector a Lorentz-invariant contribution to $\gamma \mathcal{L}$, which would be also proportional to the first power of the particle's velocity (to account for the magnetic component of the Lorentz force), is evidently

$$\gamma \mathcal{L} = -mc^2 + \text{const} \times u^\alpha A_\alpha, \quad (9.181)$$

where u^α is the 4-velocity (63). To comply with Eq. (180) at $u \ll c$, the constant factor should be equal to $(-q)$, so that Eq. (181) becomes

$$\gamma \mathcal{L} = -mc^2 - qu^\alpha A_\alpha, \quad (9.182)$$

and with the account of Eqs. (63) and the second of Eqs. (116), we get very important equality

$$\mathcal{L} = -\frac{mc^2}{\gamma} - q\phi + q\mathbf{u} \cdot \mathbf{A},$$

(9.183)
Particle's
Lagrangian
function

whose Cartesian form is

$$\mathcal{L} = -mc^2 \left(1 - \frac{u_x^2 + u_y^2 + u_z^2}{c^2} \right)^{1/2} - q\phi + q(u_x A_x + u_y A_y + u_z A_z). \quad (9.184)$$

Let us see whether this relation (which admittedly was derived by an educated guess rather than by a strict derivation) passes a natural sanity check. For the case of an unconstrained motion of a particle, we can select its three Cartesian coordinates r_j ($j = 1, 2, 3$) as the generalized coordinates, and its linear velocity components u_j as the corresponding generalized velocities. In this case, the Lagrange equations of motion are

$$\frac{d}{dt} \frac{\partial \mathcal{L}}{\partial u_j} - \frac{\partial \mathcal{L}}{\partial r_j} = 0. \quad (9.185)$$

For example, for $r_1 = x$, Eq. (184) yields

$$\frac{\partial \mathcal{L}}{\partial u_x} = \frac{mu_x}{(1 - u^2/c^2)^{1/2}} + qA_x \equiv p_x + qA_x, \quad \frac{\partial \mathcal{L}}{\partial x} = -q \frac{\partial \phi}{\partial x} + q\mathbf{u} \cdot \frac{\partial \mathbf{A}}{\partial x}, \quad (9.186)$$

⁶¹ See, e.g., CM Sec. 2.2 and on.

so that Eq. (185) takes the form

$$\frac{dp_x}{dt} = -q \frac{\partial \phi}{\partial x} + q\mathbf{u} \cdot \frac{\partial \mathbf{A}}{\partial x} - q \frac{dA_x}{dt}. \quad (9.187)$$

In the equations of motion, the field values have to be taken at the instant position of the particle, so that the last (full) derivative has components due to both the actual field's change (at a fixed point of space) and the particle's motion. Such addition is described by the so-called *convective derivative*⁶²

Convective derivative

$$\boxed{\frac{d}{dt} = \frac{\partial}{\partial t} + \mathbf{u} \cdot \nabla}. \quad (9.188)$$

Spelling out both scalar products, we may group the terms remaining after cancellations as follows:

$$\frac{dp_x}{dt} = q \left[\left(-\frac{\partial \phi}{\partial x} - \frac{\partial A_x}{\partial t} \right) + u_y \left(\frac{\partial A_y}{\partial x} - \frac{\partial A_x}{\partial y} \right) - u_z \left(\frac{\partial A_x}{\partial z} - \frac{\partial A_z}{\partial x} \right) \right]. \quad (9.189)$$

But taking into account the relations (121) between the electric and magnetic fields and potentials, this expression is nothing more than

$$\frac{dp_x}{dt} = q(E_x + u_y B_z - u_z B_y) = q(\mathbf{E} + \mathbf{u} \times \mathbf{B})_x, \quad (9.190)$$

i.e. the x -component of Eq. (144). Since other Cartesian coordinates participate in Eq. (184) similarly, it is evident that the Lagrangian equations of motion along other coordinates yield other components of the same vector equation of motion.

So, Eq. (183) does indeed give the correct Lagrangian function, and we can use it for further analysis, in particular to discuss the first of Eqs. (186). This relation shows that in the electromagnetic field, the generalized momentum corresponding to the particle's coordinate x is *not* $p_x = m\gamma u_x$, but⁶³

$$P_x \equiv \frac{\partial \mathcal{L}}{\partial u_x} = p_x + qA_x. \quad (9.191)$$

Thus, as was already discussed (at that point, without proof) in Sec. 6.4, the particle's motion in a magnetic field may be described by two different linear momentum vectors: the *kinetic momentum* \mathbf{p} defined by Eq. (70), and the *canonical* (or “conjugate”) *momentum*⁶⁴

Particle's canonical momentum

$$\boxed{\mathbf{P} = \mathbf{p} + q\mathbf{A}}. \quad (9.192)$$

In order to facilitate discussion of this notion, let us generalize Eq. (72) for the Hamiltonian function \mathcal{H} of a free particle to the case of a particle in the field:

$$\mathcal{H} \equiv \mathbf{P} \cdot \mathbf{u} - \mathcal{L} = (\mathbf{p} + q\mathbf{A}) \cdot \mathbf{u} - \left(-\frac{mc^2}{\gamma} + q\mathbf{u} \cdot \mathbf{A} - q\phi \right) \equiv \mathbf{p} \cdot \mathbf{u} + \frac{mc^2}{\gamma} + q\phi. \quad (9.193)$$

⁶² Alternatively called the “Lagrangian derivative”; for its (rather simple) derivation see, e.g., CM Sec. 8.3.

⁶³ With regrets, I have to use for the generalized momentum the same (very common) notation as was used earlier in the course for the electric polarization – which will not be discussed here and in the balance of these notes.

⁶⁴ In the Gaussian units, Eq. (192) has the form $\mathbf{P} = \mathbf{p} + q\mathbf{A}/c$.

Merging the first two terms of the last expression exactly as it was done in Eq. (72), we get an extremely simple result,

$$\mathcal{H} = \gamma mc^2 + q\phi, \quad (9.194a)$$

which may be spelled out as

$$\mathcal{H} = \left[1 + \left(\frac{p}{mc} \right)^2 \right]^{1/2} mc^2 + q\phi, \quad \text{i.e. } (\mathcal{H} - q\phi)^2 = (mc^2)^2 + c^2 p^2. \quad (9.194b)$$

These expressions may leave the reader wondering: where is the vector potential \mathbf{A} here – and the magnetic field effects it has to describe? The resolution of this puzzle is easy: as we know from analytical mechanics,⁶⁵ for most applications, for example for an alternative derivation of the equations of motion, \mathcal{H} has to be represented as a function of the particle's generalized coordinates (in the case of unconstrained motion, these may be the Cartesian components of the vector \mathbf{r} that serves as an argument for the potentials \mathbf{A} and ϕ), and the generalized momenta, i.e. the components of the vector \mathbf{P} – generally, plus time. For that, the kinematic momentum \mathbf{p} in Eq. (194b) has to be expressed via these variables. This may be done using Eq. (192), giving us the following generalization of Eq. (78):⁶⁶

$$(\mathcal{H} - q\phi)^2 = (mc^2)^2 + c^2 (\mathbf{P} - q\mathbf{A})^2.$$

(9.195)

Particle's
Hamiltonian
function

It is straightforward to verify that the Hamilton equations of motion for three Cartesian coordinates of the particle, obtained in a regular way from this \mathcal{H} , may be merged into the same vector equation (144). In the non-relativistic limit, performing the expansion of Eqs. (194b) into the Taylor series in p^2 , and limiting it to two leading terms, we get the following generalization of Eq. (74):

$$\mathcal{H} \approx mc^2 + \frac{p^2}{2m} + q\phi, \quad \text{i.e. } \mathcal{H} - mc^2 \approx \frac{1}{2m} (\mathbf{P} - q\mathbf{A})^2 + U, \quad \text{with } U = q\phi. \quad (9.196)$$

These expressions for \mathcal{H} , and Eq. (183) for \mathcal{L} , give a clear view of the electromagnetic field effects' description in analytical mechanics. The electric part $q\mathbf{E}$ of the total Lorentz force can perform mechanical work on the particle, i.e. change its kinetic energy – see Eq. (148) and its discussion. As a result, the scalar potential ϕ , whose gradient gives a contribution to \mathbf{E} , may be directly associated with the potential energy $U = q\phi$ of the particle. On the contrary, the magnetic component $q\mathbf{u} \times \mathbf{B}$ of the Lorentz force is always perpendicular to the particle's velocity \mathbf{u} , and cannot perform a non-zero work on it, and as a result, cannot be described by a contribution to U . However, if \mathbf{A} did not participate in the functions \mathcal{L} and/or \mathcal{H} at all, the analytical mechanics would be unable to describe effects of the magnetic field $\mathbf{B} = \nabla \times \mathbf{A}$ on the particle's motion. The relations (183) and (195)-(196) show the wonderful way in which physics (with some help from Mother Nature herself :-) solves this problem: the vector potential gives such contributions to the functions \mathcal{L} and \mathcal{H} that cannot be uniquely attributed to either kinetic or potential energy, but ensure both the Lagrange and Hamilton formalisms yield the correct equation of motion (144) – including the magnetic field effects.

⁶⁵ See, e.g., CM Sec. 10.1.

⁶⁶ Alternatively, this relation may be obtained from the expression for the Lorentz-invariant norm, $p^\alpha p_\alpha = (mc)^2$, of the 4-momentum (75), $p^\alpha = \{\mathcal{E}/c, \mathbf{p}\} = \{(\mathcal{H} - q\phi)/c, \mathbf{P} - q\mathbf{A}\}$.

I believe I still owe the reader some discussion of the physical sense of the canonical momentum \mathbf{P} . For that, let us consider a charged particle moving near a region of localized magnetic field $\mathbf{B}(\mathbf{r}, t)$, but not entering this region (see Fig. 14), so that on its trajectory $\nabla \times \mathbf{A} \equiv \mathbf{B} = 0$.

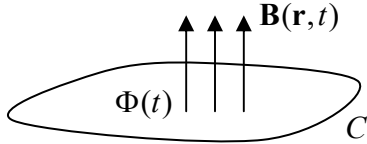


Fig. 9.14. Particle's motion around a localized magnetic field with a time-dependent flux.

If there is no electrostatic fields affecting the particle (i.e. no other electric charges nearby), we may select such a local gauge that $\phi(\mathbf{r}, t) = 0$ and $\mathbf{A} = \mathbf{A}(t)$, so that Eq. (144) is reduced to

$$\frac{d\mathbf{p}}{dt} = q\mathbf{E} = -q \frac{d\mathbf{A}}{dt}, \quad (9.197)$$

and Eq. (192) immediately gives

$$\frac{d\mathbf{P}}{dt} \equiv \frac{d\mathbf{p}}{dt} + q \frac{d\mathbf{A}}{dt} = 0. \quad (9.198)$$

Hence, even if the magnetic field is changed in time, so that the induced electric field \mathbf{E} does accelerate the particle, its canonical momentum does not change. Hence \mathbf{P} is a variable more stable to magnetic field changes than its kinetic counterpart \mathbf{p} . This conclusion may be criticized because it relies on a specific gauge, and generally $\mathbf{P} \equiv \mathbf{p} + q\mathbf{A}$ is not gauge-invariant, because the vector potential \mathbf{A} is not.⁶⁷ However, as was already discussed in Sec. 5.3, the integral $\int \mathbf{A} \cdot d\mathbf{r}$ over a closed contour is gauge-invariant and is equal to the magnetic flux Φ through the area limited by the contour – see Eq. (5.65). So, integrating Eq. (197) over a closed trajectory of a particle (Fig. 14), and over the time of one orbit, we get

$$\Delta \oint_C \mathbf{p} \cdot d\mathbf{r} = -q\Delta\Phi, \quad \text{so that } \Delta \oint_C \mathbf{P} \cdot d\mathbf{r} = 0, \quad (9.199)$$

where $\Delta\Phi$ is the change of flux during that time. This gauge-invariant result confirms the above conclusion about the stability of the canonical momentum to magnetic field variations.

Generally, Eq. (199) is invalid if a particle moves inside a magnetic field and/or changes its trajectory at the field variation. However, if the field is *almost* uniform, i.e. its gradient is small in the sense of Eq. (177), this result is (approximately) applicable. Indeed, analytical mechanics⁶⁸ tells us that for any canonical coordinate-momentum pair $\{q_j, p_j\}$, the corresponding *action variable*,

$$J_j \equiv \frac{1}{2\pi} \oint p_j dq_j, \quad (9.200)$$

remains virtually constant at slow variations of motion conditions. According to Eq. (191), for a particle in a magnetic field, the generalized momentum corresponding to the Cartesian coordinate r_j is P_j rather than p_j . Thus forming the net action variable $J \equiv J_x + J_y + J_z$, we may write

⁶⁷ In contrast, the kinetic momentum $\mathbf{p} = M\mathbf{u}$ is evidently gauge- (though not Lorentz-) invariant.

⁶⁸ See, e.g., CM Sec. 10.2.

$$2\pi J = \oint \mathbf{P} \cdot d\mathbf{r} = \oint \mathbf{p} \cdot d\mathbf{r} + q\Phi = \text{const.} \quad (9.201)$$

Let us apply this relation to the motion of a non-relativistic particle in an almost uniform magnetic field, with a relatively small longitudinal velocity, $u_{||}/u_{\perp} \rightarrow 0$ – see Fig. 15.

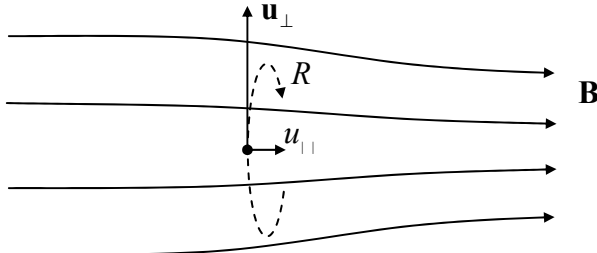


Fig. 9.15. Particle in a magnetic field with a small longitudinal gradient $\nabla B \parallel \mathbf{B}$.

In this case, Φ in Eq. (201) is the flux encircled by the particle's cyclotron orbit, $\Phi = -\pi R^2 B$, where R is its radius given by Eq. (153), and the negative sign accounts for the fact that in our case, the “correct” direction of the normal vector \mathbf{n} in the definition of flux, $\Phi = \int \mathbf{B} \cdot \mathbf{n} d^2 r$, is antiparallel to the vector \mathbf{B} . At $u \ll c$, the kinetic momentum is just $p_{\perp} = mu_{\perp}$, while Eq. (153) yields

$$mu_{\perp} = qBR. \quad (9.202)$$

Plugging these relations into Eq. (201), we get

$$2\pi J = mu_{\perp} 2\pi R - q\pi R^2 B = m \frac{qRB}{m} 2\pi R - q\pi R^2 B \equiv (2-1)q\pi R^2 B \equiv -q\Phi. \quad (9.203)$$

This means that even if the circular orbit slowly moves through the magnetic field, the flux encircled by the cyclotron orbit should remain virtually constant. One manifestation of this effect is the result already mentioned at the end of Sec. 6: if a small gradient of the magnetic field is perpendicular to the field itself, then the particle orbit's drift direction is perpendicular to ∇B , so that Φ stays constant.

Now let us analyze the case of a small longitudinal gradient, $\nabla B \parallel \mathbf{B}$ (Fig. 15). If a small initial longitudinal velocity $u_{||}$ is directed toward the higher field region, the cyclotron orbit has to gradually shrink to keep Φ constant. Rewriting Eq. (202) as

$$mu_{\perp} = q \frac{\pi R^2 B}{\pi R} = q \frac{|\Phi|}{\pi R}, \quad (9.204)$$

we see that this reduction of R (at constant Φ) increases the orbiting speed u_{\perp} . But since the magnetic field cannot perform any work on the particle, its kinetic energy,

$$\mathcal{E} = \frac{m}{2} (u_{||}^2 + u_{\perp}^2), \quad (9.205)$$

should stay constant, so that the longitudinal velocity $u_{||}$ has to decrease. Hence eventually the orbit's drift has to stop, and then it has to start moving back toward the region of lower fields, being essentially repulsed from the high-field region. This effect is very important, in particular, for plasma confinement systems. In the simplest of such systems, two coaxial magnetic coils, inducing magnetic fields of the same direction (Fig. 16), naturally form a “magnetic bottle”, which traps charged particles injected, with sufficiently low longitudinal velocities, into the region between the coils. More complex systems of this

type, but working on the same basic principle, are the most essential components of the persisting large-scale efforts to achieve controllable nuclear fusion.⁶⁹

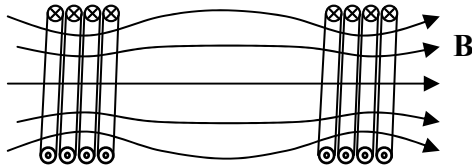


Fig. 9.16. A simple magnetic bottle (schematically).

Returning to the constancy of the magnetic flux encircled by free particles, it reminds us of the Meissner-Ochsenfeld effect, which was discussed in Sec. 6.4, and gives a motivation for a brief revisit of the electrodynamics of superconductivity. As was emphasized in that section, superconductivity is a substantially quantum phenomenon; nevertheless, the classical notion of the conjugate momentum \mathbf{P} helps to understand its theoretical description. Indeed, the general rule of quantization of physical systems⁷⁰ is that each canonical pair $\{q_j, p_j\}$ of a generalized coordinate q_j and the corresponding generalized momentum p_j is described by quantum-mechanical operators that obey the following commutation relation:

$$[\hat{q}_j, \hat{p}_{j'}] = i\hbar\delta_{jj'}. \quad (9.206)$$

According to Eq. (191), for the Cartesian coordinates r_j of a particle in the magnetic field, the corresponding generalized momenta are P_j , so that their operators should obey the similar commutation relations:

$$[\hat{r}_j, \hat{P}_{j'}] = i\hbar\delta_{jj'}. \quad (9.207)$$

In the coordinate representation of quantum mechanics, the canonical operators of the Cartesian components of the linear momentum are described by the corresponding components of the vector operator $-i\hbar\nabla$. As a result, ignoring the rest energy mc^2 (which gives an inconsequential phase factor $\exp\{-imc^2t/\hbar\}$ in the wavefunction), we can use Eq. (196) to rewrite the usual non-relativistic Schrödinger equation,

$$i\hbar\frac{\partial\psi}{\partial t} = \hat{\mathcal{H}}\psi, \quad (9.208)$$

as follows:

$$i\hbar\frac{\partial\psi}{\partial t} = \left(\frac{\hat{p}^2}{2m} + U \right)\psi \equiv \left[\frac{1}{2m}(-i\hbar\nabla - q\mathbf{A})^2 + q\phi \right]\psi. \quad (9.209)$$

Thus, I believe I have finally delivered on my promise to justify the replacement (6.50), which had been used in Secs. 6.4 and 6.5 to discuss the electrodynamics of superconductors, including the Meissner-Ochsenfeld effect. The Schrödinger equation (209) may be also used as the basis for the quantum-mechanical description of other magnetic field phenomena, including the so-called Aharonov-Bohm and quantum Hall effects – see, e.g., QM Secs. 3.1-3.2.

⁶⁹ For further reading on this technology, the reader may be referred, for example, to the simple monograph by F. Chen, *Introduction to Plasma Physics and Controllable Fusion*, vol. 1, 2nd ed., Springer, 1984, and/or the graduate-level theoretical treatment by R. Hazeltine and J. Meiss, *Plasma Confinement*, Dover, 2003.

⁷⁰ See, e.g., CM Sec. 10.1.

9.8. Analytical mechanics of the electromagnetic field

We have just seen that the analytical mechanics of a *particle* in an electromagnetic field may be used to get some important results. The same is true for the analytical mechanics of the electromagnetic *field* as such, and the *field-particle system* as a whole. For such space-distributed systems as fields, governed by local dynamics laws (in our case, the Maxwell equations), we need to apply analytical mechanics to the *local densities* ℓ and \mathcal{H} of the Lagrangian and Hamiltonian functions, defined by relations

$$\mathcal{L} = \int \ell d^3r, \quad \mathcal{H} = \int \mathcal{H} d^3r. \quad (9.210)$$

Let us start, as usual, from the Lagrange formalism. Some clues on the possible structure of the Lagrangian function density ℓ may be obtained from that of the particle-field interaction description in this formalism, discussed in the last section. As we have seen, for the case of a single particle, the interaction is described by the last two terms of Eq. (183):

$$\mathcal{L}_{\text{int}} = -q\phi - q\mathbf{u} \cdot \mathbf{A}. \quad (9.211)$$

Obviously, if the charge q is continuously distributed over some volume, we may represent this \mathcal{L}_{int} as a volume integral of the following Lagrangian function density:

$$\ell_{\text{int}} = -\rho\phi + \mathbf{j} \cdot \mathbf{A} \equiv -j_\alpha A^\alpha. \quad (9.212)$$

Interaction
Lagrangian
density

Notice that this density (in contrast to \mathcal{L}_{int} itself!) is Lorentz-invariant. (This is due to the contraction of the longitudinal coordinate, and hence volume, at the Lorentz transform.) Hence we may expect the density of the *field's* part of the Lagrangian to be Lorentz-invariant as well. Moreover, given the local structure of the Maxwell equations (containing only the first spatial and temporal derivatives of the fields), ℓ_{field} should be a function of the potential's 4-vector and its 4-derivative:

$$\ell_{\text{field}} = \ell_{\text{field}}(A^\alpha, \partial_\alpha A^\beta). \quad (9.213)$$

Also, the density should be selected in such a way that the 4-vector analog of the Lagrangian equation of motion,

$$\partial_\alpha \frac{\partial \ell_{\text{field}}}{\partial (\partial_\alpha A^\beta)} - \frac{\partial \ell_{\text{field}}}{\partial A^\beta} = 0, \quad (9.214)$$

gave us the correct inhomogeneous Maxwell equations (127).⁷¹ The field part ℓ_{field} of the total Lagrangian density ℓ should be a scalar and a quadratic form of the field strengths, i.e. of the tensor $F^{\alpha\beta}$, so that the natural choice is

$$\ell_{\text{field}} = \text{const} \times F_{\alpha\beta} F^{\alpha\beta}. \quad (9.215)$$

with the implied summation over both indices. Indeed, adding to this expression the interaction Lagrangian (212),

$$\ell = \ell_{\text{field}} + \ell_{\text{int}} = \text{const} \times F_{\alpha\beta} F^{\alpha\beta} - j_\alpha A^\alpha, \quad (9.216)$$

⁷¹ Here the implicit summation over the index α plays a role similar to the convective derivative (188) in replacing the full derivative over time, in a way that reflects the symmetry of time and space in special relativity. I do not want to spend more time justifying Eq. (214), because of the reasons that will be clear imminently.

and performing the differentiations, we see that Eqs. (214)-(215) indeed yield Eqs. (127), provided that the constant factor equals $(-1/4\mu_0)$.⁷² So, the field's Lagrangian density is

Field's
Lagrangian
density

$$\mathcal{L}_{\text{field}} = -\frac{1}{4\mu_0} F_{\alpha\beta} F^{\alpha\beta} = \frac{1}{2\mu_0} \left(\frac{E^2}{c^2} - B^2 \right) \equiv \frac{\epsilon_0}{2} E^2 - \frac{B^2}{2\mu_0} \equiv u_e - u_m, \quad (9.217)$$

where u_e is the electric field energy density (1.65), and u_m is the magnetic field energy density (5.57). Let me hope the reader agrees that Eq. (217) is a wonderful result because the Lagrangian function has a structure absolutely similar to the well-known expression $\mathcal{L} = T - U$ of classical mechanics. So, for the field alone, the “potential” and “kinetic” energies are separable again.⁷³

Now let us explore whether we can calculate the 4-form of the field's Hamiltonian function \mathcal{H} . In the generic analytical mechanics,

$$\mathcal{H} = \sum_j \frac{\partial \mathcal{L}}{\partial \dot{q}_j} \dot{q}_j - \mathcal{L}. \quad (9.218)$$

However, just as for the Lagrangian function, for a field we should find the spatial density \mathbf{h} of the Hamiltonian, defined by the second of Eqs. (210), for which the natural 4-form of Eq. (218) is

$$\mathbf{h}^{\alpha\beta} = \frac{\partial \mathcal{L}}{\partial (\partial_\alpha A^\beta)} \partial^\beta A^\gamma - g^{\alpha\beta} \mathcal{L}. \quad (9.219)$$

Calculated for the field alone, i.e. using Eq. (217) for \mathcal{L} , this definition yields

$$\mathbf{h}_{\text{field}}^{\alpha\beta} = \theta^{\alpha\beta} - \tau_D^{\alpha\beta}, \quad (9.220)$$

where the tensor

Symmetric
energy-
momentum
tensor

$$\theta^{\alpha\beta} \equiv \frac{1}{\mu_0} \left(g^{\alpha\gamma} F_{\gamma\delta} F^{\delta\beta} + \frac{1}{4} g^{\alpha\beta} F_{\gamma\delta} F^{\gamma\delta} \right), \quad (9.221)$$

is gauge-invariant, while the remaining term,

$$\tau_D^{\alpha\beta} \equiv \frac{1}{\mu_0} g^{\alpha\gamma} F_{\gamma\delta} \partial^\delta A^\beta, \quad (9.222)$$

is not, so that it cannot correspond to any measurable variables. Fortunately, it is straightforward to verify that the last tensor may be represented in the form

$$\tau_D^{\alpha\beta} = \frac{1}{\mu_0} \partial_\gamma (F^{\gamma\alpha} A^\beta), \quad (9.223)$$

and as a result, obeys the following relations:

$$\partial_\alpha \tau_D^{\alpha\beta} = 0, \quad \int \tau_D^{0\beta} d^3 r = 0, \quad (9.224)$$

⁷² In the Gaussian units, this coefficient is $(-1/16\pi)$.

⁷³ Since the Lagrange equations of motion are homogeneous, the simultaneous change of the signs of T and U does not change them. Thus, it is not important which of the two energy densities, u_e or u_m , we count as the potential energy, and which as the kinetic energy. (Actually, such duality of the two energy components is typical for all analytical mechanics – see, e.g., the discussion of this issue in CM Sec. 2.2.)

so it does not interfere with the conservation properties of the gauge-invariant, symmetric *energy-momentum tensor* (also called the *symmetric stress tensor*) $\theta^{\alpha\beta}$, to be discussed below.

Let us use Eqs. (125) to express the elements of the latter tensor via the electric and magnetic fields. For $\alpha = \beta = 0$, we get

$$\theta^{00} = \frac{\epsilon_0}{2} E^2 + \frac{B^2}{2\mu_0} = u_e + u_m \equiv u, \quad (9.225)$$

i.e. the expression for the total energy density u – see Eq. (6.113). The other 3 elements of the same row/column turn out to be just the Cartesian components of the Poynting vector (6.114), divided by c :

$$\theta^{j0} = \frac{1}{\mu_0} \left(\frac{\mathbf{E}}{c} \times \mathbf{B} \right)_j = \left(\frac{\mathbf{E}}{c} \times \mathbf{H} \right)_j \equiv \frac{S_j}{c}, \quad \text{for } j = 1, 2, 3. \quad (9.226)$$

The remaining 9 elements $\theta_{jj'}$ of the tensor, with $j, j' = 1, 2, 3$, are usually represented as

$$\theta^{jj'} = -\tau_{jj'}^{(M)}, \quad (9.227)$$

where $\tau^{(M)}$ is the so-called *Maxwell stress tensor*:

$$\tau_{jj'}^{(M)} = \epsilon_0 \left(E_j E_{j'} - \frac{\delta_{jj'}}{2} E^2 \right) + \frac{1}{\mu_0} \left(B_j B_{j'} - \frac{\delta_{jj'}}{2} B^2 \right), \quad (9.228)$$

Maxwell
stress
tensor

so that the whole symmetric energy-momentum tensor (221) may be conveniently represented in the following symbolic way:

$$\theta^{\alpha\beta} = \begin{pmatrix} u & \leftarrow & \mathbf{S}/c & \rightarrow \\ \uparrow & & & \\ \mathbf{S}/c & & -\tau_{jj'}^{(M)} & \\ \downarrow & & & \end{pmatrix}. \quad (9.229)$$

The physical meaning of this tensor may be revealed in the following way. Considering Eq. (221) as the *definition* of the tensor $\theta^{\alpha\beta}$,⁷⁴ and using the 4-vector form of Maxwell equations given by Eqs. (127) and (129), it is straightforward to verify an extremely simple result for the 4-derivative of the symmetric tensor:

$$\partial_\alpha \theta^{\alpha\beta} = -F^{\beta\gamma} j_\gamma. \quad (9.230)$$

This expression is valid in the presence of electromagnetic field sources, e.g., for any system of charged particles and the fields they have created. Of these four equations (for four values of the index β), the temporal one (with $\beta = 0$) may be simply expressed via the energy density (225) and the Poynting vector (226):

$$\frac{\partial u}{\partial t} + \nabla \cdot \mathbf{S} = -\mathbf{j} \cdot \mathbf{E}, \quad (9.231)$$

while three spatial equations (with $\beta = j = 1, 2, 3$) may be represented in the form

⁷⁴ In this way, we are using Eq. (219) just as a useful guess, which has led us to the definition of $\theta^{\alpha\beta}$, and may leave its strict justification for more in-depth field theory courses.

$$\frac{\partial}{\partial t} \frac{S_j}{c^2} - \sum_{j'=1}^3 \frac{\partial}{\partial r_{j'}} \tau_{jj'}^{(M)} = -(\rho \mathbf{E} + \mathbf{j} \times \mathbf{B})_j. \quad (9.232)$$

If integrated over a volume V limited by surface S , with the account of the divergence theorem, Eq. (231) returns us to the Poynting theorem (6.111):

$$\int_V \left(\frac{\partial u}{\partial t} + \mathbf{j} \cdot \mathbf{E} \right) d^3r + \oint_S S_n d^2r = 0, \quad (9.233)$$

while Eq. (232) yields⁷⁵

$$\int_V \left[\frac{\partial}{\partial t} \frac{\mathbf{S}}{c^2} + \mathbf{f} \right]_j d^3r = \sum_{j'=1}^3 \oint_S \tau_{jj'}^{(M)} dA_{j'}, \quad \text{with } \mathbf{f} \equiv \rho \mathbf{E} + \mathbf{j} \times \mathbf{B}, \quad (9.234)$$

where $dA_j = n_j dA = n_j d^2r$ is the j^{th} component of the elementary area vector $d\mathbf{A} = \mathbf{n} dA = \mathbf{n} d^2r$ that is normal to the volume's surface, and directed out of the volume – see Fig. 17.⁷⁶

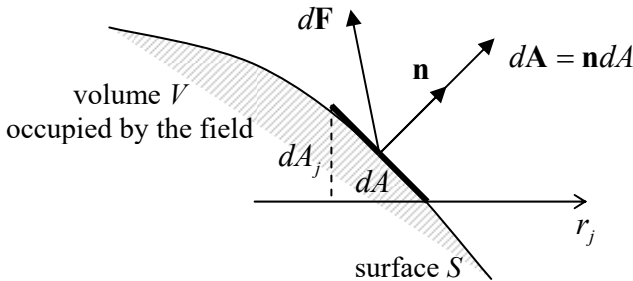


Fig. 9.17. The force $d\mathbf{F}$ exerted on a boundary element $d\mathbf{A}$ of the volume V occupied by the field.

Since, according to Eq. (5.10), the vector \mathbf{f} in Eq. (234) is nothing other than the density of volume-distributed Lorentz forces exerted by the field on the charged particles, we can use the 2nd Newton law, in its relativistic form (144), to rewrite Eq. (234), for a stationary volume V , as

$$\frac{d}{dt} \left[\int_V \frac{\mathbf{S}}{c^2} d^3r + \mathbf{p}_{\text{part}} \right] = \mathbf{F}, \quad (9.235)$$

where \mathbf{p}_{part} is the total mechanical (relativistic) momentum of all particles in the volume V , and the vector \mathbf{F} is defined by its Cartesian components:

$$F_j = \sum_{j'=1}^3 \oint_S \tau_{jj'}^{(M)} dA_{j'}. \quad (9.236)$$

Relations (235)-(236) are our main new results. The first of them shows that the vector

⁷⁵ Just like the Poynting theorem (233), Eq. (234) may be obtained directly from the Maxwell equations, without resorting to the 4-vector formalism – see, e.g., Sec. 8.2.2 in D. Griffiths, *Introduction to Electrodynamics*, 3rd ed., Prentice-Hall, 1999. However, the derivation discussed above is superior because it shows the wonderful unity between the laws of conservation of energy and momentum.

⁷⁶ The same notions are used in the mechanical stress theory – see, e.g., CM Sec. 7.2.

$$\mathbf{g} \equiv \frac{\mathbf{S}}{c^2}, \quad (9.237)$$

already discussed in Sec. 6.8 without derivation, may be indeed interpreted as the density of momentum of the electromagnetic field (per unit volume). This classical relation is consistent with the quantum-mechanical picture of photons as ultra-relativistic particles, with a momentum of magnitude \mathcal{E}/c , because then the flux of the momentum carried by photons through a unit normal area per unit time may be represented either as S_n/c or as $g_n c$. It also allows us to revisit the Poynting vector paradox that was discussed in Sec. 6.8 – see Fig. 6.11 and its discussion. As was emphasized in that discussion, in this case, the vector $\mathbf{S} = \mathbf{E} \times \mathbf{H}$ does not correspond to any measurable energy flow. However, the corresponding momentum of the field, equal to the integral of the density (237) over a volume of interest,⁷⁷ is not only real but may be measured by the recoil impulse it gives to the field sources – say, to a magnetic coil inducing the field \mathbf{H} , or to the capacitor plates creating the field \mathbf{E} .

Now let us turn to our second result, Eq. (236). It tells us that the 3×3 -element Maxwell stress tensor complies with the general definition of the stress tensor⁷⁸ characterizing the forces exerted on the boundaries of a volume, in our current case the volume occupied by the electromagnetic field (Fig. 17). Let us use this important result to analyze two simple examples of static fields.

(i) *Electrostatic field's effect on a perfect conductor*. Since Eq. (235) has been derived for a free space region, we have to select volume V outside the conductor, but we may align one of its faces with the conductor's surface (Fig. 18).

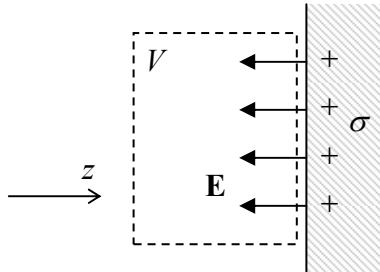


Fig. 9.18. The electrostatic field near a conductor's surface.

From Chapter 2, we know that the electrostatic field just outside the conductor's surface has to be normal to it. Selecting the z -axis in this direction, we have $E_x = E_y = 0$, $E_z = \pm E$, so that only diagonal elements of the tensor (228) are not equal to zero:

$$\tau_{xx}^{(M)} = \tau_{yy}^{(M)} = -\frac{\epsilon_0}{2} E^2, \quad \tau_{zz}^{(M)} = \frac{\epsilon_0}{2} E^2, \quad (9.238)$$

Since the elementary surface area vector has just one non-zero component, dA_z , according to Eq. (236), only the last component (that is positive regardless of the sign of E) gives a contribution to the surface force \mathbf{F} . We see that the force exerted *by the conductor* (and eventually by the external forces that hold the conductor in its equilibrium position) on the field is normal to the conductor and directed out of the field volume: $dF_z \geq 0$. Hence, by the 3rd Newton law, the force exerted *by the field* on the conductor's surface is directed toward the field-filled space:

⁷⁷ It is sometimes called *hidden momentum*.

⁷⁸ See, e.g., CM Sec. 7.2.

Electric
field's
pull

$$dF_{\text{surface}} = -dF_z = -\frac{\epsilon_0}{2} E^2 dA. \quad (9.239)$$

This important result could be obtained by simpler means as well. (Actually, this was the task of one of the exercise problems assigned in Chapter 2.) For example, one could argue, quite convincingly, that the local relation between the force and the field should not depend on the global configuration creating the field, and thus consider the simplest configuration, a planar capacitor (see, e.g. Fig. 2.3) with surfaces of both plates charged by equal and opposite charges of density $\sigma = \pm \epsilon_0 E$. According to the Coulomb law, the charges should attract each other, pulling each plate toward the field region, so that the Maxwell-tensor result gives the correct direction of the force. Now the force's magnitude given by Eq. (239) may be verified either by the direct integration of the Coulomb law or by the following simple reasoning. In the plane capacitor, the inner field $E_z = \sigma/\epsilon_0$ is equally contributed by two surface charges; hence the field created by the negative charge of the counterpart plate (not shown in Fig. 18) is $E_- = -\sigma/2\epsilon_0$, and the force it exerts of the elementary surface charge $dQ = \sigma dA$ of the positively charged plate is $dF_{\text{surface}} = EdQ = -\sigma^2 dA/2\epsilon_0 = \epsilon_0 E^2 dA/2$, in accordance with Eq. (239).⁷⁹

Quantitatively, even for such a high electric field as $E = 10^5$ V/m (close to the electric breakdown's threshold in the air at a frequency of 10 GHz⁸⁰), the “negative pressure” (dF/dA) given by Eq. (239) is of the order of 0.05 Pa (N/m²), i.e. many orders below the ambient atmospheric pressure of 1 bar $\approx 10^5$ Pa. Still, this negative pressure may be substantial (well above 1 bar) in some cases, for example in good dielectrics (such as the high-quality SiO₂ grown at high temperature, which is broadly used in integrated circuits), which can withstand electric fields up to $\sim 10^9$ V/m.

(ii) *Static magnetic field's effect on its source*⁸¹ – say a solenoid's wall or a superconductor's surface (Fig. 19). With the Cartesian coordinates' choice shown in that figure, we have $B_x = B$, $B_y = B_z = 0$, so that the Maxwell stress tensor (228) is diagonal again:

$$\tau_{xx}^{(M)} = \frac{1}{2\mu_0} B^2, \quad \tau_{yy}^{(M)} = \tau_{zz}^{(M)} = -\frac{1}{2\mu_0} B^2. \quad (9.240)$$

However, since for this geometry, only dA_z differs from 0 in Eq. (236), the sign of the resulting force is opposite to that in electrostatics: $dF_z \leq 0$, and the force exerted by the magnetic field upon the conductor's surface,

$$dF_{\text{surface}} = -dF_z = \frac{1}{2\mu_0} B^2 dA, \quad (9.241)$$

Magnetic
field's
push

⁷⁹ By the way, repeating these arguments for a plane capacitor filled with a linear dielectric, we may readily see that Eq. (239) may be generalized for this case by replacing ϵ_0 with ϵ . A similar replacement ($\mu_0 \rightarrow \mu$) is valid for Eq. (241) in a linear magnetic medium.

⁸⁰ Note that the breakdown field E_t in is a strong function of frequency. In the ambient air, it drops from its dc value of $\sim 3 \times 10^6$ V/m to $\sim 1.5 \times 10^5$ V/m at microwave frequencies and then rises to as much as $\sim 6 \times 10^9$ V/m at optical frequencies. The reason of the rise is that at very high frequencies, the amplitude of the field-induced oscillations of the rare free electrons becomes much smaller than their mean free path, inhibiting the bulk impact-ionization of neutral atoms. (Because of this reason, E_t also depends on the air's pressure.)

⁸¹ The causal relation is not important here. Especially in the case of a superconductor, the magnetic field may be induced by another source, with the surface supercurrent \mathbf{j} just shielding the superconductor's bulk from its penetration – see Sec. 6.

corresponds to positive pressure. For good laboratory magnets ($B \sim 10$ T), this pressure is of the order of 4×10^7 Pa ≈ 400 bars, i.e. is very substantial, so the magnets require solid mechanical design.

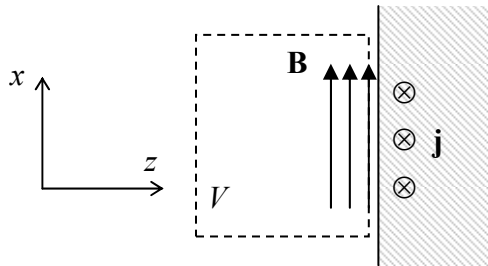


Fig. 9.19. The magnetostatic field near a current-carrying surface.

The direction of the force (241) could be also readily predicted using elementary magnetostatics arguments. Indeed, we can imagine the magnetic field volume limited by another, parallel wall with the opposite direction of surface current. According to the starting point of magnetostatics, Eq. (5.1), such surface currents of opposite directions have to repulse each other – doing that via the magnetic field.

Another explanation of the fundamental sign difference between the electric and magnetic field pressures may be provided using the electric circuit language. As we know from Chapter 2, the potential energy of the electric field stored in a capacitor may be represented in two equivalent forms,

$$U_e = \frac{CV^2}{2} = \frac{Q^2}{2C}. \quad (9.242)$$

Similarly, the magnetic field energy of an inductive coil is

$$U_m = \frac{LI^2}{2} = \frac{\Phi^2}{2L}. \quad (9.243)$$

If we do not want to consider the work of external sources at a virtual change of the system dimensions, we should use the last forms of these relations, i.e. consider a galvanically detached capacitor ($Q = \text{const}$) and an externally-shorted inductance ($\Phi = \text{const}$).⁸² Now if we let the electric field forces (239) drag the capacitor's plates in the direction they “want”, i.e. toward each other, this would lead to a *reduction* of the capacitor thickness, and hence to an *increase* of its capacitance C , and hence to a *decrease* of U_e . Similarly, for a solenoid, allowing the positive pressure (241) to move its walls from each other would lead to an *increase* of the solenoid's volume, and hence of its inductance L , so that the potential energy U_m would be also *reduced* – as it should be. It is remarkable (actually, beautiful!) how the local field formulas (239) and (241) “know” about these global circumstances.

Finally, let us see whether the major results (237) and (241) obtained in this section, match each other. For that, let us return to the normal incidence of a plane, monochromatic wave from the free space upon the plane surface of a perfect conductor (see, e.g., Fig. 7.8 and its discussion), and use those results to calculate the time average of the pressure dF_{surface}/dA imposed by the wave on the surface. At elastic reflection from the conductor's surface, the electromagnetic field's momentum retains its amplitude but reverses its sign, so that the average momentum transferred to a unit area of the surface in a unit time (i.e. the average pressure) is

⁸² Of course, this condition may hold “forever” only for solenoids with superconducting wiring, but even in normal-metal solenoids with practicable inductances, the flux relaxation constants L/R may be rather large (practically, up to a few minutes), quite sufficient to carry out the force measurement.

$$\overline{\frac{dF_{\text{surface}}}{dA}} = 2cg_{\text{incident}} = 2c \frac{\overline{S_{\text{incident}}}}{c^2} = 2c \frac{\overline{EH}}{c^2} = E_\omega H_\omega^*, \quad (9.244)$$

where E_ω and H_ω are complex amplitudes of the incident wave. Using the relation (7.7) between these amplitudes (for $\epsilon = \epsilon_0$ and $\mu = \mu_0$ giving $E_\omega = cB_\omega$), we get

$$\overline{\frac{dF_{\text{surface}}}{dA}} = \frac{1}{c} c B_\omega \frac{B_\omega^*}{\mu_0} \equiv \frac{|B_\omega|^2}{\mu_0}. \quad (9.245)$$

On the other hand, as was discussed in Sec. 7.3, at the surface of a perfect mirror the electric field vanishes while the magnetic field doubles, so that we can use Eq. (241) with $B \rightarrow B(t) = 2\text{Re}[B_\omega e^{-i\omega t}]$. Averaging the pressure given by Eq. (241) over time, we get

$$\overline{\frac{dF_{\text{surface}}}{dA}} = \frac{1}{2\mu_0} \overline{(2\text{Re}[B_\omega e^{-i\omega t}])^2} = \frac{|B_\omega|^2}{\mu_0}, \quad (9.246)$$

i.e. the same result as Eq. (245).

For physics intuition development, it is useful to evaluate the electromagnetic radiation pressure. Even for a relatively high wave intensity S_n of 1 kW/m^2 (close to that of the direct sunlight at the Earth's surface), the pressure $2cg_n = 2S_n/c$ is somewhat below $10^{-5} \text{ Pa} \sim 10^{-10} \text{ bar}$. Still, this extremely small effect was experimentally observed (by P. Lebedev) as early as 1899, giving one more confirmation of Maxwell's theory. Currently, there are ongoing attempts to use the pressure of the Sun's light for propelling small spacecraft, e.g., the *LightSail 2* satellite with a 32-m^2 sail, launched in 2019.

9.9. Exercise problems

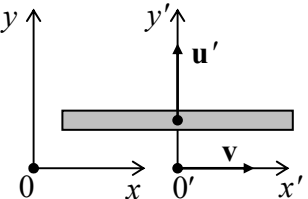
9.1. Use the pre-relativistic picture of the Doppler effect, in which light propagates with velocity c in a Sun-bound aether, to derive Eq. (4).

9.2. Show that two successive Lorentz space/time transforms in the same direction, with velocities u' and v , are equivalent to a single transform with the velocity u given by Eq. (25).

9.3. $N + 1$ reference frames, numbered by index n (taking values $0, 1, \dots, N$), move in the same direction as a particle. Express the particle's velocity in the frame number 0 via its velocity u_N in the frame number N and the set of velocities v_n of the frame number n relative to the frame number $(n - 1)$.

9.4. A spaceship moving with a constant velocity v directly from the Earth, sends back brief flashes of light with a period Δt_s – as measured by the spaceship's clock. Calculate the period with that Earth-based observers may receive these signals – as measured by their clock.

9.5. From the point of view of observers in a “moving” reference frame $0'$, a straight thin rod, parallel to the x' -axis, is moving without rotation with a constant velocity \mathbf{u}' directed along the y' -axis. The reference frame $0'$ is itself moving relative to another (“lab”) reference frame 0 with a constant velocity \mathbf{v} along the x -axis, also without rotation – see the figure on the right.



Calculate:

- (i) the direction of the rod's velocity, and
- (ii) the orientation of the rod on the $[x, y]$ plane,

both as observed from the lab reference frame. Is the velocity, in this frame, perpendicular to the rod?

9.6. Starting from the rest at $t = 0$, a spaceship moves directly from the Earth, with a constant acceleration as measured in its *instantaneous rest frame*. Find its displacement $x(t)$ from the Earth, as measured from Earth's reference frame, and interpret the result.

Hint: The instantaneous rest frame of a moving particle is the inertial reference frame that, at the considered moment of time, has the same velocity as the particle.

9.7. Analyze the twin paradox for the simplest case of 1D travel with a piecewise-constant acceleration.

Hint: You may use an intermediate result of the solution of the previous problem.

9.8. Suggest a natural definition of the 4-vector of linear acceleration (commonly called the *4-acceleration*) of a point, and use it to calculate the acceleration of a relativistic point moving with velocity $\mathbf{u} = \mathbf{u}(t)$.

9.9. Calculate the first relativistic correction to the frequency of a harmonic oscillator as a function of its amplitude.

9.10. An atom, with an initial rest mass m , has been excited to an internal state with an additional energy $\Delta\mathcal{E}$, still being at rest. Next, it returns to its initial state, emitting a photon. Calculate the photon's frequency, taking into account the relativistic recoil of the atom.

Hint: In this problem, and also in Problems 11-13, treat photons as classical ultra-relativistic point particles with zero rest mass, energy $\mathcal{E} = \hbar\omega$, and momentum $\mathbf{p} = \hbar\mathbf{k}$.

9.11. A particle of mass m , initially at rest, decays into two particles with rest masses m_1 and m_2 . Calculate the total energy of the first decay product, in the reference frame moving with that particle.

9.12. A relativistic particle with a rest mass m , moving with velocity u , decays into two particles with zero rest mass.

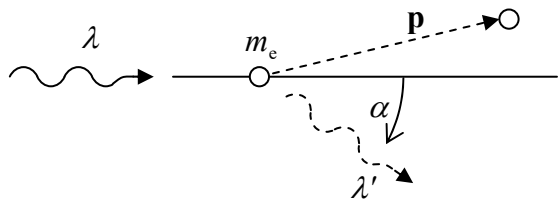
(i) Calculate the smallest possible angle between the decay product velocities (in the lab frame, in that the velocity u is measured).

(ii) What is the largest possible energy of one product particle?

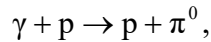
9.13. A relativistic particle flying in free space with velocity \mathbf{u} , decays into two photons.⁸³ Calculate the angular dependence of the probability of photon detection, as measured in the lab frame.

⁸³ Such a decay may happen, for example, with a neutral pion.

9.14. A photon with wavelength λ is scattered by an electron, initially at rest. Calculate the wavelength λ' of the scattered photon as a function of the scattering angle α – see the figure on the right.⁸⁴



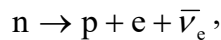
9.15. Calculate the threshold energy of a γ -photon for the reaction



if the proton was initially at rest.

Hint: For protons, $m_p c^2 \approx 938$ MeV, while for neutral pions, $m_\pi c^2 \approx 135$ MeV.

9.16. Calculate the largest possible velocity of the electrons provided at the so-called β -decays,



of neutrons at rest.

Hint: Electron neutrinos and antineutrinos are virtually massless (on the energy scale of this problem); the rest energies $\mathcal{E} \equiv mc^2$ of the other involved particles are: 939.565 MeV for the neutron, 938.272 MeV for the proton, 0.511 MeV for the electron.

9.17. A relativistic particle with a rest mass m and energy \mathcal{E} , collides with a similar particle, initially at rest in the laboratory reference frame. Calculate:

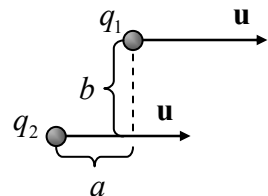
- (i) the final velocity of the center of mass of the system, in the lab frame,
- (ii) the total energy of the system, in the center-of-mass frame, and
- (iii) the final velocities of both particles (in the lab frame), if they move along the same direction.

9.18. A “primed” reference frame moves, relative to the “lab” frame, with a reduced velocity $\beta \equiv v/c = \mathbf{n}_x \beta$. Use Eq. (109) to express the elements T^{00} and T^{0j} (with $j = 1, 2, 3$) of an arbitrary contravariant 4-tensor $T^{\mu\nu}$ via its elements in the lab frame.

9.19. Prove that quantities $E^2 - c^2 B^2$ and $\mathbf{E} \cdot \mathbf{B}$ are Lorentz-invariant.

9.20. Static fields \mathbf{E} and \mathbf{B} are uniform but arbitrary (both in magnitude and in direction). What should be the velocity of an inertial reference frame to have the vectors \mathbf{E}' and \mathbf{B}' , observed from that frame, parallel? Is this solution unique?

9.21. Two charged particles, moving with equal constant velocities \mathbf{u} , are offset by distance $\mathbf{R} = \{a, b\}$ (see the figure on the right), as measured in the lab frame. Calculate the forces between the particles – also in the lab frame.



⁸⁴ This is the famous *Compton scattering* effect, whose discovery in 1923 was one of the major motivations for the development of quantum mechanics – see, e.g., QM Sec. 1.1.

9.22. Each of two thin, long, parallel particle beams of the same velocity \mathbf{u} , separated by distance d , carries electric charge with a constant density λ per unit length, as measured in the reference frame moving with the particles.

(i) Calculate the distribution of the electric and magnetic fields in the system (outside the beams), as measured in the lab reference frame.

(ii) Calculate the interaction force between the beams (per particle) and the resulting acceleration, both in the lab reference frame and in the frame moving with the particles. Compare the results and give a brief discussion of their relation.

9.23. Spell out the Lorentz transform of the scalar-potential and vector-potential components, and use the result to calculate the potentials of a point charge q moving with a constant velocity \mathbf{u} , as measured in the lab reference frame.

9.24. Calculate the scalar and vector potentials created by a time-independent electric dipole \mathbf{p} , as measured in a reference frame that moves relative to the dipole with a constant velocity \mathbf{v} , with the shortest distance (“impact parameter”) equal to b .

9.25. Solve the previous problem, in the limit $v \ll c$, for a time-independent magnetic dipole \mathbf{m} .

9.26. Assuming that the magnetic monopole does exist and has a magnetic charge g , calculate the change $\Delta\Phi$ of the magnetic flux in a superconductor ring due to the passage of a single monopole through it. Evaluate $\Delta\Phi$ for the monopole charge conjectured by P. Dirac, $g = ng_0 \equiv n(2\pi\hbar/e)$, where n is an integer; compare the result with the magnetic flux quantum Φ_0 (6.62) with $|q| = e$, and discuss their relationship.

Hint: For simplicity, you may consider the monopole’s passage along the symmetry axis of a thin, round superconducting ring, in otherwise free space.

9.27. Re-derive Eq. (9.161) of the lecture notes for the simplest case $\mathbf{p}(0) = 0$, using the 4-vector form (9.145) of the equation of motion and the notion of rapidity $\varphi \equiv \tanh^{-1}\beta$ that was briefly discussed in Sec. 9.2.

9.28.* Calculate the trajectory of a relativistic particle in a uniform electrostatic field \mathbf{E} , for an arbitrary direction of its initial velocity $\mathbf{u}(0)$, using two different approaches – at least one of them different from the approach used in Sec. 6 for the case $\mathbf{u}(0) \perp \mathbf{E}$.

9.29. A charged relativistic particle with velocity u performs planar cyclotron rotation in a uniform external magnetic field of magnitude B . How much would the velocity and the orbit’s radius change at a slow change of the field to a new magnitude B' ?

9.30.* Analyze the motion of a relativistic particle in uniform, mutually perpendicular fields \mathbf{E} and \mathbf{B} , for the particular case when E is *exactly* equal to cB .

9.31.* Find the law of motion of a relativistic particle in uniform, parallel, static fields \mathbf{E} and \mathbf{B} .

9.32. An external Lorentz force \mathbf{F} is exerted on a relativistic particle with an electric charge q and a rest mass m , moving with velocity \mathbf{u} relatively some “lab” frame. Calculate its acceleration as observed from that frame.

9.33. Neglecting relativistic kinetic effects, calculate the smallest voltage V that has to be applied between the anode and cathode of a magnetron (see Fig. 13 and its discussion) to enable electrons to reach the anode, at negligible electron-electron interactions (including the space-charge effects) and collisions with the residual gas molecules. You may:

- (i) model the cathode and anode as two coaxial round cylinders, of radii R_1 and R_2 , respectively;
- (ii) assume that the magnetic field \mathbf{B} is uniform and directed along their common axis; and
- (iii) neglect the initial velocity of the electrons emitted by the cathode.

(After the solution, estimate the validity of the last assumption and of the non-relativistic approximation, for reasonable values of parameters.)

9.34. A charged relativistic particle has been injected into a uniform electric field whose magnitude oscillates in time with frequency ω . Calculate the time dependence of the particle’s velocity, as observed from the lab reference frame.

9.35.* A plane, linearly-polarized electromagnetic wave of frequency ω is incident on an otherwise free relativistic particle with electric charge q . Analyze the dynamics of the particle’s momentum and compare the result with those of the previous problem and Problem 7.5.

9.36. Analyze the motion of a non-relativistic particle in a region where the electric and magnetic fields are both uniform and constant in time, but not necessarily parallel or perpendicular to each other.

9.37. A static distribution of electric charge in otherwise free space has created a time-independent distribution $\mathbf{E}(\mathbf{r})$ of the electric field. Use two different approaches to express the field energy density u' and the Poynting vector \mathbf{S}' , as observed from a reference frame moving with constant velocity \mathbf{v} , via the components of the vector \mathbf{E} . In particular, is \mathbf{S}' equal to $(-\mathbf{v}u')$?

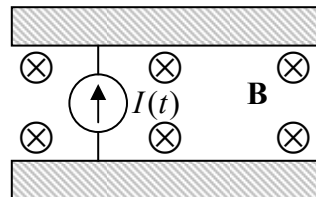
9.38. A plane wave of frequency ω and intensity S , is normally incident on a perfect mirror moving with velocity v in the same direction as the wave.

- (i) Calculate the reflected wave’s frequency, and
- (ii) use the Lorentz transform of the fields to calculate the reflected wave’s intensity – both as observed from the lab reference frame.

9.39. Perform the second task of the previous problem by using general relations between the wave’s energy, power, and momentum.

Hint: As a byproduct, this approach should also give you the pressure exerted by the wave on the moving mirror.

9.40. Consider the simple model of a capacitor's charging by a lumped current source, shown in the figure on the right, and prove that the momentum given by the constant, uniform external magnetic field \mathbf{B} to the current-carrying conductor is equal and opposite to the momentum of the electromagnetic field that the current $I(t)$ builds up in the capacitor. (You may assume that the capacitor is plane and very broad, and neglect the fringe field effects.)



9.41. Consider an electromagnetic plane wave packet propagating in free space, with its electric field represented as the Fourier integral

$$\mathbf{E}(\mathbf{r}, t) = \text{Re} \int_{-\infty}^{+\infty} \mathbf{E}_k e^{i\psi_k} dk, \quad \text{with } \psi_k \equiv kz - \omega_k t, \text{ and } \omega_k \equiv c|k|.$$

Express the full linear momentum (per unit area of wave's front) of the packet via the complex amplitudes \mathbf{E}_k of its Fourier components. Does the momentum depend on time? (In contrast with Problem 7.8, in this case the wave packet is not necessarily narrow.)

9.42. Calculate the forces exerted on well-conducting walls of a waveguide with a rectangular ($a \times b$) cross-section, by a wave propagating along it in the fundamental (H_{10}) mode. Give an interpretation of the results.

Chapter 10. Radiation by Relativistic Charges

The discussion of special relativity in the previous chapter enables us to revisit the analysis of electromagnetic radiation by charged particles, now for arbitrary velocities. For a single point particle, it turns out to be possible to calculate the radiated wave fields in an explicit form and analyze the results for such important particular cases as synchrotron radiation and the “Bremsstrahlung” (brake radiation). After that, we will discuss the apparently unrelated effect of the so-called Coulomb losses of energy by a particle moving in condensed matter, because this discussion will naturally lead us to such important phenomena as the Cherenkov radiation and the transitional radiation. At the end of the chapter, I will briefly review the effects of the back action of the emitted radiation on the emitting particle, whose analysis reveals some limitations of classical electrodynamics.

10.1. Liénard-Wiechert potentials

A convenient starting point for the discussion of radiation by relativistic charges is provided by Eqs. (8.17) for the retarded potentials. In free space, these formulas with the integration variable notation changed from \mathbf{r}' to \mathbf{r}'' for the clarity of what follows, are reduced to

$$\phi(\mathbf{r}, t) = \frac{1}{4\pi\epsilon_0} \int \frac{\rho(\mathbf{r}'', t - R/c)}{R} d^3 r'', \quad \mathbf{A}(\mathbf{r}, t) = \frac{\mu_0}{4\pi} \int \frac{\mathbf{j}(\mathbf{r}'', t - R/c)}{R} d^3 r'', \quad \text{with } \mathbf{R} \equiv \mathbf{r} - \mathbf{r}''. \quad (10.1a)$$

As a reminder, Eqs. (1a) were derived from the Maxwell equations without any restrictions, and are very natural for situations with continuous distributions of the electric charge and/or current. However, for a single charged particle, whose charge and current distributions may be described as

$$\rho(\mathbf{r}, t) = q\delta(\mathbf{r} - \mathbf{r}'), \quad \mathbf{j}(\mathbf{r}, t) = q\mathbf{u}\delta(\mathbf{r} - \mathbf{r}'), \quad \text{with } \mathbf{u} \equiv \dot{\mathbf{r}}', \quad (10.1b)$$

where $\mathbf{r}' = \mathbf{r}'(t)$ is the instantaneous position of the charge, it is more convenient to recast Eqs. (1a) into an explicit form that would not require integration in each particular case. Indeed, as Eqs. (1) show, the potentials at a given observation point $\{\mathbf{r}, t\}$ are contributed by only one specific point $\{\mathbf{r}'(t_{\text{ret}}), t_{\text{ret}}\}$ of the particle's 4D trajectory (called its *world line*), which satisfies the following condition:

$$t_{\text{ret}} \equiv t - \frac{R_{\text{ret}}}{c}, \quad (10.2)$$

where t_{ret} is called the *retarded time*, and R_{ret} is the length of the following distance vector

$$\mathbf{R}_{\text{ret}} \equiv \mathbf{r}(t) - \mathbf{r}'(t_{\text{ret}}) \quad (10.3)$$

– physically, the distance covered by the electromagnetic wave from its emission to observation.

The reduction of Eqs. (1a) to such a simpler form, however, requires some care. Their naïve integration over \mathbf{r}'' would yield the following apparent but wrong results:

$$\phi(\mathbf{r}, t) = \frac{1}{4\pi\epsilon_0} \frac{q}{R_{\text{ret}}}, \quad \text{i.e. } \frac{\phi(\mathbf{r}, t)}{c} = \frac{\mu_0}{4\pi} \frac{qc}{R_{\text{ret}}}; \quad \mathbf{A}(\mathbf{r}, t) = \frac{\mu_0}{4\pi} \frac{q\mathbf{u}_{\text{ret}}}{R_{\text{ret}}}, \quad (\text{WRONG!}) \quad (10.4)$$

where \mathbf{u}_{ret} is the particle's velocity at the retarded point $\mathbf{r}'(t_{\text{ret}})$. Eqs. (4) is a good example of how the relativity theory (even the special one :-)) cannot be taken too lightly. Indeed, the strings (9.84)-(9.85), formed from the apparent potentials (4), would not obey the Lorentz transform rule (9.91), because according to Eqs. (2)-(3), the distance R_{ret} also depends on the reference frame it is measured in.

In order to correct the error, we need, first of all, to discuss the conditions (2)-(3). Combining them by eliminating R_{ret} , we get the following equation for t_{ret} :

$$c(t - t_{\text{ret}}) = |\mathbf{r}(t) - \mathbf{r}'(t_{\text{ret}})|. \quad (10.5)$$

Retarded time

Figure 1 depicts the graphical solution of this self-consistency equation as the only¹ point of intersection of the light cone of the observation point (see Fig. 9.9 and its discussion) and the particle's world line.

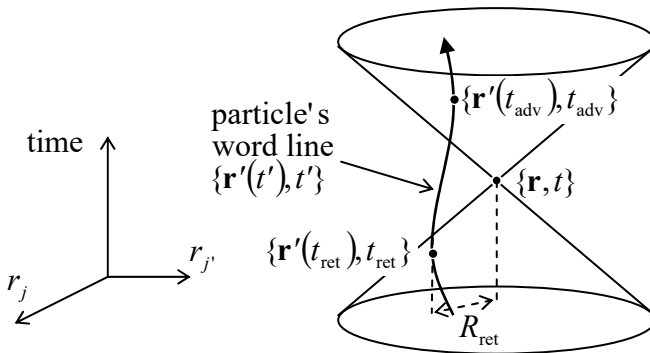


Fig. 10.1. Graphical solution of Eq. (5).

In Eq. (5), just as in Eqs. (1)-(3), all variables have to be measured in the inertial (“lab”) reference frame in which the observation point \mathbf{r} rests. Now let us write Eqs. (1) for a point charge in another inertial frame the frame $0'$ whose velocity (as measured in the lab frame) coincides, at the moment $t' = t_{\text{ret}}$, with the velocity \mathbf{u}_{ret} of the charge.² In that frame, the charge rests, so that, as we know from the electro- and magnetostatics,

$$\phi' = \frac{q}{4\pi\epsilon_0 R'}, \quad \mathbf{A}' = 0. \quad (10.6a)$$

(Remember that this R' may not be equal to R_{ret} , because the latter distance is measured in the “lab” reference frame.) Let us use the identity $1/\epsilon_0 \equiv \mu_0 c^2$ again to rewrite Eqs. (6a) in the form of components of a 4-vector similar in structure to the last two of Eqs. (4):

$$\frac{\phi'}{c} = \frac{\mu_0}{4\pi} \frac{qc}{R'}, \quad \mathbf{A}' = 0. \quad (10.6b)$$

Now it is easy to guess the correct answer for the 4-potential for an arbitrary reference frame:

¹ As Fig. 1 shows, there is always another, “advanced” point $\{\mathbf{r}'(t_{\text{adv}}), t_{\text{adv}}\}$ of the particle’s world line, with $t_{\text{adv}} > t$, which is also a solution of Eq. (5), but it does not fit Eqs. (1), because the observation, at the point $\{\mathbf{r}, t < t_{\text{adv}}\}$, of the field induced at the advanced point, would violate the causality principle.

² This is just a particular case of *the instantaneous reference frame* – the notion that was encountered in several exercise problems of the previous chapter, and indeed was implied (though admittedly not sufficiently advertised) as the derivation of the key Eq. (9.60).

$$A^\alpha = \frac{\mu_0}{4\pi} \frac{qc u^\alpha}{u_\beta R^\beta}, \quad (10.7)$$

where (as a reminder) $A^\alpha \equiv \{\phi/c, \mathbf{A}\}$, $u^\alpha \equiv \gamma\{c, \mathbf{u}\}$, and R^α is the 4-vector of the inter-event distance, formed similarly to that of a single event – cf. Eq. (9.48):

$$R^\alpha \equiv \{c(t - t'), \mathbf{R}'\} \equiv \{c(t - t'), \mathbf{r} - \mathbf{r}'\}. \quad (10.8)$$

Indeed, we needed the 4-vector A^α that would:

- (i) obey the Lorentz transform,
- (ii) have its spatial components A_j scaling, at low velocity, as u_j , and
- (iii) be reduced to the correct result (6) in the instantaneous reference frame of the charge.

Eq. (7) evidently satisfies all these requirements, because the scalar product in its denominator is just

$$u_\beta R^\beta = \gamma\{c, -\mathbf{u}\} \cdot \{c(t - t'), \mathbf{R}'\} \equiv \gamma[c^2(t - t') - \mathbf{u} \cdot \mathbf{R}] = \gamma c(R - \boldsymbol{\beta} \cdot \mathbf{R}) \equiv \gamma cR(1 - \boldsymbol{\beta} \cdot \mathbf{n}), \quad (10.9)$$

where $\mathbf{n} \equiv \mathbf{R}/R$ is a unit vector in the observer's direction, $\boldsymbol{\beta} \equiv \mathbf{u}/c$ is the normalized velocity of the particle, and $\gamma \equiv 1/(1 - u^2/c^2)^{1/2}$. In the instantaneous reference frame of the charge (in which $\boldsymbol{\beta} = 0$ and $\gamma = 1$), the expression (9) is reduced to cR , so that Eq. (7) is correctly reduced to Eq. (6b). Now let us spell out the components of Eq. (7) for the lab frame (in which $t' = t_{\text{ret}}$ and $R = R_{\text{ret}}$):

$$\phi(\mathbf{r}, t) = \frac{1}{4\pi\epsilon_0} \frac{q}{(R - \boldsymbol{\beta} \cdot \mathbf{R})_{\text{ret}}} \equiv \frac{1}{4\pi\epsilon_0} q \left[\frac{1}{R(1 - \boldsymbol{\beta} \cdot \mathbf{n})} \right]_{\text{ret}}, \quad (10.10a)$$

$$\mathbf{A}(\mathbf{r}, t) = \frac{\mu_0}{4\pi} q \left(\frac{\mathbf{u}}{R - \boldsymbol{\beta} \cdot \mathbf{R}} \right)_{\text{ret}} \equiv \frac{\mu_0}{4\pi} qc \left[\frac{\boldsymbol{\beta}}{R(1 - \boldsymbol{\beta} \cdot \mathbf{n})} \right]_{\text{ret}} \equiv \phi(\mathbf{r}, t) \frac{\mathbf{u}_{\text{ret}}}{c^2}. \quad (10.10b)$$

Liénard-Wiechert potentials

These formulas are called the *Liénard-Wiechert potentials*.³ In the non-relativistic limit, they coincide with the naïve guess (4), but in the general case include the additional factor $1/(1 - \boldsymbol{\beta} \cdot \mathbf{n})_{\text{ret}}$. Its physical origin may be illuminated by one more formal calculation – whose result we will need anyway. Let us differentiate the geometric relation (5), rewritten as

$$R_{\text{ret}} = c(t - t_{\text{ret}}), \quad (10.11)$$

over t_{ret} and then, independently, over t , assuming that \mathbf{r} is fixed. For that, let us first differentiate, over t_{ret} , both sides of the identity $R_{\text{ret}}^2 = \mathbf{R}_{\text{ret}} \cdot \mathbf{R}_{\text{ret}}$:

$$2R_{\text{ret}} \frac{\partial R_{\text{ret}}}{\partial t_{\text{ret}}} = 2\mathbf{R}_{\text{ret}} \cdot \frac{\partial \mathbf{R}_{\text{ret}}}{\partial t_{\text{ret}}}. \quad (10.12)$$

If \mathbf{r} is fixed, then $\partial \mathbf{R}_{\text{ret}} / \partial t_{\text{ret}} \equiv \partial(\mathbf{r} - \mathbf{r}') / \partial t_{\text{ret}} = -\partial \mathbf{r}' / \partial t_{\text{ret}} \equiv -\mathbf{u}_{\text{ret}}$, and Eq. (12) yields

$$\frac{\partial R_{\text{ret}}}{\partial t_{\text{ret}}} = \frac{\mathbf{R}_{\text{ret}}}{R_{\text{ret}}} \cdot \frac{\partial \mathbf{R}_{\text{ret}}}{\partial t_{\text{ret}}} = -(\mathbf{n} \cdot \mathbf{u})_{\text{ret}}. \quad (10.13)$$

Now let us differentiate the same R_{ret} over t . On one hand, Eq. (11) yields

³ They were derived in 1898 by Alfred-Marie Liénard and (independently) in 1900 by Emil Wiechert.

$$\frac{\partial R_{\text{ret}}}{\partial t} = c - c \frac{\partial t_{\text{ret}}}{\partial t}. \quad (10.14)$$

On the other hand, according to Eq. (5), at the partial differentiation over time, i.e. if \mathbf{r} is fixed, t_{ret} is a function of t alone, so that (using Eq. (13) at the second step), we may write

$$\frac{\partial R_{\text{ret}}}{\partial t_{\text{ret}}} = \frac{\partial R_{\text{ret}}}{\partial t_{\text{ret}}} \frac{\partial t_{\text{ret}}}{\partial t} = -(\mathbf{n} \cdot \mathbf{u})_{\text{ret}} \frac{\partial t_{\text{ret}}}{\partial t}. \quad (10.15)$$

Now requiring Eqs. (14) and (15) to give the same result, we get:⁴

$$\frac{\partial t_{\text{ret}}}{\partial t} = \frac{c}{c - (\mathbf{n} \cdot \mathbf{u})_{\text{ret}}} \equiv \left(\frac{1}{1 - \beta \cdot \mathbf{n}} \right)_{\text{ret}}. \quad (10.16) \quad \text{blue} \frac{\partial t_{\text{ret}}}{\partial t}$$

This important relation may be readily re-derived (and more clearly understood) for the particular case when the charge's velocity is directed straight toward the observation point. In this case, its vector \mathbf{u} resides in the same space-time plane as the observation point's world line $\mathbf{r} = \text{const}$ – say, the plane $[x, t]$ shown in Fig. 2.

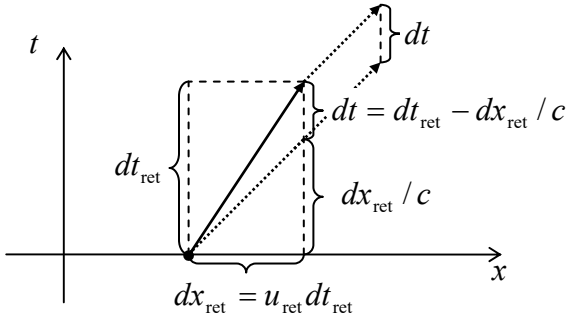


Fig. 10.2. Deriving Eq. (16)
for the case $\beta \cdot \mathbf{n} = \beta$.

Let us consider an elementary time interval $dt_{\text{ret}} \equiv dt'$, during which the particle would travel the space interval $dx_{\text{ret}} = u_{\text{ret}} dt_{\text{ret}}$. In Fig. 2, the corresponding segment of its world line is shown with a solid vector. The dotted vectors in this figure show the world lines of the radiation emitted by the particle in the beginning and at the end of this interval, and propagating with the speed of light c . As it follows from the drawing, the time interval dt between the instants of the arrival of the radiation from these two points to any time-independent spatial point of observation is

$$dt = dt_{\text{ret}} - \frac{dx_{\text{ret}}}{c} = dt_{\text{ret}} - \frac{u_{\text{ret}}}{c} dt_{\text{ret}}, \quad \text{so that } \frac{dt_{\text{ret}}}{dt} = \frac{1}{1 - u_{\text{ret}}/c} \equiv \frac{1}{1 - \beta_{\text{ret}}}. \quad (10.17)$$

This expression coincides with Eq. (16) for our particular case when the directions of the vectors $\beta \equiv \mathbf{u}/c$ and $\mathbf{n} \equiv \mathbf{R}/R$ (both taken at time t_{ret}) coincide, and hence $(\beta \cdot \mathbf{n})_{\text{ret}} = \beta_{\text{ret}}$. The difference between Eqs. (16) and (17) may be interpreted by saying that the particle's velocity in the transverse directions (normal to the vector \mathbf{n}) is not important for this kinematic effect⁵ – the fact almost evident from Fig. 1.

⁴ This relation may be used for an alternative derivation of Eqs. (10) directly from Eqs (1) – the exercise highly recommended to the reader.

⁵ Note that this effect (linear in β) has nothing to do with the Lorentz time dilation (9.21), which is quadratic in β . (Indeed, all our arguments above referred to the same, lab frame.) Rather, it is close in nature to the Doppler effect.

So, the additional factor in the Liénard-Wiechert potentials is just the derivative $\partial t_{\text{ret}}/\partial t$. The reason for its appearance in Eqs. (10) is usually interpreted along the following lines. Let the charge q be spread along the direction of the vector \mathbf{R}_{ret} (in Fig. 2, along the x -axis) by an infinitesimal speed-independent interval δx_{ret} , so that the linear density λ of its charge is proportional to $1/\delta x_{\text{ret}}$. Then the time rate of *charge's* arrival at some spatial point is $\lambda u_{\text{ret}} = \lambda dx_{\text{ret}}/dt_{\text{ret}}$, i.e. scales as $1/dt_{\text{ret}}$. However, the rate of *radiation's* arrival at the observation point scales as $1/dt$, so that due to the non-zero velocity \mathbf{u}_{ret} of the particle, this rate differs from the charge arrival rate by the factor of dt_{ret}/dt , given by Eq. (16). (If the particle moves toward the observation point, $(\beta \cdot \mathbf{n})_{\text{ret}} > 0$, as shown in Fig. 2, this factor is larger than 1.) This radiation compression effect leads to the field change (at $(\beta \cdot \mathbf{n})_{\text{ret}} > 0$, its enhancement) by the same factor (16) – as described by Eqs. (10).

So, the 4-vector formalism was very instrumental for the calculation of field potentials. It may be also used to calculate the fields \mathbf{E} and \mathbf{B} – by plugging Eq. (7) into Eq. (9.124) to calculate the field strength tensor. This calculation yields

$$F^{\alpha\beta} = \frac{\mu_0 q}{4\pi} \frac{1}{u_\gamma R^\gamma} \frac{d}{d\tau} \left[\frac{R^\alpha u^\beta - R^\beta u^\alpha}{u_\delta R^\delta} \right]. \quad (10.18)$$

Now using Eq. (9.125) to identify the elements of this tensor with the field components, we may bring the result to the following vector form:⁶

$$\mathbf{E} = \frac{q}{4\pi\epsilon_0} \left[\frac{\mathbf{n} - \boldsymbol{\beta}}{\gamma^2 (1 - \boldsymbol{\beta} \cdot \mathbf{n})^3 R^2} + \frac{\mathbf{n} \times \{(\mathbf{n} - \boldsymbol{\beta}) \times \dot{\boldsymbol{\beta}}\}}{(1 - \boldsymbol{\beta} \cdot \mathbf{n})^3 c R} \right]_{\text{ret}}, \quad (10.19)$$

$$\mathbf{B} = \frac{\mathbf{n}_{\text{ret}} \times \mathbf{E}}{c}, \quad \text{i.e. } \mathbf{H} = \frac{\mathbf{n}_{\text{ret}} \times \mathbf{E}}{Z_0}. \quad (10.20)$$

Thus the magnetic and electric fields of a relativistic particle are always proportional and perpendicular to each other, and related just as in a plane wave – cf. Eq. (7.6), with the difference that now the vector \mathbf{n}_{ret} may be a function of time. Superficially, this result contradicts the electro- and magnetostatics, because for a particle at rest, \mathbf{B} should vanish while \mathbf{E} stays finite. However, note that according to the Coulomb law for a point charge, in this case $\mathbf{E} = E\mathbf{n}_{\text{ret}}$, so that $\mathbf{B} \propto \mathbf{n}_{\text{ret}} \times \mathbf{E} \propto \mathbf{n}_{\text{ret}} \times \mathbf{n}_{\text{ret}} = 0$. (Actually, in these relations, the subscript “ret” is unnecessary.)

As a sanity check, let us use Eq. (19) as an alternative way to find the electric field of a charge moving without acceleration, i.e. uniformly, along a straight line – see Fig. 9.11a reproduced, with minor changes, in Fig. 3. (This calculation will also illustrate the technical challenges of practical applications of the Liénard-Wiechert formulas for even simple cases.) In this case, the vector $\boldsymbol{\beta}$ does not change in time, so that the second term in Eq. (19) vanishes, and all we need to do is to spell out the Cartesian components of the first term.

⁶ An alternative way of deriving these formulas (highly recommended to the reader as an exercise) is to plug Eqs. (10) into the general relations (9.121), and carry out the required temporal and spatial differentiations directly, using Eq. (16) and its spatial counterpart (which may be derived absolutely similarly):

$$\nabla t_{\text{ret}} = - \left[\frac{\mathbf{n}}{c(1 - \boldsymbol{\beta} \cdot \mathbf{n})} \right]_{\text{ret}}.$$

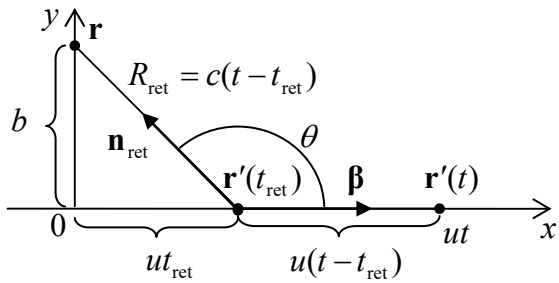


Fig. 10.3. The linearly moving charge problem.

Let us select the coordinate axes and the time origin as shown in Fig. 3, and make a clear distinction between the actual position, $\mathbf{r}'(t) = \{ut, 0, 0\}$ of the charged particle at the instant t we are considering, and its position $\mathbf{r}'(t_{\text{ret}})$ at the retarded instant defined by Eq. (5), i.e. the moment when the particle's field had to be radiated to reach the observation point \mathbf{r} at the given time t , propagating with the speed of light. In these coordinates

$$\boldsymbol{\beta} = \{\beta, 0, 0\}, \quad \mathbf{r} = \{0, b, 0\}, \quad \mathbf{r}'(t_{\text{ret}}) = \{ut_{\text{ret}}, 0, 0\}, \quad \mathbf{n}_{\text{ret}} = \{\cos \theta, \sin \theta, 0\}, \quad (10.21)$$

with $\cos \theta = -ut_{\text{ret}}/R_{\text{ret}}$, so that $[(\mathbf{n} - \boldsymbol{\beta})_x]_{\text{ret}} = -ut_{\text{ret}}/R_{\text{ret}} - \beta$, and Eq. (19) yields, in particular:

$$E_x = \frac{q}{4\pi\epsilon_0} \frac{-ut_{\text{ret}}/R_{\text{ret}} - \beta}{\gamma^2 [(1 - \boldsymbol{\beta} \cdot \mathbf{n})^3 R^2]_{\text{ret}}} \equiv \frac{q}{4\pi\epsilon_0} \frac{-ut_{\text{ret}} - \beta R_{\text{ret}}}{\gamma^2 [(1 - \boldsymbol{\beta} \cdot \mathbf{n})^3 R^3]_{\text{ret}}}. \quad (10.22)$$

But according to Eq. (5), the product βR_{ret} may be represented as $\beta c(t - t_{\text{ret}}) \equiv u(t - t_{\text{ret}})$. Plugging this expression into Eq. (22), we may eliminate the explicit dependence of E_x on time t_{ret} :

$$E_x = \frac{q}{4\pi\epsilon_0} \frac{-ut}{\gamma^2 [(1 - \boldsymbol{\beta} \cdot \mathbf{n}) R]_{\text{ret}}^3}. \quad (10.23)$$

The only non-zero transverse component of the field also has a similar form:

$$E_y = \frac{q}{4\pi\epsilon_0} \left[\frac{\sin \theta}{\gamma^2 (1 - \boldsymbol{\beta} \cdot \mathbf{n})^3 R^2} \right]_{\text{ret}} = \frac{q}{4\pi\epsilon_0} \frac{b}{\gamma^2 [(1 - \boldsymbol{\beta} \cdot \mathbf{n}) R]_{\text{ret}}^3}, \quad (10.24)$$

while $E_z = 0$. From Fig. 3, $\boldsymbol{\beta} - \mathbf{n}_{\text{ret}} = \beta \cos \theta = -\beta ut_{\text{ret}}/R_{\text{ret}}$, so that $(1 - \boldsymbol{\beta} \cdot \mathbf{n}) R_{\text{ret}} \equiv R_{\text{ret}} + \beta ut_{\text{ret}}$, and we may again use Eq. (5) to get $(1 - \boldsymbol{\beta} \cdot \mathbf{n}) R_{\text{ret}} = c(t - t_{\text{ret}}) + \beta ut_{\text{ret}} \equiv ct - ct_{\text{ret}}/\gamma^2$. What remains is to calculate t_{ret} from the self-consistency equation (5), whose square in our current case (Fig. 3) takes the form

$$R_{\text{ret}}^2 \equiv b^2 + (ut_{\text{ret}})^2 = c^2(t - t_{\text{ret}})^2. \quad (10.25)$$

This is a simple quadratic equation for t_{ret} , which (with the appropriate negative sign before the square root, to get $t_{\text{ret}} < t$) yields:

$$t_{\text{ret}} = \gamma^2 t - \left[(\gamma^2 t)^2 - \gamma^2 (t^2 - b^2/c^2) \right]^{1/2} \equiv \gamma^2 t - \frac{\gamma}{c} (u^2 \gamma^2 t^2 + b^2)^{1/2}, \quad (10.26)$$

so that the only retarded-function combination that participates in Eqs. (23)-(24) is

$$[(1 - \boldsymbol{\beta} \cdot \mathbf{n}) R]_{\text{ret}} = \frac{c}{\gamma^2} (u^2 \gamma^2 t^2 + b^2)^{1/2}, \quad (10.27)$$

and, finally, the electric field components are

$$E_x = -\frac{q}{4\pi\epsilon_0} \frac{\gamma ut}{(b^2 + \gamma^2 u^2 t^2)^{3/2}}, \quad E_y = \frac{q}{4\pi\epsilon_0} \frac{\gamma b}{(b^2 + \gamma^2 u^2 t^2)^{3/2}}, \quad E_z = 0. \quad (10.28)$$

But these are exactly Eqs. (9.139),⁷ which had been obtained in Sec. 9.5 by much simpler means, without the necessity to solve the self-consistency equation (5). However, that alternative approach was essentially based on the inertial motion of the particle, and cannot be used in problems in which it moves with acceleration. In such problems, the second term in Eq. (19), dropping with distance more slowly, as $1/R_{\text{ret}}$, and hence describing wave radiation, is frequently the most important one.

10.2. Radiation power

Let us calculate the angular distribution of the particle's radiation. For that, we need to return to Eqs. (19)-(20) to find the Poynting vector $\mathbf{S} = \mathbf{E} \times \mathbf{H}$, and in particular, its radial component $S_n = \mathbf{S} \cdot \mathbf{n}_{\text{ret}}$, at large distances R from the particle. Following tradition,⁸ let us express the result as the energy radiated into unit solid angle per unit time interval dt_{rad} of the *radiation*, rather than that (dt) of its *measurement*. (We will need to return to the measurement time t in the next section to calculate the observed radiation spectrum.) Using Eq. (16), we get

$$\frac{d\mathcal{P}}{d\Omega} = -\frac{d\mathcal{E}}{d\Omega dt_{\text{ret}}} = (R^2 S_n)_{\text{ret}} \frac{\partial t}{\partial t_{\text{ret}}} = (\mathbf{E} \times \mathbf{H}) \cdot [R^2 \mathbf{n} (1 - \boldsymbol{\beta} \cdot \mathbf{n})]_{\text{ret}}. \quad (10.29)$$

At sufficiently large distances from the particle, i.e. in the limit $R_{\text{ret}} \rightarrow \infty$ (in the *radiation zone*), the contribution of the first (essentially, the Coulomb-field) term in the square brackets of Eq. (19) vanishes as $1/R^2$, and the substitution of the remaining term into Eqs. (20) and then Eq. (29) yields the following formula, which is valid for an arbitrary law of the particle's motion:⁹

Radiation power density

$$\frac{d\mathcal{P}}{d\Omega} = \frac{Z_0 q^2}{(4\pi)^2} \frac{|\mathbf{n} \times [(\mathbf{n} - \boldsymbol{\beta}) \times \dot{\boldsymbol{\beta}}]|^2}{(1 - \mathbf{n} \cdot \boldsymbol{\beta})^5}. \quad (10.30)$$

Now, let us apply this important result to some simple cases. First of all, Eq. (30) says that a charge moving with a constant velocity $\boldsymbol{\beta}$ does not radiate at all. This might be expected from our analysis of this case in Sec. 9.5 because in the reference frame moving with the charge it produces only the Coulomb electrostatic field, i.e. no radiation.

Next, let us consider a linear motion of a point charge with a non-zero acceleration directed along the straight line of the motion. In this case, with the coordinate axes selected as shown in Fig. 4a, each of the vectors involved in Eq. (30) has at most two non-zero Cartesian components:

⁷ A similar calculation of magnetic field components from Eq. (20) gives results identical to Eqs. (9.140).

⁸ This tradition may be reasonably justified. Indeed, we may say that the radiation field "detaches" from the particle at times close to t_{ret} , while the observation time t depends on the detector's position, and hence is less relevant for the radiation process as such.

⁹ If the direction of radiation, \mathbf{n} , does not change in time, this formula does not depend on the observer's position \mathbf{R} . Hence, from this point on, the index "ret" may be safely dropped for brevity, though we should always remember that $\boldsymbol{\beta}$ in Eq. (30) is the reduced velocity of the particle at the instant of the radiation's *emission*, not of its observation.

$$\mathbf{n} = \{\sin \theta, 0, \cos \theta\}, \quad \mathbf{p} = \{0, 0, \beta\}, \quad \dot{\mathbf{p}} = \{0, 0, \dot{\beta}\}, \quad (10.31)$$

where θ is the angle between the directions of the particle's motion and of the radiation's propagation. Plugging these expressions into Eq. (30) and performing the vector multiplications, we readily get

$$\frac{d\mathcal{P}}{d\Omega} = \frac{Z_0 q^2}{(4\pi)^2} \dot{\beta}^2 \frac{\sin^2 \theta}{(1 - \beta \cos \theta)^5}. \quad (10.32)$$

Figure 4b shows the angular distribution of such radiation, for three values of the particle's speed u .

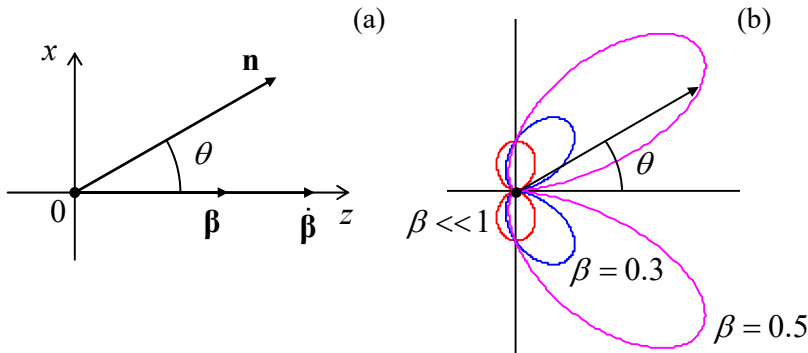


Fig. 10.4. Particle's radiation at its linear acceleration: (a) the problem's geometry, and (b) the last fraction of Eq. (32) as a function of the angle θ .

If the speed is relatively low ($u \ll c$, i.e. $\beta \ll 1$), the denominator in Eq. (32) is very close to 1 for all observation angles θ , so that the angular distribution of the radiation power is close to $\sin^2 \theta$ – just as it follows from the general non-relativistic Larmor formula (8.26), for our current case with $\Theta = \theta$. However, as the velocity is increased, the denominator becomes less than 1 for $\theta < \pi/2$, i.e. for the forward-looking directions, and larger than 1 for back directions. As a result, the radiation in the direction of the particle's motion is increased (somewhat counter-intuitively, regardless of the acceleration's sign!), while that in the back direction is suppressed. For ultra-relativistic particles ($\beta \rightarrow 1$), this trend is strongly exacerbated, and radiation to very small forward angles dominates. To describe this main part of the angular distribution, we may expand the trigonometric functions of θ participating in Eq. (32) in the Taylor series in small θ , and keep only their leading terms: $\sin \theta \approx \theta$, $\cos \theta \approx 1 - \theta^2/2$, so that $(1 - \beta \cos \theta) \approx (1 + \gamma^2 \theta^2)/2\gamma^2$. The resulting expression,

$$\frac{d\mathcal{P}}{d\Omega} \approx \frac{2Z_0 q^2}{\pi^2} \dot{\beta}^2 \gamma^8 \frac{(\gamma \theta)^2}{(1 + \gamma^2 \theta^2)^5}, \quad \text{for } \gamma \gg 1, \quad (10.33)$$

describes a narrow “hollow cone” distribution of radiation, with its maximum at the angle

$$\theta_0 = \frac{1}{2\gamma} \ll 1. \quad (10.34)$$

Another important aspect of Eq. (33) is how extremely fast (as γ^8) the radiation density grows with the Lorentz factor γ , i.e. with the particle's energy $E = \gamma mc^2$.

Still, the total radiated power \mathcal{P} (into all observation angles) at linear acceleration is not too high for any practicable values of parameters. To show this, let us first calculate \mathcal{P} for an arbitrary motion of the particle. To start, let me demonstrate how \mathcal{P} may be found (or rather guessed) from the general relativistic arguments. In Sec. 8.2, we have derived Eq. (8.27) for the power of the electric dipole radiation for a non-relativistic particle motion. That result is valid, in particular, for one charged particle,

whose electric dipole moment's derivative over time may be expressed as $d(q\mathbf{r})/dt = (q/m)\mathbf{p}$, where \mathbf{p} is the particle's linear mechanical momentum (*not* its electric dipole moment). As the result, the Larmor formula (8.27) in free space, i.e. with $v = c$ (but $u \ll c$) reduces to

$$\mathcal{P} = \frac{Z_0}{6\pi c^2} \left(\frac{q}{m} \frac{dp}{dt} \right)^2 \equiv \frac{Z_0 q^2}{6\pi m^2 c^2} \left(\frac{d\mathbf{p}}{dt} \cdot \frac{d\mathbf{p}}{dt} \right), \quad \text{for } u \ll c. \quad (10.35)$$

This is evidently not a Lorentz-invariant result, but it gives a clear hint of how such an invariant, that would be reduced to Eq. (35) in the non-relativistic limit, may be formed:

$$\mathcal{P} = -\frac{Z_0 q^2}{6\pi m^2 c^2} \left(\frac{dp_\alpha}{d\tau} \cdot \frac{dp^\alpha}{d\tau} \right) \equiv \frac{Z_0 q^2}{6\pi m^2 c^2} \left[\left(\frac{d\mathbf{p}}{d\tau} \right)^2 - \frac{1}{c^2} \left(\frac{d\mathcal{E}}{d\tau} \right)^2 \right]. \quad (10.36)$$

Using the relativistic expressions $\mathbf{p} = \gamma mc\beta$, $\mathcal{E} = \gamma mc^2$, and $d\tau = dt/\gamma$, the last formula may be recast into the so-called *Liénard extension* of the Larmor formula:¹⁰

$$\mathcal{P} = \frac{Z_0 q^2}{6\pi} \gamma^6 \left[(\dot{\beta})^2 - (\beta \times \dot{\beta})^2 \right] \equiv \frac{Z_0 q^2}{6\pi} \gamma^4 \left[(\dot{\beta})^2 + \gamma^2 (\beta \cdot \dot{\beta})^2 \right]. \quad (10.37)$$

Total radiation power via β

It may be also obtained by direct integration of Eq. (30) over the full solid angle, thus confirming our guess.

However, for some applications, it is beneficial to express \mathcal{P} via the time evolution of the particle's momentum alone. For that, we may differentiate the fundamental relativistic relation (9.78), $\mathcal{E}^2 = (mc^2)^2 + (pc)^2$, over the proper time τ to get

$$2\mathcal{E} \frac{d\mathcal{E}}{d\tau} = 2c^2 p \frac{dp}{d\tau}, \quad \text{i.e. } \frac{d\mathcal{E}}{d\tau} = \frac{c^2 p}{\mathcal{E}} \frac{dp}{d\tau} = u \frac{dp}{d\tau}, \quad (10.38)$$

where the last step used the relativistic relation $c^2 \mathbf{p}/\mathcal{E} = \mathbf{u}$ mentioned in Sec. 9.3. Plugging Eq. (38) into Eq. (36), we may rewrite it as

$$\mathcal{P} = \frac{Z_0 q^2}{6\pi m^2 c^2} \left[\left(\frac{d\mathbf{p}}{d\tau} \right)^2 - \beta^2 \left(\frac{dp}{d\tau} \right)^2 \right]. \quad (10.39)$$

Total radiation power via \mathbf{p}

Please note the difference between the squared derivatives in this expression: in the first of them we have to differentiate the momentum's vector \mathbf{p} first, and only then form a scalar by squaring the resulting vector derivative, while in the second case, only the magnitude of the vector has to be differentiated. For example, for circular motion with a constant speed (to be analyzed in detail in the next section), the second term vanishes, while the first one does not.

However, if we return to the simplest case of linear acceleration (Fig. 4), then $(d\mathbf{p}/d\tau)^2 = (dp/d\tau)^2$, and Eq. (39) is reduced to

¹⁰ The second form of Eq. (10.37), which is frequently more convenient for applications, may be readily obtained from the first one by applying MA Eq. (7.7a) to the vector product.

$$\mathcal{P} = \frac{Z_0 q^2}{6\pi m^2 c^2} \left(\frac{dp}{d\tau} \right)^2 (1 - \beta^2) \equiv \frac{Z_0 q^2}{6\pi m^2 c^2} \left(\frac{dp}{d\tau} \right)^2 \frac{1}{\gamma^2} \equiv \frac{Z_0 q^2}{6\pi m^2 c^2} \left(\frac{dp}{dt_{\text{ret}}} \right)^2, \quad (10.40)$$

i.e. formally coincides with the non-relativistic relation (35). To get a better feeling of the magnitude of this radiation, we may combine Eq. (9.144) with $\mathbf{B} = 0$, and Eq. (9.148) with $\mathbf{E} \parallel \mathbf{u}$ to get $dp/dt_{\text{ret}} = d\mathcal{E}/dz'$, where z' is the particle's coordinate at the moment t_{ret} . The last relation allows us to rewrite Eq. (40) in the following form:

$$\mathcal{P} = \frac{Z_0 q^2}{6\pi m^2 c^2} \left(\frac{d\mathcal{E}}{dz} \right)^2 \equiv \frac{Z_0 q^2}{6\pi m^2 c^2} \frac{d\mathcal{E}}{dz'} \frac{d\mathcal{E}}{dt_{\text{ret}}} \frac{dt_{\text{ret}}}{dz'} \equiv \frac{Z_0 q^2}{6\pi m^2 c^2 u} \frac{d\mathcal{E}}{dz'} \frac{d\mathcal{E}}{dt_{\text{ret}}}. \quad (10.41)$$

For the most important case of ultra-relativistic motion ($u \rightarrow c$), this result reduces to

$$\frac{\mathcal{P}}{d\mathcal{E}/dt_{\text{ret}}} \approx \frac{2}{3} \frac{d(\mathcal{E}/mc^2)}{d(z'/r_c)}, \quad (10.42)$$

where r_c is the classical radius of the particle, defined by Eq. (8.41). This formula shows that the radiated power, i.e. the change of the particle's energy due to radiation, is much smaller than that due to the accelerating field unless energy as large as $\sim mc^2$ is gained on the classical radius of the particle. For example, for an electron, with $r_c \approx 3 \times 10^{-15}$ m and $mc^2 = m_e c^2 \approx 0.5$ MeV, such an acceleration would require the accelerating electric field of the order of $(0.5 \text{ MV})/(3 \times 10^{-15} \text{ m}) \sim 10^{14}$ MV/m, while practicable accelerating fields are below 10^2 MV/m – limited by the electric breakdown effects. (As described by the factor m^2 in the denominator of Eq. (41), for heavier particles such as protons, the relative losses are even lower.) Such negligible radiative losses of energy are actually a large advantage of linear accelerators – such as the famous two-mile-long SLAC,¹¹ which can accelerate electrons or positrons to energies up to 50 GeV, i.e. to $\gamma \approx 10^5$. If obtaining radiation from the accelerated particles is the goal, it may be readily achieved by bending their trajectories using additional magnetic fields – see the next section.

10.3. Synchrotron radiation

Now let us consider a charged particle being accelerated in the direction perpendicular to its velocity \mathbf{u} (for example by the magnetic component of the Lorentz force), so that its speed u , and hence the magnitude p of its momentum, do not change. In this case, the second term in the square brackets of Eq. (39) vanishes, and it yields

$$\mathcal{P} = \frac{Z_0 q^2}{6\pi m^2 c^2} \left(\frac{d\mathbf{p}}{d\tau} \right)^2 = \frac{Z_0 q^2}{6\pi m^2 c^2} \left(\frac{d\mathbf{p}}{dt_{\text{ret}}} \right)^2 \gamma^2. \quad (10.43)$$

Comparing this expression with Eq. (40), we see that for the same acceleration magnitude, the electromagnetic radiation is a factor of γ^2 larger. For modern accelerators, with $\gamma \sim 10^4$ - 10^5 , such a factor creates an enormous difference. For example, if a particle is on a cyclotron orbit in a constant magnetic field (as was analyzed in Sec. 9.6), both \mathbf{u} and $\mathbf{p} = \gamma m \mathbf{u}$ obey Eq. (9.150), so that

¹¹ See, e.g., <https://www6.slac.stanford.edu/>.

$$\left| \frac{d\mathbf{p}}{dt_{\text{ret}}} \right| = \omega_c p = \frac{u}{R} p = \beta^2 \gamma \frac{mc^2}{R}, \quad (10.44)$$

(where R is the orbit's radius), so that for the power of this *synchrotron radiation*, Eq. (43) yields

Synchrotron
radiation:
total power

$$\boxed{\mathcal{P} = \frac{Z_0 q^2}{6\pi} \beta^4 \gamma^4 \frac{c^2}{R^2} \equiv \frac{1}{4\pi\epsilon_0} \frac{2}{3} \frac{q^4 B^2}{m^2 c} \beta^2 \gamma^2.} \quad (10.45)$$

Note that for ultrarelativistic particles ($\beta \approx 1$), the power grows as γ^2 , i.e. as the square of the particle's energy $\mathcal{E} \propto \gamma$. For example, for typical parameters of the first electron cyclotrons (such as the General Electric's machine in which the synchrotron radiation was first noticed in 1947), $R \sim 1$ m, $\mathcal{E} \sim 0.3$ GeV ($\gamma \sim 600$), Eq. (45) gives a very modest electron energy loss per one revolution: $\mathcal{PT} \equiv \mathcal{P}(2\pi R/u) \approx 2\pi\mathcal{P}R/c \sim 1$ keV. However, already by the mid-1970s, electron accelerators, with $R \sim 100$ m, could give each particle energy $\mathcal{E} \sim 10$ GeV, and the energy loss per revolution grew to ~ 10 MeV, becoming the major energy loss mechanism. For proton accelerators, such energy loss is much less of a problem, because the γ of an ultra-relativistic particle (at fixed \mathcal{E}) is proportional to $1/m$, so that the estimates, at the same R , should be scaled back by $(m_p/m_e)^4 \sim 10^{13}$. Nevertheless, in the giant modern accelerators such as the LHC (with $R \approx 4.3$ km and \mathcal{E} up to 7 TeV), the synchrotron radiation loss per revolution is rather noticeable ($\mathcal{PT} \sim 6$ keV), leading not as much to particle deceleration as to a substantial photoelectron emission from the beam tube's walls, creating harmful defocusing effects.

However, what is bad for particle accelerators and storage rings is good for the so-called *synchrotron light sources* – the electron accelerators designed specially for the generation of intensive synchrotron radiation – with the spectrum extending well beyond the visible light range. Let us analyze the angular and spectral distributions of such radiation. To calculate the angular distribution, let us select the coordinate axes as shown in Fig. 5, with the origin at the current location of the orbiting particle, the z -axis directed along its instant velocity (i.e. the vector β), and the x -axis, toward the orbit's center.

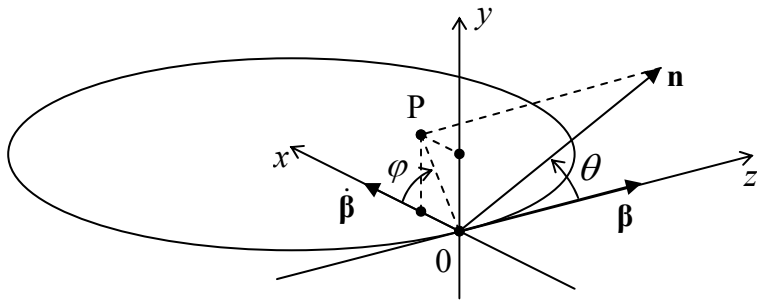


Fig. 10.5. The synchrotron radiation problem's geometry.

In the general case, when the unit vector \mathbf{n} toward the radiation's observer is not within any of the coordinate planes, it has to be described by two angles – the polar angle θ , and the azimuthal angle φ between the x -axis and the projection OP of the vector \mathbf{n} onto the $[x, y]$ -plane. Since the length of the segment OP is $\sin\theta$, the Cartesian components of the relevant vectors are as follows:

$$\mathbf{n} = \{\sin\theta \cos\varphi, \sin\theta \sin\varphi, \cos\theta\}, \quad \beta = \{0, 0, \beta\}, \quad \text{and } \dot{\beta} = \{\dot{\beta}, 0, 0\}. \quad (10.46)$$

Plugging these expressions into the general Eq. (30), we get

$$\frac{d\mathcal{P}}{d\Omega} = \frac{2Z_0 q^2}{\pi^2} |\beta|^2 \gamma^6 f(\theta, \varphi), \quad \text{where}$$

$$f(\theta, \varphi) \equiv \frac{1}{8\gamma^6 (1 - \beta \cos \theta)^3} \left[1 - \frac{\sin^2 \theta \cos^2 \varphi}{\gamma^2 (1 - \beta \cos \theta)^2} \right], \quad (10.47)$$

Synchrotron
radiation:
angular
distribution

According to this result, just as at the linear acceleration, in the ultra-relativistic limit, most radiation goes into a narrow cone (of a width $\Delta\theta \sim \gamma^{-1} \ll 1$) around the vector β , i.e. around the instant direction of the particle's propagation. For such small angles, and $\gamma \gg 1$,

$$f(\theta, \varphi) \approx \frac{1}{(1 + \gamma^2 \theta^2)^3} \left[1 - \frac{4\gamma^2 \theta^2 \cos^2 \varphi}{(1 + \gamma^2 \theta^2)^2} \right]. \quad (10.48)$$

The left panel of Fig. 6 shows a color-coded contour map of this angular distribution $f(\theta, \varphi)$, as observed on a distant plane normal to the particle's instant velocity (in Fig. 5, parallel to the $[x, y]$ -plane), while its right panel shows the factor f as a function of θ in two perpendicular directions: within the particle's rotation plane (in the direction parallel to the x -axis, i.e. at $\varphi = 0$) and perpendicular to this plane (along the y -axis, i.e. at $\varphi = \pm\pi/2$). The result shows, first of all, that, in contrast to the case of linear acceleration, the narrow radiation cone is now not hollow: the intensity maximum is reached at $\theta = 0$, i.e. exactly in the direction of the particle's motion direction. Second, the radiation cone is not axially symmetric: within the particle rotation plane, the intensity drops faster (and even has nodes at $\theta = \pm 1/\gamma$).

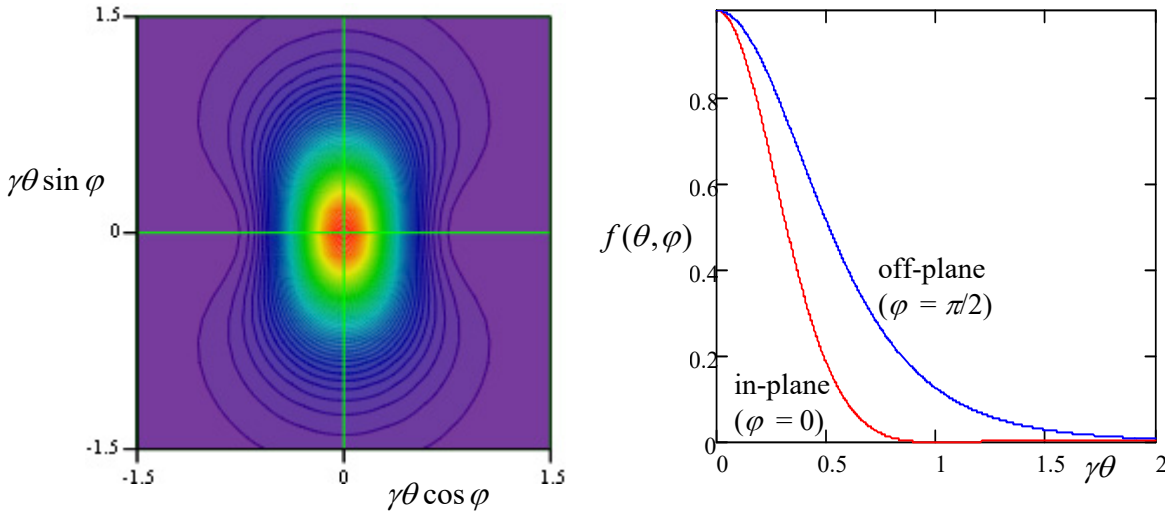


Fig. 10.6. The angular distribution of the synchrotron radiation at $\gamma \gg 1$.

The angular distribution (47) of the synchrotron radiation was calculated for the (inertial) reference frame whose origin coincides with the particle's position at this particular instant, i.e. its radiation pattern is time-independent in the frame moving with the particle. This pattern enables a semi-quantitative description of the radiation by an ultra-relativistic particle from the point of view of a stationary observer: if the observation point is on (or very close to) the rotation plane,¹² it is being

¹² It is easy (and hence is left for the reader's exercise) to show that if the observation point is much off-plane (say, is located on the particle orbit's axis), the radiation is virtually monochromatic, with frequency ω_c . (As we know from Sec. 8.2, in the non-relativistic limit $u \ll c$, this is true for *any* observation point.)

“struck” by the narrow radiation cone once each rotation period $\tau \approx 2\pi R/c$, each “strike” giving a field pulse of a short duration $\Delta t_{\text{ret}} \ll 1/\omega_c$ – see Fig. 7.¹³

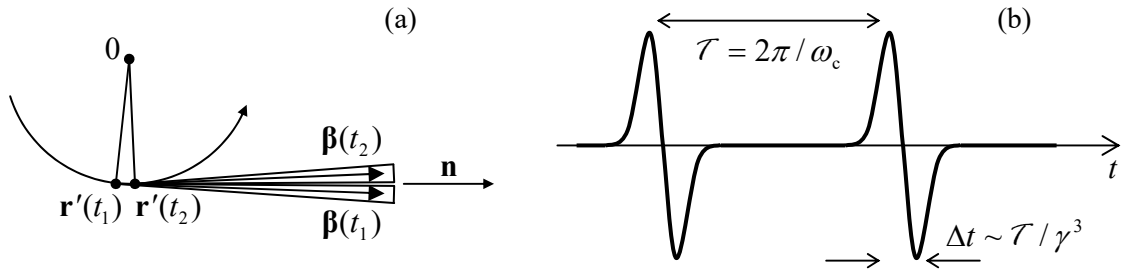


Fig. 10.7. (a) The synchrotron radiation cones (at $\gamma \gg 1$) for two close values of t_{ret} , and (b) the in-plane component of the electric field observed in the rotation plane, as a function of time t – schematically.

The evaluation of the time duration Δt of each pulse requires some care: its estimate $\Delta t_{\text{ret}} \sim 1/\gamma\omega_c$ is correct for the duration of the retarded time interval during which its cone is aimed at the observer. However, due to the time compression effect discussed in detail in Sec. 1 and described by Eq. (16), the pulse duration as seen by the observer is a factor of $1/(1 - \beta)$ shorter, so that

$$\Delta t = (1 - \beta)\Delta t_{\text{ret}} \sim \frac{1 - \beta}{\gamma\omega_c} \sim \frac{1}{\gamma^3\omega_c} \sim \gamma^{-3}\tau, \quad \text{for } \gamma \gg 1. \quad (10.49)$$

From the Fourier theorem, we can expect the frequency spectrum of such radiation to consist of numerous ($N \sim \gamma^3 \gg 1$) harmonics of the particle rotation frequency ω_c , with comparable amplitudes. However, if the orbital frequency fluctuates even slightly ($\delta\omega_c/\omega_c > 1/N \sim 1/\gamma^3$), as it happens in most practical systems, the radiation pulses are not coherent, so that the average radiation power spectrum may be calculated as that of one pulse, multiplied by the number of pulses per second. In this case, the spectrum is continuous, extending from low frequencies all the way to approximately

$$\omega_{\text{max}} \sim 1/\Delta t \sim \gamma^3\omega_c. \quad (10.50)$$

In order to verify and quantify this result, let us calculate the spectrum of radiation due to a single pulse. For that, we should first make the general notion of the radiation spectrum quantitative. Let us represent an arbitrary electric field (say that of the synchrotron radiation we are studying now) observed at a fixed point \mathbf{r} , as a function of the *observation* time t , as a Fourier integral:¹⁴

$$\mathbf{E}(t) = \int_{-\infty}^{+\infty} \mathbf{E}_\omega e^{-i\omega t} dt. \quad (10.51)$$

¹³ The fact that the in-plane component of each electric field’s pulse $\mathbf{E}(t)$ is antisymmetric with respect to its central point, and hence vanishes at that point (as Fig. 7b shows), readily follows from Eq. (19).

¹⁴ In contrast to the single-frequency case (i.e. a monochromatic wave), we may avoid taking the real part of the complex function ($\mathbf{E}_\omega e^{-i\omega t}$) by requiring that in Eq. (51), $\mathbf{E}_{-\omega} = \mathbf{E}_\omega^*$. However, it is important to remember the factor $1/2$ required for the transition to a monochromatic wave of frequency ω_0 and with real amplitude \mathbf{E}_0 : $\mathbf{E}_\omega = \mathbf{E}_0 [\delta(\omega - \omega_0) + \delta(\omega + \omega_0)]/2$.

This expression may be plugged into the formula for the total energy of the radiation pulse (i.e. of the loss of particle's energy \mathcal{E}) per unit solid angle:¹⁵

$$-\frac{d\mathcal{E}}{d\Omega} \equiv \int_{-\infty}^{+\infty} S_n(t) R^2 dt = \frac{R^2}{Z_0} \int_{-\infty}^{+\infty} |\mathbf{E}(t)|^2 dt. \quad (10.52)$$

This substitution, followed by a natural change of the integration order, yields

$$-\frac{d\mathcal{E}}{d\Omega} = \frac{R^2}{Z_0} \int_{-\omega}^{+\omega} d\omega \int_{-\omega}^{+\omega} d\omega' \mathbf{E}_\omega \cdot \mathbf{E}_{\omega'} \int_{-\infty}^{+\infty} dt e^{-i(\omega+\omega')t}. \quad (10.53)$$

But the inner integral (over t) is just $2\pi\delta(\omega + \omega')$.¹⁶ This delta function kills one of the frequency integrals (say, one over ω'), and Eq. (53) gives us a result that may be recast as

$$-\frac{d\mathcal{E}}{d\Omega} = \int_0^{+\infty} I(\omega) d\omega, \quad \text{with } I(\omega) \equiv \frac{4\pi R^2}{Z_0} \mathbf{E}_\omega \cdot \mathbf{E}_{-\omega} \equiv \frac{4\pi R^2}{Z_0} \mathbf{E}_\omega \cdot \mathbf{E}_\omega^*, \quad (10.54)$$

where the evident frequency symmetry of the scalar product $\mathbf{E}_\omega \cdot \mathbf{E}_{-\omega}$ has been utilized to fold the integral of $I(\omega)$ to positive frequencies only. The first of Eqs. (54) makes the physical sense of the function $I(\omega)$ very clear: this is the so-called *spectral density* of the electromagnetic radiation (per unit solid angle).¹⁷

To calculate the spectral density, we can express the function \mathbf{E}_ω via $\mathbf{E}(t)$ using the Fourier transform reciprocal to Eq. (51):

$$\mathbf{E}_\omega = \frac{1}{2\pi} \int_{-\infty}^{+\infty} \mathbf{E}(t) e^{i\omega t} dt. \quad (10.55)$$

In the particular case of radiation by a single point charge, we may use here the second (radiative) term of Eq. (19):

$$\mathbf{E}_\omega = \frac{1}{2\pi} \frac{q}{4\pi\epsilon_0} \frac{1}{cR} \int_{-\infty}^{+\infty} \left[\frac{\mathbf{n} \times \{(\mathbf{n} - \boldsymbol{\beta}) \times \dot{\boldsymbol{\beta}}\}}{(1 - \boldsymbol{\beta} \cdot \mathbf{n})^3} \right]_{\text{ret}} e^{i\omega t} dt. \quad (10.56)$$

Since the vectors \mathbf{n} and $\boldsymbol{\beta}$ are more natural functions of the radiation's emission (retarded) time t_{ret} , let us use Eqs. (5) and (16) to exclude the observation time t from this integral:

$$\mathbf{E}_\omega = \frac{q}{4\pi\epsilon_0} \frac{1}{2\pi} \frac{1}{cR} \int_{-\infty}^{+\infty} \left[\frac{\mathbf{n} \times \{(\mathbf{n} - \boldsymbol{\beta}) \times \dot{\boldsymbol{\beta}}\}}{(1 - \boldsymbol{\beta} \cdot \mathbf{n})^2} \right]_{\text{ret}} \exp \left\{ i\omega \left(t_{\text{ret}} + \frac{R_{\text{ret}}}{c} \right) \right\} dt_{\text{ret}}. \quad (10.57)$$

Assuming that the observer is sufficiently far from the particle,¹⁸ we may treat the unit vector \mathbf{n} as a constant and also use the approximation (8.19) to reduce Eq. (57) to

¹⁵ Note that the expression under this integral differs from $d\mathcal{P}/d\Omega$ defined by Eq. (29) by the absence of the term $(1 - \boldsymbol{\beta} \cdot \mathbf{n}) = \partial t_{\text{ret}}/\partial t$ – see Eq. (16). This is natural because now we are calculating the wave energy arriving at the observation point \mathbf{r} during the time interval dt rather than dt_{ret} .

¹⁶ See, e.g. MA Eq. (14.4).

¹⁷ The notion of spectral density may be readily generalized to random processes – see, e.g., SM Sec. 5.4.

¹⁸ According to the estimate (49), for a synchrotron radiation's pulse, this restriction requires the observer to be much farther than $\Delta r' \sim c\Delta t \sim R/\gamma^3$ from the particle. With the values $R \sim 10^4$ m and $\gamma \sim 10^5$ mentioned above, $\Delta r' \sim 10^{-11}$ m, so that this requirement is satisfied for any realistic radiation detector.

$$\mathbf{E}_\omega = \frac{1}{2\pi} \frac{q}{4\pi\epsilon_0} \frac{1}{cR} \exp\left\{\frac{i\omega r}{c}\right\} \int_{-\infty}^{+\infty} \left[\frac{\mathbf{n} \times \{(\mathbf{n} - \boldsymbol{\beta}) \times \dot{\boldsymbol{\beta}}\}}{(1 - \boldsymbol{\beta} \cdot \mathbf{n})^2} \exp\left\{i\omega\left(t - \frac{\mathbf{n} \cdot \mathbf{r}'}{c}\right)\right\} \right]_{\text{ret}} dt_{\text{ret}} . \quad (10.58)$$

Plugging this expression into Eq. (54), and then using the definitions $c \equiv 1/(\epsilon_0\mu_0)^{1/2}$ and $Z_0 \equiv (\mu_0/\epsilon_0)^{1/2}$, we get¹⁹

$$I(\omega) = \frac{Z_0 q^2}{16\pi^3} \left| \int_{-\infty}^{+\infty} \left[\frac{\mathbf{n} \times \{(\mathbf{n} - \boldsymbol{\beta}) \times \dot{\boldsymbol{\beta}}\}}{(1 - \boldsymbol{\beta} \cdot \mathbf{n})^2} \exp\left\{i\omega\left(t - \frac{\mathbf{n} \cdot \mathbf{r}'}{c}\right)\right\} \right]_{\text{ret}} dt_{\text{ret}} \right|^2 . \quad (10.59)$$

This result may be further simplified by noticing that the fraction before the exponent may be represented as a full derivative over t_{ret} ,

$$\left[\frac{\mathbf{n} \times \{(\mathbf{n} - \boldsymbol{\beta}) \times \dot{\boldsymbol{\beta}}\}}{(1 - \boldsymbol{\beta} \cdot \mathbf{n})^2} \right]_{\text{ret}} \equiv \left[\frac{\mathbf{n} \times \{(\mathbf{n} - \boldsymbol{\beta}) \times d\boldsymbol{\beta}/dt\}}{(1 - \boldsymbol{\beta} \cdot \mathbf{n})^2} \right]_{\text{ret}} \equiv \frac{d}{dt} \left[\frac{\mathbf{n} \times (\mathbf{n} \times \boldsymbol{\beta})}{1 - \boldsymbol{\beta} \cdot \mathbf{n}} \right]_{\text{ret}} , \quad (10.60)$$

and working out the resulting integral by parts. At this operation, the time differentiation of the parentheses in the exponent gives $d[t_{\text{ret}} - \mathbf{n} \cdot \mathbf{r}'(t_{\text{ret}})/c]/dt_{\text{ret}} = (1 - \mathbf{n} \cdot \mathbf{u}/c)_{\text{ret}} \equiv (1 - \boldsymbol{\beta} \cdot \mathbf{n})_{\text{ret}}$, leading to the cancellation of the remaining factor in the denominator and hence to a very simple general result:²⁰

$$I(\omega) = \frac{Z_0 q^2 \omega^2}{16\pi^3} \left| \int_{-\infty}^{+\infty} \left[\mathbf{n} \times (\mathbf{n} \times \boldsymbol{\beta}) \exp\left\{i\omega\left(t - \frac{\mathbf{n} \cdot \mathbf{r}'}{c}\right)\right\} \right]_{\text{ret}} dt_{\text{ret}} \right|^2 . \quad (10.61)$$

Relativistic radiation: spectral density

Now returning to the particular case of the synchrotron radiation, it is beneficial to choose the origin of time t_{ret} so that at $t_{\text{ret}} = 0$, the angle θ between the vectors \mathbf{n} and $\boldsymbol{\beta}$ takes its smallest value θ_0 , i.e., in terms of Fig. 5, the vector \mathbf{n} is within the $[y, z]$ -plane. Fixing this direction of the axes so that they do not move, we can redraw that figure as shown in Fig. 8.

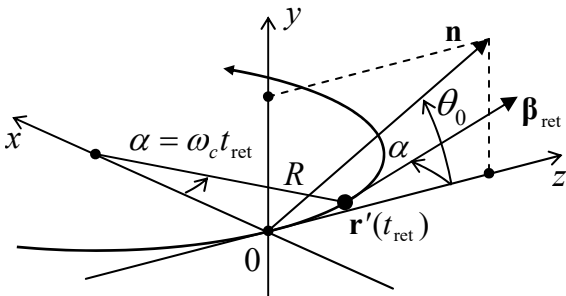


Fig. 10.8. Deriving the synchrotron radiation's spectral density. The vector \mathbf{n} is static within the $[y, z]$ -plane, while the vectors $\mathbf{r}'(t_{\text{ret}})$ and $\boldsymbol{\beta}_{\text{ret}}$ rotate, within the $[x, z]$ -plane, with the angular velocity ω_c of the particle.

In this “lab” reference frame, the vector \mathbf{n} does not depend on time, while the vectors $\mathbf{r}'(t_{\text{ret}})$ and $\boldsymbol{\beta}_{\text{ret}}$ do depend on it via the angle $\alpha \equiv \omega_c t_{\text{ret}}$:

¹⁹ Note that for our current purposes of calculation of the spectral density of radiation by a single particle, the factor $\exp\{i\omega r/c\}$ has got canceled. However, as we have seen in Chapter 8, this factor plays a central role in the interference of radiation from several (many) sources. Such interference is important, in particular, in *undulators* and *free-electron lasers* – the devices to be (qualitatively) discussed below.

²⁰ Actually, this simplification is not occasional. According to Eq. (10b), the expression under the derivative in the last form of Eq. (60) is just the transverse component of the vector potential \mathbf{A} (give or take a constant factor), and from the discussion in Sec. 8.2 we know that this component determines the electric dipole radiation of a system, which dominates the radiation in our current case of a single particle with a non-zero electric charge.

$$\mathbf{n} = \{0, \sin \theta_0, \cos \theta_0\}, \quad \mathbf{r}'(t_{\text{ret}}) = \{R(1 - \cos \alpha), 0, R \sin \alpha\}, \quad \mathbf{\beta}_{\text{ret}} \equiv \{\beta \sin \alpha, 0, \beta \cos \alpha\}. \quad (10.62)$$

Now an easy multiplication yields

$$[\mathbf{n} \times (\mathbf{n} \times \mathbf{\beta})]_{\text{ret}} = \beta \{\sin \alpha, \sin \theta_0 \cos \theta_0 \cos \alpha, -\sin^2 \theta_0 \sin \alpha\}, \quad (10.63)$$

$$\left[\exp \left\{ i\omega \left(t - \frac{\mathbf{n} \cdot \mathbf{r}'}{c} \right) \right\} \right]_{\text{ret}} = \exp \left\{ i\omega \left(t_{\text{ret}} - \frac{R}{c} \cos \theta_0 \sin \alpha \right) \right\}. \quad (10.64)$$

As we already know, in the (most interesting) ultra-relativistic limit $\gamma \gg 1$, most radiation is confined to short pulses, so that only small angles $\alpha \sim \omega_c \Delta t_{\text{ret}} \sim \gamma^{-1}$ may contribute to the integral in Eq. (61). Moreover, since most radiation goes to small angles $\theta \sim \theta_0 \sim \gamma^{-1}$, it makes sense to consider only such small angles. Expanding both trigonometric functions of these small angles, participating in parentheses of Eq. (64), into the Taylor series, and keeping only the leading terms, we get

$$t_{\text{ret}} - \frac{R}{c} \cos \theta_0 \sin \alpha \approx t_{\text{ret}} - \frac{R}{c} \omega_c t_{\text{ret}} + \frac{R \theta_0^2}{c} \omega_c t_{\text{ret}} + \frac{R \omega_c^3}{c} t_{\text{ret}}^3. \quad (10.65)$$

Since $(R/c)\omega_c = u/c = \beta \approx 1$, in the two last terms we may approximate this parameter by 1. However, it is crucial to distinguish the difference between the two first terms, proportional to $(1 - \beta)t_{\text{ret}}$, from zero; as we have done before, we may approximate it with $t_{\text{ret}}/2\gamma^2$. On the right-hand side of Eq. (63), which does not have such a critical difference, we may be bolder, taking²¹

$$\beta \{\sin \alpha, \sin \theta_0 \cos \theta_0 \cos \alpha, -\sin^2 \theta_0 \sin \alpha\} \approx \{\alpha, \theta_0, 0\} \equiv \{\omega_c t_{\text{ret}}, \theta_0, 0\}. \quad (10.66)$$

As a result, Eq. (61) is reduced to

$$I(\omega) = \frac{Z_0 q^2}{16\pi^3} |a_x \mathbf{n}_x + a_y \mathbf{n}_y|^2 \equiv \frac{Z_0 q^2}{16\pi^3} (|a_x|^2 + |a_y|^2), \quad (10.67)$$

where a_x and a_y are the following dimensionless factors:

$$\begin{aligned} a_x &\equiv \omega \int_{-\infty}^{+\infty} \omega_c t_{\text{ret}} \exp \left\{ \frac{i\omega}{2} \left((\theta_0^2 + \gamma^{-2}) t_{\text{ret}} + \frac{\omega_c^2}{3} t_{\text{ret}}^3 \right) \right\} dt_{\text{ret}}, \\ a_y &\equiv \omega \int_{-\infty}^{+\infty} \theta_0 \exp \left\{ \frac{i\omega}{2} \left((\theta_0^2 + \gamma^{-2}) t_{\text{ret}} + \frac{\omega_c^2}{3} t_{\text{ret}}^3 \right) \right\} dt_{\text{ret}}, \end{aligned} \quad (10.68)$$

that describe the frequency spectra of two components of the synchrotron radiation, with mutually perpendicular polarization planes. Defining the following dimensionless parameter

$$\nu \equiv \frac{\omega}{3\omega_c} (\theta_0^2 + \gamma^{-2})^{3/2}, \quad (10.69)$$

²¹ This expression confirms that the in-plane (x) component of the electric field is an odd function of t_{ret} and hence of $t - t_0$ (see its sketch in Fig. 7b), while the normal (y) component is an even function of this difference. Also, note that for an observer exactly in the rotation plane ($\theta_0 = 0$) the latter component equals zero for all times – the fact which could be predicted from the very beginning because of the evident mirror symmetry of the problem with respect to the particle's rotation plane.

which is proportional to the observation frequency, and changing the integration variable to $\xi \equiv \omega_{ct_{\text{ret}}} / (\theta_0^2 + \gamma^2)^{1/2}$, the integrals (68) may be reduced to the modified Bessel functions of the second kind, but with fractional indices:

$$a_x = \frac{\omega}{\omega_c} \left(\theta_0^2 + \gamma^{-2} \right)^{1/2} \int_{-\infty}^{+\infty} \xi \exp \left\{ \frac{3}{2} i \nu \left(\xi + \frac{\xi^3}{3} \right) \right\} d\xi = \frac{2\sqrt{3} i}{(\theta_0^2 + \gamma^{-2})^{1/2}} \nu K_{2/3}(\nu),$$

$$a_y = \frac{\omega}{\omega_c} \theta_0 \left(\theta_0^2 + \gamma^{-2} \right)^{1/2} \int_{-\infty}^{+\infty} \exp \left\{ \frac{3}{2} i \nu \left(\xi + \frac{\xi^3}{3} \right) \right\} d\xi = \frac{2\sqrt{3} \theta_0}{\theta_0^2 + \gamma^{-2}} \nu K_{1/3}(\nu)$$
(10.70)

Figure 9a shows the dependence of the Bessel factors defining the amplitudes a_x and a_y on the normalized observation frequency ν . It shows that the radiation intensity changes with frequency relatively slowly (note the log-log scale of the plot!) until the normalized frequency defined by Eq. (69) is increased beyond ~ 1 . For the most important observation angles $\theta_0 \sim \gamma$, this means that our estimate (50) is indeed correct, though formally the frequency spectrum extends to infinity.²²

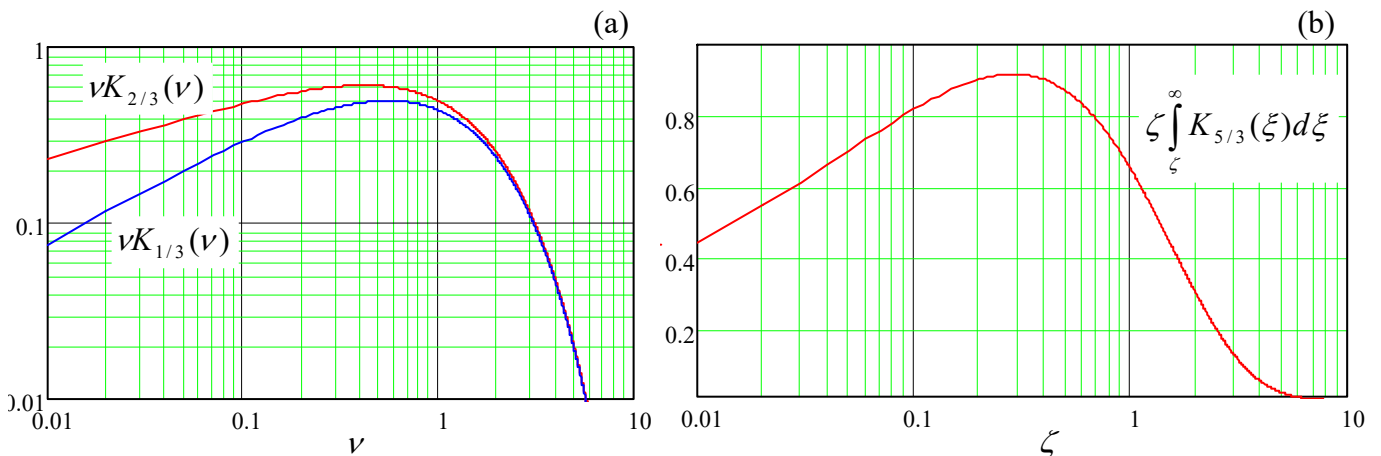


Fig. 10.9. The frequency spectra of: (a) two components of the synchrotron radiation, at a fixed angle θ_0 , and
 (b) its total (polarization- and angle-averaged) intensity.

Naturally, the spectral density integrated over the full solid angle exhibits a similar frequency behavior. Without performing the integration,²³ let me just give the result (also valid for $\gamma \gg 1$ only) for the reader's reference:

$$\oint_{\frac{4\pi}{\omega}} I(\omega) d\Omega = \frac{\sqrt{3}}{4\pi} q^2 \gamma \zeta \int_{-\infty}^{\infty} K_{5/3}(\xi) d\xi, \quad \text{where } \zeta \equiv \frac{2}{3} \frac{\omega}{\omega_c \gamma^3}. \quad (10.71)$$

Figure 9b shows the dependence of this integral on the normalized frequency ζ . (This plot is sometimes called the “universal flux curve”.) In accordance with the estimate (50), it reaches the maximum at

²² The law of the spectral density decrease at large ν may be readily obtained from the second of Eqs. (2.158), which is valid even for any (even non-integer) Bessel function index n : $a_x \propto a_y \propto \nu^{1/2} \exp\{-\nu\}$. Here the exponential factor is certainly the most important one.

²³ For that, and many other details, the interested reader may be referred, for example, to the fundamental review collection by E. Koch *et al.* (eds.) *Handbook on Synchrotron Radiation* (in 5 vols.), North-Holland, 1983-1991, or to a more concise monograph by A. Hofmann, *The Physics of Synchrotron Radiation*, Cambridge U. Press, 2007.

$$\zeta_{\max} \approx 0.3, \text{ i.e. } \omega_{\max} \approx \frac{\omega_c}{2} \gamma^3. \quad (10.72)$$

For example, in the National Synchrotron Light Source (NSLS-II) in the Brookhaven National Laboratory near our SBU campus, with its ring's circumference of 792 m, the electron revolution period \mathcal{T} is $2.64 \mu\text{s}$. With $\omega_c = 2\pi/\mathcal{T} \approx 2.4 \times 10^6 \text{ s}^{-1}$, for the achieved $\gamma \approx 6 \times 10^3$ ($\mathcal{E} \approx 3 \text{ GeV}$), we get $\omega_{\max} \sim 3 \times 10^{17} \text{ s}^{-1}$, i.e. the photon energy $\hbar\omega_{\max} \sim 200 \text{ eV}$ corresponding to soft X-rays. In light of this estimate, the reader may be surprised by Fig. 10, which shows the calculated spectra of the radiation that this facility was designed to produce, with the intensity maxima at photon energies up to a few keV.

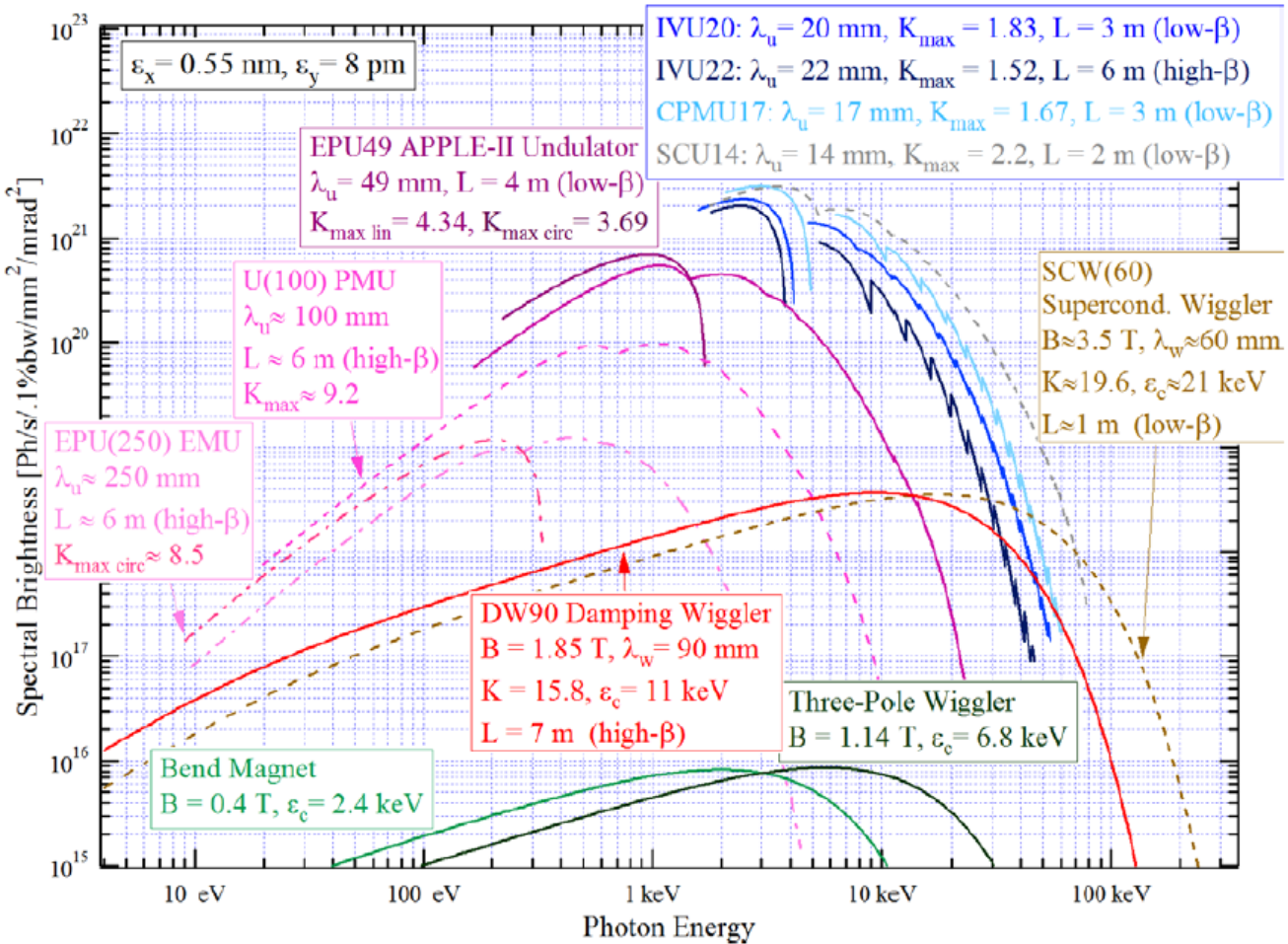


Fig. 10.10. Design brightness of various synchrotron radiation sources of the NSLS-II facility. For the bend magnets and wigglers, the “brightness” may be obtained by multiplication of the one-pulse spectral density $I(\omega)$ calculated above, by the number of electrons passing the source per second. (Note the non-SI units used by the synchrotron radiation community.) However, for undulators, there is an additional factor due to the partial coherence of radiation – see below. (Adapted from the document *NSLS-II Source Properties and Floor Layout* that was available online at <https://www.bnl.gov/ps/docs/pdf/SourceProperties.pdf> in 2011-2020.)

The reason for this discrepancy is that in the NSLS-II, and in all modern synchrotron light sources, most radiation is produced not by the circular orbit itself (which is, by the way, not exactly

circular, but consists of a series of straight and bend-magnet sections), but by such bend sections, and the devices called *wigglers* and *undulators*: strings of several strong magnets with alternating field direction (Fig. 11), that induce periodic bending (“wiggling”) of the electron’s trajectory, with the synchrotron radiation emitted at each bend.

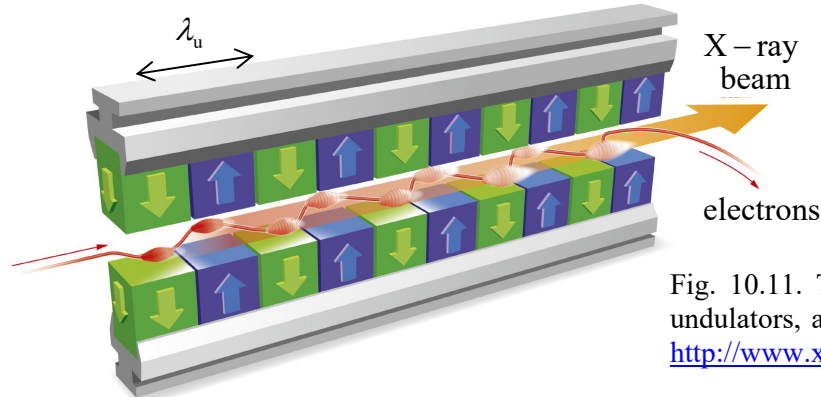


Fig. 10.11. The generic structure of the wigglers, undulators, and free-electron lasers. (Adapted from http://www.xfel.eu/overview/how_does_it_work/.)

The difference between the wigglers and the undulators is more quantitative than qualitative: the former devices have a larger spatial period λ_u (the distance between the adjacent magnets of the same polarity, see Fig. 11), giving enough space for the electron beam to bend by an angle larger than γ^{-1} , i.e. larger than the radiation cone’s width. As a result, the radiation reaches an in-plane observer as a periodic sequence of individual pulses – see Fig. 12a.

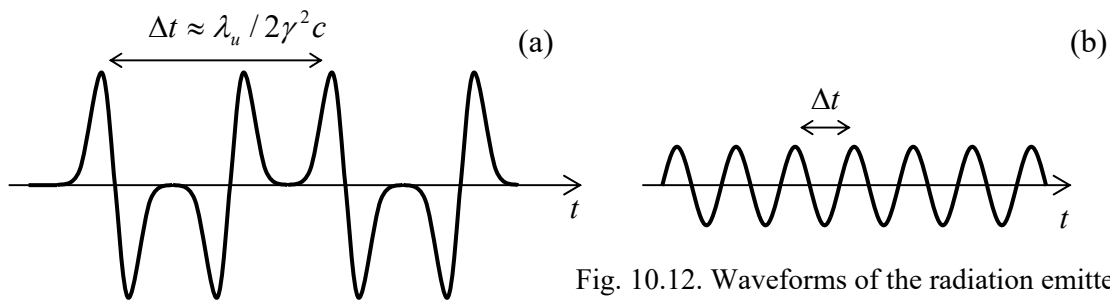


Fig. 10.12. Waveforms of the radiation emitted by (a) a wiggler and (b) an undulator – schematically.

The shape of each pulse, and hence its frequency spectrum, are essentially similar to those discussed above,²⁴ but with much higher local values of ω_c and hence ω_{\max} – see Fig. 10. Another difference is a much higher frequency of the pulses. Indeed, the fundamental Eq. (16) allows us to calculate the time distance between them, for the observer, as

$$\Delta t \approx \frac{\partial t}{\partial t_{\text{ret}}} \Delta t_{\text{ret}} \approx (1 - \beta) \frac{\lambda_u}{u} \approx \frac{1}{2\gamma^2} \frac{\lambda_u}{c} \ll \frac{\lambda_u}{c}, \quad (10.73)$$

²⁴ Indeed, the period λ_u is typically a few centimeters (see the numbers in Fig. 10), i.e. is much larger than the interval $\Delta r' \sim R/\gamma^3$ estimated above. Hence the synchrotron radiation results may be applied locally, to each electron beam’s bend. (In this context, a simple problem for the reader: use Eqs. (19) and (63) to explain the difference between shapes of the in-plane electric field pulses emitted at opposite magnetic poles of the wiggler, which is schematically shown in Fig. 12a.)

where the first two relations are valid at $\lambda_u \ll R$ (the relation typically satisfied very well, see the numbers in Fig. 10), and the last two relations assume the ultra-relativistic limit. As a result, the radiation intensity, which is proportional to the number of the poles, is much higher than that from the bend magnets – see Fig. 10 again.

The situation is different in undulators – similar structures with a smaller spatial period λ_u , in which the electron's velocity vector oscillates with an angular amplitude smaller than γ^{-1} . As a result, the radiation pulses overlap (Fig. 12b), and the radiation waveform is closer to the sinusoidal one. As a result, the radiation spectrum narrows to the central frequency²⁵

$$\omega_0 = \frac{2\pi}{\Delta t} \approx 2\gamma^2 \frac{2\pi c}{\lambda_u}. \quad (10.74)$$

For example, for the LSNL-II undulators with $\lambda_u = 2$ cm, this formula predicts a radiation peak at phonon energy $\hbar\omega_0 \approx 4$ keV, in reasonable agreement with the quantitative calculation results shown in Fig. 10.²⁶ Due to the spectrum narrowing, the undulator's radiation intensity is higher than that of wigglers using the same electron beam.

This spectrum-narrowing trend is brought to its logical conclusion in the so-called *free-electron lasers*²⁷ whose basic structure is the same as that of wigglers and undulators (Fig. 11), but the radiation at each beam bend is so intense and narrow-focused that it affects the electron motion downstream of the radiation cone. As a result, the radiation spectrum narrows around the central frequency (74), and its power grows as a square of the number N of electrons in the structure (rather than proportionately to N in wigglers and undulators).

Finally, note that wigglers, undulators, and free-electron lasers may be also used at the end of a linear electron accelerator (such as SLAC) which, as was noted above, may provide extremely high values of γ , and hence radiation frequencies, due to the smallness of radiation energy losses at the electron acceleration stage. Very unfortunately, I do not have time/space to discuss the (very interesting) physics of these devices in more detail.²⁸

10.4. Bremsstrahlung and Coulomb losses

Surprisingly, a very similar mechanism of radiation by charged particles works on a much smaller spatial scale, namely at their scattering by charged particles of the propagation medium. This

²⁵ This important formula may be also derived in the following way. Due to the relativistic length contraction (9.20), the undulator structure period as perceived by beam electrons is $\lambda' = \lambda_u/\gamma$, so that the central frequency of the radiation in the reference frame moving with the electrons is $\omega_0' = 2\pi c/\lambda' = 2\pi c/\lambda_u$. For the lab-frame observer, this frequency is Doppler-upshifted in accordance with Eq. (9.44): $\omega_0 = \omega_0'[(1 + \beta)/(1 - \beta)]^{1/2} \approx 2\gamma\omega_0'$, giving the same result as Eq. (74).

²⁶ Some of the difference is due to the fact that those plots show the spectral density of the number of photons $n = \mathcal{E}/\hbar\omega$ per second, which peaks at a frequency below that of the density of power, i.e. of the energy \mathcal{E} per second.

²⁷ This name is somewhat misleading, because in contrast to the usual (“quantum”) lasers, a free-electron laser is essentially a classical device, and the dynamics of electrons in it is very similar to that in vacuum-tube microwave generators, such as the magnetrons briefly discussed in Sec. 9.6.

²⁸ The interested reader may be referred, for example, to either P. Luchini and H. Motz, *Undulators and Free-electron Lasers*, Oxford U. Press, 1990; or E. Salin *et al.*, *The Physics of Free Electron Lasers*, Springer, 2000.

effect, traditionally called by its German name *bremsstrahlung* (“brake radiation”), is responsible, in particular, for the continuous part of the frequency spectrum of the radiation produced in standard vacuum X-ray tubes, at the electron collisions with a metallic “anticathode”.²⁹

The bremsstrahlung in condensed matter is generally a rather complicated phenomenon because of the simultaneous involvement of many particles, and (frequently) some quantum electrodynamic effects. This is why I will give only a very brief glimpse at the theoretical description of this effect, for the simplest case when the scattering of incoming, relatively light charged particles (such as electrons, protons, α -particles, etc.) is produced by atomic nuclei, which remain virtually immobile during the scattering event (Fig. 13a). This is a reasonable approximation if the energy of incoming particles is not too low; otherwise, most scattering is produced by atomic electrons whose dynamics is substantially quantum – see below.

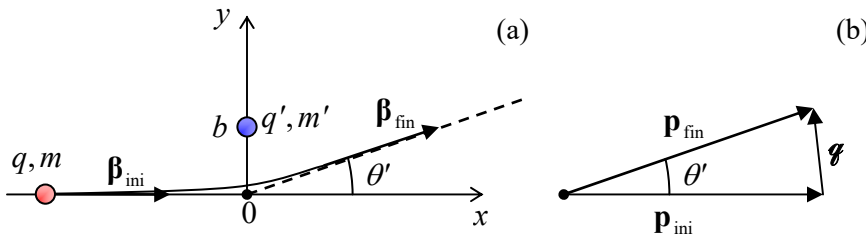


Fig. 10.13. The basic geometry of the bremsstrahlung and the Coulomb loss problems in the (a) direct and (b) reciprocal spaces.

To calculate the frequency spectrum of the radiation emitted during a single scattering event, it is convenient to use a byproduct of the last section’s analysis, namely Eq. (59) with the replacement (60):³⁰

$$I(\omega) = \frac{1}{4\pi^2 c} \frac{q^2}{4\pi\epsilon_0} \left| \int_{-\infty}^{+\infty} \left[\frac{d}{dt} \frac{\mathbf{n} \times (\mathbf{n} \times \boldsymbol{\beta})}{1 - \boldsymbol{\beta} \cdot \mathbf{n}} \exp \left\{ i\omega \left(t - \frac{\mathbf{n} \cdot \mathbf{r}'}{c} \right) \right\} \right]_{\text{ret}} dt \right|^2. \quad (10.75)$$

A typical duration τ of a single scattering event we are discussing is of the order of $\tau \equiv a_0/c \sim (10^{-10} \text{ m})/(3 \times 10^8 \text{ m/s}) \sim 10^{-18} \text{ s}$ in solids, and only an order of magnitude longer in gases at ambient conditions. This is why for most frequencies of interest, from zero all the way up to at least soft X-rays,³¹ we can use the so-called *low-frequency approximation*, taking the exponent in Eq. (75) for 1 through the whole collision event, i.e. the integration interval. This approximation immediately yields

Bremsstrahlung:
single collision

$$I(\omega) = \frac{1}{4\pi^2 c} \frac{q^2}{4\pi\epsilon_0} \left| \frac{\mathbf{n} \times (\mathbf{n} \times \boldsymbol{\beta}_{\text{fin}})}{1 - \boldsymbol{\beta}_{\text{fin}} \cdot \mathbf{n}} - \frac{\mathbf{n} \times (\mathbf{n} \times \boldsymbol{\beta}_{\text{ini}})}{1 - \boldsymbol{\beta}_{\text{ini}} \cdot \mathbf{n}} \right|^2. \quad (10.76)$$

²⁹ Such X-ray radiation had been first observed experimentally (though not correctly interpreted) by N. Tesla in 1887, i.e. before it was rediscovered and studied in detail by W. Röntgen.

³⁰ In publications on this topic (whose development peak was in the 1920s-1930s), the Gaussian units are more common, and the uppercase letter Z is usually reserved for expressing charges as multiples of the fundamental charge e , rather than for the wave impedance. This is why, in order to avoid confusion and facilitate the comparison with other texts, in this section I (while still staying with the SI units used throughout my series) will use the fraction $1/\epsilon_0 c$, instead of its equivalent Z_0 , for the free-space wave impedance, and write the coefficients in a form that makes the transfer to the Gaussian units elementary: it is sufficient to replace all $(qq'/4\pi\epsilon_0)_\text{SI}$ with $(qq')_\text{Gaussian}$. In the (rare) cases when I spell out the charge values, I will use a different font: $q \equiv \mathcal{Z}e$, $q' \equiv \mathcal{Z}'e$.

³¹ A more careful analysis shows that this approximation is actually quite reasonable up to much higher frequencies, of the order of γ^2/τ .

In the non-relativistic limit ($\beta_{\text{ini}}, \beta_{\text{fin}} \ll 1$), this formula is reduced to the following result:

$$I(\omega) = \frac{1}{4\pi^2 c} \frac{q^2}{4\pi\epsilon_0} \frac{\mathbf{q}^2}{m^2 c^2} \sin^2 \theta \quad (10.77)$$

(which may be derived from Eq. (8.27) as well), where \mathbf{q} is the momentum transferred from the scattering center to the scattered charge (Fig. 13b):³²

$$\mathbf{q} \equiv \mathbf{p}_{\text{fin}} - \mathbf{p}_{\text{ini}} = m\Delta\mathbf{u} = mc\Delta\mathbf{v} = mc(\mathbf{v}_{\text{fin}} - \mathbf{v}_{\text{ini}}), \quad (10.78)$$

and θ (not to be confused with the particle scattering angle θ' shown in Fig. 13!) is the angle between the vector \mathbf{q} and the direction \mathbf{n} toward the observer – at the collision moment.

The most important feature of the result (77)-(78) is the frequency-independent (“white”) spectrum of the radiation, very typical for any rapid pulses that may be approximated as delta functions of time.³³ (Note, however, that Eq. (77) implies a fixed value of \mathbf{q} , so that the statistics of this parameter, to be discussed in a minute, may “color” the radiation.)

Note also the “doughnut-shaped” angular distribution of the radiation, typical for non-relativistic systems, with the symmetry axis directed along the momentum transfer vector \mathbf{q} . In particular, this means that in typical cases when $|\theta'| \ll 1$, i.e. $\mathbf{q} \ll \mathbf{p}$, when the vector \mathbf{q} is nearly normal to the vector \mathbf{p}_{ini} (see, e.g., the example shown in Fig. 13b), the bremsstrahlung produces a significant radiation flow in the direction back to the particle source – the fact significant for the operation of X-ray tubes.

Now integrating Eq. (77) over all wave propagation angles, just as we did for the instant radiation power in Sec. 8.2, we get the following spectral density of the particle energy loss,

$$-\frac{d\mathcal{E}}{d\omega} = \oint_{4\pi} I(\omega) d\Omega = \frac{2}{3\pi c} \frac{q^2}{4\pi^2 \epsilon_0} \frac{\mathbf{q}^2}{m^2 c^2}. \quad (10.79)$$

In most applications of the bremsstrahlung theory (as in most scattering problems³⁴), the impact parameter b (Fig. 13a), and hence the scattering angle θ' and the transferred momentum \mathbf{q} , have to be

³² Please note the font-marked difference between this variable (\mathbf{q}) and the particle’s electric charge (q).

³³ This is the basis, in particular, of the so-called *High-Harmonic Generation* (HHG) effect, discovered in 1977, which takes place at the irradiation of gases by intensive laser beams. The high electric field of the beam strips valent electrons from initially neutral atoms, and accelerates them away from the remaining ions, just to slam them back into the ions as the field’s polarity changes in time. The electrons change their momentum sharply during their recombination with the ions, resulting in bremsstrahlung-like radiation. The spectrum of radiation from each such event obeys Eq. (77), but since the ionization/acceleration/recombination cycles repeat periodically with the frequency ω_0 of the laser field, the final spectrum consists of many equidistant lines, with frequencies $n\omega_0$. The classical theory of the bremsstrahlung does not give a cutoff $\omega_{\text{max}} = n_{\text{max}}\omega_0$ of the spectrum; this limit is imposed by quantum mechanics: $\hbar\omega_{\text{max}} \sim \mathcal{E}_p$, where the so-called *ponderomotive energy* $\mathcal{E}_p = (eE_0/\omega_0)^2/4m_e$ is the average kinetic energy given to a free electron by the periodic electric field of the laser beam, with amplitude E_0 . In practice, n_{max} may be as high as ~ 100 , enabling alternative compact sources of X-ray radiation. For a detailed quantitative theory of this effect, see, for example, M. Lewenstein *et al.*, *Phys. Rev. A* **49**, 2117 (1994).

³⁴ See, e.g., CM Sec. 3.5 and QM Sec. 3.3.

considered random. For elastic ($\beta_{\text{ini}} = \beta_{\text{fin}} \equiv \beta$) Coulomb collisions we can use the so-called *Rutherford formula* for the differential cross-section of scattering³⁵

$$\frac{d\sigma}{d\Omega'} = \left(\frac{qq'}{4\pi\epsilon_0} \right)^2 \left(\frac{1}{2pc\beta} \right)^2 \frac{1}{\sin^4(\theta'/2)}. \quad (10.80)$$

Here $d\sigma = 2\pi bdb$ is the elementary area of the sample cross-section (as visible from the direction of the incident particles) corresponding to their scattering into an elementary body angle³⁶

$$d\Omega' = 2\pi \sin \theta' |d\theta'|. \quad (10.81)$$

Differentiating the geometric relation, which is evident from Fig. 13b,

$$q = 2p \sin \frac{\theta'}{2}, \quad (10.82)$$

we may represent Eq. (80) in a more convenient form

$$\frac{d\sigma}{dq} = 8\pi \left(\frac{qq'}{4\pi\epsilon_0} \right)^2 \frac{1}{u^2 q^3}. \quad (10.83)$$

Now combining Eqs. (79) and (83), we get

$$-\frac{d\mathcal{E}}{d\omega} \frac{d\sigma}{dq} = \frac{16}{3} \frac{q^2}{4\pi\epsilon_0} \left(\frac{qq'}{4\pi\epsilon_0 mc^2} \right)^2 \frac{1}{c\beta^2} \frac{1}{q}. \quad (10.84)$$

This product is called the *differential radiation cross-section*. When integrated over all values of q (which is equivalent to averaging over all values of the impact parameter), it gives a convenient measure of the radiation intensity. Indeed, after the multiplication by the volume density n of independent scattering centers, such integral yields the particle's energy loss per unit bandwidth of radiation per unit path length, $-d^2\mathcal{E}/d\omega dx$. A minor problem here is that the integral of $1/q$ formally diverges at both infinite and zero values of q . However, these divergences are very weak (logarithmic), and the integral converges due to virtually any reason unaccounted for in our simple analysis. The standard (though slightly approximate) way to account for these effects is to write

$$-\frac{d^2\mathcal{E}}{d\omega dx} \approx \frac{16}{3} n \frac{q^2}{4\pi\epsilon_0} \left(\frac{qq'}{4\pi\epsilon_0 mc^2} \right)^2 \frac{1}{c\beta^2} \ln \frac{q_{\max}}{q_{\min}}, \quad (10.85)$$

Bremsstrahlung:
intensity

and then plug, instead of q_{\max} and q_{\min} , the scales of the most important effects limiting the range of the transferred momentum's magnitude. In the classical-mechanics analysis, according to Eq. (82), $q_{\max} = 2p \equiv 2mu$. To estimate q_{\min} , let us note that the very small momentum transfer takes place when the impact parameter b is very large, and hence the effective scattering time $\tau \sim b/v$ is very long. Recalling the condition of the low-frequency approximation, we may associate q_{\min} with $\tau \sim 1/\omega$ and hence with $b \sim$

³⁵ See, e.g., CM Eq. (3.73) with $\alpha = qq'/4\pi\epsilon_0$. In the form used in Eq. (80), the Rutherford formula is also valid for the small-angle scattering of relativistic particles, the criterion being $|\Delta\beta| \ll 2/\gamma$.

³⁶ Again, the angle θ' and the differential $d\Omega'$, describing the scattered particles (see Fig. 13) should not be confused with the parameters θ and $d\Omega$ describing the *radiation* emitted at the scattering event.

$ut \sim v/\omega$. Since for the small scattering angles, γ is close to the impulse $F\tau \sim (qq'/4\pi\epsilon_0 b^2)\tau$ of the Coulomb force, we get the estimate $\gamma_{\min} \sim (qq'/4\pi\epsilon_0)\omega/u^2$, and Eq. (85) should be used with

$$\ln \frac{\gamma_{\max}}{\gamma_{\min}} = \ln \left(\frac{2mu^3}{\omega} \Big/ \frac{qq'}{4\pi\epsilon_0} \right). \quad (10.86)$$

Classical
brems-
strahlung

This is *Bohr's formula* for what is called the *classical bremsstrahlung*. We see that the low momentum cutoff indeed makes the spectrum slightly colored, with more energy going to lower frequencies. There is even a formal divergence at $\omega \rightarrow 0$; however, this divergence is integrable, so it does not present a problem for finding the total energy radiative losses ($-dE/dx$) as an integral of Eq. (86) over all radiated frequencies ω . A larger problem for this procedure is the upper integration limit, $\omega \rightarrow \infty$, at which the integral diverges. This means that our approximate description, which considers the collision as an elastic process, becomes invalid and needs to be amended by taking into account the difference between the initial and final kinetic energies of the particle due to radiation of the energy quantum $\hbar\omega$ of the emitted photon, so that

$$\frac{p_{\text{ini}}^2}{2m} - \frac{p_{\text{fin}}^2}{2m} = \hbar\omega, \quad \text{i.e. } \frac{p_{\text{ini}}^2}{2m} = E, \quad \frac{p_{\text{fin}}^2}{2m} = E - \hbar\omega, \quad . \quad (10.87)$$

As a result, taking into account that the minimum and maximum values of γ correspond to, respectively, the parallel and antiparallel alignments of the vectors \mathbf{p}_{ini} and \mathbf{p}_{fin} , we get

$$\ln \frac{\gamma_{\max}}{\gamma_{\min}} = \ln \frac{p_{\text{ini}} + p_{\text{fin}}}{p_{\text{ini}} - p_{\text{fin}}} \equiv \ln \frac{(p_{\text{ini}} + p_{\text{fin}})^2 / 2m}{(p_{\text{ini}}^2 - p_{\text{fin}}^2) / 2m} = \ln \frac{[E^{1/2} + (E - \hbar\omega)^{1/2}]^2}{\hbar\omega}, \quad (10.88)$$

Quantum
brems-
strahlung

Plugged into Eq. (85), this expression yields the so-called *Bethe-Heitler formula* for *quantum bremsstrahlung*.³⁷ Note that at this approach, γ_{\max} is close to that of the classical approximation, but γ_{\min} is of the order of $\hbar\omega/u$, so that

$$\frac{\gamma_{\min}|_{\text{classical}}}{\gamma_{\min}|_{\text{quantum}}} \sim \frac{\alpha \mathcal{T} \mathcal{T}'}{\beta}, \quad (10.89)$$

where \mathcal{T} and \mathcal{T}' are the particles' charges in the units of e , and α is the dimensionless *fine structure* ("Sommerfeld") *constant*,

$$\alpha \equiv \frac{e^2}{4\pi\epsilon_0 \hbar c}|_{\text{SI}} = \frac{e^2}{\hbar c}|_{\text{Gaussian}} \approx \frac{1}{137} \ll 1, \quad (10.90)$$

which is one of the basic notions of quantum mechanics.³⁸ Due to the smallness of the constant, the ratio (89) is below 1 for most cases of practical interest, and since the integral of (84) over γ is limited by the largest of all possible cutoffs γ_{\min} , it is the Bethe-Heitler formula that should be used.

³⁷ The modifications of this formula necessary for the relativistic description are surprisingly minor – see, e.g., Chapter 15 in J. Jackson, *Classical Electrodynamics*, 3rd ed., Wiley 1999. For even more detail, the standard reference monograph on bremsstrahlung is W. Heitler, *The Quantum Theory of Radiation*, 3rd ed., Oxford U. Press 1954 (reprinted in 1984 and 2010 by Dover).

³⁸ See, e.g., QM Secs. 4.4, 6.3, 6.4, 9.3, 9.5, and 9.7.

Now nothing prevents us from calculating the total radiative losses of energy per unit length:

$$-\frac{d\mathcal{E}}{dx} = \int_0^\infty \left(-\frac{d^2\mathcal{E}}{d\omega dz} \right) d\omega = \frac{16}{3} n \frac{q^2}{4\pi\epsilon_0 c} \left(\frac{qq'}{4\pi\epsilon_0 mc^2} \right)^2 \frac{1}{\beta^2} 2 \int_0^{\omega_{\max}} \ln \frac{\mathcal{E}^{1/2} - (\mathcal{E} - \hbar\omega)^{1/2}}{(\hbar\omega)^{1/2}} d\omega, \quad (10.91)$$

where $\hbar\omega_{\max} = \mathcal{E}$ is the maximum energy of the radiation quantum. By introducing the dimensionless integration variable $\xi \equiv \hbar\omega/\mathcal{E} = 2\hbar\omega/(mu^2/2)$, this integral is reduced to a table one,³⁹ and we get

$$-\frac{d\mathcal{E}}{dx} = \frac{16}{3} n \frac{q^2}{4\pi\epsilon_0 c} \left(\frac{qq'}{4\pi\epsilon_0 mc^2} \right)^2 \frac{1}{\beta^2} \frac{u^2}{\hbar} \equiv \frac{16}{3} n \left(\frac{q'^2}{4\pi\epsilon_0 \hbar c} \right) \left(\frac{q^2}{4\pi\epsilon_0} \right)^2 \frac{1}{mc^2}. \quad (10.92)$$

Following my usual style, at this point I would give you an estimate of the losses for a typical case; however, let me first discuss a parallel particle energy loss mechanism, the so-called *Coulomb losses*, due to the transfer of mechanical impulse from the scattered particle to the scattering centers. (This energy eventually goes into an increase of the thermal energy of the scattering medium, rather than to the electromagnetic radiation.)

Using Eqs. (9.139) for the electric field of a linearly moving charge q , we can readily find the momentum it transfers to the counterpart charge q' :⁴⁰

$$\Delta p' = |(\Delta p')_y| = \left| \int_{-\infty}^{+\infty} (\dot{p}')_y dt \right| = \left| \int_{-\infty}^{+\infty} q'E_y dt \right| = \frac{qq'}{4\pi\epsilon_0} \int_{-\infty}^{+\infty} \frac{\gamma b}{(b^2 + \gamma^2 u^2 t^2)^{3/2}} dt = \frac{qq'}{4\pi\epsilon_0} \frac{2}{bu}. \quad (10.93)$$

Hence, the kinetic energy acquired by the scattering particle (and hence to the loss of the energy \mathcal{E} of the incident particle) is

$$-\Delta\mathcal{E} = \frac{(\Delta p')^2}{2m'} = \left(\frac{qq'}{4\pi\epsilon_0} \right)^2 \frac{2}{m'u^2 b^2}. \quad (10.94)$$

Such elementary energy losses have to be summed up over all collisions, with random values of the impact parameter b . At the scattering center density n , the number of collisions per small path length dx per small range db is $dN = n 2\pi b db dx$, so that

Coulomb losses

$$-\frac{d\mathcal{E}}{dx} = - \int \Delta\mathcal{E} dN = n \left(\frac{qq'}{4\pi\epsilon_0} \right)^2 \frac{2}{m'u^2} 2\pi \int_{b_{\min}}^{b_{\max}} \frac{db}{b} = 4\pi n \left(\frac{qq'}{4\pi\epsilon_0} \right)^2 \frac{\ln B}{m'u^2}, \quad \text{where } B \equiv \frac{b_{\max}}{b_{\min}}. \quad (10.95)$$

Here, at the last step, the logarithmic integral over b was treated similarly to that over q in the bremsstrahlung theory. This approximation is adequate because the ratio b_{\max}/b_{\min} is much larger than 1. Indeed, b_{\min} may be estimated from $(\Delta p')_{\max} \sim p = \gamma mu$. For this value, Eq. (93) with $q' \sim q$ gives $b_{\min} \sim r_c$ (see Eq. (8.41) and its discussion), which, for elementary particles, is of the order of 10^{-15} m. On the other hand, for the most important case when the Coulomb energy absorbers are electrons (which, according to Eq. (94), are the most efficient ones, due to their very low mass m'), b_{\max} may be estimated from the condition $\tau = b/\gamma u \sim 1/\omega_{\min}$, where $\omega_{\min} \sim 10^{16}$ s⁻¹ is the characteristic frequency of electron

³⁹ See, e.g., MA Eq. (6.14).

⁴⁰ According to Eq. (9.139), $E_z = 0$, while the net impulse of the longitudinal force $q'E_x$ is zero, so that Eq. (93) gives the full momentum transfer.

transitions in atoms. (Quantum mechanics forbids such energy transfer at lower frequencies.) From here, we have the estimate $b_{\max} \sim \gamma u / \omega_{\min}$, so that

$$B \equiv \frac{b_{\max}}{b_{\min}} \sim \frac{\gamma u}{r_c \omega_{\min}}, \quad (10.96)$$

for $\gamma \sim 1$ and $u \sim c \approx 3 \times 10^8$ m/s giving $b_{\max} \sim 3 \times 10^{-8}$ m, so that $B \sim 10^9$ (give or take a couple of orders of magnitude – this does not change the estimate $\ln B \approx 20$ too much).⁴¹

Now we can compare the non-radiative Coulomb losses (95) with the radiative losses due to the bremsstrahlung, given by Eq. (92):

$$\frac{-d\mathcal{E}|_{\text{radiation}}}{-d\mathcal{E}|_{\text{Coulomb}}} \sim \alpha \mathcal{F} \frac{m'}{m} \beta^2 \frac{1}{\ln B}, \quad (10.97)$$

Since $\alpha \sim 10^{-2} \ll 1$, for non-relativistic particles ($\beta \ll 1$) the bremsstrahlung losses of energy are much lower (that is why I did not want to rush with their estimates), and only for ultra-relativistic particles, the relation may be opposite.

According to Eqs. (95)-(96), for electron-electron scattering ($q = q' = -e$, $m = m' = m_e$),⁴² at the value $n = 6 \times 10^{26}$ m⁻³ typical for air at ambient conditions, the characteristic length of energy loss,

$$l_c \equiv \frac{\mathcal{E}}{(-d\mathcal{E}/dx)}, \quad (10.98)$$

for electrons with kinetic energy $\mathcal{E} = 6$ keV is close to 2×10^{-4} m $\equiv 0.2$ mm. (This is why we need high vacuum in electron microscope columns and other vacuum electron devices.) Since $l_c \propto \mathcal{E}^2$, more energetic particles penetrate to matter deeper, until the bremsstrahlung steps in, and limits this trend at very high energies.

10.5. Density effects and the Cherenkov radiation

For condensed matter, the Coulomb loss estimate made in the last section is not quite suitable, because it is based on the upper cutoff $b_{\max} \sim \gamma u / \omega_{\min}$. For the example given above, the incoming electron velocity u is close to 5×10^7 m/s, and for the typical value $\omega_{\min} \sim 10^{16}$ s⁻¹ ($\hbar \omega_{\min} \sim 10$ eV), this cutoff b_{\max} is of the order of $\sim 5 \times 10^{-9}$ m = 5 nm. Even for air at ambient conditions, this is somewhat larger than the average distance (~ 2 nm) between the molecules, so that at the high end of the impact parameter range, at $b \sim b_{\max}$, the Coulomb loss events in adjacent molecules are not quite independent, and the theory needs some corrections. For condensed matter, with much higher particle density n , most collisions satisfy the following condition:

⁴¹ A quantum analysis (carried out by Hans Bethe in 1940) replaces, in Eq. (95), $\ln B$ with $\ln(2\gamma^2 m u^2 / \hbar \langle \omega \rangle) - \beta^2$, where $\langle \omega \rangle$ is the average frequency of the atomic quantum transitions weight by their oscillator strength. This refinement does not change the estimate given below. Note that both the classical and quantum formulas describe a fast increase (as $1/\beta$) of the energy loss rate ($-d\mathcal{E}/dx$) at $\gamma \rightarrow 1$, and its slow increase (as $\ln \gamma$) at $\gamma \rightarrow \infty$, so that the losses have a minimum at $(\gamma - 1) \sim 1$.

⁴² Actually, the above analysis has neglected the change of momentum of the incident particle. This is legitimate at $m' \ll m$, but for $m = m'$ the change approximately doubles the energy losses. Still, this does not change the order of magnitude of the estimate.

$$nb^3 \gg 1, \quad (10.99)$$

and the treatment of Coulomb collisions as a set of independent events is inadequate. However, this condition enables the opposite approach: treating the medium as a continuum. In the time-domain formulation used in the previous sections of this chapter, this would be a very complex problem, because it would require an explicit description of the medium dynamics. Here the frequency-domain approach, based on the Fourier transform in both time and space, helps a lot, provided that the functions $\epsilon(\omega)$ and $\mu(\omega)$ are considered known – either calculated or taken from experiment. Let us have a good look at this approach because it gives some interesting (and practically important) results.

In Chapter 6, we have used the macroscopic Maxwell equations to derive Eqs. (6.118), which describe the time evolution of electrodynamic potentials in a linear medium with frequency-independent ϵ and μ . Looking for all functions participating in Eqs. (6.118) in the plane-wave expansion form⁴³

$$f(\mathbf{r}, t) = \int d^3k \int d\omega f_{\mathbf{k}, \omega} e^{i(\mathbf{k} \cdot \mathbf{r} - \omega t)}, \quad (10.100)$$

and requiring all coefficients at similar exponents to be balanced, we get their Fourier images:⁴⁴

$$(k^2 - \omega^2 \epsilon \mu) \phi_{\mathbf{k}, \omega} = \frac{\rho_{\mathbf{k}, \omega}}{\epsilon}, \quad (k^2 - \omega^2 \epsilon \mu) \mathbf{A}_{\mathbf{k}, \omega} = \mu \mathbf{j}_{\mathbf{k}, \omega}. \quad (10.101)$$

As was discussed in Chapter 7, in such a Fourier form, the macroscopic Maxwell theory remains valid even for dispersive (but isotropic and linear!) media, so that Eqs. (101) may be generalized as

$$[k^2 - \omega^2 \epsilon(\omega) \mu(\omega)] \phi_{\mathbf{k}, \omega} = \frac{\rho_{\mathbf{k}, \omega}}{\epsilon(\omega)}, \quad [k^2 - \omega^2 \epsilon(\omega) \mu(\omega)] \mathbf{A}_{\mathbf{k}, \omega} = \mu(\omega) \mathbf{j}_{\mathbf{k}, \omega}, \quad (10.102)$$

An evident advantage of these equations is that their formal solution is elementary:

$$\phi_{\mathbf{k}, \omega} = \frac{\rho_{\mathbf{k}, \omega}}{\epsilon(\omega) [k^2 - \omega^2 \epsilon(\omega) \mu(\omega)]}, \quad \mathbf{A}_{\mathbf{k}, \omega} = \frac{\mu(\omega) \mathbf{j}_{\mathbf{k}, \omega}}{[k^2 - \omega^2 \epsilon(\omega) \mu(\omega)]}, \quad (10.103)$$

Field
potentials
in a linear
medium

so that the “only” remaining things to do is, first, to calculate the Fourier transforms of the functions $\rho(\mathbf{r}, t)$ and $\mathbf{j}(\mathbf{r}, t)$, describing stand-alone charges and currents, using the transform reciprocal to Eq. (100), with one factor $1/2\pi$ per each scalar dimension,

$$f_{\mathbf{k}, \omega} = \frac{1}{(2\pi)^4} \int d^3r \int dt f(\mathbf{r}, t) e^{-i(\mathbf{k} \cdot \mathbf{r} - \omega t)}, \quad (10.104)$$

and then to carry out the integration (100) of Eqs. (103).

For our problem of a single charge q uniformly moving through a medium with velocity \mathbf{u} ,

$$\rho(\mathbf{r}, t) = q \delta(\mathbf{r} - \mathbf{u}t), \quad \mathbf{j}(\mathbf{r}, t) = q \mathbf{u} \delta(\mathbf{r} - \mathbf{u}t), \quad (10.105)$$

⁴³ All integrals here and below are in infinite limits unless specified otherwise.

⁴⁴ As was discussed in Sec. 7.2, the Ohmic conductivity of the medium (generally, also a function of frequency) may be readily incorporated into the dielectric permittivity: $\epsilon(\omega) \rightarrow \epsilon_{\text{ef}}(\omega) + i\sigma(\omega)/\omega$. In this section, I will assume that such incorporation, which is especially natural for high frequencies, has been performed, so that the current density $\mathbf{j}(\mathbf{r}, t)$ describes only stand-alone currents – for example, the current (105) of the incident particle.

the first task is easy:

$$\rho_{\mathbf{k},\omega} = \frac{q}{(2\pi)^4} \int d^3r \int dt q \delta(\mathbf{r} - \mathbf{u}t) e^{-i(\mathbf{k}\cdot\mathbf{r} - \omega t)} = \frac{q}{(2\pi)^4} \int e^{i(\omega t - \mathbf{k}\cdot\mathbf{u}t)} dt = \frac{q}{(2\pi)^3} \delta(\omega - \mathbf{k}\cdot\mathbf{u}). \quad (10.106)$$

Since the expressions (105) for $\rho(\mathbf{r}, t)$ and $\mathbf{j}(\mathbf{r}, t)$ differ only by a constant factor \mathbf{u} , it is clear that the absolutely similar calculation for the current gives

$$\mathbf{j}_{\mathbf{k},\omega} = \frac{q\mathbf{u}}{(2\pi)^3} \delta(\omega - \mathbf{k}\cdot\mathbf{u}). \quad (10.107)$$

Let us summarize what we have got by now, by plugging Eqs. (106)-(107) into Eqs. (103):

$$\phi_{\mathbf{k},\omega} = \frac{1}{(2\pi)^3} \frac{q\delta(\omega - \mathbf{k}\cdot\mathbf{u})}{\varepsilon(\omega)[k^2 - \omega^2\varepsilon(\omega)\mu(\omega)]}, \quad \mathbf{A}_{\mathbf{k},\omega} = \frac{1}{(2\pi)^3} \frac{\mu(\omega)q\mathbf{u}\delta(\omega - \mathbf{k}\cdot\mathbf{u})}{[k^2 - \omega^2\varepsilon(\omega)\mu(\omega)]} \equiv \varepsilon(\omega)\mu(\omega)\mathbf{u}\phi_{\mathbf{k},\omega}. \quad (10.108)$$

Now, at the last calculation step, namely the integration (100), we are starting to pay a heavy price for the easiness of the first steps. This is why let us think well about what exactly we need from it. First of all, for the calculation of power losses, the electric field is more convenient to use than the potentials, so let us calculate the Fourier images of \mathbf{E} and \mathbf{B} . Plugging the expansion (100) into the basic relations (6.7), and again requiring the balance of exponent's coefficients, we get

$$\mathbf{E}_{\mathbf{k},\omega} = -i\mathbf{k}\phi_{\mathbf{k},\omega} + i\omega\mathbf{A}_{\mathbf{k},\omega} = i[\omega\varepsilon(\omega)\mu(\omega)\mathbf{u} - \mathbf{k}]\phi_{\mathbf{k},\omega}, \quad \mathbf{B}_{\mathbf{k},\omega} = i\mathbf{k} \times \mathbf{A}_{\mathbf{k},\omega} = i\varepsilon(\omega)\mu(\omega)\mathbf{k} \times \mathbf{u}\phi_{\mathbf{k},\omega}, \quad (10.109)$$

so that Eqs. (100) and (108) yield

$$\mathbf{E}(\mathbf{r}, t) = \int d^3k \int d\omega \mathbf{E}_{\mathbf{k},\omega} e^{i(\mathbf{k}\cdot\mathbf{r} - \omega t)} = \frac{iq}{(2\pi)^3} \int d^3k \int d\omega \frac{[\omega\varepsilon(\omega)\mu(\omega)\mathbf{u} - \mathbf{k}]\delta(\omega - \mathbf{k}\cdot\mathbf{u})}{\varepsilon(\omega)[k^2 - \omega^2\varepsilon(\omega)\mu(\omega)]} e^{i(\mathbf{k}\cdot\mathbf{r} - \omega t)}. \quad (10.110)$$

This formula may be rewritten as the temporal Fourier integral (51), with the following \mathbf{r} -dependent complex amplitude:

$$\mathbf{E}_\omega(\mathbf{r}) = \int \mathbf{E}_{\mathbf{k},\omega} e^{i\mathbf{k}\cdot\mathbf{r}} d^3k = \frac{iq}{(2\pi)^3} \int \frac{[\omega\varepsilon(\omega)\mu(\omega)\mathbf{u} - \mathbf{k}]\delta(\omega - \mathbf{k}\cdot\mathbf{u})}{\varepsilon(\omega)[k^2 - \omega^2\varepsilon(\omega)\mu(\omega)]} e^{i\mathbf{k}\cdot\mathbf{r}} d^3k. \quad (10.111)$$

Let us calculate the Cartesian components of this partial Fourier image \mathbf{E}_ω , at a point separated by distance b from the particle's trajectory. Selecting the coordinates and time origin as shown in Fig. 3, we have $\mathbf{r} = \{0, b, 0\}$ and $\mathbf{u} = \{u, 0, 0\}$, so that only E_x and E_y are different from zero. In particular, according to Eq. (111),

$$(E_x)_\omega = \frac{iq}{(2\pi)^3\varepsilon(\omega)} \int dk_x \int dk_y \int dk_z \frac{\omega\varepsilon(\omega)\mu(\omega)u - k_x}{k^2 - \omega^2\varepsilon(\omega)\mu(\omega)} \delta(\omega - k_x u) \exp\{ik_y b\}. \quad (10.112)$$

The delta function kills one integral (over k_x) of the three, and we get

$$(E_x)_\omega = \frac{iq}{(2\pi)^3\varepsilon(\omega)u} \left[\omega\varepsilon(\omega)\mu(\omega)u - \frac{\omega}{u} \right] \int \exp\{ik_y b\} dk_y \int \frac{dk_z}{\omega^2/u^2 + k_y^2 + k_z^2 - \omega^2\varepsilon(\omega)\mu(\omega)}. \quad (10.113)$$

The internal integral (over k_z) may be readily reduced to the table integral $\int d\xi/(1 + \xi^2)$ in infinite limits, equal to π ,⁴⁵ and result represented as

$$(E_x)_\omega = -\frac{i\pi q\kappa^2}{(2\pi)^3 \omega \epsilon(\omega)} \int \frac{\exp\{ik_y b\}}{(k_y^2 + \kappa^2)^{1/2}} dk_y, \quad (10.114)$$

where the parameter κ (generally, a complex function of frequency) is defined as⁴⁶

Function $\kappa(\omega)$

$$\kappa^2(\omega) \equiv \omega^2 \left(\frac{1}{u^2} - \epsilon(\omega) \mu(\omega) \right). \quad (10.115)$$

The last integral may be expressed via the modified Bessel function of the second kind:⁴⁷

$$(E_x)_\omega = -\frac{iqu\kappa^2}{(2\pi)^2 \omega \epsilon(\omega)} K_0(\kappa b). \quad (10.116)$$

A very similar calculation yields

$$(E_y)_\omega = \frac{q\kappa}{(2\pi)^2 \epsilon(\omega)} K_1(\kappa b). \quad (10.117)$$

Now, instead of rushing to make the final integration (51) over ω to calculate $\mathbf{E}(t)$, let us realize that what we need most is the total energy loss through the whole time of the particle's passage over an elementary distance dx . According to Eq. (4.38), the energy loss per unit volume is

$$-\frac{d\mathcal{E}}{dV} = \int \mathbf{j} \cdot \mathbf{E} dt, \quad (10.118)$$

where \mathbf{j} is the current of the bound charges in the medium, and should not be confused with the stand-alone incident-particle current (105). This integral may be readily expressed via the partial Fourier image \mathbf{E}_ω and the similarly defined image \mathbf{j}_ω , just as it was done at the derivation of Eq. (54):

$$-\frac{d\mathcal{E}}{dV} = \int dt \int d\omega e^{-i\omega t} \int d\omega' e^{-i\omega' t} \mathbf{j}_\omega \cdot \mathbf{E}_{\omega'} = 2\pi \int d\omega \int d\omega' \mathbf{j}_\omega \cdot \mathbf{E}_{\omega'} \delta(\omega + \omega') = 2\pi \int \mathbf{j}_\omega \cdot \mathbf{E}_{-\omega} d\omega. \quad (10.119)$$

Let us incorporate the effective Ohmic conductivity $\sigma_{\text{ef}}(\omega)$ into the complex permittivity $\epsilon(\omega)$ just as this was discussed in Sec. 7.2, using Eq. (7.46) to write

$$\mathbf{j}_\omega = \sigma_{\text{ef}}(\omega) \mathbf{E}_\omega = -i\omega \epsilon(\omega) \mathbf{E}_\omega. \quad (10.120)$$

As a result, Eq. (119) yields

$$-\frac{d\mathcal{E}}{dV} = -2\pi i \int \epsilon(\omega) \mathbf{E}_\omega \cdot \mathbf{E}_{-\omega} \omega d\omega = 4\pi \text{Im} \int_0^\infty \epsilon(\omega) |E_\omega|^2 \omega d\omega. \quad (10.121)$$

(The last step was possible due to the property $\epsilon(-\omega) = \epsilon^*(\omega)$, which was discussed in Sec. 7.2.)

⁴⁵ See, e.g., MA Eq. (6.5a).

⁴⁶ The frequency-dependent parameter $\kappa(\omega)$ should not be confused with the dc low-frequency dielectric constant $\kappa \equiv \epsilon(0)/\epsilon_0$ that was discussed in Chapter 3.

⁴⁷ As a reminder, the main properties of these functions are listed in Sec. 2.7 – see, in particular, Fig. 2.22 and Eqs. (2.157)-(2.158).

Finally, just as in the last section, we have to average the energy loss rate over random values of the impact parameter b :

$$-\frac{d\mathcal{E}}{dx} = \int \left(-\frac{d\mathcal{E}}{dV} \right) d^2 b \approx 2\pi \int_{b_{\min}}^{\infty} \left(-\frac{d\mathcal{E}}{dV} \right) b db = 8\pi^2 \int_{b_{\min}}^{\infty} b db \int_0^{\infty} \left(|E_x|^2 + |E_y|^2 \right) \text{Im } \varepsilon(\omega) \omega d\omega. \quad (10.122)$$

Due to the (weak) divergence of the functions $K_0(\xi)$ and $K_1(\xi)$ at $\xi \rightarrow 0$, we have to cut the resulting integral over b at some b_{\min} where our theory loses legitimacy. (On that limit, we are not doing much better than in the past section). Plugging in the calculated expressions (116) and (117) for the field components, swapping the integrals over ω and b , and using the recurrence relations (2.142), which are valid for all Bessel functions, we finally get:

$$-\frac{d\mathcal{E}}{dx} = \frac{2}{\pi} q^2 \text{Im} \int_0^{\infty} (\kappa^* b_{\min}) K_1(\kappa^* b_{\min}) K_0(\kappa^* b_{\min}) \frac{d\omega}{\omega \varepsilon(\omega)}. \quad (10.123)$$

Radiation intensity

This general result is valid for a linear medium with arbitrary dispersion relations $\varepsilon(\omega)$ and $\mu(\omega)$. (The last function participates in Eq. (123) only via Eq. (115) that defines the parameter κ .) To get more concrete results, some particular model of the medium should be used. Let us explore the Lorentz-oscillator model that was discussed in Sec. 7.2, in its form (7.33) suitable for the transition to the quantum-mechanical description of atoms:

$$\varepsilon(\omega) = \varepsilon_0 + \frac{nq'^2}{m} \sum_j \frac{f_j}{(\omega_j^2 - \omega^2) - 2i\omega\delta_j}, \quad \text{with } \sum_j f_j = 1; \quad \mu(\omega) = \mu_0. \quad (10.124)$$

If the damping of the effective atomic oscillators is low, $\delta_j \ll \omega_j$, as it typically is, and the particle's speed u is much lower than the typical wave's phase velocity v (and hence than c !), then for most frequencies Eq. (115) gives

$$\kappa^2(\omega) \equiv \omega^2 \left(\frac{1}{u^2} - \frac{1}{v^2(\omega)} \right) \approx \frac{\omega^2}{u^2}, \quad (10.125)$$

i.e. $\kappa \approx \kappa^* \approx \omega/u$ is virtually real. In this case, Eq. (123) may be reduced to Eq. (95) with

$$b_{\max} = \frac{1.123u}{\langle \omega \rangle}. \quad (10.126)$$

The good news here is that both approaches (the microscopic analysis of Sec. 4 and the macroscopic analysis of this section) give essentially the same result. The same fact may be also perceived as bad news: the treatment of the medium as a continuum does not give any new results here. The situation somewhat changes at relativistic velocities, at which such treatment provides noticeable corrections (called *density effects*), in particular reducing the energy loss estimates.

Let me, however, leave these details for special topic courses and focus on a much more important effect described by our formulas. Consider the dependence of the electric field components on the impact parameter b , i.e. on the closest distance between the particle's trajectory and the field observation point. At $b \rightarrow \infty$, we can use, in Eqs. (116)-(117), the asymptotic formula (2.158),

$$K_n(\xi) \rightarrow \left(\frac{\pi}{2\xi} \right)^{1/2} e^{-\xi}, \quad \text{at } \xi \rightarrow \infty, \quad (10.127)$$

to conclude that if $\kappa^2 > 0$, i.e. if κ is real, the complex amplitudes E_ω of both components E_x and E_y of the electric field decrease with b exponentially. However, let us consider what happens at frequencies where $\kappa^2(\omega) < 0$,⁴⁸ i.e.

$$\varepsilon(\omega)\mu(\omega) \equiv \frac{1}{v^2(\omega)} < \frac{1}{u^2} < \frac{1}{c^2} \equiv \varepsilon_0\mu_0. \quad (10.128)$$

(This condition means that the particle's velocity is larger than the phase velocity of the waves at this particular frequency.) In this case, the parameter $\kappa(\omega)$ is purely imaginary, so that the functions $\exp\{kb\}$ in the asymptotes (127) of Eqs. (116)-(117) become just phase factors, and the field component amplitudes fall very slowly:

$$|E_x(\omega)| \propto |E_y(\omega)| \propto \frac{1}{b^{1/2}}. \quad (10.129)$$

This means that the Poynting vector drops as $1/b$, so that its flux through a surface of a round cylinder of radius b , with its axis on the particle trajectory (i.e. the power flow from the particle), does not depend on b at all. This is an electromagnetic wave emission – the famous *Cherenkov radiation*.⁴⁹

The direction \mathbf{n} of its propagation may be readily found taking into account that at large distances from the particle's trajectory, the emitted wave has to be locally planar and transverse ($\mathbf{n} \perp \mathbf{E}$), so that the so-called *Cherenkov angle* θ between the vector \mathbf{n} and the particle's velocity \mathbf{u} may be simply found from the ratio of the electric field components – see Fig. 14a:

$$\tan \theta = -\frac{E_x}{E_y}. \quad (10.130)$$

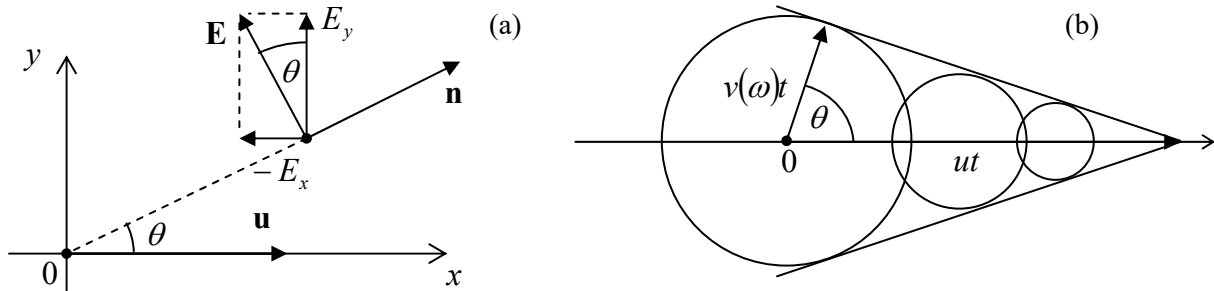


Fig. 10.14. (a) The Cherenkov radiation's propagation angle θ , and (b) its interpretation.

The ratio on the right-hand side of this relation may be calculated by plugging the asymptotic formula (127) into Eqs. (116) and (117) and calculating their ratio:

⁴⁸ Strictly speaking, the inequality $\kappa^2(\omega) < 0$ does not make sense for a medium with a complex product $\varepsilon(\omega)\mu(\omega)$, and hence complex $\kappa^2(\omega)$. However, in a typical medium where particles can propagate over substantial distances, the imaginary part of the product $\varepsilon(\omega)\mu(\omega)$ does not vanish only in very limited frequency intervals, much more narrow than the intervals that we are discussing now – please have one more look at Fig. 7.5.

⁴⁹ This radiation was observed experimentally by Pavel Alekseevich Cherenkov (in older Western texts, “Čerenkov”) in 1934, with the observations explained by Ilya Mikhailovich Frank and Igor Yevgenyevich Tamm in 1937. Note, however, that the effect had been predicted theoretically as early as 1889 by the same Oliver Heaviside whose name was mentioned in this course so many times – and whose genius I believe is still underappreciated.

$$\tan \theta = -\frac{E_x}{E_y} = \frac{i\kappa u}{\omega} = [\epsilon(\omega)\mu(\omega)u^2 - 1]^{1/2} \equiv \left(\frac{u^2}{v^2(\omega)} - 1 \right)^{1/2}, \quad (10.131a)$$

so that

$$\cos \theta = \frac{v(\omega)}{u} < 1. \quad (10.131b)$$

Cherenkov
radiation:
angle

Remarkably, this direction does not depend on the emission time t_{ret} , so that the radiation of frequency ω , at each instant, forms a hollow cone led by the particle. This simple result allows an evident interpretation (Fig. 14b): the cone's interior is just the set of all observation points that have already been reached by the radiation, propagating with the speed $v(\omega) < u$, emitted from all previous points of the particle's trajectory by the given time t . This phenomenon is an analog of the so-called *Mach cone* in fluid dynamics,⁵⁰ besides that in the Cherenkov radiation, there is a separate cone for each frequency (of the range in which $v(\omega) < u$): the smaller is the $\epsilon(\omega)\mu(\omega)$ product, i.e. the higher is the wave velocity $v(\omega) = 1/[\epsilon(\omega)\mu(\omega)]^{1/2}$, the broader is the cone, so that the earlier the corresponding “shock wave” arrives to an observer. Please note that the Cherenkov radiation is a unique radiative phenomenon: it takes place even if a particle moves without acceleration, and (in agreement with our analysis in Sec. 2), is impossible in free space, where $v(\omega) = c = \text{const}$ is larger than u for any particle.

The Cherenkov radiation's intensity may be also readily found by plugging the asymptotic expression (127), with imaginary κ , into Eq. (123). The result is

$$-\frac{d\mathcal{E}}{dx} \approx \left(\frac{3e}{4\pi} \right)^2 \int_{v(\omega) < u} \omega \left(1 - \frac{v^2(\omega)}{u^2} \right) d\omega. \quad (10.132)$$

Cherenkov
radiation:
intensity

For non-relativistic particles ($u \ll c$), the Cherenkov radiation condition $u > v(\omega)$ is fulfilled only in relatively narrow frequency intervals where the product $\epsilon(\omega)\mu(\omega)$ is very large (usually, due to optical resonance peaks of the electric permittivity – see Fig. 7.5 and its discussion). In this case, the emitted light consists of a few nearly-monochromatic components. On the contrary, if the condition $u > v(\omega)$, i.e. $u^2/\epsilon(\omega)\mu(\omega) > 1$ is fulfilled in a broad frequency range, as it is for ultra-relativistic particles in condensed media, then the radiated power, according to Eq. (132), is dominated by higher frequencies of the range – hence the famous bluish color of the Cherenkov radiation glow from water-filled nuclear reactors – see Fig. 15.

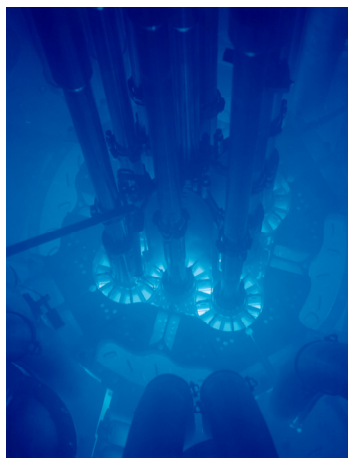


Fig. 10.15. The Cherenkov radiation glow in the Advanced Test Reactor of the Idaho National Laboratory in Arco, ID. (Adapted from http://en.wikipedia.org/wiki/Cherenkov_radiation under the Creative Commons CC-BY-SA-2.0 license.)

⁵⁰ Its brief discussion may be found in CM Sec. 8.6.

The Cherenkov radiation is broadly used in high-energy experiments for particle identification and speed measurement (since it is easy to pass the particles through layers of different densities and hence with different dielectric constants) – for example, in the so-called Ring Imaging Cherenkov (RICH) detectors that have been designed for the DELPHI experiment⁵¹ at the Large Electron-Positron Collider (LEP) in CERN.

A little bit counter-intuitively, the formalism described in this section is also very useful for the description of an apparently rather different effect – the so-called *transition radiation* that takes place when a charged particle crosses a border between two media.⁵² The effect may be interpreted as the result of the time dependence of the electric dipole formed by the moving charge q and its mirror image q' in the counterpart medium – see Fig. 16.

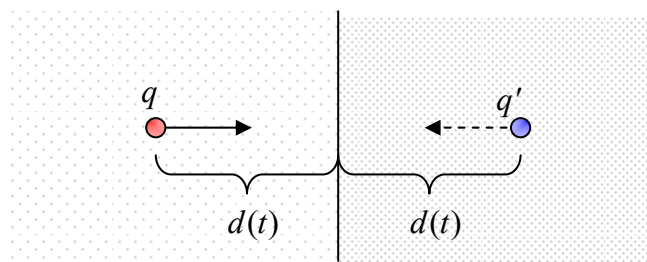


Fig. 10.16. The transition radiation's physics.

In the non-relativistic limit, this effect allows a straightforward description combining the electrostatics picture of Sec. 3.4 (see Fig. 3.9 and its discussion), and Eq. (8.27), corrected for the media polarization effects. However, if the particle's velocity u is comparable with the phase velocity of waves in either medium, the adequate theory of the transition radiation becomes very close to that of the Cherenkov radiation.

In comparison with the Cherenkov radiation, the transition radiation is rather weak, and its practical use (mostly for the measurement of the Lorentz factor γ , to which the radiation intensity is nearly proportional) requires multi-layered stacks.⁵³ In these systems, the radiation emitted at sequential borders may be coherent, and the system's physics may become close to that of the free-electron lasers mentioned in Sec. 4.

10.6. Radiation's back-action

An attentive and critically-minded reader could notice that so far our treatment of charged particle dynamics has never been fully self-consistent. Indeed, in Sec. 9.6 we have analyzed particle's motion in various external fields, ignoring those radiated by the particle itself, while in Sec. 8.2 and earlier in this chapter these fields have been calculated (admittedly, just for a few simple cases), but, again, their back-action on the emitting particle has been ignored. Only in very few cases we have taken

⁵¹ See, e.g., <http://delphiwww.cern.ch/offline/physics/delphi-detector.html>. For an in-depth review of radiation detectors (including the Cherenkov ones), the reader may be referred, for example, to the classical text by G. F. Knoll, *Radiation Detection and Measurement*, 4th ed., Wiley, 2010, and a newer treatment by K. Kleinknecht, *Detectors for Particle Radiation*, Cambridge U. Press, 1999.

⁵² The effect was predicted theoretically in 1946 by V. Ginzburg and I. Frank, and only later observed experimentally.

⁵³ See, e.g., Sec. 5.3 in K. Kleinknecht's monograph cited above.

the back effects of the radiation implicitly, via the energy conservation arguments. However, even in these cases, the near-field effects, such as the first term in Eq. (19), which affect the moving particle most, have been ignored.

At the same time, it is clear that in sharp contrast with electrostatics, the interaction of a moving point charge with its own field cannot be always ignored. As the simplest example, if an electron is made to fly through a resonant cavity, thus inducing electromagnetic oscillations in it, and then is forced (say, by an appropriate static field) to return into the cavity before the oscillations have decayed, its motion will certainly be affected by the oscillating fields, just as if they had been induced by another source. There is no conceptual problem with applying the Maxwell theory to such “field-particle rendezvous” effects; moreover, it is the basis of the engineering design of such vacuum electron devices as klystrons, magnetrons, and free-electron lasers.

A problem arises only when no clear “rendezvous” points are enforced by boundary conditions, so that the most important self-field effects are at $R \equiv |\mathbf{r} - \mathbf{r}'| \rightarrow 0$, the most evident example being the charged particle’s radiation into free space, described earlier in this chapter. We already know that such radiation takes away a part of the charge’s kinetic energy, i.e. has to cause its deceleration. One should wonder, however, whether such self-action effects might be described in a more direct, non-perturbative way.

As the first attempt, let us try a phenomenological approach based on the already derived formulas for the radiation power \mathcal{P} . For the sake of simplicity, let us consider a non-relativistic point charge q in free space, so that \mathcal{P} is described by Eq. (8.27), with the electric dipole moment’s derivative over time equal to $q\dot{\mathbf{u}}$:

$$\mathcal{P} = \frac{Z_0 q^2}{6\pi c^2} \dot{u}^2 \equiv \frac{2}{3c^3} \frac{q^2}{4\pi\epsilon_0} \dot{u}^2. \quad (10.133)$$

The most naïve approach would be to write the equation of the particle’s motion in the form

$$m\ddot{\mathbf{u}} = \mathbf{F}_{\text{ext}} + \mathbf{F}_{\text{self}}, \quad (10.134)$$

and try to calculate the radiation back-action force \mathbf{F}_{self} by requiring its instant power, $-\mathbf{F}_{\text{self}} \cdot \mathbf{u}$, to be equal to \mathcal{P} . However, this approach (say, for a 1D motion) would give a very unnatural result,

$$F_{\text{self}} \propto \frac{\dot{u}^2}{u}, \quad (10.135)$$

that might diverge at some points of the particle’s trajectory. This failure is clearly due to the retardation effect: as the reader may recall, Eq. (133) results from the analysis of radiation fields in the far-field zone, i.e. at *large* distances R from the particle, e.g., from the second term in Eq. (19), i.e. when the non-radiative first term (which is much larger at *small* distances, $R \rightarrow 0$) is ignored.

Before exploring the effects of this term, let us, however, make one more attempt at Eq. (133), considering its *average* effect on some periodic motion of the particle. (A possible argument for this step is that at the periodic motion, the retardation effects should be averaged out – just as at the transfer from Eq. (8.27) to Eq. (8.28).) To calculate the average, let us write the identity

$$\overline{\dot{u}^2} \equiv \frac{1}{T} \int_0^T \dot{\mathbf{u}} \cdot \dot{\mathbf{u}} dt, \quad (10.136)$$

and carry out the integration on the right-hand side of Eq. (133) by parts over the motion period τ :

$$\overline{\mathcal{P}} = \frac{2}{3c^3} \frac{q^2}{4\pi\epsilon_0} \overline{(\ddot{\mathbf{u}})^2} = \frac{2}{3c^3} \frac{q^2}{4\pi\epsilon_0} \frac{1}{\tau} \left(\dot{\mathbf{u}} \cdot \mathbf{u} \Big|_0^\tau - \int_0^\tau \ddot{\mathbf{u}} \cdot \mathbf{u} dt \right) = -\frac{1}{\tau} \int_0^\tau \frac{2}{3c^3} \frac{q^2}{4\pi\epsilon_0} \ddot{\mathbf{u}} \cdot \mathbf{u} dt. \quad (10.137)$$

On the other hand, the back-action force should give

$$\overline{\mathcal{P}} = -\frac{1}{\tau} \int_0^\tau \mathbf{F}_{\text{self}} \cdot \mathbf{u} dt. \quad (10.138)$$

These two averages coincide if⁵⁴

Abraham-Lorentz force

$$\boxed{\mathbf{F}_{\text{self}} = \frac{2}{3c^3} \frac{q^2}{4\pi\epsilon_0} \ddot{\mathbf{u}}}. \quad (10.139)$$

This is the so-called *Abraham-Lorentz force* of back-action. Before going after a more serious derivation of this formula, let us estimate its scale, representing Eq. (139) as

$$\mathbf{F}_{\text{self}} = m\tau\ddot{\mathbf{u}}, \quad \text{with } \tau \equiv \frac{2}{3mc^3} \frac{q^2}{4\pi\epsilon_0}, \quad (10.140)$$

where the constant τ evidently has the dimension of time. Recalling the definition (8.41) of the classical radius r_c of the particle, Eq. (140) for τ may be rewritten as

$$\tau = \frac{2}{3} \frac{r_c}{c}. \quad (10.141)$$

For the electron, τ is of the order of 10^{-23} s, so that the right-hand side of Eq. (140) is very small. This means that in most cases the Abraham-Lorentz force is either negligible or leads to the same results as the perturbative treatments of energy loss we have used earlier in this chapter.

However, Eq. (140) brings some unpleasant surprises. For example, let us consider a 1D oscillator with frequency ω_0 . For it, Eq. (134), with the back-action force given by Eq. (140), takes the form

$$m\ddot{x} + m\omega_0^2 x = m\tau\ddot{x}. \quad (10.142)$$

Looking for the solution of this linear differential equation in the usual exponential form, $x(t) \propto \exp\{\lambda t\}$, we get the following characteristic equation,

$$\lambda^2 + \omega_0^2 = \tau\lambda^3. \quad (10.143)$$

It may look like that for any “reasonable” value of $\omega_0 \ll 1/\tau \sim 10^{23}$ s⁻¹, the right-hand side of this nonlinear algebraic equation may be treated as a perturbation. Indeed, looking for its solutions in the

⁵⁴ Just for the reader’s reference, this formula may be readily generalized to the relativistic case, in the 4-form:

$$F_{\text{self}}^\alpha = \frac{2}{3mc^3} \frac{q^2}{4\pi\epsilon_0} \left[\frac{d^2 p^\alpha}{d\tau^2} + \frac{p^\alpha}{(mc)^2} \left(\frac{dp_\beta}{d\tau} \frac{dp^\beta}{d\tau} \right) \right],$$

– the so-called *Abraham-Lorentz-Dirac force*.

natural form $\lambda_{\pm} = \pm i\omega_0 + \lambda'$, with $|\lambda'| \ll \omega_0$, expanding both parts of Eq. (143) in the Taylor series in the small parameter λ' , and keeping only the terms linear in λ' , we get

$$\lambda' \approx -\frac{\omega_0^2 \tau}{2}. \quad (10.144)$$

This means that the energy of free oscillations decreases in time as $\exp\{2\lambda' t\} = \exp\{-\omega_0^2 \tau t\}$; this is exactly the radiative damping analyzed earlier. However, Eq. (143) is deceiving; it has the third root corresponding to unphysical, exponentially growing (so-called *run-away*) solutions. It is easiest to see this for a free particle, with $\omega_0 = 0$. Then Eq. (143) becomes very simple,

$$\lambda^2 = \tau \lambda^3, \quad (10.145)$$

and it is easy to find all its three roots explicitly: $\lambda_1 = \lambda_2 = 0$ and $\lambda_3 = 1/\tau$. While the first two roots correspond to the values λ_{\pm} found earlier, the last one describes an exponential (and extremely rapid!) acceleration.

In order to remove this artifact, let us try to develop a self-consistent approach to the back-action effects, taking into account the near-field terms of particle fields. For that, we need to somehow overcome the divergence of Eqs. (10) and (19) at $R \rightarrow 0$. The most reasonable way to do this is to spread the particle's charge over a ball of radius a , with a spherically symmetric (but not necessarily constant) density $\rho(r)$, and at the end of the calculations trace the limit $a \rightarrow 0$.⁵⁵ Again sticking to the non-relativistic case (so that the magnetic component of the Lorentz force is not important), we should calculate

$$\mathbf{F}_{\text{self}} = \int_V \rho(\mathbf{r}) \mathbf{E}(\mathbf{r}, t) d^3 r, \quad (10.146)$$

where the electric field is that of the charge itself, with the field of any elementary charge $dq = \rho(r)d^3r$ described by Eq. (19).

To enable an analytical calculation of the force, we need to make the assumption $a \ll r_c$, treat the ratio $R/r_c \sim a/r_c$ as a small parameter, and expand the resulting right-hand side of Eq. (146) into the Taylor series in small R . This procedure yields

$$\mathbf{F}_{\text{self}} = -\frac{2}{3} \frac{1}{4\pi\epsilon_0} \sum_{n=0}^{\infty} \frac{(-1)^n}{c^{n+2} n!} \frac{d^{n+1} \mathbf{u}}{dt^{n+1}} \int_V d^3 r \int_V d^3 r' \rho(r) R^{n-1} \rho(r'). \quad (10.147)$$

The distance R cancels only in the term with $n = 1$,

$$\mathbf{F}_1 = \frac{2}{3c^3} \frac{\ddot{\mathbf{u}}}{4\pi\epsilon_0} \int_V d^3 r \int_V d^3 r' \rho(r) \rho(r') \equiv \frac{2}{3c^3} \frac{q^2}{4\pi\epsilon_0} \ddot{\mathbf{u}}, \quad (10.148)$$

showing that we have recovered (now in an *apparently* legitimate fashion) Eq. (139) for the Abrahams-Lorentz force. One could argue that in the limit $a \rightarrow 0$ the terms higher in $R \sim a$ (with $n > 1$) could be

⁵⁵ Note: this operation cannot be interpreted as describing a quantum spread due to the finite extent of the point particle's wavefunction. In quantum mechanics, different parts of the wavefunction of the same charged particle do *not* interact with each other!

ignored. However, we have to notice that the main contribution to the series (147) is *not* described by Eq. (148) for $n = 1$, but is given by the much larger term with $n = 0$:

$$\mathbf{F}_0 = -\frac{2}{3} \frac{1}{4\pi\epsilon_0} \frac{\dot{\mathbf{u}}}{c^2} \int_V d^3r \int_V d^3r' \frac{\rho(r)\rho(r')}{R} \equiv -\frac{4}{3} \frac{\dot{\mathbf{u}}}{c^2} \frac{1}{4\pi\epsilon_0} \frac{1}{2} \int_V d^3r \int_V d^3r' \frac{\rho(r)\rho(r')}{R} \equiv -\frac{4}{3c^2} \dot{\mathbf{u}} U, \quad (10.149)$$

where U is the electrostatic energy (1.59) of the static charge's self-interaction. This term may be interpreted as the inertial "force"⁵⁶ ($-m_{\text{ef}}\mathbf{a}$) with the following effective *electromagnetic mass*:

Electro-magnetic mass

$$m_{\text{ef}} = \frac{4}{3} \frac{U}{c^2}, \quad (10.150)$$

which is a factor of $4/3$ larger than it should be according to Einstein's formula (9.73). This is the famous (or rather infamous :–) *4/3 problem* that does not allow one to interpret the electron's mass as that of its electric field. Some (admittedly, rather formal) resolution of this paradox is possible only in quantum electrodynamics with its renormalization techniques – beyond the framework of this course.

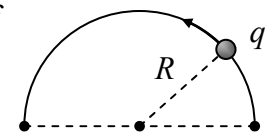
Note, however, that all these issues are only important for motions with frequencies of the order of $1/\tau \sim 10^{23} \text{ s}^{-1}$, i.e. at energies $\mathcal{E} \sim \hbar/\tau \sim 10^8 \text{ eV}$, while other quantum electrodynamics effects may be observed at much lower frequencies, starting from $\sim 10^{10} \text{ s}^{-1}$. Hence the $4/3$ problem is by no means the only motivation for the transfer from classical to quantum electrodynamics. However, the reader should not think that their time spent on this course has been lost: quantum electrodynamics is heavily based on classical electrodynamics, incorporates virtually all its results, and the basic transition between them is surprisingly straightforward.⁵⁷ So, I look forward to welcoming the reader to the next, quantum-mechanics part of this series.

10.6. Exercise problems

10.1. Derive Eqs. (10) from Eqs. (1) by a direct (but careful!) integration.

10.2. Derive the radiation-related parts of Eqs. (19)-(20) from the Liénard-Wiechert potentials (10) by direct differentiation.

10.3. A point charge q that had been in a stationary position on a circle of radius R is carried over, along the circle, to the opposite position on the same diameter (see the figure on the right) as fast as only physically possible, and then is kept steady at this new position. Calculate and sketch the time dependence of its electric field \mathbf{E} at the center of the circle.



10.4. Express the instantaneous power of electromagnetic radiation by a relativistic particle with electric charge q and rest mass m , moving with velocity \mathbf{u} , via the external Lorentz force \mathbf{F} exerted on it.

⁵⁶ See, e.g., CM Sec. 4.6.

⁵⁷ See, e.g., QM Secs. 9.1-9.4.

10.5. A relativistic particle with rest mass m and electric charge q , initially at rest, is accelerated by a constant force \mathbf{F} until it reaches a certain velocity u , and then moves by inertia. Calculate the total energy radiated during the acceleration.

10.6. A charged relativistic particle with initial momentum \mathbf{p}_0 flies ballistically from a free-space region into a region of a constant, uniform electric field \mathbf{E} , whose force is directed opposite to \mathbf{p}_0 . Calculate the energy radiated by the particle during its motion in the field, assuming that it is small in comparison with the particle's initial kinetic energy.

10.7. Calculate

- (i) the instantaneous power, and
- (ii) the power spectrum

of the radiation emitted, into a unit solid angle, by a relativistic particle with charge q , performing 1D harmonic oscillations with frequency ω_0 and displacement amplitude a .

10.8. Analyze the polarization and the spectral contents of the synchrotron radiation propagating in the direction normal to the particle's rotation plane. How do the results change if not one, but $N > 1$ similar particles move around the circle, at equal angular distances?

10.9. Calculate and analyze the time dependence of the energy of a charged relativistic particle performing synchrotron motion in a constant and uniform magnetic field \mathbf{B} , and hence emitting the synchrotron radiation. Qualitatively, what is the particle's trajectory?

Hint: You may assume that the energy loss is relatively slow ($-d\mathcal{E}/dt \ll \omega_c \mathcal{E}$), but should spell out the condition of validity of this assumption.

10.10. Analyze the polarization of the synchrotron radiation propagating within the particle's rotation plane.

10.11.* The basic quantum theory of radiation shows that the electric dipole radiation by a particle is allowed only if the change of its angular momentum's magnitude L at the transition is of the order of Planck's constant \hbar .

(i) Estimate the change of L of an ultra-relativistic particle due to its emission of a typical single photon of the synchrotron radiation.

(ii) Do you think quantum mechanics forbid such radiation? If not, why?

10.12. A relativistic particle moves along the z -axis, with velocity u_z , through an undulator – a system of permanent magnets providing (in the simplest model) a perpendicular magnetic field, whose distribution near the axis is sinusoidal:⁵⁸

$$\mathbf{B} = \mathbf{n}_y B_0 \cos k_0 z .$$

⁵⁸ As the Maxwell equation for $\nabla \times \mathbf{H}$ shows, this field distribution cannot be created in any non-zero volume of free space. However, it may be created on a line – e.g., on the particle's trajectory.

Assuming that the field is so weak that it causes negligible deviations of the particle's trajectory from the straight line, calculate the angular distribution of the resulting radiation. What condition does the above assumption impose on the system's parameters?

10.13. Discuss possible effects of the interference of the undulator radiation from different periods of its static field distribution. In particular, calculate the angular positions of the power density maxima.

10.14. An electron launched directly toward a plane surface of a perfect conductor is instantly absorbed by it at the collision. Calculate the angular distribution and the frequency spectrum of the electromagnetic waves radiated at this collision if the initial kinetic energy T of the particle is much larger than the conductor's workfunction ψ .⁵⁹ Is your result valid near the conductor's surface?

10.15. A relativistic particle, with rest mass m and electric charge q , flies ballistically, with velocity u , by an immobile point charge q' , with an impact parameter b so large that the deviations of its trajectory from the straight line are negligible. Calculate the total energy loss due to the electromagnetic radiation during the passage. Formulate the conditions of validity of your result.

⁵⁹ See Sec. 2.9, in particular Fig. 2.27a.

This page is
intentionally left
blank



Konstantin K. Likharev
Essential Graduate Physics
Lecture Notes and Problems

Beta version

Open online access at
<http://commons.library.stonybrook.edu/egp/>
and
<https://sites.google.com/site/likharevegp/>

Part QM: Quantum Mechanics

Last corrections: September 2, 2022

A version of this material was published in 2019 under the title

Quantum Mechanics: Lecture notes

IOPP, Essential Advanced Physics – Volume 5, ISBN 978-0-7503-1411-4,
with the model solutions of the exercise problems published under the title

Quantum Mechanics: Problems with solutions

IOPP, Essential Advanced Physics – Volume 6, ISBN 978-0-7503-1414-5

However, by now this online version of the lecture notes, as well as the problem solutions available from the author, have been much better corrected

About the author:

<https://you.stonybrook.edu/likharev/>

Table of Contents

Chapter 1. Introduction (28 pp.)

- 1.1. Experimental motivations
- 1.2. Wave mechanics postulates
- 1.3. Postulates' discussion
- 1.4. Continuity equation
- 1.5. Eigenstates and eigenvalues
- 1.6. Time evolution
- 1.7. Space dependence
- 1.8. Dimensionality reduction
- 1.9. Exercise problems (15)

Chapter 2. 1D wave mechanics (76 pp.)

- 2.1. Basic relations
- 2.2. Free particle: Wave packets
- 2.3. Particle reflection and tunneling
- 2.4. Motion in soft potentials
- 2.5. Resonant tunneling, and metastable states
- 2.6. Localized state coupling, and quantum oscillations
- 2.7. Periodic systems: Energy bands and gaps
- 2.8. Periodic systems: Particle dynamics
- 2.9. Harmonic oscillator: Brute force approach
- 2.10. Exercise problems (43)

Chapter 3. Higher Dimensionality Effects (64 pp.)

- 3.1. Quantum interference and the AB effect
- 3.2. Landau levels and the quantum Hall effect
- 3.3. Scattering and diffraction
- 3.4. Energy bands in higher dimensions
- 3.5. Axially-symmetric systems
- 3.6. Spherically-symmetric systems: Brute force approach
- 3.7. Atoms
- 3.8. Spherically-symmetric scatterers
- 3.9. Exercise problems (40)

Chapter 4. Bra-ket Formalism (52 pp.)

- 4.1. Motivation
- 4.2. States, state vectors, and linear operators
- 4.3. State basis and matrix representation
- 4.4. Change of basis, and matrix diagonalization
- 4.5. Observables: Expectation values and uncertainties
- 4.6. Quantum dynamics: Three pictures
- 4.7. Coordinate and momentum representations
- 4.8. Exercise problems (34)

Chapter 5. Some Exactly Solvable Problems (48 pp.)

- 5.1. Two-level systems
- 5.2. The Ehrenfest theorem
- 5.3. The Feynman path integral
- 5.4. Revisiting harmonic oscillator
- 5.5. Glauber states and squeezed states
- 5.6. Revisiting spherically-symmetric problems
- 5.7. Spin and its addition to orbital angular momentum
- 5.8. Exercise problems (48)

Chapter 6. Perturbative Approaches (36 pp.)

- 6.1. Time-independent perturbations
- 6.2. The linear Stark effect
- 6.3. Fine structure of atomic levels
- 6.4. The Zeeman effect
- 6.5. Time-dependent perturbations
- 6.6. Quantum-mechanical Golden Rule
- 6.7. Golden Rule for step-like perturbations
- 6.8. Exercise problems (31)

Chapter 7. Open Quantum Systems (50 pp.)

- 7.1. Open systems, and the density matrix
- 7.2. Coordinate representation, and the Wigner function
- 7.3. Open system dynamics: Dephasing
- 7.4. Fluctuation-dissipation theorem
- 7.5. The Heisenberg-Langevin approach
- 7.6. Density matrix approach
- 7.7. Exercise problems (14)

Chapter 8. Multiparticle Systems (52 pp.)

- 8.1. Distinguishable and indistinguishable particles
- 8.2. Singlets, triplets, and the exchange interaction
- 8.3. Multiparticle systems
- 8.4. Perturbative approaches
- 8.5. Quantum computation and cryptography
- 8.6. Exercise problems (31)

Chapter 9. Elements of Relativistic Quantum Mechanics (36 pp.)

- 9.1. Electromagnetic field quantization
- 9.2. Photon absorption and counting
- 9.3. Photon emission: spontaneous and stimulated
- 9.4. Cavity QED
- 9.5. The Klein-Gordon and relativistic Schrödinger equations
- 9.6. Dirac's theory
- 9.7. Low energy limit
- 9.8. Exercise problems (21)

Chapter 10. Making Sense of Quantum Mechanics (16 pp.)

- 10.1. Quantum measurements
- 10.2. QND measurements
- 10.3. Hidden variables, the Bell theorem, and local reality
- 10.4. Interpretations of quantum mechanics

* * *

Additional file (available from the author upon request):

Exercise and Test Problems with Model Solutions ($277 + 70 = 347$ problems; 518 pp.)

Chapter 1. Introduction

This introductory chapter briefly reviews the major experimental motivations for quantum mechanics, and then discusses its simplest formalism – Schrödinger’s wave mechanics. Much of this material (besides the last section) may be found in undergraduate textbooks,¹ so that the discussion is rather brief, and focused on the most important conceptual issues.

1.1. Experimental motivations

By the beginning of the 1900s, physics (which by that time included what we now call non-relativistic classical mechanics, classical thermodynamics and statistics, and classical electrodynamics including the geometric and wave optics) looked like an almost completed discipline, with most human-scale phenomena reasonably explained, and just a couple of mysterious “dark clouds”² on the horizon. However, rapid technological progress and the resulting development of more refined scientific instruments have led to a fast multiplication of observed phenomena that could not be explained on a classical basis. Let me list the most consequential of those experimental findings.

(i) The blackbody radiation measurements, pioneered by G. Kirchhoff in 1859, have shown that in the thermal equilibrium, the power of electromagnetic radiation by a fully absorbing (“black”) surface, per unit frequency interval, drops exponentially at high frequencies. This is not what could be expected from the combination of classical electrodynamics and statistics, which predicted an infinite growth of the radiation density with frequency. Indeed, classical electrodynamics shows³ that electromagnetic field modes evolve in time just as harmonic oscillators, and that the number dN of these modes in a large free-space volume $V \gg \lambda^3$, within a small frequency interval $d\omega \ll \omega$ near some frequency ω , is

$$dN = 2V \frac{d^3 k}{(2\pi)^3} = 2V \frac{4\pi k^2 dk}{(2\pi)^3} = V \frac{\omega^2}{\pi^2 c^3} d\omega, \quad (1.1)$$

where $c \approx 3 \times 10^8$ m/s is the free-space speed of light, $k = \omega/c$ the free-space wave number, and $\lambda = 2\pi/k$ is the radiation wavelength. On the other hand, classical statistics⁴ predicts that in the thermal equilibrium at temperature T , the average energy E of each 1D harmonic oscillator should be equal to $k_B T$, where k_B is the Boltzmann constant.⁵

Combining these two results, we readily get the so-called *Rayleigh-Jeans formula* for the average electromagnetic wave energy per unit volume:

¹ See, for example, D. Griffith, *Quantum Mechanics*, 2nd ed., Cambridge U. Press, 2016.

² This famous expression was used in a 1900 talk by Lord Kelvin (born William Thomson), in reference to the results of blackbody radiation measurements and the Michelson-Morley experiments, i.e. the precursors of quantum mechanics and relativity theory.

³ See, e.g., EM Sec. 7.8, in particular Eq. (7.211).

⁴ See, e.g., SM Sec. 2.2.

⁵ In the SI units, used throughout this series, $k_B \approx 1.38 \times 10^{-23}$ J/K – see *Appendix CA: Selected Physical Constants* for the exact value.

$$u \equiv \frac{1}{V} \frac{dE}{d\omega} = \frac{k_B T}{V} \frac{dN}{d\omega} = \frac{\omega^2}{\pi^2 c^3} k_B T, \quad (1.2)$$

that diverges at $\omega \rightarrow \infty$ (Fig. 1) – the so-called *ultraviolet catastrophe*. On the other hand, the blackbody radiation measurements, improved by O. Lummer and E. Pringsheim, and also by H. Rubens and F. Kurlbaum to reach a 1%-scale accuracy, were compatible with the phenomenological law suggested in 1900 by Max Planck:

$$u = \frac{\omega^2}{\pi^2 c^3} \frac{\hbar \omega}{\exp\{\hbar \omega / k_B T\} - 1}. \quad (1.3a)$$

Planck's
radiation
law

This law may be reconciled with the fundamental Eq. (1) if the following replacement is made for the average energy of each field oscillator:

$$k_B T \rightarrow \frac{\hbar \omega}{\exp(\hbar \omega / k_B T) - 1}, \quad (1.3b)$$

with a factor

$$\hbar \approx 1.055 \times 10^{-34} \text{ J} \cdot \text{s}, \quad (1.4)$$

Planck's
constant

now called the *Planck's constant*.⁶ At low frequencies ($\hbar \omega \ll k_B T$), the denominator in Eq. (3) may be approximated as $\hbar \omega / k_B T$, so that the average energy (3b) tends to its classical value $k_B T$, and the Planck's law (3a) reduces to the Rayleigh-Jeans formula (2). However, at higher frequencies ($\hbar \omega \gg k_B T$), Eq. (3) describes the experimentally observed rapid decrease of the radiation density – see Fig. 1.

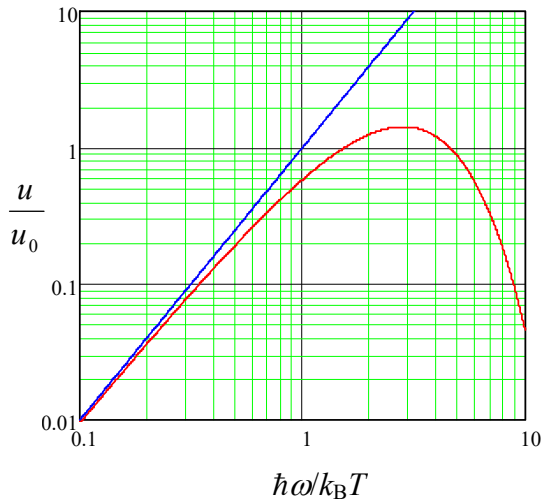


Fig. 1.1. The blackbody radiation density u , in units of $u_0 \equiv (k_B T)^3 / (\pi^2 \hbar^2 c^3)$, as a function of frequency, according to the Rayleigh-Jeans formula (blue line) and the Planck's law (red line).

(ii) The photoelectric effect, discovered in 1887 by H. Hertz, shows a sharp lower boundary for the frequency of the incident light that may kick electrons out from metallic surfaces, independent of the light's intensity. Albert Einstein, in one of his three famous 1905 papers, noticed that this threshold ω_{\min} could be explained assuming that light consisted of certain particles (now called *photons*) with energy

⁶ Max Planck himself wrote $\hbar \omega$ as $h\nu$, where $\nu = \omega/2\pi$ is the “cyclic” frequency (the number of periods per second) so that in early texts on quantum mechanics the term “Planck's constant” referred to $h \equiv 2\pi\hbar$, while \hbar was called “the Dirac constant” for a while. I will use the contemporary terminology, and abstain from using the “old Planck's constant” h at all, to avoid confusion.

Energy
vs
frequency

$$E = \hbar\omega, \quad (1.5)$$

with the same Planck's constant that participates in Eq. (3).⁷ Indeed, with this assumption, at the photon absorption by an electron, its energy $E = \hbar\omega$ is divided between a fixed energy U_0 (nowadays called the *workfunction*) of electron's binding inside the metal, and the excess kinetic energy $m_e v^2/2 > 0$ of the freed electron – see Fig. 2. In this picture, the frequency threshold finds a natural explanation as $\omega_{\min} = U_0/\hbar$.⁸ Moreover, as was shown by Satyendra Nath Bose in 1924,⁹ Eq. (5) explains Planck's law (3).

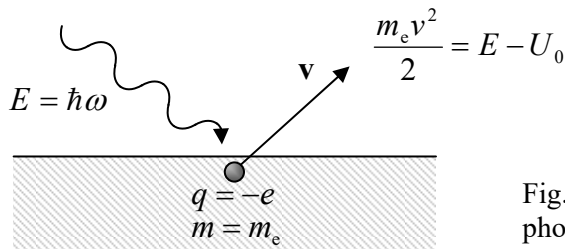


Fig. 1.2. Einstein's explanation of the photoelectric effect's frequency threshold.

(iii) The discrete frequency spectra of the electromagnetic radiation by excited atomic gases could not be explained by classical physics. (Applied to the planetary model of atoms, proposed by Ernst Rutherford, classical electrodynamics predicts the collapse of electrons on nuclei in $\sim 10^{-10}$ s, due to the electric-dipole radiation of electromagnetic waves.¹⁰) Especially challenging was the observation by Johann Jacob Balmer (in 1885) that the radiation frequencies of simple atoms may be well described by simple formulas. For example, for the lightest, hydrogen atom, all radiation frequencies may be numbered with just two positive integers n and n' :

$$\omega_{n,n'} = \omega_0 \left(\frac{1}{n^2} - \frac{1}{n'^2} \right), \quad (1.6)$$

with $\omega_0 \equiv \omega_{1,\infty} \approx 2.07 \times 10^{16}$ s⁻¹. This observation, and the experimental value of ω_0 , have found its first explanation in the famous 1913 theory by Niels Henrik David Bohr, which was a phenomenological precursor of the present-day quantum mechanics. In this theory, $\omega_{n,n'}$ was interpreted as the frequency of a photon that obeys Einstein's formula (5), with its energy $E_{n,n'} = \hbar\omega_{n,n'}$ being the difference between two *quantized* (discrete) energy levels of the atom (Fig. 3):

$$E_{n,n'} = E_{n'} - E_n > 0. \quad (1.7)$$

Bohr showed that Eq. (6) may be obtained from Eqs. (5) and (7), and non-relativistic¹¹ classical mechanics, augmented with just one additional postulate, equivalent to the assumption that the angular

⁷ As a reminder, A. Einstein received his only Nobel Prize (in 1921) for exactly this work, rather than for his relativity theory, i.e. essentially for jumpstarting the same quantum theory which he later questioned.

⁸ For most metals, U_0 is between 4 and 5 electron-volts (eV), so that the threshold corresponds to $\lambda_{\max} = 2\pi c/\omega_{\min} = 2\pi c/(U_0/\hbar) \approx 300$ nm – approximately at the border between the visible light and the ultraviolet radiation.

⁹ See, e.g., SM Sec. 2.5.

¹⁰ See, e.g., EM Sec. 8.2.

¹¹ The non-relativistic approach to the problem may be justified *a posteriori* by the fact the resulting energy scale E_H , given by Eq. (13), is much smaller than the electron's rest energy, $m_e c^2 \approx 0.5$ MeV.

momentum $L = m_e v r$ of an electron moving with velocity v on a circular orbit of radius r about the hydrogen's nucleus (the proton, assumed to be at rest because of its much higher mass), is quantized as

$$L = \hbar n, \quad (1.8)$$

where \hbar is again the same Planck's constant (4), and n is an integer. (In Bohr's theory, n could not be equal to zero, though in the genuine quantum mechanics, it can.)

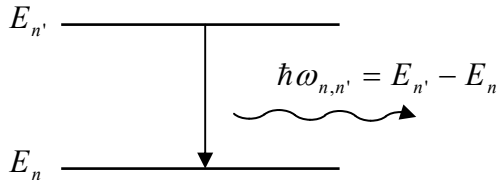


Fig. 1.3. The electromagnetic radiation of a system at a result of the transition between its quantized energy levels.

Indeed, it is sufficient to solve Eq. (8), $m_e v r = \hbar n$, together with the equation

$$m_e \frac{v^2}{r} = \frac{e^2}{4\pi\epsilon_0 r^2}, \quad (1.9)$$

which expresses the 2nd Newton's law for an electron rotating in the Coulomb field of the nucleus. (Here $e \approx 1.6 \times 10^{-19} \text{ C}$ is the fundamental electric charge, and $m_e \approx 0.91 \times 10^{-30} \text{ kg}$ is the electron's rest mass.) The result for r is

$$r = n^2 r_B, \quad \text{where } r_B \equiv \frac{\hbar^2 / m_e}{e^2 / 4\pi\epsilon_0} \approx 0.0529 \text{ nm}. \quad (1.10)$$

Bohr radius

The constant r_B , called the *Bohr radius*, is the most important spatial scale of phenomena in atomic, molecular, and condensed-matter physics – and hence in all chemistry and biochemistry.

Now plugging these results into the non-relativistic expression for the full electron energy (with its rest energy taken for reference),

$$E = \frac{m_e v^2}{2} - \frac{e^2}{4\pi\epsilon_0 r}, \quad (1.11)$$

we get the following simple expression for the electron's energy levels:

$$E_n = -\frac{E_H}{2n^2} < 0, \quad (1.12)$$

Hydrogen atom's energy levels

which, together with Eqs. (5) and (7), immediately gives Eq. (6) for the radiation frequencies. Here E_H is called the so-called *Hartree energy constant* (or just the “Hartree energy”)¹²

$$E_H \equiv \frac{(e^2 / 4\pi\epsilon_0)^2}{\hbar^2 / m_e} \approx 4.360 \times 10^{-18} \text{ J} \approx 27.21 \text{ eV}. \quad (1.13a)$$

Hartree energy constant

(Note the useful relations, which follow from Eqs. (10) and (13a):

¹² Unfortunately, another name, the “Rydberg constant”, is sometimes used for either this energy unit or its half, $E_H/2 \approx 13.6 \text{ eV}$. To add to the confusion, the same term “Rydberg constant” is used in some sub-fields of physics for the reciprocal free-space wavelength ($1/\lambda_0 = \omega_0/2\pi c$) corresponding to the frequency $\omega_0 = E_H/2\hbar$.

$$E_H = \frac{e^2}{4\pi\epsilon_0 r_B} = \frac{\hbar^2}{m_e r_B^2}, \quad \text{i.e. } r_B = \frac{e^2 / 4\pi\epsilon_0}{E_H} = \left(\frac{\hbar^2 / m_e}{E_H} \right)^{1/2}; \quad (1.13b)$$

the first of them shows, in particular, that r_B is the distance at which the natural scales of the electron's potential and kinetic energies are equal.)

Note also that Eq. (8), in the form $pr = \hbar n$, where $p = m_e v$ is the electron momentum's magnitude, may be rewritten as the condition than an integer number (n) of wavelengths λ of certain (before the late 1920s, hypothetic) waves¹³ fits the circular orbit's perimeter: $2\pi r \equiv 2\pi\hbar n/p = n\lambda$. Dividing both parts of the last equality by n , we see that for this statement to be true, the wave number $k \equiv 2\pi/\lambda$ of the de Broglie waves should be proportional to the electron's momentum $p = mv$:

Momentum
vs wave
number

$$p = \hbar k, \quad (1.14)$$

again with the same Planck's constant as in Eq. (5).

(iv) The Compton effect¹⁴ is the reduction of frequency of X-rays at their scattering on free (or nearly-free) electrons – see Fig. 4.

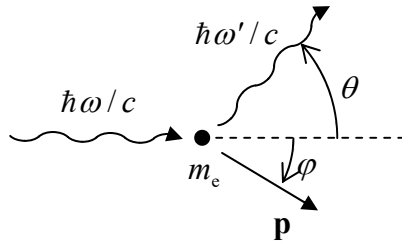


Fig. 1.4. The Compton effect.

The effect may be explained assuming that the X-ray photon also has a momentum that obeys the vector-generalized version of Eq. (14):

$$\mathbf{p}_{\text{photon}} = \hbar \mathbf{k} = \frac{\hbar \omega}{c} \mathbf{n}, \quad (1.15)$$

where \mathbf{k} is the wavevector (whose magnitude is equal to the wave number k , and whose direction coincides with the unit vector \mathbf{n} directed along the wave propagation¹⁵), and that the momenta of both the photon and the electron are related to their energies E by the classical relativistic formula¹⁶

$$E^2 = (cp)^2 + (mc^2)^2. \quad (1.16)$$

(For a photon, the rest energy m is zero, and this relation is reduced to Eq. (5): $E = cp = c\hbar k = \hbar\omega$.) Indeed, a straightforward solution of the following system of three equations,

¹³ This fact was first noticed and discussed in 1924 by Louis Victor Pierre Raymond de Broglie (in his PhD thesis!), so that instead of speaking of wavefunctions, we are still frequently speaking of the *de Broglie waves*, especially when free particles are discussed.

¹⁴ This effect was observed in 1922, and explained a year later by Arthur Holly Compton, using Eqs. (5) and (15).

¹⁵ See, e.g., EM Sec. 7.1.

¹⁶ See, e.g., EM Sec. 9.3, in particular Eq. (9.78).

$$\hbar\omega + m_e c^2 = \hbar\omega' + [(cp)^2 + (m_e c^2)^2]^{1/2}, \quad (1.17)$$

$$\frac{\hbar\omega}{c} = \frac{\hbar\omega'}{c} \cos\theta + p \cos\varphi, \quad (1.18)$$

$$0 = \frac{\hbar\omega'}{c} \sin\theta - p \sin\varphi, \quad (1.19)$$

(which express the conservation of, respectively, the full energy of the system and the two relevant Cartesian components of its full momentum, at the scattering event – see Fig. 4), yields the result:

$$\frac{1}{\hbar\omega'} = \frac{1}{\hbar\omega} + \frac{1}{m_e c^2} (1 - \cos\theta), \quad (1.20a)$$

which is traditionally represented as the relation between the initial and final values of the photon's wavelength $\lambda = 2\pi/k = 2\pi(\omega/c)$:¹⁷

$$\lambda' = \lambda + \frac{2\pi\hbar}{m_e c} (1 - \cos\theta) \equiv \lambda + \lambda_C (1 - \cos\theta), \quad \text{with } \lambda_C \equiv \frac{2\pi\hbar}{m_e c}, \quad (1.20b)$$

Compton effect

and is in agreement with experiment.

(v) De Broglie wave diffraction. In 1927, Clinton Joseph Davisson and Lester Germer, and independently George Paget Thomson succeeded to observe the diffraction of electrons on solid crystals (Fig. 5). Specifically, they have found that the intensity of the elastic reflection of electrons from a crystal increases sharply when the angle α between the incident beam of electrons and the crystal's atomic planes, separated by distance d , satisfies the following relation:

$$2d \sin\alpha = n\lambda, \quad (1.21)$$

Bragg condition

where $\lambda = 2\pi/k = 2\pi\hbar/p$ is the de Broglie wavelength of the electrons, and n is an integer. As Fig. 5 shows, this is just the well-known condition¹⁸ that the path difference $\Delta l = 2ds\sin\alpha$ between the de Broglie waves reflected from two adjacent crystal planes coincides with an integer number of λ , i.e. of the constructive interference of the waves.¹⁹

To summarize, all the listed experimental observations could be explained starting from two very simple (and similarly looking) formulas: Eq. (5) (at that stage, for photons only), and Eq. (15) for both photons and electrons – both relations involving the same Planck's constant. This fact might give an impression of experimental evidence sufficient to declare the light consisting of discrete particles

¹⁷ The constant λ_C that participates in this relation, is close to 2.46×10^{-12} m, and is called the electron's *Compton wavelength*. This term is somewhat misleading: as the reader can see from Eqs. (17)-(19), no wave in the Compton problem has such a wavelength – either before or after the scattering.

¹⁸ See, e.g., EM Sec. 8.4, in particular Fig. 8.9 and Eq. (8.82). Frequently, Eq. (21) is called the *Bragg condition*, due to the pioneering experiments by W. Bragg on X-ray scattering from crystals, which were started in 1912.

¹⁹ Later, spectacular experiments on diffraction and interference of heavier particles (with the correspondingly smaller de Broglie wavelength), e.g., neutrons and even C₆₀ molecules, have also been performed – see, e.g., the review by A. Zeilinger *et al.*, *Rev. Mod. Phys.* **60**, 1067 (1988) and a later publication by O. Nairz *et al.*, *Am. J. Phys.* **71**, 319 (2003). Nowadays, such interference of heavy particles is used, for example, for ultrasensitive measurements of gravity – see, e.g., a popular review by M. Arndt, *Phys. Today* **67**, 30 (May 2014), and more recent experiments by S. Abend *et al.*, *Phys. Rev. Lett.* **117**, 203003 (2016).

(photons), and, on the contrary, electrons being some “matter waves” rather than particles. However, by that time (the mid-1920s), physics has accumulated overwhelming evidence of *wave* properties of light, such as interference and diffraction.²⁰ In addition, there was also strong evidence for the lumped-particle (“corpuscular”) behavior of electrons. It is sufficient to mention the famous oil-drop experiments by Robert Andrew Millikan and Harvey Fletcher (1909–1913), in which only single (and whole!) electrons could be added to an oil drop, changing its total electric charge by multiples of electron’s charge ($-e$) – and never its fraction. It was apparently impossible to reconcile these observations with a purely wave picture, in which an electron and hence its charge need to be spread over the wave’s extension, so that its arbitrary part of it could be cut off using an appropriate experimental setup.

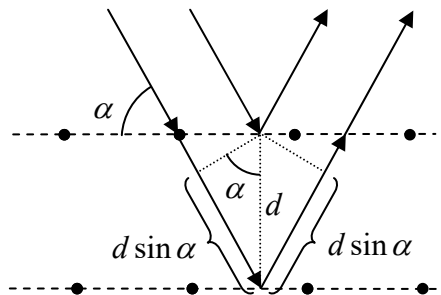


Fig. 1.5. The De Broglie wave interference at electron scattering from a crystal lattice.

Thus the founding fathers of quantum mechanics faced a formidable task of reconciling the wave and corpuscular properties of electrons and photons – and other particles. The decisive breakthrough in that task has been achieved in 1926 by Ervin Schrödinger and Max Born, who formulated what is now known either formally as the *Schrödinger picture of non-relativistic quantum mechanics of the orbital motion*²¹ in the coordinate representation (this term will be explained later in the course), or informally just as the *wave mechanics*. I will now formulate the main postulates of this theory.

1.2. Wave mechanics postulates

Let us consider a spinless,²² non-relativistic point-like particle, whose classical dynamics may be described by a certain Hamiltonian function $H(\mathbf{r}, \mathbf{p}, t)$,²³ where \mathbf{r} is the particle’s radius-vector and \mathbf{p} is its momentum. (This condition is important because it excludes from our current discussion the systems whose interaction with their environment results in *irreversible* effects, in particular the friction leading to particle energy’s decay. Such “open” systems need a more general description, which will be discussed in Chapter 7.) Wave mechanics of such *Hamiltonian particles* may be based on the following set of postulates that are comfortingly elegant – though their final justification is given only by the agreement of all their corollaries with experiment.²⁴

²⁰ See, e.g., EM Sec. 8.4.

²¹ The *orbital motion* is the historic (and rather misleading) term used for *any* motion of the particle as a whole.

²² Actually, in wave mechanics, the spin of the described particle has not to be equal to zero. Rather, it is assumed that the particle spin’s *effects* on its orbital motion are negligible.

²³ As a reminder, for many systems (including those whose kinetic energy is a quadratic-homogeneous function of generalized velocities, like $mv^2/2$), H coincides with the total energy E – see, e.g., CM Sec. 2.3. In what follows, I will assume that $H = E$.

²⁴ Quantum mechanics, like any theory, may be built on different sets of postulates/axioms leading to the same final conclusions. In this text, I will not try to beat down the number of postulates to the absolute possible

(i) Wavefunction and probability. Such variables as \mathbf{r} or \mathbf{p} cannot be always measured exactly, even at “perfect conditions” when all external uncertainties, including measurement instrument imperfection, varieties of the initial state preparation, and unintended particle interactions with its environment, have been removed.²⁵ Moreover, \mathbf{r} and \mathbf{p} of the same particle can *never* be measured exactly simultaneously. Instead, the *most detailed* description of the particle’s state allowed by Nature, is given by a certain complex function $\Psi(\mathbf{r}, t)$, called the *wavefunction* (or “wave function”), which generally enables only *probabilistic* predictions of the measured values of \mathbf{r} , \mathbf{p} , and other directly measurable variables – in quantum mechanics, usually called *observables*.

Specifically, the probability dW of finding a particle inside an elementary volume $dV \equiv d^3r$ is proportional to this volume, and hence may be characterized by a volume-independent *probability density* $w \equiv dW/d^3r$, which in turn is related to the wavefunction as

$$w = |\Psi(\mathbf{r}, t)|^2 \equiv \Psi^*(\mathbf{r}, t)\Psi(\mathbf{r}, t), \quad (1.22a)$$

where the sign * denotes the usual complex conjugation. As a result, the total probability of finding the particle somewhere inside a volume V may be calculated as

$$W = \int_V w d^3r = \int_V \Psi^* \Psi d^3r. \quad (1.22b)$$

In particular, if volume V contains the particle *definitely* (i.e. with the 100% probability, $W = 1$), Eq. (22b) is reduced to the so-called *wavefunction normalization condition*

$$\int_V \Psi^* \Psi d^3r = 1. \quad (1.22c)$$

Probability
via
wavefunction

Normalization
condition

(ii) Observables and operators. With each observable A , quantum mechanics associates a certain *linear operator* \hat{A} , such that (in the perfect conditions mentioned above) the average measured value of A (usually called the *expectation value*) is expressed as²⁶

$$\langle A \rangle = \int_V \Psi^* \hat{A} \Psi d^3r, \quad (1.23)$$

Observable's
expectation
value

where $\langle \dots \rangle$ means the statistical average, i.e. the result of averaging the measurement results over a large *ensemble* (set) of macroscopically similar experiments, and Ψ is the normalized wavefunction that obeys Eq. (22c). Note immediately that for Eqs. (22) and (23) to be compatible, the *identity* (or “unit”) *operator* defined by the relation

$$\hat{I}\Psi = \Psi, \quad (1.24)$$

Identity
operator

has to be associated with a particular type of measurement, namely with the particle’s detection.

minimum, not only because that would require longer argumentation, but chiefly because such attempts typically result in making certain implicit assumptions hidden from the reader – the practice as common as regrettable.

²⁵ I will imply such perfect conditions in the further narrative, until the discussion of the system’s interaction with its environment in Chapter 7.

²⁶ This key measurement postulate is sometimes called the *Born rule*, though sometimes this term is used for the (less general) Eqs. (22).

(iii) The Hamiltonian operator and the Schrödinger equation. Another particular operator, *Hamiltonian* \hat{H} , whose observable is the particle's energy E , also plays in wave mechanics a very special role, because it participates in the *Schrödinger equation*,

Schrödinger equation

$$i\hbar \frac{\partial \Psi}{\partial t} = \hat{H}\Psi, \quad (1.25)$$

that determines the wavefunction's dynamics, i.e. its time evolution.

(iv) The radius-vector and momentum operators. In wave mechanics (in the “coordinate representation”), the vector operator of particle’s radius-vector \mathbf{r} just multiples the wavefunction by this vector, while the operator of the particle’s momentum is proportional to the spatial derivative:

$$\hat{\mathbf{r}} = \mathbf{r}, \quad \hat{\mathbf{p}} = -i\hbar\nabla, \quad (1.26a)$$

Operators of coordinate and momentum

where ∇ is the *del* (or “nabla”) vector operator.²⁷ Thus in the Cartesian coordinates,

$$\hat{\mathbf{r}} = \mathbf{r} = \{x, y, z\}, \quad \hat{\mathbf{p}} = -i\hbar \left\{ \frac{\partial}{\partial x}, \frac{\partial}{\partial y}, \frac{\partial}{\partial z} \right\}. \quad (1.26b)$$

(v) The correspondence principle. In the limit when quantum effects are insignificant, e.g., when the characteristic scale of action²⁸ (i.e. the product of the relevant energy and time scales of the problem) is much larger than Planck’s constant \hbar , all wave mechanics results have to tend to those given by classical mechanics. Mathematically, this correspondence is achieved by duplicating the classical relations between various observables by similar relations between the corresponding operators. For example, for a free particle, the Hamiltonian (which in this particular case corresponds to the kinetic energy $T = p^2/2m$ alone) has the form

$$\hat{H} = \hat{T} = \frac{\hat{p}^2}{2m} = -\frac{\hbar^2}{2m} \nabla^2. \quad (1.27)$$

Free particle's Hamiltonian

Now, even before a deeper discussion of the postulates’ physics (offered in the next section), we may immediately see that they indeed provide a formal way toward resolution of the apparent contradiction between the wave and corpuscular properties of particles. Indeed, for a free particle, the Schrödinger equation (25), with the substitution of Eq. (27), takes the form

Free particle's Schrödinger equation

$$i\hbar \frac{\partial \Psi}{\partial t} = -\frac{\hbar^2}{2m} \nabla^2 \Psi, \quad (1.28)$$

Plane wave

whose particular, but the most important solution is a plane, single-frequency (“monochromatic”) traveling wave,²⁹

$$\Psi(\mathbf{r}, t) = ae^{i(\mathbf{k} \cdot \mathbf{r} - \omega t)}, \quad (1.29)$$

²⁷ If you need, see, e.g., Secs. 8-10 of the *Selected Mathematical Formulas* appendix – below, referred to as MA. Note that according to those formulas, the del operator follows all the rules of the usual (geometric) vectors. This is, by definition, true for other quantum-mechanical vector operators to be discussed below.

²⁸ See, e.g., CM Sec. 10.3.

²⁹ See, e.g., CM Sec. 6.4 and/or EM Sec. 7.1.

where a , \mathbf{k} and ω are constants. Indeed, plugging Eq. (29) into Eq. (28), we immediately see that such plane wave, with an arbitrary complex amplitude a , is indeed a solution of this Schrödinger equation, provided a specific *dispersion relation* between the wave number $k \equiv |\mathbf{k}|$ and the frequency ω :

$$\hbar\omega = \frac{(\hbar k)^2}{2m}. \quad (1.30)$$

Free
particle's
dispersion
relation

The constant a may be calculated, for example, assuming that the wave (29) is extended over a certain volume V , while beyond it, $\Psi = 0$. Then from the normalization condition (22c) and Eq. (29), we get³⁰

$$|a|^2 V = 1. \quad (1.31)$$

Let us use Eqs. (23), (26), and (27) to calculate the expectation values of the particle's momentum \mathbf{p} and energy $E = H$ in the state (29). The result is

$$\langle \mathbf{p} \rangle = \hbar \mathbf{k}, \quad \langle E \rangle = \langle H \rangle = \frac{(\hbar k)^2}{2m}; \quad (1.32)$$

according to Eq. (30), the last equality may be rewritten as $\langle E \rangle = \hbar\omega$.

Next, Eq. (23) enables calculation of not only the average (in the math speak, the *first moment*) of an observable but also its higher moments, notably the *second moment* – in physics, usually called *variance*:

$$\langle \tilde{A}^2 \rangle \equiv \langle (A - \langle A \rangle)^2 \rangle = \langle A^2 \rangle - \langle A \rangle^2, \quad (1.33)$$

Observable's
variance

and hence its *uncertainty*, alternatively called the “root-mean-square (r.m.s.) fluctuation”,

$$\delta A \equiv \langle \tilde{A}^2 \rangle^{1/2}. \quad (1.34)$$

Observable's
uncertainty

The uncertainty is a scale of deviations $\tilde{A} \equiv A - \langle A \rangle$ of measurement results from their average. In the particular case when the uncertainty δA equals zero, every measurement of the observable A will give the same value $\langle A \rangle$; such a state is said to have a *definite value* of the variable. For example, in application to the state with wavefunction (29), these relations yield $\delta E = 0$, $\delta \mathbf{p} = 0$. This means that in this plane-wave, monochromatic state, the energy and momentum of the particle have definite values, so that the statistical average signs in Eqs. (32) might be removed. Thus, these relations are reduced to the experimentally-inferred Eqs. (5) and (15).

Hence the wave mechanics postulates indeed may describe the observed wave properties of non-relativistic particles. (For photons, we would need its relativistic generalization – see Chapter 9 below.) On the other hand, due to the linearity of the Schrödinger equation (25), any sum of its solutions is also a solution – the so-called *linear superposition principle*. For a free particle, this means that any set of plane waves (29) is also a solution to this equation. Such sets, with close values of \mathbf{k} and hence $\mathbf{p} = \hbar \mathbf{k}$ (and, according to Eq. (30), of ω as well), may be used to describe spatially localized “pulses”, called *wave packets* – see Fig. 6. In Sec. 2.1, I will prove (or rather reproduce H. Weyl's proof :-) that the wave packet's extension δx in any direction (say, x) is related to the width δk_x of the distribution of the

³⁰ For infinite space ($V \rightarrow \infty$), Eq. (31) yields $a \rightarrow 0$, i.e. wavefunction (29) vanishes. This formal problem may be readily resolved considering sufficiently long wave packets – see Sec. 2.2 below.

corresponding component of its wave vector as $\delta x \delta k_x \geq \frac{1}{2}$, and hence, according to Eq. (15), to the width δp_x of the momentum component distribution as

Heisenberg's
uncertainty
relation

$$\delta x \cdot \delta p_x \geq \frac{\hbar}{2}. \quad (1.35)$$

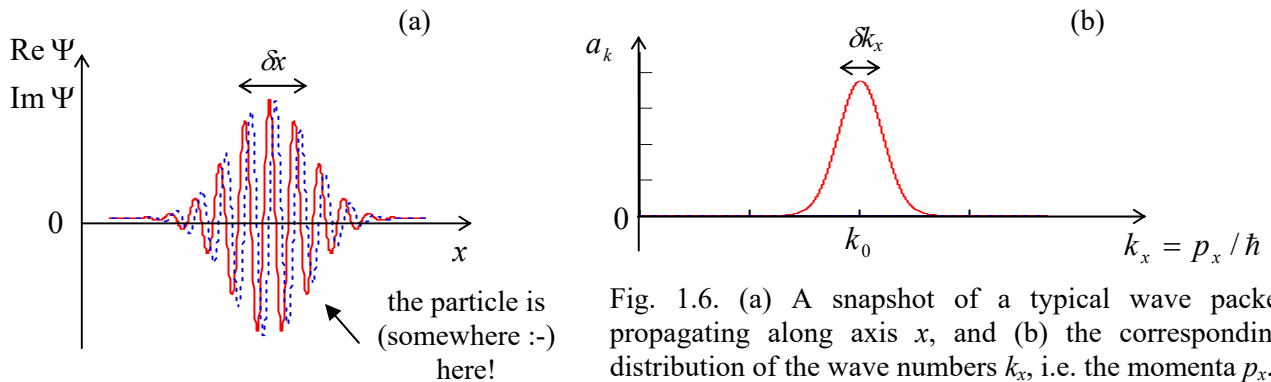


Fig. 1.6. (a) A snapshot of a typical wave packet propagating along axis x , and (b) the corresponding distribution of the wave numbers k_x , i.e. the momenta p_x .

This is the famous *Heisenberg's uncertainty principle*, which quantifies the first postulate's point that the coordinate and the momentum cannot be defined exactly simultaneously. However, since the Planck's constant, $\hbar \sim 10^{-34}$ J·s, is extremely small on the human scale of things, it still allows for particle localization in a very small volume even if the momentum spread in a wave packet is also small on that scale. For example, according to Eq. (35), a 0.1% spread of momentum of a 1 keV electron ($p \sim 1.7 \times 10^{-24}$ kg·m/s) allows its wave packet to be as small as $\sim 3 \times 10^{-10}$ m. (For a heavier particle such as a proton, the packet would be even tighter.) As a result, wave packets may be used to describe the particles that are quite point-like from the macroscopic point of view.

In a nutshell, this is the main idea of wave mechanics, and the first part of this course (Chapters 1-3) will be essentially a discussion of various effects described by this approach. During this discussion, however, we will not only witness wave mechanics' many triumphs within its applicability domain but also gradually accumulate evidence for its handicaps, which will force an eventual transfer to a more general formalism – to be discussed in Chapter 4 and beyond.

1.3. Postulates' discussion

The wave mechanics' postulates listed in the previous section (hopefully, familiar to the reader from their undergraduate studies) may look very simple. However, the physics of these axioms is very deep, leading to some counter-intuitive conclusions, and their in-depth discussion requires solutions of several key problems of wave mechanics. This is why in this section I will give only an initial, admittedly superficial discussion of the postulates, and will be repeatedly returning to the conceptual foundations of quantum mechanics throughout the course, especially in Chapter 10.

First of all, the fundamental uncertainty of observables, which is in the core of the first postulate, is very foreign to the basic ideas of classical mechanics, and historically has made quantum mechanics so hard to swallow for many star physicists, notably including Albert Einstein – despite his 1905 work, which essentially launched the whole field! However, this fact has been confirmed by numerous

experiments, and (more importantly) there has not been a single confirmed experiment that would contradict this postulate, so that quantum mechanics was long ago promoted from a theoretical hypothesis to the rank of a reliable scientific theory.

One more remark in this context is that Eq. (25) itself is *deterministic*, i.e. conceptually enables an *exact* calculation of the wavefunction's distribution in space at any instant t , provided that its initial distribution, and the particle's Hamiltonian, are known exactly. Note that in the classical statistical mechanics, the probability density distribution $w(\mathbf{r}, t)$ may be also calculated from deterministic differential equations, for example, the Liouville equation.³¹ The quantum-mechanical description differs from that situation in two important aspects. First, in the perfect conditions outlined above (the best possible initial state preparation and measurements), the Liouville equation is reduced to the 2nd Newton law of classical mechanics, i.e. the statistical uncertainty of its results disappears. In quantum mechanics this is not true: the quantum uncertainty, such as described by Eq. (35), persists even in this limit. Second, the wavefunction $\Psi(\mathbf{r}, t)$ gives more information than just $w(\mathbf{r}, t)$, because besides the modulus of Ψ , involved in Eq. (22), this complex function also has the *phase* $\varphi \equiv \arg \Psi$, which may affect some observables, describing, in particular, interference of the de Broglie waves.

Next, it is very important to understand that the relation between the quantum mechanics and experiment, given by the second postulate, necessarily involves another key notion: that of the corresponding *statistical ensemble*, in this case, a set of many experiments carried out at apparently (*macroscopically*) similar conditions, including the initial conditions – which nevertheless may lead to different measurement results (*outcomes*). Indeed, the probability of a certain (n^{th}) outcome of an experiment may be only defined for a certain statistical ensemble, as the limit

$$W_n \equiv \lim_{M \rightarrow \infty} \frac{M_n}{M}, \quad \text{with } M \equiv \sum_{n=1}^N M_n, \quad (1.36)$$

Probability:
definition

where M is the total number of experiments, M_n is the number of outcomes of the n^{th} type, and N is the number of different outcomes.

Note that a particular choice of statistical ensemble may affect probabilities W_n very significantly. For example, if we pull out playing cards at random from a standard pack of 52 different cards of 4 suits, the probability W_n of getting a certain card (e.g., the queen of spades) is 1/52. However, if the cards of a certain suit (say, hearts) had been taken out from the pack in advance, the probability of getting the queen of spades is higher, 1/39. It is important that we would also get the last number for the probability even if we had used the full 52-card pack, but by some reason discarded results of all experiments giving us any rank of hearts. Hence, the ensemble definition (or its *redefinition* in the middle of the game) may change outcome probabilities.

In wave mechanics, with its fundamental relation (22) between w and Ψ , this means that not only the outcome probabilities, but the wavefunction itself also may depend on the statistical ensemble we are using, i.e. not only on the preparation of the system and the experimental setup, but also on the subset of outcomes taken into account. The sometimes accounted attribution of the wavefunction to a single experiment, both before and after the measurement, may lead to very unphysical interpretations of the results, including some wavefunction's evolution which is not described by the Schrödinger equation (the so-called *wave packet reduction*), subluminal action on distance, etc. Later in the course, we will see that minding the fundamentally statistical nature of quantum mechanics, and in particular the

³¹ See, e.g., SM Sec. 6.1.

dependence of wavefunctions on the statistical ensembles' definition (or redefinition), readily resolves some, though not all, paradoxes of quantum measurements.

Note, however, again that the standard quantum mechanics, as discussed in Chapters 1-6 of this course, is limited to statistical ensembles with *the least possible uncertainty* of the considered systems, i.e. with the best possible knowledge of their state.³² This condition requires, first, the least uncertain initial preparation of the system, and second, its total isolation from the rest of the world, or at least from its disordered part (the “environment”), in the course of its evolution in time. Only such ensembles may be described by certain wavefunctions. A detailed discussion of more general ensembles, which are necessary if these conditions are not satisfied, will be given in Chapters 7, 8, and 10.

Finally, regarding Eq. (23): a better feeling of this definition may be obtained by its comparison with the general definition of the expectation value (i.e. the statistical average) in the probability theory. Namely, let each of N possible outcomes in a set of M experiments give a certain value A_n of observable A ; then

Definition
of statistical
average

$$\langle A \rangle \equiv \lim_{M \rightarrow \infty} \frac{1}{M} \sum_{n=1}^N A_n M_n = \sum_{n=1}^N A_n W_n. \quad (1.37)$$

Taking into account Eq. (22), which relates W and Ψ , the structures of Eq. (23) and the final form of Eq. (37) are similar. Their exact relation will be further discussed in Sec. 4.1.

1.4. Continuity equation

The wave mechanics postulates survive one more sanity check: they satisfy the natural requirement that the particle does not appear or vanish in the course of the quantum evolution.³³ Indeed, let us use Eq. (22b) to calculate the rate of change of the probability W to find a particle within a certain volume V :

$$\frac{dW}{dt} = \frac{d}{dt} \int_V \Psi \Psi^* d^3r. \quad (1.38)$$

Assuming for simplicity that the boundaries of the volume V do not move, it is sufficient to carry out the partial differentiation of the product $\Psi \Psi^*$ inside the integral. Using the Schrödinger equation (25), together with its complex conjugate,

$$-i\hbar \frac{\partial \Psi^*}{\partial t} = (\hat{H}\Psi)^*, \quad (1.39)$$

we readily get

$$\frac{dW}{dt} = \int_V \frac{\partial}{\partial t} (\Psi \Psi^*) d^3r \equiv \int_V \left(\Psi^* \frac{\partial \Psi}{\partial t} + \Psi \frac{\partial \Psi^*}{\partial t} \right) d^3r = \frac{1}{i\hbar} \int_V [\Psi^* (\hat{H}\Psi) - \Psi (\hat{H}\Psi)^*] d^3r. \quad (1.40)$$

³² The reader should not be surprised by the use of the notion of “knowledge” (or “information”) in this context. Indeed, due to the statistical character of experiment outcomes, quantum mechanics (or at least its relation to experiment) is intimately related to information theory. In contrast to much of classical physics, which may be discussed without any reference to information, in quantum mechanics, as in classical statistical physics, such abstraction is possible only in some very special (and not the most interesting) cases.

³³ Note that this requirement may be violated in the *relativistic* quantum theory – see Chapter 9.

Let the particle move in a field of external forces (not necessarily constant in time), so that its classical Hamiltonian function H is the sum of the particle's kinetic energy $T = p^2/2m$ and its potential energy $U(\mathbf{r}, t)$.³⁴ According to the correspondence principle, and Eq. (27), the Hamiltonian operator may be represented as the sum³⁵:

$$\hat{H} = \hat{T} + \hat{U} = \frac{\hat{p}^2}{2m} + U(\mathbf{r}, t) = -\frac{\hbar^2}{2m} \nabla^2 + U(\mathbf{r}, t). \quad (1.41)$$

Potential field:
Hamiltonian

At this stage, we should notice that this operator, when acting on a real function, returns a real function.³⁶ Hence, the result of its action on an arbitrary complex function $\Psi = a + ib$ (where a and b are real) is

$$\hat{H}\Psi = \hat{H}(a + ib) = \hat{H}a + i\hat{H}b, \quad (1.42)$$

where $\hat{H}a$ and $\hat{H}b$ are also real, while

$$(\hat{H}\Psi)^* = (\hat{H}a + i\hat{H}b)^* = \hat{H}a - i\hat{H}b = \hat{H}(a - ib) = \hat{H}\Psi^*. \quad (1.43)$$

This means that Eq. (40) may be rewritten as

$$\frac{dW}{dt} = \frac{1}{i\hbar} \int_V [\Psi^* \hat{H}\Psi - \Psi \hat{H}\Psi^*] d^3r = -\frac{\hbar^2}{2m} \frac{1}{i\hbar} \int_V [\Psi^* \nabla^2 \Psi - \Psi \nabla^2 \Psi^*] d^3r. \quad (1.44)$$

Now let us use general rules of vector calculus³⁷ to write the following identity:

$$\nabla \cdot (\Psi^* \nabla \Psi - \Psi \nabla \Psi^*) = \Psi^* \nabla^2 \Psi - \Psi \nabla^2 \Psi^*, \quad (1.45)$$

A comparison of Eqs. (44) and (45) shows that we may write

$$\frac{dW}{dt} = - \int_V (\nabla \cdot \mathbf{j}) d^3r, \quad (1.46)$$

where the vector \mathbf{j} is defined as

$$\mathbf{j} \equiv \frac{i\hbar}{2m} (\Psi \nabla \Psi^* - \text{c.c.}) \equiv \frac{\hbar}{m} \text{Im}(\Psi^* \nabla \Psi), \quad (1.47)$$

Probability
current
density

where c.c. means the complex conjugate of the previous expression – in this case, $(\Psi \nabla \Psi^*)^*$, i.e. $\Psi^* \nabla \Psi$. Now using the well-known divergence theorem,³⁸ Eq. (46) may be rewritten as the *continuity equation*

$$\frac{dW}{dt} + I = 0, \quad \text{with } I \equiv \int_S j_n d^2r, \quad (1.48)$$

Continuity
equation:
integral
form

³⁴ As a reminder, such description is valid not only for conservative forces (in that case U has to be time-independent), but also for any force $\mathbf{F}(\mathbf{r}, t)$ that may be expressed via the gradient of $U(\mathbf{r}, t)$ – see, e.g., CM Chapters 2 and 10. (A good example when such a description is *impossible* is given by the magnetic component of the Lorentz force – see, e.g., EM Sec. 9.7, and also Sec. 3.1 below.)

³⁵ Historically, this was the main step made (in 1926) by E. Schrödinger on the background of L. de Broglie's idea. The probabilistic interpretation of the wavefunction was put forward, almost simultaneously, by M. Born.

³⁶ In Chapter 4, we will discuss a more general family of *Hermitian operators*, which have this property.

³⁷ See, e.g., MA Eq. (11.4a), combined with the del operator's definition $\nabla^2 \equiv \nabla \cdot \nabla$.

³⁸ See, e.g., MA Eq. (12.2).

where j_n is the component of the vector \mathbf{j} , along the outwardly directed normal to the closed surface S that limits the volume V , i.e. the scalar product $\mathbf{j} \cdot \mathbf{n}$, where \mathbf{n} is the unit vector along this normal.

Equalities (47) and (48) show that if the wavefunction on the surface vanishes, the total probability W of finding the particle within the volume does not change, providing the intended sanity check. In the general case, Eq. (48) says that dW/dt equals the flux I of the vector \mathbf{j} through the surface, with the minus sign. It is clear that this vector may be interpreted as the *probability current density* – and I , as the total *probability current* through the surface S . This interpretation may be further supported by rewriting Eq. (47) for the wavefunction represented in the polar form $\Psi = ae^{i\varphi}$, with real a and φ :

$$\mathbf{j} = a^2 \frac{\hbar}{m} \nabla \varphi. \quad (1.49)$$

Note that for a real wavefunction, or even for a wavefunction with an arbitrary but space-constant phase φ , the probability current density vanishes. On the contrary, for the traveling wave (29), with a constant probability density $w = a^2$, Eq. (49) yields a non-zero (and physically very transparent) result:

$$\mathbf{j} = w \frac{\hbar}{m} \mathbf{k} = w \frac{\mathbf{p}}{m} = w \mathbf{v}, \quad (1.50)$$

where $\mathbf{v} = \mathbf{p}/m$ is particle's velocity. If multiplied by the particle's mass m , the probability density w turns into the (average) mass density ρ , and the probability current density, into the *mass flux density* $\rho \mathbf{v}$. Similarly, if multiplied by the total electric charge q of the particle, with w turning into the *charge density* σ , \mathbf{j} becomes the electric current density. As the reader (hopefully :-) knows, both these currents satisfy classical continuity equations similar to Eq. (48).³⁹

Finally, let us recast the continuity equation, rewriting Eq. (46) as

$$\int_V \left(\frac{\partial w}{\partial t} + \nabla \cdot \mathbf{j} \right) d^3 r = 0. \quad (1.51)$$

Now we may argue that this equality may be true for any choice of the volume V only if the expression under the integral vanishes everywhere, i.e. if

$$\frac{\partial w}{\partial t} + \nabla \cdot \mathbf{j} = 0. \quad (1.52)$$

This differential form of the continuity equation may be more convenient than its integral form (48).

1.5. Eigenstates and eigenvalues

Now let us discuss the most important corollaries of wave mechanics' *linearity*. First of all, it uses only *linear operators*. This term means that the operators must obey the following two rules:⁴⁰

$$(\hat{A}_1 + \hat{A}_2)\Psi = \hat{A}_1\Psi + \hat{A}_2\Psi, \quad (1.53)$$

³⁹ See, e.g., respectively, CM 8.3 and EM Sec. 4.1.

⁴⁰ By the way, if any equality involving operators is valid for an arbitrary wavefunction, the latter is frequently dropped from notation, resulting in an *operator equality*. In particular, Eq. (53) may be readily used to prove that the linear operators are *commutative*: $\hat{A}_2 + \hat{A}_1 = \hat{A}_1 + \hat{A}_2$, and *associative*: $(\hat{A}_1 + \hat{A}_2) + \hat{A}_3 = \hat{A}_1 + (\hat{A}_2 + \hat{A}_3)$.

$$\hat{A}(c_1 \Psi_1 + c_2 \Psi_2) = \hat{A}(c_1 \Psi_1) + \hat{A}(c_2 \Psi_2) = c_1 \hat{A}\Psi_1 + c_2 \hat{A}\Psi_2, \quad (1.54)$$

where Ψ_n are arbitrary wavefunctions, while c_n are arbitrary constants (in quantum mechanics, frequently called *c-numbers*, to distinguish them from operators and wavefunctions). The most important examples of linear operators are given by:

- (i) the multiplication by a function, such as for the operator $\hat{\mathbf{r}}$ given by Eq. (26), and
- (ii) the spatial or temporal differentiation, such as in Eqs. (25)-(27).

Next, it is of key importance that the Schrödinger equation (25) is also linear. (This fact was already used in the discussion of wave packets in the last section.) This means that if each of several functions Ψ_n are (particular) solutions of Eq. (25) with a certain Hamiltonian, then their arbitrary linear combination,

$$\Psi = \sum_n c_n \Psi_n, \quad (1.55)$$

is also a solution of the same equation.⁴¹

Let us use the linearity to accomplish an apparently impossible feat: immediately find the *general* solution of the Schrödinger equation for the most important case when the system's Hamiltonian does not depend on time explicitly – for example, like in Eq. (41) with time-independent potential energy $U = U(\mathbf{r})$, when the Schrödinger equation has the form

$$i\hbar \frac{\partial \Psi}{\partial t} = -\frac{\hbar^2}{2m} \nabla^2 \Psi + U(\mathbf{r}) \Psi. \quad (1.56)$$

Potential field:
Schrödinger equation

First of all, let us prove that the following product,

$$\Psi_n = a_n(t) \psi_n(\mathbf{r}), \quad (1.57)$$

Variable separation

qualifies as a (particular) solution of such an equation. Indeed, plugging Eq. (57) into Eq. (25) with *any* time-independent Hamiltonian, using the fact that in this case

$$\hat{H}a_n(t)\psi_n(\mathbf{r}) = a_n(t)\hat{H}\psi_n(\mathbf{r}), \quad (1.58)$$

and dividing both parts of the equation by $a_n \psi_n$, we get

$$\frac{i\hbar}{a_n} \frac{da_n}{dt} = \frac{\hat{H}\psi_n}{\psi_n}. \quad (1.59)$$

The left-hand side of this equation may depend only on time, while the right-hand side, only on coordinates. These facts may be only reconciled if we assume that each of these parts is equal to (the same) constant of the dimension of energy, which I will denote as E_n .⁴² As a result, we are getting two separate equations for the temporal and spatial parts of the wavefunction:

⁴¹ At the first glance, it may seem strange that the *linear* Schrödinger equation correctly describes quantum properties of systems whose classical dynamics is described by *nonlinear* equations of motion (e.g., an anharmonic oscillator – see, e.g., CM Sec. 5.2). Note, however, that statistical equations of classical dynamics (see, e.g., SM Chapters 5 and 6) also have this property, so it is not specific to quantum mechanics.

⁴² This argumentation, leading to *variable separation*, is very common in mathematical physics – see, e.g., its discussion in CM Sec. 6.5, and in EM Sec. 2.5 and beyond.

Stationary
Schrödinger
equation

$$\hat{H}\psi_n = E_n\psi_n, \quad (1.60)$$

$$i\hbar \frac{da_n}{dt} = E_n a_n. \quad (1.61a)$$

The latter of these equations, rewritten in the form

$$\frac{da_n}{a_n} = -i \frac{E_n}{\hbar} dt, \quad (1.61b)$$

is readily integrable, giving

Stationary
state:
time
evolution

$$\ln a_n = -i\omega_n t + \text{const}, \quad \text{so that } a_n = \text{const} \times \exp\{-i\omega_n t\}, \quad \text{with } \omega_n \equiv \frac{E_n}{\hbar}. \quad (1.62)$$

Now plugging Eqs. (57) and (62) into Eq. (22), we see that in the quantum state described by Eqs. (57)-(62), the probability w of finding the particle at a certain location does not depend on time:

$$w \equiv \psi_n^*(\mathbf{r})\psi_n(\mathbf{r}) = w(\mathbf{r}). \quad (1.63)$$

With the same substitution, Eq. (23) shows that the expectation value of any operator that does not depend on time explicitly is also time-independent:

$$\langle A \rangle \equiv \int \psi_n^*(\mathbf{r})\hat{A}\psi_n(\mathbf{r})d^3r = \text{const}. \quad (1.64)$$

Due to this property, the states described by Eqs. (57)-(62) are called *stationary*; they are fully defined by the possible solutions of the *stationary* (or “time-independent”) Schrödinger equation (60).⁴³ Note that for the time-independent Hamiltonian (41), the stationary Schrödinger equation (60),

Potential field:
stationary
Schrödinger
equation

$$-\frac{\hbar^2}{2m}\nabla^2\psi_n + U(\mathbf{r})\psi_n = E_n\psi_n, \quad (1.65)$$

is a linear, homogeneous differential equation for the function ψ_n , with *a priori* unknown parameter E_n . Such equations fall into the mathematical category of *eigenproblems*,⁴⁴ whose *eigenfunctions* ψ_n and *eigenvalues* E_n should be found simultaneously, i.e. self-consistently.⁴⁵

Mathematics⁴⁶ tells us that for such equations with space-confined eigenfunctions ψ_n , tending to zero at $r \rightarrow \infty$, the spectrum of eigenvalues is *discrete*. It also proves that the eigenfunctions corresponding to different eigenvalues are *orthogonal*, i.e. that space integrals of the products $\psi_n\psi_{n'}^*$ vanish for all pairs with $n \neq n'$. Due to the Schrödinger equation’s linearity, each of these functions may be multiplied by a proper constant coefficient to make their set *orthonormal*:

$$\int \psi_n^*\psi_{n'}d^3r = \delta_{n,n'} \equiv \begin{cases} 1, & \text{for } n = n', \\ 0, & \text{for } n \neq n'. \end{cases} \quad (1.66)$$

⁴³ In contrast, the *full* Schrödinger equation (25) is frequently called *time-dependent* or *non-stationary*.

⁴⁴ From the German root *eigen*, meaning “particular” or “characteristic”.

⁴⁵ Eigenvalues of energy are frequently called *eigenenergies*, and it is often said that the eigenfunction ψ_n and the corresponding eigenenergy E_n together determine the n^{th} *stationary eigenstate* of the system.

⁴⁶ See, e.g., Sec. 9.3 of the wonderful handbook by G. Korn and T. Korn, listed in MA Sec. 16(ii).

Moreover, the eigenfunctions $\psi_n(\mathbf{r})$ form a *full set*, meaning that an arbitrary function $\psi(\mathbf{r})$, in particular the actual wavefunction Ψ of the system in the initial moment of its evolution (which I will always, with a few clearly marked exceptions, take for $t = 0$) may be represented as a unique expansion over the eigenfunction set:

$$\Psi(\mathbf{r},0) = \sum_n c_n \psi_n(\mathbf{r}). \quad (1.67)$$

The expansion coefficients c_n may be readily found by multiplying both sides of Eq. (67) by $\psi_n^*(\mathbf{r})$, integrating the results over the space, and using Eq. (66). The result is

$$c_n = \int \psi_n^*(\mathbf{r}) \Psi(\mathbf{r},0) d^3 r. \quad (1.68)$$

Now let us consider the following wavefunction

$$\Psi(\mathbf{r},t) = \sum_n c_n a_k(t) \psi_k(\mathbf{r}) = \sum_n c_n \exp\left\{-i \frac{E_n}{\hbar} t\right\} \psi_n(\mathbf{r}). \quad (1.69)$$

General solution for $U = U(\mathbf{r})$

Since each term of the sum has the form (57) and satisfies the Schrödinger equation, so does the sum as the whole. Moreover, if the coefficients c_n are derived in accordance with Eq. (68), then the solution (69) satisfies the initial conditions as well. At this moment we can use one more bit of help from mathematicians, who tell us that the linear, partial differential equation of type (65), with fixed initial conditions, may have only one (*unique*) solution. This means that in our case of time-independent potential Hamiltonian, Eq. (69) gives the *general* solution of the Schrödinger equation (25).

So, we have succeeded in our apparently over-ambitious goal. Now let us pause this mad mathematical dash for a minute, and discuss this key result.

1.6. Time evolution

For the time-dependent factor, $a_n(t)$, of each component (57) of the general solution (69), our procedure gave a very simple and universal result (62), describing a linear change of the phase $\varphi_n \equiv \arg(a_n)$ of this complex function in time, with the constant rate

$$\frac{d\varphi_n}{dt} = -\omega_n = -\frac{E_n}{\hbar}, \quad (1.70)$$

so that the real and imaginary parts of a_n oscillate sinusoidally with this frequency. The relation (70) coincides with Einstein's conjecture (5), but could these oscillations of the wavefunctions represent a physical reality? Indeed, for photons, described by Eq. (5), E may be (and as we will see in Chapter 9, is) the actual, well-defined energy of one photon, and ω is the frequency of the radiation so quantized. However, for non-relativistic particles, described by wave mechanics, the potential energy U , and hence the full energy E , are defined to an arbitrary constant, because we may measure them from an arbitrary reference level. How can such a change of the energy reference level (which may be made just in our mind) alter the frequency of oscillations of a variable?

According to Eqs. (22)-(23), this time evolution of a wavefunction does not affect the particle's probability distribution, or even any observable (including the energy E , provided that it is always referred to the same origin as U), in any stationary state. However, let us combine Eq. (5) with Bohr's assumption (7):

$$\hbar\omega_{nn'} = E_{n'} - E_n. \quad (1.71)$$

The *difference* $\omega_{nn'}$ of the eigenfrequencies ω_n and $\omega_{n'}$, participating in this formula, is evidently independent of the energy reference, and as will be proved later in the course, determines the measurable frequency of the electromagnetic radiation (or possibly of a wave of a different physical nature) emitted or absorbed at the quantum transition between the states.

As another but related example, consider two similar particles 1 and 2, each in the same (say, the lowest-energy) eigenstate, but with their potential energies (and hence the ground state energies $E_{1,2}$) different by a constant $\Delta U \equiv U_1 - U_2$. Then, according to Eq. (70), the difference $\varphi \equiv \varphi_1 - \varphi_2$ of their wavefunction phases evolves in time with the reference-independent rate

$$\frac{d\varphi}{dt} = -\frac{\Delta U}{\hbar}. \quad (1.72)$$

Certain measurement instruments, weakly coupled to the particles, may allow observation of this evolution, while keeping the particle's quantum dynamics virtually unperturbed, i.e. Eq. (70) intact. Perhaps the most dramatic measurement of this type is possible using the *Josephson effect* in weak links between two superconductors – see Fig. 7.⁴⁷

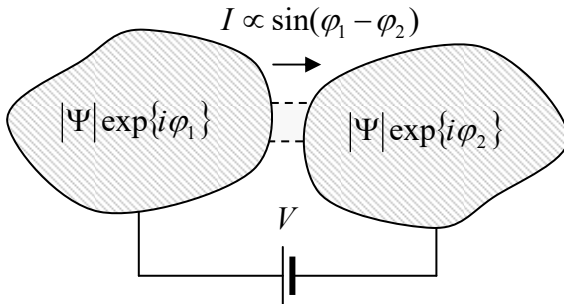


Fig. 1.7. The Josephson effect in a weak link between two bulk superconductor electrodes.

As a brief reminder,⁴⁸ superconductivity may be explained by a specific coupling between conduction electrons in solids, that leads, at low temperatures, to the formation of the so-called *Cooper pairs*. Such pairs, each consisting of two electrons with opposite spins and momenta, behave as Bose particles and form a coherent *Bose-Einstein condensate*.⁴⁹ Most properties of such a condensate may be described by a single, common wavefunction Ψ , evolving in time just as that of a free particle, with the effective potential energy $U = q\phi = -2e\phi$, where ϕ is the electrochemical potential,⁵⁰ and $q = -2e$ is the electric charge of a Cooper pair. As a result, for the system shown in Fig. 7, in which externally applied voltage V fixes the difference $\phi_1 - \phi_2$ between the electrochemical potentials of two superconductors, Eq. (72) takes the form

$$\frac{d\varphi}{dt} = \frac{2e}{\hbar}V. \quad (1.73)$$

Eq. (72) for
Josephson
effect

If the link between the superconductors is weak enough, the electric current I of the Cooper pairs (called the *supercurrent*) through the link may be approximately described by the following simple relation,

⁴⁷ The effect was predicted in 1962 by Brian Josephson (then a graduate student!) and observed soon after that.

⁴⁸ For a more detailed discussion, including the derivation of Eq. (75), see e.g. EM Chapter 6.

⁴⁹ A detailed discussion of the Bose-Einstein condensation may be found, e.g., in SM Sec. 3.4.

⁵⁰ For more on this notion see, e.g. SM Sec. 6.3.

$$I = I_c \sin \varphi, \quad (1.74)$$

where I_c is some constant, dependent on the weak link's strength.⁵¹ Now combining Eqs. (73) and (74), we see that if the applied voltage V is constant in time, the current oscillates sinusoidally, with the so-called *Josephson frequency*

$$\omega_J \equiv \frac{2e}{\hbar} V, \quad (1.75)$$

as high as ~ 484 MHz per microvolt of applied dc voltage. This effect may be readily observed experimentally: though its direct detection is a bit tricky, it is easy to observe the *phase locking* (synchronization)⁵² of the Josephson oscillations by an external microwave signal of frequency ω . Such phase locking results in the relation $\omega_J = n\omega$ fulfilled within certain dc current intervals, and hence in the formation, on the weak link's dc I - V curve, of virtually vertical current steps at dc voltages

$$V_n = n \frac{\hbar\omega}{2e}, \quad (1.76)$$

where n is an integer.⁵³ Since frequencies may be stabilized and measured with very high precision, this effect is being used in highly accurate standards of dc voltage.

1.7. Spatial dependence

In contrast to the simple and universal time dependence (62) of the stationary states, the spatial distributions of their wavefunction $\psi_n(\mathbf{r})$ need to be calculated from the problem-specific stationary Schrödinger equation (65). The solution of this equation for various particular cases is a major focus of the next two chapters. For now, let us consider just the simplest example, which nevertheless will be the basis for our discussion of more complex problems: let a particle be confined inside a rectangular hard-wall box. Such confinement may be described by the following potential energy profile:⁵⁴

$$U(\mathbf{r}) = \begin{cases} 0, & \text{for } 0 < x < a_x, \quad 0 < y < a_y, \quad \text{and } 0 < z < a_z, \\ +\infty, & \text{otherwise.} \end{cases} \quad (1.77)$$

Hard-wall box:
potential

The only way to keep the product $U(\mathbf{r})\psi_n$ in Eq. (65) finite outside the box, is to have $\psi = 0$ in these regions. Also, the function has to be continuous everywhere, to avoid the divergence of the

⁵¹ In some cases, the function $I(\varphi)$ may somewhat deviate from Eq. (74), but these deviations do not affect its fundamental 2π -periodicity, and hence the fundamental relations (75)-(76). (No corrections to them have been found yet.)

⁵² For the discussion of this very general effect, see, e.g., CM Sec. 5.4.

⁵³ The size of these dc current steps may be readily calculated from Eqs. (73) and (74). Let me leave this task for the reader's exercise.

⁵⁴ Another common name for such potentials, especially of lower dimensionality, is the *potential well*, in our current case "rectangular" one: with a flat "bottom" and vertical, infinitely high "walls". Note that sometimes, very unfortunately, such potential profiles are called "quantum wells". (This term seems to imply that the particle's confinement in such a well is a phenomenon specific for quantum mechanics. However, as we will repeatedly see in this course, the opposite is true: quantum effects do as much as they only can to *overcome* the particle's confinement in a potential well, letting it partly penetrate in the "classically forbidden" regions beyond the well's walls.)

kinetic-energy term $(-\hbar^2/2m)\nabla^2\psi_n$. Hence, in this case we may solve the stationary Schrödinger equation (60) just inside the box, i.e. with $U=0$, so that it takes a simple form

$$-\frac{\hbar^2}{2m}\nabla^2\psi_n = E_n\psi_n, \quad (1.78a)$$

with zero boundary conditions on all the walls.⁵⁵ For our particular geometry, it is natural to express the Laplace operator in the Cartesian coordinates $\{x, y, z\}$ aligned with the box sides, with the origin at one of the corners of its rectangular $a_x \times a_y \times a_z$ volume, so that our boundary problem becomes:

$$-\frac{\hbar^2}{2m}\left(\frac{\partial^2}{\partial x^2} + \frac{\partial^2}{\partial y^2} + \frac{\partial^2}{\partial z^2}\right)\psi_n = E_n\psi_n, \quad \text{for } 0 < x < a_x, \quad 0 < y < a_y, \quad \text{and } 0 < z < a_z, \quad (1.78b)$$

$$\text{with } \psi_n = 0 \text{ for: } x = 0 \text{ and } a_x; \quad y = 0 \text{ and } a_y; \quad z = 0 \text{ and } a_z.$$

This problem may be readily solved using the same variable separation method as was used in Sec. 5 – now to separate the Cartesian spatial variables from each other, by looking for a partial solution of Eq. (78) in the form

$$\psi(\mathbf{r}) = X(x)Y(y)Z(z). \quad (1.79)$$

(Let us postpone assigning function indices for a minute.) Plugging this expression into Eq. (78b) and dividing all terms by the product XYZ , we get

$$-\frac{\hbar^2}{2m}\frac{1}{X}\frac{d^2X}{dx^2} - \frac{\hbar^2}{2m}\frac{1}{Y}\frac{d^2Y}{dy^2} - \frac{\hbar^2}{2m}\frac{1}{Z}\frac{d^2Z}{dz^2} = E. \quad (1.80)$$

Now let us repeat the standard argumentation of the variable separation method: since each term on the left-hand side of this equation may be only a function of the corresponding argument, the equality is possible only if each of them is a constant – in our case, with the dimensionality of energy. Calling these constants E_x , etc., we get three similar 1D equations

$$-\frac{\hbar^2}{2m}\frac{1}{X}\frac{d^2X}{dx^2} = E_x, \quad -\frac{\hbar^2}{2m}\frac{1}{Y}\frac{d^2Y}{dy^2} = E_y, \quad -\frac{\hbar^2}{2m}\frac{1}{Z}\frac{d^2Z}{dz^2} = E_z, \quad (1.81)$$

with Eq. (80) turning into the following energy-matching condition:

$$E_x + E_y + E_z = E. \quad (1.82)$$

All three ordinary differential equations (81), and their solutions, are similar. For example, for $X(x)$, we have the following 1D Helmholtz equation

$$\frac{d^2X}{dx^2} + k_x^2X = 0, \quad \text{with } k_x^2 \equiv \frac{2mE_x}{\hbar^2}, \quad (1.83)$$

and simple boundary conditions: $X(0) = X(a_x) = 0$. Let me hope that the reader knows how to solve this well-known 1D boundary problem – describing, for example, the usual mechanical waves on a guitar string. The problem allows an infinite number of sinusoidal standing-wave eigenfunctions,⁵⁶

⁵⁵ Rewritten as $\nabla^2f + k^2f = 0$, Eq. (78a) is just the *Helmholtz equation*, which describes waves of any nature (with the wave vector \mathbf{k}) in a uniform, isotropic, linear medium – see, e.g., EM Secs. 7.5-7.9 and 8.5.

⁵⁶ The front coefficient in the last expression for X ensures the (ortho)normality condition (66).

$$X \propto \sin k_x x, \quad \text{with } k_x = \frac{\pi n_x}{a_x}, \quad \text{so that } X = \left(\frac{2}{a_x} \right)^{1/2} \sin \frac{\pi n_x x}{a_x}, \quad \text{with } n_x = 1, 2, \dots, \quad (1.84)$$

Rectangular potential well:
1D eigenfunctions

corresponding to the following eigenenergies:

$$E_x = \frac{\hbar^2}{2m} k_x^2 = \frac{\pi^2 \hbar^2}{2ma_x^2} n_x^2 \equiv E_{x1} n_x^2. \quad (1.85)$$

Figure 8 shows these simple results, using a somewhat odd but very graphic and common representation, in that the eigenenergy values (frequently called the *energy levels*) are used as horizontal axes for plotting the eigenfunctions – despite their completely different dimensionality.

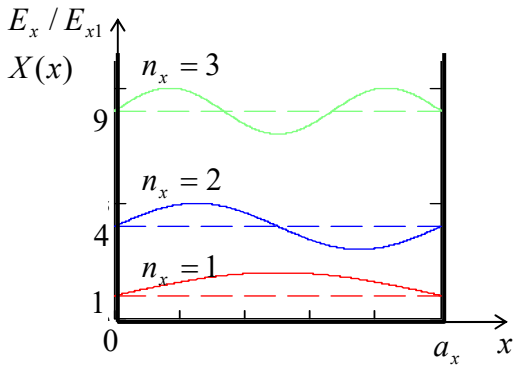


Fig. 1.8. The lowest eigenfunctions (solid lines) and eigenvalues (dashed lines) of Eq. (83) for a potential well of length a_x . Solid black lines show the effective potential of this 1D eigenproblem.

Due to the similarity of all Eqs. (81), $Y(y)$ and $Z(z)$ are absolutely similar functions of their arguments, and may also be numbered by integers (say, n_y and n_z) independent of n_x , so that the spectrum of values of the total energy (82) is

$$E_{n_x, n_y, n_z} = \frac{\pi^2 \hbar^2}{2m} \left(\frac{n_x^2}{a_x^2} + \frac{n_y^2}{a_y^2} + \frac{n_z^2}{a_z^2} \right). \quad (1.86)$$

Rectangular potential well:
energy levels

Thus, in this 3D problem, the role of the index n in the general Eq. (69) is played by a set of three independent integers $\{n_x, n_y, n_z\}$. In quantum mechanics, such integers play a key role and thus have a special name, the *quantum numbers*. Using them, that general solution, for our current simple problem may be represented as the sum

$$\Psi(\mathbf{r}, t) = \sum_{n_x, n_y, n_z=1}^{\infty} c_{n_x, n_y, n_z} \sin \frac{\pi n_x x}{a_x} \sin \frac{\pi n_y y}{a_y} \sin \frac{\pi n_z z}{a_z} \exp \left\{ -i \frac{E_{n_x, n_y, n_z}}{\hbar} t \right\}, \quad (1.87)$$

Rectangular potential well:
general solution

with the front coefficients that may be readily calculated from the initial wavefunction $\Psi(\mathbf{r}, 0)$, using Eq. (68) – again with the replacement $n \rightarrow \{n_x, n_y, n_z\}$.

This simplest problem is a good illustration of typical results the wave mechanics gives for spatially-confined motion, including the discrete energy spectrum, and (in this case, evidently) orthogonal eigenfunctions. Perhaps most importantly, its solution shows that the lowest value of the particle's kinetic energy (86), reached in the so-called *ground state* (in our case, the state with $n_x = n_y = n_z = 1$) is above zero for any finite size of the confining box.

An example of the opposite case of a *continuous spectrum* for the *unconfined motion* of a free particle is given by the plane waves (29). With the account of relations $E = \hbar\omega$ and $\mathbf{p} = \hbar\mathbf{k}$, such wavefunction may be viewed as the product of the time-dependent factor (62) by the eigenfunction,

Free
particle:
eigen-
functions

$$\psi_{\mathbf{k}} = a_{\mathbf{k}} \exp\{i\mathbf{k} \cdot \mathbf{r}\}, \quad (1.88)$$

which is the solution of the stationary Schrödinger equation (78a) if it is valid in the whole space.⁵⁷ The reader should not be worried too much by the fact that the fundamental solution (86) in free space is a *traveling* wave (having, in particular, a non-zero value of the probability current \mathbf{j}), while those inside a quantum box are *standing* waves, with $\mathbf{j} = 0$, even though the free space may be legitimately considered as the ultimate limit of a quantum box with volume $V = a_x \times a_y \times a_z \rightarrow \infty$. Indeed, due to the linearity of wave mechanics, two traveling-wave solutions (88) with equal and opposite values of the momentum (and hence with the same energy) may be readily combined to give a standing-wave solution,⁵⁸ for example, $\exp\{i\mathbf{k} \cdot \mathbf{r}\} + \exp\{-i\mathbf{k} \cdot \mathbf{r}\} = 2\cos(\mathbf{k} \cdot \mathbf{r})$, with the net current $\mathbf{j} = 0$. Thus, depending on the convenience for a particular problem, we may represent its general solution as a sum of either traveling-wave or standing-wave eigenfunctions. Since in the unlimited free space, there are no boundary conditions to satisfy, the Cartesian components of the wave vector \mathbf{k} in Eq. (88) can take any real values. (This is why it is more convenient to label these wavefunctions, and the corresponding eigenenergies,

Free
particle:
eigen-
energies

$$E_{\mathbf{k}} = \frac{\hbar^2 k^2}{2m} \geq 0, \quad (1.89)$$

with their wave vector \mathbf{k} rather than an integer index.)

However, one aspect of continuous-spectrum systems requires a bit more caution with mathematics: the summation (69) should be replaced by the integration over a continuous index or indices – in our current case, the three Cartesian components of the vector \mathbf{k} . The main rule of such replacement may be readily extracted from Eq. (84): according to this relation, for standing-wave solutions, the eigenvalues of k_x are *equidistant*, i.e. separated by equal intervals $\Delta k_x = \pi/a_x$, with similar relations for other two Cartesian components of vector \mathbf{k} . Hence the number of different eigenvalues of the standing-wave vector \mathbf{k} (with $k_x, k_y, k_z \geq 0$), within a volume $d^3 k \gg 1/V$ of the \mathbf{k} space is $dN = d^3 k / (\Delta k_x \Delta k_y \Delta k_z) = (V/\pi^3) d^3 k$. Frequently, it is more convenient to work with traveling waves (88); in this case we should take into account that, as was just discussed, there are two different traveling wave numbers (say, $+k_x$ and $-k_x$) corresponding to each standing wave vector's $k_x > 0$. Hence the same number of physically different states corresponds to a $2^3 = 8$ -fold larger \mathbf{k} space or, equivalently, to an 8-fold smaller number of states per unit volume $d^3 k$:

Number
of 3D states

$$dN = \frac{V}{(2\pi)^3} d^3 k. \quad (1.90)$$

⁵⁷ In some systems (e.g., a particle interacting with a potential well of a finite depth), a discrete energy spectrum within a certain energy interval may coexist with a continuous spectrum in a complementary interval. However, the conceptual philosophy of eigenfunctions and eigenvalues remains the same even in this case.

⁵⁸ This is, of course, the general property of waves of any physical nature, propagating in a linear medium – see, e.g., CM Sec. 6.5 and/or EM Sec. 7.3.

For $dN \gg 1$, this expression is independent of the boundary conditions, and is frequently represented as the following *summation rule*

$$\lim_{k^3 V \rightarrow \infty} \sum_{\mathbf{k}} f(\mathbf{k}) = \int f(\mathbf{k}) dN = \frac{V}{(2\pi)^3} \int f(\mathbf{k}) d^3 k, \quad (1.91)$$

Summation over 3D states

where $f(\mathbf{k})$ is an arbitrary function of \mathbf{k} . Note that if the same wave vector \mathbf{k} corresponds to several internal quantum states (such as spin – see Chapter 4), the right-hand side of Eq. (91) requires its multiplication by the corresponding *degeneracy factor* of orbital states.⁵⁹

1.8. Dimensionality reduction

To conclude this introductory chapter, let me discuss the conditions when the spatial dimensionality of a wave-mechanical problem may be reduced.⁶⁰ Naively, one may think that if the particle's potential energy depends on just one spatial coordinate, say $U = U(x, t)$, then its wavefunction has to be one-dimensional as well: $\psi = \psi(x, t)$. Our discussion of the particular case $U = \text{const}$ in the previous section shows that this assumption is wrong. Indeed, though this potential⁶¹ is just a special case of the potential $U(x, t)$, most of its eigenfunctions, given by Eqs. (87) or (88), do depend on the other two coordinates. This is why the solutions $\psi(x, t)$ of the 1D Schrödinger equation

$$i\hbar \frac{\partial \Psi}{\partial t} = -\frac{\hbar^2}{2m} \frac{\partial^2}{\partial x^2} \Psi + U(x, t)\Psi, \quad (1.92)$$

1D time-dependent Schrödinger equation

which follows from Eq. (65) by assuming $\partial\Psi/\partial y = \partial\Psi/\partial z = 0$, are insufficient to form the general solution of Eq. (65) for this case.

This fact is easy to understand physically for the simplest case of a stationary 1D potential: $U = U(x)$. The absence of the y - and z -dependence of the potential energy U may be interpreted as a potential well that is flat in two directions, y and z . Repeating the arguments of the previous section for this case, we see that the eigenfunctions of a particle in such a well have the form

$$\psi(\mathbf{r}) = X(x) \exp\{i(k_y y + k_z z)\}, \quad (1.93)$$

where $X(x)$ is an eigenfunction of the following stationary 1D Schrödinger equation:

$$-\frac{\hbar^2}{2m} \frac{d^2 X}{dx^2} + U_{\text{ef}}(x)X = EX, \quad (1.94)$$

where $U_{\text{ef}}(x)$ is *not* the full potential energy of the particle, as it would follow from Eq. (92), but rather its effective value including the kinetic energy of the lateral motion:

$$U_{\text{ef}} \equiv U + (E_y + E_z) = U + \frac{\hbar^2}{2m} (k_y^2 + k_z^2). \quad (1.95)$$

⁵⁹ Such factor is similar to the front factor 2 in Eq. (1) for the number of electromagnetic wave modes, in that case describing two different polarizations of the waves with the same wave vector.

⁶⁰ Most textbooks on quantum mechanics jump to the formal solution of 1D problems without such discussion, ignoring the fact that such dimensionality restriction is adequate only under very specific conditions.

⁶¹ Following tradition, I will frequently use this shorthand for “potential energy”, returning to the full term in cases where there is any chance of confusion of this notion with another (say, electrostatic) potential.

In plain English, the particle's partial wavefunction $X(x)$ and its full energy, depend on its transverse momenta, which have continuous spectrum – see the discussion of Eq. (89). This means that Eq. (92) is adequate only if the condition $k_y = k_z = 0$ is somehow enforced, and in most physical problems, it is not. For example, if a de Broglie (or any other) plane wave $\Psi(x, t)$ is incident on a potential step, it would be reflected exactly back, i.e. with $k_y = k_z = 0$, only if the wall's surface is perfectly plane and exactly normal to the axis x . Any imperfection (and they are so many of them in real physical systems –:) may cause excitation of waves with non-zero values of k_y and k_z , due to the continuous character of the functions $E_y(k_y)$ and $E_z(k_z)$.⁶²

There is essentially one, perhaps counter-intuitive way to make the 1D solutions “robust” to small perturbations: it is to provide a *rigid lateral confinement*⁶³ in two other directions. As the simplest example, consider a narrow *quantum wire* (Fig. 9a), described by the following potential:

$$U(\mathbf{r}) = \begin{cases} U(x), & \text{for } 0 < y < a_y, \text{ and } 0 < z < a_z, \\ +\infty, & \text{otherwise.} \end{cases} \quad (1.96)$$

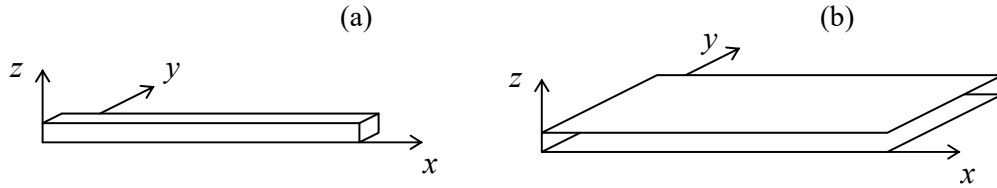


Fig. 1.9. Partial confinement in: (a) two dimensions, and (b) one dimension.

Performing the standard variable separation (79), we see that the corresponding stationary Schrödinger equation is satisfied if the partial wavefunction $X(x)$ obeys Eqs. (94)-(95), but now with a discrete energy spectrum in the transverse directions:

$$U_{\text{ef}} = U + \frac{\pi^2 \hbar^2}{2m} \left(\frac{n_y^2}{a_y^2} + \frac{n_z^2}{a_z^2} \right). \quad (1.97)$$

If the lateral confinement is tight, $a_y, a_z \rightarrow 0$, then there is a large energy gap,

$$\Delta U \sim \frac{\pi^2 \hbar^2}{2ma_{y,z}^2}, \quad (1.98)$$

between the ground-state energy of the lateral motion (with $n_y = n_z = 1$) and that for all its excited states. As a result, if the particle is initially placed into the lateral ground state, and its energy E is much smaller than ΔU , it would stay in such state, i.e. may be described by a 1D Schrödinger equation similar to Eq. (92) – even in the time-dependent case, if the characteristic frequency of energy variations is much smaller than $\Delta U/\hbar$. Absolutely similarly, the strong lateral confinement in just one dimension (say, z , see Fig. 9b) enables systems with a robust 2D evolution of the particle's wavefunction.

⁶² This problem is not specific to quantum mechanics. The classical motion of a particle in a 1D potential may be also unstable with respect to lateral perturbations, especially if the potential is time-dependent, i.e. capable of exciting low-energy lateral modes.

⁶³ The term “quantum confinement”, sometimes used to describe this phenomenon, is as unfortunate as the “quantum well” term discussed above, because of the same reason: the confinement is a purely classical effect, and as we will repeatedly see in this course, the quantum-mechanical effects reduce, rather than enable it.

The tight lateral confinement may ensure the dimensionality reduction even if the potential well is not exactly rectangular in the lateral direction(s), as described by Eq. (96), but is described by some x - and t -independent profile, if it still provides a sufficiently large energy gap ΔU . For example, many 2D quantum phenomena, such as the quantum Hall effect,⁶⁴ have been studied experimentally using electrons confined at semiconductor heterojunctions (e.g., epitaxial interfaces GaAs/Al_xGa_{1-x}As), where the potential well in the direction perpendicular to the interface has a nearly triangular shape, and provides an energy gap ΔU of the order of 10⁻² eV.⁶⁵ This gap corresponds to $k_B T$ with $T \sim 100$ K, so that careful experimentation at liquid helium temperatures (4K and below) may keep the electrons performing purely 2D motion in the “lowest subband” ($n_z = 1$).

Finally, note that in systems with reduced dimensionality, Eq. (90) for the number of states at large \mathbf{k} (i.e., for an essentially free particle motion) should be replaced accordingly: in a 2D system of area $A \gg 1/k^2$,

$$dN = \frac{A}{(2\pi)^2} d^2 k, \quad (1.99)$$
Number of 2D states

while in a 1D system of length $l \gg 1/k$,

$$dN = \frac{l}{2\pi} dk, \quad (1.100)$$
Number of 1D states

with the corresponding changes of the summation rule (91). This change has important implications for the density of states on the energy scale, dN/dE : it is straightforward (and hence left for the reader :-)) to use Eqs. (90), (99), and (100) to show that for free 3D particles the density increases with E (proportionally to $E^{1/2}$), for free 2D particles it does not depend on energy at all, while for free 1D particles it scales as $E^{1/2}$, i.e. decreases with energy.

1.9. Exercise problems

1.1. The actual postulate made by N. Bohr in his original 1913 paper was not directly Eq. (8), but the assumption that at quantum leaps between adjacent large (quasiclassical) orbits with $n \gg 1$, the hydrogen atom either emits or absorbs energy $\Delta E = \hbar\omega$, where ω is its classical radiation frequency – according to classical electrodynamics, equal to the angular velocity of electron’s rotation.⁶⁶ Prove that this postulate is indeed compatible with Eqs. (7)-(8).

1.2. Use Eq. (53) to prove that the linear operators of quantum mechanics are commutative: $\hat{A}_2 + \hat{A}_1 = \hat{A}_1 + \hat{A}_2$, and associative: $(\hat{A}_1 + \hat{A}_2) + \hat{A}_3 = \hat{A}_1 + (\hat{A}_2 + \hat{A}_3)$.

1.3. Prove that for any time-independent Hamiltonian operator \hat{H} and two arbitrary complex functions $f(\mathbf{r})$ and $g(\mathbf{r})$,

$$\int f(\mathbf{r}) \hat{H} g(\mathbf{r}) d^3 r = \int \hat{H} f(\mathbf{r}) g(\mathbf{r}) d^3 r.$$

⁶⁴ To be discussed in Sec. 3.2.

⁶⁵ See, e.g., P. Harrison, *Quantum Wells, Wires, and Dots*, 3rd ed., Wiley, 2010.

⁶⁶ See, e.g., EM Sec. 8.2.

1.4. Prove that the Schrödinger equation (25) with the Hamiltonian operator given by Eq. (41), is Galilean form-invariant, provided that the wavefunction is transformed as

$$\Psi'(\mathbf{r}', t') = \Psi(\mathbf{r}, t) \exp \left\{ -i \frac{m\mathbf{v} \cdot \mathbf{r}}{\hbar} + i \frac{mv^2 t}{2\hbar} \right\},$$

where the prime sign marks the variables measured in the reference frame 0' that moves, without rotation, with a constant velocity \mathbf{v} relatively to the “lab” frame 0. Give a physical interpretation of this transformation.

1.5.* Prove the so-called *Hellmann-Feynman theorem*:⁶⁷

$$\frac{\partial E_n}{\partial \lambda} = \left\langle \frac{\partial H}{\partial \lambda} \right\rangle_n,$$

where λ is some c -number parameter, on which the time-independent Hamiltonian \hat{H} , and hence its eigenenergies E_n , depend.

1.6.* Use Eqs. (73) and (74) to analyze the effect of phase locking of Josephson oscillations on the dc current flowing through a weak link between two superconductors (frequently called the *Josephson junction*), assuming that an external source applies to the junction a sinusoidal ac voltage with frequency ω and amplitude A .

1.7. Calculate $\langle x \rangle$, $\langle p_x \rangle$, δx , and δp_x for the eigenstate $\{n_x, n_y, n_z\}$ of a particle in a rectangular hard-wall box described by Eq. (77), and compare the product $\delta x \delta p_x$ with the Heisenberg’s uncertainty relation.

1.8. Looking at the lower (red) line in Fig. 8, it seems plausible that the 1D ground-state function (84) of the simple potential well (77) may be well approximated with an inverted quadratic parabola:

$$X_{\text{trial}}(x) = C x (a_x - x),$$

where C is a normalization constant. Explore how good this approximation is.

1.9. A particle placed in a hard-wall rectangular box with sides a_x , a_y , and a_z , is in its ground state. Calculate the average force acting on each face of the box. Can the forces be characterized by a certain pressure?

1.10. A 1D quantum particle was initially in the ground state of a very deep, rectangular potential well of width a :

$$U(x) = \begin{cases} 0, & \text{for } -a/2 < x < +a/2, \\ +\infty, & \text{otherwise.} \end{cases}$$

⁶⁷ Despite this common name, H. Hellmann (in 1937) and R. Feynman (in 1939) were not the first ones in the long list of physicists who had (apparently, independently) discovered this equality. Indeed, it has been traced back to a 1922 paper by W. Pauli, and was carefully proved by P. Güttinger in 1931.

At some instant, the well's width is abruptly increased to a new value $a' > a$, leaving the potential symmetric with respect to the point $x = 0$, and then left constant. Calculate the probability that after the change, the particle is still in the ground state of the system.

1.11. At $t = 0$, a 1D particle of mass m is placed into a hard-wall, flat-bottom potential well

$$U(x) = \begin{cases} 0, & \text{for } 0 < x < a, \\ +\infty, & \text{otherwise,} \end{cases}$$

in a 50/50 linear superposition of the lowest (ground) state and the first excited state. Calculate:

- (i) the normalized wavefunction $\Psi(x, t)$ for arbitrary time $t \geq 0$, and
- (ii) the time evolution of the expectation value $\langle x \rangle$ of the particle's coordinate.

1.12. Calculate the potential profiles $U(x)$ for that the following wavefunctions,

- (i) $\Psi = c \exp\{-ax^2 - ibt\}$, and
- (ii) $\Psi = c \exp\{-a|x| - ibt\}$

(with real coefficients $a > 0$ and b), satisfy the 1D Schrödinger equation for a particle with mass m . For each case, calculate $\langle x \rangle$, $\langle p_x \rangle$, δx , and δp_x , and compare the product $\delta x \delta p_x$ with the Heisenberg's uncertainty relation.

1.13. A 1D particle of mass m , moving in the field of a stationary potential $U(x)$, has the following eigenfunction

$$\psi(x) = \frac{C}{\cosh \kappa x},$$

where C is the normalization constant, and κ is a real constant. Calculate the function $U(x)$ and the state's eigenenergy E .

1.14. Calculate the density dN/dE of traveling-wave quantum states in large rectangular potential wells of various dimensions: $d = 1, 2$, and 3 .

1.15.* Use the finite-difference method with steps $a/2$ and $a/3$ to find as many eigenenergies as possible for a 1D particle in the infinitely deep, hard-wall 1D potential well of width a . Compare the results with each other, and with the exact formula.⁶⁸

⁶⁸ You may like to start by reading about the finite-difference method – see, e.g., CM Sec. 8.5 or EM Sec. 2.11.

Chapter 2. 1D Wave Mechanics

Even the simplest, 1D version of wave mechanics enables quantitative analysis of many important quantum-mechanical effects. The order of their discussion in this chapter is dictated mostly by mathematical convenience – going from the simplest potential profiles to more complex ones, so that we may build upon the previous results. However, I would advise the reader to focus more not on the math, but rather on the physics of the non-classical phenomena it describes, ranging from particle penetration into classically-forbidden regions, to quantum-mechanical tunneling, to the metastable state decay, to covalent bonding and quantum oscillations, to energy bands and gaps.

2.1. Basic relations

As was discussed at the end of Chapter 1, in several cases (in particular, at strong confinement within the $[y, z]$ plane), the general (3D) Schrödinger equation may be reduced to its 1D version, similar to Eq. (1.92):

$$\text{Schrödinger equation} \quad i\hbar \frac{\partial \Psi(x, t)}{\partial t} = -\frac{\hbar^2}{2m} \frac{\partial^2 \Psi(x, t)}{\partial x^2} + U(x, t)\Psi(x, t). \quad (2.1)$$

It is important, however, to remember that according to the discussion in Sec. 1.8, $U(x, t)$ in this equation is generally *effective* potential energy, which may include the energy of the lateral motion, while $\Psi(x, t)$ may be just one factor in the complete wavefunction $\Psi(x, t)\chi(y, z)$. If the transverse factor $\chi(y, z)$ is normalized to 1, then the integration of Eq. (1.22a) over the 3D space within a segment $[x_1, x_2]$ gives the following probability to find the particle on this segment:

$$\text{Probability} \quad W(t) \equiv \int_{x_1}^{x_2} \Psi(x, t)\Psi^*(x, t)dx. \quad (2.2)$$

If the particle under analysis is definitely somewhere inside the system, the normalization of its 1D wavefunction $\Psi(x, t)$ is provided by extending integral (2) to the whole axis x :

$$\text{Normalization} \quad \int_{-\infty}^{+\infty} w(x, t)dx = 1, \quad \text{where } w(x, t) \equiv \Psi(x, t)\Psi^*(x, t). \quad (2.3)$$

A similar integration of Eq. (1.23) shows that the expectation value of any observable depending only on the coordinate x (and possibly time), may be expressed as

$$\text{Expectation value} \quad \langle A \rangle(t) = \int_{-\infty}^{+\infty} \Psi^*(x, t)\hat{A}\Psi(x, t)dx. \quad (2.4)$$

It is also useful to introduce the notion of the *probability current* along the x -axis (a scalar):

$$\text{Probability current} \quad I(x, t) \equiv \int j_x dy dz = \frac{\hbar}{m} \text{Im} \left(\Psi^* \frac{\partial}{\partial x} \Psi \right) = \frac{\hbar}{m} |\Psi(x, t)|^2 \frac{\partial \varphi}{\partial x}, \quad (2.5)$$

where j_x is the x -component of the current density vector $\mathbf{j}(\mathbf{r}, t)$. Then the continuity equation (1.48) for any segment $[x_1, x_2]$ takes the form

$$\frac{dW}{dt} + I(x_2) - I(x_1) = 0. \quad (2.6)$$

Continuity
equation

The above formulas are sufficient for analysis of 1D problems of wave mechanics, but before proceeding to particular cases, let me deliver on my earlier promise to prove that Heisenberg's uncertainty relation (1.35) is indeed valid for any wavefunction $\Psi(x, t)$. For that, let us consider the following positive (or at least non-negative) integral

$$J(\lambda) \equiv \int_{-\infty}^{+\infty} \left| x\Psi + \lambda \frac{\partial\Psi}{\partial x} \right|^2 dx \geq 0, \quad (2.7)$$

where λ is an arbitrary real constant, and assume that at $x \rightarrow \pm\infty$ the wavefunction vanishes, together with its first derivative – as we will see below, a very common case. Then the left-hand side of Eq. (7) may be recast as

$$\begin{aligned} J(\lambda) &\equiv \int_{-\infty}^{+\infty} \left| x\Psi + \lambda \frac{\partial\Psi}{\partial x} \right|^2 dx = \int_{-\infty}^{+\infty} \left(x\Psi + \lambda \frac{\partial\Psi}{\partial x} \right) \left(x\Psi + \lambda \frac{\partial\Psi}{\partial x} \right)^* dx \\ &= \int_{-\infty}^{+\infty} x^2 \Psi \Psi^* dx + \lambda \int_{-\infty}^{+\infty} x \left(\Psi \frac{\partial\Psi^*}{\partial x} + \frac{\partial\Psi}{\partial x} \Psi^* \right) dx + \lambda^2 \int_{-\infty}^{+\infty} \frac{\partial\Psi}{\partial x} \frac{\partial\Psi^*}{\partial x} dx. \end{aligned} \quad (2.8)$$

According to Eq. (4), the first term in the last form of Eq. (8) is just $\langle x^2 \rangle$, while the second and the third integrals may be worked out by parts:

$$\int_{-\infty}^{+\infty} x \left(\Psi \frac{\partial\Psi^*}{\partial x} + \frac{\partial\Psi}{\partial x} \Psi^* \right) dx \equiv \int_{-\infty}^{+\infty} x \frac{\partial}{\partial x} (\Psi \Psi^*) dx = \int_{x=-\infty}^{x=+\infty} x d(\Psi \Psi^*) = \Psi \Psi^* x \Big|_{x=-\infty}^{x=+\infty} - \int_{-\infty}^{+\infty} \Psi \Psi^* dx = -1, \quad (2.9)$$

$$\int_{-\infty}^{+\infty} \frac{\partial\Psi}{\partial x} \frac{\partial\Psi^*}{\partial x} dx = \int_{x=-\infty}^{x=+\infty} \frac{\partial\Psi}{\partial x} d\Psi^* = \frac{\partial\Psi}{\partial x} \Psi^* \Big|_{x=-\infty}^{x=+\infty} - \int_{-\infty}^{+\infty} \Psi^* \frac{\partial^2\Psi}{\partial x^2} dx = \frac{1}{\hbar^2} \int_{-\infty}^{+\infty} \Psi^* \hat{p}_x^2 \Psi dx = \frac{\langle p_x^2 \rangle}{\hbar^2}. \quad (2.10)$$

As a result, Eq. (7) takes the following form:

$$J(\lambda) = \langle x^2 \rangle - \lambda + \lambda^2 \frac{\langle p_x^2 \rangle}{\hbar^2} \geq 0, \quad \text{i.e. } \lambda^2 + a\lambda + b \geq 0, \quad \text{with } a \equiv -\frac{\hbar^2}{\langle p_x^2 \rangle}, \quad b \equiv \frac{\hbar^2 \langle x^2 \rangle}{\langle p_x^2 \rangle}. \quad (2.11)$$

This inequality should be valid for any real λ , so that the corresponding quadratic equation, $\lambda^2 + a\lambda + b = 0$, can have either one (degenerate) real root – or no real roots at all. This is only possible if its determinant, $\text{Det} = a^2 - 4b$, is non-positive, leading to the following requirement:

$$\langle x^2 \rangle \langle p_x^2 \rangle \geq \frac{\hbar^2}{4}. \quad (2.12)$$

In particular, if $\langle x \rangle = 0$ and $\langle p_x \rangle = 0$,¹ then according to Eq. (1.33), Eq. (12) takes the form

¹ Eq. (13) may be proved even if $\langle x \rangle$ and $\langle p_x \rangle$ are not equal to zero, by making the following replacements: $x \rightarrow x - \langle x \rangle$ and $\partial/\partial x \rightarrow \partial/\partial x + i\langle p \rangle/\hbar$ in Eq. (7), and then repeating all the calculations – which in this case become somewhat bulky. In Chapter 4, equipped with the bra-ket formalism, we will derive a more general uncertainty relation, which includes the Heisenberg's relation (13) as a particular case, in a more efficient way.

Heisenberg's
uncertainty
relation

$$\langle \tilde{x}^2 \rangle \langle \tilde{p}_x^2 \rangle \geq \frac{\hbar^2}{4}, \quad (2.13)$$

which, according to the definition (1.34) of the r.m.s. uncertainties, is equivalent to Eq. (1.35).

Now let us notice that the Heisenberg's uncertainty relation looks very similar to the *commutation relation* between the corresponding operators:

$$[\hat{x}, \hat{p}_x] \Psi \equiv (\hat{x}\hat{p}_x - \hat{p}_x\hat{x})\Psi = x \left(-i\hbar \frac{\partial \Psi}{\partial x} \right) - \left(-i\hbar \frac{\partial}{\partial x} \right) (x\Psi) = i\hbar\Psi. \quad (2.14a)$$

Coordinate/
momentum
operators'
commutator

Since this relation is valid for any wavefunction $\Psi(x, t)$, it may be represented as an operator equality:

$$[\hat{x}, \hat{p}_x] = i\hbar \neq 0. \quad (2.14b)$$

In Sec. 4.5 we will see that the relation between Eqs. (13) and (14) is just a particular case of a general relation between the expectation values of non-commuting operators, and their commutators.

2.2. Free particle: Wave packets

Let us start our discussion of particular problems with the free 1D motion, i.e. with $U(x, t) = 0$. From Eq. (1.29), it is evident that in the 1D case, a similar “fundamental” (i.e. a particular but the most important) solution of the Schrödinger equation (1) is a sinusoidal (“monochromatic”) wave

$$\Psi_0(x, t) = \text{const} \times \exp\{i(k_0 x - \omega_0 t)\}. \quad (2.15)$$

According to Eqs. (1.32), it describes a particle with definite momentum² $p_0 = \hbar k_0$ and energy $E_0 = \hbar\omega_0 = \hbar^2 k_0^2 / 2m$. However, for this wavefunction, the product $\Psi^* \Psi$ does not depend on either x or t , so that the particle is completely delocalized, i.e. the probability to find it the same along all axis x , at all times.

In order to describe a space-localized state, let us form, at the initial moment of time ($t = 0$), a wave packet of the type shown in Fig. 1.6, by multiplying the sinusoidal waveform (15) by some smooth *envelope function* $A(x)$. As the most important particular example, consider the *Gaussian wave packet*

$$\Psi(x, 0) = A(x) e^{ik_0 x}, \quad \text{with } A(x) = \frac{1}{(2\pi)^{1/4} (\delta x)^{1/2}} \exp\left\{-\frac{x^2}{(2\delta x)^2}\right\}. \quad (2.16)$$

Gaussian
wave
packet:
 $t = 0$

(By the way, Fig. 1.6a shows exactly such a packet.) The pre-exponential factor in this envelope function has been selected in the way to have the initial probability density,

$$w(x, 0) \equiv \Psi^*(x, 0)\Psi(x, 0) = A^*(x)A(x) = \frac{1}{(2\pi)^{1/2} \delta x} \exp\left\{-\frac{x^2}{2(\delta x)^2}\right\}, \quad (2.17)$$

normalized as in Eq. (3), for any parameters δx and k_0 .³

² From this point on to the end of this chapter, I will drop the index x in the x -components of the vectors \mathbf{k} and \mathbf{p} .

³ This fact may be readily proven using the well-known integral of the Gaussian function (17), in infinite limits – see, e.g., MA Eq. (6.9b). It is also straightforward to use MA Eq. (6.9c) to prove that for the wave packet (16), the parameter δx is indeed the r.m.s. uncertainty (1.34) of the coordinate x , thus justifying its notation.

To explore the evolution of this wave packet in time, we could try to solve Eq. (1) with the initial condition (16) directly, but in the spirit of the discussion in Sec. 1.5, it is easier to proceed differently. Let us first represent the initial wavefunction (16) as a sum (1.67) of the eigenfunctions $\psi_k(x)$ of the corresponding stationary 1D Schrödinger equation (1.60), in our current case

$$-\frac{\hbar^2}{2m} \frac{d^2\psi_k}{dx^2} = E_k \psi_k, \quad \text{with } E_k \equiv \frac{\hbar^2 k^2}{2m}, \quad (2.18)$$

which are simply monochromatic waves,

$$\psi_k = a_k e^{ikx}. \quad (2.19)$$

Since (as was discussed in Sec. 1.7) at the unconstrained motion the spectrum of possible wave numbers k is continuous, the sum (1.67) should be replaced with an integral:⁴

$$\Psi(x,0) = \int a_k e^{ikx} dk. \quad (2.20)$$

Now let us notice that from the point of view of mathematics, Eq. (20) is just the usual Fourier transform from the variable k to the “conjugate” variable x , and we can use the well-known formula of the reciprocal Fourier transform to write

$$a_k = \frac{1}{2\pi} \int \Psi(x,0) e^{-ikx} dx = \frac{1}{2\pi} \frac{1}{(2\pi)^{1/4} (\delta x)^{1/2}} \int \exp\left\{-\frac{x^2}{(2\delta x)^2} - i\tilde{k}x\right\} dx, \quad \text{where } \tilde{k} \equiv k - k_0. \quad (2.21)$$

This *Gaussian integral* may be worked out by the following standard method, which will be used many times in this course. Let us complement the exponent to the full square of a linear combination of x and k , adding a compensating term independent of x :

$$-\frac{x^2}{(2\delta x)^2} - i\tilde{k}x \equiv -\frac{1}{(2\delta x)^2} [x + 2i(\delta x)^2 \tilde{k}]^2 - \tilde{k}^2 (\delta x)^2. \quad (2.22)$$

Since the integration in the right-hand side of Eq. (21) should be performed at constant \tilde{k} , in the infinite limits of x , its result would not change if we replace dx by $dx' \equiv d[x + 2i(\delta x)^2 \tilde{k}]$. As a result, we get:⁵

$$\begin{aligned} a_k &= \frac{1}{2\pi} \frac{1}{(2\pi)^{1/4} (\delta x)^{1/2}} \exp\left\{-\tilde{k}^2 (\delta x)^2\right\} \int \exp\left\{-\frac{x'^2}{(2\delta x)^2}\right\} dx' \\ &= \left(\frac{1}{2\pi}\right)^{1/2} \frac{1}{(2\pi)^{1/4} (\delta k)^{1/2}} \exp\left\{-\frac{\tilde{k}^2}{(2\delta k)^2}\right\}, \end{aligned} \quad (2.23)$$

so that a_k also has a Gaussian distribution, now along the k -axis, centered to the value k_0 (Fig. 1.6b), with the constant δk defined as

⁴ For the notation brevity, from this point on the infinite limit signs will be dropped in all 1D integrals.

⁵ The fact that the argument's shift is imaginary is not important. Indeed, since the function under the integral tends to zero at $\text{Re } x' \equiv \text{Re } x \rightarrow \pm\infty$, the difference between infinite integrals of this function along axes of x and x' is equal to its contour integral around the rectangular area $x \leq \text{Im} z \leq x'$. Since the function is also analytical, it obeys the Cauchy theorem MA Eq. (15.1), which says that this contour integral equals zero.

$$\delta k \equiv 1/2\delta x. \quad (2.24)$$

Thus we may represent the initial wave packet (16) as

$$\Psi(x,0) = \left(\frac{1}{2\pi}\right)^{1/2} \frac{1}{(2\pi)^{1/4}(\delta k)^{1/2}} \int \exp\left\{-\frac{(k-k_0)^2}{(2\delta k)^2}\right\} e^{ikx} dk. \quad (2.25)$$

From the comparison of this formula with Eq. (16), it is evident that the r.m.s. uncertainty of the wave number k in this packet is indeed equal to δk defined by Eq. (24), thus justifying the notation. The comparison of the last relation with Eq. (1.35) shows that the Gaussian packet represents the ultimate case in which the product $\delta x \delta p = \delta x (\hbar \delta k)$ has the lowest possible value ($\hbar/2$); for any other envelope's shape, the uncertainty product may only be larger. We could of course get the same result for δk from Eq. (16) using the definitions (1.23), (1.33), and (1.34); the real advantage of Eq. (25) is that it can be readily generalized to $t > 0$. Indeed, we already know that the time evolution of the wavefunction is always given by Eq. (1.69), for our current case⁶

Gaussian
wave
packet:
arbitrary
time

$$\Psi(x,t) = \left(\frac{1}{2\pi}\right)^{1/2} \frac{1}{(2\pi)^{1/4}(\delta k)^{1/2}} \int \exp\left\{-\frac{(k-k_0)^2}{(2\delta k)^2}\right\} e^{ikx} \exp\left\{-i\frac{\hbar k^2}{2m}t\right\} dk. \quad (2.26)$$

Fig. 1 shows several snapshots of the real part of the wavefunction (26), for a particular case $\delta k = 0.1 k_0$.

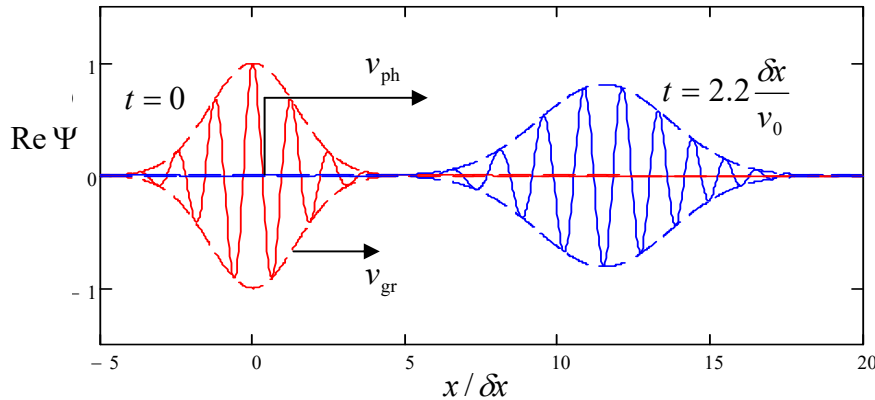
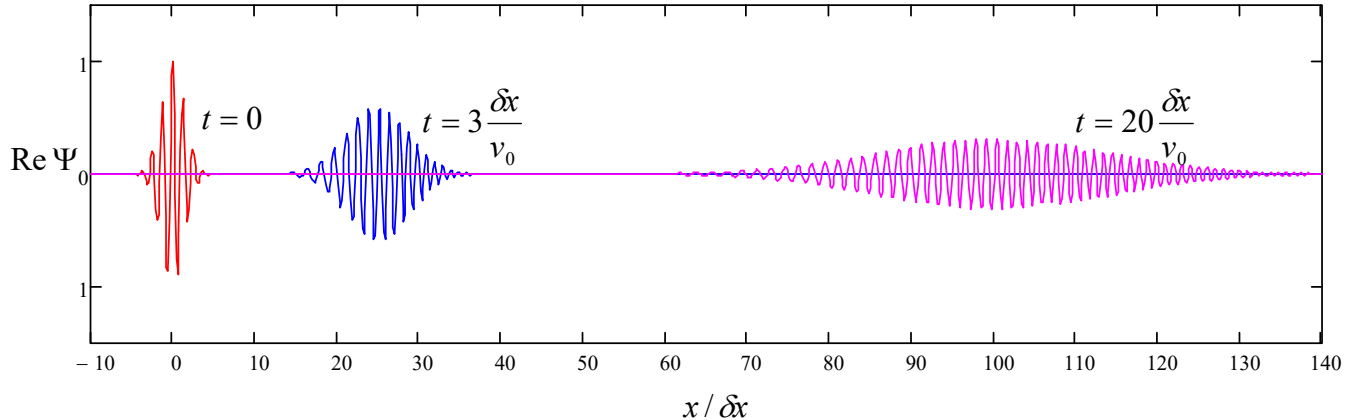


Fig. 2.1. Typical time evolution of a 1D wave packet on (a) smaller and (b) larger time scales. The dashed lines show the packet envelopes, i.e. $\pm |\Psi|$.



⁶ Note that Eq. (26) differs from Eq. (16) only by an exponent of a purely imaginary number, and hence this wavefunction is also properly normalized to 1 – see Eq. (3). Hence the wave packet introduction offers a natural solution to the problem of traveling de Broglie wave's normalization, which was mentioned in Sec. 1.2.

The plots clearly show the following effects:

- (i) the wave packet as a whole (as characterized by its envelope) moves along the x -axis with a certain *group velocity* v_{gr} ,
- (ii) the “carrier” quasi-sinusoidal wave inside the packet moves with a different, *phase velocity* v_{ph} , which may be defined as the velocity of the spatial points where the wave’s phase $\varphi(x, t) \equiv \arg \Psi$ takes a certain fixed value (say, $\varphi = \pi/2$, where $\text{Re} \Psi$ vanishes), and
- (iii) the wave packet’s spatial width gradually increases with time – the packet *spreads*.

All these effects are common for waves of any physical nature.⁷ Indeed, let us consider a 1D wave packet of the type (26), but more general:

$$\Psi(x, t) = \int a_k e^{i(kx - \omega t)} dk, \quad (2.27)$$

Arbitrary
1D wave
packet

propagating in a medium with an arbitrary (but smooth!) dispersion relation $\omega(k)$, and assume that the wave number distribution a_k is narrow: $\delta k \ll \langle k \rangle \equiv k_0$ – see Fig. 1.6b. Then we may expand the function $\omega(k)$ into the Taylor series near the central wave number k_0 , and keep only three of its leading terms:

$$\omega(k) \approx \omega_0 + \frac{d\omega}{dk} \tilde{k} + \frac{1}{2} \frac{d^2\omega}{dk^2} \tilde{k}^2, \quad \text{where } \tilde{k} \equiv k - k_0, \quad \omega_0 \equiv \omega(k_0), \quad (2.28)$$

where both derivatives have to be evaluated at the point $k = k_0$. In this approximation,⁸ the expression in the parentheses on the right-hand side of Eq. (27) may be rewritten as

$$\begin{aligned} kx - \omega(k)t &\approx k_0 x + \tilde{k}x - \left(\omega_0 + \frac{d\omega}{dk} \tilde{k} + \frac{1}{2} \frac{d^2\omega}{dk^2} \tilde{k}^2 \right) t \\ &\equiv (k_0 x - \omega_0 t) + \tilde{k} \left(x - \frac{d\omega}{dk} t \right) - \frac{1}{2} \frac{d^2\omega}{dk^2} \tilde{k}^2 t, \end{aligned} \quad (2.29)$$

so that Eq. (27) becomes

$$\Psi(x, t) \approx e^{i(k_0 x - \omega_0 t)} \int a_k \exp \left\{ i \left[\tilde{k} \left(x - \frac{d\omega}{dk} t \right) - \frac{1}{2} \frac{d^2\omega}{dk^2} \tilde{k}^2 t \right] \right\} d\tilde{k}. \quad (2.30)$$

First, let neglect the last term in square brackets (which is much smaller than the first term if the dispersion relation is smooth enough and/or the time interval t is sufficiently small), and compare the result with the initial form of the wave packet (27):

$$\Psi(x, 0) = \int a_k e^{ikx} dk = A(x) e^{ik_0 x}, \quad \text{with } A(x) \equiv \int a_k e^{i\tilde{k}x} d\tilde{k}. \quad (2.31)$$

The comparison shows that in this approximation, Eq. (30) is reduced to

$$\Psi(x, t) = A(x - v_{\text{gr}} t) e^{ik_0(x - v_{\text{ph}} t)}, \quad (2.32)$$

where v_{gr} and v_{ph} are two constants with the dimension of velocity:

⁷ See, e.g., brief discussions in CM Sec. 6.3 and EM Sec. 7.2.

⁸ By the way, in the particular case of de Broglie waves described by the dispersion relation (1.30), Eq. (28) is exact, because $\omega = E/\hbar$ is a quadratic function of $k = p/\hbar$, and all higher derivatives of ω over k vanish for any k_0 .

Group
and phase
velocities

$$v_{\text{gr}} \equiv \frac{d\omega}{dk} \Big|_{k=k_0}, \quad v_{\text{ph}} \equiv \frac{\omega}{k} \Big|_{k=k_0}. \quad (2.33a)$$

Clearly, Eq. (32) describes the effects (i) and (ii) listed above. For the particular case of the de Broglie waves, whose dispersion law is given by Eq. (1.30),

$$v_{\text{gr}} \equiv \frac{d\omega}{dk} \Big|_{k=k_0} = \frac{\hbar k_0}{m} \equiv v_0, \quad v_{\text{ph}} \equiv \frac{\omega}{k} \Big|_{k=k_0} = \frac{\hbar k_0}{2m} = \frac{v_{\text{gr}}}{2}. \quad (2.33b)$$

We see that (very fortunately :-) the velocity of the wave packet's envelope is equal to v_0 – the classical velocity of the same particle.

Next, the last term in the square brackets of Eq. (30) describes the effect (iii), the wave packet's spread. It may be readily evaluated if the packet (27) is initially Gaussian, as in our example (25):

$$a_k = \text{const} \times \exp \left\{ -\frac{\tilde{k}^2}{(2\delta k)^2} \right\}. \quad (2.34)$$

In this case the integral (30) is Gaussian, and may be worked out exactly as the integral (21), i.e. by representing the merged exponents under the integral as a full square of a linear combination of x and k :

$$\begin{aligned} & -\frac{\tilde{k}^2}{(2\delta k)^2} + i\tilde{k}(x - v_{\text{gr}}t) - \frac{i}{2} \frac{d^2\omega}{dk^2} \tilde{k}^2 t \\ & \equiv -\Delta(t) \left(\tilde{k} + i \frac{x - v_{\text{gr}}t}{2\Delta(t)} \right)^2 - \frac{(x - v_{\text{gr}}t)^2}{4\Delta(t)} + ik_0 x - \frac{i}{2} \frac{d^2\omega}{dk^2} k_0^2 t, \end{aligned} \quad (2.35)$$

where I have introduced the following complex function of time:

$$\Delta(t) \equiv \frac{1}{4(\delta k)^2} + \frac{i}{2} \frac{d^2\omega}{dk^2} t = (\delta x)^2 + \frac{i}{2} \frac{d^2\omega}{dk^2} t, \quad (2.36)$$

and used Eq. (24). Now integrating over \tilde{k} , we get

$$\Psi(x, t) \propto \exp \left\{ -\frac{(x - v_{\text{gr}}t)^2}{4\Delta(t)} + i \left(k_0 x - \frac{1}{2} \frac{d^2\omega}{dk^2} k_0^2 t \right) \right\}. \quad (2.37)$$

The imaginary part of the ratio $1/\Delta(t)$ in this exponent gives just an additional contribution to the wave's phase and does not affect the resulting probability distribution

$$w(x, t) = \Psi^* \Psi \propto \exp \left\{ -\frac{(x - v_{\text{gr}}t)^2}{2} \operatorname{Re} \frac{1}{\Delta(t)} \right\}. \quad (2.38)$$

This is again a Gaussian distribution over axis x , centered to point $\langle x \rangle = v_{\text{gr}}t$, with the r.m.s. width

$$(\delta x')^2 \equiv \left\{ \operatorname{Re} \left[\frac{1}{\Delta(t)} \right] \right\}^{-1} = (\delta x)^2 + \left(\frac{1}{2} \frac{d^2\omega}{dk^2} t \right)^2 \frac{1}{(\delta x)^2}. \quad (2.39a)$$

In the particular case of de Broglie waves, $d^2\omega/dk^2 = \hbar/m$, so that

$$(\delta x')^2 = (\delta x)^2 + \left(\frac{\hbar t}{2m} \right)^2 \frac{1}{(\delta x)^2}. \quad (2.39b)$$

Wave packet's spread

The physics of the packet spreading is very simple: if $d^2\omega/dk^2 \neq 0$, the group velocity $d\omega/dk$ of each small group dk of the monochromatic components of the wave is different, resulting in the gradual (eventually, linear) accumulation of the differences of the distances traveled by the groups. The most curious feature of Eq. (39) is that the packet width at $t > 0$ depends on its initial width $\delta x'(0) = \delta x$ in a non-monotonic way, tending to infinity at both $\delta x \rightarrow 0$ and $\delta x \rightarrow \infty$. Because of that, for a given time interval t , there is an optimal value of δx that minimizes $\delta x'$:

$$(\delta x')_{\min} = \sqrt{2} (\delta x)_{\text{opt}} = \left(\frac{\hbar t}{m} \right)^{1/2}. \quad (2.40)$$

This expression may be used for estimates of the spreading effect. Due to the smallness of the Planck constant \hbar on the human scale of things, for macroscopic bodies this effect is extremely small even for very long time intervals; however, for light particles it may be very noticeable: for an electron ($m = m_e \approx 10^{-30}$ kg), and $t = 1$ s, Eq. (40) yields $(\delta x')_{\min} \sim 1$ cm.

Note also that for any $t \neq 0$, the wave packet retains its Gaussian envelope, but the ultimate relation (24) is *not* satisfied, $\delta x' \delta p > \hbar/2$ – due to a gradually accumulated phase shift between the component monochromatic waves. The last remark on this topic: in quantum mechanics, the wave packet spreading is *not* a ubiquitous effect! For example, in Chapter 5 we will see that in a quantum oscillator, the spatial width of a Gaussian packet (for that system, called the *Glauber state* of the oscillator) does not grow monotonically but rather either stays constant or oscillates in time.

Now let us briefly discuss the case when the initial wave packet is not Gaussian but is described by an arbitrary initial wavefunction. To make the forthcoming result more aesthetically pleasing, it is beneficial to generalize our calculations to an arbitrary initial time t_0 ; it is evident that if U does not depend on time explicitly, it is sufficient to replace t with $(t - t_0)$ in all above formulas. With this replacement, Eq. (27) becomes

$$\Psi(x, t) = \int a_k e^{i[kx - \omega(t - t_0)]} dk, \quad (2.41)$$

and the reciprocal transform (21) reads

$$a_k = \frac{1}{2\pi} \int \Psi(x, t_0) e^{-ikx} dx. \quad (2.42)$$

If we want to express these two formulas with one relation, i.e. plug Eq. (42) into Eq. (41), we should give the integration variable x some other name, e.g., x_0 . (Such notation is appropriate because this variable describes the coordinate argument in the initial wave packet.) The result is

$$\Psi(x, t) = \frac{1}{2\pi} \int dk \int dx_0 \Psi(x_0, t_0) e^{i[k(x-x_0) - \omega(t-t_0)]}. \quad (2.43)$$

Changing the order of integration, this expression may be rewritten in the following general form:

$$\Psi(x, t) = \int G(x, t; x_0, t_0) \Psi(x_0, t_0) dx_0, \quad (2.44)$$

1D propagator: definition

where the function G , usually called *kernel* in mathematics, in quantum mechanics is called the *propagator*.⁹ Its physical sense may be understood by considering the following special initial condition:¹⁰

$$\Psi(x_0, t_0) = \delta(x_0 - x'), \quad (2.45)$$

where x' is a certain point within the domain of particle's motion. In this particular case, Eq. (44) gives

$$\Psi(x, t) = G(x, t; x', t_0). \quad (2.46)$$

Hence, the propagator, considered as a function of its arguments x and t only, is just the wavefunction of the particle, at the δ -functional initial conditions (45). Thus just as Eq. (41) may be understood as a mathematical expression of the linear superposition principle in the momentum (i.e., reciprocal) space domain, Eq. (44) is an expression of this principle in the direct space domain: the system's "response" $\Psi(x, t)$ to an arbitrary initial condition $\Psi(x_0, t_0)$ is just a sum of its responses to its elementary spatial "slices" of this initial function, with the propagator $G(x, t; x_0, t_0)$ representing the weight of each slice in the final sum.

According to Eqs. (43) and (44), in the particular case of a free particle the propagator is equal to

$$G(x, t; x_0, t_0) = \frac{1}{2\pi} \int e^{i[k(x-x_0)-\omega(t-t_0)]} dk, \quad (2.47)$$

Calculating this integral, one should remember that here ω is not a constant but a function of k , given by the dispersion relation for the partial waves. In particular, for the de Broglie waves, with $\hbar\omega = \hbar^2 k^2 / 2m$,

$$G(x, t; x_0, t_0) \equiv \frac{1}{2\pi} \int \exp\left\{i\left[k(x-x_0) - \frac{\hbar k^2}{2m}(t-t_0)\right]\right\} dk. \quad (2.48)$$

This is a Gaussian integral again, and may be readily calculated just it was done (twice) above, by completing the exponent to the full square. The result is

$$G(x, t; x_0, t_0) = \left(\frac{m}{2\pi i\hbar(t-t_0)} \right)^{1/2} \exp\left\{-\frac{m(x-x_0)^2}{2i\hbar(t-t_0)}\right\}. \quad (2.49)$$

Free
particle's
propagator

Please note the following features of this complex function (plotted in Fig. 2):

(i) It depends only on the differences $(x - x_0)$ and $(t - t_0)$. This is natural because the free-particle propagation problem is *translation-invariant* both in space and time.

(ii) The function's shape does not depend on its arguments – they just rescale the same function: its snapshot (Fig. 2), if plotted as a function of un-normalized x , just becomes broader and lower with time. It is curious that the spatial broadening scales as $(t - t_0)^{1/2}$ – just as at the classical diffusion, as a result of a deep mathematical analogy between quantum mechanics and classical statistics – to be discussed further in Chapter 7.

⁹ Its standard notation by letter G stems from the fact that the propagator is essentially the spatial-temporal *Green's function*, defined very similarly to Green's functions of other ordinary and partial differential equations describing various physics systems – see, e.g., CM Sec. 5.1 and/or EM Sec. 2.7 and 7.3.

¹⁰ Note that such initial condition is mathematically *not* equivalent to a δ -functional initial probability density (3).

(iii) In accordance with the uncertainty relation, the ultimately compressed wave packet (45) has an infinite width of momentum distribution, and the quasi-sinusoidal tails of the free-particle propagator, clearly visible in Fig. 2, are the results of the free propagation of the fastest (highest-momentum) components of that distribution, in both directions from the packet center.

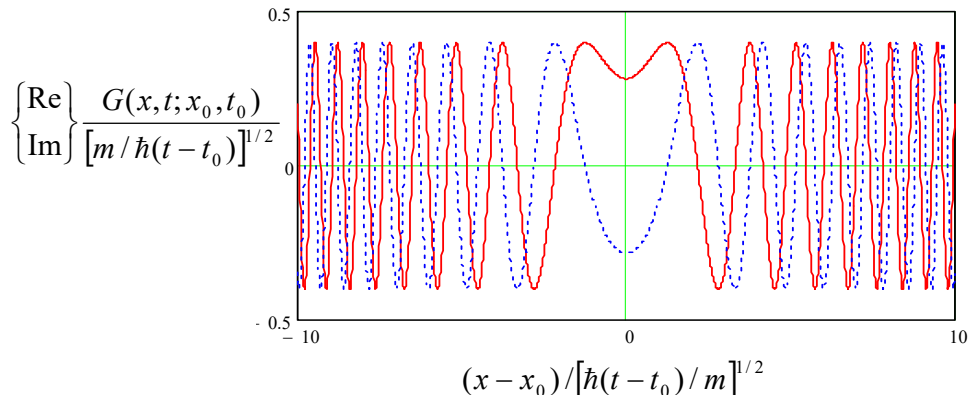


Fig. 2.2. The real (solid line) and imaginary (dotted line) parts of the 1D free particle's propagator (49).

In the following sections, I will mostly focus on monochromatic wavefunctions (that, for unconfined motion, may be interpreted as wave packets of a very large spatial width δx), and only rarely discuss wave packets. My best excuse is the linear superposition principle, i.e. our conceptual ability to restore the general solution from that of monochromatic waves of all possible energies. However, the reader should not forget that, as the above discussion has illustrated, mathematically such restoration is not always trivial.

2.3. Particle reflection and tunneling

Now, let us proceed to the cases when a 1D particle moves in various potential profiles $U(x)$ that are constant in time. Conceptually, the simplest of such profiles is a potential step – see Fig. 3.

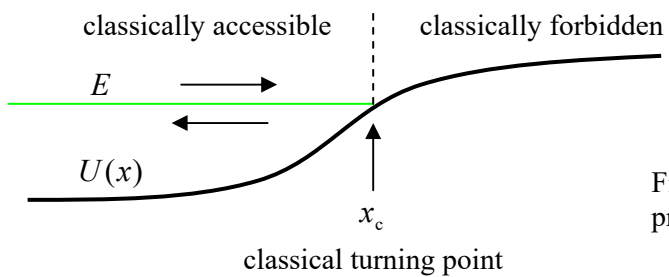


Fig. 2.3. Classical 1D motion in a potential profile $U(x)$.

As I am sure the reader knows, in classical mechanics the particle's kinetic energy $p^2/2m$ cannot be negative, so if the particle is incident on such a step (in Fig. 3, from the left), it can only travel through the *classically accessible* region, where its (conserved) full energy,

$$E = \frac{p^2}{2m} + U(x), \quad (2.50)$$

is larger than the local value $U(x)$. Let the initial velocity $v = p/m$ be positive, i.e. directed toward the step. Before it has reached the *classical turning point* x_c , defined by equality

$$U(x_c) = E, \quad (2.51)$$

the particle's kinetic energy $p^2/2m$ is positive, so that it continues to move in the initial direction. On the other hand, a classical particle cannot penetrate that *classically forbidden region* $x > x_c$, because there its kinetic energy would be negative. Hence when the particle reaches the point $x = x_c$, its velocity has to change its sign, i.e. the particle is reflected back from the classical turning point.

In order to see what does the wave mechanics say about this situation, let us start from the simplest, sharp potential step shown with the bold black line in Fig. 4:

$$U(x) = U_0 \theta(x) \equiv \begin{cases} 0, & \text{at } x < 0, \\ U_0, & \text{at } 0 < x. \end{cases} \quad (2.52)$$

For this choice, and any energy within the interval $0 < E < U_0$, the classical turning point is $x_c = 0$.

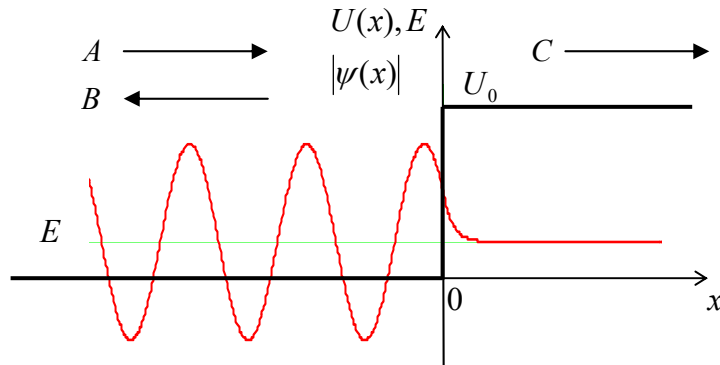


Fig. 2.4. The reflection of a monochromatic wave from a potential step $U_0 > E$. (This particular wavefunction's shape is for $U_0 = 5E$.) The wavefunction is plotted with the same schematic vertical offset by E as those in Fig. 1.8.

Let us represent an incident particle with a wave packet so long that the spread $\delta k \sim 1/\delta x$ of its wave-number spectrum is sufficiently small to make the energy uncertainty $\delta E = \hbar\delta\omega = \hbar(d\omega/dk)\delta k$ negligible in comparison with its average value $E < U_0$, as well as with $(U_0 - E)$. In this case, E may be considered as a given constant, the time dependence of the wavefunction is given by Eq. (1.62), and we can calculate its spatial factor $\psi(x)$ from the 1D version of the stationary Schrödinger equation (1.65):¹¹

$$-\frac{\hbar^2}{2m} \frac{d^2\psi}{dx^2} + U(x)\psi = E\psi. \quad (2.53)$$

At $x < 0$, i.e. at $U = 0$, the equation is reduced to the Helmholtz equation (1.78), and may be satisfied with either of two traveling waves, proportional to $\exp\{+ikx\}$ and $\exp\{-ikx\}$ correspondingly, with k satisfying the dispersion equation (1.30):

$$k^2 \equiv \frac{2mE}{\hbar^2}. \quad (2.54)$$

Thus the general solution of Eq. (53) in this region may be represented as

$$\psi_-(x) = Ae^{+ikx} + Be^{-ikx}. \quad (2.55)$$

Incident
and
reflected
waves

¹¹ Note that this is *not* the eigenproblem like the one we have solved in Sec. 1.4 for a potential well. Indeed, now the energy E is considered given – e.g., by the initial conditions that launch a long wave packet upon the potential step – in Fig. 4, from the left.

The second term on the right-hand side of Eq. (55) evidently describes a (formally, infinitely long) wave packet traveling to the left, arising because of the particle's reflection from the potential step. If $B = -A$, this solution is reduced to Eq. (1.84) for the potential well with infinitely high walls, but for our current case of a finite step height U_0 , the relation between the coefficients B and A may be different.

To show this, let us solve Eq. (53) for $x > 0$, where $U = U_0 > E$. In this region the equation may be rewritten as

$$\frac{d^2\psi_+}{dx^2} = \kappa^2 \psi_+, \quad (2.56)$$

where κ is a real and positive constant defined by a formula similar in structure to Eq. (54):

$$\kappa^2 \equiv \frac{2m(U_0 - E)}{\hbar^2} > 0. \quad (2.57)$$

The general solution of Eq. (56) is the sum of $\exp\{+\kappa x\}$ and $\exp\{-\kappa x\}$, with arbitrary coefficients. However, in our particular case the wavefunction should be finite at $x \rightarrow +\infty$, so only the latter exponent is acceptable:

$$\psi_+(x) = Ce^{-\kappa x}. \quad (2.58)$$

Decay in classically forbidden region

Such penetration of the wavefunction to the classically forbidden region, and hence a non-zero probability to find the particle there, is one of the most fascinating predictions of quantum mechanics, and has been repeatedly observed in experiment – e.g., via tunneling experiments – see the next section.¹² From Eq. (58), it is evident that the constant κ , defined by Eqs. (57), may be interpreted as the reciprocal penetration depth. Even for the lightest particles, this depth is usually very small. Indeed, for $E \ll U_0$ that relation yields

$$\delta \equiv \frac{1}{\kappa} \Big|_{E \rightarrow 0} = \frac{\hbar}{(2mU_0)^{1/2}}. \quad (2.59)$$

For example, let us consider a conduction electron in a typical metal, which runs, at the metal's surface, into a sharp potential step whose height is equal to metal's workfunction $U_0 \approx 5$ eV – see the discussion of the photoelectric effect in Sec. 1.1. In this case, according to Eq. (59), δ is close to 0.1 nm, i.e. is close to a typical size of an atom. For heavier elementary particles (e.g., protons) the penetration depth is correspondingly lower, and for macroscopic bodies, it is hardly measurable.

Returning to Eqs. (55) and (58), we still should relate the coefficients B and C to the amplitude A of the incident wave, using the boundary conditions at $x = 0$. Since E is a finite constant, and $U(x)$ is a finite function, Eq. (53) says that $d^2\psi/dx^2$ should be finite as well. This means that the first derivative should be continuous:

$$\lim_{\varepsilon \rightarrow 0} \left(\frac{d\psi}{dx} \Big|_{x=+\varepsilon} - \frac{d\psi}{dx} \Big|_{x=-\varepsilon} \right) = \lim_{\varepsilon \rightarrow 0} \int_{-\varepsilon}^{+\varepsilon} \frac{d^2\psi}{dx^2} dx = \frac{2m}{\hbar^2} \lim_{\varepsilon \rightarrow 0} \int_{-\varepsilon}^{+\varepsilon} [U(x) - E] \psi dx = 0. \quad (2.60)$$

Repeating such calculation for the wavefunction $\psi(x)$ itself, we see that it also should be continuous at all points, including the border point $x = 0$, so that the boundary conditions in our problem are

¹² Note that this effect is pertinent to waves of any type, including mechanical waves (see, e.g., CM Secs. 6.4 and 7.7) and electromagnetic waves (see, e.g., EM Secs. 7.3-7.7).

$$\psi_-(0) = \psi_+(0), \quad \frac{d\psi_-}{dx}(0) = \frac{d\psi_+}{dx}(0). \quad (2.61)$$

Plugging Eqs. (55) and (58) into Eqs. (61), we get a system of two linear equations

$$A + B = C, \quad ikA - ikB = -\kappa C, \quad (2.62)$$

whose (easy :-) solution allows us to express B and C via A :

$$B = A \frac{k - i\kappa}{k + i\kappa}, \quad C = A \frac{2k}{k + i\kappa}. \quad (2.63)$$

We immediately see that the numerator and denominator in the first of these fractions have equal moduli, so that $|B| = |A|$. This means that, as we could expect, a particle with energy $E < U_0$ is totally reflected from the step – just as in classical mechanics. As a result, at $x < 0$ our solution (55) may be represented as a standing wave

$$\psi_- = 2iAe^{i\theta} \sin(kx - \theta), \quad \text{with } \theta \equiv \tan^{-1} \frac{k}{\kappa}. \quad (2.64)$$

Note that the shift $\Delta x \equiv \theta/k = (\tan^{-1} k/\kappa)/k$ of the standing wave to the right, due to the partial penetration of the wavefunction under the potential step, is commensurate with, but generally not equal to the penetration depth $\delta \equiv 1/\kappa$. The red line in Fig. 4 shows the exact behavior of the wavefunction, for a particular case $E = U_0/5$, at which $k/\kappa \equiv [E/(U_0-E)]^{1/2} = 1/2$.

According to Eq. (59), as the particle's energy E is increased to approach U_0 , the penetration depth $1/\kappa$ diverges. This raises an important issue: what happens at $E > U_0$, i.e. if there is no classically forbidden region in the problem? In classical mechanics, the incident particle would continue to move to the right, though with a reduced velocity, corresponding to the new kinetic energy $E - U_0$, so there would be no reflection. In quantum mechanics, however, the situation is different. To analyze it, it is not necessary to re-solve the whole problem; it is sufficient to note that all our calculations, and hence Eqs. (63) are still valid if we take¹³

$$\kappa = -ik', \quad \text{with} \quad k'^2 \equiv \frac{2m(E - U_0)}{\hbar^2} > 0. \quad (2.65)$$

With this replacement, Eq. (63) becomes¹⁴

$$B = A \frac{k - k'}{k + k'}, \quad C = A \frac{2k}{k + k'}. \quad (2.66)$$

The most important result of this change is that now the particle's reflection is *not* total: $|B| < |A|$. To evaluate this effect quantitatively, it is fairer to use not the B/A or C/A ratios, but rather that of the probability currents (5) carried by the de Broglie waves traveling to the right, with amplitudes C and A , in the corresponding regions (respectively, for $x > 0$ and $x < 0$):

¹³ Our earlier discarding of the particular solution $\exp\{\kappa x\}$, now becoming $\exp\{-ik'x\}$, is still valid, but now on different grounds: this term would describe a wave packet incident on the potential step from the right, and this is not the problem under our current consideration.

¹⁴ These formulas are completely similar to those describing the partial reflection of classical waves from a sharp interface between two uniform media, at normal incidence (see, e.g., CM Sec. 6.4 and EM Sec. 7.4), with the effective impedance Z of de Broglie waves being proportional to their wave number k .

$$\mathcal{T} \equiv \frac{I_C}{I_A} = \frac{k' |C|^2}{k |A|^2} = \frac{4kk'}{(k+k')^2} \equiv \frac{4[E(E-U_0)]^{1/2}}{[E^{1/2} + (E-U_0)^{1/2}]^2}. \quad (2.67)$$

Potential
step's
transparency

(The parameter \mathcal{T} so defined is called the *transparency* of the system, in our current case of the potential step of height U_0 , at particle's energy E .) The result given by Eq. (67) is plotted in Fig. 5a as a function of the U_0/E ratio. Note its most important features:

- (i) At $U_0 = 0$, the transparency is full, $\mathcal{T} = 1$ – naturally, because there is no step at all.
- (ii) At $U_0 \rightarrow E$, the transparency drops to zero, giving a proper connection to the case $E < U_0$.
- (iii) Nothing in our solution's procedure prevents us from using Eq. (67) even for $U_0 < 0$, i.e. for the *step-down* (or “cliff”) potential profile – see Fig. 5b. Very counter-intuitively, the particle is (partly) reflected even from such a cliff, and the transmission diminishes (though rather slowly) at $U_0 \rightarrow -\infty$.

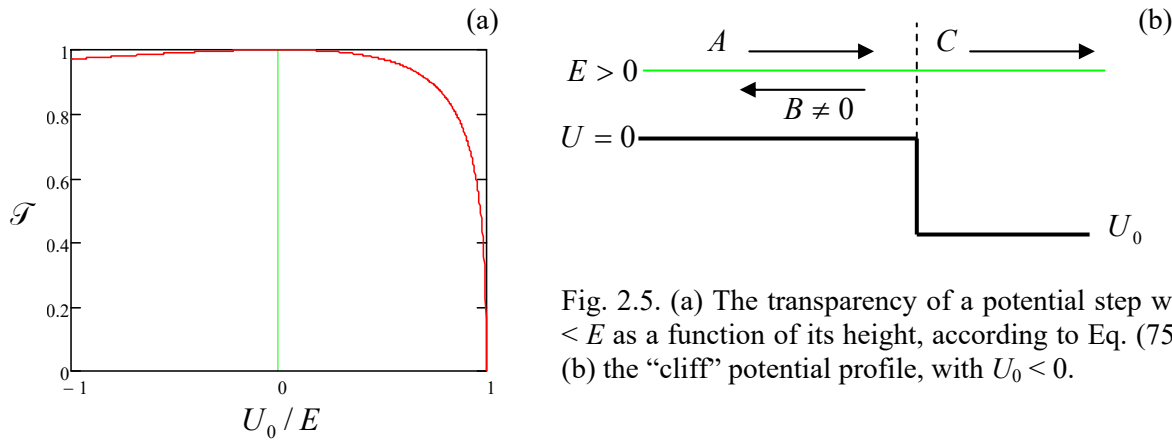


Fig. 2.5. (a) The transparency of a potential step with $U_0 < E$ as a function of its height, according to Eq. (75), and (b) the “cliff” potential profile, with $U_0 < 0$.

The most important conceptual conclusion of this analysis is that the quantum particle is *partly reflected* from a potential step with $U_0 < E$, in the sense that there is a non-zero probability $\mathcal{T} < 1$ to find it passed over the step, while there is also some probability, $(1 - \mathcal{T}) > 0$, to have it reflected.

The last property is exhibited, but for *any* relation between E and U_0 , by another simple potential profile $U(x)$, the famous *potential* (or “tunnel”) *barrier*. Fig. 6 shows its simple, “rectangular” version:

$$U(x) = \begin{cases} 0, & \text{for } x < -d/2, \\ U_0, & \text{for } -d/2 < x < +d/2, \\ 0, & \text{for } +d/2 < x. \end{cases} \quad (2.68)$$

To analyze this problem, it is sufficient to look for the solution to the Schrödinger equation in the form (55) at $x \leq -d/2$. At $x > +d/2$, i.e., behind the barrier, we may use the arguments presented above (no wave source on the right!) to keep just one traveling wave, now with the same wave number:

$$\psi_+(x) = Fe^{ikx}. \quad (2.69)$$

However, under the barrier, i.e. at $-d/2 \leq x \leq +d/2$, we should generally keep both exponential terms,

$$\psi_b(x) = Ce^{-kx} + De^{+kx}, \quad (2.70)$$

because our previous argument, used in the potential step problem's solution, is no longer valid. (Here k and κ are still defined, respectively, by Eqs. (54) and (57).) In order to express the coefficients B , C , D , and F via the amplitude A of the incident wave, we need to plug these solutions into the boundary conditions similar to Eqs. (61), but now at two boundary points, $x = \pm d/2$.

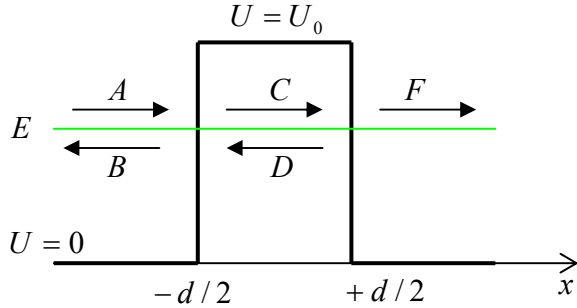


Fig. 2.6. A rectangular potential barrier, and the de Broglie waves taken into account in its analysis.

Solving the resulting system of 4 linear equations, we get four ratios B/A , C/A , etc.; in particular,

$$\frac{F}{A} = \left[\cosh \kappa d + \frac{i}{2} \left(\frac{\kappa}{k} - \frac{k}{\kappa} \right) \sinh \kappa d \right]^{-1} e^{-ikd}, \quad (2.71a)$$

and hence the barrier's transparency

$$\mathcal{T} \equiv \left| \frac{F}{A} \right|^2 = \left[\cosh^2 \kappa d + \left(\frac{\kappa^2 - k^2}{2\kappa k} \right)^2 \sinh^2 \kappa d \right]^{-1}. \quad (2.71b)$$

So, quantum mechanics indeed allows particles with energies $E < U_0$ to pass “through” the potential barrier – see Fig. 6 again. This is the famous effect of *quantum-mechanical tunneling*. Fig. 7a shows the barrier transparency as a function of the particle energy E , for several characteristic values of its thickness d , or rather of the ratio d/δ , with δ defined by Eq. (59).

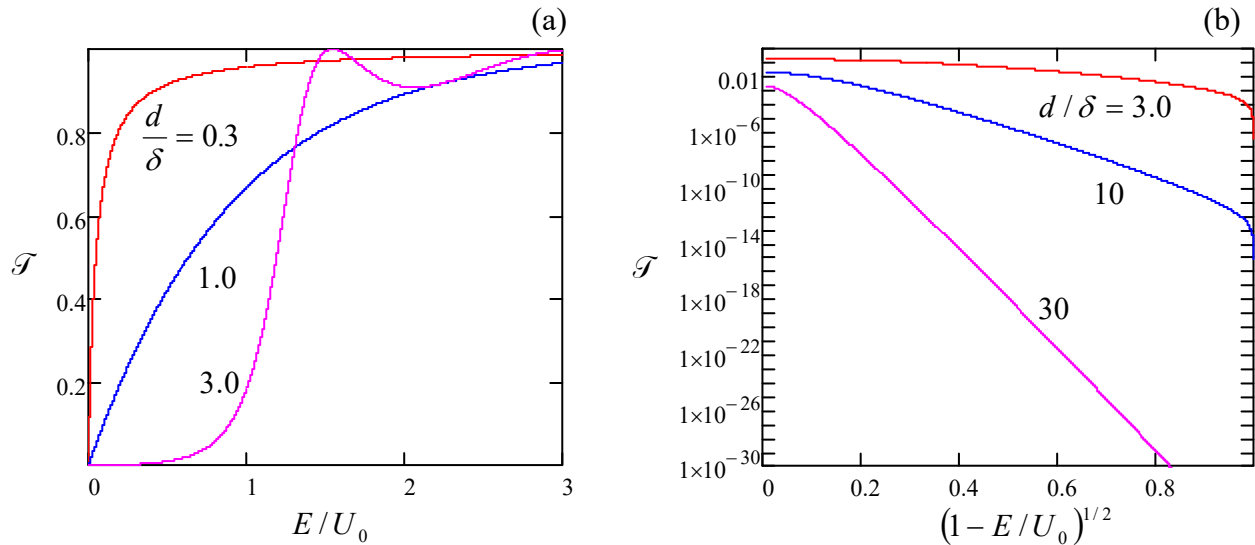


Fig. 2.7. The transparency of a rectangular potential barrier as a function of the particle's energy E .

The plots show that generally, the transparency grows gradually with the particle's energy. This growth is natural because the penetration constant κ decreases with the growth of E , i.e., the wavefunction penetrates more and more into the barrier, so that more and more of it is “picked up” at the second interface ($x = +d/2$) and transferred into the wave $F \exp\{ikx\}$ propagating behind the barrier.

Now let us consider the important limit of a very thin and high rectangular barrier, $d \ll \delta, E \ll U_0$, giving $k \ll \kappa \ll 1/d$. In this limit, Eq. (71) yields

$$\mathcal{T} \equiv \left| \frac{F}{A} \right|^2 \rightarrow \frac{1}{|1+i\alpha|^2} = \frac{1}{1+\alpha^2}, \quad \text{where } \alpha \equiv \frac{1}{2} \left(\frac{\kappa^2 - k^2}{\kappa k} \right) \kappa d \approx \frac{1}{2} \frac{\kappa^2 d}{k} \approx \frac{m}{\hbar^2 k} U_0 d, \quad (2.72)$$

The last product, $U_0 d$, is just the “energy area” (or the “weight”)

$$w \equiv \int_{U(x)>E} U(x) dx \quad (2.73)$$

of the barrier. This fact implies that the very simple result (72) may be correct for a barrier of any shape, provided that it is sufficiently thin and high.

To confirm this guess, let us consider the tunneling problem for a very thin barrier with $\kappa d, kd \ll 1$, approximating it with the Dirac's δ -function (Fig. 8):

$$U(x) = w\delta(x), \quad (2.74)$$

so that the parameter w satisfies Eq. (73).

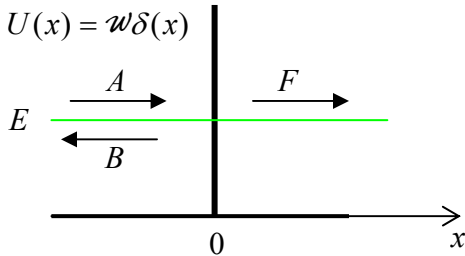


Fig. 2.8. A delta-functional potential barrier.

The solutions of the tunneling problem at all points but $x = 0$ still may be taken in the form of Eqs. (55) and (69), so we only need to analyze the boundary conditions at that point. However, due to the special character of the δ -function, we should be careful here. Indeed, instead of Eq. (60) we now get

$$\begin{aligned} \lim_{\varepsilon \rightarrow 0} \left(\frac{d\psi}{dx} \Big|_{x=+\varepsilon} - \frac{d\psi}{dx} \Big|_{x=-\varepsilon} \right) &= \lim_{\varepsilon \rightarrow 0} \int_{-\varepsilon}^{+\varepsilon} \frac{d^2\psi}{dx^2} dx = \lim_{\varepsilon \rightarrow 0} \frac{2m}{\hbar^2} \int_{-\varepsilon}^{+\varepsilon} [U(x) - E] \psi dx \\ &= \frac{2m}{\hbar^2} w \psi(0). \end{aligned} \quad (2.75)$$

According to this relation, at a finite w , the derivatives $d\psi/dx$ are also finite, so that the wavefunction itself is still continuous:

$$\lim_{\varepsilon \rightarrow 0} (\psi \Big|_{x=+\varepsilon} - \psi \Big|_{x=-\varepsilon}) = \lim_{\varepsilon \rightarrow 0} \int_{-\varepsilon}^{+\varepsilon} \frac{d\psi}{dx} dx = 0. \quad (2.76)$$

Using these two boundary conditions, we readily get the following system of two linear equations,

$$A + B = F, \quad ikF - (ikA - ikB) = \frac{2m\omega}{\hbar^2} F, \quad (2.77)$$

whose solution yields

$$\frac{B}{A} = \frac{-i\alpha}{1+i\alpha}, \quad \frac{F}{A} = \frac{1}{1+i\alpha}, \quad \text{where } \alpha \equiv \frac{m\omega}{\hbar^2 k}. \quad (2.78)$$

(Taking Eq. (73) into account, this definition of α coincides with that in Eq. (72).) For the barrier transparency $\mathcal{T} \equiv |F/A|^2$, this result again gives the first of Eqs. (72), which is therefore general for such thin barriers. That formula may be recast to give the following simple expression (valid only for $E \ll U_{\max}$):

Thin barrier:
transparency

$$\boxed{\mathcal{T} = \frac{1}{1+\alpha^2} \equiv \frac{E}{E+E_0}, \quad \text{where } E_0 \equiv \frac{m\omega^2}{2\hbar^2 k},} \quad (2.79)$$

which shows that as energy becomes larger than the constant E_0 , the transparency approaches 1.

Now proceeding to another important limit of thick barriers ($d \gg \delta$), Eq. (71) shows that in this case, the transparency is dominated by what is called the *tunnel exponent*:

Thick barrier:
transparency

$$\boxed{\mathcal{T} = \left(\frac{4k\kappa}{k^2 + \kappa^2} \right)^2 e^{-2\kappa d}} \quad (2.80)$$

– the behavior which may be clearly seen as the straight-line segments in semi-log plots (Fig. 7b) of \mathcal{T} as a function of the combination $(1 - E/U_0)^{1/2}$, which is proportional to κ – see Eq. (57). This exponential dependence on the barrier thickness is the most important factor for various applications of quantum-mechanical tunneling – from the field emission of electrons to vacuum¹⁵ to the scanning tunneling microscopy.¹⁶ Note also very substantial negative implications of the effect for the electronic technology progress, most importantly imposing limits on the so-called *Dennard scaling* of field-effect transistors in semiconductor integrated circuits (which is the technological basis of the well-known *Moore's law*), due to the increase of tunneling both through the gate oxide and along the channel of the transistors, from source to drain.¹⁷

Finally, one more feature visible in Fig. 7a (for case $d = 3\delta$) are the oscillations of the transparency as a function of energy, at $E > U_0$, with $\mathcal{T} = 1$, i.e. the reflection completely vanishing, at some points.¹⁸ This is our first glimpse at one more interesting quantum effect: *resonant tunneling*. This effect will be discussed in more detail in Sec. 5 below, using another potential profile where it is more clearly pronounced.

¹⁵ See, e.g., G. Fursey, *Field Emission in Vacuum Microelectronics*, Kluwer, New York, 2005.

¹⁶ See, e.g., G. Binning and H. Rohrer, *Helv. Phys. Acta* **55**, 726 (1982).

¹⁷ See, e.g., V. Sverdlov *et al.*, *IEEE Trans. on Electron Devices* **50**, 1926 (2003), and references therein. (A brief discussion of the field-effect transistors, and literature for further reading, may be found in SM Sec. 6.4.)

¹⁸ Let me mention in passing the curious case of the potential well $U(x) = -(\hbar^2/2m)\nu(\nu+1)/\cosh^2(x/a)$, with any positive integer ν and any real a , which is reflection-free ($\mathcal{T} = 1$) for the incident de Broigle wave of *any* energy E , and hence for any incident wave packet. Unfortunately, a proof of this fact would require more time/space than I can afford. (Note that it was first described in a 1930 paper by Paul Sophus Epstein, before the 1933 publication by G. Pöschl and E. Teller, which is responsible for the common name of this *Pöschl-Teller potential*.)

2.4. Motion in soft potentials

Before moving on to exploring other quantum-mechanical effects, let us see how the results discussed in the previous section are modified in the opposite limit of the so-called *soft* (also called “smooth”) potential profiles, like the one sketched in Fig. 3.¹⁹ The most efficient analytical tool to study this limit is the so-called *WKB* (or “JWKB”, or “quasiclassical”) *approximation* developed by H. Jeffrey, G. Wentzel, A. Kramers, and L. Brillouin in 1925-27. In order to derive its 1D version, let us rewrite the Schrödinger equation (53) in a simpler form

$$\frac{d^2\psi}{dx^2} + k^2(x)\psi = 0, \quad (2.81)$$

where the local wave number $k(x)$ is defined similarly to Eq. (65),

$$k^2(x) \equiv \frac{2m[E - U(x)]}{\hbar^2}; \quad (2.82)$$

Local
wave
number

besides that now it may be a function of x . We already know that for $k(x) = \text{const}$, the fundamental solutions of this equation are $A\exp\{+ikx\}$ and $B\exp\{-ikx\}$, which may be represented in a single form

$$\psi(x) = e^{i\Phi(x)}, \quad (2.83)$$

where $\Phi(x)$ is a complex function, in these two simplest cases being equal, respectively, to $(kx - i\ln A)$ and $(-kx - i\ln B)$. This is why we may try use Eq. (83) to look for solution of Eq. (81) even in the general case, $k(x) \neq \text{const}$. Differentiating Eq. (83) twice, we get

$$\frac{d\psi}{dx} = i \frac{d\Phi}{dx} e^{i\Phi}, \quad \frac{d^2\psi}{dx^2} = \left[i \frac{d^2\Phi}{dx^2} - \left(\frac{d\Phi}{dx} \right)^2 \right] e^{i\Phi}. \quad (2.84)$$

Plugging the last expression into Eq. (81) and requiring the factor before $\exp\{i\Phi(x)\}$ to vanish, we get

$$i \frac{d^2\Phi}{dx^2} - \left(\frac{d\Phi}{dx} \right)^2 + k^2(x) = 0. \quad (2.85)$$

This is still an exact, general equation. At the first sight, it looks harder to solve than the initial equation (81), because Eq. (85) is nonlinear. However, it is ready for simplification in the limit when the potential profile is very soft, $dU/dx \rightarrow 0$. Indeed, for a uniform potential, $d^2\Phi/dx^2 = 0$. Hence, in the so-called 0^{th} *approximation*, $\Phi(x) \rightarrow \Phi_0(x)$, we may try to keep that result, so that Eq. (85) is reduced to

$$\left(\frac{d\Phi_0}{dx} \right)^2 = k^2(x), \quad \text{i.e. } \frac{d\Phi_0}{dx} = \pm k(x), \quad \Phi_0(x) = \pm i \int_x^x k(x') dx', \quad (2.86)$$

so that its general solution is a linear superposition of two functions (83), with Φ replaced with Φ_0 :

$$\psi_0(x) = A \exp \left\{ +i \int_x^x k(x') dx' \right\} + B \exp \left\{ -i \int_x^x k(x') dx' \right\}, \quad (2.87)$$

¹⁹ Quantitative conditions of the “softness” will be formulated later in this section.

where the choice of the lower limits of integration affects only the constants A and B . The physical sense of this result is simple: it is a sum of the forward- and back-propagating de Broglie waves, with the coordinate-dependent local wave number $k(x)$ that self-adjusts to the potential profile.

Let me emphasize the non-trivial nature of this approximation.²⁰ First, any attempt to address the problem with the standard perturbation approach (say, $\psi = \psi_0 + \psi_1 + \dots$, with ψ_n proportional to the n^{th} power of some small parameter) would fail for most potentials, because as Eq. (86) shows, even a slight but persisting deviation of $U(x)$ from a constant leads to a gradual accumulation of the phase Φ_0 , impossible to describe by any small perturbation of ψ . Second, the dropping of the term $d^2\Phi/dx^2$ in Eq. (85) is not too easy to justify. Indeed, since we are committed to the “soft potential limit” $dU/dx \rightarrow 0$, we should be ready to assume the characteristic length a of the spatial variation of Φ to be large, and neglect the terms that are the smallest ones in the limit $a \rightarrow \infty$. However, both first terms in Eq. (85) are apparently of the same order in a , namely $O(a^{-2})$; why have we neglected just one of them?

The price we have paid for such a “sloppy” treatment is substantial: Eq. (87) does *not* satisfy the fundamental property of the Schrödinger equation solutions, the probability current’s conservation. Indeed, since Eq. (81) describes a fixed-energy (stationary) spatial part of the general Schrödinger equation, its probability density $w = \Psi\Psi^* = \psi\psi^*$, and should not depend on time. Hence, according to Eq. (6), we should have $I(x) = \text{const}$. However, this is not true for any component of Eq. (87); for example for the first, forward-propagating component on its right-hand side, Eq. (5) yields

$$I_0(x) = \frac{\hbar}{m} |A|^2 k(x), \quad (2.88)$$

evidently not a constant if $k(x) \neq \text{const}$. The brilliance of the WKB theory is that the problem may be fixed without a full revision of the 0th approximation, just by amending it. Indeed, let us explore the next, 1st approximation:

$$\Phi(x) \rightarrow \Phi_{\text{WKB}}(x) \equiv \Phi_0(x) + \Phi_1(x), \quad (2.89)$$

where Φ_0 still obeys Eq. (86), while Φ_1 describes a 0th approximation’s correction that is small in the following sense:²¹

$$\left| \frac{d\Phi_1}{dx} \right| \ll \left| \frac{d\Phi_0}{dx} \right| = k(x). \quad (2.90)$$

Plugging Eq. (89) into Eq. (85), with the account of the definition (86), we get

$$i \left(\frac{d^2\Phi_0}{dx^2} + \frac{d^2\Phi_1}{dx^2} \right) - \frac{d\Phi_1}{dx} \left(2 \frac{d\Phi_0}{dx} + \frac{d\Phi_1}{dx} \right) = 0. \quad (2.91)$$

Using the condition (90), we may neglect $d^2\Phi_1/dx^2$ in comparison with $d^2\Phi_0/dx^2$ inside the first parentheses, and $d\Phi_1/dx$ in comparison with $2d\Phi_0/dx$ inside the second parentheses. As a result, we get the following (still approximate!) result:

²⁰ Philosophically, this space-domain method is very close to the time-domain *van der Pol method* in classical mechanics, and the very similar *rotating wave approximation* (RWA) in quantum mechanics – see, e.g., CM Secs. 5.2-5.5, and also Secs. 6.5, 7.6, 9.2, and 9.4 of this course.

²¹ For certainty, I will use the discretion given by Eq. (82) to define $k(x)$ as the *positive* root of its right-hand side.

$$\frac{d\Phi_1}{dx} = \frac{i}{2} \frac{d^2\Phi_0}{dx^2} / \frac{d\Phi_0}{dx} = \frac{i}{2} \frac{d}{dx} \left(\ln \frac{d\Phi_0}{dx} \right) = \frac{i}{2} \frac{d}{dx} [\ln k(x)] = i \frac{d}{dx} [\ln k^{1/2}(x)], \quad (2.92)$$

$$i\Phi|_{\text{WKB}} \equiv i\Phi_0 + i\Phi_1 = \pm i \int^x k(x') dx' + \ln \frac{1}{k^{1/2}(x)}, \quad (2.93)$$

$$\psi_{\text{WKB}}(x) = \frac{a}{k^{1/2}(x)} \exp \left\{ i \int^x k(x') dx' \right\} + \frac{b}{k^{1/2}(x)} \exp \left\{ -i \int^x k(x') dx' \right\}. \quad \text{for } k^2(x) > 0. \quad (2.94)$$

WKB
wave-
function

(Again, the lower integration limit is arbitrary, because its choice may be incorporated into the complex constants a and b .) This modified approximation overcomes the problem of current continuity; for example, for the forward-propagating wave, Eq. (5) gives

$$I_{\text{WKB}}(x) = \frac{\hbar}{m} |a|^2 = \text{const.} \quad (2.95)$$

WKB
probability
current

Physically, the factor $k^{1/2}$ in the denominator of the WKB wavefunction's pre-exponent is easy to understand. The smaller the local group velocity (32) of the wave packet, $v_{\text{gr}}(x) = \hbar k(x)/m$, the "easier" (more probable) it should be to find the particle within a certain interval dx . This is exactly the result that the WKB approximation gives: $w(x) = \psi\psi^* \propto 1/k(x) \propto 1/v_{\text{gr}}$. Another value of the 1st approximation is a clarification of the WKB theory's validity condition: it is given by Eq. (90). Plugging into this relation the first form of Eq. (92), and estimating $|d^2\Phi_0/dx^2|$ as $|d\Phi_0/dx|/a$, where a is the spatial scale of a substantial change of $|d\Phi_0/dx| = k(x)$, we may write the condition as

$$ka \gg 1. \quad (2.96)$$

WKB:
first
condition
of validity

In plain English, this means that the region where $U(x)$, and hence $k(x)$, change substantially should contain many de Broglie wavelengths $\lambda = 2\pi/k$.

So far I have implied that $k^2(x) \propto E - U(x)$ is positive, i.e. particle moves in the classically accessible region. Now let us extend the WKB approximation to situations where the difference $E - U(x)$ may change sign, for example to the reflection problem sketched in Fig. 3. Just as we did for the sharp potential step, we first need to find the appropriate solution in the classically forbidden region, in this case for $x > x_c$. For that, there is again no need to redo our calculations, because they are still valid if we, just as in the sharp-step problem, take $k(x) = i\kappa(x)$, where

$$\kappa^2(x) \equiv \frac{2m[U(x) - E]}{\hbar^2} > 0, \quad \text{for } x > x_c, \quad (2.97)$$

and keep just one of two possible solutions (with $\kappa > 0$), in analogy with Eq. (58). The result is

$$\psi_{\text{WKB}}(x) = \frac{c}{\kappa^{1/2}(x)} \exp \left\{ - \int^x \kappa(x') dx' \right\}, \quad \text{for } k^2 < 0, \text{ i.e. } \kappa^2 > 0, \quad (2.98)$$

with the lower limit at some point with $\kappa^2 > 0$ as well. This is a really wonderful formula! It describes the quantum-mechanical penetration of the particle into the classically forbidden region and provides a natural generalization of Eq. (58) – leaving intact our estimates of the depth $\delta \sim 1/\kappa$ of such penetration.

Now we have to do what we have done for the sharp-step problem in Sec. 2: use the boundary conditions at classical turning point $x = x_c$ to relate the constants a , b , and c . However, now this operation is a tad more complex, because both WKB functions (94) and (98) diverge, albeit weakly, at the point, because here both $k(x)$ and $\kappa(x)$ tend to zero. This *connection problem* may be solved in the following way.²²

Let us use our commitment of the potential's "softness", assuming that it allows us to keep just two leading terms in the Taylor expansion of the function $U(x)$ at the point x_c :

$$U(x) \approx U(x_c) + \frac{dU}{dx} \Big|_{x=x_c} (x - x_c) \equiv E + \frac{dU}{dx} \Big|_{x=x_c} (x - x_c). \quad (2.99)$$

Using this truncated expansion, and introducing the following dimensionless variable for the coordinate's deviation from the classical turning point,

$$\zeta \equiv \frac{x - x_c}{x_0}, \quad \text{with } x_0 \equiv \left[\frac{\hbar^2}{2m(dU/dx)_{x=x_c}} \right]^{1/3}, \quad (2.100)$$

we reduce the Schrödinger equation (81) to the so-called *Airy equation*

Airy equation

$$\frac{d^2\psi}{d\zeta^2} - \zeta \psi = 0. \quad (2.101)$$

This simple linear, ordinary, homogenous differential equation of the second order has been very well studied. Its general solution may be represented as a linear combination of two fundamental solutions, the *Airy functions* $\text{Ai}(\zeta)$ and $\text{Bi}(\zeta)$, shown in Fig. 9a.²³

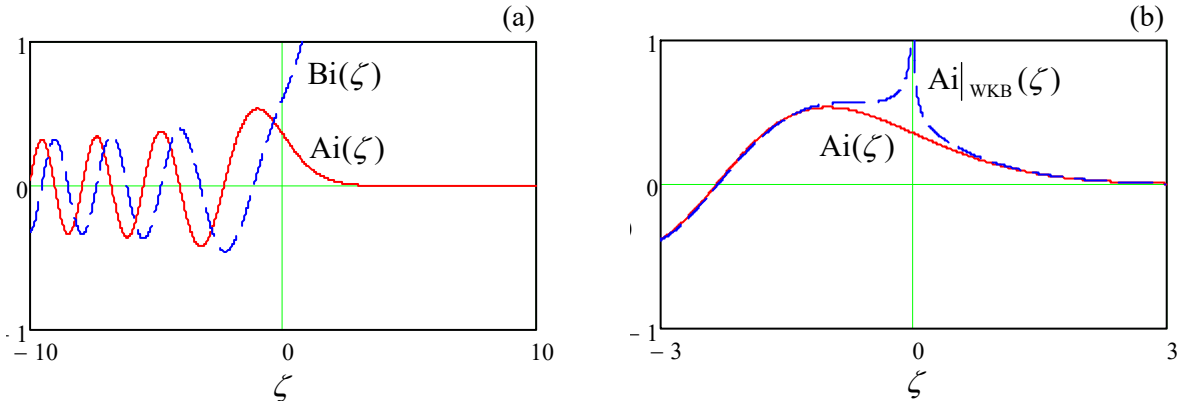


Fig. 2.9. (a) The Airy functions Ai and Bi , and (b) the WKB approximation for the function $\text{Ai}(\zeta)$.

²² An alternative way to solve the connection problem, without involving the Airy functions but using an analytical extension of WKB formulas to the complex-argument plane, may be found, e.g., in Sec. 47 of the textbook by L. Landau and E. Lifshitz, *Quantum Mechanics, Non-Relativistic Theory*, 3rd ed. Pergamon, 1977.

²³ Note the following (exact) integral formulas,

$$\text{Ai}(\zeta) = \frac{1}{\pi} \int_0^\infty \cos\left(\frac{\xi^3}{3} + \zeta\xi\right) d\xi, \quad \text{Bi}(\zeta) = \frac{1}{\pi} \int_0^\infty \left[\exp\left(-\frac{\xi^3}{3} + \zeta\xi\right) + \sin\left(\frac{\xi^3}{3} + \zeta\xi\right) \right] d\xi,$$

frequently more convenient for practical calculations of the Airy functions than the differential equation (101).

The latter function diverges at $\zeta \rightarrow +\infty$, and thus is not suitable for our current problem (Fig. 3), while the former function has the following asymptotic behaviors at $|\zeta| \gg 1$:

$$\text{Ai}(\zeta) \rightarrow \frac{1}{\pi^{1/2} |\zeta|^{1/4}} \times \begin{cases} \frac{1}{2} \exp\left\{-\frac{2}{3} \zeta^{3/2}\right\}, & \text{for } \zeta \rightarrow +\infty, \\ \sin\left\{\frac{2}{3}(-\zeta)^{3/2} + \frac{\pi}{4}\right\}, & \text{for } \zeta \rightarrow -\infty. \end{cases} \quad (2.102)$$

Now let us apply the WKB approximation to the Airy equation (101). Taking the classical turning point ($\zeta = 0$) for the lower limit, for $\zeta > 0$ we get

$$\kappa^2(\zeta) = \zeta, \quad \kappa(\zeta) = \zeta^{1/2}, \quad \int_0^\zeta \kappa(\zeta') d\zeta' = \frac{2}{3} \zeta^{3/2}, \quad (2.103)$$

i.e. exactly the exponent in the top line of Eq. (102). Making a similar calculation for $\zeta < 0$, with the natural assumption $|b| = |a|$ (full reflection from the potential step), we arrive at the following result:

$$\text{Ai}_{\text{WKB}}(\zeta) = \frac{1}{|\zeta|^{1/4}} \times \begin{cases} c' \exp\left\{-\frac{2}{3} \zeta^{3/2}\right\}, & \text{for } \zeta > 0, \\ a' \sin\left\{\frac{2}{3}(-\zeta)^{3/2} + \varphi\right\}, & \text{for } \zeta < 0. \end{cases} \quad (2.104)$$

This approximation differs from the exact solution at small values of ζ , i.e. close to the classical turning point – see Fig. 9b. However, at $|\zeta| \gg 1$, Eqs. (104) describe the Airy function exactly, provided that

$$\varphi = \frac{\pi}{4}, \quad c' = \frac{a'}{2}. \quad (2.105)$$

WKB:
connection
formulas

These *connection formulas* may be used to rewrite Eq. (104) as

$$\text{Ai}_{\text{WKB}}(\zeta) = \frac{a'}{2|\zeta|^{1/4}} \times \begin{cases} \exp\left\{-\frac{2}{3} \zeta^{3/2}\right\}, & \text{for } \zeta > 0, \\ \frac{1}{i} \left[\exp\left\{i \frac{2}{3} \zeta^{3/2} + i \frac{\pi}{4}\right\} - \exp\left\{-i \frac{2}{3} \zeta^{3/2} - i \frac{\pi}{4}\right\} \right], & \text{for } \zeta < 0, \end{cases} \quad (2.106)$$

and hence may be described by the following two simple mnemonic rules:

(i) If the classical turning point is taken for the lower limit in the WKB integrals in the classically allowed and the classically forbidden regions, then the moduli of the quasi-amplitudes of the exponents are equal.

(ii) Reflecting from a “soft” potential step, the wavefunction acquires an additional phase shift $\Delta\varphi = \pi/2$, if compared with its reflection from a “hard”, infinitely high potential wall located at point x_c (for which, according to Eq. (63) with $\kappa = 0$, we have $B = -A$).

In order for the connection formulas (105)-(106) to be valid, deviations from the linear approximation (99) of the potential profile should be relatively small within the region where the WKB approximation differs from the exact Airy function: $|\zeta| \sim 1$, i.e. $|x - x_c| \sim x_0$. These deviations may be estimated using the next term of the Taylor expansion, dropped in Eq. (99): $(d^2 U / d^2 x)(x - x_c)^2 / 2$. As a result, the condition of validity of the connection formulas (i.e. of the “softness” of the reflecting

potential profile) may be expressed as $|d^2U/dx^2| \ll |dU/dx|$ at $x \approx x_c$ – meaning the $\sim x_0$ -wide vicinity of the point x_c). With the account of Eq. (100) for x_0 , this condition becomes

$$\left| \frac{d^2U}{dx^2} \right|_{x \approx x_c}^3 \ll \frac{2m}{\hbar^2} \left(\frac{dU}{dx} \right)_{x \approx x_c}^4. \quad (2.107)$$

Connection formulas' validity

As an example of a very useful application of the WKB approximation, let us use the connection formulas to calculate the energy spectrum of a 1D particle in a soft 1D potential well (Fig. 10).

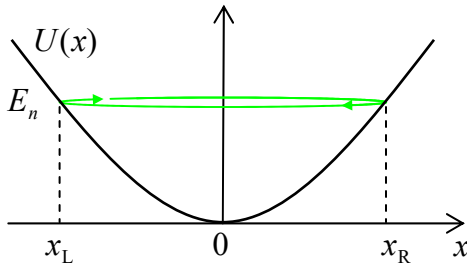


Fig. 2.10. The WKB treatment of an eigenstate of a particle in a soft 1D potential well.

As was discussed in Sec. 1.7, we may consider the standing wave describing an eigenfunction ψ_n (corresponding to an eigenenergy E_n) as a sum of two traveling de Broglie waves going back and forth between the walls, being sequentially reflected from each of them. Let us apply the WKB approximation to such traveling waves. First, according to Eq. (94), propagating from the left classical turning point x_L to the right such point x_R , it acquires the phase change

$$\Delta\varphi_{\rightarrow} = \int_{x_L}^{x_R} k(x) dx. \quad (2.108)$$

At the reflection from the soft wall at x_R , according to the mnemonic rule (ii), the wave acquires an additional shift $\pi/2$. Now, traveling back from x_R to x_L , the wave gets a shift similar to one given by Eq. (108): $\Delta\varphi_{\leftarrow} = \Delta\varphi_{\rightarrow}$. Finally, at the reflection from x_L it gets one more $\pi/2$ -shift. Summing up all these contributions at the wave's roundtrip, we may write the self-consistency condition (that the wavefunction “catches its own tail with its teeth”) in the form

$$\Delta\varphi_{\text{total}} \equiv \Delta\varphi_{\rightarrow} + \frac{\pi}{2} + \Delta\varphi_{\leftarrow} + \frac{\pi}{2} \equiv 2 \int_{x_L}^{x_R} k(x) dx + \pi = 2\pi n, \quad \text{with } n = 1, 2, \dots \quad (2.109)$$

Rewriting this result in terms of the particle's momentum $p(x) = \hbar k(x)$, we arrive at the so-called *Wilson-Sommerfeld* (or “Bohr-Sommerfeld”) *quantization rule*

$$\oint_C p(x) dx = 2\pi\hbar \left(n - \frac{1}{2} \right), \quad (2.110)$$

Wilson-Sommerfeld quantization rule

where the closed path C means the full period of classical motion.²⁴

²⁴ Note that at the motion in more than one dimension, a closed classical trajectory may have no classical turning points. In this case, the constant $1/2$, arising from the turns, should be dropped from Eqs. (110) written for the scalar product $\mathbf{p}(\mathbf{r}) \cdot d\mathbf{r}$ – the so-called *Bohr quantization rule*. It was suggested by N. Bohr as early as 1913 as an interpretation of Eq. (1.8) for the circular motion of the electron around the proton, while its 1D modification (110) is due to W. Wilson (1915) and A. Sommerfeld (1916).

Let us see what does this quantization rule give for the very important particular case of a quadratic potential profile of a harmonic oscillator of frequency ω_0 . In this case,

$$U(x) = \frac{m}{2} \omega_0^2 x^2, \quad (2.111)$$

and the classical turning points (where $U(x) = E$) are the roots of a simple equation

$$\frac{m}{2} \omega_0^2 x_c^2 = E_n, \quad \text{so that } x_R = \frac{1}{\omega_0} \left(\frac{2E_n}{m} \right)^{1/2} > 0, \quad x_L = -x_R < 0. \quad (2.112)$$

Due to the potential's symmetry, the integration required by Eq. (110) is also simple:

$$\begin{aligned} \int_{x_L}^{x_R} p(x) dx &= \int_{x_L}^{x_R} \{2m[E_n - U(x)]\}^{1/2} dx \equiv (2mE_n)^{1/2} 2 \int_0^{x_R} \left(1 - \frac{x^2}{x_R^2}\right)^{1/2} dx \\ &\equiv (2mE_n)^{1/2} 2x_R \int_0^1 (1 - \xi^2)^{1/2} d\xi = (2mE_n)^{1/2} 2x_R \frac{\pi}{4} \equiv \frac{\pi E_n}{\omega_0}, \end{aligned} \quad (2.113)$$

so that Eq. (110) yields

$$E_n = \hbar\omega_0 \left(n' + \frac{1}{2} \right), \quad \text{with } n' \equiv n - 1 = 0, 1, 2, \dots. \quad (2.114)$$

To estimate the validity of this result, we have to check the condition (96) at all points of the classically allowed region, and Eq. (107) at the turning points. The checkup shows that both conditions are valid only for $n \gg 1$. However, we will see in Sec. 9 below that Eq. (114) is actually exactly correct for *all* energy levels – thanks to special properties of the potential profile (111).

Now let us use the mnemonic rule (i) to examine particle's penetration into the classically forbidden region of an abrupt potential step of a height $U_0 > E$. For this case, the rule, i.e. the second of Eqs. (105), yields the following relation of the quasi-amplitudes in Eqs. (94) and (98): $|c| = |a|/2$. If we now naively applied this relation to the sharp step sketched in Fig. 4, forgetting that it does not satisfy Eq. (107), we would get the following relation of the full amplitudes, defined by Eqs. (55) and (58):

$$\left| \frac{C}{\kappa} \right| = \frac{1}{2} \left| \frac{A}{k} \right|. \quad (\text{WRONG!}) \quad (2.115)$$

This result differs from the correct Eq. (63), and hence we may expect that the WKB approximation's prediction for more complex potentials, most importantly for tunneling through a soft potential barrier (Fig. 11) should be also different from the exact result (71) for the rectangular barrier shown in Fig. 6.

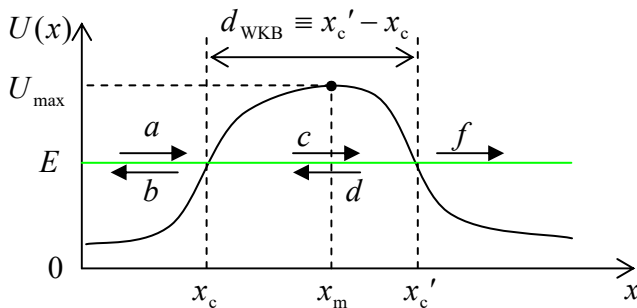


Fig. 2.11. Tunneling through a soft 1D potential barrier.

In order to analyze tunneling through such a soft barrier, we need (just as in the case of a rectangular barrier) to take unto consideration five partial waves, but now they should be taken in the WKB form:

$$\psi_{\text{WKB}} = \begin{cases} \frac{a}{k^{1/2}(x)} \exp\left\{i \int_{x'}^x k(x') dx'\right\} + \frac{b}{k^{1/2}(x)} \exp\left\{-i \int_{x'}^x k(x') dx'\right\}, & \text{for } x < x_c, \\ \frac{c}{\kappa^{1/2}(x)} \exp\left\{- \int_{x_c}^x \kappa(x') dx'\right\} + \frac{d}{\kappa^{1/2}(x)} \exp\left\{\int_{x_c}^x \kappa(x') dx'\right\}, & \text{for } x_c < x < x_c', \\ \frac{f}{k^{1/2}(x)} \exp\left\{i \int_{x_c}^x k(x') dx'\right\}, & \text{for } x_c' < x, \end{cases} \quad (2.116)$$

where the lower limits of integrals are arbitrary (each within the corresponding range of x). Since on the right of the left classical point, we have two exponents rather than one, and on the right of the second point, one traveling waves rather than two, the connection formulas (105) have to be generalized, using asymptotic formulas not only for $\text{Ai}(\zeta)$, but also for the second Airy function, $\text{Bi}(\zeta)$. The analysis, absolutely similar to that carried out above (though naturally a bit bulkier),²⁵ gives a remarkably simple result:

Soft potential barrier:
transparency

$$\mathcal{T}_{\text{WKB}} \equiv \left| \frac{f}{a} \right|^2 = \exp\left\{ -2 \int_{x_c}^{x_c'} \kappa(x) dx \right\} \equiv \exp\left\{ -\frac{2}{\hbar} \int_{x_c}^{x_c'} (2m[U(x) - E])^{1/2} dx \right\}, \quad (2.117)$$

with the pre-exponential factor equal to 1 – the fact which might be readily expected from the mnemonic rule (i) of the connection formulas.

This formula is broadly used in applied quantum mechanics, despite the approximate character of its pre-exponential coefficient for insufficiently soft barriers that do not satisfy Eq. (107). For example, Eq. (80) shows that for a rectangular barrier with thickness $d \gg \delta$, the WKB approximation (117) with $d_{\text{WKB}} = d$ underestimates \mathcal{T} by a factor of $[4k\kappa/(k^2 + \kappa^2)]^2$ – equal, for example, 4, if $k = \kappa$, i.e. if $U_0 = 2E$. However, on the appropriate logarithmic scale (see Fig. 7b), such a factor, smaller than an order of magnitude, is just a small correction.

Note also that when E approaches the barrier's top U_{\max} (Fig. 11), the points x_c and x_c' merge, so that according to Eq. (117), $\mathcal{T}_{\text{WKB}} \rightarrow 1$, i.e. the particle reflection vanishes at $E = U_{\max}$. So, the WKB approximation does not describe the effect of the over-barrier reflection at $E > U_{\max}$. (This fact could be noticed already from Eq. (95): in the absence of the classical turning points, the WKB probability current is constant for any barrier profile.) This conclusion is incorrect even for apparently smooth barriers where one could naively expect the WKB approximation to work perfectly. Indeed, near the point $x = x_m$ where the potential reaches maximum (i.e. $U(x_m) = U_{\max}$), we may always approximate any smooth function $U(x)$ with the quadratic term of the Taylor expansion, i.e. with an inverted parabola:

$$U(x) \approx U_{\max} - \frac{m\omega_0^2(x - x_m)^2}{2}. \quad (2.118)$$

²⁵ For the most important case $\mathcal{T}_{\text{WKB}} \ll 1$, Eq. (117) may be simply derived from Eqs. (105)-(106) – the exercise left for the reader.

Calculating derivatives dU/dx and d^2U/dx^2 of this function and plugging them into the condition (107), we may see that the WKB approximation is only valid if $|U_{\max} - E| \gg \hbar\omega_0$. Just for the reader's reference, an exact analysis of tunneling through the barrier (118) gives the following *Kemble formula*:²⁶

$$\mathcal{T} = \frac{1}{1 + \exp\{-2\pi(E - U_{\max})/\hbar\omega_0\}}, \quad (2.119)$$

Kemble formula

valid for any sign of the difference $(E - U_{\max})$. This formula describes a gradual approach of \mathcal{T} to 1, i.e. a *gradual* reduction of reflection, at the particle energy's increase, with $\mathcal{T} = \frac{1}{2}$ at $E = U_{\max}$.

The last remark of this section: the WKB approximation opens a straight way toward an alternative formulation of quantum mechanics, based on the *Feynman path integral*. However, I will postpone its discussion until a more compact notation has been introduced in Chapter 4.

2.5. Resonant tunneling, and metastable states

Now let us move to other, conceptually different quantum effects, taking place in more elaborate potential profiles. Neither piecewise-constant nor smooth-potential models of $U(x)$ are convenient for their quantitative description because they both require "stitching" partial de Broglie waves at each classical turning point, which may lead to cumbersome calculations. However, we may get a very good insight of the physics of quantum effects that may take place in such profiles, using their approximation by sets of Dirac's delta functions.

Additional help in studying such effects is provided by the notions of the *scattering* and *transfer matrices*, very useful for other cases as well. Consider an arbitrary but finite-length potential "bump" (formally called a *scatterer*), localized somewhere between points x_1 and x_2 , on the flat potential background, say $U = 0$ (Fig. 12).

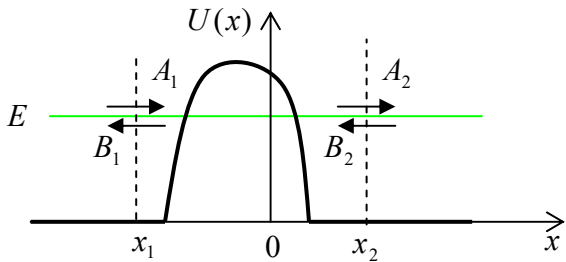


Fig. 2.12. De Broglie wave amplitudes near a single 1D scatterer.

From Sec. 2, we know that the general solutions of the stationary Schrödinger equation, with a certain energy E , outside the interval $[x_1, x_2]$ are sets of two sinusoidal waves, traveling in the opposite directions. Let us represent them in the form

$$\psi_j = A_j e^{ik(x-x_j)} + B_j e^{-ik(x-x_j)}, \quad (2.120)$$

²⁶ This formula was derived (in a more general form, valid for an arbitrary soft potential barrier) by E. Kemble in 1935. In some communities, it is known as the "Hill-Wheeler formula", after D. Hill and J. Wheeler's 1953 paper in that the Kemble formula was spelled out for the quadratic profile (118). Note that mathematically Eq. (119) is similar to the Fermi distribution in statistical physics, with an effective temperature $T_{\text{ef}} = \hbar\omega_0/2\pi k_B$. This coincidence has some curious implications for the Fermi particle tunneling statistics.

where the index j (for now) is equal to either 1 or 2, and $(\hbar k)^2/2m = E$. Note that each of the two wave pairs (129) has, in this notation, its own reference point x_j , because this is very convenient for what follows. As we have already discussed, if the de Broigle wave/particle is incident from the left (i.e. $B_2 = 0$), the solution of the linear Schrödinger equation within the scatterer range ($x_1 < x < x_2$) can provide only linear expressions for the transmitted (A_2) and reflected (B_1) wave amplitudes via the incident wave amplitude A_1 :

$$A_2 = S_{21}A_1, \quad B_1 = S_{11}A_1, \quad (2.121)$$

where S_{11} and S_{21} are certain (generally, complex) coefficients. Alternatively, if a wave, with amplitude B_2 , is incident on the scatterer from the right (i.e. if $A_1 = 0$), it can induce a transmitted wave (B_1) and a reflected wave (A_2), with amplitudes

$$B_1 = S_{12}B_2, \quad A_2 = S_{22}B_2, \quad (2.122)$$

where the coefficients S_{22} and S_{12} are generally different from S_{11} and S_{21} . Now we can use the linear superposition principle to argue that if the waves A_1 and B_2 are simultaneously incident on the scatterer (say, because the wave B_2 has been partly reflected back by some other scatterer located at $x > x_2$), the resulting *scattered wave* amplitudes A_2 and B_1 are just the sums of their values for separate incident waves:

$$\begin{aligned} B_1 &= S_{11}A_1 + S_{12}B_2, \\ A_2 &= S_{21}A_1 + S_{22}B_2. \end{aligned} \quad (2.123)$$

These linear relations may be conveniently represented using the so-called *scattering matrix* S :

Scattering
matrix:
definition

$$\begin{pmatrix} B_1 \\ A_2 \end{pmatrix} = S \begin{pmatrix} A_1 \\ B_2 \end{pmatrix}, \quad \text{with } S \equiv \begin{pmatrix} S_{11} & S_{12} \\ S_{21} & S_{22} \end{pmatrix}. \quad (2.124)$$

Scattering matrices, duly generalized, are an important tool for the analysis of wave scattering in more dimensions than one; for 1D problems, however, another matrix is often more convenient to represent the same linear relations (123). Indeed, let us solve this system for A_2 and B_2 . The result is

Transfer
matrix:
definition

$$\begin{aligned} A_2 &= T_{11}A_1 + T_{12}B_1, \quad \text{i.e. } \begin{pmatrix} A_2 \\ B_2 \end{pmatrix} = T \begin{pmatrix} A_1 \\ B_1 \end{pmatrix}, \\ B_2 &= T_{21}A_1 + T_{22}B_1, \end{aligned} \quad (2.125)$$

where T is the *transfer matrix*, with the following elements:

$$T_{11} = S_{21} - \frac{S_{11}S_{22}}{S_{12}}, \quad T_{12} = \frac{S_{22}}{S_{12}}, \quad T_{21} = -\frac{S_{11}}{S_{21}}, \quad T_{22} = \frac{1}{S_{12}}. \quad (2.126)$$

The matrices S and T have some universal properties, valid for an arbitrary (but time-independent) scatterer; they may be readily found from the probability current conservation and the time-reversal symmetry of the Schrödinger equation. Let me leave finding these relations for the reader's exercise. The results show, in particular, that the scattering matrix may be rewritten in the following form:

$$S = e^{i\theta} \begin{pmatrix} re^{i\varphi} & t \\ t & -re^{-i\varphi} \end{pmatrix}, \quad (2.127a)$$

where four real parameters r , t , θ , and φ satisfy the following universal relation:

$$r^2 + t^2 = 1, \quad (2.127b)$$

so that only 3 of these parameters are independent. As a result of this symmetry, T_{11} may be also represented in a simpler form, similar to T_{22} : $T_{11} = \exp\{i\theta\}/t = 1/S_{12}^* = 1/S_{21}^*$. The last form allows a ready expression of the scatterer's transparency via just one coefficient of the transfer matrix:

$$\mathcal{T} \equiv \left| \frac{A_2}{A_1} \right|_{B_2=0}^2 = |S_{21}|^2 = |T_{11}|^{-2}. \quad (2.128)$$

In our current context, the most important property of the 1D transfer matrices is that to find the total transfer matrix T of a system consisting of several (say, N) sequential arbitrary scatterers (Fig. 13), it is sufficient to multiply their matrices.

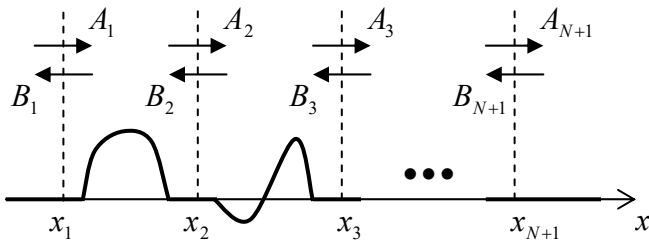


Fig. 2.13. A sequence of several 1D scatterers.

Indeed, extending the definition (125) to other points x_j ($j = 1, 2, \dots, N+1$), we can write

$$\begin{pmatrix} A_2 \\ B_2 \end{pmatrix} = T_1 \begin{pmatrix} A_1 \\ B_1 \end{pmatrix}, \quad \begin{pmatrix} A_3 \\ B_3 \end{pmatrix} = T_2 \begin{pmatrix} A_2 \\ B_2 \end{pmatrix} = T_2 T_1 \begin{pmatrix} A_1 \\ B_1 \end{pmatrix}, \quad \text{etc.} \quad (2.129)$$

(where the matrix indices correspond to the scatterers' order on the x -axis), so that

$$\begin{pmatrix} A_{N+1} \\ B_{N+1} \end{pmatrix} = T_N T_{N-1} \dots T_1 \begin{pmatrix} A_1 \\ B_1 \end{pmatrix}. \quad (2.130)$$

But we can also define the *total transfer matrix* similarly to Eq. (125), i.e. as

$$\begin{pmatrix} A_{N+1} \\ B_{N+1} \end{pmatrix} \equiv T \begin{pmatrix} A_1 \\ B_1 \end{pmatrix}, \quad (2.131)$$

so that comparing Eqs. (130) and (131) we get

$$T = T_N T_{N-1} \dots T_1. \quad (2.132)$$

This formula is valid even if the flat-potential gaps between component scatterers are shrunk to zero, so that it may be applied to a scatterer with an arbitrary profile $U(x)$, by fragmenting its length into many small segments $\Delta x = x_{j+1} - x_j$, and treating each fragment as a rectangular barrier of the average height $(U_j)_{\text{ef}} = [U(x_{j+1}) - U(x_j)]/2$ – see Fig. 14. Since very efficient numerical algorithms are readily available for fast multiplication of matrices (especially as small as 2×2 in our case), this approach is broadly used in practice for the computation of transparency of potential barriers with complicated profiles $U(x)$. (Computationally, this procedure is much more efficient than the direct numerical solution of the stationary Schrödinger equation.)

Transfer matrix:
composite scatterer

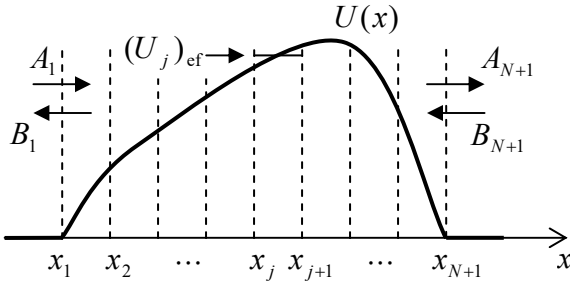


Fig. 2.14. The transfer matrix approach to a potential barrier with an arbitrary profile.

In order to apply this approach to several particular, conceptually important systems, let us calculate the transfer matrices for a few elementary scatterers, starting from the delta-functional barrier located at $x = 0$ – see Fig. 8. Taking $x_1, x_2 \rightarrow 0$, we can merely change the notation of the wave amplitudes in Eq. (78) to get

$$S_{11} = \frac{-i\alpha}{1+i\alpha}, \quad S_{21} = \frac{1}{1+i\alpha}. \quad (2.133)$$

An absolutely similar analysis of the wave incidence from the left yields

$$S_{22} = \frac{-i\alpha}{1+i\alpha}, \quad S_{12} = \frac{1}{1+i\alpha}, \quad (2.134)$$

and using Eqs. (126), we get

$$T_\alpha = \begin{pmatrix} 1-i\alpha & -i\alpha \\ i\alpha & 1+i\alpha \end{pmatrix}. \quad (2.135)$$

As a sanity check, Eq. (128) applied to this result, immediately brings us back to Eq. (79).

The next example may seem strange at the first glance: what if there is no scatterer at all between the points x_1 and x_2 ? If the points coincide, the answer is indeed trivial and can be obtained, e.g., from Eq. (135) by taking $w=0$, i.e. $\alpha=0$:

$$T_0 = \begin{pmatrix} 1 & 0 \\ 0 & 1 \end{pmatrix} \equiv I \quad (2.136)$$

- the so-called *identity matrix*. However, we are free to choose the reference points $x_{1,2}$ participating in Eq. (120) as we wish. For example, what if $x_2 - x_1 = a$? Let us first take the forward-propagating wave alone: $B_2 = 0$ (and hence $B_1 = 0$); then

$$\psi_2 = \psi_1 = A_1 e^{ik(x-x_1)} \equiv A_1 e^{ik(x_2-x_1)} e^{ik(x-x_2)}. \quad (2.137)$$

The comparison of this expression with the definition (120) for $j=2$ shows that $A_2 = A_1 \exp\{ik(x_2-x_1)\} = A_1 \exp\{ika\}$, i.e. $T_{11} = \exp\{ika\}$. Repeating the calculation for the back-propagating wave, we see that $T_{22} = \exp\{-ika\}$, and since the space interval provides no particle reflection, we finally get

$$T_a = \begin{pmatrix} e^{ika} & 0 \\ 0 & e^{-ika} \end{pmatrix}, \quad (2.138)$$

independently of a common shift of points x_1 and x_2 . At $a=0$, we naturally recover the special case (136).

Transfer matrix:
short scatterer

Identity matrix

Transfer matrix:
spatial interval

Now let us use these simple results to analyze the *double-barrier system* shown in Fig. 15. We could of course calculate its properties as before, writing down explicit expressions for all five traveling waves shown by arrows in Fig. 15, then using the boundary conditions (124) and (125) at each of points $x_{1,2}$ to get a system of four linear equations, and finally, solving it for four amplitude ratios.

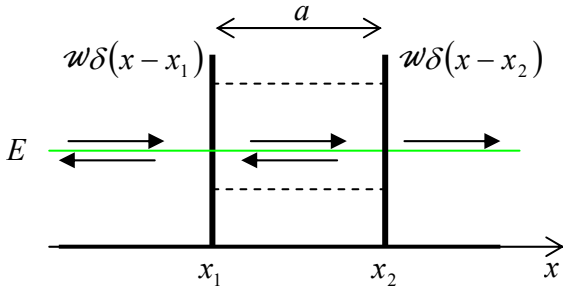


Fig. 2.15. The double-barrier system. The dashed lines show (schematically) the quasi-levels of the metastable-state energies.

However, the transfer matrix approach simplifies the calculations, because we may immediately use Eqs. (132), (135), and (138) to write

$$T = T_\alpha T_a T_\alpha = \begin{pmatrix} 1-i\alpha & -i\alpha \\ i\alpha & 1+i\alpha \end{pmatrix} \begin{pmatrix} e^{ika} & 0 \\ 0 & e^{-ika} \end{pmatrix} \begin{pmatrix} 1-i\alpha & -i\alpha \\ i\alpha & 1+i\alpha \end{pmatrix}. \quad (2.139)$$

Let me hope that the reader remembers the “row by column” rule of the multiplication of square matrices;²⁷ using it for the last two matrices, we may reduce Eq. (139) to

$$T = \begin{pmatrix} 1-i\alpha & -i\alpha \\ i\alpha & 1+i\alpha \end{pmatrix} \begin{pmatrix} (1-i\alpha)e^{ika} & -i\alpha e^{ika} \\ i\alpha e^{-ika} & (1+i\alpha)e^{-ika} \end{pmatrix}. \quad (2.140)$$

Now there is no need to calculate all elements of the full product T , because, according to Eq. (128), for the calculation of barrier’s transparency T we need only one its element, T_{11} :

$$\mathcal{T} = \frac{1}{|T_{11}|^2} = \frac{1}{|\alpha^2 e^{-ika} + (1-i\alpha)^2 e^{ika}|^2}. \quad (2.141)$$

Double barrier: transparency

This result is somewhat similar to that following from Eq. (71) for $E > U_0$: the transparency is a π -periodic function of the product ka , reaching its maximum ($\mathcal{T} = 1$) at some point of each period – see Fig. 16a. However, Eq. (141) is different in that for $\alpha \gg 1$, the resonance peaks of the transparency are very narrow, reaching their maxima at $ka \approx k_n a \equiv n\pi$, with $n = 1, 2, \dots$

The physics of this *resonant tunneling* effect²⁸ is the so-called *constructive interference*, absolutely similar to that of electromagnetic waves (for example, light) in a *Fabry-Perot resonator* formed by two parallel semi-transparent mirrors.²⁹ Namely, the incident de Broglie wave may either

²⁷ In an analytical form: $(AB)_{jj'} = \sum_{j''=1}^N A_{jj''} B_{j''j'}$, where N is the matrix rank (in our current case, $N = 2$).

²⁸ In older literature, it is sometimes called the *Townsend* (or “Ramsauer-Townsend”) effect. However, it is more common to use that term only for a similar effect at 3D scattering – to be discussed in Chapter 3.

²⁹ See, e.g., EM Sec. 7.9.

tunnel through the two barriers or undertake, on its way, several sequential reflections from these semi-transparent walls. At $k = k_n$, i.e. at $2ka = 2k_n a = 2\pi n$, the phase differences between all these partial waves are multiples of 2π , so that they add up in phase – “constructively”. Note that the same constructive interference of numerous reflections from the walls may be used to interpret the standing-wave eigenfunctions (1.84), so that the resonant tunneling at $\alpha \gg 1$ may be also considered as a result of the incident wave’s resonance induction of such a standing wave, with a very large amplitude, in the space between the barriers, with the transmitted wave’s amplitude proportionately increased.

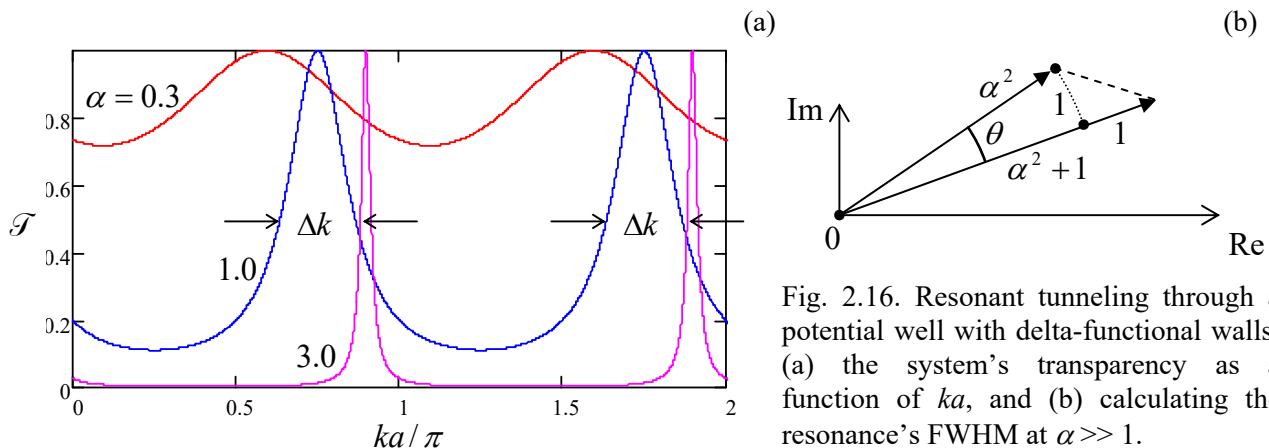


Fig. 2.16. Resonant tunneling through a potential well with delta-functional walls: (a) the system’s transparency as a function of ka , and (b) calculating the resonance’s FWHM at $\alpha \gg 1$.

As a result of this resonance, the maximum transparency of the system is *perfect* ($\mathcal{T}_{\max} = 1$) even at $\alpha \rightarrow \infty$, i.e. in the case of very *low* transparency of each of the two component barriers. Indeed, the denominator in Eq. (141) may be interpreted as the squared length of the difference between two 2D vectors, one of length α^2 , and another of length $|1 - i\alpha|^2 = 1 + \alpha^2$, with the angle $\theta = 2ka + \text{const}$ between them – see Fig. 16b. At the resonance, the vectors are aligned, and their difference is smallest (equal to 1) so that $\mathcal{T}_{\max} = 1$. (This result is exact only if the two barriers are exactly equal.)

The same vector diagram may be used to calculate the so-called FWHM, a common acronym for the *Full Width* [of the resonance curve at its] *Half-Maximum*. By definition, this is the difference $\Delta k = k_+ - k_-$ between such two values of k , on the opposite slopes of the same resonance, at that $\mathcal{T} = \mathcal{T}_{\max}/2$ – see the arrows in Fig. 16a. Let the vectors in Fig. 16b, drawn for $\alpha \gg 1$, be misaligned by a small angle $\theta \sim 1/\alpha^2 \ll 1$, so that the length of the difference vector is much smaller than the length of each vector. To double its length squared, and hence to reduce \mathcal{T} by a factor of two in comparison with its maximum value 1, the arc between the vectors, equal to $\alpha^2\theta$, should also become equal to ± 1 , i.e. $\alpha^2(2k_{\pm}a + \text{const}) = \pm 1$. Subtracting these two equalities from each other, we get

$$\Delta k \equiv k_+ - k_- = \frac{1}{a\alpha^2} \ll k_{\pm}. \quad (2.142)$$

Now let us use the simple system shown in Fig. 15 to discuss an issue of large conceptual significance. For that, consider what would happen if at some initial moment (say, $t = 0$) we have placed a 1D quantum particle inside the double-barrier well with $\alpha \gg 1$, and left it there alone, without any incident wave. To simplify the analysis, let us assume that the initial state of the particle coincides with one of the stationary states of the infinite-wall well of the same size – see Eq. (1.84):

$$\Psi(x,0) = \psi_n(x) = \left(\frac{2}{a}\right)^{1/2} \sin[k_n(x - x_1)], \quad \text{where } k_n = \frac{\pi n}{a}, \quad n = 1, 2, \dots \quad (2.143)$$

At $\alpha \rightarrow \infty$, this is just an eigenstate of the system, and from our analysis in Sec. 1.5 we know the time evolution of its wavefunction:

$$\Psi(x,t) = \psi_n(x) \exp\{-i\omega_n t\} = \left(\frac{2}{a}\right)^{1/2} \sin[k_n(x - x_1)] \exp\{-i\omega_n t\}, \quad \text{with } \omega_n = \frac{E_n}{\hbar} = \frac{\hbar k_n^2}{2m}, \quad (2.144)$$

telling us that the particle remains in the well at all times with constant probability $W(t) = W(0) = 1$.

However, if the parameter α is large but finite, the de Broglie wave would slowly “leak out” from the well, so that $W(t)$ would slowly decrease. Such a state is called *metastable*. Let us derive the law of its time evolution, assuming that at the slow leakage, with a characteristic time $\tau \gg 1/\omega_n$, does not affect the instant wave distribution inside the well, besides the gradual, slow reduction of W .³⁰ Then we can generalize Eq. (144) as

$$\Psi(x,t) = \left(\frac{2W}{a}\right)^{1/2} \sin[k_n(x - x_1)] \exp\{-i\omega_n t\} \equiv A \exp\{i(k_n x - \omega_n t)\} + B \exp\{-i(k_n x + \omega_n t)\}, \quad (2.145)$$

making the probability of finding the particle in the well equal to $W \leq 1$. As the last form of Eq. (145) shows, this function is the sum of two traveling waves, with equal magnitudes of their amplitudes and equal but opposite probability currents (5):

$$|A| = |B| = \left(\frac{W}{2a}\right)^{1/2}, \quad I_A = \frac{\hbar}{m} |A|^2 k_n = \frac{\hbar W}{m 2a} \frac{\pi n}{a}, \quad I_B = -I_A. \quad (2.146)$$

But we already know from Eq. (79) that at $\alpha \gg 1$, the delta-functional wall’s transparency \mathcal{T} equals $1/\alpha^2$, so that the wave carrying current I_A , incident on the right wall from the inside, induces an outgoing wave outside of the well (Fig. 17) with the following probability current:

$$I_R = \mathcal{T} I_A = \frac{1}{\alpha^2} I_A = \frac{1}{\alpha^2} \frac{\pi n \hbar W}{2ma^2}. \quad (2.147)$$

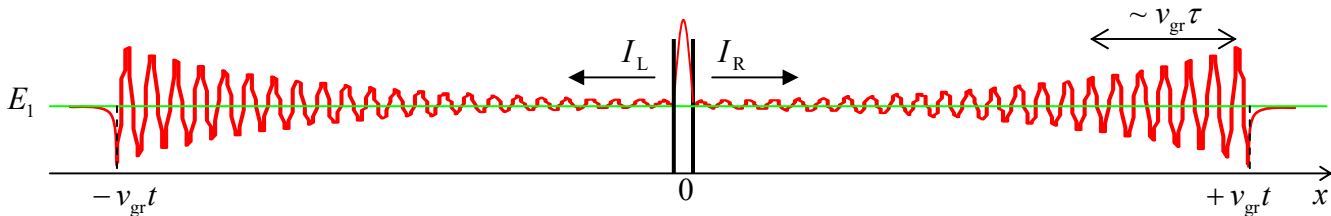


Fig. 2.17. Metastable state’s decay in the simple model of a 1D potential well formed by two low-transparent walls – schematically.

Absolutely similarly,

$$I_L = \frac{1}{\alpha^2} I_B = -I_R. \quad (2.148)$$

³⁰ This virtually evident assumption finds its formal justification in the perturbation theory to be discussed in Chapter 6.

Now we may combine the 1D version (6) of the probability conservation law for the well's interior:

$$\frac{dW}{dt} + I_R - I_L = 0, \quad (2.149)$$

with Eqs. (147)-(148) to write

$$\frac{dW}{dt} = -\frac{1}{\alpha^2} \frac{\pi n \hbar}{ma^2} W. \quad (2.150)$$

This is just the standard differential equation,

$$\boxed{\frac{dW}{dt} = -\frac{1}{\tau} W}, \quad (2.151)$$

of the exponential decay, $W(t) = W(0)\exp\{-t/\tau\}$, where the constant τ , in our case equal to

$$\tau = \frac{ma^2}{\pi n \hbar} \alpha^2, \quad (2.152)$$

is called the *metastable state's lifetime*. Using Eq. (2.33b) for the de Broglie waves' group velocity, for our particular wave vector giving $v_{gr} = \hbar k_n/m = \pi n \hbar / ma$, Eq. (152) may be rewritten in a more general form,

$$\boxed{\tau = \frac{t_a}{\mathcal{T}}}, \quad (2.153)$$

where the *attempt time* t_a is equal to a/v_{gr} , and (in our particular case) $\mathcal{T} = 1/\alpha^2$, in which it is valid for a broad class of similar metastable systems.³¹ Equality may be interpreted in the following semi-classical way. The particle travels back and forth between the confining potential barriers, with the time interval t_a between the sequential moments of incidence, each time attempting to leak through the wall, with the success probability equal to \mathcal{T} , so the reduction of W per each incidence is $\Delta W = -W\mathcal{T}$, in the limit $\alpha \gg 1$ (i.e. $\mathcal{T} \ll 1$) immediately leading to the decay equation (151) with the lifetime (153).

Another useful look at Eq. (152) may be taken by returning to the resonant tunneling problem in the same system, and expressing the resonance width (142) in terms of the incident particle's energy:

$$\Delta E = \Delta \left(\frac{\hbar^2 k^2}{2m} \right) \approx \frac{\hbar^2 k_n}{m} \Delta k = \frac{\hbar^2 k_n}{m} \frac{1}{a \alpha^2} = \frac{\pi n \hbar^2}{m a^2 \alpha^2}. \quad (2.154)$$

Comparing Eqs. (152) and (154), we get a remarkably simple, parameter-independent formula³²

$$\boxed{\Delta E \cdot \tau = \hbar}. \quad (2.155)$$

³¹ Essentially the only requirement is to have the attempt time Δt_A to be much longer than the effective time (the *instanton time*, see Sec. 5.3 below) of tunneling through the barrier. In the delta-functional approximation for the barrier, the latter time is equal to zero, so that this requirement is always fulfilled.

³² Note that the metastable state's decay (2.151) may be formally obtained from the basic Schrödinger equation (1.61) by adding an imaginary part, equal to $(-\Delta E/2)$, to its eigenenergy E_n . Indeed, in this case Eq. (1.62) becomes $a_n(t) = \text{const} \times \exp\{-i(E_n - i\Delta E/2)t/\hbar\} \equiv \text{const} \times \exp\{-iE_n t/\hbar\} \times \exp\{-\Delta E t/2\hbar\} = \text{const} \times \exp\{-iE_n t/\hbar\} \times \exp\{-t/2\tau\}$, so that $W(t) \propto |a_n(t)|^2 \propto \exp\{-t/\tau\}$. Such formalism, which hides the physical origin of the state's decay, may be convenient for some calculations, but misleading in other cases, and I will not use it in this course.

This *energy-time uncertainty relation* is certainly *more* general than our simple model; for example, it is valid for the lifetime and resonance tunneling width of any metastable state in the potential profile of any shape. This seems very natural, since because of the energy identification with frequency, $E = \hbar\omega$, typical for quantum mechanics, Eq. (155) may be rewritten as $\Delta\omega\tau = 1$ and seems to follow directly from the Fourier transform in time, just as the Heisenberg's uncertainty relation (1.35) follows from the Fourier transform in space. In some cases, these two relations are indeed interchangeable; for example, Eq. (24) for the Gaussian wave packet width may be rewritten as $\delta E \cdot \Delta t = \hbar$, where $\delta E = \hbar(d\omega/dk)\delta k = \hbar v_{\text{gr}}\delta k$ is the r.m.s. spread of energies of monochromatic components of the packet, while $\Delta t \equiv \delta x/v_{\text{gr}}$ is the time scale of packet's passage through a fixed observation point x .

However, Eq. (155) is much *less* general than Heisenberg's uncertainty relation (1.35). Indeed, in the non-relativistic quantum mechanics we are studying now, the Cartesian coordinates of a particle, the Cartesian components of its momentum, and the energy E are regular observables, represented by operators. In contrast, time is treated as a *c*-number argument, and is *not* represented by an operator, so that Eq. (155) cannot be derived in such general assumptions as Eq. (1.35). Thus the time-energy uncertainty relation should be used with caution. Unfortunately, not everybody is so careful. One can find, for example, wrong claims that due to this relation, the energy dissipated by any system performing an elementary (single-bit) calculation during a time interval Δt has to be larger than $\hbar/\Delta t$.³³ Another incorrect statement is that the energy of a system cannot be measured, during a time interval Δt , with an accuracy better than $\hbar/\Delta t$.³⁴

Now that we have a quantitative mathematical description of the metastable state's decay (valid, again, only if $\alpha \gg 1$, i.e. if $\tau \gg t_a$), we may use it for discussion of two important conceptual issues of quantum mechanics. First, this is one of the simplest examples of systems that may be considered, from two different points of view, as either Hamiltonian (and hence *time-reversible*), or open (and hence *irreversible*). Indeed, from the former point of view, our particular system is certainly described by a time-independent Hamiltonian of the type (1.41), with the potential energy

$$U(x) = w[\delta(x - x_1) + \delta(x - x_2)] \quad (2.156)$$

- see Fig. 15 again. In this point of view, the total probability of finding the particle *somewhere* on the axis x remains equal to 1, and the full system's energy, calculated from Eq. (1.23),

$$\langle E \rangle = \int_{-\infty}^{+\infty} \Psi^*(x, t) \hat{H} \Psi(x, t) d^3x, \quad (2.157)$$

remains constant and completely definite ($\delta E = 0$). On the other hand, since the "emitted" wave packets would never return to the potential well,³⁵ it makes sense to look at the well's region alone. For such a

³³ On this issue, I dare to refer the reader to my own old work K. Likharev, *Int. J. Theor. Phys.* **21**, 311 (1982), which provided a constructive proof (for a particular system) that at *reversible computation*, whose idea had been put forward in 1973 by C. Bennett (see, e.g., SM Sec. 2.3), energy dissipation may be lower than this apparent "quantum limit".

³⁴ See, e.g., a discussion of this issue in the monograph by V. Braginsky and F. Khalili, *Quantum Measurement*, Cambridge U. Press, 1992.

³⁵ For more realistic 2D and 3D systems, this statement is true even if the system as a whole is confined inside some closed volume, much larger than the potential well housing the metastable states. Indeed, if the walls

truncated, *open* system (for which the space beyond the interval $[x_1, x_2]$ serves as its *environment*), the probability W of finding the particle inside this interval, and hence its energy $\langle E \rangle = WE_n$, decay exponentially per Eq. (151) – the decay equation typical for irreversible systems. We will return to the discussion of the dynamics of such open quantum systems in Chapter 7.

Second, the same model enables a preliminary discussion of one important aspect of quantum measurements. As Eq. (151) and Fig. 17 show, at $t \gg \tau$, the well becomes virtually empty ($W \approx 0$), and the whole probability is localized in two clearly separated wave packets with equal amplitudes, moving from each other with the speed v_{gr} , each “carrying the particle away” with a probability of 50%. Now assume that an experiment has detected the particle on the left side of the well. Though the formalisms suitable for quantitative analysis of the detection process will not be discussed until Chapter 7, due to the wide separation $\Delta x = 2v_{\text{gr}}t \gg 2v_{\text{gr}}\tau$ of the packets, we may safely assume that such detection may be done without any actual physical effect on the counterpart wave packet.³⁶ But if we know that the particle has been found on the left side, there is no chance to find it on the right side. If we attributed the full wavefunction to all stages of this particular experiment, this situation might be rather confusing. Indeed, that would mean that the wavefunction at the right packet’s location should instantly turn into zero – the so-called *wave packet reduction* (or “collapse”) – a hypothetical, irreversible process that cannot be described by the Schrödinger equation for this system, even including the particle detectors.

However, if (as was already discussed in Sec. 1.3) we attribute the wavefunction to a certain statistical ensemble of similar experiments, there is no need to involve such an artificial notion. The two-packet picture we have calculated (Fig. 17) describes the full ensemble of experiments with all systems prepared in the initial state (143), i.e. does not depend on the particle detection results. On the other hand, the “reduced packet” picture (with no wave packet on the right of the well) describes only a sub-ensemble of such experiments, in which the particles have been detected on the left side. As was discussed on classical examples in Sec. 1.3, for such redefined ensemble the probability distribution is rather different. So, the “wave packet reduction” is just a result of a purely accounting decision of the observer.³⁷ I will return to this important discussion in Sec. 10.1 – on the basis of the forthcoming discussion of open systems in Chapters 7 and 8.

2.6. Localized state coupling, and quantum oscillations

Now let us discuss one more effect specific to quantum mechanics. Its mathematical description may be simplified using a model potential consisting of two very short and deep potential wells. For that, let us first analyze the properties of a single well of this type (Fig. 18), which may be modeled similarly to the short and high potential barrier – see Eq. (74), but with a negative “weight”:

$$U(x) = -w\delta(x), \quad \text{with } w > 0. \quad (2.158)$$

providing such confinement are even slightly uneven, the emitted plane-wave packets will be reflected from them, but would never return to the well intact. (See SM Sec. 2.1 for a more detailed discussion of this issue.)

³⁶ This argument is especially convincing if the particle’s detection time is much shorter than the time $t_c = 2v_{\text{gr}}t/c$, where c is the speed of light in vacuum, i.e. the maximum velocity of any information transfer.

³⁷ “The collapse of the wavefunction after measurement represents nothing more than the updating of that scientist’s expectations.” N. D. Mermin, *Phys. Today*, **72**, 53 (Jan. 2013).

In contrast to its tunnel-barrier counterpart (74), such potential sustains a stationary state with a negative eigenenergy $E < 0$, and a *localized* eigenfunction ψ , with $|\psi| \rightarrow 0$ at $x \rightarrow \pm\infty$.

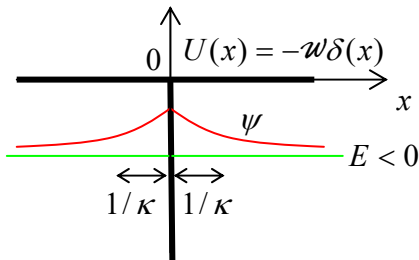


Fig. 2.18. Delta-functional potential well and its localized eigenstate (schematically).

Indeed, at $x \neq 0$, $U(x) = 0$, so the 1D Schrödinger equation is reduced to the Helmholtz equation (1.83), whose localized solutions with $E < 0$ are single exponents, vanishing at large distances:³⁸

$$\psi(x) = \psi_0(x) \equiv \begin{cases} Ae^{-\kappa x}, & \text{for } x > 0, \\ Ae^{+\kappa x}, & \text{for } x < 0, \end{cases} \quad \text{with } \frac{\hbar^2 \kappa^2}{2m} = -E, \quad \kappa > 0. \quad (2.159)$$

(The coefficients before the exponents have been selected equal to satisfy the boundary condition (76) of the wavefunction's continuity at $x = 0$.) Plugging Eq. (159) into the second boundary condition, given by Eq. (75), but now with the negative sign before w , we get

$$(-\kappa A) - (+\kappa A) = -\frac{2m w}{\hbar^2} A, \quad (2.160)$$

in which the common factor $A \neq 0$ may be canceled. This equation³⁹ has one solution for any $w > 0$:

$$\kappa = \kappa_0 \equiv \frac{m w}{\hbar^2}, \quad (2.161)$$

and hence the system has only one (ground) localized state, with the following eigenenergy:⁴⁰

$$E = E_0 \equiv -\frac{\hbar^2 \kappa_0^2}{2m} = -\frac{m w^2}{2\hbar^2}. \quad (2.162)$$

Now we are ready to analyze localized states of the two-well potential shown in Fig. 19:

$$U(x) = -w \left[\delta\left(x - \frac{a}{2}\right) + \delta\left(x + \frac{a}{2}\right) \right], \quad \text{with } w > 0. \quad (2.163)$$

Here we may still use the single-exponent solutions, similar to Eq. (159), for the wavefunction outside the interval $[-a/2, +a/2]$, but inside the interval, we need to take into account both possible exponents:

$$\psi = C_+ e^{\kappa x} + C_- e^{-\kappa x} \equiv C_A \sinh \kappa x + C_S \cosh \kappa x, \quad \text{for } -\frac{a}{2} \leq x \leq +\frac{a}{2}, \quad (2.164)$$

³⁸ See Eqs. (56)-(58), with $U_0 = 0$.

³⁹ Such algebraic equations for linear differential equations are frequently called *characteristic*.

⁴⁰ Note that this E_0 is equal, by magnitude, to the constant E_0 that participates in Eq. (79). Note also that this result was actually already obtained, “backward”, in the solution of Problem 1.12(ii), but that solution did not address the issue of whether the calculated potential (158) could sustain any other localized eigenstates.

with the parameter κ defined as in Eq. (159). The last of these equivalent expressions is more convenient because due to the symmetry of the potential (163) to the central point $x = 0$, the system's eigenfunctions should be either symmetric (even) or antisymmetric (odd) functions of x (see Fig. 19), so that they may be analyzed separately, only for one half of the system, say $x \geq 0$, and using just one of the hyperbolic function (164) in each case.

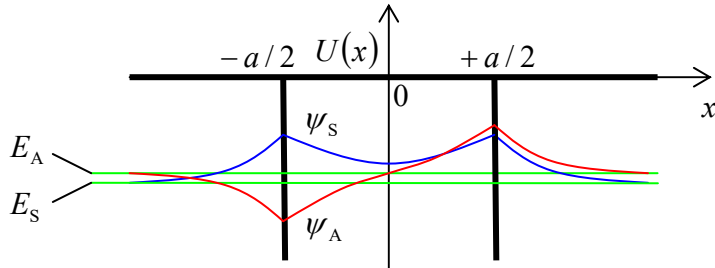


Fig. 2.19. A system of two coupled potential wells, and its localized eigenstates (schematically).

For the *antisymmetric* eigenfunction, Eqs. (159) and (164) yield

$$\psi_A \equiv C_A \times \begin{cases} \sinh \kappa x, & \text{for } 0 \leq x \leq \frac{a}{2}, \\ \sinh \frac{\kappa a}{2} \exp\left\{-\kappa\left(x - \frac{a}{2}\right)\right\}, & \text{for } \frac{a}{2} \leq x, \end{cases} \quad (2.165)$$

where the front coefficient in the lower line has been selected to satisfy the condition (76) of the wavefunction's continuity at $x = +a/2$ – and hence at $x = -a/2$. What remains is to satisfy the condition (75), with a negative sign before w , for the derivative's jump at that point. This condition yields the following characteristic equation:

$$\sinh \frac{\kappa a}{2} + \cosh \frac{\kappa a}{2} = \frac{2m w}{\hbar^2 \kappa} \sinh \frac{\kappa a}{2}, \quad \text{i.e. } 1 + \coth \frac{\kappa a}{2} = 2 \frac{(\kappa_0 a)}{(\kappa a)}, \quad (2.166)$$

where κ_0 , given by Eq. (161), is the value of κ for a single well, i.e. the reciprocal spatial width of its localized eigenfunction – see Fig. 18.

Figure 20a shows both sides of Eq. (166) as functions of the dimensionless product κa , for several values of the parameter $\kappa_0 a$, i.e. of the normalized distance between the two wells. The plots show, first of all, that as the parameter $\kappa_0 a$ is decreased, the LHS and RHS plots cross (i.e. Eq. (166) has a solution) at lower and lower values of κa . At $\kappa a \ll 1$, the left-hand side of the last form of this equation may be approximated as $2/\kappa a$. Comparing this expression with the right-hand side of the characteristic equation, we see that this transcendental equation has a solution (i.e. the system has an antisymmetric localized state) only if $\kappa_0 a > 1$, i.e. if the distance a between the two narrow potential wells is larger than the following value,

$$a_{\min} = \frac{1}{\kappa_0} \equiv \frac{\hbar^2}{m w}, \quad (2.167)$$

which is equal to the characteristic spread of the wavefunction in a single well – see Fig. 18. (At $a \rightarrow a_{\min}$, $\kappa a \rightarrow 0$, meaning that the state's localization becomes weaker and weaker.)

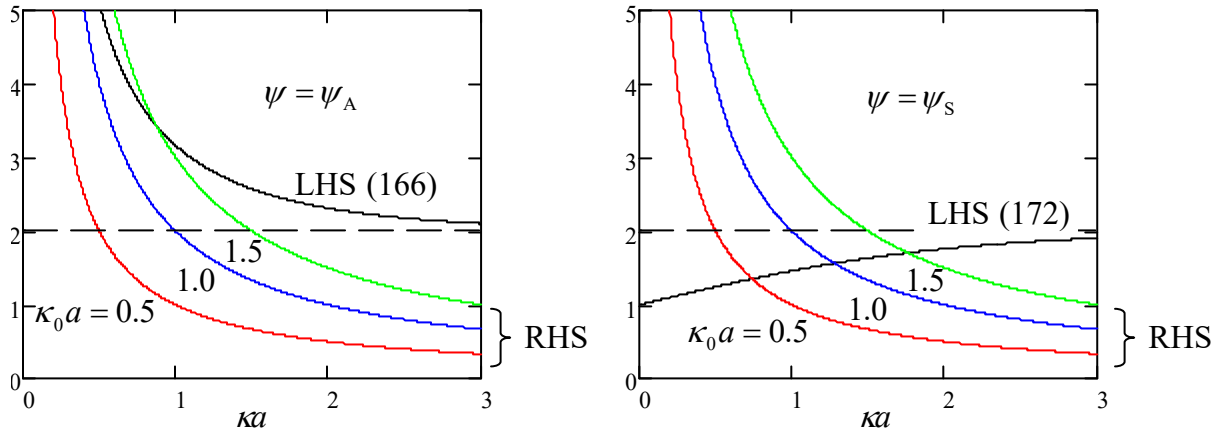


Fig. 2.20. Graphical solutions of the characteristic equations of the two-well system, for:
(a) the antisymmetric eigenstate (165), and (b) the symmetric eigenstate (171).

In the opposite limit of large distances between the potential wells, i.e. $\kappa_0 a \gg 1$, Eq. (166) shows that $\kappa a \gg 1$ as well, so that its left-hand side may be approximated as $2(1 + \exp\{-\kappa a\})$, and the equation yields

$$\kappa \approx \kappa_0 (1 - \exp\{-\kappa_0 a\}) \approx \kappa_0 . \quad (2.168)$$

This result means that the eigenfunction is an antisymmetric superposition of two virtually unperturbed wavefunctions (159) of each partial potential well:

$$\psi_A(x) \approx \frac{1}{\sqrt{2}} [\psi_R(x) - \psi_L(x)], \quad \text{where } \psi_R(x) \equiv \psi_0\left(x - \frac{a}{2}\right), \quad \psi_L(x) \equiv \psi_0\left(x + \frac{a}{2}\right), \quad (2.169)$$

and the front coefficient is selected in such a way that if the eigenfunction ψ_0 of each well is normalized, so is ψ_A . Plugging the middle (more exact) form of Eq. (168) into the last of Eqs. (159), we can see that in this limit the antisymmetric state's energy is only slightly higher than the eigenenergy E_0 of a single well, given by Eq. (162):

$$E_A \approx E_0 (1 - 2 \exp\{-\kappa_0 a\}) \equiv E_0 + \delta, \quad \text{where } \delta \equiv \frac{2m\omega^2}{\hbar^2} \exp\{-\kappa_0 a\} > 0 . \quad (2.170)$$

The *symmetric* eigenfunction has a form reminding Eq. (165), but still different from it:

$$\psi = \psi_S \equiv C_S \times \begin{cases} \cosh \kappa x, & \text{for } 0 \leq x \leq \frac{a}{2}, \\ \cosh \frac{\kappa a}{2} \exp\left\{-\kappa\left(x - \frac{a}{2}\right)\right\}, & \text{for } \frac{a}{2} \leq x, \end{cases} \quad (2.171)$$

giving a characteristic equation similar in structure to Eq. (166), but with a different left-hand side:

$$1 + \tanh \frac{\kappa a}{2} = 2 \frac{(\kappa_0 a)}{(\kappa a)} . \quad (2.172)$$

Figure 20b shows both sides of this equation for several values of the parameter $\kappa_0 a$. It is evident that in contrast to Eq. (166), Eq. (172) has a unique solution (and hence the system has a localized symmetric

eigenstate) for *any* value of the parameter $\kappa_0 a$, i.e. for any distance between the partial wells. In the limit of very close wells (i.e. their strong coupling), $\kappa_0 a \ll 1$, we get $\kappa a \ll 1$, $\tanh(\kappa a/2) \rightarrow 0$, and Eq. (172) yields $\kappa \rightarrow 2\kappa_0$, leading to a four-fold increase of the eigenenergy's magnitude in comparison with that of the single well:

$$E_S \approx 4E_0 \equiv -\frac{m(2w)^2}{2\hbar^2}, \quad \text{for } \kappa_0 a \ll 1. \quad (2.173)$$

The physical meaning of this result is very simple: two very close potential wells act (on the symmetric eigenfunction only!) together, so that their “weights” $w \equiv \int U(x)dx$ just add up.

In the opposite, weak coupling limit, i.e. $\kappa_0 a \gg 1$, Eq. (172) shows that $\kappa a \gg 1$ as well, so that its left-hand side may be approximated as $2(1 - \exp\{-\kappa a\})$, and the equation yields

$$\kappa \approx \kappa_0 (1 + \exp\{-\kappa_0 a\}) \approx \kappa_0. \quad (2.174)$$

In this limit, the eigenfunction is a symmetric superposition of two virtually unperturbed wavefunctions (159) of each partial potential well:

$$\psi_S(x) \approx \frac{1}{\sqrt{2}} [\psi_R(x) + \psi_L(x)], \quad (2.175)$$

and the eigenenergy is also close to the energy E_0 of a partial well, but is slightly lower:

$$E_S \approx E_0 (1 + 2 \exp\{-\kappa_0 a\}) \equiv E_0 - \delta, \quad \text{so that } E_A - E_S = 2\delta, \quad (2.176)$$

where δ is again given by the last of Eqs. (170).

So, the eigenenergy of the symmetric state is always lower than that of the antisymmetric state. The physics of this effect (which remains qualitatively the same in more complex two-component systems, most importantly in diatomic molecules such as H₂) is evident from the sketch of the wavefunctions ψ_A and ψ_S , given by Eqs. (165) and (171), in Fig. 19. In the antisymmetric mode, the wavefunction has to vanish at the center of the system, so that each its half is squeezed to one half of the system's spatial extension. Such a squeeze increases the function's gradient, and hence its kinetic energy (1.27), and hence its total energy. On the contrary, in the symmetric mode, the wavefunction effectively spreads into the counterpart well. As a result, it changes in space slower, and hence its kinetic energy is also lower.

Even more importantly, the symmetric state's energy decreases as the distance a is decreased, corresponding to the effective attraction of the partial wells. This is a good toy model of the strongest (and most important) type of atomic cohesion – the *covalent* (or “chemical”) *bonding*.⁴¹ In the simplest case of the H₂ molecule, each of two electrons of the system, in its ground state,⁴² reduces its kinetic energy by spreading its wavefunction around both hydrogen nuclei (protons), rather than being confined near one of them – as it had to be in a single atom. The resulting bonding is very strong: in chemical units, 429 kJ/mol, i.e. 18.6 eV per molecule. Perhaps counter-intuitively, this quantum-mechanical

⁴¹ Historically, the development of the quantum theory of such bonding in the H₂ molecule (by Walter Heinrich Heitler and Fritz Wolfgang London in 1927) was the breakthrough decisive for the acceptance of the then-emerging quantum mechanics by the community of chemists.

⁴² Due to the opposite spins of these electrons, the Pauli principle allows them to be in the same orbital ground state – see Chapter 8.

covalent bonding is even stronger than the strongest classical (*ionic*) bonding due to electron transfer between atoms, leading to the Coulomb attraction of the resulting ions. (For example, the atomic cohesion in the NaCl molecule is just 3.28 eV.)

Now let us analyze the dynamic properties of our model system (Fig. 19) because such a pair of weakly coupled potential wells is our first example of the very important class of *two-level systems*.⁴³ It is easiest to do in the weak-coupling limit $\kappa_0 a \gg 1$, when the simple results (168)-(170) and (174)-(176) are quantitatively valid. In particular, Eqs. (169) and (175) enable us to represent the quasi-localized states of the particle in each partial well as linear combinations of its two eigenstates:

$$\psi_R(x) = \frac{1}{\sqrt{2}} [\psi_S(x) + \psi_A(x)], \quad \psi_L(x) = \frac{1}{\sqrt{2}} [\psi_S(x) - \psi_A(x)]. \quad (2.177)$$

Let us perform the following thought (“gedanken”) experiment: place a particle, at $t = 0$, into one of these quasi-localized states, say $\psi_R(x)$, and leave the system alone to evolve, so that

$$\Psi(x, 0) = \psi_R(x) = \frac{1}{\sqrt{2}} [\psi_S(x) + \psi_A(x)]. \quad (2.178)$$

According to the general solution (1.69) of the time-independent Schrödinger equation, the time dynamics of this wavefunction may be obtained simply by multiplying each eigenfunction by the corresponding complex-exponential time factor:

$$\Psi(x, t) = \frac{1}{\sqrt{2}} \left[\psi_S(x) \exp\left\{-i \frac{E_S}{\hbar} t\right\} + \psi_A(x) \exp\left\{-i \frac{E_A}{\hbar} t\right\} \right]. \quad (2.179)$$

From here, using Eqs. (170) and (176), and then Eqs. (169) and (175) again, we get

$$\begin{aligned} \Psi(x, t) &= \frac{1}{\sqrt{2}} \left(\psi_S(x) \exp\left\{\frac{i\delta t}{\hbar}\right\} + \psi_A(x) \exp\left\{-\frac{i\delta t}{\hbar}\right\} \right) \exp\left\{-\frac{iE_0 t}{\hbar}\right\} \\ &= \left(\psi_R(x) \cos \frac{\delta t}{\hbar} + i \psi_L(x) \sin \frac{\delta t}{\hbar} \right) \exp\left\{-i \frac{E_0 t}{\hbar}\right\}. \end{aligned} \quad (2.180)$$

This result implies, in particular, that the probabilities W_R and W_L to find the particle, respectively, in the right and left wells change with time as

$$W_R = \cos^2 \frac{\delta t}{\hbar}, \quad W_L = \sin^2 \frac{\delta t}{\hbar},$$

(2.181)

Quantum oscillations

mercifully leaving the total probability constant: $W_R + W_L = 1$. (If our calculation had not passed this sanity check, we would be in big trouble.)

This is the famous effect of *quantum oscillations*⁴⁴ of the particle’s wavefunction between two similar, coupled subsystems, with the frequency

⁴³ As we will see later in Chapter 4, these properties are similar to those of spin-½ particles; hence two-level systems are frequently called the *spin-½-like* systems.

⁴⁴ Sometimes they are called the *Bloch oscillations*, but more commonly the last term is reserved for a related but different effect in spatially-periodic systems – to be discussed in Sec. 8 below.

$$\omega = \frac{2\delta}{\hbar} \equiv \frac{E_A - E_S}{\hbar}. \quad (2.182)$$

In its last form, this result does not depend on the assumption of weak coupling, though the simple form (181) of the oscillations, with its 100% probability variations, does. (Indeed, at a strong coupling of two subsystems, the very notion of the quasi-localized states ψ_R and ψ_L is ambiguous.) Qualitatively, this effect may be interpreted as follows: the particle, placed into one of the potential wells, tries to escape from it via tunneling through the potential barrier separating the wells. (In our particular system, shown in Fig. 17, the barrier is formed by the spatial segment of length a , which has the potential energy, $U = 0$, higher than the eigenstate energy $-E_0$.) However, in the two-well system, the particle can only escape into the adjacent well. After the tunneling into that counterpart well, the particle tries to escape from it, and hence comes back, etc. – very much as a classical 1D oscillator, initially deflected from its equilibrium position, at negligible damping.

Some care is required at using such interpretation for quantitative conclusions. In particular, let us compare the period $\mathcal{T} \equiv 2\pi/\omega$ of the oscillations (181) with the metastable state's lifetime discussed in the previous section. For our particular model, we may use the second of Eqs. (170) to write

$$\omega = \frac{4|E_0|}{\hbar} \exp\{-\kappa_0 a\}, \quad \mathcal{T} = \frac{\pi\hbar}{\delta} = \frac{\pi\hbar}{2|E_0|} \exp\{\kappa_0 a\} \equiv \frac{t_a}{2} \exp\{\kappa_0 a\}, \quad \text{for } \kappa_0 a \gg 1, \quad (2.183)$$

where $t_a \equiv 2\pi/\omega_0 \equiv 2\pi\hbar/|E_0|$ is the effective attempt time. On the other hand, according to Eq. (80), the transparency \mathcal{T} of our potential barrier, in this limit, scales as $\exp\{-2\kappa_0 a\}$,⁴⁵ so that according to the general relation (153), the lifetime τ is of the order of $t_a \exp\{2\kappa_0 a\} \gg \mathcal{T}$. This is a rather counter-intuitive result: the speed of particle tunneling into a similar adjacent well is much higher than that, through a similar barrier, to the free space!

In order to show that this important result is not an artifact of our delta-functional model of the potential barrier, and also compare \mathcal{T} and τ more directly, let us analyze the quantum oscillations between two weakly coupled wells, now assuming that the (symmetric) potential profile $U(x)$ is sufficiently soft (Fig. 21), so that all its eigenfunctions ψ_S and ψ_A are at least differentiable at all points.⁴⁶ If the barrier's transparency is low, the quasi-localized wavefunctions $\psi_R(x)$ and $\psi_L(x) = \psi_R(-x)$ and their eigenenergies may be found approximately by solving the Schrödinger equations in one of the wells, neglecting the tunneling through the barrier, but the calculation of δ requires a little bit more care. Let us write the stationary Schrödinger equations for the symmetric and antisymmetric solutions in the form

$$[E_A - U(x)]\psi_A = -\frac{\hbar^2}{2m} \frac{d^2\psi_A}{dx^2}, \quad [E_S - U(x)]\psi_S = -\frac{\hbar^2}{2m} \frac{d^2\psi_S}{dx^2}, \quad (2.184)$$

⁴⁵ It is hard to use Eq. (80) for a more exact evaluation of \mathcal{T} in our current system, with its infinitely deep potential wells, because the meaning of the wave number k is not quite clear. However, this is not too important, because in the limit $\kappa_0 a \gg 1$, the tunneling exponent makes the dominant contribution into the transparency – see, again, Fig. 2.7b.

⁴⁶ Such a smooth well may have more than one quasi-localized eigenstate, so that the proper state (and energy) index n is implied in all remaining formulas of this section.

multiply the former equation by ψ_S and the latter one by ψ_A , subtract them from each other, and then integrate the result from 0 to ∞ . The result is

$$(E_A - E_S) \int_0^\infty \psi_S \psi_A dx = \frac{\hbar^2}{2m} \int_0^\infty \left(\frac{d^2 \psi_S}{dx^2} \psi_A - \frac{d^2 \psi_A}{dx^2} \psi_S \right) dx. \quad (2.185)$$

If $U(x)$, and hence $d^2 \psi_{A,S}/dx^2$, are finite for all x , we may integrate the right-hand side by parts to get

$$(E_A - E_S) \int_0^\infty \psi_S \psi_A dx = \frac{\hbar^2}{2m} \left(\frac{d\psi_S}{dx} \psi_A - \frac{d\psi_A}{dx} \psi_S \right)_0^\infty. \quad (2.186)$$

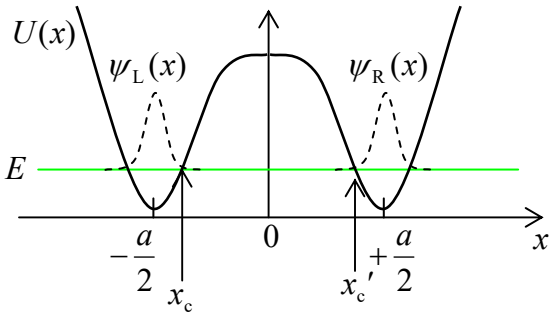


Fig. 2.21. Weak coupling between two similar, soft potential wells.

So far, this result is exact (provided that the derivatives participating in it are finite at each point); for *weakly* coupled wells, it may be further simplified. Indeed, in this case, the left-hand side of Eq. (186) may be approximated as

$$(E_A - E_S) \int_0^\infty \psi_S \psi_A dx \approx \frac{E_A - E_S}{2} \equiv \delta, \quad (2.187)$$

because this integral is dominated by the vicinity of point $x = a/2$, where the second terms in each of Eqs. (169) and (175) are negligible, and the integral is equal to $1/2$, assuming the proper normalization of the function $\psi_R(x)$. On the right-hand side of Eq. (186), the substitution at $x = \infty$ vanishes (due to the wavefunction's decay in the classically forbidden region), and so does the first term at $x = 0$, because for the antisymmetric solution, $\psi_A(0) = 0$. As a result, the energy half-split δ may be expressed in any of the following (equivalent) forms:

$$\delta = \frac{\hbar^2}{2m} \psi_S(0) \frac{d\psi_A}{dx}(0) = \frac{\hbar^2}{m} \psi_R(0) \frac{d\psi_R}{dx}(0) = -\frac{\hbar^2}{m} \psi_L(0) \frac{d\psi_L}{dx}(0). \quad (2.188)$$

It is straightforward (and hence left for the reader's exercise) to show that within the limits of the WKB approximation's validity, Eq. (188) may be reduced to

$$\delta = \frac{\hbar}{t_a} \exp \left\{ - \int_{x_c}^{x_c'} \kappa(x') dx' \right\}, \quad \text{so that } \tau \equiv \frac{\pi \hbar}{\delta} = \frac{t_a}{2} \exp \left\{ \int_{x_c}^{x_c'} \kappa(x') dx' \right\}, \quad (2.189)$$

where t_a is the time period of the classical motion of the particle, with the energy $E \approx E_A \approx E_S$, inside each well, the function $\kappa(x)$ is defined by Eq. (82), and x_c and x_c' are the classical turning points limiting the potential barrier at the level E of the particle's eigenenergy – see Fig. 21. The result (189) is evidently a natural generalization of Eq. (183), so that the strong relationship between the times of

particle tunneling into the continuum of states and into a discrete eigenstate, is indeed not specific for the delta-functional model. We will return to this fact, in its more general form, at the end of Chapter 6.

2.7. Periodic systems: Energy bands and gaps

Let us now proceed to the discussion of one of the most important issues of wave mechanics: particle motion through a periodic system. As a precursor to this discussion, let us calculate the transparency of the potential profile shown in Fig. 22 (frequently called the *Dirac comb*): a sequence of N similar, equidistant delta-functional potential barriers, separated by $(N - 1)$ potential-free intervals a .

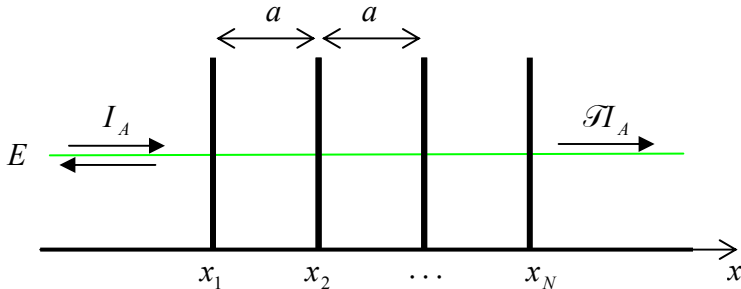


Fig. 2.22. Tunneling through a Dirac comb: a system of N similar, equidistant barriers, i.e. $(N - 1)$ similar coupled potential wells.

According to Eq. (132), its transfer matrix is the following product

$$T = \underbrace{T_\alpha T_a T_\alpha \dots T_a T_\alpha}_{(N-1)+N \text{ terms}}, \quad (2.190)$$

with the component matrices given by Eqs. (135) and (138), and the barrier height parameter α defined by the last of Eqs. (78). Remarkably, this multiplication may be carried out analytically,⁴⁷ giving

$$\mathcal{T} \equiv |T_{11}|^{-2} = \left[(\cos Nqa)^2 + \left(\frac{\sin ka - \alpha \cos ka}{\sin qa} \sin Nqa \right)^2 \right]^{-1}, \quad (2.191a)$$

where q is a new parameter, with the wave number dimensionality, defined by the following relation:

$$\cos qa \equiv \cos ka + \alpha \sin ka. \quad (2.191b)$$

For $N = 1$, Eqs. (191) immediately yield our old result (79), while for $N = 2$ they may be readily reduced to Eq. (141) – see Fig. 16a. Fig. 20 shows its predictions for two larger numbers N , and several values of the dimensionless parameter α .

Let us start the discussion of the plots from the case $N = 3$, when three barriers limit two coupled potential wells between them. Comparison of Fig. 23a and Fig. 16a shows that the transmission patterns, and their dependence on the parameter α , are very similar, besides that in the coupled-well system, each resonant tunneling peak splits into two, with the ka -difference between them scaling as $1/\alpha$. From the discussion in the last section, we may now readily interpret this result: each pair of resonance peaks of transparency corresponds to the alignment of the incident particle's energy E with the pair of energy levels E_A, E_S of the symmetric and antisymmetric states of the system. However, in contrast to the

⁴⁷ This formula will be easier to prove after we have discussed the properties of Pauli matrices in Chapter 4.

system shown in Fig. 19, these states are metastable, because the particle may leak out from these states just as it could in the system studied in Sec. 5 – see Fig. 15 and its discussion. As a result, each of the resonant peaks has a non-zero energy width ΔE , obeying Eq. (155).

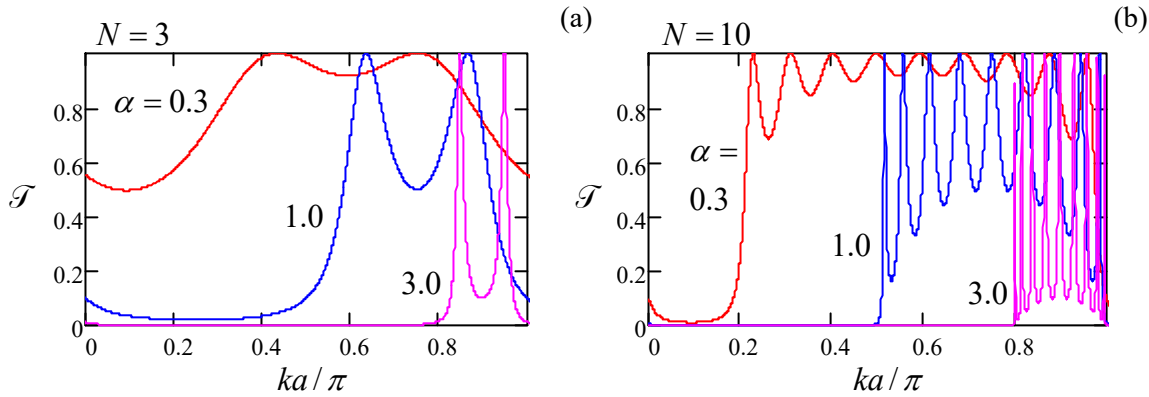


Fig. 2.23. The Dirac comb's transparency as a function of the product ka for three values of α . Since the function $\mathcal{T}(ka)$ is π -periodic (just like it is for $N = 2$, see Fig. 16a), only one period is shown.

A further increase of N (see Fig. 23b) results in the increase of the number of resonant peaks per period to $(N - 1)$, and at $N \rightarrow \infty$ the peaks merge into the so-called *allowed energy bands* (frequently called just the “energy bands”) with average transparency $\mathcal{T} \sim 1$, separated from similar bands in the adjacent periods of function $\mathcal{T}(ka)$ by *energy gaps*⁴⁸ where $\mathcal{T} \rightarrow 0$. Notice the following important features of the pattern:

- (i) at $N \rightarrow \infty$, the band/gap edges become sharp for any α , and tend to fixed positions (determined by α but independent of N);
- (ii) the larger is well coupling (the smaller is α), the broader are the allowed energy bands and the narrower are the gaps between them.

Our previous discussion of the resonant tunneling gives us a clue for a semi-quantitative interpretation of this pattern: if $(N - 1)$ potential wells are weakly coupled by tunneling through the potential barriers separating them, the system's energy spectrum consists of groups of $(N - 1)$ metastable energy levels, each group being close to one of the unperturbed eigenenergies of the well. (According to Eq. (1.84), for our current example shown in Fig. 22, with its rectangular potential wells, these eigenenergies correspond to $k_n a = \pi n$.)

Now let us recall that in the case $N = 2$, analyzed in the previous section, the eigenfunctions (169) and (175) differed only by the phase shift $\Delta\varphi$ between their localized components $\psi_R(x)$ and $\psi_L(x)$, with $\Delta\varphi = 0$ for one of them (ψ_S) and $\Delta\varphi = \pi$ for its counterpart. Hence it is natural to expect that for other N as well, each metastable energy level corresponds to an eigenfunction that is a superposition of similar localized functions in each potential well, but with certain phase shifts $\Delta\varphi$ between them.

Moreover, we may expect that at $N \rightarrow \infty$, i.e. for *periodic structures*,⁴⁹ with

⁴⁸ In solid-state (especially semiconductor) physics and electronics, the term *bandgaps* is more common.

⁴⁹ This is a reasonable 1D model, for example, for solid-state crystals, whose samples may feature up to $\sim 10^9$ similar atoms or molecules in each direction of the crystal lattice.

$$U(x+a) = U(x), \quad (2.192)$$

when the system does not have the ends that could affect its properties, the phase shifts $\Delta\varphi$ between the localized wavefunctions in all couples of adjacent potential wells should be equal, i.e.

$$\psi(x+a) = \psi(x)e^{i\Delta\varphi} \quad (2.193a)$$

for all x .⁵⁰ This equality is the (1D version of the) much-celebrated *Bloch theorem*.⁵¹ Mathematical rigor aside,⁵² it is a virtually evident fact because the particle's density $w(x) = \psi^*(x)\psi(x)$, which has to be periodic in this a -periodic system, may be so only if $\Delta\varphi$ is constant. For what follows, it is more convenient to represent the real constant $\Delta\varphi$ in the form qa , so that the Bloch theorem takes the form

Bloch
theorem:
1D version

$$\psi(x+a) = \psi(x)e^{iqa}. \quad (2.193b)$$

The physical sense of the parameter q will be discussed in detail below, but we may immediately notice that according to Eq. (193b), an addition of $(2\pi/a)$ to this parameter yields the same wavefunction; hence all observables have to be $(2\pi/a)$ -periodic functions of q .⁵³

Now let us use the Bloch theorem to calculate the eigenfunctions and eigenenergies for the infinite version of the system shown in Fig. 22, i.e. for an infinite set of delta-functional potential barriers – see Fig. 24.

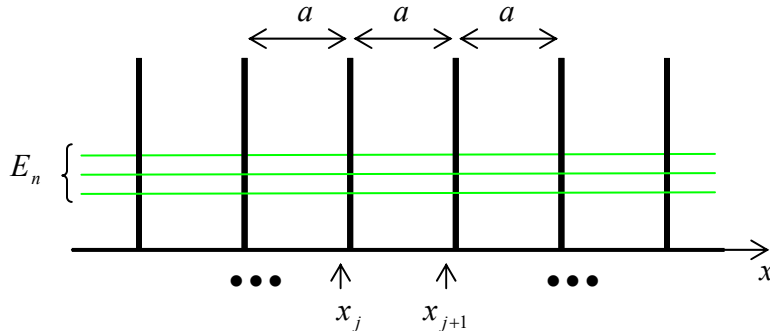


Fig. 2.24. The simplest periodic potential: an infinite Dirac comb.

To start, let us consider two points separated by one period a : one of them, x_j , just left of the position of one of the barriers, and another one, x_{j+1} , just left of the following barrier – see Fig. 24 again.

⁵⁰ A reasonably fair classical image of $\Delta\varphi$ is the geometric angle between similar objects – e.g., similar paper clips – attached at equal distances to a long, uniform rubber band. If the band's ends are twisted, the twist is equally distributed between the structure's periods, representing the constancy of $\Delta\varphi$. (I have to confess that, due to the lack of time, this was the only “lecture demonstration” in my Stony Brook QM courses.)

⁵¹ Named after F. Bloch who applied this concept to the wave mechanics in 1929, i.e. very soon after its formulation. Note, however, that an equivalent statement in mathematics, called the *Floquet theorem*, has been known since at least 1883.

⁵² I will recover this rigor in two steps. Later in this section, we will see that the function obeying Eq. (193) is indeed a solution to the Schrödinger equation. However, to save time/space, it will be better for us to postpone until Chapter 4 the proof that *any* eigenfunction of the equation, with periodic boundary conditions, obeys the Bloch theorem. As a partial reward for this delay, that proof will be valid for an arbitrary spatial dimensionality.

⁵³ The product $\hbar q$, which has the dimensionality of linear momentum, is called either the *quasimomentum* or (especially in solid-state physics) the “crystal momentum” of the particle. Informally, it is very convenient (and common) to use the name “quasimomentum” for the bare q as well, despite its evidently different dimensionality.

The eigenfunctions at each of the points may be represented as linear superpositions of two simple waves $\exp\{\pm ikx\}$, and the amplitudes of their components should be related by a 2×2 transfer matrix T of the potential fragment separating them. According to Eq. (132), this matrix may be found as the product of the matrix (135) of one delta-functional barrier by the matrix (138) of one zero-potential interval a :

$$\begin{pmatrix} A_{j+1} \\ B_{j+1} \end{pmatrix} = T_a T_\alpha \begin{pmatrix} A_j \\ B_j \end{pmatrix} = \begin{pmatrix} e^{ika} & 0 \\ 0 & e^{-ika} \end{pmatrix} \begin{pmatrix} 1-i\alpha & -i\alpha \\ i\alpha & 1+i\alpha \end{pmatrix} \begin{pmatrix} A_j \\ B_j \end{pmatrix}. \quad (2.194)$$

However, according to the Bloch theorem (193b), the component amplitudes should be also related as

$$\begin{pmatrix} A_{j+1} \\ B_{j+1} \end{pmatrix} = e^{iqa} \begin{pmatrix} A_j \\ B_j \end{pmatrix} \equiv \begin{pmatrix} e^{iqa} & 0 \\ 0 & e^{iqa} \end{pmatrix} \begin{pmatrix} A_j \\ B_j \end{pmatrix}. \quad (2.195)$$

The condition of self-consistency of these two equations gives the following characteristic equation:

$$\left| \begin{pmatrix} e^{ika} & 0 \\ 0 & e^{-ika} \end{pmatrix} \begin{pmatrix} 1-i\alpha & -i\alpha \\ i\alpha & 1+i\alpha \end{pmatrix} - \begin{pmatrix} e^{iqa} & 0 \\ 0 & e^{iqa} \end{pmatrix} \right| = 0. \quad (2.196)$$

In Sec. 5, we have already calculated the matrix product participating in this equation – see the second operand in Eq. (140). Using it, we see that Eq. (196) is reduced to the same simple Eq. (191b) that has jumped at us from the solution of the somewhat different (resonant tunneling) problem. Let us explore that simple result in detail. First of all, the left-hand side of Eq. (191b) is a sinusoidal function of the product qa with unit amplitude, while its right-hand side is a sinusoidal function of the product ka , with amplitude $(1 + \alpha^2)^{1/2} > 1$ – see Fig. 25,

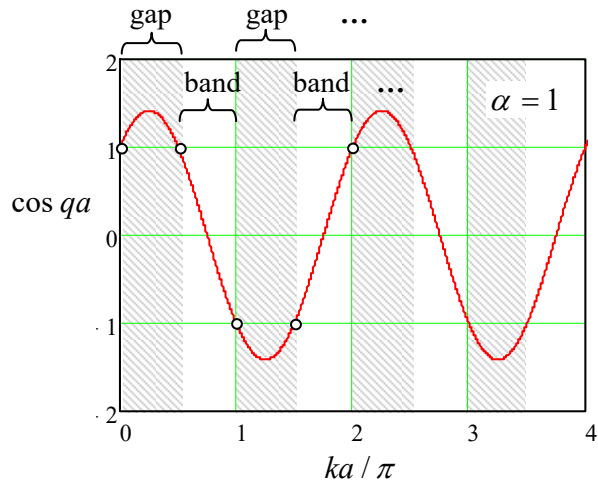


Fig. 2.25. The graphical representation of the characteristic equation (191b) for a fixed value of the parameter α . The ranges of ka that yield $|\cos qa| < 1$, correspond to allowed energy bands, while those with $|\cos qa| > 1$, correspond to energy gaps between them.

As a result, within each half-period $\Delta(ka) = \pi$ of the right-hand side, there is an interval where the magnitude of the right-hand side is larger than 1, so that the characteristic equation does not have a real solution for q . These intervals correspond to the energy gaps (see Fig. 23 again), while the complementary intervals of ka , where a real solution for q exists, correspond to the allowed energy bands. In contrast, the parameter q can take *any* real values, so it is more convenient to plot the eigenenergy $E = \hbar^2 k^2 / 2m$ as the function of the quasimomentum $\hbar q$ (or, even more conveniently, of the

dimensionless parameter qa) rather than ka .⁵⁴ Before doing that, we need to recall that the parameter α , defined by the last of Eqs. (78), depends on the wave vector k as well, so that if we vary q (and hence k), it is better to characterize the structure by another, k -independent dimensionless parameter, for example

$$\beta \equiv (ka)\alpha \equiv \frac{w}{\hbar^2 / ma}, \quad (2.197)$$

so that our characteristic equation (191b) becomes

Dirac comb:
 q vs k

$$\cos qa \equiv \cos ka + \beta \frac{\sin ka}{ka}. \quad (2.198)$$

Fig. 26 shows the plots of k and E , following from Eq. (198), as functions of qa , for a particular, moderate value of the parameter β . The first evident feature of the pattern is the 2π -periodicity of the pattern in the argument qa , which we have already predicted from the general Bloch theorem arguments. (Due to this periodicity, the complete band/gap pattern may be studied, for example, on just one interval $-\pi \leq qa \leq +\pi$, called the *1st Brillouin zone* – the so-called *reduced zone picture*. For some applications, however, it is more convenient to use the *extended zone picture* with $-\infty \leq qa \leq +\infty$ – see, e.g., the next section.)

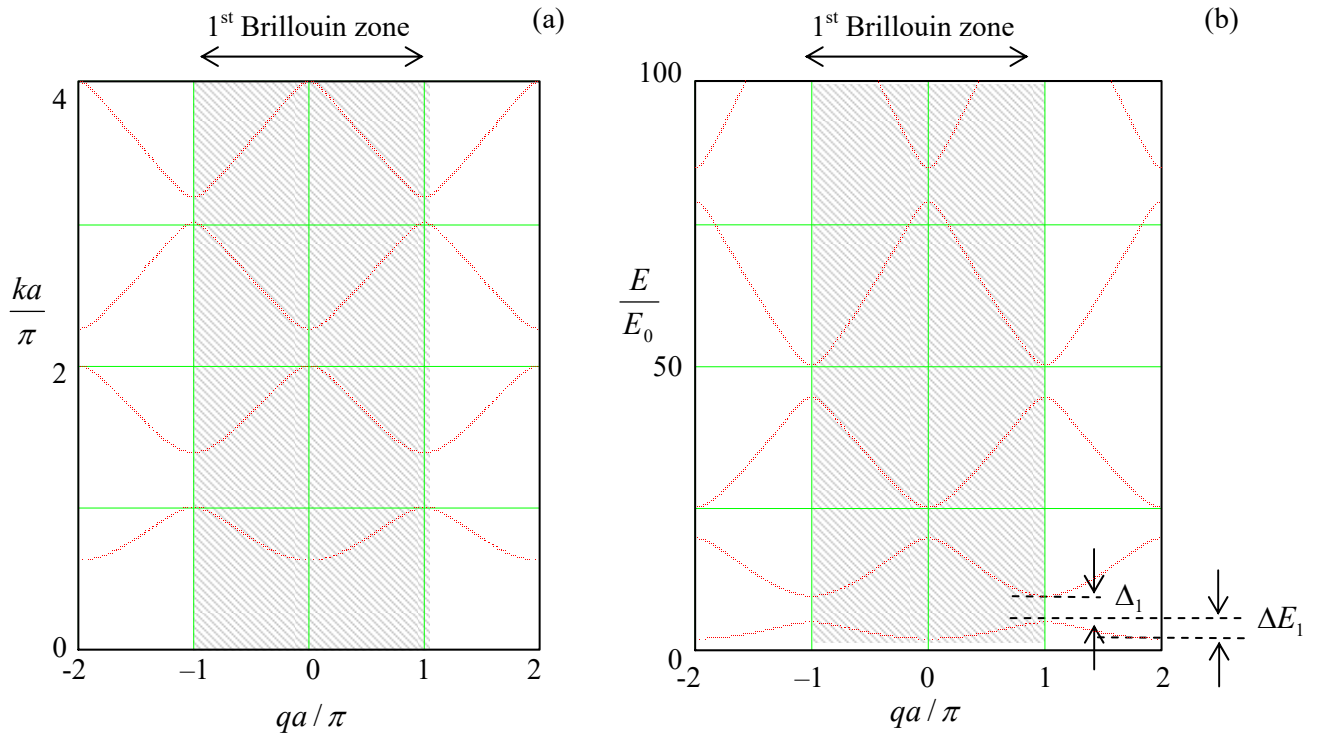


Fig. 2.26. (a) The “genuine” momentum k of a particle in an infinite Dirac comb (Fig. 24), and (b) its energy $E = \hbar^2 k^2 / 2m$ (in the units of $E_0 \equiv \hbar^2 / 2ma^2$), as functions of normalized quasimomentum, for a particular value ($\beta = 3$) of the dimensionless parameter defined by Eq. (197). Arrows in the lower right corner of panel (b) illustrate the definition of energy band (ΔE_n) and energy gap (Δ_n) widths.

⁵⁴ A more important reason for taking q as the argument is that for a general periodic potential $U(x)$, the particle’s momentum $\hbar k$ is not uniquely related to E , while (according to the Bloch theorem) the quasimomentum $\hbar q$ is.

However, maybe the most important fact, clearly visible in Fig. 26, is that there is an infinite number of energy bands, with different energies $E_n(q)$ for the same value of q . Mathematically, it is evident from Eq. (198) – or alternatively from Fig. 25. Indeed, for each value of qa , there is a solution ka to this equation on each half-period $\Delta(ka) = \pi$. Each of such solutions (see Fig. 26a) gives a specific value of particle's energy $E = \hbar^2 k^2 / 2m$. A continuous set of similar solutions for various qa forms a particular energy band.

Since the energy band picture is one of the most practically important results of quantum mechanics, it is imperative to understand its physics. It is natural to describe this physics in two different ways in two opposite potential strength limits. In parallel, we will use this discussion to obtain simpler expressions for the energy band/gap structure in each limit. An important advantage of this approach is that both analyses may be carried out for an arbitrary periodic potential $U(x)$ rather than for the particular model shown in Fig. 24.

(i) Tight-binding approximation. This approximation works well when the eigenenergy E_n of the states quasi-localized at the energy profile minima is much lower than the height of the potential barriers separating them – see Fig. 27. As should be clear from our discussion in Sec. 6, essentially the only role of coupling between these states (via tunneling through the potential barriers separating the minima) is to establish a certain phase shift $\Delta\varphi \equiv qa$ between the adjacent quasi-localized wavefunctions $u_n(x - x_j)$ and $u_n(x - x_{j+1})$.

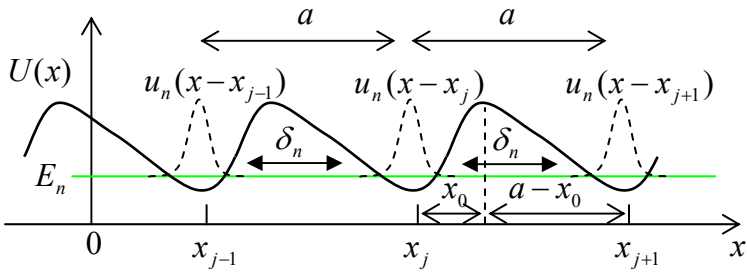


Fig. 2.27. The tight-binding approximation (schematically).

To describe this effect quantitatively, let us first return to the problem of two coupled wells considered in Sec. 6, and recast the result (180), with restored eigenstate index n , as

$$\Psi_n(x, t) = [a_R(t)\psi_R(x) + a_L(t)\psi_L(x)]\exp\left\{-i\frac{E_n}{\hbar}t\right\}, \quad (2.199)$$

where the probability amplitudes a_R and a_L oscillate sinusoidally in time:

$$a_R(t) = \cos\frac{\delta_n}{\hbar}t, \quad a_L(t) = i\sin\frac{\delta_n}{\hbar}t. \quad (2.200)$$

This evolution satisfies the following system of two equations whose structure is similar to Eq. (1.61a):

$$i\hbar\dot{a}_R = -\delta_n a_L, \quad i\hbar\dot{a}_L = -\delta_n a_R. \quad (2.201)$$

Eq. (199) may be readily generalized to the case of many similar coupled wells:

$$\Psi_n(x, t) = \left[\sum_j a_j(t)u_n(x - x_j) \right] \exp\left\{-i\frac{E_n}{\hbar}t\right\}, \quad (2.202)$$

where E_n are the eigenenergies and u_n the eigenfunctions of each well. In the tight-binding limit, only the adjacent wells are coupled, so that instead of Eq. (201) we should write an infinite system of similar equations

$$i\hbar \dot{a}_j = -\delta_n a_{j-1} - \delta_n a_{j+1}, \quad (2.203)$$

for each well number j , where parameters δ_n describe the coupling between two adjacent potential wells. Repeating the calculation outlined at the end of the last section for our new situation, for a smooth potential we may get an expression essentially similar to the last form of Eq. (188):

Tight-binding limit:
coupling energy

$$\delta_n = \frac{\hbar^2}{m} u_n(x_0) \frac{du_n}{dx}(a - x_0), \quad (2.204)$$

where x_0 is the distance between the well bottom and the middle of the potential barrier on the right of it – see Fig. 27. The only substantial new feature of this expression in comparison with Eq. (188) is that the sign of δ_n alternates with the level number n : $\delta_1 > 0$, $\delta_2 < 0$, $\delta_3 > 0$, etc. Indeed, the number of zeros (and hence, “wiggles”) of the eigenfunctions $u_n(x)$ of any potential well increases as n – see, e.g., Fig. 1.8,⁵⁵ so that the difference of the exponential tails of the functions, sneaking under the left and right barriers limiting the well also alternates with n .

The infinite system of ordinary differential equations (203) enables solutions of many important problems (such as the spread of the wavefunction that was initially localized in one well, etc.), but our task right now is just to find its stationary states, i.e. the solutions proportional to $\exp\{-i(\varepsilon_n/\hbar)t\}$, where ε_n is a still unknown, q -dependent addition to the background energy E_n of the n^{th} energy level. To satisfy the Bloch theorem (193) as well, such a solution should have the following form:

$$a_j(t) = a \exp\left\{iqx_j - i\frac{\varepsilon_n}{\hbar}t + \text{const}\right\}. \quad (2.205)$$

Plugging this solution into Eq. (203) and canceling the common exponent, we get

Tight-binding limit:
energy bands

$$E = E_n + \varepsilon_n = E_n - \delta_n (e^{-iqa} + e^{iqa}) \equiv E_n - 2\delta_n \cos qa, \quad (2.206)$$

so that in this approximation, the energy band width ΔE_n (see Fig. 26b) equals $4|\delta_n|$.

The relation (206), whose validity is restricted to $|\delta_n| \ll E_n$, describes the lowest energy bands plotted in Fig. 26b reasonably well. (For larger β , the agreement would be even better.) So, this calculation explains what the energy bands really are: in the tight-binding limit they are best interpreted as isolated well’s energy levels E_n , broadened into bands by the interwell interaction. Also, this result gives clear proof that the energy band extremes correspond to $qa = 2\pi l$ and $qa = 2\pi(l + \frac{1}{2})$, with integer l . Finally, the sign alteration of the coupling coefficient δ_n (204) explains why the energy maxima of one band are aligned, on the qa axis, with energy minima of the adjacent bands – see Fig. 26.

(ii) *Weak-potential limit*. Amazingly, the energy-band structure is also compatible with a completely different physical picture that may be developed in the opposite limit. Let the particle’s energy E be so high that the periodic potential $U(x)$ may be treated as a small perturbation. Naively, in

⁵⁵ Below, we will see several other examples of this behavior. This alternation rule is also described by the Wilson-Sommerfeld quantization condition (110).

this limit we could expect a slightly and smoothly deformed parabolic dispersion relation $E = \hbar^2 k^2 / 2m$. However, if we are plotting the stationary-state energy as a function of q rather than k , we need to add $2\pi l/a$, with an arbitrary integer l , to the argument. Let us show this by expanding all variables into the 1D-spatial Fourier series. For the potential energy $U(x)$ that obeys Eq. (192), such an expansion is straightforward:⁵⁶

$$U(x) = \sum_{l''} U_{l''} \exp\left\{-i \frac{2\pi x}{a} l''\right\}, \quad (2.207)$$

where the summation is over all integers l'' , from $-\infty$ to $+\infty$. However, for the wavefunction we should show due respect to the Bloch theorem (193), which shows that strictly speaking, $\psi(x)$ is *not* periodic.

To overcome this difficulty, let us define another function:

$$u(x) \equiv \psi(x) e^{-iqx}, \quad (2.208)$$

and study its periodicity:

$$u(x+a) = \psi(x+a) e^{-iq(x+a)} = \psi(x) e^{-iqx} = u(x). \quad (2.209)$$

We see that the new function is a -periodic, and hence we can use Eqs. (208)-(209) to rewrite the Bloch theorem in a different form:

$$\psi(x) = u(x) e^{iqx}, \quad \text{with } u(x+a) = u(x). \quad (2.210)$$

1D Bloch theorem:
alternative form

Now it is safe to expand the periodic function $u(x)$ exactly as $U(x)$:

$$u(x) = \sum_{l'} u_{l'} \exp\left\{-i \frac{2\pi x}{a} l'\right\}, \quad (2.211)$$

so that, according to Eq. (210),

$$\psi(x) = e^{iqx} \sum_{l'} u_{l'} \exp\left\{-i \frac{2\pi x}{a} l'\right\} = \sum_{l'} u_{l'} \exp\left\{i\left(q - \frac{2\pi}{a} l'\right)x\right\}. \quad (2.212)$$

The only nontrivial part of plugging Eqs. (207) and (212) into the stationary Schrödinger equation (53) is how to handle the product term,

$$U(x)\psi = \sum_{l', l''} U_{l''} u_{l'} \exp\left\{i\left[q - \frac{2\pi}{a}(l' + l'')\right]x\right\}. \quad (2.213)$$

At fixed l' , we may change the summation over l'' to that over $l \equiv l' + l''$ (so that $l'' \equiv l - l'$), and write:

$$U(x)\psi = \sum_l \exp\left\{i\left(q - \frac{2\pi}{a} l\right)x\right\} \sum_{l'} u_{l'} U_{l-l'}. \quad (2.214)$$

Now plugging Eq. (212) (with the summation index l' replaced with l) and Eq. (214) into the stationary Schrödinger equation (53), and requiring the coefficients of each spatial exponent to match, we get an infinite system of linear equations for u_l :

⁵⁶ The benefits of such an unusual notation of the summation index (l'' instead of, say, l) will be clear in a few lines.

$$\sum_l U_{l-l'} u_{l'} = \left[E - \frac{\hbar^2}{2m} \left(q - \frac{2\pi}{a} l \right)^2 \right] u_l. \quad (2.215)$$

(Note that by this calculation we have essentially proved that the Bloch wavefunction (210) is indeed a solution of the Schrödinger equation, provided that the quasimomentum q is selected in a way to make the system of linear equation (215) compatible, i.e. is a solution of its characteristic equation.)

So far, the system of equations (215) is an equivalent alternative to the initial Schrödinger equation, for any potential's strength.⁵⁷ In the weak-potential limit, i.e. if all Fourier coefficients U_n are small,⁵⁸ we can complete all the calculations analytically.⁵⁹ Indeed, in the so-called 0th approximation we can ignore *all* U_n , so that in order to have at least one u_l different from 0, Eq. (215) requires that

$$E \rightarrow E_l \equiv \frac{\hbar^2}{2m} \left(q - \frac{2\pi l}{a} \right)^2. \quad (2.216)$$

(u_l itself should be obtained from the normalization condition). This result means that in this approximation, the dispersion relation $E(q)$ has an infinite number of similar quadratic branches numbered by integer l – see Fig. 28.

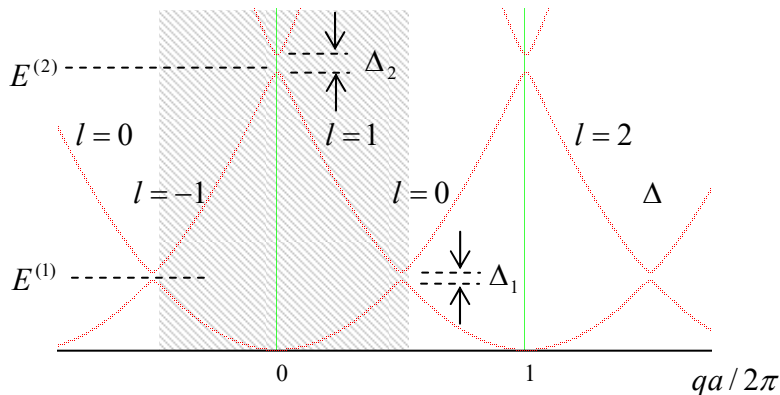


Fig. 2.28. The energy band/gap picture in the weak potential limit ($\Delta_n \ll E^{(n)}$), with the shading showing the 1st Brillouin zone.

On every branch, such eigenfunction has just one Fourier coefficient, i.e. is a monochromatic traveling wave

$$\psi_l \rightarrow u_l e^{ikx} = u_l \exp \left\{ i \left(q - \frac{2\pi l}{a} \right) x \right\}. \quad (2.217)$$

Next, the above definition of E_l allows us to rewrite Eq. (215) in a more transparent form

⁵⁷ By the way, the system is very efficient for fast numerical solution of the stationary Schrödinger equation for any periodic profile $U(x)$, even though to describe potentials with large U_n , this approach may require taking into account a correspondingly large number of Fourier amplitudes u_l .

⁵⁸ Besides, possibly, a constant potential U_0 , which, as was discussed in Chapter 1, may be always taken for the energy reference. As a result, in the following calculations, I will take $U_0 = 0$ to simplify the formulas.

⁵⁹ This method is so powerful that its multi-dimensional version is not much more complex than the 1D version described here – see, e.g., Sec. 3.2 in the classical textbook by J. Ziman, *Principles of the Theory of Solids*, 2nd ed., Cambridge U. Press, 1979.

$$\sum_{l' \neq l} U_{l-l'} u_{l'} = (E - E_l) u_l, \quad (2.218)$$

which may be formally solved for u_l :

$$u_l = \frac{1}{E - E_l} \sum_{l' \neq l} U_{l-l'} u_{l'}. \quad (2.219)$$

This formula shows that if the Fourier coefficients U_n are non-zero but small, the wavefunctions do acquire other Fourier components (besides the main one, with the index corresponding to the branch number), but these additions are all small, besides narrow regions near the points $E_l = E_{l'}$ where two branches (216) of the dispersion relation $E(q)$, with some specific numbers l and l' , cross. According to Eq. (216), this happens when

$$\left(q - \frac{2\pi}{a} l \right) \approx - \left(q - \frac{2\pi}{a} l' \right), \quad (2.220)$$

i.e. at $q \approx q_m \equiv \pi m/a$ (with the integer $m \equiv l + l'$)⁶⁰ corresponding to

$$E_l \approx E_{l'} \approx \frac{\hbar^2}{2ma^2} [\pi(l+l') - 2\pi l]^2 = \frac{\pi^2 \hbar^2}{2ma^2} n^2 \equiv E^{(n)}, \quad (2.221)$$

Weak-potential limit:
energy gap positions

with integer $n \equiv l - l'$. (According to their definitions, the index n is just the number of the branch crossing on the energy scale, while the index m numbers the position of the crossing points on the q -axis – see Fig. 28.) In such a region, E has to be close to both E_l and $E_{l'}$, so that the denominator in just one of the infinite number of terms in Eq. (219) is very small, making the term substantial despite the smallness of U_n . Hence we can take into account only one term in each of the sums (written for l and l'):

$$\begin{aligned} U_n u_{l'} &= (E - E_l) u_l, \\ U_{-n} u_l &= (E - E_{l'}) u_{l'}. \end{aligned} \quad (2.222)$$

Taking into account that for any real function $U(x)$, the Fourier coefficients in its Fourier expansion (207) have to be related as $U_{-n} = U_n^*$, Eq. (222) yields the following simple characteristic equation

$$\begin{vmatrix} E - E_l & -U_n \\ -U_n^* & E - E_{l'} \end{vmatrix} = 0, \quad (2.223)$$

with the following solution:

$$E_{\pm} = E_{\text{ave}} \pm \left[\left(\frac{E_l - E_{l'}}{2} \right)^2 + U_n U_n^* \right]^{1/2}, \quad \text{with } E_{\text{ave}} \equiv \frac{E_l + E_{l'}}{2} = E^{(n)}. \quad (2.224)$$

Weak-potential limit:
level anticrossing

According to Eq. (216), close to the branch crossing point $q_m = \pi(l + l')/a$, the fraction participating in this result may be approximated as⁶¹

$$\frac{E_l - E_{l'}}{2} \approx \gamma \tilde{q}, \quad \text{with } \gamma \equiv \frac{dE_l}{dq} \Big|_{q=q_m} = \frac{\pi \hbar^2 n}{ma} = \frac{2aE^{(n)}}{\pi n}, \quad \text{and } \tilde{q} \equiv q - q_m, \quad (2.225)$$

⁶⁰ Let me hope that the difference between this new integer and the particle's mass, both called m , is absolutely clear from the context.

⁶¹ Physically, $\gamma \hbar \equiv \hbar(\pi n/a)/m = \hbar k^{(n)}/m$ is just the velocity of a free classical particle with energy $E^{(n)}$.

while the parameters $E_{\text{ave}} = E^{(n)}$ and $U_n U_n^* = |U_n|^2$ do not depend on \tilde{q} , i.e. on the distance from the central point q_m . This is why Eq. (224) may be plotted as the famous *level anticrossing* (also called “avoided crossing”, or “intended crossing”, or “non-crossing”) *diagram* (Fig. 29), with the energy gap width Δ_n equal to $2|U_n|$, i.e. just twice the magnitude of the n -th Fourier harmonic of the periodic potential $U(x)$. Such anticrossings are also clearly visible in Fig. 28, which shows the result of the exact solution of Eq. (198) for the particular case $\beta = 0.5$.⁶²

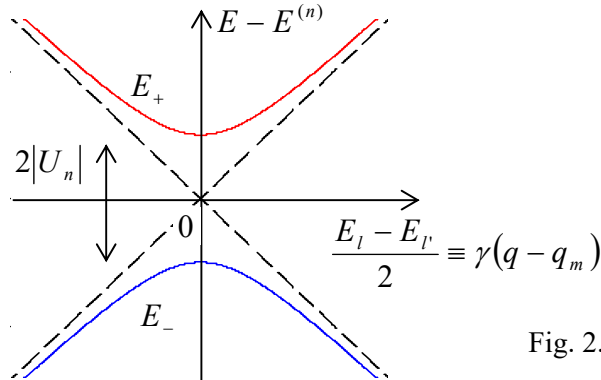


Fig. 2.29. The level anticrossing diagram.

We will run into the anticrossing diagram again and again in the course, notably at the discussion of spin- $\frac{1}{2}$ and other two-level systems. It is also repeatedly met in classical mechanics, for example at the calculation of frequencies of coupled oscillators.^{63,64} In our current case of the weak potential limit of the band theory, the diagram describes the interaction of two traveling de Broglie waves (217), with oppositely directed wave vectors, l and $-l'$, via the $(l - l')$ th (i.e. the n th) Fourier harmonic of the potential profile $U(x)$.⁶⁵ This effect exists also in the classical wave theory and is known as the *Bragg reflection*, describing, for example, the 1D model of the X-wave reflection by a crystal lattice (see, e.g. Fig. 1.5) in the limit of weak interaction between the incident wave and each atom.

The anticrossing diagram shows that rather counter-intuitively, even a weak periodic potential changes the topology of the initially parabolic dispersion relation radically, connecting its different branches, and thus creating the energy gaps. Let me hope that the reader has enjoyed the elegant description of this effect, discussed above, as well as one more illustration of the wonderful ability of physics to give completely different interpretations (and different approximate approaches) to the same effect in opposite limits.

So, we have explained analytically (though only in two limits) the particular band structure shown in Fig. 26. Now we may wonder how general this structure is, i.e. how much of it is independent of the Dirac comb model (Fig. 24). For that, let us represent the band pattern, such as that shown in Fig.

⁶² From that figure, it is also clear that in the weak potential limit, the width ΔE_n of the n th energy band is just $E^{(n)} - E^{(n-1)}$ – see Eq. (221). Note that this is exactly the distance between the adjacent energy levels of the simplest 1D potential well of infinite depth – cf. Eq. (1.85).

⁶³ See, e.g., CM Sec. 6.1 and in particular Fig. 6.2.

⁶⁴ Actually, we could readily obtain this diagram in the previous section, for the system of two weakly coupled potential wells (Fig. 21), if we assumed the wells to be slightly dissimilar.

⁶⁵ In the language of the de Broglie wave scattering, to be discussed in Sec. 3.3, Eq. (220) may be interpreted as the condition that each of these waves, scattered on the n th Fourier harmonic of the potential profile, constructively interferes with its counterpart, leading to a strong enhancement of their interaction.

26b (plotted for a particular value of the parameter β , characterizing the potential barrier strength) in a more condensed form, which would allow us to place the results for a range of β values on a single comprehensible plot. The way to do this should be clear from Fig. 26b: since the dependence of energy on the quasimomentum in each energy band is not too eventful, we may plot just the highest and the smallest values of the particle's energy $E = \hbar^2 k^2 / 2m$ as functions of $\beta \equiv ma\omega/\hbar^2$ – see Fig. 30, which may be obtained from Eq. (198) with $qa = 0$ and $qa = \pi$.

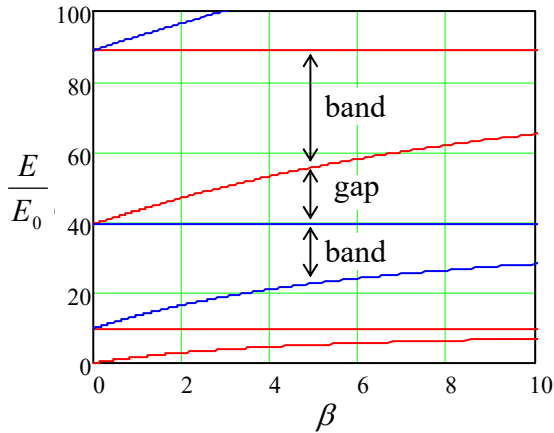


Fig. 2.30. Characteristic curves of the Schrödinger equation for the infinite Dirac comb (Fig. 24).

These plots (in mathematics, commonly called *characteristic curves*, while in applied physics, *band-edge diagrams*) show, first of all, that at small β , all energy gap widths are equal and proportional to this parameter, and hence to ω . This feature is in a full agreement with the main conclusion (224) of our general analysis of the weak-potential limit, because for the Dirac comb potential (Fig. 24),

$$U(x) = \omega \sum_{j=-\infty}^{+\infty} \delta(x - ja + \text{const}), \quad (2.226)$$

all Fourier harmonic amplitudes, defined by Eq. (207), are equal by magnitude: $|U_l| = \omega/a$. As β is further increased, the gaps grow and the allowed energy bands shrink, but rather slowly. This is also natural, because, as Eq. (79) shows, transparency \mathcal{T} of the delta-functional barriers separating the quasi-localized states (and hence the coupling parameters $\delta_n \propto \mathcal{T}^{1/2}$ participating in the general tight-binding limit's theory) decrease with $\omega \propto \beta$ very gradually.

These features may be compared with those for more realistic and relatively simple periodic functions $U(x)$, for example the sinusoidal potential $U(x) = A \cos(2\pi x/a)$ – see Fig. 31a. For this potential, the stationary Schrödinger equation (53) takes the following form:

$$-\frac{\hbar^2}{2m} \frac{d^2\psi}{dx^2} + A \cos \frac{2\pi x}{a} \psi = E \psi. \quad (2.227)$$

By introduction of dimensionless variables⁶⁶

$$\xi \equiv \frac{\pi x}{a}, \quad \alpha \equiv \frac{E}{E^{(1)}}, \quad 2\beta \equiv \frac{A}{E^{(1)}}, \quad (2.228)$$

⁶⁶ Note that this definition of β is quantitatively different from that for the Dirac comb (226), but in both cases, this parameter is proportional to the amplitude of the potential modulation.

where $E^{(1)}$ is defined by Eq. (221) with $n = 1$, Eq. (227) is reduced to the canonical form of the well-studied *Mathieu equation*⁶⁷

Mathieu
equation

$$\frac{d^2\psi}{d\xi^2} + (\alpha - 2\beta \cos 2\xi)\psi = 0. \quad (2.229)$$

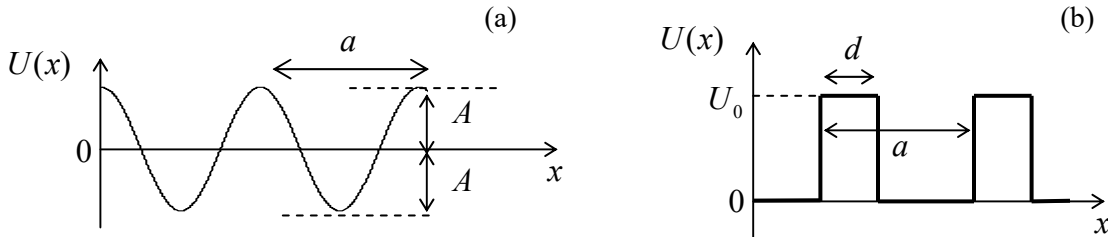


Fig. 2.31. Two other simple periodic potential profiles: (a) the sinusoidal (“Mathieu”) potential and (b) the Kronig-Penney potential.

Figure 32 shows the characteristic curves of this equation. We see that now at small β the first energy gap grows much faster than the higher ones: $\Delta_n \propto \beta^n$. This feature is in accord with the weak-coupling result $\Delta_1 = 2|U_1|$, which is valid only in the linear approximation in U_n , because for the Mathieu potential, $U_l = A(\delta_{l+1} + \delta_{l-1})/2$. Another clearly visible feature is the exponentially fast shrinkage of the allowed energy bands at $2\beta > \alpha$ (in Fig. 32, on the right from the dashed line), i.e. at $E < A$. It may be readily explained by our tight-binding approximation result (206): as soon as the eigenenergy drops significantly below the potential maximum $U_{\max} = A$ (see Fig. 31a), the quantum states in the adjacent potential wells are connected only by tunneling through relatively high potential barriers separating these wells, so that the coupling amplitudes δ_n become exponentially small – see, e.g., Eq. (189).

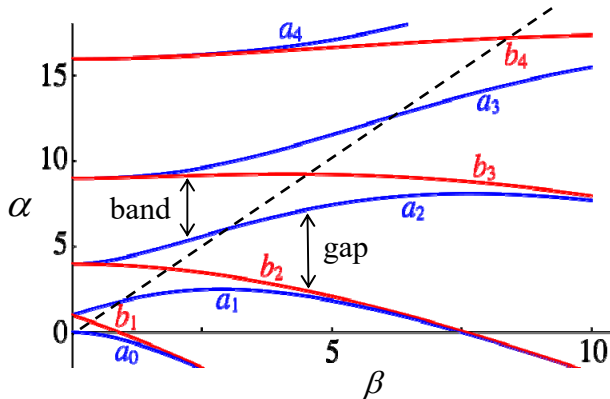


Fig. 2.32. Characteristic curves of the Mathieu equation. The dashed line corresponds to the equality $\alpha = 2\beta$, i.e. $E = A \equiv U_{\max}$, separating the regions of under-barrier tunneling and over-barrier motion. Adapted from Fig. 28.2.1 at <http://dlmf.nist.gov>. (Contribution by US Government, not subject to copyright).

Another simple periodic profile is the *Kronig-Penney potential*, shown in Fig. 31b, which gives relatively simple analytical expressions for the characteristic curves. Its advantage is a more realistic law of the decrease of the Fourier harmonics U_l at $l \gg 1$, and hence of the energy gaps in the weak-potential limit:

⁶⁷ This equation, first studied in the 1860s by É. Mathieu in the context of a rather practical problem of vibrating elliptical drumheads (!), has many other important applications in physics and engineering, notably including the parametric excitation of oscillations – see, e.g., CM Sec. 5.5.

$$\Delta_n \approx 2|U_n| \propto \frac{U_0}{n}, \quad \text{at } E \sim E^{(n)} \gg U_0. \quad (2.230)$$

Leaving a detailed analysis of the Kronig-Penney potential for the reader's exercise, let me conclude this section by addressing the effect of potential modulation on the number of eigenstates in 1D systems of a large but finite length $l \gg a, k^{-1}$. Surprisingly, the Bloch theorem makes the analysis of this problem elementary, for arbitrary $U(x)$. Indeed, let us assume that l is comprised of an integer number of periods a , and its ends are described by similar boundary conditions – both assumptions evidently inconsequential for $l \gg a$. Then, according to Eq. (210), the boundary conditions impose, on the quasimomentum q , exactly the same quantization condition as we had for k for a free 1D motion. Hence, instead of Eq. (1.100), we can write

$$dN = \frac{l}{2\pi} dq, \quad (2.231)$$

1D number
of states

with the corresponding change of the summation rule:

$$\sum_q f(q) \rightarrow \frac{l}{2\pi} \int f(q) dk. \quad (2.232)$$

As a result, the density of states in the 1D *q-space*, $dN/dq = l/2\pi$, does not depend on the potential profile at all! Note, however, that the profile does affect the density of states on the *energy* scale, dN/dE . As an extreme example, on the bottom and at the top of each energy band we have $dE/dq \rightarrow 0$, and hence

$$\frac{dN}{dE} = \frac{dN}{dq} \Big/ \frac{dE}{dq} = \frac{l}{2\pi} \Big/ \frac{dE}{dq} \rightarrow \infty. \quad (2.233)$$

This effect of state concentration at the band/gap edges (which survives in higher spatial dimensionalities as well) has important implications for the operation of several important electronic and optical devices, in particular semiconductor lasers and light-emitting diodes.

2.8. Periodic systems: Particle dynamics

The band structure of the energy spectrum of a particle moving in a periodic potential has profound implications not only for its density of states but also for its dynamics. Indeed, let us consider the simplest case of a wave packet composed of the Bloch functions (210), all belonging to the same (say, n^{th}) energy band. Similarly to Eq. (27) for a free particle, we can describe such a packet as

$$\Psi(x, t) = \int a_q u_q(x) e^{i[qx - \omega(q)t]} dq, \quad (2.234)$$

where the a -periodic functions $u(x)$, defined by Eq. (208), are now indexed to emphasize their dependence on the quasimomentum, and $\omega(q) = E_n(q)/\hbar$ is the function of q describing the shape of the corresponding energy band – see, e.g., Fig. 26b or Fig. 28. If the packet is narrow in the *q-space*, i.e. if the width δq of the distribution a_q is much smaller than all the characteristic *q*-scales of the dispersion relation $\omega(q)$, in particular of π/a , we may simplify Eq. (234) exactly as it was done in Sec. 2 for a free particle, despite the presence of the periodic factors $u_q(x)$ under the integral. In the linear approximation of the Taylor expansion, we get a full analog of Eq. (32), but now with q rather than k , and

$$v_{\text{gr}} = \frac{d\omega}{dq} \Big|_{q=q_0}, \quad \text{and} \quad v_{\text{ph}} = \frac{\omega}{q} \Big|_{q=q_0}, \quad (2.235)$$

where q_0 is the central point of the quasimomentum distribution. Despite the formal similarity with Eqs. (33) for the free particle, this result is much more eventful. For example, as evident from the dispersion relation's topology (see Figs. 26b, 28), the group velocity vanishes not only at $q = 0$, but at all values of q that are multiples of (π/a) , at the bottom and on the top of each energy band. Even more intriguing is that the group velocity's sign changes periodically with q .

This group velocity alternation leads to fascinating, counter-intuitive phenomena if a particle placed in a periodic potential is the subject of an additional external force $F(t)$. (For electrons in a crystal, this may be, for example, the force of the applied electric field.) Let the force be relatively weak, so that the product Fa (i.e. the scale of the energy increment from the additional force per one lattice period) is much smaller than both relevant energy scales of the dispersion relation $E(q)$ – see Fig. 26b:

$$Fa \ll \Delta E_n, \Delta_n. \quad (2.236)$$

This strong relationship allows one to neglect the force-induced interband transitions, so that the wave packet (234) includes the Bloch eigenfunctions belonging to only one (initial) energy band at all times. For the time evolution of its center q_0 , theory yields⁶⁸ an extremely simple equation of motion

$$\dot{q}_0 = \frac{1}{\hbar} F(t). \quad (2.237)$$

Time
evolution
of quasi-
momentum

This equation is physically very transparent: it is essentially the 2nd Newton law for the time evolution of the quasimomentum $\hbar q$ under the effect of the additional force $F(t)$ only, excluding the periodic force $-\partial U(x)/\partial x$ of the background potential $U(x)$. This is very natural, because as Eq. (210) implies, $\hbar q$ is essentially the particle's momentum averaged over the potential's period, and the periodic force effect drops out at such an averaging.

Despite the simplicity of Eq. (237), the results of its solution may be highly nontrivial. First, let us use Eqs. (235) and (237) to find the instant *group acceleration* of the particle (i.e. the acceleration of its wave packet's envelope):

$$a_{\text{gr}} \equiv \frac{dv_{\text{gr}}}{dt} \equiv \frac{d}{dt} \frac{d\omega(q_0)}{dq_0} \equiv \frac{d}{dq_0} \frac{d\omega(q_0)}{dq_0} \frac{dq_0}{dt} = \frac{d^2\omega(q_0)}{dq_0^2} \frac{dq_0}{dt} = \frac{1}{\hbar} \frac{d^2\omega}{dq^2} \Big|_{q=q_0} F(t). \quad (2.238)$$

This means that the second derivative of the dispersion $\omega(q)$ relation (specific for each energy band) plays the role of the effective reciprocal mass of the particle at this particular value of q_0 :

$$m_{\text{ef}} = \frac{\hbar}{d^2\omega/dq^2} \equiv \frac{\hbar^2}{d^2E_n/dq^2}. \quad (2.239)$$

Effective
mass

For the particular case of a free particle, for which Eq. (216) is exact, this expression is reduced to the original (and constant) mass m , but generally, the effective mass depends on the wave packet's

⁶⁸ The proof of Eq. (237) is not difficult, but becomes more compact in the bra-ket formalism, to be discussed in Chapter 4. This is why I recommend to the reader its proof as an exercise after reading that chapter. For a generalization of this theory to the case of essential interband transitions see, e.g., Sec. 55 in E. Lifshitz and L. Pitaevskii, *Statistical Physics, Part 2*, Pergamon, 1980.

momentum. According to Eq. (239), at the bottom of any energy band, m_{ef} is always positive but depends on the strength of the particle's interaction with the periodic potential. In particular, according to Eq. (206), in the tight-binding limit, the effective mass is very large:

$$|m_{\text{ef}}|_{q=(\pi/a)n} = \frac{\hbar^2}{2\delta_n a^2} \equiv m \frac{E^{(1)}}{\pi^2 \delta_n} \gg m . \quad (2.240)$$

On the contrary, in the weak-potential limit, the effective mass is close to m at most points of each energy band, but at the edges of the (narrow) bandgaps, it is much smaller. Indeed, expanding Eq. (224) in the Taylor series near point $q = q_m$, we get

$$E_{\pm}|_{E \approx E^{(n)}} - E_{\text{ave}} \approx \pm |U_n| \pm \frac{1}{2|U_n|} \left(\frac{dE_l}{dq} \right)^2_{q=q_m} \tilde{q}^2 = \pm |U_n| \pm \frac{\gamma^2}{2|U_n|} \tilde{q}^2 , \quad (2.241)$$

where γ and \tilde{q} are defined by Eq. (225), so that

$$|m_{\text{ef}}|_{q=q_m} = |U_n| \frac{\hbar^2}{\gamma^2} \equiv m \frac{|U_n|}{2E^{(n)}} \ll m . \quad (2.242)$$

The effective mass effects in real atomic crystals may be very significant. For example, the charge carriers in silicon have $m_{\text{ef}} \approx 0.19 m_e$ in the lowest, normally-empty energy band (traditionally called the *conduction band*), and $m_{\text{ef}} \approx 0.98 m_e$ in the adjacent lower, normally-filled *valence band*. In some semiconducting compounds, the conduction-band mass may be even smaller – down to $0.0145 m_e$ in InSb!

However, the effective mass' magnitude is not the most surprising effect. A more fascinating corollary of Eq. (239) is that on the top of each energy band the effective mass is *negative* – please revisit Figs. 26b, 28, and 29 again. This means that the particle (or more strictly, its wave packet's envelope) is accelerated in the direction *opposite* to the applied force. This is exactly what electronic engineers, working with electrons in semiconductors, call *holes*, characterizing them by a *positive mass* $|m_{\text{ef}}|$, but compensating this sign change by taking their charge e positive. If the particle stays in close vicinity of the energy band's top (say, due to frequent scattering effects, typical for the semiconductors used in engineering practice), such double sign flip does not lead to an error in calculations of hole's dynamics, because the electric field's force is proportional to the particle's charge, so that the particle's acceleration a_{gr} is proportional to the charge-to-mass ratio.⁶⁹

However, in some phenomena such simple representation is unacceptable.⁷⁰ For example, let us form a narrow wave packet at the bottom of the lowest energy band,⁷¹ and then exert on it a constant force $F > 0$ – say, due to a constant external electric field directed along the x -axis. According to Eq. (237), this force would lead to linear growth of q_0 in time, so that in the quasimomentum space, the

⁶⁹ More discussion of this issue may be found in SM Sec. 6.4.

⁷⁰ The balance of this section describes effects that are not discussed in most quantum mechanics textbooks. Though, in my opinion, every educated physicist should be aware of them, some readers may skip them at the first reading, jumping directly to the next Sec. 9.

⁷¹ Physical intuition tells us (and the theory of open systems, to be discussed in Chapter 7, confirms) that this may be readily done, for example, by weakly coupling the system to a relatively low-temperature environment, and letting it relax to the lowest possible energy.

packet's center would slide, with a constant speed, along the q axis – see Fig. 33a. Close to the energy band's bottom, this motion would correspond to a positive effective mass (possibly, somewhat different than the genuine particle's mass m), and hence be close to the free particle's acceleration. However, as soon as q_0 has reached the inflection point where $d^2E_1/dq^2 = 0$, the effective mass, and hence its acceleration (238) change signs to negative, i.e. the packet starts to slow down (in the direct space), while still moving ahead with the same velocity in the quasimomentum space. Finally, at the energy band's top, the particle stops at a certain x_{\max} , while continuing to move forward in the q -space.

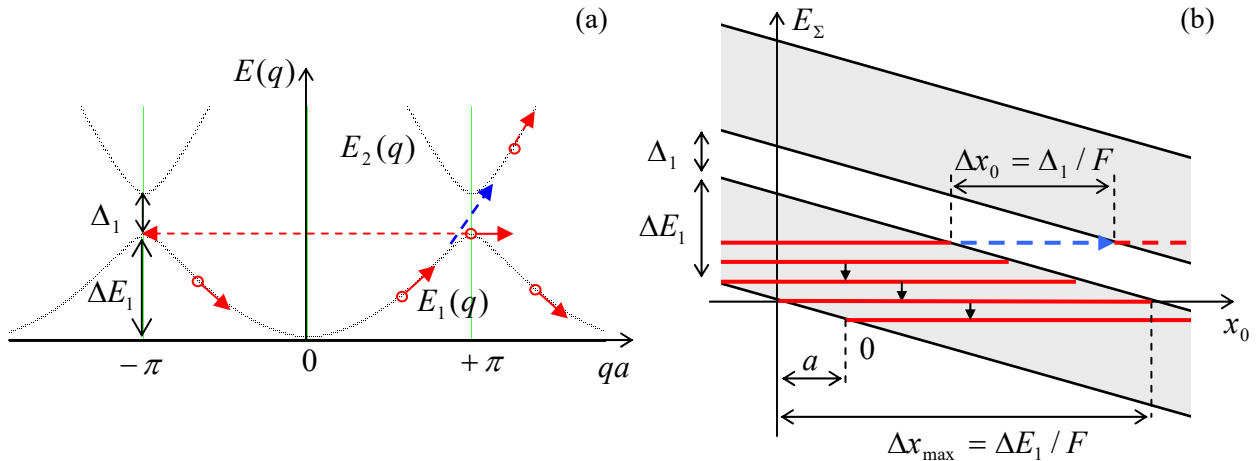


Fig. 2.33. The Bloch oscillations (red lines) and the Landau-Zener tunneling (blue arrows) represented in: (a) the reciprocal space of q , and (b) the direct space. On panel (b), the tilted gray strips show the allowed energy bands, while the bold red lines, the Wannier-Stark ladder's steps.

Now we have two alternative ways to look at the further time evolution of the wave packet along the quasimomentum's axis. From the extended zone picture (which is the simplest for this analysis, see Fig. 33a),⁷² we may say that the particle crosses the 1st Brillouin zone boundary and continues to go forward in q -space, i.e. down the lowest energy band. According to Eq. (235), this region (up to the next energy minimum at $qa = 2\pi$) corresponds to a negative group velocity. After q_0 has reached that minimum, the whole process repeats again – and again, and again.

These are the famous *Bloch oscillations* – the effect which had been predicted, by the same F. Bloch, as early as 1929 but evaded experimental observation until the 1980s (see below) due to the strong scattering effects in real solid-state crystals. The time period of the oscillations may be readily found from Eq. (237):

$$\Delta t_B = \frac{\Delta q}{dq/dt} = \frac{2\pi/a}{F/\hbar} = \frac{2\pi\hbar}{Fa}, \quad (2.243)$$

so that their frequency may be expressed by a very simple formula

⁷² This phenomenon may be also discussed from the point of view of the reduced zone picture, but then it requires the introduction of instant jumps between the Brillouin zone boundary points (see the dashed red line in Fig. 33) that correspond to physically equivalent states of the particle. Evidently, for the description of this particular phenomenon, this language is more artificial.

$$\omega_B \equiv \frac{2\pi}{\Delta t_B} = \frac{Fa}{\hbar}, \quad (2.244)$$

Bloch oscillations: frequency

and hence is independent of any peculiarities of the energy band/gap structure.

The direct-space motion of the wave packet's center $x_0(t)$ during the Bloch oscillation process may be analyzed by integrating the first of Eqs. (235) over some time interval Δt , and using Eq. (237):

$$\Delta x_0(t) \equiv \int_0^{\Delta t} v_{\text{gr}} dt = \int_0^{\Delta t} \frac{d\omega(q_0)}{dq_0} dt \equiv \int_0^{\Delta t} \frac{d\omega(q_0)}{dq_0 / dt} dt = \frac{\hbar}{F} \int_{t=0}^{t=\Delta t} d\omega = \frac{\hbar}{F} \Delta\omega(q_0). \quad (2.245)$$

If the interval Δt is equal to the Bloch oscillation period Δt_B (243), the initial and final values of $E(q_0) = \hbar\omega(q_0)$ are equal, giving $\Delta x_0 = 0$: in the end of the period, the wave packet returns to its initial position in space. However, if we carry out this integration only from the smallest to the largest values of $\omega(q_0)$, i.e. the adjacent points where the group velocity vanishes, we get the following Bloch oscillation swing:

$$\Delta x_{\max} = \frac{\hbar}{F} (\omega_{\max} - \omega_{\min}) \equiv \frac{\Delta E_1}{F}. \quad (2.246)$$

Bloch oscillations: spatial swing

This simple result may be interpreted using an alternative energy diagram (Fig. 33b), which results from the following arguments. The additional force F may be described not only via the 2nd Newton law's version (237), but, alternatively, by its contribution $-Fx$ to the Gibbs potential energy⁷³

$$U_{\Sigma}(x) = U(x) - Fx \quad (2.247)$$

The exact solution of the Schrödinger equation (61) with such a potential may be hard to find directly, but if the force F is sufficiently weak, as we are assuming throughout this discussion, the second term in Eq. (247) may be considered as a constant on the scale of $a \ll \Delta x_{\max}$. In this case, our quantum-mechanical treatment of the periodic potential $U(x)$ is still virtually correct, but with an energy shift depending on the “global” position x_0 of the packet's center. In this approximation, the total energy of the wave packet is

$$E_{\Sigma} = E(q_0) - Fx_0. \quad (2.248)$$

In a plot of such energy as a function of x_0 (Fig. 33b), the energy dependence on q_0 is hidden, but as was discussed above, it is rather uneventful and may be well characterized by the position of band-gap edges on the energy axis.⁷⁴ In this representation, the Bloch oscillations keep the full energy E_{Σ} of the particle constant, i.e. follow a horizontal line in Fig. 33b, limited by the classical turning points corresponding to the bottom and the top of the allowed energy band. The distance Δx_{\max} between these points is evidently given by Eq. (246).

Besides this alternative look at the Bloch oscillation swing, the total energy diagram shown in Fig. 33b enables one more remarkable result. Let a wave packet be so narrow in the momentum space

⁷³ Physically, this is just the relevant part of the potential energy of the total system comprised of our particle (in the periodic potential) and the source of the force F – see, e.g., CM Sec. 1.4.

⁷⁴ In semiconductor physics and engineering, such spatial *band-edge diagrams* are virtually unavoidable components of almost every discussion/publication. In this series, a few more examples of such diagrams may be found in SM Sec. 6.4.

that $\delta x \sim 1/\delta q \gg \Delta x_{\max}$; then it may be well represented by definite energy, i.e. by a horizontal line in Fig. 33b. But Eq. (247) is exactly invariant with respect to the following simultaneous translation of the coordinate and the energy:

$$x \rightarrow x + a, \quad E \rightarrow E - Fa. \quad (2.249)$$

This means that it is satisfied by an infinite set of similar solutions, each corresponding to one of the horizontal red lines shown in Fig. 33b. This is the famous *Wannier-Stark ladder*,⁷⁵ with the step height

$$\Delta E_{\text{ws}} = Fa. \quad (2.250)$$

Wannier-Stark ladder

The importance of this alternative representation of the Bloch oscillations is due to the following fact. In most experimental realizations, the power of the electromagnetic radiation with frequency (244), that may be extracted from the oscillations of a charged particle, is very low, so that their direct detection represents a hard problem.⁷⁶ However, let us apply to a Bloch oscillator an additional ac field at frequency $\omega \approx \omega_B$. As these frequencies are brought close together, the external signal should synchronize (“phase-lock”) the Bloch oscillations,⁷⁷ resulting in certain changes of time-independent observables – for example, a resonant change of absorption of the external radiation. Now let us notice that the combination of Eqs. (244) and (250) yield the following simple relation:

$$\Delta E_{\text{ws}} = \hbar \omega_B. \quad (2.251)$$

This means that the phase-locking at $\omega \approx \omega_B$ allows for an alternative (but equivalent) interpretation – as the result of ac-field-induced quantum transitions⁷⁸ between the steps of the Wannier-Stark ladder. (Again, such occasions when two very different languages may be used for alternative interpretations of the same effect is one of the most beautiful features of physics.)

This phase-locking effect has been used for the first experimental confirmations of the Bloch oscillation theory.⁷⁹ For this purpose, the natural periodic structures, solid-state crystals, are inconvenient due to their very small period $a \sim 10^{-10}$ m. Indeed, according to Eq. (244), such structures require very high forces F (and hence very high electric fields $\mathcal{E} = F/e$) to bring ω_B to an experimentally convenient range. This problem has been overcome using artificial periodic structures (*superlattices*) of certain semiconductor compounds, such as $\text{Ga}_{1-x}\text{Al}_x\text{As}$ with various degrees x of the gallium-to-aluminum atom replacement, whose layers may be grown over each other epitaxially, i.e., with very few crystal structure violations. Such superlattices, with periods $a \sim 10$ nm, have enabled a clear observation of the resonance at $\omega \approx \omega_B$, and hence a measurement of the Bloch oscillation frequency, in particular its proportionality to the applied dc electric field, predicted by Eq. (244).

⁷⁵ This effect was first discussed in detail by Gregory Hugh Wannier in his 1959 monograph on solid-state physics, while the name of Johannes Stark is traditionally associated with virtually any electric field effect on atomic systems, after he had discovered the first of such effects in 1913.

⁷⁶ In systems with many independent particles (such as electrons in semiconductors), the detection problem is exacerbated by the phase incoherence of the Bloch oscillations performed by each particle. This drawback is absent in atomic Bose-Einstein condensates whose Bloch oscillations (in a periodic potential created by standing optical waves) were eventually observed by M. Ben Dahan *et al.*, *Phys. Rev. Lett.* **76**, 4508 (1996).

⁷⁷ A simple analysis of phase locking of a classical oscillator may be found, e.g., in CM Sec. 5.4. (See also the brief discussion of the phase locking of the Josephson oscillations at the end of Sec. 1.6 of this course.)

⁷⁸ A quantitative theory of such transitions will be discussed in Sec. 6.6 and then in Chapter 7.

⁷⁹ E. Mendez *et al.*, *Phys. Rev. Lett.* **60**, 2426 (1988).

Very soon after this discovery, the Bloch oscillations were observed⁸⁰ in small Josephson junctions, where they result from the quantum dynamics of the Josephson phase difference φ in a 2π -periodic potential profile, created by the junction. A straightforward translation of Eq. (244) to this case (left for the reader's exercise) shows that the frequency of such Bloch oscillations is

$$\omega_B = \frac{\pi \bar{I}}{2e}, \quad \text{i.e. } f_B \equiv \frac{\omega_B}{2\pi} = \frac{\bar{I}}{2e}, \quad (2.252)$$

where \bar{I} is the dc current passed through the junction – the effect not to be confused with the “classical” Josephson oscillations with frequency (1.75). It is curious that Eq. (252) may be legitimately interpreted as a result of a periodic transfer, through the Josephson junction, of discrete Cooper pairs (of charge $-2e$), between two coherent Bose-Einstein condensates in the superconducting electrodes of the junction.⁸¹

Next, our discussion of the Bloch oscillations was based on the premise that the wave packet of the particle stays within one (say, the lowest) energy band. However, just one look at Fig. 28 shows that this assumption becomes unrealistic if the energy gap separating this band from the next one becomes very small, $\Delta_1 \rightarrow 0$. Indeed, in the weak-potential approximation, which is adequate in this limit, $|U_1| \rightarrow 0$, the two dispersion curve branches (216) cross without any interaction, so that if our particle (meaning its the wave packet) is driven to approach that point, it should continue to move up in energy – see the dashed blue arrow in Fig. 33a. Similarly, in the real-space representation shown in Fig. 33b, it is intuitively clear that at $\Delta_1 \rightarrow 0$, the particle residing at one of the steps of the Wannier-Stark ladder should be able to somehow overcome the vanishing spatial gap $\Delta x_0 = \Delta_1/F$ and to “leak” into the next band – see the horizontal dashed blue arrow on that panel.

This process, called the *Landau-Zener* (or “interband”, or “band-to-band”) *tunneling*,⁸² is indeed possible. To analyze it, let us first take $F = 0$, and consider what happens if a quantum particle, described by an x -long (i.e. E -narrow) wave packet, is incident from free space upon a periodic structure of a large but finite length $l = Na \gg a$ – see, e.g., Fig. 22. If the packet’s energy E is within one of the energy bands, it may evidently propagate through the structure (though may be partly reflected from its ends). The corresponding quasimomentum may be found by solving the dispersion relation for q ; for example, in the weak-potential limit, Eq. (224) (which is valid near the gap) yields

$$q = q_m + \tilde{q}, \quad \text{with} \quad \tilde{q} = \pm \frac{1}{\gamma} \left[\tilde{E}^2 - |U_n|^2 \right]^{1/2}, \quad \text{for} |U_n|^2 \leq \tilde{E}^2, \quad (2.253)$$

where $\tilde{E} \equiv E_{\pm} - E^{(n)}$ and $\gamma = 2aE^{(n)}/\pi n$ – see the second of Eqs. (225).

Now, if the energy E is inside one of the energy gaps Δ_n , the wave packet’s propagation in an infinite periodic lattice is impossible, so that it is completely reflected from it. However, our analysis of the potential step problem in Sec. 3 implies that the packet’s wavefunction should still have an exponential tail protruding into the structure and decaying on some length δ – see Eq. (58) and Fig. 2.4.

⁸⁰ D. Haviland *et al.*, *Z. Phys. B* **85**, 339 (1991).

⁸¹ See, e.g., D. Averin *et al.*, *Sov. Phys. – JETP* **61**, 407 (1985). This effect is qualitatively similar to the transfer of single electrons, with a similar frequency $f = \bar{I}/e$, in tunnel junctions between normal (non-superconducting) metals – see, e.g., EM Sec. 2.9 and references therein.

⁸² It was predicted independently by L. Landau, C. Zener, E. Stueckelberg, and E. Majorana in 1932.

Indeed, a straightforward review of the calculations leading to Eq. (253) shows that it remains valid for energies within the gap as well, if the quasimomentum is understood as a purely imaginary number:

$$\tilde{q} \rightarrow \pm i\kappa, \quad \text{where } \kappa \equiv \frac{1}{\gamma} \left[|U_n|^2 - \tilde{E}^2 \right]^{1/2}, \quad \text{for } \tilde{E}^2 \leq |U_n|^2. \quad (2.254)$$

With this replacement, the Bloch solution (193b) indeed describes an exponential decay of the wavefunction at length $\delta \sim 1/\kappa$.

Returning to the effects of weak force F , in the real-space approach described by Eq. (248) and illustrated in Fig. 33b, we may recast Eq. (254) as

$$\kappa \rightarrow \kappa(x) = \frac{1}{\gamma} \left[|U_n|^2 - (F\tilde{x})^2 \right]^{1/2}, \quad (2.255)$$

where \tilde{x} is the particle's (i.e. its wave packet center's) deviation from the mid-gap point. Thus the gap creates a potential barrier of a finite width $\Delta x_0 = 2|U_n|/F$, through which the wave packet may tunnel with a non-zero probability. As we already know, in the WKB approximation (in our case requiring $\kappa\Delta x_0 \gg 1$) this probability is just the potential barrier's transparency \mathcal{T} , which may be calculated from Eq. (117):

$$-\ln \mathcal{T} = 2 \int_{\kappa(x)^2 > 0} \kappa(x) dx = \frac{2}{\gamma} \int_{-x_c}^{x_c} \left[|U_n|^2 - (F\tilde{x})^2 \right]^{1/2} d\tilde{x} = \frac{2|U_n|}{\gamma} 2x_c \int_0^1 (1 - \xi^2)^{1/2} d\xi. \quad (2.256)$$

where $\pm x_c \equiv \pm \Delta x_0/2 = \pm |U_n|/F$ are the classical turning points. Working out this simple integral (or just noticing that it is a quarter of the unit circle's area, and hence is equal to $\pi/4$), we get

$$\mathcal{T} = \exp \left\{ -\frac{\pi |U_n|^2}{\gamma F} \right\}. \quad (2.257)$$

This famous result may be also obtained in a more complex way, whose advantage is a constructive proof that Eq. (257) is valid for an arbitrary relation between γF and $|U_n|^2$, i.e. arbitrary \mathcal{T} , while our simple derivation was limited to the WKB approximation, valid only at $\mathcal{T} \ll 1$.⁸³ Using Eq. (225), we may rewrite the product γF participating in Eq. (257), as

$$\gamma F = \frac{1}{2} \left| \frac{d(E_l - E_{l'})}{dq_0} \right|_{E_l = E_{l'} = E^{(n)}} \hbar \frac{dq_0}{dt} = \frac{\hbar}{2} \left| \frac{d(E_l - E_{l'})}{dt} \right|_{E_l = E_{l'} = E^{(n)}} \equiv \frac{\hbar u}{2}, \quad (2.258)$$

where u has the meaning of the “speed” of the energy level crossing in the absence of the gap. Hence, Eq. (257) may be rewritten in the form

$$\mathcal{T} = \exp \left\{ -\frac{2\pi |U_n|^2}{\hbar u} \right\}, \quad (2.259)$$

which is more transparent physically. Indeed, the fraction $2|U_n|/u = \Delta_n u$ gives the time scale Δt of the energy's crossing the gap region, and according to the Fourier transform, its reciprocal, $\omega_{\max} \sim 1/\Delta t$

⁸³ In Chapter 6 below, Eq. (257) will be derived using a different method, based on the so-called *Golden Rule* of quantum mechanics, but also in the weak-potential limit, i.e. for hyperbolic dispersion law (253).

gives the upper cutoff of the frequencies essentially involved in the Bloch oscillation process. Hence Eq. (259) means that

$$-\ln \mathcal{T} \approx \frac{\Delta_n}{\hbar\omega_{\max}}. \quad (2.260)$$

This formula allows us to interpret the Landau-Zener tunneling as the system's excitation across the energy gap Δ_n by the highest-energy quantum $\hbar\omega_{\max}$ available from the Bloch oscillation process. This interpretation remains valid even in the opposite, tight-binding limit, in which, according to Eqs. (206) and (237), the Bloch oscillations are purely sinusoidal, so that the Landau-Zener tunneling is completely suppressed at $\hbar\omega_B < \Delta_1$.

Interband tunneling is an important ingredient of several physical phenomena and even some practical electron devices, for example, the *tunneling* (or “Esaki”) *diodes*. This simple device is just a junction of two semiconductor electrodes, one of them so strongly *n*-doped by electron donors that some electrons form a degenerate Fermi gas at the bottom of the conduction band.⁸⁴ Similarly, the counterpart semiconductor electrode is *p*-doped so strongly that the Fermi level in the valence band is shifted below the band edge – see Fig. 34.

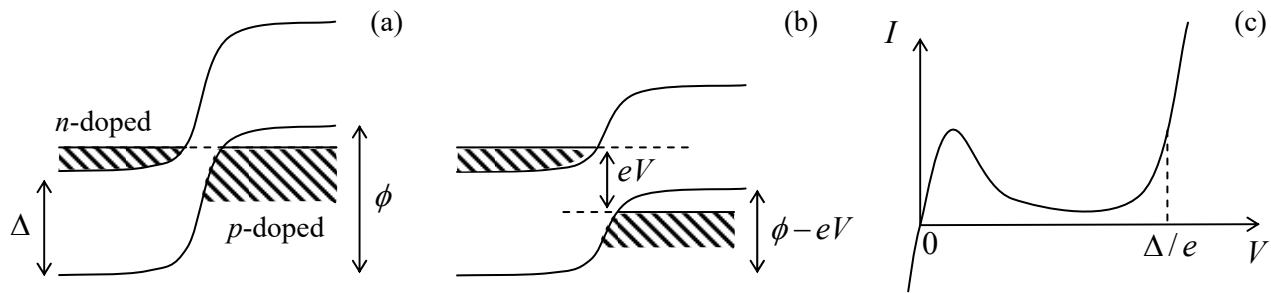


Fig. 2.34. The tunneling (“Esaki”) diode: (a) the band-edge diagram of the device at zero bias; (b) the same diagram at a modest positive bias $eV \sim \Delta/2$, and (c) the I - V curve of the device (schematically). Dashed lines on panels (a) and (b) show the Fermi level positions.

In thermal equilibrium, and in the absence of external voltage bias, the Fermi levels of the two electrodes self-align, leading to the build-up of the *contact potential difference* ϕ/e , with ϕ a bit larger than the energy bandgap Δ – see Fig. 34a. This potential difference creates an internal electric field that tilts the energy bands (just as the external field did in Fig. 33b), and leads to the formation of the so-called *depletion layer*, in which the Fermi level is located within the energy gap and hence there are no charge carriers ready to move. In the usual *p-n* junctions, this layer is broad and prevents any current at applied voltages V lower than $\sim \Delta/e$. In contrast, in a tunneling diode the depletion layer is so thin (below ~ 10 nm) that the interband tunneling is possible and provides a substantial Ohmic current at small applied voltages – see Fig. 34c. However, at larger positive biases, with $eV \sim \Delta/2$, the conduction band is aligned with the middle of the energy gap in the *p*-doped electrode, and electrons cannot tunnel there. Similarly, there are no electrons in the *n*-doped semiconductor to tunnel into the available states just above the Fermi level in the *p*-doped electrode – see Fig. 34b. As a result, at such voltages the current

⁸⁴ Here I have to rely on the reader’s background knowledge of basic semiconductor physics; it will be discussed in more detail in SM Sec. 6.4.

drops significantly, to grow again only when eV exceeds $\sim\Delta$, enabling electron motion within each energy band. Thus the tunnel junction's I - V curve has a part with a *negative differential resistance* ($dV/dI < 0$) – see Fig. 34c. This phenomenon, equivalent in its effect to negative kinematic friction in mechanics, may be used for amplification of weak analog signals, for self-excitation of electronic oscillators⁸⁵ (i.e. an ac signal generation), and for signal swing restoration in digital electronics.

2.9. Harmonic oscillator: Brute force approach

To complete our review of the basic 1D wave mechanics, we have to consider the famous harmonic oscillator, i.e. a 1D particle moving in the quadratic-parabolic potential (111), so that the stationary Schrödinger equation (53) is

$$-\frac{\hbar^2}{2m} \frac{d^2\psi}{dx^2} + \frac{m\omega_0^2 x^2}{2} \psi = E\psi. \quad (2.261)$$

Conceptually, on the background of the fascinating quantum effects discussed in the previous sections, this is not a very interesting system: Eq. (261) is a standard 1D eigenproblem, resulting in a discrete energy spectrum E_n , with smooth eigenfunctions $\psi_n(x)$ vanishing at $x \rightarrow \pm\infty$ (because the potential energy tends to infinity there).⁸⁶ However, as we will repeatedly see later in the course, this problem's solutions have an enormous range of applications, so we have to know their basic properties.

The direct analytical solution of the problem is not very simple (see below), so let us start by trying some indirect approaches to it. First, as was discussed in Sec. 4, the WKB-approximation-based Wilson-Sommerfeld quantization rule (110), applied to this potential, yields the eigenenergy spectrum (114). With the common quantum number convention, this result is

$$E_n = \hbar\omega_0 \left(n + \frac{1}{2} \right), \quad \text{with } n = 0, 1, 2, \dots, \quad (2.262)$$

so that (in contrast to the 1D rectangular potential well) the ground-state energy corresponds to $n = 0$. However, as was discussed in the end of Sec. 4, for the quadratic potential (111) the WKB approximation's conditions are strictly satisfied only at $E_n \gg \hbar\omega_0$, so that so far we can only trust Eq. (262) for high levels, with $n \gg 1$, rather than for the (most important) ground state.

This is why let me use Eq. (261) to demonstrate another approximate approach, called the *variational method*, whose simplest form is aimed at finding ground states. The method is based on the following observation. (Here I am presenting its 1D wave mechanics form, though the method is much more general.) Let ψ_n be the exact, full, and orthonormal set of stationary wavefunctions of the system under study, and E_n the set of the corresponding energy levels, satisfying Eq. (1.60):

$$\hat{H}\psi_n = E_n\psi_n. \quad (2.263)$$

Then we may use this set for the unique expansion of an arbitrary *trial wavefunction* ψ_{trial} :

⁸⁵ See, e.g., CM Sec. 5.4.

⁸⁶ The stationary state of the harmonic oscillator (which, as will be discussed in Secs. 5.4 and 7.1, may be considered as the state with a definite number of identical bosonic excitations) are sometimes called *Fock states* – after Vladimir Aleksandrovich Fock. (This term is also used in a more general sense, for definite-particle-number states of systems with indistinguishable bosons of any kind – see Sec. 8.3.)

$$\psi_{\text{trial}} = \sum_n \alpha_n \psi_n, \quad \text{so that } \psi_{\text{trial}}^* = \sum_n \alpha_n^* \psi_n^*, \quad (2.264)$$

where α_n are some (generally, complex) coefficients. Let us require the trial function to be normalized, using the condition (1.66) of orthonormality of the eigenfunctions ψ_n :

$$\int \psi_{\text{trial}}^* \psi_{\text{trial}} d^3x \equiv \sum_{n,n'} \int \alpha_n^* \psi_n^* \alpha_{n'} \psi_{n'} d^3x \equiv \sum_{n,n'} \alpha_{n'} \alpha_n^* \int \psi_n^* \psi_{n'} d^3x \equiv \sum_{n,n'} \alpha_{n'} \alpha_n^* \delta_{n,n'} \equiv \sum_n W_n = 1, \quad (2.265)$$

where each of the coefficients W_n , defined as

$$W_n \equiv \alpha_n^* \alpha_n \equiv |\alpha_n|^2 \geq 0, \quad (2.266)$$

may be interpreted as the probability for the particle, in the n^{th} trial state, to be found in the n^{th} genuine stationary state. Now let us use Eq. (1.23) for a similar calculation of the expectation value of the system's Hamiltonian in the trial state:⁸⁷

$$\begin{aligned} \langle H \rangle_{\text{trial}} &= \int \psi_{\text{trial}}^* \hat{H} \psi_{\text{trial}} d^3x \equiv \sum_{n,n'} \int \alpha_n^* \psi_n^* \hat{H} \alpha_{n'} \psi_{n'} d^3x \equiv \sum_{n,n'} \alpha_{n'} \alpha_n^* E_{n'} \int \psi_n^* \psi_{n'} d^3x \\ &\equiv \sum_{n,n'} \alpha_{n'} \alpha_n^* E_{n'} \delta_{n,n'} \equiv \sum_n W_n E_n. \end{aligned} \quad (2.267)$$

Since the exact ground state energy E_g is, by definition, the lowest one of the set E_n , i.e. $E_n \geq E_g$, Eqs. (265) and (267) yield the following inequality:

$$\boxed{\langle H \rangle_{\text{trial}} \geq \sum_n W_n E_g \equiv E_g \sum_n W_n = E_g.} \quad (2.268)$$

Variational method's justification

Thus, the genuine ground state energy of the system is always lower than (or equal to) its energy in any trial state. Hence, if we make several attempts with reasonably selected trial wavefunctions, we may expect the lowest of the results to approximate the genuine ground state energy reasonably well. Even more conveniently, if we select some reasonable class of trial wavefunctions dependent on a free parameter λ , then we may use the necessary condition of the minimum of $\langle H \rangle_{\text{trial}}$,

$$\frac{\partial \langle H \rangle_{\text{trial}}}{\partial \lambda} = 0, \quad (2.269)$$

to find the closest of them to the genuine ground state. Even better results may be obtained using trial wavefunctions dependent on several parameters. Note, however, that the variational method does not tell us how exactly the trial function should be selected, or how close its final result is to the genuine ground-state function. In this sense, this method has “uncontrollable accuracy”, and differs from both the WKB approximation and the perturbation methods (to be discussed in Chapter 6), for which we have certain accuracy criteria. Because of this drawback, the variational method is typically used as the last resort – though sometimes (as in the example that follows) it works remarkably well.⁸⁸

⁸⁷ It is easy (and hence left for the reader) to show that the uncertainty δH in *any* state of a Hamiltonian system, including the trial state (264), vanishes, so that the $\langle H \rangle_{\text{trial}}$ may be interpreted as the definite energy of the state. For our current goals, however, this fact is not important.

⁸⁸ The variational method may be used also to estimate the first excited state (or even a few lowest excited states) of the system, by requiring the new trial function to be orthogonal to the previously calculated eigenfunctions of the lower-energy states. However, the method's error typically grows with the state number.

Let us apply this method to the harmonic oscillator. Since the potential (111) is symmetric with respect to point $x = 0$, and continuous at all points (so that, according to Eq. (261), $d^2\psi/dx^2$ has to be continuous as well), the most natural selection of the ground-state trial function is the Gaussian function

$$\psi_{\text{trial}}(x) = C \exp\{-\lambda x^2\}, \quad (2.270)$$

with some real $\lambda > 0$. The normalization coefficient C may be immediately found either from the standard Gaussian integration of $|\psi_{\text{trial}}|^2$, or just from the comparison of this expression with Eq. (16), in which $\lambda = 1/(2\delta x)^2$, i.e. $\delta x = 1/2\lambda^{1/2}$, giving $|C|^2 = (2\lambda/\pi)^{1/2}$. Now the expectation value of the particle's Hamiltonian,

$$\hat{H} = \frac{\hat{p}^2}{2m} + U(x) = -\frac{\hbar^2}{2m} \frac{d^2}{dx^2} + \frac{m\omega_0^2 x^2}{2}, \quad (2.271)$$

in the trial state, may be calculated as

$$\begin{aligned} \langle H \rangle_{\text{trial}} &\equiv \int_{-\infty}^{+\infty} \psi_{\text{trial}}^* \left(-\frac{\hbar^2}{2m} \frac{d^2}{dx^2} + \frac{m\omega_0^2 x^2}{2} \right) \psi_{\text{trial}} dx \\ &= \left(\frac{2\lambda}{\pi} \right)^{1/2} \left[\frac{\hbar^2 \lambda}{m} \int_0^{\infty} \exp\{-2\lambda x^2\} dx + \left(\frac{m\omega_0^2}{2} - \frac{2\hbar^2 \lambda^2}{m} \right) \int_0^{\infty} x^2 \exp\{-2\lambda x^2\} dx \right]. \end{aligned} \quad (2.272)$$

Both involved integrals are of the same well-known Gaussian type,⁸⁹ giving

$$\langle H \rangle_{\text{trial}} = \frac{\hbar^2}{2m} \lambda + \frac{m\omega_0^2}{8\lambda}. \quad (2.273)$$

As a function of λ , this expression has a single minimum at the value λ_{opt} that may be found from the requirement (269), giving $\lambda_{\text{opt}} = m\omega_0/2\hbar$. The resulting minimum of $\langle H \rangle_{\text{trial}}$ is *exactly* equal to ground-state energy following from Eq. (262),

$$E_0 = \frac{\hbar\omega_0}{2}. \quad (2.274)$$

Such a coincidence of results of the WKB approximation and the variational method is rather unusual, and implies (though does not strictly prove) that Eq. (274) is exact. As a minimum, this coincidence gives a strong motivation to plug the trial wavefunction (270), with $\lambda = \lambda_{\text{opt}}$, i.e.

$$\psi_0 = \left(\frac{m\omega_0}{\pi\hbar} \right)^{1/4} \exp\left\{ -\frac{m\omega_0 x^2}{2\hbar} \right\}, \quad (2.275)$$

and the energy (274), into the Schrödinger equation (261). Such substitution⁹⁰ shows that the equation is indeed exactly satisfied.

According to Eq. (275), the characteristic scale of the wavefunction's spatial spread⁹¹ is

⁸⁹ See, e.g., MA Eqs. (6.9b) and (6.9c).

⁹⁰ Actually, this is a twist of one of the tasks of Problem 1.12.

⁹¹ Quantitatively, as was already mentioned in Sec. 2.1, $x_0 = \sqrt{2}\delta x = \langle 2x^2 \rangle^{1/2}$.

$$x_0 \equiv \left(\frac{\hbar}{m\omega_0} \right)^{1/2}. \quad (2.276)$$

Due to the importance of this scale, let us give its crude estimates for several representative systems:⁹²

(i) For atom-bound electrons in solids and fluids, $m \sim 10^{-30}$ kg, and $\omega_0 \sim 10^{15}$ s⁻¹, giving $x_0 \sim 0.3$ nm, of the order of the typical inter-atomic distances in condensed matter. As a result, classical mechanics is not valid at all for the analysis of their motion.

(ii) For atoms in solids, $m \approx 10^{-24}$ - 10^{-26} kg, and $\omega_0 \sim 10^{13}$ s⁻¹, giving $x_0 \sim 0.01$ – 0.1 nm, i.e. somewhat smaller than inter-atomic distances. Because of that, the methods based on classical mechanics (e.g., molecular dynamics) are approximately valid for the analysis of atomic motion, though they may miss some fine effects exhibited by lighter atoms – e.g., the so-called *quantum diffusion* of hydrogen atoms, due to their tunneling through the energy barriers of the potential profile created by other atoms.

(iii) Recently, the progress of patterning technologies has enabled the fabrication of high-quality *micromechanical* oscillators consisting of zillions of atoms. For example, the oscillator used in one of the pioneering experiments in this field⁹³ was a ~ 1 -μm thick membrane with a 60-μm diameter, and had $m \sim 2 \times 10^{-14}$ kg and $\omega_0 \sim 3 \times 10^{10}$ s⁻¹, so that $x_0 \sim 4 \times 10^{-16}$ m. It is remarkable that despite such extreme smallness of x_0 (much smaller than not only any atom but even any atomic nucleus!), quantum states of such oscillators may be manipulated and measured, using their coupling to electromagnetic (in particular, optical) resonant cavities.⁹⁴

Returning to the Schrödinger equation (261), in order to analyze its higher eigenstates, we will need more help from mathematics. Let us recast this equation into a dimensionless form by introducing the dimensionless variable $\xi \equiv x/x_0$. This gives

$$-\frac{d^2\psi}{d\xi^2} + \xi^2\psi = \varepsilon\psi, \quad (2.277)$$

where $\varepsilon \equiv 2E/\hbar\omega_0 = E/E_0$. In this notation, the ground-state wavefunction (275) is proportional to $\exp\{-\xi^2/2\}$. Using this clue, let us look for solutions to Eq. (277) in the form

$$\psi = C \exp\left\{-\frac{\xi^2}{2}\right\} H(\xi), \quad (2.278)$$

where $H(\xi)$ is a new function, and C is the normalization constant. With this substitution, Eq. (277) yields

$$\frac{d^2H}{d\xi^2} - 2\xi \frac{dH}{d\xi} + (\varepsilon - 1)H = 0. \quad (2.279)$$

⁹² By order of magnitude, such estimates are valid even for the systems whose dynamics is substantially different from that of harmonic oscillators, if a typical frequency of quantum transitions is taken for ω_0 .

⁹³ A. O'Connell *et al.*, *Nature* **464**, 697 (2010).

⁹⁴ See a review of such experiments by M. Aspelmeyer *et al.*, *Rev. Mod. Phys.* **86**, 1391 (2014), and also recent experiments with nanoparticles placed in much “softer” potential wells – e.g., by U. Delić *et al.*, *Science* **367**, 892 (2020).

It is evident that $H = \text{const}$ and $\varepsilon = 1$ is one of its solutions, describing the ground-state eigenfunction (275) and energy (274), but what are the other eigenstates and eigenvalues? Fortunately, the linear differential equation (274) was studied in detail in the mid-1800s by C. Hermite who has shown that all its eigenvalues are given by the set

$$\varepsilon_n - 1 = 2n, \quad \text{with } n = 0, 1, 2, \dots, \quad (2.280)$$

so that Eq. (262) is indeed exact for any n .⁹⁵ The eigenfunction of Eq. (279), corresponding to the eigenvalue ε_n , is a polynomial (called the *Hermite polynomial*) of degree n , which may be most conveniently calculated using the following explicit formula:

Hermite polynomials

$$H_n = (-1)^n \exp\{\xi^2\} \frac{d^n}{d\xi^n} \exp\{-\xi^2\}. \quad (2.281)$$

It is easy to use this formula to spell out several lowest-degree polynomials – see Fig. 35a:

$$H_0 = 1, \quad H_1 = 2\xi, \quad H_2 = 4\xi^2 - 2, \quad H_3 = 8\xi^3 - 12\xi, \quad H_4 = 16\xi^4 - 48\xi^2 + 12, \dots \quad (2.282)$$

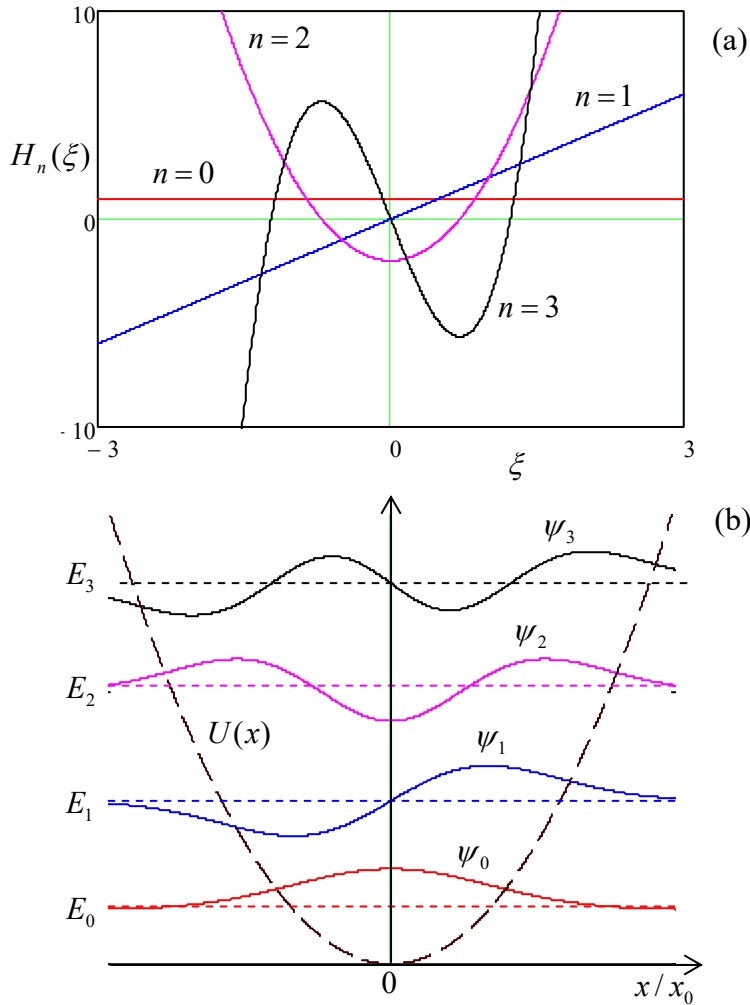


Fig. 2.35. (a) A few lowest Hermite polynomials and (b) the corresponding eigenenergies (horizontal dashed lines) and eigenfunctions (solid lines) of the harmonic oscillator. The black dashed curve shows the potential profile $U(x)$ drawn on the same scale as the energies E_n , so that its crossings with the energy levels correspond to classical turning points.

⁹⁵ Perhaps the most important property of this energy spectrum is that it is equidistant: $E_{n+1} - E_n = \hbar\omega_0 = \text{const}$.

The properties of these polynomials, which most important for applications, are as follows:

- (i) the function $H_n(\xi)$ has exactly n zeros (its plot crosses the ξ -axis exactly n times); as a result, the “parity” (symmetry-antisymmetry) of these functions alternates with n , and
- (ii) the polynomials are mutually orthonormal in the following sense:

$$\int_{-\infty}^{+\infty} H_n(\xi) H_{n'}(\xi) \exp\{-\xi^2\} d\xi = \pi^{1/2} 2^n n! \delta_{n,n'}. \quad (2.283)$$

Using the last property, we may readily calculate, from Eq. (278), the normalized eigenfunctions $\psi_n(x)$ of the harmonic oscillator – see Fig. 35b:

$$\psi_n(x) = \frac{1}{(2^n n!)^{1/2} \pi^{1/4} x_0^{1/2}} \exp\left\{-\frac{x^2}{2x_0^2}\right\} H_n\left(\frac{x}{x_0}\right). \quad (2.284)$$

Harmonic oscillator:
eigen-functions

At this point, it is instructive to compare these eigenfunctions with those of a 1D rectangular potential well, with its ultimately hard walls – see Fig. 1.8. Let us list their *common* features:

- (i) The wavefunctions oscillate in the classically allowed regions with $E_n > U(x)$, while dropping exponentially beyond the boundaries of that region. (For the rectangular well with infinite walls, the latter regions are infinitesimally narrow.)
- (ii) Each step up the energy level ladder increases the number of the oscillation half-waves (and hence the number of its zeros), by one.⁹⁶

And here are the major features *specific* for soft (e.g., the quadratic-parabolic) confinement:

- (i) The spatial spread of the wavefunction grows with n , following the gradual widening of the classically allowed region.
- (ii) Correspondingly, E_n exhibits a slower growth than the $E_n \propto n^2$ law given by Eq. (1.85), because the gradual reduction of spatial confinement moderates the kinetic energy’s growth.

Unfortunately, the “brute-force” approach to the harmonic oscillator problem, discussed above, is not too appealing. First, the proof of Eq. (281) is rather longish – so I do not have time/space for it. More importantly, it is hard to use Eq. (284) for the calculation of the expectation values of observables including the so-called *matrix elements* of the system – as we will see in Chapter 4, virtually the only numbers important for most applications. Finally, it is also almost evident that there has to be some straightforward math leading to any formula as simple as Eq. (262) for E_n . Indeed, there is a much more efficient, operator-based approach to this problem; it will be described in Sec. 5.4.

2.10. Exercise problems

2.1. The initial wave packet of a free 1D particle is described by Eq. (20):

$$\Psi(x,0) = \int a_k e^{ikx} dk.$$

⁹⁶ In mathematics, a slightly more general statement, valid for a broader class of ordinary linear differential equations, is frequently called the *Sturm oscillation theorem*, and is a part of the *Sturm-Liouville theory* of such equations – see, e.g., Chapter 10 in the handbook by G. Arfken *et al.*, cited in MA Sec. 16.

(i) Obtain a compact expression for the expectation value $\langle p \rangle$ of the particle's momentum at an arbitrary moment $t > 0$.

(ii) Calculate $\langle p \rangle$ for the case when the function $|a_k|^2$ is symmetric with respect to some value k_0 .

2.2. Calculate the function a_k defined by Eq. (20), for the wave packet with a rectangular spatial envelope:

$$\Psi(x,0) = \begin{cases} C \exp\{ik_0 x\}, & \text{for } -a/2 \leq x \leq +a/2, \\ 0, & \text{otherwise.} \end{cases}$$

Analyze the result in the limit $k_0 a \rightarrow \infty$.

2.3. Prove Eq. (49) for the 1D propagator of a free quantum particle, starting from Eq. (48).

2.4. Express the 1D propagator defined by Eq. (44), via the eigenfunctions and eigenenergies of a particle moving in an arbitrary stationary potential $U(x)$.

2.5. Calculate the change of the wavefunction of a 1D particle, resulting from a short pulse of an external classical force that may be approximated by the delta function:⁹⁷

$$F(t) = P\delta(t).$$

2.6. Calculate the transparency \mathcal{T} of the rectangular potential barrier (68),

$$U(x) = \begin{cases} 0, & \text{for } x < -d/2, \\ U_0, & \text{for } -d/2 < x < +d/2, \\ 0, & \text{for } d/2 < x, \end{cases}$$

for a particle of energy $E > U_0$. Analyze and interpret the result, taking into account that U_0 may be either positive or negative. (In the latter case, we are speaking about the particle's passage over a rectangular potential well of a finite depth $|U_0|$.)

2.7. Prove Eq. (117) for the case $\mathcal{T}_{\text{WKB}} \ll 1$, using the connection formulas (105).

2.8. Spell out the stationary wavefunctions of a harmonic oscillator in the WKB approximation, and use them to calculate the expectation values $\langle x^2 \rangle$ and $\langle x^4 \rangle$ for the eigenstate number $n \gg 1$.

2.9. Use the WKB approximation to express the expectation value of the kinetic energy of a 1D particle confined in a soft potential well, in its n^{th} stationary state, via the derivative dE_n/dn , for $n \gg 1$.

2.10. Use the WKB approximation to calculate the transparency \mathcal{T} of the following triangular potential barrier:

$$U(x) = \begin{cases} 0, & \text{for } x < 0, \\ U_0 - Fx, & \text{for } x > 0, \end{cases}$$

⁹⁷ The constant P is called the force's *impulse*. (In higher dimensionalities, it is a vector – just as the force is.)

with $F, U_0 > 0$, as a function of the incident particle's energy E .

Hint: Be careful with the sharp potential step at $x = 0$.

2.11.* Prove that the symmetry of the 1D scattering matrix S describing an arbitrary time-independent scatterer, allows its representation in the form (127).

2.12. Prove the universal relations between elements of the 1D transfer matrix T of a stationary (but otherwise arbitrary) scatterer, mentioned in Sec. 5.

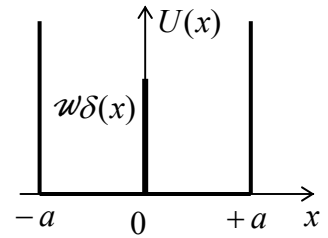
2.13. A 1D particle had been localized in a very narrow and deep potential well, with the “energy area” $\int U(x)dx$ equal to $-w$, where $w > 0$. Then (say, at $t = 0$) the well’s bottom is suddenly lifted up, so that the particle becomes completely free. Calculate the probability density, $w(k)$, to find the particle in a state with a certain wave number k at $t > 0$, and the total final energy of the system.

2.14. Calculate the lifetime of the metastable localized state of a 1D particle in the potential

$$U(x) = -w\delta(x) - Fx, \quad \text{with } w > 0,$$

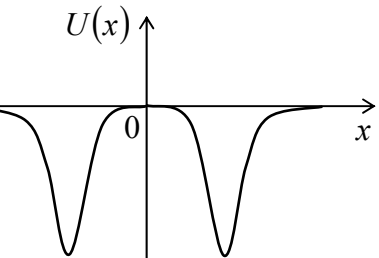
using the WKB approximation. Formulate the condition of validity of the result.

2.15. Calculate the energy levels and the corresponding eigenfunctions of a 1D particle placed into a flat-bottom potential well of width $2a$, with infinitely-high hard walls, and a transparent, short potential barrier in the middle – see the figure on the right. Discuss particle dynamics in the limit when w is very large but still finite.



2.16.* Consider a symmetric system of two potential wells of the type shown in Fig. 21, but with $U(0) = U(\pm\infty) = 0$ – see the figure on the right. What is the sign of the well interaction force due to their sharing a quantum particle of mass m , for the cases when the particle is in:

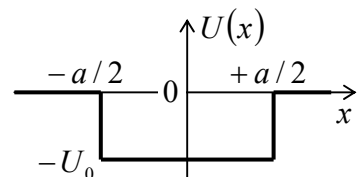
- (i) a symmetric localized eigenstate: $\psi_S(-x) = \psi_S(x)$?
- (ii) an antisymmetric localized eigenstate: $\psi_A(-x) = -\psi_A(x)$?



Use an alternative approach to verify your result for the particular case of delta-functional wells.

2.17. Derive and analyze the characteristic equation for localized eigenstates of a 1D particle in a rectangular potential well of a finite depth (see the figure on the right):

$$U(x) = \begin{cases} -U_0, & \text{for } |x| \leq a/2, \\ 0, & \text{otherwise.} \end{cases}$$



In particular, calculate the number of localized states as a function of well’s width a , and explore the limit $U_0 \ll \hbar^2/2ma^2$.

2.18. Calculate the energy of a 1D particle localized in a potential well of an arbitrary shape $U(x)$, provided that its width a is finite, and the average depth is very small:

$$|\bar{U}| \ll \frac{\hbar^2}{2ma^2}, \quad \text{where } \bar{U} \equiv \frac{1}{a} \int_{\text{well}} U(x) dx$$

2.19. A particle of mass m is moving in a field with the following potential:

$$U(x) = U_0(x) + w\delta(x),$$

where $U_0(x)$ is a smooth, symmetric function with $U_0(0) = 0$, growing monotonically at $x \rightarrow \pm\infty$.

- (i) Use the WKB approximation to derive the characteristic equation for the particle's energy spectrum, and
- (ii) semi-quantitatively describe the spectrum's evolution at the increase of $|w|$, for both signs of this parameter.

Make both results more specific for the quadratic-parabolic potential (111): $U_0(x) = m\omega_0^2 x^2/2$.

2.20. Prove Eq. (189), starting from Eq. (188).

2.21. For the problem discussed at the beginning of Sec. 7, i.e. the 1D particle's motion in an infinite Dirac comb potential shown in Fig. 24,

$$U(x) = w \sum_{j=-\infty}^{+\infty} \delta(x - ja), \quad \text{with } w > 0,$$

(where j takes integer values), write explicit expressions for the eigenfunctions at the very bottom and at the very top of the lowest energy band. Sketch both functions.

2.22. A 1D particle of mass m moves in an infinite periodic system of very narrow and deep potential wells that may be described by delta functions:

$$U(x) = w \sum_{j=-\infty}^{+\infty} \delta(x - ja), \quad \text{with } w < 0.$$

- (i) Sketch the energy band structure of the system for very small and very large values of the potential well's "weight" $|w|$, and
- (ii) calculate explicitly the ground state energy of the system in these two limits.

2.23. For the system discussed in the previous problem, write explicit expressions for the eigenfunctions of the system, corresponding to:

- (i) the bottom of the lowest energy band,
- (ii) the top of that band, and
- (iii) the bottom of each higher energy band.

Sketch these functions.

2.24.* The 1D "crystal" analyzed in the last two problems, now extends only to $x > 0$, with a sharp step to a flat potential plateau at $x < 0$:

$$U(x) = \begin{cases} w \sum_{j=1}^{+\infty} \delta(x - ja), & \text{with } w < 0, \\ U_0 > 0, & \text{for } x < 0. \end{cases} \quad \text{for } x > 0,$$

Prove that the system can have a set of the so-called *Tamm states*, localized near the “surface” $x = 0$, and calculate their energies in the limit when U_0 is very large but finite. (Quantify this condition.)⁹⁸

2.25. Calculate the whole transfer matrix of the rectangular potential barrier, specified by Eq. (68), for particle energies both below and above U_0 .

2.26. Use the results of the previous problem to calculate the transfer matrix of one period of the periodic Kronig-Penney potential shown in Fig. 31b.

2.27. Using the results of the previous problem, derive the characteristic equations for particle's motion in the periodic Kronig-Penney potential, for both $E < U_0$ and $E > U_0$. Try to bring the equations to a form similar to that obtained in Sec. 7 for the delta-functional barriers – see Eq. (198). Use the equations to formulate the conditions of applicability of the tight-binding and weak-potential approximations, in terms of the system's parameters, and the particle's energy E .

2.28. For the Kronig-Penney potential, use the tight-binding approximation to calculate the widths of the allowed energy bands. Compare the results with those of the previous problem (in the corresponding limit).

2.29. For the same Kronig-Penney potential, use the weak-potential limit formulas to calculate the energy gap widths. Again, compare the results with those of Problem 27, in the corresponding limit.

2.30. 1D periodic chains of atoms may exhibit what is called the *Peierls instability*, leading to the *Peierls transition* to a phase in which atoms are slightly displaced, from the exact periodicity, by alternating displacements $\Delta x_j = (-1)^j \Delta x$, with $\Delta x \ll a$, where j is the atom's number in the chain, and a is its initial period. These displacements lead to the alternation of the coupling amplitudes δ_n (see Eq. (204)) between close values δ_n^+ and δ_n^- . Use the tight-binding approximation to calculate the resulting change of the n^{th} energy band, and discuss the result.

2.31.* Use Eqs. (1.73)-(1.74) of the lecture notes to derive Eq. (252), and discuss the relation between these Bloch oscillations and the Josephson oscillations of frequency (1.75).

2.32. A 1D particle of mass m is placed to the following triangular potential well:

$$U(x) = \begin{cases} +\infty, & \text{for } x < 0, \\ Fx, & \text{for } x > 0, \end{cases} \quad \text{with } F > 0.$$

(i) Calculate its energy spectrum using the WKB approximation.

⁹⁸ In applications to electrons in solid-state crystals, the delta-functional potential wells model the attractive potentials of atomic nuclei, while U_0 represents the workfunction, i.e. the energy necessary for the extraction of an electron from the crystal to the free space – see, e.g., Sec. 1.1(ii), and also EM Sec. 2.6 and SM Sec. 6.3.

(ii) Estimate the ground state energy using the variational method, with two different trial functions.

(iii) Calculate the three lowest energy levels, and also the 10th level, with an accuracy better than 0.1%, from the exact solution of the problem.

(iv) Compare and discuss the results.

Hint: The values of the first zeros of the Airy function, necessary for Task (iii), may be found in many math handbooks, for example, in Table 9.9.1 of the online version of the collection edited by Abramowitz and Stegun – see MA Sec. 16(i).

2.33. Use the variational method to estimate the ground state energy E_g of a particle in the following potential well:

$$U(x) = -U_0 \exp\{-\alpha x^2\}, \quad \text{with } \alpha > 0, \text{ and } U_0 > 0.$$

Spell out the results in the limits of small and large U_0 , and give their interpretation.

2.34. For a 1D particle of mass m , placed to a potential well with the following profile,

$$U(x) = ax^{2s}, \quad \text{with } a > 0, \text{ and } s > 0,$$

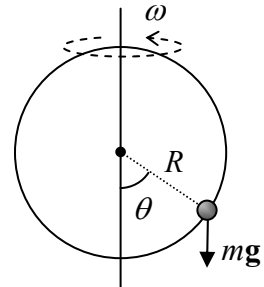
- (i) calculate its energy spectrum using the WKB approximation, and
- (ii) estimate the ground state energy using the variational method.

Compare the ground-state energy results for the parameter s equal to 1, 2, 3, and 100.

2.35. Use the variational method to estimate the 1st excited state of the 1D harmonic oscillator.

2.36. Assuming the quantum effects to be small, calculate the lower part of the energy spectrum of the following system: a small bead of mass m , free to move without friction along a ring of radius R , which is rotated about its vertical diameter with a constant angular velocity ω – see the figure on the right. Formulate a quantitative condition of validity of your results.

Hint: This system was used as the analytical mechanics' “testbed problem” in the CM part of this series, and the reader is welcome to use any relations derived there.



2.37. A 1D harmonic oscillator, with mass m and frequency ω_0 , had been in its ground state; then an additional force F was suddenly applied, and after that kept constant. Calculate the probability of the oscillator staying in its ground state.

2.38. A 1D particle of mass m has been placed to a quadratic potential well (111),

$$U(x) = \frac{m\omega_0^2 x^2}{2},$$

and allowed to relax into the ground state. At $t = 0$, the well was fast accelerated to move with velocity v , without changing its profile, so that at $t \geq 0$ the above formula for U is valid with the replacement $x \rightarrow x' \equiv x - vt$. Calculate the probability for the system to still be in the ground state at $t > 0$.

2.39. Initially, a 1D harmonic oscillator was in its ground state. At a certain moment of time, its spring constant κ is abruptly increased so that its frequency $\omega_0 = (\kappa/m)^{1/2}$ is increased by a factor of α , and then is kept constant at the new value. Calculate the probability that after the change, the oscillator is still in its ground state.

2.40. A 1D particle is placed into the following potential well:

$$U(x) = \begin{cases} +\infty, & \text{for } x < 0, \\ m\omega_0^2 x^2 / 2, & \text{for } x \geq 0. \end{cases}$$

(i) Find its eigenfunctions and eigenenergies.

(ii) This system had been let to relax into its ground state, and then the potential wall at $x < 0$ was rapidly removed so that the system was instantly turned into the usual harmonic oscillator (with the same m and ω_0). Find the probability for the oscillator to remain in its ground state.

2.41. Prove the following formula for the propagator of the 1D harmonic oscillator:

$$G(x, t; x_0, t_0) = \left(\frac{m\omega_0}{2\pi i\hbar \sin[\omega_0(t - t_0)]} \right)^{1/2} \exp \left\{ \frac{i m \omega_0}{2\hbar \sin[\omega_0(t - t_0)]} \left[(x^2 + x_0^2) \cos[\omega_0(t - t_0)] - 2x x_0 \right] \right\}.$$

Discuss the relation between this formula and the propagator of a free 1D particle.

2.42. In the context of the Sturm oscillation theorem mentioned in Sec. 9, prove that the number of eigenfunction's zeros of a particle confined in an arbitrary but finite potential well always increases with the corresponding eigenenergy.

Hint: You may like to use the suitably modified Eq. (186).

2.43.* Use the WKB approximation to calculate the lifetime of the metastable ground state of a 1D particle of mass m in the “pocket” of the potential profile

$$U(x) = \frac{m\omega_0^2}{2} x^2 - \alpha x^3.$$

Contemplate the significance of this problem.

Chapter 3. Higher Dimensionality Effects

The description of the basic quantum-mechanical effects, given in the previous chapter, may be extended to higher dimensions in an obvious way. This is why this chapter is focused on the phenomena (such as the AB effect and the Landau levels) that cannot take place in one dimension due to topological reasons, and also on a few key 3D problems (such as the Born approximation in the scattering theory, and the axially- and spherically-symmetric systems) that are important for numerous applications.

3.1. Quantum interference and the AB effect

In the past two chapters, we have already discussed some effects of the de Broglie wave interference. For example, standing waves inside a potential well, or even on the top of a potential barrier, may be considered as a result of interference of incident and reflected waves. However, there are some remarkable new effects made possible by spatial separation of such waves, and such separation requires a higher (either 2D or 3D) dimensionality. A good example of wave separation is provided by the Young-type experiment (Fig. 1) in which particles, emitted by the same source, are passed through two narrow holes (or slits) in an otherwise opaque partition.

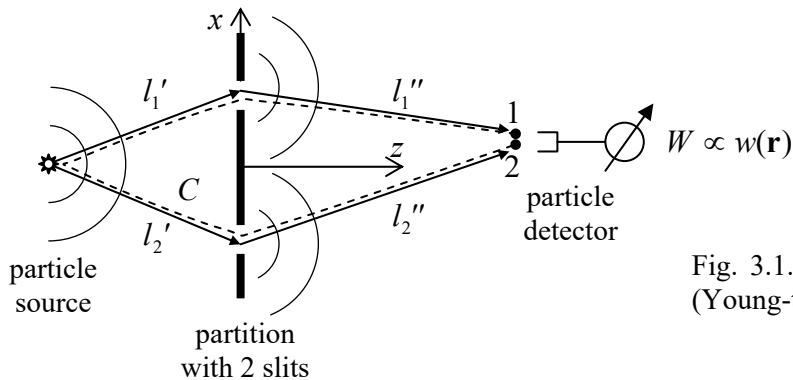


Fig. 3.1. The scheme of the “two-slit” (Young-type) interference experiment.

According to Eq. (1.22), if particle interactions are negligible (which is always true if the emission rate is sufficiently low), the average rate of particle counting by the detector is proportional to the probability density $w(\mathbf{r}, t) = \Psi(\mathbf{r}, t) \Psi^*(\mathbf{r}, t)$ to find a single particle at the detector’s location \mathbf{r} , where $\Psi(\mathbf{r}, t)$ is the solution of the single-particle Schrödinger equation (1.25) for the system. Let us calculate the rate for the case when the incident particles may be represented by virtually-monochromatic waves of energy E (e.g., very long wave packets), so that their wavefunction may be taken in the form given by Eqs. (1.57) and (1.62): $\Psi(\mathbf{r}, t) = \psi(\mathbf{r}) \exp\{-iEt/\hbar\}$. In this case, in the free-space parts of the system, where $U(\mathbf{r}) = 0$, $\psi(\mathbf{r})$ satisfies the stationary Schrödinger equation (1.78a):

$$-\frac{\hbar^2}{2m} \nabla^2 \psi = E \psi . \quad (3.1a)$$

With the standard definition $k \equiv (2mE)^{1/2}/\hbar$, it may be rewritten as the 3D Helmholtz equation:

$$\nabla^2 \psi + k^2 \psi = 0 . \quad (3.1b)$$

The opaque parts of the partition may be well described as classically forbidden regions, so if their size scale a is much larger than the wavefunction penetration depth δ described by Eq. (2.59), we may use on their surface S the same boundary conditions as for the well's walls of infinite height:

$$\psi|_S = 0. \quad (3.2)$$

Eqs. (1) and (2) describe the standard boundary problem of the theory of propagation of scalar waves of any nature. For an arbitrary geometry, this problem does not have a simple analytical solution. However, for a conceptual discussion of wave interference, we may use certain natural assumptions that will allow us to find its particular, approximate solution.

First, let us discuss the wave emission, into free space, by a small-size, isotropic source located at the origin of our reference frame. Naturally, the emitted wave should be spherically symmetric: $\psi(\mathbf{r}) = \psi(r)$. Using the well-known expression for the Laplace operator in spherical coordinates,¹ we may reduce Eq. (1) to the following ordinary differential equation:

$$\frac{1}{r^2} \frac{d}{dr} \left(r^2 \frac{d\psi}{dr} \right) + k^2 \psi = 0. \quad (3.3)$$

Let us introduce a new function, $f(r) \equiv r\psi(r)$. Plugging the reciprocal relation $\psi = f/r$ into Eq. (3), we see that it is reduced to the 1D wave equation,

$$\frac{d^2 f}{dr^2} + k^2 f = 0. \quad (3.4)$$

As was discussed in Sec. 2.2, for a fixed k , the general solution of Eq. (4) may be represented in the form of two traveling waves:

$$f = f_+ e^{ikr} + f_- e^{-ikr} \quad (3.5)$$

so that the full wavefunction is

$$\psi(\mathbf{r}) = \frac{f_+}{r} e^{ikr} + \frac{f_-}{r} e^{-ikr}, \quad \text{i.e. } \Psi(\mathbf{r}, t) = \frac{f_+}{r} e^{i(kr - \omega t)} + \frac{f_-}{r} e^{-i(kr + \omega t)}, \quad \text{with } \omega \equiv \frac{E}{\hbar} = \frac{\hbar k^2}{2m}. \quad (3.6)$$

If the source is located at point $\mathbf{r}' \neq 0$, the obvious generalization of Eq. (6) is

$$\Psi(\mathbf{r}, t) = \frac{f_+}{R} e^{i(kR - \omega t)} + \frac{f_-}{R} e^{-i(kR + \omega t)}, \quad \text{with } R \equiv |\mathbf{R}|, \quad \mathbf{R} \equiv \mathbf{r} - \mathbf{r}'. \quad (3.7)$$

The first term of this solution describes a spherically-symmetric wave propagating from the source outward, while the second one, a wave converging onto the source point \mathbf{r}' from large distances. Though the latter solution is possible at some very special circumstances (say, when the outgoing wave is reflected back from a spherical shell), for our current problem, only the outgoing waves are relevant, so that we may keep only the first term (proportional to f_+) in Eq. (7). Note that the factor R is the denominator (that was absent in the 1D geometry) has a simple physical sense: it provides the independence of the full probability current $I = 4\pi R^2 j(R)$, with $j(R) \propto k\Psi\Psi^* \propto 1/R^2$, of the distance R between the observation point and the source.

¹ See, e.g., MA Eq. (10.9) with $\partial/\partial\theta = \partial/\partial\varphi = 0$.

Now let us assume that the partition's geometry is not too complicated – for example, it is either planar as shown in Fig. 1, or nearly-planar, and consider the region of the particle detector location far behind the partition (at $z \gg 1/k$), and at a relatively small angle to it: $|x| \ll z$. Then it should be physically clear that the spherical waves (7) emitted by each point inside the slit cannot be perturbed too much by the opaque parts of the partition, and their only role is the restriction of the set of such emitting points to the area of the slits. Hence, an approximate solution of the boundary problem is given by the following *Huygens principle*: the wave behind the partition looks as if it was the sum of contributions (7) of point sources located in the slits, with each source's strength f_+ proportional to the amplitude of the wave arriving at this pseudo-source from the real source – see Fig. 1. This principle finds its confirmation in the strict wave theory, which shows that with our assumptions, the solution of the boundary problem (1)-(2) may be represented as the following *Kirchhoff integral*:²

Kirchhoff integral

$$\psi(\mathbf{r}) = c \int_{\text{slits}} \frac{\psi(\mathbf{r}')}{R} e^{ikR} d^2 r', \quad \text{with } c = \frac{k}{2\pi i}. \quad (3.8)$$

If the source is also far from the partition, its wave's front is almost parallel to the slit plane, and if the slits are not too broad, we can take $\psi(\mathbf{r}')$ constant ($\psi_{1,2}$) at each slit, so that Eq. (8) is reduced to

$$\psi(\mathbf{r}) = a''_1 \exp\{ikl''_1\} + a''_2 \exp\{ikl''_2\}, \quad \text{with } a''_{1,2} = \frac{cA_{1,2}}{l''_{1,2}} \psi_{1,2}, \quad (3.9)$$

where $A_{1,2}$ are the slit areas, and $l''_{1,2}$ are the distances from the slits to the detector. The wavefunctions on the slits may be calculated approximately³ by applying the same Eq. (7) to the region *before* the slits: $\psi_{1,2} \approx (f_+/l'_{1,2}) \exp\{ikl'_{1,2}\}$, where $l'_{1,2}$ are the distances from the source to the slits – see Fig. 1. As a result, Eq. (9) may be rewritten as

Wave-function superposition

$$\psi(\mathbf{r}) = a_1 \exp\{ikl_1\} + a_2 \exp\{ikl_2\}, \quad \text{with } l_{1,2} \equiv l'_{1,2} + l''_{1,2}; \quad a_{1,2} \equiv \frac{c f_+ A_{1,2}}{l'_{1,2} l''_{1,2}}. \quad (3.10)$$

(As Fig. 1 shows, each of $l_{1,2}$ is the full length of the classical path of the particle from the source, through the corresponding slit, and further to the observation point \mathbf{r} .)

According to Eq. (10), the resulting rate of particle counting at point \mathbf{r} is proportional to

$$w(\mathbf{r}) = \psi(\mathbf{r}) \psi^*(\mathbf{r}) = |a_1|^2 + |a_2|^2 + 2|a_1 a_2| \cos \varphi_{12}, \quad (3.11)$$

where

$$\varphi_{12} \equiv k(l_2 - l_1) \quad (3.12)$$

is the difference of the total wave phase accumulations along each of two alternative paths. The last expression may be evidently generalized as

² For the proof and a detailed discussion of Eq. (8), see, e.g., EM Sec. 8.5.

³ A possible (and reasonable) concern about the application of Eq. (7) to the field in the slits is that it ignores the effect of opaque parts of the partition. However, as we know from Chapter 2, the main role of the classically forbidden region is reflecting the incident wave toward its source (i.e. to the left in Fig. 1). As a result, the contribution of this reflection to the field inside the slits is insignificant if $A_{1,2} \gg \lambda^2$, and even in the opposite case provides just some rescaling of the amplitudes $a_{1,2}$, which is not important for our conceptual discussion.

$$\varphi_{12} = \oint_C \mathbf{k} \cdot d\mathbf{r}, \quad (3.13)$$

with integration along the virtually closed contour C (see the dashed line in Fig. 1), i.e. from point 1, in the positive (i.e. counterclockwise) direction all the way to point 2. (From our discussion of the 1D WKB approximation in Sec. 2.4, we may expect such generalization to be valid even if k changes, sufficiently slowly, along the paths.)

Our result (11)-(12) shows that the particle counting rate oscillates as a function of the difference $(l_2 - l_1)$, which in turn changes with the detector's position, giving the famous interference pattern, with the amplitude proportional to the product $|a_1 a_2|$, and hence vanishing if any of the slits is closed. For the wave theory, this is a well-known result,⁴ but for particle physics, it was (and still is :-:) rather shocking. Indeed, our analysis is valid for a very low particle emission rate, so that there is no other way to interpret the pattern other than resulting from a particle's interference *with itself* – or rather the interference of its de Broglie waves passing through each of two slits.⁵ Nowadays, such interference is reliably observed not only for electrons but also for much heavier particles: atoms and molecules, including very complex organic ones;⁶ moreover, atomic interferometers are used as ultra-sensitive instruments for measurements of gravity, rotation, and tilt.⁷

Let us now discuss a very interesting effect of magnetic field on quantum interference. To simplify our discussion, let us consider a slightly different version of the two-slit experiment, in which each of the two alternative paths is constricted to a narrow channel using partial confinement – see Fig. 2. (In this arrangement, moving the particle detector without changing channels' geometry, and hence local values of k may be more problematic experimentally, so let us think about its position \mathbf{r} as fixed.) In this case, because of the effect of the walls providing the path confinement, we cannot use Eqs. (10) for the amplitudes $a_{1,2}$. However, from the discussions in Sec. 1.6 and Sec. 2.2, it should be clear that the first of the expressions (10) remains valid, though maybe with a value of k specific for each channel.

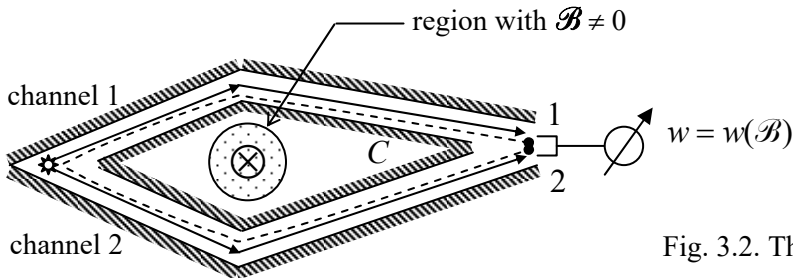


Fig. 3.2. The AB effect.

In this geometry, we can apply some local magnetic field \mathcal{B} , say normal to the plane of particle motion, whose lines would pierce, but not touch the contour C drawn along the particle propagation

⁴ See, e.g., a detailed discussion in EM Sec. 8.4.

⁵ Here I have to mention the fascinating experiments (first performed in 1987 by C. Hong *et al.* with photons, and recently, in 2015, by R. Lopes *et al.*, with non-relativistic particles – helium atoms) on the interference of de Broglie waves of *independent* but *identical* particles, in the same internal quantum state and virtually the same values of E and k . These experiments raise the important issue of particle *indistinguishability*, which will be discussed in Sec. 8.1.

⁶ See, e.g., the recent demonstration of the quantum interference of oligo-porphyrin molecules, consisting of ~2,000 atoms, with a total mass above $25,000 m_p$ – Y. Fein *et al.*, *Nature Physics* **15**, 1242 (2019).

⁷ See, e.g., the review paper by A. Cronin, J. Schmiedmayer, and D. Pritchard, *Rev. Mod. Phys.* **81**, 1051 (2009).

channels – see the dashed line in Fig. 2. In classical electrodynamics,⁸ the external magnetic field's effect on a particle with electric charge q is described by the *Lorentz force*

$$\mathbf{F}_{\mathcal{B}} = q\mathbf{v} \times \mathcal{B}, \quad (3.14)$$

where \mathcal{B} is the field value at the point of its particle's location, so that for the experiment shown in Fig. 2, $\mathbf{F}_{\mathcal{B}} = 0$, and the field would not affect the particle motion at all. In quantum mechanics, this is not so, and the field does affect the probability density w , even if $\mathcal{B} = 0$ at all points where the wavefunction $\psi(\mathbf{r})$ is not equal to zero.

In order to describe this surprising effect, let us first develop a general framework for an account of electromagnetic field effects on a quantum particle, which will also give us some by-product results important for forthcoming discussions. To do that, we need to calculate the Hamiltonian of a charged particle in electric and magnetic fields. For an electrostatic field, this is easy. Indeed, from classical electrodynamics we know that such field may be represented as a gradient of its electrostatic potential ϕ ,

$$\mathcal{E} = -\nabla\phi(\mathbf{r}), \quad (3.15)$$

so that the force exerted by the field on a particle with electric charge q ,

$$\mathbf{F}_{\mathcal{E}} = q\mathcal{E}, \quad (3.16)$$

may be described by adding the field-induced potential energy,

$$U(\mathbf{r}) = q\phi(\mathbf{r}), \quad (3.17)$$

to other (possible) components of the full potential energy of the particle. As was already discussed in Sec. 1.4, such potential energy may be included in the particle's Hamiltonian operator just by adding it to the kinetic energy operator – see Eq. (1.41).

However, the magnetic field's effect is peculiar: since its Lorentz force (14) cannot do any work on a classical particle:

$$d\mathcal{W}_{\mathcal{B}} \equiv \mathbf{F}_{\mathcal{B}} \cdot d\mathbf{r} = \mathbf{F}_{\mathcal{B}} \cdot \mathbf{v} dt = q(\mathbf{v} \times \mathcal{B}) \cdot \mathbf{v} dt = 0, \quad (3.18)$$

the field cannot be represented by any potential energy, so it may not be immediately clear how to account for it in the Hamiltonian. The crucial help comes from the analytical-mechanics approach to classical electrodynamics:⁹ in the non-relativistic limit, the Hamiltonian function of a particle in an electromagnetic field looks like that in the electric field only:

$$H = \frac{mv^2}{2} + U = \frac{p^2}{2m} + q\phi; \quad (3.19)$$

however, the momentum $\mathbf{p} \equiv mv$ that participates in this expression is now the difference

$$\mathbf{p} = \mathbf{P} - q\mathbf{A}. \quad (3.20)$$

Here \mathbf{A} is the vector potential, defined by the well-known relations for the electric and magnetic fields:¹⁰

⁸ See, e.g., EM Sec. 5.1. Note that Eq. (14), as well as all other formulas of this course, are in the SI units.

⁹ See, e.g., EM Sec. 9.7, in particular Eq. (9.196).

¹⁰ See, e.g., EM Sec. 6.1, in particular Eqs. (6.7).

$$\mathcal{E} = -\nabla\phi - \frac{\partial\mathbf{A}}{\partial t}, \quad \mathcal{B} = \nabla \times \mathbf{A}, \quad (3.21)$$

while \mathbf{P} is the *canonical momentum*, whose Cartesian components may be calculated (in classics) from the Lagrangian function L using the standard formula of analytical mechanics,

$$P_j \equiv \frac{\partial L}{\partial v_j}. \quad (3.22)$$

To emphasize the difference between the two momenta, $\mathbf{p} = m\mathbf{v}$ is frequently called the *kinematic momentum* (or “ $m\mathbf{v}$ -momentum”). The distinction between \mathbf{p} and $\mathbf{P} = \mathbf{p} + q\mathbf{A}$ becomes more clear if we notice that the vector potential is not *gauge-invariant*: according to the second of Eqs. (21), at the so-called *gauge transformation*

$$\mathbf{A} \rightarrow \mathbf{A} + \nabla\chi, \quad (3.23)$$

with an arbitrary single-valued scalar *gauge function* $\chi = \chi(\mathbf{r}, t)$, the magnetic field does not change. Moreover, according to the first of Eqs. (21), if we make the simultaneous replacement

$$\phi \rightarrow \phi - \frac{\partial\chi}{\partial t}, \quad (3.24)$$

the gauge transformation does not affect the electric field either. With that, the gauge function’s choice does not affect the classical particle’s equation of motion, and hence the velocity \mathbf{v} and momentum \mathbf{p} . Hence, the kinematic momentum is gauge-invariant, while \mathbf{P} is not, because according to Eqs. (20) and (23), the introduction of χ changes it by $q\nabla\chi$.

Now the standard way of transfer to quantum mechanics is to treat the canonical rather than kinematic momentum as prescribed by the correspondence postulate discussed in Sec. 1.2. This means that in the wave mechanics, the operator of this variable is still given by Eq. (1.26):¹¹

$$\hat{\mathbf{P}} = -i\hbar\nabla. \quad (3.25)$$

Canonical momentum operator

Hence the Hamiltonian operator corresponding to the classical function (19) is

$$\hat{H} = \frac{1}{2m}(-i\hbar\nabla - q\mathbf{A})^2 + q\phi \equiv -\frac{\hbar^2}{2m}\left(\nabla - \frac{iq}{\hbar}\mathbf{A}\right)^2 + q\phi, \quad (3.26)$$

Charged particle in EM field

so that the stationary Schrödinger equation (1.60) of a particle moving in an electromagnetic field (but otherwise free) is

$$-\frac{\hbar^2}{2m}\left(\nabla - \frac{iq}{\hbar}\mathbf{A}\right)^2\psi + q\phi\psi = E\psi, \quad (3.27)$$

We may now repeat all the calculations of Sec. 1.4 for the case $\mathbf{A} \neq 0$, and get the following generalized expression for the probability current density:

¹¹ The validity of this choice is clear from the fact that if the *kinetic* momentum was described by this differential operator, the Hamiltonian operator corresponding to the classical Hamiltonian function (19), and the corresponding Schrödinger equation would not describe the magnetic field effects at all.

$$\mathbf{j} = \frac{\hbar}{2im} \left[\psi^* \left(\nabla - \frac{iq}{\hbar} \mathbf{A} \right) \psi - \text{c.c.} \right] \equiv \frac{1}{2m} [\psi^* \hat{\mathbf{p}} \psi - \text{c.c.}] \equiv \frac{\hbar}{m} |\psi|^2 \left(\nabla \varphi - \frac{q}{\hbar} \mathbf{A} \right). \quad (3.28)$$

We see that the current density is gauge-invariant (as required for any observable) only if the wavefunction's phase φ changes as

$$\varphi \rightarrow \varphi + \frac{q}{\hbar} \chi. \quad (3.29)$$

This may be a point of conceptual concern: since quantum interference is described by the spatial dependence of the phase φ , can the observed interference pattern depend on the gauge function's choice? (That would not make any sense, because we may change the gauge in our mind.) Fortunately, this is not true, because the spatial phase *difference* between two interfering paths, participating in Eq. (12), is gauge-transformed as

$$\varphi_{12} \rightarrow \varphi_{12} + \frac{q}{\hbar} (\chi_2 - \chi_1). \quad (3.30)$$

But χ has to be a single-valued function of coordinates, hence in the limit when the points 1 and 2 coincide, $\chi_1 = \chi_2$, so that $\Delta\varphi$ gauge-invariant, and so is the interference pattern.

However, the difference φ *may be* affected by the magnetic field, even if it is localized outside the channels in which the particle propagates. Indeed, in this case, the field cannot affect the particle's velocity \mathbf{v} and the probability current density \mathbf{j} :

$$\mathbf{j}(\mathbf{r})|_{\mathcal{B} \neq 0} = \mathbf{j}(\mathbf{r})|_{\mathcal{B}=0}, \quad (3.31)$$

so that the last form of Eq. (28) yields

$$\nabla \varphi(\mathbf{r})|_{\mathcal{B} \neq 0} = \nabla \varphi(\mathbf{r})|_{\mathcal{B}=0} + \frac{q}{\hbar} \mathbf{A}. \quad (3.32)$$

Integrating this equation along the contour C (Fig. 2), for the phase difference between points 1 and 2 we get

$$\varphi_{12}|_{\mathcal{B} \neq 0} = \varphi_{12}|_{\mathcal{B}=0} + \frac{q}{\hbar} \oint_C \mathbf{A} \cdot d\mathbf{r}, \quad (3.33)$$

where the integral should be taken along the same contour C as before (in Fig. 2, from point 1, counterclockwise along the dashed line to point 2). But from classical electrodynamics we know¹² that as points 1 and 2 tend to each other, i.e. the contour C becomes closed, the last integral is just the magnetic flux $\Phi \equiv \int \mathcal{B}_n d^2 r$ through any smooth surface limited by the contour, so that Eq. (33) may be rewritten as

$$\boxed{\varphi_{12}|_{\mathcal{B} \neq 0} = \varphi_{12}|_{\mathcal{B}=0} + \frac{q}{\hbar} \Phi.} \quad (3.34a)$$

In terms of the interference pattern, this means a shift of interference fringes, proportional to the magnetic flux (Fig. 3).

AB
effect

¹² See, e.g., EM Sec. 5.3.

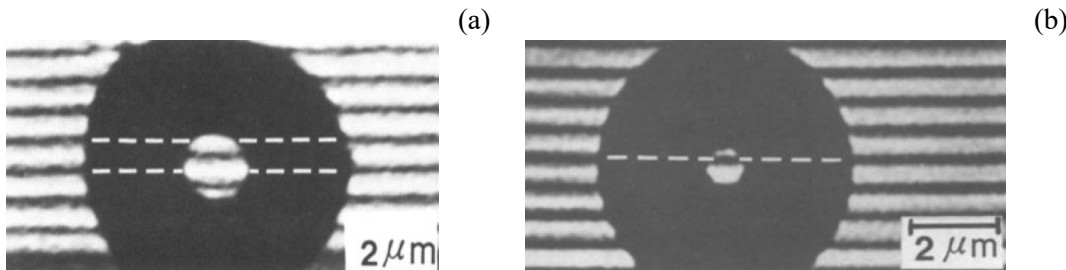


Fig. 3.3. Typical results of a two-paths interference experiment by A. Tonomura *et al.*, *Phys. Rev. Lett.* **56**, 792 (1986), showing the AB effect for electrons well shielded from the applied magnetic field. In this particular experimental geometry, the AB effect produces a relative shift of the interference patterns inside and outside the dark ring. (a) $\Phi = \Phi_0'/2$, (b) $\Phi = \Phi_0'$. © 1986 APS.

This phenomenon is usually called the “Aharonov-Bohm” (or just the *AB*) effect.¹³ For particles with a single elementary charge, $q = \pm e$, this result is frequently represented as

$$\varphi_{12} \Big|_{\mathcal{B} \neq 0} = \varphi_{12} \Big|_{\mathcal{B} = 0} \pm 2\pi \frac{\Phi}{\Phi_0'}, \quad (3.34b)$$

where the fundamental constant $\Phi_0' \equiv 2\pi\hbar/e \approx 4.14 \times 10^{-15}$ Wb has the meaning of the magnetic flux necessary to change φ_{12} by 2π , i.e. to shift the interference pattern (11) by one period, and is called the *normal magnetic flux quantum* – “normal” because of the reasons we will soon discuss.

The AB effect may be “almost explained” classically, in terms of Faraday’s electromagnetic induction. Indeed, a change $\Delta\Phi$ of magnetic flux in time induces a vortex-like electric field $\Delta\mathcal{E}$ around it. That field is *not* restricted to the magnetic field’s location, i.e. may reach the particle’s trajectories. The field’s magnitude (or rather of its integral along the contour C) may be readily calculated by integration of the first of Eqs. (21):

$$\Delta V \equiv \oint_C \Delta\mathcal{E} \cdot d\mathbf{r} = -\frac{d\Phi}{dt}. \quad (3.35)$$

I hope that in this expression the reader readily recognizes the integral (“undergraduate”) form of Faraday’s induction law.¹⁴ To calculate the effect of this electric field of the particles, let us assume that the variable separation described by Eq. (1.57) may be applied to the end points 1 and 2 of particle’s alternative trajectories as two independent systems,¹⁵ and that the magnetic flux’ change by a certain amount $\Delta\Phi$ does not change the spatial factors $\psi_{1,2}$, with the phases $\varphi_{1,2}$ included into the time-dependent factors $a_{1,2}$. Then we may repeat the arguments that were used in Sec. 1.6 at the discussion of

¹³ I prefer the latter, less personable name, because the effect had been actually predicted by Werner Ehrenberg and Raymond Siday in 1949, before it was rediscovered (also theoretically) by Y Aharonov and D. Bohm in 1959. To be fair to Aharonov and Bohm, it was their work that triggered a wave of interest in the phenomenon, resulting in its first experimental observation by Robert G. Chambers in 1960 and several other groups soon after that. Later, the experiments were improved using ferromagnetic cores and/or superconducting shielding to provide a better separation between the electrons and the applied field – as in the work whose result is shown in Fig. 3.

¹⁴ See, e.g., EM Sec. 6.1.

¹⁵ This assumption may seem a little bit of a stretch, but the resulting relation (37) may be indeed proven for a rather realistic model, though that would take more time/space than I can afford.

the Josephson effect, and since the change (35) leads to the change of the potential energy difference $\Delta U = q\Delta V$ between the two points, we may rewrite Eq. (1.72) as

$$\frac{d\varphi_{12}}{dt} = -\frac{\Delta U}{\hbar} = -\frac{q}{\hbar} \Delta V = \frac{q}{\hbar} \frac{d\Phi}{dt}. \quad (3.36)$$

Integrating this relation over the time of the magnetic field's change, we get

$$\Delta\varphi_{12} = \frac{q}{\hbar} \Delta\Phi, \quad (3.37)$$

- superficially, the same result as given by Eq. (34).

However, this interpretation of the AB effect is limited. Indeed, it requires the particle to be in the system (on the way from the source to the detector) during the flux change, i.e. when the induced electric field \mathcal{E} may affect its dynamics. On the contrary, Eq. (34) predicts that the interference pattern would shift even if the field change has been made when there was no particle in the system, and hence the field \mathcal{E} could not be felt by it. Experiment confirms the latter conclusion. Hence, there is *something* in the space where a particle propagates (i.e., outside of the magnetic field region), that transfers the information about even the static magnetic field to the particle. The standard interpretation of this surprising fact is as follows: the vector potential \mathbf{A} is not just a convenient mathematical tool, but a physical reality (just as its scalar counterpart ϕ), despite the large freedom of choice we have in prescribing specific spatial and temporal dependences of these potentials without affecting any observable – see Eqs. (23)-(24).

To conclude this section, let me briefly discuss the very interesting form taken by the AB effect in superconductivity. To be applied to this case, our results require two changes. The first one is simple: since superconductivity may be interpreted as the Bose-Einstein condensate of Cooper pairs with electric charge $q = -2e$, Φ_0 has to be replaced by the so-called *superconducting flux quantum*¹⁶

$$\Phi_0 \equiv \frac{\pi\hbar}{e} \approx 2.07 \times 10^{-15} \text{ Wb} = 2.07 \times 10^{-7} \text{ Gs} \cdot \text{cm}^2.$$

(3.38)

Superconducting flux quantum

Second, since the pairs are Bose particles and are all condensed in the same (ground) quantum state, described by the same wavefunction, the total electric current density, proportional to the probability current density j , may be extremely large – in practical superconducting materials, up to $\sim 10^{12} \text{ A/m}^2$. In these conditions, one cannot neglect the contribution of that current into the magnetic field and hence into its flux Φ , which (according to the Lenz rule of the Faraday induction law) tries to compensate for changes in external flux. To see possible results of this contribution, let us consider a closed superconducting loop (Fig. 4). Due to the Meissner effect (which is just another version of the flux self-compensation), the current and magnetic field penetrate into a superconductor by only a small distance (called the *London penetration depth*) $\delta_L \sim 10^{-7} \text{ m}$.¹⁷ If the loop is made of a superconducting “wire” that is considerably thicker than δ_L , we may draw a contour deep inside the wire, at that the current density is negligible. According to the last form of Eq. (28), everywhere at the contour,

$$\nabla\varphi - \frac{q}{\hbar} \mathbf{A} = 0. \quad (3.39)$$

¹⁶ One more bad, though common term: a metallic wire may (super)conduct, but a quantum hardly can!

¹⁷ For more detail, see EM Sec. 6.4.

Integrating this equation along the contour as before (in Fig. 4, from some point 1, all the way around the ring to the virtually coinciding point 2), we need to have the phase difference φ_{12} equal to $2\pi n$, because the wavefunction $\psi \propto \exp\{i\varphi\}$ in the initial and final points 1 and 2 should be “essentially” the same, i.e. produce the same observables. As a result, we get

$$\Phi \equiv \oint_C \mathbf{A} \cdot d\mathbf{r} = \frac{\hbar}{q} 2\pi n \equiv n\Phi_0. \quad (3.40)$$

Flux quantization

This is the famous *flux quantization effect*,¹⁸ which justifies the term “magnetic flux quantum” for the constant Φ_0 given by Eq. (38).

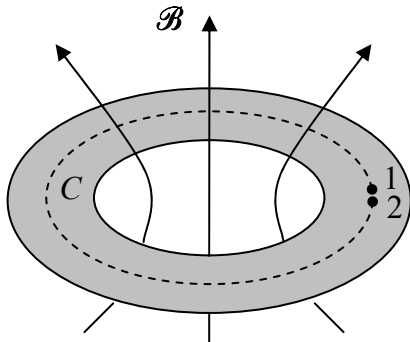


Fig. 3.4. The magnetic flux quantization in a superconducting loop (schematically).

Unfortunately, in this course I have no space/time to discuss the very interesting effects of “partial flux quantization” that arise when a superconductor loop is closed with a Josephson junction, forming the so-called *Superconductor QUantum Interference Device* – “SQUID”. Such devices are used, in particular, for supersensitive magnetometry and ultrafast, low-power computing.¹⁹

3.2. Landau levels and quantum Hall effect

In the last section, we have used the Schrödinger equation (27) for an analysis of static magnetic field effects in “almost-1D”, circular geometries shown in Figs. 1, 2, and 4. However, this equation describes very interesting effects in fully-higher-dimensions as well, especially in the 2D case. Let us consider a quantum particle free to move in the $[x, y]$ plane only (say, due to its strong confinement in the perpendicular direction z – see the discussion in Sec. 1.8). Taking the confinement energy for the reference, we may reduce Eq. (27) to a similar equation, but with the Laplace operator acting only in the directions x and y :

$$-\frac{\hbar^2}{2m} \left(\mathbf{n}_x \frac{\partial}{\partial x} + \mathbf{n}_y \frac{\partial}{\partial y} - i \frac{q}{\hbar} \mathbf{A} \right)^2 \psi = E \psi. \quad (3.41)$$

Let us find its solutions for the simplest case when the applied static magnetic field is uniform and perpendicular to the motion plane:

$$\mathcal{B} = \mathcal{B} \mathbf{n}_z. \quad (3.42)$$

¹⁸ It was predicted in 1949 by Fritz London and experimentally discovered (independently and virtually simultaneously) in 1961 by two experimental groups: B. Deaver and W. Fairbank, and R. Doll and M. Nähauer.

¹⁹ A brief review of these effects, and recommendations for further reading may be found in EM Sec. 6.5.

According to the second of Eqs. (21), this relation imposes the following restriction on the choice of the vector potential:

$$\frac{\partial A_y}{\partial x} - \frac{\partial A_x}{\partial y} = \mathcal{B}, \quad (3.43)$$

but the gauge transformations still give us a lot of freedom in its choice. The “natural” axially-symmetric form, $\mathbf{A} = \mathbf{n}_\phi \rho \mathcal{B}/2$, where $\rho = (x^2 + y^2)^{1/2}$ is the distance from some z -axis, leads to cumbersome math. In 1930, L. Landau realized that the energy spectrum of Eq. (41) may be obtained by making a much simpler, though very counter-intuitive choice:

$$A_x = 0, \quad A_y = \mathcal{B}(x - x_0), \quad (3.44)$$

(with arbitrary x_0), which evidently satisfies Eq. (43), though ignores the physical symmetry of the x and y directions for the field (42).

Now, expanding the eigenfunction into the Fourier integral in the y -direction:

$$\psi(x, y) = \int X_k(x) \exp\{ik(y - y_0)\} dk, \quad (3.45)$$

we see that for each component of this integral, Eq. (41) yields a specific equation

$$-\frac{\hbar^2}{2m} \left\{ \mathbf{n}_x \frac{d}{dx} + i \mathbf{n}_y \left[k - \frac{q}{\hbar} \mathcal{B}(x - x_0) \right] \right\}^2 X_k = E X_k. \quad (3.46)$$

Since the two vectors inside the curly brackets are mutually perpendicular, its square has no cross-terms, so that Eq. (46) reduces to

$$-\frac{\hbar^2}{2m} \frac{d^2}{dx^2} X_k + \frac{q^2}{2m} \mathcal{B}^2 (x - x_0')^2 X_k = E X_k, \quad \text{where } x_0' \equiv x_0 + \frac{\hbar k}{q \mathcal{B}}. \quad (3.47)$$

But this 1D Schrödinger equation is identical to Eq. (2.261) for a 1D harmonic oscillator,²⁰ with the center at point x_0' , and frequency ω_0 equal to

$$\omega_c = \frac{|q\mathcal{B}|}{m}. \quad (3.48)$$

In the last expression, it is easy to recognize the *cyclotron frequency* of the classical particle’s rotation in the magnetic field. (It may be readily obtained using the 2nd Newton law for a circular orbit of radius r ,

$$m \frac{v^2}{r} = F_\mathcal{B} \equiv qv\mathcal{B}, \quad (3.49)$$

and noting that the resulting ratio $v/r = |q\mathcal{B}|/m$ is just the radius-independent angular velocity ω_c of the particle’s rotation.) Hence, the energy spectrum for each Fourier component of the expansion (45) is the same:

²⁰ This result may become a bit less puzzling if we recall that at the classical circular cyclotron motion of a particle, each of its Cartesian coordinates, including x , performs sinusoidal oscillations with frequency (48), just as a 1D harmonic oscillator with this frequency.

$$E_n = \hbar\omega_c \left(n + \frac{1}{2} \right), \quad (3.50)$$

Landau levels

independent of either x_0 , or y_0 , or k .

This is a good example of a highly *degenerate* system: for each eigenvalue E_n , there are many similar eigenfunctions that differ only by the positions $\{x_0, y_0\}$ of their centers, and the rate k of their phase change along the y -axis. They may be used to assemble a large variety of linear combinations, including 2D wave packets whose centers move along classical circular orbits. Note, however, that the radius of such rotation cannot be smaller than the so-called *Landau radius*,

$$r_L \equiv \left(\frac{\hbar}{m\omega_c} \right)^{1/2} \equiv \left(\frac{\hbar}{|q\mathcal{B}|} \right)^{1/2}, \quad (3.51)$$

Landau radius

which characterizes the minimum size of the wave packet, and follows from Eq. (2.276) after the replacement $\omega_0 \rightarrow \omega_c$. This radius is remarkably independent of the particle mass, and may be interpreted in the following way: the scale $\mathcal{B}A_{\min}$ of the applied magnetic field's flux through the effective area $A_{\min} = 2\pi r_L^2$ of the smallest wave packet is just one normal flux quantum $\Phi_0' \equiv 2\pi\hbar/|q\mathcal{B}|$.

A detailed analysis of such wave packets (for which we would not have time in this course), in particular proves the virtually evident fact: the applied magnetic field does not change the *average* density dN_2/dE of different 2D states on the energy scale, following from Eq. (1.99), but just “assembles” them on the Landau levels (see Fig. 5a), so that the number of different orbital states on each Landau level (per unit area) is

$$n_L \equiv \frac{N_2}{A} = \frac{1}{A} \frac{dN_2}{dE} \Big|_{\mathcal{B}=0} \Delta E \equiv \frac{1}{A} \frac{dN_2}{d^2k} \Big|_{\mathcal{B}=0} \frac{d^2k}{dk} \frac{1}{dE/dk} \Delta E = \frac{1}{A} \frac{A}{(2\pi)^2} 2\pi k \frac{1}{\hbar^2 k/m} \hbar\omega_c \equiv \frac{|q\mathcal{B}|}{2\pi\hbar}. \quad (3.52)$$

This expression may again be interpreted in terms of magnetic flux quanta: $n_L\Phi_0' = \mathcal{B}$, i.e. there is one particular state on each Landau level per each normal flux quantum.

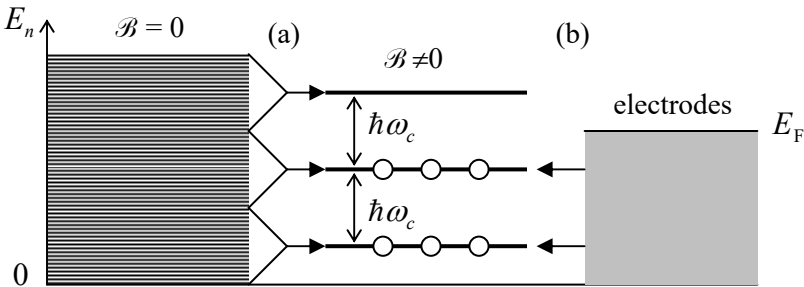


Fig. 3.5. (a) The “assembly” of 2D states on Landau levels, and (b) filling the levels with electrons at the quantum Hall effect.

The most famous application of the Landau levels picture is the explanation of the *quantum Hall effect*²¹. It is usually observed in the “Hall bar” geometry sketched in Fig. 6, where electric current I is passed through a rectangular conducting sample placed into magnetic field \mathcal{B} perpendicular to the

²¹ It was first observed in 1980 by a group led by Klaus von Klitzing, while the classical version (54) of the effect was first observed by Edwin Hall a century earlier – in 1879.

sample's plane. The classical analysis of the effect is based on the notion of the Lorentz force (14). As the magnetic field is turned on, this force starts to deviate the effective charge carriers (electrons or holes) from their straight motion between the electrodes, bending them toward the insulated sides of the bar (in Fig. 6, parallel to the x -axis). Here the carriers accumulate, generating a gradually increasing electric field \mathcal{E} until its force (16) exactly balances the Lorentz force (14):

$$q\mathcal{E}_y = qv_x\mathcal{B}, \quad (3.53)$$

where v_x is the drift velocity of the carriers along the bar (Fig. 6), providing the sustained balance condition $\mathcal{E}_y/v_x = \mathcal{B}$ at each point of the sample.

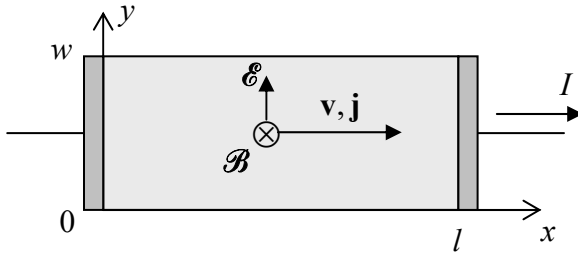


Fig. 3.6. The Hall bar geometry. Darker rectangles show external (3D) electrodes.

With n_2 carriers per unit area, in a sample of width w , this condition yields the following classical expression for the so-called *Hall resistance* R_H , remarkably independent of w and l :

$$R_H \equiv \frac{V_y}{I_x} = \frac{\mathcal{E}_y w}{qn_2 v_x w} = \frac{\mathcal{B}}{qn_2}. \quad (3.54)$$

This formula is broadly used in practice for the measurement of the 2D density n_2 of the charge carriers, and of the carrier type – electrons with $q = -e < 0$, or holes with the effective charge $q = +e > 0$.

However, in experiments with high-quality (low-defect) 2D well structures, at sub-kelvin temperatures²² and high magnetic fields, the linear growth of R_H with \mathcal{B} , described by Eq. (54), is interrupted by virtually horizontal plateaus (Fig. 7). Most remarkably, the experimental values of R_H on these plateaus are reproduced with extremely high accuracy (up to $\sim 10^{-9}$) from experiment to experiment and, even more remarkably, from sample to sample.²³ They are described by the following formula:

$$R_H = \frac{1}{i} R_K, \quad \text{where } R_K \equiv \frac{2\pi\hbar}{e^2}, \quad (3.55)$$

so that

$$R_K \approx 25.812\,807\,459\,304\dots \text{k}\Omega, \quad (3.56)$$

and i is (only until the end of this section, following tradition!) the plateau number, i.e. a real integer.

²² In some systems, such as the *graphene* (virtually perfect 2D sheets of carbon atoms – see Sec. 4 below), the effect may be more stable to thermal fluctuations, due to their topological properties, so that it may be observed even at room temperature – see, e.g., K. Novoselov *et al.*, *Science* **315**, 1379 (2007). Also note that in some thin ferromagnetic layers, the quantum Hall effects may be observed in the absence of an external magnetic field – see, e.g., M. Götz *et al.*, *Appl. Phys. Lett.* **112**, 072102 (2018) and references therein.

²³ Due to this high accuracy (which is a rare exception in solid-state physics!), since 2018 the *von Klitzing constant* R_K is used in metrology for the “legal” ohm’s definition, with its value (56) considered fixed – see Appendix CA: Selected Physical Constants.

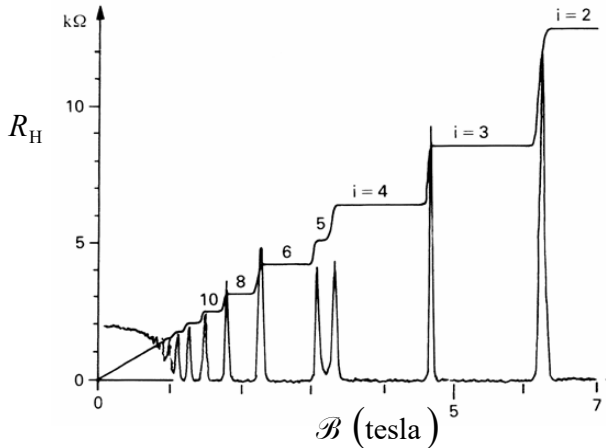


Fig. 3.7. A typical record of the integer quantum Hall effect. The lower trace (with sharp peaks) shows the diagonal element, V_x/I_x , of the resistance tensor. (Adapted from https://www.nobelprize.org/nobel_prizes/physics/laureates/1998/press.html).

This effect may be explained using the Landau level picture. The 2D sample is typically in a weak contact with 3D electrodes whose conductivity electrons, at low temperatures, fill all states with energies below a certain Fermi energy E_F – see Fig. 5b. According to Eqs. (48) and (50), as \mathcal{B} is increased, the spacing $\hbar\omega_c$ between the Landau levels increases proportionately, so that fewer and fewer of these levels are below E_F (and hence all their states are filled in equilibrium), and within certain ranges of field variations, the number i of the filled levels is constant. (In Fig. 5b, $i = 2$.) So, plugging $n_2 = in_L$ and $q = -e$ into Eq. (54), and using Eq. (52) for n_L , we get

$$R_H = \frac{1}{i} \frac{\mathcal{B}}{qn_L} = \frac{1}{i} \frac{2\pi\hbar}{e^2}, \quad (3.57)$$

i.e. exactly the experimental result (55).

This admittedly oversimplified explanation of the quantum Hall effect does not take into account at least two important factors:

- (i) the nonuniformity of the background potential $U(x, y)$ in realistic Hall bar samples, and the role of the quasi-1D *edge channels* this nonuniformity produces,²⁴ and
- (ii) the Coulomb interaction of the electrons, in high-quality samples leading to the formation of R_H plateaus with not only integer but also fractional values of i ($1/3, 2/5, 3/7$, etc.).²⁵

Unfortunately, a thorough discussion of these very interesting features is well beyond the framework of this course.²⁶²⁷

²⁴ Such quasi-1D regions, with the width of the order of r_L , form along the lines where the Landau levels cross the Fermi surface, and are actually responsible for all the electron transfer at the quantum Hall effect (giving the pioneering example of what is nowadays called the *topological insulators*). The particle motion along these channels is effectively one-dimensional; because of this, it cannot be affected by modest unintentional nonuniformities of the potential $U(x, y)$. This fact is responsible for the extraordinary accuracy of Eq. (55).

²⁵ This *fractional quantum Hall effect* was discovered in 1982 by D. Tsui, H. Stormer, and A. Gossard. In contrast, the effect described by Eq. (55) with an integer i (Fig. 7) is now called the *integer quantum Hall effect*.

²⁶ For a comprehensive discussion of these effects, I can recommend, e.g., either the monograph by D. Yoshioka, *The Quantum Hall Effect*, Springer, 1998, or the review by D. Yennie, *Rev. Mod. Phys.* **59**, 781 (1987). (See also the later publications cited above.)

²⁷ Note also that the quantum Hall effect is sometimes discussed in terms of the so-called *Berry phase*, one of the *geometric phases* – the notion apparently pioneered by S. Pancharatnam in 1956. However, in the “usual”

3.3. Scattering and diffraction

The second class of quantum effects, which becomes richer in multi-dimensional spaces, is typically referred to as either *diffraction* or *scattering* – depending on the context. In classical physics, these two terms are used to describe very different effects. The term “diffraction” is used for the interference of the waves re-emitted by elementary components of extended objects, under the effect of a single incident wave.²⁸ On the other hand, the term “scattering” is used in classical mechanics to describe the result of the interaction of a beam of incident *particles*²⁹ with such an extended object, called the *scatterer* – see Fig. 8.

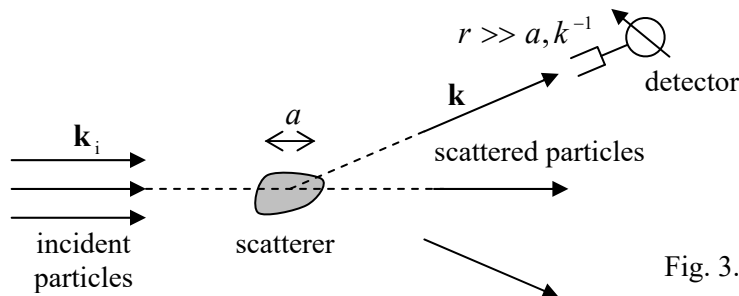


Fig. 3.8. Scattering (schematically).

Most commonly, the detector of the scattered particles is located at a large distance $r \gg a$ from the scatterer. In this case, the main observable independent of r is the *flux* (the number per unit time) of particles scattered in a certain direction, i.e. their flux per unit solid angle Ω . Since it is proportional to the incident flux of particles per unit area, the efficiency of scattering in a particular direction may be characterized by the ratio of these two fluxes. This ratio has is called the *differential cross-section* of the scatterer:

Differential cross-section

$$\frac{d\sigma}{d\Omega} \equiv \frac{\text{flux of scattered particles per unit solid angle}}{\text{flux of incident particles per unit area}}. \quad (3.58)$$

Such terminology and notation stem from the fact that the integral of $d\sigma/d\Omega$ over all scattering angles,

Total cross-section

$$\sigma \equiv \oint \frac{d\sigma}{d\Omega} d\Omega = \frac{\text{total flux of scattered particles}}{\text{incident flux per per unit area}}, \quad (3.59)$$

evidently having the dimensionality of area, has a simple interpretation as the *total cross-section* of scattering. For the simplest case when a solid object scatters all classical particles hitting its surface, but does not affect the particles flying by it, σ is just the geometric area of the scatterer, as observed from the direction of the incident particles. In classical mechanics, we first calculate the particle’s scattering

quantum Hall effect the Berry phase equals zero, and I believe that this concept should be saved for the discussion of more topologically involved systems. Unfortunately, I will have no time/space for a discussion of such systems in this course, and have to refer the interested reader to special literature – see, e.g., either the key papers collected by A. Shapere and F. Wilczek, *Geometric Phases in Physics*, World Scientific, 1992, or the monograph by A. Bohm *et al.*, *The Geometric Phase in Quantum Systems*, Springer, 2003.

²⁸ The notion of interference is very close to diffraction, but the former term is typically reserved for the wave re-emission by just a few components, such as two slits in the Young experiment – see Figs. 1 and 2. A detailed discussion of diffraction and interference of electromagnetic waves may be found in EM Secs. 8.3-8.8.

²⁹ In the context of classical waves, the term “scattering” is typically reserved for wave interaction with disordered sets of small objects – see, e.g., EM Sec. 8.3.

angle as a function of its *impact parameter* b and then average the result over all values of b , considered random.³⁰

In quantum mechanics, due to the particle/wave duality, a relatively broad, parallel beam of incident particles of the same energy E may be fairly represented with a plane de Broglie wave (1.88):

$$\psi_i = |\psi_i| \exp\{i\mathbf{k}_i \cdot \mathbf{r}\}, \quad (3.60)$$

with the free-space wave number $k_i = k = (2mE)^{1/2}/\hbar$. As a result, the particle scattering becomes a synonym of the de Broglie wave diffraction, and (somewhat counter-intuitively) the description of the effect becomes simpler, excluding the notion of the impact parameter. Indeed, the wave (60) corresponds to a constant probability current density (1.49):

$$\mathbf{j}_i = |\psi_i|^2 \frac{\hbar}{m} \mathbf{k}_i, \quad (3.61)$$

which is exactly the flux of incident particles per unit area that is used in the denominator of Eq. (58), while the numerator of that fraction may be simply expressed via the probability current density \mathbf{j}_s of the scattered de Broglie waves:

$$\frac{d\sigma}{d\Omega} = \frac{j_s r^2}{j_i}, \quad \text{at } r \gg a. \quad (3.62)$$

Hence our task is reduced to the calculation of j_s at sufficiently large distances r from the scatterer. For that, let us rewrite the stationary Schrödinger equation for the *elastic* scattering problem (when the energy E of the scattered particles is the same as that of the incident particles) in the form

$$(E - \hat{H}_0) \psi = U(\mathbf{r}) \psi, \quad \text{with } \hat{H}_0 \equiv -\frac{\hbar^2}{2m} \nabla^2, \quad \text{and } E = \frac{\hbar^2 k^2}{2m}, \quad (3.63)$$

where the potential energy $U(\mathbf{r})$ describes the effect of the scatterer. Looking for the solution of Eq. (62) in the natural form

$$\psi = \psi_i + \psi_s, \quad (3.64)$$

where ψ_i is the incident wave (60) and ψ_s has the sense of the scattered wave, and taking into account that the former wave satisfies the free-space Schrödinger equation

$$\hat{H}_0 \psi_i = E \psi_i, \quad (3.65)$$

we may reduce Eq. (63) to either of the following equivalent forms:

$$(E - \hat{H}_0) \psi_s = U(\mathbf{r})(\psi_i + \psi_s), \quad (\nabla^2 + k^2) \psi_s = \frac{2m}{\hbar^2} U(\mathbf{r}) \psi. \quad (3.66)$$

For applications, an integral form of this equation is more convenient. To derive it, we may look at the second of Eqs. (66) as a linear, inhomogeneous differential equation for the function ψ_s , thinking of its right-hand side as a known “source”. The solution of such an equation obeys the linear superposition principle, i.e. we may represent it as the sum of the waves outgoing from all elementary volumes d^3r' of the scatterer. Mathematically, this sum may be expressed as either

³⁰ See, e.g., CM Sec. 3.5.

$$\psi_s(\mathbf{r}) = \frac{2m}{\hbar^2} \int U(\mathbf{r}') \psi(\mathbf{r}') G(\mathbf{r}, \mathbf{r}') d^3 r', \quad (3.67a)$$

or, equivalently, as³¹

$$\psi(\mathbf{r}) = \psi_i(\mathbf{r}) + \frac{2m}{\hbar^2} \int U(\mathbf{r}') \psi(\mathbf{r}') G(\mathbf{r}, \mathbf{r}') d^3 r', \quad (3.67b)$$

where $G(\mathbf{r}, \mathbf{r}')$ is the *spatial Green's function*, defined as such an elementary, spherically-symmetric response of the 3D Helmholtz equation to a point source, i.e. the outward-propagating solution of the following equation³²

$$(\nabla^2 + k^2)G = \delta(\mathbf{r} - \mathbf{r}'). \quad (3.68)$$

But we already know such solution of this equation – see Eq. (7) and its discussion:

$$G(\mathbf{r}, \mathbf{r}') = \frac{f_+}{R} e^{ikR}, \quad \text{where } \mathbf{R} \equiv \mathbf{r} - \mathbf{r}', \quad (3.69)$$

so that we need just to calculate the coefficient f_+ for Eq. (68). This can be done in several ways, for example by noticing that at $R \ll k^{-1}$, the second term on the left-hand side of Eq. (68) is negligible, so that it is reduced to the well-known Poisson equation with a delta-functional right-hand side, which describes, for example, the electrostatic potential induced by a point electric charge. Either recalling the Coulomb law or applying the Gauss theorem,³³ we readily get the asymptote

$$G \rightarrow -\frac{1}{4\pi R}, \quad \text{at } kR \ll 1, \quad (3.70)$$

which is compatible with Eq. (69) only if $f_+ = -1/4\pi$, i.e. if

$$G(\mathbf{r}, \mathbf{r}') = -\frac{1}{4\pi R} e^{ikR}. \quad (3.71)$$

Plugging this result into Eq. (67a), we get the following formal solution of Eq. (66):

$$\psi_s(\mathbf{r}) = -\frac{m}{2\pi\hbar^2} \int U(\mathbf{r}') \frac{\psi(\mathbf{r}')}{R} e^{ikR} d^3 r'. \quad (3.72)$$

Note that if the function $U(\mathbf{r})$ is smooth, the singularity in the denominator is integrable (i.e. not dangerous); indeed, the contribution of a sphere with some radius $\mathcal{R} \rightarrow 0$, with the center at point \mathbf{r}' , into this integral scales as

³¹ This formula is sometimes called the *Lipmann-Schwinger equation*, though more frequently this term is reserved for either its operator form or the resulting equation for the spatial Fourier components of ψ and ψ_i .

³² Please notice both the similarity and difference between this Green's function and the propagator discussed in Sec. 2.1. In both cases, we use the linear superposition principle to solve wave equations, but while Eq. (67) gives the solution of the *inhomogeneous* equation (66), Eq. (2.44) does that for a *homogeneous* Schrödinger equation. In the latter case, the elementary wave sources are the elementary parts of the initial wavefunction, rather than of the equation's right-hand side as in our current problem.

³³ See, e.g., EM Sec. 1.2.

$$\int_{R < \mathcal{R}} \frac{d^3 R}{R} \equiv 4\pi \int_0^{\mathcal{R}} \frac{R^2 dR}{R} \equiv 4\pi \int_0^{\mathcal{R}} R dR = 2\pi \mathcal{R}^2 \rightarrow 0. \quad (3.73)$$

So far, our result (72) is exact, but its apparent simplicity is deceiving, because the wavefunction ψ on its right-hand side generally includes not only the incident wave ψ_i but also the scattered wave ψ_s – see Eq. (64). The most straightforward, and most common simplification of this problem, called the *Born approximation*,³⁴ is possible if the scattering potential $U(\mathbf{r})$ is in some sense small. (We will derive the quantitative condition of this smallness in a minute.) Since at $U(\mathbf{r}) = 0$ the scattering wave ψ_s has to disappear, at small but non-zero $U(\mathbf{r})$, $|\psi_s|$ has to be much smaller than $|\psi_i|$. In this case, on the right-hand side of Eq. (73) we may ignore ψ_s in comparison with ψ_i , getting

$$\psi_s(\mathbf{r}) = -\frac{m}{2\pi\hbar^2} |\psi_i| \int U(\mathbf{r}') \frac{\exp\{i\mathbf{k}_i \cdot \mathbf{r}'\}}{R} e^{ikR} d^3 r'. \quad (3.74)$$

Born approximation

Actually, Eq. (74) gives us even *more* than we wanted: it evaluates the scattered wave at *any* point, including those within of the scattering object, while to spell out Eq. (62), we only need to find the wave *far* from the scatterer, at $r \rightarrow \infty$. However, before going to that limit, we can use this general formula to find a quantitative criterion of the Born approximation's validity. For that, let us estimate the magnitude of the right-hand side of this equation for a scatterer of a linear size $\sim a$, and the potential magnitude's scale U_0 . The results are different in the following two limits:

(i) If $ka \ll 1$, then inside the scatterer (i.e., at distances $\Delta r' \sim a$), both $\exp\{i\mathbf{k} \cdot \mathbf{r}'\}$ and the second exponent under the integral in Eq. (74) change little, so that a crude but fair estimate of the solution's magnitude is

$$|\psi_s| \sim \frac{m}{2\pi\hbar^2} |\psi_i| U_0 a^2. \quad (3.75)$$

(ii) In the opposite limit $ka \gg 1$, the function under the integral is nearly periodic in one of the spatial directions (that of the scattered wave propagation), so that the net integral accumulates only on distances of the order of the de Broglie wavelength, $\sim k^{-1}$, and the integral is correspondingly smaller:

$$|\psi_s| \sim \frac{m}{2\pi\hbar^2} |\psi_i| U_0 \frac{a^2}{ka}. \quad (3.76)$$

These relations allow us to spell out the Born approximation's condition, $|\psi_s| \ll |\psi_i|$, as

$$U_0 \ll \frac{\hbar^2}{ma^2} \max[ka, 1]. \quad (3.77)$$

In the fraction on the right-hand side, we may readily recognize the scale of the kinetic (quantum-confinement) energy E_a of the particle inside a potential well of a size of the order of a , so that the Born approximation is valid essentially if the potential energy of particle's interaction with the scatterer is

³⁴ Named after M. Born, who was the first to apply this approximation in quantum mechanics. However, the basic idea of this approach had been developed much earlier (in 1881) by Lord Rayleigh in the context of electromagnetic wave scattering – see, e.g., EM Sec. 8.3. Note also that the contents of that section repeat some aspects of our current discussion – perhaps regrettably but unavoidably so, because the Born approximation is a centerpiece of the theory of scattering/diffraction for both the electromagnetic waves and the de Broglie waves. Hence I felt I had to cover it in this course for the benefit of the readers who skipped the EM part of my series.

smaller than E_a . Note, however, that the estimates (75) and (76) are not valid in some special situations when the effects of scattering *accumulate* in some direction. This is frequently the case for small angles θ of scattering by extended objects, when $ka \gg 1$, but $ka\theta \lesssim 1$.

Now let us proceed to large distances $r \gg r' \sim a$, and simplify Eq. (74) using an approximation similar to the dipole expansion in electrodynamics.³⁵ Namely, in the denominator's R , we may ignore r' in comparison with the much larger r , but the exponents require more care, because even if $r' \sim a \ll r$, the product $kr' \sim ka$ may still be of the order of 1. In the first approximation in r' , we can take (Fig. 9a):

$$R \equiv |\mathbf{r} - \mathbf{r}'| \approx r - \mathbf{n}_r \cdot \mathbf{r}', \quad (3.78)$$

and since directions of the vectors \mathbf{k} and \mathbf{r} coincide, i.e. $\mathbf{k} = k\mathbf{n}_r$, we get

$$kR \approx kr - \mathbf{k} \cdot \mathbf{r}', \quad \text{so that } e^{ikR} \approx e^{ikr} e^{-i\mathbf{k} \cdot \mathbf{r}'}. \quad (3.79)$$

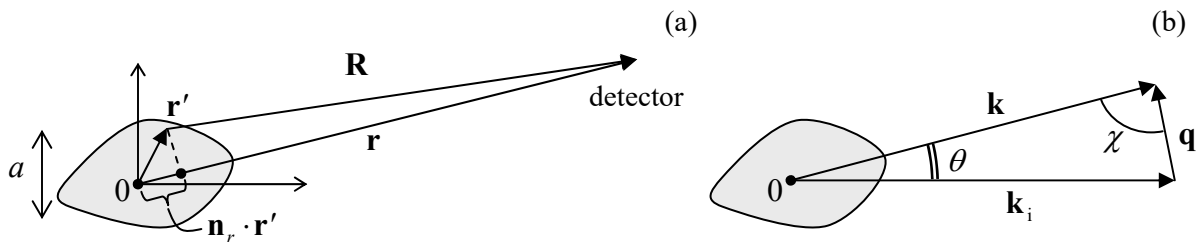


Fig. 3.9. (a) The long-range expansion of R , and (b) the definitions of \mathbf{q} , χ , and θ .

With this replacement, Eq. (74) yields

$$\psi_s(\mathbf{r}) = -\frac{m}{2\pi\hbar^2} \frac{|\psi_i|}{r} e^{ikr} \int U(\mathbf{r}') \exp\{-i(\mathbf{k} - \mathbf{k}_i) \cdot \mathbf{r}'\} d^3 r'. \quad (3.80)$$

This relation is a particular case of a more general formula³⁶

$$\psi_s = |\psi_i| \frac{f(\mathbf{k}, \mathbf{k}_i)}{r} e^{ikr}, \quad (3.81)$$

where $f(\mathbf{k}, \mathbf{k}_i)$ is called the *scattering function*.³⁷ The physical sense of this function becomes clear from the calculation of the corresponding probability current density \mathbf{j}_s . For that, generally, we need to use Eq. (1.47) with the gradient operator having all spherical-coordinate components.³⁸ However, at $kr \gg 1$, the main contribution to $\nabla \psi_s$, proportional to $k \gg 1/r$, is provided by differentiating the factor e^{ikr} , which changes in the common direction of vectors \mathbf{r} and \mathbf{k} , so that

³⁵ See, e.g., EM Sec. 8.2.

³⁶ It is easy to prove that this form is an asymptotic form of *any* solution ψ_s of the scattering problem (even that beyond the Born approximation) at sufficiently large distances $r \gg a, k^{-1}$.

³⁷ Note that the function f has the dimension of length, and does not account for the incident wave. This is why sometimes a dimensionless function, $S = 1 + 2ikf$, is used instead. This function S is called the *scattering matrix*, because it may be considered a natural generalization of the 1D matrix S defined by Eq. (2.124), to higher dimensionality.

³⁸ See, e.g., MA Eq. (10.8).

$$\nabla \psi_s \approx \mathbf{n}_r \frac{\partial}{\partial r} \psi_s \approx \mathbf{k} \psi_s, \quad \text{at } kr \gg 1, \quad (3.82)$$

and Eq. (1.47) yields

$$\mathbf{j}_s(\theta) \approx \frac{\hbar}{m} |\psi_i|^2 \frac{|f(\mathbf{k}, \mathbf{k}_i)|^2}{r^2} \mathbf{k}. \quad (3.83)$$

Plugging this expression, and also Eq. (61) into Eq. (62), for the differential cross-section we get simply

$$\frac{d\sigma}{d\Omega} = |f(\mathbf{k}, \mathbf{k}_i)|^2, \quad (3.84)$$

while the total cross-section is

$$\sigma = \oint |f(\mathbf{k}, \mathbf{k}_i)|^2 d\Omega, \quad (3.85)$$

so that the scattering function $f(\mathbf{k}, \mathbf{k}_i)$ gives us everything we need – and in fact more, because the function also contains information about the phase of the scattered wave.

According to Eq. (80), in the Born approximation the scattering function is reduced to the so-called *Born integral*

$$f(\mathbf{k}, \mathbf{k}_i) = -\frac{m}{2\pi\hbar^2} \int U(\mathbf{r}) e^{-i\mathbf{q} \cdot \mathbf{r}} d^3 r, \quad (3.86)$$

Born integral

where for the notation simplicity \mathbf{r}' is replaced with \mathbf{r} , and the following *scattering vector* is introduced:

$$\mathbf{q} \equiv \mathbf{k} - \mathbf{k}_i, \quad (3.87)$$

with the length $q = 2k \sin(\theta/2)$, where θ is the *scattering angle* between the vectors \mathbf{k} and \mathbf{k}_i – see Fig. 9b. For the differential cross-section, Eqs. (84) and (86) yield³⁹

$$\frac{d\sigma}{d\Omega} = \left(\frac{m}{2\pi\hbar^2} \right)^2 \left| \int U(\mathbf{r}) e^{-i\mathbf{q} \cdot \mathbf{r}} d^3 r \right|^2. \quad (3.88)$$

Differential cross-section: Born approximation

This is the main result of this section; it may be further simplified for spherically-symmetric scatterers, with

$$U(\mathbf{r}) = U(r). \quad (3.89)$$

In this case, it is convenient to represent the exponent in the Born integral as $\exp\{-iqr' \cos \chi\}$, where χ is the angle between the vectors \mathbf{k} (i.e. the direction \mathbf{n}_r toward the detector) and \mathbf{q} (rather than the incident wave vector \mathbf{k}_i !) – see Fig. 9b. Now, for a fixed \mathbf{q} , we can take this vector's direction for the polar axis of a spherical coordinate system, and reduce Eq. (86) to a 1D integral:

$$f(\mathbf{k}, \mathbf{k}_i) = -\frac{m}{2\pi\hbar^2} \int_0^\infty r^2 dr U(r) \int_0^{2\pi} d\phi \int_0^\pi \sin \chi d\chi \exp\{-iqr' \cos \chi\}$$

³⁹ Note that according to Eq. (88), in the Born approximation the scattering intensity does not depend on the sign of the potential U , and also that scattering in a certain direction is completely determined by a specific Fourier component of the function $U(\mathbf{r})$, namely by its harmonic with the wave vector equal to the scattering vector \mathbf{q} .

$$\equiv -\frac{m}{2\pi\hbar^2} \int_0^\infty r^2 dr U(r) 2\pi \frac{2\sin qr}{qr} \equiv -\frac{2m}{\hbar^2 q} \int_0^\infty U(r) \sin(qr) r dr. \quad (3.90)$$

As a simple example, let us use the Born approximation to analyze scattering on the following spherically-symmetric potential:

$$U(\mathbf{r}) = U_0 \exp\left\{-\frac{r^2}{2a^2}\right\}. \quad (3.91)$$

In this particular case, it is better to avoid the temptation to exploit the spherical symmetry by using Eq. (90), and instead, use the general Eq. (88), because it may be represented as a product of three similar Cartesian factors:

$$f(\mathbf{k}, \mathbf{k}_i) = -\frac{mU_0}{2\pi\hbar^2} I_x I_y I_z, \quad \text{with } I_x \equiv \int_{-\infty}^{+\infty} \exp\left\{-\left(\frac{x^2}{2a^2} + iq_x x\right)\right\} dx, \quad (3.92)$$

and similar integrals for I_y and I_z . From Chapter 2, we already know that the Gaussian integrals like I_x may be readily worked out by complementing the exponent to the full square, in our current case giving

$$\begin{aligned} I_x &= (2\pi)^{1/2} a \exp\left\{-\frac{q_x^2 a^2}{2}\right\}, \quad \text{etc.,} \\ \frac{d\sigma}{d\Omega} &= \left(\frac{mU_0}{2\pi\hbar^2} I_x I_y I_z \right)^2 = 2\pi a^2 \left(\frac{mU_0 a^2}{\hbar^2} \right)^2 e^{-q^2 a^2}. \end{aligned} \quad (3.93)$$

Now, the total cross-section σ is an integral of $d\sigma/d\Omega$ over all directions of the vector \mathbf{k} . Since in our case the scattering intensity does not depend on the azimuthal angle φ , the only nontrivial integration is over the scattering angle θ – see Fig. 9b:

$$\begin{aligned} \sigma &\equiv \oint \frac{d\sigma}{d\Omega} d\Omega = 2\pi \int_0^\pi \frac{d\sigma}{d\Omega} \sin\theta d\theta = 4\pi^2 a^2 \left(\frac{mU_0 a^2}{\hbar^2} \right)^2 \int_0^\pi \exp\left\{-\left(2k \sin\frac{\theta}{2}\right)^2 a^2\right\} \sin\theta d\theta \\ &\equiv 4\pi^2 a^2 \left(\frac{mU_0 a^2}{\hbar^2} \right)^2 \int_{\theta=0}^{\theta=\pi} \exp\{-2k^2 a^2 (1 - \cos\theta)\} d(1 - \cos\theta) = \frac{2\pi^2}{k^2} \left(\frac{mU_0 a^2}{\hbar^2} \right)^2 \left(1 - e^{-4k^2 a^2} \right). \end{aligned} \quad (3.94)$$

Let us analyze these results. In the low-energy limit, $ka \ll 1$ (and hence $qa \ll 1$ for any scattering angle), the scattered wave is virtually isotropic: $d\sigma/d\Omega \approx \text{const}$ – a very typical feature of a scalar-wave scattering⁴⁰ by small objects, in any approximation. Note that according to Eq. (77), the Born expression for σ , following from Eq. (94) in this limit,

$$\sigma = 8\pi^2 a^2 \left(\frac{mU_0 a^2}{\hbar^2} \right)^2, \quad (3.95)$$

⁴⁰ Note that this is only true for scalar (e.g., the de Broglie) waves, and different for vector ones, in particular the electromagnetic waves, where the intensity of the dipole radiation, and hence the scattering by small objects vanishes in the direction of the incident field's polarization – see, e.g., EM Eqs. (8.26) and (8.139).

is only valid if σ is much smaller than the scale a^2 of the physical cross-section of the scatterer. In the opposite, high-energy limit $ka \gg 1$, the scattering is dominated by small angles $\theta \approx q/k \sim 1/ka \sim \lambda/a$:

$$\frac{d\sigma}{d\Omega} \approx 2\pi a^2 \left(\frac{mU_0 a^2}{\hbar^2} \right)^2 \exp\{-k^2 a^2 \theta^2\}. \quad (3.96)$$

This is, again, very typical for diffraction. Note, however, that due to the smooth character of the Gaussian potential (91), the diffraction pattern (98) exhibits no oscillations of $d\sigma/d\Omega$ as a function of the diffraction angle θ .

Such oscillations naturally appear for scatterers with sharp borders. Indeed, let us consider a uniform spherical scatterer, described by the potential

$$U(\mathbf{r}) = \begin{cases} U_0, & \text{for } r < R, \\ 0, & \text{otherwise.} \end{cases} \quad (3.97)$$

In this case, integration by parts of Eq. (90) readily yields

$$f(\mathbf{k}, \mathbf{k}_i) = \frac{2mU_0}{\hbar^2 q^3} (qR \cos qR - \sin qR), \quad \text{so that } \frac{d\sigma}{d\Omega} = \left(\frac{2mU_0}{\hbar^2 q^3} \right)^2 (qR \cos qR - \sin qR)^2. \quad (3.98)$$

According to this result, the scattered wave's intensity drops very fast with q , so that one needs a semi-log plot (such as shown in Fig. 10) to reveal small diffraction fringes,⁴¹ with the n^{th} destructive interference (zero-intensity) point tending to $qR = \pi(n + \frac{1}{2})$ at $n \rightarrow \infty$. Since, as Fig. 9b shows, q may only change from 0 to $2k$, these intensity minima are only observable at sufficiently large values of the parameter kR , when they correspond to real values of the scattering angle θ . (At $kR \gg 1$, approximately kR/π of these minima, i.e. “dark rings” of low scattering probability, are observable.) On the contrary, at $kR \ll 1$ all allowed values of qR are much smaller than 1, and in this limit, the differential cross-section does not depend on qR , i.e. the scattering by the sphere (as by *any* object in this limit) is isotropic.

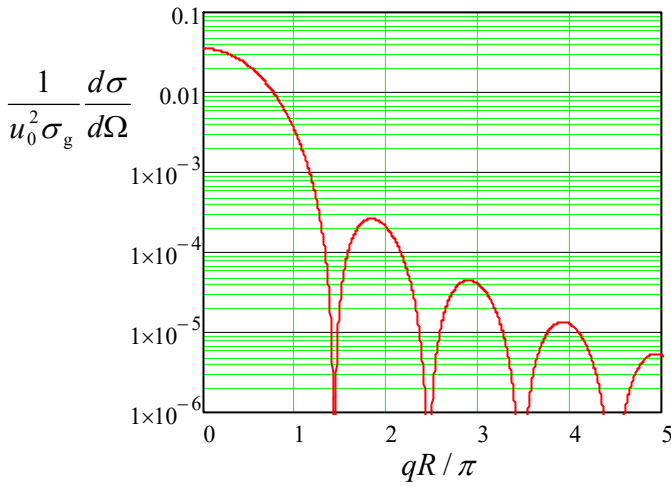


Fig. 3.10. The differential cross-section of the Born scattering of a particle by a “hard” (sharp-border) sphere (97), normalized to its geometric cross-section $\sigma_g \equiv \pi R^2$ and the square of the potential’s magnitude parameter $u_0 \equiv U_0/(\hbar^2/2mR^2)$, as a function of the normalized magnitude of the scattering vector \mathbf{q} .

This example shows that in quantum mechanics the notions of particle scattering and diffraction are essentially inseparable.

⁴¹ Their physics is very similar to that of the Fraunhofer diffraction on a 1D scatterer – see, e.g., EM Sec. 8.4.

The Born approximation, while being very simple and used more than any other scattering theory, is not without substantial shortcomings, as becomes clear from the following example. It is not too difficult to prove the so-called *optical theorem*, strictly valid for an arbitrary scatterer:

Optical theorem

$$\text{Im } f(\mathbf{k}_i, \mathbf{k}_i) = \frac{k}{4\pi} \sigma. \quad (3.99)$$

However, Eq. (86) shows that in the Born approximation, the function f is purely real at $q = 0$ (i.e. for $\mathbf{k} = \mathbf{k}_i$), and hence cannot satisfy the optical theorem. Even more evidently, it cannot describe such a simple effect as a dark shadow ($\psi \approx 0$) cast by a virtually opaque object (say, with $U \gg E$). There are several ways to improve the Born approximation, while still keeping its general idea of an approximate treatment of U .

(i) Instead of the main assumption $\psi_s \propto U_0$, we may use a complete perturbation series:

$$\psi_s = \psi_1 + \psi_2 + \dots \quad (3.100)$$

with $\psi_n \propto U_0^n$, and find successive approximations ψ_n one by one. In the 1st approximation we return to the Born formula, but already the 2nd approximation yields

$$\text{Im } f_2(\mathbf{k}_i, \mathbf{k}_i) = \frac{k}{4\pi} \sigma_1, \quad (3.101)$$

where σ_1 is the total cross-section calculated in the 1st approximation, so that the optical theorem (99) is “almost satisfied”.

(ii) As was mentioned above, the Born approximation does not work very well for the objects stretching along the direction (say, x) of the initial wave vector \mathbf{k}_i . This deficiency may be corrected by the so-called *eikonal*⁴² approximation, which replaces the plane-wave representation (60) of the incident wave with a WKB-like exponent, though still in the 1st approximation in $U \rightarrow 0$:

$$\begin{aligned} \exp\{ik_0x\} &\rightarrow \exp\left\{i\int_0^x k(\mathbf{r}')dx'\right\} \equiv \exp\left\{i\int_0^x \frac{\{2m[E-U(\mathbf{r}')]\}^{1/2}}{\hbar} dx'\right\} \\ &\approx \exp\left\{i\left[k_0x - \frac{m}{\hbar^2 k_0} \int_0^x U(\mathbf{r}')dx'\right]\right\}. \end{aligned} \quad (3.102)$$

Results of this approach satisfy the optical theorem (99) already in the 1st approximation.

Another way toward quantitative results in the theory of scattering, beyond the Born approximation, may be pursued for spherically-symmetric potentials (89); I will discuss it in Sec. 8, after a general discussion of particle motion in such potentials in Sec. 7.

3.4. Energy bands in higher dimensions

In Sec. 2.7, we have discussed the 1D band theory for potential profiles $U(x)$ that obey the periodicity condition (2.192). For what follows, let us notice that the condition may be rewritten as

$$U(x + X) = U(x), \quad (3.103)$$

⁴² From the Greek word εἰκόνα, meaning “image”. In our current context, this term is purely historic.

where $X = \tau a$, with τ being an arbitrary integer. One may say that the set of points X forms a periodic *1D lattice* in the direct (\mathbf{r} -) space. We have also seen that each Bloch state (i.e., each eigenstate of the Schrödinger equation for such periodic potential) is characterized by the quasimomentum $\hbar q$, and its energy does not change if q is changed by a multiple of $2\pi/a$. Hence if we form, in the reciprocal (\mathbf{q} -) space, a 1D lattice of points $Q = lb$, with $b \equiv 2\pi/a$ and integer l , any pair of points from these two mutually reciprocal lattices satisfies the following rule:

$$\exp\{iQX\} = \exp\left\{il\frac{2\pi}{a}\tau a\right\} \equiv e^{2\pi i \tau l} = 1. \quad (3.104)$$

In this form, the results of Sec. 2.7 may be readily extended to d -dimensional periodic potentials whose translational symmetry obeys the following natural generalization of Eq. (103):

$$U(\mathbf{r} + \mathbf{R}) = U(\mathbf{r}), \quad (3.105)$$

where the points \mathbf{R} , which may be numbered by d integers τ_j , form the so-called *Bravais lattice*:⁴³

$$\mathbf{R} = \sum_{j=1}^d \tau_j \mathbf{a}_j,$$

Bravais
lattice
(3.106)

with d primitive vectors \mathbf{a}_j . The simplest example of a 3D Bravais lattice is given by the *simple cubic* lattice (Fig. 11a), which may be described by a system of mutually perpendicular primitive vectors \mathbf{a}_j of equal length. However, not in any lattice these vectors are perpendicular; for example, Figs. 11b and 11c show possible sets of the primitive vectors describing, respectively, the *face-centered cubic* (fcc) lattice and the *body-centered cubic* (bcc) lattice. In 3D, the science of crystallography, based on group theory, distinguishes, by their symmetry properties, 14 Bravais lattices grouped into 7 different *lattice systems*.⁴⁴

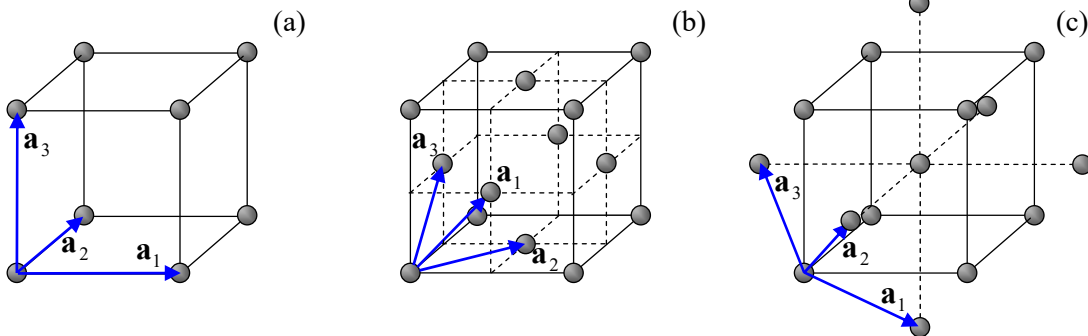


Fig. 3.11. The simplest (and most common) 3D Bravais lattices: (a) simple cubic, (b) face-centered cubic (fcc), and (c) body-centered cubic (bcc), and possible choices of their primitive vector sets (blue arrows).

Note, however, not all highly symmetric sets of points form Bravais lattices. As probably the most striking example, the nodes of a very simple 2D *honeycomb lattice* (Fig. 12a)⁴⁵ cannot be

⁴³ Named after Auguste Bravais, the crystallographer who introduced this notion in 1850.

⁴⁴ A very clear, well-illustrated introduction to the Bravais lattices is given in Chapters 4 and 7 of the famous textbook by N. Ashcroft and N. Mermin, *Solid State Physics*, Saunders College, 1976.

⁴⁵ This structure describes, for example, the now-famous *graphene*: isolated monolayer sheets of carbon atoms arranged in a honeycomb lattice with an interatomic distance of 0.142 nm.

described by a Bravais lattice – while those of the 2D hexagonal lattice shown in Fig. 12b, can. The most prominent 3D case of such a lattice is the diamond structure (Fig. 12c), which describes, in particular, silicon crystals.⁴⁶ In cases like these, the band theory is much facilitated by the fact that the Bravais lattices using some point groups (called *primitive unit cells*) may describe these systems.⁴⁷ For example, Fig. 12a shows a possible choice of the primitive vectors for the honeycomb lattice, with the primitive unit cell formed by any two adjacent points of the original lattice (say, within the dashed ovals on that panel). Similarly, the diamond lattice may be described as an fcc Bravais lattice with a two-point primitive unit cell – see Fig. 12c.

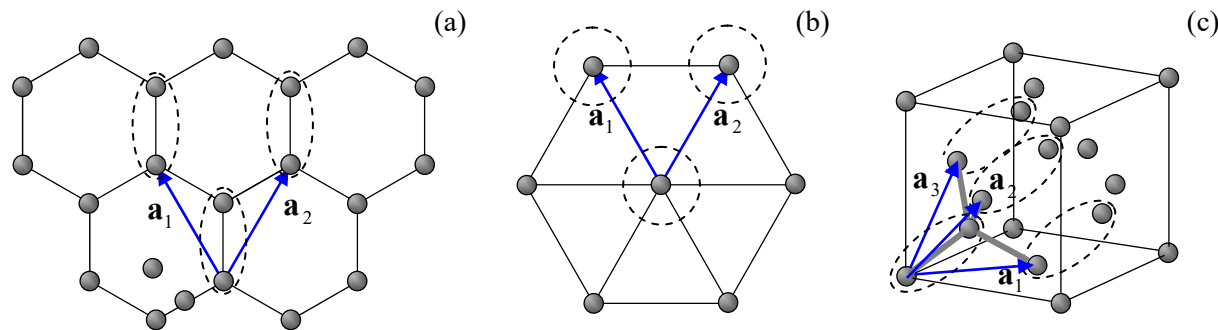


Fig. 3.12. Two important periodic structures that require two-point primitive cells for their Bravais lattice representation: (a) 2D honeycomb lattice and (c) 3D diamond lattice, and their primitive vectors. For contrast, panel (b) shows the 2D hexagonal structure which forms a Bravais lattice with a single-point primitive cell.

Now we are ready for the following generalization of the 1D Bloch theorem, given by Eqs. (2.193) and (2.210), to higher dimensions: any eigenfunction of the Schrödinger equation describing particle's motion in the spatially-unlimited periodic potential (105) may be represented either as

$$\psi(\mathbf{r} + \mathbf{R}) = \psi(\mathbf{r})e^{i\mathbf{q} \cdot \mathbf{R}}, \quad (3.107)$$

3D Bloch theorem

or as

$$\psi(\mathbf{r}) = u(\mathbf{r})e^{i\mathbf{q} \cdot \mathbf{r}}, \quad \text{with } u(\mathbf{r} + \mathbf{R}) = u(\mathbf{r}), \quad (3.108)$$

where the quasimomentum $\hbar\mathbf{q}$ is again a constant of motion, but now it is a vector. The key notion of the band theory in d dimensions is the *reciprocal lattice* in the wave-vector (\mathbf{q}) space, formed as

$$\mathbf{Q} = \sum_{j=1}^d l_j \mathbf{b}_j, \quad (3.109)$$

with integer l_j , and vectors \mathbf{b}_j selected in such a way that the following natural generalization of Eq. (104) is valid for any pair of points of the direct and reciprocal lattices:

⁴⁶ This diamond structure may be best understood as an overlap of two fcc lattices of side a , mutually shifted by the vector $\{1, 1, 1\} \times a/4$, so that the distances between each point of the combined lattice and its 4 nearest neighbors (see the solid gray lines in Fig. 12c) are all equal.

⁴⁷ A harder case is presented by so-called *quasicrystals* (whose idea may be traced down to medieval Islamic tilings, but was discovered in natural crystals, by D. Shechtman *et al.*, only in 1984), which obey a high (say, the 5-fold) rotational symmetry, but cannot be described by a Bravais lattice with *any* finite primitive unit cell. For a popular review of quasicrystals see, for example, P. Stephens and A. Goldman, *Sci. Amer.* **264**, #4, 24 (1991).

$$e^{i\mathbf{Q}\cdot\mathbf{R}} = 1. \quad (3.110)$$

One way to describe the physical sense of the lattice \mathbf{Q} is to say that according to Eqs. (80) and/or (86), it gives the set of the vectors $\mathbf{q} \equiv \mathbf{k} - \mathbf{k}_i$ for that the interference of the waves scattered by all Bravais lattice points is constructive, and hence strongly enhanced.⁴⁸ Another way to look at the reciprocal lattice follows from the first formulation of the Bloch theorem, given by Eq. (107): if we add to the quasimomentum \mathbf{q} of a particle any vector \mathbf{Q} of the reciprocal lattice, the wavefunction does not change. This means, in particular, that all information about the system's eigenfunctions is contained in just one elementary cell of the reciprocal space \mathbf{q} . Its most frequent choice, called the *1st Brillouin zone*, is the set of all points \mathbf{q} that are closer to the origin than to any other point of the lattice \mathbf{Q} . (Evidently, the 1st Brillouin zone in one dimension, discussed in Sec. 2.7, falls under this definition – see, e.g., Figs. 2.26 and 2.28.)

It is easy to see that the primitive vectors \mathbf{b}_j of the reciprocal lattice may be constructed as

$$\mathbf{b}_1 = 2\pi \frac{\mathbf{a}_2 \times \mathbf{a}_3}{\mathbf{a}_1 \cdot (\mathbf{a}_2 \times \mathbf{a}_3)}, \quad \mathbf{b}_2 = 2\pi \frac{\mathbf{a}_3 \times \mathbf{a}_1}{\mathbf{a}_1 \cdot (\mathbf{a}_2 \times \mathbf{a}_3)}, \quad \mathbf{b}_3 = 2\pi \frac{\mathbf{a}_1 \times \mathbf{a}_2}{\mathbf{a}_1 \cdot (\mathbf{a}_2 \times \mathbf{a}_3)}. \quad (3.111)$$

Reciprocal
lattice:
primitive
vectors

Indeed, from the “operand rotation rule” of the vector algebra⁴⁹ it is evident that $\mathbf{a}_j \cdot \mathbf{b}_{j'} = 2\pi\delta_{jj'}$. Hence, with the account of Eq. (109), the exponent on the left-hand side of Eq. (110) is reduced to

$$e^{i\mathbf{Q}\cdot\mathbf{R}} = \exp\{2\pi i(l_1\tau_1 + l_2\tau_2 + l_3\tau_3)\}. \quad (3.112)$$

Since all l_j and all τ_j are integers, the expression in the parentheses is also an integer, so that the exponent indeed equals 1, thus satisfying the definition of the reciprocal lattice given by Eq. (110).

As the simplest example, let us return to the simple cubic lattice of a period a (Fig. 11a), oriented in space so that

$$\mathbf{a}_1 = a\mathbf{n}_x, \quad \mathbf{a}_2 = a\mathbf{n}_y, \quad \mathbf{a}_3 = a\mathbf{n}_z, \quad (3.113)$$

According to Eq. (111), its reciprocal lattice is also cubic:

$$\mathbf{Q} = \frac{2\pi}{a}(l_x\mathbf{n}_x + l_y\mathbf{n}_y + l_z\mathbf{n}_z), \quad (3.114)$$

so that the 1st Brillouin zone is a cube with the side $b = 2\pi/a$.

Almost equally simple calculations show that the reciprocal lattice of fcc is bcc, and vice versa. Figure 13 shows the resulting 1st Brillouin zone of the fcc lattice.

The notion of the reciprocal lattice makes the multi-dimensional band theory not much more complex than that in 1D, especially for numerical calculations, at least for the single-point Bravais lattices. Indeed, repeating all the steps that have led us to Eq. (2.218), but now with a d -dimensional Fourier expansion of the functions $U(\mathbf{r})$ and $u(\mathbf{r})$, we readily get its generalization:

⁴⁸ This is why the notion of the \mathbf{Q} -lattice is also the main starting point of X-ray diffraction studies of crystals. Indeed, it allows rewriting the well-known Bragg condition for diffraction peaks in an extremely simple form: $\mathbf{k} = \mathbf{k}_i + \mathbf{Q}$, where \mathbf{k}_i and \mathbf{k} are the wave vectors of the, respectively, incident and diffracted waves – see, e.g., EM Sec. 8.4 (where it was more convenient for me to use the notation \mathbf{k}_0 for \mathbf{k}_i).

⁴⁹ See, e.g., MA Eq. (7.6).

$$\sum_{l' \neq l} U_{l'-l} u_{l'} = (E - E_l) u_l, \quad (3.115)$$

where \mathbf{l} is now a d -dimensional vector of integer indices l_j . The summation in Eq. (115) should be carried over all essential components of this vector (i.e. over all relevant nodes of the reciprocal lattice), so that writing a corresponding computer code requires a bit more care than in 1D. However, this is just a homogeneous system of linear equations, and numerous routines of finding its eigenvalues E are readily available from both public sources and commercial software packages.

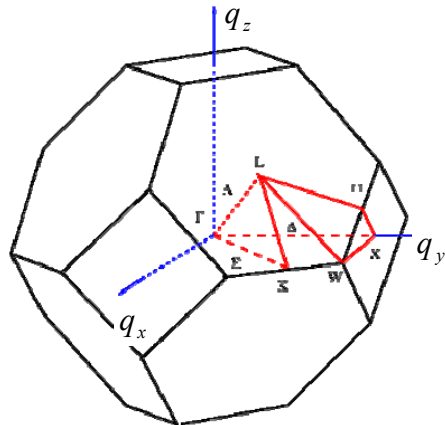


Fig. 3.13. The 1st Brillouin zone of the fcc lattice, and the traditional notation of its main directions. Adapted from http://en.wikipedia.org/wiki/Band_structure, as a public domain material.

What is indeed more complex than in 1D is representation (and hence comprehension :-), of the calculated results and experimental data. Typically, the representation is limited to plotting the Bloch state eigenenergy as a function of components of the vector q along certain special directions the reciprocal space of quasimomentum (see, e.g., the red lines in Fig. 13), typically on a single panel. Fig. 14 shows perhaps the most famous (and certainly the most practically important) of such plots, the band structure of electrons in crystalline silicon. The dashed horizontal lines mark the so-called *indirect gap* of the width ~ 1.12 eV between the “valence” (nominally occupied) and the next “conduction” (nominally unoccupied) energy bands.

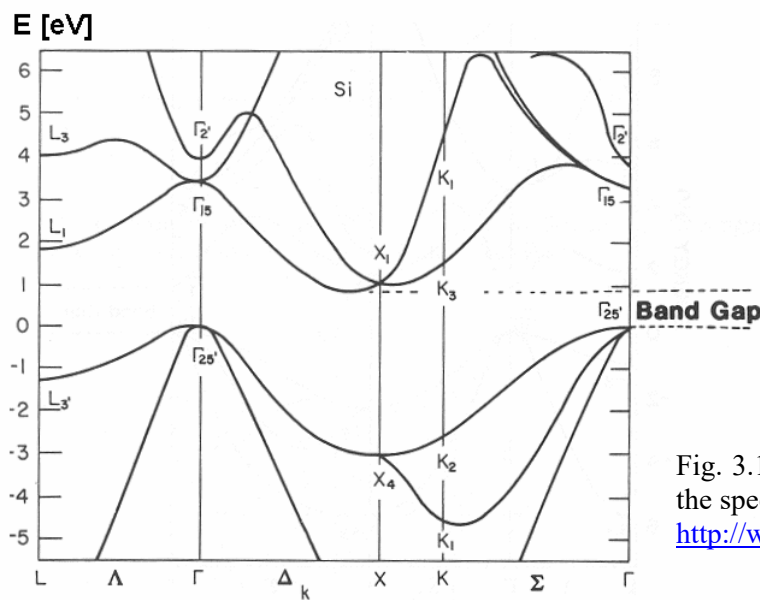


Fig. 3.14. The band structure of silicon, plotted along the special directions shown in Fig. 13. (Adapted from http://www.tf.uni-kiel.de/matwis/amat/semi_en/.)

In order to understand the reason for such complexity, let us see how we would start to calculate such a picture in the weak-potential approximation, for the simplest case of a 2D square lattice – which is a subset of the cubic lattice (106), with $\tau_3 = 0$. Its 1st Brillouin zone is of course also a square, of the area $(2\pi/a)^2$ – see the dashed lines in Fig. 15. Let us draw the lines of the constant energy of a free particle ($U = 0$) in this zone. Repeating the arguments of Sec. 2.7 (see especially Fig. 2.28 and its discussion), we may conclude that Eq. (2.216) should be now generalized as follows,

$$E = \frac{\hbar^2 k^2}{2m} = \frac{\hbar^2}{2m} \left[\left(q_x - \frac{2\pi l_x}{a} \right)^2 + \left(q_y - \frac{2\pi l_y}{a} \right)^2 \right], \quad (3.116)$$

with all possible integers l_x and l_y . Considering this result only within the 1st Brillouin zone, we see that as the particle's energy E grows, the lines of equal energy, for the lowest energy band, evolve as shown in Fig. 15. Just like in 1D, the weak-potential effects are only important at the Brillouin zone boundaries, and may be crudely considered as the appearance of narrow energy gaps, but one can see that the band structure in \mathbf{q} -space is complex enough even without these effects – and becomes even more involved at higher E .

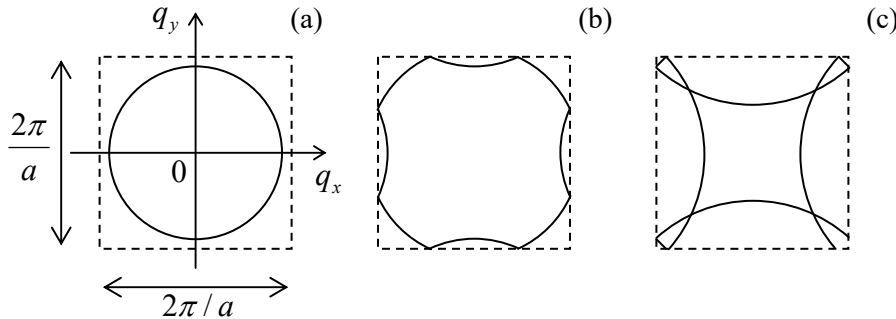


Fig. 3.15. The lines of constant energy E of a free particle, within the 1st Brillouin zone of a square Bravais lattice, for: (a) $E/E_1 \approx 0.95$, (b) $E/E_1 \approx 1.05$; and (c) $E/E_1 \approx 2.05$, where $E_1 \equiv \pi^2 \hbar^2 / 2ma^2$.

The tight-binding approximation is usually easier to follow. For example, for the same square 2D lattice, we may repeat the arguments that have led us to Eq. (2.203), to write⁵⁰

$$i\hbar \dot{a}_{0,0} = -\delta_n (a_{-1,0} + a_{+1,0} + a_{0,+1} + a_{0,-1}), \quad (3.117)$$

where the indices correspond to the deviations of the integers τ_x and τ_y from an arbitrarily selected minimum of the potential energy – and hence of the wavefunction's “hump”, quasi-localized at this minimum. Now, looking for the stationary solution of these equations, that would obey the Bloch theorem (107), instead of Eq. (2.206) we get

$$E = E_n + \varepsilon_n = E_n - \delta_n \left(e^{iq_x a} + e^{-iq_x a} + e^{iq_y a} + e^{-iq_y a} \right) \equiv E_n - 2\delta_n (\cos q_x a + \cos q_y a). \quad (3.118)$$

Figure 16 shows this result, within the 1st Brillouin zone, in two forms: as color-coded lines of equal energy, and as a 3D plot (also enhanced by color). It is evident that the plots of this function along different lines on the \mathbf{q} -plane, for example along one of the axes (say, q_x) and along a diagonal of the 1st Brillouin zone (say, with $q_x = q_y$) give different curves $E(q)$, qualitatively similar to those of silicon (Fig.

⁵⁰ Actually, using the same values of δ_n in both directions (x and y) implies some sort of symmetry of the quasi-localized states. For example, the s -states of axially-symmetric potentials (see the next section) always have such symmetry.

14). However, the latter structure is further complicated by the fact that the primitive cell of its Bravais lattice contains 2 atoms – see Fig. 12c and its discussion. In this case, even the tight-binding picture becomes more complex. Indeed, even if the atoms at different positions of the primitive unit cell are similar (as they are, for example, in both graphene and silicon), and hence the potential wells near those points and the corresponding local wavefunctions $u(\mathbf{r})$ are similar as well, the Bloch theorem (which only pertains to Bravais lattices!) does not forbid them to have different complex probability amplitudes $a(t)$ whose time evolution should be described by a specific differential equation.

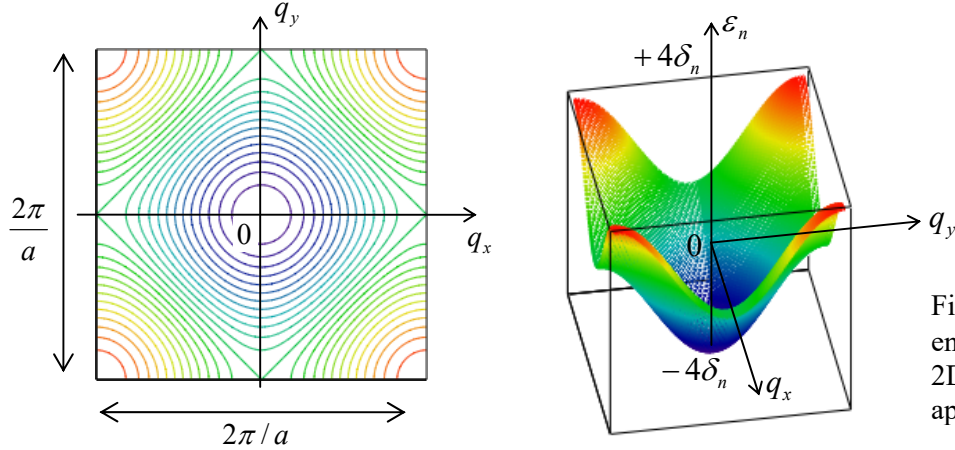


Fig. 3.16. The allowed band energy $\varepsilon_n \equiv E - E_n$ for a square 2D lattice, in the tight-binding approximation.

As the simplest example, to describe the honeycomb lattice shown in Fig. 12a, we have to prescribe different probability amplitudes to the “top” and “bottom” points of its primitive cell – say, α and β , correspondingly. Since each of these points is surrounded (and hence weakly interacts) with three neighbors of the opposite type, instead of Eq. (117) we have to write two equations:

$$i\hbar\dot{\alpha} = -\delta_n \sum_{j=1}^3 \beta_j, \quad i\hbar\dot{\beta} = -\delta_n \sum_{j'=1}^3 \alpha_{j'}, \quad (3.119)$$

where each summation is over three next-neighbor points. (In these two sums, I am using different summation indices just to emphasize that these directions are different for the “top” and “bottom” points of the primitive cell – see Fig. 12a.) Now using the Bloch theorem (107) in the form similar to Eq. (2.205), we get two coupled systems of linear algebraic equations:

$$(E - E_n)\alpha = -\delta_n \beta \sum_{j=1}^3 e^{i\mathbf{q}\cdot\mathbf{r}_j}, \quad (E - E_n)\beta = -\delta_n \alpha \sum_{j'=1}^3 e^{i\mathbf{q}\cdot\mathbf{r}'_{j'}}, \quad (3.120)$$

where \mathbf{r}_j and $\mathbf{r}'_{j'}$ are the next-neighbor positions, as seen from the top and bottom points, respectively. Writing the condition of consistency of this system of homogeneous linear equations, we get two equal and opposite values for energy correction for each value of \mathbf{q} :

$$E_{\pm} = E_n \pm \delta_n \Sigma^{1/2}, \quad \text{where } \Sigma \equiv \sum_{j,j'=1}^3 e^{i\mathbf{q}\cdot(\mathbf{r}_j + \mathbf{r}'_{j'})}. \quad (3.121)$$

According to Eq. (120), these two energy bands correspond to the phase shifts (on the top of the regular Bloch shift $\mathbf{q}\cdot\Delta\mathbf{r}$) of either 0 or π between the adjacent quasi-localized wavefunctions $u(\mathbf{r})$.

The most interesting corollary of such energy symmetry, augmented by the honeycomb lattice's symmetry, is that for certain values \mathbf{q}_D of the vector \mathbf{q} (that turn out to be in each of six corners of the honeycomb-shaped 1st Brillouin zone), the double sum Σ vanishes, i.e. the two band surfaces $E_{\pm}(\mathbf{q})$ touch each other. As a result, in the vicinities of these so-called *Dirac points*,⁵¹ the dispersion relation is linear:

$$E_{\pm}|_{\mathbf{q} \approx \mathbf{q}_D} \approx E_n \pm \hbar v_n |\tilde{\mathbf{q}}|, \quad \text{where } \tilde{\mathbf{q}} \equiv \mathbf{q} - \mathbf{q}_D, \quad (3.122)$$

with $v_n \propto \delta_n$ being a constant with the dimension of velocity – for graphene, close to 10^6 m/s. Such a linear dispersion relation ensures several interesting transport properties of graphene, in particular of the quantum Hall effect in it – as was already mentioned in Sec. 2. For their more detailed discussion, I have to refer the reader to special literature.⁵²

3.5. Axially-symmetric systems

I cannot conclude this chapter (and hence our review of wave mechanics) without addressing the exact solutions of the stationary Schrödinger equation⁵³ possible in the cases of highly symmetric functions $U(\mathbf{r})$. Such solutions are very important, in particular, for atomic and nuclear physics, and will be used in the later chapters of this course.

In some rare cases, such symmetries may be exploited by the separation of variables in Cartesian coordinates. The most famous (and rather important) example is the d -dimensional harmonic oscillator – a particle moving inside the potential

$$U = \frac{m\omega_0^2}{2} \sum_{j=1}^d r_j^2. \quad (3.123)$$

Separating the variables exactly as we did in Sec. 1.7 for the rectangular hard-wall box (1.77), for each degree of freedom we get the Schrödinger equation (2.261) of a 1D oscillator, whose eigenfunctions are

⁵¹ This term is based on a (rather indirect) analogy with the Dirac theory of relativistic quantum mechanics, to be discussed in Chapter 9 below.

⁵² See, e.g., the reviews by A. Castro Neto *et al.*, *Rev. Mod. Phys.* **81**, 109 (2009) and by X. Lu *et al.*, *Appl. Phys. Rev.* **4**, 021306 (2017). Note that the transport properties of graphene are determined by coupling of $2p$ -state electrons of its carbon atoms (see Secs. 6 and 7 below), whose wavefunctions are proportional to $\exp\{\pm i\varphi\}$ rather than are axially-symmetric as implied by Eqs. (120). However, due to the lattice symmetry, this fact does not affect the above dispersion relation $E(\mathbf{q})$.

⁵³ This is my best chance to mention, in passing, that the eigenfunctions $\psi_n(\mathbf{r})$ of any such problem do not feature the instabilities typical for the *deterministic chaos* effects of classical mechanics – see, e.g., CM Chapter 9. (This is why the term *quantum mechanics of classically chaotic systems* is preferable to the occasionally used term “quantum chaos”.) It is curious that at the initial stages of the time evolution of the wavefunctions of such systems, their certain correlation functions still grow exponentially, reminding the *Lyapunov exponents* λ of their classical chaotic dynamics. This growth stops at the so-call *Ehrefect times* $t_E \sim \lambda^{-1} \ln(S/\hbar)$, where S is the action scale of the problem – see, e.g., I. Aleiner and A. Larkin, *Phys. Rev. E* **55**, R1243 (1997). In a stationary quantum state, the most essential trace of the classical chaos in a system is an unusual statistics of its eigenvalues, in particular of the energy spectra. We will have a chance for a brief look at such statistics in Chapter 5, but unfortunately, I will not have time/space to discuss this field in much detail. Perhaps the best available book for further reading is the monograph by M. Gutzwiller, *Chaos in Classical and Quantum Mechanics*, Springer, 1991.

given by Eq. (2.284), and the energy spectrum is described by Eq. (2.162). As a result, the total energy spectrum may be indexed by a vector $\mathbf{n} = \{n_1, n_2, \dots, n_d\}$ of d independent integer quantum numbers n_j :

$$E_{\mathbf{n}} = \hbar\omega_0 \left(\sum_{j=1}^d n_j + \frac{d}{2} \right), \quad (3.124)$$

each ranging from 0 to ∞ . Note that every energy level of this system, with the only exception of its ground state,

$$\psi_g = \prod_{j=1}^d \psi_0(r_j) = \frac{1}{\pi^{d/4} x_0^{d/2}} \exp \left\{ -\frac{1}{2x_0^2} \sum_{j=1}^d r_j^2 \right\}, \quad (3.125)$$

is *degenerate*: several different wavefunctions, each with its own different set of quantum numbers n_j , but the same value of their sum, have the same energy.

However, the harmonic oscillator problem is an exception: for other central- and spherically-symmetric problems the solution is made easier by using more appropriate curvilinear coordinates. Let us start with the simplest axially-symmetric problem: the so-called *planar rigid rotator* (or “rotor”), i.e. a particle of mass m ,⁵⁴ constrained to move along a plane circle of radius R (Fig. 17).⁵⁵

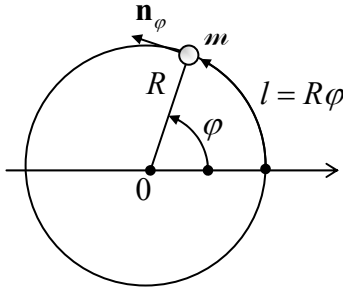


Fig. 3.17. A planar rigid rotator.

The classical planar rotator may be described by just *one* degree of freedom, say the angle displacement φ (or equivalently the arc displacement $l \equiv R\varphi$) from some reference direction, with the energy (and the Hamiltonian function) $H = p^2/2m$, where $\mathbf{p} \equiv m\mathbf{v} = m\mathbf{n}_\varphi (dl/dt)$, \mathbf{n}_φ being the unit vector in the azimuthal direction – see Fig. 17. This function is similar to that of a free 1D particle (with the replacement $x \rightarrow l \equiv R\varphi$), and hence the rotator’s quantum properties may be described by a similar Hamiltonian operator:

$$\hat{H} = \frac{\hat{p}^2}{2m}, \quad \text{with } \hat{\mathbf{p}} = -i\hbar\mathbf{n}_\varphi \frac{\partial}{\partial l} \equiv -i\frac{\hbar}{R}\mathbf{n}_\varphi \frac{\partial}{\partial\varphi}, \quad (3.126)$$

whose eigenfunctions have a similar structure:

$$\psi = Ce^{ikl} \equiv Ce^{ikR\varphi}. \quad (3.127)$$

⁵⁴ From this point on (until the chapter’s end), I will use this exotic font for the particle’s mass, to avoid any chance of its confusion with the impending “magnetic” quantum number m , traditionally used in axially-symmetric problems.

⁵⁵ This is a reasonable model for the confinement of light atoms, notably hydrogen, in some organic compounds, but I am addressing this system mostly as the basis for the following, more complex problems.

The “only” new feature is that in the rotator, all observables should be 2π -periodic functions of the angle φ . Hence, as we have already discussed in the context of the magnetic flux quantization (see Fig. 4 and its discussion), as the particle makes one turn around the central point 0, its wavefunction’s phase $kR\varphi$ may only change by $2\pi m$, with an arbitrary integer m (ranging from $-\infty$ to $+\infty$):

$$\psi_m(\varphi + 2\pi) = \psi_m(\varphi)e^{2\pi im}. \quad (3.128)$$

With the eigenfunctions (127), this periodicity condition immediately gives $2\pi kR = 2\pi m$. Thus, the wave number k can take only quantized values $k_m = m/R$, so that the eigenfunctions should be indexed by this *magnetic quantum number* m :

$$\psi_m = C_m \exp\left\{im \frac{l}{R}\right\} \equiv C_m \exp\{im\varphi\},$$

(3.129) Planar rotator:
eigenfunctions

and the energy spectrum is discrete:

$$E_m = \frac{p_m^2}{2m} = \frac{\hbar^2 k_m^2}{2m} = \frac{\hbar^2 m^2}{2mR^2}.$$

(3.130) Planar rotator:
eigenenergies

This simple model allows exact analysis of the external magnetic field effects on a confined motion of an electrically charged particle. Indeed, in the simplest case when this field is axially symmetric (or just uniform) and directed normally to the rotator’s plane, it does not violate the axial symmetry of the system. According to Eq. (26), in this case, we have to generalize Eq. (126) as

$$\hat{H} = \frac{1}{2m} \left(-i\hbar \mathbf{n}_\varphi \frac{\partial}{\partial l} - q\mathbf{A} \right)^2 \equiv \frac{1}{2m} \left(-i \frac{\hbar}{R} \mathbf{n}_\varphi \frac{\partial}{\partial \varphi} - q\mathbf{A} \right)^2. \quad (3.131)$$

Here, in contrast to the Cartesian gauge choice (44), which was so instrumental for the solution of the Landau level problem, it is beneficial to take the vector potential in the axially-symmetric form $\mathbf{A} = A(\rho)\mathbf{n}_\varphi$, where $\rho = \{x, y\}$ is the 2D radius-vector, with the magnitude $\rho = (x^2 + y^2)^{1/2}$. Using the well-known expression for the curl operator in the cylindrical coordinates,⁵⁶ we can readily check that the requirement $\nabla \times \mathbf{A} = \mathcal{B}\mathbf{n}_z$, with $\mathcal{B} = \text{const}$, is satisfied by the following function:

$$\mathbf{A} = \mathbf{n}_\varphi \frac{\mathcal{B}\rho}{2}. \quad (3.132)$$

For the planar rotator, $\rho = R = \text{const}$, so that the stationary Schrödinger equation becomes

$$\frac{1}{2m} \left(-i \frac{\hbar}{R} \frac{\partial}{\partial \varphi} - q \frac{\mathcal{B}R}{2} \right)^2 \psi_m = E_n \psi_m. \quad (3.133)$$

A little bit surprisingly, this equation is still satisfied with the eigenfunctions (127). Moreover, since the periodicity condition (128) is also unaffected by the applied magnetic field, we return to the periodic eigenfunctions (129), independent of \mathcal{B} . However, the field does affect the system’s eigenenergies:

⁵⁶ See, e.g., MA Eq. (10.5).

Planar rotator:
magnetic field's effect

$$E_m = \frac{1}{\psi_m} \frac{1}{2m} \left(-i \frac{\hbar}{R} \frac{\partial}{\partial \varphi} - q \frac{\mathcal{B}R}{2} \right)^2 \psi_m = \frac{1}{2m} \left(\frac{\hbar m}{R} - q \frac{\mathcal{B}R}{2} \right)^2 \equiv \frac{\hbar^2}{2mR^2} \left(m - \frac{\Phi}{\Phi_0'} \right)^2, \quad (3.134)$$

where $\Phi = \pi R^2 \mathcal{B}$ is the magnetic flux through the particle's trajectory, and $\Phi_0' = 2\pi\hbar/q$ is the “normal” magnetic flux quantum we have already met in the AB effect’s context – see Eq. (34) and its discussion. The field also changes the electric current of the particle in each eigenstate:

$$I_m = q \frac{\hbar}{2imR} \left[\psi_m^* \left(\frac{\partial}{\partial \varphi} - \frac{iqR\mathcal{B}}{2\hbar} \right) \psi_m - \text{c.c.} \right] = q \frac{\hbar}{mR} |C_m|^2 \left(m - \frac{\Phi}{\Phi_0'} \right). \quad (3.135)$$

Normalizing the wavefunction (129) to have $W_m = 1$, we get $|C_m|^2 = 1/2\pi R$, so that Eq. (135) becomes

$$I_m = \left(m - \frac{\Phi}{\Phi_0'} \right) I_0, \quad \text{with } I_0 \equiv \frac{\hbar q}{2\pi m R^2}. \quad (3.136)$$

The functions $E_m(\Phi)$ and $I_m(\Phi)$ are shown in Fig. 18. Note that since $\Phi_0' \propto 1/q$, for any sign of the particle’s charge q , $dI_m/d\Phi < 0$. It is easy to verify that this means that the current is *diamagnetic* for any sign of q :⁵⁷ the field-induced current flows in the direction that its own magnetic field tries to compensate for the external magnetic flux applied to the loop. This result may be interpreted as a different manifestation of the AB effect.⁵⁸ In contrast to the interference experiment that was discussed in Sec. 1, in the situation shown in Fig. 17 the particle is not absorbed by the detector but travels around the ring continuously. As a result, its wavefunction is “rigid”: due to the periodicity condition (128), the quantum number m is discrete, and the applied magnetic field cannot change the wavefunction gradually. In this sense, the system is similar to a superconducting loop – see Fig. 4 and its discussion. The difference between these systems is two-fold:

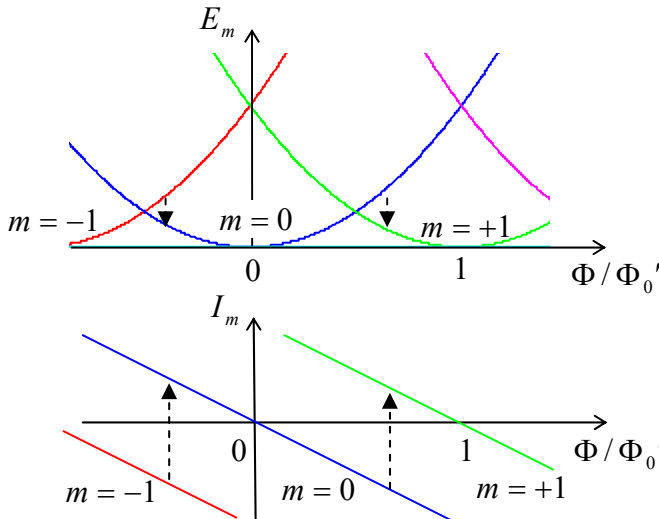


Fig. 3.18. The magnetic field effect on a charged planar rotator. Dashed arrows show possible inelastic transitions between metastable and ground states, due to weak interaction with the environment, as the external magnetic field is slowly increased.

⁵⁷ This effect, whose qualitative features remain the same for all 2D or 3D localized states (see Chapter 6 below), is frequently referred to as *orbital diamagnetism*. In magnetic materials consisting of particles with uncompensated spins, this effect competes with an opposite effect, *spin paramagnetism* – see, e.g., EM Sec. 5.5.

⁵⁸ It is straightforward to check that the final forms of Eqs. (134)-(136) remain valid even if the magnetic field is localized well inside the rotator’s circumference so that its lines do not touch the particle’s trajectory.

(i) For a single charged particle, in macroscopic systems with practicable values of q , R , and m , the scale I_0 of the induced current is very small. For example, for $m = m_e$, $q = -e$, and $R = 1 \mu\text{m}$, Eq. (136) yields $I_0 \approx 3 \text{ pA}$.⁵⁹ With the ring's inductance \mathcal{L} of the order of $\mu_0 R$,⁶⁰ the contribution $\Phi_I = \mathcal{L}I \sim \mu_0 R I_0 \sim 10^{-24} \text{ Wb}$ of such a small current into the net magnetic flux Φ is negligible in comparison with $\Phi_0' \sim 10^{-15} \text{ Wb}$, so that the wavefunction quantization does not lead to the constancy of the total magnetic flux.

(ii) As soon as the magnetic field raises the eigenstate energy E_m above that of another eigenstate $E_{m'}$, the former state becomes metastable, and a weak interaction of the system with its environment (which is neglected in our simple model, but will be discussed in Chapter 7) may induce a quantum transition of the system to the lower-energy state, thus reducing the diamagnetic current's magnitude – see the dashed lines in Fig. 18. The flux quantization in superconductors is much more robust to such perturbations.⁶¹

Now let us return, once again, to the key Eq. (129), and see what does it give for one more important observable, the particle's angular momentum

$$\mathbf{L} \equiv \mathbf{r} \times \mathbf{p}, \quad (3.137)$$

In this particular geometry, the vector \mathbf{L} has just one component, normal to the rotator plane:

$$L_z = Rp. \quad (3.138)$$

In classical mechanics, L_z of the rotator should be conserved (due to the absence of external torque), but it may take arbitrary values. In quantum mechanics, the situation changes: with $p = \hbar k$, our result $k_m = m/R$ for the m^{th} eigenstate may be rewritten as

$(L_z)_m = R\hbar k_m = \hbar m.$

(3.139)
Angular momentum quantization

Thus, the angular momentum is quantized: it may be only a multiple of the Planck constant \hbar – confirming the N. Bohr's guess – see Eq. (1.8). As we will see in Chapter 5, this result is very general (though it may be modified by spin effects), and the wavefunctions (129) may be interpreted as eigenfunctions of the angular momentum operator.

Let us see whether this quantization persists in more general, but still axial-symmetric systems. To implement the planar rotator in our 3D world, we needed to provide rigid confinement of the particle both in the motion plane and along the 2D radius ρ . Let us consider a more general situation when only the former confinement is strict, i.e. to the case when a 2D particle moves in an arbitrary centrally-symmetric potential

$$U(\mathbf{p}) = U(\rho). \quad (3.140)$$

⁵⁹ Such weak persistent, macroscopic diamagnetic currents in non-superconducting systems have been experimentally observed by measuring the weak magnetic field induced by the currents, in systems of a large number ($\sim 10^7$) of similar conducting rings – see, e.g., L. Lévy *et al.*, *Phys. Rev. Lett.* **64**, 2074 (1990). Due to the dephasing effects of electron scattering by phonons and other electrons (unaccounted for in our simple theory), the effect's observation requires submicron rings and millikelvin temperatures.

⁶⁰ See, e.g., EM Sec. 5.3.

⁶¹ Interrupting a superconducting ring with a weak link (Josephson junction), i.e. forming a SQUID, we may get a switching behavior similar to that shown with dashed arrows in Fig. 18 – see, e.g., EM Sec. 6.5.

Using the well-known expression for the 2D Laplace operator in polar coordinates,⁶² we may represent the 2D stationary Schrödinger equation in the form

$$-\frac{\hbar^2}{2m} \left[\frac{1}{\rho} \frac{\partial}{\partial \rho} \left(\rho \frac{\partial}{\partial \rho} \right) + \frac{1}{\rho^2} \frac{\partial^2}{\partial \varphi^2} \right] \psi + U(\rho) \psi = E \psi. \quad (3.141)$$

Separating the radial and angular variables as⁶³

$$\psi = \mathcal{R}(\rho) \mathcal{A}(\varphi), \quad (3.142)$$

we get, after the division of all terms by ψ and their multiplication by ρ^2 , the following equation:

$$-\frac{\hbar^2}{2m} \left[\frac{\rho}{\mathcal{R}} \frac{d}{d\rho} \left(\rho \frac{d\mathcal{R}}{d\rho} \right) + \frac{1}{\mathcal{A}} \frac{d^2\mathcal{A}}{d\varphi^2} \right] + \rho^2 U(\rho) = \rho^2 E. \quad (3.143)$$

The fraction $(d^2\mathcal{A}/d\varphi^2)/\mathcal{A}$ should be a constant (because all other terms of the equation may be functions only of ρ), so that for the function $\mathcal{A}(\varphi)$ we get an ordinary differential equation,

$$\frac{d^2\mathcal{A}}{d\varphi^2} + \nu^2 \mathcal{A} = 0, \quad (3.144)$$

where ν^2 is the variable separation constant. The fundamental solutions of Eq. (144) are evidently $\mathcal{A} \propto \exp\{\pm i \nu \varphi\}$. Now requiring, as we did for the planar rotator, the 2π periodicity of any observable, i.e.

$$\mathcal{A}(\varphi + 2\pi) = \mathcal{A}(\varphi) e^{2\pi i m}, \quad (3.145)$$

where m is an integer, we see that the constant ν has to be equal to m , and get, for the angular factor, the same result as for the full wavefunction of the planar rotator – cf. Eq. (129):

$$\mathcal{A}_m = C_m e^{im\varphi}, \quad \text{with } m = 0, \pm 1, \pm 2, \dots \quad (3.146)$$

Plugging the resulting relation $(d^2\mathcal{A}/d\varphi^2)/\mathcal{A} = -m^2$ back into Eq. (143), we may rewrite it as

$$-\frac{\hbar^2}{2m} \left[\frac{1}{\rho \mathcal{R}} \frac{d}{d\rho} \left(\rho \frac{d\mathcal{R}}{d\rho} \right) - \frac{m^2}{\rho^2} \right] + U(\rho) = E. \quad (3.147)$$

The physical interpretation of this equation is that the full energy is a sum,

$$E = E_\rho + E_\varphi, \quad (3.148)$$

of the radial-motion part

$$E_\rho = -\frac{\hbar^2}{2m} \frac{1}{\rho} \frac{d}{d\rho} \left(\rho \frac{d\mathcal{R}}{d\rho} \right) + U(\rho). \quad (3.149)$$

and the angular-motion part

⁶² See, e.g., MA Eq. (10.3) with $\partial/\partial z = 0$.

⁶³ At this stage, I do not want to mark the particular solution (eigenfunction) ψ and corresponding eigenenergy E with any single index, because based on our experience in Sec. 1.7, we already may expect that in a 2D problem the role of this index will be played by *two* integers – two quantum numbers.

$$E_\varphi = \frac{\hbar^2 m^2}{2m\rho^2}. \quad (3.150)$$

Now let us recall that a similar separation exists in classical mechanics,⁶⁴ because the total energy of a particle moving in a central field may be represented as

$$E = \frac{m}{2} v^2 + U(\rho) = \frac{m}{2} (\dot{\rho}^2 + \rho^2 \dot{\varphi}^2) + U(\rho) \equiv E_\rho + E_\varphi, \quad (3.151)$$

$$\text{with } E_\rho \equiv \frac{p_\rho^2}{2m} + U(\rho), \quad \text{and } E_\varphi \equiv \frac{m}{2} \rho^2 \dot{\varphi}^2 \equiv \frac{p_\varphi^2}{2m} \equiv \frac{L_z^2}{2m\rho^2}. \quad (3.152)$$

The comparison of the latter relation with Eqs. (139) and (150) gives us grounds to expect that the quantization rule $L_z = m\hbar$ may be valid not only for this 2D problem but in 3D cases as well. In Sec. 5.6, we will see that this is indeed the case.

Returning to Eq. (147), with our 1D wave mechanics experience we may expect that any fixed m this ordinary, linear, second-order differential equation should have (for a motion confined to a certain final region of its argument ρ) a discrete energy spectrum described by another integer quantum number – say, n . This means that the eigenfunctions (142) and corresponding eigenenergies (148) and $\mathcal{R}(\rho)$ should be indexed by two quantum numbers, m and n . So, the variable separation is not so “clean” as it was for the rectangular potential well. Normalizing the angular function \mathcal{F} to the full circle, $\Delta\varphi = 2\pi$, we may rewrite Eq. (142) as

$$\psi_{m,n} = \mathcal{R}_{m,n}(\rho)\mathcal{F}_m(\varphi) = \frac{1}{(2\pi)^{1/2}} \mathcal{R}_{m,n}(\rho)e^{im\varphi}. \quad (3.153)$$

A good (and important) example of an analytically solvable problem of this type is a 2D particle whose motion is rigidly confined to a disk of radius R , but otherwise free:

$$U(\rho) = \begin{cases} 0, & \text{for } 0 \leq \rho < R, \\ +\infty, & \text{for } R < \rho. \end{cases} \quad (3.154)$$

In this case, the solutions $\mathcal{R}_{m,n}(\rho)$ of Eq. (147) are proportional to the first-order Bessel functions $J_m(k_n\rho)$,⁶⁵ with the spectrum of possible values k_n following from the boundary condition $\mathcal{R}_{m,n}(R) = 0$. Let me leave a detailed analysis of this problem for the reader’s exercise.

3.6. Spherically-symmetric systems: Brute force approach

Now let us proceed to the mathematically more involved, but practically even more important case of the 3D motion, in a spherically-symmetric potential

$$U(\mathbf{r}) = U(r). \quad (3.155)$$

⁶⁴ See, e.g., CM Sec. 3.5.

⁶⁵ A short summary of properties of these functions, including the most important plots and a useful table of values, may be found in EM Sec. 2.7.

Let us start, again, with solving the eigenproblem for a rigid rotator – now a *spherical rotator*, i.e. a particle confined to move on the spherical surface of radius R . The rotator has two degrees of freedom because its position on the surface is completely described by two coordinates – say, the polar angle θ and the azimuthal angle φ . In this case, the kinetic energy we need to consider is limited to its angular part, so that in the Laplace operator in spherical coordinates⁶⁶ we may keep only those parts, with fixed $r = R$. Because of this, the stationary Schrödinger equation becomes

$$-\frac{\hbar^2}{2mR^2} \left[\frac{1}{\sin \theta} \frac{\partial}{\partial \theta} \left(\sin \theta \frac{\partial}{\partial \theta} \right) + \frac{1}{\sin^2 \theta} \frac{\partial^2}{\partial \varphi^2} \right] \psi = E \psi. \quad (3.156)$$

(Again, we will attach indices to ψ and E in a minute.) With the natural variable separation,

$$\psi = \Theta(\theta) \mathcal{F}(\varphi), \quad (3.157)$$

Eq. (156), with all terms multiplied by $\sin^2 \theta / \Theta \mathcal{F}$, yields

$$-\frac{\hbar^2}{2mR^2} \left[\frac{\sin \theta}{\Theta} \frac{d}{d\theta} \left(\sin \theta \frac{d\Theta}{d\theta} \right) + \frac{1}{\mathcal{F}} \frac{d^2 \mathcal{F}}{d\varphi^2} \right] = E \sin^2 \theta. \quad (3.158)$$

Just as in Eq. (143), the fraction $(d^2 \mathcal{F}/d\varphi^2)/\mathcal{F}$ may be a function of φ only, and hence has to be constant, giving Eq. (144) for it. So, with the same periodicity condition (145), the azimuthal functions are expressed by (146) again; in the normalized form,

$$\mathcal{F}_m(\varphi) = \frac{1}{(2\pi)^{1/2}} e^{im\varphi}. \quad (3.159)$$

With that, the fraction $(d^2 \mathcal{F}/d\varphi^2)/\mathcal{F}$ in Eq. (158) equals $(-m^2)$, and after the multiplication of all terms of that equation by $\Theta/\sin^2 \theta$, it is reduced to the following ordinary linear differential equation for the polar eigenfunctions $\Theta(\theta)$:

$$-\frac{1}{\sin \theta} \frac{d}{d\theta} \left(\sin \theta \frac{d\Theta}{d\theta} \right) + \frac{m^2}{\sin^2 \theta} \Theta = \varepsilon \Theta, \quad \text{with } \varepsilon \equiv E / \frac{\hbar^2}{2mR^2}. \quad (3.160)$$

It is common to recast it into an equation for a new function $P(\xi) \equiv \Theta(\theta)$, with $\xi \equiv \cos \theta$:

$$\frac{d}{d\xi} \left[(1 - \xi^2) \frac{dP}{d\xi} \right] + \left[l(l+1) - \frac{m^2}{1 - \xi^2} \right] P = 0, \quad (3.161)$$

where a new notation for the normalized energy is introduced: $l(l+1) \equiv \varepsilon$. The motivation for such notation is that, according to the mathematical analysis of Eq. (161) with integer m ,⁶⁷ it has solutions only if the parameter l is an integer: $l = 0, 1, 2, \dots$, and only if that integer is not smaller than $|m|$, i.e. if

$$-l \leq m \leq +l. \quad (3.162)$$

This fact immediately gives the following spectrum of the spherical rotator's energy E – and, as we will see later, the angular part of the energy of any spherically-symmetric system:

⁶⁶ See, e.g., MA Eq. (10.9).

⁶⁷ This analysis was first carried out by A.-M. Legendre (1752-1833). Just as a historic note: besides many original mathematical achievements, Dr. Legendre had authored a famous textbook, *Éléments de Géométrie*, which dominated teaching geometry through the 19th century.

$$E_l = \frac{\hbar^2 l(l+1)}{2mR^2}, \quad (3.163)$$

Angular energy spectrum

so that the only effect of the magnetic quantum number m here is imposing the restriction (162) on the non-negative integer l – the so-called *orbital quantum number*. This means, in particular, that each energy (163) corresponds to $(2l+1)$ different values of m , i.e. is $(2l+1)$ -degenerate.

To understand the nature of this degeneracy, we need to explore the corresponding eigenfunctions of Eq. (161). They are naturally numbered by two integers, m and l , and are called the associated *Legendre functions* P_l^m . (Note that here m is an upper index, not a power!) For the particular, simplest case $m = 0$, these functions are the so-called *Legendre polynomials* $P_l(\xi) \equiv P_l^0(\xi)$, which may be defined as the solutions of the following *Legendre equation*, resulting from Eq. (161) at $m = 0$:

$$\frac{d}{d\xi} \left[(1 - \xi^2) \frac{d}{d\xi} P \right] + l(l+1)P = 0, \quad (3.164)$$

Legendre equation

but also may be calculated explicitly from the following *Rodrigues formula*:⁶⁸

$$P_l(\xi) = \frac{1}{2^l l!} \frac{d^l}{d\xi^l} (\xi^2 - 1)^l, \quad l = 0, 1, 2, \dots \quad (3.165)$$

Legendre polynomials

Using this formula, it is easy to spell out a few lowest Legendre polynomials:

$$P_0(\xi) = 1, \quad P_1(\xi) = \xi, \quad P_2(\xi) = \frac{1}{2}(3\xi^2 - 1), \quad P_3(\xi) = \frac{1}{2}(5\xi^3 - 3\xi), \dots, \quad (3.166)$$

though such explicit expressions become bulkier and bulkier as l is increased. As these expressions (and Fig. 19) show, as the argument ξ is increased, all these functions end up at the same point, $P_l(+1) = +1$, while starting at either at the same point or at the opposite point: $P_l(-1) = (-1)^l$. On the way between these two end points, the l^{th} polynomial crosses the horizontal axis exactly l times, i.e. Eq. (164) has l roots.⁶⁹

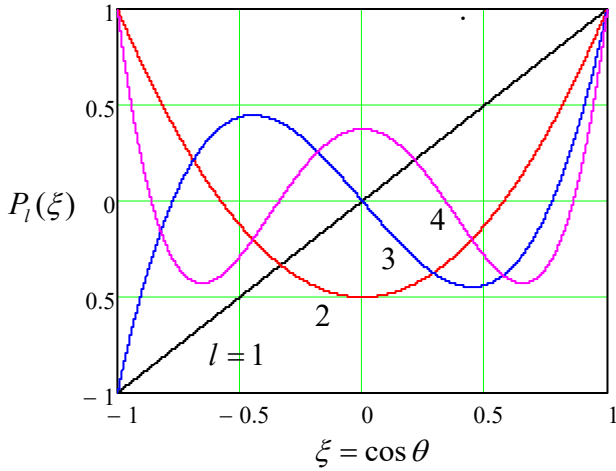


Fig. 3.19. A few lowest Legendre polynomials.

⁶⁸ This wonderful formula may be readily proved by plugging it into Eq. (164), but was not so easy to discover! This was done (independently) by B. O. Rodrigues in 1816, J. Ivory in 1824, and C. Jacobi in 1827.

⁶⁹ In this behavior, we may readily recognize the “standing wave” pattern typical for all 1D eigenproblems – cf. Figs. 1.8 and 2.35, as well as the discussion of the Sturm oscillation theorem at the end of Sec. 2.9.

It is also easy to use the Rodrigues formula (165) and the integration by parts to show that on the segment $-1 \leq \xi \leq +1$, the Lagrange polynomials form a full orthogonal set of functions, with the following normalization rule:

$$\int_{-1}^{+1} P_l(\xi) P_{l'}(\xi) d\xi = \frac{2}{2l+1} \delta_{ll'}, \quad (3.167)$$

For $m > 0$, the associated Legendre functions (now *not* necessarily polynomials!), may be expressed via the Legendre polynomials (165) using the following formula:⁷⁰

$$P_l^m(\xi) = (-1)^m (1 - \xi^2)^{m/2} \frac{d^m}{d\xi^m} P_l(\xi), \quad (3.168)$$

while the functions with a negative magnetic quantum number may be found as

$$P_l^{-m}(\xi) = (-1)^m \frac{(l-m)!}{(l+m)!} P_l^m(\xi), \quad \text{for } m > 0. \quad (3.169)$$

On the segment $-1 \leq \xi \leq +1$, the associated Legendre functions with a fixed index m form a full orthogonal set, with the normalization relation,

$$\int_{-1}^{+1} P_l^m(\xi) P_{l'}^m(\xi) d\xi = \frac{2}{2l+1} \frac{(l+m)!}{(l-m)!} \delta_{ll'}, \quad (3.170)$$

which is evidently a generalization of Eq. (167) for arbitrary m .

Since the difference between the angles θ and φ is to large extent artificial (due to an arbitrary direction of the polar axis), physicists prefer to use not the functions $\Theta(\theta) \propto P_l^m(\cos \theta)$ and $\mathcal{Z}_m(\varphi) \propto e^{im\varphi}$ separately, but normalized products of the type (157), which are called the *spherical harmonics*:

$$Y_l^m(\theta, \varphi) = \left[\frac{(2l+1)}{4\pi} \frac{(l-m)!}{(l+m)!} \right]^{1/2} P_l^m(\cos \theta) e^{im\varphi}. \quad (3.171)$$

The specific front factor in Eq. (171) is chosen in a way to simplify the following two expressions: the relation of the spherical harmonics with opposite signs of the magnetic quantum number,

$$Y_l^{-m}(\theta, \varphi) = (-1)^m [Y_l^m(\theta, \varphi)]^*, \quad (3.172)$$

and the following normalization relation:

$$\oint_{4\pi} Y_l^m(\theta, \varphi) [Y_{l'}^{m'}(\theta, \varphi)]^* d\Omega = \delta_{ll'} \delta_{mm'}, \quad (3.173)$$

with the integration over the whole solid angle. The last formula shows that on a spherical surface, the spherical harmonics form an orthonormal set of functions. This set is also full, so that any function defined on the surface, may be uniquely represented as a linear combination of Y_l^m .

Despite a somewhat intimidating character of the formulas given above, they yield quite simple expressions for the lowest spherical harmonics, which are most important for applications:

⁷⁰ Note that some texts use different choices for the front factor (called the *Condon-Shortley phase*) in the functions P_l^m , which do not affect the final results for the spherical harmonics Y_l^m .

$$l=0 : \quad Y_0^0 = (1/4\pi)^{1/2}, \quad (3.174)$$

$$l=1 : \quad \begin{cases} Y_1^{-1} = (3/8\pi)^{1/2} \sin \theta e^{-i\varphi}, \\ Y_1^0 = (3/4\pi)^{1/2} \cos \theta, \\ Y_1^1 = -(3/8\pi)^{1/2} \sin \theta e^{i\varphi}, \end{cases} \quad (3.175)$$

$$l=2 : \quad \begin{cases} Y_2^{-2} = -(15/32\pi)^{1/2} \sin^2 \theta e^{-2i\varphi}, \\ Y_2^{-1} = (15/8\pi)^{1/2} \sin \theta \cos \theta e^{-i\varphi}, \\ Y_2^0 = (3/16\pi)^{1/2} (3 \cos^2 \theta - 1), \quad \text{etc.} \\ Y_2^1 = -(15/8\pi)^{1/2} \sin \theta \cos \theta e^{i\varphi}, \\ Y_2^2 = (15/32\pi)^{1/2} \sin^2 \theta e^{2i\varphi}, \end{cases} \quad (3.176)$$

It is important to understand the general structure and symmetry of these functions. Since the spherical harmonics with $m \neq 0$ are complex, the most popular way of their graphical representation is to normalize their real and imaginary parts as⁷¹

$$Y_{lm} \equiv \sqrt{2}(-1)^m \times \begin{cases} \text{Im}(Y_l^{|m|}) \propto \sin m\varphi, & \text{for } m < 0, \\ \text{Re}(Y_l^{|m|}) \propto \cos m\varphi, & \text{for } m > 0, \end{cases} \quad (3.177)$$

(for $m = 0$, $Y_{l0} \equiv Y_l^0$), and then plot the magnitude of these real functions in the spherical coordinates as the distance from the origin, while using two colors to show their sign – see Fig. 20.

Let us start from the simplest case $l = 0$. According to Eq. (162), for this lowest orbital quantum number, there may be only one magnetic quantum number, $m = 0$. According to Eq. (174), the spherical harmonic corresponding to that state is just a constant, so that the wavefunction of this so-called *s state*⁷² is uniformly distributed over the sphere. Since this function has no gradient in any angular direction, it is only natural that the angular kinetic energy (163) of the particle equals zero.

According to the same Eq. (162), for $l = 1$, there are 3 different *p states*, with $m = -1$, $m = 0$, and $m = +1$ – see Eq. (175). As the second row of Fig. 20 shows, these states are essentially identical in structure and are just differently oriented in space, thus readily explaining the 3-fold degeneracy of the kinetic energy (163). Such a simple explanation, however, is not valid for the 5 different *d states* ($l = 2$), shown in the third row of Fig. 20, as well as the states with higher l : despite their equal energies, they differ not only by their spatial orientation but their structure as well. All states with $m = 0$ have a nonzero gradient only in the θ direction. On the contrary, the states with the ultimate values of m ($\pm l$), change only monotonically (as $\sin^l \theta$) in the polar direction, while oscillating in the azimuthal direction. The states with intermediate values of m provide a gradual transition between these two extremes, oscillating in both directions, stronger and stronger in the azimuthal direction as $|m|$ is increased. Still, the magnetic quantum number, surprisingly, does not affect the angular energy for any l .

⁷¹ Such real functions Y_{lm} , which also form a full orthonormal set, and are frequently called the *real* (or “tesseral”) *spherical harmonics*, are more convenient than the complex harmonics Y_l^m for several applications, especially when the variables of interest are real by definition.

⁷² The letter names for the states with various values of l stem from the history of optical spectroscopy – for example, the letter “s” used for states with $l = 0$, originally denoted the “sharp” optical line series, etc. The sequence of the letters is as follows: *s, p, d, f, g*, and then continuing in alphabetical order.

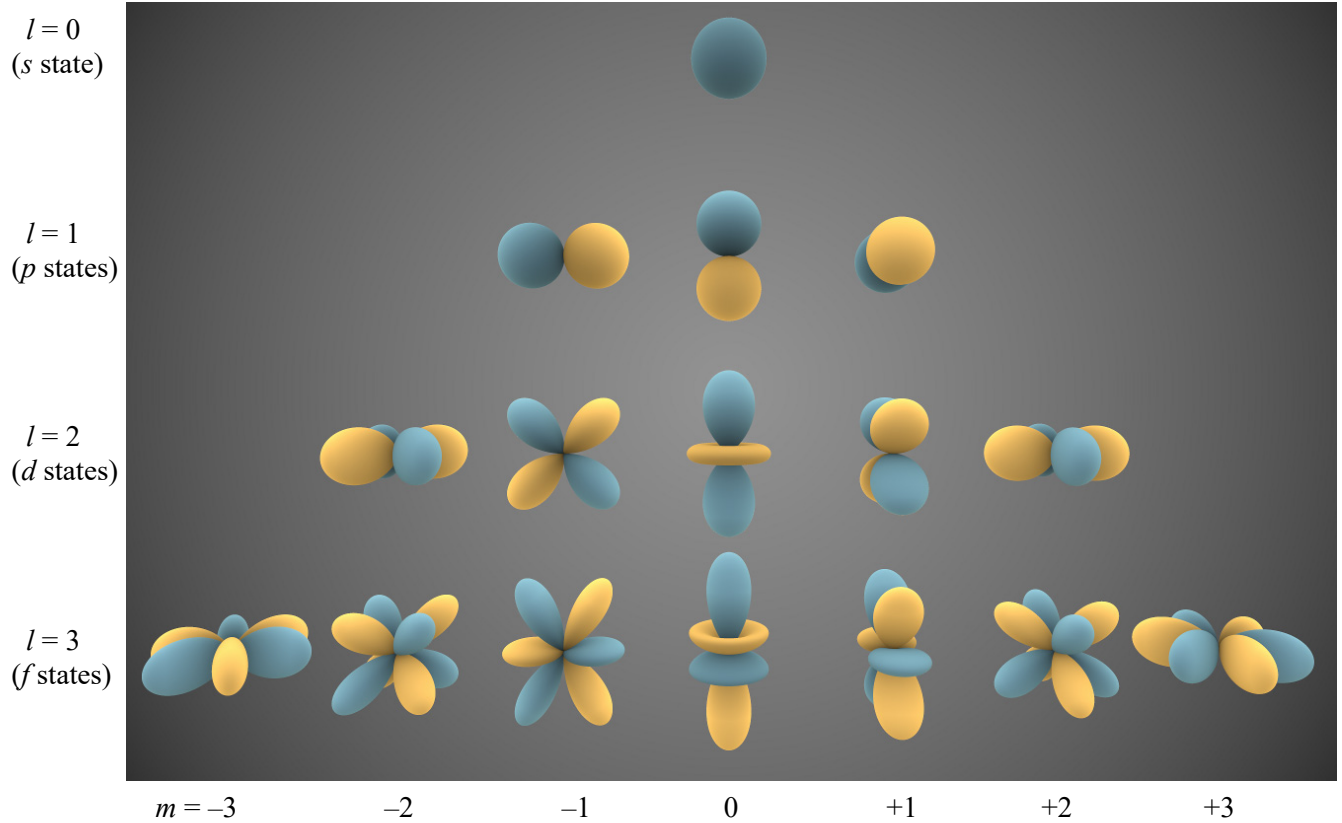


Fig. 3.20. Radial plots of several lowest real spherical harmonics Y_{lm} . (Adapted from https://en.wikipedia.org/wiki/Spherical_harmonics under the CC BY-SA 3.0 license.)

Another counter-intuitive feature of the spherical harmonics follows from the comparison of Eq. (163) with the second of the classical relations (152). These expressions coincide if we interpret the constant

$$L^2 \equiv \hbar^2 l(l+1), \quad (3.178)$$

as the value of the full angular momentum squared, $L^2 = |\mathbf{L}|^2$ (including its both θ and φ components) in the eigenstate with eigenfunction Y_l^m . On the other hand, the structure (159) of the azimuthal component $\mathcal{H}(\varphi)$ of the wavefunction is exactly the same as in 2D axially-symmetric problems, implying that Eq. (139) still gives correct values $L_z = m\hbar$ for the z -component of the angular momentum. This fact invites a question: why for any state with $l > 0$, $(L_z)^2 = m^2\hbar^2 \leq l^2\hbar^2$ is always less than $L^2 = l(l+1)\hbar^2$? In other words, what prevents the angular momentum vector to be fully aligned with the axis z ?

Besides the difficulty of answering this question using the above formulas, this analysis (though mathematically complete), is as intellectually unsatisfactory as the harmonic oscillator analysis in Sec. 2.9. In particular, it does not explain the meaning of the extremely simple relations for the eigenvalues of the energy and the angular momentum, coexisting with rather complicated eigenfunctions.

We will obtain natural answers to all these questions and concerns in Sec. 5.6 below, and now proceed to the extension of our wave-mechanical analysis to the 3D motion in an *arbitrary* spherically-symmetric potential (155). In this case, we have to use the full form of the Laplace operator in spherical

coordinates.⁷³ The variable separation procedure is an evident generalization of what we have done before, with the particular solutions of the type

$$\psi = \mathcal{R}(\rho)\Theta(\theta)\mathcal{F}(\phi), \quad (3.179)$$

whose substitution into the stationary Schrödinger equation yields

$$-\frac{\hbar^2}{2mr^2} \left[\frac{1}{\mathcal{R}} \frac{d}{dr} \left(r^2 \frac{d\mathcal{R}}{dr} \right) + \frac{1}{\Theta \sin \theta} \frac{d}{d\theta} \left(\sin \theta \frac{d\Theta}{d\theta} \right) + \frac{1}{\sin^2 \theta} \frac{1}{\mathcal{F}} \frac{d^2\mathcal{F}}{d\phi^2} \right] + U(r) = E. \quad (3.180)$$

It is evident that the angular part of the left-hand side (the two last terms in the square brackets) separates from the radial part, and that for the former part we get Eq. (156) again, with the only change, $R \rightarrow r$. This change does not affect the fact that the eigenfunctions of that equation are still the spherical harmonics (171), which obey Eq. (164). As a result, Eq. (180) gives the following equation for the radial function $\mathcal{R}(r)$:

$$-\frac{\hbar^2}{2mr^2} \left[\frac{1}{\mathcal{R}} \frac{d}{dr} \left(r^2 \frac{d\mathcal{R}}{dr} \right) - l(l+1) \right] + U(r) = E. \quad (3.181)$$

Note that no information about the magnetic quantum number m has crept into this radial equation (besides setting the limitation (162) for the possible values of l) so that it includes only the orbital quantum number l .

Let us explore the radial equation for the simplest case when $U(r) = 0$ – for example, to solve the eigenproblem for a 3D particle free to move only inside the sphere of radius R – say, confined there by the potential⁷⁴

$$U = \begin{cases} 0, & \text{for } 0 \leq r < R, \\ +\infty, & \text{for } R < r. \end{cases} \quad (3.182)$$

In this case, Eq. (181) is reduced to

$$-\frac{\hbar^2}{2mr^2} \left[\frac{1}{\mathcal{R}} \frac{d}{dr} \left(r^2 \frac{d\mathcal{R}}{dr} \right) - l(l+1) \right] = E. \quad (3.183)$$

Multiplying both parts of this equality by $r^2 \mathcal{R}$, and introducing the dimensionless argument $\xi \equiv kr$, where k^2 is defined by the usual relation $\hbar^2 k^2 / 2m = E$, we obtain the canonical form of this equation,

$$\xi^2 \frac{d^2\mathcal{R}}{d\xi^2} + 2\xi \frac{d\mathcal{R}}{d\xi} + [\xi^2 - l(l+1)]\mathcal{R} = 0, \quad (3.184)$$

Satisfied by so-called *spherical Bessel functions* of the first and second kind, $j_l(\xi)$ and $y_l(\xi)$.⁷⁵ These functions are directly related to the Bessel functions of semi-integer order,⁷⁶

⁷³ Again, see MA Eq. (10.9).

⁷⁴ This problem, besides giving a simple example of the quantization in spherically-symmetric systems, is also an important precursor for the discussion of scattering by spherically-symmetric potentials in Sec. 8.

⁷⁵ Alternatively, $y_l(\xi)$ are called “spherical Weber functions” or “spherical Neumann functions”.

⁷⁶ Note that the Bessel functions $J_v(\xi)$ and $Y_v(\xi)$ of *any* order v obey the universal recurrence relations and asymptotic formulas (discussed, e.g., in EM Sec. 2.7), so that many properties of the functions $j_l(\xi)$ and $y_l(\xi)$ may be readily derived from these relations and Eqs. (185).

$$j_l(\xi) = \left(\frac{\pi}{2\xi} \right)^{1/2} J_{l+\frac{1}{2}}(\xi), \quad y_l(\xi) = \left(\frac{\pi}{2\xi} \right)^{1/2} Y_{l+\frac{1}{2}}(\xi), \quad (3.185)$$

but are actually much simpler than even the “usual” Bessel functions, such as $J_n(\xi)$ and $Y_n(\xi)$ of an integer order n , because the former ones may be directly expressed via elementary functions:

$$\begin{aligned} j_0(\xi) &= \frac{\sin \xi}{\xi}, & j_1(\xi) &= \frac{\sin \xi}{\xi^2} - \frac{\cos \xi}{\xi}, & j_2(\xi) &= \left(\frac{3}{\xi^3} - \frac{1}{\xi} \right) \sin \xi - \frac{3}{\xi^2} \cos \xi, \dots, \\ y_0(\xi) &= -\frac{\cos \xi}{\xi}, & y_1(\xi) &= -\frac{\cos \xi}{\xi^2} - \frac{\sin \xi}{\xi}, & y_2(\xi) &= -\left(\frac{3}{\xi^3} - \frac{1}{\xi} \right) \cos \xi - \frac{3}{\xi^2} \sin \xi, \dots, \end{aligned} \quad (3.186)$$

A few lowest-order spherical Bessel functions are plotted in Fig. 21.

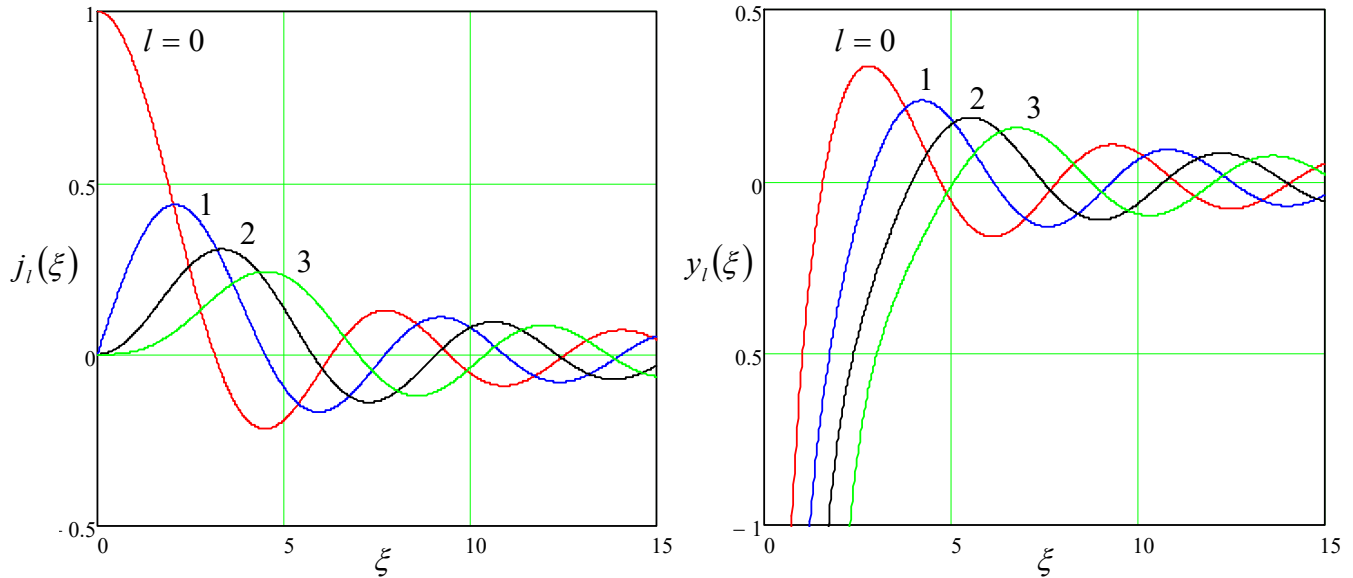


Fig. 3.21. Several lowest-order spherical Bessel functions.

As these formulas and plots show, the functions $y_l(\xi)$ are diverging at $\xi \rightarrow 0$, and thus cannot be used in the solution of our current problem (182), so that we have to take

$$\mathcal{R}_l(r) = \text{const} \times j_l(kr). \quad (3.187)$$

Still, even for these functions, with the sole exception of the simplest function $j_0(\xi)$, the characteristic equation $j_l(kR) = 0$, resulting from the boundary condition $\mathcal{R}(R) = 0$, can be solved only numerically. However, the roots $\xi_{l,n}$ of the equation $j_l(\xi) = 0$, where the integer $n (= 1, 2, 3, \dots)$ is the root’s number, are tabulated in virtually any math handbook, and we may express the eigenvalues we are interested in,

$$k_{l,n} = \frac{\xi_{l,n}}{R}, \quad E_{l,n} = \frac{\hbar^2 k_{l,n}^2}{2m} \equiv \frac{\hbar^2 \xi_{l,n}^2}{2m R^2}, \quad (3.188)$$

via these tabulated numbers. The table below lists several smallest roots, and the corresponding eigenenergies (normalized to their natural unit $E_0 \equiv \hbar^2/2mR^2$), in the order of their growth. It shows a

very interesting effect: going up the energy spectrum, first the eigenenergies grow because of increases of the orbital quantum number l , at the same (lowest) radial quantum number $n = 1$, due to the growth of the first roots of functions $j_l(\xi)$, but then suddenly the second root of $j_0(\xi)$ cuts into this orderly sequence, just to be followed by the first root of $j_3(\xi)$. With the further growth of energy, the sequences of l and n become even more entangled.

l	n	$\xi_{l,n}$	$E_{l,n}/E_0 = (\xi_{l,n})^2$
0	1	$\pi \approx 3.1415$	$\pi^2 \approx 9.87$
1	1	4.493	20.19
2	1	5.763	33.21
0	2	$2\pi \approx 6.283$	$4\pi^2 \approx 39.48$
3	1	6.988	48.83

To complete the discussion of our current problem (182), note again that the energy levels, listed in the table above, are $(2l + 1)$ -degenerate because each of them corresponds to $(2l + 1)$ different eigenfunctions, each with a specific value of the magnetic quantum number m :

$$\psi_{n,l,m} = C_{l,n} j_l \left(\frac{\xi_{l,n} r}{R} \right) Y_l^m(\theta, \varphi), \quad \text{with } -l \leq m \leq +l. \quad (3.189)$$

3.7 Atoms

Now we are ready to discuss atoms, starting from the simplest, exactly solvable *Bohr atom problem*, i.e. that of a single particle's motion in the so-called *attractive Coulomb potential*⁷⁷

$$U(r) = -\frac{C}{r}, \quad \text{with } C > 0. \quad (3.190)$$

Attractive Coulomb potential

The natural scales of E and r in this problem are commonly defined by the requirement of equality of the kinetic and potential energy magnitude scales (dropping all numerical coefficients):

$$E_0 \equiv \frac{\hbar^2}{mr_0^2} \equiv \frac{C}{r_0}, \quad (3.191)$$

similar to its particular case (1.13b). Solving this system of two equations, we get⁷⁸

$$E_0 \equiv \frac{\hbar^2}{mr_0^2} \equiv m \left(\frac{C}{\hbar} \right)^2, \quad \text{and} \quad r_0 \equiv \frac{\hbar^2}{mC}. \quad (3.192)$$

⁷⁷ Historically, the solution of this problem in 1928, that reproduced the main result (1.12)-(1.13) of the “old” quantum theory developed by N. Bohr in 1912, without its phenomenological assumptions, was the decisive step toward the general acceptance of Schrödinger’s wave mechanics.

⁷⁸ For the most important case of the hydrogen atom, with $C = e^2/4\pi\varepsilon_0$, these scales are reduced, respectively, to the Bohr radius r_B (1.10) and the Hartree energy E_H (1.13a). Note also that according to Eq. (192), for the so-called *hydrogen-like atom* (actually, a positive ion) with $C = Z(e^2/4\pi\varepsilon_0)$, these two key parameters are rescaled as $r_0 = r_B/Z$ and $E_0 = Z^2 E_H$.

In the normalized units $\varepsilon \equiv E/E_0$ and $\xi \equiv r/r_0$, equation (181) for our current case (190), looks relatively simple,

$$\frac{d^2\mathcal{R}}{d\xi^2} + \frac{2}{\xi} \frac{d\mathcal{R}}{d\xi} - l(l+1)\mathcal{R} + 2\left(\varepsilon + \frac{1}{\xi}\right)\mathcal{R} = 0, \quad (3.193)$$

but unfortunately, its eigenfunctions may be called elementary only in the most generous meaning of the word. With the adequate normalization,

$$\int_0^\infty \mathcal{R}_{n,l} \mathcal{R}_{n',l'} r^2 dr = \delta_{nn'}, \quad (3.194)$$

these (mutually orthogonal) functions may be represented as

$$\mathcal{R}_{n,l}(r) = -\left\{\left(\frac{2}{nr_0}\right)^3 \frac{(n-l-1)!}{2n[(n+l)!]^3}\right\}^{1/2} \exp\left\{-\frac{r}{nr_0}\right\} \left(\frac{2r}{nr_0}\right)^l L_{n-l-1}^{2l+1}\left(\frac{2r}{nr_0}\right). \quad (3.195)$$

Here $L_p^q(\xi)$ are the so-called *associated Laguerre polynomials*, which may be calculated as

$$L_p^q(\xi) = (-1)^q \frac{d^q}{d\xi^q} L_{p+q}(\xi). \quad (3.196)$$

from the *simple Laguerre polynomials* $L_p(\xi) \equiv L_p^0(\xi)$.⁷⁹ In turn, the easiest way to obtain $L_p(\xi)$ is to use the following *Rodrigues formula*:⁸⁰

$$L_p(\xi) = e^\xi \frac{d^p}{d\xi^p} (\xi^p e^{-\xi}). \quad (3.197)$$

Note that in contrast with the associated Legendre *functions* P_l^m , participating in the spherical harmonics, all L_p^q are just *polynomials*, and those with small indices p and q are indeed quite simple:

$$\begin{aligned} L_0^0(\xi) &= 1, & L_1^0(\xi) &= -\xi + 1, & L_2^0(\xi) &= \xi^2 - 4\xi + 2, \\ L_0^1(\xi) &= 1, & L_1^1(\xi) &= -2\xi + 4, & L_2^1(\xi) &= 3\xi^2 - 18\xi + 18, \\ L_0^2(\xi) &= 2, & L_1^2(\xi) &= -6\xi + 18, & L_2^2(\xi) &= 12\xi^2 - 96\xi + 144, \end{aligned} \quad (3.198)$$

Returning to Eq. (195), we see that the natural quantization of the radial equation (193) has brought us a new integer quantum number n . To understand its range, we should notice that according to Eq. (197), the highest power of terms in the polynomial L_{p+q} is $(p + q)$, and hence, according to Eq. (196), that of L_p^q is p , so that the highest power in the polynomial participating in Eq. (195) is $(n - l - 1)$. Since the power cannot be negative to avoid the unphysical divergence of wavefunctions at $r \rightarrow 0$, the radial quantum number n has to obey the restriction $n \geq l + 1$. Since l , as we already know, may take values $l = 0, 1, 2, \dots$, we may conclude n may only take the following values:

⁷⁹ In Eqs. (196)-(197), p and q are non-negative integers, with no relation whatsoever to the particle's momentum or electric charge. Sorry for this notation, but it is absolutely common, and can hardly result in any confusion.

⁸⁰ Named after the same B. O. Rodrigues, and belonging to the same class as his other famous result, Eq. (165) for the Legendre polynomials.

$$n = 1, 2, 3, \dots \quad (3.199)$$

What makes this relation very important is the following, most surprising result: the eigenenergies corresponding to the wavefunctions (179), which are indexed with three quantum numbers:

$$\psi_{n,l,m} = \mathcal{R}_{n,l}(r)Y_l^m(\theta, \varphi), \quad (3.200)$$

depend *only on one of them*, n :

$$\varepsilon = \varepsilon_n = -\frac{1}{2n^2}, \quad \text{i.e. } E_n = -\frac{E_0}{2n^2} = -\frac{1}{2n^2} \frac{m}{\hbar} \left(\frac{C}{\hbar} \right)^2. \quad (3.201)$$

i.e. agree with Bohr's formula (1.12). Because of this reason, n is usually called the *principal quantum number*, and the above relation between it and the "more subordinate" orbital quantum number l is rewritten as

$$l \leq n - 1. \quad (3.202)$$

Together with the inequality (162), this gives us the following, very important hierarchy of the three quantum numbers involved in the Bohr atom problem:

$$1 \leq n \leq \infty \Rightarrow 0 \leq l \leq n - 1 \Rightarrow -l \leq m \leq +l. \quad (3.203)$$

Bohr
atom:
quantum
numbers

Taking into account the $(2l+1)$ -degeneracy related to the magnetic number m , and using the well-known formula for the arithmetic progression,⁸¹ we see that the n^{th} energy level (201) has the following *orbital degeneracy*:

$$g = \sum_{l=0}^{n-1} (2l+1) \equiv 2 \sum_{l=0}^{n-1} l + \sum_{l=0}^{n-1} 1 = 2 \frac{n(n-1)}{2} + n \equiv n^2. \quad (3.204)$$

Due to its importance for atoms, let us spell out the hierarchy (203) of a few lowest-energy states, using the traditional state notation, in which the value of n is followed by the letter that denotes the value of l :

$$n = 1: \quad l = 0 \quad (\text{one } 1s \text{ state}) \quad m = 0. \quad (3.205)$$

$$\begin{aligned} n = 2: \quad l = 0 &\quad (\text{one } 2s \text{ state}) & m = 0, \\ &\quad l = 1 & (\text{three } 2p \text{ states}) & m = 0, \pm 1. \end{aligned} \quad (3.206)$$

$$\begin{aligned} n = 3: \quad l = 0 &\quad (\text{one } 3s \text{ state}) & m = 0, \\ &\quad l = 1 & (\text{three } 3p \text{ states}) & m = 0, \pm 1, \\ &\quad l = 2 & (\text{five } 3d \text{ states}) & m = 0, \pm 1, \pm 2. \end{aligned} \quad (3.207)$$

Figure 22 shows plots of the radial functions (195) of the listed states. The most important of them is of course the ground ($1s$) state with $n = 1$ and hence $E = -E_0/2$. According to Eqs. (195) and (198), its radial function is just a simple decaying exponent

$$\mathcal{R}_{1,0}(r) = \frac{2}{r_0^{3/2}} e^{-r/r_0}, \quad (3.208)$$

Ground
state:
radial
function

⁸¹ See, e.g., MA Eq. (2.5a).

while its angular distribution is uniform – see Eq. (174). The gap between the ground energy and the energy $E = -E_0/8$ of the lowest excited states (with $n = 2$) in a hydrogen atom (in which $E_0 = E_H \approx 27.2$ eV) is as large as ~ 10 eV, so that their thermal excitation requires temperatures as high as $\sim 10^5$ K, and the overwhelming part of all hydrogen atoms in the visible Universe are in their ground state. Since the atomic hydrogen makes up about 75% of the “normal” matter,⁸² we are very fortunate that such simple formulas as Eqs. (174) and (208) describe the atomic states prevalent in Mother Nature!

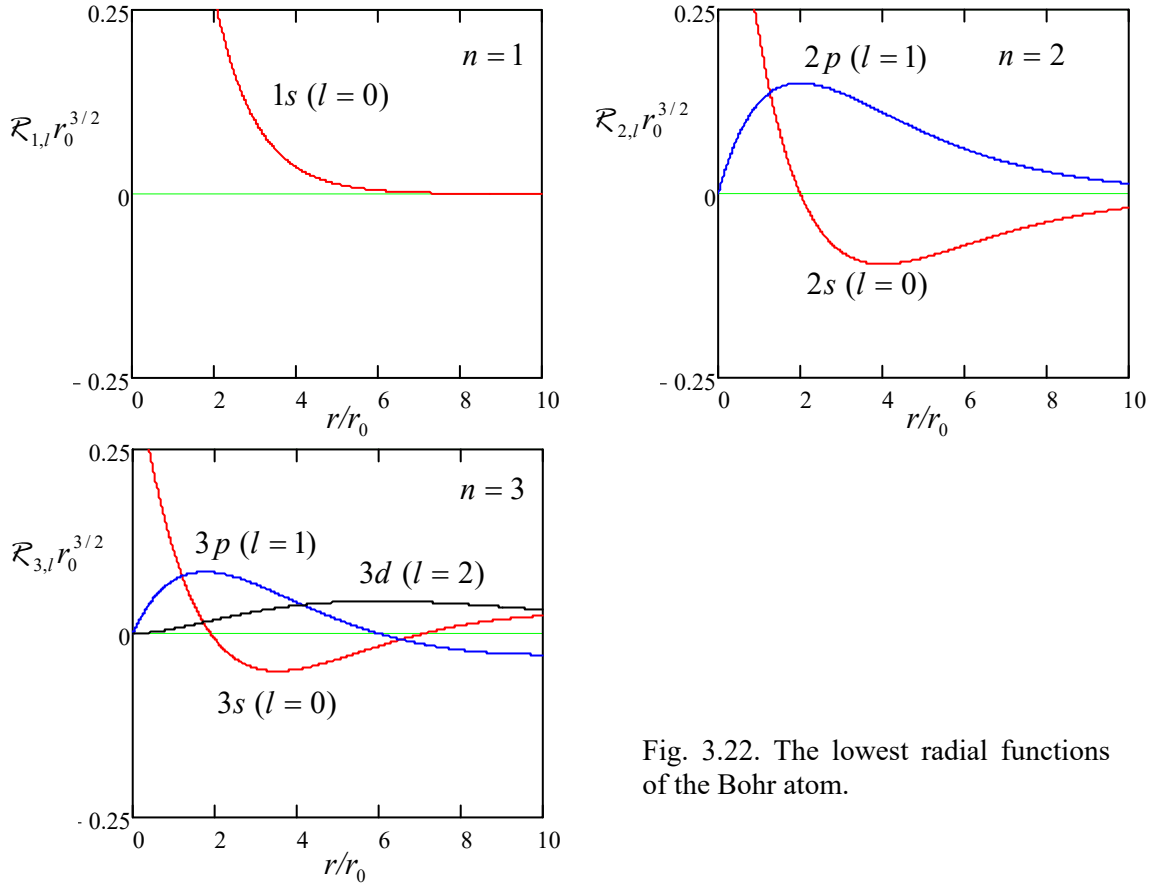


Fig. 3.22. The lowest radial functions of the Bohr atom.

According to Eqs. (195) and (198), the radial functions of the lowest excited states, $2s$ (with $n = 2$ and $l = 0$), and $2p$ (with $n = 2$ and $l = 1$) are also not too complicated:

$$\mathcal{R}_{2,0}(r) = \frac{1}{(2r_0)^{3/2}} \left(2 - \frac{r}{r_0} \right) e^{-r/2r_0}, \quad \mathcal{R}_{2,1}(r) = \frac{1}{(2r_0)^{3/2}} \frac{r}{3^{1/2} r_0} e^{-r/2r_0}, \quad (3.209)$$

with the former of these states ($2s$) having a uniform angular distribution, and the three latter ($2p$) states, with different $m = 0, \pm 1$, having simple angular distributions, which differ only by their spatial orientation – see Eq. (175) and the second row of Fig. 20. The most important trend here, clearly visible from the comparison of the two top panels of Fig. 22 as well, is a larger radius of the decay exponent in

⁸² Excluding the so-far hypothetical *dark matter* and *dark energy*.

the radial functions ($2r_0$ for $n = 2$ instead of r_0 for $n = 1$), and hence a larger radial extension of the states. This trend is confirmed by the following general formula:⁸³

$$\langle r \rangle_{n,l} = \frac{r_0}{2} [3n^2 - l(l+1)]. \quad (3.210)$$

The second important trend is that at a fixed n , the orbital quantum number l determines how fast does the wavefunction change with r near the origin, and how much it oscillates in the radial direction at larger values of r . For example, the $2s$ eigenfunction $\mathcal{R}_{2,0}(r)$ is different from zero at $r = 0$, and “makes one wiggle” (has one root) in the radial direction, while the eigenfunctions $2p$ equal zero at $r = 0$ but do not cross the horizontal axis after that. Instead, those wavefunctions oscillate as the functions of an angle – see the second row of Fig. 20. The same trend is clearly visible for $n = 3$ (see the bottom panel of Fig. 22), and continues for the higher values of n .

The states with $l = l_{\max} \equiv n - 1$ may be viewed as crude analogs of the circular motion of a particle in a plane whose orientation defines the quantum number m . On the other hand, the best classical image of the s -state ($l = 0$) is a purely radial, spherically-symmetric motion of the particle to and from the attracting center. (The latter image is especially imperfect because the motion needs to happen simultaneously in all radial directions.) The classical language becomes reasonable only for the highly degenerate *Rydberg states*, with $n \gg 1$, whose linear superpositions may be used to compose wave packets closely following the classical (circular or elliptic) trajectories of the particle – just as was discussed in Sec. 2.2 for the free 1D motion.

Besides Eq. (210), mathematics gives us several other simple relations for the radial functions $\mathcal{R}_{n,l}$ (and, since the spherical harmonics are normalized to 1, for the eigenfunctions as the whole), including those that we will use later in the course:⁸⁴

$$\left\langle \frac{1}{r} \right\rangle_{n,l} = \frac{1}{n^2 r_0}, \quad \left\langle \frac{1}{r^2} \right\rangle_{n,l} = \frac{1}{n^3 (l + \frac{1}{2}) r_0^2}, \quad \left\langle \frac{1}{r^3} \right\rangle_{n,l} = \frac{1}{n^3 l (l + \frac{1}{2}) (l + 1) r_0^3}. \quad (3.211)$$

In particular, the first of these formulas means that for *any* eigenfunction $\psi_{n,l,m}$, with all its complicated radial and angular dependencies, there is a simple relation between the potential and full energies:

$$\langle U \rangle_{n,l} = -C \left\langle \frac{1}{r} \right\rangle_{n,l} = -\frac{C}{n^2 r_0} = -\frac{E_0}{n^2} = 2E_n, \quad (3.212)$$

so that the average kinetic energy of the particle, $\langle T \rangle_{n,l} = E_n - \langle U \rangle_{n,l}$, is equal to $E_n - 2E_n = |E_n| > 0$.

As in the several previous cases we have met, simple results (201), (210)-(212) are in sharp contrast with the rather complicated expressions for the corresponding eigenfunctions. Historically this contrast gave an additional motivation for the development of more general approaches to quantum mechanics, that would replace, or at least complement our brute-force (wave-mechanics) analysis. A discussion of such an approach will be the main topic of the next chapter.

⁸³ Note that even at the largest value of l , equal to $(n - 1)$, the second term $l(l + 1)$ in Eq. (210) is equal to $(n^2 - n)$, and hence cannot over-compensate the first term $3n^2$.

⁸⁴ The first of these relations may be readily proved using the Heller-Feynman theorem (see Chapter 1); this proof will be offered for the reader’s exercise after a more general form of this theorem has been proved in Chapter 6.

Rather strikingly, the above classification of the quantum numbers, with minor steals from the later chapters of this course, allows a semi-quantitative explanation of the whole system of chemical elements. The “only” two additions we need are the following facts:

(i) due to their unavoidable interaction with relatively low-temperature environments, atoms tend to relax into their lowest-energy state, and

(ii) due to the Pauli principle (valid for electrons as the Fermi particles), each *orbital eigenstate* discussed above may be occupied by two electrons with opposite spins.

Of course, atomic electrons do interact, so that their quantitative description requires quantum mechanics of multiparticle systems, which is rather complex. (Its main concepts will be discussed in Chapter 8.) However, the lion’s share of this interaction is reduced to simple electrostatic *screening*, i.e. a partial compensation of the electric charge of the atomic nucleus, as felt by a particular electron, by other electrons of the atom. This screening changes quantitative results (such as the energy scale E_0) dramatically; however, the quantum number hierarchy, and hence their classification, is not affected.

The hierarchy of atoms is most often represented as the famous *periodic table of chemical elements*,⁸⁵ whose simple version is shown in Fig. 23. (The table in Fig. 24 presents a sequential list of the elements and their electron configurations, following the convention already used in Eqs. (205)-(207), with the additional upper index showing the number of electrons with the indicated values of quantum numbers n and l .) The number in each table’s cell, and in the first column of the list, is the so-called *atomic number Z*, which physically is the number of protons in the particular atomic nucleus, and hence the number of electrons in an electrically-neutral atom.

1 H	Property legend:												2 He				
3 Li	4 Be	alkali metals		transition metals		metalloids		5 B	6 C	7 N	8 O	9 F	10 Ne				
11 Na	12 Mg	alkali-earth metals		nonmetals		halogens		13 Al	14 Si	15 P	16 S	17 Cl	18 Ar				
19 K	20 Ca	rare-earth metals		other metals		noble gases		31 Ga	32 Ge	33 As	34 Se	35 Br	36 Kr				
37 Rb	38 Sr	Y	40 Zr	41 Nb	42 Mo	43 Tc	44 Ru	45 Rh	46 Pd	47 Ag	48 Cd	49 In	50 Sn	51 Sb	52 Te	53 I	54 Xe
55 Cs	56 Ba	71	57- Hf	72 Ta	73 W	74 Re	75 Os	77 Ir	78 Pt	79 Au	80 Hg	81 Tl	82 Pb	83 Bi	84 Po	85 At	86 Rn
87 Fr	88 Ra	89- 102	104 Rf	105 Db	106 Sg	107 Bh	108 Hs	109 Mt	110 Ds	111 Rg	112 Cn	113 Uut	114 Fl	115 Uup	116 Lv	117 Uus	118 Uuo
Lanthanides:		57 La	58 Ce	59 Pr	60 Nd	61 Pm	62 Sm	63 Eu	64 Gd	65 Tb	66 Dy	67 Ho	68 Er	69 Tm	70 Yb	71 Lu	
Actinides:		89 Ac	89 Ac	90 Th	91 Pa	92 U	93 Np	94 Pu	95 Am	96 Cm	97 Bk	98 Cf	99 Es	100 Fm	101 Md	102 Lr	

Fig. 3. 23. The periodic table of elements, showing their atomic numbers and chemical symbols, as well as their color-coded basic physical/chemical properties at the so-called *ambient* (meaning usual laboratory) conditions.

⁸⁵ Also called the *Mendeleev table*, after Dmitri Ivanovich Mendeleev who put forward the concept of the quasi-periodicity of chemical element properties as functions of Z phenomenologically in 1869. (The explanation of this periodicity had to wait for 60 more years until the advent of quantum mechanics in the late 1920s.)

Atomic number	Atomic symbol	Electron states	Atomic number	Atomic symbol	Electron states	Atomic number	Atomic symbol	Electron states					
Period 1													
1	H	$1s^1$	37	Rb	$5s^1$	77	Ir	$4f^{14}5d^76s^2$					
2	He	$1s^2$	38	Sr	$5s^2$	78	Pt	$4f^{14}5d^96s^1$					
Period 2													
		[He] shell, plus:	39	Y	$4d^15s^2$	79	Au	$4f^{14}5d^{10}6s^1$					
3	Li	$2s^1$	40	Zr	$4d^25s^2$	80	Hg	$4f^{14}5d^{10}6s^2$					
4	Be	$2s^2$	41	Nb	$4d^45s^1$	81	Tl	$4f^{14}5d^{10}6s^26p^1$					
5	B	$2s^22p^1$	42	Mo	$4d^55s^1$	82	Pb	$4f^{14}5d^{10}6s^26p^2$					
6	C	$2s^22p^2$	43	Tc	$4d^65s^1$	83	Bi	$4f^{14}5d^{10}6s^26p^3$					
7	N	$2s^22p^3$	44	Ru	$4d^75s^1$	84	Po	$4f^{14}5d^{10}6s^26p^4$					
8	O	$2s^22p^4$	45	Rh	$4d^85s^1$	85	At	$4f^{14}5d^{10}6s^26p^5$					
9	F	$2s^22p^5$	46	Pd	$4d^{10}$	86	Rn	$4f^{14}5d^{10}6s^26p^6$					
10	Ne	$2s^22p^6$	47	Ag	$4d^{10}5s^1$	Period 7							
Period 3								[Rn] shell, plus:					
		[Ne] shell, plus:	48	Cd	$4d^{10}5s^2$	87	Fr	$7s^1$					
11	Na	$3s^1$	49	In	$4d^{10}5s^25p^1$	88	Ra	$7s^2$					
12	Mg	$3s^2$	50	Sn	$4d^{10}5s^25p^2$	89	Ac	$6d^17s^2$					
13	Al	$3s^23p^1$	51	Sb	$4d^{10}5s^25p^3$	90	Th	$6d^27s^2$					
14	Si	$3s^23p^2$	52	Te	$4d^{10}5s^25p^4$	91	Pa	$5f^26d^17s^2$					
15	P	$3s^23p^3$	53	I	$4d^{10}5s^25p^5$	92	U	$5f^26d^17s^2$					
16	S	$3s^23p^4$	54	Xe	$4d^{10}5s^25p^6$	93	Np	$5f^46d^17s^2$					
17	Cl	$3s^23p^5$	Period 6										
18	Ar	$3s^23p^6$	55	Cs	$6s^1$	94	Pu	$5f^67s^2$					
Period 4			56	Ba	$6s^2$	95	Am	$5f^77s^2$					
		[Ar] shell, plus:	57	La	$5d^16s^2$	96	Cm	$5f^66d^17s^2$					
19	K	$4s^1$	58	Ce	$4f^15d^16s^2$	97	Bk	$5f^97s^2$					
20	Ca	$4s^2$	59	Pr	$4f^26s^2$	98	Cf	$5f^{10}7s^2$					
21	Sc	$3d^14s^2$	60	Nd	$4f^46s^2$	99	Es	$5f^{11}7s^2$					
22	Ti	$3d^24s^2$	61	Pm	$4f^56s^2$	100	Fm	$5f^{12}7s^2$					
23	V	$3d^34s^2$	62	Sm	$4f^66s^2$	101	Md	$5f^{13}7s^2$					
24	Cr	$3d^44s^2$	63	Eu	$4f^76s^2$	102	No	$5f^{14}7s^2$					
25	Mn	$3d^54s^2$	64	Gd	$4f^75d^16s^2$	103	Lr	$5f^{14}6d^17s^2$					
26	Fe	$3d^64s^2$	65	Tb	$4f^86s^2$	104	Rf	$5f^{14}6d^27s^2$					
27	Co	$3d^74s^2$	66	Dy	$4f^{10}6s^2$	105	Db	$5f^{14}6d^37s^2$					
28	Ni	$3d^84s^2$	67	Ho	$4f^{11}6s^2$	106	Sg	$5f^{14}6d^47s^2$					
29	Cu	$3d^94s^1$	68	Er	$4f^{12}6s^2$	107	Bh	$5f^{14}6d^57s^2$					
30	Zn	$3d^{10}4s^2$	69	Tm	$4f^{13}6s^2$	108	Hs	$5f^{14}6d^67s^2$					
31	Ga	$3d^{10}4s^24p^1$	70	Yb	$4f^{14}6s^2$	109	Mt	$5f^{14}6d^77s^2$					
32	Ge	$3d^{10}4s^24p^2$	71	Lu	$4f^{14}5d^16s^2$	110	Ds	$5f^{14}6d^87s^2$					
33	As	$3d^{10}4s^24p^3$	72	Hf	$4f^{14}5d^26s^2$	111	Rg	$5f^{14}6d^97s^2$					
34	Se	$3d^{10}4s^24p^4$	73	Ta	$4f^{14}5d^36s^2$	112	Cn	$5f^{14}6d^{10}7s^2$					
35	Br	$3d^{10}4s^24p^5$	74	W	$4f^{14}5d^46s^2$	113	Uut	$5f^{14}6d^{10}7s^27p^1$					
36	Kr	$3d^{10}4s^24p^6$	75	Re	$4f^{14}5d^56s^2$	114	Fl	$5f^{14}6d^{10}7s^27p^2$					
			76	Os	$4f^{14}5d^66s^2$	115	Uup	$5f^{14}6d^{10}7s^27p^3$					
						116	Lv	$5f^{14}6d^{10}7s^27p^4$					
						117	Uus	$5f^{14}6d^{10}7s^27p^5$					
						118	Uuo	$5f^{14}6d^{10}7s^27p^6$					

Fig. 3.24. Atomic electron configurations. The upper index shows the number of electrons in the states with the indicated quantum numbers n (the first digit) and l (letter-coded as was discussed above).

The simplest atom, with $Z = 1$, is hydrogen (chemical symbol H) – the only atom for that the theory discussed above is quantitatively correct.⁸⁶ According to Eq. (191), the $1s$ ground state of its only electron corresponds to the quantum number values $n = 1$, $l = 0$, and $m = 0$ – see Eq. (205). In most versions of the periodic table, the cell of H is placed in the top left corner.

In the next atom, helium (symbol He, $Z = 2$), the same orbital quantum state ($1s$) is filled with two electrons. As will be discussed in detail in Chapter 8, electrons of the same atom are actually *indistinguishable*, so that their quantum states are not independent and may be *entangled*. These factors are important for several properties of helium atoms (and heavier elements as well); however, a bit counter-intuitively, for the atom classification purposes, they are not crucial, and we may pretend that two electrons of a helium atom just have “opposite spins”. Due to the twice higher electric charge of the nucleus of the helium atom, i.e. the twice higher value of the constant C in Eq. (190), resulting in a 4-fold increase of the constant E_0 given by Eq. (192), the binding energy of each electron is crudely 4 times higher than that of the hydrogen atom – though the electron interaction decreases it by about 25% – see Sec. 8.2. This is why taking one electron away (i.e. the *positive ionization* of a helium atom) requires relatively high energy, ~ 23.4 eV, which is not available in the usual chemical reactions. On the other hand, a neutral helium atom cannot bind one more electron (i.e. form a *negative ion*) either. As a result, the helium, and all other elements with fully completed electron *shells* (the term meaning the sets of states with eigenenergies well separated from higher energy levels) is a chemically inert *noble gas*, thus starting the whole right-most column of the periodic table, allocated for such elements.

The situation changes rather dramatically as we move to the next element, lithium (Li), with $Z = 3$ electrons. Two of them are still accommodated by the inner shell with $n = 1$ (listed in Fig. 24 as the *helium shell* [He]), but the third one has to reside in the next shell with $n = 2$, $l = 0$, and $m = 0$, i.e. in the $2s$ state. According to Eq. (201), the binding energy of this electron is much lower, especially if we take into account that according to Eqs. (210)-(211), the $1s$ electrons of the [He] shell are much closer to the nucleus and almost completely compensate two-thirds of its electric charge $+3e$. As a result, the $2s$ -state electron is approximately, but reasonably well described by Eq. (201) with $Z = 1$ and $n = 2$, giving binding energy close to just 3.4 eV (experimentally, ~ 5.39 eV), so that a lithium atom can give out that electron rather easily – to either an atom/ion of another element to form a chemical compound, or to the common conduction band of the solid-state lithium; as a result, at the ambient conditions, it is a typical *alkali metal*. The similarity of chemical properties of lithium and hydrogen, with the *chemical valence* of one,⁸⁷ places Li as the starting element of the second *period* (row), with the first period limited to only H and He – see Fig. 23.

In the next element, beryllium (symbol Be, $Z = 4$), the $2s$ state ($n = 2$, $l = 0$, $m = 0$) houses one more electron, with the “opposite spin”. Due to the higher electric charge of the nucleus, $Q = +4e$, with only half of it compensated by $1s$ electrons of the [He] shell, the binding energy of the $2s$ electrons is somewhat higher than that in lithium, so that the ionization energy increases to ~ 9.32 eV. As a result, beryllium is also chemically active with the valence of two, but not as active as lithium, and is also is metallic in its solid-state phase, but with a lower electric conductivity than lithium.

⁸⁶ Besides very small *fine-structure* and *hyperfine-splitting* corrections – to be discussed, respectively, in Chapters 6 and 8.

⁸⁷ The chemical valence (or “valency”) is a not very precise term describing the number of atom’s electrons involved in chemical reactions. For the same atom, especially with a large number of electrons in its outer, unfilled shell, this number may depend on the chemical compound formed. (For example, the valence of iron is two in the *ferrous oxide*, FeO, and three in the *ferric oxide*, Fe₂O₃.)

Moving in this way along the second row of the periodic table (from $Z = 3$ to $Z = 10$), we see a gradual filling of the rest of the total $2n^2 = 2 \times 2^2 = 8$ different electron states of the $n = 2$ shell (see Eq. (204), with the additional spin degeneracy factor of 2), including two $2s$ states with $m = 0$, and six $2p$ states with $m = 0, \pm 1$,⁸⁸ with a gradually growing ionization potential (up to ~ 21.6 eV in Ne with $Z = 10$), i.e. a growing reluctance to conduct electricity or form *positive* ions. However, the last elements of the row, such as oxygen (O, with $Z = 8$) and especially fluorine (F, with $Z = 9$) can readily pick up extra electrons to fill up their $2p$ states, i.e. form *negative* ions. As a result, these elements are chemically active, with a double valence for oxygen and a single valence for fluorine. However, the final element of this row, neon, has its $n = 2$ shell completely full, and cannot form a stable negative ion. This is why it is a noble gas, like helium. Traditionally, in the periodic table, such elements are placed right under helium (Fig. 23), to emphasize the similarity of their chemical properties. But this necessitates making an at least 6-cell gap in the 1st row. (Actually, the gap is often made larger, to accommodate the next rows – keep reading.)

Period 3, i.e. the 3rd row of the table, starts exactly like period 2, with sodium (Na, with $Z = 11$), also a chemically active alkali metal whose atom features 10 electrons filling the shells with $n = 1$ and $n = 2$ (in Fig. 24, collectively called the neon shell [Ne]), plus one electron in the $3s$ state ($n = 3, l = 0, m = 0$), which may be again reasonably well described by the hydrogen atom theory – see, e.g., the red curve on the last panel of Fig. 22. Continuing along this row, we could naively expect that, according to Eq. (204), and with the account of double spin degeneracy, this period of the table should have $2n^2 = 2 \times 3^2 = 18$ elements, with a gradual, sequential filling of two $3s$ states, then six $3p$ states, and then ten $3d$ states. However, here we run into a big surprise: after argon (Ar, with $Z = 18$), a relatively inert element with the ionization energy of ~ 15.7 eV due to the fully filled $3s$ and $3p$ shells, the next element, potassium (K, with $Z = 19$) is an alkali metal again!

The reason for that is the difference of the actual electron energies from those of the hydrogen atom, which is due mostly to inter-electron interactions, and gradually accumulates with the growth of Z . It may be semi-quantitatively understood from the results of Sec. 6. In hydrogen-like atoms/ions, the electron state energies do not depend on the quantum number l (as well as m) – see Eq. (201). However, the orbital quantum number does affect the wavefunction of an electron. As Fig. 22 shows, the larger l the less the probability for an electron to be close to the nucleus, where its positive charge is less compensated by other electrons. As a result of this effect (and also the relativistic corrections to be discussed in Sec. 6.3), the electron's energy grows with l . Actually, this effect is visible already in period 2 of the table: it manifests itself in the filling order – the p states after the s states. However, for potassium (K, with $Z = 19$) and calcium (Ca, with $Z = 20$), the energies of the $3d$ states become so high that the energies of the two $4s$ states are lower, and the latter states are filled first. As described by Eq. (210), and also by the first of Eqs. (211), the effect of the principal number n on the distance from the nucleus is much stronger than that of l , so that the $4s$ wavefunctions of K and Ca are relatively far from the nucleus, and determine the chemical valence (equal to 1 and 2, correspondingly) of these elements. The next atoms, from Sc ($Z = 21$) to Zn ($Z = 30$), with the gradually filled “internal” $3d$ states, are the so-called *transition metals* whose (comparable) ionization energies and chemical properties are determined by the $4s$ electrons.

This fact is the origin of the difference between various forms of the “periodic” table. In its most popular option, shown in Fig. 23, K is used to start the next period 4, and then a new period is started

⁸⁸ The specific order of filling of the states within each shell follows the so-called *Hund rules* – see Sec. 8.3.

each time and only when the first electron with the next principal quantum number (n) appears.⁸⁹ This topology of the table provides a very clear match of the chemical properties of the first element of each period (an alkali metal), as well as its last element (a noble gas). It also automatically means making gaps in all previous rows. Usually, this gap is made between the atoms with completely filled s states and with those with the first electron in a p state, because here the properties of the elements make a somewhat larger step. (For example, the step from Be to B makes the material an insulator, but the step from Mg to Al makes a smaller difference.) As a result, the elements of the same column have only *approximately* similar chemical valences and physical properties.

In order to accommodate the lower, longer rows, such representation is inconvenient, because the whole table would be too broad. This is why the so-called *rare earth* elements, including *lanthanides* (with Z from 57 to 70, of the 6th row, with a gradual filling of the 4 f and 5 d states) and *actinides* (Z from 89 to 103, of the 7th row, with a gradual filling of the 5 f and 6 d states), are usually represented as outlet rows – see Fig. 23. This is quite acceptable for basic chemistry, because the chemical properties of the elements within each such group are rather close.

To summarize my very short review of this extremely important topic,⁹⁰ the “periodic table of elements” is not periodic in the strict sense of the word. Nevertheless, it has had an enormous historic significance for chemistry, as well as atomic and solid-state physics, and is still very convenient for many purposes. For our course, the most important aspect of its discussion is the surprising possibility to describe, at least for classification purposes, such a complex multi-electron system as an atom as a set of quasi-independent electrons in certain quantum states indexed with the same quantum numbers n , l , and m as those of the hydrogen atom. This fact enables the use of various *perturbation theories*, which give a more quantitative description of atomic properties. Some of these techniques will be reviewed in Chapters 6 and 8.

3.8. Spherically-symmetric scatterers

The machinery of the Legendre polynomials and the spherical Bessel functions, discussed in Sec. 6, may also be used for analysis of particle scattering by spherically-symmetric potentials (155) beyond the Born approximation (Sec. 3), provided that such a potential $U(r)$ is also localized, i.e. reduces sufficiently fast at $r \rightarrow \infty$. (The quantification of this condition is left for the reader’s exercise.)

Indeed, directing the z -axis along the propagation of the incident plane de Broglie wave ψ_i , and taking its origin in the center of the scatterer, we may expect the scattered wave ψ_s to be axially symmetric, so that its expansion in the series over the spherical harmonics includes only the terms with $m = 0$. Hence, the solution (64) of the stationary Schrödinger equation (63) in this case may be represented as⁹¹

$$\psi = \psi_i + \psi_s = a_i \left[e^{ikz} + \sum_{l=0}^{\infty} R_l(r) P_l(\cos \theta) \right], \quad (3.213)$$

⁸⁹ Another popular option is to return to the first column as soon an atom has one electron in the s state (like it is in Cu, Ag, and Au, in addition to the alkali metals).

⁹⁰ For a bit more detailed (but still succinct) discussion of the valence and other chemical aspects of atomic structure, I can recommend Chapter 5 of the very clear text by L. Pauling, *General Chemistry*, Dover, 1988.

⁹¹ The particular terms in this sum are frequently called *partial waves*.

where $k \equiv (2mE)^{1/2}/\hbar$ is defined by the energy E of the incident particle, while the radial functions $\mathcal{R}_l(r)$ have to satisfy Eq. (181), and be finite at $r \rightarrow 0$. At large distances $r \gg R$, where R is the effective radius of the scatterer, the potential $U(r)$ is negligible, and Eq. (181) is reduced to Eq. (183). In contrast to its analysis in Sec. 6, we should look for its solution using a linear superposition of the spherical Bessel functions of both kinds:

$$\mathcal{R}_l(r) = A_l j_l(kr) + B_l y_l(kr), \quad \text{at } r \gg R, \quad (3.214)$$

because Eq. (183) is now invalid at $r \rightarrow 0$, and our former argument for dropping the functions $y_l(kr)$ is no more valid. In Eq. (214), A_l and B_l are some complex coefficients, determined by the scattering potential $U(r)$, i.e. by the solution of Eq. (181) at $r \sim R$.

As the explicit expressions (186) show, the spherical Bessel functions $j_l(\xi)$ and $y_l(\xi)$ represent *standing* de Broglie waves, with equal real amplitudes, so that their simple linear combinations (called the *spherical Hankel functions of the first and second kind*),

$$h_l^{(1)}(\xi) \equiv j_l(\xi) + iy_l(\xi), \quad \text{and} \quad h_l^{(2)}(\xi) \equiv j_l(\xi) - iy_l(\xi), \quad (3.215)$$

represent *traveling* spherical waves propagating, respectively, from the origin (i.e. from the center of the scatterer), and toward the origin. In particular, at $\xi \gg 1, l$, i.e. at large distances $r \gg 1/k, l/k$,⁹²

$$h_l^{(1)}(kr) \rightarrow \frac{(-i)^{l+1}}{kr} e^{ikr} \quad h_l^{(2)}(kr) \rightarrow \frac{i^{l+1}}{kr} e^{-ikr}. \quad (3.216)$$

But using the same physical argument as at the beginning of Sec. 1, we may argue that in the case of a localized scatterer, there should be no latter waves at $r \gg R$; hence, we have to require the amplitude of the term proportional to $h_l^{(2)}$ to be zero. With the relations reciprocal to Eqs. (215),

$$j_l(\xi) = \frac{1}{2} [h_l^{(1)}(\xi) + h_l^{(2)}(\xi)], \quad y_l(\xi) = \frac{1}{2i} [h_l^{(1)}(\xi) - h_l^{(2)}(\xi)], \quad (3.217)$$

which enable us to rewrite Eq. (214) as

$$\begin{aligned} \mathcal{R}_l(r) &= \frac{A_l}{2} [h_l^{(1)}(\xi) + h_l^{(2)}(\xi)] + \frac{B_l}{2i} [h_l^{(1)}(\xi) - h_l^{(2)}(\xi)] \\ &\equiv \left(\frac{A_l - iB_l}{2} \right) h_l^{(1)}(\xi) + \left(\frac{A_l + iB_l}{2} \right) h_l^{(2)}(\xi), \end{aligned} \quad (3.218)$$

this means that the combination $(A_l + iB_l)$ has to be equal zero, so that $B_l = iA_l$. Hence we have just one unknown coefficient (say, A_l) for each l ,⁹³ and may rewrite Eq. (218) in an even simpler form:

$$\mathcal{R}_l(r) = A_l [j_l(kr) + iy_l(kr)] \equiv A_l h_l^{(1)}(kr), \quad \text{at } r \gg R, \quad (3.219)$$

Spherically-symmetric scatterer: A_l

⁹² For arbitrary l , this result may be confirmed using Eqs. (185) and the asymptotic formulas for the “usual” Bessel functions – see, e.g., EM Eqs. (2.135) and (2.152), valid for an arbitrary (not necessarily integer) index n .

⁹³ Moreover, using the conservation of the orbital momentum, to be discussed in Sec. 5.6, it is possible to show that this *complex* coefficient may be further reduced to just one *real* parameter, usually recast as the *partial phase shift* δ_l between the l^{th} spherical harmonics of the incident and scattered waves. However, I will not use this notion, because practical calculations are more physically transparent (and not more complex) without it.

and use Eqs. (213) and (216) to write the following expression for the scattered wave at large distances:

$$\psi_s \approx \frac{a_i}{kr} e^{ikr} \sum_{l=0}^{\infty} (-i)^{l+1} A_l P_l(\cos \theta), \quad \text{at } r \gg R, \frac{1}{k}, \frac{l}{k}. \quad (3.220)$$

Comparing this expression with the general Eq. (81), we see that for a spherically-symmetric, localized scatterer,

$$f = \frac{1}{k} \sum_{l=0}^{\infty} (-i)^{l+1} A_l P_l(\cos \theta), \quad (3.221)$$

so that the differential cross-section (84) is

$$\frac{d\sigma}{d\Omega} = \frac{1}{k^2} \left| \sum_{l=0}^{\infty} (-i)^{l+1} A_l P_l(\cos \theta) \right|^2 \equiv \frac{1}{k^2} \sum_{l,l'=0}^{\infty} i^{l'-l} A_l A_{l'}^* P_l(\cos \theta) P_{l'}(\cos \theta). \quad (3.222)$$

The last expression is more convenient for the calculation of the total cross-section (59):

$$\sigma = \oint \frac{d\sigma}{d\Omega} d\Omega = 2\pi \int_{-1}^{+1} d\Omega d(\cos \theta) = \frac{2\pi}{k^2} \sum_{l,l'=0}^{\infty} i^{l'-l} A_l A_{l'}^* \int_{-1}^{+1} P_l(\xi) P_{l'}(\xi) d\xi, \quad (3.223)$$

where $\xi \equiv \cos \theta$, because this result may be much simplified by using Eq. (167):⁹⁴

$$\sigma = \sum_{l=0}^{\infty} \sigma_l, \quad \text{with } \sigma_l = \frac{4\pi}{k^2} \frac{|A_l|^2}{2l+1}. \quad (3.224)$$

Hence the solution of the scattering problem is reduced to the calculation of the partial wave amplitudes A_l defined by Eq. (219) – and for the total cross-section, merely of their magnitudes. This task is much facilitated by using the following *Rayleigh formula* for the expansion of the incident plane wave's exponent into a series over the Legendre polynomials,⁹⁵

$$e^{ikz} \equiv e^{ikr \cos \theta} = \sum_{l=0}^{\infty} i^l (2l+1) j_l(kr) P_l(\cos \theta). \quad (3.225)$$

As the simplest example, let us calculate scattering by a completely opaque and “hard” (meaning sharp-boundary) sphere, which may be described by the following potential:

$$U(r) = \begin{cases} +\infty, & \text{for } r < R, \\ 0, & \text{for } R < r. \end{cases} \quad (3.226)$$

In this case, the total wavefunction has to vanish at $r \leq R$, and hence for the external problem ($r \geq R$) the sphere enforces the boundary condition $\psi = \psi_0 + \psi_s = 0$ for all values of θ , at $r = R$. With Eqs. (213), (220) and (225), this condition becomes

$$a_i \sum_{l=0}^{\infty} [\mathcal{R}_l(R) + i^l (2l+1) j_l(kR)] P_l(\cos \theta) = 0. \quad (3.227)$$

⁹⁴ Physically, this reduction of the double sum to a single one means that due to the orthogonality of the spherical harmonics, the total scattering probability flows due to each partial wave just add up.

⁹⁵ It may be proved using the Rodrigues formula (165) and integration by parts – the task left for the reader's exercise.

Due to the orthogonality of the Legendre polynomials, this condition may be satisfied for all angles θ only if all the coefficients before all $P_l(\cos\theta)$ vanish, i.e. if

$$\mathcal{R}_l(R) = -i^l (2l+1) j_l(kR). \quad (3.228)$$

On the other hand, for $r > R$, $U(r) = 0$, so that Eq. (183) is valid, and its outward-wave solution (219) has to be valid even at $r \rightarrow R$, giving

$$\mathcal{R}_l(R) = A_l [j_l(kR) + iy_l(kR)]. \quad (3.229)$$

Requiring the two last expressions to give the same result, we get

$$A_l = -i^l (2l+1) \frac{j_l(kR)}{j_l(kR) + iy_l(kR)}, \quad (3.230)$$

so that Eqs. (222) and (224) yield:

$$\frac{d\sigma}{d\Omega} = \frac{1}{k^2} \left| \sum_{l=0}^{\infty} (2l+1) \frac{j_l(kR)}{j_l(kR) + iy_l(kR)} P_l(\cos\theta) \right|^2, \quad \sigma_l = \frac{4\pi(2l+1)}{k^2} \frac{j_l^2(kR)}{j_l^2(kR) + y_l^2(kR)}. \quad (3.231)$$

As Fig. 25a shows, the first of these results describes an angular structure of the scattered de Broglie wave, which is qualitatively similar to that given by the Born approximation – cf. Eq. (98) and Fig. 10.

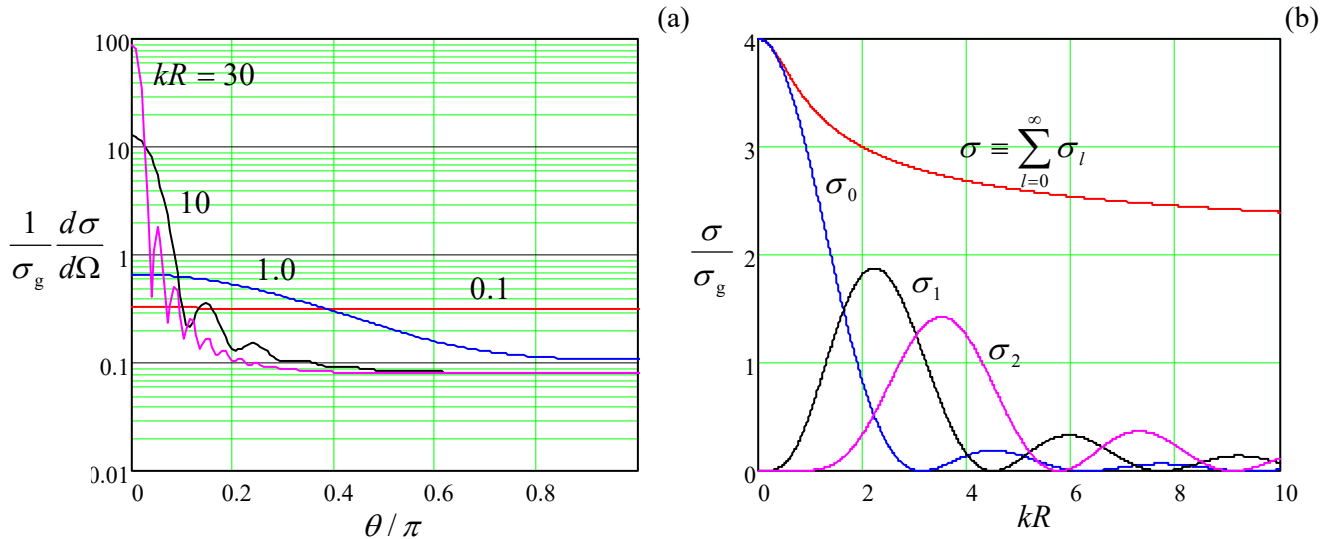


Fig. 3.25. Particle scattering by an opaque, hard sphere: (a) the differential cross-section normalized to the geometric cross-section $\sigma_g \equiv \pi R^2$ of the sphere, as a function of the scattering angle θ , and (b) the (similarly normalized) total cross-section and its lowest spherical components, as functions of the dimensionless product $kR \propto E^{1/2}$.

Namely, at low particle's energies ($kR \ll 1$), the scattering is essentially isotropic, while in the opposite, high-energy limit $kR \gg 1$, it is mostly confined to small angles $\theta \sim \pi/kR \ll 1$, and exhibits numerous local destructive-interference minima at angles $\theta_n \sim \pi n/kR$. However, in our current (exact!) theory, these minima are always finite, because the theory describes effective bending of the de Broglie waves along the back side of the sphere, which smears the interference pattern.

The same bending is also responsible for a rather counter-intuitive fact, described by the second of Eqs. (231) and clearly visible in Fig. 25b: even at $kR \rightarrow \infty$, the total cross-section σ of scattering tends to $2\sigma_g \equiv 2\pi R^2$, rather than to σ_g as in the purely-classical scattering theory. First discovered for optical wave scattering, this fact (common for all large non-absorbing scatterers) is sometimes interpreted as a manifestation of the so-called *wave extinction paradox*.

The fact that at $kR \ll 1$, the cross-section is also larger than σ_g , approaching $4\sigma_g$ at $kR \rightarrow 0$, is much less surprising, because in this limit the de Broglie wavelength $\lambda = 2\pi/k$ is much longer than the sphere's radius R , so that the wave's propagation is affected by the whole sphere.

The above analysis may be readily generalized to the case a step-like (*sharp* but finite) potential (97) – the problem left for the reader's exercise. On the other hand, for a finite and *smooth* scattering potential $U(r)$, plugging Eq. (225) into Eq. (213) and the result into Eq. (66), requiring the coefficients before each angular function $P_l(\cos\theta)$ to be balanced, and canceling the common coefficient a_0 , we get the following inhomogeneous generalization of Eq. (181) for the radial functions defined by Eq. (213):

$$[E - U(r)]\mathcal{R}_l + \frac{\hbar^2}{2mr^2} \left[\frac{d}{dr} \left(r^2 \frac{d}{dr} \right) - l(l+1) \right] \mathcal{R}_l(r) = U(r) i^l (2l+1) j_l(kr). \quad (3.232)$$

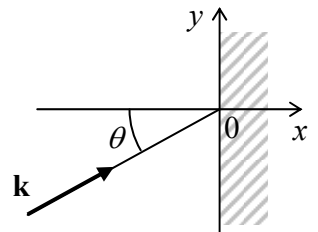
This differential equation has to be solved in the whole scatterer volume (i.e. for all $r \sim R$) with the boundary conditions for the functions $\mathcal{R}_l(r)$ to be finite at $r \rightarrow 0$, and to tend to the asymptotic form (219) at $r \gg R$. The last requirement enables the evaluation of the coefficients A_l that are needed for spelling out Eqs. (222) and (224). Unfortunately, due to the lack of time, I have to refer the reader interested in such cases to special literature.⁹⁶

3.9. Exercise Problems

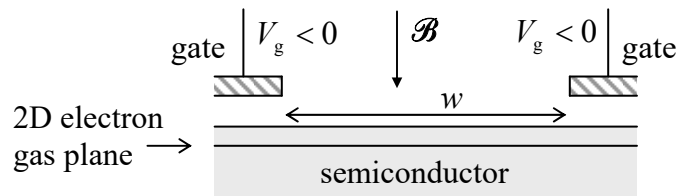
3.1. A particle of energy E is incident (in the figure on the right, within the plane of the drawing) on a sharp potential step:

$$U(\mathbf{r}) = \begin{cases} 0, & \text{for } x < 0, \\ U_0, & \text{for } 0 < x. \end{cases}$$

Calculate the particle reflection probability \mathcal{R} as a function of the incidence angle θ ; sketch and discuss this function for various magnitudes and signs of U_0 .



3.2.* Analyze how are the Landau levels (50) modified by an additional uniform electric field \mathcal{E} directed along the plane of the particle's motion. Contemplate the physical meaning of your result and its implications for the quantum Hall effect in a gate-defined Hall bar. (The area



⁹⁶ See, e.g., J. Taylor, *Scattering Theory*, Dover, 2006.

$l \times w$ of such a bar [see Fig. 6] is defined by metallic gate electrodes parallel to the 2D electron gas plane – see the figure on the right. The negative voltage V_g , applied to the gates, squeezes the 2D gas from the area under them into the complementary, Hall-bar part of the plane.)

3.3. Analyze how are the Landau levels (50) modified if a 2D particle is confined in an additional 1D potential well $U(x) = m\omega_0^2 x^2/2$.

3.4. Find the stationary states of a spinless, charged 3D particle moving in “crossed” (mutually perpendicular), uniform electric and magnetic fields, with $\mathcal{E} \ll c\mathcal{B}$. For such states, calculate the expectation values of the particle’s velocity in the direction perpendicular to both fields, and compare the result with the solution of the corresponding classical problem.

Hint: You may like to generalize Landau’s solution for 2D particles, discussed in Sec. 2.

3.5. Use the Born approximation to calculate the angular dependence and the total cross-section of scattering of an incident plane wave propagating along the x -axis, by the following pair of similar point inhomogeneities:

$$U(\mathbf{r}) = \mathcal{W} \left[\delta\left(\mathbf{r} - \mathbf{n}_z \frac{\mathbf{a}}{2}\right) + \delta\left(\mathbf{r} + \mathbf{n}_z \frac{\mathbf{a}}{2}\right) \right].$$

Analyze the results in detail. Derive the condition of the Born approximation’s validity for such delta-functional scatterers.

3.6. Complete the analysis of the Born scattering by a uniform spherical potential (97), started in Sec. 3, by calculation of its total cross-section. Analyze the result in the limits $kR \ll 1$ and $kR \gg 1$.

3.7. Use the Born approximation to calculate the differential cross-section of particle scattering by a very thin spherical shell, whose potential may be approximated as

$$U(r) = \mathcal{W} \delta(r - R).$$

Analyze the results in the limits $kR \ll 1$ and $kR \gg 1$, and compare them with those for a uniform sphere considered in Sec. 3.

3.8. Use the Born approximation to calculate the differential and total cross-sections of electron scattering by a screened Coulomb field of a point charge Ze , with the electrostatic potential

$$\phi(\mathbf{r}) = \frac{Ze}{4\pi\epsilon_0 r} e^{-\lambda r},$$

neglecting spin interaction effects, and analyze the result’s dependence on the screening parameter λ . Compare the results with those given by the classical (“Rutherford”) formula⁹⁷ for the unscreened Coulomb potential ($\lambda \rightarrow 0$), and formulate the condition of Born approximation’s validity in this limit.

3.9. A quantum particle with electric charge Q is scattered by a localized distributed charge with a spherically-symmetric density $\rho(r)$, and zero total charge. Use the Born approximation to calculate the

⁹⁷ See, e.g., CM Sec. 3.5, in particular Eq. (3.73).

differential cross-section of the *forward scattering* (with the scattering angle $\theta = 0$), and evaluate it for the scattering of electrons by a hydrogen atom in its ground state.

3.10. Reformulate the Born approximation for the 1D case. Use the result to find the scattering and transfer matrices of a “rectangular” (flat-top) scatterer

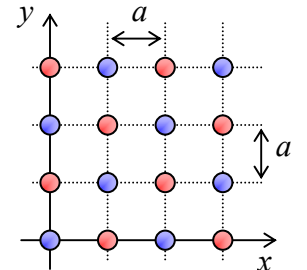
$$U(x) = \begin{cases} U_0, & \text{for } |x| < d/2, \\ 0, & \text{otherwise.} \end{cases}$$

Compare the results with those of the exact calculations carried out earlier in Chapter 2, and analyze how does their relationship change in the eikonal approximation.

3.11. In the tight-binding approximation, find the lowest stationary states of a particle placed into a system of three similar, weakly coupled potential wells located in the vertices of an equilateral triangle.

3.12. The figure on the right shows a fragment of a periodic 2D lattice, with the red and blue points showing the positions of different local potentials.

- (i) Find the reciprocal lattice and the 1st Brillouin zone of the system.
- (ii) Calculate the wave number k of the monochromatic de Broglie wave incident along axis x , at that the lattice creates the lowest-order diffraction peak within the $[x, y]$ plane, and the direction toward this peak.
- (iii) Semi-quantitatively, describe the evolution of the intensity of the peak when the local potentials, represented by the different points, become similar.



Hint: The *order of diffraction* on a multidimensional Bravais lattice is a somewhat ambiguous notion, usually associated with the sum of magnitudes of all integers l_j in Eq. (109), for the vector \mathbf{Q} that is equal to $\mathbf{q} \equiv \mathbf{k} - \mathbf{k}_i$.

3.13. For the 2D hexagonal lattice (Fig. 12b):

- (i) find the reciprocal lattice \mathbf{Q} and the 1st Brillouin zone;
- (ii) use the tight-binding approximation to calculate the dispersion relation $E(\mathbf{q})$ for a 2D particle moving through a potential profile with such periodicity, with an energy close to the energy of the axially-symmetric states quasi-localized at the potential minima;
- (iii) analyze and sketch (or plot) the resulting dispersion relation $E(\mathbf{q})$ inside the 1st Brillouin zone.

3.14. Complete the tight-binding-approximation calculation of the band structure of the honeycomb lattice, started at the end of Sec. 4. Analyze the results; in particular prove that the Dirac points \mathbf{q}_D are located in the corners of the 1st Brillouin zone, and express the velocity v_n participating in Eq. (122), in terms of the coupling energy δ_n . Show that the final results do not change if the quasi-localized wavefunctions are not axially-symmetric, but are proportional to $\exp\{im\varphi\}$ – as they are, with $m = 1$, for the $2p_z$ electrons of carbon atoms in graphene, that are responsible for its transport properties.

3.15. Examine basic properties of the so-called *Wannier functions* defined as

$$\phi_{\mathbf{R}}(\mathbf{r}) \equiv \text{const} \times \int_{\text{BZ}} \psi_{\mathbf{q}}(\mathbf{r}) e^{-i\mathbf{q}\cdot\mathbf{R}} d^3q,$$

where $\psi_{\mathbf{q}}(\mathbf{r})$ is the Bloch wavefunction (108), \mathbf{R} is any vector of the Bravais lattice, and the integration over the quasimomentum \mathbf{q} is extended over any (e.g., the first) Brillouin zone.

3.16. Evaluate the long-range interaction (the so-called *London dispersion force*) between two similar, electrically-neutral atoms or molecules, modeling each of them as an isotropic 3D harmonic oscillator with the electric dipole moment $\mathbf{d} = q\mathbf{s}$, where \mathbf{s} is the oscillator's displacement from its equilibrium position.

Hint: Represent the total Hamiltonian of the system as a sum of Hamiltonians of independent 1D harmonic oscillators, and calculate their total ground-state energy as a function of the distance between the dipoles.⁹⁸

3.17. Derive expressions for the stationary wavefunctions and the corresponding energies of a 2D particle of mass m , free to move inside a round disk of radius R . What is the degeneracy of each energy level? Calculate the five lowest energy levels with an accuracy better than 1%.

3.18. Calculate the ground-state energy of a 2D particle of mass m , localized in a very shallow flat-bottom potential well

$$U(\rho) = \begin{cases} -U_0, & \text{for } \rho < R, \\ 0, & \text{for } \rho > R, \end{cases} \quad \text{with } 0 < U_0 \ll \frac{\hbar^2}{mR^2}.$$

3.19. Estimate the energy E of the localized ground state of a particle of mass m , in an axially-symmetric 2D potential well of a finite radius R , with an arbitrary but very small potential $U(\rho)$. (Quantify this condition.)

3.20. Spell out the explicit form of the spherical harmonics $Y_4^0(\theta, \varphi)$ and $Y_4^4(\theta, \varphi)$.

3.21. Calculate $\langle x \rangle$ and $\langle x^2 \rangle$ in the ground states of the planar and spherical rotators of radius R . What can you say about $\langle p_x \rangle$ and $\langle p_x^2 \rangle$?

3.22. A spherical rotator, with $r \equiv (x^2 + y^2 + z^2)^{1/2} = R = \text{const}$, of mass m is in a state with the following wavefunction: $\psi = \text{const} \times (\frac{1}{3} + \sin^2 \theta)$. Calculate its energy.

3.23. According to the discussion at the beginning of Sec. 5, stationary wavefunctions of a 3D harmonic oscillator may be calculated as products of three 1D “Cartesian oscillators” – see, in particular Eq. (125), with $d = 3$. However, according to the discussion in Sec. 6, the wavefunctions of the type (200), proportional to the spherical harmonics Y_l^m , also describe stationary states of this spherically-symmetric system. Represent the wavefunctions (200) of:

⁹⁸ This explanation of the interaction between electrically-neutral atoms was put forward in 1930 by F. London, on the background of a prior (1928) work by C. Wang. Note that in some texts this interaction is (rather inappropriately) referred to as the “van der Waals force”, though it is only one, long-range component of the van der Waals model – see, e.g. SM Sec. 4.1.

- (i) the ground state of the oscillator, and
- (ii) each of its lowest excited states,

as linear combinations of products of 1D oscillator's stationary wavefunctions. Also, calculate the degeneracy of the n^{th} energy level of the oscillator.

3.24. Calculate the smallest depth U_0 of a spherical, flat-bottom potential well

$$U(\mathbf{r}) = \begin{cases} -U_0, & \text{for } r < R, \\ 0, & \text{for } R < r, \end{cases}$$

at that it has a bound (localized) stationary state. Does such a state exist for a very narrow and deep well $U(\mathbf{r}) = -w\delta(\mathbf{r})$, with a positive and finite w ?

3.25. A 3D particle of mass m is placed into a spherically-symmetric potential well with $-\infty < U(r) \leq U(\infty) = 0$. Relate its ground-state energy to that of a 1D particle of the same mass, moving in the following potential well:

$$U'(x) = \begin{cases} U(x), & \text{for } x \geq 0, \\ +\infty, & \text{for } x \leq 0. \end{cases}$$

In the light of the found relation, discuss the origin of the difference between the solutions of the previous problem and Problem 2.17.

3.26. Calculate the smallest value of the parameter U_0 , for that the following spherically-symmetric potential well,

$$U(r) = -U_0 e^{-r/R}, \quad \text{with } U_0, R > 0,$$

has a bound (localized) eigenstate.

Hint: You may like to introduce the following new variables: $f \equiv rR$ and $\xi \equiv Ce^{-r/2R}$, with an appropriate choice of the constant C .

3.27. A particle moving in a certain central potential $U(r)$ has a stationary state with the following wavefunction:

$$\psi = Cr^\alpha e^{-\beta r} \cos \theta,$$

where C , α , and $\beta > 0$ are constants. Calculate:

- (i) the probabilities of all possible values of the quantum numbers m and l , and
- (ii) the confining potential and the state's energy.

3.28. Use the variational method to estimate the ground-state energy of a particle of mass m , moving in the following spherically-symmetric potential:

$$U(\mathbf{r}) = ar^4.$$

3.29. Use the variational method, with the trial wavefunction $\psi_{\text{trial}} = A/(r + a)^b$, where both $a > 0$ and $b > 1$ are fitting parameters, to estimate the ground-state energy of the hydrogen-like atom/ion with the nuclear charge $+Ze$. Compare the solution with the exact result.

3.30. Calculate the energy spectrum of a particle moving in a monotonic, but otherwise arbitrary attractive spherically-symmetric potential $U(r) < 0$, in the approximation of very large orbital quantum numbers l . Formulate the quantitative condition(s) of validity of your theory. Check that for the Coulomb potential $U(r) = -C/r$, your result agrees with Eq. (201).

Hint: Try to solve Eq. (181) approximately, introducing the same new function, $f(r) \equiv r\mathcal{R}(r)$, that was already used in Sec. 1 and in the solutions of a few earlier problems.

3.31. An electron had been in the ground state of a hydrogen-like atom/ion with nuclear charge Ze , when the charge suddenly changed to $(Z + 1)e$.⁹⁹ Calculate the probabilities for the electron of the changed system to be:

- (i) in the ground state, and
- (ii) in the lowest excited state.

3.32. Due to a very short pulse of an external force, the nucleus of a hydrogen-like atom/ion, initially at rest in its ground state, starts moving with velocity v . Calculate the probability W_g that the atom remains in its ground state. Evaluate the energy to be given, by the pulse, to a hydrogen atom in order to reduce W_g to 50%.

3.33. Calculate $\langle x^2 \rangle$ and $\langle p_x^2 \rangle$ in the ground state of a hydrogen-like atom/ion. Compare the results with Heisenberg's uncertainty relation. What do these results tell about the electron's velocity in the system?

3.34. Use the Hellmann-Feynman theorem (see Problem 1.5) to prove:

- (i) the first of Eqs. (211), and
- (ii) the fact that for a spinless particle in an arbitrary spherically-symmetric attractive potential $U(r)$, the ground state is always an s -state (with the orbital quantum number $l = 0$).

3.35. For the ground state of a hydrogen atom, calculate the expectation values of \mathcal{E} and \mathcal{E}^2 , where \mathcal{E} is the electric field created by the atom, at distances $r \gg r_0$ from its nucleus. Interpret the resulting relation between $\langle \mathcal{E} \rangle^2$ and $\langle \mathcal{E}^2 \rangle$, at the same observation point.

3.36. Calculate the condition at that a particle of mass m , moving in the field of a very thin spherically-symmetric shell, with

$$U(\mathbf{r}) = w\delta(r - R),$$

and $w < 0$, has at least one localized ("bound") stationary state.

⁹⁹ Such a fast change happens, for example, at the beta-decay, when one of the nucleus' neutrons spontaneously turns into a proton, emitting a high-energy electron and a neutrino, which leave the system very fast (instantly on the atomic time scale), and do not affect directly the atom transition's dynamics.

3.37. Calculate the lifetime of the lowest metastable state of a particle in the same spherical-shell potential as in the previous problem, but now with $w > 0$, for sufficiently large w . (Quantify this condition.)

3.38. A particle of mass m and energy E is incident on a very thin spherical shell of radius R , whose localized states were the subject of two previous problems, with an arbitrary “weight” w .

(i) Derive general expressions for the differential and total cross-sections of scattering for this geometry.

(ii) Spell out the contribution σ_0 to the total cross-section σ , due to the spherically-symmetric component of the scattered de Broglie wave.

(iii) Analyze the result for σ_0 in the limits of very small and very large magnitudes of w , for both signs of this parameter. In particular, in the limit $w \rightarrow +\infty$, relate the result to the metastable state’s lifetime τ calculated in the previous problem.

3.39. Calculate the spherically-symmetric contribution σ_0 to the total cross-section of particle scattering by a uniform sphere of radius R , described by the following potential:

$$U(r) = \begin{cases} U_0, & \text{for } r < R, \\ 0, & \text{otherwise,} \end{cases}$$

with an arbitrary U_0 . Analyze the result in detail, and give an interpretation of its most remarkable features.

3.40. Use the finite difference method with the step $h = a/2$ to calculate as many energy levels as possible, for a particle confined to the interior of:

- (i) a square with side a , and
- (ii) a cube with side a ,

with hard walls. For the square, repeat the calculations, using a finer step: $h = a/3$. Compare the results for different values of h with each other and with the exact formulas.

Hint: It is advisable to either first solve (or review the solution of) the similar 1D Problem 1.15, or start from reading about the finite difference method.¹⁰⁰ Also: try to exploit the symmetry of the systems.

¹⁰⁰ See, e.g., CM Sec. 8.5 or EM Sec. 2.11.

This page is
intentionally left
blank

Chapter 4. Bra-ket Formalism

The objective of this chapter is to describe Dirac's "bra-ket" formalism of quantum mechanics, which not only overcomes some inconveniences of wave mechanics but also allows a natural description of such intrinsic properties of particles as their spin. In the course of the formalism's discussion, I will give only a few simple examples of its application, leaving more involved cases for the following chapters.

4.1. Motivation

As the reader could see from the previous chapters of these notes, wave mechanics gives many results of primary importance. Moreover, it is mostly sufficient for many applications, for example, solid-state electronics and device physics. However, in the course of our survey, we have filed several grievances about this approach. Let me briefly summarize these complaints:

- (i) Attempts to analyze the *temporal* evolution of quantum systems, beyond the trivial time behavior of the stationary states, described by Eq. (1.62), run into technical difficulties. For example, we could derive Eq. (2.151) describing the metastable state's decay and Eq. (2.181) describing the quantum oscillations in coupled wells, only for the simplest potential profiles, though it is intuitively clear that such simple results should be common for all problems of this kind. Solving such problems for more complex potential profiles would entangle the time evolution analysis with the calculation of the spatial distribution of the evolving wavefunctions – which (as we could see in Secs. 2.9 and 3.6) may be rather complex even for simple time-independent potentials. Some separation of the spatial and temporal dependencies is possible using perturbation approaches (to be discussed in Chapter 6), but even those would lead, in the wavefunction language, to very cumbersome formulas.
- (ii) The last statement can also be made concerning other issues that are conceptually addressable within the wave mechanics, e.g., the Feynman path integral approach, coupling to the environment, etc. Pursuing them in the wave mechanics language would lead to formulas so bulky that I had postponed their discussion until we would have a more compact formalism on hand.
- (iii) In the discussion of several key problems (for example the harmonic oscillator and spherically-symmetric potentials), we have run into rather complicated eigenfunctions coexisting with very simple energy spectra – that infer some simple background physics. It is very important to get this physics revealed.
- (iv) In the wave-mechanics postulates formulated in Sec. 1.2, the quantum mechanical operators of the coordinate and momentum are treated rather unequally – see Eqs. (1.26b). However, some key expressions, e.g., for the fundamental eigenfunction of a free particle,

$$\exp\left\{i\frac{\mathbf{p}\cdot\mathbf{r}}{\hbar}\right\}, \quad (4.1)$$

or the harmonic oscillator's Hamiltonian,

$$\hat{H} = \frac{1}{2m}\hat{p}^2 + \frac{m\omega_0^2}{2}\hat{r}^2, \quad (4.2)$$

just beg for a similar treatment of coordinates and momenta.

However, the strongest motivation for a more general formalism comes from wave mechanics' conceptual inability to describe elementary particles' *spins*¹ and other internal quantum degrees of freedom, such as quark flavors or lepton numbers. In this context, let us review the basic facts on spin (which is very representative and experimentally the most accessible of all internal quantum numbers), to understand what a more general formalism has to explain – as a minimum.

Figure 1 shows the conceptual scheme of the simplest spin-revealing experiment, first conceived by Otto Stern in 1921 and implemented by Walther Gerlach in 1922. A collimated beam of electrons from a natural source, such as a heated cathode, is passed through a gap between the poles of a strong magnet, whose magnetic field \mathcal{B} , (in Fig. 1, directed along the z -axis) is nonuniform, so that both \mathcal{B}_z and $d\mathcal{B}_z/dz$ are not equal to zero. The experiment shows that the beam splits into two beams of equal intensity.

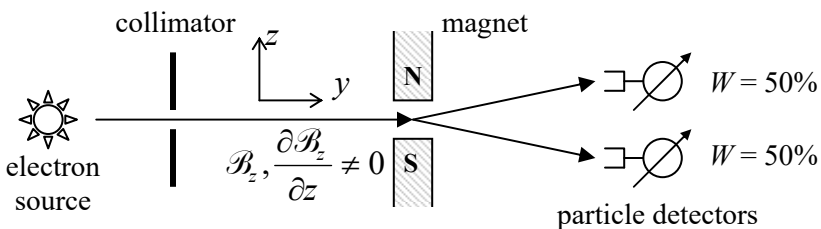


Fig. 4.1. The simplest Stern-Gerlach experiment.

This result may be semi-quantitatively explained on classical if somewhat phenomenological grounds, by assuming that each electron has an intrinsic, permanent magnetic dipole moment \mathbf{m} . Indeed, classical electrodynamics² tells us that the potential energy U of a magnetic dipole in an external magnetic field \mathcal{B} is equal to $(-\mathbf{m} \cdot \mathcal{B})$, so that the force acting on the electron,

$$\mathbf{F} = -\nabla U = -\nabla(-\mathbf{m} \cdot \mathcal{B}), \quad (4.3)$$

has a non-zero vertical component

$$F_z = -\frac{\partial}{\partial z}(-m_z \cdot \mathcal{B}_z) \equiv m_z \frac{\partial \mathcal{B}_z}{\partial z}. \quad (4.4)$$

Hence if we further assume that electron's magnetic moment may take only two equally probable discrete values of $m_z = \pm\mu$ (though such discreteness does not follow from any classical model of the particle), this may explain the original Stern-Gerlach effect qualitatively. The quantitative explanation of the beam splitting angle requires the magnitude of μ to be equal (or very close) to the so-called *Bohr magneton*³

$$\mu_B \equiv \frac{\hbar e}{2m_e} \approx 0.9274 \times 10^{-23} \frac{\text{J}}{\text{T}}. \quad (4.5)$$

Bohr
magneton

¹ To the best of my knowledge, the concept of spin as a measure of the internal rotation of a particle was first suggested by Ralph Kronig, then a 20-year-old student, in January 1925, a few months before two other students, G. Uhlenbeck and S. Goudsmit – to whom the idea is usually attributed. The concept was then accepted (rather reluctantly) and developed quantitatively by Wolfgang Pauli.

² See, e.g., EM Sec. 5.4, in particular Eq. (5.100).

³ A good mnemonic rule is that it is close to 1 K/T. In the Gaussian units, $\mu_B \equiv \hbar e/2m_e c \approx 0.9274 \times 10^{-20}$ erg/G.

However, as we will see below, this value cannot be explained by any internal motion of the electron, say its rotation about the z -axis. More importantly, this semi-classical phenomenology cannot explain, even qualitatively, other experimental results, for example those of the set of multi-stage Stern-Gerlach experiments shown in Fig. 2. In the first of the experiments, the electron beam is first passed through a magnetic field (and its gradient) oriented along the z -axis, just as in Fig. 1. Then one of the two resulting beams is absorbed (or removed from the setup in some other way), while the other one is passed through a similar but x -oriented field. The experiment shows that this beam is split again into two components of equal intensity. A classical explanation of this experiment would require an even more unnatural additional assumption that the initial electrons had random but discrete components of the magnetic moment simultaneously in *two* directions, z and x .

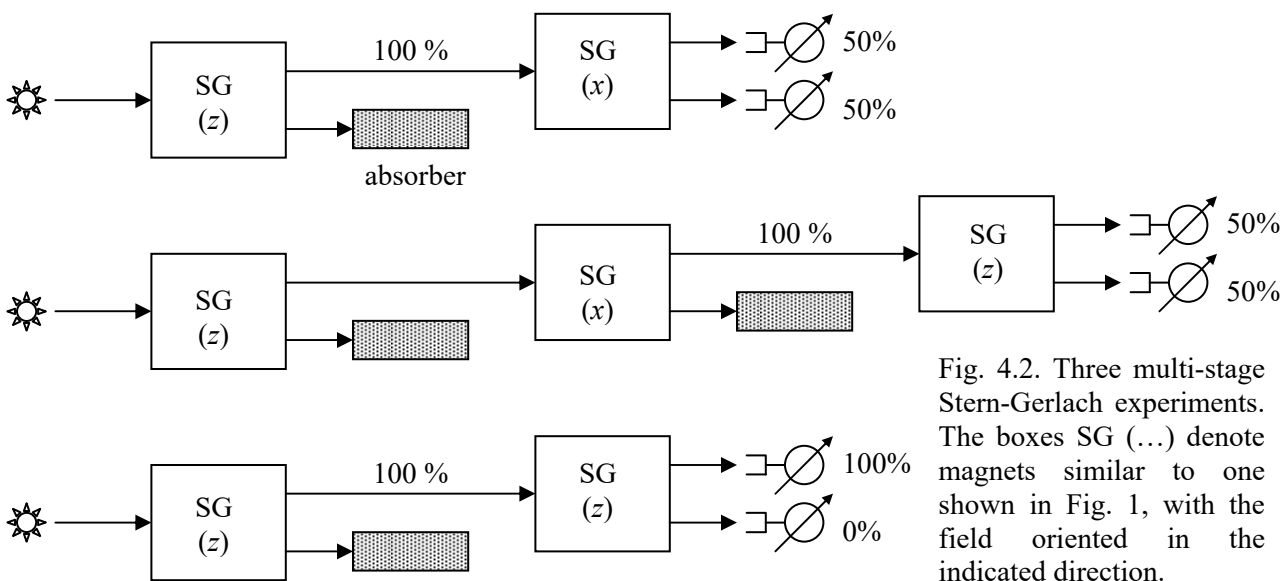


Fig. 4.2. Three multi-stage Stern-Gerlach experiments. The boxes SG (...) denote magnets similar to one shown in Fig. 1, with the field oriented in the indicated direction.

However, even this assumption cannot explain the results of the three-stage Stern-Gerlach experiment shown on the middle panel of Fig. 2. Here, the previous two-state setup is complemented with one more absorber and one more magnet, now with the z -orientation again. Completely counter-intuitively, it again gives two beams of equal intensity, as if we have not yet filtered out the electrons with m_z corresponding to the lower beam, at the first z -stage. The only way to save the classical explanation here is to say that maybe, electrons *somewhat* interact with the magnetic field so that the x -polarized (non-absorbed) beam becomes spontaneously depolarized again somewhere between the two last stages. But any hope for such an explanation is ruined by the control experiment shown on the bottom panel of Fig. 2, whose results indicate that no such depolarization happens.

We will see below that all these (and many more) results find a natural explanation in the so-called *matrix mechanics* pioneered by Werner Heisenberg, Max Born, and Pascual Jordan in 1925. However, the matrix formalism is rather inconvenient for the solution of most problems discussed in Chapters 1-3, and for a short time, it was eclipsed by E. Schrödinger's wave mechanics, which had been put forward just a few months later. However, very soon Paul Adrien Maurice Dirac introduced a more general *bra-ket formalism* of quantum mechanics, which provides a generalization of both approaches and proves their equivalence. Let me describe it, begging for the reader's patience, because (in a contrast with my usual style), I will not be able to give particular examples of its application for a while – until all the basic notions of the formalism have been introduced.

4.2. States, state vectors, and linear operators

The basic notion of the general formulation of quantum mechanics is the *quantum state* of a system.⁴ To get some gut feeling of this notion, if a quantum state α of a particle may be adequately described by wave mechanics, this description is given by the corresponding wavefunction $\Psi_\alpha(\mathbf{r}, t)$. Note, however, a quantum state as such is *not* a mathematical object,⁵ and can participate in mathematical formulas only as a “label” – e.g., the index of the wavefunction Ψ_α . On the other hand, such wavefunction is *not* a state, but a mathematical object (a complex function of space and time) giving a quantitative description of the state – just as the classical radius vector \mathbf{r}_α and velocity \mathbf{v}_α as real functions of time are mathematical objects describing the motion of the particle in its classical description – see Fig. 3. Similarly, in the Dirac formalism, a certain quantum state α is described by either of two mathematical objects, called the *state vectors*: the *ket-vector* $|\alpha\rangle$ and *bra-vector* $\langle\alpha|$,⁶ whose relationship is close to that between the wavefunction Ψ_α and its complex conjugate Ψ_α^* .

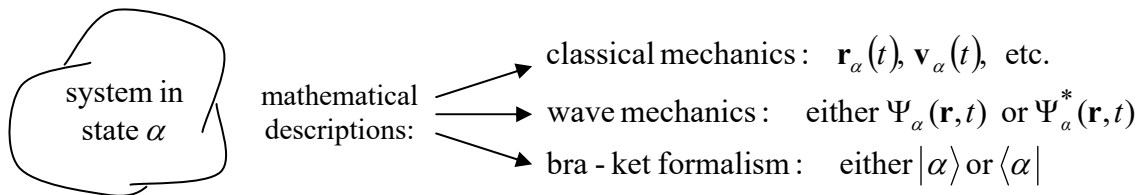


Fig. 4.3. Physical state of a system and its descriptions.

One should be cautious with the term “vector” here. The usual geometric vectors, such as \mathbf{r} and \mathbf{v} , are defined in the usual geometric (say, Euclidean) space. In contrast, the bra- and ket-vectors are defined in a more abstract *Hilbert space* – the full set of its possible bra- and ket-vectors of a given system.⁷ So, despite certain similarities with the geometric vectors, the bra- and ket-vectors are different mathematical objects, and we need to define the rules of their handling. The primary rules are essentially postulates and are justified only by the correct description of all experimental observations of the rule corollaries. While there is a general consensus among physicists what the corollaries are, there are many possible ways to carve from them the basic postulate sets. Just as in Sec. 1.2, I will not try too hard to beat the number of the postulates to the smallest possible minimum, trying instead to keep their physical meaning transparent.

(i) Ket-vectors. Let us start with *ket-vectors* – sometimes called just *kets* for short. Their most important property is the *linear superposition*. Namely, if several ket-vectors $|\alpha_j\rangle$ describe possible states of a quantum system, numbered by the index j , then any linear combination (*superposition*)

$$|\alpha\rangle = \sum_j c_j |\alpha_j\rangle, \quad (4.6)$$

Linear
superposition
of ket-vectors

⁴ An attentive reader could notice my smuggling the term “system” instead of “particle”, which was used in the previous chapters. Indeed, the bra-ket formalism allows the description of quantum systems much more complex than a single spinless particle that is a typical (though not the only possible) subject of wave mechanics.

⁵ As was expressed nicely by Asher Peres, one of the pioneers of the quantum information theory, “quantum phenomena do not occur in the Hilbert space, they occur in a laboratory”.

⁶ The terms *bra* and *ket* were suggested to reflect the fact that the pair $\langle\beta|$ and $|\alpha\rangle$ may be considered as the parts of the combinations like $\langle\beta|\alpha\rangle$ (see below), which remind expressions in the usual angle brackets.

⁷ I have to confess that this is a bit loose definition; it will be refined soon.

where c_j are any (possibly complex) c -numbers, also describes a possible state of the same system.⁸ Actually, since ket-vectors are new mathematical objects, the exact meaning of the right-hand side of Eq. (6) becomes clear only after we have postulated the following rules of summation of these vectors,

$$|\alpha_j\rangle + |\alpha_{j'}\rangle = |\alpha_{j'}\rangle + |\alpha_j\rangle, \quad (4.7)$$

and their multiplication by an arbitrary c -number:

$$c|\alpha_j\rangle = |\alpha_j\rangle c. \quad (4.8)$$

Note that in the set of wave mechanics postulates, the statements parallel to Eqs. (7) and (8) were unnecessary, because the wavefunctions are the usual (albeit complex) functions of space and time, and we know from the usual algebra that such relations are indeed valid.

As evident from Eq. (6), the complex coefficient c_j may be interpreted as the “weight” of the state α_j in the linear superposition α . One important particular case is $c_j = 0$, showing that the state α_j does not participate in the superposition α . The corresponding term of the sum (6), i.e. the product

Null-state vector

$$0|\alpha_j\rangle, \quad (4.9)$$

has a special name: the *null-state* vector. (It is important to avoid confusion between the null-state corresponding to vector (9), and the ground state of the system, which is frequently denoted by ket-vector $|0\rangle$. In some sense, the null-state does not exist at all, while the ground state not only does exist but frequently is the most important quantum state of the system.)

(ii) Bra-vectors and inner products. Bra-vectors $\langle\alpha|$, which obey the rules similar to Eqs. (7) and (8), are not new, independent objects: a ket-vector $|\alpha\rangle$ and the corresponding bra-vector $\langle\alpha|$ describe the same state. In other words, there is a *unique dual correspondence* between $|\alpha\rangle$ and $\langle\alpha|$,⁹ very similar (though not identical) to that between a wavefunction Ψ and its complex conjugate Ψ^* . The correspondence between these vectors is described by the following rule: if a ket-vector of a linear superposition is described by Eq. (6), then the corresponding bra-vector is

Linear superposition of bra-vectors

$$\langle\alpha| = \sum_j c_j^* \langle\alpha_j| = \sum_j \langle\alpha_j| c_j^*. \quad (4.10)$$

The mathematical convenience of using two types of vectors rather than just one becomes clear from the notion of their *inner product* (due to its second, shorthand form, also called the *short bracket*):

Short bracket (inner product)

$$(\langle\beta|)(\langle\alpha|) \equiv \langle\beta|\alpha\rangle, \quad (4.11)$$

which is a scalar c -number, in a certain but limited analogy with the scalar product of the usual geometric vectors. (For one difference, the product (11) may be a complex number.)

The main property of the inner product is its linearity with respect to any of its component vectors. For example, if a linear superposition α is described by the ket-vector (6), then

⁸ One may express the same statement by saying that the vector $|\alpha\rangle$ belongs to the same Hilbert space as all $|\alpha_j\rangle$.

⁹ Mathematicians like to say that the ket- and bra-vectors of the same quantum system are defined in two *isomorphic* Hilbert spaces.

$$\langle \beta | \alpha \rangle = \sum_j c_j \langle \beta | \alpha_j \rangle, \quad (4.12)$$

while if Eq. (10) is true, then

$$\langle \alpha | \beta \rangle = \sum_j c_j^* \langle \alpha_j | \beta \rangle. \quad (4.13)$$

In plain English, c -number factors may be moved either into or out of the inner products.

The second key property of the inner product is

$$\langle \alpha | \beta \rangle = \langle \beta | \alpha \rangle^*. \quad (4.14)$$

Inner product:: complex conjugate

It is compatible with Eq. (10); indeed, the complex conjugation of both parts of Eq. (12) gives:

$$\langle \beta | \alpha \rangle^* = \sum_j c_j^* \langle \beta | \alpha_j \rangle^* = \sum_j c_j^* \langle \alpha_j | \beta \rangle = \langle \alpha | \beta \rangle. \quad (4.15)$$

Finally, one more rule: the inner product of the bra- and ket-vectors describing the same state (called the *norm squared*) is real and non-negative,

$$\| \alpha \|^2 \equiv \langle \alpha | \alpha \rangle \geq 0. \quad (4.16)$$

State's norm squared

In order to give the reader some feeling about the meaning of this rule: we will see below that if some state α may be described by the wavefunction $\Psi_\alpha(\mathbf{r}, t)$, then

$$\langle \alpha | \alpha \rangle = \int \Psi_\alpha^* \Psi_\alpha d^3 r \geq 0. \quad (4.17)$$

Hence the role of the bra- and ket-vectors of the same state is very similar to that of complex-conjugate pairs of its wavefunctions.

(iii) Operators. One more key notion of the Dirac formalism is quantum-mechanical *linear operators*. Just as for the operators discussed in wave mechanics, the function of an operator is to “generate” of one state from another: if $|\alpha\rangle$ is a possible ket of the system, and \hat{A} is a legitimate¹⁰ operator, then the following combination,

$$\hat{A}|\alpha\rangle, \quad (4.18)$$

is also a ket-vector describing a possible state of the system, i.e. a ket-vector in the same Hilbert space as the initial vector $|\alpha\rangle$. An alternative formulation of the same rule is the following clarification of the notion of the Hilbert space: for the given set of linear operators of a system, its Hilbert state includes all vectors that may be obtained from each other using the operations of the type (18). In this context, let me note that the operator set, and hence the Hilbert space of a system, usually (if not always) implies its certain approximate model. For example, if the coupling of orbital degrees of freedom of a particle to its spin may be ignored (as it may be for a non-relativistic particle in the absence of an external magnetic

¹⁰ Here the term “legitimate” means “having a clear sense in the bra-ket formalism”. Some examples of “illegitimate” expressions are: $|\alpha\rangle \hat{A}$, $\hat{A} \langle \alpha|$, $|\alpha\rangle |\beta\rangle$, and $\langle \alpha| \langle \beta|$. Note, however, that the last two expressions may be legitimate if α and β are states of different systems, i.e. if their state vectors belong to different Hilbert spaces. We will run into such *direct products* of the bra- and ket-vectors (sometimes denoted, respectively, as $|\alpha\rangle \otimes |\beta\rangle$ and $\langle \alpha| \otimes \langle \beta|$) in Chapters 6-10.

field), we may describe the dynamics of the particle using spin operators only. In this case, the set of all possible spin vectors of the particle forms a Hilbert space separate from that of the orbital-state vectors of that particle.

As the adjective “linear” in the operator definition implies, the main rules governing the operators is their linearity with respect to both any superposition of vectors:

$$\hat{A}\left(\sum_j c_j |\alpha_j\rangle\right) = \sum_j c_j \hat{A}|\alpha_j\rangle, \quad (4.19)$$

and any superposition of operators:

$$\left(\sum_j c_j \hat{A}_j\right)|\alpha\rangle = \sum_j c_j \hat{A}_j|\alpha\rangle. \quad (4.20)$$

These rules are evidently similar to Eqs. (1.53)-(1.54) of wave mechanics.

The above rules imply that an operator “acts” on the ket-vector on its right; however, a combination of the type $\langle\alpha|\hat{A}$ is also legitimate and represents a new bra-vector. It is important that, generally, this vector does *not* represent the same state as the ket-vector (18); instead, the bra-vector isomorphic to the ket-vector (18) is

$$\langle\alpha|\hat{A}^\dagger. \quad (4.21)$$

Conjugate operator

This statement serves as the definition of the *Hermitian conjugate* (also called “Hermitian adjoint”) \hat{A}^\dagger of the initial operator \hat{A} . For an important class of operators, called the *Hermitian operators*, the conjugation is inconsequential, i.e. for them

$$\hat{A}^\dagger = \hat{A}. \quad (4.22)$$

Hermitian operator

(This equality, as well as any other operator equation below, means that these operators act similarly on any bra- or ket-vector of the given Hilbert space.)¹¹

To proceed further, we need one more additional postulate, sometimes called the *associative axiom of multiplication*: just as an ordinary product of scalars, *any* legitimate bra-ket expression, not including explicit summations, does not change from an insertion or removal of a pair of parentheses – meaning as usual that the operation inside them has to be performed first. The first two examples of this postulate are given by Eqs. (19) and (20), but the associative axiom is more general and means, for example, that

$$\langle\beta|\left(\hat{A}|\alpha\rangle\right) = \left(\langle\beta|\hat{A}\right)|\alpha\rangle \equiv \langle\beta|\hat{A}|\alpha\rangle, \quad (4.23)$$

Long bracket:
definition

This last equality serves as the definition of the last form, called the *long bracket* (evidently, also a scalar), with an operator sandwiched between a bra-vector and a ket-vector. This definition, when combined with the definition of the Hermitian conjugate and Eq. (14), yields an important corollary:

¹¹ If we consider *c*-numbers as a particular type of operators (which is legitimate for any Hilbert space), then according to Eqs. (11) and (21), for them the Hermitian conjugation is equivalent to the simple complex conjugation, so that only real *c*-numbers may be considered as a particular type of the Hermitian operators (22).

$$\langle \beta | \hat{A} | \alpha \rangle = \langle \beta | (\hat{A} | \alpha \rangle) = \left(\left(\langle \alpha | \hat{A}^\dagger \right) | \beta \rangle \right)^* = \left(\langle \alpha | \hat{A}^\dagger | \beta \rangle \right)^*, \quad (4.24)$$

which is most frequently rewritten as

$$\langle \alpha | \hat{A} | \beta \rangle^* = \langle \beta | \hat{A}^\dagger | \alpha \rangle. \quad (4.25)$$

Long bracket:
complex conjugate

The associative axiom also enables us to comprehend the following definition of one more, *outer* product of bra- and ket-vectors:

$$| \beta \rangle \langle \alpha |. \quad (4.26)$$

Outer
bra-ket
product

In contrast to the inner product (11), which is a *scalar*, this mathematical construct is an *operator*. Indeed, the associative axiom allows us to remove parentheses in the following expression:

$$(\langle \beta | \langle \alpha |) | \gamma \rangle = \langle \beta | \langle \alpha | \gamma \rangle. \quad (4.27)$$

But the last short bracket is just a scalar; hence the mathematical object (26), acting on a ket-vector (in this case, $|\gamma\rangle$), gives a new ket-vector, which is the essence of the operator's action. Very similarly,

$$\langle \delta | (\langle \beta | \langle \alpha |) = \langle \delta | \beta \rangle \langle \alpha | \quad (4.28)$$

– again a typical operator's action on a bra-vector. So, Eq. (26) defines an operator.

Now let us perform the following calculation. We may use the parentheses' insertion into the bra-ket equality following from Eq. (14),

$$\langle \gamma | \alpha \rangle \langle \beta | \delta \rangle = (\langle \delta | \beta \rangle \langle \alpha | \gamma \rangle)^*, \quad (4.29)$$

to transform it to the following form:

$$\langle \gamma | (\langle \alpha | \langle \beta |) | \delta \rangle = (\langle \delta | (\langle \beta | \langle \alpha |) | \gamma \rangle)^*. \quad (4.30)$$

Since this equality should be valid for any state vectors $\langle \gamma |$ and $| \beta \rangle$, its comparison with Eq. (25) gives the following operator equality

$$(\langle \alpha | \langle \beta |)^\dagger = | \beta \rangle \langle \alpha |. \quad (4.31)$$

Outer
product:
Hermitian
conjugate

This is the conjugate rule for outer products; it reminds the rule (14) for inner products but involves the Hermitian (rather than the usual complex) conjugation.

The associative axiom is also valid for the operator “multiplication”:

$$(\hat{A} \hat{B}) | \alpha \rangle = \hat{A} (\hat{B} | \alpha \rangle), \quad \langle \beta | (\hat{A} \hat{B}) = (\langle \beta | \hat{A}) \hat{B}, \quad (4.32)$$

showing that the action of an operator product on a state vector is nothing more than the sequential action of its operands. However, we have to be careful with the operator products; generally, they do not commute: $\hat{A} \hat{B} \neq \hat{B} \hat{A}$. This is why the *commutator* – the operator defined as

$$[\hat{A}, \hat{B}] \equiv \hat{A} \hat{B} - \hat{B} \hat{A}, \quad (4.33)$$

Commutator

is a non-trivial and very useful notion. Another similar notion is the *anticommutator*:¹²

$$\{\hat{A}, \hat{B}\} \equiv \hat{A}\hat{B} + \hat{B}\hat{A}. \quad (4.34)$$

Finally, the bra-ket formalism broadly uses two special operators. The *null-operator* $\hat{0}$ is defined by the following relations:

$$\hat{0}|\alpha\rangle \equiv 0|\alpha\rangle, \quad \langle\alpha|\hat{0} \equiv \langle\alpha|0, \quad (4.35)$$

where α is an arbitrary state; we may say that the null-operator “kills” *any* state, turning it into the null-state. Another useful notion is the *identity operator*, which is defined by the following action (or rather “inaction” :-)) on an arbitrary state vector:

$$\hat{I}|\alpha\rangle \equiv |\alpha\rangle, \quad \langle\alpha|\hat{I} \equiv \langle\alpha|. \quad (4.36)$$

These definitions show that the null-operator and the identity operator are Hermitian.

4.3. State basis and matrix representation

While some operations in quantum mechanics may be carried out in the general bra-ket formalism outlined above, many calculations are performed for quantum systems that feature a *full and orthonormal* set $\{u\} \equiv \{u_1, u_2, \dots, u_j, \dots\}$ of its states u_j , frequently called a *basis*. The first of these terms means that any possible state vector of the system (i.e. of its Hilbert space) may be represented as a unique sum of the type (6) or (10) over its basis vectors:

$$|\alpha\rangle = \sum_j \alpha_j |u_j\rangle, \quad \langle\alpha| = \sum_j \alpha_j^* \langle u_j|, \quad (4.37)$$

so that, in particular, if α is one of the basis states, say $u_{j'}$, then $\alpha_j = \delta_{jj'}$. The second term means that

$$\langle u_j | u_{j'} \rangle = \delta_{jj'}. \quad (4.38)$$

For the systems that may be described by wave mechanics, examples of the full orthonormal bases are represented by any full and orthonormal set of eigenfunctions calculated in the previous three chapters of this course – for the simplest example, see Eq. (1.87).

Due to the uniqueness of the expansion (37), the full set of the coefficients α_j involved in the expansion of a state α in certain basis $\{u\}$ gives its complete description – just as the Cartesian components A_x , A_y , and A_z of a usual geometric 3D vector \mathbf{A} in certain reference frame give its complete description. Still, let me emphasize some differences between such representations of the quantum-mechanical state vectors and 3D geometric vectors:

- (i) a quantum state basis may have a large or even infinite number of states u_j , and
- (ii) the expansion coefficients α_j may be complex.

¹² Another popular notation for the anticommutator (34) is $[\hat{A}, \hat{B}]_+$; it will not be used in these notes.

With these reservations in mind, the analogy with geometric vectors may be pushed further on. Let us inner-multiply both parts of the first of Eqs. (37) by a bra-vector $\langle u_j |$ and then transform the resulting relation using the linearity rules discussed in the previous section, and Eq. (38):

$$\langle u_{j'} | \alpha \rangle = \langle u_{j'} | \sum_j \alpha_j | u_j \rangle = \sum_j \alpha_j \langle u_{j'} | u_j \rangle = \alpha_{j'}. \quad (4.39)$$

Together with Eq. (14), this means that any of the expansion coefficients in Eq. (37) may be represented as an inner product:

$$\alpha_j = \langle u_j | \alpha \rangle, \quad \alpha_j^* = \langle \alpha | u_j \rangle; \quad (4.40)$$

Expansion coefficients as inner products

these important equalities relations are analogs of equalities $A_j = \mathbf{n}_j \cdot \mathbf{A}$ of the usual vector algebra, and will be used on numerous occasions in this course. With them, the expansions (37) may be rewritten as

$$|\alpha\rangle = \sum_j |u_j\rangle \langle u_j| \alpha \rangle \equiv \sum_j \hat{\Lambda}_j |\alpha\rangle, \quad \langle \alpha| = \sum_j \langle \alpha| u_j \rangle \langle u_j| \equiv \sum_j \langle \alpha| \hat{\Lambda}_j, \quad (4.41)$$

where

$$\hat{\Lambda}_j \equiv |u_j\rangle \langle u_j|. \quad (4.42)$$

Projection operator

Eqs. (41) show that $\hat{\Lambda}_j$ so defined is a legitimate linear operator. This operator, acting on any state vector of the type (37), singles out just one of its components, for example,

$$\hat{\Lambda}_j |\alpha\rangle = |u_j\rangle \langle u_j| \alpha \rangle = \alpha_j |u_j\rangle, \quad (4.43)$$

i.e. “kills” all components of the linear superposition but one. In the geometric analogy, such operator “projects” the state vector on the j^{th} “direction”, hence its name – the *projection operator*. Probably, the most important property of the projection operators, called the *closure* (or “completeness”) *relation*, immediately follows from Eq. (41): their sum over the full basis is equivalent to the identity operator

$$\sum_j |u_j\rangle \langle u_j| = \hat{I}. \quad (4.44)$$

Closure relation

This means in particular that we may insert the left-hand side of Eq. (44), for any basis, into any bra-ket relation, at any place – the trick that we will use again and again.

Now let us see how the expansions (37) transform the key notions introduced in the last section, starting from the short bracket (11), i.e. the inner product of two state vectors:

$$\langle \beta | \alpha \rangle = \sum_{j,j'} \langle u_j | \beta_j^* \alpha_{j'} | u_{j'} \rangle = \sum_{j,j'} \beta_j^* \alpha_{j'} \delta_{jj'} = \sum_j \beta_j^* \alpha_j. \quad (4.45)$$

Besides the complex conjugation, this expression is similar to the scalar product of the usual, geometric vectors. Now, let us explore the long bracket (23):

$$\langle \beta | \hat{A} | \alpha \rangle = \sum_{j,j'} \beta_j^* \langle u_j | \hat{A} | u_{j'} \rangle \alpha_{j'} = \sum_{j,j'} \beta_j^* A_{jj'} \alpha_{j'}. \quad (4.46)$$

Here, the last step uses the very important notion of *matrix elements* of the operator, defined as

Operator's
matrix
elements

$$A_{jj'} \equiv \langle u_j | \hat{A} | u_{j'} \rangle. \quad (4.47)$$

As evident from Eq. (46), the full set of the matrix elements completely characterizes the operator, just as the full set of the expansion coefficients (40) fully characterizes a quantum state. The term “matrix” means, first of all, that it is convenient to represent the full set of $A_{jj'}$ as a square table (*matrix*), with the linear dimension equal to the number of basis states u_j of the system under the consideration. By the way, this number (which may be infinite) is called the *dimensionality* of its Hilbert space.

As two simplest examples, all matrix elements of the null-operator, defined by Eqs. (35), are evidently equal to zero (in any basis), and hence it may be represented as a matrix of zeros (called the *null-matrix*):

Null
matrix

$$0 \equiv \begin{pmatrix} 0 & 0 & \dots \\ 0 & 0 & \dots \\ \dots & \dots & \dots \end{pmatrix}, \quad (4.48)$$

while for the identity operator \hat{I} , defined by Eqs. (36), we readily get

$$I_{jj'} = \langle u_j | \hat{I} | u_{j'} \rangle = \langle u_j | u_{j'} \rangle = \delta_{jj'}, \quad (4.49)$$

i.e. its matrix (naturally called the *identity matrix*) is diagonal – also in any basis:

Identity
matrix

$$I \equiv \begin{pmatrix} 1 & 0 & \dots \\ 0 & 1 & \dots \\ \dots & \dots & \dots \end{pmatrix}. \quad (4.50)$$

The convenience of the matrix language extends well beyond the representation of particular operators. For example, let us use the definition (47) to calculate matrix elements of a product of two operators:

$$(AB)_{jj''} = \langle u_j | \hat{A} \hat{B} | u_{j''} \rangle. \quad (4.51)$$

Matrix
element
of an
operator
product

Here we may use Eq. (44) for the first (but not the last!) time, inserting the identity operator between the two operators, and then expressing it via a sum of projection operators:

$$(AB)_{jj''} = \langle u_j | \hat{A} \hat{B} | u_{j''} \rangle = \langle u_j | \hat{A} \hat{I} \hat{B} | u_{j''} \rangle = \sum_{j'} \langle u_j | \hat{A} | u_{j'} \rangle \langle u_{j'} | \hat{B} | u_{j''} \rangle = \sum_{j'} A_{jj'} B_{j'j''}. \quad (4.52)$$

This result corresponds to the standard “row by column” rule of calculation of an arbitrary element of the matrix product

$$AB = \begin{pmatrix} A_{11} & A_{12} & \dots \\ A_{21} & A_{22} & \dots \\ \dots & \dots & \dots \end{pmatrix} \begin{pmatrix} B_{11} & B_{12} & \dots \\ B_{21} & B_{22} & \dots \\ \dots & \dots & \dots \end{pmatrix}. \quad (4.53)$$

Hence a product of operators may be represented (in a fixed basis!) by that of their matrices (in the same basis).

This is so convenient that the same language is often used to represent not only long brackets,

$$\langle \beta | \hat{A} | \alpha \rangle = \sum_{j'} \beta_j^* A_{jj'} \alpha_{j'} = \left(\beta_1^*, \beta_2^*, \dots \right) \begin{pmatrix} A_{11} & A_{12} & \dots \\ A_{21} & A_{22} & \dots \\ \dots & \dots & \dots \end{pmatrix} \begin{pmatrix} \alpha_1 \\ \alpha_2 \\ \dots \end{pmatrix}, \quad (4.54)$$

Long bracket as a matrix product

but even short brackets:

$$\langle \beta | \alpha \rangle = \sum_j \beta_j^* \alpha_j = \left(\beta_1^*, \beta_2^*, \dots \right) \begin{pmatrix} \alpha_1 \\ \alpha_2 \\ \dots \end{pmatrix}, \quad (4.55)$$

Short bracket as a matrix product

although these equalities require the use of non-square matrices: rows of (complex-conjugate!) expansion coefficients for the representation of bra-vectors, and columns of these coefficients for the representation of ket-vectors. With that, the mapping of quantum states and operators on matrices becomes completely general.

Now let us have a look at the outer product operator (26). Its matrix elements are just

$$(\langle \alpha | \beta \rangle)_{jj'} = \langle u_j | \alpha \rangle \langle \beta | u_{j'} \rangle = \alpha_j \beta_{j'}^*. \quad (4.56)$$

These are the elements of a very special square matrix, whose filling requires the knowledge of just $2N$ scalars (where N is the basis size), rather than N^2 scalars as for an arbitrary operator. However, a simple generalization of such an outer product may represent an arbitrary operator. Indeed, let us insert two identity operators (44), with different summation indices, on both sides of an arbitrary operator:

$$\hat{A} = \hat{I} \hat{A} \hat{I} = \left(\sum_j |u_j\rangle \langle u_j| \right) \hat{A} \left(\sum_{j'} |u_{j'}\rangle \langle u_{j'}| \right), \quad (4.57)$$

and then use the associative axiom to rewrite this expression as

$$\hat{A} = \sum_{j,j'} |u_j\rangle \langle u_j | \hat{A} | u_{j'} \rangle \langle u_{j'}|. \quad (4.58)$$

But the expression in the middle long bracket is just the matrix element (47), so that we may write

$$\hat{A} = \sum_{j,j'} |u_j\rangle A_{jj'} \langle u_{j'}|. \quad (4.59)$$

Operator via its matrix elements

The reader has to agree that this formula, which is a natural generalization of Eq. (44), is extremely elegant.

The matrix representation is so convenient that it makes sense to extend it to one level lower – from state vector products to the “bare” state vectors resulting from the operator’s action upon a given state. For example, let us use Eq. (59) to represent the ket-vector (18) as

$$|\alpha'\rangle \equiv \hat{A}|\alpha\rangle = \left(\sum_{j,j'} |u_j\rangle A_{jj'} \langle u_{j'}| \right) |\alpha\rangle = \sum_{j,j'} |u_j\rangle A_{jj'} \langle u_{j'}| \alpha\rangle. \quad (4.60)$$

According to Eq. (40), the last short bracket is just α_j , so that

$$|\alpha'\rangle = \sum_{j,j'} |u_j\rangle A_{jj'} \alpha_{j'} = \sum_j \left(\sum_{j'} A_{jj'} \alpha_{j'} \right) |u_j\rangle \quad (4.61)$$

But the expression in the parentheses is just the coefficient α'_j of the expansion (37) of the resulting ket-vector (60) in the same basis, so that

$$\alpha'_j = \sum_{j'} A_{jj'} \alpha_{j'} . \quad (4.62)$$

This result corresponds to the usual rule of multiplication of a matrix by a column, so that we may represent any ket-vector by its column matrix, with the operator's action looking like

$$\begin{pmatrix} \alpha'_1 \\ \alpha'_2 \\ \dots \end{pmatrix} = \begin{pmatrix} A_{11} & A_{12} & \dots \\ A_{21} & A_{22} & \dots \\ \dots & \dots & \dots \end{pmatrix} \begin{pmatrix} \alpha_1 \\ \alpha_2 \\ \dots \end{pmatrix} . \quad (4.63)$$

Absolutely similarly, the operator action on the bra-vector (21), represented by its row-matrix, is

$$\left(\alpha'^*_1, \alpha'^*_2, \dots \right) = \left(\alpha^*_1, \alpha^*_2, \dots \right) \begin{pmatrix} \left(A^\dagger \right)_{11} & \left(A^\dagger \right)_{12} & \dots \\ \left(A^\dagger \right)_{21} & \left(A^\dagger \right)_{22} & \dots \\ \dots & \dots & \dots \end{pmatrix} . \quad (4.64)$$

By the way, Eq. (64) naturally raises the following question: what are the elements of the matrix on its right-hand side, or more exactly, what is the relation between the matrix elements of an operator and its Hermitian conjugate? The simplest way to answer it is to use Eq. (25) with two arbitrary states (say, u_j and $u_{j'}$) of the same basis in the role of α and β . Together with the orthonormality relation (38), this immediately gives¹³

$$\left(\hat{A}^\dagger \right)_{jj'} = \left(A_{j'j} \right)^* . \quad (4.65)$$

Hermitian
conjugate:
matrix
elements

Thus, the matrix of the Hermitian-conjugate operator is the *complex conjugated and transposed* matrix of the initial operator. This result exposes very clearly the difference between the Hermitian and the complex conjugation. It also shows that for the Hermitian operators, defined by Eq. (22),

$$A_{jj'} = A_{j'j}^*, \quad (4.66)$$

i.e. any pair of their matrix elements, symmetric with respect to the main diagonal, should be the complex conjugate of each other. As a corollary, their main-diagonal elements have to be real:

$$A_{jj} = A_{jj}^*, \quad \text{i.e. } \operatorname{Im} A_{jj} = 0. \quad (4.67)$$

¹³ For the sake of formula compactness, below I will use the shorthand notation in that the operands of this equality are just $A^\dagger_{jj'}$ and $A^*_{jj'}$. I believe that it leaves little chance for confusion, because the Hermitian conjugation sign \dagger may pertain only to an operator (or its matrix), while the complex conjugation sign $*$, to a scalar – say a matrix element.

In order to fully appreciate the special role played by Hermitian operators in quantum theory, let us introduce the key notions of *eigenstates* a_j (described by their *eigenvectors* $\langle a_j |$ and $| a_j \rangle$) and *eigenvalues* (*c-numbers*) A_j of an operator \hat{A} , both defined by the equation they have to satisfy:¹⁴

$$\hat{A} | a_j \rangle = A_j | a_j \rangle. \quad (4.68)$$

Let us prove that eigenvalues of any Hermitian operator are real,¹⁵

$$A_j = A_j^*, \quad \text{for } j = 1, 2, \dots, N, \quad (4.69)$$

while the eigenstates corresponding to different eigenvalues are orthogonal:

$$\langle a_j | a_{j'} \rangle = 0, \quad \text{if } A_j \neq A_{j'}. \quad (4.70)$$

The proof of both statements is surprisingly simple. Let us inner-multiply both sides of Eq. (68) by the bra-vector $\langle a_{j'} |$. On the right-hand side of the result, the eigenvalue A_j , as a *c-number*, may be taken out of the bracket, giving

$$\langle a_{j'} | \hat{A} | a_j \rangle = A_j \langle a_{j'} | a_j \rangle. \quad (4.71)$$

This equality has to hold for any pair of eigenstates, so that we may swap the indices in Eq. (71), and write the complex-conjugate of the result:

$$\langle a_j | \hat{A} | a_{j'} \rangle^* = A_{j'}^* \langle a_j | a_{j'} \rangle^*. \quad (4.72)$$

Now using Eqs. (14) and (25), together with the Hermitian operator's definition (22), we may transform Eq. (72) into the following form:

$$\langle a_{j'} | \hat{A} | a_j \rangle = A_{j'}^* \langle a_{j'} | a_j \rangle. \quad (4.73)$$

Subtracting this equation from Eq. (71), we get

$$0 = (A_j - A_{j'}^*) \langle a_{j'} | a_j \rangle. \quad (4.74)$$

There are two possibilities to satisfy this relation. If the indices j and j' are equal (denote the same eigenstate), then the bracket is the state's norm squared, and cannot be equal to zero. In this case, the left parentheses (with $j = j'$) have to be zero, proving Eq. (69). On the other hand, if j and j' correspond to different eigenvalues of A , the parentheses cannot equal zero (we have just proved that all A_j are real!), and hence the state vectors indexed by j and j' should be orthogonal, e.g., Eq. (70) is valid.

As will be discussed below, these properties make Hermitian operators suitable, in particular, for the description of physical observables.

Operator:
eigenstates
and
eigenvalues

Hermitian
operator:
eigenvalues

Hermitian
operator:
eigenvectors

¹⁴ This equation should look familiar to the reader – see the stationary Schrödinger equation (1.60), which was the focus of our studies in the first three chapters. We will see soon that that equation is just a particular (coordinate) representation of Eq. (68) for the Hamiltonian as the operator of energy.

¹⁵ The reciprocal statement is also true: if all eigenvalues of an operator are real, it is Hermitian (in any basis). This statement may be readily proved by applying Eq. (93) below to the case when $A_{kk'} = A_k \delta_{kk'}$, with $A_k^* = A_k$.

4.4. Change of basis, and matrix diagonalization

From the discussion of the last section, it may look that the matrix language is fully similar to, and in many instances more convenient than the general bra-ket formalism. In particular, Eqs. (54)-(55) and (63)-(64) show that any part of any bra-ket expression may be directly mapped on the similar matrix expression, with the only slight inconvenience of using not only columns but also rows (with their elements complex-conjugated), for state vector representation. This invites the question: why do we need the bra-ket language at all? The answer is that the elements of the matrices depend on the particular choice of the basis set, very much like the Cartesian components of a usual geometric vector depend on the particular choice of reference frame orientation (Fig. 4), and very frequently, at problem solution, it is convenient to use two or more different basis sets for the same system. (Just a bit more patience – numerous examples will follow soon.)

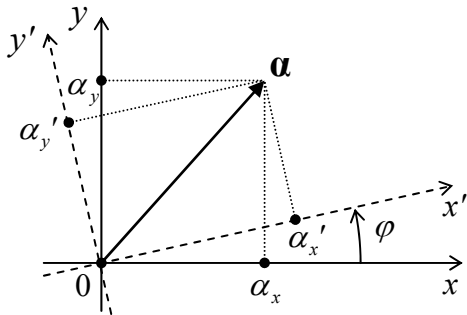


Fig. 4.4. The transformation of components of a 2D vector at a reference frame's rotation.

With this motivation, let us explore what happens at the transform from one basis, $\{u\}$, to another one, $\{v\}$ – both full and orthonormal. First of all, let us prove that for each such pair of bases, and an arbitrary numbering of the states of each base, there exists such an operator \hat{U} that, first,

$$|v_j\rangle = \hat{U}|u_j\rangle, \quad (4.75)$$

and, second,

$$\hat{U}\hat{U}^\dagger = \hat{U}^\dagger\hat{U} = \hat{I}. \quad (4.76)$$

(Due to the last property,¹⁶ \hat{U} is called a *unitary operator*, and Eq. (75), a *unitary transformation*.)

A very simple proof of both statements may be achieved by construction. Indeed, let us take

$$\hat{U} \equiv \sum_{j'} |v_{j'}\rangle \langle u_{j'}|, \quad (4.77)$$

- an evident generalization of Eq. (44). Then, using Eq. (38), we obtain

$$\hat{U}|u_j\rangle = \sum_{j'} |v_{j'}\rangle \langle u_{j'}|u_j\rangle = \sum_{j'} |v_{j'}\rangle \delta_{jj'} = |v_j\rangle, \quad (4.78)$$

so that Eq. (75) has been proved. Now, applying Eq. (31) to each term of the sum (77), we get

$$\hat{U}^\dagger \equiv \sum_{j'} |u_{j'}\rangle \langle v_{j'}|, \quad (4.79)$$

¹⁶ An alternative way to express Eq. (76) is to write $\hat{U}^\dagger = \hat{U}^{-1}$, but I will try to avoid this language.

so that

$$\hat{U}\hat{U}^\dagger = \sum_{j,j'} |v_j\rangle\langle u_j|u_{j'}\rangle\langle v_{j'}| = \sum_{j,j'} |v_j\rangle\delta_{jj'}\langle v_{j'}| = \sum_j |v_j\rangle\langle v_j|. \quad (4.80)$$

But according to the closure relation (44), the last expression is just the identity operator, so that one of Eqs. (76) has been proved. (The proof of the second equality is absolutely similar.) As a by-product of our proof, we have also got another important expression – Eq. (79). It implies, in particular, that while, according to Eq. (75), the operator \hat{U} performs the transform from the “old” basis u_j to the “new” basis v_j , its Hermitian adjoint \hat{U}^\dagger performs the reciprocal transform:

$$\hat{U}^\dagger |v_j\rangle = \sum_{j'} |u_{j'}\rangle\delta_{jj'} = |u_j\rangle. \quad (4.81)$$

Reciprocal basis transform

Now let us see how do the matrix elements of the unitary transform operators look like. Generally, as was discussed above, the operator’s elements may depend on the basis we calculate them in, so let us be specific – at least initially. For example, let us calculate the desired matrix elements $U_{jj'}$ in the “old” basis $\{u\}$, using Eq. (77):

$$U_{jj'}|_{in\ u} \equiv \langle u_j | \hat{U} | u_{j'} \rangle = \langle u_j | \left(\sum_{j''} |v_{j''}\rangle\langle u_{j''}| \right) | u_{j'} \rangle = \langle u_j | \sum_{j''} |v_{j''}\rangle\delta_{j''j'} = \langle u_j | v_{j'} \rangle. \quad (4.82)$$

Now performing a similar calculation in the “new” basis $\{v\}$, we get

$$U_{jj'}|_{in\ v} \equiv \langle v_j | \hat{U} | v_{j'} \rangle = \langle v_j | \left(\sum_{j''} |v_{j''}\rangle\langle u_{j''}| \right) | v_{j'} \rangle = \sum_{j''} \delta_{jj''} \langle u_{j''} | v_{j'} \rangle = \langle u_j | v_{j'} \rangle. \quad (4.83)$$

Surprisingly, the result is the same! This is of course true for the Hermitian conjugate (79) as well:

$$U_{jj'}^\dagger|_{in\ u} = U_{jj'}^\dagger|_{in\ v} = \langle v_j | u_{j'} \rangle. \quad (4.84)$$

These expressions may be used, first of all, to rewrite Eq. (75) in a more direct form. Applying the first of Eqs. (41) to any state $v_{j'}$ of the “new” basis, and then Eq. (82), we get

$$|v_{j'}\rangle = \sum_j |u_j\rangle\langle u_j|v_{j'}\rangle = \sum_j U_{jj'}|u_j\rangle. \quad (4.85)$$

Basis transforms: matrix form

Similarly, the reciprocal transform is

$$|u_{j'}\rangle = \sum_j |v_j\rangle\langle v_j|u_{j'}\rangle = \sum_j U_{jj'}^\dagger|v_j\rangle. \quad (4.86)$$

These formulas are very convenient for applications; we will use them already in this section.

Next, we may use Eqs. (83)-(84) to express the effect of the unitary transform on the expansion coefficients α_j of the vectors of an *arbitrary* state α , defined by Eq. (37). As a reminder, in the “old” basis $\{u\}$ they are given by Eqs. (40). Similarly, in the “new” basis $\{v\}$,

$$\alpha_j|_{in\ v} = \langle v_j | \alpha \rangle. \quad (4.87)$$

Again inserting the identity operator in its closure form (44) with the internal index j' , and then using Eqs. (84) and (40), we get

$$\alpha_j|_{\text{in } v} = \left\langle v_j \left| \left(\sum_{j'} |u_{j'}\rangle \langle u_{j'}| \right) \right| \alpha \right\rangle = \sum_{j'} \langle v_j | u_{j'} \rangle \langle u_{j'} | \alpha \rangle = \sum_{j'} U_{jj'}^\dagger \langle u_{j'} | \alpha \rangle = \sum_{j'} U_{jj'}^\dagger \alpha_{j'}|_{\text{in } u}. \quad (4.88)$$

The reciprocal transform is performed by matrix elements of the operator \hat{U} :

$$\alpha_j|_{\text{in } u} = \sum_{j'} U_{jj'} \alpha_{j'}|_{\text{in } v}. \quad (4.89)$$

So, if the transform (75) from the “old” basis $\{u\}$ to the “new” basis $\{v\}$ is performed by a unitary operator, the change (88) of state vectors components at this transformation requires its Hermitian conjugate. This fact is similar to the transformation of components of a usual vector at coordinate frame rotation. For example, for a 2D vector whose actual position in space is fixed (Fig. 4):

$$\begin{pmatrix} \alpha_x' \\ \alpha_y' \end{pmatrix} = \begin{pmatrix} \cos \varphi & \sin \varphi \\ -\sin \varphi & \cos \varphi \end{pmatrix} \begin{pmatrix} \alpha_x \\ \alpha_y \end{pmatrix}, \quad (4.90)$$

but the reciprocal transform is performed by a different matrix, which may be obtained from that participating in Eq. (90) by the replacement $\varphi \rightarrow -\varphi$. This replacement has a clear geometric sense: if the “new” reference frame $\{x', y'\}$ is obtained from the “old” frame $\{x, y\}$ by a *councclockwise* rotation by angle φ , the reciprocal transformation requires angle $-\varphi$. (In this analogy, the unitary property (76) of the unitary transform operators corresponds to the equality of the determinants of both rotation matrices to 1.)

Due to the analogy between expressions (88) and (89) on one hand, and our old friend Eq. (62) on the other hand, it is tempting to skip indices in these new results by writing

$$|\alpha\rangle_{\text{in } v} = \hat{U}^\dagger |\alpha\rangle_{\text{in } u}, \quad |\alpha\rangle_{\text{in } u} = \hat{U} |\alpha\rangle_{\text{in } v}. \quad (\text{SYMBOLIC ONLY!}) \quad (4.91)$$

Since the matrix elements of \hat{U} and \hat{U}^\dagger do not depend on the basis, such language is not too bad and is mnemonically useful. However, since in the bra-ket formalism (or at least its version presented in this course), the state vectors are basis-independent, Eq. (91) has to be treated as a symbolic one, and should not be confused with the strict Eqs. (88)-(89), and with the rigorous basis-independent vector and operator equalities discussed in Sec. 2.

Now let us use the same trick of identity operator insertion, repeated twice, to find the transformation rule for matrix elements of an arbitrary operator:

$$A_{jj'}|_{\text{in } v} \equiv \langle v_j | \hat{A} | v_{j'} \rangle = \left\langle v_j \left| \left(\sum_k |u_k\rangle \langle u_k| \right) \hat{A} \left(\sum_{k'} |u_{k'}\rangle \langle u_{k'}| \right) \right| v_{j'} \right\rangle = \sum_{k,k'} U_{jk}^\dagger A_{kk'}|_{\text{in } u} U_{kj'}; \quad (4.92)$$

Matrix
elements'
transforms

absolutely similarly, we may also get

$$A_{jj'}|_{\text{in } u} \equiv \sum_{k,k'} U_{jk} A_{kk'}|_{\text{in } v} U_{kj'}^\dagger. \quad (4.93)$$

In the spirit of Eq. (91), we may represent these results symbolically as well, in a compact form:

$$\hat{A}|_{\text{in } v} = \hat{U}^\dagger \hat{A}|_{\text{in } u} \hat{U}, \quad \hat{A}|_{\text{in } u} = \hat{U} \hat{A}|_{\text{in } v} \hat{U}^\dagger. \quad (\text{SYMBOLIC ONLY!}) \quad (4.94)$$

As a sanity check, let us apply Eq. (93) to the identity operator:

$$\hat{I}|_{\text{in } v} = \left(\hat{U}^\dagger \hat{I} \hat{U} \right)_{\text{in } u} = \left(\hat{U}^\dagger \hat{U} \right)_{\text{in } u} = \hat{I}|_{\text{in } u} \quad (4.95)$$

- as it should be. One more (strict rather than symbolic) invariant of the basis change is the *trace* of any operator, defined as the sum of the diagonal terms of its matrix:

$$\text{Tr } \hat{A} \equiv \text{Tr } A \equiv \sum_j A_{jj}. \quad (4.96)$$

Operator's/
matrix'
trace

The (easy) proof of this fact, using previous relations, is left for the reader's exercise.

So far, I have implied that both state bases $\{u\}$ and $\{v\}$ are known, and the natural question is where does this information come from in quantum mechanics of actual physical systems. To get a partial answer to this question, let us return to Eq. (68), which defines the eigenstates and the eigenvalues of an operator. Let us assume that the eigenstates a_j of a certain operator \hat{A} form a full and orthonormal set, and calculate the matrix elements of the operator in the basis $\{a\}$ of these states, at their arbitrary numbering. For that, it is sufficient to inner-multiply both sides of Eq. (68), written for some index j' , by the bra-vector of an arbitrary state $a_{j'}$ of the same set:

$$\langle a_j | \hat{A} | a_{j'} \rangle = \langle a_j | A_{j'} | a_{j'} \rangle. \quad (4.97)$$

The left-hand side of this equality is the matrix element $A_{jj'}$ we are looking for, while its right-hand side is just $A_j \delta_{jj'}$. As a result, we see that the matrix is diagonal, with the diagonal consisting of the operator's eigenvalues:

$$A_{jj'} = A_j \delta_{jj'}. \quad (4.98)$$

Matrix
elements in
eigenstate
basis

In particular, in the eigenstate basis (but not necessarily in an arbitrary basis!), A_{jj} means the same as A_j . Thus the important problem of finding the eigenvalues and eigenstates of an operator is equivalent to the *diagonalization* of its matrix,¹⁷ i.e. finding the basis in which the operator's matrix acquires the diagonal form (98); then the diagonal elements are the eigenvalues, and the basis itself is the desirable set of eigenstates.

To see how this is done in practice, let us inner-multiply Eq. (68) by a bra-vector of the basis (say, $\{u\}$) in that we have happened to know the matrix elements A_{jj} :

$$\langle u_k | \hat{A} | a_j \rangle = \langle u_k | A_j | a_j \rangle. \quad (4.99)$$

On the left-hand side, we can (as usual :-) insert the identity operator between the operator \hat{A} and the ket-vector, and then use the closure relation (44) in the same basis $\{u\}$, while on the right-hand side, we can move the eigenvalue A_j (a *c*-number) out of the bracket, and then insert a summation over the same index as in the closure, compensating it with the proper Kronecker delta symbol:

$$\langle u_k | \hat{A} \sum_{k'} | u_{k'} \rangle \langle u_{k'} | a_j \rangle = A_j \sum_{k'} \langle u_{k'} | a_j \rangle \delta_{kk'}. \quad (4.100)$$

Moving out the signs of summation over k' , and using the definition (47) of the matrix elements, we get

¹⁷ Note that the expression "matrix diagonalization" is a very common but dangerous jargon. (Formally, a matrix is just a matrix, an ordered set of *c*-numbers, and cannot be "diagonalized".) It is OK to use this jargon if you remember clearly what it actually means – see the definition above.

$$\sum_{k'} (A_{kk'} - A_j \delta_{kk'}) \langle u_{k'} | a_j \rangle = 0. \quad (4.101)$$

But the set of such equalities, for all N possible values of the index k , is just a system of linear, homogeneous equations for unknown c -numbers $\langle u_k | a_j \rangle$. According to Eqs. (82)-(84), these numbers are nothing else than the matrix elements U_{kj} of a unitary matrix providing the required transformation from the initial basis $\{u\}$ to the basis $\{a\}$ that diagonalizes the matrix A . This system may be represented in the matrix form:

Matrix diagonalization

$$\begin{pmatrix} A_{11} - A_j & A_{12} & \dots \\ A_{21} & A_{22} - A_j & \dots \\ \dots & \dots & \dots \end{pmatrix} \begin{pmatrix} U_{1j} \\ U_{2j} \\ \dots \end{pmatrix} = 0, \quad (4.102)$$

and the condition of its consistency,

Characteristic equation for eigenvalues

$$\begin{vmatrix} A_{11} - A_j & A_{12} & \dots \\ A_{21} & A_{22} - A_j & \dots \\ \dots & \dots & \dots \end{vmatrix} = 0, \quad (4.103)$$

plays the role of the characteristic equation of the system. This equation has N roots A_j – the eigenvalues of the operator \hat{A} ; after they have been calculated, plugging any of them back into the system (102), we can use it to find N matrix elements U_{kj} ($k = 1, 2, \dots, N$) corresponding to this particular eigenvalue. However, since the equations (103) are homogeneous, they allow finding U_{kj} only to a constant multiplier. To ensure their normalization, i.e. enforce the unitary character of the matrix U , we may use the condition that all eigenvectors are normalized (just as the basis vectors are):

$$\langle a_j | a_j \rangle \equiv \sum_k \langle a_j | u_k \rangle \langle u_k | a_j \rangle \equiv \sum_k |U_{kj}|^2 = 1, \quad (4.104)$$

for each j . This normalization completes the diagonalization.¹⁸

Now (at last!) I can give the reader some examples. As a simple but very important case, let us diagonalize each of the operators described (in a certain two-function basis $\{u\}$, i.e. in two-dimensional Hilbert space) by the so-called *Pauli matrices*

Pauli matrices

$$\sigma_x \equiv \begin{pmatrix} 0 & 1 \\ 1 & 0 \end{pmatrix}, \quad \sigma_y \equiv \begin{pmatrix} 0 & -i \\ i & 0 \end{pmatrix}, \quad \sigma_z \equiv \begin{pmatrix} 1 & 0 \\ 0 & -1 \end{pmatrix}. \quad (4.105)$$

Though introduced by a physicist, with a specific purpose to describe electron's spin, these matrices have a general mathematical significance, because together with the 2×2 identity matrix, they provide a full, linearly-independent system – meaning that an arbitrary 2×2 matrix may be represented as

$$\begin{pmatrix} A_{11} & A_{12} \\ A_{21} & A_{22} \end{pmatrix} = bI + c_x \sigma_x + c_y \sigma_y + c_z \sigma_z, \quad (4.106)$$

¹⁸ A possible slight complication here is that the characteristic equation may give equal eigenvalues for certain groups of different eigenvectors. In such cases, the requirement of the mutual orthogonality of these *degenerate states* should be additionally enforced.

with a unique set of four *c*-number coefficients b , c_x , c_y , and c_z .

Since the matrix σ_z is already diagonal, with the evident eigenvalues ± 1 , let us start with diagonalizing the matrix σ_x . For it, the characteristic equation (103) is evidently

$$\begin{vmatrix} -A_j & 1 \\ 1 & -A_j \end{vmatrix} = 0, \quad \text{i.e. } A_j^2 - 1 = 0, \quad (4.107)$$

and has two roots, $A_{1,2} = \pm 1$. (Again, the state numbering is arbitrary!) So the eigenvalues of the matrix σ_x are the same as of the matrix σ_z . (The reader may readily check that the eigenvalues of the matrix σ_y are also the same.) However, the eigenvectors of the operators corresponding to these three matrices are different. To find them for σ_x , let us plug its first eigenvalue, $A_1 = +1$, back into equations (101) spelled out for this particular case ($j = 1$; $k, k' = 1, 2$):

$$\begin{aligned} -\langle u_1 | a_1 \rangle + \langle u_2 | a_1 \rangle &= 0, \\ \langle u_1 | a_1 \rangle - \langle u_2 | a_1 \rangle &= 0. \end{aligned} \quad (4.108)$$

These two equations are compatible (of course, because the used eigenvalue $A_1 = +1$ satisfies the characteristic equation), and any of them gives

$$\langle u_1 | a_1 \rangle = \langle u_2 | a_1 \rangle, \quad \text{i.e. } U_{11} = U_{21}. \quad (4.109)$$

With that, the normalization condition (104) yields

$$|U_{11}|^2 = |U_{21}|^2 = \frac{1}{2}. \quad (4.110)$$

Although the normalization is insensitive to the simultaneous multiplication of U_{11} and U_{21} by the same phase factor $\exp\{i\varphi\}$ with any real φ , it is convenient to keep the coefficients real, for example taking $\varphi = 0$, to get

$$U_{11} = U_{21} = \frac{1}{\sqrt{2}}. \quad (4.111)$$

Performing an absolutely similar calculation for the second characteristic value, $A_2 = -1$, we get $U_{12} = -U_{22}$, and we may choose the common phase to have

$$U_{12} = -U_{22} = \frac{1}{\sqrt{2}}, \quad (4.112)$$

so that the whole unitary matrix for diagonalization of the operator corresponding to σ_x is¹⁹

$$U_x = U_x^\dagger = \frac{1}{\sqrt{2}} \begin{pmatrix} 1 & 1 \\ 1 & -1 \end{pmatrix},$$

(4.113)

Unitary matrix
diagonalizing
 σ_x

For what follows, it will be convenient to have this result expressed in the ket-relation form – see Eqs. (85)-(86):

$$|a_1\rangle = U_{11}|u_1\rangle + U_{21}|u_2\rangle = \frac{1}{\sqrt{2}}(|u_1\rangle + |u_2\rangle), \quad |a_2\rangle = U_{12}|u_1\rangle + U_{22}|u_2\rangle = \frac{1}{\sqrt{2}}(|u_1\rangle - |u_2\rangle), \quad (4.114a)$$

¹⁹ Note that though this particular unitary matrix is Hermitian, this is not true for an arbitrary choice of phases φ .

$$|u_1\rangle = U_{11}^\dagger |a_1\rangle + U_{21}^\dagger |a_2\rangle = \frac{1}{\sqrt{2}}(|a_1\rangle + |a_2\rangle), \quad |u_2\rangle = U_{12}^\dagger |a_1\rangle + U_{22}^\dagger |a_2\rangle = \frac{1}{\sqrt{2}}(|a_1\rangle - |a_2\rangle) \quad (4.114b)$$

Now let me show that these results are already sufficient to understand the Stern-Gerlach experiments described in Sec. 1 – but with two additional postulates. The first of them is that the interaction of a particle with the external magnetic field, besides that due to its orbital motion, may be described by the following *vector operator* of its spin dipole magnetic moment:²⁰

Spin
magnetic
moment

$$\hat{\mathbf{m}} = \gamma \hat{\mathbf{S}}, \quad (4.115a)$$

where the constant coefficient γ , specific for every particle type, is called the *gyromagnetic ratio*,²¹ and $\hat{\mathbf{S}}$ is the *vector operator of spin*, with three Cartesian components:

$$\hat{\mathbf{S}} = \mathbf{n}_x \hat{S}_x + \mathbf{n}_y \hat{S}_y + \mathbf{n}_z \hat{S}_z. \quad (4.115b)$$

Spin
vector
operator

Here $\mathbf{n}_{x,y,z}$ are the usual Cartesian unit vectors in the 3D geometric space (in the quantum-mechanics sense, just *c*-numbers, or rather “*c*-vectors”), while $\hat{S}_{x,y,z}$ are the “usual” (scalar) operators.

For the so-called *spin-½ particles* (including the electron), these components may be simply, as

$$\hat{S}_{x,y,z} = \frac{\hbar}{2} \hat{\sigma}_{x,y,z}, \quad (4.116a)$$

Spin-½
operator

expressed via those of the *Pauli vector operator* $\hat{\boldsymbol{\sigma}} \equiv \mathbf{n}_x \hat{\sigma}_x + \mathbf{n}_y \hat{\sigma}_y + \mathbf{n}_z \hat{\sigma}_z$, so that we may also write

$$\hat{\mathbf{S}} = \frac{\hbar}{2} \hat{\boldsymbol{\sigma}}. \quad (4.116b)$$

In turn, in the so-called *z-basis*, each Cartesian component of the latter operator is just the corresponding Pauli matrix (105), so that it may be also convenient to use the following 3D vector of these matrices:

Pauli
matrix
vector

$$\boldsymbol{\sigma} \equiv \mathbf{n}_x \sigma_x + \mathbf{n}_y \sigma_y + \mathbf{n}_z \sigma_z \equiv \begin{pmatrix} \mathbf{n}_z & \mathbf{n}_x - i\mathbf{n}_y \\ \mathbf{n}_x + i\mathbf{n}_y & -\mathbf{n}_z \end{pmatrix}. \quad (4.117)$$

The *z-basis*, in which such matrix representation of $\hat{\boldsymbol{\sigma}}$ is valid, is *defined* as an orthonormal basis of certain two states, commonly denoted \uparrow an \downarrow , in that the matrix of the operator $\hat{\sigma}_z$ is diagonal, with eigenvalues, respectively, $+1$ and -1 , and hence the matrix $S_z \equiv (\hbar/2)\sigma_z$ of \hat{S}_z is also diagonal, with the eigenvalues $+\hbar/2$ and $-\hbar/2$. Note that we do not “understand” what exactly the states \uparrow and \downarrow are,²² but

²⁰ This was the key point in the electron spin’s description, developed by W. Pauli in 1925-1927.

²¹ For the electron, with its negative charge $q = -e$, the gyromagnetic ratio is negative: $\gamma_e = -g_e e/2m_e$, where $g_e \approx 2$ is the dimensionless *g-factor*. Due to quantum-electrodynamic (relativistic) effects, this *g*-factor is slightly higher than 2: $g_e = 2(1 + \alpha/2\pi + \dots) \approx 2.002319304\dots$, where $\alpha \equiv e^2/4\pi\epsilon_0\hbar c \equiv (E_H/m_e c^2)^{1/2} \approx 1/137$ is the so-called *fine structure constant*. (The origin of its name will be clear from the discussion in Sec. 6.3.)

²² If you think about it, the word “understand” typically means that we can express a new, more complex notion in terms of those discussed earlier and considered “known”. In our current case, we cannot describe the spin states by some wavefunction $\psi(\mathbf{r})$, or any other mathematical notion discussed in the previous three chapters. The bracket formalism has been invented exactly to enable mathematical analyses of such “new” quantum states we do not

loosely associate them with some internal rotation of a spin- $\frac{1}{2}$ particle about the z -axis, with either positive or negative angular momentum component S_z . However, attempts to use such classical interpretation for quantitative predictions runs into fundamental difficulties – see Sec. 6 below.

The second necessary postulate describes the general relation between the bra-ket formalism and experiment. Namely, in quantum mechanics, each real observable A is represented by a Hermitian operator $\hat{A} = \hat{A}^\dagger$, and the result of its measurement,²³ in a quantum state α described by a linear superposition of the eigenstates a_j of the operator,

$$|\alpha\rangle = \sum_j \alpha_j |a_j\rangle, \quad \text{with } \alpha_j = \langle a_j | \alpha \rangle, \quad (4.118)$$

may be only one of the corresponding eigenvalues A_j .²⁴ Specifically, if the ket (118) and all eigenkets $|a_j\rangle$ are normalized to 1,

$$\langle \alpha | \alpha \rangle = 1, \quad \langle a_j | a_j \rangle = 1, \quad (4.119)$$

then the probability of a certain measurement outcome A_j is²⁵

$$W_j = |\alpha_j|^2 \equiv \alpha_j^* \alpha_j \equiv \langle \alpha | a_j \rangle \langle a_j | \alpha \rangle,$$

(4.120)

Quantum measurement postulate

This relation is evidently a generalization of Eq. (1.22) in wave mechanics. As a sanity check, let us assume that the set of the eigenstates a_j is full, and calculate the sum of the probabilities to find the system in one of these states:

$$\sum_j W_j = \sum_j \langle \alpha | a_j \rangle \langle a_j | \alpha \rangle = \langle \alpha | \hat{I} | \alpha \rangle = 1. \quad (4.121)$$

Now returning to the Stern-Gerlach experiment, conceptually the description of the first (z -oriented) experiment shown in Fig. 1 is the hardest for us, because the statistical ensemble describing the unpolarized electron beam at its input is *mixed* (“incoherent”), and cannot be described by a *pure* (“coherent”) superposition of the type (6) that have been the subject of our studies so far. (We will discuss such mixed ensembles in Chapter 7.) However, it is intuitively clear that its results are compatible with the description of the two output beams as sets of electrons in the pure states \uparrow and \downarrow , respectively. The absorber following that first stage (Fig. 2) just takes all spin-down electrons out of the picture, producing an output beam of polarized electrons in the definite \uparrow state. For such a beam, the probabilities (120) are $W_\uparrow = 1$ and $W_\downarrow = 0$. This is certainly compatible with the result of the “control” experiment shown on the bottom panel of Fig. 2: the repeated SG (z) stage does not split such a beam, keeping the probabilities the same.

initially “understand”. Gradually we get *accustomed* to these notions, and eventually, as we know more and more about their properties, start treating them as “known” ones.

²³ Here again, just like in Sec. 1.2, the statement implies the abstract notion of “ideal experiments”, deferring the discussion of real (physical) measurements until Chapter 10.

²⁴ As a reminder, at the end of Sec. 3 we have already proved that such eigenstates corresponding to different values A_j are orthogonal. If any of these values is degenerate, i.e. corresponds to several different eigenstates, they should be also selected orthogonal, in order for Eq. (118) to be valid.

²⁵ This key relation, in particular, explains the most common term for the (generally, complex) coefficients α_j , the *probability amplitudes*.

Now let us discuss the double Stern-Gerlach experiment shown on the top panel of Fig. 2. For that, let us represent the z -polarized beam in another basis – of the two states (I will denote them as \rightarrow and \leftarrow) in that, by definition, the matrix S_x is diagonal. But this is exactly the set we called $a_{1,2}$ in the σ_x matrix diagonalization problem solved above. On the other hand, the states \uparrow and \downarrow are exactly what we called $u_{1,2}$ in that problem, because in this basis, we know matrix σ explicitly – see Eq. (117). Hence, in the application to the electron spin problem, we may rewrite Eqs. (114) as

$$|\rightarrow\rangle = \frac{1}{\sqrt{2}}(|\uparrow\rangle + |\downarrow\rangle), \quad |\leftarrow\rangle = \frac{1}{\sqrt{2}}(|\uparrow\rangle - |\downarrow\rangle), \quad (4.122)$$

$$|\uparrow\rangle = \frac{1}{\sqrt{2}}(|\rightarrow\rangle + |\leftarrow\rangle), \quad |\downarrow\rangle = \frac{1}{\sqrt{2}}(|\rightarrow\rangle - |\leftarrow\rangle), \quad (4.123)$$

Relation between eigenvectors of S_x and S_z

Currently for us the first of Eqs. (123) is most important, because it shows that the quantum state of electrons entering the SG (x) stage may be represented as a coherent superposition of electrons with $S_x = +\hbar/2$ and $S_x = -\hbar/2$. Notice that the beams have equal probability amplitude moduli, so that according to Eq. (122), the split beams \rightarrow and \leftarrow have equal intensities, in accordance with experimental results. (The minus sign before the second ket-vector is of no consequence here, but it may have an impact on outcomes of other experiments – for example, if coherently split beams are brought together again.)

Now, let us discuss the most mysterious (from the classical point of view) multi-stage SG experiment shown on the middle panel of Fig. 2. After the second absorber has taken out all electrons in, say, the \leftarrow state, the remaining electrons, all in the state \rightarrow , are passed to the final, SG (z), stage. But according to the first of Eqs. (122), this state may be represented as a (coherent) linear superposition of the \uparrow and \downarrow states, with equal probability amplitudes. The final stage separates electrons in these two states into separate beams, with equal probabilities $W_\uparrow = W_\downarrow = \frac{1}{2}$ to find an electron in each of them, thus explaining the experimental results.

To conclude our discussion of the multistage Stern-Gerlach experiment, let me note that though it cannot be explained in terms of wave mechanics (which operates with *scalar* de Broglie waves), it has an analogy in classical theories of *vector* fields, such as the classical electrodynamics. Indeed, let a plane electromagnetic wave propagate normally to the plane of the drawing in Fig. 5, and pass through the linear polarizer 1.

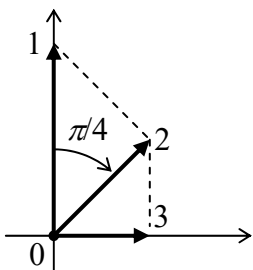


Fig. 4.5. A light polarization sequence similar to the three-stage Stern-Gerlach experiment shown on the middle panel of Fig. 2.

Similarly to the output of the initial SG (z) stages (including the absorbers) shown in Fig. 2, the output wave is linearly polarized in one direction – the vertical direction in Fig. 5. Now its electric field vector has no horizontal component – as may be revealed by the wave's full absorption in a perpendicular polarizer 3. However, let us pass the wave through polarizer 2 first. In this case, the

output wave does acquire a horizontal component, as can be, again, revealed by passing it through polarizer 3. If the angles between the polarization directions 1 and 2, and between 2 and 3, are both equal to $\pi/4$, each polarizer reduces the wave amplitude by a factor of $\sqrt{2}$, and hence the intensity by a factor of 2, exactly like in the multistage SG experiment, with the polarizer 2 playing the role of the SG (x) stage. The “only” difference is that the necessary angle is $\pi/4$, rather than by $\pi/2$ for the Stern-Gerlach experiment. In quantum electrodynamics (see Chapter 9 below), which confirms classical predictions for this experiment, this difference may be interpreted by that between the *integer* spin of electromagnetic field quanta (photons) and the *half-integer* spin of electrons.

4.5. Observables: Expectation values and uncertainties

After this particular (and hopefully inspiring) example, let us discuss the general relation between the Dirac formalism and experiment in more detail. The expectation value of an observable over *any* statistical ensemble (not necessarily coherent) may be always calculated using the general statistical rule (1.37). For the particular case of a coherent superposition (118), we can combine that rule with Eq. (120) and the second of Eqs. (118):

$$\langle A \rangle = \sum_j A_j W_j = \sum_j \alpha_j^* A_j \alpha_j = \sum_j \langle \alpha | a_j \rangle A_j \langle a_j | \alpha \rangle \equiv \langle \alpha | \left(\sum_j |a_j \rangle A_j \langle a_j| \right) | \alpha \rangle. \quad (4.124)$$

Now using Eq. (59) for the particular case of the eigenstate basis $\{a\}$, for which Eq. (98) is valid, we arrive at a very simple and important formula²⁶

$$\langle A \rangle = \langle \alpha | \hat{A} | \alpha \rangle. \quad (4.125)$$

Expectation
value
as a long
bracket

This is a clear analog of the wave-mechanics formula (1.23) – and as we will see soon, may be used to derive it. A big advantage of Eq. (125) is that it does not explicitly involve the eigenvector set of the corresponding operator, and allows the calculation to be performed in any convenient basis.²⁷

For example, let us consider an arbitrary coherent state α of spin- $1/2$,²⁸ and calculate the expectation values of its components. The calculations are easiest in the z -basis because we know the matrix elements of the spin operator components in that basis. Representing the ket- and bra-vectors of the given state as linear superpositions of the corresponding vectors of the basis states \uparrow and \downarrow ,

$$|\alpha\rangle = \alpha_{\uparrow} |\uparrow\rangle + \alpha_{\downarrow} |\downarrow\rangle, \quad \langle \alpha | = \langle \uparrow | \alpha_{\uparrow}^* + \langle \downarrow | \alpha_{\downarrow}^*. \quad (4.126)$$

and plugging these expressions to Eq. (125) written for the observable S_z , we get

²⁶ This equality reveals the full beauty of Dirac’s notation. Indeed, initially in this chapter the quantum-mechanical brackets just *reminded* the angular brackets used for the statistical averaging. Now we see that in this particular (but most important) case, the angular brackets of these two types may be indeed *equal* to each other!

²⁷ Note also that Eq. (120) may be rewritten in a form similar to Eq. (125): $W_j = \langle \alpha | \hat{\Lambda}_j | \alpha \rangle$, where $\hat{\Lambda}_j$ is the operator (42) of the state’s projection upon the j^{th} eigenstate a_j .

²⁸ For clarity, the noun “spin- $1/2$ ” is used, here and below, to denote the spin degree of freedom of a spin- $1/2$ particle, independent of its orbital motion.

$$\begin{aligned}\langle S_z \rangle &= \left(\langle \uparrow | \alpha_{\uparrow}^* + \langle \downarrow | \alpha_{\downarrow}^* \right) \hat{S}_z \left(\alpha_{\uparrow} | \uparrow \rangle + \alpha_{\downarrow} | \downarrow \rangle \right) \\ &= \alpha_{\uparrow} \alpha_{\uparrow}^* \langle \uparrow | \hat{S}_z | \uparrow \rangle + \alpha_{\downarrow} \alpha_{\downarrow}^* \langle \downarrow | \hat{S}_z | \downarrow \rangle + \alpha_{\uparrow} \alpha_{\downarrow}^* \langle \downarrow | \hat{S}_z | \uparrow \rangle + \alpha_{\downarrow} \alpha_{\uparrow}^* \langle \uparrow | \hat{S}_z | \downarrow \rangle.\end{aligned}\quad (4.127)$$

Now there are two equivalent ways (both very simple) to calculate the long brackets in this expression. The first one is to represent each of them in the matrix form in the z -basis, in which the bra- and ket-vectors of states \uparrow and \downarrow are the matrix-rows $(1, 0)$ and $(0, 1)$, or similar matrix-columns – the exercise highly recommended to the reader. Another (perhaps more elegant) way is to use the general Eq. (59), in the z -basis, together with the spin- $1/2$ -specific Eqs. (116a) and (105) to write

$$\hat{S}_x = \frac{\hbar}{2} (\langle \uparrow | \langle \downarrow | + \langle \downarrow | \langle \uparrow |), \quad \hat{S}_y = -i \frac{\hbar}{2} (\langle \uparrow | \langle \downarrow | - \langle \downarrow | \langle \uparrow |), \quad \hat{S}_z = \frac{\hbar}{2} (\langle \uparrow | \langle \uparrow | - \langle \downarrow | \langle \downarrow |). \quad (4.128)$$

For our particular calculation, we may plug the last of these expressions into Eq. (127), and use the orthonormality conditions (38):

$$\langle \uparrow | \uparrow \rangle = \langle \downarrow | \downarrow \rangle = 1, \quad \langle \uparrow | \downarrow \rangle = \langle \downarrow | \uparrow \rangle = 0. \quad (4.129)$$

Both approaches give (of course) the same result:

$$\langle S_z \rangle = \frac{\hbar}{2} \left(\alpha_{\uparrow} \alpha_{\uparrow}^* - \alpha_{\downarrow} \alpha_{\downarrow}^* \right). \quad (4.130)$$

This particular result might be also obtained using Eq. (120) for the probabilities $W_{\uparrow} = \alpha_{\uparrow} \alpha_{\uparrow}^*$ and $W_{\downarrow} = \alpha_{\downarrow} \alpha_{\downarrow}^*$, namely:

$$\langle S_z \rangle = W_{\uparrow} \left(+ \frac{\hbar}{2} \right) + W_{\downarrow} \left(- \frac{\hbar}{2} \right) = \alpha_{\uparrow} \alpha_{\uparrow}^* \left(+ \frac{\hbar}{2} \right) + \alpha_{\downarrow} \alpha_{\downarrow}^* \left(- \frac{\hbar}{2} \right). \quad (4.131)$$

The formal way (127), based on using Eq. (125), has, however, an advantage of being applicable, without any change, to finding the observables whose operators are *not* diagonal in the z -basis, as well. In particular, absolutely similar calculations give

$$\langle S_x \rangle = \alpha_{\uparrow} \alpha_{\uparrow}^* \langle \uparrow | \hat{S}_x | \uparrow \rangle + \alpha_{\downarrow} \alpha_{\downarrow}^* \langle \downarrow | \hat{S}_x | \downarrow \rangle + \alpha_{\uparrow} \alpha_{\downarrow}^* \langle \downarrow | \hat{S}_x | \uparrow \rangle + \alpha_{\downarrow} \alpha_{\uparrow}^* \langle \uparrow | \hat{S}_x | \downarrow \rangle = \frac{\hbar}{2} \left(\alpha_{\uparrow} \alpha_{\downarrow}^* + \alpha_{\downarrow} \alpha_{\uparrow}^* \right), \quad (4.132)$$

$$\langle S_y \rangle = \alpha_{\uparrow} \alpha_{\uparrow}^* \langle \uparrow | \hat{S}_y | \uparrow \rangle + \alpha_{\downarrow} \alpha_{\downarrow}^* \langle \downarrow | \hat{S}_y | \downarrow \rangle + \alpha_{\uparrow} \alpha_{\downarrow}^* \langle \downarrow | \hat{S}_y | \uparrow \rangle + \alpha_{\downarrow} \alpha_{\uparrow}^* \langle \uparrow | \hat{S}_y | \downarrow \rangle = i \frac{\hbar}{2} \left(\alpha_{\uparrow} \alpha_{\downarrow}^* - \alpha_{\downarrow} \alpha_{\uparrow}^* \right), \quad (4.133)$$

Let us have a good look at a particular spin state, for example the spin-up state \uparrow . According to Eq. (126), in this state $\alpha_{\uparrow} = 1$ and $\alpha_{\downarrow} = 0$, so that Eqs. (130)-(133) yield:

$$\langle S_z \rangle = \frac{\hbar}{2}, \quad \langle S_x \rangle = \langle S_y \rangle = 0. \quad (4.134)$$

Now let us use the same Eq. (125) to calculate the spin component uncertainties. According to Eqs. (105) and (116)-(117), the operator of each spin component squared is equal to $(\hbar/2)^2 \hat{I}$, so that the general Eq. (1.33) yields

$$(\delta S_z)^2 = \langle S_z^2 \rangle - \langle S_z \rangle^2 = \langle \uparrow | \hat{S}_z^2 | \uparrow \rangle - \left(\frac{\hbar}{2} \right)^2 = \left(\frac{\hbar}{2} \right)^2 \langle \uparrow | \hat{I} | \uparrow \rangle - \left(\frac{\hbar}{2} \right)^2 = 0, \quad (4.135a)$$

$$(\delta S_x)^2 = \langle S_x^2 \rangle - \langle S_x \rangle^2 = \langle \uparrow | \hat{S}_x^2 | \uparrow \rangle - 0 = \left(\frac{\hbar}{2} \right)^2 \langle \uparrow | \hat{I} | \uparrow \rangle = \left(\frac{\hbar}{2} \right)^2, \quad (4.135b)$$

$$(\delta S_y)^2 = \langle S_y^2 \rangle - \langle S_y \rangle^2 = \langle \uparrow | \hat{S}_y^2 | \uparrow \rangle - 0 = \left(\frac{\hbar}{2} \right)^2 \langle \uparrow | \hat{I} | \uparrow \rangle = \left(\frac{\hbar}{2} \right)^2. \quad (4.135c)$$

While Eqs. (134) and (135a) are compatible with the classical notion of the angular momentum of magnitude $\hbar/2$ being directed exactly along the z -axis, this correspondence should not be overstretched, because such classical picture cannot explain Eqs. (135b) and (135c). The best (but still imprecise!) classical image I can offer is the spin vector \mathbf{S} oriented, on average, in the z -direction, but still having its x - and y -components strongly “wobbling” (fluctuating) about their zero average values.

It is straightforward to verify that in the x -polarized and y -polarized states the situation is similar, with the corresponding change of axis indices. Thus, in neither of these states all three spin components have definite values. Let me show that this is not just an occasional fact, but reflects the perhaps most profound property of quantum mechanics, the *uncertainty relations*. For that, let us consider two measurable observables, A and B , of the same quantum system. There are two possibilities here. If the operators corresponding to these observables commute,

$$[\hat{A}, \hat{B}] = 0, \quad (4.136)$$

then all matrix elements of the commutator in any orthogonal basis (in particular, in the basis of eigenstates a_j of the operator \hat{A}) have to equal zero:

$$\langle a_j | [\hat{A}, \hat{B}] | a_{j'} \rangle \equiv \langle a_j | \hat{A} \hat{B} | a_{j'} \rangle - \langle a_j | \hat{B} \hat{A} | a_{j'} \rangle = 0. \quad (4.137)$$

In the first bracket of the middle expression, let us act by the (Hermitian!) operator \hat{A} on the bra-vector, while in the second one, on the ket-vector. According to Eq. (68), such action turns the operators into the corresponding eigenvalues, which may be taken out of the long brackets, so that we get

$$A_j \langle a_j | \hat{B} | a_{j'} \rangle - A_{j'} \langle a_j | \hat{B} | a_{j'} \rangle \equiv (A_j - A_{j'}) \langle a_j | \hat{B} | a_{j'} \rangle = 0. \quad (4.138)$$

This means that if all eigenstates of operator \hat{A} are non-degenerate (i.e. $A_j \neq A_{j'}$ if $j \neq j'$), the matrix of operator \hat{B} has to be diagonal in the basis $\{a\}$, i.e., the eigenstate sets of the operators \hat{A} and \hat{B} coincide. Such pairs of observables (and their operators) that share their eigenstates, are called *compatible*. For example, in the wave mechanics of a particle, its momentum (1.26) and kinetic energy (1.27) are compatible, sharing their eigenfunctions (1.29). Now we see that this is not occasional, because each Cartesian component of the kinetic energy is proportional to the square of the corresponding component of the momentum, and any operator commutes with an arbitrary integer power of itself:

$$[\hat{A}, \hat{A}^n] \equiv \left[\hat{A}, \underbrace{\hat{A} \hat{A} \dots \hat{A}}_n \right] = \hat{A} \underbrace{\hat{A} \hat{A} \dots \hat{A}}_n - \underbrace{\hat{A} \hat{A} \dots \hat{A}}_n \hat{A} = 0. \quad (4.139)$$

Now, what if operators \hat{A} and \hat{B} do *not* commute? Then the following *general uncertainty relation* is valid:

General uncertainty relation

$$\delta A \delta B \geq \frac{1}{2} \left| \langle [\hat{A}, \hat{B}] \rangle \right|, \quad (4.140)$$

where all expectation values are for the same but arbitrary state of the system. The proof of Eq. (140) may be divided into two steps, the first one proving the so-called *Schwartz inequality* for any two possible states, say α and β :²⁹

Schwartz inequality

$$\langle \alpha | \alpha \rangle \langle \beta | \beta \rangle \geq |\langle \alpha | \beta \rangle|^2. \quad (4.141)$$

Its proof may be readily achieved by applying the postulate (16) – that the norm of any legitimate state of the system cannot be negative – to the state with the following ket-vector:

$$|\delta\rangle \equiv |\alpha\rangle - \frac{\langle \beta | \alpha \rangle}{\langle \beta | \beta \rangle} |\beta\rangle, \quad (4.142)$$

where α and β are possible, non-null states of the system, so that the denominator in Eq. (142) is not equal to zero. For this case, Eq. (16) gives

$$\left(\langle \alpha | - \frac{\langle \alpha | \beta \rangle}{\langle \beta | \beta \rangle} \langle \beta | \right) \left(|\alpha\rangle - \frac{\langle \beta | \alpha \rangle}{\langle \beta | \beta \rangle} |\beta\rangle \right) \geq 0. \quad (4.143)$$

Opening the parentheses, we get

$$\langle \alpha | \alpha \rangle - \frac{\langle \alpha | \beta \rangle}{\langle \beta | \beta \rangle} \langle \beta | \alpha \rangle - \frac{\langle \beta | \alpha \rangle}{\langle \beta | \beta \rangle} \langle \alpha | \beta \rangle + \frac{\langle \alpha | \beta \rangle \langle \beta | \alpha \rangle}{\langle \beta | \beta \rangle^2} \langle \beta | \beta \rangle \geq 0. \quad (4.144)$$

After the cancellation of one inner product $\langle \beta | \beta \rangle$ in the numerator and the denominator of the last term, it cancels with the 2nd (or the 3rd) term. What remains is the Schwartz inequality (141).

Now let us apply this inequality to states

$$|\alpha\rangle \equiv \hat{A}|\gamma\rangle \quad \text{and} \quad |\beta\rangle \equiv \hat{B}|\gamma\rangle, \quad (4.145)$$

where, in both relations, γ is the same (but otherwise arbitrary) possible state of the system, and the deviation operators are defined similarly to the deviations of the observables (see Sec. 1.2):

$$\hat{\tilde{A}} \equiv \hat{A} - \langle \hat{A} \rangle, \quad \hat{\tilde{B}} \equiv \hat{B} - \langle \hat{B} \rangle. \quad (4.146)$$

With this substitution, and taking into account again that the observable operators \hat{A} and \hat{B} are Hermitian, Eq. (141) yields

$$\langle \gamma | \hat{\tilde{A}}^2 | \gamma \rangle \langle \gamma | \hat{\tilde{B}}^2 | \gamma \rangle \geq \left| \langle \gamma | \hat{\tilde{A}} \hat{\tilde{B}} | \gamma \rangle \right|^2. \quad (4.147)$$

Since the state γ is arbitrary, we may use Eq. (125) to rewrite this relation as an operator inequality:

²⁹ This inequality is the quantum-mechanical analog of the usual vector algebra's result $\alpha^2 \beta^2 \geq |\alpha \cdot \beta|^2$.

$$\delta A \delta B \geq \left| \langle \hat{A} \hat{B} \rangle \right|. \quad (4.148)$$

Actually, this is already an uncertainty relation, even “better” (stronger) than its standard form (140); moreover, it is more convenient in some cases. To prove Eq. (140), we need a couple of more steps. First, let us notice that the operator product participating in Eq. (148) may be recast as

$$\hat{A} \hat{B} = \frac{1}{2} \left\{ \hat{A}, \hat{B} \right\} - \frac{i}{2} \hat{C}, \quad \text{where } \hat{C} \equiv i \left[\hat{A}, \hat{B} \right]. \quad (4.149)$$

Any anticommutator of Hermitian operators, including that in Eq. (149), is a Hermitian operator, and its eigenvalues are purely real, so that its expectation value (in any state) is also purely real. On the other hand, the commutator part of Eq. (149) is just

$$\hat{C} \equiv i \left[\hat{A}, \hat{B} \right] = i \left(\hat{A} - \langle A \rangle \right) \left(\hat{B} - \langle B \rangle \right) - i \left(\hat{B} - \langle B \rangle \right) \left(\hat{A} - \langle A \rangle \right) = i \left(\hat{A} \hat{B} - \hat{B} \hat{A} \right) = i \left[\hat{A}, \hat{B} \right]. \quad (4.150)$$

Second, according to Eqs. (52) and (65), the Hermitian conjugate of any product of the Hermitian operators \hat{A} and \hat{B} is just the product of these operators swapped. Using the fact, we may write

$$\hat{C}^\dagger = \left(i \left[\hat{A}, \hat{B} \right] \right)^\dagger = -i (\hat{A} \hat{B})^\dagger + i (\hat{B} \hat{A})^\dagger = -i \hat{B} \hat{A} + i \hat{A} \hat{B} = i \left[\hat{A}, \hat{B} \right] = \hat{C}, \quad (4.151)$$

so that the operator \hat{C} is also Hermitian, i.e. its eigenvalues are also real, and thus its expectation value is purely real as well. As a result, the square of the expectation value of the operator product (149) may be represented as

$$\left\langle \hat{A} \hat{B} \right\rangle^2 = \left\langle \frac{1}{2} \left\{ \hat{A}, \hat{B} \right\} \right\rangle^2 + \left\langle \frac{1}{2} \hat{C} \right\rangle^2. \quad (4.152)$$

Since the first term on the right-hand side of this equality cannot be negative, we may write

$$\left\langle \hat{A} \hat{B} \right\rangle^2 \geq \left\langle \frac{1}{2} \hat{C} \right\rangle^2 = \left\langle \frac{i}{2} \left[\hat{A}, \hat{B} \right] \right\rangle^2, \quad (4.153)$$

and hence continue Eq. (148) as

$$\delta A \delta B \geq \left| \langle \hat{A} \hat{B} \rangle \right| \geq \frac{1}{2} \left| \langle \left[\hat{A}, \hat{B} \right] \rangle \right|, \quad (4.154)$$

thus proving Eq. (140).

For the particular case of operators \hat{x} and \hat{p}_x (or a similar pair of operators for another Cartesian coordinate), we may readily combine Eq. (140) with Eq. (2.14b) and to prove the original Heisenberg’s uncertainty relation (2.13). For the spin- $\frac{1}{2}$ operators defined by Eq. (116)-(117), it is very simple (and highly recommended to the reader) to show that

$$[\hat{\sigma}_j, \hat{\sigma}_{j'}] = 2i \varepsilon_{jj'j''} \hat{\sigma}_{j''}, \quad \text{i.e. } [\hat{S}_j, \hat{S}_{j'}] = i \varepsilon_{jj'j''} \hbar \hat{S}_{j''}, \quad (4.155)$$

Spin- $\frac{1}{2}$:
commutation
relations

where $\varepsilon_{jj'j''}$ is the *Levi-Civita permutation symbol* – see, e.g., MA Eq. (13.2). As a result, the uncertainty relations (140) for all Cartesian components of spin- $\frac{1}{2}$ systems are similar, for example

$$\delta S_x \delta S_y \geq \frac{\hbar}{2} |\langle S_z \rangle|, \text{ etc.} \quad (4.156)$$

Spin- $\frac{1}{2}$:
uncertainty
relations

In particular, as we already know, in the \uparrow state the right-hand side of this relation equals $(\hbar/2)^2 > 0$, so that neither of the uncertainties δS_x , δS_y can equal zero. As a reminder, our direct calculation earlier in this section has shown that each of these uncertainties is equal to $\hbar/2$, i.e. their product is equal to the lowest value allowed by the uncertainty relation (156) – just as the Gaussian wave packets (2.16) provide the lowest possible value of the product $\delta x \delta p_x$, allowed by the Heisenberg relation (2.13).

4.6. Quantum dynamics: Three pictures

So far in this chapter, I shied away from the discussion of the system's dynamics, implying that the bra- and ket-vectors were just their “snapshots” at a certain instant t . Now we are sufficiently prepared to examine their evolution in time. One of the most beautiful features of quantum mechanics is that this evolution may be described using either of three alternative “pictures”, giving exactly the same final results for the expectation values of all observables.

From the standpoint of our wave-mechanics experience, the *Schrödinger picture* is the most natural one. In this picture, the operators corresponding to time-independent observables (e.g., to the Hamiltonian function H of an isolated system) are also constant in time, while the bra- and ket-vectors evolve in time as

$$\langle \alpha(t) | = \langle \alpha(t_0) | \hat{u}^\dagger(t, t_0), \quad | \alpha(t) \rangle = \hat{u}(t, t_0) | \alpha(t_0) \rangle. \quad (4.157a)$$

Here $\hat{u}(t, t_0)$ is the *time-evolution operator*, which obeys the following differential equation:

$$i\hbar \frac{\partial}{\partial t} \hat{u} = \hat{H} \hat{u}, \quad (4.157b)$$

where \hat{H} is the Hamiltonian operator of the system – which is always Hermitian: $\hat{H}^\dagger = \hat{H}$, and t_0 is the initial moment of time. (Note that Eqs. (157) remain valid even if the Hamiltonian depends on time explicitly.) Differentiating the second of Eqs. (157a) over time t , and then using Eq. (157b) twice, we can merge these two relations into a single equation, without explicit use of the time-evolution operator:

$i\hbar \frac{\partial}{\partial t} | \alpha(t) \rangle = \hat{H} | \alpha(t) \rangle,$

(4.158)

Schrödinger
equation

which is frequently more convenient. (However, for some purposes the notion of the time-evolution operator, together with Eq. (157b), are useful – as we will see in a minute.) While Eq. (158) is a very natural generalization of the wave-mechanical equation (1.25), and is also frequently called the *Schrödinger equation*,³⁰ it still should be considered as a new, more general postulate, which finds its final justification (as it is usual in physics) in the agreement of its corollaries with experiment – more exactly, in the absence of a single credible contradiction to an experiment.

Starting the discussion of Eq. (158), let us first consider the case of a time-independent Hamiltonian, whose eigenstates a_n and eigenvalues E_n obey Eq. (68) for this operator:³¹

$$\hat{H} | a_n \rangle = E_n | a_n \rangle, \quad (4.159)$$

³⁰ Moreover, we will be able to *derive* Eq. (1.25) from Eq. (158) – see below.

³¹ I have switched the state index notation from j to n , which was used for numbering stationary states in Chapter 1, to emphasize the special role played by the stationary states a_n in quantum dynamics.

and hence are also time-independent. (Similarly to the wavefunctions ψ_n defined by Eq. (1.60), a_n are called the *stationary states* of the system.) Let us use Eqs. (158)-(159) to calculate the law of time evolution of the expansion coefficients α_n (i.e. the probability amplitudes) defined by Eq. (118), in a stationary state basis, using Eq. (158):

$$\dot{\alpha}_n(t) = \frac{d}{dt} \langle a_n | \alpha(t) \rangle = \langle a_n | \frac{d}{dt} | \alpha(t) \rangle = \langle a_n | \frac{1}{i\hbar} \hat{H} | \alpha(t) \rangle = \frac{E_n}{i\hbar} \langle a_n | \alpha(t) \rangle = -\frac{i}{\hbar} E_n \alpha_n. \quad (4.160)$$

This is the same simple equation as Eq. (1.61), and its integration, with the initial moment t_0 taken for 0, yields a similar result – cf. Eq. (1.62), just with the initial time t_0 rather than 0:

$$\alpha_n(t) = \alpha_n(t_0) \exp\left\{-\frac{i}{\hbar} E_n t\right\}. \quad (4.161)$$

Time
evolution
of probability
amplitudes

In order to illustrate how this result works, let us consider the dynamics of a spin-½ in a time-independent, uniform external magnetic field \mathcal{B} . To construct the system's Hamiltonian, we may apply the correspondence principle to the classical expression for the energy of a magnetic moment \mathbf{m} in the external magnetic field \mathcal{B} ,³²

$$U = -\mathbf{m} \cdot \mathcal{B}. \quad (4.162)$$

In quantum mechanics, the operator corresponding to the moment \mathbf{m} is given by Eq. (115) (suggested by W. Pauli), so that the spin-field interaction is described by the so-called *Pauli Hamiltonian*, which may be, due to Eqs. (116)-(117), represented in several equivalent forms:

$$\hat{H} = -\hat{\mathbf{m}} \cdot \mathcal{B} \equiv -\gamma \hat{\mathbf{S}} \cdot \mathcal{B} \equiv -\gamma \frac{\hbar}{2} \hat{\mathbf{\sigma}} \cdot \mathcal{B}. \quad (4.163a)$$

Pauli
Hamiltonian:
operator

If the z -axis is aligned with the field's direction, this expression is reduced to

$$\hat{H} = -\gamma \mathcal{B} \hat{S}_z \equiv -\gamma \mathcal{B} \frac{\hbar}{2} \hat{\sigma}_z. \quad (4.163b)$$

According to Eq. (117), in the z -basis of the spin states \uparrow and \downarrow , the matrix of the operator (163b) is

$$H = -\frac{\gamma \hbar \mathcal{B}}{2} \sigma_z \equiv \frac{\hbar \Omega}{2} \sigma_z, \quad \text{where } \Omega \equiv -\gamma \mathcal{B}. \quad (4.164)$$

Pauli
Hamiltonian:
 z -basis matrix

The constant Ω so defined coincides with the classical frequency of the precession, about the z -axis, of an axially-symmetric rigid body (the so-called *symmetric top*), with an angular momentum \mathbf{S} and the magnetic moment $\mathbf{m} = \gamma \mathbf{S}$, induced by the external torque $\tau = \mathbf{m} \times \mathcal{B}$.³³ (For an electron, with its negative gyromagnetic ratio $\gamma_e = -g_e e / 2m_e$, neglecting the tiny difference of the g_e -factor from 2, we get

$$\Omega = \frac{e}{m_e} \mathcal{B}, \quad (4.165)$$

so that according to Eq. (3.48), the frequency Ω coincides with the electron's cyclotron frequency ω_c .)

³² See, e.g., EM Eq. (5.100). As a reminder, we have already used this expression for the derivation of Eq. (3).

³³ See, e.g., CM Sec. 4.5, in particular Eq. (4.72), and EM Sec. 5.5, in particular Eq. (5.114) and its discussion.

In order to apply the general Eq. (161) to this case, we need to find the eigenstates a_n and eigenenergies E_n of our Hamiltonian. However, with our (smart :-) choice of the z -axis, the Hamiltonian matrix is already diagonal:

$$H = \frac{\hbar\Omega}{2} \sigma_z \equiv \frac{\hbar\Omega}{2} \begin{pmatrix} 1 & 0 \\ 0 & -1 \end{pmatrix}, \quad (4.166)$$

meaning that the states \uparrow and \downarrow are the eigenstates of this system, with the eigenenergies, respectively,

Spin-½ in magnetic field: eigenenergies

$$E_{\uparrow} = +\frac{\hbar\Omega}{2} \quad \text{and} \quad E_{\downarrow} = -\frac{\hbar\Omega}{2}. \quad (4.167)$$

Note that their difference,

$$\Delta E \equiv |E_{\uparrow} - E_{\downarrow}| = \hbar|\Omega| = \hbar|\gamma\mathcal{B}|, \quad (4.168)$$

corresponds to the classical energy $2|m\mathcal{B}|$ of flipping a magnetic dipole with the moment's magnitude $m = \gamma\hbar/2$, oriented along the direction of the field \mathcal{B} . Note also that if the product $\gamma\mathcal{B}$ is positive, then Ω is negative, so that E_{\uparrow} is negative, while E_{\downarrow} is positive. This is in the agreement with the classical picture of a magnetic dipole **m** having negative potential energy when it is aligned with the external magnetic field \mathcal{B} – see Eq. (162) again.

So, for the time evolution of the probability amplitudes of these states, Eq. (161) immediately yields the following expressions:

$$\alpha_{\uparrow}(t) = \alpha_{\uparrow}(0) \exp\left\{-\frac{i}{2}\Omega t\right\}, \quad \alpha_{\downarrow}(t) = \alpha_{\downarrow}(0) \exp\left\{+\frac{i}{2}\Omega t\right\}, \quad (4.169)$$

allowing a ready calculation of the time evolution of the expectation values of any observable. In particular, we can calculate the expectation value of S_z as a function of time by applying Eq. (130) to the (arbitrary) time moment t :

$$\langle S_z \rangle(t) = \frac{\hbar}{2} \left[\alpha_{\uparrow}(t)\alpha_{\uparrow}^*(t) - \alpha_{\downarrow}(t)\alpha_{\downarrow}^*(t) \right] = \frac{\hbar}{2} \left[\alpha_{\uparrow}(0)\alpha_{\uparrow}^*(0) - \alpha_{\downarrow}(0)\alpha_{\downarrow}^*(0) \right] = \langle S_z \rangle(0). \quad (4.170)$$

Thus the expectation value of the spin component parallel to the applied magnetic field remains constant in time, regardless of the initial state of the system. However, this is not true for the components perpendicular to the field. For example, Eq. (132), applied to the moment t , gives

$$\langle S_x \rangle(t) = \frac{\hbar}{2} \left[\alpha_{\uparrow}(t)\alpha_{\downarrow}^*(t) + \alpha_{\downarrow}(t)\alpha_{\uparrow}^*(t) \right] = \frac{\hbar}{2} \left[\alpha_{\uparrow}(0)\alpha_{\downarrow}^*(0)e^{-i\Omega t} + \alpha_{\downarrow}(0)\alpha_{\uparrow}^*(0)e^{+i\Omega t} \right]. \quad (4.171)$$

Clearly, this expression describes sinusoidal oscillations with frequency (164). The amplitude and the phase of these oscillations depend on initial conditions. Indeed, solving Eqs. (132)-(133) for the probability amplitude products, we get the following relations:

$$\hbar\alpha_{\downarrow}(t)\alpha_{\uparrow}^*(t) = \langle S_x \rangle(t) + i\langle S_y \rangle(t), \quad \hbar\alpha_{\uparrow}(t)\alpha_{\downarrow}^*(t) = \langle S_x \rangle(t) - i\langle S_y \rangle(t), \quad (4.172)$$

valid for any time t . Plugging their values for $t = 0$ into Eq. (171), we get

$$\begin{aligned}\langle S_x \rangle(t) &= \frac{1}{2} [\langle S_x \rangle(0) + i\langle S_y \rangle(0)] e^{+i\Omega t} + \frac{1}{2} [\langle S_x \rangle(0) - i\langle S_y \rangle(0)] e^{-i\Omega t} \\ &\equiv \langle S_x \rangle(0) \cos \Omega t - \langle S_y \rangle(0) \sin \Omega t.\end{aligned}\quad (4.173)$$

An absolutely similar calculation using Eq. (133) gives

$$\langle S_y \rangle(t) = \langle S_y \rangle(0) \cos \Omega t + \langle S_x \rangle(0) \sin \Omega t. \quad (4.174)$$

These formulas show, for example, that if at moment $t = 0$ the spin's state was \uparrow , i.e. $\langle S_x \rangle(0) = \langle S_y \rangle(0) = 0$, then the oscillation amplitudes of the both “lateral” components of the spin vanish. On the other hand, if the spin was initially in the state \rightarrow , i.e. had the definite, largest possible value of S_x , equal to $\hbar/2$ (in classics, we would say “the spin- $\frac{1}{2}$ was oriented in the x -direction”), then both expectation values $\langle S_x \rangle$ and $\langle S_y \rangle$ oscillate in time³⁴ with this amplitude, and with the phase shift $\pi/2$ between them.

So, the quantum-mechanical results for the expectation values of the Cartesian components of spin- $\frac{1}{2}$ are indistinguishable from the classical results for the precession, with the frequency $\Omega = -\gamma \mathcal{B}$,³⁵ of a symmetric top with the angular momentum of magnitude $S = \hbar/2$, about the field's direction (our axis z), under the effect of an external torque $\tau = \mathbf{m} \times \mathcal{B}$ exerted by the field \mathcal{B} on the magnetic moment $\mathbf{m} = \gamma \mathbf{S}$. Note, however, that the classical language does not describe the large quantum-mechanical uncertainties of the components, obeying Eqs. (156), which are absent in the classical picture – at least when it starts from a definite orientation of the angular momentum vector. Also, as we have seen in Sec. 3.5, the component L_z of the angular momentum at the orbital motion of particles is always a multiple of \hbar – see, e.g., Eq. (3.139). As a result, the angular momentum of a spin- $\frac{1}{2}$ particle, with $S_z = \pm \hbar/2$, cannot be explained by any summation of orbital angular moments of its hypothetical components, i.e. by any internal rotation of the particle about its axis.

After this illustration, let us return to the discussion of the general Schrödinger equation (157b) and prove the following fascinating fact: it is possible to write the general solution of this *operator* equation. In the easiest case when the Hamiltonian is time-independent, this solution is an exact analog of Eq. (161),

$$\hat{u}(t, t_0) = \hat{u}(t_0, t_0) \exp\left\{-\frac{i}{\hbar} \hat{H}(t-t_0)\right\} = \exp\left\{-\frac{i}{\hbar} \hat{H}(t-t_0)\right\}. \quad (4.175)$$

To start its proof we should, first of all, understand what a function (in this particular case, the exponent) of an operator means. In the operator (and matrix) algebra, such nonlinear functions are *defined* by their Taylor expansions; in particular, Eq. (175) means that

³⁴ This is one more (hopefully, redundant :-) illustration of the difference between the averaging over the statistical ensemble and that over time: in Eqs. (170), (173)-(174), and also in quite a few relations below, only the former averaging has been performed, so the results are still functions of time.

³⁵ Note that according to this relation, the gyromagnetic ratio γ may be interpreted just as the angular frequency of the spin precession per unit magnetic field – hence the name. In particular, for electrons, $|\gamma_e| \approx 1.761 \times 10^{11} \text{ s}^{-1}\text{T}^{-1}$; for protons, the ratio is much smaller, $\gamma_p \equiv g_p e/2m_p \approx 2.675 \times 10^8 \text{ s}^{-1}\text{T}^{-1}$, mostly because of their larger mass m_p , at a g -factor of the same order as for the electron: $g_p \approx 5.586$. For heavier spin- $\frac{1}{2}$ particles, e.g., atomic nuclei with such spin, the values of γ are correspondingly smaller – e.g., $\gamma \approx 8.681 \times 10^6 \text{ s}^{-1}\text{T}^{-1}$ for the ${}^{57}\text{Fe}$ nucleus.

$$\begin{aligned}\hat{u}(t, t_0) &= \hat{I} + \sum_{k=1}^{\infty} \frac{1}{k!} \left[-\frac{i}{\hbar} \hat{H}(t-t_0) \right]^k \\ &\equiv \hat{I} + \frac{1}{1!} \left(-\frac{i}{\hbar} \right) \hat{H}(t-t_0) + \frac{1}{2!} \left(-\frac{i}{\hbar} \right)^2 \hat{H}^2(t-t_0)^2 + \frac{1}{3!} \left(-\frac{i}{\hbar} \right)^3 \hat{H}^3(t-t_0)^3 + \dots,\end{aligned}\quad (4.176)$$

where $\hat{H}^2 \equiv \hat{H}\hat{H}$, $\hat{H}^3 \equiv \hat{H}\hat{H}\hat{H}$, etc. Working with such series of operator products is not as hard as one could imagine, due to their regular structure. For example, let us differentiate both sides of Eq. (176) over t , at constant t_0 , at the last stage using this equality again – backward:

$$\begin{aligned}\frac{\partial}{\partial t} \hat{u}(t, t_0) &= \hat{0} + \frac{1}{1!} \left(-\frac{i}{\hbar} \right) \hat{H} + \frac{1}{2!} \left(-\frac{i}{\hbar} \right)^2 \hat{H}^2 2(t-t_0) + \frac{1}{3!} \left(-\frac{i}{\hbar} \right)^2 \hat{H}^3 3(t-t_0)^2 + \dots \\ &\equiv \left(-\frac{i}{\hbar} \right) \hat{H} \left[\hat{I} + \frac{1}{1!} \left(-\frac{i}{\hbar} \right) \hat{H}(t-t_0) + \frac{1}{2!} \left(-\frac{i}{\hbar} \right)^2 \hat{H}^2(t-t_0)^2 \right] + \dots \equiv -\frac{i}{\hbar} \hat{H} \hat{u}(t, t_0),\end{aligned}\quad (4.177)$$

so that the differential equation (158) is indeed satisfied. On the other hand, Eq. (175) also satisfies the initial condition

$$\hat{u}(t_0, t_0) = \hat{u}^\dagger(t_0, t_0) = \hat{I} \quad (4.178)$$

that immediately follows from the definition (157a) of the evolution operator. Thus, Eq. (175) indeed gives the (unique) solution for the time evolution operator – in the Schrödinger picture.

Now let us allow the operator \hat{H} to be a function of time, but with the condition that its “values” (in fact, operators) at different instants commute with each other:

$$[\hat{H}(t'), \hat{H}(t'')] = 0, \quad \text{for any } t', t''. \quad (4.179)$$

(An important non-trivial example of such a Hamiltonian is the time-dependent part of the Hamiltonian of a particle, due to the effect of a classical, time-dependent, but position-independent force $\mathbf{F}(t)$,

$$\hat{H}_F = -\mathbf{F}(t) \cdot \hat{\mathbf{r}}. \quad (4.180)$$

Indeed, the radius vector’s operator $\hat{\mathbf{r}}$ does not depend explicitly on time and hence commutes with itself, as well as with the c -numbers $\mathbf{F}(t')$ and $\mathbf{F}(t'')$.) In this case, it is sufficient to replace, in all the above formulas, the product $\hat{H}(t-t_0)$ with the corresponding integral over time; in particular, Eq. (175) is generalized as

$$\hat{u}(t, t_0) = \exp \left\{ -\frac{i}{\hbar} \int_{t_0}^t \hat{H}(t') dt' \right\}.$$

(4.181)

Evolution operator:
explicit expression

This replacement means that the first form of Eq. (176) should be replaced with

$$\hat{u}(t, t_0) = \hat{I} + \sum_{k=1}^{\infty} \frac{1}{k!} \left(-\frac{i}{\hbar} \right)^k \left(\int_{t_0}^t \hat{H}(t') dt' \right)^k$$

$$\equiv \hat{I} + \sum_{k=1}^{\infty} \frac{1}{k!} \left(-\frac{i}{\hbar} \right)^k \int_{t_0}^t dt_1 \int_{t_0}^{t_1} dt_2 \dots \int_{t_0}^{t_{k-1}} dt_k \hat{H}(t_1) \hat{H}(t_2) \dots \hat{H}(t_k). \quad (4.182)$$

The proof that Eq. (182) satisfies Eq. (158) is absolutely similar to the one carried out above.

We may now use Eq. (181) to show that the time-evolution operator remains unitary at any moment, even for a time-dependent Hamiltonian, if it satisfies Eq. (179). Indeed, Eq. (181) yields

$$\hat{u}(t, t_0) \hat{u}^\dagger(t, t_0) = \exp \left\{ -\frac{i}{\hbar} \int_{t_0}^t \hat{H}(t') dt' \right\} \exp \left\{ +\frac{i}{\hbar} \int_{t_0}^t \hat{H}(t'') dt'' \right\}. \quad (4.183)$$

Since each of these exponents may be represented with the Taylor series (182), and, thanks to Eq. (179), different components of these sums may be swapped at will, the expression (183) may be manipulated exactly as the product of *c*-number exponents, for example rewritten as

$$\hat{u}(t, t_0) \hat{u}^\dagger(t, t_0) = \exp \left\{ -\frac{i}{\hbar} \left[\int_{t_0}^t \hat{H}(t') dt' - \int_{t_0}^t \hat{H}(t'') dt'' \right] \right\} = \exp \{ \hat{0} \} = \hat{I}. \quad (4.184)$$

This property ensures, in particular, that the system state's normalization does not depend on time:

$$\langle \alpha(t) | \alpha(t) \rangle = \langle \alpha(t_0) | \hat{u}^\dagger(t, t_0) \hat{u}(t, t_0) | \alpha(t_0) \rangle = \langle \alpha(t_0) | \alpha(t_0) \rangle. \quad (4.185)$$

The most difficult cases for the explicit solution of Eq. (158) are those where Eq. (179) is violated.³⁶ It may be proven that in these cases the integral limits in the last form of Eq. (182) should be truncated, giving the so-called *Dyson series*

$$\hat{u}(t, t_0) = \hat{I} + \sum_{k=1}^{\infty} \frac{1}{k!} \left(-\frac{i}{\hbar} \right)^k \int_{t_0}^t dt_1 \int_{t_0}^{t_1} dt_2 \dots \int_{t_0}^{t_{k-1}} dt_k \hat{H}(t_1) \hat{H}(t_2) \dots \hat{H}(t_k). \quad (4.186)$$

Since we would not have time/space to use this relation in our course, I will skip its proof.³⁷

Let me now return to the general discussion of quantum dynamics to outline its alternative, *Heisenberg picture*. For its introduction, let us recall that according to Eq. (125), in quantum mechanics the expectation value of any observable *A* is a long bracket. Let us explore an even more general form of such bracket:

$$\langle \alpha | \hat{A} | \beta \rangle. \quad (4.187)$$

(In some applications, the states α and β may be different.) As was discussed above, in the Schrödinger picture the bra- and ket-vectors of the states evolve in time, while the operators of observables remain time-independent (if they do not explicitly depend on time), so that Eq. (187), applied to a moment *t*, may be represented as

$$\langle \alpha(t) | \hat{A}_S | \beta(t) \rangle, \quad (4.188)$$

where the index “S” is added to emphasize the Schrödinger picture. Let us apply the evolution law (157a) to the bra- and ket-vectors in this expression:

³⁶ We will run into such situations in Chapter 7, but will not need to apply Eq. (186) there.

³⁷ It may be found, for example, in Chapter 5 of J. Sakurai’s textbook – see References.

$$\langle \alpha(t) | \hat{A}_s | \beta(t) \rangle = \langle \alpha(t_0) | \hat{u}^\dagger(t, t_0) \hat{A}_s \hat{u}(t, t_0) | \beta(t_0) \rangle. \quad (4.189)$$

This equality means that if we form a long bracket with bra- and ket-vectors of the initial-time states, together with the following time-dependent *Heisenberg operator*³⁸

$$\hat{A}_H(t) \equiv \hat{u}^\dagger(t, t_0) \hat{A}_s \hat{u}(t, t_0) = \hat{u}^\dagger(t, t_0) \hat{A}_H(t_0) \hat{u}(t, t_0), \quad (4.190)$$

all experimentally measurable results will remain the same as in the Schrödinger picture:

$$\langle \alpha(t) | \hat{A} | \beta(t) \rangle = \langle \alpha(t_0) | \hat{A}_H(t, t_0) | \beta(t_0) \rangle. \quad (4.191)$$

For full clarity, let us see how does the Heisenberg picture work for the same simple (but very important!) problem of the spin-½ precession in a *z*-oriented magnetic field, described (in the *z*-basis) by the Hamiltonian matrix (164). In that basis, Eq. (157b) for the time-evolution operator becomes

$$i\hbar \frac{\partial}{\partial t} \begin{pmatrix} u_{11} & u_{12} \\ u_{21} & u_{22} \end{pmatrix} = \frac{\hbar\Omega}{2} \begin{pmatrix} 1 & 0 \\ 0 & -1 \end{pmatrix} \begin{pmatrix} u_{11} & u_{12} \\ u_{21} & u_{22} \end{pmatrix} \equiv \frac{\hbar\Omega}{2} \begin{pmatrix} u_{11} & u_{12} \\ -u_{21} & -u_{22} \end{pmatrix}. \quad (4.192)$$

We see that in this simple case the differential equations for different matrix elements of the evolution operator matrix are decoupled, and readily solvable, using the universal initial conditions (178):³⁹

$$u(t, 0) = \begin{pmatrix} e^{-i\Omega t/2} & 0 \\ 0 & e^{i\Omega t/2} \end{pmatrix} \equiv I \cos \frac{\Omega t}{2} - i\sigma_z \sin \frac{\Omega t}{2}. \quad (4.193)$$

Now let us use them in Eq. (190) to calculate the Heisenberg-picture operators of spin components – still in the *z*-basis. Dropping the index “H” for the notation brevity (the Heisenberg-picture operators are clearly marked by their dependence on time anyway), we get

$$\begin{aligned} S_x(t) &= u^\dagger(t, 0) S_x(0) u(t, 0) = \frac{\hbar}{2} u^\dagger(t, 0) \sigma_x u(t, 0) \\ &= \frac{\hbar}{2} \begin{pmatrix} e^{i\Omega t/2} & 0 \\ 0 & e^{-i\Omega t/2} \end{pmatrix} \begin{pmatrix} 0 & 1 \\ 1 & 0 \end{pmatrix} \begin{pmatrix} e^{-i\Omega t/2} & 0 \\ 0 & e^{i\Omega t/2} \end{pmatrix} \\ &= \frac{\hbar}{2} \begin{pmatrix} 0 & e^{i\Omega t} \\ e^{-i\Omega t} & 0 \end{pmatrix} = \frac{\hbar}{2} (\sigma_x \cos \Omega t - \sigma_y \sin \Omega t) \equiv S_x(0) \cos \Omega t - S_y(0) \sin \Omega t. \end{aligned} \quad (4.194)$$

Absolutely similar calculations of the other spin components yield

³⁸ Note that this *strict* relation is similar in structure to the first of the *symbolic* Eqs. (94), with the state bases $\{v\}$ and $\{u\}$ loosely associated with the time moments, respectively, t and t_0 .

³⁹ We could of course use this solution, together with Eq. (157), to obtain all the above results for this system within the Schrödinger picture. In our simple case, the use of Eqs. (161) for this purpose was more straightforward, but in some cases, e.g., for some time-dependent Hamiltonians, an explicit calculation of the time-evolution matrix may be the best (or even only practicable) way to proceed.

$$\mathbf{S}_y(t) = \frac{\hbar}{2} \begin{pmatrix} 0 & -ie^{i\Omega t} \\ ie^{-i\Omega t} & 0 \end{pmatrix} = \frac{\hbar}{2} (\sigma_y \cos \Omega t + \sigma_x \sin \Omega t) \equiv \mathbf{S}_y(0) \cos \Omega t + \mathbf{S}_x(0) \sin \Omega t, \quad (4.195)$$

$$\mathbf{S}_z(t) = \frac{\hbar}{2} \begin{pmatrix} 1 & 0 \\ 0 & -1 \end{pmatrix} = \frac{\hbar}{2} \sigma_z = S_z(0). \quad (4.196)$$

One practical advantage of these formulas is that they describe the system's evolution for *arbitrary* initial conditions, thus making the analysis of initial state effects very simple. Indeed, since in the Heisenberg picture the expectation values of observables are calculated using Eq. (191) (with $\beta = \alpha$), with time-independent bra- and ket-vectors, such averaging of Eqs. (194)-(196) immediately returns us to Eqs. (170), (173), and (174), which were obtained above in the Schrödinger picture. Moreover, these equations for the Heisenberg operators formally coincide with the classical equations of the torque-induced precession for *c*-number variables. (Below we will see that the same exact correspondence is valid for the Heisenberg picture of the orbital motion.)

In order to see that the last fact is by no means a coincidence, let us combine Eqs. (157b) and (190) to form an explicit differential equation of the Heisenberg operator's evolution. For that, let us differentiate Eq. (190) over time:

$$\frac{d}{dt} \hat{A}_H = \frac{\partial \hat{u}^\dagger}{\partial t} \hat{A}_S \hat{u} + \hat{u}^\dagger \frac{\partial \hat{A}_S}{\partial t} \hat{u} + \hat{u}^\dagger \hat{A}_S \frac{\partial \hat{u}}{\partial t}. \quad (4.197)$$

Plugging in the derivatives of the time evolution operator from Eq. (157b) and its Hermitian conjugate, and multiplying both sides of the equation by $i\hbar$, we get

$$i\hbar \frac{d}{dt} \hat{A}_H = -\hat{u}^\dagger \hat{H} \hat{A}_S \hat{u} + i\hbar \hat{u}^\dagger \frac{\partial \hat{A}_S}{\partial t} \hat{u} + \hat{u}^\dagger \hat{A}_S \hat{H} \hat{u}. \quad (4.198a)$$

If for the Schrödinger-picture's Hamiltonian the condition similar to Eq. (179) is satisfied, then, according to Eqs. (177) or (182), the Hamiltonian commutes with the time evolution operator and its Hermitian conjugate, and may be swapped with any of them.⁴⁰ Hence, we may rewrite Eq. (198a) as

$$i\hbar \frac{d}{dt} \hat{A}_H = -\hat{H} \hat{u}^\dagger \hat{A}_S \hat{u} + i\hbar \hat{u}^\dagger \frac{\partial \hat{A}_S}{\partial t} \hat{u} + \hat{u}^\dagger \hat{A}_S \hat{H} \hat{u} \equiv i\hbar \hat{u}^\dagger \frac{\partial \hat{A}_S}{\partial t} \hat{u} + [\hat{u}^\dagger \hat{A}_S \hat{u}, \hat{H}]. \quad (4.198b)$$

Now using the definition (190) again, for both terms on the right-hand side, we may write

$$i\hbar \frac{d}{dt} \hat{A}_H = i\hbar \left(\frac{\partial \hat{A}}{\partial t} \right)_H + [\hat{A}_H, \hat{H}].$$

(4.199)

Heisenberg
equation
of motion

This is the so-called *Heisenberg equation of motion*.

Let us see how this equation looks for the same problem of the spin-1/2 precession in a *z*-oriented, time-independent magnetic field, described in the *z*-basis by the Hamiltonian matrix (164), which does not depend on time. In this basis, Eq. (199) for the vector operator of spin reads⁴¹

⁴⁰ Due to the same reason, $\hat{H}_H \equiv \hat{u}^\dagger \hat{H}_S \hat{u} = \hat{u}^\dagger \hat{u} \hat{H}_S = \hat{H}_S$; this is why the Hamiltonian operator's index may be dropped in Eqs. (198)-(199).

$$i\hbar \begin{pmatrix} \dot{\mathbf{S}}_{11} & \dot{\mathbf{S}}_{12} \\ \dot{\mathbf{S}}_{21} & \dot{\mathbf{S}}_{22} \end{pmatrix} = \frac{\hbar\Omega}{2} \left[\begin{pmatrix} \mathbf{S}_{11} & \mathbf{S}_{12} \\ \mathbf{S}_{21} & \mathbf{S}_{22} \end{pmatrix}, \begin{pmatrix} 1 & 0 \\ 0 & -1 \end{pmatrix} \right] = \hbar\Omega \begin{pmatrix} 0 & -\mathbf{S}_{12} \\ \mathbf{S}_{21} & 0 \end{pmatrix}. \quad (4.200)$$

Once again, the equations for different matrix elements are decoupled, and their solution is elementary:

$$\begin{aligned} \mathbf{S}_{11}(t) &= \mathbf{S}_{11}(0) = \text{const}, & \mathbf{S}_{22}(t) &= \mathbf{S}_{22}(0) = \text{const}, \\ \mathbf{S}_{12}(t) &= \mathbf{S}_{12}(0)e^{+i\Omega t}, & \mathbf{S}_{21}(t) &= \mathbf{S}_{21}(0)e^{-i\Omega t}. \end{aligned} \quad (4.201)$$

According to Eq. (190), the initial values of the Heisenberg-picture matrix elements are just the Schrödinger-picture ones, so that using Eq. (117) we may rewrite this solution in either of two forms:

$$\begin{aligned} \mathbf{S}(t) &= \frac{\hbar}{2} \left[\mathbf{n}_x \begin{pmatrix} 0 & e^{+i\Omega t} \\ e^{-i\Omega t} & 0 \end{pmatrix} + \mathbf{n}_y \begin{pmatrix} 0 & -ie^{+i\Omega t} \\ ie^{-i\Omega t} & 0 \end{pmatrix} + \mathbf{n}_z \begin{pmatrix} 1 & 0 \\ 0 & -1 \end{pmatrix} \right] \\ &\equiv \frac{\hbar}{2} \begin{pmatrix} \mathbf{n}_z & \mathbf{n}_-e^{+i\Omega t} \\ \mathbf{n}_+e^{-i\Omega t} & -\mathbf{n}_z \end{pmatrix}, \quad \text{where } \mathbf{n}_\pm \equiv \mathbf{n}_x \pm i\mathbf{n}_y. \end{aligned} \quad (4.202)$$

The simplicity of the last expression is spectacular. (Remember, it covers *any* initial conditions and *all* three spatial components of spin!) On the other hand, for some purposes the previous form may be more convenient; in particular, its Cartesian components give our earlier results (194)-(196).⁴²

One of the advantages of the Heisenberg picture is that it provides a more clear link between classical and quantum mechanics, found by P. Dirac. Indeed, analytical classical mechanics may be used to derive the following equation of time evolution of an arbitrary function $A(q_j, p_j, t)$ of the generalized coordinates q_j and momenta p_j of the system, and time t :⁴³

$$\frac{dA}{dt} = \frac{\partial A}{\partial t} - \{A, H\}_P, \quad (4.203)$$

where H is the classical Hamiltonian function of the system, and $\{....\}$ is the so-called *Poisson bracket* defined, for two arbitrary functions $A(q_j, p_j, t)$ and $B(q_j, p_j, t)$, as

Poisson
bracket

$$\{A, B\}_P \equiv \sum_j \left(\frac{\partial A}{\partial p_j} \frac{\partial B}{\partial q_j} - \frac{\partial A}{\partial q_j} \frac{\partial B}{\partial p_j} \right). \quad (4.204)$$

Comparing Eq. (203) with Eq. (199), we see that the correspondence between the classical and quantum mechanics (in the Heisenberg picture) is provided by the following symbolic relation

⁴¹ Using the commutation relations (155), this equation may be readily generalized to the case of an arbitrary magnetic field $\mathcal{B}(t)$ and an arbitrary state basis – the exercise highly recommended to the reader.

⁴² Note that the “values” of the same Heisenberg operator at different moments of time may or may not commute. For example, consider a free 1D particle, with the time-independent Hamiltonian $\hat{H} = \hat{p}^2/2m$. In this case, Eq. (199) yields the following equations: $i\hbar\dot{\hat{x}} = [\hat{x}, \hat{H}] = i\hbar\hat{p}/m$ and $i\hbar\dot{\hat{p}} = [\hat{p}, \hat{H}] = 0$, with simple solutions (similar to those for the classical motion): $\hat{p}(t) = \text{const} = \hat{p}(0)$ and $\hat{x}(t) = \hat{x}(0) + \hat{p}(0)t/m$, so that $[\hat{x}(0), \hat{x}(t)] = [\hat{x}(0), \hat{p}(0)]t/m \equiv [\hat{x}_S, \hat{p}_S]t/m = i\hbar t/m \neq 0$, for $t \neq 0$.

⁴³ See, e.g., CM Eq. (10.17). The notation there does not use the subscript “P” that is employed in Eqs. (203)-(205) to distinguish the classical Poisson bracket (204) from the quantum anticommutator (34).

$$\{A, B\}_P \leftrightarrow \frac{i}{\hbar} [\hat{A}, \hat{B}]. \quad (4.205)$$

This relation may be used, in particular, for finding appropriate operators for the system's observables, if their form is not immediately evident from the correspondence principle.

Finally, let us discuss one more alternative picture of quantum dynamics. It is also attributed to Dirac, and is called either the "Dirac picture", or (more frequently) the *interaction picture*. The last name stems from the fact that this picture is very useful for the *perturbative* (approximate) approaches to systems whose Hamiltonians may be partitioned into two parts,

$$\hat{H} = \hat{H}_0 + \hat{H}_{\text{int}}, \quad (4.206)$$

where \hat{H}_0 is the sum of relatively simple Hamiltonians of the component subsystems, while the second term in Eq. (206) represents their weak interaction. (Note, however, that all relations in the balance of this section are exact and not directly based on the interaction weakness.) In this case, it is natural to consider, together with the full operator $\hat{u}(t, t_0)$ of the system's evolution, which obeys Eq. (157b), a similarly defined unitary operator $\hat{u}_0(t, t_0)$ of evolution of the "unperturbed system" described by the Hamiltonian \hat{H}_0 alone:

$$i\hbar \frac{\partial}{\partial t} \hat{u}_0 = \hat{H}_0 \hat{u}_0, \quad (4.207)$$

and also the following *interaction evolution operator*,

$$\hat{u}_I \equiv \hat{u}_0^\dagger \hat{u}. \quad (4.208)$$

The motivation for these definitions become more clear if we insert the reciprocal relation,

$$\hat{u} \equiv \hat{u}_0 \hat{u}_0^\dagger \hat{u} = \hat{u}_0 \hat{u}_1, \quad (4.209)$$

and its Hermitian conjugate,

$$\hat{u}^\dagger = (\hat{u}_0 \hat{u}_1)^\dagger = \hat{u}_1^\dagger \hat{u}_0^\dagger, \quad (4.210)$$

into the basic Eq. (189):

$$\begin{aligned} \langle \alpha | \hat{A} | \beta \rangle &= \langle \alpha(t_0) | \hat{u}^\dagger(t, t_0) \hat{A}_S \hat{u}(t, t_0) | \beta(t_0) \rangle \\ &= \langle \alpha(t_0) | \hat{u}_1^\dagger(t, t_0) \hat{u}_0^\dagger(t, t_0) \hat{A}_S \hat{u}_0(t, t_0) \hat{u}_1(t, t_0) | \beta(t_0) \rangle. \end{aligned} \quad (4.211)$$

This relation shows that any long bracket (187), i.e. any experimentally verifiable result of quantum mechanics, may be expressed as

$$\langle \alpha | \hat{A} | \beta \rangle = \langle \alpha_I(t) | \hat{A}_I(t) | \beta_I(t) \rangle, \quad (4.212)$$

if we assume that both the state vectors and the operators depend on time, with the vectors evolving only due to the *interaction operator* \hat{u}_I ,

$$\langle \alpha_I(t) | \equiv \langle \alpha(t_0) | \hat{u}_I^\dagger(t, t_0), \quad | \beta_I(t) \rangle \equiv \hat{u}_I(t, t_0) | \beta(t_0) \rangle, \quad (4.213)$$

while the operators' evolution being governed by the *unperturbed operator* \hat{u}_0 :

$$\hat{A}_I(t) \equiv \hat{u}_0^\dagger(t, t_0) \hat{A}_S \hat{u}_0(t, t_0). \quad (4.214)$$

These relations describe the interaction picture of quantum dynamics. Let me defer an example of its use until the perturbative analysis of open quantum systems in Sec. 7.6, and end this section with a proof that the interaction evolution operator (208) satisfies the following natural equation,

$$i\hbar \frac{\partial}{\partial t} \hat{u}_I = \hat{H}_I \hat{u}_I, \quad (4.215)$$

where \hat{H}_I is the interaction Hamiltonian formed from \hat{H}_{int} in accordance with the same rule (214):

$$\hat{H}_I(t) \equiv \hat{u}_0^\dagger(t, t_0) \hat{H}_{\text{int}} \hat{u}_0(t, t_0). \quad (4.216)$$

The proof is very straightforward: first using the definition (208), and then Eqs. (157b) and the Hermitian conjugate of Eq. (207), we may write

$$\begin{aligned} i\hbar \frac{\partial}{\partial t} \hat{u}_I &\equiv i\hbar \frac{\partial}{\partial t} (\hat{u}_0^\dagger \hat{u}) \equiv i\hbar \frac{\partial \hat{u}_0^\dagger}{\partial t} \hat{u} + \hat{u}_0^\dagger i\hbar \frac{\partial \hat{u}}{\partial t} = -\hat{H}_0 \hat{u}_0^\dagger \hat{u} + \hat{u}_0^\dagger \hat{H} \hat{u} = -\hat{H}_0 \hat{u}_0^\dagger \hat{u} + \hat{u}_0^\dagger (\hat{H}_0 + \hat{H}_{\text{int}}) \hat{u} \\ &\equiv -\hat{H}_0 \hat{u}_0^\dagger \hat{u} + \hat{u}_0^\dagger \hat{H}_0 \hat{u} + \hat{u}_0^\dagger \hat{H}_{\text{int}} \hat{u} \equiv (-\hat{H}_0 \hat{u}_0^\dagger + \hat{u}_0^\dagger \hat{H}_0) \hat{u} + \hat{u}_0^\dagger \hat{H}_{\text{int}} \hat{u}. \end{aligned} \quad (4.217)$$

Since \hat{u}_0^\dagger may be represented as an integral of an exponent of \hat{H}_0 over time (similar to Eq. (181) relating \hat{u} and \hat{H}), these operators commute, so that the parentheses in the last form of Eq. (217) vanish. Now plugging \hat{u} from the last form of Eq. (209), we get the equation,

$$i\hbar \frac{\partial}{\partial t} \hat{u}_I = \hat{u}_0^\dagger \hat{H}_{\text{int}} \hat{u}_0 u_I \equiv (\hat{u}_0^\dagger \hat{H}_{\text{int}} \hat{u}_0) \hat{u}_I, \quad (4.218)$$

which is clearly equivalent to the combination of Eqs. (215) and (216).

As Eq. (215) shows, if the energy scale of the interaction H_{int} is much smaller than that of the background Hamiltonian H_0 , the interaction evolution operators \hat{u}_I and \hat{u}_I^\dagger , and hence the state vectors (213) evolve relatively slowly, without fast background oscillations. This is very convenient for the perturbative approaches to complex interacting systems, in particular to the “open” quantum systems that weakly interact with their environment – see Sec. 7.6.

4.7. Coordinate and momentum representations

Now let me show that in application to the orbital motion of a particle, the bra-ket formalism naturally reduces to the notions and postulates of wave mechanics, which were discussed in Chapter 1. For that, we first have to modify some of the above formulas for the case of a basis with a continuous spectrum of eigenvalues. In that case, it is more appropriate to replace discrete indices, such as j, j' , etc. broadly used above, with the corresponding eigenvalue – just as it was done earlier for functions of the wave vector – see, e.g., Eqs. (1.88), (2.20), etc. For example, the key Eq. (68), defining the eigenkets and eigenvalues of an operator, may be conveniently rewritten in the form

$$\hat{A}|a_A\rangle = A|a_A\rangle. \quad (4.219)$$

More substantially, all sums over such continuous eigenstate sets should be replaced with integrals. For example, for a full and orthonormal set of the continuous eigenstates $|a_A\rangle$, the closure relation (44) should be replaced with

$$\int dA |a_A\rangle\langle a_A| = \hat{I}, \quad (4.220)$$

Continuous spectrum:
closure relation

where the integral is over the whole interval of possible eigenvalues of the observable A .⁴⁴ Applying this relation to the ket-vector of an arbitrary state α , we get the following replacement of Eq. (37):

$$|\alpha\rangle \equiv \hat{I}|\alpha\rangle = \int dA |a_A\rangle\langle a_A|\alpha\rangle = \int dA \langle a_A|\alpha\rangle|a_A\rangle. \quad (4.221)$$

For the particular case when $|\alpha\rangle = |a_{A'}\rangle$, this relation requires that

$$\langle a_A|a_{A'}\rangle = \delta(A - A'); \quad (4.222)$$

Continuous spectrum:
state ortho-normality

this formula replaces the orthonormality condition (38).

According to Eq. (221), in the continuous case the bracket $\langle a_A|\alpha\rangle$ still the role of probability amplitude, i.e. a complex c -number whose modulus squared determines the state a_A 's probability – see the last form of Eq. (120). However, for a continuous observable, the probability to find the system exactly in a particular state is infinitesimal; instead, we should speak about the probability $dW = w(A)dA$ of finding the observable within a small interval $dA \ll A$ near the value A , with *probability density* $w(A) \propto |\langle a_A|\alpha\rangle|^2$. The coefficient in this relation may be found by making a similar change from the summation to integration in the normalization condition (121):

$$\int dA \langle \alpha|a_A\rangle\langle a_A|\alpha\rangle = 1. \quad (4.223)$$

Since the total probability of the system to be in *some* state should be equal to $\int w(A)dA$, this means that

$$w(A) = \langle \alpha|a_A\rangle\langle a_A|\alpha\rangle = |\langle \alpha|a_A\rangle|^2. \quad (4.224)$$

Continuous spectrum:
probability density

Now let us see how we can calculate the expectation values of continuous observables, i.e. their ensemble averages. If we speak about the same observable A whose eigenstates are used as the continuous basis (or any compatible observable), everything is simple. Indeed, inserting Eq. (224) into the general statistical relation

$$\langle A \rangle = \int w(A)AdA, \quad (4.225)$$

which is just the obvious continuous version of Eq. (1.37), we get

$$\langle A \rangle = \int \langle \alpha|a_A\rangle A \langle a_A|\alpha\rangle dA. \quad (4.226)$$

Inserting a delta-function to represent this expression as a formally double integral,

$$\langle A \rangle = \int dA \int dA' \langle \alpha|a_A\rangle A \delta(A - A') \langle a_{A'}|\alpha\rangle, \quad (4.227)$$

and using the continuous-spectrum version of Eq. (98),

⁴⁴ The generalization to cases when the eigenvalue spectrum consists of both a continuum interval plus some set of discrete values, is straightforward, though leads to somewhat cumbersome formulas.

$$\langle a_A | \hat{A} | a_{A'} \rangle = A \delta(A - A'), \quad (4.228)$$

we may write

$$\langle A \rangle = \int dA \int dA' \langle \alpha | a_A \rangle \langle a_A | \hat{A} | a_{A'} \rangle \langle a_{A'} | \alpha \rangle \equiv \langle \alpha | \hat{A} | \alpha \rangle, \quad (4.229)$$

so that Eq. (4.125) remains valid in the continuous-spectrum case without any changes.

The situation is a bit more complicated for the expectation values of an operator that does not commute with the basis-generating operator, because its matrix in that basis may not be diagonal. We will consider (and overcome :-) this technical difficulty very soon, but otherwise we are ready for a discussion of the relation between the bra-ket formalism and the wave mechanics. (For the notation simplicity I will discuss its 1D version; its generalization to 2D and 3D cases is straightforward.)

Let us postulate the (intuitively almost evident) existence of a quantum state basis, whose ket-vectors will be called $|x\rangle$, corresponding to a certain definite value x of the particle's coordinate. Writing the following trivial identity:

$$x|x\rangle = x|x\rangle, \quad (4.230)$$

and comparing this relation with Eq. (219), we see that they do not contradict each other if we assume that x on the left-hand side of this relation is the (Hermitian) operator \hat{x} of particle's coordinate, whose action on a ket- (or bra-) vector is just its multiplication by the c -number x . (This looks like a proof, but is actually a separate, independent postulate, no matter how plausible.) Hence we may consider vectors $|x\rangle$ as the eigenstates of the operator \hat{x} . Let me hope that the reader will excuse me if I do not pursue here a strict proof that this set is full and orthogonal,⁴⁵ so that we may apply to them Eq. (222):

$$\langle x | x' \rangle = \delta(x - x'). \quad (4.231)$$

Using this basis is called the *coordinate representation* – the term which was already used at the end of Sec. 1.1, but without explanation.

In the basis of the x -states, the inner product $\langle a_A | \alpha(t) \rangle$ becomes $\langle x | \alpha(t) \rangle$, and Eq. (223) takes the following form:

$$w(x, t) = \langle \alpha(t) | x \rangle \langle x | \alpha(t) \rangle \equiv \langle x | \alpha(t) \rangle^* \langle x | \alpha(t) \rangle. \quad (4.232)$$

Comparing this formula with the basic postulate (1.22) of wave mechanics, we see that they coincide if the wavefunction of a time-dependent state α is identified with that short bracket:⁴⁶

$$\Psi_\alpha(x, t) \equiv \langle x | \alpha(t) \rangle. \quad (4.233)$$

This key formula provides the desired connection between the bra-ket formalism and the wave mechanics, and should not be too surprising for the (thoughtful :-) reader. Indeed, Eq. (45) shows that any inner product of two state vectors describing two states is a measure of their coincidence – just as the scalar product of two geometric vectors is; the orthonormality condition (38) is a particular manifestation of this fact. In this language, the particular value (233) of a wavefunction Ψ_α at some

⁴⁵Such proof is rather involved mathematically, but physically this fact should be evident.

⁴⁶I do not quite like expressions like $\langle x | \Psi \rangle$ used in some papers and even textbooks. Of course, one is free to replace α with any other letter (Ψ including) to denote a quantum state, but then it is better not to use the same letter to denote the wavefunction, i.e. an inner product of two state vectors, to avoid confusion.

point x and moment t characterizes “how much of a particular coordinate x ” does the state α contain at time t . (Of course, this informal language is too crude to reflect the fact that $\Psi_\alpha(x, t)$ is a complex function, which has not only a modulus but also an argument – the quantum-mechanical phase.)

Now let us rewrite the most important formulas of the bra-ket formalism in the wave mechanics notation. Inner-multiplying both parts of Eq. (219) by the ket-vector $\langle x|$, and then inserting into the left-hand side of that relation the identity operator in the form (220) for coordinate x' , we get

$$\int dx' \langle x | \hat{A} | x' \rangle \langle x' | a_A \rangle = A \langle x | a_A \rangle, \quad (4.234)$$

i.e., using the wavefunction’s definition (233),

$$\int dx' \langle x | \hat{A} | x' \rangle \Psi_A(x') = A \Psi_A(x), \quad (4.235)$$

where, for the notation brevity, the time dependence of the wavefunction is just implied (with the capital Ψ serving as a reminder of this fact), and will be restored when needed.

For a general operator, we would have to stop here, because if it does not commute with the coordinate operator, its matrix in the x -basis is not diagonal, and the integral on the left-hand side of Eq. (235) cannot be worked out explicitly. However, virtually all quantum-mechanical operators discussed in this course⁴⁷ are (*space-*) *local*: they depend on only one spatial coordinate, say x . For such operators, the left-hand side of Eq. (235) may be further transformed as

$$\int \langle x | \hat{A} | x' \rangle \Psi(x') dx' = \int \langle x | x' \rangle \hat{A} \Psi(x') dx' \equiv \hat{A} \int \delta(x - x') \Psi(x') dx' = \hat{A} \Psi(x). \quad (4.236)$$

The first step in this transformation may appear as elementary as the last two, with the ket-vector $|x'\rangle$ swapped with the operator depending only on x ; however, due to the delta-functional character of the bracket (231), this step is, in fact, an additional postulate, so that the second equality in Eq. (236) essentially *defines* the coordinate representation of the local operator, whose explicit form still needs to be determined.

Let us consider, for example, the 1D version of the Hamiltonian (1.41),

$$\hat{H} = \frac{\hat{p}_x^2}{2m} + U(\hat{x}), \quad (4.237)$$

which was the basis of all our discussions in Chapter 2. Its potential-energy part U (which may be time-dependent as well) commutes with the operator \hat{x} , i.e. its matrix in the x -basis has to be diagonal. For such an operator, the transformation (236) is indeed trivial, and its coordinate representation is given merely by the *c*-number function $U(x)$.

The situation the momentum operator \hat{p}_x (and hence the kinetic energy $\hat{p}_x^2/2m$), not commuting with \hat{x} , is less evident. Let me show that its coordinate representation is given by the 1D version of Eq. (1.26), if we *postulate* that the commutation relation (2.14),

$$[\hat{x}, \hat{p}] = i\hbar \hat{I}, \quad \text{i.e. } \hat{x}\hat{p}_x - \hat{p}_x\hat{x} = i\hbar \hat{I}, \quad (4.238)$$

⁴⁷ The only substantial exception is the statistical operator $\hat{w}(x, x')$, to be discussed in Chapter 7.

is valid in *any* representation.⁴⁸ For that, let us consider the following matrix element, $\langle x | \hat{x}\hat{p}_x - \hat{p}_x\hat{x} | x' \rangle$. On one hand, we may use Eq. (238), and then Eq. (231), to write

$$\langle x | \hat{x}\hat{p}_x - \hat{p}_x\hat{x} | x' \rangle = \langle x | i\hbar\hat{I} | x' \rangle = i\hbar\langle x | x' \rangle = i\hbar\delta(x - x'). \quad (4.239)$$

On the other hand, since $\hat{x}|x'\rangle = x'|x'\rangle$ and $\langle x|\hat{x} = \langle x|x$, we may represent the same matrix element as

$$\langle x | \hat{x}\hat{p}_x - \hat{p}_x\hat{x} | x' \rangle = \langle x | x\hat{p}_x - \hat{p}_x x' | x' \rangle = (x - x')\langle x | \hat{p}_x | x' \rangle. \quad (4.240)$$

Comparing Eqs. (239) and (240), we get

$$\langle x | \hat{p}_x | x' \rangle = i\hbar \frac{\delta(x - x')}{x - x'}. \quad (4.241)$$

As it follows from the definition of the delta function,⁴⁹ all expressions involving it acquire final sense only at their integration, in our current case, at that described by Eq. (236). Plugging Eq. (241) into the left-hand side of that relation, we get

$$\int \langle x | \hat{p}_x | x' \rangle \Psi(x') dx' = i\hbar \int \frac{\delta(x - x')}{x - x'} \Psi(x') dx'. \quad (4.242)$$

Since the right-hand-part integral is contributed only by an infinitesimal vicinity of the point $x' = x$, we may calculate it by expanding the continuous wavefunction $\Psi(x')$ into the Taylor series in small $(x' - x)$, and keeping only two leading terms of the series, so that Eq. (242) is reduced to

$$\int \langle x | \hat{p}_x | x' \rangle \Psi(x') dx' = i\hbar \left[\Psi(x) \int \frac{\delta(x - x')}{x - x'} dx' - \int \delta(x - x') \frac{\partial \Psi(x')}{\partial x'} \Big|_{x'=x} dx' \right]. \quad (4.243)$$

Since the delta function may be always understood as an even function of its argument, in our case of $(x - x')$, the first term on the right-hand side is proportional to an integral of an odd function in symmetric limits and is equal to zero, and we get⁵⁰

$$\int \langle x | \hat{p}_x | x' \rangle \Psi(x') dx' = -i\hbar \frac{\partial \Psi}{\partial x}. \quad (4.244)$$

Comparing this expression with the right-hand side of Eq. (236), we see that in the coordinate representation we indeed get the 1D version of Eq. (1.26), which was used so much in Chapter 2,⁵¹

$$\hat{p}_x = -i\hbar \frac{\partial}{\partial x}. \quad (4.245)$$

⁴⁸ Another possible approach to the wave mechanics axiomatics is to *derive* Eg. (238) by *postulating* the form, $\hat{T}_X = \exp\{-ip_x X / \hbar\}$, of the operator that shifts any wavefunction by distance X along the axis x . In my approach, this expression will be *derived* when we need it (in Sec. 5.5), while Eq. (238) is *postulated*.

⁴⁹ If necessary, please revisit MA Sec. 14.

⁵⁰ One more useful expression of this type, which may be proved similarly, is $(\partial/\partial x)\delta(x - x') = \delta(x - x')\partial/\partial x'$.

⁵¹ This means, in particular, that in the sense of Eq. (236), the operator of differentiation is local, despite the fact that its action on a function f may be interpreted as the limit of the fraction $\Delta f / \Delta x$, involving *two* points. (In some axiomatic systems, local operators are *defined* as arbitrary polynomials of functions and their derivatives.)

It is straightforward to show (and is virtually evident) that the coordinate representation of any operator function $f(\hat{p}_x)$ is

$$f\left(-i\hbar \frac{\partial}{\partial x}\right). \quad (4.246)$$

In particular, this pertains to the kinetic energy operator in Eq. (237), so the coordinate representation of this Hamiltonian also takes the very familiar form:

$$\hat{H} = \frac{1}{2m} \left(-i\hbar \frac{\partial}{\partial x} \right)^2 + U(x, t) \equiv -\frac{\hbar^2}{2m} \frac{\partial^2}{\partial x^2} + U(x, t). \quad (4.247)$$

Now returning to the discussion of the general Eq. (235), and comparing its last form with that of Eq. (236), we see that for a local operator in the coordinate representation, the eigenproblem (219) takes the form

$$\hat{A}\Psi_\alpha(x) = A\Psi_\alpha(x), \quad (4.248)$$

Eigenproblem
in x-
representation

even if the operator \hat{A} does not commute with the operator \hat{x} . The most important case of this coordinate-representation form of the eigenproblem (68) is the familiar Eq. (1.60) for the eigenvalues E_n of the energy of a system with a time-independent Hamiltonian.

The operator locality also simplifies the expression for its expectation value. Indeed, plugging the closure relation in the form (231) into the general Eq. (125) twice (written in the first case for x and in the second case for x'), we get

$$\langle A \rangle = \int dx \int dx' \langle \alpha(t) | x \rangle \langle x | \hat{A} | x' \rangle \langle x' | \alpha(t) \rangle = \int dx \int dx' \Psi_\alpha^*(x, t) \langle x | \hat{A} | x' \rangle \Psi_\alpha(x', t). \quad (4.249)$$

Now, Eq. (236) reduces this result to just

$$\langle A \rangle = \int dx \int dx' \Psi_\alpha^*(x, t) \hat{A} \Psi_\alpha(x, t) \delta(x - x') \equiv \int \Psi_\alpha^*(x, t) \hat{A} \Psi_\alpha(x, t) dx. \quad (4.250)$$

i.e. to Eq. (1.23), which had to be postulated in Chapter 1.

Finally, let us discuss the time evolution of the wavefunction, in the Schrödinger picture. For that, we may use Eq. (233) to calculate the (partial) time derivative of the wavefunction of some state α :

$$i\hbar \frac{\partial \Psi_\alpha}{\partial t} = i\hbar \frac{\partial}{\partial t} \langle x | \alpha(t) \rangle. \quad (4.251)$$

Since the coordinate operator \hat{x} does not depend on time explicitly, its eigenstates x are stationary, and we can swap the time derivative and the time-independent bra-vector $\langle x |$. Now using the Schrödinger-picture equation (158), and then inserting the identity operator in the continuous form (220) of the closure relation, written for the coordinate eigenstates,

$$\int dx' |x'\rangle \langle x'| = \hat{I}, \quad (4.252)$$

we may continue to develop the right-hand side of Eq. (251) as

$$\langle x | i\hbar \frac{\partial}{\partial t} | \alpha(t) \rangle = \langle x | \hat{H} | \alpha(t) \rangle = \int dx' \langle x | \hat{H} | x' \rangle \langle x' | \alpha(t) \rangle = \int dx' \langle x | \hat{H} | x' \rangle \Psi_\alpha(x'), \quad (4.253)$$

If the Hamiltonian operator is local, we may apply Eq. (236) to the last expression, to get the familiar form (1.28) of the Schrödinger equation:

$$i\hbar \frac{\partial \Psi_\alpha}{\partial t} = \hat{H}\Psi_\alpha, \quad (4.254)$$

in which the coordinate representation of the operator \hat{H} is implied.

So, for the local operators that obey Eq. (236), we have been able to derive all the basic notions and postulates of the wave mechanics from the bra-ket formalism. Moreover, the formalism has allowed us to get the very useful equation (248) for an arbitrary local operator, which will be repeatedly used below. (In the first three chapters of this course, we have only used its particular case (1.60) for the Hamiltonian operator.)

Now let me deliver on my promise to develop a more balanced view at the monochromatic de Broglie waves (1), which would be more respectful to the evident $\mathbf{r} \leftrightarrow \mathbf{p}$ symmetry of the coordinate and momentum. Let us do this for the 1D case when the wave may be represented as

$$\psi_p(x) = a_p \exp\left\{i \frac{px}{\hbar}\right\}, \quad \text{for all } -\infty < x < +\infty. \quad (4.255)$$

(For the sake of brevity, from this point to the end of the section, I am dropping the index x in the notation of the momentum – just as it was done in Chapter 2.) Let us have a good look at this function. Since it satisfies Eq. (248) for the 1D momentum operator (245),

$$\hat{p}\psi_p = p\psi_p, \quad (4.256)$$

ψ_p is an eigenfunction of that operator. But this means that we can also write Eq. (219) for the corresponding ket-vector:

$$\hat{p}|p\rangle = p|p\rangle, \quad (4.257)$$

and according to Eq. (233), the wavefunction (255) may be represented as

$$\psi_p(x) = \langle x|p\rangle. \quad (4.258)$$

This expression is quite remarkable in its $x \leftrightarrow p$ symmetry – which may be pursued further on. Before doing that, however, we have to discuss the normalization of such wavefunctions. Indeed, in this case, the probability density $w(x)$ (18) is constant, so that its integral

$$\int_{-\infty}^{+\infty} w(x)dx = \int_{-\infty}^{+\infty} \psi_p(x)\psi_p^*(x)dx \quad (4.259)$$

diverges if $a_p \neq 0$. Earlier in the course, we discussed two ways to avoid this divergence. One is to use a very large but finite integration volume – see Eq. (1.31). Another way is to work with wave packets of the type (2.20), possibly of a very large length and hence a very narrow spread of the momentum values. Then the integral (259) may be required to equal 1 without any conceptual problem.

However, both these methods, convenient for the solution of many particular problems, violate the $x \leftrightarrow p$ symmetry and hence are inconvenient for our current conceptual discussion. Instead, let us continue to identify the eigenvectors $\langle p|$ and $|p\rangle$ of the momentum with the bra- and ket-vectors $\langle a_p|$ and

$|a_A\rangle$ of the general theory described at the beginning of this section. Then the normalization condition (222) becomes

$$\langle p | p' \rangle = \delta(p - p'). \quad (4.260)$$

Inserting the identity operator in the form (252), with the integration variable x' replaced by x , into the left-hand side of this equation, and using Eq. (258), we can translate this normalization rule to the wavefunction language:

$$\int dx \langle p | x \rangle \langle x | p' \rangle \equiv \int dx \psi_p^*(x) \psi_{p'}(x) = \delta(p - p'). \quad (4.261)$$

For the wavefunction (255), this requirement turns into the following condition:

$$a_p^* a_{p'} \int_{-\infty}^{+\infty} \exp\left\{i \frac{(p-p')x}{\hbar}\right\} dx \equiv |a_p|^2 2\pi\hbar \delta(p - p') = \delta(p - p'), \quad (4.262)$$

so that, finally, $a_p = e^{i\phi}/(2\pi\hbar)^{1/2}$, where ϕ is an arbitrary (real) phase, and Eq. (255) becomes⁵²

$$\psi_p(x) = \langle x | p \rangle = \frac{1}{(2\pi\hbar)^{1/2}} \exp\left\{i\left(\frac{px}{\hbar} + \phi\right)\right\}, \quad (4.263)$$

Now let us represent an arbitrary wavefunction $\psi(x)$ as a wave packet of the type (2.20), based on the wavefunctions (263), taking $\phi = 0$ for the notation brevity, because the phase may be incorporated into the (generally, complex) envelope function $\varphi(p)$:

$$\psi(x) = \frac{1}{(2\pi\hbar)^{1/2}} \int \varphi(p) \exp\left\{i \frac{px}{\hbar}\right\} dp. \quad (4.264)$$

x-
representation:
wavefunctions

From the mathematical point of view, this is just a 1D Fourier spatial transform, and its reciprocal is

$$\varphi(p) \equiv \frac{1}{(2\pi\hbar)^{1/2}} \int \psi(x) \exp\left\{-i \frac{px}{\hbar}\right\} dx. \quad (4.265)$$

p-
representation:
wavefunctions

These expressions are completely symmetric, and represent the same wave packet; this is why the functions $\psi(x)$ and $\varphi(p)$ are frequently called the *reciprocal representations* of a quantum state of the particle: respectively, its *coordinate (x-) and momentum (p-) representations*. Using Eq. (258), and Eq. (263) with $\phi = 0$, they may be recast into simpler forms,

$$\psi(x) = \int \varphi(p) \langle x | p \rangle dp, \quad \varphi(p) = \int \psi(x) \langle p | x \rangle dx, \quad (4.266)$$

in which the inner products satisfy the basic postulate (14) of the bra-ket formalism:

$$\langle p | x \rangle = \frac{1}{(2\pi\hbar)^{1/2}} \exp\left\{-i \frac{px}{\hbar}\right\} = \langle x | p \rangle^*. \quad (4.267)$$

⁵² Repeating such calculation for each Cartesian component of a plane monochromatic wave of arbitrary dimensionality d , we get $\psi_p = (2\pi\hbar)^{-d/2} \exp\{i(\mathbf{p} \cdot \mathbf{r}/\hbar + \phi)\}$.

Next, we already know that in the x -representation, i.e. in the usual wave mechanics, the coordinate operator \hat{x} is reduced to the multiplication by x , and the momentum operator is proportional to the partial derivative over the coordinate:

x-representation:
operators

$$\hat{x}|_{\text{in } x} = x, \quad \hat{p}|_{\text{in } x} = -i\hbar \frac{\partial}{\partial x}. \quad (4.268)$$

It is natural to guess that in the p -representation, the expressions for operators would be reciprocal:

p-representation:
operators

$$\hat{x}|_{\text{in } p} = +i\hbar \frac{\partial}{\partial p}, \quad \hat{p}|_{\text{in } p} = p, \quad (4.269)$$

with the only difference of one sign, which is due to the opposite signs of the Fourier exponents in Eqs. (264) and (265). The proof of Eqs. (269) is straightforward; for example, acting by the momentum operator on the arbitrary wavefunction (264), we get

$$\hat{p}\psi(x) = -i\hbar \frac{\partial}{\partial x} \psi(x) = \frac{1}{(2\pi\hbar)^{1/2}} \int \varphi(p) \left(-i\hbar \frac{\partial}{\partial x} \exp\left\{i \frac{px}{\hbar}\right\} \right) dp = \frac{1}{(2\pi\hbar)^{1/2}} \int p \varphi(p) \exp\left\{i \frac{px}{\hbar}\right\} dp, \quad (4.270)$$

and similarly for the operator \hat{x} acting on the function $\varphi(p)$. Comparing the final form of Eq. (270) with the initial Eq. (264), we see that the action of the operators (268) on the wavefunction ψ (i.e. the state's x -representation) gives the same results as the action of the operators (269) on the function φ (i.e. its p -representation).

It is illuminating to have one more, different look at this coordinate-momentum duality. For that, notice that according to Eqs. (82)-(84), we may consider the bracket $\langle x|p\rangle$ as an element of the (infinite-size) matrix U_{xp} of the unitary transform from the x -basis to the p -basis. Let us use this fact to derive the general operator transform rule that would be a continuous version of Eq. (92). Say, we want to calculate the general matrix element of some operator, known in the x -representation, in the p -representation:

$$\langle p|\hat{A}|p'\rangle. \quad (4.271)$$

Inserting two identity operators (252), written for x and x' , into this bracket, and then using Eq. (258) and its complex conjugate, and also Eq. (236) (again, valid only for space-local operators!), we get

$$\begin{aligned} \langle p|\hat{A}|p'\rangle &= \int dx \int dx' \langle p|x\rangle \langle x|\hat{A}|x'\rangle \langle x'|p'\rangle = \int dx \int dx' \psi_p^*(x) \langle x|\hat{A}|x'\rangle \psi_{p'}(x') \\ &= \frac{1}{2\pi\hbar} \int dx \int dx' \exp\left\{-i \frac{px}{\hbar}\right\} \delta(x-x') \hat{A} \exp\left\{+i \frac{p'x'}{\hbar}\right\} = \frac{1}{2\pi\hbar} \int dx \exp\left\{-i \frac{px}{\hbar}\right\} \hat{A} \exp\left\{+i \frac{p'x}{\hbar}\right\}. \end{aligned} \quad (4.272)$$

As a sanity check, for the momentum operator itself, this relation yields:

$$\langle p|\hat{p}|p'\rangle = \frac{1}{2\pi\hbar} \int dx \exp\left\{-i \frac{px}{\hbar}\right\} \left(-i\hbar \frac{\partial}{\partial x}\right) \exp\left\{i \frac{p'x}{\hbar}\right\} = \frac{p'}{2\pi\hbar} \int_{-\infty}^{+\infty} \exp\left\{i \frac{(p'-p)x}{\hbar}\right\} dx = p' \delta(p'-p). \quad (4.273)$$

Due to Eq. (257), this result is equivalent to the second of Eqs. (269).

From a thoughtful reader, I anticipate the following natural question: why is the momentum representation used much less frequently than the coordinate representation – i.e. wave mechanics? The answer is purely practical: besides the important special case of the 1D harmonic oscillator (to be

revisited in Sec. 5.4), in most systems the orbital-motion Hamiltonian (237) is not $x \leftrightarrow p$ symmetric, with the potential energy $U(\mathbf{r})$ typically being a more complex function than the kinetic energy $p^2/2m$. Because of that, it is easier to analyze such systems treating such potential energy operator just a c -number multiplier, as it is in the coordinate representation – as it was done in Chapters 1-3.

The most significant exception from this practice is the motion in a periodic potential in presence of a coordinate-independent external force $\mathbf{F}(t)$. As was discussed in Secs. 2.7 and 3.4, in such periodic systems the eigenenergies $E_n(\mathbf{q})$, playing the role of the effective kinetic energy of the particle, may be rather involved functions of its quasimomentum $\hbar\mathbf{q}$, while its effective potential energy $U_{\text{ef}} = -\mathbf{F}(t) \cdot \mathbf{r}$, due to the additional force $\mathbf{F}(t)$, is a very simple function of coordinates. This is why detailed analyses of the quantum effects briefly discussed in Sec. 2.8 (the Bloch oscillations, etc.) and also such statistical phenomena as drift, diffusion, etc.,⁵³ in solid-state theory are typically based on the momentum (or rather quasimomentum) representation.

4.8. Exercise problems

4.1. Prove that if \hat{A} and \hat{B} are linear operators, and C is a c -number, then:

- (i) $(\hat{A}^\dagger)^\dagger = \hat{A}$;
- (ii) $(C\hat{A})^\dagger = C^* \hat{A}^\dagger$;
- (iii) $(\hat{A}\hat{B})^\dagger = \hat{B}^\dagger \hat{A}^\dagger$;
- (iv) the operators $\hat{A}\hat{A}^\dagger$ and $\hat{A}^\dagger\hat{A}$ are Hermitian.

4.2. Prove that for any linear operators $\hat{A}, \hat{B}, \hat{C}$, and \hat{D} ,

$$[\hat{A}\hat{B}, \hat{C}\hat{D}] = \hat{A}\{\hat{B}, \hat{C}\}\hat{D} - \hat{A}\hat{C}\{\hat{B}, \hat{D}\} + \{\hat{A}, \hat{C}\}\hat{D}\hat{B} - \hat{C}\{\hat{A}, \hat{D}\}\hat{B}.$$

4.3. Calculate all possible binary products $\sigma_j\sigma_{j'}$ (for $j, j' = x, y, z$) of the Pauli matrices, defined by Eqs. (105), and their commutators and anticommutators (defined similarly to those of the corresponding operators). Summarize the results, using the Kronecker delta and Levi-Civita permutation symbols.⁵⁴

4.4. Calculate the following expressions,

- (i) $(\mathbf{c} \cdot \boldsymbol{\sigma})^n$, and then
- (ii) $(b\mathbf{I} + \mathbf{c} \cdot \boldsymbol{\sigma})^n$,

for the scalar product $\mathbf{c} \cdot \boldsymbol{\sigma}$ of the Pauli matrix vector $\boldsymbol{\sigma} \equiv \mathbf{n}_x\sigma_x + \mathbf{n}_y\sigma_y + \mathbf{n}_z\sigma_z$ by an arbitrary c -number geometric vector \mathbf{c} , where $n \geq 0$ is an integer, and b is an arbitrary scalar c -number.

Hint: For task (ii), you may like to use the binomial theorem,⁵⁵ and then transform the result in a way enabling you to use the same theorem backward.

⁵³ In this series, a brief discussion of these effects may be found in SM Chapter 6.

⁵⁴ See, e.g., MA Eqs. (13.1) and (13.2).

⁵⁵ See, e.g. MA Eq. (2.9).

4.5. Use the solution of the previous problem to derive Eqs. (2.191) for the transparency \mathcal{T} of a system of N similar, equidistant, delta-functional potential barriers.

4.6. Use the solution of Problem 4(i) to spell out the following matrix: $\exp\{i\theta \mathbf{n} \cdot \boldsymbol{\sigma}\}$, where $\boldsymbol{\sigma}$ is the 3D vector (117) of the Pauli matrices, \mathbf{n} is a c -number geometric vector of unit length, and θ is a c -number scalar.

4.7. Use the solution of Problem 4(ii) to calculate $\exp\{A\}$, where A is an arbitrary 2×2 matrix.

4.8. Express all elements of the matrix $B \equiv \exp\{A\}$ explicitly via those of the 2×2 matrix A . Spell out your result for the following matrices:

$$A = \begin{pmatrix} a & a \\ a & a \end{pmatrix}, \quad A' = \begin{pmatrix} i\varphi & i\varphi \\ i\varphi & i\varphi \end{pmatrix},$$

with real a and φ .

4.9. Prove that for arbitrary square matrices A and B ,

$$\text{Tr}(AB) = \text{Tr}(BA).$$

Is each diagonal element $(AB)_{jj}$ necessarily equal to $(BA)_{jj}$?

4.10. Calculate the trace of the following 2×2 matrix:

$$A \equiv (\mathbf{a} \cdot \boldsymbol{\sigma})(\mathbf{b} \cdot \boldsymbol{\sigma})(\mathbf{c} \cdot \boldsymbol{\sigma}),$$

where $\boldsymbol{\sigma}$ is the Pauli matrix vector, while \mathbf{a} , \mathbf{b} , and \mathbf{c} are arbitrary c -number vectors.

4.11. Prove that the matrix trace of an arbitrary operator does not change at its arbitrary unitary transformation.

4.12. Prove that for any two full and orthonormal bases $\{u\}$ and $\{v\}$ of the same Hilbert space,

$$\text{Tr}\left(\left|u_j\right\rangle\left\langle v_{j'}\right|\right) = \left\langle v_{j'}\left|u_j\right\rangle\right.$$

4.13. Is the 1D scattering matrix S , defined by Eq. (2.124), unitary? What about the 1D transfer matrix T defined by Eq. (2.125)?

4.14. Calculate the trace of the following matrix:

$$\exp\{i\mathbf{a} \cdot \boldsymbol{\sigma}\} \exp\{i\mathbf{b} \cdot \boldsymbol{\sigma}\},$$

where $\boldsymbol{\sigma}$ is the Pauli matrix vector, while \mathbf{a} and \mathbf{b} are c -number geometric vectors.

4.15. Prove the following vector-operator identity:

$$(\boldsymbol{\sigma} \cdot \hat{\mathbf{r}})(\boldsymbol{\sigma} \cdot \hat{\mathbf{p}}) = I \hat{\mathbf{r}} \cdot \hat{\mathbf{p}} + i\boldsymbol{\sigma} \cdot (\hat{\mathbf{r}} \times \hat{\mathbf{p}}),$$

where $\boldsymbol{\sigma}$ is the Pauli matrix vector, and I is the 2×2 identity matrix.

Hint: Take into account that the vector operators $\hat{\mathbf{r}}$ and $\hat{\mathbf{p}}$ are defined in the orbital-motion Hilbert space, different from that of the Pauli vector-matrix σ , and hence commute with it – even though they do not commute with each other.

4.16. Let A_j be eigenvalues of some operator \hat{A} . Express the following two sums,

$$\Sigma_1 \equiv \sum_j A_j, \quad \Sigma_2 \equiv \sum_j A_j^2,$$

via the matrix elements $A_{jj'}$ of this operator in an arbitrary basis.

4.17. Calculate $\langle \sigma_z \rangle$ of a spin- $1/2$ in the quantum state with the following ket-vector:

$$|\alpha\rangle = \text{const} \times (\left| \uparrow \right\rangle + \left| \downarrow \right\rangle + \left| \rightarrow \right\rangle + \left| \leftarrow \right\rangle),$$

where (\uparrow, \downarrow) and $(\rightarrow, \leftarrow)$ are the eigenstates of the Pauli matrices σ_z and σ_x , respectively.

Hint: Double-check whether your solution is general.

4.18. A spin- $1/2$ is fully polarized in the positive z -direction. Calculate the probabilities of the alternative outcomes of a perfect Stern-Gerlach experiment with the magnetic field oriented in an arbitrary different direction, performed on a particle in this spin state.

4.19. In a certain basis, the Hamiltonian of a two-level system is described by the matrix

$$H = \begin{pmatrix} E_1 & 0 \\ 0 & E_2 \end{pmatrix}, \quad \text{with } E_1 \neq E_2,$$

while the operator of some observable A of this system, by the matrix

$$A = \begin{pmatrix} 1 & 1 \\ 1 & 1 \end{pmatrix}.$$

For the system's state with the energy definitely equal to E_1 , find the possible results of measurements of the observable A and the probabilities of the corresponding measurement outcomes.

4.20. Certain states $u_{1,2,3}$ form an orthonormal basis of a system with the following Hamiltonian

$$\hat{H} = -\delta (\left| u_1 \right\rangle \langle u_2 | + \left| u_2 \right\rangle \langle u_3 | + \left| u_3 \right\rangle \langle u_1 |) + \text{h.c.},$$

where δ is a real constant, and h.c. means the Hermitian conjugate of the previous expression. Calculate its stationary states and energy levels. Can you relate this system to any other(s) discussed earlier in the course?

4.21. Guided by Eq. (2.203), and by the solutions of Problems 3.11 and 4.20, suggest a Hamiltonian describing particle's dynamics in an infinite 1D chain of similar potential wells in the tight-binding approximation, in the bra-ket formalism. Verify that its eigenstates and eigenvalues correspond to those discussed in Sec. 2.7.

4.22. Calculate eigenvectors and eigenvalues of the following matrices:

$$A = \begin{pmatrix} 0 & 1 & 0 \\ 1 & 0 & 1 \\ 0 & 1 & 0 \end{pmatrix}, \quad B = \begin{pmatrix} 0 & 0 & 0 & 1 \\ 0 & 0 & 1 & 0 \\ 0 & 1 & 0 & 0 \\ 1 & 0 & 0 & 0 \end{pmatrix}.$$

4.23. A certain state γ is an eigenstate of each of two operators, \hat{A} and \hat{B} . What can be said about the corresponding eigenvalues a and b , if the operators anticommute?

4.24. Derive the differential equation for the time evolution of the expectation value of an observable, using both the Schrödinger picture and the Heisenberg picture of quantum dynamics.

4.25. At $t = 0$, a spin- $\frac{1}{2}$ whose interaction with an external field is described by the Hamiltonian

$$\hat{H} = \mathbf{c} \cdot \hat{\mathbf{\sigma}} \equiv c_x \hat{\sigma}_x + c_y \hat{\sigma}_y + c_z \hat{\sigma}_z$$

(where $c_{x,y,z}$ are real c -number constants, and $\hat{\sigma}_{x,y,z}$ are the Pauli operators), was in the state \uparrow , one of the two eigenstates of $\hat{\sigma}_z$. In the Schrödinger picture, calculate the time evolution of:

- (i) the ket-vector $|\alpha\rangle$ of the spin (in any time-independent basis you like),
- (ii) the probabilities to find the spin in the states \uparrow and \downarrow , and
- (iii) the expectation values of all three Cartesian components (\hat{S}_x , etc.) of the spin vector.

Analyze and interpret the results for the particular case $c_y = c_z = 0$.

Hint: Think about the best basis to use for the solution.

4.26. For the same system as in the previous problem, use the Heisenberg picture to calculate the time evolution of:

- (i) all three Cartesian components of the spin operator $\hat{S}_H(t)$, and
- (ii) the expectation values of the spin components.

Compare the latter results with those of the previous problem.

4.27. For the same system as in the two last problems, calculate matrix elements of the operator $\hat{\sigma}_z$ in the basis of the stationary states of the system.

4.28. In the Schrödinger picture of quantum dynamics, certain three operators satisfy the following commutation relation:

$$[\hat{A}, \hat{B}] = \hat{C}.$$

What is their relation in the Heisenberg picture, at a certain time instant t ?

4.29. Prove the Bloch theorem given by either Eq. (3.107) or Eq. (3.108).

Hint: Consider the *translation operator* $\hat{\tau}_{\mathbf{R}}$ defined by the following result of its action on an arbitrary function $f(\mathbf{r})$:

$$\hat{\tau}_{\mathbf{R}} f(\mathbf{r}) = f(\mathbf{r} + \mathbf{R}),$$

for the case when \mathbf{R} is an arbitrary vector of the Bravais lattice (3.106). In particular, analyze the commutation properties of this operator, and apply them to an eigenfunction $\psi(\mathbf{r})$ of the stationary Schrödinger equation for a particle moving in the 3D periodic potential described by Eq. (3.105).

4.30. A constant force F is applied to an (otherwise free) 1D particle of mass m . Calculate the stationary wavefunctions of the particle in:

- (i) the coordinate representation, and
- (ii) the momentum representation.

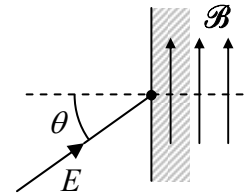
Discuss the relation between the results.

4.31. Use the momentum representation to re-solve the problem discussed at the beginning of Sec. 2.6, i.e. calculate the eigenenergy of a 1D particle of mass m , localized in a very short potential well of “weight” w .

4.32. The momentum representation of a certain operator of 1D orbital motion is p^{-1} . Find its coordinate representation.

4.33.* For a particle moving in a 3D periodic potential, develop the bra-ket formalism for the \mathbf{q} -representation, in which a complex amplitude similar to a_q in Eq. (2.234) (but generalized to 3D and all energy bands) plays the role of the wavefunction. In particular, calculate the operators \mathbf{r} and \mathbf{v} in this representation, and use the result to prove Eq. (2.237) for the 1D case in the low-field limit.

4.34. A uniform, time-independent magnetic field \mathcal{B} is induced in one semi-space, while the other semi-space is field-free, with a sharp, plane boundary between these two regions. A monochromatic beam of non-relativistic, electrically-neutral spin- $1/2$ particles with a gyromagnetic ratio $\gamma \neq 0$,⁵⁶ in a certain spin state and with a kinetic energy E , is incident on this boundary, from the field-free side, under angle θ – see figure on the right. Calculate the coefficient of particle reflection from the boundary.



⁵⁶ The fact that γ may be different from zero even for electrically-neutral particles, such as neutrons, is explained by the Standard Model of the elementary particles, in which a neutron “consists” (in a broad sense of the word) of three electrically-charged quarks with zero net charge.

Chapter 5. Some Exactly Solvable Problems

The objective of this chapter is to describe several relatively simple but very important applications of the bra-ket formalism, including a few core problems of wave mechanics we have already started to discuss in Chapters 2 and 3.

5.1. Two-level systems

The discussion of the bra-ket formalism in the previous chapter was peppered with numerous illustrations of its main concepts on the example of “spins-½” – systems with the smallest non-trivial (two-dimensional) Hilbert space, in which the bra- and ket-vectors of an arbitrary quantum state α may be represented as a linear superposition of just two basis vectors, for example

$$|\alpha\rangle = \alpha_{\uparrow}|\uparrow\rangle + \alpha_{\downarrow}|\downarrow\rangle, \quad (5.1)$$

where the states \uparrow and \downarrow were defined as the eigenstates of the Pauli matrix σ_z – see Eq. (4.105). For the genuine spin-½ particles, such as electrons, placed in a z -oriented time-independent magnetic field, these states are the stationary “spin-up” and “spin-down” stationary states of the Pauli Hamiltonian (4.163), with the corresponding two energy levels (4.167). However, an approximate but reasonable quantum description of some other important systems may also be given in such Hilbert space.

For example, as was discussed in Sec. 2.6, two weakly coupled space-localized orbital states of a spin-free particle are sufficient for an approximate description of its quantum oscillations between two potential wells. A similar coupling of two traveling waves explains the energy band splitting in the weak-potential approximation of the band theory – Sec. 2.7. As will be shown in the next chapter, in systems with time-independent Hamiltonians, such situation almost unavoidably appears each time when two energy levels are much closer to each other than to other levels. Moreover, as will be shown in Sec. 6.5, a similar truncated description is adequate even in cases when two levels E_n and $E_{n'}$ of an unperturbed system are not close to each other, but the corresponding states become coupled by an applied ac field of a frequency ω very close to the difference $(E_n - E_{n'})/\hbar$. Such *two-level systems* (alternatively called “spin-½-like” systems) are nowadays the focus of additional attention in the view of prospects of their use for quantum information processing and encryption.¹ This is why let me spend a bit more time reviewing the main properties of an arbitrary two-level system.

First, the most general form of the Hamiltonian of a two-level system is represented, in an arbitrary basis, by a 2×2 matrix

$$H = \begin{pmatrix} H_{11} & H_{12} \\ H_{21} & H_{22} \end{pmatrix}. \quad (5.2)$$

According to the discussion in Secs. 4.3-4.5, since the Hamiltonian operator has to be Hermitian, the diagonal elements of the matrix H have to be real, and its off-diagonal elements be complex conjugates

¹ In the last context, to be discussed in Sec. 8.5, the two-level systems are usually called *qubits*.

of each other: $H_{21} = H_{12}^*$. As a result, we may not only represent H as a linear combination (4.106) of the identity matrix and the Pauli matrices but also reduce it to a more specific form:

$$H = bI + \mathbf{c} \cdot \boldsymbol{\sigma} = \begin{pmatrix} b + c_z & c_x - ic_y \\ c_x + ic_y & b - c_z \end{pmatrix} \equiv \begin{pmatrix} b + c_z & c_- \\ c_+ & b - c_z \end{pmatrix}, \quad c_\pm \equiv c_x \pm ic_y, \quad (5.3)$$

where the scalar b and the Cartesian components of the vector \mathbf{c} are *real* c -number coefficients:

$$b = \frac{H_{11} + H_{22}}{2}, \quad c_x = \frac{H_{12} + H_{21}}{2} \equiv \text{Re } H_{21}, \quad c_y = \frac{H_{21} - H_{12}}{2i} \equiv \text{Im } H_{21}, \quad c_z = \frac{H_{11} - H_{22}}{2}. \quad (5.4)$$

If such Hamiltonian does not depend on time, the corresponding characteristic equation (4.103) for the system's energy levels E_\pm ,

$$\begin{vmatrix} b + c_z - E & c_- \\ c_+ & b - c_z - E \end{vmatrix} = 0, \quad (5.5)$$

is a simple quadratic equation, with the following solutions:

$$E_\pm = b \pm c \equiv b \pm (c_+ c_- + c_z^2)^{1/2} \equiv b \pm (c_x^2 + c_y^2 + c_z^2)^{1/2} \equiv \frac{H_{11} + H_{22}}{2} \pm \left[\left(\frac{H_{11} - H_{22}}{2} \right)^2 + |H_{21}|^2 \right]^{1/2}. \quad (5.6)$$

The parameter $b \equiv (H_{11} + H_{22})/2$ evidently gives the average energy $E^{(0)}$ of the system, which does not contribute to the level splitting

$$\Delta E \equiv E_+ - E_- = 2c \equiv 2(c_x^2 + c_y^2 + c_z^2)^{1/2} \equiv \left[(H_{11} - H_{22})^2 + 4|H_{21}|^2 \right]^{1/2}. \quad (5.7)$$

So, the splitting is a hyperbolic function of the coefficient $c_z \equiv (H_{11} - H_{22})/2$. A plot of this function is the famous level-anticrossing diagram (Fig. 1), which has already been discussed in Sec. 2.7 in the particular context of the weak-potential limit of the 1D band theory.

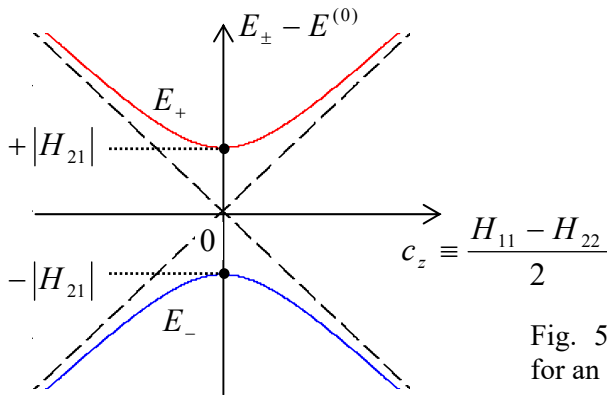


Fig. 5.1. The level-anticrossing diagram for an arbitrary two-level system.

The physics of the diagram becomes especially clear if the two states of the basis used to spell out the matrix (2), may be interpreted as the stationary states of two potentially independent subsystems, with the energies, respectively, H_{11} and H_{22} . (For example, in the case of two weakly coupled potential wells discussed in Sec. 2.6, these are the ground-state energies of two distant wells.) Then the off-diagonal elements $c_- \equiv H_{12}$ and $c_+ \equiv H_{21} = H_{12}^*$ describe the subsystem coupling, and the level

anticrossing diagram shows how do the eigenenergies of the coupled system depend (at fixed coupling) on the difference of the subsystem energies. As was already discussed in Sec. 2.7, the most striking feature of the diagram is that any non-zero coupling $|c_{\pm}| \equiv (c_x^2 + c_y^2)^{1/2}$ changes the topology of the eigenstate energies, creating a gap of the width ΔE .

As it follows from our discussions of particular two-level systems in Secs. 2.6 and 4.6, their dynamics also has a general feature – the quantum oscillations. Namely, if we put any two-level system into any initial state different from one of its eigenstates \pm , and then let it evolve on its own, the probability of its finding the system in any of the “partial” states exhibits oscillations with the frequency

$$\Omega = \frac{\Delta E}{\hbar} \equiv \frac{E_+ - E_-}{\hbar} = 2c, \quad (5.8)$$

lowest at the exact subsystem symmetry ($c_z = 0$, i.e. $H_{11} = H_{22}$), when it is proportional to the coupling strength: $\Omega_{\min} = 2|c_{\pm}|/\hbar \equiv 2|H_{12}|/\hbar = 2|H_{21}|/\hbar$.

In the case discussed in Sec. 2.6, these are the oscillations of a particle between the two coupled potential wells (or rather of the probabilities to find it in either well) – see, e.g., Eqs. (2.181). On the other hand, for a spin-½ particle in an external magnetic field, these oscillations take the form of spin precession in the plane normal to the field, with periodic oscillations of its Cartesian components (or rather their expectation values) – see, e.g., Eqs. (4.173)-(4.174). Some other examples of the quantum oscillations in two-level systems may be rather unexpected; for example, the ammonium molecule NH₃ (Fig. 2) has two symmetric states that differ by the inversion of the nitrogen atom relative to the plane of the three hydrogen atoms, which are weakly coupled due to quantum-mechanical tunneling of the nitrogen atom through the plane of the hydrogen atoms.² Since for this particular molecule, in the absence of external fields, the level splitting ΔE corresponds to an experimentally convenient frequency $\Omega/2\pi \approx 24$ GHz, it played an important historic role at the initial development of the atomic frequency standards and microwave quantum generators (*masers*) in the early 1950s,³ which paved the way toward laser technology.

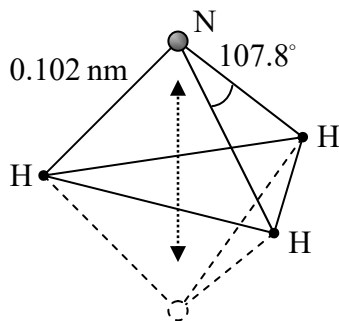


Fig. 5.2. An ammonia molecule and its inversion.

Now let us now discuss a very convenient geometric representation of an arbitrary state α of (any!) two-level system. As Eq. (1) shows, such state is completely described by two complex

² Since the hydrogen atoms are much lighter, it would be fairer to speak about the tunneling of their triangle around the (nearly immobile) nitrogen atom.

³ In particular, these molecules were used in the demonstration of the first maser by C. Townes' group in 1954.

coefficients (*c*-numbers) – say, α_{\uparrow} and α_{\downarrow} . If the vectors of the basis states \uparrow and \downarrow are normalized, then these coefficients must obey the following restriction:

$$W_{\Sigma} = \langle \alpha | \alpha \rangle = (\langle \uparrow | \alpha_{\uparrow}^* + \langle \downarrow | \alpha_{\downarrow}^* \rangle (\alpha_{\uparrow} | \uparrow \rangle + \alpha_{\downarrow} | \downarrow \rangle) = \alpha_{\uparrow}^* \alpha_{\uparrow} + \alpha_{\downarrow}^* \alpha_{\downarrow} = |\alpha_{\uparrow}|^2 + |\alpha_{\downarrow}|^2 = 1. \quad (5.9)$$

This requirement is automatically satisfied if we take the moduli of α_{\uparrow} and α_{\downarrow} equal to the sine and cosine of the same (real) angle. Thus we may write, for example,

$$\alpha_{\uparrow} = \cos \frac{\theta}{2} e^{i\gamma}, \quad \alpha_{\downarrow} = \sin \frac{\theta}{2} e^{i(\gamma+\varphi)}. \quad (5.10)$$

Moreover, according to the general Eq. (4.125), if we deal with just one system,⁴ the common phase factor $\exp\{i\gamma\}$ drops out of the calculation of any expectation value, so that we may take $\gamma = 0$, and Eq. (10) is reduced to

$$\alpha_{\uparrow} = \cos \frac{\theta}{2}, \quad \alpha_{\downarrow} = \sin \frac{\theta}{2} e^{i\varphi}. \quad (5.11)$$

Bloch
sphere
representation

The reason why the argument of these sine and cosine functions is usually taken in the form $\theta/2$, becomes clear from Fig. 3a: Eq. (11) conveniently maps each state α of a two-level system on a certain *representation point* on a unit-radius *Bloch sphere*,⁵ with the polar angle θ and the azimuthal angle φ .

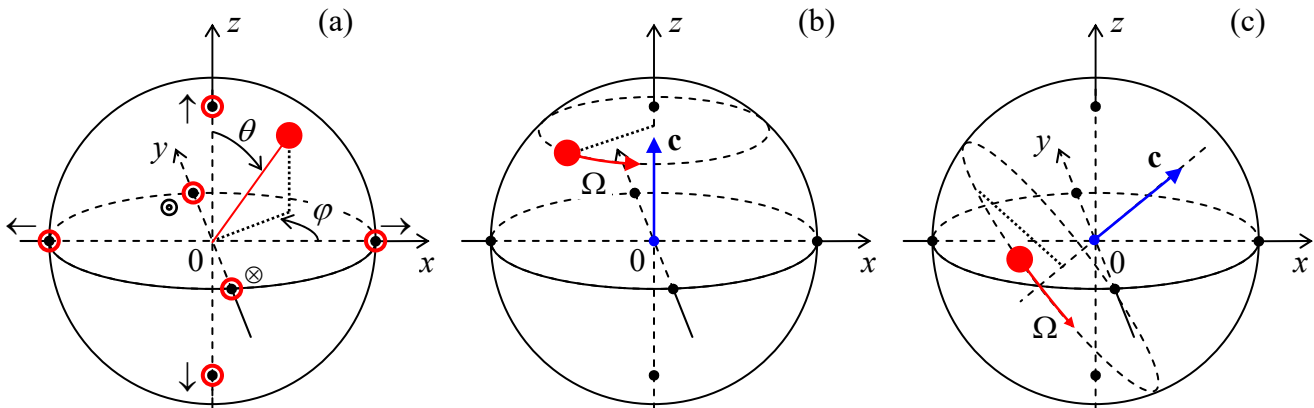


Fig. 5.3. The Bloch sphere: (a) the representation of an arbitrary state (solid red point) and the eigenstates of the Pauli matrices (dotted points), and (b, c) the two-level system's evolution: (b) in a constant “field” \mathbf{c} directed along the z -axis, and (c) in a field of arbitrary orientation.

In particular, the basis state \uparrow , described by Eq. (1) with $\alpha_{\uparrow} = 1$ and $\alpha_{\downarrow} = 0$, corresponds to the North Pole of the sphere ($\theta = 0$), while the opposite state \downarrow , with $\alpha_{\uparrow} = 0$ and $\alpha_{\downarrow} = 1$, to its South Pole ($\theta = \pi$). Similarly, the eigenstates \rightarrow and \leftarrow of the matrix σ_x , described by Eqs. (4.122), i.e. having $\alpha_{\uparrow} =$

⁴ If you need a reminder of why this condition is crucial, please revisit the discussion at the end of Sec. 1.6. Note also that the mutual phase shifts between different qubits are important, in particular, for quantum information processing (see Sec. 8.5 below), so that most discussions of these applications have to start from Eq. (10) rather than Eq. (11).

⁵ This representation was suggested in 1946 by the same Felix Bloch who has pioneered the energy band theory discussed in Chapters 2-3.

$1/\sqrt{2}$ and $\alpha_{\downarrow} = \pm 1/\sqrt{2}$, correspond to the equator ($\theta = \pi/2$) points with, respectively, $\varphi = 0$ and $\varphi = \pi$. Two more special points (denoted in Fig. 3a as \odot and \otimes) are also located on the sphere's equator, at $\theta = \pi/2$ and $\varphi = \pm\pi/2$; it is easy to check that they correspond to the eigenstates of the matrix σ_y (in the same z -basis).

To understand why such mutually perpendicular location of these three special point pairs on the Bloch sphere is not occasional, let us plug Eqs. (11) into Eqs. (4.131)-(4.133) for the expectation values of the spin- $1/2$ components. In terms of the Pauli vector operator (4.117), $\boldsymbol{\sigma} \equiv \mathbf{S}/(\hbar/2)$, the result is

$$\langle \sigma_x \rangle = \sin \theta \cos \varphi, \quad \langle \sigma_y \rangle = \sin \theta \sin \varphi, \quad \langle \sigma_z \rangle = \cos \theta, \quad (5.12)$$

showing that the radius vector of any representation point is just the expectation value of $\boldsymbol{\sigma}$.

Now let us use Eq. (3) to see how does the representation point moves in various cases, ignoring the term bI – which, again, describes the offset of the total energy of the system relative to some reference level, and does not affect its dynamics. First of all, according to Eq. (4.158), in the case $\mathbf{c} = 0$ (when the Hamiltonian operator turns to zero, and hence the state vectors do not depend on time) the point does not move at all, and its position is determined by initial conditions, i.e. by the system's preparation. If $\mathbf{c} \neq 0$, we may re-use some results of Sec. 4.6, obtained for the Pauli Hamiltonian (4.163a), which coincides with Eq. (3) if⁶

$$\mathbf{c} = -\gamma \mathcal{B} \frac{\hbar}{2}. \quad (5.13)$$

In particular, if the field \mathcal{B} , and hence the vector \mathbf{c} , is directed along the z -axis and is time-independent, Eqs. (4.170) and (4.173)-(4.174) show that the representation point $\langle \boldsymbol{\sigma} \rangle$ on the Bloch sphere rotates within a plane normal to this axis (see Fig. 3b) with the angular velocity

$$\frac{d\varphi}{dt} \equiv \Omega = -\gamma \mathcal{B}_z \equiv \frac{2c_z}{\hbar}. \quad (5.14)$$

Almost evidently, since the selection of the coordinate axes is arbitrary, this picture should remain valid for any orientation of the vector \mathbf{c} , with the representation point rotating, on the Bloch sphere, around its direction, with the angular speed $|\Omega| = 2c/\hbar$ – see Fig. 3c. This fact may be proved using any picture of the quantum dynamics, discussed in Sec. 4.6. Actually, the reader may already have done that by solving Problems 4.25 and 4.26, just to see that even for the particular, simple initial state of the system (\uparrow), the final results for the Cartesian components of the vector $\langle \boldsymbol{\sigma} \rangle$ are somewhat bulky. However, this description may be readily simplified, even for arbitrary time dependence of the “field” vector $\mathbf{c}(t)$ in Eq. (3), using the (geometric) vector language.

Indeed, let us rewrite Eq. (3) (again, with $b = 0$) in the operator form,

$$\hat{H} = \mathbf{c}(t) \cdot \hat{\boldsymbol{\sigma}}, \quad (5.15)$$

valid in an arbitrary basis. According to Eq. (4.199), the corresponding Heisenberg equation of motion for the j^{th} Cartesian components of the vector-operator $\hat{\boldsymbol{\sigma}}$ (which does not depend on time explicitly, so that $\partial \hat{\sigma} / \partial t = 0$) is

⁶ This correspondence justifies using the use of term “field” for the vector \mathbf{c} .

$$i\hbar\dot{\hat{\sigma}}_j = [\hat{\sigma}_j, \hat{H}] \equiv [\hat{\sigma}_j, \mathbf{c}(t) \cdot \hat{\boldsymbol{\sigma}}] \equiv \left[\hat{\sigma}_j, \sum_{j'=1}^3 c_{j'}(t) \hat{\sigma}_{j'} \right] \equiv \sum_{j'=1}^3 c_{j'}(t) [\hat{\sigma}_j, \hat{\sigma}_{j'}]. \quad (5.16)$$

Now using the commutation relations (4.155), which remain valid in any basis and in any picture of time evolution,⁷ we get

$$i\hbar\dot{\hat{\sigma}}_j = 2i \sum_{j'=1}^3 c_{j'}(t) \hat{\sigma}_{j''} \epsilon_{jj''}, \quad (5.17)$$

where j'' is the index, or the same set $\{1, 2, 3\}$, complementary to j and j' ($j'' \neq j, j'$), and $\epsilon_{jj''}$ is the Levi-Civita symbol.⁸ But it is straightforward to verify that the usual vector product of two 3D vectors may be represented in a similar Cartesian-component form:

$$(\mathbf{a} \times \mathbf{b})_j = \begin{vmatrix} \mathbf{n}_1 & \mathbf{n}_2 & \mathbf{n}_3 \\ a_1 & a_2 & a_3 \\ b_1 & b_2 & b_3 \end{vmatrix}_j = \sum_{j'=1}^3 a_{j'} b_{j''} \epsilon_{jj''}, \quad (5.18)$$

As a result, Eq. (17) may be rewritten in a vector form – or rather several equivalent forms:

$$i\hbar\dot{\hat{\sigma}}_j = 2i[\mathbf{c}(t) \times \hat{\boldsymbol{\sigma}}]_j, \quad \text{i.e. } i\hbar\dot{\hat{\boldsymbol{\sigma}}} = 2i\mathbf{c}(t) \times \hat{\boldsymbol{\sigma}}, \quad \text{or } \dot{\hat{\boldsymbol{\sigma}}} = \frac{2}{\hbar} \mathbf{c}(t) \times \hat{\boldsymbol{\sigma}}, \quad \text{or } \dot{\hat{\boldsymbol{\sigma}}} = \boldsymbol{\Omega}(t) \times \hat{\boldsymbol{\sigma}}, \quad (5.19)$$

where the vector $\boldsymbol{\Omega}$ is defined as

$$\hbar\boldsymbol{\Omega}(t) \equiv 2\mathbf{c}(t) \quad (5.20)$$

– an evident generalization of Eq. (14).⁹ As we have seen in Sec. 4.6, any linear relation between two Heisenberg operators is also valid for the expectation values of the corresponding observables, so that the last form of Eq. (19) yields:

$$\langle \hat{\boldsymbol{\sigma}} \rangle = \boldsymbol{\Omega}(t) \times \langle \boldsymbol{\sigma} \rangle. \quad (5.21)$$

But this is the well-known kinematic formula¹⁰ for the rotation of a constant-length classical 3D vector $\langle \boldsymbol{\sigma} \rangle$ around the instantaneous direction of the vector $\boldsymbol{\Omega}(t)$, with the instantaneous angular velocity $\boldsymbol{\Omega}(t)$. So, the time evolution of the representation point on the Bloch sphere is quite simple, especially in the case of a time-independent \mathbf{c} , and hence $\boldsymbol{\Omega}$ – see Fig. 3c.¹¹ Note that it is sufficient to turn off the field to stop the precession instantly. (Since Eq. (21) is the first-order differential equation, the

⁷ Indeed, if some three operators in the Schrödinger picture are related as $[\hat{A}_S, \hat{B}_S] = \hat{C}_S$, then according to Eq. (4.190), in the Heisenberg picture:

$$[\hat{A}_H, \hat{B}_H] = [\hat{u}^\dagger \hat{A}_H \hat{u}, \hat{u}^\dagger \hat{B}_H \hat{u}] \equiv \hat{u}^\dagger \hat{A}_H \hat{u} \hat{u}^\dagger \hat{B}_H \hat{u} - \hat{u}^\dagger \hat{B}_H \hat{u} \hat{u}^\dagger \hat{A}_H \hat{u} \equiv \hat{u}^\dagger [\hat{A}_S, \hat{B}_S] \hat{u} \equiv \hat{u}^\dagger \hat{C}_S \hat{u} = \hat{C}_H.$$

⁸ See, e.g., MA Eq. (9.2). Note that in Eqs. (17)-(18) and similar expressions below, the condition $j'' \neq j, j'$ may be (and frequently is) replaced by the summation over not only j' , but also j'' , in their right-hand sides.

⁹ It is also easy to verify that in the particular case $\boldsymbol{\Omega} = \Omega \mathbf{n}_z$, Eqs. (19) are reduced, in the z -basis, to Eqs. (4.200) for the spin- $1/2$ vector matrix $\mathbf{S} = (\hbar/2)\boldsymbol{\sigma}$.

¹⁰ See, e.g., CM Sec. 4.1, in particular Eq. (4.8).

¹¹ The bulkiness of the solutions of Problems 4.25 and 4.26 (which were offered just as useful exercises in quantum dynamic formalisms) reflects the awkward expression of the resulting circular motion of the vector $\langle \boldsymbol{\sigma} \rangle$ (see Fig. 3c) via its Cartesian components.

representation point has no effective inertia.¹²⁾ Hence, changing the direction and the magnitude of the effective external field, it is possible to drive the representation point of a two-level system from any initial position to any final position on the Bloch sphere, i.e. make the system take any of its possible quantum states.

In the particular case of a spin- $\frac{1}{2}$ in a magnetic field $\mathcal{B}(t)$, it is more customary to use Eqs. (13) and (20) to rewrite Eq. (21) as the following equation for the expectation value of the spin vector $\mathbf{S} = (\hbar/2)\boldsymbol{\sigma}$:

$$\langle \dot{\mathbf{S}} \rangle \equiv \gamma \langle \mathbf{S} \rangle \times \mathcal{B}(t). \quad (5.22)$$

As we know from the discussion in Chapter 4, such a classical description of the spin's evolution does not give a full picture of the quantum reality; in particular, it does not describe the possible large uncertainties of its components – see, e.g., Eqs. (4.135). The situation, however, is different for a collection of $N \gg 1$ similar, non-interacting spins, initially prepared to be in the same state – for example by polarizing all spins with a strong external field \mathcal{B}_0 , at relatively low temperatures T , with $k_B T \ll \gamma \mathcal{B}_0 \hbar$. (A practically important example of such a collection is a set of nuclear spins in macroscopic condensed-matter samples, where the spin interaction with each other and the environment is typically very small.) For such a collection, Eq. (22) is still valid, while the relative uncertainty of the resulting sample's magnetization $\mathbf{M} = n\langle \mathbf{m} \rangle = n\gamma \langle \mathbf{S} \rangle$ (where $n \equiv N/V$ is the spin density) is proportional to $1/N^{1/2} \ll 1$. Thus, the evolution of magnetization may be described, with good precision, by the essentially classical equation (valid for any spin, not necessarily spin- $\frac{1}{2}$):

$$\dot{\mathbf{M}} = \gamma \mathbf{M} \times \mathcal{B}(t). \quad (5.23)$$

This equation, or the equivalent set of three *Bloch equations*¹³ for its Cartesian components, with the right-hand side augmented with small terms describing the effects of dephasing and relaxation (to be discussed in Chapter 7), is used, in particular, to describe the *magnetic resonance*, taking place when the frequency (4.164) of the spin's precession in a strong dc magnetic field approaches the frequency of an additionally applied (and usually weak) ac field.¹⁴⁾

5.2. The Ehrenfest theorem

In Sec. 4.7, we have derived all the basic relations of wave mechanics from the bra-ket formalism, which will also enable us to get some important additional results in that area. One of them is a pair of very interesting relations, together called the *Ehrenfest theorem*. To derive them, for the simplest case of 1D orbital motion, let us calculate the following commutator:

$$[\hat{x}, \hat{p}_x^2] \equiv \hat{x}\hat{p}_x\hat{p}_x - \hat{p}_x\hat{p}_x\hat{x}. \quad (5.24)$$

Let us apply the commutation relation (4.238) in the following form:

$$\hat{x}\hat{p}_x = \hat{p}_x\hat{x} + i\hbar\hat{I}, \quad (5.25)$$

¹² This is also true for the classical angular momentum \mathbf{L} at its torque-induced precession – see, e.g., CM Sec. 4.5.

¹³ They were introduced by F. Bloch in the same 1946 paper as the Bloch-sphere representation.

¹⁴ The quantum theory of this effect will be discussed in the next chapter.

to the first term of the right-hand side of Eq. (24) twice, with the goal to move the coordinate operator to the rightmost position:

$$\hat{x}\hat{p}_x\hat{p}_x = (\hat{p}_x\hat{x} + i\hbar\hat{I})\hat{p}_x \equiv \hat{p}_x\hat{x}\hat{p}_x + i\hbar\hat{p}_x = \hat{p}_x(\hat{p}_x\hat{x} + i\hbar\hat{I}) + i\hbar\hat{p}_x \equiv \hat{p}_x\hat{p}_x\hat{x} + 2i\hbar\hat{p}_x. \quad (5.26)$$

The first term of this result cancels with the last term of Eq. (24), so that the commutator becomes quite simple:

$$[\hat{x}, \hat{p}_x^2] = 2i\hbar\hat{p}_x. \quad (5.27)$$

Let us use this equality to calculate the Heisenberg-picture equation of motion of the operator \hat{x} , by applying the general Heisenberg equation (4.199) to the 1D orbital motion described by the Hamiltonian (4.237), but possibly with a more general, time-dependent potential energy U :

$$\frac{d\hat{x}}{dt} = \frac{1}{i\hbar} [\hat{x}, \hat{H}] = \frac{1}{i\hbar} \left[\hat{x}, \frac{\hat{p}_x^2}{2m} + U(\hat{x}, t) \right]. \quad (5.28)$$

The potential energy operator is a function of the coordinate operator and hence, as we know, commutes with it. Thus, the right-hand side of Eq. (28) is proportional to the commutator (27), and we get

$$\frac{d\hat{x}}{dt} = \frac{\hat{p}_x}{m}.$$

(5.29)

Heisenberg
equation
for
coordinate

In this *operator* equality, we readily recognize the full analog of the classical relation between the particle's momentum and its velocity.

Now let us see what a similar procedure gives for the momentum's derivative:

$$\frac{d\hat{p}_x}{dt} = \frac{1}{i\hbar} [\hat{p}_x, \hat{H}] = \frac{1}{i\hbar} \left[\hat{p}_x, \frac{\hat{p}_x^2}{2m} + U(\hat{x}, t) \right]. \quad (5.30)$$

The kinetic energy operator commutes with the momentum operator and hence drops from the right-hand side of this equation. To calculate the remaining commutator of the momentum and potential energy, let us use the fact that any smooth (infinitely differentiable) function may be represented by its Taylor expansion:

$$U(\hat{x}, t) = \sum_{k=0}^{\infty} \frac{1}{k!} \frac{\partial^k U}{\partial \hat{x}^k} \hat{x}^k, \quad (5.31)$$

where the derivatives of U may be understood as *c*-numbers (evaluated at $x = 0$, and the given time t), so that we may write

$$[\hat{p}_x, U(\hat{x}, t)] = \sum_{k=0}^{\infty} \frac{1}{k!} \frac{\partial^k U}{\partial \hat{x}^k} [\hat{p}_x, \hat{x}^k] = \sum_{k=0}^{\infty} \frac{1}{k!} \frac{\partial^k U}{\partial \hat{x}^k} \left(\hat{p}_x \underbrace{\hat{x}\hat{x}\dots\hat{x}}_{k \text{ times}} - \underbrace{\hat{x}\hat{x}\dots\hat{x}}_{k \text{ times}} \hat{p}_x \right). \quad (5.32a)$$

Applying Eq. (25) k times to the last term in the parentheses, exactly as we did it in Eq. (26), we get

$$[\hat{p}_x, U(\hat{x}, t)] = - \sum_{k=1}^{\infty} \frac{1}{k!} \frac{\partial^k U}{\partial \hat{x}^k} ik\hbar\hat{x}^{k-1} \equiv -i\hbar \sum_{k=1}^{\infty} \frac{1}{(k-1)!} \frac{\partial^k U}{\partial \hat{x}^k} \hat{x}^{k-1}. \quad (5.32b)$$

But the last sum is just the Taylor expansion of the derivative $\partial U / \partial x$. Indeed,

$$\frac{\partial U}{\partial \hat{x}} = \sum_{k=0}^{\infty} \frac{1}{k!} \frac{\partial^{k'}}{\partial \hat{x}^{k'}} \left(\frac{\partial U}{\partial \hat{x}} \right) \hat{x}^{k'} = \sum_{k=0}^{\infty} \frac{1}{k'!} \frac{\partial^{k'+1} U}{\partial \hat{x}^{k'+1}} \hat{x}^{k'} = \sum_{k=1}^{\infty} \frac{1}{(k-1)!} \frac{\partial^k U}{\partial \hat{x}^k} \hat{x}^{k-1}, \quad (5.33)$$

where at the last step the summation index was changed from k' to $k - 1$. As a result, we may rewrite Eq. (5.32b) as

$$[\hat{p}_x, U(\hat{x}, t)] = -i\hbar \frac{\partial}{\partial \hat{x}} U(\hat{x}, t), \quad (5.34)$$

so that Eq. (30) yields:

Heisenberg
equation
for
momentum

$$\frac{d\hat{p}_x}{dt} = -\frac{\partial}{\partial \hat{x}} U(\hat{x}, t). \quad (5.35)$$

This equation also coincides with the classical equation of motion! Moreover, averaging Eqs. (29) and (35) over the initial state (as Eq. (4.191) prescribes), we get similar results for the expectation values:¹⁵

Ehrenfest
theorem

$$\frac{d\langle x \rangle}{dt} = \frac{\langle p_x \rangle}{m}, \quad \frac{d\langle p_x \rangle}{dt} = -\left\langle \frac{\partial U}{\partial x} \right\rangle. \quad (5.36)$$

However, it is important to remember that the equivalence between these quantum-mechanical equations and similar equations of classical mechanics is superficial, and the degree of the similarity between the two mechanics very much depends on the problem. As one extreme, let us consider the case when a particle's state, at any moment between t_0 and t , may be accurately represented by one, relatively p_x -narrow wave packet. Then we may interpret Eqs. (36) as the equations of the essentially classical motion of the wave packet's center, in accordance with the correspondence principle. However, even in this case, it is important to remember the purely quantum mechanical effects of non-zero wave packet width and its spread in time, which were discussed in Sec. 2.2.

As an opposite extreme, let us revisit the “leaky” potential well discussed in Sec. 2.5 – see Fig. 2.15. Since both the potential $U(x)$ and the initial wavefunction of that system are symmetric relative to point $x = 0$ at all times, the right-hand sides of both Eqs. (36) identically equal zero. Of course, the result they predict (that the average values of the coordinate and the momentum stay equal to zero at all times) is correct, but this fact does not tell us much about the rich dynamics of the system: the finite lifetime of the metastable state, the formation of two wave packets, their waveform and propagation speed (see Fig. 2.17), and about the insights the full solution gives for the quantum measurement theory and the system's irreversibility. Another similar example is the energy band theory (Sec. 2.7), with its purely quantum effect of the allowed energy bands and forbidden energy gaps, of which Eqs. (36) give no clue.

To summarize, the Ehrenfest theorem is important as an illustration of the correspondence principle, but its predictive power should not be exaggerated.

5.3. The Feynman path integral

As has been already mentioned, even within the realm of wave mechanics, the bra-ket language may simplify some calculations that would be very bulky using the notation used in Chapters 1-3. Probably the best example is the famous alternative, *path-integral* formulation of quantum mechanics.¹⁶

¹⁵ The equation set (36) constitutes the *Ehrenfest theorem*, named after its author, P. Ehrenfest.

¹⁶ This formulation was developed in 1948 by Richard Phillips Feynman. (According to his memories, this work was motivated by a “mysterious” remark by P. Dirac in his pioneering 1930 textbook on quantum mechanics.)

I will review this important concept, cutting one math corner for the sake of brevity.¹⁷ (This shortcut will be clearly marked below.)

Let us inner-multiply both parts of Eq. (4.157a), which is essentially the definition of the time-evolution operator, by the bra-vector of state x ,

$$\langle x | \alpha(t) \rangle = \langle x | \hat{u}(t, t_0) | \alpha(t_0) \rangle, \quad (5.37)$$

insert the identity operator before the ket-vector on the right-hand side, and then use the closure condition in the form of Eq. (4.252), with x' replaced with x_0 :

$$\langle x | \alpha(t) \rangle = \int dx_0 \langle x | \hat{u}(t, t_0) | x_0 \rangle \langle x_0 | \alpha(t_0) \rangle. \quad (5.38)$$

According to Eq. (4.233), this equality may be represented as

$$\Psi_\alpha(x, t) = \int dx_0 \langle x | \hat{u}(t, t_0) | x_0 \rangle \Psi_\alpha(x_0, t_0). \quad (5.39)$$

Comparing this expression with Eq. (2.44), we see that the long bracket in this relation is nothing other than the 1D propagator, which was discussed in Sec. 2.2, i.e.

$$G(x, t; x_0, t_0) = \langle x | \hat{u}(t, t_0) | x_0 \rangle. \quad (5.40)$$

Let me hope that the reader sees that this equality corresponds to the physical sense of the propagator.

Now let us break the time segment $[t_0, t]$ into N (for the time being, not necessarily equal) parts, by inserting $(N - 1)$ intermediate points (Fig. 4) with

$$t_0 < t_1 < \dots < t_k < \dots < t_{N-1} < t, \quad (5.41)$$

and use the definition (4.157) of the time evolution operator to write

$$\hat{u}(t, t_0) = \hat{u}(t, t_{N-1}) \hat{u}(t_{N-1}, t_{N-2}) \dots \hat{u}(t_2, t_1) \hat{u}(t_1, t_0). \quad (5.42)$$

After plugging Eq. (42) into Eq. (40), let us insert the identity operator, again in the closure form (4.252), but written for x_k rather than x' , between each two partial evolution operators including the time argument t_k . The result is

$$G(x, t; x_0, t_0) = \int dx_{N-1} \int dx_{N-2} \dots \int dx_1 \langle x | \hat{u}(t, t_{N-1}) | x_{N-1} \rangle \langle x_{N-1} | \hat{u}(t_{N-1}, t_{N-2}) | x_{N-2} \rangle \dots \langle x_1 | \hat{u}(t_1, t_0) | x_0 \rangle. \quad (5.43)$$

The physical sense of each integration variable x_k is the wavefunction's argument at time t_k – see Fig. 4.

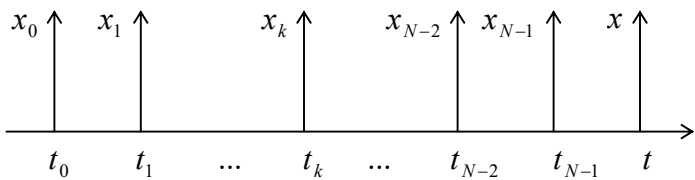


Fig. 5.4. Time partition and coordinate notation at the initial stage of the Feynman path integral's derivation.

¹⁷ A more thorough discussion of the path-integral approach may be found in the famous text by R. Feynman and A. Hibbs, *Quantum Mechanics and Path Integrals*, first published in 1965. (For its latest edition by Dover in 2010, the book was emended by D. Styler.) For a more recent monograph, which reviews more applications, see L. Schulman, *Techniques and Applications of Path Integration*, Wiley, 1981.

The key Feynman's breakthrough was the realization that if all intervals are taken similar and sufficiently small, $t_k - t_{k-1} = d\tau \rightarrow 0$, all the partial brackets participating in Eq. (43) may be expressed via the free-particle's propagator, given by Eq. (2.49), even if the particle is not free, but moves in a stationary potential profile $U(x)$. To show that, let us use either Eq. (4.175) or Eq. (4.181), which, for a small time interval $d\tau$, give the same result:

$$\hat{u}(\tau + d\tau, \tau) = \exp\left\{-\frac{i}{\hbar} \hat{H}d\tau\right\} = \exp\left\{-\frac{i}{\hbar}\left(\frac{\hat{p}^2}{2m}d\tau + U(\hat{x})d\tau\right)\right\}. \quad (5.44)$$

Generally, an exponent of a sum of two operators may be treated as that of *c*-number arguments, and in particular factored into a product of two exponents, only if the operators commute. (In this case, we can use all the standard algebra for the exponents of *c*-number arguments.) In our case, this is not so, because the operator $\hat{p}^2/2m$ does not commute with \hat{x} , and hence with $U(\hat{x})$. However, it may be shown¹⁸ that for an infinitesimal time interval $d\tau$, the non-zero commutator

$$\left[\frac{\hat{p}^2}{2m}d\tau, U(\hat{x})d\tau\right] \neq 0, \quad (5.45)$$

proportional to $(d\tau)^2$, may be ignored in the first, linear approximation in $d\tau$. As a result, we may factorize the right-hand side in Eq. (44) by writing

$$\hat{u}(\tau + d\tau, \tau)_{d\tau \rightarrow 0} \rightarrow \exp\left\{-\frac{i}{\hbar} \frac{\hat{p}^2}{2m}d\tau\right\} \exp\left\{-\frac{i}{\hbar} U(\hat{x})d\tau\right\}. \quad (5.46)$$

(This approximation is very much similar in spirit to the trapezoidal-rule approximation in the usual 1D integration,¹⁹ which is also asymptotically impeccable.)

Since the second exponential function on the right-hand side of Eq. (46) commutes with the coordinate operator, we may move it out of each partial bracket participating in Eq. (43), with $U(x)$ turning into a *c*-number function:

$$\langle x_{\tau+d\tau} | \hat{u}(\tau + d\tau, \tau) | x_\tau \rangle = \langle x_{\tau+d\tau} | \exp\left\{-\frac{i}{\hbar} \frac{\hat{p}^2}{2m}d\tau\right\} | x_\tau \rangle \exp\left\{-\frac{i}{\hbar} U(x)d\tau\right\}. \quad (5.47)$$

But the remaining bracket is just the propagator of a free particle, so that for it we may use Eq. (2.49):

$$\langle x_{\tau+d\tau} | \exp\left\{-\frac{i}{\hbar} \frac{\hat{p}^2}{2m}d\tau\right\} | x_\tau \rangle = \left(\frac{m}{2\pi i \hbar d\tau}\right)^{1/2} \exp\left\{i \frac{m(dx)^2}{2\hbar d\tau}\right\}. \quad (5.48)$$

As the result, the full propagator (43) takes the form

$$G(x, t; x_0, t_0) = \lim_{\substack{d\tau \rightarrow 0 \\ N \rightarrow \infty}} \int dx_{N-1} \int dx_{N-2} \dots \int dx_1 \left(\frac{m}{2\pi i \hbar d\tau}\right)^{N/2} \exp\left\{\sum_{k=1}^N \left[i \frac{m(dx)^2}{2\hbar d\tau} - i \frac{U(x)}{\hbar} d\tau\right]\right\}. \quad (5.49)$$

¹⁸ This is exactly the corner I am going to cut because a strict mathematical proof of this (intuitively evident) statement would take more time/space than I can afford.

¹⁹ See, e.g., MA Eq. (5.2).

At $N \rightarrow \infty$ and hence $d\tau \equiv (t - t_0)/N \rightarrow 0$, the sum under the exponent in this expression may be approximated with the corresponding integral:

$$\sum_{k=1}^N \frac{i}{\hbar} \left[\frac{m}{2} \left(\frac{dx}{d\tau} \right)^2 - U(x) \right]_{\tau=t_k} d\tau \rightarrow \frac{i}{\hbar} \int_{t_0}^t \left[\frac{m}{2} \left(\frac{dx}{d\tau} \right)^2 - U(x) \right] d\tau, \quad (5.50)$$

and the expression in the square brackets is just the particle's Lagrangian function \mathcal{L} .²⁰ The integral of this function over time is the classical action \mathcal{S} calculated along a particular "path" $x(\tau)$.²¹ As a result, defining the (1D) *path integral* as

$$\int (\dots) D[x(\tau)] \equiv \lim_{\substack{d\tau \rightarrow 0 \\ N \rightarrow \infty}} \left(\frac{m}{2\pi i \hbar d\tau} \right)^{N/2} \int dx_{N-1} \int dx_{N-2} \dots \int dx_1 (\dots), \quad (5.51a)$$

1D path integral:
definition

we can bring our result to the following (superficially simple) form:

$$G(x, t; x_0, t_0) = \int \exp \left\{ \frac{i}{\hbar} \mathcal{S}[x(\tau)] \right\} D[x(\tau)]. \quad (5.51b)$$

1D propagator
via path integral

The name "path integral" for the mathematical construct (51a) may be readily explained if we keep the number N of time intervals large but finite, and also approximate each of the enclosed integrals with a sum over $M \gg 1$ discrete points along the coordinate axis – see Fig. 5a.

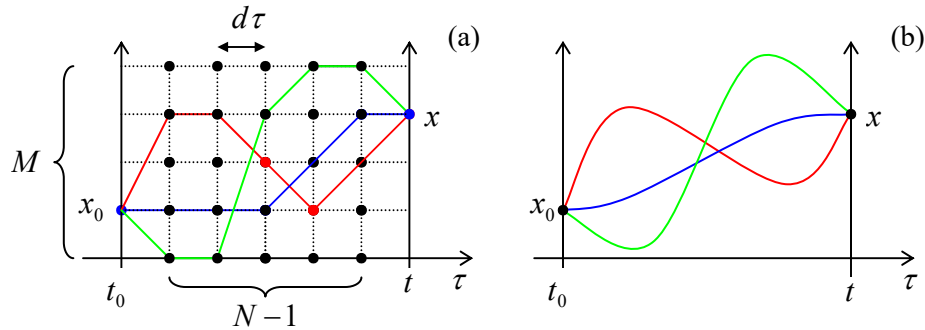


Fig. 5.5. Several 1D classical paths: (a) in the discrete approximation and (b) in the continuous limit.

Then the path integral (51a) is the product of $(N - 1)$ sums corresponding to different values of time τ , each of them with M terms, each of those representing the function under the integral at a particular spatial point. Multiplying those $(N - 1)$ sums, we get a sum of $(N - 1)M$ terms, each evaluating the function at a specific spatial-temporal point $[x, \tau]$. These terms may be now grouped to represent all possible different continuous classical paths $x[\tau]$ from the initial point $[x_0, t_0]$ to the finite point $[x, t]$. It is evident that the last interpretation remains true even in the continuous limit $N, M \rightarrow \infty$ – see Fig. 5b.

Why does such path representation of the sum make sense? This is because in the classical limit the particle follows just a certain path, corresponding to the minimum of the action \mathcal{S} . As a result, for all close trajectories, the difference $(\mathcal{S} - \mathcal{S}_{\text{cl}})$ is proportional to the square of the deviation from the

²⁰ See, e.g., CM Sec. 2.1.

²¹ See, e.g., CM Sec. 10.3.

classical trajectory. Hence, for a quasiclassical motion, with $\mathcal{S}_{\text{cl}} \gg \hbar$, there is a bunch of close trajectories, with $(\mathcal{S} - \mathcal{S}_{\text{cl}}) \ll \hbar$, that give substantial contributions to the path integral. On the other hand, strongly non-classical trajectories, with $(\mathcal{S} - \mathcal{S}_{\text{cl}}) \gg \hbar$, give phases $\mathcal{S}\hbar$ rapidly oscillating from one trajectory to the next one, and their contributions to the path integral are averaged out.²² As a result, for a quasi-classical motion, the propagator's exponent may be evaluated on the classical path only:

$$G_{\text{cl}} \propto \exp\left\{\frac{i}{\hbar} \mathcal{S}_{\text{cl}}\right\} = \exp\left\{\frac{i}{\hbar} \int_{t_0}^t \left[\frac{m}{2} \left(\frac{dx}{d\tau} \right)^2 - U(x) \right] d\tau\right\}. \quad (5.52)$$

The sum of the kinetic and potential energies is the full energy E of the particle, that remains constant for motion in a stationary potential $U(x)$, so that we may rewrite the expression under this integral as²³

$$\left[\frac{m}{2} \left(\frac{dx}{d\tau} \right)^2 - U(x) \right] d\tau = \left[m \left(\frac{dx}{d\tau} \right)^2 - E \right] d\tau = m \frac{dx}{d\tau} dx - Ed\tau. \quad (5.53)$$

With this replacement, Eq. (52) yields

$$G_{\text{cl}} \propto \exp\left\{\frac{i}{\hbar} \int_{x_0}^x m \frac{dx}{d\tau} dx\right\} \exp\left\{-\frac{i}{\hbar} E(t - t_0)\right\} = \exp\left\{\frac{i}{\hbar} \int_{x_0}^x p(x) dx\right\} \exp\left\{-\frac{i}{\hbar} E(t - t_0)\right\}, \quad (5.54)$$

where p is the classical momentum of the particle. But (at least, leaving the pre-exponential factor alone) this is the WKB approximation result that was derived and studied in detail in Chapter 2!

One may question the value of such a complicated calculation, which yields the results that could be readily obtained from Schrödinger's wave mechanics. Feynman's approach is indeed not used too often, but it has its merits. First, it has an important philosophical (and hence heuristic) value. Indeed, Eq. (51) may be interpreted by saying that the essence of quantum mechanics is the exploration, by the system, of all possible paths $x(\tau)$, each of them classical-like, in the sense that the particle's coordinate x and velocity $dx/d\tau$ are exactly defined simultaneously at each point. The resulting contributions to the path integral are added up coherently to form the actual propagator G , and via it, the final probability $W \propto |G|^2$ of the particle's propagation from $[x_0, t_0]$ to $[x, t]$. As the scale of the action \mathcal{S} of the motion decreases and becomes comparable to \hbar , more and more paths produce substantial contributions to this sum, and hence to W , providing a larger and larger difference between the quantum and classical properties of the system.

Second, the path integral provides a justification for some simple explanations of quantum phenomena. A typical example is the quantum interference effects discussed in Sec. 3.1 – see, e.g., Fig. 3.1 and the corresponding text. At that discussion, we used the Huygens principle to argue that at the two-slit interference, the WKB approximation might be restricted to contributions from two paths that pass through different slits, but otherwise consisting of straight-line segments. To have another look at

²² This fact may be proved by expanding the difference $(\mathcal{S} - \mathcal{S}_{\text{cl}})$ in the Taylor series in the path variation (leaving only the leading quadratic terms) and working out the resulting Gaussian integrals. This integration, together with the pre-exponential coefficient in Eq. (51a), gives exactly the pre-exponential factor that we have already found refining the WKB approximation in Sec. 2.4.

²³ The same trick is often used in analytical classical mechanics – say, for proving the Hamilton principle, and for the derivation of the Hamilton – Jacobi equations (see, e.g., CM Secs. 10.3-4).

that assumption, let us generalize the path integral to multi-dimensional geometries. Fortunately, the simple structure of Eq. (51b) makes such generalization virtually evident:

$$G(\mathbf{r}, t; \mathbf{r}_0, t_0) = \int \exp\left\{\frac{i}{\hbar} \mathcal{S}[\mathbf{r}(\tau)]\right\} D[\mathbf{r}(\tau)], \quad \mathcal{S} = \int_{t_0}^t \mathcal{L}\left(\mathbf{r}, \frac{d\mathbf{r}}{d\tau}\right) d\tau = \int_{t_0}^t \left[\frac{m}{2} \left(\frac{d\mathbf{r}}{d\tau} \right)^2 - U(\mathbf{r}) \right] d\tau. \quad (5.55)$$

3D
propagator
as a path
integral

where the definition (51a) of the path integral should be also modified correspondingly. (I will not go into these technical details.) For the Young-type experiment (Fig. 3.1), where a classical particle could reach the detector only after passing through one of the slits, the classical paths are the straight-line segments shown in Fig. 3.1, and if they are much longer than the de Broglie wavelength, the propagator may be well approximated by the sum of two integrals of $\mathcal{L}d\tau = i\mathbf{p}(\mathbf{r}) \cdot d\mathbf{r}/\hbar$ – as it was done in Sec. 3.1.

Last but not least, the path integral allows simple solutions to some problems that would be hard to obtain by other methods. As the simplest example, let us consider the problem of tunneling in multi-dimensional space, sketched in Fig. 6 for the 2D case – just for the graphics' simplicity. Here, the potential profile $U(x, y)$ has a saddle-like shape. (Another helpful image is a mountain path between two summits, in Fig. 6 located on the top and at the bottom of the shown region.) A particle of energy E may move classically in the left and right regions with $U(x, y) < E$, but if E is not sufficiently high, it can pass from one of these regions to another one only via the quantum-mechanical tunneling under the pass. Let us calculate the transparency of this potential barrier in the WKB approximation, ignoring the possible pre-exponential factor.²⁴

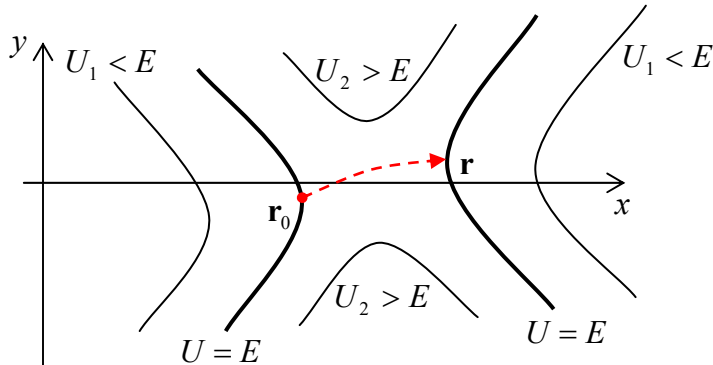


Fig. 5.6. A saddle-type 2D potential profile and the instanton trajectory of a particle of energy E (schematically).

According to the evident multi-dimensional generalization Eq. (54), for the classically forbidden region, where $E < U(x, y)$, and hence $\mathbf{p}(\mathbf{r})/\hbar = i\boldsymbol{\kappa}(\mathbf{r})$, the contributions to the propagator (55) are proportional to

$$e^{-I} \exp\left\{-\frac{i}{\hbar} E(t - t_0)\right\}, \quad \text{where } I \equiv \int_{\mathbf{r}_0}^{\mathbf{r}} \boldsymbol{\kappa}(\mathbf{r}) \cdot d\mathbf{r}, \quad (5.56)$$

where $\boldsymbol{\kappa} \equiv \boldsymbol{\kappa}$ may be calculated just in the 1D case – cf. Eq. (2.97):

$$\frac{\hbar^2 \boldsymbol{\kappa}^2(\mathbf{r})}{2m} = U(\mathbf{r}) - E. \quad (5.57)$$

²⁴ Actually, one can argue that the pre-exponential factor should be close to 1, just like in Eq. (2.117), especially if the potential is smooth, in the sense of Eq. (2.107), in all spatial directions. (Let me remind the reader that for most practical applications of quantum tunneling, the pre-exponential factor is of minor importance.)

Hence the path integral in this region is much simpler than in the classically allowed region, because the spatial exponents are purely real and there is no complex interference between them. Due to the minus sign before I in the exponent (56), the *largest* contribution to G evidently comes from the trajectory (or a narrow bundle of close trajectories) for which the integral I has the *smallest* value, so that the barrier transparency may be calculated as

3D
tunneling
in WKB
limit

$$\mathcal{T} \approx |G|^2 \approx e^{-2I} \equiv \exp \left\{ -2 \int_{\mathbf{r}_0}^{\mathbf{r}} \mathbf{k}(\mathbf{r}') \cdot d\mathbf{r}' \right\}, \quad (5.58)$$

where \mathbf{r} and \mathbf{r}_0 are certain points on the opposite classical turning-point surfaces: $U(\mathbf{r}) = U(\mathbf{r}_0) = E$ – see Fig. 6.

Thus the barrier transparency problem is reduced to finding the trajectory (including the points \mathbf{r} and \mathbf{r}_0) that connects the two surfaces and minimizes the functional I . This is of course a well-known problem of the calculus of variations,²⁵ but it is interesting that the path integral provides a simple alternative way of solving it. Let us consider an auxiliary problem of particle's motion in the potential profile $U_{\text{inv}}(\mathbf{r})$ that is *inverted* relative to the particle's energy E , i.e. is defined by the following equality:

$$U_{\text{inv}}(\mathbf{r}) - E \equiv E - U(\mathbf{r}). \quad (5.59)$$

As was discussed above, at fixed energy E , the path integral for the WKB motion in the classically allowed region of potential $U_{\text{inv}}(x, y)$ (that coincides with the classically forbidden region of the original problem) is dominated by the classical trajectory corresponding to the minimum of

$$\mathcal{S}_{\text{inv}} = \int_{\mathbf{r}_0}^{\mathbf{r}} \mathbf{p}_{\text{inv}}(\mathbf{r}') \cdot d\mathbf{r}' = \hbar \int_{\mathbf{r}_0}^{\mathbf{r}} \mathbf{k}_{\text{inv}}(\mathbf{r}') \cdot d\mathbf{r}, \quad (5.60)$$

where \mathbf{k}_{inv} should be determined from the WKB relation

$$\frac{\hbar^2 k_{\text{inv}}^2(\mathbf{r})}{2m} \equiv E - U_{\text{inv}}(\mathbf{r}). \quad (5.61)$$

But comparing Eqs. (57), (59), and (61), we see that $\mathbf{k}_{\text{inv}} = \mathbf{k}$ at each point! This means that the tunneling path (in the WKB limit) corresponds to the classical (so-called *instanton*²⁶) trajectory of the same particle moving in the inverted potential $U_{\text{inv}}(\mathbf{r})$. If the initial point \mathbf{r}_0 is fixed, this trajectory may be readily found by the means of classical mechanics. (Note that the initial kinetic energy, and hence the initial velocity of the instanton launched from point \mathbf{r}_0 should be zero because by the classical turning point definition, $U_{\text{inv}}(\mathbf{r}_0) = U(\mathbf{r}_0) = E$.) Thus the problem is further reduced to a simpler task of maximizing the transparency (58) by choosing the optimal position of \mathbf{r}_0 on the equipotential surface $U(\mathbf{r}_0) = E$ – see Fig. 6. Moreover, for many symmetric potentials, the position of this point may be readily guessed even without calculations – as it is in Problems 6 and 7, left for the reader's exercise.

Note that besides the calculation of the potential barrier's transparency, the instanton trajectory has one more important implication: the so-called *traversal time* τ_i of the classical motion along it, from

²⁵ For a concise introduction to the field see, e.g., I. Gelfand and S. Fomin, *Calculus of Variations*, Dover, 2000, or L. Elsgolc, *Calculus of Variations*, Dover, 2007.

²⁶ In the quantum field theory, the instanton concept may be formulated somewhat differently, and has more complex applications – see, e.g. R. Rajaraman, *Solitons and Instantons*, North-Holland, 1987.

the point \mathbf{r}_0 to the point \mathbf{r} , in the inverted potential defined by Eq. (59), plays the role of the most important (though not the only one) time scale of the particle's tunneling under the barrier.²⁷

5.4. Revisiting harmonic oscillator

Let us return to the 1D harmonic oscillator, now understood as any system, regardless of its physical nature, described by the Hamiltonian (4.237) with the potential energy (2.111):

$$\hat{H} = \frac{\hat{p}^2}{2m} + \frac{m\omega_0^2 \hat{x}^2}{2}. \quad (5.62)$$

Harmonic oscillator:
Hamiltonian

In Sec. 2.9 we have used a “brute-force” (wave-mechanics) approach to analyze the eigenfunctions $\psi_n(x)$ and eigenvalues E_n of this Hamiltonian, and found that, unfortunately, this approach required relatively complex mathematics, which does not enable an easy calculation of its key characteristics. Fortunately, the bra-ket formalism helps to make such calculations.

First, introducing normalized (dimensionless) operators of coordinates and momentum:²⁸

$$\hat{\xi} \equiv \frac{\hat{x}}{x_0}, \quad \hat{\zeta} \equiv \frac{\hat{p}}{m\omega_0 x_0}, \quad (5.63)$$

where $x_0 \equiv (\hbar/m\omega_0)^{1/2}$ is the natural coordinate scale discussed in detail in Sec. 2.9, we can represent the Hamiltonian (62) in a very simple and $x \leftrightarrow p$ symmetric form:

$$\hat{H} = \frac{\hbar\omega_0}{2} \left(\hat{\xi}^2 + \hat{\zeta}^2 \right). \quad (5.64)$$

This symmetry, as well as our discussion of the very similar coordinate and momentum representations in Sec. 4.7, hints that much may be gained by treating the operators $\hat{\xi}$ and $\hat{\zeta}$ on equal footing. Inspired by this clue, let us introduce a new operator

$$\hat{a} \equiv \frac{\hat{\xi} + i\hat{\zeta}}{\sqrt{2}} \equiv \left(\frac{m\omega_0}{2\hbar} \right)^{1/2} \left(\hat{x} + i\frac{\hat{p}}{m\omega_0} \right). \quad (5.65a)$$

Annihilation operator:
definition

Since both operators $\hat{\xi}$ and $\hat{\zeta}$ correspond to real observables, i.e. have real eigenvalues and hence are Hermitian (self-adjoint), the Hermitian conjugate of the operator \hat{a} is simply its complex conjugate:

$$\hat{a}^\dagger \equiv \frac{\hat{\xi} - i\hat{\zeta}}{\sqrt{2}} \equiv \left(\frac{m\omega_0}{2\hbar} \right)^{1/2} \left(\hat{x} - i\frac{\hat{p}}{m\omega_0} \right). \quad (5.65b)$$

Creation operator:
definition

Because of the reason that will be clear very soon, \hat{a}^\dagger and \hat{a} (in this order!) are called the *creation and annihilation operators*.

²⁷ For more on this interesting issue see, e.g., M. Buttiker and R. Landauer, *Phys. Rev. Lett.* **49**, 1739 (1982), and references therein.

²⁸ This normalization is not really necessary, it just makes the following calculations less bulky – and thus more aesthetically appealing.

Now solving the simple system of two linear equations (65) for $\hat{\xi}$ and $\hat{\zeta}$, we get the following reciprocal relations:

$$\hat{\xi} = \frac{\hat{a} + \hat{a}^\dagger}{\sqrt{2}}, \quad \hat{\zeta} = \frac{\hat{a} - \hat{a}^\dagger}{\sqrt{2} i}, \quad \text{i.e. } \hat{x} = \left(\frac{\hbar}{m\omega_0} \right)^{1/2} \frac{\hat{a} + \hat{a}^\dagger}{\sqrt{2}}, \quad \hat{p} = (\hbar m \omega_0)^{1/2} \frac{\hat{a} - \hat{a}^\dagger}{\sqrt{2} i}. \quad (5.66)$$

Our Hamiltonian (64) includes squares of these operators. Calculating them, we have to be careful to avoid swapping the new operators, because they do not commute. Indeed, for the normalized operators (63), Eq. (2.14) gives

$$[\hat{\xi}, \hat{\zeta}] \equiv \frac{1}{x_0^2 m \omega_0} [\hat{x}, \hat{p}] = i\hat{I}, \quad (5.67)$$

so that Eqs. (65) yield

$$[\hat{a}, \hat{a}^\dagger] = \frac{1}{2} [(\hat{\xi} + i\hat{\zeta}), (\hat{\xi} - i\hat{\zeta})] = -\frac{i}{2} ([\hat{\xi}, \hat{\zeta}] - [\hat{\zeta}, \hat{\xi}]) = \hat{I}. \quad (5.68)$$

With such due caution, Eq. (66) gives

$$\hat{\xi}^2 = \frac{1}{2} \left(\hat{a}^2 + \hat{a}^{\dagger 2} + \hat{a}\hat{a}^\dagger + \hat{a}^\dagger\hat{a} \right), \quad \hat{\zeta}^2 = -\frac{1}{2} \left(\hat{a}^2 + \hat{a}^{\dagger 2} - \hat{a}\hat{a}^\dagger - \hat{a}^\dagger\hat{a} \right). \quad (5.69)$$

Plugging these expressions back into Eq. (64), we get

$$\hat{H} = \frac{\hbar\omega_0}{2} (\hat{a}\hat{a}^\dagger + \hat{a}^\dagger\hat{a}). \quad (5.70)$$

This expression is elegant enough, but may be recast into an even more convenient form. For that, let us rewrite the commutation relation (68) as

$$\hat{a}\hat{a}^\dagger = \hat{a}^\dagger\hat{a} + \hat{I}, \quad (5.71)$$

and plug it into Eq. (70). The result is

$$\hat{H} = \frac{\hbar\omega_0}{2} (2\hat{a}^\dagger\hat{a} + \hat{I}) \equiv \hbar\omega_0 \left(\hat{N} + \frac{1}{2} \hat{I} \right), \quad (5.72)$$

where, in the last form, one more (evidently, Hermitian) operator,

$$\hat{N} \equiv \hat{a}^\dagger\hat{a}, \quad (5.73)$$

has been introduced. Since, according to Eq. (72), the operators \hat{H} and \hat{N} differ only by the addition of the identity operator and multiplication by a c -number, these operators commute. Hence, according to the general arguments of Sec. 4.5, they share a set of stationary eigenstates n (they are frequently called the *Fock states*), and we can write the standard eigenproblem (4.68) for the new operator as

$$\hat{N}|n\rangle = N_n|n\rangle, \quad (5.74)$$

where N_n are some eigenvalues that, according to Eq. (72), determine also the energy spectrum of the oscillator:

$$E_n = \hbar\omega_0 \left(N_n + \frac{1}{2} \right). \quad (5.75)$$

So far, we know only that all eigenvalues N_n are real; to calculate them, let us carry out the following calculation – splendid in its simplicity and efficiency. Consider the result of the action of the operator \hat{N} on the ket-vector $\hat{a}^\dagger|n\rangle$. Using the definition (73) and then the associative rule of the bra-ket formalism, we may write

$$\hat{N}(\hat{a}^\dagger|n\rangle) = (\hat{a}^\dagger \hat{a})(\hat{a}^\dagger|n\rangle) = \hat{a}^\dagger(\hat{a}\hat{a}^\dagger)|n\rangle. \quad (5.76)$$

Now using the commutation relation (71), and then Eq. (74), we may continue as

$$\hat{a}^\dagger(\hat{a}\hat{a}^\dagger)|n\rangle = \hat{a}^\dagger(\hat{a}^\dagger \hat{a} + \hat{I})|n\rangle = \hat{a}^\dagger(\hat{N} + \hat{I})|n\rangle = \hat{a}^\dagger(N_n + 1)|n\rangle = (N_n + 1)(\hat{a}^\dagger|n\rangle). \quad (5.77)$$

For clarity, let us summarize the result of this calculation:

$$\hat{N}(\hat{a}^\dagger|n\rangle) = (N_n + 1)(\hat{a}^\dagger|n\rangle). \quad (5.78)$$

Performing a similar calculation for the operator \hat{a} , we get a similar formula:

$$\hat{N}(\hat{a}|n\rangle) = (N_n - 1)(\hat{a}|n\rangle). \quad (5.79)$$

It is time to stop calculations for a minute, and translate these results into plain English: if $|n\rangle$ is an eigenket of the operator \hat{N} with the eigenvalue N_n , then $\hat{a}^\dagger|n\rangle$ and $\hat{a}|n\rangle$ are also eigenkets of that operator, with the eigenvalues $(N_n + 1)$, and $(N_n - 1)$, respectively. This statement may be vividly represented on the so-called *ladder diagram* shown in Fig. 7.

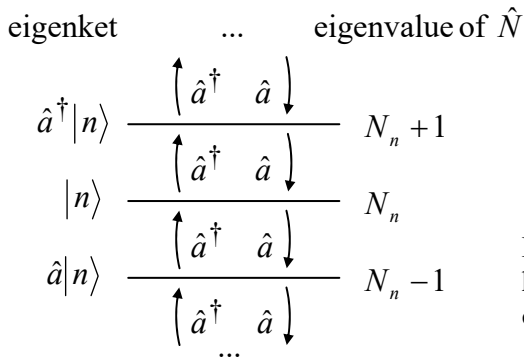


Fig. 5.7. The “ladder diagram” of eigenstates of a 1D harmonic oscillator. Arrows show the actions of the creation and annihilation operators on the eigenstates.

The operator \hat{a}^\dagger moves the system one step up this ladder, while the operator \hat{a} brings it one step down. In other words, the former operator creates a new *excitation* of the system,²⁹ while the latter operator kills (“annihilates”) such excitation.³⁰ On the other hand, according to Eq. (74) inner-multiplied by the bra-vector $\langle n|$, the operator \hat{N} does not change the state of the system, but “counts” its position on the ladder:

²⁹ For electromagnetic field oscillators, such excitations are called *photons*; for mechanical wave oscillators, *phonons*, etc.

³⁰ This is exactly why \hat{a}^\dagger is called the *creation* operator, and \hat{a} , the *annihilation* operator.

$$\langle n | \hat{N} | n \rangle = \langle n | N_n | n \rangle = N_n. \quad (5.80)$$

This is why \hat{N} is called the *number operator*, in our current context meaning the number of the elementary excitations of the oscillator.

This calculation still needs completion. Indeed, we still do not know whether the ladder shown in Fig. 7 shows *all* eigenstates of the oscillator, and what exactly the numbers N_n are. Fascinating enough, both questions may be answered by exploring just one paradox. Let us start with some state n (read a step of the ladder), and keep going down the ladder, applying the operator \hat{a} again and again. According to Eq. (79), at each step the eigenvalue N_n is decreased by one, so that eventually it should become negative. However, this cannot happen, because any actual eigenstate, including the states represented by kets $|d\rangle \equiv \hat{a}|n\rangle$ and $|n\rangle$, should have a positive norm – see Eq. (4.16). Comparing the norms,

$$\|n\|^2 = \langle n | n \rangle, \quad \|d\|^2 = \langle n | \hat{a}^\dagger a | n \rangle = \langle n | \hat{N} | n \rangle = N_n \langle n | n \rangle, \quad (5.81)$$

we see that both of them cannot be positive simultaneously if N_n is negative.

To resolve this paradox let us notice that the action of the creation and annihilation operators on the stationary states n may consist of not only their promotion to an adjacent step of the ladder diagram but also by their multiplication by some c -numbers:

$$\hat{a}|n\rangle = A_n |n-1\rangle, \quad \hat{a}^\dagger |n\rangle = A'_n |n+1\rangle. \quad (5.82)$$

(The linear relations (78)-(79) clearly allow that.) Let us calculate the coefficients A_n assuming, for convenience, that all eigenstates, including the states n and $(n-1)$, are normalized:

$$\langle n | n \rangle = 1, \quad \langle n-1 | n-1 \rangle = \langle n | \frac{\hat{a}^\dagger}{A_n^*} \frac{\hat{a}}{A_n} | n \rangle = \frac{1}{A_n^* A_n} \langle n | \hat{N} | n \rangle = \frac{N_n}{A_n^* A_n} \langle n | n \rangle = 1. \quad (5.83)$$

From here, we get $|A_n| = (N_n)^{1/2}$, i.e.

$$\hat{a}|n\rangle = N_n^{1/2} e^{i\varphi_n} |n-1\rangle, \quad (5.84)$$

where φ_n is an arbitrary real phase. Now let us consider what happens if all numbers N_n are integers. (Because of the definition of N_n , given by Eq. (74), it is convenient to call these integers n , i.e. to use the same letter as for the corresponding eigenstate.) Then when we have come down to the state with $n = 0$, an attempt to make one more step down gives

$$\hat{a}|0\rangle = | -1 \rangle. \quad (5.85)$$

But according to Eq. (4.9), the state on the right-hand side of this equation is the “null-state”, i.e. does not exist.³¹ This gives the (only known :-) resolution of the state ladder paradox: the ladder has the lowest step with $N_n = n = 0$.

As a by-product of our discussion, we have obtained a very important relation $N_n = n$, which means, in particular, that the state ladder shown in Fig. 7 includes *all* eigenstates of the oscillator.

³¹ Please note again the radical difference between the null-state on the right-hand side of Eq. (85) and the state described by the ket-vector $|0\rangle$ on the left-hand side of that relation. The latter state *does* exist and, moreover, represents the most important, ground state of the system, with $n = 0$ – see Eqs. (2.274)-(2.275).

Plugging this relation into Eq. (75), we see that the *full* spectrum of eigenenergies of the harmonic oscillator is described by the simple formula

$$E_n = \hbar\omega_0 \left(n + \frac{1}{2} \right), \quad n = 0, 1, 2, \dots, \quad (5.86)$$

which was already discussed in Sec. 2.9. It is rather remarkable that the bra-ket formalism has allowed us to derive it without calculating the corresponding (rather cumbersome) wavefunctions $\psi_n(x)$ – see Eqs. (2.284).

Moreover, this formalism may be also used to calculate virtually any matrix element of the oscillator, without using $\psi_n(x)$. However, to do that, we should first calculate the coefficient A'_n participating in the second of Eqs. (82). This may be done similarly to the above calculation of A_n ; alternatively, since we already know that $|A_n| = (N_n)^{1/2} = n^{1/2}$, we may notice that according to Eqs. (73) and (82), the eigenproblem (74), which in our new notation for N_n becomes

$$\hat{N}|n\rangle = n|n\rangle, \quad (5.87)$$

may be rewritten as

$$n|n\rangle = \hat{a}^\dagger \hat{a}|n\rangle = \hat{a}^\dagger A_n |n-1\rangle = A_n A'_{n-1} |n\rangle. \quad (5.88)$$

Comparing the first and the last form of this equality, we see that $|A'_{n-1}| = n/|A_n| = n^{1/2}$, so that $A'_n = (n+1)^{1/2} \exp(i\varphi_n')$. Taking all phases φ_n and φ_n' equal to zero for simplicity, we may spell out Eqs. (82) as³²

$$\hat{a}^\dagger |n\rangle = (n+1)^{1/2} |n+1\rangle, \quad \hat{a}|n\rangle = n^{1/2} |n-1\rangle. \quad (5.89)$$

Fock state ladder

Now we can use these formulas to calculate, for example, the matrix elements of the operator \hat{x} in the Fock state basis:

$$\begin{aligned} \langle n'|\hat{x}|n\rangle &\equiv x_0 \langle n'|\hat{\xi}|n\rangle = \frac{x_0}{\sqrt{2}} \langle n'|\left(\hat{a} + \hat{a}^\dagger\right)|n\rangle = \frac{x_0}{\sqrt{2}} \left(\langle n'|\hat{a}|n\rangle + \langle n'|\hat{a}^\dagger|n\rangle \right) \\ &= \frac{x_0}{\sqrt{2}} \left[n^{1/2} \langle n'|n-1\rangle + (n+1)^{1/2} \langle n'|n-1\rangle \right]. \end{aligned} \quad (5.90)$$

Taking into account the Fock state orthonormality:

$$\langle n'|n\rangle = \delta_{n'n}, \quad (5.91)$$

this result becomes

$$\langle n'|\hat{x}|n\rangle = \frac{x_0}{\sqrt{2}} \left[n^{1/2} \delta_{n',n-1} + (n+1)^{1/2} \delta_{n',n+1} \right] \equiv \left(\frac{\hbar}{2m\omega_0} \right)^{1/2} \left[n^{1/2} \delta_{n',n-1} + (n+1)^{1/2} \delta_{n',n+1} \right]. \quad (5.92)$$

Coordinate's matrix elements

Acting absolutely similarly, for the momentum's matrix elements we get a similar expression:

$$\langle n'|\hat{p}|n\rangle = i \left(\frac{\hbar m \omega_0}{2} \right)^{1/2} \left[-n^{1/2} \delta_{n',n-1} + (n+1)^{1/2} \delta_{n',n+1} \right] \quad (5.93)$$

³² A useful mnemonic rule for these key relations is that the *c*-number coefficient in any of them is equal to the square root of the *largest* number of the two states it relates.

Hence the matrices of both operators in the Fock-state basis have only two diagonals, adjacent to the main diagonal; all other elements (including the main-diagonal ones) are zeros.

The matrix elements of higher powers of these operators, as well as their products, may be handled similarly, though the higher the power, the bulkier the result. For example,

$$\begin{aligned}\langle n' | \hat{x}^2 | n \rangle &= \langle n' | \hat{x} \hat{x} | n \rangle = \sum_{n''=0}^{\infty} \langle n' | \hat{x} | n'' \rangle \langle n'' | \hat{x} | n \rangle \\ &= \frac{x_0^2}{2} \sum_{n''=0}^{\infty} [(n'')^{1/2} \delta_{n',n''-1} + (n''+1)^{1/2} \delta_{n',n''+1}] [n^{1/2} \delta_{n'',n-1} + (n+1)^{1/2} \delta_{n'',n+1}] \\ &= \frac{x_0^2}{2} \left\{ [n(n-1)]^{1/2} \delta_{n',n-2} + [(n+1)(n+2)]^{1/2} \delta_{n',n+2} + (2n+1) \delta_{n',n} \right\}.\end{aligned}\quad (5.94)$$

For applications, the most important of these matrix elements are those on its main diagonal:

$$\langle x^2 \rangle \equiv \langle n | \hat{x}^2 | n \rangle = \frac{x_0^2}{2} (2n+1). \quad (5.95)$$

This expression shows, in particular, that the expectation value of the oscillator's potential energy in the n^{th} Fock state is

$$\langle U \rangle \equiv \frac{m\omega_0^2}{2} \langle x^2 \rangle = \frac{m\omega_0^2 x_0^2}{2} \left(n + \frac{1}{2} \right) \equiv \frac{\hbar\omega_0}{2} \left(n + \frac{1}{2} \right). \quad (5.96)$$

This is exactly one-half of the total energy (86) of the oscillator. As a sanity check, an absolutely similar calculation for the momentum squared, and hence for the kinetic energy $p^2/2m$, yields

$$\langle p^2 \rangle = \langle n | \hat{p}^2 | n \rangle = (m\omega_0 x_0)^2 \left(n + \frac{1}{2} \right) \equiv \hbar m \omega_0 \left(n + \frac{1}{2} \right), \quad \text{so that } \langle \frac{p^2}{2m} \rangle = \frac{\hbar\omega_0}{2} \left(n + \frac{1}{2} \right), \quad (5.97)$$

i.e. both partial energies are equal to $E_n/2$, just as in a classical oscillator.³³

Note that according to Eqs. (92) and (93), the expectation values of both x and p in any Fock state are equal to zero:

$$\langle x \rangle \equiv \langle n | \hat{x} | n \rangle = 0, \quad \langle p \rangle \equiv \langle n | \hat{p} | n \rangle = 0, \quad (5.98)$$

This is why, according to the general Eqs. (1.33)-(1.34), the results (95) and (97) also give the variances of the coordinate and the momentum, i.e. the squares of their uncertainties, $(\delta x)^2$ and $(\delta p)^2$. In particular, for the ground state ($n = 0$), these uncertainties are

$$\delta x = \frac{x_0}{\sqrt{2}} \equiv \left(\frac{\hbar}{2m\omega_0} \right)^{1/2}, \quad \delta p = \frac{m\omega_0 x_0}{\sqrt{2}} \equiv \left(\frac{\hbar m \omega_0}{2} \right)^{1/2}. \quad (5.99)$$

In the theory of precise measurements (to be reviewed in brief in Chapter 10), these expressions are often called the *standard quantum limit*.

³³ Still note that operators of the partial (potential and kinetic) energies do *not* commute with either each other or with the full-energy (Hamiltonian) operator, so that the Fock states n are *not* their eigenstates. This fact maps on the well-known oscillations of these partial energies (with the frequency $2\omega_0$) in a classical oscillator, at the full energy staying constant.

5.5. Glauber states and squeezed states

There is a huge difference between a quantum stationary (Fock) state of the oscillator and its classical state. Indeed, let us write the well known classical equations of motion of the oscillator (using capital letters to distinguish classical variables from the arguments of quantum wavefunctions):³⁴

$$\dot{X} = \frac{P}{m}, \quad \dot{P} = -\frac{\partial U}{\partial x} = -m\omega_0^2 X. \quad (5.100)$$

On the so-called *phase plane*, with the Cartesian coordinates x and p , these equations describe a clockwise rotation of the representation point $\{X(t), P(t)\}$ along an elliptic trajectory starting from the initial point $\{X(0), P(0)\}$. (The normalization of the momentum by $m\omega_0$, similar to the one performed by the second of Eqs. (63), makes this trajectory pleasingly circular, with a constant radius equal to the oscillations amplitude A , corresponding to the constant full energy

$$E = \frac{m\omega_0^2}{2} A^2, \quad \text{with } A^2 = [X(t)]^2 + \left[\frac{P(t)}{m\omega_0} \right]^2 = \text{const} = [X(0)]^2 + \left[\frac{P(0)}{m\omega_0} \right]^2, \quad (5.101)$$

determined by the initial conditions – see Fig. 8.)

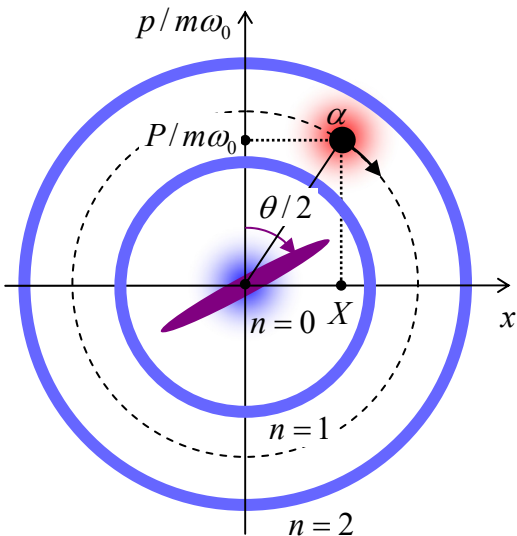


Fig. 5.8. Representations of various states of a harmonic oscillator on the phase plane. The bold black point represents a classical state with the complex amplitude α , with the dashed line showing its trajectory. The (very imperfect) classical images of the Fock states with $n = 0, 1$, and 2 are shown in blue. The blurred red spot is the (equally schematic) image of the Glauber state α . Finally, the magenta elliptical spot is a classical image of a *squeezed* ground state – see below. Arrows show the direction of the states' evolution in time.

For the forthcoming comparison with quantum states, it is convenient to describe this classical motion by the following dimensionless complex variable

$$\alpha(t) = \frac{1}{\sqrt{2}x_0} \left[X(t) + i \frac{P(t)}{m\omega_0} \right], \quad (5.102)$$

which is essentially the standard complex-number representation of the representing point's position on the 2D phase plane, with $|\alpha| \equiv A/\sqrt{2}x_0$. With this definition, Eqs. (100) are conveniently merged into one equation,

$$\dot{\alpha} = -i\omega_0\alpha, \quad (5.103)$$

³⁴ If Eqs. (100) are not evident, please consult a classical mechanics course – e.g., CM Sec. 3.2 and/or Sec. 10.1.

with an evident, very simple solution

$$\alpha(t) = \alpha(0) \exp\{-i\omega_0 t\}, \quad (5.104)$$

where the constant $\alpha(0)$ may be complex, and is just the (normalized) classical complex amplitude of oscillations.³⁵ This equation describes sinusoidal oscillations of both $X(t) \propto \text{Re}[\alpha(t)]$ and $P \propto \text{Im}[\alpha(t)]$, with a phase shift of $\pi/2$ between them.

On the other hand, according to the basic Eq. (4.161), the time dependence of a Fock state, as of a stationary state of the oscillator, is limited to the phase factor $\exp\{-iE_n t/\hbar\}$. This factor drops out at the averaging (4.125) for any observable. As a result, in this state the expectation values of x , p , or of any function thereof are time-independent. (Moreover, as Eqs. (98) show, $\langle x \rangle = \langle p \rangle = 0$.) Taking into account Eqs. (96)-(97), the closest (though very imperfect) geometric image³⁶ of such a state on the phase plane is a static circle of the radius $A_n = x_0(2n + 1)^{1/2}$, along which the wavefunction is uniformly spread – see the blue rings in Fig. 8. For the ground state ($n = 0$), with the wavefunction (2.275), a better image may be a blurred round spot, of a radius $\sim x_0$, at the origin. (It is easy to criticize such blurring, intended to represent the non-vanishing spreads (99), because it fails to reflect the fact that the total energy of the oscillator in the state, $E_0 = \hbar\omega_0/2$ is defined exactly, without any uncertainty.)

So, the difference between a classical state of the oscillator and its Fock state n is very profound. However, the Fock states are not the only possible quantum states of the oscillator: according to the basic Eq. (4.6), any state described by the ket-vector

$$|\alpha\rangle = \sum_{n=0}^{\infty} \alpha_n |n\rangle \quad (5.105)$$

with an arbitrary set of (complex) c -numbers α_n , is also its legitimate state, subject only to the normalization condition $\langle \alpha | \alpha \rangle = 1$, giving

$$\sum_{n=0}^{\infty} |\alpha_n|^2 = 1. \quad (5.106)$$

It is natural to ask: could we select the coefficients α_n in such a special way that the state properties would be closer to the classical one; in particular the expectation values $\langle x \rangle$ and $\langle p \rangle$ of the coordinate and momentum would evolve in time as the classical values $X(t)$ and $P(t)$, while the uncertainties of these observables would be, just as in the ground state, given by Eqs. (99), and hence have the smallest possible uncertainty product, $\delta x \delta p = \hbar/2$. Let me show that such a *Glauber state*,³⁷ which is

³⁵ See, e.g., CM Chapter 5, especially Eqs. (5.4).

³⁶ I have to confess that such geometric mapping of a quantum state on the phase plane $[x, p]$ is not exactly defined; you may think about colored areas in Fig. 8 as the regions of the observable pairs $\{x, p\}$ most probably obtained in measurements. A quantitative definition of such a mapping will be given in Sec. 7.3 using the Wigner function, though, as we will see, even such imaging has certain internal contradictions. Still, such cartoons as Fig. 8 have a substantial heuristic value, provided that their limitations are kept in mind.

³⁷ Named after Roy Jay Glauber who studied these states in detail in the mid-1960s, though they had been discussed in brief by Ervin Schrödinger as early as in 1926. Another popular adjective, “coherent”, for the Glauber states is very misleading, because *all* quantum states of *all* systems we have studied so far (including the Fock states of the harmonic oscillator) may be represented as coherent (pure) superpositions of the basis states. This is why I will not use this term for the Glauber states.

schematically represented in Fig. 8 by a blurred red spot around the classical point $\{X(t), P(t)\}$, is indeed possible.

Conceptually the simplest way to find the corresponding coefficients α_n would be to calculate $\langle x \rangle$, $\langle p \rangle$, δx , and δp for an arbitrary set of α_n , and then try to optimize these coefficients to reach our goal. However, this problem may be solved much easier using wave mechanics. Indeed, let us consider the following wavefunction:

$$\Psi_\alpha(x, t) = \left(\frac{m\omega_0}{\pi\hbar} \right)^{1/2} \exp \left\{ -\frac{m\omega_0}{2\hbar} [x - X(t)]^2 + i \frac{P(t)x}{\hbar} \right\}, \quad (5.107)$$

Glauber state:
coordinate representation

Its comparison with Eqs. (2.275) shows that this is just the ground-state wavefunction, but with the center shifted from the origin into the classical point $\{X(t), P(t)\}$. A straightforward (though a bit bulky) differentiation over x and t shows that it satisfies the oscillator's Schrödinger equation, provided that the c -number functions $X(t)$ and $P(t)$ obey the classical equations (100). Moreover, a similar calculation shows that the wavefunction (107) also satisfies the Schrödinger equation of an oscillator under the effect of a pulse of a classical force $F(t)$, provided that the oscillator initially was in its ground state, and that the classical evolution law $\{X(t), P(t)\}$ in Eq. (107) takes this force into account.³⁸ Since for many experimental implementations of the harmonic oscillator, the ground state may be readily formed (for example, by providing a weak coupling of the oscillator to a low-temperature environment), the Glauber state is usually easier to form than any Fock state with $n > 0$. This is why the Glauber states are so important and deserve much discussion.

In such a discussion, there is a substantial place for the bra-ket formalism. For example, to calculate the corresponding coefficients in the expansion (105) by wave-mechanical means,

$$\alpha_n(t) \equiv \langle n | \alpha(t) \rangle = \int dx \langle n | x \rangle \langle x | \alpha(t) \rangle = \int \psi_n^*(x) \Psi_\alpha(x, t) dx, \quad (5.108)$$

we would need to use not only the simple Eq. (107), but also the Fock state wavefunctions $\psi_n(x)$, which are not very appealing – see Eq. (2.284) again. Instead, this calculation may be readily done in the bra-ket formalism, giving us one important byproduct result as well.

Let us start by expressing the double shift of the ground state (by X and P), which has led us to Eq. (107), in the operator language. Forgetting about the P for a minute, let us find the *translation operator* $\hat{\mathcal{T}}_X$ that would produce the desired shift of an arbitrary wavefunction $\psi(x)$ by a c -number distance X along the coordinate argument x . This means

$$\hat{\mathcal{T}}_X \psi(x) \equiv \psi(x - X). \quad (5.109)$$

Representing the wavefunction ψ as the standard wave packet (4.264), we see that

$$\hat{\mathcal{T}}_X \psi(x) = \frac{1}{(2\pi\hbar)^{1/2}} \int \phi(p) \exp \left\{ i \frac{p(x - X)}{\hbar} \right\} dp \equiv \frac{1}{(2\pi\hbar)^{1/2}} \int \left[\phi(p) \exp \left\{ -i \frac{pX}{\hbar} \right\} \right] \exp \left\{ i \frac{px}{\hbar} \right\} dp. \quad (5.110)$$

³⁸ For its description, it is sufficient to solve Eqs. (100), with $F(t)$ added to the right-hand side of the second of these equations.

Hence, the shift may be achieved by the multiplication of each Fourier component of the packet, with the momentum p , by $\exp\{-ipX/\hbar\}$. This gives us a hint that the general form of the translation operator, valid in *any* representation, should be

$$\hat{\mathcal{T}}_x = \exp\left\{-i\frac{\hat{p}X}{\hbar}\right\}. \quad (5.111)$$

The proof of this formula is provided merely by the fact that, as we know from Chapter 4, any operator is uniquely determined by the set of its matrix elements in any full and orthogonal basis, in particular the basis of momentum states p . According to Eq. (110), the analog of Eq. (4.235) for the p -representation, applied to the translation operator (which is evidently local), is

$$\int dp \langle p | \hat{\mathcal{T}}_x | p' \rangle \phi(p') = \exp\left\{-i\frac{pX}{\hbar}\right\} \phi(p), \quad (5.112)$$

so that the operator (111) does exactly the job we need it to.

The operator that provides the shift of momentum by a *c*-number P is absolutely similar – with the opposite sign under the exponent, due to the opposite sign of the exponent in the reciprocal Fourier transform, so that the simultaneous shift by both X and P may be achieved by the following translation operator:

$$\hat{\mathcal{T}}_\alpha = \exp\left\{i\frac{P\hat{x} - \hat{p}X}{\hbar}\right\}. \quad (5.113)$$

Translation operator

As we already know, for a harmonic oscillator the creation-annihilation operators are more natural, so that we may use Eqs. (66) to recast Eq. (113) as

$$\hat{\mathcal{T}}_\alpha = \exp\left\{\alpha\hat{a}^\dagger - \alpha^*\hat{a}\right\}, \quad \text{so that } \hat{\mathcal{T}}_\alpha^\dagger = \exp\left\{\alpha^*\hat{a} - \alpha\hat{a}^\dagger\right\}, \quad (5.114)$$

where α (which, generally, may be a function of time) is the *c*-number defined by Eq. (102). Now, according to Eq. (107), we may form the Glauber state's ket-vector just as

$$|\alpha\rangle = \hat{\mathcal{T}}_\alpha |0\rangle. \quad (5.115)$$

This formula, valid in any representation, is very elegant, but using it for practical calculations (say, of the expectation values of observables) is not too easy because of the exponent-of-operators form of the translation operator. Fortunately, it turns out that a much simpler representation for the Glauber state is possible. To show this, let us start with the following general (and very useful) property of exponential functions of an operator argument: if

$$[\hat{A}, \hat{B}] = \mu\hat{l}, \quad (5.116)$$

(where \hat{A} and \hat{B} are arbitrary linear operators, and μ is a *c*-number), then³⁹

$$\exp\{+\hat{A}\}\hat{B}\exp\{-\hat{A}\} = \hat{B} + \mu\hat{l}. \quad (5.117)$$

³⁹ A proof of Eq. (117) may be readily achieved by expanding the operator $\hat{f}(\lambda) \equiv \exp\{+\lambda\hat{A}\}\hat{B}\exp\{-\lambda\hat{A}\}$ in the Taylor series with respect to the *c*-number parameter λ , and then evaluating the result for $\lambda = 1$. This simple exercise is left for the reader.

Let us apply Eqs. (116)-(117) to two cases, both with

$$\hat{A} = \alpha^* \hat{a} - \alpha \hat{a}^\dagger, \quad \text{so that } \exp\{\hat{A}\} = \hat{\mathcal{T}}_\alpha^\dagger, \quad \exp\{-\hat{A}\} = \hat{\mathcal{T}}_\alpha. \quad (5.118)$$

First, let us take $\hat{B} = \hat{I}$; then Eq. (116) is valid with $\mu = 0$, and Eq. (117) yields

$$\hat{\mathcal{T}}_\alpha^\dagger \hat{\mathcal{T}}_\alpha = \hat{I}, \quad (5.119)$$

This equality means that the translation operator is unitary – not a big surprise, because if we shift a classical point on the phase plane by a complex number ($+\alpha$) and then by ($-\alpha$), we certainly must come back to the initial position. Eq. (119) means merely that this fact is true for any quantum state as well.

Second, let us take $\hat{B} = \hat{a}$; in order to find the corresponding parameter μ , we must calculate the commutator on the left-hand side of Eq. (116) for this case. Using, at the due stage of the calculation, Eq. (68), we get

$$[\hat{A}, \hat{B}] = [\alpha^* \hat{a} - \alpha \hat{a}^\dagger, \hat{a}] = -\alpha [\hat{a}^\dagger, \hat{a}] = \alpha \hat{I}, \quad (5.120)$$

so that in this case $\mu = \alpha$, and Eq. (117) yields

$$\hat{\mathcal{T}}_\alpha^\dagger \hat{a} \hat{\mathcal{T}}_\alpha = \hat{a} + \alpha \hat{I}. \quad (5.121)$$

We have approached the summit of this beautiful calculation. Let us consider the following operator:

$$\hat{\mathcal{T}}_\alpha \hat{\mathcal{T}}_\alpha^\dagger \hat{a} \hat{\mathcal{T}}_\alpha. \quad (5.122)$$

Using Eq. (119), we may reduce this product to $\hat{a} \hat{\mathcal{T}}_\alpha$, while the application of Eq. (121) to the same expression (122) yields $\hat{\mathcal{T}}_\alpha \hat{a} + \alpha \hat{\mathcal{T}}_\alpha$. Hence, we get the following operator equality:

$$\hat{a} \hat{\mathcal{T}}_\alpha = \hat{\mathcal{T}}_\alpha \hat{a} + \alpha \hat{\mathcal{T}}_\alpha, \quad (5.123)$$

which may be applied to any state. Now acting by both sides of this equality on the ground state's ket $|0\rangle$, and using the fact that $\hat{a}|0\rangle$ is the null-state, while according to Eq. (115), $\hat{\mathcal{T}}_\alpha|0\rangle \equiv |\alpha\rangle$, we finally get a very simple and elegant result:⁴⁰

$\hat{a}|\alpha\rangle = \alpha|\alpha\rangle. \quad (5.124)$

Glauber
state as
eigenstate

Thus any Glauber state α is one of the eigenstates of the annihilation operator, namely the one with the eigenvalue equal to the *c*-number parameter α of the state, i.e. to the complex representation (102) of the classical point which is the center of the Glauber state's wavefunction.⁴¹ This fact makes the

⁴⁰ This result is also rather counter-intuitive. Indeed, according to Eq. (89), the annihilation operator \hat{a} , acting upon a Fock state n , “beats it down” to the lower-energy state $(n - 1)$. However, according to Eq. (124), the action of the same operator on a Glauber state α does *not* lead to the state change and hence to any energy change! The resolution of this paradox is given by the representation of the Glauber state as a series of Fock states – see Eq. (134) below. The operator \hat{a} indeed transfers each Fock component of this series to a lower-energy state, but it also re-weights each term, so that the complete energy of the Glauber state remains constant.

⁴¹ This fact means that the spectrum of eigenvalues α in Eq. (124), viewed as an eigenproblem, is continuous – it may be *any* complex number.

calculations of all Glauber state properties much simpler. As an example, let us calculate $\langle x \rangle$ in the Glauber state with some c -number α :

$$\langle x \rangle = \langle \alpha | \hat{x} | \alpha \rangle = \frac{x_0}{\sqrt{2}} \langle \alpha | \left(\hat{a} + \hat{a}^\dagger \right) | \alpha \rangle \equiv \frac{x_0}{\sqrt{2}} \left(\langle \alpha | \hat{a} | \alpha \rangle + \langle \alpha | \hat{a}^\dagger | \alpha \rangle \right). \quad (5.125)$$

In the first term in the parentheses, we can apply Eq. (124) directly, while in the second term, we can use the bra-counterpart of that relation, $\langle \alpha | \hat{a}^\dagger = \langle \alpha | \alpha^*$. Now assuming that the Glauber state is normalized, $\langle \alpha | \alpha \rangle = 1$, and using Eq. (102), we get

$$\langle x \rangle = \frac{x_0}{\sqrt{2}} \left(\langle \alpha | \alpha | \alpha \rangle + \langle \alpha | \dots \alpha^* | \alpha \rangle \right) = \frac{x_0}{\sqrt{2}} (\alpha + \alpha^*) = X, \quad (5.126)$$

Acting absolutely similarly, we may verify that $\langle p \rangle = P$, and that δx and δp do indeed obey Eqs. (99).

As the last sanity check, let us use Eq. (124) to re-calculate the Glauber state's wavefunction (107). Inner-multiplying both sides of that relation by the bra-vector $\langle x |$, and using the definition (65a) of the annihilation operator, we get

$$\frac{1}{\sqrt{2}x_0} \langle x | \left(\hat{x} + i \frac{\hat{p}}{m\omega_0} \right) | \alpha \rangle = \alpha \langle x | \alpha \rangle. \quad (5.127)$$

Since $\langle x |$ is the bra-vector of the eigenstate of the Hermitian operator \hat{x} , they may be swapped, with the operator giving its eigenvalue x ; acting on that bra-vector by the (local!) operator of momentum, we have to use it in the coordinate representation – see Eq. (4.245). As a result, we get

$$\frac{1}{\sqrt{2}x_0} \left(x \langle x | \alpha \rangle + \frac{\hbar}{m\omega_0} \frac{\partial}{\partial x} \langle x | \alpha \rangle \right) = \alpha \langle x | \alpha \rangle. \quad (5.128)$$

But $\langle x | \alpha \rangle$ is nothing else than the Glauber state's wavefunction Ψ_α so that Eq. (128) gives for it a first-order differential equation

$$\frac{1}{\sqrt{2}x_0} \left(x \Psi_\alpha + \frac{\hbar}{m\omega_0} \frac{\partial}{\partial x} \Psi_\alpha \right) = \alpha \Psi_\alpha. \quad (5.129)$$

Chasing Ψ_α and x to the opposite sides of the equation, and using the definition (102) of the parameter α , we can bring this equation to the form (valid at fixed t , and hence fixed X and P):

$$\frac{d\Psi_\alpha}{\Psi_\alpha} = \frac{m\omega_0}{\hbar} \left[-x + \left(X + i \frac{P}{m\omega_0} \right) \right] dx. \quad (5.130)$$

Integrating both parts, we return to Eq. (107).

Now we can use Eq. (124) for finding the coefficients α_n in the expansion (105) of the Glauber state α in the series over the Fock states n . Plugging Eq. (105) into both sides of Eq. (124), using the second of Eqs. (89) on the left-hand side, and requiring the coefficients at each ket-vector $|n\rangle$ in both parts of the resulting relation to be equal, we get the following recurrence relation:

$$\alpha_{n+1} = \frac{\alpha}{(n+1)^{1/2}} \alpha_n. \quad (5.131)$$

Applying this relation sequentially for $n = 0, 1, 2, \dots$, we get

$$\alpha_n = \frac{\alpha^n}{(n!)^{1/2}} \alpha_0. \quad (5.132)$$

Now we can find α_0 from the normalization requirement (106), getting

$$|\alpha_0|^2 \sum_{n=0}^{\infty} \frac{|\alpha|^{2n}}{n!} = 1. \quad (5.133)$$

In this sum, we may readily recognize the Taylor expansion of the function $\exp\{|\alpha|^2\}$, so that the final result (besides an arbitrary common phase multiplier) is

$$|\alpha\rangle = \exp\left\{-\frac{|\alpha|^2}{2}\right\} \sum_{n=0}^{\infty} \frac{\alpha^n}{(n!)^{1/2}} |n\rangle. \quad (5.134)$$

Glauber state vs Fock states

Hence, if the oscillator is in the Glauber state α , the probabilities $W_n \equiv \alpha_n \alpha_n^*$ of finding the system on the n^{th} energy level (86) obey the well-known *Poisson distribution* (Fig. 9):

$$W_n = \frac{\langle n \rangle^n}{n!} e^{-\langle n \rangle}, \quad (5.135)$$

Poisson distribution

where $\langle n \rangle$ is the statistical average of n – see Eq. (1.37):

$$\langle n \rangle = \sum_{n=0}^{\infty} n W_n. \quad (5.136)$$

The result of such summation is not necessarily integer! In our particular case, Eqs. (134)-(136) yield

$$\langle n \rangle = |\alpha|^2. \quad (5.137)$$

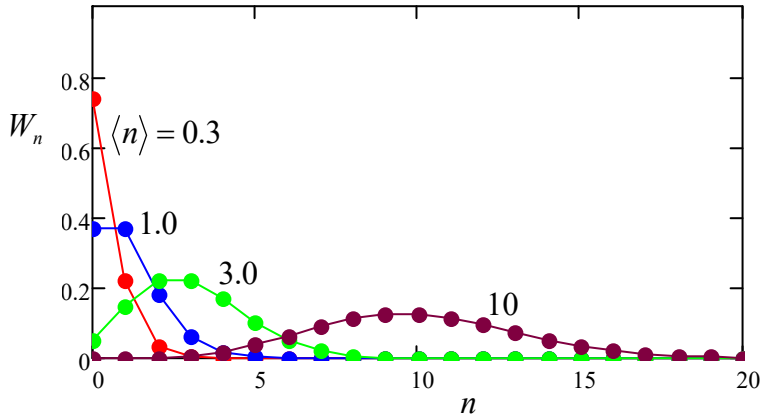


Fig. 5.9. The Poisson distribution (135) for several values of $\langle n \rangle$. Note that W_n are defined only for integer values of n ; the lines are only guides for the eye.

For applications, perhaps the most important mathematical property of this distribution is

$$\langle \tilde{n}^2 \rangle \equiv \langle (n - \langle n \rangle)^2 \rangle = \langle n \rangle, \quad \text{so that } \delta n \equiv \langle \tilde{n}^2 \rangle^{1/2} = \langle n \rangle^{1/2}. \quad (5.138)$$

Glauber state: r.m.s. uncertainty

Another important property is that at $\langle n \rangle \gg 1$, the Poisson distribution approaches the Gaussian (“normal”) one, with a small relative r.m.s. uncertainty: $\delta n / \langle n \rangle \ll 1$ – the trend clearly visible in Fig. 9.

Now let us discuss the Glauber state's evolution in time. In the wave-mechanics language, it is completely described by the dynamics (100) of the *c*-number shifts $X(t)$ and $P(t)$ participating in the wavefunction (107). Note again that, in contrast to the spread of the wave packet of a free particle, discussed in Sec. 2.2, in the harmonic oscillator the Gaussian packet of the special width (99) does not spread at all!

An alternative and equivalent way of dynamics description is to use the Heisenberg equation of motion. As Eqs. (29) and (35) tell us, such equations for the Heisenberg operators of coordinate and momentum have to be similar to the classical equations (100):

$$\dot{\hat{x}}_H = \frac{\hat{p}_H}{m}, \quad \dot{\hat{p}}_H = -m\omega_0^2 \hat{x}_H. \quad (5.139)$$

Now using Eqs. (66), for the Heisenberg-picture creation and annihilation operators we get the equations

$$\dot{\hat{a}}_H = -i\omega_0 \hat{a}_H, \quad \dot{\hat{a}}_H^\dagger = +i\omega_0 \hat{a}_H^\dagger, \quad (5.140)$$

which are completely similar to the classical equation (103) for the *c*-number parameter α and its complex conjugate, and hence have the solutions identical to Eq. (104):

$$\hat{a}_H(t) = \hat{a}_H(0)e^{-i\omega_0 t}, \quad \hat{a}_H^\dagger(t) = \hat{a}_H^\dagger(0)e^{i\omega_0 t}. \quad (5.141)$$

As was discussed in Sec. 4.6, such equations are very convenient, because they enable simple calculation of time evolution of observables for any initial state of the oscillator (Fock, Glauber, or any other) using Eq. (4.191). In particular, Eq. (141) shows that regardless of the initial state, the oscillator always returns to it *exactly* with the period $2\pi/\omega_0$.⁴² Applied to the Glauber state with $\alpha = 0$, i.e. the ground state of the oscillator, such calculation confirms that the Gaussian wave packet of the special width (99) does not spread in time at all – even temporarily.

Now let me briefly mention the states whose initial wave packets are still Gaussian, but have different widths, say $\delta x < x_0/\sqrt{2}$. As we already know from Sec. 2.2, the momentum spread δp will be correspondingly larger, still with the smallest possible uncertainty product: $\delta x \delta p = \hbar/2$. Such *squeezed ground state* ζ , with zero expectation values of x and p , may be generated from the Fock/Glauber ground state:

$$|\zeta\rangle = \hat{\mathcal{S}}_\zeta |0\rangle, \quad (5.142a)$$

using the so-called *squeezing operator*,

$$\hat{\mathcal{S}}_\zeta \equiv \exp\left\{\frac{1}{2}\left(\zeta^* \hat{a} \hat{a} - \zeta \hat{a}^\dagger \hat{a}^\dagger\right)\right\}, \quad (5.142b)$$

which depends on a complex *c*-number parameter $\zeta = re^{i\theta}$, where r and θ are real. The parameter's modulus r determines the squeezing degree; if ζ is real (i.e. $\theta = 0$), then

⁴² Actually, this fact is also evident from the Schrödinger picture of the oscillator's time evolution: due to the exactly equal distances $\hbar\omega_0$ between the eigenenergies (86), the time functions $a_n(t)$ in the fundamental expansion (1.69) of its wavefunction oscillate with frequencies $n\omega_0$, and hence they all share the same time period $2\pi/\omega_0$.

Squeezed
ground
state

Squeezing
operator

$$\delta x = \frac{x_0}{\sqrt{2}} e^{-r}, \quad \delta p = \frac{m\omega_0 x_0}{\sqrt{2}} e^r, \quad \text{so that } \delta x \delta p = \frac{m\omega_0 x_0^2}{2} = \frac{\hbar}{2}. \quad (5.143)$$

On the phase plane (Fig. 8), this state, with $r > 0$, may be represented by an oval spot squeezed along one of two mutually perpendicular axes (hence the state's name), and stretched by the same factor e^r along the counterpart axis; the same formulas but with $r < 0$ describe squeezing along the other axis. On the other hand, the phase θ of the squeezing parameter ζ determines the angle $\theta/2$ of the squeezing/stretching axes about the phase plane origin – see the magenta ellipse in Fig. 8. If $\theta \neq 0$, Eqs. (143) are valid for the variables $\{x', p'\}$ obtained from $\{x, p\}$ via clockwise rotation by that angle. For any of such origin-centered squeezed ground states, the time evolution is reduced to an increase of the angle with the rate ω_0 , i.e. to the clockwise rotation of the ellipse, without its deformation, with the angular velocity ω_0 – see the magenta arrows in Fig. 8. As a result, the uncertainties δx and δp oscillate in time with the double frequency $2\omega_0$. Such squeezed ground states may be formed, for example, by a parametric excitation of the oscillator,⁴³ with a parameter modulation depth close to, but still below the threshold of the excitation of degenerate parametric oscillations.

By action of an additional external force, the center of a squeezed state may be displaced from the origin to an arbitrary point $\{X, P\}$. Such displaced squeezed state may be described by the action of the translation operator (113) upon the ground squeezed state, i.e. by the action of the operator product $\hat{T}_\alpha \hat{\zeta}_\zeta$ on the usual (Fock / Glauber, i.e. non-squeezed) ground state. Calculations similar to those that led us from Eq. (114) to Eq. (124), show that such displaced squeezed state is an eigenstate of the following mixed operator:

$$\hat{b} \equiv \hat{a} \cosh r + \hat{a}^\dagger e^{i\theta} \sinh r, \quad (5.144)$$

with the same parameters r and θ , with the eigenvalue

$$\beta = \alpha \cosh r + \alpha^* e^{i\theta} \sinh r, \quad (5.145)$$

thus generalizing Eq. (124), which corresponds to $r = 0$. For the particular case $\alpha = 0$, Eq. (145) yields $\beta = 0$, i.e. the action of the operator (144) on the squeezed ground state ζ yields the null-state. Just as Eq. (124) in the case of the Glauber states, Eqs. (144)-(145) make the calculation of the basic properties of the squeezed states (for example, the proof of Eqs. (143) for the case $\alpha = \theta = 0$) very straightforward.

Unfortunately, I do not have more time/space for a further discussion of the squeezed states in this section, but their importance for precise quantum measurements will be discussed in Sec. 10.2 below.⁴⁴

⁴³ For a discussion and classical theory of this effect, see, e.g., CM Sec. 5.5.

⁴⁴ For more on the squeezed states see, e.g., Chapter 7 in the monograph by C. Gerry and P. Knight, *Introductory Quantum Optics*, Cambridge U. Press, 2005. Also, note the spectacular measurements of the Glauber and squeezed states of electromagnetic (optical) oscillators by G. Breitenbach *et al.*, *Nature* **387**, 471 (1997), a large (ten-fold) squeezing achieved in such oscillators by H. Vahlbruch *et al.*, *Phys. Rev. Lett.* **100**, 033602 (2008), and the first results on the ground state squeezing in micromechanical oscillators, with resonance frequencies $\omega_0/2\pi$ as low as a few MHz, using their parametric coupling to microwave electromagnetic oscillators – see, e.g., E. Wollman *et al.*, *Science* **349**, 952 (2015) and/or J.-M. Pirkkalainen *et al.*, *Phys. Rev. Lett.* **115**, 243601 (2015).

5.6. Revisiting spherically-symmetric systems

One more blank spot to fill has been left by our study, in Sec. 3.6, of wave mechanics of particle motion in spherically-symmetric 3D potentials. Indeed, while the azimuthal components of the eigenfunctions (the spherical harmonics) of such systems are very simple,

$$\psi_m = (2\pi)^{-1/2} e^{im\varphi}, \quad \text{with } m = 0, \pm 1, \pm 2, \dots, \quad (5.146)$$

their polar components include the associated Legendre functions $P_l^m(\cos\theta)$, which may be expressed via elementary functions only indirectly – see Eqs. (3.165) and (3.168). This makes all the calculations less than transparent and, in particular, does not allow a clear insight into the origin of the very simple energy spectrum of such systems – see, e.g., Eq. (3.163). The bra-ket formalism, applied to the angular momentum operator, not only enables such insight and produces a very convenient tool for many calculations involving spherically-symmetric potentials, but also opens a clear way toward the unification of the orbital momentum with the particle's spin – the latter task to be addressed in the next section.

Let us start by using the correspondence principle to spell out the quantum-mechanical vector operator of the orbital angular momentum $\mathbf{L} \equiv \mathbf{r} \times \mathbf{p}$ of a point particle:

Angular momentum operator

$$\hat{\mathbf{L}} \equiv \hat{\mathbf{r}} \times \hat{\mathbf{p}} = \begin{vmatrix} \mathbf{n}_x & \mathbf{n}_y & \mathbf{n}_z \\ \hat{r}_1 & \hat{r}_2 & \hat{r}_3 \\ \hat{p}_1 & \hat{p}_2 & \hat{p}_3 \end{vmatrix}, \quad \text{i.e. } \hat{L}_j \equiv \sum_{j'=1}^3 \hat{r}_{j'} \hat{p}_{j''} \varepsilon_{jj''},$$

(5.147)

where each of the indices j , j' , and j'' may take values 1, 2, and 3 (with $j'' \neq j, j'$), and $\varepsilon_{jj''}$ is the Levi-Civita permutation symbol, which we have already used in Sec. 4.5, and also in Sec. 1 of this chapter, in similar expressions (17)-(18). From this definition, we can readily calculate the commutation relations for all Cartesian components of operators $\hat{\mathbf{L}}$, $\hat{\mathbf{r}}$, and $\hat{\mathbf{p}}$; for example,

$$[\hat{L}_j, \hat{r}_{j''}] = \left[\sum_{k=1}^3 \hat{r}_k \hat{p}_{j''} \varepsilon_{jk''}, \hat{r}_{j''} \right] \equiv - \sum_{k=1}^3 \hat{r}_k [\hat{r}_{j'}, \hat{p}_{j''}] \varepsilon_{jk''} = -i\hbar \sum_{k=1}^3 \hat{r}_k \delta_{j'j''} \varepsilon_{jk''} \equiv i\hbar \sum_{k=1}^3 \hat{r}_k \varepsilon_{jj'k} \equiv i\hbar \hat{r}_{j''} \varepsilon_{jj''}, \quad (5.148)$$

The summary of all these calculations may be represented in similar compact forms:

Key commutation relations

$$[\hat{L}_j, \hat{r}_{j''}] = i\hbar \hat{r}_{j''} \varepsilon_{jj''}, \quad [\hat{L}_j, \hat{p}_{j''}] = i\hbar \hat{p}_{j''} \varepsilon_{jj''}, \quad [\hat{L}_j, \hat{L}_{j''}] = i\hbar \hat{L}_{j''} \varepsilon_{jj''};$$

(5.149)

the last of them shows that the commutator of two different Cartesian components of the vector-operator $\hat{\mathbf{L}}$ is proportional to its complementary component.

Also introducing, in a natural way, the (scalar!) operator of the observable $L^2 \equiv |\mathbf{L}|^2$,

Operator of L^2

$$\hat{L}^2 \equiv \hat{L}_x^2 + \hat{L}_y^2 + \hat{L}_z^2 \equiv \sum_{j=1}^3 \hat{L}_j^2,$$

(5.150)

it is straightforward to check that this operator commutes with each of the Cartesian components:

$$[\hat{L}^2, \hat{L}_j] = 0. \quad (5.151)$$

This result, at the first sight, may seem to contradict the last of Eqs. (149). Indeed, haven't we learned in Sec. 4.5 that commuting operators (e.g., \hat{L}^2 and any of \hat{L}_j) share their eigenstate sets? If yes, shouldn't this set has to be common for all four angular momentum operators? The resolution in this paradox may be found in the condition that was mentioned just after Eq. (4.138), but (sorry!) was not sufficiently emphasized there. According to that relation, if an operator has *degenerate* eigenstates (i.e. if some $A_j = A_{j'}$ even for $j \neq j'$), they should not be necessarily all shared by another compatible operator.

This is exactly the situation with the orbital angular momentum operators, which may be schematically shown on a *Venn diagram* (Fig. 10):⁴⁵ the eigenstates of the operator \hat{L}^2 are highly degenerate,⁴⁶ and their set is broader than those of any component operator \hat{L}_j (that, as will be shown below, are non-degenerate – until we consider particle's spin).

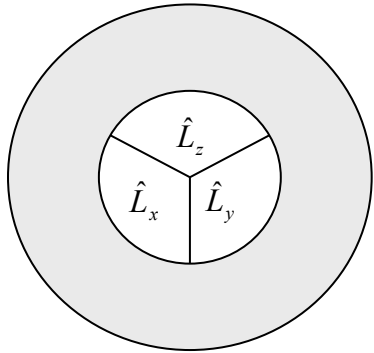


Fig. 5.10. The Venn diagram showing the partitioning of the set of eigenstates of the operator \hat{L}^2 . Each inner sector corresponds to the states shared with one of the Cartesian component operators \hat{L}_j , while the outer (shaded) ring represents the eigenstates of \hat{L}^2 that are not shared with either of \hat{L}_j – for example, all linear combinations of the eigenstates of different component operators.

Let us focus on just one of these three joint sets of eigenstates – by tradition, of the operators \hat{L}_z and \hat{L}_x . (This tradition stems from the canonical form of the spherical coordinates, in which the polar angle is measured from the z -axis. Indeed, in the coordinate representation we may write

$$\hat{L}_z \equiv \hat{x}p_y - \hat{y}p_x = x\left(-i\hbar \frac{\partial}{\partial y}\right) - y\left(-i\hbar \frac{\partial}{\partial x}\right) = -i\hbar \frac{\partial}{\partial \varphi}. \quad (5.152)$$

Writing the standard eigenproblem for the operator in this representation, $\hat{L}_z \psi_m = L_z \psi_m$, we see that it is satisfied by the eigenfunctions (146), with eigenvalues $L_z = \hbar m$ – which was already conjectured in Sec. 3.5.) More specifically, let us consider a set of eigenstates $\{l, m\}$ corresponding to a certain degenerate eigenvalue of the operator \hat{L}^2 , and all possible eigenvalues of the operator \hat{L}_z , i.e. all possible quantum numbers m . (At this point, l is just some label of the eigenvalue of the operator \hat{L}^2 ; it will be defined more explicitly in a minute.) To analyze this set, it is instrumental to introduce the so-called *ladder* (also called, respectively, “raising” and “lowering”) *operators*⁴⁷

⁴⁵ This is just a particular example of the Venn diagrams (introduced in the 1880s by John Venn) that show possible relations (such as intersections, unions, complements, etc.) between various sets of objects, and are very useful tool in the general set theory.

⁴⁶ Note that this particular result is consistent with the classical picture of the angular momentum vector: even when its length is fixed, the vector may be oriented in various directions, corresponding to different values of its Cartesian components. However, in the classical picture, all these components may be fixed simultaneously, while in the quantum picture this is not true.

⁴⁷ Note a substantial similarity between this definition and Eqs. (65) for the creation/annihilation operators.

Ladder
operators

$$\hat{L}_{\pm} \equiv \hat{L}_x \pm i\hat{L}_y. \quad (5.153)$$

It is simple (and hence left for the reader's exercise) to use this definition and the last of Eqs. (149) to calculate the following commutators:

Important
commutation
relations

$$[\hat{L}_+, \hat{L}_-] = 2\hbar\hat{L}_z, \quad \text{and} \quad [\hat{L}_z, \hat{L}_{\pm}] = \pm\hbar\hat{L}_{\pm}, \quad (5.154)$$

and also to use Eqs. (149)-(150) to prove two other important operator relations:

$$\hat{L}^2 = \hat{L}_z^2 + \hat{L}_+ \hat{L}_- - \hbar \hat{L}_z, \quad \hat{L}^2 = \hat{L}_z^2 + \hat{L}_- \hat{L}_+ + \hbar \hat{L}_z. \quad (5.155)$$

Now let us rewrite the last of Eqs. (154) as

$$\hat{L}_z \hat{L}_{\pm} = \hat{L}_{\pm} \hat{L}_z \pm \hbar \hat{L}_{\pm}, \quad (5.156)$$

and act by its both sides upon the ket-vector $|l, m\rangle$ of an arbitrary common eigenstate:

$$\hat{L}_z \hat{L}_{\pm} |l, m\rangle = \hat{L}_{\pm} \hat{L}_z |l, m\rangle \pm \hbar \hat{L}_{\pm} |l, m\rangle. \quad (5.157)$$

Since the eigenvalues of the operator \hat{L}_z are equal to $\hbar m$, in the first term of the right-hand side of Eq. (157) we may write

$$\hat{L}_z |l, m\rangle = \hbar m |l, m\rangle. \quad (5.158)$$

With that, Eq. (157) may be recast as

$$\hat{L}_z (\hat{L}_{\pm} |l, m\rangle) = \hbar(m \pm 1) (\hat{L}_{\pm} |l, m\rangle). \quad (5.159)$$

In a spectacular similarity with Eqs. (78)-(79) for the harmonic oscillator, Eq. (159) means that the states $\hat{L}_{\pm} |l, m\rangle$ are also eigenstates of the operator \hat{L}_z , corresponding to eigenvalues $\hbar(m \pm 1)$. Thus the ladder operators act exactly as the creation and annihilation operators of a harmonic oscillator, moving the system up or down a ladder of eigenstates – see Fig. 11.

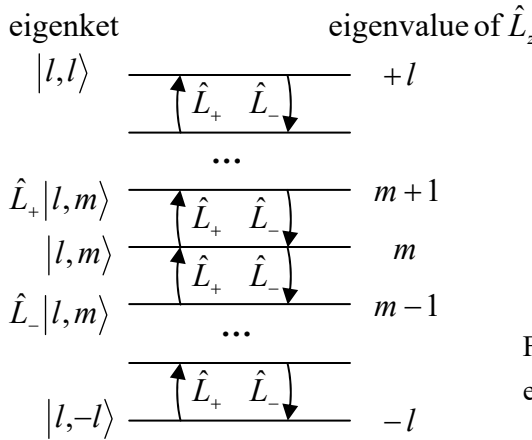


Fig. 5.11. The ladder diagram of the common eigenstates of the operators \hat{L}^2 and \hat{L}_z .

The most significant difference is that now the state ladder must end in both directions, because an infinite increase of $|m|$, with whichever sign of m , would cause the expectation values of the operator

$$\hat{L}_x^2 + \hat{L}_y^2 \equiv \hat{L}^2 - \hat{L}_z^2, \quad (5.160)$$

which corresponds to a non-negative observable, to become negative. Hence there have to be two states at both ends of the ladder, with such ket-vectors $|l, m_{\max}\rangle$ and $|l, m_{\min}\rangle$ that

$$\hat{L}_+|l, m_{\max}\rangle = 0, \quad \hat{L}_-|l, m_{\min}\rangle = 0. \quad (5.161)$$

Due to the symmetry of the whole problem with respect to the replacement $m \rightarrow -m$, we should have $m_{\min} = -m_{\max}$. This m_{\max} is exactly the quantum number traditionally called l , so that

$$-l \leq m \leq +l. \quad (5.162)$$

Relation between m and l

Evidently, this relation of quantum numbers m and l is semi-quantitatively compatible with the classical image of the angular momentum vector \mathbf{L} , of the same length L , pointing in various directions, thus affecting the value of its component L_z . In this classical picture, however, L^2 would be equal to the square of $(L_z)_{\max}$, i.e. to $(\hbar l)^2$; however, in quantum mechanics, this is not so. Indeed, applying both parts of the second of the operator equalities (155) to the top state's vector $|l, m_{\max}\rangle \equiv |l, l\rangle$, we get

$$\begin{aligned} \hat{L}^2|l, l\rangle &= \hbar \hat{L}_z|l, l\rangle + \hat{L}_z^2|l, l\rangle + \hat{L}_- \hat{L}_+|l, l\rangle = \hbar^2 l |l, l\rangle + \hbar^2 l^2 |l, l\rangle + 0 \\ &= \hbar^2 l(l+1)|l, l\rangle. \end{aligned} \quad (5.163)$$

Eigenvalues of L^2

Since by our initial assumption, all eigenvectors $|l, m\rangle$ correspond to the same eigenvalue of \hat{L}^2 , this result means that all these eigenvalues are equal to $\hbar^2 l(l+1)$. Just as in the case of the spin- $\frac{1}{2}$ vector operators discussed in Sec. 4.5, the deviation of this result from $\hbar^2 l^2$ may be interpreted as the result of unavoidable uncertainties (“fluctuations”) of the x - and y -components of the angular momentum, which give non-zero positive contributions to $\langle L_x^2 \rangle$ and $\langle L_y^2 \rangle$, and hence to $\langle L^2 \rangle$, even if the angular momentum vector is aligned with the z -axis in the best possible way.

(For various applications of the ladder operators (153), one more relation is convenient:

$$\hat{L}_{\pm}|l, m\rangle = \hbar [l(l+1) - m(m \pm 1)]^{1/2} |l, m \pm 1\rangle. \quad (5.164)$$

This equality, valid to the multiplier $e^{i\varphi}$ with an arbitrary real phase φ , may be readily proved from the above relations in the same way as the parallel Eqs. (89) for the harmonic-oscillator operators (65) were proved in Sec. 4; due to this similarity, the proof is also left for the reader's exercise.⁴⁸⁾

Now let us compare our results with those of Sec. 3.6. Using the expression of Cartesian coordinates via the spherical ones exactly as this was done in Eq. (152), we get the following expressions for the ladder operators (153) in the coordinate representation:

⁴⁸ The reader is also challenged to use the commutation relations discussed above to prove one more important property of the common eigenstates of \hat{L}_z and \hat{L}^2 :

$$\langle l, m | \hat{r}_j | l', m' \rangle = 0, \quad \text{unless } l' = l \pm 1 \text{ and } m' = \text{either } m \pm 1 \text{ or } m.$$

This property gives the *selection rule* for the orbital electric-dipole quantum transitions, to be discussed later in the course, especially in Sec. 9.3. (The final selection rules at these transitions may be affected by the particle's spin – see the next section.)

$$\hat{L}_\pm = \hbar e^{\pm i\varphi} \left(\pm \frac{\partial}{\partial \theta} + i \cotan \theta \frac{\partial}{\partial \varphi} \right). \quad (5.165)$$

Now plugging this relation, together with Eq. (152), into any of Eqs. (155), we get

$$\hat{L}^2 = -\hbar^2 \left[\frac{1}{\sin \theta} \frac{\partial}{\partial \theta} \left(\sin \theta \frac{\partial}{\partial \theta} \right) + \frac{1}{\sin^2 \theta} \frac{\partial^2}{\partial \varphi^2} \right]. \quad (5.166)$$

But this is exactly the operator (besides its division by the constant parameter $2mR^2$) that stands on the left-hand side of Eq. (3.156). Hence that equation, which was explored by the “brute-force” (wave-mechanical) approach in Sec. 3.6, may be understood as the eigenproblem for the operator \hat{L}^2 in the coordinate representation, with the eigenfunctions $Y_l^m(\theta, \varphi)$ corresponding to the eigenkets $|l, m\rangle$, and the eigenvalues $\hat{L}^2 = 2mR^2E$. As a reminder, the main result of that, rather involved analysis was expressed by Eq. (3.163), which now may be rewritten as

$$L_l^2 \equiv 2mR^2 E_l = \hbar^2 l(l+1), \quad (5.167)$$

in full agreement with Eq. (163), which was obtained by much more efficient means based on the bracket formalism. In particular, it is fascinating to see how easy it is to operate with the eigenvectors $|l, m\rangle$, while the coordinate representations of these ket-vectors, the spherical harmonics $Y_l^m(\theta, \varphi)$, may be only expressed by rather complicated functions – please have one more look at Eq. (3.171) and Fig. 3.20.

Note that all relations discussed in this section are not conditioned by any particular Hamiltonian of the system under analysis, though they (as well as those discussed in the next section) are especially important for particles moving in spherically-symmetric potentials.

5.7. Spin and its addition to orbital angular momentum

The theory described in the last section is useful for much more than orbital motion analysis. In particular, it helps to generalize the spin-½ results discussed in Chapter 4 to other values of spin s – the parameter still to be quantitatively defined. For that, let us notice that the commutation relations (4.155) for spin-½, which were derived from the Pauli matrix properties, may be rewritten in exactly the same form as Eqs. (149) and (151) for the orbital momentum:

$$[\hat{S}_j, \hat{S}_{j'}] = i\hbar \hat{S}_{j''} \epsilon_{jj''}, \quad [\hat{S}^2, \hat{S}_j] = 0. \quad (5.168)$$

It had been postulated (and then confirmed by numerous experiments) that these relations hold for quantum particles with any spin. Now notice that all the calculations of the last section have been based *almost* exclusively on such relations – the only exception will be discussed imminently. Hence, we may repeat them for the spin operators, and get the relations similar to Eqs. (158) and (163):

$$\hat{S}_z |s, m_s\rangle = \hbar m_s |s, m_s\rangle, \quad \hat{S}^2 |s, m_s\rangle = \hbar^2 s(s+1) |s, m_s\rangle, \quad 0 \leq s, \quad -s \leq m_s \leq +s, \quad (5.169)$$

where m_s is a quantum number parallel to the orbital magnetic number m , and the non-negative constant s is defined as the maximum value of $|m_s|$. The *c*-number s is exactly what is called the *particle’s spin*.

Now let us return to the only part of our orbital moment calculations that has *not* been derived from the commutation relations. This was the fact, based on the solution (146) of the orbital motion problems, that the quantum number m (the analog of m_s) may be only an integer. For spin, we do not have such a solution, so that the spectrum of numbers m_s (and hence its limits $\pm s$) should be found from the more loose requirement that the eigenstate ladder, extending from $-s$ to $+s$, has an integer number of steps. Hence, $2s$ has to be an integer, i.e. the spin s of a quantum particle may be either *integer* (as it is, for example, for photons, gluons, and massive bosons W^\pm and Z^0), or *half-integer* (e.g., for all quarks and leptons, notably including electrons).⁴⁹ For $s = \frac{1}{2}$, this picture yields all the properties of the spin- $\frac{1}{2}$ that were derived in Chapter 4 from Eqs. (4.115)-(4.117). In particular, the operators \hat{S}^2 and \hat{S}_z have two common eigenstates (\uparrow and \downarrow), with $S_z = \hbar m_s = \pm \hbar/2$, both with $S^2 = s(s+1)\hbar^2 = (3/4)\hbar^2$.

Note that this analogy with the angular momentum sheds new light on the symmetry properties of spin- $\frac{1}{2}$. Indeed, the fact that m in Eq. (146) is integer was derived in Sec. 3.5 from the requirement that making a full circle around axis z , we should find a similar value of wavefunction ψ_m , which differs from the initial one by an inconsequential factor $\exp\{2\pi im\} = +1$. With the replacement $m \rightarrow m_s = \pm \frac{1}{2}$, such operation would multiply the wavefunction by $\exp\{\pm\pi i\} = -1$, i.e. reverse its sign. Of course, spin properties cannot be described by a usual wavefunction, but this *odd parity* of electrons, shared by all other spin- $\frac{1}{2}$ particles, is clearly revealed in properties of multiparticle systems (see Chapter 8 below), and as a result, in their statistics (see, e.g., SM Chapter 2).

Now we are sufficiently equipped to analyze the situations in which a particle has both the orbital momentum and the spin – as an electron in an atom. In classical mechanics, such an object, with the spin \mathbf{S} interpreted as the angular moment of its internal rotation, would be characterized by the *total angular momentum* vector $\mathbf{J} = \mathbf{L} + \mathbf{S}$. Following the correspondence principle, we may assume that quantum-mechanical properties of this observable may be described by the similarly defined vector operator:

$$\hat{\mathbf{J}} \equiv \hat{\mathbf{L}} + \hat{\mathbf{S}}, \quad (5.170)$$

Total
angular
momentum

with Cartesian components

$$\hat{J}_z \equiv \hat{L}_z + \hat{S}_z, \text{ etc.}, \quad (5.171)$$

and the magnitude squared equal to

$$\hat{J}^2 \equiv \hat{J}_x^2 + \hat{J}_y^2 + \hat{J}_z^2. \quad (5.172)$$

Let us examine the properties of this vector operator. Since its two components (170) describe different degrees of freedom of the particle, i.e. belong to different Hilbert spaces, they have to be completely commuting:

$$[\hat{L}_j, \hat{S}_{j'}] = 0, \quad [\hat{L}^2, \hat{S}^2] = 0, \quad [\hat{L}_j, \hat{S}^2] = 0, \quad [\hat{L}^2, \hat{S}_j] = 0. \quad (5.173)$$

The above equalities are sufficient to derive the commutation relations for the operator $\hat{\mathbf{J}}$, and unsurprisingly, they turn out to be absolutely similar to those of its components:

⁴⁹ As a reminder, in the Standard Model of particle physics, such hadrons as mesons and baryons (notably including protons and neutrons) are essentially composite particles. However, at non-relativistic energies, protons and neutrons may be considered fundamental particles with $s = \frac{1}{2}$.

Total
momentum:
commutation
relations

Total
momentum:
eigenstates,
and
eigenvalues

$$[\hat{J}_j, \hat{J}_{j'}] = i\hbar \hat{J}_{j''} \epsilon_{jj''}, \quad [\hat{J}^2, \hat{J}_j] = 0. \quad (5.174)$$

Now repeating all the arguments of the last section, we may derive the following expressions for the common eigenstates of the operators \hat{J}^2 and \hat{J}_z :

$$J_z |j, m_j\rangle = \hbar m_j |j, m_j\rangle, \quad \hat{J}^2 |j, m_j\rangle = \hbar^2 j(j+1) |j, m_j\rangle, \quad 0 \leq j, \quad -j \leq m_j \leq +j, \quad (5.175)$$

where j and m_j are new quantum numbers.⁵⁰ Repeating the arguments just made for s and m_s , we may conclude that j and m_j may be either integer or half-integer.

Before we proceed, one remark on notation: it is very convenient to use the same letter m for numbering eigenstates of all momentum components participating in Eq. (171), with corresponding indices (j , l , and s), in particular, to replace what we called m with m_l . With this replacement, the main results of the last section may be summarized in a form similar to Eqs. (168), (169), (174), and (175):

$$[\hat{L}_j, \hat{L}_{j'}] = i\hbar \hat{L}_{j''} \epsilon_{jj''}, \quad [\hat{L}^2, \hat{L}_j] = 0, \quad (5.176)$$

$$\hat{L}_z |l, m_l\rangle = \hbar m_l |l, m_l\rangle, \quad \hat{L}^2 |l, m_l\rangle = \hbar^2 l(l+1) |l, m_l\rangle, \quad 0 \leq l, \quad -l \leq m_l \leq +l. \quad (5.177)$$

In order to understand which eigenstates participating in Eqs. (169), (175), and (177) are compatible with each other, it is straightforward to use Eq. (172), together with Eqs. (168), (173), (174), and (176) to get the following relations:

$$[\hat{J}^2, \hat{L}^2] = 0, \quad [\hat{J}^2, \hat{S}^2] = 0, \quad (5.178)$$

$$[\hat{J}^2, \hat{L}_z] \neq 0, \quad [\hat{J}^2, \hat{S}_z] \neq 0. \quad (5.179)$$

This result is represented schematically on the Venn diagram shown in Fig. 12, in which the crossed arrows indicate the only *non-commuting* pairs of operators.

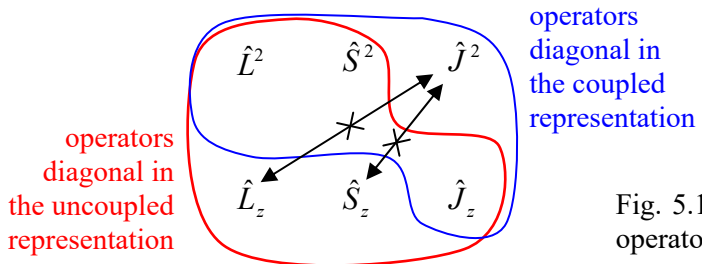


Fig. 5.12. The Venn diagram of angular momentum operators, and their mutually-commuting groups.

This means that there are eigenstates shared by two operator groups encircled with colored lines in Fig. 12. The first group (encircled red), consists of all these operators but \hat{J}^2 . Hence there are eigenstates shared by the five remaining operators, and these states correspond to definite values of the corresponding quantum numbers: l , m_l , s , m_s , and m_j . Actually, only four of these numbers are

⁵⁰ Let me hope that the difference between the quantum number j , and the indices j, j', j'' numbering the Cartesian components in the relations like Eqs. (168) or (174), is absolutely clear from the context.

independent, because due to Eq. (171) for these compatible operators, for each eigenstate of this group, their “magnetic” quantum numbers m have to satisfy the following relation:

$$m_j = m_l + m_s. \quad (5.180)$$

Hence the common eigenstates of the operators of this group are fully defined by just four quantum numbers, for example, l , m_l , s , and m_s . For some calculations, especially those for the systems whose Hamiltonians include only the operators of this group, it is convenient⁵¹ to use this set of eigenstates as the basis; frequently this approach is called the *uncoupled representation*.

However, in some situations we cannot ignore interactions between the orbital and spin degrees of freedom (in the common jargon, the *spin-orbit coupling*), which leads in particular to splitting (called the *fine structure*) of the atomic energy levels even in the absence of external magnetic field. I will discuss these effects in detail in the next chapter, and now will only note that they may be described by a term proportional to the product $\hat{\mathbf{L}} \cdot \hat{\mathbf{S}}$, in the system’s Hamiltonian. If this term is substantial, the uncoupled representation becomes inconvenient. Indeed, writing

$$\hat{J}^2 = (\hat{\mathbf{L}} + \hat{\mathbf{S}})^2 = \hat{L}^2 + \hat{S}^2 + 2\hat{\mathbf{L}} \cdot \hat{\mathbf{S}}, \quad \text{so that } 2\hat{\mathbf{L}} \cdot \hat{\mathbf{S}} = \hat{J}^2 - \hat{L}^2 - \hat{S}^2, \quad (5.181)$$

and looking at Fig. 12 again, we see that operator $\hat{\mathbf{L}} \cdot \hat{\mathbf{S}}$, describing the spin-orbit coupling, does not commute with operators \hat{L}_z and \hat{S}_z . This means that stationary states of the system with such term in the Hamiltonian do not belong to the uncoupled representation’s basis. On the other hand, Eq. (181) shows that the operator $\hat{\mathbf{L}} \cdot \hat{\mathbf{S}}$ does commute with all four operators of another group, encircled blue in Fig. 12. According to Eqs. (178), (179), and (181), all operators of that group also commute with each other, so that they have common eigenstates, described by the quantum numbers, l , s , j , and m_j . This group is the basis for the so-called *coupled representation* of particle states.

Excluding, for the notation brevity, the quantum numbers l and s , common for both groups, it is convenient to denote the common ket-vectors of each group as, respectively,

$ m_l, m_s\rangle$, for the uncoupled representation's basis, $ j, m_j\rangle$, for the coupled representation's basis.	Coupled and uncoupled bases
------------------------------------------------------------------------------------------------------------------------------	---------------------------------------------------------------

(5.182)

As we will see in the next chapter, for the solution of some important problems (e.g., the fine structure of atomic spectra and the Zeeman effect), we will need the relation between the kets $|j, m_j\rangle$ and the kets $|m_l, m_s\rangle$. This relation may be represented as the usual linear superposition,

$ j, m_j\rangle = \sum_{m_l, m_s} m_l, m_s\rangle \langle m_l, m_s j, m_j \rangle.$	Clebsch-Jordan coefficients: definition
----------------------------------------------------------------------------------------	---------------------------------------------------------------------------

(5.183)

The short brackets in this relation, essentially the elements of the unitary matrix of the transformation between two eigenstate bases (182), are called the *Clebsch-Gordan coefficients*.

The best (though imperfect) classical interpretation of Eq. (183) I can offer is as follows. If the lengths of the vectors \mathbf{L} and \mathbf{S} (in quantum mechanics associated with the numbers l and s , respectively),

⁵¹ This is especially true for motion in spherically-symmetric potentials, whose stationary states correspond to definite l and m_l ; however, the relations discussed in this section are important for some other problems as well.

and also their scalar product $\mathbf{L} \cdot \mathbf{S}$, are all fixed, then so is the length of the vector $\mathbf{J} = \mathbf{L} + \mathbf{S}$ – whose length in quantum mechanics is described by the number j . Hence, the classical image of a specific eigenket $|j, m_j\rangle$, in which l , s , j , and m_j are all fixed, is a state in which L^2 , S^2 , J^2 , and J_z are fixed. However, this fixation still allows for arbitrary rotation of the pair of vectors \mathbf{L} and \mathbf{S} (with a fixed angle between them, and hence fixed $\mathbf{L} \cdot \mathbf{S}$ and J^2) about the direction of the vector \mathbf{J} – see Fig. 13.

Hence the components L_z and S_z in these conditions are *not* fixed, and in classical mechanics may take a continuum of values, two of which (with the largest and the smallest possible values of S_z) are shown in Fig. 13. In quantum mechanics, these components are quantized, with their states represented by eigenkets $|m_l, m_s\rangle$, so that a linear combination of such kets is necessary to represent a ket $|j, m_j\rangle$. This is exactly what Eq. (183) does.

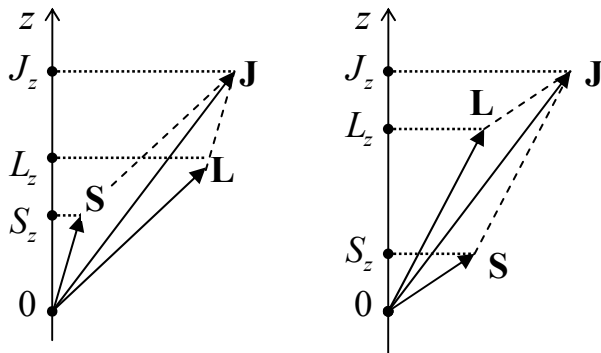


Fig. 5.13. A classical image of two different quantum states with the same quantum numbers l , s , j , and m_j , but different m_l and m_s .

Some properties of the Clebsch-Gordan coefficients $\langle m_l, m_s | j, m_j \rangle$ may be readily established. For example, the coefficients do not vanish only if the involved magnetic quantum numbers satisfy Eq. (180). In our current case, this relation is not an elementary corollary of Eq. (171), because in the Clebsch-Gordan coefficients, with the quantum numbers m_l , m_s in one state vector, and m_j in the other state vector, characterize the relation between different groups of the basis states, so we need to prove this fact. All matrix elements of the null-operator

$$\hat{J}_z - (\hat{L}_z + \hat{S}_z) = \hat{0} \quad (5.184)$$

should equal zero in any basis; in particular

$$\langle j, m_j | \hat{J}_z - (\hat{L}_z + \hat{S}_z) | m_l, m_s \rangle = 0. \quad (5.185)$$

Acting by the operator \hat{J}_z upon the bra-vector, and by the sum $(\hat{L}_z + \hat{S}_z)$ upon the ket-vector, we get

$$[m_j - (m_l + m_s)] \langle j, m_j | m_l, m_s \rangle = 0, \quad (5.186)$$

thus proving that

$$\langle m_l, m_s | j, m_j \rangle \equiv \langle j, m_j | m_l, m_s \rangle^* = 0, \quad \text{if } m_j \neq m_l + m_s. \quad (5.187)$$

For the most important case of spin- $\frac{1}{2}$ particles (with $s = \frac{1}{2}$, and hence $m_s = \pm\frac{1}{2}$), whose uncoupled representation basis includes $2(2l+1)$ states, the restriction (187) enables the representation of all non-zero Clebsch-Gordan coefficients on the simple “rectangular” diagram shown in Fig. 14. Indeed, each coupled-representation eigenket $|j, m_j\rangle$, with $m_j = m_l + m_s = m_l \pm \frac{1}{2}$, may be related by non-zero Clebsch-Gordan coefficients to at most two uncoupled-representation eigenstates $|m_l, m_s\rangle$. Since m_l

may only take integer values from $-l$ to $+l$, m_j may only take semi-integer values on the interval $[-l - \frac{1}{2}, l + \frac{1}{2}]$. Hence, by the definition of j as $(m_j)_{\max}$, its maximum value has to be $l + \frac{1}{2}$, and for $m_j = l + \frac{1}{2}$, this is the only possible value with this j . This means that the uncoupled state with $m_l = l$ and $m_s = \frac{1}{2}$ should be identical to the coupled-representation state with $j = l + \frac{1}{2}$ and $m_j = l + \frac{1}{2}$:

$$|j = l + \frac{1}{2}, m_j = l + \frac{1}{2}\rangle = |m_l = m_j - \frac{1}{2}, m_s = +\frac{1}{2}\rangle. \quad (5.188)$$

In Fig. 14, these two identical states are represented with the top-rightmost point (the uncoupled representation) and the sloped line passing through it (the coupled representation).

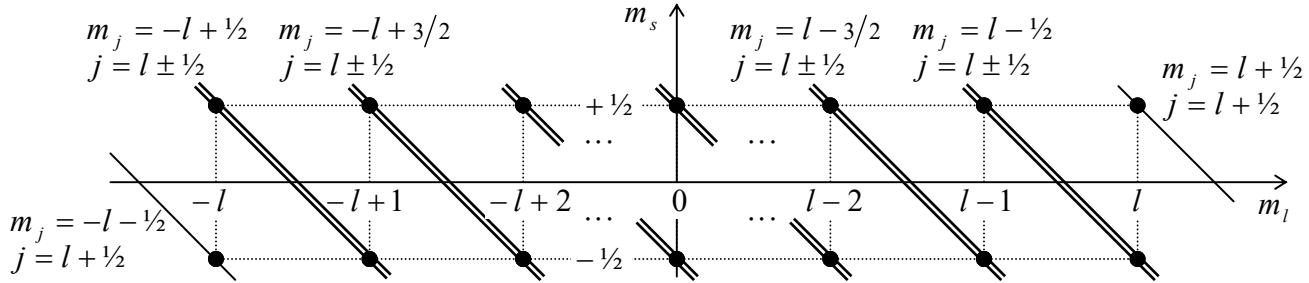


Fig. 5.14. A graphical representation of possible basis states of a spin- $\frac{1}{2}$ particle with a fixed l . Each dot corresponds to an uncoupled-representation ket-vector $|m_l, m_s\rangle$, while each sloped line corresponds to one coupled-representation ket-vector $|j, m_j\rangle$, related by Eq. (183) to the kets $|m_l, m_s\rangle$ whose dots it connects.

However, already the next value of this quantum number, $m_j = l - \frac{1}{2}$, is compatible with two values of j , so that each $|m_l, m_s\rangle$ ket has to be related to two $|j, m_j\rangle$ kets by two Clebsch-Gordan coefficients. Since j changes in unit steps, these values of j have to be $l \pm \frac{1}{2}$. This choice,

$$j = l \pm \frac{1}{2}, \quad (5.189)$$

evidently satisfies all lower values of m_j as well – see Fig. 14.⁵² (Again, only one value, $j = l + \frac{1}{2}$, is necessary to represent the state with the lowest $m_j = -l - \frac{1}{2}$ – see the bottom-leftmost point of that diagram.) Note that the total number of the coupled-representation states is $1 + 2 \times 2l + 1 \equiv 2(2l + 1)$, i.e. is the same as those in the uncoupled representation. So, for spin- $\frac{1}{2}$ systems, each sum (183), for fixed j and m_j (plus the fixed common parameter l , plus the common $s = \frac{1}{2}$), has at most two terms, i.e. involves at most two Clebsch-Gordan coefficients.

These coefficients may be calculated in a few steps, all but the last one rather simple even for an arbitrary spin s . First, the similarity of the vector operators $\hat{\mathbf{J}}$ and $\hat{\mathbf{S}}$ to the operator $\hat{\mathbf{L}}$, expressed by Eqs. (169), (175), and (177), may be used to argue that the matrix elements of the operators \hat{S}_\pm and \hat{J}_\pm , defined similarly to \hat{L}_\pm , have the matrix elements similar to those given by Eq. (164). Next, acting by the operator $\hat{J}_\pm = \hat{L}_\pm + \hat{S}_\pm$ upon both parts of Eq. (183), and then inner-multiplying the result by the bra

⁵² Eq. (5.189) allows a semi-qualitative classical interpretation in terms of the vector diagrams shown in Fig. 13: since, according to Eq. (169), $\hbar s$ gives the scale of the length of the vector \mathbf{S} , if it is small ($s = \frac{1}{2}$), the length of vector \mathbf{J} (similarly scaled by $\hbar j$) cannot deviate much from the length of the vector \mathbf{L} (scaled by $\hbar l$) for any spatial orientation of these vectors, so that j cannot differ from l too much. Note also that for a fixed m_j , the alternating sign in Eq. (189) is independent of the sign of m_s – see also Eqs. (190).

vector $\langle m_l, m_s |$ and using the above matrix elements, we may get recurrence relations for the Clebsch-Gordan coefficients with adjacent values of m_l , m_s , and m_j . Finally, these relations may be sequentially applied to the adjacent states in both representations, starting from any of the two states common for them – for example, from the state with the ket-vector (188), corresponding to the top right point in Fig. 14.

Let me leave these straightforward but a bit tedious calculations for the reader's exercise, and just cite the final result of this procedure for $s = \frac{1}{2}$:⁵³

Clebsch –
Gordan
coefficients
for $s = \frac{1}{2}$

$$\langle m_l = m_j - \frac{1}{2}, m_s = +\frac{1}{2} | j = l \pm \frac{1}{2}, m_j \rangle = \pm \left(\frac{l \pm m_j + \frac{1}{2}}{2l+1} \right)^{1/2},$$

$$\langle m_l = m_j + \frac{1}{2}, m_s = -\frac{1}{2} | j = l \pm \frac{1}{2}, m_j \rangle = + \left(\frac{l \mp m_j + \frac{1}{2}}{2l+1} \right)^{1/2}.$$

(5.190)

In this course, these relations will be used mostly in Sec. 6.4 for an analysis of the anomalous Zeeman effect. Moreover, the angular momentum addition theory described above is also valid for the addition of angular momenta of multiparticle system components, so we will revisit it in Chapter 8.

To conclude this section, I have to note that the Clebsch-Gordan coefficients (for arbitrary s) participate also in the so-called *Wigner-Eckart theorem* that expresses the matrix elements of *spherical tensor operators*, in the coupled-representation basis $|j, m_j\rangle$, via a reduced set of matrix elements. This theorem may be useful, for example, for the calculation of the rate of quantum transitions to/from high- n states in spherically-symmetric potentials. Unfortunately, a discussion of this theorem and its applications would require a higher mathematical background than I can expect from my readers, and more time/space than I can afford.⁵⁴

5.8. Exercise problems

5.1. Use the discussion in Sec. 1 to find an alternative solution of Problem 4.18.

5.2. A spin- $\frac{1}{2}$ is placed into an external magnetic field, with a time-independent orientation, its magnitude $\mathcal{B}(t)$ being an arbitrary function of time. Find explicit expressions for the Heisenberg operators and the expectation values of all three Cartesian components of the spin, as functions of time, in a coordinate system of your choice.

5.3. A two-level system is in the quantum state α described by the ket-vector $|\alpha\rangle = \alpha|\uparrow\rangle + \alpha|\downarrow\rangle$, with given (generally, complex) c -number coefficients $\alpha_{\uparrow\downarrow}$. Prove that we can always select such a geometric c -number vector $\mathbf{c} = \{c_x, c_y, c_z\}$, that α is an eigenstate of $\mathbf{c} \cdot \hat{\mathbf{\sigma}}$, where $\hat{\mathbf{\sigma}}$ is the Pauli vector operator. Find all possible values of \mathbf{c} satisfying this condition, and the second eigenstate (orthogonal to α) of the operator $\mathbf{c} \cdot \hat{\mathbf{\sigma}}$. Give a Bloch-sphere interpretation of your result.

⁵³ For arbitrary spin s , the calculations and even the final expressions for the Clebsch-Gordan coefficients are rather bulky. They may be found, typically in a table form, mostly in special monographs – see, e.g., A. Edmonds, *Angular Momentum in Quantum Mechanics*, Princeton U. Press, 1957.

⁵⁴ For the interested reader, I can recommend either Sec. 17.7 in E. Merzbacher, *Quantum Mechanics*, 3rd ed., Wiley, 1998, or Sec. 3.10 in J. Sakurai, *Modern Quantum Mechanics*, Addison-Wesley, 1994.

5.4.* Analyze statistics of the spacing $S \equiv E_+ - E_-$ between energy levels of a two-level system, assuming that all elements $H_{jj'}$ of its Hamiltonian matrix (2) are independent random numbers, with equal and constant probability densities within the energy interval of interest. Compare the result with that for a purely diagonal Hamiltonian matrix, with the similar probability distribution of its random diagonal elements.

5.5. For a periodic motion of a single particle in a confining potential $U(\mathbf{r})$, the *virial theorem* of non-relativistic classical mechanics⁵⁵ is reduced to the following equality:

$$\bar{T} = \frac{1}{2} \overline{\mathbf{r} \cdot \nabla U},$$

where T is the particle's kinetic energy, and the top bar means averaging over the time period of motion. Prove the following quantum-mechanical version of the theorem for an arbitrary stationary quantum state, in the absence of spin effects:

$$\langle T \rangle = \frac{1}{2} \langle \mathbf{r} \cdot \nabla U \rangle,$$

where the angular brackets mean the expectation values of the observables.

Hint: Mimicking the proof of the classical virial theorem, consider the time evolution of the following operator:

$$\hat{G} \equiv \hat{\mathbf{r}} \cdot \hat{\mathbf{p}}.$$

5.6. Calculate, in the WKB approximation, the transparency \mathcal{T} of the following saddle-shaped potential barrier:

$$U(x, y) = U_0 \left(1 + \frac{xy}{a^2} \right),$$

where $U_0 > 0$ and a are real constants, for tunneling of a 2D particle with energy $E < U_0$.

5.7. Calculate the so-called *Gamow factor*⁵⁶ for the alpha decay of atomic nuclei, i.e. the exponential factor in the transparency of the potential barrier resulting from the following simple model for the alpha-particle's potential energy as a function of its distance from the nuclear center:

$$U(r) = \begin{cases} U_0 < 0, & \text{for } r < R, \\ \frac{ZZ'e^2}{4\pi\epsilon_0 r}, & \text{for } R < r, \end{cases}$$

(where $Ze = 2e > 0$ is the charge of the particle, $Z'e > 0$ is that of the nucleus after the decay, and R is the nucleus' radius), in the WKB approximation.

5.8. Use the WKB approximation to calculate the average time of ionization of a hydrogen atom, initially in its ground state, made metastable by application of an additional weak, uniform, time-independent electric field \mathcal{E} . Formulate the conditions of validity of your result.

⁵⁵ See, e.g., CM Problem 1.12.

⁵⁶ Named after G. Gamow, who made this calculation as early as in 1928.

5.9. For a 1D harmonic oscillator with mass m and frequency ω_0 , calculate:

- (i) all matrix elements $\langle n | \hat{x}^3 | n' \rangle$, and
- (ii) the diagonal matrix elements $\langle n | \hat{x}^4 | n \rangle$,

where n and n' are arbitrary Fock states.

5.10. Calculate the sum (over all $n > 0$) of the so-called *oscillator strengths*,

$$f_n \equiv \frac{2m}{\hbar^2} (E_n - E_0) |\langle n | \hat{x} | 0 \rangle|^2,$$

- (i) for a 1D harmonic oscillator, and
- (ii) for a 1D particle confined in an arbitrary stationary potential.

5.11. Prove the so-called *Bethe sum rule*,

$$\sum_{n'} (E_{n'} - E_n) \left| \langle n | e^{ik\hat{x}} | n' \rangle \right|^2 = \frac{\hbar^2 k^2}{2m},$$

valid for a 1D particle moving in an arbitrary time-independent potential $U(x)$, and discuss its relation with the *Thomas-Reiche-Kuhn sum rule* whose derivation was the subject of the previous problem.

Hint: Calculate the expectation value, in a stationary state n , of the following double commutator,

$$\hat{D} = [\hat{H}, e^{ik\hat{x}}], e^{-ik\hat{x}},$$

in two ways: first, just spelling out both commutators, and, second, using the commutation relations between operators \hat{p}_x and $e^{ik\hat{x}}$, and compare the results.

5.12. Given Eq. (116), prove Eq. (117), using the hint given in the accompanying footnote.

5.13. Use Eqs. (116)-(117) to simplify the following operators:

- (i) $\exp\{+ia\hat{x}\} \hat{p}_x \exp\{-ia\hat{x}\}$, and
- (ii) $\exp\{+ia\hat{p}_x\} \hat{x} \exp\{-ia\hat{p}_x\}$,

where a is a *c*-number.

5.14. For a 1D harmonic oscillator, calculate:

- (i) the expectation value of energy, and
- (ii) the time evolution of the expectation values of the coordinate and momentum,

provided that in the initial moment ($t = 0$) it was in the state described by the following ket-vector:

$$|\alpha\rangle = \frac{1}{\sqrt{2}} (|31\rangle + |32\rangle),$$

where $|n\rangle$ are the ket-vectors of the stationary (Fock) states of the oscillator.

5.15.* Re-derive the London dispersion force's potential of the interaction of two isotropic 3D harmonic oscillators (already calculated in Problem 3.16), using the language of mutually-induced polarization.

5.16. An external force pulse $F(t)$, of a finite time duration \mathcal{T} , has been exerted on a 1D harmonic oscillator, initially in its ground state. Use the Heisenberg-picture equations of motion to calculate the expectation value of the oscillator's energy at the end of the pulse.

5.17. Use Eqs. (144)-(145) to calculate the uncertainties δx and δp for a harmonic oscillator in its squeezed ground state, and in particular, to prove Eqs. (143) for the case $\theta = 0$.

5.18. Calculate the energy of a harmonic oscillator in the squeezed ground state ζ .

5.19.* Prove that the squeezed ground state, described by Eqs. (142) and (144)-(145), may be sustained by a sinusoidal modulation of a harmonic oscillator's parameter, and calculate the squeezing factor r as a function of the parameter modulation depth, assuming that the depth is small, and the oscillator's damping is negligible.

5.20. Use Eqs. (148) to prove that the operators \hat{L}_j and \hat{L}^2 commute with the Hamiltonian of a spinless particle placed in any central potential field.

5.21. Use Eqs. (149)-(150) and (153) to prove Eqs. (155).

5.22. Derive Eq. (164), using any of the prior formulas.

5.23. In the basis of common eigenstates of the operators \hat{L}_z and \hat{L}^2 , described by kets $|l, m\rangle$:

(i) calculate the matrix elements $\langle l, m_1 | \hat{L}_x | l, m_2 \rangle$ and $\langle l, m_1 | \hat{L}_x^2 | l, m_2 \rangle$;

(ii) spell out your results for diagonal matrix elements (with $m_1 = m_2$) and their y -axis counterparts; and

(iii) calculate the diagonal matrix elements $\langle l, m | \hat{L}_x \hat{L}_y | l, m \rangle$ and $\langle l, m | \hat{L}_y \hat{L}_x | l, m \rangle$.

5.24. For the state described by the common eigenket $|l, m\rangle$ of the operators \hat{L}_z and \hat{L}^2 in a reference frame $\{x, y, z\}$, calculate the expectation values $\langle L_z \rangle$ and $\langle L_z^2 \rangle$ in the reference frame whose z' -axis forms angle θ with the z -axis.

5.25. Write down the matrices of the following angular momentum operators: $\hat{L}_x, \hat{L}_y, \hat{L}_z$, and \hat{L}_\pm , in the z -basis of the $\{l, m\}$ states with $l = 1$.

5.26. Calculate the angular factor of the orbital wavefunction of a particle with a definite value of L^2 , equal to $6\hbar^2$, and the largest possible value of L_x . What is this value?

5.27. For the state with the wavefunction $\psi = Cxye^{-\lambda r}$, with a real, positive λ , calculate:

- (i) the expectation values of the observables L_x , L_y , L_z , and L^2 , and
- (ii) the normalization constant C .

5.28. An angular state of a spinless particle is described by the following ket-vector:

$$|\alpha\rangle = \frac{1}{\sqrt{2}}(|l=3, m=0\rangle + |l=3, m=1\rangle).$$

Calculate the expectation values of the x - and y -components of its angular momentum. Is the result sensitive to a possible phase shift between the component eigenkets?

5.29. A particle is in a quantum state α with the orbital wavefunction proportional to the spherical harmonic $Y_1^1(\theta, \phi)$. Find the angular dependence of the wavefunctions corresponding to the following ket-vectors:

- (i) $\hat{L}_x|\alpha\rangle$, (ii) $\hat{L}_y|\alpha\rangle$, (iii) $\hat{L}_z|\alpha\rangle$, (iv) $\hat{L}_+ \hat{L}_- |\alpha\rangle$, and (v) $\hat{L}^2|\alpha\rangle$.

5.30. A charged, spinless 2D particle of mass m is trapped in a soft potential well $U(x, y) = m\omega_0^2(x^2 + y^2)/2$. Calculate its energy spectrum in the presence of a uniform magnetic field \mathcal{B} , normal to the $[x, y]$ -plane of particle's motion.

5.31. Solve the previous problem for a spinless 3D particle, placed (in addition to a uniform magnetic field \mathcal{B}) into a spherically-symmetric potential well $U(\mathbf{r}) = m\omega_0^2 r^2/2$.

5.32. Calculate the spectrum of rotational energies of an axially-symmetric, rigid body.

5.33. Simplify the following double commutator:

$$[\hat{r}_j, [\hat{L}^2, \hat{r}_{j'}]].$$

5.34. Prove the following commutation relation:

$$[\hat{L}^2, [\hat{L}^2, \hat{r}_j]] = 2\hbar^2 (\hat{r}_j \hat{L}^2 + \hat{L}^2 \hat{r}_j).$$

5.35. Use the commutation relation proved in the previous problem, and Eq. (148), to prove the orbital electric-dipole selection rules mentioned in Sec. 5.6 of the lecture notes.

5.36. Express the commutators listed in Eq. (179), $[\hat{J}^2, \hat{L}_z]$ and $[\hat{J}^2, \hat{S}_z]$, via \hat{L}_j and \hat{S}_j .

5.37. Find the operator $\hat{\mathcal{T}}_\phi$ describing a quantum state's rotation by angle ϕ about a certain axis, using the similarity of this operation with the shift of a Cartesian coordinate, discussed in Sec. 5. Then use this operator to calculate the probabilities of measurements of spin- $1/2$ components of a beam of

particles with z -polarized spin, by a Stern-Gerlach instrument turned by angle θ within the $[z, x]$ plane, where y is the axis of particle propagation – see Fig. 4.1.⁵⁷

5.38. The rotation (“angular translation”) operator $\hat{\mathcal{T}}_\phi$ analyzed in the previous problem, and the linear translation operator $\hat{\mathcal{T}}_x$ discussed in Sec. 5, have a similar structure:

$$\hat{\mathcal{T}}_\lambda = \exp\left\{-i\hat{C}\lambda/\hbar\right\},$$

where λ is a real c -number, characterizing the shift, and \hat{C} is a Hermitian operator, which does not explicitly depend on time.

(i) Prove that such operators $\hat{\mathcal{T}}_\lambda$ are unitary.

(ii) Prove that if the shift by λ , induced by the operator $\hat{\mathcal{T}}_\lambda$, leaves the Hamiltonian of some system unchanged for any λ , then $\langle C \rangle$ is a constant of motion for any initial state of the system.

(iii) Discuss what the last conclusion means for the particular operators $\hat{\mathcal{T}}_x$ and $\hat{\mathcal{T}}_\phi$.

5.39. A particle with spin s is in a state with definite quantum numbers l and j . Prove that the observable $\mathbf{L} \cdot \mathbf{S}$ also has a definite value, and calculate it.

5.40. For a spin- $\frac{1}{2}$ particle in a state with definite quantum numbers l , m_l , and m_s , calculate the expectation value of the observable J^2 , and the probabilities of all its possible values. Interpret your results in the terms of the Clebsh-Gordan coefficients (190).

5.41. Derive general recurrence relations for the Clebsh-Gordan coefficients.

Hint: Using the similarity of the commutation relations discussed in Sec. 7, write the relations similar to Eqs. (164) for other components of the angular momentum, and apply them to Eq. (170).

5.42. Use the recurrence relations derived in the previous problem to prove Eqs. (190) for the spin- $\frac{1}{2}$ Clebsh-Gordan coefficients.

5.43. A spin- $\frac{1}{2}$ particle is in a state with definite values of L^2 , J^2 , and J_z . Find all possible values of the observables S^2 , S_z , and L_z , the probability of each listed value, and the expectation value for each of these observables.

5.44. Re-solve the Landau-level problem discussed in Sec. 3.2, for a spin- $\frac{1}{2}$ particle. Discuss the result for the particular case of an electron, with the g -factor equal to 2.

5.45. In the Heisenberg picture of quantum dynamics, find an explicit relation between the operators of velocity $\hat{\mathbf{v}} \equiv d\hat{\mathbf{r}}/dt$ and acceleration $\hat{\mathbf{a}} \equiv d\hat{\mathbf{v}}/dt$ of a spin- $\frac{1}{2}$ particle with electric charge q , moving in an arbitrary external electromagnetic field. Compare the result with the corresponding classical expression.

Hint: For the orbital motion’s description, you may use Eq. (3.26).

⁵⁷ Note that the last task is just a particular case of Problem 4.18 (see also Problem 1).

5.46. A byproduct of the solution of Problem 41 is the following relation for the spin operators (valid for any spin s):

$$\langle m_s \pm 1 | \hat{S}_\pm | m_s \rangle = \hbar [(s \pm m_s + 1)(s \mp m_s)]^{1/2}.$$

Use this result to spell out the matrices S_x , S_y , S_z , and S^2 of a particle with $s = 1$, in the z -basis – defined as the basis in which the matrix S_z is diagonal.

5.47.* For a particle with an arbitrary spin s , moving in a spherically-symmetric field, find the ranges of the quantum numbers m_j and j that are necessary to describe, in the coupled-representation basis:

- (i) all states with a definite quantum number l , and
- (ii) a state with definite values of not only l , but also m_l and m_s .

Give an interpretation of your results in terms of the classical geometric vector diagram (Fig. 13).

5.48. A particle of mass m , with electric charge q and spin s , free to move along a plane ring of a radius R , is placed into a constant, uniform magnetic field \mathcal{B} , directed normally to the ring's plane. Calculate the energy spectrum of the system. Explore and interpret the particular form the result takes when the particle is an electron with the g-factor $g_e = 2$.

This page is
intentionally left
blank

Chapter 6. Perturbative Approaches

This chapter discusses several perturbative approaches to problems of quantum mechanics, and their simplest but important applications including the fine structure of atomic energy levels, and the effects of external dc and ac electric and magnetic fields on these levels. It continues with a discussion of the perturbation theory of transitions to continuous spectrum and the Golden Rule of quantum mechanics, which naturally brings us to the issue of open quantum systems – to be discussed in the next chapter.

6.1. Time-independent perturbations

Unfortunately, only a few problems of quantum mechanics may be solved exactly in an analytical form. Actually, in the previous chapters we have solved a substantial part of such problems for a single particle, while for multiparticle systems, the exactly solvable cases are even more rare. However, most practical problems of physics feature a certain small parameter, and this smallness may be exploited by various approximate analytical methods giving *asymptotically correct* results – i.e. the results whose error tends to zero at the reduction of the small parameter(s). Earlier in the course, we have explored one of them, the WKB approximation, which is adequate for a particle moving through a soft potential profile. In this chapter, we will discuss other techniques that are more suitable for other cases. The historic name for these techniques is *the perturbation theory*, though it is more fair to speak about several *perturbative approaches*, because they are substantially different for different situations.

The simplest version of the perturbation theory addresses the problem of stationary states and energy levels of systems described by time-independent Hamiltonians of the type

$$\hat{H} = \hat{H}^{(0)} + \hat{H}^{(1)}, \quad (6.1)$$

where the operator $\hat{H}^{(1)}$, describing the system's “perturbation”, is relatively small – in the sense that its addition to the unperturbed operator $\hat{H}^{(0)}$ results in a relatively small change of the eigenenergies E_n of the system, and the corresponding eigenstates. A typical problem of this type is the 1D *weakly anharmonic oscillator* (Fig. 1), described by the Hamiltonian (1) with

$$\hat{H}^{(0)} = \frac{\hat{p}^2}{2m} + \frac{m\omega_0^2 \hat{x}^2}{2}, \quad \hat{H}^{(1)} = \alpha \hat{x}^3 + \beta \hat{x}^4 + \dots \quad (6.2)$$

Weakly
anharmonic
oscillator

with sufficiently small coefficients α, β, \dots

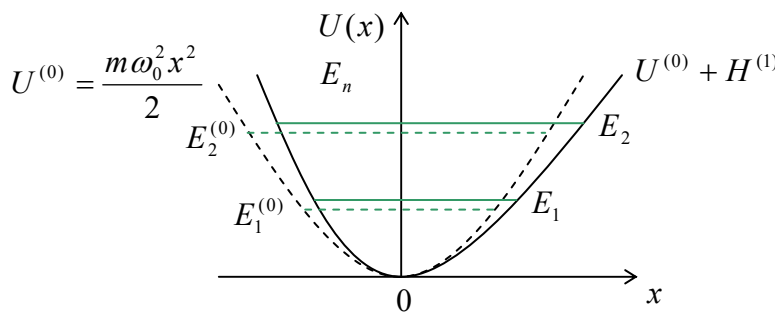


Fig. 6.1. The simplest application of the perturbation theory: a weakly anharmonic 1D oscillator. (Dashed lines characterize the unperturbed, harmonic oscillator.)

I will use this system as our first example, but let me start by describing the perturbative approach to the general time-independent Hamiltonian (1). In the bra-ket formalism, the eigenproblem (4.68) for the perturbed Hamiltonian, i.e. the stationary Schrödinger equation of the system, is

$$(\hat{H}^{(0)} + \hat{H}^{(1)})|n\rangle = E_n |n\rangle. \quad (6.3)$$

Let the eigenstates and eigenvalues of the unperturbed Hamiltonian, which satisfy the equation

$$\hat{H}^{(0)}|n^{(0)}\rangle = E_n^{(0)}|n^{(0)}\rangle, \quad (6.4)$$

be considered as known. In this case, the solution of problem (3) means finding, first, its perturbed eigenvalues E_n and, second, the coefficients $\langle n',^{(0)}|n\rangle$ of the expansion of the perturbed state's vectors $|n\rangle$ in the following series over the unperturbed ones, $|n',^{(0)}\rangle$:

$$|n\rangle = \sum_{n'} |n',^{(0)}\rangle \langle n',^{(0)}|n\rangle. \quad (6.5)$$

Let us plug Eq. (5), with the summation index n' replaced with n'' (just to have a more compact notation in our forthcoming result), into both sides of Eq. (3):

$$\sum_{n''} \langle n'',^{(0)}|n\rangle \hat{H}^{(0)}|n'',^{(0)}\rangle + \sum_{n''} \langle n'',^{(0)}|n\rangle \hat{H}^{(1)}|n'',^{(0)}\rangle = \sum_{n''} \langle n'',^{(0)}|n\rangle E_n |n'',^{(0)}\rangle. \quad (6.6)$$

and then inner-multiply all terms by an arbitrary unperturbed bra-vector $\langle n',^{(0)}|$ of the system. Assuming that the unperturbed eigenstates are orthonormal, $\langle n',^{(0)}|n'',^{(0)}\rangle = \delta_{n'n''}$, and using Eq. (4) in the first term on the left-hand side, we get the following system of linear equations

$$\sum_{n''} \langle n'',^{(0)}|n\rangle H_{n'n''}^{(1)} = \langle n',^{(0)}|n\rangle (E_n - E_{n'}^{(0)}), \quad (6.7)$$

where the matrix elements of the perturbation are calculated, by definition, in the *unperturbed* brackets:

$H_{n'n''}^{(1)} \equiv \langle n',^{(0)}|\hat{H}^{(1)}|n'',^{(0)}\rangle.$

(6.8)

Perturbation's
matrix
elements

The linear equation system (7) is still exact,¹ and is frequently used for numerical calculations. (Since the matrix coefficients (8) typically decrease when n' and/or n'' become sufficiently large, the sum on the left-hand side of Eq. (7) may usually be truncated, still giving an acceptable accuracy of the solution.) To get analytical results, we need to make approximations. In the simple perturbation theory we are discussing now, this is achieved by the expansion of both the eigenenergies and the expansion coefficients into the Taylor series in a certain small parameter μ of the problem:

$$E_n = E_n^{(0)} + E_n^{(1)} + E_n^{(2)} \dots, \quad (6.9)$$

$$\langle n',^{(0)}|n\rangle = \langle n',^{(0)}|n\rangle^{(0)} + \langle n',^{(0)}|n\rangle^{(1)} + \langle n',^{(0)}|n\rangle^{(2)} \dots, \quad (6.10)$$

where

¹ Please note the similarity of Eq. (7) with Eq. (2.215) of the 1D band theory. Indeed, the latter equation is not much more than a particular form of Eq. (7) for the 1D wave mechanics, and a specific (periodic) potential $U(x)$ considered as the perturbation Hamiltonian. Moreover, the whole approximate treatment of the weak-potential limit in Sec. 2.7 is essentially a particular case of the perturbation theory we are discussing now (in its 1st order).

$$E_n^{(k)} \propto \langle n'^{(0)} | n \rangle^{(k)} \propto \mu^k. \quad (6.11)$$

In order to explore the 1st-order approximation, which ignores all terms $O(\mu^2)$ and higher, let us plug only the two first terms of the expansions (9) and (10) into the basic equation (7):

$$\sum_{n''} H_{n'n''}^{(1)} \left(\delta_{n''n} + \langle n''^{(0)} | n \rangle^{(1)} \right) = \left(\delta_{n'n} + \langle n'^{(0)} | n \rangle^{(1)} \right) (E_n^{(0)} + E_n^{(1)} - E_{n'}^{(0)}). \quad (6.12)$$

Now let us open the parentheses, and disregard all the remaining terms $O(\mu^2)$. The result is

$$H_{n'n}^{(1)} = \delta_{n'n} E_n^{(1)} + \langle n'^{(0)} | n \rangle^{(1)} (E_n^{(0)} - E_{n'}^{(0)}), \quad (6.13)$$

This relation is valid for any set of indices n and n' ; let us start from the case $n = n'$, immediately getting a very simple (and practically, the most important!) result:

Energy:
1st-order
correction

$$E_n^{(1)} = H_{nn}^{(1)} \equiv \langle n^{(0)} | \hat{H}^{(1)} | n^{(0)} \rangle. \quad (6.14)$$

For example, let us see what this result gives for two first perturbation terms in the weakly anharmonic oscillator (2):

$$E_n^{(1)} = \alpha \langle n^{(0)} | \hat{x}^3 | n^{(0)} \rangle + \beta \langle n^{(0)} | \hat{x}^4 | n^{(0)} \rangle. \quad (6.15)$$

As the reader knows (or should know :-) from the solution of Problem 5.9, the first bracket equals zero, while the second one yields²

$$E_n^{(1)} = \frac{3}{4} \beta x_0^4 (2n^2 + 2n + 1). \quad (6.16)$$

Naturally, there should be some non-vanishing contribution to the energies from the (typically, larger) perturbation proportional to α , so that for its calculation we need to explore the 2nd order of the theory. However, before doing that, let us complete our discussion of its 1st order.

For $n' \neq n$, Eq. (13) may be used to calculate the eigenstates rather than the eigenvalues:

$$\langle n'^{(0)} | n \rangle^{(1)} = \frac{H_{n'n}^{(1)}}{E_n^{(0)} - E_{n'}^{(0)}}, \quad \text{for } n' \neq n. \quad (6.17)$$

This means that the eigenket's expansion (5), in the 1st order, may be represented as

States:
1st-order
result

$$| n^{(1)} \rangle = C | n^{(0)} \rangle + \sum_{n' \neq n} \frac{H_{n'n}^{(1)}}{E_n^{(0)} - E_{n'}^{(0)}} | n'^{(0)} \rangle. \quad (6.18)$$

The coefficient $C \equiv \langle n^{(0)} | n^{(1)} \rangle$ cannot be found from Eq. (17); however, requiring the final state n to be normalized, we see that other terms may provide only corrections $O(\mu^2)$, so that in the 1st order we should take $C = 1$. The most important feature of Eq. (18) is its denominators: the closer are the unperturbed eigenenergies of two states, the larger is their mutual “interaction” due to the perturbation.

² A useful exercise for the reader: analyze the relation between Eq. (16) and the result of the classical theory of such weakly anharmonic (“nonlinear”) oscillator – see, e.g., CM Sec. 5.2, in particular, Eq. (5.49).

This feature also affects the 1st-order's validity condition, which may be quantified using Eq. (17): the magnitudes of the brackets it describes have to be much less than the unperturbed bracket $\langle n|n \rangle^{(0)} = 1$, so that all elements of the perturbation matrix have to be much less than the difference between the corresponding unperturbed energies. For the anharmonic oscillator's energy corrections (16), this requirement is reduced to $E_n^{(1)} \ll \hbar\omega_0$.

Now we are ready for going after the 2nd-order approximation to Eq. (7). Let us focus on the case $n' = n$, because as we already know, only this term will give us a correction to the eigenenergies. Moreover, since the left-hand side of Eq. (7) already has a small factor $H_{n'n}^{(1)} \propto \mu$, the bracket coefficients in that part may be taken from the 1st-order result (17). As a result, we get

$$E_n^{(2)} = \sum_{n''} \langle n''^{(0)} | n \rangle^{(1)} H_{nn''}^{(1)} = \sum_{n'' \neq n} \frac{H_{n''n}^{(1)} H_{nn''}^{(1)}}{E_n^{(0)} - E_{n''}^{(0)}}. \quad (6.19)$$

Since $\hat{H}^{(1)}$ has to be Hermitian, we may rewrite this expression as

$$E_n^{(2)} = \sum_{n' \neq n} \frac{|H_{n'n}^{(1)}|^2}{E_n^{(0)} - E_{n'}^{(0)}} \equiv \sum_{n' \neq n} \frac{|\langle n'^{(0)} | \hat{H}^{(1)} | n^{(0)} \rangle|^2}{E_n^{(0)} - E_{n'}^{(0)}}. \quad (6.20)$$

Energy:
2nd-order
correction

This is the much-celebrated 2nd-order perturbation result, which frequently (in sufficiently symmetric problems) is the first non-vanishing correction to the state energy – for example, from the cubic term (proportional to α) in our weakly anharmonic oscillator problem (2). To calculate the corresponding correction, we may use another result of the solution of Problem 5.9:

$$\begin{aligned} \langle n' | \hat{x}^3 | n \rangle &= \left(\frac{x_0}{\sqrt{2}} \right)^3 \\ &\times \left\{ [n(n-1)(n-2)]^{1/2} \delta_{n',n-3} + 3n^{3/2} \delta_{n',n-1} + 3(n+1)^{3/2} \delta_{n',n+1} + [(n+1)(n+2)(n+3)]^{1/2} \delta_{n',n+3} \right\}. \end{aligned} \quad (6.21)$$

So, according to Eq. (20), we need to calculate

$$\begin{aligned} E_n^{(2)} &= \alpha^2 \left(\frac{x_0}{\sqrt{2}} \right)^6 \\ &\times \sum_{n' \neq n} \frac{\left\{ [n(n-1)(n-2)]^{1/2} \delta_{n',n-3} + 3n^{3/2} \delta_{n',n-1} + 3(n+1)^{3/2} \delta_{n',n+1} + [(n+1)(n+2)(n+3)]^{1/2} \delta_{n',n+3} \right\}^2}{\hbar\omega_0(n-n')}. \end{aligned} \quad (6.22)$$

The summation is not as cumbersome as may look, because at the curly brackets' squaring, all mixed products are proportional to the products of different Kronecker deltas and hence vanish, so that we need to sum up only the squares of each term, finally getting

$$E_n^{(2)} = -\frac{15}{4} \frac{\alpha^2 x_0^6}{\hbar\omega_0} \left(n^2 + n + \frac{11}{30} \right). \quad (6.23)$$

This formula shows that all energy level corrections are negative, regardless of the sign of α .³ On the contrary, the 1st order correction $E_n^{(1)}$, given by Eq. (16), does depend on the sign of β , so that the net correction, $E_n^{(1)} + E_n^{(2)}$, may be of any sign.

³ Note that this is correct for the ground-state energy correction $E_g^{(2)}$ of *any* system, because for this state, the denominators of all terms of the sum (20) are negative, while their numerators are always non-negative.

The results (18) and (20) are clearly inapplicable to the degenerate case where, in the absence of perturbation, several states correspond to the same energy level, because of the divergence of their denominators.⁴ This divergence hints that in this case, the largest effect of the perturbation is the *degeneracy lifting*, e.g., some splitting of the initially degenerate energy level $E^{(0)}$ (Fig. 2), and that for the analysis of this case we can, in the first approximation, ignore the effect of all other energy levels. (A careful analysis shows that this is indeed the case until the level splitting becomes comparable with the distance to other energy levels.)

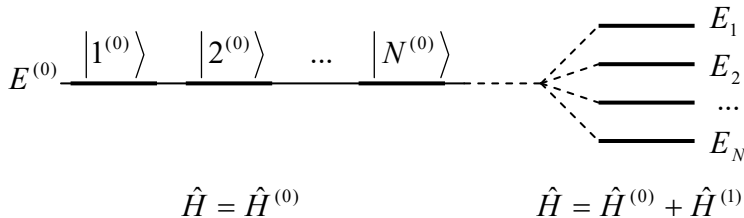


Fig. 5.2. Lifting the energy level degeneracy by a perturbation (schematically).

Limiting the summation in Eq. (7) to the group of N degenerate states with equal $E_{n'}^{(0)} \equiv E^{(0)}$, we reduce it to

$$\sum_{n''=1}^N \langle n''^{(0)} | n \rangle H_{n'n''}^{(1)} = \langle n'^{(0)} | n \rangle (E_n - E^{(0)}), \quad (6.24)$$

where now n' and n'' number the N states of the degenerate group.⁵ For $n = n'$, Eq. (24) may be rewritten as

$$\sum_{n''=1}^N (H_{n'n''}^{(1)} - E_{n''}^{(1)} \delta_{n'n''}) \langle n''^{(0)} | n' \rangle = 0, \quad \text{where } E_n^{(1)} \equiv E_n - E^{(0)}. \quad (6.25)$$

For each $n' = 1, 2, \dots, N$, this is a system of N linear, homogenous equations (with N terms each) for N unknown coefficients $\langle n''^{(0)} | n' \rangle$. In this problem, we may readily recognize the problem of diagonalization of the perturbation matrix $H^{(1)}$ – cf. Sec. 4.4 and in particular Eq. (4.101). As in the general case, the condition of self-consistency of the system is:

Initially
degenerate
system:
energy levels

$$\begin{vmatrix} H_{11}^{(1)} - E_n^{(1)} & H_{12}^{(1)} & \dots \\ H_{21}^{(1)} & H_{22}^{(1)} - E_n^{(1)} & \dots \\ \dots & \dots & \dots \end{vmatrix} = 0, \quad (6.26)$$

where now the index n numbers the N roots of this equation, in an arbitrary order. According to the definition (25) of $E_n^{(1)}$, the resulting N energy levels E_n may be found as $E^{(0)} + E_n^{(1)}$. If the perturbation matrix is diagonal in the chosen basis $n''^{(0)}$, the result is extremely simple,

$$E_n - E^{(0)} \equiv E_n^{(1)} = H_{nn}^{(1)}, \quad (6.27)$$

⁴ This is exactly the reason why such simple perturbation approach runs into serious problems for systems with a continuous spectrum, and other techniques (such as the WKB approximation) are often necessary.

⁵ Note that here the choice of the basis is to some extent arbitrary, because due to the linearity of equations of quantum mechanics, any linear combination of the states $n''^{(0)}$ is also an eigenstate of the unperturbed Hamiltonian. However, for using Eq. (25), these combinations have to be orthonormal, as was supposed at the derivation of Eq. (7).

and formally coincides with Eq. (14) for the non-degenerate case, but now it may give a different result for each of N previously degenerate states n .

Now let us see what this general theory gives for several important examples. First of all, let us consider a system with just two degenerate states with energy sufficiently far from all other levels. Then, in the basis of these two degenerate states, the most general perturbation matrix is

$$\mathbf{H}^{(1)} = \begin{pmatrix} H_{11} & H_{12} \\ H_{21} & H_{22} \end{pmatrix} \quad (6.28)$$

This matrix coincides with the general matrix (5.2) of a two-level system. Hence, we come to the very important conclusion: for a weak perturbation, all properties of any double-degenerate system are identical to those of the genuine two-level systems, which were the subject of numerous discussions in Chapter 4 and again in Sec. 5.1. In particular, its eigenenergies are given by Eq. (5.6), and may be described by the level-anticrossing diagram shown in Fig. 5.1.

6.2. The linear Stark effect

As a more involved example of the level degeneracy lifting by a perturbation, let us discuss the *Stark effect*⁶ – the atomic level splitting by an external electric field. Let us study this effect, in the linear approximation, for a hydrogen-like atom/ion. Taking the direction of the external electric field \mathcal{E} (which is practically always uniform on the atomic scale) for the z -axis, the perturbation may be represented by the following Hamiltonian:

$$\hat{H}^{(1)} = -F\hat{z} = -q\mathcal{E}\hat{z} = -q\mathcal{E}r \cos\theta. \quad (6.29)$$

(In the last form, the operator sign is dropped, because we will work in the coordinate representation.)

As you (should :-) remember, energy levels of a hydrogen-like atom/ion depend only on the principal quantum number n – see Eq. (3.201); hence all the states, besides the ground $1s$ state in which $n = 1$ and $l = m = 0$, have some orbital degeneracy, which grows rapidly with n . Let us consider the lowest degenerate level with $n = 2$. Since, according to Eq. (3.203), $0 \leq l \leq n-1$, at this level the orbital quantum number l may equal either 0 (one $2s$ state, with $m = 0$) or 1 (three $2p$ states, with $m = 0, \pm 1$). Due to this 4-fold degeneracy, $\mathbf{H}^{(1)}$ is a 4×4 matrix with 16 elements:

$$\mathbf{H}^{(1)} = \underbrace{\begin{matrix} l=0 \\ m=0 & m=0 & m=+1 & m=-1 \end{matrix}}_{\text{m=0}} \left\{ \begin{array}{ll} \left(\begin{matrix} H_{11} & H_{12} & H_{13} & H_{14} \\ H_{21} & H_{22} & H_{23} & H_{24} \\ H_{31} & H_{32} & H_{33} & H_{34} \\ H_{41} & H_{42} & H_{43} & H_{44} \end{matrix} \right) & \begin{array}{l} m=0, \\ m=0, \\ m=+1, \\ m=-1, \end{array} \\ \left. \begin{array}{l} l=0, \\ l=0, \\ l=1, \\ l=1. \end{array} \right\} & \end{array} \right. \quad (6.30)$$

⁶ This effect was discovered experimentally in 1913 by Johannes Stark and independently by Antonio Lo Surdo, so it is sometimes (and more fairly) called the “Stark – Lo Surdo effect”. Sometimes this name is used with the qualifier “dc” to distinguish it from the *ac* Stark effect – the energy level shift under the effect of an ac field – see Sec. 5 below.

However, there is no need to be scared. First, due to the Hermitian nature of the operator, only ten of these matrix elements (four diagonal and six off-diagonal ones) may be substantially different from each other. Moreover, due to a high symmetry of the problem, there are a lot of zeros even among these elements. Indeed, let us have a look at the angular components Y_l^m of the corresponding wavefunctions, with $l = 0$ and $l = 1$, described by Eqs. (3.174)-(3.175). For the states with $m = \pm 1$, the azimuthal parts of wavefunctions are proportional to $\exp\{\pm i\varphi\}$; hence the off-diagonal elements H_{34} and H_{43} of the matrix (30), relating these functions, are proportional to

$$\oint d\Omega Y_1^\pm * \hat{H}^{(1)} Y_1^\mp \propto \int_0^{2\pi} d\varphi \left(e^{\pm i\varphi} \right)^* \left(e^{\mp i\varphi} \right) = 0. \quad (6.31)$$

The azimuthal-angle symmetry also kills the off-diagonal elements $H_{13}, H_{14}, H_{23}, H_{24}$ (and hence their complex conjugates H_{31}, H_{41}, H_{32} , and H_{42}), because they relate states with $m = 0$ and $m = \pm 1$, and hence are proportional to

$$\oint d\Omega Y_1^0 * \hat{H}^{(1)} Y_1^{\pm 1} \propto \int_0^{2\pi} d\varphi e^{\pm i\varphi} = 0. \quad (6.32)$$

For the diagonal matrix elements H_{33} and H_{44} , corresponding to $l = 1$ and $m = \pm 1$, the azimuthal-angle integrals do not vanish, but since the corresponding spherical harmonics depend on the polar angle as $\sin\theta$, these elements are proportional to

$$\oint d\Omega Y_1^{\pm 1} * \hat{H}^{(1)} Y_1^{\pm 1} \propto \int_0^\pi \sin\theta d\theta \sin\theta \cos\theta \sin\theta = \int_{-1}^{+1} \cos\theta (1 - \cos^2\theta) d(\cos\theta), \quad (6.33)$$

and hence are equal to zero – as any limit-symmetric integral of an odd function. Finally, for the states $2s$ and $2p$ with $m = 0$, the diagonal elements H_{11} and H_{22} are also killed by the polar-angle integration:

$$\oint d\Omega Y_0^0 * \hat{H}^{(1)} Y_0^0 \propto \int_0^\pi \sin\theta d\theta \cos\theta = \int_{-1}^1 \cos\theta d(\cos\theta) = 0, \quad (6.34)$$

$$\oint d\Omega Y_0^1 * \hat{H}^{(1)} Y_0^1 \propto \int_0^\pi \sin\theta d\theta \cos^3\theta = \int_{-1}^{+1} \cos^3\theta d(\cos\theta) = 0. \quad (6.35)$$

Hence, the only non-zero elements of the matrix (30) are two off-diagonal elements H_{12} and H_{21} , which relate two states with the same $m = 0$, but different $l = \{0, 1\}$, because they are proportional to

$$\oint d\Omega Y_0^0 * \cos\theta Y_1^0 = \frac{\sqrt{3}}{4\pi} \int_0^{2\pi} d\varphi \int_0^\pi \sin\theta d\theta \cos^2\theta = \frac{1}{\sqrt{3}} \neq 0. \quad (6.36)$$

What remains is to use Eqs. (3.209) for the radial parts of these functions to complete the calculation of those two matrix elements:

$$H_{12} = H_{21} = -\frac{q\mathcal{E}}{\sqrt{3}} \int_0^\infty r^2 dr \mathcal{R}_{2,0}(r) r \mathcal{R}_{2,1}(r). \quad (6.37)$$

Due to the additive structure of the function $\mathcal{R}_{2,0}(r)$, the integral falls into a sum of two table integrals, both of the type MA Eq. (6.7d), finally giving

$$H_{12} = H_{21} = 3q\mathcal{E}r_0, \quad (6.38)$$

where r_0 is the spatial scale (3.192); for the hydrogen atom, it is just the Bohr radius r_B – see Eq. (1.10).

Thus, the perturbation matrix (30) is reduced to

$$H^{(1)} = \begin{pmatrix} 0 & 3q\epsilon r_0 & 0 & 0 \\ 3q\epsilon r_0 & 0 & 0 & 0 \\ 0 & 0 & 0 & 0 \\ 0 & 0 & 0 & 0 \end{pmatrix}, \quad (6.39)$$

so that the condition (26) of self-consistency of the system (25),

$$\begin{vmatrix} -E_2^{(1)} & 3q\epsilon r_0 & 0 & 0 \\ 3q\epsilon r_0 & -E_2^{(1)} & 0 & 0 \\ 0 & 0 & -E_2^{(1)} & 0 \\ 0 & 0 & 0 & -E_2^{(1)} \end{vmatrix} = 0, \quad (6.40)$$

gives a very simple characteristic equation

$$(E_2^{(1)})^2 [(E_2^{(1)})^2 - (3q\epsilon r_0)^2] = 0. \quad (6.41)$$

with four roots:

$$(E_2^{(1)})_{1,2} = 0, \quad (E_2^{(1)})_{3,4} = \pm 3q\epsilon r_0. \quad (6.42)$$

Linear Stark effect for $n = 2$

so that the degeneracy is only partly lifted – see the levels in Fig. 3.⁷

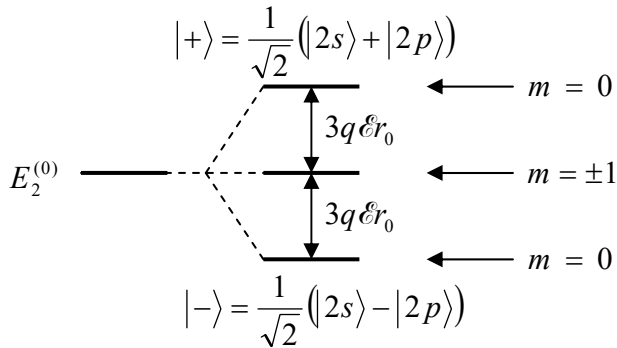


Fig. 6.3. The linear Stark effect for the level $n = 2$ of a hydrogen-like atom.

Generally, in order to understand the nature of states corresponding to these levels, we should return to Eq. (25) with each calculated value of $E_2^{(1)}$, and find the corresponding expansion coefficients $\langle n''|n' \rangle$ that describe the perturbed states. However, in our simple case, the outcome of this procedure is clear in advance. Indeed, since the states with $\{l = 1, m = \pm 1\}$ are not affected by the perturbation at all (in the linear approximation in the electric field), their degeneracy is not lifted, and energy is not affected – see the middle line in Fig. 3. On the other hand, the partial perturbation matrix connecting the states $2s$ and $2p$, i.e. the top left 2×2 part of the full matrix (39), is proportional to the Pauli matrix σ_x , and we already know the result of its diagonalization – see Eqs. (4.113)-(4.114). This means that the

⁷ The proportionality of this splitting to the small field is responsible for the qualifier “linear” in the name of this effect. If observable effects grow only as ϵ^2 (see, e.g., Problem 9), the term *quadratic Stark effect* is used instead.

upper and lower split levels correspond to very simple linear combinations of the previously degenerate states with $m = 0$,

$$|\pm\rangle = \frac{1}{\sqrt{2}}(|2s\rangle \pm |2p\rangle). \quad (6.43)$$

Finally, let us estimate the magnitude of the linear Stark effect for a hydrogen atom. For a very high electric field of $\mathcal{E} = 3 \times 10^6 \text{ V/m}$,⁸ $|q| = e \approx 1.6 \times 10^{-19} \text{ C}$, and $r_0 = r_B \approx 0.5 \times 10^{-10} \text{ m}$, we get a level splitting of $3q\mathcal{E}r_0 \approx 0.8 \times 10^{-22} \text{ J} \approx 0.5 \text{ meV}$. This number is much lower than the unperturbed energy of the level, $E_2 = -E_H/(2 \times 2^2) \approx -3.4 \text{ eV}$, so that the perturbative result is quite applicable. On the other hand, the calculated splitting is much larger than the resolution limit imposed by the line's natural width ($\sim 10^{-7} E_2$, see Chapter 9), so that the effect is quite observable even in substantially lower electric fields. Note, however, that our simple results are quantitatively correct only when the Stark splitting (42) is much larger than the fine-structure splitting of the same level in the absence of the field— see the next section.

6.3. Fine structure of atomic levels

Now let us use the same perturbation theory to analyze, also for the simplest case of a hydrogen-like atom/ion, the so-called *fine structure* of atomic levels – their degeneracy lifting even in the absence of external fields. Since the effective speed v of the electron motion in atoms is much smaller than the speed of light c , the fine structure may be analyzed as a sum of two independent relativistic effects. To analyze the first of them, let us expand the well-known classical relativistic expression⁹ for the kinetic energy $T = E - mc^2$ of a free particle with the rest mass m ,¹⁰

$$T = (m^2 c^4 + p^2 c^2)^{1/2} - mc^2 \equiv mc^2 \left[\left(1 + \frac{p^2}{m^2 c^2} \right)^{1/2} - 1 \right], \quad (6.44)$$

into the Taylor series with respect to the small ratio $(p/mc)^2 \approx (v/c)^2$:

$$T = mc^2 \left[1 + \frac{1}{2} \left(\frac{p}{mc} \right)^2 - \frac{1}{8} \left(\frac{p}{mc} \right)^4 + \dots - 1 \right] \equiv \frac{p^2}{2m} - \frac{p^4}{8m^3 c^2} + \dots, \quad (6.45)$$

and drop all the terms besides the two spelled-out terms. Of them, the first term is non-relativistic, while the second one represents the first relativistic correction to T .

Following the correspondence principle, the quantum-mechanical problem in this approximation may be described by the perturbative Hamiltonian (1), whose unperturbed part (whose eigenstates and eigenenergies were discussed in Sec. 3.5) is

$$\hat{H}^{(0)} = \frac{\hat{p}^2}{2m} + \hat{U}(r), \quad \hat{U}(r) = -\frac{C}{r}, \quad (6.46)$$

while the kinetic-relativistic perturbation

⁸ This value approximately corresponds to the threshold of electric breakdown in air at ambient conditions, due to the impact ionization. As a result, experiments with higher dc fields are rather difficult.

⁹ See, e.g., EM Eq. (9.78) – or any undergraduate text on special relativity.

¹⁰ This fancy font is used, as in Secs. 3.5-3.8, to distinguish the mass m from the magnetic quantum number m .

$$\hat{H}^{(1)} = -\frac{\hat{p}^4}{8m^3c^2} \equiv -\frac{1}{2mc^2} \left(\frac{\hat{p}^2}{2m} \right)^2. \quad (6.47)$$

Kinetic-relativistic perturbation

Using Eq. (46), we may rewrite the last formula as

$$\hat{H}^{(1)} = -\frac{1}{2mc^2} (\hat{H}^{(0)} - \hat{U}(r))^2, \quad (6.48)$$

so that its matrix elements participating in the characteristic equation (25) for a given degenerate energy level (3.201), i.e. a given principal quantum number n , are

$$\langle nlm | \hat{H}^{(1)} | nl'm' \rangle = -\frac{1}{2mc^2} \langle nlm | (\hat{H}^{(0)} - \hat{U}(r)) (\hat{H}^{(0)} - \hat{U}(r)) | nl'm' \rangle, \quad (6.49)$$

where the bra- and ket-vectors describe the unperturbed eigenstates, whose eigenfunctions (in the coordinate representation) are given by Eq. (3.200): $\psi_{n,l,m} = \mathcal{R}_{n,l}(r)Y_l^m(\theta, \phi)$.

It is straightforward (and hence left for the reader :-) to prove that all off-diagonal elements of the set (49) are equal to 0. Thus we may use Eq. (27) for each set of the quantum numbers $\{n, l, m\}$:

$$\begin{aligned} E_{n,l,m}^{(1)} &\equiv E_{n,l,m} - E_n^{(0)} = \langle nlm | \hat{H}^{(1)} | nlm \rangle = -\frac{1}{2mc^2} \left\langle (\hat{H}^{(0)} - \hat{U}(r))^2 \right\rangle_{n,l,m} \\ &= -\frac{1}{2mc^2} \left(E_n^2 - 2E_n \langle \hat{U} \rangle_{n,l} + \langle \hat{U}^2 \rangle_{n,l} \right) = -\frac{1}{2mc^2} \left(\frac{E_0^2}{4n^4} - \frac{E_0}{n^2} C \left\langle \frac{1}{r} \right\rangle_{n,l} + C^2 \left\langle \frac{1}{r^2} \right\rangle_{n,l} \right), \end{aligned} \quad (6.50)$$

where the index m has been dropped, because the radial wavefunctions $\mathcal{R}_{n,l}(r)$, which affect these expectation values, do not depend on that quantum number. Now using Eqs. (3.191), (3.201) and the first two of Eqs. (3.211), we finally get

$$E_{n,l}^{(1)} = -\frac{mc^2}{2\hbar^2 c^2 n^4} \left(\frac{n}{l + \frac{1}{2}} - \frac{3}{4} \right) \equiv -\frac{2E_n^2}{mc^2} \left(\frac{n}{l + \frac{1}{2}} - \frac{3}{4} \right). \quad (6.51)$$

Kinetic-relativistic energy correction

Let us discuss this result. First of all, its last form confirms that the correction (51) is indeed much smaller than the unperturbed energy E_n (and hence the perturbation theory is valid) if the latter is much smaller than the relativistic rest energy mc^2 of the particle – as it is for the hydrogen atom. Next, since in the Bohr problem’s solution $n \geq l + 1$, the first fraction in the parentheses of Eq. (51) is always larger than 1, and hence than 3/4, so that the kinetic relativistic correction to energy is negative for all n and l . (Actually, this fact could be predicted already from Eq. (47), which shows that the perturbation’s Hamiltonian is a negatively defined form.) Finally, for a fixed principal number n , the negative correction’s magnitude decreases with the growth of l . This fact may be interpreted using the second of Eqs. (3.211): the larger is l (at fixed n), the larger is the particle’s effective distance from the center, and hence the smaller is its effective velocity, i.e. the smaller is the magnitude of the quantum-mechanical average of the negative relativistic correction (47) to the kinetic energy.

The result (51) is valid for the Coulomb interaction $U(r) = -C/r$ of any physical nature. However, if we speak specifically about hydrogen-like atoms/ions, there is also another relativistic correction to energy, due to the so-called *spin-orbit interaction* (alternatively called the “spin-orbit coupling”). Its physics may be understood from the following semi-quantitative classical reasoning: from the “the point of view” of an electron rotating about the nucleus at distance r with velocity v , it is the nucleus, of the

electric charge Ze , that rotates about the electron with the velocity $(-\mathbf{v})$ and hence the time period $\mathcal{T} = 2\pi r/v$. From the point of view of magnetostatics, such circular motion of the electric charge $Q = Ze$, is equivalent to a circular dc electric current $I = Q/\mathcal{T} = (Ze)(v/2\pi r)$, which creates, at the electron's location, i.e. in the center of the current loop, the magnetic field with the following magnitude:¹¹

$$\mathcal{B}_a = \frac{\mu_0}{2r} I = \frac{\mu_0}{2r} \frac{Zev}{2\pi r} \equiv \frac{\mu_0 Zev}{4\pi r^2}. \quad (6.52)$$

The field's direction \mathbf{n} is perpendicular to the apparent plane of the nucleus' rotation (i.e. that of the real rotation of the electron), and hence its vector may be readily expressed via the similarly directed vector $\mathbf{L} = m_e v r n$ of the electron's angular (orbital) momentum:

$$\mathcal{B}_a = \frac{\mu_0 Zev}{4\pi r^2} \mathbf{n} \equiv \frac{\mu_0 Ze}{4\pi r^3 m_e} m_e v r n \equiv \frac{\mu_0 Ze}{4\pi r^3 m_e} \mathbf{L} \equiv \frac{Ze}{4\pi \epsilon_0 r^3 m_e c^2} \mathbf{L}, \quad (6.53)$$

where the last step used the basic relation between the SI-unit constants: $\mu_0 \equiv 1/c^2 \epsilon_0$.

A more careful (but still classical) analysis of the problem¹² brings both good and bad news. The bad news is that the result (53) is wrong by the so-called *Thomas factor* of two even for the circular motion, because the electron moves with acceleration, and the reference frame bound to it cannot be inertial (as was implied in the above reasoning), so that the effective magnetic field felt by the electron is actually

$$\mathcal{B} = \frac{Ze}{8\pi \epsilon_0 r^3 m_e c^2} \mathbf{L}. \quad (6.54)$$

The good news is that this result is valid not only for circular but an arbitrary orbital motion in the Coulomb field $U(r)$. Hence from the discussion in Sec. 4.1 and Sec. 4.4 we may expect that the quantum-mechanical description of the interaction between this effective magnetic field and the electron's spin moment (4.115) is given by the following perturbation Hamiltonian¹³

$$\hat{H}^{(1)} = -\hat{\mathbf{m}} \cdot \hat{\mathcal{B}} = -\gamma_e \hat{\mathbf{S}} \cdot \left(\frac{Ze}{8\pi \epsilon_0 r^3 m_e c^2} \hat{\mathbf{L}} \right) \equiv \frac{1}{2m_e^2 c^2} \frac{Ze^2}{4\pi \epsilon_0} \frac{1}{r^3} \hat{\mathbf{S}} \cdot \hat{\mathbf{L}}, \quad (6.55)$$

where at spelling out the electron's gyromagnetic ratio $\gamma_e \equiv -g_e e/2m_e$, the small correction to the value $g_e = 2$ of the electron's *g*-factor (see Sec. 4.4) is ignored, because Eq. (55) is already a small correction. This expectation is confirmed by the fully-relativistic Dirac theory, to be discussed in Sec. 9.7 below: it yields, for an arbitrary central potential $U(r)$, the following spin-orbit coupling Hamiltonian:

$$\hat{H}^{(1)} = \frac{1}{2m_e^2 c^2} \frac{1}{r} \frac{dU(r)}{dr} \hat{\mathbf{S}} \cdot \hat{\mathbf{L}}. \quad (6.56)$$

For the Coulomb potential $U(r) = -Ze^2/4\pi \epsilon_0 r$, this formula is reduced to Eq. (55).

¹¹ See, e.g., EM Sec. 5.1, in particular, Eq. (5.24). Note that such effective magnetic field is induced by any motion of electrons, in particular that in solids, leading to a variety of spin-orbit effects there – see, e.g., a concise review by R. Winkler *et al.*, in B. Kramer (ed.), *Advances in Solid State Physics* **41**, 211 (2001).

¹² It was carried out first by Llewellyn Thomas in 1926; for a simple review see, e.g., R. Harr and L. Curtis, *Am. J. Phys.* **55**, 1044 (1987).

¹³ In the Gaussian units, Eq. (55) is valid without the factor $4\pi \epsilon_0$ in the denominator; while Eq. (56), “as is”.

As we already know from the discussion in Sec. 5.7, the angular factor of this Hamiltonian commutes with all the operators of the coupled-representation group (inside the blue line in Fig. 5.12): \hat{L}^2 , \hat{S}^2 , \hat{J}^2 , and \hat{J}_z , and hence is diagonal in the coupled-representation basis with definite quantum numbers l , j , and m_j (and of course $s = \frac{1}{2}$). Hence, using Eq. (5.181) to rewrite Eq. (56) as

$$\hat{H}^{(1)} = \frac{1}{2m_e^2 c^2} \frac{Ze^2}{4\pi\epsilon_0} \frac{1}{r^3} \frac{1}{2} (\hat{J}^2 - \hat{L}^2 - \hat{S}^2), \quad (6.57)$$

we may again use Eq. (27) for each set $\{s, l, j, m_j\}$, with common n :

$$E_{n,j,l}^{(1)} = \frac{1}{2m_e^2 c^2} \frac{Ze^2}{4\pi\epsilon_0} \left\langle \frac{1}{r^3} \right\rangle_{n,l} \frac{1}{2} \langle \hat{J}^2 - \hat{L}^2 - \hat{S}^2 \rangle_{j,s}, \quad (6.58)$$

where the indices irrelevant for each particular factor have been dropped. Now using the last of Eqs. (3.211), and similar expressions (5.169), (5.175), and (5.177) for eigenvalues of the involved operators, we get an explicit expression for the spin-orbit corrections¹⁴

$$E_{n,j,l}^{(1)} = \frac{1}{2m_e^2 c^2} \frac{Ze^2}{4\pi\epsilon_0} \frac{\hbar^2}{2r_0^3} \frac{j(j+1) - l(l+1) - \frac{3}{4}}{n^3 l(l+\frac{1}{2})(l+1)} \equiv \frac{E_n^2}{m_e c^2} n \frac{j(j+1) - l(l+1) - \frac{3}{4}}{l(l+\frac{1}{2})(l+1)}, \quad (6.59)$$

Spin-orbit energy correction

with l and j related by Eq. (5.189): $j = l \pm \frac{1}{2}$.

The last form of its result shows clearly that this correction has the same scale as the kinetic correction (51).¹⁵ In the 1st order of the perturbation theory, they may be just added (with $m = m_e$), giving a surprisingly simple formula for the net fine structure of the n^{th} energy level:

$$E_{\text{fine}}^{(1)} = \frac{E_n^2}{2m_e c^2} \left(3 - \frac{4n}{j + \frac{1}{2}} \right). \quad (6.60)$$

Fine structure of atomic levels

This simplicity, as well as the independence of the result of the orbital quantum number l , will become less surprising when (in Sec. 9.7) we see that this formula follows in one shot from the Dirac theory, in which the Bohr atom's energy spectrum is numbered only with n and j , but not l . Let us recall that for an electron ($s = \frac{1}{2}$), according to Eq. (5.189) with $0 \leq l \leq n-1$, the quantum number j may take n positive half-integer values, from $\frac{1}{2}$ to $n - \frac{1}{2}$. Hence, Eq. (60) shows that the fine structure of the n^{th} Bohr's energy level has n sub-levels – see Fig. 4.

Please note that according to Eq. (5.175), each of these sub-levels is still $(2j + 1)$ -times degenerate in the quantum number m_j . This degeneracy is very natural, because in the absence of an external field the system is still isotropic. Moreover, on each fine-structure level (besides the highest one with $j = n - \frac{1}{2}$), each of the m_j -states is doubly-degenerate in the orbital quantum number $l = j \mp \frac{1}{2}$ – see the labels of l in Fig. 4. (According to Eq. (5.190), each of these states, with fixed j and m_j , may be

¹⁴ The factor l in the denominator does not give a divergence at $l = 0$, because in this case $j = s = \frac{1}{2}$, so that $j(j+1) = \frac{3}{4}$, and the numerator turns into 0 as well. A careful analysis of this case (which may be found, e.g., in G. Woolgate, *Elementary Atomic Structure*, 2nd ed., Oxford, 1983), as well as the exact analysis of the hydrogen atom using the Dirac theory (see Sec. 9.7), show that Eq. (60), which does not include l , is valid even in this case.

¹⁵ This is natural, because the magnetic interaction of charged particles is essentially a relativistic effect, of the same order ($\sim v^2/c^2$) as the kinetic correction (47) – see, e.g., EM Sec. 5.1, in particular Eq. (5.3).

represented as a linear combination of two states with adjacent values of l , and hence different electron spin orientations, $m_s = \pm \frac{1}{2}$, weighed with the Clebsch-Gordan coefficients.)

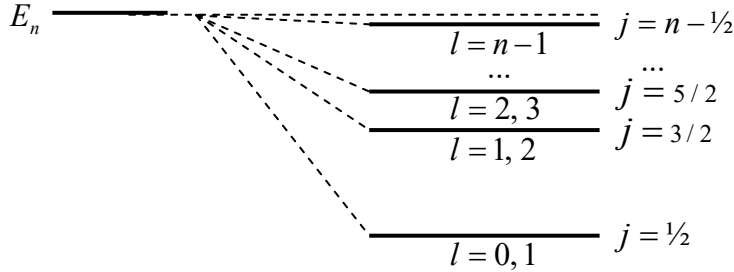


Fig. 6.4. The fine structure of a hydrogen-like atom's level.

These details aside, one may crudely say that the relativistic corrections combined make the total eigenenergy grow with l , contributing to the effect already mentioned at our analysis of the periodic table of elements in Sec. 3.7. The relative scale of this increase may be scaled by the largest deviation from the unperturbed energy E_n , reached for s -states (with $l = 0, j = \frac{1}{2}$):

$$\left| \frac{E_{\max}^{(1)}}{E_n} \right| = \frac{E_n}{m_e c^2} \left(2n - \frac{3}{2} \right) \equiv \left(\frac{Ze^2}{4\pi\epsilon_0 \hbar c} \right)^2 \left(\frac{1}{n} - \frac{3}{4n^2} \right) \equiv Z^2 \alpha^2 \left(\frac{1}{n} - \frac{3}{4n^2} \right). \quad (6.61)$$

where α is the *fine-structure* (“Sommerfeld’s”) *constant*,

$$\alpha \equiv \frac{e^2}{4\pi\epsilon_0 \hbar c} \approx \frac{1}{137}, \quad (6.62)$$

(already mentioned in Sec. 4.4), which characterizes the relative strength (or rather weakness :-)) of the electromagnetic effects in quantum mechanics – which in particular makes the perturbative quantum electrodynamics possible.¹⁶ These expressions show that the fine-structure splitting is a very small effect ($\sim \alpha^2 \sim 10^{-6}$) for the hydrogen atom, but it rapidly grows (as Z^2) with the nuclear charge (i.e. the atomic number) Z , and becomes rather substantial for the heaviest stable atoms with $Z \sim 10^2$.

6.4. The Zeeman effect

Now, we are ready to review the *Zeeman effect* – the atomic level splitting by an external magnetic field.¹⁷ Using Eq. (3.26), with $q = -e$, for the description of the electron’s orbital motion in the field, and the Pauli Hamiltonian (4.163), with $\gamma = -e/m_e$, for the electron spin’s interaction with the field, we see that even for a hydrogen-like (i.e. single-electron) atom/ion, neglecting the relativistic effects, the full Hamiltonian is rather involved:

$$\hat{H} = \frac{1}{2m_e} (\hat{\mathbf{p}} + e\hat{\mathbf{A}})^2 - \frac{Ze^2}{4\pi\epsilon_0 r} + \frac{e}{m_e} \mathcal{B} \cdot \hat{\mathbf{S}}. \quad (6.63)$$

¹⁶ The expression $\alpha^2 = E_H/m_e c^2$, where E_H is the Hartree energy (1.13), i.e. the scale of energies E_n , is also very revealing.

¹⁷ It was discovered experimentally in 1896 by Pieter Zeeman who, amazingly, was fired from the University of Leiden for unauthorized use of lab equipment for this work – just to receive a Nobel Prize for it in a few years!

There are several simplifications we may make. First, let us assume that the external field is spatial-uniform on the atomic scale (which is a very good approximation for most cases), so that we can take its vector potential in an axially-symmetric gauge – cf. Eq. (3.132):

$$\mathbf{A} = \frac{1}{2} \mathcal{B} \times \mathbf{r}. \quad (6.64)$$

Second, let us neglect the terms proportional to \mathcal{B}^2 , which are small in practical magnetic fields of the order of a few teslas.¹⁸ The remaining term in the effective kinetic energy, describing the interaction with the magnetic field, is linear in the momentum operator, so that we may repeat the standard classical calculation¹⁹ to reduce it to the product of \mathcal{B} by the orbital magnetic moment's component $m_z = -eL_z/2m_e$ – besides that both m_z and L_z should be understood as operators now. As a result, the Hamiltonian (63) reduces to Eq. (1), $\hat{H}^{(0)} + \hat{H}^{(1)}$, where $\hat{H}^{(0)}$ is that of the atom at $\mathcal{B} = 0$, and

$$\hat{H}^{(1)} = \frac{e\mathcal{B}}{2m_e} (\hat{L}_z + 2\hat{S}_z). \quad (6.65)$$

Zeeman effect's perturbation

This expression immediately reveals the major complication with the Zeeman effect's analysis. Namely, in comparison with the equal orbital and spin contributions to the total angular momentum (5.170) of the electron, its spin produces a twice larger contribution to the magnetic moment, so that the right-hand side of Eq. (65) is *not* proportional to the total angular moment \mathbf{J} . As a result, the effect's description is simple only in two limits.

If the magnetic field is so *high* that its effects are much stronger than the relativistic (fine-structure) effects discussed in the previous section, we may treat the two terms in Eq. (65) as independent perturbations of different (orbital and spin) degrees of freedom. Since each of the perturbation matrices is diagonal in its own z -basis, we can again use Eq. (27) to write

$$E - E^{(0)} = \frac{e\mathcal{B}}{2m_e} (\langle n, l, m_l | \hat{L}_z | n, l, m_l \rangle + 2\langle m_s | \hat{S}_z | m_s \rangle) = \frac{e\mathcal{B}}{2m_e} (\hbar m_l + 2\hbar m_s) = \mu_B \mathcal{B} (m_l \pm 1). \quad (6.66)$$

Paschen-Back effect

This result describes splitting of each $2 \times (2l + 1)$ -degenerate energy level, with certain n and l , into $(2l + 3)$ levels (Fig. 5), with the adjacent level distance of $\mu_B \mathcal{B}$, of the order of 10^{-4} eV per tesla.

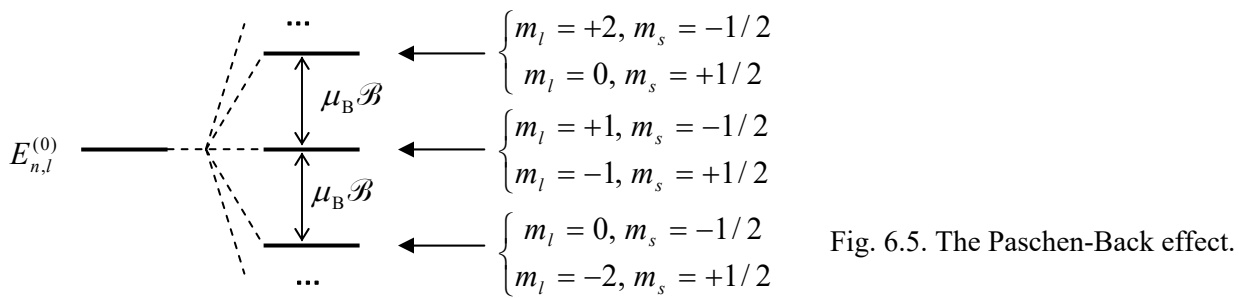


Fig. 6.5. The Paschen-Back effect.

¹⁸ Despite its smallness, the quadratic term is necessary for a description of the negative contribution of the orbital motion to the magnetic susceptibility χ_m (the so-called *orbital diamagnetism*, see EM Sec. 5.5), whose analysis, using Eq. (63), is left for the reader's exercise.

¹⁹ See, e.g., EM Sec. 5.4, in particular Eqs. (5.95) and (5.100).

Note that all the levels, these besides the top and bottom ones, remain doubly degenerate. This limit of the Zeeman effect is sometimes called the *Paschen-Back effect* – whose simplicity was recognized only in the 1920s, due to the need in very high magnetic fields for its observation.

In the opposite limit of relatively *low* magnetic fields, the Zeeman effect takes place on the background of the much larger fine-structure splitting. As was discussed in Sec. 3, at $\mathcal{B} = 0$ each split sub-level has a $2 \times (2j + 1)$ -fold degeneracy corresponding to $(2j + 1)$ different values of the half-integer quantum number m_j , ranging from $-j$ to $+j$, and two values of the integer $l = j \mp \frac{1}{2}$ – see Fig. 4.²⁰ The magnetic field lifts this degeneracy. Indeed, in the coupled representation discussed in Sec. 5.7, the perturbation (65) is described by the matrix with elements

$$\begin{aligned} H^{(1)} &= \frac{e\mathcal{B}}{2m_e} \langle j, m_j | \hat{L}_z + 2\hat{S}_z | j', m_{j'} \rangle \equiv \frac{e\mathcal{B}}{2m_e} \langle j, m_j | \hat{J}_z + \hat{S}_z | j', m_{j'} \rangle \\ &= \frac{e\mathcal{B}}{2m_e} \left(\hbar m_j \delta_{m_j m_{j'}} + \langle j, m_j | \hat{S}_z | j', m_{j'} \rangle \right). \end{aligned} \quad (6.67)$$

To spell out the second term, let us use the general expansion (5.183) for the particular case $s = \frac{1}{2}$, when (as was discussed in the end of Sec. 5.7) it has at most two non-vanishing terms, with the Clebsch-Gordan coefficients (5.190):

$$\begin{aligned} &|j = l \pm \frac{1}{2}, m_j\rangle \\ &= \pm \left(\frac{l \pm m_j + \frac{1}{2}}{2l+1} \right)^{1/2} |m_l = m_j - \frac{1}{2}, m_s = +\frac{1}{2}\rangle + \left(\frac{l \mp m_j + \frac{1}{2}}{2l+1} \right)^{1/2} |m_l = m_j + \frac{1}{2}, m_s = -\frac{1}{2}\rangle. \end{aligned} \quad (6.68)$$

Taking into account that the operator \hat{S}_z gives non-zero brackets only for $m_s = m_{s'}$, the 2×2 matrix of elements $\langle m_l = m_j \pm \frac{1}{2}, m_s = \mp \frac{1}{2} | \hat{S}_z | m_l = m_j \pm \frac{1}{2}, m_s = \mp \frac{1}{2} \rangle$ is diagonal, so we may use Eq. (27) to get

$$\begin{aligned} E - E^{(0)} &= \frac{e\mathcal{B}}{2m_e} \left[\hbar m_j + \frac{\hbar (l \pm m_j + \frac{1}{2})}{2l+1} - \frac{\hbar (l \mp m_j + \frac{1}{2})}{2l+1} \right] \\ &\equiv \frac{e\mathcal{B}}{2m_e} \hbar m_j \left(1 \pm \frac{1}{2l+1} \right) \equiv \mu_B \mathcal{B} m_j \left(1 \pm \frac{1}{2l+1} \right), \quad \text{for } -j \leq m_j \leq +j, \end{aligned} \quad (6.69)$$

Anomalous
Zeeman
effect
for $s = 1/2$

where the two signs correspond to the two possible values of $l = j \mp \frac{1}{2}$ – see Fig. 6.

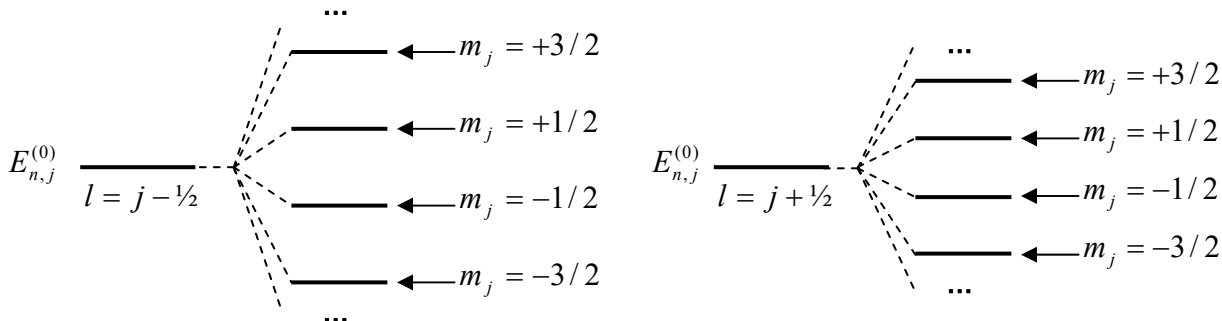


Fig. 6.6. The anomalous Zeeman effect in a hydrogen-like atom/ion.

²⁰ In the almost-hydrogen-like, but more complex atoms (such as those of alkali metals), the degeneracy in l may be lifted by electron-electron Coulomb interaction even in the absence of external magnetic field.

We see that the magnetic field splits each sub-level of the fine structure, with a given l , into $2j + 1$ equidistant levels, with the distance between the levels depending on l . In the late 1890s, when the Zeeman effect was first observed, there was no notion of spin at all, so that this puzzling result was called the *anomalous Zeeman effect*. (In this terminology, the *normal Zeeman effect* is the one with no spin splitting, i.e. without the second terms in the parentheses of Eqs. (66), (67), and (69); it was first observed in 1898 by Preston Thomas in atoms with zero net spin.)

The strict quantum-mechanical analysis of the anomalous Zeeman effect for arbitrary s (which is important for applications to multi-electron atoms) is conceptually not complex, but requires explicit expressions for the corresponding Clebsch-Gordan coefficients, which are rather bulky. Let me just cite the unexpectedly simple result of this analysis:

$$\Delta E = \mu_B \mathcal{B} m_j g, \quad (6.70a)$$

where g is the so-called *Lande factor*:²¹

$$g = 1 + \frac{j(j+1) + s(s+1) - l(l+1)}{2j(j+1)}. \quad (6.70b)$$

Anomalous
Zeeman
effect
for arbitrary s

For $s = \frac{1}{2}$ (and hence $j = l \pm \frac{1}{2}$), this factor is reduced to the parentheses in the last forms of Eq. (69).

It is remarkable that Eqs. (70) may be readily derived using very plausible classical arguments, similar to those used in Sec. 5.7 – see Fig. 5.13 and its discussion. As was discussed in Sec. 5.6, in the absence of spin, the quantization of the observable L_z is an extension of the classical picture of the torque-induced precession of the vector \mathbf{L} about the magnetic field's direction, so that the interaction energy, proportional to $\mathcal{B}L_z = \mathcal{B} \cdot \mathbf{L}$, remains constant – see Fig. 7a. On the other hand, at the spin-orbit interaction without an external magnetic field, the Hamiltonian function of the system includes the product $\mathbf{S} \cdot \mathbf{L}$, so that in the stationary state it has to be constant, together with J^2 , L^2 , and S^2 . Hence, this system's classical image is a joint precession of the vectors \mathbf{S} and \mathbf{L} about the direction of the vector $\mathbf{J} = \mathbf{L} + \mathbf{S}$, in such a manner that the spin-orbit interaction energy, proportional to the product $\mathbf{L} \cdot \mathbf{S}$, remains constant (Fig. 7b). On this backdrop, the anomalous Zeeman effect in a relatively weak magnetic field $\mathcal{B} = \mathcal{B}n_z$ corresponds to a much slower precession of the vector \mathbf{J} about the z -axis, “dragging” with it the vectors \mathbf{L} and \mathbf{S} , rapidly rotating around it.

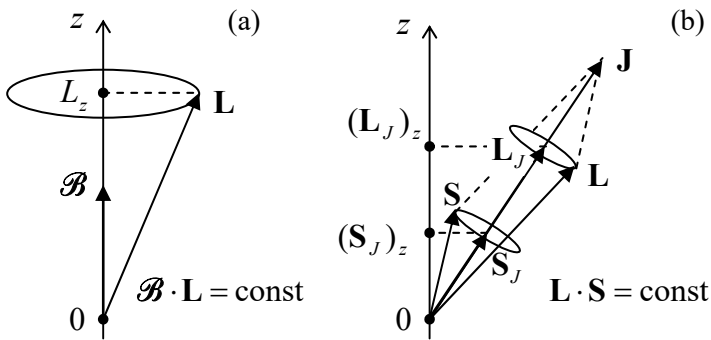


Fig. 6.7. Classical images of (a) the orbital angular momentum's quantization in a magnetic field, and (b) the fine-structure level splitting.

²¹ This formula is frequently used with capital letters J , S , and L , which denote the quantum numbers of the atom as a whole.

This physical picture allows us to conjecture that what is important for the slow precession rate are only the vectors \mathbf{L} and \mathbf{S} averaged over the period of their much faster precession around vector \mathbf{J} – in other words, only their components \mathbf{L}_J and \mathbf{S}_J along the vector \mathbf{J} . Classically, these components may be calculated as

$$\mathbf{L}_J = \frac{\mathbf{L} \cdot \mathbf{J}}{J^2} \mathbf{J}, \quad \text{and} \quad \mathbf{S}_J = \frac{\mathbf{S} \cdot \mathbf{J}}{J^2} \mathbf{J}. \quad (6.71)$$

The scalar products participating in these expressions may be readily expressed via the squared lengths of the vectors, using the following geometric formulas:

$$S^2 = (\mathbf{J} - \mathbf{L})^2 \equiv J^2 + L^2 - 2\mathbf{L} \cdot \mathbf{J}, \quad L^2 = (\mathbf{J} - \mathbf{S})^2 \equiv J^2 + S^2 - 2\mathbf{J} \cdot \mathbf{S}. \quad (6.72)$$

As a result, we get the following time average:

$$\begin{aligned} \overline{L_z + 2S_z} &= (\mathbf{L}_J + 2\mathbf{S}_J)_z = \left(\frac{\mathbf{L} \cdot \mathbf{J}}{J^2} \mathbf{J} + 2 \frac{\mathbf{S} \cdot \mathbf{J}}{J^2} \mathbf{J} \right)_z = \frac{J_z}{J^2} (\mathbf{L} \cdot \mathbf{J} + 2\mathbf{S} \cdot \mathbf{J}) \\ &= J_z \frac{(J^2 + L^2 - S^2) + 2(J^2 + S^2 - L^2)}{2J^2} \equiv J_z \left(1 + \frac{J^2 + S^2 - L^2}{2J^2} \right). \end{aligned} \quad (6.73)$$

The last move is to smuggle in some quantum mechanics by using, instead of the vector lengths squared and the z -component of J_z , their eigenvalues given by Eqs. (5.169), (5.175), and (5.177). As a result, we immediately arrive at the exact Eqs. (70). This coincidence encourages thinking about quantum mechanics of angular momenta in the classical terms of torque-induced precession, which turns out to be very fruitful in some more complex problems of atomic and molecular physics.

The high-field limit and low-field limits of the Zeeman effect, described respectively by Eqs. (66) and (69), are separated by a medium field range, in which the Zeeman splitting is of the order of the fine-structure splitting analyzed in Sec. 3. There is no time in this course for a quantitative analysis of this crossover.²²

6.5. Time-dependent perturbations

Now let us proceed to the case when the perturbation $\hat{H}^{(1)}$ in Eq. (1) is a function of time, while $\hat{H}^{(0)}$ is time-independent. The adequate perturbative approach to this problem, and its results, depend critically on the relation between the characteristic frequency ω of the perturbation and the distance between the initial system's energy levels:

$$\hbar\omega \leftrightarrow |E_n - E_{n'}|. \quad (6.74)$$

In the case when all essential frequencies of a perturbation are very small in the sense of Eq. (74), we are dealing with the so-called *adiabatic* change of parameters, that may be treated essentially as a time-independent perturbation – see the previous sections of this chapter). The most interesting observation here is that the adiabatic perturbation does not allow any significant transfer of system's

²² For a more complete discussion of the Stark, Zeeman, and fine-structure effects in atoms, I can recommend, for example, either the monograph by G. Woolgate cited above, or the one by I. Sobelman, *Theory of Atomic Spectra*, Alpha Science, 2006.

probability from one eigenstate to another. For example, in the WKB limit of the orbital motion, the Bohr quantization rule and its Wilson-Sommerfeld modification (2.110) guarantee that the integral

$$\oint_C \mathbf{p} \cdot d\mathbf{r}, \quad (6.75)$$

taken along the particle's classical trajectory, is an *adiabatic invariant*, i.e. does not change at a slow change of system's parameters. (It is curious that classical mechanics also guarantees the invariance of the integral (75), but its proof there²³ is much harder than the quantum-mechanical derivation of this fact, carried out in Sec. 2.4.) This is why even if the perturbation becomes large with time (while changing sufficiently slowly), we can expect the classification of eigenstates and eigenvalues to persist.

Let us proceed to the harder case when both sides of Eq. (74) are comparable, using for this discussion the Schrödinger picture of quantum dynamics, given by Eq. (4.158). Combining it with Eq. (1), we get the Schrödinger equation in the form

$$i\hbar \frac{\partial}{\partial t} |\alpha(t)\rangle = (\hat{H}^{(0)} + H^{(1)}(t)) |\alpha(t)\rangle. \quad (6.76)$$

Very much in the spirit of our treatment of the time-independent case in Sec. 1, let us represent the time-dependent ket-vector of the system with its expansion,

$$|\alpha(t)\rangle = \sum_n |n\rangle \langle n| \alpha(t)\rangle, \quad (6.77)$$

over the full and orthonormal set of the unperturbed, stationary ket-vectors defined by equation

$$\hat{H}^{(0)} |n\rangle = E_n |n\rangle. \quad (6.78)$$

(Note that these kets $|n\rangle$ are exactly what was called $|n^{(0)}\rangle$ in Sec. 1; we may afford a less bulky notation in this section, because only the lowest orders of the perturbation theory will be discussed.) Plugging the expansion (77), with n replaced with n' , into both sides of Eq. (76), and then inner-multiplying both its sides by the bra-vector $\langle n|$ of another unperturbed (and hence time-independent) state of the system, we get the following set of linear, ordinary differential equations for the expansion coefficients:

$$i\hbar \frac{d}{dt} \langle n| \alpha(t)\rangle = E_n \langle n| \alpha(t)\rangle + \sum_{n'} H_{nn'}^{(1)}(t) \langle n'| \alpha(t)\rangle, \quad (6.79)$$

where the matrix elements of the perturbation, in the *unperturbed* state basis, defined similarly to Eq. (8), are now functions of time:

$$H_{nn'}^{(1)}(t) \equiv \langle n| \hat{H}^{(1)}(t) |n'\rangle. \quad (6.80)$$

The set of differential equations (79), which are still exact, may be useful for numerical calculations.²⁴ However, it has a certain technical inconvenience, which becomes clear if we consider its (evident) solution in the absence of perturbation:²⁵

²³ See, e.g., CM Sec. 10.2.

²⁴ Even if the problem under analysis may be described by the wave-mechanics Schrödinger equation (1.25), a direct numerical integration of that *partial* differential equation is typically less convenient than that of the *ordinary* differential equations (79).

²⁵ This is of course just a more general form of Eq. (1.62) of the wave mechanics of time-independent systems.

$$\langle n | \alpha(t) \rangle = \langle n | \alpha(0) \rangle \exp \left\{ -i \frac{E_n}{\hbar} t \right\}. \quad (6.81)$$

We see that these solutions oscillate very fast, and their numerical modeling may represent a challenge for even the fastest computers. These spurious oscillations (whose frequency, in particular, depends on the energy reference level) may be partly tamed by looking for the general solution of Eqs. (79) in a form inspired by Eq. (81):

$$\langle n | \alpha(t) \rangle \equiv a_n(t) \exp \left\{ -i \frac{E_n}{\hbar} t \right\}. \quad (6.82)$$

Here $a_n(t)$ are new functions of time (essentially, the stationary states' probability amplitudes), which may be used, in particular, to calculate the time-dependent *level occupancies*, i.e. the probabilities W_n to find the perturbed system on the corresponding energy levels of the unperturbed system:

$$W_n(t) = |\langle n | \alpha(t) \rangle|^2 = |a_n(t)|^2. \quad (6.83)$$

Plugging Eq. (82) into Eq. (79), for these functions we readily get a slightly modified system of equations:

$$i\hbar \dot{a}_n = \sum_{n'} a_{n'} H_{nn'}^{(1)}(t) e^{i\omega_{nn'} t}, \quad (6.84)$$

where the factors $\omega_{nn'}$, defined by the relation

$$\hbar \omega_{nn'} \equiv E_n - E_{n'}, \quad (6.85)$$

have the physical sense of frequencies of *potential* quantum transitions between the n^{th} and n'^{th} energy levels of the unperturbed system. (The conditions when such transitions indeed take place will be clear soon.) The advantages of Eq. (84) over Eq. (79), for both analytical and numerical calculations, is their independence of the energy reference, and lower frequencies of oscillations of the right-hand side terms, especially when the energy levels of interest are close to each other.²⁶

In order to continue our analytical treatment, let us focus on a particular but very important problem of a sinusoidal perturbation *turned on* at some moment – which may be taken for $t = 0$:

$$\hat{H}^{(1)}(t) = \begin{cases} 0, & \text{for } t < 0, \\ \hat{A}e^{-i\omega t} + \hat{A}^\dagger e^{+i\omega t}, & \text{for } t \geq 0, \end{cases} \quad (6.86)$$

where the *perturbation amplitude operators* \hat{A} and \hat{A}^\dagger ,²⁷ and hence their matrix elements,

²⁶ Note that the relation of Eq. (84) to the initial Eq. (79) is very close to the relation of the interaction picture of quantum dynamics, discussed at the end of Sec. 4.6, to its Schrödinger picture, with the perturbation Hamiltonian playing the role of the interaction one – compare Eqs. (1) and Eq. (4.206). Indeed, Eq. (84) could be readily obtained from the interaction picture, and I did not do this just to avoid using this heavy bra-ket artillery for our current (relatively) simple problem, and hence to keep its physics more transparent.

²⁷ The notation of the amplitude operators in Eq. (86) is justified by the fact that the perturbation Hamiltonian has to be self-adjoint (Hermitian), and hence each term on the right-hand side of that relation has to be a Hermitian conjugate of its counterpart, which is evidently true only if the amplitude operators are also the Hermitian conjugates of each other. Note, however, that each of these amplitude operators is generally *not* Hermitian.

$$\langle n | \hat{A} | n' \rangle = A_{nn'}, \quad \langle n | \hat{A}^\dagger | n' \rangle = A_{n'n}^*, \quad (6.87)$$

are time-independent after the turn-on moment. In this case, Eq. (84) yields

$$i\hbar \dot{a}_n = \sum_{n'} a_{n'} \left[A_{nn'} e^{i(\omega_{nn'} - \omega)t} + A_{n'n}^* e^{i(\omega_{nn'} + \omega)t} \right], \quad \text{for } t > 0. \quad (6.88)$$

This is, generally, still a nontrivial system of coupled differential equations; however, it allows simple and explicit solutions in two very important limits. First, let us assume that our system initially was definitely in one eigenstate n' (usually, though not necessarily, in the ground state), and that the occupancies W_n of all other levels stay very low all the time. (We will find the condition when the second assumption is valid *a posteriori* – from the solution.) With these assumptions,

$$a_{n'} = 1; \quad |a_n| \ll 1, \quad \text{for } n \neq n', \quad (6.89)$$

Eq. (88) may be readily integrated, giving

$$a_n = -\frac{A_{nn'}}{\hbar(\omega_{nn'} - \omega)} \left[e^{i(\omega_{nn'} - \omega)t} - 1 \right] - \frac{A_{n'n}^*}{\hbar(\omega_{nn'} + \omega)} \left[e^{i(\omega_{nn'} + \omega)t} - 1 \right], \quad \text{for } n \neq n'. \quad (6.90)$$

This expression describes what is colloquially called the *ac excitation of (other) energy levels*. Qualitatively, it shows that the probability W_n (83) of finding the system in each state (“on each energy level”) of the system does not tend to any constant value but rather oscillates in time. It also shows that that the ac-field-induced transfer of the system from one state to the other one has a clearly resonant character: the maximum occupancy W_n of a level number $n \neq n'$ grows infinitely when the corresponding *detuning*²⁸

$$\Delta_{nn'} \equiv \omega - \omega_{nn'}, \quad (6.91)$$

tends to zero. This conclusion is clearly unrealistic, and is an artifact of our initial assumption (89); according to Eq. (90), it is satisfied only if²⁹

$$|A_{nn'}| \ll \hbar |\omega \pm \omega_{nn'}|, \quad (6.92)$$

and hence which does not allow a more deep analysis of the resonant excitation.

In order to overcome this limitation, we may perform the following trick – very similar to the one we used for the transfer to the degenerate case in Sec. 1. Let us assume that for a certain level n ,

$$|\Delta_{nn'}| \ll \omega, |\omega \pm \omega_{n''n}|, |\omega \pm \omega_{n''n'}|, \quad \text{for all } n'' \neq n, n' \quad (6.93)$$

– the condition illustrated in Fig. 8. Then, according to Eq. (90), we may ignore the occupancy of all but two levels, n and n' , and also the second, non-resonant term with frequency $\omega_{nn'} + \omega \approx 2\omega \gg |\Delta_{nn'}|$ in Eqs. (88),³⁰ now written for two probability amplitudes, a_n and $a_{n'}$.

²⁸ The notion of detuning is also very useful in the classical theory of oscillations (see, e.g., CM Chapter 5), where the role of $\omega_{nn'}$ is played by the own frequency ω_0 of the oscillator.

²⁹ Strictly speaking, one more condition is that the number of “resonance” levels is also not too high – see Sec. 6.

³⁰ The second assumption, i.e. the omission of non-resonant terms in the equations for amplitudes is called the *Rotating Wave Approximation* (RWA); the same idea in the classical theory of oscillations is the basis of what is usually called the *van der Pol method*, and its result, the *reduced equations* – see, e.g., CM Secs. 5.3-5.5.

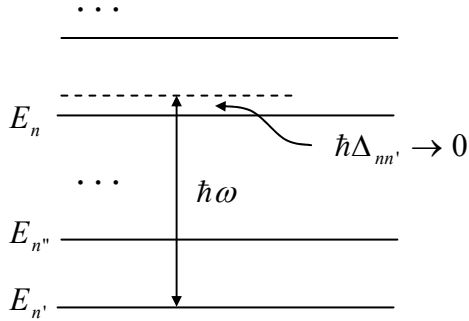


Fig. 6.8. The resonant excitation of an energy level.

The result is the following system of two linear equations:

$$i\hbar\dot{a}_n = a_{n'} A e^{-i\Delta t}, \quad i\hbar\dot{a}_{n'} = a_n A^* e^{i\Delta t}, \quad (6.94)$$

which uses the shorthand notation $A \equiv A_{nn'}$ and $\Delta \equiv \Delta_{nn'}$. (I will use this notation for a while – until other energy levels become involved, at the beginning of the next section). This system may be readily reduced to a form without explicit time dependence of the right-hand parts – for example, by introducing the following new probability amplitudes, with the same moduli:

$$b_n \equiv a_n e^{i\Delta t/2}, \quad b_{n'} \equiv a_{n'} e^{-i\Delta t/2}, \quad (6.95)$$

so that

$$a_n = b_n e^{-i\Delta t/2}, \quad a_{n'} = b_{n'} e^{i\Delta t/2}. \quad (6.96)$$

Plugging these relations into Eq. (94), we get two usual linear first-order differential equations:

$$i\hbar\dot{b}_n = -\frac{\hbar\Delta}{2}b_n + Ab_{n'}, \quad i\hbar\dot{b}_{n'} = A^*b_n + \frac{\hbar\Delta}{2}b_{n'}. \quad (6.97)$$

As the reader knows very well by now, the general solution of such a system is a linear combination of two exponential functions, $\exp\{\lambda_{\pm}t\}$, with the exponents λ_{\pm} that may be found by plugging any of these functions into Eq. (97), and requiring the consistency of the two resulting linear algebraic equations. In our case, the consistency condition (i.e. the characteristic equation of the system) is

$$\begin{vmatrix} -\hbar\Delta/2 - i\hbar\lambda & A \\ A^* & \hbar\Delta/2 - i\hbar\lambda \end{vmatrix} = 0, \quad (6.98)$$

and has two solutions $\lambda_{\pm} = \pm i\Omega$, where

$$\Omega \equiv \left(\frac{\Delta^2}{4} + \frac{|A|^2}{\hbar^2} \right)^{1/2}, \quad \text{i.e. } 2\Omega = \left(\Delta^2 + 4 \frac{|A|^2}{\hbar^2} \right)^{1/2}. \quad (6.99)$$

The coefficients at the exponents are determined by initial conditions. If, as was assumed before, the system was completely on the level n' initially (at $t = 0$), i.e. if $a_{n'}(0) = 1$, $a_n(0) = 0$, so that $b_{n'}(0) = 1$, $b_n(0) = 0$ as well, then Eqs. (97) yield, in particular:

$$b_n(t) = -i \frac{A}{\hbar\Omega} \sin \Omega t, \quad (6.100)$$

so that the n^{th} level occupancy is

$$W_n = |b_n|^2 = \frac{|A|^2}{\hbar^2 \Omega^2} \sin^2 \Omega t \equiv \frac{|A|^2}{|A|^2 + (\hbar \Delta / 2)^2} \sin^2 \Omega t. \quad (6.101)$$

Rabi formula

This is the famous *Rabi oscillation formula*.³¹ If the detuning is large in comparison with $|A|/\hbar$, though still small in the sense of Eq. (93), the frequency 2Ω of the Rabi oscillations is completely determined by the detuning, and their amplitude is small:

$$W_n(t) = 4 \frac{|A|^2}{\hbar^2 \Delta^2} \sin^2 \frac{\Delta t}{2} \ll 1, \quad \text{for } |A|^2 \ll (\hbar \Delta)^2, \quad (6.102)$$

– the result which could be obtained directly from Eq. (90), just neglecting the second term on its right-hand side. However, now we may also analyze the results of an increase of the perturbation amplitude: it leads not only to an increase of the amplitude of the probability oscillations, but also of their frequency – see Fig. 9. Ultimately, at $|A| \gg \hbar|\Delta|$ (for example, at the exact resonance, $\Delta = 0$, i.e. $\omega_{nn'} = \omega$, so that $E_n = E_{n'} + \hbar\omega$), Eqs. (101)-(102) give $\Omega = |A|/\hbar$ and $(W_n)_{\max} = 1$, i.e. describe a periodic, full “repumping” of the system from one level to another and back, with a frequency proportional to the perturbation amplitude.³²

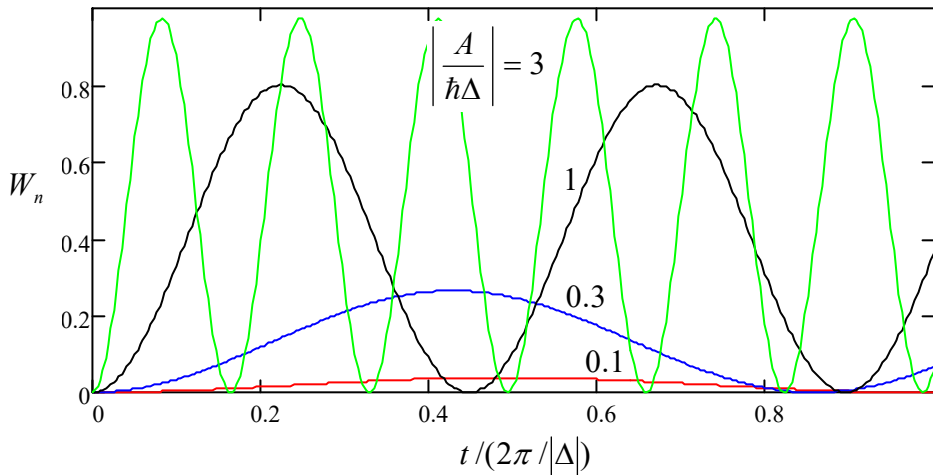


Fig. 6.9. The Rabi oscillations for several values of the normalized amplitude of ac perturbation.

This effect is a close analog of the quantum oscillations in two-level systems with time-independent Hamiltonians, which were discussed in Secs. 2.6 and 5.1. Indeed, let us revisit, for a moment, their discussion started at the end of Sec. 1 of this chapter, now paying more attention to the time evolution of the system under the perturbation. As was argued in that section, the most general perturbation Hamiltonian lifting the two-fold degeneracy of an energy level, in an arbitrary basis, has the matrix (28). Let us describe the system’s dynamics using, again, the Schrödinger picture, representing the ket-vector of an arbitrary state of the system in the form (5.1), where \uparrow and \downarrow are the

³¹ It was derived in 1952 by Isaac Rabi, in the context of his group’s pioneering experiments with the ac (practically, microwave) excitation of quantum states, using molecular beams in vacuum.

³² As Eqs. (82), (96), and (99) show, the lowest frequency in the system is $\omega_l = \omega_{n'} - \Delta/2 + \Omega$, so that at $A \rightarrow 0$, $\hbar\omega_l \approx \hbar\omega_{n'} + 2|A|^2/\hbar\Delta$. This effective shift of the lowest energy level (which may be measured by another “probe” field of a different frequency) is a particular case of the *ac Stark effect*, which was already mentioned in Sec. 2.

time-independent states of the basis in that Eq. (28) is written (now without any obligation to associate these states with the z -basis of any spin- $\frac{1}{2}$.) Then, the Schrödinger equation (4.158) yields

$$i\hbar \begin{pmatrix} \dot{\alpha}_\uparrow \\ \dot{\alpha}_\downarrow \end{pmatrix} = H^{(1)} \begin{pmatrix} \alpha_\uparrow \\ \alpha_\downarrow \end{pmatrix} \equiv \begin{pmatrix} H_{11} & H_{12} \\ H_{21} & H_{22} \end{pmatrix} \begin{pmatrix} \alpha_\uparrow \\ \alpha_\downarrow \end{pmatrix} \equiv \begin{pmatrix} H_{11}\alpha_\uparrow + H_{12}\alpha_\downarrow \\ H_{21}\alpha_\uparrow + H_{22}\alpha_\downarrow \end{pmatrix}. \quad (6.103)$$

As we know (for example, from the discussion in Sec. 5.1), the average of the diagonal elements of the matrix gives just a common shift of the system's energy; for the purpose of the dynamics analysis, it may be absorbed into the energy reference level. Also, the Hamiltonian operator has to be Hermitian, so that the off-diagonal elements of its matrix have to be complex-conjugate. With this, Eqs. (103) are reduced to the form,

$$i\hbar \dot{\alpha}_\uparrow = -\frac{\xi}{2} \alpha_\uparrow + H_{12} \alpha_\downarrow, \quad i\hbar \dot{\alpha}_\downarrow = H_{12}^* \alpha_\uparrow + \frac{\xi}{2} \alpha_\downarrow, \quad \text{with } \hbar\xi \equiv H_{22} - H_{11}, \quad (6.104)$$

which is absolutely similar to Eqs. (97). In particular, these equations describe the quantum oscillations of the probabilities $W_\uparrow = |\alpha_\uparrow|^2$ and $W_\downarrow = |\alpha_\downarrow|^2$ with the frequency³³

$$2\Omega = \left(\xi^2 + 4 \frac{|H_{12}|^2}{\hbar^2} \right)^{1/2}. \quad (6.105)$$

The similarity of Eqs. (97) and (104), and hence of Eqs. (99) and (105), shows that the “usual” quantum oscillations and the Rabi oscillations have essentially the same physical nature, besides that in the latter case the external ac signal quantum $\hbar\omega$ bridges the separated energy levels, effectively reducing their difference $(E_n - E_{n'})$ to a much smaller difference $-\Delta \equiv (E_n - E_{n'}) - \hbar\omega$. Also, since the Hamiltonian (28) is similar to that given by Eq. (5.2), the dynamics of such a system with two ac-coupled energy levels, within the limits (93) of the perturbation theory, is completely similar to that of a time-independent two-level system. In particular, its state may be similarly represented by a point on the Bloch sphere shown in Fig. 5.3, with its dynamics described, in the Heisenberg picture, by Eq. (5.19). This fact is very convenient for the experimental implementation of quantum information systems (to be discussed in more detail in Sec. 8.5), because it enables qubit manipulations in a broad variety of physical systems with well-separated energy levels, using external ac (usually either microwave or optical) sources.

Note, however, that according to Eq. (90), if the system has energy levels other than n and n' , they also become occupied to some extent. Since the sum of all occupancies equals 1, this means that $(W_n)_{\max}$ may approach 1 only if the other excitation amplitude is very small, and hence the state manipulation time scale $\mathcal{T} = 2\pi/\Omega = 2\pi\hbar/|A|$ is very long. The ultimate limit in this sense is provided by the harmonic oscillator where all energy levels are equidistant, and the probability repumping between all of them occurs at comparable rates. In particular, in this system the implementation of the full Rabi oscillations is impossible even at the exact resonance.³⁴

³³ By the way, Eq. (105) gives a natural generalization of the relations obtained for the frequency of such oscillations in Sec. 2.6, where the coupled potential wells were assumed to be exactly similar, so that $\xi = 0$. Moreover, Eqs. (104) gives a long-promised proof of Eqs. (2.201), and hence a better justification of Eqs. (2.203).

³⁴ From Sec. 5.5, we already know what happens to the ground state of an oscillator at its external sinusoidal (or any other) excitation: it turns into a Glauber state, i.e. a superposition of *all* Fock states – see Eq. (5.134).

However, I would not like these the quantitative details to obscure from the reader the most important qualitative (OK, maybe semi-quantitative :-) conclusion of this section's analysis: a resonant increase of the interlevel transition intensity at $\omega \rightarrow \omega_{nn'}$. As will be shown later in the course, in a quantum system coupled to its environment at least slightly (hence in reality, in *any* quantum system), such increase is accompanied by a sharp increase of the external field's *absorption*, which may be measured. This effect has numerous practical applications including spectroscopies based on the electron paramagnetic resonance (EPR) and nuclear magnetic resonance (NMR), which are broadly used in material science, chemistry, and medicine. Unfortunately, I will not have time to discuss the related technical issues and methods (in particular, interesting ac pulsing techniques, including the so-called *Ramsey interferometry*) in detail, and have to refer the reader to special literature.³⁵

6.6. Quantum-mechanical Golden Rule

One of the results of the past section, Eq. (102), may be used to derive one of the most important and nontrivial results of quantum mechanics. For that, let us consider the case when the perturbation causes quantum transitions from a *discrete* energy level E_n into a group of eigenstates with a very dense (essentially *continuous*) spectrum $E_{n'}$ – see Fig. 10a.

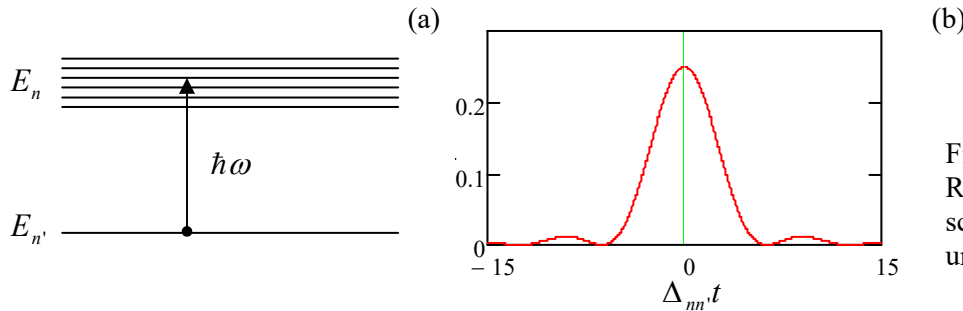


Fig. 6.10. Deriving the Golden Rule: (a) the energy level scheme, and (b) the function under the integral (108).

If, for all states n of the group, the following conditions are satisfied

$$|A_{nn'}|^2 \ll (\hbar\Delta_{nn'})^2 \ll (\hbar\omega_{nn'})^2, \quad (6.106)$$

then Eq. (102) coincides with the result that would follow from Eq. (90). This means that we may apply Eq. (102), with the indices n and n' duly restored, to any level n of our tight group. As a result, the total probability of having our system transferred from the initial level n' to that group is

$$W_\Sigma(t) = \sum_n W_n(t) = \frac{4}{\hbar^2} \sum_n \frac{|A_{nn'}|^2}{\Delta_{nn'}^2} \sin^2 \frac{\Delta_{nn'} t}{2}. \quad (6.107)$$

Now comes the main, absolutely beautiful trick: let us assume that the summation over n is limited to a tight group of very similar states whose matrix elements $A_{nn'}$ are virtually similar (we will check the validity of this assumption later on), so that we can take $|A_{nn'}|^2$ out of the sum in Eq. (107) and then replace the sum with the corresponding integral:

³⁵ For introductions see, e.g., J. Wertz and J. Bolton, *Electron Spin Resonance*, 2nd ed., Wiley, 2007; J. Keeler, *Understanding NMR Spectroscopy*, 2nd ed., Wiley, 2010.

$$W_{\Sigma}(t) = \frac{4|A_{nn'}|^2}{\hbar^2} \int \frac{1}{\Delta_{nn'}^2} \sin^2 \frac{\Delta_{nn'} t}{2} d_n \equiv \frac{4|A_{nn'}|^2 \rho_n t}{\hbar} \int \frac{1}{(\Delta_{nn'} t)^2} \sin^2 \frac{\Delta_{nn'} t}{2} d(-\Delta_{nn'} t), \quad (6.108)$$

where ρ_n is the density of the states n on the energy axis:

$$\boxed{\rho_n \equiv \frac{dn}{dE_n}}. \quad (6.109)$$

Density of states
This density and the matrix element $A_{nn'}$ have to be evaluated at $\Delta_{nn'} = 0$, i.e. at energy $E_n = E_{n'} + \hbar\omega$, and are assumed to be constant within the final state group. At fixed $E_{n'}$, the function under integral (108) is even and decreases fast at $|\Delta_{nn'} t| \gg 1$ – see Fig. 10b. Hence we may introduce a dimensionless integration variable $\xi \equiv \Delta_{nn'} t$, and extend the integration over it formally from $-\infty$ to $+\infty$. Then the integral in Eq. (108) is reduced to a table one,³⁶ and yields

$$W_{\Sigma}(t) = \frac{4|A_{nn'}|^2 \rho_n t}{\hbar} \int_{-\infty}^{+\infty} \frac{1}{\xi^2} \sin^2 \frac{\xi}{2} d\xi = \frac{4|A_{nn'}|^2 \rho_n t}{\hbar} \frac{\pi}{2} \equiv \Gamma t, \quad (6.110)$$

where the constant

$$\boxed{\Gamma = \frac{2\pi}{\hbar} |A_{nn'}|^2 \rho_n} \quad (6.111)$$

Golden Rule
is called the *transition rate*.³⁷ This is one of the most famous and useful results of quantum mechanics, its *Golden Rule*³⁸, which deserves much discussion.

First of all, let us reproduce the reasoning already used in Sec. 2.5 to show that the meaning of the rate Γ is much deeper than Eq. (110) seems to imply. Indeed, due to the conservation of the total probability, $W_{n'} + W_{\Sigma} = 1$, we can rewrite that equation as

$$\dot{W}_{n'}|_{t=0} = -\Gamma. \quad (6.112)$$

Evidently, this result cannot be true for all times, otherwise the probability $W_{n'}$ would become negative. The reason for this apparent contradiction is that Eq. (110) was obtained in the assumption that initially, the system was completely on level n' : $W_{n'}(0) = 1$. Now, if at the initial moment the value of $W_{n'}$ is different, the result (110) has to be multiplied by that number, due to the linear relation (88) between da_n/dt and a_n . Hence, instead of Eq. (112) we get a differential equation similar to Eq. (2.159),

$$\dot{W}_{n'}|_{t \geq 0} = -\Gamma W_{n'}, \quad (6.113)$$

which, for a time-independent Γ , has the evident solution,

³⁶ See, e.g., MA Eq. (6.12).

³⁷ In some texts, the density of states in Eq. (111) is replaced with a formal expression $\Sigma_n \delta(E_n - E_{n'} - \hbar\omega)$. Indeed, applied to a finite energy interval ΔE_n with $\Delta n \gg 1$ levels, it gives the same result: $\Delta n \equiv (dn/dE_n)\Delta E_n \equiv \rho_n \Delta E_n$. Such replacement may be technically useful in some cases, but is incorrect for $\Delta n \sim 1$, and hence should be used with the utmost care, so that for most applications the more explicit form (111) is preferable.

³⁸ Sometimes Eq. (111) is called “Fermi’s Golden Rule”. This is rather unfair, because this result was developed mostly by the same P. A. M. Dirac in 1927, and Enrico Fermi’s role was not much more than advertising it, under the name of “Golden Rule No. 2”, in his influential lecture notes on nuclear physics, which were published much later, in 1950. (To be fair to Fermi, he has never tried to pose as the Golden Rule’s author.)

$$W_{n'}(t) = W_{n'}(0)e^{-\Gamma t}, \quad (6.114)$$

Initial occupancy's decay

describing the exponential decay of the initial state's occupancy, with the time constant $\tau = 1/\Gamma$.

I am inviting the reader to review this fascinating result again: by the summation of *periodic oscillations* (102) over many levels n , we have got an *exponential decay* (114) of the probability. This trick becomes possible because the effective range ΔE_n of the state energies E_n giving substantial contributions to the integral (108), shrinks with time: $\Delta E_n \sim \hbar/t$.³⁹ However, since most of the decay (114) takes place within the time interval of the order of $\tau \equiv 1/\Gamma$, the range of the participating final energies may be estimated as

$$\Delta E_n \sim \frac{\hbar}{\tau} \equiv \hbar\Gamma. \quad (6.115)$$

This estimate is very instrumental for the formulation of conditions of the Golden Rule's validity. First, we have assumed that the matrix elements of the perturbation and the density of states are independent of the energy within the interval (115). This gives the following requirement

$$\Delta E_n \sim \hbar\Gamma \ll E_n - E_{n'} \sim \hbar\omega, \quad (6.116)$$

Second, for the transfer from the sum (107) to the integral (108), we need the number of states within that energy interval, $\Delta N_n = \rho_n \Delta E_n$, to be much larger than 1. Merging Eq. (116) with Eq. (92) for all the energy levels $n'' \neq n, n'$ not participating in the resonant transition, we may summarize all conditions of the Golden Rule validity as

$$\rho_n^{-1} \ll \hbar\Gamma \ll \hbar|\omega \pm \omega_{n'n''}|. \quad (6.117)$$

Golden Rule's validity

(The reader may ask whether I have neglected the condition expressed by the first of Eqs. (106). However, for $\Delta_{nn'} \sim \Delta E_n / \hbar \sim \Gamma$, this condition is just $|A_{nn'}|^2 \ll (\hbar\Gamma)^2$, so that plugging it into Eq. (111),

$$\Gamma \ll \frac{2\pi}{\hbar}(\hbar\Gamma)^2 \rho_n, \quad (6.118)$$

and canceling one Γ and one \hbar , we see that it coincides with the first relation in Eq. (117) above.)

Let us have a look at whether these conditions may be satisfied in practice, at least in some cases. For example, let us consider the optical ionization of an atom, with the released electron confined in a volume of the order of $1 \text{ cm}^3 \equiv 10^{-6} \text{ m}^3$. According to Eq. (1.90), with E of the order of the atomic ionization energy $E_n - E_{n'} = \hbar\omega \sim 1 \text{ eV}$, the density of electron states in that volume is of the order of 10^{21} 1/eV , while the right-hand side of Eq. (117) is of the order of $E_n \sim 1 \text{ eV}$. Thus the conditions (117) provide an approximately 20-orders-of magnitude range for acceptable values of $\hbar\Gamma$. This illustration should give the reader a taste of why the Golden Rule is applicable to so many situations.

Finally, the physical picture of the initial state's decay (which will also be the key to our discussion of quantum-mechanical “open” systems in the next chapter) is also very important. According to Eq. (114), the external excitation transfers the system into the continuous spectrum of levels n , and it never comes back to the initial level n' . However, it was derived from the quantum mechanics of Hamiltonian systems, whose equations are invariant with respect to time reversal. This

³⁹ This is one more appearance of the “energy-time uncertainty relation”, which was discussed in Sec. 2.5.

paradox is a result of our generalization (113) of the exact result (112). This trick, breaking the time-reversal symmetry, is absolutely adequate for the physics under study. Indeed, some gut feeling of the physical sense of this irreversibility may be obtained from the following observation. As Eq. (1.86) illustrates, the distance between the adjacent orbital energy levels tends to zero only if the system's size goes to infinity. This means that our assumption of the continuous energy spectrum of the final states n essentially requires these states to be broadly extended in space – being either free, or essentially free de Broglie waves. Thus the Golden Rule corresponds to the (physically justified) assumption that in an infinitely large system, the traveling de Broglie waves excited by a local source and propagating outward from it, would never come back, and even if they did, unpredictable phase shifts introduced by minor uncontrollable perturbations on their way would never allow them to sum up in the coherent way necessary to bring the system back into the initial state n' . (This is essentially the same situation which was discussed, for a particular 1D wave-mechanical system, in Sec. 2.5.)⁴⁰

To get a feeling of the Golden Rule at work, let us apply it to the following simple problem – which is a toy model of the photoelectric effect, briefly discussed in Sec. 1.1(ii). A 1D particle is initially trapped in the ground state of a narrow potential well, described by Eq. (2.158):

$$U(x) = -\omega \delta(x), \quad \text{with } \omega > 0. \quad (6.119)$$

Let us calculate the rate Γ of the particle's “ionization” (i.e. its excitation into a group of extended, delocalized states) by a weak classical sinusoidal force of amplitude F_0 and frequency ω , suddenly turned on at some instant, say $t = 0$.

As a reminder, the initial localized state (in our current notation, n') of such a particle was already found in Sec. 2.6:

$$\psi_{n'}(x) = \kappa^{1/2} \exp\{-\kappa|x|\}, \quad \text{with } \kappa \equiv \frac{m\omega}{\hbar^2}, \quad E_{n'} \equiv -\frac{\hbar^2 \kappa^2}{2m} = -\frac{m\omega^2}{2\hbar^2}. \quad (6.120)$$

The final, extended states n , with a continuous spectrum, for this problem exist only at energies $E_n > 0$, so that the excitation rate is different from zero only for frequencies

$$\omega > \omega_{\min} \equiv \frac{|E_{n'}|}{\hbar} = \frac{m\omega^2}{2\hbar^3}. \quad (6.121)$$

The weak sinusoidal force may be described by the following perturbation Hamiltonian,

$$\hat{H}^{(1)} = -F(t)\hat{x} = -F_0 \hat{x} \cos \omega t \equiv -\frac{F_0}{2} \hat{x} \left(e^{i\omega t} + e^{-i\omega t} \right), \quad \text{for } t > 0, \quad (6.122)$$

so that according to Eq. (86), which serves as the amplitude operator's definition, in this case

$$\hat{A} = \hat{A}^\dagger = -\frac{F_0}{2} \hat{x}. \quad (6.123)$$

The matrix elements $A_{nn'}$ that participate in Eq. (111) may be readily calculated in the coordinate representation:

⁴⁰ This situation is also similar to the irreversible increase of entropy of macroscopic systems, despite the fact that their microscopic components obey reversible laws of motion, which is postulated in thermodynamics and explained in statistical physics – see, e.g., SM Secs. 1.2 and 2.2.

$$A_{nn'} = \int_{-\infty}^{+\infty} \psi_n^*(x) \hat{A}(x) \psi_{n'}(x) dx = -\frac{F_0}{2} \int_{-\infty}^{+\infty} \psi_n^*(x) x \psi_{n'}(x) dx. \quad (6.124)$$

Since, according to Eq. (120), the initial ψ_n is a *symmetric* function of x , non-vanishing contributions to this integral are given only by *antisymmetric* functions $\psi_n(x)$, proportional to $\sin k_n x$, with the wave number k_n related to the final energy by the well-familiar equality (1.89):

$$\frac{\hbar^2 k_n^2}{2m} = E_n. \quad (6.125)$$

As we know from Sec. 2.6 (see in particular Eq. (2.167) and its discussion), such antisymmetric functions, with $\psi_n(0) = 0$, are not affected by the zero-centered delta-functional potential (119), so that their density ρ_n is the same as that in completely free space, and we could use Eq. (1.100). However, since that relation was derived for traveling waves, it is more prudent to repeat its derivation for standing waves, confining them to an artificial segment $[-l/2, +l/2]$ – long in the sense

$$k_n l, \kappa l \gg 1, \quad (6.126)$$

so it does not affect the initial localized state and the excitation process. Then the confinement requirement $\psi_n(\pm l/2) = 0$ immediately yields the condition $k_n l/2 = n\pi$, so that Eq. (1.100) is indeed valid, but only for positive values of k_n , because $\sin k_n x$ with $k_n \rightarrow -k_n$ does not describe an independent standing-wave eigenstate. Hence the final state density is

$$\rho_n \equiv \frac{dn}{dE_n} \equiv \frac{dn}{dk_n} \Big/ \frac{dE_n}{dk_n} = \frac{l}{2\pi} \Big/ \frac{\hbar^2 k_n}{m} \equiv \frac{lm}{2\pi\hbar^2 k_n}. \quad (6.127)$$

It may look troubling that the density of states depends on the artificial segment's length l , but the same l also participates in the final wavefunctions' normalization factor,⁴¹

$$\psi_n = \left(\frac{2}{l} \right)^{1/2} \sin k_n x, \quad (6.128)$$

and hence in the matrix element (124):

$$A_{nn'} = -\frac{F_0}{2} \left(\frac{2\kappa}{l} \right)^{1/2} \int_{-l}^{+l} \sin k_n x e^{-\kappa|x|} x dx = -\frac{F_0}{2i} \left(\frac{2\kappa}{l} \right)^{1/2} \left(\int_0^l e^{(ik_n - \kappa)x} x dx - \int_0^l e^{-(ik_n + \kappa)x} x dx \right). \quad (6.129)$$

These two integrals may be readily worked out by parts. Taking into account that due to the condition (126), their upper limits may be extended to ∞ , the result is

$$A_{nn'} = -\left(\frac{2\kappa}{l} \right)^{1/2} F_0 \frac{2k_n \kappa}{(k_n^2 + \kappa^2)^2}. \quad (6.130)$$

Note that the matrix element is a smooth function of k_n (and hence of E_n), so that an important condition of the Golden Rule, the virtual constancy of $A_{nn'}$ on the interval $\Delta E_n \sim \hbar\Gamma \ll E_n$, is satisfied. So, the general Eq. (111) is reduced, for our problem, to the following expression:

⁴¹ The normalization to infinite volume, using Eq. (4.263), is also possible, but physically less transparent.

$$\Gamma = \frac{2\pi}{\hbar} \left[\left(\frac{2\kappa}{l} \right)^{1/2} F_0 \frac{2k_n \kappa}{(k_n^2 + \kappa^2)^2} \right]^2 \frac{lm}{2\pi\hbar^2 k_n} \equiv \frac{8F_0^2 m k_n \kappa^3}{\hbar^3 (k_n^2 + \kappa^2)^4}, \quad (6.131)$$

which is independent of the artificially introduced l – thus justifying its use.

Note that due to the above definitions of k_n and κ , the expression in the parentheses in the denominator of the last expression does not depend on the potential well's "weight" \mathcal{W} , and is a function of only the excitation frequency ω (and the particle's mass):

$$\frac{\hbar^2 (k_n^2 + \kappa^2)}{2m} = E_n - E_{n'} = \hbar\omega. \quad (6.132)$$

As a result, Eq. (131) may be recast simply as

$$\hbar\Gamma = \frac{F_0^2 \mathcal{W}^3 k_n}{2(\hbar\omega)^4}. \quad (6.133)$$

What is hidden here is that k_n , defined by Eq. (125) with $E_n = E_{n'} + \hbar\omega$, is a function of the external force's frequency, changing as $\omega^{1/2}$ at $\omega \gg \omega_{\min}$ (so that Γ drops as $\omega^{-7/2}$ at $\omega \rightarrow \infty$), and as $(\omega - \omega_{\min})^{1/2}$ when ω approaches the "red boundary" (121) of the ionization effect, so that $\Gamma \propto (\omega - \omega_{\min})^{1/2} \rightarrow 0$ in that limit as well.

A conceptually very similar, but a bit more involved analysis of such effect in a more realistic 3D case, namely the hydrogen atom's ionization by an optical wave, is left for the reader's exercise.

6.7. Golden Rule for step-like perturbations

Now let us reuse some of our results for a perturbation being turned on at $t = 0$, but after that time-independent:

Step-like perturbation

$$\hat{H}^{(1)}(t) = \begin{cases} 0, & \text{for } t < 0, \\ \hat{H} = \text{const}, & \text{for } t \geq 0. \end{cases} \quad (6.134)$$

A superficial comparison of this equality and the former Eq. (86) seems to indicate that we may use all our previous results, taking $\omega = 0$ and replacing $\hat{A} + \hat{A}^\dagger$ with $\hat{H}^{(1)}$. However, that conclusion (which would give us a wrong factor of 2 in the result) does not take into account the fact that analyzing both the two-level approximation in Sec. 5, and the Golden Rule in Sec. 6, we have dropped the second (non-resonant) term in Eq. (90). In our current case (134), with $\omega = 0$, there is no such difference between these terms. This why it is more prudent to use the general Eq. (84),

$$i\hbar\dot{a}_n = \sum_{n'} a_{n'} H_{nn'} e^{i\omega_{nn'} t}, \quad (6.135)$$

in which the matrix element of the perturbation is now time-independent at $t > 0$. We see that it is formally equivalent to Eq. (88) with only the first (resonant) term kept, if we make the following replacements:

$$\hat{A} \rightarrow \hat{H}, \quad \Delta_{nn'} \equiv \omega - \omega_{nn'} \rightarrow -\omega_{nn'}. \quad (6.136)$$

Let us use this equivalency to consider the results of coupling between a discrete-energy state n' , into which the particle is initially placed, and a dense group of states with a quasi-continuum spectrum, in the same energy range. Figure 11a shows an example of such a system: a particle is initially (say, at $t = 0$) placed into a potential well separated by a penetrable potential barrier from a formally infinite region with a continuous energy spectrum. Let me hope that the physical discussion in the last section makes the outcome of such an experiment evident: the particle will gradually and irreversibly tunnel out of the well, so that the probability $W_n(t)$ of its still residing in the well will decay in accordance with Eq. (114). The rate of this decay may be found by making the replacements (136) in Eq. (111):

$$\Gamma = \frac{2\pi}{\hbar} |H_{nn'}|^2 \rho_n, \quad (6.137)$$

where the states n and n' now have virtually the same energy.⁴²

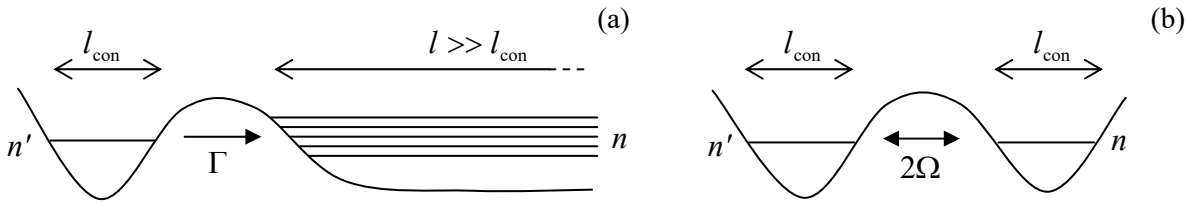


Fig. 6.11. Tunneling from a discrete-energy state n' : (a) to a state continuum, and (b) to another discrete-energy state n .

It is very informative to compare this result, semi-quantitatively, with Eq. (105) for a symmetric ($E_n = E_{n'}$) system of two potential wells separated by a similar potential barrier – see Fig. 11b. For the symmetric case, i.e. $\xi = 0$, Eq. (105) is reduced to simply

$$\Omega = \frac{1}{\hbar} |H_{nn'}|_{\text{con}}. \quad (6.138)$$

Here I have used the index “con” (from “confinement”) to emphasize that this matrix element is somewhat different from the one participating in Eq. (137), even if the potential barriers are similar. Indeed, in the latter case, the matrix element,

$$H_{nn'} = \langle n | \hat{H} | n' \rangle = \int \psi_{n'}^* \hat{H} \psi_n dx, \quad (6.139)$$

has to be calculated for two wavefunctions ψ_n and $\psi_{n'}$ confined to spatial intervals of the same scale l_{con} , while in Eq. (137), the wavefunctions ψ_n are extended over a much larger distance $l \gg l_{\text{con}}$ – see Fig. 11. As Eq. (128) tells us, in the 1D model this means an additional small factor of the order of $(l_{\text{con}}/l)^{1/2}$. Now using Eq. (128) as a crude but suitable model for the final-state wavefunctions, we arrive at the following estimate, independent of the artificially introduced length l :

$$\hbar\Gamma \sim 2\pi |H_{nn'}|_{\text{con}}^2 \frac{l_{\text{con}}}{l} \rho_n \sim 2\pi |H_{nn'}|_{\text{con}}^2 \frac{l_{\text{con}}}{l} \frac{lm}{2\pi\hbar^2 k_n} \sim \frac{|H_{nn'}|_{\text{con}}^2}{\Delta E_{n'}} \equiv \frac{(\hbar\Omega)^2}{\Delta E_{n'}}, \quad (6.140)$$

where $\Delta E_{n'} \sim \hbar^2/ml_{\text{con}}^2$ is the scale of the differences between the eigenenergies of the particle in an unperturbed potential well. Since the condition of validity of Eq. (138) is $\hbar\Omega \ll \Delta E_{n'}$, we see that

⁴² The condition of validity of Eq. (137) is again given by Eq. (117), just with $\omega = 0$ in the upper limit for Γ .

$$\hbar\Gamma \sim \frac{\hbar\Omega}{\Delta E_n} \hbar\Omega \ll \hbar\Omega.. \quad (6.141)$$

This (sufficiently general⁴³) perturbative result confirms the conclusion of a more particular analysis carried out in the end of Sec. 2.6: the rate of the (irreversible) quantum tunneling into a state continuum is always *much lower* than the frequency of (reversible) quantum oscillations between discrete states separated with the same potential barrier – at least for the case when both are much lower than $\Delta E_n/\hbar$, so that the perturbation theory is valid. A very handwaving interpretation of this result is that the particle oscillates between the confined state in the well and the space-extended states behind the barrier many times before finally “deciding to perform” an irreversible transition into the unconfined continuum. This qualitative picture is consistent with experimentally observable effects of dispersive electromagnetic environments on electron tunneling.⁴⁴

Let me conclude this section (and this chapter) with the application of Eq. (137) to a very important case, which will provide a smooth transition to the next chapter’s topic. Consider a *composite* system consisting of two *component* systems, *a* and *b*, with the energy spectra sketched in Fig. 12.

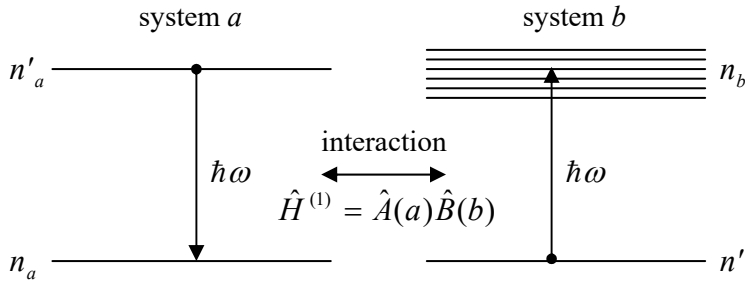


Fig. 6.12. Energy relaxation in system *a* due to its weak coupling to system *b* (which serves as the environment of *a*).

Let the systems be completely independent initially. The independence means that in the absence of their coupling, the total Hamiltonian of the system may be represented as a sum of two operators:

$$\hat{H}^{(0)} = \hat{H}_a(a) + \hat{H}_b(b), \quad (6.142)$$

where the arguments *a* and *b* symbolize the non-overlapping sets of the degrees of freedom of the two systems. Such operators, belonging to their individual, different Hilbert spaces, naturally commute. Similarly, the eigenkets of the system may be naturally factored as

$$|n\rangle = |n_a\rangle \otimes |n_b\rangle. \quad (6.143)$$

The *direct product* sign \otimes is used here (and below) to denote the formation of a joint ket-vector from the kets of the independent systems, belonging to different Hilbert spaces. Evidently, the order of operands in such a product may be changed at will. As a result, its eigenenergies separate into a sum, just as the Hamiltonian (142) does:

$$\hat{H}^{(0)}|n\rangle = (\hat{H}_a + \hat{H}_b)|n_a\rangle \otimes |n_b\rangle \equiv (\hat{H}_a|n_a\rangle) \otimes |n_b\rangle + (\hat{H}_b|n_b\rangle) \otimes |n_a\rangle = (E_{na} + E_{nb})|n\rangle. \quad (6.144)$$

⁴³ It is straightforward to verify that the estimate (141) is valid for similar problems of any spatial dimensionality, not just for the 1D case we have analyzed.

⁴⁴ See, e.g., P. Delsing *et al.*, *Phys. Rev. Lett.* **63**, 1180 (1989).

In such composite systems, the relatively weak interaction of its components may be usually represented as a *bilinear* product of two Hermitian operators, each depending only on the degrees of freedom of one component system:

$$\hat{H}^{(1)} = \hat{A}(a)\hat{B}(b). \quad (6.145)$$

A very common example of such an interaction is the electric-dipole interaction between an atomic-scale system (with a linear size of the order of the Bohr radius $r_B \sim 10^{-10}$ m) and the electromagnetic field at optical frequencies $\omega \sim 10^{16}$ s⁻¹, with the wavelength $\lambda = 2\pi c/\omega \sim 10^{-6}$ m $>> r_B$:⁴⁵

$$\hat{H}^{(1)} = -\hat{\mathbf{d}} \cdot \hat{\mathcal{E}}, \quad \text{with } \hat{\mathbf{d}} \equiv \sum_k q_k \hat{\mathbf{r}}_k, \quad (6.146)$$

where the dipole electric moment \mathbf{d} depends only on the positions \mathbf{r}_k of the charged particles (numbered with index k) of the atomic system, while that of electric field \mathcal{E} is a function of only the electromagnetic field's degrees of freedom – to be discussed in Chapter 9 below.

Returning to the general situation shown in Fig. 12, if the component system a was initially in an excited state n'_a , the interaction (145), turned on at some moment of time, may bring it into another discrete state n_a of a lower energy – for example, the ground state. In the process of this transition, the released energy, in the form of an energy quantum

$$\hbar\omega \equiv E_{n'a} - E_{na}, \quad (6.147)$$

is picked up by the system b :

$$E_{nb} = E_{n'b} + \hbar\omega \equiv E_{n'b} + (E_{n'a} - E_{na}), \quad (6.148)$$

so that the total energy $E = E_a + E_b$ of the system does not change. (If the states n_a and n'_b are the ground states of the two component systems, as they are in most applications of this analysis, and we take the ground state energy $E_g = E_{na} + E_{n'b}$ of the composite system for the reference, then Eq. (148) gives merely $E_{nb} = E_{n'a}$.) If the final state n_b of the system b is inside a state group with a quasi-continuous energy spectrum (Fig. 12), the process has the exponential character (114)⁴⁶ and may be interpreted as the effect of *energy relaxation* of the system a , with the released energy quantum $\hbar\omega$ absorbed by the system b . Note that since the quasi-continuous spectrum essentially requires a system of large spatial size, such a model is very convenient for description of the *environment* b of the quantum system a . (In physics, the “environment” typically means all the Universe – less the system under consideration.)

If the relaxation rate Γ is sufficiently low, it may be described by the Golden Rule (137). Since the perturbation (145) does not depend on time explicitly, and the total energy E does not change, this relation, with the account of Eqs. (143) and (145), takes the form

$$\Gamma = \frac{2\pi}{\hbar} |A_{nn'}|^2 |B_{nn'}|^2 \rho_n, \quad \text{where } A_{nn'} \equiv \langle n_a | \hat{A} | n'_a \rangle, \quad \text{and } B_{nn'} = \langle n_b | \hat{B} | n'_b \rangle, \quad (6.149)$$

Golden
Rule
for coupled
systems

where ρ_n is the density of the final states of the system b at the relevant energy (147). In particular, Eq. (149), with the dipole Hamiltonian (146), enables a very straightforward calculation of the natural linewidth of atomic electric-dipole transitions. However, such calculation has to be postponed until Chapter 9, in which we will discuss the electromagnetic field quantization – i.e., the exact nature of the

⁴⁵ See, e.g., EM Sec. 3.1, in particular Eq. (3.16), in which letter \mathbf{p} is used for the electric dipole moment.

⁴⁶ Such process is *spontaneous*: it does not require any external agent, and starts as soon as either the interaction (145) has been turned on, or (if it is always on) as soon as the system a is placed into the excited state n'_a .

states n_b and $n_{\bar{b}}$ for this problem, and hence will be able to calculate $B_{nn'}$ and ρ_n . Instead, I will now proceed to a general discussion of the effects of quantum systems interaction with their environment, toward which the situation shown in Fig. 12 provides a clear conceptual path.

6.8. Exercise problems

6.1. Use Eq. (14) to prove the following general form of the Hellmann-Feynman theorem (whose proof in the wave-mechanics domain was the task of Problem 1.5):

$$\frac{\partial E_n}{\partial \lambda} = \left\langle n \left| \frac{\partial \hat{H}}{\partial \lambda} \right| n \right\rangle,$$

where λ is an arbitrary *c*-number parameter.

6.2. Establish a relation between Eq. (16) and the result of the classical theory of weakly anharmonic (“nonlinear”) oscillations at negligible damping.

Hint: You may like to use N. Bohr’s reasoning discussed in Problem 1.1.

6.3. A weak, time-independent force F is exerted on a 1D particle that was placed into a hard-wall potential well

$$U(x) = \begin{cases} 0, & \text{for } 0 < x < a, \\ +\infty, & \text{otherwise.} \end{cases}$$

Calculate, sketch, and discuss the 1st-order perturbation of its ground-state wavefunction.

6.4. A time-independent force $\mathbf{F} = \mu(\mathbf{n}_x y + \mathbf{n}_y x)$, where μ is a small constant, is applied to a 3D harmonic oscillator of mass m and frequency ω_0 , located at the origin. Calculate, in the first order of the perturbation theory, the effect of the force upon the ground state energy of the oscillator, and its lowest excited energy level. How small should the constant μ be for your results to be quantitatively correct?

6.5. A 1D particle of mass m is localized at a narrow potential well that may be approximated with a delta function:

$$U(x) = -w\delta(x), \quad \text{with } w > 0.$$

Calculate the change of its ground state energy by an additional weak, time-independent force F , in the first non-vanishing approximation of the perturbation theory. Discuss the limits of validity of this result, taking into account that at $F \neq 0$, the localized state of the particle is metastable.

6.6. Use the perturbation theory to calculate the eigenvalues of the operator \hat{L}^2 in the limit $|m| \approx l \gg 1$, by purely wave-mechanical means.

Hint: Try the following substitution: $\Theta(\theta) = f(\theta)/\sin^{1/2}\theta$.

6.7. In the lowest non-vanishing order of the perturbation theory, calculate the shift of the ground-state energy of an electrically charged spherical rotator (i.e. a particle of mass m , free to move over a spherical surface of radius R) due to a weak, uniform, time-independent electric field \mathcal{E} .

6.8. Use the perturbation theory to evaluate the effect of a time-independent, uniform electric field \mathcal{E} on the ground state energy E_g of a hydrogen atom. In particular:

- (i) calculate the 2nd-order shift of E_g , neglecting the extended unperturbed states with $E > 0$, and bring the result to the simplest analytical form you can,
- (ii) find the lower and the upper bounds on the shift, and
- (iii) discuss the simplest experimental manifestations of this *quadratic Stark effect*.

6.9. A particle of mass m , with electric charge q , is in its ground s -state with a given energy $E_g < 0$, being localized by a very short-range, spherically-symmetric potential well. Calculate its static electric polarizability α .

6.10. In some atoms, the charge-screening effect of other electrons on the motion of each of them may be reasonably well approximated by the replacement of the Coulomb potential (3.190), $U = -C/r$, with the so-called *Hulthén potential*

$$U = -\frac{C/a}{\exp\{r/a\}-1} \rightarrow -C \times \begin{cases} 1/r, & \text{for } r \ll a, \\ \exp\{-r/a\}/a, & \text{for } a \ll r. \end{cases}$$

Assuming that the effective screening radius a is much larger than $r_0 \equiv \hbar^2/mC$, use the perturbation theory to calculate the energy spectrum of a single particle of mass m , moving in this potential, in the lowest order needed to lift the l -degeneracy of the levels.

6.11. In the lowest non-vanishing order of the perturbation theory, calculate the correction to energies of the ground state and all lowest excited states of a hydrogen-like atom/ion, due to electron's penetration into its nucleus, modeling it as a spinless, uniformly charged sphere of radius $R \ll r_B/Z$.

6.12. Prove that the kinetic-relativistic correction operator (48) indeed has only diagonal matrix elements in the basis of unperturbed Bohr atom states (3.200).

6.13. Calculate the lowest-order relativistic correction to the ground-state energy of a 1D harmonic oscillator.

6.14. Use the perturbation theory to calculate the contribution to the magnetic susceptibility χ_m of a dilute gas, that is due to the orbital motion of a single electron inside each gas particle. Spell out your result for a spherically-symmetric ground state of the electron, and give an estimate of the magnitude of this *orbital susceptibility*.

6.15. How to calculate the energy level degeneracy lifting, by a time-independent perturbation, in the 2nd order of the perturbation in $\hat{H}^{(1)}$, assuming that it is not lifted in the 1st order? Carry out such calculation for a plane rotator of mass m and radius R , carrying electric charge q , and placed into a weak, uniform, constant electric field \mathcal{E} .

6.16.* The Hamiltonian of a quantum system is slowly changed in time.

- (i) Develop a theory of quantum transitions in the system, and spell out its result in the 1st order in the speed of the change.

- (ii) Use the 1st-order result to calculate the probability that a finite-time pulse of a slowly changing force $F(t)$ drives a 1D harmonic oscillator, initially in its ground state, into an excited state.
 (iii) Compare the last result with the exact one.

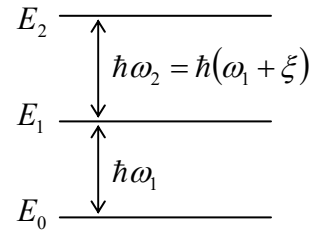
6.17. Use the single-particle model to calculate the complex electric permittivity $\alpha(\omega)$ of a dilute gas of similar atoms, due to their induced electric polarization by a weak external ac field, for a field frequency ω very close to one of quantum transition frequencies $\omega_{nn'}$. Based on the result, calculate and estimate the absorption cross-section of each atom.

Hint: In the single-particle model, atom's properties are determined by Z similar, non-interacting electrons, each moving in a similar static attracting potential, generally different from the Coulomb one, because it is contributed not only by the nucleus, but also by other electrons.

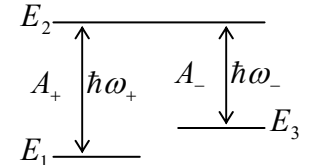
6.18. Use the solution of the previous problem to generalize the expression for the London dispersion force between two atoms (whose calculation in the harmonic-oscillator model was the subject of Problems 3.16 and 5.15) to the single-particle model with an arbitrary energy spectrum.

6.19. Use the solution of the previous problem to calculate the potential energy of interaction of two hydrogen atoms, both in their ground state, separated by distance $r \gg r_B$.

6.20. In a certain quantum system, distances between the three lowest energy levels are slightly different – see the figure on the right ($|\xi| \ll \omega_{1,2}$). Assuming that the involved matrix elements of the perturbation Hamiltonian are known, and are all proportional to the external ac field's amplitude, find the time necessary to populate the first excited level almost completely (with a given precision $\varepsilon \ll 1$), using the Rabi oscillation effect, if at $t = 0$ the system is completely in its ground state.



6.21.* Analyze the possibility of a slow transfer of a system from one of its energy levels to another one (in the figure on the right, from level 1 to level 3), using the scheme shown in that figure, in which the monochromatic external excitation amplitudes A_+ and A_- may be slowly changed at will.



6.22. A weak external force pulse $F(t)$, of a finite time duration, is applied to a 1D harmonic oscillator that initially was in its ground state.

- (i) Calculate, in the lowest non-vanishing order of the perturbation theory, the probability that the pulse drives the oscillator into its lowest excited state.
- (ii) Compare the result with the exact solution of the problem.
- (iii) Spell out the perturbative result for a Gaussian-shaped waveform,

$$F(t) = F_0 \exp\left\{-t^2 / \tau^2\right\},$$

and analyze its dependence on the scale τ of the pulse duration.

6.23. A spatially-uniform, but time-dependent external electric field $\mathcal{E}(t)$ is applied, starting from $t = 0$, to a charged plane rotator, initially in its ground state.

(i) Calculate, in the lowest non-vanishing order in the field's strength, the probability that by time $t > 0$, the rotator is in its n^{th} excited state.

(ii) Spell out and analyze your results for a constant-magnitude field rotating, with a constant angular velocity ω , within the rotator's plane.

(iii) Do the same for a monochromatic field of frequency ω , with a fixed polarization.

6.24. A spin- $\frac{1}{2}$ with a gyromagnetic ratio γ is placed into a magnetic field including a time-independent component \mathcal{B}_0 , and a perpendicular field of a constant magnitude \mathcal{B}_r , rotated with a constant angular velocity ω . Can this *magnetic resonance* problem be reduced to one already discussed in Chapter 6?

6.25. Develop general theory of quantum excitations of the higher levels of a discrete-spectrum system, initially in the ground state, by a weak time-dependent perturbation, up to the 2nd order. Spell out and discuss the result for the case of monochromatic excitation, with a nearly perfect tuning of its frequency ω to *the half* of a certain quantum transition frequency $\omega_{n0} \equiv (E_n - E_0)/\hbar$.

6.26. A heavy, relativistic particle, with electric charge $q = Ze$, passes by a hydrogen atom, initially in its ground state, with an impact parameter b within the range $r_B \ll b \ll r_B/\alpha$, where $\alpha \approx 1/137$ is the fine structure constant. Calculate the probabilities of the atom's transition to its lowest excited states.

6.27. A particle of mass m is initially in the localized ground state, with energy $E_g < 0$, of a very small, spherically-symmetric potential well. Calculate the rate of its delocalization by an applied classical force $\mathbf{F}(t) = \mathbf{n}F_0\cos\omega t$ with a time-independent direction \mathbf{n} .

6.28.* Calculate the rate of ionization of a hydrogen atom, initially in its ground state, by a classical, linearly polarized electromagnetic wave with an electric field's amplitude \mathcal{E}_0 , and a frequency ω within the range

$$\hbar/m_e r_B^2 \ll \omega \ll c/r_B,$$

where r_B is the Bohr radius. Recast your result in terms of the cross-section of electromagnetic wave absorption. Discuss briefly what changes of the theory would be necessary if either of the above conditions had been violated.

6.29.* Use the quantum-mechanical Golden Rule to derive the general expression for the electric current I through a weak tunnel junction between two conductors, biased with dc voltage V , treating the conductors as degenerate Fermi gases of electrons with negligible direct interaction. Simplify the result in the low-voltage limit.

Hint: The electric current flowing through a weak tunnel junction is so low that it does not substantially perturb the electron states inside each conductor.

6.30.* Generalize the result of the previous problem to the case when a weak tunnel junction is biased with voltage $V(t) = V_0 + A\cos\omega t$, with $\hbar\omega$ generally comparable with eV_0 and eA .

6.31.* Use the quantum-mechanical Golden Rule to derive the Landau-Zener formula (2.257).

Chapter 7. Open Quantum Systems

This chapter discusses the effects of a weak interaction of a quantum system with its environment. Some part of this material is on the fine line between quantum mechanics and (quantum) statistical physics. Here I will only cover those aspects of the latter field¹ that are of key importance for the major goals of this course, including the discussion of quantum measurements in Chapter 10.

7.1. Open systems, and the density matrix

All the way until the last part of the previous chapter, we have discussed quantum systems isolated from their environment. Indeed, from the very beginning, we have assumed that we are dealing with the statistical ensembles of systems as similar to each other as only allowed by the laws of quantum mechanics. Each member of such an ensemble, called *pure* or *coherent*, may be described by the same state vector $|\alpha\rangle$ – in the wave mechanics case, by the same wavefunction Ψ_α . Even the discussion at the end of the last chapter, in which one component system (in Fig. 6.13, system *b*) may be used as a model of the environment of its counterpart (system *a*), was still based on the assumption of a pure initial state (6.143) of the composite system. If the interaction of the two components of such a system is described by a certain Hamiltonian (the one given by Eq. (6.145) for example), and the energy spectrum of each component system is discrete, for state α of the composite system at an arbitrary instant we may write

$$|\alpha\rangle = \sum_n \alpha_n |n\rangle = \sum_n \alpha_n |n_a\rangle \otimes |n_b\rangle, \quad (7.1)$$

with a *unique* correspondence between the eigenstates n_a and n_b .

However, in many important cases, our knowledge of a quantum system's state is even less complete.² These cases fall into two categories. The first case is when a relatively simple quantum system *s* of our interest (say, an electron or an atom) is in a weak³ but substantial contact with its environment *e* – here understood in the most general sense, say, as all the whole Universe less system *s* – see Fig. 1. Then there is virtually no chance of making two or more experiments with exactly the same composite system because that would imply a repeated preparation of the whole environment (including the experimenter :-) in a certain quantum state – a rather challenging task, to put it mildly. Then it makes much more sense to consider a statistical ensemble of another kind – a *mixed ensemble*, with *random* states of the environment, though possibly with its macroscopic parameters (e.g., temperature, pressure, etc.) known with high precision. Such ensembles will be the focus of the analysis in this chapter.

Much of this analysis will pertain also to another category of cases – when the system of our interest is isolated from its environment, at present, with acceptable precision, but our knowledge of its state is still incomplete for some other reason. Most typically, the system could be in contact with its

¹ A broader discussion of statistical mechanics and physical kinetics, including those of quantum systems, may be found in the SM part of this series.

² Indeed, a system, possibly apart from our Universe as a whole (who knows? – see below), is never *exactly* coherent, though in many cases, such as the ones discussed in the previous chapters, deviations from the coherence may be ignored with *acceptable accuracy*.

³ If the interaction between a system and its environment is very strong, their very partition is impossible.

environment at earlier times, and its reduction to a pure state is impracticable. So, this second category of cases may be considered as a particular case of the first one, and may be described by the results of its analysis, with certain simplifications – which will be spelled out in appropriate places of my narrative.

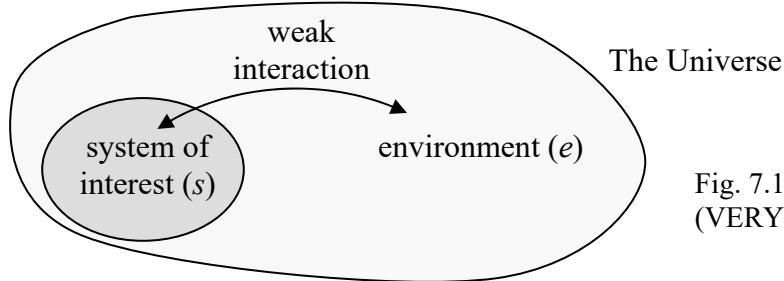


Fig. 7.1. A quantum system and its environment (VERY schematically :-).

In classical physics, the analysis of mixed statistical ensembles is based on the notion of the probability W (or the probability density w) of each detailed (“microscopic”) state of the system of interest.⁴ Let us see how such an ensemble may be described in quantum mechanics. In the case when the coupling between the system of our interest and its environment is so weak that they may be clearly separated, we can still use state vectors of their states, defined in completely different Hilbert spaces. Then the most general quantum state of the whole Universe, still assumed to be pure,⁵ may be described as the following linear superposition:

$$|\alpha\rangle = \sum_{j,k} \alpha_{jk} |s_j\rangle \otimes |e_k\rangle. \quad (7.2)$$

Universe:
quantum
state

The “only” difference of such a state from the superposition described by Eq. (1), is that there is no one-to-one correspondence between the states of our system and its environment. In other words, a certain quantum state s_j of the system of interest may coexist with different states e_k of its environment. This is exactly the quantum-mechanical description of a *mixed state* of the system s .

Of course, the huge size of the Hilbert space of the environment, i.e. of the number of the $|e_k\rangle$ factors in the superposition (2), strips us of any practical opportunity to make direct calculations using that sum. For example, according to the basic Eq. (4.125), to find the expectation value of an arbitrary observable A in the state (2), we would need to calculate the long bracket

$$\langle A \rangle = \langle \alpha | \hat{A} | \alpha \rangle \equiv \sum_{j,j';k,k'} \alpha_{jk}^* \alpha_{j'k'} \langle e_k | \otimes \langle s_j | \hat{A} | s_{j'} \rangle \otimes | e_{k'} \rangle. \quad (7.3)$$

Even if we assume that each of the sets $\{s\}$ and $\{e\}$ is full and orthonormal, Eq. (3) still includes a double sum over the enormous basis state set of the environment!

However, let us consider a limited, but the most important subset of operators – those of *intrinsic* observables, which depend only on the degrees of freedom of the system of our interest (s). These operators do not act upon the environment’s degrees of freedom, and hence in Eq. (3), we may move the environment’s bra-vectors $\langle e_k |$ over all the way to the ket-vectors $| e_k \rangle$. Assuming, again, that the set of environmental eigenstates is full and orthonormal, Eq. (3) is now reduced to

⁴ See, e.g., SM Sec. 2.1.

⁵ Whether this assumption is true is an interesting issue, still being debated (more by philosophers than by physicists), but it is widely believed that its solution is not critical for the validity of the results of this approach.

$$\langle A \rangle = \sum_{j,j';k,k'} \alpha_{jk}^* \alpha_{j'k'} \langle s_j | \hat{A} | s_{j'} \rangle \langle e_k | e_{k'} \rangle = \sum_{jj'} A_{jj'} \sum_k \alpha_{jk}^* \alpha_{j'k}. \quad (7.4)$$

This is already a big relief because we have “only” a single sum over k , but the main trick is still ahead. After the summation over k , the second sum in the last form of Eq. (4) is some function w of the indices j and j' , so that, according to Eq. (4.96), this relation may be represented as

$$\langle A \rangle = \sum_{jj'} A_{jj'} w_{j'j} \equiv \text{Tr}(Aw), \quad (7.5)$$

where the matrix w , with the elements

$$w_{jj'} \equiv \sum_k \alpha_{jk}^* \alpha_{j'k}, \quad \text{i.e. } w_{jj'} \equiv \sum_k \alpha_{jk} \alpha_{j'k}^*, \quad (7.6)$$

is called the *density matrix* of the system.⁶ Most importantly, Eq. (5) shows that the knowledge of this matrix allows the calculation of the expectation value of *any* intrinsic observable A (and, according to the general Eqs. (1.33)-(1.34), its r.m.s. fluctuation as well, if needed), even for the very general state (2). This is why let us have a good look at the density matrix.

First of all, we know from the general discussion in Chapter 4, fully applicable to the pure state (2), the expansion coefficients in superpositions of this type may be always expressed as short brackets of the type (4.40); in our current case, we may write

$$\alpha_{jk} = (\langle e_k | \otimes \langle s_j |) |\alpha\rangle. \quad (7.7)$$

Plugging this expression into Eq. (6), we get

$$w_{jj'} \equiv \sum_k \alpha_{jk} \alpha_{j'k}^* = \langle s_j | \otimes \left(\sum_k \langle e_k | \alpha \rangle \langle \alpha | e_k \rangle \right) \otimes |s_{j'} \rangle = \langle s_j | \hat{w} | s_{j'} \rangle. \quad (7.8)$$

We see that from the point of our system (i.e. in its Hilbert space whose basis states may be numbered by the index j only), the density matrix is indeed just the matrix of some construct,⁷

$$\hat{w} \equiv \sum_k \langle e_k | \alpha \rangle \langle \alpha | e_k \rangle, \quad (7.9)$$

which is called the *density* (or “statistical”) *operator*. As it follows from the definition (9), in contrast to the density matrix this operator does not depend on the choice of a particular basis s_j – just as all linear operators considered earlier in this course. However, in contrast to them, the density operator *does* depend on the composite system’s state α , including the state of the system s as well. Still, in the j -space it is mathematically just an operator whose matrix elements obey all relations of the bra-ket formalism.

In particular, due to its definition (6), the density operator is Hermitian:

$$w_{jj'}^* = \sum_k \alpha_{jk}^* \alpha_{j'k} = \sum_k \alpha_{j'k} \alpha_{jk}^* = w_{j'j}, \quad (7.10)$$

⁶ This notion was suggested in 1927 by John von Neumann.

⁷ Note that the “short brackets” in this expression are not *c*-numbers, because the state α is defined in a larger Hilbert space (of the environment plus the system of interest) than the basis states e_k (of the environment only).

so that according to the general analysis of Sec. 4.3, in the Hilbert space of the system s , there should be a certain basis $\{w\}$ in that the matrix of this operator is diagonal:

$$w_{jj'}|_{in w} = w_j \delta_{jj'}. \quad (7.11)$$

Since any operator, in any basis, may be represented in the form (4.59), in the basis $\{w\}$ we may write

$$\hat{w} = \sum_j |w_j\rangle w_j \langle w_j|. \quad (7.12)$$

Statistical operator in w -basis

This expression reminds, but is not equivalent to Eq. (4.44) for the identity operator, that has been used so many times in this course, and in the basis w_j has the form

$$\hat{I} = \sum_j |w_j\rangle \langle w_j|. \quad (7.13)$$

In order to comprehend the meaning of the coefficients w_j participating in Eq. (12), let us use Eq. (5) to calculate the expectation value of any observable A whose eigenstates coincide with those of the special basis $\{w\}$, and whose matrix is, therefore, diagonal in this basis:

$$\langle A \rangle = \text{Tr}(Aw) = \sum_{jj'} A_{jj'} w_j \delta_{jj'} = \sum_j A_j w_j, \quad (7.14)$$

Expectation value of w_j -compatible variable

where A_j is just the expectation value of the observable A in the state w_j . Hence, to comply with the general Eq. (1.37), the real c -number w_j must have the physical sense of the probability W_j of finding the system in the state j . As the result, we may rewrite Eq. (12) in the form

$$\hat{w} = \sum_j |w_j\rangle W_j \langle w_j|. \quad (7.15)$$

In the ultimate case when only one of the probabilities (say, $W_{j''}$) is different from zero,

$$W_j = \delta_{jj''}, \quad (7.16)$$

the system is in a coherent (pure) state $w_{j''}$. Indeed, it is fully described by one ket-vector $|w_{j''}\rangle$, and we can use the general rule (4.86) to represent it in another (arbitrary) basis $\{s\}$ as a coherent superposition

$$|w_{j''}\rangle = \sum_{j'} U_{j''j'}^\dagger |s_{j'}\rangle = \sum_{j'} U_{j''j'}^* |s_{j'}\rangle, \quad (7.17)$$

where U is the unitary matrix of transform from the basis $\{w\}$ to the basis $\{s\}$. According to Eqs. (11) and (16), in such a pure state the density matrix is diagonal in the $\{w\}$ basis,

$$w_{jj'}|_{in w} = \delta_{j,j''} \delta_{j',j''}, \quad (7.18a)$$

but not in an arbitrary basis. Indeed, using the general rule (4.92), we get

$$w_{jj'}|_{in s} = \sum_{l,l'} U_{jl}^\dagger w_{ll'}|_{in w} U_{l'j'} = U_{jj''}^\dagger U_{j''j'} = U_{jj''}^* U_{j''j'}, \quad (7.18b)$$

To make this result more transparent, let us denote the matrix elements $U_{j''j} \equiv \langle w_{j''}|s_j\rangle$ (which, for a fixed j'' , depend on just one index j) by α_j ; then

$$w_{jj'}|_{in s} = \alpha_j^* \alpha_{j'}, \quad (7.19)$$

Density matrix: pure state

so that N^2 elements of the whole $N \times N$ matrix is determined by just *one* string of N *c-numbers* α_j . For example, for a two-level system ($N = 2$),

$$\mathbf{w}|_{\text{in } s} = \begin{pmatrix} \alpha_1 \alpha_1^* & \alpha_2 \alpha_1^* \\ \alpha_1 \alpha_2^* & \alpha_2 \alpha_2^* \end{pmatrix}. \quad (7.20)$$

We see that the off-diagonal terms are, colloquially, “as large as the diagonal ones”, in the following sense:

$$w_{12} w_{21} = w_{11} w_{22}. \quad (7.21)$$

Since the diagonal terms have the sense of the probabilities $W_{1,2}$ to find the system in the corresponding state, we may represent Eq. (20) in the form

$$\mathbf{w}|_{\text{pure state}} = \begin{pmatrix} W_1 & (W_1 W_2)^{1/2} e^{i\varphi} \\ (W_1 W_2)^{1/2} e^{-i\varphi} & W_2 \end{pmatrix}. \quad (7.22)$$

The physical sense of the (real) constant φ is the phase shift between the coefficients in the linear superposition (17), which represents the pure state w_j in the basis $\{s_{1,2}\}$.

Now let us consider a different statistical ensemble of two-level systems, that includes the member states identical in all aspects (including similar probabilities $W_{1,2}$ in the same basis $s_{1,2}$), besides that the phase shifts φ are random, with the phase probability uniformly distributed over the trigonometric circle. Then the ensemble averaging is equivalent to the averaging over φ from 0 to 2π ,⁸ which kills the off-diagonal terms of the density matrix (22), so that the matrix becomes diagonal:

$$\mathbf{w}|_{\text{classical mixture}} = \begin{pmatrix} W_1 & 0 \\ 0 & W_2 \end{pmatrix}. \quad (7.23)$$

The mixed statistical ensemble with the density matrix diagonal in the stationary state basis is called the *classical mixture* and represents the limit opposite to the pure (coherent) state.

After this example, the reader should not be much shocked by the main claim⁹ of statistical mechanics that any large ensemble of similar systems in *thermodynamic* (or “thermal”) *equilibrium* is exactly such a *classical mixture*. Moreover, for systems in the thermal equilibrium with a much larger environment of a fixed temperature T (such an environment is usually called a *heat bath*) the statistical physics gives a very simple expression, called the *Gibbs distribution*, for the probabilities W_n :¹⁰

$$W_n = \frac{1}{Z} \exp\left\{-\frac{E_n}{k_B T}\right\}, \quad \text{with } Z \equiv \sum_n \exp\left\{-\frac{E_n}{k_B T}\right\}. \quad (7.24)$$

⁸ For a system with a time-independent Hamiltonian, such averaging is especially plausible in the basis of the stationary states n of the system, in which the phase φ is just the difference of integration constants in Eq. (4.158), and its randomness may be naturally produced by minor fluctuations of the energy difference $E_1 - E_2$. In Sec. 3 below, we will study the dynamics of this *dephasing* process.

⁹ This fact follows from the basic postulate of statistical physics, called the *microcanonical distribution* – see, e.g., SM Sec. 2.2.

¹⁰ See, e.g., SM Sec. 2.4. The Boltzmann constant k_B is only needed if the temperature is measured in non-energy units – say in kelvins.

where E_n is the eigenenergy of the corresponding stationary state, and the normalization coefficient Z is called the *statistical sum*.

A detailed analysis of classical and quantum ensembles in thermodynamic equilibrium is a major focus of statistical physics courses (such as the SM of this series) rather than this course of quantum mechanics. However, I would still like to attract the reader's attention to the key fact that, in contrast with the similarly-looking Boltzmann distribution for single particles,¹¹ the Gibbs distribution is *general, not limited to classical statistics*. In particular, for a quantum gas of indistinguishable particles, it is absolutely compatible with the quantum statistics (such as the Bose-Einstein or Fermi-Dirac distributions) of the component particles. For example, if we use Eq. (24) to calculate the average energy of a 1D harmonic oscillator of frequency ω_0 in thermal equilibrium, we easily get¹²

$$W_n = \exp\left\{-n \frac{\hbar\omega_0}{k_B T}\right\} \left(1 - \exp\left\{-\frac{\hbar\omega_0}{k_B T}\right\}\right), \quad Z = \exp\left\{-\frac{\hbar\omega_0}{2k_B T}\right\} / \left(1 - \exp\left\{-\frac{\hbar\omega_0}{k_B T}\right\}\right). \quad (7.25)$$

$$\langle E \rangle \equiv \sum_{n=0}^{\infty} W_n E_n = \frac{\hbar\omega_0}{2} \coth \frac{\hbar\omega_0}{2k_B T} \equiv \frac{\hbar\omega_0}{2} + \frac{\hbar\omega_0}{\exp\{\hbar\omega_0/k_B T\} - 1}. \quad (7.26a)$$

The final form of the last result,

$$\langle E \rangle = \frac{\hbar\omega_0}{2} + \hbar\omega_0 \langle n \rangle, \quad \text{with } \langle n \rangle = \frac{1}{\exp\{\hbar\omega_0/k_B T\} - 1} \rightarrow \begin{cases} 0, & \text{for } k_B T \ll \hbar\omega_0, \\ k_B T / \hbar\omega_0, & \text{for } \hbar\omega_0 \ll k_B T, \end{cases} \quad (7.26b)$$

may be interpreted as an addition, to the ground-state energy $\hbar\omega_0/2$, of the average number $\langle n \rangle$ of thermally-induced excitations, with the energy $\hbar\omega_0$ each. In the harmonic oscillator, whose energy levels are equidistant, such a language is completely appropriate, because the transfer of the system from any level to the one just above it adds the same amount of energy, $\hbar\omega_0$. Note that the above expression for $\langle n \rangle$ is actually the Bose-Einstein distribution (for the particular case of zero chemical potential); we see that it does not contradict the Gibbs distribution (24) of the total energy of the system, but rather immediately follows from it.

Because of the fundamental importance of Eq. (26) for virtually all fields of physics, let me draw the reader's attention to its main properties. At low temperatures, $k_B T \ll \hbar\omega_0$, there are virtually no excitations, $\langle n \rangle \rightarrow 0$, and the average energy of the oscillator is dominated by that of its ground state. In the opposite limit of high temperatures, $\langle n \rangle \rightarrow k_B T / \hbar\omega_0 \gg 1$, and $\langle E \rangle$ approaches the classical value $k_B T$.

7.2. Coordinate representation, and the Wigner function

For many applications of the density operator, its coordinate representation is convenient. (I will only discuss it for the 1D case; the generalization to multi-dimensional cases is straightforward.) Following Eq. (4.47), it is natural to define the following function of two arguments (traditionally, also called the *density matrix*):

¹¹ See, e.g., SM Sec. 2.8.

¹² See, e.g., SM Sec. 2.5 – but mind a different energy reference level, $E_0 = \hbar\omega_0/2$, used for example in SM Eqs. (2.68)-(2.69), affecting the expression for Z . Actually, the calculation, using Eqs. (24) and (5.86), is so straightforward that it is highly recommended to the reader as a simple exercise.

$$w(x, x') \equiv \langle x | \hat{w} | x' \rangle. \quad (7.27)$$

Inserting, into the right-hand side of this definition, two closure conditions (4.44) for an arbitrary (but full and orthonormal) basis $\{s\}$, and then using Eq. (4.233),¹³ we get

$$w(x, x') = \sum_{j, j'} \langle x | s_j \rangle \langle s_j | \hat{w} | s_{j'} \rangle \langle s_{j'} | x' \rangle = \sum_{j, j'} \psi_j(x) w_{jj'}|_{in_s} \psi_{j'}^*(x'). \quad (7.28)$$

In the special basis $\{w\}$, in which the density matrix is diagonal, this expression is reduced to

$$w(x, x') = \sum_j \psi_j(x) W_j \psi_j^*(x'). \quad (7.29)$$

Let us discuss the properties of this function. At coinciding arguments, $x' = x$, this is just the probability density:¹⁴

$$w(x, x) = \sum_j \psi_j(x) W_j \psi_j^*(x) = \sum_j w_j(x) W_j = w(x). \quad (7.30)$$

However, the density matrix gives more information about the system than just the probability density. As the simplest example, let us consider a pure quantum state, with $W_j = \delta_{jj'}$, so that $\psi(x) = \psi_j(x)$, and

$$w(x, x') = \psi_{j'}(x) \psi_{j'}^*(x') \equiv \psi(x) \psi^*(x'). \quad (7.31)$$

We see that the density matrix carries the information not only about the modulus but also the phase of the wavefunction. (Of course one may argue rather convincingly that in this ultimate limit the density-matrix description is redundant because all this information is contained in the wavefunction itself.)

How may be the density matrix interpreted? In the simple case (31), we can write

$$|w(x, x')|^2 \equiv w(x, x') w^*(x, x') = \psi(x) \psi^*(x) \psi(x') \psi^*(x') = w(x) w(x'), \quad (7.32)$$

so that the modulus squared of the density matrix is just as the joint probability density to find the system at the point x and the point x' . For example, for a simple wave packet with a spatial extent δx , $w(x, x')$ has an appreciable magnitude only if both points are not farther than $\sim \delta x$ from the packet center, and hence from each other. The interpretation becomes more complex if we deal with an incoherent mixture of several wavefunctions, for example, the classical mixture describing the thermodynamic equilibrium. In this case, we can use Eq. (24) to rewrite Eq. (29) as follows:

$$w(x, x') = \sum_n \psi_n(x) W_n \psi_n^*(x') = \frac{1}{Z} \sum_n \psi_n(x) \exp\left\{-\frac{E_n}{k_B T}\right\} \psi_n^*(x'). \quad (7.33)$$

As the simplest example, let us see what is the density matrix of a *free* (1D) particle in the thermal equilibrium. As we know very well by now, in this case, the set of energies $E_p = p^2/2m$ of stationary states (monochromatic waves) forms a continuum, so that we need to replace the sum (33) with an integral, using for example the “delta-normalized” traveling-wave eigenfunctions (4.264):

¹³ For now, I will focus on a fixed time instant (say, $t = 0$), and hence write $\psi(x)$ instead of $\Psi(x, t)$.

¹⁴ This fact is the origin of the density matrix’s name.

$$w(x, x') = \frac{1}{2\pi\hbar Z} \int_{-\infty}^{+\infty} \exp\left\{-\frac{ipx}{\hbar}\right\} \exp\left\{-\frac{p^2}{2mk_B T}\right\} \exp\left\{\frac{ipx'}{\hbar}\right\} dp. \quad (7.34)$$

This is a usual Gaussian integral, and may be worked out, as we have done repeatedly in Chapter 2 and beyond, by complementing the exponent to the full square of the momentum p plus a constant. The statistical sum Z may be also readily calculated,¹⁵

$$Z = (2\pi m k_B T)^{1/2}, \quad (7.35)$$

However, for what follows it is more useful to write the result for the product wZ (the so-called *un-normalized density matrix*):

$$w(x, x')Z = \left(\frac{mk_B T}{2\pi\hbar^2}\right)^{1/2} \exp\left\{-\frac{mk_B T(x - x')^2}{2\hbar^2}\right\}. \quad (7.36)$$

Free
particle:
thermal
equilibrium

This is a very interesting result: the density matrix depends only on the difference of its arguments, dropping to zero fast as the distance between the points x and x' exceeds the following characteristic scale (called the *correlation length*)

$$x_c \equiv \langle (x - x')^2 \rangle^{1/2} = \frac{\hbar}{(mk_B T)^{1/2}}. \quad (7.37)$$

Correlation
length

This length may be interpreted in the following way. It is straightforward to use Eq. (24) to verify that the average energy $\langle E \rangle = \langle p^2/2m \rangle$ of a free particle in the thermal equilibrium, i.e. in the classical mixture (33), equals $k_B T/2$. Hence the average magnitude of the particle's momentum may be estimated as

$$p_c \equiv \langle p^2 \rangle^{1/2} = (2m\langle E \rangle)^{1/2} = (mk_B T)^{1/2}, \quad (7.38)$$

so that x_c is of the order of the minimal length allowed by the Heisenberg-like “uncertainty relation”:

$$x_c = \hbar / p_c. \quad (7.39)$$

Note that with the growth of temperature, the correlation length (37) goes to zero, and the density matrix (36) tends to a delta function:

$$w(x, x')Z \Big|_{T \rightarrow \infty} \rightarrow \delta(x - x'). \quad (7.40)$$

Since in this limit the average kinetic energy of the particle is not smaller than its potential energy in *any* fixed potential profile, Eq. (40) is the general property of the density matrix (33).

Let us discuss the following curious feature of Eq. (36): if we replace $k_B T$ with $\hbar/i(t - t_0)$, and x' with x_0 , the un-normalized density matrix wZ for a free particle turns into the particle's propagator – cf. Eq. (2.49). This is not just an occasional coincidence. Indeed, in Chapter 2 we saw that the propagator of a system with an arbitrary stationary Hamiltonian may be expressed via the stationary eigenfunctions as

¹⁵ Due to the delta-normalization of the eigenfunction, the density matrix (34) for the free particle (and any system with a continuous eigenvalue spectrum) is normalized as

$$\int_{-\infty}^{+\infty} w(x, x')Z dx' = \int_{-\infty}^{+\infty} w(x, x')Z dx = 1.$$

$$G(x, t; x_0, t_0) = \sum_n \psi_n(x) \exp\left\{-i \frac{E_n}{\hbar}(t - t_0)\right\} \psi_n^*(x_0). \quad (7.41)$$

Comparing this expression with Eq. (33), we see that the replacements

$$\frac{i(t - t_0)}{\hbar} \rightarrow \frac{1}{k_B T}, \quad x_0 \rightarrow x', \quad (7.42)$$

turn the pure-state propagator G into the un-normalized density matrix wZ of the same system in thermodynamic equilibrium. This important fact, rooted in the formal similarity of the Gibbs distribution (24) with the Schrödinger equation's solution (1.69), enables a theoretical technique of the so-called *thermodynamic Green's functions*, which is especially productive in condensed matter physics.¹⁶

For our current purposes, we can employ Eq. (42) to re-use some of the wave mechanics results, in particular, the following formula for the harmonic oscillator's propagator

$$G(x, t; x_0, t_0) = \left(\frac{m\omega_0}{2\pi i \hbar \sin[\omega_0(t - t_0)]} \right)^{1/2} \exp\left\{ -\frac{m\omega_0[(x^2 + x_0^2)\cos[\omega_0(t - t_0)] - 2xx_0]}{2i\hbar \sin[\omega_0(t - t_0)]} \right\}. \quad (7.43)$$

which may be readily proved to satisfy the Schrödinger equation for the Hamiltonian (5.62), with the appropriate initial condition: $G(x, t_0; x_0, t_0) = \delta(x - x_0)$. Making the substitution (42), we immediately get

Harmonic oscillator in thermal equilibrium

$$w(x, x')Z = \left[\frac{m\omega_0}{2\pi i \hbar \sinh(\hbar\omega_0/k_B T)} \right]^{1/2} \exp\left\{ -\frac{m\omega_0[(x^2 + x'^2)\cosh(\hbar\omega_0/k_B T) - 2xx']}{2\hbar \sinh(\hbar\omega_0/k_B T)} \right\}. \quad (7.44)$$

As a sanity check, at very low temperatures, $k_B T \ll \hbar\omega_0$, both hyperbolic functions participating in this expression are very large and nearly equal, and it yields

$$w(x, x')Z|_{T \rightarrow 0} \rightarrow \left[\left(\frac{m\omega_0}{\pi\hbar} \right)^{1/4} \exp\left\{ -\frac{m\omega_0 x^2}{\hbar} \right\} \right] \times \exp\left\{ -\frac{\hbar\omega_0}{2k_B T} \right\} \times \left[\left(\frac{m\omega_0}{\pi\hbar} \right)^{1/4} \exp\left\{ -\frac{m\omega_0 x'^2}{\hbar} \right\} \right]. \quad (7.45)$$

In each of the expressions in square brackets we can readily recognize the ground state's wavefunction (2.275) of the oscillator, while the middle exponent is just the statistical sum (24) in the low-temperature limit when it is dominated by the ground-level contribution:

$$Z|_{T \rightarrow 0} \rightarrow \exp\left\{ -\frac{\hbar\omega_0}{2k_B T} \right\}. \quad (7.46)$$

As a result, Z in both parts of Eq. (45) may be canceled, and the density matrix in this limit is described by Eq. (31), with the ground state as the only state of the system. This is natural when the temperature is too low for the thermal excitation of any other state.

¹⁶ I will have no time to discuss this technique and have to refer the interested reader to special literature. Probably, the most famous text of that field is A. Abrikosov, L. Gor'kov, and I. Dzyaloshinski, *Methods of Quantum Field Theory in Statistical Physics*, Prentice-Hall, 1963. (Later reprintings are available from Dover.)

Returning to arbitrary temperatures, Eq. (44) in coinciding arguments gives the following expression for the probability density:¹⁷

$$w(x, x)Z \equiv w(x)Z = \left[\frac{m\omega_0}{2\pi\hbar \sinh(\hbar\omega_0/k_B T)} \right]^{1/2} \exp\left\{ -\frac{m\omega_0 x^2}{\hbar} \tanh \frac{\hbar\omega_0}{2k_B T} \right\}. \quad (7.47)$$

This is just a Gaussian function of x , with the following variance:

$$\langle x^2 \rangle = \frac{\hbar}{2m\omega_0} \coth \frac{\hbar\omega_0}{2k_B T}. \quad (7.48)$$

To compare this result with our earlier ones, it is useful to recast it as

$$\langle U \rangle = \frac{m\omega_0^2}{2} \langle x^2 \rangle = \frac{\hbar\omega_0}{4} \coth \frac{\hbar\omega_0}{2k_B T}. \quad (7.49)$$

Comparing this expression with Eq. (26), we see that the average value of potential energy is exactly one-half of the total energy – the other half being the average kinetic energy. This is what we could expect, because according to Eqs. (5.96)-(5.97), such relation holds for each Fock state and hence should also hold for their classical mixture.

Unfortunately, besides the trivial case (30) of coinciding arguments, it is hard to give a straightforward interpretation of the density function in terms of the system's measurements. This is a fundamental difficulty, which has been well explored in terms of the *Wigner function* (sometimes called the “Wigner-Ville distribution”)¹⁸ defined as

$$W(X, P) \equiv \frac{1}{2\pi\hbar} \int w\left(X + \frac{\tilde{X}}{2}, X - \frac{\tilde{X}}{2}\right) \exp\left\{-\frac{iP\tilde{X}}{\hbar}\right\} d\tilde{X}. \quad (7.50)$$

[Wigner function: definition](#)

From the mathematical standpoint, this is just the Fourier transform of the density matrix in one of two new coordinates defined by the following relations (see Fig. 2):

$$X \equiv \frac{x+x'}{2}, \quad \tilde{X} \equiv x-x', \quad \text{so that } x \equiv X + \frac{\tilde{X}}{2}, \quad x' \equiv X - \frac{\tilde{X}}{2}. \quad (7.51)$$

Physically, the new argument X may be interpreted as the average position of the particle during the time interval $(t-t')$, while \tilde{X} , as the distance passed by it during that time interval, so that P characterizes the momentum of the particle during that motion. As a result, the Wigner function is a mathematical construct intended to characterize the system's probability distribution simultaneously in the coordinate and the momentum space – for 1D systems, on the phase plane $[X, P]$, which we had discussed earlier – see Fig. 5.8. Let us see how fruitful this intention is.

¹⁷ I have to confess that this notation is imperfect, because strictly speaking, $w(x, x')$ and $w(x)$ are different functions, and so are the functions $w(p, p')$ and $w(p)$ used below. In the perfect world, I would use different letters for them all, but I desperately want to stay with “ w ” for all the probability densities, and there are not so many good fonts for this letter. Let me hope that the difference between these functions is clear from their arguments and the context.

¹⁸ It was introduced in 1932 by Eugene Wigner on the basis of a general (*Weyl-Wigner*) transform suggested by Hermann Weyl in 1927 and re-derived in 1948 by Jean Ville on a different mathematical basis.

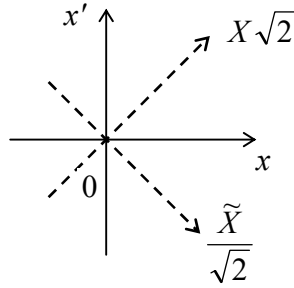


Fig. 7.2. The coordinates X and \tilde{X} employed in the Weyl-Wigner transform (50). They differ from the coordinates obtained by the rotation of the reference frame by the angle $\pi/4$ only by factors $\sqrt{2}$ and $1/\sqrt{2}$, describing scale stretch.

First of all, we may write the Fourier transform reciprocal to Eq. (50):

$$w\left(X + \frac{\tilde{X}}{2}, X - \frac{\tilde{X}}{2}\right) = \int W(X, P) \exp\left\{\frac{iP\tilde{X}}{\hbar}\right\} dP. \quad (7.52)$$

For the particular case $\tilde{X} = 0$, this relation yields

$$w(X) \equiv w(X, X) = \int W(X, P) dP. \quad (7.53)$$

Hence the integral of the Wigner function over the momentum P gives the probability density to find the system at point X – just as it does for a classical distribution function $w_{\text{cl}}(X, P)$.¹⁹

Next, the Wigner function has the similar property for integration over X . To prove this fact, we may first introduce the momentum representation of the density matrix, in full analogy with its coordinate representation (27):

$$w(p, p') \equiv \langle p | \hat{w} | p' \rangle. \quad (7.54)$$

Inserting, as usual, two identity operators, in the form given by Eq. (4.252), into the right-hand side of this equality, we get the following relation between the momentum and coordinate representations:

$$w(p, p') = \iint dx dx' \langle p | x \rangle \langle x | \hat{w} | x' \rangle \langle x' | p' \rangle = \frac{1}{2\pi\hbar} \iint dx dx' \exp\left\{-\frac{ipx}{\hbar}\right\} w(x, x') \exp\left\{+\frac{ip'x'}{\hbar}\right\}. \quad (7.55)$$

This is of course nothing else than the unitary transform of an operator from the x -basis to the p -basis, similar to the first form of Eq. (4.272). For coinciding arguments, $p = p'$, Eq. (55) is reduced to

$$w(p) \equiv w(p, p) = \frac{1}{2\pi\hbar} \iint dx dx' w(x, x') \exp\left\{-\frac{ip(x-x')}{\hbar}\right\}. \quad (7.56)$$

Now using Eq. (29) and then Eq. (4.265), this function may be represented as

$$w(p) = \frac{1}{2\pi\hbar} \sum_j W_j \iint dx dx' \psi_j(x) \psi_j^*(x) \exp\left\{-\frac{ip(x-x')}{\hbar}\right\} = \sum_j W_j \varphi_j(p) \varphi_j^*(p), \quad (7.57)$$

and hence interpreted as the probability density of the particle's momentum at value p . Now, in the variables (51), Eq. (56) has the form

¹⁹ Such function, used to express the probability dW to find the system in a small area of the phase plane as $dW = w_{\text{cl}}(X, P)dXdP$, is a major notion of the (1D) classical statistics – see, e.g., SM Sec. 2.1.

$$w(p) = \frac{1}{2\pi\hbar} \int \int w\left(X + \frac{\tilde{X}}{2}, X - \frac{\tilde{X}}{2}\right) \exp\left\{-\frac{ip\tilde{X}}{\hbar}\right\} d\tilde{X} dX. \quad (7.58)$$

Comparing this equality with the definition (50) of the Wigner function, we see that

$$w(P) = \int W(X, P) dX. \quad (7.59)$$

Thus, according to Eqs. (53) and (59), the integrals of the Wigner function over either the coordinate or momentum give the probability densities to find the system at a certain value of the counterpart variable. This is of course the main requirement to any quantum-mechanical candidate for the best analog of the classical probability density, $w_c(X, P)$.

Let us see at how does the Wigner function look for the simplest systems at thermodynamic equilibrium. For a free 1D particle, we can use Eq. (34), ignoring for simplicity the normalization issues:

$$W(X, P) \propto \int_{-\infty}^{+\infty} \exp\left\{-\frac{mk_B T \tilde{X}^2}{2\hbar^2}\right\} \exp\left\{-\frac{iP\tilde{X}}{\hbar}\right\} d\tilde{X}. \quad (7.60)$$

The usual Gaussian integration yields:

$$W(X, P) = \text{const} \times \exp\left\{-\frac{P^2}{2mk_B T}\right\}. \quad (7.61)$$

We see that the function is independent of X (as it should be for this translational-invariant system), and coincides with the Gibbs distribution (24). We could get the same result directly from classical statistics. This is natural because as we know from Sec. 2.2, the free motion is essentially not quantized – at least in terms of its energy and momentum.

Now let us consider a substantially quantum system, the harmonic oscillator. Plugging Eq. (44) into Eq. (50), for that system in thermal equilibrium it is easy to show (and hence is left for reader's exercise) that the Wigner function is also Gaussian, now in both its arguments:

$$W(X, P) = \text{const} \times \exp\left\{-C\left[\frac{m\omega_0^2 X^2}{2} + \frac{P^2}{2m}\right]\right\}, \quad (7.62)$$

though the coefficient C is now different from $1/k_B T$, and tends to that limit only at high temperatures, $k_B T \gg \hbar\omega_0$. Moreover, for a Glauber state, the Wigner function also gives a very plausible result – a Gaussian distribution similar to Eq. (62), but properly shifted from the origin to the central point of the state – see Sec. 5.5.²⁰

Unfortunately, for some other possible states of the harmonic oscillator, e.g., any pure Fock state with $n > 0$, the Wigner function takes negative values in some regions of the $[X, P]$ plane – see Fig. 3.²¹ (Such plots were the basis of my, admittedly very imperfect, classical images of the Fock states in Fig. 5.8.)

²⁰ Please note that in the notation of Sec. 5.5, the capital letters X and P mean not the arguments of the Wigner function, but the Cartesian coordinates of the central point (5.102), i.e. the classical complex amplitude of the oscillations.

²¹ Spectacular experimental measurements of this function (for $n = 0$ and $n = 1$) were carried out recently by E. Bimbard *et al.*, *Phys. Rev. Lett.* **112**, 033601 (2014).

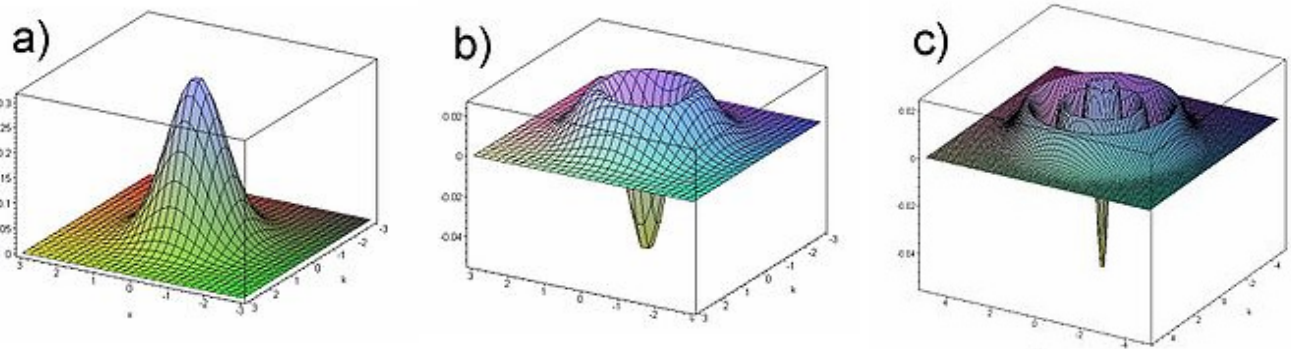


Fig. 7.3. The Wigner functions $W(X, P)$ of a harmonic oscillator, in a few of its stationary (Fock) states n : (a) $n = 0$, (b) $n = 1$; (c) $n = 5$. Graphics by J. S. Lundeen; adapted from http://en.wikipedia.org/wiki/Wigner_function as a public-domain material.

The same is true for most other quantum systems and their states. Indeed, this fact could be predicted just by looking at the definition (50) applied to a pure quantum state, in which the density function may be factored – see Eq. (31):

$$W(X, P) = \frac{1}{2\pi\hbar} \int \psi\left(X + \frac{\tilde{X}}{2}\right) \psi^*\left(X - \frac{\tilde{X}}{2}\right) \exp\left\{-\frac{iP\tilde{X}}{\hbar}\right\} d\tilde{X}. \quad (7.63)$$

Changing the argument P (say, at fixed X), we are essentially changing the spatial “frequency” (wave number) of the wavefunction product’s Fourier component we are calculating, and we know that their Fourier images typically change sign as the frequency is changed. Hence the wavefunctions should have some high-symmetry properties to avoid this effect. Indeed, the Gaussian functions (describing, for example, the Glauber states, and in their particular case, the ground state of the harmonic oscillator) have such symmetry, but many other functions do not.

Hence if the Wigner function was taken seriously as the quantum-mechanical analog of the classical probability density $w_{\text{cl}}(X, P)$, we would need to interpret the negative probability of finding the particle in certain elementary intervals $dXdP$ – which is hard to do. However, the function is still used for a semi-quantitative interpretation of mixed states of quantum systems.

7.3. Open system dynamics: Dephasing

So far we have discussed the density operator as something *given* at a particular time instant. Now let us discuss how it *formed*, i.e. its evolution in time, starting from the simplest case when the probabilities W_j participating in Eq. (15) are *time-independent* – by this or that reason, to be discussed in a moment. In this case, in the Schrödinger picture, we may rewrite Eq. (15) as

$$\hat{w}(t) = \sum_j |w_j(t)\rangle W_j \langle w_j(t)|. \quad (7.64)$$

Taking a time derivative of both sides of this equation, multiplying them by $i\hbar$, and applying Eq. (4.158) to the basis states w_j , with the account of the fact that the Hamiltonian operator is Hermitian, we get

$$\begin{aligned}
i\hbar\dot{\hat{w}} &= i\hbar \sum_j \left(|\dot{w}_j(t)\rangle W_j \langle w_j(t)| + |w_j(t)\rangle W_j \langle \dot{w}_j(t)| \right) \\
&= \sum_j \left(\hat{H} |w_j(t)\rangle W_j \langle w_j(t)| - |w_j(t)\rangle W_j \langle w_j(t)| \hat{H} \right) \\
&\equiv \hat{H} \sum_j |w_j(t)\rangle W_j \langle w_j(t)| - \sum_j |w_j(t)\rangle W_j \langle w_j(t)| \hat{H}.
\end{aligned} \tag{7.65}$$

Now using Eq. (64) again (twice), we get the so-called *von Neumann equation*²²

$$i\hbar\dot{\hat{w}} = [\hat{H}, \hat{w}]. \tag{7.66}$$
von Neumann
equation

Note that this equation is similar in structure to Eq. (4.199) describing the time evolution of time-independent operators in the Heisenberg picture operators:

$$i\hbar\dot{\hat{A}} = [\hat{A}, \hat{H}], \tag{7.67}$$

besides the opposite order of the operators in the commutator – equivalent to the change of sign of the right-hand side. This should not be too surprising, because Eq. (66) belongs to the Schrödinger picture of quantum dynamics, while Eq. (67), to its Heisenberg picture.

The most important case when the von Neumann equation is (approximately) valid is when the “own” Hamiltonian \hat{H}_s of the system s of our interest is time-independent, and its interaction with the environment is so small that its effect on the system’s evolution during the considered time interval is negligible, but it had lasted so long that it gradually put the system into a non-pure state – for example, but not necessarily, into the classical mixture (24).²³ (This is an example of the second case discussed in Sec. 1, when we need the mixed-ensemble description of the system even if its current interaction with the environment is negligible.) If the interaction with the environment is stronger, and hence is not negligible at the considered time interval, Eq. (66) is generally *not* valid,²⁴ because the probabilities W_j may change in time. However, this equation may still be used for a discussion of one major effect of the environment, namely *dephasing* (also called “decoherence”), within a simple model.

Let us start with the following general model a system interacting with its environment, which will be used throughout this chapter:

$$\hat{H} = \hat{H}_s + \hat{H}_e \{\lambda\} + \hat{H}_{\text{int}}, \tag{7.68}$$
Interaction
with
environment

²² In some texts, it is called the “Liouville equation”, due to its philosophical proximity to the classical Liouville theorem for the classical distribution function $w_{\text{cl}}(X, P)$ – see, e.g., SM Sec. 6.1 and in particular Eq. (6.5).

²³ In the last case, the statistical operator is diagonal in the stationary state basis and hence commutes with the Hamiltonian. Hence the right-hand side of Eq. (66) vanishes, and it shows that in this basis, the density matrix is completely time-independent.

²⁴ Very unfortunately, this fact is not explained in some textbooks, which quote the von Neumann equation without proper qualifications.

where $\{\lambda\}$ denotes the (huge) set of degrees of freedom of the environment.²⁵ Evidently, this model is useful only if we may somehow tame the enormous size of the Hilbert space of these degrees of freedom, and so work out the calculations all way to a practicably simple result. This turns out to be possible mostly if the elementary act of interaction of the system and its environment is in some sense small. Below, I will describe several cases when this is true; the classical example is the *Brownian particle* interacting with the molecules of the surrounding gas or fluid.²⁶ (In this example, a single hit by a molecule changes the particle's momentum by a minor fraction.) On the other hand, the model (68) is not very productive for a particle interacting with the environment consisting of *similar* particles, when a single collision may change its momentum dramatically. In such cases, the methods discussed in the next chapter are more relevant.

Now let us analyze a very simple model of an open two-level quantum system, with its intrinsic Hamiltonian having the form

$$\hat{H}_s = c_z \hat{\sigma}_z, \quad (7.69)$$

similar to the Pauli Hamiltonian (4.163),²⁷ and a factorable, bilinear interaction – cf. Eq. (6.145) and its discussion:

$$\hat{H}_{\text{int}} = \hat{f}\{\lambda\} \hat{\sigma}_z, \quad (7.70)$$

where \hat{f} is a Hermitian operator depending only on the set $\{\lambda\}$ of environmental degrees of freedom (“coordinates”), defined in their Hilbert space – different from that of the two-level system. As a result, the operators $\hat{f}\{\lambda\}$ and $\hat{H}_e\{\lambda\}$ commute with $\hat{\sigma}_z$ – and with any other intrinsic operator of the two-level system. Of course, any realistic $\hat{H}_e\{\lambda\}$ is extremely complex, so that how much we will be able to achieve without specifying it, may be a pleasant surprise for the reader.

Before we proceed to the analysis, let us recognize two examples of two-level systems that may be described by this model. The first example is a spin- $1/2$ in an external magnetic field of a fixed direction (taken for the axis z), which includes both an average component $\bar{\mathcal{B}}$ and a random (fluctuating) component $\tilde{\mathcal{B}}_z(t)$ induced by the environment. As it follows from Eq. (4.163b), it may be described by the Hamiltonian (68)-(70) with

$$c_z = -\frac{\hbar\gamma}{2} \bar{\mathcal{B}}_z, \quad \text{and} \quad \hat{f} = -\frac{\hbar\gamma}{2} \hat{\tilde{\mathcal{B}}}_z(t). \quad (7.71)$$

²⁵ Note that by writing Eq. (68), we are treating the whole system, including the environment, as a Hamiltonian one. This can always be done if the accounted part of the environment is large enough so that the processes in the system s of our interest do not depend on the type of boundary between this part and the “external” (even larger) environment; in particular, we may assume the total system to be closed, i.e. Hamiltonian.

²⁶ The theory of the Brownian motion, the effect first observed experimentally by biologist Robert Brown in the 1820s, was pioneered by Albert Einstein in 1905 and developed in detail by Marian Smoluchowski in 1906-1907 and Adriaan Fokker in 1913. Due to this historic background, in some older texts, the approach described in the balance of this chapter is called the “quantum theory of the Brownian motion”. Let me, however, emphasize that due to the later progress of experimental techniques, quantum-mechanical behaviors, including the environmental effects in them, have been observed in a rapidly growing number of various quasi-macroscopic systems, for which this approach is quite applicable. In particular, this is true for most systems being explored as possible qubits of prospective quantum computing and encryption systems – see Sec. 8.5 below.

²⁷ As we know from Secs. 4.6 and 5.1, such Hamiltonian is sufficient to lift the energy level degeneracy.

Another example is a particle in a symmetric double-well potential $U_s(x)$ (Fig. 4), with a barrier between them sufficiently high to be practically impenetrable, and an additional force $F(t)$, exerted by the environment, so that the total potential energy is $U(x, t) = U_s(x) - F(t)x$. If the force, including its static part \bar{F} and fluctuations $\tilde{F}(t)$, is sufficiently weak, we can neglect its effects on the shape of potential wells and hence on the localized wavefunctions $\psi_{L,R}$, so that the force effect is reduced to the variation of the difference $E_L - E_R = F(t)\Delta x$ between the eigenenergies. As a result, the system may be described by Eqs. (68)-(70) with

$$c_z = -\bar{F}\Delta x/2; \quad \hat{f} = -\tilde{F}(t)\Delta x/2. \quad (7.72)$$

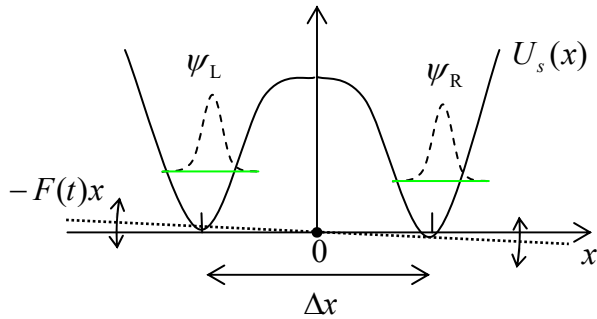


Fig. 7.4. Dephasing in a double-well system.

Let us start our general analysis of the model described by Eqs. (68)-(70) by writing the equation of motion for the Heisenberg operator $\hat{\sigma}_z(t)$:

$$i\hbar\dot{\hat{\sigma}}_z = [\hat{\sigma}_z, \hat{H}] = (c_z + \hat{f})[\hat{\sigma}_z, \hat{\sigma}_z] = 0, \quad (7.73)$$

showing that in our simple model (68)-(70), the operator $\hat{\sigma}_z$ does not evolve in time. What does this mean for the observables? For an arbitrary density matrix of any two-level system,

$$w = \begin{pmatrix} w_{11} & w_{12} \\ w_{21} & w_{22} \end{pmatrix}, \quad (7.74)$$

we can readily calculate the trace of operator $\hat{\sigma}_z w$. Indeed, since the operator traces are basis-independent, we can do this in any basis, in particular in the usual z -basis:

$$\text{Tr}(\hat{\sigma}_z w) = \text{Tr}(\sigma_z w) = \text{Tr} \left[\begin{pmatrix} 1 & 0 \\ 0 & -1 \end{pmatrix} \begin{pmatrix} w_{11} & w_{12} \\ w_{21} & w_{22} \end{pmatrix} \right] = w_{11} - w_{22} = W_1 - W_2. \quad (7.75)$$

Since, according to Eq. (5), $\hat{\sigma}_z$ may be considered the operator for the difference of the number of particles in the basis states 1 and 2, in the case (73) the difference $W_1 - W_2$ does not depend on time, and since the sum of these probabilities is also fixed, $W_1 + W_2 = 1$, both of them are constant. The physics of this simple result is especially clear for the model shown in Fig. 4: since the potential barrier separating the potential wells is so high that tunneling through it is negligible, the interaction with the environment cannot move the system from one well into another one.

It may look like nothing interesting may happen in such a simple situation, but in a minute we will see that this is not true. Due to the time independence of W_1 and W_2 , we may use the von Neumann equation (66) to describe the density matrix evolution. In the usual z -basis:

$$\begin{aligned} i\hbar \dot{\mathbf{w}} &\equiv i\hbar \begin{pmatrix} \dot{w}_{11} & \dot{w}_{12} \\ \dot{w}_{21} & \dot{w}_{22} \end{pmatrix} = [\mathbf{H}, \mathbf{w}] \equiv (c_z + \hat{f})[\sigma_z, \mathbf{w}] \\ &\equiv (c_z + \hat{f}) \left[\begin{pmatrix} 1 & 0 \\ 0 & -1 \end{pmatrix}, \begin{pmatrix} w_{11} & w_{12} \\ w_{21} & w_{22} \end{pmatrix} \right] = (c_z + \hat{f}) \begin{pmatrix} 0 & 2w_{12} \\ -2w_{21} & 0 \end{pmatrix}. \end{aligned} \quad (7.76)$$

This result means that while the diagonal elements, i.e., the probabilities of the states, do not evolve in time (as we already know), the off-diagonal elements do change; for example,

$$i\hbar \dot{w}_{12} = 2(c_z + \hat{f})w_{12}, \quad (7.77)$$

with a similar but complex-conjugate equation for w_{21} . The solution of this linear differential equation (77) is straightforward, and yields

$$w_{12}(t) = w_{12}(0) \exp \left\{ -i \frac{2c_z}{\hbar} t \right\} \exp \left\{ -i \frac{2}{\hbar} \int_0^t \hat{f}(t') dt' \right\}. \quad (7.78)$$

The first exponent is a deterministic c -number factor, while in the second one $\hat{f}(t) \equiv \hat{f}\{\lambda(t)\}$ is still an operator in the Hilbert space of the environment, but from the point of view of the two-level system of our interest, it is a random function of time. The time-average part of this function may be included in c_z , so in what follows, we will assume that it equals zero.

Let us start from the limit when the environment behaves classically.²⁸ In this case, the operator in Eq. (78) may be considered as a *classical* random function of time $f(t)$, provided that we average its effects over a statistical ensemble of many functions $f(t)$ describing many (macroscopically similar) experiments. For a small time interval $t = dt \rightarrow 0$, we can use the Taylor expansion of the exponent, truncating it after the quadratic term:

$$\begin{aligned} \left\langle \exp \left\{ -i \frac{2}{\hbar} \int_0^t f(t') dt' \right\} \right\rangle &\approx 1 + \left\langle -i \frac{2}{\hbar} \int_0^t f(t') dt' \right\rangle + \left\langle \frac{1}{2} \left(-i \frac{2}{\hbar} \int_0^t f(t') dt' \right) \left(-i \frac{2}{\hbar} \int_0^t f(t'') dt'' \right) \right\rangle \\ &\equiv 1 - i \frac{2}{\hbar} \int_0^t \langle f(t') \rangle dt' - \frac{2}{\hbar^2} \int_0^t dt' \int_0^t dt'' \langle f(t') f(t'') \rangle \equiv 1 - \frac{2}{\hbar^2} \int_0^t dt' \int_0^t dt'' K_f(t' - t''). \end{aligned} \quad (7.79)$$

Here we have used the facts that the statistical average of $f(t)$ is equal to zero, while the second average, called the *correlation function*, in a statistically- (i.e. macroscopically-) stationary state of any environment may only depend on the time difference $\tau \equiv t' - t''$:

$$\langle f(t') f(t'') \rangle = K_f(t' - t'') \equiv K_f(\tau). \quad (7.80)$$

If this difference is much larger than some time scale τ_c , called the *correlation time* of the environment, the values $f(t')$ and $f(t'')$ are completely independent (*uncorrelated*), as illustrated in Fig. 5a, so that at $\tau \rightarrow \infty$, the correlation function has to tend to zero. On the other hand, at $\tau = 0$, i.e. $t' = t''$, the correlation function is just the variance of f :

²⁸ This assumption is not in contradiction with the need for the quantum treatment of the two-level system s , because a typical environment is large, and hence has a very dense energy spectrum, with the distances adjacent levels that may be readily bridged by thermal excitations of small energies, often making it essentially classical.

$$K_f(0) = \langle f^2 \rangle, \quad (7.81)$$

and has to be positive. As a result, the function looks (semi-quantitatively) as shown in Fig. 5b.

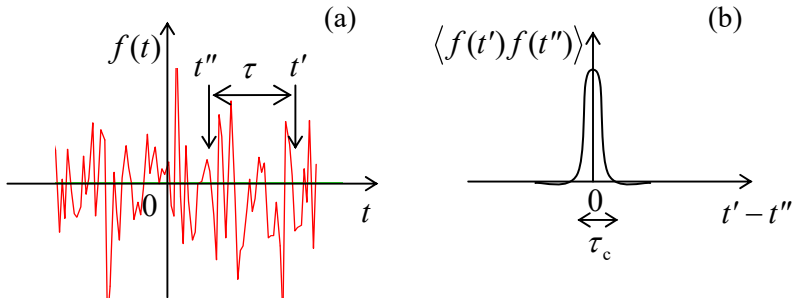


Fig. 7.5. (a) A typical random process and (b) its correlation function – schematically.

Hence, if we are only interested in time differences τ much longer than τ_c , which is typically very short, we may approximate $K_f(\tau)$ well with a delta function of the time difference. Let us take it in the following form, convenient for later discussion:

$$K_f(\tau) \approx \hbar^2 D_\phi \delta(\tau), \quad (7.82)$$

Phase diffusion coefficient

where D_ϕ is a positive constant called the *phase diffusion coefficient*. The origin of this term stems from the very similar effect of classical diffusion of Brownian particles in a highly viscous medium. Indeed, the particle's velocity in such a medium is approximately proportional to the external force. Hence, if the random hits of a particle by the medium's molecules may be described by a force that obeys a law similar to Eq. (82), the velocity (along any Cartesian coordinate) is also *delta-correlated*:

$$\langle v(t) \rangle = 0, \quad \langle v(t')v(t'') \rangle = 2D\delta(t' - t''). \quad (7.83)$$

Now we can integrate the kinematic relation $\dot{x} = v$, to calculate particle's displacement from its initial position during a time interval $[0, t]$ and its variance:

$$x(t) - x(0) = \int_0^t v(t') dt', \quad (7.84)$$

$$\langle (x(t) - x(0))^2 \rangle = \left\langle \int_0^t v(t') dt' \int_0^t v(t'') dt'' \right\rangle = \int_0^t dt' \int_0^t dt'' \langle v(t')v(t'') \rangle = \int_0^t dt' \int_0^t dt'' 2D\delta(t' - t'') = 2Dt. \quad (7.85)$$

This is the famous law of diffusion, showing that the r.m.s. deviation of the particle from the initial point grows with time as $(2Dt)^{1/2}$, where the constant D is called the *diffusion coefficient*.

Returning to the diffusion of the quantum-mechanical phase, with Eq. (82) the last double integral in Eq. (79) yields $\hbar^2 D_\phi dt$, so that the statistical average of Eq. (78) is

$$\langle w_{12}(dt) \rangle = w_{12}(0) \exp \left\{ -i \frac{2c_z}{\hbar} dt \right\} (1 - 2D_\phi dt). \quad (7.86)$$

Applying this formula to sequential time intervals,

$$\langle w_{12}(2dt) \rangle = \langle w_{12}(dt) \rangle \exp \left\{ -i \frac{2c_z}{\hbar} dt \right\} (1 - 2D_\phi dt) = w_{12}(0) \exp \left\{ -i \frac{2c_z}{\hbar} 2dt \right\} (1 - 2D_\phi dt)^2, \quad (7.87)$$

etc., for a finite time $t = Ndt$, in the limit $N \rightarrow \infty$ and $dt \rightarrow 0$ (at fixed t) we get

$$\langle w_{12}(t) \rangle = w_{12}(0) \exp\left\{-i \frac{2c_z}{\hbar} t\right\} \times \lim_{N \rightarrow \infty} \left(1 - 2D_\phi t \frac{1}{N}\right)^N. \quad (7.88)$$

By the definition of the natural logarithm base e ,²⁹ this limit is just $\exp\{-2D_\phi t\}$, so that, finally:

Two-level system:
dephasing

$$\langle w_{12}(t) \rangle = w_{12}(0) \exp\left\{-i \frac{2a}{\hbar} t\right\} \exp\{-2D_\phi t\} \equiv w_{12}(0) \exp\left\{-i \frac{2a}{\hbar} t\right\} \exp\left\{-\frac{t}{T_2}\right\}. \quad (7.89)$$

So, due to coupling to the environment, the off-diagonal elements of the density matrix decay with some *dephasing time* $T_2 = 1/2D_\phi$, providing a natural evolution from the density matrix (22) of a pure state to the diagonal matrix (23), with the same probabilities $W_{1,2}$, describing a fully dephased (incoherent) classical mixture.³⁰

This simple model offers a very clear look at the nature of the decoherence: the random “force” $f(t)$, exerted by the environment, “shakes” the energy difference between two eigenstates of the system and hence the instantaneous velocity $2(c_z + f)/\hbar$ of their mutual phase shift $\phi(t)$ – cf. Eq. (22). Due to the randomness of the force, $\phi(t)$ performs a random walk around the trigonometric circle, so that the average of its trigonometric functions $\exp\{\pm i\phi\}$ over time gradually tends to zero, killing the off-diagonal elements of the density matrix. Our analysis, however, has left open two important issues:

- (i) Is this approach valid for a *quantum* description of a typical environment?
- (ii) If yes, what is physically the D_ϕ that was formally defined by Eq. (82)?

7.4. Fluctuation-dissipation theorem

Similar questions may be asked about a more general situation, when the Hamiltonian \hat{H}_s of the system of interest (s), in the composite Hamiltonian (68), is not specified at all, but the interaction between that system and its environment still has a bilinear form similar to Eqs. (70) and (6.130):

$$\hat{H}_{\text{int}} = -\hat{F}\{\lambda\} \hat{x}, \quad (7.90)$$

where x is some observable of our system s – say, its generalized coordinate or generalized momentum. It may look incredible that in this very general situation one still can make a very simple and powerful statement about the statistical properties of the generalized force F , under only two (interrelated) conditions – which are satisfied in a huge number of cases of interest:

- (i) the coupling of system s of interest to its environment e is weak – in the sense that the perturbation theory (see Chapter 6) is applicable, and

²⁹ See, e.g., MA Eq. (1.2a) with $n = -N/2D_\phi t$.

³⁰ Note that this result is valid only if the approximation (82) may be applied at time interval dt which, in turn, should be much smaller than the T_2 in Eq. (88), i.e. if the dephasing time is much longer than the environment’s correlation time τ_c . This requirement may be always satisfied by making the coupling to the environment sufficiently weak. In addition, in typical environments, τ_c is very short. For example, in the original Brownian motion experiments with a-few-μm pollen grains in water, it is of the order of the average interval between sequential molecular impacts, of the order of 10^{-21} s.

(ii) the environment may be considered as staying in thermodynamic equilibrium, with a certain temperature T , regardless of the process in the system of interest.³¹

This famous statement is called the *fluctuation-dissipation theorem* (FDT).³² Due to the importance of this fundamental result, let me derive it.³³ Since by writing Eq. (68) we treat the whole system ($s + e$) as a Hamiltonian one, we may use the Heisenberg equation (4.199) to write

$$i\hbar \dot{\hat{F}} = [\hat{F}, \hat{H}] = [\hat{F}, \hat{H}_e], \quad (7.91)$$

because, as was discussed in the last section, operator $\hat{F}\{\lambda\}$ commutes with both \hat{H}_s and \hat{x} . Generally, very little may be done with this equation, because the time evolution of the environment's Hamiltonian depends, in turn, on that of the force. This is where the perturbation theory becomes indispensable. Let us decompose the force operator into the following sum:

$$\hat{F}\{\lambda\} = \langle \hat{F} \rangle + \hat{\tilde{F}}(t), \quad \text{with } \langle \hat{\tilde{F}}(t) \rangle = 0, \quad (7.92)$$

where (here and on, until further notice) the sign $\langle \dots \rangle$ means the statistical averaging *over the environment alone*, i.e. over an ensemble with absolutely similar evolutions of the system s , but random states of its environment.³⁴ From the point of view of the system s , the first term of the sum (still an operator!) describes the average response of the environment to the system dynamics (possibly, including such irreversible effects as friction), and has to be calculated with a proper account of their interaction – as we will do later in this section. On the other hand, the last term in Eq. (92) represents random *fluctuations* of the environment, which exist even in the absence of the system s . Hence, in the first non-zero approximation in the interaction strength, the fluctuation part may be calculated ignoring the interaction, i.e. treating the environment as being in thermodynamic equilibrium:

$$i\hbar \dot{\hat{\tilde{F}}} = \left[\hat{\tilde{F}}, \hat{H}_e \Big|_{\text{eq}} \right]. \quad (7.93)$$

Since in this approximation the environment's Hamiltonian does not have an explicit dependence on time, the solution of this equation may be written by combining Eqs. (4.190) and (4.175):

³¹ The most frequent example of the violation of this condition is the environment's overheating by the energy flow from system s . Let me leave it to the reader to estimate the overheating of a standard physical laboratory room by a typical dissipative quantum process – the emission of an optical photon by an atom. (*Hint*: it is extremely small.)

³² The FDT was first derived by Herbert Callen and Theodore Allen Welton in 1951, on the background of an earlier derivation of its classical limit by Harry Nyquist in 1928.

³³ The FDT may be proved in several ways that are shorter than the one given below – see, e.g., either the proof in SM Secs. 5.5 and 5.6 (based on H. Nyquist's arguments), or the original paper by H. Callen and T. Welton, *Phys. Rev.* **83**, 34 (1951) – wonderful in its clarity. The longer approach I will describe here, besides giving the important *Green-Kubo formula* (109) as a byproduct, is a very useful exercise in the operator manipulation and the perturbation theory in its integral form – different from the differential forms used in Chapter 6. If the reader is not interested in this exercise, they may skip the derivation and jump straight to the result expressed by Eq. (134), which uses the notions defined by Eqs. (114) and (123).

³⁴ For usual (“ergodic”) environments, without intrinsic long-term memories, this statistical averaging over an ensemble of environments is equivalent to averaging over intermediate times – much longer than the correlation time τ_c of the environment, but still much shorter than the characteristic time of evolution of the system under analysis, such as the dephasing time T_2 and the energy relaxation time T_1 – both still to be calculated.

$$\hat{F}(t) = \exp\left\{ +\frac{i}{\hbar} \hat{H}_e |_{\text{eq}} t \right\} \hat{F}(0) \exp\left\{ -\frac{i}{\hbar} \hat{H}_e |_{\text{eq}} t \right\}. \quad (7.94)$$

Let us use this relation to calculate the correlation function of the fluctuations $F(t)$, defined similarly to Eq. (80), but taking care of the order of the time arguments (very soon we will see why):

$$\langle \tilde{F}(t)\tilde{F}(t') \rangle = \left\langle \exp\left\{ +\frac{i}{\hbar} \hat{H}_e t \right\} \hat{F}(0) \exp\left\{ -\frac{i}{\hbar} \hat{H}_e t \right\} \exp\left\{ +\frac{i}{\hbar} \hat{H}_e t' \right\} \hat{F}(0) \exp\left\{ -\frac{i}{\hbar} \hat{H}_e t' \right\} \right\rangle. \quad (7.95)$$

(Here, for the notation brevity, the thermal equilibrium of the environment is just implied.) We may calculate this expectation value in any basis, and the best choice for it is evident: in the environment's stationary-state basis, the density operator of the environment, its Hamiltonian, and hence the exponents in Eq. (95) are all represented by diagonal matrices. Using Eq. (5), the correlation function becomes

$$\begin{aligned} \langle \tilde{F}(t)\tilde{F}(t') \rangle &= \text{Tr} \left[\hat{w} \exp\left\{ +\frac{i}{\hbar} \hat{H}_e t \right\} \hat{F}(0) \exp\left\{ -\frac{i}{\hbar} \hat{H}_e t \right\} \exp\left\{ +\frac{i}{\hbar} \hat{H}_e t' \right\} \hat{F}(0) \exp\left\{ -\frac{i}{\hbar} \hat{H}_e t' \right\} \right] \\ &\equiv \sum_n \left[\hat{w} \exp\left\{ +\frac{i}{\hbar} \hat{H}_e t \right\} \hat{F}(0) \exp\left\{ -\frac{i}{\hbar} \hat{H}_e t \right\} \exp\left\{ +\frac{i}{\hbar} \hat{H}_e t' \right\} \hat{F}(0) \exp\left\{ -\frac{i}{\hbar} \hat{H}_e t' \right\} \right]_{nn} \\ &= \sum_{n,n'} W_n \exp\left\{ +\frac{i}{\hbar} E_n t \right\} \hat{F}_{nn'} \exp\left\{ -\frac{i}{\hbar} E_n t \right\} \exp\left\{ +\frac{i}{\hbar} E_{n'} t' \right\} \hat{F}_{n'n} \exp\left\{ -\frac{i}{\hbar} E_{n'} t' \right\} \\ &\equiv \sum_{n,n'} W_n |F_{nn'}|^2 \exp\left\{ +\frac{i}{\hbar} (E_n - E_{n'}) (t - t') \right\}. \end{aligned} \quad (7.96)$$

Here W_n are the Gibbs distribution probabilities given by Eq. (24), with the environment's temperature T , and $F_{nn'} \equiv F_{nn'}(0)$ are the Schrödinger-picture matrix elements of the interaction force operator.

We see that though the correlator (96) is a function of the difference $\tau \equiv t - t'$ only (as it should be for fluctuations in a macroscopically stationary system), it may depend on the order of its arguments. This is why let us mark this particular correlation function with the upper index “+”,

$$K_F^+(\tau) \equiv \langle \tilde{F}(t)\tilde{F}(t') \rangle = \sum_{n,n'} W_n |F_{nn'}|^2 \exp\left\{ +\frac{i\tilde{E}\tau}{\hbar} \right\}, \quad \text{where } \tilde{E} \equiv E_n - E_{n'}, \quad (7.97)$$

while its counterpart, with the swapped times t and t' , with the upper index “-”:

$$K_F^-(\tau) \equiv K_F^+(-\tau) = \langle \tilde{F}(t')\tilde{F}(t) \rangle = \sum_{n,n'} W_n |F_{nn'}|^2 \exp\left\{ -\frac{i\tilde{E}\tau}{\hbar} \right\}. \quad (7.98)$$

So, in contrast with classical processes, in quantum mechanics the correlation function of fluctuations \tilde{F} is not necessarily time-symmetric:

$$K_F^+(\tau) - K_F^-(\tau) \equiv K_F^+(\tau) - K_F^+(-\tau) = \langle \tilde{F}(t)\tilde{F}(t') - \tilde{F}(t')\tilde{F}(t) \rangle = 2i \sum_{n,n'} W_n |F_{nn'}|^2 \sin \frac{\tilde{E}\tau}{\hbar} \neq 0, \quad (7.99)$$

so that $\hat{F}(t)$ gives one more example of a Heisenberg-picture operator whose “values”, taken in different moments of time, generally do not commute – see Footnote 49 in Chapter 4. (A good sanity check here is that at $\tau = 0$, i.e. at $t = t'$, the difference (99) between K_F^+ and K_F^- vanishes.)

Now let us return to the force operator's decomposition (92), and calculate its first (average) component. To do that, let us write the formal solution of Eq. (91) as follows:

$$\hat{F}(t) = \frac{1}{i\hbar} \int_{-\infty}^t [\hat{F}(t'), \hat{H}_e(t')] dt'. \quad (7.100)$$

On the right-hand side of this relation, we still cannot treat the Hamiltonian of the environment as an unperturbed (equilibrium) one, even if the effect of our system (s) on the environment is very weak, because this would give zero statistical average of the force $F(t)$. Hence, we should make one more step of our perturbative treatment, taking into account the effect of the force on the environment. To do this, let us use Eqs. (68) and (90) to write the (so far, exact) Heisenberg equation of motion for the environment's Hamiltonian,

$$i\hbar \dot{\hat{H}}_e = [\hat{H}_e, \hat{H}] = -\hat{x} [\hat{H}_e, \hat{F}], \quad (7.101)$$

and its formal solution, similar to Eq. (100), but for time t' rather than t :

$$\hat{H}_e(t') = -\frac{1}{i\hbar} \int_{-\infty}^{t'} \hat{x}(t'') [\hat{H}_e(t''), \hat{F}(t'')] dt''. \quad (7.102)$$

Plugging this equality into the right-hand side of Eq. (100), and averaging the result (again, over the environment only!), we get

$$\langle \hat{F}(t) \rangle = \frac{1}{\hbar^2} \int_{-\infty}^t dt' \int_{-\infty}^{t'} dt'' \hat{x}(t'') \langle [\hat{F}(t'), [\hat{H}_e(t''), \hat{F}(t'')]] \rangle. \quad (7.103)$$

This is still an exact result, but now it is ready for an approximate treatment, implemented by averaging in its right-hand side over the unperturbed (thermal-equilibrium) state of the environment. This may be done absolutely similarly to that in Eq. (96), at the last step using Eq. (94):

$$\begin{aligned} \langle [\hat{F}(t'), [\hat{H}_e(t''), \hat{F}(t'')]] \rangle &= \text{Tr}\{w[F(t'), [H_e F(t'')]]\} \\ &\equiv \text{Tr}\{w[F(t') H_e F(t'') - F(t') F(t'') H_e - H_e F(t'') F(t') + F(t'') H_e F(t')]\} \\ &= \sum_{n,n'} W_n [F_{nn'}(t') E_{n'} F_{n'n}(t'') - F_{nn'}(t') F_{n'n}(t'') E_n - E_n F_{nn'}(t'') F_{n'n}(t') + F_{nn'}(t'') E_{n'} F_{n'n}(t'')] \\ &\equiv -\sum_{n,n'} W_n \tilde{E} |F_{nn'}|^2 \left[\exp\left\{\frac{i\tilde{E}(t'-t'')}{\hbar}\right\} + \text{c.c.} \right]. \end{aligned} \quad (7.104)$$

Now, if we try to integrate each term of this sum, as Eq. (103) seems to require, we will see that the lower-limit substitution (at $t', t'' \rightarrow -\infty$) is uncertain because the exponents oscillate without decay. This mathematical difficulty may be overcome by the following physical reasoning. As illustrated by the example considered in the previous section, coupling to a disordered environment makes the “memory horizon” of the system of our interest (s) finite: its current state does not depend on its history beyond a certain time scale.³⁵ As a result, the function under the integrals of Eq. (103), i.e. the sum (104), should

³⁵ Actually, this is true for virtually any real physical system – in contrast to idealized models such as a dissipation-free oscillator that swings for ever and ever with the same amplitude and phase, thus “remembering” the initial conditions.

self-average at a certain finite time. A simplistic technique for expressing this fact mathematically is just dropping the lower-limit substitution; this would give the correct result for Eq. (103). However, a better (mathematically more acceptable) trick is to first multiply the functions under the integrals by, respectively, $\exp\{\varepsilon(t-t')\}$ and $\exp\{\varepsilon(t'-t'')\}$, where ε is a very small positive constant, then carry out the integration, and after that follow the limit $\varepsilon \rightarrow 0$. The physical justification of this procedure may be provided by saying that the system's behavior should not be affected if its interaction with the environment was not kept constant but rather turned on gradually – say, exponentially with an infinitesimal rate ε . With this modification, Eq. (103) becomes

$$\langle \hat{F}(t) \rangle = -\frac{1}{\hbar^2} \sum_{n,n'} W_n \tilde{E} |F_{nn'}|^2 \lim_{\varepsilon \rightarrow 0} \int_{-\infty}^t dt' \int_{-\infty}^{t'} dt'' \hat{x}(t'') \left[\exp\left\{ \frac{i\tilde{E}(t'-t'')}{\hbar} + \varepsilon(t''-t) \right\} + \text{c.c.} \right]. \quad (7.105)$$

This double integration is over the area shaded in Fig. 6, which makes it obvious that the order of integration may be changed to the opposite one as

$$\int_{-\infty}^t dt' \int_{-\infty}^{t'} dt'' \dots = \int_{-\infty}^{t''} dt'' \int_{t''}^{t'} dt' \dots = \int_{-\infty}^{t''} dt'' \int_{t''-t}^0 d(t'-t) \dots \equiv \int_{-\infty}^{t''} dt'' \int_0^\tau d\tau' \dots, \quad (7.106)$$

where $\tau' \equiv t - t'$, and $\tau \equiv t - t''$.

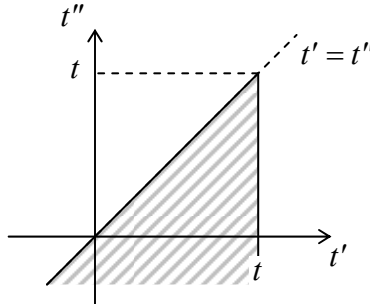


Fig. 7.6. The 2D integration area in Eqs. (105) and (106).

As a result, Eq. (105) may be rewritten as a single integral,

$$\langle \hat{F}(t) \rangle = \int_{-\infty}^t G(t-t'') \hat{x}(t'') dt'' \equiv \int_0^\infty G(\tau) \hat{x}(t-\tau) d\tau, \quad (7.107)$$

whose kernel,

$$\begin{aligned} G(\tau > 0) &\equiv -\frac{1}{\hbar^2} \sum_{n,n'} W_n \tilde{E} |F_{nn'}|^2 \lim_{\varepsilon \rightarrow 0} \int_0^\tau \left[\exp\left\{ \frac{i\tilde{E}(\tau-\tau')}{\hbar} - \varepsilon\tau \right\} + \text{c.c.} \right] d\tau' \\ &= \lim_{\varepsilon \rightarrow 0} \frac{2}{\hbar} \sum_{n,n'} W_n |F_{nn'}|^2 \sin \frac{\tilde{E}\tau}{\hbar} e^{-\varepsilon\tau} \equiv \frac{2}{\hbar} \sum_{n,n'} W_n |F_{nn'}|^2 \sin \frac{\tilde{E}\tau}{\hbar}, \end{aligned} \quad (7.108)$$

does not depend on the particular law of evolution of the system (s) under study, i.e. provides a general characterization of its coupling to the environment.

In Eq. (107) we may readily recognize the most general form of the linear response of a system (in our case, the environment), taking into account the causality principle, where $G(\tau)$ is the *response function* (also called the “temporal Green’s function”) of the environment. Now comparing Eq. (108) with Eq. (99), we get a wonderfully simple universal relation,

$$\left\langle \left[\hat{F}(\tau), \hat{F}(0) \right] \right\rangle = i\hbar G(\tau). \quad (7.109)$$

Green-Kubo formula

that emphasizes once again the quantum nature of the correlation function's time asymmetry. (This relation, called the *Green-Kubo* (or just “Kubo”) *formula* after the works by Melville Green (1954) and Ryogo Kubo (1957), does not come up in the easier derivations of the FDT, mentioned in the beginning of this section.)

However, for us the relation between the function $G(\tau)$ and the force's *anti-commutator*,

$$\left\langle \left[\hat{F}(t+\tau), \hat{F}(t) \right] \right\rangle \equiv \left\langle \hat{F}(t+\tau)\hat{F}(t) + \hat{F}(t)\hat{F}(t+\tau) \right\rangle \equiv K_F^+(\tau) + K_F^-(\tau), \quad (7.110)$$

is much more important, because of the following reason. Eqs. (97)-(98) show that the so-called *symmetrized correlation function*,

$$\begin{aligned} K_F(\tau) &\equiv \frac{K_F^+(\tau) + K_F^-(\tau)}{2} = \frac{1}{2} \left\langle \left[\hat{F}(\tau), \hat{F}(0) \right] \right\rangle = \lim_{\varepsilon \rightarrow 0} \sum_{n,n'} W_n |F_{nn'}|^2 \cos \frac{\tilde{E}\tau}{\hbar} e^{-2\varepsilon|\tau|} \\ &\equiv \sum_{n,n'} W_n |F_{nn'}|^2 \cos \frac{\tilde{E}\tau}{\hbar}, \end{aligned} \quad (7.111)$$

Symmetrized correlation function

which is an even function of the time difference τ , looks very similar to the response function (108), “only” with another trigonometric function under the sum, and a constant front factor.³⁶ This similarity may be used to obtain a direct algebraic relation between the Fourier images of these two functions of τ . Indeed, the function (111) may be represented as the Fourier integral³⁷

$$K_F(\tau) = \int_{-\infty}^{+\infty} S_F(\omega) e^{-i\omega\tau} d\omega = 2 \int_0^{+\infty} S_F(\omega) \cos \omega\tau d\omega, \quad (7.112)$$

with the reciprocal transform

$$S_F(\omega) = \frac{1}{2\pi} \int_{-\infty}^{+\infty} K_F(\tau) e^{i\omega\tau} d\tau = \frac{1}{\pi} \int_0^{+\infty} K_F(\tau) \cos \omega\tau d\tau, \quad (7.113)$$

of the *symmetrized spectral density* of the variable F , defined as

$$S_F(\omega) \delta(\omega - \omega') \equiv \frac{1}{2} \left\langle \hat{F}_\omega \hat{F}_{-\omega'} + \hat{F}_{-\omega'} \hat{F}_\omega \right\rangle \equiv \frac{1}{2} \left\langle \left\{ \hat{F}_\omega, \hat{F}_{-\omega'} \right\} \right\rangle, \quad (7.114)$$

Symmetrized spectral density

where the function \hat{F}_ω (also a Heisenberg operator rather than a *c*-number!) is defined as

$$\hat{F}_\omega \equiv \frac{1}{2\pi} \int_{-\infty}^{+\infty} \hat{F}(t) e^{i\omega t} dt, \quad \text{so that } \hat{F}(t) = \int_{-\infty}^{+\infty} \hat{F}_\omega e^{-i\omega t} d\omega. \quad (7.115)$$

The physical meaning of the function $S_F(\omega)$ becomes clear if we write Eq. (112) for the particular case $\tau = 0$:

³⁶ For the heroic reader who has suffered through the calculations up to this point: our conceptual work is done! What remains is just some simple math to bring the relation between Eqs. (108) and (111) to an explicit form.

³⁷ Due to their practical importance, and certain mathematical issues of their justification for random functions, Eqs. (112)-(113) have their own grand name, the *Wiener-Khinchin theorem*, though the math rigor aside, they are just a straightforward corollary of the standard Fourier integral transform (115).

$$K_F(0) \equiv \left\langle \hat{F}^2 \right\rangle = \int_{-\infty}^{+\infty} S_F(\omega) d\omega = 2 \int_0^{+\infty} S_F(\omega) d\omega. \quad (7.116)$$

This formula infers that if we pass the function $F(t)$ through a linear filter cutting from its frequency spectrum a narrow band $d\omega$ of physical (positive) frequencies, then the variance $\langle F_f^2 \rangle$ of the filtered signal $F_f(t)$ would be equal to $2S_F(\omega)d\omega$ – hence the name “spectral density”.³⁸

Let us use Eqs. (111) and (113) to calculate the spectral density of fluctuations $\tilde{F}(t)$ in our model, using the same ε -trick as at the deviation of Eq. (108), to quench the upper-limit substitution:

$$\begin{aligned} S_F(\omega) &= \sum_{n,n'} W_n |F_{nn'}|^2 \frac{1}{2\pi} \lim_{\varepsilon \rightarrow 0} \int_{-\infty}^{+\infty} \cos \frac{\tilde{E}\tau}{\hbar} e^{-\varepsilon|\tau|} e^{i\omega\tau} d\tau \\ &\equiv \frac{1}{2\pi} \sum_{n,n'} W_n |F_{nn'}|^2 \lim_{\varepsilon \rightarrow 0} \int_0^{+\infty} \left[\exp \left\{ \frac{i\tilde{E}\tau}{\hbar} \right\} + \text{c.c.} \right] e^{-\varepsilon\tau} e^{i\omega\tau} d\tau \\ &= \frac{1}{2\pi} \sum_{n,n'} W_n |F_{nn'}|^2 \lim_{\varepsilon \rightarrow 0} \left[\frac{1}{i(\tilde{E}/\hbar + \omega) - \varepsilon} + \frac{1}{i(-\tilde{E}/\hbar + \omega) - \varepsilon} \right]. \end{aligned} \quad (7.117)$$

Now it is a convenient time to recall that each of the two summations here is over the eigenenergies of the environment, whose spectrum is virtually continuous because of its large size, so that we may transform each sum into an integral – just as this was done in Sec. 6.6:

$$\sum_n \dots \rightarrow \int \dots dn = \int \dots \rho(E_n) dE_n, \quad (7.118)$$

where $\rho(E) \equiv dn/dE$ is the environment’s density of states at a given energy. This transformation yields

$$S_F(\omega) = \frac{1}{2\pi} \lim_{\varepsilon \rightarrow 0} \int dE_n W(E_n) \rho(E_n) \int dE_{n'} \rho(E_{n'}) |F_{nn'}|^2 \left[\frac{1}{i(\tilde{E}/\hbar - \omega) - \varepsilon} + \frac{1}{i(-\tilde{E}/\hbar - \omega) - \varepsilon} \right]. \quad (7.119)$$

Since the expression inside the square bracket depends only on a specific linear combination of two energies, namely on $\tilde{E} \equiv E_n - E_{n'}$, it is convenient to introduce also another, linearly-independent combination of the energies, for example, the average energy $\bar{E} \equiv (E_n + E_{n'})/2$, so that the state energies may be represented as

$$E_n = \bar{E} + \frac{\tilde{E}}{2}, \quad E_{n'} = \bar{E} - \frac{\tilde{E}}{2}. \quad (7.120)$$

With this notation, Eq. (119) becomes

$$\begin{aligned} S_F(\omega) &= -\frac{\hbar}{2\pi} \lim_{\varepsilon \rightarrow 0} \int d\bar{E} \left[\int d\tilde{E} W\left(\bar{E} + \frac{\tilde{E}}{2}\right) \rho\left(\bar{E} + \frac{\tilde{E}}{2}\right) \rho\left(\bar{E} - \frac{\tilde{E}}{2}\right) |F_{nn'}|^2 \frac{1}{i(\tilde{E}/\hbar - \omega) - \hbar\varepsilon} \right. \\ &\quad \left. + \int d\tilde{E} W\left(\bar{E} + \frac{\tilde{E}}{2}\right) \rho\left(\bar{E} + \frac{\tilde{E}}{2}\right) \rho\left(\bar{E} - \frac{\tilde{E}}{2}\right) |F_{nn'}|^2 \frac{1}{i(-\tilde{E}/\hbar - \omega) - \hbar\varepsilon} \right]. \end{aligned} \quad (7.121)$$

³⁸ An alternative popular measure of the spectral density of a process $F(t)$ is $S_F(\nu) \equiv \langle F_f^2 \rangle / d\nu = 4\pi S_F(\omega)$, where $\nu = \omega/2\pi$ is the “cyclic” frequency (measured in Hz).

Due to the smallness of the parameter $\hbar\omega$ (which should be much smaller than all genuine energies of the problem, including $k_B T$, $\hbar\omega$, E_n , and $E_{n'}$), each of the internal integrals in Eq. (121) is dominated by an infinitesimal vicinity of one point, $\tilde{E}_\pm = \pm\hbar\omega$. In these vicinities, the state densities, the matrix elements, and the Gibbs probabilities do not change considerably, and may be taken out of the integral, which may be then worked out explicitly:³⁹

$$\begin{aligned} S_F(\omega) &= -\frac{\hbar}{2\pi} \lim_{\varepsilon \rightarrow 0} \int d\tilde{E} \rho_+ \rho_- \left[W_+ |F_+|^2 \int_{-\infty}^{+\infty} \frac{d\tilde{E}}{i(\tilde{E} - \hbar\omega) - \hbar\varepsilon} + W_- |F_-|^2 \int_{-\infty}^{+\infty} \frac{d\tilde{E}}{i(-\tilde{E} - \hbar\omega) - \hbar\varepsilon} \right] \\ &\equiv -\frac{\hbar}{2\pi} \lim_{\varepsilon \rightarrow 0} \int d\tilde{E} \rho_+ \rho_- \left[W_+ |F_+|^2 \int_{-\infty}^{+\infty} \frac{-i(\tilde{E} - \hbar\omega) - \hbar\varepsilon}{\tilde{E}^2 + (\hbar\varepsilon)^2} d\tilde{E} + W_- |F_-|^2 \int_{-\infty}^{+\infty} \frac{i(\tilde{E} + \hbar\omega) - \hbar\varepsilon}{\tilde{E}^2 + (\hbar\varepsilon)^2} d\tilde{E} \right] \\ &= \frac{\hbar}{2} \int \rho_+ \rho_- [W_+ |F_+|^2 + W_- |F_-|^2] d\tilde{E}, \end{aligned} \quad (7.122)$$

where the indices \pm mark the functions' values at the special points $\tilde{E}_\pm = \pm\hbar\omega$, i.e. $E_n = E_{n'} \pm \hbar\omega$. The physics of these points becomes simple if we interpret the state n , for which the equilibrium Gibbs distribution function equals W_n , as the initial state of the environment, and n' as its final state. Then the top-sign point corresponds to $E_{n'} = E_n - \hbar\omega$, i.e. to the result of emission of one energy quantum $\hbar\omega$ of the "observation" frequency ω by the environment to the system s of our interest, while the bottom-sign point $E_{n'} = E_n + \hbar\omega$, corresponds to the absorption of such quantum by the environment. As Eq. (122) shows, both processes give similar, positive contributions into the force fluctuations.

The situation is different for the Fourier image of the response function $G(\tau)$,⁴⁰

$$\chi(\omega) \equiv \int_0^{+\infty} G(\tau) e^{i\omega\tau} d\tau,$$

(7.123) Generalized susceptibility

that is usually called either the *generalized susceptibility* or the *response function* – in our case, of the environment. Its physical meaning is that according to Eq. (107), the complex function $\chi(\omega) = \chi'(\omega) + i\chi''(\omega)$ relates the Fourier amplitudes of the generalized coordinate and the generalized force:⁴¹

$$\langle \hat{F}_\omega \rangle = \chi(\omega) \hat{x}_\omega. \quad (7.124)$$

The physics of its imaginary part $\chi''(\omega)$ is especially clear. Indeed, if x_ω represents a sinusoidal classical process, say

$$x(t) = x_0 \cos \omega t \equiv \frac{x_0}{2} e^{-i\omega t} + \frac{x_0}{2} e^{+i\omega t}, \quad \text{i.e. } x_\omega = x_{-\omega} = \frac{x_0}{2}, \quad (7.125)$$

³⁹ Using, e.g., MA Eq. (6.5a). (The imaginary parts of the integrals vanish, because the integration in infinite limits may be always re-centered to the finite points $\pm\hbar\omega$.) A math-enlightened reader may have noticed that the integrals might be taken without the introduction of small ε , using the Cauchy theorem – see MA Eq. (15.1).

⁴⁰ The integration in Eq. (123) may be extended to the whole time axis, $-\infty < \tau < +\infty$, if we complement the definition (107) of the function $G(\tau)$ for $\tau > 0$ with its definition as $G(\tau) = 0$ for $\tau < 0$, in correspondence with the causality principle.

⁴¹ In order to prove this relation, it is sufficient to plug expression $\hat{x}_s = \hat{x}_\omega e^{-i\omega t}$, or any sum of such exponents, into Eqs. (107) and then use the definition (123). This (simple) exercise is highly recommended to the reader.

then, in accordance with the correspondence principle, Eq. (124) should hold for the *c*-number complex amplitudes F_ω and x_ω , enabling us to calculate the time dependence of the force as

$$\begin{aligned} F(t) &= F_\omega e^{-i\omega t} + F_{-\omega} e^{+i\omega t} = \chi(\omega)x_\omega e^{-i\omega t} + \chi(-\omega)x_{-\omega} e^{+i\omega t} = \frac{x_0}{2} [\chi(\omega)e^{-i\omega t} + \chi^*(\omega)e^{+i\omega t}] \\ &= \frac{x_0}{2} [(\chi' + i\chi'')e^{-i\omega t} + (\chi' - i\chi'')e^{+i\omega t}] \equiv x_0 [\chi'(\omega)\cos\omega t + \chi''(\omega)\sin\omega t]. \end{aligned} \quad (7.126)$$

We see that $\chi''(\omega)$ weighs the force's part (frequently called *quadrature*) that is $\pi/2$ -shifted from the coordinate x , i.e. is in phase with its velocity, and hence characterizes the time-average power flow from the system into its environment, i.e. the *energy dissipation* rate:⁴²

$$\overline{\mathcal{P}} = \overline{-F(t)\dot{x}(t)} = \overline{-x_0[\chi'(\omega)\cos\omega t + \chi''(\omega)\sin\omega t]}(-\omega x_0 \sin\omega t) = \frac{x_0^2}{2}\omega\chi''(\omega). \quad (7.127)$$

Let us calculate this function from Eqs. (108) and (123), just as we have done for the spectral density of fluctuations:

$$\begin{aligned} \chi''(\omega) &= \text{Im} \int_0^{+\infty} G(\tau) e^{i\omega\tau} d\tau = \frac{2}{\hbar} \sum_{n,n'} W_n |F_{nn'}|^2 \lim_{\varepsilon \rightarrow 0} \text{Im} \int_0^{+\infty} \frac{1}{2i} \left(\exp \left\{ i \frac{\tilde{E}\tau}{\hbar} \right\} - \text{c.c.} \right) e^{i\omega\tau} e^{-\varepsilon\tau} d\tau \\ &= \sum_{n,n'} W_n |F_{nn'}|^2 \lim_{\varepsilon \rightarrow 0} \text{Im} \left(\frac{1}{-\tilde{E} - \hbar\omega - i\hbar\varepsilon} - \frac{1}{\tilde{E} - \hbar\omega - i\hbar\varepsilon} \right) \\ &\equiv \sum_{n,n'} W_n |F_{nn'}|^2 \lim_{\varepsilon \rightarrow 0} \left(\frac{\hbar\varepsilon}{(\tilde{E} + \hbar\omega)^2 + (\hbar\varepsilon)^2} - \frac{\hbar\varepsilon}{(\tilde{E} - \hbar\omega)^2 + (\hbar\varepsilon)^2} \right). \end{aligned} \quad (7.128)$$

Making the transfer (118) from the double sum to the double integral, and then the integration variable transfer (120), we get

$$\begin{aligned} \chi''(\omega) &= \lim_{\varepsilon \rightarrow 0} \int d\tilde{E} \left[\int_{-\infty}^{+\infty} W \left(\tilde{E} + \frac{\tilde{E}}{2} \right) \rho \left(\tilde{E} + \frac{\tilde{E}}{2} \right) \rho \left(\tilde{E} - \frac{\tilde{E}}{2} \right) |F_{nn'}|^2 \frac{\hbar\varepsilon}{(\tilde{E} + \hbar\omega)^2 + (\hbar\varepsilon)^2} d\tilde{E} \right. \\ &\quad \left. - \int_{-\infty}^{+\infty} W \left(\tilde{E} + \frac{\tilde{E}}{2} \right) \rho \left(\tilde{E} + \frac{\tilde{E}}{2} \right) \rho \left(\tilde{E} - \frac{\tilde{E}}{2} \right) |F_{nn'}|^2 \frac{\hbar\varepsilon}{(\tilde{E} - \hbar\omega)^2 + (\hbar\varepsilon)^2} d\tilde{E} \right]. \end{aligned} \quad (7.129)$$

Now using the same argument about the smallness of parameter ε as above, we may take the spectral densities, the matrix elements of force, and the Gibbs probabilities out of the integrals, and work out the remaining integrals, getting a result very similar to Eq. (122):

$$\chi''(\omega) = \pi \int \rho_+ \rho_- [W_- |F_-|^2 - W_+ |F_+|^2] d\tilde{E}. \quad (7.130)$$

⁴² The sign minus in Eq. (127) is due to the fact that according to Eq. (90), F is the force exerted *on* our system (s) by the environment, so that the force exerted *by* our system on the environment is $-F$. With this sign clarification, the expression $\mathcal{P} = -F\dot{x} = -Fv$ for the instant power flow is evident if x is the usual Cartesian coordinate of a 1D particle. However, according to analytical mechanics (see, e.g., CM Chapters 2 and 10), it is also valid for any {generalized coordinate, generalized force} pair which forms the interaction Hamiltonian (90).

In order to relate these two results, it is sufficient to notice that according to Eq. (24), the Gibbs probabilities W_{\pm} are related by a coefficient depending on only the temperature T and observation frequency ω :

$$W_{\pm} \equiv W\left(\bar{E} + \frac{\tilde{E}_{\pm}}{2}\right) \equiv W\left(\bar{E} \pm \frac{\hbar\omega}{2}\right) = \frac{1}{Z} \exp\left\{-\frac{\bar{E} \pm \hbar\omega/2}{k_B T}\right\} = W(\bar{E}) \exp\left\{\mp \frac{\hbar\omega}{2k_B T}\right\}, \quad (7.131)$$

so that both the spectral density (122) and the dissipative part (130) of the generalized susceptibility may be expressed via the same integral over the environment energies:

$$S_F(\omega) = \hbar \cosh\left(\frac{\hbar\omega}{2k_B T}\right) \int \rho_+ \rho_- W(\bar{E}) [|F_+|^2 + |F_-|^2] d\bar{E}, \quad (7.132)$$

$$\chi''(\omega) = 2\pi \sinh\left(\frac{\hbar\omega}{2k_B T}\right) \int \rho_+ \rho_- W(\bar{E}) [|F_+|^2 + |F_-|^2] d\bar{E}, \quad (7.133)$$

and hence are universally related as

$$S_F(\omega) = \frac{\hbar}{2\pi} \chi''(\omega) \coth \frac{\hbar\omega}{2k_B T}. \quad (7.134)$$

Fluctuation-dissipation theorem

This is, finally, the much-celebrated Callen-Welton's fluctuation-dissipation theorem (FDT). It reveals a fundamental, intimate relationship between these two effects of the environment ("no dissipation without fluctuation") – hence the name. A curious feature of the FDT is that Eq. (134) includes the same function of temperature as the average energy (26) of a quantum oscillator of frequency ω , though, as the reader could witness, the notion of the oscillator was by no means used in its derivation. As will see in the next section, this fact leads to rather interesting consequences and even conceptual opportunities.

In the classical limit, $\hbar\omega \ll k_B T$, the FDT is reduced to

$$S_F(\omega) = \frac{\hbar}{2\pi} \chi''(\omega) \frac{2k_B T}{\hbar\omega} = \frac{k_B T}{\pi} \frac{\text{Im } \chi(\omega)}{\omega}. \quad (7.135)$$

In most systems of interest, the last fraction is close to a finite (positive) constant within a substantial range of relatively low frequencies. Indeed, expanding the right-hand side of Eq. (123) into the Taylor series in small ω , we get

$$\chi(\omega) = \chi(0) + i\omega\eta + \dots, \quad \text{with } \chi(0) = \int_0^\infty G(\tau) d\tau, \quad \text{and } \eta \equiv \int_0^\infty G(\tau) \tau d\tau. \quad (7.136)$$

Since the temporal Green's function G is real by definition, the Taylor expansion of $\chi''(\omega) \equiv \text{Im } \chi(\omega)$ at $\omega = 0$ starts with the linear term $i\omega\eta$, where η is a certain real coefficient, and unless $\eta = 0$, is dominated by this term at small ω . The physical sense of the constant η becomes clear if we consider an environment that provides a force described by a simple, well-known kinematic friction law

$$\langle \hat{F} \rangle = -\eta \dot{\hat{x}}, \quad \text{with } \eta \geq 0, \quad (7.137)$$

where η is usually called the *drag coefficient*. For the Fourier images of coordinate and force, this gives the relation $F_\omega = i\omega\eta x_\omega$, so that according to Eq. (124),

Ohmic
dissipation

$$\chi(\omega) = i\omega\eta, \quad \text{i.e. } \frac{\chi''(\omega)}{\omega} \equiv \frac{\text{Im } \chi(\omega)}{\omega} = \eta \geq 0. \quad (7.138)$$

With this approximation, and in the classical limit, the FDT (134) is reduced to the well-known *Nyquist formula*:⁴³

Nyquist
formula

$$S_F(\omega) = \frac{k_B T}{\pi} \eta, \quad \text{i.e. } \langle F_f^2 \rangle = 4k_B T \eta d\nu. \quad (7.139)$$

According to Eq. (112), if such a constant spectral density⁴⁴ persisted at all frequencies, it would correspond to a delta-correlated process $F(t)$, with

$$K_F(\tau) = 2\pi S_F(0)\delta(\tau) = 2k_B T \eta \delta(\tau) \quad (7.140)$$

- cf. Eqs. (82) and (83). Since in the classical limit the right-hand side of Eq. (109) is negligible, and the correlation function may be considered an even function of time, the symmetrized function under the integral in Eq. (113) may be rewritten just as $\langle F(\tau)F(0) \rangle$. In the limit of relatively low observation frequencies (in the sense that ω is much smaller than not only the quantum frontier $k_B T/\hbar$ but also the frequency scale of the function $\chi''(\omega)/\omega$), Eq. (138) may be used to recast Eq. (135) in the form⁴⁵

$$\eta \equiv \lim_{\omega \rightarrow 0} \frac{\chi''(\omega)}{\omega} = \frac{1}{k_B T} \int_0^\infty \langle F(\tau)F(0) \rangle d\tau. \quad (7.141)$$

To conclude this section, let me return for a minute to the questions formulated in our earlier discussion of dephasing in the two-level model. In that problem, the dephasing time scale is $T_2 = 1/2D_\phi$. Hence the classical approach to the dephasing, used in Sec. 3, is adequate if $\hbar D_\phi \ll k_B T$. Next, we may identify the operators \hat{f} and $\hat{\sigma}_z$ participating in Eq. (70) with, respectively, $(-\hat{F})$ and \hat{x} participating in the general Eq. (90). Then the comparison of Eqs. (82), (89), and (140) yields

$$\frac{1}{T_2} \equiv 2D_\phi = \frac{4k_B T}{\hbar^2} \eta, \quad (7.142)$$

Classical
dephasing

⁴³ Actually, the 1928 work by H. Nyquist was about the electronic noise in resistors, just discovered experimentally by his Bell Labs colleague John Bertrand Johnson. For an Ohmic resistor, as the dissipative “environment” of the electric circuit it is connected with, Eq. (137) is just the Ohm’s law, and may be recast as either $\langle V \rangle = -R(dQ/dt) = RI$, or $\langle I \rangle = -G(d\Phi/dt) = GV$. Thus for the voltage V across an open circuit, η corresponds to its resistance R , while for current I in a short circuit, to its conductance $G = 1/R$. In this case, the fluctuations described by Eq. (139) are referred to as the *Johnson-Nyquist noise*. (Because of this important application, any model leading to Eq. (138) is commonly referred to as the *Ohmic dissipation*, even if the physical nature of the variables x and F is quite different from voltage and current.)

⁴⁴ A random process whose spectral density may be reasonably approximated by a constant is frequently called the *white noise*, because it is a random mixture of all possible sinusoidal components with equal weights, reminding the spectral composition of the natural white light.

⁴⁵ Note that in some fields (especially in physical kinetics and chemical physics), this particular limit of the Nyquist formula is called the Green-Kubo (or just “Kubo”) formula. However, in the view of the FDT development history (described above), it is much more reasonable to associate these names with Eq. (109) – as it is done in most fields of physics.

so that, for the model described by Eq. (137) with a temperature-independent drag coefficient η , the rate of dephasing by a classical environment is proportional to its temperature.

7.5. The Heisenberg-Langevin approach

The fluctuation-dissipation theorem offers a very simple and efficient, though limited approach to the analysis of the system of interest (s in Fig. 1). It is to write its Heisenberg equations (4.199) of motion of the relevant operators, which would now include the environmental force operator, and explore these equations using the Fourier transform and the Wiener-Khinchin theorem (112)-(113). This approach to classical equations of motion is commonly associated with the name of Langevin,⁴⁶ so that its extension to dynamics of Heisenberg-picture operators is frequently referred to as the *Heisenberg-Langevin* (or “quantum Langevin”, or “Langevin-Lax”⁴⁷) *approach* to open system analysis.

Perhaps the best way to describe this method is to demonstrate how it works for the very important case of a 1D harmonic oscillator, so that the generalized coordinate x of Sec. 4 is just the oscillator’s coordinate. For the sake of simplicity, let us assume that the environment provides the simple Ohmic dissipation described by Eq. (137) – which is a very good approximation in many cases. As we already know from Chapter 5, the Heisenberg equations of motion for operators of coordinate and momentum of the oscillator, in the presence of an external force $F(t)$, are

$$\dot{\hat{x}} = \frac{\hat{p}}{m}, \quad \dot{\hat{p}} = -m\omega_0^2 \hat{x} + \hat{F}, \quad (7.143)$$

so that using Eqs. (92) and (137), we get

$$\dot{\hat{x}} = \frac{\hat{p}}{m}, \quad \dot{\hat{p}} = -m\omega_0^2 \hat{x} - \eta \dot{\hat{x}} + \hat{F}(t). \quad (7.144)$$

Combining Eqs. (144), we may write their system as a single differential equation

$$m\ddot{\hat{x}} + \eta \dot{\hat{x}} + m\omega_0^2 \hat{x} = \hat{F}(t), \quad (7.145)$$

which is similar to the well-known classical equation of motion of a damped oscillator under the effect of an external force. In the view of Eqs. (5.29) and (5.35), whose corollary the Ehrenfest theorem (5.36) is, this may look not surprising, but please note again that the approach discussed in the previous section justifies such quantitative description of the drag force in quantum mechanics – necessarily in parallel with the accompanying fluctuation force.

For the Fourier images of the operators, defined similarly to Eq. (115), Eq. (145) gives the following relation,

⁴⁶ A 1908 work by Paul Langevin was the first systematic development of Einstein’s ideas (1905) on the Brownian motion, using the random force language, as an alternative to Smoluchowski’s approach using the probability density language – see Sec. 6 below.

⁴⁷ Indeed, perhaps the largest credit for the extension of the Langevin approach to quantum systems belongs to Melvin J. Lax, whose work in the early 1960s was motivated mostly by quantum electronics applications – see, e.g., his monograph M. Lax, *Fluctuation and Coherent Phenomena in Classical and Quantum Physics*, Gordon and Breach, 1968, and references therein.

$$\hat{x}_\omega = \frac{F_\omega}{m(\omega_0^2 - \omega^2) - i\eta\omega}, \quad (7.146)$$

which should be also well known to the reader from the classical theory of forced oscillations.⁴⁸ However, since these Fourier components are still Heisenberg-picture operators, and their “values” for different ω generally do not commute, we have to tread carefully. The best way to proceed is to write a copy of Eq. (146) for frequency ($-\omega$), and then combine these equations to form a symmetrical combination similar to that used in Eq. (114). The result is

$$\frac{1}{2} \langle \hat{x}_\omega \hat{x}_{-\omega} + \hat{x}_{-\omega} \hat{x}_\omega \rangle = \frac{1}{|m(\omega_0^2 - \omega^2) - i\eta\omega|^2} \frac{1}{2} \langle \hat{F}_\omega \hat{F}_{-\omega} + \hat{F}_{-\omega} \hat{F}_\omega \rangle. \quad (7.147)$$

Since the spectral density definition similar to Eq. (114) is valid for any observable, in particular for x , Eq. (147) allows us to relate the symmetrized spectral densities of coordinate and force:

$$S_x(\omega) = \frac{S_F(\omega)}{|m(\omega_0^2 - \omega^2) - i\eta\omega|^2} \equiv \frac{S_F(\omega)}{m^2(\omega_0^2 - \omega^2)^2 + (\eta\omega)^2}. \quad (7.148)$$

Now using an analog of Eq. (116) for x , we can calculate the coordinate’s variance:

$$\langle x^2 \rangle = K_x(0) = \int_{-\infty}^{+\infty} S_x(\omega) d\omega = 2 \int_0^{+\infty} \frac{S_F(\omega) d\omega}{m^2(\omega_0^2 - \omega^2)^2 + (\eta\omega)^2}, \quad (7.149)$$

where now, in contrast to the notation used in Sec. 4, the sign $\langle \dots \rangle$ means averaging over the usual statistical ensemble of many systems of interest – in our current case, of many harmonic oscillators.

If the coupling to the environment is so weak that the drag coefficient η is small (in the sense that the oscillator’s dimensionless *Q-factor* is large, $Q \equiv m\omega_0/\eta \gg 1$), this integral is dominated by the resonance peak in a narrow vicinity, $|\omega - \omega_0| \equiv |\xi| \ll \omega_0$, of its resonance frequency, and we can take the relatively smooth function $S_F(\omega)$ out of the integral, thus reducing it to a table form:⁴⁹

$$\begin{aligned} \langle x^2 \rangle &\approx 2S_F(\omega_0) \int_0^{+\infty} \frac{d\omega}{m^2(\omega_0^2 - \omega^2)^2 + (\eta\omega)^2} \approx 2S_F(\omega_0) \int_{-\infty}^{+\infty} \frac{d\xi}{(2m\omega_0\xi)^2 + (\eta\omega_0)^2} \\ &\equiv 2S_F(\omega_0) \frac{1}{(\eta\omega_0)^2} \int_{-\infty}^{+\infty} \frac{d\xi}{(2m\xi/\eta)^2 + 1} = 2S_F(\omega_0) \frac{1}{(\eta\omega_0)^2} \frac{\pi\eta}{2m} = \frac{\pi S_F(\omega_0)}{\eta m \omega_0^2}. \end{aligned} \quad (7.150)$$

With the account of the FDT (134) and of Eq. (138), this gives⁵⁰

$$\langle x^2 \rangle = \frac{\pi}{\eta m \omega_0^2} \frac{\hbar}{2\pi} \eta \omega_0 \coth \frac{\hbar \omega_0}{2k_B T} \equiv \frac{\hbar}{2m\omega_0} \coth \frac{\hbar \omega_0}{2k_B T}. \quad (7.151)$$

⁴⁸ If necessary, see CM Sec. 5.1.

⁴⁹ See, e.g., MA Eq. (6.5a).

⁵⁰ Note that this calculation remains correct even if the dissipation’s dispersion law deviates from the Ohmic model (138), provided that the drag coefficient η is replaced with its effective value $\text{Im}\chi(\omega_0)/\omega_0$, because the effects of the environment are only felt, by the oscillator, at its oscillation frequency.

But this is exactly Eq. (48), which was derived in Sec. 2 from the Gibbs distribution, without any explicit account of the environment – though keeping it in mind by using the notion of the thermally-equilibrium ensemble.⁵¹

Notice that in the final form of Eq. (151) the coefficient η , which characterizes the oscillator-to-environment interaction strength, has canceled! Does this mean that in Sec. 4 we toiled in vain? By no means. First of all, the result (150), augmented by the FDT (134), has an important conceptual value. For example, let us consider the low-temperature limit $k_B T \ll \hbar\omega_0$ where Eq. (151) is reduced to

$$\langle x^2 \rangle = \frac{\hbar}{2m\omega_0} \equiv \frac{x_0^2}{2}. \quad (7.152)$$

Let us ask a naïve question: what exactly is the origin of this coordinate's uncertainty? From the point of view of the usual quantum mechanics of absolutely closed (Hamiltonian) systems, there is no doubt: this non-vanishing variance of the coordinate is the result of the final spatial extension of the ground-state wavefunction (2.275), reflecting Heisenberg's uncertainty relation – which in turn results from the fact that the operators of coordinate and momentum do not commute. However, from the point of view of the Heisenberg-Langevin equation (145), the variance (152) is an inalienable part of the oscillator's response to the fluctuation force $\tilde{F}(t)$ exerted by the environment at frequencies $\omega \approx \omega_0$. Though it is impossible to refute the former, absolutely legitimate point of view, in many applications it is easier to subscribe to the latter standpoint and treat the coordinate's uncertainty as the result of the so-called *quantum noise* of the environment, which, in equilibrium, obeys the FTD (134). This notion has received numerous confirmations in experiments that did not include *any* oscillators with their own frequencies ω_0 close to the noise measurement frequency ω .⁵²

The second advantage of the Heisenberg-Langevin approach is that it is possible to use Eq. (148) to calculate the (experimentally measurable!) distribution $S_x(\omega)$, i.e. decompose the fluctuations into their spectral components. This procedure is not restricted to the limit of small η (i.e. of large Q); for any damping, we may just plug the FDT (134) into Eq. (148). For example, let us have a look at the so-called *quantum diffusion*. A free 1D particle, moving in a viscous medium providing it with the Ohmic damping (137), may be considered as the particular case of a 1D harmonic oscillator (145), but with $\omega_0 = 0$, so that combining Eqs. (134) and (149), we get

$$\langle x^2 \rangle = 2 \int_0^{+\infty} \frac{S_F(\omega)d\omega}{(m\omega^2)^2 + (\eta\omega)^2} = 2\eta \int_0^{+\infty} \frac{1}{(m\omega^2)^2 + (\eta\omega)^2} \frac{\hbar\omega}{2\pi} \coth \frac{\hbar\omega}{2k_B T} d\omega. \quad (7.153)$$

This integral has two divergences. The first one, of the type $\int d\omega/\omega^2$ at the lower limit, is just a classical effect: according to Eq. (85), the particle's displacement variance grows with time, so it cannot have a finite time-independent value that Eq. (153) tries to calculate. However, we still can use that result to single out the quantum effects on diffusion – say, by comparing it with a similar but purely classical case. These effects are prominent at high frequencies, especially if the quantum noise overcomes the thermal noise before the dynamic cut-off, i.e. if

⁵¹ By the way, the simplest way to calculate $S_F(\omega)$, i.e. to derive the FDT, is to *require* that Eqs. (48) and (150) give the same result for an oscillator with any eigenfrequency ω . This is exactly the approach used by H. Nyquist (for the classical case) – see also SM Sec. 5.5.

⁵² See, for example, R. Koch *et al.*, *Phys. Lev. B* **26**, 74 (1982).

$$\frac{k_B T}{\hbar} \ll \frac{\eta}{m}. \quad (7.154)$$

In this case, there is a broad range of frequencies where the quantum noise gives a substantial contribution to the integral:

Quantum diffusion

$$\langle x^2 \rangle_Q \approx 2\eta \int_{k_B T / \hbar}^{\eta / m} \frac{1}{(\eta\omega)^2} \frac{\hbar\omega}{2\pi} d\omega \equiv \frac{\hbar}{\pi\eta} \int_{k_B T / \hbar}^{\eta / m} \frac{d\omega}{\omega} = \frac{\hbar}{\pi\eta} \ln \frac{\hbar\eta}{mk_B T} \sim \frac{\hbar}{\eta}. \quad (7.155)$$

Formally, this contribution diverges at either $m \rightarrow 0$ or $T \rightarrow 0$, but this logarithmic (i.e. extremely weak) divergence is readily quenched by almost any change of the environment model at very high frequencies, where the “Ohmic” approximation (136) becomes unrealistic.

The Heisenberg-Langevin approach is very powerful, because its straightforward generalizations enable analyses of fluctuations in virtually arbitrary linear systems, i.e. the systems described by linear differential (or integro-differential) equations of motion, including those with many degrees of freedom, and distributed systems (*continua*), and such systems prevail in many fields of physics. However, this approach also has its limitations. The main of them is that if the equations of motion of the Heisenberg operators are *not* linear, there is no linear relation, such as Eq. (146), between the Fourier images of the generalized forces and the generalized coordinates, and as the result, there is no simple relation, such as Eq. (148), between their spectral densities. In other words, if the Heisenberg equations of motion are nonlinear, there is no regular simple way to use them to calculate the statistical properties of the observables.

For example, let us return to the dephasing problem described by Eqs. (68)-(70), and assume that the deterministic and fluctuating parts of the effective force \dot{f} exerted by the environment, are characterized by relations similar, respectively, to Eqs. (124) and (134). Now writing the Heisenberg equations of motion for the two remaining spin operators, and using the commutation relations between them, we get

$$\dot{\hat{\sigma}}_x = \frac{1}{i\hbar} [\hat{\sigma}_x, \hat{H}] = \frac{1}{i\hbar} [\hat{\sigma}_x, (c_z + \hat{f}) \hat{\sigma}_z] = -\frac{2}{\hbar} \hat{\sigma}_y (c_z + \hat{f}) = -\frac{2}{\hbar} \hat{\sigma}_y (c_z + \eta \hat{\sigma}_z + \hat{f}), \quad (7.156)$$

and a similar equation for $\dot{\hat{\sigma}}_y$. Such nonlinear equations cannot be used to calculate the statistical properties of the Pauli operators in this system exactly – at least analytically.

For some calculations, this problem may be circumvented by *linearization*: if we are only interested in small fluctuations of the observables, their nonlinear Heisenberg equations of motion, such as Eq. (156), may be linearized with respect to small deviations of the operators about their (generally, time-dependent) deterministic “values”, and then the resulting linear equations for the operator variations may be solved either as has been demonstrated above, or (if the deterministic “values” evolve in time) using their Fourier expansions. Sometimes such approach gives relatively simple and important results,⁵³ but for many other problems, this approach is insufficient, leaving a lot of space for alternative methods.

⁵³ For example, the formula used for processing the experimental results by R. Koch *et al.* (mentioned above), had been derived in this way. (This derivation will be suggested to the reader as an exercise.)

7.6. Density matrix approach

The main alternative approach to the dynamics of open quantum systems, which is essentially a generalization of the one discussed in Sec. 2, is to extract the final results of interest from the dynamics of the density operator of our system s . Let us discuss this approach in detail.⁵⁴

We already know that the density matrix allows the calculation of the expectation value of any observable of the system s – see Eq. (5). However, our initial recipe (6) for the density matrix element calculation, which requires the knowledge of the exact state (2) of the whole Universe, is not too practicable, while the von Neumann equation (66) for the density matrix evolution is limited to cases in which probabilities W_j of the system states are fixed – thus excluding such important effects as the energy relaxation. However, such effects may be analyzed using a different assumption – that the system of interest interacts only with a *local environment* that is very close to its thermally-equilibrium state described, in the stationary-state basis, by a diagonal density matrix with the elements (24).

This calculation is facilitated by the following general observation. Let us number the basis states of the full local system (the system of our interest plus its local environment) by l , and use Eq. (5) to write

$$\langle A \rangle = \text{Tr}(\hat{A}\hat{w}_l) \equiv \sum_{l,l'} A_{ll'} w_{ll'} = \sum_{l,l'} \langle l | \hat{A} | l' \rangle \langle l' | \hat{w}_l | l \rangle, \quad (7.157)$$

where \hat{w}_l is the density operator of this local system. At a weak interaction between the system s and the local environment e , their states reside in different Hilbert spaces, so that we can write

$$|l\rangle = |s_j\rangle \otimes |e_k\rangle, \quad (7.158)$$

and if the observable A depends only on the coordinates of the system s of our interest, we may reduce Eq. (157) to the form similar to Eq. (5):

$$\begin{aligned} \langle A \rangle &= \sum_{j,j';k,k'} \langle e_k | \otimes \langle s_j | \hat{A} | s_{j'} \rangle \otimes | e_{k'} \rangle \langle e_{k'} | \otimes \langle s_{j'} | \hat{w}_l | s_j \rangle \otimes | e_k \rangle \\ &= \sum_{j,j'} A_{jj'} \left\langle s_{j'} \left(\sum_k \otimes \langle e_k | \hat{w}_l | e_k \rangle \otimes \right) \right| s_j \rangle = \text{Tr}_j(\hat{A}\hat{w}), \end{aligned} \quad (7.159)$$

where

$$\hat{w} \equiv \sum_k \langle e_k | \hat{w}_l | e_k \rangle = \text{Tr}_k \hat{w}_l, \quad (7.160)$$

showing how exactly the density operator \hat{w} of the system s may be calculated from \hat{w}_l .

Now comes the key physical assumption of this approach: since we may select the local environment e to be much larger than the system s of our interest, we may consider the composite system l as a Hamiltonian one, with time-independent probabilities of its stationary states, so that for the description of the evolution in time of *its* full density operator \hat{w}_l (again, in contrast to that, \hat{w} , of the system of our interest) we *may* use the von Neumann equation (66). Partitioning its right-hand side in accordance with Eq. (68), we get:

$$i\hbar \dot{\hat{w}}_l = [\hat{H}_s, \hat{w}_l] + [\hat{H}_e, \hat{w}_l] + [\hat{H}_{\text{int}}, \hat{w}_l]. \quad (7.161)$$

⁵⁴ As in Sec. 4, the reader not interested in the derivation of the basic equation (181) of the density matrix evolution may immediately jump to the discussion of this equation and its applications.

The next step is to use the perturbation theory to solve this equation in the lowest order in \hat{H}_{int} , which would yield, for the evolution of w , a non-vanishing contribution due to the interaction. For that, Eq. (161) is not very convenient, because its right-hand side contains two other terms, of a much larger scale than the interaction Hamiltonian. To mitigate this technical difficulty, the interaction picture that was discussed at the end of Sec. 4.6, is very natural. (It is not necessary though, and I will use this picture mostly as an exercise of its application – unfortunately, the only example I can afford in this course.)

As a reminder, in that picture (whose entities will be marked with index “I”, with the unmarked operators assumed to be in the Schrödinger picture), both the operators *and* the state vectors (and hence the density operator) depend on time. However, the time evolution of the operator of any observable A is described by an equation similar to Eq. (67), but with the *unperturbed* part of the Hamiltonian only – see Eq. (4.214). In model (68), this means

$$i\hbar\dot{\hat{A}}_I = [\hat{A}_I, \hat{H}_0]. \quad (7.162)$$

where the unperturbed Hamiltonian consists of two parts defined in different Hilbert spaces:

$$\hat{H}_0 \equiv \hat{H}_s + \hat{H}_e. \quad (7.163)$$

On the other hand, the state vector’s dynamics is governed by the interaction evolution operator \hat{u}_I that obeys Eqs. (4.215). Since this equation, using the interaction-picture Hamiltonian (4.216),

$$\hat{H}_I \equiv \hat{u}_0^\dagger \hat{H}_{\text{int}} \hat{u}_0, \quad (7.164)$$

is absolutely similar to the ordinary Schrödinger equation using the full Hamiltonian, we may repeat all arguments given at the beginning of Sec. 3 to prove that the dynamics of the density operator in the interaction picture of a Hamiltonian system is governed by the following analog of the von Neumann equation (66):

$$i\hbar\dot{\hat{w}}_I = [\hat{H}_I, \hat{w}_I], \quad (7.165)$$

where the index I is dropped for the notation simplicity. Since this equation is similar in structure (with the opposite sign) to the Heisenberg equation (67), we may use the solution Eq. (4.190) of the latter equation to write its analog:

$$\hat{w}_I(t) = \hat{u}_I(t, 0)\hat{w}_I(0)\hat{u}_I^\dagger(t, 0). \quad (7.166)$$

It is also straightforward to verify that in this picture, the expectation value of any observable A may be found from an expression similar to the basic Eq. (5):

$$\langle A \rangle = \text{Tr}(\hat{A}_I \hat{w}_I). \quad (7.167)$$

showing again that the interaction and Schrödinger pictures give the same final results.

In the most frequent case of factorable interaction (90),⁵⁵ Eq. (162) is simplified for both operators participating in that product – for each one in its own way. In particular, for $\hat{A} = \hat{x}$, it yields

⁵⁵ A similar analysis of a more general case, when the interaction with the environment has to be represented as a sum of products of the type (90), may be found, for example, in the monograph by K. Blum, *Density Matrix Theory and Applications*, 3rd ed., Springer, 2012.

$$i\hbar\dot{\hat{x}}_I = [\hat{x}_I, \hat{H}_0] = [\hat{x}_I, \hat{H}_s] + [\hat{x}_I, \hat{H}_e]. \quad (7.168)$$

Since the coordinate operator is defined in the Hilbert space of our system s , it commutes with the Hamiltonian of the environment, so that we finally get

$$i\hbar\dot{\hat{x}}_I = [\hat{x}_I, \hat{H}_s]. \quad (7.169)$$

On the other hand, if $\hat{A} = \hat{F}$, this operator is defined in the Hilbert space of the environment, and commutes with the Hamiltonian of the unperturbed system s . As a result, we get

$$i\hbar\dot{\hat{F}}_I = [\hat{F}_I, \hat{H}_e]. \quad (7.170)$$

This means that with our time-independent unperturbed Hamiltonians, \hat{H}_s and \hat{H}_e , the time evolution of the interaction-picture operators is rather simple. In particular, the analogy between Eq. (170) and Eq. (93) allows us to immediately write the following analog of Eq. (94):

$$\hat{F}_I(t) = \exp\left\{+\frac{i}{\hbar}\hat{H}_e t\right\} \hat{F}(0) \exp\left\{-\frac{i}{\hbar}\hat{H}_e t\right\}, \quad (7.171)$$

so that in the stationary-state basis n of the environment,

$$(\hat{F}_I)_{nn'}(t) = \exp\left\{+\frac{i}{\hbar}E_n t\right\} F_{nn'}(0) \exp\left\{-\frac{i}{\hbar}E_n t\right\} \equiv F_{nn'}(0) \exp\left\{-i\frac{E_n - E_{n'}}{\hbar} t\right\}, \quad (7.172)$$

and similarly (but in the basis of the stationary states of system s) for operator \hat{x} . As a result, the right-hand side of Eq. (164) may be also factored:

$$\begin{aligned} \hat{H}_I(t) &\equiv \hat{u}_0^\dagger(t, 0) \hat{H}_{\text{int}} \hat{u}_0(t, 0) = \exp\left\{+\frac{i}{\hbar}(\hat{H}_s + \hat{H}_e)t\right\} (-\hat{x}\hat{F}) \exp\left\{-\frac{i}{\hbar}(\hat{H}_s + \hat{H}_e)t\right\} \\ &= -\left(\exp\left\{+\frac{i}{\hbar}\hat{H}_s t\right\} \hat{x} \exp\left\{-\frac{i}{\hbar}\hat{H}_s t\right\} \right) \left(\exp\left\{+\frac{i}{\hbar}\hat{H}_e t\right\} \hat{F}(0) \exp\left\{-\frac{i}{\hbar}\hat{H}_e t\right\} \right) \equiv -\hat{x}_I(t)\hat{F}_I(t). \end{aligned} \quad (7.173)$$

So, the transfer to the interaction picture has taken some time, but now it enables a smooth ride.⁵⁶ Indeed, just as in Sec. 4, we may rewrite Eq. (165) in the integral form:

$$\hat{w}_I(t) = \frac{1}{i\hbar} \int_{-\infty}^t [\hat{H}_I(t'), \hat{w}_I(t')] dt'; \quad (7.174)$$

plugging this result into the right-hand side of Eq. (165), we get

$$\dot{\hat{w}}_I(t) = -\frac{1}{\hbar^2} \int_{-\infty}^t [\hat{H}_I(t), [\hat{H}_I(t'), \hat{w}_I(t')]] dt' = -\frac{1}{\hbar^2} \int_{-\infty}^t [\hat{x}(t)\hat{F}(t), [\hat{x}(t')\hat{F}(t'), \hat{w}_I(t')]] dt', \quad (7.175)$$

where, for the notation's brevity, from this point on I will strip the operators \hat{x} and \hat{F} of their index "I". (I hope their time dependence indicates the interaction picture clearly enough.)

⁵⁶ If we used either the Schrödinger or the Heisenberg picture instead, the forthcoming Eq. (175) would pick up a rather annoying multitude of fast-oscillating exponents, of different time arguments, on its right-hand side.

So far, this equation is exact (and cannot be solved analytically), but this is a good time to notice that even if we approximate the density operator on its right-hand side by its unperturbed, factorable “value” (corresponding to no interaction between the system s and its thermally-equilibrium environment e),⁵⁷

$$\hat{w}_I(t') \rightarrow \hat{w}(t')\hat{w}_e, \quad \text{with } \langle e_n | \hat{w}_e | e_{n'} \rangle = W_n \delta_{nn'}, \quad (7.176)$$

where e_n are the stationary states of the environment and W_n are the Gibbs probabilities (24), Eq. (175) still describes nontrivial time evolution of the density operator. This is exactly the first non-vanishing approximation (in the weak interaction) we have been looking for. Now using Eq. (160), we find the equation of evolution of the density operator of the system of our interest:

$$\dot{\hat{w}}(t) = -\frac{1}{\hbar^2} \int_{-\infty}^t \text{Tr}_n [\hat{x}(t)\hat{F}(t), [\hat{x}(t')\hat{F}(t'), \hat{w}(t')\hat{w}_e]] dt', \quad (7.177)$$

where the trace is over the stationary states of the environment. To spell out the right-hand side of Eq. (177), note again that the coordinate and force operators commute with each other (but not with themselves at different time moments!) and hence may be swapped at will, so that we may write

$$\begin{aligned} \text{Tr}_n [...] &= \hat{x}(t)\hat{x}(t')\hat{w}(t')\text{Tr}_n [\hat{F}(t)\hat{F}(t')\hat{w}_e] - \hat{x}(t)\hat{w}(t')\hat{x}(t')\text{Tr}_n [\hat{F}(t)\hat{w}_e\hat{F}(t')] \\ &\quad - \hat{x}(t')\hat{w}(t')\hat{x}(t)\text{Tr}_n [\hat{F}(t')\hat{w}_e\hat{F}(t)] + \hat{w}(t')\hat{x}(t')\hat{x}(t)\text{Tr}_n [\hat{w}_e\hat{F}(t')\hat{F}(t)] \\ &= \hat{x}(t)\hat{x}(t')\hat{w}(t') \sum_{n,n'} F_{nn'}(t)F_{n'n}(t')W_n - \hat{x}(t)\hat{w}(t')\hat{x}(t') \sum_{n,n'} F_{nn'}(t)W_{n'}F_{n'n}(t') \\ &\quad - \hat{x}(t')\hat{w}(t')\hat{x}(t) \sum_{n,n'} F_{nn'}(t')W_{n'}F_{n'n}(t) + \hat{w}(t')\hat{x}(t')\hat{x}(t) \sum_{n,n'} W_n F_{nn'}(t')F_{n'n}(t). \end{aligned} \quad (7.178)$$

Since the summation over both indices n and n' in this expression is over the same energy level set (of all stationary states of the environment), we may swap these indices in any of the sums. Doing this only in the terms including the factors $W_{n'}$, we turn them into W_n , so that this factor becomes common:

$$\begin{aligned} \text{Tr}_n [...] &= \sum_{n,n'} W_n [\hat{x}(t)\hat{x}(t')\hat{w}(t')F_{nn'}(t)F_{n'n}(t') - \hat{x}(t)\hat{w}(t')\hat{x}(t')F_{n'n}(t)F_{nn'}(t')] \\ &\quad - \hat{x}(t')\hat{w}\hat{x}(t)F_{n'n}(t')F_{nn'}(t) + \hat{w}\hat{x}(t')\hat{x}(t)F_{nn'}(t')F_{n'n}(t)]. \end{aligned} \quad (7.179)$$

Now using Eq. (172), we get

$$\begin{aligned} \text{Tr}_n [...] &= \sum_{n,n'} W_n |F_{nn'}|^2 \times \left[\begin{aligned} &\hat{x}(t)\hat{x}(t')\hat{w}(t')\exp\left\{+\frac{i\tilde{E}(t-t')}{\hbar}\right\} - \hat{x}(t)\hat{w}(t')\hat{x}(t')\exp\left\{-\frac{i\tilde{E}(t-t')}{\hbar}\right\} \\ &- \hat{x}(t')\hat{w}(t')\hat{x}(t)\exp\left\{+\frac{i\tilde{E}(t-t')}{\hbar}\right\} + \hat{w}(t')\hat{x}(t')\hat{x}(t)\exp\left\{-\frac{i\tilde{E}(t-t')}{\hbar}\right\} \end{aligned} \right] \\ &\equiv \sum_{n,n'} W_n |F_{nn'}|^2 \cos \frac{\tilde{E}(t-t')}{\hbar} [\hat{x}(t), [\hat{x}(t'), \hat{w}(t')]] + i \sum_{n,n'} W_n |F_{nn'}|^2 \sin \frac{\tilde{E}(t-t')}{\hbar} [\hat{x}(t), \{\hat{x}(t'), \hat{w}(t')\}]. \end{aligned} \quad (7.180)$$

Comparing the two double sums participating in this expression with Eqs. (108) and (111), we see that they are nothing else than, respectively, the symmetrized correlation function and the temporal Green’s

⁵⁷ For the notation simplicity, the fact that here (and in all following formulas) the density operator \hat{w} of the system s of our interest is taken in the interaction picture, is just implied.

function (multiplied by $\hbar/2$) of the time-difference argument $\tau = t - t' \geq 0$. As the result, Eq. (177) takes a compact form:

$$\dot{\hat{w}}(t) = -\frac{1}{\hbar^2} \int_{-\infty}^t K_F(t-t') [\hat{x}(t), [\hat{x}(t'), \hat{w}(t')]] dt' - \frac{i}{2\hbar} \int_{-\infty}^t G(t-t') [\hat{x}(t), \{\hat{x}(t'), \hat{w}(t')\}] dt'. \quad (7.181)$$

Density matrix:
time evolution

Let me hope that the readers (especially the ones who have braved through this derivation) enjoy this beautiful result as much as I do. It gives an equation for the time evolution of the density operator of the system of our interest (s), with the effects of its environment represented only by two real, c -number functions of τ : one (K_F) describing the fluctuation force exerted by the environment, and the other one (G) representing its ensemble-averaged environment's response to the system's evolution. And most spectacularly, these are exactly the same functions that participate in the alternative, Heisenberg-Langevin approach to the problem, and hence related to each other by the fluctuation-dissipation theorem (134).

After a short celebration, let us acknowledge that Eq. (181) is still an integro-differential equation, and needs to be solved together with Eq. (169) for the system coordinate's evolution. Such equations do not allow explicit analytical solutions, besides a few very simple (and not very interesting) cases. For most applications, further simplifications should be made. One of them is based on the fact (which was already discussed in Sec. 3) that both environmental functions participating in Eq. (181) tend to zero when their argument τ becomes much larger than the environment's correlation time τ_c , independent of the system-to-environment coupling strength. If the coupling is sufficiently weak, the time scales $T_{nn'}$ of the evolution of the density matrix elements, following from Eq. (181), are much longer than this correlation time, and also the characteristic time scale of the coordinate operator's evolution. In this limit, all arguments t' of the density operator, giving substantial contributions to the right-hand side of Eq. (181), are so close to t that it does not matter whether its argument is t' or just t . This simplification, $w(t') \approx w(t)$, is known as the *Markov approximation*.⁵⁸

However, this approximation alone is still insufficient for finding the general solution of Eq. (181). Substantial further progress is possible in two important cases. The most important of them is when the intrinsic Hamiltonian \hat{H}_s of the system s of our interest does not depend on time explicitly and has a *discrete* eigenenergy spectrum E_n ,⁵⁹ with well-separated levels:

$$|E_n - E_{n'}| \gg \frac{\hbar}{T_{nn'}}. \quad (7.182)$$

Let us see what does this condition yield for Eq. (181), rewritten for the matrix elements in the stationary state basis, in the Markov approximation:

⁵⁸ Named after Andrey Andreyevich Markov (1856-1922; in older Western literature, “Markoff”), a mathematician famous for his general theory of the so-called *Markov processes*, whose future development is completely determined by its present state, but not its pre-history.

⁵⁹ Here, rather reluctantly, I will use this standard notation, E_n , for the eigenenergies of our system of interest (s), in hope that the reader would not confuse these discrete energy levels with the quasi-continuous energy levels of its environment (e), participating in particular in Eqs. (108) and (111). As a reminder, by this stage of our calculations, the environment levels have disappeared from our formulas, leaving behind their functionals $K_F(\tau)$ and $G(\tau)$.

$$\dot{w}_{nn'} = -\frac{1}{\hbar^2} \int_{-\infty}^t K_F(t-t') [\hat{x}(t), [\hat{x}(t'), \hat{w}]]_{nn'} dt' - \frac{i}{2\hbar} \int_{-\infty}^t G(t-t') [\hat{x}(t), \{\hat{x}(t'), \hat{w}\}]_{nn'} dt'. \quad (7.183)$$

After spelling out the commutators, the right-hand side of this expression includes four operator products, which differ “only” by the operator order. Let us first have a look at one of these products,

$$[\hat{x}(t)\hat{x}(t')\hat{w}]_{nn'} \equiv \sum_{m,m'} x_{nm}(t)x_{mm'}(t')w_{m'n'}, \quad (7.184)$$

where the indices m and m' run over the same set of stationary states of the system s of our interest as the indices n and n' . According to Eq. (169) with a time-independent H_s , the matrix elements $x_{nn'}$ (in the stationary state basis) oscillate in time as $\exp\{i\omega_{nn'}t\}$, so that

$$[\hat{x}(t)\hat{x}(t')\hat{w}]_{nn'} = \sum_{m,m'} x_{nm}x_{mm'} \exp\{i(\omega_{nm}t + \omega_{mm'}t')\} w_{m'n'}, \quad (7.185)$$

where on the right-hand side, the coordinate matrix elements are in the Schrödinger picture, and the usual notation (6.85) is used for the quantum transition frequencies:

$$\hbar\omega_{nn'} \equiv E_n - E_{n'}. \quad (7.186)$$

According to the condition (182), frequencies $\omega_{nn'}$ with $n \neq n'$ are much higher than the speed of evolution of the density matrix elements (in the interaction picture!) – on both the left-hand and right-hand sides of Eq. (183). Hence, on the right-hand side of Eq. (183), we may keep only the terms that do not oscillate with these frequencies $\omega_{nn'}$, because rapidly-oscillating terms would give negligible contributions to the density matrix dynamics.⁶⁰ For that, in the double sum (185) we should save only the terms proportional to the difference $(t - t')$ because they will give (after the integration over t') a slowly changing contribution to the right-hand side.⁶¹ These terms should have $\omega_{nm} + \omega_{mm'} = 0$, i.e. $(E_n - E_m) + (E_m - E_{m'}) \equiv E_n - E_{m'} = 0$. For a non-degenerate energy spectrum, this requirement means $m' = n$; as a result, the double sum is reduced to a single one:

$$[\hat{x}(t)\hat{x}(t')\hat{w}]_{nn'} \approx w_{nn'} \sum_m x_{nm}x_{mn} \exp\{i\omega_{nm}(t-t')\} \equiv w_{nn'} \sum_m |x_{nm}|^2 \exp\{i\omega_{nm}(t-t')\}. \quad (7.187)$$

Another product, $[\hat{w}\hat{x}(t')\hat{x}(t)]_{nn'}$, which appears on the right-hand side of Eq. (183), may be simplified absolutely similarly, giving

$$[\hat{w}\hat{x}(t')\hat{x}(t)]_{nn'} \approx \sum_m |x_{n'm}|^2 \exp\{i\omega_{n'm}(t'-t)\} w_{nn'}. \quad (7.188)$$

These expressions hold whether n and n' are equal or not. The situation is different for two other products on the right-hand side of Eq. (183), with w sandwiched between $x(t)$ and $x(t')$. For example,

$$[\hat{x}(t)\hat{w}\hat{x}(t')]_{nn'} = \sum_{m,m'} x_{nm}(t)w_{mm'}x_{m'n'}(t') = \sum_{m,m'} x_{nm}w_{mm'}x_{m'n'} \exp\{i(\omega_{nm}t + \omega_{m'n'}t')\}. \quad (7.189)$$

⁶⁰ This is essentially the same rotating-wave approximation (RWA) as was used in Sec. 6.5.

⁶¹ As was already discussed in Sec. 4, the lower-limit substitution ($t' = -\infty$) in the integrals participating in Eq. (183) gives zero, due to the finite-time “memory” of the system, expressed by the decay of the correlation and response functions at large values of the time delay $\tau = t - t'$.

For this term, the same requirement of having a fast oscillating function of $(t - t')$ only, yields a different condition: $\omega_{nm} + \omega_{m'n'} = 0$, i.e.

$$(E_n - E_m) + (E_{m'} - E_{n'}) = 0. \quad (7.190)$$

Here the double sum's reduction is possible only if we make an additional assumption that all interlevel energy distances are unique, i.e. our system of interest has no equidistant levels (such as in the harmonic oscillator). For the diagonal elements ($n = n'$), the RWA requirement is reduced to $m = m'$, giving sums over all diagonal elements of the density matrix:

$$[\hat{x}(t)\hat{w}\hat{x}(t')]_{nn} = \sum_m |x_{nm}|^2 \exp\{i\omega_{nm}(t-t')\} w_{mm}. \quad (7.191)$$

(Another similar term, $[\hat{x}(t')\hat{w}\hat{x}(t)]_{nn}$, is just a complex conjugate of (191).) However, for off-diagonal matrix elements ($n \neq n'$), the situation is different: Eq. (190) may be satisfied only if $m = n$ and also $m' = n'$, so that the double sum is reduced to just one, non-oscillating term:

$$[\hat{x}(t)\hat{w}\hat{x}(t')]_{nn'} = x_{nn} w_{nn'} x_{n'n'}, \quad \text{for } n \neq n'. \quad (7.192)$$

The second similar term, $[\hat{x}(t')\hat{w}\hat{x}(t)]_{nn'}$, is exactly the same, so that in one of the integrals of Eq. (183), these terms add up, while in the second one, they cancel.

This is why the final equations of evolution look differently for diagonal and off-diagonal elements of the density matrix. For the former case ($n = n'$), Eq. (183) is reduced to the so-called *master equation*⁶² relating diagonal elements w_{nn} of the density matrix, i.e. the energy level occupancies W_n :⁶³

$$\begin{aligned} \dot{W}_n = \sum_{m \neq n} |x_{nm}|^2 \int_0^\infty & \left[-\frac{1}{\hbar^2} K_F(\tau)(W_n - W_m)(\exp\{i\omega_{nm}\tau\} + \exp\{-i\omega_{nm}\tau\}) \right. \\ & \left. - \frac{i}{2\hbar} G(\tau)(-W_n - W_m)(\exp\{i\omega_{nm}\tau\} - \exp\{-i\omega_{nm}\tau\}) \right] d\tau, \end{aligned} \quad (7.193)$$

where $\tau \equiv t - t'$. Changing the summation index notation from m to n' , we may rewrite the master equation in its canonical form

$$\boxed{\dot{W}_n = \sum_{n' \neq n} (\Gamma_{n' \rightarrow n} W_{n'} - \Gamma_{n \rightarrow n'} W_n)}, \quad (7.194) \quad \text{Master equation}$$

where the coefficients

$$\boxed{\Gamma_{n' \rightarrow n} \equiv |x_{nn'}|^2 \int_0^\infty \left[\frac{2}{\hbar^2} K_F(\tau) \cos \omega_{nn'} \tau - \frac{1}{\hbar} G(\tau) \sin \omega_{nn'} \tau \right] dt'}, \quad (7.195) \quad \text{Interlevel transition rates}$$

are called the *interlevel transition rates*.⁶⁴ Eq. (194) has a very clear physical meaning of the level occupancy dynamics (i.e. the balance of the probability flows ΓW) due to quantum transitions between

⁶² The master equations, first introduced to quantum mechanics in 1928 by W. Pauli, are sometimes called the “Pauli master equations”, or “kinetic equations”, or “rate equations”.

⁶³ As Eq. (193) shows, the term with $m = n$ would vanish and thus may be legitimately excluded from the sum.

⁶⁴ As Eq. (193) shows, the result for $\Gamma_{n \rightarrow n'}$ is described by Eq. (195) as well, provided that the indices n and n' are swapped in all components of its right-hand side, including the swap $\omega_{nn'} \rightarrow \omega_{n'n} = -\omega_{nn'}$.

the energy levels (see Fig. 7), in our current case caused by the interaction between the system of our interest and its environment.

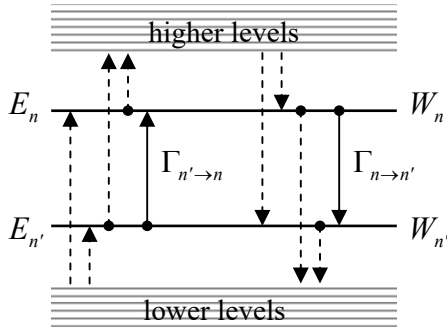


Fig. 7.7. Probability flows in a discrete-spectrum system. Solid arrows: the exchange between the two energy levels, n and n' , described by one term in the master equation (194); dashed arrows: other transitions to/from these two levels.

The Fourier transforms (113) and (123) enable us to express the two integrals in Eq. (195) via, respectively, the symmetrized spectral density $S_F(\omega)$ of environment force fluctuations and the imaginary part $\chi''(\omega)$ of the generalized susceptibility, both at frequency $\omega = \omega_{nn'}$. After that we may use the fluctuation-dissipation theorem (134) to exclude the former function, getting finally⁶⁵

Transition rates via $\chi''(\omega)$

$$\Gamma_{n' \rightarrow n} = \frac{1}{\hbar} |x_{nn'}|^2 \chi''(\omega_{nn'}) \left(\coth \frac{\hbar \omega_{nn'}}{2k_B T} - 1 \right) \equiv \frac{2}{\hbar} |x_{nn'}|^2 \frac{\chi''(\omega_{nn'})}{\exp\{(E_n - E_{n'})/k_B T\} - 1}. \quad (7.196)$$

Note that since the imaginary part χ'' of the generalized susceptibility is an odd function of frequency, Eq. (196) is in compliance with the Gibbs distribution for arbitrary temperature. Indeed, according to this equation, the ratio of the “up” and “down” rates for each pair of levels equals

$$\frac{\Gamma_{n' \rightarrow n}}{\Gamma_{n \rightarrow n'}} = \frac{\chi''(\omega_{nn'})}{\exp\{(E_n - E_{n'})/k_B T\} - 1} / \frac{\chi''(\omega_{n'n})}{\exp\{(E_{n'} - E_n)/k_B T\} - 1} \equiv \exp\left\{-\frac{E_n - E_{n'}}{k_B T}\right\}. \quad (7.197)$$

On the other hand, according to the Gibbs distribution (24), in thermal equilibrium the level populations should be in the same proportion. Hence, Eq. (196) complies with the so-called *detailed balance equation*,

$$W_n \Gamma_{n \rightarrow n'} = W_{n'} \Gamma_{n' \rightarrow n}, \quad (7.198)$$

valid in the equilibrium for each pair $\{n, n'\}$, so that all right-hand sides of all Eqs. (194), and hence the time derivatives of all W_n vanish – as they should. Thus, the stationary solution of the master equations indeed describes the thermal equilibrium correctly.

The system of master equations (194), frequently complemented by additional terms on their right-hand sides, describing interlevel transitions due to other factors (e.g., by an external ac force with a frequency close to one of $\omega_{nn'}$), is the key starting point for practical analyses of many quantum systems, notably including optical quantum amplifiers and generators (lasers). It is important to remember that

⁶⁵ It is straightforward (and highly recommended to the reader) to show that at low temperatures ($k_B T \ll |E_{n'} - E_n|$), Eq. (196) gives the same result as the Golden Rate formula (6.111), with $A = x$. (The low-temperature condition ensures that the initial occupancy of the excited level n is negligible, as was assumed at the derivation of Eq. (6.111).)

they are strictly valid only in the rotating-wave approximation, i.e. if Eq. (182) is well satisfied for all n and n' of substance.

For a particular but very important case of a two-level system (with, say, $E_1 > E_2$), the rate $\Gamma_{1 \rightarrow 2}$ may be interpreted (especially in the low-temperature limit $k_B T \ll \hbar\omega_{12} = E_1 - E_2$, when $\Gamma_{1 \rightarrow 2} \gg \Gamma_{2 \rightarrow 1}$) as the reciprocal characteristic time $1/T_1 \equiv \Gamma_{1 \rightarrow 2}$ of the *energy relaxation* process that brings the *diagonal* elements of the density matrix to their thermally-equilibrium values (24). For the Ohmic dissipation described by Eqs. (137)-(138), Eq. (196) yields

$$\frac{1}{T_1} \equiv \Gamma_{1 \rightarrow 2} = \frac{2}{\hbar^2} |x_{12}|^2 \eta \times \begin{cases} \hbar\omega_{12}, & \text{for } k_B T \ll \hbar\omega_{12}, \\ k_B T, & \text{for } \hbar\omega_{12} \ll k_B T. \end{cases} \quad (7.199)$$

Energy
relaxation
time

This relaxation time T_1 should not be confused with the characteristic time T_2 of the *off-diagonal* element decay, i.e. dephasing, which was already discussed in Sec. 3. In this context, let us see what do Eqs. (183) have to say about the dephasing rates. Taking into account our intermediate results (187)-(192), and merging the non-oscillating components (with $m = n$ and $m = n'$) of the sums Eq. (187) and (188) with the terms (192), which also do not oscillate in time, we get the following equation:⁶⁶

$$\dot{w}_{nn'} = - \left\{ \int_0^\infty \left[\frac{1}{\hbar^2} K_F(\tau) \left(\sum_{m \neq n} |x_{nm}|^2 \exp\{i\omega_{nm}\tau\} + \sum_{m \neq n'} |x_{n'm}|^2 \exp\{-i\omega_{n'm}\tau\} + (x_{nn} - x_{n'n'})^2 \right) \right. \right. \\ \left. \left. + \frac{i}{2\hbar} G(\tau) \left(\sum_{m \neq n} |x_{nm}|^2 \exp\{i\omega_{nm}\tau\} - \sum_{m \neq n'} |x_{n'm}|^2 \exp\{-i\omega_{n'm}\tau\} \right) \right] d\tau \right\} w_{nn'}, \text{ for } n \neq n'. \quad (7.200)$$

In contrast with Eq. (194), the right-hand side of this equation includes both a real and an imaginary part, and hence it may be represented as

$$\dot{w}_{nn'} = -(1/T_{nn'} + i\Delta_{nn'}) w_{nn'}, \quad (7.201)$$

where both factors $1/T_{nn'}$ and $\Delta_{nn'}$ are real. As Eq. (201) shows, the second term in the right-hand side of this equation causes slow oscillations of the matrix elements $w_{nn'}$, which, after returning to the Schrödinger picture, add just small corrections⁶⁷ to the unperturbed frequencies (186) of their oscillations, and are not important for most applications. More important is the first term, proportional to

$$\frac{1}{T_{nn'}} = \int_0^\infty \left[\frac{1}{\hbar^2} K_F(\tau) \left(\sum_{m \neq n} |x_{nm}|^2 \cos \omega_{nm}\tau + \sum_{m \neq n'} |x_{n'm}|^2 \cos \omega_{n'm}\tau + (x_{nn} - x_{n'n'})^2 \right) \right]$$

⁶⁶ Sometimes Eq. (200) (in any of its numerous alternative forms) is called the *Redfield equation*, after the 1965 work by A. Redfield. Note, however, that in the mid-1960s several other authors, notably including (in the alphabetical order) H. Haken, W. Lamb, M. Lax, W. Louisell, and M. Scully, also made major contributions to the very fast development of the density-matrix approach to open quantum systems.

⁶⁷ Such corrections are sometimes called *Lamb shifts*, due to their conceptual similarity to the genuine Lamb shift – the effect first observed experimentally in 1947 by Willis Lamb and Robert Rutherford: a minor difference between energy levels of the $2s$ and $2p$ states of hydrogen, due to the electric-dipole coupling of hydrogen atoms to the free-space electromagnetic environment. (These energies are equal not only in the non-relativistic theory described in Sec. 3.6 but also in the relativistic theory (see Secs. 6.3, 9.7), if the electromagnetic environment is ignored.) The explanation of the Lamb shift by H. Bethe, in the same 1947, essentially launched the whole field of quantum electrodynamics – to be briefly discussed in Chapter 9.

$$-\frac{1}{2\hbar}G(\tau)\left(\sum_{m \neq n}|x_{nm}|^2 \sin \omega_{nm}\tau + \sum_{m \neq n'}|x_{n'm}|^2 \sin \omega_{n'm}\tau\right)d\tau, \quad \text{for } n \neq n', \quad (7.202)$$

because it describes the effect completely absent without the environment coupling: exponential decay of the off-diagonal matrix elements, i.e. the dephasing. Comparing the first two terms of Eq. (202) with Eq. (195), we see that the dephasing rates may be described by a very simple formula:

Dephasing rate

$$\begin{aligned} \frac{1}{T_{nn'}} &= \frac{1}{2}\left(\sum_{m \neq n}\Gamma_{n \rightarrow m} + \sum_{m \neq n'}\Gamma_{n' \rightarrow m}\right) + \frac{\pi}{\hbar^2}(x_{nn} - x_{n'n'})^2 S_F(0) \\ &= \frac{1}{2}\left(\sum_{m \neq n}\Gamma_{n \rightarrow m} + \sum_{m \neq n'}\Gamma_{n' \rightarrow m}\right) + \frac{k_B T}{\hbar^2}\eta(x_{nn} - x_{n'n'})^2, \quad \text{for } n \neq n', \end{aligned} \quad (7.203)$$

where the low-frequency drag coefficient η is again defined as $\lim_{\omega \rightarrow 0}\chi''(\omega)/\omega$ – see Eq. (138).

This result shows that two effects yield independent contributions to the dephasing. The first of them may be interpreted as a result of “virtual” transitions of the system, from the levels n and n' of our interest, to other energy levels m ; according to Eq. (195), this contribution is proportional to the strength of coupling to the environment at relatively high frequencies ω_{nm} and $\omega_{n'm}$. (If the energy quanta $\hbar\omega$ of these frequencies are much larger than the thermal fluctuation scale $k_B T$, then only the lower levels, with $E_m < \max[E_n, E_{n'}]$ are important.) On the contrary, the second contribution is due to low-frequency, essentially classical fluctuations of the environment, and hence to the low-frequency dissipative susceptibility. In the Ohmic dissipation case, when the ratio $\eta \equiv \chi''(\omega)/\omega$ is frequency-independent, both contributions are of the same order, but their exact relation depends on the matrix elements $x_{nn'}$ of a particular system.

For example, returning for a minute to the two-level system discussed in Sec. 3, described by our current theory with the replacement $\hat{x} \rightarrow \hat{\sigma}_z$, the high-frequency contributions to dephasing vanish because of the absence of transitions between energy levels, while the low-frequency contribution yields

$$\frac{1}{T_2} \equiv \frac{1}{T_{12}} = \frac{k_B T}{\hbar^2}\eta(x_{nn} - x_{n'n'})^2 \rightarrow \frac{k_B T}{\hbar^2}\eta[(\sigma_z)_{11} - (\sigma_z)_{22}]^2 = \frac{4k_B T}{\hbar^2}\eta, \quad (7.204)$$

thus exactly reproducing the result (142) of the Heisenberg-Langevin approach.⁶⁸ Note also that the expression for T_2 is very close in structure to Eq. (199) for T_1 (in the high-temperature limit). However, for the simple interaction model (70) that was explored in Sec. 3, the off-diagonal elements of the operator $\hat{x} = \hat{\sigma}_z$ in the stationary-state z -basis vanish, so that $T_1 \rightarrow \infty$, while T_2 says finite. The physics of this result is very clear, for example, for the two-well implementation of the model (see Fig. 4 and its discussion): it is suitable for the case of a very high energy barrier between the wells, which inhibits tunneling, and hence any change of the well occupancies. However, T_1 may become finite, and comparable with T_2 , if tunneling between the wells is substantial.⁶⁹

⁶⁸ The first form of Eq. (203), as well as the analysis of Sec. 3, implies that low-frequency fluctuations of any other origin, not taken into account in own current analysis (say, an unintentional noise from experimental equipment), may also contribute to dephasing; such “technical fluctuations” are indeed a very serious challenge for the experimental implementation of coherent qubit systems – see Sec. 8.5 below.

⁶⁹ As was discussed in Sec. 5.1, the tunneling may be described by using, instead of Eq. (70), the full two-level Hamiltonian (5.3). Let me leave for the reader’s exercise to spell out the equations for the time evolution of the density matrix elements of this system, and of the expectation values of the Pauli operators, for this case.

Because of the reason explained above, the derivation of Eqs. (200)-(204) is not valid for systems with equidistant energy spectra – for example, the harmonic oscillator. For this particular, but very important system, with its simple matrix elements $x_{nn'}$ given by Eqs. (5.92), it is longish but straightforward to repeat the above calculations, starting from (183), to obtain an equation similar in structure to Eq. (200), but with two other terms, proportional to $w_{n\pm 1,n'\pm 1}$, on its right-hand side. Neglecting the minor Lamb-shift term, the equation reads

$$\dot{w}_{nn'} = -\delta \left\{ \begin{aligned} & [(n_e + 1)(n + n') + n_e(n + n' + 2)]w_{nn'} \\ & - 2(n_e + 1)[(n + 1)(n' + 1)]^{1/2} w_{n+1,n'+1} - 2n_e(nn')^{1/2} w_{n-1,n'-1} \end{aligned} \right\}. \quad (7.205)$$

Here δ is the effective damping coefficient,⁷⁰

$$\delta \equiv \frac{x_0^2}{2\hbar} \text{Im } \chi(\omega_0) \equiv \frac{\text{Im } \chi(\omega_0)}{2m\omega_0}, \quad (7.206)$$

equal to just $\eta/2m$ for the Ohmic dissipation, and n_e is the equilibrium number of oscillator's excitations, given by Eq. (26b), with the environment's temperature T . (I am using this new notation because in dynamics, the instant expectation value $\langle n \rangle$ may be time-dependent, and is generally different from its equilibrium value n_e .)

As a remark: the derivation of Eq. (205) might be started at a bit earlier point, from the Markov approximation applied to Eq. (181), expressing the coordinate operator via the creation-annihilation operators (5.65). This procedure gives the result in the operator (i.e. basis-independent) form:⁷¹

$$\dot{\hat{w}} = -\delta \left[(n_e + 1) \left(\left\{ \hat{a}^\dagger \hat{a}, \hat{w} \right\} - 2\hat{a}\hat{w}\hat{a}^\dagger \right) + n_e \left(\left\{ \hat{a}\hat{a}^\dagger, \hat{w} \right\} - 2\hat{a}^\dagger\hat{w}\hat{a} \right) \right]. \quad (7.207)$$

In the Fock state basis, this equation immediately reduces to Eq. (205); however, Eq. (207) may be more convenient for some applications.

Returning to Eq. (205), we see that it relates only the elements $w_{nn'}$ located at the same distance ($n - n'$) from the principal diagonal of the density matrix. This means, in particular, that the dynamics of the diagonal elements w_{nn} of the matrix, i.e. the Fock state probabilities W_n , is independent of the off-diagonal elements, and may be represented in the form (194), truncated to the transitions between the adjacent energy levels only ($n' = n \pm 1$):

⁷⁰ This coefficient participates prominently in the classical theory of damped oscillations (see, e.g., CM Sec. 5.1), in particular defining the oscillator's Q -factor as $Q \equiv \omega_0/2\delta$, and the decay time of the amplitude A and the energy E of free oscillations: $A(t) = A(0)\exp\{-\delta t\}$, $E(t) = E(0)\exp\{-2\delta t\}$.

⁷¹ Sometimes Eq. (207) is called the *Lindblad equation*, but I believe this terminology is inappropriate. It is true that its structure falls into a general category of equations, suggested by G. Lindblad in 1976 for the density operators in the Markov approximation, whose diagonalized form in the interaction picture is

$$\dot{\hat{w}} = \sum_j \gamma_j \left(2\hat{L}_j \hat{w} \hat{L}_j^\dagger - \left\{ \hat{L}_j \hat{L}_j^\dagger, \hat{w} \right\} \right).$$

However, Eq. (207) was derived much earlier (by L. Landau in 1927 for zero temperature, and by M. Lax in 1960 for an arbitrary temperature), and in contrast to the general Lindblad equation, spells out the participating operators \hat{L}_j and coefficients γ_j for a particular physical system – the harmonic oscillator.

$$\dot{W}_n = (\Gamma_{n+1 \rightarrow n} W_{n+1} - \Gamma_{n \rightarrow n+1} W_n) + (\Gamma_{n-1 \rightarrow n} W_{n-1} - \Gamma_{n \rightarrow n-1} W_n), \quad (7.208)$$

with the following rates:

$$\begin{aligned} \Gamma_{n+1 \rightarrow n} &= 2\delta(n+1)(n_e + 1), & \Gamma_{n \rightarrow n+1} &= 2\delta(n+1)n_e, \\ \Gamma_{n-1 \rightarrow n} &= 2\delta n n_e, & \Gamma_{n \rightarrow n-1} &= 2\delta n(n_e + 1). \end{aligned} \quad (7.209)$$

Since according to the definition of n_e , given by Eq. (26b),

$$n_e = \frac{1}{\exp\{\hbar\omega_0/k_B T\} - 1}, \quad \text{so that } n_e + 1 = \frac{\exp\{\hbar\omega_0/k_B T\}}{\exp\{\hbar\omega_0/k_B T\} - 1} = -\frac{1}{\exp\{-\hbar\omega_0/k_B T\} - 1}, \quad (7.210)$$

taking into account Eqs. (5.92), (186), (206), and the asymmetry of the function $\chi''(\omega)$, we see that these rates are again described by Eq. (196), even though the last formula was derived for non-equidistant energy spectra.

Hence the only substantial new feature of the master equation for the harmonic oscillator, is that the decay of the off-diagonal elements of its density matrix is scaled by the same parameter (2δ) as that of the decay of its diagonal elements, i.e. there is no radical difference between the dephasing and energy-relaxation times T_2 and T_1 . This fact may be interpreted as the result of the independence of the energy level distances, $\hbar\omega_0$, of the fluctuations $F(t)$ exerted on the oscillator by the environment, so that their low-frequency density, $S_F(0)$, does not contribute to the dephasing. (This fact formally follows also from Eq. (203) as well, taking into account that for the oscillator, $x_{nn} = x_{n'n'} = 0$.)

The simple equidistant structure of the oscillator's spectrum makes it possible to readily solve the system of Eqs. (208), with $n = 0, 1, 2, \dots$, for some important cases. In particular, if the initial state of the oscillator is a classical mixture, with no off-diagonal elements, its further relaxation proceeds as such a mixture: $w_{nn'}(t) = 0$ for all $n' \neq n$.⁷² In particular, it is straightforward to use Eq. (208) to verify that if the initial classical mixture obeys the Gibbs distribution (25), but with a temperature T_i different from that of the environment (T_e), then the relaxation process is reduced to a simple exponential transient of the effective temperature from T_i to T_e :

$$W_n(t) = \exp\left\{-n \frac{\hbar\omega_0}{k_B T_{\text{ef}}(t)}\right\} \left(1 - \exp\left\{-\frac{\hbar\omega_0}{k_B T_{\text{ef}}(t)}\right\}\right), \quad \text{with } T_{\text{ef}}(t) = T_i e^{-2\delta t} + T_e (1 - e^{-2\delta t}), \quad (7.211)$$

with the corresponding evolution of the expectation value of the full energy E – cf. Eq. (26b):

$$\langle E \rangle(t) = \frac{\hbar\omega_0}{2} + \hbar\omega_0 \langle n \rangle(t), \quad \langle n \rangle(t) = \frac{1}{\exp\{\hbar\omega_0/k_B T_{\text{ef}}(t)\} - 1} \xrightarrow{t \rightarrow \infty} n_e. \quad (7.212)$$

However, if the initial state of the oscillator is different (say, corresponds to some upper Fock state), the relaxation process, described by Eqs. (208)-(209), is more complex – see, e.g., Fig. 8. At low temperatures (Fig. 8a), it may be interpreted as a gradual “roll” of the probability distribution down the energy staircase, with a gradually decreasing velocity $dn/dt \propto n$. However, at substantial temperatures,

⁷² Note, however, that this is not true for many applications, in which a damped oscillator is also under the effect of an external time-dependent field, which may be described by additional, typically off-diagonal terms on the right-hand side of Eqs. (205).

with $k_B T \sim \hbar\omega_0$ (Fig. 8b), this “roll-down” is saturated when the level occupancies $W_n(t)$ approach their equilibrium values (25).⁷³

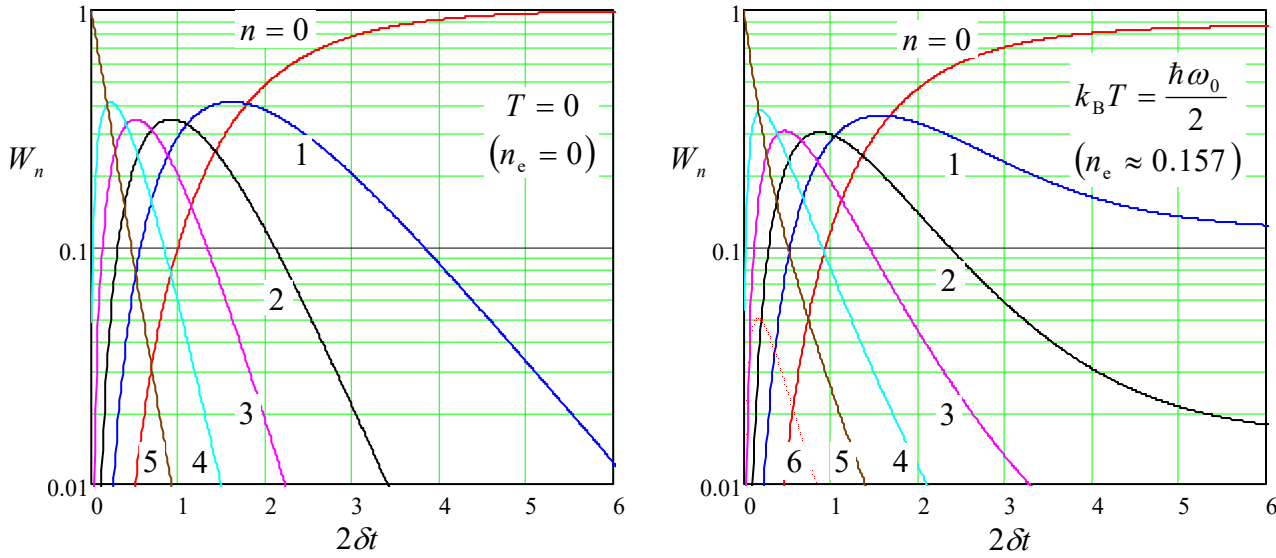


Fig. 7.8. Relaxation of a harmonic oscillator, initially in its 5th Fock state, at: (a) $T = 0$, and (b) $T > 0$. Note that in the latter case, even the energy levels with $n > 5$ get populated, due to their thermal excitation.

The analysis of this process may be simplified in the case when $W(n, t) \equiv W_n(t)$ is a smooth function of the energy level number n , limited to high levels: $n \gg 1$. In this limit, we may use the Taylor expansion of this function (written for the points $\Delta n = \pm 1$), truncated to three leading terms:

$$W_{n\pm 1}(t) \equiv W(n \pm 1, t) \approx W(n, t) \pm \frac{\partial W(n, t)}{\partial n} + \frac{1}{2} \frac{\partial^2 W(n, t)}{\partial n^2}. \quad (7.213)$$

Plugging this expression into Eqs. (208)-(209), we get for the function $W(n, t)$ a partial differential equation, which may be recast in the following form:

$$\frac{\partial W}{\partial t} = -\frac{\partial}{\partial n} [f(n)W] + \frac{\partial^2}{\partial n^2} [d(n)W], \quad \text{with } f(n) \equiv 2\delta(n_e - n), \quad d(n) \equiv 2\delta(n_e + \frac{1}{2})n. \quad (7.214)$$

Since at $n \gg 1$, the oscillator’s energy E is close to $\hbar\omega_0 n$, this *energy diffusion equation* (sometimes incorrectly called the Fokker-Planck equation – see below) essentially describes the time evolution of the continuous probability density $w(E, t)$, which may be defined as $w(E, t) \equiv W(E/\hbar\omega_0, t)/\hbar\omega_0$.⁷⁴

⁷³ The reader may like to have a look at the results of nice measurements of such functions $W_n(t)$ in microwave oscillators, performed using their coupling with Josephson-junction circuits: H. Wang *et al.*, *Phys. Rev. Lett.* **101**, 240401 (2008), and with Rydberg atoms: M. Brune *et al.*, *Phys. Rev. Lett.* **101**, 240402 (2008).

⁷⁴ In the classical limit $n_e \gg 1$, Eq. (214) is analytically solvable for any initial conditions – see, e.g., the paper by B. Zeldovich *et al.*, *Sov. Phys. JETP* **28**, 308 (1969), which also gives some more intricate solutions of Eqs. (208)-(209). Note, however, that the most important properties of the damped harmonic oscillator (including its relaxation dynamics) may be analyzed simpler by using the Heisenberg-Langevin approach discussed in the previous section.

This continuous approximation naturally reminds us of the need to discuss dissipative systems with a *continuous* spectrum. Unfortunately, for such systems the few (relatively :-) simple results that may be obtained from the basic Eq. (181), are essentially classical in nature and are discussed in detail in the SM part of this series. Here, I will give only a simple illustration. Let us consider a 1D particle that interacts weakly with a thermally-equilibrium environment, but otherwise is free to move along the x -axis. As we know from Chapters 2 and 5, in this case, the most convenient basis is that of the momentum eigenstates p . In the momentum representation, the density matrix is just the c -number function $w(p, p')$, defined by Eq. (54), which was already discussed in brief in Sec. 2. On the other hand, the coordinate operator, which participates in the right-hand side of Eq. (181), has the form given by the first of Eqs. (4.269),

$$\hat{x} = i\hbar \frac{\partial}{\partial p}, \quad (7.215)$$

dual to the coordinate-representation formula (4.268). As we already know, such operators are local – see, e.g., Eq. (4.244). Due to this locality, the whole right-hand side of Eq. (181) is local as well, and hence (within the framework of our perturbative treatment) the interaction with the environment affects only the diagonal values $w(p, p)$ of the density matrix, i.e. the momentum probability density $w(p)$.

Let us find the equation governing the evolution of this function in time in the Markov approximation, when the time scale of the density matrix evolution is much longer than the correlation time τ_c of the environment, i.e. the time scale of the functions $K_F(\tau)$ and $G(\tau)$. In this approximation, we may take the matrix elements out of the first integral of Eq. (181),

$$\begin{aligned} -\frac{1}{\hbar^2} \int_{-\infty}^t K_F(t-t') dt' [\hat{x}(t), [\hat{x}(t'), \hat{w}(t')]] &\approx -\frac{1}{\hbar^2} \int_0^\infty K_F(\tau) d\tau [\hat{x}, [\hat{x}, \hat{w}]] \\ &= -\frac{\pi}{\hbar^2} S_F(0) [\hat{x}, [\hat{x}, \hat{w}]] = -\frac{k_B T}{\hbar^2} \eta [\hat{x}, [\hat{x}, \hat{w}]], \end{aligned} \quad (7.216)$$

and calculate the last double commutator in the Schrödinger picture. This may be done either using an explicit expression for the matrix elements of the coordinate operator or in a simpler way – using the same trick as at the derivation of the Ehrenfest theorem in Sec. 5.2. Namely, expanding an arbitrary function $f(p)$ into the Taylor series in p ,

$$f(p) = \sum_{k=0}^{\infty} \frac{1}{k!} \frac{\partial^k f}{\partial p^k} p^k, \quad (7.217)$$

and using Eq. (215), we can prove the following simple commutation relation:

$$[\hat{x}, f] = \sum_{k=0}^{\infty} \frac{1}{k!} \frac{\partial^k f}{\partial p^k} [\hat{x}, p^k] = \sum_{k=0}^{\infty} \frac{1}{k!} \frac{\partial^k f}{\partial p^k} (i\hbar k p^{k-1}) = i\hbar \sum_{k=1}^{\infty} \frac{1}{(k-1)!} \frac{\partial^{k-1}}{\partial p^{k-1}} \left(\frac{\partial f}{\partial p} \right) p^{k-1} = i\hbar \frac{\partial f}{\partial p}. \quad (7.218)$$

Now applying this result sequentially, first to w and then to the resulting commutator, we get

$$[\hat{x}, [\hat{x}, w]] = \left[\hat{x}, i\hbar \frac{\partial w}{\partial p} \right] = i\hbar \frac{\partial}{\partial p} \left(i\hbar \frac{\partial w}{\partial p} \right) = -\hbar^2 \frac{\partial^2 w}{\partial p^2}. \quad (7.219)$$

It may look like the second integral in Eq. (181) might be simplified similarly. However, it vanishes at $p' \rightarrow p$, and $t' \rightarrow t$, so that to calculate the first non-vanishing contribution from that integral for $p = p'$, we have to take into account the small difference $\tau \equiv t - t' \sim \tau_c$ between the arguments of the

coordinate operators under that integral. This may be done using Eq. (169) with the free-particle's Hamiltonian consisting of the kinetic-energy contribution alone:

$$\hat{x}(t') - \hat{x}(t) \approx -\tau \dot{\hat{x}} = -\tau \frac{1}{i\hbar} [\hat{x}, \hat{H}_s] = -\tau \frac{1}{i\hbar} \left[\hat{x}, \frac{\hat{p}^2}{2m} \right] = -\tau \frac{\hat{p}}{m}, \quad (7.220)$$

where the exact argument of the operator on the right-hand side is already unimportant and may be taken for t . As a result, we may use the last of Eqs. (136) to reduce the second term on the right-hand side of Eq. (181) to

$$-\frac{i}{2\hbar} \int_{-\infty}^t G(t-t')[\hat{x}(t), \{\hat{x}(t'), \hat{w}(t')\}] dt' \approx \frac{i}{2\hbar} \int_0^\infty G(\tau) \tau d\tau \left[\hat{x}, \left\{ \frac{\hat{p}}{m}, \hat{w} \right\} \right] = \frac{\eta}{2i\hbar} \left[\hat{x}, \left\{ \frac{\hat{p}}{m}, \hat{w} \right\} \right]. \quad (7.221)$$

In the momentum representation, the momentum operator and the density matrix w are just c -numbers and commute, so that, applying Eq. (218) to the product pw , we get

$$\left[\hat{x}, \left\{ \frac{\hat{p}}{m}, \hat{w} \right\} \right] = \left[\hat{x}, 2 \frac{p}{m} w \right] = 2i\hbar \frac{\partial}{\partial p} \left(\frac{p}{m} w \right), \quad (7.222)$$

and may finally reduce the integro-differential equation Eq. (181) to a partial differential equation:

$$\frac{\partial w}{\partial t} = -\frac{\partial}{\partial p} (Fw) + \eta k_B T \frac{\partial^2 w}{\partial p^2}, \quad \text{with } F \equiv -\eta \frac{p}{m}. \quad (7.223)$$

Fokker –
Planck
equation:
free
1D particle

This is the 1D form of the famous *Fokker-Planck equation* describing the classical statistics of motion of a particle (in our particular case, of a free particle) in an environment providing a linear drag characterized by the coefficient η ; it belongs to the same drift-diffusion type as Eq. (214). The first, *drift* term on its right-hand side describes the particle's deceleration due to the drag force (137), $F = -\eta p/m = -\eta v$, provided by the environment. The second, *diffusion* term on the right-hand side of Eq. (223) describes the effect of fluctuations: the particle's momentum' random walk around its average (drift-affected, and hence time-dependent) value. The walk obeys the law similar to Eq. (85), but with the *momentum-space* diffusion coefficient

$$D_p = \eta k_B T. \quad (7.224)$$

This is the reciprocal-space version of the fundamental Einstein relation between the dissipation (friction) and fluctuations, in this classical limit represented by their thermal energy scale $k_B T$.⁷⁵

Just for the reader's reference, let me note that the Fokker-Planck equation (223) may be readily generalized to the 3D motion of a particle under the effect of an additional external force,⁷⁶ and in this

⁷⁵ Note that Eq. (224), as well as the original Einstein's relation between the diffusion coefficient D in the direct space and temperature, may be derived much simpler by other means – for example, from the Nyquist formula (139). These issues are discussed in detail in SM Chapter 5.

⁷⁶ Moreover, Eq. (223) may be generalized to the motion of a *quantum* particle in an additional periodic potential $U(\mathbf{r})$. In this case, due to the band structure of the energy spectrum (which was discussed in Secs. 2.7 and 3.4), the coupling to the environment produces not only a continuous drift-diffusion of the probability density in the space of the quasimomentum $\hbar\mathbf{q}$ but also quantum transitions between different energy bands at the same $\hbar\mathbf{q}$ – see, e.g., K. Likharev and A. Zorin, *J. Low Temp. Phys.* **59**, 347 (1985).

more general form is the basis for many important applications; however, due to its classical character, its discussion is also left for the SM part of this series.⁷⁷

To summarize our discussion of the two alternative approaches to the analysis of quantum systems interacting with a thermally-equilibrium environment, described in the last three sections, let me emphasize again that they give different descriptions of the same phenomena, and are characterized by the same two functions $G(\tau)$ and $K_F(\tau)$. Namely, in the Heisenberg-Langevin approach, we describe the system by operators that change (fluctuate) in time, even in the thermal equilibrium, while in the density-matrix approach, the system is described by non-fluctuating probability functions, such as $W_n(t)$ or $w(p, t)$, which are stationary in equilibrium. In the cases when a problem may be solved analytically to the end by both methods (for example, for a harmonic oscillator), they give identical results.

7.8. Exercise problems

7.1. Calculate the density matrix of a two-level system whose Hamiltonian is described, in a certain basis, by the following matrix:

$$H = \mathbf{c} \cdot \boldsymbol{\sigma} \equiv c_x \sigma_x + c_y \sigma_y + c_z \sigma_z,$$

where σ_k are the Pauli matrices and c_j are c -numbers, in thermodynamic equilibrium at temperature T .

7.2. In the usual z -basis, spell out the density matrix of a spin- $\frac{1}{2}$ with gyromagnetic ratio γ :

- (i) in the pure state with the spin definitely directed along the z -axis,
- (ii) in the pure state with the spin definitely directed along the x -axis,
- (iii) in thermal equilibrium at temperature T , in a magnetic field directed along the z -axis, and
- (iv) in thermal equilibrium at temperature T , in a magnetic field directed along the x -axis.

7.3. Calculate the Wigner function of a harmonic oscillator in:

- (i) in thermodynamic equilibrium at temperature T ,
- (ii) in the ground state, and
- (ii) in the Glauber state with dimensionless complex amplitude α .

Discuss the relation between the first of the results and the Gibbs distribution.

7.4. Calculate the Wigner function of a harmonic oscillator, with mass m and frequency ω_0 , in its first excited stationary state ($n = 1$).

7.5.* A harmonic oscillator is weakly coupled to an Ohmic environment.

- (i) Use the rotating-wave approximation to write the reduced equations of motion for the Heisenberg operators of the complex amplitude of oscillations.

⁷⁷ See SM Secs. 5.6-5.7. For a more detailed discussion of *quantum* effects in dissipative systems with continuous spectra see, e. g., either U. Weiss, *Quantum Dissipative Systems*, 2nd ed., World Scientific, 1999, or H.-P. Breuer and F. Petruccione, *The Theory of Open Quantum Systems*, Oxford U. Press, 2007.

(ii) Calculate the expectation values of the correlators of the fluctuation force operators participating in these equations, and express them via the average number $\langle n \rangle$ of thermally-induced excitations in equilibrium, given by the second of Eqs. (26b).

7.6. Calculate the average potential energy of long-range electrostatic interaction between two similar isotropic, 3D harmonic oscillators, each with the electric dipole moment $\mathbf{d} = q\mathbf{s}$, where \mathbf{s} is the oscillator's displacement from its equilibrium position, at arbitrary temperature T .

7.7. A semi-infinite string with mass μ per unit length is attached to a wall and stretched with a constant force (tension) \mathcal{T} . Calculate the spectral density of the transverse force exerted on the wall, in thermal equilibrium at temperature T .

7.8.* Calculate the low-frequency spectral density of small fluctuations of the voltage V across a Josephson junction, shunted with an Ohmic conductor, and biased with a dc external current $\bar{I} > I_c$.

Hint: You may use Eqs. (1.73)-(1.74) to describe the junction's dynamics, and assume that the shunting conductor remains in thermal equilibrium.

7.9. Prove that in the interaction picture of quantum dynamics, the expectation value of an arbitrary observable A may be indeed calculated using Eq. (167).

7.10. Show that the quantum-mechanical Golden Rule (6.149) and the master equation (196) give the same results for the rate of spontaneous quantum transitions $n' \rightarrow n$ in a system with a discrete energy spectrum, weakly coupled to a low-temperature heat bath (with $k_B T \ll \hbar\omega_{nn'}$).

Hint: You may start by establishing a relation between the function $\chi''(\omega_{nn'})$, which participates in Eq. (196), and the density of states ρ_n , which participates in the Golden Rule formula, using the particular case of sinusoidal classical oscillations in the system of interest.

7.11. For a harmonic oscillator with weak Ohmic dissipation, use Eqs. (208)-(209) to find the time evolution of the expectation value $\langle E \rangle$ of oscillator's energy for an arbitrary initial state, and compare the result with that following from the Heisenberg-Langevin approach.

7.12. Derive Eq. (219) in an alternative way, using an expression dual to Eq. (4.244).

7.13. A particle in a system of two coupled potential wells (see, e.g., Fig. 7.4 in the lecture notes) is weakly coupled to an Ohmic environment.

(i) Derive equations describing the time evolution of the density matrix elements.

(ii) Solve these equations in the low-temperature limit, when the energy level splitting is much larger than $k_B T$, to calculate the time evolution of the probability of finding the particle in one of the wells, after it had been placed there at $t = 0$.

7.14.* A spin- $\frac{1}{2}$ with gyromagnetic ratio γ is placed into the magnetic field $\mathcal{B}(t) = \mathcal{B}_0 + \tilde{\mathcal{B}}(t)$ with an arbitrary but relatively small time-dependent component, and is also weakly coupled to a dissipative environment. Derive differential equations describing the time evolution of the expectation values of spin's Cartesian components, at arbitrary temperature.

Chapter 8. Multiparticle Systems

This chapter provides a brief introduction to quantum mechanics of systems of similar particles, with special attention to the case when they are indistinguishable. For such systems, theory predicts (and experiment confirms) very specific effects even in the case of negligible explicit (“direct”) interactions between the particles. These effects notably include the Bose-Einstein condensation of bosons and the exchange interaction of fermions.

8.1. Distinguishable and indistinguishable particles

The importance of quantum systems of many similar particles is probably self-evident; just the very fact that most atoms include several/many electrons is sufficient to attract our attention. There are also important systems where the total number of electrons is much higher than in one atom; for example, a cubic centimeter of a typical metal houses $\sim 10^{23}$ conduction electrons that cannot be attributed to particular atoms, and have to be considered as common parts of the system as the whole. Though quantum mechanics offers virtually no exact analytical results for systems of substantially interacting particles,¹ it reveals very important new quantum effects even in the simplest cases when particles do not interact, and least explicitly (*directly*).

If non-interacting particles are either different from each other by their nature, or physically similar but still distinguishable because of other reasons, everything is simple – at least, conceptually. Then, as was already discussed in Sec. 6.7, a system of two particles, 1 and 2, each in a pure quantum state, may be described by a state vector which is a direct product,

$$|\alpha\rangle = |\beta\rangle_1 \otimes |\beta'\rangle_2, \quad (8.1a)$$

Distinguishable particles of single-particle vectors, describing their states β and β' defined in different Hilbert spaces. (Below, I will frequently use, for such direct product, the following convenient shorthand:

$$|\alpha\rangle = |\beta\beta'\rangle, \quad (8.1b)$$

in which the particle’s number is coded by the state symbol’s position.) Hence the *permuted state*

$$\hat{\mathcal{P}} |\beta\beta'\rangle = |\beta'\beta\rangle = |\beta'\rangle_1 \otimes |\beta\rangle_2, \quad (8.2)$$

where $\hat{\mathcal{P}}$ is the *permutation operator* defined by Eq. (2), is clearly different from the initial one.

This operator may be also used for states of systems of *identical particles*. In physics, the last term may be used to describe:

(i) the “really elementary” particles like electrons, which (at least at this stage of development of physics) are considered as structure-less entities, and hence are all identical;

¹ As was emphasized in Sec. 7.3, for such systems of similar particles the powerful methods discussed in the last chapter, based on the separation of the whole Universe into a “system of our interest” and its “environment”, typically do not work well – mostly because the quantum state of the “particle of interest” may be substantially correlated (in particular, entangled) with those of similar particles forming its “environment” – see below.

(ii) any objects (e.g., hadrons or mesons) that may be considered as a system of “more elementary” particles (e.g., quarks and gluons), but are placed in the same internal quantum state – most simply, though not necessarily, in the ground state.²

It is important to note that *identical* particles still may be *distinguishable* – say by their clear spatial separation. Such systems of similar but distinguishable particles (or subsystems) are broadly discussed nowadays in the context of quantum computing and encryption – see Sec. 5 below. This is why it is insufficient to use the term “identical particles” if we want to say that they are genuinely *indistinguishable*, so I below I will use the latter term, despite it being rather unpleasant grammatically.

It turns out that for a quantitative description of systems of indistinguishable particles we need to use, instead of direct products of the type (1), linear combinations of such products, for example of $|\beta\beta'\rangle$ and $|\beta'\beta\rangle$.³ To see this, let us discuss the properties of the permutation operator defined by Eq. (2). Consider an observable A , and a system of eigenstates of its operator:

$$\hat{A}|\alpha_j\rangle = A_j|\alpha_j\rangle. \quad (8.3)$$

If the particles are indistinguishable, the observable’s expectation value should not be affected by their permutation. Hence the operators \hat{A} and $\hat{\mathcal{P}}$ have to commute and share their eigenstates. This is why the eigenstates of the operator $\hat{\mathcal{P}}$ are so important: in particular, they include the eigenstates of the Hamiltonian, i.e. the stationary states of a system of indistinguishable particles.

Let us have a look at the action of the permutation operator squared, on an elementary ket-vector product:

$$\hat{\mathcal{P}}^2|\beta\beta'\rangle = \hat{\mathcal{P}}(\hat{\mathcal{P}}|\beta\beta'\rangle) = \hat{\mathcal{P}}|\beta'\beta\rangle = |\beta\beta'\rangle, \quad (8.4)$$

i.e. $\hat{\mathcal{P}}^2$ brings the state back to its original form. Since any pure state of a two-particle system may be represented as a linear combination of such products, this result does not depend on the state, and may be represented as the following operator relation:

$$\hat{\mathcal{P}}^2 = \hat{I}. \quad (8.5)$$

Now let us find the possible eigenvalues \mathcal{P}_j of the permutation operator. Acting by both sides of Eq. (5) on any of eigenstates $|\alpha_j\rangle$ of the permutation operator, we get a very simple equation for its eigenvalues:

$$\mathcal{P}_j^2 = 1, \quad (8.6)$$

² Note that from this point of view, even complex atoms or molecules, in the same internal quantum state, may be considered on the same footing as the “really elementary” particles. For example, the already mentioned recent spectacular interference experiments by R. Lopes *et al.*, which require particle identity, were carried out with couples of ⁴He atoms in the same internal quantum state.

³ A very legitimate question is why, in this situation, we need to introduce the particles’ numbers to start with. A partial answer is that in this approach, it is much simpler to derive (or guess) the system Hamiltonians from the correspondence principle – see, e.g., Eq. (27) below. Later in this chapter, we will discuss an alternative approach (the so-called “second quantization”), in which particle numbering is avoided. While that approach is more logical, writing adequate Hamiltonians (which, in particular, would avoid spurious self-interaction of the particles) within it is more challenging – see Sec. 3 below.

with two possible solutions:

$$\mathcal{P}_j = \pm 1. \quad (8.7)$$

Let us find the eigenstates of the permutation operator in the simplest case when each of the component particles can be only in one of two single-particle states – say, β and β' . Evidently, none of the simple products $|\beta\beta'\rangle$ and $|\beta'\beta\rangle$, taken alone, does qualify for the eigenstate – unless the states β and β' are identical. This is why let us try their linear combination

$$|\alpha_j\rangle = a|\beta\beta'\rangle + b|\beta'\beta\rangle, \quad (8.8)$$

so that

$$\hat{\mathcal{P}}|\alpha_j\rangle = \mathcal{P}_j|\alpha_j\rangle = a|\beta'\beta\rangle + b|\beta\beta'\rangle. \quad (8.9)$$

For the case $\mathcal{P}_j = +1$ we have to require the states (8) and (9) to be the same, so that $a = b$, giving the so-called *symmetric eigenstate*⁴

$$|\alpha_+\rangle = \frac{1}{\sqrt{2}}(|\beta\beta'\rangle + |\beta'\beta\rangle), \quad (8.10)$$

where the front coefficient guarantees the orthonormality of the two-particle state vectors, provided that the single-particle vectors are orthonormal. Similarly, for $\mathcal{P}_j = -1$ we get $a = -b$, i.e. an *antisymmetric eigenstate*

$$|\alpha_-\rangle = \frac{1}{\sqrt{2}}(|\beta\beta'\rangle - |\beta'\beta\rangle). \quad (8.11)$$

These are the simplest (two-particle, two-state) examples of *entangled states*, defined as multiparticle system states whose vectors cannot be factored into a direct product (1) of single-particle vectors.

So far, our math does not preclude either sign of \mathcal{P}_j , in particular the possibility that the sign would depend on the state (i.e. on the index j). Here, however, comes in a crucial fact: all indistinguishable particles fall into two groups:⁵

- (i) *bosons*, particles with integer spin s , for whose states $\mathcal{P}_j = +1$, and
- (ii) *fermions*, particles with half-integer spin, with $\mathcal{P}_j = -1$.

In the non-relativistic theory we are discussing now, this key fact should be considered as an experimental one. (The relativistic quantum theory, whose elements will be discussed in Chapter 9, offers proof that the half-integer-spin particles cannot be bosons and the integer-spin ones cannot be fermions.) However, our discussion of spin in Sec. 5.7 enables the following handwaving *interpretation* of the difference between these two particle species. In the free space, the permutation of particles 1 and 2 may be viewed as a result of their pair's common rotation by angle $\phi = \pm\pi$ about a properly selected z -

⁴ As in many situations we have met earlier, the kets given by Eqs. (10) and (11) may be multiplied by $\exp\{i\varphi\}$ with an arbitrary real phase φ . However, until we discuss coherent superpositions of various states α , there is no good motivation for taking the phase different from 0; that would only clutter the notation.

⁵ Sometimes this fact is described as having two different “statistics”: the *Bose-Einstein statistics* of bosons and *Fermi-Dirac statistics* of fermions, because their statistical distributions in thermal equilibrium are indeed different – see, e.g., SM Sec. 2.8. However, this difference is actually deeper: we are dealing with *two different quantum mechanics*.

axis. As we have seen in Sec. 5.7, at the rotation by this angle, the state vector $|\beta\rangle$ of a particle with a definite quantum number m_s acquires an extra factor $\exp\{\pm im_s\pi\}$. As we know, the quantum number m_s ranges from $-s$ to $+s$, in unit steps. As a result, for bosons, with integer s , m_s can take only integer values, so that $\exp\{\pm im_s\pi\} = \pm 1$, so that the product of two such factors in the state product $|\beta\beta'\rangle$ is equal to $+1$. On the contrary, for the fermions with their half-integer s , all m_s are half-integer as well, so that $\exp\{\pm im_s\pi\} = \pm i$ so that the product of two such factors in vector $|\beta\beta'\rangle$ is equal to $(\pm i)^2 = -1$.

The most impressive corollaries of Eqs. (10) and (11) are for the case when the partial states of the two particles are the same: $\beta = \beta'$. The corresponding Bose state α_+ , defined by Eq. (10), is possible; in particular, at sufficiently low temperatures, a set of non-interacting Bose particles condenses on the ground state – the so-called *Bose-Einstein condensate* (“BEC”).⁶ The most fascinating feature of the condensates is that their dynamics is governed by quantum mechanical laws, which may show up in the behavior of their observables with virtually no quantum uncertainties⁷ – see, e.g., Eqs. (1.73)-(1.74).

On the other hand, if we take $\beta = \beta'$ in Eq. (11), we see that state α_- becomes the null-state, i.e. *cannot exist* at all. This is the mathematical expression of the *Pauli exclusion principle*:⁸ two indistinguishable fermions cannot be placed into the same quantum state. (As will be discussed below, this is true for systems with more than two fermions as well.) Probably, the key importance of this principle is self-evident: if it was not valid for electrons (that are fermions), all electrons of each atom would condense on in their ground (1s-like) state, and all the usual chemistry (and biochemistry, and biology, including dear us!) would not exist. The Pauli principle makes fermions implicitly interacting even if they do not interact *directly*, i.e. in the usual sense of this word.

8.2. Singlets, triplets, and the exchange interaction

Now let us discuss possible approaches to quantitative analyses of identical particles, starting from a simple case of two spin-½ particles (say, electrons), whose explicit interaction with each other and the external world does not involve spin. The description of such a system may be based on factorable states with ket-vectors

$$|\alpha_-\rangle = |o_{12}\rangle \otimes |s_{12}\rangle, \quad (8.12)$$

with the orbital state vector $|o_{12}\rangle$ and the spin vector $|s_{12}\rangle$ belonging to different Hilbert spaces. It is frequently convenient to use the coordinate representation of such a state, sometimes called the *spinor*:

$\langle \mathbf{r}_1, \mathbf{r}_2 | \alpha_-\rangle = \langle \mathbf{r}_1, \mathbf{r}_2 | o_{12}\rangle \otimes |s_{12}\rangle \equiv \psi(\mathbf{r}_1, \mathbf{r}_2) |s_{12}\rangle.$

(8.13)
2-particle
spinor

Since the spin-½ particles are fermions, the particle permutation has to change the sign:

⁶ For a quantitative discussion of the Bose-Einstein condensation see, e.g., SM Sec. 3.4. Examples of such condensates include *superfluids* like helium, Cooper-pair condensates in superconductors, and BECs of weakly interacting atoms.

⁷ For example, for a coherent condensate of $N \gg 1$ particles, Heisenberg's uncertainty relation takes the form $\delta x \delta p = \delta x \delta(Nmv) \geq \hbar/2$, so that its coordinate x and velocity v may be measured simultaneously with much higher precision than those of a single particle.

⁸ It was first formulated for electrons by Wolfgang Pauli in 1925, on the background of less general rules suggested by Gilbert Lewis (1916), Irving Langmuir (1919), Niels Bohr (1922), and Edmund Stoner (1924) for the explanation of experimental spectroscopic data.

$$\hat{\mathcal{P}}\psi(\mathbf{r}_1, \mathbf{r}_2)|s_{12}\rangle \equiv \psi(\mathbf{r}_2, \mathbf{r}_1)|s_{21}\rangle = -\psi(\mathbf{r}_1, \mathbf{r}_2)|s_{12}\rangle, \quad (8.14)$$

of either the orbital factor or the spin factor.

In particular, in the case of symmetric orbital factor,

$$\psi(\mathbf{r}_2, \mathbf{r}_1) = \psi(\mathbf{r}_1, \mathbf{r}_2), \quad (8.15)$$

the spin factor has to obey the relation

$$|s_{21}\rangle = -|s_{12}\rangle. \quad (8.16)$$

Let us use the ordinary z -basis (where z , in the absence of an external magnetic field, is an arbitrary spatial axis) for both spins. In this basis, the ket-vector of any two spins- $\frac{1}{2}$ may be represented as a linear combination of the following four basis vectors:

$$|\uparrow\uparrow\rangle, |\downarrow\downarrow\rangle, |\uparrow\downarrow\rangle, \text{ and } |\downarrow\uparrow\rangle. \quad (8.17)$$

The first two kets evidently do not satisfy Eq. (16), and cannot participate in the state. Applying to the remaining kets the same argumentation as has resulted in Eq. (11), we get

Singlet state

$$|s_{12}\rangle = |s_-\rangle \equiv \frac{1}{\sqrt{2}}(|\uparrow\downarrow\rangle - |\downarrow\uparrow\rangle). \quad (8.18)$$

Such an orbital-symmetric and spin-antisymmetric state is called the *singlet*.

The origin of this term becomes clear from the analysis of the opposite (orbital-antisymmetric and spin-symmetric) case:

$$\psi(\mathbf{r}_2, \mathbf{r}_1) = -\psi(\mathbf{r}_1, \mathbf{r}_2), \quad |s_{12}\rangle = |s_+\rangle. \quad (8.19)$$

For the composition of such a symmetric spin state, the first two kets of Eq. (17) are completely acceptable (with arbitrary weights), and so is an entangled spin state that is the symmetric combination of the two last kets, similar to Eq. (10):

$$|s_+\rangle \equiv \frac{1}{\sqrt{2}}(|\uparrow\downarrow\rangle + |\downarrow\uparrow\rangle), \quad (8.20)$$

so that the general spin state is a *triplet*:

Triplet state

$$|s_{12}\rangle = c_+|\uparrow\uparrow\rangle + c_-|\downarrow\downarrow\rangle + c_0\frac{1}{\sqrt{2}}(|\uparrow\downarrow\rangle + |\downarrow\uparrow\rangle). \quad (8.21)$$

Note that any such state (with any values of the coefficients c satisfying the normalization condition), corresponds to the same orbital wavefunction and hence the same energy. However, each of these three states has a specific value of the z -component of the net spin – evidently equal to, respectively, $+\hbar$, $-\hbar$, and 0. Because of this, even a small external magnetic field lifts their degeneracy, splitting the energy level in three; hence the term “triplet”.

In the particular case when the particles do not interact at all, for example

$$\hat{H} = \hat{h}_1 + \hat{h}_2, \quad \hat{h}_k = \frac{\hat{p}_k^2}{2m} + \hat{u}(\mathbf{r}_k), \quad \text{with } k = 1, 2, \quad (8.22)$$

the two-particle Schrödinger equation for the symmetrical orbital wavefunction (15) is obviously satisfied by the direct products,

$$\psi(\mathbf{r}_1, \mathbf{r}_2) = \psi_n(\mathbf{r}_1)\psi_{n'}(\mathbf{r}_2), \quad (8.23)$$

of single-particle eigenfunctions, with arbitrary sets n, n' of quantum numbers. For the particular but very important case $n = n'$, this means that the eigenenergy of the (only acceptable) singlet state,

$$\frac{1}{\sqrt{2}}(\lvert \uparrow \downarrow \rangle - \lvert \downarrow \uparrow \rangle)\psi_n(\mathbf{r}_1)\psi_n(\mathbf{r}_2), \quad (8.24)$$

is just $2\varepsilon_n$, where ε_n is the single-particle energy level.⁹ In particular, for the ground state of the system, such singlet spin state gives the lowest energy $E_g = 2\varepsilon_g$, while any triplet spin state (19) would require one of the particles to be in a different orbital state, i.e. in a state of higher energy, so that the total energy of the system would be also higher.

Now moving to the systems in which two indistinguishable spin- $\frac{1}{2}$ particles do interact, let us consider, as their simplest but important¹⁰ example, the lower energy states of a neutral atom¹¹ of helium – more exactly, ${}^4\text{He}$. Such an atom consists of a nucleus with two protons and two neutrons, with the total electric charge $q = +2e$, and two electrons “rotating” about the nucleus. Neglecting the small relativistic effects that were discussed in Sec. 6.3, the Hamiltonian describing the electron motion may be expressed as

$$\hat{H} = \hat{h}_1 + \hat{h}_2 + \hat{U}_{\text{int}}, \quad \hat{h}_k = \frac{\hat{p}_k^2}{2m} - \frac{2e^2}{4\pi\varepsilon_0 r_k}, \quad \hat{U}_{\text{int}} = \frac{e^2}{4\pi\varepsilon_0 |\mathbf{r}_1 - \mathbf{r}_2|}. \quad (8.25)$$

As with most problems of multiparticle quantum mechanics, the eigenvalue/eigenstate problem for this Hamiltonian does not have an exact analytical solution, so let us carry out its approximate analysis considering the electron-electron interaction U_{int} as a perturbation. As was discussed in Chapter 6, we have to start with the “0th-order” approximation in which the perturbation is ignored, so that the Hamiltonian is reduced to the sum (22). In this approximation, the ground state of the atom is the singlet (24), with the orbital factor

$$\psi_g(\mathbf{r}_1, \mathbf{r}_2) = \psi_{100}(\mathbf{r}_1)\psi_{100}(\mathbf{r}_2), \quad (8.26)$$

and energy $2\varepsilon_g$. Here each factor $\psi_{100}(\mathbf{r})$ is the single-particle wavefunction of the ground (1s) state of the hydrogen-like atom with $Z = 2$, with quantum numbers $n = 1, l = 0$, and $m = 0$ – hence the wavefunctions’ indices. According to Eqs. (3.174) and (3.208),

$$\psi_{100}(\mathbf{r}) = Y_0^0(\theta, \varphi)\mathcal{R}_{1,0}(r) = \frac{1}{\sqrt{4\pi}} \frac{2}{r_0^{3/2}} e^{-r/r_0}, \quad \text{with } r_0 = \frac{r_B}{Z} = \frac{r_B}{2}, \quad (8.27)$$

and according to Eqs. (3.191) and (3.201), in this approximation the total ground state energy is

⁹ In this chapter, I try to use lower-case letters for all *single-particle* observables (in particular, ε for their energies), in order to distinguish them as clearly as possible from the *system’s* observables (including the total energy E of the system), which are typeset in capital letters.

¹⁰ Indeed, helium makes up more than 20% of all “ordinary” matter of our Universe.

¹¹ Note that the positive ion He^{+1} of this atom, with just one electron, is fully described by the hydrogen-like atom theory with $Z = 2$, whose ground-state energy, according to Eq. (3.191), is $-Z^2 E_H/2 = -2E_H \approx -55.4 \text{ eV}$.

$$E_g^{(0)} = 2\epsilon_g^{(0)} = 2 \left(-\frac{\epsilon_0}{2n^2} \right)_{n=1, Z=2} = 2 \left(-\frac{Z^2 E_H}{2} \right)_{Z=2} = -4E_H \approx -109 \text{ eV}. \quad (8.28)$$

This is still somewhat far (though not terribly far!) from the experimental value $E_g \approx -78.8 \text{ eV}$ – see the bottom level in Fig. 1a.

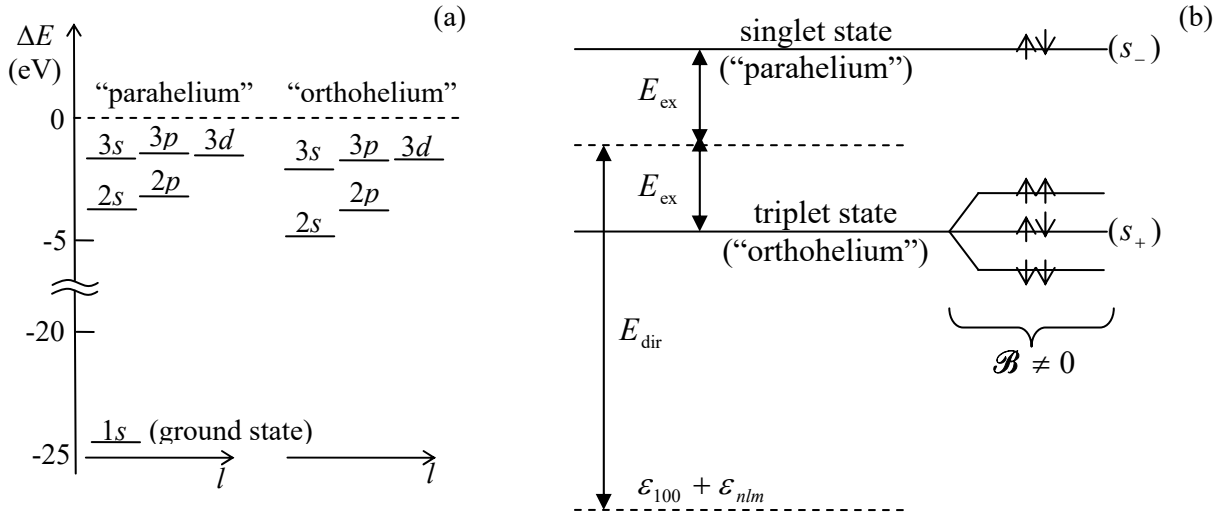


Fig. 8.1. The lower energy levels of a helium atom: (a) experimental data and (b) a schematic structure of an excited state in the first order of the perturbation theory. On panel (a), all energies are referred to that ($-2E_H \approx -55.4 \text{ eV}$) of the ground state of the positive ion He^{+1} , so that their magnitudes are the (readily measurable) energies of the atom's single ionization starting from the corresponding state of the neutral atom. Note that the “spin direction” nomenclature on panel (b) is rather crude: it does not reflect the difference between the entangled states s_+ and s_- .

Making a minor (but very useful) detour from our main topic, let us note that we can get a much better agreement with experiment by calculating the electron interaction energy in the 1st order of the perturbation theory. Indeed, in application to our system, Eq. (6.14) reads

$$E_g^{(1)} = \langle g | \hat{U}_{\text{int}} | g \rangle = \int d^3 r_1 \int d^3 r_2 \psi_g^*(\mathbf{r}_1, \mathbf{r}_2) U_{\text{int}}(\mathbf{r}_1, \mathbf{r}_2) \psi_g(\mathbf{r}_1, \mathbf{r}_2). \quad (8.29)$$

Plugging in Eqs. (25)-(27), we get

$$E_g^{(1)} = \left(\frac{1}{4\pi} \frac{4}{r_0^3} \right)^2 \int d^3 r_1 \int d^3 r_2 \frac{e^2}{4\pi\epsilon_0 |\mathbf{r}_1 - \mathbf{r}_2|} \exp \left\{ -\frac{2(r_1 + r_2)}{r_0} \right\}. \quad (8.30)$$

As may be readily evaluated analytically (this exercise is left for the reader), this expression equals $(5/4)E_H$, so that the corrected ground state energy,

$$E_g \approx E_g^{(0)} + E_g^{(1)} = (-4 + 5/4)E_H = -74.8 \text{ eV}, \quad (8.31)$$

is much closer to experiment.

There is still room here for a ready improvement, using the variational method discussed in Sec. 2.9. For our particular case of the ${}^4\text{He}$ atom, we may try to use, as the trial state, the orbital wavefunction given by Eqs. (26)-(27), but with the atomic number Z considered as an adjustable

parameter $Z_{\text{ef}} < Z = 2$ rather than a fixed number. The physics behind this approach is that the electric charge density $\rho(\mathbf{r}) = -e|\psi(\mathbf{r})|^2$ of each electron forms a negatively charged “cloud” that reduces the effective charge of the nucleus, as seen by the other electron, to $Z_{\text{ef}}e$, with some $Z_{\text{ef}} < 2$. As a result, the single-particle wavefunction spreads further in space (with the scale $r_0 = r_B/Z_{\text{ef}} > r_B/Z$), while keeping its functional form (27) nearly intact. Since the kinetic energy T in the system’s Hamiltonian (25) is proportional to $r_0^{-2} \propto Z_{\text{ef}}^{-2}$, while the potential energy is proportional to $r_0^{-1} \propto Z_{\text{ef}}^{-1}$, we can write

$$E_g(Z_{\text{ef}}) = \left(\frac{Z_{\text{ef}}}{2}\right)^2 \langle T_g \rangle_{Z=2} + \frac{Z_{\text{ef}}}{2} \langle U_g \rangle_{Z=2}. \quad (8.32)$$

Now we can use the fact that according to Eq. (3.212), for any stationary state of a hydrogen-like atom (just as for the classical circular motion in the Coulomb potential), $\langle U \rangle = 2E$, and hence $\langle T \rangle = E - \langle U \rangle = -E$. Using Eq. (30), and adding the correction (31) to the potential energy, we get

$$E_g(Z_{\text{ef}}) = \left[4\left(\frac{Z_{\text{ef}}}{2}\right)^2 + \left(-8 + \frac{5}{4}\right) \frac{Z_{\text{ef}}}{2} \right] E_H. \quad (8.33)$$

This expression allows an elementary calculation of the optimal value of Z_{ef} , and the corresponding minimum of the function $E_g(Z_{\text{ef}})$:

$$(Z_{\text{ef}})_{\text{opt}} = 2\left(1 - \frac{5}{32}\right) = 1.6875, \quad (E_g)_{\text{min}} \approx -2.85E_H \approx -77.5 \text{ eV}. \quad (8.34)$$

Given the trial state’s crudeness, this number is in surprisingly good agreement with the experimental value cited above, with a difference of the order of 1%.

Now let us return to the main topic of this section – the effects of particle (in this case, electron) indistinguishability. As we have just seen, the ground-level energy of the helium atom is not affected directly by this fact, but the situation is different for its excited states – even the lowest ones. The reasonably good precision of the perturbation theory, which we have seen for the ground state, tells us that we can base our analysis of wavefunctions (ψ_e) of the lowest excited state orbitals, on products like $\psi_{100}(\mathbf{r}_k)\psi_{nlm}(\mathbf{r}_{k'})$, with $n > 1$. To satisfy the fermion permutation rule, $\mathcal{P}_j = -1$, we have to take the orbital factor of the state in either the symmetric or the antisymmetric form:

$$\psi_e(\mathbf{r}_1, \mathbf{r}_2) = \frac{1}{\sqrt{2}} [\psi_{100}(\mathbf{r}_1)\psi_{nlm}(\mathbf{r}_2) \pm \psi_{nlm}(\mathbf{r}_1)\psi_{100}(\mathbf{r}_2)], \quad (8.35)$$

Orthohelium
and
parahelium:
orbital
wavefunctions

with the proper total permutation asymmetry provided by the corresponding spin factor (18) or (21), so that the upper/lower sign in Eq. (35) corresponds to the singlet/triplet spin state. Let us calculate the expectation values of the total energy of the system in the first order of the perturbation theory. Plugging Eq. (35) into the 0th-order expression

$$\langle E_e \rangle^{(0)} = \int d^3r_1 \int d^3r_2 \psi_e^*(\mathbf{r}_1, \mathbf{r}_2) (\hat{h}_1 + \hat{h}_2) \psi_e(\mathbf{r}_1, \mathbf{r}_2), \quad (8.36)$$

we get two groups of similar terms that differ only by the particle index. We can merge the terms of each pair by changing the notation as $(\mathbf{r}_1 \rightarrow \mathbf{r}, \mathbf{r}_2 \rightarrow \mathbf{r}')$ in one of them, and $(\mathbf{r}_1 \rightarrow \mathbf{r}', \mathbf{r}_2 \rightarrow \mathbf{r})$ in the counterpart term. Using Eq. (25), and the mutual orthogonality of the wavefunctions $\psi_{100}(\mathbf{r})$ and $\psi_{nlm}(\mathbf{r})$, we get the following result:

$$\langle E_e \rangle^{(0)} = \int \psi_{100}^*(\mathbf{r}) \left(-\frac{\hbar^2 \nabla_r^2}{2m} - \frac{2e^2}{4\pi\epsilon_0 r} \right) \psi_{100}(\mathbf{r}) d^3r + \int \psi_{nlm}^*(\mathbf{r}') \left(-\frac{\hbar^2 \nabla_{r'}^2}{2m} - \frac{2e^2}{4\pi\epsilon_0 r'} \right) \psi_{nlm}(\mathbf{r}') d^3r' \quad (8.37)$$

$\equiv \epsilon_{100} + \epsilon_{nlm}, \quad \text{with } n > 1.$

It may be interpreted as the sum of eigenenergies of two separate single particles, one in the ground state 100, and another in the excited state nlm – although actually the electron states are entangled. Thus, in the 0th order of the perturbation theory, the electron entanglement does not affect their energy.

However, the potential energy of the system also includes the interaction term U_{int} , which does not allow such separation. Indeed, in the 1st approximation of the perturbation theory, the total energy E_e of the system may be expressed as $\epsilon_{100} + \epsilon_{nlm} + E_{\text{int}}^{(1)}$, with

$$E_{\text{int}}^{(1)} = \langle U_{\text{int}} \rangle = \int d^3r_1 \int d^3r_2 \psi_e^*(\mathbf{r}_1, \mathbf{r}_2) U_{\text{int}}(\mathbf{r}_1, \mathbf{r}_2) \psi_e(\mathbf{r}_1, \mathbf{r}_2), \quad (8.38)$$

Plugging Eq. (35) into this result, using the symmetry of the function U_{int} with respect to the particle number permutation, and the same particle coordinate re-numbering as above, we get

$$E_{\text{int}}^{(1)} = E_{\text{dir}} \pm E_{\text{ex}}, \quad (8.39)$$

with the following, deceptively similar expressions for the two components of this sum/difference:

Direct
interaction
energy

Exchange
interaction
energy

$$E_{\text{dir}} \equiv \int d^3r \int d^3r' \psi_{100}^*(\mathbf{r}) \psi_{nlm}^*(\mathbf{r}') U_{\text{int}}(\mathbf{r}, \mathbf{r}') \psi_{100}(\mathbf{r}) \psi_{nlm}(\mathbf{r}'), \quad (8.40)$$

$$E_{\text{ex}} \equiv \int d^3r \int d^3r' \psi_{100}^*(\mathbf{r}) \psi_{nlm}^*(\mathbf{r}') U_{\text{int}}(\mathbf{r}, \mathbf{r}') \psi_{nlm}(\mathbf{r}) \psi_{100}(\mathbf{r}'). \quad (8.41)$$

Since the single-particle orbitals can be always made real, both components are positive – or at least non-negative. However, their physics and magnitude are different. The integral (40), called the *direct interaction energy*, allows a simple semi-classical interpretation as the Coulomb energy of interacting electrons, each distributed in space with the electric charge density $\rho(\mathbf{r}) = -e\psi^*(\mathbf{r})\psi(\mathbf{r})$:¹²

$$E_{\text{dir}} = \int d^3r \int d^3r' \frac{\rho_{100}(\mathbf{r})\rho_{nlm}(\mathbf{r}')}{4\pi\epsilon_0 |\mathbf{r} - \mathbf{r}'|} \equiv \int \rho_{100}(\mathbf{r})\phi_{nlm}(\mathbf{r}) d^3r \equiv \int \rho_{nlm}(\mathbf{r})\phi_{100}(\mathbf{r}) d^3r, \quad (8.42)$$

where $\phi(\mathbf{r})$ are the electrostatic potentials created by the electron “charge clouds”:¹³

$$\phi_{100}(\mathbf{r}) = \frac{1}{4\pi\epsilon_0} \int d^3r' \frac{\rho_{100}(\mathbf{r}')}{|\mathbf{r} - \mathbf{r}'|}, \quad \phi_{nlm}(\mathbf{r}) = \frac{1}{4\pi\epsilon_0} \int d^3r' \frac{\rho_{nlm}(\mathbf{r}')}{|\mathbf{r} - \mathbf{r}'|}. \quad (8.43)$$

However, the integral (41), called the *exchange interaction energy*, evades a classical interpretation, and (as it is clear from its derivation) is the direct corollary of electrons’ indistinguishability. The magnitude of E_{ex} is also very much different from E_{dir} because the function under the integral (41) disappears in the regions where the single-particle wavefunctions $\psi_{100}(\mathbf{r})$ and $\psi_{nlm}(\mathbf{r})$ do not overlap. This is in full agreement with the discussion in Sec. 1: if two particles are identical but well separated, i.e. their wavefunctions do not overlap, the exchange interaction disappears,

¹² See, e.g., EM Sec. 1.3, in particular Eq. (1.54).

¹³ Note that the result for E_{dir} correctly reflects the basic fact that a charged particle does not interact with itself, even if its wavefunction is quantum-mechanically spread over a finite space volume. Unfortunately, this is not true for some popular approximate theories of multiparticle systems – see Sec. 4 below.

i.e. measurable effects of particle indistinguishability vanish. (In contrast, the integral (40) decreases with the growing electron separation only slowly, due to the long-range Coulomb interaction.)

Figure 1b shows the structure of an excited energy level, with certain quantum numbers $n > 1$, l , and m , given by Eqs. (39)-(41). The upper, so-called *parahelium*¹⁴ level, with the energy

$$E_{\text{para}} = (\varepsilon_{100} + \varepsilon_{nlm}) + E_{\text{dir}} + E_{\text{ex}} > \varepsilon_{100} + \varepsilon_{nlm}, \quad (8.44)$$

corresponds to the symmetric orbital state and hence to the singlet spin state (18), while the lower, *orthohelium* level, with

$$E_{\text{orth}} = (\varepsilon_{100} + \varepsilon_{nlm}) + E_{\text{dir}} - E_{\text{ex}} < E_{\text{para}}, \quad (8.45)$$

corresponds to the degenerate triplet spin state (21).

This degeneracy may be lifted by an external magnetic field, whose effect on the electron spins¹⁵ is described by the following evident generalization of the Pauli Hamiltonian (4.163),

$$\hat{H}_{\text{field}} = -\gamma \hat{\mathbf{s}}_1 \cdot \mathcal{B} - \gamma \hat{\mathbf{s}}_2 \cdot \mathcal{B} \equiv -\gamma \hat{\mathbf{S}} \cdot \mathcal{B}, \quad \text{with } \gamma = \gamma_e \equiv -\frac{e}{m_e} \equiv -2 \frac{\mu_B}{\hbar}, \quad (8.46)$$

where

$$\hat{\mathbf{S}} \equiv \hat{\mathbf{s}}_1 + \hat{\mathbf{s}}_2, \quad (8.47)$$

is the operator of the (vector) sum of the system of two spins.¹⁶ To analyze this effect, we need first to make one more detour, to address the general issue of *spin addition*. The main rule¹⁷ here is that in a full analogy with the net spin of a single particle, defined by Eq. (5.170), the net spin operator (47) of *any* system of two spins, and its component \hat{S}_z along the (arbitrarily selected) z -axis, obey the same commutation relations (5.168) as the component operators, and hence have the properties similar to those expressed by Eqs. (5.169) and (5.175):

$$\hat{S}^2 |S, M_S\rangle = \hbar^2 S(S+1) |S, M_S\rangle, \quad \hat{S}_z |S, M_S\rangle = \hbar M_S |S, M_S\rangle, \quad \text{with } -S \leq M_S \leq +S, \quad (8.48)$$

where the ket vectors correspond to the coupled basis of joint eigenstates of the operators of S^2 and S_z (but not necessarily all component operators – see again the Venn shown in Fig. 5.12 and its discussion, with the replacements \mathbf{S} , $\mathbf{L} \rightarrow \mathbf{s}_{1,2}$ and $\mathbf{J} \rightarrow \mathbf{S}$). Repeating the discussion of Sec. 5.7 with these replacements, we see that in both coupled and uncoupled bases, the net magnetic number M_S is simply expressed via those of the components

¹⁴ This terminology reflects the historic fact that the observation of two different hydrogen-like spectra, corresponding to the opposite signs in Eq. (39), was first taken as evidence for two different species of ${}^4\text{He}$, which were called, respectively, the “orthohelium” and the “parahelium”.

¹⁵ As we know from Sec. 6.4, the field also affects the orbital motion of the electrons, so that the simple analysis based on Eq. (46) is strictly valid only for the s excited state ($l = 0$, and hence $m = 0$). However, the orbital effects of a weak magnetic field do not affect the triplet level splitting we are analyzing now.

¹⁶ Note that similarly to Eqs. (22) and (25), here the uppercase notation of the component spins is replaced with their lowercase notation, to avoid any possibility of their confusion with the total spin of the system.

¹⁷ Since we already know that the spin of a particle is physically nothing more than a (specific) part of its angular momentum, the similarity of the properties (48) of the sum (47) of spins of different particles to those of the sum (5.170) of different spin components of the same particle is very natural, but still has to be considered as a new fact – confirmed by a vast body of experimental data.

$$M_S = (m_s)_1 + (m_s)_2. \quad (8.49)$$

However, the net spin quantum number S (in contrast to the Nature-given spins $s_{1,2}$ of its elementary components) is not universally definite, and we may immediately say only that it has to obey the following analog of the relation $|l - s| \leq j \leq (l + s)$ discussed in Sec. 5.7:

$$|s_1 - s_2| \leq S \leq s_1 + s_2. \quad (8.50)$$

What exactly S is (within these limits), depends on the spin state of the system.

For the simplest case of two spin- $\frac{1}{2}$ components, each with $s = \frac{1}{2}$ and $m_s = \pm\frac{1}{2}$, Eq. (49) gives three possible values of M_S , equal to 0 and ± 1 , while Eq. (50) limits the possible values of S to just either 0 or 1. Using the last of Eqs. (48), we see that the possible combinations of the quantum numbers are

$$\begin{cases} S = 0, \\ M_S = 0, \end{cases} \quad \text{and} \quad \begin{cases} S = 1, \\ M_S = 0, \pm 1. \end{cases} \quad (8.51)$$

It is virtually evident that the singlet spin state s_- belongs to the first class, while the simple (separable) triplet states $\uparrow\uparrow$ and $\downarrow\downarrow$ belong to the second class, with $M_S = +1$ and $M_S = -1$, respectively. However, for the entangled triplet state s_+ , evidently with $M_S = 0$, the value of S is less obvious. Perhaps the easiest way to recover it¹⁸ to use the “rectangular diagram”, similar to that shown in Fig. 5.14, but redrawn for our case of two spins, i.e., with the replacements $m_l \rightarrow (m_s)_1 = \pm\frac{1}{2}$, $m_s \rightarrow (m_s)_2 = \pm\frac{1}{2}$ – see Fig. 2.

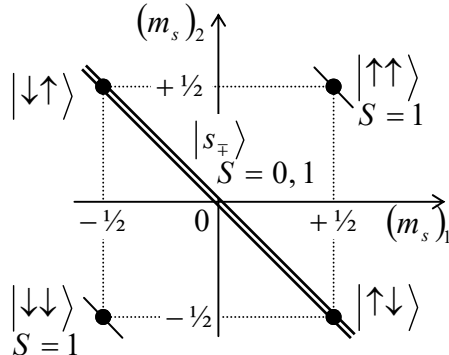


Fig. 8.2. The “rectangular diagram” showing the relation between the uncoupled-representation states (dots) and the coupled-representation states (straight lines) of a system of two spins- $\frac{1}{2}$ – cf. Fig. 5.14.

Just as at the addition of various angular momenta of a single particle, the top-right and bottom-left corners of this diagram correspond to the factorable triplet states $\uparrow\uparrow$ and $\downarrow\downarrow$, which participate in both the uncoupled-representation and coupled-representation bases, and have the largest value of S , i.e. 1. However, the entangled states s_+ , which are linear combinations of the uncoupled-representation states $\uparrow\downarrow$ and $\downarrow\uparrow$, cannot have the same value of S , so that for the triplet state s_+ , S has to take the value different from that (0) of the singlet state, i.e. 1. With that, the first of Eqs. (48) gives the following expectation values for the square of the net spin operator:

$$\langle S^2 \rangle = \begin{cases} 2\hbar^2, & \text{for each triplet state,} \\ 0, & \text{for the singlet state.} \end{cases} \quad (8.52)$$

¹⁸ Another, a bit longer but perhaps a more prudent way is to directly calculate the expectation values of \hat{S}^2 for the states s_+ , and then find S by comparing the results with the first of Eqs. (48); it is highly recommended to the reader as a useful exercise.

Note that for the entangled triplet state s_+ , whose ket-vector (20) is a linear superposition of two kets of states with *opposite* spins, this result is highly counter-intuitive, and shows how careful we should be interpreting entangled quantum states. (As will be discussed in Chapter 10, the entanglement brings even more surprises for quantum measurements.)

Now we may return to the particular issue of the magnetic field effect on the triplet state of the ${}^4\text{He}$ atom. Directing the z -axis along the field, we may reduce Eq. (46) to

$$\hat{H}_{\text{field}} = -\gamma_e \hat{S}_z \mathcal{B} \equiv 2\mu_B \mathcal{B} \frac{\hat{S}_z}{\hbar}. \quad (8.53)$$

Since all three triplet states (21) are eigenstates, in particular, of the operator \hat{S}_z , and hence of the Hamiltonian (53), we may use the second of Eqs. (48) to calculate their energy change simply as

$$\Delta E_{\text{field}} = 2\mu_B \mathcal{B} M_S = 2\mu_B \mathcal{B} \times \begin{cases} +1, & \text{for the factorable triplet state } \uparrow\uparrow, \\ 0, & \text{for the entangled triplet state } s_+, \\ -1, & \text{for the factorable triplet state } \downarrow\downarrow. \end{cases} \quad (8.54)$$

This splitting of the “orthohelium” level is schematically shown in Fig. 1b.¹⁹

8.3. Multiparticle systems

Leaving several other problems on two-particle systems for the reader’s exercise, let me proceed to the discussion of systems with $N > 2$ indistinguishable particles, whose list notably includes atoms, molecules, and condensed-matter systems. In this case, Eq. (7) for fermions is generalized as

$$\hat{\mathcal{P}}_{kk'} |\alpha_- \rangle = -|\alpha_- \rangle, \quad \text{for all } k, k' = 1, 2, \dots, N, \quad (8.55)$$

where the operator $\hat{\mathcal{P}}_{kk'}$ permutes particles with numbers k and k' . As a result, for systems with non-directly-interacting fermions, the Pauli principle forbids any state in which *any* two particles have similar single-particle wavefunctions. Nevertheless, it permits two fermions to have similar *orbital* wavefunctions, provided that their spins are in the singlet state (18), because this satisfies the permutation requirement (55). This fact is of paramount importance for the ground state of the systems whose Hamiltonians do not depend on spin because it allows the fermions to be in their orbital single-particle ground states, with two electrons of the spin singlet sharing the same orbital state. Hence, for the limited (but very important!) goal of finding ground-state energies of multi-fermion systems with negligible direct interaction, we may ignore the actual singlet spin structure, and reduce the Pauli

¹⁹ It is interesting that another very important two-electron system, the hydrogen (H_2) molecule, which was briefly discussed in Sec. 2.6, also has two similarly named forms, *parahydrogen* and *orthohydrogen*. However, their difference is due to two possible (respectively, singlet and triplet) states of the system of two spins of the two hydrogen nuclei – protons, which are also spin- $1/2$ particles. The resulting energy of the parahydrogen is lower than that of the orthohydrogen by only ~ 45 meV per molecule – the difference comparable with $k_B T$ at room temperature (~ 26 meV). As a result, at the ambient conditions, the equilibrium ratio of these two *spin isomers* is close to 3:1. Curiously, the theoretical prediction of this minor effect by W. Heisenberg (together with F. Hund) in 1927 was cited in his 1932 Nobel Prize award as the most noteworthy application of quantum theory.

exclusion principle to the simple picture of single-particle orbital energy levels, each “occupied with two fermions”.

As a very simple example, let us find the ground energy of five fermions, confined in a hard-wall, cubic-shaped 3D volume of side a , ignoring their direct interaction. From Sec. 1.7, we know the single-particle energy spectrum of the system:

$$\varepsilon_{n_x, n_y, n_z} = \varepsilon_0 (n_x^2 + n_y^2 + n_z^2), \quad \text{with } \varepsilon_0 \equiv \frac{\pi^2 \hbar^2}{2ma^2}, \quad \text{and } n_x, n_y, n_z = 1, 2, \dots \quad (8.56)$$

so that the lowest-energy states are:

- one ground state with $\{n_x, n_y, n_z\} = \{1, 1, 1\}$, and energy $\varepsilon_{111} = (1^2 + 1^2 + 1^2) \varepsilon_0 = 3 \varepsilon_0$, and
- three excited states, with $\{n_x, n_y, n_z\}$ equal to either $\{2, 1, 1\}$, or $\{1, 2, 1\}$, or $\{1, 1, 2\}$, with equal energies $\varepsilon_{211} = \varepsilon_{121} = \varepsilon_{112} = (2^2 + 1^2 + 1^2) \varepsilon_0 = 6 \varepsilon_0$.

According to the above simple formulation of the Pauli principle, each of these orbital energy levels can accommodate up to two fermions. Hence the lowest-energy (ground) state of the five-fermion system is achieved by placing two of them on the ground level $\varepsilon_{111} = 3 \varepsilon_0$, and the remaining three particles, in any of the degenerate “excited” states of energy $6 \varepsilon_0$, so that the ground-state energy of the system is

$$E_g = 2 \times 3 \varepsilon_0 + 3 \times 6 \varepsilon_0 \equiv 24 \varepsilon_0 \equiv \frac{12 \pi^2 \hbar^2}{ma^2}. \quad (8.57)$$

Moreover, in many cases, relatively weak interaction between fermions does not blow up such a simple quantum state classification scheme qualitatively, and the Pauli principle allows tracing the order of single-particle state filling. This is exactly the simple approach that has been used in our discussion of atoms in Sec. 3.7. Unfortunately, it does not allow for a more specific characterization of the ground states of most atoms, in particular the evaluation of the corresponding values of the quantum numbers S , L , and J that characterize the net angular momenta of the atom, and hence its response to an external magnetic field. These numbers are defined by relations similar to Eqs. (48), each for the corresponding vector operator of the net angular momenta:

$$\hat{\mathbf{S}} \equiv \sum_{k=1}^N \hat{\mathbf{s}}_k, \quad \hat{\mathbf{L}} \equiv \sum_{k=1}^N \hat{\mathbf{l}}_k, \quad \hat{\mathbf{J}} \equiv \sum_{k=1}^N \hat{\mathbf{j}}_k; \quad (8.58)$$

note that these definitions are consistent with Eq. (5.170) applied both to the angular momenta \mathbf{s}_k , \mathbf{l}_k , and \mathbf{j}_k of each particle, and to the full vectors \mathbf{S} , \mathbf{L} , and \mathbf{J} . When the numbers S , L , and J for a state are known, they are traditionally recorded in the form of the so-called *Russell-Saunders symbols*:²⁰

$$^{2S+1}\mathcal{L}_J, \quad (8.59)$$

where S and J are the corresponding values of these quantum numbers, while \mathcal{L} is a capital *letter*, encoding the quantum number L – via the same spectroscopic notation as for single particles (see Sec. 3.6): $\mathcal{L} = S$ for $L = 0$, $\mathcal{L} = P$ for $L = 1$, $\mathcal{L} = D$ for $L = 2$, etc. (The reason why the front superscript of the Russel-Saunders symbol lists $2S + 1$ rather than just S , is that according to the last of Eqs. (48), it

²⁰ Named after H. Russell and F. Saunders, whose pioneering (circa 1925) processing of experimental spectral-line data has established the very idea of vector addition of the electron spins, described by the first of Eqs. (58).

shows the number of possible values of the quantum number M_S , which characterizes the state's spin degeneracy, and is called its *multiplicity*.)

For example, for the simplest, hydrogen atom ($Z = 1$), with its single electron in the ground $1s$ state, $L = l = 0$, $S = s = \frac{1}{2}$, and $J = S = \frac{1}{2}$, so that its Russell-Saunders symbol is $2S_{1/2}$. Next, the discussion of the helium atom ($Z = 2$) in the previous section has shown that in its ground state $L = 0$ (because of the $1s$ orbital state of both electrons), and $S = 0$ (because of the singlet spin state), so that the total angular momentum also vanishes: $J = 0$. As a result, the Russell-Saunders symbol is 1S_0 . The structure of the next atom, lithium ($Z = 3$) is also easy to predict, because, as was discussed in Sec. 3.7, its ground-state electron configuration is $1s^22s^1$, i.e. includes two electrons in the “helium shell”, i.e. on the $1s$ orbitals (now we know that they are actually in a singlet spin state), and one electron in the $2s$ state, of higher energy, also with zero orbital momentum, $l = 0$. As a result, the total L in this state is evidently equal to 0, and S is equal to $\frac{1}{2}$, so that $J = \frac{1}{2}$, meaning that the Russell-Saunders symbol of lithium is $^2P_{1/2}$. Even in the next atom, beryllium ($Z = 4$), with the ground state configuration $1s^22s^2$, the symbol is readily predictable, because none of its electrons has non-zero orbital momentum, giving $L = 0$. Also, each electron pair is in the singlet spin state, i.e. we have $S = 0$, so that $J = 0$ – the quantum number set described by the Russell-Saunders symbol 1S_0 – just as for helium.

However, for the next, boron atom ($Z = 5$), with its ground-state electron configuration $1s^22s^22p^1$ (see, e.g., Fig. 3.24), there is no obvious way to predict the result. Indeed, this atom has two pairs of electrons, with opposite spins, on its two lowest s -orbitals, giving zero contributions to the net S , L , and J . Hence these total quantum numbers may be only contributed by the last, fifth electron with $s = \frac{1}{2}$ and $l = 1$, giving $S = \frac{1}{2}$, $L = 1$. As was discussed in Sec. 5.7 for the single-particle case, the vector addition of the angular momenta \mathbf{S} and \mathbf{L} enables two values of the quantum number J : either $L + S = \frac{3}{2}$ or $L - S = \frac{1}{2}$. Experiment shows that the difference between the energies of these two states is very small (~ 2 meV), so that at room temperature (with $k_B T \approx 26$ meV) they are both occupied, with the genuine ground state having $J = \frac{1}{2}$, so that its Russell-Saunders symbol is $^2P_{1/2}$.

Such energy differences, which become larger for heavier atoms, are determined both by the Coulomb and spin-orbit²¹ interactions between the electrons. Their quantitative analysis is rather involved (see below), but the results tend to follow simple phenomenological *Hund rules*, with the following hierarchy:

Rule 1. For a given electron configuration, the ground state has the *largest* possible S , and hence the largest multiplicity $2S + 1$.

Rule 2. For a given S , the ground state has the *largest* possible L .

Rule 3. For given S and L , J has its *smallest* possible value, $|L - S|$, if the given sub-shell $\{n, l\}$ is filled not more than by half, while in the opposite case, J has its *largest* possible value, $L + S$.

Let us see how these rules work for the boron atom we have just discussed. For it, the Hund Rules 1 and 2 are satisfied automatically, while the sub-shell $\{n = 2, l = 1\}$, which can house up to $2(2l + 1) = 6$ electrons, is filled with just one $2p$ electron, i.e. by less than a half of the maximum value. As a result, the Hund Rule 3 predicts the ground state's value $J = \frac{1}{2}$, in agreement with experiment.

²¹ In light atoms, the spin-orbit interaction is so weak that it may be reasonably well described as an interaction of the total momenta \mathbf{L} and \mathbf{S} of the system – the so-called LS (or “Russell-Saunders”) coupling. On the other hand, in very heavy atoms, the interaction is effectively between the net momenta $\mathbf{j}_k = \mathbf{l}_k + \mathbf{s}_k$ of the individual electrons – the so-called jj coupling. This is the reason why in such atoms the Hund rule 3 may be violated.

Generally, for lighter atoms, the Hund rules are well obeyed. However, the lower down the Hund rule hierarchy, the less “powerful” the rules are, i.e. the more often they are violated in heavier atoms.

Now let us discuss possible approaches to a quantitative theory of multiparticle systems – not only atoms. As was discussed in Sec. 1, if fermions do not interact directly, the stationary states of the system have to be the antisymmetric eigenstates of the permutation operator, i.e. satisfy Eq. (55). To understand how such states may be formed from the single-electron ones, let us return for a minute to the case of two electrons, and rewrite Eq. (11) in the following compact form:

$$|\alpha_-\rangle \equiv \frac{1}{\sqrt{2}}(|\beta\rangle \otimes |\beta'\rangle - |\beta'\rangle \otimes |\beta\rangle) = \frac{1}{\sqrt{2}} \begin{vmatrix} |\beta\rangle & |\beta'\rangle \\ |\beta'\rangle & |\beta\rangle \end{vmatrix} \begin{array}{l} \text{state 1} \\ \downarrow \end{array} \begin{array}{l} \text{state 2} \\ \downarrow \end{array} \quad (8.60a)$$

← particle number 1,
← particle number 2,

where the direct product signs are just implied. In this way, the Pauli principle is mapped on the well-known property of matrix determinants: if any of two columns of a matrix coincide, its determinant vanishes. This *Slater determinant* approach²² may be readily generalized to N fermions occupying any N (not necessarily the lowest-energy) single-particle states $\beta, \beta', \beta'', \dots$, etc:

Slater determinant

$$|\alpha_-\rangle = \frac{1}{(N!)^{1/2}} \left| \begin{array}{cccc} |\beta\rangle & |\beta'\rangle & |\beta''\rangle & \dots \\ |\beta\rangle & |\beta'\rangle & |\beta''\rangle & \dots \\ |\beta\rangle & |\beta'\rangle & |\beta''\rangle & \dots \\ \dots & \dots & \dots & \dots \end{array} \right|_{\overbrace{N}}^{\text{state list} \rightarrow \text{particle list}} \quad (8.60b)$$

The Slater determinant form is extremely nice and compact – in comparison with direct writing of a sum of $N!$ products, each of N ket factors. However, there are two major problems with using it for practical calculations:

(i) For the calculation of any bra-ket product (say, within the perturbation theory) we still need to spell out each bra- and ket-vector as a sum of component terms. Even for a limited number of electrons (say $N \sim 10^2$ in a typical atom), the number $N! \sim 10^{160}$ of terms in such a sum is impractically large for any analytical or numerical calculation.

(ii) In the case of interacting fermions, the Slater determinant does not describe the eigenvectors of the system; rather the stationary state is a *superposition* of such basis functions, i.e. of the Slater determinants – each for a specific selection of N states from the full set of single-particle states – that is generally larger than N .

For atoms and simple molecules, whose filled-shell electrons may be excluded from an explicit analysis (by describing their effects, approximately, with effective *pseudo-potentials*), the effective number N may be reduced to a smaller number N_{ef} of the order of 10, so that $N_{\text{ef}}! < 10^6$, and the Slater determinants may be used for numerical calculations – for example, in the Hartree-Fock theory – see the next section. However, for condensed-matter systems, such as metals and semiconductors, with the

²² It was suggested in 1929 by John C. Slater.

number of free electrons is of the order of 10^{23} per cm³, this approach is generally unacceptable, though with some smart tricks (such as using the crystal's periodicity) it may be still used for some approximate (also mostly numerical) calculations.

These challenges make the development of a more general theory that would not use particle numbers (which are superficial for indistinguishable particles to start with) a must for getting any final analytical results for multiparticle systems. The most effective formalism for this purpose, which avoids particle numbering at all, is called the *second quantization*.²³ Actually, we have already discussed a particular version of this formalism, for the case of the 1D harmonic oscillator, in Sec. 5.4. As a reminder, after the definition (5.65) of the “creation” and “annihilation” operators via those of the particle’s coordinate and momentum, we have derived their key properties (5.89),

$$\hat{a}|n\rangle = n^{1/2}|n-1\rangle, \quad \hat{a}^\dagger|n\rangle = (n+1)^{1/2}|n+1\rangle, \quad (8.61)$$

where n are the stationary (Fock) states of the oscillator. This property allows an interpretation of the operators’ actions as the creation/annihilation of a single *excitation* with the energy $\hbar\omega_0$ – thus justifying the operator names. In the next chapter, we will show that such excitation of an electromagnetic field mode may be interpreted as a massless *boson* with $s = 1$, called the *photon*.

In order to generalize this approach to *arbitrary bosons*, not appealing to a specific system, we may use relations similar to Eq. (61) to *define* the creation and annihilation operators. The definitions look simple in the language of the so-called *Dirac states*, described by ket-vectors

$$|N_1, N_2, \dots, N_j, \dots\rangle, \quad (8.62)$$

Dirac state

where N_j is the state *occupancy*, i.e. the number of bosons in the single-particle state j . Let me emphasize that here the indices $1, 2, \dots, j, \dots$ number single-particle *states* (including their spin parts) rather than *particles*. Thus the very notion of an individual particle’s number is completely (and for indistinguishable particles, very relevantly) absent from this formalism. Generally, the set of single-particle states participating in the Dirac state may be selected arbitrarily, provided that it is full and orthonormal in the sense

$$\langle N'_1, N'_2, \dots, N'_{j'}, \dots | N_1, N_2, \dots, N_j, \dots \rangle = \delta_{N_1 N'_1} \delta_{N_2 N'_2} \dots \delta_{N_j N'_{j'}}, \quad (8.63)$$

though for systems of non- (or weakly) interacting bosons, using the stationary states of individual particles in the system under analysis is almost always the best choice.

Now we can define the *particle annihilation operator* as follows:

$$\hat{a}_j |N_1, N_2, \dots, N_j, \dots\rangle \equiv N_j^{1/2} |N_1, N_2, \dots, N_j - 1, \dots\rangle. \quad (8.64)$$

Boson annihilation operator

Note that the pre-ket coefficient, similar to that in the first of Eqs. (61), guarantees that any attempt to annihilate a particle in an initially unpopulated state gives the non-existing (“null”) state:

$$\hat{a}_j |N_1, N_2, \dots, 0_j, \dots\rangle = 0, \quad (8.65)$$

²³ It was invented (first for photons and then for arbitrary bosons) by P. Dirac in 1927, and then modified in 1928 for fermions by E. Wigner and P. Jordan. Note that the term “second quantization” is rather misleading for the non-relativistic applications we are discussing here, but finds certain justification in the quantum field theory.

where the symbol 0_j means zero occupancy of the j^{th} state. According to Eq. (63), an equivalent way to write Eq. (64) is

$$\langle N'_1, N'_2, \dots, N'_j, \dots | \hat{a}_j | N_1, N_2, \dots, N_j, \dots \rangle = N_j^{1/2} \delta_{N_1 N'_1} \delta_{N_2 N'_2} \dots \delta_{N_j N'_j} \dots \quad (8.66)$$

According to the general Eq. (4.65), the matrix element of the Hermitian conjugate operator \hat{a}_j^\dagger is

$$\begin{aligned} \langle N'_1, N'_2, \dots, N'_j, \dots | \hat{a}_j^\dagger | N_1, N_2, \dots, N_j, \dots \rangle &= \langle N_1, N_2, \dots, N_j, \dots | \hat{a}_j | N'_1, N'_2, \dots, N'_j, \dots \rangle^* \\ &= \langle N_1, N_2, \dots, N_j, \dots | (N'_j)^{1/2} | N'_1, N'_2, \dots, N'_j - 1, \dots \rangle = (N'_j)^{1/2} \delta_{N_1 N'_1} \delta_{N_2 N'_2} \dots \delta_{N_j N'_j - 1} \dots \\ &= (N_j + 1)^{1/2} \delta_{N_1 N'_1} \delta_{N_2 N'_2} \dots \delta_{N_j + 1, N'_j}, \end{aligned} \quad (8.67)$$

meaning that

Boson
creation
operator

$$\hat{a}_j^\dagger | N_1, N_2, \dots, N_j, \dots \rangle = (N_j + 1)^{1/2} | N_1, N_2, \dots, N_j + 1, \dots \rangle, \quad (8.68)$$

in total compliance with the second of Eqs. (61). In particular, this *particle creation operator* allows the description of the generation of a single particle from the *vacuum* (not null!) state $|0, 0, \dots\rangle$:

$$\hat{a}_j^\dagger | 0, 0, \dots, 0_j, \dots, 0 \rangle = | 0, 0, \dots, 1_j, \dots, 0 \rangle, \quad (8.69)$$

and hence a product of such operators may create, from the vacuum, a multiparticle state with an arbitrary set of occupancies:²⁴

$$\underbrace{\hat{a}_1^\dagger \hat{a}_1^\dagger \dots \hat{a}_1^\dagger}_{N_1 \text{ times}} \underbrace{\hat{a}_2^\dagger \hat{a}_2^\dagger \dots \hat{a}_2^\dagger}_{N_2 \text{ times}} \dots | 0, 0, \dots \rangle = (N_1! N_2! \dots)^{1/2} | N_1, N_2, \dots \rangle. \quad (8.70)$$

Next, combining Eqs. (64) and (68), we get

$$\hat{a}_j^\dagger \hat{a}_j | N_1, N_2, \dots, N_j, \dots \rangle = N_j | N_1, N_2, \dots, N_j, \dots \rangle, \quad (8.71)$$

so that, just as for the particular case of harmonic oscillator excitations, the operator

$$\hat{N}_j \equiv \hat{a}_j^\dagger \hat{a}_j \quad (8.72)$$

“counts” the number of particles in the j^{th} single-particle state, while preserving the whole multiparticle state. Acting on a state by the creation-annihilation operators in the reverse order, we get

$$\hat{a}_j \hat{a}_j^\dagger | N_1, N_2, \dots, N_j, \dots \rangle = (N_j + 1) | N_1, N_2, \dots, N_j, \dots \rangle. \quad (8.73)$$

Eqs. (71) and (73) show that for *any* state of a multiparticle system (which may be represented as a linear superposition of Dirac states with all possible sets of numbers N_j), we may write

$$\hat{a}_j \hat{a}_j^\dagger - \hat{a}_j^\dagger \hat{a}_j \equiv [\hat{a}_j, \hat{a}_j^\dagger] = \hat{I}, \quad (8.74)$$

²⁴ The resulting Dirac state is *not* an eigenstate of every multiparticle Hamiltonian. However, we will see below that for a set of non-interacting particles it *is* a stationary state, so that the full set of such states may be used as a good basis in perturbation theories of systems of weakly interacting particles.

again in agreement with what we had for the 1D oscillator – cf. Eq. (5.68). According to Eqs. (63), (64), and (68), the creation and annihilation operators corresponding to different single-particle states do commute, so that Eq. (74) may be generalized as

$$\left[\hat{a}_j, \hat{a}_{j'}^\dagger \right] = \hat{I} \delta_{jj'}, \quad (8.75)$$

while the similar operators commute, regardless of which states do they act upon:

$$\left[\hat{a}_j^\dagger, \hat{a}_{j'}^\dagger \right] = \left[\hat{a}_j, \hat{a}_{j'} \right] = \hat{0}. \quad (8.76)$$

Bosonic operators:
commutation relations

As was mentioned earlier, a major challenge in the Dirac approach is to rewrite the Hamiltonian of a multiparticle system, that naturally carries particle numbers k (see, e.g., Eq. (22) for $k = 1, 2$), in the second quantization language, in which there are no these numbers. Let us start with *single-particle* components of such Hamiltonians, i.e. operators of the type

$$\hat{F} = \sum_{k=1}^N \hat{f}_k. \quad (8.77)$$

Single-particle operator

where all N operators \hat{f}_k are similar, besides that each of them acts on one specific (k^{th}) particle, and N is the total number of particles in the system, which is evidently equal to the sum of single-particle state occupancies:

$$N = \sum_j N_j. \quad (8.78)$$

The most important examples of such operators are the kinetic energy of N similar single particles, and their potential energy in an external field:

$$\hat{T} = \sum_{k=1}^N \frac{\hat{p}_k^2}{2m}, \quad \hat{U} = \sum_{k=1}^N \hat{u}(\mathbf{r}_k). \quad (8.79)$$

For bosons, instead of the Slater determinant (60), we have to write a similar expression, but without the sign alternation at permutations:

$$\left| N_1, \dots, N_j, \dots \right\rangle = \left(\frac{N_1! \dots N_j! \dots}{N!} \right)^{1/2} \sum_P \left| \underbrace{\dots \beta \beta' \beta'' \dots}_{N \text{ operands}} \right\rangle, \quad (8.80)$$

sometimes called the *permanent*. Note again that the left-hand side of this relation is written in the Dirac notation (that does not use particle numbering), while on its right-hand side, just in relations of Secs. 1 and 2, the particle numbers are coded with the positions of the single-particle states inside the state vectors, and the summation is over all different permutations of the states in the ket – cf. Eq. (10). (According to the basic combinatorics,²⁵ there are $N!/(N_1! \dots N_j! \dots)$ such permutations, so that the front coefficient in Eq. (80) ensures the normalization of the Dirac state, provided that the single-particle states β, β', \dots are normalized.) Let us use Eq. (80) to spell out the following matrix element for a system with $(N-1)$ particles:

²⁵ See, e.g., MA Eq. (2.3).

$$\begin{aligned} & \langle \dots N_j, \dots N_{j'} - 1, \dots | \hat{F} | \dots N_j - 1, \dots N_{j'}, \dots \rangle \\ &= \frac{N_1! \dots (N_j - 1)! \dots (N_{j'} - 1)! \dots}{(N - 1)!} (N_j N_{j'})^{1/2} \sum_{P(N-1)} \sum_{P(N-1)} \langle \dots \beta \beta' \beta'' \dots | \sum_{k=1}^{N-1} \hat{f}_k | \dots \beta \beta' \beta'' \dots \rangle, \end{aligned} \quad (8.81)$$

where all non-specified occupation numbers in the corresponding positions of the bra- and ket-vectors are equal to each other. Each single-particle operator \hat{f}_k participating in the operator sum, acts on the bra- and ket-vectors of states only in one (k^{th}) position, giving the following result, independent of the position number:

$$\langle \beta_j |_{\text{in } k^{\text{th}} \text{ position}} \hat{f}_k | \beta_{j'} \rangle_{\text{in } k^{\text{th}} \text{ position}} = \langle \beta_j | \hat{f} | \beta_{j'} \rangle \equiv f_{jj'}. \quad (8.82)$$

Since in both permutation sets participating in Eq. (81), with $(N - 1)$ state vectors each, all positions are equivalent, we can fix the position (say, take the first one) and replace the sum over k with the multiplication by of the bracket by $(N - 1)$. The fraction of permutations with the necessary bra-vector (with number j) in that position is $N_j/(N - 1)$, while that with the necessary ket-vector (with number j') in the same position is $N_{j'}/(N - 1)$. As the result, the permutation sum in Eq. (81) reduces to

$$(N - 1) \frac{N_j}{N - 1} \frac{N_{j'}}{N - 1} f_{jj'} \sum_{P(N-2)} \sum_{P(N-2)} \langle \dots \beta \beta' \beta'' \dots | \dots \beta \beta' \beta'' \dots \rangle, \quad (8.83)$$

where our specific position k is now excluded from both the bra- and ket-vector permutations. Each of these permutations now includes only $(N_j - 1)$ states j and $(N_{j'} - 1)$ states j' , so that, using the state orthonormality, we finally arrive at a very simple result:

$$\begin{aligned} & \langle \dots N_j, \dots N_{j'} - 1, \dots | \hat{F} | \dots N_j - 1, \dots N_{j'}, \dots \rangle \\ &= \frac{N_1! \dots (N_j - 1)! \dots (N_{j'} - 1)! \dots}{(N - 1)!} (N_j N_{j'})^{1/2} (N - 1) \frac{N_j}{N - 1} \frac{N_{j'}}{N - 1} f_{jj'} \frac{(N - 2)!}{N_1! \dots (N_j - 1)! \dots (N_{j'} - 1)! \dots} \\ & \equiv (N_j N_{j'})^{1/2} f_{jj'}. \end{aligned} \quad (8.84)$$

On the other hand, let us calculate matrix elements of the following operator:

$$\sum_{j,j'} f_{jj'} \hat{a}_j^\dagger \hat{a}_{j'} . \quad (8.85)$$

A direct application of Eqs. (64) and (68) shows that the only non-vanishing of the elements are

$$\langle \dots N_j, \dots N_{j'} - 1, \dots | f_{jj'} \hat{a}_j^\dagger \hat{a}_{j'} | \dots N_j - 1, \dots, N_{j'}, \dots \rangle = (N_j N_{j'})^{1/2} f_{jj'} . \quad (8.86)$$

But this is exactly the last form of Eq. (84), so that in the basis of Dirac states, the operator (77) may be represented as

$$\hat{F} = \sum_{j,j'} f_{jj'} \hat{a}_j^\dagger \hat{a}_{j'} . \quad (8.87)$$

This beautifully simple relation is the key formula of the second quantization theory, and is essentially the Dirac-language analog of Eq. (4.59) of the single-particle quantum mechanics. Each term of the sum (87) may be described by a very simple mnemonic rule: for each pair of single-particle states

j and j' , annihilate a particle in the state j' , create one in the state j , and weigh the result with the corresponding single-particle matrix element. One of the corollaries of Eq. (87) is that the expectation value of an operator whose eigenstates coincide with the Dirac states is

$$\langle F \rangle \equiv \langle \dots N_j, \dots | \hat{F} | \dots N_j, \dots \rangle = \sum_j f_{jj} N_j, \quad (8.88)$$

with an evident physical interpretation as the sum of single-particle expectation values over all states, weighed by the occupancy of each state.

Proceeding to *fermions*, which have to obey the Pauli principle, we immediately notice that any occupation number N_j may only take two values, 0 or 1. To account for that, and also make the key relation (87) valid for fermions as well, the creation-annihilation operators are defined by the following relations:

$$\hat{a}_j |N_1, N_2, \dots, 0_j, \dots\rangle = 0, \quad \hat{a}_j |N_1, N_2, \dots, 1_j, \dots\rangle = (-1)^{\Sigma(1, j-1)} |N_1, N_2, \dots, 0_j, \dots\rangle, \quad (8.89)$$

$$\hat{a}_j^\dagger |N_1, N_2, \dots, 0_j, \dots\rangle = (-1)^{\Sigma(1, j-1)} |N_1, N_2, \dots, 1_j, \dots\rangle, \quad \hat{a}_j^\dagger |N_1, N_2, \dots, 1_j, \dots\rangle = 0, \quad (8.90)$$

Fermion
creation-
annihilation
operators

where the symbol $\Sigma(J, J')$ means the sum of all occupancy numbers in the states with numbers from J to J' , including the border points:

$$\Sigma(J, J') \equiv \sum_{j=J}^{J'} N_j, \quad (8.91)$$

so that the sum participating in Eqs. (89)-(90) is the total occupancy of all states with the numbers below j . (The states are supposed to be numbered in a fixed albeit arbitrary order.) As a result, these relations may be conveniently summarized in the following verbal form: if an operator replaces the j^{th} state's occupancy with the opposite one (either 1 with 0, or vice versa), it also changes the sign before the result if (and only if) the total number of particles in the states with $j' < j$ is odd.

Let us use this (perhaps somewhat counter-intuitive) sign alternation rule to spell out the ket-vector $|11\rangle$ of a completely filled two-state system, formed from the vacuum state $|00\rangle$ in two different ways. If we start by creating a fermion in the state 1, we get

$$\hat{a}_1^\dagger |0, 0\rangle = (-1)^0 |1, 0\rangle \equiv |1, 0\rangle, \quad \hat{a}_2^\dagger \hat{a}_1^\dagger |0, 0\rangle = \hat{a}_2^\dagger |1, 0\rangle = (-1)^1 |1, 1\rangle \equiv -|1, 1\rangle, \quad (8.92a)$$

while if the operator order is different, the result is

$$\hat{a}_2^\dagger |0, 0\rangle = (-1)^0 |0, 1\rangle \equiv |0, 1\rangle, \quad \hat{a}_1^\dagger \hat{a}_2^\dagger |0, 0\rangle = \hat{a}_1^\dagger |0, 1\rangle = (-1)^0 |1, 1\rangle \equiv |1, 1\rangle, \quad (8.92b)$$

so that

$$(\hat{a}_1^\dagger \hat{a}_2^\dagger + \hat{a}_2^\dagger \hat{a}_1^\dagger) |0, 0\rangle = 0. \quad (8.93)$$

Since the action of any of these operator products on any initial state rather than the vacuum one also gives the null ket, we may write the following operator equality:

$$\hat{a}_1^\dagger \hat{a}_2^\dagger + \hat{a}_2^\dagger \hat{a}_1^\dagger \equiv \left\{ \hat{a}_1^\dagger, \hat{a}_2^\dagger \right\} = \hat{0}. \quad (8.94)$$

It is straightforward to check that this result is valid for Dirac vectors of an arbitrary length, and does not depend on the occupancy of other states, so that we may generalize it as

$$\left\{ \hat{a}_j^\dagger, \hat{a}_{j'}^\dagger \right\} = \left\{ \hat{a}_j, \hat{a}_{j'} \right\} = \hat{0}; \quad (8.95)$$

Fermionic operators:
commutation relations

these equalities hold for $j = j'$ as well. On the other hand, an absolutely similar calculation shows that the mixed creation-annihilation commutators do depend on whether the states are different or not:²⁶

$$\left\{ \hat{a}_j, \hat{a}_{j'}^\dagger \right\} = \hat{I} \delta_{jj'}. \quad (8.96)$$

These equations look very much like Eqs. (75)-(76) for bosons, “only” with the replacement of commutators with anticommutators. Since the core laws of quantum mechanics, including the operator compatibility (Sec. 4.5) and the Heisenberg equation (4.199) of operator evolution in time, involve commutators rather than anticommutators, one might think that all the behavior of bosonic and fermionic multiparticle systems should be dramatically different. However, the difference is not as big as one could expect; indeed, a straightforward check shows that the sign factors in Eqs. (89)-(90) just compensate those in the Slater determinant, and thus make the key relation (87) valid for the fermions as well. (Indeed, this is the very goal of the introduction of these factors.)

To illustrate this fact on the simplest example, let us examine what does the second quantization formalism say about the dynamics of non-interacting particles in the system whose single-particle properties we have discussed repeatedly, namely two nearly-similar potential wells, coupled by tunneling through the separating potential barrier – see, e.g., Figs. 2.21 or 7.4. If the coupling is so small that the states localized in the wells are only weakly perturbed, then in the basis of these states, the single-particle Hamiltonian of the system may be represented by the 2×2 matrix (5.3). With the energy reference selected at the middle between the energies of unperturbed states, the coefficient b vanishes, this matrix is reduced to

$$h = \mathbf{c} \cdot \boldsymbol{\sigma} \equiv \begin{pmatrix} c_z & c_- \\ c_+ & -c_z \end{pmatrix}, \quad \text{with } c_\pm \equiv c_x \pm i c_y, \quad (8.97)$$

and its eigenvalues to

$$\varepsilon_\pm = \pm c, \quad \text{with } c \equiv |\mathbf{c}| \equiv (c_x^2 + c_y^2 + c_z^2)^{1/2}. \quad (8.98)$$

Now following the recipe (87), we can use Eq. (97) to represent the Hamiltonian of the whole system of particles in terms of the creation-annihilation operators:

$$\hat{H} = c_z \hat{a}_1^\dagger \hat{a}_1 + c_- \hat{a}_1^\dagger \hat{a}_2 + c_+ \hat{a}_2^\dagger \hat{a}_1 - c_z \hat{a}_2^\dagger \hat{a}_2, \quad (8.99)$$

where $\hat{a}_{1,2}^\dagger$ and $\hat{a}_{1,2}$ are the operators of creation and annihilation of a particle in the corresponding *potential well*. (Again, in the second quantization approach the *particles* are not numbered at all!) As Eq. (72) shows, the first and the last terms of the right-hand side of Eq. (99) describe the particle energies $\varepsilon_{1,2} = \pm c_z$ in uncoupled wells,

$$c_z \hat{a}_1^\dagger \hat{a}_1 = c_z \hat{N}_1 \equiv \varepsilon_1 \hat{N}_1, \quad -c_z \hat{a}_2^\dagger \hat{a}_2 = -c_z \hat{N}_2 \equiv \varepsilon_2 \hat{N}_2, \quad (8.100)$$

²⁶ A by-product of this calculation is proof that the operator defined by Eq. (72) counts the number of particles N_j (now equal to either 1 or 0), just as it does for bosons.

while the sum of the middle two terms is the second-quantization description of tunneling between the wells.

Now we can use the general Eq. (4.199) of the Heisenberg picture to spell out the equations of motion of the creation-annihilation operators. For example,

$$i\hbar\dot{\hat{a}}_1 = [\hat{a}_1, \hat{H}] = c_z \left[\hat{a}_1, \hat{a}_1^\dagger \hat{a}_1 \right] + c_- \left[\hat{a}_1, \hat{a}_1^\dagger \hat{a}_2 \right] + c_+ \left[\hat{a}_1, \hat{a}_2^\dagger \hat{a}_1 \right] - c_z \left[\hat{a}_1, \hat{a}_2^\dagger \hat{a}_2 \right]. \quad (8.101)$$

Since the Bose and Fermi operators satisfy different commutation relations, one could expect the right-hand side of this equation to be different for bosons and fermions. However, it is not so. Indeed, all commutators on the right-hand side of Eq. (101) have the following form:

$$\left[\hat{a}_j, \hat{a}_{j'}^\dagger \hat{a}_{j''} \right] \equiv \hat{a}_j \hat{a}_{j'}^\dagger \hat{a}_{j''} - \hat{a}_{j'}^\dagger \hat{a}_{j''} \hat{a}_j. \quad (8.102)$$

As Eqs. (74) and (94) show, the first pair product of operators on the right-hand side may be recast as

$$\hat{a}_j \hat{a}_{j'}^\dagger = \hat{I} \delta_{jj'} \pm \hat{a}_{j'}^\dagger \hat{a}_j, \quad (8.103)$$

where the upper sign pertains to bosons and the lower one to fermions, while according to Eqs. (76) and (95), the very last pair product in Eq. (102) is

$$\hat{a}_{j''} \hat{a}_j = \pm \hat{a}_j \hat{a}_{j''}, \quad (8.104)$$

with the same sign convention. Plugging these expressions into Eq. (102), we see that regardless of the particle type, there is a universal (and generally very useful) commutation relation

$$\left[\hat{a}_j, \hat{a}_{j'}^\dagger \hat{a}_{j''} \right] = \hat{a}_{j''} \delta_{jj'}, \quad (8.105)$$

valid for both bosons and fermions. As a result, the Heisenberg equation of motion for the operator \hat{a}_1 , and the equation for \hat{a}_2 (which may be obtained absolutely similarly), are also universal:²⁷

$$\begin{aligned} i\hbar\dot{\hat{a}}_1 &= c_z \hat{a}_1 + c_- \hat{a}_2, \\ i\hbar\dot{\hat{a}}_2 &= c_+ \hat{a}_1 - c_z \hat{a}_2. \end{aligned} \quad (8.106)$$

This is a system of two coupled, linear differential equations, which is similar to the equations for the c -number probability amplitudes of single-particle wavefunctions of a two-level system – see, e.g., Eq. (2.201) and the model solution of Problem 4.25. Their general solution is a linear superposition

$$\hat{a}_{1,2}(t) = \sum_{\pm} \hat{\alpha}_{1,2}^{(\pm)} \exp\{\lambda_{\pm} t\}. \quad (8.107)$$

As usual, to find the exponents λ_{\pm} , it is sufficient to plug in a particular solution $\hat{a}_{1,2}(t) = \hat{\alpha}_{1,2} \exp\{\lambda t\}$ into Eq. (106) and require that the determinant of the resulting homogeneous, linear system for the “coefficients” (actually, time-independent operators) $\hat{\alpha}_{1,2}$ equals zero. This gives us the following characteristic equation

²⁷ Equations of motion for the creation operators $\hat{a}_{1,2}^\dagger$ are just the Hermitian-conjugates of Eqs. (106), and do not add any new information about the system’s dynamics.

$$\begin{vmatrix} c_z - i\hbar\lambda & c_- \\ c_+ & -c_z - i\hbar\lambda \end{vmatrix} = 0, \quad (8.108)$$

with two roots $\lambda_{\pm} = \pm i\Omega/2$, where $\Omega \equiv 2c/\hbar$ – cf. Eq. (5.20). Now plugging each of the roots, one by one, into the system of equations for $\hat{\alpha}_{1,2}$, we can find these operators, and hence the general solution of system (98) for arbitrary initial conditions.

Let us consider the simple case $c_y = c_z = 0$ (meaning in particular that the wells are exactly aligned, see Fig. 2.21), so that $\hbar\Omega/2 \equiv c = c_x$; then the solution of Eq. (106) is

$$\hat{a}_1(t) = \hat{a}_1(0) \cos \frac{\Omega t}{2} - i\hat{a}_2(0) \sin \frac{\Omega t}{2}, \quad \hat{a}_2(t) = -i\hat{a}_1(0) \sin \frac{\Omega t}{2} + \hat{a}_2(0) \cos \frac{\Omega t}{2}. \quad (8.109)$$

Multiplying the first of these relations by its Hermitian conjugate, and ensemble-averaging the result, we get

$$\langle N_1 \rangle \equiv \left\langle \hat{a}_1^\dagger(t) \hat{a}_1(t) \right\rangle = \left\langle \hat{a}_1^\dagger(0) \hat{a}_1(0) \right\rangle \cos^2 \frac{\Omega t}{2} + \left\langle \hat{a}_2^\dagger(0) \hat{a}_2(0) \right\rangle \sin^2 \frac{\Omega t}{2} - i \left\langle \hat{a}_1^\dagger(0) \hat{a}_2(0) + \hat{a}_2^\dagger(0) \hat{a}_1(0) \right\rangle \sin \frac{\Omega t}{2} \cos \frac{\Omega t}{2}. \quad (8.110)$$

Quantum oscillations:
second quantization form

Let the initial state of the system be a single Dirac state, i.e. have a definite number of particles in each well; in this case, only the two first terms on the right-hand side of Eq. (110) are different from zero, giving:²⁸

$$\langle N_1 \rangle = N_1(0) \cos^2 \frac{\Omega t}{2} + N_2(0) \sin^2 \frac{\Omega t}{2}. \quad (8.111)$$

For one particle, initially placed in either well, this gives us our old result (2.181) describing the usual quantum oscillations of the particle between two wells with the frequency Ω . However, Eq. (111) is valid for *any* set of initial occupancies; let us use this fact. For example, starting from two particles, with initially one particle in each well, we get $\langle N_1 \rangle = 1$, regardless of time. So, the occupancies do not oscillate, and no experiment may detect the quantum oscillations, though their frequency Ω is still formally present in the time evolution equations. This fact may be interpreted as the simultaneous quantum oscillations of two particles between the wells, exactly in anti-phase. For bosons, we can go on to even larger occupancies by preparing the system, for example, in the state with $N_1(0) = N$, $N_2(0) = 0$. The result (111) says that in this case, we see that the quantum oscillation amplitude increases N -fold; this is a particular manifestation of the general fact that bosons can be (and evolve in time) in the same quantum state. On the other hand, for fermions we cannot increase the initial occupancies beyond 1, so that the largest oscillation amplitude we can get is if we initially fill just one well.

The Dirac approach may be readily generalized to more complex systems. For example, Eq. (99) implies that an arbitrary system of potential wells with weak tunneling coupling between the adjacent wells may be described by the Hamiltonian

$$\hat{H} = \sum_j \varepsilon_j a_j^\dagger \hat{a}_j + \sum_{\{j,j'\}} \delta_{jj'} a_j^\dagger \hat{a}_{j'} + \text{h.c.}, \quad (8.112)$$

²⁸ For the second well's occupancy, the result is complementary, $N_2(t) = N_1(0)\sin^2\Omega t + N_2(0)\cos^2\Omega t$, giving in particular a good sanity check: $N_1(t) + N_2(t) = N_1(0) + N_2(0) = \text{const.}$

where the symbol $\{j, j'\}$ means that the second sum is restricted to pairs of next-neighbor wells – see, e.g., Eq. (2.203) and its discussion. Note that this Hamiltonian is still a quadratic form of the creation-annihilation operators, so the Heisenberg-picture equations of motion of these operators are still linear, and its exact solutions, though possibly cumbersome, may be studied in detail. Due to this fact, the Hamiltonian (112) is widely used for the study of some phenomena, for example, the very interesting *Anderson localization* effects, in which a random distribution of the localized-site energies ε_j prevents tunneling particles, within a certain energy range, from spreading to unlimited distances.²⁹

8.4. Perturbative approaches

The situation becomes much more difficult if we need to account for direct interactions between the particles. Let us assume that the interaction may be reduced to that between their pairs (as it is the case at their Coulomb interaction and most other interactions³⁰), so that it may be described by the following “pair-interaction” Hamiltonian

$$\hat{U}_{\text{int}} = \frac{1}{2} \sum_{\substack{k,k'=1 \\ k \neq k'}}^N \hat{u}_{\text{int}}(\mathbf{r}_k, \mathbf{r}_{k'}), \quad (8.113)$$

with the front factor of $1/2$ compensating the double-counting of each particle pair. The translation of this operator to the second-quantization form may be done absolutely similarly to the derivation of Eq. (87), and gives a similar (though naturally more involved) result

$$\hat{U}_{\text{int}} = \frac{1}{2} \sum_{j,j',l,l'} u_{jj'll'} \hat{a}_j^\dagger \hat{a}_{j'}^\dagger \hat{a}_l \hat{a}_{l'}, \quad (8.114)$$

Pair-interaction Hamiltonian: two forms

where the two-particle matrix elements are defined similarly to Eq. (82):

$$u_{jj'll'} \equiv \langle \beta_j \beta_{j'} | \hat{u}_{\text{int}} | \beta_l \beta_{l'} \rangle. \quad (8.115)$$

The only new feature of Eq. (114) is a specific order of the indices of the creation operators. Note the mnemonic rule of writing this expression, similar to that for Eq. (87): each term corresponds to moving a pair of particles from states l and l' to states j' and j (in this order!) factored with the corresponding two-particle matrix element (115).

However, with the account of such term, the resulting Heisenberg equations of the time evolution of the creation/annihilation operators are nonlinear, so that solving them and calculating observables from the results is usually impossible, at least analytically. The only case when some general results may be obtained is the *weak interaction* limit. In this case, the unperturbed Hamiltonian contains only single-particle terms such as (79), and we can always (at least conceptually :-) find such a basis of orthonormal single-particle states β_j in which that Hamiltonian is diagonal in the Dirac representation:

²⁹ For a review of the 1D version of this problem, see, e.g., J. Pendry, *Adv. Phys.* **43**, 461 (1994).

³⁰ A simple but important example from the condensed matter theory is the so-called *Hubbard model*, in which particle repulsion limits their number on each of localized sites to either 0, or 1, or 2, with negligible interaction of the particles on different sites – though the next-neighbor sites are still connected by tunneling – as in Eq. (112).

$$\hat{H}^{(0)} = \sum_j \varepsilon_j^{(0)} \hat{a}_j^\dagger \hat{a}_j . \quad (8.116)$$

Now we can use Eq. (6.14), in this basis, to calculate the interaction energy as a first-order perturbation:

$$\begin{aligned} E_{\text{int}}^{(1)} &= \langle N_1, N_2, \dots | \hat{U}_{\text{int}} | N_1, N_2, \dots \rangle = \frac{1}{2} \langle N_1, N_2, \dots | \sum_{j,j',l,l'} u_{jj'll'} \hat{a}_j^\dagger \hat{a}_{j'}^\dagger \hat{a}_l \hat{a}_l | N_1, N_2, \dots \rangle \\ &\equiv \frac{1}{2} \sum_{j,j',l,l'} u_{jj'll'} \langle N_1, N_2, \dots | \hat{a}_j^\dagger \hat{a}_{j'}^\dagger \hat{a}_l \hat{a}_l | N_1, N_2, \dots \rangle. \end{aligned} \quad (8.117)$$

Since, according to Eq. (63), the Dirac states with different occupancies are orthogonal, the last long bracket is different from zero only for three particular subsets of its indices:

(i) $j \neq j'$, $l = j$, and $l' = j'$. In this case, the four-operator product in Eq. (117) is equal to $\hat{a}_j^\dagger \hat{a}_{j'}^\dagger \hat{a}_{j'} \hat{a}_j$, and applying the commutation rules twice, we can bring it to the so-called *normal ordering*, with each creation operator standing to the right of the corresponding annihilation operator, thus forming the particle number operator (72):

$$\hat{a}_j^\dagger \hat{a}_{j'}^\dagger \hat{a}_{j'} \hat{a}_j = \pm \hat{a}_j^\dagger \hat{a}_j^\dagger \hat{a}_j \hat{a}_{j'} = \pm \hat{a}_j^\dagger (\pm \hat{a}_j \hat{a}_{j'}^\dagger) \hat{a}_{j'} = \hat{a}_j^\dagger \hat{a}_j \hat{a}_{j'}^\dagger \hat{a}_{j'} = \hat{N}_j \hat{N}_{j'}, \quad (8.118)$$

with a similar sign of the final result for bosons and fermions.

(ii) $j \neq j'$, $l = j'$, and $l' = j$. In this case, the four-operator product is equal to $\hat{a}_j^\dagger \hat{a}_{j'}^\dagger \hat{a}_j \hat{a}_{j'}$, and bringing it to the form $\hat{N}_j \hat{N}_{j'}$ requires only one commutation:

$$\hat{a}_j^\dagger \hat{a}_{j'}^\dagger \hat{a}_j \hat{a}_{j'} = \hat{a}_j^\dagger (\pm \hat{a}_j \hat{a}_{j'}^\dagger) \hat{a}_{j'} = \pm \hat{a}_j^\dagger \hat{a}_j \hat{a}_{j'}^\dagger \hat{a}_{j'} = \pm \hat{N}_j \hat{N}_{j'}, \quad (8.119)$$

with the upper sign for bosons and the lower sign for fermions.

(iii) All indices are equal to each other, giving $\hat{a}_j^\dagger \hat{a}_{j'}^\dagger \hat{a}_l \hat{a}_l = \hat{a}_j^\dagger \hat{a}_j^\dagger \hat{a}_j \hat{a}_j$. For fermions, such an operator (that “tries” to create or to kill two particles in a row, in the same state) immediately gives the null-vector. In the case of bosons, we may use Eq. (74) to commute the internal pair of operators, getting

$$\hat{a}_j^\dagger \hat{a}_j^\dagger \hat{a}_j \hat{a}_j = \hat{a}_j^\dagger (\hat{a}_j \hat{a}_j^\dagger - \hat{I}) \hat{a}_j = \hat{N}_j (\hat{N}_j - \hat{I}). \quad (8.120)$$

Note, however, that this expression formally covers the fermion case as well (always giving zero). As a result, Eq. (117) may be rewritten in the following universal form:

$$E_{\text{int}}^{(1)} = \frac{1}{2} \sum_{\substack{j,j' \\ j \neq j'}} N_j N_{j'} (u_{jj'jj'} \pm u_{jj'jj}) + \frac{1}{2} \sum_j N_j (N_j - 1) u_{jjjj}. \quad (8.121)$$

Particle interaction:
1st-order
energy
correction

The corollaries of this important result are very different for bosons and fermions. In the former case, the last term usually dominates, because the matrix elements (115) are typically the largest when all basis functions coincide. Note that this term allows a very simple interpretation: the number of the diagonal matrix elements it sums up for each state (j) is just the number of interacting particle pairs residing in that state.

In contrast, for fermions the last term is zero, and the interaction energy is proportional to the difference of the two terms inside the first parentheses. To spell them out, let us consider the case when there is no direct spin-orbit interaction. Then the vectors $|\beta_j\rangle$ of the single-particle state basis may be represented as direct products $|o_j\rangle \otimes |m_j\rangle$ of their orbital and spin-orientation parts. (Here, for the brevity of notation, I am using m instead of m_s .) For spin- $\frac{1}{2}$ particles, including electrons, m_j may equal only either $+\frac{1}{2}$ or $-\frac{1}{2}$; in this case the spin part of the first matrix element, proportional to $u_{jj'jj'}$, equals

$$\langle m| \otimes \langle m' | m \rangle \otimes | m' \rangle, \quad (8.122)$$

where, as in the general Eq. (115), the position of a particular state vector in each direct product is encoding the particle's number. Since the spins of different particles are defined in different Hilbert spaces, we may move their state vectors around to get

$$\langle m| \otimes \langle m' | m \rangle \otimes | m' \rangle = (\langle m | m \rangle)_1 \times (\langle m' | m' \rangle)_2 = 1, \quad (8.123)$$

for any pair of j and j' . On the other hand, the second matrix element, $u_{jj'jj'}$, is factored by

$$\langle m| \otimes \langle m' | m' \rangle \otimes | m \rangle = (\langle m | m' \rangle)_1 \times (\langle m' | m \rangle)_2 = \delta_{mm'}. \quad (8.124)$$

In this case, it is convenient to rewrite Eq. (121) in the coordinate representation, using single-particle wavefunctions called *spin-orbitals*

$$\psi_j(\mathbf{r}) \equiv \langle \mathbf{r} | \beta_j \rangle = (\langle \mathbf{r} | o \rangle \otimes | m \rangle)_j. \quad (8.125)$$
Spin-orbital

They differ from the spatial parts of the usual orbital wavefunctions of the type (4.233) only in that their index j should be understood as the set of the orbital-state and the spin-orientation indices.³¹ Also, due to the Pauli-principle restriction of numbers N_j to either 0 or 1, Eq. (121) may be also rewritten without the explicit occupancy numbers, with the understanding that the summation is extended only over the pairs of occupied states. As a result, it becomes

$$E_{\text{int}}^{(1)} = \frac{1}{2} \sum_{\substack{j,j' \\ j \neq j'}} \int d^3 r \int d^3 r' \left[\psi_j^*(\mathbf{r}) \psi_{j'}^*(\mathbf{r}') u_{\text{int}}(\mathbf{r}, \mathbf{r}') \psi_j(\mathbf{r}) \psi_{j'}(\mathbf{r}') - \psi_j^*(\mathbf{r}) \psi_{j'}^*(\mathbf{r}') u_{\text{int}}(\mathbf{r}, \mathbf{r}') \psi_{j'}(\mathbf{r}) \psi_j(\mathbf{r}') \right]. \quad (8.126)$$
Energy correction due to fermion interaction

In particular, for a system of two electrons, we may limit the summation to just two states ($j, j' = 1, 2$). As a result, we return to Eqs. (39)-(41), with the bottom (minus) sign in Eq. (39), corresponding to the triplet spin states. Hence, Eq. (126) may be considered as the generalization of the direct and exchange interaction balance picture to an arbitrary number of orbitals and an arbitrary total number N of electrons. Note, however, that this formula cannot correctly describe the energy of the singlet spin states, corresponding to the plus sign in Eq. (39), and also of the entangled triplet states.³² The reason is

³¹ The spin-orbitals (125) are also close to spinors (13), besides that the former definition takes into account that the spin s of a single particle is fixed, so that the spin-orbital may be indexed by the spin's orientation $m \equiv m_s$ only. Also, if an orbital index is used, it should be clearly distinguished from j , i.e. the set of the orbital and spin indices. This is why I believe that the frequently met notation of spin-orbitals as $\psi_{j,s}(\mathbf{r})$ may lead to confusion.

³² Indeed, due to the condition $j' \neq j$, and Eq. (124), the calculated negative exchange interaction is limited to electron state pairs with the same spin direction – such as the factorable triplet states ($\uparrow\uparrow$ and $\downarrow\downarrow$) of a two-electron system, in which the contribution of E_{ex} , given by Eq. (41), to the total energy is also negative.

that the description of entangled spin states, given in particular by Eqs. (18) and (20), requires linear *superpositions* of different Dirac states. (A proof of this fact is left for the reader's exercise.)

Now comes a very important fact: the *approximate* result (126), added to the sum of unperturbed energies $\varepsilon_j^{(0)}$, equals the sum of *exact* eigenenergies of the so-called *Hartree-Fock equation*:³³

Hartree-Fock equation

$$\left(-\frac{\hbar^2}{2m} \nabla^2 + u(\mathbf{r}) \right) \psi_j(\mathbf{r}) + \sum_{j' \neq j} \int \left[\psi_{j'}^*(\mathbf{r}') u_{\text{int}}(\mathbf{r}, \mathbf{r}') \psi_j(\mathbf{r}) \psi_{j'}(\mathbf{r}') - \psi_{j'}^*(\mathbf{r}') u_{\text{int}}(\mathbf{r}, \mathbf{r}') \psi_{j'}(\mathbf{r}) \psi_j(\mathbf{r}) \right] d^3 r' = \varepsilon_j \psi_j(\mathbf{r}), \quad (8.127)$$

where $u(\mathbf{r})$ is the external-field potential acting on each particle separately – see the second of Eqs. (79). An advantage of this equation in comparison with Eq. (126) is that it allows the (approximate) calculation of not only the energy spectrum of the system, but also the corresponding spin-orbitals, taking into account their electron-electron interaction. Of course, Eq. (127) is an *integro-differential* rather than just a differential equation. There are, however, efficient methods of numerical solution of such equations, typically based on iterative methods. One more important practical trick is the exclusion of the filled internal electron shells (see Sec. 3.7) from the explicit calculations, because the shell states are virtually unperturbed by the valence electron effects involved in typical atomic phenomena and chemical reactions. In this approach, the Coulomb field of the shells, described by fixed, pre-calculated, and tabulated *pseudo-potentials*, is added to that of the nuclei. This approach dramatically cuts the computing resources necessary for systems of relatively heavy atoms, enabling a pretty accurate simulation of electronic and chemical properties of rather complex molecules, with thousands of electrons.³⁴ As a result, the Hartree-Fock approximation has become the de-facto baseline of all so-called *ab-initio* (“first-principle”) calculations in the very important field of quantum chemistry.³⁵

In departures from this baseline, there are two opposite trends. For larger accuracy (and typically smaller systems), several “post-Hartree-Fock methods”, notably including the *configuration interaction* method,³⁶ that are more complex but may provide higher accuracy, have been developed.

There is also a strong opposite trend of extending such *ab initio* (“first-principle”) methods to larger systems while sacrificing some of the results’ accuracy and reliability. The ultimate limit of this trend is applicable when the single-particle wavefunction overlaps are small and hence the exchange interaction is negligible. In this limit, the last term in the square brackets in Eq. (127) may be ignored, and the multiplier $\psi_j(\mathbf{r})$ taken out of the integral, which is thus reduced to a differential equation – formally just the Schrödinger equation for a single particle in the following self-consistent effective potential:

³³ This equation was suggested in 1929 by Douglas Hartree for the direct interaction and extended to the exchange interaction by Vladimir Fock in 1930. To verify its compliance with Eq. (126), it is sufficient to multiply all terms of Eq. (127) by $\psi_j^*(\mathbf{r})$, integrate them over all \mathbf{r} -space (so that the right-hand side would give ε_j), and then sum these single-particle energies over all occupied states j .

³⁴ For condensed-matter systems, this and other computational methods are applied to single elementary spatial cells, with a limited number of electrons in them, using cyclic boundary conditions.

³⁵ See, e.g., A. Szabo and N. Ostlund, *Modern Quantum Chemistry*, Revised ed., Dover, 1996.

³⁶ That method, in particular, allows the calculation of proper linear superpositions of the Dirac states (such as the entangled states for $N = 2$, discussed above) which are missing in the generic Hartree-Fock approach – see, e.g., the just-cited monograph by Szabo and Ostlund.

$$u_{\text{ef}}(\mathbf{r}) = u(\mathbf{r}) + u_{\text{dir}}(\mathbf{r}), \quad u_{\text{dir}}(\mathbf{r}) = \sum_{j' \neq j} \int \psi_{j'}^*(\mathbf{r}') u_{\text{int}}(\mathbf{r}, \mathbf{r}') \psi_{j'}(\mathbf{r}') d^3 r'. \quad (8.128)$$

Hartree approximation

This is the so-called *Hartree approximation* – that gives reasonable results for some systems,³⁷ especially those with low electron density.

However, in dense electron systems (such as typical atoms, molecules, and condensed matter) the exchange interaction, described by the second term in the square brackets of Eqs. (126)-(127), may be as high as $\sim 30\%$ of the direct interaction, and frequently cannot be ignored. The tendency of taking this interaction in the simplest possible form is currently dominated by the *Density Functional Theory*,³⁸ universally known by its acronym DFT. In this approach, the equation solved for each eigenfunction $\psi_j(\mathbf{r})$ is a differential, Schrödinger-like *Kohn-Sham equation*

$$\left[-\frac{\hbar^2}{2m} \nabla^2 + u(\mathbf{r}) + u_{\text{dir}}^{\text{KS}}(\mathbf{r}) + u_{\text{xc}}(\mathbf{r}) \right] \psi_j(\mathbf{r}) = \varepsilon_j \psi_j(\mathbf{r}), \quad (8.129)$$

Kohn-Sham equation

where

$$u_{\text{dir}}^{\text{KS}}(\mathbf{r}) = -e\phi(\mathbf{r}), \quad \phi(\mathbf{r}) = \frac{1}{4\pi\varepsilon_0} \int d^3 r' \frac{\rho(\mathbf{r}')}{|\mathbf{r} - \mathbf{r}'|}, \quad \rho(\mathbf{r}) = -en(\mathbf{r}), \quad (8.130)$$

and $n(\mathbf{r})$ is the total electron density in a particular point, calculated as

$$n(\mathbf{r}) \equiv \sum_j \psi_j^*(\mathbf{r}) \psi_j(\mathbf{r}). \quad (8.131)$$

The most important feature of the Kohn-Sham Hamiltonian is the simplified description of the exchange and correlation effects by the effective *exchange-correlation potential* $u_{\text{xc}}(\mathbf{r})$. This potential is calculated in various approximations, most of them valid only in the limit when the number of electrons in the system is very high. The simplest of them (proposed by Kohn *et al.* in the 1960s) is the *Local Density Approximation* (LDA) in which the effective exchange potential at each point is a function only of the electron density n at the same point \mathbf{r} , taken from the theory of a *uniform* gas of free electrons.³⁹ However, for many tasks of quantum chemistry, the accuracy given by the LDA is insufficient, because inside molecules the density n typically changes very fast. As a result, DFT has become widely accepted in that field only after the introduction, in the 1980s, of more accurate, though more cumbersome models for $u_{\text{xc}}(\mathbf{r})$, notably the so-called *Generalized Gradient Approximations* (GGAs). Due to its relative simplicity, DFT enables the calculation, with the same computing resources and reasonable precision, some properties of much larger systems than the methods based on the Hartree-Fock theory. As the result, it has become a very popular tool of ab initio calculations. This popularity is enhanced by the availability of several advanced DFT software packages, some of them in the public domain.

³⁷ An extreme example of the Hartree approximation is the *Thomas-Fermi model* of heavy atoms (with $Z \gg 1$), in which atomic electrons, at each distance r from the nucleus, are treated as an ideal, uniform Fermi gas, with a certain density $n(r)$ corresponding to the local value $u_{\text{ef}}(r)$, but a global value of their highest full single-particle energy, $\varepsilon = 0$, to ensure the equilibrium. (The analysis of this model is left for the reader's exercise.)

³⁸ It had been developed by Walter Kohn and his associates (notably Pierre Hohenberg) in 1965-66, and eventually (in 1998) was marked with a Nobel Prize in Chemistry for W. Kohn.

³⁹ Just for the reader's reference: for a uniform, degenerate Fermi-gas of electrons (with the Fermi energy $\varepsilon_F \gg k_B T$), the most important, exchange part u_x of u_{xc} may be calculated analytically: $u_x = -(3/4\pi) e^2 k_F / 4\pi\varepsilon_0$, where the Fermi momentum $k_F = (2m_e\varepsilon_F)^{1/2}/\hbar$ is defined by the electron density: $n = 2(4\pi/3)k_F^3/(2\pi)^3 \equiv k_F^3/3\pi^2$.

Please note, however, that despite this undisputable success, this approach has its problems. From my personal point of view, the most offensive of them is the implicit assumption of the unphysical Coulomb interaction of an electron with itself (by dropping, on the way from Eq. (128) to Eq. (130), the condition $j' \neq j$ at the calculation of $u_{\text{dir}}^{\text{KS}}$). As a result, for a reasonable description of some effects, the available DFT packages are either inapplicable at all or require substantial artificial tinkering.⁴⁰

Unfortunately, because of lack of time/space, for details I have to refer the interested reader to specialized literature.⁴¹

8.5. Quantum computation and cryptography

Now I have to review the emerging fields of *quantum computation* and *encryption*. (Since these fields are much related, they are often referred to under the common title of “quantum information science”, though this term is somewhat misleading, de-emphasizing physical aspects of the topic.) These fields are currently the subject of intensive research and development efforts, which has already brought, besides an enormous body of hype, some results of general importance. My coverage, by necessity short, will focus on these results, referring the reader interested in details to special literature.⁴² Because of the very active stage of the fields, I will also provide quite a few references to recent publications, making the style of this section closer to a brief literature review than to a textbook’s section.

Presently, most work on quantum computation and encryption is based on systems of spatially separated (and hence *distinguishable*) two-level systems – in this context, universally called *qubits*.⁴³ Due to this distinguishability, the issues that were the focus of the first sections of this chapter, including the second quantization approach, are irrelevant here. On the other hand, systems of qubits have some interesting properties that have not been discussed in this course yet.

First of all, a system of $N \gg 1$ qubits may contain much more information than the same number of N classical bits. Indeed, according to the discussions in Chapter 4 and Sec. 5.1, an arbitrary pure state of a single qubit may be represented by its ket vector (4.37) – see also Eq. (5.1):

$$|\alpha\rangle_{N=1} = \alpha_1|u_1\rangle + \alpha_2|u_2\rangle, \quad (8.132)$$

where $\{u_j\}$ is any orthonormal two-state basis. It is natural and common to employ, as u_j , the eigenstates a_j of the observable A that is eventually measured in the particular physical implementation of the qubit – say, a certain Cartesian component of spin-½. It is also common to write the kets of these base states as $|0\rangle$ and $|1\rangle$, so that Eq. (132) takes the form

⁴⁰ As just a few examples, see N. Simonian *et al.*, *J. Appl. Phys.* **113**, 044504 (2013); M. Medvedev *et al.*, *Science* **355**, 49 (2017); A. Hutama *et al.*, *J. Phys. Chem. C* **121**, 14888 (2017).

⁴¹ See, e.g., either the monograph by R. Parr and W. Yang, *Density-Functional Theory of Atoms and Molecules*, Oxford U. Press, 1994, or the later textbook J. A. Steckel and D. Sholl, *Density Functional Theory: Practical Introduction*, Wiley, 2009. For a popular review and references to more recent work in this still-developing field, see A. Zangwill, *Phys. Today* **68**, 34 (July 2015).

⁴² Despite the recent flood of new books on the field, one of its first surveys, by M. Nielsen and I. Chuang, *Quantum Computation and Quantum Information*, Cambridge U. Press, 2000, is perhaps still the best one.

⁴³ In some texts, the term qubit (or “Qbit”, or “Q-bit”) is used instead for the *information contents* of a two-level system – very much like the classical bit of information (in this context, frequently called “Cbit” or “C-bit”) describes the information contents of a classical bistable system – see, e.g., SM Sec. 2.2.

$$|\alpha\rangle_{N=1} = a_0|0\rangle + a_1|1\rangle \equiv \sum_{j=0,1} a_j |j\rangle. \quad (8.133)$$

Single qubit state's representation

(Here, and in the balance of this section, the letter j is used to denote an integer equal to either 0 or 1.) According to this relation, any state α of a qubit is completely defined by two complex c -numbers a_j , i.e. by 4 real numbers. Moreover, due to the normalization condition $|a_0|^2 + |a_1|^2 = 1$, we need just 3 independent real numbers – say, the Bloch sphere coordinates θ and φ (see Fig. 5.3), plus the common phase γ , which becomes important only when we consider coherent states of a several-qubit system.

This is a good time to note that a qubit is very much different from any classical bistable system used to store single bits of information – such as two possible voltage states of the usual SRAM cell (essentially, a positive-feedback loop of two transistor-based inverters). Namely, the stationary states of a classical bistable system, due to its nonlinearity, are stable with respect to small perturbations, so that they may be very robust to unintentional interaction with their environment. In contrast, the qubit's state may be disturbed (i.e. its representation point on the Bloch sphere shifted) by even minor perturbations, because it does not have such an internal state stabilization mechanism.⁴⁴ Due to this reason, qubit-based systems are rather vulnerable to environment-induced drifts, including the dephasing and relaxation discussed in the previous chapter, creating major experimental challenges – see below.

Now, if we have a system of 2 qubits, the vectors of its arbitrary pure state may be represented as a sum of $2^2 = 4$ terms,⁴⁵

$$|\alpha\rangle_{N=2} = a_{00}|00\rangle + a_{01}|01\rangle + a_{10}|10\rangle + a_{11}|11\rangle \equiv \sum_{j_1, j_2=0,1} a_{j_1 j_2} |j_1 j_2\rangle, \quad (8.134)$$

Two-qubit state's representation

with four complex coefficients, i.e. eight real numbers, subject to just one normalization condition, which follows from the requirement $\langle\alpha|\alpha\rangle = 1$:

$$\sum_{j_1, j_2=0,1} \left| a_{j_1 j_2} \right|^2 = 1. \quad (8.135)$$

The evident generalization of Eqs. (133)-(134) to an arbitrary pure state of an N -qubit system is a sum of 2^N terms:

$$|\alpha\rangle_N = \sum_{j_1, j_2, \dots, j_N=0,1} a_{j_1 j_2 \dots j_N} |j_1 j_2 \dots j_N\rangle, \quad (8.136)$$

including all possible combinations of 0s and 1s for indices j , so that the state is fully described by 2^N complex numbers, i.e. $2 \cdot 2^N \equiv 2^{N+1}$ real numbers, with only one constraint, similar to Eq. (135), imposed by the normalization condition. Let me emphasize that this exponential growth of the information contents would not be possible without the qubit state entanglement. Indeed, in the particular case when qubit states are not entangled, i.e. are factorable:

⁴⁴ In this aspect as well, the information processing systems based on qubits are closer to classical analog computers (which were popular once, but nowadays are used for a few special applications only) rather than classical digital ones.

⁴⁵ Here and in most instances below I use the same shorthand notation as was used at the beginning of this chapter – cf. Eq. (1b). In this short form, qubit's number is coded by the order of its state index inside a full ket-vector, while in the long form, such as in Eq. (137), it is coded by the order of its single-qubit vector in a full direct product.

$$|\alpha\rangle_N = |\alpha_1\rangle|\alpha_2\rangle\cdots|\alpha_N\rangle, \quad (8.137)$$

where each $|\alpha_n\rangle$ is described by an equality similar to Eq. (133) with its individual expansion coefficients, the system state description requires only $3N - 1$ real numbers – e.g., N sets $\{\theta, \varphi, \gamma\}$ less one common phase.

However, it would be wrong to project this exponential growth of information contents directly on the capabilities of quantum computation, because this process has to include the output information readout, i.e. qubit state measurements. Due to the fundamental intrinsic uncertainty of quantum systems, the measurement of a single qubit even in a pure state (133) generally may give either of two results, with probabilities $W_0 = |a_0|^2$ and $W_1 = |a_1|^2$. To comply with the general notion of computation, any quantum computer has to provide certain (or virtually certain) results, and hence the probabilities W_j have to be very close to either 0 or 1, so that before the measurement, each measured qubit has to be in a basis state – either 0 or 1. This means that the computational system with N output qubits, just before the final readout, has to be in one of the factorable states

$$|\alpha\rangle_N = |j_1\rangle|j_2\rangle\cdots|j_N\rangle \equiv |j_1 j_2 \dots j_N\rangle, \quad (8.138)$$

which is a very small subset even of the set of all unentangled states (137), and whose maximum information contents is just N classical bits.

Now the reader may start thinking that this constraint strips quantum computations of any advantages over their classical counterparts, but such a view is also superficial. To show that, let us consider the scheme of the most actively explored type of quantum computation, shown in Fig. 3.⁴⁶

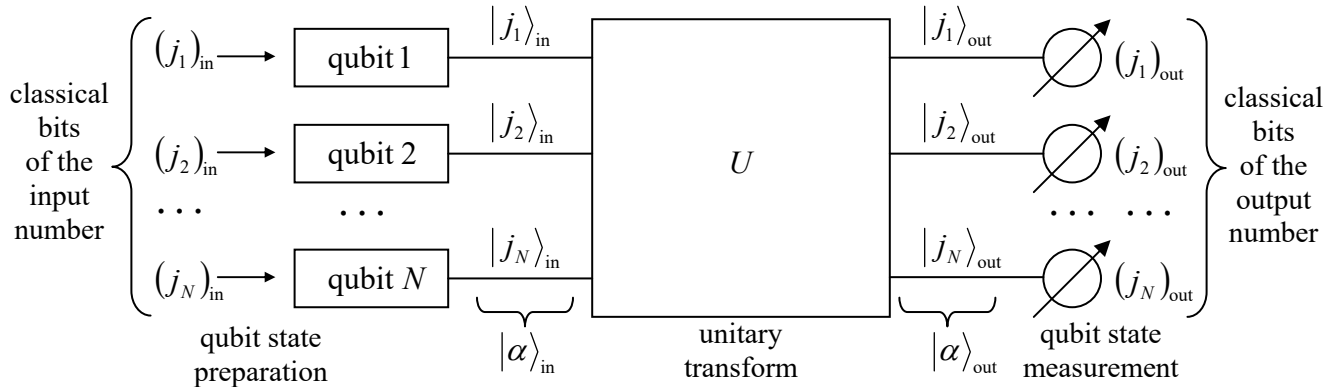


Fig. 8.3. The baseline scheme of quantum computation.

Here each horizontal line (sometimes called a “wire”⁴⁷) corresponds to a single qubit, tracing its time evolution in the same direction as at the usual time function plots: from left to right. This means

⁴⁶ Numerous modifications of this “baseline” scheme have been suggested, for example with the number of output qubits different from that of input qubits, etc. Some other options are discussed at the end of this section.

⁴⁷ The notion of “wires” stems from the similarity between such quantum schemes and the drawings describing classical computation circuits – see, e.g., Fig. 4a below. In the classical case, the lines may be indeed understood as physical wires connecting physical devices: logic gates and/or memory cells. In this context, note that classical computer components also have non-zero time delays, so that even in this case the left-to-right device ordering is useful to indicate the timing of (and frequently the causal relation between) the signals.

that the left column $|\alpha\rangle_{\text{in}}$ of ket-vectors describes the initial state of the qubits,⁴⁸ while the right column $|\alpha\rangle_{\text{out}}$ describes their final (but pre-measurement) state. The box labeled U represents the qubit evolution in time due to their specially arranged interactions between each other and/or external drive “forces”. Besides these forces, during this evolution the system is supposed to be ideally isolated from the dephasing and energy-dissipating environment, so that the process may be described by a unitary operator defined in the 2^N -dimensional Hilbert space of N qubits:

$$|\alpha\rangle_{\text{out}} = \hat{U}|\alpha\rangle_{\text{in}}. \quad (8.139)$$

With the condition that the input and output states have the simple form (138), this equality reads

$$|(j_1)_{\text{out}}(j_2)_{\text{out}}\dots(j_N)_{\text{out}}\rangle = \hat{U}|(j_1)_{\text{in}}(j_2)_{\text{in}}\dots(j_N)_{\text{in}}\rangle. \quad (8.140)$$

The art of quantum computer design consists of selecting such unitary operators \hat{U} that would:

- satisfy Eq. (140),
- be physically implementable, and
- enable substantial performance advantages of the quantum computation over its classical counterparts with similar functionality, at least for some digital functions (algorithms).

I will have time/space to demonstrate the possibility of such advantages on just one, perhaps the simplest example – the so-called *Deutsch problem*,⁴⁹ on the way discussing several common notions and issues of this field. Let us consider the family of single-bit classical Boolean functions $j_{\text{out}} = f(j_{\text{in}})$. Since both j are Boolean variables, i.e. may take only values 0 and 1, there are evidently only 4 such functions – see the first four columns of the following table:

f	$f(0)$	$f(1)$	class	F	$f(1)-f(0)$
f_1	0	0	constant	0	0
f_2	0	1	balanced	1	1
f_3	1	0	balanced	1	-1
f_4	1	1	constant	0	0

(8.141)

Of them, the functions f_1 and f_4 , whose values are independent of their arguments, are called *constants*, while the functions f_2 (called “YES” or “IDENTITY”) and f_3 (“NOT” or “INVERSION”) are called *balanced*. The Deutsch problem is to determine the class of a single-bit function, implemented in a “black box”, as being either constant or balanced, using just one experiment.

⁴⁸ As was discussed in Chapter 7, the preparation of a pure state (133) is (conceptually :-) straightforward. Placing a qubit into a weak contact with an environment of temperature $T \ll \Delta/k_B$, where Δ is the difference between energies of the eigenstates 0 and 1, we may achieve its relaxation into the lowest-energy state. Then, if the qubit must be set into a different pure state, it may be driven there by the application of a pulse of a proper external classical “force”. For example, if an actual spin-½ is used as the qubit, a pulse of a magnetic field, with proper direction and duration, may be applied to arrange its precession to the required Bloch sphere point – see Fig. 5.3c. However, in most physical implementations of qubits, a more practicable way for that step is to use a proper part of the Rabi oscillation period – see Sec. 6.5.

⁴⁹ It is named after David Elieser Deutsch, whose 1985 paper (motivated by an inspirational but not very specific publication by Richard Feynman in 1982) launched the whole field of quantum computation.

Classically, this is clearly impossible, and the simplest way to perform the function's classification involves two similar black boxes f – see Fig. 4a.⁵⁰ It also uses the so-called *exclusive-OR* (XOR for short) *gate* whose output is described by the following function F of its two Boolean arguments j_1 and j_2 :⁵¹

$$F(j_1, j_2) = j_1 \oplus j_2 \equiv \begin{cases} 0, & \text{if } j_1 = j_2, \\ 1, & \text{if } j_1 \neq j_2. \end{cases} \quad (8.142)$$

In the particular circuit shown in Fig. 4a, the gate produces the following output:

$$F = f(0) \oplus f(1), \quad (8.143)$$

which is equal to 1 if $f(0) \neq f(1)$, i.e. if the function f is balanced, and to 0 in the opposite case – see column F in the table of Eq. (141).

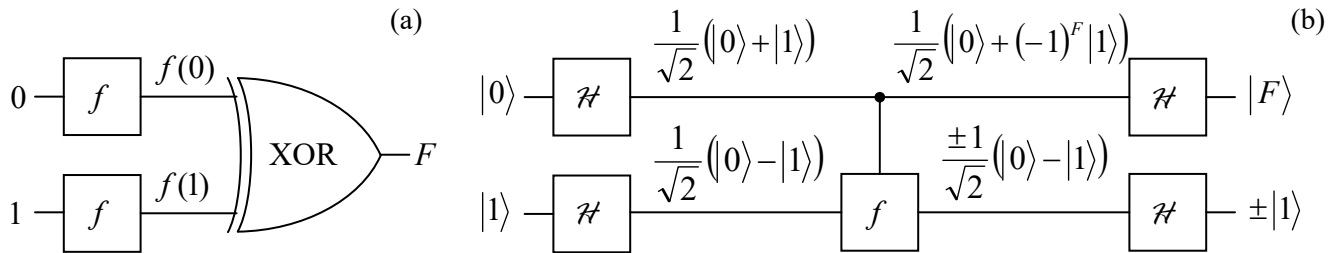


Fig. 8.4. The simplest (a) classical and (b) quantum ways to classify a single-bit Boolean function f .

On the other hand, as will be shown below, any of four functions f may be implemented quantum-mechanically, for example (Fig. 5a) as a unitary transform of two input qubits, acting as follows on each basis component $|j_1 j_2\rangle \equiv |j_1\rangle |j_2\rangle$ of the general input state (134):

$$\hat{f}|j_1\rangle |j_2\rangle = |j_1\rangle |j_2 \oplus f(j_1)\rangle, \quad (8.144)$$

where f is the corresponding classical Boolean function – see the table in Eq. (141).

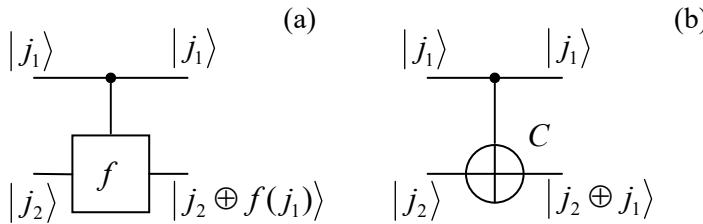


Fig. 8.5. Two-qubit quantum gates: (a) a two-qubit function f and (b) its particular case C (CNOT), and their actions on a basis state.

In the particular case when f in Eq. (144) is just the YES function: $f(j) = f_2(j) = j$, this “circuit” is reduced to the so-called *CNOT gate*, a key ingredient of many other quantum computation schemes, performing the following two-qubit transform:

⁵⁰ Alternatively, we may perform two sequential experiments on the same black box f , first recording, and then recalling the first experiment's result. However, the Deutsch problem calls for a single-shot experiment.

⁵¹ The XOR sign \oplus should not be confused with the sign \otimes of the direct product of state vectors (which in this section is just implied).

$$\hat{C}|j_1 j_2\rangle = |j_1\rangle|j_2 \oplus j_1\rangle.$$

(8.145a) CNOT function

Let us use Eq. (142) to spell out this function for all four possible input qubit combinations:

$$\hat{C}|00\rangle = |00\rangle, \quad \hat{C}|01\rangle = |01\rangle, \quad \hat{C}|10\rangle = |11\rangle, \quad \hat{C}|11\rangle = |10\rangle. \quad (8.145b)$$

In plain English, this means that acting on a basis state $j_1 j_2$, the CNOT gate leaves the state of the first, *source* qubit (shown by the upper horizontal line in Fig. 5) intact, but flips the state of the second, *target* qubit if the first one is in the basis state 1. In even simpler words, the state j_1 of the source qubit controls the NOT function acting on the target qubit; hence the gate's name CNOT – the semi-acronym of “Controlled NOT”.

For the quantum function (144), with an arbitrary and unknown f , the Deutsch problem may be solved within the general scheme shown in Fig. 3, with the particular structure of the unitary-transform box U spelled out in Fig. 4b, which involves just one implementation of the function f . Here the single-qubit quantum gate $\hat{\mathcal{H}}$ performs the *Hadamard* (or “Walsh-Hadamard” or “Walsh”) transform,⁵² whose operator is defined by the following actions on the qubit’s basis states:

$$\hat{\mathcal{H}}|0\rangle = \frac{1}{\sqrt{2}}(|0\rangle + |1\rangle), \quad \hat{\mathcal{H}}|1\rangle = \frac{1}{\sqrt{2}}(|0\rangle - |1\rangle), \quad (8.146) \quad \text{Hadamard transform}$$

- see also the two leftmost state label columns in Fig. 4b.⁵³ Since this operator has to be linear (to be quantum-mechanically realistic), it needs to perform the action (146) on the basis states even when they are parts of a linear superposition – as they are, for example, for the two right Hadamard gates in Fig. 4b. For example, as immediately follows from Eqs. (146) and the operator’s linearity,

$$\hat{\mathcal{H}}(\hat{\mathcal{H}}|0\rangle) = \hat{\mathcal{H}}\left(\frac{1}{\sqrt{2}}(|0\rangle + |1\rangle)\right) = \frac{1}{\sqrt{2}}\hat{\mathcal{H}}(|0\rangle + \hat{\mathcal{H}}|1\rangle) = \frac{1}{\sqrt{2}}\left(\frac{1}{\sqrt{2}}(|0\rangle + |1\rangle) + \frac{1}{\sqrt{2}}(|0\rangle - |1\rangle)\right) = |0\rangle. \quad (8.147a)$$

Absolutely similarly, we may get⁵⁴

$$\hat{\mathcal{H}}(\hat{\mathcal{H}}|1\rangle) = |1\rangle. \quad (8.147b)$$

Now let us carry out a sequential analysis of the “circuit” shown in Fig. 4b. Since the input states of the gate f in this particular circuit are described by Eqs. (146), its output state’s ket is

$$\hat{f}(\hat{\mathcal{H}}|0\rangle\hat{\mathcal{H}}|1\rangle) = \hat{f}\left(\frac{1}{\sqrt{2}}(|0\rangle + |1\rangle)\frac{1}{\sqrt{2}}(|0\rangle - |1\rangle)\right) = \frac{1}{2}(\hat{f}|00\rangle - \hat{f}|01\rangle + \hat{f}|10\rangle - \hat{f}|11\rangle). \quad (8.148)$$

Now we may apply Eq. (144) to each component in the parentheses:

⁵² Named after mathematicians J. Hadamard (1865-1963) and J. Walsh (1895-1973). To avoid any chance of confusion between the Hadamard transform’s operator $\hat{\mathcal{H}}$ and the general Hamiltonian operator \hat{H} , in these notes they are typeset using different fonts.

⁵³ Note that according to Eq. (146), the operator $\hat{\mathcal{H}}$ does *not* belong to the class of transforms \hat{U} described by Eq. (140) – while the whole “circuit” shown in Fig. 4b, does – see below.

⁵⁴ Since the states 0 and 1 form a full basis of a single qubit, both Eqs. (147) may be summarized as an operator equality: $\hat{\mathcal{H}}^2 = \hat{I}$. It is also easy to verify that the Hadamard transform of an arbitrary state may be represented on the Bloch sphere (Fig. 5.3) as a π -rotation about the direction that bisects the angle between the x - and z -axes.

$$\begin{aligned}
\hat{f}|00\rangle - \hat{f}|01\rangle + \hat{f}|10\rangle - \hat{f}|11\rangle &\equiv \hat{f}|0\rangle|0\rangle - \hat{f}|0\rangle|1\rangle + \hat{f}|1\rangle|0\rangle - \hat{f}|1\rangle|1\rangle \\
&= |0\rangle|0 \oplus f(0)\rangle - |0\rangle|1 \oplus f(0)\rangle + |1\rangle|0 \oplus f(1)\rangle - |1\rangle|1 \oplus f(1)\rangle \quad (8.149) \\
&\equiv |0\rangle(|0 \oplus f(0)\rangle - |1 \oplus f(0)\rangle) + |1\rangle(|0 \oplus f(1)\rangle - |1 \oplus f(1)\rangle).
\end{aligned}$$

Note that the contents of the first parentheses of the last expression, characterizing the state of the target qubit, is equal to $(|0\rangle - |1\rangle) \equiv (-1)^0 (|0\rangle - |1\rangle)$ if $f(0) = 0$ (and hence $0 \oplus f(0) = 0$ and $1 \oplus f(0) = 1$), and to $(|1\rangle - |0\rangle) \equiv (-1)^1 (|0\rangle - |1\rangle)$ in the opposite case $f(0) = 1$, so that both cases may be described in one shot by rewriting the parentheses as $(-1)^{f(0)} (|0\rangle - |1\rangle)$. The second parentheses is absolutely similarly controlled by the value of $f(1)$, so that the outputs of the gate f are unentangled:

$$\hat{f}(\hat{\mathcal{H}}|0\rangle\hat{\mathcal{H}}|1\rangle) = \frac{1}{2}((-1)^{f(0)}|0\rangle + (-1)^{f(1)}|1\rangle)(|0\rangle - |1\rangle) = \pm \frac{1}{\sqrt{2}}(|0\rangle + (-1)^F|1\rangle) \frac{1}{\sqrt{2}}(|0\rangle - |1\rangle), \quad (8.150)$$

where the last step has used the fact that the classical Boolean function F , defined by Eq. (142), is equal to $\pm[f(1) - f(0)]$ – please compare the last two columns in Eq. (141). The front sign \pm in Eq. (150) may be prescribed to any of the component ket-vectors – for example to that of the target qubit, as shown by the third column of state labels in Fig. 4b.

This intermediate result is already rather remarkable. Indeed, it shows that, despite the superficial impression one could get from Fig. 5, the gates f and C , being “controlled” by the source qubit, may change that qubit’s state as well! This fact (partly reflected by the vertical direction of the control lines in Figs. 4 and 5, symbolizing the same stage of the system’s time evolution) shows how careful one should be interpreting quantum-computational “circuits”, thriving on qubits’ entanglement, because the “signals” on different sections of a “wire” may differ – see Fig. 4b again.

At the last stage of the circuit shown in Fig. 4b, the qubit components of the state (150) are fed into one more pair of Hadamard gates, whose outputs therefore are

$$\hat{\mathcal{H}} \frac{1}{\sqrt{2}}(|0\rangle + (-1)^F|1\rangle) = \frac{1}{\sqrt{2}}(\hat{\mathcal{H}}|0\rangle + (-1)^F \hat{\mathcal{H}}|1\rangle), \quad \text{and} \quad \hat{\mathcal{H}} \left(\pm \frac{1}{\sqrt{2}}(|0\rangle - |1\rangle) \right) = \pm \frac{1}{\sqrt{2}}(\hat{\mathcal{H}}|1\rangle - \hat{\mathcal{H}}|0\rangle). \quad (8.151)$$

Now using Eqs. (146) again, we see that the output state ket-vectors of the source and target qubits are, respectively,

$$\frac{1+(-1)^F}{2}|0\rangle + \frac{1-(-1)^F}{2}|1\rangle, \quad \text{and} \quad \pm|1\rangle. \quad (8.152)$$

Since, according to Eq. (142), the Boolean function F may take only values 0 or 1, the final state of the source qubit is always one of its basis states j , namely the one with $j = F$. Its measurement tells us whether the function f , participating in Eq. (144), is constant or balanced – see Eq. (141) again.⁵⁵

Thus, the quantum circuit shown in Fig. 4b indeed solves the Deutsch problem in one shot. Reviewing our analysis, we may see that this is possible because the unitary transform performed by the quantum gate f is applied to the entangled states (146) rather than to the basis states. Due to this trick, the quantum state components depending on $f(0)$ and $f(1)$ are processed simultaneously, in parallel. This

⁵⁵ Note that the last Hadamard transform of the target qubit (i.e. the Hadamard gate shown in the lower right corner of Fig. 4b) is not necessary for the Deutsch problem’s solution – though it should be included if we want the whole circuit to satisfy the condition (140).

quantum parallelism may be extended to circuits with many ($N \gg 1$) qubits and, for some tasks, provide a dramatic performance increase – for example, reducing the necessary circuit component number from $O(2^N)$ to $O(N^p)$, where p is a finite (and not very big) number.

However, this efficiency comes at a high price. Indeed, let us discuss the possible physical implementation of quantum gates, starting from the single-qubit case, on an example of the Hadamard gate (146). With the linearity requirement, its action on the arbitrary state (133) should be

$$\hat{\mathcal{H}}|\alpha\rangle = a_0\hat{\mathcal{H}}|0\rangle + a_1\hat{\mathcal{H}}|1\rangle = a_0 \frac{1}{\sqrt{2}}(|0\rangle + |1\rangle) + a_1 \frac{1}{\sqrt{2}}(|0\rangle - |1\rangle) = \frac{1}{\sqrt{2}}(a_0 + a_1)|0\rangle + \frac{1}{\sqrt{2}}(a_0 - a_1)|1\rangle, \quad (8.153)$$

meaning that the state probability amplitudes in the end ($t = \mathcal{T}$) and in the beginning ($t = 0$) of the qubit evolution in time have to be related as

$$a_0(\mathcal{T}) = \frac{a_0(0) + a_1(0)}{\sqrt{2}}, \quad a_1(\mathcal{T}) = \frac{a_0(0) - a_1(0)}{\sqrt{2}}. \quad (8.154)$$

This task may be again performed using the Rabi oscillations, which were discussed in Sec. 6.5, i.e. by applying to the qubit (a two-level system), for a limited time period \mathcal{T} , a weak sinusoidal external signal of frequency ω equal to the intrinsic quantum oscillation frequency $\omega_{nn'}$ defined by Eq. (6.85). The analysis of the Rabi oscillations was carried out in Sec. 6.5, even for non-vanishing (though small) detuning $\Delta = \omega - \omega_{nn'}$, but only for the particular initial conditions when at $t = 0$ the system was fully in one on the basis states (there labeled as n'), i.e. the counterpart state (there labeled n) was empty. For our current purposes we need to find the amplitudes $a_{0,1}(t)$ for arbitrary initial conditions $a_{0,1}(0)$, subject only to the time-independent normalization condition $|a_0|^2 + |a_1|^2 = 1$. For the case of exact tuning, $\Delta = 0$, the solution of the system (6.94) is elementary,⁵⁶ and gives the following solution:⁵⁷

$$\begin{aligned} a_0(t) &= a_0(0) \cos \Omega t - i a_1(0) e^{i\varphi} \sin \Omega t, \\ a_1(t) &= a_1(0) \cos \Omega t - i a_0(0) e^{-i\varphi} \sin \Omega t, \end{aligned} \quad (8.155)$$

where Ω is the Rabi oscillation frequency (6.99), in the exact-tuning case proportional to the amplitude $|A|$ of the external ac drive $A = |A|\exp\{i\varphi\}$ – see Eq. (6.86). Comparing these expressions with Eqs. (154), we see that for $t = \mathcal{T} = \pi/4\Omega$ and $\varphi = \pi/2$ they “almost” coincide, besides the opposite sign of $a_1(\mathcal{T})$. Conceptually the simplest way to correct this deficiency is to follow the *ac* “ $\pi/4$ -pulse”, just discussed, by a short *dc* “ π -pulse” of the duration $\mathcal{T} = \pi/\delta$, which temporarily creates a small additional energy difference δ between the basis states 0 and 1. According to the basic Eq. (1.62), such difference creates an additional phase difference $\mathcal{T}\delta/\hbar$ between the states, equal to π for the “ π -pulse”.

Another way (that may be also useful for two-qubit operations) is to use another, auxiliary energy level E_2 whose distances from the basic levels E_1 and E_0 are significantly different from the difference $(E_1 - E_0)$ – see Fig. 6a. In this case, the weak external ac field tuned to any of the three potential quantum transition frequencies $\omega_{nn'} \equiv (E_n - E_{n'})/\hbar$ initiates such transitions between the corresponding states only, with a negligible perturbation of the third state. (Such transitions may be

⁵⁶ An alternative way to analyze the qubit evolution is to use the Bloch equation (5.21), with an appropriate function $\mathbf{Q}(t)$ describing the control field.

⁵⁷ To comply with our current notation, the coefficients $a_{n'}$ and a_n of Sec. 6.5 are replaced with a_0 and a_1 .

again described by Eqs. (155), with the appropriate index changes.) For the Hadamard transform implementation, it is sufficient to apply (after the already discussed $\pi/4$ -pulse of frequency ω_{10} , and with the initially empty level E_2), an additional π -pulse of frequency ω_{20} , with any phase φ . Indeed, according to the first of Eqs. (155), with the due replacement $a_1(0) \rightarrow a_2(0) = 0$, such pulse flips the sign of the amplitude $a_0(t)$, while the amplitude $a_1(t)$, not involved in this additional transition, remains unchanged.

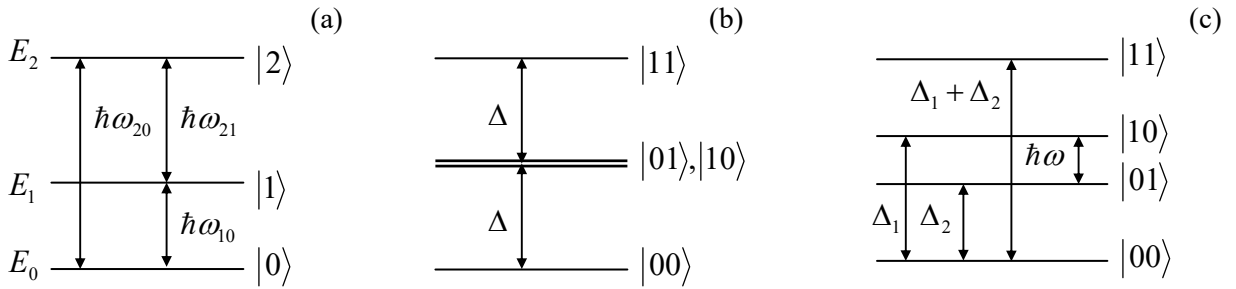


Fig. 8.6. Energy-level schemes used for unitary transformations of (a) single qubits and (b, c) two-qubit systems.

Now let me describe the conceptually simplest (though, for some qubit types, not the most practically convenient) scheme for the implementation of two-qubit gates, on an example of the CNOT gate whose operation is described by Eq. (145). For that, evidently, the involved qubits have to interact for some time \mathcal{T} . As was repeatedly discussed in the two last chapters, in most cases such interaction of two subsystems is factorable – see Eq. (6.145). For qubits, i.e. two-level systems, each of the component operators may be represented by a 2×2 matrix in the basis of states 0 and 1. According to Eq. (4.106), such matrix may be always expressed as a linear combination ($bI + \mathbf{c} \cdot \boldsymbol{\sigma}$), where b and three Cartesian components of the vector \mathbf{c} are c -numbers. Let us consider the simplest form of such factorable interaction Hamiltonian:

$$\hat{H}_{\text{int}}(t) = \begin{cases} \kappa \hat{\sigma}_z^{(1)} \hat{\sigma}_z^{(2)}, & \text{for } 0 < t < \mathcal{T}, \\ 0, & \text{otherwise,} \end{cases} \quad (8.156)$$

where the upper index is the qubit number and κ is a c -number constant.⁵⁸ According to Eq. (4.175), by the end of the interaction period, this Hamiltonian produces the following unitary transform:

$$\hat{U}_{\text{int}} = \exp \left\{ -\frac{i}{\hbar} \hat{H}_{\text{int}} \mathcal{T} \right\} \equiv \exp \left\{ -\frac{i}{\hbar} \kappa \hat{\sigma}_z^{(1)} \hat{\sigma}_z^{(2)} \mathcal{T} \right\}. \quad (8.157)$$

Since in the basis of unperturbed two-bit basis states $|j_1 j_2\rangle$, the product operator $\hat{\sigma}_z^{(1)} \hat{\sigma}_z^{(2)}$ is diagonal, so is the unitary operator (157), with the following action on these states:

⁵⁸ The assumption of simultaneous time independence of the basis state vectors and the interaction operator (within the time interval $0 < t < \mathcal{T}$) is possible only if the basis state energy difference Δ of both qubits is exactly the same. In this case, the simple physical explanation of the time evolution (156) follows from Figs. 6b,c, which show the spectrum of the total energy $E = E_1 + E_2$ of the two-bit system. In the absence of interaction (Fig. 6b), the energies of two basis states, $|01\rangle$ and $|10\rangle$, are equal, enabling even a weak qubit interaction to cause their substantial evolution in time – see Sec. 6.7. If the qubit energies are different (Fig. 6c), the interaction may still be reduced, in the rotating-wave approximation, to Eq. (156), by compensating the energy difference ($\Delta_1 - \Delta_2$) with an external ac signal of frequency $\omega = (\Delta_1 - \Delta_2)/\hbar$ – see Sec. 6.5.

$$\hat{U}_{\text{int}}|j_1 j_2\rangle = \exp\left\{i\theta\sigma_z^{(1)}\sigma_z^{(2)}\right\}|j_1 j_2\rangle, \quad (8.158)$$

where $\theta \equiv -\kappa\mathcal{T}\hbar$, and σ_z are the eigenvalues of the Pauli matrix σ_z for the basis states of the corresponding qubit: $\sigma_z = +1$ for $|j\rangle = |0\rangle$, and $\sigma_z = -1$ for $|j\rangle = |1\rangle$. Let me, for clarity, spell out Eq. (158) for the particular case $\theta = -\pi/4$ (corresponding to the qubit coupling time $\mathcal{T} = \pi\hbar/4\kappa$):

$$\hat{U}_{\text{int}}|00\rangle = e^{-i\pi/4}|00\rangle, \quad \hat{U}_{\text{int}}|01\rangle = e^{i\pi/4}|01\rangle, \quad \hat{U}_{\text{int}}|10\rangle = e^{i\pi/4}|10\rangle, \quad \hat{U}_{\text{int}}|11\rangle = e^{-i\pi/4}|11\rangle. \quad (8.159)$$

In order to compensate the undesirable parts of this joint phase shift of the basis states, let us now apply similar individual “rotations” of each qubit by angle $\theta' = +\pi/4$, using the following product of two independent operators, plus (just for the result’s clarity) a common, and hence inconsequential, phase shift $\theta'' = -\pi/4$:⁵⁹

$$\hat{U}_{\text{com}} = \exp\left\{i\theta'\left(\hat{\sigma}_z^{(1)} + \hat{\sigma}_z^{(2)}\right) + i\theta''\right\} \equiv \exp\left\{i\frac{\pi}{4}\hat{\sigma}_z^{(1)}\right\} \exp\left\{i\frac{\pi}{4}\hat{\sigma}_z^{(2)}\right\} e^{-i\pi/4}. \quad (8.160)$$

Since this operator is also diagonal in the $|j_1 j_2\rangle$ basis, it is easy to calculate the change of the basis states by the total unitary operator $\hat{U}_{\text{tot}} \equiv \hat{U}_{\text{com}} \hat{U}_{\text{int}}$:

$$\hat{U}_{\text{tot}}|00\rangle = |00\rangle, \quad \hat{U}_{\text{tot}}|01\rangle = |01\rangle, \quad \hat{U}_{\text{tot}}|10\rangle = |10\rangle, \quad \hat{U}_{\text{tot}}|11\rangle = -|11\rangle. \quad (8.161)$$

This result already shows the main “miracle action” of two-qubit gates, such as the one shown in Fig. 4b: the source qubit is left intact (only if it is in one of the basis states!), while the state of the target qubit is altered. True, this change (of the sign) is still different from the CNOT operator’s action (145), but may be readily used for its implementation by sandwiching of the transform U_{tot} between two Hadamard transforms of the target qubit alone:

$$\hat{C} = \frac{1}{2}\hat{\mathcal{H}}^{(2)}\hat{U}_{\text{tot}}\hat{\mathcal{H}}^{(2)}. \quad (8.162)$$

So, we have spent quite a bit of time on the discussion of the CNOT gate,⁶⁰ and now I can reward the reader for their effort with a bit of good news: it has been proved that an *arbitrary* unitary transform that satisfies Eq. (140), i.e. may be used within the general scheme outlined in Fig. 3, may be decomposed into a set of CNOT gates, possibly augmented with simpler single-qubit gates – for example, the Hadamard gate plus the $\pi/2$ rotation discussed above.⁶¹ Unfortunately, I have no time for a

⁵⁹ As Eq. (4.175) shows, each of the component unitary transforms $\exp\{i\theta'\hat{\sigma}_z\}$ may be created by applying to each qubit, for time interval $\mathcal{T} = \hbar\theta'/\kappa'$, a constant external field described by Hamiltonian $\hat{H} = -\kappa'\hat{\sigma}_z$. We already know that for a charged, spin-½ particle, such Hamiltonian may be created by applying a z-oriented external dc magnetic field – see Eq. (4.163). For most other physical implementations of qubits, the organization of such a Hamiltonian is also straightforward – see, e.g., Fig. 7.4 and its discussion.

⁶⁰ As was discussed above, this gate is identical to the two-qubit gate shown in Fig. 5a for $f = f_3$, i.e. $f(j) = j$. The implementation of the gate of f for 3 other possible functions f requires straightforward modifications, whose analysis is left for the reader’s exercise.

⁶¹ This fundamental importance of the CNOT gate was perhaps a major reason why David Wineland, the leader of the NIST group that had demonstrated its first experimental implementation in 1995 (following the theoretical suggestion by J. Cirac and P. Zoller), was awarded the 2012 Nobel Prize in Physics – shared with Serge Haroche, the leader of another group working towards quantum computation.

detailed discussion of more complex circuits.⁶² The most famous of them is the scheme for integer number factoring, suggested in 1994 by Peter Winston Shor.⁶³ Due to its potential practical importance for breaking broadly used communication encryption schemes such as the RSA code,⁶⁴ this opportunity has incited much enthusiasm and triggered experimental efforts to implement quantum gates and circuits using a broad variety of two-level quantum systems. By now, the following experimental options have given the most significant results:⁶⁵

(i) Trapped ions. The first experimental demonstrations of quantum state manipulation (including the already mentioned first CNOT gate) have been carried out using deeply cooled atoms in optical traps, similar to those used in frequency and time standards. Their total spins are natural qubits, whose states may be manipulated using the Rabi transfers excited by suitably tuned lasers. The spin interactions with the environment may be very weak, resulting in large dephasing times T_2 – up to a few seconds. Since the distances between ions in the traps are relatively large (of the order of a micron), their direct spin-spin interaction is even weaker, but the ions may be made effectively interacting either via their mechanical oscillations about the potential minima of the trapping field, or via photons in external electromagnetic resonators (“cavities”).⁶⁶ Perhaps the main challenge of using this approach for quantum computation is poor “scalability”, i.e. the enormous experimental difficulty of creating and managing large ordered systems of individually addressable qubits. So far, only a-few-qubit systems have been demonstrated.⁶⁷

(ii) Nuclear spins are also typically very weakly connected to their environment, with dephasing times T_2 exceeding 10 seconds in some cases. Their eigenenergies E_0 and E_1 may be split by external dc magnetic fields (typically, of the order of 10 T), while the interstate Rabi transfers may be readily achieved by using the nuclear magnetic resonance, i.e. the application of external ac fields with frequencies $\omega = (E_1 - E_0)/\hbar$ – typically, of a few hundred MHz. The challenges of this option include the weakness of spin-spin interactions (typically mediated through molecular electrons), resulting in a very slow spin evolution, whose time scale \hbar/κ may become comparable with T_2 , and also very small level separations $E_1 - E_0$, corresponding to a few K, i.e. much smaller than the room temperature, creating a challenge of qubit state preparation.⁶⁸ Despite these challenges, the nuclear spin option was used for the first implementation of the Shor algorithm for factoring of a small number ($15 = 5 \times 3$) as early as 2001.⁶⁹ However, the extension of this success to larger systems, beyond the set of spins inside one molecule, is extremely challenging.

⁶² For that, the reader may be referred to either the monographs by Nielsen-Chuang and Reiffel-Polak, cited above, or to a shorter (but much more formal) textbook by N. Mermin, *Quantum Computer Science*, Cambridge U. Press, 2007.

⁶³ A clear description of this algorithm may be found in several accessible sources, including *Wikipedia* – see the article *Shor's Algorithm*.

⁶⁴ Named after R. Rivest, A. Shamir, and L. Adleman, the authors of the first open publication of the code in 1977, but actually invented earlier (in 1973) by C. Cocks.

⁶⁵ For a discussion of other possible implementations (such as quantum dots and dopants in crystals) see, e.g., T. Ladd *et al.*, *Nature* **464**, 45 (2010), and references therein.

⁶⁶ A brief discussion of such interactions (so-called *Cavity QED*) will be given in Sec. 9.4 below.

⁶⁷ See, e.g., S. Debnath *et al.*, *Nature* **536**, 63 (2016). Note also the related work on arrays of trapped, optically-coupled neutral atoms – see, e.g., J. Perczel *et al.*, *Phys. Rev. Lett.* **119**, 023603 (2017) and references therein.

⁶⁸ This challenge may be partly mitigated using ingenious spin manipulation techniques such as *refocusing* – see, e.g., either Sec. 7.7 in Nielsen and Chuang, or the J. Keeler's monograph cited at the end of Sec. 6.5.

⁶⁹ B. Lanyon *et al.*, *Phys. Rev. Lett.* **99**, 250505 (2001).

(iii) Josephson-junction devices. Much better scalability may be achieved with solid-state devices, especially using superconductor integrated circuits including weak contacts – Josephson junctions (see their brief discussion in Sec. 1.6). The qubits of this type are based on the fact that the energy U of such a junction is a highly nonlinear function of the Josephson phase difference φ – see Sec. 1.6. Indeed, combining Eqs. (1.73) and (1.74), we can readily calculate $U(\varphi)$ as the work \mathcal{W} of an external circuit increasing the phase from, say, zero to some value φ :

$$U(\varphi) - U(0) = \int_{\varphi'=0}^{\varphi'=\varphi} d\mathcal{W} = \int_{\varphi'=0}^{\varphi'=\varphi} IVdt = \frac{2eI_c}{\hbar} \int_{\varphi'=0}^{\varphi'=\varphi} \sin \varphi' \frac{d\varphi'}{dt} dt = \frac{2eI_c}{\hbar} (1 - \cos \varphi). \quad (8.163)$$

There are several options of using this nonlinearity for creating qubits;⁷⁰ currently the leading option, called the *phase qubit*, is using two lowest eigenstates localized in one of the potential wells of the periodic potential (163). A major problem of such qubits is that at the very bottom of this well the potential $U(\varphi)$ is almost quadratic, so that the energy levels are nearly equidistant – cf. Eqs. (2.262), (6.16), and (6.23). This is even more true for the so-called “transmons” (and “Xmons”, and “Gatemons”, and several other very similar devices⁷¹) – the currently used phase qubits versions, where a Josephson junction is made a part of an external electromagnetic oscillator, making its relative total nonlinearity (anharmonism) even smaller. As a result, the external rf drive of frequency $\omega = (E_1 - E_0)/\hbar$, used to arrange the state transforms described by Eq. (155), may induce simultaneous undesirable transitions to (and between) higher energy levels. This effect may be mitigated by a reduction of the ac drive amplitude, but at a price of the proportional increase of the operation time and hence of dephasing – see below. (I am leaving a quantitative estimate of such an increase for the reader’s exercise.)

Since the coupling of Josephson-junction qubits may be most readily controlled (and, very importantly, kept stable if so desired), they have been used to demonstrate the largest prototype quantum computing systems to date, despite quite modest dephasing times T_2 – for purely integrated circuits, in the tens of microseconds at best, even at operating temperatures in tens of mK. By the time of this writing (mid-2019), several groups have announced chips with a few dozen of such qubits, but to the best of my knowledge, only their smaller subsets could be used for high-fidelity quantum operations.⁷²

(iv) Optical systems, attractive because of their inherently enormous bandwidth, pose a special challenge for quantum computation: due to the virtual linearity of most electromagnetic media at reasonable light power, the implementation of qubits (i.e. two-level systems), and interaction Hamiltonians such as the one given by Eq. (156), is problematic. In 2001, a very smart way around this

⁷⁰ The “most quantum” option in this technology is to use Josephson junctions very weakly coupled to their dissipative environment (so that the effective resistance shunting the junction is much higher than the quantum resistance unit $R_Q \equiv (\pi/2) \hbar/e^2 \sim 10^4 \Omega$). In this case, the Josephson phase variable φ behaves as a coordinate of a 1D quantum particle, moving in the 2π -periodic potential (163), forming the energy band structure $E(q)$ similar to those discussed in Sec. 2.7. Both theory and experiment show that in this case, the quantum states in adjacent Brillouin zones differ by the charge of one Cooper pair $2e$. (This is exactly the effect responsible for the Bloch oscillations of frequency (2.252).) These two states may be used as the basis states of *charge qubits*. Unfortunately, such qubits are rather sensitive to charged impurities, randomly located in the junction’s vicinity, causing uncontrollable changes of its parameters, so that currently, to the best of my knowledge, this option is not actively pursued.

⁷¹ For a recent review of these devices see, e.g., G. Wendum, *Repts. Progr. Phys.* **80**, 106001 (2017), and references therein.

⁷² See, e.g., C. Song *et al.*, *Phys. Rev. Lett.* **119**, 180511 (2017) and references therein.

hurdle was invented.⁷³ In this *KLM scheme* (also called the “linear optical quantum computing”), nonlinear elements are not needed at all, and quantum gates may be composed just of linear devices (such as optical waveguides, mirrors, and beam splitters), plus single-photon sources and detectors. However, estimates show that this approach requires a much larger number of physical components than those using nonlinear quantum systems such as usual qubits,⁷⁴ so that right now it is not very popular.

So, despite more than two decades of large-scale efforts, the progress of quantum computing development has been rather modest. The main culprit here is the unintentional coupling of qubits to their environment, leading most importantly to their state dephasing, and eventually to errors. Let me discuss this major issue in detail.

Of course, some error probability exists in classical digital logic gates and memory cells as well.⁷⁵ However, in this case, there is no conceptual problem with the device state measurement, so that the error may be detected and corrected in many ways. Conceptually,⁷⁶ the simplest of them is the so-called *majority voting logic* – using several similar logic circuits working in parallel and fed with identical input data. Evidently, two such devices can detect a single error in one of them, while three devices in parallel may correct such error, by taking two coinciding output signals for the genuine one.

For quantum computation, the general idea of using several devices (say, qubits) for coding the same information remains valid; however, there are two major complications. First, as we know from Chapter 7, the environment’s dephasing effect may be described as a slow random drift of the probability amplitudes a_j , leading to the deviation of the output state α_{fin} from the required form (140), and hence to a non-vanishing probability of wrong qubit state readout – see Fig. 3. Hence the quantum error correction has to protect the result not against possible random state flips $0 \leftrightarrow 1$, as in classical digital computers, but against these “creeping” analog errors.

Second, the qubit state is impossible to copy exactly (*clone*) without disturbing it, as follows from the following simple calculation.⁷⁷ Cloning some state α of one qubit to another qubit that is initially in an independent state (say, the basis state $|0\rangle$), without any change of α , means the following transformation of the two-qubit ket: $|\alpha 0\rangle \rightarrow |\alpha\alpha\rangle$. If we want such transform to be performed by a real quantum system, whose evolution is described by a unitary operator \hat{u} , and to be correct for an arbitrary state α , it has to work not only for both basis states of the qubit:

$$\hat{u}|00\rangle = |00\rangle, \quad \hat{u}|10\rangle = |11\rangle, \quad (8.164)$$

but also for their arbitrary linear combination (133). Since the operator \hat{u} has to be linear, we may use that relation, and then Eq. (164) to write

⁷³ E. Knill *et al.*, *Nature* **409**, 46 (2001).

⁷⁴ See, e.g., Y. Li *et al.*, *Phys. Rev. X* **5**, 041007 (2015).

⁷⁵ In modern integrated circuits, such “soft” (runtime) errors are created mostly by the high-energy neutron component of cosmic rays, and also by the α -particles emitted by radioactive impurities in silicon chips and their packaging.

⁷⁶ Practically, the majority voting logic increases circuit complexity and power consumption, so that it is used only in most critical points. Since in modern digital integrated circuits the bit error rate is very small ($< 10^{-5}$), in most of them, less radical but also less penalizing schemes are used – if used at all.

⁷⁷ Amazingly, this simple *no-cloning theorem* was discovered as late as 1982 (to the best of my knowledge, independently by W. Wootters and W. Zurek, and by D. Dieks), in the context of work toward quantum cryptography – see below.

$$\hat{u}|\alpha 0\rangle \equiv \hat{u}(a_0|0\rangle + a_1|1\rangle)|0\rangle \equiv a_0\hat{u}|00\rangle + a_1\hat{u}|10\rangle = a_0|00\rangle + a_1|11\rangle. \quad (8.165)$$

On the other hand, the desired result of the state cloning is

$$|\alpha\alpha\rangle = (a_0|0\rangle + a_1|1\rangle)(a_0|0\rangle + a_1|1\rangle) \equiv a_0^2|00\rangle + a_0a_1(|10\rangle + |01\rangle) + a_1^2|11\rangle, \quad (8.166)$$

i.e. is evidently different, so that, for an arbitrary state α , and an arbitrary unitary operator \hat{u} ,

$$\hat{u}|\alpha 0\rangle \neq |\alpha\alpha\rangle, \quad \text{No-cloning theorem} \quad (8.167)$$

meaning that the qubit state cloning is indeed impossible.⁷⁸ This problem may be, however, indirectly circumvented – for example, in the way shown in Fig. 7a.

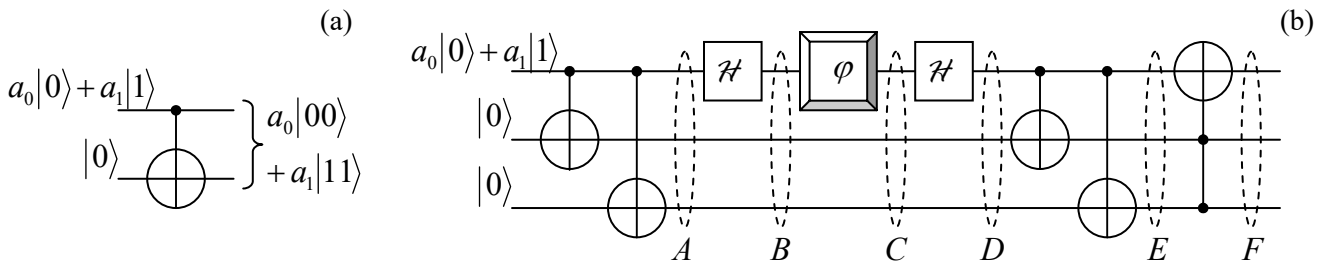


Fig. 8.7. (a) Quasi-cloning, and (b) detection and correction of dephasing errors in a single qubit.

Here the CNOT gate, whose action is described by Eq. (145), entangles an arbitrary input state (133) of the source qubit with a basis initial state of an ancillary target qubit – frequently called the *ancilla*. Using Eq. (145), we can readily calculate the output two-qubit state's vector:

$$|\alpha\rangle_{N=2} = \hat{C}(a_0|0\rangle + a_1|1\rangle)|0\rangle \equiv a_0\hat{C}|00\rangle + a_1\hat{C}|10\rangle = a_0|00\rangle + a_1|11\rangle. \quad \text{Quasi-cloning} \quad (8.168)$$

We see that this circuit does perform the operation (165), i.e. gives the initial source qubit's probability amplitudes a_0 and a_1 equally to two qubits, i.e. duplicates the input information. However, in contrast with the “genuine” cloning, it changes the state of the source qubit as well, making it entangled with the target (ancilla) qubit. Such “quasi-cloning” is the key element of most suggested quantum error correction techniques.

Consider, for example, the three-qubit “circuit” shown in Fig. 7b, which uses two ancilla qubits – see the two lower “wires”. At its first two stages, the double application of the quasi-cloning produces an intermediate state A with the following ket-vector:

$$|A\rangle = a_0|000\rangle + a_1|111\rangle, \quad (8.169)$$

which is an evident generalization of Eq. (168).⁷⁹ Next, subjecting the source qubit to the Hadamard transform (146), we get the three-qubit state B represented by the state vector

⁷⁸ Note that this does not mean that two (or several) qubits cannot be put into the same, arbitrary quantum state – theoretically, with arbitrary precision. Indeed, they may be first set into their lowest-energy stationary states, and then driven into the same arbitrary state (133) by exerting on them similar classical external fields. So, the no-cloning theorem pertains only to qubits in *unknown* states α – but this is exactly what we need for error correction – see below.

$$|B\rangle = a_0 \frac{1}{\sqrt{2}}(|0\rangle + |1\rangle)|00\rangle + a_1 \frac{1}{\sqrt{2}}(|0\rangle - |1\rangle)|11\rangle. \quad (8.170)$$

Now let us assume that at this stage, the source qubit comes into contact with a dephasing environment – in Fig. 7b, symbolized by the single-qubit “gate” φ . As we know from Chapter 7 (see Eq. (7.22) and its discussion, and also Sec. 7.3), its effect may be described by a random shift of the relative phase of two states:⁸⁰

$$|0\rangle \rightarrow e^{i\varphi}|0\rangle, \quad |1\rangle \rightarrow e^{-i\varphi}|1\rangle. \quad (8.171)$$

As a result, for the intermediate state C (see Fig. 7b) we may write

$$|C\rangle = a_0 \frac{1}{\sqrt{2}}(e^{i\varphi}|0\rangle + e^{-i\varphi}|1\rangle)|00\rangle + a_1 \frac{1}{\sqrt{2}}(e^{i\varphi}|0\rangle - e^{-i\varphi}|1\rangle)|11\rangle. \quad (8.172)$$

At this stage, in this simple theoretical model, the coupling with the environment is completely stopped (ahh, if this could be possible! we might have quantum computers by now :-), and the source qubit is fed into one more Hadamard gate. Using Eqs. (146) again, for the state D after this gate we get

$$|D\rangle = a_0(\cos\varphi|0\rangle + i\sin\varphi|1\rangle)|00\rangle + a_1(i\sin\varphi|0\rangle + \cos\varphi|1\rangle)|11\rangle. \quad (8.173)$$

Now the qubits are passed through the second, similar pair of CNOT gates – see Fig. 7b. Using Eq. (145), for the resulting state E we readily get the following expression:

$$|E\rangle = a_0 \cos\varphi|000\rangle + a_0 i \sin\varphi|111\rangle + a_1 i \sin\varphi|011\rangle + a_1 \cos\varphi|100\rangle, \quad (8.174a)$$

whose right-hand side may be evidently grouped as

$$|E\rangle = (a_0|0\rangle + a_1|1\rangle)\cos\varphi|00\rangle + (a_1|0\rangle + a_0|1\rangle)i\sin\varphi|11\rangle. \quad (8.174b)$$

This is already a rather remarkable result. It shows that if we measured the ancilla qubits at stage E , and both results corresponded to states 0, we might be 100% sure that the source qubit (which is not affected by these measurements!) is in its initial state even after the interaction with the environment. The only result of an increase of this unintentional interaction (as quantified by the r.m.s. magnitude of the random phase shift φ) is the growth of the probability,

$$W = \sin^2 \varphi, \quad (8.175)$$

of getting the opposite result, which signals a dephasing-induced error in the source qubit. Such implicit measurement, without disturbing the source qubit, is called *quantum error detection*.

An even more impressive result may be achieved by the last component of the circuit, the so-called *Toffoli* (or “CCNOT”) gate, denoted by the rightmost symbol in Fig. 7b. This three-qubit gate is conceptually similar to the CNOT gate discussed above, besides that it flips the basis state of its target qubit only if *both* source qubits are in state 1. (In the circuit shown in Fig. 7b, the former role is played

⁷⁹ Such state is also the 3-qubit example of the so-called *Greeenberger-Horne-Zeilinger (GHZ) states*, which are frequently called the “most entangled” states of a system of $N > 2$ qubits.

⁸⁰ Let me emphasize again that Eq. (171) is strictly valid only if the interaction with the environment is a pure dephasing, i.e. does not include the energy relaxation of the qubit or its thermal activation to the higher-energy eigenstate; however, it is a reasonable description of errors in the frequent case when $T_2 \ll T_1$.

by our source qubit, while the latter role, by the two ancilla qubits.) According to its definition, the Toffoli gate does not affect the first parentheses in Eq. (174b), but flips the source qubit's states in the second parentheses, so that for the output three-qubit state F we get

$$|F\rangle = (a_0|0\rangle + a_1|1\rangle) \cos \varphi |00\rangle + (a_0|0\rangle + a_1|1\rangle) i \sin \varphi |11\rangle. \quad (8.176a)$$

Obviously, this result may be factored as

$$|F\rangle = (a_0|0\rangle + a_1|1\rangle)(\cos \varphi |00\rangle + i \sin \varphi |11\rangle), \quad (8.176b)$$

showing that now the source qubit is again fully unentangled from the ancilla qubits. Moreover, calculating the norm squared of the second operand, we get

$$(\cos \varphi |00\rangle - i \sin \varphi |11\rangle)(\cos \varphi |00\rangle + i \sin \varphi |11\rangle) = \cos^2 \varphi + \sin^2 \varphi = 1, \quad (8.177)$$

so that the final state of the source qubit *exactly* coincides with its initial state. This is the famous miracle of *quantum state correction*, taking place “automatically” – without any qubit measurements, and for any random phase shift φ .

The circuit shown in Fig. 7b may be further improved by adding Hadamard gate pairs, similar to that used for the source qubit, to the ancilla qubits as well. It is straightforward to show that if the dephasing is small in the sense that the W given by Eq. (175) is much less than 1, this modified circuit may provide a substantial error probability reduction (to $\sim W^2$) even if the ancilla qubits are also subjected to a similar dephasing and the source qubits, at the same stage – i.e. between the two Hadamard gates. Such perfect automatic correction of *any* error (not only of an inner dephasing of a qubit and its relaxation/excitation, but also of the mutual dephasing between qubits) of *any* used qubit needs even more parallelism. The first circuit of that kind, based on nine parallel qubits, which is a natural generalization of the circuit discussed above, was invented in 1995 by the same P. Shor. Later, five-qubit circuits enabling similar error correction were suggested. (The further parallelism reduction has been proved impossible.)

However, all these results assume that the error correction circuits as such are perfect, i.e. completely isolated from the environment. In the real world, this cannot be done. Now the key question is what maximum level W_{\max} of the error probability in each gate (including those in the used error correction scheme) can be automatically corrected, and how many qubits with $W < W_{\max}$ would be required to implement quantum computers producing important practical results – first of all, factoring of large numbers.⁸¹ To the best of my knowledge, estimates of these two related numbers have been made only for some very specific approaches, and they are rather pessimistic. For example, using the so-called *surface codes*, which employ many physical qubits for coding an informational one, and hence increase its fidelity, W_{\min} may be increased to a few times 10^{-3} , but then we would need $\sim 10^8$ physical qubits for the Shor’s algorithm implementation.⁸² This is very far from what currently looks doable using the existing approaches.

Because of this hard situation, the current development of quantum computing is focused on finding at least *some* problems that could be within the reach of either the existing systems, or their immediate extensions, and simultaneously would present some practical interest – a typical example of a

Quantum
error
correction

⁸¹ In order to compete with the existing classical factoring algorithms, such numbers should have at least 10^3 bits.

⁸² A. Fowler *et al.*, *Phys. Rev. A* **86**, 032324 (2012).

technology in the search for applications. Currently, to the best of my knowledge, all suggested problems of this kind address either specially crafted mathematical problems,⁸³ or properties of some simple physical systems – such as the molecular hydrogen⁸⁴ or the deuteron (the deuterium’s nucleus, i.e. the proton-neutron system).⁸⁵ In the latter case, the interaction between the qubits of the computational system is organized so that the system’s Hamiltonian is similar to that of the quantum system of interest. (For this work, *quantum simulation* is a more adequate name than “quantum computation”.)⁸⁶

Such simulations are pursued by some teams using schemes different from that shown in Fig. 3. Of those, the most developed is the so-called *adiabatic quantum computation*,⁸⁷ which drops the hardest requirement of negligible interaction with the environment. In this approach, the qubit system is first prepared in a certain initial state, and then is let evolve on its own, with no effort to couple-uncouple qubits by external control signals during the evolution.⁸⁸ Due to the interaction with the environment, in particular the dephasing and the energy dissipation it imposes, the system eventually relaxes to a final incoherent state, which is then measured. (This reminds the scheme shown in Fig. 3, with the important difference that the transform U should not necessarily be unitary.) From numerous runs of such an experiment, the outcome statistics may be revealed. Thus, at this approach the interaction with the environment is allowed to play a certain role in the system evolution, though every effort is made to reduce it, thus slowing down the relaxation process – hence the word “adiabatic” in the name of this approach. This slowness allows the system to exhibit *some* quantum properties, in particular quantum tunneling⁸⁹ *through* the energy barriers separating close energy minima in the multi-dimensional space of states. This tunneling creates a substantial difference in the finite state statistics from that in purely classical systems, where such barriers may be overcome only by thermally-activated jumps *over* them.⁹⁰

Due to technical difficulties of the organization and precise control of long-range interaction in multi-qubit systems, the adiabatic quantum computing demonstrations so far have been limited to a few simple arrays described by the so-called *extended quantum Ising* (“spin-glass”) model

$$\hat{H} = -J \sum_{\{j,j'\}} \hat{\sigma}_z^{(j)} \hat{\sigma}_z^{(j')} - \sum_j h_j \hat{\sigma}_z^{(j)}, \quad (8.178)$$

where the curly brackets denote the summation over pairs of close (though not necessarily closest) neighbors. Though the Hamiltonian (178) is the traditional playground of phase transitions theory (see,

⁸³ F. Arute *et al.*, *Nature* **574**, 505 (2019). Note that the claim of the first achievement of “quantum supremacy”, made in this paper, refers only to an artificial, specially crafted mathematical problem, and does not change my assessment of the current status of this technology.

⁸⁴ P. O’Malley *et al.*, *Phys. Rev. X* **6**, 031007 (2016).

⁸⁵ E. Dumitrescu *et al.*, *Phys. Lett. Lett.* **120**, 210501 (2018).

⁸⁶ To the best of my knowledge, this idea was first put forward by Yuri I. Malin in his book *Computable and Incomputable* published in 1980, i.e. before the famous 1982 paper by Richard Feynman. Unfortunately, since the book was in Russian, this suggestion was acknowledged by the international community only much later.

⁸⁷ Note that the qualifier “quantum” is important in this term, to distinguish this research direction from the *classical* adiabatic (or “reversible”) computation – see, e.g., SM Sec. 2.3 and references therein.

⁸⁸ Recently, some hybrids of this approach with the “usual” scheme of quantum computation have been demonstrated, in particular, using some control of inter-bit coupling during the relaxation process – see, e.g., R. Barends *et al.*, *Nature* **534**, 222 (2016).

⁸⁹ As a reminder, this process was repeatedly discussed in this course, starting from Sec. 2.3.

⁹⁰ A quantitative discussion of such jumps may be found in SM Sec. 5.6.

e.g., SM Chapter 4), to the best of my knowledge there are not many practically important tasks that could be achieved by studying the statistics of its solutions. Moreover, even for this limited task, the speed of the largest experimental adiabatic quantum “computers”, with several hundreds of Josephson-junction qubits⁹¹ is still comparable with that of classical, off-the-shelf semiconductor processors (with the dollar cost lower by many orders of magnitude), and no dramatic change of this comparison is predicted for realistic larger systems.

To summarize the current (circa mid-2019) situation with the quantum computation development, it faces a very hard challenge of mitigating the effects of unintentional coupling with the environment. This problem is exacerbated by the lack of algorithms, beyond Shor’s factoring, that would give quantum computation a substantial advantage over the classical competition in solving real-world problems, and hence a much broader potential customer base that would provide the field with the necessary long-term motivation and resources. So far, even the leading experts in this field abstain from predictions on when quantum computation may become a self-supporting commercial technology.⁹²

There seem to be somewhat better prospects for another application of entangled qubit systems, namely to telecommunication cryptography.⁹³ The goal here is more modest: to replace the currently dominating classical encryption, based on the public-key RSA code mentioned above, that may be broken by factoring very large numbers, with a quantum encryption system that would be fundamentally unbreakable. The basis of this opportunity is the measurement postulate and the no-cloning theorem: if a message is carried over by a qubit, it is impossible for an eavesdropper (in cryptography, traditionally called *Eve*) to either measure or copy it faithfully, without also disturbing its state. However, as we have seen from the discussion of Fig. 7a, state *quasi*-cloning using entangled qubits is possible, so that the issue is far from being simple, especially if we want to use a publicly distributed quantum key, in some sense similar to the classical public key used at the RSA encryption. Unfortunately, I would not have time/space to discuss various options for quantum encryption, but cannot help demonstrating how counter-intuitive they may be, on the famous example of the so-called *quantum teleportation* (Fig. 8).⁹⁴

Suppose that some party A (in cryptography, traditionally called *Alice*) wants to send to party B (*Bob*) the full information about the pure quantum state α of a qubit, unknown to either party. Instead of sending her qubit directly to Bob, Alice asks *him* to send *her* one qubit (β) of a pair of other qubits, prepared in a certain entangled state, for example in the singlet state described by Eq. (11); in our current notation

$$|\beta\beta'\rangle = \frac{1}{\sqrt{2}}(|01\rangle - |10\rangle). \quad (8.179)$$

The initial state of the whole three-qubit system may be represented in the form

⁹¹ See, e.g., R. Harris *et al.*, *Science* **361**, 162 (2018). Similar demonstrations with trapped-ion systems so far have been on a smaller scale, with a few tens of qubits – see, e.g., J. Zhang *et al.*, *Nature* **551**, 601 (2017).

⁹² See the publication *Quantum Computing: Progress and Prospects*, The National Academies Press, 2019.

⁹³ This field was pioneered in the 1970s by S. Wiesner. Its important theoretical aspect (which I, unfortunately, also will not be able to cover) is the distinguishability of different but close quantum states – for example, of an original qubit set, and that slightly corrupted by noise. A good introduction to this topic may be found, for example, in Chapter 9 of the monograph by Nielsen and Chuang, cited above.

⁹⁴ This procedure had been first suggested in 1993 by Charles Henry Bennett, and then repeatedly demonstrated experimentally – see, e.g., L. Steffen *et al.*, *Nature* **500**, 319 (2013), and literature therein.

$$|\alpha\beta\beta'\rangle = (a_0|0\rangle + a_1|1\rangle)|\beta\beta'\rangle = \frac{a_0}{\sqrt{2}}|001\rangle - \frac{a_0}{\sqrt{2}}|010\rangle + \frac{a_1}{\sqrt{2}}|010\rangle - \frac{a_1}{\sqrt{2}}|111\rangle, \quad (8.180a)$$

which may be equivalently rewritten as the following linear superposition,

$$\begin{aligned} |\alpha\beta\beta'\rangle &= \frac{1}{2}|\alpha\beta\rangle_s^+(-a_1|0\rangle + a_0|1\rangle) + \frac{1}{2}|\alpha\beta\rangle_s^- (a_1|0\rangle + a_0|1\rangle) \\ &\quad + \frac{1}{2}|\alpha\beta\rangle_e^+(-a_0|0\rangle + a_1|1\rangle) + \frac{1}{2}|\alpha\beta\rangle_e^- (-a_0|0\rangle - a_1|1\rangle), \end{aligned} \quad (8.180b)$$

of the following four states of the qubit pair $\alpha\beta$:

$$|\alpha\beta\rangle_s^\pm \equiv \frac{1}{\sqrt{2}}(|00\rangle \pm |11\rangle), \quad |\alpha\beta\rangle_e^\pm \equiv \frac{1}{\sqrt{2}}(|01\rangle \pm |10\rangle). \quad (8.181)$$

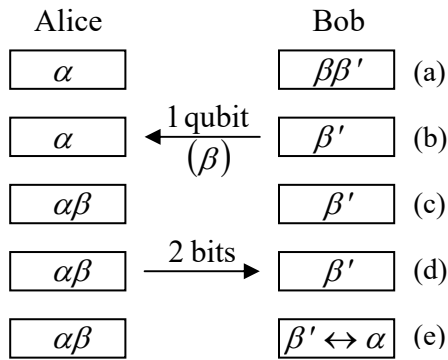


Fig. 8.8. Sequential stages of a “quantum teleportation” procedure: (a) the initial state with entangled qubits β and β' , (b) the back transfer of the qubit β , (c) the measurement of the pair $\alpha\beta$, (d) the forward transfer of two classical bits with the measurement results, and (e) the final state, with the state of the qubit β' mirroring the initial state of the qubit α .

After having received qubit β from Bob, Alice measures which of these four states does the pair $\alpha\beta$ have. This may be achieved, for example, by measurement of one observable represented by the operator $\hat{\sigma}_z^{(\alpha)}\hat{\sigma}_z^{(\beta)}$ and another one corresponding to $\hat{\sigma}_x^{(\alpha)}\hat{\sigma}_x^{(\beta)}$ – cf. Eq. (156). (Since all four states (181) are eigenstates of both these operators, these two measurements do not affect each other and may be performed in any order.) The measured eigenvalue of the former operator enables distinguishing the couples of states (181) with different values of the lower index, while the latter measurement distinguishes the states with different upper indices.

Then Alice reports the measurement result (which may be coded with just two classical bits) to Bob over a classical communication channel. Since the measurement places the pair $\alpha\beta$ *definitely* into the corresponding state, the remaining Bob’s bit β' is now *definitely* in the unentangled single-qubit state that is represented by the corresponding parentheses in Eq. (180b). Note that each of these parentheses contains both coefficients $a_{0,1}$, i.e. the whole information about the initial state that the qubit α had initially. If Bob likes, he may now use appropriate single-qubit operations, similar to those discussed earlier in this section, to move his qubit β' into the state *exactly* similar to the initial state of qubit α . (This fact does not violate the no-cloning theorem (167), because the measurement has already changed the state of α .) This is, of course, a “teleportation” only in a very special sense of this term, but a good example of the importance of qubit entanglement’s preservation at their spatial transfer. For this course, this was also a good primer for the forthcoming discussion of the *EPR paradox* and *Bell’s inequalities* in Chapter 10.

Returning for just a minute to quantum cryptography: since its most common quantum key distribution protocols⁹⁵ require just a few simple quantum gates, whose experimental implementation is not a large technological challenge, the main focus of the current effort is on decreasing the single-photon dephasing in long electromagnetic-wave transmission channels,⁹⁶ with sufficiently high qubit transfer fidelity. The recent progress was rather impressive, with the demonstrated transfer of entangled qubits over landlines longer than 100 km,⁹⁷ and over at least one satellite-based line longer than 1,000 km;⁹⁸ and also the whole quantum key distribution over a comparable distance, though for now at a very low rate yet.⁹⁹ Let me hope that if not the author of this course, then its readers will see this technology used in practical secure telecommunication systems.

8.6. Exercise problems

8.1. Prove that Eq. (30) indeed yields $E_g^{(1)} = (5/4)E_H$.

8.2. For a dilute gas of helium atoms in their ground state, with n atoms per unit volume, calculate its:

- (i) electric susceptibility χ_e , and
- (ii) magnetic susceptibility χ_m ,

and compare the results.

Hint: You may use the model solution of Problems 6.8 and 6.14, and the results of the variational description of the helium atom's ground state in Sec. 2.

8.3. Calculate the expectation values of the following observables: $\mathbf{s}_1 \cdot \mathbf{s}_2$, $S^2 \equiv (\mathbf{s}_1 + \mathbf{s}_2)^2$, and $S_z \equiv s_{1z} + s_{2z}$, for the singlet and triplet states of the system of two spins- $1/2$, defined by Eqs. (18) and (21), directly, without using the general Eq. (48). Compare the results with those for the system of two classical geometric vectors of length $\hbar/2$ each.

8.4. Discuss the factors $\pm 1/\sqrt{2}$ that participate in Eqs. (18) and (20) for the entangled states of the system of two spins- $1/2$, in terms of Clebsch-Gordan coefficients similar to those discussed in Sec. 5.7.

8.5.* Use the perturbation theory to calculate the contribution into the so-called *hyperfine splitting* of the ground energy of the hydrogen atom,¹⁰⁰ due to the interaction between the spins of its nucleus (proton) and electron.

⁹⁵ Two of them are the BB84 suggested in 1984 by C. Bennett and G. Brassard, and the EPRBE suggested in 1991 by A. Ekert. For details, see, e.g., either Sec. 12.6 in the repeatedly cited monograph by Nielsen and Chuang, or the review by N. Gisin *et al.*, *Rev. Mod. Phys.* **74**, 145 (2002).

⁹⁶ For their quantitative discussion see, e.g., EM Sec. 7.8.

⁹⁷ See, e.g., T. Herbst *et al.*, *Proc. Natl. Acad. Sci.* **112**, 14202 (2015), and references therein.

⁹⁸ J. Yin *et al.*, *Science* **356**, 1140 (2017).

⁹⁹ H.-L. Yin *et al.*, *Phys. Rev. Lett.* **117**, 190501 (2016).

¹⁰⁰ This effect was discovered experimentally by A. Michelson in 1881 and explained theoretically by W. Pauli in 1924.

Hint: The proton's magnetic moment operator is described by the same Eq. (4.115) as the electron, but with a positive gyromagnetic factor $\gamma_p = g_p e / 2m_p \approx 2.675 \times 10^8 \text{ s}^{-1}\text{T}^{-1}$, whose magnitude is much smaller than that of the electron ($|\gamma_e| \approx 1.761 \times 10^{11} \text{ s}^{-1}\text{T}^{-1}$), due to the much higher mass, $m_p \approx 1.673 \times 10^{-27} \text{ kg} \approx 1,835 m_e$. (The *g*-factor of the proton is also different, $g_p \approx 5.586$.¹⁰¹)

8.6. In the simple case of just two similar spin-interacting particles, distinguishable by their spatial location, the famous *Heisenberg model* of ferromagnetism¹⁰² is reduced to the following Hamiltonian:

$$H = -J \hat{\mathbf{s}}_1 \cdot \hat{\mathbf{s}}_2 - \gamma \mathcal{B} \cdot (\hat{\mathbf{s}}_1 + \hat{\mathbf{s}}_2),$$

where J is the spin interaction constant, γ is the gyromagnetic ratio of each particle, and \mathcal{B} is the external magnetic field. Find the stationary states and energies of this system for spin- $\frac{1}{2}$ particles.

8.7. Two particles, both with spin- $\frac{1}{2}$ but different gyromagnetic ratios γ_1 and γ_2 , are placed to external magnetic field \mathcal{B} . In addition, their spins interact as in the Heisenberg model:

$$\hat{H}_{\text{int}} = -J \hat{\mathbf{s}}_1 \cdot \hat{\mathbf{s}}_2.$$

Find the eigenstates and eigenenergies of the system.

8.8. Two similar spin- $\frac{1}{2}$ particles, with gyromagnetic ratio γ , localized at two points separated by distance a , interact via the field of their magnetic dipole moments. Calculate stationary states and energies of the system.

8.9. Consider the permutation of two identical particles, each of spin s . How many different symmetric and antisymmetric spin states can the system have?

8.10. For a system of two identical particles with $s = 1$:

- (i) List all spin states forming the uncoupled-representation basis.
- (ii) List all possible pairs $\{S, M_S\}$ of the quantum numbers describing the states of the coupled-representation basis – see Eq. (48).
- (iii) Which of the $\{S, M_S\}$ pairs describe the states symmetric, and which the states antisymmetric, with respect to the particle permutation?

8.11. Represent the operators of the total kinetic energy and the total orbital angular momentum of a system of two particles, with masses m_1 and m_2 , as combinations of terms describing the center-of-mass motion and the relative motion. Use the results to calculate the energy spectrum of the so-called

¹⁰¹ The anomalously large value of the proton's *g*-factor results from the composite quark-gluon structure of this particle. (An exact calculation of g_p remains a challenge for quantum chromodynamics.)

¹⁰² It was suggested in 1926, independently by W. Heisenberg and P. Dirac. A discussion of thermal motion effects on this and other similar systems (especially the Ising model of ferromagnetism) may be found in SM Chapter 4.

positronium – a metastable “atom”¹⁰³ consisting of one electron and its positively charged antiparticle, the positron.

8.12. Two particles with similar masses m and charges q are free to move along a round, plane ring of radius R . In the limit of strong Coulomb interaction of the particles, find the lowest eigenenergies of the system, and sketch the system of its energy levels. Discuss possible effects of particle indistinguishability.

8.13. Low-energy spectra of many diatomic molecules may be well described by modeling the molecule as a system of two particles connected with a light and elastic, but very stiff spring. Calculate the energy spectrum of a molecule within this model. Discuss possible effects of nuclear spins on spectra of the so-called *homonuclear* diatomic molecules, formed by two similar atoms.

8.14. Two indistinguishable spin- $\frac{1}{2}$ particles are attracting each other at contact:

$$U(x_1, x_2) = -w\delta(x_1 - x_2), \quad \text{with } w > 0,$$

but are otherwise free to move along the x -axis. Find the energy and the orbital wavefunction of the ground state of the system.

8.15. Calculate the energy spectrum of the system of two identical spin- $\frac{1}{2}$ particles, moving along the x -axis, which is described by the following Hamiltonian:

$$\hat{H} = \frac{\hat{p}_1^2}{2m_0} + \frac{\hat{p}_2^2}{2m_0} + \frac{m_0\omega_0^2}{2}(x_1^2 + x_2^2 + \alpha x_1 x_2),$$

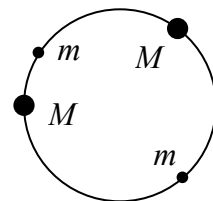
and the degeneracy of each energy level.

8.16.* Two indistinguishable spin- $\frac{1}{2}$ particles are confined to move around a circle of radius R , and interact only at a very short arc distance $l = R\varphi \equiv R(\varphi_1 - \varphi_2)$ between them, so that the interaction potential U may be well approximated with a delta function of φ . Find the ground state and its energy, for the following two cases:

- (i) the “orbital” (spin-independent) repulsion: $\hat{U} = w\delta(\varphi)$,
- (ii) the spin-spin interaction: $\hat{U} = -w\hat{\mathbf{s}}_1 \cdot \hat{\mathbf{s}}_2\delta(\varphi)$,

both with constant $w > 0$. Analyze the trends of your results in the limits $w \rightarrow 0$ and $w \rightarrow \infty$.

8.17. Two particles of mass M , separated by two much lighter particles of mass $m \ll M$, are placed on a ring of radius R – see the figure on the right. The particles strongly repulse at contact, but otherwise, each of them is free to move along the ring. Calculate the lower part of the energy spectrum of the system.



¹⁰³ Its lifetime (either 0.124 ns or 138 ns, depending on the parallel or antiparallel configuration of the component spins), is limited by the weak interaction of its components, which causes their annihilation with the emission of several gamma-ray photons.

8.18. N indistinguishable spin- $\frac{1}{2}$ particles move in a spherically-symmetric quadratic potential $U(\mathbf{r}) = m\omega_0^2 r^2/2$. Neglecting the direct interaction of the particles, find the ground-state energy of the system.

8.19. Use the Hund rules to find the values of the quantum numbers L , S , and J in the ground states of the atoms of carbon and nitrogen. Write down the Russell-Saunders symbols for these states.

8.20. $N \gg 1$ indistinguishable, non-interacting quantum particles are placed in a hard-wall, rectangular box with sides a_x , a_y , and a_z . Calculate the ground-state energy of the system, and the average forces it exerts on each face of the box. Can we characterize the forces by certain pressure P ?

Hint: Consider separately the cases of bosons and fermions.

8.21.* Explore the *Thomas-Fermi model*¹⁰⁴ of a heavy atom, with the nuclear charge $Q = Ze \gg e$, in which the interaction between electrons is limited to their contribution to the common electrostatic potential $\phi(\mathbf{r})$. In particular, derive the ordinary differential equation obeyed by the radial distribution of the potential, and use it to estimate the effective radius of the atom.

8.22.* Use the Thomas-Fermi model, explored in the previous problem, to calculate the total binding energy of a heavy atom. Compare the result with that for the simpler model, in that the Coulomb electron-electron interaction is completely ignored.

8.23. A system of three similar spin- $\frac{1}{2}$ particles is described by the Heisenberg Hamiltonian (cf. Problems 6 and 7):

$$\hat{H} = -J(\hat{\mathbf{s}}_1 \cdot \hat{\mathbf{s}}_2 + \hat{\mathbf{s}}_2 \cdot \hat{\mathbf{s}}_3 + \hat{\mathbf{s}}_3 \cdot \hat{\mathbf{s}}_1),$$

where J is the spin interaction constant. Find the stationary states and energies of this system, and give an interpretation of your results.

8.24. For a system of three spins- $\frac{1}{2}$, find the common eigenstates and eigenvalues of the operators \hat{S}_z and \hat{S}^2 , where

$$\hat{\mathbf{S}} \equiv \hat{\mathbf{s}}_1 + \hat{\mathbf{s}}_2 + \hat{\mathbf{s}}_3$$

is the vector operator of the total spin of the system. Do the corresponding quantum numbers S and M_S obey Eqs. (48)?

8.25. Explore basic properties of the Heisenberg model (which was the subject of Problems 6, 7, and 23), for a 1D chain of N spins- $\frac{1}{2}$:

$$\hat{H} = -J \sum_{\{j,j'\}} \hat{\mathbf{s}}_j \cdot \hat{\mathbf{s}}_{j'} - \gamma \mathcal{B} \cdot \sum_j \hat{\mathbf{s}}_j, \quad \text{with } J > 0,$$

where the summation is over all N spins, with the symbol $\{j,j'\}$ meaning that the first sum is only over the adjacent spin pairs. In particular, find the ground state of the system and its lowest excited states in the absence of external magnetic field \mathcal{B} , and also the dependence of their energies on the field.

¹⁰⁴ It was suggested in 1927, independently, by L. Thomas and E. Fermi.

Hint: For the sake of simplicity, you may assume that the first sum includes the term $\hat{\mathbf{s}}_N \cdot \hat{\mathbf{s}}_1$ as well. (Physically, this means that the chain is bent into a closed loop.¹⁰⁵)

8.26. Compose the simplest model Hamiltonians, in terms of the second quantization formalism, for systems of indistinguishable particles moving in the following external potentials:

- (i) two weakly coupled potential wells, with on-site particle interactions (giving additional energy J per each pair of particles in the same potential well), and
- (ii) a periodic 1D potential, with the same particle interactions, in the tight-binding limit.

8.27. For each of the Hamiltonians composed in the previous problem, derive the Heisenberg equations of motion for particle creation/annihilation operators:

- (i) for bosons, and
- (ii) for fermions.

8.28. Express the ket-vectors of all possible Dirac states for the system of three indistinguishable

- (i) bosons, and
- (ii) fermions,

via those of the single-particle states β , β' , and β'' they occupy.

8.29. Explain why the general perturbative result (8.126), when applied to the ${}^4\text{He}$ atom, gives the correct¹⁰⁶ expression (8.29) for the ground singlet state, and correct Eqs. (8.39)-(8.42) (with the minus sign in the first of these relations) for the excited triplet states, but cannot describe these results, with the plus sign in Eq. (8.39), for the excited singlet state.

8.30. For a system of two distinct qubits (i.e. two-level systems), introduce a reasonable uncoupled-representation z -basis, and write in this basis the 4×4 matrix of the operator that swaps their states.

8.31. Find a time-independent Hamiltonian that can cause the qubit evolution described by Eqs. (155). Discuss the relation between your result and the time-dependent Hamiltonian (6.86).

¹⁰⁵ Note that for dissipative spin systems, differences between low-energy excitations of open-end and closed-end 1D chains may be substantial even in the limit $N \rightarrow \infty$ – see, e.g., SM Sec. 4.5. However, for our Hamiltonian (and hence dissipation-free) system, the differences are relatively small.

¹⁰⁶ Correct in the sense of the first order of the perturbation theory.

Chapter 9. Introduction to Relativistic Quantum Mechanics

The brief introduction to relativistic quantum mechanics, presented in this chapter, consists of two very different parts. Its first part is a discussion of the basic elements of the quantum theory of the electromagnetic field (usually called quantum electrodynamics, QED), including the field quantization scheme, photon statistics, radiative atomic transitions, the spontaneous and stimulated radiation, and so-called cavity QED. We will see, in particular, that the QED may be considered as the relativistic quantum theory of particles with zero rest mass – photons. The second part of the chapter is a brief review of the relativistic quantum theory of particles with non-zero rest mass, including the Dirac theory of spin-½ particles. These theories mark the point of entry into a more complete relativistic quantum theory – the quantum field theory – which is beyond the scope of this course.¹

9.1. Electromagnetic field quantization²

Classical physics gives us³ the following general relativistic relation between the momentum \mathbf{p} and energy E of a free particle with rest mass m , which may be simplified in two limits – non-relativistic and ultra-relativistic:

$$E = \left[(pc)^2 + (mc^2)^2 \right]^{1/2} \rightarrow \begin{cases} mc^2 + p^2 / 2m, & \text{for } p \ll mc, \\ pc, & \text{for } p \gg mc. \end{cases} \quad (9.1)$$

Free
particle's
relativistic
energy

In both limits, the transfer from classical to quantum mechanics is easier than in the arbitrary case. Since all the previous part of this course was committed to the first, non-relativistic limit, I will now jump to a brief discussion of the ultra-relativistic limit $p \gg mc$, for a particular but very important system – the electromagnetic field. Since the excitations of this field, called *photons*, are currently believed to have zero rest mass m ,⁴ the ultra-relativistic relation $E = pc$ is exactly valid for any photon energy E , and the quantization scheme is rather straightforward.

As usual, the quantization has to be based on the classical theory of the system – in this case, the Maxwell equations. As the simplest case, let us consider the electromagnetic field inside a finite free-space volume limited by ideal walls, which reflect incident waves perfectly.⁵ Inside the volume, the Maxwell equations give a simple wave equation⁶ for the electric field

$$\nabla^2 \mathcal{E} - \frac{1}{c^2} \frac{\partial^2 \mathcal{E}}{\partial t^2} = 0, \quad (9.2)$$

¹ Note that some material covered in this chapter is frequently taught as a part of the quantum field theory. I will focus on the most important results that may be obtained without starting the heavy engines of that theory.

² The described approach was pioneered by the same P. A. M. Dirac as early as 1927.

³ See, e.g., EM Chapter 9.

⁴ By now this fact has been verified experimentally with an accuracy of at least $\sim 10^{-22} m_e$ – see S. Eidelman *et al.*, *Phys. Lett. B* **592**, 1 (2004).

⁵ In the case of finite energy absorption in the walls, or in the wave propagation media (say, described by complex constants ϵ and μ), the system is not energy-conserving (Hamiltonian), i.e. interacts with some dissipative environment. Specific cases of such interaction will be considered in Sections 2 and 3 below.

⁶ See, e.g., EM Eq. (7.3), for the particular case $\epsilon = \epsilon_0$, $\mu = \mu_0$, so that $v^2 \equiv 1/\epsilon\mu = 1/\epsilon_0\mu_0 \equiv c^2$.

and an absolutely similar equation for the magnetic field \mathcal{B} . We may look for the general solution of Eq. (2) in the variable-separating form

$$\mathcal{E}(\mathbf{r}, t) = \sum_j p_j(t) \mathbf{e}_j(\mathbf{r}). \quad (9.3)$$

Physically, each term of this sum is a standing wave whose spatial distribution and polarization (“mode”) are described by the vector function $\mathbf{e}_j(\mathbf{r})$, while the temporal dynamics, by the function $p_j(t)$. Plugging an arbitrary term of this sum into Eq. (2), and separating the variables exactly as we did, for example, in the Schrödinger equation in Sec. 1.5, we get

$$\frac{\nabla^2 \mathbf{e}_j}{\mathbf{e}_j} = \frac{1}{c^2} \frac{\ddot{p}_j}{p_j} = \text{const} \equiv -k_j^2, \quad (9.4)$$

so that the spatial distribution of the mode satisfies the 3D Helmholtz equation:

$$\boxed{\nabla^2 \mathbf{e}_j + k_j^2 \mathbf{e}_j = 0.} \quad (9.5)$$

Equation
for spatial
distribution

The set of solutions of this equation, with appropriate boundary conditions, determines the set of the functions \mathbf{e}_j , and simultaneously the spectrum of the wave number magnitudes k_j . The latter values determine the mode eigenfrequencies, following from Eq. (4):

$$\ddot{p}_j + \omega_j^2 p_j = 0, \quad \text{with } \omega_j \equiv k_j c. \quad (9.6)$$

There is a big philosophical difference between the quantum-mechanical approach to Eqs. (5) and (6), despite their single origin (4). The first (Helmholtz) equation may be rather difficult to solve in realistic geometries,⁷ but it remains intact in the basic quantum electrodynamics, with the scalar components of the vector functions $\mathbf{e}_j(\mathbf{r})$ still treated (at each point \mathbf{r}) as c -numbers. In contrast, the classical Eq. (6) is readily solvable (giving sinusoidal oscillations with frequency ω_j), but this is exactly where we can make the transfer to quantum mechanics, because we already know how to quantize a mechanical 1D harmonic oscillator, which in classics obeys the same equation.

As usual, we need to start with the appropriate Hamiltonian – the operator corresponding to the classical Hamiltonian function H of the proper set of generalized coordinates and momenta. The electromagnetic field’s Hamiltonian function (which in this case coincides with the field’s energy) is⁸

$$H = \int d^3 r \left(\frac{\epsilon_0 \mathcal{E}^2}{2} + \frac{\mathcal{B}^2}{2\mu_0} \right). \quad (9.7)$$

Let us represent the magnetic field in a form similar to Eq. (3),⁹

⁷ See, e.g., various problems discussed in EM Chapter 7, especially in Sec. 7.9.

⁸ See, e.g., EM Sec. 9.8, in particular, Eq. (9.225). Here I am using SI units, with $\epsilon_0 \mu_0 \equiv c^2$; in the Gaussian units, the coefficients ϵ_0 and μ_0 disappear, but there is an additional common factor $1/4\pi$ in the equation for energy. However, if we modify the normalization conditions (see below) accordingly, all the subsequent results, starting from Eq. (10), look similar in any system of units.

⁹ Here I am using the letter q_j instead of x_j , for the generalized coordinate of the field oscillator, in order to emphasize the difference between the former variable, and one of the Cartesian coordinates, i.e. one of the arguments of the c -number functions \mathbf{e} and \mathbf{b} .

$$\mathcal{B}(\mathbf{r}, t) = -\sum_j \omega_j q_j(t) \mathbf{b}_j(\mathbf{r}). \quad (9.8)$$

Since, according to the Maxwell equations, in our case the magnetic field satisfies the equation similar to Eq. (2), the time-dependent amplitude q_j of each of its modes $\mathbf{b}_j(\mathbf{r})$ obeys an equation similar to Eq. (6), i.e. in the classical theory also changes in time sinusoidally, with the same frequency ω_j . Plugging Eqs. (3) and (8) into Eq. (7), we may recast it as

$$H = \sum_j \left[\frac{p_j^2}{2} \int \epsilon_0 e_j^2(\mathbf{r}) d^3 r + \frac{\omega_j^2 q_j^2}{2} \int \frac{1}{\mu_0} b_j^2(\mathbf{r}) d^3 r \right]. \quad (9.9)$$

Since the distribution of constant factors between two multiplication operands in each term of Eq. (3) is so far arbitrary, we may fix it by requiring the first integral in Eq. (9) to equal 1. It is straightforward to check that according to the Maxwell equations, which give a specific relation between vectors \mathcal{E} and \mathcal{B} ,¹⁰ this normalization makes the second integral in Eq. (9) equal 1 as well, and Eq. (9) becomes

$$H = \sum_j H_j, \quad H_j = \frac{p_j^2}{2} + \frac{\omega_j^2 q_j^2}{2}. \quad (9.10a)$$

Note that that p_j is the legitimate generalized momentum corresponding to the generalized coordinate q_j , because it is equal to $\partial L / \partial \dot{q}_j$, where L is the Lagrangian function of the field – see EM Eq. (9.217):

$$L = \int d^3 r \left(\frac{\epsilon_0 \mathcal{E}^2}{2} - \frac{\mathcal{B}^2}{2 \mu_0} \right) = \sum_j L_j, \quad L_j = \frac{p_j^2}{2} - \frac{\omega_j^2 q_j^2}{2}. \quad (9.10b)$$

Hence we can carry out the standard quantization procedure, namely declare H_j , p_j , and q_j the quantum-mechanical operators related exactly as in Eq. (10a),

$$\hat{H}_j = \frac{\hat{p}_j^2}{2} + \frac{\omega_j^2 \hat{q}_j^2}{2}. \quad (9.11)$$

Electro-
magnetic
mode's
Hamiltonian

We see that this Hamiltonian coincides with that of a 1D harmonic oscillator with the mass m_j formally equal to 1,¹¹ and the eigenfrequency equal to ω_j . However, in order to use Eq. (11) in the general Eq. (4.199) for the time evolution of Heisenberg-picture operators \hat{p}_j and \hat{q}_j , we need to know the commutation relation between these operators. To find them, let us calculate the Poisson bracket (4.204) for the functions $A = q_{j'}$ and $B = p_{j''}$, taking into account that in the classical Hamiltonian mechanics, all generalized coordinates q_j and the corresponding momenta p_j have to be considered independent arguments of H , only one term (with $j = j' = j''$) in only one of the sums (12) (namely, with $j' = j''$), gives a non-zero value (-1), so that

$$\{q_{j'}, p_{j''}\}_P \equiv \sum_j \left(\frac{\partial q_{j'}}{\partial p_j} \frac{\partial p_{j''}}{\partial q_j} - \frac{\partial q_{j'}}{\partial q_j} \frac{\partial p_{j''}}{\partial p_j} \right) = -\delta_{jj''}. \quad (9.12)$$

Hence, according to the general quantization rule (4.205), the commutation relation of the operators corresponding to $q_{j'}$ and $p_{j''}$ is

¹⁰ See, e.g., EM Eq. (7.6).

¹¹ Selecting a different normalization of the functions $\mathbf{e}_j(\mathbf{r})$ and $\mathbf{b}_j(\mathbf{r})$, we could readily arrange any value of m_j , and the choice corresponding to $m_j = 1$ is the best one just for the notation simplicity.

$$[\hat{q}_{j'}, \hat{p}_{j''}] = i\hbar\delta_{jj''}, \quad (9.13)$$

i.e. is exactly the same as for the usual Cartesian components of the radius-vector and momentum of a mechanical particle – see Eq. (2.14).

As the reader already knows, Eqs. (11) and (13) open for us several alternative ways to proceed:

(i) Use the Schrödinger-picture wave mechanics based on wavefunctions $\Psi_j(q_j, t)$. As we know from Sec. 2.9, this way is inconvenient for most tasks, because the eigenfunctions of the harmonic oscillator are rather clumsy.

(ii) A substantially better way (for the harmonic oscillator case) is to write the equations of the time evolution of the operators $\hat{q}_j(t)$ and $\hat{p}_j(t)$ in the Heisenberg picture of quantum dynamics.

(iii) An even more convenient approach is to use equations similar to Eqs. (5.65) to decompose the Heisenberg operators $\hat{q}_j(t)$ and $\hat{p}_j(t)$ into the creation-annihilation operators $\hat{a}_j^\dagger(t)$ and $\hat{a}_j(t)$, and work with these operators.

In this chapter, I will mostly use the last route. Replacing m with $m_j \equiv 1$, and ω_0 with ω_j , the last forms of Eqs. (5.65) become

$$\hat{a}_j = \left(\frac{\omega_j}{2\hbar} \right)^{1/2} \left(\hat{q}_j + i \frac{\hat{p}_j}{\omega_j} \right), \quad \hat{a}_j^\dagger = \left(\frac{\omega_j}{2\hbar} \right)^{1/2} \left(\hat{q}_j - i \frac{\hat{p}_j}{\omega_j} \right). \quad (9.14)$$

Due to Eq. (13), the creation-annihilation operators obey the commutation similar to Eq. (5.68),

$$[\hat{a}_j, \hat{a}_{j'}^\dagger] = \hat{I}\delta_{jj'}. \quad (9.15)$$

As a result, according to Eqs. (3) and (8), the quantum-mechanical operators of the electric and magnetic fields are sums over all *field oscillators*:

$$\hat{\mathcal{E}}(\mathbf{r}, t) = i \sum_j \left(\frac{\hbar\omega_j}{2} \right)^{1/2} \mathbf{e}_j(\mathbf{r}) \left(\hat{a}_j^\dagger - \hat{a}_j \right), \quad (9.16a)$$

$$\hat{\mathcal{B}}(\mathbf{r}, t) = \sum_j \left(\frac{\hbar\omega_j}{2} \right)^{1/2} \mathbf{b}_j(\mathbf{r}) \left(\hat{a}_j^\dagger + \hat{a}_j \right), \quad (9.16b)$$

Electro-magnetic fields' operators

and Eq. (11) for the j^{th} mode's Hamiltonian becomes

$$\hat{H}_j = \hbar\omega_j \left(\hat{a}_j^\dagger \hat{a}_j + \frac{1}{2} \hat{I} \right) = \hbar\omega_j \left(\hat{n}_j + \frac{1}{2} \hat{I} \right), \quad \text{with } \hat{n}_j \equiv \hat{a}_j^\dagger \hat{a}_j, \quad (9.17)$$

absolutely similar to Eq. (5.72) for a mechanical oscillator.

Now comes a very important conceptual step. From Sec. 5.4 we know that the eigenfunctions (Fock states) n_j of the Hamiltonian (17) have energies

$$E_j = \hbar\omega_j \left(n_j + \frac{1}{2} \right), \quad n_j = 0, 1, 2, \dots \quad (9.18)$$

Electro-magnetic mode's eigen-energies

and, according to Eq. (5.89), the operators \hat{a}_j^\dagger and \hat{a}_j act on the eigenkets of these partial states as

$$\hat{a}_j |n_j\rangle = (n_j)^{1/2} |n_j - 1\rangle, \quad \hat{a}_j^\dagger |n_j\rangle = (n_j + 1)^{1/2} |n_j + 1\rangle, \quad (9.19)$$

regardless of the quantum states of other modes. These rules coincide with the definitions (8.64) and (8.68) of bosonic creation-annihilation operators, and hence their action may be considered as the creation/annihilation of certain bosons. Such a “particle” (actually, an *excitation*, with energy $\hbar\omega_j$, of an electromagnetic field oscillator) is exactly what is, strictly speaking, called a *photon*. Note immediately that according to Eq. (16), such an excitation does not change the spatial distribution of the j^{th} mode of the field. So, such a “global” photon is an excitation created simultaneously at all points of the field confinement region.

If this picture is too contrary to the intuitive image of a particle, please recall that in Chapter 2, we discussed a similar situation with the fundamental solutions of the Schrödinger equation of a free non-relativistic particle: they represent sinusoidal de Broglie waves existing simultaneously in all points of the particle confinement region. The (partial :-) reconciliation with the classical picture of a moving particle might be obtained by using the linear superposition principle to assemble a quasi-localized wave packet, as a group of sinusoidal waves with close wave numbers. Very similarly, we may form a similar wave packet using a linear superposition of the “global” photons with close values of \mathbf{k}_j (and hence ω_j), to form a quasi-localized photon. An additional simplification here is that the dispersion relation for electromagnetic waves (at least in free space) is linear:

$$\frac{\partial\omega_j}{\partial k_j} = c = \text{const}, \quad \text{i.e. } \frac{\partial^2\omega_j}{\partial k_j^2} = 0, \quad (9.20)$$

so that, according to Eq. (2.39a), the electromagnetic wave packets (i.e. space-localized photons) do not spread out during their propagation. Note also that due to the fundamental classical relations $\mathbf{p} = \mathbf{n}E/c$ for the linear momentum of the traveling electromagnetic wave packet of energy E , propagating along the direction $\mathbf{n} \equiv \mathbf{k}/k$, and $\mathbf{L} = \pm\mathbf{n}E/\omega_j$ for its angular momentum,¹² such photon may be prescribed the linear momentum $\mathbf{p} = \mathbf{n}\hbar\omega_j/c \equiv \hbar\mathbf{k}$ and the angular momentum $\mathbf{L} = \pm\mathbf{n}\hbar$, with the sign depending on the direction of its circular polarization (“helicity”).

This electromagnetic field quantization scheme should look very straightforward, but it raises an important conceptual issue of the ground state energy. Indeed, Eq. (18) implies that the total ground-state (i.e., the lowest) energy of the field is

$$E_g = \sum_j (E_g)_j = \sum_j \frac{\hbar\omega_j}{2}. \quad (9.21)$$

Ground-state energy of EM field

Since for any realistic model of the field-confining volume, either infinite or not, the density of electromagnetic field modes only grows with frequency,¹³ this sum diverges on its upper limit, leading to infinite ground-state energy per unit volume. This infinite-energy paradox cannot be dismissed by declaring the ground-state energy of field oscillators unobservable, because this would contradict numerous experimental observations – starting perhaps from the famous *Casimir effect*.¹⁴ The

¹² See, e.g., EM Sections 7.7 and 9.8.

¹³ See, e.g., Eq. (1.1), which is similar to Eq. (1.90) for the de Broglie waves, derived in Sec. 1.7.

¹⁴ This effect was predicted in 1948 by Hendrik Casimir and Dirk Polder, and confirmed semi-quantitatively in experiments by M. Spaarnay, *Nature* **180**, 334 (1957). After this, and several other experiments, a decisive error bar reduction (to about $\sim 5\%$), providing a quantitative confirmation of the Casimir formula (23), was achieved by

conceptually simplest implementation of this effect involves two parallel, perfectly conducting plates of area A , separated by a vacuum gap of thickness $t \ll A^{1/2}$ (Fig. 1).



Fig. 9.1. The simplest geometry of the Casimir effect manifestation.

Rather counter-intuitively, the plates attract each other with a force F proportional to the area A and rapidly increasing with the decrease of t , even in the absence of any explicit electromagnetic field sources. The effect's explanation is that the energy of each electromagnetic field mode, including its ground-state energy, exerts average pressure,

$$\langle \mathcal{P}_j \rangle = -\frac{\partial E_j}{\partial V}, \quad (9.22)$$

on the walls constraining it to volume V . While the field's pressure on the external surfaces on the plates is due to the contributions (22) of all free-space modes, with arbitrary values of k_z (the z -component of the wave vector \mathbf{k}_j), in the gap between the plates the spectrum of k_z is limited to the multiples of π/t , so that the pressure on the internal surfaces is lower. This is why the net force exerted on the plates may be calculated as the sum of the contributions (22) from all "missing" low-frequency modes in the gap, with the minus sign. In the simplest model when the plates are made of an ideal conductor, which provides boundary conditions $\mathcal{E}_\tau = \mathcal{B}_n = 0$ on their surfaces,¹⁵ such calculation is quite straightforward (and is hence left for the reader's exercise), and its result is

$$F = -\frac{\pi^2 A \hbar c}{240 t^4}. \quad (9.23)$$

Casimir
effect

Note that for such calculation, the high-frequency divergence of Eq. (21) is not important, because it participates in the forces exerted on all surfaces of each plate, and cancels out from the net pressure. In this way, the Casimir effect not only confirms Eq. (21), but also teaches us an important lesson on how to deal with the divergences of such sums at $\omega_j \rightarrow \infty$. The lesson is: just get accustomed to the idea that the divergence exists, and ignore this fact while you can, i.e. if the final result you are interested in is finite. However, for some more complex problems of quantum electrodynamics (and the

S. Lamoreaux, *Phys. Rev. Lett.* **78**, 5 (1997) and by U. Mohideen and A. Roy, *Phys. Rev. Lett.* **81**, 004549 (1998). Note also that there are other experimental confirmations of the reality of the ground-state electromagnetic field, including, for example, the experiments by R. Koch *et al.* already discussed in Sec. 7.5, and the recent spectacular direct observations by C. Riek *et al.*, *Science* **350**, 420 (2015).

¹⁵ For realistic conductors, the reduction of t below $\sim 1 \mu\text{m}$ causes significant deviations from this simple model, and hence from Eq. (23). The reason is that for gaps so narrow, the depth of field penetration into the conductors (see, e.g., EM Sec. 6.2), at the important frequencies $\omega \sim c/t$, becomes comparable with t , and an adequate theory of the Casimir effect has to involve a certain model of the penetration. (It is curious that in-depth analyses of this problem, pioneered in 1956 by E. Lifshitz, have revealed a deep relation between the Casimir effect and the London dispersion force which was the subject of Problems 3.16, 5.15, and 6.18 – for a review see, e.g., either I. Dzhalyoshinskii *et al.*, *Sov. Phys. Uspekhi* **4**, 153 (1961), or K. Milton, *The Casimir Effect*, World Scientific, 2001. Recent experiments in the $100 \text{ nm} - 2 \mu\text{m}$ range of t , with an accuracy better than 1%, have allowed not only to observe the effects of field penetration on the Casimir force, but even to make a selection between some approximate models of the penetration – see D. Garcia-Sanchez *et al.*, *Phys. Rev. Lett.* **109**, 027202 (2012)).

quantum theory of any other fields), this simplest approach becomes impossible, and then more complex, *renormalization* techniques become necessary. For their study, I have to refer the reader to a quantum field theory course – see the references at the end of this chapter.

9.2. Photon absorption and counting

As a matter of principle, the Casimir effect may be used to measure quantum effects in not only the free-space electromagnetic field but also that the field arriving from active sources – lasers, etc. However, usually such studies may be done by simpler detectors, in which the absorption of a photon by a single atom leads to its ionization. This ionization, i.e. the emission of a free electron, triggers an avalanche reaction (e.g., an electric discharge in a Geiger-type counter), which may be readily registered using appropriate electronic circuitry. In good photon counters, the first step, the “trigger” atom ionization, is the bottleneck of the whole process (the *photon count*), so that to analyze their statistics, it is sufficient to consider the field’s interaction with just this atom.

Its ionization is a quantum transition from a discrete initial state of the atom to its final, ionized state with a continuous energy spectrum, induced by an external electromagnetic field. This is exactly the situation shown in Fig. 6.12, so we may apply to it the Golden Rule of quantum mechanics in the form (6.149), with the system *a* associated with the electromagnetic field, and system *b* with the trigger atom. The atom’s size is typically much smaller than the radiation wavelength, so that the field-atom interaction may be adequately described in the electric dipole approximation (6.146)

$$\hat{H}_{\text{int}} = -\hat{\mathcal{E}} \cdot \hat{\mathbf{d}}, \quad (9.24)$$

where $\hat{\mathbf{d}}$ is the dipole moment’s operator. Hence we may associate this operator with the operand \hat{B} in Eqs. (6.145)-(6.149), while the electric field operator $\hat{\mathcal{E}}$ is associated with the operand \hat{A} in those relations. First, let us assume that our field consists of only one mode $\mathbf{e}_j(\mathbf{r})$ of frequency ω . Then we can keep only one term in the sum (16a), and drop the index *j*, so that Eq. (6.149) may be rewritten as

$$\begin{aligned} \Gamma &= \frac{2\pi}{\hbar} \left| \langle \text{fin} | \hat{\mathcal{E}}(\mathbf{r}, t) | \text{ini} \rangle \right|^2 \left| \langle \text{fin} | \hat{\mathbf{d}}(t) \cdot \mathbf{n}_e | \text{ini} \rangle \right|^2 \rho_a \\ &= \frac{2\pi}{\hbar} \frac{\hbar\omega}{2} \left| \langle \text{fin} | [\hat{a}^\dagger(t) - \hat{a}(t)] \mathbf{e}(\mathbf{r}) | \text{ini} \rangle \right|^2 \left| \langle \text{fin} | \hat{\mathbf{d}}(t) \cdot \mathbf{n}_e | \text{ini} \rangle \right|^2 \rho_a, \end{aligned} \quad (9.25)$$

where $\mathbf{n}_e \equiv \mathbf{e}(\mathbf{r})/e(\mathbf{r})$ is the local direction of the vector $\mathbf{e}(\mathbf{r})$, symbols “ini” and “fin” denote the initial and final states of the corresponding system (the electromagnetic field in the first long bracket, and the atom in the second bracket), and the density ρ_a of the continuous atomic states should be calculated at its final energy $E_{\text{fin}} = E_{\text{ini}} + \hbar\omega$.

As a reminder, in the Heisenberg picture of quantum dynamics, the initial and final states are time-independent, while the creation-annihilation operators are functions of time. In the Golden Rule formula (25), as in any perturbative result, this time dependence has to be calculated ignoring the perturbation – in this case, the field-atom interaction. For the field’s creation-annihilation operators, this dependence coincides with that of the usual 1D oscillator – see Eq. (5.141), in which ω_0 should be, in our current notation, replaced with ω :

$$\hat{a}(t) = \hat{a}(0)e^{-i\omega t}, \quad \hat{a}^\dagger(t) = \hat{a}^\dagger(0)e^{+i\omega t}. \quad (9.26)$$

Hence Eq. (25) becomes

$$\Gamma = \pi\omega \left| \left\langle \text{fin} \left[\hat{a}^\dagger(0)e^{i\omega t} - \hat{a}(0)e^{-i\omega t} \right] e(\mathbf{r}) \right| \text{ini} \right\rangle^2 \left| \left\langle \text{fin} |\hat{\mathbf{d}}(t) \cdot \mathbf{n}_e| \right| \text{ini} \right\rangle^2 \rho_a. \quad (9.27a)$$

Now let us multiply the first long bracket by $\exp\{i\omega t\}$, and the second one by $\exp\{-i\omega t\}$:

$$\Gamma = \pi\omega \left| \left\langle \text{fin} \left[\hat{a}^\dagger(0)e^{2i\omega t} - \hat{a}(0) \right] e(\mathbf{r}) \right| \text{ini} \right\rangle^2 \left| \left\langle \text{fin} |\hat{\mathbf{d}}(t) \cdot \mathbf{n}_e e^{-i\omega t}| \right| \text{ini} \right\rangle^2 \rho_a. \quad (9.27b)$$

This, mathematically equivalent form of the previous relation shows more clearly that at resonant photon absorption, only the *annihilation* operator gives a significant time-averaged contribution to the first bracket matrix element. (As a reminder, the quantum-mechanical Golden Rule for time-dependent perturbations is a result of averaging over a time interval much larger than $1/\omega$ – see Sec. 6.6.) Similarly, according to Eq. (4.199), the Heisenberg operator of the dipole moment, corresponding to the *increase* of atom's energy by $\hbar\omega$, has the Fourier components that differ in frequency from ω only by $\sim\Gamma \ll \omega$, so that its time dependence virtually compensates the additional factor in the second bracket of Eq. (27b), and this bracket also may have a substantial time average. Hence, in the first bracket we may neglect the fast-oscillating term, whose average over time interval $\sim 1/\Gamma$ is very close to zero.¹⁶

Now let us assume, first, that we use the same detector, characterized by the same matrix element of the quantum transition, i.e. the same second bracket in Eq. (27), and the same final state density ρ_a , for measurement of various electromagnetic fields – or just of the same field at different points \mathbf{r} . Then we are only interested in the behavior of the first, field-related bracket, and may write

$$\Gamma \propto \left| \left\langle \text{fin} |\hat{a}e(\mathbf{r})| \text{ini} \right\rangle \right|^2 \equiv \left\langle \text{fin} |\hat{a}e(\mathbf{r})| \text{ini} \right\rangle \left\langle \text{fin} |\hat{a}e(\mathbf{r})| \text{ini} \right\rangle^* \equiv \left\langle \text{ini} |\hat{a}^\dagger e^*(\mathbf{r})| \text{fin} \right\rangle \left\langle \text{fin} |\hat{a}e(\mathbf{r})| \text{ini} \right\rangle, \quad (9.28)$$

where the creation-annihilation operators are implied to be taken at $t = 0$, i.e. in the Schrödinger picture, and the initial and final states are those of the field alone. Second, let us now calculate the *total* rate of transitions to *all* available final states of the given mode $e(\mathbf{r})$. If such states formed a full and orthonormal set, we could use the closure relation (4.44), applied to the final states, to write

$$\Gamma \propto \sum_{\text{fin}} \left\langle \text{ini} |\hat{a}^\dagger e^*(\mathbf{r})| \text{fin} \right\rangle \left\langle \text{fin} |\hat{a}e(\mathbf{r})| \text{ini} \right\rangle = \left\langle \text{ini} |\hat{a}^\dagger \hat{a}| \text{ini} \right\rangle e^*(\mathbf{r}) e(\mathbf{r}) = \langle n \rangle_{\text{ini}} |e(\mathbf{r})|^2, \quad (9.29)$$

Photon
counting
rate

where, for a given field mode, $\langle n \rangle_{\text{ini}}$ is the expectation value of the operator $\hat{n} \equiv \hat{a}^\dagger \hat{a}$ for the initial state of the electromagnetic field. In the more realistic case of fields in relatively large volumes, $V \gg \lambda^3$, with their virtually continuous spectrum of final states, the middle equality in this relation is not strictly valid, but it is correct to a constant multiplier,¹⁷ which we are currently not interested in. Note, however, that Eq. (29) may be substantially wrong for high- Q electromagnetic resonators (“cavities”), which may make just one (or a few) modes available for transitions. (Quantum electrodynamics of such cavities will be briefly discussed in Sec. 4 below.)

Let us apply Eq. (29) to several possible quantum states of the mode.

¹⁶ This is essentially the same rotating wave approximation (RWA), which was already used in Sec. 6.5 and beyond – see, e.g., the transition from Eq. (6.90) to the first of Eqs. (6.94).

¹⁷ As the Golden Rule shows, this multiplier is proportional to the density ρ_f of the final states of the field.

(i) First, as a sanity check, the ground initial state, $n = 0$, gives no photon absorption at all. The interpretation is easy: the ground state field, cannot emit a photon that would ionize an atom in the counter. Again, this does not mean that the ground-state “motion” is not observable (if you still think so, please review the Casimir effect discussion in Sec. 1), just that it cannot ionize the trigger atom – because it does not have any *spare* energy for doing that.

(ii) All other coherent states (Fock, Glauber, squeezed, etc.) of the field oscillator give the same counting rate, provided that their $\langle n \rangle_{\text{ini}}$ is the same. This result may be less evident if we apply Eq. (29) to the interference of two light beams from the same source – say, in the double-slit or the Bragg-scattering configurations. In this case, we may represent the spatial distribution of the field as a sum

$$e(\mathbf{r}) = e_1(\mathbf{r}) + e_2(\mathbf{r}). \quad (9.30)$$

Here each term describes one possible wave path, so that the operator product in Eq. (29) may be a rapidly changing function of the detector position. For this configuration, our result (29) means that the interference pattern (and its contrast) are independent of the particular state of the electromagnetic field’s mode.

(iii) Surprisingly, the last statement is also valid for a classical mixture of the different eigenstates of the same field mode, for example for its thermal-equilibrium state. Indeed, in this case we need to average Eq. (29) over the corresponding classical ensemble, but it would only result in a different meaning of averaging n in that equation; the field part describing the interference pattern is not affected.

The last result may look a bit counter-intuitive because common sense tells us that the stochasticity associated with thermal equilibrium has to suppress the interference pattern contrast. These expectations are (partly :-) justified because a typical thermal source of radiation produces many field modes j , rather than one mode we have analyzed. These modes may have different wave numbers k_j and hence different field distribution functions $e_j(\mathbf{r})$, resulting in shifted interference patterns. Their summation would indeed smear the interference, suppressing its contrast.

So the use of one photon detector is not the best way to distinguish different quantum states of an electromagnetic field mode. This task, however, may be achieved using the photon counting correlation technique shown in Fig. 2.¹⁸

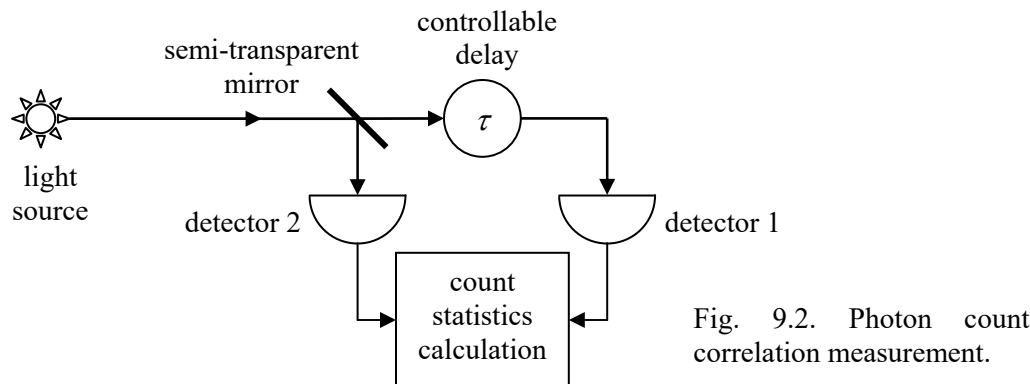


Fig. 9.2. Photon count correlation measurement.

¹⁸ It was pioneered as early as the mid-1950s (i.e. before the advent of lasers), by Robert Hanbury Brown and Richard Twiss. Their second experiment was also remarkable for the rather unusual light source – the star Sirius! (Their work was an effort to improve astrophysics interferometry techniques.)

In this experiment, the counter rate correlation may be characterized by the so-called *second-order correlation function* of the counting rates,

$$g^{(2)}(\tau) \equiv \frac{\langle \Gamma_1(t)\Gamma_2(t-\tau) \rangle}{\langle \Gamma_1(t) \rangle \langle \Gamma_2(t) \rangle}, \quad (9.31)$$

Second-order correlation function

where the averaging may be carried out either over many similar experiments, or over a relatively long time interval $t \gg \tau$, with usual field sources – due to their ergodicity. Using the normalized correlation function (31) is very convenient because the characteristics of both detectors and the beam splitter (e.g., a semi-transparent mirror, see Fig. 2) drop out from this fraction.

Very unexpectedly for the mid-1950s, Hanbury Brown and Twiss discovered that the correlation function depends on time delay τ in the way shown (schematically) with the solid line in Fig. 3. It is evident from Eq. (31) that if the counting events are completely independent, $g^{(2)}(\tau)$ should be equal to 1 – which is always the case in the limit $\tau \rightarrow \infty$. (As will be shown in the next section, the characteristic time of this approach is usually between 10^{-11} s and 10^{-8} s, so that for its measurement, the delay time control may be provided just by moving one of the detectors by a human-scale distance between a few millimeters to a few meters.) Hence, the observed behavior at $\tau \rightarrow 0$ corresponds to a *positive* correlation of detector counts at small time delays, i.e. to a *higher* probability of the nearly simultaneous arrival of photons to both counters. This counter-intuitive effect is called *photon bunching*.

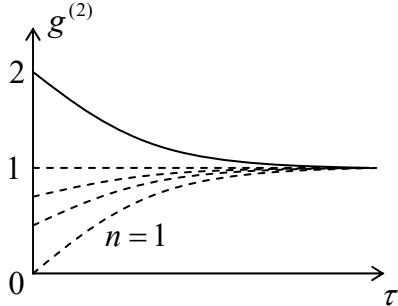


Fig. 9.3. Photon bunching (solid line) and antibunching for various n (dashed lines). The lines approach level $g^{(2)} = 1$ at $\tau \rightarrow \infty$ (on the time scale depending on the light source).

Let us use our simple single-mode model to analyze this experiment. Now the elementary quantum process characterized by the numerator of Eq. (31), is the correlated, simultaneous ionization of two trigger atoms, at two spatial-temporal points $\{\mathbf{r}_1, t\}$ and $\{\mathbf{r}_2, t - \tau\}$, by the same field mode, so that we need to make the following replacement in the first of Eqs. (25):

$$\hat{\mathcal{E}}(\mathbf{r}, t) \rightarrow \text{const} \times \hat{\mathcal{E}}(\mathbf{r}_1, t) \hat{\mathcal{E}}^*(\mathbf{r}_2, t - \tau). \quad (9.32)$$

Repeating all the manipulations done above for the single-counter case, we get

$$\langle \Gamma_1(t)\Gamma_2(t-\tau) \rangle \propto \langle \text{ini} | \hat{a}(t)^\dagger \hat{a}(t-\tau)^\dagger \hat{a}(t-\tau) \hat{a}(t) | \text{ini} \rangle e^*(\mathbf{r}_1) e^*(\mathbf{r}_2) e(\mathbf{r}_1) e(\mathbf{r}_2). \quad (9.33)$$

Plugging this expression, as well as Eq. (29) for single-counter rates, into Eq. (31), we see that the field distribution factors (as well as the detector-specific brackets and the density of states ρ_a) cancel, giving a very simple final expression:

$$g^{(2)}(\tau) = \frac{\langle \hat{a}^\dagger(t) \hat{a}^\dagger(t-\tau) \hat{a}(t-\tau) \hat{a}(t) \rangle}{\langle \hat{a}^\dagger(t) \hat{a}(t) \rangle^2}, \quad (9.34)$$

where the averaging should be carried out, as before, over the initial state of the field.

Still, the calculation of this expression for arbitrary τ may be quite complex, because in many cases the relaxation of the correlation function to the asymptotic value $g^{(2)}(\infty)$ is due to the interaction of the light source with the environment, and hence requires the open-system techniques that were discussed in Chapter 7. However, the zero-delay value $g^{(2)}(0)$ may be calculated straightforwardly, because the time arguments of all operators are equal, so that we may write

Zero-delay correlation

$$g^{(2)}(0) = \frac{\langle \hat{a}^\dagger \hat{a}^\dagger \hat{a} \hat{a} \rangle}{\langle \hat{a}^\dagger \hat{a} \rangle^2}. \quad (9.35)$$

Let us evaluate this ratio for the simplest states of the field.

(i) The n^{th} Fock state. In this case, it is convenient to act with the annihilation operators upon the ket-vectors, and by the creation operators, upon the bra-vectors, using Eqs. (19):

Photon anti-bunching

$$g^{(2)}(0) = \frac{\langle n | \hat{a}^\dagger \hat{a}^\dagger \hat{a} \hat{a} | n \rangle}{\langle n | \hat{a}^\dagger \hat{a} | n \rangle^2} = \frac{\langle n-2 | [n(n-1)]^{1/2} [n(n-1)]^{1/2} | n-2 \rangle}{\langle n-1 | n^{1/2} n^{1/2} | n-1 \rangle^2} = \frac{n(n-1)}{n^2} \equiv 1 - \frac{1}{n}. \quad (9.36)$$

We see that the correlation function at small delays is suppressed rather than enhanced – see the dashed lines in Fig. 3. This *photon antibunching* effect has a very simple handwaving explanation: a single photon emitted by the wave source may be absorbed by just one of the detectors. For the initial state $n = 1$, this is the only option, and it is very natural that Eq. (36) predicts no simultaneous counts at $\tau = 0$. Despite this theoretical simplicity, reliable observations of the antibunching have not been carried out until 1977,¹⁹ due to the experimental difficulty of driving electromagnetic field oscillators into their Fock states – see Sec. 4 below.

(ii) The Glauber state α . A similar procedure, but now using Eq. (5.124) and its Hermitian conjugate, $\langle \alpha | \hat{a}^\dagger = \langle \alpha | \alpha^*$, yields

Glauber field statistics

$$g^{(2)}(0) = \frac{\langle \alpha | \hat{a}^\dagger \hat{a}^\dagger \hat{a} \hat{a} | \alpha \rangle}{\langle \alpha | \hat{a}^\dagger \hat{a} | \alpha \rangle^2} = \frac{\alpha^* \alpha^* \alpha \alpha}{(\alpha^* \alpha)^2} \equiv 1, \quad (9.37)$$

for any parameter α . We see that the result is different from that for the Fock states, unless in the latter case $n \rightarrow \infty$. (We know that the Fock and Glauber properties should also coincide for the ground state, but at that state the correlation function's value is uncertain, because there are no photon counts at all.)

(iii) Classical mixture. From Chapter 7, we know that such statistical ensembles cannot be described by single state vectors, and require the density matrix w for their description. Here, we may combine Eqs. (35) and (7.5) to write

$$g^{(2)}(0) = \frac{\text{Tr}(\hat{w} \hat{a}^\dagger \hat{a}^\dagger \hat{a} \hat{a})}{\left[\text{Tr}(\hat{w} \hat{a}^\dagger \hat{a}) \right]^2}. \quad (9.38)$$

¹⁹ By H. J. Kimble *et al.*, *Phys. Rev. Lett.* **39**, 691 (1977). For a detailed review of phonon antibunching, see, e.g., H. Paul, *Rev. Mod. Phys.* **54**, 1061 (1982).

Spelling out this expression is easy for the field in thermal equilibrium at some temperature T , because its density matrix is diagonal in the basis of Fock states n – see Eqs. (7.24):

$$w_{nn'} = W_n \delta_{nn'}, \quad W_n = \exp\left\{-\frac{E_n}{k_B T}\right\} / Z \equiv \lambda^n / \sum_{n=0}^{\infty} \lambda^n, \quad \text{where } \lambda \equiv \exp\left\{-\frac{\hbar\omega}{k_B T}\right\}. \quad (9.39)$$

So, for the operators in the numerator and denominator of Eq. (38) we also need just the diagonal terms of the operator products, which have already been calculated – see Eq. (36). As a result, we get

$$g^{(2)}(0) = \frac{\sum_{n=0}^{\infty} W_n n(n-1)}{\left(\sum_{n=0}^{\infty} W_n n\right)^2} = \frac{\sum_{n=0}^{\infty} \lambda^n n(n-1) \times \sum_{n=0}^{\infty} \lambda^n}{\left(\sum_{n=0}^{\infty} \lambda^n n\right)^2}. \quad (9.40)$$

One of the three series involved in this expression is just the usual geometric progression,

$$\sum_{n=0}^{\infty} \lambda^n = \frac{1}{1-\lambda}, \quad (9.41)$$

and the remaining two series may be readily calculated by its differentiation over the parameter λ :

$$\begin{aligned} \sum_{n=0}^{\infty} \lambda^n n &\equiv \lambda \sum_{n=0}^{\infty} \lambda^{n-1} n = \lambda \frac{d}{d\lambda} \sum_{n=0}^{\infty} \lambda^n = \lambda \frac{d}{d\lambda} \frac{1}{1-\lambda} = \frac{\lambda}{(1-\lambda)^2}, \\ \sum_{n=0}^{\infty} \lambda^n n(n-1) &\equiv \lambda^2 \sum_{n=0}^{\infty} \lambda^{n-2} n(n-1) = \lambda^2 \frac{d^2}{d\lambda^2} \left(\sum_{n=0}^{\infty} \lambda^n \right) = \lambda^2 \frac{d^2}{d\lambda^2} \frac{1}{1-\lambda} = \frac{2\lambda^2}{(1-\lambda)^3}, \end{aligned} \quad (9.42)$$

and for the correlation function we get an extremely simple result independent of the parameter λ and hence of temperature:

$$g^{(2)}(0) = \frac{[2\lambda^2/(1-\lambda)^3][1/(1-\lambda)]}{[\lambda/(1-\lambda)^2]^2} \equiv 2. \quad (9.43)$$

Photon bunching

This is exactly the photon bunching effect first observed by Hanbury Brown and Twiss – see Fig. 3. We see that in contrast to antibunching, this is an essentially classical (statistical) effect. Indeed, Eq. (43) allows a purely classical derivation. In the classical theory, the counting rate (of a single counter) is proportional to the wave intensity I , so that Eq. (31) with $\tau = 0$ is reduced to

$$g^{(2)}(0) = \frac{\langle I^2 \rangle}{\langle I \rangle^2}, \quad \text{with } I \propto \overline{E^2(t)} \propto E_\omega E_\omega^*. \quad (9.44)$$

For a sinusoidal field, the intensity is constant, and $g^{(2)}(0) = 1$. (This is also evident from Eq. (37), because the classical state may be considered as a Glauber state with $\alpha \rightarrow \infty$.) On the other hand, if the intensity fluctuates (either in time, or from one experiment to another), the averages in Eq. (44) should be calculated as

$$\langle I^k \rangle = \int_0^\infty w(I) I^k dI, \quad \text{with } \int_0^\infty w(I) dI = 1, \quad \text{and } k = 1, 2, \quad (9.45)$$

where $w(I)$ is the probability density. For classical statistics, the probability is an exponential function of the electromagnetic field energy, and hence its intensity:

$$w(I) = Ce^{-\beta I}, \quad \text{where } \beta \propto 1/k_B T, \quad (9.46)$$

so that Eqs. (45) yield:²⁰

$$\begin{aligned} \int_0^\infty C \exp\{-\beta I\} dI &\equiv C/\beta = 1, \quad \text{and hence } C = \beta, \\ \langle I^k \rangle &= \int_0^\infty w(I) I^k dI = C \int_0^\infty \exp\{-\beta I\} I^k dI = \frac{1}{\beta^k} \int_0^\infty \exp\{-\xi\} \xi^k d\xi = \begin{cases} 1/\beta, & \text{for } k=1, \\ 2/\beta^2, & \text{for } k=2. \end{cases} \end{aligned} \quad (9.47)$$

Plugging these results into Eq. (44), we get $g^{(2)}(0) = 0$, in complete agreement with Eq. (43).

For some field states, including the squeezed ground states ζ discussed at the end of Sec. 5.5, values $g^{(2)}(0)$ may be even higher than 2 – the so-called *super-bunching*. Analyses of two cases of such super-bunching are offered for the reader’s exercise – see the problem list in the chapter’s end.

9.3. Photon emission: spontaneous and stimulated

In our simple model of photon counting, considered in the last section, the trigger atom in the counter *absorbed* a photon. Now let us have a look at the opposite process of *spontaneous emission* of photons by an atom in an excited state, still using the same electric-dipole approximation (24) for the atom-to-field interaction. For this, we may still use the Golden Rule for the model depicted in Fig. 6.12, but now the roles have changed: we have to associate the operator \hat{A} with the electric dipole moment of the atom, while the operator \hat{B} , with the electric field, so that the continuous spectrum of the system b represents the plurality of the electromagnetic field modes into which the spontaneous radiation may happen. Since now the transition *increases* the energy of the electromagnetic field, and *decreases* that of the atom, after the multiplication of the field bracket in Eq. (27a) by $\exp\{-i\omega t\}$, and the second, by $\exp\{+i\omega t\}$, we may keep only the photon *creation* operator whose time evolution (26) compensates this additional fast “rotation”. As a result, the Golden Rule takes the following form:

$$\Gamma_s = \pi\omega \left| \langle \text{fin} | \hat{a}^\dagger | 0 \rangle \right|^2 \left| \langle \text{fin} | \hat{\mathbf{d}} \cdot \mathbf{e}(\mathbf{r}) | \text{ini} \rangle \right|^2 \rho_f, \quad (9.48)$$

Spontaneous
photon
emission
rate

where all operators and states are time-independent (i.e. taken in the Schrödinger picture), and ρ_f is the density of final states of the electromagnetic field – which in this problem plays the role of the atom’s environment.²¹ Here the electromagnetic field oscillator has been assumed to be initially in the ground state – the assumption that will be changed later in this section.

This relation, together with Eq. (19), shows that for the field’s matrix element be different from zero, the final state of the field has to be the first excited Fock state, $n = 1$. (By the way, *this* is exactly

²⁰ See, e.g., MA Eq. (6.7c) with $n = 0$ and $n = 1$.

²¹ Here the sum over all electromagnetic field modes j may be smuggled back. Since in the quasi-static approximation $k_j a \ll 1$, which is necessary for the interaction representation by Eq. (24), the matrix elements in Eq. (48) are virtually independent on the direction of the wave vectors, and their magnitudes are fixed by ω , the summation is reduced to the calculation of the total ρ_f for all modes, and the averaging of $e^2(\mathbf{r})$ – see below.

the most practicable way of generating an excited Fock state of a field oscillator.) With that, Eq. (48) yields

$$\Gamma_s = \pi\omega \left| \langle \text{fin} | \hat{\mathbf{d}} \cdot \mathbf{e}(\mathbf{r}) | \text{ini} \rangle \right|^2 \rho_f \equiv \pi\omega \left| \langle \text{fin} | \hat{d}e_d(\mathbf{r}) | \text{ini} \rangle \right|^2 \rho_f, \quad (9.49)$$

where the density ρ_f of the excited electromagnetic field states should be calculated at the energy $E = \hbar\omega$, and e_d is the Cartesian component of the vector $\mathbf{e}(\mathbf{r})$ along the electric dipole's direction. The expression for the density ρ_f was our first formula in this course – see Eq. (1.1).²² From it, we get

$$\rho_f \equiv \frac{dN}{dE} = V \frac{\omega^2}{\pi^2 \hbar c^3}, \quad (9.50)$$

where the bounding volume V should be large enough to ensure spectrum's virtual continuity: $V \gg \lambda^3 = (2\pi c/\omega)^3$. Because of that, in the normalization condition used to simplify Eq. (9), we may consider $e^2(\mathbf{r})$ constant. Let us represent this square as a sum of squares of the three Cartesian components of the vector $\mathbf{e}(\mathbf{r})$: one of those (e_d) aligned with the dipole's direction; due to the space isotropy we may write

$$e^2 \equiv e_d^2 + e_{\perp 1}^2 + e_{\perp 2}^2 = 3e_d^2. \quad (9.51)$$

As a result, the normalization condition yields

$$e_d^2 = \frac{1}{3\epsilon_0 V}. \quad (9.52)$$

and Eq. (49) gives the famous (and very important) formula²³

$$\Gamma_s = \frac{1}{4\pi\epsilon_0} \frac{4\omega^3}{3\hbar c^3} \left| \langle \text{fin} | \hat{\mathbf{d}} | \text{ini} \rangle \right|^2 \equiv \frac{1}{4\pi\epsilon_0} \frac{4\omega^3}{3\hbar c^3} \langle \text{fin} | \hat{\mathbf{d}} | \text{ini} \rangle \cdot \langle \text{ini} | \hat{\mathbf{d}} | \text{fin} \rangle^*. \quad (9.53)$$

Free-space spontaneous emission rate

Leaving a comparison of this formula with the classical theory of radiation,²⁴ and the exact evaluation of Γ_s for a particular transition in the hydrogen atom, for reader's exercises, let me just estimate its order of magnitude. Assuming that $d \sim er_B \equiv eh^2/m_e(e^2/4\pi\epsilon_0)$ and $\hbar\omega \sim E_H \equiv m_e(e^2/4\pi\epsilon_0)^2/h^2$, and taking into account the definition (6.62) of the fine structure constant $\alpha \approx 1/137$, we get

$$\frac{\Gamma}{\omega} \sim \left(\frac{e^2}{4\pi\epsilon_0 \hbar c} \right)^3 \equiv \alpha^3 \sim 3 \times 10^{-7}. \quad (9.54)$$

This estimate shows that the emission lines at atomic transitions are typically very sharp. With the present-day availability of high-speed electronics, it also makes sense to evaluate the time scale $\tau = 1/\Gamma$ of the typical quantum transition: for a typical optical frequency $\omega \sim 3 \times 10^{15} \text{ s}^{-1}$, it is close to 1 ns. This is

²² If the same atom is placed into a high- Q resonant cavity (see, e.g., EM 7.9), the rate of its photon emission is strongly suppressed at frequencies between the cavity resonances (where $\rho_f \rightarrow 0$) – see, e.g., the review by S. Haroche and D. Kleppner, *Phys. Today* **42**, 24 (Jan. 1989). On the other hand, the emission is strongly (by a factor $\sim (\lambda^3/V)Q$, where V is cavity's volume) enhanced at resonance frequencies – the so-called *Purcell effect*, discovered by E. Purcell in the 1940s. For a brief discussion of this and other quantum electrodynamic effects in cavities, see the next section.

²³ This was the breakthrough result obtained by P. Dirac in 1927, which jumpstarted the whole field of quantum electrodynamics. An equivalent expression was obtained from more formal arguments in 1930 by V. Weisskopf and E. Wigner, so that sometimes Eq. (53) is (very unfairly) called the “Weisskopf-Wigner formula”.

²⁴ See, e.g., EM Sec. 8.2, in particular Eq. (8.29).

exactly the time constant that determines the time-delay dependence of the photon counting statistics of the spontaneously emitted radiation – see Fig. 3. Colloquially, this is the temporal scale of the photon emitted by an atom.²⁵

Note, however, that the above estimate of τ is only valid for a transition with a non-zero electric-dipole matrix element. If it equals zero, i.e. the transition does not satisfy the *selection rules*,²⁶ – say, due to the initial and final state symmetry – it is “forbidden”. The “forbidden” transition may still take place due to a different, smaller interaction (say, via a magnetic dipole field of the atom, or its quadrupole electric field²⁷), but takes much longer. In some cases the increase of τ is rather dramatic – sometimes to hours! Such long-lasting radiation is called the *luminescence* – or the *fluorescence* if the initial atom’s excitation was due to external radiation of a higher frequency, followed first by non-radiative transitions down the ladder of energy levels.

Now let us consider a more general case when the electromagnetic field mode of frequency ω is initially in an arbitrary Fock state n , and from it may either get energy $\hbar\omega$ from the atomic system (*photon emission*) or, vice versa, give such energy back to the atom (*photon absorption*). For the photon emission rate, an evident generalization of Eq. (48) gives

$$\frac{\Gamma_e}{\Gamma_s} \equiv \frac{\Gamma_{n \rightarrow \text{fin}}}{\Gamma_{0 \rightarrow 1}} = \frac{\left| \langle \text{fin} | \hat{a}^\dagger | n \rangle \right|^2}{\left| \langle 1 | \hat{a}^\dagger | 0 \rangle \right|^2}, \quad (9.55)$$

where both brackets should be calculated in the Schrödinger picture, and Γ_s is the spontaneous emission rate (48) of the same atomic system. According to the second of Eqs. (19), at the photon emission, the final field state has to be the Fock state with $n' = n + 1$, and Eq. (55) yields

$$\boxed{\Gamma_e = (n + 1)\Gamma_s}. \quad (9.56)$$

Thus the initial field increases the photon emission rate; this effect is called the *stimulated emission of radiation*. Note that the spontaneous emission may be considered as a particular case of the stimulated emission for $n = 0$, and hence interpreted as the emission stimulated by the ground state of the electromagnetic field – one more manifestation of the non-trivial nature of this “vacuum” state.

On the other hand, following the arguments of Sec. 2,²⁸ for the description of radiation *absorption*, the photon creation operator has to be replaced with the annihilation operator, giving the rate ratio

²⁵ The scale $c\tau$ of the spatial extension of the corresponding wave packet is surprisingly macroscopic – in the range of a few millimeters. Such a “human” size of spontaneously emitted photons makes the usual optical table, with its 1-cm-scale components, the key equipment for many optical experiments – see, e.g., Fig. 2.

²⁶ As was already discussed in Sec. 5.6, for a single spin-less particle moving in a spherically-symmetric potential (e.g., a hydrogen-like atom), the orbital selection rules are simple: the only allowed electric-dipole transitions are those with $\Delta l \equiv l_{\text{fin}} - l_{\text{ini}} = \pm 1$ and $\Delta m \equiv m_{\text{fin}} - m_{\text{ini}} = 0$ or ± 1 . The simplest example of the transition that does *not* satisfy this rule, i.e. is “forbidden”, is that between the *s*-states ($l = 0$) with $n = 2$ and $n = 1$; because of that, the lifetime of the lowest excited *s*-state of a hydrogen atom is as long as ~ 0.15 s.

²⁷ See, e.g., EM Sec. 8.9.

²⁸ Note, however, a major difference between the rate Γ discussed in Sec. 2, and Γ_a in Eq. (57). In our current case, the atomic transition is still between two *discrete* energy levels (see Fig. 4 below), so that the rate Γ_a is

$$\frac{\Gamma_a}{\Gamma_s} = \frac{|\langle \text{fin} | \hat{a} | n \rangle|^2}{|\langle 1 | \hat{a}^\dagger | 0 \rangle|^2}. \quad (9.57)$$

According to this relation and the first of Eqs. (19), the final state of the field at the photon absorption has to be the Fock state with $n' = n - 1$, and Eq. (57) yields

$$\Gamma_a = n \Gamma_s. \quad (9.58)$$

Photon absorption rate

The results (56) and (58) are usually formulated in terms of relations between the *Einstein coefficients* A and B defined in the way shown in Fig. 4, where the two energy levels are those of the atom, Γ_a is the rate of energy absorption from the electromagnetic field in its n^{th} Fock state, and Γ_e is that of energy emission into the field, initially in the same state. In this notation, Eqs. (56) and (58) yield²⁹

$$A_{21} = B_{21} = B_{12}, \quad (9.59)$$

Einstein coefficients' relation

because each of these coefficients equals the spontaneous emission rate Γ_s .

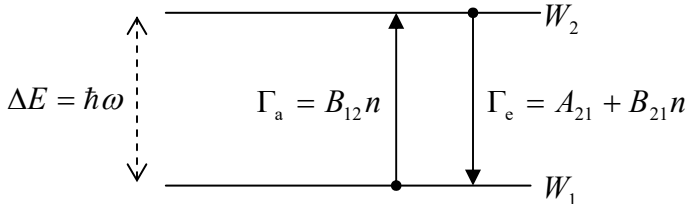


Fig. 9.4. The Einstein coefficients on the atomic quantum transition diagram – cf. Fig. 7.6.

I cannot resist the temptation to use this point for a small detour – an alternative derivation of the Bose-Einstein statistics for photons. Indeed, in the thermodynamic equilibrium, the average probability flows between levels 1 and 2 (see Fig. 4 again) should be equal:³⁰

$$W_2 \langle \Gamma_e \rangle = W_1 \langle \Gamma_a \rangle, \quad (9.60)$$

where W_1 and W_2 are the probabilities for the atomic system to occupy the corresponding levels, so that Eqs. (56) and (58) yield

$$W_2 \Gamma_s \langle 1+n \rangle = W_1 \Gamma_s \langle n \rangle, \quad \text{i.e. } \frac{W_2}{W_1} = \frac{\langle n \rangle}{\langle n \rangle + 1}, \quad (9.61)$$

where $\langle n \rangle$ is the average number of photons in the field causing the interstate transitions. But, on the other hand, for an atomic subsystem only weakly coupled to its electromagnetic environment, we ought to have the Gibbs distribution of these probabilities:

$$\frac{W_2}{W_1} = \frac{\exp\{-E_2/k_B T\}}{\exp\{-E_1/k_B T\}} = \exp\left\{-\frac{\Delta E}{k_B T}\right\} = \exp\left\{-\frac{\hbar\omega}{k_B T}\right\}. \quad (9.62)$$

proportional to ρ_f , the density of final states of the electromagnetic field, i.e. the same density as in Eq. (48) and beyond, while the rate (27) is proportional to ρ_a , the density of final (ionized) states of the “trigger” atom – more exactly, of it’s the electron released at its ionization.

²⁹ These relations were conjectured, from very general arguments, by Albert Einstein as early as 1916.

³⁰ This is just a particular embodiment of the detailed balance equation (7.198).

Requiring Eqs. (61) and (62) to give the same result for the probability ratio, we get the Bose-Einstein distribution for the electromagnetic field in thermal equilibrium:

$$\langle n \rangle = \frac{1}{\exp\{\hbar\omega/k_B T\} - 1} \quad (9.63)$$

- the same result as that obtained in Sec. 7.1 by other means – see Eq. (7.26b).

Now returning to the discussion of Eqs. (56) and (58), their very important implication is the possibility to achieve the stimulated emission of coherent radiation using the level *occupancy inversion*. Indeed, if the ratio W_2/W_1 is larger than that given by Eq. (62), the net power flow from the atomic system into the electromagnetic field,

$$\text{power} = \hbar\omega \times \Gamma_s [W_2(\langle n \rangle + 1) - W_1\langle n \rangle], \quad (9.64)$$

may be positive. The necessary inversion may be produced using several ways, notably by intensive quantum transitions to level 2 from an even higher energy level (which, in turn, is populated, e.g., by absorption of external radiation, usually called *pumping*, at a higher frequency.)

A less obvious, but crucial feature of the stimulated emission is spelled out by Eq. (55): as was mentioned above, it shows that the final state of the field after the absorption of energy $\hbar\omega$ from the atom is a pure (coherent) Fock state $(n + 1)$. Colloquially, one may say that the new, $(n + 1)^{\text{st}}$ photon emitted from the atom is automatically in phase with the n photons that had been in the field mode initially, i.e. joins them coherently.³¹ The idea of stimulated emission of coherent radiation using population inversion³² was first implemented in the early 1950s in the microwave range (*masers*) and in 1960 in the optical range (*lasers*). Nowadays, lasers are ubiquitous components of almost all high-tech systems and constitute one of the cornerstones of our technological civilization.

A quantitative discussion of laser operation is well beyond the framework of this course, and I have to refer the reader to special literature,³³ but still would like to briefly mention two key points:

(i) In a typical laser, each generated electromagnetic field mode is in its Glauber (rather than the Fock) state, so that Eqs. (56) and (58) are applicable only for the n averaged over the Fock-state decomposition of the Glauber state – see Eq. (5.134).

(ii) Since in a typical laser $\langle n \rangle \gg 1$, its operation may be well described using quasiclassical theories that use Eq. (64) to describe the electromagnetic energy balance (with the addition of a term describing the energy loss due to field absorption in external components of the laser, including the useful load), plus the equation describing the balance of occupancies $W_{1,2}$ due to all interlevel transitions – similar to Eq. (60), but including also the contribution(s) from the particular population inversion mechanism used in the laser. At this approach, the role of quantum mechanics in laser science is essentially reduced to the calculation of the parameter Γ_s for the particular system.

This role becomes more prominent when one needs to describe *fluctuations* of the laser field. Here two approaches are possible, following the two options discussed in Chapter 7. If the fluctuations

³¹ It is straightforward to show that this fact is also true if the field is initially in the Glauber state – which is more typical for modes in practical lasers.

³² This idea may be traced back at least to an obscure 1939 publication by V. Fabrikant.

³³ I can recommend, for example, P. Milloni and J. Eberly, *Laser Physics*, 2nd ed., Wiley, 2010, and a less technical text by A. Yariv, *Quantum Electronics*, 3rd ed., Wiley, 1989.

are relatively small, one can linearize the Heisenberg equations of motion of the field oscillator operators near their stationary-lasing “values”, with the Langevin “forces” (also time-dependent operators) describing the fluctuation sources, and use these Heisenberg-Langevin equations to calculate the radiation fluctuations, just as was described in Sec. 7.5. On the other hand, near the lasing threshold, the field fluctuations are relatively large, smearing the phase transition between the no-lasing and lasing states. Here the linearization is not an option, but one can use the density-matrix approach described in Sec. 7.6, for the fluctuation analysis.³⁴ Note that while the laser fluctuations may look like a peripheral issue, pioneering research in that field has led to the development of the general theory of open quantum systems, which was discussed in Chapter 7.

9.4. Cavity QED

Now I have to visit, at least in passing, the field of *cavity quantum electrodynamics* (usually called *cavity QED* for short) – the art and science of creating and using the entanglement between quantum states of an atomic system (either an atom, or an ion, or a molecule, etc.) and the electromagnetic field in a macroscopic volume called the *resonant cavity* (or just “resonator”, or just “cavity”). This field is very popular nowadays, especially in the context of the quantum computation and communication research discussed in Sec. 8.5.³⁵

The discussion in the previous section was based on the implicit assumption that the energy spectrum of the electromagnetic field interacting with an atomic subsystem is essentially continuous, so that its final state is spread among many field modes, effectively losing its coherence with the quantum state of the atomic subsystem. This assumption has justified using the quantum-mechanical Golden Rule for the calculation of the spontaneous and stimulated transition rates. However, the assumption becomes invalid if the electromagnetic field is contained inside a relatively small volume, with its linear size comparable with the radiation wavelength. If the walls of such a cavity mostly reflect, rather than absorb, radiation, then the 0th approximation the energy dissipation may be disregarded, and the particular solutions $\mathbf{e}_j(\mathbf{r})$ of the Helmholtz equation (5) correspond to discrete, well-separated mode wave numbers k_j and hence well-separated frequencies ω_j .³⁶ Due to the energy conservation, an atomic transition corresponding to energy $\Delta E = |E_{\text{ini}} - E_{\text{fin}}|$ may be effective only if the corresponding quantum transition frequency $\Omega \equiv \Delta E/\hbar$ is close to one of these resonance frequencies.³⁷ As a result of such resonant interaction, the quantum states of the atomic system and the resonant electromagnetic mode may become entangled.

A very popular approximation for the quantitative description of this effect is the so-called *Rabi model*,³⁸ in which the atom is treated as a two-level system interacting with a single electromagnetic field mode of the resonant cavity. (As was shown in Sec. 6.5, this model is justified, e.g., if transitions

³⁴ This path has been developed (also in the mid-1960s), by several researchers, notably including M. Sully and W. Lamb – see, e.g., M. Sargent III, M. Scully, and W. Lamb, Jr., *Laser Physics*, Westview, 1977.

³⁵ This popularity was demonstrated, for example, by the award of the 2012 Nobel Prize in Physics to cavity QED experimentalists S. Haroche and D. Wineland.

³⁶ The calculation of such modes and corresponding frequencies for several simple cavity geometries was the subject of EM Sec. 7.8 of this series.

³⁷ On the contrary, if Ω is far from any ω_j , the interaction is suppressed; in particular, the spontaneous emission rate may be much lower than that given by Eq. (53) – so that this result is not as fundamental as it may look.

³⁸ After the pioneering work by I. Rabi in 1936-37.

between all other energy level pairs have considerably different frequencies.) As the reader knows well from Chapters 4-6 (see in particular Sec. 5.1), any two-level system may be described, just as a spin- $\frac{1}{2}$, by the Hamiltonian $b\hat{I} + \mathbf{c} \cdot \hat{\mathbf{\sigma}}$. Since we may always select the energy origin that $b = 0$, and the state basis in which $\mathbf{c} = c\mathbf{n}_z$, the Hamiltonian of the atomic subsystem may be taken in the diagonal form

$$\hat{H}_a = c\hat{\sigma}_z \equiv \frac{\hbar\Omega}{2}\hat{\sigma}_z, \quad (9.65)$$

where $\hbar\Omega \equiv 2c = \Delta E$ is the difference between the energy levels in the absence of interaction with the field. Next, according to Eq. (17), ignoring the constant ground-state energy $\hbar\omega/2$ (which may be always added to the energy at the end – if necessary), the contribution of a single field mode of frequency ω to the total Hamiltonian of the system is

$$\hat{H}_f = \hbar\omega\hat{a}^\dagger\hat{a}. \quad (9.66)$$

Finally, according to Eq. (16a), the electric field of the mode may be represented as

$$\hat{\mathcal{E}}(\mathbf{r}, t) = \frac{1}{i} \left(\frac{\hbar\omega}{2} \right)^{1/2} \mathbf{e}(\mathbf{r}) \left(\hat{a} - \hat{a}^\dagger \right), \quad (9.67)$$

so that in the electric-dipole approximation (24), the cavity-atom interaction may be represented as a product of the field by some (say, y -) Cartesian component³⁹ of the Pauli spin- $\frac{1}{2}$ operator:

$$\hat{H}_{int} = \text{const} \times \hat{\sigma}_y \times \hat{\mathcal{E}} = \text{const} \times \hat{\sigma}_y \times \left(\frac{\hbar\omega}{2} \right)^{1/2} \frac{1}{i} \left(\hat{a} - \hat{a}^\dagger \right) = i\hbar\kappa\hat{\sigma}_y \left(\hat{a} - \hat{a}^\dagger \right), \quad (9.68)$$

where κ is a coupling constant (with the dimension of frequency). The sum of these three terms,

$$\hat{H} \equiv \hat{H}_a + \hat{H}_f + \hat{H}_{int} = \frac{\hbar\Omega}{2}\hat{\sigma}_z + \hbar\omega\hat{a}^\dagger\hat{a} + i\hbar\kappa\hat{\sigma}_y \left(\hat{a} - \hat{a}^\dagger \right). \quad (9.69)$$

Rabi Hamiltonian

giving a very reasonable description of the system, is called the *Rabi Hamiltonian*. Despite its apparent simplicity, using this Hamiltonian for calculations is not that straightforward.⁴⁰ Only in the case when the electromagnetic field is large and hence may be treated classically, the results following from Eq. (69) are reduced to Eqs. (6.94) describing, in particular, the Rabi oscillations discussed in Sec. 6.3.

The situation becomes simpler in the most important case when the frequencies Ω and ω are very close, enabling an effective interaction between the cavity field and the atom even if the coupling constant κ is relatively small. Indeed, if both the κ and the so-called *detuning* (defined similarly to the parameter Δ used in Sec. 6.5),

$$\xi \equiv \Omega - \omega, \quad (9.70)$$

³⁹ The exact component is not important for final results, while intermediate formulas simplify if the interaction is proportional to either pure $\hat{\sigma}_x$ or pure $\hat{\sigma}_y$.

⁴⁰ For example, an exact quasi-analytical expression for its eigenenergies (as zeros of a Taylor series in the parameter κ , with coefficients determined by a recurrence relation) was found only recently – see D. Braak, *Phys. Rev. Lett.* **107**, 100401 (2011).

are much smaller than $\Omega \approx \omega$, the Rabi Hamiltonian may be simplified using the rotating-wave approximation, already used several times in this course. For this, it is convenient to use the *spin ladder operators*, defined absolutely similarly for those of the orbital angular momentum – see Eqs. (5.153):

$$\hat{\sigma}_{\pm} \equiv \hat{\sigma}_x \pm i\hat{\sigma}_y, \quad \text{so that } \hat{\sigma}_y = \frac{\hat{\sigma}_+ - \hat{\sigma}_-}{2i}. \quad (9.71)$$

From Eq. (4.105), it is very easy to find the matrices of these operators in the standard z -basis,

$$\sigma_+ = \begin{pmatrix} 0 & 2 \\ 0 & 0 \end{pmatrix}, \quad \sigma_- = \begin{pmatrix} 0 & 0 \\ 2 & 0 \end{pmatrix}, \quad (9.72)$$

and their commutation rules – which turn out to be naturally similar to Eqs. (5.154):

$$[\hat{\sigma}_+, \hat{\sigma}_-] = 4\hat{\sigma}_z, \quad [\hat{\sigma}_z, \hat{\sigma}_{\pm}] = \pm 2\hat{\sigma}_{\pm}. \quad (9.73)$$

In this notation, the Rabi Hamiltonian becomes

$$\hat{H} = \frac{\hbar\Omega}{2}\hat{\sigma}_z + \hbar\omega\hat{a}^\dagger\hat{a} + \frac{\hbar\kappa}{2}(\hat{\sigma}_+ - \hat{\sigma}_-)(\hat{a} - \hat{a}^\dagger), \quad (9.74)$$

and it is straightforward to use Eq. (4.199) and (73) to derive the Heisenberg-picture equations of motion for the involved operators. (Doing this, we have to remember that operators of the “spin” subsystem, on one hand, and of the field mode, on the other hand, are defined in different Hilbert spaces and hence commute – at least at coinciding time moments.) The result (so far, exact!) is

$$\begin{aligned} \dot{\hat{a}} &= -i\omega\hat{a} + \frac{i\kappa}{2}(\hat{\sigma}_+ - \hat{\sigma}_-), & \dot{\hat{a}}^\dagger &= i\omega\hat{a}^\dagger + \frac{i\kappa}{2}(\hat{\sigma}_+ - \hat{\sigma}_-), \\ \dot{\hat{\sigma}}_{\pm} &= \pm i\Omega\hat{\sigma}_{\pm} + 2i\kappa(\hat{a} - \hat{a}^\dagger)\hat{\sigma}_z, & \dot{\hat{\sigma}}_z &= i\kappa(\hat{a}^\dagger - \hat{a})(\hat{\sigma}_+ + \hat{\sigma}_-). \end{aligned} \quad (9.75)$$

At negligible coupling, $\kappa \rightarrow 0$, these equations have simple solutions,

$$\hat{a}(t) \propto e^{-i\omega t}, \quad \hat{a}^\dagger(t) \propto e^{i\omega t}, \quad \hat{\sigma}_{\pm}(t) \propto e^{\pm i\Omega t}, \quad \hat{\sigma}_z(t) \approx \text{const}, \quad (9.76)$$

and the small terms proportional to κ on the right-hand sides of Eqs. (75) cannot affect these time evolution laws dramatically even if κ is not exactly zero. Of those terms, ones with frequencies close to the “basic” frequency of each variable would act in resonance and hence may have a substantial impact on the system’s dynamics, while non-resonant terms may be ignored. In this rotating-wave approximation, Eqs. (75) are reduced to a much simpler system of equations:

$$\begin{aligned} \dot{\hat{a}} &= -i\omega\hat{a} - \frac{i\kappa}{2}\hat{\sigma}_-, & \dot{\hat{a}}^\dagger &= i\omega\hat{a}^\dagger + \frac{i\kappa}{2}\hat{\sigma}_+, \\ \dot{\hat{\sigma}}_+ &= i\Omega\hat{\sigma}_+ + 2i\kappa\hat{a}^\dagger\hat{\sigma}_z, & \dot{\hat{\sigma}}_- &= -i\Omega\hat{\sigma}_- - 2i\kappa\hat{a}\hat{\sigma}_z, & \dot{\hat{\sigma}}_z &= i\kappa(\hat{a}^\dagger\hat{\sigma}_- - \hat{a}\hat{\sigma}_+). \end{aligned} \quad (9.77)$$

Alternatively, these equations of motion may be obtained *exactly* from the Rabi Hamiltonian (74), if it is preliminary cleared of the terms proportional to $\hat{\sigma}_+\hat{a}^\dagger$ and $\hat{\sigma}_-\hat{a}$, that oscillate fast and hence self-average to produce virtually zero effect:

Jaynes-
Cummings
Hamiltonian

$$\hat{H} = \frac{\hbar\Omega}{2}\hat{\sigma}_z + \hbar\omega\hat{a}^\dagger\hat{a} + \frac{\hbar\kappa}{2}\left(\hat{\sigma}_+\hat{a} + \hat{\sigma}_-\hat{a}^\dagger\right), \quad \text{at } \kappa, |\xi| \ll \omega, \Omega. \quad (9.78)$$

This is the famous *Jaynes-Cummings Hamiltonian*,⁴¹ which is basic model used in the cavity QED and its applications.⁴² To find its eigenstates and eigenenergies, let us note that at negligible interaction ($\kappa \rightarrow 0$), the spectrum of the total energy E of the system, which in this limit is the sum of two independent contributions from the atomic and cavity-field subsystems,

$$E|_{\kappa=0} = \pm \frac{\hbar\Omega}{2} + \hbar\omega n \equiv E_n \pm \frac{\hbar\xi}{2}, \quad \text{with } n = 1, 2, \dots, \quad (9.79)$$

consists⁴³ of close level pairs (Fig. 5) centered to values

$$E_n \equiv \hbar\omega\left(n - \frac{1}{2}\right). \quad (9.80)$$

(At the exact resonance $\omega = \Omega$, i.e. at $\xi = 0$, each pair merges into one double-degenerate level E_n .) Since at $\kappa \rightarrow 0$ the two subsystems do not interact, the eigenstates corresponding to the sublevels of the n^{th} pair may be represented by direct products of their independent state vectors:

$$|+\rangle \equiv |\uparrow\rangle \otimes |n-1\rangle \quad \text{and} \quad |-\rangle \equiv |\downarrow\rangle \otimes |n\rangle, \quad (9.81)$$

where the first ket of each product represents the state of the two-level (spin-½-like) atomic subsystem, and the second ket, that of the field oscillator.

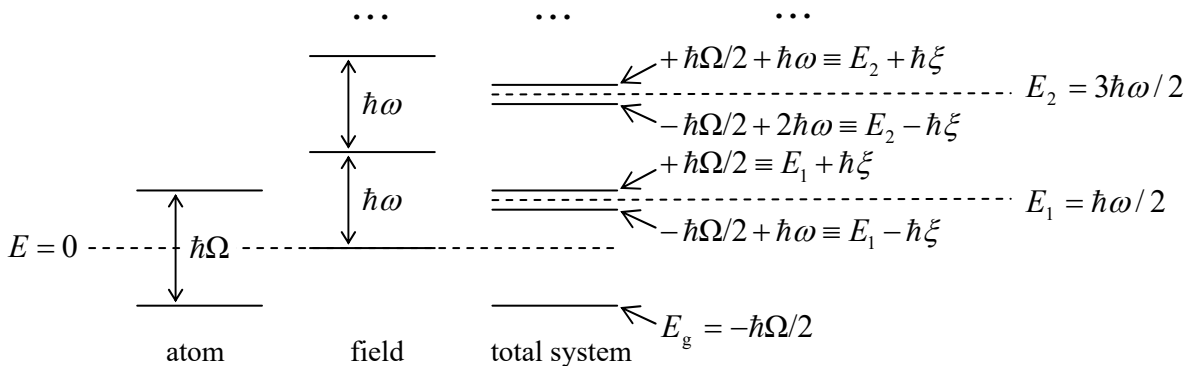


Fig. 9.5. The energy spectrum (79) of the Jaynes-Cummings Hamiltonian in the limit $\kappa \ll |\xi|$. Note again that the energy is referred to the ground-state energy $\hbar\omega/2$ of the cavity field.

As we know from Chapter 6, even weak interaction may lead to strong coherent mixing⁴⁴ of quantum states with close energies (in this case, the two states (81) within each pair with the same n),

⁴¹ It was first proposed and analyzed in 1963 by two engineers, Edwin Jaynes and Fred Cummings, in a *Proc. IEEE* publication, and it took the physics community a while to recognize and acknowledge the fundamental importance of that work.

⁴² For most applications, the baseline Hamiltonian (78) has to be augmented by additional term(s) describing, for example, the incoming radiation and/or the system's coupling to the environment, for example, due to the electromagnetic energy loss in a finite- Q -factor cavity – see Eq. (7.68).

⁴³ Only the ground state level $E_g = -\hbar\Omega/2$ is non-degenerate – see Fig. 5.

while their mixing with the states with farther energies is still negligible. Hence, at $0 < \kappa, |\xi| \ll \omega \approx \Omega$, a good approximation of the eigenstate with $E \approx E_n$ is given by a linear superposition of the states (81):

$$|\alpha_n\rangle = c_+ |+\rangle + c_- |-\rangle \equiv c_+ |\uparrow\rangle \otimes |n-1\rangle + c_- |\downarrow\rangle \otimes |n\rangle, \quad (9.82)$$

Jaynes-Cummings eigenstates

with certain c -number coefficients c_{\pm} . This relation describes the entanglement of the atomic eigenstates \uparrow and \downarrow with the Fock states number n and $n - 1$ of the field mode. Let me leave the (straightforward) calculation of the coefficients $(c_{\pm})^{\pm}$ for each of two entangled states (for each n) for the reader's exercise. (The result for the corresponding two eigenenergies $(E_n)_{\pm}$ may be again represented by the same anticrossing diagram as shown in Figs. 2.29 and 5.1, now with the detuning ξ as the argument.) This calculation shows, in particular, that at $\xi = 0$ (i.e. at $\omega = \Omega$), $|c_+| = |c_-| = 1/\sqrt{2}$ for both states of the pair. This fact may be interpreted as a (coherent!) equal sharing of an energy quantum $\hbar\omega = \hbar\Omega$ by the atom and the cavity field at the exact resonance.

As a (hopefully, self-evident) by-product of the calculation of c_{\pm} is the fact that the dynamics of the state α_n described by Eq. (82), is similar to that of the generic two-level system that was repeatedly discussed in this course – the first time in Sec. 2.6 and then in Chapters 4-6. In particular, if the composite system had been initially prepared to be in one component state, for example $|\uparrow\rangle \otimes |0\rangle$ (i.e. with the atom excited, while the cavity in its ground state), and then allowed to evolve on its own, after some time interval $\Delta t \sim 1/\kappa$ it may be found definitely in the counterpart state $|\downarrow\rangle \otimes |1\rangle$, including the first excited Fock state $n = 1$ of the field mode. If the process is allowed to continue, after the equal time interval Δt , the system returns to the initial state $|\uparrow\rangle \otimes |0\rangle$, etc. This most striking prediction of the Jaynes-Cummings model was directly observed, by G. Rempe *et al.*, only in 1987, although less directly this model was repeatedly confirmed by numerous experiments carried out in the 1960s and 1970s.

This quantized version of the Rabi oscillations can only persist in time if the inevitable electromagnetic energy losses (not described by the basic Jaynes-Cummings Hamiltonian) are somehow compensated – for example, by passing a beam of particles, externally excited into the higher-energy state \uparrow , through the cavity. If the losses become higher, the dissipation suppresses quantum coherence, in our case the coherence between two components of each pair (82), as was discussed in Chapter 7. As a result, the transition from the higher-energy atomic state \uparrow to the lower-energy state \downarrow , giving energy $\hbar\omega$ to the cavity ($n - 1 \rightarrow n$), which is then rapidly drained into the environment, becomes incoherent, so that the system's dynamics is reduced to the Purcell effect, already mentioned in Sec. 3. A quantitative analysis of this effect is left for the reader's exercise.

The number of interesting physics games one can play with such systems – say by adding external sources of radiation at a frequency close to ω and Ω , in particular with manipulated time-dependent amplitude and/or phase, is always unlimited.⁴⁵ Unfortunately, my time/space allowance for the cavity QED is over, and for further discussion, I have to refer the interested reader to special literature.⁴⁶

⁴⁴ In some fields, especially chemistry, such mixing is frequently called *hybridization*.

⁴⁵ Most of them may be described by adding new terms to the basic Jaynes-Cummings Hamiltonian (78).

⁴⁶ I can recommend, for example, either C. Gerry and P. Knight, *Introductory Quantum Optics*, Cambridge U. Press, 2005, or G. Agarwal, *Quantum Optics*, Cambridge U. Press, 2012.

9.5. The Klein-Gordon and relativistic Schrödinger equations

Now let me switch gears and discuss the basics of relativistic quantum mechanics of particles with a non-zero rest mass m . In the ultra-relativistic limit $pc \gg mc^2$ the quantization scheme of such particles may be essentially the same as for electromagnetic waves, but for the intermediate energy range, $pc \sim mc^2$, a more general approach is necessary. Historically, the first attempts⁴⁷ to extend the non-relativistic wave mechanics into the relativistic energy range were based on performing the same transitions from classical observables to their quantum-mechanical operators as in the non-relativistic limit:

$$\mathbf{p} \rightarrow \hat{\mathbf{p}} = -i\hbar\nabla, \quad E \rightarrow \hat{H} = i\hbar \frac{\partial}{\partial t}. \quad (9.83)$$

The substitution of these operators, acting on the Schrödinger-picture wavefunction $\Psi(\mathbf{r},t)$, into the classical relation (1) between the energy E and momentum \mathbf{p} (for of a free particle) leads to the following formulas:

Table 9.1. Deriving the Klein-Gordon equation for a free relativistic particle.⁴⁸

	Non-relativistic limit	Relativistic case
Classical mechanics	$E = \frac{1}{2m} p^2$	$E^2 = c^2 p^2 + (mc^2)^2$
Wave mechanics	$i\hbar \frac{\partial}{\partial t} \Psi = \frac{1}{2m} (-i\hbar\nabla)^2 \Psi$	$\left(i\hbar \frac{\partial}{\partial t}\right)^2 \Psi = c^2 (-i\hbar\nabla)^2 \Psi + (mc^2)^2 \Psi$

The resulting equation for the non-relativistic limit, in the left-bottom cell of the table, is just the usual Schrödinger equation (1.28) for a free particle. Its relativistic generalization, in the right-bottom cell, usually rewritten as

Klein-Gordon equation

$$\left(\frac{1}{c^2} \frac{\partial^2}{\partial t^2} - \nabla^2 \right) \Psi + \mu^2 \Psi = 0, \quad \text{with } \mu \equiv \frac{mc}{\hbar}, \quad (9.84)$$

is called the *Klein-Gordon* (or sometimes “Klein-Gordon-Fock”) *equation*. The fundamental solutions of this equation are the same plane, monochromatic waves

$$\Psi(\mathbf{r},t) \propto \exp\{i(\mathbf{k} \cdot \mathbf{r} - \omega t)\}. \quad (9.85)$$

as in the non-relativistic case. Indeed, such waves are eigenstates of the operators (83), with eigenvalues, respectively,

$$\mathbf{p} = \hbar\mathbf{k}, \quad \text{and } E = \hbar\omega, \quad (9.86)$$

so that their substitution into Eq. (84) immediately returns us to Eq. (1) with the replacements (86):

⁴⁷ This approach was suggested in 1926-1927, i.e. virtually simultaneously, by (at least) V. Fock, E. Schrödinger, O. Klein and W. Gordon, J. Kudar, T. de Donder and F.-H. van der Dungen, and L. de Broglie.

⁴⁸ Note that in the left, non-relativistic column of this table, the energy is referred to the rest energy mc^2 , while in its right, relativistic column, it is referred to zero – see Eq. (1).

$$E_{\pm} = \hbar\omega_{\pm} = \pm \left[(\hbar ck)^2 + (mc^2)^2 \right]^{1/2}. \quad (9.87)$$

Though one may say that this dispersion relation is just a simple combination of the classical relation (1) and the same basic quantum-mechanical relations (86) as in non-relativistic limit, it attracts our attention to the fact that the energy $\hbar\omega$ as a function of the momentum $\hbar k$ has two branches, with $E_-(\mathbf{p}) = -E_+(\mathbf{p})$ – see Fig. 6a. Historically, this fact has played a very important role in spurring the fundamental idea of *particle-antiparticle pairs*. In this idea (very similar to the concept of electrons and holes in semiconductors, which was discussed in Sec. 2.8), what we call the “vacuum” actually corresponds to all quantum states of the lower branch, with energies $E_-(\mathbf{p}) < 0$, being completely filled, while the states on the upper branch, with energies $E_+(\mathbf{p}) > 0$, being empty. Then an externally supplied energy,

$$\Delta E = E_+ - E_- \equiv E_+ + (-E_-) \geq 2mc^2 > 0, \quad (9.88)$$

may bring the system from the lower branch to the upper one (Fig. 6b). The resulting excited state is interpreted as a combination of a particle (formally, of the infinite spatial extension) with the energy E_+ and the momentum \mathbf{p} , and a “hole” (antiparticle) of the *positive* energy ($-E_-$) and the momentum $-\mathbf{p}$. This idea⁴⁹ has led to a search for, and discovery of the positron: the electron’s antiparticle with charge $q = +e$, in 1932, and later of the antiproton and other antiparticles.

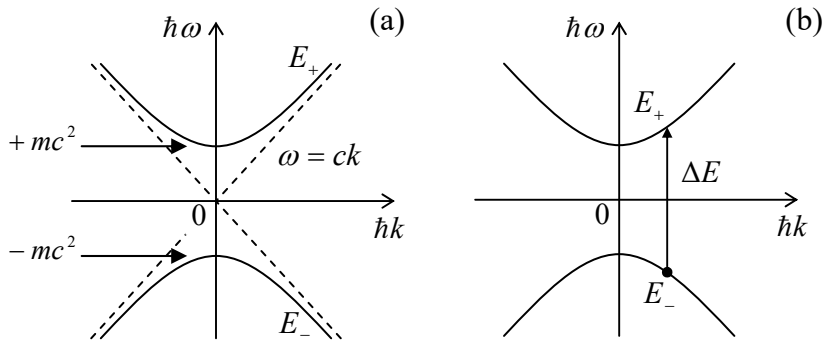


Fig. 9.6. (a) The free-particle dispersion relation resulting from the Klein-Gordon and Dirac equations, and (b) the scheme of creation of a particle-antiparticle pair from the vacuum.

Free particles of a finite spatial extension may be described, in this approach, just as in the non-relativistic Schrödinger equation, by wave packets, i.e. linear superpositions of the de Broglie waves (85) with close wave vectors \mathbf{k} , and the corresponding values of ω given by Eq. (87), with the positive sign for the “usual” particles, and negative sign for antiparticles – see Fig. 6a above. Note that to form, from a particle’s wave packet, a similar wave packet for the antiparticle, with the same phase and group velocities (2.33a) in each direction, we need to change the sign not only before ω , but also before \mathbf{k} , i.e. to replace all component wavefunctions (85), and hence the full wavefunction, with their complex conjugates.

Of more formal properties of Eq. (84), it is easy to prove that its solutions satisfy the same continuity equation (1.52), with the probability current density \mathbf{j} still given by Eq. (1.47), but a different expression for the probability density w – which becomes very similar to that for \mathbf{j} :

$$w = \frac{i\hbar}{2mc^2} \left(\Psi^* \frac{\partial \Psi}{\partial t} - c.c. \right), \quad \mathbf{j} = \frac{i\hbar}{2m} \left(\Psi \nabla \Psi^* - c.c. \right) \quad (9.89)$$

⁴⁹ Due to the same P. A. M. Dirac!

– very much in the spirit of the relativity theory, treating space and time on equal footing. (In the non-relativistic limit $p/mc \rightarrow 0$, Eq. (84) allows the reduction of this expression for w to the non-relativistic Eq. (1.22): $w \rightarrow \Psi\Psi^*$.)

The Klein-Gordon equation may be readily generalized to describe a particle moving in external fields; for example, the electromagnetic field effects on a particle with charge q may be described by the same replacement as in the non-relativistic limit (see Sec. 3.1):

$$\hat{\mathbf{p}} \rightarrow \hat{\mathbf{P}} - q\mathbf{A}(\mathbf{r}, t), \quad \hat{H} \rightarrow \hat{H} - q\phi(\mathbf{r}, t), \quad (9.90)$$

where $\hat{\mathbf{P}} = -i\hbar\nabla$ is the canonical momentum operator (3.25), and the vector- and scalar potentials, \mathbf{A} and ϕ , should be treated appropriately – either as c -number functions if the electromagnetic field quantization is not important for the particular problem, or as operators (see Secs. 1-4 above) if it is.

However, the practical value of the resulting *relativistic Schrödinger equation* is rather limited, for two main reasons. First of all, it does not give the correct description of particles with spin. For example, for the hydrogen-like atom/ion problem, i.e. the motion of an electron with the electric charge $-e$, in the Coulomb central field of an immobile nucleus with charge $+Ze$, the equation may be readily solved exactly⁵⁰ and yields the following spectrum of (doubly-degenerate) energy levels:

$$E = mc^2 \left(1 + \frac{Z^2\alpha^2}{\lambda^2} \right)^{-1/2}, \quad \text{with } \lambda \equiv n + \left[(l + \tfrac{1}{2})^2 - Z^2\alpha^2 \right]^{1/2} - (l + \tfrac{1}{2}), \quad (9.91)$$

where $n = 1, 2, \dots$ and $l = 0, 1, \dots, n - 1$ are the same quantum numbers as in the non-relativistic theory (see Sec. 3.6), and $\alpha \approx 1/137$ is the fine structure constant (6.62). The three leading terms of the Taylor expansion of this result in the small parameter $Z\alpha$ are as follows:

$$E \approx mc^2 \left[1 - \frac{Z^2\alpha^2}{2n^2} - \frac{Z^4\alpha^4}{2n^4} \left(\frac{n}{l + \tfrac{1}{2}} - \frac{3}{4} \right) \right]. \quad (9.92)$$

The first of these terms is just the rest energy of the particle. The second term,

$$E_n = -mc^2 \frac{Z^2\alpha^2}{2n^2} \equiv -\frac{mZ^2e^4}{(4\pi\epsilon_0)^2\hbar^2} \frac{1}{2n^2} \equiv -\frac{E_0}{2n^2}, \quad \text{with } E_0 = Z^2 E_H, \quad (9.93)$$

reproduces the non-relativistic Bohr's formula (3.201). Finally, the third term,

$$-\frac{mc^2}{2n^4} \frac{Z^4\alpha^4}{2n^4} \left(\frac{n}{l + \tfrac{1}{2}} - \frac{3}{4} \right) \equiv -\frac{2E_n^2}{mc^2} \left(\frac{n}{l + \tfrac{1}{2}} - \frac{3}{4} \right), \quad (9.94)$$

is just the perturbative kinetic-relativistic contribution (6.51) to the fine structure of the Bohr levels (93). However, as we already know from Sec. 6.3, for a spin- $\frac{1}{2}$ particle such as the electron, the spin-orbit interaction (6.55) gives an additional contribution to the fine structure, of the same order, so that the net result, confirmed by experiment, is given by Eq. (6.60), i.e. is different from Eq. (94). This is very natural, because the relativistic Schrödinger equation does not have the very notion of spin.

Second, even for massive spinless particles (such as the Z^0 bosons), for which this equation is believed to be valid, the most important problems are related to particle interactions at high energies of

⁵⁰ This task is left for the reader's exercise.

the order of $\Delta E \sim 2mc^2$ and beyond – see Eq. (88). Due to the possibility of creation and annihilation of particle-antiparticle pairs at such energies, the number of particles participating in such interactions is typically considerable (and variable), and the adequate description of the system is given not by the relativistic Schrödinger equation (which is formulated in single-particle terms), but by the *quantum field theory* – to which I will devote only a few sentences in the very end of this chapter.

9.6. Dirac's theory

The real breakthrough toward the quantum relativistic theory of electrons (and other spin- $\frac{1}{2}$ fermions) was achieved in 1928 by P. A. M. Dirac. For that time, the structure of his theory was highly nontrivial. Namely, while formally preserving, in the coordinate representation, the same Schrödinger-picture equation of quantum dynamics as in the non-relativistic quantum mechanics,⁵¹

$$i\hbar \frac{\partial \Psi}{\partial t} = \hat{H}\Psi, \quad (9.95)$$

it postulates that the wavefunction Ψ it describes is not a scalar complex function of time and coordinates, but a *four-component* column-vector (sometimes called the *bispinor*) of such functions, its Hermitian-conjugate bispinor Ψ^\dagger being a 4-component row-vector of their complex conjugates:

$$\Psi = \begin{pmatrix} \Psi_1(\mathbf{r}, t) \\ \Psi_2(\mathbf{r}, t) \\ \Psi_3(\mathbf{r}, t) \\ \Psi_4(\mathbf{r}, t) \end{pmatrix}, \quad \Psi^\dagger = (\Psi_1^*(\mathbf{r}, t), \ \Psi_2^*(\mathbf{r}, t), \ \Psi_3^*(\mathbf{r}, t), \ \Psi_4^*(\mathbf{r}, t)), \quad (9.96)$$

and that the Hamiltonian participating in Eq. (95) is a 4×4 matrix defined in the Hilbert space of bispinors Ψ . For a free particle, the postulated Hamiltonian looks amazingly simple:⁵²

⁵¹ After the “naturally-relativistic” form of the Klein-Gordon equation (84), this apparent return to the non-relativistic Schrödinger equation may look very counter-intuitive. However, it becomes a bit less surprising taking into account the fact (whose proof is left for the reader’s exercise) that Eq. (84) may be also recast into the form (95) for a *two-component* column-vector Ψ (sometimes called *spinor*), with a Hamiltonian which may be represented by a 2×2 matrix – and hence expressed via the Pauli matrices (4.105) and the identity matrix I.

⁵² Moreover, if the time derivative participating in Eq. (95), and the three coordinate derivatives participating (via the momentum operator) in Eq. (97), are merged into one 4-vector operator $\partial/\partial x_k \equiv \{\nabla, \partial/\partial(ct)\}$, the Dirac equation (95) may be rewritten in an even simpler, manifestly Lorentz-invariant 4-vector form (with the implied summation over the repeated index $k = 1, \dots, 4$ – see, e.g., EM Sec. 9.4):

$$\left(\hat{\gamma}_k \frac{\partial}{\partial x_k} + \mu \right) \Psi = 0, \quad \text{where } \hat{\gamma} \equiv \{\hat{\gamma}_1, \hat{\gamma}_2, \hat{\gamma}_3\} = \begin{pmatrix} 0 & -i\hat{\sigma} \\ i\hat{\sigma} & 0 \end{pmatrix}, \quad \hat{\gamma}_4 = \hat{\beta},$$

where $\mu \equiv mc/\hbar$ – just as in Eq. (84). Note also that, very counter-intuitively, the Dirac Hamiltonian (97) is *linear* in the momentum, while the non-relativistic Hamiltonian of a particle, as well as the relativistic Schrödinger equation, are *quadratic* in \mathbf{p} . In my humble opinion, the Dirac theory (including the concept of antiparticles it has inspired) may compete for the title of the most revolutionary theoretical idea in physics of all times, despite such strong contenders as Newton’s laws, Maxwell’s equations, Gibbs’ statistical distribution, Bohr’s theory of the hydrogen atom, and Einstein’s general relativity.

$$\hat{H} = c\hat{\mathbf{a}} \cdot \hat{\mathbf{p}} + \hat{\beta}mc^2. \quad (9.97)$$

where $\hat{\mathbf{p}} = -i\hbar\nabla$ is the same 3D vector operator of momentum as in the non-relativistic case, while the operators $\hat{\mathbf{a}}$ and $\hat{\beta}$ may be represented in the following shorthand 2×2 form:

$$\hat{\mathbf{a}} \equiv \begin{pmatrix} \hat{0} & \hat{\sigma} \\ \hat{\sigma} & \hat{0} \end{pmatrix}, \quad \hat{\beta} \equiv \begin{pmatrix} \hat{I} & \hat{0} \\ \hat{0} & -\hat{I} \end{pmatrix}. \quad (9.98a)$$

The operator $\hat{\mathbf{a}}$, composed of the Pauli vector operators $\hat{\sigma}$, is also a vector in the usual 3D space, with each of its 3 Cartesian components being a 4×4 matrix. The particular form of the 2×2 matrices corresponding to the operators $\hat{\sigma}$ and \hat{I} in Eq. (98a) depends on the basis selected for the spin state representation; for example, in the standard z -basis, in which the Cartesian components of $\hat{\sigma}$ are represented by the Pauli matrices (4.105), the 4×4 matrix form of Eq. (98a) is

$$\alpha_x = \begin{pmatrix} 0 & 0 & 0 & 1 \\ 0 & 0 & 1 & 0 \\ 0 & 1 & 0 & 0 \\ 1 & 0 & 0 & 0 \end{pmatrix}, \quad \alpha_y = \begin{pmatrix} 0 & 0 & 0 & -i \\ 0 & 0 & i & 0 \\ 0 & -i & 0 & 0 \\ i & 0 & 0 & 0 \end{pmatrix}, \quad \alpha_z = \begin{pmatrix} 0 & 0 & 1 & 0 \\ 0 & 0 & 0 & -1 \\ 1 & 0 & 0 & 0 \\ 0 & -1 & 0 & 0 \end{pmatrix}, \quad \beta = \begin{pmatrix} 1 & 0 & 0 & 0 \\ 0 & 1 & 0 & 0 \\ 0 & 0 & -1 & 0 \\ 0 & 0 & 0 & -1 \end{pmatrix}. \quad (9.98b)$$

It is straightforward to use Eqs. (98) to verify that the matrices α_x , α_y , α_z and β satisfy the following relations:

$$\alpha_x^2 = \alpha_y^2 = \alpha_z^2 = \beta^2 = I, \quad (9.99)$$

$$\alpha_x\alpha_y + \alpha_y\alpha_x = \alpha_y\alpha_z + \alpha_z\alpha_y = \alpha_z\alpha_x + \alpha_x\alpha_z = \alpha_x\beta + \beta\alpha_x = \alpha_y\beta + \beta\alpha_y = \alpha_z\beta + \beta\alpha_z = 0, \quad (9.100)$$

i.e. anticommute.

Using these commutation relations, and acting essentially as in Sec. 1.4, it is straightforward to show that any solution to the Dirac equation obeys the probability conservation law, i.e. the continuity equation (1.52), with the probability density:

$$w = \Psi^\dagger \Psi, \quad (9.101)$$

and the probability current,

$$\mathbf{j} = \Psi^\dagger c\hat{\mathbf{a}} \Psi, \quad (9.102)$$

looking *almost* as in the non-relativistic wave mechanics – cf. Eqs. (1.22) and (1.47). Note, however, the Hermitian conjugation used in these formulas instead of the complex conjugation, to form the scalars w , j_x , j_y , and j_z from the 4-component state vectors (96).

This close similarity is extended to the fundamental, plane-wave solutions of the Dirac equations in free space. Indeed, plugging such solution, in the form

$$\Psi = ue^{i(\mathbf{k}\cdot\mathbf{r}-\omega t)} \equiv \begin{pmatrix} u_1 \\ u_2 \\ u_3 \\ u_4 \end{pmatrix} e^{i(\mathbf{k}\cdot\mathbf{r}-\omega t)}, \quad (9.103)$$

into Eqs. (95) and (97), we see that they are indeed satisfied, provided that a system of four coupled, linear algebraic equations for four complex *c*-number amplitudes $u_{1,2,3,4}$ is satisfied. The condition of its consistency yields the same dispersion relation (87), i.e. the same two-branch diagram shown in Fig. 6, as follows from the Klein-Gordon equation. The difference is that plugging each value of ω , given by Eq. (87), back into the system of the linear equations for four amplitudes u , we get two solutions for their vector $\mathbf{u} \equiv (u_1, u_2, u_3, u_4)$ for each of the two energy branches – see Fig. 6 again. In the standard *z*-basis of spin operators, they may be represented as follows:

$$\text{for } E = E_+ > 0 : \quad \mathbf{u}_{+\uparrow} = c_{+\uparrow} \begin{pmatrix} 1 \\ 0 \\ \frac{cp_z}{E_+ + mc^2} \\ \frac{cp_+}{E_+ + mc^2} \end{pmatrix}, \quad \mathbf{u}_{+\downarrow} = c_{+\downarrow} \begin{pmatrix} 0 \\ 1 \\ \frac{cp_-}{E_+ + mc^2} \\ \frac{-cp_z}{E_+ + mc^2} \end{pmatrix}, \quad (9.104a)$$

$$\text{for } E = E_- < 0 : \quad \mathbf{u}_{-\uparrow} = c_{-\uparrow} \begin{pmatrix} \frac{cp_z}{E_- - mc^2} \\ \frac{cp_+}{E_- - mc^2} \\ 1 \\ 0 \end{pmatrix}, \quad \mathbf{u}_{-\downarrow} = c_{-\downarrow} \begin{pmatrix} \frac{cp_-}{E_- - mc^2} \\ \frac{-cp_z}{E_- - mc^2} \\ 0 \\ 1 \end{pmatrix}, \quad (9.104b)$$

where $p_{\pm} \equiv p_x \pm ip_y$, and c_{\pm} are normalization coefficients.

The simplest interpretation of these solutions is that Eq. (103), with the vectors \mathbf{u}_+ given by Eq. (104a), represents a spin-½ particle (say, an electron), while with the vectors \mathbf{u}_- given by Eq. (104b), it represents an antiparticle (a positron), and the two solutions for each particle, indexed with opposite arrows, correspond to two possible directions of the spin-½, $\sigma_z = \pm 1$, i.e. $S_z = \pm \hbar/2$. This interpretation is indeed solid in the non-relativistic limit, when two last components of the vector (104a), and two first components of the vector (104b) are negligibly small:

$$\mathbf{u}_{+\uparrow} \rightarrow \begin{pmatrix} 1 \\ 0 \\ 0 \\ 0 \end{pmatrix}, \quad \mathbf{u}_{+\downarrow} \rightarrow \begin{pmatrix} 0 \\ 1 \\ 0 \\ 0 \end{pmatrix}, \quad \mathbf{u}_{-\uparrow} \rightarrow \begin{pmatrix} 0 \\ 0 \\ 1 \\ 0 \end{pmatrix}, \quad \mathbf{u}_{-\downarrow} \rightarrow \begin{pmatrix} 0 \\ 0 \\ 0 \\ 1 \end{pmatrix}, \quad \text{for } \frac{p_{x,y,z}}{mc} \rightarrow 0. \quad (9.105)$$

However, at arbitrary energies, the physical picture is more complex. To show this, let us use the Dirac equation to calculate the Heisenberg-picture law of time evolution of the operator of some Cartesian component of the orbital angular momentum $\mathbf{L} \equiv \mathbf{r} \times \mathbf{p}$, for example of $L_x = yp_z - zp_y$, taking into account that the Dirac operators (98a) commute with those of \mathbf{r} and \mathbf{p} , and also the Heisenberg commutation relations (2.14):

$$i\hbar \frac{\partial \hat{L}_x}{\partial t} = [\hat{L}_x, \hat{H}] = c\hat{\mathbf{a}} \cdot [(\hat{y}\hat{p}_z - \hat{z}\hat{p}_y), \hat{\mathbf{p}}] = -i\hbar c (\hat{\alpha}_z \hat{p}_y - \hat{\alpha}_y \hat{p}_z), \quad (9.106)$$

with similar relations for two other Cartesian components. Since the right-hand side of these equations is different from zero, the orbital momentum is generally *not* conserved – even for a free particle! Let us, however, consider the following vector operator,

$$\hat{\mathbf{S}} \equiv \frac{\hbar}{2} \begin{pmatrix} \hat{\boldsymbol{\sigma}} & \hat{0} \\ \hat{0} & \hat{\boldsymbol{\sigma}} \end{pmatrix}. \quad (9.107a)$$

Spin operator in Dirac's theory

According to Eqs. (4.105), its Cartesian components, in the z -basis, are represented by 4×4 matrices

$$\mathbf{S}_x = \frac{\hbar}{2} \begin{pmatrix} 0 & 1 & 0 & 0 \\ 1 & 0 & 0 & 0 \\ 0 & 0 & 0 & 1 \\ 0 & 0 & 1 & 0 \end{pmatrix}, \quad \mathbf{S}_y = \frac{\hbar}{2} \begin{pmatrix} 0 & -i & 0 & 0 \\ i & 0 & 0 & 0 \\ 0 & 0 & 0 & -i \\ 0 & 0 & i & 0 \end{pmatrix}, \quad \mathbf{S}_z = \frac{\hbar}{2} \begin{pmatrix} 1 & 0 & 0 & 0 \\ 0 & -1 & 0 & 0 \\ 0 & 0 & 1 & 0 \\ 0 & 0 & 0 & -1 \end{pmatrix}. \quad (9.107b)$$

Let us calculate the Heisenberg-picture law of time evolution of these components, for example

$$i\hbar \frac{\partial \hat{S}_x}{\partial t} = [\hat{S}_x, \hat{H}] = c[\hat{S}_x, (\hat{\alpha}_x \hat{p}_x + \hat{\alpha}_y \hat{p}_y + \hat{\alpha}_z \hat{p}_z)]. \quad (9.108)$$

A direct calculation of the commutators of the matrices (98) and (107) yields

$$[\hat{S}_x, \hat{\alpha}_x] = 0, \quad [\hat{S}_x, \hat{\alpha}_y] = i\hbar \hat{\alpha}_z, \quad [\hat{S}_x, \hat{\alpha}_z] = -i\hbar \hat{\alpha}_y, \quad (9.109)$$

so that we finally get

$$i\hbar \frac{\partial \hat{S}_x}{\partial t} = i\hbar c(\hat{\alpha}_z \hat{p}_y - \hat{\alpha}_y \hat{p}_z), \quad (9.110)$$

with similar expressions for the other two components of the operator. Comparing this result with Eq. (106), we see that any Cartesian component of the operator defined similarly to Eq. (5.170),

$$\hat{\mathbf{J}} \equiv \hat{\mathbf{L}} + \hat{\mathbf{S}}, \quad (9.111)$$

is an integral of motion,⁵³ so that this operator may be interpreted as the one representing the total angular momentum of the particle. Hence, the operator (107) *may* be interpreted as the spin operator of a spin-½ particle (e.g., electron). As it follows from the last of Eq. (107b), in the non-relativistic limit the columns (105) represent the eigenkets of the z -component of that operator, with eigenstates $S_z = \pm\hbar/2$, with the sign corresponding to on the arrow index. So, the Dirac theory provides a justification for spin-½ – or, somewhat more humbly, replaces the Pauli Hamiltonian postulate (4.163) with that of a simpler (and hence more plausible), Lorentz-invariant Hamiltonian (97).

Note, however, that this simple interpretation, fully separating a particle from its antiparticle, is not valid for the exact solutions (103)-(104), so that generally the eigenstates of the Dirac Hamiltonian are certain linear (coherent) superpositions of the components describing the particle and its antiparticle – each with both directions of spin. This fact leads to several interesting effects, including the so-called *Klien paradox* at the reflection of a relativistic electron from a potential barrier.⁵⁴

⁵³ It is straightforward to show that this result remains valid for a particle in any central field $U(r)$.

⁵⁴ See, e.g., A. Calogeracos and N. Dombey, *Contemp. Phys.* **40**, 313 (1999).

9.7. Low-energy limit

The generalization of Dirac's theory to the case of a (spin-1/2) particle with an electric charge q , moving in a classically-described electromagnetic field, may be obtained using the same replacement (90). As a result, Eq. (95) turns into

$$\boxed{[c\hat{\mathbf{a}} \cdot (-i\hbar\nabla - q\mathbf{A}) + mc^2\hat{\beta} + (q\phi - \hat{H})]\Psi = 0,} \quad (9.112)$$

Dirac equation
in EM field

where the Hamiltonian operator \hat{H} is understood in the sense of Eq. (95), i.e. as the partial time derivative with the multiplier $i\hbar$. Let us prepare this equation for a low-energy approximation by acting on its left-hand side by a similar square bracket but with the opposite sign before the last parentheses – also an operator! Using Eqs. (99) and (100), and the fact that the space- and time-independent operators $\hat{\mathbf{a}}$ and $\hat{\beta}$ commute with the spin-independent, c -number functions $\mathbf{A}(\mathbf{r}, t)$ and $\phi(\mathbf{r}, t)$, as well as with the Hamiltonian operator $i\hbar\partial/\partial t$, the result is

$$\left\{ c^2[\hat{\mathbf{a}} \cdot (-i\hbar\nabla - q\mathbf{A})]^2 + (mc^2)^2 - c[\hat{\mathbf{a}} \cdot (-i\hbar\nabla - q\mathbf{A}), (q\phi - \hat{H})] - (q\phi - \hat{H})^2 \right\} \Psi = 0. \quad (9.113)$$

A direct calculation of the first square bracket, using Eqs. (98) and (107), yields

$$[\hat{\mathbf{a}} \cdot (-i\hbar\nabla - q\mathbf{A})]^2 \equiv (-i\hbar\nabla - q\mathbf{A})^2 - 2q\hat{\mathbf{S}} \cdot \nabla \times \mathbf{A}. \quad (9.114)$$

But the last vector product on the right-hand side is just the magnetic field – see, e.g., Eqs. (3.21):

$$\mathcal{B} = \nabla \times \mathbf{A}. \quad (9.115)$$

Similarly, we may use the first of Eqs. (3.21), for the electric field,

$$\mathcal{E} = -\nabla\phi - \frac{\partial\mathbf{A}}{\partial t}, \quad (9.116)$$

to simplify the commutator participating in Eq. (9.113):

$$[\hat{\mathbf{a}} \cdot (-i\hbar\nabla - q\mathbf{A}), (q\phi - \hat{H})] \equiv -q\hat{\mathbf{a}} \cdot [\hat{H}, \mathbf{A}] - i\hbar q\hat{\mathbf{a}} \cdot [\nabla, \phi] \equiv -i\hbar q \frac{\partial\mathbf{A}}{\partial t} - i\hbar\hat{\mathbf{a}} \cdot \nabla\phi \equiv i\hbar q\hat{\mathbf{a}} \cdot \mathcal{E}. \quad (9.117)$$

As a result, Eq. (113) becomes

$$\left\{ c^2(-i\hbar\nabla - q\mathbf{A})^2 + (q\phi - \hat{H})^2 - (mc^2)^2 - 2qc^2\hat{\mathbf{S}} \cdot \mathcal{B} + i\hbar c q\hat{\mathbf{a}} \cdot \mathcal{E} \right\} \Psi = 0. \quad (9.118)$$

So far, this is an exact result, equivalent to Eq. (112), but it is more convenient for an analysis of the low-energy limit, in which not only the energy offset $E - mc^2$ (which is just the energy used in the non-relativistic mechanics), but also the electrostatic energy of the particle, $|q\langle\phi\rangle|$, are much smaller than the rest energy mc^2 . In this limit, the second and third terms of Eq. (118) almost cancel, and introducing the offset Hamiltonian

$$\hat{H} \equiv \hat{H} - mc^2\hat{I}. \quad (9.119)$$

we may approximate their difference, up to the first non-zero term, as

$$(q\phi\hat{I} - \hat{H})^2 - (mc^2)^2\hat{I} \equiv \left(q\phi\hat{I} - mc^2\hat{I} - \hat{H} \right)^2 - (mc^2)^2\hat{I} \approx 2mc^2\left(\hat{H} - q\phi\hat{I} \right). \quad (9.120)$$

As a result, after the division of all terms by $2mc^2$, Eq. (118) may be approximated as

$$\hat{H}\Psi = \left[\frac{1}{2m}(-i\hbar\nabla - q\mathbf{A})^2 + q\phi - \frac{q}{m}\hat{\mathbf{S}} \cdot \mathcal{B} + \frac{i\hbar q}{2mc}\hat{\mathbf{a}} \cdot \mathcal{E} \right] \Psi. \quad (9.121)$$

Let us discuss this important result. The first two terms in the square brackets give the non-relativistic Hamiltonian (3.26), which was extensively used in Chapter 3 for the discussion of charged particle motion. Note again that the contribution of the vector potential \mathbf{A} into that Hamiltonian is essentially relativistic, in the following sense: when used for the description of magnetic interaction of two charged particles, due to their *orbital* motion with speed $v \ll c$, the magnetic interaction is a factor of $(v/c)^2$ smaller than the electrostatic interaction of the particles.⁵⁵ The reason why we did discuss the effects of \mathbf{A} in Chapter 3 was that it was used there to describe *external* magnetic fields, keeping our analysis valid even for the cases when that field is strong because of being produced by relativistic effects – such as aligned spins of a permanent magnet.

The next, third term in the square brackets of Eq. (121) should be also familiar to the reader: this is the Pauli Hamiltonian – see Eqs. (4.3), (4.5), and (4.163). When justifying this form of interaction in Chapter 4, I referred mostly to the results of Stern-Gerlach-type experiments, but it is extremely pleasing that this result⁵⁶ follows from such a fundamental relativistic treatment as Dirac's theory. As we already know from the discussion of the Zeeman effect in Sec. 6.4, the magnetic field effects on the orbital motion of an electron (described by the orbital angular momentum \mathbf{L}) and its spin \mathbf{S} are of the same order, though quantitatively different.

Finally, the last term in the square brackets of Eq. (121) is also not quite new for us: in particular, it describes the spin-orbit interaction. Indeed, in the case of a classical, spherical-symmetric electric field \mathcal{E} corresponding to the potential $\phi(r) = U(r)/q$, this term may be reduced to Eq. (6.56):

$$\hat{H}_{\text{so}} = \frac{1}{2m^2c^2}\hat{\mathbf{S}} \cdot \hat{\mathbf{L}} \frac{1}{r} \frac{dU}{dr} \equiv -\frac{q}{2m^2c^2}\hat{\mathbf{S}} \cdot \hat{\mathbf{L}} \frac{1}{r}\mathcal{E}. \quad (9.122)$$

The proof of this correspondence requires a bit of additional work.⁵⁷ Indeed, in Eq. (121), the term responsible for the spin-orbit interaction acts on 4-component wavefunctions, while the Hamiltonian (122) is supposed to act on non-relativistic state vectors with an account of spin, whose coordinate representation may be given by 2-component spinors:⁵⁸

⁵⁵ This difference may be traced by classical means – see, e.g., EM Sec. 5.1.

⁵⁶ Note that in this result, the g -factor of the particle is still equal to exactly 2 – see Eq. (4.115) and its discussion in Sec. 4.4. In order to describe the small deviation of g_e from 2, the electromagnetic field should be quantized (just as this was discussed in Secs. 1-4 of this chapter), and its potentials \mathbf{A} and ϕ , participating in Eq. (121), should be treated as operators – rather than as c -number functions as was assumed above.

⁵⁷ The only facts immediately evident from Eq. (121) are that the term we are discussing is proportional to the electric field, as required by Eq. (122), and that it is of the proper order of magnitude. Indeed, Eqs. (101)-(102) imply that in the Dirac theory, $c\hat{\mathbf{a}}$ plays the role of the velocity operator, so that the expectation values of the term are of the order of $\hbar q v \mathcal{E}/2mc^2$. Since the expectation values of the operators participating in the Hamiltonian (122) scale as $S \sim \hbar/2$ and $L \sim mvr$, the spin-orbit interaction energy has the same order of magnitude.

⁵⁸ In this course, the notion of spinor (popular in some textbooks) was not used much; it was introduced earlier only for two-particle states – see Eq. (8.13). For a single particle, such definition is reduced to $\psi(\mathbf{r})|s\rangle$, whose representation in a particular spin-½ basis is the column (123). Note that such spinors may be used as a basis for an expansion of the spin-orbitals $\psi_j(\mathbf{r})$ defined by Eq. (8.125), where the index j is used for numbering both the spin's orientation (i.e. the particular component of the spinor's column) and the orbital eigenfunction.

$$\psi = \begin{pmatrix} \psi_{\uparrow} \\ \psi_{\downarrow} \end{pmatrix}. \quad (9.123)$$

The simplest way to prove the equivalence of these two expressions is not to use Eq. (121) directly, but to return to the Dirac equation (112), for the particular case of motion in a static electric field but no magnetic field, when Dirac's Hamiltonian is reduced to

$$\hat{H} = c\hat{\mathbf{a}} \cdot \hat{\mathbf{p}} + \hat{\beta}mc^2 + U(\mathbf{r}), \quad \text{with } U = q\phi. \quad (9.124)$$

Since this Hamiltonian is time-independent, we may look for its 4-component eigenfunctions in the form

$$\Psi(\mathbf{r}, t) = \begin{pmatrix} \psi_+(\mathbf{r}) \\ \psi_-(\mathbf{r}) \end{pmatrix} \exp\left(-i\frac{E}{\hbar}t\right), \quad (9.125)$$

where each of ψ_{\pm} is a 2-component column of the type (123), representing two spin states of the particle (index +) and its antiparticle (index -). Plugging Eq. (125) into Eq. (95) with the Hamiltonian (124), and using Eq. (98a), we get the following system of two linear equations:

$$[E - mc^2 - U(\mathbf{r})]\psi_+ - c\hat{\mathbf{a}} \cdot \hat{\mathbf{p}}\psi_- = 0, \quad [E + mc^2 - U(\mathbf{r})]\psi_- - c\hat{\mathbf{a}} \cdot \hat{\mathbf{p}}\psi_+ = 0. \quad (9.126)$$

Expressing ψ_- from the latter equation, and plugging the result into the former one, we get the following single equation for the particle's spinor:

$$\left[E - mc^2 - U(\mathbf{r}) - c^2\hat{\mathbf{a}} \cdot \hat{\mathbf{p}} \frac{1}{E + mc^2 - U(\mathbf{r})}\hat{\mathbf{a}} \cdot \hat{\mathbf{p}} \right] \psi_+ = 0. \quad (9.127)$$

So far, this is an exact equation for eigenstates and eigenvalues of the Hamiltonian (124), but it may be substantially simplified in the low-energy limit when both the potential energy⁵⁹ and the non-relativistic eigenenergy

$$\tilde{E} \equiv E - mc^2 \quad (9.128)$$

are much lower than mc^2 . Indeed, in this case, the expression in the denominator of the last term in the brackets of Eq. (127) is close to $2mc^2$. Since $\sigma^2 = 1$, with that replacement, Eq. (127) is reduced to the non-relativistic Schrödinger equation, similar for both spin components of ψ_+ , and hence giving spin-degenerate energy levels. To recover small relativistic and spin-orbit effects, we need a slightly more accurate approximation:

$$\frac{1}{E + mc^2 - U(\mathbf{r})} \equiv \frac{1}{2mc^2 + \tilde{E} - U(\mathbf{r})} \equiv \frac{1}{2mc^2} \left[1 + \frac{\tilde{E} - U(\mathbf{r})}{2mc^2} \right]^{-1} \approx \frac{1}{2mc^2} \left[1 - \frac{\tilde{E} - U(\mathbf{r})}{2mc^2} \right], \quad (9.129)$$

in which Eq. (127) is reduced to

$$\left[\tilde{E} - U(\mathbf{r}) - \frac{\hat{\mathbf{p}}^2}{2m} + \hat{\mathbf{a}} \cdot \hat{\mathbf{p}} \frac{\tilde{E} - U(\mathbf{r})}{(2mc^2)^2} \hat{\mathbf{a}} \cdot \hat{\mathbf{p}} \right] \psi_+ = 0. \quad (9.130)$$

As Eqs. (5.34) shows, the operators of the momentum and of a function of coordinates commute as

$$[\hat{\mathbf{p}}, U(\mathbf{r})] = -i\hbar \nabla U, \quad (9.131)$$

⁵⁹ Strictly speaking, this requirement is imposed on the expectation values of $U(\mathbf{r})$ in the eigenstates to be found.

so that the last term in the square brackets of Eq. (130) may be rewritten as

$$\hat{\sigma} \cdot \hat{p} \frac{\tilde{E} - U(\mathbf{r})}{(2mc)^2} \hat{\sigma} \cdot \hat{p} \equiv \frac{\tilde{E} - U(\mathbf{r})}{(2mc)^2} \hat{p}^2 - \frac{i\hbar}{(2mc)^2} (\hat{\sigma} \cdot \nabla U)(\hat{\sigma} \cdot \hat{p}). \quad (9.132)$$

Since in the low-energy limit, both terms on the right-hand side of this relation are much smaller than the three leading terms of Eq. (130), we may replace the first term's numerator with its non-relativistic approximation $\hat{p}^2 / 2m$. With this replacement, the term coincides with the first relativistic correction to the kinetic energy operator – see Eq. (6.47). The second term, proportional to the electric field $\mathcal{E} = -\nabla\phi = -\nabla U/q$, may be transformed further on, using a readily verifiable identity

$$(\hat{\sigma} \cdot \nabla U)(\hat{\sigma} \cdot \hat{p}) \equiv (\nabla U) \cdot \hat{p} + i\hat{\sigma} \cdot [(\nabla U) \times \hat{p}]. \quad (9.133)$$

Of the two terms on the right-hand side of this relation, only the second one depends on spin,⁶⁰ giving the following spin-orbital interaction contribution to the Hamiltonian,

$$\hat{H}_{\text{so}} = \frac{\hbar}{(2mc)^2} \hat{\sigma} \cdot [(\nabla U) \times \hat{p}] \equiv \frac{q}{2m^2 c^2} \hat{\mathbf{S}} \cdot [(\nabla\phi) \times \hat{p}]. \quad (9.134)$$

For a central potential $\phi(r)$, its gradient has only the radial component: $\nabla\phi = (d\phi/dr)\mathbf{r}/r = -\mathcal{E}\mathbf{r}/r$, and with the angular momentum definition (5.147), Eq. (134) is (finally!) reduced to Eq. (122).

As was shown in Sec. 6.3, the perturbative treatment of Eq. (122), together with the kinetic-relativistic correction (6.47), in the hydrogen-like atom/ion problem, leads to the fine structure of each Bohr level E_n , given by Eq. (6.60):

$$\Delta E_{\text{fine}} = -\frac{2E_n}{mc^2} \left(3 - \frac{4n}{j + \frac{1}{2}} \right). \quad (9.135)$$

This result receives a confirmation from the surprising fact that for the hydrogen-like atom/ion problem, the Dirac equation may be solved *exactly* – without any assumptions. I would not have time/space to reproduce the solution,⁶¹ and will only list the final result for the energy spectrum:

$$\frac{E}{mc^2} = \left\{ 1 + \frac{Z^2 \alpha^2}{\left[n + \left\{ (j + \frac{1}{2})^2 - Z^2 \alpha^2 \right\}^{1/2} - (j + \frac{1}{2}) \right]^2} \right\}^{-1/2}. \quad (9.136)$$

Here $n = 1, 2, \dots$ is the same principal quantum number as in Bohr's theory, while j is the quantum number specifying the eigenvalues (5.175) of J^2 , in our case of a spin-½ particle taking half-integer values: $j = l \pm \frac{1}{2} = 1/2, 3/2, 5/2, \dots$ – see Eq. (5.189). This is natural, because due to the spin-orbit interaction, the orbital momentum and spin are not conserved, while their vector sum, $\mathbf{J} = \mathbf{L} + \mathbf{S}$, is – at least in the absence of an external field. Each energy level (136) is doubly-degenerate, with two eigenstates representing two directions of the spin. (In the low-energy limit, we may say: corresponding to two values of $l = j \mp \frac{1}{2}$, at fixed j .)

⁶⁰ The first term gives a small spin-independent energy shift, which is very difficult to verify experimentally.

⁶¹ Good descriptions of the solution are available in many textbooks (the older the better :-) – see, e.g., Sec. 53 in L. Schiff, *Quantum Mechanics*, 3rd ed., McGraw-Hill (1968).

Speaking of that limit (when $E - mc^2 \sim E_H \ll mc^2$): since according to Eq. (1.13) for E_H , the square of the fine-structure constant $\alpha \equiv e^2/4\pi\epsilon_0\hbar c$ may be represented as the ratio E_H/mc^2 , we may follow this limit expanding Eq. (136) into the Taylor series in $(Z\alpha)^2 \ll 1$. The result,

$$E \approx mc^2 \left[1 - \frac{Z^2 \alpha^2}{2n^2} - \frac{Z^4 \alpha^4}{2n^4} \left(\frac{n}{|j + \frac{1}{2}|} - \frac{3}{4} \right) \right], \quad (9.137)$$

has the same structure, and allows the same interpretation as Eq. (92), but with the last term coinciding with Eq. (6.60) – and with experimental results. Historically, this correct description of the fine structure of the atomic levels provided the decisive proof of Dirac's theory.

However, even such an impressive theory does not have too many direct applications. The main reason for that was already discussed in brief in the end of Sec. 5: due to the possibility of creation and annihilation of particle-antiparticle pairs by an energy influx higher than $2mc^2$, the number of particles participating in high-energy interactions is not fixed. An adequate general description of such situations is given by the quantum field theory, in which the particle's wavefunction is treated as a field to be quantized, using so-called *field operators* $\hat{\Psi}(\mathbf{r}, t)$ – very much similar to the electromagnetic field operators (16). The Dirac equation follows from such theory in the single-particle approximation.

As was mentioned above on several occasions, the quantum field theory is well beyond the time/space limits of this course, and I have to stop here, referring the interested reader to one of several excellent textbooks on this discipline.⁶² However, I would strongly encourage the students going in this direction to start by playing with the field operators on their own, taking clues from Eqs. (16), but replacing the creation/annihilations operators \hat{a}_j^\dagger and \hat{a}_j of the electromagnetic field oscillators with those of the general second quantization formalism outlined in Sec. 8.3.

9.8. Exercise problems

9.1. Prove the Casimir formula, given by Eq. (23), by calculating the net force $F = \mathcal{P}A$ exerted by the electromagnetic field, in its ground state, on two perfectly conducting parallel plates of area A , separated by a vacuum gap of width $t \ll A^{1/2}$.

Hint: Calculate the field energy in the gap volume with and without the account of the plate effect, and then apply the Euler-Maclaurin formula⁶³ to the difference between these two results.

9.2. Electromagnetic radiation by some single-mode quantum sources may have such a high degree of coherence that it is possible to observe the interference of waves from two independent sources with virtually the same frequency, incident on one detector.

(i) Generalize Eq. (29) to this case.

⁶² For a gradual introduction see, e.g., either L. Brown, *Quantum Field Theory*, Cambridge U. Press (1994) or R. Klauber, *Student Friendly Quantum Field Theory*, Sandtrove (2013). On the other hand, M. Srednicki, *Quantum Field Theory*, Cambridge U. Press (2007) and A. Zee, *Quantum Field Theory in a Nutshell*, 2nd ed., Princeton (2010), among others, offer steeper learning curves.

⁶³ See, e.g., MA Eq. (2.12a).

(ii) Use this generalized expression to show that incident waves in different Fock states do not create an interference pattern.

9.3. Calculate the zero-delay value $g^{(2)}(0)$ of the second-order correlation function of a single-mode electromagnetic field in the so-called *Schrödinger-cat state*:⁶⁴ a coherent superposition of two Glauber states, with equal but sign-opposite parameters α , and a certain phase shift between them.

9.4. Calculate the zero-delay value $g^{(2)}(0)$ of the second-order correlation function of a single-mode electromagnetic field in the squeezed ground state ζ defined by Eq. (5.142).

9.5. Calculate the rate of spontaneous photon emission (into unrestricted free space) by a hydrogen atom, initially in the $2p$ state ($n = 2, l = 1$) with $m = 0$. Would the result be different for $m = \pm 1$ for the $2s$ state ($n = 2, l = 0, m = 0$)? Discuss the relation between these quantum-mechanical results and those given by the classical theory of radiation for the simplest classical model of the atom.

9.6. An electron has been placed on the lowest excited level of a spherically-symmetric, quadratic potential well $U(\mathbf{r}) = m_e\omega^2 r^2/2$. Calculate the rate of its relaxation to the ground state, with the emission of a photon (into unrestricted free space). Compare the rate with that for a similar transition of the hydrogen atom, for the case when the radiation frequencies of these two systems are equal.

9.7. Derive an analog of Eq. (53) for the spontaneous photon emission into the free space, due to a change of the *magnetic* dipole moment \mathbf{m} of a small-size system.

9.8. A spin- $1/2$ particle, with a gyromagnetic ratio γ , is in its orbital ground state in dc magnetic field \mathcal{B}_0 . Calculate the rate of its spontaneous transition from the higher to the lower energy level, with the emission of a photon into the free space. Evaluate this rate for an electron in a field of 10 T, and discuss the implications of this result for laboratory experiments with electron spins.

9.9. Calculate the rate of spontaneous transitions between the two sublevels of the ground state of a hydrogen atom, formed as a result of its hyperfine splitting. Discuss the implications of the result for the width of the 21-cm spectral line of hydrogen.

9.10. Find the eigenstates and eigenvalues of the Jaynes-Cummings Hamiltonian (78), and discuss their behavior near the resonance point $\omega = \Omega$.

9.11. Analyze the Purcell effect, mentioned in Secs. 3 and 4, quantitatively; in particular, calculate the so-called *Purcell factor* F_P defined as the ratio of the rate Γ_s of atom's spontaneous emission into a resonant cavity tuned exactly to the quantum transition frequency, to that into the free space.

9.12. Prove that the Klein-Gordon equation (84) may be rewritten in the form similar to the non-relativistic Schrödinger equation (1.25), but for a two-component wavefunction, with the Hamiltonian represented (in the usual z -basis) by the following 2×2 -matrix:

⁶⁴ Its name stems from the well-known *Schrödinger cat paradox*, which is (very briefly) discussed in Sec. 10.1.

$$H = -(\sigma_z + i\sigma_y) \frac{\hbar^2}{2m} \nabla^2 + mc^2 \sigma_z.$$

Use your solution to discuss the physical meaning of the wavefunction's components.

9.13. Calculate and discuss the energy spectrum of a relativistic, spinless, charged particle placed into an external uniform, time-independent magnetic field \mathcal{B} . Use the result to formulate the condition of validity of the non-relativistic theory in this situation.

9.14. Prove Eq. (91) for the energy spectrum of a hydrogen-like atom/ion, starting from the relativistic Schrödinger equation.

Hint: A mathematical analysis of Eq. (3.193) shows that its eigenvalues are given by Eq. (3.201), $\varepsilon_n = -1/2n^2$, with $n = l + 1 + n_r$, where $n_r = 0, 1, 2, \dots$, even if the parameter l is not integer.

9.15. Derive a general expression for the differential cross-section of elastic scattering of a spinless relativistic particle by a static potential $U(\mathbf{r})$, in the Born approximation, and formulate the conditions of its validity. Use these results to calculate the differential cross-section of scattering of a particle with the electric charge $-e$ by the Coulomb electrostatic potential $\phi(\mathbf{r}) = Ze/4\pi\varepsilon_0 r$.

9.16. Starting from Eqs. (95)-(98), prove that the probability density w given by Eq. (101) and the probability current density \mathbf{j} defined by Eq. (102) do indeed satisfy the continuity equation (1.52): $\partial w/\partial t + \nabla \cdot \mathbf{j} = 0$.

9.17. Calculate the commutator of the operator \hat{L}^2 and Dirac's Hamiltonian of a free particle. Compare the result with that for the non-relativistic Hamiltonian, and interpret the difference.

9.18. Calculate commutators of the operators \hat{S}^2 and \hat{J}^2 with Dirac's Hamiltonian (97), and give an interpretation of the results.

9.19. In the Heisenberg picture of quantum dynamics, derive an equation describing the time evolution of free electron's velocity in the Dirac theory. Solve the equation for the simplest state, with definite energy and momentum, and discuss the solution.

9.20. Calculate the eigenstates and eigenenergies of a relativistic spin- $1/2$ particle with charge q , placed into a uniform, time-independent external magnetic field \mathcal{B} . Compare the calculated energy spectrum with those following from the non-relativistic theory and the relativistic Schrödinger equation.

9.21.* Following the discussion at the very end of Section 7, introduce quantum field operators $\hat{\psi}$ that would be related to the usual wavefunctions ψ just as the electromagnetic field operators (16) are related to the classical electromagnetic fields, and explore basic properties of these operators. (For this preliminary study, consider the fixed-time situation.)

Chapter 10. Making Sense of Quantum Mechanics

This (rather brief) chapter addresses some conceptually important issues of quantum measurements and quantum state interpretation. Please note that some of these issues are still subjects of debate¹ – fortunately not affecting quantum mechanics' practical results, discussed in the previous chapters.

10.1. Quantum measurements

The knowledge base outlined in the previous chapters gives us a sufficient background for a (by necessity, very brief) discussion of *quantum measurements*.² Let me start by reminding the reader of the only postulate of the quantum theory that relates it to experiment – so far, meaning *perfect* measurements. In the simplest case when the system is in a coherent (pure) quantum state, its ket-vector may be represented as a linear superposition

$$|\alpha\rangle = \sum_j \alpha_j |a_j\rangle, \quad (10.1)$$

where a_j are the eigenstates of the operator of an observable A , related to its eigenvalues A_j by Eq. (4.68):

$$\hat{A}|a_j\rangle = A_j|a_j\rangle. \quad (10.2)$$

In such a state, the outcome of every single measurement of the observable A may be uncertain, but is restricted to the set of eigenvalues A_j , with the j^{th} outcome probability equal to

$$W_j = |\alpha_j|^2. \quad (10.3)$$

As was discussed in Chapter 7, the state of the system (or rather of the statistical ensemble of macroscopically similar systems we are using for this particular series of similar experiments) may be not coherent, and hence even more uncertain than the state described by Eq. (1). Hence, the measurement postulate means that even if the system is in this (the least uncertain) state, the measurement outcomes are *still* probabilistic.³

If we believe that a particular measurement may be done perfectly, and do not worry too much how exactly, we are subscribing to the *mathematical* notion of measurement, that was, rather reluctantly, used in these notes – up to this point. However, the actual (*physical*) measurements are *always* imperfect, first of all because of the huge gap between the energy-time scale $\hbar \sim 10^{-34}$ J·s of the quantum phenomena in “microscopic” systems such as atoms, and the “macroscopic” scale of the direct human perception, so that the role of the instruments bridging this gap (Fig. 1), is highly nontrivial.

¹ For an excellent review of these controversies, as presented in a few leading textbooks, I highly recommend J. Bell's paper in the collection by A. Miller (ed.), *Sixty-Two Years of Uncertainty*, Plenum, 1989.

² “Quantum measurements” is a very unfortunate and misleading term; it would be more sensible to speak about “measurements of observables in quantum mechanical systems”. However, the former term is so common and compact that I will use it – albeit rather reluctantly.

³ The measurement outcomes become definite only in the trivial case when the system is definitely in one of the eigenstates a_j , say a_0 ; then $\alpha_j = \delta_{j,0} \exp\{i\varphi\}$, and $W_j = \delta_{j,0}$.

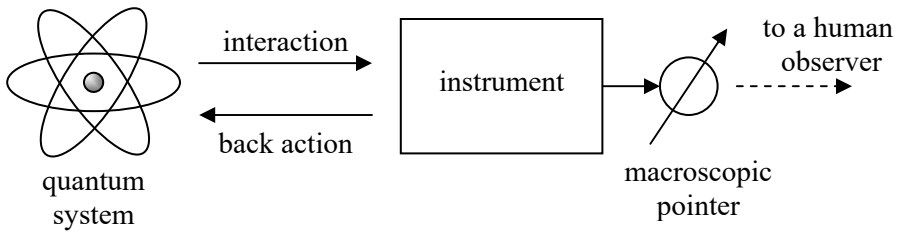


Fig.10.1. The general scheme of a quantum measurement.

Besides the famous Bohr-Einstein discussion in the mid-1930s, which will be briefly reviewed in Sec. 3, the founding fathers of quantum mechanics have not paid much attention to these issues, apparently because of the following reason. At that time it looked like the experimental instruments (at least the best of them :-) were doing exactly what the measurement postulate was telling. For example, the z-oriented Stern-Gerlach experiment (Fig. 4.1) turns two complex coefficients $\alpha\uparrow$ and $\alpha\downarrow$, describing the spin state of the incoming electrons, into a set of particle-counter clicks, with the rates proportional to, respectively, $|\alpha\uparrow|^2$ and $|\alpha\downarrow|^2$. The crude internal nature of these instruments makes more detailed questions unnatural. For example, each click of a Geiger counter involves an effective disappearance of one observed electron in a zillion-particle electric discharge avalanche it has triggered. A century ago, it looked much more important to extend the newly born quantum mechanics to more complex systems (such as atomic nuclei, etc.) than to think about the physics of such instruments.

However, since that time the experimental techniques, notably including high-vacuum and low-temperature systems, micro- and nano-fabrication, and low-noise electronics, have improved quite dramatically. In particular, we now may observe quantum-mechanical behavior of more and more macroscopic objects – such as the micromechanical oscillators mentioned in Sec. 2.9. Moreover, some “macroscopic quantum systems” (in particular, special systems of Josephson junctions, see below) have properties enabling their use as essential parts of measurement setups. Such developments are making the line separating the “micro” and “macro” worlds finer and finer, so that more inquisitive inquiries into the physical nature of quantum measurements are not so hopeless now. In my personal scheme of things,⁴ these inquiries may be grouped as follows:

(i) Does a quantum measurement involve any laws besides those of quantum mechanics? In particular, should it necessarily involve a human/intelligent observer? (The last question is not as laughable as it may look – see below.)

(ii) What is the state of the measured system *just after a single-shot* measurement – meaning a measurement process limited to a time interval much shorter than the time scale of the measured system’s evolution? (This question is a necessary part of any discussion of *repeated measurements* and of their ultimate form – *continuous monitoring* of a certain observable.)

(iii) If a measurement of an observable A has produced a certain outcome A_j , what statements may be made about the state of the system *just before* the measurement? (This question is most closely related to various interpretations of quantum mechanics.)

Let me discuss these issues in the listed order. First of all, I am happy to report that there is a virtual consensus of physicists on some aspects of these issues. According to this consensus, any reasonable quantum measurement needs to result in a certain, distinguishable state of a *macroscopic* output component of the measurement instrument – see Fig. 1. (Traditionally, its component is called a

⁴ Again, this list and some other issues discussed in the balance of this section are still controversial.

pointer, though its role may be played by a printer or a plotter, an electronic circuit sending out the result as a number, etc.). This requirement implies that the measurement process should have the following features:

- provide a large “signal gain”, i.e. some means of mapping the quantum state with its \hbar -scale of action (i.e. of the energy-by-time product) onto a macroscopic position of the pointer with a much larger action scale, and
- if we want to approach the fundamental limit of uncertainty, given by Eq. (3), the instrument should introduce as little additional fluctuations (“noise”) as permitted by the laws of physics.

Both these requirements *are* fulfilled in a well-designed Stern-Gerlach experiment – see Fig. 4.1 again. Indeed, the magnetic field gradient, splitting the electron beam, turns the minuscule (microscopic) energy difference (4.167) between two spin-polarized states into a macroscopic difference between the final positions of two output beams, where their detectors may be located. However, as was noted above, the internal physics of the particle detectors (say, Geiger counters) at this measurement is rather complex, and would not allow us to discuss some aspects of the measurement, in particular to answer the second of inquiries we are working on.

This is why let me describe the scheme of an almost similar “single-shot” measurement of a two-level quantum system, which shares the simplicity, high gain, and low internal noise of the Stern-Gerlach apparatus, but has an advantage that at its certain hardware implementations,⁵ the measurement process allows a thorough, quantitative theoretical description. Let us measure a particle trapped in a double-well potential (Fig. 2), where x is some continuous generalized coordinate – not necessarily a mechanical displacement. Let the particle be initially in a pure quantum state, with the energy close to the well’s bottom. Then, as we know from the discussion of such systems in Secs. 2.6 and 5.1, the state may be described by a ket-vector similar to that of spin-½:

$$|\alpha\rangle = \alpha_{\rightarrow} |\rightarrow\rangle + \alpha_{\leftarrow} |\leftarrow\rangle, \quad (10.4)$$

where the component states \rightarrow and \leftarrow is described by wavefunctions localized near the potential well bottoms at $x \approx \pm x_0$ – see the blue lines in Fig. 2. Our goal is to measure in which well the particle resides at a certain time instant, say at $t = 0$. For that, let us rapidly change, at that moment, the potential profile of the system, so that at $t > 0$, near the origin, it may be well described by an inverted parabola:

$$U(x) \approx -\frac{m\lambda^2}{2} x^2, \quad \text{for } t > 0, \quad |x| \ll x_f. \quad (10.5)$$

⁵ The scheme may be implemented, for example, using a simple Josephson-junction circuit called the *balanced comparator* – see, e.g., T. Walls *et al.*, *IEEE Trans. on Appl. Supercond.* **17**, 136 (2007), and references therein. Experiments have demonstrated that this system may have a measurement variance dominated by the theoretically expected quantum-mechanical uncertainty, at practicable experimental conditions (at temperatures below $\sim 1\text{K}$). A conceptual advantage of this system is that it is based on externally-shunted Josephson junctions, i.e. the devices whose quantum-mechanical model, including its part describing the coupling to the environment, is in a quantitative agreement with experiment – see, e.g., D. Schwartz *et al.*, *Phys. Rev. Lett.* **55**, 1547 (1985). Colloquially, the balanced comparator is a high-gain instrument with a “well-documented Hamiltonian”, eliminating the need for speculations about the environmental effects. In particular, the dephasing process in it, and its time T_2 , are well described by Eqs. (7.89) and (7.142), with the coefficients η equal to the Ohmic conductances G of the shunts.

It is straightforward to verify that the Heisenberg equations of motion in such an inverted potential describe exponential growth of operator \hat{x} in time (proportional to $\exp\{\lambda t\}$) and hence a similar, proportional growth of the expectation value $\langle x \rangle$ and its r.m.s. uncertainty δx .⁶ At this “inflation” stage, the coherence between the two component states \rightarrow and \leftarrow is still preserved, i.e. the time evolution of the system is, in principle, reversible.

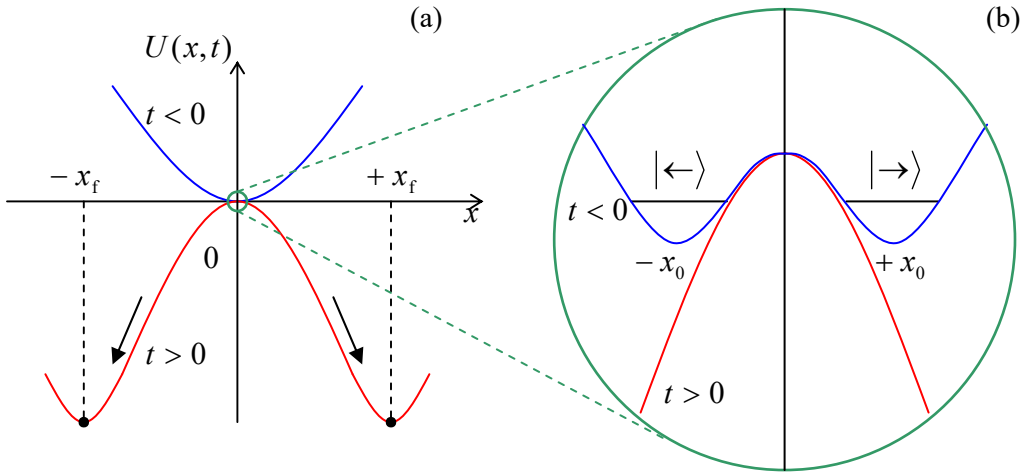


Fig. 10.2. The potential inversion, as viewed on the (a) “macroscopic” and (b) “microscopic” scales of the generalized coordinate x .

Now let the system be weakly coupled, also at $t > 0$, to a dissipative (e.g., Ohmic) environment. As we know from Chapter 7, such coupling ensures the state’s dephasing on some time scale T_2 . If

$$x_0 \ll x_0 \exp\{\lambda T_2\}, x_f, \quad (10.6)$$

then the process, after the potential inversion, consists of two stages, well separated in time:

- the already discussed “inflation” stage, preserving the component the state’s coherence, and
- the dephasing stage, at which the coherence of the component states \rightarrow and \leftarrow is gradually suppressed as described by Eq. (7.89), i.e. the density matrix of the system is gradually reduced to the diagonal form describing a classical mixture of two probability packets with the probabilities (3) equal to, respectively, $W_{\rightarrow} = |\alpha_{\rightarrow}|^2$ and $W_{\leftarrow} = |\alpha_{\leftarrow}|^2 \equiv 1 - |\alpha_{\rightarrow}|^2$.

Besides dephasing, the environment gives the motion certain kinematic friction, with the drag coefficient η (7.141), so that the system eventually settles to rest at one of the macroscopically separated minima $x = \pm x_f$ of the inverted potential (Fig. 2a), thus ensuring a high “signal gain” $x_f/x_0 \gg 1$. As a result, the final probability density distribution $w(x)$ along the x -axis has two narrow, well-separated peaks. But this is just the situation that was discussed in Sec. 2.5 – see, in particular, Fig. 2.17. Since that discussion is very important, let me repeat – or rather rephrase it. The final state of the system is a classical mixture of two well-separated states, with the respective probabilities W_{\leftarrow} and W_{\rightarrow} , whose sum equals 1. Now let us use some detector to test whether the system is in one of these states – say the right

⁶ Somewhat counter-intuitively, the latter growth *improves* the measurement’s fidelity. Indeed, it does not affect the intrinsic “signal-to-noise ratio” $\delta x/\langle x \rangle$, while making the intrinsic (say, quantum-mechanical) uncertainty much larger than the possible noise contribution by the later measurement stage(s).

one. (If x_f is sufficiently large, the noise contribution of this detector into the measurement uncertainty is negligible,⁷ and its physics is unimportant.) If the system has been found at this location (again, the probability of this outcome is $W_{\rightarrow} = |\alpha_{\rightarrow}|^2$), the probability to find it at the counterpart (left) location at a consequent detection turns to zero.

This probability “reduction” is a purely classical (or if you like, mathematical) effect of the statistical ensemble’s re-definition: W_{\leftarrow} equals zero not in the initial ensemble of all similar experiments (where is equals $|\alpha_{\leftarrow}|^2$), but only in the re-defined ensemble of experiments in that the system had been found at the right location. Of course, which ensemble to use, i.e. what probabilities to register/publish is a purely accounting decision, which should be made by a human (or otherwise intelligent :-) observer. If we are only interested in an objective recording of results of a pre-fixed sequence of experiments (i.e. the members of a pre-defined, fixed statistical ensemble), there is no need to include such an observer in any discussion. In any case, this detection/registration process, very common in classical statistics, leaves no space for any mysterious “wave packet reduction” – understood as a hypothetical process that would not obey the regular laws of quantum mechanical evolution.

The state dephasing and ensemble re-definition at measurements are in the core of several paradoxes, of which the so-called *quantum Zeno paradox* is perhaps the most spectacular.⁸ Let us return to a two-level system with the unperturbed Hamiltonian given by Eq. (4.166), the quantum oscillation period $2\pi/\Omega$ much longer than the single-shot measurement time, and the system initially (at $t = 0$) definitely in one of the partial quantum states – for example, a certain potential well of the double-well potential. Then, as we know from Secs. 2.6 and 4.6, the probability to find the system in this initial state at time $t > 0$ is

$$W(t) = \cos^2 \frac{\Omega t}{2} \equiv 1 - \sin^2 \frac{\Omega t}{2}. \quad (10.7)$$

If the time is small enough ($t = dt \ll 1/\Omega$), we may use the Taylor expansion to write

$$W(dt) \approx 1 - \frac{\Omega^2 dt^2}{4}. \quad (10.8)$$

Now, let us use some good measurement scheme (say, the potential inversion discussed above) to measure whether the system is still in this initial state. If it is (as Eq. (8) shows, the probability of such an outcome is nearly 100%), then the system, after the measurement, is in the same state. Let us allow it to evolve again, with the same Hamiltonian. Then the evolution of W will follow the same law

⁷ At the balanced-comparator implementation mentioned above, the final state detection may be readily performed using a “SQUID” magnetometer based on the same Josephson junction technology – see, e.g., EM Sec. 6.5. In this case, the distance between the potential minima $\pm x_f$ is close to one superconducting flux quantum (3.38), while the additional uncertainty induced by the SQUID may be as low as a few millionths of that amount.

⁸ This name, coined by E. Sudarshan and B. Mishra in 1997 (though the paradox had been discussed in detail by A. Turing in 1954) is due to its superficial similarity to the classical paradoxes by the ancient Greek philosopher Zeno of Elea. By the way, just for fun, let us have a look at what happens when Mother Nature is discussed by people that do not understand math and physics. The most famous of the classical Zeno paradoxes is the case of *Achilles and Tortoise*: the fast runner Achilles can apparently never overtake the slower Tortoise, because (in Aristotle’s words) “the pursuer must first reach the point whence the pursued started, so that the slower must always hold a lead”. For a physicist, the paradox has a trivial, obvious resolution, but here is what a philosopher writes about it – not in some year BC, but in the 2010 AD: “Given the history of ‘final resolutions’, from Aristotle onwards, it’s probably foolhardy to think we’ve reached the end.” For me, this is a sad symbol of modern philosophy.

as in Eq. (7). Thus, when the system is measured again at time $2dt$, the probability to find it in the same state both times is

$$W(2dt) \approx W(dt) \left(1 - \frac{\Omega^2 dt^2}{4}\right) = \left(1 - \frac{\Omega^2 dt^2}{4}\right)^2. \quad (10.9)$$

After repeating this cycle N times (with the total time $t = Ndt$ still much less than $N^{1/2}/\Omega$), the probability that the system is still in its initial state is

$$W(Ndt) \equiv W(t) \approx \left(1 - \frac{\Omega^2 dt^2}{4}\right)^N = \left(1 - \frac{\Omega^2 t^2}{4N^2}\right)^N \approx 1 - \frac{\Omega^2 t^2}{4N}. \quad (10.10)$$

Comparing this result with Eq. (7), we see that the process of system's transfer to the opposite partial state has been slowed down rather dramatically, and in the limit $N \rightarrow \infty$ (at fixed t), its evolution is virtually stopped by the measurement process. There is of course nothing mysterious here; the evolution slowdown is due to the quantum state dephasing at each measurement.

This may be the only acceptable occasion for me to mention, very briefly, one more famous – or rather infamous *Schrödinger cat paradox*, so much overplayed in popular publications.⁹ For this thought experiment, there is no need to discuss the (rather complicated :-) physics of the cat. As soon as the charged particle, produced at the radioactive decay, reaches the Geiger counter, the initial coherent superposition of the two possible quantum states (“the decay has happened”)/“the decay has not happened”) of the system is rapidly dephased, i.e. reduced to their classical mixture, leading, correspondingly, to the classical mixture of the final macroscopic states “cat dead”/“cat alive”. So, despite attempts by numerous authors, without a proper physics background, to represent this situation as a mystery whose discussion needs involvement of professional philosophers, hopefully the reader knows enough about dephasing from Chapter 7, to ignore all this babble.

10.2. QND measurements

I hope that the above discussion has sufficiently illuminated the issues of the group (i), so let me proceed to the question group (ii), in particular to the general issue of the *back action* of the instrument upon the system under measurement – symbolized with the back arrow in Fig. 1. In the instruments like the Geiger counter, such back action is large: the instrument essentially destroys (“demolishes”) the state of the system under measurement. Even the “cleaner” potential-inversion measurement, shown in Fig. 2, fully destroys the initial coherence of the system, i.e. perturbs it rather substantially.

However, in the 1970s it was understood that this is not really necessary. For example, in Sec. 7.3, we have already discussed an example of a two-level system coupled with its environment and described by the Hamiltonian (7.68)-(7.70):

$$\hat{H} = \hat{H}_s + \hat{H}_{\text{int}} + \hat{H}_e \{\lambda\}, \quad \text{with } \hat{H}_s = c_z \hat{\sigma}_z, \text{ and } \hat{H}_{\text{int}} = -f \{\lambda\} \hat{\sigma}_z, \quad (10.11)$$

so that

$$[\hat{H}_s, \hat{H}_{\text{int}}] = 0. \quad (10.12)$$

⁹ I fully agree with S. Hawking who has been quoted to say, “When I hear about the Schrödinger cat, I reach for my gun.” The only good aspect of this popularity is that the formulation of this paradox should be so well known to the reader that I do not need to waste time/space repeating it.

Comparing this equality with Eq. (4.199), applied to the explicitly-time-independent Hamiltonian \hat{H}_s ,

$$i\hbar \dot{\hat{H}}_s = [\hat{H}_s, \hat{H}] \equiv [\hat{H}_s, (\hat{H}_s + \hat{H}_{\text{int}} + \hat{H}_e \{\lambda\})] = [\hat{H}_s, \hat{H}_{\text{int}}] = 0, \quad (10.13)$$

we see that in the Heisenberg picture, the Hamiltonian operator (and hence the energy) of the system of our interest does not change in time. On the other hand, if the “environment” in this discussion is the instrument used for the measurement (see Fig. 1 again), the interaction can change its state, so it may be used to measure the system’s energy – or another observable whose operator commutes with the interaction Hamiltonian. Such a trick is called the *quantum non-demolition* (QND), or sometimes “back-action-evading” measurements.¹⁰ Due to the lack of back action of the instrument on the corresponding variable, such measurements allow its continuous monitoring. Let me present a fine example of an actual measurement of this kind – see Fig. 3.¹¹

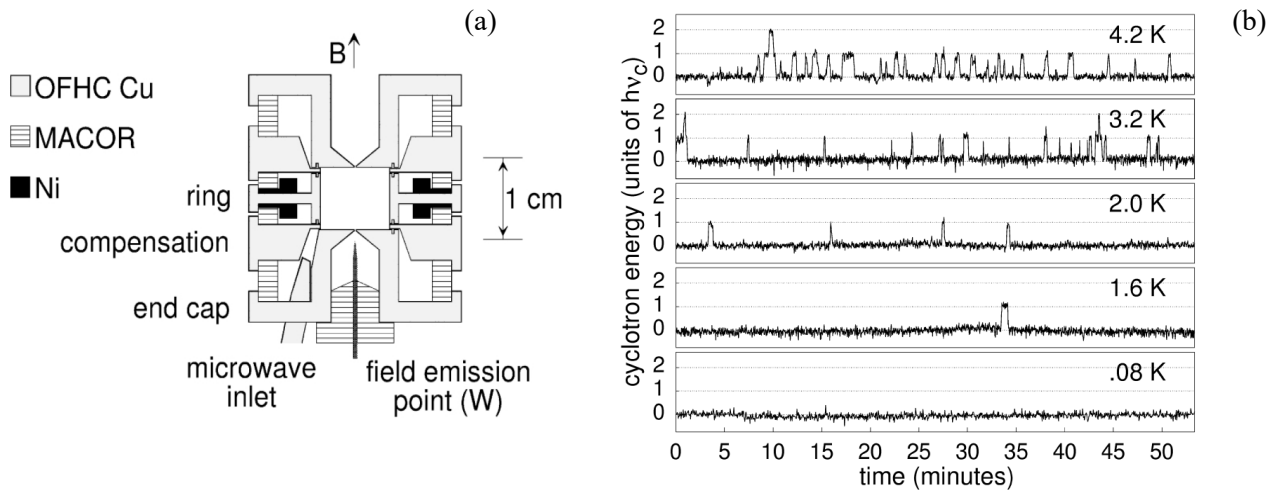


Fig. 10.3. QND measurements of single electron’s energy by Peil and Gabrielse: (a) the experimental setup’s core, and (b) a record of the thermal excitation and spontaneous relaxation of the Fock states. © 1999 APS; reproduced with permission.

In this experiment, a single electron is captured in a *Penning trap* – a combination of a (virtually) uniform magnetic field \mathcal{B} and a quadrupole electric field.¹² This electric field stabilizes the cyclotron orbits but does not have any noticeable effect on electron motion in the plane perpendicular to the magnetic field, and hence on its Landau level energies – see Eq. (3.50):

$$E_n = \hbar \omega_c \left(n + \frac{1}{2} \right), \quad \text{with } \omega_c = \frac{e\mathcal{B}}{m_e}. \quad (10.14)$$

(In the cited work, with $\mathcal{B} \approx 5.3$ T, the cyclic frequency $\omega_c/2\pi$ was about 147 GHz, so that the Landau level splitting $\hbar\omega_c$ was close to 10^{-22} J, i.e. corresponded to $k_B T$ at $T \sim 10$ K, while the physical temperature of the system might be reduced well below that, down to 80 mK). Now note that the

¹⁰ For a detailed discussion of this field see, e.g., V. Braginsky and F. Khalili (ed. by K. Thorne), *Quantum Measurement*, Cambridge U. Press, 1992; for an earlier review, see V. Braginsky *et al.*, *Science* **209**, 547 (1980).

¹¹ S. Peil and G. Gabrielse, *Phys. Rev. Lett.* **83**, 1287 (1999).

¹² It is similar to the 2D system discussed in EM Sec. 2.7, but with additional rotation about one of the axes.

analogy between a Landau-level particle and a harmonic oscillator goes beyond the energy spectrum (14). Indeed, since the Hamiltonian of a 2D particle in a perpendicular magnetic field may be reduced to Eq. (3.47), similar to that of a 1D oscillator, we may repeat all procedures of Sec. 5.4 and rewrite this effective Hamiltonian in the terms of the creation-annihilation operators – see Eq. (5.72):

$$\hat{H}_s = \hbar\omega_c \left(\hat{a}^\dagger \hat{a} + \frac{1}{2} \right). \quad (10.15)$$

In the Peil and Gabrielse experiment, the trapped electron had one more degree of freedom – along the magnetic field. The electric field of the Penning trap created a soft confining potential along this direction (vertical in Fig. 3a; I will take it for the z -axis), so that small electron oscillations along that axis could be well described as those of a 1D harmonic oscillator of much lower eigenfrequency, in that particular experiment with $\omega_z/2\pi \approx 64$ MHz. This frequency could be measured very accurately (with error ~ 1 Hz) by sensitive electronics whose electric field does affect the z -motion of the electron, but not its motion in the perpendicular plane. In an exactly uniform magnetic field, the two modes of electron motion would be completely uncoupled. However, the experimental setup included two special superconducting rings made of niobium (see Fig. 3a), which slightly distorted the magnetic field and created an interaction between the modes, which might be well approximated by the Hamiltonian¹³

$$\hat{H}_{\text{int}} = \text{const} \times \left(\hat{a}^\dagger \hat{a} + \frac{1}{2} \right) \hat{z}^2, \quad (10.16)$$

so that the main condition (12) of a QND measurement was very closely satisfied. At the same time, the coupling (16) ensured that a change of the Landau level number n by 1 changed the z -oscillation eigenfrequency by ~ 12.4 Hz. Since this shift was substantially larger than electronics' noise, rare spontaneous changes of n (due to a weak uncontrolled coupling of the electron to the environment) could be readily measured – moreover, continuously monitored – see Fig. 3b. The record shows spontaneous excitations of the electron to higher Landau levels, with its sequential relaxation, just as described by Eqs. (7.208)-(7.210). The detailed data statistics analysis showed that there was virtually no effect of the measuring instrument on these processes – at least on the scale of minutes, i.e. as many as $\sim 10^{13}$ cyclotron orbit periods.¹⁴

It is important, however, to note that any measurement – QND or not – cannot avoid the uncertainty relations between incompatible variables; in the particular case described above, continuous monitoring of the Landau state number n does not allow the simultaneous monitoring of its quantum phase (which may be defined exactly as in the harmonic oscillator). In this context, it is natural to wonder whether the QND measurement concept may be extended from quadratic-form variables like energy to “usual” observables such as coordinates and momenta, whose uncertainties are bound by the ordinary Heisenberg’s relation (1.35). The answer is yes, but the required methods are a bit more tricky.

For example, let us place an electrically charged particle into a uniform electric field $\mathcal{E} = \mathbf{n}_x \mathcal{E}(t)$ of an instrument, so that their interaction Hamiltonian is

¹³ Here I have simplified the real situation a bit. Actually, in that experiment, there was an electron spin’s contribution to the interaction Hamiltonian as well, but since the used high magnetic field polarized the spins quite reliably, their only effect was a constant shift of the frequency ω_z , which is not important for our discussion.

¹⁴ See also the conceptually similar experiments, performed by different means: G. Nogues *et al.*, *Nature* **400**, 239 (1999).

$$\hat{H}_{\text{int}} = -q\hat{\mathcal{E}}(t)\hat{x}. \quad (10.17)$$

Such interaction may certainly pass the information on the time evolution of the coordinate x to the instrument. However, in this case, Eq. (12) is *not* satisfied – at least for the kinetic-energy part of the particle's Hamiltonian; as a result, the interaction distorts its time evolution. Indeed, writing the Heisenberg equation (4.199) for the x -component of the momentum, we get

$$\dot{\hat{p}} - \dot{\hat{p}} \Big|_{\mathcal{E}=0} = q\hat{\mathcal{E}}(t). \quad (10.18)$$

On the other hand, integrating Eq. (5.139) for the coordinate operator evolution,¹⁵ we get the expression

$$\hat{x}(t) = \hat{x}(t_0) + \frac{1}{m} \int_{t_0}^t \hat{p}(t') dt', \quad (10.19)$$

which shows that the perturbations (18) of the momentum eventually find their way to the coordinate evolution, not allowing its unperturbed sequential measurements.

However, for such an important particular system as a harmonic oscillator, the following trick is possible. For this system, Eqs. (5.139) with the addition (18) may be readily combined to give a second-order differential equation for the coordinate operator, that is absolutely similar to the classical equation of motion of the system, and has a similar solution:¹⁶

$$\hat{x}(t) = \hat{x}(t) \Big|_{\mathcal{E}=0} + \frac{q}{m\omega_0} \int_{-\infty}^t \hat{\mathcal{E}}(t') \sin \omega_0(t-t') dt'. \quad (10.20)$$

This formula confirms that generally, the external field $\mathcal{E}(t)$ (in our case, the sensing field of the measurement instrument) affects the time evolution law – of course. However, Eq. (20) shows that if the field is applied only at moments t'_n separated by intervals $\mathcal{T}/2$, where $\mathcal{T} \equiv 2\pi/\omega_0$ is the oscillation period, its effect on coordinate vanishes at similarly spaced observation instants $t_n = t_{n'} + (m+1/2)\mathcal{T}$. This is the idea of *stroboscopic* QND measurements. Of course, according to Eq. (18), even such measurement strongly perturbs the oscillator momentum, so that even if the values x_n are measured with high accuracy, the Heisenberg's uncertainty relation is not violated.

A direct implementation of the stroboscopic measurements is technically complicated, but this initial idea has opened a way to more practicable solutions. For example, it is straightforward to use the Heisenberg equations of motion to show that if the coupling of two harmonic oscillators, with coordinates x and X , and unperturbed frequencies ω and Ω , is modulated in time as

$$\hat{H}_{\text{int}} \propto \hat{x}\hat{X} \cos \omega t \cos \Omega t, \quad (10.21)$$

¹⁵ This simple relation is limited to 1D systems with Hamiltonians of the type (1.41), but by now the reader certainly knows enough to understand that this discussion may be readily generalized to many other systems.

¹⁶ Note in particular that the function $\sin \omega_0 \tau$ (with $\tau \equiv t - t'$) under the integral, divided by ω_0 , is nothing more than the temporal Green's function $G(\tau)$ of a loss-free harmonic oscillator – see, e.g., CM Sec. 5.1.

then the process in one of the oscillators (say, that with frequency Ω) does not affect dynamics of one of the *quadrature components* of the counterpart oscillator, defined by relations¹⁷

$$\hat{x}_1 \equiv \hat{x} \cos \omega t - \frac{\hat{p}}{m\omega} \sin \omega t, \quad \hat{x}_2 \equiv \hat{x} \sin \omega t + \frac{\hat{p}}{m\omega} \cos \omega t, \quad (10.22)$$

while this component's motion does affect the dynamics of one of the quadrature components of the counterpart oscillator. (For the counterpart couple of quadrature components, the information transfer goes in the opposite direction.) This scheme has been successfully used for QND measurements.¹⁸

Please note that the last two QND measurement examples are based on the idea of a periodic change of a certain parameter in time – either in the short-pulse form or the sinusoidal form. If the only goal of a QND measurement is a sensitive measurement of a weak *classical force* acting on a quantum *probe system*, i.e. a 1D oscillator of eigenfrequency ω_0 , it may be implemented much simpler – just by modulating an oscillator's parameter with a frequency $\omega \approx 2\omega_0$. From the classical dynamics, we know that if the depth of such modulation exceeds a certain threshold value, it results in the excitation of the so-called degenerate parametric oscillations with frequency $\omega/2 \approx \omega_0$, and one of two opposite phases.¹⁹ In the language of Eq. (22), the parametric excitation means exponential growth of one of the quadrature components (with its sign depending on initial conditions), while the counterpart component is suppressed. Close to, but below the excitation threshold, the parameter modulation boosts all fluctuations of the almost-excited component, including its quantum-mechanical uncertainty, and suppresses (*squeezes*) those of the counterpart component. The result is a squeezed state, already discussed in Sec. 5.5 of this course (see in particular Eqs. (5.143) and Fig. 5.8), which allows one to notice the effect of an external force on the oscillator on the backdrop of a quantum uncertainty much smaller than the standard quantum limit (5.99).

In electrical engineering, this fact may be conveniently formulated in terms of *noise parameter* Θ_N of a *linear amplifier* – essentially the tool for continuous monitoring of an input “signal” – e.g., a microwave or optical waveform.²⁰ Namely, Θ_N of “usual” (say, transistor or maser) amplifiers which are equally sensitive to both quadrature components of the signal, Θ_N has the minimum value $\hbar\omega/2$, due to the quantum uncertainty pertinent to the quantum state of the amplifier itself (which therefore plays the role of its “quantum noise”) – the fact that was recognized in the early 1960s.²¹ On the other hand, a

¹⁷ The physical sense of these relations should be clear from Fig. 5.8: they define a system of coordinates rotating clockwise with the angular velocity equal to ω , so that the point representing unperturbed classical oscillations with that frequency is at rest in this rotating frame. (The “probability cloud” representing a Glauber state is also stationary in the coordinates $[x_1, x_2]$.) The reader familiar with the classical theory oscillations may notice that the observables x_1 and x_2 so defined are just the *Poincaré plane* coordinates (“RWA variables”) – see, e.g., CM Sec. 5.3-5.6, and especially Fig. 5.9, where these coordinates are denoted as u and v .

¹⁸ The first, initially imperfect QND experiments were reported by R. Slusher *et al.*, *Phys. Rev. Lett.* **55**, 2409 (1985), and other groups soon after this, using nonlinear interactions of optical waves. Later, the results were much improved – see, e.g., P. Grangier *et al.*, *Nature* **396**, 537 (1998), and references therein. Recently, such experiments were extended to mechanical systems – see, e.g., F. Lecocq *et al.*, *Phys. Rev. X* **5**, 041037 (2015).

¹⁹ See, e.g., CM Sec. 5.5, and also Fig. 5.8 and its discussion in Sec. 5.6.

²⁰ For a quantitative definition of the latter parameter, suitable for the quantum sensitivity range ($\Theta_N \sim \hbar\omega$) as well, see, e.g., I. Devyatov *et al.*, *J. Appl. Phys.* **60**, 1808 (1986). In the classical noise limit ($\Theta_N \gg \hbar\omega$), it coincides with $k_B T_N$, where T_N is a more popular measure of electronics' noise, called the *noise temperature*.

²¹ See, e.g., H. Haus and J. Mullen, *Phys. Rev.* **128**, 2407 (1962).

degenerate parametric amplifier, sensitive to just one quadrature component, may have Θ_N well below $\hbar\omega/2$, due to its ground state squeezing.²²

Let me note that the parameter-modulation schemes of the QND measurements are not limited to harmonic oscillators, and may be applied to other important quantum systems, notably including two-level (i.e. spin-½-like) systems.²³ Such measurements may be an important tool for the further progress of quantum computation and cryptography.²⁴

Finally, let me mention that the composite systems consisting of a quantum subsystem, and a classical subsystem performing its continuous weakly-perturbing measurement and using its results for providing a specially crafted feedback to the quantum subsystem, may have some curious properties, in particular mock a quantum system detached from the environment.²⁵

10.3. Hidden variables and local reality

Now we are ready to proceed to the discussion of the last, hardest group (iii) of the questions posed in Sec. 1, namely on the state of a quantum system *just before* its measurement. After a very important but inconclusive discussion of this issue by Albert Einstein and his collaborators on one side, and Niels Bohr on the other side, in the mid-1930s, such discussions have resumed in the 1950s.²⁶ They have led to a key contribution by John Stewart Bell in the early 1960s, summarized as so-called *Bell's inequalities*, and then to experimental work on better and better verification of these inequalities. (Besides that work, the recent progress, in my humble view, has been rather marginal.)

The central question may be formulated as follows: what *had been* the “real” state of a quantum-mechanical system *just before* a virtually perfect single-shot measurement was performed on it, and gave a certain, documented outcome? To be specific, let us focus again on the example of Stern-Gerlach measurements of spin-½ particles – because of their conceptual simplicity.²⁷ For a single-component system (in this case a single spin-½) the answer to the posed question may look evident. Indeed, as we know, if the spin is in a pure (least-uncertain) state α , i.e. its ket-vector may be expressed in the form similar to Eq. (4),

$$|\alpha\rangle = \alpha_{\uparrow}|\uparrow\rangle + \alpha_{\downarrow}|\downarrow\rangle, \quad (10.23)$$

where, as usual, \uparrow and \downarrow denote the states with definite spin orientations along the z -axis, the probabilities of the corresponding outcomes of the z -oriented Stern-Gerlach experiment are $W_{\uparrow} = |\alpha_{\uparrow}|^2$ and $W_{\downarrow} = |\alpha_{\downarrow}|^2$. Then it looks natural to suggest that if a particular experiment gave the outcome corresponding to the state \uparrow , the spin had been in that state just before the experiment. For a classical

²² See, e.g., the spectacular experiments by B. Yurke *et al.*, *Phys. Rev. Lett.* **60**, 764 (1988). Note also that the squeezed ground states of light are now used to improve the sensitivity of interferometers in gravitational wave detectors – see, e.g., the recent review by R. Schnabel, *Phys. Repts.* **684**, 1 (2017), and the later paper by F. Acernese *et al.*, *Phys. Rev. Lett.* **123**, 231108 (2019).

²³ See, e.g., D. Averin, *Phys. Rev. Lett.* **88**, 207901 (2002).

²⁴ See, e.g., G. Jaeger, *Quantum Information: An Overview*, Springer, 2006.

²⁵ See, e.g., the monograph by H. Wiseman and G. Milburn, *Quantum Measurement and Control*, Cambridge U. Press (2009), more recent experiments by R. Vijay *et al.*, *Nature* **490**, 77 (2012), and references therein.

²⁶ See, e.g., J. Wheeler and W. Zurek (eds.), *Quantum Theory and Measurement*, Princeton U. Press, 1983.

²⁷ As was discussed in Sec. 1, the Stern-Gerlach-type experiments may be readily made virtually perfect, provided that we do not care about the evolution of the system *after* the single-shot measurement.

system such answer would be certainly correct, and the fact that the probability $W_{\uparrow} = |\alpha_{\uparrow}|^2$, defined for the statistical ensemble of *all* experiments (regardless of their outcome), may be less than 1, would merely reflect our ignorance about the *real state* of this particular system before the measurement – which just *reveals* the real situation.

However, as was first argued in the famous *EPR paper* published in 1935 by A. Einstein, B. Podolsky, and N. Rosen, such an answer becomes impossible in the case of an entangled quantum system, if only one of its components is measured with an instrument. The original EPR paper discussed thought experiments with a pair of 1D particles prepared in a quantum state in that both the *sum* of their momenta and the *difference* of their coordinates simultaneously have definite values: $p_1 + p_2 = 0$, $x_1 - x_2 = a$.²⁸ However, usually this discussion is recast into an equivalent Stern-Gerlach experiment shown in Fig. 4a.²⁹ A source emits rare pairs of spin-½ particles, propagating in opposite directions. The particle spin states are random, but with the net spin of the pair definitely equal to zero. After the spatial separation of the particles has become sufficiently large (see below), the spin state of each of them is measured with a Stern-Gerlach detector, with one of them (in Fig. 1, SG₁) somewhat closer to the particle source, so it makes the measurement first, at a time $t_1 < t_2$.

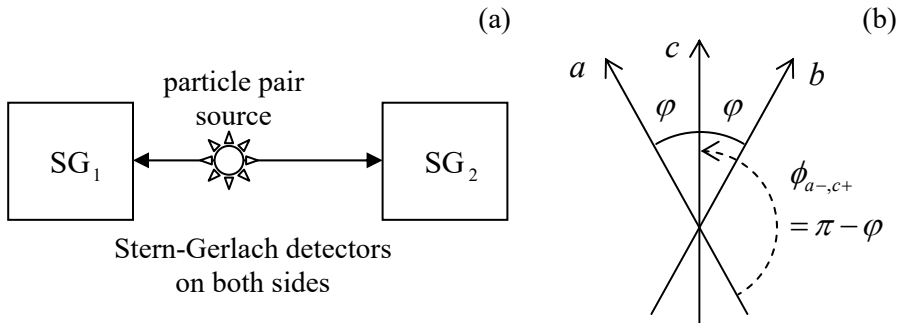


Fig. 10.4. (a) General scheme of two-particle Stern-Gerlach experiments, and (b) the orientation of the detectors, assumed at Wigner's deviation of Bell's inequality (36).

First, let the detectors be oriented say along the same direction, say the z -axis. Evidently, the probability of each detector to give any of the values $s_z = \pm \hbar/2$ is 50%. However, if the first detector had given the result $S_z = -\hbar/2$, then even before the second detector's measurement, we know that the latter will give the result $S_z = +\hbar/2$ with the 100% probability. So far, this situation still allows for a classical interpretation, just as for the single-particle measurements: we may fancy that the second particle has a definite spin before the measurement, and the first measurement just removes our ignorance about that reality. In other words, the change of the probability of the outcome $S_z = +\hbar/2$ at the second detection from 50% to 100% is due to the statistical ensemble re-definition: the 50% probability of this detection belongs to the ensemble of all experiments, while the 100% probability, to the sub-ensemble of experiments with the $S_z = -\hbar/2$ outcome of the first experiment.

However, let the source generate the spin pairs in the entangled, singlet state (8.18),

$$|s_{12}\rangle = \frac{1}{\sqrt{2}}(|\uparrow\downarrow\rangle - |\downarrow\uparrow\rangle), \quad (10.24)$$

²⁸ This is possible because the corresponding operators commute: $[\hat{p}_1 + \hat{p}_2, \hat{x}_1 - \hat{x}_2] = [\hat{p}_1, \hat{x}_1] - [\hat{p}_2, \hat{x}_2] = 0$.

²⁹ Another equivalent but experimentally more convenient (and as a result, frequently used) technique is the degenerate parametric excitation of entangled optical photon pairs – see, e.g., the publications cited at the end of this section.

that certainly satisfies the above assumptions: the probability of each value of S_z of any particle is 50%, and the sum of both S_z is definitely zero, so that if the first detector's result is $S_z = -\hbar/2$, then the state of the remaining particle is \uparrow , with zero uncertainty. Now let us use Eqs. (4.123) to represent the same state (24) in a different form:

$$|s_{12}\rangle = \frac{1}{\sqrt{2}} \left[\frac{1}{\sqrt{2}}(|\rightarrow\rangle + |\leftarrow\rangle) \frac{1}{\sqrt{2}}(|\rightarrow\rangle - |\leftarrow\rangle) - \frac{1}{\sqrt{2}}(|\rightarrow\rangle - |\leftarrow\rangle) \frac{1}{\sqrt{2}}(|\rightarrow\rangle + |\leftarrow\rangle) \right]. \quad (10.25)$$

Opening the parentheses (carefully, without swapping the ket-vector order, which encodes the particle numbers!), we get an expression similar to Eq. (24), but now for the x -basis:

$$|s_{12}\rangle = \frac{1}{\sqrt{2}}(|\rightarrow\leftarrow\rangle - |\leftarrow\rightarrow\rangle). \quad (10.26)$$

Hence if we use the first detector (closest to the particle source) to measure S_x rather than S_z , then after it had given a certain result (say, $S_x = -\hbar/2$), we know for sure, before the second particle spin's measurement, that its S_x component definitely equals $+\hbar/2$.

So, depending on the experiment performed on the first particle, the second particle, before its measurement, may be in one of two states – either with a definite component S_z or with a definite component S_x , in each case with zero uncertainty. Evidently, this situation cannot be interpreted in classical terms if the particles do not interact during the measurements. A. Einstein was deeply unhappy with such situation because it did not satisfy what, in his view, was the general requirement to any theory, which nowadays is called the *local reality*. His definition of this requirement was as follows: “The real factual situation of system 2 is independent of what is done with system 1 that is spatially separated from the former”. (Here the term “spatially separated” is not defined, but from the context, it is clear that Einstein meant the detector separation by a *superluminal interval*, i.e. by distance

$$|\mathbf{r}_1 - \mathbf{r}_2| > c|t_1 - t_2|, \quad (10.27)$$

where the measurement time difference on the right-hand side includes the measurement duration.) In Einstein's view, since quantum mechanics did not satisfy the local reality condition, it could not be considered a complete theory of Nature.

This situation naturally raises the question of whether *something* (usually called *hidden variables*) may be added to the quantum-mechanical description to enable it to satisfy the local reality requirement. The first definite statement in this regard was John von Neumann's “proof”³⁰ (first famous, then infamous :-) that such variables cannot be introduced; for a while, his work satisfied the quantum mechanics practitioners, who apparently did not pay much attention.³¹ A major new contribution to the problem was made only in the 1960s by J. Bell.³² First of all, he has found an elementary (in his words, “foolish”) error in von Neumann's logic, which voids his “proof”. Second, he has demonstrated that Einstein's local reality condition is *incompatible* with conclusions of quantum mechanics – that had been, by that time, confirmed by too many experiments to be seriously questioned.

³⁰ In his very early book J. von Neumann, *Mathematische Grundlagen der Quantenmechanik* [Mathematical Foundations of Quantum Mechanics], Springer, 1932. (The first English translation was published only in 1955.)

³¹ Perhaps it would not satisfy A. Einstein, but reportedly he did not know about the von Neumann's publication before signing the EPR paper.

³² See, e. g., either J. Bell, *Rev. Mod. Phys.* **38**, 447 (1966) or J. Bell, *Foundations of Physics* **12**, 158 (1982).

Let me describe a particular version of the Bell's result (suggested by E. Wigner), using the same EPR pair experiment (Fig. 4a), in that each SG detector may be oriented in any of 3 directions: a , b , or c – see Fig. 4b. As we already know from Chapter 4, if a fully-polarized beam of spin- $\frac{1}{2}$ particles is passed through a Stern-Gerlach apparatus forming angle ϕ with the polarization axis, the probabilities of two alternative outcomes of the experiment are

$$W(\phi_+) = \cos^2 \frac{\phi}{2}, \quad W(\phi_-) = \sin^2 \frac{\phi}{2}. \quad (10.28)$$

Let us use this formula to calculate all joint probabilities of measurement outcomes, starting from the detectors 1 and 2 oriented, respectively, in the directions a and c . Since the angle between the *negative* direction of the a -axis and the *positive* direction of the c -axis is $\phi_{a-,c+} = \pi - \varphi$ (see the dashed arrow in Fig. 4b), we get

$$W(a_+ \wedge c_+) \equiv W(a_+)W(c_+ | a_+) = W(a_+)W(\phi_{a-,c+}) = \frac{1}{2} \cos^2 \frac{\pi - \varphi}{2} \equiv \frac{1}{2} \sin^2 \frac{\varphi}{2}, \quad (10.29)$$

where $W(x \wedge y)$ is the joint probability of both outcomes x and y , while $W(x | y)$ is the conditional probability of the outcome x , provided that the outcome y has happened. (The first equality in Eq. (29) is the well-known identity of the probability theory.) Absolutely similarly,

$$W(c_+ \wedge b_+) \equiv W(c_+)W(b_+ | c_+) = \frac{1}{2} \sin^2 \frac{\varphi}{2}, \quad (10.30)$$

$$W(a_+ \wedge b_+) \equiv W(a_+)W(b_+ | a_+) = \frac{1}{2} \cos^2 \frac{\pi - 2\varphi}{2} \equiv \frac{1}{2} \sin^2 \varphi. \quad (10.31)$$

Now note that for any angle φ smaller than $\pi/2$ (as in the case shown in Fig. 4b), trigonometry gives

$$\frac{1}{2} \sin^2 \varphi \geq \frac{1}{2} \sin^2 \frac{\varphi}{2} + \frac{1}{2} \sin^2 \frac{\varphi}{2} \equiv \sin^2 \frac{\varphi}{2}. \quad (10.32)$$

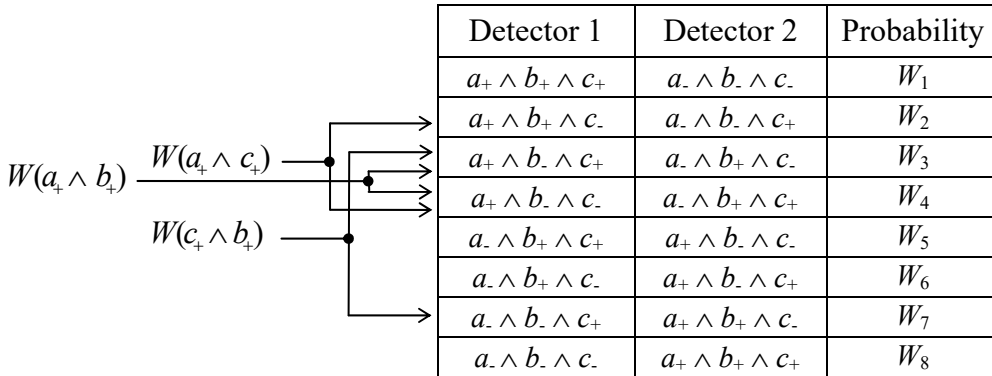
(For example, for $\varphi \rightarrow 0$ the left-hand side of this inequality tends to $\varphi^2/2$, while the right-hand side, to $\varphi^2/4$.) Hence the quantum-mechanical result gives, in particular,

$$W(a_+ \wedge b_+) \geq W(a_+ \wedge c_+) + W(c_+ \wedge b_+), \quad \text{for } |\varphi| \leq \pi/2.$$

(10.33)

Quantum-mechanical result

On the other hand, we can get a different inequality for these probabilities without calculating them from any particular theory, but using the local reality assumption. For that, let us prescribe some probability to each of $2^3 = 8$ possible outcomes of a set of three spin measurements. (Due to zero net spin of particle pairs, the probabilities of the sets shown in both columns of the table have to be equal.)



From the local-reality point of view, these measurement options are independent, so we may write (see the arrows on the left of the table):

$$W(a_+ \wedge c_+) = W_2 + W_4, \quad W(c_+ \wedge b_+) = W_3 + W_7, \quad W(a_+ \wedge b_+) = W_3 + W_4. \quad (10.34)$$

On the other hand, since no probability may be negative (by its very definition), we may always write

$$W_3 + W_4 \leq (W_2 + W_4) + (W_3 + W_7). \quad (10.35)$$

Plugging into this inequality the values of these two parentheses, given by Eq. (34), we get

$$W(a_+ \wedge b_+) \leq W(a_+ \wedge c_+) + W(c_+ \wedge b_+). \quad (10.36)$$

Bell's
inequality
(local-reality
theory)

This is the *Bell's inequality*, which has to be satisfied by *any* local-reality theory; it directly contradicts the quantum-mechanical result (33) – opening the issue to direct experimental testing. Such tests were started in the late 1960s, but the first results were vulnerable to two criticisms:

(i) The detectors were not fast enough and not far enough to have the relation (27) satisfied. This is why, as a matter of principle, there was a chance that information on the first measurement outcome had been transferred (by some, mostly implausible) means to particles before the second measurement – the so-called *locality loophole*.

(ii) The particle/photon detection efficiencies were too low to have sufficiently small error bars for both parts of the inequality – the *detection loophole*.

Gradually, these loopholes have been closed.³³ As expected, substantial violations of the Bell inequalities (36) (or their equivalent forms) have been proved, essentially rejecting any possibility to reconcile quantum mechanics with Einstein's local reality requirement.

10.4. Interpretations of quantum mechanics

The fact that quantum mechanics is incompatible with local reality, makes it reconciliation with our (classically-bred) “common sense” rather challenging. Here is a brief list of the major interpretations of quantum mechanics, that try to provide at least a partial reconciliation of this kind.

(i) The so-called *Copenhagen interpretation* – to which most physicists adhere. This “interpretation” does not really interpret anything; it just accepts the intrinsic stochasticity of measurement results in quantum mechanics, and the absence of local reality, essentially saying: “Do not worry; this is just how it is; live with it”. I generally subscribe to this school of thought, with the following qualification. While the Copenhagen interpretation implies statistical ensembles (otherwise, how would you define the probability? – see Sec. 1.3), its most frequently stated formulations³⁴ do not put a sufficient emphasis on their role, in particular on the ensemble re-definition as the only point of human observer’s involvement in a nearly-perfect measurement process – see Sec. 1 above. The most

³³ Important milestones in that way were the experiments by A. Aspect *et al.*, *Phys. Rev. Lett.* **49**, 91 (1982) and M. Rowe *et al.*, *Nature* **409**, 791 (2001). Detailed reviews of the experimental situation were given, for example, by M. Genovese, *Phys. Repts.* **413**, 319 (2005) and A. Aspect, *Physics* **8**, 123 (2015); see also the later paper by J. Handsteiner *et al.*, *Phys. Rev. Lett.* **118**, 060401 (2017). Presently, a high-fidelity demonstration of the Bell inequality violation has become a standard test in virtually every experiment with entangled qubits used for quantum encryption research – see Sec. 8.5, in particular the paper by J. Lin cited there.

³⁴ With certain pleasant exceptions – see, e.g. L. Ballentine, *Rev. Mod. Phys.* **42**, 358 (1970).

famous objection to the Copenhagen interpretation belongs to A. Einstein: “God does not play dice.” OK, when Einstein speaks, we all should listen, but perhaps when God speaks (through experimental results), we have to pay even more attention.

(ii) *Non-local reality*. After the dismissal of J. von Neumann’s “proof” by J. Bell, to the best of my knowledge, there has been *no* proof that hidden parameters *could not* be introduced, provided that they do not imply the local reality. Of constructive approaches, perhaps the most notable contribution was made by David Joseph Bohm,³⁵ who developed the initial Louis de Broglie’s interpretation of the wavefunction as a “pilot wave”, making it quantitative. In the wave-mechanics version of this concept, the wavefunction governed by the Schrödinger equation, just guides a “real”, point-like classical particle whose coordinates serve as hidden variables. However, this concept does not satisfy the notion of local reality. For example, the measurement of the particle’s coordinate at a certain point \mathbf{r}_1 has to *instantly* change the wavefunction everywhere in space, including the points \mathbf{r}_2 in the superluminal range (27). After A. Einstein’s private criticism, D. Bohm essentially abandoned his theory.³⁶

(iii) The *many-world interpretation*, introduced in 1957 by Hugh Everett and popularized in the 1960s and 1970s by Bruce de Witt. In this interpretation, *all* possible measurement outcomes *do* happen, splitting the Universe into the corresponding number of “parallel multiverses”, so that from one of them, other multiverses and hence other outcomes cannot be observed. Let me leave to the reader an estimate of the rate at which the parallel multiverses have to be constantly generated (say, per second), taking into account that such generation should take place not only at explicit lab experiments but at every irreversible process – such as fission of every atomic nucleus or an absorption/emission of every photon, everywhere in each multiverse – whether its result is formally recorded or not. Nicolaas van Kampen has called this a “mind-boggling fantasy”.³⁷ Even the main proponent of this interpretation, B. de Witt has confessed: “The idea is not easy to reconcile with common sense.” I agree.

(iv) *Quantum logic*. In desperation, some physicists turned philosophers have decided to dismiss the formal logic we are using – in science and elsewhere. From what (admittedly, very little) I have read about this school of thought, it seems that from its point of view, definite statements like “the SG detector has found the spin to be directed along the magnetic field” should not necessarily be either true or false. OK, if we dismiss the formal logic, I do not know how we can use any scientific theory to make any predictions – until the quantum logic experts tell us what to replace it with. To the best of my knowledge, so far they have not done that. I personally trust the opinion by J. Bell, who certainly gave more thought to these issues: “It is my impression that the whole vast subject of Quantum Logic has arisen [...] from the misuse of a word.”

As far as I know, neither of these interpretations has yet provided a suggestion on how it might be tested experimentally to exclude other ones. On the positive side, there is a virtual consensus that quantum mechanics makes correct (if sometimes probabilistic) predictions, which do not contradict any reliable experimental results we are aware of. Maybe, this is not that bad for a scientific theory.³⁸

³⁵ D. Bohm, *Phys. Rev.* **85**, 165; 180 (1952).

³⁶ See, e.g., Sec. 22.19 of his (generally very good) textbook D. Bohm, *Quantum Theory*, Dover, 1979.

³⁷ N. van Kampen, *Physica A* **153**, 97 (1988). By the way, I highly recommend the very reasonable summary of the quantum measurement issues, given in this paper, though believe that the quantitative theory of dephasing, discussed in Chapter 7 of this course, might give additional clarity to some of van Kampen’s statements.

³⁸ For the reader who is not satisfied with this “positivistic” approach, and wants to improve the situation, my earnest advice is to start not from square one, but from reading what other (including some very clever!) people thought about it. The review collection by J. Wheeler and W. Zurek, cited above, may be a good starting point.



Konstantin K. Likharev
Essential Graduate Physics
Lecture Notes and Problems

Beta version

Open online access at
<http://commons.library.stonybrook.edu/egp/>
and
<https://sites.google.com/site/likharevegp/>

Part SM: Statistical Mechanics

Last corrections: October 15, 2021

A version of this material was published in 2019 under the title
Statistical Mechanics: Lecture notes
IOPP, Essential Advanced Physics – Volume 7, ISBN 978-0-7503-1416-6,
with the model solutions of the exercise problems published under the title
Statistical Mechanics: Problems with solutions
IOPP, Essential Advanced Physics – Volume 8, ISBN 978-0-7503-1420-6

However, by now this online version of the lecture notes
and the problem solutions available from the author, have been better corrected

See also the author's list
<https://you.stonybrook.edu/likharev/essential-books-for-young-physicist/>
of other essential reading recommended to young physicists

Table of Contents

Chapter 1. Review of Thermodynamics (24 pp.)

- 1.1. Introduction: Statistical physics and thermodynamics
- 1.2. The 2nd law of thermodynamics, entropy, and temperature
- 1.3. The 1st and 3rd laws of thermodynamics, and heat capacity
- 1.4. Thermodynamic potentials
- 1.5. Systems with a variable number of particles
- 1.6. Thermal machines
- 1.7. Exercise problems (16)

Chapter 2. Principles of Physical Statistics (44 pp.)

- 2.1. Statistical ensemble and probability
- 2.2. Microcanonical ensemble and distribution
- 2.3. Maxwell's Demon, information, and computing
- 2.4. Canonical ensemble and the Gibbs distribution
- 2.5. Harmonic oscillator statistics
- 2.6. Two important applications
- 2.7. Grand canonical ensemble and distribution
- 2.8. Systems of independent particles
- 2.9. Exercise problems (32)

Chapter 3. Ideal and Not-so-Ideal Gases (34 pp.)

- 3.1. Ideal classical gas
- 3.2. Calculating μ
- 3.3. Degenerate Fermi gas
- 3.4. The Bose-Einstein condensation
- 3.5. Gases of weakly interacting particles
- 3.6. Exercise problems (29)

Chapter 4. Phase Transitions (36 pp.)

- 4.1. First order phase transitions
- 4.2. Continuous phase transitions
- 4.3. Landau's mean-field theory
- 4.4. Ising model: Weiss molecular-field theory
- 4.5. Ising model: Exact and numerical results
- 4.6. Exercise problems (18)

Chapter 5. Fluctuations (44 pp.)

- 5.1. Characterization of fluctuations
- 5.2. Energy and the number of particles
- 5.3. Volume and temperature
- 5.4. Fluctuations as functions of time
- 5.5. Fluctuations and dissipation

- 5.6. The Kramers problem and the Smoluchowski equation
- 5.7. The Fokker-Planck equation
- 5.8. Back to the correlation function
- 5.9. Exercise problems (21)

Chapter 6. Elements of Kinetics (38 pp.)

- 6.1. The Liouville theorem and the Boltzmann equation
- 6.2. The Ohm law and the Drude formula
- 6.3. Electrochemical potential and drift-diffusion equation
- 6.4. Charge carriers in semiconductors: Statics and kinetics
- 6.5. Thermoelectric effects
- 6.6. Exercise problems (15)

* * *

Additional file (available from the author upon request):

Exercise and Test Problems with Model Solutions (131 + 23 = 154 problems; 232 pp.)

This page is
intentionally left
blank

Chapter 1. Review of Thermodynamics

This chapter starts with a brief discussion of the subject of statistical physics and thermodynamics, and the relation between these two disciplines. Then I proceed to a review of the basic notions and relations of thermodynamics. Most of this material is supposed to be known to the reader from their undergraduate studies,¹ so the discussion is rather brief.

1.1. Introduction: Statistical physics and thermodynamics

Statistical physics (alternatively called “statistical mechanics”) and *thermodynamics* are two different but related approaches to the same goal: an approximate description of the “internal”² properties of large physical systems, notably those consisting of $N \gg 1$ identical particles – or other components. The traditional example of such a system is a human-scale portion of gas, with the number N of atoms/molecules³ of the order of the Avogadro number $N_A \sim 10^{23}$ (see Sec. 4 below).

The motivation for the statistical approach to such systems is straightforward: even if the laws governing the dynamics of each particle and their interactions were exactly known, and we had infinite computing resources at our disposal, calculating the exact evolution of the system in time would be impossible, at least because it is completely impracticable to measure the exact initial state of each component – in the classical case, the initial position and velocity of each particle. The situation is further exacerbated by the phenomena of chaos and turbulence,⁴ and the quantum-mechanical uncertainty, which do not allow the exact calculation of final positions and velocities of the component particles even if their initial state is known with the best possible precision. As a result, in most situations, only statistical predictions about the behavior of such systems may be made, with the *probability theory* becoming a major tool of the mathematical arsenal.

However, the statistical approach is not as bad as it may look. Indeed, it is almost self-evident that any measurable *macroscopic* variable characterizing a stationary system of $N \gg 1$ particles as a whole (think, e.g., about the stationary pressure P of the gas contained in a fixed volume V) is almost constant in time. Indeed, as we will see below, besides certain exotic exceptions, the relative magnitude of fluctuations – either in time, or among many macroscopically similar systems – of such a variable is of the order of $1/N^{1/2}$, and for $N \sim N_A$ is extremely small. As a result, the *average values* of appropriate macroscopic variables may characterize the state of the system quite well – satisfactory for nearly all practical purposes. The calculation of relations between such average values is the only task of thermodynamics and the main task of statistical physics. (Fluctuations may be important, but due to their smallness, in most cases their analysis may be based on perturbative approaches – see Chapter 5.)

¹ For remedial reading, I can recommend, for example (in the alphabetical order): C. Kittel and H. Kroemer, *Thermal Physics*, 2nd ed., W. H. Freeman (1980); F. Reif, *Fundamentals of Statistical and Thermal Physics*, Waveland (2008); D. V. Schroeder, *Introduction to Thermal Physics*, Addison Wesley (1999).

² Here “internal” is an (admittedly loose) term meaning all the physics unrelated to the motion of the system as a whole. The most important example of internal dynamics is the thermal motion of atoms and molecules.

³ This is perhaps my best chance for a reverent mention of Democritus (circa 460-370 BC) – the Ancient Greek genius who was apparently the first one to conjecture the atomic structure of matter.

⁴ See, e.g., CM Chapters 8 and 9.

Now let us have a fast look at the typical macroscopic variables the statistical physics and thermodynamics should operate with. Since I have already mentioned pressure P and volume V , let me start with this famous pair of variables. First of all, note that volume is an *extensive variable*, i.e. a variable whose value for a system consisting of several non-interacting parts is the sum of those of its parts. On the other hand, pressure is an example of an *intensive variable* whose value is the same for different parts of a system – if they are in equilibrium. To understand why P and V form a natural pair of variables, let us consider the classical playground of thermodynamics, a portion of a gas contained in a cylinder, closed with a movable piston of area A (Fig. 1).

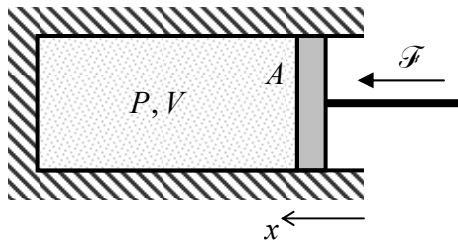


Fig. 1.1. Compressing gas.

Neglecting the friction between the walls and the piston, and assuming that it is being moved so slowly that the pressure P is virtually the same for all parts of the volume at any instant, the elementary work of the external force $\mathcal{F} = PA$, compressing the gas, at a small piston displacement $dx = -dV/A$, is

$$d\mathcal{W} = \mathcal{F}dx \equiv \left(\frac{\mathcal{F}}{A}\right)(Adx) \equiv -PdV. \quad (1.1)$$

Work
on a gas

Of course, the last expression is more general than the model shown in Fig. 1, and does not depend on the particular shape of the system's surface.⁵ (Note that in the notation of Eq. (1), which will be used through the course, the elementary work done *by* the gas *on* the external system equals $-d\mathcal{W}$.)

From the point of analytical mechanics,⁶ V and $(-P)$ is just one of many possible *canonical pairs* of generalized coordinates q_j and generalized forces \mathcal{F}_j , whose products $d\mathcal{W}_j = \mathcal{F}_j dq_j$ give independent contributions to the total work of the environment on the system under analysis. For example, the reader familiar with the basics of electrostatics knows that if the spatial distribution $\mathcal{E}(\mathbf{r})$ of an external electric field does not depend on the electric polarization $\mathcal{P}(\mathbf{r})$ of a dielectric medium placed into the field, its elementary work on the medium is

$$d\mathcal{W} = \int \mathcal{E}(\mathbf{r}) \cdot d\mathcal{P}(\mathbf{r}) d^3r \equiv \int \sum_{j=1}^3 \mathcal{E}_j(\mathbf{r}) d\mathcal{P}_j(\mathbf{r}) d^3r. \quad (1.2a)$$

The most important cases when this condition is fulfilled (and hence Eq. (2a) is valid) are, first, long cylindrical samples in a parallel external field (see, e.g., EM Fig. 3.13) and, second, the polarization of a sample (of any shape) due to that of discrete electric dipoles \mathbf{p}_k , whose electric interaction is negligible. In the latter case, Eq. (2a) may be also rewritten as the sum over the single dipoles, located at points \mathbf{r}_k :⁷

⁵ In order to prove that, it is sufficient to integrate the scalar product $d\mathcal{W} = d\mathcal{F} \cdot d\mathbf{r}$, with $d\mathcal{F} = -\mathbf{n} P d^2r$, where $d\mathbf{r}$ is the surface displacement vector (see, e.g., CM Sec. 7.1), and \mathbf{n} is the outer normal, over the surface.

⁶ See, e.g., CM Chapters 2 and 10.

⁷ Some of my students needed an effort to reconcile the positive signs in Eqs. (2) with the negative sign in the well-known relation $dU_k = -\mathcal{E}(\mathbf{r}_k)d\mathbf{p}_k$ for the potential energy of a dipole in an external electric field – see, e.g.,

$$d\mathcal{W} = \sum_k d\mathcal{W}_k, \quad \text{with } d\mathcal{W}_k = \mathcal{E}(\mathbf{r}_k) \cdot d\mathbf{p}_k. \quad (1.2b)$$

Very similarly, and at the similar conditions on the external magnetic field $\mathcal{H}(\mathbf{r})$, its elementary work on a magnetic medium may be also represented in either of two forms:⁸

$$d\mathcal{W} = \mu_0 \int \mathcal{H}(\mathbf{r}) \cdot d\mathcal{M}(\mathbf{r}) d^3 r \equiv \mu_0 \int \sum_{j=1}^3 \mathcal{H}_j(\mathbf{r}) d\mathcal{M}_j(\mathbf{r}) d^3 r, \quad (1.3a)$$

$$d\mathcal{W} = \sum_k d\mathcal{W}_k, \quad \text{with } d\mathcal{W}_k = \mu_0 \mathcal{H}(\mathbf{r}_k) \cdot d\mathbf{m}_k. \quad (1.3b)$$

where \mathcal{M} and \mathbf{m} are the vectors of, respectively, the medium's magnetization and the magnetic moment of a single dipole. Formulas (2) and (3) show that the roles of generalized coordinates may be played by Cartesian components of the vectors \mathcal{P} (or \mathbf{p}) and \mathcal{M} (or \mathbf{m}), with the components of the electric and magnetic fields playing the roles of the corresponding generalized forces. This list may be extended to other interactions (such as gravitation, surface tension in fluids, etc.). Following tradition, I will use the $\{-P, V\}$ pair in almost all the formulas below, but the reader should remember that they all are valid for any other pair $\{\mathcal{F}_j, q_j\}$.⁹

Again, the specific relations between the variables of each pair listed above may depend on the statistical properties of the system under analysis, but their definitions are not based on statistics. The situation is very different for a very specific pair of variables, *temperature T* and *entropy S*, although these “sister variables” participate in many formulas of thermodynamics exactly as if they were just one more canonical pair $\{\mathcal{F}_j, q_j\}$. However, the very existence of these two notions is due to statistics. Namely, temperature T is an intensive variable that characterizes the degree of thermal “agitation” of the system’s components. On the contrary, the entropy S is an extensive variable that in most cases evades immediate perception by human senses; it is a qualitative measure of the *disorder* of the system, i.e. the degree of our ignorance about its exact microscopic state.¹⁰

The reason for the appearance of the $\{T, S\}$ pair of variables in formulas of thermodynamics and statistical mechanics is that the statistical approach to large systems of particles brings some qualitatively new results, most notably the notion of the *irreversible* time evolution of collective (*macroscopic*) variables describing the system. On one hand, the irreversibility looks absolutely natural in such phenomena as the diffusion of an ink drop in a glass of water. In the beginning, the ink molecules are located in a certain small part of the system’s volume, i.e. to some extent ordered, while at the late stages of diffusion, the position of each molecule in the glass is essentially random. However, as a second thought, the irreversibility is rather surprising, taking into account that the laws governing the

EM Eqs. (3.15). The resolution of this paradox is simple: each term of Eq. (2b) describes the work $d\mathcal{W}_k$ of the electric field on the *internal* degrees of freedom of the k^{th} dipole, changing its *internal* energy E_k : $dE_k = d\mathcal{W}_k$. This energy change may be viewed as coming from the dipole’s potential energy in the field: $dE_k = -dU_k$.

⁸ Here, as in all my series, I am using the SI units; for their translation to the Gaussian units, I have to refer the reader to the EM part of the series.

⁹ Note that in systems of discrete particles, most generalized forces, including the fields \mathcal{E} and \mathcal{H} , differ from the pressure P in the sense that their work may be explicitly partitioned into single-particle components – see Eqs. (2b) and (3b). This fact gives some discretion for the calculations based on thermodynamic potentials – see Sec.4.

¹⁰ The notion of entropy was introduced into thermodynamics in 1865 by Rudolf Julius Emanuel Clausius on a purely phenomenological basis. In the absence of a clue about the entropy’s microscopic origin (which had to wait for the works by L. Boltzmann and J. Maxwell), this was an amazing intellectual achievement.

motion of the system's components are *time-reversible* – such as the Newton laws or the basic laws of quantum mechanics.¹¹ Indeed, if at a late stage of the diffusion process, we reversed the velocities of all molecules exactly and simultaneously, the ink molecules would again gather (for a moment) into the original spot.¹² The problem is that getting the *information* necessary for the exact velocity reversal is not practicable. This example shows a deep connection between statistical mechanics and information theory.

A qualitative discussion of the reversibility-irreversibility dilemma requires a strict definition of the basic notion of statistical mechanics (and indeed of the probability theory), the *statistical ensemble*, and I would like to postpone it until the beginning of Chapter 2. In particular, in that chapter, we will see that the basic law of irreversible behavior is an increase of the entropy S in any closed system. Thus, the statistical mechanics, without defying the “microscopic” laws governing the evolution of system's components, introduces on top of them some new “macroscopic” laws, intrinsically related to the evolution of *information*, i.e. the degree of our knowledge of the microscopic state of the system.

To conclude this brief discussion of variables, let me mention that as in all fields of physics, a very special role in statistical mechanics is played by the *energy* E . To emphasize the commitment to disregard the motion of the system as a whole in this subfield of physics, the E considered in thermodynamics it is frequently called the *internal energy*, though just for brevity, I will skip this adjective in most cases. The simplest example of such E is the sum of kinetic energies of molecules in a dilute gas at their thermal motion, but in general, the internal energy also includes not only the individual energies of the system's components but also their interactions with each other. Besides a few “pathological” cases of very-long-range interactions, these interactions may be treated as local; in this case the internal energy is proportional to N , i.e. is an extensive variable. As will be shown below, other extensive variables with the dimension of energy are often very useful as well, including the (Helmholtz) *free energy* F , the *Gibbs energy* G , the *enthalpy* H , and the *grand potential* Ω . (The collective name for such variables is *thermodynamic potentials*.)

Now, we are ready for a brief discussion of the relationship between *statistical physics* and *thermodynamics*. While the task of statistical physics is to calculate the macroscopic variables discussed above¹³ for various microscopic models of the system, the main role of thermodynamics is to derive some general relations between the average values of the macroscopic variables (also called *thermodynamic variables*) that do not depend on specific models. Surprisingly, it is possible to accomplish such a feat using just a few either evident or very plausible general assumptions (sometimes called the *laws of thermodynamics*), which find their proof in statistical physics.¹⁴ Such general relations allow for a substantial reduction of the number of calculations we have to do in statistical physics: in most cases, it is sufficient to calculate from the statistics just one or two variables, and then use general

¹¹ Because of that, the possibility of the irreversible macroscopic behavior of microscopically reversible systems was questioned by some serious scientists as recently as in the late 19th century – notably by J. Loschmidt in 1876.

¹² While quantum-mechanical effects, with their intrinsic uncertainty, may be quantitatively important in this example, our qualitative discussion does not depend on them. Another classical example is the chaotic motion of a ball on a 2D Sinai billiard – see CM Chapter 9 and in particular Fig. 9.8 and its discussion.

¹³ Several other quantities, for example the heat capacity C , may be calculated as partial derivatives of the basic variables discussed above. Also, at certain conditions, the number of particles N in a certain system may be not fixed and also considered as an (extensive) variable – see Sec. 5 below.

¹⁴ Admittedly, some of these proofs are based on other plausible but deeper postulates, for example the central statistical hypothesis (Sec. 2.2), whose best proof, to my knowledge, is just the whole body of experimental data.

thermodynamic relations to get all other properties of interest. Thus the thermodynamics, sometimes snubbed as a phenomenology, deserves every respect not only as a useful theoretical tool but also as a discipline more general than any particular statistical model. This is why the balance of this chapter is devoted to a brief review of thermodynamics.

1.2. The 2nd law of thermodynamics, entropy, and temperature

Thermodynamics accepts a phenomenological approach to the entropy S , postulating that there is such a unique extensive measure of the aggregate disorder, and that in a *closed system* (defined as a system completely isolated from its environment, i.e. the system with its internal energy fixed) it may only grow in time, reaching its constant (maximum) value at equilibrium:¹⁵

2nd law of
thermo-
dynamics

$$dS \geq 0. \quad (1.4)$$

This postulate is called the *2nd law of thermodynamics* – arguably its only substantial new law.¹⁶

Rather surprisingly, this law, together with the additivity of S in composite systems of non-interacting parts (as an extensive variable), is sufficient for a formal definition of temperature, and a derivation of its basic properties that comply with our everyday notion of this key variable. Indeed, let us consider a closed system consisting of two fixed-volume subsystems (Fig. 2) whose internal relaxation is very fast in comparison with the rate of the thermal flow (i.e. the energy and entropy exchange) between the parts. In this case, on the latter time scale, each part is always in some quasi-equilibrium state, which may be described by a unique relation $E(S)$ between its energy and entropy.¹⁷

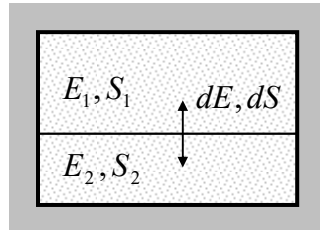


Fig. 1.2. A. composite thermodynamic system.

Neglecting the energy of interaction between the parts (which is always possible at $N \gg 1$, and in the absence of long-range interactions), we may use the extensive character of the variables E and S to write

$$E = E_1(S_1) + E_2(S_2), \quad S = S_1 + S_2, \quad (1.5)$$

for the full energy and entropy of the system. Now let us use them to calculate the following derivative:

¹⁵ Implicitly, this statement also postulates the existence, in a closed system, of *thermodynamic equilibrium*, an asymptotically reached state in which all macroscopic variables, including entropy, remain constant. Sometimes this postulate is called the 0th law of thermodynamics.

¹⁶ Two initial formulations of this law, later proved equivalent, were put forward independently by Lord Kelvin (born William Thomson) in 1851 and by Rudolf Clausius in 1854.

¹⁷ Here we strongly depend on a very important (and possibly the least intuitive) aspect of the 2nd law, namely that the entropy is a *unique* measure of disorder.

$$\frac{dS}{dE_1} = \frac{dS_1}{dE_1} + \frac{dS_2}{dE_1} \equiv \frac{dS_1}{dE_1} + \frac{dS_2}{dE_2} \frac{dE_2}{dE_1} = \frac{dS_1}{dE_1} + \frac{dS_2}{dE_2} \frac{d(E - E_1)}{dE_1}. \quad (1.6)$$

Since the total energy E of the closed system is fixed and hence independent of its re-distribution between the subsystems, we have to take $dE/dE_1 = 0$, and Eq. (6) yields

$$\frac{dS}{dE_1} = \frac{dS_1}{dE_1} - \frac{dS_2}{dE_2}. \quad (1.7)$$

According to the 2nd law of thermodynamics, when the two parts have reached the thermodynamic equilibrium, the total entropy S reaches its maximum, so that $dS/dE_1 = 0$, and Eq. (7) yields

$$\frac{dS_1}{dE_1} = \frac{dS_2}{dE_2}. \quad (1.8)$$

This equality shows that if a thermodynamic system may be partitioned into weakly interacting macroscopic parts, their derivatives dS/dE should be equal in the equilibrium. The reciprocal of this derivative is called *temperature*. Taking into account that our analysis pertains to the situation (Fig. 2) when both volumes $V_{1,2}$ are fixed, we may write this definition as

$$\left(\frac{\partial E}{\partial S} \right)_V \equiv T, \quad (1.9)$$

Definition of temperature

the subscript V meaning that volume is kept constant at the differentiation. (Such notation is common and very useful in thermodynamics, with its broad range of variables.)

Note that according to Eq. (9), if the temperature is measured in energy units¹⁸ (as I will do in this course for the brevity of notation), then S is dimensionless. The transfer to the SI or Gaussian units, i.e. to the temperature T_K measured in kelvins (not “Kelvins”, and not “degrees Kelvin”, please!), is given by the relation $T = k_B T_K$, where the *Boltzmann constant* $k_B \approx 1.38 \times 10^{-23}$ J/K = 1.38×10^{-16} erg/K.¹⁹ In those units, the entropy becomes dimensional: $S_K = k_B S$.

The definition of temperature, given by Eq. (9), is of course in sharp contrast with the popular notion of T as a measure of the average energy of one particle. However, as we will repeatedly see below, in many cases these two notions may be reconciled, with Eq. (9) being more general. In particular, the so-defined T is in semi-quantitative agreement with our everyday notion of temperature:²⁰

(i) according to Eq. (9), the temperature is an intensive variable (since both E and S are extensive), i.e., in a system of similar particles, it is independent of the particle number N ;

¹⁸ Here I have to mention a traditional unit of thermal energy, the calorie, still being used in some applied fields. In the most common modern definition (as the so-called *thermochemical calorie*) it equals exactly 4.148 J.

¹⁹ For the more exact values of this and other constants, see appendix CA: *Selected Physical Constants*. Note that both T and T_K define the natural *absolute* (also called “thermodynamic”) *scale* of temperature, vanishing at the same point – in contrast to such artificial scales as the degrees Celsius (“centigrades”), defined as $T_C \equiv T_K + 273.15$, or the degrees Fahrenheit: $T_F \equiv (9/5)T_C + 32$.

²⁰ Historically, such notion was initially qualitative – just as something distinguishing “hot” from “cold”. After the invention of thermometers (the first one by Galileo Galilei in 1592), mostly based on thermal expansion of fluids, this notion had become quantitative but not very deep: being understood as something “what the thermometer measures” – until its physical sense as a measure of thermal motion’s intensity, was revealed in the 19th century.

- (ii) temperatures of all parts of a system are equal at equilibrium – see Eq. (8);
- (iii) in a closed system whose parts are *not* in equilibrium, thermal energy (*heat*) always flows from a warmer part (with higher T) to the colder part.

In order to prove the last property, let us revisit the closed, composite system shown in Fig. 2, and consider another derivative:

$$\frac{dS}{dt} = \frac{dS_1}{dt} + \frac{dS_2}{dt} \equiv \frac{dS_1}{dE_1} \frac{dE_1}{dt} + \frac{dS_2}{dE_2} \frac{dE_2}{dt}. \quad (1.10)$$

If the internal state of each part is very close to equilibrium (as was assumed from the very beginning) at each moment of time, we can use Eq. (9) to replace the derivatives $dS_{1,2}/dE_{1,2}$ with $1/T_{1,2}$, getting

$$\frac{dS}{dt} = \frac{1}{T_1} \frac{dE_1}{dt} + \frac{1}{T_2} \frac{dE_2}{dt}. \quad (1.11)$$

Since in a closed system $E = E_1 + E_2 = \text{const}$, these time derivatives are related as $dE_2/dt = -dE_1/dt$, and Eq. (11) yields

$$\frac{dS}{dt} = \left(\frac{1}{T_1} - \frac{1}{T_2} \right) \frac{dE_1}{dt}. \quad (1.12)$$

But according to the 2nd law of thermodynamics, this derivative cannot be negative: $dS/dt \geq 0$. Hence,

$$\left(\frac{1}{T_1} - \frac{1}{T_2} \right) \frac{dE_1}{dt} \geq 0. \quad (1.13)$$

For example, if $T_1 > T_2$, then $dE_1/dt \leq 0$, i.e. the warmer part gives energy to its colder counterpart.

Note also that at such a heat exchange, at fixed volumes $V_{1,2}$, and $T_1 \neq T_2$, increases the total system's entropy, without performing any “useful” mechanical work – see Eq. (1).

1.3. The 1st and 3rd laws of thermodynamics, and heat capacity

Now let us consider a *thermally insulated* system whose volume V may be changed by force – see, for example, Fig. 1. Such a system is different from the fully closed one, because its energy E may be changed by the external force's work – see Eq. (1):

$$dE = d\mathcal{W} = -PdV. \quad (1.14)$$

Let the volume change be so slow ($dV/dt \rightarrow 0$) that the system is virtually at equilibrium at any instant. Such a slow process is called *reversible*, and in the particular case of a thermally insulated system, it is also called *adiabatic*. If the pressure P (or any generalized external force \mathcal{F}_j) is deterministic, i.e. is a predetermined function of time, independent of the state of the system under analysis, it may be considered as coming from a fully ordered system, i.e. the one having zero entropy, with the total system (the system under our analysis plus the source of the force) completely closed. Since the entropy of the total closed system should stay constant (see the second of Eqs. (5) above), S of the system under analysis should stay constant on its own. Thus we arrive at a very important conclusion: at an adiabatic process, the entropy of a system cannot change. (Sometimes such a process is called *isentropic*.) This means that we may use Eq. (14) to write

$$P = -\left(\frac{\partial E}{\partial V}\right)_S. \quad (1.15)$$

Now let us consider a more general thermodynamic system that may also exchange thermal energy (“heat”) with its environment (Fig. 3).

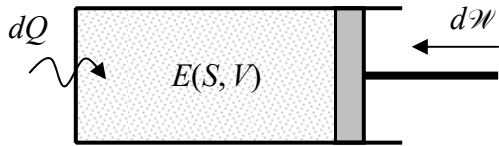


Fig. 1.3. An example of the thermodynamic process involving both the mechanical work by the environment, and the heat exchange with it.

For such a system, our previous conclusion about the entropy’s constancy is not valid, so that S , in equilibrium, may be a function of not only the system’s energy E , but also of its volume: $S = S(E, V)$. Let us consider this relation resolved for energy: $E = E(S, V)$, and write the general mathematical expression for the full differential of E as a function of these two independent arguments:

$$dE = \left(\frac{\partial E}{\partial S}\right)_V dS + \left(\frac{\partial E}{\partial V}\right)_S dV. \quad (1.16)$$

This formula, based on the stationary relation $E = E(S, V)$, is evidently valid not only in equilibrium but also for all very slow, reversible²¹ processes. Now, using Eqs. (9) and (15), we may rewrite Eq. (16) as

$$dE = TdS - PdV. \quad (1.17)$$

Energy:
differential

According to Eq. (1), the second term on the right-hand side of this equation is just the work of the external force, so that due to the conservation of energy,²² the first term has to be equal to the *heat* dQ transferred from the environment to the system (see Fig. 3):

$$dE = dQ + dW, \quad (1.18)$$

$$dQ = TdS. \quad (1.19)$$

1st law of
thermo-
dynamics

The last relation, divided by T and then integrated along an arbitrary (but reversible!) process,

$$S = \int \frac{dQ}{T} + \text{const}, \quad (1.20)$$

is sometimes used as an alternative definition of entropy S – provided that temperature is defined not by Eq. (9), but in some independent way. It is useful to recognize that entropy (like energy) may be defined

²¹ Let me emphasize again that any adiabatic process is reversible, but not vice versa.

²² Such conservation, expressed by Eqs. (18)-(19), is commonly called the *1st law of thermodynamics*. While it (in contrast with the 2nd law) does not present any new law of nature, and in particular was already used de-facto to write the first of Eqs. (5) and also Eq. (14), such a grand name was absolutely justified in the 19th century when the mechanical nature of the internal energy (the thermal motion) was not at all clear. In this context, the names of three scientists, Benjamin Thompson (who gave, in 1799, convincing arguments that heat cannot be anything but a form of particle motion), Julius Robert von Mayer (who conjectured the conservation of the sum of the thermal and macroscopic mechanical energies in 1841), and James Prescott Joule (who proved this conservation experimentally two years later), have to be reverently mentioned.

to an arbitrary constant, which does not affect any other thermodynamic observables. The common convention is to take

$$S \rightarrow 0, \quad \text{at } T \rightarrow 0. \quad (1.21)$$

This condition is sometimes called the “3rd law of thermodynamics”, but it is important to realize that this is just a convention rather than a real law.²³ Indeed, the convention corresponds well to the notion of the full order at $T = 0$ in some systems (e.g., separate atoms or perfect crystals), but creates ambiguity for other systems, e.g., amorphous solids (like the usual glasses) that may remain highly disordered for “astronomic” times, even at $T \rightarrow 0$.

Now let us discuss the notion of *heat capacity* that, by definition, is the ratio dQ/dT , where dQ is the amount of heat that should be given to a system to raise its temperature by a small amount dT .²⁴ (This notion is important because the heat capacity may be most readily measured experimentally.) The heat capacity depends, naturally, on whether the heat dQ goes only into an increase of the internal energy dE of the system (as it does if its volume V is constant), or also into the mechanical work ($-dW$) performed by the system at its expansion – as it happens, for example, if the pressure P , rather than the volume V , is fixed (the so-called *isobaric* process – see Fig. 4).

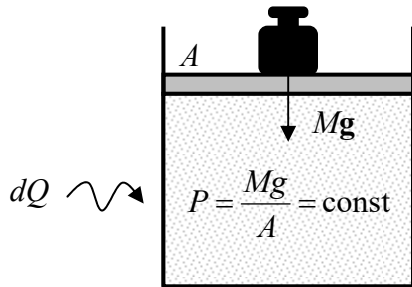


Fig. 1.4. The simplest example of the isobaric process.

Hence we should discuss at least two different quantities,²⁵ the *heat capacity at fixed volume*,

$$C_V \equiv \left(\frac{\partial Q}{\partial T} \right)_V \quad (1.22)$$

Heat capacity: definitions

and the *heat capacity at fixed pressure*

$$C_P \equiv \left(\frac{\partial Q}{\partial T} \right)_P, \quad (1.23)$$

²³Actually, the 3rd law (also called the *Nernst theorem*) as postulated by Walter Hermann Nernst in 1912 was different – and really meaningful: “It is impossible for any procedure to lead to the isotherm $T = 0$ in a finite number of steps.” I will discuss this theorem at the end of Sec. 6.

²⁴By this definition, the full heat capacity of a system is an extensive variable, but it may be used to form such intensive variables as the heat capacity per particle, called the *specific heat capacity*, or just the *specific heat*. (Please note that the last terms are rather ambiguous: they are used for the heat capacity per unit mass, per unit volume, and sometimes even for the heat capacity of the system as the whole, so that some caution is in order.)

²⁵Dividing both sides of Eq. (19) by dT , we get the general relation $dQ/dT = TdS/dT$, which may be used to rewrite the definitions (22) and (23) in the following forms:

$$C_V = T \left(\frac{\partial S}{\partial T} \right)_V, \quad C_P = T \left(\frac{\partial S}{\partial T} \right)_P,$$

more convenient for some applications.

and expect that for all “normal” (mechanically stable) systems, $C_P \geq C_V$. The difference between C_P and C_V is rather minor for most liquids and solids, but may be very substantial for gases – see Sec. 4.

1.4. Thermodynamic potentials

Since for a fixed volume, $d\mathcal{W} = -PdV = 0$, and Eq. (18) yields $dQ = dE$, we may rewrite Eq. (22) in another convenient form

$$C_V = \left(\frac{\partial E}{\partial T} \right)_V . \quad (1.24)$$

so that to calculate C_V from a certain statistical-physics model, we only need to calculate E as a function of temperature and volume. If we want to obtain a similarly convenient expression for C_P , the best way is to introduce a new notion of so-called *thermodynamic potentials* – whose introduction and effective use is perhaps one of the most impressive techniques of thermodynamics. For that, let us combine Eqs. (1) and (18) to write the 1st law of thermodynamics in its most common form

$$dQ = dE + PdV. \quad (1.25)$$

At an isobaric process (Fig. 4), i.e. at $P = \text{const}$, this expression is reduced to

$$(dQ)_P = dE_P + d(PV)_P = d(E + PV)_P. \quad (1.26)$$

Thus, if we introduce a new function with the dimensionality of energy:²⁶

$$H \equiv E + PV, \quad (1.27)$$

Enthalpy:
definition

called *enthalpy* (or, sometimes, the “heat function” or the “heat contents”),²⁷ we may rewrite Eq. (23) as

$$C_P = \left(\frac{\partial H}{\partial T} \right)_P . \quad (1.28)$$

Comparing Eqs. (28) and (24) we see that for the heat capacity, the enthalpy H plays the same role at fixed pressure as the internal energy E plays at fixed volume.

Now let us explore properties of the enthalpy at an *arbitrary* reversible process, i.e. lifting the restriction $P = \text{const}$, but keeping the definition (27). Differentiating this equality, we get

$$dH = dE + PdV + VdP. \quad (1.29)$$

Plugging into this relation Eq. (17) for dE , we see that the terms $\pm PdV$ cancel, yielding a very simple expression

$$dH = TdS + VdP, \quad (1.30)$$

Enthalpy:
differential

whose right-hand side differs from Eq. (17) only by the swap of P and V in the second term, with the simultaneous change of its sign. Formula (30) shows that if H has been found (say, experimentally

²⁶ From the point of view of mathematics, Eq. (27) is a particular case of the so-called *Legendre transformations*.

²⁷ This function (as well as the Gibbs free energy G , see below), had been introduced in 1875 by J. Gibbs, though the term “enthalpy” was coined (much later) by H. Onnes.

measured or calculated for a certain microscopic model) as a function of the entropy S and the pressure P of a system, we can calculate its temperature T and volume V by simple partial differentiation:

$$T = \left(\frac{\partial H}{\partial S} \right)_P, \quad V = \left(\frac{\partial H}{\partial P} \right)_S. \quad (1.31)$$

The comparison of the first of these relations with Eq. (9) shows that not only for the heat capacity but for temperature as well, enthalpy plays the same role at fixed pressure, as played by internal energy at fixed volume.

This success immediately raises the question of whether we could develop this idea further on, by defining other useful thermodynamic potentials – the variables with the dimensionality of energy that would have similar properties – first of all, a potential that would enable a similar swap of T and S in its full differential, in comparison with Eq. (30). We already know that an adiabatic process is the reversible process with fixed entropy, inviting analysis of a reversible process with fixed temperature. Such an *isothermal process* may be implemented, for example, by placing the system under consideration into thermal contact with a much larger system (called either the *heat bath*, or “heat reservoir”, or “thermostat”) that remains in thermodynamic equilibrium at all times – see Fig. 5.

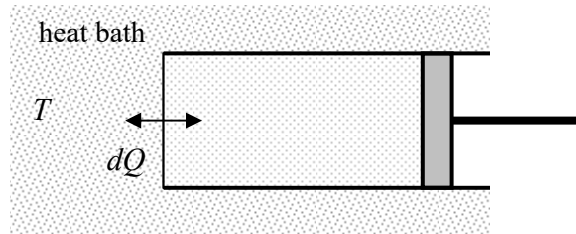


Fig. 1.5. The simplest example of the isothermal process.

Due to its very large size, the heat bath temperature T does not depend on what is being done with our system, and if the change is being done sufficiently slowly (i.e. reversibly), that this temperature is also the temperature of our system – see Eq. (8) and its discussion. Let us calculate the elementary mechanical work $d\mathcal{W}$ (1) at such a reversible isothermal process. According to the general Eq. (18), $d\mathcal{W} = dE - dQ$. Plugging dQ from Eq. (19) into this equality, for $T = \text{const}$ we get

$$(d\mathcal{W})_T = dE - TdS = d(E - TS) \equiv dF, \quad (1.32)$$

where the following combination,

Free energy:
definition

$$F \equiv E - TS, \quad (1.33)$$

is called the *free energy* (or the “Helmholtz free energy”, or just the “Helmholtz energy”²⁸). Just as we have done for the enthalpy, let us establish properties of this new thermodynamic potential for an arbitrarily small, reversible (now not necessarily isothermal!) variation of variables, while keeping the definition (33). Differentiating this relation and then using Eq. (17), we get

Free energy:
differential

$$dF = -SdT - PdV. \quad (1.34)$$

²⁸ It was named after Hermann von Helmholtz (1821-1894). The last of the listed terms for F was recommended by the most recent (1988) IUPAC’s decision, but I will use the first term, which prevails in physics literature. The origin of the adjective “free” stems from Eq. (32): F is may be interpreted as the internal energy’s part that is “free” to be transferred to the mechanical work, at the (most common) reversible, isothermal process.

Thus, if we know the function $F(T, V)$, we can calculate S and P by simple differentiation:

$$S = -\left(\frac{\partial F}{\partial T}\right)_V, \quad P = -\left(\frac{\partial F}{\partial V}\right)_T. \quad (1.35)$$

Now we may notice that the system of all partial derivatives may be made full and symmetric if we introduce one more thermodynamic potential. Indeed, we have already seen that each of the three already introduced thermodynamic potentials (E , H , and F) has an especially simple full differential if it is considered as a function of its two *canonical* arguments: one of the “thermal variables” (either S or T) and one of the “mechanical variables” (either P or V):²⁹

$$E = E(S, V); \quad H = H(S, P); \quad F = F(T, V). \quad (1.36)$$

In this list of pairs of four arguments, only one pair is missing: $\{T, P\}$. The thermodynamic function of this pair, which gives the two remaining variables (S and V) by simple differentiation, is called the *Gibbs energy* (or sometimes the “Gibbs free energy”): $G = G(T, P)$. The way to define it in a symmetric way is evident from the so-called *circular diagram* shown in Fig. 6.

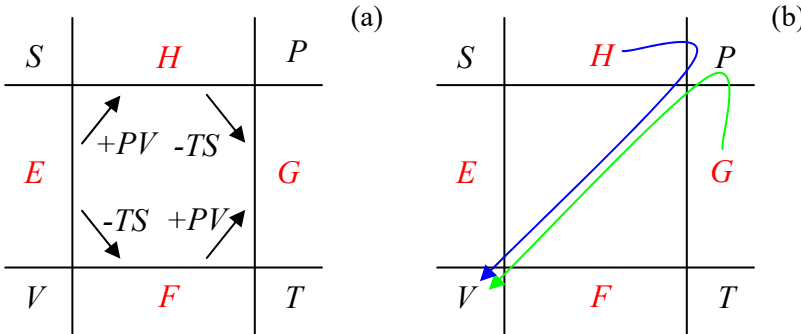


Fig. 1.6. (a) The circular diagram and (b) an example of its use for variable calculation. The thermodynamic potentials are typeset in red, each flanked with its two canonical arguments.

In this diagram, each thermodynamic potential is placed between its two canonical arguments – see Eq. (36). The left two arrows in Fig. 6a show the way the potentials H and F have been obtained from energy E – see Eqs. (27) and (33). This diagram hints that G has to be defined as shown by either of the two right arrows on that panel, i.e. as

$$G \equiv F + PV \equiv H - TS \equiv E - TS + PV. \quad (1.37)$$

Gibbs energy:
definition

In order to verify this idea, let us calculate the full differential of this new thermodynamic potential, using, e.g., the first form of Eq. (37) together with Eq. (34):

$$dG = dF + d(PV) = (-SdT - PdV) + (PdV + VdP) \equiv -SdT + VdP, \quad (1.38)$$

Gibbs energy:
differential

so that if we know the function $G(T, P)$, we can indeed readily calculate both entropy and volume:

$$S = -\left(\frac{\partial G}{\partial T}\right)_P, \quad V = \left(\frac{\partial G}{\partial P}\right)_T. \quad (1.39)$$

²⁹ Note the similarity of this situation with that in analytical mechanics (see, e.g., CM Chapters 2 and 10): the Lagrangian function may be used to derive the equations of motion if it is expressed as a function of generalized coordinates and their *velocities*, while to use the Hamiltonian function in a similar way, it has to be expressed as a function of the generalized coordinates and the corresponding *momenta*.

The circular diagram completed in this way is a good mnemonic tool for describing Eqs. (9), (15), (31), (35), and (39), which express thermodynamic variables as partial derivatives of the thermodynamic potentials. Indeed, the variable in any corner of the diagram may be found as a partial derivative of any of two potentials that are not its immediate neighbors, over the variable in the opposite corner. For example, the green line in Fig. 6b corresponds to the second of Eqs. (39), while the blue line, to the second of Eqs. (31). At this procedure, all the derivatives giving the variables of the upper row (S and P) have to be taken with negative signs, while those giving the variables of the bottom row (V and T), with positive signs.³⁰

Now I have to justify the collective name “thermodynamic potentials” used for E , H , F , and G . For that, let us consider an *irreversible* process, for example, a direct thermal contact of two bodies with different initial temperatures. As was discussed in Sec. 2, at such a process, the entropy may grow even without the external heat flow: $dS \geq 0$ at $dQ = 0$ – see Eq. (12). This means that at a more general process with $dQ \neq 0$, the entropy may grow faster than predicted by Eq. (19), which has been derived for a reversible process, so that

$$dS \geq \frac{dQ}{T}, \quad (1.40)$$

with the equality approached in the reversible limit. Plugging Eq. (40) into Eq. (18) (which, being just the energy conservation law, remains valid for irreversible processes as well), we get

$$dE \leq TdS - PdV. \quad (1.41)$$

We can use this relation to have a look at the behavior of other thermodynamic potentials in irreversible situations, still keeping their definitions given by Eqs. (27), (33), and (37). Let us start from the (very common) case when both the temperature T and the volume V of a system are kept constant. If the process is reversible, then according to Eq. (34), the full time derivative of the free energy F would equal zero. Eq. (41) says that at an irreversible process, this is not necessarily so: if $dT = dV = 0$, then

$$\frac{dF}{dt} = \frac{d}{dt}(E - TS)_T = \frac{dE}{dt} - T \frac{dS}{dt} \leq 0. \quad (1.42)$$

Hence, in the general (irreversible) situation, F can only decrease, but not increase in time. This means that F eventually approaches its minimum value $F(T, S)$, given by the equations of reversible thermodynamics. To re-phrase this important conclusion, in the case $T = \text{const}$, $V = \text{const}$, the free energy F , i.e. the difference $E - TS$, plays the role of the potential energy in the classical mechanics of dissipative processes: its minimum corresponds to the (in the case of F , thermodynamic) equilibrium of the system. This is one of the key results of thermodynamics, and I invite the reader to give it some thought. One of its possible handwaving interpretations of this fact is that the heat bath with fixed $T > 0$, i.e. with a substantial thermal agitation of its components, “wants” to impose thermal disorder in the system immersed into it, by “rewarding” it with lower F for any increase of disorder.

³⁰ There is also a wealth of other relations between thermodynamic variables that may be represented as second derivatives of the thermodynamic potentials, including four *Maxwell relations* such as $(\partial S/\partial V)_T = (\partial P/\partial T)_V$, etc. (They may be readily recovered from the well-known property of a function of two independent arguments, say, $f(x, y)$: $\partial(\partial f/\partial x)/\partial y = \partial(\partial f/\partial y)/\partial x$.) In this chapter, I will list only the thermodynamic relations that will be used later in the course; a more complete list may be found, e.g., in Sec. 16 of the book by L. Landau and E. Lifshitz, *Statistical Physics, Part 1*, 3rd ed., Pergamon, 1980 (and its later re-printings).

Repeating the calculation for a different case, $T = \text{const}$, $P = \text{const}$, it is easy to see that in this case the same role is played by the Gibbs energy:

$$\frac{dG}{dt} \equiv \frac{d}{dt}(E - TS + PV) = \frac{dE}{dt} - T \frac{dS}{dt} + P \frac{dV}{dt} \leq (T \frac{dS}{dt} - P \frac{dV}{dt}) - T \frac{dS}{dt} + P \frac{dV}{dt} \equiv 0, \quad (1.43)$$

so that the thermal equilibrium now corresponds to the minimum of G rather than F .

For the two remaining thermodynamic potentials, E and H , the calculations similar to Eqs. (42) and (43) make less sense because that would require keeping $S = \text{const}$ (with $V = \text{const}$ for E , and $P = \text{const}$ for H) for an irreversible process, but it is usually hard to prevent the entropy from growing if initially it had been lower than its equilibrium value, at least on the long-term basis.³¹ Thus the circular diagram is not so symmetric after all: G and F are somewhat more useful for most practical calculations than E and H .

Note that the difference $G - F = PV$ between the two “more useful” potentials has very little to do with thermodynamics at all because this difference exists (although is not much advertised) in classical mechanics as well.³² Indeed, the difference may be generalized as $G - F = -\mathcal{F}q$, where q is a generalized coordinate, and \mathcal{F} is the corresponding generalized force. The minimum of F corresponds to the equilibrium of an autonomous system (with $\mathcal{F} = 0$), while the equilibrium position of the same system under the action of external force \mathcal{F} is given by the minimum of G . Thus the external force “wants” the system to subdue to its effect, “rewarding” it with lower G .

Moreover, the difference between F and G becomes a bit ambiguous (approach-dependent) when the product $\mathcal{F}q$ may be partitioned into single-particle components – just as it is done in Eqs. (2b) and (3b) for the electric and magnetic fields. Here the applied field may be taken into account on the microscopic level, including its effect directly into the energy ε_k of each particle. In this case, the field contributes to the total internal energy E directly, and hence the thermodynamic equilibrium (at $T = \text{const}$) is described as the minimum of F . (We may say that in this case $F = G$, unless a difference between these thermodynamic potentials is created by the actual mechanical pressure P .) However, in some cases, typically for condensed systems, with their strong interparticle interactions, the easier (and sometimes the only one practicable³³) way to account for the field is on the macroscopic level, taking $G = F - \mathcal{F}q$. In this case, the same equilibrium state is described as the minimum of G . (Several examples of this dichotomy will be given later in this course.) Whatever the choice, one should mind not take the same field effect into account twice.

³¹ There are a few practicable systems, notably including the so-called *adiabatic magnetic refrigerators* (to be discussed in Chapter 2), where the unintentional growth of S is so slow that the condition $S = \text{const}$ may be closely approached.

³² It is convenient to describe it as the difference between the “usual” (internal) potential energy U of the system to its “Gibbs potential energy” U_G – see CM Sec. 1.4. For the readers who skipped that discussion: my pet example is the usual elastic spring with $U = kx^2/2$, under the effect of an external force \mathcal{F} , whose equilibrium position ($x_0 = \mathcal{F}/k$) evidently corresponds to the minimum of $U_G = U - \mathcal{F}x$, rather than just U .

³³ An example of such an extreme situation is the case when an external magnetic field \mathcal{H} is applied to a superconductor in its so-called *intermediate state*, in which the sample partitions into domains of the “normal” phase with $\mathcal{B} = \mu_0 \mathcal{H}$, and the superconducting phase with $\mathcal{B} = 0$. In this case, the field is effectively applied to the interfaces between the domains, very similarly to the mechanical pressure applied to a gas portion via a piston – see Fig. 1 again.

One more important conceptual question I would like to discuss here is why usually statistical physics pursues the calculation of thermodynamic potentials, rather than just of a relation between P , V , and T . (Such relation is called the *equation of state* of the system.) Let us explore this issue on the particular but important example of an *ideal classical gas* in thermodynamic equilibrium, for which the equation of state should be well known to the reader from undergraduate physics:³⁴

Ideal gas:
equation
of state

$$PV = NT, \quad (1.44)$$

where N is the number of particles in volume V . (In Chapter 3, we will derive Eq. (44) from statistics.) Let us try to use it for the calculation of all thermodynamic potentials, and all other thermodynamic variables discussed above. We may start, for example, from the calculation of the free energy F . Indeed, integrating the second of Eqs. (35) with the pressure calculated from Eq. (44), $P = NT/V$, we get

$$F = -\int PdV \Big|_{T=\text{const}} = -NT \int \frac{dV}{V} \equiv -NT \int \frac{d(V/N)}{(V/N)} = -NT \ln \frac{V}{N} + Nf(T), \quad (1.45)$$

where V has been divided by N in both instances just to represent F as a manifestly extensive variable, in this uniform system proportional to N . The integration “constant” $f(T)$ is some function of temperature, which cannot be recovered from the equation of state. This function affects all other thermodynamic potentials, and the entropy as well. Indeed, using the first of Eqs. (35) together with Eq. (45), we get

$$S = -\left(\frac{\partial F}{\partial T}\right)_V = N \left[\ln \frac{V}{N} - \frac{df(T)}{dT} \right], \quad (1.46)$$

and now may combine Eqs. (33) with (46) to calculate the (internal) energy of the gas,³⁵

$$E = F + TS = \left[-NT \ln \frac{V}{N} + Nf(T) \right] + T \left[N \ln \frac{V}{N} - N \frac{df(T)}{dT} \right] \equiv N \left[f(T) - T \frac{df(T)}{dT} \right], \quad (1.47)$$

then use Eqs. (27), (44) and (47) to calculate its enthalpy,

$$H = E + PV = E + NT = N \left[f(T) - T \frac{df(T)}{dT} + T \right], \quad (1.48)$$

and, finally, plug Eqs. (44) and (45) into Eq. (37) to calculate the Gibbs energy

$$G = F + PV = N \left[-T \ln \frac{V}{N} + f(T) + T \right]. \quad (1.49)$$

³⁴ The long history of the gradual discovery of this relation includes the very early (circa 1662) work by R. Boyle and R. Townely, followed by contributions from H. Power, E. Mariotte, J. Charles, J. Dalton, and J. Gay-Lussac. It was fully formulated by Benoît Paul Émile Clapeyron in 1834, in the form $PV = nRT_K$, where n is the number of moles in the gas sample, and $R \approx 8.31 \text{ J/mole}\cdot\text{K}$ is the so-called *gas constant*. This form is equivalent to Eq. (44), taking into account that $R \equiv k_B N_A$, where $N_A = 6.022\ 140\ 76 \times 10^{23} \text{ mole}^{-1}$ is the *Avogadro number*, i.e. the number of molecules per mole. (By the mole’s definition, N_A is just the reciprocal mass, in grams, of the 1/12th part of the ¹²C atom, which is close to the mass of one proton or neutron – see *Appendix CA: Selected Physical Constants*.) Historically, this equation of state was the main argument for the introduction of the absolute temperature T , because only with it, the equation acquires the spectacularly simple form (44).

³⁵ Note that Eq. (47), in particular, describes a very important property of the ideal classical gas: its energy depends only on temperature (and the number of particles), but not on volume or pressure.

One might ask whether the function $f(T)$ is physically significant, or it is something like the inconsequential, arbitrary constant – like the one that may be always added to the potential energy in non-relativistic mechanics. In order to address this issue, let us calculate, from Eqs. (24) and (28), both heat capacities, which are evidently measurable quantities:

$$C_V = \left(\frac{\partial E}{\partial T} \right)_V = -NT \frac{d^2 f}{dT^2}, \quad (1.50)$$

$$C_P = \left(\frac{\partial H}{\partial T} \right)_P = N \left(-T \frac{d^2 f}{dT^2} + 1 \right) = C_V + N. \quad (1.51)$$

We see that the function $f(T)$, or at least its second derivative, is measurable.³⁶ (In Chapter 3, we will calculate this function for two simple “microscopic” models of the ideal classical gas.) The meaning of this function is evident from the physical picture of the ideal gas: the pressure P exerted on the walls of the containing volume is produced only by the translational motion of the gas molecules, while their internal energy E (and hence other thermodynamic potentials) may be also contributed by the internal dynamics of the molecules – their rotations, vibrations, etc. Thus, the equation of state does *not* give us the full thermodynamic description of a system, while the thermodynamic potentials do.

1.5. Systems with a variable number of particles

Now we have to consider one more important case: when the number N of particles in a system is not rigidly fixed, but may change as a result of a thermodynamic process. A typical example of such a system is a gas sample separated from the environment by a penetrable partition – see Fig. 7.³⁷

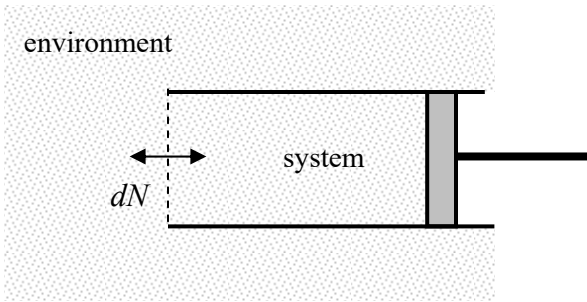


Fig. 1.7. An example of a system with a variable number of particles.

Let us analyze this situation for the simplest case when all the particles are similar. (In Sec. 4.1, this analysis will be extended to systems with particles of several sorts). In this case, we may consider N as an independent thermodynamic variable whose variation may change the energy E of the system, so that (for a slow, reversible process) Eq. (17) should be now generalized as

$$dE = TdS - PdV + \mu dN, \quad (1.52)$$

Chemical potential:
definition

³⁶ Note, however, that the difference $C_P - C_V = N$ is independent of $f(T)$. (If the temperature is measured in kelvins, this relation takes a more familiar form $C_P - C_V = nR$.) It is straightforward (and hence left for the reader’s exercise) to show that the difference $C_P - C_V$ of *any* system is fully determined by its equation of state.

³⁷ Another important example is a gas in a contact with the open-surface liquid of similar molecules.

where μ is a new function of state, called the *chemical potential*.³⁸ Keeping the definitions of other thermodynamic potentials, given by Eqs. (27), (33), and (37), intact, we see that the expressions for their differentials should be generalized as

$$dH = TdS + VdP + \mu dN, \quad (1.53a)$$

$$dF = -SdT - PdV + \mu dN, \quad (1.53b)$$

$$dG = -SdT + VdP + \mu dN, \quad (1.53c)$$

so that the chemical potential may be calculated as either of the following partial derivatives:³⁹

$$\mu = \left(\frac{\partial E}{\partial N} \right)_{S,V} = \left(\frac{\partial H}{\partial N} \right)_{S,P} = \left(\frac{\partial F}{\partial N} \right)_{T,V} = \left(\frac{\partial G}{\partial N} \right)_{T,P}. \quad (1.54)$$

Despite the formal similarity of all Eqs. (54), one of them is more consequential than the others. Indeed, the Gibbs energy G is the only thermodynamic potential that is a function of two *intensive* parameters, T and P . However, as all thermodynamic potentials, G has to be *extensive*, so that in a system of similar particles it has to be proportional to N :

$$G = Ng, \quad (1.55)$$

where g is some function of T and P . Plugging this expression into the last of Eqs. (54), we see that μ equals exactly this function, so that

$$\boxed{\mu = \frac{G}{N}}, \quad (1.56)$$

i.e. the chemical potential is just the Gibbs energy per particle.

In order to demonstrate how vital the notion of chemical potential may be, let us consider the situation (parallel to that shown in Fig. 2) when a system consists of two parts, with equal pressure and temperature, that can exchange particles at a relatively slow rate (much slower than the speed of the internal relaxation of each part). Then we can write two equations similar to Eqs. (5):

$$N = N_1 + N_2, \quad G = G_1 + G_2, \quad (1.57)$$

where $N = \text{const}$, and Eq. (56) may be used to describe each component of G :

$$G = \mu_1 N_1 + \mu_2 N_2. \quad (1.58)$$

Plugging the N_2 expressed from the first of Eqs. (57), $N_2 = N - N_1$, into Eq. (58), we see that

$$\frac{dG}{dN_1} = \mu_1 - \mu_2, \quad (1.59)$$

so that the minimum of G is achieved at $\mu_1 = \mu_2$. Hence, in the conditions of fixed temperature and pressure, i.e. when G is the appropriate thermodynamic potential, the chemical potentials of the system parts should be equal – the so-called *chemical equilibrium*.

³⁸ This name, of a historic origin, is misleading: as evident from Eq. (52), μ has a clear *physical* sense of the average energy cost of adding one more particle to the system of $N \gg 1$ particles.

³⁹ Note that strictly speaking, Eqs. (9), (15), (31), (35), and (39) should be now generalized by adding another lower index, N , to the corresponding derivatives; I will just imply this.

Finally, later in the course, we will also run into several cases when the volume V of a system, its temperature T , and the chemical potential μ are all fixed. (The last condition may be readily implemented by allowing the system of our interest to exchange particles with an environment so large that its μ stays constant.) The thermodynamic potential appropriate for this case may be obtained by subtraction of the product μN from the free energy F , resulting in the so-called *grand thermodynamic* (or “Landau”) *potential*:

$$\Omega \equiv F - \mu N = F - \frac{G}{N} N \equiv F - G = -PV. \quad (1.60)$$

Grand potential: definition

Indeed, for a reversible process, the full differential of this potential is

$$d\Omega = dF - d(\mu N) = (-SdT - PdV + \mu dN) - (\mu dN + Nd\mu) = -SdT - PdV - Nd\mu, \quad (1.61)$$

Grand potential: differential

so that if Ω has been calculated as a function of T , V , and μ , other thermodynamic variables may be found as

$$S = -\left(\frac{\partial\Omega}{\partial T}\right)_{V,\mu}, \quad P = -\left(\frac{\partial\Omega}{\partial V}\right)_{T,\mu}, \quad N = -\left(\frac{\partial\Omega}{\partial\mu}\right)_{T,V}. \quad (1.62)$$

Now acting exactly as we have done for other potentials, it is straightforward to prove that an irreversible process with fixed T , V , and μ , provides $d\Omega/dt \leq 0$, so that system’s equilibrium indeed corresponds to the minimum of the grand potential Ω . We will repeatedly use this fact in this course.

1.6. Thermal machines

In order to complete this brief review of thermodynamics, I cannot completely pass the topic of *thermal machines* – not because it will be used much in this course, but mostly because of its practical and historic significance.⁴⁰ Figure 8a shows the generic scheme of a thermal machine that may perform mechanical work on its environment (in our notation, equal to $-\mathcal{W}$) during each cycle of the expansion/compression of some “working gas”, by transferring different amounts of heat from a high-temperature heat bath (Q_H) and to the low-temperature bath (Q_L).

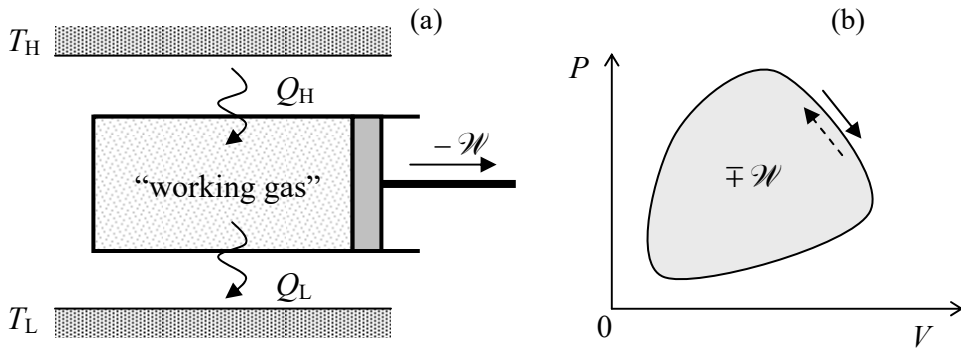


Fig. 1.8. (a) The simplest implementation of a thermal machine, and (b) the graphic representation of the mechanical work it performs. On panel (b), the solid arrow indicates the heat engine cycle direction, while the dashed arrow, the refrigerator cycle direction.

⁴⁰ The whole field of thermodynamics was spurred by the famous 1824 work by Nicolas Léonard Sadi Carnot, in which he, in particular, gave an alternative, indirect form of the 2nd law of thermodynamics – see below.

One relation between the three amounts Q_H , Q_L , and \mathcal{W} is immediately given by the energy conservation (i.e. by the 1st law of thermodynamics):

$$Q_H - Q_L = -\mathcal{W}. \quad (1.63)$$

From Eq. (1), the mechanical work during the cycle may be calculated as

$$-\mathcal{W} = \oint P dV, \quad (1.64)$$

and hence represented by the area circumvented by the state-representing point on the $[P, V]$ plane – see Fig. 8b. Note that the sign of this circular integral depends on the direction of the point's rotation; in particular, the work ($-\mathcal{W}$) done by the working gas is positive at its clockwise rotation (pertinent to *heat engines*) and negative in the opposite case (implemented in *refrigerators* and *heat pumps* – see below). Evidently, the work depends on the exact form of the cycle, which in turn may depend not only on T_H and T_L , but also on the working gas' properties.

An exception from this rule is the famous *Carnot cycle*, consisting of two isothermal and two adiabatic processes (all reversible!). In its heat engine's form, the cycle may start, for example, from an isothermic expansion of the working gas in contact with the hot bath (i.e. at $T = T_H$). It is followed by its additional adiabatic expansion (with the gas being disconnected from both heat baths) until its temperature drops to T_L . Then an isothermal compression of the gas is performed in its contact with the cold bath (at $T = T_L$), followed by its additional adiabatic compression to raise T to T_H again, after which the cycle is repeated again and again. Note that during this cycle the working gas is never in contact with both heat baths simultaneously, thus avoiding the irreversible heat transfer between them. The cycle's shape on the $[V, P]$ plane (Fig. 9a) depends on the exact properties of the working gas and may be rather complicated. However, since the system's entropy is constant at any adiabatic process, the Carnot cycle's shape on the $[S, T]$ plane is always rectangular – see Fig. 9b.

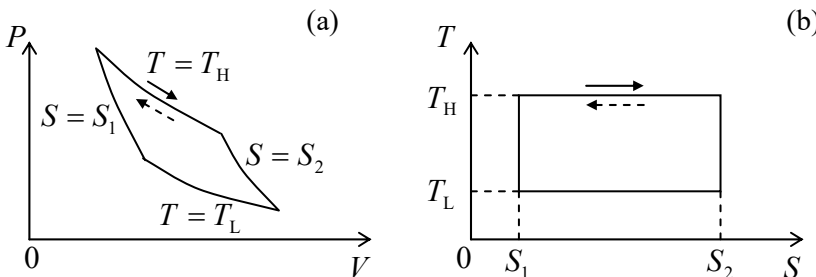


Fig. 1.9. Representation of the Carnot cycle: (a) on the $[V, P]$ plane (schematically), and (b) on the $[S, T]$ plane. The meaning of the arrows is the same as in Fig. 8.

Since during each isotherm, the working gas is brought into thermal contact only with the corresponding heat bath, i.e. its temperature is constant, the relation (19), $dQ = TdS$, may be immediately integrated to yield

$$Q_H = T_H(S_2 - S_1), \quad Q_L = T_L(S_2 - S_1). \quad (1.65)$$

Hence the ratio of these two heat flows is completely determined by their temperature ratio:

$$\frac{Q_H}{Q_L} = \frac{T_H}{T_L}, \quad (1.66)$$

regardless of the working gas properties. Formulas (63) and (66) are sufficient to find the ratio of the work ($-\mathcal{W}$) to any of Q_H and Q_L . For example, the main figure-of-merit of a thermal machine used as a heat engine ($Q_H > 0, Q_L > 0, -\mathcal{W} = |\mathcal{W}| > 0$), is its *efficiency*

$$\eta \equiv \frac{|\mathcal{W}|}{Q_H} = \frac{Q_H - Q_L}{Q_H} \equiv 1 - \frac{Q_L}{Q_H} \leq 1. \quad (1.67)$$

Heat
engine's
efficiency:
definition

For the Carnot cycle, this definition, together with Eq. (66), immediately yield the famous relation⁴¹

$$\eta_{\text{Carnot}} = 1 - \frac{T_L}{T_H}, \quad (1.68)$$

Carnot
cycle's
efficiency

which shows that at a given T_L (that is typically the ambient temperature ~ 300 K), the efficiency may be increased, ultimately to 1, by raising the temperature T_H of the heat source.⁴²

The unique nature of the Carnot cycle (see Fig. 9b again) makes its efficiency (68) the upper limit for any heat engine.⁴³ Indeed, in this cycle, the transfer of heat between any heat bath and the working gas is performed reversibly, when their temperatures are equal. (If this is not so, some heat might flow from a hotter to colder bath without performing any work.) In particular, it shows that $\eta_{\max} = 0$ at $T_H = T_L$, i.e., no heat engine can perform mechanical work in the absence of temperature gradients.⁴⁴

On the other hand, if the cycle is reversed (see the dashed arrows in Figs. 8 and 9), the same thermal machine may serve as a *refrigerator*, providing heat removal from the low-temperature bath ($Q_L < 0$) at the cost of consuming external mechanical work: $\mathcal{W} > 0$. This reversal does not affect the basic relation (63), which now may be used to calculate the relevant figure-of-merit, called the *cooling coefficient of performance* (COP_{cooling}):

$$\text{COP}_{\text{cooling}} \equiv \frac{|Q_L|}{\mathcal{W}} = \frac{Q_L}{Q_H - Q_L}. \quad (1.69)$$

Notice that this coefficient may be above unity; in particular, for the Carnot cycle we may use Eq. (66) (which is also unaffected by the cycle reversal) to get

$$(\text{COP}_{\text{cooling}})_{\text{Carnot}} = \frac{T_L}{T_H - T_L}, \quad (1.70)$$

⁴¹ Curiously, S. Carnot derived his key result still believing that heat is some specific fluid (“caloric”), whose flow is driven by the temperature difference, rather than just a form of particle motion.

⁴² Semi-quantitatively, such trend is valid also for other, less efficient but more practicable heat engine cycles – see Problems 13-16. This trend is the leading reason why internal combustion engines, with T_H of the order of 1,500 K, are more efficient than steam engines, with the difference $T_H - T_L$ of at most a few hundred K.

⁴³ In some alternative axiomatic systems of thermodynamics, this fact is postulated and serves the role of the 2nd law. This is why it is under persisting (dominantly, theoretical) attacks by suggestions of more efficient heat engines – recently, mostly of quantum systems using sophisticated protocols such as the so-called *shortcut-to-adiabaticity* – see, e.g., the recent paper by O. Abah and E. Lutz, *Europhysics Lett.* **118**, 40005 (2017), and references therein. To the best of my knowledge, reliable analyses of all the suggestions put forward so far have confirmed that the Carnot efficiency (68) is the highest possible even in quantum systems.

⁴⁴ Such a hypothetical heat engine, which would violate the 2nd law of thermodynamics, is called the “perpetual motion machine of the 2nd kind” – in contrast to any (also hypothetical) “perpetual motion machine of the 1st kind” that would violate the 1st law, i.e., the energy conservation.

so that this value is larger than 1 at $T_H < 2T_L$, and even may be much larger than that when the temperature difference $(T_H - T_L)$ sustained by the refrigerator, tends to zero. For example, in a typical air-conditioning system, this difference is of the order of 10 K, while $T_L \sim 300$ K, so that $(T_H - T_L) \sim T_L/30$, i.e. the Carnot value of $\text{COP}_{\text{cooling}}$ is as high as ~ 30 . (In the state-of-the-art commercial HVAC systems it is within the range of 3 to 4.) This is why the term “cooling efficiency”, used in some textbooks instead of $(\text{COP})_{\text{cooling}}$, may be misleading.

Since in the reversed cycle $Q_H = -\mathcal{W} + Q_L < 0$, i.e. the system provides heat flow into the high-temperature heat bath, it may be used as a *heat pump* for heating purposes. The figure-of-merit appropriate for this application is different from Eq. (69):

$$\text{COP}_{\text{heating}} \equiv \frac{|Q_H|}{\mathcal{W}} = \frac{Q_H}{Q_H - Q_L}, \quad (1.71)$$

so that for the Carnot cycle, using Eq. (66) again, we get

$$(\text{COP}_{\text{heating}})_{\text{Carnot}} = \frac{T_H}{T_H - T_L}. \quad (1.72)$$

Note that this COP is *always* larger than 1, meaning that the Carnot heat pump is always more efficient than the direct conversion of work into heat (when $Q_H = -\mathcal{W}$, so that $\text{COP}_{\text{heating}} = 1$), though practical electricity-driven heat pumps are substantially more complex, and hence more expensive than simple electric heaters. Such heat pumps, with the typical $\text{COP}_{\text{heating}}$ values around 4 in summer and 2 in winter, are frequently used for heating large buildings.

Finally, note that according to Eq. (70), the $\text{COP}_{\text{cooling}}$ of the Carnot cycle tends to zero at $T_L \rightarrow 0$, making it impossible to reach the absolute zero of temperature, and hence illustrating the meaningful (Nernst's) formulation of the 3rd law of thermodynamics, cited in Sec. 3. Indeed, let us prescribe a finite but very large heat capacity $C(T)$ to the low-temperature bath, and use the definition of this variable to write the following expression for the relatively small change of its temperature as a result of dn similar refrigeration cycles:

$$C(T_L)dT_L = Q_L dn. \quad (1.73)$$

Together with Eq. (66), this relation yields

$$\frac{C(T_L)dT_L}{T_L} = -\frac{|Q_H|}{T_H} dn. \quad (1.74)$$

If $T_L \rightarrow 0$, so that $T_H \gg T_L$ and $|Q_H| \approx -\mathcal{W} = \text{const}$, the right-hand side of this equation does not depend on T_L , so that if we integrate it over many ($n \gg 1$) cycles, getting the following simple relation between the initial and final values of T_L :

$$\int_{T_{\text{ini}}}^{T_{\text{fin}}} \frac{C(T)dT}{T} = -\frac{|Q_H|}{T_H} n. \quad (1.75)$$

For example, if $C(T)$ is a constant, Eq. (75) yields an exponential law,

$$T_{\text{fin}} = T_{\text{ini}} \exp \left\{ -\frac{|Q_H|}{CT_H} n \right\}, \quad (1.76)$$

with the absolute zero of temperature not reached as any finite n . Even for an arbitrary function $C(T)$ that does not vanish at $T \rightarrow 0$, Eq. (74) proves the Nernst theorem, because dn diverges at $T_L \rightarrow 0$.⁴⁵

1.7. Exercise problems

1.1. Two bodies, with temperature-independent heat capacities C_1 and C_2 , and different initial temperatures T_1 and T_2 , are placed into a weak thermal contact. Calculate the change of the total entropy of the system before it reaches the thermal equilibrium.

1.2. A gas portion has the following properties:

- (i) its heat capacity $C_V = aT^b$, and
- (ii) the work \mathcal{W}_T needed for its isothermal compression from V_2 to V_1 equals $cT\ln(V_2/V_1)$,

where a , b , and c are some constants. Find the equation of state of the gas, and calculate the temperature dependence of its entropy S and thermodynamic potentials E , H , F , G , and Ω .

1.3. A closed volume with an ideal classical gas of similar molecules is separated with a partition in such a way that the number N of molecules in each part is the same, but their volumes are different. The gas is initially in thermal equilibrium, and its pressure in one part is P_1 , and in the other part, P_2 . Calculate the change of entropy resulting from a fast removal of the partition, and analyze the result.

1.4. An ideal classical gas of N particles is initially confined to volume V , and is in thermal equilibrium with a heat bath of temperature T . Then the gas is allowed to expand to volume $V' > V$ in one of the following ways:

- (i) The expansion is slow, so that due to the sustained thermal contact with the heat bath, the gas temperature remains equal to T .
- (ii) The partition separating the volumes V and $(V' - V)$ is removed very fast, allowing the gas to expand rapidly.

For each process, calculate the eventual changes of pressure, temperature, energy, and entropy of the gas at its expansion.

1.5. For an ideal classical gas with temperature-independent specific heat, derive the relation between P and V at an adiabatic expansion/compression.

1.6. Calculate the speed and the wave impedance of acoustic waves propagating in an ideal classical gas with temperature-independent specific heat, in the limits when the propagation may be treated as:

- (i) an isothermal process, and
- (ii) an adiabatic process.

⁴⁵ Note that for such metastable systems as glasses the situation may be more complicated. (For a detailed discussion of this issue see, e.g., J. Wilks, *The Third Law of Thermodynamics*, Oxford U. Press, 1961.) Fortunately, this issue does not affect other aspects of statistical physics – at least those to be discussed in this course.

Which of these limits is achieved at higher wave frequencies?

1.7. As will be discussed in Sec. 3.5, the so-called “hardball” models of classical particle interaction yield the following equation of state of a gas of such particles:

$$P = T\varphi(n),$$

where $n = N/V$ is the particle density, and the function $\varphi(n)$ is generally different from that ($\varphi_{\text{ideal}}(n) = n$) of the ideal gas, but still independent of temperature. For such a gas, with temperature-independent c_V , calculate:

- (i) the energy of the gas, and
- (ii) its pressure as a function of n at the adiabatic compression.

1.8. For an arbitrary thermodynamic system with a fixed number of particles, prove the following four *Maxwell relations* (already mentioned in Sec. 4):

$$\begin{aligned} \text{(i)}: \left(\frac{\partial S}{\partial V}\right)_T &= \left(\frac{\partial P}{\partial T}\right)_V, & \text{(ii)}: \left(\frac{\partial V}{\partial S}\right)_P &= \left(\frac{\partial T}{\partial P}\right)_S, \\ \text{(iii)}: \left(\frac{\partial S}{\partial P}\right)_T &= -\left(\frac{\partial V}{\partial T}\right)_P, & \text{(iv)}: \left(\frac{\partial P}{\partial S}\right)_V &= -\left(\frac{\partial T}{\partial V}\right)_S, \end{aligned}$$

and also the following relation:

$$\left(\frac{\partial E}{\partial V}\right)_T = T\left(\frac{\partial P}{\partial T}\right)_V - P.$$

1.9. Express the heat capacity difference, $C_P - C_V$, via the equation of state $P = P(V, T)$ of the system.

1.10. Prove that the *isothermal compressibility*⁴⁶

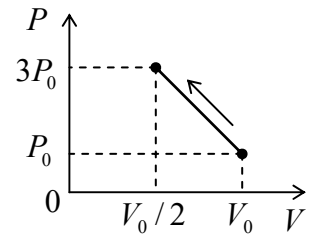
$$\kappa_T \equiv -\frac{1}{V}\left(\frac{\partial V}{\partial P}\right)_{T,N}$$

in a single-phase system may be expressed in two different ways:

$$\kappa_T = \frac{V^2}{N^2}\left(\frac{\partial^2 P}{\partial \mu^2}\right)_T = \frac{V}{N^2}\left(\frac{\partial N}{\partial \mu}\right)_{T,V}.$$

1.11. A reversible process, performed with a fixed portion of an ideal classical gas, may be represented on the $[V, P]$ plane with the straight line shown in the figure on the right. Find the point at which the heat flow into/out of the gas changes its direction.

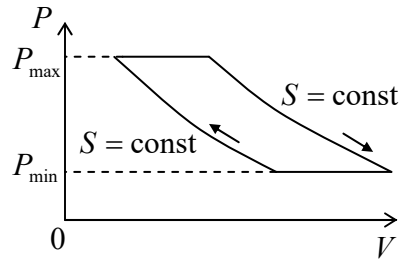
1.12. Two bodies have equal, temperature-independent heat capacities



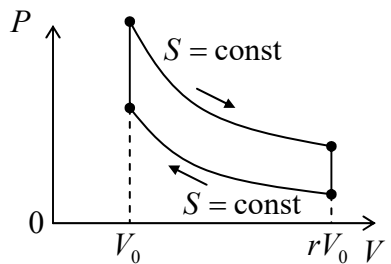
⁴⁶ Note that the compressibility is just the reciprocal bulk modulus, $\kappa = 1/K$ – see, e.g., CM Sec. 7.3.

C , but different temperatures, T_1 and T_2 . Calculate the maximum mechanical work obtainable from this system, using a heat engine.

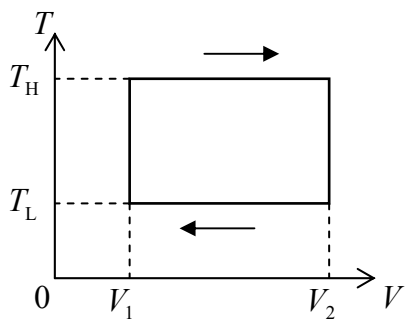
1.13. Express the efficiency η of a heat engine that uses the so-called *Joule cycle*, consisting of two adiabatic and two isobaric processes (see the figure on the right), via the minimum and maximum values of pressure, and compare the result with η_{Carnot} . Assume an ideal classical working gas with temperature-independent C_P and C_V .



1.14. Calculate the efficiency of a heat engine using the *Otto cycle*,⁴⁷ which consists of two adiabatic and two isochoric (constant-volume) reversible processes – see the figure on the right. Explore how the efficiency depends on the ratio $r \equiv V_{\max}/V_{\min}$, and compare it with the Carnot cycle's efficiency. Assume an ideal classical working gas with temperature-independent heat capacity.



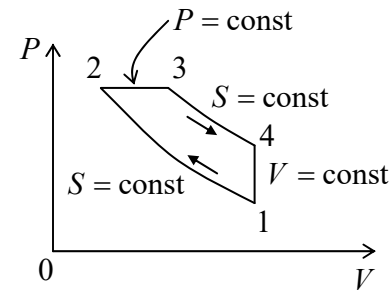
1.15. A heat engine's cycle consists of two isothermal ($T = \text{const}$) and two isochoric ($V = \text{const}$) reversible processes – see the figure on the right.⁴⁸



(i) Assuming that the working gas is an ideal classical gas of N particles, calculate the mechanical work performed by the engine during one cycle.

(ii) Are the specified conditions sufficient to calculate the engine's efficiency? (Justify your answer.)

1.16. The *Diesel cycle* (an approximate model of the Diesel internal combustion engine's operation) consists of two adiabatic processes, one isochoric process, and one isobaric process – see the figure on the right. Assuming an ideal working gas with temperature-independent C_V and C_P , express the efficiency η of the heat engine using this cycle via the gas temperature values in its transitional states corresponding to the corners of the cycle diagram.



⁴⁷ This name stems from the fact that the cycle is an approximate model of operation of the four-stroke internal combustion engine, which was improved and made practicable (though not invented!) by N. Otto in 1876.

⁴⁸ The reversed cycle of this type is a reasonable approximation for the operation of the *Stirling* and *Gifford-McMahon* (GM) refrigerators, broadly used for *cryocooling* – for a recent review see, e.g., A. de Waele, *J. Low Temp. Phys.* **164**, 179 (2011).

Chapter 2. Principles of Physical Statistics

This chapter is the keystone of this course. It starts with a brief discussion of such basic notions of statistical physics as statistical ensembles, probability, and ergodicity. Then the so-called microcanonical distribution postulate is formulated, simultaneously with the statistical definition of the entropy. This allows a derivation of the famous Gibbs (“canonical”) distribution – the most frequently used tool of statistical physics. Then we will discuss one more, “grand canonical” distribution, which is more convenient for some tasks. In particular, it is immediately used for the derivation of the most important Boltzmann, Fermi-Dirac, and Bose-Einstein statistics of independent particles, which will be repeatedly utilized in the following chapters.

2.1. Statistical ensembles and probability

As has been already discussed in Sec. 1.1, statistical physics deals with situations when either unknown initial conditions, or system’s complexity, or the laws of its motion (as in the case of quantum mechanics) do not allow a definite prediction of measurement results. The main formalism for the analysis of such systems is the probability theory, so let me start with a very brief review of its basic concepts, using an informal “physical” language – less rigorous but (hopefully) more transparent than standard mathematical treatments,¹ and quite sufficient for our purposes.

Consider $N \gg 1$ independent similar experiments carried out with *apparently* similar systems (i.e. systems with identical *macroscopic* parameters such as volume, pressure, etc.), but still giving, by any of the reasons listed above, different results of measurements. Such a collection of experiments, together with a fixed method of result processing, is a good example of a *statistical ensemble*. Let us start from the case when the experiments may have M different *discrete* outcomes, and the number of experiments giving the corresponding different results is N_1, N_2, \dots, N_M , so that

$$\sum_{m=1}^M N_m = N. \quad (2.1)$$

The *probability* of each outcome, for the given statistical ensemble, is then defined as

Probability

$$W_m \equiv \lim_{N \rightarrow \infty} \frac{N_m}{N}. \quad (2.2)$$

Though this definition is so close to our everyday experience that it is almost self-evident, a few remarks may still be relevant.

First, the probabilities W_m depend on the exact statistical ensemble they are defined for, notably including the method of result processing. As the simplest example, consider throwing the standard cubic-shaped dice many times. For the ensemble of all thrown and counted dice, the probability of each outcome (say, “1”) is $1/6$. However, nothing prevents us from defining another statistical ensemble of dice-throwing experiments in which all outcomes “1” are discounted. Evidently, the probability of

¹ For the reader interested in a more rigorous approach, I can recommend, for example, Chapter 18 of the handbook by G. Korn and T. Korn – see MA Sec. 16(ii).

finding outcomes “1” in this modified (but legitimate) ensemble is 0, while for all other five outcomes (“2” to “6”), it is $1/5$ rather than $1/6$.

Second, a statistical ensemble does not necessarily require N similar physical systems, e.g., N distinct dice. It is intuitively clear that tossing the same die N times constitutes an ensemble with similar statistical properties. More generally, a set of N experiments with the same system gives a statistical ensemble equivalent to the set of experiments with N different systems, provided that the experiments are kept independent, i.e. that outcomes of past experiments do not affect those of the experiments to follow. Moreover, for many physical systems of interest, no special preparation of each experiment is necessary, and N experiments separated by sufficiently long time intervals, form a “good” statistical ensemble – the property called *ergodicity*.²

Third, the reference to infinite N in Eq. (2) does not strip the notion of probability from its practical relevance. Indeed, it is easy to prove (see Chapter 5) that, at very general conditions, at finite but sufficiently large N , the numbers N_m are approaching their *average* (or *expectation*) values³

$$\langle N_m \rangle \equiv W_m N, \quad (2.3)$$

with the relative deviations decreasing as $\sim 1/\langle N_m \rangle^{1/2}$, i.e. as $1/N^{1/2}$.

Now let me list those properties of probabilities that we will immediately need. First, dividing both sides of Eq. (1) by N and following the limit $N \rightarrow \infty$, we get the well-known *normalization condition*

$$\sum_{m=1}^M W_m = 1; \quad (2.4)$$

just remember that it is true only if each experiment definitely yields one of the outcomes N_1, N_2, \dots, N_M .

Second, if we have an additive function of the results,

$$f = \frac{1}{N} \sum_{m=1}^M N_m f_m, \quad (2.5)$$

where f_m are some definite (deterministic) coefficients, the *statistical average* (also called the *expectation value*) of the function is naturally defined as

² The most popular counter-example is an energy-conserving system. Consider, for example, a system of particles placed in a potential that is a quadratic form of its coordinates. The theory of oscillations tells us (see, e.g., CM Sec. 6.2) that this system is equivalent to a set of non-interacting harmonic oscillators. Each of these oscillators conserves its own initial energy E_j forever, so that the statistics of N measurements of one such system may differ from that of N different systems with a random distribution of E_j , even if the total energy of the system, $E = \sum_j E_j$, is the same. Such non-ergodicity, however, is a rather feeble phenomenon and is readily destroyed by any of many mechanisms, such as weak interaction with the environment (leading, in particular, to oscillation damping), potential anharmonicity (see, e.g., CM Chapter 5), and chaos (CM Chapter 9), all of them strongly enhanced by increasing the number of particles in the system, i.e. the number of its degrees of freedom. This is why an overwhelming part of real-life systems are ergodic; for the readers interested in non-ergodic exotics, I can recommend the monograph by V. Arnold and A. Avez, *Ergodic Problems of Classical Mechanics*, Addison-Wesley, 1989.

³ Here, and everywhere in this series, angle brackets $\langle \dots \rangle$ mean averaging over a statistical ensemble, which is generally different from averaging over time – as it will be the case in quite a few examples considered below.

$$\langle f \rangle \equiv \lim_{N \rightarrow \infty} \frac{1}{N} \sum_{m=1}^M \langle N_m \rangle f_m, \quad (2.6)$$

so that using Eq. (3) we get

Expectation
value via
probabilities

$$\langle f \rangle = \sum_{m=1}^M W_m f_m. \quad (2.7)$$

Notice that Eq. (3) may be considered as the particular form of this general result, when all $f_m = 1$.

Next, the spectrum of possible experimental outcomes is frequently continuous for all practical purposes. (Think, for example, about the set of positions of the marks left by bullets fired into a target from afar.) The above formulas may be readily generalized to this case; let us start from the simplest situation when all different outcomes may be described by just one continuous scalar variable q – which replaces the discrete index m in Eqs. (1)-(7). The basic relation for this case is the self-evident fact that the probability dW of having an outcome within a small interval dq near some point q is proportional to the magnitude of that interval:

$$dW = w(q)dq, \quad (2.8)$$

where $w(q)$ is some function of q , which does not depend on dq . This function is called *probability density*. Now all the above formulas may be recast by replacing the probabilities W_m with the products (8), and the summation over m , with the integration over q . In particular, instead of Eq. (4) the normalization condition now becomes

$$\int w(q)dq = 1, \quad (2.9)$$

where the integration should be extended over the whole range of possible values of q . Similarly, instead of the discrete values f_m participating in Eq. (5), it is natural to consider a function $f(q)$. Then instead of Eq. (7), the expectation value of the function may be calculated as

$$\langle f \rangle = \int w(q)f(q)dq. \quad (2.10)$$

Expectation
value via
probability
density

It is also straightforward to generalize these formulas to the case of more variables. For example, the state of a classical particle with three degrees of freedom may be fully described by the probability density w defined in the 6D space of its generalized radius-vector \mathbf{q} and momentum \mathbf{p} . As a result, the expectation value of a function of these variables may be expressed as a 6D integral

$$\langle f \rangle = \int w(\mathbf{q}, \mathbf{p})f(\mathbf{q}, \mathbf{p})d^3qd^3p. \quad (2.11)$$

Some systems considered in this course consist of components whose quantum properties cannot be ignored, so let us discuss how $\langle f \rangle$ should be calculated in this case. If by f_m we mean measurement results, then Eq. (7) (and its generalizations) remains valid, but since these numbers themselves may be affected by the intrinsic quantum-mechanical uncertainty, it may make sense to have a bit deeper look into this situation. Quantum mechanics tells us⁴ that the most general expression for the expectation value of an observable f in a certain ensemble of macroscopically similar systems is

$$\langle f \rangle = \sum_{m,m'} W_{mm'} f_{m'm} \equiv \text{Tr}(Wf). \quad (2.12)$$

⁴ See, e.g., QM Sec. 7.1.

Here $f_{mm'}$ are the matrix elements of the quantum-mechanical operator \hat{f} corresponding to the observable f , in a full basis of orthonormal states m ,

$$f_{mm'} = \langle m | \hat{f} | m' \rangle, \quad (2.13)$$

while the coefficients $W_{mm'}$ are the elements of the so-called *density matrix* W , which represents, in the same basis, the *density operator* \hat{W} describing properties of this ensemble. Eq. (12) is evidently more general than Eq. (7), and is reduced to it only if the density matrix is diagonal:

$$W_{mm'} = W_m \delta_{mm'} \quad (2.14)$$

(where $\delta_{mm'}$ is the Kronecker symbol), when the diagonal elements W_m play the role of probabilities of the corresponding states.

Thus formally, the largest difference between the quantum and classical description is the presence, in Eq. (12), of the off-diagonal elements of the density matrix. They have the largest values in the *pure* (also called “coherent”) ensemble, in which the state of the system may be described with *state vectors*, e.g., the *ket-vector*

$$|\alpha\rangle = \sum_m \alpha_m |m\rangle, \quad (2.15)$$

where α_m are some (generally, complex) coefficients. In this case, the density matrix elements are merely

$$W_{mm'} = \alpha_m^* \alpha_{m'}, \quad (2.16)$$

so that the off-diagonal elements are of the same order as the diagonal elements. For example, in the very important particular case of a *two-level system*, the pure-state density matrix is

$$W = \begin{pmatrix} \alpha_1^* \alpha_1 & \alpha_1^* \alpha_2 \\ \alpha_2^* \alpha_1 & \alpha_2^* \alpha_2 \end{pmatrix}, \quad (2.17)$$

so that the product of its off-diagonal components is as large as that of the diagonal components.

In the most important basis of stationary states, i.e. the eigenstates of the system’s time-independent Hamiltonian, the coefficients α_m oscillate in time as⁵

$$\alpha_m(t) = \alpha_m(0) \exp\left\{-i \frac{E_m}{\hbar} t\right\} \equiv |\alpha_m| \exp\left\{-i \frac{E_m}{\hbar} t + i\varphi_m\right\}, \quad (2.18)$$

where E_m are the corresponding eigenenergies, and φ_m are constant phase shifts. This means that while the diagonal terms of the density matrix (16) remain constant, its off-diagonal components are oscillating functions of time:

$$W_{mm'} = \alpha_{m'}^* \alpha_m = |\alpha_{m'} \alpha_m| \exp\left\{i \frac{E_m - E_{m'}}{\hbar} t\right\} \exp\{i(\varphi_{m'} - \varphi_m)\}. \quad (2.19)$$

⁵ Here I use the Schrödinger picture of quantum dynamics, in which the matrix elements $f_{nn'}$ representing quantum-mechanical operators, do not evolve in time. The final results of this discussion do not depend on the particular picture – see, e.g., QM Sec. 4.6.

Due to the extreme smallness of the Planck constant (on the human scale of things), minuscule random perturbations of eigenenergies are equivalent to substantial random changes of the phase multipliers, so that the time average of any off-diagonal matrix element tends to zero. Moreover, even if our statistical ensemble consists of systems with exactly the same E_m , but different values φ_m (which are typically hard to control at the initial preparation of the system), the average values of all $W_{mm'}$ (with $m \neq m'$) vanish again.

This is why, besides some very special cases, typical statistical ensembles of quantum particles are far from being pure, and in most cases (certainly including the thermodynamic equilibrium), a good approximation for their description is given by the opposite limit of the so-called *classical mixture*, in which all off-diagonal matrix elements of the density matrix equal zero, and its diagonal elements W_{mm} are merely the probabilities W_m of the corresponding eigenstates. In this case, for the observables compatible with energy, Eq. (12) is reduced to Eq. (7), with f_m being the eigenvalues of the variable f , so that we may base our further discussion on this key relation and its continuous extensions (10)-(11).

2.2. Microcanonical ensemble and distribution

Now we move to the now-standard approach to statistical mechanics, based on the three statistical ensembles introduced in the 1870s by Josiah Willard Gibbs.⁶ The most basic of them is the so-called *microcanonical statistical ensemble*⁷ defined as a set of macroscopically similar closed (isolated) systems with *virtually* the same total energy E . Since in quantum mechanics the energy of a closed system is quantized, in order to make the forthcoming discussion suitable for quantum systems as well, it is convenient to include to the ensemble all systems with energies E_m within a relatively narrow interval $\Delta E \ll E$ (see Fig. 1) that is nevertheless much larger than the average distance δE between the energy levels, so that the number M of different quantum states within the interval ΔE is large, $M \gg 1$. Such choice of ΔE is only possible if $\delta E \ll E$; however, the reader should not worry too much about this condition, because the most important applications of the microcanonical ensemble are for very large systems (and/or very high energies) when the energy spectrum is very dense.⁸

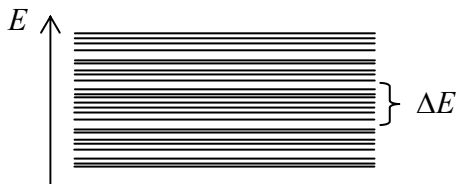


Fig. 2.1. A very schematic image of the microcanonical ensemble. (Actually, the ensemble deals with quantum states rather than energy levels. An energy level may be degenerate, i.e. correspond to several states.)

This ensemble serves as the basis for the formulation of the postulate which is most frequently called the *microcanonical distribution* (or, more adequately, “the main statistical postulate” or “the main

⁶ Personally, I believe that the genius of J. Gibbs, praised by Albert Einstein as the “greatest mind in the American history”, is still insufficiently recognized, and agree with R. Millikan that Gibbs “did for statistical mechanics and thermodynamics what [...] Maxwell did for electrodynamics”.

⁷ The terms “microcanonical”, as well as “canonical” (see Sec. 4 below) are apparently due to Gibbs and I was unable to find out his motivation for the former name. (“Canonical” in the sense of “standard” or “common” is quite appropriate, but why “micro”? Perhaps to reflect the smallness of ΔE ?)

⁸ Formally, the main result of this section, Eq. (20), is valid for any M (including $M = 1$); it is just less informative for small M – and trivial for $M = 1$.

statistical hypothesis"): *in the thermodynamic equilibrium of a microcanonical ensemble, all its states have equal probabilities,*

$$W_m = \frac{1}{M} = \text{const.} \quad (2.20)$$

Micro-canonical distribution

Though in some constructs of statistical mechanics this equality is derived from other axioms, which look more plausible to their authors, I believe that Eq. (20) may be taken as the starting point of the statistical physics, supported "just" by the compliance of all its corollaries with experimental observations.

Note that the postulate (20) is closely related to the macroscopic irreversibility of the systems that are microscopically virtually reversible (closed): if such a system was initially in a certain state, its time evolution with just minuscule interactions with the environment (which is necessary for reaching the thermodynamic equilibrium) eventually leads to the uniform distribution of its probability among all states with essentially the same energy. Each of these states is not "better" than the initial one; rather, in a macroscopic system, there are just so many of these states that the chance to find the system in the initial state is practically nil – again, think about the ink drop diffusion into a glass of water.⁹

Now let us find a suitable definition of the entropy S of a microcanonical ensemble's member – for now, in the thermodynamic equilibrium only. This was done in 1877 by another giant of statistical physics, Ludwig Eduard Boltzmann – on the basis of the prior work by James Clerk Maxwell on the kinetic theory of gases – see Sec. 3.1 below. In the present-day terminology, since S is a measure of *disorder*, it should be related to the amount of information¹⁰ *lost* when the system went irreversibly from the full order to the full disorder, i.e. from one definite state to the microcanonical distribution (20). In an even more convenient formulation, this is the amount of information necessary to find the exact state of your system in a microcanonical ensemble.

In the information theory, the amount of information necessary to make a definite choice between two options with equal probabilities (Fig. 2a) is defined as

$$I(2) \equiv \log_2 2 = 1. \quad (2.21)$$

This unit of information is called a *bit*.

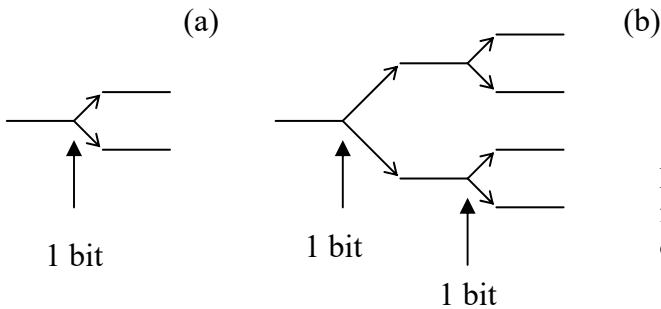


Fig. 2.2. "Logarithmic trees" of binary decisions for choosing between (a) $M = 2$, and (b) $M = 4$ opportunities with equal probabilities.

⁹ Though I have to move on, let me note that the microcanonical distribution (20) is a very nontrivial postulate, and my advice to the reader is to find some time to give additional thought to this keystone of the whole building of statistical mechanics.

¹⁰ I will rely on the reader's common sense and intuitive understanding of what information is, because even in the formal information theory, this notion is essentially postulated – see, e.g., the wonderfully clear text by J. Pierce, *An Introduction to Information Theory*, Dover, 1980.

Now, if we need to make a choice between four equally probable opportunities, it can be made in two similar steps (Fig. 2b), each requiring one bit of information, so that the total amount of information necessary for the choice is

$$I(4) = 2I(2) = 2 \equiv \log_2 4. \quad (2.22)$$

An obvious extension of this process to the choice between $M = 2^m$ states gives

$$I(M) = mI(2) = m \equiv \log_2 M. \quad (2.23)$$

This measure, if extended naturally to any integer M is quite suitable for the definition of entropy at equilibrium, with the only difference that, following tradition, the binary logarithm is replaced with the natural one:¹¹

$$S \equiv \ln M. \quad (2.24a)$$

Using Eq. (20), we may recast this definition in its most frequently used form

$$S = \ln \frac{1}{W_m} \equiv -\ln W_m. \quad (2.24b)$$

(Again, please note that Eq. (24) is valid in thermodynamic equilibrium only!)

Note that Eq. (24) satisfies the major properties of the entropy discussed in thermodynamics. First, it is a unique characteristic of the disorder. Indeed, according to Eq. (20), M (at fixed ΔE) is the only possible measure characterizing the microcanonical distribution, and so is its unique function $\ln M$. This function also satisfies another thermodynamic requirement to the entropy, of being an extensive variable. Indeed, for several independent systems, the joint probability of a certain state is just a product of the partial probabilities, and hence, according to Eq. (24), their entropies just add up.

Now let us see whether Eqs. (20) and (24) are compatible with the 2nd law of thermodynamics. For that, we need to generalize Eq. (24) for S to an arbitrary state of the system (generally, out of thermodynamic equilibrium), with an arbitrary set of state probabilities W_m . Let us first recognize that M in Eq. (24) is just the number of possible ways to commit a particular system to a certain state m ($m = 1, 2, \dots, M$), in a statistical ensemble where each state is equally probable. Now let us consider a more general ensemble, still consisting of a large number $N \gg 1$ of similar systems, but with a certain number $N_m = W_m N \gg 1$ of systems in each of M states, with the factors W_m not necessarily equal. In this case, the evident generalization of Eq. (24) is that the entropy S_N of the whole ensemble is

$$S_N \equiv \ln M(N_1, N_2, \dots), \quad (2.25)$$

where $M(N_1, N_2, \dots)$ is the number of ways to commit a particular system to a certain state m while keeping all numbers N_m fixed. This number $M(N_1, N_2, \dots)$ is clearly equal to the number of ways to distribute N distinct balls between M different boxes, with the fixed number N_m of balls in each box, but

¹¹ This is of course just the change of a constant factor: $S(M) = \ln M = \ln 2 \times \log_2 M = \ln 2 \times I(M) \approx 0.693 I(M)$. A review of Chapter 1 shows that nothing in thermodynamics prevents us from choosing such a constant coefficient arbitrarily, with the corresponding change of the temperature scale – see Eq. (1.9). In particular, in the SI units, where Eq. (24b) becomes $S = -k_B \ln W_m$, one bit of information corresponds to the entropy change $\Delta S = k_B \ln 2 \approx 0.693 k_B \approx 0.965 \times 10^{-23}$ J/K. By the way, the formula “ $S = k \log W$ ” is engraved on L. Boltzmann’s tombstone in Vienna.

in no particular order within it. Comparing this description with the definition of the so-called *multinomial coefficients*,¹² we get

$$M(N_1, N_2, \dots) = {}^N C_{N_1, N_2, \dots, N_M} \equiv \frac{N!}{N_1! N_2! \dots N_M!}, \quad \text{with } N = \sum_{m=1}^M N_m. \quad (2.26)$$

To simplify the resulting expression for S_N , we can use the famous *Stirling formula*, in its crudest, de Moivre's form,¹³ whose accuracy is suitable for most purposes of statistical physics:

$$\ln(N!)_{N \rightarrow \infty} \rightarrow N(\ln N - 1). \quad (2.27)$$

When applied to our current problem, this formula gives the following average entropy per system,¹⁴

$$\begin{aligned} S \equiv \frac{S_N}{N} &= \frac{1}{N} \left[\ln(N!) - \sum_{m=1}^M \ln(N_m!) \right]_{N_m \rightarrow \infty} \rightarrow \frac{1}{N} \left[N(\ln N - 1) - \sum_{m=1}^M N_m (\ln N_m - 1) \right] \\ &\equiv -\sum_{m=1}^M \frac{N_m}{N} \ln \frac{N_m}{N}, \end{aligned} \quad (2.28)$$

and since this result is only valid in the limit $N_m \rightarrow \infty$ anyway, we may use Eq. (2) to represent it as

$$S = -\sum_{m=1}^M W_m \ln W_m = \sum_{m=1}^M W_m \ln \frac{1}{W_m}. \quad (2.29)$$

Entropy
out of
equilibrium

This extremely important result¹⁵ may be interpreted as the average of the entropy values given by Eq. (24), weighed with specific probabilities W_m per the general formula (7).¹⁶

Now let us find what distribution of probabilities W_m provides the largest value of the entropy (29). The answer is almost evident from a good glance at Eq. (29). For example, if for a subgroup of $M' \leq M$ states the coefficients W_m are constant and equal to $1/M'$, so that $W_m = 0$ for all other states, all M' non-zero terms in the sum (29) are equal to each other, so that

$$S = M' \frac{1}{M'} \ln M' \equiv \ln M', \quad (2.30)$$

and the closer M' to its maximum value M the larger S . Hence, the maximum of S is reached at the uniform distribution given by Eq. (24).

¹² See, e.g., MA Eq. (2.3). Despite the intimidating name, Eq. (26) may be very simply derived. Indeed, $N!$ is just the number of all possible permutations of N balls, i.e. the ways to place them in *certain* positions – say, inside M boxes. Now to take into account that the particular order of the balls in each box is not important, that number should be divided by all numbers $N_m!$ of possible permutations of balls within each box – that's it.

¹³ See, e.g., MA Eq. (2.10).

¹⁴ Strictly speaking, I should use the notation $\langle S \rangle$ here. However, following the style accepted in thermodynamics, I will drop the averaging signs until we will really need them to avoid confusion. Again, this shorthand is not too bad because the relative fluctuations of entropy (as those of any macroscopic variable) are very small at $N \gg 1$.

¹⁵ With the replacement of $\ln W_m$ with $\log_2 W_m$ (i.e. division of both sides by $\ln 2$), Eq. (29) becomes the famous *Shannon* (or “Boltzmann-Shannon”) *formula* for the average information I per symbol in a long communication string using M different symbols, with probability W_m each.

¹⁶ In some textbooks, this interpretation is even accepted as the derivation of Eq. (29); however, it is evidently less strict than the one outlined above.

In order to prove this important fact more strictly, let us find the maximum of the function given by Eq. (29). If its arguments W_1, W_2, \dots, W_M were completely independent, this could be done by finding the point (in the M -dimensional space of the coefficients W_m) where all partial derivatives $\partial S/\partial W_m$ equal zero. However, since the probabilities are constrained by the condition (4), the differentiation has to be carried out more carefully, taking into account this interdependence:

$$\left[\frac{\partial}{\partial W_m} S(W_1, W_2, \dots) \right]_{\text{cond}} = \frac{\partial S}{\partial W_m} + \sum_{m' \neq m} \frac{\partial S}{\partial W_{m'}} \frac{\partial W_{m'}}{\partial W_m}. \quad (2.31)$$

At the maximum of the function S , all such expressions should be equal to zero simultaneously. This condition yields $\partial S/\partial W_m = \lambda$, where the so-called *Lagrange multiplier* λ is independent of m . Indeed, at such point Eq. (31) becomes

$$\left[\frac{\partial}{\partial W_m} S(W_1, W_2, \dots) \right]_{\text{cond}} = \lambda + \sum_{m' \neq m} \lambda \frac{\partial W_{m'}}{\partial W_m} \equiv \lambda \left(\frac{\partial W_m}{\partial W_m} + \sum_{m' \neq m} \frac{\partial W_{m'}}{\partial W_m} \right) \equiv \lambda \frac{\partial}{\partial W_m} (1) = 0. \quad (2.32)$$

For our particular expression (29), the condition $\partial S/\partial W_m = \lambda$ yields

$$\frac{\partial S}{\partial W_m} \equiv \frac{d}{d W_m} [-W_m \ln W_m] \equiv -\ln W_m - 1 = \lambda. \quad (2.33)$$

The last equality holds for all m (and hence the entropy reaches its maximum value) only if W_m is independent on m . Thus the entropy (29) indeed reaches its maximum value (24) at equilibrium.

To summarize, we see that the statistical definition (24) of entropy does fit all the requirements imposed on this variable by thermodynamics. In particular, we have been able to *prove* the 2nd law of thermodynamics using that definition together with the fundamental postulate (20).

Now let me discuss one possible point of discomfort with that definition: the values of M , and hence W_m , depend on the accepted energy interval ΔE of the microcanonical ensemble, for whose choice no exact guidance is offered. However, if the interval ΔE contains many states, $M \gg 1$, as was assumed before, then with a very small relative error (vanishing in the limit $M \rightarrow \infty$), M may be represented as

$$M = g(E)\Delta E, \quad (2.34)$$

where $g(E)$ is the *density of states* of the system:

$$g(E) \equiv \frac{d\Sigma(E)}{dE}, \quad (2.35)$$

$\Sigma(E)$ being the total number of states with energies *below* E . (Note that the average interval δE between energy levels, mentioned at the beginning of this section, is just $\Delta E/M = 1/g(E)$.) Plugging Eq. (34) into Eq. (24), we get

$$S = \ln M = \ln g(E) + \ln \Delta E, \quad (2.36)$$

so that the only effect of a particular choice of ΔE is an offset of the entropy by a constant, and in Chapter 1 we have seen that such constant shift does not affect any measurable quantity. Of course, Eq. (34), and hence Eq. (36) are only precise in the limit when the density of states $g(E)$ is so large that the range available for the appropriate choice of ΔE :

$$g^{-1}(E) \ll \Delta E \ll E, \quad (2.37)$$

is sufficiently broad: $g(E)E = E/\delta E \gg 1$.

In order to get some feeling of the functions $g(E)$ and $S(E)$ and the feasibility of the condition (37), and also to see whether the microcanonical distribution may be directly used for calculations of thermodynamic variables in particular systems, let us apply it to a microcanonical ensemble of many sets of $N \gg 1$ independent, similar harmonic oscillators with frequency ω . (Please note that the requirement of a virtually fixed energy is applied, in this case, to the total energy E_N of each set of oscillators, rather to energy E of a single oscillator – which may be virtually arbitrary, though certainly much less than $E_N \sim NE \gg E$.) Basic quantum mechanics tells us¹⁷ that the eigenenergies of such an oscillator form a discrete, equidistant spectrum:

$$E_m = \hbar\omega \left(m + \frac{1}{2} \right), \quad \text{where } m = 0, 1, 2, \dots \quad (2.38)$$

If ω is kept constant, the ground-state energy $\hbar\omega/2$ does not contribute to any thermodynamic properties of the system,¹⁸ so that for the sake of simplicity we may take that point as the energy origin, and replace Eq. (38) with $E_m = m\hbar\omega$. Let us carry out an approximate analysis of the system for the case when its average energy per oscillator,

$$E = \frac{E_N}{N}, \quad (2.39)$$

is much larger than the energy quantum $\hbar\omega$.

For one oscillator, the number of states with energy ε_1 below a certain value $E_1 \gg \hbar\omega$ is evidently $\Sigma(E_1) \approx E_1/\hbar\omega \equiv (E_1/\hbar\omega)/1!$ (Fig. 3a). For two oscillators, all possible values of the total energy ($\varepsilon_1 + \varepsilon_2$) below some level E_2 correspond to the points of a 2D square grid within the right triangle shown in Fig. 3b, giving $\Sigma(E_2) \approx (1/2)(E_2/\hbar\omega)^2 \equiv (E_2/\hbar\omega)^2/2!$. For three oscillators, the possible values of the total energy ($\varepsilon_1 + \varepsilon_2 + \varepsilon_3$) correspond to those points of the 3D cubic grid, that fit inside the right pyramid shown in Fig. 3c, giving $\Sigma(E_3) \approx (1/3)[(1/2)(E_3/\hbar\omega)^3] \equiv (E_3/\hbar\omega)^3/3!$, etc.

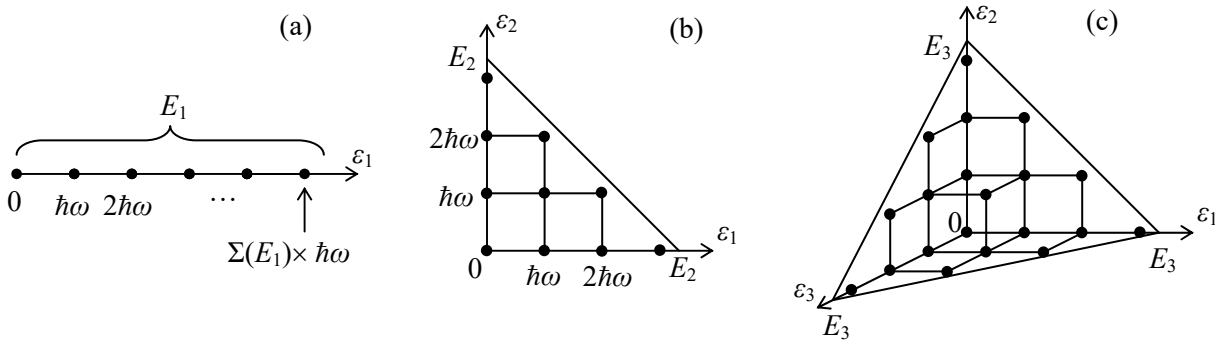


Fig. 2.3. Calculating functions $\Sigma(E_N)$ for systems of (a) one, (b) two, and (c) three harmonic oscillators.

¹⁷ See, e.g., QM Secs. 2.9 and 5.4.

¹⁸ Let me hope that the reader knows that the ground-state energy *is* experimentally measurable – for example, using the famous *Casimir effect* – see, e.g., QM Sec. 9.1. (In Sec. 5.5 below I will briefly discuss another method of experimental observation of that energy.)

An evident generalization of these formulas to arbitrary N gives the number of states¹⁹

$$\Sigma(E_N) \approx \frac{1}{N!} \left(\frac{E_N}{\hbar\omega} \right)^N. \quad (2.40)$$

Differentiating this expression over the energy, we get

$$g(E_N) \equiv \frac{d\Sigma(E_N)}{dE_N} = \frac{1}{(N-1)!} \frac{E_N^{N-1}}{(\hbar\omega)^N}, \quad (2.41)$$

so that

$$S_N(E_N) = \ln g(E_N) + \text{const} = -\ln[(N-1)!] + (N-1)\ln E_N - N\ln(\hbar\omega) + \text{const}. \quad (2.42)$$

For $N \gg 1$ we can ignore the difference between N and $(N-1)$ in both instances, and use the Stirling formula (27) to simplify this result as

$$S_N(E) - \text{const} \approx N \left(\ln \frac{E_N}{N\hbar\omega} + 1 \right) \approx N \left(\ln \frac{E}{\hbar\omega} \right) \equiv \ln \left[\left(\frac{E}{\hbar\omega} \right)^N \right]. \quad (2.43)$$

(The second, approximate step is only valid at very high $E/\hbar\omega$ ratios, when the logarithm in Eq. (43) is substantially larger than 1.) Returning for a second to the density of states, we see that in the limit $N \rightarrow \infty$, it is exponentially large:

$$g(E_N) = e^{S_N} \approx \left(\frac{E}{\hbar\omega} \right)^N, \quad (2.44)$$

so that the conditions (37) may be indeed satisfied within a very broad range of ΔE .

Now we can use Eq. (43) to find all thermodynamic properties of the system, though only in the limit $E \gg \hbar\omega$. Indeed, according to thermodynamics, if the system's volume and the number of particles in it are fixed, the derivative dS/dE is nothing else than the reciprocal temperature in thermal equilibrium – see Eq. (1.9). In our current case, we imply that the harmonic oscillators are distinct, for example by their spatial positions. Hence, even if we can speak of some volume of the system, it is certainly fixed.²⁰ Differentiating Eq. (43) over energy E , we get

$$\frac{1}{T} \equiv \frac{dS_N}{dE_N} = \frac{N}{E_N} = \frac{1}{E}. \quad (2.45)$$

Classical oscillator:
average energy

Reading this result backward, we see that the average energy E of a harmonic oscillator equals T (i.e. $k_B T_K$ is SI units). At this point, the first-time student of thermodynamics should be very much relieved to see that the counter-intuitive thermodynamic definition (1.9) of temperature does indeed correspond to what we all have known about this notion from our kindergarten physics courses.

The result (45) may be readily generalized. Indeed, in quantum mechanics, a harmonic oscillator with eigenfrequency ω may be described by the Hamiltonian operator

¹⁹ The coefficient $1/N!$ in this formula has the geometrical meaning of the (hyper)volume of the N -dimensional right pyramid with unit sides.

²⁰ For the same reason, the notion of pressure P in such a system is not clearly defined, and neither are any thermodynamic potentials but E and F .

$$\hat{H} = \frac{\hat{p}^2}{2m} + \frac{\kappa\hat{q}^2}{2}, \quad (2.46)$$

where q is some generalized coordinate, p is the corresponding generalized momentum, m is oscillator's mass,²¹ and κ is the spring constant, so that $\omega = (\kappa/m)^{1/2}$. Since in the thermodynamic equilibrium the density matrix is always diagonal in the basis of stationary states m (see Sec. 1 above), the quantum-mechanical averages of the kinetic and potential energies may be found from Eq. (7):

$$\left\langle \frac{p^2}{2m} \right\rangle = \sum_{m=0}^{\infty} W_m \langle m | \frac{\hat{p}^2}{2m} | m \rangle, \quad \left\langle \frac{\kappa q^2}{2} \right\rangle = \sum_{m=0}^{\infty} W_m \langle m | \frac{\kappa \hat{q}^2}{2} | m \rangle, \quad (2.47)$$

where W_m is the probability to occupy the m^{th} energy level, and bra- and ket-vectors describe the stationary state corresponding to that level.²² However, both classical and quantum mechanics teach us that for any m , the bra-ket expressions under the sums in Eqs. (47), which represent the average kinetic and mechanical energies of the oscillator on its m^{th} energy level, are equal to each other, and hence each of them is equal to $E_m/2$. Hence, even though we do not know the probability distribution W_m yet (it will be calculated in Sec. 5 below), we may conclude that in the “classical limit” $T \gg \hbar\omega$,

$$\left\langle \frac{p^2}{2m} \right\rangle = \left\langle \frac{\kappa q^2}{2} \right\rangle = \frac{T}{2}. \quad (2.48)$$

Equipartition theorem

Now let us consider a system with an arbitrary number of degrees of freedom, described by a more general Hamiltonian:²³

$$\hat{H} = \sum_j \hat{H}_j, \quad \text{with } \hat{H}_j = \frac{\hat{p}_j^2}{2m_j} + \frac{\kappa_j \hat{q}_j^2}{2}, \quad (2.49)$$

with (generally, different) frequencies $\omega_j = (\kappa_j/m_j)^{1/2}$. Since the “modes” (effective harmonic oscillators) contributing to this Hamiltonian, are independent, the result (48) is valid for each of the modes. This is the famous *equipartition theorem*: at thermal equilibrium with $T \gg \hbar\omega_j$, the average energy of each so-called *half-degree of freedom* (which is defined as any variable, either p_j or q_j , giving a quadratic contribution to the system's Hamiltonian), is equal to $T/2$.²⁴ In particular, for each of three Cartesian component contributions to the kinetic energy of a free-moving particle, this theorem is valid for *any* temperature, because such components may be considered as 1D harmonic oscillators with vanishing potential energy, i.e. $\omega_j = 0$, so that condition $T \gg \hbar\omega_j$ is fulfilled at any temperature.

²¹ I am using this fancy font for the mass to avoid any chance of its confusion with the state number.

²² Note again that while we have committed the energy E_N of N oscillators to be fixed (to apply Eq. (36), valid only for a microcanonical ensemble at thermodynamic equilibrium), the single oscillator's energy E in our analysis may be arbitrary – within the limits $\hbar\omega \ll E \leq E_N \sim NT$.

²³ As a reminder, the Hamiltonian of any system whose classical Lagrangian function is an arbitrary quadratic form of its generalized coordinates and the corresponding generalized velocities, may be brought to the form (49) by an appropriate choice of “normal coordinates” q_j which are certain linear combinations of the original coordinates – see, e.g., CM Sec. 6.2.

²⁴ This also means that in the classical limit, the heat capacity of a system is equal to one-half of the number of its half-degrees of freedom (in the SI units, multiplied by k_B).

I believe that this case study of harmonic oscillator systems was a fair illustration of both the strengths and the weaknesses of the microcanonical ensemble approach.²⁵ On one hand, we could readily calculate virtually everything we wanted in the classical limit $T \gg \hbar\omega$, but calculations for an arbitrary $T \sim \hbar\omega$, though possible, are rather unpleasant because for that, all vertical steps of the function $\Sigma(E_N)$ have to be carefully counted. In Sec. 4, we will see that other statistical ensembles are much more convenient for such calculations.

Let me conclude this section with a short notice on deterministic classical systems with just a few degrees of freedom (and even simpler mathematical objects called “maps”) that may exhibit essentially disordered behavior, called the *deterministic chaos*.²⁶ Such chaotic system may be approximately characterized by an entropy defined similarly to Eq. (29), where W_m are the probabilities to find it in different small regions of phase space, at well-separated small time intervals. On the other hand, one can use an expression slightly more general than Eq. (29) to define the so-called *Kolmogorov* (or “Kolmogorov-Sinai”) *entropy K* that characterizes the speed of loss of the information about the initial state of the system, and hence what is called the “chaos depth”. In the definition of K , the sum over m is replaced with the summation over all possible permutations $\{m\} = m_0, m_1, \dots, m_{N-1}$ of small space regions, and W_m is replaced with $W_{\{m\}}$, the probability of finding the system in the corresponding regions m at time moment t_m , with $t_m = m\tau$, in the limit $\tau \rightarrow 0$, with $N\tau = \text{const}$. For chaos in the simplest objects, 1D maps, K is equal to the Lyapunov exponent $\lambda > 0$.²⁷ For systems of higher dimensionality, which are characterized by several Lyapunov exponents λ , the Kolmogorov entropy is equal to the phase-space average of the sum of all positive λ . These facts provide a much more practicable way of (typically, numerical) calculation of the Kolmogorov entropy than the direct use of its definition.²⁸

2.3. Maxwell’s Demon, information, and computation

Before proceeding to other statistical distributions, I would like to make a detour to address one more popular concern about Eq. (24) – the direct relation between entropy and information. Some physicists are still uneasy with entropy being nothing else than the (deficit of) information, though to the best of my knowledge, nobody has yet been able to suggest any experimentally verifiable difference between these two notions. Let me give one example of their direct relation.²⁹ Consider a cylinder containing just one molecule (considered as a point particle), and separated into two halves by a movable partition with a door that may be opened and closed at will, at no energy cost – see Fig. 4a. If the door is open and the system is in thermodynamic equilibrium, we do not know on which side of the partition the molecule is. Here the disorder, i.e. the entropy has the largest value, and there is no way to get, from a large ensemble of such systems in equilibrium, any useful mechanical energy.

²⁵ The reader is strongly urged to solve Problem 2, whose task is to do a similar calculation for another key (“two-level”) physical system, and compare the results.

²⁶ See, e.g., CM Chapter 9 and literature therein.

²⁷ For the definition of λ , see, e.g., CM Eq. (9.9).

²⁸ For more discussion, see, e.g., either Sec. 6.2 of the monograph H. G. Schuster and W. Just, *Deterministic Chaos*, 4th ed., Wiley-VHS, 2005, or the monograph by Arnold and Avez, cited in Sec. 1.

²⁹ This system is frequently called the *Szilard engine*, after L. Szilard who published its detailed theoretical discussion in 1929, but is essentially a straightforward extension of the thought experiment suggested by J. Maxwell as early as 1867.

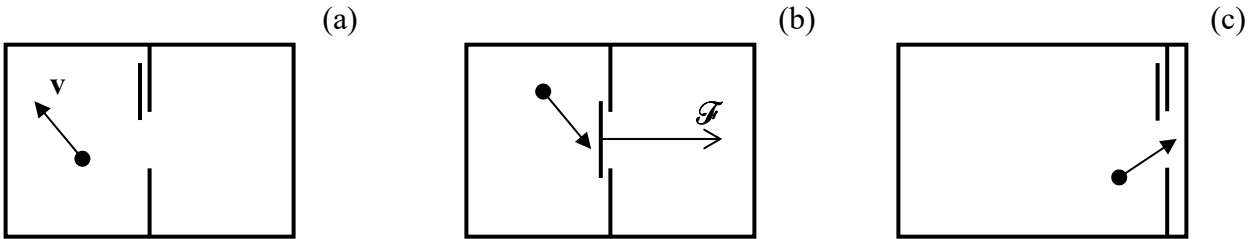


Fig. 2.4. The Szilard engine: a cylinder with a single molecule and a movable partition: (a) before and (b) after closing the door, and (c) after opening the door at the end of the expansion stage.

Now, let us consider that we know (as instructed by, in Lord Kelvin's formulation, an omniscient *Maxwell's Demon*) on which side of the partition the molecule is currently located. Then we may close the door, trapping the molecule, so that its repeated impacts on the partition create, on average, a pressure force \mathcal{F} directed toward the empty part of the volume (in Fig. 4b, the right one). Now we can get from the molecule some mechanical work, say by allowing the force \mathcal{F} to move the partition to the right, and picking up the resulting mechanical energy by some deterministic (zero-entropy) external mechanism. After the partition has been moved to the right end of the volume, we can open the door again (Fig. 4c), equalizing the molecule's average pressure on both sides of the partition, and then slowly move the partition back to the middle of the volume – without its resistance, i.e. without doing any substantial work. With the continuing help by the Maxwell's Demon, we can repeat the cycle again and again, and hence make the system perform unlimited mechanical work, fed “only” by the molecule's thermal motion, and the information about its position – thus implementing the perpetual motion machine of the 2nd kind – see Sec. 1.6. The fact that such heat engines do not exist means that getting any *new* information, at non-zero temperature (i.e. at a substantial thermal agitation of particles) has a non-zero energy cost.

In order to evaluate this cost, let us calculate the maximum work per cycle that can be made by the Szilard engine (Fig. 4), assuming that it is constantly in the thermal equilibrium with a heat bath of temperature T . Formula (21) tells us that the information supplied by the demon (on what exactly half of the volume contains the molecule) is exactly one bit, $I(2) = 1$. According to Eq. (24), this means that by getting this information we are changing the entropy of our system by

$$\Delta S_I = -\ln 2. \quad (2.50)$$

Now, it would be a mistake to plug this (negative) entropy change into Eq. (1.19). First, that relation is only valid for slow, reversible processes. Moreover (and more importantly), this equation, as well as its irreversible version (1.41), is only valid for a fixed statistical ensemble. The change ΔS_I does not belong to this category and may be formally described by the change of the statistical ensemble – from the one consisting of all similar systems (experiments) with an unknown location of the molecule, to a new ensemble consisting of the systems with the molecule in its certain (in Fig. 4, left) half.³⁰

Now let us consider a slow expansion of the “gas” after the door had been closed. At this stage, we do not need the Demon's help any longer (i.e. the statistical ensemble may be fixed), and can indeed use the relation (1.19). At the assumed isothermal conditions ($T = \text{const}$), this relation may be integrated

³⁰ This procedure of the *statistical ensemble re-definition* is the central point of the connection between physics and information theory, and is crucial in particular for any (or rather any meaningful :-) discussion of measurements in quantum mechanics – see, e.g., QM Secs. 2.5 and 10.1.

over the whole expansion process, getting $\Delta Q = T\Delta S$. At the final position shown in Fig. 4c, the system's entropy should be the same as initially, i.e. before the door had been opened, because we again do not know where in the volume the molecule is. This means that the entropy was replenished, during the reversible expansion, from the heat bath, by $\Delta S = -\Delta S_I = +\ln 2$, so that $\Delta Q = T\Delta S = T\ln 2$. Since by the end of the whole cycle the internal energy E of the system is the same as before, all this heat could have gone into the mechanical energy obtained during the expansion. Thus the maximum obtained work per cycle (i.e. for each obtained information bit) is $T\ln 2$ ($k_B T_K \ln 2$ in the SI units), about 4×10^{-21} Joule at room temperature. This is exactly the energy cost of getting one bit of *new* information about a system at temperature T . The smallness of that amount on the everyday human scale has left the Szilard engine an academic theoretical exercise for almost a century. However, recently several such devices, of various physical nature, were implemented experimentally (with the Demon's role played by an instrument measuring the position of the particle without a substantial effect on its motion), and the relation $\Delta Q = T\ln 2$ was proved, with a gradually increasing precision.³¹

Actually, discussion of another issue closely related to Maxwell's Demon, namely of energy consumption at numerical calculations, was started earlier, in the 1960s. It was motivated by the exponential (*Moore's-law*) progress of the digital integrated circuits, which has led in particular, to a fast reduction of the energy ΔE "spent" (turned into heat) per one binary logic operation. In the recent generations of semiconductor digital integrated circuits, the typical ΔE is still above 10^{-17} J, i.e. still exceeds the room-temperature value of $T\ln 2 \approx 4 \times 10^{-21}$ J by several orders of magnitude. Still, some engineers believe that thermodynamics imposes this important lower limit on ΔE and hence presents an insurmountable obstacle to the future progress of computation. Unfortunately, in the 2000s this delusion resulted in a substantial and unjustified shift of electron device research resources toward using "non-charge degrees of freedom" such as spin (as if they do not obey the general laws of statistical physics!), so that the issue deserves at least a brief discussion.

Let me believe that the reader of these notes understands that, in contrast to naïve popular talk, computers *do not create* any new information; all they can do is reshaping ("processing") the input information, *losing* most of it on the go. Indeed, any digital computation algorithm may be decomposed into simple, binary logical operations, each of them performed by a circuit called the *logic gate*. Some of these gates (e.g., the logical NOT performed by inverters, as well as memory READ and WRITE operations) do not change the amount of information in the computer. On the other hand, such *information-irreversible* logic gates as two-input NAND (or NOR, or XOR, etc.) erase one bit at each operation, because they turn two input bits into one output bit – see Fig. 5a.

In 1961, Rolf Landauer argued that each logic operation should turn into heat at least energy

$$\Delta E_{\min} = T \ln 2 \equiv k_B T_K \ln 2 . \quad (2.51)$$

Irreversible computation:
energy cost

This result may be illustrated with the Szilard engine (Fig. 4), operated in a reversed cycle. At the first stage, with the door closed, it uses external mechanical work $\Delta E = T\ln 2$ to reduce the volume in that the molecule is confined, from V to $V/2$, pumping heat $\Delta Q = \Delta E$ into the heat bath. To model a logically irreversible logic gate, let us now open the door in the partition, and thus lose one bit of information about the molecule's position. Then we will never get the work $T\ln 2$ back, because moving the partition

³¹ See, for example, A. Bérut *et al.*, *Nature* **483**, 187 (2012); J. Koski *et al.*, *PNAS USA* **111**, 13786 (2014); Y. Jun *et al.*, *Phys. Rev. Lett.* **113**, 190601 (2014); J. Peterson *et al.*, *Proc. Roy. Soc. A* **472**, 20150813 (2016).

back to the right, with the door open, takes place at zero average pressure. Hence, Eq. (51) gives a fundamental limit for energy loss (per bit) at the logically irreversible computation.

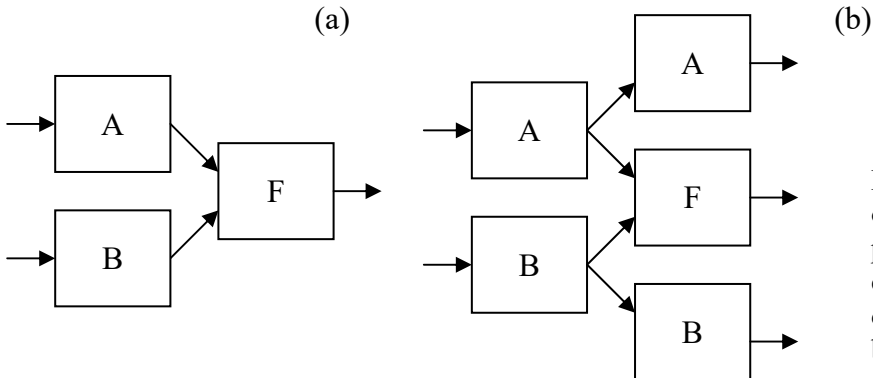


Fig. 2.5. Simple examples of (a) irreversible and (b) potentially reversible logic circuits. Each rectangle denotes a circuit storing one bit of information.

However, in 1973 Charles Bennett came up with convincing arguments that it is possible to avoid such energy loss by using only operations that are *reversible* not only physically, but also logically.³² For that, one has to avoid any loss of information, i.e. any erasure of intermediate results, for example in the way shown in Fig. 5b.³³ At the end of all calculations, after the result has been copied into memory, the intermediate results may be “rolled back” through reversible gates to be eventually merged into a copy of input data, again without erasing a single bit. The minimal energy dissipation at such reversible calculation tends to zero as the operation speed is decreased, so that the average energy loss per bit may be less than the perceived “fundamental thermodynamic limit” (51). The price to pay for this ultralow dissipation is a very high complexity of the hardware necessary for the storage of all intermediate results. However, using irreversible gates sparsely, it may be possible to reduce the complexity dramatically, so that in the future such *mostly* reversible computation may be able to reduce energy consumption in practical digital electronics.³⁴

Before we leave Maxwell’s Demon behind, let me use it to revisit, for one more time, the relation between the reversibility of the classical and quantum mechanics of Hamiltonian systems and the irreversibility possible in thermodynamics and statistical physics. In the gedanken experiment shown in Fig. 4, the laws of mechanics governing the motion of the molecule are reversible at all times. Still, at partition’s motion to the right, driven by molecular impacts, the entropy grows, because the molecule picks up the heat $\Delta Q > 0$, and hence the entropy $\Delta S = \Delta Q/T > 0$, from the heat bath. The physical mechanism of this irreversible entropy (read: disorder) growth is the interaction of the molecule with uncontrollable components of the heat bath, and the resulting loss of information about the motion of the molecule. Philosophically, such emergence of irreversibility in large systems is a strong argument against *reductionism* – a naïve belief that knowing the exact laws of Nature at the lowest, most fundamental level of its complexity, we can readily understand all phenomena on the higher levels of its

³² C. Bennett, *IBM J. Res. Devel.* **17**, 525 (1973); see also C. Bennett, *Int. J. Theor. Phys.* **21**, 905 (1982).

³³ For that, all gates have to be *physically reversible*, with no static power consumption. Such logic devices do exist, though they are still not very practicable – see, e.g., K. Likharev, *Int. J. Theor. Phys.* **21**, 311 (1982). (Another reason for citing, rather reluctantly, my own paper is that it also gave constructive proof that the reversible computation may also beat the perceived “fundamental quantum limit”, $\Delta E \Delta t > \hbar$, where Δt is the time of the binary logic operation.)

³⁴ Many currently explored schemes of *quantum computing* are also reversible – see, e.g., QM Sec. 8.5 and references therein.

organization. In reality, the macroscopic irreversibility of large systems is a good example³⁵ of a new law (in this case, the 2nd law of thermodynamics) that becomes relevant on a substantially new, higher level of complexity – without defying the lower-level laws. Without such new laws, very little of the higher-level organization of Nature may be understood.

2.4. Canonical ensemble and the Gibbs distribution

As was shown in Sec. 2 (see also a few problems of the list given in the end of this chapter), the microcanonical distribution may be directly used for solving some simple problems. However, its further development, also due to J. Gibbs, turns out to be much more convenient for calculations.

Let us consider a statistical ensemble of macroscopically similar systems, each in thermal equilibrium with a heat bath of the same temperature T (Fig. 6a). Such an ensemble is called *canonical*.

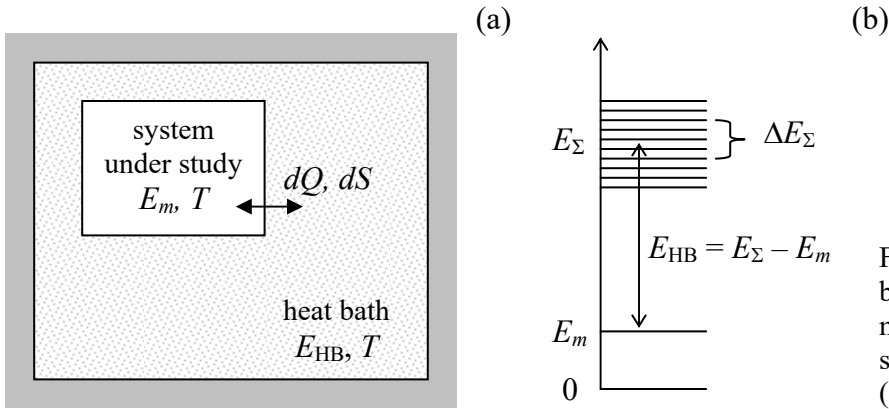


Fig. 2.6. (a) A system in a heat bath (i.e. a canonical ensemble's member) and (b) the energy spectrum of the composite system (including the heat bath).

It is intuitively evident that if the heat bath is sufficiently large, any thermodynamic variables characterizing the system under study should not depend on the *heat bath's* environment. In particular, we may assume that the heat bath is thermally insulated, so that the total energy E_Σ of the *composite* system, consisting of the system of our interest plus the heat bath, does not change in time. For example, if the system of our interest is in a certain (say, m^{th}) quantum state, then the sum

$$E_\Sigma = E_m + E_{\text{HB}} \quad (2.52)$$

is time-independent. Now let us partition the considered *canonical* ensemble of such systems into much smaller sub-ensembles, each being a *microcanonical* ensemble of composite systems whose total, time-independent energies E_Σ are the same – as was discussed in Sec. 2, within a certain small energy interval $\Delta E_\Sigma \ll E_\Sigma$ – see Fig. 6b. Due to the very large size of each heat bath in comparison with that of the system under study, the heat bath's density of states g_{HB} is very high, and ΔE_Σ may be selected so that

$$\frac{1}{g_{\text{HB}}} \ll \Delta E_\Sigma \ll |E_m - E_{m'}| \ll E_{\text{HB}}, \quad (2.53)$$

where m and m' are any states of the system of our interest.

³⁵ Another famous example is Charles Darwin's theory of biological evolution.

According to the microcanonical distribution, the probabilities to find the composite system, within each of these microcanonical sub-ensembles, in any state are equal. Still, the heat bath energies $E_{\text{HB}} = E_{\Sigma} - E_m$ (Fig. 6b) of the members of this sub-ensemble may be different – due to the difference in E_m . The probability $W(E_m)$ to find the system of our interest (within the selected sub-ensemble) in a state with energy E_m is proportional to the number ΔM of the corresponding heat baths in the sub-ensemble. As Fig. 6b shows, in this case we may write $\Delta M = g_{\text{HB}}(E_{\text{HB}})\Delta E_{\Sigma}$. As a result, within the microcanonical sub-ensemble with the total energy E_{Σ} ,

$$W_m \propto \Delta M = g_{\text{HB}}(E_{\text{HB}})\Delta E_{\Sigma} = g_{\text{HB}}(E_{\Sigma} - E_m)\Delta E_{\Sigma}. \quad (2.54)$$

Let us simplify this expression further, using the Taylor expansion with respect to relatively small $E_m \ll E_{\Sigma}$. However, here we should be careful. As we have seen in Sec. 2, the density of states of a large system is an extremely fast growing function of energy, so that if we applied the Taylor expansion directly to Eq. (54), the Taylor series would converge for very small E_m only. A much broader applicability range may be obtained by taking logarithms of both parts of Eq. (54) first:

$$\ln W_m = \text{const} + \ln[g_{\text{HB}}(E_{\Sigma} - E_m)] + \ln \Delta E_{\Sigma} = \text{const} + S_{\text{HB}}(E_{\Sigma} - E_m), \quad (2.55)$$

where the last equality results from the application of Eq. (36) to the heat bath, and $\ln \Delta E_{\Sigma}$ has been incorporated into the (inconsequential) constant. Now, we can Taylor-expand the (much more smooth) function of energy on the right-hand side, and limit ourselves to the two leading terms of the series:

$$\ln W_m \approx \text{const} + S_{\text{HB}} \Big|_{E_m=0} - \frac{dS_{\text{HB}}}{dE_{\text{HB}}} \Big|_{E_m=0} E_m. \quad (2.56)$$

But according to Eq. (1.9), the derivative participating in this expression is nothing else than the reciprocal temperature of the heat bath, which (due to the large bath size) does not depend on whether E_m is equal to zero or not. Since our system of interest is in the thermal equilibrium with the bath, this is also the temperature T of the system – see Eq. (1.8). Hence Eq. (56) is merely

$$\ln W_m = \text{const} - \frac{E_m}{T}. \quad (2.57)$$

This equality describes a substantial decrease of W_m as E_m is increased by $\sim T$, and hence our linear approximation (56) is virtually exact as soon as E_{HB} is much larger than T – the condition that is rather easy to satisfy, because as we have seen in Sec. 2, the average energy per one degree of freedom of the system of the heat bath is also of the order of T , so that its total energy is much larger because of its much larger size.

Now we should be careful again because so far Eq. (57) was only derived for a sub-ensemble with a certain fixed E_{Σ} . However, since the second term on the right-hand side of Eq. (57) includes only E_m and T , which are independent of E_{Σ} , this relation, perhaps with different constant terms, is valid for all sub-ensembles of the canonical ensemble, and hence for that ensemble as the whole. Hence for the total probability to find our system of interest in a state with energy E_m , in the canonical ensemble with temperature T , we can write

$$W_m = \text{const} \times \exp \left\{ -\frac{E_m}{T} \right\} \equiv \frac{1}{Z} \exp \left\{ -\frac{E_m}{T} \right\}. \quad (2.58)$$

Gibbs
distribution

. This is the famous *Gibbs distribution*,³⁶ sometimes called the “canonical distribution”, which is arguably the summit of statistical physics,³⁷ because it may be used for a straightforward (or at least conceptually straightforward :-) calculation of all statistical and thermodynamic variables of a vast range of systems.

Before illustrating this, let us first calculate the coefficient Z participating in Eq. (58) for the general case. Requiring, per Eq. (4), the sum of all W_m to be equal 1, we get

$$\text{Statistical sum} \quad Z = \sum_m \exp\left\{-\frac{E_m}{T}\right\}, \quad (2.59)$$

where the summation is formally extended to all quantum states of the system, though in practical calculations, the sum may be truncated to include only the states that are noticeably occupied. The apparently humble normalization coefficient Z turns out to be so important for applications that it has a special name – or actually, two names: either the *statistical sum* or the *partition function* of the system. To appreciate the importance of Z , let us use the general expression (29) for entropy to calculate it for the particular case of the canonical ensemble, i.e. the Gibbs distribution (58) of the probabilities W_n :

$$S = -\sum_m W_m \ln W_m = \frac{\ln Z}{Z} \sum_m \exp\left\{-\frac{E_m}{T}\right\} + \frac{1}{ZT} \sum_m E_m \exp\left\{-\frac{E_m}{T}\right\}. \quad (2.60)$$

On the other hand, according to the general rule (7), the thermodynamic (i.e. ensemble-averaged) value E of the internal energy of the system is

$$E = \sum_m W_m E_m = \frac{1}{Z} \sum_m E_m \exp\left\{-\frac{E_m}{T}\right\}, \quad (2.61a)$$

so that the second term on the right-hand side of Eq. (60) is just E/T , while the first term equals $\ln Z$, due to Eq. (59). (By the way, using the notion of *reciprocal temperature* $\beta \equiv 1/T$, with the account of Eq. (59), Eq. (61a) may be also rewritten as

$$E = -\frac{\partial(\ln Z)}{\partial\beta}. \quad (2.61b)$$

This formula is very convenient for calculations if our prime interest is the average internal energy E rather than F or W_n .) With these substitutions, Eq. (60) yields a very simple relation between the statistical sum and the entropy of the system:

$$S = \frac{E}{T} + \ln Z. \quad (2.62)$$

Now using Eq. (1.33), we see that Eq. (62) gives a straightforward way to calculate the free energy F of the system from nothing other than its statistical sum (and temperature):

³⁶ The temperature dependence of the type $\exp\{-\text{const}/T\}$, especially when showing up in rates of certain events, e.g., chemical reactions, is also frequently called the *Arrhenius law* – after chemist S. Arrhenius who has noticed this law in numerous experimental data. In all cases I am aware of, the Gibbs distribution is the underlying reason of the Arrhenius law. (We will see several examples of that later in this course.)

³⁷ This is the opinion of many physicists, including Richard Feynman – who climbs on this “summit” already on the first page of his brilliant book *Statistical Mechanics*, CRC Press, 1998. (This is a collection of lectures on a few diverse, mostly advanced topics of statistical physics, rather than its systematic course, so that it can hardly be used as the first textbook on the subject. However, I can highly recommend its first chapter to all my readers.)

$$F \equiv E - TS = -T \ln Z. \quad (2.63) \quad F \text{ from } Z$$

The relations (61b) and (63) play the key role in the connection of statistics to thermodynamics, because they enable the calculation, from Z alone, of the thermodynamic potentials of the system in equilibrium, and hence of all other variables of interest, using the general thermodynamic relations – see especially the circular diagram shown in Fig. 1.6, and its discussion in Sec. 1.4. Let me only note that to calculate the pressure P , e.g., from the second of Eqs. (1.35), we would need to know the explicit dependence of F , and hence of the statistical sum Z on the system's volume V . This would require the calculation, by appropriate methods of either classical or quantum mechanics, of the dependence of the eigenenergies E_m on the volume. Numerous examples of such calculations will be given later in the course.

Before proceeding to first such examples, let us notice that Eqs. (59) and (63) may be readily combined to give an elegant equality,

$$\exp\left\{-\frac{F}{T}\right\} = \sum_m \exp\left\{-\frac{E_m}{T}\right\}. \quad (2.64)$$

This equality, together with Eq. (59), enables us to rewrite the Gibbs distribution (58) in another form:

$$W_m = \exp\left\{\frac{F - E_m}{T}\right\}, \quad (2.65)$$

more convenient for some applications. In particular, this expression shows that since all probabilities W_m are below 1, F is always *lower* than the lowest energy level. Also, Eq. (65) clearly shows that the probabilities W_m do not depend on the energy reference, i. e. on an arbitrary constant added to all E_m – and hence to E and F .

2.5. Harmonic oscillator statistics

The last property may be immediately used in our first example of the Gibbs distribution application to a particular, but very important system – the harmonic oscillator, for a much more general case than was done in Sec. 2, namely for an arbitrary relation between T and $\hbar\omega$.³⁸ Let us consider a canonical ensemble of similar oscillators, each in a contact with a heat bath of temperature T . Selecting the ground-state energy $\hbar\omega/2$ for the origin of E , the oscillator eigenenergies (38) become $E_m = m\hbar\omega$ (with $m = 0, 1, \dots$), so that the Gibbs distribution (58) for probabilities of these states is

$$W_m = \frac{1}{Z} \exp\left\{-\frac{E_m}{T}\right\} = \frac{1}{Z} \exp\left\{-\frac{m\hbar\omega}{T}\right\}, \quad (2.66)$$

with the following statistical sum:

$$Z = \sum_{m=0}^{\infty} \exp\left\{-\frac{m\hbar\omega}{T}\right\} \equiv \sum_{m=0}^{\infty} \lambda^m, \quad \text{where } \lambda \equiv \exp\left\{-\frac{\hbar\omega}{T}\right\} \leq 1. \quad (2.67)$$

This is just the well-known infinite geometric progression (the “geometric series”),³⁹ with the sum

³⁸ The task of making a similar (and even simpler) calculation for another key quantum-mechanical object, the two-level system, is left for the reader's exercise.

³⁹ See, e.g., MA Eq. (2.8b).

so that Eq. (66) yields

$$Z = \frac{1}{1-\lambda} \equiv \frac{1}{1-e^{-\hbar\omega/T}}, \quad (2.68)$$

$$W_m = (1-e^{-\hbar\omega/T}) e^{-m\hbar\omega/T}. \quad (2.69)$$

Figure 7a shows W_m for several lower energy levels, as functions of temperature, or rather of the $T/\hbar\omega$ ratio. The plots show that the probability to find the oscillator in each particular state (except for the ground one, with $m = 0$) vanishes in both low- and high-temperature limits, and reaches its maximum value $W_m \sim 0.3/m$ at $T \sim m\hbar\omega$, so that the contribution $m\hbar\omega W_m$ of each excited level to the average oscillator energy E is always smaller than $\hbar\omega$.

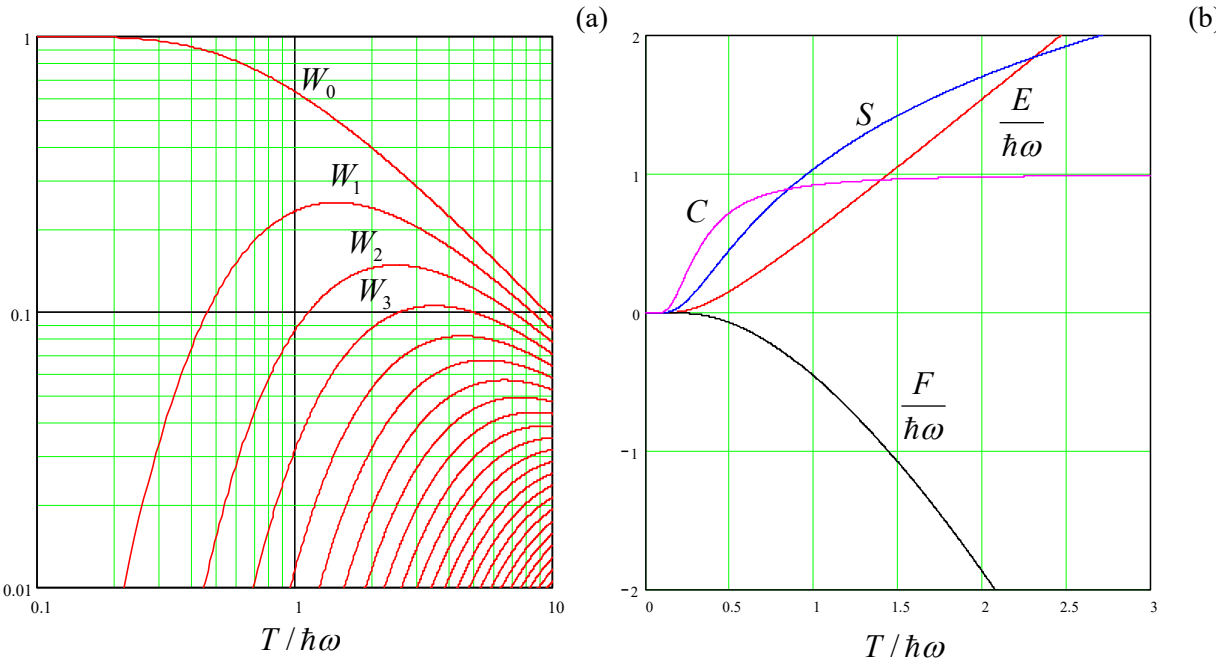


Fig. 2.7. Statistical and thermodynamic parameters of a harmonic oscillator, as functions of temperature.

This average energy may be calculated in either of two ways: either using Eq. (61a) directly:

$$E = \sum_{m=0}^{\infty} E_m W_m = (1 - e^{-\hbar\omega/T}) \sum_{m=0}^{\infty} m\hbar\omega e^{-m\hbar\omega/T}, \quad (2.70)$$

or (simpler) using Eq. (61b), as

$$E = -\frac{\partial}{\partial \beta} \ln Z = \frac{\partial}{\partial \beta} \ln(1 - \exp\{-\beta\hbar\omega\}), \quad \text{where } \beta \equiv \frac{1}{T}. \quad (2.71)$$

Both methods give (of course) the same result,⁴⁰

⁴⁰ It was first obtained in 1924 by S. Bose and is sometimes called the *Bose distribution* – a particular case of the *Bose-Einstein distribution* to be discussed in Sec. 8 below.

$$E = E(\omega, T) = \hbar\omega \frac{1}{e^{\hbar\omega/T} - 1}, \quad (2.72)$$

Quantum oscillator:
average energy

which is valid for arbitrary temperature and plays a key role in many fundamental problems of physics. The red line in Fig. 7b shows this result as a function of the normalized temperature. At relatively low temperatures, $T \ll \hbar\omega$, the oscillator is predominantly in its lowest (ground) state, and its energy (on top of the constant zero-point energy $\hbar\omega/2$, which was used in our calculation as the reference) is exponentially small: $E \approx \hbar\omega \exp\{-\hbar\omega/T\} \ll T, \hbar\omega$. On the other hand, in the high-temperature limit, the energy tends to T . This is exactly the result (a particular case of the equipartition theorem) that was obtained in Sec. 2 from the microcanonical distribution. Please note how much simpler is the calculation using the Gibbs distribution, even for an arbitrary ratio $T/\hbar\omega$.

To complete the discussion of the thermodynamic properties of the harmonic oscillator, we can calculate its free energy using Eq. (63):

$$F = T \ln \frac{1}{Z} = T \ln \left(1 - e^{-\hbar\omega/T} \right). \quad (2.73)$$

Now the entropy may be found from thermodynamics: either from the first of Eqs. (1.35), $S = -(\partial F / \partial T)_V$, or (even more easily) from Eq. (1.33): $S = (E - F)/T$. Both relations give, of course, the same result:

$$S = \frac{\hbar\omega}{T} \frac{1}{e^{\hbar\omega/T} - 1} - \ln \left(1 - e^{-\hbar\omega/T} \right). \quad (2.74)$$

Finally, since in the general case the dependence of the oscillator properties (essentially, of ω) on volume V is not specified, such variables as P , μ , G , W , and Ω are not defined, and what remains is to calculate the average heat capacity C per one oscillator:

$$C = \frac{\partial E}{\partial T} = \left(\frac{\hbar\omega}{T} \right)^2 \frac{e^{\hbar\omega/T}}{(e^{\hbar\omega/T} - 1)^2} \equiv \left[\frac{\hbar\omega/2T}{\sinh(\hbar\omega/2T)} \right]^2. \quad (2.75)$$

The calculated thermodynamic variables are plotted in Fig. 7b. In the low-temperature limit ($T \ll \hbar\omega$), they all tend to zero. On the other hand, in the high-temperature limit ($T \gg \hbar\omega$), $F \rightarrow -T \ln(T/\hbar\omega) \rightarrow -\infty$, $S \rightarrow \ln(T/\hbar\omega) \rightarrow +\infty$, and $C \rightarrow 1$ (in the SI units, $C \rightarrow k_B$). Note that the last limit is the direct corollary of the equipartition theorem: each of the two “half-degrees of freedom” of the oscillator gives, in the classical limit, the same contribution $C = \frac{1}{2}$ into its heat capacity.

Now let us use Eq. (69) to discuss the statistics of the quantum oscillator described by Hamiltonian (46), in the coordinate representation. Again using the density matrix’ diagonality in thermodynamic equilibrium, we may use a relation similar to Eqs. (47) to calculate the probability density to find the oscillator at coordinate q :

$$w(q) = \sum_{m=0}^{\infty} W_m w_m(q) = \sum_{m=0}^{\infty} W_m |\psi_m(q)|^2 = \left(1 - e^{-\hbar\omega/T} \right) \sum_{m=0}^{\infty} e^{-m\hbar\omega/T} |\psi_m(q)|^2, \quad (2.76)$$

where $\psi_m(q)$ is the normalized eigenfunction of the m^{th} stationary state of the oscillator. Since each $\psi_m(q)$ is proportional to the Hermite polynomial⁴¹ that requires at least m elementary functions for its

⁴¹ See, e.g., QM Sec. 2.10.

representation, working out the sum in Eq. (76) is a bit tricky,⁴² but the final result is rather simple: $w(q)$ is just a normalized *Gaussian distribution* (the “bell curve”),

$$w(q) = \frac{1}{(2\pi)^{1/2} \delta q} \exp\left\{-\frac{q^2}{2(\delta q)^2}\right\}, \quad (2.77)$$

with $\langle q \rangle = 0$, and

$$\langle q^2 \rangle = (\delta q)^2 = \frac{\hbar}{2m\omega} \coth \frac{\hbar\omega}{2T}. \quad (2.78)$$

Since the function $\coth \xi$ tends to 1 at $\xi \rightarrow \infty$, and diverges as $1/\xi$ at $\xi \rightarrow 0$, Eq. (78) shows that the width δq of the coordinate distribution is nearly constant (and equal to that, $(\hbar/2m\omega)^{1/2}$, of the ground-state wavefunction ψ_0) at $T \ll \hbar\omega$, and grows as $(T/m\omega^2)^{1/2} \equiv (T/\kappa)^{1/2}$ at $T/\hbar\omega \rightarrow \infty$.

As a sanity check, we may use Eq. (78) to write the following expression,

$$U \equiv \left\langle \frac{\kappa q^2}{2} \right\rangle = \frac{\hbar\omega}{4} \coth \frac{\hbar\omega}{2T} \rightarrow \begin{cases} \hbar\omega/4, & \text{for } T \ll \hbar\omega, \\ T/2, & \text{for } \hbar\omega \ll T, \end{cases} \quad (2.79)$$

for the average potential energy of the oscillator. To comprehend this result, let us recall that Eq. (72) for the average full energy E was obtained by counting it from the ground state energy $\hbar\omega/2$ of the oscillator. If we add this reference energy to that result, we get

$$E = \frac{\hbar\omega}{e^{\hbar\omega/T} - 1} + \frac{\hbar\omega}{2} \equiv \frac{\hbar\omega}{2} \coth \frac{\hbar\omega}{2T}. \quad (2.80)$$

We see that for arbitrary temperature, $U = E/2$, as was already discussed in Sec. 2. This means that the average kinetic energy, equal to $E - U$, is also the same:⁴³

$$\left\langle \frac{p^2}{2m} \right\rangle = \left\langle \frac{\kappa q^2}{2} \right\rangle = \frac{E}{2} = \frac{\hbar\omega}{4} \coth \frac{\hbar\omega}{2T}. \quad (2.81)$$

In the classical limit $T \gg \hbar\omega$, both energies equal $T/2$, reproducing the equipartition theorem result (48).

2.6. Two important applications

The results of the previous section, especially Eq. (72), have innumerable applications in physics and related disciplines, but here I have time for a brief discussion of only two of them.

(i) Blackbody radiation. Let us consider a free-space volume V limited by non-absorbing (i.e. ideally reflecting) walls. Electrodynamics tells us⁴⁴ that the electromagnetic field in such a “cavity” may be represented as a sum of “modes” with the time evolution similar to that of the usual harmonic

⁴² The calculation may be found, e.g., in QM Sec. 7.2.

⁴³ As a reminder: the equality of these two averages, at arbitrary temperature, was proved already in Sec. 2.

⁴⁴ See, e.g., EM Sec. 7.8.

oscillator. If the volume V is large enough,⁴⁵ the number of these modes within a small range dk of the wavevector magnitude k is

$$dN = \frac{gV}{(2\pi)^3} d^3k = \frac{gV}{(2\pi)^3} 4\pi k^2 dk, \quad (2.82)$$

where for electromagnetic waves, the degeneracy factor g is equal to 2, due to their two different independent (e.g., linear) polarizations of waves with the same wave vector \mathbf{k} . With the linear, isotropic dispersion relation for waves in vacuum, $k = \omega/c$, Eq. (82) yields

$$dN = \frac{2V}{(2\pi)^3} 4\pi \frac{\omega^2 d\omega}{c^3} \equiv V \frac{\omega^2}{\pi^2 c^3} d\omega. \quad (2.83)$$

On the other hand, quantum mechanics says⁴⁶ that the energy of such a “field oscillator” is quantized per Eq. (38), so that at thermal equilibrium its average energy is described by Eq. (72). Plugging that result into Eq. (83), we see that the spectral density of the electromagnetic field’s energy, per unit volume, is

$$u(\omega) \equiv \frac{E}{V} \frac{dN}{d\omega} = \frac{\hbar\omega^3}{\pi^2 c^3} \frac{1}{e^{\hbar\omega/T} - 1}. \quad (2.84)$$

Planck's
radiation
law

This is the famous *Planck's blackbody radiation law*.⁴⁷ To understand why its common name mentions radiation, let us consider a small planar part, of area dA , of a surface that completely absorbs electromagnetic waves incident from any direction. (Such “perfect black body” approximation may be closely approached using special experimental structures, especially in limited frequency intervals.) Figure 8 shows that if the arriving wave was planar, with the incidence angle θ , then the power $d\mathcal{P}_\theta(\omega)$ absorbed by the surface of small area dA , within a small frequency interval $d\omega$, i.e. the energy incident at that area in unit time, would be equal to the radiation energy within the same frequency interval, contained inside an imaginary cylinder (shaded in Fig. 8) of height c , base area $dA\cos\theta$, and hence volume $dV = c dA\cos\theta$:

$$d\mathcal{P}_\theta(\omega) = u(\omega)d\omega dV = u(\omega)d\omega c dA\cos\theta. \quad (2.85)$$

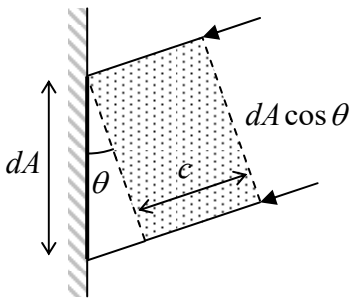


Fig. 2.8. Calculating the relation between $d\mathcal{P}(\omega)$ and $u(\omega)d\omega$.

⁴⁵ In our current context, the volume should be much larger than $(c\hbar/T)^3$, where $c \approx 3 \times 10^8$ m/s is the speed of light. For the room temperature ($T \approx k_B \times 300K \approx 4 \times 10^{-21}$ J), this lower bound is of the order of 10^{-16} m³.

⁴⁶ See, e.g., QM Sec. 9.1.

⁴⁷ Let me hope the reader knows that this law was first suggested in 1900 by Max Planck as an empirical fit for the experimental data on blackbody radiation, and this was the historic point at which the Planck constant \hbar (or rather $\hbar \equiv 2\pi\hbar$) was introduced – see, e.g., QM Sec. 1.1.

Since the thermally-induced field is isotropic, i.e. propagates equally in all directions, this result should be averaged over all solid angles within the polar angle interval $0 \leq \theta \leq \pi/2$:

$$\frac{d\mathcal{P}(\omega)}{dAd\omega} = \frac{1}{4\pi} \int \frac{d\mathcal{P}_\theta(\omega)}{dAd\omega} d\Omega = cu(\omega) \frac{1}{4\pi} \int_0^{\pi/2} \sin \theta d\theta \int_0^{2\pi} d\varphi \cos \theta = \frac{c}{4} u(\omega). \quad (2.86)$$

Hence the Planck's expression (84), multiplied by $c/4$, gives the power absorbed by such a “blackbody” surface. But at thermal equilibrium, this absorption has to be exactly balanced by the surface's own radiation, due to its non-zero temperature T .

I hope the reader is familiar with the main features of the Planck law (84), including its general shape (Fig. 9), with the low-frequency asymptote $u(\omega) \propto \omega^2$ (due to its historic significance bearing the special name of the *Rayleigh-Jeans law*), the exponential drop at high frequencies (the *Wien law*), and the resulting maximum of the function $u(\omega)$, reached at the frequency ω_{\max} with

$$\hbar\omega_{\max} \approx 2.82T, \quad (2.87)$$

i.e. at the wavelength $\lambda_{\max} = 2\pi/k_{\max} = 2\pi c/\omega_{\max} \approx 2.22 \text{ cm}/T$.

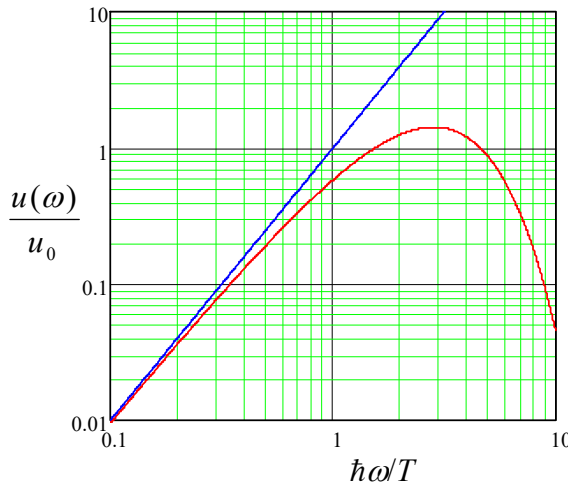


Fig. 2.9. The frequency dependence of the blackbody radiation density, normalized by $u_0 \equiv T^3/\pi^2\hbar^2c^3$, according to the Planck law (red line) and the Rayleigh-Jeans law (blue line).

Still, I cannot help mentioning a few important particular values: one corresponding to the visible light ($\lambda_{\max} \sim 500 \text{ nm}$) for the Sun's effective surface temperature $T_K \approx 6,000 \text{ K}$, and another one corresponding to the mid-infrared range ($\lambda_{\max} \sim 10 \mu\text{m}$) for the Earth's surface temperature $T_K \approx 300 \text{ K}$. The balance of these two radiations, absorbed and emitted by the Earth, determines its surface temperature and hence has the key importance for all life on our planet. This is why it is at the front and center of the current climate change discussions. As one more example, the cosmic microwave background (CMB) radiation, closely following the Planck law with $T_K = 2.725 \text{ K}$ (and hence having the maximum density at $\lambda_{\max} \approx 1.9 \text{ mm}$), and in particular its (very small) anisotropy, is a major source of data for modern cosmology.

Now let us calculate the total energy E of the blackbody radiation inside some volume V . It may be found from Eq. (84) by its integration over all frequencies:⁴⁸⁻⁴⁹

⁴⁸ The last step in Eq. (88) uses a table integral, equal to $\Gamma(4)\zeta(4) = (3!)(\pi^4/90) = \pi^4/15$ – see, e.g., MA Eq. (6.8b), with $s = 4$, and then MA Eqs. (6.7e), and (2.7b).

$$E = V \int_0^\infty u(\omega) d\omega = V \int_0^\infty \frac{\hbar\omega^3}{\pi^2 c^3} \frac{d\omega}{e^{\hbar\omega/T} - 1} = \frac{VT^4}{\pi^2 \hbar^3 c^3} \int_0^\infty \frac{\xi^3 d\xi}{e^{\xi} - 1} = V \frac{\pi^2}{15\hbar^3 c^3} T^4. \quad (2.88)$$

Using Eq. (86) to recast Eq. (88) into the total power radiated by a blackbody surface, we get the well-known *Stefan* (or “Stefan-Boltzmann”) law⁵⁰

$$\boxed{\frac{d\mathcal{P}}{dA} = \frac{\pi^2}{60\hbar^3 c^2} T^4 \equiv \sigma T_K^4,} \quad (2.89a) \quad \text{Stefan law}$$

where σ is the *Stefan-Boltzmann constant*

$$\boxed{\sigma \equiv \frac{\pi^2}{60\hbar^3 c^2} k_B^4 \approx 5.67 \times 10^{-8} \frac{\text{W}}{\text{m}^2 \text{K}^4}.} \quad (2.89b) \quad \text{Stefan-Boltzmann constant}$$

By this point, the thoughtful reader should have an important concern ready: Eq. (84) and hence Eq. (88) are based on Eq. (72) for the average energy of each oscillator, referred to its ground-state energy $\hbar\omega/2$. However, the radiation power should not depend on the energy origin; why have not we included the ground energy of each oscillator into the integration (88), as we have done in Eq. (80)? The answer is that usual radiation detectors only measure the *difference* between the power \mathcal{P}_{in} of the incident radiation (say, that of a blackbody surface with temperature T) and their own back-radiation power \mathcal{P}_{out} , corresponding to some effective temperature T_d of the detector – see Fig. 10. But however low T_d is, the temperature-independent contribution $\hbar\omega/2$ of the ground-state energy to the back radiation is always there. Hence, the term $\hbar\omega/2$ drops out from the balance, and cannot be detected – at least in this simple way. This is the reason why we had the right to ignore this contribution in Eq. (88) – very fortunately, because it would lead to the integral’s divergence at its upper limit. However, let me repeat that the ground-state energy of the electromagnetic field oscillators is physically real – and important – see Sec. 5.5 below.

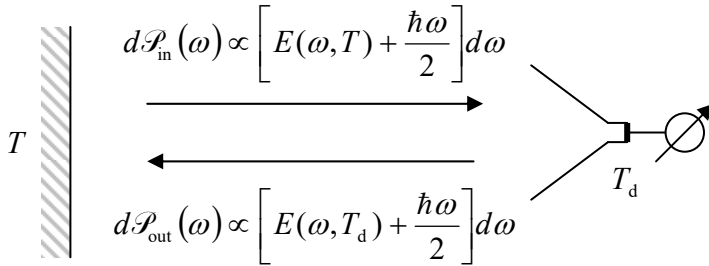


Fig. 2.10. The power balance at the electromagnetic radiation power measurement.

One more interesting result may be deduced from the free energy F of the electromagnetic radiation, which may be calculated by integration of Eq. (73) over all the modes, with the appropriate weight (83):

⁴⁹ Note that the heat capacity $C_V \equiv (\partial E / \partial T)_V$, following from Eq. (88), is proportional to T^3 at any temperature, and hence does not obey the trend $C_V \rightarrow \text{const}$ at $T \rightarrow \infty$. This is the result of the unlimited growth, with temperature, of the number of thermally-excited field oscillators with frequencies ω below T/\hbar .

⁵⁰ Its functional part ($E \propto T^4$) was deduced in 1879 by Joseph Stefan from earlier experiments by John Tyndall. Theoretically, it was proved in 1884 by L. Boltzmann, using a result derived earlier by Adolfo Bartoli from the Maxwell equations for the electromagnetic field – all well before Max Planck’s work.

$$F = \sum_{\omega} T \ln(1 - e^{-\hbar\omega/T}) \rightarrow \int_0^{\infty} T \ln(1 - e^{-\hbar\omega/T}) \frac{dN}{d\omega} d\omega = \int_0^{\infty} T \ln(1 - e^{-\hbar\omega/T}) \left(V \frac{\omega^2}{\pi^2 c^3} \right) d\omega. \quad (2.90)$$

Representing $\omega^2 d\omega$ as $d(\omega^3)/3$, we can readily work out this integral by parts, reducing it to a table integral similar to that in Eq. (88), and getting a surprisingly simple result:

$$F = -V \frac{\pi^2}{45\hbar^3 c^3} T^4 \equiv -\frac{E}{3}. \quad (2.91)$$

Now we can use the second of the general thermodynamic relations (1.35) to calculate the pressure exerted by the radiation on the walls of the containing volume V :⁵¹

$$P = -\left(\frac{\partial F}{\partial V}\right)_T = \frac{\pi^2}{45\hbar^3 c^3} T^4 = \frac{E}{3V}. \quad (2.92a)$$

Rewritten in the form,

Photon gas:
PV vs. E

$$PV = \frac{E}{3}, \quad (2.92b)$$

this result may be considered as the equation of state of the electromagnetic field, i.e. from the quantum-mechanical point of view, of the *photon gas*. Note that the equation of state (1.44) of the ideal classical gas may be represented in a similar form, but with a coefficient generally different from Eq. (92). Indeed, according to the equipartition theorem, for an ideal gas of non-relativistic particles whose internal degrees of freedom are in a fixed (say, ground) state, the temperature-dependent energy is that of the three translational “half-degrees of freedom”, $E = 3N(T/2)$. Expressing from here the product $NT = (2E/3)$, and plugging it into Eq. (1.44), we get a relation similar to Eq. (92), but with a twice larger factor before E . On the other hand, a *relativistic* treatment of the classical gas shows that Eq. (92) is valid for any gas in the ultra-relativistic limit, $T \gg mc^2$, where m is the rest mass of the gas’ particle. Evidently, photons (i.e. particles with $m = 0$) satisfy this condition at any energy.⁵²

Finally, let me note that Eq. (92) allows for the following interesting interpretation. The last of Eqs. (1.60), being applied to Eq. (92), shows that in this particular case the grand thermodynamic potential Ω equals $(-E/3)$, so that according to Eq. (91), it is equal to F . But according to the definition of Ω , i.e. the first of Eqs. (1.60), this means that the chemical potential of the electromagnetic field excitations (photons) vanishes:

$$\mu = \frac{F - \Omega}{N} = 0. \quad (2.93)$$

In Sec. 8 below, we will see that the same result follows from the comparison of Eq. (72) and the general Bose-Einstein distribution for arbitrary bosons. So, from the statistical point of view, photons may be considered as bosons with zero chemical potential.

(ii) Specific heat of solids. The heat capacity of solids is readily measurable, and in the early 1900s, its experimentally observed temperature dependence served as an important test for the then-

⁵¹ This formula may be also derived from the expression for the forces exerted by the electromagnetic radiation on the walls (see, e.g. EM Sec. 9.8), but the above calculation is much simpler.

⁵² Note that according to Eqs. (1.44), (88), and (92), the difference between the equations of state of the photon gas and an ideal gas of non-relativistic particles, expressed in the more usual form $P = P(V, T)$, is much more dramatic: $P \propto T^4 V^0$ vs. $P \propto T^1 V^1$.

emerging quantum theories. However, the theoretical calculation of C_V is not simple⁵³ – even for insulators, whose specific heat at realistic temperatures is due to thermally-induced vibrations of their crystal lattice alone.⁵⁴ Indeed, at relatively low frequencies, a solid may be treated as an elastic continuum. Such a continuum supports three different modes of mechanical waves with the same frequency ω , that all obey linear dispersion laws, $\omega = vk$, but the velocity $v = v_l$ for one of these modes (the *longitudinal sound*) is higher than that (v_t) of two other modes (the *transverse sound*).⁵⁵ At such frequencies, the wave mode density may be described by an evident generalization of Eq. (83):

$$dN = V \frac{1}{(2\pi)^3} \left(\frac{1}{v_l^3} + \frac{2}{v_t^3} \right) 4\pi\omega^2 d\omega. \quad (2.94a)$$

For what follows, it is convenient to rewrite this relation in a form similar to Eq. (83):

$$dN = \frac{3V}{(2\pi)^3} 4\pi \frac{\omega^2 d\omega}{v^3}, \quad \text{with } v \equiv \left[\frac{1}{3} \left(\frac{1}{v_l^3} + \frac{2}{v_t^3} \right) \right]^{-1/3}. \quad (2.94b)$$

However, the basic wave theory shows⁵⁶ that as the frequency ω of a sound wave in a periodic structure is increased so that its half-wavelength π/k approaches the crystal period d , the dispersion law $\omega(k)$ becomes nonlinear before the frequency reaches its maximum at $k = \pi/d$. To make things even more complex, 3D crystals are generally anisotropic, so that the dispersion law is different in different directions of the wave propagation. As a result, the exact statistics of thermally excited sound waves, and hence the heat capacity of crystals, is rather complex and specific for each particular crystal type.

In 1912, P. Debye suggested an approximate theory of the specific heat's temperature dependence, which is in a surprisingly good agreement with experiment for many insulators, including polycrystalline and amorphous materials. In his model, the linear (*acoustic*) dispersion law $\omega = vk$, with the effective sound velocity v defined by the second of Eqs. (94b), is assumed to be exact all the way up to some cutoff frequency ω_D , the same for all three wave modes. This *Debye frequency* may be defined by the requirement that the total number of acoustic modes, calculated within this model from Eq. (94b),

$$N = V \frac{1}{(2\pi)^3} \frac{3}{v^3} \int_0^{\omega_D} 4\pi\omega^2 d\omega = \frac{V\omega_D^3}{2\pi^2 v^3}, \quad (2.95)$$

is equal to the universal number $N = 3nV$ of the degrees of freedom (and hence of independent oscillation modes) in a 3D system of nV elastically coupled particles, where n is the atomic density of the crystal, i.e. the number of atoms per unit volume.⁵⁷ For this model, Eq. (72) immediately yields the following expression for the average energy and specific heat (in thermal equilibrium at temperature T):

$$E = V \frac{1}{(2\pi)^3} \frac{3}{v^3} \int_0^{\omega_D} \frac{\hbar\omega}{e^{\hbar\omega/T} - 1} 4\pi\omega^2 d\omega \equiv 3nVT D(x)_{x=T_D/T}, \quad (2.96)$$

⁵³ Due to a rather low temperature expansion of solids, the difference between their C_V and C_P is small.

⁵⁴ In good conductors (e.g., metals), specific heat is contributed (and at low temperatures, dominated) by free electrons – see Sec. 3.3 below.

⁵⁵ See, e.g., CM Sec. 7.7.

⁵⁶ See, e.g., CM Sec. 6.3, in particular Fig. 6.5 and its discussion.

⁵⁷ See, e.g., CM Sec. 6.2.

Debye
law

$$c_V \equiv \frac{C_V}{nV} = \frac{1}{nV} \left(\frac{\partial E}{\partial T} \right)_V = 3 \left[D(x) - x \frac{dD(x)}{dx} \right]_{x=T_D/T}, \quad (2.97)$$

where $T_D \equiv \hbar\omega_D$ is called the *Debye temperature*,⁵⁸ and

$$D(x) \equiv \frac{3}{x^3} \int_0^x \frac{\xi^3 d\xi}{e^{\xi} - 1} \rightarrow \begin{cases} 1, & \text{for } x \rightarrow 0, \\ \pi^4 / 5x^3, & \text{for } x \rightarrow \infty, \end{cases} \quad (2.98)$$

is the *Debye function*. Red lines in Fig. 11 show the temperature dependence of the specific heat c_V (per particle) within the Debye model. At high temperatures, it approaches a constant value of three, corresponding to the energy $E = 3nVT$, in agreement with the equipartition theorem for each of three degrees of freedom (i.e. six half-degrees of freedom) of each mode. (This value of c_V is known as the *Dulong-Petit law*.) In the opposite limit of low temperatures, the specific heat is much smaller:

$$c_V \approx \frac{12\pi^4}{5} \left(\frac{T}{T_D} \right)^3 \ll 1, \quad (2.99)$$

reflecting the reduction of the number of excited phonons with $\hbar\omega < T$ as the temperature is decreased.

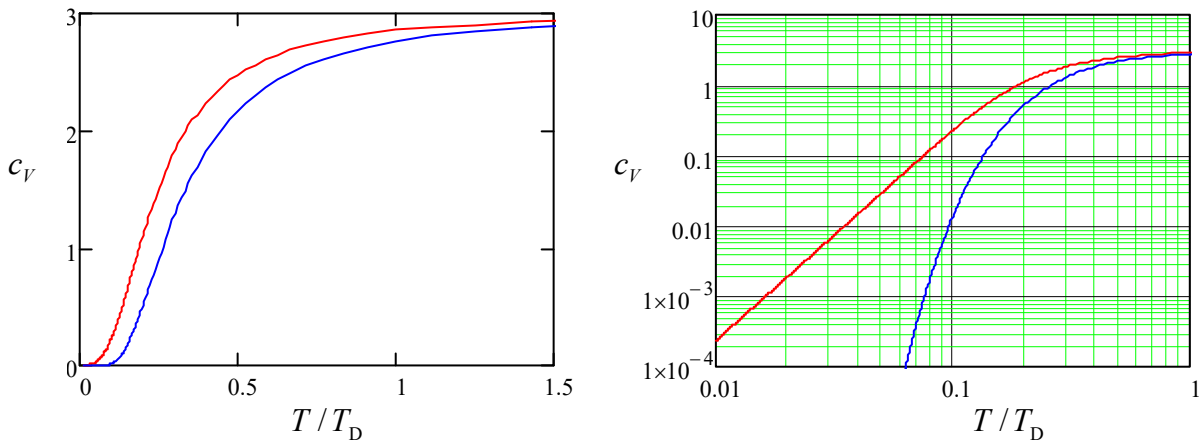


Fig. 2.11. The specific heat as a function of temperature in the Debye (red lines) and Einstein (blue lines) models.

As a historic curiosity, P. Debye's work followed one by A. Einstein, who had suggested (in 1907) a simpler model of crystal vibrations. In his model, all $3nV$ independent oscillatory modes of nV atoms of the crystal have approximately the same frequency, say ω_E , and Eq. (72) immediately yields

$$E = 3nV \frac{\hbar\omega_E}{e^{\hbar\omega_E/T} - 1}, \quad (2.100)$$

so that the specific heat is functionally similar to Eq. (75):

⁵⁸ In the SI units, the Debye temperature T_D is of the order of a few hundred K for most simple solids (e.g., ~430 K for aluminum and ~340 K for copper), with somewhat lower values for crystals with heavy atoms (~105 K for lead), and reaches its highest value ~2200 K for diamond, with its relatively light atoms and very stiff lattice.

$$c_V \equiv \frac{1}{nV} \left(\frac{\partial E}{\partial T} \right)_V = 3 \left[\frac{\hbar\omega_E / 2T}{\sinh(\hbar\omega_E / 2T)} \right]^2. \quad (2.101)$$

This dependence $c_V(T)$ is shown with blue lines in Fig. 11 (assuming, for the sake of simplicity, that $\hbar\omega_E = T_D$). At high temperatures, this result does satisfy the universal Dulong-Petit law ($c_V = 3$), but for $T \ll T_D$, Einstein's model predicts a much faster (exponential) drop of the specific heat as the temperature is reduced. (The difference between the Debye and Einstein models is not too spectacular on the linear scale, but in the log-log plot, shown on the right panel of Fig. 11, it is rather dramatic.⁵⁹⁾ The Debye model is in a much better agreement with experimental data for simple, monoatomic crystals, thus confirming the conceptual correctness of his wave-based approach.

Note, however, that when a genius such as Albert Einstein makes an error, there is usually some deep and important background under it. Indeed, crystals with the basic cell consisting of atoms of two or more types (such as NaCl, etc.), feature two or more separate branches of the dispersion law $\omega(k)$ – see, e.g., Fig. 12. While the lower, “acoustic” branch is virtually similar to those for monoatomic crystals and may be approximated by the Debye model, $\omega = v k$, reasonably well, the upper (“optical”⁶⁰⁾ branch does not approach $\omega = 0$ at any k . Moreover, for large values of the atomic mass ratio r , the optical branches are almost flat, with virtually k -independent frequencies ω_0 , which correspond to simple oscillations of each light atom between its heavy neighbors. For thermal excitations of such oscillations, and their contribution to the specific heat, Einstein's model (with $\omega_E = \omega_0$) gives a very good approximation, so that for such solids, the specific heat may be well described by a sum of the Debye and Einstein laws (97) and (101), with appropriate weights.

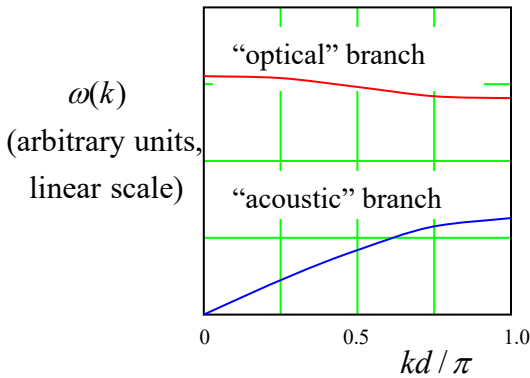


Fig. 2.12. The dispersion relation for mechanical waves in a simple 1D model of a solid, with similar interparticle distances d , but alternating particle masses, plotted for a particular mass ratio $r = 5$ – see CM Chapter 6.

2.7. Grand canonical ensemble and distribution

As we have seen, the Gibbs distribution is a very convenient way to calculate the statistical and thermodynamic properties of systems with a fixed number N of particles. However, for systems in which N may vary, another distribution is preferable for applications. Several examples of such situations (as

⁵⁹⁾ This is why there is the following general “rule of thumb” in quantitative sciences: if you plot your data on a linear rather than log scale, you better have a good excuse ready. (An example of a valid excuse: the variable you are plotting changes its sign within the range you want to exhibit.)

⁶⁰⁾ This term stems from the fact that at $k \rightarrow 0$, the mechanical waves corresponding to these branches have phase velocities $v_{ph} \equiv \omega(k)/k$ that are much higher than that of the acoustic waves, and may approach the speed of light. As a result, these waves can strongly interact with electromagnetic (practically, optical) waves of the same frequency, while acoustic waves cannot.

well as the basic thermodynamics of such systems) have already been discussed in Sec. 1.5. Perhaps even more importantly, statistical distributions for systems with variable N are also applicable to some ensembles of independent particles in certain single-particle states even if the number of the particles is fixed – see the next section.

With this motivation, let us consider what is called the *grand canonical ensemble* (Fig. 13). It is similar to the canonical ensemble discussed in Sec. 4 (see Fig. 6) in all aspects, besides that now the system under study and the heat bath (in this case more often called the *environment*) may exchange not only heat but also particles. In this ensemble, all environments are in both the thermal and chemical equilibrium, with their temperatures T and chemical potentials μ the same for all members.

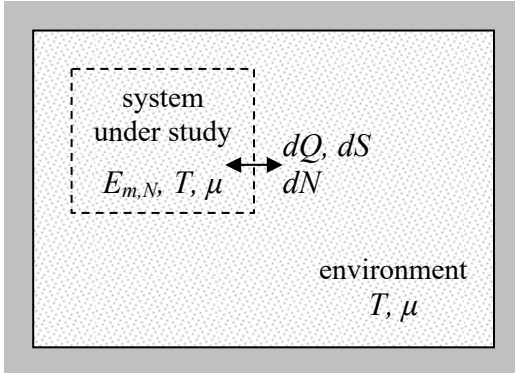


Fig. 2.13. A member of the grand canonical ensemble.

Let us assume that the system of interest is also in the chemical and thermal equilibrium with its environment. Then using exactly the same arguments as in Sec. 4 (including the specification of microcanonical sub-ensembles with fixed E_Σ and N_Σ), we may generalize Eq. (55), taking into account that the entropy S_{env} of the environment is now a function of not only its energy $E_{\text{env}} = E_\Sigma - E_{m,N}$,⁶¹ but also of the number of particles $N_{\text{env}} = N_\Sigma - N$, with E_Σ and N_Σ fixed:

$$\begin{aligned} \ln W_{m,N} &\propto \ln M = \ln g_{\text{env}}(E_\Sigma - E_{m,N}, N_\Sigma - N) + \ln \Delta E_\Sigma = S_{\text{env}}(E_\Sigma - E_{m,N}, N_\Sigma - N) + \text{const} \\ &\approx S_{\text{env}} \Big|_{E_\Sigma, N_\Sigma} - \frac{\partial S_{\text{env}}}{\partial E_{\text{env}}} \Big|_{E_\Sigma, N_\Sigma} E_{m,N} - \frac{\partial S_{\text{env}}}{\partial N_{\text{env}}} \Big|_{E_\Sigma, N_\Sigma} N + \text{const}. \end{aligned} \quad (2.102)$$

To simplify this relation, let us rewrite Eq. (1.52) in the following equivalent form:

$$dS = \frac{1}{T} dE + \frac{P}{T} dV - \frac{\mu}{T} dN. \quad (2.103)$$

Hence, if the entropy S of a system is expressed as a function of E , V , and N , then

$$\left(\frac{\partial S}{\partial E} \right)_{V,N} = \frac{1}{T}, \quad \left(\frac{\partial S}{\partial V} \right)_{E,N} = \frac{P}{T}, \quad \left(\frac{\partial S}{\partial N} \right)_{E,V} = -\frac{\mu}{T}. \quad (2.104)$$

Applying the first one and the last one of these relations to the last form of Eq. (102), and using the equality of the temperatures T and chemical potentials μ in the system under study and its environment, at equilibrium (as was discussed in Sec. 1.5), we get

⁶¹ The additional index in the new notation $E_{m,N}$ for the energy of the system of interest reflects the fact that its spectrum is generally dependent on the number N of particles in it.

$$\ln W_{m,N} = S_{\text{env}}(E_\Sigma, N_\Sigma) - \frac{1}{T} E_{m,N} + \frac{\mu}{T} N + \text{const.} \quad (2.105)$$

Again, exactly as at the derivation of the Gibbs distribution in Sec. 4, we may argue that since $E_{m,N}$, T , and μ do not depend on the choice of environment's size, i.e. on E_Σ and N_Σ , the probability $W_{m,N}$ for a system to have N particles and be in m^{th} quantum state in the whole grand canonical ensemble should also obey Eq. (105). As a result, we get the so-called *grand canonical distribution*:

$$W_{m,N} = \frac{1}{Z_G} \exp \left\{ \frac{\mu N - E_{m,N}}{T} \right\}. \quad (2.106)$$

Grand
canonical
distribution

Just as in the case of the Gibbs distribution, the constant Z_G (most often called the *grand statistical sum*, but sometimes the “grand partition function”) should be determined from the probability normalization condition, now with the summation of probabilities $W_{m,N}$ over all possible values of both m and N :

$$Z_G = \sum_{m,N} \exp \left\{ \frac{\mu N - E_{m,N}}{T} \right\}. \quad (2.107)$$

Grand
canonical
sum

Now, using the general Eq. (29) to calculate the entropy for the distribution (106) (exactly like we did it for the canonical ensemble), we get the following expression,

$$S = - \sum_{m,N} W_{m,N} \ln W_{m,N} = \frac{E}{T} - \frac{\mu \langle N \rangle}{T} + \ln Z_G, \quad (2.108)$$

which is evidently a generalization of Eq. (62).⁶² We see that now the grand thermodynamic potential Ω (rather than the free energy F) may be expressed directly via the normalization coefficient Z_G :

$$\Omega \equiv F - \mu \langle N \rangle = E - TS - \mu \langle N \rangle = T \ln \frac{1}{Z_G} = -T \ln \sum_{m,N} \exp \left\{ \frac{\mu N - E_{m,N}}{T} \right\}. \quad (2.109)$$

Ω from Z_G

Finally, solving the last equality for Z_G , and plugging the result back into Eq. (106), we can rewrite the grand canonical distribution in the form

$$W_{m,N} = \exp \left\{ \frac{\Omega + \mu N - E_{m,N}}{T} \right\}, \quad (2.110)$$

similar to Eq. (65) for the Gibbs distribution. Indeed, in the particular case when the number N of particles is fixed, $N = \langle N \rangle$, so that $\Omega + \mu N = \Omega + \mu \langle N \rangle \equiv F$, Eq. (110) is reduced to Eq. (65).

2.8. Systems of independent particles

Now let us apply the general statistical distributions discussed above to a simple but very important case when the system we are considering consists of many similar particles whose explicit (“direct”) interaction is negligible. As a result, each particular energy value $E_{m,N}$ of such a system may

⁶² The average number of particles $\langle N \rangle$ is exactly what was called N in thermodynamics (see Chapter 1), but I keep this explicit notation here to make a clear distinction between this average value of the variable, and its particular values participating in Eqs. (102)-(110).

be represented as a sum of energies ε_k of the particles, where the index k numbers single-particle states – rather than those of the whole system, as the index m does.

Let us start with the classical limit. In classical mechanics, the energy quantization effects are negligible, i.e. there is a formally infinite number of quantum states k within each finite energy interval. However, it is convenient to keep, for the time being, the discrete-state language, with the understanding that the average number $\langle N_k \rangle$ of particles in each of these states, usually called the *state occupancy*, is very small. In this case, we may apply the Gibbs distribution to the canonical ensemble of *single particles*, and hence use it with the substitution $E_m \rightarrow \varepsilon_k$, so that Eq. (58) becomes

$$\langle N_k \rangle = c \exp\left\{-\frac{\varepsilon_k}{T}\right\} \ll 1, \quad (2.111)$$

Boltzmann distribution

where the constant c should be found from the normalization condition:

$$\sum_k \langle N_k \rangle = 1. \quad (2.112)$$

This is the famous *Boltzmann distribution*.⁶³ Despite its formal similarity to the Gibbs distribution (58), let me emphasize the conceptual difference between these two important formulas. The Gibbs distribution describes the probability to find the *whole system* on one of its states with energy E_m , and it is *always* valid – more exactly, for a canonical ensemble of systems in thermodynamic equilibrium. On the other hand, the Boltzmann distribution describes the occupancy of an energy level of a *single particle*, and, as we will see in just a minute, is valid for quantum particles *only in the classical limit* $\langle N_k \rangle \ll 1$, even if they do not interact directly.

The last fact may be surprising, because it may seem that as soon as particles of the system are independent, nothing prevents us from using the Gibbs distribution to derive Eq. (111), regardless of the value of $\langle N_k \rangle$. This is indeed true if the particles are *distinguishable*, i.e. may be distinguished from each other – say by their fixed spatial positions, or by the states of certain internal degrees of freedom (say, spin), or by any other “pencil mark”. However, it is an experimental fact that elementary particles of each particular type (say, electrons) are *identical* to each other, i.e. cannot be “pencil-marked”.⁶⁴ For such particles we have to be more careful: even if they do not interact *explicitly*, there is still some *implicit* dependence in their behavior, which is especially evident for the so-called *fermions* (elementary particles with semi-integer spin): they obey the *Pauli exclusion principle* that forbids two identical particles to be in the same quantum state, even if they do not interact explicitly.⁶⁵

⁶³ The distribution was first suggested in 1877 by L. Boltzmann. For the particular case when ε is the kinetic energy of a free classical particle (and hence has a continuous spectrum), it is reduced to the *Maxwell distribution* (see Sec. 3.1 below), which was derived earlier – in 1860.

⁶⁴ This invites a natural question: what particles are “elementary enough” for their identity? For example, protons and neutrons have an internal structure, in some sense consisting of quarks and gluons; can they be considered elementary? Next, if protons and neutrons are elementary, are atoms? molecules? What about *really* large molecules (such as proteins)? viruses? The general answer to these questions, given by quantum mechanics (or rather experiment :-), is that any particles/systems, no matter how large and complex they are, are identical if they not only have the same internal structure but also are exactly in the same internal quantum state – for example, in the ground state of all their internal degrees of freedom.

⁶⁵ For a more detailed discussion of this issue, see, e.g., QM Sec. 8.1.

Note that the term “the same quantum state” carries a heavy meaning load here. For example, if two particles are confined to stay at different spatial positions (say, reliably locked in different boxes), they are *distinguishable* even if they are internally *identical*. Thus the Pauli principle, as well as other particle identity effects such as the Bose-Einstein condensation to be discussed in the next chapter, are important only when identical particles may move in the same spatial region. To emphasize this fact, it is common to use, instead of “identical”, a more precise (though grammatically rather unpleasant) adjective *indistinguishable*.

In order to take these effects into account, let us examine statistical properties of a system of many non-interacting but indistinguishable particles (at the first stage of calculation, either fermions or bosons) in equilibrium, applying the grand canonical distribution (109) to a very unusual grand canonical ensemble: a subset of particles in the same quantum state k (Fig. 14).

single-particle energy levels:

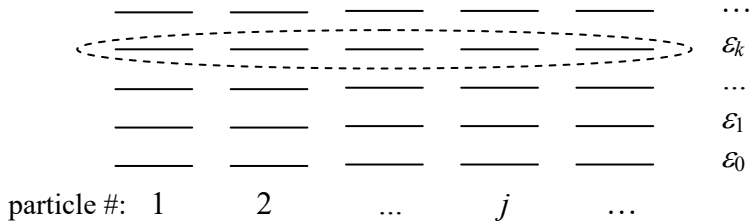


Fig. 2.14. The grand canonical ensemble of particles in the same quantum state with energy ε_k – schematically.

In this ensemble, the role of the environment may be played just by the set of particles in all other states $k' \neq k$, because due to infinitesimal interactions, the particles may gradually change their states. In the resulting equilibrium, the chemical potential μ and temperature T of the system should not depend on the state number k , though the grand thermodynamic potential Ω_k of the chosen particle subset may. Replacing N with N_k – the particular (not average!) number of particles in the selected k^{th} state, and the particular energy value $E_{m,N}$ with $\varepsilon_k N_k$, we reduce the final form of Eq. (109) to

$$\Omega_k = -T \ln \left(\sum_{N_k} \exp \left\{ \frac{\mu N_k - \varepsilon_k N_k}{T} \right\} \right) \equiv -T \ln \left[\sum_{N_k} \left(\exp \left\{ \frac{\mu - \varepsilon_k}{T} \right\} \right)^{N_k} \right], \quad (2.113)$$

where the summation should be carried out over all possible values of N_k . For the final calculation of this sum, the elementary particle type is essential.

On one hand, for *fermions*, obeying the Pauli principle, the numbers N_k in Eq. (113) may take only two values, either 0 (the state k is unoccupied) or 1 (the state is occupied), and the summation gives

$$\Omega_k = -T \ln \left[\sum_{N_k=0,1} \left(\exp \left\{ \frac{\mu - \varepsilon_k}{T} \right\} \right)^{N_k} \right] \equiv -T \ln \left(1 + \exp \left\{ \frac{\mu - \varepsilon_k}{T} \right\} \right). \quad (2.114)$$

Now the state occupancy may be calculated from the last of Eqs. (1.62) – in this case, with the (average) N replaced with $\langle N_k \rangle$:

$$\langle N_k \rangle = - \left(\frac{\partial \Omega_k}{\partial \mu} \right)_{T,V} = \frac{1}{e^{(\varepsilon_k - \mu)/T} + 1}. \quad (2.115)$$

Fermi-
Dirac
distribution

This is the famous *Fermi-Dirac distribution*, derived in 1926 independently by Enrico Fermi and Paul Dirac.

On the other hand, *bosons* do not obey the Pauli principle, and for them the numbers N_k can take any non-negative integer values. In this case, Eq. (113) turns into the following equality:

$$\Omega_k = -T \ln \left[\sum_{N_k=0}^{\infty} \left(\exp \left\{ \frac{\mu - \varepsilon_k}{T} \right\} \right)^{N_k} \right] \equiv -T \ln \sum_{N_k=0}^{\infty} \lambda^{N_k}, \quad \text{with } \lambda \equiv \exp \left\{ \frac{\mu - \varepsilon_k}{T} \right\}. \quad (2.116)$$

This sum is just the usual geometric series, which converges if $\lambda < 1$, giving

$$\Omega_k = -T \ln \frac{1}{1-\lambda} \equiv T \ln \left(1 - \exp \left\{ \frac{\mu - \varepsilon_k}{T} \right\} \right), \quad \text{for } \mu < \varepsilon_k. \quad (2.117)$$

In this case, the average occupancy, again calculated using Eq. (1.62) with N replaced with $\langle N_k \rangle$, obeys the *Bose-Einstein distribution*,

$$\langle N_k \rangle = - \left(\frac{\partial \Omega_k}{\partial \mu} \right)_{T,V} = \frac{1}{e^{(\varepsilon_k - \mu)/T} - 1}, \quad \text{for } \mu < \varepsilon_k, \quad (2.118)$$

which was derived in 1924 by Satyendra Nath Bose (for the particular case $\mu = 0$) and generalized in 1925 by Albert Einstein for an arbitrary chemical potential. In particular, comparing Eq. (118) with Eq. (72), we see that harmonic oscillator's *excitations*,⁶⁶ each with energy $\hbar\omega$, may be considered as bosons, with the chemical potential equal to zero. As a reminder, we have already obtained this equality ($\mu = 0$) in a different way – see Eq. (93). Its physical interpretation is that the oscillator excitations may be created inside the system, so that there is no energy cost μ of moving them into the system under consideration from its environment.

The simple form of Eqs. (115) and (118), and their similarity (besides “only” the difference of the signs before the unity in their denominators), is one of the most beautiful results of physics. This similarity, however, should not disguise the fact that the energy dependences of the occupancies $\langle N_k \rangle$ given by these two formulas are very different – see their linear and semi-log plots in Fig. 15.

In the Fermi-Dirac statistics, the level occupancy is not only finite, but below 1 at any energy, while in the Bose-Einstein it may be above 1, and diverges at $\varepsilon_k \rightarrow \mu$. However, as the temperature is increased, it eventually becomes much larger than the difference $(\varepsilon_k - \mu)$. In this limit, $\langle N_k \rangle \ll 1$, both quantum distributions coincide with each other, as well as with the classical Boltzmann distribution (111) with $c = \exp \{ \mu/T \}$:

$$\langle N_k \rangle \rightarrow \exp \left\{ \frac{\mu - \varepsilon_k}{T} \right\}, \quad \text{for } \langle N_k \rangle \rightarrow 0. \quad (2.119)$$

This distribution (also shown in Fig. 15) may be, therefore, understood also as the high-temperature limit for indistinguishable particles of both sorts.

Bose-Einstein distribution

Boltzmann distribution:
identical particles

⁶⁶ As the reader certainly knows, for the electromagnetic field oscillators, such excitations are called *photons*; for mechanical oscillation modes, *phonons*. It is important, however, not to confuse these mode *excitations* with the oscillators as such, and be very careful in prescribing to them certain spatial locations – see, e.g., QM Sec. 9.1.

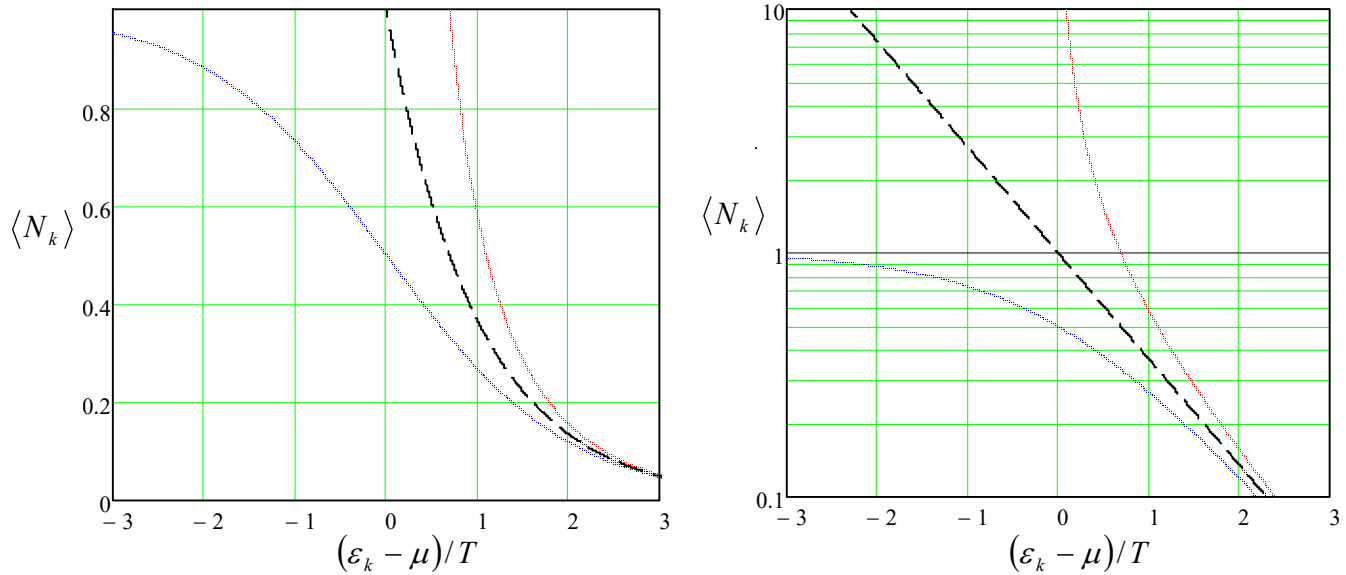


Fig. 2.15. The Fermi-Dirac (blue line), Bose-Einstein (red line), and Boltzmann (dashed line) distributions for indistinguishable quantum particles. (The last distribution is valid only asymptotically, at $\langle N_k \rangle \ll 1$.)

A natural question now is how to find the chemical potential μ participating in Eqs. (115), (118), and (119). In the grand canonical ensemble as such (Fig. 13), with the number of particles variable, the value of μ is imposed by the system's environment. However, both the Fermi-Dirac and Bose-Einstein distributions are also *approximately* applicable (in thermal equilibrium) to systems with a *fixed but very large* number N of particles. In these conditions, the role of the environment for some subset of $N' \ll N$ particles is essentially played by the remaining $N - N'$ particles. In this case, μ may be found by the calculation of $\langle N \rangle$ from the corresponding probability distribution, and then requiring it to be equal to the genuine number of particles in the system. In the next section, we will perform such calculations for several particular systems.

For that and other applications, it will be convenient for us to have ready formulas for the entropy S of a general (i.e. not necessarily equilibrium) state of systems of independent Fermi or Bose particles, expressed not as a function of W_m of the whole system, as in Eq. (29), but via the occupancy numbers $\langle N_k \rangle$. For that, let us consider an ensemble of *composite systems*, each consisting of $M \gg 1$ similar but distinct *component systems*, numbered by index $m = 1, 2, \dots, M$, with independent (i.e. not directly interacting) particles. We will assume that though in each of M component systems the number $N_k^{(m)}$ of particles in their k^{th} quantum state may be different (Fig. 16), their total number $N_k^{(\Sigma)}$ in the composite system is fixed. As a result, the total energy of the composite system is fixed as well,

$$\sum_{m=1}^M N_k^{(m)} = N_k^{(\Sigma)} = \text{const}, \quad E_k = \sum_{m=1}^M N_k^{(m)} \varepsilon_k = N_k^{(\Sigma)} \varepsilon_k = \text{const}, \quad (2.120)$$

so that an ensemble of many such composite systems (with the same k), in equilibrium, is microcanonical.

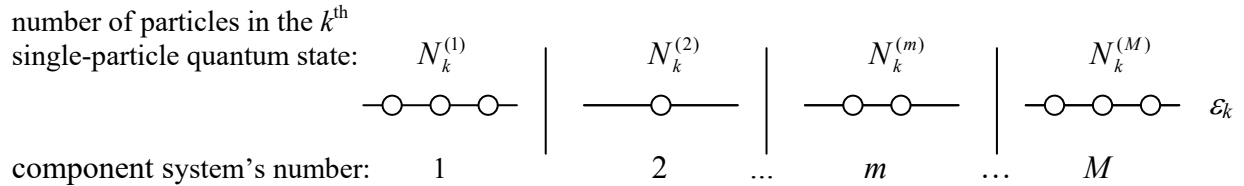


Fig. 2.16. A composite system of $N_k^{(\Sigma)}$ particles in the k^{th} quantum state, distributed between M component systems.

According to Eq. (24a), the average entropy S_k per component system in this microcanonical ensemble may be calculated as

$$S_k = \lim_{M \rightarrow \infty} \frac{\ln M_k}{M}, \quad (2.121)$$

where M_k is the number of possible different ways such a composite system (with fixed $N_k^{(\Sigma)}$) may be implemented. Let us start the calculation of M_k for Fermi particles – for which the Pauli principle is valid. Here the level occupancies $N_k^{(m)}$ may be only equal to either 0 or 1, so that the distribution problem is solvable only if $N_k^{(\Sigma)} \leq M$, and evidently equivalent to the choice of $N_k^{(\Sigma)}$ balls (in *arbitrary* order) from the total number of M *distinct* balls. Comparing this formulation with the definition of the binomial coefficient,⁶⁷ we immediately get

$$M_k = {}^M C_{N_k^{(\Sigma)}} = \frac{M!}{(M - N_k^{(\Sigma)})! N_k^{(\Sigma)}!}. \quad (2.122)$$

From here, using the Stirling formula (again, in its simplest form (27)), we get

Fermions:
entropy

$$S_k = -\langle N_k \rangle \ln \langle N_k \rangle - (1 - \langle N_k \rangle) \ln (1 - \langle N_k \rangle), \quad (2.123)$$

where

$$\langle N_k \rangle \equiv \lim_{M \rightarrow \infty} \frac{N_k^{(\Sigma)}}{M} \quad (2.124)$$

is exactly the average occupancy of the k^{th} single-particle state in each system, which was discussed earlier in this section. Since for a Fermi system, $\langle N_k \rangle$ is always somewhere between 0 and 1, its entropy (123) is always positive.

In the Bose case, where the Pauli principle is not valid, the number $N_k^{(m)}$ of particles on the k^{th} energy level in each of the systems is an arbitrary (non-negative) integer. Let us consider $N_k^{(\Sigma)}$ particles and $(M - 1)$ partitions (shown by vertical lines in Fig. 16) between M systems as $(M - 1 + N_k^{(\Sigma)})$ mathematical objects ordered along one axis. Each specific location of the partitions evidently fixes all $N_k^{(m)}$. Hence M_k may be calculated as the number of possible ways to distribute the $(M - 1)$ indistinguishable partitions among these $(M - 1 + N_k^{(\Sigma)})$ ordered objects, i.e. as the following binomial coefficient:⁶⁸

⁶⁷ See, e.g., MA Eq. (2.2).

⁶⁸ See also MA Eq. (2.4).

$$M_k = {}^{M+N_k-1}C_{M-1} = \frac{(M-1+N_k^{(\Sigma)})!}{(M-1)!N_k^{(\Sigma)}!}. \quad (2.125)$$

Applying the Stirling formula (27) again, we get the following result,

$$S_k = -\langle N_k \rangle \ln \langle N_k \rangle + (1 + \langle N_k \rangle) \ln (1 + \langle N_k \rangle), \quad (2.126)$$
Bosons:
entropy

which again differs from the Fermi case (123) “only” by the signs in the second term, and is valid for any positive $\langle N_k \rangle$.

Expressions (123) and (126) are valid for an arbitrary (possibly non-equilibrium) case; they may be also used for an alternative derivation of the Fermi-Dirac (115) and Bose-Einstein (118) distributions, which are valid only in equilibrium. For that, we may use the method of Lagrange multipliers, requiring (just like it was done in Sec. 2) the total entropy of a system of N independent, similar particles,

$$S = \sum_k S_k, \quad (2.127)$$

considered as a function of state occupancies $\langle N_k \rangle$, to attain its maximum, under the conditions of the fixed total number of particles N and total energy E :

$$\sum_k \langle N_k \rangle = N = \text{const}, \quad \sum_k \langle N_k \rangle \varepsilon_k = E = \text{const}. \quad (2.128)$$

The completion of this calculation is left for the reader’s exercise.

In the classical limit, when the average occupancies $\langle N_k \rangle$ of all states are small, the Fermi and Bose expressions for S_k tend to the same limit

$$S_k = -\langle N_k \rangle \ln \langle N_k \rangle, \quad \text{for } \langle N_k \rangle \ll 1. \quad (2.129)$$
Boltzmann
entropy

This expression, frequently referred to as the *Boltzmann* (or “classical”) *entropy*, might be also obtained, for arbitrary $\langle N_k \rangle$, directly from the functionally similar Eq. (29), by considering an ensemble of systems, each consisting of just one classical particle, so that $E_m \rightarrow \varepsilon_k$ and $W_m \rightarrow \langle N_k \rangle$. Let me emphasize again that for indistinguishable particles, such identification is generally (i.e. at $\langle N_k \rangle \sim 1$) illegitimate even if the particles do not interact explicitly. As we will see in the next chapter, indistinguishability may affect the statistical properties of identical particles even in the classical limit.

2.9. Exercise problems

2.1. A famous example of macroscopic irreversibility was suggested in 1907 by P. Ehrenfest. Two dogs share $2N \gg 1$ fleas. Each flea may jump onto another dog, and the rate Γ of such events (i.e. the probability of jumping per unit time) does not depend either on time or on the location of other fleas. Find the time evolution of the average number of fleas on a dog, and of the flea-related part of the total dogs’ entropy (at arbitrary initial conditions), and prove that the entropy can only grow.⁶⁹

⁶⁹ This is essentially a simpler (and funnier :-) version of the particle scattering model used by L. Boltzmann to prove his famous *H-theorem* (1872). Besides the historic significance of that theorem, the model used in it (see Sec. 6.2 below) is as cartoonish, and not more general.

2.2. Use the microcanonical distribution to calculate thermodynamic properties (including the entropy, all relevant thermodynamic potentials, and the heat capacity), of a two-level system in thermodynamic equilibrium with its environment, at temperature T that is comparable with the energy gap Δ . For each variable, sketch its temperature dependence, and find its asymptotic values (or trends) in the low-temperature and high-temperature limits.

Hint: The two-level system is any quantum system with just two different stationary states, whose energies (say, E_0 and E_1) are separated by a gap $\Delta \equiv E_1 - E_0$. Its most popular (but by no means the only!) example is the spin- $\frac{1}{2}$ of a particle, e.g., an electron, in an external magnetic field.⁷⁰

2.3. Solve the previous problem using the Gibbs distribution. Also, calculate the probabilities of the energy level occupation, and give physical interpretations of your results, in both temperature limits.

2.4. Calculate low-field magnetic susceptibility χ of a quantum spin- $\frac{1}{2}$ particle with a gyromagnetic ratio γ , in thermal equilibrium with an environment at temperature T , neglecting its orbital motion. Compare the result with that for a classical spontaneous magnetic dipole \mathbf{m} of a fixed magnitude m_0 , free to change its direction in space.

Hint: The low-field magnetic susceptibility of a single particle is defined⁷¹ as

$$\chi = \left. \frac{\partial \langle m_z \rangle}{\partial \mathcal{H}} \right|_{\mathcal{H} \rightarrow 0},$$

where the z -axis is aligned with the direction of the external magnetic field \mathcal{H} .

2.5. Calculate the low-field magnetic susceptibility of a particle with an arbitrary (either integer or semi-integer) spin s , neglecting its orbital motion. Compare the result with the solution of the previous problem.

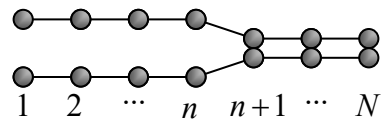
Hint: Quantum mechanics⁷² tells us that the Cartesian component m_z of the magnetic moment of such a particle, in the direction of the applied field, has $(2s + 1)$ stationary values:

$$m_z = \gamma \hbar m_s, \quad \text{with } m_s = -s, -s+1, \dots, s-1, s,$$

where γ is the gyromagnetic ratio of the particle, and \hbar is Planck's constant.

2.6.* Analyze the possibility of using a system of non-interacting spin- $\frac{1}{2}$ particles, placed into a strong, controllable external magnetic field, for refrigeration.

2.7. The rudimentary “zipper” model of DNA replication is a chain of N links that may be either open or closed – see the figure on the right. Opening a link increases the system's energy by $\Delta > 0$; a link may change its state (either open or closed) only if all links to the left of it are



⁷⁰ See, e.g., QM Secs. 4.6 and 5.1, for example, Eq. (4.167).

⁷¹ This “atomic” (or “molecular”) susceptibility should be distinguished from the “volumic” susceptibility $\chi_m \equiv \partial M_z / \partial \mathcal{H}$, where M_z is the magnetization, i.e. the magnetic moment of a unit volume of a system – see, e.g., EM Eq. (5.111). For a uniform medium with $n \equiv N/V$ non-interacting dipoles per unit volume, $\chi_m = n\chi$.

⁷² See, e.g., QM Sec. 5.7, in particular Eq. (5.169).

open, while those on the right of it, are closed. Calculate the average number of open links at thermal equilibrium, and analyze its temperature dependence, especially for the case $N \gg 1$.

2.8. Use the microcanonical distribution to calculate the average entropy, energy, and pressure of a classical particle of mass m , with no internal degrees of freedom, free to move in volume V , at temperature T .

Hint: Try to make a more accurate calculation than has been done in Sec. 2.2 for the system of N harmonic oscillators. For that, you will need to know the volume V_d of a d -dimensional hypersphere of the unit radius. To avoid being too cruel, I am giving it to you:

$$V_d = \pi^{d/2} / \Gamma\left(\frac{d}{2} + 1\right),$$

where $\Gamma(\xi)$ is the gamma function.⁷³

2.9. Solve the previous problem starting from the Gibbs distribution.

2.10. Calculate the average energy, entropy, free energy, and the equation of state of a classical 2D particle (without internal degrees of freedom), free to move within area A , at temperature T , starting from:

- (i) the microcanonical distribution, and
- (ii) the Gibbs distribution.

Hint: For the equation of state, make the appropriate modification of the notion of pressure.

2.11. A quantum particle of mass m is confined to free motion along a 1D segment of length a . Using any approach you like, calculate the average force the particle exerts on the “walls” (ends) of such “1D potential well” in thermal equilibrium, and analyze its temperature dependence, focusing on the low-temperature and high-temperature limits.

Hint: You may consider the series $\Theta(\xi) \equiv \sum_{n=1}^{\infty} \exp\{-\xi n^2\}$ a known function of ξ .⁷⁴

2.12.* Rotational properties of diatomic molecules (such as N_2 , CO , etc.) may be reasonably well described by the so-called *dumbbell model*: two point particles, of masses m_1 and m_2 , with a fixed distance d between them. Ignoring the translational motion of the molecule as the whole, use this model to calculate its heat capacity, and spell out the result in the limits of low and high temperatures. Discuss whether your solution is valid for the so-called *homonuclear* molecules, consisting of two similar atoms, such as H_2 , O_2 , N_2 , etc.

2.13. Calculate the heat capacity of a heteronuclear diatomic molecule, using the simple model described in the previous problem, but now assuming that the rotation is confined to one plane.⁷⁵

⁷³ For its definition and main properties, see, e.g., MA Eqs. (6.6)-(6.9).

⁷⁴ It may be reduced to the so-called elliptic theta-function $\theta_3(z, \tau)$ for a particular case $z = 0$ – see, e.g., Sec. 16.27 in the Abramowitz-Stegun handbook cited in MA Sec. 16(ii). However, you do not need that (or any other) handbook to solve this problem.

⁷⁵ This is a reasonable model of the constraints imposed on small atomic groups (e.g., ligands) by their atomic environment inside some large molecules.

2.14. A classical, rigid, strongly elongated body (such as a thin needle), is free to rotate about its center of mass, and is in thermal equilibrium with its environment. Are the angular velocity vector ω and the angular momentum vector \mathbf{L} , on average, directed along the elongation axis of the body, or normal to it?

2.15. Two similar classical electric dipoles, of a fixed magnitude d , are separated by a fixed distance r . Assuming that each dipole moment \mathbf{d} may take any spatial direction and that the system is in thermal equilibrium, write the general expressions for its statistical sum Z , average interaction energy E , heat capacity C , and entropy S , and calculate them explicitly in the high-temperature limit.

2.16. A classical 1D particle of mass m , residing in the potential well

$$U(x) = \alpha|x|^\gamma, \quad \text{with } \gamma > 0,$$

is in thermal equilibrium with its environment, at temperature T . Calculate the average values of its potential energy U and the full energy E , using two approaches:

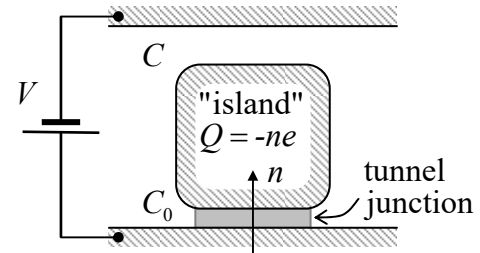
- (i) directly from the Gibbs distribution, and
- (ii) using the virial theorem of classical mechanics.⁷⁶

2.17. For a thermally-equilibrium ensemble of slightly anharmonic classical 1D oscillators, with mass m and potential energy

$$U(q) = \frac{\kappa}{2}x^2 + \alpha x^3,$$

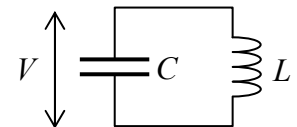
with a small coefficient α , calculate $\langle x \rangle$ in the first approximation in low temperature T .

2.18.^{*} A small conductor (in this context, usually called the *single-electron island*) is placed between two conducting electrodes, with voltage V applied between them. The gap between one of the electrodes and the island is so narrow that electrons may tunnel quantum-mechanically through this gap (the “weak tunnel junction”) – see the figure on the right. Calculate the average charge of the island as a function of V at temperature T .



Hint: The quantum-mechanical tunneling of an electron through a weak junction⁷⁷ between two macroscopic conductors and their subsequent energy relaxation, may be considered as a single inelastic (energy-dissipating) event, so that the only energy relevant for the thermal equilibrium of the system is its electrostatic potential energy.

2.19. An LC circuit (see the figure on the right) is in thermodynamic equilibrium with its environment. Calculate the r.m.s. fluctuation $\delta V \equiv \langle V^2 \rangle^{1/2}$



⁷⁶ See, e.g., CM Problem 1.12.

⁷⁷ In this particular context, the adjective “weak” denotes a junction with the tunneling transparency so low that the tunneling electron’s wavefunction loses its quantum-mechanical coherence before the electron has a chance to tunnel back. In a typical junction of a macroscopic area this condition is fulfilled if its effective resistance is much higher than the quantum unit of resistance (see, e.g., QM Sec. 3.2), $R_Q \equiv \pi\hbar/2e^2 \approx 6.5 \text{ k}\Omega$.

of the voltage across it, for an arbitrary ratio $T/\hbar\omega$, where $\omega = (LC)^{-1/2}$ is the resonance frequency of this “tank circuit”.

2.20. Derive Eq. (92) from simplistic arguments, representing the blackbody radiation as an ideal gas of photons treated as classical ultra-relativistic particles. What do similar arguments give for an ideal gas of classical but non-relativistic particles?

2.21. Calculate the enthalpy, the entropy, and the Gibbs energy of blackbody electromagnetic radiation with temperature T inside volume V , and then use these results to find the law of temperature and pressure drop at an adiabatic expansion.

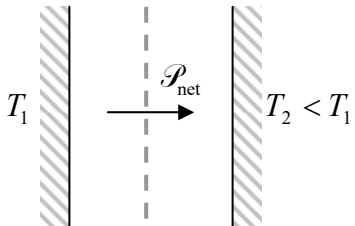
2.22. As was mentioned in Sec. 6(i), the relation between the temperatures T_{\oplus} of the visible Sun’s surface and that (T_0) of the Earth’s surface follows from the balance of the thermal radiation they emit. Prove that the experimentally observed relation indeed follows, with good precision, from a simple model in which the surfaces radiate as perfect black bodies with constant temperatures.

Hint: You may pick up the experimental values you need from any (reliable :-) source.

2.23. If a surface is not perfectly radiation-absorbing (“black”), the electromagnetic power of its thermal radiation differs from the Planck radiation law by a frequency-dependent factor $\varepsilon < 1$, called the *emissivity*. Prove that such surface reflects the $(1 - \varepsilon)$ fraction of the incident radiation.

2.24. If two black surfaces, facing each other, have different temperatures (see the figure on the right), then according to the Stefan radiation law (89), there is a net flow of thermal radiation, from a warmer surface to the colder one:

$$\frac{\mathcal{P}_{\text{net}}}{A} = \sigma(T_1^4 - T_2^4).$$



For many applications, notably including most low-temperature experiments, this flow is detrimental. One way to suppress it is to reduce the emissivity ε (for its definition, see the previous problem) of both surfaces – say by covering them with shiny metallic films. An alternative way toward the same goal is to place, between the surfaces, a thin layer (usually called the *thermal shield*), with a low emissivity of both surfaces – see the dashed line in Fig. above. Assuming that the emissivity is the same in both cases, find out which way is more efficient.

2.25. Two parallel, well-conducting plates of area A are separated by a free-space gap of a constant thickness $t \ll A^{1/2}$. Calculate the energy of the thermally-induced electromagnetic field inside the gap at thermal equilibrium with temperature T in the range

$$\frac{\hbar c}{A^{1/2}} \ll T \ll \frac{\hbar c}{t}.$$

Does the field push the plates apart?

2.26. Use the Debye theory to estimate the specific heat of aluminum at room temperature (say, 300 K), and express the result in the following popular units:

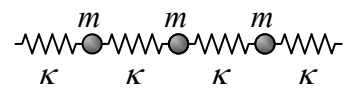
- (i) eV/K per atom,
- (ii) J/K per mole, and
- (iii) J/K per gram.

Compare the last number with the experimental value (from a reliable book or online source).

2.27. Low-temperature specific heat of some solids has a considerable contribution from thermal excitation of spin waves, whose dispersion law scales as $\omega \propto k^2$ at $\omega \rightarrow 0$.⁷⁸ Neglecting anisotropy, calculate the temperature dependence of this contribution to C_V at low temperatures, and discuss conditions of its experimental observation.

Hint: Just as the photons and phonons discussed in section 2.6, the quantum excitations of spin waves (called *magnons*) may be considered as non-interacting bosonic quasiparticles with zero chemical potential, whose statistics obeys Eq. (2.72).

2.28. Derive a general expression for the specific heat of a very long, straight chain of similar particles of mass m , confined to move only in the direction of the chain, and elastically interacting with effective spring constants κ – see the figure on the right. Spell out the result in the limits of very low and very high temperatures.



Hint: You may like to use the following integral:⁷⁹

$$\int_0^{+\infty} \frac{\xi^2 d\xi}{\sinh^2 \xi} = \frac{\pi^2}{6}.$$

2.29. Calculate the r.m.s. thermal fluctuation of the middle point of a uniform guitar string of length l , stretched by force \mathcal{T} , at temperature T . Evaluate your result for $l = 0.7$ m, $\mathcal{T} = 10^3$ N, and room temperature.

Hint: You may like to use the following series:

$$1 + \frac{1}{3^2} + \frac{1}{5^2} + \dots \equiv \sum_{m=0}^{\infty} \frac{1}{(2m+1)^2} = \frac{\pi^2}{8}.$$

2.30. Use the general Eq. (123) to re-derive the Fermi-Dirac distribution (115) for a system in equilibrium.

2.31. Each of two identical particles, not interacting directly, may be in any of two quantum states, with single-particle energies ε equal to 0 and Δ . Write down the statistical sum Z of the system, and use it to calculate its average total energy E at temperature T , for the cases when the particles are:

- (i) distinguishable (say, by their positions);
- (ii) indistinguishable fermions;
- (iii) indistinguishable bosons.

Analyze and interpret the temperature dependence of E for each case, assuming that $\Delta > 0$.

2.32. Calculate the chemical potential of a system of $N \gg 1$ independent fermions, kept at a fixed temperature T , if each particle has two non-degenerate energy levels separated by gap Δ .

⁷⁸ Note that the same dispersion law is typical for bending waves in thin elastic rods – see, e.g., CM Sec. 7.8.

⁷⁹ It may be reduced, via integration by parts, to the table integral MA Eq. (6.8d) with $n = 1$.

This page is
intentionally left
blank

Chapter 3. Ideal and Not-So-Ideal Gases

In this chapter, the general principles of thermodynamics and statistics, discussed in the previous two chapters, are applied to examine the basic physical properties of gases, i.e. collections of identical particles (for example, atoms or molecules) that are free to move inside a certain volume, either not interacting or weakly interacting with each other. We will see that due to the quantum statistics, properties of even the simplest, so-called ideal gases, with negligible direct interactions between particles, may be highly nontrivial.

3.1. Ideal classical gas

Direct interactions of typical atoms and molecules are well localized, i.e. rapidly decreasing with distance r between them and becoming negligible at a certain distance r_0 . In a gas of N particles inside volume V , the average distance r_{ave} between the particles is $(V/N)^{1/3}$. As a result, if the gas density $n \equiv N/V = (r_{\text{ave}})^{-3}$ is much lower than r_0^{-3} , i.e. if $nr_0^{-3} \ll 1$, the chance for its particles to approach each other and interact is rather small. The model in which such direct interactions are completely ignored is called the *ideal gas*.

Let us start with a *classical* ideal gas, which may be defined as the ideal gas in whose behavior the quantum effects are also negligible. As was discussed in Sec. 2.8, the condition of that is to have the average occupancy of each quantum state low:

$$\langle N_k \rangle \ll 1. \quad (3.1)$$

It may seem that we have already found all properties of such a system, in particular the equilibrium occupancy of its states – see Eq. (2.111):

$$\langle N_k \rangle = \text{const} \times \exp\left\{-\frac{\varepsilon_k}{T}\right\}. \quad (3.2)$$

In some sense this is true, but we still need, first, to see what exactly Eq. (2) means for the gas, a system with an essentially continuous energy spectrum, and, second, to show that, rather surprisingly, the particles' indistinguishability affects some properties of even classical gases.

The first of these tasks is evidently easiest for gas out of any external fields, and with no internal degrees of freedom.¹ In this case, ε_k is just the kinetic energy of the particle, which is an isotropic and parabolic function of p :

$$\varepsilon_k = \frac{p^2}{2m} = \frac{p_x^2 + p_y^2 + p_z^2}{2m}. \quad (3.3)$$

Now we have to use two facts from other fields of physics, hopefully well known to the reader. First, in quantum mechanics, the linear momentum \mathbf{p} is associated with the wavevector \mathbf{k} of the de Broglie wave,

¹ In more realistic cases when particles do have internal degrees of freedom, but they are all in a certain (say, ground) quantum state, Eq. (3) is valid as well, with ε_k referred to the internal ground-state energy. The effect of thermal excitation of the internal degrees of freedom will be briefly discussed at the end of this section.

$\mathbf{p} = \hbar\mathbf{k}$. Second, the eigenvalues of \mathbf{k} for *any* waves (including the de Broglie waves) in free space are uniformly distributed in the momentum space, with a constant density of states, given by Eq. (2.82):

$$\frac{dN_{\text{states}}}{d^3 k} = \frac{gV}{(2\pi)^3}, \quad \text{i.e. } \frac{dN_{\text{states}}}{d^3 p} = \frac{gV}{(2\pi\hbar)^3}, \quad (3.4)$$

where g is the degeneracy of particle's internal states (for example, for all spin- $\frac{1}{2}$ particles, the spin degeneracy $g = 2s + 1 = 2$). Even regardless of the exact proportionality coefficient between dN_{states} and $d^3 p$, the very fact that this coefficient does not depend on \mathbf{p} means that the probability dW to find the particle in a small region $d^3 p = dp_1 dp_2 dp_3$ of the momentum space is proportional to the right-hand side of Eq. (2), with ε_k given by Eq. (3):

$$dW = C \exp\left\{-\frac{p^2}{2mT}\right\} d^3 p = C \exp\left\{-\frac{p_1^2 + p_2^2 + p_3^2}{2mT}\right\} dp_1 dp_2 dp_3. \quad (3.5)$$

Maxwell distribution

This is the famous *Maxwell distribution*.² The normalization constant C may be readily found from the last form of Eq. (5), by requiring the integral of dW over all the momentum space to equal 1. Indeed, the integral is evidently a product of three similar 1D integrals over each Cartesian component p_j of the momentum ($j = 1, 2, 3$), which may be readily reduced to the well-known dimensionless Gaussian integral,³ so that we get

$$C = \left[\int_{-\infty}^{+\infty} \exp\left\{-\frac{p_j^2}{2mT}\right\} dp_j \right]^{-3} \equiv \left[(2mT)^{1/2} \int_{-\infty}^{+\infty} e^{-\xi^2} d\xi \right]^{-3} = (2\pi mT)^{-3/2}. \quad (3.6)$$

As a sanity check, let us use the Maxwell distribution to calculate the average energy corresponding to each half-degree of freedom:

$$\begin{aligned} \left\langle \frac{p_j^2}{2m} \right\rangle &= \int \frac{p_j^2}{2m} dW = \left[C^{1/3} \int_{-\infty}^{+\infty} \frac{p_j^2}{2m} \exp\left\{-\frac{p_j^2}{2mT}\right\} dp_j \right] \times \left[C^{1/3} \int_{-\infty}^{+\infty} \exp\left\{-\frac{p_{j'}^2}{2mT}\right\} dp_{j'} \right]^2 \\ &= \frac{T}{\pi^{1/2}} \int_{-\infty}^{+\infty} \xi^2 e^{-\xi^2} d\xi. \end{aligned} \quad (3.7)$$

The last, dimensionless integral equals $\sqrt{\pi}/2$,⁴ so that, finally,

$$\left\langle \frac{p_j^2}{2m} \right\rangle \equiv \left\langle \frac{mv_j^2}{2} \right\rangle = \frac{T}{2}. \quad (3.8)$$

² This formula had been suggested by J. C. Maxwell as early as 1860, i.e. well before the Boltzmann and Gibbs distributions were developed. Note also that the term “Maxwell distribution” is often associated with the distribution of the particle momentum (or velocity) *magnitude*,

$$dW = 4\pi C p^2 \exp\left\{-\frac{p^2}{2mT}\right\} dp = 4\pi C m^3 v^2 \exp\left\{-\frac{mv^2}{2T}\right\} dv, \quad \text{with } 0 \leq p, v < \infty,$$

which immediately follows from the first form of Eq. (5), combined with the expression $d^3 p = 4\pi p^2 dp$ due to the spherical symmetry of the distribution in the momentum/velocity space.

³ See, e.g., MA Eq. (6.9b).

⁴ See, e.g., MA Eq. (6.9c).

This result is (fortunately :-) in agreement with the equipartition theorem (2.48). It also means that the r.m.s. velocity of each particle is

$$\delta v \equiv \langle v^2 \rangle^{1/2} = \left\langle \sum_{j=1}^3 v_j^2 \right\rangle^{1/2} = \langle 3v_j^2 \rangle^{1/2} = \left(3 \frac{T}{m} \right)^{1/2}. \quad (3.9)$$

For a typical gas (say, for N₂, the air's main component), with $m \approx 28m_p \approx 4.7 \times 10^{-26}$ kg, this velocity, at room temperature ($T = k_B T_K \approx k_B \times 300$ K $\approx 4.1 \times 10^{-21}$ J) is about 500 m/s, comparable with the sound velocity in the same gas – and with the muzzle velocity of a typical handgun bullet. Still, it is measurable using even the simple table-top equipment (say, a set of two concentric, rapidly rotating cylinders with a thin slit collimating an atomic beam emitted at the axis) that was available in the end of the 19th century. Experiments using such equipment gave convincing early confirmations of the Maxwell distribution.

This is all very simple (isn't it?), but actually the thermodynamic properties of a classical gas, especially its entropy, are more intricate. To show that, let us apply the Gibbs distribution to a gas portion consisting of N particles, rather than just one of them. If the particles are exactly similar, the eigenenergy spectrum $\{\varepsilon_k\}$ of each of them is also exactly the same, and each value E_m of the total energy is just the sum of particular energies $\varepsilon_{k(l)}$ of the particles, where $k(l)$, with $l = 1, 2, \dots, N$, is the number of the energy level on which the l^{th} particle resides. Moreover, since the gas is classical, $\langle N_k \rangle \ll 1$, the probability of having two or more particles in any state may be ignored. As a result, we can use Eq. (2.59) to write

$$Z \equiv \sum_m \exp \left\{ -\frac{E_m}{T} \right\} = \sum_{k(1)} \exp \left\{ -\frac{1}{T} \sum_l \varepsilon_{k(l)} \right\} = \sum_{k(1)} \sum_{k(2)} \dots \sum_{k(N)} \prod_l \exp \left\{ -\frac{\varepsilon_{k(l)}}{T} \right\}, \quad (3.10)$$

where the summation has to be carried over all possible states of each particle. Since the summation over each set $\{k(l)\}$ concerns only one of the operands of the product of exponents under the sum, it is tempting to complete the calculation as follows:

$$Z \rightarrow Z_{\text{dist}} = \sum_{k(1)} \exp \left\{ -\frac{\varepsilon_{k(1)}}{T} \right\} \cdot \sum_{k(2)} \exp \left\{ -\frac{\varepsilon_{k(2)}}{T} \right\} \dots \sum_{k(N)} \exp \left\{ -\frac{\varepsilon_{k(N)}}{T} \right\} = \left(\sum_k \exp \left\{ -\frac{\varepsilon_k}{T} \right\} \right)^N, \quad (3.11)$$

where the final summation is over all states of one particle. This formula is indeed valid for distinguishable particles.⁵ However, if the particles are indistinguishable (again, meaning that they are internally identical *and* free to move within the same spatial region), Eq. (11) has to be modified by what is called the *correct Boltzmann counting*:

$$Z = \frac{1}{N!} \left(\sum_k \exp \left\{ -\frac{\varepsilon_k}{T} \right\} \right)^N, \quad (3.12)$$

Correct
Boltzmann
counting

that considers all quantum states different only by particle permutations, as the same state.

⁵ Since, by our initial assumption, each particle belongs to the same portion of gas, i.e. cannot be distinguished from others by its spatial position, this requires some internal “pencil mark” for each particle – for example, a specific structure or a specific quantum state of its internal degrees of freedom.

This expression is valid for any set $\{\varepsilon_k\}$ of eigenenergies. Now let us use it for the translational 3D motion of free particles, taking into account that the fundamental relation (4) implies the following rule for the replacement of a sum over quantum states of such motion with an integral:⁶

$$\sum_k (\dots) \rightarrow \int (\dots) dN_{\text{states}} = \frac{gV}{(2\pi)^3} \int (\dots) d^3k = \frac{gV}{(2\pi\hbar)^3} \int (\dots) d^3p. \quad (3.13)$$

In application to Eq. (12), this rule yields

$$Z = \frac{1}{N!} \left(\frac{gV}{(2\pi\hbar)^3} \left[\int_{-\infty}^{+\infty} \exp \left\{ -\frac{p_j^2}{2mT} \right\} dp_j \right]^3 \right)^N. \quad (3.14)$$

The integral in the square brackets is the same one as in Eq. (6), i.e. is equal to $(2\pi mT)^{1/2}$, so that finally

$$Z = \frac{1}{N!} \left(\frac{gV}{(2\pi\hbar)^3} (2\pi mT)^{3/2} \right)^N \equiv \frac{1}{N!} \left[gV \left(\frac{mT}{2\pi\hbar^2} \right)^{3/2} \right]^N. \quad (3.15)$$

Now, assuming that $N \gg 1$,⁷ and applying the Stirling formula, we can calculate the gas' free energy:

$$F = T \ln \frac{1}{Z} = -NT \ln \frac{V}{N} + Nf(T), \quad (3.16a)$$

with

$$f(T) \equiv -T \left\{ \ln \left[g \left(\frac{mT}{2\pi\hbar^2} \right)^{3/2} \right] + 1 \right\}. \quad (3.16b)$$

The first of these relations exactly coincides with Eq. (1.45), which was derived in Sec. 1.4 from the equation of state $PV = NT$, using thermodynamic identities. At that stage, this equation of state was just postulated, but now we can *derive* it by calculating the pressure from the second of Eqs. (1.35), and Eq. (16a):

$$P = - \left(\frac{\partial F}{\partial V} \right)_T = \frac{NT}{V}. \quad (3.17)$$

So, the equation of state of the ideal classical gas, with density $n \equiv N/V$, is indeed given by Eq. (1.44):

$$P = \frac{NT}{V} \equiv nT. \quad (3.18)$$

Hence we may use Eqs. (1.46)-(1.51), derived from this equation of state, to calculate all other thermodynamic variables of the gas. For example, using Eq. (1.47) with $f(T)$ given by Eq. (16b), for the internal energy and the specific heat of the gas we immediately get

⁶ As a reminder, we have already used this rule (twice) in Sec. 2.6, with particular values of g .

⁷ For the opposite limit when $N = g = 1$, Eq. (15) yields the results obtained, by two alternative methods, in the solutions of Problems 2.8 and 2.9. Indeed, for $N = 1$, the “correct Boltzmann counting” factor $N!$ equals 1, so that the particle distinguishability effects vanish – naturally.

$$E = N \left[f(T) - T \frac{df(T)}{dT} \right] = \frac{3}{2} NT, \quad c_v \equiv \frac{C_v}{N} = \frac{1}{N} \left(\frac{\partial E}{\partial T} \right)_v = \frac{3}{2}, \quad (3.19)$$

in full agreement with Eq. (8) and hence with the equipartition theorem.

Much less trivial is the result for entropy, which may be obtained by combining Eqs. (1.46) and (16a):

$$S = - \left(\frac{\partial F}{\partial T} \right)_V = N \left[\ln \frac{V}{N} - \frac{df(T)}{dT} \right]. \quad (3.20)$$

This formula,⁸ in particular, provides the means to resolve the following *gas mixing paradox* (sometimes called the “Gibbs paradox”). Consider two volumes, V_1 and V_2 , separated by a partition, each filled with the same gas, with the same density n , at the same temperature T , and hence with the same pressure P . Now let us remove the partition and let the gas portions mix; would the total entropy change? According to Eq. (20), it would not, because the ratio $V/N = n$, and hence the expression in the square brackets is the same in the initial and the final state, so that the entropy is additive, as any extensive variable should be. This makes full sense if the gas particles in both parts of the volume are truly identical, i.e. the partition’s removal does not change our information about the system. However, let us assume that all particles are distinguishable; then the entropy should clearly increase because the mixing would decrease our information about the system, i.e. increase its disorder. A quantitative description of this effect may be obtained using Eq. (11). Repeating for Z_{dist} the calculations made above for Z , we readily get a different formula for entropy:

$$S_{\text{dist}} = N \left[\ln V - \frac{df_{\text{dist}}(T)}{dT} \right], \quad f_{\text{dist}}(T) \equiv -T \ln \left[g \left(\frac{mT}{2\pi\hbar^2} \right)^{3/2} \right]. \quad (3.21)$$

Please notice that in contrast to the S given by Eq. (20), this entropy includes the term $\ln V$ instead of $\ln(V/N)$, so that S_{dist} is *not* proportional to N (at fixed temperature T and density N/V). While for distinguishable particles this fact does not present any conceptual problem, for indistinguishable particles it would mean that entropy was not an extensive variable, i.e. would contradict the basic assumptions of thermodynamics. This fact emphasizes again the necessity of the correct Boltzmann counting in the latter case.

Using Eq. (21), we can calculate the change of entropy due to mixing two gas portions, with N_1 and N_2 distinguishable particles, at a fixed temperature T (and hence at unchanged function f_{dist}):

$$\Delta S_{\text{dist}} = (N_1 + N_2) \ln(V_1 + V_2) - (N_1 \ln V_1 + N_2 \ln V_2) = N_1 \ln \frac{V_1 + V_2}{V_1} + N_2 \ln \frac{V_1 + V_2}{V_2} > 0. \quad (3.22)$$

Note that for a particular case, $V_1 = V_2 = V/2$, Eq. (22) reduces to the simple result, $\Delta S_{\text{dist}} = (N_1 + N_2) \ln 2$, which may be readily understood in terms of the information theory. Indeed, allowing each particle of the total number $N = N_1 + N_2$ to spread to a twice larger volume, we lose one bit of information per particle, i.e. $\Delta I = (N_1 + N_2)$ bits for the whole system. Let me leave it for the reader to show that Eq. (22) is also valid if particles in each sub-volume are indistinguishable from each other, but different from

⁸ The result represented by Eq. (20), with the function f given by Eq. (16b), was obtained independently by O. Sackur and H. Tetrode as early as in 1911, i.e. well before the final formulation of quantum mechanics in the late 1920s.

those in another sub-volume, i.e. for mixing of two different gases.⁹ However, it is certainly *not* applicable to the system where *all* particles are identical, stressing again that the correct Boltzmann counting (12) does indeed affect the gas entropy, even though it may be not as consequential as the Maxwell distribution (5), the equation of state (18), and the average energy (19).

In this context, one may wonder whether the change (22) (called the *mixing entropy*) is experimentally observable. The answer is yes. For example, after free mixing of two different gases, and hence boosting their total entropy by ΔS_{dist} , one can use a thin movable membrane that is *semipermeable*, i.e. whose pores are penetrable for particles of one type only, to separate them again, thus reducing the entropy back to the initial value, and measure either the necessary mechanical work $\Delta \mathcal{W} = T\Delta S_{\text{dist}}$ or the corresponding heat discharge into the heat bath. Practically, measurements of this type are easier in *weak solutions*¹⁰ – systems with a small concentration $c \ll 1$ of particles of one sort (*solute*) within much more abundant particles of another sort (*solvent*). The mixing entropy also affects the thermodynamics of chemical reactions in gases and liquids.¹¹ Note that besides purely thermal-mechanical measurements, the mixing entropy in some conducting solutions (*electrolytes*) is also measurable by a purely electrical method, called *cyclic voltammetry*, in which a low-frequency ac voltage, applied between two solid-state electrodes embedded in the solution, is used to periodically separate different ions, and then mix them again.¹²

Now let us briefly discuss two generalizations of our results for ideal classical gases. First, let us consider such gas in an external field of potential forces. It may be described by replacing Eq. (3) with

$$\varepsilon_k = \frac{p_k^2}{2m} + U(\mathbf{r}_k), \quad (3.23)$$

where \mathbf{r}_k is the position of the k^{th} particular particle, and $U(\mathbf{r})$ is the potential energy of the particle. If the potential $U(\mathbf{r})$ is changing in space sufficiently slowly,¹³ Eq. (4) is still applicable, but only to small volumes, $V \rightarrow dV = d^3r$ whose linear size is much smaller than the spatial scale of substantial variations of the function $U(\mathbf{r})$. Hence, instead of Eq. (5), we may only write the probability dW of finding the particle in a small volume d^3rd^3p of the 6-dimensional phase space:

⁹ By the way, if an ideal classical gas consists of particles of several different sorts, its full pressure is a sum of independent *partial pressures* exerted by each component – the so-called *Dalton law*. While this fact was an important experimental discovery in the early 1800s, for statistical physics this is just a straightforward corollary of Eq. (18), because in an ideal gas, the component particles do not interact.

¹⁰ Interestingly, the statistical mechanics of weak solutions is very similar to that of ideal gases, with Eq. (18) recast into the following formula (derived in 1885 by J. van 't Hoff), $PV = cNT$, for the partial pressure of the solute. One of its corollaries is that the net force (called the *osmotic pressure*) exerted on a semipermeable membrane is proportional to the difference of the solute concentrations it is supporting.

¹¹ Unfortunately, I do not have time for even a brief introduction into this important field, and have to refer the interested reader to specialized textbooks – for example, P. A. Rock, *Chemical Thermodynamics*, University Science Books, 1983; or P. Atkins, *Physical Chemistry*, 5th ed., Freeman, 1994; or G. M. Barrow, *Physical Chemistry*, 6th ed., McGraw-Hill, 1996.

¹² See, e.g., either Chapter 6 in A. Bard and L. Falkner, *Electrochemical Methods*, 2nd ed., Wiley, 2000 (which is a good introduction to electrochemistry as the whole); or Sec. II.8.3.1 in F. Scholz (ed.), *Electroanalytical Methods*, 2nd ed., Springer, 2010.

¹³ Quantitatively, the effective distance of substantial variations of the potential, $T/|\nabla U(\mathbf{r})|$, has to be much larger than the *mean free path* l of the gas particles, i.e. the average distance a particle passes its successive collisions with its counterparts. (For more on this notion, see Chapter 6 below.)

$$dW = w(\mathbf{r}, \mathbf{p}) d^3 r d^3 p, \quad w(\mathbf{r}, \mathbf{p}) = \text{const} \times \exp \left\{ -\frac{p^2}{2mT} - \frac{U(\mathbf{r})}{T} \right\}. \quad (3.24)$$

Hence, the Maxwell distribution of particle velocities is still valid at each point \mathbf{r} , so that the equation of state (18) is also valid locally. A new issue here is the spatial distribution of the total density,

$$n(\mathbf{r}) \equiv N \int w(\mathbf{r}, \mathbf{p}) d^3 p, \quad (3.25)$$

of all gas particles, regardless of their momentum/velocity. For this variable, Eq. (24) yields¹⁴

$$n(\mathbf{r}) = n(0) \exp \left\{ -\frac{U(\mathbf{r})}{T} \right\}, \quad (3.26)$$

where the potential energy at the origin ($\mathbf{r} = 0$) is used as the reference of U , and the local gas pressure may be still calculated from the local form of Eq. (18):

$$P(\mathbf{r}) = n(\mathbf{r})T = P(0) \exp \left\{ -\frac{U(\mathbf{r})}{T} \right\}. \quad (3.27)$$

A simple example of numerous applications of Eq. (27) is an approximate description of the Earth's atmosphere. At all heights $h \ll R_E \sim 6 \times 10^6$ m above the Earth's surface (say, above the sea level), we may describe the Earth gravity effect by the potential $U = mgh$, and Eq. (27) yields the so-called *barometric formula*

$$P(h) = P(0) \exp \left\{ -\frac{h}{h_0} \right\}, \quad \text{with } h_0 \equiv \frac{T}{mg} = \frac{k_B T_K}{mg}. \quad (3.28)$$

For the same N_2 , the main component of the atmosphere, at $T_K = 300$ K, $h_0 \approx 7$ km. This gives the correct order of magnitude of the atmosphere's thickness, though the exact law of the pressure change differs somewhat from Eq. (28), because the flow of radiation from Sun and Earth cause a relatively small deviation of the atmospheric air from the thermal equilibrium: a drop of its temperature T with height, with the so-called *lapse rate* of about 2% (~ 6.5 K) per km.

The second generalization I need to discuss is to particles with internal degrees of freedom. Now ignoring the potential energy $U(\mathbf{r})$, we may describe them by replacing Eq. (3) with

$$\varepsilon_k = \frac{p^2}{2m} + \varepsilon'_k, \quad (3.29)$$

where ε'_k describes the internal energy spectrum of the k^{th} particle. If the particles are similar, we may repeat all the above calculations, and see that all their results (including the Maxwell distribution, and the equation of state) are still valid, with the only exception of Eq. (16), which now becomes

$$f(T) = -T \left\{ \ln \left[g \left(\frac{mT}{2\pi\hbar^2} \right)^{3/2} \right] + 1 + \ln \left[\sum_{\varepsilon'_k} \exp \left\{ -\frac{\varepsilon'_k}{T} \right\} \right] \right\}. \quad (3.30)$$

¹⁴ In some textbooks, Eq. (26) is also called the *Boltzmann distribution*, though it certainly should be distinguished from Eq. (2.111).

As we already know from Eqs. (1.50)-(1.51), this change may affect both specific heats of the ideal gas – though not their difference, $c_V - c_P = 1$. They may be readily calculated for usual atoms and molecules, at not very high temperatures (say the room temperature of ~ 25 meV), because in these conditions, $\varepsilon_k' \gg T$ for most their internal degrees of freedom, including the electronic and vibrational ones. (The typical energy of the lowest electronic excitations is of the order of a few eV, and that of the lowest vibrational excitations is only an order of magnitude lower.) As a result, these degrees of freedom are “frozen out”: they are in their ground states, so that their contributions $\exp\{-\varepsilon_k'/T\}$ to the sum in Eq. (30), and hence to the heat capacity, are negligible. In monoatomic gases, this is true for all degrees of freedom besides those of the translational motion, already taken into account by the first term in Eq. (30), i.e. by Eq. (16b), so that their specific heat is typically well described by Eq. (19).

The most important exception is the rotational degrees of freedom of diatomic and polyatomic molecules. As quantum mechanics shows,¹⁵ the excitation energy of these degrees of freedom scales as $\hbar^2/2I$, where I is the molecule’s relevant moment of inertia. In the most important molecules, this energy is rather low (e.g. for N₂, it is close to 0.25 meV, i.e. $\sim 1\%$ of the room temperature), so that at usual conditions they are well excited and, moreover, behave virtually as classical degrees of freedom, each giving a quadratic contribution to the molecule’s energy, and hence obeying the equipartition theorem, i.e. giving an extra contribution of $T/2$ to the energy, i.e. $1/2$ to the specific heat.¹⁶ In polyatomic molecules, there are three such classical degrees of freedom (corresponding to their rotations about three principal axes¹⁷), but in diatomic molecules, only two.¹⁸ Hence, these contributions may be described by the following generalization of Eq. (19):

$$c_V = \begin{cases} 3/2, & \text{for monoatomic gases,} \\ 5/2, & \text{for gases of diatomic molecules,} \\ 3, & \text{for gases of polyatomic molecules.} \end{cases} \quad (3.31)$$

Please keep in mind, however, that as the above discussion shows, this simple result is invalid at very low and very high temperatures; its most notable violation is that the thermal activation of vibrational degrees of freedom for many important molecules at temperatures of a few thousand K.

3.2. Calculating μ

Now let us discuss properties of ideal gases of free, indistinguishable particles in more detail, paying special attention to the chemical potential μ – which, for some readers, may still be a somewhat mysterious aspect of the Fermi and Bose distributions. Note again that particle indistinguishability *requires* the absence of thermal excitations of their internal degrees of freedom, so that in the balance of this chapter such excitations will be ignored, and the particle’s energy ε_k will be associated with its “external” energy alone: for a free particle in an ideal gas, with its kinetic energy (3).

¹⁵ See, e.g., either the model solution of Problem 2.12 (and references therein), or QM Secs. 3.6 and 5.6.

¹⁶ This result may be readily obtained again from the last term of Eq. (30) by treating it exactly like the first one was and then applying the general Eq. (1.50).

¹⁷ See, e.g., CM Sec. 4.1.

¹⁸ This conclusion of the quantum theory may be interpreted as the indistinguishability of the rotations about the molecule’s symmetry axis.

Let us start from the classical gas, and recall the conclusion of thermodynamics that μ is just the Gibbs potential per unit particle – see Eq. (1.56). Hence we can calculate $\mu = G/N$ from Eqs. (1.49) and (16b). The result,

$$\mu = -T \ln \frac{V}{N} + f(T) + T = T \ln \left[\frac{N}{gV} \left(\frac{2\pi\hbar^2}{mT} \right)^{3/2} \right], \quad (3.32a)$$

which may be rewritten as

$$\exp \left\{ \frac{\mu}{T} \right\} = \frac{N}{gV} \left(\frac{2\pi\hbar^2}{mT} \right)^{3/2}, \quad (3.32b)$$

gives us some information about μ not only for a classical gas but for quantum (Fermi and Bose) gases as well. Indeed, we already know that for indistinguishable particles, the Boltzmann distribution (2.111) is valid only if $\langle N_k \rangle \ll 1$. Comparing this condition with the quantum statistics (2.115) and (2.118), we see again that the condition of the gas behaving classically may be expressed as

$$\exp \left\{ \frac{\mu - \varepsilon_k}{T} \right\} \ll 1 \quad (3.33)$$

for all ε_k . Since the lowest value of ε_k given by Eq. (3) is zero, Eq. (33) may be satisfied only if $\exp\{\mu/T\} \ll 1$. This means that the chemical potential of a classical gas has to be not just negative, but also “strongly negative” in the sense

$$-\mu \gg T. \quad (3.34a)$$

According to Eq. (32), this important condition may be represented as

$$T \gg T_0, \quad (3.34b)$$

with T_0 defined as

$$T_0 \equiv \frac{\hbar^2}{m} \left(\frac{N}{gV} \right)^{2/3} \equiv \frac{\hbar^2}{m} \left(\frac{n}{g} \right)^{2/3} \equiv \frac{\hbar^2}{g^{2/3} m r_{\text{ave}}^2}, \quad (3.35)$$

where r_{ave} is the average distance between the gas particles:

$$r_{\text{ave}} \equiv \frac{1}{n^{1/3}} = \left(\frac{V}{N} \right)^{1/3}. \quad (3.36)$$

In this form, the condition (34) is very transparent physically: disregarding the factor $g^{2/3}$ (which is typically of the order of 1), it means that the average thermal energy of a particle, which is always of the order of T , has to be much larger than the energy of quantization of particle's motion at the length r_{ave} . An alternative form of the same condition is¹⁹

$$r_{\text{ave}} \gg g^{-1/3} r_c, \quad \text{where } r_c \equiv \frac{\hbar}{(mT)^{1/2}}. \quad (3.37)$$

For a typical gas (say, N₂, with $m \approx 14m_p \approx 2.3 \times 10^{-26}$ kg) at the standard room temperature ($T = k_B \times 300\text{K} \approx 4.1 \times 10^{-21}$ J), the correlation length r_c is close to 10^{-11} m, i.e. is significantly smaller than the

¹⁹ In quantum mechanics, the parameter r_c so defined is frequently called the *correlation length* – see, e.g., QM Sec. 7.2 and in particular Eq. (7.37).

physical size $a \sim 3 \times 10^{-10}$ m of the molecule. This estimate shows that at room temperature, as soon as any practical gas is rare enough to be ideal ($r_{\text{ave}} \gg a$), it is classical, i.e. the only way to observe quantum effects in the translational motion of molecules is very deep refrigeration. According to Eq. (37), for the same nitrogen molecule, taking $r_{\text{ave}} \sim 10^2 a \sim 10^{-8}$ m (to ensure that direct interaction effects are negligible), the temperature should be well below 1 mK.

In order to analyze quantitatively what happens with gases when T is reduced to such low values, we need to calculate μ for an arbitrary ideal gas of indistinguishable particles. Let us use the lucky fact that the Fermi-Dirac and the Bose-Einstein statistics may be represented with one formula:

$$\langle N(\varepsilon) \rangle = \frac{1}{e^{(\varepsilon-\mu)/T} \pm 1}, \quad (3.38)$$

where (and everywhere in the balance of this section) the top sign stands for fermions and the lower one for bosons, to discuss fermionic and bosonic ideal gases in one shot.

If we deal with a member of the *grand canonical* ensemble (Fig. 2.13), in which not only T but also μ is externally fixed, we may use Eq. (38) to calculate the *average* number N of particles in volume V . If the volume is so large that $N \gg 1$, we may use the general state counting rule (13) to get

$$N = \frac{gV}{(2\pi)^3} \int \langle N(\varepsilon) \rangle d^3k = \frac{gV}{(2\pi\hbar)^3} \int \frac{d^3p}{e^{[\varepsilon(p)-\mu]/T} \pm 1} = \frac{gV}{(2\pi\hbar)^3} \int_0^\infty \frac{4\pi p^2 dp}{e^{[\varepsilon(p)-\mu]/T} \pm 1}. \quad (3.39)$$

In most practical cases, however, the number N of gas particles is fixed by particle confinement (i.e. the gas portion under study is a member of a *canonical* ensemble – see Fig. 2.6), and hence μ rather than N should be calculated. Let us use the trick already mentioned in Sec. 2.8: if N is very large, the relative fluctuation of the particle number, at fixed μ , is negligibly small ($\delta N/N \sim 1/\sqrt{N} \ll 1$), and the relation between the *average* values of N and μ should not depend on which of these variables is exactly fixed. Hence, Eq. (39), with μ having the sense of the *average* chemical potential, should be valid even if N is *exactly* fixed, so that the small fluctuations of N are replaced with (equally small) fluctuations of μ . Physically, in this case the role of the μ -fixing environment for any sub-portion of the gas is played by the rest of it, and Eq. (39) expresses the condition of self-consistency of such chemical equilibrium.

So, at $N \gg 1$, Eq. (39) may be used for calculating the average μ as a function of two independent parameters: N (i.e. the gas density $n = N/V$) and temperature T . For carrying out this calculation, it is convenient to convert the right-hand side of Eq. (39) to an integral over the particle's energy $\varepsilon(p) = p^2/2m$, so that $p = (2m\varepsilon)^{1/2}$, and $dp = (m/2\varepsilon)^{1/2} d\varepsilon$, getting

$$N = \frac{gVm^{3/2}}{\sqrt{2\pi^2\hbar^3}} \int_0^\infty \frac{\varepsilon^{1/2} d\varepsilon}{e^{(\varepsilon-\mu)/T} \pm 1}. \quad (3.40)$$

Basic equation for μ

This key result may be represented in two other, more convenient forms. First, Eq. (40), derived for our current (3D, isotropic and parabolic-dispersion) approximation (3), is just a particular case of the following self-evident state-counting relation

$$N = \int_0^\infty g(\varepsilon) \langle N(\varepsilon) \rangle d\varepsilon, \quad (3.41)$$

where

$$g(\varepsilon) \equiv dN_{\text{states}}/d\varepsilon \quad (3.42)$$

is the temperature-independent density of all quantum states of a particle – regardless of whether they are occupied or not. Indeed, according to the general Eq. (4), for our simple model (3),

$$g(\varepsilon) = g_3(\varepsilon) \equiv \frac{dN_{\text{states}}}{d\varepsilon} = \frac{d}{d\varepsilon} \left(\frac{gV}{(2\pi\hbar)^3} \frac{4\pi}{3} p^3 \right) = \frac{gVm^{3/2}}{\sqrt{2\pi^2\hbar^3}} \varepsilon^{1/2}, \quad (3.43)$$

so that we return to Eq. (39).

On the other hand, for some calculations, it is convenient to introduce the following dimensionless energy variable: $\xi \equiv \varepsilon/T$, to express Eq. (40) via a dimensionless integral:

$$N = \frac{gV(mT)^{3/2}}{\sqrt{2\pi^2\hbar^3}} \int_0^\infty \frac{\xi^{1/2} d\xi}{e^{\xi - \mu/T} \pm 1}. \quad (3.44)$$

As a sanity check, in the classical limit (34), the exponent in the denominator of the fraction under the integral is much larger than 1, and Eq. (44) reduces to

$$N = \frac{gV(mT)^{3/2}}{\sqrt{2\pi^2\hbar^3}} \int_0^\infty \frac{\xi^{1/2} d\xi}{e^{\xi - \mu/T}} \approx \frac{gV(mT)^{3/2}}{\sqrt{2\pi^2\hbar^3}} \exp\left\{\frac{\mu}{T}\right\} \int_0^\infty \xi^{1/2} e^{-\xi} d\xi, \quad \text{at } -\mu \gg T. \quad (3.45)$$

By the definition of the gamma function $\Gamma(\xi)$,²⁰ the last integral is just $\Gamma(3/2) = \pi^{1/2}/2$, and we get

$$\exp\left\{\frac{\mu}{T}\right\} = N \frac{\sqrt{2\pi^2\hbar^3}}{gV(mT)^{3/2}} \frac{2}{\sqrt{\pi}} = \left(2\pi \frac{T_0}{T}\right)^{3/2}, \quad (3.46)$$

which is exactly the same result as given by Eq. (32), obtained earlier in a rather different way – from the Boltzmann distribution and thermodynamic identities.

Unfortunately, in the general case of arbitrary μ , the integral in Eq. (44) cannot be worked out analytically.²¹ The best we can do is to use T_0 , defined by Eq. (35), to rewrite Eq. (44) in the following convenient, fully dimensionless form:

$$\frac{T}{T_0} = \left[\frac{1}{\sqrt{2\pi^2}} \int_0^\infty \frac{\xi^{1/2} d\xi}{e^{\xi - \mu/T} \pm 1} \right]^{-2/3}, \quad (3.47)$$

and then use this relation to calculate the ratios T/T_0 and $\mu/T_0 \equiv (\mu/T) \times (T/T_0)$, as functions of μ/T numerically. After that, we may plot the results versus each other, now considering the first ratio as the argument. Figure 1 below shows the resulting plots, for both particle types. They show that at high temperatures, $T \gg T_0$, the chemical potential is negative and approaches the classical behavior given by Eq. (46) for both fermions and bosons – just as we could expect. However, at temperatures $T \sim T_0$ the type of statistics becomes crucial. For fermions, the reduction of temperature leads to μ changing its

²⁰ See, e.g., MA Eq. (6.7a).

²¹ For the reader's reference only: for the upper sign, the integral in Eq. (40) is a particular form (for $s = 1/2$) of a special function called the *complete Fermi-Dirac integral* F_s , while for the lower sign, it is a particular case (for $s = 3/2$) of another special function called the *polylogarithm* Li_s . (In what follows, I will not use these notations.)

sign from negative to positive, and then approaching a constant positive value called the *Fermi energy*, $\varepsilon_F \approx 7.595 T_0$ at $T \rightarrow 0$. On the contrary, the chemical potential of a bosonic gas stays negative, and then turns into zero at a certain *critical temperature* $T_c \approx 3.313 T_0$. Both these limits, which are very important for applications, may (and will be :-) explored analytically, separately for each statistics.

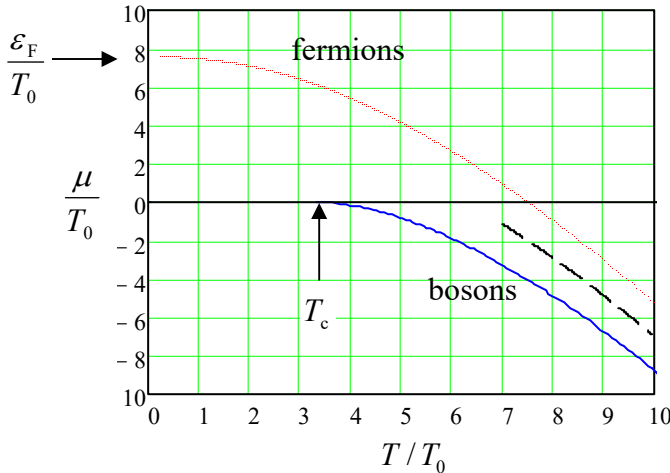


Fig. 3.1. The chemical potential of an ideal gas of $N \gg 1$ indistinguishable quantum particles, as a function of temperature at a fixed gas density $n \equiv N/V$ (i.e. fixed $T_0 \propto n^{2/3}$), for two different particle types. The dashed line shows the classical approximation (46), valid only at $T \gg T_0$.

Before carrying out such studies (in the next two sections), let me show that, rather surprisingly, for any non-relativistic, ideal quantum gas, the relation between the product PV and the energy,

$$PV = \frac{2}{3} E, \quad (3.48)$$
Ideal gas:
 PV vs. E

is exactly the same as follows from Eqs. (18) and (19) for the classical gas, and hence does *not* depend on the particle statistics. To prove this, it is sufficient to use Eqs. (2.114) and (2.117) for the grand thermodynamic potential of each quantum state, which may be conveniently represented by a single formula,

$$\Omega_k = \mp T \ln \left(1 \pm e^{(\mu - \varepsilon_k)/T} \right), \quad (3.49)$$

and sum them over all states k , using the general summation formula (13). The result for the total grand potential of a 3D gas with the dispersion law (3) is

$$\Omega = \mp T \frac{gV}{(2\pi\hbar)^3} \int_0^\infty \ln \left(1 \pm e^{(\mu - p^2/2m)/T} \right) 4\pi p^2 dp = \mp T \frac{gVm^{3/2}}{\sqrt{2\pi^2\hbar^3}} \int_0^\infty \ln \left(1 \pm e^{(\mu - \varepsilon)/T} \right) \varepsilon^{1/2} d\varepsilon. \quad (3.50)$$

Working out this integral by parts, exactly as we did it with the one in Eq. (2.90), we get

$$\Omega = -\frac{2}{3} \frac{gVm^{3/2}}{\sqrt{2\pi^2\hbar^3}} \int_0^\infty \frac{\varepsilon^{3/2} d\varepsilon}{e^{(\varepsilon - \mu)/T} \pm 1} = -\frac{2}{3} \int_0^\infty \varepsilon g_3(\varepsilon) \langle N(\varepsilon) \rangle d\varepsilon. \quad (3.51)$$

But the last integral is just the total energy E of the gas:

$$E = \frac{gV}{(2\pi\hbar)^3} \int_0^\infty \frac{p^2}{2m} \frac{4\pi p^2 dp}{e^{[\varepsilon(p) - \mu]/T} \pm 1} = \frac{gVm^{3/2}}{\sqrt{2\pi^2\hbar^3}} \int_0^\infty \frac{\varepsilon^{3/2} d\varepsilon}{e^{(\varepsilon - \mu)/T} \pm 1} = \int_0^\infty \varepsilon g_3(\varepsilon) \langle N(\varepsilon) \rangle d\varepsilon, \quad (3.52)$$
Ideal
gas:
energy

so that for any temperature and any particle type, $\Omega = -(2/3)E$. But since, from thermodynamics, $\Omega = -PV$, we have Eq. (48) proved. This universal relation²² will be repeatedly used below.

3.3. Degenerate Fermi gas

Analysis of low-temperature properties of a *Fermi gas* is very simple in the limit $T = 0$. Indeed, in this limit, the Fermi-Dirac distribution (2.115) is just the step function:

$$\langle N(\varepsilon) \rangle = \begin{cases} 1, & \text{for } \varepsilon < \mu, \\ 0, & \text{for } \mu < \varepsilon, \end{cases} \quad (3.53)$$

- see by the bold line in Fig. 2a. Since $\varepsilon = p^2/2m$ is isotropic in the momentum space, in that space the particles, at $T = 0$, fully occupy all possible quantum states inside a sphere (frequently called either the *Fermi sphere* or the *Fermi sea*) with some radius p_F (Fig. 2b), while all states above the sea surface are empty. Such *degenerate Fermi gas* is a striking manifestation of the Pauli principle: though in thermodynamic equilibrium at $T = 0$ all particles try to lower their energies as much as possible, only g of them may occupy each translational (“orbital”) quantum state. As a result, the sphere’s volume is proportional to the particle number N , or rather to their density $n = N/V$.

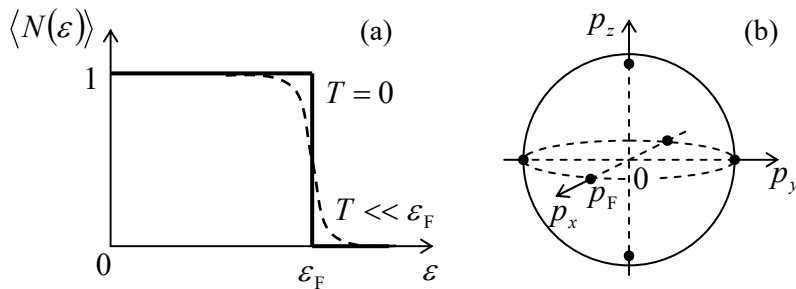


Fig. 3.2. Representations of the Fermi sea: (a) on the Fermi distribution plot, and (b) in the momentum space.

Indeed, the radius p_F may be readily related to the number of particles N using Eq. (39), with the upper sign, whose integral in this limit is just the Fermi sphere’s volume:

$$N = \frac{gV}{(2\pi\hbar)^3} \int_0^{p_F} 4\pi p^2 dp = \frac{gV}{(2\pi\hbar)^3} \frac{4\pi}{3} p_F^3. \quad (3.54)$$

Now we can use Eq. (3) to express via N the chemical potential μ (which, in the limit $T = 0$, it bears the special name of the *Fermi energy* ε_F)²³:

Fermi energy

$$\varepsilon_F \equiv \mu|_{T=0} = \frac{p_F^2}{2m} = \frac{\hbar^2}{2m} \left(6\pi^2 \frac{N}{gV} \right)^{2/3} \equiv \left(\frac{9\pi^4}{2} \right)^{1/3} T_0 \approx 7.595 T_0, \quad (3.55a)$$

where T_0 is the quantum temperature scale defined by Eq. (35). This formula quantifies the low-temperature trend of the function $\mu(T)$, clearly visible in Fig. 1, and in particular, explains the ratio ε_F/T_0 mentioned in Sec. 2. Note also a simple and very useful relation,

²² For gases of diatomic and polyatomic molecules at relatively high temperatures, when some of their internal degrees of freedom are thermally excited, Eq. (48) is valid only for the translational-motion energy.

²³ Note that in the electronic engineering literature, μ is usually called the *Fermi level*, for any temperature.

$$\varepsilon_F = \frac{3}{2} \frac{N}{g_3(\varepsilon_F)}, \quad \text{i.e. } g_3(\varepsilon_F) = \frac{3}{2} \frac{N}{\varepsilon_F}, \quad (3.55b)$$

that may be obtained immediately from the comparison of Eqs. (43) and (54).

The total energy of the degenerate Fermi gas may be (equally easily) calculated from Eq. (52):

$$E = \frac{gV}{(2\pi\hbar)^3} \int_0^{p_F} \frac{p^2}{2m} 4\pi p^2 dp = \frac{gV}{(2\pi\hbar)^3} \frac{4\pi}{2m} \frac{p_F^5}{5} = \frac{3}{5} \varepsilon_F N, \quad (3.56)$$

showing that the average energy, $\langle \varepsilon \rangle \equiv E/N$, of a particle inside the Fermi sea is equal to 3/5 of that (ε_F) of the particles in the most energetic occupied states, on the Fermi surface. Since, according to the formulas of Chapter 1, at zero temperature $H = G = N\mu$, and $F = E$, the only thermodynamic variable still to be calculated is the gas pressure P . For it, we could use any of the thermodynamic relations $P = (H - E)/V$ or $P = -(\partial F/\partial V)_T$, but it is even easier to use our recent result (48). Together with Eq. (56), it yields

$$P = \frac{2}{3} \frac{E}{V} = \frac{2}{5} \varepsilon_F \frac{N}{V} = \left(\frac{36\pi^4}{125} \right)^{1/3} P_0 \approx 3.035 P_0, \quad \text{where } P_0 \equiv nT_0 = \frac{\hbar^2 n^{5/3}}{mg^{2/3}}. \quad (3.57)$$

From here, it is straightforward to calculate the *bulk modulus* (reciprocal compressibility),²⁴

$$K \equiv -V \left(\frac{\partial P}{\partial V} \right)_T = \frac{2}{3} \varepsilon_F \frac{N}{V}, \quad (3.58)$$

which may be simpler to measure experimentally than P .

Perhaps the most important example²⁵ of the degenerate Fermi gas is the *conduction electrons* in metals – the electrons that belong to outer shells of the isolated atoms but become shared in solid metals, and as a result, can move through the crystal lattice almost freely. Though the electrons (which are fermions with spin $s = 1/2$ and hence with the spin degeneracy $g = 2s + 1 = 2$) are negatively charged, the Coulomb interaction of the conduction electrons with each other is substantially compensated by the positively charged ions of the atomic lattice, so that they follow the simple model discussed above, in which the interaction is disregarded, reasonably well. This is especially true for alkali metals (forming Group 1 of the periodic table of elements), whose experimentally measured Fermi surfaces are spherical within 1% – even within 0.1% for Na.

Table 1 lists, in particular, the experimental values of the bulk modulus for such metals, together with the values given by Eq. (58) using the ε_F calculated from Eq. (55) with the experimental density of the conduction electrons. The agreement is pretty impressive, taking into account that the simple theory

²⁴ For a general discussion of this notion, see, e.g., CM Eqs. (7.32) and (7.36).

²⁵ Recently, nearly degenerate gases (with $\varepsilon_F \sim 5T$) have been formed of weakly interacting Fermi atoms as well – see, e.g., K. Aikawa *et al.*, *Phys. Rev. Lett.* **112**, 010404 (2014), and references therein. Another interesting example of the system that may be approximately treated as a degenerate Fermi gas is the set of $Z \gg 1$ electrons in a heavy atom. However, in this system the account of electron interaction via the electrostatic field they create is important. Since for this *Thomas-Fermi model* of atoms, the thermal effects are unimportant, it was discussed already in the quantum-mechanical part of this series (see QM Chapter 8). However, its analysis may be streamlined using the notion of the chemical potential, introduced only in this course – the problem left for the reader's exercise.

described above completely ignores the Coulomb and exchange interactions of the electrons. This agreement implies that, surprisingly, the experimentally observed rigidity of solids (or at least metals) is predominantly due to the kinetic energy (3) of the conduction electrons, rather than any electrostatic interactions – though, to be fair, these interactions are the crucial factor defining the equilibrium value of n . Numerical calculations using more accurate approximations (e.g., the Density Functional Theory²⁶), which agree with experiment with a few-percent accuracy, confirm this conclusion.²⁷

Table 3.1. Experimental and theoretical parameters of electrons' Fermi sea in some alkali metals²⁸

Metal	ε_F (eV) Eq. (55)	K (GPa) Eq. (58)	K (GPa) experiment	γ (mcal/mole-K ²) Eq. (69)	γ (mcal/mole-K ²) experiment
Na	3.24	923	642	0.26	0.35
K	2.12	319	281	0.40	0.47
Rb	1.85	230	192	0.46	0.58
Cs	1.59	154	143	0.53	0.77

Looking at the values of ε_F listed in this table, note that room temperatures ($T_K \sim 300$ K) correspond to $T \sim 25$ meV. As a result, virtually all experiments with metals, at least in their solid or liquid form, are performed in the limit $T \ll \varepsilon_F$. According to Eq. (39), at such temperatures, the occupancy step described by the Fermi-Dirac distribution has a non-zero but relatively small width of the order of T – see the dashed line in Fig. 2a. Calculations for this case are much facilitated by the so-called *Sommerfeld expansion formula*²⁹ for the integrals like those in Eqs. (41) and (52):

$$I(T) \equiv \int_0^\infty \varphi(\varepsilon) \langle N(\varepsilon) \rangle d\varepsilon \approx \int_0^\mu \varphi(\varepsilon) d\varepsilon + \frac{\pi^2}{6} T^2 \frac{d\varphi(\mu)}{d\mu}, \quad \text{for } T \ll \mu, \quad (3.59)$$

Sommerfeld expansion

where $\varphi(\varepsilon)$ is an arbitrary function that is sufficiently smooth at $\varepsilon = \mu$ and integrable at $\varepsilon = 0$. To prove this formula, let us introduce another function,

$$f(\varepsilon) \equiv \int_0^\varepsilon \varphi(\varepsilon') d\varepsilon', \quad \text{so that } \varphi(\varepsilon) = \frac{df(\varepsilon)}{d\varepsilon}, \quad (3.60)$$

and work out the integral $I(T)$ by parts:

$$I(T) \equiv \int_0^\infty \frac{df(\varepsilon)}{d\varepsilon} \langle N(\varepsilon) \rangle d\varepsilon = \int_{\varepsilon=0}^{\varepsilon=\infty} \langle N(\varepsilon) \rangle df$$

²⁶ See, e.g., QM Sec. 8.4.

²⁷ Note also a huge difference between the very high bulk modulus of metals ($K \sim 10^{11}$ Pa) and its very low values in usual, atomic gases (for them, at ambient conditions, $K \sim 10^5$ Pa). About four orders of magnitude of this difference is due to that in the particle density N/V , but the balance is due to the electron gas' degeneracy. Indeed, in an ideal classical gas, $K = P = T(N/V)$, so that the factor $(2/3)\varepsilon_F$ in Eq. (58), of the order of a few eV in metals, should be compared with the factor $T \approx 25$ meV in the classical gas at room temperature.

²⁸ Data from N. Ashcroft and N. D. Mermin, *Solid State Physics*, W. B. Saunders, 1976.

²⁹ Named after Arnold Sommerfeld, who was the first (in 1927) to apply quantum mechanics to degenerate Fermi gases, in particular to electrons in metals, and may be credited for most of the results discussed in this section.

$$= \left[\langle N(\varepsilon) \rangle f(\varepsilon) \right]_{\varepsilon=0}^{\varepsilon=\infty} - \int_{\varepsilon=0}^{\varepsilon=\infty} f(\varepsilon) d\langle N(\varepsilon) \rangle = \int_0^{\infty} f(\varepsilon) \left[-\frac{\partial \langle N(\varepsilon) \rangle}{\partial \varepsilon} \right] d\varepsilon. \quad (3.61)$$

As evident from Eq. (2.115) and/or Fig. 2a, at $T \ll \mu$ the function $-\partial \langle N(\varepsilon) \rangle / \partial \varepsilon$ is close to zero for all energies, besides a narrow peak of the unit area, at $\varepsilon \approx \mu$. Hence, if we expand the function $f(\varepsilon)$ in the Taylor series near this point, just a few leading terms of the expansion should give us a good approximation:

$$\begin{aligned} I(T) &\approx \int_0^{\infty} \left[f(\mu) + \frac{df}{d\varepsilon} \Big|_{\varepsilon=\mu} (\varepsilon - \mu) + \frac{1}{2} \frac{d^2 f}{d\varepsilon^2} \Big|_{\varepsilon=\mu} (\varepsilon - \mu)^2 \right] \left[-\frac{\partial \langle N(\varepsilon) \rangle}{\partial \varepsilon} \right] d\varepsilon \\ &= \int_0^{\mu} \varphi(\varepsilon') d\varepsilon' \int_0^{\infty} \left(-\frac{\partial \langle N(\varepsilon) \rangle}{\partial \varepsilon} \right) d\varepsilon + \varphi(\mu) \int_0^{\infty} (\varepsilon - \mu) \left[-\frac{\partial \langle N(\varepsilon) \rangle}{\partial \varepsilon} \right] d\varepsilon \\ &\quad + \frac{1}{2} \frac{d\varphi(\mu)}{d\mu} \int_0^{\infty} (\varepsilon - \mu)^2 \left[-\frac{\partial \langle N(\varepsilon) \rangle}{\partial \varepsilon} \right] d\varepsilon. \end{aligned} \quad (3.62)$$

In the last form of this relation, the first integral over ε equals $\langle N(\varepsilon=0) \rangle - \langle N(\varepsilon=\infty) \rangle = 1$, the second one vanishes (because the function under it is antisymmetric with respect to the point $\varepsilon = \mu$), and only the last one needs to be dealt with explicitly, by working it out by parts and then using a table integral:³⁰

$$\int_0^{\infty} (\varepsilon - \mu)^2 \left[-\frac{\partial \langle N(\varepsilon) \rangle}{\partial \varepsilon} \right] d\varepsilon \approx T^2 \int_{-\infty}^{+\infty} \xi^2 \frac{d}{d\xi} \left(-\frac{1}{e^\xi + 1} \right) d\xi = 4T^2 \int_0^{+\infty} \frac{\xi d\xi}{e^\xi + 1} = 4T^2 \frac{\pi^2}{12}. \quad (3.63)$$

Being plugged into Eq. (62), this result proves the Sommerfeld formula (59).

The last preparatory step we need to make is to account for a possible small difference (as we will see below, also proportional to T^2) between the temperature-dependent chemical potential $\mu(T)$ and the Fermi energy defined as $\varepsilon_F \equiv \mu(0)$, in the largest (first) term on the right-hand side of Eq. (59), to write

$$I(T) \approx \int_0^{\varepsilon_F} \varphi(\varepsilon) d\varepsilon + (\mu - \varepsilon_F) \varphi(\mu) + \frac{\pi^2}{6} T^2 \frac{d\varphi(\mu)}{d\mu} \equiv I(0) + (\mu - \varepsilon_F) \varphi(\mu) + \frac{\pi^2}{6} T^2 \frac{d\varphi(\mu)}{d\mu}. \quad (3.64)$$

Now, applying this formula to Eq. (41) and the last form of Eq. (52), we get the following results (which are valid for any dispersion law $\varepsilon(\mathbf{p})$ and even any dimensionality of the gas):

$$N(T) = N(0) + (\mu - \varepsilon_F) g(\mu) + \frac{\pi^2}{6} T^2 \frac{dg(\mu)}{d\mu}, \quad (3.65)$$

$$E(T) = E(0) + (\mu - \varepsilon_F) \mu g(\mu) + \frac{\pi^2}{6} T^2 \frac{d}{d\mu} [\mu g(\mu)]. \quad (3.66)$$

If the number of particles does not change with temperature, $N(T) = N(0)$, as in most experiments, Eq. (65) gives the following formula for finding the temperature-induced change of μ :

³⁰ See, e.g., MA Eqs. (6.8c) and (2.12b), with $n = 1$.

$$\mu - \varepsilon_F = -\frac{\pi^2}{6} T^2 \frac{1}{g(\mu)} \frac{dg(\mu)}{d\mu}. \quad (3.67)$$

Note that the change is quadratic in T and negative, in agreement with the numerical results shown with the red line in Fig. 1. Plugging this expression (which is only valid when the magnitude of the change is much smaller than ε_F) into Eq. (66), we get the following temperature correction to the energy:

$$E(T) - E(0) = \frac{\pi^2}{6} g(\mu) T^2, \quad (3.68)$$

where within the accuracy of our approximation, μ may be replaced with ε_F . (Due to the universal relation (48), this result also gives the temperature correction to the Fermi gas' pressure.) Now we may use Eq. (68) to calculate the heat capacity of the degenerate Fermi gas:

Low-T
heat
capacity

$$C_V \equiv \left(\frac{\partial E}{\partial T} \right)_V = \gamma T, \quad \text{with } \gamma = \frac{\pi^2}{3} g(\varepsilon_F). \quad (3.69)$$

According to Eq. (55b), in the particular case of a 3D gas with the isotropic and parabolic dispersion law (3), Eq. (69) reduces to

$$\gamma = \frac{\pi^2}{2} \frac{N}{\varepsilon_F}, \quad \text{i.e. } c_V \equiv \frac{C_V}{N} = \frac{\pi^2}{2} \frac{T}{\varepsilon_F} \ll 1. \quad (3.70)$$

This important result deserves a discussion. First, note that within the range of validity of the Sommerfeld approximation ($T \ll \varepsilon_F$), the specific heat of the degenerate gas is much smaller than that of the classical gas, even without internal degrees of freedom: $c_V = 3/2$ – see Eq. (19). The physical reason for such a low heat capacity is that the particles deep inside the Fermi sea cannot pick up thermal excitations with available energies of the order of $T \ll \varepsilon_F$, because the states immediately above them are already occupied. The only particles (or rather quantum states, due to the particle indistinguishability) that may be excited with such small energies are those at the Fermi surface, more exactly within a surface layer of thickness $\Delta\varepsilon \sim T \ll \varepsilon_F$, and Eq. (70) presents a very vivid manifestation of this fact.

The second important feature of Eqs. (69)-(70) is the linear dependence of the heat capacity on temperature, which decreases with a reduction of T much slower than that of crystal vibrations – see Eq. (2.99). This means that in metals the specific heat at temperatures $T \ll T_D$ is dominated by the conduction electrons. Indeed, experiments confirm not only the linear dependence (70) of the specific heat,³¹ but also the values of the proportionality coefficient $\gamma \equiv C_V/T$ for cases when ε_F can be calculated independently, for example for alkali metals – see the two rightmost columns of Table 1 above. More typically, Eq. (69) is used for the experimental measurement of the density of states on the Fermi surface, $g(\varepsilon_F)$ – the factor which participates in many theoretical results, in particular in transport properties of degenerate Fermi gases (see Chapter 6 below).

³¹ Solids, with their low thermal expansion coefficients, provide a virtually-fixed-volume confinement for the electron gas, so that the specific heat measured at ambient conditions may be legitimately compared with the calculated c_V .

3.4. Bose-Einstein condensation

Now let us explore what happens at the cooling of an ideal gas of bosons. Figure 3a shows the same plot as Fig. 1b, i.e. the result of a numerical solution of Eq. (47) with the appropriate (lower) sign in the denominator, on a more appropriate, log-log scale. One can see that the chemical potential μ indeed tends to zero at some finite “critical temperature” T_c . This temperature may be found by taking $\mu = 0$ in Eq. (47), reducing it to a table integral:³²

$$T_c = T_0 \left[\frac{1}{\sqrt{2\pi^2}} \int_0^\infty \frac{\xi^{1/2} d\xi}{e^\xi - 1} \right]^{-2/3} = T_0 \left[\frac{1}{\sqrt{2\pi^2}} \Gamma\left(\frac{3}{2}\right) \zeta\left(\frac{3}{2}\right) \right]^{-2/3} \approx 3.313 T_0, \quad (3.71)$$

BEC:
critical
temperature

the result explaining the T_c/T_0 ratio mentioned in Sec. 2 and indicated in Fig. 1.

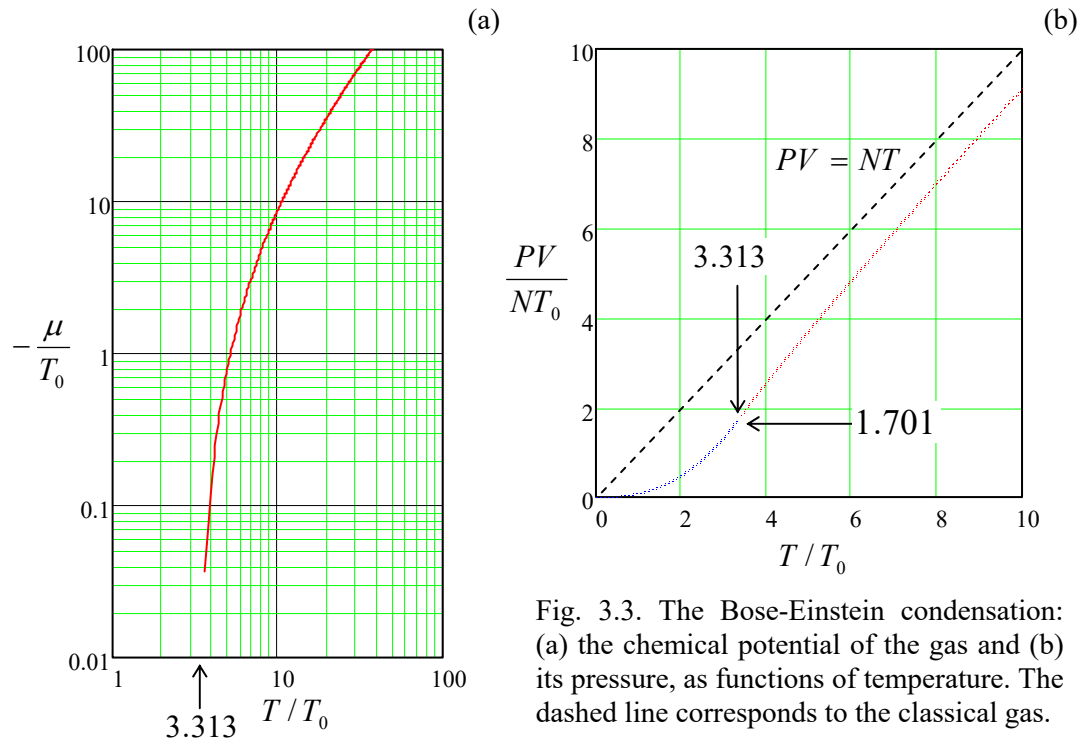


Fig. 3.3. The Bose-Einstein condensation: (a) the chemical potential of the gas and (b) its pressure, as functions of temperature. The dashed line corresponds to the classical gas.

Let us have a good look at the temperature interval $0 < T < T_c$, which cannot be directly described by Eq. (40) (with the appropriate negative sign in the denominator), and hence may look rather mysterious. Indeed, within this range, the chemical potential μ , cannot either be negative or equal zero, because according to Eq. (71), in this case, Eq. (40) would give a value of N smaller than the number of particles we actually have. On the other hand, μ cannot be positive either, because the integral (40) would diverge at $\varepsilon \rightarrow \mu$ due to the divergence of $\langle N(\varepsilon) \rangle$ – see, e.g., Fig. 2.15. The only possible resolution of the paradox, suggested by A. Einstein in 1925, is as follows: at $T < T_c$, the chemical potential of each particle of the system still equals exactly zero, but a certain number (N_0 of N) of them are in the ground state (with $\varepsilon \equiv p^2/2m = 0$), forming the so-called *Bose-Einstein condensate*, usually referred to as the BEC. Since the condensate particles do not contribute to Eq. (40) (because of

³² See, e.g., MA Eq. (6.8b) with $s = 3/2$, and then Eqs. (2.7b) and (6.7e).

the factor $\varepsilon^{1/2} = 0$), their number N_0 may be calculated by using that formula (or, equivalently, Eq. (44)), with $\mu = 0$, to find the number $(N - N_0)$ of particles still remaining in the gas, i.e. having energy $\varepsilon > 0$:

$$N - N_0 = \frac{gV(mT)^{3/2}}{\sqrt{2\pi^2\hbar^3}} \int_0^\infty \frac{\xi^{1/2} d\xi}{e^\xi - 1}. \quad (3.72)$$

This result is even simpler than it may look. Indeed, let us write it for the case $T = T_c$, when $N_0 = 0$:³³

$$N = \frac{gV(mT_c)^{3/2}}{\sqrt{2\pi^2\hbar^3}} \int_0^\infty \frac{\xi^{1/2} d\xi}{e^\xi - 1}. \quad (3.73)$$

Dividing both sides of Eqs. (72) and (73), we get an extremely simple and elegant result:

$$\frac{N - N_0}{N} = \left(\frac{T}{T_c} \right)^{3/2}, \quad \text{so that } N_0 = N \left[1 - \left(\frac{T}{T_c} \right)^{3/2} \right], \quad \text{for } T \leq T_c. \quad (3.74a)$$

Please note that this result is only valid for the particles whose motion, within the volume V , is free – in other words, for a system of free particles confined within a rigid-wall box of volume V . In most experiments with the Bose-Einstein condensation of dilute gases of neutral (and hence very weakly interacting) atoms, they are held not in such a box, but at the bottom of a “soft” potential well, which may be well approximated by a 3D quadratic parabola: $U(\mathbf{r}) = m\omega^2 r^2/2$. It is straightforward (and hence left for the reader’s exercise) to show that in this case, the dependence of $N_0(T)$ is somewhat different:

$$N_0 = N \left[1 - \left(\frac{T}{T_c^*} \right)^3 \right], \quad \text{for } T \leq T_c^*, \quad (3.74b)$$

where T_c^* is a different critical temperature, which now depends on $\hbar\omega$, i.e. on the confining potential’s “steepness”. (In this case, V is not exactly fixed; however, the effective volume occupied by the particles at $T = T_c^*$ is related to this temperature by a formula close to Eq. (71), so that all estimates given above are still valid.) Figure 4 shows one of the first sets of experimental data for the Bose-Einstein condensation of a dilute gas of neutral atoms. Taking into account the finite number of particles in the experiment, the agreement with the simple theory is surprisingly good.

Returning to the spatially-uniform Bose system, let us explore what happens below the critical temperature with its other parameters. Formula (52) with the appropriate (lower) sign shows that approaching T_c from higher temperatures, the gas energy and hence its pressure do not vanish – see the red line in Fig. 3b. Indeed, at $T = T_c$ (where $\mu = 0$), that formula yields³⁴

$$E(T_c) = gV \frac{m^{3/2} T_c^{5/2}}{\sqrt{2\pi^2\hbar^3}} \int_0^\infty \frac{\xi^{3/2} d\xi}{e^\xi - 1} = gV \frac{m^{3/2} T_c^{5/2}}{\sqrt{2\pi^2\hbar^3}} \Gamma\left(\frac{5}{2}\right) \zeta\left(\frac{5}{2}\right) \approx 0.7701 NT_c, \quad (3.75)$$

so that using the universal relation (48), we get the pressure value,

$$P(T_c) = \frac{2}{3} \frac{E(T_c)}{V} = \frac{\zeta(5/2)}{\zeta(3/2)} \frac{N}{V} T_c \approx 0.5134 \frac{N}{V} T_c \approx 1.701 P_0, \quad (3.76)$$

³³ This is, of course, just another form of Eq. (71).

³⁴ For the involved dimensionless integral see, e.g., MA Eqs. (6.8b) with $s = 5/2$, and then (2.7b) and (6.7c).

which is somewhat lower than, but comparable to $P(0)$ for the fermions – cf. Eq. (57).

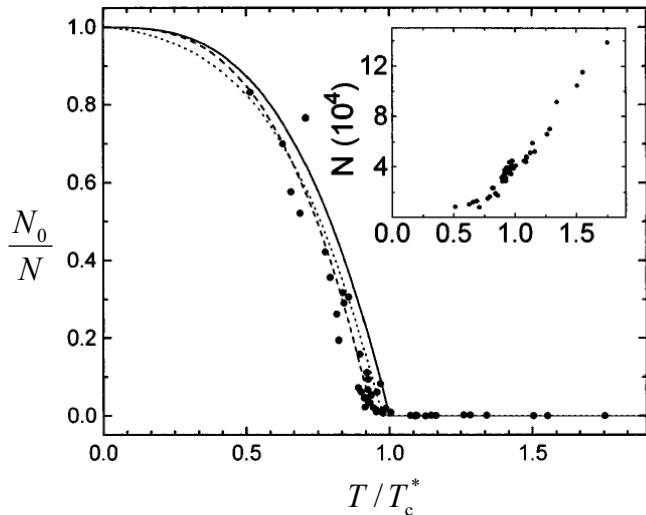


Fig. 3.4. The total number N of trapped ^{87}Rb atoms (inset) and their ground-state fraction N_0/N , as functions of the ratio T/T_c , as measured in one of the pioneering experiments – see J. Ensher *et al.*, *Phys. Rev. Lett.* **77**, 4984 (1996). In this experiment, T_c^* was as low as 0.28×10^{-6} K. The solid line shows the simple theoretical dependence $N(T)$ given by Eq. (74b), while other lines correspond to more detailed theories taking into account the finite number N of trapped atoms. © 1996 APS, reproduced with permission.

Now we can use the same Eq. (52), also with $\mu = 0$, to calculate the energy of the gas at $T < T_c$,

$$E(T) = gV \frac{m^{3/2} T^{5/2}}{\sqrt{2\pi^2 \hbar^3}} \int_0^\infty \frac{\xi^{3/2} d\xi}{e^\xi - 1}. \quad (3.77)$$

Comparing this relation with the first form of Eq. (75), which features the same integral, we immediately get one more simple temperature dependence:

$$E(T) = E(T_c) \left(\frac{T}{T_c} \right)^{5/2}, \quad \text{for } T \leq T_c. \quad (3.78)$$

BEC:
energy

From the universal relation (48), we immediately see that the gas pressure follows the same dependence:

$$P(T) = P(T_c) \left(\frac{T}{T_c} \right)^{5/2}, \quad \text{for } T \leq T_c. \quad (3.79)$$

BEC:
pressure

This temperature dependence of pressure is shown with the blue line in Fig. 3b. The plot shows that for all temperatures (both below and above T_c) the pressure is lower than that of the classical gas of the same density. Now note also that since, according to Eqs. (57) and (76), $P(T_c) \propto P_0 \propto V^{5/3}$, while according to Eqs. (35) and (71), $T_c \propto T_0 \propto V^{2/3}$, the pressure (79) is proportional to $V^{5/3}/(V^{2/3})^{5/2} = V^0$, i.e. does not depend on the volume at all! The physics of this result (which is valid at $T < T_c$ only) is that as we decrease the volume at a fixed total number N of particles, more and more of them go to the condensate, decreasing the number $(N - N_0)$ of particles in the gas phase, but not changing its spatial density pressure. Such behavior is very typical for the coexistence of two different phases of the same matter – see, in particular, the next chapter.

The last thermodynamic variable of major interest is heat capacity, because it may be most readily measured. For temperatures $T \leq T_c$, it may be easily calculated from Eq. (78):

$$C_V(T) \equiv \left(\frac{\partial E}{\partial T} \right)_{N,V} = E(T_c) \frac{5}{2} \frac{T^{3/2}}{T_c^{5/2}}, \quad (3.80)$$

so that below T_c , the capacity *increases* with temperature, at the critical temperature reaching the value

$$C_V(T_c) = \frac{5}{2} \frac{E(T_c)}{T_c} \approx 1.925 N, \quad (3.81)$$

which is approximately 28% above that ($3N/2$) of the classical gas. (As a reminder, in both cases we ignore possible contributions from the internal degrees of freedom.) The analysis for $T \geq T_c$ is a little bit more cumbersome because differentiating E over temperature – say, using Eq. (52) – one should also take into account the temperature dependence of μ that follows from Eq. (40) – see also Fig. 1. However, the most important feature of the result may be predicted without the calculation (which is being left for the reader's exercise). Namely, since at $T \gg T_c$ the heat capacity has to approach the classical value $1.5N$, starting from the value (81), it must *decrease* with temperature at $T > T_c$, thus forming a sharp maximum (a “cusp”) at the critical point $T = T_c$ – see Fig. 5.

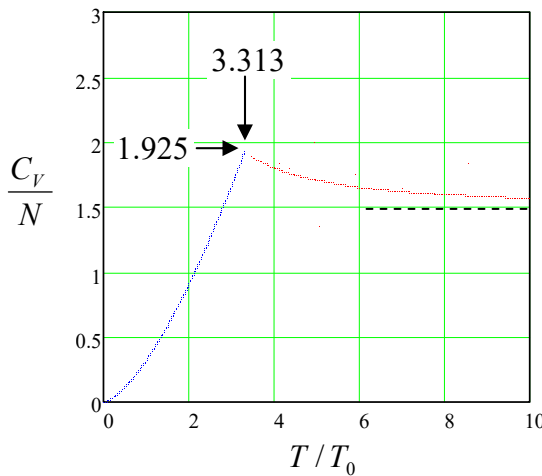


Fig. 3.5. Temperature dependences of the heat capacity of an ideal Bose-Einstein gas, numerically calculated from Eqs. (52) and (40) for $T \geq T_c$, and given by Eq. (80) for $T \leq T_c$.

Such a cusp is a good indication of the Bose-Einstein condensation in virtually any experimental system, especially because inter-particle interactions (unaccounted for in our simple discussion) typically make this feature even more substantial, frequently turning it into a weak (logarithmic) singularity. Historically, such a singularity was the first noticed, though not immediately understood sign of the Bose-Einstein condensation, observed in 1931 by W. Keesom and K. Clusius in liquid ^4He at its λ -point (called so exactly because of the characteristic shape of the $C_V(T)$ dependence) $T = T_c \approx 2.17$ K. Other milestones of the Bose-Einstein condensation studies include:

- the experimental discovery of superconductivity (which was later explained as the result of the Bose-Einstein condensation of electron pairs) by H. Kamerlingh-Onnes in 1911;
- the development of the Bose-Einstein statistics, and predicting the condensation, by S. Bose and A. Einstein, in 1924-1925;
- the discovery of superfluidity in liquid ^4He by P. Kapitza and (independently) by J. Allen and D. Misener in 1937, and its explanation as a result of the Bose-Einstein condensation by F. and H. Londons and L. Titza, with further significant elaborations by L. Landau – all in 1938;
- the explanation of superconductivity as a result of electron binding into *Cooper pairs*, with a simultaneous Bose-Einstein condensation of the resulting bosons, by J. Bardeen, L. Cooper, and J. Schrieffer in 1957;

- the discovery of superfluidity of two different phases of ^3He , due to the similar Bose-Einstein condensation of pairs of its fermion atoms, by D. Lee, D. Osheroff, and R. Richardson in 1972;

- the first observation of the Bose-Einstein condensation in dilute gases (^{87}Ru by E. Cornell, C. Wieman, *et al.*, and ^{23}Na by W. Ketterle *et al.*) in 1995.

The importance of the last achievement stems from the fact that in contrast to other Bose-Einstein condensates, in dilute gases (with the typical density n as low as $\sim 10^{14} \text{ cm}^{-3}$) the particles interact very weakly, and hence many experimental results are very close to the simple theory described above and its straightforward elaborations – see, e.g., Fig. 4.³⁵ On the other hand, the importance of other Bose-Einstein condensates, which involve more complex and challenging physics, should not be underestimated – as it sometimes is.

Perhaps the most important feature of any Bose-Einstein condensate is that all N_0 condensed particles are in the same quantum state, and hence are described by exactly the same wavefunction. This wavefunction is substantially less “feeble” than that of a single particle – in the following sense. In the second quantization language,³⁶ the well-known Heisenberg’s uncertainty relation may be rewritten for the creation/annihilation operators; in particular, for bosons,

$$|\delta\hat{a}\delta\hat{a}^\dagger| \geq 1. \quad (3.82)$$

Since \hat{a} and \hat{a}^\dagger are the quantum-mechanical operators of the complex amplitude $a = A\exp\{i\varphi\}$ and its complex conjugate $a^* = A\exp\{-i\varphi\}$, where A and φ are real amplitude and phase of the wavefunction, Eq. (82) yields the following approximate uncertainty relation (strict in the limit $\delta\varphi \ll 1$) between the number of particles $N = AA^*$ and the phase φ :

$$\delta N \delta\varphi \geq \frac{1}{2}. \quad (3.83)$$

This means that a condensate of $N \gg 1$ bosons may be in a state with both phase and amplitude of the wavefunction behaving virtually as *c*-numbers, with very small relative uncertainties: $\delta N \ll N$, $\delta\varphi \ll 1$. Moreover, such states are much less susceptible to perturbations by experimental instruments. For example, the electric current carried along a superconducting wire by a coherent Bose-Einstein condensate of Cooper pairs may be as high as hundreds of amperes. As a result, the “strange” behaviors predicted by the quantum mechanics are not averaged out as in the usual particle ensembles (see, e.g., the discussion of the density matrix in Sec. 2.1), but may be directly revealed in macroscopic, measurable dynamics of the condensate.

For example, the density \mathbf{j} of the electric “supercurrent” of the Cooper pairs may be described by the same formula as the well-known usual probability current density of a single quantum particle,³⁷ just multiplied by the electric charge $q = -2e$ of a single pair, and the pair density n :

³⁵ Such controllability of theoretical description has motivated the use of dilute-gas BECs for modeling of renowned problems of many-body physics – see, e.g. the review by I. Bloch *et al.*, *Rev. Mod. Phys.* **80**, 885 (2008). These efforts are assisted by the development of better techniques for reaching the necessary sub- μK temperatures – see, e.g., the recent work by J. Hu *et al.*, *Science* **358**, 1078 (2017). For a more general, detailed discussion see, e.g., C. Pethick and H. Smith, *Bose-Einstein Condensation in Dilute Gases*, 2nd ed., Cambridge U. Press, 2008.

³⁶ See, e.g., QM Sec. 8.3.

³⁷ See, e.g., QM Eq. (3.28).

$$\mathbf{j} = qn \frac{\hbar}{m} \left(\nabla \varphi - \frac{q}{\hbar} \mathbf{A} \right), \quad (3.84)$$

where \mathbf{A} is the vector potential of the (electro)magnetic field. If a superconducting wire is not extremely thin, the supercurrent does not penetrate into its interior.³⁸ As a result, the integral of Eq. (84), taken along a closed superconducting loop, inside its interior (where $\mathbf{j} = 0$), yields

$$\frac{q}{\hbar} \oint_C \mathbf{A} \cdot d\mathbf{r} = \Delta\varphi = 2\pi M, \quad (3.85)$$

where M is an integer. But, according to the basic electrodynamics, the integral on the left-hand side of this relation is nothing more than the flux Φ of the magnetic field \mathcal{B} piercing the wire loop area A . Thus we immediately arrive at the famous *magnetic flux quantization* effect:

$$\Phi \equiv \int_A \mathcal{B}_n d^2 r = M\Phi_0, \quad \text{where } \Phi_0 \equiv \frac{2\pi\hbar}{|q|} \approx 2.07 \times 10^{-15} \text{ Wb}, \quad (3.86)$$

which was theoretically predicted in 1950 and experimentally observed in 1961. Amazingly, this effect holds even “over miles of dirty lead wire”, citing H. Casimir’s famous expression, sustained by the coherence of the Bose-Einstein condensate of Cooper pairs.

Other prominent examples of such *macroscopic quantum effects* in Bose-Einstein condensates include not only the superfluidity and superconductivity as such, but also the Josephson effect, quantized Abrikosov vortices, etc. Some of these effects are briefly discussed in other parts of this series.³⁹

3.5. Gases of weakly interacting particles

Now let us discuss the effects of weak particle interaction effects on properties of their gas. (Unfortunately, I will have time to do that only very briefly, and only for classical gases.⁴⁰) In most cases of interest, particle interaction may be well described by a certain potential energy U , so that in the simplest model, the total energy is

$$E = \sum_{k=1}^N \frac{p_k^2}{2m} + U(\mathbf{r}_1, \dots, \mathbf{r}_j, \dots, \mathbf{r}_N), \quad (3.87)$$

where \mathbf{r}_k is the radius-vector of the k^{th} particle’s center.⁴¹ First, let us see how far would the statistical physics allow us to proceed for an arbitrary potential U . For $N \gg 1$, at the calculation of the Gibbs statistical sum (2.59), we may perform the usual transfer from the summation over all quantum states of the system to the integration over the $6N$ -dimensional space, with the correct Boltzmann counting:

³⁸ This is the *Meissner-Ochsenfeld* (or just “Meissner”) effect which may be also readily explained using Eq. (84) combined with the Maxwell equations – see, e.g., EM Sec. 6.4.

³⁹ See EM Secs. 6.4-6.5, and QM Secs. 1.6 and 3.1.

⁴⁰ A concise discussion of the effects of weak interactions on the properties of *quantum* gases may be found, for example, in Chapter 10 of the textbook by K. Huang, *Statistical Mechanics*, 2nd ed., Wiley, 2003.

⁴¹ One of the most significant effects *neglected* by Eq. (87) is the influence of atomic/molecular angular orientations on their interactions.

$$\begin{aligned}
Z = \sum_m e^{-E_m/T} &\rightarrow \frac{1}{N!} \frac{g^N}{(2\pi\hbar)^{3N}} \int \exp \left\{ -\sum_{k=1}^N \frac{p_j^2}{2mT} \right\} d^3 p_1 \dots d^3 p_N \int \exp \left\{ -\frac{U(\mathbf{r}_1, \dots, \mathbf{r}_N)}{T} \right\} d^3 r_1 \dots d^3 r_N \\
&\equiv \left(\frac{1}{N!} \frac{g^N V^N}{(2\pi\hbar)^{3N}} \int \exp \left\{ -\sum_{k=1}^N \frac{p_j^2}{2mT} \right\} d^3 p_1 \dots d^3 p_N \right) \times \left(\frac{1}{V^N} \int \exp \left\{ -\frac{U(\mathbf{r}_1, \dots, \mathbf{r}_N)}{T} \right\} d^3 r_1 \dots d^3 r_N \right).
\end{aligned} \tag{3.88}$$

But according to Eq. (14), the first operand in the last product is just the statistical sum of an ideal gas (with the same g , N , V , and T), so that we may use Eq. (2.63) to write

$$F = F_{\text{ideal}} - T \ln \left[\frac{1}{V^N} \int d^3 r_1 \dots d^3 r_N e^{-U/T} \right] \equiv F_{\text{ideal}} - T \ln \left[1 + \frac{1}{V^N} \int d^3 r_1 \dots d^3 r_N (e^{-U/T} - 1) \right], \tag{3.89}$$

where F_{ideal} is the free energy of the ideal gas (i.e. the same gas but with $U=0$), given by Eq. (16).

I believe that Eq. (89) is a very convincing demonstration of the enormous power of statistical physics methods. Instead of trying to solve an impossibly complex problem of classical dynamics of $N \gg 1$ (think of $N \sim 10^{23}$) interacting particles, and only then calculating appropriate ensemble averages, the Gibbs approach reduces finding the free energy (and then, from thermodynamic relations, all other thermodynamic variables) to the calculation of just one integral on its right-hand side of Eq. (89). Still, this integral is $3N$ -dimensional and may be worked out analytically only if the particle interactions are weak in some sense. Indeed, the last form of Eq. (89) makes it especially evident that if $U \rightarrow 0$ everywhere, the term in the parentheses under the integral vanishes, and so does the integral itself, and hence the addition to F_{ideal} .

Now let us see what would this integral yield for the simplest, *short-range* interactions, in which the potential U is substantial only when the mutual distance $\mathbf{r}_{kk'} \equiv \mathbf{r}_k - \mathbf{r}_{k'}$ between the centers of two particles is smaller than certain value $2r_0$, where r_0 may be interpreted as the particle's radius. If the gas is sufficiently dilute, so that the radius r_0 is much smaller than the average distance r_{ave} between the particles, the integral in the last form of Eq. (89) is of the order of $(2r_0)^{3N}$, i.e. much smaller than $(r_{\text{ave}})^{3N} = V^N$. Then we may expand the logarithm in that expression into the Taylor series with respect to the small second term in the square brackets, and keep only its first non-zero term:

$$F \approx F_{\text{ideal}} - \frac{T}{V^N} \int d^3 r_1 \dots d^3 r_N (e^{-U/T} - 1). \tag{3.90}$$

Moreover, if the gas density is so low, the chances for three or more particles to come close to each other and interact (collide) simultaneously are typically very small, so that *pair collisions* are the most important. In this case, we may recast the integral in Eq. (90) as a sum of $N(N-1)/2 \approx N^2/2$ similar terms describing such pair interactions, each of the type

$$V^{N-2} \int (e^{-U(\mathbf{r}_{kk'})/T} - 1) d^3 r_k d^3 r_{k'}. \tag{3.91}$$

It is convenient to think about the $\mathbf{r}_{kk'} \equiv \mathbf{r}_k - \mathbf{r}_{k'}$ as the radius-vector of the particle number k in the reference frame with the origin placed at the center of the particle number k' – see Fig. 6a.

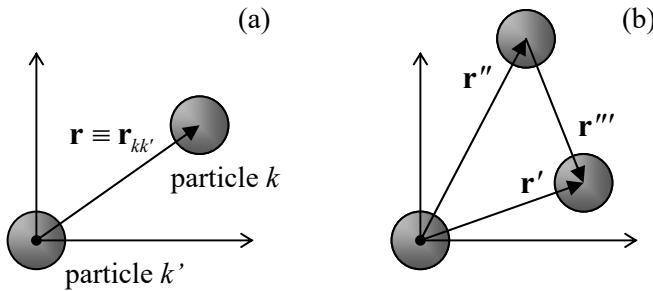


Fig. 3.6. The definition of the interparticle distance vectors at their (a) pair and (b) triple interactions.

Then in Eq. (91), we may first calculate the integral over \mathbf{r}_k , while keeping the distance vector $\mathbf{r}_{kk'}$, and hence $U(\mathbf{r}_{kk'})$, constant, getting one more factor V . Moreover, since all particle pairs are similar, in the remaining integral over $\mathbf{r}_{kk'}$ we may drop the radius-vector's index, so that Eq. (90) becomes

$$F = F_{\text{ideal}} - \frac{T}{V^N} \frac{N^2}{2} V^{N-1} \int (e^{-U(\mathbf{r})/T} - 1) d^3 r \equiv F_{\text{ideal}} + \frac{T}{V} N^2 B(T), \quad (3.92)$$

where the function $B(T)$, called the *second virial coefficient*,⁴² has an especially simple form for spherically-symmetric interactions:

Second
virial
coefficient

$$B(T) \equiv \frac{1}{2} \int (1 - e^{-U(\mathbf{r})/T}) d^3 r \rightarrow \frac{1}{2} \int_0^\infty 4\pi r^2 dr (1 - e^{-U(r)/T}). \quad (3.93)$$

From Eq. (92), and the second of the thermodynamic relations (1.35), we already know something particular about the equation of state $P(V, T)$:

$$P = -\left(\frac{\partial F}{\partial V}\right)_{T,N} = P_{\text{ideal}} + \frac{N^2 T}{V^2} B(T) = T \left[\frac{N}{V} + B(T) \frac{N^2}{V^2} \right]. \quad (3.94)$$

We see that at a fixed gas density $n = N/V$, the pair interaction creates additional pressure, proportional to $(N/V)^2 = n^2$ and a function of temperature, $B(T)T$.

Let us calculate $B(T)$ for a few simple models of particle interactions. The solid curve in Fig. 7 shows (schematically) a typical form of the interaction potential between electrically neutral atoms/molecules. At large distances the interaction of particles that do not have their own permanent electrical dipole moment \mathbf{p} , is dominated by the attraction (the so-called *London dispersion force*) between the correlated components of the spontaneously induced dipole moments, giving $U(r) \rightarrow r^{-6}$ at $r \rightarrow \infty$.⁴³ At closer distances the potential is repulsive, growing very fast at $r \rightarrow 0$, but its quantitative

⁴² The term “virial”, from Latin *viris* (meaning “force”), was introduced to molecular physics by R. Clausius. The motivation for the adjective “second” for $B(T)$ is evident from the last form of Eq. (94), with the “first virial coefficient”, standing before the N/V ratio and sometimes denoted $A(T)$, equal to 1 – see also Eq. (100) below.

⁴³ Indeed, independent fluctuation-induced components $\mathbf{p}(t)$ and $\mathbf{p}'(t)$ of dipole moments of two particles have random mutual orientation, so that the time average of their interaction energy, proportional to $\mathbf{p}(t) \cdot \mathbf{p}'(t)/r^3$, vanishes. However, the electric field \mathcal{E} of each dipole \mathbf{p} , proportional to r^{-3} , induces a correlated component of \mathbf{p}' , also proportional to r^{-3} , giving interaction energy proportional to $\mathbf{p}' \cdot \mathcal{E} \propto r^{-6}$, with a non-zero statistical average. Quantitative discussions of this effect, within several models, may be found, for example, in QM Chapters 3, 5, and 6.

form is specific for particular atoms/molecules.⁴⁴ The crudest description of such repulsion is given by the so-called *hardball model*:

$$U(r) = \begin{cases} +\infty, & \text{for } 0 < r < 2r_0, \\ 0, & \text{for } 2r_0 < r < \infty, \end{cases} \quad (3.95)$$

– see the dashed line and the inset in Fig. 7.

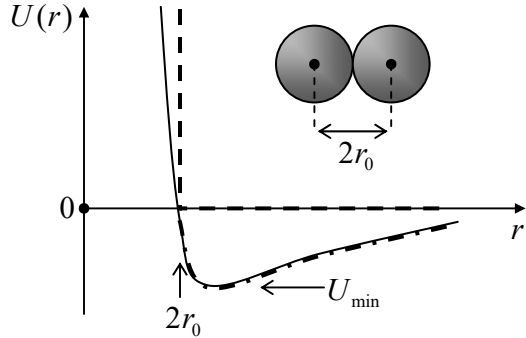


Fig. 3.7. Pair interactions of particles. Solid line: a typical interaction potential; dashed line: its hardball model (95); dash-dotted line: the improved model (97) – all schematically. The inset illustrates the hardball model’s physics.

As Eq. (93) shows, in this model the second virial coefficient is temperature-independent:

$$B(T) = b \equiv \frac{1}{2} \int_0^{2r_0} 4\pi r^2 dr = \frac{2\pi}{3} (2r_0)^3 \equiv 4V_0, \quad \text{where } V_0 \equiv \frac{4\pi}{3} r_0^3, \quad (3.96)$$

so that the equation of state (94) still gives a linear dependence of pressure on temperature.

A correction to this result may be obtained by the following approximate account of the long-range attraction (see the dash-dotted line in Fig. 7):⁴⁵

$$U(r) = \begin{cases} +\infty, & \text{for } 0 < r < 2r_0, \\ U(r), & \text{with } |U| \ll T, \quad \text{for } 2r_0 < r < \infty. \end{cases} \quad (3.97)$$

For this improved model, Eq. (93) yields:

$$B(T) = b + \frac{1}{2} \int_{2r_0}^{\infty} 4\pi r^2 dr \frac{U(r)}{T} \equiv b - \frac{a}{T}, \quad \text{with } a \equiv 2\pi \int_{2r_0}^{\infty} r^2 dr |U(r)|. \quad (3.98)$$

In this model, the equation of state (94) acquires a temperature-independent term:

⁴⁴ Note that the particular form of the first term in the approximation $U(r) = a/r^{12} - b/r^6$ (called either the *Lennard-Jones potential* or the “12-6 potential”), that had been suggested in 1924, lacks physical justification, and in professional physics was soon replaced with other approximations, including the so-called *exp-6 model*, which fits most experimental data much better. However, the Lennard-Jones potential still keeps creeping from one undergraduate textbook to another one, apparently for a not better reason than enabling a simple analytical calculation of the equilibrium distance between the particles at $T \rightarrow 0$.

⁴⁵ The strong inequality $|U| \ll T$ in this model is necessary not only to make the calculations simpler. A deeper reason is that if $(-U_{\min})$ becomes comparable with T , particles may become trapped in this potential well, forming a different phase – a liquid or a solid. In such phases, the probability of finding more than two particles interacting simultaneously is high, so that Eq. (92), on which Eqs. (93)-(94) and Eqs. (98)-(99) are based, becomes invalid.

$$P = T \left[\frac{N}{V} + \left(\frac{N}{V} \right)^2 \left(b - \frac{a}{T} \right) \right] \equiv T \left[\frac{N}{V} + b \left(\frac{N}{V} \right)^2 \right] - a \left(\frac{N}{V} \right)^2. \quad (3.99)$$

Still, the correction to the ideal-gas pressure is proportional to $(N/V)^2$ and has to be relatively small for this result to be valid.

Generally, the right-hand side of Eq. (99) may be considered as the sum of two leading terms in the general expansion of P into the Taylor series in the density $n = N/V$ of the gas:

Pressure:
virial
expansion

$$P = T \left[\frac{N}{V} + B(T) \left(\frac{N}{V} \right)^2 + C(T) \left(\frac{N}{V} \right)^3 + \dots \right], \quad (3.100)$$

where $C(T)$ is called the *third virial coefficient*. It is natural to ask how can we calculate $C(T)$ and the higher virial coefficients. This may be done, first of all, just by a careful direct analysis of Eq. (90),⁴⁶ but I would like to use this occasion to demonstrate a different, very interesting and counter-intuitive approach, called the *cluster expansion method*,⁴⁷ which allows streamlining such calculations.

Let us apply to our system, with the energy given by Eq. (87), the grand canonical distribution. (Just as in Sec. 2, we may argue that if the average number $\langle N \rangle$ of particles in a member of a grand canonical ensemble, with fixed μ and T , is much larger than 1, the relative fluctuations of N are small, so that all its thermodynamic properties should be similar to those when N is exactly fixed.) For our current case, Eq. (2.109) takes the form

$$\Omega = -T \ln \sum_{N=0}^{\infty} Z_N, \quad \text{with } Z_N \equiv e^{\mu N/T} \sum_m e^{-E_{m,N}/T}, \quad E_{m,N} = \sum_{k=1}^N \frac{p_k^2}{2m} + U(r_1, \dots, r_N). \quad (3.101)$$

(Notice that here, as at all discussions of the grand canonical distribution, N means a particular rather than the average number of particles.) Now let us try to forget for a minute that in real systems of interest the number of particles is extremely large, and start to calculate, one by one, the first terms Z_N .

In the term with $N = 0$, both contributions to $E_{m,N}$ vanish, and so does the factor $\mu N/T$, so that $Z_0 = 1$. In the next term, with $N = 1$, the interaction term vanishes, so that $E_{m,1}$ is reduced to the kinetic energy of one particle, giving

$$Z_1 = e^{\mu/T} \sum_k \exp \left\{ -\frac{p_k^2}{2mT} \right\}. \quad (3.102)$$

Making the usual transition from the summation to integration, we may write

$$Z_1 = Z I_1, \quad \text{where } Z \equiv e^{\mu/T} \frac{gV}{(2\pi\hbar)^3} \int \exp \left\{ -\frac{p^2}{2mT} \right\} d^3 p, \quad \text{and } I_1 \equiv 1. \quad (3.103)$$

This is the same simple (Gaussian) integral as in Eq. (6), giving

⁴⁶ L. Boltzmann has used that way to calculate the 3rd and 4th virial coefficients for the hardball model – as much as can be done analytically.

⁴⁷ This method was developed in 1937-38 by J. Mayer and collaborators for the classical gas, and generalized to quantum systems in 1938 by B. Kahn and G. Uhlenbeck.

$$Z = e^{\mu/T} \frac{gV}{(2\pi\hbar)^3} (2\pi mT)^{3/2} = e^{\mu/T} gV \left(\frac{mT}{2\pi\hbar^2} \right)^{3/2}. \quad (3.104)$$

Now let us explore the next term, with $N=2$, which describes, in particular, pair interactions $U=U(\mathbf{r})$, with $\mathbf{r} = \mathbf{r} - \mathbf{r}'$. Due to the assumed particle indistinguishability, this term needs the “correct Boltzmann counting” factor $1/2!$ – cf. Eqs. (12) and (88):

$$Z_2 = e^{2\mu/T} \frac{1}{2!} \sum_{k,k'} \left[\exp \left\{ -\frac{p_k^2}{2mT} - \frac{p_{k'}^2}{2mT} \right\} e^{-U(\mathbf{r})/T} \right]. \quad (3.105)$$

Since U is coordinate-dependent, here the transfer from the summation to integration should be done more carefully than in the first term – cf. Eqs. (24) and (88):

$$Z_2 = e^{2\mu/T} \frac{1}{2!} \frac{(gV)^2}{(2\pi\hbar)^6} \int \exp \left\{ -\frac{p^2}{2mT} \right\} d^3 p \times \int \exp \left\{ -\frac{p'^2}{2mT} \right\} d^3 p' \times \frac{1}{V} \int e^{-U(\mathbf{r})/T} d^3 r. \quad (3.106)$$

Comparing this expression with the Eq. (104) for the parameter Z , we get

$$Z_2 = \frac{Z^2}{2!} I_2, \quad \text{where } I_2 \equiv \frac{1}{V} \int e^{-U(\mathbf{r})/T} d^3 r. \quad (3.107)$$

Acting absolutely similarly, for the third term of the grand canonical sum we may get

$$Z_3 = \frac{Z^3}{3!} I_3, \quad \text{where } I_3 \equiv \frac{1}{V^2} \int e^{-U(\mathbf{r}', \mathbf{r}'')/T} d^3 r' d^3 r'', \quad (3.108)$$

where \mathbf{r}' and \mathbf{r}'' are the vectors characterizing the mutual positions of 3 particles – see Fig. 6b.

These results may be extended by induction to an arbitrary N . Plugging the expression for Z_N into the first of Eqs. (101) and recalling that $\Omega = -PV$, we get the equation of state of the gas in the form

$$P = \frac{T}{V} \ln \left(1 + ZI_1 + \frac{Z^2}{2!} I_2 + \frac{Z^3}{3!} I_3 + \dots \right). \quad (3.109)$$

As a sanity check: at $U=0$, all integrals I_N are equal to 1, and the expression under the logarithm is just the Taylor expansion of the function e^Z , giving $P = TZ/V$, and $\Omega = -PV = -TZ$. In this case, according to the last of Eqs. (1.62), the *average* number of particles of particles in the system is $\langle N \rangle = -(\partial\Omega/\partial\mu)_{T,V} = Z$, because since $Z \propto \exp\{\mu/T\}$, $\partial Z/\partial\mu = Z/T$.⁴⁸ Thus, in this limit, we have happily recovered the equation of state of the ideal gas.

Returning to the general case of non-zero interactions, let us assume that the logarithm in Eq. (109) may be also represented as a direct Taylor expansion in Z :

$$P = \frac{T}{V} \sum_{l=1}^{\infty} \frac{J_l}{l!} Z^l. \quad (3.110)$$

Cluster expansion: pressure

⁴⁸ Actually, the fact that in that case $Z = \langle N \rangle$ could have been noted earlier – just by comparing Eq. (104) with Eq. (32).

(The lower limit of the sum reflects the fact that according to Eq. (109), at $Z = 0$, $P = (T/V) \ln 1 = 0$, so that the coefficient J_0 in a more complete version of Eq. (110) would equal 0 anyway.) According to Eq. (1.60), this expansion corresponds to the grand potential

$$\Omega = -PV = -T \sum_{l=1}^{\infty} \frac{J_l}{l!} Z^l. \quad (3.111)$$

Again using the last of Eqs. (1.62), and the definition (104) of the parameter Z , we get

Cluster
expansion:
 $\langle N \rangle$

$$\langle N \rangle = \sum_{l=1}^{\infty} \frac{J_l}{(l-1)!} Z^l. \quad (3.112)$$

This equation may be used for finding Z for the given $\langle N \rangle$, and hence for the calculation of the equation of state from Eq. (110). The only remaining conceptual action item is to express the coefficients J_l via the integrals I_N participating in the expansion (109). This may be done using the well-known Taylor expansion of the logarithm function,⁴⁹

$$\ln(1 + \xi) = \sum_{l=1}^{\infty} (-1)^{l+1} \frac{\xi^l}{l}. \quad (3.113)$$

Using it together with Eq. (109), we get a Taylor series in Z , starting as

$$P = \frac{T}{V} \left[Z + \frac{Z^2}{2!} (I_2 - 1) + \frac{Z^3}{3!} [(I_3 - 1) - 3(I_2 - 1)] + \dots \right]. \quad (3.114)$$

Comparing this expression with Eq. (110), we see that

$$\begin{aligned} J_1 &= 1, \\ J_2 &= I_2 - 1 = \frac{1}{V} \int (e^{-U(\mathbf{r})/T} - 1) d^3 r, \\ J_3 &= (I_3 - 1) - 3(I_2 - 1) \\ &= \frac{1}{V^2} \int (e^{-U(\mathbf{r}', \mathbf{r}'')/T} - e^{-U(\mathbf{r}')/T} - e^{-U(\mathbf{r}'')/T} - e^{-U(\mathbf{r}'')/T} + 2) d^3 r' d^3 r'', \dots \end{aligned} \quad (3.115)$$

where $\mathbf{r}''' \equiv \mathbf{r}' - \mathbf{r}''$ - see Fig. 6b. The expression of J_2 , describing the pair interactions of particles, is (besides a different numerical factor) equal to the second virial coefficient $B(T)$ - see Eq. (93). As a reminder, the subtraction of 1 from the integral I_2 in the second of Eqs. (115) makes the contribution of each elementary 3D volume $d^3 r$ into the integral J_2 different from zero only if at this \mathbf{r} two particles interact ($U \neq 0$). Very similarly, in the last of Eqs. (115), the subtraction of three pair-interaction terms from $(I_3 - 1)$ makes the contribution from an elementary 6D volume $d^3 r' d^3 r''$ into the integral J_3 different from zero only if at that mutual location of particles, all *three* of them interact simultaneously, etc.

⁴⁹ Looking at Eq. (109), one may think that since $\xi = Z + Z^2 I_2 / 2 + \dots$ is of the order of at least $Z \sim \langle N \rangle \gg 1$, the expansion (113), which converges only if $|\xi| < 1$, is illegitimate. However, the expansion is justified by its result (114), in which the n^{th} term is of the order of $\langle N \rangle^n (V_0/V)^{n-1} / n!$, so that the series does converge if the gas density is sufficiently low: $\langle N \rangle / V \ll 1 / V_0$, i.e. $r_{\text{ave}} \gg r_0$. This is the very beauty of the cluster expansion, whose few first terms, rather unexpectedly, give good approximation even for a gas with $\langle N \rangle \gg 1$ particles.

In order to illustrate the cluster expansion method at work, let us eliminate the factor Z from the system of equations (110) and (112), with accuracy to terms $O(Z^2)$. For that, let us spell out these equations up to the terms $O(Z^3)$:

$$\frac{PV}{T} = J_1 Z + \frac{J_2}{2} Z^2 + \frac{J_3}{6} Z^3 + \dots, \quad (3.116)$$

$$\langle N \rangle = J_1 Z + J_2 Z^2 + \frac{J_3}{2} Z^3 + \dots, \quad (3.117)$$

and then divide these two expressions. We get the following result:

$$\frac{PV}{\langle N \rangle T} = \frac{1 + (J_2 / 2J_1)Z + (J_3 / 6J_1)Z^2 + \dots}{1 + (J_2 / J_1)Z + (J_3 / 2J_1)Z^2 + \dots} \approx 1 - \frac{J_2}{2J_1}Z + \left(\frac{J_2^2}{2J_1^2} - \frac{J_3}{3J_1} \right) Z^2, \quad (3.118)$$

whose final form is accurate to terms $O(Z^2)$. In this approximation, we may again use Eq. (117), now solved for Z with the same accuracy:

$$Z \approx \langle N \rangle - \frac{J_2}{J_1} \langle N \rangle^2. \quad (3.119)$$

Plugging this expression into Eq. (118), we get the virial expansion (100) with

$$B(T) = -\frac{J_2}{2J_1}V, \quad C(T) = \left(\frac{J_2^2}{2J_1^2} - \frac{J_3}{3J_1} \right) V^2. \quad (3.120)$$

2nd and 3rd virial coefficients

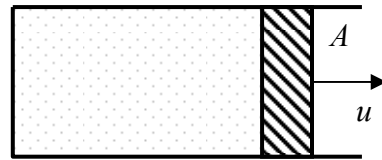
The first of these relations, combined with the first two of Eqs. (115), yields for the 2nd virial coefficient the same Eq. (96), $B(T) = 4V_0$, that was obtained from the Gibbs distribution. The second of these relations enables the calculation of the 3rd virial coefficient $C(T)$. (Let me leave the calculation of J_3 and $C(T)$, for the hardball model, for the reader's exercise.) Evidently, a more complete solution of Eqs. (114), (116), and (117) may be used to calculate an arbitrary virial coefficient, though starting from the 5th coefficient, such calculations may be completed only numerically even in the simplest hardball model.

3.6. Exercise problems

3.1. Use the Maxwell distribution for an alternative (statistical) calculation of the mechanical work performed by the Szilard engine discussed in Sec. 2.3.

Hint: You may assume the simplest geometry of the engine – see Fig. 2.4.

3.2. Use the Maxwell distribution to calculate the *drag coefficient* $\eta \equiv -\partial \langle \mathcal{F} \rangle / \partial u$, where \mathcal{F} is the force exerted by an ideal classical gas on a piston moving with a low velocity u , in the simplest geometry shown in the figure on the right, assuming that collisions of gas particles with the piston are elastic.



3.3. Derive the equation of state of the ideal classical gas from the grand canonical distribution.

3.4. Prove that Eq. (22),

$$\Delta S = N_1 \ln \frac{V_1 + V_2}{V_1} + N_2 \ln \frac{V_1 + V_2}{V_2},$$

derived for the change of entropy at mixing of two ideal classical gases of completely distinguishable particles (that initially had equal densities N/V and temperatures T), is also valid if particles in each of the initial volumes are indistinguishable from each other but different from those in the counterpart volume. For simplicity, you may assume that masses and internal degeneracy factors of all particles are equal.

3.5. A round cylinder of radius R and length L , containing an ideal classical gas of $N \gg 1$ particles of mass m each, is rotated about its symmetry axis with angular velocity ω . Assuming that the gas as the whole rotates with the cylinder, and is in thermal equilibrium at temperature T ,

- (i) calculate the gas pressure distribution along its radius, and analyze its temperature dependence, and
- (ii) neglecting the internal degrees of freedom of the particles, calculate the total energy of the gas and its heat capacity in the high- and low-temperature limits.

3.6. $N \gg 1$ classical, non-interacting, indistinguishable particles of mass m are confined in a parabolic, spherically-symmetric 3D potential well $U(\mathbf{r}) = \kappa r^2/2$. Use two different approaches to calculate all major thermodynamic characteristics of the system, in thermal equilibrium at temperature T , including its heat capacity. Which of the results should be changed if the particles are distinguishable, and how?

Hint: Suggest a replacement of the notions of volume and pressure, appropriate for this system.

3.7. In the simplest model of thermodynamic equilibrium between the liquid and gas phases of the same molecules, temperature and pressure do not affect the molecule's condensation energy Δ . Calculate the concentration and pressure of such *saturated vapor*, assuming that it behaves as an ideal gas of classical particles.

3.8. An ideal classical gas of $N \gg 1$ particles is confined in a container of volume V and wall surface area A . The particles may condense on container walls, releasing energy Δ per particle, and forming an ideal 2D gas. Calculate the equilibrium number of condensed particles and the gas pressure, and discuss their temperature dependences.

3.9. The inner surfaces of the walls of a closed container of volume V , filled with $N \gg 1$ particles, have $N_S \gg 1$ similar traps (small potential wells). Each trap can hold only one particle, at potential energy $-\Delta < 0$. Assuming that the gas of the particles in the volume is ideal and classical, derive an equation for the chemical potential μ of the system in equilibrium, and use it to calculate the potential and the gas pressure in the limits of small and large values of the N/N_S ratio.

3.10. Calculate the magnetic response (the *Pauli paramagnetism*) of a degenerate ideal gas of spin- $1/2$ particles to a weak external magnetic field, due to a partial spin alignment with the field.

3.11. Calculate the magnetic response (the *Landau diamagnetism*) of a degenerate ideal gas of electrically charged fermions to a weak external magnetic field, due to their orbital motion.

3.12.* Explore the *Thomas-Fermi model* of a heavy atom, with nuclear charge $Q = Ze \gg e$, in which the electrons are treated as a degenerate Fermi gas, interacting with each other only via their contribution to the common electrostatic potential $\phi(\mathbf{r})$. In particular, derive the ordinary differential equation obeyed by the radial distribution of the potential, and use it to estimate the effective radius of the atom.⁵⁰

3.13.* Use the Thomas-Fermi model, explored in the previous problem, to calculate the total binding energy of a heavy atom. Compare the result with that for a simpler model, in that the Coulomb electron-electron interaction of electrons is completely ignored.

3.14. Calculate the characteristic *Thomas-Fermi length* λ_{TF} of weak electric field's screening by conduction electrons in a metal, modeling their ensemble as an ideal, degenerate, isotropic Fermi gas.

Hint: Assume that λ_{TF} is much larger than the Bohr radius r_B .

3.15. For a degenerate ideal 3D Fermi gas of N particles, confined in a rigid-wall box of volume V , calculate the temperature dependencies of its pressure P and the heat capacity difference $(C_P - C_V)$, in the leading approximation in $T \ll \varepsilon_F$. Compare the results with those for the ideal classical gas.

Hint: You may like to use the solution of Problem 1.9.

3.16. How would the Fermi statistics of an ideal gas affect the barometric formula (28)?

3.17. Derive general expressions for the energy E and the chemical potential μ of a uniform Fermi gas of $N \gg 1$ non-interacting, indistinguishable, ultra-relativistic particles.⁵¹ Calculate E , and also the gas pressure P explicitly in the degenerate gas limit $T \rightarrow 0$. In particular, is Eq. (48) valid in this case?

3.18. Use Eq. (49) to calculate the pressure of an ideal gas of ultra-relativistic, indistinguishable quantum particles, for an arbitrary temperature, as a function of the total energy E of the gas, and its volume V . Compare the result with the corresponding relations for the electromagnetic blackbody radiation and for an ideal gas of non-relativistic particles.

3.19.* Calculate the speed of sound in an ideal gas of ultra-relativistic fermions of density n at negligible temperature.

⁵⁰ Since this problem, and the next one, are important for atomic physics, and at their solution, thermal effects may be ignored, they were given in Chapter 8 of the QM part of the series as well, for the benefit of readers who would not take this SM part. Note, however, that the argumentation in their solutions may be streamlined by using the notion of the chemical potential μ , which was introduced only in this course.

⁵¹ This is, for example, an approximate but reasonable model for electrons in white dwarf stars, whose Coulomb interaction is mostly compensated by the charge of nuclei of fully ionized helium atoms.

3.20. Calculate basic thermodynamic characteristics, including all relevant thermodynamic potentials, specific heat, and the surface tension of a uniform, non-relativistic 2D electron gas with given areal density $n \equiv N/A$:

- (i) at $T = 0$, and
- (ii) at low temperatures (in the lowest order in $T/\varepsilon_F \ll 1$, giving a nonzero result),

neglecting the Coulomb interaction effects.⁵²

3.21. Calculate the effective latent heat $\Lambda_{\text{ef}} \equiv -N(\partial Q/\partial N_0)_{N,V}$ of evaporation of the spatially-uniform Bose-Einstein condensate as a function of temperature T . Here Q is the heat absorbed by the (condensate + gas) system of $N \gg 1$ particles as a whole, while N_0 is the number of particles in the condensate alone.

3.22.* For an ideal, spatially-uniform Bose gas, calculate the law of the chemical potential's disappearance at $T \rightarrow T_c$, and use the result to prove that the heat capacity C_V is a continuous function of temperature at the critical point $T = T_c$.

3.23. In Chapter 1 of these notes, several thermodynamic relations involving entropy have been discussed, including the first of Eqs. (1.39):

$$S = -(\partial G / \partial T)_P.$$

If we combine this expression with Eq. (1.56), $G = \mu N$, it looks like that for the Bose-Einstein condensate, whose chemical potential μ equals zero at temperatures below the critical point T_c , the entropy should vanish as well. On the other hand, dividing both parts of Eq. (1.19) by dT , and assuming that at this temperature change the volume is kept constant, we get

$$C_V = T(\partial S / \partial T)_V.$$

(This equality was also mentioned in Chapter 1.) If the C_V is known as a function of temperature, the last relation may be integrated over T to calculate S :

$$S = \int_{V=\text{const}} \frac{C_V(T)}{T} dT + \text{const.}$$

According to Eq. (80), the specific heat for the Bose-Einstein condensate is proportional to $T^{3/2}$, so that the integration gives a non-zero entropy $S \propto T^{3/2}$. Resolve this apparent contradiction, and calculate the genuine entropy at $T = T_c$.

3.24. The standard analysis of the Bose-Einstein condensation, outlined in Sec. 4, may seem to ignore the energy quantization of the particles confined in volume V . Use the particular case of a cubic confining volume $V = a \times a \times a$ with rigid walls to analyze whether the main conclusions of the standard theory, in particular Eq. (71) for the critical temperature of the system of $N \gg 1$ particles, are affected by such quantization.

⁵² This condition may be approached reasonably well, for example, in 2D electron gases formed in semiconductor heterostructures (see, e.g., the discussion in QM Sec. 1.6, and the solution of Problem 3.2 of that course), due to the electron field's compensation by background ionized atoms, and its screening by highly doped semiconductor bulk.

3.25.* $N \gg 1$ non-interacting bosons are confined in a soft, spherically-symmetric potential well $U(\mathbf{r}) = m\omega^2 r^2/2$. Develop the theory of the Bose-Einstein condensation in this system; in particular, prove Eq. (74b), and calculate the critical temperature T_c^* . Looking at the solution, what is the most straightforward way to detect the condensation in experiment?

3.26. Calculate the chemical potential of an ideal, uniform 2D gas of spin-0 Bose particles as a function of its areal density n (the number of particles per unit area), and find out whether such gas can condense at low temperatures. Review your result for the case of a large ($N \gg 1$) but finite number of particles.

3.27. Can the Bose-Einstein condensation be achieved in a 2D system of $N \gg 1$ non-interacting bosons placed into a soft, axially-symmetric potential well, whose potential may be approximated as $U(\mathbf{r}) = m\omega^2 \rho^2/2$, where $\rho^2 \equiv x^2 + y^2$, and $\{x, y\}$ are the Cartesian coordinates in the particle confinement plane? If yes, calculate the critical temperature of the condensation.

3.28. Use Eqs. (115) and (120) to calculate the third virial coefficient $C(T)$ for the hardball model of particle interactions.

3.29. Assuming the hardball model, with volume V_0 per molecule, for the liquid phase, describe how the results of Problem 3.7 change if the liquid forms spherical drops of radius $R \gg V_0^{1/3}$. Briefly discuss the implications of the result for water cloud formation.

Hint: Surface effects in macroscopic volumes of liquids may be well described by attributing an additional energy γ (equal to the surface tension) to the unit surface area.⁵³

⁵³ See, e.g., CM Sec. 8.2.

Chapter 4. Phase Transitions

This chapter gives a rather brief discussion of coexistence between different states (“phases”) of collections of many similar particles, and transitions between these phases. Due to the complexity of these phenomena, which involve particle interactions, quantitative analytical results in this field have been obtained only for a few very simple models, typically giving only a very approximate description of real systems.

4.1. First-order phase transitions

From our everyday experience, say with water ice, liquid water, and water vapor, we know that one chemical substance (i.e. a set of many similar particles) may exist in different stable states – *phases*. A typical substance may have:

- (i) a dense *solid phase*, in which interatomic forces keep all atoms/molecules in virtually fixed relative positions, with just small thermal fluctuations about them;
- (ii) a *liquid phase*, of comparable density, in which the relative distances between atoms or molecules are almost constant, but the particles are virtually free to move around each other, and
- (iii) a *gas phase*, typically of a much lower density, in which the molecules are virtually free to move all around the containing volume.¹

Experience also tells us that at certain conditions, two different phases may be in thermal and chemical equilibrium – say, ice floating on water with the freezing-point temperature. Actually, in Sec. 3.4 we already discussed a qualitative theory of one such equilibrium: the Bose-Einstein condensate’s coexistence with the uncondensed “vapor” of similar particles. However, this is a rather exceptional case when the phase coexistence is due to the quantum nature of the particles (bosons) that may not interact directly. Much more frequently, the formation of different phases, and transitions between them, are due to particle repulsive and attractive interactions, briefly discussed in Sec. 3.5.

Phase transitions are sometimes classified by their *order*.² I will start their discussion with the so-called *first-order phase transitions* that feature non-zero *latent heat* Λ – the amount of heat that is necessary to turn one phase into another phase completely, even if temperature and pressure are kept constant.³ Unfortunately, even the simplest “microscopic” models of particle interaction, such as those discussed in Sec. 3.5, give rather complex equations of state. (As a reminder, even the simplest hardball model leads to the series (3.100), whose higher virial coefficients defy analytical calculation.) This is

¹ The plasma phase, in which atoms are partly or completely ionized, is frequently mentioned on one more phase, on equal footing with the three phases listed above, but one has to remember that in contrast to them, a typical electroneutral plasma consists of particles of two very different sorts – positive ions and electrons.

² Such classification schemes, started by Paul Ehrenfest in the early 1930s, have been repeatedly modified to accommodate new results for particular systems, and by now only the “first-order phase transition” is still a generally accepted term, but with a definition different from the original one.

³ For example, for water the latent heat of vaporization at the ambient pressure is as high as $\sim 2.2 \times 10^6$ J/kg, i.e. ~ 0.4 eV per molecule, making this ubiquitous liquid indispensable for effective fire fighting. (The latent heat of water ice’s melting is an order of magnitude lower.)

why I will follow the tradition to discuss the first-order phase transitions using a simple phenomenological model suggested in 1873 by Johannes Diderik van der Waals.

For its introduction, it is useful to recall that in Sec. 3.5 we have derived Eq. (3.99) – the equation of state for a classical gas of weakly interacting particles, which takes into account (albeit approximately) both interaction components necessary for a realistic description of gas condensation/liquefaction: the long-range attraction of the particles and their short-range repulsion. Let us rewrite that result as follows:

$$P + a \frac{N^2}{V^2} = \frac{NT}{V} \left(1 + \frac{Nb}{V}\right). \quad (4.1)$$

As we saw at the derivation of this formula, the physical meaning of the constant b is the effective volume of space taken by a particle pair collision – see Eq. (3.96). The relation (1) is quantitatively valid only if the second term in the parentheses is small, $Nb \ll V$, i.e. if the total volume excluded from particles' free motion because of their collisions is much smaller than the whole volume V . In order to describe the condensed phase (which I will call “liquid”⁴), we need to generalize this relation to the case $Nb \sim V$. Since the effective volume left for particles' motion is $V - Nb$, it is very natural to make the following replacement: $V \rightarrow V - Nb$, in the equation of state of the ideal gas. If we also keep on the left-hand side the term aN^2/V^2 , which describes the long-range attraction of particles, we get the *van der Waals equation of state*:

$$P + a \frac{N^2}{V^2} = \frac{NT}{V - Nb}. \quad (4.2)$$

Van der
Waals
equation

One advantage of this simple model is that in the rare gas limit, $Nb \ll V$, it reduces back to the microscopically-justified Eq. (1). (To verify this, it is sufficient to Taylor-expand the right-hand side of Eq. (2) in small $Nb/V \ll 1$, and retain only two leading terms.) Let us explore the basic properties of this model.

It is frequently convenient to discuss any equation of state in terms of its isotherms, i.e. the $P(V)$ curves plotted at constant T . As Eq. (2) shows, in the van der Waals model such a plot depends on four parameters: a , b , N , and T , complicating general analysis of the model. To simplify the task, it is convenient to introduce dimensionless variables: pressure $p \equiv P/P_c$, volume $v \equiv V/V_c$, and temperature $t \equiv T/T_c$, normalized to their so-called *critical values*,

$$P_c \equiv \frac{1}{27} \frac{a}{b^2}, \quad V_c \equiv 3Nb, \quad T_c \equiv \frac{8}{27} \frac{a}{b}, \quad (4.3)$$

whose meaning will be clear in a minute. In this notation, Eq. (2) acquires the following form,

$$p + \frac{3}{v^2} = \frac{8t}{3v - 1}, \quad (4.4)$$

so that the normalized isotherms $p(v)$ depend on only one parameter, the normalized temperature t – see Fig. 1.

⁴ Due to the phenomenological character of the van der Waals model, one cannot say for sure whether the condensed phase it predicts corresponds to a liquid or a solid. However, in most real substances at ambient conditions, gas coexists with liquid, hence the name.

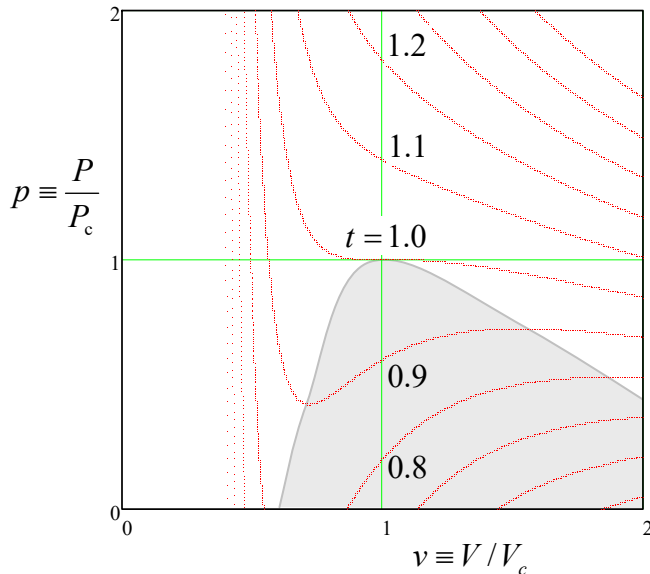


Fig. 4.1. The van der Waals equation of state, plotted on the $[p, v]$ plane for several values of the reduced temperature $t \equiv T/T_c$. Shading shows the single-phase instability range in that $(\partial P / \partial V)_T > 0$.

The most important property of these plots is that the isotherms have qualitatively different shapes in two temperature regions. At $t > 1$, i.e. $T > T_c$, pressure increases monotonically at gas compression (qualitatively, as in an ideal classical gas, with $P = NT/V$, to which the van der Waals system tends at $T \gg T_c$), i.e. with $(\partial P / \partial V)_T < 0$ at all points of the isotherm.⁵ However, below the critical temperature T_c , any isotherm features a segment with $(\partial P / \partial V)_T > 0$. It is easy to understand that, as least in a constant-pressure experiment (see, for example, Fig. 1.5),⁶ these segments describe a mechanically unstable equilibrium. Indeed, if due to a random fluctuation, the volume deviated upward from the equilibrium value, the pressure would also increase, forcing the environment (say, the heavy piston in Fig. 1.5) to allow further expansion of the system, leading to even higher pressure, etc. A similar deviation of volume downward would lead to a similar avalanche-like decrease of the volume. Such avalanche instability would develop further and further until the system has reached one of the stable branches with a negative slope $(\partial P / \partial V)_T$. In the range where the single-phase equilibrium state is unstable, the system as a whole may be stable only if it consists of the two phases (one with a smaller, and another with a higher density $n = N/V$) that are described by the two stable branches – see Fig. 2.

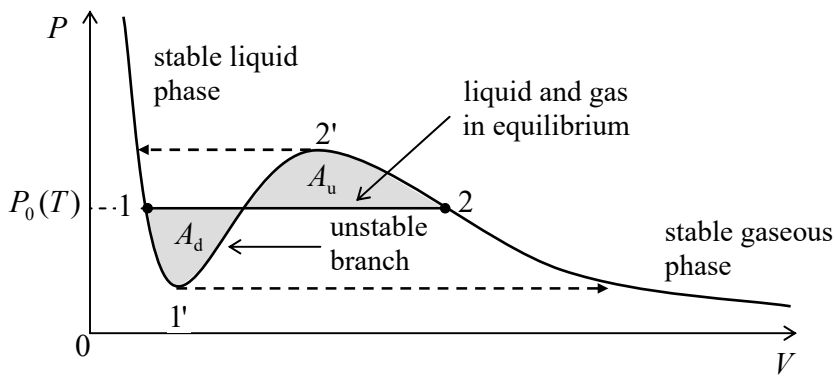


Fig. 4.2. Phase equilibrium at $T < T_c$ (schematically).

⁵ The special choice of numerical coefficients in Eq. (3) makes the border between these two regions to take place exactly at $t = 1$, i.e. at the temperature equal to T_c , with the critical point's coordinates equal to P_c and V_c .

⁶ Actually, this assumption is not crucial for our analysis of mechanical stability, because if a fluctuation takes place in a small part of the total volume V , its other parts play the role of pressure-fixing environment.

In order to understand the basic properties of this two-phase system, let us recall the general conditions of the thermodynamic equilibrium of two systems, which have been discussed in Chapter 1:

$$T_1 = T_2 \text{ (thermal equilibrium),} \quad (4.5)$$

$$\mu_1 = \mu_2 \text{ (“chemical” equilibrium),} \quad (4.6)$$

the latter condition meaning that the average energy of a single (“probe”) particle in both systems has to be the same. To those, we should add the evident condition of mechanical equilibrium,

$$P_1 = P_2 \text{ (mechanical equilibrium),} \quad (4.7)$$

which immediately follows from the balance of normal forces exerted on an inter-phase boundary.

If we discuss isotherms, Eq. (5) is fulfilled automatically, while Eq. (7) means that the effective isotherm $P(V)$ describing a two-phase system should be a horizontal line – see Fig. 2:

$$P = P_0(T). \quad (4.8)$$

Along this line,⁷ internal properties of each phase do not change; only the particle distribution is: it evolves gradually from all particles being in the liquid phase at point 1 to all particles being in the gas phase at point 2.⁸ In particular, according to Eq. (6), the chemical potentials μ of the phases should be equal at each point of the horizontal line (8). This fact enables us to find the line’s position: it has to connect points 1 and 2 in that the chemical potentials of the two phases are equal to each other. Let us recast this condition as

$$\int_1^2 d\mu = 0, \quad \text{i.e.} \quad \int_1^2 dG = 0, \quad (4.9)$$

where the integral may be taken along the single-phase isotherm. (For this mathematical calculation, the mechanical instability of states on some part of this curve is not important.) By its construction, along that curve, $N = \text{const}$ and $T = \text{const}$, so that according to Eq. (1.53c), $dG = -SdT + VdP + \mu dN$, for a slow (reversible) change, $dG = VdP$. Hence Eq. (9) yields

$$\int_1^2 VdP = 0. \quad (4.10)$$

This equality means that in Fig. 2, the shaded areas A_d and A_u should be equal.⁹

⁷ Frequently, $P_0(T)$ is called the *saturated vapor pressure*.

⁸ A natural question: is the two-phase state with $P = P_0(T)$ the only state existing between points 1 and 2? Indeed, the branches 1-1' and 2-2' of the single-phase isotherm also have negative derivatives $(\partial P/\partial V)_T$ and hence are mechanically stable with respect to small perturbations. However, these branches are actually *metastable*, i.e. have larger Gibbs energy per particle (i.e. μ) than the counterpart phase and are hence unstable to *larger* perturbations – such as foreign microparticles (say, dust), protrusions on the confining walls, etc. In very controlled conditions, these single-phase “superheated” and “supercooled” states can survive almost all the way to the zero-derivative points 1' and 2', leading to sudden jumps of the system into the counterpart phase. (At fixed pressure, such jumps go as shown by dashed lines in Fig. 2.) In particular, at the atmospheric pressure, purified water may be supercooled to almost -50°C , and superheated to nearly $+270^\circ\text{C}$. However, at more realistic conditions, perturbations result in the two-phase coexistence formation close to points 1 and 2.

⁹ This *Maxwell equal-area rule* (also called “Maxwell’s construct”) was suggested by J. C. Maxwell in 1875 using more complex reasoning.

As the same Fig. 2 figure shows, the Maxwell rule may be rewritten in a different form,

Maxwell
equal-area
rule

$$\int_1^2 [P - P_0(T)] dV = 0. \quad (4.11)$$

which is more convenient for analytical calculations than Eq. (10) if the equation of state may be explicitly solved for P – as it is in the van der Waals model (2). Such calculation (left for the reader’s exercise) shows that for that model, the temperature dependence of the saturated vapor pressure at low T is exponential,¹⁰

$$P_0(T) \propto P_c \exp\left\{-\frac{\Delta}{T}\right\}, \quad \text{with } \Delta = \frac{a}{b} \equiv \frac{27}{8} T_c, \quad \text{for } T \ll T_c, \quad (4.12)$$

corresponding very well to the physical picture of particle’s thermal activation from a potential well of depth Δ .

The signature parameter of a first-order phase transition, the latent heat of evaporation

Latent
heat:
definition

$$\Lambda \equiv \int_1^2 dQ, \quad (4.13)$$

may also be found by a similar integration along the single-phase isotherm. Indeed, using Eq. (1.19), $dQ = TdS$, we get

$$\Lambda = \int_1^2 TdS = T(S_2 - S_1). \quad (4.14)$$

Let us express the right-hand side of Eq. (14) via the equation of state. For that, let us take the full derivative of both sides of Eq. (6) over temperature, considering the value of $G = N\mu$ for each phase as a function of P and T , and taking into account that according to Eq. (7), $P_1 = P_2 = P_0(T)$:

$$\left(\frac{\partial G_1}{\partial T}\right)_P + \left(\frac{\partial G_1}{\partial P}\right)_T \frac{dP_0}{dT} = \left(\frac{\partial G_2}{\partial T}\right)_P + \left(\frac{\partial G_2}{\partial P}\right)_T \frac{dP_0}{dT}. \quad (4.15)$$

According to the first of Eqs. (1.39), the partial derivative $(\partial G/\partial T)_P$ is just minus the entropy, while according to the second of those equalities, $(\partial G/\partial P)_T$ is the volume. Thus Eq. (15) becomes

$$-S_1 + V_1 \frac{dP_0}{dT} = -S_2 + V_2 \frac{dP_0}{dT}. \quad (4.16)$$

Solving this equation for $(S_2 - S_1)$, and plugging the result into Eq. (14), we get the following *Clapeyron-Clausius formula*:

$$\Lambda = T(V_2 - V_1) \frac{dP_0}{dT}. \quad (4.17)$$

For the van der Waals model, this formula may be readily used for the analytical calculation of Λ in two limits: $T \ll T_c$ and $(T_c - T) \ll T_c$ – the exercises left for the reader. In the latter limit, $\Lambda \propto (T_c - T)^{1/2}$, naturally vanishing at the critical temperature.

¹⁰ It is fascinating how well is this Arrhenius exponent hidden in the polynomial van der Waals equation (2)!

Finally, some important properties of the van der Waals' model may be revealed more easily by looking at the set of its isochores $P = P(T)$ for $V = \text{const}$, rather than at the isotherms. Indeed, as Eq. (2) shows, all single-phase isochores are straight lines. However, if we interrupt these lines at the points when the single phase becomes metastable, and complement them with the (very nonlinear!) dependence $P_0(T)$, we get the pattern (called the *phase diagram*) shown schematically in Fig. 3a.

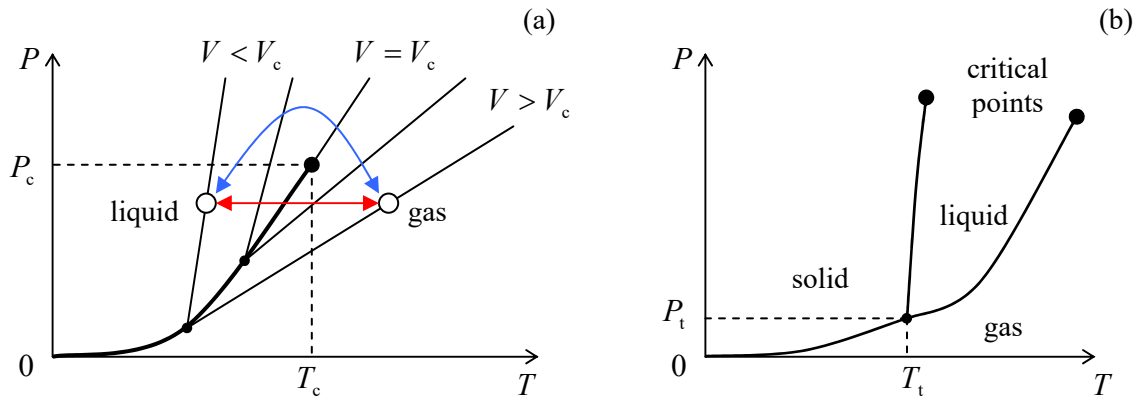


Fig. 4.3. (a) Van der Waals model's isochores, the saturated gas pressure diagram, and the critical point, and (b) the phase diagram of a typical three-phase system (all schematically).

At this plot, one more meaning of the critical point $\{P_c, T_c\}$ becomes very vivid. At fixed pressure $P < P_c$, the liquid and gaseous phases are clearly separated by the saturated pressure line $P_0(T)$, so if we achieve the transition between the phases just by changing temperature (see the red horizontal line in Fig. 3a), we have to pass through the phase equilibrium point, being delayed there to either give to the system the latent heat or take it out. However, if we perform the transition between the same initial and final points by changing both the pressure and temperature, going around the critical point (see the blue line in Fig. 3a), no definite point of transition may be observed: the substance stays in a single phase, and it is a subjective judgment of the observer in which region that phase should be called the liquid, and in which region – the gas. For water, the critical point corresponds to the temperature of 647 K (374°C), and $P_c \approx 22.1$ MPa (i.e. ~200 bars), so that a lecture demonstration of its critical behavior would require substantial safety precautions. This is why such demonstrations are typically carried out with other substances such as either diethyl ether,¹¹ with its much lower T_c (194°C) and P_c (3.6 MPa), or the now-infamous carbon dioxide CO₂, with even lower T_c (31.1°C), though higher P_c (7.4 MPa). Though these substances are colorless and clear in both gas and liquid phases, their separation (by gravity) is still visible, due to small differences in the optical refraction coefficient, at $P < P_c$, but not above P_c .¹²

Thus, in the van der Waals model, two phases may coexist, though only at certain conditions – in particular, $T < T_c$. Now a natural, more general question is whether the coexistence of more than two

¹¹ (CH₃-CH₂)-O-(CH₂-CH₃), historically the first popular general anesthetic.

¹² It is interesting that very close to the critical point the substance suddenly becomes opaque – in the case of ether, whitish. The qualitative explanation of this effect, called the *critical opalescence*, is simple: at this point, the difference of the Gibbs energies per particle (i.e. the chemical potentials) of the two phases becomes so small that unavoidable thermal fluctuations lead to spontaneous appearance and disappearance of relatively large (a few-μm-scale) single-phase regions in all the volume. A large concentration of boundaries of such randomly-shaped regions leads to strong light scattering.

phases of the same substance is possible. For example, can the water ice, the liquid water, and the water vapor (steam) all be in thermodynamic equilibrium? The answer is essentially given by Eq. (6). From thermodynamics, we know that for a uniform system (i.e. a single phase), pressure and temperature completely define the chemical potential $\mu(P, T)$. Hence, dealing with two phases, we had to satisfy just *one* chemical equilibrium condition (6) for *two* common arguments P and T . Evidently, this leaves us with one extra degree of freedom, so that the two-phase equilibrium is possible within a certain range of P at fixed T (or vice versa) – see again the horizontal line in Fig. 2 and the bold line in Fig. 3a. Now, if we want *three* phases to be in equilibrium, we need to satisfy *two* equations for these variables:

$$\mu_1(P, T) = \mu_2(P, T) = \mu_3(P, T). \quad (4.18)$$

Typically, the functions $\mu(P, T)$ are monotonic, so that the two equations (18) have just one solution, the so-called *triple point* $\{P_t, T_t\}$. Of course, the triple point $\{P_t, T_t\}$ of equilibrium between *three* phases should not be confused with the critical points $\{P_c, T_c\}$ of transitions between each of *two*-phase pairs. Fig. 3b shows, very schematically, their relation for a typical three-phase system solid-liquid-gas. For example, water, ice, and water vapor are at equilibrium at a triple point corresponding to $P_t \approx 0.612$ kPa¹³ and $T_t = 273.16$ K. The practical importance of this particular temperature point is that by an international agreement it has been accepted for the definition of not only the Kelvin temperature scale, but also of the Celsius scale's reference, as 0.01°C , so that the absolute temperature zero corresponds to exactly -273.15°C .¹⁴ More generally, triple points of purified simple substances (such as H₂, N₂, O₂, Ar, Hg, and H₂O) are broadly used for thermometer calibration, defining the so-called *international temperature scales* including the currently accepted scale ITS-90.

This analysis may be readily generalized to multi-component systems consisting of particles of several (say, L) sorts.¹⁵ If such a mixed system is in a single phase, i.e. is macroscopically uniform, its chemical potential may be defined by a natural generalization of Eq. (1.53c):

$$dG = -SdT + VdP + \sum_{l=1}^L \mu^{(l)} dN^{(l)}. \quad (4.19)$$

The last term reflects the fact that usually, each single phase is not a pure chemical substance, but has certain concentrations of all other components, so that $\mu^{(l)}$ may depend not only on P and T but also on the *concentrations* $c^{(l)} \equiv N^{(l)}/N$ of particles of each sort. If the total number N of particles is fixed, the number of independent concentrations is $(L - 1)$. For the chemical equilibrium of R phases, all R values of $\mu_r^{(l)}$ ($r = 1, 2, \dots, R$) have to be equal for particles of each sort: $\mu_1^{(l)} = \mu_2^{(l)} = \dots = \mu_R^{(l)}$, with each $\mu_r^{(l)}$ depending on $(L - 1)$ concentrations $c_r^{(l)}$, and also on P and T . This requirement gives $L(R - 1)$ equations for $(L - 1)R$ concentrations $c_r^{(l)}$, plus two common arguments P and T , i.e. for $[(L - 1)R + 2]$ independent variables. This means that the number of phases has to satisfy the limitation

Gibbs
phase
rule

$$L(R - 1) \leq (L - 1)R + 2, \quad \text{i.e. } R \leq L + 2, \quad (4.20)$$

¹³ Please note that for water, P_t is much lower than the normal atmospheric pressure (101.325 kPa).

¹⁴ Note the recent (2018) re-definition of the “legal” kelvin via joule (see, appendix CA: *Selected Physical Constants*); however, the new definition is compatible, within experimental accuracy, with that mentioned above.

¹⁵ Perhaps the most practically important example is the air/water system. For its detailed discussion, based on Eq. (19), the reader may be referred, e.g., to Sec. 3.9 in F. Schwabl, *Statistical Mechanics*, Springer (2000). Other important applications include liquid solutions, and metallic *alloys* – solid solutions of metal elements.

where the equality sign may be reached in just one point in the whole parameter space. This is the *Gibbs phase rule*. As a sanity check, for a single-component system, $L = 1$, the rule yields $R \leq 3$ – exactly the result we have already discussed.

4.2. Continuous phase transitions

As Fig. 2 illustrates, if we fix pressure P in a system with a first-order phase transition, and start changing its temperature, then the complete crossing of the transition-point line, defined by the equation $P_0(T) = P$, requires the insertion (or extraction) some non-zero latent heat Λ . Eqs. (14) and (17) show that Λ is directly related to non-zero differences between the entropies and volumes of the two phases (at the same pressure). As we know from Chapter 1, both S and V may be represented as the first derivatives of appropriate thermodynamic potentials. This is why P. Ehrenfest called such transitions, involving jumps of potentials' first derivatives, the *first-order* phase transitions.

On the other hand, there are phase transitions that have no first derivative jumps at the transition temperature T_c , so that the temperature point may be clearly marked, for example, by a jump of the second derivative of a thermodynamic potential – for example, the derivative $\partial C/\partial T$ which, according to Eq. (1.24), equals to $\partial^2 E/\partial T^2$. In the initial Ehrenfest classification, this was an example of a *second-order* phase transition. However, most features of such phase transitions are also pertinent to some systems in which the second derivatives of potentials are continuous as well. Due to this reason, I will use a more recent terminology (suggested in 1967 by M. Fisher), in which all phase transitions with $\Lambda = 0$ are called *continuous*.

Most (though not all) continuous phase transitions result from particle interactions. Here are some representative examples:

(i) At temperatures above ~ 490 K, the crystal lattice of barium titanate (BaTiO_3) is cubic, with a Ba ion in the center of each Ti-cornered cube (or vice versa) – see Fig. 4a. However, as the temperature is being lowered below that critical value, the sublattice of Ba ions starts moving along one of six sides of the TiO_3 sublattice, leading to a small deformation of both lattices – which become tetragonal. This is a typical example of a *structural transition*, in this particular case combined with a *ferroelectric transition*, because (due to the positive electric charge of the Ba ions) below the critical temperature the BaTiO_3 crystal acquires a spontaneous electric polarization even in the absence of external electric field.

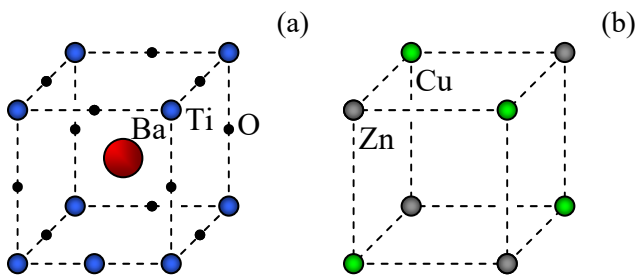


Fig. 4.4. Single cells of crystal lattices of (a) BaTiO_3 and (b) CuZn .

(ii) A different kind of phase transition happens, for example, in $\text{Cu}_x\text{Zn}_{1-x}$ alloys – so-called *brasses*. Their crystal lattice is always cubic, but above certain critical temperature T_c (which depends on x) any of its nodes may be occupied by either a copper or a zinc atom, at random. At $T < T_c$, a trend toward ordered atom alternation arises, and at low temperatures, the atoms are fully ordered, as shown in Fig. 4b for the stoichiometric case $x = 0.5$. This is a good example of an *order-disorder* transition.

(iii) At *ferromagnetic* transitions (such as the one taking place, for example, in Fe at 1,388 K) and *antiferromagnetic* transitions (e.g., in MnO at 116 K), lowering of temperature below the critical value¹⁶ does not change atom positions substantially, but results in a partial ordering of atomic spins, eventually leading to their full ordering (Fig. 5).

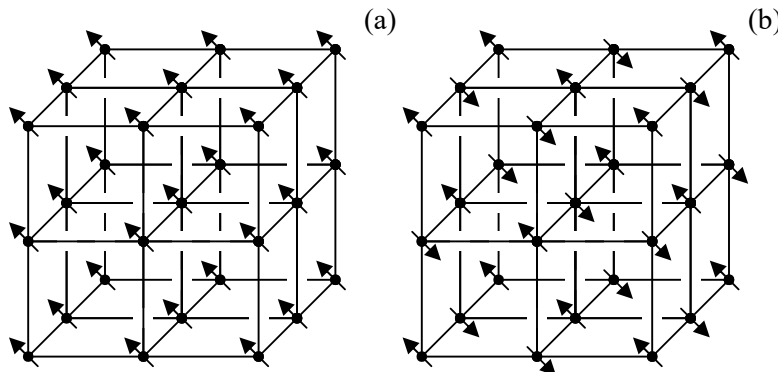


Fig. 4.5. Classical images of fully ordered phases: (a) a ferromagnet, and (b) an antiferromagnet.

Note that, as it follows from Eqs. (1.1)-(1.3), at ferroelectric transitions the role of pressure is played by the external electric field \mathcal{E} , and at the ferromagnetic transitions, by the external magnetic field \mathcal{H} . As we will see very soon, even in systems with continuous phase transitions, a gradual change of such an external field, at a fixed temperature, may induce jumps between metastable states, similar to those in systems with first-order phase transitions (see, e.g., the dashed arrows in Fig. 2), with non-zero decreases of the appropriate free energy.

Besides these standard examples, some other threshold phenomena, such as the formation of a coherent optical field in a laser, and even the self-excitation of oscillators with negative damping (see, e.g., CM Sec. 5.4), may be treated, at certain conditions, as continuous phase transitions.¹⁷

The general feature of all these transitions is the gradual formation, at $T < T_c$, of certain *ordering*, which may be characterized by some *order parameter* $\eta \neq 0$. The simplest example of such an order parameter is the magnetization at the ferromagnetic transitions, and this is why the continuous phase transitions are usually discussed on certain models of ferromagnetism. (I will follow this tradition, while mentioning in passing other important cases that require a substantial modification of the theory.) Most of such models are defined on an infinite 3D cubic lattice (see, e.g., Fig. 5), with evident generalizations to lower dimensions. For example, the *Heisenberg model* of a ferromagnet (suggested in 1928) is defined by the following Hamiltonian:

Heisenberg model

$$\hat{H} = -J \sum_{\{k,k'\}} \hat{\sigma}_k \cdot \hat{\sigma}_{k'} - \sum_k \mathbf{h} \cdot \hat{\sigma}_k , \quad (4.21)$$

where $\hat{\sigma}_k$ is the Pauli vector operator¹⁸ acting on the k^{th} spin, and \mathbf{h} is the normalized external magnetic field:

¹⁶ For ferromagnets, this point is usually referred to at the *Curie temperature*, and for antiferromagnets, as the *Néel temperature*.

¹⁷ Unfortunately, I will have no time/space for these interesting (and practically important) generalizations, and have to refer the interested reader to the famous monograph by R. Stratonovich, *Topics in the Theory of Random Noise*, in 2 vols., Gordon and Breach, 1963 and 1967, and/or the influential review by H. Haken, *Ferstkörperprobleme* **10**, 351 (1970).

$$\mathbf{h} \equiv m_0 \mu_0 \mathcal{H} . \quad (4.22)$$

(Here m_0 is the magnitude of the spin's magnetic moment; for the Heisenberg model to be realistic, it should be of the order of the *Bohr magneton* $\mu_B \equiv e\hbar/2m_e \approx 0.927 \times 10^{-23}$ J/T.) The figure brackets $\{j, j'\}$ in Eq. (21) denote the summation over the pairs of adjacent lattice sites, so that the magnitude of the constant J may be interpreted as the maximum coupling energy per “bond” between two adjacent particles. At $J > 0$, the coupling tries to keep spins aligned, i.e. to install the ferromagnetic ordering.¹⁹ The second term in Eq. (21) describes the effect of the external magnetic field, which tries to orient all spin magnetic moments along its direction.²⁰

However, even the Heisenberg model, while being rather approximate (in particular because its standard form (21) is only valid for spins- $\frac{1}{2}$), is still rather complex for analysis. This is why most theoretical results have been obtained for its classical twin, the *Ising model*:²¹

$$E_m = -J \sum_{\{k, k'\}} s_k s_{k'} - h \sum_k s_k . \quad (4.23)$$
Ising
model

Here E_m are the particular values of the system's energy in each of its 2^N possible states with all possible combinations of the binary classical variables $s_k = \pm 1$, while h is the normalized external magnetic field's magnitude – see Eq. (22). (Despite its classical character, the variable s_k , modeling the field-oriented Cartesian component of the real spin, is usually called “spin” for brevity, and I will follow this tradition.) Somewhat shockingly, even for this toy model, no exact analytical 3D solution that would be valid at arbitrary temperature has been found yet, and the solution of its 2D version by L. Onsager in 1944 (see Sec. 5 below) is still considered one of the top intellectual achievements of statistical physics. Still, Eq. (23) is very useful for the introduction of basic notions of continuous phase transitions, and methods of their analysis, so that for my brief discussion I will mostly use this model.²²

Evidently, if $T = 0$ and $h = 0$, the lowest possible energy,

$$E_{\min} = -JNd , \quad (4.24)$$

where d is the lattice dimensionality, is achieved in the “ferromagnetic” phase in which all spins s_k are equal to either $+1$ or -1 , so that $\langle s_k \rangle = \pm 1$ as well. On the other hand, at $J = 0$, the spins are independent, and if $h = 0$ as well, all s_k are completely random, with the 50% probability to take either of values ± 1 , so that $\langle s_k \rangle = 0$. Hence in the general case (with arbitrary J and h), we may use the average

$$\eta = \langle s_k \rangle \quad (4.25)$$
Ising
model:
order
parameter

¹⁸ See, e.g., QM Sec. 4.4.

¹⁹ At $J < 0$, the first term of Eq. (21) gives a reasonable model of an antiferromagnet, but in this case, the external magnetic field effects are more subtle; I will not have time to discuss them.

²⁰ See, e.g., QM Eq. (4.163).

²¹ Named after Ernst Ising who explored the 1D version of the model in detail in 1925, though a similar model was discussed earlier (in 1920) by Wilhelm Lenz.

²² For more detailed discussions of phase transition theories (including other popular models of the ferromagnetic phase transition, e.g., the *Potts model*), see, e.g., either H. Stanley, *Introduction to Phase Transitions and Critical Phenomena*, Oxford U. Press, 1971; or A. Patashinskii and V. Pokrovskii, *Fluctuation Theory of Phase Transitions*, Pergamon, 1979; or B. McCoy, *Advanced Statistical Mechanics*, Oxford U. Press, 2010. For a very concise text, I can recommend J. Yeomans, *Statistical Mechanics of Phase Transitions*, Clarendon, 1992.

as a good measure of spin ordering, i.e. as the order parameter. Since in a real ferromagnet, each spin carries a magnetic moment, the order parameter η is proportional to the Cartesian component of the system's magnetization, in the direction of the applied magnetic field.

Now that the Ising model gave us a very clear illustration of the order parameter, let me use this notion for quantitative characterization of continuous phase transitions. Due to the difficulty of theoretical analyses of most models of the transitions at arbitrary temperatures, their theoretical discussions are focused mostly on a close vicinity of the critical point T_c . Both experiment and theory show that in the absence of an external field, the function $\eta(T)$ is close to a certain power,

$$\eta \propto \tau^\beta, \quad \text{for } \tau > 0, \text{ i.e. } T < T_c, \quad (4.26)$$

of the small deviation from the critical temperature – which is conveniently normalized as

$$\tau \equiv \frac{T_c - T}{T_c}. \quad (4.27)$$

Remarkably, most other key variables follow a similar temperature behavior, with *critical exponents* being the same for both signs of τ . In particular, the heat capacity at a fixed magnetic field behaves as²³

$$c_h \propto |\tau|^{-\alpha}. \quad (4.28)$$

Similarly, the (normalized) low-field *susceptibility*²⁴

$$\chi \equiv \frac{\partial \eta}{\partial h} \Big|_{h=0} \propto |\tau|^{-\gamma}. \quad (4.29)$$

Two other important critical exponents, ζ and ν , describe the temperature behavior of the *correlation function* $\langle s_k s_{k'} \rangle$, whose dependence on the distance $r_{kk'}$ between two spins may be well fitted by the following law,

$$\langle s_k s_{k'} \rangle \propto \frac{1}{r_{kk'}^{d-2+\zeta}} \exp\left\{-\frac{r_{kk'}}{r_c}\right\}, \quad (4.30)$$

with the *correlation radius*

$$r_c \propto |\tau|^{-\nu}. \quad (4.31)$$

Finally, three more critical exponents, usually denoted ε , δ , and μ , describe the external field dependences of, respectively, c , η , and r_c at $\tau > 0$. For example, δ is defined as

$$\eta \propto h^{1/\delta}. \quad (4.32)$$

(Other field exponents are used less frequently, and for their discussion, the interested reader is referred to the special literature that was cited above.)

The leftmost column of Table 1 shows the ranges of experimental values of the critical exponents for various 3D physical systems featuring continuous phase transitions. One can see that their values vary from system to system, leaving no hope for a universal theory that would describe them all

²³ The forms of this and other functions of τ are selected to make all critical exponents non-negative.

²⁴ In most models of ferromagnetic phase transitions, this variable is proportional to the genuine low-field magnetic susceptibility χ_m of the material – see, e.g., EM Eq. (5.111).

exactly. However, certain combinations of the exponents are much more reproducible – see the four bottom lines of the table.

Table 4.1. Major critical exponents of continuous phase transitions

Exponents and combinations	Experimental range (3D) ^(a)	Landau's theory	2D Ising model	3D Ising model	3D Heisenberg Model ^(d)
α	0 – 0.14	0 ^(b)	(c)	0.12	-0.14
β	0.32 – 0.39	1/2	1/8	0.31	0.3
γ	1.3 – 1.4	1	7/4	1.25	1.4
δ	4-5	3	15	5	?
ν	0.6 – 0.7	1/2	1	0.64	0.7
ζ	0.05	0	1/4	0.05	0.04
$(\alpha + 2\beta + \gamma)/2$	1.00 ± 0.005	1	1	1	1
$\delta - \gamma/\beta$	0.93 ± 0.08	1	1	1	?
$(2 - \zeta)\nu/\gamma$	1.02 ± 0.05	1	1	1	1
$(2 - \alpha)/\nu d$?	4/d	1	1	1

(a) Experimental data are from the monograph by A. Patashinskii and V. Pokrovskii, cited above.

(b) Discontinuity at $\tau = 0$ – see below.

(c) Instead of following Eq. (28), in this case c_h diverges as $\ln|\tau|$.

(d) With the order parameter η defined as $\langle \mathbf{\sigma}_j \cdot \mathbf{B} \rangle / \mathcal{B}$.

Historically the first (and perhaps the most fundamental) of these *universal relations* was derived in 1963 by J. Essam and M. Fisher:

$$\alpha + 2\beta + \gamma = 2. \quad (4.33)$$

It may be proved, for example, by finding the temperature dependence of the magnetic field value, h_τ , that changes the order parameter by the same amount as a finite temperature deviation $\tau > 0$ gives at $h = 0$. Comparing Eqs. (26) and (29), we get

$$h_\tau \propto \tau^{\beta+\gamma}. \quad (4.34)$$

By the physical sense of h_τ , we may expect that such a field has to affect the system's free energy F by an amount comparable to the effect of a bare temperature change τ . Ensemble-averaging the last term of Eq. (23) and using the definition (25) of the order parameter η , we see that the change of F (per particle) due to the field equals $-h_\tau \eta$ and, according to Eq. (26), scales as $h_\tau \tau^\beta \propto \tau^{(2\beta+\gamma)}$ ²⁵

²⁵ As was already discussed in Secs. 1.4 and 2.4, there is some dichotomy of terminology for free energies in literature. In models (21) and (23), the magnetic field effects are accounted for at the microscopic level, by the inclusion of the corresponding term into each particular value E_m . From this point of view, the list of macroscopic variables in these systems does not include either P and V or their magnetic analogs, so that we may take $G \equiv F +$

In order to estimate the thermal effect on F , let me first elaborate a bit more on the useful thermodynamic formula already mentioned in Sec. 1.3:

$$C_X = T \left(\frac{\partial S}{\partial T} \right)_X , \quad (4.35)$$

where X means the variable(s) maintained constant at the temperature variation. In the standard “ P - V ” thermodynamics, we may use Eqs. (1.35) for $X = V$, and Eqs. (1.39) for $X = P$, to write

$$C_V = T \left(\frac{\partial S}{\partial T} \right)_{V,N} = -T \left(\frac{\partial^2 F}{\partial T^2} \right)_{V,N} , \quad C_P = T \left(\frac{\partial S}{\partial T} \right)_{P,N} = -T \left(\frac{\partial^2 G}{\partial T^2} \right)_{P,N} . \quad (4.36)$$

As was just discussed, in the ferromagnetic models of the type (21) or (23), at a constant field h , the role of G is played by F , so that Eq. (35) yields

$$C_h = T \left(\frac{\partial S}{\partial T} \right)_{h,N} = -T \left(\frac{\partial^2 F}{\partial T^2} \right)_{h,N} . \quad (4.37)$$

The last form of this relation means that F may be found by double integration of $(-C_h/T)$ over temperature. With Eq. (28) for $c_h \propto C_h$, this means that near T_c , the free energy scales as the double integral of $c_h \propto \tau^{-\alpha}$ over τ . In the limit $\tau \ll 1$, the factor T may be treated as a constant; as a result, the change of F due to $\tau > 0$ alone scales as $\tau^{2-\alpha}$. Requiring this change to be proportional to the same power of τ as the field-induced part of the energy, we finally get the Essam-Fisher relation (33).

Using similar reasoning, it is straightforward to derive a few other universal relations of critical exponents, including the *Widom relation*,

$$\delta - \frac{\gamma}{\beta} = 1 , \quad (4.38)$$

very similar relations for other high-field exponents ε and μ (which I do not have time to discuss), and the *Fisher relation*

$$\nu(2-\zeta) = \gamma . \quad (4.39)$$

A slightly more complex reasoning, involving the so-called *scaling hypothesis*, yields the following dimensionality-dependent *Josephson relation*

$$\nu d = 2 - \alpha . \quad (4.40)$$

The second column of Table 1 shows that at least three of these relations are in a very reasonable agreement with experiment, so that we may use their set as a testbed for various theoretical approaches to continuous phase transitions.

4.3. Landau’s mean-field theory

The highest-level approach to continuous phase transitions, formally not based on any particular microscopic model (though in fact implying either the Ising model (23) or one of its siblings), is the *mean-field theory* developed in 1937 by L. Landau, on the basis of prior ideas by P. Weiss – to be

$PV = F + \text{const}$, and the equilibrium (at fixed h , T and N) corresponds to the minimum of the *Helmholtz* free energy F .

discussed in the next section. The main idea of this phenomenological approach is to represent the free energy's change ΔF at the phase transition as an explicit function of the order parameter η (25). Since at $T \rightarrow T_c$, the order parameter has to tend to zero, this change,

$$\Delta F \equiv F(T) - F(T_c), \quad (4.41)$$

may be expanded into the Taylor series in η , and only a few, most important first terms of that expansion retained. In order to keep the symmetry between two possible signs of the order parameter (i.e. between two possible spin directions in the Ising model) in the absence of external field, at $h = 0$ this expansion should include only even powers of η :

$$\Delta f|_{h=0} \equiv \frac{\Delta F}{V}|_{h=0} = A(T)\eta^2 + \frac{1}{2}B(T)\eta^4 + \dots, \quad \text{at } T \approx T_c. \quad (4.42)$$

As Fig. 6 shows, at $A(T) < 0$, and $B(T) > 0$, these two terms are sufficient to describe the minimum of the free energy at $\eta^2 > 0$, i.e. to calculate stationary values of the order parameter; this is why Landau's theory ignores higher terms of the Taylor expansion – which are much smaller at $\eta \rightarrow 0$.

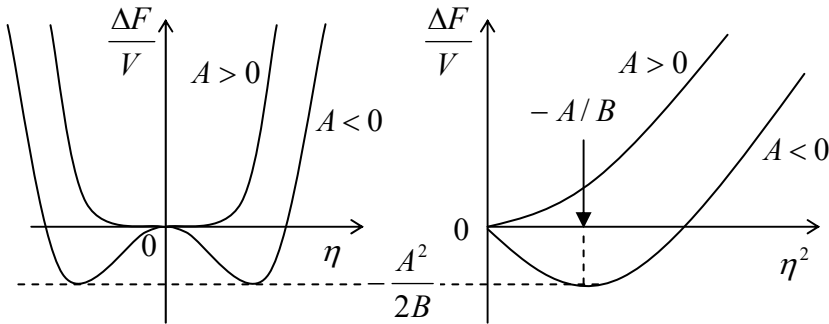


Fig. 4.6. The Landau free energy (42) as a function of (a) η and (b) η^2 , for two signs of the coefficient $A(T)$, both for $B(T) > 0$.

Now let us discuss the temperature dependencies of the coefficients A and B . As Eq. (42) shows, first of all, the coefficient $B(T)$ has to be positive for any sign of $\tau \propto (T_c - T)$, to ensure the equilibrium at a finite value of η^2 . Thus, it is reasonable to ignore the temperature dependence of B near the critical temperature altogether, i.e. use the approximation

$$B(T) = b > 0. \quad (4.43)$$

On the other hand, as Fig. 6 shows, the coefficient $A(T)$ has to change sign at $T = T_c$, to be positive at $T > T_c$ and negative at $T < T_c$, to ensure the transition from $\eta = 0$ at $T > T_c$ to a certain non-zero value of the order parameter at $T < T_c$. Assuming that A is a smooth function of temperature, we may approximate it by the leading term of its Taylor expansion in τ :

$$A(T) = -a\tau, \quad \text{with } a > 0, \quad (4.44)$$

so that Eq. (42) becomes

$$\Delta f|_{h=0} = -a\tau\eta^2 + \frac{1}{2}b\eta^4. \quad (4.45)$$

In this rudimentary form, the Landau theory may look almost trivial, and its main strength is the possibility of its straightforward extension to the effects of the external field and of spatial variations of the order parameter. First, as the field terms in Eqs. (21) or (23) show, the applied field gives such

systems, on average, the energy addition of $-h\eta$ per particle, i.e. $-nh\eta$ per unit volume, where n is the particle density. Second, since according to Eq. (31) (with $\nu > 0$, see Table 1) the correlation radius diverges at $\tau \rightarrow 0$, in this limit the spatial variations of the order parameter should be slow, $|\nabla\eta| \rightarrow 0$. Hence, the effects of the gradient on ΔF may be approximated by the first non-zero term of its expansion into the Taylor series in $(\nabla\eta)^2$.²⁶ As a result, Eq. (45) may be generalized as

Landau theory:
free energy

$$\Delta F = \int \Delta f d^3 r, \quad \text{with } \Delta f = -a\tau\eta^2 + \frac{1}{2}b\eta^4 - nh\eta + c(\nabla\eta)^2, \quad (4.46)$$

where c is a coefficient independent of η . To avoid the unphysical effect of spontaneous formation of spatial variations of the order parameter, that factor has to be positive at all temperatures and hence may be taken for a constant in a small vicinity of T_c – the only region where Eq. (46) may be expected to provide quantitatively correct results.

Let us find out what critical exponents are predicted by this phenomenological approach. First of all, we may find the equilibrium values of the order parameter from the condition of F having a minimum, $\partial F / \partial \eta = 0$. At $h = 0$, it is easier to use the equivalent equation $\partial F / \partial (\eta^2) = 0$, where F is given by Eq. (45) – see Fig. 6b. This immediately yields

$$|\eta| = \begin{cases} (a\tau/b)^{1/2}, & \text{for } \tau > 0, \\ 0, & \text{for } \tau < 0. \end{cases} \quad (4.47)$$

Comparing this result with Eq. (26), we see that in the Landau theory, $\beta = 1/2$. Next, plugging the result (47) back into Eq. (45), for the equilibrium (minimal) value of the free energy, we get

$$\Delta f = \begin{cases} -a^2\tau^2/2b, & \text{for } \tau > 0, \\ 0, & \text{for } \tau < 0. \end{cases} \quad (4.48)$$

From here and Eq. (37), the specific heat,

$$\frac{C_h}{V} = \begin{cases} a^2/bT_c, & \text{for } \tau > 0, \\ 0, & \text{for } \tau < 0, \end{cases} \quad (4.49)$$

has, at the critical point, a discontinuity rather than a singularity, so that we need to prescribe zero value to the critical exponent α .

In the presence of a uniform field, the equilibrium order parameter should be found from the condition $\partial f / \partial \eta = 0$ applied to Eq. (46) with $\nabla\eta = 0$, giving

$$\frac{\partial f}{\partial \eta} \equiv -2a\tau\eta + 2b\eta^3 - nh = 0. \quad (4.50)$$

In the limit of a small order parameter, $\eta \rightarrow 0$, the term with η^3 is negligible, and Eq. (50) gives

$$\eta = -\frac{nh}{2a\tau}, \quad (4.51)$$

²⁶ Historically, the last term belongs to the later (1950) extension of the theory by V. Ginzburg and L. Landau – see below.

so that according to Eq. (29), $\gamma = 1$. On the other hand, at $\tau = 0$ (or at relatively high fields at other temperatures), the cubic term in Eq. (50) is much larger than the linear one, and this equation yields

$$\eta = \left(\frac{nh}{2b} \right)^{1/3}, \quad (4.52)$$

so that comparison with Eq. (32) yields $\delta = 3$. Finally, according to Eq. (30), the last term in Eq. (46) scales as $c\eta^2/r_c^2$. (If $r_c \neq \infty$, the effects of the pre-exponential factor in Eq. (30) are negligible.) As a result, the gradient term's contribution is comparable²⁷ with the two leading terms in Δf (which, according to Eq. (47), are of the same order), if

$$r_c \approx \left(\frac{c}{a|\tau|} \right)^{1/2}, \quad (4.53)$$

so that according to the definition (31) of the critical exponent ν , in the Landau theory it is equal to $\frac{1}{2}$.

The third column in Table 1 summarizes the critical exponents and their combinations in Landau's theory. It shows that these values are somewhat out of the experimental ranges, and while some of their “universal” relations are correct, some are not; for example, the Josephson relation would be only correct at $d = 4$ (not the most realistic spatial dimensionality :-). The main reason for this disappointing result is that describing the spin interaction with the field, the Landau mean-field theory neglects spin randomness, i.e. fluctuations. Though a quantitative theory of fluctuations will be discussed only in the next chapter, we can readily perform their crude estimate. Looking at Eq. (46), we see that its first term is a quadratic function of the effective “half-degree of freedom”, η . Hence per the equipartition theorem (2.28), we may expect that the average square of its thermal fluctuations, within a d -dimensional volume with a linear size of the order of r_c , should be of the order of $T/2$ (close to the critical temperature, $T_c/2$ is a good enough approximation):

$$a|\tau| \langle \tilde{\eta}^2 \rangle r_c^d \sim \frac{T_c}{2}. \quad (4.54)$$

In order to be negligible, the variance has to be small in comparison with the average $\eta^2 \sim a\tau/b$ – see Eq. (47). Plugging in the τ -dependences of the operands of this relation, and values of the critical exponents in the Landau theory, for $\tau > 0$ we get the so-called *Levanyuk-Ginzburg criterion* of its validity:

$$\frac{T_c}{2a\tau} \left(\frac{a\tau}{c} \right)^{d/2} \ll \frac{a\tau}{b}. \quad (4.55)$$

We see that for any realistic dimensionality, $d < 4$, at $\tau \rightarrow 0$ the order parameter's fluctuations grow faster than its average value, and hence the theory becomes invalid.

Thus the Landau mean-field theory is not a perfect approach to finding critical indices at continuous phase transitions in Ising-type systems with their next-neighbor interactions between the particles. Despite that fact, this theory is very much valued because of the following reason. Any long-range interactions between particles increase the correlation radius r_c , and hence suppress the order

²⁷ According to Eq. (30), the correlation radius may be interpreted as the distance at which the order parameter η relaxes to its equilibrium value, if it is deflected from that value at some point. Since the law of such spatial change may be obtained by a variational differentiation of F , for the actual relaxation law, all major terms of (46) have to be comparable.

parameter fluctuations. As one example, at laser self-excitation, the emerging coherent optical field couples essentially *all* photon-emitting particles in the electromagnetic cavity (resonator). As another example, in superconductors the role of the correlation radius is played by the Cooper-pair size ξ_0 , which is typically of the order of 10^{-6} m, i.e. much larger than the average distance between the pairs ($\sim 10^{-8}$ m). As a result, the mean-field theory remains valid at all temperatures besides an extremely small temperature interval near T_c – for bulk superconductors, of the order of 10^{-6} K.

Another strength of Landau's *classical* mean-field theory (46) is that it may be readily generalized for a description of Bose-Einstein condensates, i.e. *quantum* fluids. Of those generalizations, the most famous is the *Ginzburg-Landau theory* of superconductivity. It was developed in 1950, i.e. even before the microscopic-level explanation of this phenomenon by J. Bardeen, L. Cooper, and R. Schrieffer in 1956-57. In this theory, the real order parameter η is replaced with the modulus of a complex function ψ , physically the wavefunction of the coherent Bose-Einstein condensate of Cooper pairs. Since each pair carries the electric charge $q = -2e$ and has zero spin, it interacts with the magnetic field in a way different from that described by the Heisenberg or Ising models. Namely, as was already discussed in Sec. 3.4, in the magnetic field, the del operator ∇ in Eq. (46) has to be complemented with the term $-i(q/\hbar)\mathbf{A}$, where \mathbf{A} is the vector potential of the total magnetic field $\mathcal{B} = \nabla \times \mathbf{A}$, including not only the external magnetic field \mathcal{H} but also the field induced by the supercurrent itself. With the account for the well-known formula for the magnetic field energy, Eq. (46) is now replaced with

GL theory:
free energy

$$\Delta f = -a\tau|\psi|^2 + \frac{1}{2}b|\psi|^4 - \frac{\hbar^2}{2m}\left|\left(\nabla - i\frac{q}{\hbar}\mathbf{A}\right)\psi\right|^2 + \frac{\mathcal{B}^2}{2\mu_0}, \quad (4.56)$$

where m is a phenomenological coefficient rather than the actual particle's mass.

The variational minimization of the resulting Gibbs energy density $\Delta g \equiv \Delta f - \mu_0\mathcal{H}\mathcal{M} \equiv \Delta f - \mathcal{H}\mathcal{B} + \text{const}^{28}$ over the variables ψ and \mathcal{B} (which is suggested for reader's exercise) yields two differential equations:

GL
equations

$$\frac{\nabla \times \mathcal{B}}{\mu_0} = q\frac{i\hbar}{2m}\left[\psi\left(\nabla - i\frac{q}{\hbar}\mathbf{A}\right)\psi^* - \text{c.c.}\right], \quad (4.57a)$$

$$a\tau\psi = b|\psi|^2\psi - \frac{\hbar^2}{2m}\left(\nabla - i\frac{q}{\hbar}\mathbf{A}\right)^2\psi. \quad (4.57b)$$

The first of these *Ginzburg-Landau equations* (57a) should be no big surprise for the reader, because according to the Maxwell equations, in magnetostatics the left-hand side of Eq. (57a) has to be equal to the electric current density, while its right-hand side is the usual quantum-mechanical probability current density multiplied by q , i.e. the density \mathbf{j} of the electric current of the Cooper pair condensate. (Indeed, after plugging $\psi = n^{1/2}\exp\{i\varphi\}$ into that expression, we come back to Eq. (3.84) which, as we already know, explains such macroscopic quantum phenomena as the magnetic flux quantization and the Meissner-Ochsenfeld effect.)

²⁸ As an immediate elementary sanity check of this relation, resulting from the analogy of Eqs. (1.1) and (1.3), the minimization of Δg in the absence of superconductivity ($\psi = 0$) gives the correct result $\mathcal{B} = \mu_0\mathcal{H}$. Note that this account of the difference between Δf and Δg is necessary here because (unlike Eqs. (21) and (23)), the Ginzburg-Landau free energy (56) does not take into account the effect of the field on each particle directly.

However, Eq. (57b) is new for us – at least for this course.²⁹ Since the last term on its right-hand side is the standard wave-mechanical expression for the kinetic energy of a particle in the presence of a magnetic field,³⁰ if this term dominates that side of the equation, Eq. (57b) is reduced to the stationary Schrödinger equation $E\psi = \hat{H}\psi$, for the ground state of free Cooper pairs, with the total energy $E = a\tau$. However, in contrast to the usual (single-particle) Schrödinger equation, in which $|\psi|$ is determined by the normalization condition, the Cooper pair condensate density $n = |\psi|^2$ is determined by the thermodynamic balance of the condensate with the ensemble of “normal” (unpaired) electrons, which plays the role of the uncondensed part of the particles in the usual Bose-Einstein condensate – see Sec. 3.4. In Eq. (57b), such balance is enforced by the first term $b|\psi|^2\psi$ on the right-hand side. As we have already seen, in the absence of magnetic field and spatial gradients, such term yields $|\psi| \propto \tau^{1/2} \propto (T_c - T)^{1/2}$ – see Eq. (47).

As a parenthetic remark, from the mathematical standpoint, the term $b|\psi|^2\psi$, which is nonlinear in ψ , makes Eq. (57b) a member of the family of the so-called *nonlinear Schrödinger equations*. Another member of this family, important for physics, is the *Gross-Pitaevskii equation*,

$$a\tau\psi = b|\psi|^2\psi - \frac{\hbar^2}{2m}\nabla^2\psi + U(\mathbf{r})\psi, \quad (4.58)$$

Gross-Pitaevskii equation

which gives a reasonable (albeit approximate) description of gradient and field effects on Bose-Einstein condensates of electrically neutral atoms at $T \approx T_c$. The differences between Eqs. (58) and (57) reflect, first, the zero electric charge q of the atoms (so that Eq. (57a) becomes trivial) and, second, the fact that the atoms forming the condensates may be readily placed in external potentials $U(\mathbf{r}) \neq \text{const}$ (including the time-averaged potentials of optical traps – see EM Chapter 7), while in superconductors such potential profiles are much harder to create due to the screening of external electric and optical fields by conductors – see, e.g., EM Sec. 2.1.

Returning to the discussion of Eq. (57b), it is easy to see that its last term increases as either the external magnetic field or the density of current passed through a superconductor are increased, increasing the vector potential. In the Ginzburg-Landau equation, this *increase* is matched by a corresponding *decrease* of $|\psi|^2$, i.e. of the condensate density n , until it is completely suppressed. This balance describes the well-documented effect of superconductivity suppression by an external magnetic field and/or the supercurrent passed through the sample. Moreover, together with Eq. (57a), naturally describing the flux quantization (see Sec. 3.4), Eq. (57b) explains the existence of the so-called *Abrikosov vortices* – thin magnetic-field tubes, each carrying one quantum Φ_0 of magnetic flux – see Eq. (3.86). At the core part of the vortex, $|\psi|^2$ is suppressed (down to zero at its central line) by the persistent, dissipation-free current of the superconducting condensate, which circulates around the core and screens the rest of the superconductor from the magnetic field carried by the vortex.³¹ The penetration of such vortices into the so-called type-II superconductors enables them to sustain zero dc resistance up to very high magnetic fields of the order of 20 T, and as a result, to be used in very compact magnets – including those used for beam bending in particle accelerators.

Moreover, generalizing Eqs. (57) to the time-dependent case, just as it is done with the usual Schrödinger equation, one can describe other fascinating quantum macroscopic phenomena such as the

²⁹ It is discussed in EM Sec. 6.5.

³⁰ See, e.g., QM Sec. 3.1.

³¹ See, e.g., EM Sec. 6.5.

Josephson effects, including the generation of oscillations with frequency $\omega_J = (q/\hbar)\mathcal{V}$ by weak links between two superconductors, biased by dc voltage \mathcal{V} . Unfortunately, time/space restrictions do not allow me to discuss these effects in any detail in this course, and I have to refer the reader to special literature.³² Let me only note that in the limit $T \rightarrow T_c$, and for not extremely pure superconductor crystals (in which the so-called non-local transport phenomena may be important), the Ginzburg-Landau equations are exact, and may be derived (and their parameters T_c , a , b , q , and m determined) from the standard “microscopic” theory of superconductivity, based on the initial work by Bardeen, Cooper, and Schrieffer.³³ Most importantly, such derivation proves that $q = -2e$ – the electric charge of a single Cooper pair.

4.4. Ising model: The Weiss molecular-field theory

The Landau mean-field theory is phenomenological in the sense that even within the range of its validity, it tells us nothing about the value of the critical temperature T_c and other parameters (in Eq. (46), the coefficients a , b , and c), so that they have to be found from a particular “microscopic” model of the system under analysis. In this course, we would have time to discuss only the Ising model (23) for various dimensionalities d .

The most simplistic way to map this model on a mean-field theory is to assume that all spins are exactly equal, $s_k = \eta$, with an additional condition $\eta^2 \leq 1$, ignoring for a minute the fact that in the genuine Ising model, s_k may equal only +1 or -1. Plugging this relation into Eq. (23), we get³⁴

$$F = -(NJd)\eta^2 - Nh\eta. \quad (4.59)$$

This energy is plotted in Fig. 7a as a function of η , for several values of h .

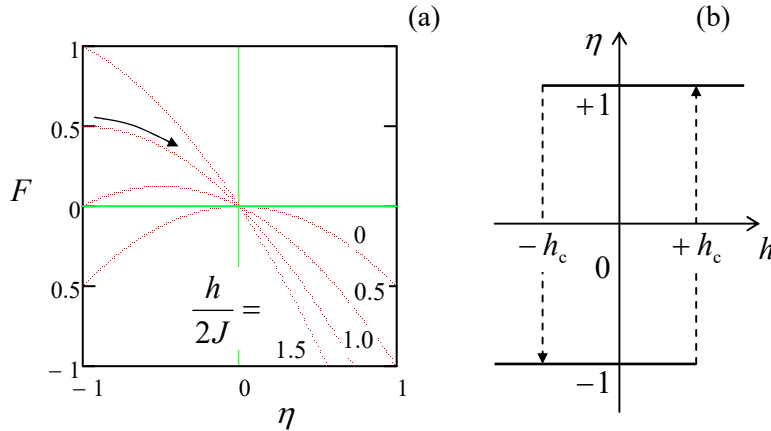


Fig. 4.7. Field dependences of (a) the free energy profile and (b) the order parameter (i.e. magnetization) in the crudest mean-field approach to the Ising model.

The plots show that at $h = 0$, the system may be in either of two stable states, with $\eta = \pm 1$, corresponding to two different spin directions (i.e. two different directions of magnetization), with equal

³² See, e.g., M. Tinkham, *Introduction to Superconductivity*, 2nd ed., McGraw-Hill, 1996. A short discussion of the Josephson effects and Abrikosov vortices may be found in QM Sec. 1.6 and EM Sec. 6.5 of this series.

³³ See, e.g., Sec. 45 in E. Lifshitz and L. Pitaevskii, *Statistical Physics*, Part 2, Pergamon, 1980.

³⁴ Since in this naïve approach we neglect the fluctuations of spin, i.e. their disorder, the assumption of full ordering implies $S = 0$, so that $F \equiv E - TS = E$, and we may use either notation for the system’s energy.

energy.³⁵ (Formally, the state with $\eta = 0$ is also stationary, because at this point $\partial F/\partial\eta = 0$, but it is unstable, because for the ferromagnetic interaction, $J > 0$, the second derivative $\partial^2 F/\partial\eta^2$ is always negative.)

As the external field is increased, it tilts the potential profile, and finally at the critical field,

$$h = h_c \equiv 2Jd, \quad (4.60)$$

the state with $\eta = -1$ becomes unstable, leading to the system's jump into the only remaining state with opposite magnetization, $\eta = +1$ – see the arrow in Fig. 7a. Application of the similar external field of the opposite polarity leads to the similar switching, back to $\eta = -1$, at the field $h = -h_c$, so that the full field dependence of η follows the hysteretic pattern shown in Fig. 7b.³⁶

Such a pattern is the most visible experimental feature of actual ferromagnetic materials, with the *coercive magnetic field* \mathcal{H}_c of the order of 10^3 A/m, and the *saturated* (or “remnant”) *magnetization* corresponding to fields \mathcal{B} of the order of a few teslas. The most important property of these materials, also called *permanent magnets*, is their stability, i.e. the ability to retain the history-determined direction of magnetization in the absence of an external field, for a very long time. In particular, this property is the basis of all magnetic systems for data recording, including the now-ubiquitous hard disk drives with their incredible information density, currently approaching 1 Terabit per square inch.³⁷

So, this simplest mean-field theory (59) does give a (crude) description of the ferromagnetic ordering. However, this theory grossly overestimates the stability of these states with respect to thermal fluctuations. Indeed, in this theory, there is no thermally-induced randomness at all, until T becomes comparable with the height of the energy barrier separating two stable states,

$$\Delta F \equiv F(\eta = 0) - F(\eta = \pm 1) = NJd, \quad (4.61)$$

which is proportional to the number of particles. At $N \rightarrow \infty$, this value diverges, and in this sense, the critical temperature is infinite, while numerical experiments and more refined theories of the Ising model show that actually its ferromagnetic phase is suppressed at $T > T_c \sim Jd$ – see below.

The accuracy of this theory may be dramatically improved by even an approximate account for thermally-induced randomness. In this approach (suggested in 1907 by Pierre-Ernest Weiss), called the *molecular-field theory*,³⁸ random deviations of individual spin values from the lattice average,

³⁵ The fact that the stable states always correspond to $\eta = \pm 1$, partly justifies the treatment, in this crude approximation, of the order parameter η as a continuous variable.

³⁶ Since these magnetization jumps are accompanied by (negative) jumps of the free energy F , they are sometimes called the first-order phase transitions. Note, however, that in this simple theory, these transitions are between two physically similar *fully-ordered* phases.

³⁷ For me, it was always shocking how little my graduate students knew about this fascinating (and very important) field of modern engineering, which involves so much interesting physics and fantastic electromechanical technology. For getting acquainted with it, I may recommend, for example, the monograph by C. Mee and E. Daniel, *Magnetic Recording Technology*, 2nd ed., McGraw-Hill, 1996.

³⁸ In some texts, this approximation is called the “mean-field theory”. This terminology may lead to confusion, because the molecular-field theory belongs to a different, deeper level of the theoretical hierarchy than, say, the (more phenomenological) Landau-style mean-field theories. For example, for a given microscopic model, the molecular-field approach may be used for the (approximate) calculation of the parameters a , b , and T_c participating in Eq. (46) – the starting point of the Landau theory.

$$\tilde{s}_k \equiv s_k - \eta, \quad \text{with } \eta \equiv \langle s_k \rangle, \quad (4.62)$$

are allowed, but considered small, $|\tilde{s}_k| \ll \eta$. This assumption allows us, after plugging the resulting expression $s_k = \eta + \tilde{s}_k$ to the first term on the right-hand side of Eq. (23),

$$E_m = -J \sum_{\{k,k'\}} (\eta + \tilde{s}_k)(\eta + \tilde{s}_{k'}) - h \sum_k s_k \equiv -J \sum_{\{k,k'\}} [\eta^2 + \eta(\tilde{s}_k + \tilde{s}_{k'}) + \tilde{s}_k \tilde{s}_{k'}] - h \sum_k s_k, \quad (4.63)$$

ignore the last term in the square brackets. Making the replacement (62) in the terms proportional to \tilde{s}_k , we may rewrite the result as

$$E_m \approx E'_m \equiv (N J d) \eta^2 - h_{\text{ef}} \sum_k s_k, \quad (4.64)$$

where h_{ef} is defined as the sum

$$h_{\text{ef}} \equiv h + (2 J d) \eta. \quad (4.65)$$

This sum may be interpreted as the *effective* external field, which takes into account (besides the genuine external field h) the effect that *would be* exerted on spin s_k by its $2d$ next neighbors if they all had non-fluctuating (but possibly continuous) spin values $s_{k'} = \eta$. Such addition to the external field,

Weiss
molecular
field

$$h_{\text{mol}} \equiv h_{\text{ef}} - h = (2 J d) \eta, \quad (4.66)$$

is called the *molecular field* – giving its name to the Weiss theory.

From the point of view of statistical physics, at fixed parameters of the system (including the order parameter η), the first term on the right-hand side of Eq. (64) is merely a constant energy offset, and h_{ef} is just another constant, so that

$$E'_m = \text{const} + \sum_k \varepsilon_k, \quad \text{with } \varepsilon_k = -h_{\text{ef}} s_k \equiv \begin{cases} -h_{\text{ef}}, & \text{for } s_k = +1, \\ +h_{\text{ef}}, & \text{for } s_k = -1. \end{cases} \quad (4.67)$$

Such separability of the energy means that in the molecular-field approximation the fluctuations of different spins are independent of each other, and their statistics may be examined individually, using the energy spectrum ε_k . But this is exactly the two-level system that was the subject of Problems 2.2-2.4. Actually, its statistics is so simple that it is easier to redo this fundamental problem starting from scratch, rather than to use the results of those exercises (which would require changing notation).

Indeed, according to the Gibbs distribution (2.58)-(2.59), the equilibrium probabilities of the states $s_k = \pm 1$ may be found as

$$W_{\pm} = \frac{1}{Z} e^{\pm h_{\text{ef}}/T}, \quad \text{with } Z = \exp\left\{+\frac{h_{\text{ef}}}{T}\right\} + \exp\left\{-\frac{h_{\text{ef}}}{T}\right\} \equiv 2 \cosh \frac{h_{\text{ef}}}{T}. \quad (4.68)$$

From here, we may readily calculate $F = -T \ln Z$ and all other thermodynamic variables, but let us immediately use Eq. (68) to calculate the statistical average of s_j , i.e. the order parameter:

$$\eta \equiv \langle s_j \rangle = (+1) W_+ + (-1) W_- = \frac{e^{+h_{\text{ef}}/T} - e^{-h_{\text{ef}}/T}}{2 \cosh(h_{\text{ef}}/T)} \equiv \tanh \frac{h_{\text{ef}}}{T}. \quad (4.69)$$

Now comes the punch line of the Weiss' approach: plugging this result back into Eq. (65), we may write the condition of *self-consistency* of the molecular-field theory:

$$h_{\text{ef}} - h = 2Jd \tanh \frac{h_{\text{ef}}}{T}. \quad (4.70)$$

Self-consistency equation

This is a transcendental equation, which evades an explicit analytical solution, but whose properties may be readily analyzed by plotting both its sides as functions of the same argument, so that the stationary state(s) of the system corresponds to the intersection point(s) of these plots.

First of all, let us explore the field-free case ($h = 0$), when $h_{\text{ef}} = h_{\text{mol}} \equiv 2dJ\eta$, so that Eq. (70) is reduced to

$$\eta = \tanh\left(\frac{2Jd}{T}\eta\right), \quad (4.71)$$

giving one of the patterns sketched in Fig. 8, depending on the dimensionless parameter $2Jd/T$.

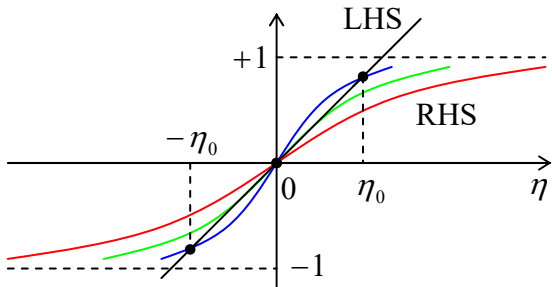


Fig. 4.8. The ferromagnetic phase transition in Weiss' molecular-field theory: two sides of Eq. (71) sketched as functions of η for three different temperatures: above T_c (red), below T_c (blue), and equal to T_c (green).

If this parameter is small, the right-hand side of Eq. (71) grows slowly with η (see the red line in Fig. 8), and there is only one intersection point with the left-hand side plot, at $\eta = 0$. This means that the spin system has no spontaneous magnetization; this is the so-called *paramagnetic phase*. However, if the parameter $2Jd/T$ exceeds 1, i.e. if T is decreased below the following critical value,

$$T_c = 2Jd, \quad (4.72)$$

Critical ("Curie") temperature

the right-hand side of Eq. (71) grows, at small η , faster than its left-hand side, so that their plots intersect it in 3 points: $\eta = 0$ and $\eta = \pm\eta_0$ – see the blue line in Fig. 8. It is almost evident that the former stationary point is unstable, while the two latter points are stable. (This fact may be readily verified by using Eq. (68) to calculate F . Now the condition $\partial F / \partial \eta|_{h=0} = 0$ returns us to Eq. (71), while calculating the second derivative, for $T < T_c$ we get $\partial^2 F / \partial \eta^2 > 0$ at $\eta = \pm\eta_0$, and $\partial^2 F / \partial \eta^2 < 0$ at $\eta = 0$). Thus, below T_c the system is in the ferromagnetic phase, with one of two possible directions of the average spontaneous magnetization, so that the critical (*Curie*³⁹) temperature, given by Eq. (72), marks the transition between the paramagnetic and ferromagnetic phases. (Since the stable minimum value of the free energy F is a continuous function of temperature at $T = T_c$, this phase transition is continuous.)

Now let us repeat this graphics analysis to examine how each of these phases responds to an external magnetic field $h \neq 0$. According to Eq. (70), the effect of h is just a horizontal shift of the

³⁹ Named after Pierre Curie, rather than his (more famous) wife Marie Skłodowska-Curie.

straight-line plot of its left-hand side – see Fig. 9. (Note a different, here more convenient, normalization of both axes.)

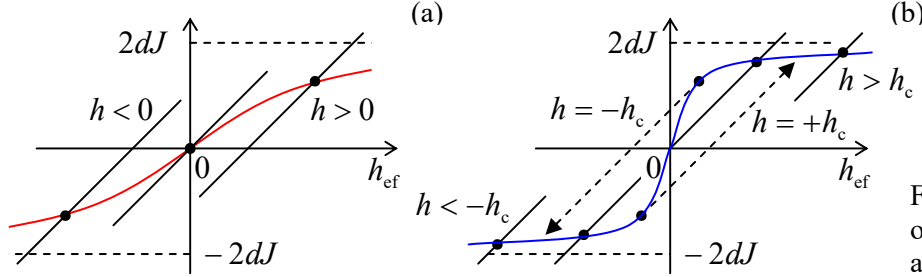


Fig. 4.9 External field effects on: (a) a paramagnet ($T > T_c$), and (b) a ferromagnet ($T < T_c$).

In the paramagnetic case (Fig. 9a) the resulting dependence $h_{\text{ef}}(h)$ is evidently continuous, but the coupling effect ($J > 0$) makes it steeper than it would be without spin interaction. This effect may be quantified by the calculation of the low-field susceptibility defined by Eq. (29). To calculate it, let us notice that for small h , and hence small h_{ef} , the function \tanh in Eq. (70) is approximately equal to its argument so that Eq. (70) is reduced to

$$h_{\text{ef}} - h = \frac{2Jd}{T} h_{\text{ef}}, \quad \text{for } \left| \frac{2Jd}{T} h_{\text{ef}} \right| \ll 1. \quad (4.73)$$

Solving this equation for h_{ef} , and then using Eq. (72), we get

$$h_{\text{ef}} = \frac{h}{1 - 2Jd/T} = \frac{h}{1 - T_c/T}. \quad (4.74)$$

Recalling Eq. (66), we can rewrite this result for the order parameter:

$$\eta = \frac{h_{\text{ef}} - h}{T_c} = \frac{h}{T - T_c}, \quad (4.75)$$

so that the low-field susceptibility

$$\chi \equiv \frac{\partial \eta}{\partial h} \Big|_{h=0} = \frac{1}{T - T_c}, \quad \text{for } T > T_c. \quad (4.76)$$

This is the famous *Curie-Weiss law*, which shows that the susceptibility diverges at the approach to the Curie temperature T_c .

In the ferromagnetic case, the graphical solution (Fig. 9b) of Eq. (70) gives a qualitatively different result. A field increase leads, depending on the spontaneous magnetization, either to the further saturation of h_{mol} (with the order parameter η gradually approaching 1), or, if the initial η was negative, to a jump to positive η at some critical (coercive) field h_c . In contrast with the crude approximation (59), at $T > 0$ the coercive field is smaller than that given by Eq. (60), and the magnetization saturation is gradual, in a good (semi-qualitative) accordance with experiment.

To summarize, the Weiss molecular-field theory gives an approximate but realistic description of the ferromagnetic and paramagnetic phases in the Ising model, and a very simple prediction (72) of the temperature of the phase transition between them, for an arbitrary dimensionality d of the cubic lattice. It also enables calculation of other parameters of Landau's mean-field theory for this model – an easy

exercise left for the reader. Moreover, the molecular-field approach allows one to obtain analytical (if approximate) results for other models of phase transitions – see, e.g., Problem 18.

4.5. Ising model: Exact and numerical results

In order to evaluate the main prediction (72) of the Weiss theory, let us now discuss the exact (analytical) and quasi-exact (numerical) results obtained for the Ising model, going from the lowest value of dimensionality, $d = 0$, to its higher values. Zero dimensionality means that the spin has no nearest neighbors at all, so that the first term of Eq. (23) vanishes. Hence Eq. (64) is exact, with $h_{\text{ef}} = h$, and so is its solution (69). Now we can simply use Eq. (76), with $J = 0$, i.e. $T_c = 0$, reducing this result to the so-called *Curie law*:

$$\chi = \frac{1}{T}. \quad (4.77)$$

Curie
law

It shows that the system is paramagnetic at any temperature. One may say that for $d = 0$ the Weiss molecular-field theory is exact – or even trivial. (However, in some sense it is more general than the Ising model, because as we know from Chapter 2, it gives the exact result for a fully quantum-mechanical treatment of any two-level system, including spin-½.) Experimentally, the Curie law is approximately valid for many so-called *paramagnetic materials*, i.e. 3D systems with sufficiently weak interaction between particle spins.

The case $d = 1$ is more complex but has an exact analytical solution. A simple (though not the simplest!) way to obtain it is to use the so-called *transfer matrix approach*.⁴⁰ For this, first of all, we may argue that most properties of a 1D system of $N \gg 1$ spins (say, put at equal distances on a straight line) should not change noticeably if we bend that line gently into a closed ring (Fig. 10), assuming that spins s_1 and s_N interact exactly as all other next-neighbor pairs. Then the energy (23) becomes

$$E_m = -(J s_1 s_2 + J s_2 s_3 + \dots + J s_N s_1) - (h s_1 + h s_2 + \dots + h s_N). \quad (4.78)$$

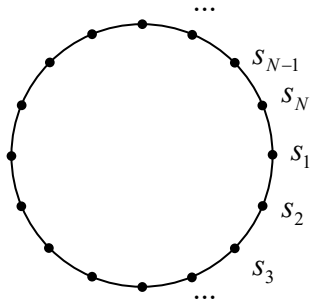


Fig. 4.10. The closed-ring version of the 1D Ising system.

Let us regroup the terms of this sum in the following way:

$$E_m = - \left[\left(\frac{h}{2} s_1 + J s_1 s_2 + \frac{h}{2} s_2 \right) + \left(\frac{h}{2} s_2 + J s_2 s_3 + \frac{h}{2} s_3 \right) + \dots + \left(\frac{h}{2} s_N + J s_N s_1 + \frac{h}{2} s_1 \right) \right], \quad (4.79)$$

⁴⁰ It was developed in 1941 by H. Kramers and G. Wannier. I am following this method here because it is very close to the one used in quantum mechanics (see, e.g., QM Sec. 2.5), and may be applied to other problems as well. For a simpler approach to the 1D Ising problem, which gives an explicit solution even for an “open-end” system with a finite number of spins, see the model solution of Problem 5.5.

so that the group inside each pair of parentheses depends only on the state of two adjacent spins. The corresponding statistical sum,

$$Z = \sum_{\substack{s_k=\pm 1, \text{for} \\ k=1,2,\dots,N}} \exp\left\{h \frac{s_1}{2T} + J \frac{s_1 s_2}{T} + h \frac{s_2}{2T}\right\} \exp\left\{h \frac{s_2}{2T} + J \frac{s_2 s_3}{T} + h \frac{s_3}{2T}\right\} \dots \exp\left\{h \frac{s_N}{2T} + J \frac{s_N s_1}{T} + h \frac{s_1}{2T}\right\}, \quad (4.80)$$

still has 2^N terms, each corresponding to a certain combination of signs of N spins. However, each operand of the product under the sum may take only four values, corresponding to four different combinations of its two arguments:

$$\exp\left\{h \frac{s_k}{2T} + J \frac{s_k s_{k+1}}{T} + h \frac{s_{k+1}}{2T}\right\} = \begin{cases} \exp\{(J+h)/T\}, & \text{for } s_k = s_{k+1} = +1, \\ \exp\{(J-h)/T\}, & \text{for } s_k = s_{k+1} = -1, \\ \exp\{-J/T\}, & \text{for } s_k = -s_{k+1} = \pm 1. \end{cases} \quad (4.81)$$

These values do not depend on the site number k ,⁴¹ and may be represented as the elements $M_{j,j'}$ (with $j, j' = 1, 2$) of the so-called *transfer matrix*

$$M \equiv \begin{pmatrix} \exp\{(J+h)/T\} & \exp\{-J/T\} \\ \exp\{-J/T\} & \exp\{(J-h)/T\} \end{pmatrix}, \quad (4.82)$$

so that the whole statistical sum (80) may be recast as a product:

$$Z = \sum_{j_k=1,2} M_{j_1 j_2} M_{j_2 j_3} \dots M_{j_{N-1} j_N} M_{j_N j_1}. \quad (4.83)$$

According to the basic rule of matrix multiplication, this sum is just

$$Z = \text{Tr}(M^N). \quad (4.84)$$

Linear algebra tells us that this trace may be represented just as

$$Z = \lambda_+^N + \lambda_-^N, \quad (4.85)$$

where λ_{\pm} are the eigenvalues of the transfer matrix M , i.e. the roots of its characteristic equation,

$$\begin{vmatrix} \exp\{(J+h)/T\} - \lambda & \exp\{-J/T\} \\ \exp\{-J/T\} & \exp\{(J-h)/T\} - \lambda \end{vmatrix} = 0. \quad (4.86)$$

A straightforward calculation yields

$$\lambda_{\pm} = \exp\left\{\frac{J}{T}\right\} \left[\cosh \frac{h}{T} \pm \left(\sinh^2 \frac{h}{T} + \exp\left\{-\frac{4J}{T}\right\} \right)^{1/2} \right]. \quad (4.87)$$

The last simplification comes from the condition $N \gg 1$ – which we need anyway, to make the ring model sufficiently close to the infinite linear 1D system. In this limit, even a small difference of the exponents, $\lambda_+ > \lambda_-$, makes the second term in Eq. (85) negligible, so that we finally get

⁴¹ This is a result of the “translational” (or rather rotational) symmetry of the system, i.e. its invariance to the index replacement $k \rightarrow k + 1$ in all terms of Eq. (78).

$$Z = \lambda_+^N = \exp\left\{\frac{NJ}{T}\right\} \left[\cosh \frac{h}{T} + \left(\sinh^2 \frac{h}{T} + \exp\left\{-\frac{4J}{T}\right\} \right)^{1/2} \right]^N. \quad (4.88)$$

From here, we can find the free energy per particle:

$$\frac{F}{N} = \frac{T}{N} \ln \frac{1}{Z} = -J - T \ln \left[\cosh \frac{h}{T} + \left(\sinh^2 \frac{h}{T} + \exp\left\{-\frac{4J}{T}\right\} \right)^{1/2} \right], \quad (4.89)$$

and then use thermodynamics to calculate such variables as entropy – see the first of Eqs. (1.35).

However, we are mostly interested in the order parameter defined by Eq. (25): $\eta \equiv \langle s_j \rangle$. The conceptually simplest approach to the calculation of this statistical average would be to use the sum (2.7), with the Gibbs probabilities $W_m = Z^{-1} \exp\{-E_m/T\}$. However, the number of terms in this sum is 2^N , so that for $N \gg 1$ this approach is completely impracticable. Here the analogy between the canonical pair $\{-P, V\}$ and other generalized force-coordinate pairs $\{\mathcal{F}, q\}$, in particular $\{\mu_0 \mathcal{H}(\mathbf{r}_k), m_k\}$ for the magnetic field, discussed in Secs. 1.1 and 1.4, becomes invaluable – see in particular Eq. (1.3b). (In our normalization (22), and for a uniform field, the pair $\{\mu_0 \mathcal{H}(\mathbf{r}_k), m_k\}$ becomes $\{h, s_k\}$.) Indeed, in this analogy the last term of Eq. (23), i.e. the sum of N products $(-hs_k)$ for all spins, with the statistical average $(-Nh\eta)$, is similar to the product PV , i.e. the difference between the thermodynamic potentials F and $G \equiv F + PV$ in the usual “ P - V thermodynamics”. Hence, the free energy F given by Eq. (89) may be understood as the Gibbs energy of the Ising system in the external field, and the equilibrium value of the order parameter may be found from the last of Eqs. (1.39) with the replacements $-P \rightarrow h$, $V \rightarrow N\eta$:

$$N\eta = -\left(\frac{\partial F}{\partial h} \right)_T, \quad \text{i.e. } \eta = -\left[\frac{\partial(F/N)}{\partial h} \right]_T. \quad (4.90)$$

Note that this formula is valid for any model of ferromagnetism, of any dimensionality, if it has the same form of interaction with the external field as the Ising model.

For the 1D Ising ring with $N \gg 1$, Eqs. (89) and (90) yield

$$\eta = \sinh \frac{h}{T} \left/ \left(\sinh^2 \frac{h}{T} + \exp\left\{-\frac{4J}{T}\right\} \right)^{1/2} \right., \quad \text{giving } \chi \equiv \frac{\partial \eta}{\partial h} \Big|_{h=0} = \frac{1}{T} \exp\left\{\frac{2J}{T}\right\}. \quad (4.91)$$

This result means that the 1D Ising model does *not* exhibit a phase transition, i.e., in this model $T_c = 0$. However, its susceptibility grows, at $T \rightarrow 0$, much faster than the Curie law (77). This gives us a hint that at low temperatures the system is “virtually ferromagnetic”, i.e. has the ferromagnetic order with some rare random violations. (Such violations are commonly called *low-temperature excitations*.) This interpretation may be confirmed by the following approximate calculation. It is almost evident that the lowest-energy excitation of the ferromagnetic state of an open-end 1D Ising chain at $h = 0$ is the reversal of signs of all spins in one of its parts – see Fig. 11.

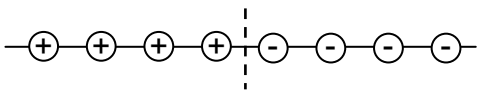


Fig. 4.11. A Bloch wall in an open-end 1D Ising system.

Indeed, such an excitation (called the *Bloch wall*⁴²) involves the change of sign of just one product $s_k s_{k'}$, so that according to Eq. (23), its energy E_W (defined as the difference between the values of E_m with and without the excitation) equals $2J$, regardless of the wall's position.⁴³ Since in the ferromagnetic Ising model, the parameter J is positive, $E_W > 0$. If the system “tried” to minimize its internal energy, having any wall in the system would be energy-disadvantageous. However, thermodynamics tells us that at $T \neq 0$, the system’s thermal equilibrium corresponds to the minimum of the free energy $F \equiv E - TS$, rather than just energy E .⁴⁴ Hence, we have to calculate the Bloch wall’s contribution F_W to the free energy. Since in an open-end linear chain of $N \gg 1$ spins, the wall can take $(N - 1) \approx N$ positions with the same energy E_W , we may claim that the entropy S_W associated with this excitation is $\ln N$, so that

$$F_W \equiv E_W - TS_W \approx 2J - T \ln N. \quad (4.92)$$

This result tells us that in the limit $N \rightarrow \infty$, and at $T \neq 0$, walls are always free-energy-beneficial, thus explaining the absence of the perfect ferromagnetic order in the 1D Ising system. Note, however, that since the logarithmic function changes extremely slowly at large values of its argument, one may argue that a large but finite 1D system should still feature a quasi-critical temperature

$$\text{"}T_c\text{"} = \frac{2J}{\ln N}, \quad (4.93)$$

below which it would be in a virtually complete ferromagnetic order. (The exponentially large susceptibility (91) is another manifestation of this fact.)

Now let us apply a similar approach to estimate T_c of a 2D Ising model, with open borders. Here the Bloch wall is a line of a certain total length L – see Fig. 12. (For the example presented in that figure, counting from the left to the right, $L = 2 + 1 + 4 + 2 + 3 = 12$ lattice periods.) Evidently, the additional energy associated with such a wall is $E_W = 2JL$, while the wall’s entropy S_W may be estimated using the following reasoning. Let the wall be formed along the path of a “Manhattan pedestrian” traveling between its nodes. (The dashed line in Fig. 12 is an example of such a path.) At each junction, the pedestrian may select 3 choices of 4 possible directions (except the one that leads backward), so that there are approximately $3^{(L-1)} \approx 3^L$ options for a walk starting from a certain point. Now taking into account that the open borders of a square-shaped lattice with N spins have a length of the order of $N^{1/2}$, and the Bloch wall may start from any of them, there are approximately $M \sim N^{1/2}3^L$ different walks between two borders. Again estimating S_W as $\ln M$, we get

$$F_W = E_W - TS_W \approx 2JL - T \ln(N^{1/2}3^L) \equiv L(2J - T \ln 3) - (T/2) \ln N. \quad (4.94)$$

(Actually, since L scales as $N^{1/2}$ or higher, at $N \rightarrow \infty$ the last term in Eq. (94) is negligible.) We see that the sign of the derivative $\partial F_W / \partial L$ depends on whether the temperature is higher or lower than the following critical value:

⁴² Named after Felix Bloch who was the first one to discuss such excitations in ferromagnetism.

⁴³ For the closed-ring model (Fig. 10) such analysis gives an almost similar prediction, with the difference that in that system, the Bloch walls may appear only in pairs, so that $E_W = 4J$, and $S_W = \ln[N(N-1)] \approx 2\ln N$.

⁴⁴ This is a very vivid application of one of the core results of thermodynamics. If the reader is still uncomfortable with it, they are strongly encouraged to revisit Eq. (1.42) and its discussion.

$$T_c = \frac{2J}{\ln 3} \approx 1.82 J. \quad (4.95)$$

At $T < T_c$, the free energy's minimum corresponds to $L \rightarrow 0$, i.e. the Bloch walls are free-energy-detrimental, and the system is in the purely ferromagnetic phase.

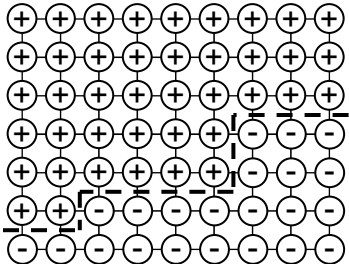


Fig. 4.12. A Bloch wall in a 2D Ising system.

So, for $d = 2$ the estimates predict a non-zero critical temperature of the same order as the Weiss theory (according to Eq. (72), in this case $T_c = 4J$). The major approximation implied in our calculation leading to Eq. (95) is disregarding possible self-crossings of the “Manhattan walk”. The accurate counting of such self-crossings is rather difficult. It had been carried out in 1944 by L. Onsager; since then his calculations have been redone in several easier ways, but even they are rather cumbersome, and I will not have time to discuss them.⁴⁵ The final result, however, is surprisingly simple:

$$T_c = \frac{2J}{\ln(1 + \sqrt{2})} \approx 2.269 J, \quad (4.96)$$

Onsager's exact result

i.e. showing that the simple estimate (95) is off the mark by only ~20%.

The Onsager solution, as well as all alternative solutions of the problem that were found later, are so “artificial” (2D-specific) that they do not give a clear way towards their generalization to other (higher) dimensions. As a result, the 3D Ising problem is still unsolved analytically. Nevertheless, we do know T_c for it with extremely high precision – at least to the 6th decimal place. This has been achieved by numerical methods; they deserve a thorough discussion because of their importance for the solution of other similar problems as well.

Conceptually, this task is rather simple: just compute, to the desired precision, the statistical sum of the system (23):

$$Z = \sum_{\substack{s_k = \pm 1, \text{ for} \\ k=1,2,\dots,N}} \exp \left\{ \frac{J}{T} \sum_{\{k,k'\}} s_k s_{k'} + \frac{h}{T} \sum_k s_k \right\}. \quad (4.97)$$

As soon as this has been done for a sufficient number of values of the dimensionless parameters J/T and h/T , everything becomes easy; in particular, we can compute the dimensionless function

$$F/T = -\ln Z, \quad (4.98)$$

⁴⁵ For that, the interested reader may be referred to either Sec. 151 in the textbook by Landau and Lifshitz, or Chapter 15 in the text by Huang, both cited above.

and then find the ratio J/T_c as the smallest value of the parameter J/T at that the ratio F/T (as a function of h/T) has a minimum at zero field. However, for any system of a reasonable size N , the “exact” computation of the statistical sum (97) is impossible, because it contains too many terms for any supercomputer to handle. For example, let us take a relatively small 3D lattice with $N = 10 \times 10 \times 10 = 10^3$ spins, which still feature substantial boundary artifacts even using the periodic boundary conditions, so that its phase transition is smeared about T_c by $\sim 3\%$. Still, even for such a crude model, Z would include $2^{1,000} \equiv (2^{10})^{100} \approx (10^3)^{100} \equiv 10^{300}$ terms. Let us suppose we are using a modern exaflops-scale supercomputer performing 10^{18} floating-point operations per second, i.e. $\sim 10^{26}$ such operations per year. With those resources, the computation of just one statistical sum would require $\sim 10^{(300-26)} = 10^{274}$ years. To call such a number “astronomic” would be a strong understatement. (As a reminder, the age of our Universe is close to 1.3×10^{10} years – a very humble number in comparison.)

This situation may be improved dramatically by noticing that any statistical sum,

$$Z = \sum_m \exp\left\{-\frac{E_m}{T}\right\}, \quad (4.99)$$

is dominated by terms with lower values of E_m . To find those lowest-energy states, we may use the following powerful approach (belonging to a broad class of numerical *Monte-Carlo techniques*), which essentially mimics one (randomly selected) path of the system’s evolution in time. One could argue that for that we would need to know the exact laws of evolution of statistical systems,⁴⁶ that may differ from one system to another, even if their energy spectra E_m are the same. This is true, but since the genuine value of Z should be independent of these details, it may be evaluated using *any* reasonable kinetic model that satisfies certain general rules. In order to reveal these rules, let us start from a system with just two states, with energies E_m and $E_{m'} = E_m + \Delta$ – see Fig. 13.

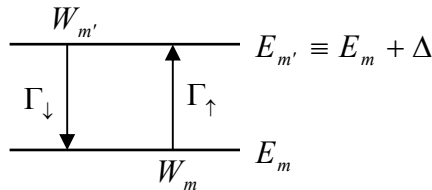


Fig. 4.13. Deriving the detailed balance relation.

In the absence of quantum coherence between the states (see Sec. 2.1), the equations for the time evolution of the corresponding probabilities W_m and $W_{m'}$ should depend only on the probabilities (plus certain constant coefficients). Moreover, since the equations of quantum mechanics are linear, these *master equations* should be also linear. Hence, it is natural to expect them to have the following form,

$$\frac{dW_m}{dt} = W_{m'}\Gamma_\downarrow - W_m\Gamma_\uparrow, \quad \frac{dW_{m'}}{dt} = W_m\Gamma_\uparrow - W_{m'}\Gamma_\downarrow, \quad (4.100)$$

where the coefficients Γ_\uparrow and Γ_\downarrow have the physical sense of the *rates* of the corresponding transitions (see Fig. 13); for example, $\Gamma_\uparrow dt$ is the probability of the system’s transition into the state m' during an infinitesimal time interval dt , provided that at the beginning of that interval it was in the state m with full certainty: $W_m = 1$, $W_{m'} = 0$.⁴⁷ Since for the system with just two energy levels, the time derivatives of the

⁴⁶ Discussion of such laws in the task of *physical kinetics*, which will be briefly reviewed in Chapter 6.

⁴⁷ The calculation of these rates for several particular cases is described in QM Secs. 6.6, 6.7, and 7.6 – see, e.g., QM Eq. (7.196), which is valid for a very general model of a quantum system.

probabilities have to be equal and opposite, Eqs. (100) describe an (irreversible) redistribution of the probabilities while keeping their sum $W = W_m + W_{m'}$ constant. According to Eqs. (100), at $t \rightarrow \infty$ the probabilities settle to their stationary values related as

$$\frac{W_{m'}}{W_m} = \frac{\Gamma_{\uparrow}}{\Gamma_{\downarrow}}. \quad (4.101)$$

Now let us require these stationary values to obey the Gibbs distribution (2.58); from it

$$\frac{W_{m'}}{W_m} = \exp\left\{\frac{E_m - E_{m'}}{T}\right\} = \exp\left\{-\frac{\Delta}{T}\right\} < 1. \quad (4.102)$$

Comparing these two expressions, we see that the rates have to satisfy the following *detailed balance relation*:

$$\frac{\Gamma_{\uparrow}}{\Gamma_{\downarrow}} = \exp\left\{-\frac{\Delta}{T}\right\}. \quad (4.103)$$
Detailed balance

Now comes the final step: since the rates of transition between two particular states should not depend on other states and their occupation, Eq. (103) has to be valid for *each* pair of states of any multi-state system. (By the way, this relation may serve as an important sanity check: the rates calculated using any reasonable model of a quantum system have to satisfy it.)

The detailed balance yields only one equation for two rates Γ_{\uparrow} and Γ_{\downarrow} ; if our only goal is the calculation of Z , the choice of the other equation is not too important. A very simple choice is

$$\Gamma(\Delta) \propto \gamma(\Delta) \equiv \begin{cases} 1, & \text{if } \Delta < 0, \\ \exp\{-\Delta/T\}, & \text{otherwise,} \end{cases} \quad (4.104)$$

where Δ is the energy change resulting from the transition. This model, which evidently satisfies the detailed balance relation (103), is very popular (despite the unphysical cusp this function has at $\Delta = 0$), because it enables the following simple *Metropolis algorithm* (Fig. 14).

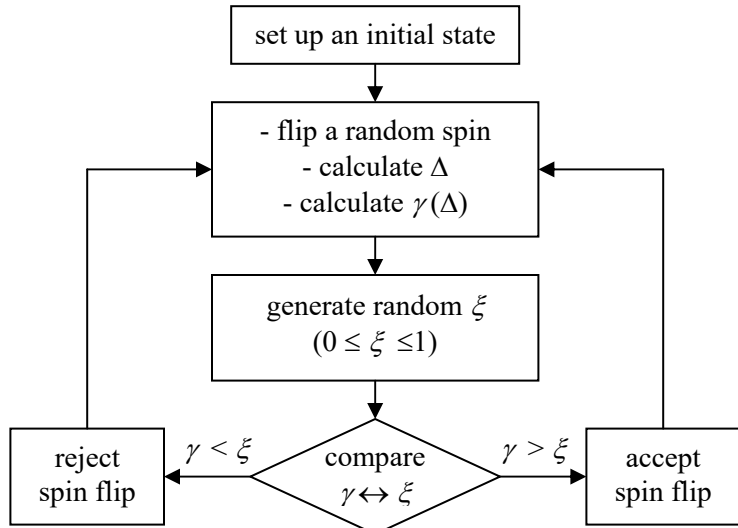


Fig. 4.14. A crude scheme of the Metropolis algorithm for the Ising model simulation.

The calculation starts by setting a certain initial state of the system. At relatively high temperatures, the state may be generated randomly; for example, in the Ising system, the initial state of each spin s_k may be selected independently, with a 50% probability. At low temperatures, starting the calculations from the lowest-energy state (in particular, for the Ising model, from the ferromagnetic state $s_k = \text{sgn}(h) = \text{const}$) may give the fastest convergence. Now one spin is flipped at random, the corresponding change Δ of the energy is calculated,⁴⁸ and plugged into Eq. (104) to calculate $\gamma(\Delta)$. Next, a pseudo-random number generator is used to generate a random number ξ , with the probability density being constant on the segment $[0, 1]$. (Such functions are available in virtually any numerical library.) If the resulting ξ is less than $\gamma(\Delta)$, the transition is accepted, while if $\xi > \gamma(\Delta)$, it is rejected. Physically, this means that any transition down the energy spectrum ($\Delta < 0$) is always accepted, while those up the energy profile ($\Delta > 0$) are accepted with the probability proportional to $\exp\{-\Delta/T\}$.⁴⁹ After sufficiently many such steps, the statistical sum (99) may be calculated approximately as a partial sum over the states passed by the system. (It may be better to discard the contributions from a few first steps, to avoid the effects of the initial state choice.)

This algorithm is extremely efficient. Even with modest computers available in the 1980s, it has allowed simulating a 3D Ising system of $(128)^3$ spins to get the following result: $J/T_c \approx 0.221650 \pm 0.000005$. For all practical purposes, this result is exact – so that perhaps the largest benefit of the possible future analytical solution of the infinite 3D Ising problem will be a virtually certain Nobel Prize for its author. Table 2 summarizes the values of T_c for the Ising model. Very visible is the fast improvement of the prediction accuracy of the molecular-field theory – which is asymptotically correct at $d \rightarrow \infty$.

Table 4.2. The critical temperature T_c (in the units of J) of the Ising model of a ferromagnet ($J > 0$), for several values of dimensionality d

d	Molecular-field theory – Eq. (72)	Exact value	Exact value's source
0	0	0	Gibbs distribution
1	2	0	Transfer matrix theory
2	4	2.269...	Onsager's solution
3	6	4.513...	Numerical simulation

Finally, I need to mention the *renormalization-group* (“RG”) approach,⁵⁰ despite its low efficiency for the Ising-type problems. The basic idea of this approach stems from the scaling law (30)–(31): at $T = T_c$ the correlation radius r_c diverges. Hence, the critical temperature may be found from the requirement for the system to be *spatially self-similar*. Namely, let us form larger and larger groups (“blocks”) of adjacent spins, and require that all properties of the resulting system of the blocks approach those of the initial system, as T approaches T_c .

⁴⁸ Note that a flip of a single spin changes the signs of only $(2d + 1)$ terms in the sum (23), i.e. does not require the re-calculation of all $(2d + 1)N$ terms of the sum, so that the computation of Δ takes just a few multiply-and-accumulate operations even at $N \gg 1$.

⁴⁹ The latter step is necessary to avoid the system’s trapping in local minima of its multidimensional energy profile $E_m(s_1, s_2, \dots, s_N)$.

⁵⁰ Initially developed in the quantum field theory in the 1950s, it was adapted to statistics by L. Kadanoff in 1966, with a spectacular solution of the so-called *Kubo problem* by K. Wilson in 1972, later awarded with a Nobel Prize.

Let us see how this idea works for the simplest nontrivial (1D) case, described by the statistical sum (80). Assuming N to be even (which does not matter at $N \rightarrow \infty$), and adding an inconsequential constant C to each exponent (for the purpose that will be clear soon), we may rewrite this expression as

$$Z = \sum_{s_k=\pm 1} \prod_{k=1,2,\dots,N} \exp \left\{ \frac{h}{2T} s_k + \frac{J}{T} s_k s_{k+1} + \frac{h}{2T} s_{k+1} + C \right\}. \quad (4.105)$$

Let us group each pair of adjacent exponents to recast this expression as a product over only *even* numbers k ,

$$Z = \sum_{s_k=\pm 1} \prod_{k=2,4,\dots,N} \exp \left\{ \frac{h}{2T} s_{k-1} + s_k \left[\frac{J}{T} (s_{k-1} + s_{k+1}) + \frac{h}{T} \right] + \frac{h}{2T} s_{k+1} + 2C \right\}, \quad (4.106)$$

and carry out the summation over two possible states of the internal spin s_k explicitly:

$$\begin{aligned} Z &= \sum_{s_k=\pm 1} \prod_{k=2,4,\dots,N} \left[\exp \left\{ \frac{h}{2T} s_{k-1} + \frac{J}{T} (s_{k-1} + s_{k+1}) + \frac{h}{T} + \frac{h}{2T} s_{k+1} + 2C \right\} \right. \\ &\quad \left. + \exp \left\{ \frac{h}{2T} s_{k-1} - \frac{J}{T} (s_{k-1} + s_{k+1}) - \frac{h}{T} + \frac{h}{2T} s_{k+1} + 2C \right\} \right] \\ &\equiv \sum_{s_k=\pm 1} \prod_{k=2,4,\dots,N} 2 \cosh \left\{ \frac{J}{T} (s_{k-1} + s_{k+1}) + \frac{h}{T} \right\} \exp \left\{ \frac{h}{2T} (s_{k-1} + s_{k+1}) + 2C \right\}. \end{aligned} \quad (4.107)$$

Now let us require this statistical sum (and hence all statistical properties of the system of 2-spin blocks) to be identical to that of the Ising system of $N/2$ spins, numbered by odd k :

$$Z' = \sum_{s_k=\pm 1} \prod_{k=2,4,\dots,N} \exp \left\{ \frac{J'}{T} s_{k-1} s_{k+1} + \frac{h'}{T} s_{k+1} + C' \right\}, \quad (4.108)$$

with some different parameters h' , J' , and C' , for all four possible values of $s_{k-1} = \pm 1$ and $s_{k+1} = \pm 1$. Since the right-hand side of Eq. (107) depends only on the sum $(s_{k-1} + s_{k+1})$, this requirement yields only three (rather than four) independent equations for finding h' , J' , and C' . Of them, the equations for h' and J' depend only on h and J (but not on C),⁵¹ and may be represented in an especially simple form,

$$x' = \frac{x(1+y)^2}{(x+y)(1+xy)}, \quad y' = \frac{y(x+y)}{1+xy}, \quad (4.109)$$

RG
equations
for 1D Ising
model

if the following notation is used:

$$x \equiv \exp \left\{ -4 \frac{J}{T} \right\}, \quad y \equiv \exp \left\{ -2 \frac{h}{T} \right\}. \quad (4.110)$$

Now the grouping procedure may be repeated, with the same result (109)-(110). Hence these equations may be considered as recurrence relations describing repeated doubling of the spin block size. Figure 15 shows (schematically) the *trajectories* of this dynamic system on the phase plane $[x, y]$. (Each trajectory is defined by the following property: for each of its points $\{x, y\}$, the point $\{x', y'\}$ defined by

⁵¹ This might be expected because physically C is just a certain constant addition to the system's energy. However, the introduction of that constant is mathematically necessary, because Eqs. (107) and (108) may be reconciled only if $C' \neq C$.

the “mapping” Eq. (109) is also on the same trajectory.) For ferromagnetic coupling ($J > 0$) and $h > 0$, we may limit the analysis to the unit square $0 \leq x, y \leq 1$. If this *flow diagram* had a stable fixed point with $x' = x = x_\infty \neq 0$ (i.e. $T/J < \infty$) and $y' = y = 1$ (i.e. $h = 0$), then the first of Eqs. (110) would immediately give us the critical temperature of the phase transition in the field-free system:

$$T_c = \frac{4J}{\ln(1/x_\infty)}. \quad (4.111)$$

However, Fig. 15 shows that the only fixed point of the 1D system is $x = y = 0$, which (at a finite coupling J) should be interpreted as $T_c = 0$. This is of course in agreement with the exact result of the transfer-matrix analysis, but does not provide any additional information.

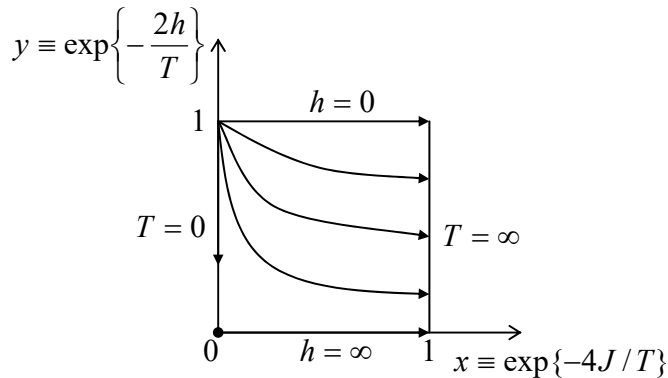


Fig. 4.15. The RG flow diagram of the 1D Ising system (schematically).

Unfortunately, for higher dimensionalities, the renormalization-group approach rapidly becomes rather cumbersome and requires certain approximations, whose accuracy cannot be easily controlled. For the 2D Ising system, such approximations lead to the prediction $T_c \approx 2.55 J$, i.e. to a substantial difference from the exact result (96).

4.6. Exercise problems

4.1. Compare the third virial coefficient $C(T)$ that follows from the van der Waals equation, with its value for the hardball model of particle interactions (whose calculation was the subject of Problem 3.28), and comment.

4.2. Calculate the entropy and the internal energy of the van der Waals gas, and discuss the results.

4.3. Use two different approaches to calculate the so-called *Joule-Thomson coefficient* $(\partial E/\partial V)_T$ for the van der Waals gas, and the change of temperature of such a gas, with a temperature-independent C_V , at its fast expansion.

4.4. Calculate the difference $C_P - C_V$ for the van der Waals gas, and compare the result with that for an ideal classical gas.

4.5. Calculate the temperature dependence of the phase-equilibrium pressure $P_0(T)$ and the latent heat $\Lambda(T)$, for the van der Waals model, in the low-temperature limit $T \ll T_c$.

4.6. Perform the same tasks as in the previous problem in the opposite limit – in close vicinity of the critical point T_c .

4.7. Calculate the critical values P_c , V_c , and T_c for the so-called *Redlich-Kwong model* of the real gas, with the following equation of state:⁵²

$$P + \frac{a}{V(V + Nb)T^{1/2}} = \frac{NT}{V - Nb},$$

with constant parameters a and b .

Hint: Be prepared to solve a cubic equation with particular (numerical) coefficients.

4.8. Calculate the critical values P_c , V_c , and T_c for the phenomenological *Dieterici model*, with the following equation of state:⁵³

$$P = \frac{NT}{V - b} \exp\left\{-\frac{a}{NTV}\right\},$$

with constant parameters a and b . Compare the value of the dimensionless factor $P_c V_c / NT_c$ with those given by the van der Waals and Redlich-Kwong models.

4.9. In the crude sketch shown in Fig. 3b, the derivatives dP/dT of the phase transitions liquid-gas (“vaporization”) and solid-gas (“sublimation”), at the triple point, are different, with

$$\left(\frac{dP_v}{dT}\right)_{T=T_t} < \left(\frac{dP_s}{dT}\right)_{T=T_t}.$$

Is this occasional? What relation between these derivatives can be obtained from thermodynamics?

4.10. Use the Clapeyron-Clausius formula (17) to calculate the latent heat Λ of the Bose-Einstein condensation, and compare the result with that obtained in the solution of Problem 3.21.

4.11.

(i) Write the effective Hamiltonian for that the usual single-particle stationary Schrödinger equation coincides with the Gross-Pitaevski equation (58).

(ii) Use this *Gross-Pitaevskii Hamiltonian*, with the trapping potential $U(\mathbf{r}) = m\omega^2 r^2/2$, to calculate the energy E of $N \gg 1$ trapped particles, assuming the trial solution $\psi \propto \exp\{-r^2/2r_0^2\}$, as a function of the parameter r_0 .⁵⁴

⁵² This equation of state, suggested in 1948, describes most real gases better than not only the original van der Waals model, but also other two-parameter alternatives, such as the *Berthelot*, *modified-Berthelot*, and *Dieterici* models, though some approximations with more fitting parameters (such as the *Soave-Redlich-Kwong model*) work even better.

⁵³ This model is currently less popular than the Redlich-Kwong one (also with two fitting parameters), whose analysis was the task of the previous problem.

⁵⁴ This task is essentially the first step of the variational method of quantum mechanics – see, e.g., QM Sec. 2.9.

(iii) Explore the function $E(r_0)$ for positive and negative values of the constant b , and interpret the results.

(iv) For small $b < 0$, estimate the largest number N of particles that may form a metastable Bose-Einstein condensate.

4.12. Superconductivity may be suppressed by a sufficiently strong magnetic field. In the simplest case of a bulk, long cylindrical sample of a type-I superconductor, placed into an external magnetic field \mathcal{H}_{ext} parallel to its surface, this suppression takes a simple form of a simultaneous transition of the whole sample from the superconducting state to the “normal” (non-superconducting) state at a certain value $\mathcal{H}_c(T)$ of the field’s magnitude. This *critical field* gradually decreases with temperature from its maximum value $\mathcal{H}_c(0)$ at $T \rightarrow 0$ to zero at the critical temperature T_c . Assuming that the function $\mathcal{H}_c(T)$ is known, calculate the latent heat of this phase transition as a function of temperature, and spell out its values at $T \rightarrow 0$ and $T = T_c$.

Hint: In this context, “bulk sample” means a sample much larger than the intrinsic length scales of the superconductor (such as the London penetration depth δ_L and the coherence length ξ).⁵⁵ For such bulk superconductors, magnetic properties of the superconducting phase may be well described just as the perfect diamagnetism, with $\mathcal{B} = 0$ inside it.

4.13. In some textbooks, the discussion of thermodynamics of superconductivity is started with displaying, as self-evident, the following formula:

$$F_n(T) - F_s(T) = \frac{\mu_0 \mathcal{H}_c^2(T)}{2} V,$$

where F_s and F_n are the free energy values in the superconducting and non-superconducting (“normal”) phases, and $\mathcal{H}_c(T)$ is the critical value of the magnetic external field. Is this formula correct, and if not, what qualification is necessary to make it valid? Assume that all conditions of the simultaneous field-induced phase transition in the whole sample, spelled out in the previous problem, are satisfied.

4.14. In Sec. 4, we have discussed Weiss’ molecular-field approach to the Ising model, in which the average $\langle s_j \rangle$ plays the role of the order parameter η . Use the results of that analysis to calculate the coefficients a and b in the corresponding Landau expansion (46) of the free energy. List the critical exponents α and β , defined by Eqs. (26) and (28), within this approach.

4.15. Consider a ring of $N = 3$ Ising “spins” ($s_k = \pm 1$), with similar ferromagnetic coupling J between all sites, in thermal equilibrium.

(i) Calculate the order parameter η and the low-field susceptibility $\chi \equiv \partial \eta / \partial h|_{h=0}$.

(ii) Use the low-temperature limit of the result for χ to predict it for a ring with an arbitrary N , and verify your prediction by a direct calculation (in this limit).

(iii) Discuss the relation between the last result, in the limit $N \rightarrow \infty$, and Eq. (91).

⁵⁵A discussion of these parameters, as well as of the difference between the type-I and type-II superconductivity, may be found in EM Secs. 6.4-6.5. However, those details are not needed for the solution of this problem.

4.16. Calculate the average energy, entropy, and heat capacity of a three-site ring of Ising-type “spins” ($s_k = \pm 1$), with *anti*-ferromagnetic coupling (of magnitude J) between the sites, in thermal equilibrium at temperature T , with no external magnetic field. Find the asymptotic behavior of its heat capacity for low and high temperatures, and give an interpretation of the results.

4.17. Using the results discussed in Sec. 5, calculate the average energy, free energy, entropy, and heat capacity (all per spin) as functions of temperature T and external field h , for the infinite 1D Ising model. Sketch the temperature dependence of the heat capacity for various values of ratio h/J , and give a physical interpretation of the result.

4.18. Use the molecular-field theory to calculate the critical temperature and the low-field susceptibility of a d -dimensional cubic lattice of spins, described by the so-called *classical Heisenberg model*:⁵⁶

$$E_m = -J \sum_{\{k, k'\}} \mathbf{s}_k \cdot \mathbf{s}_{k'} - \sum_k \mathbf{h} \cdot \mathbf{s}_k .$$

Here, in contrast to the (otherwise, very similar) Ising model (23), the spin of each site is modeled by a classical 3D vector $\mathbf{s}_k = \{s_{xk}, s_{yk}, s_{zk}\}$ of unit length: $s_k^2 = 1$.

⁵⁶ This classical model is formally similar to the generalization of the genuine (quantum) Heisenberg model (21) to arbitrary spin s , and serves as its infinite-spin limit.

Chapter 5. Fluctuations

This chapter discusses fluctuations of macroscopic variables, mostly at thermodynamic equilibrium. In particular, it describes the intimate connection between fluctuations and dissipation (damping) in dynamic systems weakly coupled to multi-particle environments, which culminates in the Einstein relation between the diffusion coefficient and mobility, the Nyquist formula, and its quantum-mechanical generalization – the fluctuation-dissipation theorem. An alternative approach to the same problem, based on the Smoluchowski and Fokker-Planck equations, is also discussed in brief.

5.1. Characterization of fluctuations

At the beginning of Chapter 2, we have discussed the notion of averaging, $\langle f \rangle$, of a variable f over a statistical ensemble – see Eqs. (2.7) and (2.10). Now, the *fluctuation* of the variable is defined simply as its deviation from such average:

$$\tilde{f} \equiv f - \langle f \rangle; \quad (5.1)$$

this deviation is, generally, also a random variable. The most important property of any fluctuation is that its average (over the same statistical ensemble) equals zero:

$$\langle \tilde{f} \rangle = \langle f - \langle f \rangle \rangle = \langle f \rangle - \langle \langle f \rangle \rangle = \langle f \rangle - \langle f \rangle = 0. \quad (5.2)$$

As a result, such an average cannot characterize fluctuations' *intensity*, and the simplest characteristic of the intensity is the *variance* (sometimes called "dispersion"):

$$\langle \tilde{f}^2 \rangle = \langle (f - \langle f \rangle)^2 \rangle. \quad (5.3)$$

The following simple property of the variance is frequently convenient for its calculation:

$$\langle \tilde{f}^2 \rangle = \langle (f - \langle f \rangle)^2 \rangle = \langle f^2 - 2f\langle f \rangle + \langle f \rangle^2 \rangle = \langle f^2 \rangle - 2\langle f \rangle^2 + \langle f \rangle^2, \quad (5.4a)$$

so that, finally:

$$\langle \tilde{f}^2 \rangle = \langle f^2 \rangle - \langle f \rangle^2. \quad (5.4b)$$

As the simplest example, consider a variable that takes only two values, ± 1 , with equal probabilities $W_j = 1/2$. For such a variable, the basic Eq. (2.7) yields

$$\begin{aligned} \langle f \rangle &= \sum_j W_j f_j = \frac{1}{2}(+1) + \frac{1}{2}(-1) = 0, \quad \text{but } \langle f^2 \rangle = \sum_j W_j f_j^2 = \frac{1}{2}(+1)^2 + \frac{1}{2}(-1)^2 = 1 \neq 0, \\ &\text{so that } \langle \tilde{f}^2 \rangle = \langle f^2 \rangle - \langle f \rangle^2 = 1. \end{aligned} \quad (5.5)$$

The square root of the variance,

$$\delta f \equiv \langle \tilde{f}^2 \rangle^{1/2}, \quad (5.6)$$

is called the *root-mean-square (r.m.s.) fluctuation*. An advantage of this measure is that it has the same dimensionality as the variable itself, so that the ratio $\delta f / \langle f \rangle$ is dimensionless, and may be used to characterize the *relative intensity* of fluctuations.

As has been mentioned in Chapter 1, all results of thermodynamics are valid only if the fluctuations of thermodynamic variables (internal energy E , entropy S , etc.) are relatively small.¹ Let us make a simple estimate of the relative intensity of fluctuations for an example of a system of N independent, similar particles, and an extensive variable

$$\mathcal{F} \equiv \sum_{k=1}^N f_k . \quad (5.7)$$

where all single-particle functions f_k are similar, besides that each of them depends on the state of only “its own” (k^{th}) particle. The statistical average of such \mathcal{F} is evidently

$$\langle \mathcal{F} \rangle = \sum_{k=1}^N \langle f \rangle = N \langle f \rangle, \quad (5.8)$$

while its fluctuation variance is

$$\langle \tilde{\mathcal{F}}^2 \rangle \equiv \langle \tilde{\mathcal{F}} \tilde{\mathcal{F}} \rangle \equiv \left\langle \sum_{k=1}^N \tilde{f}_k \sum_{k'=1}^N \tilde{f}_{k'} \right\rangle \equiv \left\langle \sum_{k,k'=1}^N \tilde{f}_k \tilde{f}_{k'} \right\rangle \equiv \sum_{k,k'=1}^N \langle \tilde{f}_k \tilde{f}_{k'} \rangle. \quad (5.9)$$

Now we may use the fact that for two independent variables

$$\langle \tilde{f}_k \tilde{f}_{k'} \rangle = 0, \quad \text{for } k' \neq k; \quad (5.10)$$

indeed, this relation may be considered as the mathematical definition of their independence. Hence, only the terms with $k' = k$ make substantial contributions to the sum (9):

$$\langle \tilde{\mathcal{F}}^2 \rangle = \sum_{k,k'=1}^N \langle \tilde{f}_k^2 \rangle \delta_{k,k'} = N \langle \tilde{f}^2 \rangle. \quad (5.11)$$

Comparing Eqs. (8) and (11), we see that the relative intensity of fluctuations of the variable \mathcal{F} ,

$$\frac{\delta \mathcal{F}}{\langle \mathcal{F} \rangle} = \frac{1}{N^{1/2}} \frac{\delta f}{\langle f \rangle}, \quad (5.12)$$

Relative fluctuation estimate

tends to zero as the system size grows ($N \rightarrow \infty$). It is this fact that justifies the thermodynamic approach to typical physical systems, with the number N of particles of the order of the Avogadro number $N_A \sim 10^{24}$. Nevertheless, in many situations even small fluctuations of variables are important, and in this chapter we will calculate their basic properties, starting with the variance.

It should be comforting for the reader to notice that for some simple (but very important) cases, such calculation has already been done in our course. In particular, for any generalized coordinate q and generalized momentum p that give quadratic contributions of the type (2.46) to the system’s

¹ Let me remind the reader that up to this point, the averaging signs $\langle \dots \rangle$ were dropped in most formulas, for the sake of notation simplicity. In this chapter, I have to restore these signs to avoid confusion. The only exception will be temperature – whose average, following (probably, bad :-) tradition, will be still called just T everywhere, besides the last part of Sec. 3, where temperature fluctuations are discussed explicitly.

Hamiltonian (as in a harmonic oscillator), we have derived the equipartition theorem (2.48), valid in the classical limit. Since the average values of these variables, in the thermodynamic equilibrium, equal zero, Eq. (6) immediately yields their r.m.s. fluctuations:

$$\delta p = (mT)^{1/2}, \quad \delta q = \left(\frac{T}{\kappa} \right)^{1/2} \equiv \left(\frac{T}{m\omega^2} \right)^{1/2}, \quad \text{where } \omega = \left(\frac{\kappa}{m} \right)^{1/2}. \quad (5.13)$$

The generalization of these classical relations to the quantum-mechanical case ($T \sim \hbar\omega_j$) is provided by Eqs. (2.78) and (2.81):

$$\delta p = \left[\frac{\hbar m \omega}{2} \coth \frac{\hbar \omega}{2T} \right]^{1/2}, \quad \delta q = \left[\frac{\hbar}{2m\omega} \coth \frac{\hbar \omega}{2T} \right]^{1/2}. \quad (5.14)$$

However, the intensity of fluctuations in other systems requires special calculations. Moreover, only a few cases allow for general, model-independent results. Let us review some of them.

5.2. Energy and the number of particles

First of all, note that fluctuations of macroscopic variables depend on particular conditions.² For example, in a mechanically- and thermally-insulated system with a fixed number of particles, i.e. a member of a *microcanonical* ensemble, the internal energy does not fluctuate: $\delta E = 0$. However, if such a system is in thermal contact with the environment, i.e. is a member of a *canonical* ensemble (Fig. 2.6), the situation is different. Indeed, for such a system we may apply the general Eq. (2.7), with W_m given by the Gibbs distribution (2.58)-(2.59), not only to E but also to E^2 . As we already know from Sec. 2.4, the first average,

$$\langle E \rangle = \sum_m W_m E_m, \quad W_m = \frac{1}{Z} \exp \left\{ -\frac{E_m}{T} \right\}, \quad Z = \sum_m \exp \left\{ -\frac{E_m}{T} \right\}, \quad (5.15)$$

yields Eq. (2.61b), which may be rewritten in the form

$$\langle E \rangle = \frac{1}{Z} \frac{\partial Z}{\partial(-\beta)}, \quad \text{where } \beta \equiv \frac{1}{T}, \quad (5.16)$$

more convenient for our current purposes. Let us carry out a similar calculation for E^2 :

$$\langle E^2 \rangle = \sum_m W_m E_m^2 = \frac{1}{Z} \sum_m E_m^2 \exp \left\{ -\beta E_m \right\}. \quad (5.17)$$

It is straightforward to verify, by double differentiation, that the last expression may be rewritten in a form similar to Eq. (16):

$$\langle E^2 \rangle = \frac{1}{Z} \frac{\partial^2}{\partial(-\beta)^2} \sum_m \exp \left\{ -\beta E_m \right\} \equiv \frac{1}{Z} \frac{\partial^2 Z}{\partial(-\beta)^2}. \quad (5.18)$$

Now it is easy to use Eqs. (4) to calculate the variance of energy fluctuations:

$$\langle \tilde{E}^2 \rangle = \langle E^2 \rangle - \langle E \rangle^2 = \frac{1}{Z} \frac{\partial^2 Z}{\partial(-\beta)^2} - \left(\frac{1}{Z} \frac{\partial Z}{\partial(-\beta)} \right)^2 \equiv \frac{\partial}{\partial(-\beta)} \left(\frac{1}{Z} \frac{\partial Z}{\partial(-\beta)} \right) = \frac{\partial \langle E \rangle}{\partial(-\beta)}. \quad (5.19)$$

² Unfortunately, even in some popular textbooks, certain formulas pertaining to fluctuations are either incorrect or given without specifying the conditions of their applicability, so that the reader's caution is advised.

Since Eqs. (15)-(19) are valid only if the system's volume V is fixed (because its change may affect the energy spectrum E_m), it is customary to rewrite this important result as follows:

$$\langle \tilde{E}^2 \rangle = \frac{\partial \langle E \rangle}{\partial (-1/T)} = T^2 \left(\frac{\partial \langle E \rangle}{\partial T} \right)_V \equiv C_V T^2. \quad (5.20)$$

Fluctuations
of E

This is a remarkably simple, fundamental result. As a sanity check, for a system of N similar, independent particles, $\langle E \rangle$ and hence C_V are proportional to N , so that $\delta E \propto N^{1/2}$ and $\delta E/\langle E \rangle \propto N^{-1/2}$, in agreement with Eq. (12). Let me emphasize that the classically-looking Eq. (20) is based on the general Gibbs distribution, and hence is valid for any system (either classical or quantum) in thermal equilibrium.

Some corollaries of this result will be discussed in the next section, and now let us carry out a very similar calculation for a system whose number N of particles in a system is not fixed, because they may go to, and come from its environment at will. If the chemical potential μ of the environment and its temperature T are fixed, i.e. we are dealing with the *grand canonical ensemble* (Fig. 2.13), we may use the grand canonical distribution (2.106)-(2.107):

$$W_{m,N} = \frac{1}{Z_G} \exp \left\{ \frac{\mu N - E_{m,N}}{T} \right\}, \quad Z_G = \sum_{N,m} \exp \left\{ \frac{\mu N - E_{m,N}}{T} \right\}. \quad (5.21)$$

Acting exactly as we did above for the internal energy, we get

$$\langle N \rangle = \frac{1}{Z_G} \sum_{m,N} N \exp \left\{ \frac{\mu N - E_{m,N}}{T} \right\} = \frac{T}{Z_G} \frac{\partial Z_G}{\partial \mu}, \quad (5.22)$$

$$\langle N^2 \rangle = \frac{1}{Z_G} \sum_{m,N} N^2 \exp \left\{ \frac{\mu N - E_{m,N}}{T} \right\} = \frac{T^2}{Z_G} \frac{\partial^2 Z_G}{\partial \mu^2}, \quad (5.23)$$

so that the particle number's variance is

$$\langle \tilde{N}^2 \rangle = \langle N^2 \rangle - \langle N \rangle^2 = \frac{T^2}{Z_G} \frac{\partial Z_G}{\partial \mu} - \frac{T^2}{Z_G^2} \left(\frac{\partial Z_G}{\partial \mu} \right)^2 = T \frac{\partial}{\partial \mu} \left(\frac{T}{Z_G} \frac{\partial Z_G}{\partial \mu} \right) = T \frac{\partial \langle N \rangle}{\partial \mu}, \quad (5.24)$$

Fluctuations
of N

in full analogy with Eq. (19).

In particular, for an ideal classical gas, we may combine the last result with Eq. (3.32b). (As was already emphasized in Sec. 3.2, though that result has been obtained for the canonical ensemble, in which the number of particles N is fixed, at $N \gg 1$ the fluctuations of N in the grand canonical ensemble should be relatively small, so that the same relation should be valid for the *average* $\langle N \rangle$ in that ensemble.) Easily solving Eq. (3.32b) for $\langle N \rangle$, we get

$$\langle N \rangle = \text{const} \times \exp \left\{ \frac{\mu}{T} \right\}, \quad (5.25)$$

where “const” means a factor constant at the partial differentiation of $\langle N \rangle$ over μ , required by Eq. (24). Performing the differentiation and then using Eq. (25) again,

$$\frac{\partial \langle N \rangle}{\partial \mu} = \text{const} \times \frac{1}{T} \exp\left\{\frac{\mu}{T}\right\} = \frac{\langle N \rangle}{T}, \quad (5.26)$$

we get from Eq. (24) a very simple result:

Fluctuations
of N :
classical gas

$$\langle \tilde{N}^2 \rangle = \langle N \rangle, \quad \text{i.e. } \delta N = \langle N \rangle^{1/2}. \quad (5.27)$$

This relation is so important that I will also show how it may be derived differently. As a by-product of this new derivation, we will prove that this result is valid for systems with an arbitrary (say, small) N , and also get more detailed information about the statistics of fluctuations of that number. Let us consider an ideal classical gas of N_0 particles in a volume V_0 , and calculate the probability W_N to have exactly $N \leq N_0$ of these particles in its part of volume $V \leq V_0$ – see Fig. 1.

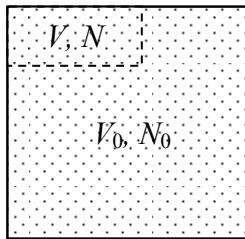


Fig. 5.1. Deriving the binomial and Poisson distributions.

For one particle such probability is $W = V/V_0 = \langle N \rangle/N_0 \leq 1$, while the probability to have that particle in the remaining part of the volume is $W' = 1 - W = 1 - \langle N \rangle/N_0$. If all particles were distinguishable, the probability of having $N \leq N_0$ specific particles in volume V and $(N - N_0)$ specific particles in volume $(V - V_0)$, would be $W^N W'^{(N_0-N)}$. However, if we do not want to distinguish the particles, we should multiply this probability by the number of possible particle combinations keeping the numbers N and N_0 constant, i.e. by the binomial coefficient $N_0!/N!(N_0 - N)!$.³ As the result, the required probability is

Binomial distribution

$$W_N = W^N W'^{(N_0-N)} \frac{N_0!}{N!(N_0 - N)!} = \left(\frac{\langle N \rangle}{N_0} \right)^N \left(1 - \frac{\langle N \rangle}{N_0} \right)^{N_0 - N} \frac{N_0!}{N!(N_0 - N)!}. \quad (5.28)$$

This is the so-called *binomial probability distribution*, valid for any $\langle N \rangle$ and N_0 .⁴

Still keeping $\langle N \rangle$ arbitrary, we can simplify the binomial distribution by assuming that the whole volume V_0 , and hence N_0 , are very large:

$$N_0 \gg N, \quad (5.29)$$

where N means all values of interest, including $\langle N \rangle$. Indeed, in this limit we can neglect N in comparison with N_0 in the second exponent of Eq. (28), and also approximate the fraction $N_0!/(N_0 - N)!$, i.e. the product of N terms, $(N_0 - N + 1)(N_0 - N + 2)\dots(N_0 - 1)N_0$, by just N_0^N . As a result, we get

$$W_N \approx \left(\frac{\langle N \rangle}{N_0} \right)^N \left(1 - \frac{\langle N \rangle}{N_0} \right)^{N_0} \frac{N_0^N}{N!} \equiv \frac{\langle N \rangle^N}{N!} \left(1 - \frac{\langle N \rangle}{N_0} \right)^{N_0} = \frac{\langle N \rangle^N}{N!} \left[(1 - W)^{\frac{1}{W}} \right]^{\langle N \rangle}, \quad (5.30)$$

³ See, e.g., MA Eq. (2.2).

⁴ It was derived by Jacob Bernoulli (1655-1705).

where, as before, $W = \langle N \rangle / N_0$. In the limit (29), $W \rightarrow 0$, so that the factor inside the square brackets tends to $1/e$, the reciprocal of the natural logarithm base.⁵ Thus, we get an expression independent of N_0 :

$$W_N = \frac{\langle N \rangle^N}{N!} e^{-\langle N \rangle}. \quad (5.31)$$

Poisson distribution

This is the much-celebrated *Poisson distribution*⁶ which describes a very broad family of random phenomena. Figure 2 shows this distribution for several values of $\langle N \rangle$ – which, in contrast to N , are not necessarily integer.

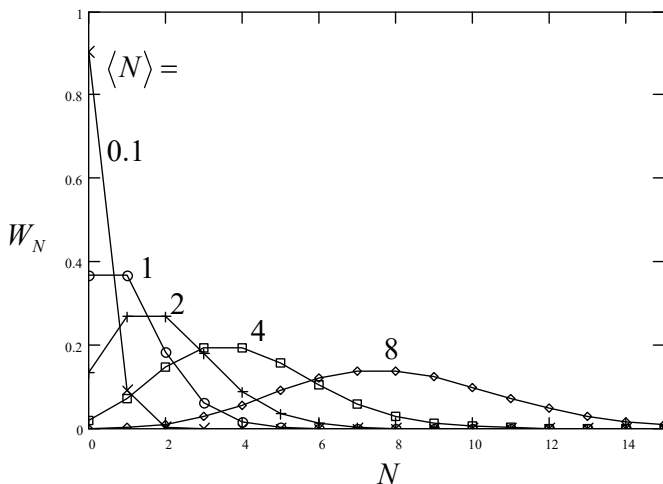


Fig. 5.2. The Poisson distribution for several values of $\langle N \rangle$. In contrast to that average, the argument N may take only integer values, so that the lines in these plots are only guides for the eye.

In the limit of very small $\langle N \rangle$, the function $W_N(N)$ is close to an exponent, $W_N \approx W^N \propto \langle N \rangle^N$, while in the opposite limit, $\langle N \rangle \gg 1$, it rapidly approaches the *Gaussian* (or “normal”) *distribution*⁷

$$W_N = \frac{1}{(2\pi)^{1/2} \delta N} \exp\left\{-\frac{(N - \langle N \rangle)^2}{2(\delta N)^2}\right\}. \quad (5.32)$$

Gaussian distribution

(Note that the Gaussian distribution is also valid if both N and N_0 are large, regardless of the relation between them – see Fig. 3.)

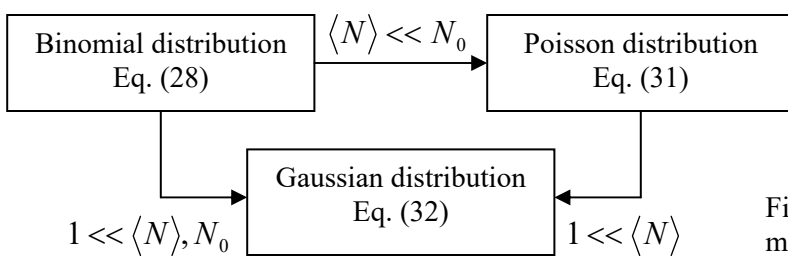


Fig. 5.3. The hierarchy of three major probability distributions.

⁵ Indeed, this is just the most popular definition of that major mathematical constant – see, e.g., MA Eq. (1.2a) with $n = -1/W$.

⁶ Named after the same Siméon Denis Poisson (1781-1840) who is also responsible for other mathematical tools and results used in this series, including the Poisson equation – see Sec. 6.4 below.

⁷ Named after Carl Friedrich Gauss (1777-1855), though Pierre-Simone Laplace (1749-1827) is credited for substantial contributions to its development.

A major property of the Poisson (and hence of the Gaussian) distribution is that it has the same variance as given by Eq. (27):

$$\langle \tilde{N}^2 \rangle \equiv \langle (N - \langle N \rangle)^2 \rangle = \langle N \rangle. \quad (5.33)$$

(This is not true for the general binomial distribution.) For our current purposes, this means that for the ideal classical gas, Eq. (27) is valid for *any* number of particles.

5.3. Volume and temperature

What are the r.m.s. fluctuations of other thermodynamic variables – like V , T , etc.? Again, the answer depends on specific conditions. For example, if the volume V occupied by a gas is externally fixed (say, by rigid walls), it evidently does not fluctuate at all: $\delta V = 0$. On the other hand, the volume may fluctuate in the situation when the average pressure is fixed – see, e.g., Fig. 1.5. A formal calculation of these fluctuations, using the approach applied in the last section, is complicated by the fact that it is physically impracticable to fix its conjugate variable, P , i.e. suppress its fluctuations. For example, the force $\mathcal{F}(t)$ exerted by an ideal classical gas on a container's wall (whose measure the pressure is) is the result of individual, independent hits of the wall by particles (Fig. 4), with the time scale $\tau_c \sim r_B/\langle v^2 \rangle^{1/2} \sim r_B/(T/m)^{1/2} \sim 10^{-16}$ s, so that its frequency spectrum extends to very high frequencies, virtually impossible to control.

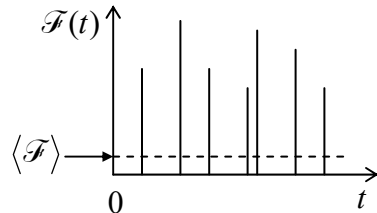


Fig. 5.4. The force exerted by gas particles on a container's wall, as a function of time (schematically).

However, we can use the following trick, very typical for the theory of fluctuations. It is almost evident that the r.m.s. fluctuations of the gas volume are independent of the shape of the container. Let us consider a particular situation similar to that shown in Fig. 1.5, with the container of a cylindrical shape, with the base area A .⁸ Then the coordinate of the piston is just $q = V/A$, while the average force exerted by the gas on the cylinder is $\mathcal{F} = PA$ – see Fig. 5. Now if the piston is sufficiently massive, its free oscillation frequency ω near the equilibrium position is small enough to satisfy the following three conditions.

First, besides balancing the average force $\langle \mathcal{F} \rangle$ and thus sustaining the average pressure $\langle P \rangle = \langle \mathcal{F} \rangle / A$ of the gas, the interaction between the heavy piston and the relatively light particles of the gas is weak, because of a relatively short duration of the particle hits (Fig. 4). As a result, the full energy of the system may be represented as a sum of those of the particles and the piston, with a quadratic contribution to the piston's potential energy by small deviations from the equilibrium:

⁸ As a math reminder, the term “cylinder” does not necessarily mean the “circular cylinder”; the shape of its base may be arbitrary; it just should not change with height.

$$U_p = \frac{\kappa}{2} \tilde{q}^2, \quad \text{where } \tilde{q} \equiv q - \langle q \rangle = \frac{\tilde{V}}{A}, \quad (5.34)$$

and κ is the effective spring constant arising from the finite compressibility of the gas.

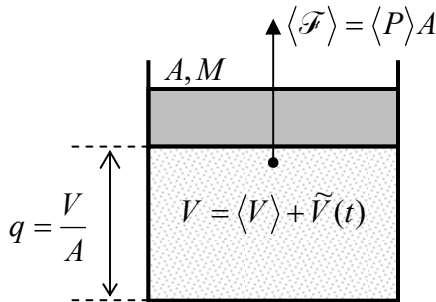


Fig. 5.5. Deriving Eq. (37).

Second, at $\omega \rightarrow 0$, this spring constant may be calculated just as for constant variations of the volume, with the gas remaining in quasi-equilibrium at all times:

$$\kappa = -\frac{\partial \langle \mathcal{F} \rangle}{\partial q} = A^2 \left(-\frac{\partial \langle P \rangle}{\partial \langle V \rangle} \right). \quad (5.35)$$

This partial derivative⁹ should be calculated at whatever the given thermal conditions are, e.g., with $S = \text{const}$ for adiabatic conditions (i.e., a thermally insulated gas), or with $T = \text{const}$ for isothermal conditions (including a good thermal contact between the gas and a heat bath), etc. With that constant denoted as X , Eqs. (34)-(35) give

$$U_p = \frac{1}{2} \left(-A^2 \frac{\partial \langle P \rangle}{\partial \langle V \rangle} \right)_X \left(\frac{\tilde{V}}{A} \right)^2 \equiv \frac{1}{2} \left(-\frac{\partial \langle P \rangle}{\partial \langle V \rangle} \right)_X \tilde{V}^2. \quad (5.36)$$

Finally, assuming that $\omega = (\kappa/M)^{1/2}$ is sufficiently small (namely, $\hbar\omega \ll T$) because of a sufficiently large piston mass M , we may apply, to the piston's fluctuations, the classical equipartition theorem: $\langle U_p \rangle = T/2$, giving¹⁰

$$\boxed{\langle \tilde{V}^2 \rangle_X = T \left(-\frac{\partial \langle V \rangle}{\partial \langle P \rangle} \right)_X.} \quad (5.37a) \quad \text{Fluctuations of } V$$

Since this result is valid for any A and ω , it should not depend on the system's geometry and piston's mass, provided that it is large in comparison with the effective mass of a single system component (say, a gas molecule) – the condition that is naturally fulfilled in most experiments. For the

⁹ As already was discussed in Sec. 4.1 in the context of the van der Waals equation, for the mechanical stability of a gas (or liquid), the derivative $\partial P/\partial V$ has to be negative, so that κ is positive.

¹⁰ One may meet statements that a similar formula,

$$\langle \tilde{P}^2 \rangle_X = T \left(-\frac{\partial \langle P \rangle}{\partial \langle V \rangle} \right)_X, \quad \text{(WRONG!)}$$

is valid for pressure fluctuations. However, a such statement does not take into account a different physical nature of pressure (Fig. 4), with its very broad frequency spectrum. This issue will be discussed later in this chapter.

particular case of fluctuations at constant temperature ($X = T$),¹¹ we may use the definition (3.58) of the isothermal bulk compressibility K_T of the gas to rewrite Eq. (37a) as

$$\langle \tilde{V}^2 \rangle_T = \frac{TV}{K_T}. \quad (5.37b)$$

For an ideal classical gas of N particles, with the equation of state $\langle V \rangle = NT/\langle P \rangle$, it is easier to use directly Eq. (37a), again with $X = T$, to get

$$\langle \tilde{V}^2 \rangle_T = -T \left(-\frac{NT}{\langle P \rangle^2} \right) = \frac{\langle V \rangle^2}{N}, \quad \text{i.e. } \frac{\delta V_T}{\langle V \rangle} = \frac{1}{N^{1/2}}, \quad (5.38)$$

in full agreement with the general trend given by Eq. (12).

Now let us proceed to fluctuations of temperature, for simplicity focusing on the case $V = \text{const}$. Let us again assume that the system we are considering is weakly coupled to a heat bath of temperature T_0 , in the sense that the time τ of temperature equilibration between the two is much larger than the time of internal equilibration, called *thermalization*. Then we may assume that, on the former time scale, T changes virtually simultaneously in the whole system, and consider it a function of time alone:

$$T = \langle T \rangle + \tilde{T}(t). \quad (5.39)$$

Moreover, due to the (relatively) large τ , we may use the stationary relation between small fluctuations of temperature and the internal energy of the system:

$$\tilde{T}(t) = \frac{\tilde{E}(t)}{C_V}, \quad \text{so that } \delta T = \frac{\delta E}{C_V}. \quad (5.40)$$

With those assumptions, Eq. (20) immediately yields the famous expression for the so-called *thermodynamic fluctuations of temperature*:

$$\delta T = \frac{\delta E}{C_V} = \frac{\langle T \rangle}{C_V^{1/2}}. \quad (5.41)$$

The most straightforward application of this result is to analyses of so-called *bolometers* – broadband detectors of electromagnetic radiation in microwave and infrared frequency bands. (In particular, they are used for measurements of the CMB radiation, which was discussed in Sec. 2.6). In such a detector (Fig. 6), the incoming radiation is focused on a small sensor (e.g., either a small piece of a germanium crystal or a superconductor thin film at temperature $T \approx T_c$, etc.), which is well isolated thermally from the environment. As a result, the absorption of an even small radiation power \mathcal{P} leads to a noticeable change ΔT of the sensor's average temperature $\langle T \rangle$ and hence of its electric resistance R , which is probed up by low-noise external electronics.¹² If the power does not change in time too fast, ΔT is a certain function of \mathcal{P} , turning to 0 at $\mathcal{P} = 0$. Hence, if ΔT is much lower than the environment temperature T_0 , we may keep only the main, linear term in its Taylor expansion in \mathcal{P} .

¹¹ In this case, we may also use the second of Eqs. (1.39) to rewrite Eq. (37) via the second derivative $(\partial^2 G / \partial P^2)_T$.

¹² Besides low internal electric noise, a good sensor should have a sufficiently large *temperature responsivity* dR/dT , making the noise contribution by the readout electronics insignificant – see below.

$$\Delta T \equiv \langle T \rangle - T_0 = \frac{\mathcal{P}}{\mathcal{G}}, \quad (5.42)$$

where the coefficient $\mathcal{G} \equiv \partial \mathcal{P} / \partial T$ is called the *thermal conductance* of the (perhaps small but unavoidable) thermal coupling between the sensor and the heat bath – see Fig. 6.

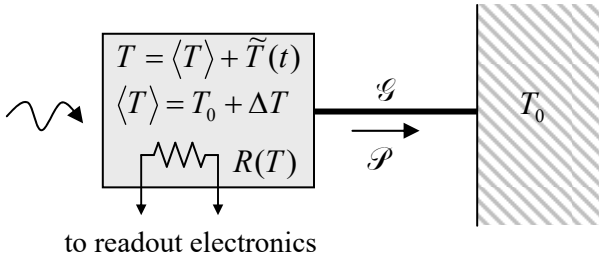


Fig. 5.6. The conceptual scheme of a bolometer.

The power may be detected if the electric signal from the sensor, which results from the change ΔT , is not drowned in spontaneous fluctuations. In practical systems, these fluctuations are contributed by several sources including electronic amplifiers. However, in modern systems, these “technical” contributions to noise are successfully suppressed,¹³ and the dominating noise source is the fundamental sensor temperature fluctuations, described by Eq. (41). In this case, the so-called *noise-equivalent power* (“NEP”), defined as the level of \mathcal{P} that produces the signal equal to the r.m.s. value of noise, may be calculated by equating the expressions (41) (with $\langle T \rangle = T_0$) and (42):

$$\text{NEP} \equiv \mathcal{P} \Big|_{\Delta T = \delta T} = \frac{T_0 \mathcal{G}}{C_V^{1/2}}. \quad (5.43)$$

This expression shows that to decrease the NEP, i.e. improve the detector’s sensitivity, both the environment temperature T_0 and the thermal conductance \mathcal{G} should be reduced. In modern receivers of radiation, their typical values are of the order of 0.1 K and 10^{-10} W/K, respectively.

On the other hand, Eq. (43) implies that to increase the bolometer’s sensitivity, i.e. to reduce the NEP, the C_V of the sensor, and hence its mass, should be *increased*. This conclusion is valid only to a certain extent, because due to technical reasons (parameter drifts and the so-called *1/f noise* of the sensor and external electronics), the incoming power has to be modulated with as high frequency ω as technically possible (in practical receivers, the cyclic frequency $\nu = \omega/2\pi$ of the modulation is between 10 and 1,000 Hz), so that the electrical signal might be picked up from the sensor at that frequency. As a result, the C_V may be increased only until the thermal constant of the sensor,

$$\tau = \frac{C_V}{\mathcal{G}}, \quad (5.44)$$

becomes close to $1/\omega$, because at $\omega\tau \gg 1$ the useful signal drops faster than noise. So, the lowest (i.e. the best) values of the NEP,

¹³ An important modern trend in this progress [see, e.g., P. Day *et al.*, *Nature* **425**, 817 (2003)] is the replacement of the resistive temperature sensors $R(T)$ with thin and narrow superconducting strips with temperature-sensitive kinetic inductance $L_k(T)$ – see the model solution of EM Problem 6.19. Such inductive sensors have zero dc resistance, and hence vanishing Johnson-Nyquist noise at typical signal pickup frequencies of a few kHz – see Eq. (81) and its discussion below.

$$(NEP)_{\min} = \alpha T_0 \mathcal{G}^{1/2} \nu^{1/2}, \quad \text{with } \alpha \sim 1, \quad (5.45)$$

are reached at $\nu\tau \approx 1$. (The exact values of the optimal product $\omega\tau$, and of the numerical constant $\alpha \sim 1$ in Eq. (45), depend on the exact law of the power modulation in time, and the readout signal processing procedure.) With the parameters cited above, this estimate yields $(NEP)_{\min}/\nu^{1/2} \sim 3 \times 10^{-17} \text{ W/Hz}^{1/2}$ – a very low power indeed.

However, perhaps counter-intuitively, the power modulation allows the bolometric (and other broadband) receivers to register radiation with power much lower than this NEP! Indeed, picking up the sensor signal at the modulation frequency ω , we can use the subsequent electronics stages to filter out all the noise besides its components within a very narrow band, of width $\Delta\nu \ll \nu$, around the modulation frequency (Fig. 7). This is the idea of a *microwave radiometer*,¹⁴ currently used in all sensitive broadband receivers of radiation.

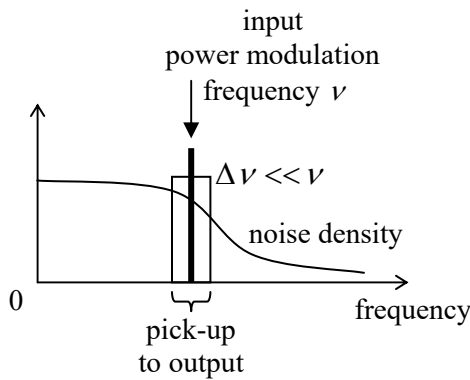


Fig. 5.7. The basic idea of the Dicke radiometer.

In order to analyze this opportunity, we need to develop theoretical tools for a quantitative description of the spectral distribution of fluctuations. Another motivation for that description is a need for analysis of variables dominated by fast (high-frequency) components, such as pressure – please have one more look at Fig. 4. Finally, during such an analysis, we will run into the fundamental relation between fluctuations and dissipation, which is one of the main results of statistical physics as a whole.

5.4. Fluctuations as functions of time

In the previous sections, the averaging $\langle \dots \rangle$ of any function was assumed to be over an appropriate statistical ensemble of many similar systems. However, as was discussed in Sec. 2.1, most physical systems of interest are ergodic. If such a system is also *stationary*, i.e. the statistical averages of its variables do not change with time, the averaging may be also understood as that over a sufficiently long time interval. In this case, we may think about fluctuations of any variable f as of a random process taking place in just one system, but developing in time: $\tilde{f} = \tilde{f}(t)$.

There are two mathematically equivalent approaches to the description of such random functions of time, called the *time-domain* picture and the *frequency-domain* picture, their relative convenience

¹⁴ It was pioneered in the 1950s by Robert Henry Dicke, so that the device is frequently called the *Dicke radiometer*. Note that the optimal strategy of using similar devices for time- and energy-resolved detection of single high-energy photons is different – though even it is essentially based on Eq. (41). For a recent brief review of such detectors see, e.g., K. Morgan, *Phys. Today* **71**, 29 (Aug. 2018), and references therein.

depending on the particular problem to be solved. In the time domain, we need to characterize a *random* fluctuation $\tilde{f}(t)$ by some *deterministic* function of time. Evidently, the average $\langle \tilde{f}(t) \rangle$ cannot be used for this purpose, because it equals zero – see Eq. (2). Of course, the variance (3) does not equal zero, but if the system is stationary, that average cannot depend on time either. Because of that, let us consider the following average:

$$\langle \tilde{f}(t)\tilde{f}(t') \rangle. \quad (5.46)$$

Generally, this is a function of two arguments. However, in a stationary system, the average like (46) may depend only on the difference,

$$\tau \equiv t' - t, \quad (5.47)$$

between the two observation times. In this case, the average (46) is called the *correlation function* of the variable f :

$$K_f(\tau) \equiv \langle \tilde{f}(t)\tilde{f}(t+\tau) \rangle. \quad (5.48)$$

Correlation
function

Again, here the averaging may be understood as that either over a statistical ensemble of macroscopically similar systems or over a sufficiently long interval of the time argument t , with the argument τ kept constant. The correlation function's name¹⁵ catches the idea of this notion very well: $K_f(\tau)$ characterizes the mutual relation between the fluctuations of the variable f at two times separated by the given interval τ . Let us list the basic properties of this function.¹⁶

First of all, $K_f(\tau)$ has to be an even function of the time delay τ . Indeed, we may write

$$K_f(-\tau) = \langle \tilde{f}(t)\tilde{f}(t-\tau) \rangle \equiv \langle \tilde{f}(t-\tau)\tilde{f}(t) \rangle = \langle \tilde{f}(t')\tilde{f}(t'+\tau) \rangle, \quad (5.49)$$

with $t' \equiv t - \tau$. For stationary processes, this average cannot depend on the common shift of two observation times, so that the averages (48) and (49) have to be equal:

$$K_f(-\tau) = K_f(\tau). \quad (5.50)$$

Second, at $\tau \rightarrow 0$ the correlation function tends to the variance:

$$K_f(0) = \langle \tilde{f}(t)\tilde{f}(t) \rangle = \langle \tilde{f}^2 \rangle \geq 0. \quad (5.51)$$

In the opposite limit, when τ is much larger than certain characteristic *correlation time* τ_c of the system,¹⁷ the correlation function has to tend to zero because the fluctuations separated by such time interval are virtually independent (*uncorrelated*). As a result, the correlation function typically looks like one of the plots sketched in Fig. 8.

¹⁵ Another term, the *autocorrelation function*, is sometimes used for the average (48) to distinguish it from the *mutual correlation function*, $\langle f_1(t)f_2(t+\tau) \rangle$, of two different stationary processes.

¹⁶ Please notice that this correlation function is the direct temporal analog of the spatial correlation function briefly discussed in Sec. 4.2 – see Eq. (4.30).

¹⁷ Note that the correlation time τ_c is the direct temporal analog of the correlation radius r_c that was discussed in Sec. 4.2 – see the same Eq. (4.30).

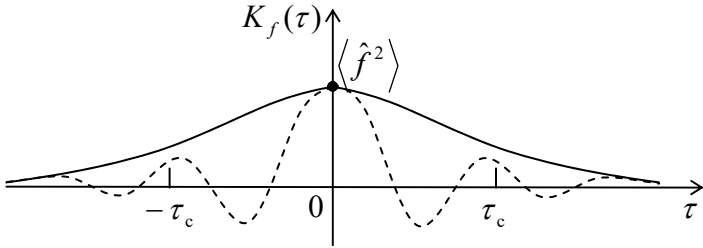


Fig. 5.8. The correlation function of fluctuations: two typical examples.

Note that on a time scale much longer than τ_c , any physically-realistic correlation function may be well approximated with a delta function of τ . (For example, for a process which is a sum of independent very short pulses, e.g., the gas pressure force exerted on the container wall (Fig. 4), such approximation is legitimate on time scales much longer than the single pulse duration, e.g., the time of particle's interaction with on the wall at the impact.)

In the reciprocal, frequency domain, the same process $\tilde{f}(t)$ is represented as a Fourier integral,¹⁸

$$\tilde{f}(t) = \int_{-\infty}^{+\infty} f_\omega e^{-i\omega t} d\omega, \quad (5.52)$$

with the reciprocal transform being

$$f_\omega = \frac{1}{2\pi} \int_{-\infty}^{+\infty} \tilde{f}(t) e^{i\omega t} dt. \quad (5.53)$$

If the function $\tilde{f}(t)$ is random (as it is in the case of fluctuations), with zero average, its Fourier transform f_ω is also a random function (now of frequency), also with a vanishing statistical average. Indeed, now thinking of the operation $\langle \dots \rangle$ as an ensemble averaging, we may write

$$\langle f_\omega \rangle = \left\langle \frac{1}{2\pi} \int_{-\infty}^{+\infty} \tilde{f}(t) e^{i\omega t} dt \right\rangle = \frac{1}{2\pi} \int_{-\infty}^{+\infty} \langle \tilde{f}(t) \rangle e^{i\omega t} dt = 0. \quad (5.54)$$

The simplest non-zero average may be formed similarly to Eq. (46), but with due respect to the complex-variable character of the Fourier images:

$$\langle f_\omega f_{\omega'}^* \rangle = \frac{1}{(2\pi)^2} \int_{-\infty}^{+\infty} dt' \int_{-\infty}^{+\infty} dt \langle \tilde{f}(t) \tilde{f}(t') \rangle e^{i(\omega' t' - \omega t)}. \quad (5.55)$$

It turns out that for a stationary process, the averages (46) and (55) are directly related. Indeed, since the integration over t' in Eq. (55) is in infinite limits, we may replace it with the integration over $\tau \equiv t' - t$ (at fixed t), also in infinite limits. Replacing t' with $t + \tau$ in the expressions under the integral, we see that the average is just the correlation function $K_f(\tau)$, while the time exponent is equal to $\exp\{i(\omega' - \omega)t\}\exp\{i\omega'\tau\}$. As a result, changing the order of integration, we get

$$\langle f_\omega f_{\omega'}^* \rangle = \frac{1}{(2\pi)^2} \int_{-\infty}^{+\infty} dt \int_{-\infty}^{+\infty} d\tau K_f(\tau) e^{i(\omega - \omega')t} e^{i\omega'\tau} \equiv \frac{1}{(2\pi)^2} \int_{-\infty}^{+\infty} K_f(\tau) e^{i\omega'\tau} d\tau \int_{-\infty}^{+\infty} e^{i(\omega - \omega')t} dt. \quad (5.56)$$

But the last integral is just $2\pi\delta(\omega - \omega')$,¹⁹ so that we finally get

¹⁸ The argument of the function f_ω is represented as its index with a purpose to emphasize that this function is different from $\tilde{f}(t)$, while (very conveniently) still using the same letter for the same variable.

$$\langle f_\omega f_{\omega'}^* \rangle = S_f(\omega) \delta(\omega - \omega'), \quad (5.57)$$

where the real function of frequency,

$$S_f(\omega) \equiv \frac{1}{2\pi} \int_{-\infty}^{+\infty} K_f(\tau) e^{i\omega\tau} d\tau = \frac{1}{\pi} \int_0^\infty K_f(\tau) \cos \omega\tau d\tau, \quad (5.58)$$

Spectral density of fluctuations

is called the *spectral density of fluctuations at frequency ω* . According to Eq. (58), the spectral density is just the Fourier image of the correlation function, and hence the reciprocal Fourier transform is:²⁰⁻²¹

$$K_f(\tau) = \int_{-\infty}^{+\infty} S_f(\omega) e^{-i\omega\tau} d\omega = 2 \int_0^\infty S_f(\omega) \cos \omega\tau d\omega. \quad (5.59)$$

Wiener-Khinchin theorem

In particular, for the fluctuation variance, Eq. (59) yields

$$\langle \tilde{f}^2 \rangle \equiv K_f(0) = \int_{-\infty}^{+\infty} S_f(\omega) d\omega \equiv 2 \int_0^\infty S_f(\omega) d\omega. \quad (5.60)$$

The last relation shows that the term “spectral density” describes the physical sense of the function $S_f(\omega)$ very well. Indeed, if a random signal $f(t)$ had been passed through a frequency filter with a small bandwidth $\Delta\nu \ll \nu$ of positive cyclic frequencies, the integral in the last form of Eq. (60) could be limited to the interval $\Delta\omega = 2\pi\Delta\nu$, i.e. the variance of the filtered signal would become

$$\langle \tilde{f}^2 \rangle_{\Delta\nu} = 2S_f(\omega)\Delta\omega \equiv 4\pi S_f(\omega)\Delta\nu. \quad (5.61)$$

(A popular alternative definition of the spectral density is $\mathcal{S}(\nu) \equiv 4\pi S_f(\omega)$, making the average (61) equal to just $\mathcal{S}(\nu)\Delta\nu$.)

To conclude this introductory (mostly mathematical) section, let me note an important particular case. If the spectral density of some process is nearly constant within all the frequency range of interest, $S_f(\omega) = \text{const} = S_f(0)$,²² Eq. (59) shows that its correlation function may be well approximated with a delta function:

$$K_f(\tau) = S_f(0) \int_{-\infty}^{+\infty} e^{-i\omega\tau} d\omega = 2\pi S_f(0) \delta(\tau). \quad (5.62)$$

From this relation stems another popular name of the white noise, the *delta-correlated process*. We have already seen that this is a very reasonable approximation, for example, for the gas pressure force fluctuations (Fig. 4). Of course, for the spectral density of a realistic, limited physical variable the approximation of constant spectral density cannot be true for *all* frequencies (otherwise, for example,

¹⁹ See, e.g., MA Eq. (14.4).

²⁰ The second form of Eq. (59) uses the fact that, according to Eq. (58), $S_f(\omega)$ is an even function of frequency – just as $K_f(\tau)$ is an even function of time.

²¹ Although Eqs. (58) and (59) look not much more than straightforward corollaries of the Fourier transform, they bear a special name of the *Wiener-Khinchin theorem* – after the mathematicians N. Wiener and A. Khinchin who have proved that these relations are valid even for the functions $f(t)$ that are not square-integrable, so that from the point of view of standard mathematics, their Fourier transforms are not well defined.

²² Such process is frequently called the *white noise*, because it consists of all frequency components with equal amplitudes, reminding the white light, which consists of many monochromatic components with close amplitudes.

the integral (60) would diverge, giving an unphysical, infinite value of its variance), and may be valid only at frequencies much lower than $1/\tau_c$.

5.5. Fluctuations and dissipation

Now we are equipped mathematically to address one of the most important issues of statistical physics, the relation between fluctuations and dissipation. This relation is especially simple for the following hierarchical situation: a relatively “heavy”, slowly moving system, weakly interacting with an environment consisting of rapidly moving, “light” components. A popular theoretical term for such a system is the *Brownian particle*, named after botanist Robert Brown who was first to notice (in 1827) the random motion of small particles (in his case, pollen grains), caused by their random hits by fluid’s molecules, under a microscope. However, the family of such systems is much broader than that of small mechanical particles. Just for a few examples, such description is valid for an atom interacting with electromagnetic field modes of the surrounding space, a clock pendulum interacting with molecules of the air around it, current and voltage in electric circuits, etc.²³

One more important assumption of this theory is that the system’s motion does not violate the thermal equilibrium of the environment – well fulfilled in many cases. (Think, for example, about a typical mechanical pendulum – its motion does not overheat the air around it to any noticeable extent.) In this case, the averaging over a statistical ensemble of *similar environments*, at a fixed, specific motion of the system of interest, may be performed assuming their thermal equilibrium.²⁴ I will denote such a “primary” averaging by the usual angle brackets $\langle \dots \rangle$. At a later stage, we may carry out additional, “secondary” averaging, over an ensemble of many similar systems of interest, coupled to similar environments. When we do, such double averaging will be denoted by double angle brackets $\langle\langle \dots \rangle\rangle$.

Let me start from a simple classical system, a 1D harmonic oscillator whose equation of evolution may be represented as

$$m\ddot{q} + \kappa q = \mathcal{F}_{\text{det}}(t) + \mathcal{F}_{\text{env}}(t) \equiv \mathcal{F}_{\text{det}}(t) + \langle \mathcal{F} \rangle + \tilde{\mathcal{F}}(t), \quad \text{with } \langle \tilde{\mathcal{F}}(t) \rangle = 0, \quad (5.63)$$

where q is the (generalized) coordinate of the oscillator, $\mathcal{F}_{\text{det}}(t)$ is the deterministic external force, while both components of the force $\mathcal{F}_{\text{env}}(t)$ represent the impact of the environment on the oscillator’s motion. Again, on the time scale of the fast-moving environmental components, the oscillator’s motion is slow. The average component $\langle \mathcal{F} \rangle$ of the force exerted by the environment on such a slowly moving object is frequently independent of its coordinate q but does depend on its velocity \dot{q} . For most such systems, the Taylor expansion of the force in small velocity has a non-zero linear term:

$$\langle \mathcal{F} \rangle = -\eta \dot{q}, \quad (5.64)$$

where the constant η is usually called the *drag* (or “kinematic friction”, or “damping”) *coefficient*, so that Eq. (63) may be rewritten as

²³ To emphasize this generality, in the forthcoming discussion of the 1D case, I will use the letter q rather than x for the system’s displacement.

²⁴ For a usual (ergodic) environment, the primary averaging may be interpreted as that over relatively short time intervals, $\tau_c \ll \Delta t \ll \tau$, where τ_c is the correlation time of the environment, while τ is the characteristic time scale of motion of our “heavy” system of interest.

$$m\ddot{q} + \eta\dot{q} + \kappa q = \mathcal{F}_{\text{det}}(t) + \tilde{\mathcal{F}}(t). \quad (5.65)$$

This method of describing the environmental effects on an otherwise Hamiltonian system is called the *Langevin equation*.²⁵ Due to the linearity of the differential equation (65), its general solution may be represented as a sum of two independent parts: the deterministic motion of the damped linear oscillator due to the external force $\mathcal{F}_{\text{det}}(t)$, and its random fluctuations due to the random force $\tilde{\mathcal{F}}(t)$ exerted by the environment. The former effects are well known from classical dynamics,²⁶ so let us focus on the latter part by taking $\mathcal{F}_{\text{det}}(t) = 0$. The remaining term on the right-hand side of Eq. (65) describes the fluctuating part of the environmental force; in contrast to the average component (64), its intensity (read: its spectral density at relevant frequencies $\omega \sim \omega_0 \equiv (\kappa/m)^{1/2}$) does not vanish at $q(t) = 0$, and hence may be evaluated ignoring the system's motion.²⁷

Plugging into Eq. (65) the representation of both variables in the Fourier form similar to Eq. (52), and requiring the coefficients before the same $\exp\{-i\omega t\}$ to be equal on both sides of the equation, for their Fourier images we get the following relation:

$$-m\omega^2 q_\omega - i\omega\eta q_\omega + \kappa q_\omega = \mathcal{F}_\omega, \quad (5.66)$$

which immediately gives us q_ω , i.e. the (random) complex amplitude of the coordinate fluctuations:

$$q_\omega = \frac{\mathcal{F}_\omega}{(\kappa - m\omega^2) - i\eta\omega} \equiv \frac{\mathcal{F}_\omega}{m(\omega_0^2 - \omega^2) - i\eta\omega}. \quad (5.67)$$

Now multiplying Eq. (67) by its complex conjugate for another frequency (say, ω'), averaging both parts of the resulting equation, and using the formulas similar to Eq. (57) for each of them,²⁸ we get the following relation between spectral densities of the oscillations and the random force:²⁹

$$S_q(\omega) = \frac{1}{m^2(\omega_0^2 - \omega^2)^2 + \eta^2\omega^2} S_{\mathcal{F}}(\omega). \quad (5.68)$$

In the so-called low-damping limit ($\eta \ll m\omega_0$), the fraction on the right-hand side of Eq. (68) has a sharp peak near the oscillator's own frequency ω_0 (describing the well-known effect of high- Q resonance), and may be well approximated in that vicinity as

²⁵ Named after Paul Langevin, whose 1908 work was the first systematic development of A. Einstein's ideas on Brownian motion (see below) using this formalism. A detailed discussion of this approach, with numerical examples of its application, may be found, e.g., in the monograph by W. Coffey, Yu. Kalmykov, and J. Waldron, *The Langevin Equation*, World Scientific, 1996.

²⁶ See, e.g., CM Sec. 5.1. Here I assume that the variable $f(t)$ is classical, with the discussion of the quantum case postponed until the end of the section.

²⁷ Note that the direct secondary statistical averaging of Eq. (65) with $\mathcal{F}_{\text{det}} = 0$ yields $\langle\langle q \rangle\rangle = 0$! This, perhaps a bit counter-intuitive result becomes less puzzling if we recognize that this is the averaging over a large statistical ensemble of random sinusoidal oscillations with all values of their phase, and that the (equally probable) oscillations with opposite phases give mutually canceling contributions to the sum in Eq. (2.6).

²⁸ At this stage, we restrict our analysis to random, stationary processes $q(t)$, so that Eq. (57) is valid for this variable as well, if the averaging in it is understood in the $\langle\langle \dots \rangle\rangle$ sense.

²⁹ Regardless of the physical sense of such a function of ω , and of whether its maximum is situated at a finite frequency ω_0 as in Eq. (68) or at $\omega = 0$, it is often referred to as the *Lorentzian* (or "Breit-Wigner") *line*.

$$\frac{1}{m^2(\omega_0^2 - \omega^2)^2 + (\eta\omega)^2} \approx \frac{1}{\eta^2\omega_0^2(\xi^2 + 1)}, \quad \text{with } \xi \equiv \frac{2m(\omega - \omega_0)}{\eta}. \quad (5.69)$$

In contrast, the spectral density $S_{\mathcal{F}}(\omega)$ of fluctuations of a typical environment is changing relatively slowly, so that for the purpose of integration over frequencies near ω_0 we may replace $S_{\mathcal{F}}(\omega)$ with $S_{\mathcal{F}}(\omega_0)$. As a result, the variance of the environment-imposed random oscillations may be calculated, using Eq. (60), as³⁰

$$\langle\langle \tilde{q}^2 \rangle\rangle = 2 \int_0^\infty S_q(\omega) d\omega \approx 2 \int_{\omega \approx \omega_0} S_q(\omega) d\omega = 2S_{\mathcal{F}}(\omega_0) \frac{1}{\eta^2\omega_0^2} \frac{\eta}{2m} \int_{-\infty}^{+\infty} \frac{d\xi}{\xi^2 + 1}. \quad (5.70)$$

This is a well-known table integral,³¹ equal to π , so that, finally:

$$\langle\langle \tilde{q}^2 \rangle\rangle = 2S_{\mathcal{F}}(\omega_0) \frac{1}{\eta^2\omega_0^2} \frac{\eta}{2m} \pi \equiv \frac{\pi}{m\omega_0^2\eta} S_{\mathcal{F}}(\omega_0) \equiv \frac{\pi}{\kappa\eta} S_{\mathcal{F}}(\omega_0). \quad (5.71)$$

But on the other hand, the weak interaction with the environment should keep the oscillator in thermodynamic equilibrium at the same temperature T . Since our analysis has been based on the classical Langevin equation (65), we may only use it in the classical limit $\hbar\omega_0 \ll T$, in which we may use the equipartition theorem (2.48). In our current notation, it yields

$$\frac{\kappa}{2} \langle\langle \tilde{q}^2 \rangle\rangle = \frac{T}{2}. \quad (5.72)$$

Comparing Eqs. (71) and (72), we see that the spectral density of the random force exerted by the environment has to be fundamentally related to the damping it provides:

$$S_{\mathcal{F}}(\omega_0) = \frac{\eta}{\pi} T. \quad (5.73a)$$

Now we may argue (rather convincingly :-) that since this relation does not depend on oscillator's parameters m and κ , and hence its eigenfrequency $\omega_0 = (\kappa/m)^{1/2}$, it should be valid at any relatively low frequency ($\omega\tau_c \ll 1$). Using Eq. (58) with $\omega \rightarrow 0$, it may be also rewritten as a formula for the effective low-frequency drag coefficient:

$$\eta = \frac{1}{T} \int_0^\infty K_{\mathcal{F}}(\tau) d\tau \equiv \frac{1}{T} \int_0^\infty \langle\langle \tilde{\mathcal{F}}(0)\tilde{\mathcal{F}}(\tau) \rangle\rangle d\tau. \quad (5.73b)$$

Formulas (73) reveal an intimate, fundamental relation between the fluctuations and the dissipation provided by a thermally-equilibrium environment. Parroting the famous political slogan, there is “no dissipation without fluctuation” – and vice versa. This means in particular that the phenomenological description of dissipation barely by the drag force in classical mechanics³² is

³⁰ Since in this case the process in the oscillator is entirely due to its environment, its variance should be obtained by statistical averaging over an ensemble of many similar (oscillator + environment) systems, and hence, following our convention, it is denoted by double angular brackets.

³¹ See, e.g. MA Eq. (6.5a).

³² See, e.g., CM Sec. 5.1.

(approximately) valid only when the energy scale of the process is much larger than T . To the best of my knowledge, this fact was first recognized in 1905 by A. Einstein,³³ for the following particular case.

Let us apply our result (73) to a free 1D Brownian particle, by taking $\kappa = 0$ and $\mathcal{F}_{\text{det}}(t) = 0$. In this case, both relations (71) and (72) give infinities. To understand the reason for that divergence, let us go back to the Langevin equation (65) with not only $\kappa = 0$ and $\mathcal{F}_{\text{det}}(t) = 0$, but also $m \rightarrow 0$ – just for the sake of simplicity. (The latter approximation, frequently called the *overdamping limit*, is quite appropriate, for example, for the motion of small particles in viscous fluids – such as in R. Brown's experiments.) In this approximation, Eq. (65) is reduced to a simple equation,

$$\eta \dot{q} = \tilde{\mathcal{F}}(t), \quad \text{with } \langle \tilde{\mathcal{F}}(t) \rangle = 0, \quad (5.74)$$

which may be readily integrated to give the particle's displacement during a finite time interval t :

$$\Delta q(t) \equiv q(t) - q(0) = \frac{1}{\eta} \int_0^t \tilde{\mathcal{F}}(t') dt'. \quad (5.75)$$

Evidently, at the full statistical averaging of the displacement, the fluctuation effects vanish, but this does not mean that the particle does not move – just that it has equal probabilities to be shifted in either of two possible directions. To see that, let us calculate the variance of the displacement:

$$\langle \langle \Delta \tilde{q}^2(t) \rangle \rangle = \frac{1}{\eta^2} \int_0^t dt' \int_0^t dt'' \langle \tilde{\mathcal{F}}(t') \tilde{\mathcal{F}}(t'') \rangle \equiv \frac{1}{\eta^2} \int_0^t dt' \int_0^t dt'' K_{\mathcal{F}}(t' - t''). \quad (5.76)$$

As we already know, at times $\tau \gg \tau_c$, the correlation function may be well approximated by the delta function – see Eq. (62). In this approximation, with $S_{\mathcal{F}}(0)$ expressed by Eq. (73a), we get

$$\langle \langle \Delta \tilde{q}^2(t) \rangle \rangle = \frac{2\pi}{\eta^2} S_{\mathcal{F}}(0) \int_0^t dt' \int_0^t dt'' \delta(t'' - t') = \frac{2\pi}{\eta^2} \frac{\eta T}{\pi} \int_0^t dt' = \frac{2T}{\eta} t \equiv 2Dt, \quad (5.77)$$

with

$$D = \frac{T}{\eta}. \quad (5.78)$$

Einstein's relation

The final form of Eq. (77) describes the well-known law of *diffusion* (“random walk”) of a 1D system, with the r.m.s. deviation from the point of origin growing as $(2Dt)^{1/2}$. The coefficient D is this relation is called the *coefficient of diffusion*, and Eq. (78) describes the extremely simple and important³⁴ *Einstein's relation* between that coefficient and the drag coefficient. Often this relation is rewritten, in the SI units of temperature, as $D = \mu k_B T_K$, where $\mu \equiv 1/\eta$ is the *mobility* of the particle. The physical sense of μ becomes clear from the expression for the deterministic velocity (particle's “drift”), which follows from the averaging of both sides of Eq. (74) after the restoration of the term $\mathcal{F}_{\text{det}}(t)$ in it:

³³ It was published in one of the three papers of Einstein's celebrated 1905 “triad”. As a reminder, another paper started the (special) relativity theory, and one more was the quantum description of the photoelectric effect, essentially starting the quantum mechanics. Not too bad for one year, one young scientist!

³⁴ In particular, in 1908, i.e. very soon after Einstein's publication, it was used by J. Perrin for an accurate determination of the Avogadro number N_A . (It was Perrin who graciously suggested naming this constant after A. Avogadro, honoring his pioneering studies of gases in the 1810s.)

$$v_{\text{drift}} \equiv \langle \langle \dot{q}(t) \rangle \rangle = \frac{1}{\eta} \mathcal{F}_{\text{det}}(t) \equiv \mu \mathcal{F}_{\text{det}}(t), \quad (5.79)$$

so that the mobility is just the drift velocity given to the particle by a unit force.³⁵

Another famous embodiment of the general Eq. (73) is the *thermal* (or “Johnson”, or “Johnson-Nyquist”, or just “Nyquist”) *noise* in resistive electron devices. Let us consider a two-terminal, dissipation-free “probe” circuit, playing the role of the harmonic oscillator in our analysis carried out above, connected to a resistive device (Fig. 9), playing the role of the probe circuit’s environment. (The noise is generated by the thermal motion of numerous electrons, randomly moving inside the resistive device.) For this system, one convenient choice of the conjugate variables (the generalized coordinate and generalized force) is, respectively, the electric charge $Q \equiv \int I(t)dt$ that has passed through the “probe” circuit by time t , and the voltage \mathcal{V} across its terminals, with the polarity shown in Fig. 9. (Indeed, the product $\mathcal{V}dQ$ is the elementary work $d\mathcal{W}$ done by the environment on the probe circuit.)

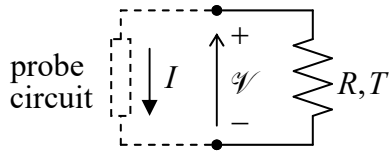


Fig. 5.9. A resistive device as a dissipative environment of a two-terminal probe circuit.

Making the corresponding replacements, $q \rightarrow Q$ and $\mathcal{F} \rightarrow \mathcal{V}$ in Eq. (64), we see that it becomes

$$\langle \mathcal{V} \rangle = -\eta \dot{Q} \equiv -\eta I. \quad (5.80)$$

Comparing this relation with Ohm’s law, $\mathcal{V} = R(-I)$,³⁶ we see that in this case, the coefficient η has the physical sense of the usual Ohmic resistance R of our dissipative device,³⁷ so that Eq. (73a) becomes

$$S_{\mathcal{V}}(\omega) = \frac{R}{\pi} T. \quad (5.81a)$$

Using last equality in Eq. (61), and transferring to the SI units of temperature ($T = k_B T_K$), we may bring this famous *Nyquist formula*³⁸ to its most popular form:

$$\langle \tilde{\mathcal{V}}^2 \rangle_{\Delta\nu} = 4k_B T_K R \Delta\nu. \quad (5.81b)$$

Nyquist formula

³⁵ Note that in solid-state physics and electronics, the charge carrier mobility is usually defined as $|\mathbf{v}_{\text{drift}}/\mathcal{E}| = e v_{\text{drift}}/|\mathcal{F}_{\text{det}}| \equiv e |\mu|$ (where \mathcal{E} is the applied electric field), and is traditionally measured in $\text{cm}^2/\text{V}\cdot\text{s}$.

³⁶ The minus sign is due to the fact that in our notation, the current flowing in the resistor, from the positive terminal to the negative one, is $(-I)$ – see Fig. 9.

³⁷ Due to this fact, Eq. (64) is often called the *Ohmic model* of the environment’s response, even if the physical nature of the variables q and \mathcal{F} is completely different from the electric charge and voltage.

³⁸ It is named after Harry Nyquist who derived this formula in 1928 (independently of the prior work by A. Einstein, M. Smoluchowski, and P. Langevin) to describe the noise that had been just discovered experimentally by his Bell Labs’ colleague John Bertrand Johnson. The derivation of Eq. (73) and hence Eq. (81) in these notes is essentially a twist of the derivation used by H. Nyquist.

Note that according to Eq. (65), this result is only valid at a negligible speed of change of the coordinate q (in our current case, negligible current I), i.e. Eq. (81) expresses the voltage fluctuations as would be measured by a virtually ideal *voltmeter*, with its input resistance much higher than R .

On the other hand, using a different choice of generalized coordinate and force, $q \rightarrow \Phi$, $\mathcal{F} \rightarrow I$ (where $\Phi \equiv \int \mathcal{V}(t)dt$ is the generalized magnetic flux, so that $d\mathcal{W} = I\mathcal{V}(t)dt \equiv Id\Phi$), we get $\eta \rightarrow 1/R$, and Eq. (73) yields the thermal fluctuations of the current through the resistive device, as measured by a virtually ideal *ammeter*, i.e. at $\mathcal{V} \rightarrow 0$:

$$S_I(\omega) = \frac{1}{\pi R} T, \quad \text{i.e. } \langle \tilde{I}^2 \rangle_{\Delta\nu} = \frac{4k_B T_K}{R} \Delta\nu. \quad (5.81c)$$

The nature of Eqs. (81) is so fundamental that they may be used, in particular, for the so-called *Johnson noise thermometry*.³⁹ Note, however, that these relations are valid for noise in thermal equilibrium only. In electric circuits that may be readily driven out of equilibrium by an applied voltage \mathcal{V} , other types of noise are frequently important, notably the *shot noise*, which arises in short conductors, e.g., tunnel junctions, at applied voltages with $|\mathcal{V}| \gg T/q$, due to the discreteness of charge carriers.⁴⁰ A straightforward analysis (left for the reader's exercise) shows that this noise may be characterized by current fluctuations with the following low-frequency spectral density:

$$S_I(\omega) = \frac{|q\bar{I}|}{2\pi}, \quad \text{i.e. } \langle \tilde{I}^2 \rangle_{\Delta\nu} = 2|q\bar{I}|\Delta\nu, \quad (5.82)$$

Schottky formula

where q is the electric charge of a single current carrier. This is the *Schottky formula*,⁴¹ valid for any relation between the average I and \mathcal{V} . The comparison of Eqs. (81c) and (82) for a device that obeys the Ohm law shows that the shot noise has the same intensity as the thermal noise with the effective temperature

$$T_{\text{ef}} = \frac{|q\mathcal{V}|}{2} \gg T. \quad (5.83)$$

This relation may be interpreted as a result of charge carrier overheating by the applied electric field, and explains why the Schottky formula (82) is only valid in conductors much shorter than the energy relaxation length l_e of the charge carriers.⁴² (Another mechanism of shot noise suppression, which may become noticeable in highly conductive nanoscale devices, is the Fermi-Dirac statistics of electrons.⁴³)

Now let us return for a minute to the bolometric Dicke radiometer (see Figs. 6-7 and their discussion in Sec. 4), and use the Langevin formalism to finalize its analysis. For this system, the Langevin equation is an extension of the usual equation of heat balance:

³⁹ See, e.g., J. Crossno *et al.*, *Appl. Phys. Lett.* **106**, 023121 (2015), and references therein.

⁴⁰ Another practically important type of fluctuations in electronic devices is the low-frequency *1/f noise* that was already mentioned in Sec. 3 above. I will briefly discuss it in Sec. 8.

⁴¹ It was derived by Walter Hans Schottky as early as 1918, i.e. even before Nyquist's work.

⁴² See, e.g., Y. Naveh *et al.*, *Phys. Rev. B* **58**, 15371 (1998). In practically used metals, l_e is of the order of 30 nm even at liquid-helium temperatures (and much shorter at room temperatures), so that the usual "macroscopic" resistors do not exhibit the shot noise.

⁴³ For a review of this effect see, e.g., Ya. Blanter and M. Büttiker, *Phys. Repts.* **336**, 1 (2000).

$$C_V \frac{dT}{dt} + \mathcal{G}(T - T_0) = \mathcal{P}_{\text{det}}(t) + \tilde{\mathcal{P}}(t), \quad (5.84)$$

where $\mathcal{P}_{\text{det}} \equiv \langle \mathcal{P} \rangle$ describes the (deterministic) power of the absorbed radiation and $\tilde{\mathcal{P}}$ represents the effective source of temperature fluctuations. Now we can use Eq. (84) to carry out a calculation of the spectral density $S_T(\omega)$ of temperature fluctuations absolutely similarly to how this was done with Eq. (65), assuming that the frequency spectrum of the fluctuation source is much broader than the intrinsic bandwidth $1/\tau = \mathcal{G}/C_V$ of the bolometer, so that its spectral density at frequencies $\omega\tau \sim 1$ may be well approximated by its low-frequency value $S_{\mathcal{P}}(0)$:

$$S_T(\omega) = \left| \frac{1}{-i\omega C_V + \mathcal{G}} \right|^2 S_{\mathcal{P}}(0). \quad (5.85)$$

Then, requiring the variance of temperature fluctuations, calculated from this formula and Eq. (60),

$$\begin{aligned} (\delta T)^2 &\equiv \langle \tilde{T}^2 \rangle = 2 \int_0^\infty S_T(\omega) d\omega = 2 S_{\mathcal{P}}(0) \int_0^\infty \left| \frac{1}{-i\omega C_V + \mathcal{G}} \right|^2 d\omega \\ &\equiv 2 S_{\mathcal{P}}(0) \frac{1}{C_V^2} \int_0^\infty \frac{d\omega}{\omega^2 + (\mathcal{G}/C_V)^2} = \frac{\pi S_{\mathcal{P}}(0)}{\mathcal{G} C_V}, \end{aligned} \quad (5.86)$$

to coincide with our earlier “thermodynamic fluctuation” result (41), we get

$$S_{\mathcal{P}}(0) = \frac{\mathcal{G}}{\pi} T_0^2. \quad (5.87)$$

The r.m.s. value of the “power noise” within a bandwidth $\Delta\nu \ll 1/\tau$ (see Fig. 7) becomes equal to the deterministic signal power \mathcal{P}_{det} (or more exactly, the main harmonic of its modulation law) at

$$\mathcal{P} = \mathcal{P}_{\text{min}} \equiv \left(\langle \tilde{\mathcal{P}}^2 \rangle_{\Delta\nu} \right)^{1/2} = (2 S_{\mathcal{P}}(0) \Delta\nu)^{1/2} = 2(\mathcal{G} \Delta\nu)^{1/2} T_0. \quad (5.88)$$

This result shows that our earlier prediction (45) may be improved by a substantial factor of the order of $(\Delta\nu/\nu)^{1/2}$, where the reduction of the output bandwidth is limited only by the signal accumulation time $\Delta t \sim 1/\Delta\nu$, while the increase of ν is limited by the speed of (typically, mechanical) devices performing the power modulation. In practical systems this factor may improve the sensitivity by a couple of orders of magnitude, enabling observation of extremely weak radiation. Maybe the most spectacular example is the recent measurements of the CMB radiation, which corresponds to blackbody temperature $T_K \approx 2.726$ K, with accuracy $\delta T_K \sim 10^{-6}$ K, using microwave receivers with the physical temperature of all their components much higher than δT . The observed weak ($\sim 10^{-5}$ K) anisotropy of the CMB radiation is a major experimental basis of all modern cosmology.⁴⁴

Returning to the discussion of our main result, Eq. (73), let me note that it may be readily generalized to the case when the environment’s response is different from the Ohmic form (64). This opportunity is virtually evident from Eq. (66): by its derivation, the second term on its left-hand side is just the Fourier component of the average response of the environment to the system’s displacement:

⁴⁴ See, e.g., a concise book by A. Balbi, *The Music of the Big Bang*, Springer, 2008.

$$\langle \hat{\mathcal{F}}_\omega \rangle = i\omega\eta q_\omega. \quad (5.89)$$

Now let the response be still linear, but have an arbitrary frequency dispersion,

$$\langle \hat{\mathcal{F}}_\omega \rangle = \chi(\omega)q_\omega, \quad (5.90)$$

where the function $\chi(\omega)$, called the *generalized susceptibility* (in our case, of the environment) may be complex, i.e. have both the imaginary and real parts:

$$\chi(\omega) = \chi'(\omega) + i\chi''(\omega). \quad (5.91)$$

Then Eq. (73) remains valid with the replacement $\eta \rightarrow \chi''(\omega)/\omega$.⁴⁵

$$S_{\hat{\mathcal{F}}}(\omega) = \frac{\chi''(\omega)}{\pi\omega} T. \quad (5.92)$$

This fundamental relation⁴⁶ may be used not only to calculate the fluctuation intensity from the known generalized responsibility (i.e. the deterministic response of the system to a small perturbation), but also in reverse – to calculate such linear response from the known fluctuations. The latter use is especially attractive at numerical simulations of complex systems, e.g., those based on molecular-dynamics approaches, because it circumvents the need in extracting a weak response to a small perturbation out of a noisy background.

Now let us discuss what generalization of Eq. (92) is necessary to make that fundamental result suitable for arbitrary temperatures, $T \sim \hbar\omega$. The calculations we had performed were based on the apparently classical equation of motion, Eq. (63). However, quantum mechanics shows⁴⁷ that a similar equation is valid for the corresponding Heisenberg-picture operators, so that repeating all the arguments leading to the Langevin equation (65), we may write its quantum-mechanical version

$$m\ddot{\hat{q}} + \eta\dot{\hat{q}} + \kappa\hat{q} = \hat{\mathcal{F}}_{\text{det}} + \hat{\mathcal{F}}. \quad (5.93)$$

Heisenberg-Langevin equation

This is the so-called *Heisenberg-Langevin* (or “quantum Langevin”) *equation* – in this particular case, for a harmonic oscillator.

The further operations, however, require certain caution, because the right-hand side of the equation is now an operator, and has some nontrivial properties. For example, the “values” of the Heisenberg operator, representing the same variable $f(t)$ at different times, do not necessarily commute:

$$\hat{f}(t)\hat{f}(t') \neq \hat{f}(t')\hat{f}(t), \quad \text{if } t' \neq t. \quad (5.94)$$

⁴⁵ Reviewing the calculations leading to Eq. (73), we may see that the possible real part $\chi'(\omega)$ of the susceptibility just adds up to $(k - m\omega^2)$ in the denominator of Eq. (67), resulting in a change of the oscillator’s frequency ω_0 . This renormalization is insignificant if the oscillator-to-environment coupling is weak, i.e. if the susceptibility $\chi(\omega)$ is small – as had been assumed at the derivation of Eq. (69) and hence Eq. (73).

⁴⁶ It is sometimes called the Green-Kubo (or just the Kubo) formula. This is hardly fair, because, as the reader could see, Eq. (92) is just an elementary generalization of the Nyquist formula (81). Moreover, the corresponding works of M. Green and R. Kubo were published, respectively, in 1954 and 1957, i.e. after the 1951 paper by H. Callen and T. Welton, where a more general result (98) had been derived. Much more adequately, the Green/Kubo names are associated with Eq. (102) below.

⁴⁷ See, e.g., QM Sec. 4.6.

As a result, the function defined by Eq. (46) may not be a symmetric function of the time delay $\tau \equiv t' - t$ even for a stationary process, making it inadequate for the representation of the actual correlation function – which has to obey Eq. (50). This technical difficulty may be overcome by the introduction of the following *symmetrized correlation function*⁴⁸

$$K_f(\tau) \equiv \frac{1}{2} \left\langle \hat{\tilde{f}}(t) \hat{\tilde{f}}(t+\tau) + \hat{\tilde{f}}(t+\tau) \hat{\tilde{f}}(t) \right\rangle \equiv \frac{1}{2} \left\langle \left\{ \hat{\tilde{f}}(t), \hat{\tilde{f}}(t+\tau) \right\} \right\rangle, \quad (5.95)$$

(where $\{ \dots, \dots \}$ denotes the anticommutator of the two operators), and, similarly, the symmetrical spectral density $S_f(\omega)$, defined by the following relation:

$$S_f(\omega) \delta(\omega - \omega') \equiv \frac{1}{2} \left\langle \hat{f}_\omega \hat{f}_{\omega'}^* + \hat{f}_{\omega'}^* \hat{f}_\omega \right\rangle \equiv \frac{1}{2} \left\langle \left\{ \hat{f}_\omega, \hat{f}_{\omega'}^* \right\} \right\rangle, \quad (5.96)$$

with $K_f(\tau)$ and $S_f(\omega)$ still related by the Fourier transform (59).

Now we may repeat all the analysis that was carried out for the classical case, and get Eq. (71) again, but now this expression has to be compared not with the equipartition theorem, but with its quantum-mechanical generalization (14), which, in our current notation, reads

$$\left\langle \left\langle \tilde{q}^2 \right\rangle \right\rangle = \frac{\hbar\omega_0}{2\kappa} \coth \frac{\hbar\omega_0}{2T}. \quad (5.97)$$

As a result, we get the following quantum-mechanical generalization of Eq. (92):

FDT

$$S_{\mathcal{F}}(\omega) = \frac{\hbar\chi''(\omega)}{2\pi} \coth \frac{\hbar\omega}{2T}. \quad (5.98)$$

This is the much-celebrated *fluctuation-dissipation theorem*, usually referred to just as the FDT, first derived in 1951 by Herbert Bernard Callen and Theodore A. Welton – in a somewhat different way.

As natural as it seems, this generalization of the relation between fluctuations and dissipation poses a very interesting conceptual dilemma. Let, for the sake of clarity, temperature be relatively low, $T \ll \hbar\omega$; then Eq. (98) gives a temperature-independent result

$$S_{\mathcal{F}}(\omega) = \frac{\hbar\chi''(\omega)}{2\pi}, \quad (5.99)$$

Quantum noise

which describes what is frequently called *quantum noise*. According to the quantum Langevin equation (93), nothing but the random force exerted by the environment, with the spectral density (99) proportional to the imaginary part of susceptibility (i.e. damping), is the source of the ground-state “fluctuations” of the coordinate and momentum of a quantum harmonic oscillator, with the r.m.s. values

$$\delta q \equiv \left\langle \left\langle \tilde{q}^2 \right\rangle \right\rangle^{1/2} = \left(\frac{\hbar}{2m\omega_0} \right)^{1/2}, \quad \delta p \equiv \left\langle \left\langle \tilde{p}^2 \right\rangle \right\rangle^{1/2} = \left(\frac{\hbar m\omega_0}{2} \right)^{1/2}, \quad (5.100)$$

⁴⁸ Here (and to the end of this section) the averaging $\langle \dots \rangle$ should be understood in the general quantum-statistical sense – see Eq. (2.12). As was discussed in Sec. 2.1, for the classical-mixture state of the system, this does not create any difference in either the mathematical treatment of the averages or their physical interpretation.

and the total energy $\hbar\omega_0/2$. On the other hand, the basic quantum mechanics tells us that exactly these formulas describe the ground state of a *dissipation-free* oscillator, not coupled to any environment, and are a direct corollary of the basic commutation relation

$$[\hat{q}, \hat{p}] = i\hbar. \quad (5.101)$$

So, what is the genuine source of the uncertainty described by Eqs. (100)?

The best resolution of this paradox I can offer is that *either* interpretation of Eqs. (100) is legitimate, with their relative convenience depending on the particular application. One may say that since the right-hand side of the quantum Langevin equation (93) is a quantum-mechanical operator, rather than a classical force, it “carries the uncertainty relation within itself”. However, this (admittedly, opportunistic :-) resolution leaves the following question open: is the quantum noise (99) of the environment’s observable \mathcal{F} directly, without any probe oscillator subjected to it? An experimental resolution of this dilemma is not quite simple, because usual scientific instruments have their own ground-state uncertainty, i.e. their own quantum fluctuations, which may be readily confused with those of the system under study. Fortunately, this difficulty may be overcome, for example, using unique frequency-mixing (“down-conversion”) properties of Josephson junctions. Special low-temperature experiments using such down-conversion⁴⁹ have confirmed that the noise (99) is real and measurable.

Finally, let me mention an alternative derivation⁵⁰ of the fluctuation-theorem (98) from the general quantum mechanics of open systems. This derivation is substantially longer than that presented above, but gives an interesting sub-product, the *Green-Kubo formula*

$$\left\langle \left[\hat{\mathcal{F}}(t), \hat{\mathcal{F}}(t + \tau) \right] \right\rangle = i\hbar \mathcal{G}(\tau), \quad (5.102)$$

where $\mathcal{G}(\tau)$ is the temporal Green’s function of the environment, defined by the following relation:

$$\langle \mathcal{F}(t) \rangle = \int_0^\infty \mathcal{G}(\tau) q(t - \tau) d\tau \equiv \int_{-\infty}^t \mathcal{G}(t - t') q(t') dt'. \quad (5.103)$$

Plugging the Fourier transforms of all three functions of time participating in Eq. (103) into this relation, it is straightforward to check that this Green’s function is just the Fourier image of the complex susceptibility $\chi(\omega)$ defined by Eq. (90):

$$\int_0^\infty \mathcal{G}(\tau) e^{i\omega\tau} d\tau = \chi(\omega); \quad (5.104)$$

here 0 is used as the lower limit instead of $(-\infty)$ just to emphasize that due to the causality principle, Green’s function has to be equal zero for $\tau < 0$.⁵¹

In order to reveal the real beauty of Eq. (102), we may use the Wiener-Khinchin theorem (59) to rewrite the fluctuation-dissipation theorem (98) in a similar time-domain form:

⁴⁹ R. Koch *et al.*, *Phys. Rev. B* **26**, 74 (1982), and references therein.

⁵⁰ See, e.g., QM Sec. 7.4.

⁵¹ See, e.g., CM Sec. 5.1.

$$\left\langle \left\{ \hat{\mathcal{F}}(t), \hat{\mathcal{F}}(t+\tau) \right\} \right\rangle = 2K_{\mathcal{F}}(\tau), \quad (5.105)$$

where the symmetrized correlation function $K_{\mathcal{F}}(\tau)$ is most simply described by its Fourier transform, which is, according to Eq. (58), equal to $\pi S_{\mathcal{F}}(\omega)$, so that using the FDT, we get

$$\int_0^\infty K_{\mathcal{F}}(\tau) \cos \omega \tau d\tau = \frac{\hbar \chi''(\omega)}{2} \coth \frac{\hbar \omega}{2T}. \quad (5.106)$$

The comparison of Eqs. (102) and (104), on one hand, and Eqs (105)-(106), on the other hand, shows that both the commutation and anticommutation properties of the Heisenberg-Langevin force operator at different moments of time are determined by the same generalized susceptibility $\chi(\omega)$ of the environment. However, the averaged anticommutator also depends on temperature, while the averaged commutator does not – at least explicitly, because the complex susceptibility of an environment may be temperature-dependent as well.

5.6. The Kramers problem and the Smoluchowski equation

Returning to the classical case, it is evident that Langevin equations of the type (65) provide means not only for the analysis of stationary fluctuations, but also for the description of arbitrary time evolution of (classical) systems coupled to their environments – which, again, may provide both dissipation and fluctuations. However, this approach to evolution analysis suffers from two major handicaps.

First, the Langevin equation does enable a straightforward calculation of the statistical average of the variable q , and its fluctuation variance – i.e., in the common mathematical terminology, the first and second *moments* of the probability density $w(q, t)$ – as functions of time, but not of the probability distribution as such. Admittedly, this is rarely a big problem, because in most cases the distribution is Gaussian – see, e.g., Eq. (2.77).

The second, more painful drawback of the Langevin approach is that it is instrumental only for “linear” systems – i.e., the systems whose dynamics may be described by linear differential equations, such as Eq. (65). However, as we know from classical dynamics, many important problems (for example, the Kepler problem of planetary motion⁵²) are reduced to motion in substantially non-harmonic potentials $U_{\text{ef}}(q)$, leading to nonlinear equations of motion. If the energy of interaction between the system and its random environment is factorable – i.e. is a product of variables belonging to these subsystems (as it is very frequently the case), we may repeat all arguments of the last section to derive the following generalized version of the 1D Langevin equation:⁵³

$$m\ddot{q} + \eta \dot{q} + \frac{\partial U(q, t)}{\partial q} = \tilde{\mathcal{F}}(t), \quad (5.107)$$

⁵² See, e.g., CM Secs. 3.4-3.6.

⁵³ The generalization of Eq. (107) to higher spatial dimensionality is also straightforward, with the scalar variable q replaced with a multi-dimensional vector \mathbf{q} , and the scalar derivative dU/dq replaced with the vector ∇U , where ∇ is the del vector-operator in the \mathbf{q} -space.

valid for an arbitrary, possibly time-dependent potential $U(q, t)$. Unfortunately, the solution of this equation may be very hard. Indeed, its Fourier analysis carried out in the last section was essentially based on the linear superposition principle, which is invalid for nonlinear equations.

If the fluctuation intensity is low, $|\delta q| \ll \langle q \rangle$, where $\langle q \rangle(t)$ is the deterministic solution of Eq. (107) in the absence of fluctuations, this equation may be linearized⁵⁴ with respect to small fluctuations $\tilde{q} \equiv q - \langle q \rangle$ to get a linear equation,

$$m\ddot{\tilde{q}} + \eta \dot{\tilde{q}} + \kappa(t)\tilde{q} = \tilde{\mathcal{F}}(t), \quad \text{with } \kappa(t) \equiv \frac{\partial^2}{\partial q^2} U(\langle q \rangle(t), t). \quad (5.108)$$

This equation differs from Eq. (65) only by the time dependence of the effective spring constant $\kappa(t)$, and may be solved by the Fourier expansion of both the fluctuations and the function $\kappa(t)$. Such calculations may be more cumbersome than those performed above, but still be doable (especially if the unperturbed motion $\langle q \rangle(t)$ is periodic), and sometimes give useful analytical results.⁵⁵

However, some important problems cannot be solved by linearization. Perhaps, the most apparent (and practically very important) example is the so-called *Kramers problem*⁵⁶ of finding the lifetime of a metastable state of a 1D classical system in a potential well separated from the region of unlimited motion with a potential barrier – see Fig. 10.

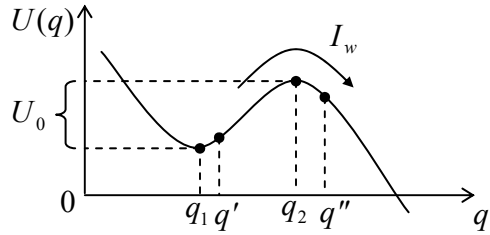


Fig. 5.10. The Kramers problem.

In the absence of fluctuations, the system, initially placed close to the well's bottom (in Fig. 10, at $q \approx q_1$), would stay there forever. Fluctuations result not only in a finite spread of the probability density $w(q, t)$ around that point but also in a gradual decrease of the total probability

$$W(t) = \int_{\text{well's bottom}} w(q, t) dq \quad (5.109)$$

to find the system in the well, because of a non-zero rate of its escape from it, over the potential barrier, due to thermal activation. What may be immediately expected of the situation is that if the barrier height,

$$U_0 \equiv U(q_2) - U(q_1), \quad (5.110)$$

⁵⁴ See, e.g., CM Secs. 3.2, 5.2, and beyond.

⁵⁵ See, e.g., QM Problem 7.8, and also Chapters 5 and 6 in the monograph by W. Coffey *et al.*, cited above.

⁵⁶ It was named after Hendrik Anthony (“Hans”) Kramers who, besides solving this conceptually important problem in 1940, has made several other seminal contributions to physics, including the famous Kramers-Kronig dispersion relations (see, e.g., EM Sec. 7.4) and the WKB (Wentzel-Kramers-Brillouin) approximation in quantum mechanics – see, e.g., QM Sec. 2.4.

is much larger than temperature T ,⁵⁷ the Boltzmann distribution $w \propto \exp\{-U(q)/T\}$ should be still approximately valid in most of the well, so that the probability for the system to overcome the barrier should scale as $\exp\{-U_0/T\}$. From these handwaving arguments, one may reasonably expect that if the probability $W(t)$ of the system's still residing in the well by time t obeys the usual “decay law”

$$\dot{W} = -\frac{W}{\tau}, \quad (5.111a)$$

then the lifetime τ has to obey the general Arrhenius law:

$$\tau = \tau_A \exp\left\{\frac{U_0}{T}\right\}. \quad (5.111b)$$

However, these relations need to be proved, and the pre-exponential coefficient τ_A (usually called the *attempt time*) needs to be calculated. This cannot be done by the linearization of Eq. (107), because this approximation is equivalent to a quadratic approximation of the potential $U(q)$, which evidently cannot describe the potential well *and* the potential barrier simultaneously – see Fig. 10 again.

This and other essentially nonlinear problems may be addressed using an alternative approach to fluctuations, dealing directly with the time evolution of the probability density $w(q, t)$. Due to the shortage of time/space, I will review this approach using mostly handwaving arguments, and refer the interested reader to special literature⁵⁸ for strict mathematical proofs. Let us start from the diffusion of a free classical 1D particle with inertial effects negligible in comparison with damping. It is described by the Langevin equation (74) with $\mathcal{F}_{\text{det}} = 0$. Let us assume that at all times the probability distribution stays Gaussian:

$$w(q, t) = \frac{1}{(2\pi)^{1/2} \delta q(t)} \exp\left\{-\frac{(q - q_0)^2}{2\delta q^2(t)}\right\}, \quad (5.112)$$

where q_0 is the initial position of the particle, and $\delta q(t)$ is the time-dependent distribution width, whose growth in time is described, as we already know, by Eq. (77):

$$\delta q(t) = (2Dt)^{1/2}. \quad (5.113)$$

Then it is straightforward to verify, by substitution, that this solution satisfies the following simple partial differential equation,⁵⁹

$$\frac{\partial w}{\partial t} = D \frac{\partial^2 w}{\partial q^2}, \quad (5.114)$$

with the delta-functional initial condition

$$w(q, 0) = \delta(q - q_0). \quad (5.115)$$

⁵⁷ If U_0 is comparable with T , the system's behavior also depends substantially on the initial probability distribution, i.e., does not follow the simple law (111).

⁵⁸ See, e.g., either R. Stratonovich, *Topics in the Theory of Random Noise*, vol. 1., Gordon and Breach, 1963, or Chapter 1 in the monograph by W. Coffey *et al.*, cited above.

⁵⁹ By the way, the goal of the traditional definition (78) of the diffusion coefficient, leading to the front coefficient 2 in Eq. (77), is exactly to have the fundamental equations (114) and (116) free of numerical coefficients.

The simple and important *equation of diffusion* (114) may be naturally generalized to the 3D motion:⁶⁰

$$\boxed{\frac{\partial w}{\partial t} = D \nabla^2 w.} \quad (5.116)$$

Equation
of diffusion

Now let us compare this equation with the probability conservation law,⁶¹

$$\frac{\partial w}{\partial t} + \nabla \cdot \mathbf{j}_w = 0, \quad (5.117a)$$

where the vector \mathbf{j}_w has the physical sense of the probability current density. (The validity of this relation is evident from its integral form,

$$\frac{d}{dt} \int_V w d^3 r + \oint_S \mathbf{j}_w \cdot d^2 \mathbf{q} = 0, \quad (5.117b)$$

which results from the integration of Eq. (117a) over an arbitrary time-independent volume V limited by surface S , and applying the divergence theorem⁶² to the second term.) The continuity relation (117a) coincides with Eq. (116), with D given by Eq. (78), only if we take

$$\mathbf{j}_w = -D \nabla w = -\frac{T}{\eta} \nabla w. \quad (5.118)$$

The first form of this relation allows a simple interpretation: the probability flow is proportional to the spatial gradient of the probability density (i.e., in application to $N \gg 1$ similar and independent particles, just to the gradient of their concentration $n = Nw$), with the sign corresponding to the flow from the higher to lower concentrations. This flow is the very essence of the effect of diffusion. The second form of Eq. (118) is also not very surprising: the diffusion speed scales as temperature and is inversely proportional to the viscous drag.

The fundamental Eq. (117) has to be satisfied also in the case of a force-driven particle at negligible diffusion ($D \rightarrow 0$); in this case

$$\mathbf{j}_w = w \mathbf{v}, \quad (5.119)$$

where \mathbf{v} is the deterministic velocity of the particle. In the high-damping limit we are considering right now, \mathbf{v} has to be just the *drift velocity*:

$$\mathbf{v} = \frac{1}{\eta} \mathcal{F}_{\text{det}} = -\frac{1}{\eta} \nabla U(\mathbf{q}), \quad (5.120)$$

where \mathcal{F}_{det} is the deterministic force described by the potential energy $U(\mathbf{q})$.

Now that we have descriptions of \mathbf{j}_w due to both the drift *and* the diffusion separately, we may rationally assume that in the general case when both effects are present, the corresponding components (118) and (119) of the probability current just add up, so that

⁶⁰ As will be discussed in Chapter 6, the equation of diffusion also describes several other physical phenomena – in particular, the heat propagation in a uniform, isotropic solid, and in this context is called the *heat conduction equation* or (rather inappropriately) just the “heat equation”.

⁶¹ Both forms of Eq. (117) are similar to the mass conservation law in classical dynamics (see, e.g., CM Sec. 8.2), the electric charge conservation law in electrodynamics (see, e.g., EM Sec. 4.1), and the probability conservation law in quantum mechanics (see, e.g., QM Sec. 1.4).

⁶² See, e.g., MA Eq. (12.2),

$$\mathbf{j}_w = \frac{1}{\eta} [w(-\nabla U) - T\nabla w], \quad (5.121)$$

and Eq. (117a) takes the form

Smoluchowski
equation

$$\eta \frac{\partial w}{\partial t} = \nabla(w\nabla U) + T\nabla^2 w. \quad (5.122)$$

This is the *Smoluchowski equation*,⁶³ which is closely related to the *drift-diffusion equation* in multi-particle kinetics – to be discussed in the next chapter.

As a sanity check, let us see what the Smoluchowski equation gives in the stationary limit, $\partial w/\partial t \rightarrow 0$ (which evidently may be eventually achieved only if the deterministic potential U is time-independent.) Then Eq. (117a) yields $\mathbf{j}_w = \text{const}$, where the constant describes the deterministic motion of the system as the whole. If such a motion is absent, $\mathbf{j}_w = 0$, then according to Eq. (121),

$$w\nabla U + T\nabla w = 0, \quad \text{i.e. } \frac{\nabla w}{w} = -\frac{\nabla U}{T}. \quad (5.123)$$

Since the left-hand side of the last relation is just $\nabla(\ln w)$, it may be easily integrated over \mathbf{q} , giving

$$\ln w = -\frac{U}{T} + \ln C, \quad \text{i.e. } w(\mathbf{r}) = C \exp\left\{-\frac{U(\mathbf{q})}{T}\right\}, \quad (5.124)$$

where C is a normalization constant. With both sides multiplied by the number N of similar, independent systems, with the spatial density $n(\mathbf{q}) = Nw(\mathbf{q})$, this equality becomes the Boltzmann distribution (3.26).

As a less trivial example of the Smoluchowski equation's applications, let us use it to solve the 1D Kramers problem (Fig. 10) in the corresponding high-damping limit, $m \ll \eta\tau_A$, where τ_A (still to be calculated) is some time scale of the particle's motion inside the well. It is straightforward to verify that the 1D version of Eq. (121),

$$I_w = \frac{1}{\eta} \left[w \left(-\frac{\partial U}{\partial q} \right) - T \frac{\partial w}{\partial q} \right], \quad (5.125a)$$

(where I_w is the probability current at a certain point q , rather than its density) is mathematically equivalent to

$$I_w = -\frac{T}{\eta} \exp\left\{-\frac{U(q)}{T}\right\} \frac{\partial}{\partial q} \left(w \exp\left\{\frac{U(q)}{T}\right\} \right), \quad (5.125b)$$

so that we may write

$$I_w \exp\left\{\frac{U(q)}{T}\right\} = -\frac{T}{\eta} \frac{\partial}{\partial q} \left(w \exp\left\{\frac{U(q)}{T}\right\} \right). \quad (5.126)$$

As was discussed above, the notion of metastable state's lifetime is well defined only for sufficiently low temperatures

⁶³ It is named after Marian Smoluchowski, who developed this formalism in 1906, apparently independently from the slightly earlier Einstein's work, but in much more detail. This equation has important applications in many fields of science – including such surprising topics as statistics of spikes in neural networks. (Note, however, that in some non-physical fields, Eq. (122) is referred to as the *Fokker-Planck equation*, while actually, the latter equation is much more general – see the next section.)

$$T \ll U_0. \quad (5.127)$$

when the lifetime is relatively long: $\tau \gg \tau_A$. Since according to Eq. (111a), the first term of the continuity equation (117b) has to be of the order of W/τ , in this limit the term, and hence the gradient of I_w , are exponentially small, so the probability current virtually does not depend on q in the potential barrier region. Let us use this fact at the integration of both sides of Eq. (126) over that region:

$$I_w \int_{q'}^{q''} \exp\left\{\frac{U(q)}{T}\right\} dq = -\frac{T}{\eta} \left(w \exp\left\{\frac{U(q)}{T}\right\} \right)_{q'}^{q''}, \quad (5.128)$$

where the integration limits q' and q'' (see Fig. 10) are selected so that

$$T \ll U(q') - U(q_1), U(q_2) - U(q'') \ll U_0. \quad (5.129)$$

(Obviously, such selection is only possible if the condition (127) is satisfied.) In this limit, the contribution from the point q'' to the right-hand side of Eq. (129) is negligible because the probability density behind the barrier is exponentially small. On the other hand, the probability at the point q' has to be close to the value given by its quasi-stationary Boltzmann distribution (124), so that

$$w(q') \exp\left\{\frac{U(q')}{T}\right\} = w(q_1) \exp\left\{\frac{U(q_1)}{T}\right\}, \quad (5.130)$$

and Eq. (128) yields

$$I_w = \frac{T}{\eta} w(q_1) \int_{q'}^{q''} \exp\left\{\frac{U(q) - U(q_1)}{T}\right\} dq. \quad (5.131)$$

Patience, my reader, we are almost done. The probability density $w(q_1)$ at the well's bottom may be expressed in terms of the total probability W of the particle being in the well by using the normalization condition

$$W = \int_{\text{well's bottom}} w(q_1) \exp\left\{\frac{U(q_1) - U(q)}{T}\right\} dq; \quad (5.132)$$

the integration here may be limited to the region where the difference $U(q) - U(q_1)$ is much smaller than U_0 – cf. Eq. (129). According to the Taylor expansion, the shape of virtually any smooth potential $U(q)$ near the point q_1 of its minimum may be well approximated with a quadratic parabola:

$$U(q \approx q_1) - U(q_1) \approx \frac{\kappa_1}{2}(q - q_1)^2, \quad \text{where } \kappa_1 \equiv \frac{d^2 U}{dq^2} \Big|_{q=q_1} > 0. \quad (5.133)$$

With this approximation, Eq. (132) is reduced to the standard Gaussian integral:⁶⁴

$$W = w(q_1) \int_{\text{well's bottom}} \exp\left\{-\frac{\kappa_1(q - q_1)^2}{2T}\right\} dq \approx w(q_1) \int_{-\infty}^{+\infty} \exp\left\{-\frac{\kappa_1 \tilde{q}^2}{2T}\right\} d\tilde{q} = w(q_1) \left(\frac{2\pi T}{\kappa_1}\right)^{1/2}. \quad (5.134)$$

To complete the calculation, we may use a similar approximation for the barrier top:

⁶⁴ If necessary, see MA Eq. (6.9b) again.

$$U(q \approx q_2) - U(q_1) \approx \left[U(q_2) - \frac{\kappa_2}{2} (q - q_2)^2 \right] - U(q_1) = U_0 - \frac{\kappa_2}{2} (q - q_2)^2, \quad (5.135)$$

where $\kappa_2 \equiv -\frac{d^2 U}{dq^2} \Big|_{q=q_2} > 0$,

and work out the remaining integral in Eq. (131), because in the limit (129) it is dominated by the contribution from a region very close to the barrier top, where the approximation (135) is asymptotically exact. As a result, we get

$$\int_{q'}^{q''} \exp\left\{-\frac{U(q) - U(q_1)}{T}\right\} dq \approx \exp\left\{-\frac{U_0}{T}\right\} \left(\frac{2\pi T}{\kappa_2}\right)^{1/2}. \quad (5.136)$$

Plugging Eq. (136), and the $w(q_1)$ expressed from Eq. (134), into Eq. (131), we finally get

$$I_w = W \frac{(\kappa_1 \kappa_2)^{1/2}}{2\pi\eta} \exp\left\{-\frac{U_0}{T}\right\}. \quad (5.137)$$

This expression should be compared with the 1D version of Eq. (117b) for the segment $[-\infty, q']$. Since this interval covers the region near q_1 where most of the probability density resides, and $I_q(-\infty) = 0$, this equation is merely

$$\frac{dW}{dt} + I_w(q') = 0. \quad (5.138)$$

In our approximation, $I_w(q')$ does not depend on the exact position of the point q' , and is given by Eq. (137), so that plugging it into Eq. (138), we recover the exponential decay law (111a), with the lifetime τ obeying the Arrhenius law (111b), and the following attempt time:

$$\tau_A = \frac{2\pi\eta}{(\kappa_1 \kappa_2)^{1/2}} \equiv 2\pi(\tau_1 \tau_2)^{1/2}, \quad \text{where } \tau_{1,2} \equiv \frac{\eta}{\kappa_{1,2}}. \quad (5.139)$$

Kramers formula for high damping

Thus the metastable state lifetime is indeed described by the Arrhenius law, with the attempt time scaling as the geometric mean of the system's "relaxation times" near the potential well bottom (τ_1) and the potential barrier top (τ_2).⁶⁵ Let me leave for the reader's exercise to prove that if the potential profile near well's bottom and/or top is sharp, the expression for the attempt time should be modified, but the Arrhenius decay law (111) is not affected.

5.7. The Fokker-Planck equation

Formula (139) is just a particular, high-damping limit of a more general result obtained by Kramers. In order to get all of it (and much more), we need to generalize the Smoluchowski equation to arbitrary values of damping η . In this case, the probability density w is a function of not only the particle's position \mathbf{q} (and time t) but also of its momentum \mathbf{p} – see Eq. (2.11). Thus the continuity equation (117) needs to be generalized to the 6D phase space $\{\mathbf{q}, \mathbf{p}\}$. Such generalization is natural:

⁶⁵ Actually, τ_2 describes the characteristic time of the exponential *growth* of small deviations from the unstable fixed point q_2 at the barrier top, rather than their *decay*, as near the stable point q_1 .

$$\frac{\partial w}{\partial t} + \nabla_q \cdot \mathbf{j}_q + \nabla_p \cdot \mathbf{j}_p = 0, \quad (5.140)$$

where \mathbf{j}_q (which was called \mathbf{j}_w in the last section) is the probability current density in the coordinate space, and ∇_q (which was denoted as ∇ in that section) is the usual vector operator in the space, while \mathbf{j}_p is the current density in the momentum space, and ∇_p is the similar vector operator in that space:

$$\nabla_q \equiv \sum_{j=1}^3 \mathbf{n}_j \frac{\partial}{\partial q_j}, \quad \nabla_p \equiv \sum_{j=1}^3 \mathbf{n}_j \frac{\partial}{\partial p_j}. \quad (5.141)$$

At negligible fluctuations ($T \rightarrow 0$), \mathbf{j}_p may be composed using the natural analogy with \mathbf{j}_q – see Eq. (119). In our new notation, that relation reads,

$$\mathbf{j}_q = w \dot{\mathbf{q}} = w \frac{\mathbf{p}}{m}, \quad (5.142)$$

so it is natural to take

$$\mathbf{j}_p = w \dot{\mathbf{p}} = w \langle \mathcal{F} \rangle, \quad (5.143a)$$

where the (statistical-ensemble) averaged force $\langle \mathcal{F} \rangle$ includes not only the contribution due to the potential's gradient, but also the drag force $-\eta \mathbf{v}$ provided by the environment – see Eq. (64) and its discussion:

$$\mathbf{j}_p = w(-\nabla_q U - \eta \mathbf{v}) = -w(\nabla_q U + \eta \frac{\mathbf{p}}{m}). \quad (5.143b)$$

As a sanity check, it is straightforward to verify that the diffusion-free equation resulting from the combination of Eqs. (140), (142) and (143),

$$\frac{\partial w}{\partial t} \Big|_{\text{drift}} = -\nabla_q \cdot \left(w \frac{\mathbf{p}}{m} \right) + \nabla_p \cdot \left[w \left(\nabla_q U + \eta \frac{\mathbf{p}}{m} \right) \right], \quad (5.144)$$

allows the following particular solution:

$$w(\mathbf{q}, \mathbf{p}, t) = \delta[\mathbf{q} - \langle \mathbf{q} \rangle(t)] \delta[\mathbf{p} - \langle \mathbf{p} \rangle(t)], \quad (5.145)$$

where the statistical-averaged coordinate and momentum satisfy the deterministic equations of motion,

$$\langle \dot{\mathbf{q}} \rangle = \frac{\langle \mathbf{p} \rangle}{m}, \quad \langle \dot{\mathbf{p}} \rangle = -\nabla_q U - \eta \frac{\langle \mathbf{p} \rangle}{m}, \quad (5.146)$$

describing the particle's drift, with the usual deterministic initial conditions.

In order to understand how the diffusion should be accounted for, let us consider a statistical ensemble of free ($\nabla_q U = 0$, $\eta \rightarrow 0$) particles that are uniformly distributed in the direct space \mathbf{q} (so that $\nabla_q w = 0$), but possibly localized in the momentum space. For this case, the right-hand side of Eq. (144) vanishes, i.e. the time evolution of the probability density w may be only due to diffusion. In the corresponding limit $\langle \mathcal{F} \rangle \rightarrow 0$, the Langevin equation (107) for each Cartesian coordinate is reduced to

$$m \ddot{q}_j = \tilde{\mathcal{F}}_j(t), \quad \text{i.e. } \dot{p}_j = \tilde{\mathcal{F}}_j(t). \quad (5.147)$$

The last equation is identical to the high-damping 1D equation (74) (with $\mathcal{F}_{\text{det}} = 0$), with the replacement $q \rightarrow p/\eta$, and hence the corresponding contribution to $\partial w/\partial t$ may be described by the last term of Eq. (122), with that replacement:

$$\frac{\partial w}{\partial t} \Big|_{\text{diffusion}} = D \nabla_{p/\eta}^2 w = \frac{T}{\eta} \eta^2 \nabla_p^2 w \equiv \eta T \nabla_p^2 w. \quad (5.148)$$

Now the reasonable assumption that in the arbitrary case the drift and diffusion contributions to $\partial w/\partial t$ just add up immediately leads us to the full *Fokker-Planck equation*:⁶⁶

Fokker-
Planck
equation

$$\frac{\partial w}{\partial t} = -\nabla_q \cdot \left(w \frac{\mathbf{p}}{m} \right) + \nabla_p \cdot \left[w \left(\nabla_q U + \eta \frac{\mathbf{p}}{m} \right) \right] + \eta T \nabla_p^2 w. \quad (5.149)$$

As a sanity check, let us use this equation to calculate the stationary probability distribution of the momentum of particles with an arbitrary damping η but otherwise free, in the momentum space, assuming (just for simplicity) their uniform distribution in the direct space, $\nabla_q = 0$. In this case, Eq. (149) is reduced to

$$\nabla_p \cdot \left[w \left(\eta \frac{\mathbf{p}}{m} \right) \right] + \eta T \nabla_p^2 w = 0, \quad \text{i.e. } \nabla_p \cdot \left(\frac{\mathbf{p}}{m} w + T \nabla_p w \right) = 0. \quad (5.150)$$

The first integration over the momentum space yields

$$\frac{\mathbf{p}}{m} w + T \nabla_p w = \mathbf{j}_w, \quad \text{i.e. } w \nabla_p \left(\frac{\mathbf{p}^2}{2m} \right) + T \nabla_p w = \mathbf{j}_w, \quad (5.151)$$

where \mathbf{j}_w is a vector constant describing a possible general probability flow in the system. In the absence of such flow, $\mathbf{j}_w = 0$, we get

$$\nabla_p \left(\frac{\mathbf{p}^2}{2m} \right) + T \frac{\nabla_p w}{w} \equiv \nabla_p \left(\frac{\mathbf{p}^2}{2m} + T \ln w \right) = 0, \quad \text{giving } w = \text{const} \times \exp \left\{ -\frac{\mathbf{p}^2}{2mT} \right\}, \quad (5.152)$$

i.e. the Maxwell distribution (3.5). However, the result (152) is more general than that obtained in Sec. 3.1, because it shows that the distribution stays the same even at non-zero damping. It is easy to verify that in the more general case of an arbitrary stationary potential $U(\mathbf{q})$, Eq. (149) is satisfied with the stationary solution (3.24), also giving $\mathbf{j}_w = 0$.

It is also straightforward to show that if the damping is large (in the sense assumed in the last section), the solution of the Fokker-Planck equation tends to the following product

$$w(\mathbf{q}, \mathbf{p}, t) \rightarrow \text{const} \times \exp \left\{ -\frac{\mathbf{p}^2}{2mT} \right\} \times \mathbf{w}(\mathbf{q}, t), \quad (5.153)$$

where the direct-space distribution $\mathbf{w}(\mathbf{q}, t)$ obeys the Smoluchowski equation (122).

Another important particular case is that of a quasi-periodic motion of a particle, with low damping, in a soft potential well. In this case, the Fokker-Planck equation describes both diffusion of the effective phase Θ of such (generally nonlinear, “anharmonic”) oscillator, and slow relaxation of its

⁶⁶ It was first derived by Adriaan Fokker in 1913 in his PhD thesis, and further elaborated by Max Planck in 1917. (Curiously, A. Fokker is more famous for his work on music theory, and the invention and construction of several new keyboard instruments, than for this and several other important contributions to theoretical physics.)

energy. If we are only interested in the latter process, Eq. (149) may be reduced to the so-called *energy diffusion equation*,⁶⁷ which is easier to solve.

However, in most practically interesting cases, solutions of Eq. (149) are rather complicated. (Indeed, the reader should remember that these solutions embody, in the particular case $T = 0$, all classical dynamics of a particle.) Because of this, I will present (rather than derive) only one more of them: the solution of the Kramers problem (Fig. 10). Acting almost exactly as in Sec. 6, one can show⁶⁸ that at virtually arbitrary damping (but still in the limit $T \ll U_0$), the metastable state's lifetime is again given by the Arrhenius formula (111b), with the attempt time again expressed by the first of Eqs. (139), but with the reciprocal time constants $1/\tau_{1,2}$ replaced with

$$\omega'_{1,2} \equiv \left[\omega_{1,2}^2 + \left(\frac{\eta}{2m} \right)^2 \right]^{1/2} - \frac{\eta}{2m} \rightarrow \begin{cases} \omega_{1,2}, & \text{for } \eta \ll m\omega_{1,2}, \\ 1/\tau_{1,2}, & \text{for } m\omega_{1,2} \ll \eta, \end{cases} \quad (5.154)$$

where $\omega_{1,2} \equiv (\kappa_{1,2}/m)^{1/2}$, and $\kappa_{1,2}$ are the effective spring constants defined by Eqs. (133) and (135). Thus, in the important particular limit of low damping, Eqs. (111b) and (154) give the famous formula

$$\tau = \frac{2\pi}{(\omega_1\omega_2)^{1/2}} \exp\left\{ \frac{U_0}{T} \right\}. \quad (5.155)$$

Kramers formula for low damping

This Kramers' result for the classical thermal activation of the dissipation-free system *over* a potential barrier may be compared with that for its quantum-mechanical tunneling *through* the barrier.⁶⁹ The WKB approximation for the latter effect gives the expression

$$\tau_Q = \tau_A \exp\left\{ -2 \int_{\kappa^2(q)>0} \kappa(q) dq \right\}, \quad \text{with } \frac{\hbar^2 \kappa^2(q)}{2m} \equiv U(q) - E, \quad (5.156)$$

showing that generally, the classical and quantum lifetimes of a metastable state have different dependences on the barrier shape. For example, for a nearly-rectangular potential barrier, the exponent that determines the classical lifetime (155) depends (linearly) only on the barrier *height* U_0 , while that defining the quantum lifetime (156) is proportional to the barrier *width* and to the square root of U_0 . However, in the important case of "soft" potential profiles, which are typical for the case of barely emerging (or nearly disappearing) quantum wells (Fig. 11), the classical and quantum results are closely related.

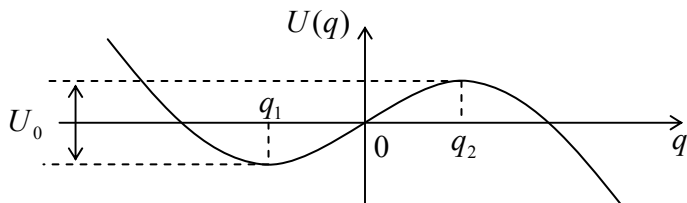


Fig. 5.11. Cubic-parabolic potential profile and its parameters.

⁶⁷ An example of such an equation, for the particular case of a harmonic oscillator, is given by QM Eq. (7.214). The Fokker-Planck equation, of course, can give only its classical limit, with $n, n_e \gg 1$.

⁶⁸ A detailed description of this calculation (first performed by H. Kramers in 1940) may be found, for example, in Sec. III.7 of the review paper by S. Chandrasekhar, *Rev. Mod. Phys.* **15**, 1 (1943).

⁶⁹ See, e.g., QM Secs. 2.4-2.6.

Indeed, such potential profile $U(q)$ may be well approximated by four leading terms of its Taylor expansion, with the highest term proportional to $(q - q_0)^3$, near any point q_0 in the vicinity of the well. In this approximation, the second derivative d^2U/dq^2 vanishes at the inflection point $q_0 = (q_1 + q_2)/2$, exactly between the well's bottom and the barrier's top (in Fig. 11, q_1 and q_2). Selecting the origin at this point, as this is done in Fig. 11, we may reduce the approximation to just two terms:⁷⁰

$$U(q) = aq - \frac{b}{3}q^3. \quad (5.157)$$

(For the particle's escape into the positive direction of the q -axis, we should have $a, b > 0$.) An easy calculation gives all essential parameters of this cubic parabola: the positions of its minimum and maximum:

$$q_2 = -q_1 = (a/b)^{1/2}, \quad (5.158)$$

the barrier height over the well's bottom:

$$U_0 \equiv U(q_2) - U(q_1) = \frac{4}{3} \left(\frac{a^3}{b} \right)^{1/2}, \quad (5.159)$$

and the effective spring constants at these points:

$$\kappa_1 = \kappa_2 \equiv \left| \frac{d^2U}{dq^2} \right|_{q_{1,2}} = 2(ab)^{1/2}. \quad (5.160)$$

The last expression shows that for this potential profile, the frequencies $\omega_{1,2}$ participating in Eq. (155) are equal to each other, so that this result may be rewritten as

$$\tau = \frac{2\pi}{\omega_0} \exp\left\{ \frac{U_0}{T} \right\}, \quad \text{with } \omega_0^2 \equiv \frac{2(ab)^{1/2}}{m}. \quad (5.161)$$

On the other hand, for the same profile, the WKB approximation (156) (which is accurate when the height of the metastable state energy over the well's bottom, $E - U(q_1) \approx \hbar\omega_0/2$, is much lower than the barrier height U_0) yields⁷¹

$$\tau_Q = \frac{2\pi}{\omega_0} \left(\frac{\hbar\omega_0}{864U_0} \right)^{1/2} \exp\left\{ \frac{36}{5} \frac{U_0}{\hbar\omega_0} \right\}. \quad (5.162)$$

The comparison of the dominating, exponential factors in these two results shows that the thermal activation yields a lower lifetime (i.e., dominates the metastable state decay) if the temperature is above the crossover value

$$T_c = \frac{36}{5} \hbar\omega_0 \equiv 7.2 \hbar\omega_0. \quad (5.163)$$

⁷⁰ As a reminder, a similar approximation arises for the $P(V)$ function, at the analysis of the van der Waals model near the critical temperature – see Problem 4.6.

⁷¹ The main, exponential factor in this result may be obtained simply by ignoring the difference between E and $U(q_1)$, but the correct calculation of the pre-exponential factor requires taking this difference, $\hbar\omega_0/2$, into account – see, e.g., the model solution of QM Problem 2.43.

This expression for the *cubic*-parabolic barrier may be compared with the similar crossover for a *quadratic*-parabolic barrier,⁷² for which $T_c = 2\pi \hbar\omega_0 \approx 6.28 \hbar\omega_0$. We see that the numerical factors for the quantum-to-classical crossover temperature for these two different soft potential profiles are close to each other – and much larger than 1, which could result from a naïve estimate.

5.8. Back to the correlation function

Unfortunately, I will not have time/space to either derive or even review solutions of other problems using the Smoluchowski and Fokker-Planck equations, but have to mention one conceptual issue. Since it is intuitively clear that the solution $w(\mathbf{q}, \mathbf{p}, t)$ of the Fokker-Planck equation for a system provides the complete statistical information about it, one may wonder how it may be used to find its temporal characteristics that were discussed in Secs. 4-5, using the Langevin formalism. For any statistical average of a function taken at the same time instant, the answer is clear – cf. Eq. (2.11):

$$\langle f[\mathbf{q}(t), \mathbf{p}(t)] \rangle = \int f(\mathbf{q}, \mathbf{p}) w(\mathbf{q}, \mathbf{p}, t) d^3 q d^3 p, \quad (5.164)$$

but what if the function depends on variables taken at *different* times, for example as in the correlation function $K(\tau)$ defined by Eq. (48)?

To answer this question, let us start from the discrete-variable case when Eq. (164) takes the form (2.7), which, for our current purposes, may be rewritten as

$$\langle f(t) \rangle = \sum_m f_m W_m(t). \quad (5.165)$$

In plain English, this is a sum of all possible values of the function, each multiplied by its probability as a function of time. But this implies that the average $\langle f(t)f(t') \rangle$ may be calculated as the sum of all possible products $f_m f_{m'}$, multiplied by the *joint probability* to measure outcome m at moment t , and outcome m' at moment t' . The joint probability may be represented as a product of $W_m(t)$ by the *conditional probability* $W(m', t' | m, t)$. Since the correlation function is well defined only for stationary systems, in the last expression we may take $t = 0$, i.e. look for the conditional probability as the solution, $W_m(\tau)$, of the equation describing the system's probability evolution, at time $\tau = t' - t$ (rather than t'), with the special initial condition

$$W_{m'}(0) = \delta_{m',m}. \quad (5.166)$$

On the other hand, since the average $\langle f(t)f(t+\tau) \rangle$ of a stationary process should not depend on t , instead of $W_m(0)$ we may take the stationary probability distribution $W_m(\infty)$, independent of the initial conditions, which may be found as the same special solution, but at time $\tau \rightarrow \infty$. As a result, we get

$$\langle f(t)f(t+\tau) \rangle = \sum_{m,m'} f_m W_m(\infty) f_{m'} W_{m'}(\tau). \quad (5.167)$$

Correlation
function:
discrete
system

This expression looks simple, but note that this recipe requires solving the time evolution equations for each $W_m(\tau)$ for all possible initial conditions (166). To see how this recipe works in practice, let us revisit the simplest two-level system (see, e.g., Fig. 4.13, which is reproduced in Fig. 12

⁷² See, e.g., QM Sec. 2.4.

below in a notation more convenient for our current purposes), and calculate the correlation function of its energy fluctuations.

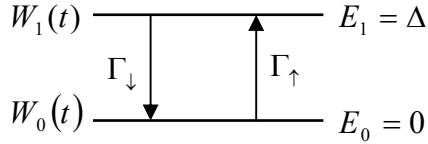


Fig. 5.12. Dynamics of a two-level system.

The stationary probabilities of the system's states (i.e. their probabilities for $\tau \rightarrow \infty$) have been calculated in problems of Chapter 2, and then again in Sec. 4.4 – see Eq. (4.68). In our current notation (Fig. 12),

$$W_0(\infty) = \frac{1}{1 + e^{-\Delta/T}}, \quad W_1(\infty) = \frac{1}{e^{\Delta/T} + 1}, \quad (5.168)$$

so that $\langle E(\infty) \rangle = W_0(\infty) \times 0 + W_1(\infty) \times \Delta = \frac{\Delta}{e^{\Delta/T} + 1}$.

To calculate the conditional probabilities $W_m(\tau)$ with the initial conditions (167) (according to Eq. (168), we need all four of them, for $\{m, m'\} = \{0, 1\}$), we may use the master equations (4.100), in our current notation reading

$$\frac{dW_1}{d\tau} = -\frac{dW_0}{d\tau} = \Gamma_\uparrow W_0 - \Gamma_\downarrow W_1. \quad (5.169)$$

Since Eq. (169) conserves the total probability, $W_0 + W_1 = 1$, only one probability (say, W_1) is an independent variable, and for it, Eq. (169) gives a simple, linear differential equation

$$\frac{dW_1}{d\tau} = \Gamma_\uparrow - \Gamma_\Sigma W_1, \quad \text{where } \Gamma_\Sigma \equiv \Gamma_\uparrow + \Gamma_\downarrow, \quad (5.170)$$

which may be readily integrated for an arbitrary initial condition:

$$W_1(\tau) = W_1(0)e^{-\Gamma_\Sigma\tau} + W_1(\infty)\left(1 - e^{-\Gamma_\Sigma\tau}\right), \quad (5.171)$$

where $W_1(\infty)$ is given by the second of Eqs. (168). (It is straightforward to verify that the solution for $W_0(\tau)$ may be represented in a similar form, with the corresponding change of the state index.)

Now everything is ready to calculate the average $\langle E(t)E(t+\tau) \rangle$ using Eq. (167), with $f_{m,m'} = E_{0,1}$. Thanks to our (smart :-) choice of the energy reference, of the four terms in the double sum (167), all three terms that include at least one factor $E_0 = 0$ vanish, and we have only one term left to calculate:

$$\begin{aligned} \langle E(t)E(t+\tau) \rangle &= E_1 W_1(\infty) E_1 W_1(\tau) \Big|_{W_1(0)=1} = E_1^2 W_1(\infty) \left[W_1(0) e^{-\Gamma_\Sigma\tau} + W_1(\infty) \left(1 - e^{-\Gamma_\Sigma\tau}\right) \right] \Big|_{W_1(0)=1} \\ &= \frac{\Delta^2}{e^{\Delta/T} + 1} \left[e^{-\Gamma_\Sigma\tau} + \frac{1}{e^{\Delta/T} + 1} \left(1 - e^{-\Gamma_\Sigma\tau}\right) \right] \equiv \frac{\Delta^2}{(e^{\Delta/T} + 1)^2} \left(1 + e^{\Delta/T} e^{-\Gamma_\Sigma\tau}\right). \end{aligned} \quad (5.172)$$

From here and the last of Eqs. (168), the correlation function of energy fluctuations is⁷³

$$\begin{aligned} K_E(\tau) &\equiv \langle \tilde{E}(t)\tilde{E}(t+\tau) \rangle = \langle (E(t) - \langle E(t) \rangle)(E(t+\tau) - \langle E(t) \rangle) \rangle \\ &= \langle E(t)E(t+\tau) \rangle - \langle E(\infty) \rangle^2 = \Delta^2 \frac{e^{\Delta/T}}{(e^{\Delta/T} + 1)^2} e^{-\Gamma_\Sigma \tau}, \end{aligned} \quad (5.173)$$

so that its variance, equal to $K_E(0)$, does not depend on the transition rates Γ_\uparrow and Γ_\downarrow . However, since the rates have to obey the detailed balance relation (4.103), $\Gamma_\downarrow/\Gamma_\uparrow = \exp\{\Delta/T\}$, for this variance we may formally write

$$\frac{K_E(0)}{\Delta^2} = \frac{e^{\Delta/T}}{(e^{\Delta/T} + 1)^2} = \frac{\Gamma_\downarrow/\Gamma_\uparrow}{(\Gamma_\downarrow/\Gamma_\uparrow + 1)^2} = \frac{\Gamma_\uparrow\Gamma_\downarrow}{(\Gamma_\uparrow + \Gamma_\downarrow)^2} \equiv \frac{\Gamma_\uparrow\Gamma_\downarrow}{\Gamma_\Sigma^2}, \quad (5.174)$$

so that Eq. (173) may be represented in a simpler form:

$$K_E(\tau) = \Delta^2 \frac{\Gamma_\uparrow\Gamma_\downarrow}{\Gamma_\Sigma^2} e^{-\Gamma_\Sigma \tau}. \quad (5.175)$$

Energy fluctuations:
two-level system

We see that the correlation function of energy fluctuations decays exponentially with time, with the net rate Γ_Σ . Now using the Wiener-Khinchin theorem (58) to calculate its spectral density, we get

$$S_E(\omega) = \frac{1}{\pi} \int_0^\infty \Delta^2 \frac{\Gamma_\uparrow\Gamma_\downarrow}{\Gamma_\Sigma^2} e^{-\Gamma_\Sigma \tau} \cos \omega \tau d\tau = \frac{\Delta^2}{\pi \Gamma_\Sigma} \frac{\Gamma_\uparrow\Gamma_\downarrow}{\Gamma_\Sigma^2 + \omega^2}. \quad (5.176)$$

Such Lorentzian dependence on frequency is very typical for discrete-state systems described by master equations. It is interesting that the most widely accepted explanation of the *1/f noise* (also called the “flicker” or “excess” noise), which was mentioned in Sec. 5, is that it is a result of thermally-activated jumps between states of two-level systems with an exponentially-broad statistical distribution of the transition rates $\Gamma_{\uparrow\downarrow}$. Such a broad distribution follows from the Kramers formula (155), which is approximately valid for the lifetimes of both states of systems with double-well potential profiles (Fig. 13), for a statistical ensemble with a smooth statistical distribution of the energy barrier heights U_0 . Such profiles are typical, in particular, for electrons in disordered (amorphous) solid-state materials, which indeed feature high *1/f* noise.

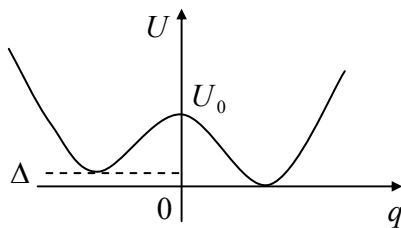


Fig. 5.13. Typical double-well potential profile.

Returning to the Fokker-Planck equation, we may use the following evident generalization of Eq. (167) to the continuous-variable case:

⁷³ The step from the first line of Eq. (173) to its second line utilizes the fact that our system is stationary, so that $\langle E(t+\tau) \rangle = \langle E(t) \rangle = \langle E(\infty) \rangle = \text{const.}$

$$\langle f(t)f(t+\tau) \rangle = \int d^3q d^3p \int d^3q' d^3p' f(\mathbf{q}, \mathbf{p}) w(\mathbf{q}, \mathbf{p}, \infty) f(\mathbf{q}', \mathbf{p}') w(\mathbf{q}', \mathbf{p}', \tau), \quad (5.177)$$

were both probability densities are particular values of the equation's solution with the delta-functional initial condition

$$w(\mathbf{q}', \mathbf{p}', 0) = \delta(\mathbf{q}' - \mathbf{q}) \delta(\mathbf{p}' - \mathbf{p}). \quad (5.178)$$

For the Smoluchowski equation valid in the high-damping limit, the expressions are similar, albeit with a lower dimensionality:

$$\langle f(t)f(t+\tau) \rangle = \int d^3q \int d^3q' f(\mathbf{q}) w(\mathbf{q}, \infty) f(\mathbf{q}') w(\mathbf{q}', \tau), \quad (5.179)$$

$$w(\mathbf{q}', 0) = \delta(\mathbf{q}' - \mathbf{q}). \quad (5.180)$$

To see this formalism in action, let us use it to calculate the correlation function $K_q(\tau)$ of a *linear relaxator*, i.e. an overdamped 1D harmonic oscillator with $m\omega_0 \ll \eta$. In this limit, as Eq. (65) shows, the oscillator's coordinate, averaged over the ensemble of environments, obeys a linear equation,

$$\eta \langle \dot{q} \rangle + \kappa \langle q \rangle = 0, \quad (5.181)$$

which describes its exponential relaxation from the initial position q_0 to the equilibrium position $q = 0$, with the reciprocal time constant $\Gamma = \kappa/\eta$:

$$\langle q \rangle(t) = q_0 e^{-\Gamma t}. \quad (5.182)$$

The deterministic equation (181) corresponds to the quadratic potential energy $U(q) = \kappa q^2/2$, so that the 1D version of the corresponding Smoluchowski equation (122) takes the form

$$\eta \frac{\partial w}{\partial t} = \kappa \frac{\partial}{\partial q} (wq) + T \frac{\partial^2 w}{\partial q^2}. \quad (5.183)$$

It is straightforward to check, by substitution, that this equation, rewritten for the function $w(q', \tau)$, with the 1D version of the delta-functional initial condition (180), $w(q', 0) = \delta(q' - q)$, is satisfied with a Gaussian function:

$$w(q', \tau) = \frac{1}{(2\pi)^{1/2} \delta q(\tau)} \exp \left\{ -\frac{(q' - \langle q \rangle(\tau))^2}{2\delta q^2(\tau)} \right\}, \quad (5.184)$$

with its center $\langle q \rangle(\tau)$ moving in accordance with Eq. (182), and a time-dependent variance

$$\delta q^2(\tau) = \delta q^2(\infty) (1 - e^{-2\Gamma\tau}), \quad \text{where } \delta q^2(\infty) = \langle q^2 \rangle = \frac{T}{\kappa}. \quad (5.185)$$

(As a sanity check, the last equality coincides with the equipartition theorem's result.) Finally, the first probability under the integral in Eq. (179) may be found from Eq. (184) in the limit $\tau \rightarrow \infty$ (in which $\langle q \rangle(\tau) \rightarrow 0$), by replacing q' with q :

$$w(q, \infty) = \frac{1}{(2\pi)^{1/2} \delta q(\infty)} \exp \left\{ -\frac{q^2}{2\delta q^2(\infty)} \right\}. \quad (5.186)$$

Now all ingredients of the recipe (179) are ready, and we can spell it out, for $f(q) = q$, as

$$\langle q(t)q(t+\tau) \rangle = \frac{1}{2\pi\delta q(\tau)\delta q(\infty)} \int_{-\infty}^{+\infty} dq \int_{-\infty}^{+\infty} dq' q \exp\left\{-\frac{q^2}{2\delta q^2(\infty)}\right\} q' \exp\left\{-\frac{(q'-qe^{-\Gamma\tau})^2}{2\delta q^2(\tau)}\right\}. \quad (5.187)$$

The integral over q' may be worked out first, by replacing this integration variable with $(q'' + qe^{-\Gamma\tau})$ and hence dq' with dq'' :

$$\langle q(t)q(t+\tau) \rangle = \frac{1}{2\pi\delta q(\tau)\delta q(\infty)} \int_{-\infty}^{+\infty} q \exp\left\{-\frac{q^2}{2\delta q^2(\infty)}\right\} dq \int_{-\infty}^{+\infty} (q'' + qe^{-\Gamma\tau}) \exp\left\{-\frac{q''^2}{2\delta q^2(\tau)}\right\} dq''. \quad (5.188)$$

The internal integral of the first term in the parentheses equals zero (as that of an odd function in symmetric integration limits), while that with the second term is the standard Gaussian integral, so that

$$\langle q(t)q(t+\tau) \rangle = \frac{1}{(2\pi)^{1/2}\delta q(\infty)} e^{-\Gamma\tau} \int_{-\infty}^{+\infty} q^2 \exp\left\{-\frac{q^2}{2\delta q^2(\infty)}\right\} dq \equiv \frac{2T}{\pi^{1/2}\kappa} e^{-\Gamma\tau} \int_{-\infty}^{+\infty} \xi^2 \exp\{-\xi^2\} d\xi. \quad (5.189)$$

The last integral⁷⁴ equals $\pi^{1/2}/2$, so that taking into account that for this stationary system centered at the coordinate origin, $\langle q(\infty) \rangle = 0$, we finally get a very simple result,

$$K_q(\tau) \equiv \langle \tilde{q}(t)\tilde{q}(t+\tau) \rangle = \langle q(t)q(t+\tau) \rangle - \langle q(\infty) \rangle^2 = \langle q(t)q(t+\tau) \rangle = \frac{T}{\kappa} e^{-\Gamma\tau}. \quad (5.190)$$

Correlation
function:
linear
relaxator

As a sanity check, for $\tau = 0$ it yields $K_q(0) \equiv \langle q^2 \rangle = T/\kappa$, in accordance with Eq. (185). As τ is increased the correlation function decreases monotonically – see the solid-line sketch in Fig. 8.

So, the solution of this very simple problem has required straightforward but somewhat bulky calculations. On the other hand, the same result may be obtained literally in one line using the Langevin formalism – namely, as the Fourier transform (59) of the spectral density (68) in the corresponding limit $m\omega \ll \eta$, with $S_A(\omega)$ given by Eq. (73a):⁷⁵

$$K_q(\tau) = 2 \int_0^\infty S_q(\omega) \cos \omega\tau d\omega = 2 \int_0^\infty \frac{\eta T}{\pi} \frac{1}{\kappa^2 + (\eta\omega)^2} \cos \omega\tau d\omega = 2 \frac{T\Gamma}{\pi} \int_0^\infty \frac{\cos \xi}{(\Gamma\tau)^2 + \xi^2} d\xi = \frac{T}{\kappa} e^{-\Gamma\tau}. \quad (5.191)$$

This example illustrates the fact that for linear systems (and small fluctuations in nonlinear systems) the Langevin approach is usually much simpler than the one based on the Fokker-Planck or Smoluchowski equations. However, again, the latter approach is indispensable for the analysis of fluctuations of arbitrary intensity in nonlinear systems.

To conclude this chapter, I have to emphasize again that the Fokker-Planck and Smoluchowski equations give a quantitative description of the time evolution of nonlinear Brownian systems with dissipation in the *classical* limit. The description of the corresponding properties of such dissipative (“open”) and nonlinear *quantum* systems is more complex,⁷⁶ and only a few simple problems of their theory have been solved analytically so far,⁷⁷ typically using a particular model of the environment, e.g.,

⁷⁴ See, e.g., MA Eq. (6.9c).

⁷⁵ The involved table integral may be found, e.g., in MA Eq. (6.11).

⁷⁶ See, e.g., QM Sec. 7.6.

⁷⁷ See, e.g., the solutions of the 1D Kramers problem for quantum systems with low damping by A. Caldeira and A. Leggett, *Phys. Rev. Lett.* **46**, 211 (1981), and with high damping by A. Larkin and Yu. Ovchinnikov, *JETP Lett.* **37**, 382 (1983).

as a large set of harmonic oscillators with different statistical distributions of their parameters, leading to different frequency dependences of the generalized susceptibility $\chi(\omega)$.

5.10. Exercise problems

5.1. Treating the first 30 digits of number $\pi = 3.1415\dots$ as a statistical ensemble of integers k (equal to 3, 1, 4, 1, 5,...), calculate the average $\langle k \rangle$ and the r.m.s. fluctuation δk . Compare the results with those for the ensemble of completely random decimal integers 0, 1, 2,..,9, and comment.

5.2. Calculate the variance of fluctuations of a magnetic moment \mathbf{m} placed into an external magnetic field \mathcal{H} , within the same two models as in Problem 2.4:

- (i) a spin- $\frac{1}{2}$ with a gyromagnetic ratio γ , and
- (ii) a classical magnetic moment \mathbf{m} , of a fixed magnitude m_0 , but an arbitrary orientation,

both in thermal equilibrium at temperature T . Discuss and compare the results.⁷⁸

Hint: Mind all three Cartesian components of the vector \mathbf{m} .

5.3. For a field-free, two-site Ising system with energy values $E_m = -J s_1 s_2$, in thermal equilibrium at temperature T , calculate the variance of energy fluctuations. Explore the low-temperature and high-temperature limits of the result.

5.4. For a uniform, three-site Ising ring with ferromagnetic coupling (and no external field), calculate the correlation coefficients $K_s \equiv \langle s_k s_k \rangle$ for both $k = k'$ and $k \neq k'$.

5.5.* For a field-free 1D Ising system of $N \gg 1$ “spins”, in thermal equilibrium at temperature T , calculate the correlation coefficient $K_s \equiv \langle s_l s_{l+n} \rangle$, where l and $(l+n)$ are the numbers of two specific spins in the chain.

Hint: You may like to start with the calculation of the statistical sum for an open-ended chain with arbitrary $N > 1$ and arbitrary coupling coefficients J_k , and then consider its mixed partial derivative over a part of these parameters.

5.6. Within the framework of the Weiss molecular-field theory, calculate the variance of spin fluctuations in the d -dimensional Ising model. Use the result to derive the conditions of its validity.

5.7. Calculate the variance of energy fluctuations in a quantum harmonic oscillator with frequency ω , in thermal equilibrium at temperature T , and express it via the average value of the energy.

5.8. The spontaneous electromagnetic field inside a closed volume V is in thermal equilibrium at temperature T . Assuming that V is sufficiently large, calculate the variance of fluctuations of the total

⁷⁸ Note that these two cases may be considered as the non-interacting limits of, respectively, the Ising model (4.23) and the classical limit of the Heisenberg model (4.21), whose analysis within the Weiss approximation was the subject of Problem 4.18.

energy of the field, and express the result via its average energy and temperature. How large should the volume V be for your results to be quantitatively valid? Evaluate this limitation for room temperature.

5.9. Express the r.m.s. uncertainty of the occupancy N_k of a certain energy level ε_k by non-interacting:

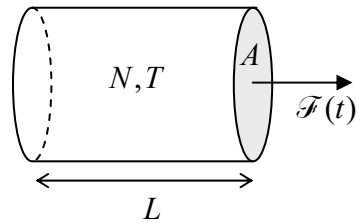
- (i) classical particles,
- (ii) fermions, and
- (iii) bosons,

in thermodynamic equilibrium, via the level's average occupancy $\langle N_k \rangle$, and compare the results.

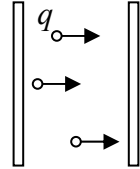
5.10. Express the variance of the number of particles, $\langle \tilde{N}^2 \rangle_{V,T,\mu}$, of a single-phase system in equilibrium, via its isothermal compressibility $\kappa_T \equiv -(1/V)(\partial V/\partial P)_{T,N}$.

5.11.* Starting from the Maxwell distribution of velocities, calculate the low-frequency spectral density of fluctuations of the pressure $P(t)$ of an ideal gas of N classical particles, in thermal equilibrium at temperature T , and estimate their variance. Compare the former result with the solution of Problem 3.2.

Hints: You may consider a cylindrically-shaped container of volume $V = LA$ (see the figure on the right), calculate fluctuations of the force $\mathcal{F}(t)$ exerted by the confined particles on its plane lid of area A , approximating it as a delta-correlated process (62), and then re-calculate the fluctuations into those of pressure $P \equiv \mathcal{F}/A$.

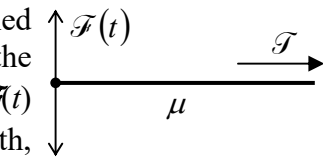


5.12. Calculate the low-frequency spectral density of fluctuations of the electric current $I(t)$ due to the random passage of charged particles between two conducting electrodes – see the figure on the right. Assume that the particles are emitted, at random times, by one of the electrodes, and are fully absorbed by the counterpart electrode. Can your result be mapped on some aspect of the electromagnetic blackbody radiation?



Hint: For the current $I(t)$, use the same delta-correlated-process approximation as for the force $\mathcal{F}(t)$ in the previous problem.

5.13.⁷⁹ A very long, uniform string, of mass μ per unit length, is attached to a firm support, and stretched with a constant force (“tension”) \mathcal{T} – see the figure on the right. Calculate the spectral density of the random force $\mathcal{F}(t)$ exerted by the string on the support point, within the plane normal to its length, in thermal equilibrium at temperature T .



Hint: You may assume that the string is so long that a transverse wave, propagating along it from the support point, never comes back.

⁷⁹ This problem, conceptually important for the quantum mechanics of open systems, was given in Chapter 7 of the QM part of this series, and is repeated here for the benefit of the readers who, by any reason, skipped that course.

5.14.⁸⁰ Each of two 3D harmonic oscillators, with mass m , resonance frequency ω_0 , and damping $\delta > 0$, has electric dipole moment $\mathbf{d} = q\mathbf{s}$, where \mathbf{s} is the vector of oscillator's displacement from its equilibrium position. Use the Langevin formalism to calculate the average potential of electrostatic interaction of these two oscillators (a particular case of the so-called *London dispersion force*), separated by distance $r \gg (T/m)^{1/2}/\omega_0$, in thermal equilibrium at temperature $T \gg \hbar\omega_0$. Also, explain why the approach used to solve a very similar Problem 2.15 is not directly applicable to this case.

Hint: You may like to use the following integral:
$$\int_0^{\infty} \frac{1 - \xi^2}{[(1 - \xi^2)^2 + (a\xi)^2]^2} d\xi = \frac{\pi}{4a}.$$

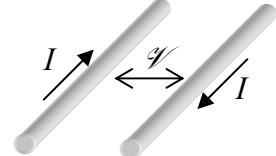
5.15.^{*} Within the van der Pol approximation,⁸¹ calculate major statistical properties of fluctuations of classical self-oscillations, at:

- (i) the free (“autonomous”) run of the oscillator, and
- (ii) their phase been locked by an external sinusoidal force,

assuming that the fluctuations are caused by a weak external noise with a smooth spectral density $S_f(\omega)$. In particular, calculate the self-oscillation linewidth.

5.16. Calculate the correlation function of the coordinate of a 1D harmonic oscillator with small Ohmic damping at thermal equilibrium. Compare the result with that for the autonomous self-oscillator (the subject of the previous problem).

5.17. Consider a very long, uniform, two-wire transmission line (see the figure on the right) with wave impedance \mathcal{Z} , which allows propagation of TEM electromagnetic waves with negligible attenuation, in thermal equilibrium at temperature T . Calculate the variance $\langle \mathcal{V}^2 \rangle_{\Delta\nu}$ of the voltage \mathcal{V} between the wires within a small interval $\Delta\nu$ of cyclic frequencies.



Hint: As an E&M reminder,⁸² in the absence of dispersive materials, TEM waves propagate with a frequency-independent velocity (equal to the speed c of light, if the wires are in free space), with the voltage \mathcal{V} and the current I (see Fig. above) related as $\mathcal{V}(x,t)/I(x,t) = \pm\mathcal{Z}$, where \mathcal{Z} is line's wave impedance.

5.18. Now consider a similar long transmission line but terminated, at one end, with an impedance-matching Ohmic resistor $R = \mathcal{Z}$. Calculate the variance $\langle \mathcal{V}^2 \rangle_{\Delta\nu}$ of the voltage across the

⁸⁰ This problem, for the case of arbitrary temperature, was the subject of QM Problem 7.6, with Problem 5.15 of that course serving as the background. However, the method used in the model solutions of those problems requires one to prescribe, to the oscillators, different frequencies ω_1 and ω_2 at first, and only after this more general problem has been solved, pursue the limit $\omega_1 \rightarrow \omega_2$, while neglecting dissipation altogether. The goal of this problem is to show that the result of that solution is valid even at non-zero damping.

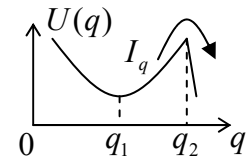
⁸¹ See, e.g., CM Secs. 5.2-5.5. Note that in quantum mechanics, a similar approach is called the *rotating-wave approximation* (RWA) – see, e.g., QM Secs. 6.5, 7.6, 9.2, and 9.4.

⁸² See, e.g., EM Sec. 7.6.

resistor, and discuss the relation between the result and the Nyquist formula (81b), including numerical factors.

Hint: A termination with resistance $R = \mathcal{F}$ absorbs incident TEM waves without reflection.

5.19. An overdamped classical 1D particle escapes from a potential well with a smooth bottom, but a sharp top of the barrier – see the figure on the right. Perform the necessary modification of the Kramers formula (139).



5.20. Perhaps the simplest model of the diffusion is the 1D *discrete random walk*: each time interval τ , a particle leaps, with equal probability, to any of two adjacent sites of a 1D lattice with spatial period a . Prove that the particle's displacement during a time interval $t \gg \tau$ obeys Eq. (77), and calculate the corresponding diffusion coefficient D .

5.21. A classical particle may occupy any of N similar sites. Its weak interaction with the environment induces random, incoherent jumps from the occupied site to any other site, with the same time-independent rate Γ . Calculate the correlation function and the spectral density of fluctuations of the instant occupancy $n(t)$ (equal to either 1 or 0) of a site.

Chapter 6. Elements of Kinetics

This chapter gives a brief introduction to the basic notions of physical kinetics. Its main focus is on the Boltzmann transport equation, especially within the simple relaxation-time approximation (RTA), which allows an approximate but reasonable and simple description of transport phenomena (such as the electric current and thermoelectric effects) in gases, including electron gases in metals and semiconductors.

6.1. The Liouville theorem and the Boltzmann equation

Physical kinetics (not to be confused with “kinematics”!) is the branch of statistical physics that deals with systems out of thermodynamic equilibrium. Major effects addressed by kinetics include:

- (i) for *autonomous* systems (those out of external fields): the transient processes (*relaxation*), that lead from an arbitrary initial state of a system to its thermodynamic equilibrium;
- (ii) for systems in time-dependent (say, sinusoidal) external fields: the field-induced periodic oscillations of the system’s variables; and
- (iii) for systems in time-independent (“dc”) external fields: dc transport.

In the last case, we are dealing with stationary ($\partial/\partial t = 0$ everywhere), but *non-equilibrium* situations, in which the effect of an external field, continuously driving the system out of equilibrium, is balanced by the simultaneous relaxation – the trend back to equilibrium. Perhaps the most important effect of this class is the dc current in conductors and semiconductors,¹ which alone justifies the inclusion of the basic notions of kinetics into any set of core physics courses.

The reader who has reached this point of the notes already has some taste of physical kinetics, because the subject of the last part of Chapter 5 was the kinetics of a “Brownian particle”, i.e. of a “heavy” system interacting with an environment consisting of many “lighter” components. Indeed, the equations discussed in that part – whether the Smoluchowski equation (5.122) or the Fokker-Planck equation (5.149) – are valid if the environment is in thermodynamic equilibrium, but the system of our interest is not necessarily so. As a result, we could use those equations to discuss such non-equilibrium phenomena as the Kramers problem of the metastable state’s lifetime.

In contrast, this chapter is devoted to the more traditional subject of kinetics: systems of many *similar* particles – generally, interacting with each other, but not too strongly, so that the energy of the system still may be partitioned into a sum of single-particle components, with the interparticle interactions considered as a weak perturbation. Actually, we have already started the job of describing such a system at the beginning of Sec. 5.7. Indeed, in the absence of particle interactions (i.e. when it is unimportant whether the particle of our interest is “light” or “heavy”), the probability current densities in the coordinate and momentum spaces are given, respectively, by Eq. (5.142) and the first form of Eq. (5.143a), so that the continuity equation (5.140) takes the form

$$\frac{\partial w}{\partial t} + \nabla_q \cdot (w \dot{\mathbf{q}}) + \nabla_p \cdot (w \dot{\mathbf{p}}) = 0. \quad (6.1)$$

¹ This topic was briefly addressed in EM Chapter 4, carefully avoiding the aspects related to the thermal effects.

If similar particles do *not* interact, this equation for the single-particle probability density $w(\mathbf{q}, \mathbf{p}, t)$ is valid for each of them, and the result of its solution may be used to calculate any ensemble-average characteristic of the system as a whole.

Let us rewrite Eq. (1) in the Cartesian-component form,

$$\frac{\partial w}{\partial t} + \sum_j \left[\frac{\partial}{\partial q_j} (w \dot{q}_j) + \frac{\partial}{\partial p_j} (w \dot{p}_j) \right] = 0, \quad (6.2)$$

where the index j lists all degrees of freedom of the particle under consideration, and assume that its motion (perhaps in an external, time-dependent field) may be described by a Hamiltonian function $\mathcal{H}(q_j, p_j, t)$. Plugging into Eq. (2) the Hamiltonian equations of motion:²

$$\dot{q}_j = \frac{\partial \mathcal{H}}{\partial p_j}, \quad \dot{p}_j = -\frac{\partial \mathcal{H}}{\partial q_j}, \quad (6.3)$$

we get

$$\frac{\partial w}{\partial t} + \sum_j \left[\frac{\partial}{\partial q_j} \left(w \frac{\partial \mathcal{H}}{\partial p_j} \right) - \frac{\partial}{\partial p_j} \left(w \frac{\partial \mathcal{H}}{\partial q_j} \right) \right] = 0. \quad (6.4)$$

After differentiation of both parentheses by parts, the equal mixed terms $w \partial^2 \mathcal{H} / \partial q_j \partial p_j$ and $w \partial^2 \mathcal{H} / \partial p_j \partial q_j$ cancel, and using Eq. (3) again, we get the so-called *Liouville theorem*³

$$\frac{\partial w}{\partial t} + \sum_j \left(\frac{\partial w}{\partial q_j} \dot{q}_j + \frac{\partial w}{\partial p_j} \dot{p}_j \right) = 0.$$

(6.5)

Liouville theorem

Since the left-hand side of this equation is just the full derivative of the probability density w considered as a function of the generalized coordinates $q_j(t)$ of a particle, its generalized momenta components $p_j(t)$, and (possibly) time t ,⁴ the Liouville theorem (5) may be represented in a surprisingly simple form:

$$\frac{dw(\mathbf{q}, \mathbf{p}, t)}{dt} = 0. \quad (6.6)$$

Physically this means that the elementary probability $dW = w d^3q d^3p$ to find a Hamiltonian particle in a small volume of the coordinate-momentum space $[\mathbf{q}, \mathbf{p}]$, with its center moving in accordance to the deterministic law (3), does not change with time – see Fig. 1.

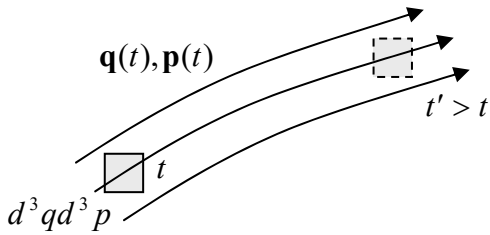


Fig. 6.1. The Liouville theorem's interpretation: probability's conservation at its flow through the $[\mathbf{q}, \mathbf{p}]$ space.

² See, e.g., CM Sec. 10.1.

³ Actually, this is just one of several theorems bearing the name of Joseph Liouville (1809-1882).

⁴ See, e.g., MA Eq. (4.2).

At the first glance, this may not look surprising because according to the fundamental Einstein relation (5.78), one needs non-Hamiltonian forces (such as the kinematic friction) to have diffusion. On the other hand, it is striking that the Liouville theorem is valid even for (Hamiltonian) systems with deterministic chaos,⁵ in which the deterministic trajectories corresponding to slightly different initial conditions become increasingly mixed with time.

For an ideal gas of 3D particles, we may use the ordinary Cartesian coordinates r_j (with $j = 1, 2, 3$) for the generalized coordinates q_j , so that p_j become the Cartesian components mv_j of the usual (linear) momentum, and the elementary volume is just $d^3r d^3p$ – see Fig. 1. In this case, Eqs. (3) are just

$$\dot{r}_j = \frac{p_j}{m} \equiv v_j, \quad \dot{p}_j = \mathcal{F}_j, \quad (6.7)$$

where \mathcal{F} is the force exerted on the particle, so that the Liouville theorem may be rewritten as

$$\frac{\partial w}{\partial t} + \sum_{j=1}^3 \left(v_j \frac{\partial w}{\partial r_j} + \mathcal{F}_j \frac{\partial w}{\partial p_j} \right) = 0, \quad (6.8)$$

and conveniently represented in the vector form

$$\frac{\partial w}{\partial t} + \mathbf{v} \cdot \nabla_r w + \mathcal{F} \cdot \nabla_p w = 0. \quad (6.9)$$

Of course, the situation becomes much more complex if the particles interact. Generally, a system of N similar particles in 3D space has to be described by the probability density being a function of $6N + 1$ arguments (3 N Cartesian coordinates, plus 3 N momentum components, plus time). An analytical or numerical solution of any equation describing the time evolution of such a function for a typical system of $N \sim 10^{23}$ particles is evidently a hopeless task. Hence, any theory of realistic systems' kinetics has to rely on making reasonable approximations that would simplify the situation.

One of the most useful approximations (sometimes called *Stosszahlansatz* – German for the “collision-number assumption”) was suggested by Ludwig Boltzmann for gas of particles that move freely most of the time but interact during short time intervals, when a particle comes close to either an immobile scattering center (say, an impurity in a conductor's crystal lattice) or to another particle of the gas. Such brief *scattering events* may change the particle's momentum. Boltzmann argued that they may be still approximately described Eq. (9), with the addition of a special term (called the *scattering integral*) to its right-hand side:

$$\frac{\partial w}{\partial t} + \mathbf{v} \cdot \nabla_r w + \mathcal{F} \cdot \nabla_p w = \frac{\partial w}{\partial t} \Big|_{\text{scattering}}. \quad (6.10)$$

Boltzmann
equation

This is the *Boltzmann equation*, also called the “Boltzmann transport equation”. As will be discussed below, it may give a very reasonable description of not only classical but also quantum particles, though it evidently neglects the quantum-mechanical coherence/entanglement effects⁶ – besides those that may be hidden inside the scattering integral.

⁵ See, e.g., CM Sec. 9.3.

⁶ Indeed, the quantum state coherence is described by off-diagonal elements of the density matrix, while the classical probability w represents only the diagonal elements of that matrix. However, at least for the ensembles close to thermal equilibrium, this is a reasonable approximation – see the discussion in Sec. 2.1.

The concrete form of the scattering integral depends on the type of particle scattering. If the scattering centers do not belong to the ensemble under consideration (an example is given, again, by impurity atoms in a conductor), then the scattering integral may be expressed as an evident generalization of the master equation (4.100):

$$\frac{\partial w}{\partial t} \Big|_{\text{scattering}} = \int d^3 p' \left[\Gamma_{\mathbf{p}' \rightarrow \mathbf{p}} w(\mathbf{r}, \mathbf{p}', t) - \Gamma_{\mathbf{p} \rightarrow \mathbf{p}'} w(\mathbf{r}, \mathbf{p}, t) \right], \quad (6.11)$$

where the physical sense of $\Gamma_{\mathbf{p} \rightarrow \mathbf{p}'}$ is the rate (i.e. the probability per unit time) for the particle to be scattered from the state with the momentum \mathbf{p} into the state with the momentum \mathbf{p}' – see Fig. 2.

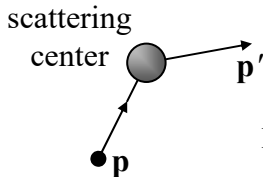


Fig. 6.2. A single-particle scattering event.

Most elastic interactions are *reciprocal*, i.e. obey the following relation (closely related to the reversibility of time in Hamiltonian systems): $\Gamma_{\mathbf{p} \rightarrow \mathbf{p}'} = \Gamma_{\mathbf{p}' \rightarrow \mathbf{p}}$, so that Eq. (11) may be rewritten as⁷

$$\frac{\partial w}{\partial t} \Big|_{\text{scattering}} = \int d^3 p' \Gamma_{\mathbf{p} \rightarrow \mathbf{p}'} [w(\mathbf{r}, \mathbf{p}', t) - w(\mathbf{r}, \mathbf{p}, t)]. \quad (6.12)$$

With such scattering integral, Eq. (10) stays linear in w but becomes an *integro-differential equation*, typically harder to solve analytically than differential equations.

The equation becomes even more complex if the scattering is due to the mutual interaction of the particle members of the system – see Fig. 3.

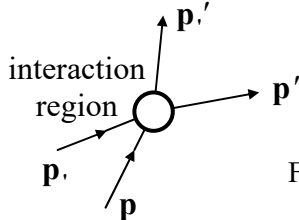


Fig. 6.3. A particle-particle scattering event.

In this case, the probability of a scattering event scales as a product of two single-particle probabilities, and the simplest reasonable form of the scattering integral is⁸

⁷ One may wonder whether this approximation may work for Fermi particles, such as electrons, for whom the Pauli principle forbids scattering into the already occupied state, so that for the scattering $\mathbf{p} \rightarrow \mathbf{p}'$, the term $w(\mathbf{r}, \mathbf{p}, t)$ in Eq. (12) has to be multiplied by the probability $[1 - w(\mathbf{r}, \mathbf{p}', t)]$ that the final state is available. This is a valid argument, but one should notice that if this modification has been done with both terms of Eq. (12), it becomes

$$\frac{\partial w}{\partial t} \Big|_{\text{scattering}} = \int d^3 p' \Gamma_{\mathbf{p} \rightarrow \mathbf{p}'} \{w(\mathbf{r}, \mathbf{p}', t)[1 - w(\mathbf{r}, \mathbf{p}, t)] - w(\mathbf{r}, \mathbf{p}, t)[1 - w(\mathbf{r}, \mathbf{p}', t)]\}.$$

Opening both square brackets, we see that the probability density products cancel, bringing us back to Eq. (12).

⁸ This was the approximation used by L. Boltzmann to prove the famous *H-theorem*, stating that entropy of the gas described by Eq. (13) may only grow (or stay constant) in time, $dS/dt \geq 0$. Since the model is very approximate, that result does not seem too fundamental nowadays, despite all its historic significance.

$$\frac{\partial w}{\partial t} \Big|_{\text{scattering}} = \int d^3 p' \int d^3 p \left[\begin{array}{l} \Gamma_{\mathbf{p}' \rightarrow \mathbf{p}, \mathbf{p}' \rightarrow \mathbf{p}, \mathbf{p}'} w(\mathbf{r}, \mathbf{p}', t) w(\mathbf{r}, \mathbf{p}', t) \\ - \Gamma_{\mathbf{p} \rightarrow \mathbf{p}', \mathbf{p} \rightarrow \mathbf{p}', \mathbf{p}'} w(\mathbf{r}, \mathbf{p}, t) w(\mathbf{r}, \mathbf{p}, t) \end{array} \right]. \quad (6.13)$$

The integration dimensionality in Eq. (13) takes into account the fact that due to the conservation of the total momentum at scattering,

$$\mathbf{p} + \mathbf{p}_+ = \mathbf{p}' + \mathbf{p}', \quad (6.14)$$

one of the momenta is not an independent argument, so that the integration in Eq. (13) may be restricted to a 6D p -space rather than the 9D one. For the reciprocal interaction, Eq. (13) may also be a bit simplified, but it still keeps Eq. (10) a *nonlinear* integro-differential transport equation, excluding such powerful solution methods as the Fourier expansion – which hinges on the linear superposition principle.

This is why most useful results based on the Boltzmann transport equation depend on its further simplifications, most notably the *relaxation-time approximation* – RTA for short.⁹ This approximation is based on the fact that in the absence of spatial gradients ($\nabla = 0$), and external forces ($\mathcal{F} = 0$), in at the thermal equilibrium, Eq. (10) yields

$$\frac{\partial w}{\partial t} = \frac{\partial w}{\partial t} \Big|_{\text{scattering}}, \quad (6.15)$$

so that the equilibrium probability distribution $w_0(\mathbf{r}, \mathbf{p}, t)$ has to turn any scattering integral to zero. Hence at a *small* deviation from the equilibrium,

$$\tilde{w}(\mathbf{r}, \mathbf{p}, t) \equiv w(\mathbf{r}, \mathbf{p}, t) - w_0(\mathbf{r}, \mathbf{p}, t) \rightarrow 0, \quad (6.16)$$

the scattering integral should be proportional to the deviation \tilde{w} , and its simplest reasonable model is

$$\frac{\partial w}{\partial t} \Big|_{\text{scattering}} = -\frac{\tilde{w}}{\tau}, \quad (6.17)$$

where τ is a phenomenological constant (which, according to Eq. (15), has to be positive for the system's stability) called the *relaxation time*. Its physical meaning will be more clear in the next section.

The relaxation-time approximation is quite reasonable if the angular distribution of the scattering rate is dominated by small angles between vectors \mathbf{p} and \mathbf{p}' – as it is, for example, for the Rutherford scattering by a Coulomb center.¹⁰ Indeed, in this case the two values of the function w , participating in Eq. (12), are close to each other for most scattering events so that the loss of the second momentum argument (\mathbf{p}') is not too essential. However, using the Boltzmann-RTA equation that results from combining Eqs. (10) and (17),

$$\frac{\partial w}{\partial t} + \mathbf{v} \cdot \nabla_r w + \mathcal{F} \cdot \nabla_p w = -\frac{\tilde{w}}{\tau}, \quad (6.18)$$

we should always remember that this is just a phenomenological model, sometimes giving completely wrong results. For example, it prescribes the same time scale (τ) to the relaxation of the net *momentum*

⁹ Sometimes this approximation is called the “BGK model”, after P. Bhatnager, E. Gross, and M. Krook who suggested it in 1954. (The same year, a similar model was considered by P. Welander.)

¹⁰ See, e.g., CM Sec. 3.7.

of the system, and to its *energy relaxation*, while in many real systems the latter process (that results from inelastic collisions) may be substantially longer. Naturally, in the following sections, I will describe only those applications of the Boltzmann-RTA equation that give a reasonable description of physical reality.

6.2. The Ohm law and the Drude formula

Despite its shortcomings, Eq. (18) is adequate for quite a few applications. Perhaps the most important of them is deriving the Ohm law for dc current in a “nearly-ideal” gas of charged particles, whose only important deviation from ideality is the rare scattering effects described by Eq. (17). As a result, in equilibrium it is described by the stationary probability w_0 of an ideal gas (see Sec. 3.1):

$$w_0(\mathbf{r}, \mathbf{p}, t) = \frac{g}{(2\pi\hbar)^3} \langle N(\varepsilon) \rangle, \quad (6.19)$$

where g is the internal degeneracy factor (say, $g = 2$ for electrons due to their spin), and $\langle N(\varepsilon) \rangle$ is the average occupancy of a quantum state with momentum \mathbf{p} , that obeys either the Fermi-Dirac or the Bose-Einstein distribution:

$$\langle N(\varepsilon) \rangle = \frac{1}{\exp\{(\varepsilon - \mu)/T\} \pm 1}, \quad \varepsilon = \varepsilon(\mathbf{p}). \quad (6.20)$$

(The following calculations will be valid, up to a point, for both statistics and hence, in the limit $\mu/T \rightarrow -\infty$, for a classical gas as well.)

Now let a uniform dc electric field \mathcal{E} be applied to the gas of particles with electric charge q , exerting force $\mathcal{F} = q\mathcal{E}$ on each of them. Then the stationary solution to Eq. (18), with $\partial/\partial t = 0$, should also be stationary and spatially-uniform ($\nabla_r = 0$), so that this equation is reduced to

$$q\mathcal{E} \cdot \nabla_p w = -\frac{\tilde{w}}{\tau}. \quad (6.21)$$

Let us require the electric field to be relatively low, so that the perturbation \tilde{w} it produces is relatively small, as required by our basic assumption (16).¹¹ Then on the left-hand side of Eq. (21), we can neglect that perturbation, by replacing w with w_0 , because that side already has a small factor (\mathcal{E}). As a result, this equation yields

$$\tilde{w} = -\tau q \mathcal{E} \cdot \nabla_p w_0 \equiv -\tau q \mathcal{E} \cdot \left(\nabla_p \varepsilon \right) \frac{\partial w_0}{\partial \varepsilon}, \quad (6.22)$$

where the second step implies isotropy of the parameters μ and T , i.e. their independence of the direction of the particle’s momentum \mathbf{p} . But the gradient $\nabla_p \varepsilon$ is nothing else than the particle’s velocity

¹¹ Since the scale of the fastest change of w_0 in the momentum space is of the order of $\partial w_0 / \partial p = (\partial w_0 / \partial \varepsilon)(d\varepsilon/dp) \sim (1/T)v$, where v is the scale of particle’s speed, the necessary condition of the linear approximation (22) is $e\mathcal{E}\tau \ll T/v$, i.e. if $e\mathcal{E}l \ll T$, where $l \equiv v\tau$ has the meaning of the effective mean-free path. Since the left-hand side of the last inequality is just the average energy given to the particle by the electric field between two scattering events, the condition may be interpreted as the smallness of the gas’ “overheating” by the applied field. However, another condition is also necessary – see the last paragraph of this section.

\mathbf{v} – for a quantum particle, its group velocity.¹² (This fact is easy to verify for the isotropic and parabolic dispersion law, pertinent to classical particles moving in free space,

$$\epsilon(\mathbf{p}) = \frac{\mathbf{p}^2}{2m} \equiv \frac{p_1^2 + p_2^2 + p_3^2}{2m}. \quad (6.23)$$

Indeed, in this case, the j^{th} Cartesian components of the vector $\nabla_p \epsilon$ is

$$(\nabla_p \epsilon)_j \equiv \frac{\partial \epsilon}{\partial p_j} = \frac{p_j}{m} = v_j, \quad (6.24)$$

so that $\nabla_p \epsilon = \mathbf{v}$.) Hence, Eq. (22) may be rewritten as

$$\tilde{w} = -\tau q \mathcal{E} \cdot \mathbf{v} \frac{\partial w_0}{\partial \epsilon}. \quad (6.25)$$

Let us use this result to calculate the electric current density \mathbf{j} . The contribution of each particle to the current density is $q\mathbf{v}$ so that the total density is

$$\mathbf{j} = \int q\mathbf{v} w d^3 p \equiv q \int \mathbf{v} (w_0 + \tilde{w}) d^3 p. \quad (6.26)$$

Since in the equilibrium state (with $w = w_0$), the current has to be zero, the integral of the first term in the parentheses has to vanish. For the integral of the second term, plugging in Eq. (25), and then using Eq. (19), we get

$$\mathbf{j} = q^2 \tau \int \mathbf{v} (\mathcal{E} \cdot \mathbf{v}) \left(-\frac{\partial w_0}{\partial \epsilon} \right) d^3 p = \frac{gq^2 \tau}{(2\pi\hbar)^3} \int \mathbf{v} (\mathcal{E} \cdot \mathbf{v}) \left[-\frac{\partial \langle N(\epsilon) \rangle}{\partial \epsilon} \right] d^2 p_{\perp} dp_{||}, \quad (6.27)$$

where $d^2 p_{\perp}$ is the elementary area of the constant energy surface in the momentum space, while $dp_{||}$ is the momentum differential's component normal to that surface. The real power of this result¹³ is that it is valid even for particles with an arbitrary dispersion law $\epsilon(\mathbf{p})$ (which may be rather complicated, for example, for particles moving in space-periodic potentials¹⁴), and gives, in particular, a fair description of conductivity's anisotropy in crystals.

For free particles whose dispersion law is isotropic and parabolic, as in Eq. (23), the constant energy surface is a sphere of radius p , so that $d^2 p_{\perp} = p^2 d\Omega = p^2 \sin\theta d\theta d\varphi$, while $dp_{||} = dp$. In the spherical coordinates, with the polar axis directed along the electric field vector \mathcal{E} , we get $(\mathcal{E} \cdot \mathbf{v}) = \mathcal{E} v \cos\theta$. Now separating the vector \mathbf{v} outside the parentheses into the component $v \cos\theta$ directed along the vector \mathcal{E} , and two perpendicular components, $v \sin\theta \cos\varphi$ and $v \sin\theta \sin\varphi$, we see that the integrals of the last two components over the angle φ give zero. Hence, as we could expect, in the isotropic case the net current is directed along the electric field and obeys the linear *Ohm law*,

$$\mathbf{j} = \sigma \mathcal{E}, \quad (6.28)$$

Ohm
law

¹² See, e.g., QM Sec. 2.1.

¹³ It was obtained by Arnold Sommerfeld in 1927.

¹⁴ See, e.g., QM Secs. 2.7, 2.8, and 3.4. (In this case, \mathbf{p} should be understood as the quasimomentum rather than the genuine momentum.)

with a field-independent, scalar¹⁵ *electric conductivity*

$$\sigma = \frac{gq^2\tau}{(2\pi\hbar)^3} \int_0^{2\pi} d\varphi \int_0^\pi \sin\theta d\theta \cos^2\theta \int_0^\infty p^2 dp v^2 \left[-\frac{\partial \langle N(\varepsilon) \rangle}{\partial \varepsilon} \right]. \quad (6.29)$$

(Note that σ is proportional to q^2 and hence does not depend on the particle charge sign.¹⁶)

Since $\sin\theta d\theta$ is just $-d(\cos\theta)$, the integral over θ equals $(2/3)$. The integral over $d\varphi$ is of course just 2π , while that over p may be readily transformed to one over the particle's energy $\varepsilon(\mathbf{p}) = p^2/2m$: $p^2 = 2m\varepsilon$, $v^2 = 2\varepsilon/m$, $p = (2m\varepsilon)^{1/2}$, so that $dp = (m/2\varepsilon)^{1/2}d\varepsilon$, and $p^2 dp v^2 = (2m\varepsilon)(m/2\varepsilon)^{1/2}d\varepsilon (2\varepsilon/m) \equiv (8m\varepsilon^3)^{1/2}d\varepsilon$. As a result, the conductivity equals

$$\sigma = \frac{gq^2\tau}{(2\pi\hbar)^3} \frac{4\pi}{3} \int_0^\infty (8m\varepsilon^3)^{1/2} \left[-\frac{\partial \langle N(\varepsilon) \rangle}{\partial \varepsilon} \right] d\varepsilon. \quad (6.30)$$

Now we may work out the integral in Eq. (30) by parts, first rewriting $[-\partial \langle N(\varepsilon) \rangle / \partial \varepsilon] d\varepsilon$ as $-d[\langle N(\varepsilon) \rangle]$. Due to the fast (exponential) decay of the factor $\langle N(\varepsilon) \rangle$ at $\varepsilon \rightarrow \infty$, its product by the factor $(8m\varepsilon^3)^{1/2}$ vanishes at both integration limits, and we get

$$\begin{aligned} \sigma &= \frac{gq^2\tau}{(2\pi\hbar)^3} \frac{4\pi}{3} \int_0^\infty \langle N(\varepsilon) \rangle d[(8m\varepsilon^3)^{1/2}] = \frac{gq^2\tau}{(2\pi\hbar)^3} \frac{4\pi}{3} (8m)^{1/2} \int_0^\infty \langle N(\varepsilon) \rangle \frac{3}{2} \varepsilon^{1/2} d\varepsilon \\ &\equiv \frac{q^2\tau}{m} \times \frac{gm^{3/2}}{\sqrt{2\pi^2\hbar^3}} \int_0^\infty \langle N(\varepsilon) \rangle \varepsilon^{1/2} d\varepsilon. \end{aligned} \quad (6.31)$$

But according to Eq. (3.40), the last factor in this expression (after the \times sign) is just the particle density $n \equiv N/V$, so that the Sommerfeld's result is reduced, for arbitrary temperature, and any particle statistics, to the very simple *Drude formula*,¹⁷

$$\sigma = \frac{q^2\tau}{m} n, \quad (6.32)$$

Drude formula

which should be well familiar to the reader from an undergraduate physics course.

As a reminder, here is its simple classical derivation.¹⁸ Let 2τ be the average time interval between two sequential scattering events that cause a particle to lose the deterministic component of its velocity, $\mathbf{v}_{\text{drift}}$, provided by the electric field \mathcal{E} on the top of particle's random thermal motion – which does not contribute to the net current. Using the 2nd Newton law to describe particle's acceleration by

¹⁵ As Eq. (27) shows, if the dispersion law $\varepsilon(\mathbf{p})$ is anisotropic, the current density direction may be different from that of the electric field. In this case, conductivity should be described by a tensor $\sigma_{jj'}$, rather than a scalar. However, in most important conducting materials, the anisotropy is rather small – see, e.g., EM Table 4.1.

¹⁶ This is why to determine the dominating type of charge carriers in semiconductors (electrons or holes, see Sec. 4 below), the Hall effect, which lacks such ambivalence (see, e.g., QM 3.2), is frequently used.

¹⁷ It was derived in 1900 by Paul Drude. Note that Drude also used the same arguments to derive a very simple (and very reasonable) approximation for the complex electric conductivity in the ac field of frequency ω : $\sigma(\omega) = \sigma(0)/(1 - i\omega\tau)$, with $\sigma(0)$ given by Eq. (32); sometimes the name “Drude formula” is used for this expression rather than for Eq. (32). Let me leave its derivation, from the Boltzmann-RTA equation, for the reader's exercise.

¹⁸ See also EM Sec. 4.2.

the field, $d\mathbf{v}_{\text{drift}}/dt = q\mathcal{E}/m$, we get $\langle \mathbf{v}_{\text{drift}} \rangle = \tau q \mathcal{E}/m$. Multiplying this result by the particle's charge q and density $n \equiv N/V$, we get the Ohm law $\mathbf{j} = \sigma \mathcal{E}$, with σ given by Eq. (32).

Sommerfeld's derivation of the Drude formula poses an important conceptual question. The structure of Eq. (30) implies that the only quantum states contributing to the electric conductivity are those whose derivative $[-\partial\langle N(\mathcal{E})\rangle/\partial\mathcal{E}]$ is significant. For the Fermi particles such as electrons, in the limit $T \ll \epsilon_F$, these are the states at the very surface of the Fermi sphere. On the other hand, Eq. (32) and the whole Drude reasoning, involves the density n of *all* electrons. So, what exactly electrons are responsible for the conductivity: all of them, or only those at the Fermi surface? For the resolution of this paradox, let us return to Eq. (22) and analyze the physical meaning of that result. Let us compare it with the following model distribution:

$$w_{\text{model}} \equiv w_0(\mathbf{r}, \mathbf{p} - \tilde{\mathbf{p}}, t), \quad (6.33)$$

where $\tilde{\mathbf{p}}$ is some constant, small vector, which describes a small shift of the unperturbed distribution w_0 as a whole, in the momentum space. Performing the Taylor expansion of Eq. (33) in this small parameter, and keeping only two leading terms, we get

$$w_{\text{model}} \approx w_0(\mathbf{r}, \mathbf{p}, t) + \tilde{w}_{\text{model}}, \quad \text{with } \tilde{w}_{\text{model}} = -\tilde{\mathbf{p}} \cdot \nabla_p w_0(\mathbf{r}, \mathbf{p}, t). \quad (6.34)$$

Comparing the last expression with the first form of Eq. (22), we see that they coincide if

$$\tilde{\mathbf{p}} = q\mathcal{E}\tau \equiv \mathcal{F}\tau. \quad (6.35)$$

This means that Eq. (22) describes a small shift of the equilibrium distribution of all particles (in the momentum space) by $q\mathcal{E}\tau$ along the electric field's direction, justifying the cartoon shown in Fig. 4.

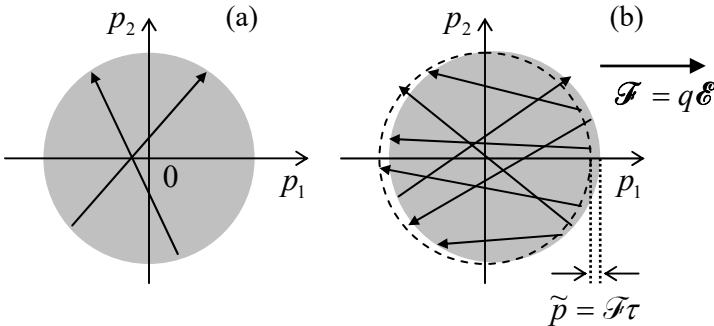


Fig. 6.4. Filling of momentum states by a degenerate electron gas: (a) in the absence and (b) in the presence of an external electric field \mathcal{E} . Arrows show representative scattering events.

At $\mathcal{E} = 0$, the system is in equilibrium, so that the quantum states inside the Fermi sphere ($p < p_F$), are occupied, while those outside of it are empty – see Fig. 4a. Electron scattering events may happen only between states within a very thin layer ($|p^2/2m - \epsilon_F| \sim T$) at the Fermi surface, because only in this layer the states are partially occupied, so that both components of the product $w(\mathbf{r}, \mathbf{p}, t)[1 - w(\mathbf{r}, \mathbf{p}', t)]$, mentioned in Sec. 1, do not vanish. These scattering events, on average, do not change the equilibrium probability distribution, because they are uniformly spread over the Fermi surface.

Now let the electric field be turned on instantly. Immediately it starts accelerating all electrons in its direction, i.e. the whole Fermi sphere starts moving in the momentum space, along the field's direction in the real space. For elastic scattering events (with $|\mathbf{p}'| = |\mathbf{p}|$), this creates an addition of occupied states at the leading edge of the accelerating sphere and an addition of free states on its trailing

edge (Fig. 4b). As a result, now there are more scattering events bringing electrons from the leading edge to the trailing edge of the sphere than in the opposite direction. This creates the average backflow of the state occupancy in the momentum space. These two trends eventually cancel each other, and the Fermi sphere approaches a stationary (though not a thermal-equilibrium!) state, with the shift (35) relatively to its thermal-equilibrium position.

Now Fig. 4b may be used to answer the question of which of the two different interpretations of the Drude formula is correct, and the answer is: *either*. On one hand, we can look at the electric current as a result of the shift (35) of *all* electrons in the momentum space. On the other hand, each filled quantum state deep inside the sphere gives exactly the same contribution to the net current density as it did without the field. All these internal contributions to the net current cancel each other so that the applied field changes the situation only at the Fermi surface. Thus it is equally legitimate to say that only the surface states are responsible for the non-zero net current.¹⁹

Let me also mention another paradox related to the Drude formula, which is often misunderstood (not only by students :-). As was emphasized above, τ is finite even at *elastic* scattering – that by itself does not change the total energy of the gas. The question is how can such scattering be responsible for the Ohmic resistivity $\rho \equiv 1/\sigma$, and hence for the Joule heat production, with the power density $p = j \cdot \mathcal{E} = \rho j^2$?²⁰ The answer is that the Drude/Sommerfeld formulas describe just the “bottleneck” of the Joule heat formation. In the scattering picture (Fig. 4b) the states filled by elastically scattered electrons are located above the (shifted) Fermi surface, and these electrons eventually need to relax onto it via some inelastic process, which releases their excessive energy in the form of heat (in solid state, described by phonons – see Sec. 2.6). The rate and other features of these inelastic phenomena do not participate in the Drude formula directly, but for keeping the theory valid (in particular, keeping the probability distribution w close to its equilibrium value w_0), their intensity has to be sufficient to avoid gas overheating by the applied field. In some poorly conducting materials, charge carrier overheating effects, resulting in deviations from the Ohm law, i.e. from the linear relation (28) between j and \mathcal{E} , may be observed already at rather practicable electric fields.

One final comment is that the Sommerfeld theory of the Ohmic conductivity works very well for the electron gas in most conductors. The scheme shown in Fig. 4 helps to understand why: for degenerate Fermi gases the energies of all particles whose scattering contributes to transport properties, are close ($\varepsilon \approx \varepsilon_F$) and prescribing them all the same relaxation time τ is very reasonable. In contrast, in classical gases, with their relatively broad distribution of ε , some results given by the Boltzmann-RTA equation (18) are valid only by the order of magnitude.

6.3. Electrochemical potential and the drift-diffusion equation

Now let us generalize our calculation to the case when the particle transport takes place in the presence of a time-independent spatial gradient of the probability distribution, $\nabla_r w \neq 0$, caused for example by that of the particle concentration $n = N/V$ (and hence, according to Eq. (3.40), of the

¹⁹ So here, as it frequently happens in physics, formulas (or graphical sketches, such as Fig. 4b) give a more clear and unambiguous description of reality than words – the privilege lacked by many “scientific” disciplines, rich with unending, shallow verbal debates. Note also that, as frequently happens in physics, the dual interpretation of σ is expressed by two different but equal integrals (30) and (31), related by the integration-by-parts rule.

²⁰ This formula is probably self-evident, but if you need you may revisit EM Sec. 4.4.

chemical potential μ), while still assuming that temperature T is constant. For this generalization, we should keep the second term on the left-hand side of Eq. (18). If the gradient of w is sufficiently small, we can repeat the arguments of the last section and replace w with w_0 in this term as well. With the applied electric field \mathcal{E} represented as $(-\nabla\phi)$,²¹ where ϕ is the electrostatic potential, Eq. (25) becomes

$$\tilde{w} = \tau \mathbf{v} \cdot \left(\frac{\partial w_0}{\partial \varepsilon} q \nabla \phi - \nabla w_0 \right). \quad (6.36)$$

Since in any of the equilibrium distributions (20), $\langle N(\varepsilon) \rangle$ is a function of ε and μ only in the combination $(\varepsilon - \mu)$, it obeys the following relation:

$$\frac{\partial \langle N(\varepsilon) \rangle}{\partial \mu} = - \frac{\partial \langle N(\varepsilon) \rangle}{\partial \varepsilon}. \quad (6.37)$$

Using this relation, the gradient of $w_0 \propto \langle N(\varepsilon) \rangle$ may be represented as²²

$$\nabla w_0 = - \frac{\partial w_0}{\partial \varepsilon} \nabla \mu, \quad \text{for } T = \text{const}, \quad (6.38)$$

so that Eq. (36) becomes

$$\tilde{w} = \tau \frac{\partial w_0}{\partial \varepsilon} \mathbf{v} \cdot (q \nabla \phi + \nabla \mu) \equiv \tau \frac{\partial w_0}{\partial \varepsilon} \mathbf{v} \cdot \nabla \mu', \quad (6.39)$$

where the following sum,

$$\mu' \equiv \mu + q\phi, \quad (6.40)$$

is called the *electrochemical potential*. Now repeating the calculation of the electric current, carried out in the last section, we get the following generalization of the Ohm law (28):

$$\mathbf{j} = \sigma(-\nabla \mu' / q) \equiv \sigma \mathcal{E}, \quad (6.41)$$

where the *effective electric field* \mathcal{E} is proportional to the gradient of the electrochemical potential, rather than the electrostatic potential:

$$\mathcal{E} \equiv -\frac{\nabla \mu'}{q} = \mathcal{E} - \frac{\nabla \mu}{q}. \quad (6.42)$$

The physics of this extremely important and general result²³ may be explained in two ways. First, let us have a look at the energy spectrum of a degenerate Fermi-gas confined in a volume of finite size, but otherwise free. To ensure such a confinement we need a piecewise-constant potential $U(\mathbf{r})$ – a “hard-wall, flat-bottom potential well” – see Fig. 5a. (For conduction electrons in a metal, such profile is

²¹ Since we will not encounter ∇_p in the balance of this chapter, from this point on, the subscript r of the operator ∇_r is dropped for the notation brevity.

²² Since we consider w_0 as a function of two *independent* arguments \mathbf{r} and \mathbf{p} , taking its gradient, i.e. the differentiation of this function over \mathbf{r} , does not involve its differentiation over the kinetic energy ε – which is a function of \mathbf{p} only.

²³ Note that Eq. (42) does not include the phenomenological parameter τ of the relaxation-time approximation, signaling that it is much more general than the RTA. Indeed, this equality is based entirely on the relation between the second and third terms on the left-hand side of the general Boltzmann equation (10), rather than on any details of the scattering integral on its right-hand side.

provided by the positively charged ions of the crystal lattice.) The well should be of a sufficient depth $U_0 > \varepsilon_F \equiv \mu|_{T=0}$ to provide the confinement of the overwhelming majority of the particles, with energies below and somewhat above the Fermi level ε_F . This means that there should be a substantial energy gap,

$$\psi \equiv U_0 - \mu \gg T, \quad (6.43)$$

between the Fermi energy of a particle inside the well, and its potential energy U_0 outside the well. (The latter value of energy is usually called the *vacuum level*.) The difference defined by Eq. (43) is called the *workfunction*,²⁴ for most metals, it is between 4 and 5 eV, so that the relation $\psi \gg T$ is well fulfilled for room temperatures ($T \sim 0.025$ eV) – and actually for all temperatures up to the metal’s evaporation point.

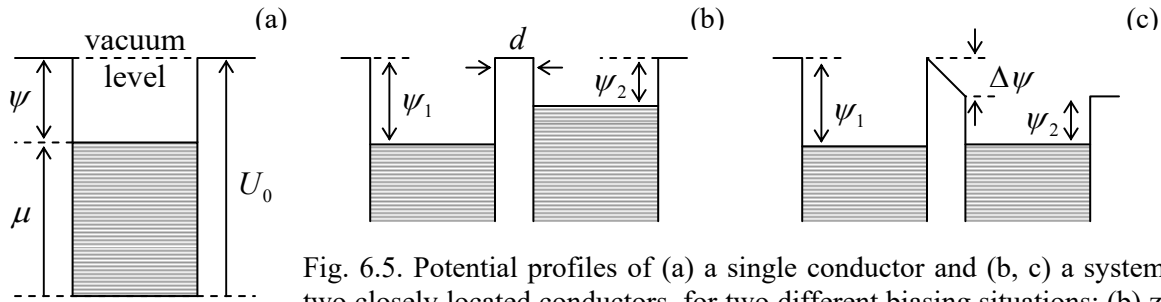


Fig. 6.5. Potential profiles of (a) a single conductor and (b, c) a system of two closely located conductors, for two different biasing situations: (b) zero electrostatic field (the “flat-band condition”), and (c) zero voltage $\Delta\mu'$.

Now let us consider two conductors, with different values of ψ , separated by a small spatial gap d – see Figs. 5b,c. Panel (b) shows the case when the electric field $\mathcal{E} = -\nabla\phi$ in the free-space gap between the conductors equals zero, i.e. their *electrostatic* potentials ϕ are equal.²⁵ If there is an opportunity for particles to cross the gap (e.g., by either the thermally-activated hopping *over* the potential barrier, discussed in Secs. 5.6-5.7, or the quantum-mechanical tunneling *through* it), there will be an average flow of particles from the conductor with the higher Fermi level to that with the lower Fermi level,²⁶ because the chemical equilibrium requires their equality – see Secs. 1.5 and 2.7. If the particles have an electric charge (as electrons do), the equilibrium will be automatically achieved by them recharging the effective capacitor formed by the conductors, until the electrostatic energy difference $q\Delta\phi$ reaches the value reproducing that of the workfunctions (Fig. 5c). So for the equilibrium potential difference²⁷ we may write

$$q\Delta\phi = \Delta\psi = -\Delta\mu. \quad (6.44)$$

At this equilibrium, the electric field in the gap between the conductors is

²⁴ Sometimes it is also called the “electron affinity”, though this term is mostly used for atoms and molecules.

²⁵ In semiconductor physics and engineering, the situation shown in Fig. 5b is called the *flat-band condition*, because any electric field applied normally to a surface of a semiconductor leads to the so-called energy *band bending* – see the next section.

²⁶ As measured from a common reference value, for example from the vacuum level – rather than from the bottom of an individual potential well as in Fig. 5a.

²⁷ In physics literature, it is usually called the *contact potential difference*, while in electrochemistry (for which it is one of the key notions), the term *Volta potential* is more common.

$$\mathcal{E} \equiv -\frac{\Delta\phi}{d} \mathbf{n} = \frac{\Delta\mu}{qd} \mathbf{n} = \frac{\nabla\mu}{q}; \quad (6.45)$$

in Fig. 5c this field is clearly visible as the tilt of the electric potential profile. Comparing Eq. (45) with the definition (42) of the effective electric field \mathcal{E} , we see that the equilibrium, i.e. the absence of current through the potential barrier, is achieved exactly when $\mathcal{E} = 0$, in accordance with Eq. (41).

The electric field dichotomy, $\mathcal{E} \leftrightarrow \mathcal{E}$, raises a natural question: which of these fields we are speaking about in the everyday and laboratory practice? Upon some contemplation, the reader should agree that most of our electric field measurements are done indirectly, by measuring corresponding voltages – with voltmeters. A vast majority of these instruments belong to the so-called *electrodynamic* variety, which is based on the measurement of a small current flowing through the voltmeter.²⁸ As Eq. (41) shows, such electrodynamic voltmeters measure the *electrochemical* potential difference $\Delta\mu'/q$. However, there exists a rare breed of *electrostatic* voltmeters (also called “electrometers”) that measure the *electrostatic* potential difference $\Delta\phi$ between two conductors. One way to implement such an instrument is to use an ordinary, electrodynamic voltmeter, but with the reference point set at the flat-band condition (Fig. 5b) between the conductors. (This condition may be detected by vanishing electric charge on the adjacent surfaces of the conductors, and hence by the absence of its modulation in time if the distance between the surfaces is periodically modulated.)

Now let me return to Eq. (41) and make two very important remarks. First, it says that in the presence of an electric field, the current vanishes only if $\nabla\mu' = 0$, i.e. that the electrochemical potential μ' , rather than the chemical potential μ , has to be position-independent in a system in thermodynamic (thermal, chemical, and electric) equilibrium of a conducting system. This result by no means contradicts the fundamental thermodynamic relations for μ discussed in Sec. 1.5, or the statistical relations involving μ , which were discussed in Sec. 2.7 and beyond. Indeed, according to Eq. (40), $\mu'(\mathbf{r})$ is “merely” the chemical potential referred to the local value of the electrostatic energy $q\phi(\mathbf{r})$, and in all previous parts of the course, this energy was assumed to be constant through the system.

Second, note another interpretation of Eq. (41), which may be achieved by modifying Eq. (38) for the particular case of the classical gas. Indeed, the local density $n \equiv N/V$ of the gas obeys Eq. (3.32), which may be rewritten as

$$n(\mathbf{r}) = \text{const} \times \exp\left\{\frac{\mu(\mathbf{r})}{T}\right\}. \quad (6.46)$$

Taking the spatial gradient of both sides of this relation (still at constant T), we get

$$\nabla n = \text{const} \times \frac{1}{T} \exp\left\{\frac{\mu}{T}\right\} \nabla \mu = \frac{n}{T} \nabla \mu, \quad (6.47)$$

so that $\nabla\mu = (T/n)\nabla n$, and Eq. (41), with σ given by Eq. (32), may be recast as

$$\mathbf{j} = \sigma \left(-\frac{\nabla\mu'}{q} \right) \equiv \frac{q^2\tau}{m} n \left(-\nabla\phi - \frac{1}{q} \nabla\mu \right) \equiv q \frac{\tau}{m} (nq\mathcal{E} - T\nabla n). \quad (6.48)$$

²⁸ The devices for such measurement may be based on the interaction between the measured current and a permanent magnet, as pioneered by A.-M. Ampère in the 1820s – see, e.g., EM Chapter 5. Such devices are sometimes called *galvanometers*, honoring another pioneer of electricity, Luigi Galvani.

Hence the current density may be viewed as consisting of two independent parts: one due to particle *drift* induced by the “usual” electric field $\mathcal{E} = -\nabla\phi$, and another due to their *diffusion* – see Eq. (5.118) and its discussion. This is exactly the physics of the “mysterious” term $\nabla\mu$ in Eq. (42), though its simple form (48) is valid only in the classical limit.

Besides being very useful for applications, Eq. (48) also gives us a pleasant surprise. Namely, plugging it into the continuity equation for electric charge,²⁹

$$\frac{\partial(qn)}{\partial t} + \nabla \cdot \mathbf{j} = 0, \quad (6.49)$$

we get (after the division of all terms by $q\tau/m$) the so-called *drift-diffusion equation*:³⁰

$$\frac{m}{\tau} \frac{\partial n}{\partial t} = \nabla(n\nabla U) + T\nabla^2 n, \quad \text{with } U \equiv q\phi. \quad (6.50)$$

Drift-diffusion equation

Comparing it with Eq. (5.122), we see that the drift-diffusion equation is identical to the Smoluchowski equation,³¹ provided that we parallel the ratio τ/m with the mobility $\mu_m = 1/\eta$ of the Brownian particle. Now using the Einstein relation (5.78), we see that the effective diffusion constant D of the classical gas of similar particles is

$$D = \frac{\tau T}{m}. \quad (6.51a)$$

This important relation is more frequently represented in either of two other forms. First, since the rare scattering events we are considering do not change the statistics of the gas in thermal equilibrium, we may still use the Maxwell-distribution result (3.9) for the average-square velocity $\langle v^2 \rangle$, to recast Eq. (51a) as

$$D = \frac{1}{3} \langle v^2 \rangle \tau. \quad (6.51b)$$

One more popular form of the same relation uses the notion of the *mean free path* l , which may be defined as the average distance passed by the particle between two sequential scattering events:

$$D = \frac{1}{3} l \langle v^2 \rangle^{1/2}, \quad \text{with } l \equiv \langle v^2 \rangle^{1/2} \tau. \quad (6.51c)$$

In the forms (51b)-(51c), the result for D makes more physical sense, because it may be readily derived (admittedly, with some uncertainty of the numerical coefficient) from simple kinematic arguments – the task left for the reader’s exercise. Note that since the definition of τ in Eq. (17) is phenomenological, so is the above definition of l ; this is why several definitions of this parameter, which may differ by a numerical factor of the order of 1, are possible.

Note also that using Eq. (51a), Eq. (48) may be rewritten as an expression for the *particle flow density* $\mathbf{j}_n \equiv n\mathbf{j}_w = \mathbf{j}/q$:

$$\mathbf{j}_n = n\mu_m q \mathcal{E} - D \nabla n, \quad (6.52)$$

²⁹ If this relation is not evident, please revisit EM Sec. 4.1.

³⁰ Sometimes this term is associated with Eq. (52). One may also run into the term “convection-diffusion equation” for Eq. (50) with the replacement (51a).

³¹ And hence, at negligible ∇U , identical to the diffusion equation (5.116).

with the first term on the right-hand side describing particles' drift, while the second one, their diffusion. I will discuss the application of this equation to the most important case of non-degenerate ("quasiclassical") gases of electrons and holes in semiconductors, in the next section.

To complete this section, let me emphasize again that the mathematically similar drift-diffusion equation (50) and the Smoluchowski equation (5.122) describe different physical situations. Indeed, our (or rather Einstein and Smoluchowski's :-) treatment of the Brownian motion in Chapter 5 was based on a strong hierarchy of the system, consisting of a large "Brownian particle" in an environment of many smaller particles – "molecules". On the other hand, in this chapter we are considering a gas of similar particles. Nevertheless, the equations describing the dynamics of their probability distribution, are the same – at least within the framework of the Boltzmann transport equation with the relaxation-time approximation (17) of the scattering integral. The origin of this similarity is the fact that Eq. (12) is clearly applicable to a Brownian particle as well, with each "scattering" event being the particle's hit by a random molecule of its environment. Since, due to the mass hierarchy, the particle momentum change at each such event is very small, the scattering integral has to be local, i.e. depend only on w at the same momentum \mathbf{p} as the left-hand side of the Boltzmann equation, so that the relaxation time approximation (17) is absolutely natural – indeed, more natural than for our current case of similar particles.

6.4. Charge carriers in semiconductors

Now let me demonstrate the application of the concepts discussed in the last section to understanding the basic kinetic properties of semiconductors and a few key semiconductor structures – which are the basis of most modern electronic and optoelectronic devices, and hence of all our IT civilization. For that, I will need to take a detour to discuss their equilibrium properties first.

I will use an approximate but reasonable picture in which the energy of the electron subsystem in a solid may be partitioned into the sum of effective energies ε of independent electrons. Quantum mechanics says³² that in such periodic structures as crystals, the stationary state energy ε of a particle interacting with the atomic lattice follows one of periodic functions $\varepsilon_n(\mathbf{q})$ of the *quasimomentum* \mathbf{q} , oscillating between two extreme values $\varepsilon_{n\text{min}}$ and $\varepsilon_{n\text{max}}$. These *allowed energy bands* are separated by *bandgaps*, of widths $\Delta_n \equiv \varepsilon_{n\text{min}} - \varepsilon_{n-1\text{max}}$, with no allowed states inside them. Semiconductors and insulators (dielectrics) are defined as such crystals that in equilibrium at $T = 0$, all electron states in several energy bands (with the highest of them called the *valence band*) are completely filled, $\langle N(\varepsilon_v) \rangle = 1$, while those in the upper bands, starting from the lowest, *conduction band*, are completely empty, $\langle N(\varepsilon_c) \rangle = 0$.^{33, 34} Since the electrons follow the Fermi-Dirac statistics (2.115), this means that at $T \rightarrow 0$,

³² See, e.g., QM Sec. 2.7 and 3.4, but the thorough knowledge of this material is not necessary for following discussions of this section. If the reader is not familiar with the notion of quasimomentum (alternatively called the "crystal momentum"), its following semi-quantitative interpretation may be useful: \mathbf{q} is the result of quantum averaging of the genuine electron momentum \mathbf{p} over the crystal lattice period. In contrast to \mathbf{p} , which is not conserved because of the electron's interaction with the atomic lattice, \mathbf{q} is an integral of motion – in the absence of other forces.

³³ This mapping of electrical properties of crystals on their band structure was pioneered in 1931-32 by Alan H. Wilson.

³⁴ In insulators, the bandgap Δ is so large (e.g., ~9 eV in SiO₂) that the conduction band remains unpopulated in all practical situations, so that the following discussion is only relevant for semiconductors, with their moderate bandgaps – such as 1.14 eV in the most important case of silicon at room temperature.

the Fermi energy $\varepsilon_F \equiv \mu(0)$ is located somewhere between the valence band's maximum $\varepsilon_{V\max}$ (usually called simply ε_V), and the conduction band's minimum $\varepsilon_{C\min}$ (called ε_C) – see Fig. 6.

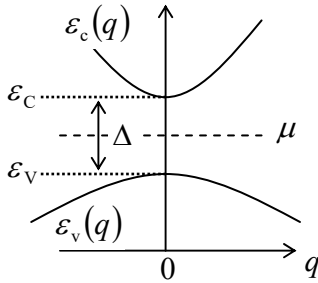


Fig. 6.6. Calculating μ in an intrinsic semiconductor.

Let us calculate the population of both branches $\varepsilon_n(\mathbf{q})$, and the chemical potential μ in equilibrium at $T > 0$. Since the functions $\varepsilon_n(\mathbf{q})$ are typically smooth, near the bandgap edges the dispersion laws $\varepsilon_c(\mathbf{q})$ and $\varepsilon_v(\mathbf{q})$ may be well approximated with quadratic parabolas. For our analysis, let us take the parabolas the simplest, isotropic form, with origins at the same quasimomentum, taking it for the reference point.³⁵

$$\varepsilon = \begin{cases} \varepsilon_C + q^2 / 2m_C, & \text{for } \varepsilon \geq \varepsilon_C, \\ \varepsilon_V - q^2 / 2m_V, & \text{for } \varepsilon \leq \varepsilon_V, \end{cases} \quad \text{with } \varepsilon_C - \varepsilon_V \equiv \Delta. \quad (6.53)$$

The positive constants m_C and m_V are usually called the effective masses of, respectively, electrons and holes. (In a typical semiconductor, m_C is a few times smaller than the free electron mass m_e , while m_V is closer to m_e .)

Due to the similarity between the top line of Eq. (53) and the dispersion law (3.3) of free particles, we may re-use Eq. (3.40), with the appropriate particle mass m , the degeneracy factor g , and the energy origin, to calculate the full spatial density of populated states (in semiconductor physics, called *electrons* in the narrow sense of the word):

$$n \equiv \frac{N_e}{V} = \int_{\varepsilon_C}^{\infty} \langle N(\varepsilon) \rangle g_3(\varepsilon) d\varepsilon \equiv \frac{g_C m_C^{3/2}}{\sqrt{2\pi^2 \hbar^3}} \int_0^{\infty} \langle N(\tilde{\varepsilon} + \varepsilon_C) \rangle \tilde{\varepsilon}^{1/2} d\tilde{\varepsilon}, \quad (6.54)$$

where $\tilde{\varepsilon} \equiv \varepsilon - \varepsilon_C \geq 0$. Similarly, the density p of “no-electron” excitations (called *holes*) in the valence band is the number of *unfilled* states in the band, and hence may be calculated as

$$p \equiv \frac{N_h}{V} = \int_{-\infty}^{\varepsilon_V} [1 - \langle N(\varepsilon) \rangle] g_3(\varepsilon) d\varepsilon \equiv \frac{g_V m_V^{3/2}}{\sqrt{2\pi^2 \hbar^3}} \int_0^{\infty} [1 - \langle N(\varepsilon_V - \tilde{\varepsilon}) \rangle] \tilde{\varepsilon}^{1/2} d\tilde{\varepsilon}, \quad (6.55)$$

where in this case, $\tilde{\varepsilon} \geq 0$ is defined as $(\varepsilon_V - \varepsilon)$. If the electrons and holes³⁶ are in the thermal and chemical equilibrium, the functions $\langle N(\varepsilon) \rangle$ in these two relations should follow the Fermi-Dirac

³⁵ It is easy (and hence is left for the reader's exercise) to verify that all equilibrium properties of charge carriers remain the same (with some effective values of m_C and m_V) if $\varepsilon_c(\mathbf{q})$ and $\varepsilon_v(\mathbf{q})$ are arbitrary quadratic forms of the Cartesian components of the quasimomentum. A mutual displacement of the branches $\varepsilon_c(\mathbf{q})$ and $\varepsilon_v(\mathbf{q})$ in the quasimomentum space is also unimportant for statistical and most transport properties of the semiconductors, though it is very important for their optical properties – which I will not have time to discuss in any detail.

³⁶ The collective name for them in semiconductor physics is *charge carriers* – or just “carriers”.

distribution (2.115) with the same temperature T and the same chemical potential μ . Moreover, in our current case of an undoped (*intrinsic*) semiconductor, these densities have to be equal,

$$n = p \equiv n_i, \quad (6.56)$$

because if this *electroneutrality condition* was violated, the volume would acquire a non-zero electric charge density $\rho = e(p - n)$, which would result, in a bulk sample, in an extremely high electric field energy. From this condition, we get a system of two equations,

$$n_i = \frac{g_C m_C^{3/2}}{\sqrt{2\pi^2 \hbar^3}} \int_0^\infty \frac{\tilde{\varepsilon}^{1/2} d\tilde{\varepsilon}}{\exp\{(\tilde{\varepsilon} + \varepsilon_C - \mu)/T\} + 1} = \frac{g_V m_V^{3/2}}{\sqrt{2\pi^2 \hbar^3}} \int_0^\infty \frac{\tilde{\varepsilon}^{1/2} d\tilde{\varepsilon}}{\exp\{(\tilde{\varepsilon} - \varepsilon_V + \mu)/T\} + 1}, \quad (6.57)$$

whose solution gives both the requested charge carrier density n_i and the Fermi level μ .

For an arbitrary ratio Δ/T , this solution may be found only numerically, but in most practical cases, this ratio is very large. (Again, for Si at room temperature, $\Delta \approx 1.14$ eV, while $T \approx 0.025$ eV.) In this case, we may use the same classical approximation as in Eq. (3.45), to reduce Eqs. (54) and (55) to simple expressions

$$n = n_C \exp\left\{\frac{\mu - \varepsilon_C}{T}\right\}, \quad p = n_V \exp\left\{\frac{\varepsilon_V - \mu}{T}\right\}, \quad \text{for } T \ll \Delta, \quad (6.58)$$

where the temperature-dependent parameters

$$n_C \equiv \frac{g_C}{\hbar^3} \left(\frac{m_C T}{2\pi} \right)^{3/2} \quad \text{and} \quad n_V \equiv \frac{g_V}{\hbar^3} \left(\frac{m_V T}{2\pi} \right)^{3/2} \quad (6.59)$$

may be interpreted as the effective numbers of states (per unit volume) available for occupation in, respectively, the conduction and valence bands, in thermal equilibrium. For usual semiconductors (with $g_C \sim g_V \sim 1$, and $m_C \sim m_V \sim m_e$), at room temperature, these numbers are of the order of $3 \times 10^{25} \text{ m}^{-3} \equiv 3 \times 10^{19} \text{ cm}^{-3}$. (Note that all results based on Eqs. (58) are only valid if both n and p are much lower than, respectively, n_C and n_V .)

With the substitution of Eqs. (58), the system of equations (56) allows a straightforward solution:

$$\mu = \frac{\varepsilon_V + \varepsilon_C}{2} + \frac{T}{2} \left(\ln \frac{g_V}{g_C} + \frac{3}{2} \ln \frac{m_V}{m_C} \right), \quad n_i = (n_C n_V)^{1/2} \exp\left\{-\frac{\Delta}{2T}\right\}. \quad (6.60)$$

Since in all practical materials the logarithms in the first of these expressions are never much larger than 1,³⁷ it shows that the Fermi level in intrinsic semiconductors never deviates substantially from the so-called *midgap value* $(\varepsilon_V + \varepsilon_C)/2$ – see the (schematic) Fig. 6. In the result for n_i , the last (exponential) factor is very small, so that the equilibrium number of charge carriers is much lower than that of the atoms – for the most important case of silicon at room temperature, $n_i \sim 10^{10} \text{ cm}^{-3}$. The exponential temperature dependence of n_i (and hence of the electric conductivity $\sigma \propto n_i$) of intrinsic semiconductors is the basis of several applications, for example simple *germanium resistance thermometers*, efficient in the whole range from $\sim 0.5\text{K}$ to $\sim 100\text{K}$. Another useful application of the same fact is the extraction of

³⁷ Note that in the case of simple electron spin degeneracy ($g_V = g_C = 2$), the first logarithm vanishes altogether. However, in many semiconductors, the degeneracy is factored by the number of similar energy bands (e.g., six similar conduction bands in silicon), and the factor $\ln(g_V/g_C)$ may slightly affect quantitative results.

the bandgap of a semiconductor from the experimental measurement of the temperature dependence of $\sigma \propto n_i$ – frequently, in just two well-separated temperature points.

However, most applications require a much higher concentration of carriers. It may be increased quite dramatically by planting into a semiconductor a relatively small number of slightly different atoms – either *donors* (e.g., phosphorus atoms for Si) or *acceptors* (e.g., boron atoms for Si). Let us analyze the first opportunity, called *n-doping*, using the same simple energy band model (53). If the donor atom is only slightly different from those in the crystal lattice, it may be easily ionized – giving an additional electron to the conduction band, and hence becoming a positive ion. This means that the effective ground state energy ε_D of the additional electrons is just slightly below the conduction band edge ε_C – see Fig. 7a.³⁸

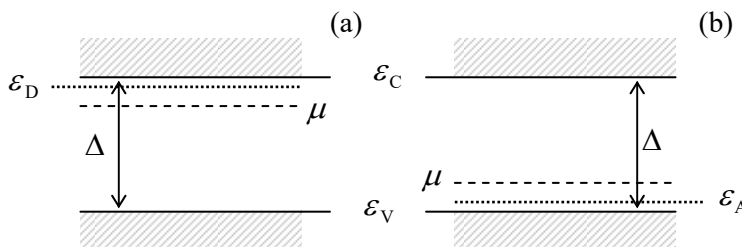


Fig. 6.7. The Fermi levels μ in (a) *n*-doped and (b) *p*-doped semiconductors. Hatching shows the ranges of unlocalized state energies.

Reviewing the arguments that have led us to Eqs. (58), we see that at relatively low doping, when the strong inequalities $n \ll n_C$ and $p \ll n_V$ still hold, these relations are not affected by the doping, so that the concentrations of electrons and holes given by these equalities still obey a universal (doping-independent) relation following from Eqs. (58) and (60):³⁹

$$np = n_i^2. \quad (6.61)$$

However, for a doped semiconductor, the electroneutrality condition looks differently from Eq. (56), because the total density of positive charges in a unit volume is not p , but rather $(p + n_+)$, where n_+ is the density of positively-ionized (“activated”) donor atoms, so that the electroneutrality condition becomes

$$n = p + n_+. \quad (6.62)$$

If virtually all dopants are activated, as it is in most practical cases,⁴⁰ then we may take $n_+ = n_D$, where n_D is the total concentration of donor atoms, i.e. their number per unit volume, and Eq. (62) becomes

$$n = p + n_D. \quad (6.63)$$

Plugging in the expression $p = n_i^2/n$, following from Eq. (61), we get a simple quadratic equation for n , with the following physically acceptable (positive) solution:

³⁸ Note that in comparison with Fig. 6, here the (for most purposes, redundant) information on the q -dependence of the energies is collapsed, leaving the horizontal axis of such a *band-edge diagram* free for showing their possible spatial dependences – see Figs. 8, 10, and 11 below.

³⁹ Very similar relations may be met in the theory of chemical reactions (where it is called the *law of mass action*), and other disciplines – including such exotic examples as the theoretical ecology.

⁴⁰ Let me leave it for the reader’s exercise to prove that this assumption is always valid unless the doping density n_D becomes comparable to n_C , and as a result, the Fermi energy μ moves into a $\sim T$ -wide vicinity of ε_D .

$$n = \frac{n_D}{2} + \left(\frac{n_D^2}{4} + n_i^2 \right)^{1/2}. \quad (6.64)$$

This result shows that the doping affects n (and hence $\mu = \varepsilon_C - T \ln(n_C/n)$ and $p = n_i^2/n$) only if the dopant concentration n_D is comparable with, or higher than the intrinsic carrier density n_i given by Eq. (60). For most applications, n_D is made *much* higher than n_i ; in this case Eq. (64) yields

$$n \approx n_D \gg n_i, \quad p = \frac{n_i^2}{n} \approx \frac{n_i^2}{n_D} \ll n, \quad \mu \approx \mu_p \equiv \varepsilon_C - T \ln \frac{n_C}{n_D}. \quad (6.65)$$

Because of the reasons to be discussed very soon, modern electron devices require doping densities above 10^{18} cm^{-3} , so that the logarithm in Eq. (65) is not much larger than 1. This means that the Fermi level rises from the midgap to a position only slightly below the conduction band edge ε_C – see Fig. 7a.

The opposite case of purely *p*-doping, with n_A acceptor atoms per unit volume, and a small activation (negative ionization) energy $\varepsilon_A - \varepsilon_V \ll \Delta$,⁴¹ may be considered absolutely similarly, using the electroneutrality condition in the form

$$n + n_- = p, \quad (6.66)$$

where n_- is the number of activated (and hence negatively charged) acceptors. For the relatively high concentration ($n_i \ll n_A \ll n_V$), virtually all acceptors are activated, so that $n_- \approx n_A$, Eq. (66) may be approximated as $n + n_A = p$, and the analysis gives the results dual to Eq. (65):

$$p \approx n_A \gg n_i, \quad n = \frac{n_i^2}{p} \approx \frac{n_i^2}{n_A} \ll p, \quad \mu \approx \mu_n \equiv \varepsilon_V + T \ln \frac{n_V}{n_A}, \quad (6.67)$$

so that in this case, the Fermi level is just slightly above the valence band edge (Fig. 7b), and the number of holes far exceeds that of electrons – again, in the narrow sense of the word. Let me leave the analysis of the simultaneous *n*- and *p*-doping (which enables, in particular, so-called *compensated semiconductors* with the sign-variable difference $n - p \approx n_D - n_A$) for the reader's exercise.

Now let us consider how a sample of a doped semiconductor (say, a *p*-doped one) responds to a static external electrostatic field \mathcal{E} applied normally to its surface.⁴² (In semiconductor integrated circuits, such field is usually created by the voltage applied to a special highly-conducting *gate electrode* separated from the semiconductor surface by a thin insulating layer.) Assuming that the field penetrates into the sample by a distance λ much larger than the crystal lattice period a (the assumption to be verified *a posteriori*), we may calculate the distribution of the electrostatic potential ϕ using the macroscopic version of the Poisson equation.⁴³ Assuming that the semiconductor occupies the semi-space $x > 0$ and that $\mathcal{E} = \mathbf{n}_x \mathcal{E}$, the equation reduces to the following 1D form⁴⁴

⁴¹ For the typical donors (P) and acceptors (B) in silicon, both ionization energies, $(\varepsilon_C - \varepsilon_D)$ and $(\varepsilon_A - \varepsilon_V)$, are close to 45 meV, i.e. are indeed much smaller than $\Delta \approx 1.14 \text{ eV}$.

⁴² A simplified version of this analysis was discussed in EM Sec. 2.1.

⁴³ See, e.g., EM Sec. 3.4.

⁴⁴ I am sorry for using, for the SI electric constant ε_0 , the same Greek letter as for single-particle energies, but both notations are traditional, and the difference between these uses will be clear from the context.

$$\frac{d^2\phi}{dx^2} = -\frac{\rho(x)}{\kappa\epsilon_0}. \quad (6.68)$$

Here κ is the dielectric constant of the semiconductor matrix – excluding the dopants and charge carriers, which in this approach are treated as explicit (“stand-alone”) charges, with the volumic density

$$\rho = e(p - n_- - n). \quad (6.69)$$

(As a sanity check, Eqs. (68)-(69) show that if $\mathcal{E} \equiv -d\phi/dx = 0$, then $\rho = 0$, bringing us back to the electroneutrality condition (66), and hence the “flat” band-edge diagrams shown in Figs. 7b and 8a.)

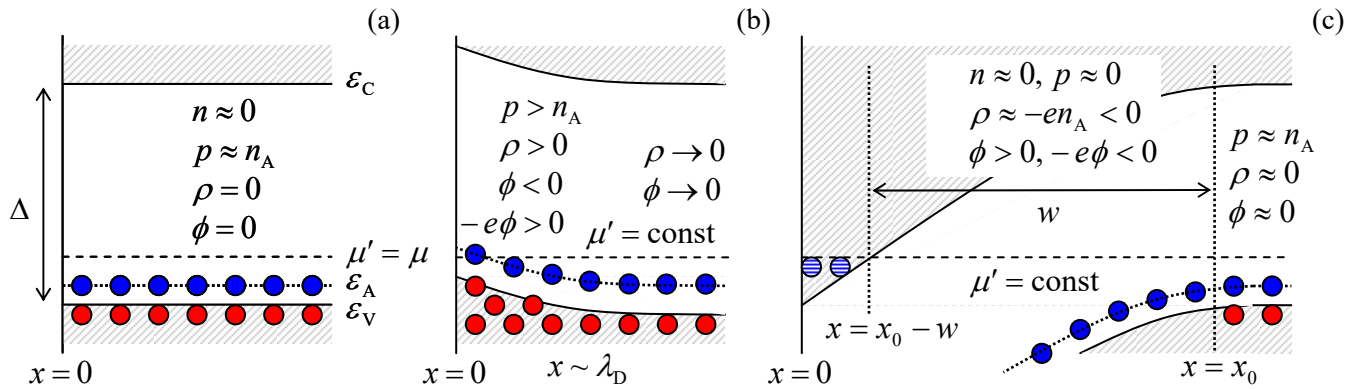


Fig. 6.8. The band-edge diagrams of the electric field penetration into a uniform p -doped semiconductor: (a) $\mathcal{E} = 0$, (b) $\mathcal{E} < 0$, and (c) $\mathcal{E} > \mathcal{E}_c > 0$. Solid red points depict positive charges; solid blue points, negative charges; and hatched blue points, possible electrons in the inversion layer – all very schematically.

In order to get a closed system of equations for the case $\mathcal{E} \neq 0$, we should take into account that the electrostatic potential $\phi \neq 0$, penetrating into the sample with the field,⁴⁵ adds the potential component $q\phi(x) = -e\phi(x)$ to the energy of each electron, and hence shifts the whole local system of single-electron energy levels “vertically” by this amount – down for $\phi > 0$, and up for $\phi < 0$. As a result, the field penetration leads to what is called *band bending* – see the band-edge diagrams schematically shown in Figs. 8b,c for two possible polarities of the applied field, which affects the distribution $\phi(x)$ via the boundary condition⁴⁶

$$\frac{d\phi}{dx}(0) = -\mathcal{E}. \quad (6.70)$$

Note that the electrochemical potential μ' (which, in accordance with the discussion in Sec. 3, replaces the chemical potential in presence of the electric field),⁴⁷ has to stay constant through the system in equilibrium, keeping the electric current equal to zero – see Eq. (41). For arbitrary doping parameters, the system of equations (58) (with the replacements $\epsilon_V \rightarrow \epsilon_V - e\phi$, and $\mu \rightarrow \mu'$) and (68)-(70), plus the

⁴⁵ It is common (though not necessary) to select the energy reference so that deep inside the semiconductor, $\phi = 0$; in what follows I will use this convention.

⁴⁶ Here \mathcal{E} is the field *just inside* the semiconductor. The free-space field necessary to create it is κ times larger – see, e.g., the same EM Sec. 3.4, in particular Eq. (3.56).

⁴⁷ In semiconductor physics literature, the value of μ' is usually called the *Fermi level*, even in the absence of the degenerate Fermi sea typical for metals – cf. Sec. 3.3. In this section, I will follow this common terminology.

relation between n_- and n_A (describing the acceptor activation), does not allow an analytical solution. However, as was discussed above, in the most practical cases $n_A \gg n_i$, we may use the approximate relations $n_- \approx n_A$ and $n \approx 0$ at virtually any values of μ' within the locally shifted bandgap [$\varepsilon_V - e\phi(x)$, $\varepsilon_C - e\phi(x)$], so that the substitution of these relations, and the second of Eqs. (58), with the mentioned replacements, into Eq. (69) yields

$$\rho \approx en_V \exp\left\{\frac{\varepsilon_V - e\phi - \mu'}{T}\right\} - en_A = en_A \left[\left(\frac{n_V}{n_A} \exp\left\{\frac{\varepsilon_V - \mu'}{T}\right\} \right) \exp\left\{-\frac{e\phi}{T}\right\} - 1 \right]. \quad (6.71)$$

The x -independent electrochemical potential (a.k.a. Fermi level) μ' in this relation should be equal to the value of the chemical potential $\mu(x \rightarrow \infty)$ in the semiconductor's bulk, given by the last of Eqs. (67), which turns the expression in the parentheses into 1. With these substitutions, Eq. (68) becomes

$$\frac{d^2\phi}{dx^2} = -\frac{en_A}{\kappa\varepsilon_0} \left[\exp\left\{-\frac{e\phi}{T}\right\} - 1 \right], \quad \text{for } \varepsilon_V - e\phi(x) < \mu' < \varepsilon_C - e\phi(x). \quad (6.72)$$

This nonlinear differential equation may be solved analytically, but in order to avoid a distraction by this (rather bulky) solution, let me first consider the case when the electrostatic potential is sufficiently small – either because the external field is small, or because we focus on the distances sufficiently far from the surface – see Fig. 8 again. In this case, in the Taylor expansion of the exponent in Eq. (72), with respect to small ϕ , we may keep only two leading terms, turning it into a linear equation:

$$\frac{d^2\phi}{dx^2} = \frac{e^2 n_A}{\kappa\varepsilon_0 T} \phi, \quad \text{i.e. } \frac{d^2\phi}{dx^2} = \frac{\phi}{\lambda_D^2}, \quad \text{where } \lambda_D \equiv \left(\frac{\kappa\varepsilon_0 T}{e^2 n_A} \right)^{1/2}, \quad (6.73)$$

with the well-known exponential solution, satisfying also the boundary condition $\phi \rightarrow 0$ at $x \rightarrow \infty$:

$$\phi = C \exp\left\{-\frac{x}{\lambda_D}\right\}, \quad \text{at } e|\phi| \ll T. \quad (6.74)$$

The constant λ_D given by the last of Eqs. (73) is called the *Debye screening length*. It may be rather substantial; for example, at $T_K = 300K$, even for the relatively high doping, $n_A \approx 10^{18} \text{ cm}^{-3}$ typical for modern silicon ($\kappa \approx 12$) integrated circuits, it is close to 4 nm – still much larger than the crystal lattice constant $a \sim 0.3$ nm, so that the above analysis is indeed quantitatively valid. Note also that λ_D does not depend on the charge's sign; hence it should be no large surprise that repeating our analysis for an n -doped semiconductor, we may find out that Eqs. (73)-(74) are valid for that case as well, with the only replacement $n_A \rightarrow n_D$.

If the applied field \mathcal{E} is weak, Eq. (74) is valid in the whole sample, and the constant C in it may be readily calculated using the boundary condition (70), giving

$$\phi|_{x=0} \equiv C = \lambda_D \mathcal{E} \equiv \left(\frac{\kappa\varepsilon_0 T}{e^2 n_A} \right)^{1/2} \mathcal{E}. \quad (6.75)$$

This formula allows us to express the condition of validity of the linear approximation leading to Eq. (74), $e|\phi| \ll T$, in terms of the applied field:

$$|\mathcal{E}| \ll \mathcal{E}_{\max}, \quad \text{with } \mathcal{E}_{\max} \equiv \frac{T}{e\lambda_D} \equiv \left(\frac{Tn_A}{\kappa\epsilon_0} \right)^{1/2}; \quad (6.76)$$

in the above example, $\mathcal{E}_{\max} \sim 60 \text{ kV/cm}$. On the lab scale, such field is not low at all (it is twice higher than the threshold of electric breakdown in the air at ambient conditions), but may be sustained by many solid-state materials that are much less prone to the breakdown.⁴⁸ This is why we should be interested in what happens if the applied field is higher than this value.

The semi-quantitative answer is relatively simple if the field is directed out of the *p*-doped semiconductor (in our nomenclature, $\mathcal{E} < 0$ – see Fig. 8b). As the valence band bends up by a few T , the local hole concentration $p(x)$, and hence the charge density $\rho(x)$, grow exponentially – see Eq. (71). Hence the effective local length of the nonlinear field's penetration, $\lambda_{\text{ef}}(x) \propto \rho^{-1/2}(x)$, shrinks exponentially. A detailed analysis of this effect using Eq. (72) does not make much sense, because as soon as $\lambda_{\text{ef}}(0)$ decreases to $\sim a$, the macroscopic Poisson equation (68) is no longer valid quantitatively. For typical semiconductors, this happens at the field that raises the edge $\epsilon_V - e\phi(0)$ of the bent valence band at the sample's surface above the Fermi level μ' . In this case, the valence-band electrons near the surface form a degenerate Fermi gas, with an “open” Fermi surface – essentially a metal, which a very small (atomic-size) *Thomas-Fermi screening length*:⁴⁹

$$\lambda_{\text{ef}}(0) \sim \lambda_{\text{TF}} \equiv \left[\frac{\kappa\epsilon_0}{e^2 g_3(\epsilon_F)} \right]^{1/2}. \quad (6.77)$$

The effects taking place at the opposite polarity of the field, $\mathcal{E} > 0$, are much more interesting – and more useful for applications. Indeed, in this case, the band bending down leads to an exponential decrease of $\rho(x)$ as soon as the valence band edge $\epsilon_V - e\phi(x)$ drops down by just a few T below its unperturbed value ϵ_V . If the applied field is large enough, $\mathcal{E} > \mathcal{E}_{\max}$ (as it is in the situation shown in Fig. 8c), it forms, on the left of such point x_0 the so-called *depletion layer*, of a certain width w . Within this layer, not only the electron density n , but the hole density p as well, are negligible, so that the only substantial contribution to the charge density ρ is given by the fully ionized acceptors: $\rho \approx -en_- \approx -en_A$, and Eq. (72) becomes very simple:

$$\frac{d^2\phi}{dx^2} = \frac{en_A}{\kappa\epsilon_0} = \text{const}, \quad \text{for } x_0 - w < x < x_0. \quad (6.78)$$

Let us use this equation to calculate the largest possible width w of the depletion layer, and the critical value, \mathcal{E}_c , of the applied field necessary for this. (By definition, at $\mathcal{E} = \mathcal{E}_c$, the left boundary of the layer, where $\epsilon_V - e\phi(x) = \epsilon_c$, i.e. $e\phi(x) = \epsilon_V - \epsilon_A \equiv \Delta$, just touches the semiconductor surface: $x_0 - w = 0$, i.e. $x_0 = w$. (Figure 8c shows the case when \mathcal{E} is slightly larger than \mathcal{E}_c .) For this, Eq. (78) has to be solved with the following boundary conditions:

$$\phi(0) = \frac{\Delta}{e}, \quad \frac{d\phi}{dx}(0) = -\mathcal{E}_c, \quad \phi(w) = 0, \quad \frac{d\phi}{dx}(w) = 0. \quad (6.79)$$

⁴⁸ Even some amorphous thin-film insulators, such as properly grown silicon and aluminum oxides, can withstand fields up to $\sim 10 \text{ MV/cm}$.

⁴⁹ As a reminder, the derivation of this formula was the task of Problem 3.14.

Note that the first of these conditions is strictly valid only if $T \ll \Delta$, i.e. at the assumption we have made from the very beginning, while the last two conditions are asymptotically correct only if $\lambda_D \ll w$ – the assumption we should not forget to check after the solution.

After all the undergraduate experience with projectile motion problems, the reader certainly knows by heart that the solution of Eq. (78) is a quadratic parabola, so that let me immediately write its final form satisfying the boundary conditions (79):

$$\phi(x) = \frac{en_A}{\kappa\varepsilon_0} \frac{(w-x)^2}{2}, \quad \text{with } w = \left(\frac{2\kappa\varepsilon_0\Delta}{e^2 n_A} \right)^{1/2}, \quad \text{at } \mathcal{E}_c = \frac{2\Delta}{e\varepsilon_0 w}. \quad (6.80)$$

Comparing the result for w with Eq. (73), we see that if our basic condition $T \ll \Delta$ is fulfilled, then $\lambda_D \ll w$, confirming the qualitative validity of the whole solution (80). For the same particular parameters as in the example before ($n_A \approx 10^{18} \text{ cm}^{-3}$, $\kappa \approx 10$), and $\Delta \approx 1 \text{ eV}$, Eqs. (80) give $w \approx 40 \text{ nm}$ and $\mathcal{E}_c \approx 600 \text{ kV/cm}$ – still a practicable field. (As Fig. 8c shows, to create it, we need a gate voltage only slightly larger than Δ/e , i.e. close to 1 V for typical semiconductors.)

Figure 8c also shows that if the applied field exceeds this critical value, near the surface of the semiconductor the conduction band edge drops below the Fermi level. This is the so-called *inversion layer*, in which electrons with energies below μ' form a highly conductive degenerate Fermi gas. However, typical rates of electron tunneling from the bulk through the depletion layer are very low, so that after the inversion layer has been created (say, by the gate voltage application), it may be only populated from another source – hence the hatched blue points in Fig. 8c. This is exactly the fact used in the workhorse device of semiconductor integrated circuits – the *field-effect transistor* (FET) – see Fig. 9.⁵⁰

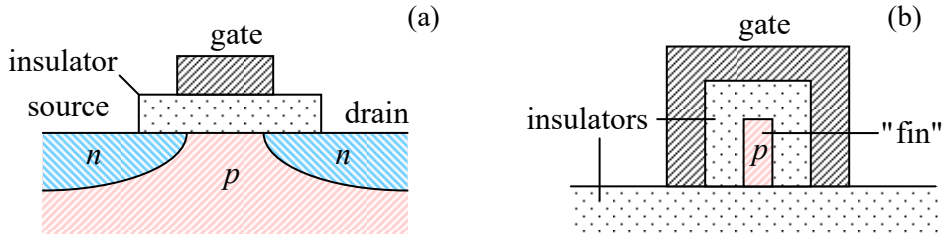


Fig. 6.9. Two main species of the *n*-FET: (a) the *bulk FET*, and (b) the *FinFET*. While on panel (a), the current flow from the source to the drain is parallel to the plane of the drawing, on panel (b) it is normal to the plane, with the *n*-doped source and drain contacting the thin “fin” from two sides off this plane.

In the “bulk” variety of this structure (Fig. 9a), a gate electrode overlaps a gap between two similar highly-*n*-doped regions near the surface, called *source* and *drain*, formed by *n*-doping inside a *p*-doped semiconductor. It is more or less obvious (and will be shown in a moment) that in the absence of gate voltage, the electrons cannot pass through the *p*-doped region, so that virtually no current flows between the source and the drain, even if a modest voltage is applied between these electrodes. However, if the gate voltage is positive and large enough to induce the electric field $\mathcal{E} > \mathcal{E}_c$ at the surface of the *p*-doped semiconductor, it creates the inversion layer as shown in Fig. 8c, and the electron current

⁵⁰ This device was invented (by Julius E. Lilienfeld) in 1930, but demonstrated only in the mid-1950s.

between the source and drain electrodes may readily flow through this *surface channel*. (Very unfortunately, in this course I would not have time/space for a detailed analysis of transport properties of this keystone electron device, and have to refer the reader to special literature.⁵¹⁾

Fig. 9a makes it obvious that another major (and virtually unavoidable) structure of semiconductor integrated circuits is the famous *p-n junction* – an interface between *p*- and *n*-doped regions. Let us analyze its simple model, in which the interface is in the plane $x = 0$, and the doping profiles $n_D(x)$ and $n_A(x)$ are step-like, making an abrupt jump at the interface:

$$n_A(x) = \begin{cases} n_A = \text{const}, & \text{at } x < 0, \\ 0, & \text{at } x > 0, \end{cases} \quad n_D(x) = \begin{cases} 0, & \text{at } x < 0, \\ n_D = \text{const}, & \text{at } x > 0. \end{cases} \quad (6.81)$$

(This model is very reasonable for modern integrated circuits, where the doping is performed by *implantation*, using high-energy ion beams.)

To start with, let us assume that no voltage is applied between the *p*- and *n*-regions, so that the system may be in thermodynamic equilibrium. In the equilibrium, the Fermi level μ' should be flat through the structure, and at $x \rightarrow -\infty$ and $x \rightarrow +\infty$, where $\phi \rightarrow 0$, the level structure has to approach the positions shown, respectively, on panels (a) and (b) of Fig. 7. In addition, the distribution of the electric potential $\phi(x)$, shifting the level structure vertically by $-e\phi(x)$, has to be continuous to avoid unphysical infinite electric fields. With that, we inevitably arrive at the band-edge diagram that is (schematically) shown in Fig. 10.

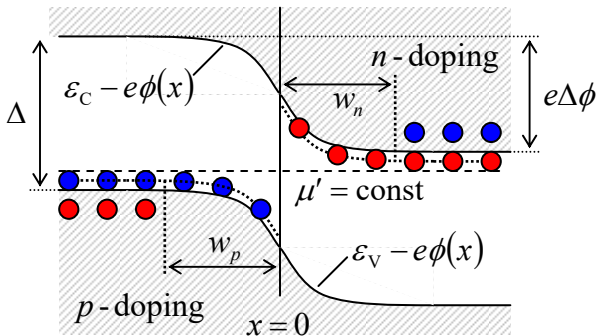


Fig. 6.10. The band-edge diagram of a *p-n* junction in thermodynamic equilibrium ($T = \text{const}$, $\mu' = \text{const}$). The notation is the same as in Figs. 7 and 8.

The diagram shows that the contact of differently doped semiconductors gives rise to a built-in electric potential difference $\Delta\phi$, equal to the difference of their values of μ in the absence of the contact – see Eqs. (65) and (67):

$$e\Delta\phi \equiv e\phi(+\infty) - e\phi(-\infty) = \mu_n - \mu_p = \Delta - T \ln \frac{n_C n_V}{n_D n_A}, \quad (6.82)$$

which is usually just slightly smaller than the bandgap.⁵² (Qualitatively, this is the same contact potential difference that was discussed, for the case of metals, in Sec. 3 – see Fig. 5.) The arising

⁵¹ The classical monograph in this field is S. Sze, *Physics of Semiconductor Devices*, 2nd ed., Wiley 1981. (The 3rd edition, circa 2006, co-authored with K. Ng, is more tilted toward technical details.) I can also recommend a detailed textbook by R. Pierret, *Semiconductor Device Fundamentals*, 2nd ed., Addison Wesley, 1996.

internal electrostatic field $\mathcal{E} = -d\phi/dx$ induces, in both semiconductors, depletion layers similar to that induced by an external field (Fig. 8c). Their widths w_p and w_n may also be calculated similarly, by solving the following boundary problem of electrostatics, mostly similar to that given by Eqs. (78)-(79):

$$\frac{d^2\phi}{dx^2} = \frac{e}{\kappa\epsilon_0} \times \begin{cases} n_A, & \text{for } -w_p < x < 0, \\ (-n_D), & \text{for } 0 < x < +w_n, \end{cases} \quad (6.83)$$

$$\phi(w_n) = \phi(-w_p) + \Delta\phi, \quad \frac{d\phi}{dx}(w_n) = \frac{d\phi}{dx}(-w_p) = 0, \quad \phi(-0) = \phi(+0), \quad \frac{d\phi}{dx}(-0) = \frac{d\phi}{dx}(+0), \quad (6.84)$$

also exact only in the limit $T \ll \Delta$, $n_i \ll n_D, n_A$. Its (easy) solution gives the result similar to Eq. (80):

$$\phi = \text{const} + \begin{cases} en_A(w_p + x)^2 / 2\kappa\epsilon_0, & \text{for } -w_p < x < 0, \\ \Delta\phi - en_D(w_n - x)^2 / 2\kappa\epsilon_0, & \text{for } 0 < x < +w_n, \end{cases} \quad (6.85)$$

with expressions for w_p and w_n giving the following formula for the full depletion layer width:

$$w \equiv w_p + w_n = \left(\frac{2\kappa\epsilon_0 \Delta\phi}{en_{\text{ef}}} \right)^{1/2}, \quad \text{with } n_{\text{ef}} \equiv \frac{n_A n_D}{n_A + n_D}, \quad \text{i.e. } \frac{1}{n_{\text{ef}}} = \frac{1}{n_A} + \frac{1}{n_D}. \quad (6.86)$$

This expression is similar to that given by Eq. (80), so that for typical highly doped semiconductors ($n_{\text{ef}} \sim 10^{18} \text{ cm}^{-3}$) it gives for w a similar estimate of a few tens nm.⁵³ Returning to Fig. 9a, we see that this scale imposes an essential limit on the reduction of bulk FETs (whose scaling down is at the heart of the well-known *Moore's law*),⁵⁴ explaining why such high doping is necessary. In the early 2010s, the problems with implementing even higher doping, plus issues with dissipated power management, have motivated the transition of advanced silicon integrated circuit technology from the bulk FETs to the *FinFET* (also called “double-gate”, or “tri-gate”, or “wrap-around-gate”) variety of these devices, schematically shown in Fig. 9b, despite their essentially 3D structure and hence a more complex fabrication technology. In the FinFETs, the role of *p-n* junctions is reduced, but these structures remain an important feature of semiconductor integrated circuits.

Now let us have a look at the *p-n* junction in equilibrium from the point of view of Eq. (52). In the simple model we are considering now (in particular, at $T \ll \Delta$), this equation is applicable separately to the electron and hole subsystems, because in this model the gases of these charge carriers are classical in all parts of the system, and the *generation-recombination* processes⁵⁵ coupling these subsystems have relatively small rates – see below. Hence, for the electron subsystem, we may rewrite Eq. (52) as

⁵² Frequently, Eq. (82) is also rewritten in the form $e\Delta\phi = T \ln(n_D n_A / n_i^2)$. In the view of the second of Eqs. (60), this equality is formally correct but may be misleading because the intrinsic carrier density n_i is an exponential function of temperature and is physically irrelevant for this particular problem.

⁵³ Note that such w is again much larger than λ_D – the fact that justifies the first two boundary conditions (84).

⁵⁴ Another important limit is quantum-mechanical tunneling through the gate insulator, whose thickness has to be scaled down in parallel with lateral dimensions of a FET, including its channel length.

⁵⁵ In the semiconductor physics lingo, the “carrier generation” event is the thermal excitation of an electron from the valence band to the conduction band, leaving a hole behind, while the reciprocal event of filling such a hole by a conduction-band electron is called the “carrier recombination”.

$$j_n = n\mu_m q\mathcal{E} - D_n \frac{\partial n}{\partial x}, \quad (6.87)$$

where $q = -e$. Let us discuss how each term of the right-hand of this equality depends on the system's parameters. Because of the n -doping at $x > 0$, there are many more electrons in this part of the system. According to the Boltzmann distribution (58), some number of them,

$$n_s \propto \exp\left\{-\frac{e\Delta\phi}{T}\right\}, \quad (6.88)$$

have energies above the conduction band edge in the p -doped part (see Fig. 11a) and try to diffuse into this part through the depletion layer; this diffusion flow of electrons from the n -side to the p -side of the structure (in Fig. 11, from the right to the left) is described by the second term on the right-hand side of Eq. (87). On the other hand, the intrinsic electric field $\mathcal{E} = -\partial\phi/\partial x$ inside the depletion layer, directed as Fig. 11a shows, exerting on the electrons the force $\mathcal{F} = q\mathcal{E} \equiv -e\mathcal{E}$ pushing them in the opposite direction (from p to n), is described by the first, "drift" term on the right-hand side of Eq. (87).⁵⁶

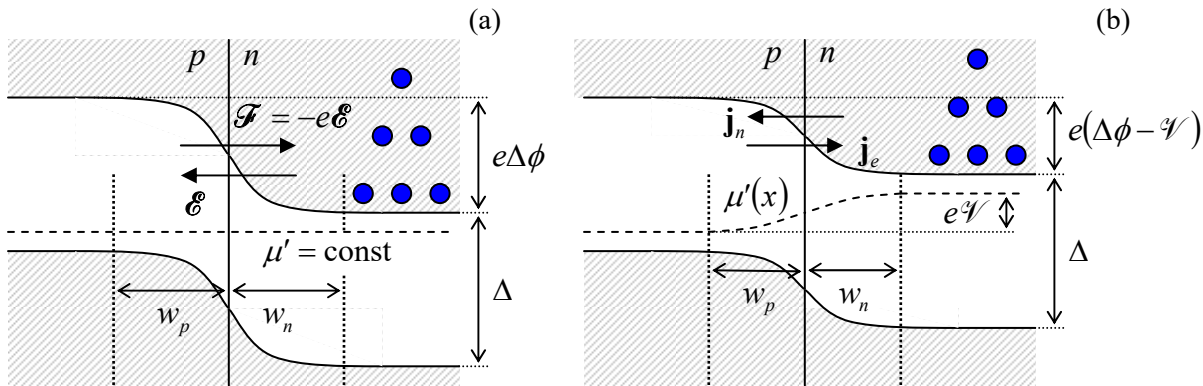


Fig. 6.11. Electrons in the conduction band of a p - n junction at: (a) $V=0$, and (b) $V>0$.

For clarity, other charges (of the holes and all ionized dopant atoms) are not shown.

The explicit calculation of these two flows⁵⁷ shows, unsurprisingly, that in the equilibrium, they are exactly equal and opposite, so that $j_n = 0$, and such analysis does not give us any new information. However, the picture of two electron counter-flows, given by Eq. (87), enables us to predict the functional dependence of j_n on a modest external voltage V , with $|V| < \Delta\phi$, applied to the junction. Indeed, since the doped semiconductor regions outside the depletion layer are much more conductive

⁵⁶ Note that if an external photon with energy $\hbar\omega > \Delta$ generates an electron-hole pair somewhere inside the depletion layer, this electric field immediately drives its electron component to the right, and the hole component to the left, thus generating a pulse of electric current through the junction. This is the physical basis of the whole vast technological field of *photovoltaics*, currently strongly driven by the demand for renewable electric power. Due to the progress of this technology, the cost of solar power systems has dropped from ~\$300 per watt in the mid-1950s to the current ~\$1 per watt, and its global generation has increased to almost 10^{15} watt-hours per year – though this is still below 2% of the whole generated electric power.

⁵⁷ I will not try to reproduce this calculation (which may be found in any of the semiconductor physics books mentioned above), because getting all its scaling factors right requires using some model of the recombination process, and in this course, there is just no time for their quantitative discussion. However, see Eq. (93) below.

than it, virtually all applied voltage (i.e. the difference of values of the electrochemical potential μ') drops across this layer, changing the total band edge shift – see Fig. 11b:⁵⁸

$$e\Delta\phi \rightarrow e\Delta\phi + \Delta\mu' \equiv e\Delta\phi + q\mathcal{V} \equiv e(\Delta\phi - \mathcal{V}). \quad (6.89)$$

This change results in an exponential change of the number of electrons able to diffuse into the *p*-side of the junction – cf. Eq. (88):

$$n_>(\mathcal{V}) \approx n_>(0) \exp\left\{\frac{e\mathcal{V}}{T}\right\}, \quad (6.90)$$

and hence in a proportional change of the diffusion flow j_n of electrons from the *n*-side to the *p*-side of the system, i.e. of the oppositely directed density of the electron current $j_e = -ej_n$ – see Fig. 11b.

On the other hand, the drift counter-flow of electrons is not altered too much by the applied voltage: though it does change the electrostatic field $\mathcal{E} = -\nabla\phi$ inside the depletion layer, and also the depletion layer width,⁵⁹ these changes are incremental, not exponential. As the result, the net density of the current carried by electrons may be approximately expressed as

$$j_e(\mathcal{V}) = j_{\text{diffusion}} - j_{\text{drift}} \approx j_e(0) \exp\left\{\frac{e\mathcal{V}}{T}\right\} - \text{const.} \quad (6.91a)$$

As was discussed above, at $\mathcal{V}=0$, the net current has to vanish, so that the constant in Eq. (91a) has to equal $j_e(0)$, and we may rewrite this equality as

$$j_e(\mathcal{V}) = j_e(0) \left(\exp\left\{\frac{e\mathcal{V}}{T}\right\} - 1 \right). \quad (6.91b)$$

Now repeating this analysis for the current j_h of the holes (the exercise highly recommended to the reader), we get a similar expression, with the *same* sign before $e\mathcal{V}$,⁶⁰ though with a different scaling factor, $j_h(0)$ instead of $j_e(0)$. As a result, the total electric current density obeys the famous *Shockley law*

$$j(\mathcal{V}) \equiv j_e(\mathcal{V}) + j_h(\mathcal{V}) = j(0) \left(\exp\left\{\frac{e\mathcal{V}}{T}\right\} - 1 \right), \quad \text{with } j(0) \equiv j_e(0) + j_h(0), \quad (6.92)$$

describing the main *p-n* junction's property as an *electric diode* – a two-terminal device passing the current more “readily” in one direction (from the *p*- to the *n*-terminal) than in the opposite one.⁶¹

⁵⁸ In our model, the positive sign of $\mathcal{V} \equiv \Delta\mu'/q \equiv -\Delta\mu'/e$ corresponds to the additional electric field, $-\nabla\mu'/q \equiv \nabla\mu'/e$, directed in the positive direction of the *x*-axis (in Fig. 11, from the left to the right), i.e. to the positive terminal of the voltage source connected to the *p*-doped semiconductor – which is the common convention.

⁵⁹ This change, schematically shown in Fig. 11b, may be readily calculated by making the replacement (89) in the first of Eqs. (86).

⁶⁰ This sign invariance may look strange, due to the opposite (positive) electric charge of the holes. However, this difference in the charge sign is compensated by the opposite direction of the hole diffusion – see Fig. 10. (Note also that the actual charge carriers in the valence band are still electrons, and the positive charge of holes is just a convenient representation of the specific dispersion law in this energy band, with a negative effective mass – see Fig. 6, the second line of Eq. (53), and a more detailed discussion of this issue in QM Sec. 2.8.)

Besides numerous practical applications in electrical and electronic engineering, such diodes have very interesting statistical properties, in particular performing very non-trivial transformations of the spectra of deterministic and random signals. Very unfortunately, I would not have time for their discussion and have to refer the interested reader to the special literature.⁶²

Still, before proceeding to our next (and last!) topic, let me give for the reader reference, without proof, the expression for the scaling factor $j(0)$ in Eq. (92), which follows from a simple, but broadly used model of the recombination process:

$$j(0) = en_i^2 \left(\frac{D_e}{l_e n_A} + \frac{D_h}{l_h n_D} \right). \quad (6.93)$$

Here l_e and l_h are the characteristic lengths of diffusion of electrons and holes before their recombination, which may be expressed by Eq. (5.113), $l_e = (2D_e\tau_e)^{1/2}$ and $l_h = (2D_h\tau_h)^{1/2}$, with τ_e and τ_h being the characteristic times of recombination of the so-called *minority carriers* – of electrons in the *p*-doped part, and of holes in the *n*-doped part of the structure. Since the recombination is an inelastic process, its times are typically rather long – of the order of 10^{-7} s, i.e. much longer than the typical times of elastic scattering of the same carriers, that define their diffusion coefficients – see Eq. (51).

6.5. Heat transfer and thermoelectric effects

Now let us return to our analysis of kinetic effects using the Boltzmann-RTA equation, and extend it even further, to the effects of a non-zero (albeit small) temperature gradient. Again, since for any of the statistics (20), the average occupancy $\langle N(\varepsilon) \rangle$ is a function of just one combination of all its arguments, $\xi \equiv (\varepsilon - \mu)/T$, its partial derivatives obey not only Eq. (37), but also the following relation:

$$\frac{\partial \langle N(\varepsilon) \rangle}{\partial T} = -\frac{\varepsilon - \mu}{T^2} \frac{\partial \langle N(\varepsilon) \rangle}{\partial \xi} = \frac{\varepsilon - \mu}{T} \frac{\partial \langle N(\varepsilon) \rangle}{\partial \mu}. \quad (6.94)$$

As a result, Eq. (38) is generalized as

$$\nabla w_0 = -\frac{\partial w_0}{\partial \varepsilon} \left(\nabla \mu + \frac{\varepsilon - \mu}{T} \nabla T \right), \quad (6.95)$$

giving the following generalization of Eq. (39):

$$\tilde{w} = \tau \frac{\partial w_0}{\partial \varepsilon} \mathbf{v} \cdot \left(\nabla \mu' + \frac{\varepsilon - \mu}{T} \nabla T \right). \quad (6.96)$$

Now, calculating current density as in Sec. 3, we get the result that is traditionally represented as

$$\mathbf{j} = \sigma \left(-\frac{\nabla \mu'}{q} \right) + \sigma \mathcal{S}(-\nabla T), \quad (6.97)$$

⁶¹ Some metal-semiconductor junctions, called *Schottky diodes*, have similar rectifying properties (and may be better fitted for high-power applications than silicon *p-n* junctions), but their properties are more complex because of the rather involved chemistry and physics of interfaces between different materials.

⁶² See, e.g., the monograph by R. Strattonovich cited in Sec. 4.2.

where the constant \mathcal{S} , called the *Seebeck coefficient*⁶³ (or the “thermoelectric power”, or just “thermopower”) is given by the following relation:

Seebeck coefficient

$$\sigma \mathcal{S} = \frac{gq\tau}{(2\pi\hbar)^3} \frac{4\pi}{3} \int_0^{\infty} (8m\varepsilon^3)^{1/2} \frac{(\varepsilon - \mu)}{T} \left[-\frac{\partial \langle N(\varepsilon) \rangle}{\partial \varepsilon} \right] d\varepsilon. \quad (6.98)$$

Working out this integral for the most important case of a degenerate Fermi gas, with $T \ll \varepsilon_F$, we have to be careful because the center of the sharp peak of the last factor under the integral coincides with the zero point of the previous factor, $(\varepsilon - \mu)/T$. This uncertainty may be resolved using the Sommerfeld expansion formula (3.59). Indeed, for a smooth function $f(\varepsilon)$ obeying Eq. (3.60), so that $f(0) = 0$, we may use Eq. (3.61) to rewrite Eq. (3.59) as

$$\int_0^{\infty} f(\varepsilon) \left[-\frac{\partial \langle N(\varepsilon) \rangle}{\partial \varepsilon} \right] d\varepsilon = f(\mu) + \frac{\pi^2 T^2}{6} \frac{d^2 f(\varepsilon)}{d\varepsilon^2} \Big|_{\varepsilon=\mu}. \quad (6.99)$$

In particular, for working out the integral (98), we may take $f(\varepsilon) \equiv (8m\varepsilon^3)^{1/2}(\varepsilon - \mu)/T$. (For this function, the condition $f(0) = 0$ is evidently satisfied.) Then $f(\mu) = 0$, $d^2f/d\varepsilon^2|_{\varepsilon=\mu} = 3(8m\mu)^{1/2}/T \approx 3(8m\varepsilon_F)^{1/2}/T$, and Eq. (98) yields

$$\sigma \mathcal{S} = \frac{gq\tau}{(2\pi\hbar)^3} \frac{4\pi}{3} \frac{\pi^2 T^2}{6} \frac{3(8m\varepsilon_F)^{1/2}}{T}. \quad (6.100)$$

Comparing the result with Eqs. (3.54) and (32), for the constant \mathcal{S} we get a simple expression independent of τ :⁶⁴

$$\mathcal{S} = \frac{\pi^2}{2q} \frac{T}{\varepsilon_F} = \frac{c_V}{q}, \quad \text{for } T \ll \varepsilon_F, \quad (6.101)$$

where $c_V \equiv C_V/N$ is the heat capacity of the gas per unit particle, in this case given by Eq. (3.70).

In order to understand the physical meaning of the Seebeck coefficient, it is sufficient to consider a conductor carrying no current. For this case, Eq. (97) yields

Seebeck effect

$$\nabla(\mu'/q + \mathcal{S}T) = 0. \quad (6.102)$$

So, at these conditions, a temperature gradient creates a proportional gradient of the electrochemical potential μ' , and hence the effective electric field \mathcal{E} defined by Eq. (42). This is the *Seebeck effect*. Figure 12 shows the standard way of its measurement, using an ordinary (electrodynamic) voltmeter that measures the difference of μ'/e at its terminals, and a pair of junctions (in this context, called the *thermocouple*) of two materials with different coefficients \mathcal{S} .

⁶³ Named after Thomas Johann Seebeck who experimentally discovered, in 1822, the effect described by the second term in Eq. (97) – and hence by Eq. (103).

⁶⁴ Again, such independence hints that Eq. (101) has a broader validity than in our simple model of an isotropic gas. This is indeed the case: this result turns out to be valid for any form of the Fermi surface, and for any dispersion law $\alpha(\mathbf{p})$. Note, however, that all calculations of this section are valid for the simplest RTA model in that τ is an energy-independent parameter; for real metals, a more accurate description of experimental results may be obtained by tweaking this model to take this dependence into account – see, e.g., Chapter 13 in the monograph by N. Ashcroft and N. D. Mermin, cited in Sec. 3.5.

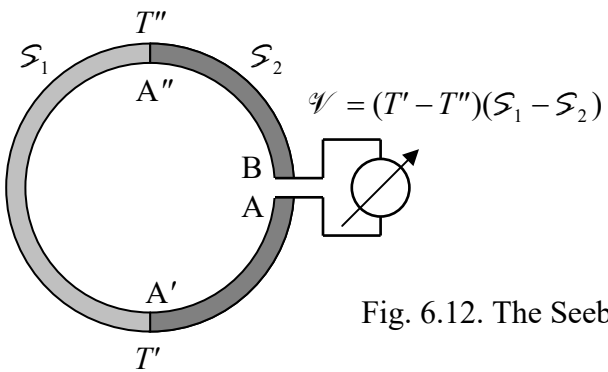


Fig. 6.12. The Seebeck effect in a thermocouple.

Integrating Eq. (102) around the loop from point A to point B , and neglecting the temperature drop across the voltmeter, we get the following simple expression for the thermally-induced difference of the electrochemical potential, usually called either the *thermoelectric power* or the “thermo e.m.f.”:

$$\begin{aligned} \mathcal{V} &\equiv \frac{\mu'_B - \mu'_A}{q} = \frac{1}{q} \int_A^B \nabla \mu' \cdot d\mathbf{r} = - \int_A^B \mathcal{S} \nabla T \cdot d\mathbf{r} = -\mathcal{S}_1 \int_{A'}^{A''} \nabla T \cdot d\mathbf{r} - \mathcal{S}_2 \left(\int_A^{A'} \nabla T \cdot d\mathbf{r} + \int_{A''}^B \nabla T \cdot d\mathbf{r} \right) \\ &= -\mathcal{S}_1(T'' - T') - \mathcal{S}_2(T' - T'') \equiv (\mathcal{S}_1 - \mathcal{S}_2)(T' - T''). \end{aligned} \quad (6.103)$$

(Note that according to Eq. (103), any attempt to measure such voltage across any two points of a *uniform* conductor would give results depending on the voltmeter wire materials, due to an unintentional gradient of temperature in them.)

Using thermocouples is a very popular, inexpensive method of temperature measurement – especially in the few-hundred-°C range where gas- and fluid-based thermometers are not too practicable, if a 1°C-scale accuracy is sufficient. The *temperature responsivity* ($\mathcal{S}_1 - \mathcal{S}_2$) of a typical popular thermocouple, chromel-constantan,⁶⁵ is about 70 $\mu\text{V}/^\circ\text{C}$. To understand why the typical values of \mathcal{S} are so small, let us discuss the Seebeck effect’s physics. Superficially, it is very simple: particles, heated by an external source, diffuse from it toward the colder parts of the conductor, carrying electrical current with them if they are electrically charged. However, this naïve argument neglects the fact that at $\mathbf{j} = 0$, there is no total flow of particles. For a more accurate interpretation, note that inside the integral (98), the Seebeck effect is described by the factor $(\varepsilon - \mu)/T$, which changes its sign at the Fermi surface, i.e. at the same energy where the term $[-\partial\langle N(\varepsilon)\rangle/\partial\varepsilon]$, describing the availability of quantum states for transport (due to their intermediate occupancy $0 < \langle N(\varepsilon)\rangle < 1$), reaches its peak. The only reason why that integral does not vanish completely, and hence $\mathcal{S} \neq 0$, is the growth of the first factor under the integral (which describes the density of available quantum states on the energy scale) with ε , so the hotter particles (with $\varepsilon > \mu$) are more numerous and hence carry more heat than the colder ones.

The Seebeck effect is not the only result of a temperature gradient; the same diffusion of particles also causes the less subtle effect of *heat flow* from the region of higher T to that with lower T , i.e. the effect of *thermal conductivity*, well known from our everyday practice. The density of this flow (i.e. that of thermal energy) may be calculated similarly to that of the electric current – see Eq. (26), with the natural replacement of the electric charge q of each particle with its thermal energy $(\varepsilon - \mu)$:

⁶⁵ Both these materials are *alloys*, i.e. solid solutions: chromel is 10% chromium in 90% nickel, while constantan is 45% nickel and 55% copper.

$$\mathbf{j}_h = \int (\varepsilon - \mu) \mathbf{v} w d^3 p. \quad (6.104)$$

(Indeed, we may look at this expression as at the difference between the total energy flow density, $\mathbf{j}_\varepsilon = [\varepsilon w d^3 p]$, and the product of the average energy needed to add a particle to the system (μ) by the particle flow density, $\mathbf{j}_n = \int w d^3 p \equiv \mathbf{j}/q$.)⁶⁶ Again, at equilibrium ($w = w_0$) the heat flow vanishes, so that w in Eq. (104) may be replaced with its perturbation \tilde{w} , which already has been calculated – see Eq. (96). The substitution of that expression into Eq. (104), and its transformation exactly similar to the one performed above for the electric current \mathbf{j} , yields

$$\mathbf{j}_h = \sigma \Pi \left(-\frac{\nabla \mu'}{q} \right) + \kappa (-\nabla T), \quad (6.105)$$

with the coefficients Π and κ given, in our approximation, by the following formulas:

Peltier coefficient

$$\sigma \Pi = \frac{g q \tau}{(2\pi\hbar)^3} \frac{4\pi}{3} \int_0^\infty (8m\varepsilon^3)^{1/2} (\varepsilon - \mu) \left[-\frac{\partial \langle N(\varepsilon) \rangle}{\partial \varepsilon} \right] d\varepsilon, \quad (6.106)$$

Thermal conductivity

$$\kappa = \frac{g \tau}{(2\pi\hbar)^3} \frac{4\pi}{3} \int_0^\infty (8m\varepsilon^3)^{1/2} \frac{(\varepsilon - \mu)^2}{T} \left[-\frac{\partial \langle N(\varepsilon) \rangle}{\partial \varepsilon} \right] d\varepsilon. \quad (6.107)$$

Besides the missing factor T in the denominator, the integral in Eq. (106) is the same as the one in Eq. (98), so that the constant Π (called the *Peltier coefficient*⁶⁷), is simply and fundamentally related to the Seebeck coefficient:

Π vs. S

$$\Pi = ST. \quad (6.108)$$

The simplicity of this relation (first discovered experimentally in 1854 by W. Thompson, a.k.a. Lord Kelvin) is not occasional. This is one of the so-called *Onsager reciprocal relations* between kinetic coefficients (suggested by L. Onsager in 1931), which are model-independent, i.e. valid within very general assumptions. Unfortunately, I have no time/space left for a discussion of this interesting topic (closely related to the fluctuation-dissipation theorem discussed in Sec. 5.5), and have to refer the interested reader to its detailed discussions available in the literature.⁶⁸

On the other hand, the integral in Eq. (107) is different, but may be readily calculated, for the most important case of a degenerate Fermi gas, using the Sommerfeld expansion in the form (99), with $f(\varepsilon) \equiv (8m\varepsilon^3)^{1/2}(\varepsilon - \mu)^2/T$, for which $f(\mu) = 0$ and $d^2f/d\varepsilon^2|_{\varepsilon=\mu} = 2(8m\mu^3)^{1/2}/T \approx 2(8m\varepsilon_F^3)^{1/2}/T$, so that

$$\kappa = \frac{g \tau}{(2\pi\hbar)^3} \frac{4\pi}{3} \frac{\pi^2}{6} T^2 \frac{2(8m\varepsilon_F^3)^{1/2}}{T} \equiv \frac{\pi^2}{3} \frac{n \tau T}{m}. \quad (6.109)$$

⁶⁶ An alternative explanation of the factor $(\varepsilon - \mu)$ in Eq. (104) is that according to Eqs. (1.37) and (1.56), for a uniform system of N particles this factor is just $(E - G)/N \equiv (TS - PV)/N$. The full differential of the numerator is $TdS + SdT - PdV - VdP$, so that in the absence of the mechanical work $dW = -PdV$, and changes of temperature and pressure, it is just $TdS \equiv dQ$ – see Eq. (1.19).

⁶⁷ Named after Jean Charles Athanase Peltier who experimentally discovered, in 1834, the effect expressed by the first term in Eq. (105) – and hence by Eq. (112).

⁶⁸ See, for example, Sec. 15.7 in R. Pathria and P. Beale, *Statistical Mechanics*, 3rd ed., Elsevier, 2011. Note, however, that the range of validity of the Onsager relations is still debated – see, e.g., K.-T. Chen and P. Lee, *Phys. Rev. B* **79**, 18 (2009).

Comparing the result with Eq. (32), we get the so-called *Wiedemann-Franz law*⁶⁹

$$\frac{\kappa}{\sigma} = \frac{\pi^2}{3} \frac{T}{q^2}. \quad (6.110)$$
Wiedemann-Franz law

This relation between the electric conductivity σ and the *thermal conductivity* κ is more general than our formal derivation might imply. Indeed, it may be shown that the Wiedemann-Franz law is also valid for an arbitrary anisotropy (i.e. an arbitrary Fermi surface shape) and, moreover, well beyond the relaxation-time approximation. (For example, it is also valid for the scattering integral (12) with an arbitrary angular dependence of rate Γ , provided that the scattering is elastic.) Experiments show that the law is well obeyed by most metals, but only at relatively low temperatures, when the thermal conductance due to electrons is well above the one due to lattice vibrations, i.e. phonons – see Sec. 2.6. Moreover, for a non-degenerate gas, Eq. (107) should be treated with the utmost care, in the context of the definition (105) of this coefficient κ . (Let me leave this issue for the reader's analysis.)

Now let us discuss the effects described by Eq. (105), starting from the less obvious, first term on its right-hand side. It describes the so-called *Peltier effect*, which may be measured in the loop geometry similar to that shown in Fig. 12, but now driven by an external voltage source – see Fig. 13.

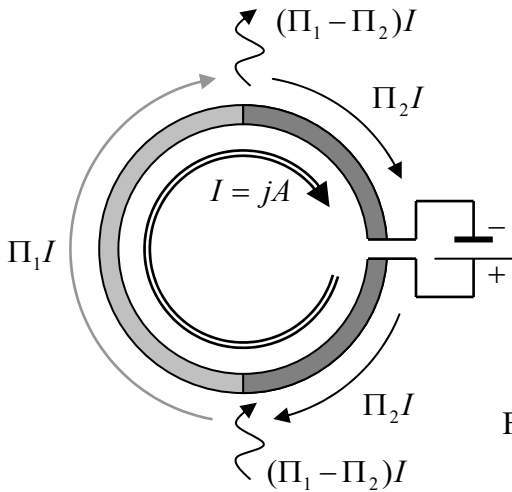


Fig. 6.13. The Peltier effect at $T = \text{const.}$

The voltage drives a certain dc current $I = jA$ (where A is the area of conductor's cross-section), necessarily the same in the whole loop. However, according to Eq. (105), if materials 1 and 2 are different, the power $\mathcal{P} = j_h A$ of the associated heat flow is different in two parts of the loop.⁷⁰ Indeed, if the whole system is kept at the same temperature ($\nabla T = 0$), the integration of that relation over the cross-sections of each part yields

⁶⁹ It was named after Gustav Wiedemann and Rudolph Franz who noticed the constancy of ratio κ/σ for various materials, at the same temperature, as early as 1853. The direct proportionality of the ratio to the absolute temperature was noticed by Ludwig Lorenz in 1872. Due to his contribution, the Wiedemann-Franz law is frequently represented, in the SI temperature units, as $\kappa/\sigma = LT_K$, where the constant $L \equiv (\pi^2/3)k_B/e^2$, called the *Lorenz number*, is close to $2.45 \times 10^{-8} \text{ W}\cdot\Omega\cdot\text{K}^{-2}$. Theoretically, Eq. (110) was derived in 1928 by A. Sommerfeld.

⁷⁰ Let me emphasize that here we are discussing the heat *transferred* through a conductor, not the Joule heat *generated* in it by the current. (The latter effect is quadratic, rather than linear, in current, and hence is much smaller at $I \rightarrow 0$.)

$$\mathcal{P}_{1,2} = \Pi_{1,2} A_{1,2} \sigma_{1,2} \left(-\frac{\nabla \mu'}{q} \right)_{1,2} = \Pi_{1,2} A_{1,2} j_{1,2} = \Pi_{1,2} I_{1,2} = \Pi_{1,2} I, \quad (6.111)$$

where, at the second step, Eq. (41) for the electric current density has been used. This equality means that to sustain a constant temperature, the following power difference,

Peltier effect

$$\Delta \mathcal{P} = (\Pi_1 - \Pi_2) I, \quad (6.112)$$

has to be extracted from one junction of the two materials (in Fig. 13, shown on the top), and inserted into the counterpart junction.

If a constant temperature is not maintained, the former junction is heated (in excess of the bulk, Joule heating), while the latter one is cooled, thus implementing a thermoelectric heat pump/refrigerator. Such *Peltier refrigerators*, which require neither moving parts nor fluids, are very convenient for modest (by a few tens °C) cooling of relatively small components of various systems – from sensitive radiation detectors on mobile platforms (including spacecraft), all the way to cold drinks in vending machines. It is straightforward to use the above formulas to show that the practical efficiency of active materials used in such thermoelectric refrigerators may be characterized by the following dimensionless figure-of-merit,

$$ZT \equiv \frac{\sigma S^2}{\kappa} T. \quad (6.113)$$

For the best thermoelectric materials found so far, the values of ZT at room temperature are in the range from 2 to 3, providing the COP_{cooling}, defined by Eq. (1.69), of the order of 0.5 – a few times lower than that of traditional, mechanical refrigerators. The search for composite materials (including those with nanoparticles) with higher values of ZT is one of very active fields of applied solid-state physics.⁷¹

Finally, let us discuss the second term of Eq. (105), in the absence of $\nabla \mu'$ (and hence of the electric current) giving

Fourier law

$$\mathbf{j}_h = -\kappa \nabla T, \quad (6.114)$$

This equality should be familiar to the reader because it describes the very common effect of *thermal conductivity*. Indeed, this linear relation is much more general than the particular expression (107) for κ : for sufficiently small temperature gradients it is valid for virtually any medium – for example, for insulators. (The left column in Table 6.1 gives typical values of κ for most common and/or representative materials.) Due to its universality and importance, Eq. (114) has deserved its own name – the *Fourier law*.⁷²

Acting absolutely similarly to the derivation of other continuity equations, such as Eqs. (5.117) for the classical probability, and Eq. (49) for the electric charge,⁷³ let us consider the conservation of the aggregate variable corresponding to \mathbf{j}_h – the internal energy E within a time-independent volume V . According to the basic Eq. (1.18), in the absence of media's expansion ($dV = 0$ and hence $dW = 0$), the

⁷¹ See, e.g., D. Rowe (ed.), *Thermoelectrics Handbook: Macro to Nano*, CRC Press, 2005.

⁷² It was suggested (in 1822) by the same universal scientific genius J.-B. J. Fourier who has not only developed such a key mathematical tool as the Fourier series but also discovered what is now called the greenhouse effect!

⁷³ They are all similar to continuity equations for other quantities – e.g., the mass (see CM Sec. 8.3) and the quantum-mechanical probability (see QM Secs. 1.4 and 9.6).

energy change⁷⁴ has only the thermal component, so its only cause may be the heat flow through its boundary surface S :

$$\frac{dE}{dt} = -\oint_S \mathbf{j}_h \cdot d^2\mathbf{r}. \quad (6.115)$$

In the simplest case of thermally-independent heat capacity C_V , we may integrate Eq. (1.22) over temperature to write⁷⁵

$$E = C_V T = \int_V c_V T d^3 r, \quad (6.116)$$

where c_V is the volumic specific heat, i.e. the heat capacity per unit volume (see the right column in Table 6.1).

Table 6.1. Approximate values of two major thermal coefficients of some materials at 20°C.

Material	κ (W·m ⁻¹ ·K ⁻¹)	c_V (J·K ⁻¹ ·m ⁻³)
Air ^{(a),(b)}	0.026	1.2×10^3
Teflon ([C ₂ F ₄] _n)	0.25	0.6×10^6
Water ^(b)	0.60	4.2×10^6
Amorphous silicon dioxide	1.1-1.4	1.5×10^6
Undoped silicon	150	1.6×10^6
Aluminum ^(c)	235	2.4×10^6
Copper ^(c)	400	3.4×10^6
Diamond	2,200	1.8×10^6

^(a) At ambient pressure.

^(b) In fluids (gases and liquids), heat flow may be much enhanced by temperature-gradient-induced turbulent circulation – *convection*, which is highly dependent on the system's geometry. The given values correspond to conditions preventing the convection.

^(c) In the context of the Wiedemann-Franz law (valid for metals only!), the values of κ for Al and Cu correspond to the Lorenz numbers, respectively, 2.22×10^{-8} W·Ω·K⁻² and 2.39×10^{-8} W·Ω·K⁻², in a pretty impressive comparison with the universal theoretical value of 2.45×10^{-8} W·Ω·K⁻² given by Eq. (110).

Now applying to the right-hand side of Eq. (115) the divergence theorem,⁷⁶ and taking into account that for a time-independent volume the full and partial derivatives over time are equivalent, we get

$$\int_V \left(c_V \frac{\partial T}{\partial t} + \nabla \cdot \mathbf{j}_h \right) d^3 r = 0, \quad (6.117)$$

⁷⁴ According to Eq. (1.25), in the case of negligible thermal expansion, it does not matter whether we speak about the internal energy E or the enthalpy H .

⁷⁵ If the dependence of c_V on temperature may be ignored only within a limited temperature interval, Eqs. (116) and (118) may be still used within that interval, for temperature deviations from some reference value.

⁷⁶ I hope the reader knows it by heart by now, but if not – see, e.g., MA Eq. (12.2).

This equality should hold for any time-independent volume V , which is possible only if the function under the integral equals zero at any point. Using Eq. (114), we get the following partial differential equation, called the *heat conduction equation* (or, rather inappropriately, the “heat equation”):

$$c_V(\mathbf{r}) \frac{\partial T}{\partial t} - \nabla \cdot [\kappa(\mathbf{r}) \nabla T] = 0, \quad (6.118)$$

Heat
conduction
equation

where the spatial arguments of the coefficients c_V and κ are spelled out to emphasize that this equation is valid even for nonuniform media. (Note, however, that Eq. (114) and hence Eq. (118) are valid only if the medium is *isotropic*.)

In a uniform medium, the thermal conductivity κ may be taken out from the external spatial differentiation, and the heat conduction equation becomes mathematically similar to the diffusion equation (5.116), and also to the drift-diffusion equation (50) in the absence of drift ($\nabla U = 0$):

$$\frac{\partial T}{\partial t} = D_T \nabla^2 T, \quad \text{with } D_T \equiv \frac{\kappa}{c_V}. \quad (6.119)$$

This means, in particular, that the solutions of these equations, discussed earlier in this course (such as Eqs. (5.112)-(5.113) for the evolution of the delta-functional initial perturbation) are valid for Eq. (119) as well, with the only replacement $D \rightarrow D_T$. This is why I will leave a few other examples of the solution of this equation for the reader’s exercise.

Let me finish this chapter (and this course as a whole) by emphasizing again that due to time/space restrictions I was able to barely scratch the surface of physical kinetics.⁷⁷

6.6. Exercise problems

6.1. Use the Boltzmann equation in the relaxation-time approximation to derive the Drude formula for the complex ac conductivity $\sigma(\omega)$, and give a physical interpretation of the result’s trend at high frequencies.

6.2. Apply the variable separation method⁷⁸ to Eq. (50) to calculate the time evolution of the particle density distribution in an unlimited uniform medium, in the absence of external forces, provided that at $t = 0$ the particles are released from their uniform distribution in a plane layer of thickness $2a$:

$$n = \begin{cases} n_0, & \text{for } -a \leq x \leq +a, \\ 0, & \text{otherwise.} \end{cases}$$

⁷⁷ A much more detailed coverage of this important part of physics may be found, for example, in the textbook by L. Pitaevskii and E. Lifshitz, *Physical Kinetics*, Butterworth-Heinemann, 1981. A deeper discussion of the Boltzmann equation is given, e.g., in the monograph by S. Harris, *An Introduction to the Theory of the Boltzmann Equation*, Dover 2011. For a discussion of applied aspects of kinetics see, e.g., T. Bergman *et al.*, *Fundamentals of Heat and Mass Transfer*, 7th ed., Wiley, 2011.

⁷⁸ A detailed introduction to this method (repeatedly used in this series) may be found, for example, in EM Sec. 2.5.

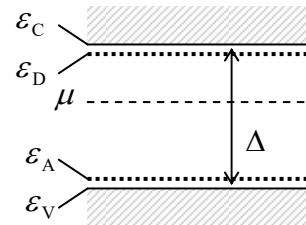
6.3. Solve the previous problem using an appropriate Green's function for the 1D version of the diffusion equation, and discuss the relative convenience of the results.

6.4.* Calculate the electric conductance of a narrow, uniform conducting link between two bulk conductors, in the low-voltage and low-temperature limit, neglecting the electron interaction and scattering inside the link.

6.5. Calculate the effective capacitance (per unit area) of a broad plane sheet of a degenerate 2D electron gas, separated by distance d from a metallic ground plane.

6.6. Give a quantitative description of the dopant atom ionization, which would be consistent with the conduction and valence band occupation statistics, using the same simple model of an n -doped semiconductor as in Sec. 4 (see Fig. 7a), and taking into account that the ground state of the dopant atom is typically doubly degenerate, due to two possible spin orientations of the bound electron. Use the results to verify Eq. (65), within the displayed limits of its validity.

6.7. Generalize the solution of the previous problem to the case when the n -doping of a semiconductor by n_D donor atoms per unit volume is complemented with its simultaneous p -doping by n_A acceptor atoms per unit volume, whose energy $\varepsilon_A - \varepsilon_V$ of activation, i.e. of accepting an additional electron and hence becoming a negative ion, is much lower than the bandgap Δ – see the figure on the right.



6.8. A nearly-ideal classical gas of N particles with mass m , was in thermal equilibrium at temperature T , in a closed container of volume V . At some moment, an orifice of a very small area A is open in one of the container's walls, allowing the particles to escape into the surrounding vacuum.⁷⁹ In the limit of very low density $n \equiv N/V$, use simple kinetic arguments to calculate the r.m.s. velocity of the escaped particles during the time period when the total number of such particles is still much smaller than N . Formulate the limits of validity of your results in terms of V, A , and the mean free path l .

Hint: Here and below, the term “nearly-ideal” means that l is so large that particle collisions do not affect the basic statistical properties of the gas.

6.9. For the system analyzed in the previous problem, calculate the rate of particle flow through the orifice – the so-called *effusion rate*. Discuss the limits of validity of your result.

6.10. Use simple kinetic arguments to estimate:

- (i) the diffusion coefficient D ,
- (ii) the thermal conductivity κ , and
- (iii) the *shear viscosity* η ,

of a nearly-ideal classical gas with mean free path l . Compare the result for D with that calculated in Sec. 3 from the Boltzmann-RTA equation.

⁷⁹ In chemistry-related fields, this process is frequently called *effusion*.

Hint: In fluid dynamics, the shear viscosity (frequently called simply "viscosity") may be defined as the coefficient η in the following relation:⁸⁰

$$\frac{d\mathcal{F}_{j'}}{dA_j} = \eta \frac{\partial v_{j'}}{\partial r_j},$$

where $d\mathcal{F}_{j'}$ is the j' th Cartesian component of the tangential force between two parts of a fluid, separated by an imaginary interface normal to some direction \mathbf{n}_j (with $j \neq j'$, and hence $\mathbf{n}_j \perp \mathbf{n}_{j'}$), exerted over an elementary area dA_j of this surface, and $\mathbf{v}(\mathbf{r})$ is the velocity of the fluid at the interface.

6.11. Use simple kinetic arguments to relate the mean free path l in a nearly-ideal classical gas, with the full cross-section σ of mutual scattering of its particles.⁸¹ Use the result to evaluate the thermal conductivity and the viscosity coefficient estimates made in the previous problem, for the molecular nitrogen, with the molecular mass $m \approx 4.7 \times 10^{-26}$ kg and the effective ("van der Waals") diameter $d_{\text{ef}} \approx 4.5 \times 10^{-10}$ m, at ambient conditions, and compare them with experimental results.

6.12. Use the Boltzmann-RTA equation to calculate the thermal conductivity of a nearly-ideal classical gas, measured in conditions when the applied thermal gradient does not create a net particle flow. Compare the result with that following from the simple kinetic arguments (Problem 6.10), and discuss their relationship.

6.13. Use the heat conduction equation (6.119) to calculate the time evolution of temperature in the center of a uniform solid sphere of radius R , initially heated to a uniformly distributed temperature T_{ini} , and at $t = 0$ placed into a heat bath that keeps its surface at temperature T_0 .

6.14. Suggest a reasonable definition of the entropy production rate (per unit volume), and calculate this rate for stationary thermal conduction, assuming that it obeys the Fourier law, in a material with negligible thermal expansion. Give a physical interpretation of the result. Does the stationary temperature distribution in a sample correspond to the minimum of the total entropy production in it?

6.15.⁸² Use the Boltzmann-RTA equation to calculate the shear viscosity of a nearly-ideal gas. Spell out the result in the classical limit, and compare it with the estimate made in the solution of Problem 10.

⁸⁰ See, e.g., CM Eq. (8.56). Please note the difference between the shear viscosity coefficient η considered in this problem and the drag coefficient η whose calculation was the task of Problem 3.2. Despite the similar (traditional) notation, and belonging to the same realm (kinematic friction), these coefficients have different definitions and even different dimensionalities.

⁸¹ I am sorry for using the same letter for the cross-section as for the electric Ohmic conductivity. (Both notations are very traditional.) Let me hope this would not lead to confusion, because the conductivity is not discussed in this problem.

⁸² This problem does not follow Problem 12 only for historic reasons.

This page is
intentionally left
blank



Konstantin K. Likharev
Essential Graduate Physics
Lecture Notes and Problems

Open online access at
<https://sites.google.com/site/likharevegp/>
and
<http://commons.library.stonybrook.edu/egp/>

Appendix MA

Selected Mathematical Formulas

that are used in this series, but not always remembered by students
(and some instructors :-)

Last corrections: 2021/08/20

1. Constants

– Euclidean circle's *length-to-diameter ratio*:

$$\pi = 3.141\ 592\ 653\dots; \quad \pi^{1/2} \approx 1.77. \quad (1.1)$$

– *Natural logarithm base*:

$$e \equiv \lim_{n \rightarrow \infty} \left(1 + \frac{1}{n}\right)^n = 2.718\ 281\ 828\dots; \quad (1.2a)$$

from that value, the logarithm base conversion factors are as follows ($\xi > 0$):

$$\frac{\ln \xi}{\log_{10} \xi} = \ln 10 \approx 2.303, \quad \frac{\log_{10} \xi}{\ln \xi} = \frac{1}{\ln 10} \approx 0.434. \quad (1.2b)$$

– The *Euler* (or “*Euler-Mascheroni*”) *constant*:

$$\gamma \equiv \lim_{n \rightarrow \infty} \left(1 + \frac{1}{2} + \frac{1}{3} + \dots + \frac{1}{n} - \ln n\right) = 0.5771566490\dots; \quad e^\gamma \approx 1.781. \quad (1.3)$$

2. Combinatorics, sums, and series

(i) Combinatorics

– The number of different *permutations*, i.e. *ordered* sequences of k elements selected from a set of n distinct elements ($n \geq k$), is

$${}^n P_k \equiv n \cdot (n-1) \cdot \dots \cdot (n-k+1) = \frac{n!}{(n-k)!}; \quad (2.1a)$$

in particular, the number of different permutations of *all* elements of the set ($n = k$) is

$${}^k P_k = k \cdot (k-1) \cdot \dots \cdot 2 \cdot 1 = k! \quad (2.1b)$$

– The number of different *combinations*, i.e. *unordered* sequences of k elements from a set of $n \geq k$ distinct elements, is equal to the *binomial coefficient*

$${}^n C_k \equiv \binom{n}{k} \equiv \frac{{}^n P_k}{{}^k P_k} = \frac{n!}{k!(n-k)!}. \quad (2.2)$$

In an alternative, very popular “ball/box language”, ${}^n C_k$ is the number of different ways to put in a box, in an arbitrary order, k balls selected from n distinct balls.

– A generalization of the binomial coefficient notion is the *multinomial coefficient*,

$${}^n C_{k_1, k_2, \dots, k_l} \equiv \frac{n!}{k_1! k_2! \dots k_l!}, \quad \text{with } n = \sum_{j=1}^l k_j, \quad (2.3)$$

which, in the standard mathematical language, is a number of different permutations in a multiset of l distinct element types from an n -element set which contains k_j ($j = 1, 2, \dots, l$) elements of each type. In the less formal “ball/box language”, the coefficient (2.3) is the number of different ways to distribute n distinct balls between l distinct boxes, each time keeping the number (k_j) of balls in the j^{th} box fixed, but ignoring their order inside the box. The binomial coefficient ${}^n C_k$, given by Eq. (2.2), is a particular case of the multinomial coefficient (2.3) for $l = 2$ – counting the explicit box for the first one, and the remaining space for the second box, so that if $k_1 \equiv k$, then $k_2 = n - k$.

– One more important combinatorial quantity is the number $M_n^{(k)}$ of different ways to place n *indistinguishable* balls into k distinct boxes. It may be readily calculated from Eq. (2.2) as the number of different ways to select $(k-1)$ partitions between the boxes in an imagined linear row of $(k-1+n)$ “objects” (balls in the boxes *and* partitions between them):

$$M_n^{(k)} = {}^{n-1+k} C_{k-1} \equiv \frac{(k-1+n)!}{(k-1)! n!}. \quad (2.4)$$

(ii) Sums and series

– *Arithmetic progression:*

$$r + 2r + \dots + nr \equiv \sum_{k=1}^n kr = \frac{n(r+nr)}{2}; \quad (2.5a)$$

in particular, at $r = 1$ it is reduced to the sum of n first natural numbers:

$$1 + 2 + \dots + n \equiv \sum_{k=1}^n k = \frac{n(n+1)}{2}. \quad (2.5b)$$

– Sums of squares and cubes of n first natural numbers:

$$1^2 + 2^2 + \dots + n^2 \equiv \sum_{k=1}^n k^2 = \frac{n(n+1)(2n+1)}{6}; \quad (2.6a)$$

$$1^3 + 2^3 + \dots + n^3 \equiv \sum_{k=1}^n k^3 = \frac{n^2(n+1)^2}{4}. \quad (2.6b)$$

– The *Riemann zeta function*:

$$\zeta(s) \equiv 1 + \frac{1}{2^s} + \frac{1}{3^s} + \dots \equiv \sum_{k=1}^{\infty} \frac{1}{k^s}; \quad (2.7a)$$

the particular values frequently met in applications are

$$\zeta\left(\frac{3}{2}\right) \approx 2.612, \quad \zeta(2) = \frac{\pi^2}{6}, \quad \zeta\left(\frac{5}{2}\right) \approx 1.341, \quad \zeta(3) \approx 1.202, \quad \zeta(4) = \frac{\pi^4}{90}, \quad \zeta(5) \approx 1.037. \quad (2.7b)$$

– Finite geometric progression (for real $\lambda \neq 1$):

$$1 + \lambda + \lambda^2 + \dots + \lambda^{n-1} \equiv \sum_{k=0}^{n-1} \lambda^k = \frac{1 - \lambda^n}{1 - \lambda}; \quad (2.8a)$$

in particular, if $\lambda^2 < 1$, the progression has a finite limit at $n \rightarrow \infty$ (called the *geometric series*):

$$\lim_{n \rightarrow \infty} \sum_{k=0}^{n-1} \lambda^k \equiv \sum_{k=0}^{\infty} \lambda^k = \frac{1}{1 - \lambda}. \quad (2.8b)$$

– *Binomial sum* (also called the “binomial theorem”):

$$(1 + a)^n = \sum_{k=0}^n {}^n C_k a^k, \quad (2.9)$$

where ${}^n C_k$ are the binomial coefficients given by Eq. (2.2).

– The *Stirling formula*:

$$\lim_{n \rightarrow \infty} \ln(n!) = n(\ln n - 1) + \frac{1}{2} \ln(2\pi n) + \frac{1}{12n} - \frac{1}{360n^3} + \dots; \quad (2.10)$$

for most applications in physics, the first term¹ is sufficient.

– The *Taylor* (or “Taylor-Maclaurin”) *series*: for any infinitely differentiable function $f(\xi)$:

$$\lim_{\tilde{\xi} \rightarrow 0} f(\xi + \tilde{\xi}) = f(\xi) + \frac{df}{d\xi}(\xi) \tilde{\xi} + \frac{1}{2!} \frac{d^2 f}{d\xi^2}(\xi) \tilde{\xi}^2 + \dots = \sum_{k=0}^{\infty} \frac{1}{k!} \frac{d^k f}{d\xi^k}(\xi) \tilde{\xi}^k; \quad (2.11a)$$

note that for many functions this series converges only within a limited, sometimes small range of deviations $\tilde{\xi}$. For a function of several arguments, $f(\xi_1, \xi_2, \dots, \xi_N)$, the first terms of the Taylor series are

$$\lim_{\tilde{\xi}_k \rightarrow 0} f(\xi_1 + \tilde{\xi}_1, \xi_2 + \tilde{\xi}_2, \dots) = f(\xi_1, \xi_2, \dots) + \sum_{k=1}^N \frac{\partial f}{\partial \xi_k}(\xi_1, \xi_2, \dots) \tilde{\xi}_k + \frac{1}{2!} \sum_{k,k'=1}^N \frac{\partial^2 f}{\partial \xi_k \partial \xi_{k'}}(\xi_1, \xi_2, \dots) \tilde{\xi}_k \tilde{\xi}_{k'} + \dots \quad (2.11b)$$

– The *Euler-Maclaurin formula*, valid for any infinitely differentiable function $f(\xi)$:

$$\sum_{k=1}^n f(k) = \int_0^n f(\xi) d\xi + \frac{1}{2} [f(n) - f(0)] + \frac{1}{6} \cdot \frac{1}{2!} \left[\frac{df}{d\xi}(n) - \frac{df}{d\xi}(0) \right]$$

¹ Actually, this leading term was conjectured by A. de Moivre in 1733, before J. Stirling’s proof of the series.

$$-\frac{1}{30} \cdot \frac{1}{4!} \left[\frac{d^3 f}{d\xi^3}(n) - \frac{d^3 f}{d\xi^3}(0) \right] + \frac{1}{42} \cdot \frac{1}{6!} \left[\frac{d^5 f}{d\xi^5}(n) - \frac{d^5 f}{d\xi^5}(0) \right] + \dots; \quad (2.12a)$$

the coefficients participating in this formula are the so-called *Bernoulli numbers*:²

$$B_1 = \frac{1}{2}, \quad B_2 = \frac{1}{6}, \quad B_3 = 0, \quad B_4 = \frac{1}{30}, \quad B_5 = 0, \quad B_6 = \frac{1}{42}, \quad B_7 = 0, \quad B_8 = \frac{1}{30}, \dots \quad (2.12b)$$

3. Basic trigonometric functions

– Trigonometric functions of the sum and the difference of two arguments:³

$$\cos(a \pm b) = \cos a \cos b \mp \sin a \sin b, \quad (3.1a)$$

$$\sin(a \pm b) = \sin a \cos b \pm \cos a \sin b. \quad (3.1b)$$

– Sums of two functions of arbitrary arguments:

$$\cos a + \cos b = 2 \cos \frac{a+b}{2} \cos \frac{b-a}{2}, \quad (3.2a)$$

$$\cos a - \cos b = 2 \sin \frac{a+b}{2} \sin \frac{b-a}{2}, \quad (3.2b)$$

$$\sin a \pm \sin b = 2 \sin \frac{a \pm b}{2} \cos \frac{\pm b - a}{2}. \quad (3.2c)$$

– Trigonometric function products:

$$2 \cos a \cos b = \cos(a+b) + \cos(a-b), \quad (3.3a)$$

$$2 \sin a \cos b = \sin(a+b) + \sin(a-b), \quad (3.3b)$$

$$2 \sin a \sin b = \cos(a-b) - \cos(a+b); \quad (3.3c)$$

for the particular case of equal arguments, $b = a$, these three formulas yield the following expressions for the squares of trigonometric functions, and their product:

$$\cos^2 a = \frac{1}{2}(1 + \cos 2a), \quad \sin a \cos a = \frac{1}{2} \sin 2a, \quad \sin^2 a = \frac{1}{2}(1 - \cos 2a). \quad (3.3d)$$

– Cubes of trigonometric functions:

$$\cos^3 a = \frac{3}{4} \cos a + \frac{1}{4} \cos 3a, \quad \sin^3 a = \frac{3}{4} \sin a - \frac{1}{4} \sin 3a. \quad (3.4)$$

– Trigonometric functions of a complex argument:

² Note that definitions of B_k (or rather their signs and indices) vary even in the most popular handbooks.

³ I am confident that the reader is quite capable of deriving the relations (3.1) by representing exponent in the elementary relation $e^{i(a \pm b)} = e^{ia} e^{\pm ib}$ as a sum of its real and imaginary parts, then Eqs. (3.3) directly from Eqs. (3.1), and then Eqs. (3.2) from Eqs. (3.3) by variable replacement; however, I am still providing these formulas to save their time. (Quite a few formulas below are included for the same reason.)

$$\begin{aligned}\sin(a+ib) &= \sin a \cosh b + i \cos a \sinh b, \\ \cos(a+ib) &= \cos a \cosh b - i \sin a \sinh b.\end{aligned}\tag{3.5}$$

– Sums of trigonometric functions of n equidistant arguments:

$$\sum_{k=1}^n \begin{Bmatrix} \sin \\ \cos \end{Bmatrix} k\xi = \begin{Bmatrix} \sin \\ \cos \end{Bmatrix} \left(\frac{n+1}{2} \xi \right) \sin \left(\frac{n}{2} \xi \right) / \sin \left(\frac{\xi}{2} \right). \tag{3.6}$$

4. General differentiation

– Full differential of a product of two functions:

$$d(fg) = (df)g + f(dg). \tag{4.1}$$

– Full differential of a function of several independent arguments, $f(\xi_1, \xi_2, \dots, \xi_n)$:

$$df = \sum_{k=1}^n \frac{\partial f}{\partial \xi_k} d\xi_k. \tag{4.2}$$

– Curvature of the Cartesian plot of a smooth function $f(\xi)$:

$$\kappa \equiv \frac{1}{R} = \frac{\left| d^2 f / d\xi^2 \right|}{\left[1 + (df / d\xi)^2 \right]^{3/2}}. \tag{4.3}$$

5. General integration

– Integration by parts:⁴

$$\int_{g(A)}^{g(B)} f \, dg = fg \Big|_A^B - \int_{f(A)}^{f(B)} g \, df. \tag{5.1}$$

– Numerical (approximate) integration of 1D functions: the simplest *trapezoidal rule*,

$$\int_a^b f(\xi) d\xi \approx h \left[f\left(a + \frac{h}{2}\right) + f\left(a + \frac{3h}{2}\right) + \dots + f\left(b - \frac{h}{2}\right) \right] = h \sum_{n=1}^N f\left(a - \frac{h}{2} + nh\right), \quad h \equiv \frac{b-a}{N}. \tag{5.2}$$

has a relatively low accuracy (error of the order of $(h^3/12)d^2f/d\xi^2$ per step), so that the following *Simpson formula*,

$$\int_a^b f(\xi) d\xi \approx \frac{h}{3} [f(a) + 4f(a+h) + 2f(a+2h) + \dots + 4f(b-h) + f(b)], \quad h \equiv \frac{b-a}{2N}, \tag{5.3}$$

whose error per step scales as $(h^5/180)d^4f/d\xi^4$, is used much more frequently.⁵

⁴ This formula immediately follows from Eq. (4.1).

⁵ Higher-order formulas (e.g., the *Bode rule*), and other guidance including ready-for-use codes for computer calculations may be found, for example, in the popular reference texts by W. H. Press *et al.*, cited in Sec. 16

6. A few 1D integrals⁶

(i) Indefinite integrals

– Integrals with $(1 + \xi^2)^{1/2}$:

$$\int (1 + \xi^2)^{1/2} d\xi = \frac{\xi}{2} (1 + \xi^2)^{1/2} + \frac{1}{2} \ln \left| \xi + (1 + \xi^2)^{1/2} \right|, \quad (6.1)$$

$$\int \frac{d\xi}{(1 + \xi^2)^{1/2}} = \ln \left| \xi + (1 + \xi^2)^{1/2} \right|, \quad (6.2a)$$

$$\int \frac{d\xi}{(1 + \xi^2)^{3/2}} = \frac{\xi}{(1 + \xi^2)^{1/2}}. \quad (6.2b)$$

– Miscellaneous indefinite integrals:

$$\int \frac{d\xi}{\xi(\xi^2 + 2a\xi - 1)^{1/2}} = \cos^{-1} \frac{a\xi - 1}{|\xi|(a^2 + 1)^{1/2}}, \quad (6.3a)$$

$$\int \frac{(\sin \xi - \xi \cos \xi)^2}{\xi^5} d\xi = \frac{2\xi \sin 2\xi + \cos 2\xi - 2\xi^2 - 1}{8\xi^4}, \quad (6.3b)$$

$$\int \frac{d\xi}{a + b \cos \xi} = \frac{2}{(a^2 - b^2)^{1/2}} \tan^{-1} \left[\frac{(a-b)}{(a^2 - b^2)^{1/2}} \tan \frac{\xi}{2} \right], \quad \text{for } a^2 > b^2. \quad (6.3c)$$

$$\int \frac{d\xi}{1 + \xi^2} = \tan^{-1} \xi. \quad (6.3d)$$

(ii) Semi-definite integrals:

– Integrals with $1/(e^\xi \pm 1)$:

$$\int_a^\infty \frac{d\xi}{e^\xi + 1} = \ln(1 + e^{-a}), \quad (6.4a)$$

$$\int_{a>0}^\infty \frac{d\xi}{e^\xi - 1} = \ln \frac{1}{1 - e^{-a}}. \quad (6.4b)$$

(iii) Definite integrals

– Integrals with $1/(1 + \xi^2)$:⁷

$$\int_0^\infty \frac{d\xi}{1 + \xi^2} = \frac{\pi}{2}, \quad (6.5a)$$

below. Besides that, some advanced codes are used as subroutines in the software packages listed in the same section. In some cases, the Euler-Maclaurin formula (2.12) also may be useful for numerical integration.

⁶ A powerful (and free :-) interactive online tool for working out indefinite 1D integrals is available at <http://integrals.wolfram.com/index.jsp>.

⁷ Eq. (6.5a) follows immediately from Eq. (6.3d), and Eq. (6.5b) from Eq. (6.2b) – a couple more examples of the (intentional) redundancies in this list.

$$\int_0^\infty \frac{d\xi}{(1+\xi^2)^{3/2}} = 1; \quad (6.5b)$$

more generally,

$$\int_0^\infty \frac{d\xi}{(1+\xi^2)^n} = \frac{\pi}{2} \frac{(2n-3)!!}{(2n-2)!!} \equiv \frac{\pi}{2} \frac{1 \cdot 3 \cdot 5 \dots (2n-3)}{2 \cdot 4 \cdot 6 \dots (2n-2)}, \quad \text{for } n = 2, 3, \dots \quad (6.5c)$$

– Integrals with $(1 - \xi^{2n})^{1/2}$:

$$\int_0^1 \frac{d\xi}{(1 - \xi^{2n})^{1/2}} = \frac{\pi^{1/2}}{2n} \Gamma\left(\frac{1}{2n}\right) / \Gamma\left(\frac{n+1}{2n}\right), \quad (6.6a)$$

$$\int_0^1 (1 - \xi^{2n})^{1/2} d\xi = \frac{\pi^{1/2}}{4n} \Gamma\left(\frac{1}{2n}\right) / \Gamma\left(\frac{3n+1}{2n}\right), \quad (6.6b)$$

where $\Gamma(s)$ is the *gamma function*, which is most often defined (for $\operatorname{Re} s > 0$) by the following integral:

$$\int_0^\infty \xi^{s-1} e^{-\xi} d\xi = \Gamma(s). \quad (6.7a)$$

The key property of this function is the recurrence relation, which is valid for any $s \neq 0, -1, -2, \dots$:

$$\Gamma(s+1) = s\Gamma(s). \quad (6.7b)$$

Since, according to Eq. (6.7a), $\Gamma(1) = 1$, Eq. (6.7b) for non-negative integers takes the form

$$\Gamma(n+1) = n!, \quad \text{for } n = 0, 1, 2, \dots \quad (6.7c)$$

(where $0! \equiv 1$). Because of this, for integer $s = n+1 \geq 1$, Eq. (6.7a) is reduced to

$$\int_0^\infty \xi^n e^{-\xi} d\xi = n!. \quad (6.7d)$$

Other frequently met values of the gamma function are those for positive semi-integer values:

$$\Gamma\left(\frac{1}{2}\right) = \pi^{1/2}, \quad \Gamma\left(\frac{3}{2}\right) = \frac{1}{2}\pi^{1/2}, \quad \Gamma\left(\frac{5}{2}\right) = \frac{1}{2} \cdot \frac{3}{2}\pi^{1/2}, \quad \Gamma\left(\frac{7}{2}\right) = \frac{1}{2} \cdot \frac{3}{2} \cdot \frac{5}{2}\pi^{1/2}, \dots . \quad (6.7e)$$

– Integrals with $1/(e^\xi \pm 1)$:

$$\int_0^\infty \frac{\xi^{s-1} d\xi}{e^\xi + 1} = (1 - 2^{1-s}) \Gamma(s) \zeta(s), \quad \text{for } s > 0, \quad (6.8a)$$

$$\int_0^\infty \frac{\xi^{s-1} d\xi}{e^\xi - 1} = \Gamma(s) \zeta(s), \quad \text{for } s > 1, \quad (6.8b)$$

where $\zeta(s)$ is the Riemann zeta-function – see Eq. (2.6). Particular cases: for $s = 2n$,

$$\int_0^\infty \frac{\xi^{2n-1} d\xi}{e^\xi + 1} = \frac{2^{2n-1} - 1}{2n} \pi^{2n} B_{2n}, \quad (6.8c)$$

$$\int_0^\infty \frac{\xi^{2n-1} d\xi}{e^\xi - 1} = \frac{(2\pi)^{2n}}{4n} B_{2n}. \quad (6.8d)$$

where B_n are the Bernoulli numbers – see Eq. (2.12). For the particular case $s = 1$ (when Eq. (6.8a) yields uncertainty),

$$\int_0^\infty \frac{d\xi}{e^\xi + 1} = \ln 2. \quad (6.8e)$$

– Integrals with $\exp\{-\xi^2\}$:

$$\int_0^\infty \xi^s e^{-\xi^2} d\xi = \frac{1}{2} \Gamma\left(\frac{s+1}{2}\right), \quad \text{for } s > -1; \quad (6.9a)$$

for applications the most important particular values of s are 0 and 2:

$$\int_0^\infty e^{-\xi^2} d\xi = \frac{1}{2} \Gamma\left(\frac{1}{2}\right) = \frac{\pi^{1/2}}{2}, \quad (6.9b)$$

$$\int_0^\infty \xi^2 e^{-\xi^2} d\xi = \frac{1}{2} \Gamma\left(\frac{3}{2}\right) = \frac{\pi^{1/2}}{4}, \quad (6.9c)$$

though we will also run into the cases $s = 4$ and $s = 6$:

$$\int_0^\infty \xi^4 e^{-\xi^2} d\xi = \frac{1}{2} \Gamma\left(\frac{5}{2}\right) = \frac{3\pi^{1/2}}{8}, \quad \int_0^\infty \xi^6 e^{-\xi^2} d\xi = \frac{1}{2} \Gamma\left(\frac{7}{2}\right) = \frac{15\pi^{1/2}}{16}; \quad (6.9d)$$

for odd integer values $s = 2n + 1$ (with $n = 0, 1, 2, \dots$), Eq. (6.9a) takes a simpler form:

$$\int_0^\infty \xi^{2n+1} e^{-\xi^2} d\xi = \frac{1}{2} \Gamma(n+1) = \frac{n!}{2}. \quad (6.9e)$$

– Integrals with cosine and sine functions:

$$\int_0^\infty \cos(\xi^2) d\xi = \int_0^\infty \sin(\xi^2) d\xi = \left(\frac{\pi}{8}\right)^{1/2}. \quad (6.10)$$

$$\int_0^\infty \frac{\cos \xi}{a^2 + \xi^2} d\xi = \frac{\pi}{2|a|} e^{-|a|}. \quad (6.11)$$

$$\int_0^\infty \left(\frac{\sin \xi}{\xi} \right)^2 d\xi = \frac{\pi}{2}. \quad (6.12)$$

– Integrals with logarithms:

$$\int_0^1 \ln \frac{a + (1 - \xi^2)^{1/2}}{a - (1 - \xi^2)^{1/2}} d\xi = \pi \left[a - (a^2 - 1)^{1/2} \right], \quad \text{for } a \geq 1. \quad (6.13)$$

$$\int_0^1 \ln \frac{1 + (1 - \xi)^{1/2}}{\xi^{1/2}} d\xi = 1. \quad (6.14)$$

– Integral representations of the Bessel functions of integer order:

$$J_n(\alpha) = \frac{1}{2\pi} \int_{-\pi}^{+\pi} e^{i(\alpha \sin \xi - n\xi)} d\xi, \quad \text{so that } e^{i\alpha \sin \xi} = \sum_{k=-\infty}^{\infty} J_k(\alpha) e^{ik\xi}; \quad (6.15a)$$

$$I_n(\alpha) = \frac{1}{\pi} \int_0^\pi e^{\alpha \cos \xi} \cos n\xi d\xi. \quad (6.15b)$$

7. 3D vector products

(i) Definitions:

– *Scalar (“dot-“) product:*

$$\mathbf{a} \cdot \mathbf{b} = \sum_{j=1}^3 a_j b_j, \quad (7.1)$$

where a_j and b_j are vector components in any orthogonal coordinate system. In particular, the vector squared (the same as its norm squared) is the following scalar:

$$a^2 \equiv \mathbf{a} \cdot \mathbf{a} = \sum_{j=1}^3 a_j^2 \equiv \|\mathbf{a}\|^2. \quad (7.2)$$

– *Vector (“cross-“) product:*

$$\mathbf{a} \times \mathbf{b} \equiv \mathbf{n}_1(a_2 b_3 - a_3 b_2) + \mathbf{n}_2(a_3 b_1 - a_1 b_3) + \mathbf{n}_3(a_1 b_2 - a_2 b_1) = \begin{vmatrix} \mathbf{n}_1 & \mathbf{n}_2 & \mathbf{n}_3 \\ a_1 & a_2 & a_3 \\ b_1 & b_2 & b_3 \end{vmatrix}, \quad (7.3)$$

where $\{\mathbf{n}_j\}$ is the set of mutually perpendicular unit vectors⁸ along the corresponding coordinate system axes.⁹ In particular, Eq. (7.3) yields

$$\mathbf{a} \times \mathbf{a} = 0. \quad (7.4)$$

(ii) Corollaries (readily verified by Cartesian components):

– Double vector product (the so-called *bac minus cab rule*):

$$\mathbf{a} \times (\mathbf{b} \times \mathbf{c}) = \mathbf{b}(\mathbf{a} \cdot \mathbf{c}) - \mathbf{c}(\mathbf{a} \cdot \mathbf{b}). \quad (7.5)$$

– Mixed scalar-vector product (the *operand rotation rule*):

$$\mathbf{a} \cdot (\mathbf{b} \times \mathbf{c}) = \mathbf{b} \cdot (\mathbf{c} \times \mathbf{a}) = \mathbf{c} \cdot (\mathbf{a} \times \mathbf{b}). \quad (7.6)$$

⁸ Other popular notations for this vector set are $\{\mathbf{e}_j\}$ and $\{\hat{\mathbf{r}}_j\}$.

⁹ It is easy to use Eq. (7.3) to check that the direction of the product vector corresponds to the well-known “right-hand rule” and to the even more convenient *corkscrew rule*: if we rotate a corkscrew’s handle from the first operand toward the second one, its axis moves in the direction of the product.

– Scalar product of vector products:

$$(\mathbf{a} \times \mathbf{b}) \cdot (\mathbf{c} \times \mathbf{d}) = (\mathbf{a} \cdot \mathbf{c})(\mathbf{b} \cdot \mathbf{d}) - (\mathbf{a} \cdot \mathbf{d})(\mathbf{b} \cdot \mathbf{c}); \quad (7.7a)$$

in the particular case of two similar operands (say, $\mathbf{a} = \mathbf{c}$ and $\mathbf{b} = \mathbf{d}$), the last formula is reduced to

$$(\mathbf{a} \times \mathbf{b})^2 = (ab)^2 - (\mathbf{a} \cdot \mathbf{b})^2. \quad (7.7b)$$

8. Differentiation in 3D Cartesian coordinates

– Definition of the *del* (or “nabla”) vector-operator ∇ :¹⁰

$$\nabla \equiv \sum_{j=1}^3 \mathbf{n}_j \frac{\partial}{\partial r_j}, \quad (8.1)$$

where r_j is a set of linear and orthogonal (*Cartesian*) coordinates along directions \mathbf{n}_j . In accordance with this definition, the operator ∇ acting on a *scalar* function of coordinates, $f(\mathbf{r})$,¹¹ gives its gradient, i.e. a new *vector*:

$$\nabla f \equiv \sum_{j=1}^3 \mathbf{n}_j \frac{\partial f}{\partial r_j} \equiv \mathbf{grad} f. \quad (8.2)$$

– The *scalar product* of del by a *vector* function of coordinates (a *vector field*),

$$\mathbf{f}(\mathbf{r}) \equiv \sum_{j=1}^3 \mathbf{n}_j f_j(\mathbf{r}), \quad (8.3)$$

compiled by formally following Eq. (7.1), is a *scalar* function – the *divergence* of the initial function:

$$\nabla \cdot \mathbf{f} \equiv \sum_{j=1}^3 \frac{\partial f_j}{\partial r_j} \equiv \text{div } \mathbf{f}, \quad (8.4)$$

while the *vector product* of ∇ and \mathbf{f} , formed in a formal accordance with Eq. (7.3), is a new vector – the **curl** (in European tradition, called *rotor* and denoted **rot**) of \mathbf{f} :

$$\nabla \times \mathbf{f} \equiv \begin{vmatrix} \mathbf{n}_1 & \mathbf{n}_2 & \mathbf{n}_3 \\ \frac{\partial}{\partial r_1} & \frac{\partial}{\partial r_2} & \frac{\partial}{\partial r_3} \\ f_1 & f_2 & f_3 \end{vmatrix} = \mathbf{n}_1 \left(\frac{\partial f_3}{\partial r_2} - \frac{\partial f_2}{\partial r_3} \right) + \mathbf{n}_2 \left(\frac{\partial f_1}{\partial r_3} - \frac{\partial f_3}{\partial r_1} \right) + \mathbf{n}_3 \left(\frac{\partial f_2}{\partial r_1} - \frac{\partial f_1}{\partial r_2} \right) \equiv \mathbf{curl} \mathbf{f}. \quad (8.5)$$

– One more frequently met “product” is $(\mathbf{f} \cdot \nabla) \mathbf{g}$, where \mathbf{f} and \mathbf{g} are two arbitrary vector functions of \mathbf{r} . This product should be also understood in the sense implied by Eq. (7.1), i.e. as a vector whose j^{th} Cartesian component is

$$[(\mathbf{f} \cdot \nabla) \mathbf{g}]_j = \sum_{j'=1}^3 f_{j'} \frac{\partial g_j}{\partial r_{j'}}. \quad (8.5)$$

¹⁰ One can run into the following notation: $\nabla \equiv \partial/\partial \mathbf{r}$, which is convenient in some cases, but may be misleading in quite a few others, so it will be not used in this series.

¹¹ In this, and four next sections, all scalar and vector functions are assumed to be differentiable.

9. The Laplace operator $\nabla^2 \equiv \nabla \cdot \nabla$

– Expression in Cartesian coordinates – in the formal accordance with Eq. (7.2):

$$\nabla^2 = \sum_{j=1}^3 \frac{\partial^2}{\partial r_j^2}. \quad (9.1)$$

– According to its definition, the Laplace operator acting on a *scalar* function of coordinates gives a new scalar function:

$$\nabla^2 f \equiv \nabla \cdot (\nabla f) = \operatorname{div}(\operatorname{grad} f) = \sum_{j=1}^3 \frac{\partial^2 f}{\partial r_j^2}. \quad (9.2)$$

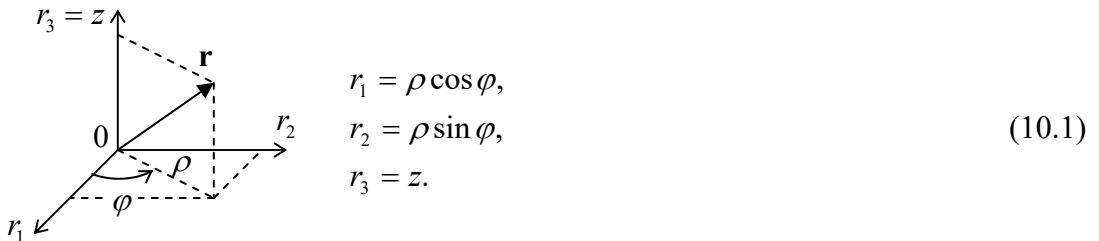
– On the other hand, acting on a *vector* function (8.3), the operator ∇^2 returns another *vector*:

$$\nabla^2 \mathbf{f} = \sum_{j=1}^3 \mathbf{n}_j \nabla^2 f_j. \quad (9.3)$$

Note that Eqs. (9.1)-(9.3) are only valid in Cartesian (i.e. orthogonal and linear) coordinates, but generally not in other orthogonal coordinates – see, e.g., Eqs. (10.3), (10.6), (10.9) and (10.12) below.

10. Operators ∇ and ∇^2 in the most important systems of orthogonal coordinates¹²

(i) Cylindrical¹³ coordinates $\{\rho, \varphi, z\}$ (see Fig. below) may be defined by their relations with the Cartesian coordinates:



– Gradient of a scalar function:

$$\nabla f = \mathbf{n}_\rho \frac{\partial f}{\partial \rho} + \mathbf{n}_\varphi \frac{1}{\rho} \frac{\partial f}{\partial \varphi} + \mathbf{n}_z \frac{\partial f}{\partial z}. \quad (10.2)$$

– The Laplace operator of a scalar function:

$$\nabla^2 f = \frac{1}{\rho} \frac{\partial}{\partial \rho} \left(\rho \frac{\partial f}{\partial \rho} \right) + \frac{1}{\rho^2} \frac{\partial^2 f}{\partial \varphi^2} + \frac{\partial^2 f}{\partial z^2}, \quad (10.3)$$

– Divergence of a vector function of coordinates ($\mathbf{f} = \mathbf{n}_\rho f_\rho + \mathbf{n}_\varphi f_\varphi + \mathbf{n}_z f_z$):

$$\nabla \cdot \mathbf{f} = \frac{1}{\rho} \frac{\partial (\rho f_\rho)}{\partial \rho} + \frac{1}{\rho} \frac{\partial f_\varphi}{\partial \varphi} + \frac{\partial f_z}{\partial z}. \quad (10.4)$$

¹² Some other orthogonal curvilinear coordinate systems are discussed in EM Sec. 2.3.

¹³ In the 2D geometry with fixed coordinate z , these coordinates are called *polar*.

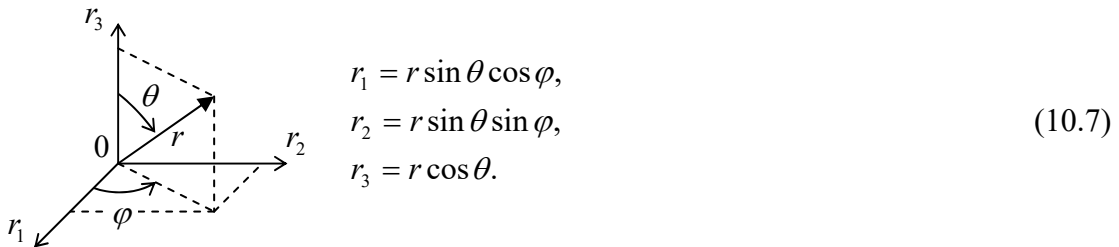
– Curl of a vector function:

$$\nabla \times \mathbf{f} = \mathbf{n}_\rho \left(\frac{1}{\rho} \frac{\partial f_z}{\partial \varphi} - \frac{\partial f_\varphi}{\partial z} \right) + \mathbf{n}_\varphi \left(\frac{\partial f_\rho}{\partial z} - \frac{\partial f_z}{\partial \rho} \right) + \mathbf{n}_z \frac{1}{\rho} \left(\frac{\partial(\rho f_\varphi)}{\partial \rho} - \frac{\partial f_\rho}{\partial \varphi} \right). \quad (10.5)$$

– The Laplace operator of a vector function:

$$\nabla^2 \mathbf{f} = \mathbf{n}_\rho \left(\nabla^2 f_\rho - \frac{1}{\rho^2} f_\rho - \frac{2}{\rho^2} \frac{\partial f_\varphi}{\partial \varphi} \right) + \mathbf{n}_\varphi \left(\nabla^2 f_\varphi - \frac{1}{\rho^2} f_\varphi + \frac{2}{\rho^2} \frac{\partial f_\rho}{\partial \varphi} \right) + \mathbf{n}_z \nabla^2 f_z. \quad (10.6)$$

(ii) Spherical coordinates $\{r, \theta, \varphi\}$ (see Fig. below) may be defined as:



– Gradient of a scalar function:

$$\nabla f = \mathbf{n}_r \frac{\partial f}{\partial r} + \mathbf{n}_\theta \frac{1}{r} \frac{\partial f}{\partial \theta} + \mathbf{n}_\varphi \frac{1}{r \sin \theta} \frac{\partial f}{\partial \varphi}. \quad (10.8)$$

– The Laplace operator of a scalar function:

$$\nabla^2 f = \frac{1}{r^2} \frac{\partial}{\partial r} \left(r^2 \frac{\partial f}{\partial r} \right) + \frac{1}{r^2 \sin \theta} \frac{\partial}{\partial \theta} \left(\sin \theta \frac{\partial f}{\partial \theta} \right) + \frac{1}{(r \sin \theta)^2} \frac{\partial^2 f}{\partial \varphi^2}. \quad (10.9)$$

– Divergence of a vector function $\mathbf{f} = \mathbf{n}_r f_r + \mathbf{n}_\theta f_\theta + \mathbf{n}_\varphi f_\varphi$:

$$\nabla \cdot \mathbf{f} = \frac{1}{r^2} \frac{\partial(r^2 f_r)}{\partial r} + \frac{1}{r \sin \theta} \frac{\partial(f_\theta \sin \theta)}{\partial \theta} + \frac{1}{r \sin \theta} \frac{\partial f_\varphi}{\partial \varphi}. \quad (10.10)$$

– Curl of the similar vector function:

$$\nabla \times \mathbf{f} = \mathbf{n}_r \frac{1}{r \sin \theta} \left(\frac{\partial(f_\varphi \sin \theta)}{\partial \theta} - \frac{\partial f_\theta}{\partial \varphi} \right) + \mathbf{n}_\theta \frac{1}{r} \left(\frac{1}{\sin \theta} \frac{\partial f_r}{\partial \varphi} - \frac{\partial(r f_\varphi)}{\partial r} \right) + \mathbf{n}_\varphi \frac{1}{r} \left(\frac{\partial(r f_\theta)}{\partial r} - \frac{\partial f_r}{\partial \theta} \right). \quad (10.11)$$

– The Laplace operator of a vector function:

$$\begin{aligned} \nabla^2 \mathbf{f} = & \mathbf{n}_r \left(\nabla^2 f_r - \frac{2}{r^2} f_r - \frac{2}{r^2 \sin \theta} \frac{\partial}{\partial \theta} (f_\theta \sin \theta) - \frac{2}{r^2 \sin \theta} \frac{\partial f_\varphi}{\partial \varphi} \right) \\ & + \mathbf{n}_\theta \left(\nabla^2 f_\theta - \frac{1}{r^2 \sin^2 \theta} f_\theta + \frac{2}{r^2} \frac{\partial f_r}{\partial \theta} - \frac{2 \cos \theta}{r^2 \sin^2 \theta} \frac{\partial f_\varphi}{\partial \varphi} \right) \\ & + \mathbf{n}_\varphi \left(\nabla^2 f_\varphi - \frac{1}{r^2 \sin^2 \theta} f_\varphi + \frac{2}{r^2 \sin \theta} \frac{\partial f_r}{\partial \varphi} + \frac{2 \cos \theta}{r^2 \sin^2 \theta} \frac{\partial f_\theta}{\partial \varphi} \right). \end{aligned} \quad (10.12)$$

11. Products involving ∇

(i) Useful zeros:

- For any scalar function $f(\mathbf{r})$,

$$\nabla \times (\nabla f) \equiv \mathbf{curl}(\mathbf{grad} f) = 0. \quad (11.1)$$

- For any vector function $\mathbf{f}(\mathbf{r})$,

$$\nabla \cdot (\nabla \times \mathbf{f}) \equiv \text{div}(\mathbf{curl} \mathbf{f}) = 0. \quad (11.2)$$

(ii) The Laplace operator expressed via the curl of a curl:

$$\nabla^2 \mathbf{f} = \nabla(\nabla \cdot \mathbf{f}) - \nabla \times (\nabla \times \mathbf{f}). \quad (11.3)$$

(iii) Spatial differentiation of a product of a scalar function by a vector function:

- The scalar 3D generalization of Eq. (4.1) is

$$\nabla \cdot (f \mathbf{g}) = (\nabla f) \cdot \mathbf{g} + f(\nabla \cdot \mathbf{g}). \quad (11.4a)$$

- Its vector generalization is similar:

$$\nabla \times (f \mathbf{g}) = (\nabla f) \times \mathbf{g} + f(\nabla \times \mathbf{g}). \quad (11.4b)$$

(iv) 3D spatial differentiation of products of two vector functions:

$$\nabla \times (\mathbf{f} \times \mathbf{g}) = \mathbf{f}(\nabla \cdot \mathbf{g}) - (\mathbf{f} \cdot \nabla) \mathbf{g} - (\nabla \cdot \mathbf{f}) \mathbf{g} + (\mathbf{g} \cdot \nabla) \mathbf{f}, \quad (11.5)$$

$$\nabla(\mathbf{f} \cdot \mathbf{g}) = (\mathbf{f} \cdot \nabla) \mathbf{g} + (\mathbf{g} \cdot \nabla) \mathbf{f} + \mathbf{f} \times (\nabla \times \mathbf{g}) + \mathbf{g} \times (\nabla \times \mathbf{f}), \quad (11.6)$$

$$\nabla \cdot (\mathbf{f} \times \mathbf{g}) = \mathbf{g} \cdot (\nabla \times \mathbf{f}) - \mathbf{f} \cdot (\nabla \times \mathbf{g}). \quad (11.7)$$

12. Integro-differential relations

(i) For an arbitrary surface S limited by closed contour C :

- The *Stokes theorem*, valid for any differentiable vector field $\mathbf{f}(\mathbf{r})$:

$$\int_S (\nabla \times \mathbf{f}) \cdot d^2 \mathbf{r} \equiv \int_S (\nabla \times \mathbf{f})_n d^2 r = \oint_C \mathbf{f} \cdot d\mathbf{r} \equiv \oint_C f_\tau dr, \quad (12.1)$$

where $d^2 \mathbf{r} \equiv \mathbf{n} d^2 r$ is the elementary area vector (normal to the surface), and $d\mathbf{r}$ is the elementary contour length vector (tangential to the contour line).

(ii) For an arbitrary volume V limited by closed surface S :

- *Divergence (or “Gauss”) theorem*, valid for any differentiable vector field $\mathbf{f}(\mathbf{r})$:

$$\int_V (\nabla \cdot \mathbf{f}) d^3 r = \oint_S \mathbf{f} \cdot d^2 \mathbf{r} \equiv \oint_S f_n d^2 r. \quad (12.2)$$

- *Green’s theorem*, valid for two differentiable scalar functions $f(\mathbf{r})$ and $g(\mathbf{r})$:

$$\int_V (f \nabla^2 g - g \nabla^2 f) d^3 r = \oint_S (f \nabla g - g \nabla f)_n d^2 r. \quad (12.3)$$

- An identity valid for any two scalar functions f and g , and a vector field \mathbf{j} with $\nabla \cdot \mathbf{j} = 0$ (all differentiable):

$$\int_V [f(\mathbf{j} \cdot \nabla g) + g(\mathbf{j} \cdot \nabla f)] d^3r = \oint_S fg j_n d^2r. \quad (12.3)$$

13. The Kronecker delta and Levi-Civita permutation symbols

- The *Kronecker delta symbol* (defined for integer indices):

$$\delta_{jj'} \equiv \begin{cases} 1, & \text{if } j' = j, \\ 0, & \text{otherwise.} \end{cases} \quad (13.1)$$

- The *Levi-Civita permutation symbol* for three integer indices (each taking one of the values 1, 2, or 3):

$$\varepsilon_{jj'j''} \equiv \begin{cases} +1, & \text{if the indices follow in any "correct" ("even") order : } 1 \rightarrow 2 \rightarrow 3 \rightarrow 1 \rightarrow 2 \dots, \\ -1, & \text{if the indices follow in any "incorrect" ("odd") order : } 1 \rightarrow 3 \rightarrow 2 \rightarrow 1 \rightarrow 3 \dots, \\ 0, & \text{if any two indices coincide.} \end{cases} \quad (13.2)$$

- Relation between the products of the Levi-Civita and Kronecker symbols:

$$\varepsilon_{jj'j''} \varepsilon_{kk'k''} = \sum_{l,l',l''=1}^3 \begin{vmatrix} \delta_{jl} & \delta_{jl'} & \delta_{jl''} \\ \delta_{j'l} & \delta_{j'l'} & \delta_{j'l''} \\ \delta_{j''l} & \delta_{j''l'} & \delta_{j''l''} \end{vmatrix}; \quad (13.3a)$$

the summation of three such relations written for three different values of $j = k$, yields the so-called *contracted epsilon identity*:

$$\sum_{j=1}^3 \varepsilon_{jj'j''} \varepsilon_{jk'k''} = \delta_{jk} \delta_{j''k''} - \delta_{jk''} \delta_{j''k}. \quad (13.3b)$$

14. Dirac's delta function, sign function, and theta function

- Definition of 1D *delta function* (for real $a < b$):

$$\int_a^b f(\xi) \delta(\xi) d\xi = \begin{cases} f(0), & \text{if } a < 0 < b, \\ 0, & \text{otherwise,} \end{cases} \quad (14.1)$$

where $f(\xi)$ is any function continuous near $\xi = 0$. In particular (if $f(\xi) = 1$ near $\xi = 0$), the definition yields

$$\int_a^b \delta(\xi) d\xi = \begin{cases} 1, & \text{if } a < 0 < b, \\ 0, & \text{otherwise.} \end{cases} \quad (14.2)$$

- Relation to the *theta function* $\theta(\xi)$ and the *sign function* $\text{sgn}(\xi)$

$$\delta(\xi) = \frac{d}{d\xi} \theta(\xi) = \frac{1}{2} \frac{d}{d\xi} \text{sgn}(\xi), \quad (14.3a)$$

where

$$\theta(\xi) \equiv \frac{\operatorname{sgn}(\xi) + 1}{2} = \begin{cases} 0, & \text{if } \xi < 0, \\ 1, & \text{if } \xi > 1, \end{cases} \quad \operatorname{sgn}(\xi) \equiv \frac{\xi}{|\xi|} = \begin{cases} -1, & \text{if } \xi < 0, \\ +1, & \text{if } \xi > 1. \end{cases} \quad (14.3b)$$

– An important integral:¹⁴

$$\int_{-\infty}^{+\infty} e^{is\xi} ds = 2\pi\delta(\xi). \quad (14.4)$$

– 3D generalization: the delta function $\delta(\mathbf{r})$ of the radius-vector is defined as

$$\int_V f(\mathbf{r})\delta(\mathbf{r})d^3r = \begin{cases} f(0), & \text{if } 0 \in V, \\ 0, & \text{otherwise;} \end{cases} \quad (14.5)$$

it may be represented as a product of 1D delta functions of Cartesian coordinates:

$$\delta(\mathbf{r}) = \delta(r_1)\delta(r_2)\delta(r_3). \quad (14.6)$$

(The 2D generalization is similar.)

15. The Cauchy theorem and integral

Let a complex function $f(z)$ be analytic within a part of the complex plane z , which is limited by a closed contour C and includes point z' . Then

$$\oint_C f(z)dz = 0, \quad (15.1)$$

$$\oint_C f(z) \frac{dz}{z - z'} = 2\pi i f(z'). \quad (15.2)$$

The first of these relations is usually called the *Cauchy integral theorem* (or the “Cauchy-Goursat theorem”), and the second one, the *Cauchy integral* (or the “Cauchy integral formula”).

16. References

(i) Properties of some *special functions* are briefly discussed at the relevant points of the lecture notes (in alphabetical order):

- *Airy functions*: QM Sec. 2.4;
- *Bessel functions*: EM Sec. 2.7;
- *Fresnel integrals*: EM Sec. 8.6;
- *Hermite polynomials*: QM Sec. 2.9;

¹⁴ The coefficient in this relation may be readily recalled by considering its left-hand side as the Fourier-integral representation of the function $f(s) \equiv 1$, and applying Eq. (14.1) to the reciprocal Fourier transform:

$$f(s) \equiv 1 = \frac{1}{2\pi} \int_{-\infty}^{+\infty} e^{-is\xi} [2\pi\delta(\xi)] d\xi.$$

- *Laguerre polynomials* (both *simple* and *associated*): QM Sec. 3.7;
- *Legendre polynomials, associated Legendre functions*: EM Sec. 2.8 and QM Sec. 3.6;
- *Spherical harmonics*: QM Sec. 3.6;
- *Spherical Bessel functions*: QM Secs. 3.6 and 3.8.

(ii) For *more formulas*, and their discussions, I can recommend the following handbooks (in alphabetical order):¹⁵

- M. Abramowitz and I. Stegun (eds.), *Handbook of Mathematical Formulas*, Dover, 1965 (and numerous later printings);¹⁶
- I. Gradshteyn and I. Ryzhik, *Tables of Integrals, Series, and Products*, 5th ed., Acad. Press, 1980;
- G. Korn and T. Korn, *Mathematical Handbook for Scientists and Engineers*, 2nd ed., Dover, 2000;
- A. Prudnikov *et al.*, *Integrals and Series*, vols. 1 and 2, CRC Press, 1986.

The popular textbook,

- G. Arfken *et al.*, *Mathematical Methods for Physicists*, 7th ed., Acad. Press, 2012,
- may be also used as a formula manual.

Many formulas are also available from the symbolic calculation parts of commercially available software packages listed in Sec. (iv) below.

(iii) Probably the most popular collection of *numerical calculation codes* are the twin manuals

- W. Press *et al.*, *Numerical Recipes in Fortran 77*, 2nd ed., Cambridge U. Press, 1992;
- W. Press *et al.*, *Numerical Recipes [in C++ – KKL]*, 3rd ed., Cambridge U. Press, 2007.

These lecture notes include very brief introductions into numerical methods of differential equation solution:

- ordinary differential equations: CM Sec. 5.7, and
- partial differential equations: CM Sec. 8.5 and EM Sec. 2.11,

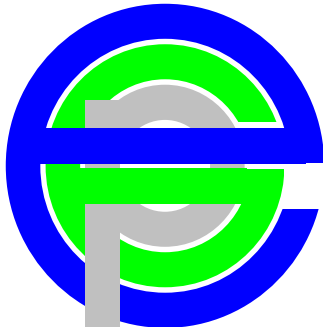
which include references to the literature for further reading.

(iv) The most popular *software packages* for numerical and symbolic calculations, all with plotting capabilities (in alphabetical order):

- *Maple* (<http://www.maplesoft.com/>);
- *MathCAD* (<http://www.ptc.com/products/mathcad/>);
- *Mathematica* (<http://www.wolfram.com/products/mathematica/index.html>);
- *MATLAB* (<http://www.mathworks.com/products/matlab/>).

¹⁵ On a personal note, perhaps 90% of all formula needs throughout my research career were satisfied by a tiny, wonderfully compiled old book: H. Dwight, *Tables of Integrals and Other Mathematical Data*, 4th ed., Macmillan, 1961, whose used copies, rather amazingly, are still available on the Web.

¹⁶ An updated version of this collection is now available online at <http://dlmf.nist.gov/>.



Konstantin K. Likharev
Essential Graduate Physics
Lecture Notes and Problems

Open online access at
<http://commons.library.stonybrook.edu/egp/>
and
<https://sites.google.com/site/likharevegp/>

Appendix CA

Selected Physical Constants

according to the 2018 International CODATA recommendation.¹

Last corrections: 2021/08/20

Symbol	Constant	SI value and unit	Gaussian value and unit	Relative r.m.s. uncertainty
c	speed of light in vacuum	$2.997\ 924\ 58 \times 10^8$ m/s	$2.997\ 924\ 58 \times 10^{10}$ cm/s	0 (defined value)
N_A	Avogadro constant	$6.022\ 140\ 76 \times 10^{23}$ 1/mol	$6.022\ 140\ 76 \times 10^{23}$ 1/mol	0 (defined value)
$2\pi\hbar$	Planck constant	$6.626\ 070\ 15 \times 10^{-34}$ J/Hz	$6.626\ 070\ 15 \times 10^{-27}$ erg/Hz	0 (defined value)
k_B	Boltzmann constant	$1.380\ 649\ 000 \times 10^{-23}$ J/K	$1.380\ 649\ 000 \times 10^{-16}$ erg/K	0 (defined value)
e	elementary electric charge	$1.602\ 176\ 634 \times 10^{-19}$ C	$4.803\ 204\ 713 \times 10^{-10}$ statcoulomb	0 (defined value)
ϵ_0	electric constant	$8.854\ 187\ 8128 \times 10^{-12}$ F/m	—	$\sim 1.5 \times 10^{-10}$
μ_0	magnetic constant	$1.256\ 637\ 062\ 12 \times 10^{-6}$ N/A ²	—	$\sim 1.5 \times 10^{-10}$
m_e	electron's rest mass	$0.910\ 938\ 370 \times 10^{-30}$ kg	$0.910\ 938\ 370 \times 10^{-27}$ g	$\sim 3 \times 10^{-10}$
m_p	proton's rest mass	$1.672\ 621\ 923 \times 10^{-27}$ kg	$1.672\ 621\ 923 \times 10^{-24}$ g	$\sim 3 \times 10^{-10}$
G	gravitation constant	$6.674\ 30 \times 10^{-11}$ m ³ /kg·s ²	$6.674\ 30 \times 10^{-8}$ cm ³ /g·s ²	$\sim 2 \times 10^{-5}$

¹ See, e.g., <http://physics.nist.gov/cuu/Constants/index.html>. CODATA is an interdisciplinary Committee on Data for Science and Technology of the International Council of Science (ISCU). Its recommendations, renewed every four years, are widely accepted by the scientific community.

Comments:

1. The fixed value of c transfers the legal definition of the second (as “the duration of 9,192,631,770 periods of the radiation corresponding to the transition between the two hyperfine levels of the ground state of the cesium-133 atom”) to that of the meter. These values are back-compatible with the legacy definitions of the meter (initially, as the 1/40,000,000th part of the Earth meridian length) and the second (for a long time, as the 1/(24×60×60) = 1/86,400th part of the Earth rotation period), within the experimental errors of those measures.

2. The exact value of the Avogadro number, prescribed by the last CODATA adjustment of fundamental constants in 2018, fixes 1 kg in the atomic units of mass (u), defined as 1/12 of the ¹²C atom’s mass, excluding the legacy etalons of the kilogram from the primary metrology – even though their masses are compatible with the new definition within the experimental accuracy.

3. The exact value of \hbar , also prescribed by CODATA in 2018, together with the fixed value of the second, enables the fundamental definition of energy units (in the SI system, the Joule) in terms of time/frequency.

4. The only role of the Boltzmann constant k_B is to express the kelvin (K) in energy units. If temperature is used in these units (as is done, for example, in the SM part of this series), this constant is unnecessary.

5. ϵ_0 and μ_0 are also not really the fundamental constants; their role is just to fix electric and magnetic units in the SI system. Their product is exactly fixed as $\epsilon_0\mu_0 \equiv 1/c^2$, and μ_0 virtually coincides with the legacy value $4\pi \times 10^{-7}$. (Before the 2018 adjustment, that value was considered exact, but the exact fixation of e in the new system of constants gives it an experimental uncertainty, if only a very small one – see the table above.)

6. The dimensionless *fine structure* (“Sommerfeld’s”) *constant* α is numerically the same in any system of units:

$$\alpha \equiv \left\{ \begin{array}{ll} e^2 / 4\pi\epsilon_0\hbar c & \text{in SI units} \\ e^2 / \hbar c & \text{in Gaussian units} \end{array} \right\} \approx 7.297\,352\,563 \times 10^{-3} \approx \frac{1}{137}.$$

The relative uncertainty of the first value is smaller than 10^{-10} .² The accuracy of the second, mnemonic value is better than 0.03%.

7. The listed proton’s rest mass m_p is close to 1.007 u, while the neutron’s rest mass is close to 1.009 u; their differences from 1 u reflect mostly the binding energy of these baryons in the ¹²C nucleus.

8. Note the relatively poor accuracy with which we know the Newtonian constant of gravitation – due to the extreme weakness of gravity on human scales of mass and distance.

² L. Morel *et al.*, *Nature* **588**, 61 (2020).



Konstantin K. Likharev
Essential Graduate Physics
Lecture Notes and Problems

Open online access at
<https://sites.google.com/site/likharevegp/>
and
<http://commons.library.stonybrook.edu/egp/>

References

(a partial list of textbooks and monographs used at work on the series¹)

CM

- A. L. Fetter and J. D. Walecka, *Theoretical Mechanics of Particles and Continua*, Dover, 2003.
H. Goldstein, C. Poole, and J. Safko, 3rd ed., *Classical Mechanics*, Addison Wesley, 2002.
R. A. Granger, *Fluid Mechanics*, Dover, 1995.
J. V. José and E. J. Saletan, *Classical Dynamics*, Cambridge U. Press, 1998.
L. D. Landau and E. Lifshitz, *Fluid Mechanics*, 2nd ed., Butterworth-Heinemann, 1987.
L. D. Landau and E. Lifshitz, *Mechanics*, 3rd ed., Butterworth-Heinemann, 1976.
L. D. Landau and E. Lifshitz, *Theory of Elasticity*, Butterworth-Heinemann, 1986.
H. G. Schuster, *Deterministic Chaos*, 3rd ed., VCH 1995.
A. Sommerfeld, *Mechanics*, Academic Press, 1964.
A. Sommerfeld, *Mechanics of Deformable Bodies*, Academic Press, 1964.

EM

- V. V. Batygin and I. N. Toptygin, *Problems in Electrodynamics*, 2nd ed., Academic Press, 1978.
D. J. Griffiths, *Introduction to Electrodynamics*, 3rd ed. Prentice-Hall, 2007.
J. D. Jackson, *Classical Electrodynamics*, 3rd ed., Wiley, 1999.
L. D. Landau and E. Lifshitz, *Electrodynamics of Continuous Media*, 2nd ed., Reed, 1984.
L. D. Landau and E. Lifshitz, *The Classical Theory of Fields*, 4th ed., Pergamon, 1975.
W. K. H. Panofsky and M. Phillips, *Classical Electricity and Magnetism*, 2nd ed., Dover, 1990.
J. A. Stratton, *Electromagnetic Theory*, Adams Press, 2007.
I. E. Tamm, *Fundamentals of the Theory of Electricity*, Mir, 1979.
A. Zangwill, *Modern Electrodynamics*, Cambridge U. Press, 2013.

QM

- E. S. Abers, *Quantum Mechanics*, Pearson, 2004.
G. Auletta, M. Fortunato, and G. Parisi, *Quantum Mechanics*, Cambridge U. Press, 2009.
L. E. Ballentine, *Quantum Mechanics: A Modern Development*, 2nd ed., World Scientific, 2014.

¹ This list does not include the numerous sources (mostly recent original publications) cited in the lecture notes and problem solutions, the open-access materials mentioned in the Preface, and the mathematics textbooks and handbooks listed in MA Sec. 16.

- A. Z. Capri, *Nonrelativistic Quantum Mechanics*, 3rd ed., World Scientific, 2002.
- C. Cohen-Tannoudji, B. Diu, and F. Laloë, *Quantum Mechanics*, in 2 vols., Wiley-VCH, 2005.
- F. Constantinescu, E. Magyari, and J. A. Spiers, *Problems in Quantum Mechanics*, Elsevier, 1971.
- V. Galitski *et al.*, *Exploring Quantum Mechanics*, Oxford U. Press, 2013.
- K. Gottfried and T.-M. Yan, *Quantum Mechanics: Fundamentals*, 2nd ed., Springer, 2004.
- D. Griffith, *Quantum Mechanics*, 2nd ed., Pearson Prentice Hall, 2005.
- L. D. Landau and E. M. Lifshitz, *Quantum Mechanics (Nonrelativistic Theory)*, 3rd ed., Pergamon, 1977.
- A. Messiah, *Quantum Mechanics*, Dover, 1999.
- E. Merzbacher, *Quantum Mechanics*, 3rd ed., Wiley, 1998.
- D. A. B. Miller, *Quantum Mechanics for Scientists and Engineers*, Cambridge U. Press, 2008.
- J. J. Sakurai, *Modern Quantum Mechanics*, Revised ed., Addison-Wesley, 1994.
- L. I. Schiff, *Quantum Mechanics*, 3rd ed., McGraw-Hill, 1968.
- R. Shankar, *Principles of Quantum Mechanics*, 2nd ed., Springer, 1980.
- F. Schwabl, *Quantum Mechanics*, 3rd ed., Springer, 2002.

SM

- R. P. Feynman, *Statistical Mechanics*, 2nd ed., Westview, 1998.
- K. Huang, *Statistical Mechanics*, 2nd ed., Wiley, 1987.
- R. Kubo, *Statistical Mechanics*, Elsevier, 1965.
- L. D. Landau and E. M. Lifshitz, *Statistical Physics, Part 1*, 3rd ed., Pergamon, 1980.
- E. M. Lifshitz and L. Pitaevskii, *Physical Kinetics*, Pergamon, 1981.
- R. K. Pathria and P. D. Beale, *Statistical Mechanics*, 3rd ed., Elsevier, 2011.
- J. R. Pierce, *An Introduction to Information Theory*, 2nd ed., Dover, 1980.
- M. Plishke and B. Bergersen, *Equilibrium Statistical Physics*, 3rd ed., World Scientific, 2006.
- F. Schwabl, *Statistical Mechanics*, Springer, 2000.
- J. M. Yeomans, *Statistical Mechanics of Phase Transitions*, Oxford U. Press, 1992.

Multidisciplinary and Specialty

- N. W. Ashcroft and N. D. Mermin, *Solid State Physics*, W. B. Saunders, 1976.
- K. Blum, *Density Matrix and Applications*, Plenum, 1981.
- H.-P. Breuer and E. Petruccione, *The Theory of Open Quantum Systems*, Oxford U. Press, 2002.
- S. B. Cahn and B. E. Nadgorny, *A Guide to Physics Problems*, Part 1, Plenum, 1994.
- S. B. Cahn, G. D. Mahan, and B. E. Nadgorny, *A Guide to Physics Problems*, Part 2, Plenum, 1997.
- J. A. Cronin, D. F. Greenberg, and V. L. Telegdi, *Graduate Problems in Physics*, U. Chicago, 1967.
- J. R. Hook and H. E. Hall, *Solid State Physics*, 2nd ed., Wiley, 1991.
- G. Joos, *Theoretical Physics*, Dover, 1986.
- A. S. Kompaneyets, *Theoretical Physics*, 2nd ed., Dover, 2012.
- M. Lax, *Fluctuations and Coherent Phenomena*, Gordon and Breach, 1968.
- N. N. Lebedev *et al.*, *Problems in Mathematical Physics*, Prentice-Hall, 1965
- E. M. Lifshitz and L. P. Pitaevskii, *Statistical Physics, Part 2*, Pergamon, 1980.
- N. Newbury *et al.*, *Princeton Problems in Physics*, Princeton U., 1991.
- L. Pauling, *General Chemistry*, 3rd ed., Dover, 1988.
- M. Tinkham, *Introduction to Superconductivity*, 2nd ed., McGraw-Hill, 1996.
- J. D. Walecka, *Introduction to Modern Physics*, World Scientific, 2008.
- J. M. Ziman, *Principles of the Theory of Solids*, 2nd ed., Cambridge U. Press, 1979.